

Echocardiography

Petros Nihoyannopoulos
Joseph Kisslo
Editors

Second Edition

Echocardiography

Petros Nihoyannopoulos · Joseph Kisslo
Editors

Echocardiography

Second Edition

 Springer

Editors

Petros Nihoyannopoulos
Hammersmith Hospital
Imperial College London National Heart
& Lung Institute
London
UK

Joseph Kisslo
Duke Heart Center
Duke University Medical Center
Durham, NC
USA

ISBN 978-3-319-71615-2 ISBN 978-3-319-71617-6 (eBook)
<https://doi.org/10.1007/978-3-319-71617-6>

Library of Congress Control Number: 2018957115

© Springer International Publishing AG, part of Springer Nature 2018

This work is subject to copyright. All rights are reserved by the Publisher, whether the whole or part of the material is concerned, specifically the rights of translation, reprinting, reuse of illustrations, recitation, broadcasting, reproduction on microfilms or in any other physical way, and transmission or information storage and retrieval, electronic adaptation, computer software, or by similar or dissimilar methodology now known or hereafter developed.

The use of general descriptive names, registered names, trademarks, service marks, etc. in this publication does not imply, even in the absence of a specific statement, that such names are exempt from the relevant protective laws and regulations and therefore free for general use.

The publisher, the authors, and the editors are safe to assume that the advice and information in this book are believed to be true and accurate at the date of publication. Neither the publisher nor the authors or the editors give a warranty, express or implied, with respect to the material contained herein or for any errors or omissions that may have been made. The publisher remains neutral with regard to jurisdictional claims in published maps and institutional affiliations.

This Springer imprint is published by the registered company Springer Nature Switzerland AG
The registered company address is: Gewerbestrasse 11, 6330 Cham, Switzerland

Preface

Echocardiography has expanded greatly over recent years to earn its place as a subspecialty in cardiology in its own right. From the original single M-mode modality of 50 years ago, it has evolved into a complex “multimodality” method for evaluating and quantifying cardiovascular lesions. In addition, the entire spectrum of hemodynamic assessment of the heart can now be performed noninvasively using echocardiography alone. Transesophageal echocardiography has added to the clarity of imaging and proved to be extremely helpful in valve surgery. Lately, three-dimensional echocardiography has added a new dimension and helped the understanding of cardiac anatomy and pathology in real time. Finally, deformation imaging and assessment of myocardial perfusion complete the global assessment of the heart by echocardiography by looking at the various contraction and perfusion patterns in patients with coronary artery disease at rest and during stress.

Echocardiography highlights the clinical utility of these evolving modalities that are now crucial to the renaissance of echocardiography. This book provides a thorough clinical review of the most revealing and adaptable echocardiographic methods of imaging a patient. The editors and their world-class group of contributors have created an essential reference for all who use echocardiography in their practice.

London, UK
Durham, NC, USA

Petros Nihoyannopoulos
Joseph Kisslo

Contents

Part I Basic Methods

1 Physical Principles of Ultrasound	3
Graham J. Leech [†] , Marti L. McCulloch, and David Adams	
2 Conducting a Cardiac Ultrasound Examination	33
Jayne Cleve and Marti L. McCulloch	
3 Machine Controls and Optimizing the Images	43
Marti L. McCulloch and Jayne Cleve	
4 Cardiac Anatomy by Three-Dimensional Echocardiography . .	59
Francesco F. Faletra, Romina Murzilli, Laura Anna Leo, and Siew Yen Ho	
5 Principles of Flow Assessment	95
Ahmed A. Alsaileek, Fatima Samad, and A. Jamil Tajik	
6 Principles of Measuring Chamber Size, Volume and Hemodynamic Assessment of the Heart	111
Carolyn M. Larsen, Carrie L. Vanden Bussche, and Sunil Mankad	
7 Myocardial Deformation Imaging	129
Alaa Mabrouk Salem Omar and Partho P. Sengupta	
8 Transesophageal Echocardiography: Principles and Application	159
Partho P. Sengupta and Bijoy K. Khandheria	

Part II Valvular Heart Disease

9 Aortic Pathology	177
Richard A. E. Wheeler	
10 Mitral Valve Disease	199
Joseph Kisslo, J. Daniel Rivera, David Adams, Burkhard G. Mackenson, Alicia Armour, Ashlee Davis, Joshua Lander, and Donald D. Glower	

11	Tricuspid and Pulmonary Valve Disease	297
	Anne Bernard and Patrizio Lancellotti	
12	The Role of Stress in Valvular Heart Disease	313
	Luc A. Pierard	
13	Replacement Heart Valves	325
	John Chambers	
14	Infective Endocarditis	345
	Trine K. Lauridsen, Joseph Kisslo, and Anna Lisa Crowley	

Part III Assessing the Right Ventricle

15	Assessing the Right Ventricle	373
	Vasileios Kamperidis, Petros Nihoyannopoulos, Jeroen J. Bax, and Victoria Delgado	
16	Pulmonary Hypertension	397
	Julia Grapsa	
17	Pulmonary Embolism	413
	David Dawson and Petros Nihoyannopoulos	

Part IV Pericardial Disease

18	Pericardial Effusion, Tamponade, and Constrictive Pericarditis	429
	Terrence D. Welch and Jae K. Oh	

Part V Ischemic Disease

19	Coronary Artery Disease: Assessing Regional Wall Motion	451
	Paramjit Jeetley, Rajdeep S. Khattar, and Roxy Senior	
20	Echocardiography for Assessing Acute Myocardial Infarction and Complications	467
	Otto Kamp	
21	Stress Echocardiography	491
	Thomas H. Marwick	
22	Assessing Myocardial Viability: Principles and the Role of Echocardiography	521
	Agnès Pasquet, Bernhard Gerber, and Jean-Louis J. Vanoverschelde	
23	Contrast Echocardiography	541
	Mehdi Eskandari and Mark J. Monaghan	

Part VI Cardiomyopathy and Heart Failure

- 24 The Cardiomyopathies** 577
Petros Nihoyannopoulos and Perry Elliott
- 25 Echocardiography in Heart Failure** 619
Manish Bansal, Partho P. Sengupta, and Bijoy K. Khandheria
- 26 Echocardiography in Cardiac Resynchronization Therapy** ... 643
Ulas Höke, Jeroen J. Bax, Nina Ajmone Marsan,
and Victoria Delgado
- 27 Assessing Atrial Function** 661
Melissa Leung, Jeroen J. Bax, Nina Ajmone Marsan,
and Victoria Delgado

Part VII Masses, Emboli and Trauma

- 28 Cardiac Masses** 685
Joseph Kisslo and Piers Barker
- 29 Aortic Disorders** 719
Ayan R. Patel, Anthony Caffarelli, and Natesa G. Pandian
- 30 Source of Embolus** 739
Wissam Alajaji, Hussain Isma'eel, Patrick J. Nash,
Ronan J. Curtin, and Allan L. Klein

Part VIII Congenital Heart Disease

- 31 Congenital Heart Disease: Simple Lesions** 767
Maria Boutsikou, George Giannakoulas,
Michael A. Gatzoulis, and Wei Li
- 32 Assessing the Patient with Congenital Heart Disease** 791
John M. Simpson and Karolina Hall
- 33 Assessing the Adult with Congenital Heart Disease** 817
Maria Boutsikou, Michael A. Gatzoulis, and Wei Li

Part IX Strain

- 34 Strain Basics and Global Longitudinal Strain** 845
Joseph Kisslo, Daniel Forsha, Minna Moreira Dias Romano,
Fawaz Abdulaziz M. Alenezi, Kasper Emerek, Zainab Samad,
and Niels Risum
- 35 Regional Strain: The Physiology of Dyssynchrony** 867
Niels Risum, Daniel Forsha, Kasper Emerek, Peter Søgaaard,
and Joseph Kisslo

- 36 Strain in Complex Congenital Heart Disease in Infants and Children** 889
Daniel Forsha, Joseph Kisslo, Niels Risum, and Piers Barker

Part X Special Applications

- 37 The Athlete's Heart** 899
Andrew D'Silva and Sanjay Sharma
- 38 Cardio-Oncology** 921
Juan Carlos Plana
- 39 Pocket-Size Hand-Held Echocardiography** 937
Vasileios F. Panoulas and Petros Nihoyannopoulos

Part XI Interventional Echocardiography

- 40 Intraoperative Echocardiography** 947
William J. Stewart and Robert M. Savage
- 41 Role of Echocardiography in Transcatheter Aortic Valve Implantation** 961
Rafal Dworakowski, Mehdi Eskandari, and Mark J. Monaghan
- 42 Echocardiography in Mitral Valve Repair** 987
Michael Bellamy and Christopher Baker
- 43 Echocardiography in Device Closure and Paravalvular Leaks** 1015
Rosita Zakeri and Nilesh Sutaria
- 44 Echocardiography in Electrophysiology** 1031
Francesco F. Faletra, Giovanni Pedrazzini, Laura Anna Leo, Romina Murzilli, Elena Pasotti, Tiziano Moccetti, and Siew Yen Ho

- Index** 1043

Contributors

David Adams, ACS, RCS, RDCS, FASE Cardiac Diagnostic Unity, Duke University Health Center, Durham, NC, USA

Wissam Alajaji, MD Department of Cardiovascular Medicine, Akron City Hospital-Summa Health System, Akron, OH, USA

Fawaz Abdulaziz M. Alenezi, MD Duke University Medical Center, Durham, NC, USA

Ahmed A. Alsaileek, MD King Saud bin Abdulaziz University for Health Sciences, Riyadh, Saudi Arabia

Adult Cardiology/Cardiac Imaging, King Abdulaziz Cardiac Center, National Guard Health Affairs, Riyadh, Saudi Arabia

Alicia Armour, RDCS Cardiac Diagnostic Unity, Duke University Health Center, Durham, NC, USA

Christopher Baker, PhD FRCP Department of Cardiology, Imperial Healthcare NHS Trust, Hammersmith Hospital, London, UK

Manish Bansal, MD, FACC, FASE Medanta – The Medicity, Gurgaon, Haryana, India

Piers Barker, MD Department of Pediatrics, Division of Pediatric Cardiology, Duke University Medical Center, Durham, NC, USA

Jeroen J. Bax, MD, PhD Department of Cardiology, Leiden University Medical Center, Leiden, The Netherlands

Michael Bellamy, MD FRCP Imperial Healthcare NHS Trust, Hammersmith Hospital, London, UK

Anne Bernard, MD University François Rabelais of Tours, Cardiology Department, Tours, France

University of Liège Hospital, GIGA Cardiovascular Sciences, Department of Cardiology, Heart Valve Clinic, Liège, Belgium

Karolina Hall, BSc (Hons) Evelina London Children's Hospital, London, UK

Maria Boutsikou, MD, PhD Adult Congenital Heart Disease, The Royal Brompton Hospital, Adult Congenital Heart Centre and Centre for Pulmonary Hypertension, London, UK

Anthony Caffarelli, MD Hoag Hospital, Newport Beach, CA, USA

Jayne Cleve, BS, RDCS Cardiac Diagnostic Unit, Duke University Hospital, Raleigh, NC, USA

John Chambers, MD Cardiothoracic Department, St Thomas' Hospital, London, UK

Anna Lisa Crowley, MD Division of Cardiology, Duke University Medical Center, Durham, NC, USA

Ronan J. Curtin, MD Department of Cardiovascular Medicine, Cleveland Clinic Foundation, Cleveland, OH, USA

J. Daniel Rivera, CVT Cardiac Diagnostic Unity, Duke University Health Center, Durham, NC, USA

Ashlee Davis, RDCS Cardiac Diagnostic Unity, Duke University Health Center, Durham, NC, USA

David Dawson, MD Department of Echocardiography, Imperial College Healthcare NHS Trust, Hammersmith Hospital, London, UK

Victoria Delgado, MD, PhD Department of Cardiology, Leiden University Medical Center, Leiden, The Netherlands

Andrew D'Silva, BSc (Hons), MRCP (UK) St George's University of London, St George's University Hospital NHS Foundation Trust, London, UK

Rafal Dworakowski, MD (Hons), PhD, FRCP Kings College Hospital, London, UK

Perry Elliott, MBBS, MD, FRCP, FESC, FACC University College London, London, UK

UCL Institute of Cardiovascular Science, London, UK

Barts Heart Centre, St. Bartholomew's Hospital, London, UK

Kasper Emerek, MD, PhD Candidate Department of Clinical Medicine, Aalborg University, Aalborg, Denmark

Mehdi Eskandari, MD, FRACP Department of Cardiology, King's College Hospital, London, UK

Francesco F. Faletra, MD Department of Cardiology, Fondazione Cardiocentro Ticino, Lugano, Switzerland

Daniel Forsha, MD Pediatric Cardiology, Children's Mercy Hospital, Kansas City, MO, USA

Michael A. Gatzoulis, MD, PhD, FACC, FESC Adult Congenital Heart Center and Center for Pulmonary Hypertension, Royal Brompton Hospital, National Heart and Lung Institute, Imperial College, London, UK

Bernhard Gerber, MD Pole of Cardiovascular Research (CARD), Institut de Recherche Expérimentale et Clinique, Division of Cardiology, Department of Cardiovascular Diseases, Cliniques Universitaires St. Luc Université Catholique, Brussels, Belgium

George Giannakoulas, MD, PhD Aristotle University of Thessaloniki, AHEPA Hospital, Cardiology Department, Thessaloniki, Greece

Donald D. Glower, MD Department of Surgery, Duke University Medical Center, Durham, NC, USA

Julia Grapsa, MD, PhD Imperial College of London, London, UK

Siew Yen Ho, MD Cardiac Morphology, Royal Brompton and Imperial College, London, UK

Ulas Höke, MD Department of Cardiology, Leiden University Medical Center, Leiden, The Netherlands

Hussain Isma'eel, MD Department of Cardiology, American University of Beirut, Beirut, Lebanon

Paramjit Jeetley, MB, ChB, MRCP Department of Cardiovascular Medicine, Northwick Park Hospital and Institute for Medical Research, Middlesex, UK

Otto Kamp, MD, PhD, FESC Department of Cardiology, VU University Medical Center, Amsterdam, The Netherlands

Vasileios Kamperidis, MD Department of Cardiology, Leiden University Medical Center, Leiden, The Netherlands

Department of Cardiology, AHEPA University Hospital, Thessaloniki, Greece

Bijoy K. Khandheria, MD, FACC University of Wisconsin School of Health, Milwaukee, WI, USA

Echocardiography, Aurora Health Care, Milwaukee, WI, USA

Global Health, Milwaukee, WI, USA

Rajdeep S. Khattar, DM FRCP FESC FACC Department of Cardiovascular Medicine, Northwick Park Hospital and Institute for Medical Research, Middlesex, UK

Joseph Kisslo, MD Division of Cardiology, Duke University Medical Center, Durham, NC, USA

Allan L. Klein, MD Department of Cardiovascular Medicine, Cleveland Clinic Foundation, Cleveland, OH, USA

Patrizio Lancellotti, MD University of Liège Hospital, GIGA Cardiovascular Sciences, Department of Cardiology, Heart Valve Clinic, Liège, Belgium

Joshua Lander, RCS Cardiac Diagnostic Unity, Duke University Health Center, Durham, NC, USA

Carolyn M. Larsen, MD Department of Cardiovascular Medicine, Mayo Clinic Arizona, Scottsdale, AZ, USA

Trine K. Lauridsen, MD, PhD Department of Cardiology, Copenhagen University Hospital Glostrup, Glostrup, Denmark

Graham J. Leech, MA Department of Cardiovascular Science, St. George's Hospital Medical School, London, UK

Laura Anna Leo, MD Department of Cardiology, Fondazione Cardiocentro Ticino, Lugano, Switzerland

Melissa Leung, MBBS, Biostat, PhD Department of Cardiology, Liverpool Hospital, University of New South Wales, Sydney, NSW, Australia

Wei Li, MD, PhD, FESC, FACC Adult Congenital Heart Disease Echocardiography, Adult Congenital Heart Centre and Centre for Pulmonary Hypertension, Royal Brompton Hospital and the National Heart and Lung Institute, London, UK

Burkhard G. Mackenson, MD Department of Anesthesia, University of Washington, Seattle, WA, USA

Sunil Mankad, MD Mayo Clinic, Rochester, MN, USA

Nina Ajmone Marsan, MD Department of Cardiology, Leiden University Medical Center, Leiden, The Netherlands

Thomas H. Marwick, MBBS, PhD, MPH Baker Heart and Diabetes Institute, Melbourne, VIC, Australia

Marti L. McCulloch, MBA, ACS, FASE CV Ultrasound, Siemens Healthcare, Siemens Medical Solutions USA, Inc., Malvern, PA, USA

Tiziano Moccetti, MD Department of Cardiology, Fondazione Cardiocentro Ticino, Lugano, Switzerland

Mark J. Monaghan, MSc, PhD Department of Cardiology, King's College Hospital, London, UK

Romina Murzilli, MD Division of Cardiology, Fondazione Cardiocentro Ticino, Lugano, Switzerland

Patrick J. Nash, MD Department of Cardiology, University Hospital Galway, Galway, Ireland

Petros Nihoyannopoulos, MD, FRCP, FESC, FACC, FAHA Imperial College London, NHLI, Hammersmith Hospital, London, UK

Jae K. Oh, MD Division of Cardiovascular Diseases, Mayo Clinic, Rochester, MN, USA

Alaa Mabrouk Salem Omar, MD, PhD Icahn School of Medicine at Mount Sinai, Division of Cardiology, New York, NY, USA

BronxCare Hospital Center, Department of Internal Medicine, Bronx, NY, USA

Natesa G. Pandian, MD Heart Valve Center, Tufts Medical Center, CardioVascular Center, Boston, MA, USA

Tufts University School of Medicine, Boston, MA, USA

Vasileios F. Panoulas, MD, MRCP, PhD, FESC Department of Cardiology, Royal Brompton and Harefield NHS Foundation Trust, London, UK

Elena Pasotti, MD Department of Cardiology, Fondazione Cardiocentro Ticino, Lugano, Switzerland

Agnès Pasquet, MD Division of Cardiology, Cliniques Universitaires St Luc, Brussels, Belgium

Ayan R. Patel, MD Cardiovascular Imaging and Hemodynamic Laboratory, Tufts Medical Center, CardioVascular Center, Boston, MA, USA

Tufts University School of Medicine, Boston, MA, USA

Giovanni Pedrazzini, MD Division of Cardiology, Fondazione Cardiocentro Ticino, Lugano, Switzerland

Luc A. Pierard, MD Cardiology Services, Domaine Universitaire du Sart Tilman, Liege, Belgium

Juan Carlos Plana, MD, FASE, FACC Cardiovascular Service Line, Baylor St. Luke's Medical Center, Section of Cardiology, Baylor College of Medicine, Houston, TX, USA

Niels Risum, MD, PhD Division of Cardiology, Rigshospitalet, Copenhagen, Denmark

Minna Moreira Dias Romano, MD, PhD Cardiology Center, Medical School of Ribeirão Preto, University of São Paulo, São Paulo, Brazil

Fatima Samad, MD St. Luke's Medical Center, Aurora Cardiovascular Services, Milwaukee, WI, USA

Zainab Samad, MD Duke University Medical Center, Durham, NC, USA

Robert M. Savage, MD, FACC Cardiothoracic Anesthesia and CVICU, Heart and Vascular Institute, McLeod Regional Medical Center, Florence, SC, USA

Department of Cardiothoracic Anesthesia, Cleveland Clinic Foundation, Cleveland, OH, USA

Partho P. Sengupta, MD, MBBS, FACC Section of Cardiology, West Virginia University Health Sciences Center, Morgantown, WV, USA

Roxy Senior, MD, DM, FRCP, FESC, FACC Department of Cardiovascular Medicine, Northwick Park Hospital, Middlesex, UK

Sanjay Sharma, MSc (Hons), MD, FRCP Department of Cardiovascular and Cell Sciences, St. George's University of London, London, UK

John M. Simpson, MD Department of Congenital Heart Disease, Evelina London Children's Hospital, London, UK

Peter Søgaard, MD Department of Cardiology, Aalborg University, Aalborg, Denmark

William J. Stewart, MD, FACC, FASE Department of Cardiovascular Medicine, The Cleveland Clinic Foundation, Cleveland, OH, USA

Nilesh Sutaria, MD, FRCP Imperial College Healthcare NHS Trust, St Mary's Hospital, London, UK

A. Jamil Tajik, MD St Luke's Medical Center, Aurora Cardiovascular Services, Milwaukee, WI, USA

Carrie L. Vanden Bussche, RDCS, ACS, BS Department of Echocardiography, Mayo Clinic, Rochester, MN, USA

Jean-Louis J. Vanoverschelde, MD Pole of Cardiovascular Research (CARD), Institut de Recherche Expérimentale et Clinique, Division of Cardiology, Department of Cardiovascular Diseases, Cliniques Universitaires St. Luc Université Catholique, Brussels, Belgium

Terrence D. Welch, MD, FACC Section of Cardiology, Dartmouth-Hitchcock Medical Center, Geisel School of Medicine at Dartmouth, Hanover, NH, USA

Richard A. E. Wheeler, MBChB, FRCP Department of Cardiology, University Hospital of Wales, Cardiff, UK

Rosita Zakeri, MBChB, PhD Royal Brompton Hospital, London, UK

Part I

Basic Methods

Physical Principles of Ultrasound

1

Graham J. Leech[†], Marti L. McCulloch,
and David Adams

Introduction

Modern ultrasound systems are very sophisticated and provide the ability to display real-time moving images of the heart, together with quantitative data on blood flow and tissue motion. The output is displayed in real time, either as two-dimensional tomographic ('slice') images or, more recently, rendered 3-dimensional 'volume' images from which individual sectional planes can be extracted.

This chapter will review the fundamental principles of ultrasound imaging necessary for clinical applications. Many regard physics as a 'necessary evil', to be endured and then forgotten once they have moved on to the clinical applications. However, understanding the physics behind the echo and Doppler images is vital in optimizing the machine settings, understanding artifacts and reaching an accurate diagnostic conclusion. Conscious of these facts, the primary aim of this chapter will be in two areas:

- (a) Basic understanding of how images and flow velocity data are obtained;
- (b) How limitations of physics and current technology can result in image distortion and artifacts that not infrequently result in serious misdiagnoses.

Basic Concepts of Sound

Echocardiography utilizes high frequency sound (pressure) waves to produce images of the heart and to study blood flow within the cardiac chambers and blood vessels. It is closely analogous to radar and the reader familiar with the way in which information from radar or a marine depth-sounder is gathered and displayed will recognise many similarities in the two techniques. Because there are fundamental differences in the physical principles underlying imaging of the heart's structure and studying blood flow, these will be considered separately, whereas in practice images and blood flow data are usually displayed and recorded superimposed or concurrently.

Sound (pressure) waves are generated by a vibrating object, and transmitted through a solid, liquid or gaseous medium as pressure fluctuations—waves of alternating compression and rarefaction. The velocity at which a medium propagates waves is primarily determined by its density, being higher in a solid, whose molecules are close together, than in a liquid or a gas.

[†](Deceased)

G. J. Leech
Department of Cardiovascular Science, St. George's
Hospital Medical School, London, UK

M. L. McCulloch
CV Ultrasound, Siemens Healthcare, Siemens
Medical Solutions USA, Inc., Malvern, PA, USA

D. Adams (✉)
Duke University Medical Center, Durham, NC, USA
e-mail: david.adams@duke.edu

The normal sound range for humans are frequencies from about 30 Hz to 15,000 Hz. Dogs and other animals have a higher range thus most people cannot hear dog whistles. The term ultrasound is used for any frequencies above the normal range for humans.

Ultrasound (pressure) waves and light waves share many properties. When a beam of light passes from one medium to another, part of the energy is reflected and the path of the transmitted portion is deviated by refraction. In the same way, when ultrasound (pressure) waves encounter an interface between two different body tissues, blood and muscle for example, some of the incident energy is reflected.

Ultrasound (pressure) waves travel in air at approximately 300 m.s^{-1} and in soft body tissues the average value is about 1540 m.s^{-1} . There is a fundamental relationship between propagation velocity, the frequency (pitch) of the waves and their wavelength (the distance between two successive maxima or minima in the train of pressure cycles) noted in the following equation.

$$\text{Propagation Velocity} = \text{Frequency} \times \text{Wavelength}$$

In soft body tissues (1540 m.s^{-1}), at a frequency of 1000 Hz (Hertz, or cycles per second), the wavelength is 1.54 m. Common sense dictates that this is too great to image the heart, which is only about 15 cm across and which contains structures less than 1 mm thick. To achieve a wavelength of 1 mm, the frequency has to be 1,540,000 Hz, or 1.54 MHz, which is in the ultrasound range as opposed to the hearing range.

Ultrasound waves are usually generated and detected by ceramic crystals, which exhibit strong piezo-electric properties. Piezo-electric means that when an electric potential is applied to the ceramic crystal they mechanically change shape or deform. The term transducer is applied to the imaging ultrasound device because they convert electric energy into mechanical, and vice-versa. The material that has been used almost exclusively for imaging transducers is Lead Zirconate Titanate. This normally is in the form of a polycrystalline ceramic material and is 'polarised' by applying an electric field to align the electrical axes of the microscopic crystals. The alignment is, however, not perfect but a new process has been introduced recently, which allows production of large, single crystals, which

have a single polarisation axis, and this promises to improve transducer performance significantly. An echocardiographic transducer comprises one or more such crystals, mounted on an absorbent backing. When electric impulses are applied to the crystal, it vibrates at a frequency determined by its mechanical dimensions, in the same way that a bell vibrates when struck by a hammer. Transducers used for echocardiography typically generate frequencies in the range 1.5–7 MHz. The same crystal is used to detect returning echoes from ultrasonic waves it has generated.

Imaging Modalities

The Ultrasound Beam

Images of cardiac structures are formed by transmitting a stream of very brief 'pulses' of ultrasonic waves into the chest. Each pulse comprises only a few waves and lasts 1–2 microseconds (μs). One to two millionth of a second! As a pulse travels through the chest wall, the pericardium and the heart, it crosses a succession of interfaces between different types of tissue: blood, muscle, fat etc. At each interface, a proportion of the incident energy is reflected, the remainder being transmitted into deeper tissue layers. When two interfaces are widespread compared to the ultrasound wavelength, the reflections become specular or mirror-like with the angle of reflection equal to the angle of incidence. When the incident angle is 90° more energy will be reflected and return to the transducer as an echo.

A 90° incident angle is not typical in clinical practice and limits the quality of echo signals from many cardiac structures. Fortunately, the fact that body tissue interfaces are not totally smooth allows the return of some echoes even if the interface is not perpendicular to the ultrasound beam. The transmitted portion of the ultrasound pulse may then encounter additional interfaces and further echoes return to the transducer.

The time delay between transmission of an ultrasound pulse and arrival of an echo back at the transducer (round-trip-time) is calculated by:

$$\text{Time Delay} = 2 \times \text{Interface Distance} / \text{Propagation Velocity}$$

Accordingly, if the propagation velocity is known and the time delay can be measured, the distance of each echo-generating interface from the transducer can be determined. It is important to note that the machine actually measures *time delay* and derives the *distance* from an assumed value for the propagation velocity in soft tissues. If, however, the ultrasound passes through an object having different transmission characteristics from soft tissue, e.g. a silicone valve prosthesis, the time delay of returning echoes will change and the derived distance measurements will be false.

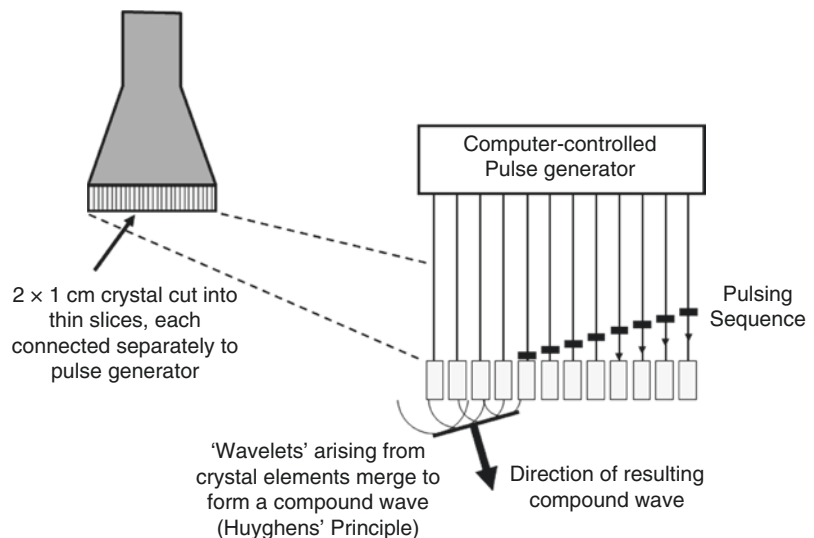
The total time for all echoes to return depends on the distance of the furthest structure of interest. This may be up to 24 cm, for which the round trip time in soft tissue is approximately 300 μs . Only then can a second ultrasound pulse be transmitted, but even so it is possible to send more than 3000 pulses each second. This stream of brief ultrasound pulses emanating from the transducer is referred to as an 'ultrasound beam.' The first echoes to return and strike the piezo-electric crystal arise from structures closest to the transducer, followed in succession by those from more distant interfaces. The electrical signals generated are amplified and processed to form a visual display illustrating the relative distances of the reflecting structures from the transducer, with the signal intensities providing some information about the nature of the interfaces.

The 2-D Sector Scan

In order to generate two-dimensional tomographic (slice) images of the heart, the ultrasound beam has to be scanned across a section of the heart. The limited access to the heart afforded by spaces between the ribs and lungs dictates that cardiac scanners are of the sector scan type. The transducer is manually positioned on the chest and held steady while the ultrasound beam sweeps rapidly back and forth across a sector of an arc to create a fan shaped sector scan, similar to a lighthouse beam that sweeps across the sea, illuminating objects in its path. In order to avoid blurring of the image by the heart's motion, at least 30 images per second are required. The maximum attainable image frame rate is primarily the result of a trade-off between the required image depth, which limits the number of pulses transmitted per second, and the sector angle and image line density, but other factors such as the display mode and imaging processing power of the machine are now involved. Image frame rate is shown on the display screen and may be as high as 150 s^{-1} or as low as 6 s^{-1} .

A single piezo-electric crystal can be sliced into as many as 256 very thin strips with each individually connected to the electric pulse generator, which activates them in a very rapid and very precisely controlled sequence, as shown in Fig. 1.1. The wavelets from each crystal element merge to form a compound ultrasound wave. By varying the electrical activation sequence, the

Fig. 1.1 How the ultrasound beam direction is controlled by pulsing the crystal elements in sequence



direction of the compound wave can be changed and a series of pulses generated to form a sector scan configuration. For a sector angle of 90° and working depth of 15 cm, each image comprises about 200 scan lines and takes about 40 ms.

Once a pulse is transmitted the echoes start to return immediately to strike the transducer and deform the crystal piezo-electric elements forming an ultrasound signal, which is first amplified then demodulated. The echo signals resulting from a single ultrasound pulse now comprise a sequence of electronic 'blips' representing the intensities of the echo reflections it generated (Fig. 1.2). To facilitate further processing the signals are digitized into a series of numbers, whose values represent the echo amplitudes at discrete intervals and allocated to a digital memory store.

The basic image data comprises a series of radial scan lines like spokes of a wheel which are relatively close together close to the transducer but tend to spread apart with increased depth (Fig. 1.3). The scan lines were evident in the

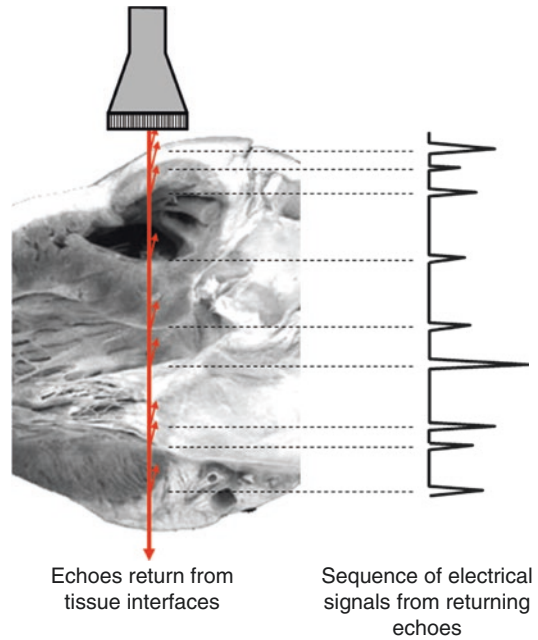


Fig. 1.2 Echoes returning from tissue interfaces are converted into electrical impulses

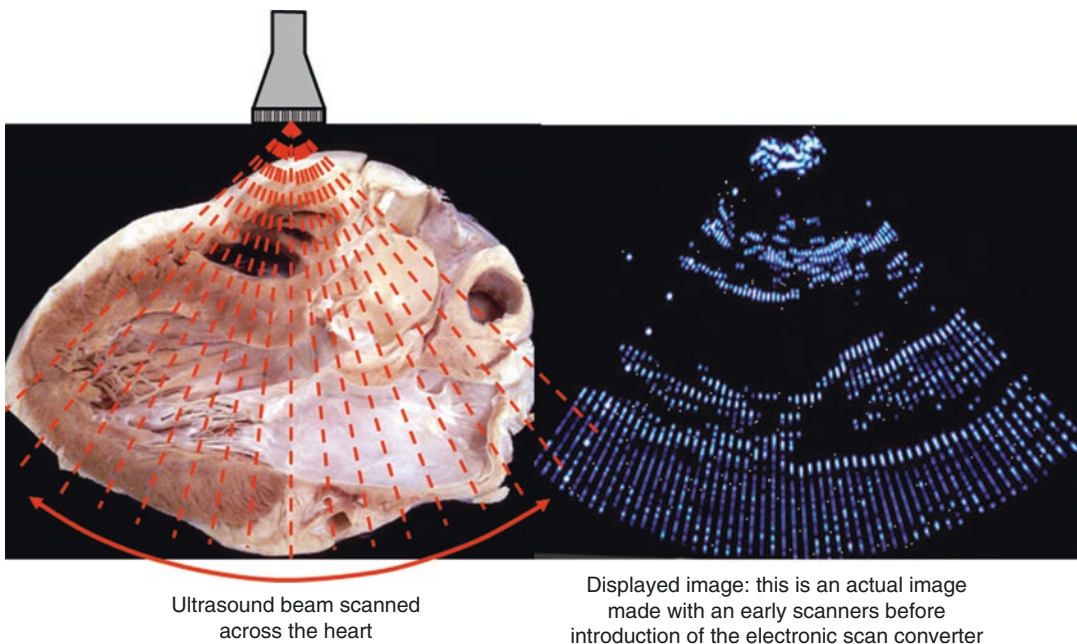


Fig. 1.3 The ultrasound beam is scanned rapidly to and fro across the heart and the echo signals are converted into an electronically generated image

early 2-D scanners of the 1970s (Fig. 1.4) but current machines use digital scan converters that assign image values to the ‘empty’ memory cells based on averages of surrounding cells. The averaging process employs proprietary algorithms specific for each vendor and accounts for some of the differences in image display. The scan lines form a sector scan image and is representative of a matrix of numbers that enable the power of digital computer processing to be harnessed to further process and form the visual ultrasound image displayed on the monitor screen.

M-Mode

M-mode (M is for motion) only interrogates structures along a single axis (think ‘ice-pick’ or ‘needle biopsy’ view) with tissue interfaces represented as dots on the display screen. In order to show motion patterns, a linear sweep is added resulting in a graphic display as shown in Fig. 1.5. M-mode can be more difficult to understand for the non-specialist but continues to have relevance due to its high temporal resolution (1000 lines.s⁻¹ compared to 25 for a 2-D image) which is superior for timing as well as the fact that several cardiac cycles can be displayed on a on a single image.

Critical Ultrasound Concepts: Attenuation, Reflection and Depth Compensation

Attenuation: The Decrease in Amplitude and Intensity as a Wave Travels Through a Medium

Ultrasound can travel great distances in water, but soft body tissues are ‘spongy’ and non-homogenous, resulting in attenuation of the ultrasound waves. The degree of attenuation depends greatly on the frequency. At 2.5 MHz, approximately half of the amplitude is lost for every 4 cm of path length, rising to half per 2 cm at 5 MHz and half in only 1 cm at 7.5 MHz. This is a cumulative effect so at 5 MHz the wave amplitude reaching a structure 16 cm distant is only $1/256$ ($\frac{1}{2} \times \frac{1}{2} \times \frac{1}{2} \times \frac{1}{2} \times \frac{1}{2} \times \frac{1}{2} \times \frac{1}{2} \times \frac{1}{2}$) of that transmitted.

Reflection: The Amount of Sound/Signal Returned from a Boundary/Medium (Echo Reflection)

The proportion reflected at a tissue interface depends mainly on the difference in density of the tissues. Where there is a large difference, such as an interface with air or bone, most of the incident energy is reflected, creating an intense echo but leaving little to penetrate further to

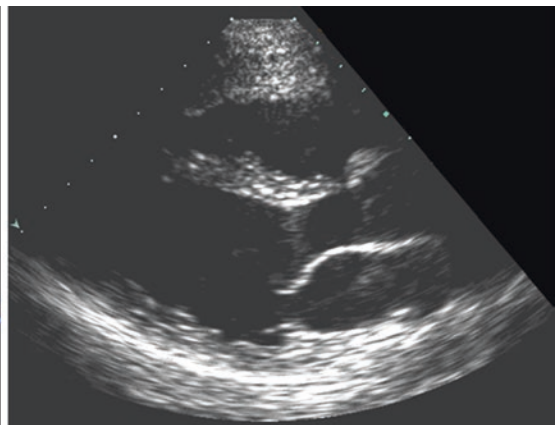
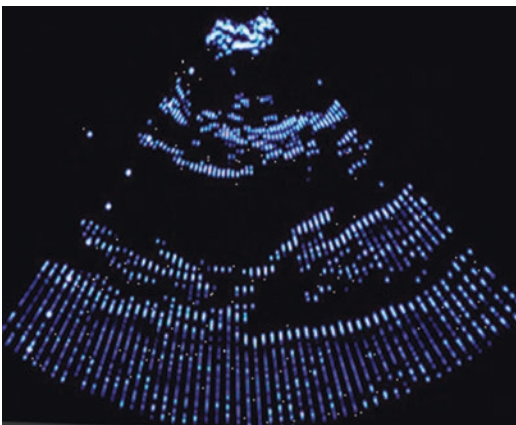


Fig. 1.4 (Left) Ultrasound image made in 1977 prior to introduction of scan converters and (Right) from a modern machine. The scan converter interpolates the spaces

between the actual scan lines and creates a more aesthetically pleasing image, but does not add new information

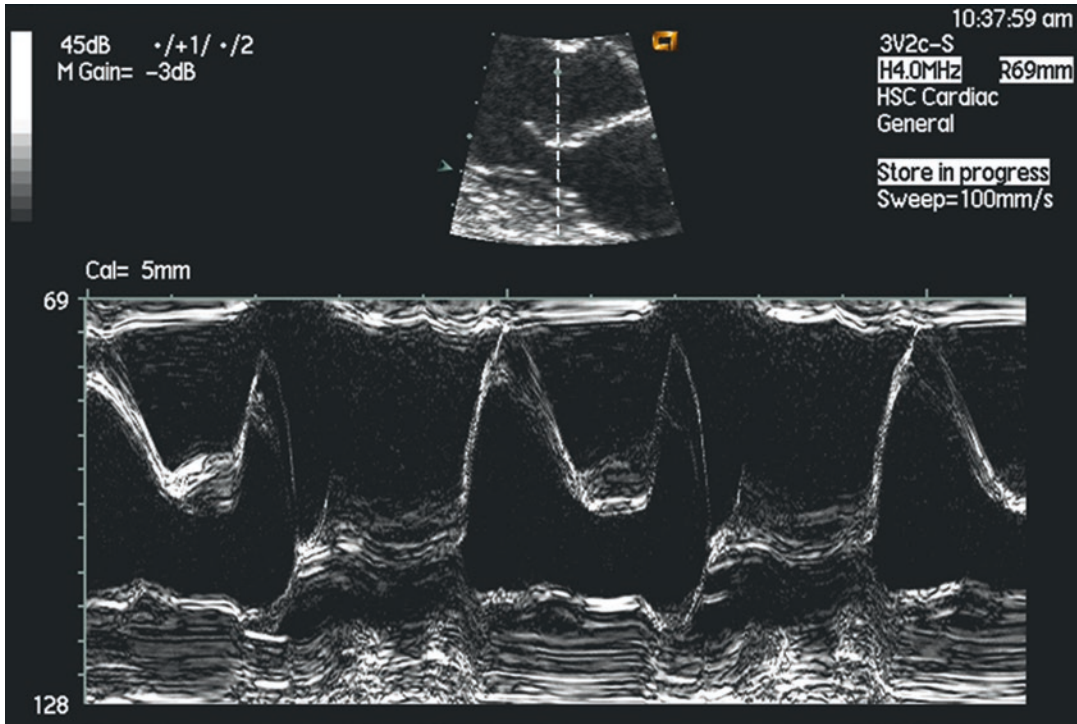


Fig. 1.5 “M-mode” display of the motion pattern of the mitral valve. The beam direction is indicated on the small image icon at the top of the display

deeper structures. It is for this reason that the operator has to manipulate the transducer to avoid ribs and lungs, and that a contact gel is used to eliminate any air between the transducer and the chest wall. In contrast, there is relatively little difference in the densities of blood, muscle and fat, so echoes from interfaces between them are very small—something like 0.1% of the incident amplitude. The echoes are then further attenuated as they return to the transducer, with the result that the amount reaching the transducer is very small indeed. In the case illustrated above, approximately $(1/256) \times (1/1000) \times (1/256)$ or just $1/65,000,000$ of the transmitted amplitude!

Time Gain Compensation (TGC or Depth Compensation): Adjusts or Equalizes the Amplitude of Received Signals to Account for Attenuation and Reflection

Not only is this a very small signal to detect, but the amplification level required would be vastly greater than that needed for the same interface at

a range of 4 cm, for which the returning signal would be approximately $(1/4) \times (1/1000) \times (1/4)$ or $1/16,000$. To overcome this problem, the machine incorporates Depth Compensation or Time-Gain Compensation (TGC). This automatically increases the amplification during the time echoes from a particular pulse return, so that the last to arrive are amplified much more than the first. Most of this compensation is built into the machine, but the user can fine-tune it by means of a bank of slider controls that adjust the amplification at selected depths (Fig. 1.6).

Resolution of Ultrasound Images

The quality of all images is affected by processing imperfections and random ‘noise’. Resolution is quantified by measuring how close together two objects can be without their images blurring into one. In an ultrasound image resolution is limited by inability to generate infinitely brief pulses and spreading of the beam by diffraction.

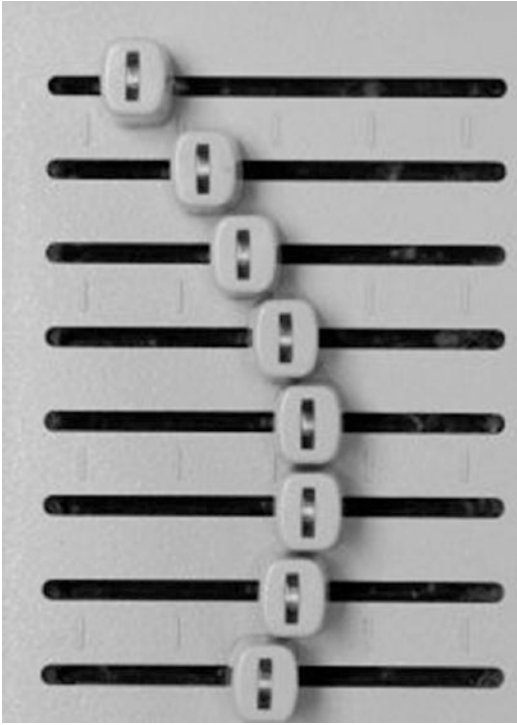


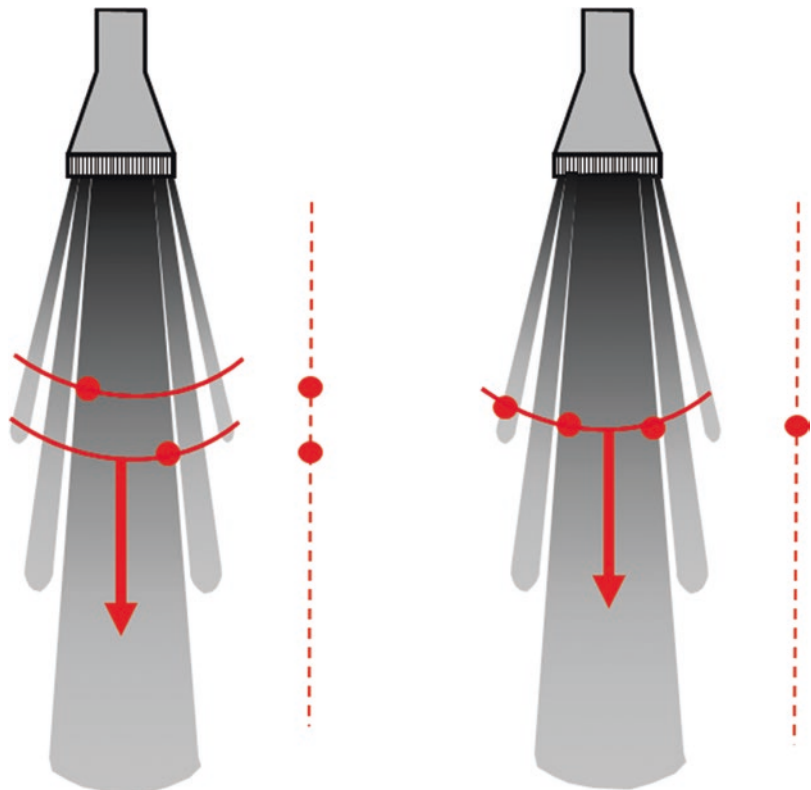
Fig. 1.6 Typical TGC control panel which allows adjustment of the returning echo images at various depths

Measurements along the direction of the beam are termed axial or range resolution and measurements of right-angles to the beam direction (beam to beam) are termed lateral resolution. Lateral resolution can further be divided into azimuthal resolution, in the plane of the scan, and elevation resolution, above and below the scan plane.

Axial resolution is determined by the pulse duration. Since each pulse comprises a short burst of waves lasting about $2\ \mu\text{s}$, with the propagation velocity $1500\ \text{m.s}^{-1}$, this means that the length of the pulse is about 3 mm. If it encounters two objects thinner than the axial length then the two objects will merge and appear as one. Axial resolution can be improved by (a) employing a higher ultrasound frequency, for which the pulse duration is corresponding shorter, and (b) reducing ‘ringing’ by lowering the transmitted power (Mechanical Index).

The ultrasound beam comprises a central main beam, which diverges with increasing distance from the transducer, surrounded by a number of smaller, secondary beams called ‘side lobes’, as shown diagrammatically in Fig. 1.7. These arise

Fig. 1.7 Lateral Resolution: (Left) the ultrasound beam detects only the time taken for echoes to return to the transducer, so only their axial separation is registered. (Right) if more than one object is illuminated by the beam at the same range, the echo signals cannot be resolved



from the physics of wave propagation, and from the fact that the ultrasound transducer comprises a number of individual crystal elements.

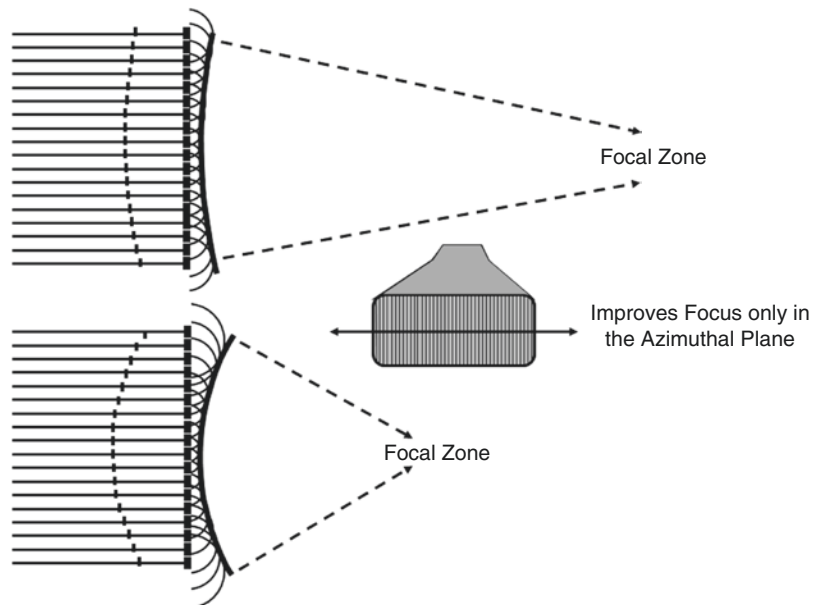
Lateral resolution is primarily determined by the ultrasound beam width. As shown in Fig. 1.7, if two objects are the same depth but very close to each other then there will be no differentiation between the two objects because they are in the same beam (or its side-lobes) and due to the lateral resolution cannot be resolved. With the image generated by scanning the beam across the image plane, this means that an object is detected over a range of beam directions, resulting in lateral ‘smearing’ on the display, or multiple representations of a small object such as a pacemaker wire. Lateral resolution is the chief factor limiting the quality of all ultrasound images and is worse than axial resolution, typically by a factor of 10. Lateral resolution can be improved by making the ultrasound beam narrower utilizing focus in both transmit and receive modes. In addition, the pulsing sequence in a phased array transducer can be modified to provide additional variable focusing as shown in Fig. 1.8. In most ultrasound systems, this improves focussing only in the azimuthal plane, but some of the more sophisticated machines have matrix arrays, in which the crystal ele-

ments are sliced in two directions, providing the ability for focussing also in the elevation plane. Even so, the beam illuminates un-wanted objects, but it is possible also to filter some of these selectively using dynamic receive focusing. As show diagrammatically in Fig. 1.9, echoes from a particular object do not arrive at all the crystal elements in the transducer simultaneously, but the electrical impulses they generate can be selectively delayed so that those from a particular distance and/or direction reinforce each other, whilst those from other sources do not.

Artifacts: Attenuation, Reverberation and Mirror (Ghost)

Attenuation Artifact: Is a Shadowing Effect or Appearance The intensity of an echo is determined by the product of the ultrasound beam intensity and the structure of the reflecting object. If the scanned region is essentially of similar material such as a blood-filled chamber then the image would appear homogenous. However, if the area within the beam is not homogeneous (silicone or bio prosthetic valves), then the image in this region will be more intense

Fig. 1.8 Modification of the electronic pulsing sequence generates a curved wavefront allowing focus in the Azimuthal plane to be adjusted by the operator



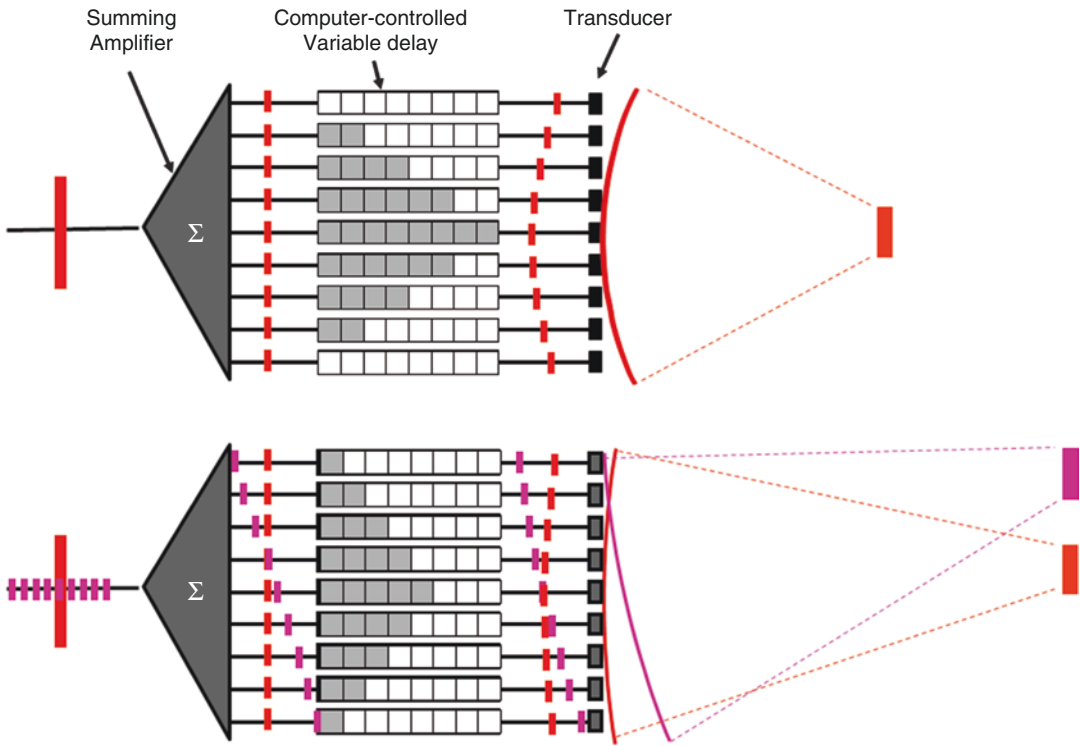


Fig. 1.9 Dynamic Receive Focussing: As echoes from more distant objects arrive, the delay is changed to keep them in focus, at the same time dispersing off-axis echoes

and generate an artefact that might be interpreted as shadowing or even mistaken as a mass within the chamber.

Reverberation Artifact: Is a Bright Display of Reflections That May/May Not Have a Ring Down Appearance The presence of structures having transmission and attenuation characteristics greatly different from soft tissue is also the cause of reverberation and multiple reflection artifacts, one of the most common sources of misinterpretation of images. Referring to Fig. 1.10, an ultrasound beam crossing a structure normally generates two echoes—one from each interface. However, the echo returning from the further interface has to cross the nearer interface, so part of it is again reflected. This secondary reflection then meets the distant interface a second time, where further reflection occurs, and so on. Under normal circumstances this effect is not seen because soft-tissue reflections are weak. For example, if the original echo is

0.1% of the incident wave, the secondary echo has undergone two further reflections and is only $(0.1\% \times 0.1\% \times 0.1\%)$ and too small to register. However, if the object is a very strong reflector such as a calcified or prosthetic valve with each reflection, say, 10% of the incident wave then the secondary or higher-order reverberation echoes are strong enough to be detected and are shown as multiple images of the object (Fig. 1.11).

Mirror Artifact: Is a Mirror Reflection or Ghost Image of a True Structure Another consequence of a high-intensity echo is that it can bounce off the transducer face, or a strongly reflecting structure like the pericardium, and back again to the object, creating a secondary ‘ghost’ image (Fig. 1.12). The clue to recognizing a mirror artifact is that they are always exactly twice as far away from the transducer as a high-intensity echo, and if the primary structure moves a certain distance, the image generated by multiple reflections moves twice as far (Table 1.1).

Fig. 1.10 Multiple reflection artifact: If an object generates intense echoes, higher-order reflections are still strong enough to register on the display

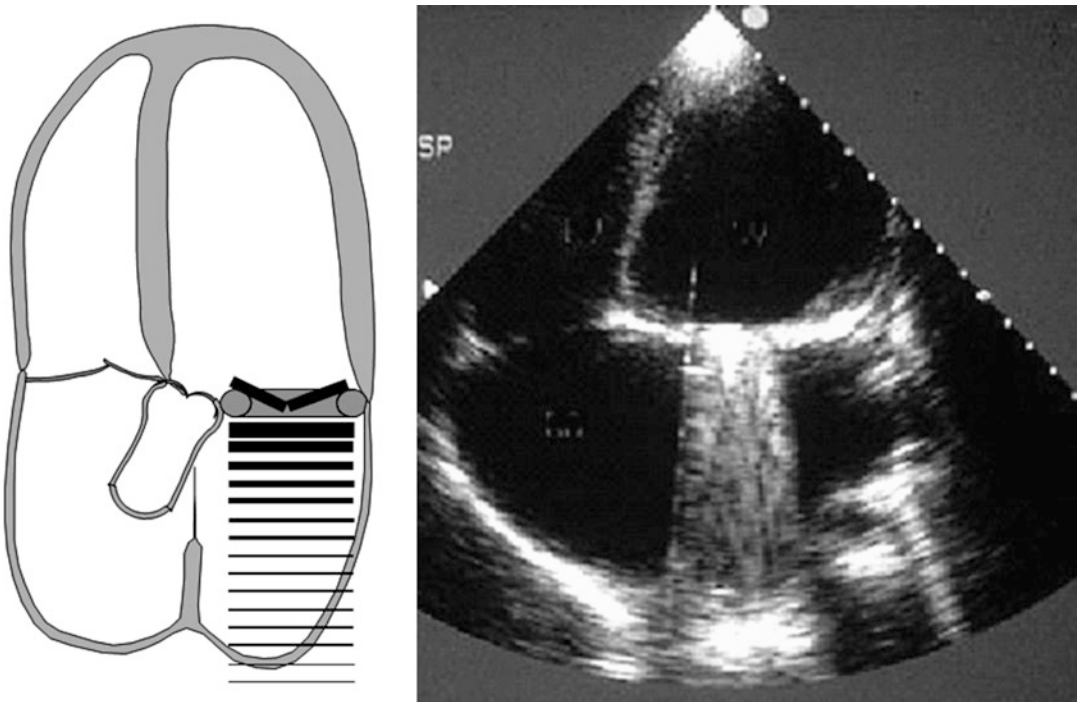
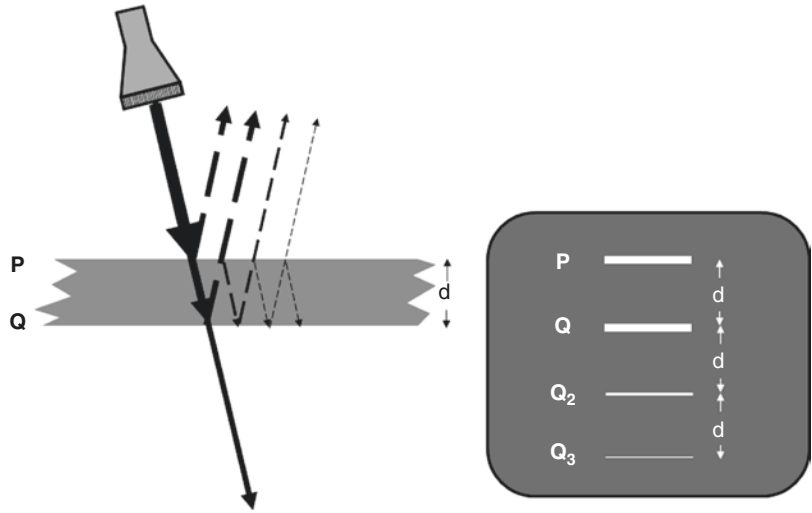


Fig. 1.11 (Left) Diagram and (Right) ultrasound image of a bi-leaflet prosthetic mitral valve showing multiple reflections from the strongly reflecting hemi-discs.

Note how the scan converter has tried to “fill in” the spaces between the echoes

Parallel Processing

So far, the emphasis has been on the formation of images by detecting the time it takes for echo signals to return to the transducer and their intensi-

ties. With this method the electrical activity is unified though the transducer contains a number of crystal elements. Image quality is constrained by the scan line density and the beam width. However, this is not the way the human eye forms an image

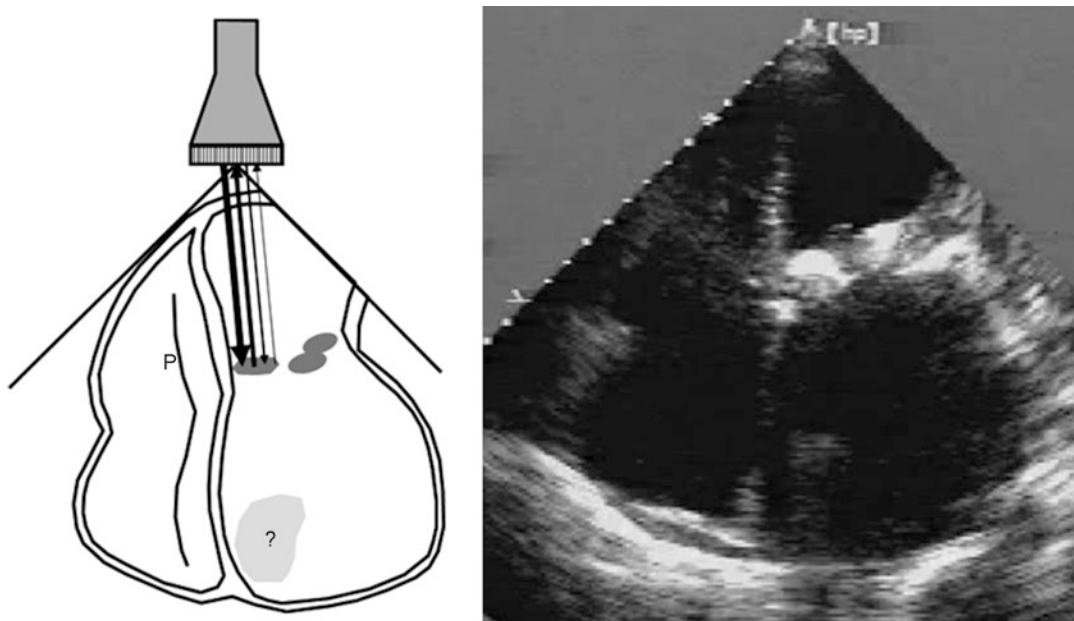


Fig. 1.12 Artifact mimicking a mass in the left atrium resulting from very strong echoes from the calcified mitral valve bouncing off the transducer face

Table 1.1 Minimising false diagnoses from image artifacts

- Always use minimum power consistent with obtaining an image
- Beware of ‘objects’ that:
 - Are twice as far from the transducer as intense reflectors
 - Lie on an arc centered at the transducer and/or have an intense reflection
 - Are in the centre of the scan sector and a few centimetres from the transducer

If in doubt, see if they are still present when transducer position and image plane are altered

(Fig. 1.13). Instead of the eye scanning across the field of view, the scene is flooded with light and image data from it is focussed onto the millions of individual receptors that comprise the retina. Impulses from these are fed simultaneously to the brain, which processes them to form an image to complete the scene. With the advances in crystal and transducer technology—parallel processing has become the norm. Currently most imaging systems operate with two or more parallel processing paths (Fig. 1.14) unless they have real-time 3D capability for which there is advanced proprietary parallel processing. Yet there is great benefit with

having multiple separate detectors because it can provide a wider/thicker image slice. With a thicker slice or wide ultrasound beam an echo from an object in the centre of the beam axis arrives simultaneously at the two detector channels, but those from off-axis objects reach one detector channel before the other. The resulting phase delay allows the computer to assign them to corresponding memory cells. As the beam direction changes, objects previously on the central beam axis are still detected, but their echoes are now out of phase, and can be assigned to the correct memory location, where they add to those from the previous pulse. Several major advantages follow:

1. It is no longer necessary to have a very narrow transmitted beam, and to have as many transmitted pulses per image, so the frame rate can be increased.
2. By detecting both amplitude and phase data, the total amount of information is doubled.
3. The image data in each memory cell is built up over several pulses, thus improving sensitivity and reducing noise and allowing higher imaging frequencies to be used with consequent improvement in resolution.

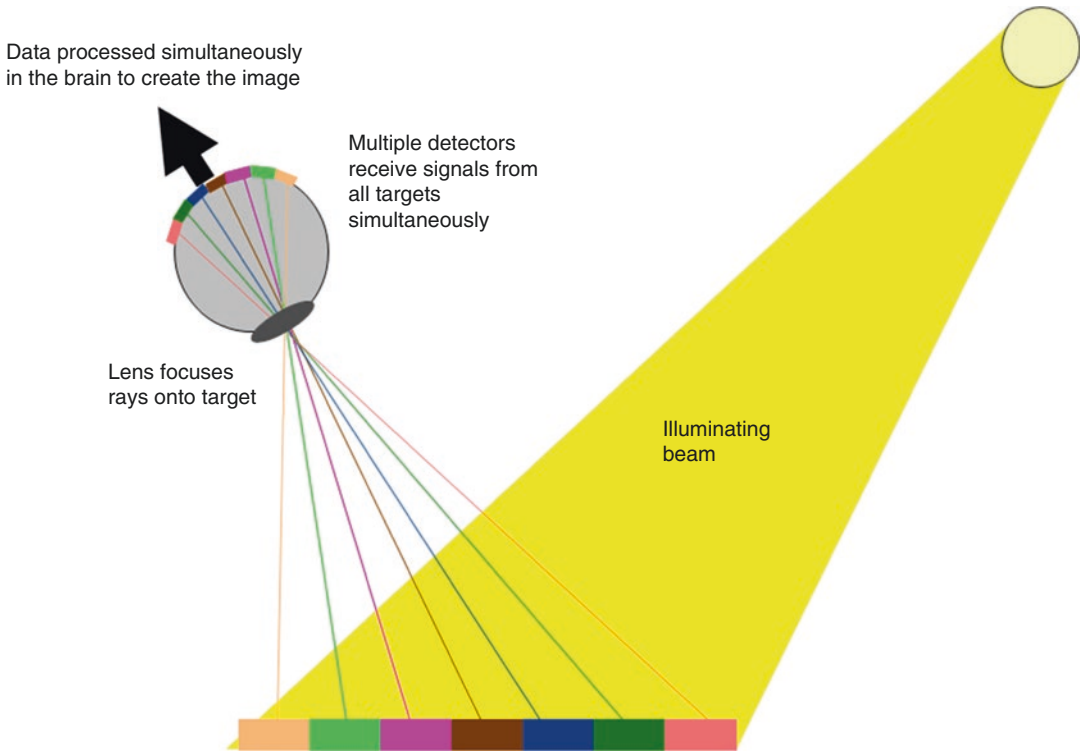


Fig. 1.13 In the eye, a lens focuses reflected light onto an array of detectors, signals from which are processed simultaneously ('Parallel Processing') by the brain to create the image

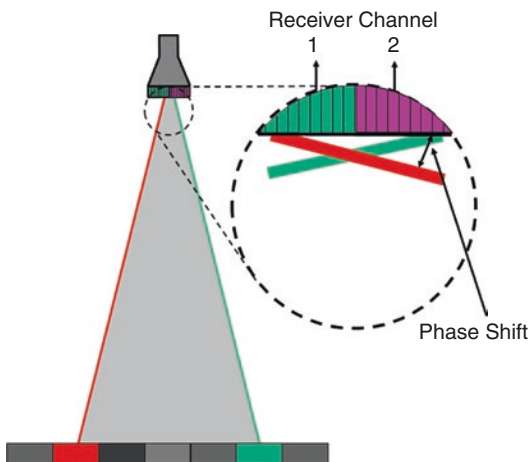


Fig. 1.14 Parallel processing: with two receiver channels, the machine can detect from which part of the illuminated region a particular echo arises

Grey Scale

The intensity of an echo depends on the nature of the tissue interface. As shown earlier, there is a wide range of echo intensities, with a calcified

structure generating an echo many thousands of times more intense than a boundary between, say, blood and newly formed thrombus. However, the ultrasound display can only represent a fraction of these specific shades of grey. The typical scan converter image memory only has a range of 64 shades of grey. As a result the image gets tagged white for all intense echoes and black for all weak echoes with almost no grey tones. This can to some extent be overcome by compressing the intensity scale to create a softer image, but at the expense of loss of boundary definition (Figs. 1.15 and 1.16).

Harmonic Imaging

Contrast Harmonic

Second Harmonic imaging was originally developed in order to enhance signals from encapsulated contrast media. These are proprietary products and comprise very small (1–3 μm) microspheres with a hard outer shell containing a gas. At very low ultrasound power levels, these act as normal scatterers,

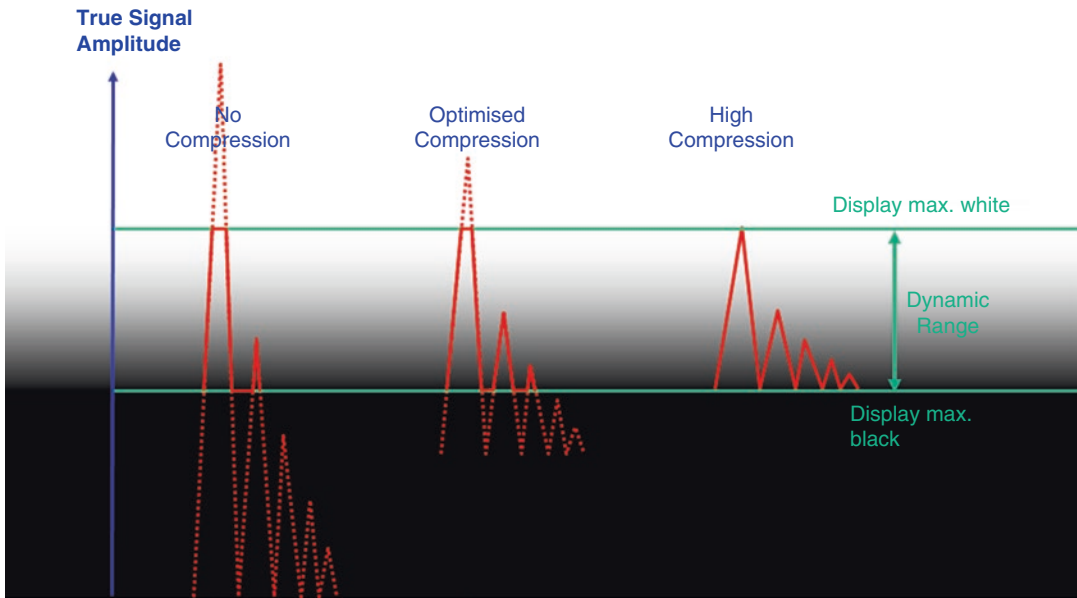


Fig. 1.15 Compression: Compressing the echo signal amplitudes helps overcome the very limited dynamic range of the display

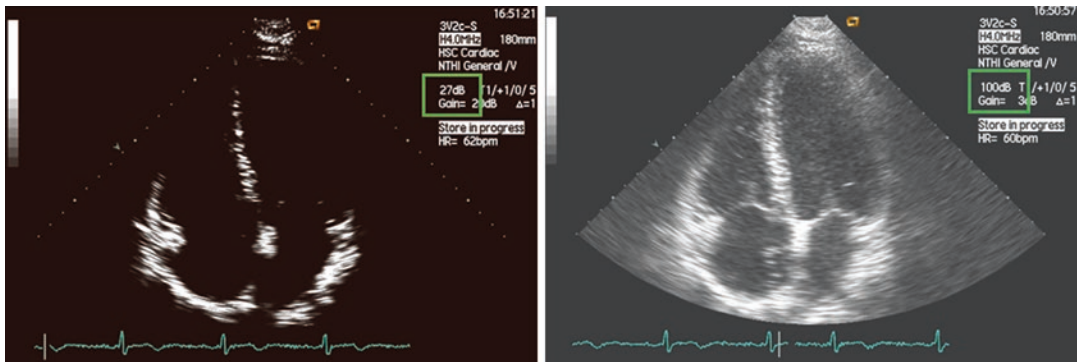


Fig. 1.16 Echo images with (left) low grey scale compression (27 dB) giving a harsh 'black and white' image and (right) high compression (100 dB) resulting in an overly 'soft' image

but with slightly greater power (but still lower than normally used for imaging) the pressure waves distort them and they vibrate, emitting energy at the second harmonic frequency. A display based only on the second harmonic Doppler frequency thus selectively comes from the microspheres rather than from tissue or blood. The addition of echo contrast greatly enhances the quality of both images of blood-filled cavities and of Doppler signals, giving a clear velocity profile for even very small jets. At high ultrasound power levels, the microspheres shatter, releasing the contained gas, and generating a brief, but very intense, echo.

Tissue Harmonic Imaging

Fourier's Theorem is a powerful mathematical tool for analysing waves. It states that any repetitive wave, of whatever shape, can be constructed by adding together a number of regular sine waves of varying frequencies and amplitudes. The basic building block for a particular complex wave is a sine wave having the same frequency, and termed the 'fundamental'. The detail that gives the complex wave its shape is provided by adding to the fundamental further sine waves having frequencies that are exact multiples of that of the fundamental. These are called

harmonics (the second harmonic has twice the frequency of the fundamental, the third harmonic three times, and so on). To form a complex wave perfectly, theory requires an infinite number of harmonics, but their contributions become smaller as the frequency increases and in practice a fundamental plus ten harmonics provides an adequate representation of the complex wave (Fig. 1.17). The reason why a violin and a trumpet playing the same note sound different is that, though they generate the same fundamental frequency, their harmonic contents are different.

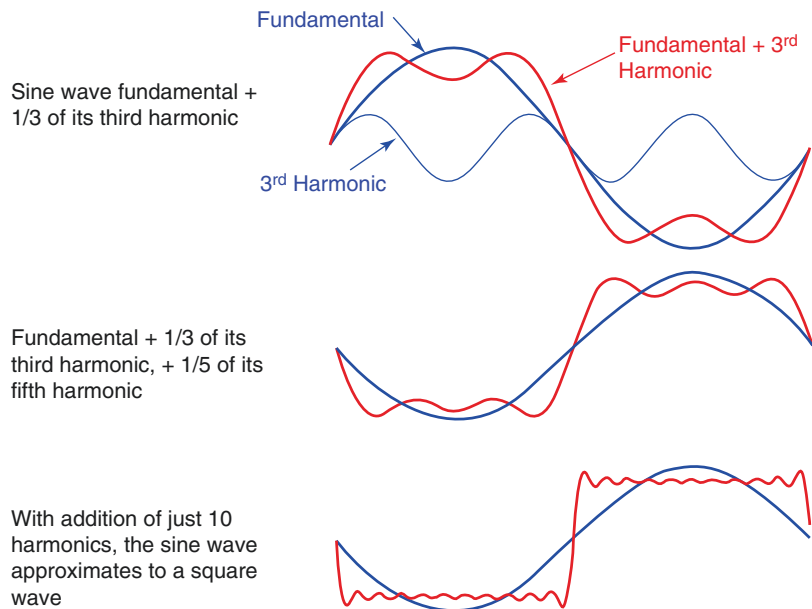
A pure sine wave contains no harmonics, but if its shape is distorted it means that harmonics have been added. This is what happens as an ultrasound pulse travels through the body, the sine wave becomes distorted and creates harmonics. As shown in Fig. 1.18, when the positive pressure region of the wave passes through the tissue, it compresses it, and the negative part of the wave vice-versa. The density of the compressed tissue increases, so the positive pressure part of the wave travels faster and conversely the negative pressure part travels more slowly. The fact that the wave shape changes as it progresses through the body means that it has acquired a harmonic component, which applied to Fourier analysis illustrates a mainly second

harmonic, with a smaller proportion of fourth harmonic, and so on.

When a 2 MHz ultrasound pulse is transmitted into the body, the echoes that return are not pure 2 MHz sine waves, but include some of its second harmonic (4 MHz), and a little of its fourth harmonic (8 MHz). By selectively filtering out the 2 MHz fundamental, it is possible to form the image from the 4 MHz second harmonic component. The second harmonic image is mainly created from the most intense central part of the beam from greater depths because wave distortion increases as the wave travels through the body. As a result, a relatively small amount of harmonics arise from proximal structures. Harmonic imaging provides the following benefits:

1. It combines the penetration power of a transmitted low fundamental frequency with the improved image resolution of the harmonic and twice the frequency.
2. The harmonic image is preferentially derived from deeper structures, and reduces artefacts from proximal objects such as ribs
3. The harmonic image away from the central beam axis is relatively weak and thus not so susceptible to off-axis artifacts.

Fig. 1.17 Fourier Analysis: the principle by which a complex wave can be created by addition of sine waves, or broken down into its sine-wave components



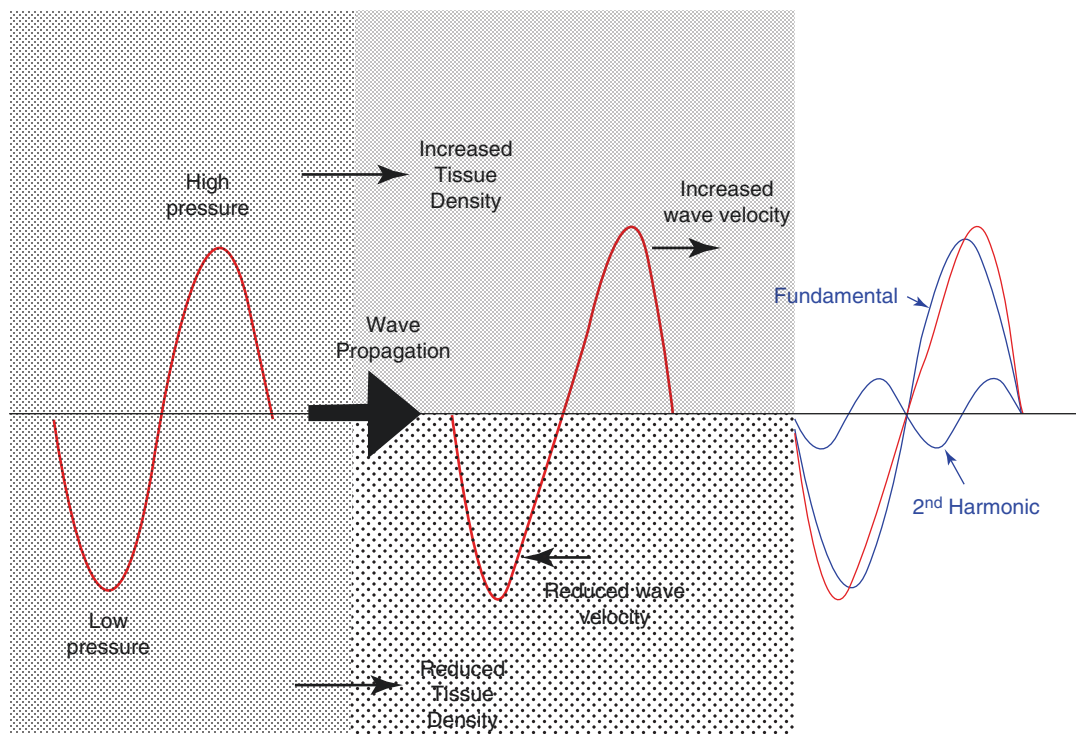


Fig. 1.18 Distortion of a wave as it travels through a compressible medium gives it a significant second-harmonic content

The improvement in image quality obtained from second harmonic imaging is such that it should be mandatory for all new machine procurement and machines without it should be regarded as obsolete.

There is one limitation associated with harmonic imaging. Because the image is now formed from echoes of a single frequency, some 'texture' is lost and structures such as valve leaflets may appear artificially thick. Therefore, it is good practice to image with high fundamental frequency provided image quality is good.

Transesophageal Imaging

2-D imaging from a phased array transducer positioned in the esophagus has been commercially available since the 1980s. The transducer (Fig. 1.19) is similar in construction to a gastro-scope, but in place of the fibre-optic bundle used

for light imaging, a miniature ultrasound transducer is mounted at its tip. Current available elements range from 64, 128 or 256 depending on the ultrasound system/vendor. Due to the insertion of the probe there is no attenuation from the chest wall and can operate at higher frequencies (up to 14 MHz) thereby producing excellent image quality. Since limited manipulation is possible within the esophagus, the complete transducer array can be rotated by a small electric motor controlled by the operator to provide image planes that correspond to the orthogonal axes of the heart despite the fact that these are not naturally aligned with the axis of the esophagus. Since the image acquisition is semi invasive, special precautions need to be taken to prevent accidental harm to the patient through heating of the transducer. The potential for it to apply 300-V electrical impulses to the back of the heart also requires it to be checked regularly to ensure integrity of the electrical insulation.



Fig. 1.19 Transoesophageal transducer

Real-Time 3D Imaging

3D imaging is similar to 2D image except, instead of acquiring frames per second there are volumes of ultrasound information acquired per second. To achieve this has required overcoming several daunting technological challenges. The first is the construction of the transducer. Instead of cutting a crystal into slices, with wires attached to their edges, the crystal now has to be cut into a matrix of minute squares, each only 2–3 times the width of a human hair, and a wire attached to each one (Fig. 1.20). Even when this is done, the total number of wires is such as to make the connecting cable too unwieldy for clinical use, so the ‘front-end’ beam forming and image processing has to be controlled by electronics built into the transducer, without making it too large or heavy for the operator to hold.

The second problem is to process the enormous amount of data in real time. In the earliest machines real-time imaging was possible only in parasternal views (where the smaller depth allows higher pulse rates), and involved significant compromises of frame rate and image depth, with a lot of inter-beam smoothing and interpolation. Currently, the image quality is not as good as that of 2-D images, but with ever-increasing computer power it is only a matter of time before this is overcome.

The final problem is that of displaying the data on two-dimensional video screens. This is done by computer-generated texturing and shadowing to emphasise closer structures and create the impression of a 3-dimensional solid which can be

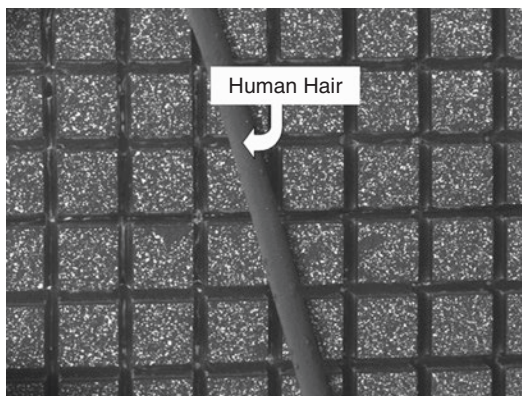


Fig. 1.20 Photomicrograph of the matrix array in a real-time 3-D imaging transducer

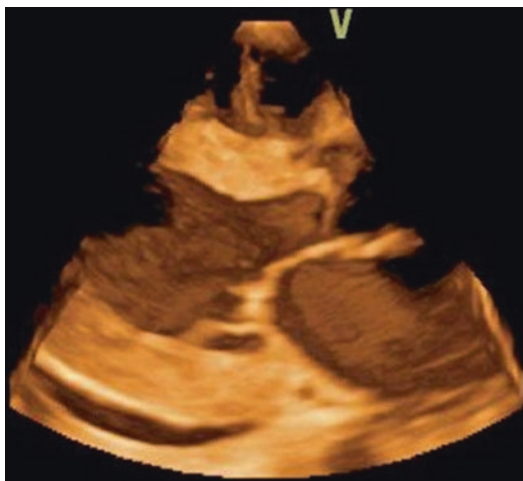


Fig. 1.21 Textured 3-D image from the parasternal window

rotated and tilted by a trackball, and from which individual 2-D sections can be extracted (Fig. 1.21). The clinical possibilities for real-time 3-D imaging are enormous and will be explored in depth in subsequent chapters.

Doppler Echocardiography

Doppler Principles

The specular ultrasound echoes used for imaging the heart are derived from relatively extensive tissue interfaces. When the ultrasound beam

encounters much smaller structures, it interacts with them in a completely different way, and instead of being reflected along a defined path, it is scattered equally in all directions just as the circular ripples formed when a small stone is thrown into a pond. The consequence is that most of the incident energy is dissipated, but a small amount returns along the incident path and can be detected, though the resulting signals are much weaker than the specular image echoes. Red blood cells are ideal scatterers; although the echo from a single cell is negligible, signals from millions of them added together can be detected and, if the blood is moving, the frequency of the backscattered echoes is modified by the Doppler effect.

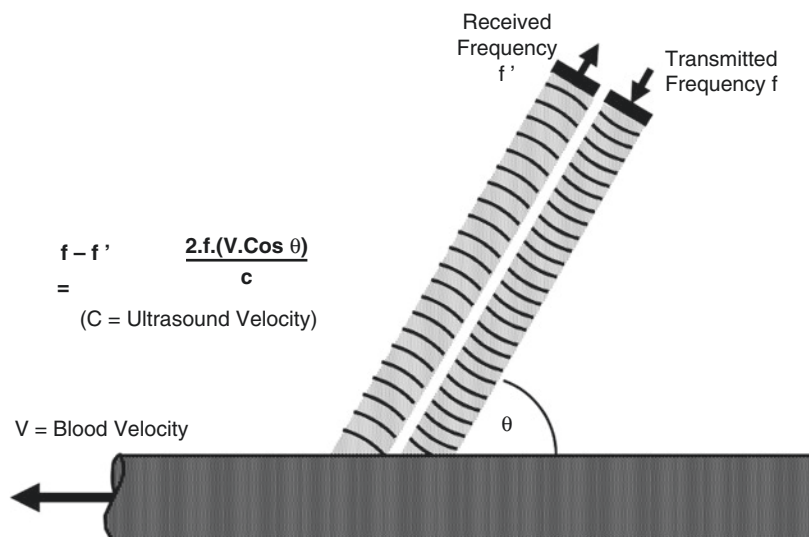
The Doppler effect was first described in 1843 by Christian Doppler, an Austrian Mathematician and scientist. He studied the light spectra of double stars and hypothesised that the shifts he observed in the hydrogen spectral lines arose from rotation of the stars about each other. If a star is moving towards the earth the spectral lines are shifted towards blue, and if its distance is increasing, the shift is towards red. Doppler's theory was confirmed by Buys Ballot in a classical experiment with two trumpeters, one on a moving train and the other on the station. Both played the same note, but observers heard the pitch of the note from

the passing train change as it first approached then receded. As the wave source moves towards the observer, the waves are compressed, decreasing the wavelength and increasing the pitch, and as the source moves away from the observer, the apparent wavelength increases and pitch lowers.

Similarly, if an ultrasound beam encounters a stream of moving blood, returning backscattered echoes have a slightly different frequency from that of the transmitted beam, the difference being known as the Doppler shift, or Doppler frequency. The Doppler equation (Fig. 1.22) shows how this can be used to calculate the blood flow velocity. For a velocity of 1 m.s^{-1} and ultrasound frequency 2.5 MHz the Doppler shift is about 3.3 kHz , only 0.1% , but readily detected and directly proportional to the blood velocity. Note, that the application of the Doppler equation requires that the angle between the beam axis and blood flow direction either must be known, or must be so small that its cosine is effectively unity. Also, the Doppler shift for a given blood velocity is related to the ultrasound frequency, so is twice as large for the same blood velocity at 5 MHz as for 2.5 MHz .

In practice, blood in an artery does not all flow at the same velocity, due to friction at the walls. Furthermore, with pulsatile flow the velocity is

Fig. 1.22 The Doppler equation, relating flow velocity to the ultrasound 'Doppler Shift'



constantly changing, resulting in complex flow patterns. The interrogating ultrasound beam does not therefore return just one Doppler shift, but a spectrum of frequencies, like the orchestra tuning up before a performance. The complex mix of Doppler shifts is analysed and the resulting velocity data is used to generate a Spectral Doppler Display (Fig. 1.23). The spectrum shows the range of velocities detected at each point in the cardiac cycle, with flow towards the transducer shown above the baseline and flow away from the transducer below it. The density of the image shows the amplitude of the signal at each Doppler shift, which depends on the number of scatterers, and the proportion of blood flow at that velocity. A line tracing the outer edge of the spectrum shows the peak velocity and a line through the centre of the band approximates to the mean velocity (Fig. 1.24).

Pulsed Wave (PW) Doppler

PW Doppler extracts flow velocity information from the echoes generated during imaging. As well as the high-amplitude, specular echoes arising from tissue interfaces, the returning signals contain backscattered echoes from blood. A movable electronic cursor on the 2-D image indicates the location of the 'sample volume' from which Doppler signals are extracted, amplified and analysed to provide velocity data (Fig. 1.25). It should be noted, however, that whereas the axial extent of the sample volume can be made quite small, its lateral extent, governed by the ultrasound beam width, is usually significantly greater than suggested by the icon on the display. PW Doppler overcomes the lack of depth discrimination of CW, but this benefit is offset by the problem of aliasing.

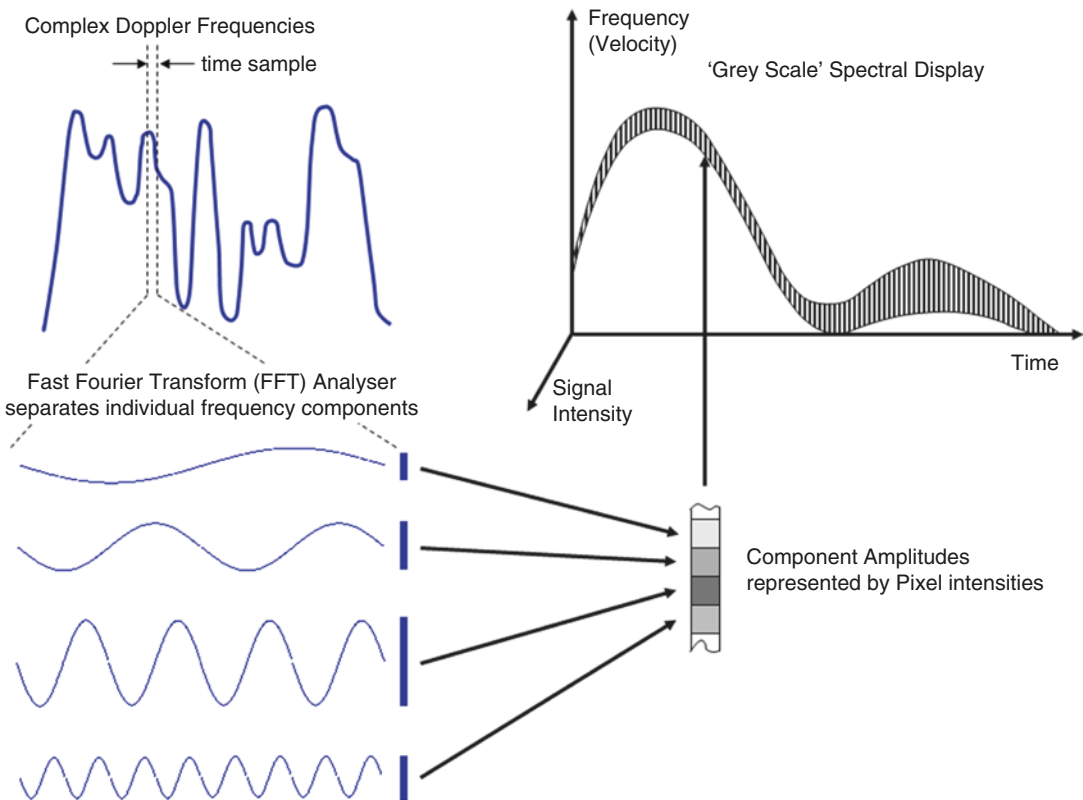


Fig. 1.23 Breaking down a complex waveform into its sine-wave components to generate a spectral Doppler display

Fig. 1.24 Spectral Doppler display of flow in a carotid artery

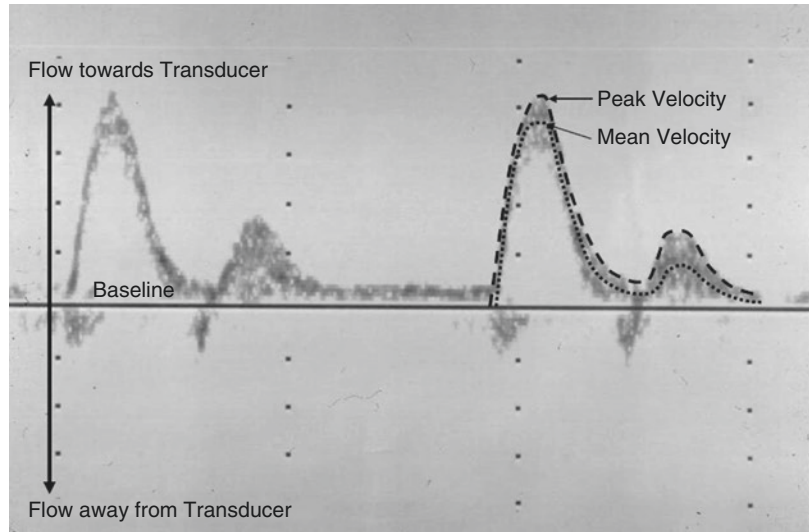
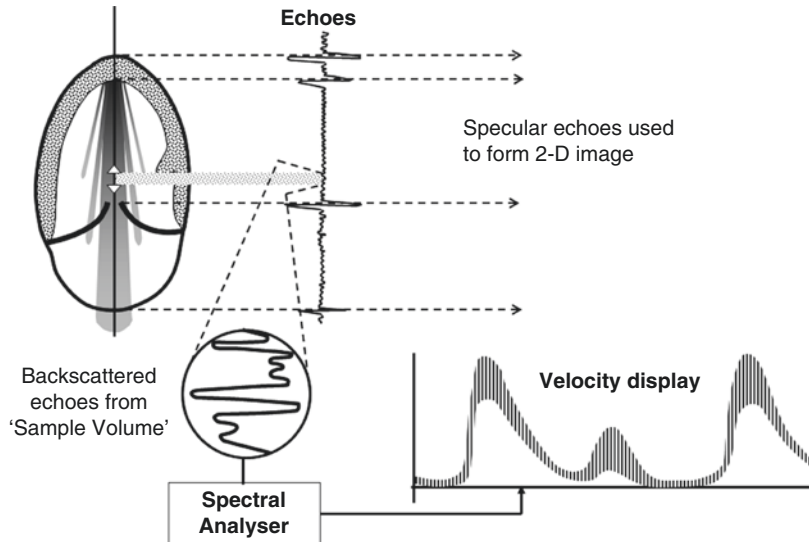


Fig. 1.25 Principle of pulsed-wave (PW) Doppler



Aliasing Effect

Although PW Doppler allows spatial localisation of the flow signals, it suffers from a fundamental technical limitation that severely restricts its clinical use. This is called 'aliasing' and it arises from the fact that there are significant time intervals between the ultrasound pulses. Most people are familiar with aliasing as it affects cinema films. The movie camera takes a sequence of individual pictures and between exposures the camera shutter is closed while the

film is advanced. Moving objects are thus seen as a sequence of 'snapshots' with time gaps between them. This causes the phenomenon typified in the 'Western' where, as the stagecoach with its spoke wheels starts to move, the wheels initially are seen to turn normally but, as its speed increases, they appear to stop moving, or rotate in reverse. The explanation of this is shown in Fig. 1.26. Provided the wheel rotates less than half a turn between images, all is well, but if it turns faster the images are ambiguous.

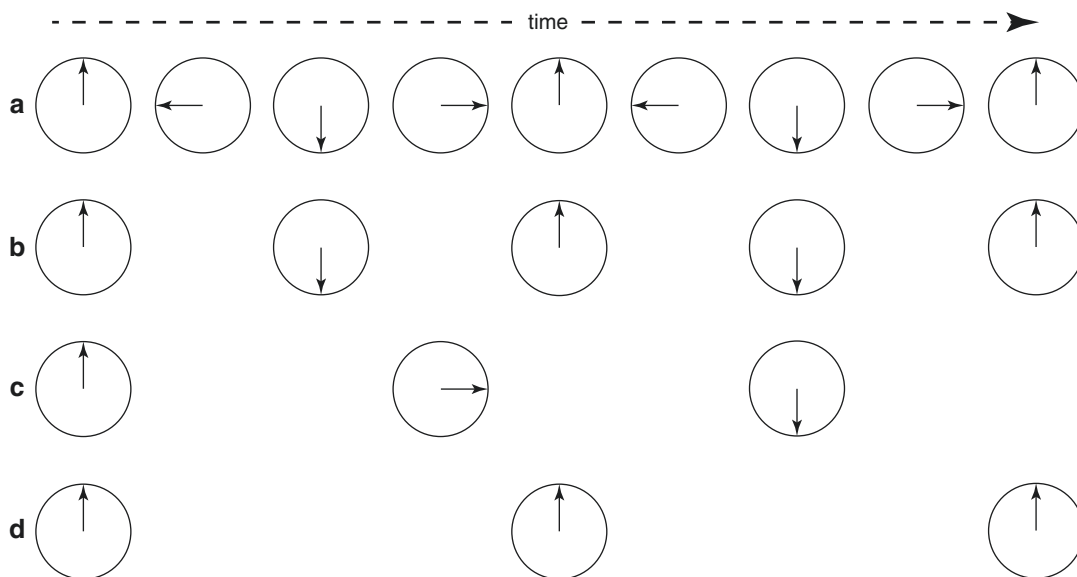


Fig. 1.26 Aliasing: (a) the imaging rate is high and the arrow is seen to rotate in a counter-clockwise direction; (b) with only two images per revolution, the direction of rotation is unknown; (c) with less than two images per

revolution, it appears to rotate in a clockwise direction; (d) with only one image per revolution, it appears to be stationary

This is an example of Nyquist's Theorem, a very powerful tool of information theory. It states that for a wave to be reproduced accurately, it has to be sampled at least twice per cycle. Applied to PW Doppler, this means that the highest blood velocity that can be detected without ambiguity is that whose Doppler shift is equal to half the pulse repetition frequency (PRF) of the imaging system. This is called the 'Nyquist Limit'. The PRF is determined by the imaging depth, so as depth increases, the PRF, and the Nyquist Limit, are correspondingly reduced. This is the basis of the so-called 'Range-Velocity Product' which has constant value for a given ultrasound frequency: doubling the sample depth halves the aliasing velocity, and *vice-versa*. Since Doppler shift is also proportional to the ultrasound frequency, aliasing can be reduced, and the Range-Velocity Product increased, by lowering the ultrasound frequency.

The practical effect of aliasing in PW Doppler is illustrated in Fig. 1.27. The tops of the positive velocities that exceed the Nyquist Limit are cut off and displayed as negative velocities,

corresponding to the stagecoach wheel turning in reverse. A simple calculation shows that aliasing occurs at quite modest blood velocities: for a working depth of 15 cm, the round-trip time is approximately 200 μs and the maximum PRF 5000 s^{-1} . For an ultrasound frequency of 2.5 MHz, the Nyquist Limit is thus 2500 Hz and aliasing occurs at blood velocities above 0.75 m.s^{-1} ; and at 5 MHz aliasing begins at only 0.375 m.s^{-1} . Provided that the flow is predominantly towards or away from the transducer, the zero velocity baseline can be shifted to favour one direction at the expense of the other, and it is thus possible to increase the aliasing velocity by a factor of up to two. Beyond this nothing can be done, and when high velocities are encountered, the display overlaps and it not possible to tell whether the flow is towards or away from the transducer, let alone measure the velocity (Fig. 1.28).

Clinical Applications of PW Doppler

The limitation imposed by aliasing makes PW Doppler generally unsuitable for quantifying obstructive valve lesions and its main clinical applications are to be found where spatial locali-

Fig. 1.27 Mild Aliasing can be removed by shifting the zero-velocity baseline

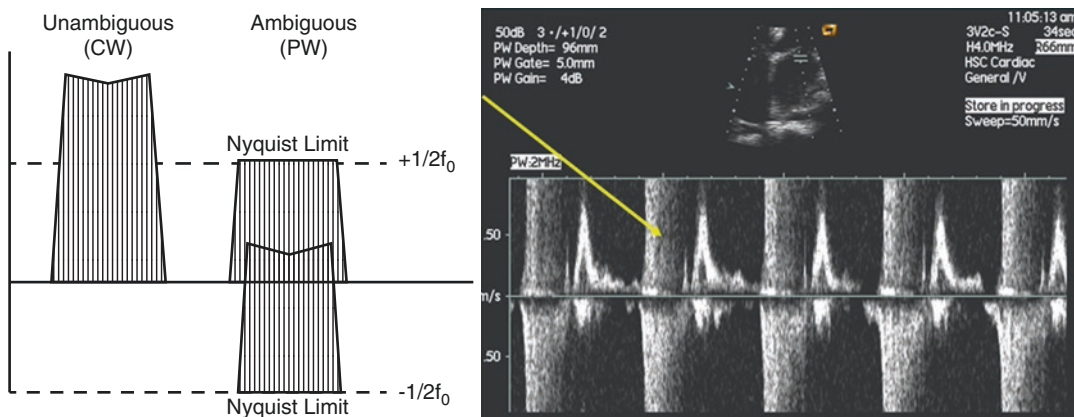
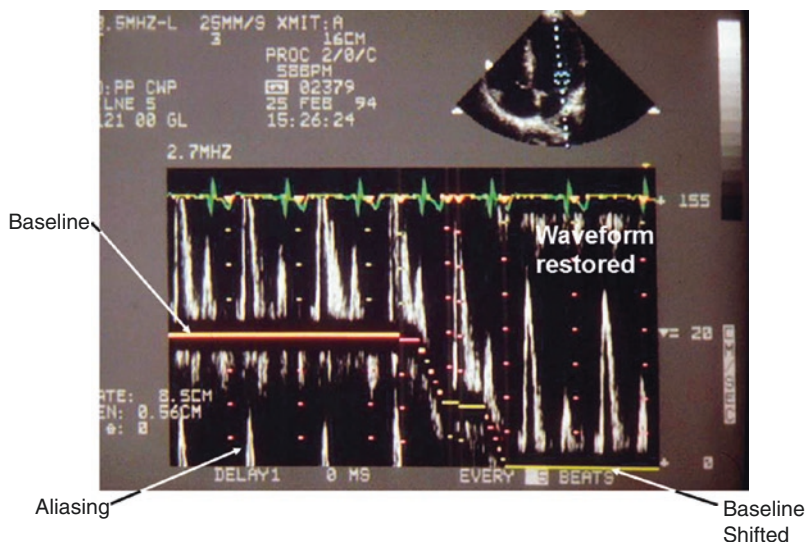


Fig. 1.28 A high velocity jet caused severe Aliasing and the PW spectral display overlaps, resulting in loss of all velocity and direction data

sation is important, and velocities are relatively low ($1\text{--}2\text{ m.s}^{-1}$ or less). Examples include:

- Flow waveforms across normal mitral and tricuspid valves (e.g. for evaluating diastolic function and respiratory flow variation)
- Flow waveforms in the left- and right-ventricular outflow tracts (e.g. for Continuity Equation calculations and for separating sub-valvular from valvular lesions)
- Calculating Stroke Volumes in the aorta and pulmonary artery (e.g. for cardiac output and Qp/Qs shunt calculations).
- Pulmonary venous flow waveforms

High PRF PW Doppler

The primary factor determining the aliasing velocity is the PRF, limited by working depth. If, the PRF is doubled, instead of Doppler shift data returning only from a single depth, it will arrive simultaneously from more than one sample volume, leading to ambiguity (Fig. 1.29). However, since the PRF has been doubled, so has the aliasing velocity. This technique, called 'High PRF' or 'Extended range' Doppler, can lead to confusion as to the origin of Doppler signals, but by judicious placement of the beam so that the additional sample volumes are not in high-velocity areas, this usually can be avoided (Table 1.2).

Fig. 1.29 High PRF Doppler reduces Aliasing, but introduces some depth ambiguity

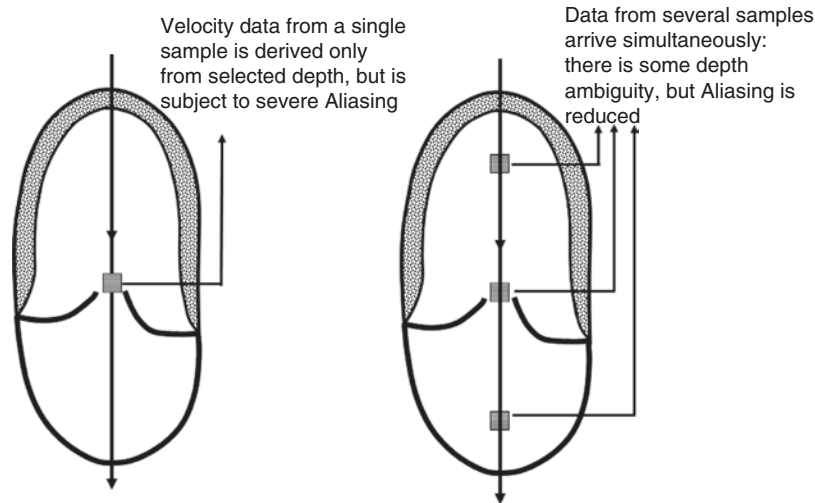


Table 1.2 Comparison of spectral Doppler modes

Mode	Velocity data	Depth data
Continuous wave (CW)	Correct	None
Pulsed wave (PW)	Limited by aliasing	Correct
High PRF	Aliasing velocity doubled, or quadrupled	May be ambiguous

Color Flow Imaging

The PW Doppler principle can be extended to detect backscattered echoes, not just from a single ‘sample volume’ but from a matrix of small ‘pixels’ on the 2-D image, or 3-dimensional ‘voxels’ on a real-time 3-D image. To analyse the Doppler shifts in real time imposes burdens on the processing system, and it is not possible to display the full spectral data from numerous sample points simultaneously, but basic velocity information can be provided in the form of a display in which the color of each pixel indicates the local flow direction and the approximate velocity. (Fig. 1.30). The color flow data are superimposed on the 2-D or M-mode image. The standard convention is for flow towards the transducer to be shown as red and flow away from the transducer in blue; this is actually opposite to the observation Doppler made when he studied the stars, but it apparently arose when

pioneering investigators looked at flow in their own carotid arteries and thought it ought to be colored red!

Advantages of Color Flow Imaging

Since its introduction in the mid-1980s, color Doppler has contributed greatly both to our understanding of blood flow patterns within the heart and great vessels, and also to diagnosis and management of heart disease. Many of these will become apparent in later Chapters, but broadly they can be listed as follows:

- It provides a rapid, comprehensive ‘overview’ of blood flow. This enables the echocardiographer rapidly to ascertain the presence of valve and shunt lesions, especially the un-expected, such as finding a persistent arterial duct in a middle-aged patient presenting with ‘left heart failure’
- It shows the spatial localization and extent of flow jets, for example the site of a VSD, or the path of an eccentric mxj jet from degenerative mitral valve disease. This also allows the operator to align the display cursor correctly for measuring the jet velocity with CW Doppler.
- When superimposed on an M-mode, it provides excellent temporal localisation, for example to show the point at which a prolapsing mitral valve starts to leak (Fig. 1.31).

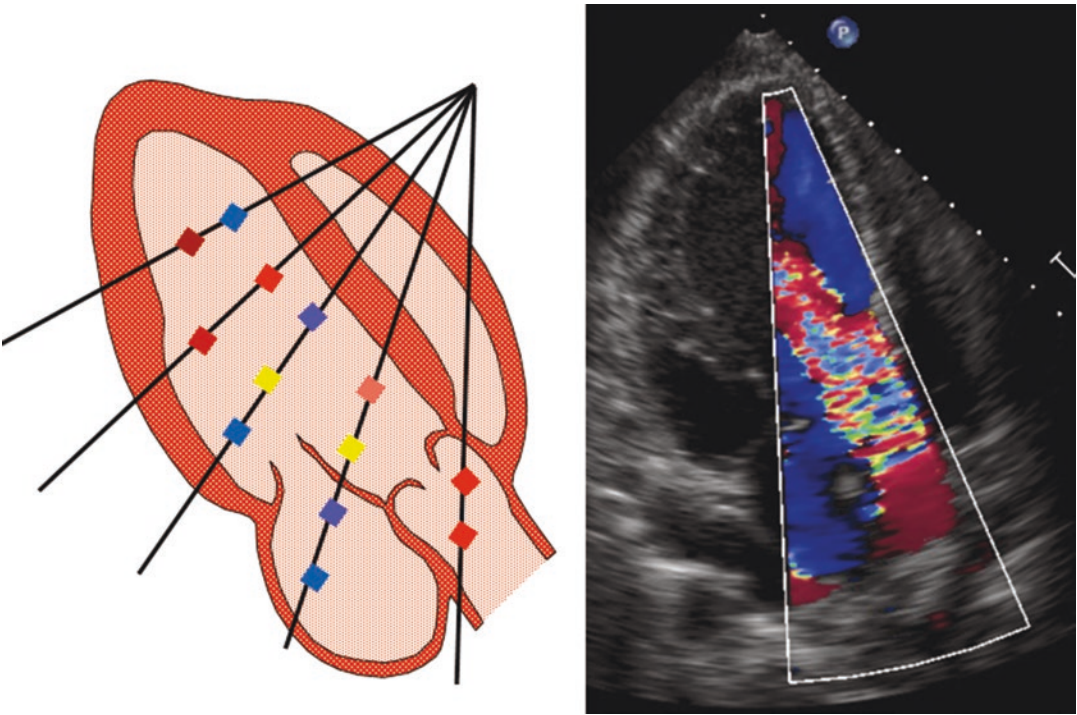
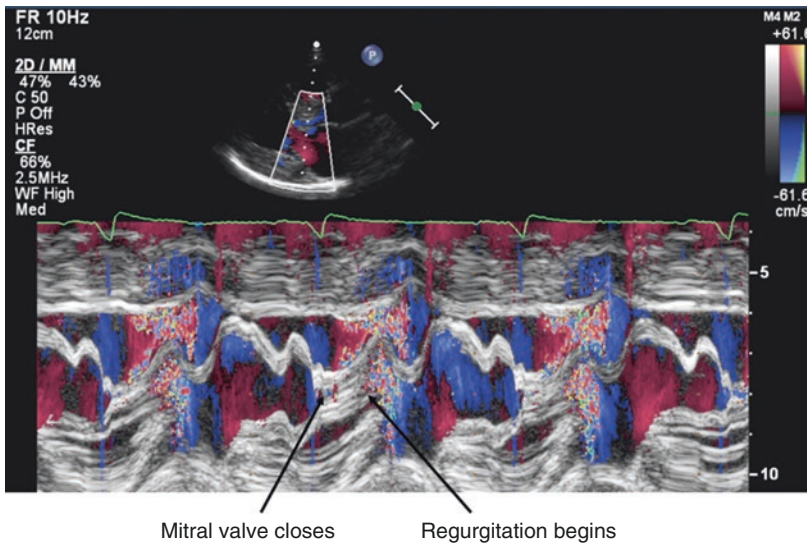


Fig. 1.30 A colour flow image is formed by sampling flow velocity at a number of points and indicating mean velocity values by coloured pixels superimposed on the 2-D image

Fig. 1.31 Superimposing color on an M-mode recording relates the timing of valve movements to blood flow in this patient with HOCM



Limitations of Color Flow Imaging

While color Doppler has undoubtedly enriched understanding of blood flow within the heart, and is invaluable for detecting valve regurgitation and shunts lesions, it does have severe technical limi-

tations, which must be understood if the images are to be interpreted correctly.

Reduced Frame Rate To form a 2-D image and superimpose color Doppler on it requires three or

more ultrasound pulses to be transmitted along each image line, with consequent reduction in frame rate and/or line density. With modern parallel-processing systems, this is less important than it used to be, but still requires the operator to minimise sector depth and angle, and restrict the color sector size if acceptable frame rates are to be maintained.

Aliasing Since color Doppler is derived from PW Doppler, it suffers from aliasing, and to an even greater degree, because the effective PRF is reduced. Aliasing in a color image typically occurs at velocities above 0.5 m.s^{-1} . It manifests on a color display as color inversion: red turning to blue, and vice-versa (Fig. 1.32). Thus, for steady flow towards the transducer, a velocity of 0.4 m.s^{-1} is represented by pale red but as it increases to 0.6 m.s^{-1} it becomes pale blue. At 1.0 m.s^{-1} (twice the aliasing velocity) the color display shows black; at 1.4 m.s^{-1} pale red again, 1.6 m.s^{-1} pale blue, and so on. There is, however, one application where the limitation imposed by aliasing has been turned into a benefit, and this is in the Proximal Isovelocity Surface Area (PISA) method for calculating instantaneous volumetric flow rates, which exploits the fact that as blood accelerates as it

approaches a restrictive orifice, the velocity at which the color aliases is precisely known.

Mean Velocity, Peak Velocity and Turbulence A color display can only show velocity at one point and at one time by a single color and it was therefore sensible that this should represent the mean velocity. Color Doppler does not attempt to show peak velocities. However, when flow is turbulent, there is a wide spectrum of local velocities: high and low, forward and reverse. This is indicated on a CW display as an increased peak velocity and broadening of the spectral band, but since the mean velocity is unchanged, it presented a challenge to color Doppler. The solution was to analyse the time-variance of local velocity, and where the same pixel detects greatly different velocities in successive images, to modify the display, for example by showing those pixels in green. This is called variance mapping, but it places further strain on frame rates and aliasing velocity so is seldom used.

Flow Angle Since the Doppler shift is the product of blood velocity and the cosine of the angle between the flow axis and the ultrasound beam, the apparent velocity on a color display is determined both by the true blood velocity and by the angle at which the flow vector is intersected by the scanning beam. Not only does this mean that constant flow velocity is represented by a range of colors, but it can additionally introduce aliasing at higher velocities (Fig. 1.33).

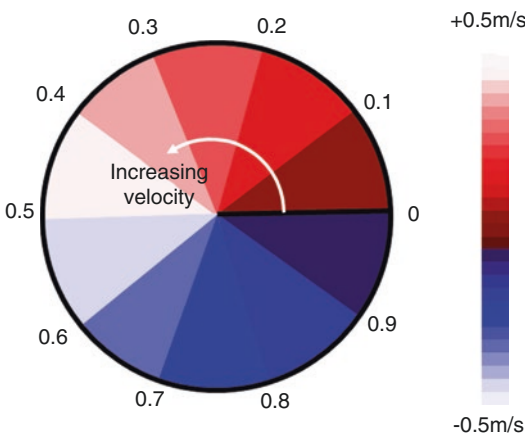


Fig. 1.32 Aliasing in color Doppler. As velocity towards the transducer increases, the display changes from dark to light red. At the Aliasing velocity, it ‘flips’ to pale blue, and thence to darker blue. With further velocity increase, this process repeats. Once Aliasing has occurred, the observer no longer knows the true velocity

Tissue Doppler Imaging (TDI)

All moving objects intersected by the ultrasound beam generate Doppler shifts. For study of blood flow, Doppler signals from moving heart structures such as valve leaflets are removed by selective filtering, since they would generate high-amplitude artefacts. The filtering is possible because the characteristics of Doppler signals from blood and tissue are markedly different: blood generally has high velocities, and relatively low signal amplitude since the red cell scatterers are relatively sparse. Conversely, muscle and

Fig. 1.33 The velocity indicated by a color display is determined both by the true velocity, and the angle at which the flow vector intersects the scanning beam

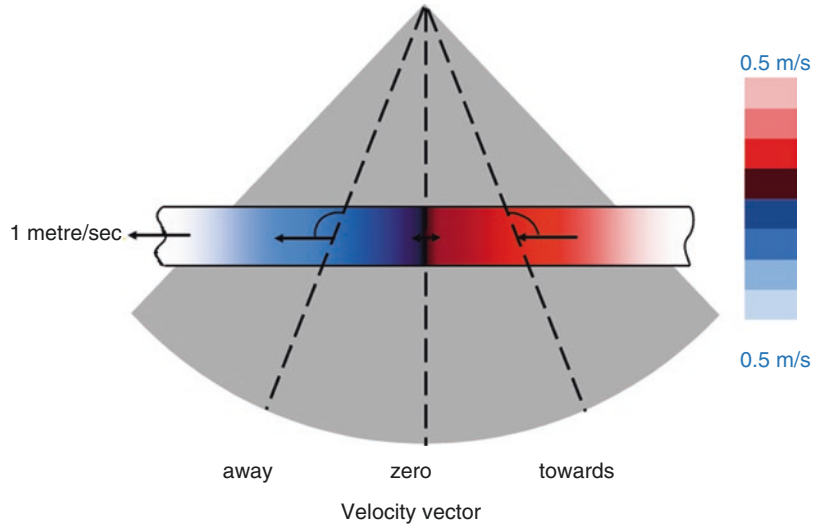
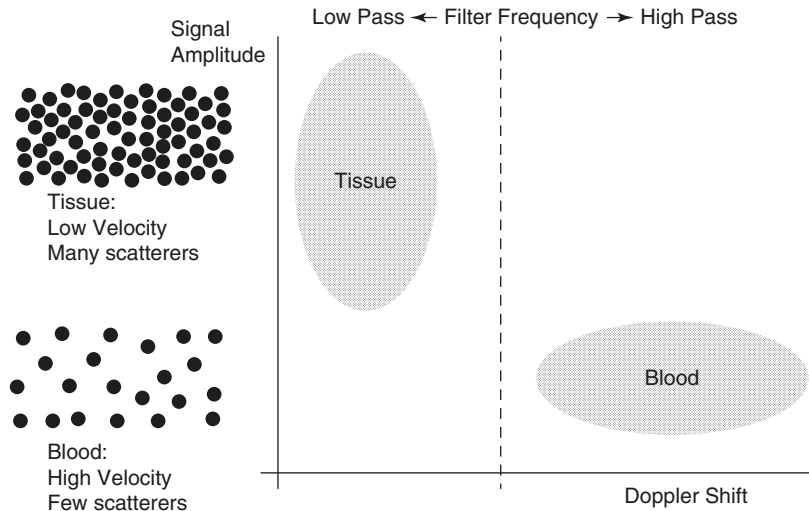


Fig. 1.34 By selectively filtering out high velocities, Doppler signals from tissue are displayed and those from blood are suppressed, and vice-versa



valve tissue have much slower velocities and higher signal amplitudes as the cells are packed together (Fig. 1.34). The extent to which low velocities are removed can be controlled by the operator; excessive low-velocity attenuation causes a dark band either side of the zero-velocity baseline and is undesirable for recording, say, venous flows.

If, instead of removing low velocities, the high velocity signals from blood are filtered out and the velocity and amplification scales suitably adjusted, Doppler signals from tissue motions can be recorded, either as PW spectral displays or in color (2-D or M-mode) (Figs. 1.35 and 1.36).

Power Mode (Amplitude) Imaging

As stated previously, the Doppler Shift is determined by velocity, but the intensity of the Doppler signal relates to the *number* of scatterers within the ultrasound beam. If there are a lot of scatterers, but they are moving in random directions, the net velocity will be zero, but the amplitude of the Doppler signal remains high (Fig. 1.37). Thus, a display showing the amplitude or power of the Doppler signal shows the *density of scatterers*, regardless of their *velocities*. This type of display is used, often in conjunction with harmonic mode, in contrast studies (Table 1.3).

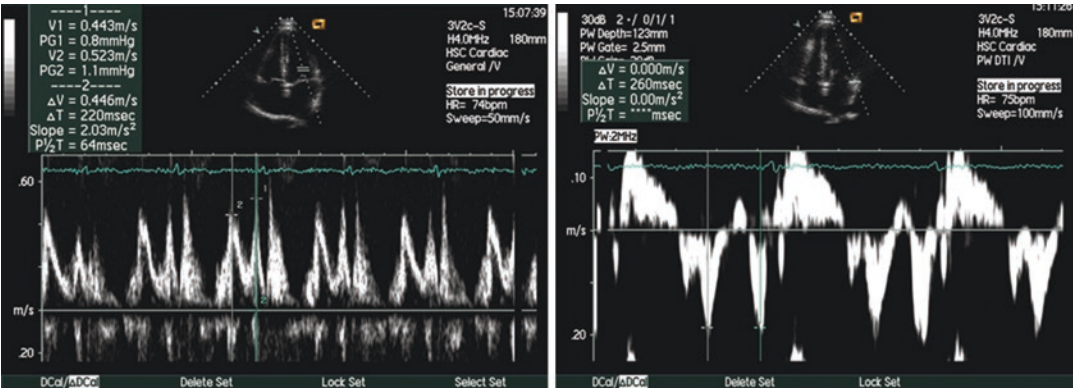


Fig. 1.35 Doppler recordings showing (Left) blood velocity through the mitral valve and (Right) the velocity of the valve annulus

Fig. 1.36 Tissue velocity shown in the form of a colour M-mode

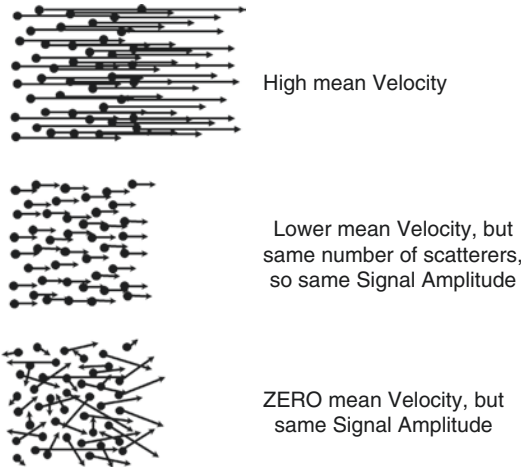
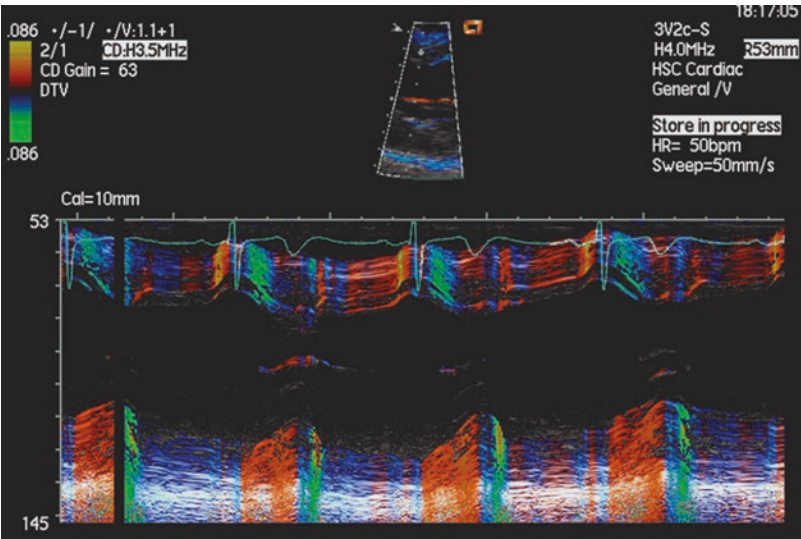


Fig. 1.37 Doppler signal Amplitude is determined by the number of scatterers, and is independent of their velocities

Table 1.3 Summary of Doppler modes

Doppler mode	Display
Spectral:	Velocity:
Continuous wave (CW)	Blood: high velocities
Pulsed wave (PW)	Tissue: low velocities
High PRF	Signal amplitude (power):
	Blood: low amplitude
Color flow mapping (2-D and M-mode)	Tissue: high amplitude
Fundamental & harmonic	Strain rate

Continuous-Wave (CW) Spectral Doppler

Instead of the brief pulses used for imaging, Continuous Wave (CW) Doppler requires transmission of a continuous train of sinusoidal ultrasound waves, and simultaneous reception of the returning backscattered echoes. This is achieved either by using a special dedicated transducer (commonly referred to as a 'pencil probe') containing two separate crystals, or by assigning the crystal elements in the imaging transducer to two groups, one for transmission and the other to detect the echoes. CW Doppler provides quantitative data on blood velocities of any magnitude, enabling flow volumes and pressure gradients to be calculated.

The Continuity Equation and Flow Through a Restricting Orifice

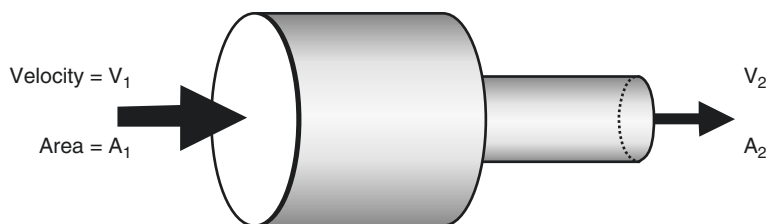
Referring to Fig. 1.38, if a fluid, which is not compressible, flows along a rigid-walled pipe, the amount entering one end of the pipe must be the same as that leaving the other end. If the

diameter of the pipe changes, this still holds true, so a reduction in cross-sectional area is compensated for by an increase in mean velocity. This principle, known as the Continuity Equation, can be expressed as $A_1 \times V_1 = A_2 \times V_2$. Provided three of the terms in the equation are known, the fourth can be derived. This is used, for example, to determine the valve orifice area in aortic stenosis. The orifice is too small and irregular to be measured directly, but if the area of the outflow tract up-stream is measured, together with the up-stream and trans-valvular velocities, then the valve area can be calculated.

Figure 1.39 shows the application of Bernoulli's Equation to the pressure-velocity relationships in mitral valve stenosis. In this example, and most clinical cases of obstructed blood flow (valve stenoses, aortic coarctation, restrictive VSD, etc.) the upstream velocity is small compared to the downstream velocity and the difference is further magnified when the values are squared, making it admissible to omit this term. In this case, the equation becomes:

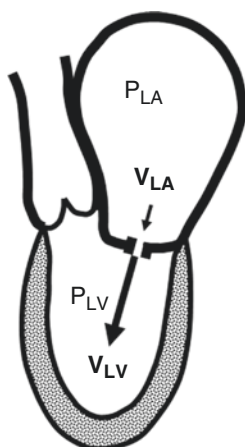
$$P_1 - P_2 = 4 V^2$$

Fig. 1.38 The Continuity Equation



Same volume per second flows in each section, therefore: $A_1 \times V_1 = A_2 \times V_2$

Fig. 1.39 Application of Bernoulli's Equation to left heart pressure-velocity relationships in mitral stenosis



	Pressure Energy	Velocity Energy
Left Atrium:	P_{LA}	$1/2 \cdot \rho \cdot (V_{LA})^2$
Left Ventricle:	P_{LV}	$1/2 \cdot \rho \cdot (V_{LV})^2$
$(\rho = \text{Blood Density})$		

Pressure Energy Lost = Velocity Energy Gained

$$P_{LA} - P_{LV} = 1/2 \cdot \rho [(V_{LV})^2 - (V_{LA})^2]$$

Since V_{LA} is usually small, $(V_{LA})^2$ can be ignored

$$P_{LA} - P_{LV} = 1/2 \cdot \rho \cdot (V_{LV})^2$$

$$\text{Pressure Gradient} = 4x(\text{Jet Velocity})^2$$

when pressure is measured in mmHg and velocity in metres/second. This is the simple, easily memorized relationship, first introduced into clinical cardiology by Dr. Liv Hatle and colleagues in 1978, has largely superseded invasive pressure measurements for evaluation of cardiac lesions.

Successful application of CW Doppler to measure pressure gradients requires some appreciation of its limitations, the greatest of which is the requirement to align the ultrasound beam with the direction of blood flow. Application of the Doppler Equation requires that the angle between the ultrasound beam and the blood flow be known, or for the angle to be sufficiently small that its cosine is effectively unity. In practice this means aligning the beam to within 15° of the flow, for which the cosine is 0.97 and the error in the value of $(\text{velocity})^2$ is $<7\%$.

One potential disadvantage of CW Doppler is that it provides no information on the distance at which a flow signal is detected, since it employs a continuous stream of waves, and cannot detect the round-trip time of any individual echo. It therefore cannot indicate the distance to any moving blood stream, and if it encounters more than one (e.g. normal ventricular inflow through the mitral valve together with a regurgitant stream from the aortic valve), it superimposes the two. Although this appears to be a major problem, it usually is not the case in clinical practice, since identification of the source of a high velocity jet is usually apparent from the image and from the flow velocity profile. It was, however, to overcome this limitation that an alternative form of Doppler display pulsed wave (PW) was developed.

Is Ultrasound Safe?

Ultrasound is a form of energy, and at high power levels can be used to coagulate tissues, heat deep muscles or clean dirty surgical instruments. Potential harmful effects are related to the beam intensity and ultrasound frequency. The energy lost through attenuation as the beam passes through tissues is converted to heat. The

peak intensity as the ultrasound pulse passes may be quite high, but in pulsed modes (but not CW), there are large gaps between pulses (pulse duration $2\ \mu\text{s}$, interval between pulses $200\ \mu\text{s}$) so the average heating is quite low. The term used to express this is Thermal Index and is the ratio of the actual beam power to that required to raise the temperature of a specific tissue by 1°C . A particular issue arises with trans-oesophageal scanning, where the transducer face is in contact with the esophagus and local heating could, in the event of a fault within the transducer, cause tissue necrosis. For this reason, the probe tip temperature is monitored and there is an automatic thermal cut-out in the event it becomes too high.

The pressure fluctuations within tissues as the ultrasound waves travel through them can be quite high. The potential for harm is quantified by the Mechanical Index, a parameter derived by dividing the peak negative wave pressure by the square root of the ultrasound frequency. Transthoracic scanning has caused hemorrhagic lesions on the lung surface of monkeys at MI 1.8. For this reason, most commercial cardiac scanners limit the maximum power to MI 1.1.

The fact is that in over almost half a century of use, involving millions of scans in a wide variety of clinical settings (including trans-vaginal fetal imaging), no case of harm to a patient from diagnostic ultrasound has ever been documented. By any standards the risk-benefit ratio of diagnostic ultrasound is negligibly low, but there is no such thing as zero-risk and to minimise it the user should always employ the 'ALARA' principle (As Low As Reasonably Achievable) for machine power levels and patient exposure times.

Conclusions

The modern echo machine derives a great deal of information from echoes generated from the ultrasound beam it transmits into the body. These include specular echoes from which real-time 2-D/3-D images and M-mode traces are formed to study cardiac structures and their motion

patterns; and Doppler signals from backscattered from blood and tissues that can be processed to provide spectral displays and color flow maps. Additional processing produces derived data such as strain rate and power mode imaging. It can be likened to a toolkit, all powered by a single source, the ultrasound beam. Each tool has its

own particular applications; to use it optimally requires appreciation of its features, strengths and weaknesses. Together they form a powerful, non-invasive diagnostic armoury, which has revolutionised cardiac diagnosis in almost every area of clinical activity from primary care to the operating room.

Conducting a Cardiac Ultrasound Examination

2

Jayne Cleve and Marti L. McCulloch

Introduction

This chapter will serve as a guide to getting started in the conduct of a two-dimensional (2D) chest wall echocardiogram. Standard views and how to obtain them will be covered while specific controls and optimization of the images will be addressed in a subsequent chapter. Echocardiography is a noninvasive procedure which illustrates the anatomy of the heart, including valves, chamber size, wall motion, masses, pericardial fluid and many other findings. Doppler echocardiography assesses the severity of valvular regurgitation, gradients across normal and stenotic valves or between cardiac chambers and the detection of intracardiac shunts.

surrounded by the lungs lying within pleural membranes. The bony structure of the ribs and the air within the lungs provide a formidable obstacle to access of the heart using ultrasound. Fortunately, there are small acoustic windows beneath the third, fourth, and fifth intercostal spaces for 2 or 3 cm to the left of the sternal border. Having the patient rotate into a left lateral decubitus position also helps with image acquisition as the heart will shift leftward from under the sternum.

A typical cardiac ultrasound transducer (probe) is seen in Fig. 2.1. Note the raised notch on the side as all probes have a notch or groove on one side of the transducer which corresponds to a symbol or icon on the ultrasound image. This helps in orienting the images correctly on the screen and with positioning/manipulating the probe on the patient's chest. Figure 2.2 shows the

Normal Cardiac Anatomy

A normal heart is comprised of four cardiac chambers and four cardiac valves. Ultrasonic access to these chambers and valves would be easy if it were not for the fact the heart is protected by the rib cage. Additionally, the heart is



Fig. 2.1 A typical cardiac ultrasound transducer. The raised indicator on one side corresponds to a marker on the image and is used to orientate the probe when scanning

J. Cleve (✉)
Cardiac Diagnostic Unit, Duke University Hospital,
Raleigh, NC, USA
e-mail: jayne.cleve@duke.edu

M. L. McCulloch
CV Ultrasound, Siemens Healthcare, Siemens
Medical Solutions USA, Inc., Malvern, PA, USA

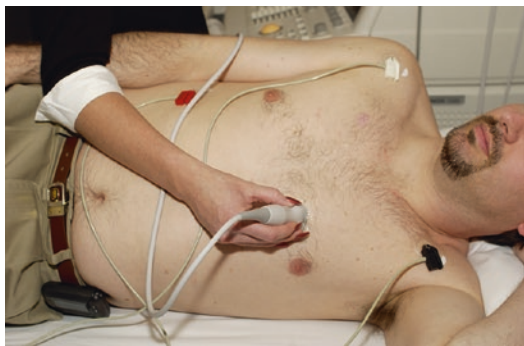


Fig. 2.2 Typical transducer position along the left sternal border. Note that the patient is turned into a left lateral decubitus position

typical transducer position on the chest along the left sternal border. Additional access can be obtained from the apical, subcostal and suprasternal approaches. Some of these approaches are more useful in Doppler echocardiography where it is important to be parallel to blood flow and not so important to be perpendicular to cardiac structures. For imaging purposes where it is important to be perpendicular to structures for the best reflections of the ultrasound, approaches such as the left parasternal window are best.

Standard Imaging Planes

Two-dimensional echocardiography allows for the detection of pathology and the ability to define spatial relationships between the valves and cardiac chambers. Through the acquisition of multiple two-dimensional ultrasound imaging planes, a three dimensional perspective of the heart can be gained. The following is a basic protocol to acquire and interrogate intracardiac structures in a standardized fashion.

Left Parasternal Window

Long-Axis View of the Left Ventricle

This is the standard view obtained at the start of a typical transthoracic echo. The position of the transducer is placed in the fourth intercostal space along the sternal border with the notch of the

transducer pointed to the patient's right shoulder. The landmarks to look for are the mitral valve in the center of the picture, the aortic root, and the left ventricular cavity aligned and open. The left ventricular apex is usually not visualized due to interference from air in the lungs. An example of this view is seen in Fig. 2.3 (a) in diastole and (b) systole. This view is used to evaluate LV chamber size, performance, septal wall thickness and motion, aortic valve and aortic root, overriding aorta, mitral valve and left atrial dimensions.

Long-Axis View of Right Ventricular Inflow

From the parasternal long-axis position view the long-axis of the right ventricular tract can be obtained with a slight counterclockwise rotation with medial angulation underneath the sternum. Figure 2.4 is an example of anatomy seen in this view which is used to evaluate right atrial and right ventricular dimensions, to detect mass lesions and tricuspid valve abnormalities. The landmarks to look for are the tricuspid valve in an oblique projection in the center of the image, dividing the RA at the bottom from the RV at the top.

Short-Axis Views of the Heart from Basis to Apex

Used for the evaluation of the aortic valve, the mitral valve and left ventricular wall motion, wall thickness, chamber size, and presence of apical masses. The aim here is to produce serial cross-sectional sections of the heart from basis to apex so that the entire left ventricular walls and thickening be evaluated. In addition, these views provide "surgical" planes for the evaluation of the aortic root and mitral leaflets.

Short Axis-Level of the Great Arteries

From the parasternal long-axis view the transducer is rotated clockwise approximately 90° with slight superior angulation up to the aortic valve in short-axis. The indicator of the transducer should now be pointing at the left shoulder of the patient. Figure 2.5 depicts the anatomy of a normal patient seen in this view during diastole with anatomic structures labeled. This view is commonly used to determine spatial orientation

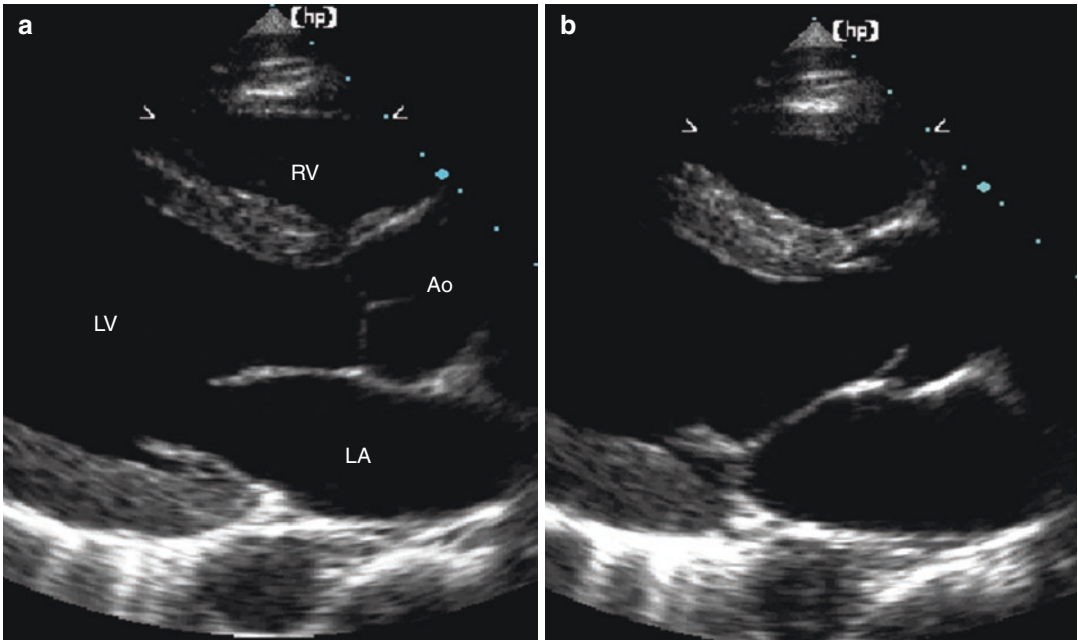


Fig. 2.3 The parasternal long-axis view in (a) diastole and (b) systole are seen in a normal patient. The anatomic chambers are labeled in (a)

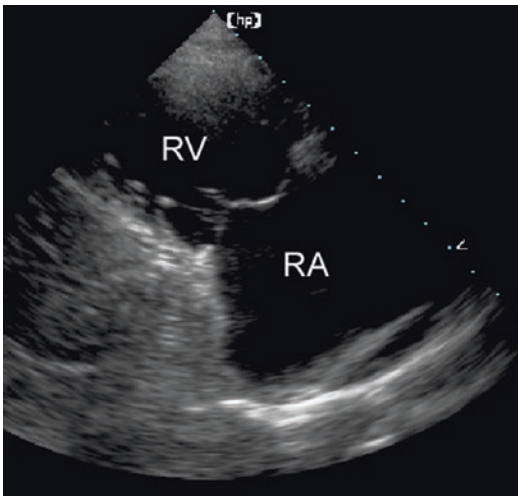


Fig. 2.4 The parasternal right ventricular inflow view is shown. Two of the tricuspid leaflets are seen between the right ventricle and atrium

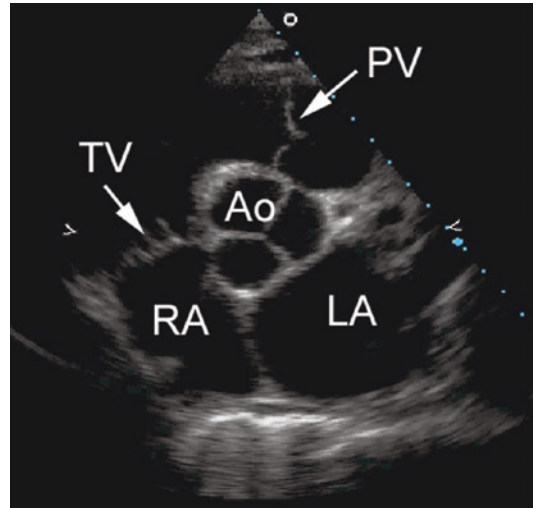


Fig. 2.5 Parasternal short-axis at the base of the heart is instrumental in determining the orientation of the semilunar valves

of the great arteries, to see enlargement and drainage of the coronary sinus, to evaluate abnormalities of the aortic, tricuspid, and pulmonic valves, and to determine location of the coronary arteries.

Short-Axis-Level of Mitral Leaflets

With the transducer in the same position as the short-axis of the aorta, a slight inferior angulation toward the patient's left hip will reveal the short-axis at the level of the mitral valve

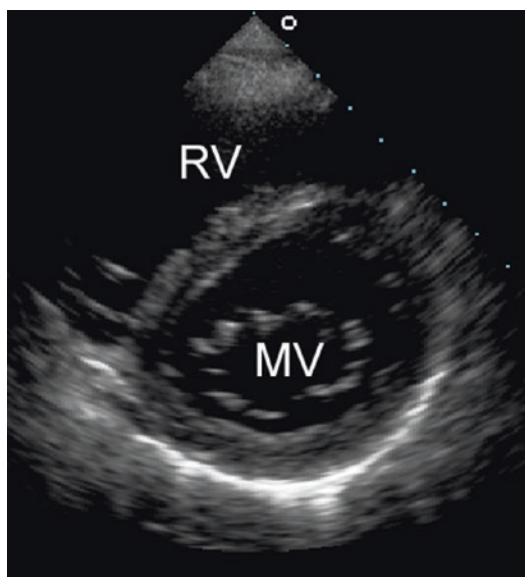


Fig. 2.6 Parasternal short-axis at the mitral valve level during diastole

leaflets. Figure 2.6 demonstrates the anatomy seen in this view, with the mitral orifice seen in diastole and labeled “MV”. This view is useful in evaluating ventricular septum, determining abnormalities of the mitral valve and tricuspid valve leaflets, and estimating the mitral orifice in mitral stenosis. This is a good view to interrogate both the anterior and posterior mitral leaflets from the anterolateral to posteromedial commissures.

Short-Axis-Level of Papillary Muscles

With a continuation of an inferior angulation of the probe from the level of the mitral valve, the papillary muscles will next appear. These anatomic landmarks can be seen in Fig. 2.7 as well as the crescent shape right ventricular cavity. Here you can locate and determine the number of papillary muscles in the left ventricle, evaluate interventricular septal motion, assess right and left ventricular chamber dimensions, detect intraventricular masses and pericardial fluid. The internal landmark here is the anterolateral papillary muscle situated at 3 o'clock and the posteromedial at 8 o'clock. It is important that the left ventricle is displayed as a circle implying that the section is truly perpendicular to the left ven-

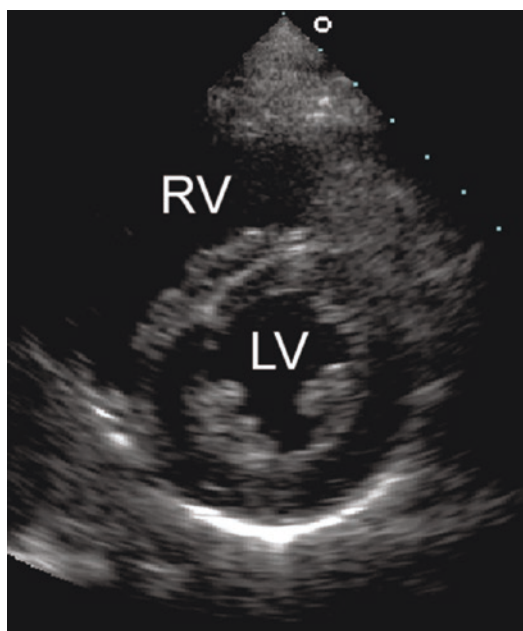


Fig. 2.7 Parasternal short-axis of the left ventricle at the level of the two papillary muscles

tricle. In some pathological conditions (RV pressure or volume overload) the septum assumes a non-circular geometry.

Apical Window

Positioning of the transducer on the patient's apex is vital for obtaining all the necessary images required for a complete transthoracic study. From the transducer position used to obtain the parasternal short-axis views, the probe is moved to the patient's axilla and placed over the point of maximum impulse (PMI). Keeping the patient in the left lateral decubitus position aids in obtaining optimal images, as seen in Fig. 2.8.

Apical Four-Chamber View

The apical four-chamber gives you the bird's-eye view of all four cardiac chambers with the atrial and ventricular septa. The indicator of the transducer is now pointing to the patient's left, downward towards the bed. This view is used for the detection of intracardiac cardiac masses, evaluation of septal defects, detection of atrial

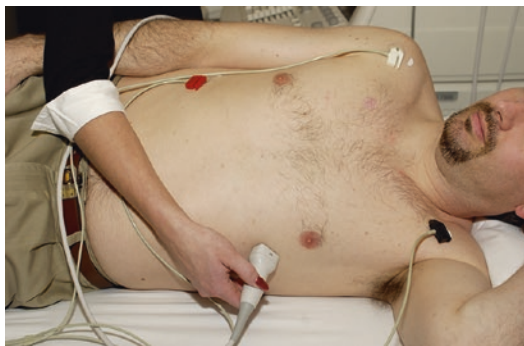


Fig. 2.8 With the patient in the left lateral decubitus position the transducer is placed at the cardiac apex or point of maximal impulse (PMI) to acquire the apical views. See text for details

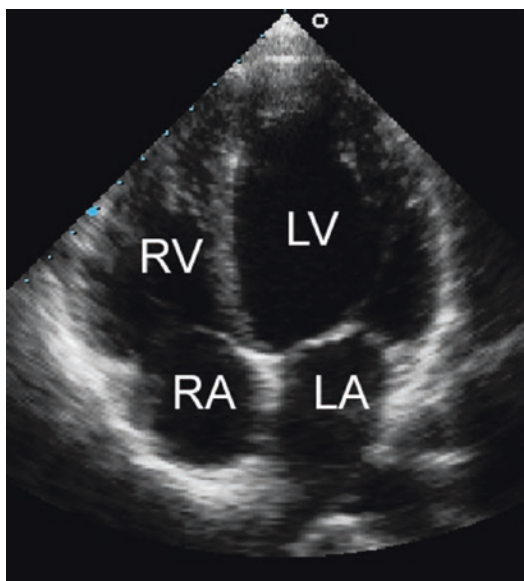


Fig. 2.9 A properly angled apical four-chamber view is shown with the chambers labeled. Adult echocardiographers display the apical views with the ventricles on to as shown. Most pediatric laboratories will electronically invert the apex so that the display is anatomically correct

and ventricular septal defects. Structural abnormalities of the atrio-ventricular valves and their tensor apparatus, evaluation of left ventricular function and imaging left ventricular apex can also be assessed. This is the best view for comparing the right versus left ventricular chamber size, as well as gauging atria size. Attention should be made to position the ventricular septum in the middle of the sector (Fig. 2.9),

although occasionally, this could be shifted more the left so that the LV free wall can better be evaluated.

Apical Two-Chamber View

From the apical four-chamber, the probe is rotated counterclockwise approximately 60° into the apical two-chamber view. With this rotation, the anterior (Fig. 2.10, arrow) and inferior wall are visualized. This view is useful in the evaluation of left ventricular function, detection of left ventricular aneurysms and intracardiac masses. The aortic valve is not visualized in this view.

Apical Long-Axis View

With an additional, approximately, 40° counterclockwise rotation, with the indicator of the probe now pointing to the patient's right shoulder, will result in the apical long-axis view, also referred to as the apical three-chamber view. Left ventricular function, imaging of the left ventricular apex, detecting left ventricular aneurysms, determining aortic override of the left ventricular septum, and detecting intracardiac masses can all be evaluated from this view. The same anatomy seen in the parasternal long-axis can be visualized here, including more of the left ventricular apex (Fig. 2.11).

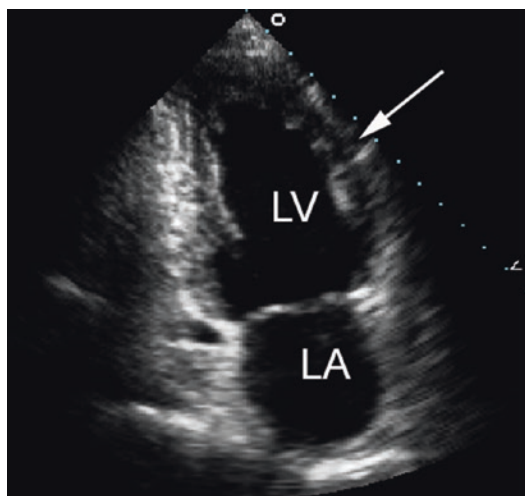


Fig. 2.10 The apical two-chamber view is seen. In this view the left ventricular anterior (arrow) and inferior walls are seen

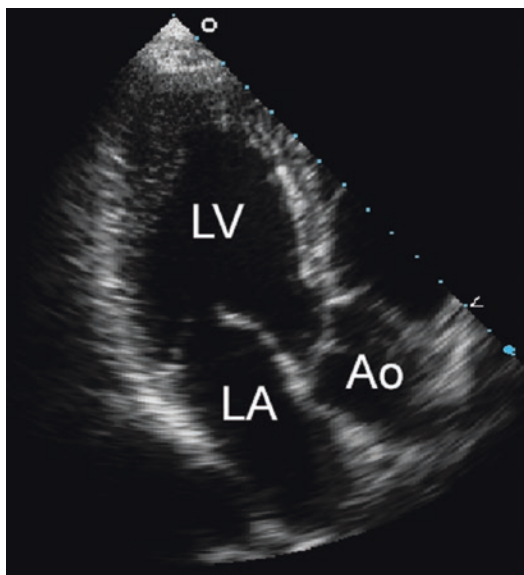


Fig. 2.11 The apical long-axis or three-chamber view demonstrates the same anatomy that is seen in the parasternal long-axis view

Subcostal Window

The subcostal approach allows visualization of the cardiac structures without obstruction from air in the lungs in many patients. With the patient supine, the probe is placed in the sub-xiphoid area, just below the sternum (Fig. 2.12), and often requires pushing down and angling the ultrasound beam under the ribcage, towards the heart.

Subcostal Long-Axis of the Inferior Vena Cava

With the probe in the subcostal window, the indicator is pointed toward the patient's head, with the probe perpendicular to the patient with a slight caudal angulation. The long-axis of the inferior vena cava (IVC) is seen coming through the liver, joining with the hepatic vein (HV) as they enter the right atrium. These anatomic landmarks are seen in Fig. 2.13. Evaluation of the inferior vena cava (size and collapsibility) and hepatic vein can be achieved, as well as the presence of a Charri network or masses within the IVC or right atrium.



Fig. 2.12 Subcostal views are obtained with the transducer positioned in the sub-xiphoid process located at the bottom of the sternum. The ultrasound beam is angled superiorly towards the heart

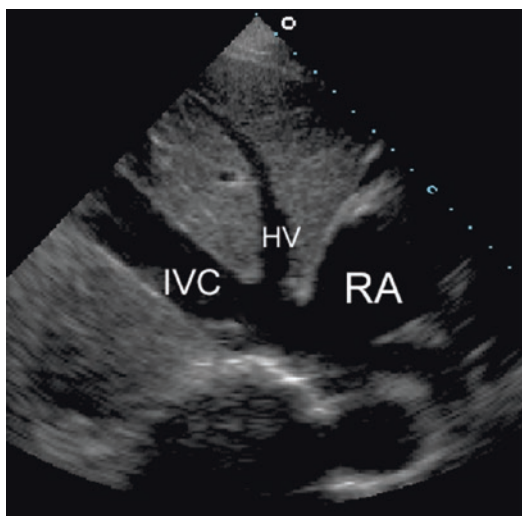


Fig. 2.13 The subcostal view is modified to show the inferior vena cava (IVC) and hepatic vein (HV) joining with the right atrium (RA)

Subcostal Four-Chamber View

From the long-axis of the IVC, the probe can be rotated clockwise 90°, flattened against the patient's skin and angled slightly laterally to obtain the subcostal four-chamber view (Fig. 2.12). The four chambers are easily seen in Fig. 2.14, which was obtained from the subcostal window. This view is useful for the evaluation of atrial septal defects, as the ultrasound beam is

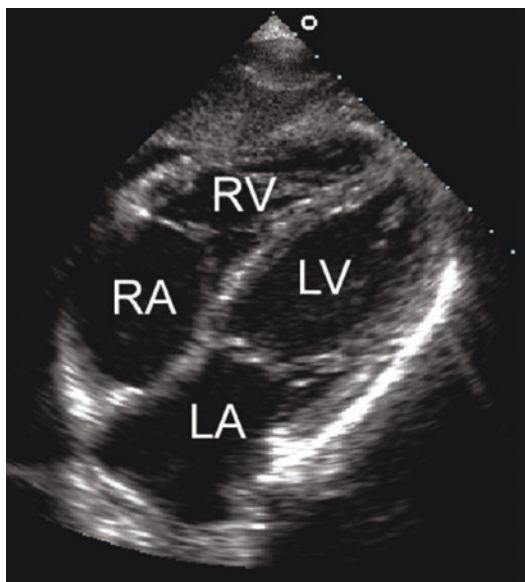


Fig. 2.14 A four-chamber view is obtained from the subcostal window. See text for details

perpendicular to interatrial septum, as well as assessing the presence of pericardial effusions.

Subcostal Short Axis-Left Ventricular Level

An approximate 50° counterclockwise rotation from the subcostal four-chamber view will bring you to a short axis view of the left ventricle. Once you obtain a short axis of the left ventricle, one can sweep from the base of the heart to the apex. Figure 2.15 is an example of the short axis of the left ventricle at the level of the papillary muscles from the subcostal window. Size and contractility of the right and left ventricles can be assessed from this position.

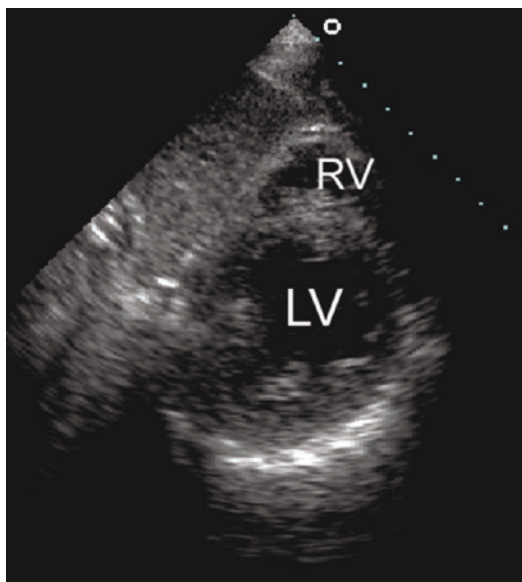


Fig. 2.15 A subcostal short-axis of the left ventricle is sometimes used when the views from the parasternal window are suboptimal



Fig. 2.16 The ultrasound transducer is positioned in the suprasternal notch. Placing a pillow underneath the shoulders and when possible, tilting the patient's neck back will allow better access to the notch

Suprasternal Window

Imaging of the aortic arch anatomy in the suprasternal window can be aided by having the patient tilting their heads slightly backwards. This position is shown in Fig. 2.16 with the patient in a supine position and the probe placed in the suprasternal notch.

Suprasternal Aortic Arch View

With the probe in the suprasternal notch and the indicator rotated towards the patient's left clavicle, the aortic arch (AA) can be visualized in long-axis. Figure 2.17 shows visualization of the aortic arch and the main branch vessels.

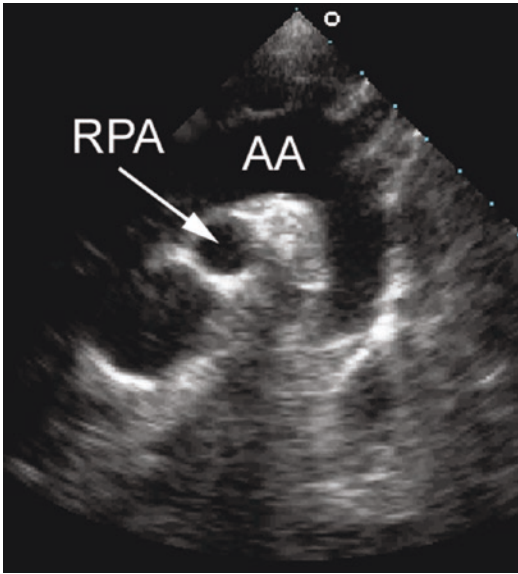


Fig. 2.17 The aortic arch (AA) and right pulmonary artery (arrow RPA) can be visualized in most patients from the suprasternal notch window

Normally, the right pulmonary artery (RPA) is seen underneath the arch in short-axis.

From here, you can determine the dimensions of the various parts of the aorta, detect and locate possible coarctation of the aorta.

Doppler Basics

Doppler analysis on the ultrasound machine, including color Doppler, are based on the Doppler effect. The Doppler effect is the perceived change in frequency that occurs between a sound source and a sound receiver. When a reflector is stationary and the transducer is stationary, no Doppler shift occurs. In the heart the constantly moving red blood cells serve as reflectors creating the Doppler effect. In cardiac ultrasound three main forms of Doppler imaging are used: color, pulsed wave with spectral display and continuous wave with spectral display of the direction and velocity of blood flow.

Color Flow Doppler

Color Doppler overlays blood flow onto a 2D or M-mode image. Figure 2.18 demonstrates flow during diastole entering the left atrium and continuing through the mitral valve into the left ventricle. The direction of flow is shown on the machine's color map seen on the right upper corner of this figure. By convention manufacturers provide a red and blue color map, with red moving toward the probe and blue moving away from the probe. In this example the flow is red since the transducer is positioned at the patient's apex. The 2D images provide a context needed to adequately interpret the color data.

Pulsed Wave Doppler

Pulsed wave Doppler samples velocities at a specific point along the beam axis. A sample gate designates the sampling point and its position within a 2D image. In Fig. 2.19 the sample gate is positioned within the right atrium just below the tricuspid valve in this apical four-chamber view. While you can sample the flow in a specific area by moving the sample gate higher velocities are subject to aliasing when they exceed the Nyquist limit. In this patient with tricuspid regurgitation the systolic spectrum has wrapped around (aliased) and you are unable to see the true velocity.

Continuous Wave Doppler

Continuous wave Doppler possesses a clear advantage over pulsed wave in its total lack of a Nyquist Limit. This means that the high velocity flows will not alias and in Fig. 2.20 the tricuspid regurgitation which aliased with pulsed Doppler can now be visualized. For accurate velocities it is also of primary importance to have the beam axis at an angle as close as possible to 0° (parallel) with blood flow. Continuous wave Doppler is not depth-specific as the machine samples all along the beam axis, sending and receiving Doppler signals constantly.

Fig. 2.18 Color Doppler example of flow during diastole entering the left atrium and continuing through the mitral valve into the left ventricle. See text for details

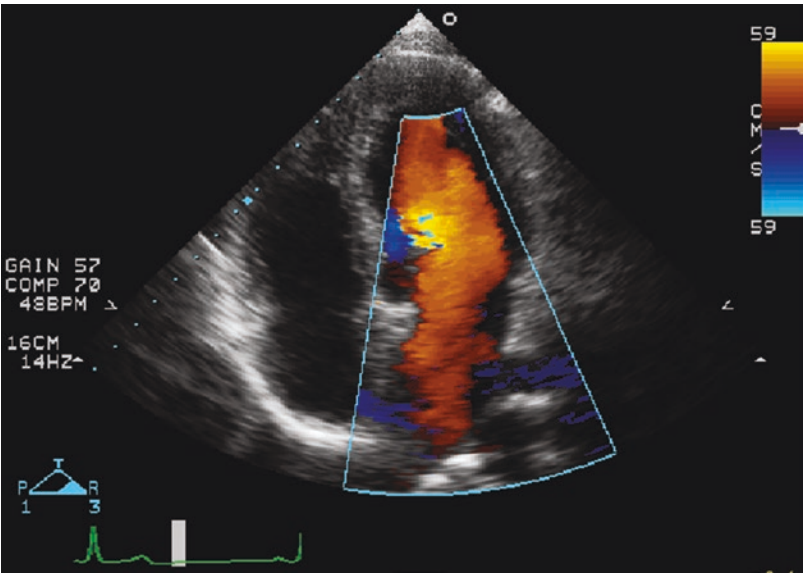


Fig. 2.19 Pulsed wave Doppler with the sample volume placed on the right atrial side of the tricuspid valve. The spectral display shows aliasing of the high velocity tricuspid regurgitation jet

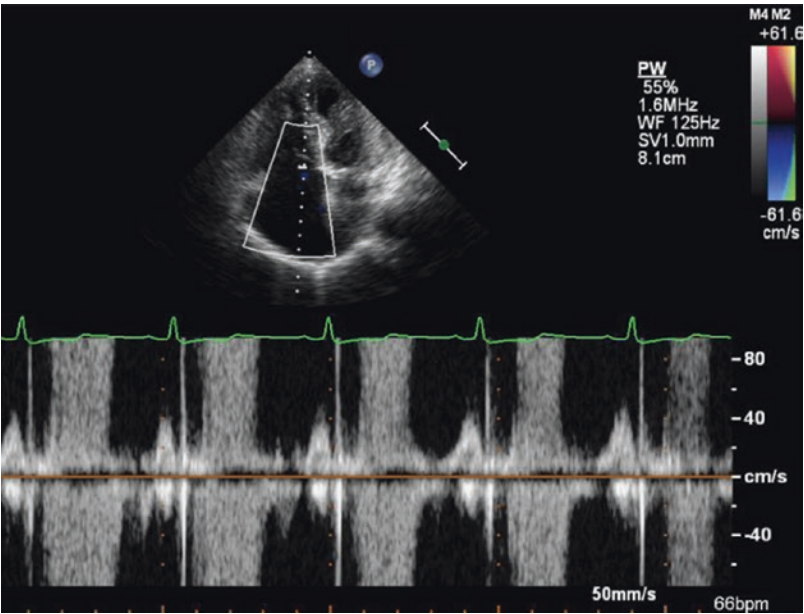
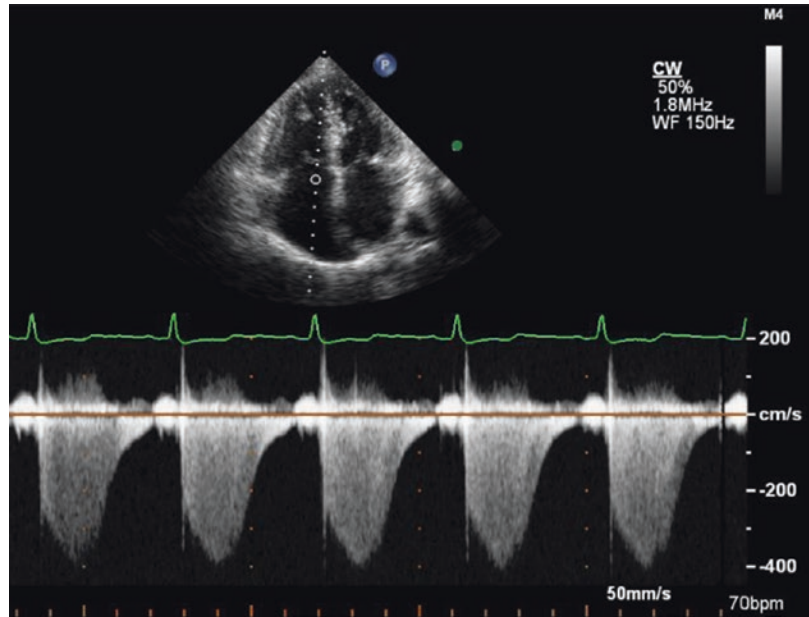


Fig. 2.20 Continuous wave Doppler in the same patient as Fig. 2.19 showing the entire spectral display without aliasing so that the peak systolic velocity can be measured



Conclusions

This chapter should serve as a starting point for the acquisition of standard 2D and Doppler transthoracic echo images. It is, by no means, comprehensive and all echocardiographic studies should include both standard and nonstandard views.

Many of these views are used in Doppler studies or in evaluating specific pathologies and will be covered in subsequent chapters. Optimizing these views requires the understanding and application of system controls which will be covered in the next chapter.

Machine Controls and Optimizing the Images

3

Marti L. McCulloch and Jayne Cleve

Introduction

It is crucial for those performing an echocardiographic examination to understand how the controls on an ultrasound machine alter the display. Without this knowledge, it is impossible to consistently optimize images. Unskilled manipulations may misrepresent diagnostic information and result in missed diagnoses. This chapter aims to describe controls found on most ultrasound machines, how they affect the image, and how they are used to optimize the ultrasound image. Table 3.1 describes the most commonly used controls for two-dimensional (2D) imaging.

Preparing the Machine

Preset

After providing power to the machine itself, be sure to define basic parameters for the test by choosing an appropriate *preset*. The preset provides a starting point for such basic machine settings as depth, gain, and process settings. The

operator can adjust all of the machine's variables from the initially fixed settings as needed. On most machines adjustments to the preset can be permanently saved under a different preset name when desired.

Patient Identification

Patient identification and any other relevant information should be entered into the machine. Relevant information outside of the patient's name and medical record number may include date of birth, sex, the person performing the examination, location (Clinic or Ward) or any number of other qualifiers for later reference.

Transducer Selection

A transducer must be connected to the machine and be selected from other possible transducer options. A high transducer frequency may be selected for most children and pediatric population (higher resolution) while for adult patients a lower frequency transducer will provide better penetration and target acquisition.

The four most common modes used during the examinations are two-dimensional gray scale imaging (2D), color Doppler (Color), pulsed wave Doppler (PW), and continuous wave Doppler (CW). The usual buttons or

M. L. McCulloch
CV Ultrasound, Siemens Healthcare, Siemens
Medical Solutions USA, Inc., Malvern, PA, USA

J. Cleve (✉)
Cardiac Diagnostic Unit, Duke University Hospital,
Raleigh, NC, USA
e-mail: jayne.cleve@duke.edu

Table 3.1 The most commonly used controls for two-dimensional (2D) imaging

2D variable	Knob(s)	Function
Gain	Gain	Amplifies returning signals before display
TGC	TGC toggles	Selectively amplifies returning signals before display (horizontally)
Compression	Compression	Changes the difference between the highest and lowest received amplitudes (shades of gray)
Power	Power (dB)	Controls rate at which energy is propagated into an imaged medium
Frequency	Dependent on probe	Determines number of times per second a sound wave completes a cycle
Focal zone	Focal zone	Alters the placement of the narrowed region that designates an area of improved resolution
Depth	Depth	Selects how shallow or deep an area is imaged
Sector size	Size, trackball	Narrows or widens the image sector
Zoom	Zoom	Magnifies a particular area of interest within the sector
Freeze	Freeze	Stops or starts live imaging
Measurement	Freeze, caliper, trace, enter, erase	Quantifies features of a 2D image
Harmonics	Harmonics	Uses frequencies created by the tissues, rather than the fundamental frequency, to create an image
Annotation	Annotation	Adds text or picture to image

markers to enable these modes are: *2D*, *Color*, *PW*, and *CW*. Other scanning modes, such as *M-mode*, *3D* and *tissue Doppler*, are often available. For simplicity, the focus in this chapter

will be on the controls that affect the four primary modes previously listed.

Monitor Setup

During a 2-D scan, cardiac function and anatomical morphology take center stage. Granted there is definitely an art to performing a cardiac ultrasound, however there are adjustments that can increase the image quality without manipulating the transducer location. First and foremost, prior to imaging, the monitor needs to be adjusted according to the ambient light within the room. Failure to do so can lead to poor quality real-time images and a mismatch between what the images look like on the machines and how they display on other workstations. Depending on the individual, the monitor can be adjusted to provide either a smooth or crisp image simply by adjusting the contrast level on the monitor. In order to achieve a smoother image appearance, decrease the contrast and for a crisper image appearance increase the contrast level on the monitor. In addition, the brightness level should be adjusted to according to the room brightness. Typically, begin with the brightness level in the middle range and increase or decrease with respect to background preference (black or gray) and according to ambient light. Additionally, it is a good idea to periodically check the reading room monitor as well. Once the monitor has been appropriately adjusted, the next step to improving image quality, other than transducer manipulation, is to adjust the control settings of the system.

2D Imaging and Basic Image Manipulation

Gain is the most important variable to adjust during a study. It is also the one control that is most often misused. Overall gain controls the degree of amplification that returning signals undergo before display. Having too little gain will lead to an image where the anatomic structures are not visualized (Fig. 3.1a). The appropriate amount of

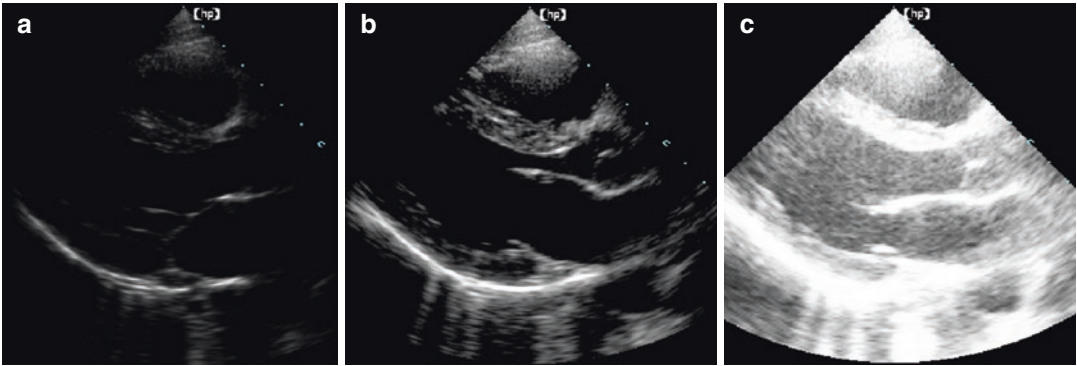


Fig. 3.1 (a–c) Parasternal long-axis view demonstrating the effect of gain on an image. Insufficient gain is seen in “a”, sufficient gain in “b” while the image in “c” is over gained destroying resolution

gain for a picture becomes apparent when reflectors and tissue interfaces can be seen, but fluid and blood appears black and echo-free (Fig. 3.1b). Myocardium should be adequately dispersed with reflectors, but the muscle should not approach the look of a solid white band. Only the pericardium, certain states of abnormal thickening, calcification, tissue infiltration, or surgically altered valves should be hyperechoic (very bright). The myocardium should display a range of grays controlled by the operator with gain (brightness) incrementally added as needed. One of the most common mistakes is to add too much gain to a picture as is demonstrated in Fig. 3.1c. While this can make the picture brighter and structures more obvious over gaining will decrease image resolution.

TGC is the second post-processing function of the receiver and is commonly known as Time Gain Compensation (*TGC*). Time Gain Compensation adjusts for the variable energy loss due to attenuation. Attenuation is the loss of intensity and amplitude of ultrasound energy as it travels deeper into the body. Strong returning signals from the near field (close to the transducer) need to be suppressed while signals from the far field (deeper depths) require higher amplification.

TGC is seen on the machine as a column of toggles that can be slid along a horizontal plane (Fig. 3.2). By sliding a toggle to the right, the operator increases the gain at that given depth. The *TGC* toggles are normally placed at a diagon-

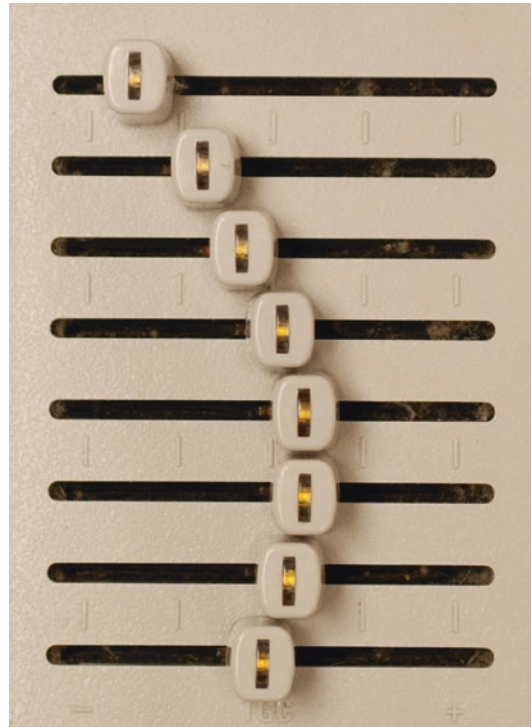


Fig. 3.2 Time Gain Compensation (*TGC*) slider controls showing an increase setting in the far field as the toggles are moved to the right

nal slope of variable steepness. The upper or near field toggles are often set at a lower degree of compensation, while the lower, far field toggles are often set to boost returning signals in the far field. A pattern of gradual change from one toggle to the next avoids a “striped” look to the ultrasound picture (Fig. 3.3).

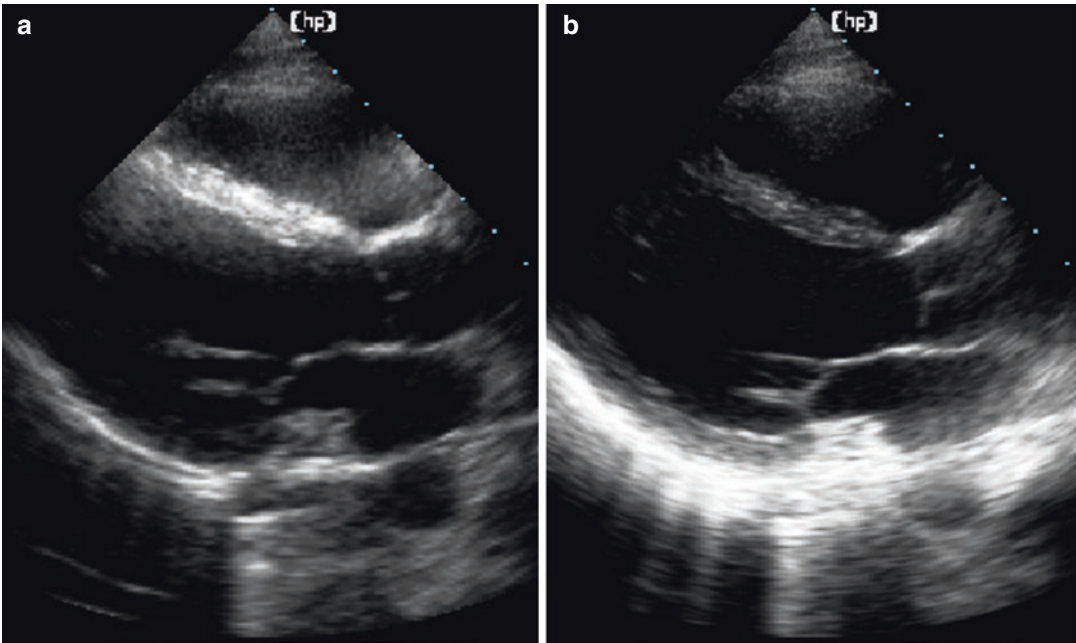


Fig. 3.3 Parasternal long-axis images showing the improper application of the TGC control. Image “a” shows excessive gain in the septum while “b” has too much gain in the posterior pericardial area

Compression/dynamic range is equivalent to the number of shades of gray seen in the image and is just as important as gain. Compression can decrease or increase the difference between the highest and lowest echo amplitudes received. Compression takes the received amplitudes and fits them into a gray scale range the machines can display. Dynamic range expresses how many shades of gray appear within the image. By increasing the compression, the image displays more shades of gray. Areas of medium amplitudes of gray, such as myocardium, may be better resolved. Decreasing the compression provides a highly contrasted image with strong white and black components. While sharply decreasing the compression may improve structure delineation, it will sacrifice low amplitude targets. Most presets start at roughly midlevel value of compression/dynamic range and gain.

Power can be indirectly assessed by *decibel (dB)* settings, *Mechanical Index (MI)* and *Thermal Index (TI)*. Power, expressed in watts (W) or milliwatts (mW), describes the rate at which energy is propagated into the imaged medium. Intensity is a concept that closely relates

to power. Intensity is power per unit area (mW/cm^2 or some unit variation). Intensity may not be entirely uniform throughout tissues but will more accurately predict risk of bioeffects than power levels. When looking at an image, simply changing the output power from the transducer appears to have a similar effect as changing the overall gain on the receive end. The difference is that gain settings do not change the amount of energy in tissues whereas power/intensity does. The overall gain works with signals that have already traveled through tissues and as a rule—you should always *work with gain variables before ever reaching to change the power*. Recognize the power knob by its unit of measurement. Most machines do not describe the power level in watts or Milliwatts. Instead, they indirectly describe power in terms of *decibels (dB)*.

Because the exact power or intensity levels are not apparent, manufacturers began to put two more variables on the screen to help clinicians to estimate power and intensity levels. The two variables are the *Mechanical Index (MI)* and the *Thermal Index (TI)*. Mechanical Index (MI) is intended to convey the likelihood

of *cavitation* resulting from the ultrasonic energy during the exam. Cavitation refers to activity of created or pre-existing gas bubbles within the tissues due to ultrasound energy. Thermal Index (TI) is the ratio of output power emitted by the transducer to the power needed to raise tissue temperature by one degree Celsius.

Frequency is defined as the number of cycles per second. The frequency of most cardiac ultrasound probes range between 2.5 and 7 mega (million) Hertz (MHz). The frequency of the ultrasound probe has a dramatic effect on image quality (Fig. 3.4). *Higher frequency transducers* have a smaller wavelength and *better axial resolution* (Fig. 3.3a). *Resolution* is the ability to detect two targets positioned closely to one another. Improved resolution generates a more accurate anatomic rendering. The lower the frequency, the more effective it is in penetrating tissue and not falling subject to attenuation. Unfortunately, *low frequency transducers* yield *poorer resolution* in their resulting images when compared to high frequency images (Fig. 3.3b).

Lower transmitted frequencies provide deeper tissue penetration but less resolution than higher frequencies. There is always a trade off and imaging at higher frequencies, while giving you images with better resolution, will have with less tissue penetration.

Echocardiograms on pediatric or easy to image adult patients should be performed using a high frequency transducer. While the imaging frequency is dependent on the transducer used, each probe has a *frequency bandwidth*. Some machines have a wide-bandwidth and allow an operator to select a part of the bandwidth spectrum to make the images.

Focal Zone

The ultrasound beam is not necessarily the same width as it travels into the depths of tissue. Many systems use a technique known as *focusing*. Focusing the ultrasound beam is a process accomplished by mechanical or electronic means. As the beam proceeds deeper into the tissue, the beam

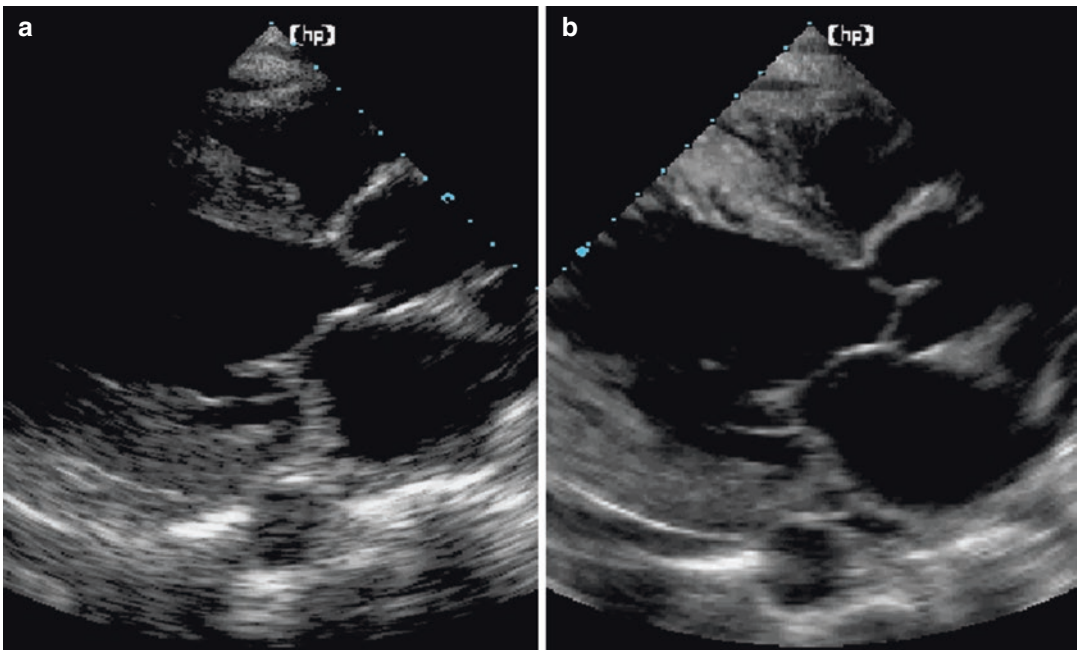


Fig. 3.4 Two images showing the effect of using a low frequency transducer on the left (a) versus a higher frequency transducer on the right (b) in the same patient. Note the improved resolution seen on the right image

gradually tapers to a narrow region known as the *focal zone*. The central point of the focal zone is the *focal point*. The focal point of a focused ultrasound beam will have the highest intensity (mW/cm^2) of the transmitted ultrasound energy from the transducer. It also produces a higher quality image because it yields better returning signals for the machine to process and display.

Depth

All machines have a control that increases or decreases the overall image depth (Fig. 3.5). Decreasing the depth increases the frame rate by reducing the amount of information that the machine has to process and shortening the time required for the beam to travel to and return from a target of interest. Regardless of frame rate, some cardiac views require a deeper field of view for adequate anatomical display.

Sector size refers to the field of view. Reducing the width of the sector is another

excellent way to increase frame rate and isolate an area of interest. Figure 3.6 shows an example of varying the width of the ultrasound image. Just as depth will reduce the amount of information needing to be processed so will narrowing the sector.

Zoom increases the size and field of interest. Zooming an area of interest is another good way to remove unwanted information from the sector. *Zoom* can be selected on the machine and an initial zoom box will appear. Change the zoom parameters using the size and the position buttons along with the trackball, until the area of interest is adequately covered.

Freeze stops a moving cine image. While the freeze button is fairly simple and straightforward, it should not be underestimated in an instrumentation overview. When measuring *2D*, *PW*, or *CW* images, an operator must first freeze an image and sometimes scroll backward or forward in time to obtain the correct frame. Individual frames can be compared and scrolled as needed.

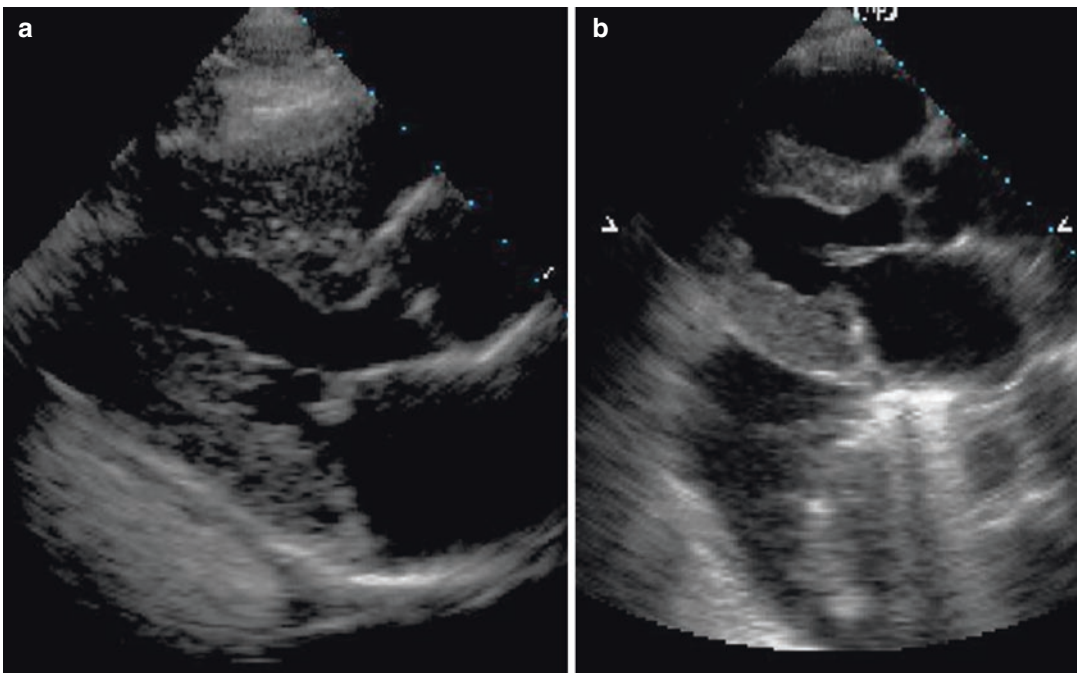


Fig. 3.5 The effect of using the Depth control is seen in these two views. Image (a) on the left was obtained at a shallower depth setting than the one on the right (b)

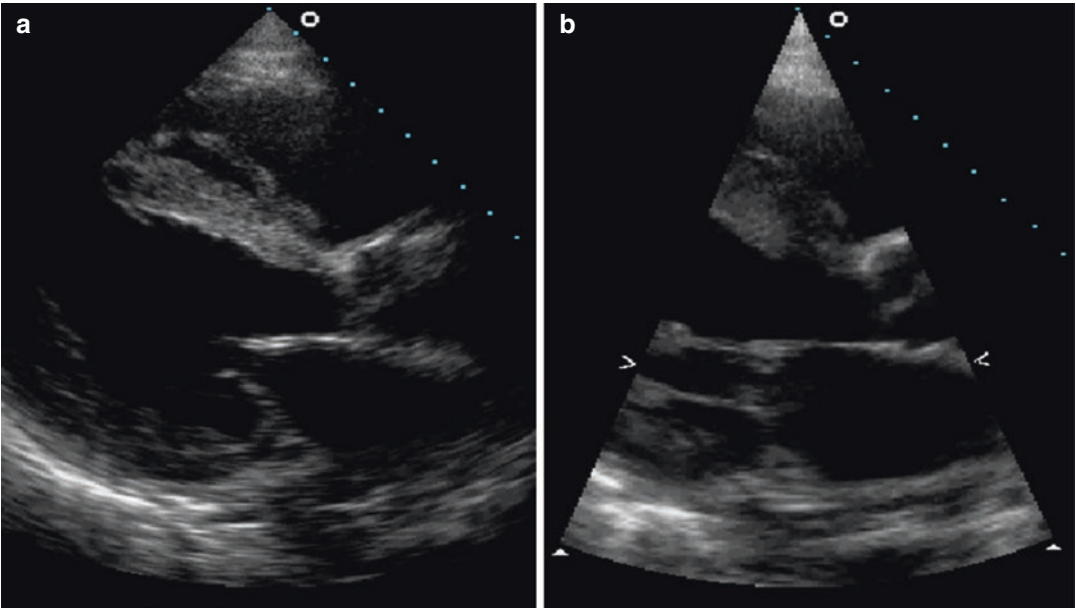
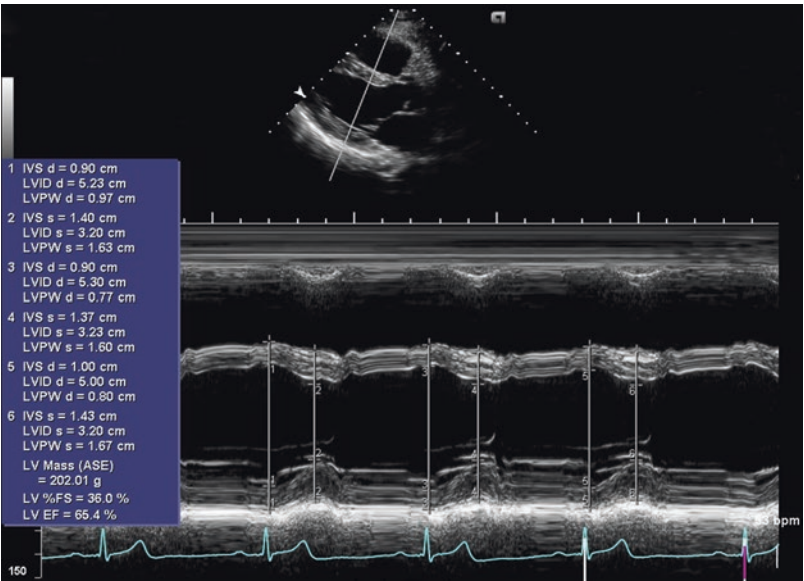


Fig. 3.6 Two images on the same patient demonstrating the machines ability to narrow the sector width. Image (a) on the left has a wider field of view than image (b) on the right

Fig. 3.7 An M-mode taken from the left parasternal long-axis view showing typical linear measurements performed on the ultrasound machine



Measurements

All echocardiographic images can be measured and quantified. Typical buttons are: *freeze*, *caliper*, *trace*, *enter*, and *erase*. Measurements of 2D and Doppler images can be made either outside

or inside of the analysis package. Figure 3.7 is an example of linear M-mode measurements made on a parasternal long-axis view. If measurements are plugged into the analysis package, the operator will need to select the *analysis* or *measurement package* button and then the proper name

for the subsequent measurement. A pair of calipers can tell you exact linear measurements of gray scale images.

Harmonics

Standard transducers transmit and receive frequencies that are the same or within a very close range. The frequency from such a transducer is known as the *fundamental frequency*. As the beam propagates through tissues, it distorts and creates additional frequencies that are multiples of the fundamental frequency. These additional frequencies are the *harmonic frequencies* and are created by the tissues themselves (Chap. 1). While the fundamental frequency may undergo a large amount of distortion, the harmonic frequencies do not. In patients with poor sound transmission due to obesity or dense muscle tissue, the harmonic frequencies may make a better image than the fundamental frequency. In fact, when using harmonics the image will likely have poorer resolution than the image created with the

fundamental frequency. During contrast studies harmonics will improve image quality whether using agitated saline or one of the new, transpulmonary contrast agents. Figure 3.8 demonstrates the differences between a fundamental image (a) and one obtained using tissue harmonics (b). Notice the increased thickness of the mitral and aortic leaflets on the harmonic image.

Annotation is an on screen text option that can label in words or pictures information related to the corresponding image. Non-standard views, unusual anatomic variations, or highly edited standard views may need some further explanation. It is also helpful to annotate when a standard view is not available or is of very poor quality. Naming anatomical landmarks, relationship to other anatomic points of reference, body positioning of the patient, or timing of events is often helpful for the interpreting physician. For example, it may be of use to label a heart as pre- or post-surgical event. Be sure to remove any comments after acquiring the specific labeled image so that later pictures do not become confusing or mislabeled labeled.

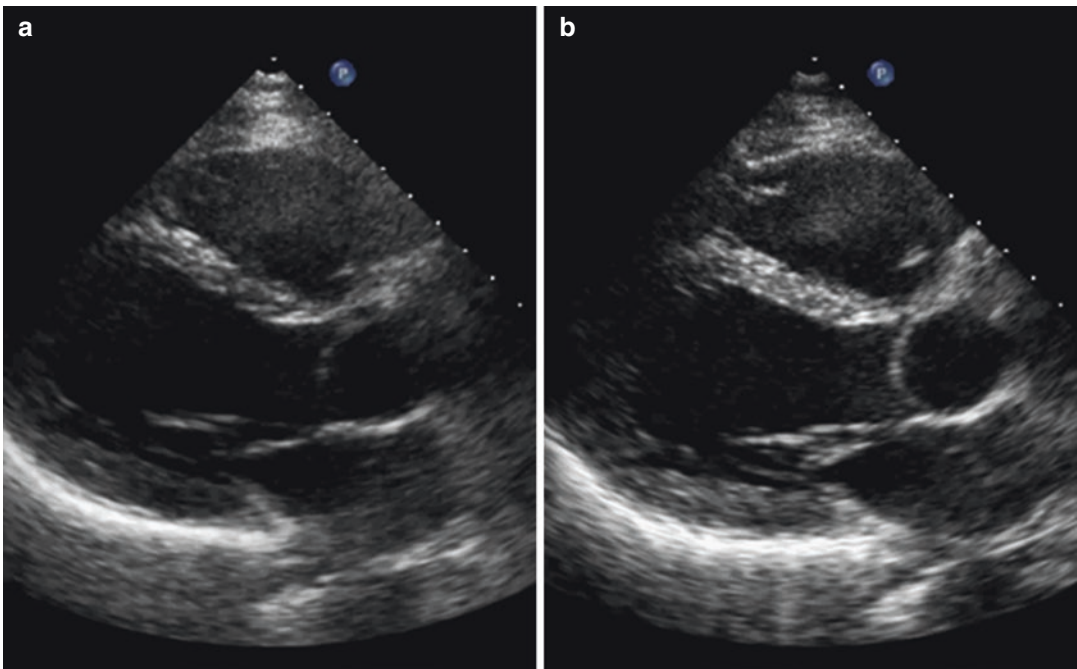


Fig. 3.8 Fundamental image on the left (a) compared to a tissue harmonic image on the right (b) in the same patient. See text for details

Color Doppler is layered over a 2D image to provide information on blood flow. All forms of Doppler on the ultrasound machine, including color flow, are based on the *Doppler effect*. The Doppler effect is the perceived change in frequency that occurs between a sound source and a sound receiver. When a reflector is stationary and the transducer is stationary, no Doppler shift occurs.

Color Doppler primarily provides data on moving reflectors of red blood cells. Stationary reflectors detected within each color packet are mostly eliminated through post processing. The machine operator can change many color display properties. The direction of flow is shown on the machine's color map. By convention manufacturers provide a red and blue color map, with red denoting flow moving towards the probe and blue for flow moving away (Fig. 3.9).

A *color invert* option will flip the color map—blue flows toward the probe, red flows away from the probe. Figure 3.10 demonstrates this color invert option but is not recommended in cardiac imaging. The *color map* can also be changed to display flows in an entirely new set of hues or intensities. Some color maps add an element of green or yellow to differentiate between laminar and turbulent flow. The color mode has an adjustable *scale*, as well. The number above and below the color map shows the range of

mean velocities that can be displayed, typically in cm/s, without aliasing.

The machine calculates an optimal scale largely based on depth. Lowering the scale number lowers the pulse repetition frequency (PRF) and therefore the Nyquist limit (Nyquist Limit = $PRF/2$). The lower scale is more sensitive to flow. Raising the scale will reduce sensitivity to flow, raise the pulse repetition frequency and Nyquist limit, and make the color display less likely to alias. Figure 3.11 demonstrates this shift in the color Doppler scale. Figure 3.11a shows flow into the left ventricle in an apical four-chamber view with the color scale set at a normal value of 61.6 cm/s. In Fig. 3.11b the color Doppler scale has been shifted to 46.2 cm/s and the normal flow into the left ventricle has now aliased. The scale should be left alone most of the time—particularly when grading valvular regurgitation. Remember that this number represents the aliasing point for the mean not the peak velocities.

The *frame rate* of the image with color Doppler is highly dependent on the machine operator. It is important to know how to raise frame rate without sacrificing diagnostic information. Use the *trackball*, *size*, and *position* controls to change the length, width, and placement of the color box. The length of the color box is of no consequence to the frame rate. However, the

Fig. 3.9 Apical four-chamber view with color Doppler showing the normal red/blue direction of the color map. Flow towards the probe is red while flow away from the probe is colored blue

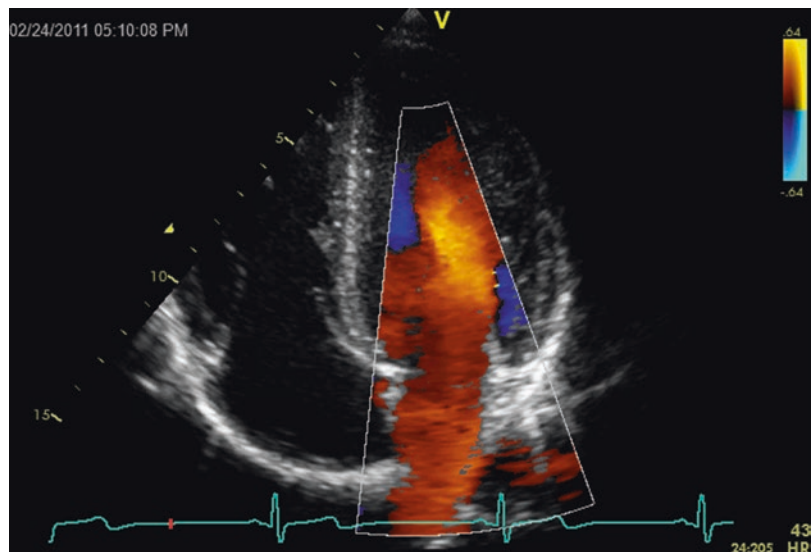


Fig. 3.10 Apical four-chamber view with color Doppler showing the color map inverted which is controlled by the user. Flow towards the probe is now blue while flow away from the probe is colored red. This is not the recommended configuration

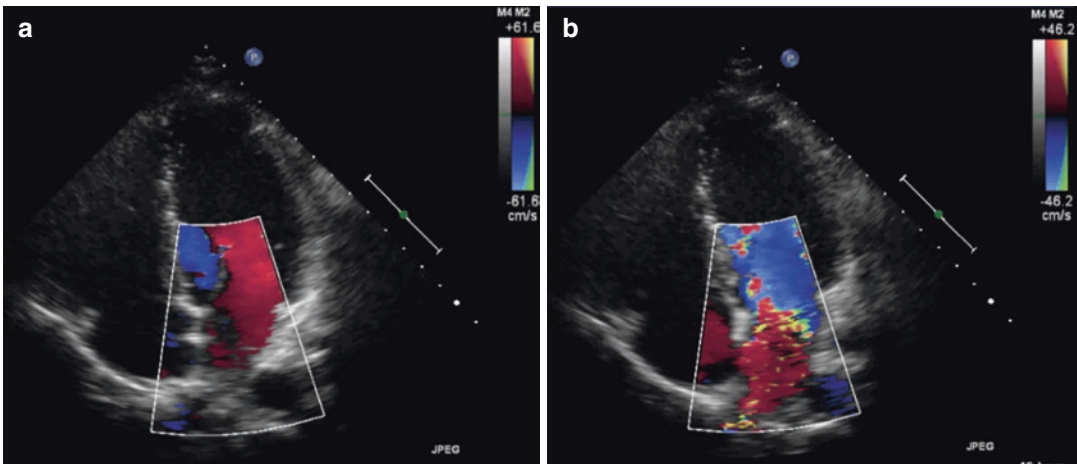
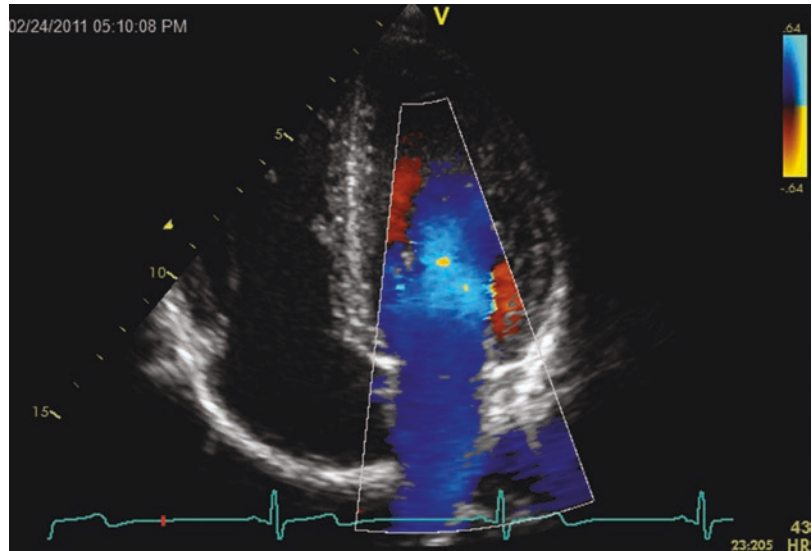


Fig. 3.11 (a and b) Flow into the left ventricle in an apical four-chamber view with the color scale set at a normal value of 61.6 cm/s (a). The color Doppler scale then is

shifted to 46.2 cm/s (b) and the normal flow into the left ventricle has now aliased. See text for details

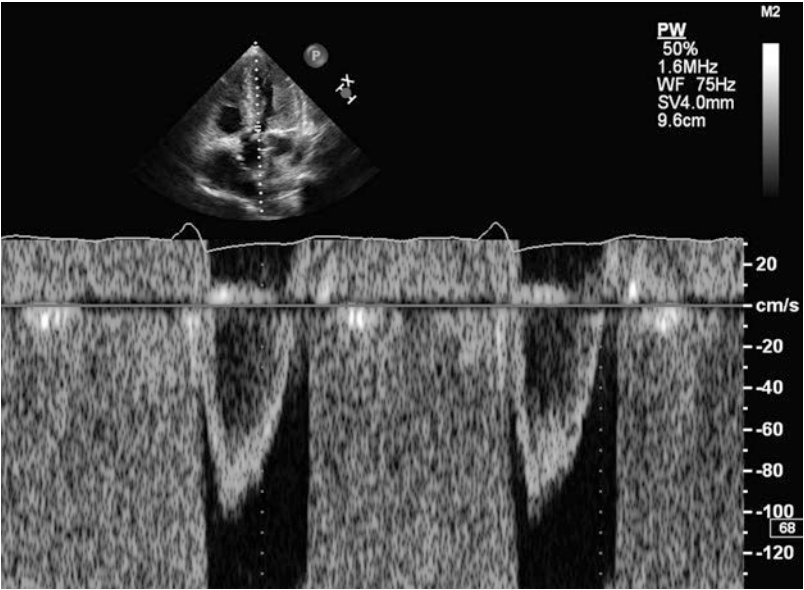
overall depth of view does affect the frame rate so keep the image as shallow as possible in order to have the highest frame rate. Wider color boxes will lower frame rate as more time is required to interrogate a flow in a larger area. The color box should be as narrow as possible while fully covering the area of interest. If the color appears bright and flashy within the color box, it may help to decrease the color gain. Table 3.2 describes the most commonly used controls for adjusting the color Doppler display.

Pulsed wave Doppler samples velocities at a specific point along the beam axis. A gate designates the sampling point and its position within a 2D image. The *trackball* moves the pulse sample gate within the ultrasound image. The disadvantage of pulsed wave lies in its susceptibility to aliasing. This type of Doppler is best for low velocity flows as higher velocity jets will alias. Figure 3.12 is an example of pulsed wave Doppler sampling the left ventricular outflow tract in a patient with aortic regurgitation (AR).

Table 3.2 The most commonly used controls for adjusting the color Doppler display

Color variable	Knob(s)	Function
Map	Map	Provides key to convert velocities into colors
Scale	Scale	Specifies range of velocities that can be expressed by color and Nyquist limit
Invert	Invert	Assigns specified color to direction of flow
Sector placement	Position, trackball	Determines placement of color box
Sector size	Size, trackball	Determines size of color box
Gain	Gain	Amplifies color Doppler signal before display
Baseline	Baseline	Shifts the zero baseline of the color scale velocities
Smoothing	Smoothing	Determines degree of separation of color packets

Fig. 3.12 An example of pulsed wave Doppler sampling the left ventricular outflow tract in a patient with aortic regurgitation. The high velocity diastolic flow has aliased



The baseline has been shifted upwards in order to see the entire systolic flow but the higher velocity AR jet is aliased.

Continuous wave Doppler possesses a clear advantage over pulsed wave in its total lack of a Nyquist Limit. This means that the high velocity flows will not alias as is seen in Fig. 3.13 where the AR jet that aliased in Fig. 3.12 is now fully resolved. If the scale on the Doppler waveform display is set too low, it may appear to wrap around in the same manner as pulsed wave Doppler. If this occurs, increase the scale (in cm/s) to the desired velocity range. Continuous wave Doppler is not depth-specific. The machine samples all along the beam axis, sending and receiving Doppler signals con-

stantly. Table 3.3 describes the most commonly used controls for pulsed and continuous wave Doppler variables.

For accurate velocities it is of primary importance to have the beam axis at an angle as close as possible to 0° (parallel) with blood flow. On the sector display, position the dotted line designating Doppler beam placement within the area of interest. This is performed using the *position* button and the *trackball*. When using pulsed wave Doppler mode, the sample gate can freely move vertically along the beam path. Only flow at the point designated by the sample gate will be displayed. Very small, incremental changes in beam axis or sample gate placement can produce significant changes in pressures, velocities, and

Fig. 3.13 Continuous wave Doppler now shows the entire spectral trace of aortic regurgitation without aliasing

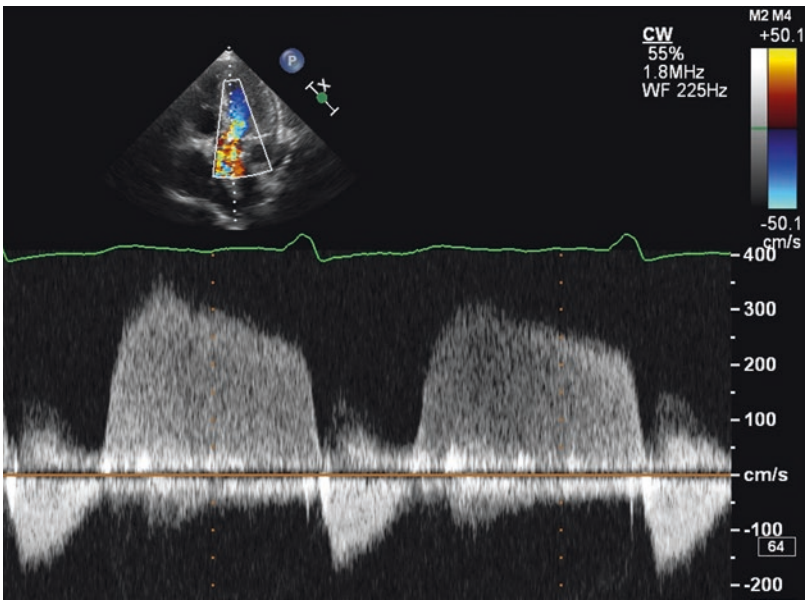


Table 3.3 The most commonly used controls for pulsed and continuous wave Doppler variables

PW/CW variable	Knob(s)	Function
Sample placement	Position, trackball	Specifies location of Doppler beam
Scale	Scale	Specifies range of velocities that can be displayed and Nyquist limit (PW)
Sweep speed	Sweep speed	Changes number of cycles that can be shown on the x-axis of the Doppler display
Gain	Gain	Amplifies PW and CW Doppler signals before display
Baseline	Baseline	Positions the zero baseline of the Doppler display
Compression	Compression	Changes the difference between the highest and lowest received amplitudes (shades of gray)
Reject	Reject	Eliminates low velocity signals near zero baseline
Invert	Invert	Determines the presentation of signals as above or below zero baseline regardless of direction of flow
Measurements	Freeze, caliper, trace, enter, erase	Quantifies features of a PW/CW Doppler spectral display

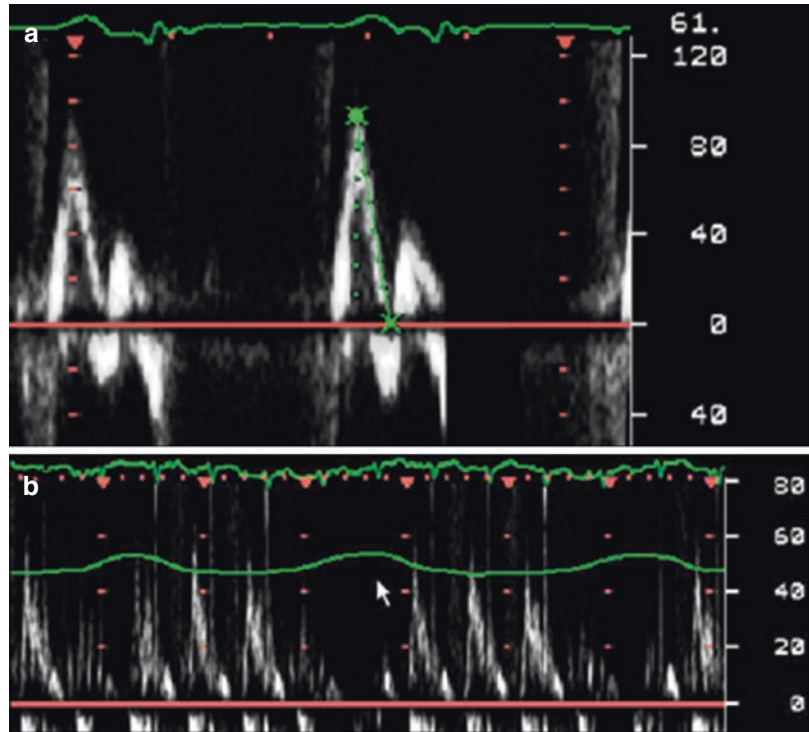
patterns of flow. In continuous wave Doppler mode, an operator can adjust only the focal point of the beam without eliminating any specific depths from the overall Doppler display.

The *spectral display* for PW and CW Doppler may need to be “cleaned up” before they are acceptable for acquisition. Relevant information should be extracted and refined from the Doppler display. Once Doppler sampling placement is optimal, the resulting Doppler signal can be easily manipulated. Common controls to manipulate

the signal include Doppler *sweep speed*, *gain*, *scale*, *baseline*, *compression*, and *reject*.

Sweep speed changes the number and width of Doppler waveforms that can be displayed in a single image acquisition/capture. Increasing the sweep speed effectively zooms on one or a few Doppler waveforms at a time and makes for more accurate measurements (Fig. 3.14a). High sweep speed is optimal for patients in normal sinus rhythm with multiple uniform Doppler readings over time. Sweep speed should be reduced for

Fig. 3.14 (a and b)
Examples of varying the sweep speed of the Doppler spectral trace. “a” demonstrates a fast sweep speed which aids in measuring velocities while “b” shows more waveforms when the speed is lowered



patient with significant Doppler variations between cardiac cycles or for arrhythmic patients (Fig. 3.14b). Other common indications for very low sweep speed include assessment of tamponade or constriction, where presence or lack of respiratory variation needs to be demonstrated.

Doppler Gain amplifies or de-amplifies the returning signal from the moving red blood cells. The gain is often preset, but it helps to change gain to compensate for low or high density red blood cell movement. The Doppler spectral signal itself should be a mid-level gray, while the Doppler background should be black. If the signal is bright white, turn down the Doppler gain. If it is very faint or totally black but present, turn the Doppler gain up. Increasing the audio volume to hear the Doppler shift maybe helpful in optimizing the spectral trace. Audio volume provides critical information when using PEDOFF probes, which produce Doppler signals with no 2D image for guidance.

The Doppler scale controls the highest and lowest velocity levels that can be presented on the spectral display (in cm/s). If the baseline is in

the center of the Doppler display y-axis, then the highest velocities that can be potentially detected above and below the baseline (towards and away from the probe) should be the same. If a flow is very high or low velocity, it may at some point be required to alter the Doppler scale.

The baseline is a horizontal line showing the zero velocity point over time. Velocities can be shown symmetrically above and below the baseline. Care should be taken to position the baseline in order to see the entire spectral display. Figure 3.15 is an example of poor positioning of the baseline since the peak velocities of the spectral display are not visualized. The alternative is to eliminate unwanted information by raising or lowering (shifting) the zero velocity point along the y-axis of the Doppler display to focus attention on flow above or below the baseline. Figure 3.16 demonstrates that shifting the baseline up now displays the entire spectral trace.

Doppler compression changes the number of shades of gray assigned to the spectral display. Increasing the numerical level of Doppler

Fig. 3.15 Pulsed wave Doppler spectral waveform with the baseline positioned too low and the peak velocity is not seen

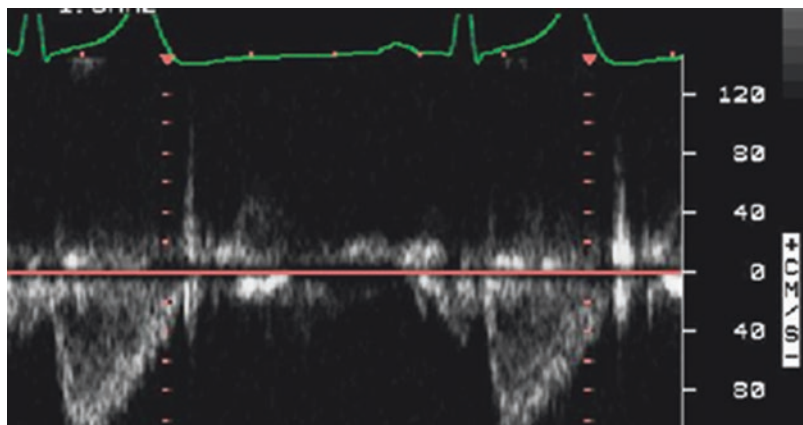
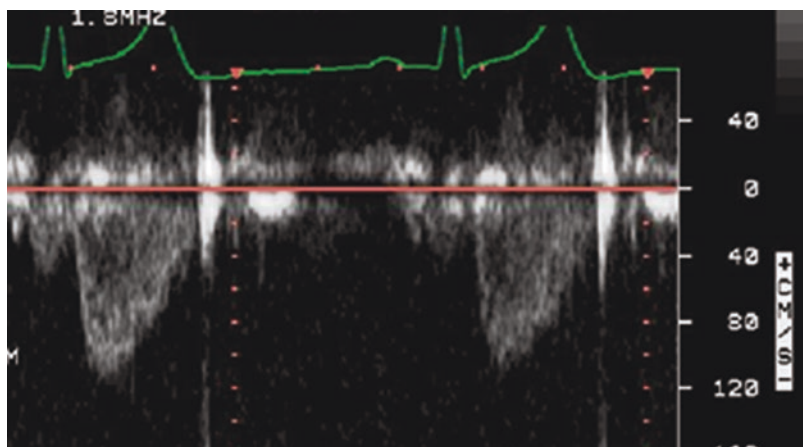


Fig. 3.16 Pulsed wave Doppler spectral waveform with the baseline shifted higher so that the peak velocity is now seen



compression creates a softer, smoother gray Doppler display. A lower numerical level of Doppler compression creates a harsh display with more black/white contrast and fewer shades of gray.

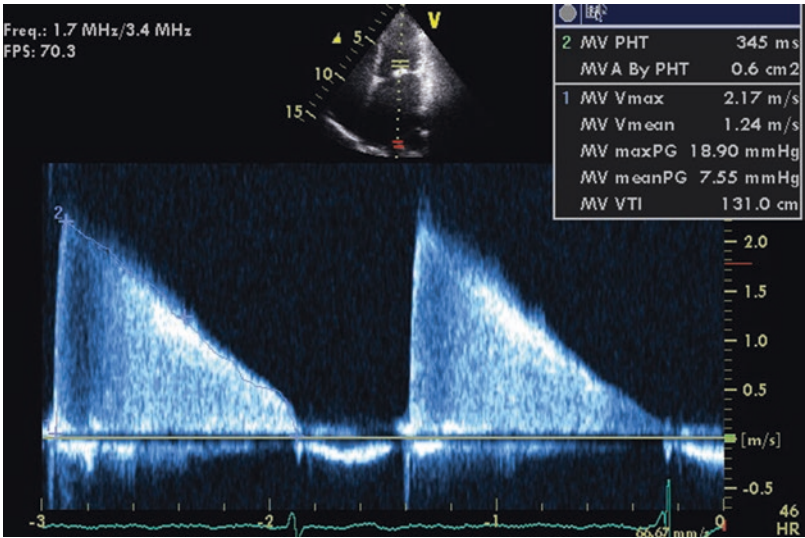
Doppler reject eliminates low velocity signals, which are usually seen near the baseline. Reject brings the Doppler background to black or close to it. Reject also helps to define the borders of the Doppler signal. When tracing or measuring, be sure that the reject is set at an acceptable level.

Doppler measurements are often necessary for a complete cardiac assessment. Relevant controls include: *freeze*, *caliper*, *trace*, *enter*, *erase*, and the *trackball*. Caliper measurements of pulsed and continuous wave Doppler can be made using the *caliper*, *trackball*, and *enter* controls. Caliper settings give rise to machine calculations of instantane-

ous velocity values and instantaneous pressure values. Tracing will provide information on peak velocity, peak pressure gradient, and mean pressure gradient. A tracing is made by using the *trace*, *trackball*, and *enter* buttons. Press the *erase* button once or more to remove one or all of the Doppler measurements from the image waveforms. Figure 3.17 shows examples of typical Doppler measurements in a patient with mitral stenosis.

Similar to 2D, Doppler measurements can be recorded inside or outside of the machine *analysis* package. The analysis package on any machine is intended to label, identify and present measurements in an organized manner. Once certain Doppler measurements are accumulated, the machine may be able to calculate further helpful values using previously programmed ultrasound equations.

Fig. 3.17 An example of Doppler measurements performed on the mitral inflow spectral trace in a patient with mitral stenosis



Conclusions

It is important to familiarize yourself with the common echocardiographic imaging modes and their controls. Image quality and diagnostic accuracy depend heavily on the knowledge and

skill of the clinician operating the ultrasound machine. Awareness of the basic knobology associated with 2D, Color Doppler, PW Doppler, and CW Doppler is absolutely essential for performing a good echocardiographic examination.

Cardiac Anatomy by Three-Dimensional Echocardiography

4

Francesco F. Faletra, Romina Murzilli,
Laura Anna Leo, and Siew Yen Ho

Introduction

Real-time three-dimensional (3D) echocardiography appeared in the clinical arena nearly a decade ago. From the beginning, it was clear that this new technology would be a milestone in the “evolution” of ultrasounds. Indeed, this technique has the following unique peculiarities:

- It generates “live” images, in other words it shows the motion of a given structure in three-dimensions at the same moment in which the motion occurs.
- Three-dimensional images appear almost identical to the anatomic specimens.
- The operator can rotate and angulate the image on and off line, in any direction and illustrate the cardiac structures from a countless number of perspectives. Moreover, as in a kind of “electronic” dissection, the operator can crop, again on and off line, the image, deleting redundant echoes and discovering hidden structures.

Currently, both transthoracic echocardiography (3D TTE) and transesophageal echocardiography (3D TEE) transducers may generate 3D images. However, 3D TEE provides images of higher quality in comparison with 3D TTE. From the esophagus, in fact, the ultrasound beams reach the heart crossing only the thin esophageal and the left atrial walls with a narrow almost “virtual” space in-between. Thus, contrarily to the transthoracic view, reverberations and aberrations due to the multiple layers of different tissues or lungs are avoided or minimized. Second, because the esophagus is very close to the heart, 3D TEE may use transducers with high pulse frequencies (up to 7.0 MHz). These transducers, producing images with high spatial resolution, enable providing fine anatomical details. For these reasons, the majority of the images shown in this chapter are obtained with 3D TEE.

It would be pretentious from our side to describe every anatomical detail of any cardiac structure proceeding systematically as in an anatomical book since in reality both 3D TTE and TEE are not able to visualize all the cardiac structures with the same clarity and finesse. Moreover, although it is true that 3D TEE may provide images of a given cardiac structure from a countless number of perspectives, only few of them are very informative and clearly show the anatomy as it is, while others are confounding and some even incomprehensible. Finally, in 3D

F. F. Faletra (✉) · R. Murzilli · L. A. Leo
Department of Cardiology, Fondazione Cardiocentro
Ticino, Lugano, Switzerland
e-mail: francesco.faletra@cardiocentro.org

S. Y. Ho
Cardiac Morphology, Royal Brompton Hospital and
Imperial College, London, UK

echocardiography, the axial resolution is superior to the lateral resolution and the lateral resolution is superior to the elevation (azimuth) resolution. Thus, the same 3D image may appear very clear in the perspective where the system primarily uses the axial resolution to reconstruct the image, and quite poor in another perspective where the system uses the lateral or azimuth resolution.

In this chapter, we present 3D echocardiographic images from perspectives that present the following characteristics:

- Perspectives that clearly illustrate anatomical details of a given structure (due to the particular acquisition or angulations that favors, for instance, the axial resolution in the reconstructed images).
- Perspectives already described in literature or suggested by the guide-lines [1].
- Perspectives that are very didactic because they look like anatomical specimens.

We call these perspectives “3D basic perspectives”. Readers should familiarize themselves with these perspectives, because they may have in the future the same relevance as the well-known two-dimensional (2D) echocardiographic sections. Keeping in mind structures that appear in a given basic perspective, will help to recognize the same structures in any other perspective used.

When useful, we also present “cross-section images” or “magnified images” to illustrate specific anatomical details. Finally, to demonstrate the reliability of 3D anatomy with the “real” anatomy, some images appear side-by-side with anatomical specimens dissected and displayed in the same perspective.

All 3D images we show in this chapter were from a Philips echo-machine (Philips Medical system, Andover, MA). Thus, readers must be aware that other echo-machines may generate images of different quality from ours. Our images are the result of a meticulous selection among thousands of studies stored in our database. Once selected, for their optimal acquisitions and clarity, images were thoroughly postprocessed (i.e., opti-

mizing gain, compression, brightness and smoothing) and manipulated (i.e., rotated, angulated and cropped) to obtain either the above-mentioned *3D basic perspectives* or specific cropped sections.

Mitral Valve

Perloff and Williams in 1972 emphasized that the mitral valve is not a mere couple of flaps of tissue closing and opening following flow and pressure gradients but rather a more complex *apparatus* consisting of several components, which move in a perfect spatial and temporal coordination to ensure an effective valve competence [2]. These components are the mitral annulus, the leaflets, the chordae tendineae and the papillary muscles. In this section, we will describe these components as they appear on 3D echocardiography.

Mitral Annulus

Medical students and young cardiologists usually perceive the mitral “annulus” as a ring of dense connective tissue that encircles the atrio-ventricular junction, anchors the leaflets and divides the left atrium from the left ventricle. However, as shown by Angelini et al. [3] in 1988, the arrangement of *left atrial wall/complete fibrous ring/left ventricular wall* is rather rare. More often, the posterior segment of mitral annulus is an incomplete arc of dense connective tissue variably interrupted by loose connective tissue separating atrial and ventricular musculature. As result, segments of posterior leaflet do not have a firm fibrous anchorage but rather directly attach on muscular tissue allowing a contraction (sphincter mechanism) of this part of annulus during the systole. A “surface rendering technique” such as 3D echocardiography, can only inconstantly show the hinge line (which make up the so-called annulus) of leaflets using “en face” perspectives (Fig. 4.1a, b) However, the “dynamic” anatomy (Fig. 4.1c, d), may show the contraction of the posterior hinge line, which moves anteriorly.

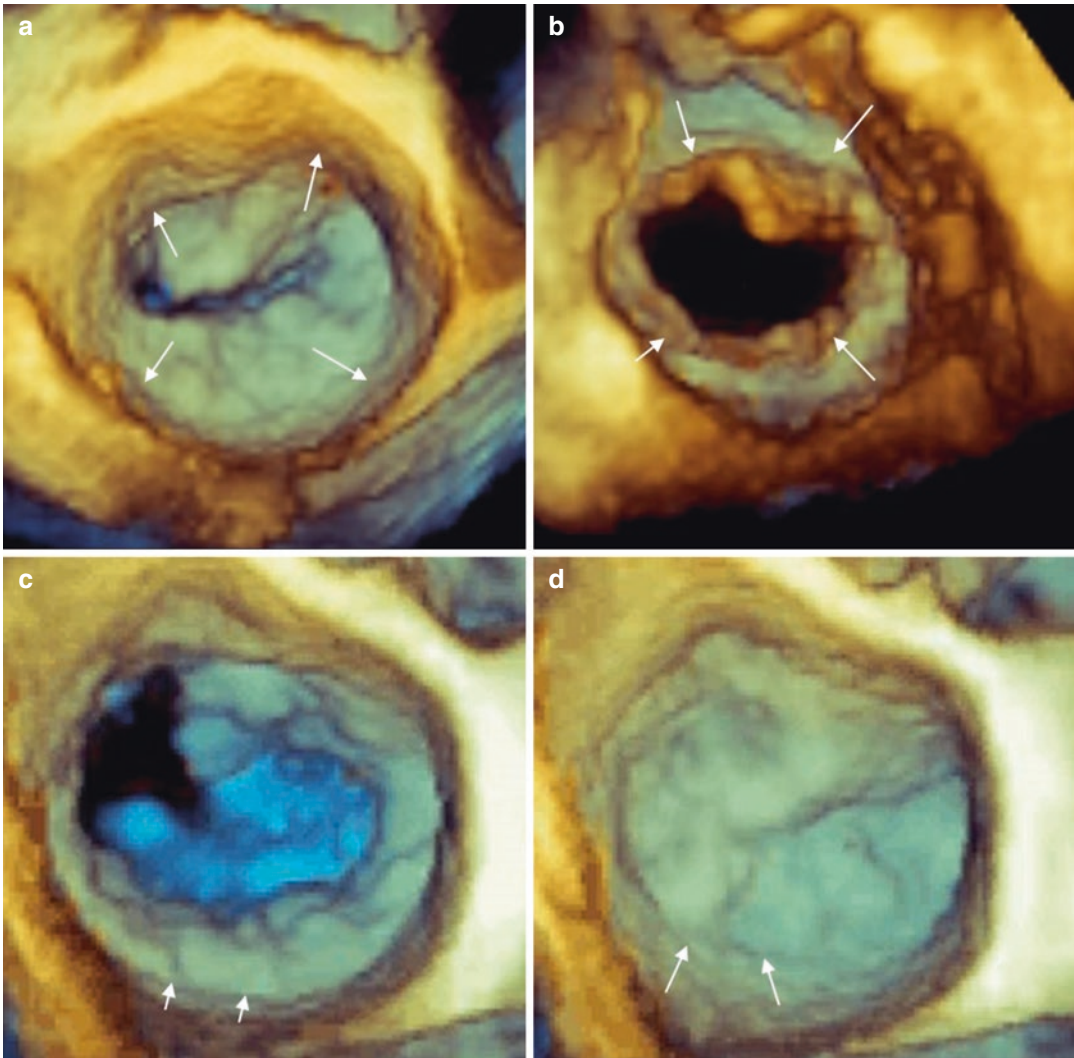


Fig. 4.1 Three-dimensional transthoracic echocardiography image of the mitral valve from (a) left atrial and (b) ventricular perspectives. Arrows point at the hinge line. (c and d) shows the posterior annulus contracts moving

anteriorly from diastole (c) to systole (d). The contraction is possible because the posterior annulus is a mix of connective tissue and muscular fibers

Similarly, the anterior mitral leaflet often continues imperceptibly with the interleaflet triangle of the aortic valve without any recognisable annulus. Cardiac surgeons call this area “mitral-aortic continuity” or “mitral-aortic curtain”. Two nodules of dense connective tissue, the trigones, are located at the medial and lateral extremities of this area.

Despite the lack of a well-defined fibrous circular/ellipsoidal structure, for practical reasons, we will continue to call the mitral hinge line as

mitral annulus. Levine et al. [4] showed in 1987 that the mitral annulus has a saddle-shaped configuration with the highest points in correspondence of the insertion of A2 and P2 and the lowest points in correspondence of the commissures. This study has led to a substantial change of the echocardiographic criteria of mitral valve prolapse [4]. Salgo et al. [5] demonstrated that this three-dimensional arrangement of mitral annulus concentrates the peak stress on the two trigones.

Mitral Leaflets

The final aim of the mitral valve apparatus is yielding a perfect closure of the mitral orifice by apposition of mitral valve leaflets in systole. Thus, for these reasons the mitral valve (MV) leaflets probably remain the most important component of the MV apparatus. Anatomists describe the mitral valve as having two leaflets separated by two deep incisures (commissures). The anterior leaflet has a triangular shape. Its insertion on the MV annulus covers approximately one third of the entire annular circumference. The posterior leaflet has a more quadrangular shape and covers the remaining two thirds of the annulus. Because the distance between the hinge line and the free margin of anterior leaflet is considerably longer than that of the posterior leaflet, the area of each leaflet is almost equal.

3D TEE provides superb images of the MV. Herein we describe four basic 3D perspectives for visualizing MV leaflets: the perspective from the left atrium, the perspective from left ventricle, the angled right-to-left perspective and the angled left-to-right perspective. The best known is certainly the perspective from left atrium or so-called “surgical view” because of similarity to the surgical inspection in the operating room [6]. Through the left atrium, the valve appears to the surgeon “en face” with the anterior leaflet sited superior, the posterior leaflet inferior and the aorta at nearly 12 o’clock. Any acquisition mode (live 3D, zoom, wide-angle single-beat, wide-angle multi-beat) may show this “surgical” view if the pyramidal data set is large enough to include the whole valve from commissure to commissure. This perspective allows imaging the atrial aspect of both leaflets with the anterior leaflet deeper and shorter around the perimeter of the orifice than the posterior leaflet. In the most frequent leaflet arrangement (present in nearly 70% of normal valves) two incisures divide the posterior leaflet into three scallops P1 (lateral), P2 (central), P3 (medial), while the anterior leaflets have no identifiable incisures. However, for practical reasons, surgeons also designate the anterior leaflet into three segments,

named A1, A2, and A3, indicating the areas opposed the corresponding scallops of the posterior leaflet (Fig. 4.2a, b).

By angulating the surgical view of 70–90°, operators can obtain the angled right-to-left and the angled left-to-right perspectives [7]. These two perspectives allow a better vision of medial and lateral commissures (Fig. 4.2b, c). Moreover, being almost tangential to the annular plane, both angled views may identify even small prolapsing segments [8].

Inspection of ventricular surface of both leaflets reveals two distinct areas: the *rough* and *clear zones*. The rough zone, receiving the insertion of chordae tendineae presents a “corrugate” surface and is thicker while the clear zone has a smoother appearance and is thinner. Interestingly, in normal MV, the rough zones correspond on their atrial aspect to the coaptation surface, the area where leaflets juxtapose each other during the systole. Thus, the vast majority of chordal attachment is therefore within the coaptation area and chordae may share the mechanical stress with the leaflets. By rotation of 180° the pyramidal data set from the surgical view and cropping the covering structures, we obtain the perspective from left ventricle. The resolution power of 3D TEE does not allow a clear distinction between rough zone and clear zone (Fig. 4.3a). A cross section through the anterior leaflet may show the difference in thickness between the two zones (Fig. 4.3b). On the other hand, this perspective is the most favourable for imaging the “mitral-aortic curtain” (Fig. 4.3c).

Chordae Tendineae and Papillary Muscles

No more than a dozen of chordae tendineae take origin by the tip of papillary muscles and before reaching the rough zone of both leaflets, they split in numerous branches and interconnections that ensure a balanced distribution of the mechanical stress. The subdivision of marginal (or first order), strut (or second order), and basal chordae (or third order) is the simplest because this nomenclature is

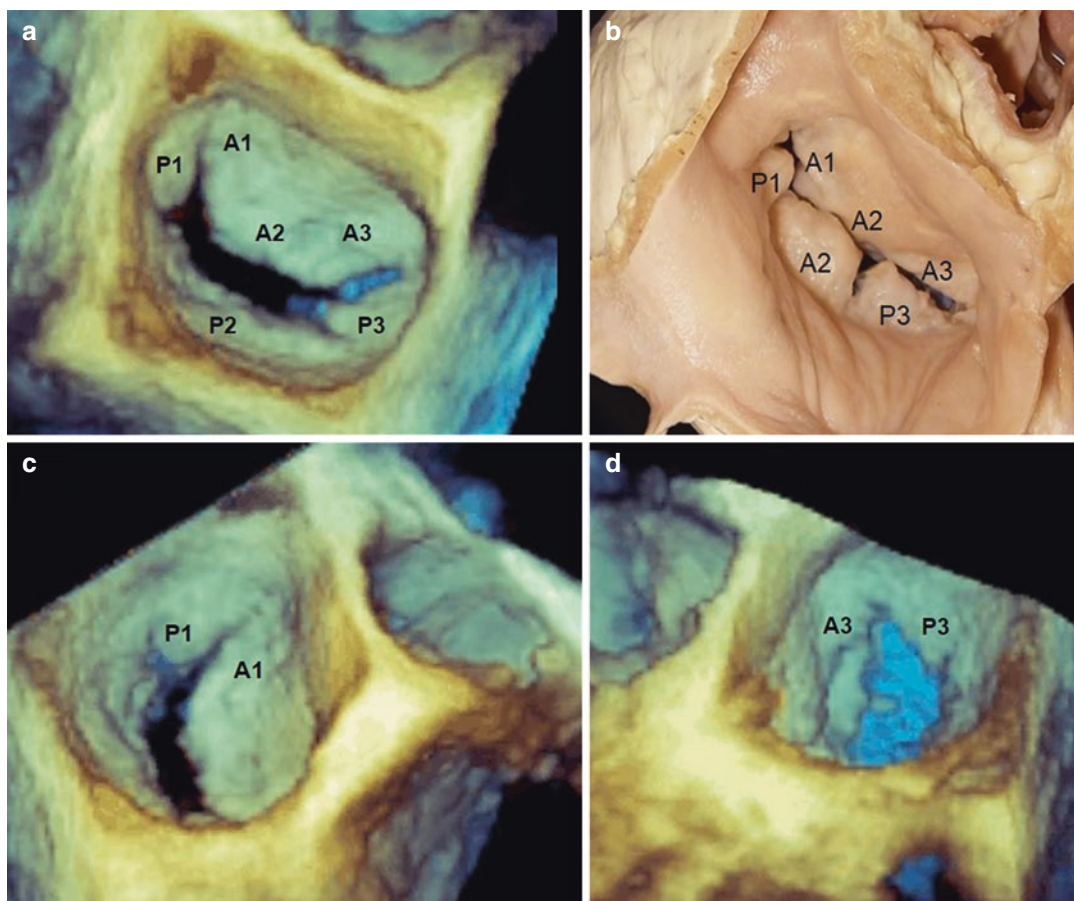


Fig. 4.2 (a) A view from above shows the atrial surface of mitral leaflets. In mid-diastole, providing clearly image of the subdivision in scallops (see text) of posterior leaflet. (b) Corresponding anatomical specimen. (c) Angled view

right-to-left showing the lateral commissure and P1, A1 segments. (d) Angled left-to-right view showing the medial commissure and A3, P3 segments

coherent with their function. Indeed, marginal chordae, inserted on the free margins of both leaflets prevent eversion of leaflets during the systole, strut chordae, usually two in number, inserted on the confines between the rough and clear zones of the anterior leaflet ensure a sort of fibrous continuity between leaflet and ventricular wall, supporting the contraction of longitudinal myocardial strands of the left ventricle. Finally, basal chordae originate directly from the ventricular wall and insert only on the posterior leaflet. Logically they should limit the motion of the posterior leaflet but their role remains unclear.

Unfortunately, 3D TEE is not able to distinguish among different types of chordae. The best

approach is probably the trans-gastric (the same view used in 2D TEE). However, the spatial resolution scarcely allows imaging individual chordae. More often, 3D TTE or 3D TEE show groups of chordae thicker than they actually are (because of “blurring” artefacts) originating from papillary muscles (Fig. 4.4a).

The papillary muscles (PMs) originate from the distal third of the ventricular wall in the posterior-medial and anterior-lateral position as a single entity or a group of two or three muscles. Contrary to that often written in anatomical textbook or in some papers [1], papillary muscles do not attach directly on the compact myocardium but arise from a network of ventricular trabeculations [9] (Fig. 4.4b).

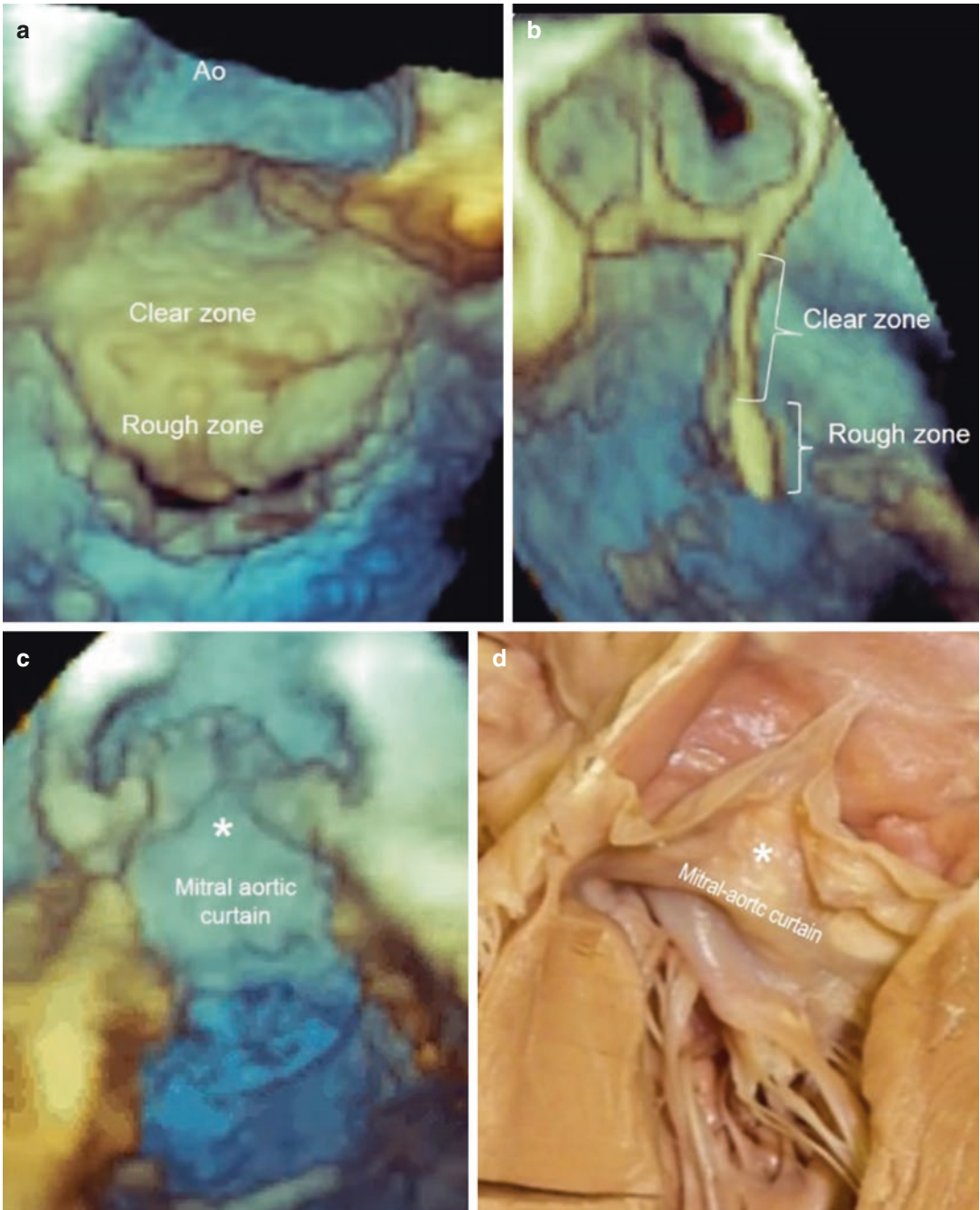


Fig. 4.3 (a) A magnified image of the ventricular aspect of MV. The resolution power does not allow distinguishing the two zones described by anatomists. (b) A cross-section through the anterior leaflet clearly shows the

different thickness, between the two zones. (c) This ventricular perspective visualizes the mitral-aortic curtain. The asterisk points at the interleaflet triangle. (d) Corresponding anatomical specimen

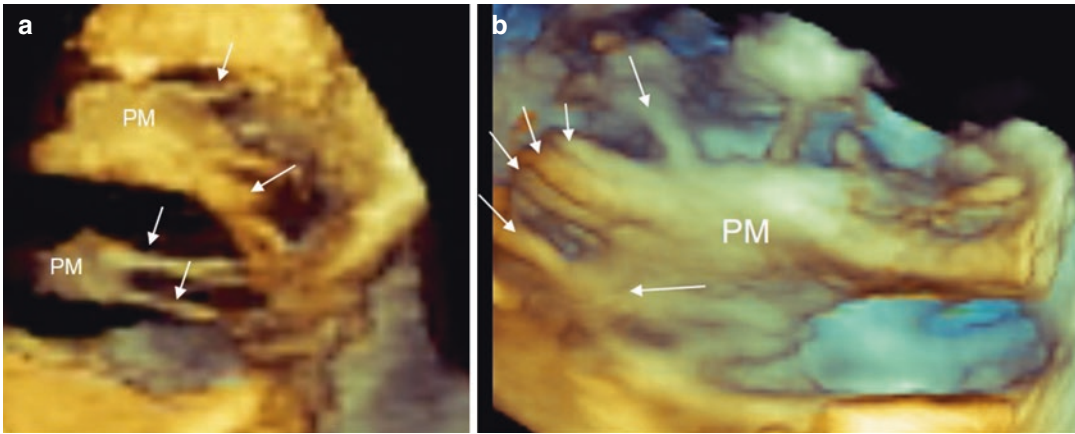


Fig. 4.4 (a) 3D images showing chordae tendineae (arrows) originating from papillary muscles (PM). Some chordae appear thicker than they actually are because of

poor spatial resolution. (b) Magnified 3D image of the base of PM arrows point at the network of trabeculations at the base of PM

Aortic Valve Anatomy

Introduction

The aortic valve, like the mitral valve, is more complex than generally thought. Indeed, what we usually call “aortic valve” comprises the following components: three sinuses, three leaflets, three interleaflet triangles, three-commissure, two coronary ostia, one so-called annulus, one ventriculoarterial junction, and one sinotubular junction. Because of its cylindrical shape and its specific role, this complex apparatus has the relevance of a “fifth chamber” of the heart and anatomists call it the “aortic root” [10]. The job of the aortic root is very demanding. In systole, it must allow the passage of a significant amount of blood in one direction with a pressure gradient of only few mm Hg, assuring, at the same time, wide flow variations (up to five times) and coronary perfusion. In diastole, the aortic root must have such robust structural configuration to bear up against the aortic pressure while preventing the back flow. Moreover, the opening and closing of aortic leaflets occur approximately three billions of times in the course of an average lifetime. The stress exerted on the leaflets for such a

long time would certainly cause premature leaflet damages. If this does not occur, it is because the leaflets are “inserted” inside the “aortic root”. The role of the aortic root is, eventually, to preserve the integrity of the leaflets distributing the stress between leaflets and sinuses. Although with less consistency than the mitral valve, 3D TEE allows nice images of the aortic root to be obtained. In this section, we will describe the components of the aortic root as they appear at 3D TEE showing three basic 3D perspectives: a longitudinal perspective, a perspective from above or aortic perspective and a perspective from below or ventricular perspective. The longitudinal perspective allows imaging of most of the components of the aortic root (Fig. 4.5).

The Ventriculoarterial Junction

The ventriculoarterial junction (Fig. 4.5) as an anatomically entity does not exist. It can be more simply defined as a “border area” (round in systole and elliptical in diastole) where the fibroelastic wall of the aorta meets partly the muscular and partly the fibrous borders of the outflow tract of the left ventricle.

The Aortic Leaflet

The aortic leaflets have a shape that resembles a “bird’s nest.” In each leaflet, we can distinguish a hinge-line, which is the line of insertion of the leaflet on the wall, a body and a surface of coaptation, in the center of which is located a fibrous nodule: the nodule of Arantius. When the valve closes, each leaflet faces with the other along the surface of coaptation, which takes the

name of “lunula.” This area of leaflet coaptation reduces the radial forces acting on the leaflets. The same *longitudinal basic perspective* may illustrate fine anatomical details of aortic leaflet (Fig. 4.6a, b).

Two other basic perspectives enable imaging the aortic leaflets. The perspective from the aorta is the most used and shows the leaflets “en face.” The European Association of Echocardiography/American Association of

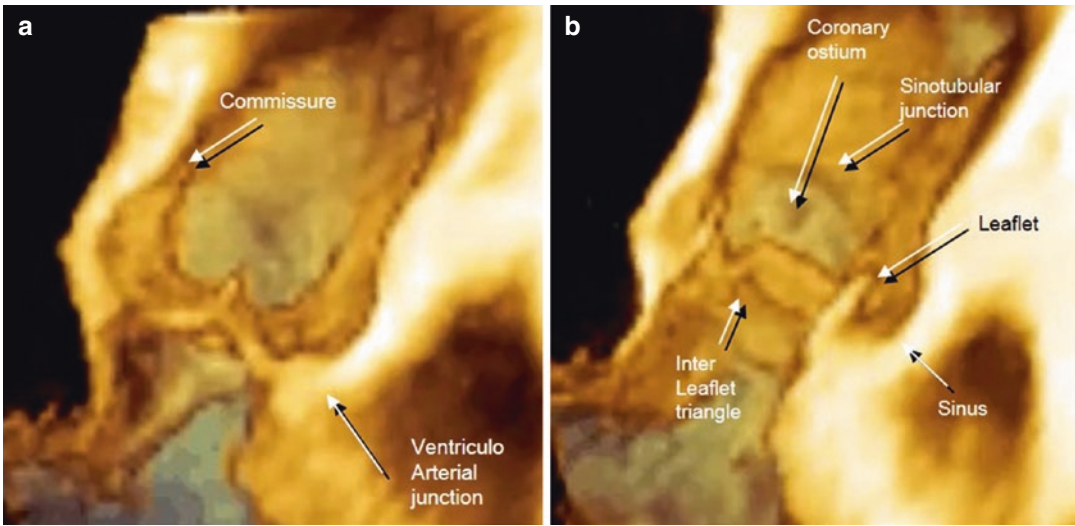


Fig. 4.5 Three-dimensional images showing a longitudinal cut of the aortic root in diastole (a) and systole (b), showing most of its components (see text)

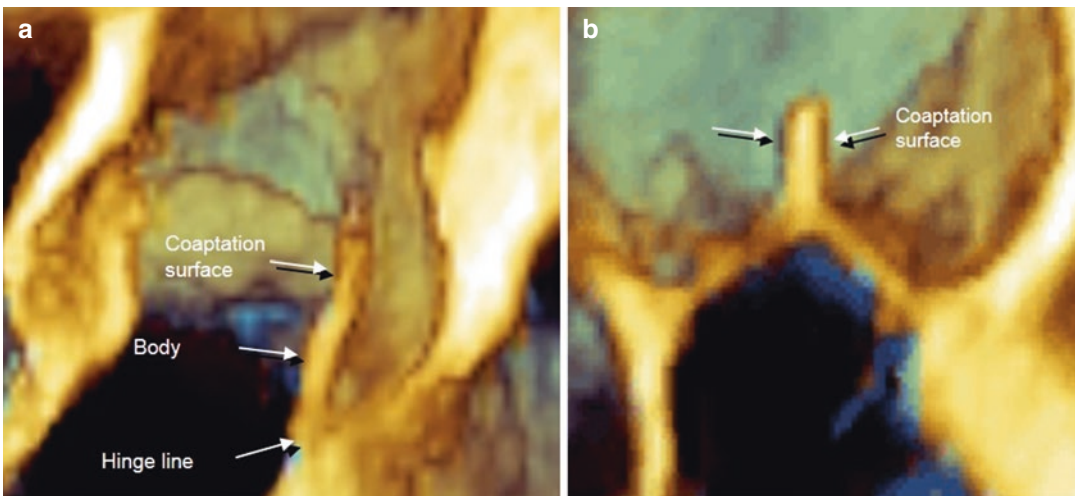


Fig. 4.6 Three-dimensional images in longitudinal basic perspective showing anatomical details of the aortic leaflet in systole (a) and diastole (b)

Echocardiography (ESE/ASE) recommendations paper [1] suggests orientating the right coronary leaflet at 6 o'clock, so that the non-coronary leaflet appears approximately at 10 o'clock and the left coronary leaflet at 2 o'clock (Fig. 4.7). The perspective from aortic root may suffer from "drop-out" artefacts. Indeed, the nearly parallel incidence of ultrasound beams (when intersect the body of the leaflets) and the thinness of the valve itself produces only weak

scattering echoes that are not enough for reconstructing the image in its entirety [11] (Fig. 4.7).

The perspective from left ventricle is less used. From this perspective, a proper cut may reveal the ventriculoarterial junction, which in diastole is elliptical, while in systole becomes more circular (Fig. 4.8). This is mainly due by the fact that the mitral-aortic curtain, which partially reflects the motion of the mitral anterior leaflet, forms part of the ventriculoarterial junction.

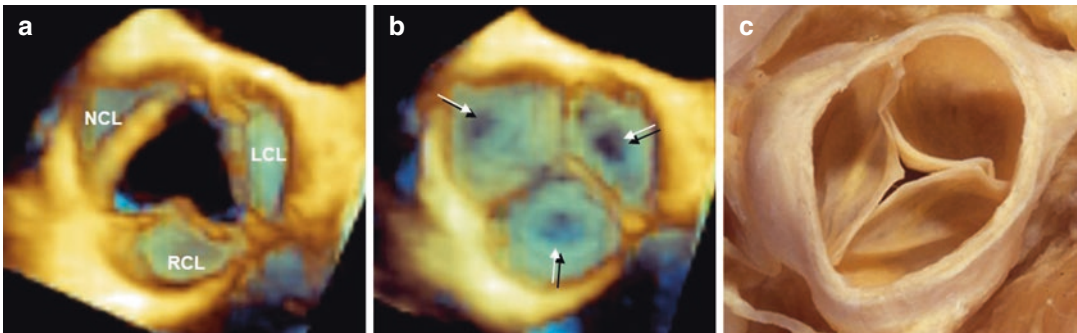


Fig. 4.7 (a) Mid systole 3D images of the aortic leaflets in "en face" view from aortic perspectives. As suggested by the guide-lines [1], the right coronary leaflet (RCL) is oriented at 6 o'clock, noncoronary leaflet (NCL) approximately at 10 o'clock and left coronary leaflet at 2 o'clock.

(b) In diastole, the dropout artefacts (arrows) appear on the body of leaflets. Please note that in diastole the aortic sinuses assume a trifoliate configuration. (c) The corresponding image of anatomic specimen

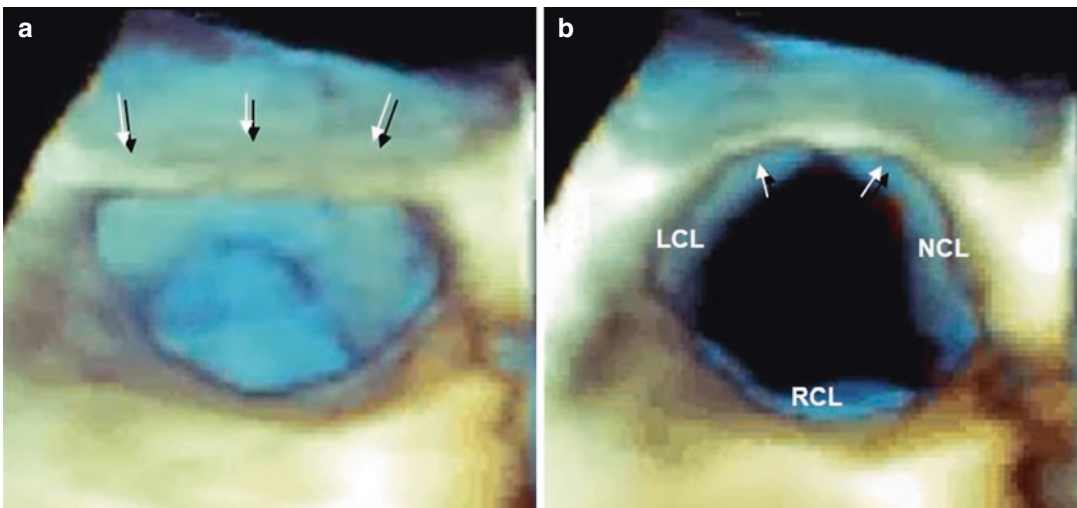


Fig. 4.8 (a) Three-dimensional image of the aortic leaflets from left ventricular perspective. In diastole, the atrial pressure pushes the mitral-aortic curtain towards the LV outflow tract (arrows), while in systole (b) towards the left atrium (arrows). This explains why in

diastole, the ventriculoarterial junction assumes a rather elliptical configuration, while in systole becomes more circular. Contrary to Fig. 4.7, the left coronary leaflet is located at 10 o'clock and the NCL approximately at 2 o'clock, while the RCL remains at 6 o'clock

Thus, in diastole, the curtain bulges towards the left ventricular outflow tract, while in systole towards the left atrium.

The aortic annulus (defined as a fibrous “string” that allows a robust attachment of each leaflet to the aortic wall) has a “crown-shape” configuration. The lowest part of the insertions (nadir) corresponds to ventriculoarterial junction and the highest part (commissure) to the sinotubular junction. At this level, the insertion of one leaflet meets and continues with that of adjacent leaflet. 3D TEE cannot visualize in a single image the entire annulus, but a dedicated cropping may show the curved insertion of the leaflet on the aortic wall (Fig. 4.9a). A magnified cropped perspective may also show the characteristic “bird’s nest” configuration of the leaflet (Fig. 4.9b).

Given the particular crown-shaped configuration of the aortic annulus, three triangles of

fibrous tissue, named *inter-leaflets triangles* (ILT), lie between leaflets [12]. The first ILT is sited between the right and left coronary leaflets (Fig. 4.10a). The second, between the left coronary and the noncoronary leaflet, is the fibrous sheet that continues with the anterior leaflet of mitral valve (the well-known mitral-aortic curtain) (Fig. 4.10b). Third triangle, located between the non-coronary and right coronary leaflet, includes the membranous septum (Fig. 4.10c).

The sinuses of Valsalva (from the Italian anatomist Antonio Valsalva) are three bulges of the aortic root and, like the leaflets, are named right, left, and non-coronary sinus. The right and left coronary sinuses include the ostia of coronary arteries. When seen in cross-section, the sinuses assume a trilobate conformation. This trilobate conformation (see Fig. 4.7b) allows a more

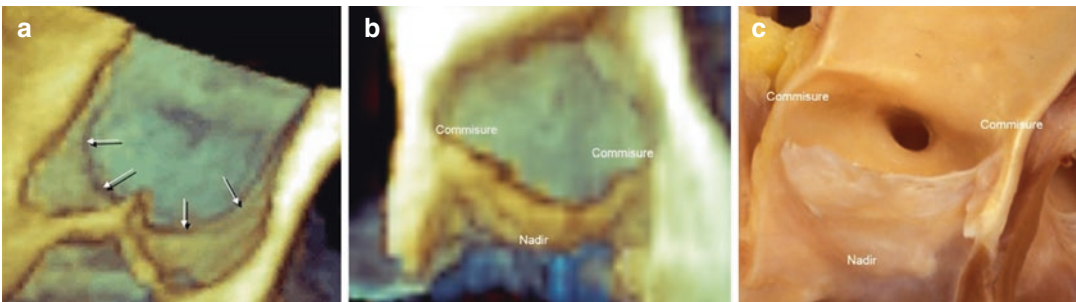


Fig. 4.9 (a) Longitudinal cropped 3D image showing the curved insertion (arrows) of one of the leaflet. (b) 3D-magnified image showing one leaflet in “en face”

view resembling a “bird’s nest.” Note the characteristic bird’s nest configuration. (c) The corresponding anatomical specimen

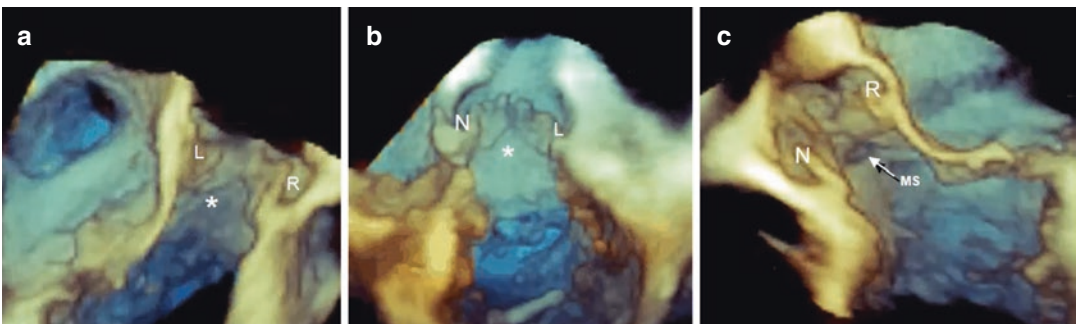


Fig. 4.10 (a) 3D image of the ILT between left (L) and right (R) aortic leaflets. This triangle is entirely muscular. (b) The ILT between non-coronary (N) and L. This trian-

gle consists of the mitral aortic curtain and is entirely fibrous. (c) The ILT between N and R, which includes the membranous septum (MS)

homogeneous distribution of the aortic pressure between the leaflets and the sinuses. In systole, the sinuses create a space between the aortic wall and the leaflets. In this space, the blood stream produces small vortices, which prevent the occlusion of coronary ostia from leaflets (thus granting a certain coronary perfusion in systole) and facilitate valve closure. Indeed, during the end-systole the vortices bring the leaflets very close to each other. Thus, when the pressure in the aorta exceeds that in the ventricle, the valve is almost closed.

The sinotubular junction is the only defined ring of the aortic root and marks the border between the aortic root and the ascending aorta. This ring supports the commissures at the peaks of leaflet insertions. Finally, the coronary ostia arise from the upper part of the aortic sinuses near the sinotubular junction. 3D TEE consistently visualizes the left coronary ostium. Being smaller, the right coronary ostium is less frequently imaged. A longitudinal cut may show both sinotubular junction (Fig. 4.11a) and left coronary ostium (Fig. 4.11b).

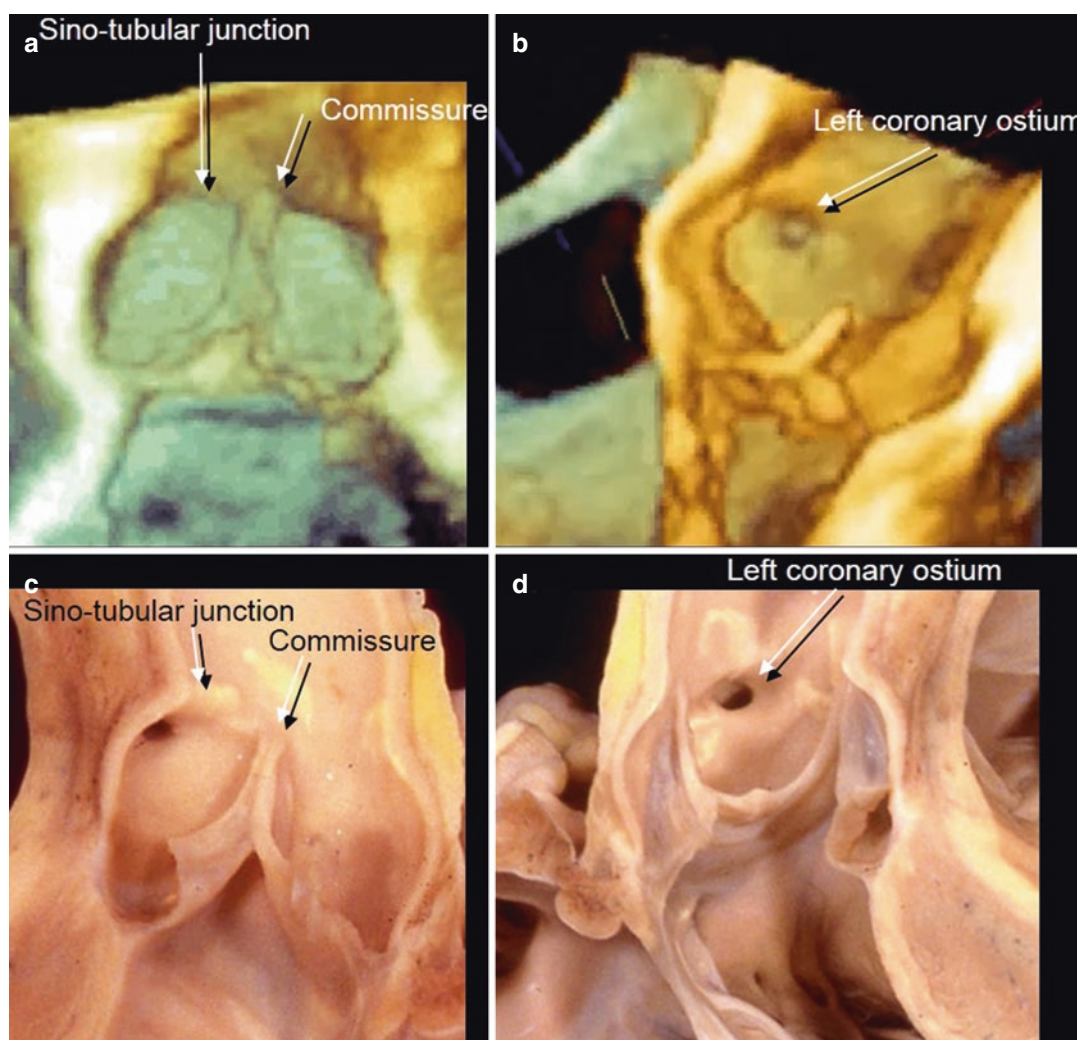


Fig. 4.11 (a) Longitudinal cut showing the sino-tubular junction and the commissure. (b) Longitudinal cut showing the left coronary ostium. (c, d) The corresponding anatomical specimens

Tricuspid Valve Anatomy

Although subjected at much lower systolic pressures than the MV, the global architecture of the tricuspid valve (TV) apparatus is surprisingly similar to the mitral valve. Indeed, just like the MV, the TV is a complex apparatus consisting of a partially fibrous annulus, three leaflets, chordae tendineae and three small papillary muscles. The normal shape of the annulus is rather elliptical and has a three-dimensional saddle-shaped configuration with the *peaks* in septal and lateral position and the *valleys* in anterior and posterior position. The three leaflets (anterior, posterior and septal) have different sizes, the anterior being the largest and the septal the smallest.

Three-dimensional TEE is less than ideal for imaging tricuspid leaflets: first, the valve is farther from the transducer than the MV; second, in normal individuals the tricuspid leaflets are thinner than the mitral leaflets; third, in normally positioned heart the ultrasound beams from the esophagus, intersect the valve nearly tangentially producing scattering rather than specular echoes. As result, rarely both 2D TEE and 3D TEE visualize the TV in its entirety:

in most cases, the leaflets suffer dropout artifacts (difficult to fill by increasing gain), which are magnified when we add the third dimensions (Fig. 4.12). Not rarely, apical 3D TTE provides better images than 3D TEE (Fig. 4.13).

Either the anterior or the posterior leaflet may have deep incisures with a further subdivision into several scallops. In some hearts, because of the absence of incisures, the anterior and posterior leaflets appears as a unique veil, inserted on the free wall of the right ventricle. In this anatomical arrangement, the tricuspid valve appears as being bicuspid with one septal and one “mural” leaflet. In some favorable cases, where for some reasons the tricuspid leaflets are more perpendicular to the ultrasound beam, 3D TEE enables visualizing both of these features (Fig. 4.14).

The septal leaflet has its own unique characteristics. Contrary to the other two leaflets, short chordae tendineae originating directly from the septum insert on its ventricular surface. Moreover, its attachment on the annulus is closer to the apex than the attachment of anterior leaflet of MV. Thus, part of the muscular ventricular wall and nearly half of the membranous septum are located in an

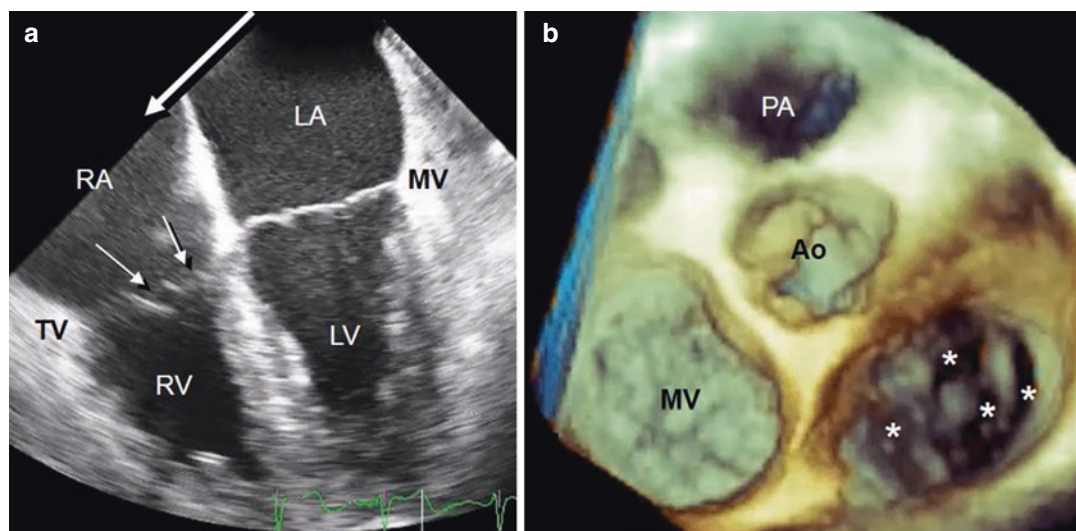


Fig. 4.12 (a) Four-chamber 2D TEE view showing as the tricuspid leaflets are nearly tangential to the ultrasound beams (large arrow). The scattered echoes back to the transducer are too feeble causing dropout artefacts (small arrows). (b) These artefacts result bigger in 3D TEE (asterisks). On the contrary, the mitral valve (MV) is

nearly perpendicular and therefore the specular echoes back to the transducer are enough strong to allow a complete 3D mitral valve (MV) reconstruction. Ao aorta, LA left atrium, LV left ventricle, PA pulmonary artery, RA right atrium, RV right ventricle

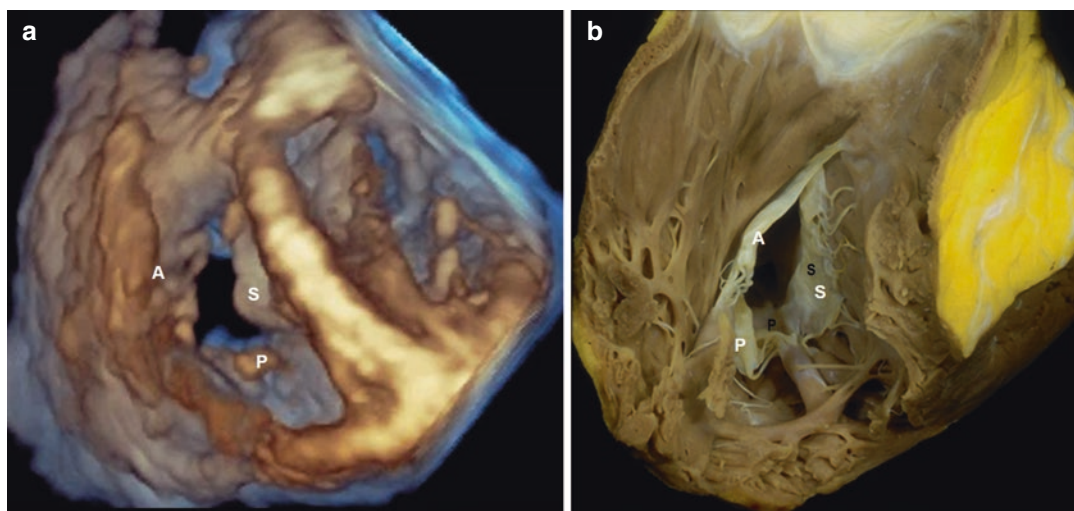


Fig. 4.13 (a) 3D TTE image, from ventricular perspective showing quite clearly the anterior (A) posterior (P) and septal (S) leaflet. (b) The corresponding anatomical specimen

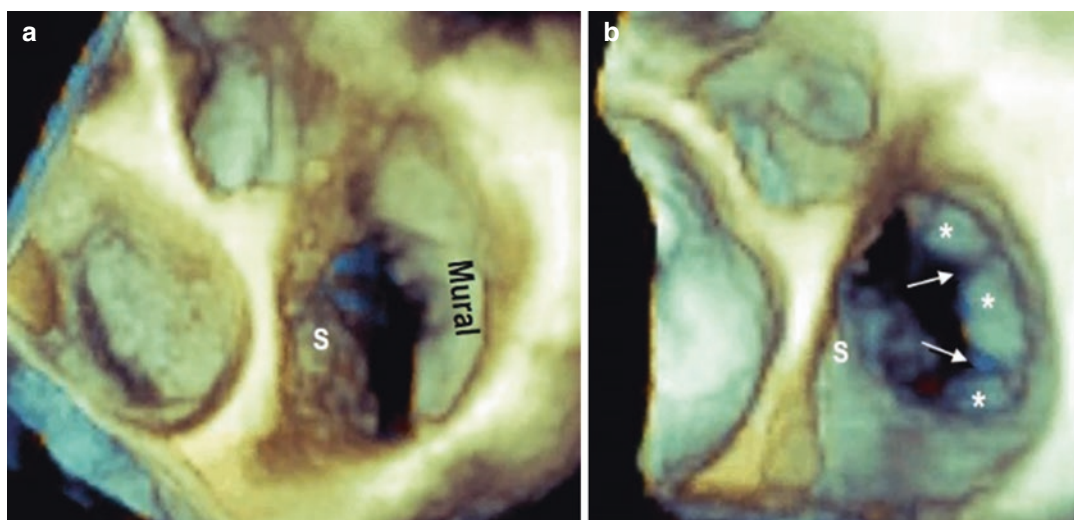


Fig. 4.14 (a) 3D TEE image from atrial perspective. In the absence of a clear incisures between the anterior and posterior leaflets, these two leaflets appears as a single

veil (mural leaflet). (b) Same perspective of the image shown in A. In this case, two incisures (arrows) divide the mural leaflet in three segments (asterisks). S septal

atrio-ventricular position (taking the name of atrioventricular septum). While imaging the chordae directly connecting the right ventricle wall to the septal leaflets is beyond the resolution power of both the 2D and 3D TEE, the insertion of the septal leaflet on the interventricular septum lower than the anterior mitral leaflet is well known to echocardiographers since the introduction of 2D echocardiography. Of course, the 3D TEE shows

the actual anatomy of the atrio-ventricular septum as a strip of membranous (anterior) and muscular (posterior) tissue interposed between the right atrium and the left ventricle (Fig. 4.15).

Compared with left ventricular PMs, the right ventricular PMs are smaller, less well defined and rather dispersed. A relatively large PM originating from the moderator band supports the anterior leaflet and the antero-posterior commissure.

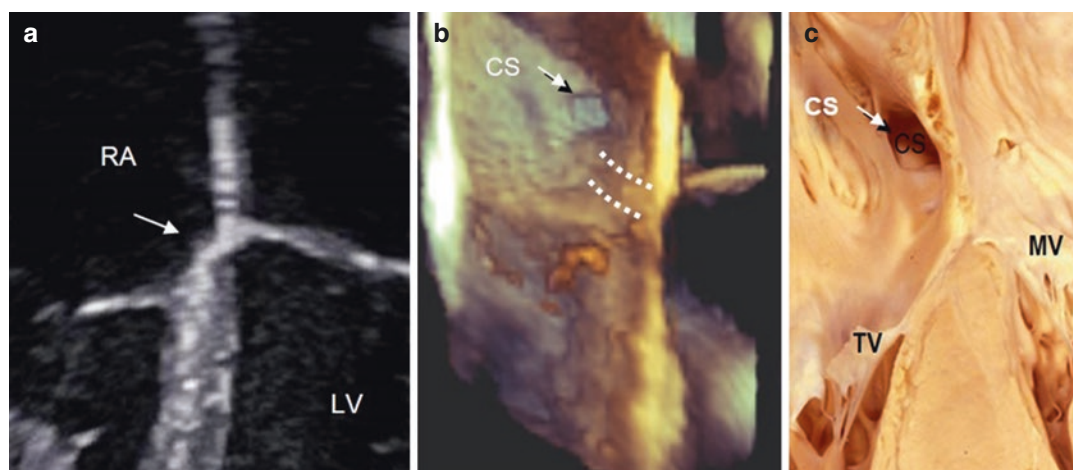


Fig. 4.15 (a) The atrioventricular septum (arrow) as imaged from 2D TTE. This septum separates the right atrium (RA) from the left ventricle (LV). (b) 3D Image of the same structure slightly rotated to illustrate the so-called septum in its posterior portion as a thin band of muscular

tissue (between the two dotted lines) of the RA wall overlying the crest of the ventricular septum. In the background the orifice of the coronary sinus (CS; arrow). (c) Anatomical specimen in a similar view as in *B* showing the offset between tricuspid (TV) and mitral (MV) valves

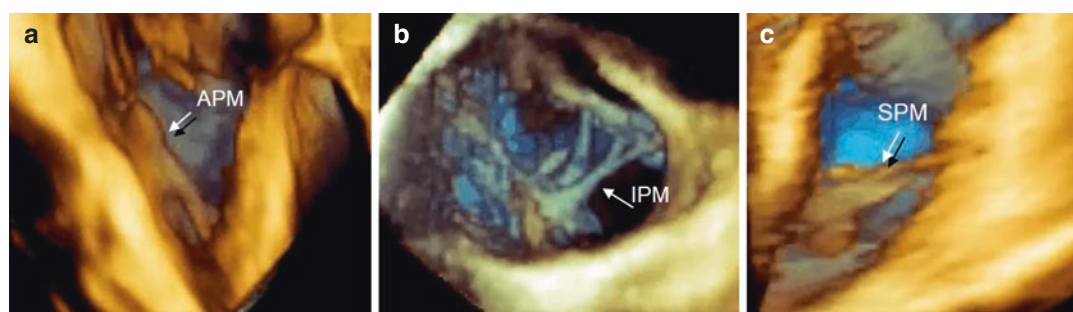


Fig. 4.16 Three-dimensional TEE images of (a) anterior (APM), (b) inferior (IPM) and (c) septal (SPM) papillary muscles

Small PMs arising from the inferior wall support the posterior leaflet. A medial PM or group of minute PMs originating from the septomarginal trabecula supports the antero-septal commissure. Usually PMs and chordae are poorly defined at 3D TEE. In a large right ventricle, a single PM can be sometimes seen (Fig. 4.16).

Pulmonary Valve Anatomy

Pulmonary valve (PV) is identical in design to the aortic root and consists of three leaflets, three sinuses of Valsalva, a crown-shaped annulus, three

commissures and three interleaflet triangles [13]. Because of the anatomical arrangement that parallels the aortic root, the anatomists describe the pulmonary valve also as “pulmonary root.” In a normal individual, the hemodynamic forces in the pulmonary circulation are five times less than that of systemic circulation; consequently, all the components of pulmonary root are thinner, more delicate and flexible than those of the aortic root. The sinotubular junction, which is the cranial border of the pulmonary trunk rather than a well-defined circular ring of dense connective tissue, is only a subtle line separating the thin wall of the sinuses from the thicker wall of the pulmonary trunk. The pulmonary

leaflets have the same “bird’s nest” shape of the aortic leaflets, and a crown-shaped insertion on the pulmonary wall. Two leaflets take the name of right and left facing leaflets with the homonymous aortic leaflets. The third leaflet is the most anterior and takes the name of non-facing or anterior leaflet. The ventriculoarterial junction is the boundary between the fibrous-elastic wall of the vessel and the muscular tissue of the infundibulum. The three interleaflet triangle consist of muscular tissue arising from the outflow tract surrounding by a thin line of fibrous tissue connecting with the base of the crown-shaped annulus. Being the furthest from the esophagus, the pulmonary trunk rarely provides images of good quality on 3D TEE. More often, a longitudinal cut through the right ventricular outflow tract shows one or two pulmonary leaflets in cross section as in 2D TEE (Fig. 4.17). The “en face” view of the valve usually shows large dropout artifacts that make the leaflets unrecognizable.

The Right Atrium

The right atrium (RA) consists of two main components: the sinus venosus and the right atrial appendage. The first, located posteriorly, derives from the

systemic venous plexus and presents a smooth internal surface. The second, derived from the embryonic primitive atrium, is a large triangular pouch that extends laterally and anterosuperiorly, and, characteristically, contains numerous pectinate muscles. Externally a groove named “sulcus terminalis” divides these two components. The *internal aspect* of RA consists of several components particularly relevant for electrophysiologists. In this section, we describe the following right atrial structures: the terminal crest, the cavo-tricuspid isthmus and surrounding structures (i.e. the Eustachian valve and the ostium of coronary sinus), the right atrial appendage, and the right side of the interatrial septum. Because the RA is very close to the oesophageal transducer, 3D TEE may image nicely all these internal anatomical structures [14].

The Terminal Crest

The terminal crest (TC) is a muscular ridge that divides the smooth wall of sinus venosus from the rough surface of the RAA. This muscular ridge originates from the anteromedial wall of the RA near the interatrial sulcus and runs adjacent to the anterior margin of superior vena cava. Then it curves

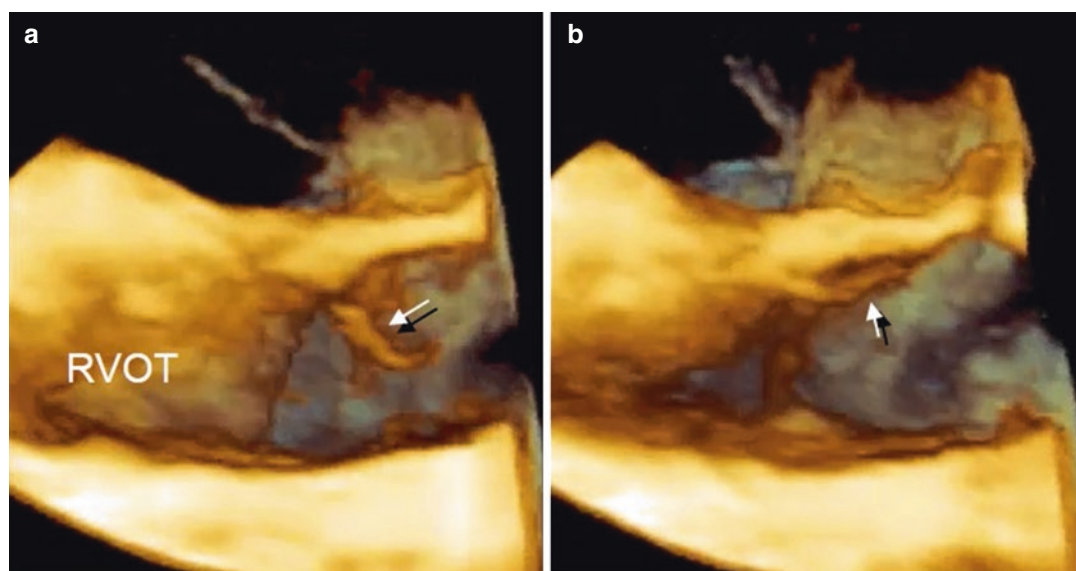


Fig. 4.17 Cross-section long axis view of the right ventricle outflow tract (RVOT), showing the pulmonary leaflets in diastole (a) and systole (b) (arrow)

descending towards the inferior of the RA where it ends into fine trabeculations. An extensive array of pectinate muscles originates perpendicularly from the TC. The TC may have variable sizes from a thin, almost invisible, protuberance to a broad-based

muscular bump miming an atrial mass. When it protrudes into the atrial cavity, the TC is easily recognisable with 3D TEE (Fig. 4.18). Starting from the bicaval 2D TEE view, any acquisition modality (i.e., live, zoom modality, width angle single beat, width

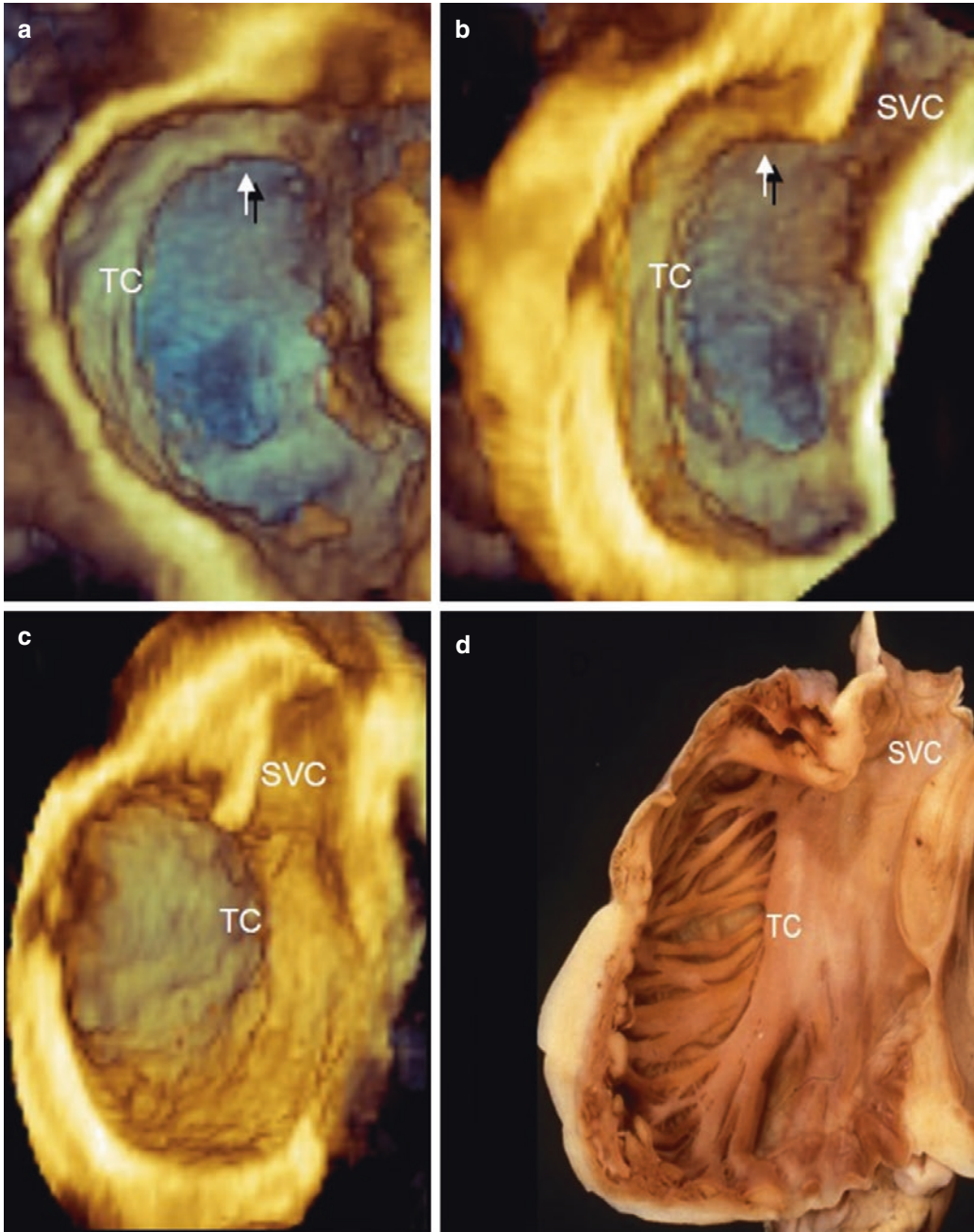


Fig. 4.18 (a–c) 3D TEE images of the terminal crest (TC) in three different perspectives. The arrow in panels A and B points at the portion of the terminal crest adjacent to

the anterior margin of the superior vena cava (SVC). (d) A corresponding anatomical specimen

angle multibeam) enables an optimal imaging of the TC. An anatomically correct orientation (i.e., superior vena cava up) may help in the understanding the anatomical course of this structure.

The Right Atrial Appendage

The right atrial appendage (RAA) is a relatively large and roughly triangular shape which lines the right border of the cardiac silhouette and extends anteriorly partially embracing the aortic root. Pectinate muscles (PMs) originating from the TC, typically line its endocardial surface. Between PMs, the atrial wall shows variable thickness, in some part having a very thin, pouch-like configuration. One of the PM, known as sagittal bundle (SB), crosses transversally the RAA. The SB may form an incomplete ring around the RAA apex, delimiting an antero-lateral pocket-shaped area of thin muscular myocardium. A zoom modality focus on RAA may provide nice images of RAA, PMs and SB (Fig. 4.19).

The Cavotricuspid Isthmus

The cavotricuspid isthmus (CVTI) is a somewhat quadrilateral-shaped region that comprises the inferior-posterior wall of the right atrium. The

hinge line of the tricuspid leaflet attachment delimits the anterior border, while the eustachian valve (EV) the posterior. The medial border corresponds to the inferior margin of coronary sinus ostium while the lateral border is rather indistinct roughly corresponding to the final ramifications of the TC. The CVTI is the target for the linear ablation of typical atrial flutter. In this regard, electrophysiologists divide the CVTI in three sectors: para-septal, inferior and inferolateral isthmus [15]. The preferred site of linear ablation is across the inferior isthmus. Starting from 2D TEE four chamber view, a 3D pyramidal data set embracing the posterior half of the RA and the posterior hinge line of the tricuspid leaflet provides beautiful images of the CVTI. We consider this perspective another *3D basic perspective* (Fig. 4.20).

The eustachian valve and the eustachian ridge can be visualized starting from a bicaval view and adjusting the volumetric data set (i.e., cropping and rotating) to obtain a cross-section of the superior vena cava. When particularly protruding, the EV can be seen in “en face” view guarding the inferior vena cava (Fig. 4.21).

The Coronary Sinus

In the past, cardiologists have totally ignored the anatomy of the coronary sinus (CS) and, in gen-

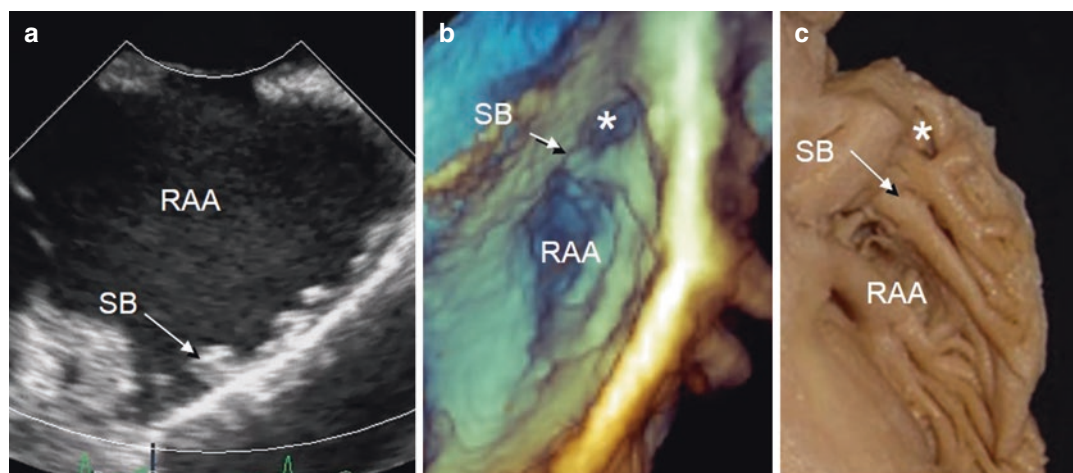


Fig. 4.19 (a) A zoom modality focused on the right atrial appendage (RAA). The arrow points at the sagittal bundle (SB) (b) 3D TEE image derived by the zoom acquisition

in panel A. The SB crosses transversally the RAA forming a pocket-shaped area (asterisk). (c) The corresponding anatomical specimen

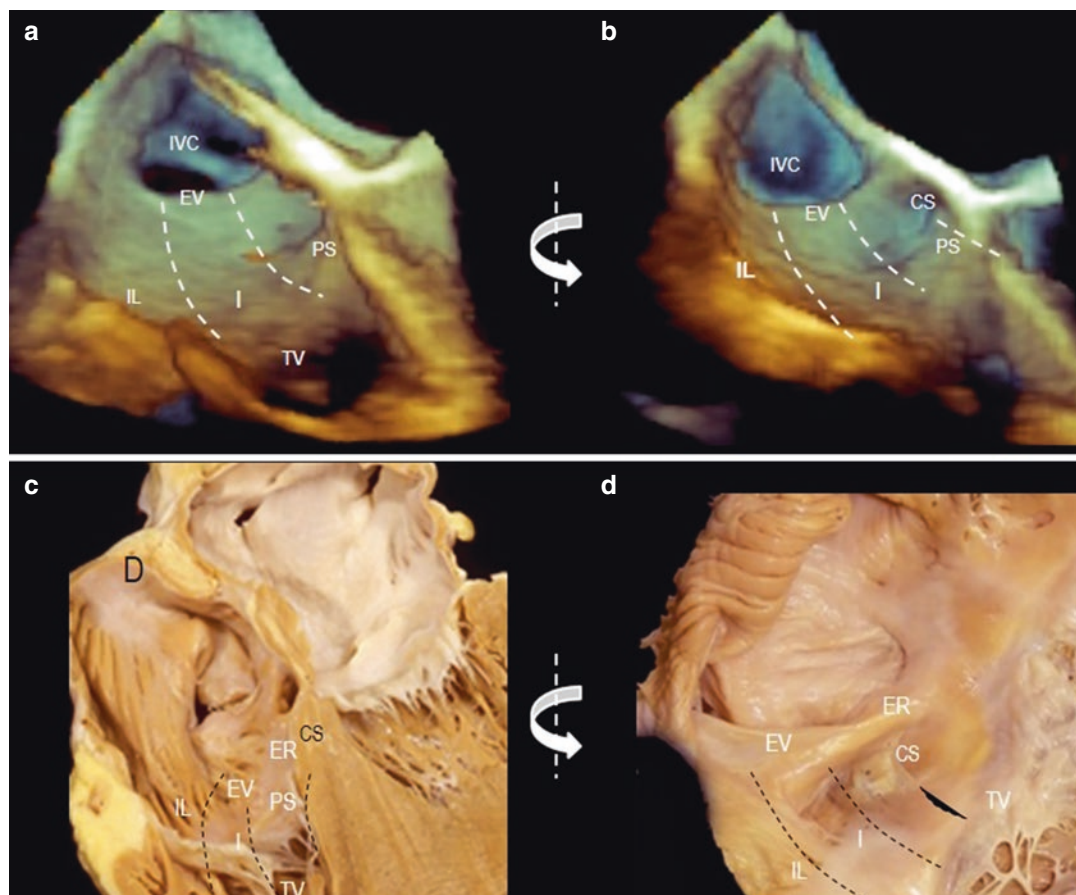


Fig. 4.20 (a) The cross-sectional four-chamber view including the posterior half of right atrium enables imaging the inferolateral (IF), the Inferior (I) and the para-septal (PS) isthmuses that are between the tricuspid valve (TV) and the orifice of the inferior caval vein (IVC). (b) A slight rotation left-to-right around the y-axis (curved

arrows) permits a more complete image of the PS isthmus. The same basic perspective shows the Eustachian valve (EV) and the coronary sinus ostium (CS). (c and d) Images of anatomical specimens replicating the views seen in A and B, respectively

eral, the anatomy of the coronary venous system, focusing their attention on the angiographic anatomy of coronary arteries circulation. In the last decade, the cardiac resynchronization therapy (CRT) has renewed the attention of cardiologists in the anatomy of coronary venous system. Indeed, CRT involves placement of pacing leads in the right atrium, right ventricle and one of venous side branches (preferably posterolateral cardiac vein) through the CS. Other techniques, in particular computed tomography, may visual-

ize the course and size of coronary sinus along the atrioventricular groove and the distribution of first- and second-order venous branches. 2D TEE may show the CS in short axis view (as a circle) and in long axis view (as two parallel lines). 3D TEE, of course, offers a more “anatomical” picture of CS, showing the coronary ostium in “en face view” and the course of a long segment along the interventricular groove. Once recognised in 3D TEE, a zoom modality may provide nice 3D images of the CS (Fig. 4.22).

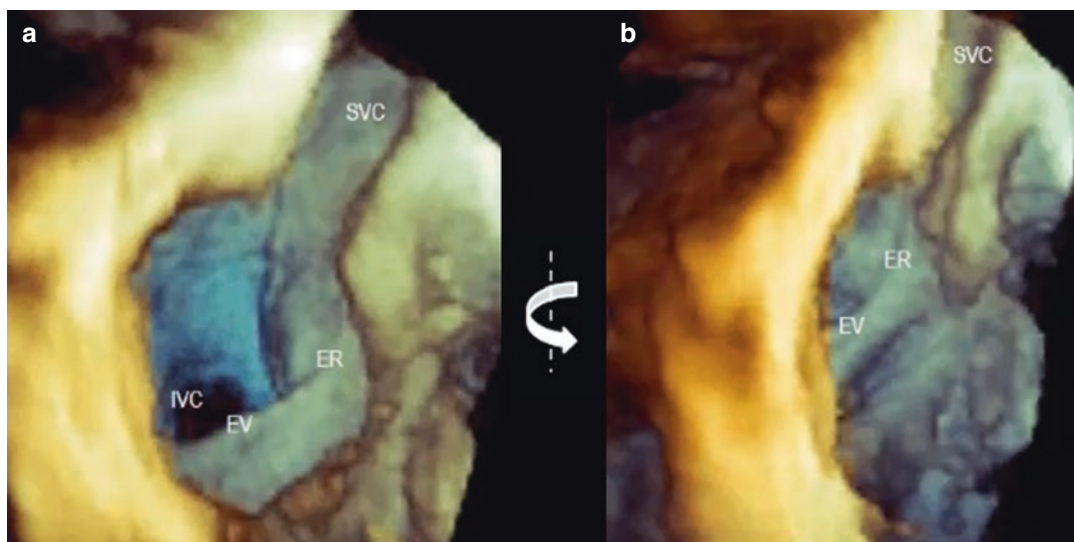


Fig. 4.21 (a) Eustachian valve (EV). (b) Eustachian ridge (ER)

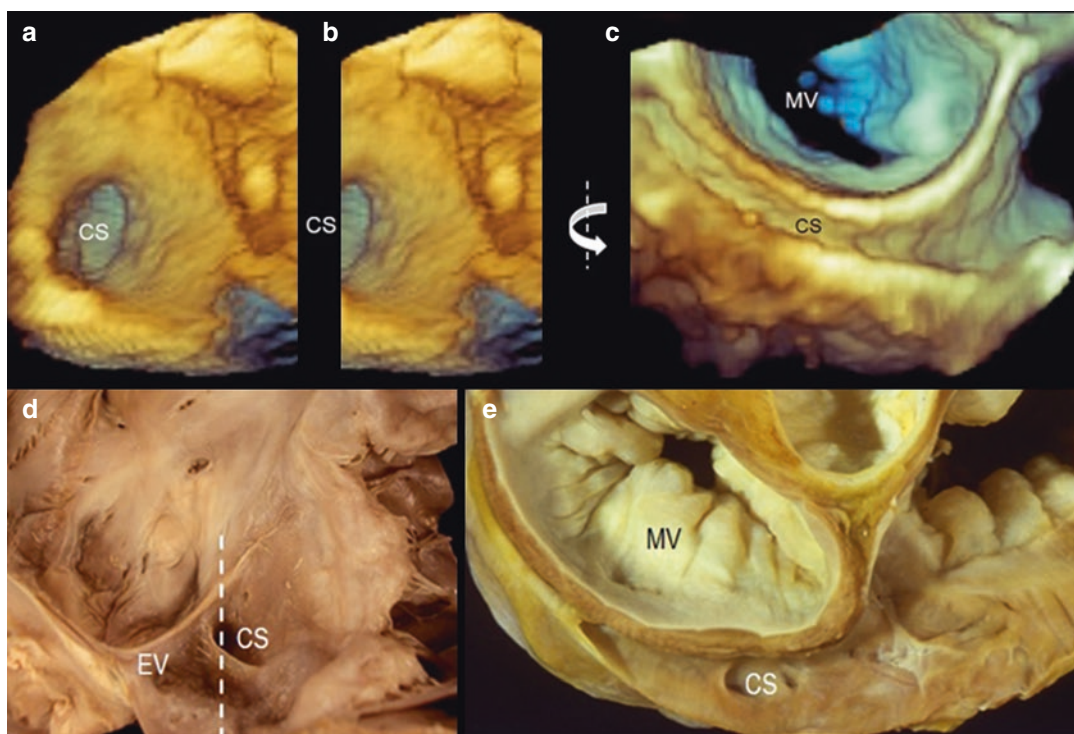


Fig. 4.22 (a) 3D-magnified image of the coronary sinus (CS) ostium. (b) Same image cropped longitudinally. (c) Same image rotated left-to-right around the Y-axis (curved arrow) to show a long segment of CS running along the atrioventricular groove. (d) Right atrial view of anatomi-

cal specimen corresponding to perspective shown in (a). The CS is cut along the broken line and the heart rotated to produce (e) that corresponds to the view shown in (c). EV Eustachian valve

The Right Side of the Interatrial Septum

The right side of the interatrial septum (IAS) comprises the fossa ovalis (FO) or septum primum, and the surrounding muscular septum secundum. The fossa ovalis (FO) essentially consists of a thin flap of connective tissue that overlaps the muscular rim on its left side. Thus, seen from a right perspective, the FO appears as an oval-shaped, crater-like depression of variable size. The septum secundum is an extensive and deep enfolding of the posterior-superior atrial wall between the vena cavae and the right pulmonary veins. This enfolding contains epicardial fat and small vessels [16]. The 3D TEE, being a “surface rendering” modality, appears particularly suitable for imaging the IAS [17]. Any 3D acquisition modality (zoom, width angle single beat, width angle multi-beat) from a 2D bicaval view may easily show both sides. An anatomically correct orientation (i.e., superior vena cava up) may help for the spatial relationship among structures. Three-dimensional TEE clearly show the fossa ovalis, the aorta and the coronary sinus (Fig. 4.23). We consider the “en face” view of right side (and of left side: see below) another *basic 3D perspectives*.

The Left Atrium

The left atrium (LA) is an ovoid-shaped chamber located posteriorly, slightly superior and to the left of the right atrium [16]. Externally the LA confines with the transverse sinus anteriorly, with the pulmonary trunk and to the right pulmonary artery superiorly and with oesophagus and descending thoracic aorta posteriorly. The internal surface is characterized by the four orifices of pulmonary veins superiorly, by the orifice of the left atrial appendage laterally and by the vestibule (i.e., an annular muscular band that surrounding the mitral orifice) inferiorly [16]. The majority of the internal surface of the LA is smooth. Only the LAA has an irregular shape presenting lobes and pectinate muscles. Because of the proximity of LA to the oesophagus, 3D TEE appears the ideal technique to illustrate the

internal surface of this cavity. Most of the LA structures shown in this section, such as the left atrial isthmus, the left lateral ridge, the orifice of pulmonary veins, are relevant from an electrophysiological viewpoint, while the shape and size of left atrial appendage are relevant for a percutaneous closure.

The left atrial isthmus (LAI) includes an area between the left lower pulmonary vein and the lateral commissure of mitral valve. Its relevance arises by the fact that a linear ablation may improve the success rate of catheter ablation of paroxysmal atrial fibrillation and may cure a subset of LA flutter. Starting by the 2D TEE long axis view at 120° a 3D TEE width angle single or multi-beat shows the lateral wall of the LA (Fig. 4.24). We consider this view another *basic 3D perspective*.

The left lateral ridge (LLR) is the most prominent structure of the LA. Echocardiographers call it “Coumadin ridge” because in the early era of 2D TEE, its Q-tip was mistaken for a thrombus. The LLR is actually an infolding of the atrial wall. Nerve bundles, small atrial arteries, and the remnant of Marshall’s vein runs within the fold. Indeed, some electrophysiologists erroneously call the LLR “ligament of Marshall.” The size of LLR may vary widely from long and thin to short and thick. Moreover, following the shape of the atrial cavity, the LLR presents a concave profile with the concavity towards the cavity. Finally, being part of the muscular atrial wall, it becomes thicker and more concave during the atrial systole. LLR is very close to the left atrial appendage and a single 3D perspective from above enables both structures to be visualised (Fig. 4.25a). This view is another *3D basic perspective*. A cross-section from this view enables imaging the infolding configuration of the LLR (Fig. 4.25b). Finally, a lateral view shows its concave shape (Fig. 4.25c).

The left atrial appendage is a well-recognised source of systemic embolism. Although several imaging techniques (i.e. CT, MRI, and intracardiac echocardiography) may visualize the LAA, for its versatility, high frame rate and spatial resolution, 2D TEE remains, in everyday practice, the first line imaging modality to rule-out LAA

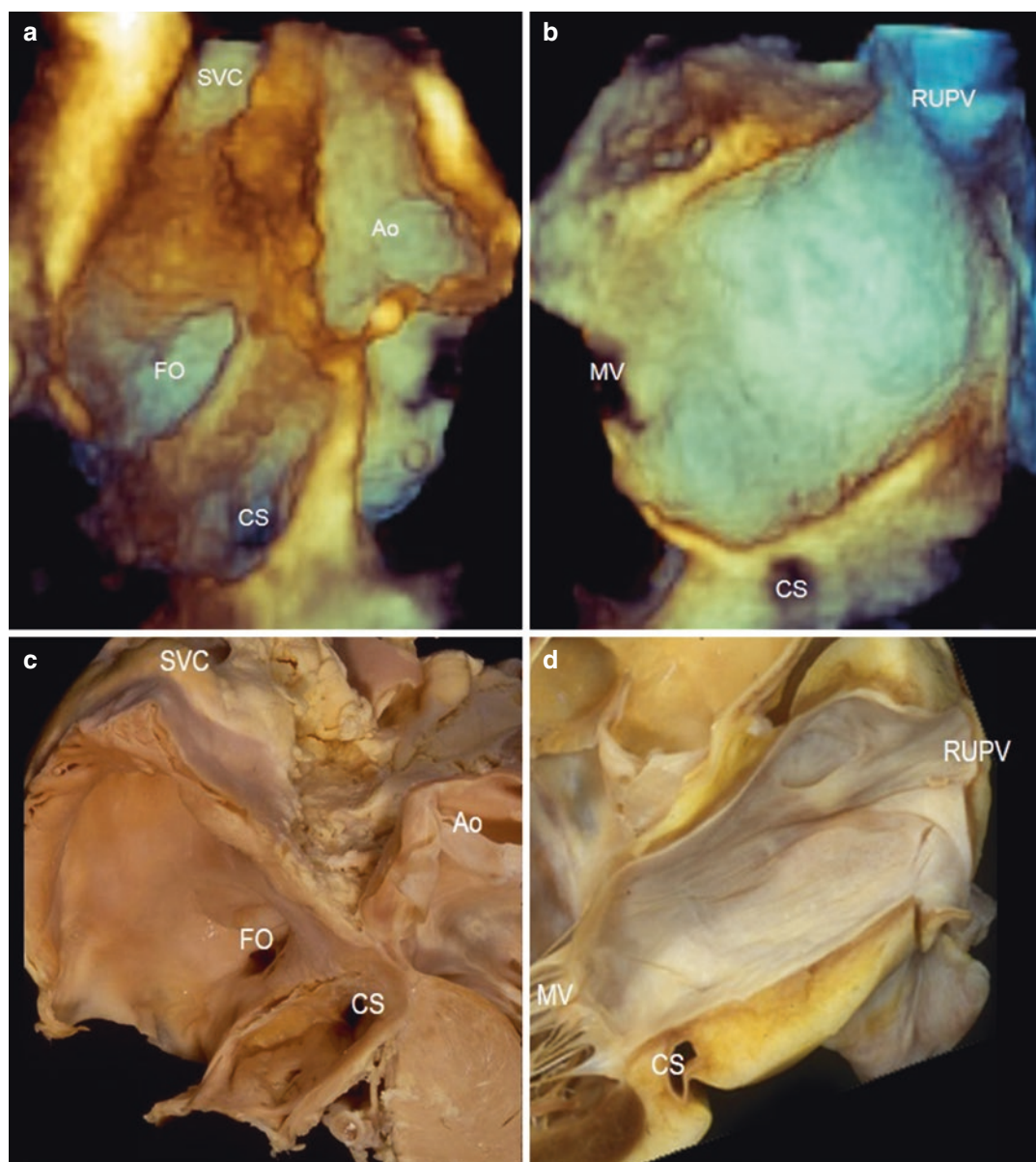


Fig. 4.23 (a) Three-dimensional TEE image of the right side of the interatrial septum (IAS) in a correct anatomical orientation, showing the fossa ovalis (FO), the superior vena cava (SVC), the coronary sinus (CS) and the aorta

(Ao). (b) The left side of the IAS. Usually this surface is featureless. (c) and (d) are corresponding views of anatomical specimens. *MV* mitral valve, *RUPV* right upper pulmonary vein

thrombi. 3D TEE is particularly appropriate for imaging LAA because it is very close to the intra-oesophageal transducer with a favourable angle with respect to the ultrasound beams. Moreover, being relatively small, a narrow 3D pyramidal data set may image the whole LAA with a high

frame rate and an optimal spatial resolution. Finally, for the first time, an ultrasound technique enables the LAA orifice to be visualised in an “en face” view.

The same *3D basic perspective* described for the LLR, enables visualization of the LAA’s

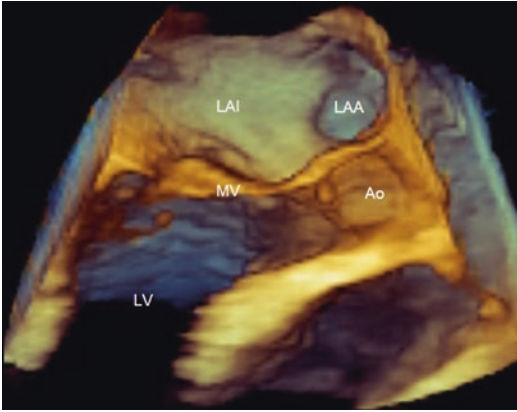


Fig. 4.24 Long axis view 3D TEE image showing the left atrial isthmus and left atrial appendage

orifice. In the normal individual, the orifice is elliptical with the pectinate muscles running perpendicular to the major axis (Fig. 4.26a). In patients with long-standing atrial fibrillation, the orifice becomes more circular [18] (Fig. 4.26b). Sporadically lobes may appear from this perspective (Fig. 4.26c). However, only a longitudinal cut allows visualization of number, size and site of the lobes (Fig. 4.26d).

Quantitative assessment of LAA size and length appear more precise with 3D TEE than with 2D TEE when using computed tomography as reference method [18]. Measurements can be done in both multi-planar reconstruction

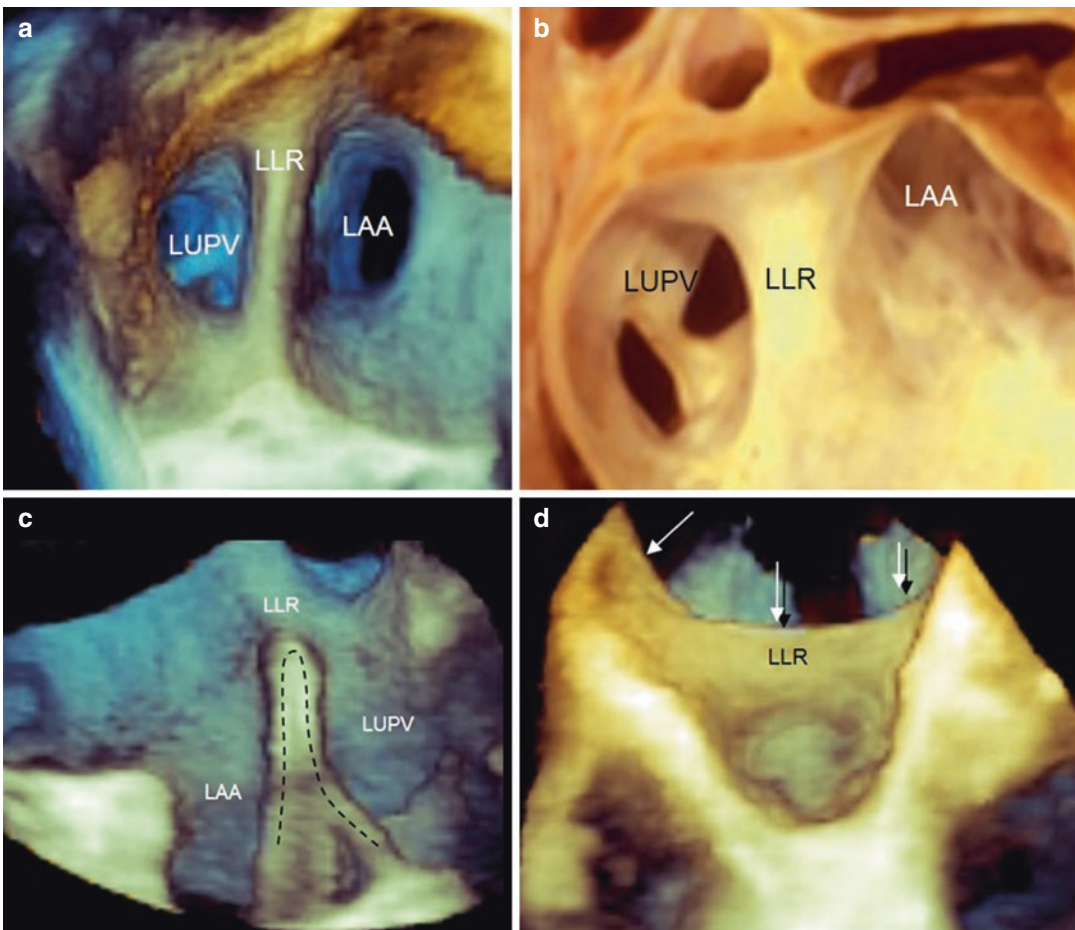


Fig. 4.25 (a) Three-dimensional basic perspective showing the orifice of the left atrial appendage (LAA) and left upper pulmonary vein (LUPV). The left lateral ridge is in between. (b) The corresponding anatomical specimen. (c)

Cross-sectional image of the LLR showing the infolding (dotted line). (d) The curved shape of LLR (arrows) seen from LA

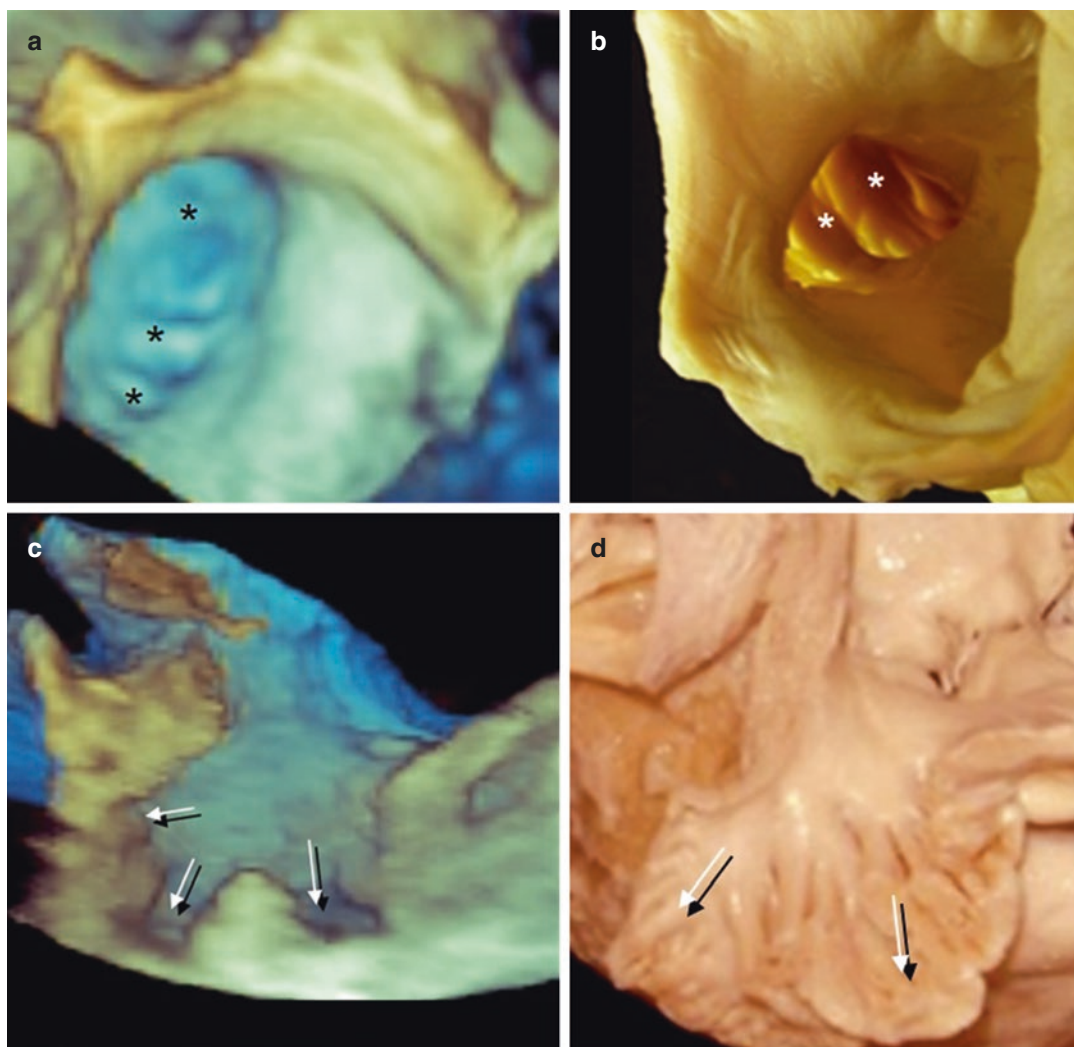


Fig. 4.26 (a) Three-dimensional perspective from above showing the elliptic shape of the left atrial appendage (LAA) and pectinate muscles (asterisks), running perpendicularly to the major axis. (b) The corresponding ana-

tomical specimen. (c) A longitudinal cut allows defining shape, size and site of the lobes (arrows). (d) The corresponding anatomical specimen

(i.e., using 2D images derived from the 3D data set) (Fig. 4.27) and directly on 3D image (Fig. 4.28).

The anterior wall of LA lies just beyond the transverse sinus and the aortic root. The wall is rather smooth, without recognisable anatomical features. Two-dimensional TEE may differentiate (in cross-section long axis view), the thin wall of LAA from the thicker wall of the aorta (Fig. 4.29a). Shifting in 3D mode, the atrial and aortic walls appear as one (Fig. 4.29b). This is

particularly true at the level of coronary sinuses, where both walls are very thin (Fig. 4.29c). Indeed, the spatial resolution of 3D TEE is not enough to differentiate the two walls.

The transverse sinus that divides the two walls is nearly virtual and can be sporadically appreciated sporadically immediately above the level of the sinotubular junction (Fig. 4.30).

Because of this proximity, prominent left and/or non-coronary aortic sinuses may cause a protuberance of the wall into the left atrial cavity,

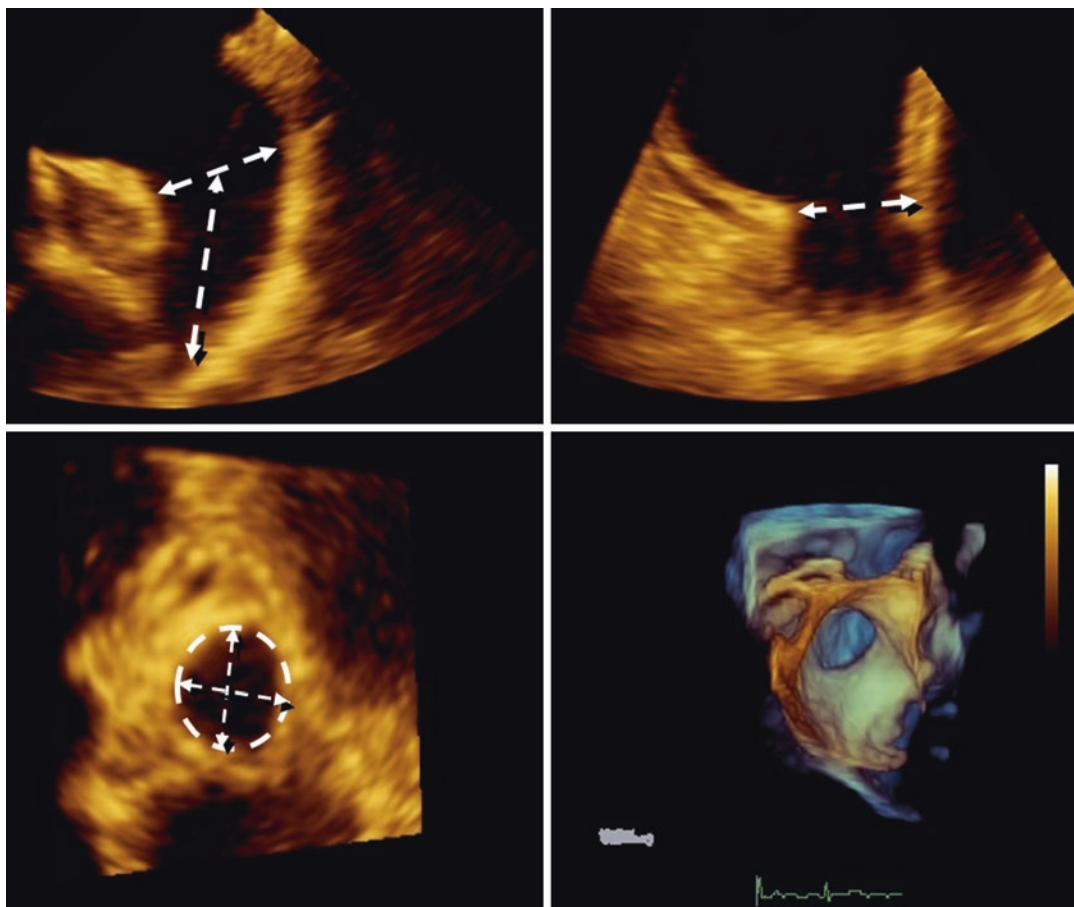


Fig. 4.27 Measurements taken in multi-planar reconstruction

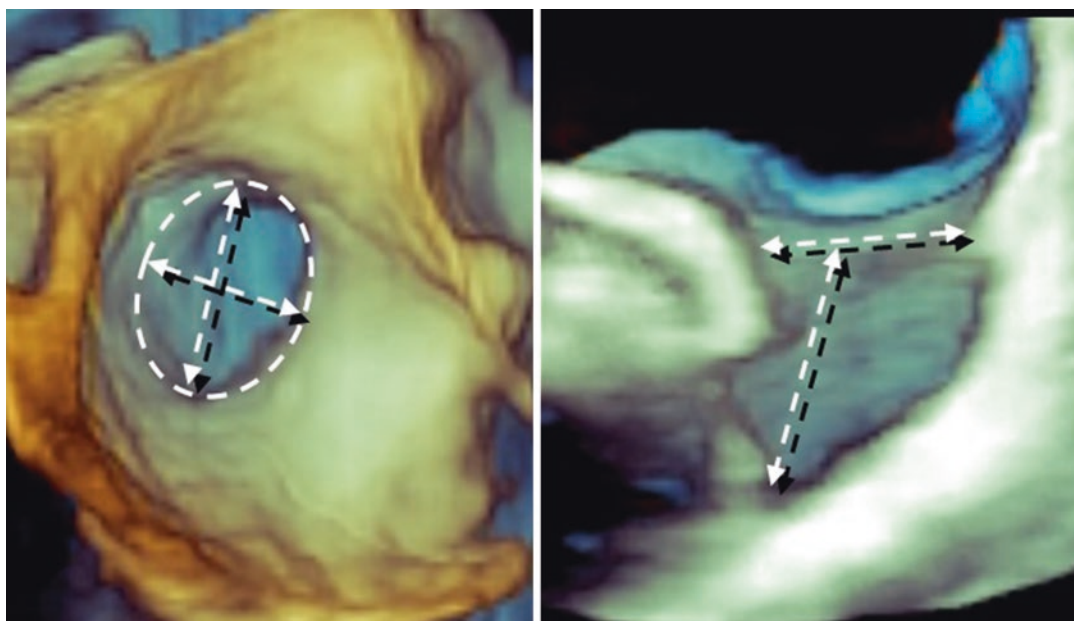


Fig. 4.28 Measurement taken directly on 3D images

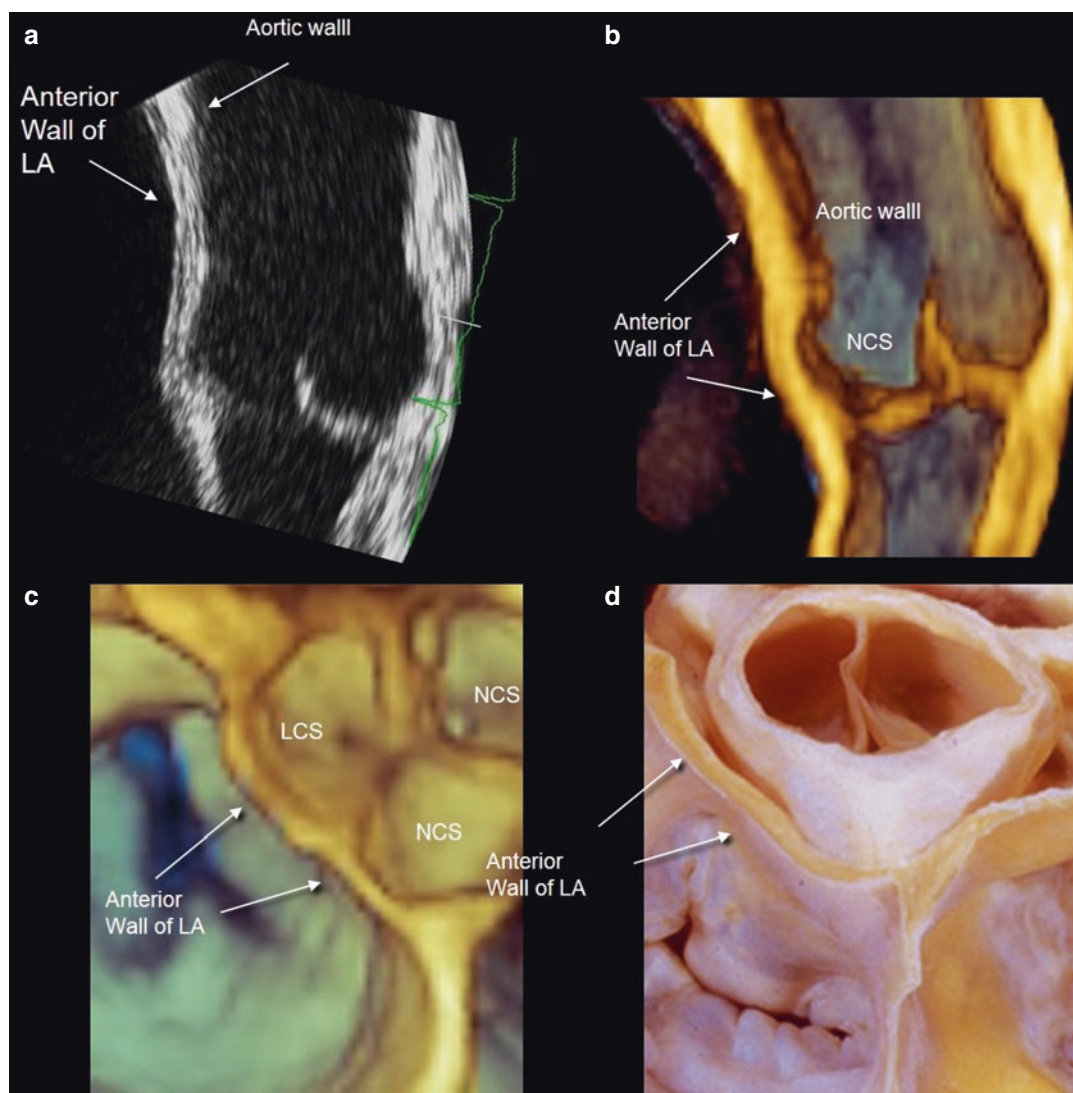


Fig. 4.29 (a) Two-dimensional TEE image of a cross-sectional long-axis view of the aorta. The high spatial resolution allows distinguishing the anterior wall of left atrium (LA) from the posterior aortic wall. (b) Same image of the panel A in 3D. The lower spatial resolution of 3D TEE does not allow separating the two walls. (c)

Particular of 3D TEE imaging illustrating as the two walls, particularly thin at the level of coronary sinuses, appear as one. (d) Conversely the anatomic specimen clearly shows the two adjacent walls. *LCS* left coronary sinus, *NCS* noncoronary sinus

which, at first glance, may be mistaken for a pathological feature (Fig. 4.31).

The “roof” of the LA is usually the thickest area (due to the presence of the Bachmann’s bundle) measuring up to 6 mm; externally, this wall relates to the bifurcation of the pulmonary trunk and to the right pulmonary artery (Fig. 4.32).

The pulmonary veins (PVs) join the LA at the posterior-superior part of the left atrial body. The PVs play a relevant role in triggering and sustaining

atrial fibrillation. Indeed, the most common interventional treatment strategy for symptomatic, drug-resistant patients with atrial fibrillation is the electrical isolation of PVs. The most common pattern is two veins from each lung, though nonpathological variations are frequent: on the left side the merger of upper and lower PVs in a common trunk occurs in around 15% of the population, while on the right side the most common variant consists of a third accessory vein entering independently.

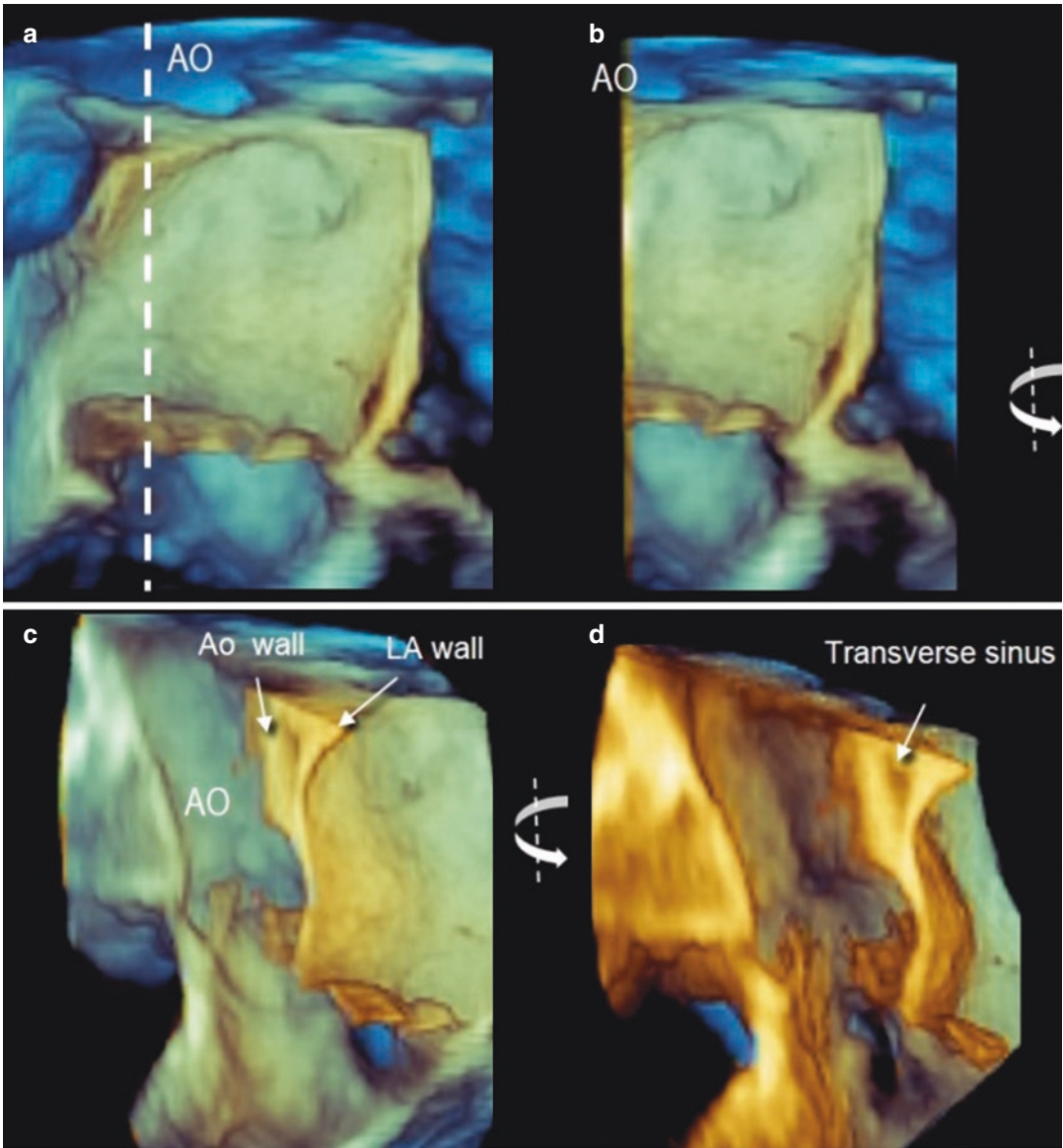


Fig. 4.30 (a) Three-dimensional image of the anterior wall of left atrium. The wall appears rather smooth without irregularities. The dotted lines mark the line of cropping to obtain the image in panel (b). A rotation

left-to-right around the y-axis (curved arrows) shows as the transverse sinus appears immediately after the sinus tubular junction (panels c and d)

The region in between two separate ipsilateral veins takes the name of inter-venous ridge. Often PVs enter gradually into the atrial cavity and the precise location of the venous-atrial junction or, in other words, the PV's orifice is difficult to delineate [19].

Theoretically, the proximity of the intra-esophageal transducer to the posterior wall of the LA should facilitate imaging of PVs and should

allow visualizing all the four PVs in a single “panoramic” view. Unfortunately, this is not the case because the left and right PVs are widely separated from each other and the pyramidal data set at such short distance is too narrow to include in a single image the four PVs orifices. Thus, the right and left PVs can be visualized using different perspectives [20].

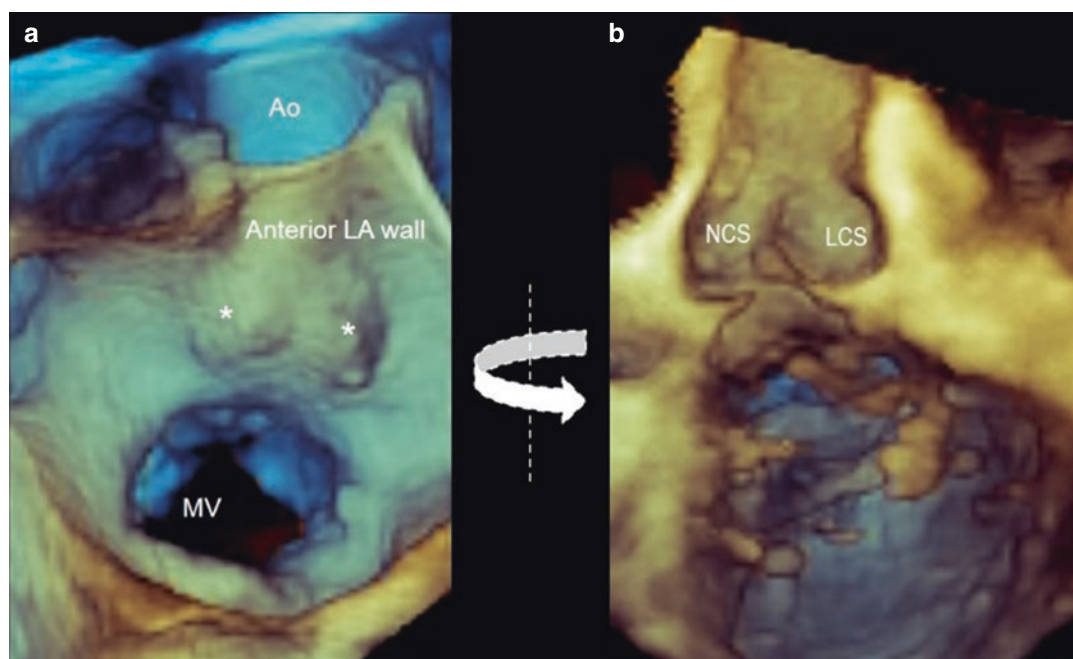


Fig. 4.31 (a) Three-dimensional image of the anterior wall of the left atrium (LA) in “en face” view. Prominent left (LCS) and noncoronary (NCS) sinuses push against the atrial wall, protruding into the cavity (asterisks). At

first glance, and using this only perspective this image may be misinterpreted as pathological. (b) A longitudinal cut and a 180° rotation left-to right around the Y-axis show the sinuses from an internal aortic perspective

The best way to visualize the left PVs is to direct the pyramidal beam on the left atrial appendage. A lateral shifting from this view and a slight drawback of the transducer enable imaging “en face” the orifice of left upper and left lower pulmonary veins (Fig. 4.33a). From this perspective, a longitudinal crop through the PVs’ lumen and a rotation of the entire 3D data set of 90° reveals the left PVs in long axis view (Fig. 4.33b). The right PVs’ orifices are adjacent to the interatrial septum. Thus, the best approach to visualize right PVs is the *3D basic perspective* used to visualize the left side interatrial septum. From this view, a clockwise rotation of the probe reveals both orifices of right PVs (Fig. 4.33c) [20]. As for the left PVs, a longitudinal crop and a 90° rotation displays the right PVs in their long-axis orientation (Fig. 4.33d).

The left surface of the interatrial septum (IAS) constitutes the medial wall of the LA. This surface is relatively featureless (Fig. 4.34a). Indeed, because the septum primum overlaps the septum secundum from this side, it becomes almost

invisible when imaged from an “en face” perspective. The distinction between septum primum and septum secundum appears evident when the IAS is shown in a cross-section perspective (Fig. 4.34b).

A small irregularity called the atrial pouch is frequently seen superiorly and anteriorly of the fossa ovalis [21]. This pouch, which resembles a kangaroo pocket, is due to a partial fusion between septum primum and septum secundum. The two septa remain fused only at their caudal border. The resulting pocket opens superior-anterior at the left side usually with a curved shape (Fig. 4.35).

The Ventricles

The Right Ventricle

The right ventricle (RV) is the most anterior chamber of the heart being located directly behind the sternum [22]. The RV has a complex

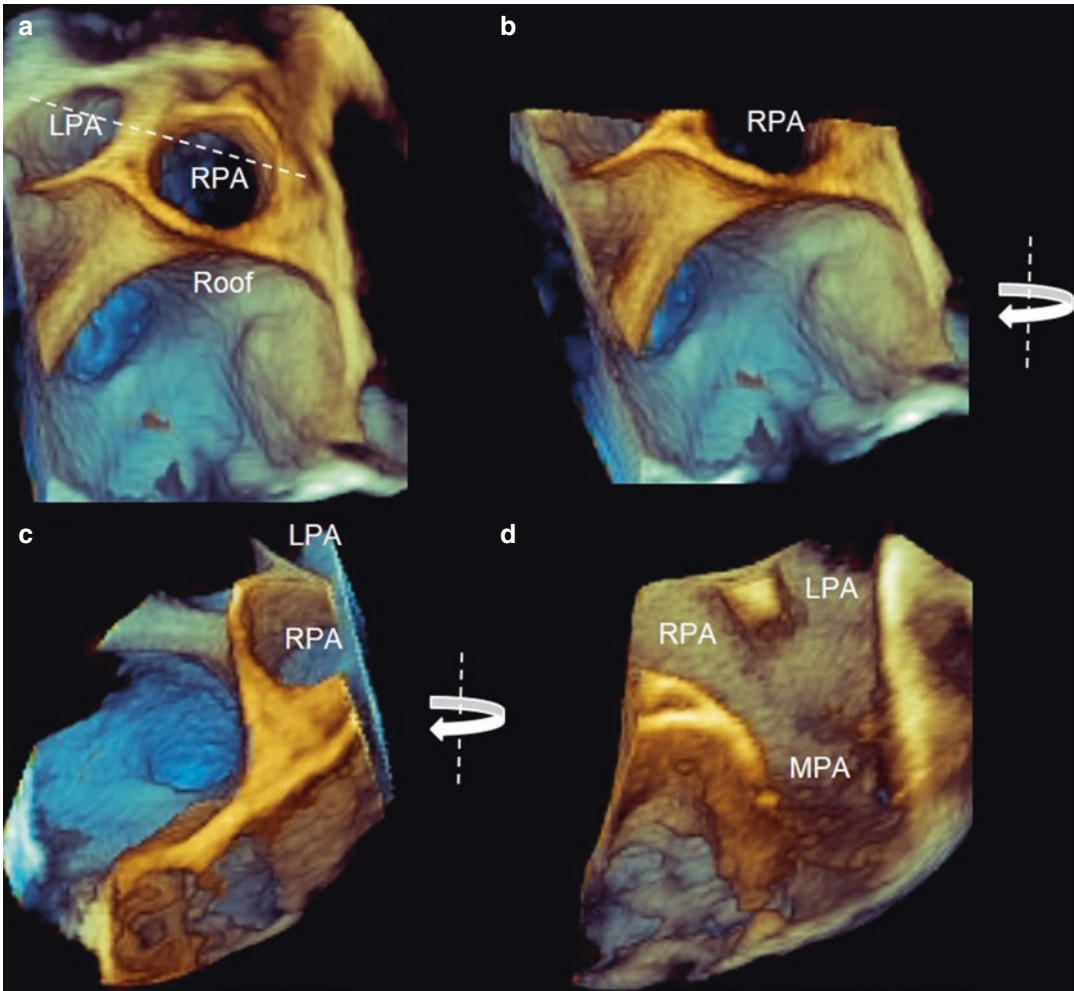


Fig. 4.32 (a) The roof of the left atrium and its strict anatomical relationship with the main pulmonary artery (MPA) and the left (LPA) and right (RPA) pulmonary

branches. (b–d) This close proximity is better appreciated, by properly cropping and rotated the volumetric data set

shape: when seen anteriorly it looks triangular, while in cross-section has a crescent-shaped aspect embracing the left ventricle. Because of this complex configuration, in four-chamber echocardiographic view, the RV may appear smaller than the left ventricle (LV), while, in reality, in normal adult heart, RV volume is larger than the LV volume (Fig. 4.36). The wall of the RV is considerably thinner than that of the left ventricle ranging from three to 7 mm, being as thin as 1.5 mm at the apex. Thus, the RV mass is about one-sixtieth that of LV mass.

Anatomists describe the cavity of the RV in terms of three components: the inlet, the apical

and the outlet. By cutting tangentially to the anterior right ventricular wall (the so-called coronal view), 3D TTE/TEE may show all these components in a single image. We consider this crop image another *3D basic perspective* (Fig. 4.37a).

The inlet component roughly extends from the hinge line of the tricuspid valve to the line of insertion of papillary muscles. The apical component characteristically consists of coarse trabeculations. A longitudinal cut of the right ventricular apex from the transgastric view is probably the best perspective for imaging these trabeculations (Fig. 4.37b). In congenital heart disease, these trabeculations help distinguishing

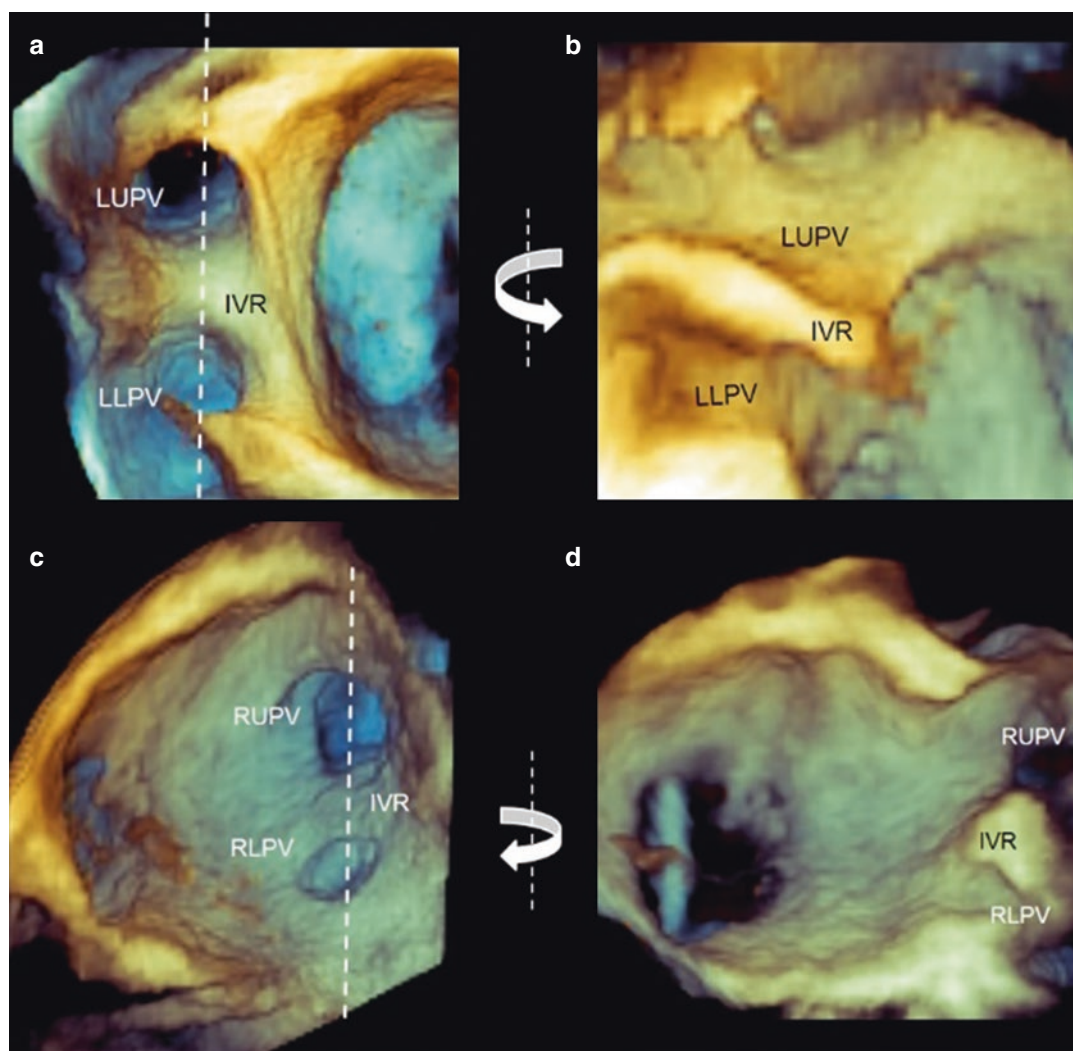


Fig. 4.33 (a) Three-dimensional TEE images of the left upper (LUPV) and left lower (LLPV) pulmonary vein orifices in “en face” view. In between there is the intervenous ridge (IVR). The dotted line marks the line of cropping. (b) A left-to-right rotation of cropped image around the Y-axis (curved arrow), of 90° reveals the left PVs in their

long axis orientation. (c) The right upper (RUPV) and right lower (RLPV) pulmonary veins orifices in “en face” view. (d) The dotted line marks the line of cropping. A right-to-left rotation of cropped image around the Y-axis (curved arrow) of 90° reveals the right PVs and their IVR in their long-axis orientation

the morphologically right ventricle from the morphologically left ventricle, which presents finer trabeculations. Finally, the outlet component is a smooth muscular cylinder that sustains the pulmonary root (Fig. 4.37c). A well-defined border, which separates the outlet from the inlet and apical components, is absent.

Three specific anatomical structures characterize the RV cavity: the crista supraventricularis

(CSV), the trabecula septomarginal (TSM) and the moderator band (MB). The CSV (or ventriculoinfundibular fold) is a prominent muscular structure, formed by the posterior wall of the infundibulum and in continuity with the ventricular septum. In cross-section, the CSV looks as a curved ridge, which appears sustaining the aortic root between tricuspid and pulmonary valve (Fig. 4.38a). The TSM is a muscular column protruding from the

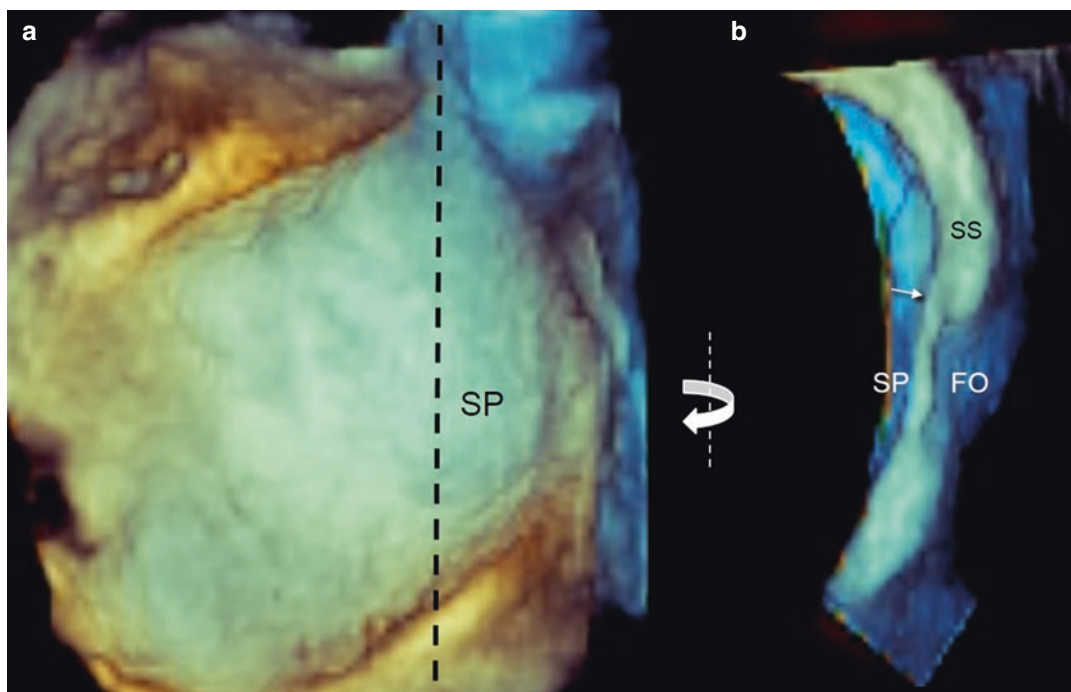


Fig. 4.34 (a) Three-dimensional TEE images showing a featureless surface of the left side of interatrial septum when seen “en face”. The septum primum (SP) is rather indistinguishable from the septum secundum. The dotted line marks the line of cropping. (b) Cross-section of the

cropped 3D image obtained by a rotation of 90° right-to-left around the y-axis (curved arrow). It appears clear as the thin septum primum (SP) overlaps (arrow) the ticker septum secundum (SS)

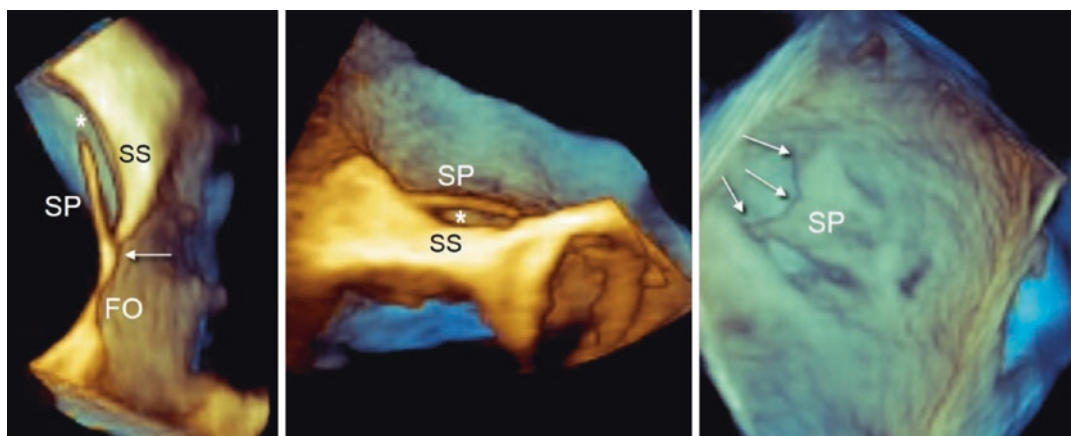


Fig. 4.35 (a) Three-dimensional TEE cross-section images showing a pouch (asterisk) due to the fusion of the septum primum (SP) with the septum secundum (SS) only at their caudal border causing a kind of

pocket (asterisk). (b) Seen en face perspective, this pouch has a narrow ovoid overture (asterisk). (c) Seen from a left perspective, the margin of SP is curved with an anterior concavity

septal surface. It bifurcates in two arms that encircles the CSV. The body of this “trabeculation” extends towards the apex, giving origin to the MB, which crosses the right ventricular cavity and ends

at the base of anterior papillary muscle (APM). The “complex” *TSM-MB-APM* forms a U-shaped structure that looks like a wide communication between the inlet and the outlet portions of the RV

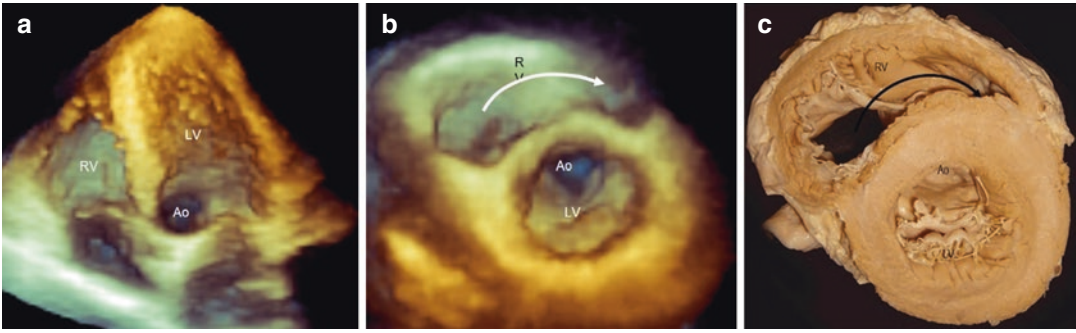


Fig. 4.36 (a, b) Three-dimensional transthoracic images. In four-chamber view (a), the right ventricle (RV) appears smaller of the left ventricle (LV). In short-axis view (b),

the RV embraces the left ventricle (curved arrow). (c) Anatomic specimen showing the same perspective as in panel (b)

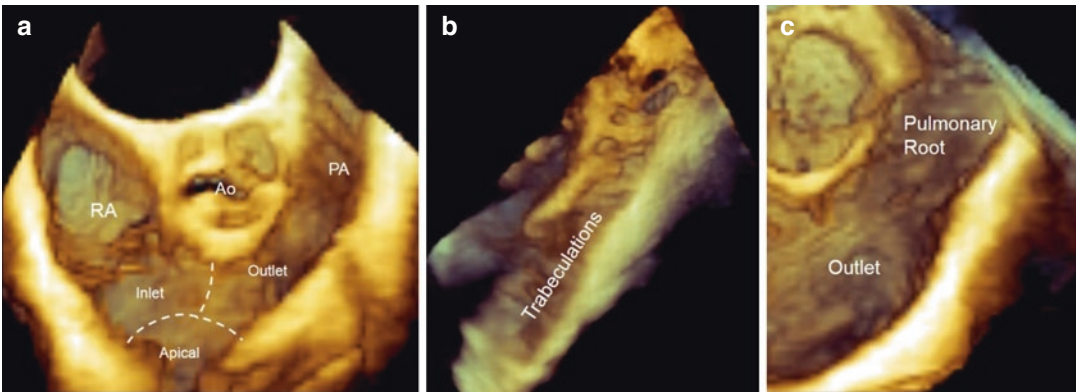


Fig. 4.37 (a), “Coronal” cut of 3D data set allows visualizing the three components of the right ventricle in a single view. The dotted lines delimit the supposed confines.

(b) A magnified image of the trabeculations of the RV apex obtained by a trans-gastric view. (c) A particular of the outlet component sustaining the pulmonary root

(Fig. 4.38b). When hypertrophied, this complex may divide the RV in two chambers, one proximal at high pressure and one distal at low pressure (double-chambered RV).

The complex nonsymmetric RV morphology makes accurate quantification of RV volume and EF with a tomographic technique such as 2D TTE/TEE (based on geometrical assumptions) problematic and unreliable. Because 3D TTE/TEE does not need of geometrical assumptions, this technique has the potential to provide accurate and reproducible quantitative data. Moreover, commercially available software may, on and off line, provide a fast reconstruction of volumes and EF. Indeed, 3D TTE and TEE echocardiography appear to improve quantitative RV size and function over the 2D echocardiography when compared with magnetic resonance [23]

(Fig. 4.39). However, poor echocardiographic transthoracic and transesophageal windows may negatively affect the quality of images and, as results, the accuracy of quantitative data.

The Left Ventricle

The left ventricle (LV) has the shape of an ellipsoid of revolution. When seen in cross-section perpendicular to its long-axis orientation, LV reveals a circular geometry. Two groups of papillary muscles, in the anterolateral and posteromedial positions, characterize the internal surface. Like the right ventricle, anatomists describe three components: the inlet, the apical trabecular and the outlet component. The inlet component extends from the mitral hinge line to

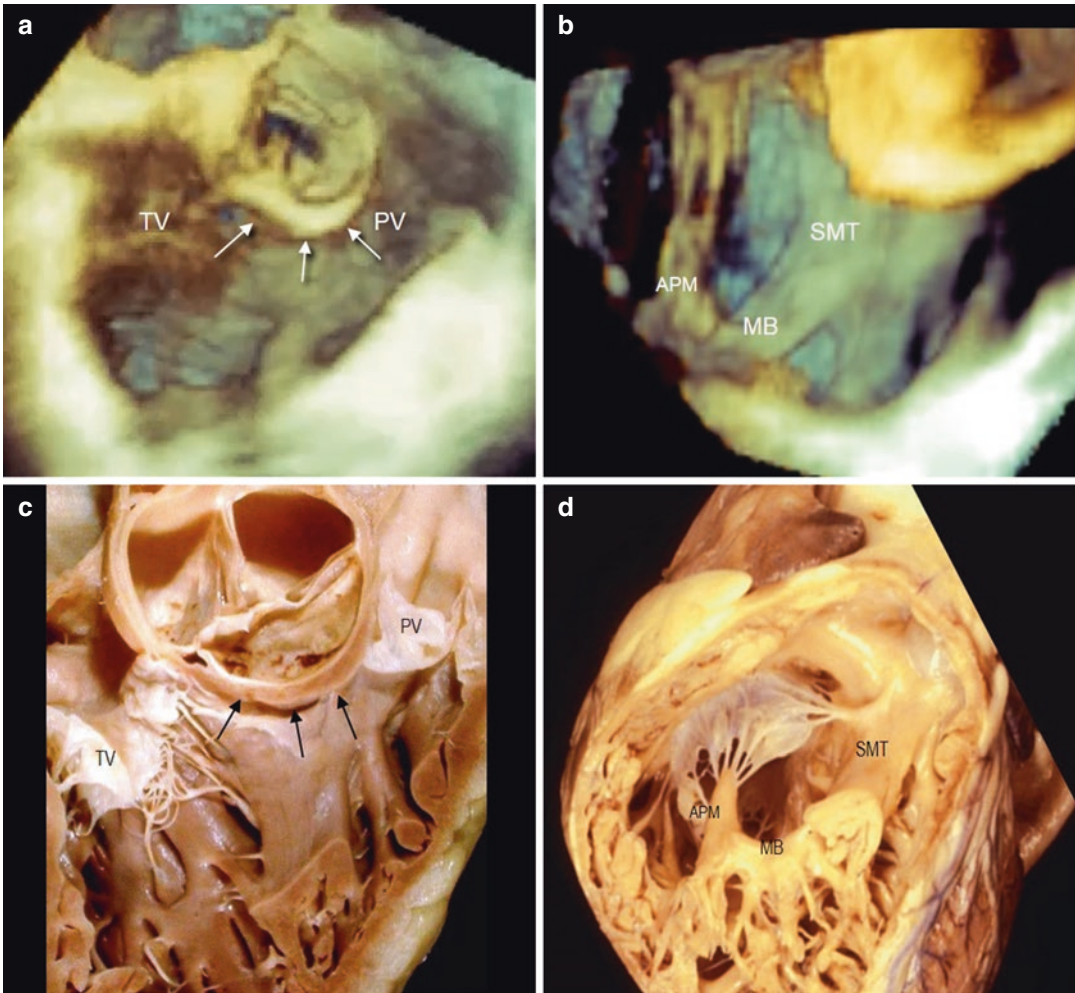


Fig. 4.38 (a) “Coronal” perspective showing the crista supraventricular (arrows) separating the tricuspid valve (TV) from the pulmonary valve (PV). (b) The complex trabecula septomarginal (TSM), moderator band (MB)

and anterior papillary muscle (APM) forming a “U-shaped” structure (*see text*). (c and d) Anatomic specimens corresponding to 3D images

the attachment of the papillary muscles. Compared to coarse apical trabeculations of RV, the apical components contain finer trabeculations. The outlet component supports the aortic valve and, contrary to the RV infundibulum, consists of both muscular and fibrous portions. Because the interventricular septum is curve with the concavity towards the LV cavity, the inlet component partially overlaps the outlet.

3D TTE and TEE allow imaging in a 3D format these morphological features (Fig. 4.40).

Probably the most remarkable advantage of 3D TTE/TEE compare with 2D TTE/TEE is the quantification of left ventricular volumes and the evaluation of “synchronicity”. In many patients, 3D TTE is more suitable than 3D TEE for assessing left ventricular size and function: the apical portion of LV are far from the transesophageal

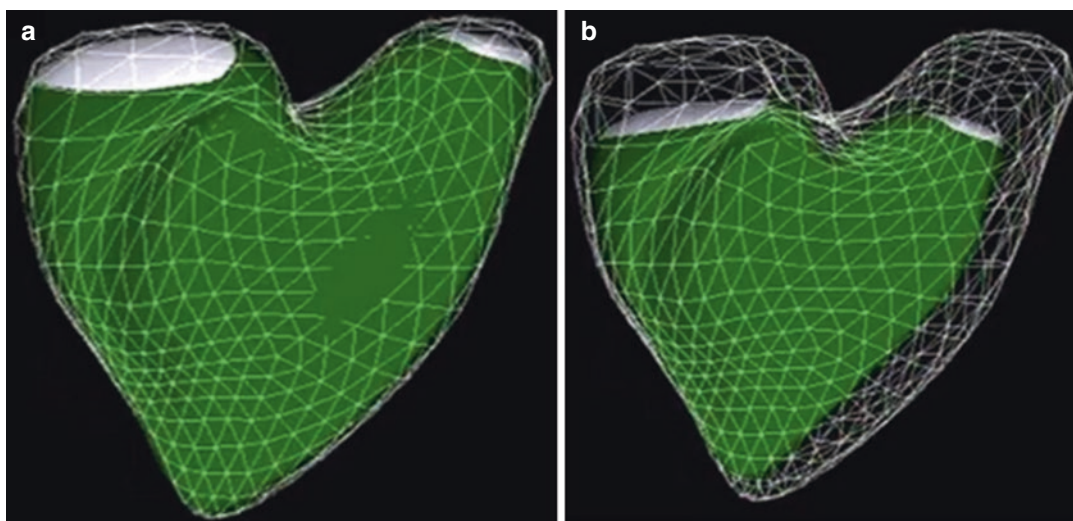


Fig. 4.39 Commercially available software, which allows a fast reconstruction of RV size and function. (a) Diastolic frame. (b) Systolic frame

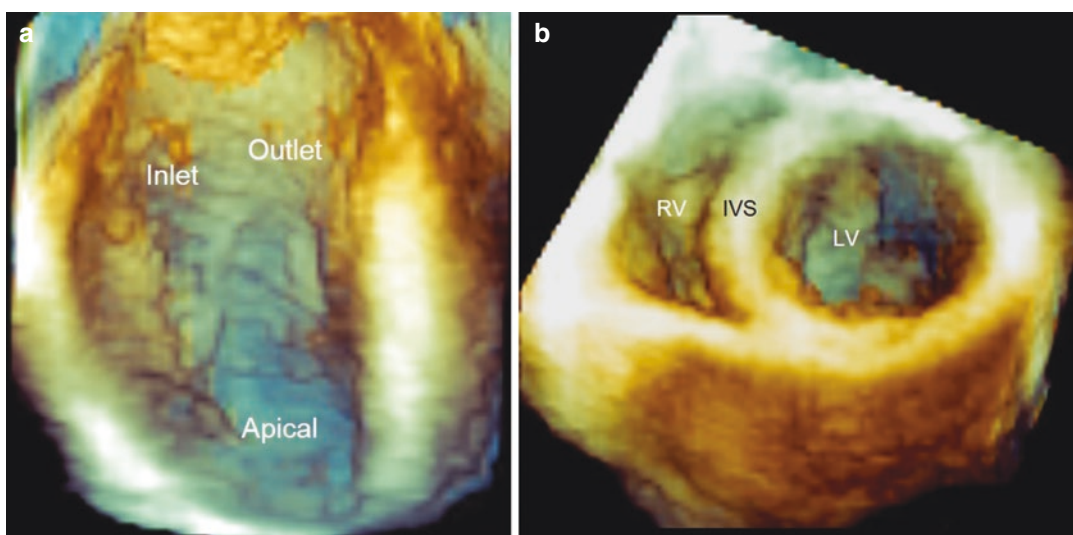


Fig. 4.40 Three-dimensional TEE images showing the elliptical shape of left ventricle (LV) when seen in longitudinal view. (a) In this view, the inlet, apical and outlet

components of the LV cavity can be roughly imaged. (b) Cross-section of the LV showing its circular shape. *IVS* interventricular septum

transducer and the quality of imaging in the far field may not be optimal. 2D TTE and TEE echocardiography have well-known limitations in measuring LV volumes and EF (e.g., dependence

on geometrical models, inaccurate measurement due to foreshortening LV). 3D TTE/TEE may overcome some of these limitations. 3D data on LV volumes and EF are more accurate and

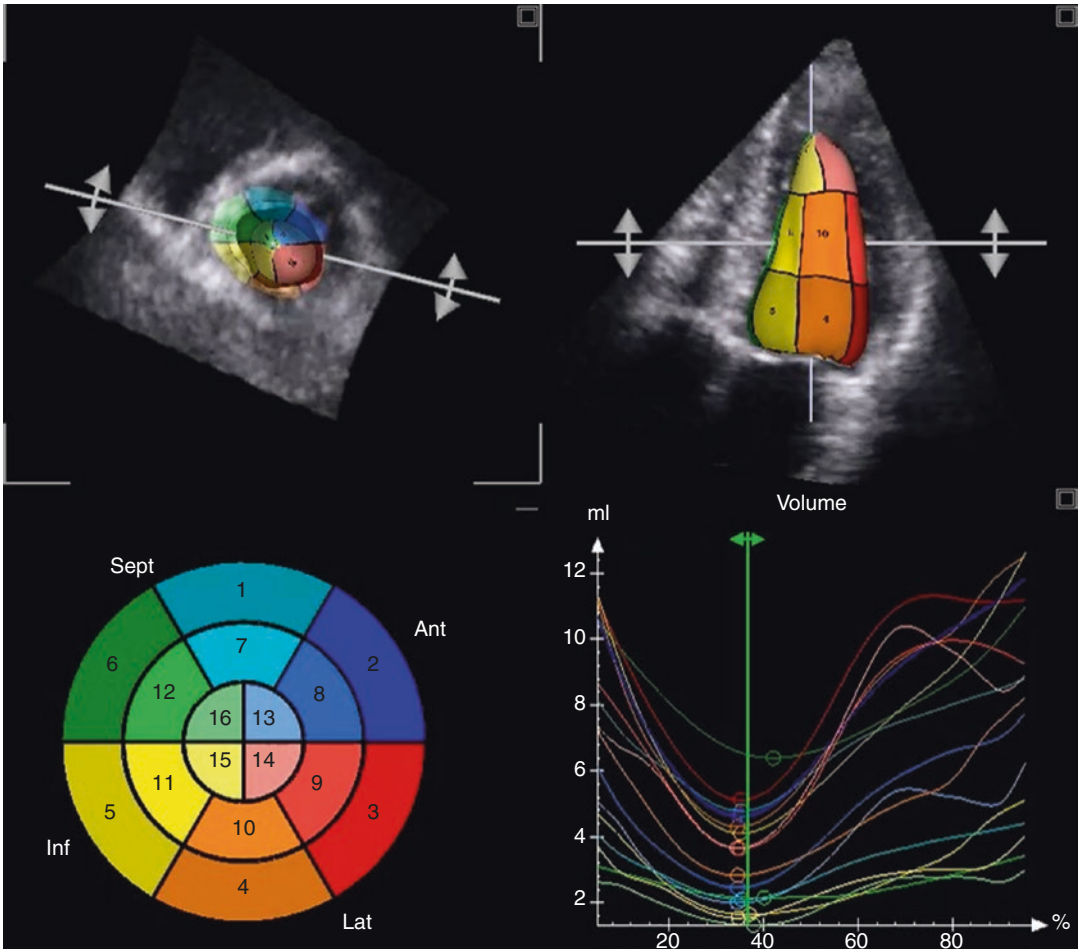


Fig. 4.41 Examples of “synchronicity” assessed by 3D TTE

reproducible than 2D data [24]. Moreover, a single perspective may capture the wall motion abnormalities and the dyssynchrony due to LBBB [25]. However, as for the right ventricle, 3D TTE/TEE have its own limitations in assessing LV volumes and function. A reliable tracing of the left ventricular contour of 3D TTE relies on the imaging quality: poor quality data affects 3D TTE more than 2D TTE. When compared with cardiac magnetic resonance (considered the gold standard) both 3D TTE and TEE may underestimate the LV volumes (probably due to the presence of trabeculations and the relatively poor resolution that not allow discrimination between trabeculations and compact myocardium [26,

27]. Current real-time 3D TTE and TEE suffer from a relative low frame rate and a fluid and natural image motion can be obtained only using full volume multi-beat (ECG gated) acquisition, which is, by definition, not a real-time (Fig. 4.41).

Conclusions

In this chapter, we showed how 3D TTE and TEE provide fine anatomic images of cardiac structures, which parallel anatomic specimens. Moreover, we described those perspectives that in our mind are the most clear and informative. We called these perspectives “basic 3D perspectives”.

We do believe that readers should familiarized with these basic perspectives. Indeed, as far as 3D TTE and TEE will be fully incorporated into the echo lab, these perspectives will assume the same relevance as the well-known 2D TTE, TEE sections.

References

- Lang RM, Badano LP, Tsang W, Adams DH, Agricola E, Buck T, et al. EAE/ASE recommendations for image acquisition and display using three-dimensional echocardiography. *J Am Soc Echocardiogr*. 2012;25:3–46.
- Perloff JK, Roberts WC. The mitral valve apparatus: functional anatomy of mitral regurgitation. *Circulation*. 1972;46:227–39.
- Angelini A, Ho SY, Anderson RH, et al. A histological study of atrio-ventricular junction in heart with normal and prolapsed leaflets of the mitral valve. *Br Heart J*. 1988;59:712–6.
- Levine RA, Handschumacher MD, Sanfilippo AJ, Hagege AA, Harrigan P, Marshall JE, Weyman AE. Three-dimensional echocardiographic reconstruction of the mitral valve, with implications for the diagnosis of mitral valve prolapse. *Circulation*. 1989;80:589–98.
- Salgo IS, Gorman JH 3rd, Gorman RC, Jackson BM, Bowen FW, Plappert T, et al. Effect of annular shape on leaflet curvature in reducing mitral valve stress. *Circulation*. 2002;106:711–7.
- Sugeng L, Shernan SK, Salgo IS, Weinert L, Shook D, Raman J, et al. Live three-dimensional transesophageal echocardiography: initial experience using the fully sampled matrix array probe. *J Am Coll Cardiol*. 2008;52:446–9.
- Biaggi P, Gruner C, Jedrzkiewicz S, Karski J, Meineri M, Vegas A, et al. Assessment of mitral valve prolapse by 3D TEE angled views are key. *JACC Cardiovasc Imaging*. 2011;4(1):94–7.
- Faletra FF, Demertzis S, Pedrazzini G, Murzilli R, Pasotti E, Muzzarelli S, et al. Three-dimensional transesophageal echocardiography in degenerative mitral regurgitation. *J Am Soc Echocardiogr*. 2015;28:437–48.
- Axel L. Papillary muscles does not attach directly to the solid heart wall. *Circulation*. 2004;109:3145–8.
- Ho Y. Structure and anatomy of the aortic root. *Eur J Echocardiogr*. 2009;10:i3–10.
- Faletra FF, Ramamurthi A, Dequarti MC, Leo LA, Moccetti T, Pandian N. Artifacts in three-dimensional transesophageal echocardiography. *J Am Soc Echocardiogr*. 2014;27:453–62.
- Sutton JP 3rd, Ho SY, Anderson RH. The forgotten interleaflet triangles: a review of the surgical anatomy of the aortic valve. *Ann Thorac Surg*. 1995;59:419–27.
- Stamm C, Anderson RH, Ho SY. Clinical anatomy of pulmonary root compared with that of isolated pulmonary valvular stenosis. *J Am Coll Cardiol*. 1998;31:1420–5.
- Faletra FF, Ho SY, Auricchio A. Anatomy of right atrial structures by real-time 3D transesophageal echocardiography. *J Am Coll Cardiol Imaging*. 2010;3:966–75.
- Cabrera JA, Sanchez-Quintana D, Farre J, Rubio JA, Ho SY. The inferior right atrial isthmus: further architectural insights for current and coming ablation technologies. *J Cardiovasc Electrophysiol*. 2005;16:402–8.
- Ho SY, Anderson RH, Sanchez-Quintana D. Atrial structure and fibres: morphological basis of atrial conduction. *Cardiovasc Res*. 2002;54:325–36.
- Faletra FF, Nucifora G, Ho SY. Imaging the atrial septum using real-time three-dimensional transesophageal echocardiography: technical tips, normal anatomy, and its role in transseptal puncture. *J Am Soc Echocardiogr*. 2011;24:593–9.
- Nucifora G, Faletra FF, Regoly F, Pasotti E, Pedrazzini G, Moccetti T, Auricchio A. Evaluation of left atrial appendage with real-time transesophageal echocardiography: implication for catheter-based left atrial appendage closure. *Circ Cardiovasc Imaging*. 2011;4:514–23.
- Ho SY, Sanchez-Quintana D, Cabrera JA, Anderson RH. Anatomy of the left atrium: implications for radiofrequency ablation of atrial fibrillation. *J Cardiovasc Electrophysiol*. 1999;10:1525–33.
- Faletra FF, Ho SY, Regoly F, Acena M, Auricchio A. Real-time three-dimensional transesophageal echocardiography in imaging key anatomical structures of the left atrium: potential role during atrial fibrillation ablation. *Heart*. 2013;99:33–42.
- Subramaniam C, Krishnan MD, Miguel Salazar MD. Septal pouch in the left atrium. A new anatomical entity with potential for embolic complications. *J Am Coll Cardiol Interv*. 2010;3:98–104.
- Ho SY, Nihoyannopoulos P. Anatomy, echocardiography and normal right ventricular dimensions. *Heart*. 2006;92(Suppl I):i2–i13.
- Van der Zwaan HB, KGeleijnse ML, McGhie JS, Boersma E, Helbing WA, Meijboom FJ, Roos-Hesselink JW. Right ventricular quantification in clinical practice: two-dimensional vs. three-dimensional echocardiography compared with cardiac magnetic resonance imaging. *Eur J Echocardiogr*. 2011;12:656–64.
- Jenkins C, Bricknell K, Hanekom L, Marwick TH. Reproducibility and accuracy of echocardiographic measurements of left ventricular parameters using real-time three-dimensional echocardiography. *J Am Coll Cardiol*. 2004;44:878–86.
- Kapetanakis S, Kearney MT, Siva A. Real-time three dimensional echocardiography: a novel technique to quantify global left ventricular mechanical dyssynchrony. *Circulation*. 2005;112:992–1000.

-
26. Sugeng L, Mor-Avi V, Weinert L, Niel J, Ebner C, Steringer-Mascherbauer R, Schmidt F, Galuschky C, Schummers G, Lang RM, Nesser HJ. Quantitative assessment of left ventricular size and function: side-by-side comparison of real-time three-dimensional echocardiography and computed tomography with magnetic resonance reference. *Circulation*. 2006;114:654–61.
 27. Mor-Avi V, Jenkins C, Kuhl HP, et al. Real-time 3-dimensional echocardiographic quantification of left ventricular volumes. Multicenter study for validation with magnetic resonance imaging and investigation of source of errors. *J Am Coll Cardiol Imaging*. 2008;1(4):413–23.

Principles of Flow Assessment

5

Ahmed A. Alsaileek, Fatima Samad,
and A. Jamil Tajik

Introduction

Hemodynamic is concerned with the physical and physiological principles governing the movement of blood through the circulatory system. In other words, hemodynamic is the science and art of the relationship among pressure, viscous resistance to flow, and the volume flow rate in the cardiovascular system. Prior to the application of Doppler echocardiography, hemodynamic assessment was obtained invasively through cardiac catheterization. For most clinical purposes and in daily practice, Doppler echocardiography has replaced cardiac catheterization and becomes the preferred method for hemodynamic assessment. Doppler principle can be applied to calculate flows through different valves, stroke volume, cardiac output, valve areas, regurgitant volumes and shunts. Several animal and clinical studies have validated these methods and have yielded excellent

correlations with simultaneously acquired invasive data [1–5].

The Doppler Principle

The Doppler principle is applied in echocardiography to enable the determination of the blood flow characteristics such as velocity and direction. In principle, the frequency of the sound waves that are reflected by a stationary object is the same as the frequency of the sound waves transmitted by the transducer. On the other hand, the transmitted frequency of sound waves is altered when reflected by a moving object. If the object is moving toward the transducer, the reflected frequency will be slightly higher and if the object is moving away from the transducer the reflected frequency is slightly lower. This phenomenon is called *Doppler Effect*. In cardiovascular imaging, the moving objects are the red blood cells. The echocardiography instruments determine the *frequency (Doppler) shift* (f_D) which is the difference between the transmitted (f_T) and the received frequency (f_R).

$$f_D = f_R - f_T$$

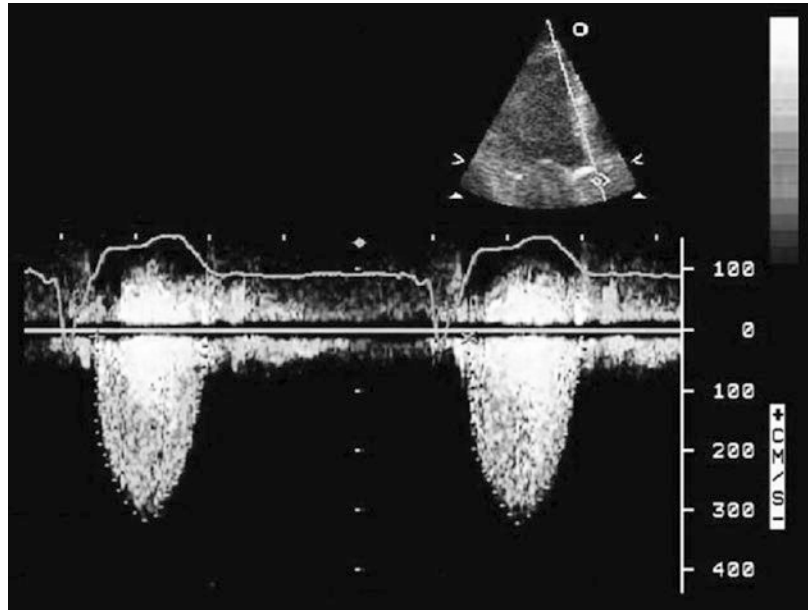
This Doppler shift is affected by speed of sound in the tissue ($c = 1540$ m/s), blood flow velocity (V), and the angle (θ) between the ultrasound

A. A. Alsaileek
King Saud bin Abdulaziz University for Health
Sciences, Riyadh, Saudi Arabia

Adult Cardiology/Cardiac Imaging, King Abdulaziz
Cardiac Center, National Guard Health Affairs,
Riyadh, Saudi Arabia

F. Samad (✉) · A. J. Tajik
St. Luke's Medical Center, Aurora Cardiovascular
Services, Milwaukee, WI, USA

Fig. 5.1 Spectral Doppler analysis, where the time is the horizontal line (baseline), the Y-axis determines the velocity of the flow, and the spectral envelop above and below the baseline determines the flow direction. In this example of aortic stenosis, the transducer is at the apex and the stenotic jet velocities are moving away from the transducer and, therefore, are displayed below the baseline



beam and the blood flow. So the equation can be restated as follows (Doppler equation):

$$f_D = 2f_T \frac{V \cos \theta}{C}$$

Frequency shift (f_D) is, therefore, directly proportional to the blood flow velocity and the equation may be more practically rewritten this way:

$$V = \frac{f_D C}{2f_T \cos \theta}$$

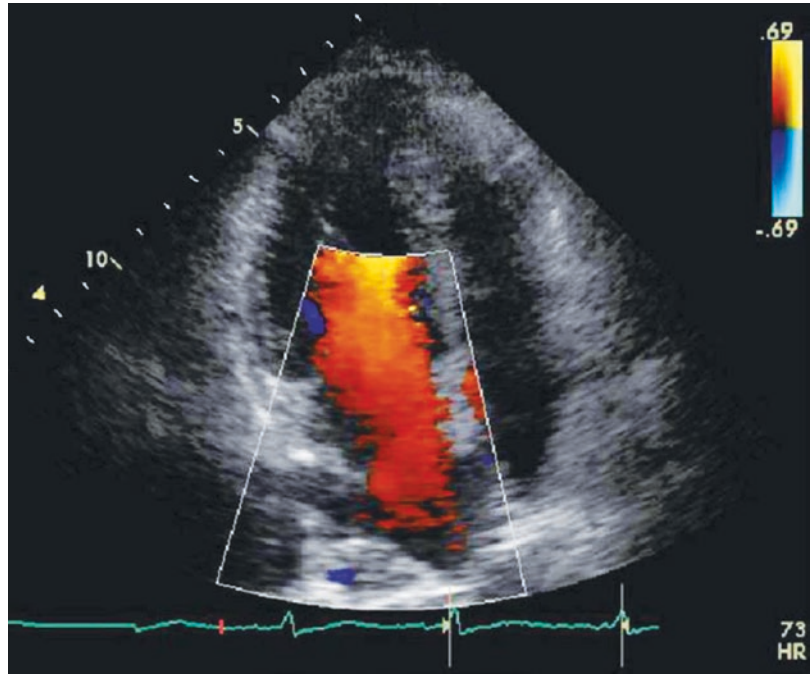
(Note that C and f_T are constant and the $\cos \theta$ (when the ultrasound beam is parallel to the flow) is equal to one). Therefore, with this equation we can easily determine the frequency shift and hence the blood flow velocity. However, this does not determine the direction of blood flow. The direction can be determined by the echo machine by calculating the frequency shift and giving a positive sign for flow toward the transducer and negative sign for that away from the transducer. In the computer screen this is shown in two ways:

- Spectral Doppler analysis, where the time is the horizontal line (baseline), the Y-axis determines the velocity of the flow. The spectral envelopes, above and below the baseline, determines the flow direction (Fig. 5.1). In this example the envelop is below the baseline which represent a flow away from the transducer.
- Color-flow Doppler analysis where the flow is color coded according to the direction of the flow. The flow toward the transducer is red and the color away from the transducer is blue (Fig. 5.2).

We will discuss the Doppler assessment of hemodynamics as follows:

- Stroke volume, cardiac output, and cardiac index determination.
- Methodology for calculation of stenotic valve area.
- Principles of calculation of regurgitant volume and effective regurgitant orifice (ERO).
- Determination of transvalvular pressure gradient.
- Estimation of intracardiac pressure and pulmonary artery pressure.

Fig. 5.2 Color Doppler analysis where the flow is color coded according to the direction of the flow. The flow toward the transducer is depicted in shade of *red* and the flow away from the transducer is in shade of *blue*. In this example of the flow across the mitral valve, the transducer is at the apex. The flow is coming toward the transducer, so it is shown as *red*



Four equations or principles are commonly used for these purposes:

1. Hydraulic equation of flow.
2. Continuity equation (law of conservation of mass).
3. Proximal isovelocity surface area (PISA) method.
4. Bernoulli equation.

Principle of Flow Assessment

Blood flow (Q) through a tube, vessel, or across a valve can be derived by a simple hydraulic equation as the product of flow velocity (V) and cross-sectional area (A) of the vessel at the site where velocity is measured. The area can be assumed to be circular and calculated as follows:

$$\begin{aligned} \text{Area} &= \pi r^2 \text{ (for circular orifice)} \\ &= \pi (D/2)^2 = 3.14 (D/2)^2 \\ &= (3.14/4) D^2 = 0.785 D^2 \end{aligned}$$

Where D is the diameter of the vessel.

And sometimes the area can be ellipsoid and calculated as follows:

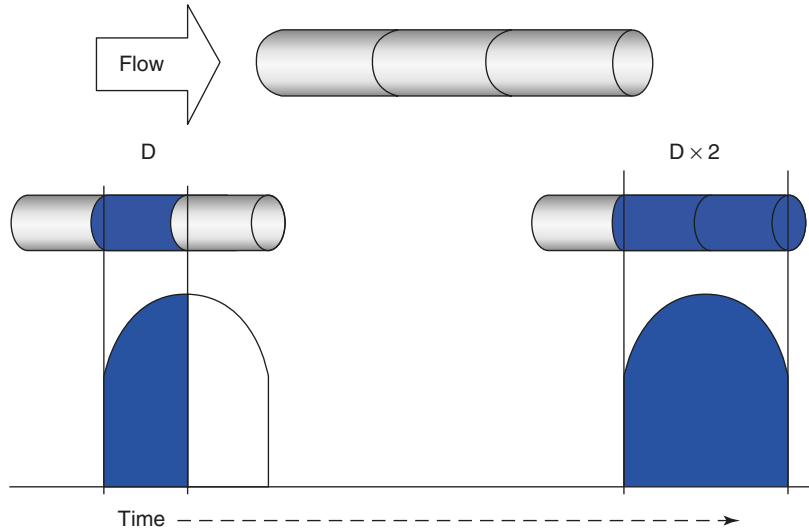
$$\begin{aligned} \text{Area} &= \pi (D_1/2 \times D_2/2) \text{ (for ellipsoid orifice)} \\ &= 0.785 D_1 D_2 \end{aligned}$$

Flow is the product of area and velocity and can be expressed as:

$$\begin{aligned} Q (\text{cc/s}) &= A (\text{cm}^2) \times V (\text{cm/s}) = 0.785 D^2 V \\ &\text{(for circular orifice)} = 0.785 D_1 D_2 V \\ &\text{(for ellipsoid orifice)} \end{aligned}$$

This equation assumes a constant flow. However, in pulsatile system (cardiovascular system), flow velocity varies throughout the ejection period and calculation of the volumetric flow is more complex. Therefore, the total flow has to be determined by integrating all individual velocities of the Doppler spectrum over time. In Doppler echocardiography this is known as time velocity

Fig. 5.3 This figure demonstrates the flow in the tube and its representation by spectral method. The relation between the distance (D) and time is also shown. The blood travels longer distance with time. In pulsatile system the flow velocity starts at zero, gradually increases to peak, then again decelerates to zero



integral (TVI), which is determined by measuring the area under the curve of the Doppler spectrum. The area under the curve is a measure of the distance the column of fluid travels (Figs. 5.3 and 5.4).

The commercially available echocardiography machines can readily obtain TVI. The modal velocity is derived using the Doppler equation and is dependent on knowing the frequency shift, the velocity of sound in tissue, and the angle between the ultrasound beam and the direction of blood flow. The latter has to be less than 20° ; otherwise, significant underestimation of velocity of calculated flow would occur using the assumption of a zero or near-zero intercept between the sound wave and the bloodstream. The area can be planimetered or calculated utilizing two-dimensional echocardiography to obtain diameter (D) with a circular ($A = 0.785 \times D^2$) or elliptic ($A = 0.785 D_1 D_2$) assumption after the diameter(s) (D) is measured.

Stroke Volume and Cardiac Output

One of the fundamental functions of the heart as a pump is to provide adequate amount of blood flow for the normal function of the human body. In the past, the cardiac output determination required invasive comprehensive and time-consuming

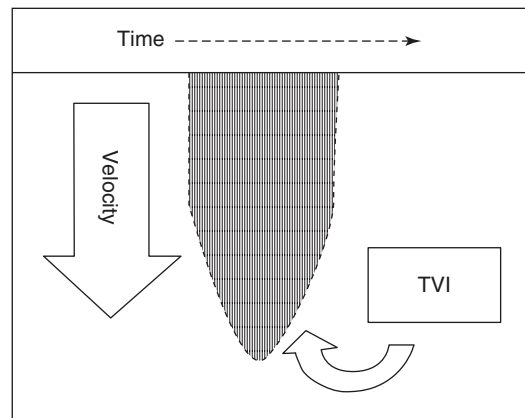


Fig. 5.4 This figure shows schematic illustration of spectral Doppler. The outer border of the spectral Doppler display is traced to determine the TVI

methods based upon Fick and indicator dilution principles. Nowadays, stroke volume and cardiac output can be noninvasively and reliably measured by 2D echo/Doppler methodology.

The forward stroke volume can be determined by the Doppler method mentioned earlier, which can basically be applied to any of the cardiac valves assuming no significant valvular regurgitation is present. Usually the flow through the aortic valve (or left ventricular outflow tract—LVOT) is calculated because the aortic annulus has the least change in size during the cardiac cycle [4, 6].

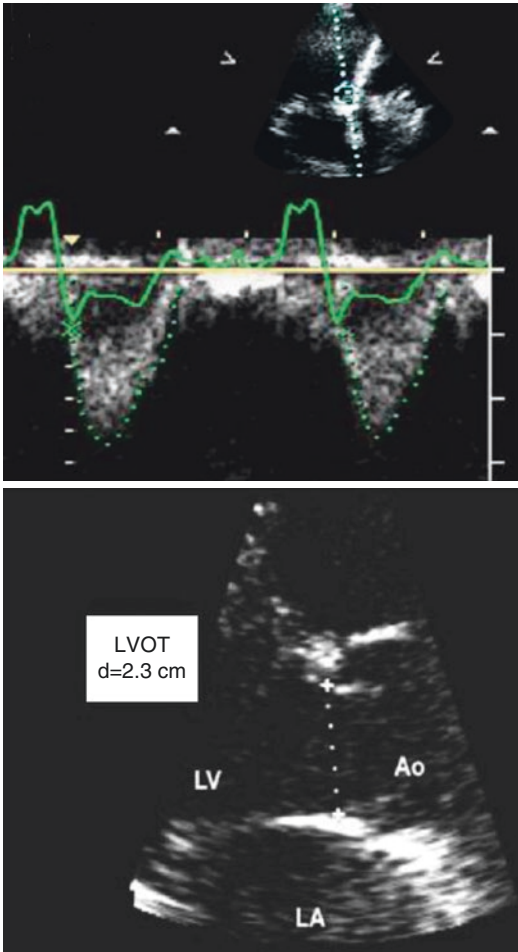


Fig. 5.5 This figure illustrates the Doppler method to determine stroke volume. The diameter of the aortic annulus is usually obtained from parasternal long-axis view (lower). In this example aortic annulus diameter is equal to 2.3 cm. The maximum diameter should be recorded. The TVI of the aortic annulus is normally obtained from apical long-axis view and occasionally utilizing 5-chamber view (upper). The TVI of LVOT is obtained by tracing the outer border of PW Doppler signal of LVOT. In this example average TVI is equal to 20.0 cm

The aortic annulus diameter is measured in the parasternal long-axis view (Fig. 5.5 -lower) and the maximum diameter is obtained. The velocity at the annulus is obtained utilizing the apical long-axis view and by placing the pulsed-wave (PW) Doppler sample volume at the level of aortic annulus. The closing click of the aortic valve should be recognized to insure good position. This velocity is then planimetered along its outer

edge to obtain the TVI (Fig. 5.5 -upper). If significant aortic regurgitation is present, the flow through this valve cannot be used to calculate the cardiac output. Errors can be incurred in the area calculation, mostly related to the diameter measurement (the error in area calculation is roughly doubled compared to the error in diameter measurement), but also includes inappropriate geometric assumptions and data acquisition at a different site from where velocity was recorded. Looking at the numbers in the figures (Fig. 5.5) we can calculate the stroke volume as follows:

$$\text{Stroke volume (SV)} = 0.785 \times D^2 \times \text{TVI} = 0.785 \times 2.3^2 \times 20.0 = 83 \text{ ml}$$

Cardiac output is the product of stroke volume and heart rate (assume the heart rate is 65 beats/min).

Cardiac output (CO) = SV × HR = 83 × 65 = 5398 ml/min = 5.40 l/min (by converting the milliliter to liter).

Cardiac index is obtained by dividing the cardiac output by body surface area (BSA).

$$\text{Cardiac index (CI)} = \text{CO} / \text{BSA} (\text{liter} / \text{min} / \text{m}^2)$$

Alternatively, but uncommonly, cardiac output can be obtained from pulmonic valve or right ventricular outflow tract. In the short axis at the level of aortic valve the ultrasound beam is almost parallel to the blood flow at the level of pulmonic valve or right ventricular outflow tract. The TVI is obtained by pulsed-wave Doppler at the same level where the right ventricular outflow tract area is measured in 2D echocardiography [7]. The cardiac output can be obtained at any valve assuming there is no regurgitation of the valve so the cardiac output is constant for any given cardiac cycle.

Continuity Equation

Continuity equation is based on the principle of conservation of mass. This principle states that, under conditions of cardiovascular stability

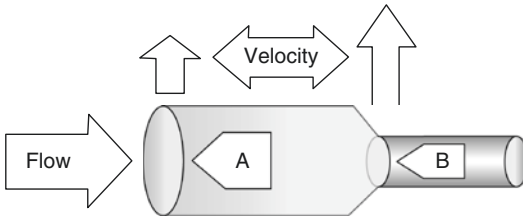


Fig. 5.6 This figure shows two tubes with different diameter in continuity. The continuity equation states that the flow volume at point A is equal to that of point B and mathematically written as follows: (Area A \times Velocity A = Area B \times Velocity B). Note that the velocity is higher with smaller area

without any regurgitation or shunt, the net blood volume at any part of circulation must equal the net blood volume at any other part next to it (what comes in must go out) (Fig. 5.6). This situation is true under certain assumptions:

- The two points are directly connected.
- Blood is neither added nor removed from the system.

Clinical Applications of Continuity Equation

In applying the continuity equation to the blood flow in and out of the heart, the mitral valve stroke volume is equal to aortic valve stroke volume provided there is no mitral or aortic regurgitation (Fig. 5.7). In the same way the aortic stroke volume is equal to pulmonic valve stroke volume provided no significant regurgitation is present in any of the valves, and no intracardiac shunt is present. The tricuspid valve stroke is not commonly used in clinical practice because of complex geometry for valve area calculation and because of the presence of tricuspid regurgitation in the majority of normal subjects. The aortic valve stroke volume is calculated by measuring the aortic annulus diameter in parasternal long-axis view at maximum valve opening in systole. The TVI is obtained utilizing pulsed-wave Doppler sample volume at the level

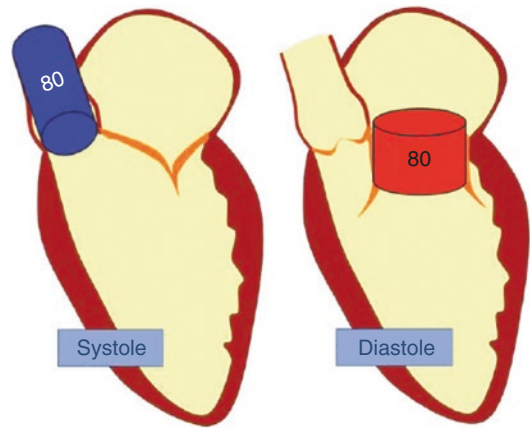


Fig. 5.7 This figure demonstrates the continuity between mitral and aortic valves' stroke volume. The volume of blood that comes in through mitral valve must go out through aortic valve

of aortic annulus on the apical long-axis or 5-chamber view. The aortic valve area (AVA) is assumed to be circular, and hence, the area is calculated from the obtained aortic annulus diameter (D_{AA}).

$$AVA = \pi (D_{AA} / 2)^2 = 0.785 D_{AA}^2$$

The stroke volume at the level of aortic valve is then calculated as follows:

$$\begin{aligned} SV_{AA} &= AVA \times TVI_{AA} \\ SV_{AA} &= 0.785 \times D_{AA}^2 \times TVI_{AA} \end{aligned}$$

In calculating the mitral valve stroke volume, the mitral valve area is calculated either by assuming a circular or ellipsoid geometry. For practical purposes, the circular shape is the most often used. The mitral annulus diameter (D_{MA}) is obtained from the apical 4-chamber view at maximum valve opening in diastole. The TVI is obtained from the same view by pulsed-wave Doppler sample volume at the level of the mitral annulus.

$$MVA = 0.785 \times D_{MA}^2$$

And therefore:

$$\begin{aligned} SV_{MA} &= MVA \times TVI_{MA} \\ SV_{MA} &= 0.785 \times D_{MA}^2 \times TVI_{MA} \end{aligned}$$

Mathematically the continuity equation means that stroke volume through mitral valve is equal to the stroke volume through aortic valve:

$$\begin{aligned} TVI1 \times \text{Area}1(\text{mitral}) &= TVI2 \times \text{Area}2(\text{aortic}) \\ 0.785 \times D_{MA}^2 \times TVI_{MA} &= 0.785 \times D_{AA}^2 \times TVI_{AA} \end{aligned}$$

The concept of continuity is very useful clinically to assess mitral or aortic regurgitant volume, regurgitant fraction, regurgitant orifice, as well as the stenotic mitral or aortic valve area.

Mitral Regurgitation

In mitral regurgitation (MR) (Figs. 5.8 and 5.9), the aortic stroke volume is less than the forward mitral stroke volume because part of the blood contained in the LV at the end of diastole is

ejected back to the left atrium through the regurgitant mitral valve.

$$\begin{aligned} \text{Aortic stroke volume} &= \\ \text{mitral stroke volume} - \text{RV}(\text{Mitral}) \end{aligned}$$

Therefore,

$$\begin{aligned} \text{Mitral RV} &= \text{mitral stroke volume} - \text{Aortic stroke volume} \\ &= (0.785 \times D_{MA}^2 \times TVI_{MA}) - (0.785 \times D_{AA}^2 \times TVI_{AA}) \end{aligned}$$

Aortic Regurgitation

In aortic regurgitation, the aortic stroke volume is more than the mitral stroke volume because the regurgitant volume through aortic valve will be added to the subsequent stroke volume from mitral valve (Figs. 5.9 and 5.10). The same methodology described to assess the mitral valve regurgitant volume is used to assess the aortic regurgitant volume. The difference is that the aortic stroke volume will be higher than that of mitral stroke volume (see earlier).

$$\begin{aligned} \text{Aortic \textbackslash stroke \textbackslash volume} &= \\ \text{mitral \textbackslash stroke \textbackslash volume} + \text{RV}(\text{Aortic}) \end{aligned}$$

Therefore,

$$\begin{aligned} \text{Aortic RV} &= \text{Aortic stroke volume} - \\ \text{mitral stroke volume} &= (0.785 \times D_{AA}^2 \times TVI_{AA}) - \\ &\quad (0.785 \times D_{MA}^2 \times TVI_{MA}) \end{aligned}$$

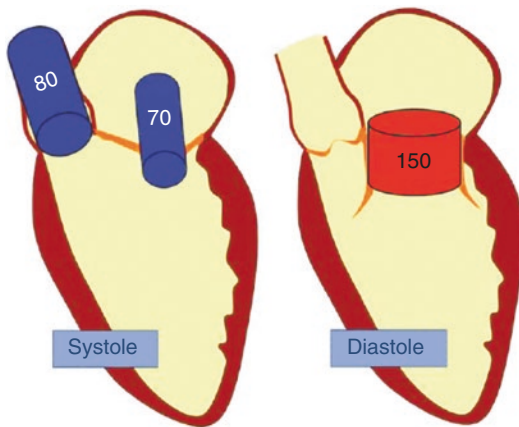


Fig. 5.8 This figure shows schematic illustration of the principle of calculating mitral regurgitant volume based on hydraulic formula. Mitral inflow volume of 150 cc (what goes in) and aortic stroke volume of 80 cc (what goes out) are calculated based on the continuity equation. The difference (150 – 80 = 70 cc) must represent the mitral regurgitation volume

Mitral Stenosis

The mitral valve area in the presence of mitral stenosis can also be estimated using the continuity equation. The stroke volume at mitral valve orifice is equal to the aortic stroke volume (the

Fig. 5.9 The measurement needed for continuity equation in mitral regurgitation and aortic regurgitation. The mitral inflow volume is calculated from the mitral inflow TVI and mitral annulus diameter ($0.785 D_{MA}^2 \times TVI_{MA} = 196 \text{ cc}$). The aortic stroke volume is calculated from the aortic TVI and aortic annulus diameter ($0.785 \times D_{AA}^2 \times TVI_{AA} = 113 \text{ cc}$). The difference ($196 - 113 = 83 \text{ cc}$) must be the MR volume

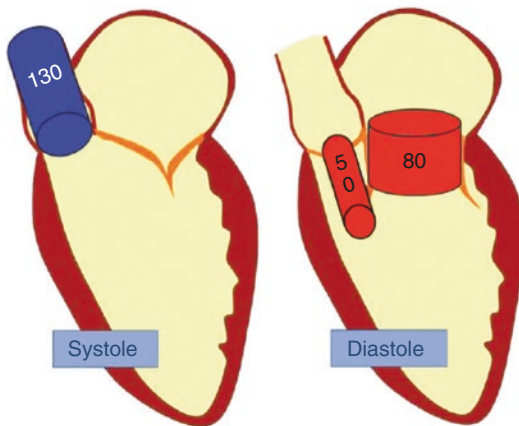
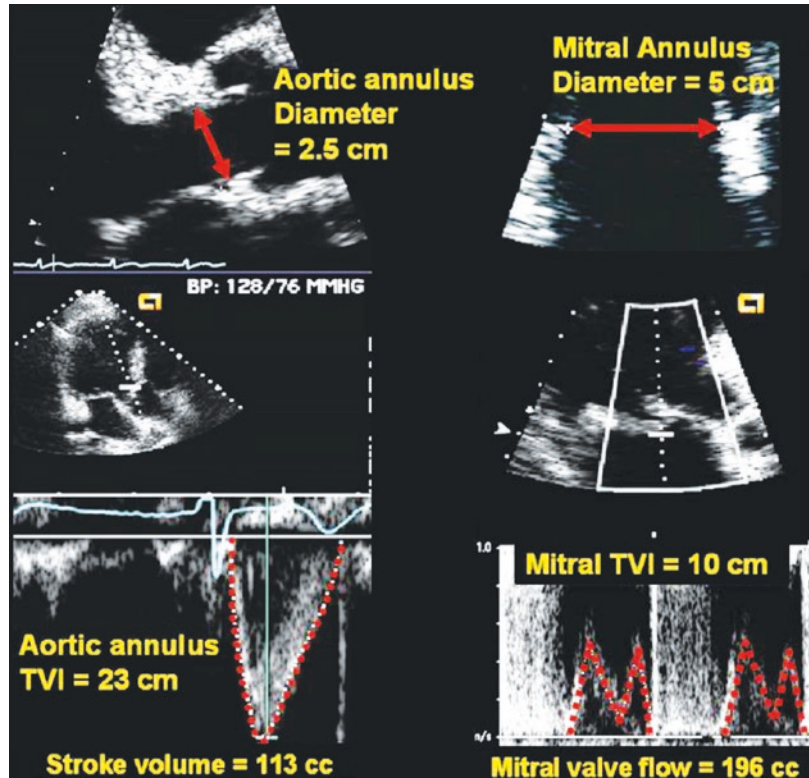


Fig. 5.10 This figure shows schematic illustration of the principle of calculating aortic regurgitant volume based of hydraulic formula. Mitral inflow volume 80 cc (what goes in) and aortic stroke volume 130 cc (what goes out) are calculated based on the continuity equation. The difference ($130 - 80 = 50 \text{ cc}$) must represent the aortic regurgitation volume

method to obtain the aortic SV is already discussed). The aortic annulus area multiplied by the aortic TVI is equal to MVA multiplied by the mitral TVI. Mitral valve TVI is obtained by

continuous-wave Doppler across the mitral valve from apical 4-chamber or apical long-axis views. The MVA can then be calculated as follows:

$$\begin{aligned} MVA \times \text{flow} &= AVA \times \text{flow} \\ MVA \times TVI_{MA} &= 0.785 \times D_{AA}^2 \times TVI_{AA} \\ MVA &= 0.785 \times D_{AA}^2 \times TVI_{AA} / TVI_{MA} \end{aligned}$$

The limitation of this method is the presence of more than trivial/mild MR, which may be present in a significant number of patients [8, 9].

Aortic Stenosis

The same principle can be applied to any two orifices connected in series or tube at two different points provided that all the flow goes in one direction. This can be applied to assess the aortic valve area in aortic stenosis (*what comes in must go out*) [10, 11] (Fig. 5.11). The volume of blood going through LVOT (proximal) should be equal to that going through a stenotic aortic valve

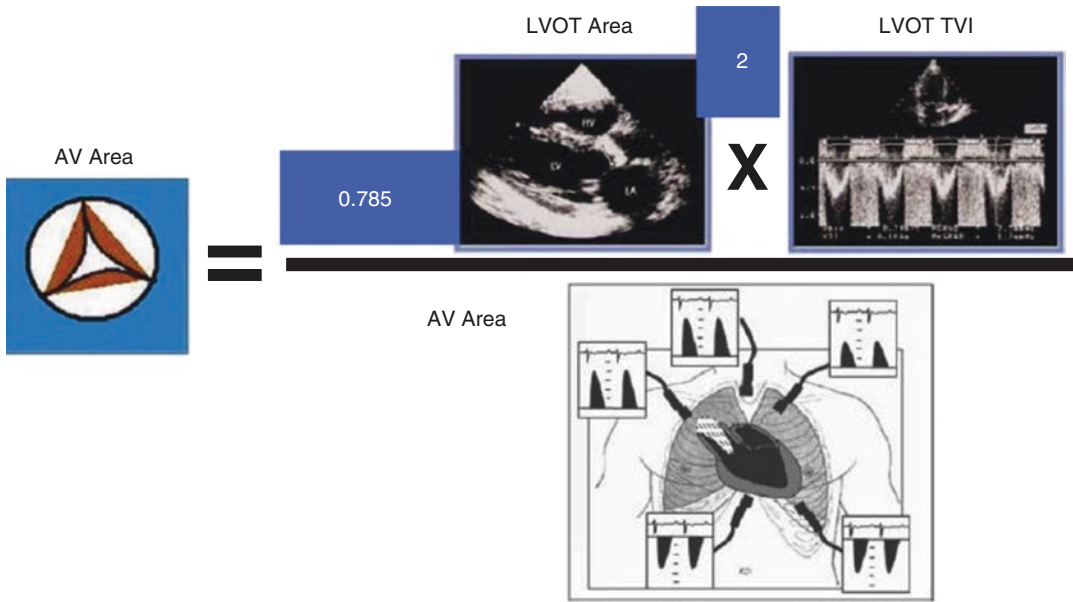


Fig. 5.11 This figure shows the continuity method to assess AS severity. The flow rates at the LVOT and AV are the same. The LVOT flow rate is calculated from the LVOT TVI and diameter (see also Fig. 5.5). The TVI of

AV is obtained by tracing the outer border of CW Doppler signal of AV. Then the AVA is calculated as: $AVA (cm^2) = (0.785 D_{LVOT}^2 \times TVI_{LVOT}) / TVI_{AA}$

(distal). The LVOT diameter and TVI (TVI_{LVOT}) is determined as discussed previously. One important point to make is to avoid the area of flow acceleration (due to severe aortic stenosis) in the LVOT TVI determination by moving the sample volume about 1 cm below the aortic annulus. The aortic TVI (TVI_{AA}) is obtained by CW Doppler across the aortic valve. This should be done from multiple locations (Fig. 5.11) and the highest velocity is used in the calculation. Aortic valve area (AVA) is calculated as:

$$AVA (cm^2) \times TVI_{AA} = (0.785 \times D_{LVOT}^2 \times TVI_{LVOT})$$

And then,

$$AVA (cm^2) = 0.785 \times D_{LVOT}^2 \times TVI_{LVOT} / TVI_{AA}$$

Echocardiographic findings of patients with tricuspid regurgitation generally mirror those found in MR. Therefore, the tricuspid valve stroke volume can be compared to the pulmonic valve stroke volume and the regurgitant volume

can be estimated, but clinically this method is less often used than the PISA method [12].

Proximal Isovelocity Surface Area Method

Proximal isovelocity surface area (PISA) method is based on the law of conservation of flow. The law states the flow rate at two consecutive points is identical. The method uses the advantage of aliasing in color Doppler imaging. In color Doppler the flow is given red or blue color if the direction of flow is toward and away from the transducer, respectively. As the flow approaches a narrowed orifice (stenotic or regurgitant), its velocity increases, in a shape of isovelocity hemispheric shell as blood flow converges from all directions toward the orifice (Fig. 5.12). The flow rate at the surface of the hemispheric shell is equal to the flow rate at the regurgitant orifice (law of conservation of the flow). As the flow converges toward the orifice, it accelerates and aliasing occurs if the velocity exceeds the Nyquist limit. This can be nicely shown using the color Doppler imaging where the color changes from red to blue in a nice hemisphere. If the Nyquist limit is

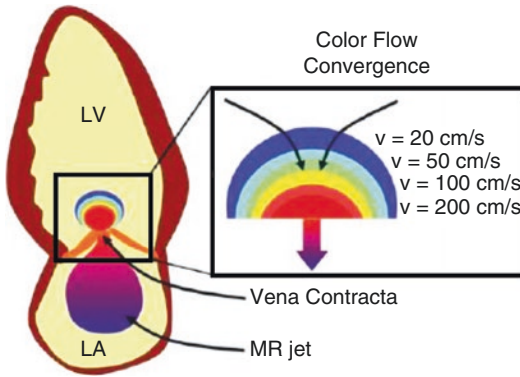


Fig. 5.12 Schematic illustration of the PISA. The flow accelerates as it approaches a narrow orifice forming hemispheric shell. This can be shown on color Doppler (as in case of MR). The flow converges as it approaches the regurgitant mitral valve. The color changes due to high velocity exceeding the Nyquist limit and forming hemispheric shell (PISA)

decreased, the aliasing occurs with lower velocity and starts further away from the regurgitant orifice making the hemisphere (PISA) larger. Using this principle, flow rate at the surface of the hemispheric shape can be estimated. The flow rate can be calculated by multiplying the area by velocity (Flow rate = Area \times Velocity). The area in case of valve is circular so it is calculated as (πr^2), but in case of hemisphere surface area is calculated as ($2\pi r^2$ or $6.28r^2$), the r is the radius of the hemisphere. The radius of the hemisphere can be measured from the surface to the narrowest area of color flow, which is closely related to the regurgitant or stenotic orifice. The flow rate at the hemisphere (PISA) surface is Flow rate = $AV = 2\pi r^2 V_{\text{aliasing}} = 6.28r^2 V_{\text{aliasing}}$.

Clinical Applications of PISA Method

Mitral Regurgitation

In MR, the apical 4-chamber view with color Doppler is commonly used (Figs. 5.12 and 5.13). However, parasternal long-axis view is sometimes used in case of eccentric jet where the PISA is better visualized. The Nyquist limit is shifted downward in the direction of the flow of MR jet. The velocity of the PISA is measured at midlate

systole (the same time the maximum MR velocity occurs) [13, 14].

$$\begin{aligned} \text{Area(ERO)} \times V_{\text{max MR}} &= 6.28r^2 V_{\text{aliasing}} \\ \text{Effective regurgitant orifice (ERO)} &= \\ &= 6.28r^2 V_{\text{aliasing}} / V_{\text{max MR}} \end{aligned}$$

As discussed in the calculation of the stroke volume, it is the product of area and TVI. The same method can be applied to calculate the regurgitant volume (RV). The area here is known (see earlier), which is the ERO of the mitral valve. The TVI is nothing but the TVI of the MR jet. Therefore:

$$\begin{aligned} \text{Mitral RV} &= \text{ERO(PISA)} \times \text{TVI}_{\text{MR}} (\text{CW Doppler}) = \\ &= (6.28r^2 V_{\text{aliasing}} / V_{\text{max MR}}) \text{TVI}_{\text{MR}} \end{aligned}$$

Width of vena contracta is another quantitative method to assess MR. It is defined as the narrowest cross-sectional area of a jet. This can be easily seen, while obtaining the zone of flow convergence, above the mitral valve on the left atrial side (Fig. 5.12). On transthoracic color-flow mapping it has been shown that vena contracta width predicts angiographic severity of MR [15]. Compared to continuity equation, vena contracta of more than 5 mm correlates well with severe MR [16].

Semiquantitative Doppler methods to evaluate the MR are less sensitive and are considered complementary in MR evaluation.

Color-flow Doppler: The features of severe MR seen on color-flow Doppler imaging arise from the high-energy transfer of a large volume of blood into the left atrium, producing “jets” in the left atrium. Color-flow Doppler remains the easiest and the best method to screen for MR. It also provides semiquantitative assessment of the MR severity. The ratio of the MR jet area to the total left atrial area has been reported to correlate well with MR severity [17]. Severe MR is characterized by large jet (>40%) and extending into the pulmonary veins. However, jets are very sensitive to

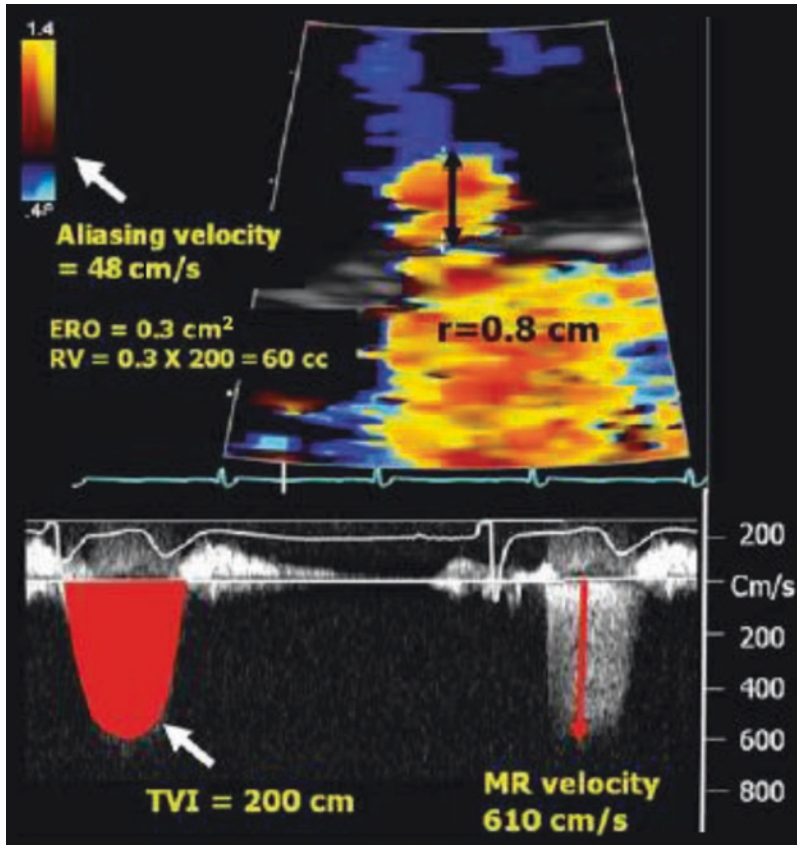


Fig. 5.13 This figure shows the PISA methods to evaluate the severity of MR. The PISA is obtained from the apical 4-chamber view. The baseline is shifted downward toward the regurgitant jet flow (arrow). Then the PISA diameter is measured from the surface of the hemisphere to the narrowest area on color Doppler (0.8 cm). The CW

Doppler is utilized to measure the mitral regurgitation TVI and peak velocity. The effective regurgitant orifice (ERO) and the regurgitant volume (RV) are calculated as follows: $ERO = 6.28 r^2 V_{aliasing} / V_{max MR} = 6.28 \times .82 \times 48 / 610 = 0.3 \text{ cm}^2$ and $RV = TVI \times ERO = 200 \times 0.3 = 60 \text{ cc}$

instrument settings, and the size of a color jet may be misleading such as in an eccentric jet; thus, reliance on these size judgments alone may not be sound practice [18–20].

Doppler of pulmonary veins: Doppler interrogation of the pulmonary veins has produced insights into hemodynamics. In MR evaluation, pulsed-wave Doppler of the left and right upper pulmonary veins is performed from the apical 4-chamber view. In hemodynamically severe MR, the flow in one or more pulmonary veins will show systolic flow reversal. This echo feature is the analog of the V wave seen in the left atrial pressure tracing and on a pulmonary artery wedge pressure tracing.

Continuous-wave Doppler of the MR jet: If the flow signal can be aligned parallel to the beam, in severe MR, the Spectral Doppler of the jet will appear uniformly dense throughout its duration and have a well-defined envelop. MR jet velocity does not correlate with the severity. Other features that are associated with severe MR include dilated or dysfunctional left ventricle, dilated left atrium, elevated pulmonary artery systolic pressure, and the presence of significant tricuspid regurgitation. In severe decompensated MR, the tricuspid regurgitation peak velocity will be increased as the result of pulmonary hypertension.

D PISA in some studies has proved to be superior to 2D measures for distinguishing moderate

from severe MR, especially for eccentric and asymmetric jets.

Tricuspid Regurgitation

As with MR, severity of tricuspid regurgitation (TR) can be estimated by effective regurgitant orifice (ERO) by measuring the size of proximal flow convergence zones (PISA) [21].

$$\text{Area(ERO)} \times V_{\max} \text{ TR} = 6.28r^2 V_{\text{aliasing}}$$

$$\text{ERO(Tricuspid)} = 6.28r^2 V_{\text{aliasing}} / V_{\max} \text{ TR}$$

And even the regurgitant volume (RV) can be calculated:

$$\text{RV(Tricuspid)} = \text{Area(ERO)} \times \text{TVI} =$$

$$(6.28r^2 V_{\text{aliasing}} / V_{\max} \text{ TR}) \times \text{TVI}_{\text{TR}}$$

Aortic Regurgitation

The severity of aortic regurgitation can be quantitatively assessed utilizing the PISA method [22]. The apical 5-chamber and apical long-axis views are used to visualize the PISA. However, parasternal long-axis view is sometimes used in case of eccentric jet where the PISA is better visualized. The Nyquist limit baseline is shifted toward the flow of the aortic regurgitation jet (Fig. 5.14). The PISA radius is measured at early diastole [23]. The maximum aortic regurgitation (AR) velocity in early diastole is measured. The ERO is calculated as follows:

$$\text{Aortic ERO} = \text{PISA flow rate} /$$

$$\text{AR regurgitant velocity}$$

$$= 6.28r^2 (V_{\text{aliasing}} / \text{AR regurgitant velocity})$$

The aortic regurgitant volume is calculated by tracing the aortic regurgitation jet outer surface to

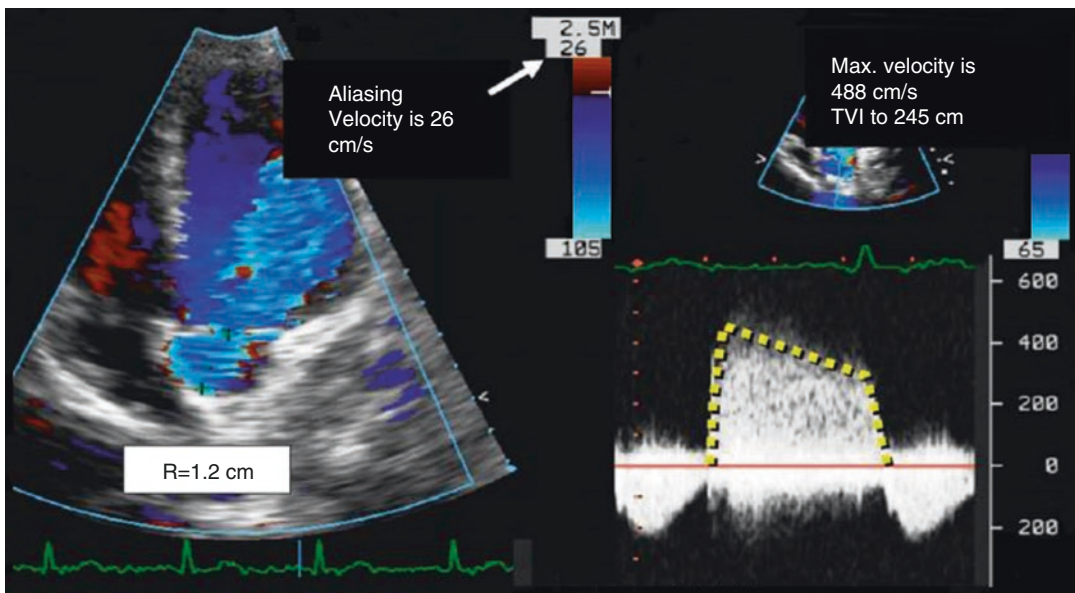


Fig. 5.14 This figure shows the PISA method for calculation of the ERO in case of aortic regurgitation. The PISA is obtained from the apical long-axis or 5-chamber view. The baseline is shifted upward toward the regurgitant jet flow (arrow regurgitant volume). Then the PISA diameter is measured from the surface of the hemisphere to the nar-

rowest area on color Doppler (1.2 cm). The CW Doppler is utilized to measure the aortic regurgitation TVI and peak velocity. The effective regurgitant orifice (ERO) and the regurgitant volume (RV) are calculated as follows: $\text{ERO} = 6.28r^2 V_{\text{aliasing}} / V_{\max} \text{ AR} = 6.28 \times 1.2 \times 1.2 \times 26 / 488 = 0.5 \text{ cm}^2$ and $\text{RV} = \text{TVI} \times \text{ERO} = 245 \times 0.5 = 118 \text{ cc}$

measure the aortic regurgitation TVI (TVIAR); therefore:

$$\text{flow volume (RV)} = \text{Area (ERO)} \times \text{TVI} = (6.28r^2 V_{\text{aliasing}} / V_{\text{max AR}}) \times \text{TVI}_{\text{AR}}$$

Vena Contracta It is the narrowest portion of the jet crossing the plane of the valve. It lies immediately next to the area of flow convergence. It can be measured from parasternal long-axis or apical long axis views. To optimize the visualization, the echo sector should be the narrowest possible and the depth decreased. Vena contracta of equal to or more than 6 mm has been shown to correlate with severe aortic regurgitation. This method was found useful even in eccentric jet [24–26]. Some investigators [27] have used the cross-sectional area of the vena contracta to evaluate aortic regurgitation severity. The approach sounds promising and 3D echo may help to further tune this approach [24].

There are several Doppler methods to evaluate aortic regurgitation severity, most of which are less accurate and should not be used alone to guide clinical decisions [25–27].

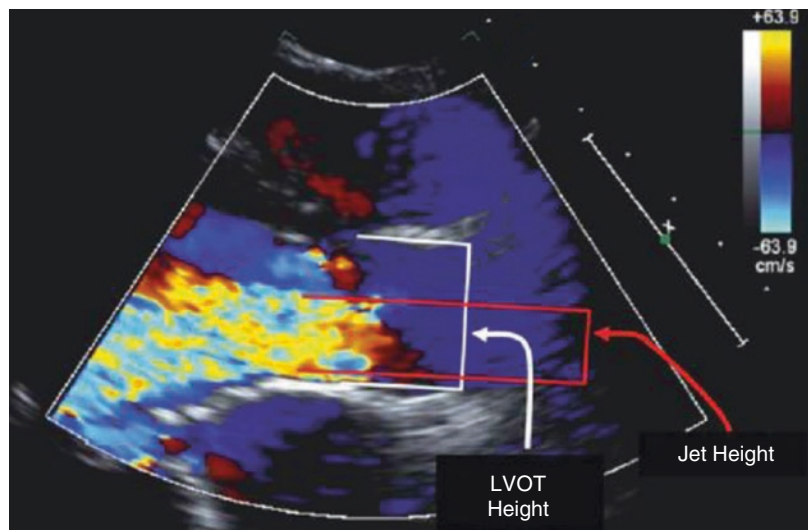
Regurgitant Jet Size Similar to most of the valvular lesions, color-flow Doppler is the initial

screening method for the aortic regurgitation. With the advent of color Doppler many investigators had attempted to use the regurgitant jet size to quantify aortic regurgitation severity. However, this method has suffered several limitations [28, 29]. The jet is frequently eccentric and appears much smaller even in the presence of significant aortic regurgitation, and its spread may be affected by the shape of the ventricular septum. Thus the size of the jet is only used as a screening tool after which other quantitative methods are used.

Jet Height to LVOT Height Ratio This method depends on using the color Doppler in parasternal long-axis view to record the jet height at the valve orifice and compare it to the LVOT height (Fig. 5.15).

This is related to the regurgitant orifice. The higher the ratio, the more severe is the aortic regurgitation. This method also has limitations. Eccentric jet may be difficult to assess. The shape of the regurgitant orifice affects the height of the jet on color Doppler images. Due to 2-Dimensional nature of the color-flow Doppler alignment on 2-Dimensional echo, they may not be perfectly aligned as they may not be in the same plane [30]. **Pressure half-time (PHT)**—Aortic regurgitation jet PHT is measured using continuous-

Fig. 5.15 Transthoracic echocardiogram at long-axis view demonstrates color Doppler method of the ratio of jet height to LVOT height to assess the severity of aortic regurgitation



wave Doppler spectral display from apical long-axis view. It represents how quickly the aortoventricular pressure gradient equalizes during diastole (Fig. 5.16) [31]. The larger the regurgitant orifice, the more quickly the pressure equalizes and the velocity falls. A group of investigators has demonstrated that this sign is useful to judge about severe aortic regurgitation. The PHT of less than 200 ms has been used to indicate severe aortic regurgitation [32]. However, it is important to keep in mind that numerous other factors can impact this, such as systemic vascular resistance and ventricular compliance [33].

Aortic Diastolic Flow Reversal One of the earliest Doppler techniques to study aortic regurgitation was to examine retrograde diastolic flow reversal in the ascending and descending aorta or arch. Different numbers had been proposed to the measurement of the flow reversal TVI trying to assess severity. In general, flow reversal throughout the entire diastole is consistent with significant aortic regurgitation [34].

Mitral Stenosis

The PISA method can also be used to estimate mitral stenosis (MS) [35, 36]. Because of the ste-

notic mitral valve, blood flow accelerates at the left atrial side and converges forming nice PISA (Fig. 5.17). With the appropriate setting (moving the Nyquist limit baseline upward the same direction of flow while interrogating the mitral valve from apical views), PISA can be optimized. The flow rate at the PISA surface is equal to the flow rate at the mitral valve orifice. The mitral valve maximum velocity is obtained by continuous Doppler through mitral valve at early diastole. Then the stenotic area (MVA) can be calculated as follows:

$$\text{MVA} = 6.28r^2 \text{Valiasing/stenotic MV max velocity}$$

The truly hemispheric shells occurs if surface of the valve is flat with the leaflets apposed at 180° . This PISA method in case of mitral stenosis is not perfect because mitral valve at maximum opening is not fl at (less than 180°) (Fig. 5.17). So the angle (alpha = a) has to be corrected for, by dividing this angle by 180° . The estimation of the angle is crude approach and a

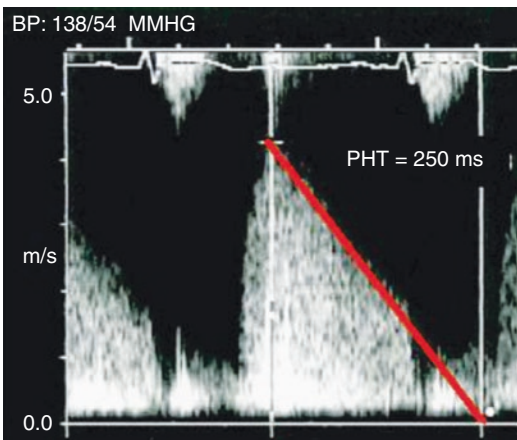


Fig. 5.16 CW spectral Doppler of the aortic regurgitation showing the slope of pressure gradient decays. The pressure halftime is then calculated to assess the severity of aortic regurgitation

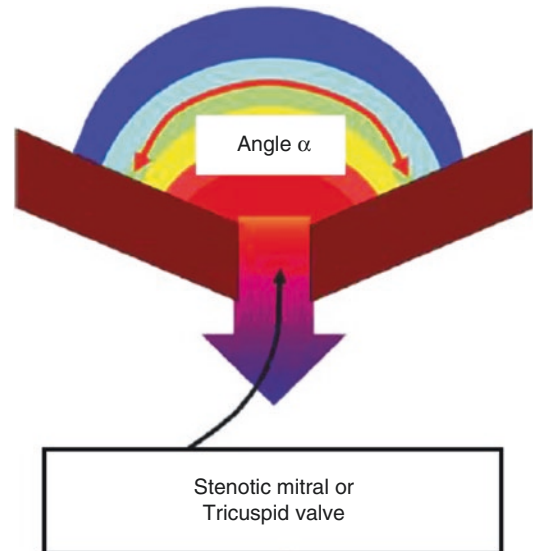


Fig. 5.17 This figure shows the PISA at the mitral or tricuspid valves in case of mitral or tricuspid stenosis. Occasionally, the valve leaflets form an angle while opening during diastole (not flat surface). This angle (a) is less than 180 and needs correction factor ($a/180$) when using the PISA to calculate stenotic lesion. This makes the method less perfect than for the regurgitant lesions

significant source of error [35–37]. MVA then calculated as:

$$\text{MVA} = 6.28r^2 \times \text{Valiasing} / \text{stenotic MV maximum velocity} (a/180)$$

The advantage of this approach is that it is not affected by coexisting mitral or aortic regurgitation [38]. The tricuspid stenosis is not common. The severity can be quantitatively estimated in an identical way as the mitral stenosis. Utilizing PISA, the flow at the PISA surface is equal to the flow rate at the tricuspid valve orifice (TVA). Because of complex valve geometry similar to the mitral stenosis, the angle needs to be corrected for ($a/180$).

$$\text{TVA} = 6.28r^2 \text{Valiasing} / \text{stenotic TV maximum velocity} \times (a/180)$$

Again this approach is not perfect and less commonly used than other methods such as mean gradient and pressure half-time.

References

- Callahan MJ, Tajik AJ, Su-Fan Q, Bove AA. Validation of instantaneous pressure gradients measured by continuous-wave Doppler in experimentally induced aortic stenosis. *Am J Cardiol.* 1985;56(15):989–93.
- Currie PJ, Seward JB, Chan KL, Fyfe DA, Hagler DJ, Mair DD, et al. Continuous wave Doppler determination of right ventricular pressure: a simultaneous Doppler-catheterization study in 127 patients. *J Am Coll Cardiol.* 1985;6(4):750–6.
- Burstow DJ, Nishimura RA, Bailey KR, Reeder GS, Holmes DR Jr, Seward JB, Tajik AJ. Continuous wave Doppler echocardiographic measurement of prosthetic valve gradients. A simultaneous Doppler-catheter correlative study. *Circulation.* 1989;80(3):504–14.
- Lewis JF, Kuo LC, Nelson JG, Limacher MC, Quinones MA. Pulsed Doppler echocardiographic determination of stroke volume and cardiac output: clinical validation of two new methods using the apical window. *Circulation.* 1984;70:425–31.
- Stewart WJ, Jiang L, Mich R, Pandian N, Guerrero JL, Weyman AE. Variable effects of changes in flow rate through the aortic, pulmonary and mitral valves on valve area and flow velocity: impact on quantitative Doppler flow calculations. *J Am Coll Cardiol.* 1985;6:653–62.
- Zoghbi WA, Quinones MA. Determination of cardiac output by Doppler echocardiography: a critical appraisal. *Herz.* 1986;11(5):258–68.
- Maslow A, Comunale ME, Haering JM, Watkins J. Pulsed wave Doppler measurement of cardiac output from the right ventricular outflow tract. *Anesth Analg.* 1996;83:466–71.
- Karp K, Teien D, Eriksson P. Doppler echocardiographic assessment of the valve area in patients with atrioventricular valve stenosis by application of the continuity equation. *J Intern Med.* 1989;225:261–6.
- Nakatani S, Masuyama T, Kodama K, Kitabatake A, Fujii K, Kamada T, et al. Value and limitations of Doppler echocardiography in the quantification of stenotic mitral valve area: comparison of the pressure half-time and the continuity equation methods. *Circulation.* 1988;77:78–85.
- Otto CM, Pearlman AS, Gardner CL, Enomoto DM, Togo T, Tsuboi H, Ivey TD. Experimental validation of Doppler echocardiographic measurement of volume flow through the stenotic aortic valve. *Circulation.* 1988;78:435–41.
- Skjaerpe T, Hegrenaes L, Hatle L. Noninvasive estimation of valve area in patients with aortic stenosis by Doppler ultrasound and two-dimensional echocardiography. *Circulation.* 1985;72:810–8.
- Miyatake K, Okamoto M, Kinoshita N, Ohta M, Kozuka T, Sakakibara H, Nimura Y. Evaluation of tricuspid regurgitation by pulsed Doppler and two-dimensional echocardiography. *Circulation.* 1982;66(4):777–84.
- Thomas L, Foster E, Hoffman JI, Schiller NB. Prospective validation of an echocardiographic index for determining the severity of chronic mitral regurgitation. *Am J Cardiol.* 2002;90:607–12.
- Enriquez-Sarano M, Miller FA Jr, Hayes SN, Bailey KR, Tajik AJ, Seward JB. Effective mitral regurgitant orifice area: clinical use and pitfalls of the proximal isovelocity surface area method. *J Am Coll Cardiol.* 1995;25(3):703–9.
- Fehske W, Omran H, Manz M, Köhler J, Hagendorff A, Lüderitz B. Color-coded Doppler imaging of the vena contracta as a basis for quantification of pure mitral regurgitation. *Am J Cardiol.* 1994;73:268–74.
- Hall SA, Brickner ME, Willett DL, Irani WN, Afridi I, Grayburn PA. Assessment of mitral regurgitation severity by Doppler color flow mapping of the vena contracta [see comment]. *Circulation.* 1997;95:636–42.
- Helmcke F, Nanda NC, Hsiung MC, Soto B, Adey CK, Goyal RG, Gatewood RP Jr. Color Doppler assessment of mitral regurgitation with orthogonal planes. *Circulation.* 1987;75:175–83.
- Utsunomiya T, Doshi R, Patel D, Nguyen D, Mehta K, Gardin JM. Regurgitant volume estimation in patients with mitral regurgitation: initial studies using color Doppler ‘proximal isovelocity surface area’ method. *Echocardiography.* 1992;9:63–70.

19. Stevenson JG. Two-dimensional color Doppler estimation of the severity of atrioventricular valve regurgitation: important effects of instrument gain setting, pulse repetition frequency, and carrier frequency. *J Am Soc Echocardiogr.* 1989;2(1):1–10.
20. Cape EG, Yoganathan AP, Weyman AE, Levine RA. Adjacent solid boundaries alter the size of regurgitant jets on Doppler color flow maps. *J Am Coll Cardiol.* 1991;17:1094–102.
21. Skjaerpe T, Hatle L. Diagnosis of tricuspid regurgitation. Sensitivity of Doppler ultrasound compared with contrast echocardiography. *Eur Heart J.* 1985;6:429–36.
22. Tribouilloy CM, Enriquez-Sarano M, Fett SL, Bailey KR, Seward JB, Tajik AJ. Application of the proximal flow convergence method to calculate the effective regurgitant orifice area in aortic regurgitation. *J Am Coll Cardiol.* 1998;32:1032–9.
23. Shiota T, Jones M, Yamada I, Heinrich RS, Ishii M, Sinclair B, Yoganathan AP, Sahn DJ. Evaluation of aortic regurgitation with digitally determined color Doppler-imaged flow convergence acceleration: a quantitative study in sheep. *J Am Coll Cardiol.* 1996;27:203–10.
24. Quere JP, Tribouilloy C, Enriquez-Sarano M. Vena contracta width measurement: theoretic basis and usefulness in the assessment of valvular regurgitation severity. *Curr Cardiol Rep.* 2003;5:110–5.
25. Tribouilloy CM, Enriquez-Sarano M, Bailey KR, Seward JB, Tajik AJ. Assessment of severity of aortic regurgitation using the width of the vena contracta: a clinical color Doppler imaging study. *Circulation.* 2000;102:558–64.
26. Willett DL, Hall SA, Jessen ME, Wait MA, Grayburn PA. Assessment of aortic regurgitation by transesophageal color Doppler imaging of the vena contracta: validation against an intraoperative aortic flow probe. *J Am Coll Cardiol.* 2001;37:1450–5.
27. Nozaki S, Mizushige K, Taminato T, Obayashi N, Matsuo H. New index for grading the severity of aortic regurgitation based on the cross-sectional area of vena contracta measured by color Doppler flow mapping. *Circ J.* 2003;67:243–7.
28. Smith MD, Grayburn PA, Spain MG, DeMaria AN. Observer variability in the quantitation of Doppler color flow jet areas for mitral and aortic regurgitation. *J Am Coll Cardiol.* 1988;11:579–84.
29. Reimold SC, Thomas JD, Lee RT. Relation between Doppler color flow variables and invasively determined jet variables in patients with aortic regurgitation. *J Am Coll Cardiol.* 1992;20:1143–8.
30. Taylor AL, Eichhorn EJ, Brickner ME, Eberhart RC, Grayburn PA. Aortic valve morphology: an important in vitro determinant of proximal regurgitant jet width by Doppler color flow mapping. *J Am Coll Cardiol.* 1990;16(2):405–12.
31. Grayburn PA, Handshoe R, Smith MD, Harrison MR, DeMaria AN. Quantitative assessment of the hemodynamic consequences of aortic regurgitation by means of continuous wave Doppler recordings. *J Am Coll Cardiol.* 1987;10(1):135–41.
32. Labovitz AJ, Ferrara RP, Kern MJ, Bryg RJ, Mrosek DG, Williams GA. Quantitative evaluation of aortic insufficiency by continuous wave Doppler echocardiography. *J Am Coll Cardiol.* 1986;8(6):1341–7.
33. Griffin BP, Flachskampf FA, Siu S, Weyman AE, Thomas JD. The effects of regurgitant orifice size, chamber compliance, and systemic vascular resistance on aortic regurgitant velocity slope and pressure half-time. *Am Heart J.* 1991;122(4 Pt 1):1049–56.
34. Quinones MA, Young JB, Waggoner AD, Ostojic MC, Ribeiro LG, Miller RR. Assessment of pulsed Doppler echocardiography in detection and quantification of aortic and mitral regurgitation. *Br Heart J.* 1980;44:612–20.
35. Rodriguez L, Thomas JD, Monterroso V, Weyman AE, Harrigan P, Mueller LN, Levine RA. Validation of the proximal flow convergence method. Calculation of orifice area in patients with mitral stenosis [see comment]. *Circulation.* 1993;88(3):1157–65.
36. Deng YB, Matsumoto M, Wang XF, Liu L, Takizawa S, Takekoshi N, Shimizu T, Mishima K. Estimation of mitral valve area in patients with mitral stenosis by the flow convergence region method: selection of aliasing velocity. *J Am Coll Cardiol.* 1994;24:683–9.
37. Rifkin RD, Harper K, Tighe D. Comparison of proximal isovelocity surface area method with pressure half-time and planimetry in evaluation of mitral stenosis. *J Am Coll Cardiol.* 1995;26:458–65.
38. Degertekin M, Basaran Y, Gencbay M, Yaymaci B, Dindar I, Turan F. Validation of flow convergence region method in assessing mitral valve area in the course of transthoracic and transesophageal echocardiographic studies. *Am Heart J.* 1998;135(2 Pt 1):207–14.

Principles of Measuring Chamber Size, Volume and Hemodynamic Assessment of the Heart

6

Carolyn M. Larsen, Carrie L. Vanden Bussche,
and Sunil Mankad

Assessment of Left Ventricular Chamber Size and Mass

Linear Assessment of Left Ventricular Chamber Size and Wall Thickness

Linear measurements of left ventricular (LV) cavity size and wall thickness are relatively quick and easy to obtain. In patients without structural heart disease, they provide a reliable representative assessment of LV size. The main limitation of these measurements is they only assess one dimension of a three-dimensional structure. In patients with structural heart disease linear measurements may not adequately reflect the true LV size and shape.

M-Mode Method

Assessment of LV size by m-mode is performed from the parasternal window. A two-dimensional (2DE) parasternal short axis image at the mid-

papillary muscle level is obtained and the m-mode cursor is placed directly through the middle of the left ventricle. Care must be taken to avoid obtaining m-mode measurements in an oblique plane as this will overestimate left ventricular cavity diameter and wall thickness measurements. An example of appropriately oriented LV end-diastolic and end-systolic diameter measurements obtained from the m-mode tracing are demonstrated in Fig. 6.1. Other measurements obtained from this view should include septal and posterior wall thickness at end diastole. The end-diastolic measurement should be taken at the time in the cardiac cycle when the LV diameter is the largest or corresponding with the QRS complex on the electrocardiogram (ECG). The end-systolic measurement should be taken at the point of maximal posterior wall excursion [1].

Two-Dimensional Method

Assessment of LV size by 2DE is performed from the parasternal long axis view. Measurements of septal and posterior wall thickness and LV cavity size at end diastole are performed perpendicular to the LV long axis at the level of the mitral valve leaflet tips. LV end diastolic measurements should be taken at the time in the cardiac cycle when the LV diameter is the largest or the frame after mitral valve closure. Examples of correctly and incorrectly

C. M. Larsen
Department of Cardiovascular Medicine,
Mayo Clinic, Rochester, AZ, USA

C. L. Vanden Bussche
Department of Echocardiography, Mayo Clinic,
Rochester, MN, USA

S. Mankad (✉)
Department of Cardiovascular Medicine,
Mayo Clinic, Rochester, MN, USA
e-mail: Mankad.Sunil@mayo.edu

positioned LV end-diastolic 2D measurements are shown in Fig. 6.2. An example of LV end-systolic cavity dimension which should be measured at the time in the cardiac cycle when the

LV diameter is the smallest is shown in Fig. 6.3 [2]. The parasternal long axis view from which these measurements are obtained should be optimized to open up the LV cavity towards the

Fig. 6.1 Shown is a parasternal short axis at the mid-papillary muscle level with the m-mode cursor through the LV; appropriately timed LV end-diastolic and end-systolic diameter measurements are demonstrated

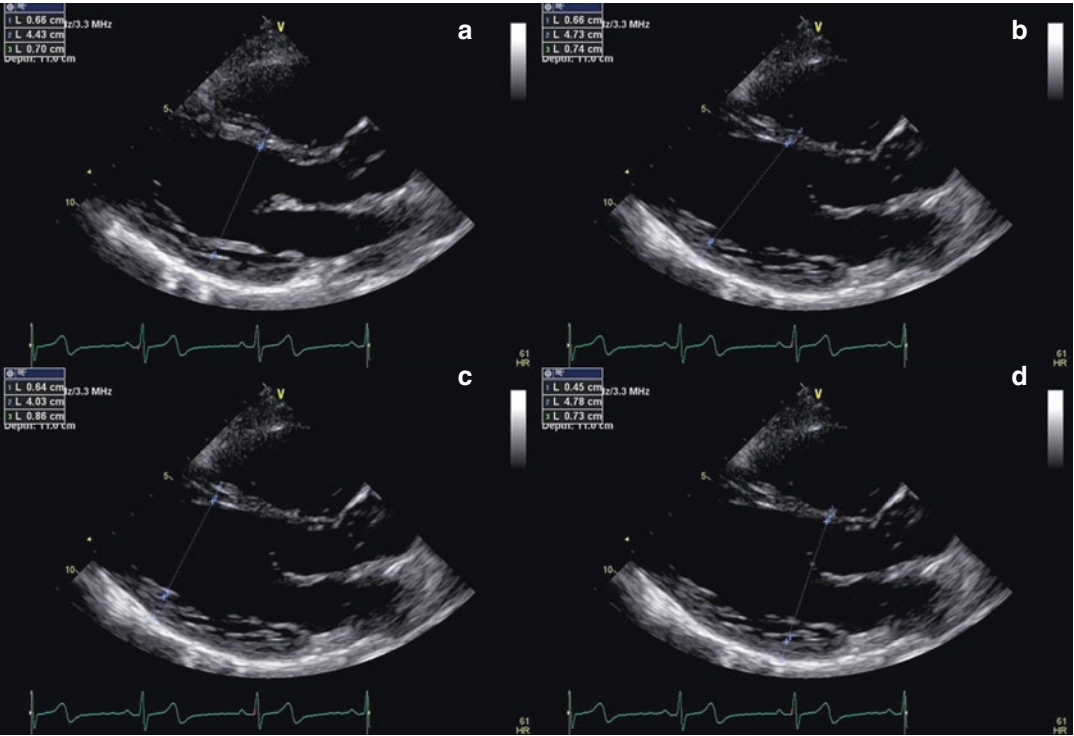
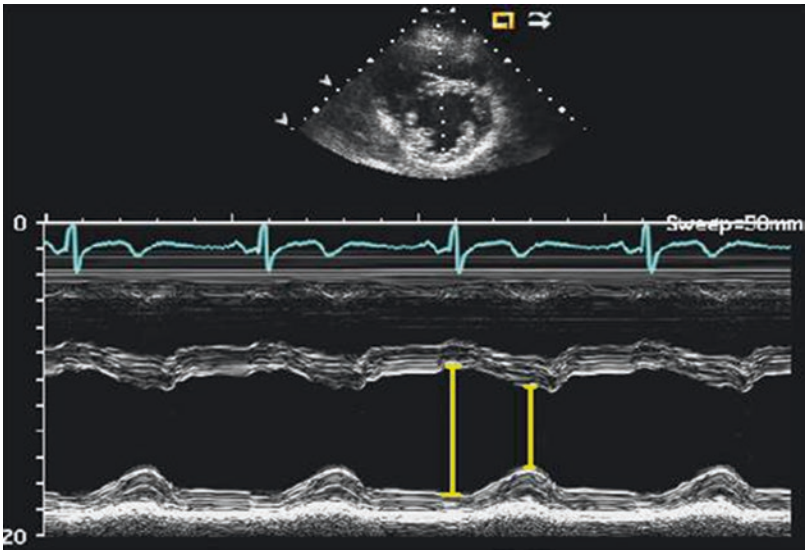
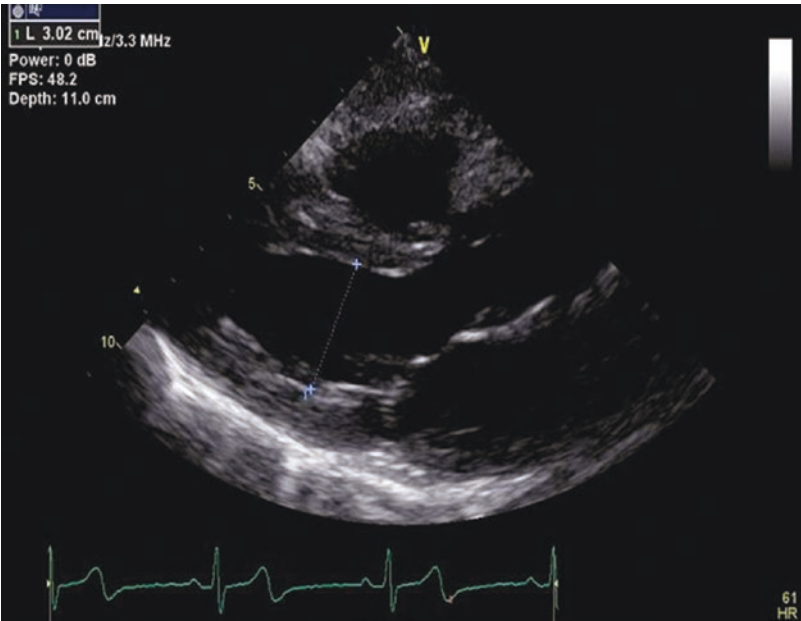


Fig. 6.2 Shown is a 2-D parasternal long-axis view of the left ventricle at end-diastole; the upper left panel **a** demonstrates the correct measurement position for LV end-diastolic diameter; the upper right panel **b** illustrates an

incorrect non-perpendicular or angulated/tangential measurement of the LV end-diastolic diameter; the lower panels **c** and **d** demonstrate incorrect apical and basally displaced measurements, respectively

Fig. 6.3 Shown is a parasternal long-axis image at end-systole with correct measurement of the LV end-systolic diameter



apex and to include the mitral and aortic valves. Papillary muscles should be included in the LV cavity and should not be measured with the LV wall. Normal values for LV wall thickness and LV cavity size by 2DE echocardiography are presented in Table 6.1 [1].

Volumetric Assessment of Left Ventricular Chamber Size

Two-Dimensional Methods

The 2DE volumetric methods for assessing left ventricular size are superior to linear methods, especially in patients with structural heart disease. However, they still make assumptions about ventricular geometry to provide an estimate of LV volume. Multiple methods for estimating LV volume from 2DE measurements have been used in the past. However, the current recommendation is to use the biplane disk summation method [1].

To calculate LV volumes from 2DE images by the biplane disk summation method, apical two-chamber and four-chamber images are obtained. The left ventricular cavity is traced at the blood tissue interface in the two-chamber and four-chamber views. If the endocardial border is difficult to define for two or more contiguous segments, ultrasound contrast can be administered to enhance border definition [1, 3]. Papillary

Table 6.1 Normal values for LV size by 2DE

	Female Mean (2-SD range)	Male Mean (2-SD range)
LV internal dimension		
Diastolic dimension (mm)	45.0 (37.8–52.2)	50.2 (42.0–58.4)
Systolic dimension (mm)	28.2 (21.6–34.8)	32.4 (25.0–39.8)

From [1]; with permission
SD standard deviation, L left ventricle

muscles should be included in the left ventricular cavity. The trace should start and end at the mitral annulus. The LV length is measured from the midpoint of the line connecting the sides of the mitral annulus to the most distant point of the LV contour. The left ventricular cavity is traced at end-diastole and end-systole, defined as the frame of largest and smallest LV dimension, respectively, to obtain LV diastolic and LV systolic volumes, respectively. An example of this is shown in Fig. 6.4. A common mistake when making biplane measurements is to use foreshortened apical images, which will underestimate LV volumes. An example of this is shown in Fig. 6.5. Normal values for 2DE biplane LV volumes indexed to body surface area (BSA) are provided in Table 6.2 [1].

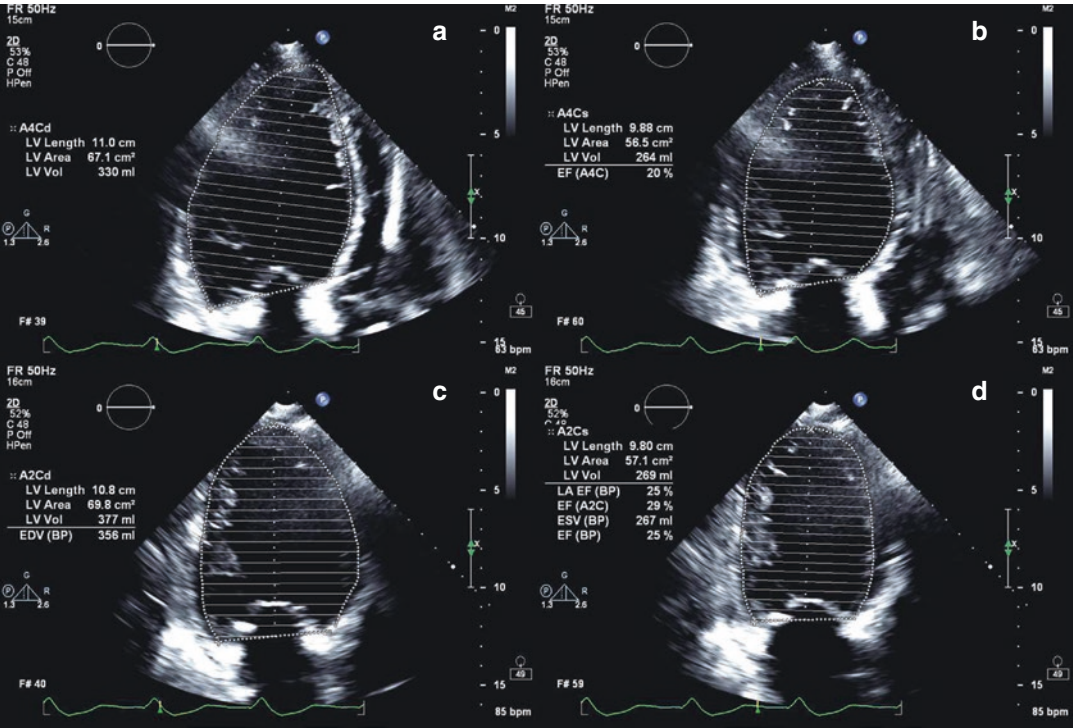


Fig. 6.4 Shown are apical four-chamber views (above, panels **a** (end-diastole) and **b** (end-systole)) in the American Society of Echocardiography type B format with the LV on the left in a patient with a dilated cardiomyopathy with appropriate tracing of the LV endocardial

border; note how the correct position requires tracing beyond the trabeculations; shown below (panels **c** (end-diastole) and **d** (end-systole)) are appropriately traced LV apical two-chamber views in the same patient

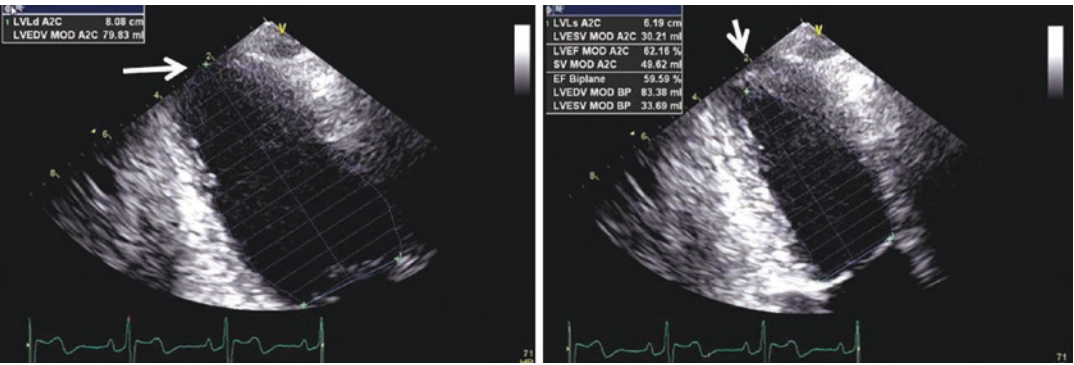


Fig. 6.5 Shown is a foreshortened apical two-chamber with the end-diastolic image on the left showing the apex out of the field of view and the end-systolic image on the

right demonstrating a truncated view of the apex due to foreshortening of the image (arrows)

Three-Dimensional Method

Left ventricular volumes can be measured from full-volume 3DE data sets and this is the preferred method for assessment of LV volumes

when feasible. The advantages of 3DE LV volumes are they make no assumptions about LV geometry and are not subject to foreshortening. Compared with 2DE, 3DE offers improved

Table 6.2 Normal values for LV size and function by biplane volumetric assessment

	Female Mean (2-SD range)	Male Mean (2-SD range)
Biplane LV volumes		
End diastolic volume (mL)	76 (46–106)	106 (62–150)
End systolic volume (mL)	28 (14–42)	41 (21–61)
Biplane LV volumes indexed to BSA		
End diastolic volume (mL/m ²)	45 (29–61)	54 (34–74)
End systolic volume (mL/m ²)	16 (8–24)	21 (11–31)
Biplane LV EF	64 (54–74)	62 (52–72)

From [1]; with permission
SD standard deviation, *LV* left ventricle, *BSA* body surface area, *EF* ejection fraction

reproducibility, accuracy, and precision in the assessment of LV volumes [4]. Limitations of the 3DE method include user familiarity with 3DE and patient body habitus, which may limit image quality and the ability to obtain 3DE data sets by transthoracic echocardiography (TTE). An example of 3DE volumetric measurements of the LV is shown in Fig. 6.6.

Assessment of Left Ventricular Mass

Left ventricular mass can be estimated or directly measured. Linear measurements of the septum and posterior wall, obtained by 2DE or 2DE-guided M-mode, can be used to estimate a calculated LV mass with the following formula,

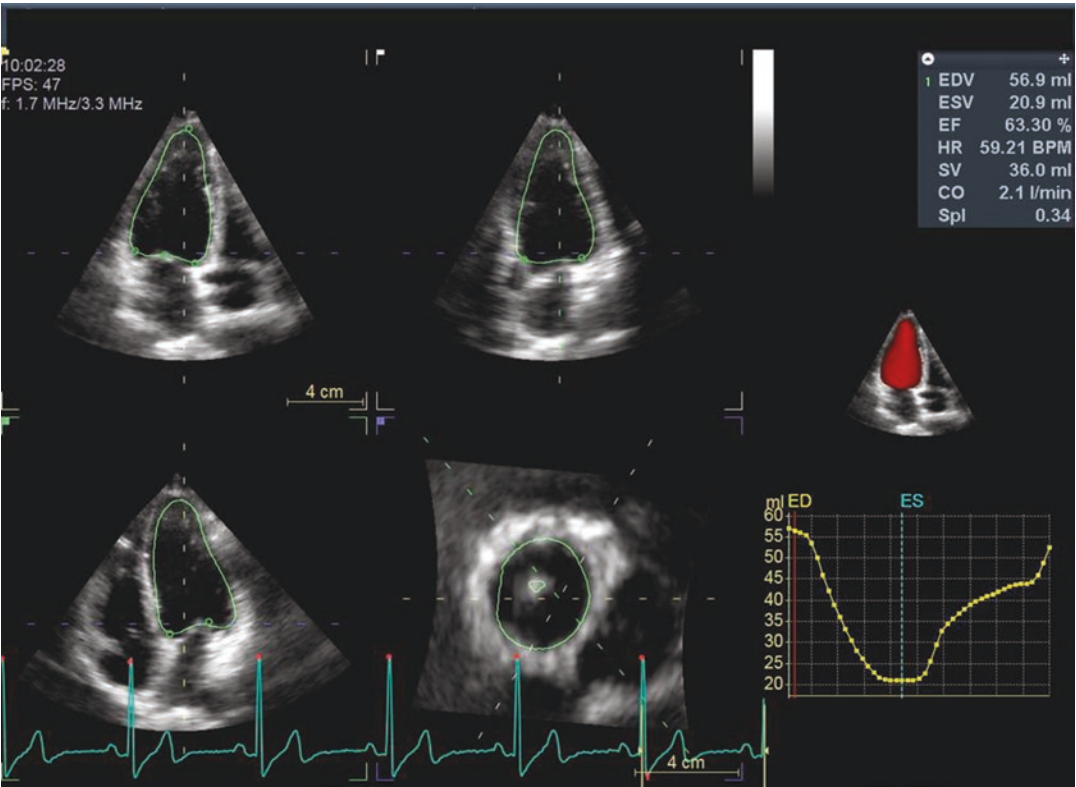


Fig. 6.6 Shown is a 3D volumetric measurement of the LV measured from a multiple beat full-volume dataset; the LV endocardial border is tracked throughout the cardiac cycle and short-axis image (middle bottom) allows

for the use to make sure that this is accurate; the time-volume curve (bottom right) can also be generated from the dataset

where *IVS* is interventricular septum, *LVIDd* is LV internal diameter at end diastole, and *PWT* is posterior wall thickness:

LV mass = 0.8 × 1.04 ×

$$\left[(IVS + LVIDd + PWT)^3 - LVID^3 \right]$$

+0.6 g

The upper limit of normal for LV mass indexed to BSA is 95 g/m² for women and 115 g/m² for men. One limitation of this method is linear measurements of LV dimensions are taken to the third power and small errors will have a large effect on the calculated LV mass. Additionally, it makes assumptions about the LV geometry that are inaccurate in presence of structural heart disease. LV mass can be directly measured by 3DE by measuring the LV myocardial volume and then multiplying it by the approximate myocardial density (1.05 g/mL). However, there is currently not enough data on LV mass by 3DE in normal subjects to propose reference values for this method [1].

Left ventricular remodeling can be described further by calculating the relative wall thickness (RWT) by the following formula, where *PWT* is

posterior wall thickness and *LVIDd* is LV internal diameter at end diastole:

RWT = (2 × PWT) / LVIDd

Left ventricular geometry can be classified as either normal, concentric remodeling, concentric hypertrophy, or eccentric hypertrophy based on the RWT and LV mass index (Fig. 6.7).

Quantification of Left Ventricular Systolic Function

The most commonly reported measurement of LV systolic function is the ejection fraction (EF). The EF can be calculated from the difference between end diastolic and end systolic M-mode, 2DE, or 3DE measurements. For the calculation of EF, end-diastolic measurements should be made in the frame after mitral valve closure or in the frame where the LV dimension or volume is the largest. End-systolic measurements should be made in the frame after aortic valve closure or the

Fig. 6.7 Characterization of left ventricular geometry by LV mass index and RWT. A normal LV mass index is ≤95 g/m² for women and ≤ 115 g/m² for men. *LV* left ventricular, *RWT* relative wall thickness. Data from Lang et al. [1]

<div>Concentric Remodeling</div> <div>Normal LV mass index</div> <div>RWT (> 0.42)</div>	<div>Concentric Hypertrophy</div> <div>Increased LV mass index</div> <div>RWT (> 0.42)</div>
<div>Normal Geometry</div> <div>Normal LV mass index</div> <div>RWT (≤ 0.42)</div>	<div>Eccentric Hypertrophy</div> <div>Increased LV mass index</div> <div>RWT (≤ 0.42)</div>

frame in which the LV dimension or volume is the smallest [1].

Linear measurements of LV systolic function suffer from the same limitations as measurements of LV chamber size. They work well in patients with normal cardiac structure but make assumptions about LV geometry that are inaccurate in the presence of structural heart disease. Biplane methods are also limited by assumptions about LV geometry but are superior to linear measurements in this regard. The biplane method is the preferred 2DE method for assessing LV EF, but assessment of LV EF by 3DE is preferred when feasible [1].

Linear Methods for Quantification of Left Ventricular Systolic Function

The LV EF can be calculated from the M-mode or 2DE measurements demonstrated previously in Figs. 6.2 and 6.3, respectively, by the following formula, where *LVEDd* is LV end-diastolic diameter and *LVESd* is LV end-systolic diameter:

$$\text{LV EF} = \left[\frac{(LVEDd^2 - LVESd^2)}{LVEDd^2} \right] \times 100$$

If apical contractility is normal, the LV EF can be adjusted by the following formula to account for normal apical function:

$$\text{Adjusted LV EF} = \text{unadjusted LV EF} + \left[(100 - \text{unadjusted LV EF}) \times 0.15 \right]$$

This method is acceptable for patients without regional wall motion abnormalities. In the presence of regional wall motion abnormalities it will not accurately reflect global LV systolic function [5]. The normal range for LV EF by 2DE is 54–74% for women and 52–72% for men [1].

Biplane Methods for Quantification of Left Ventricular Systolic Function

The LV EF can be calculated from the LV end-diastolic and LV end-systolic biplane volumes as

shown in Fig. 6.4 by the following formula, where *EDV* is end-diastolic volume and *ESV* is end-systolic volume:

$$\text{LV EF} = (EDV - ESV) / EDV \times 100$$

The LV EF by the biplane method is the preferred over linear methods for assessing LV EF because it makes fewer assumptions about LV geometry than the linear methods. Normal values for biplane LV EF are provided in Table 6.2.

Three-Dimensional Method for Quantification of Left Ventricular Systolic Function

The LV EF can also be calculated from 3DE end-diastolic and systolic volumes as shown in Fig. 6.6 by the following formula:

$$\text{LV EF} = (EDV - ESV) / EDV \times 100$$

This is the preferred method for assessment of LV EF when feasible. Compared with 2DE methods, 3DE offers improved precision in LV EF assessment [4].

Measurements of the Left Ventricular Outflow Tract and Aorta

Measurements of the left ventricular outflow tract (LVOT), the aortic root (sinus of Valsalva and sinotubular junction), and the ascending aorta can be acquired from the parasternal long axis view and/or the right parasternal window. From the parasternal long axis view, zoom in to focus on the LVOT and the aortic root. The aortic valve should be in the center of the image with the LVOT and aortic root in a horizontal position on the image display. The image should be optimized to show the maximal diameter of the aortic root perpendicular to the long axis of the aorta. In patients with tricuspid aortic valves, the closure point of the aortic valve cusps should be in the

center of a line drawn between the points of leaflet insertion. If this is not the case, the aortic root is likely not displayed in maximal diameter. The transducer may need to be moved closer to the sternum or to a different intercostals space to optimize the image [1].

The guidelines recommend measurement of the LVOT diameter from inner edge to inner edge (septal endocardium to anterior mitral valve leaflet) in mid-systole parallel to the aortic valve (Fig. 6.8). This measurement should be made at the same distance from the valve that the LVOT velocity is measured and just proximal to the location at which flow acceleration through the valve occurs (usually within 0.5–1.0 cm of the aortic valve) [6].

Measurements of the Sinus of Valsalva, sinotubular junction, and ascending aorta are made perpendicular to the long axis of the aorta from leading edge to leading edge at end diastole, as identified by the peak of the R wave of the QRS complex. These measurements are demonstrated in Fig. 6.9. By going up an intercostal space from the parasternal long axis image, the image of the mid-ascending aorta can frequently be optimized. Alternatively, the mid-ascending aorta can be imaged from the right parasternal view. Normal values for measurements of the aorta vary by age and body surface area (BSA) [1].

Assessment of Left Atrial Size

The recommended method for reporting left atrial (LA) size is LA volume because it takes into account remodeling in multiple dimensions. LA volume can either be calculated by the

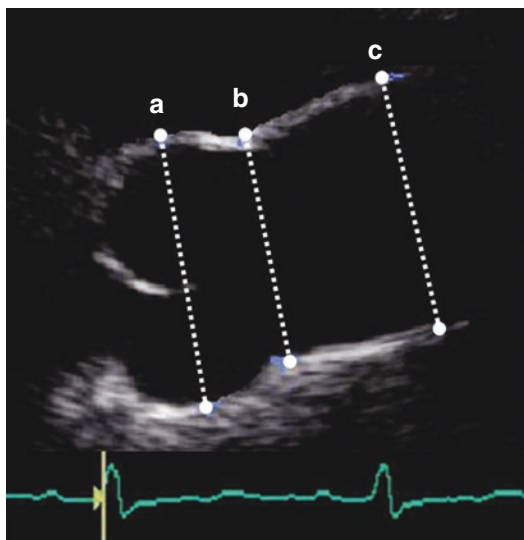
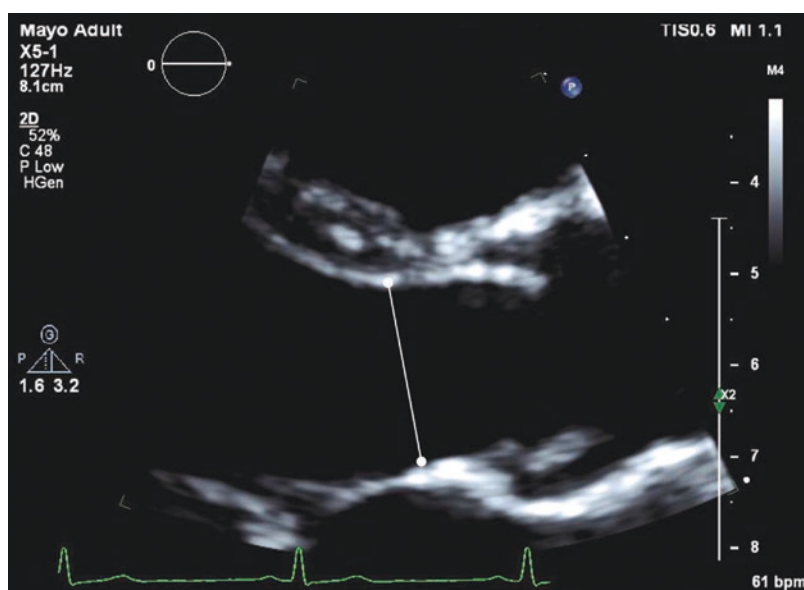


Fig. 6.9 Shown is the parasternal long-axis view of the aortic root and proximal ascending aorta; measurement of the sinus of Valsalva (A), the sinotubular junction (B), and proximal ascending aorta (C) are designated to be “leading edge to leading edge”

Fig. 6.8 Shown is the correct location for measurement of the LVOT from the zoomed in parasternal long axis view; the line illustrates the correct position for the recommended measurement of the LVOT from inner edge to inner edge (septal endocardium to anterior mitral valve leaflet) in mid-systole parallel to the aortic valve



area-length technique (Fig. 6.10) or the biplane method of disks (Fig. 6.11). The biplane method is preferred because it makes fewer assumptions about the geometry of the LA [1]. If adequate images of the LA cannot be obtained in both the two- and four-chamber views, a single-plane volume can be reported [1].

For either method, dedicated apical two- and four-chamber views are obtained which avoid foreshortening and maximize LA area. The LA is traced at the blood tissue interface at end systole excluding the left atrial appendage and the pulmonary veins. The LA length is measured along

the long axis of the LA and is the distance from the middle of a line connecting the two sides of the mitral annulus to the opposite side of the LA. The measured LA length from the apical two- and four-chamber views should not differ by more than 5 mm [1].

Using the area length technique, an estimated LA volume is calculated by the following formula where A_1 and A_2 are the LA areas from the two- and four-chamber apical views and L is the shorter of the two measured LA lengths:

$$\text{LA volume} = (8/3\pi) \times [(A_1 \times A_2)/L]$$

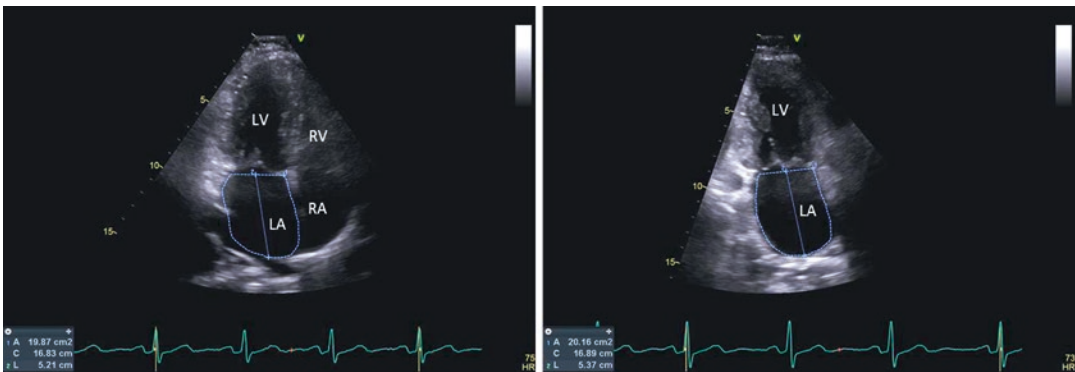


Fig. 6.10 Shown is an example of measurement of the LA by the area-length technique from dedicated apical two- and four-chamber views (American Society of Echocardiography type B format with the left ventricle on the left); care must be taken to avoid foreshortening and to

maximize LA area. The LA is traced at the blood tissue interface at end systole excluding the left atrial appendage and the pulmonary veins (LA left atrium, RA right atrium, LV left ventricle, RV right ventricle)

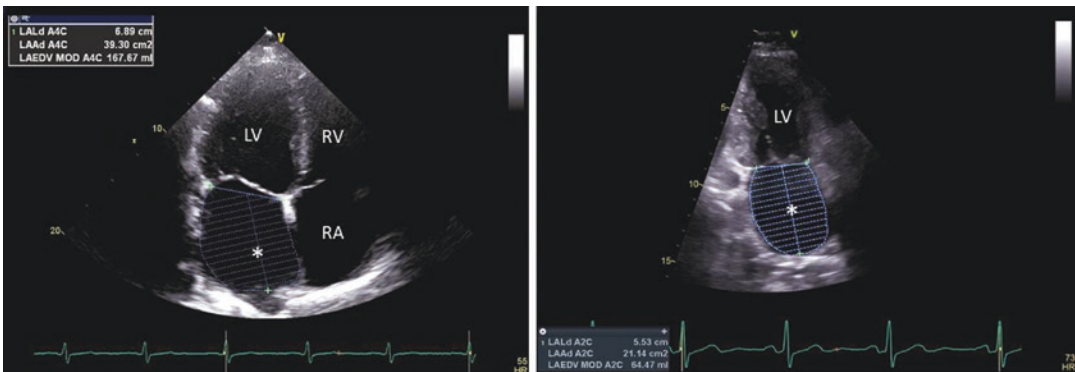


Fig. 6.11 Shown is an example of measurement of the LA by the disc summation technique from dedicated apical two- and four-chamber views (American Society of Echocardiography type B format with the left ventricle on the left); care must be taken to avoid foreshortening and to

maximize LA area. The LA is traced at the blood tissue interface at end systole excluding the left atrial appendage and the pulmonary veins (* designates the left atrium; RA right atrium, LV left ventricle, RV right ventricle)

The biplane disk summation method estimates LA volume by adding the volumes of a stack of cylinders using the following formula where h is the cylinder height and $D1$ and $D2$ are the diameters of the cylinder measured from the apical two- and four-chamber views:

$$\text{LA volume} = \pi / 4 (h) \Sigma (D1)(D2)$$

LA volumes are indexed to BSA. The upper limit of normal for left atrial volume index (LAVI) by 2DE is 34 mL/m² for males and females. An LAVI of 35–41 mL/m² is mildly enlarged, 42–48 mL/m² moderately enlarged, and more than 48 mL/m² severely enlarged. LA volume can also be assessed by 3DE. This technique has the advantage of directly measuring the LA and therefore not making geometric assumptions about LA shape. However, limited data are available on normal values for LA volume by 3DE [1].

Assessment of the Inferior Vena Cava

An estimation of right atrial (RA) pressure can be made from the size and inspiratory collapse of the inferior vena cava (IVC). The IVC is assessed in long axis from the subcostal view. It can be imaged with the patient lying supine or in the left lateral decubitus position. If the IVC appears dilated with the patient supine, additional images should be taken with the patient in the left lateral decubitus

position to confirm whether the IVC is dilated. If inadequate images of the IVC are obtained from the traditional subcostal window, it can also be imaged from a transhepatic window [7].

Measurements of the IVC diameter should be made just proximal to the junction with the hepatic vein (Fig. 6.12). The IVC diameter should be measured during expiration and during an inspiratory sniff. The normal IVC diameter during expiration is less than 2.1 cm and the normal IVC collapses more than 50% with inspiration. If the IVC diameter is normal and it collapses more than 50% with a sniff, the RA pressure is estimated at 3 mmHg. If the IVC diameter is more than 2.1 cm and collapses less than 50% with inspiration, the RA pressure is estimated at 15 mmHg. With any other combination of these two measurements, an RA pressure of 8 mmHg is estimated [7].

Assessment of Left Ventricular Diastolic Function

Assessment of LV diastolic function involves integration of data from multiple measurements. The first abnormality to develop with diastolic dysfunction is impaired relaxation of the LV. This is followed by development of increased LV filling pressures. In the following sections, first individual measurements and their implications for LV filling pressures and diastolic function

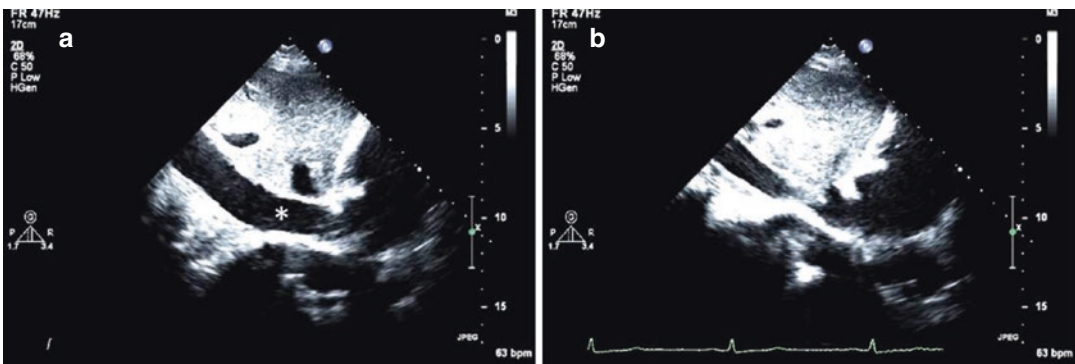


Fig. 6.12 Shown is a sub-costal view of the inferior vena cava (IVC) with the patient supine; the left hand panel (a) demonstrates the appropriate location to measure the IVC

(asterisk) and the right hand panel (b) demonstrates >50% collapse of the IVC with inspiration

will be reviewed. Then, a stepwise approach to integrating this data to classify LV diastolic function will be presented [8].

Mitral Inflow

Diastolic flow through the mitral valve is assessed by pulsed-wave (PW) Doppler with a 1- to 3-mm sample volume placed between the mitral valve leaflet tips. Continuous wave (CW) Doppler should be performed prior to PW Doppler to ensure maximal inflow velocities are obtained. Color flow Doppler can be used as a reference to verify the Doppler beam is centered and parallel to flow (Fig. 6.13) [8].

Mitral inflow should initially be assessed at a sweep speed of 25–50 mm/s to assess for respiratory variation in mitral inflow velocities, as can be seen in patients with significant pulmonary or pericardial disease. Then the sweep speed should be increased to 100 mm/s and recordings taken at end expiration for measurement of peak early filling (E-wave), late diastolic filling (A-wave), and the deceleration time (DT) of early diastolic filling. These measurements should be averaged over three cardiac cycles. Normal values for mitral inflow are

affected by age. With increasing age, the E-wave decreases while the A-wave and deceleration time increase [8].

The pattern of mitral inflow defined by the E/A ratio and the deceleration time can provide valuable clues as to the state of myocardial relaxation and LA pressure (Fig. 6.14) [8]. Patients with impaired LV relaxation generally have a normal LA pressure and the pseudonormal and restrictive LV filling patterns are seen as LA pressures rise. The Valsalva maneuver can be performed to help differentiate normal from pseudonormal patterns of mitral inflow. The Valsalva maneuver results in a decrease in preload (decrease in LA pressure) and can transiently convert a pseudonormal pattern of LV filling to a pattern of impaired relaxation. A decrease in the E/A ratio of 50% or greater is specific for increased LV filling pressures. However, if the E/A ratio decreases by less than 50%, this does not always indicate normal diastolic function (Fig. 6.15) [8, 9].

The deceleration time first prolongs when LV relaxation is impaired. Subsequently it shortens as LV filling pressures rise. With a restrictive pattern of LV filling, the deceleration time is

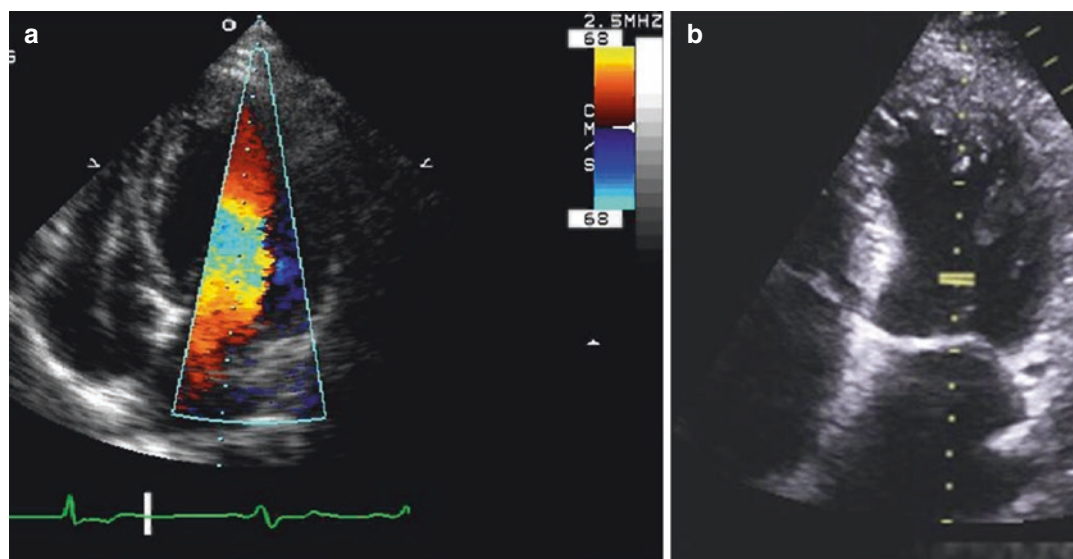
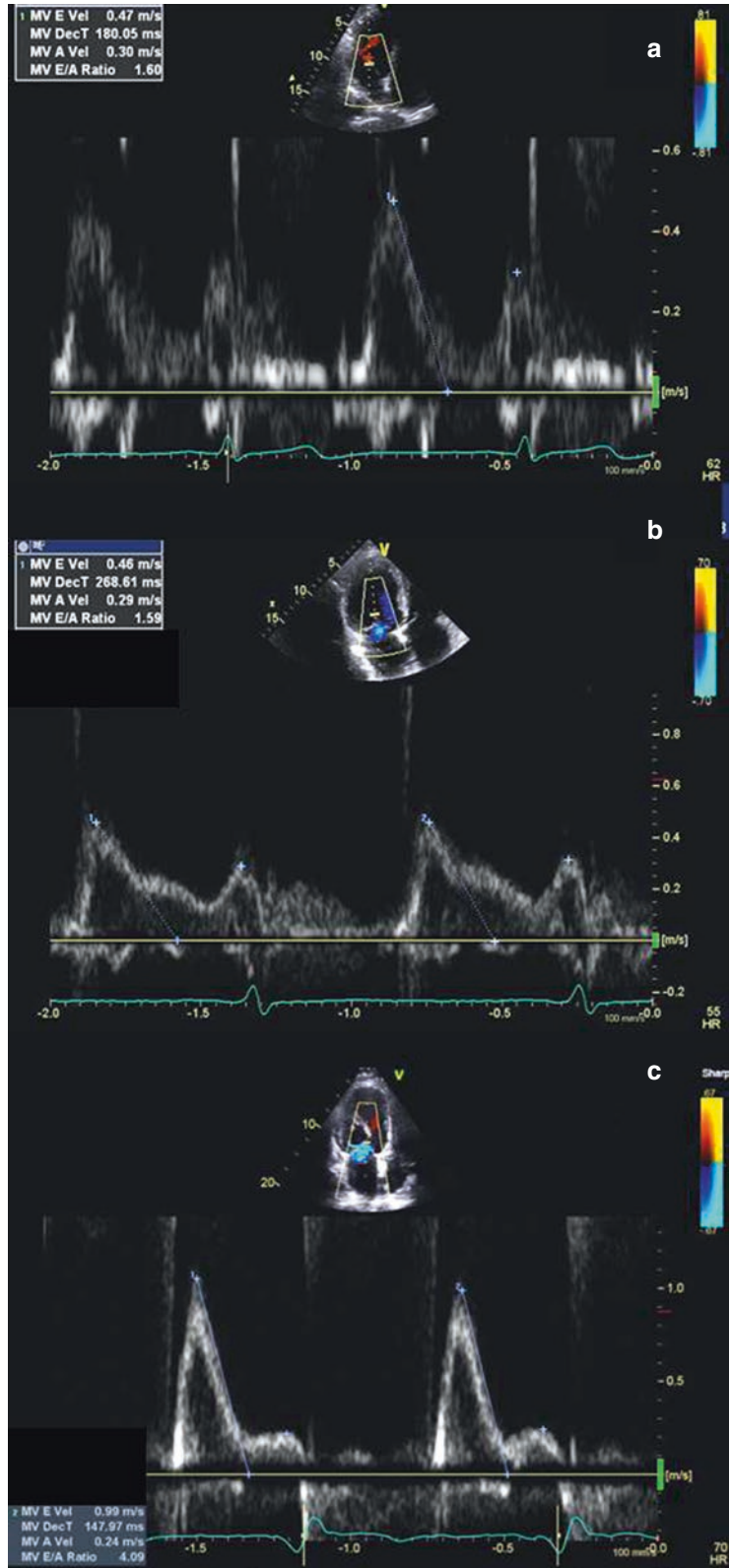


Fig. 6.13 Shown on the left hand panel (a) is the use of color Doppler echocardiography to align the pulse Doppler sample volume/cursor to be parallel to left ventricular inflow; the right hand panel (b) demonstrates the

location of the pulse Doppler sample volume/cursor at the mitral valve leaflet tips for appropriate mitral inflow measurements to assess LV diastolic function

Fig. 6.14 Shown in the top panel (a) is a normal pattern diastolic mitral inflow pattern with a deceleration time of 180 ms; the middle panel (b) demonstrates diastolic mitral inflow in a patient with grade 2 LV diastolic dysfunction and the deceleration time is >200 ms and there is persistent forward inflow during diastasis representing elevated filling pressures or an “L” wave; the lower panel (c) demonstrates mitral inflow in a patient with restrictive pattern of diastolic function with a rapid deceleration time of <150 ms



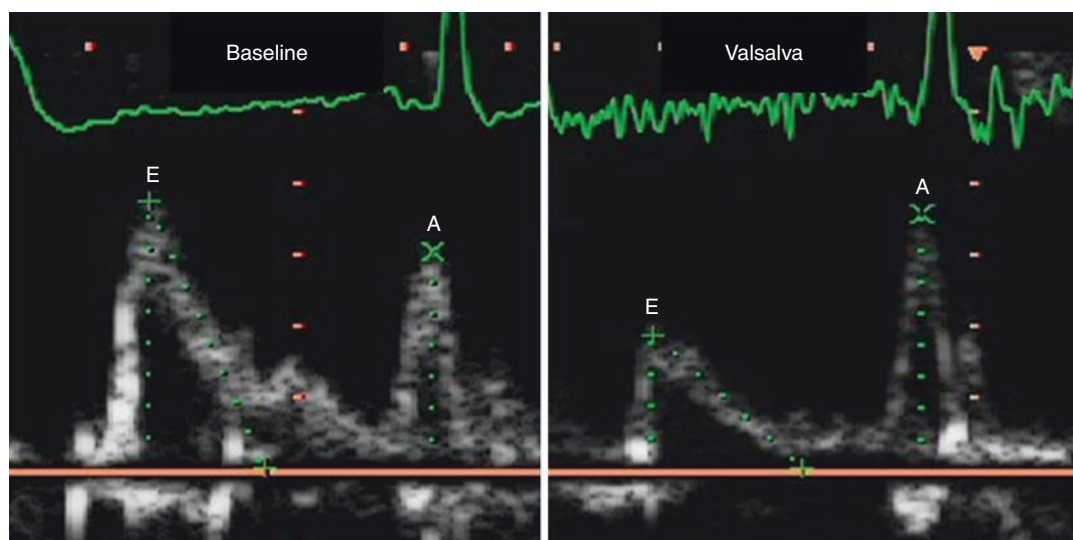


Fig. 6.15 Shown is mitral inflow pulsed Doppler with the sample volume at the leaflet tips; the left panel demonstrates what is a “pseudonormal” pattern that is unmasked with the Valsalva maneuver on the right panel; note the change in the early mitral inflow velocity (E wave) from

0.8 m/s to 0.4 m/s, the change in deceleration time from 220 ms to 285 ms, the change in the late diastolic atrial contraction velocity (A wave) from 0.6 m/s to 0.7 m/s, and the change in E/A ratio from 1.3 to 0.6 (>70% change)

short (Fig. 6.14). A stepwise approach to integrating echocardiographic data to grade diastolic function is outlined in elsewhere.

Mitral Annular Tissue Doppler

Tissue Doppler measurements at the level of the mitral annulus aid in the assessment of LV diastolic function. These measurements should be obtained with PW Doppler tissue imaging (DTI). Mitral annular tissue Doppler measurements are obtained from the apical four-chamber view by placing the sample volume at the level of the septal and lateral insertion of the mitral valve leaflets or 1 cm within. The sample volume placement should be adjusted as needed so that it covers the systolic and diastolic longitudinal excursion of the mitral annulus. DTI measurements are angle dependent. To optimize measurements, the angle between the ultrasound beam and the plane of cardiac motion should be less than 20°. A velocity scale of 20 cm/s is a good starting point but may need to be reduced in the setting of severe LV dysfunction. Recordings should be obtained at end-expiration with a sweep speed of 50–100 cm/s and measurements should be averaged over three cardiac cycles [8].

For diastolic function assessment, early (e') and late (a') diastolic annular velocities are measured (Fig. 6.16). Normal values for e' and a' are influenced by age, with e' decreasing with age and a' increasing. The left atrial pressure can be estimated from the E/e' in patients with cardiac disease. The average of the DTI measurements from the medial and lateral mitral annulus should be used for the E/e'. An E/e' > 14 is associated with elevated left atrial pressure. The E/e' does not correlate well with LV filling pressures in patients with heavy annular calcification, mitral valve disease, and constrictive pericarditis and should not be used to estimate LV filling pressure in these settings [8, 10].

Pulmonary Venous Inflow

The left atrium (LA) has three roles during the cardiac cycle. During systole, it functions as a reservoir, during early diastole as a conduit, and during late diastole (atrial contraction) as a pump [11]. The pattern of pulmonary venous inflow to the LA provides information about LV diastolic function.

Pulmonary venous inflow to the LA can be measured from the apical four-chamber view

with PW Doppler. The sample volume should be set at 2–3 mm and placed greater than 0.5 cm into the right upper pulmonary vein. Color flow Doppler guidance can be utilized for localization when placing the sample volume. Doppler recordings can often be optimized by angulating the transducer anteriorly from the standard apical 4-chamber view. Recordings should be made at end expiration with a sweep speed of 50–100 mm/s and averaged over three cardiac cycles [8].

Four measurements are commonly obtained from the pulmonary venous inflow signal including peak systolic velocity (S), peak diastolic velocity (D), peak atrial reversal velocity (Ar), and the duration of Ar (Fig. 6.17). There are two systolic velocities that can be measured (S1 and S2). S1 is a reflection of left atrial relaxation. S2 should be measured and used in comparisons with D. The normal pattern of pulmonary venous inflow is influenced by age. In normal patients younger than 40 years of age, D is greater than S. With increasing

Fig. 6.16 Shown is tissue Doppler imaging of the lateral mitral annulus (American Society of Echocardiography type B format with the LV on the left) and the pulse Doppler tracing; the E' represents the early diastolic tissue Doppler longitudinal relaxation velocity and the a' represents the late diastolic relaxation velocity

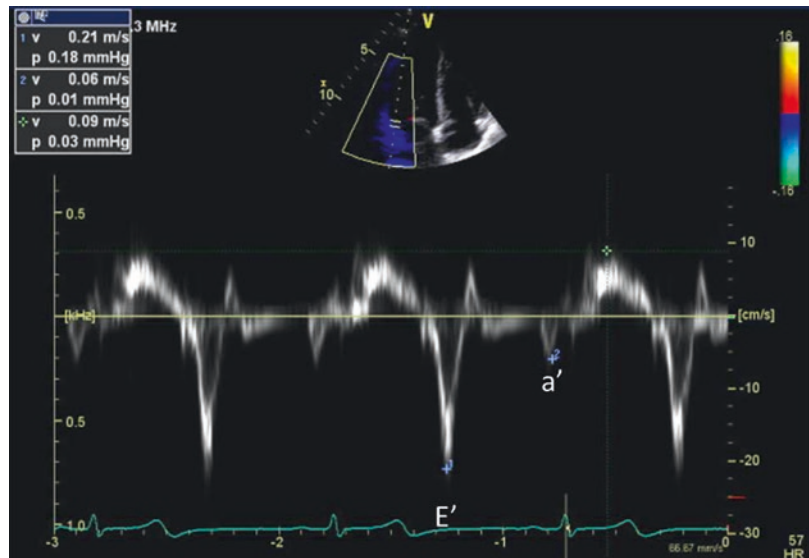
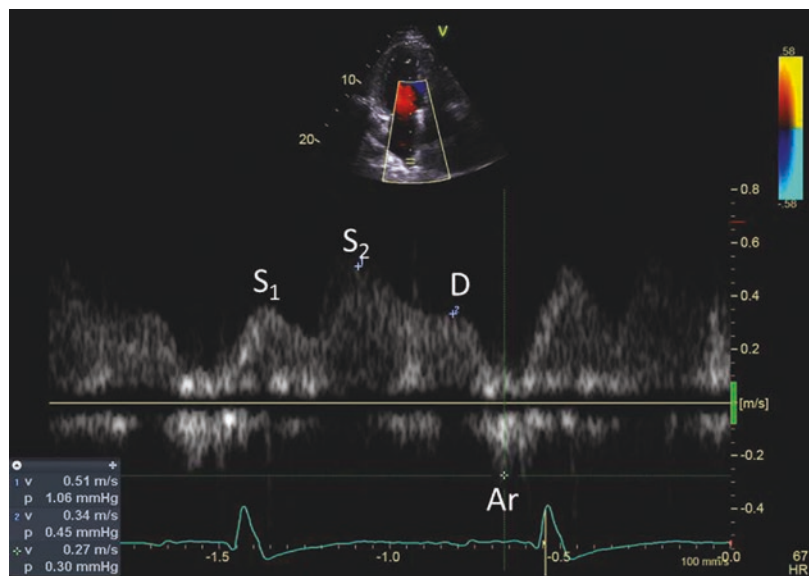


Fig. 6.17 Shown is the pulmonary vein Doppler from the apical view; four measurements are commonly obtained from the pulmonary venous inflow signal including peak systolic velocity (S), peak diastolic velocity (D), peak atrial reversal velocity (Ar), and the duration of Ar; there are two systolic velocities that can be measured (S1 and S2); S1 is a reflection of left atrial relaxation; S2 should be measured and used in comparisons with D



age, the S/D ratio increases. The S2 velocity decreases in the setting of decreased LA compliance and increased LA pressure. Changes in the D velocity parallel changes in the mitral inflow E velocity because the D velocity depends on LV compliance and filling pressures [8].

The pulmonary venous inflow atrial reversal velocity and duration provide information about the LV end diastolic pressure (LVEDP). If the Ar velocity is greater than 35 cm/s, this suggests the LVEDP is increased [8, 12]. The Ar velocity duration also increases with increased LVEDP. An Ar – A velocity duration >30 ms is an indication of increased LVEDP (Fig. 6.18) [8].

Step-Wise Approach to Grading Left Ventricular Diastolic Function

The first step in grading diastolic function requires identifying whether the patient has a reduced LV EF or myocardial disease versus a normal LV EF and normal myocardium. Then one of two algorithms can be followed to assign a diastolic function grade by integrating data from the assessment of mitral inflow and mitral annular tissue Doppler as well as the LAVI and the peak tricuspid regurgitation (TR) velocity. The peak TR velocity should be obtained with CW Doppler from the window (right ventricular [RV] inflow, parasternal short axis at the aortic valve level, apical four-chamber,

or para-apical RV focused view) that optimizes Doppler alignment parallel to flow within the regurgitant jet. See Sect. “Assessment of Left Atrial Size” for a discussion of measurement of LAVI. Patients with a normal LV EF and normal myocardium are classified as having normal diastolic function, indeterminate diastolic function, or diastolic dysfunction as outlined in Fig. 6.19a. Patients with a reduced LV EF and/or known myocardial disease are classified as having either normal or increased left atrial pressure and grade 1, 2, or 3 diastolic dysfunction as outlined in Fig. 6.19b [10]. In patients with a reduced LV EF and/or myocardial disease who have an indeterminate left atrial pressure and indeterminate diastolic function grade after following the algorithm, mitral inflow with the Valsalva maneuver and pulmonary venous inflow can be evaluated to further assess for evidence of elevated left atrial pressure or left ventricular end diastolic pressure, respectively.

Principles of Hemodynamics and Flow

Doppler echocardiography enables the noninvasive quantification of many aspects of cardiac function including: stroke volume, cardiac output, estimated chamber pressures, gradients

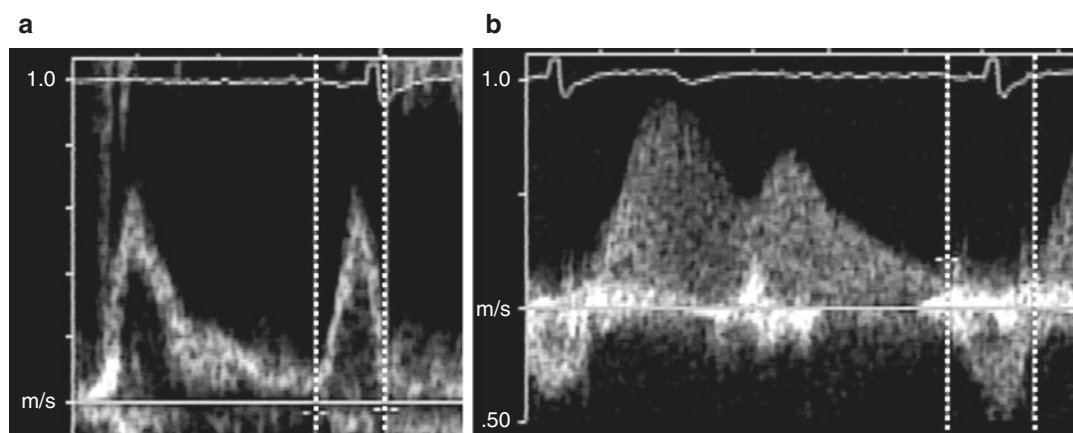


Fig. 6.18 Shown is an example of pulmonary venous inflow atrial reversal velocity (Ar) duration (right hand panel **b**) in comparison with the mitral inflow atrial velocity duration (left hand panel **a**); the Ar velocity dura-

tion increases with increased LVEDP and an Ar – A velocity duration >30 ms is an indication of increased LVEDP

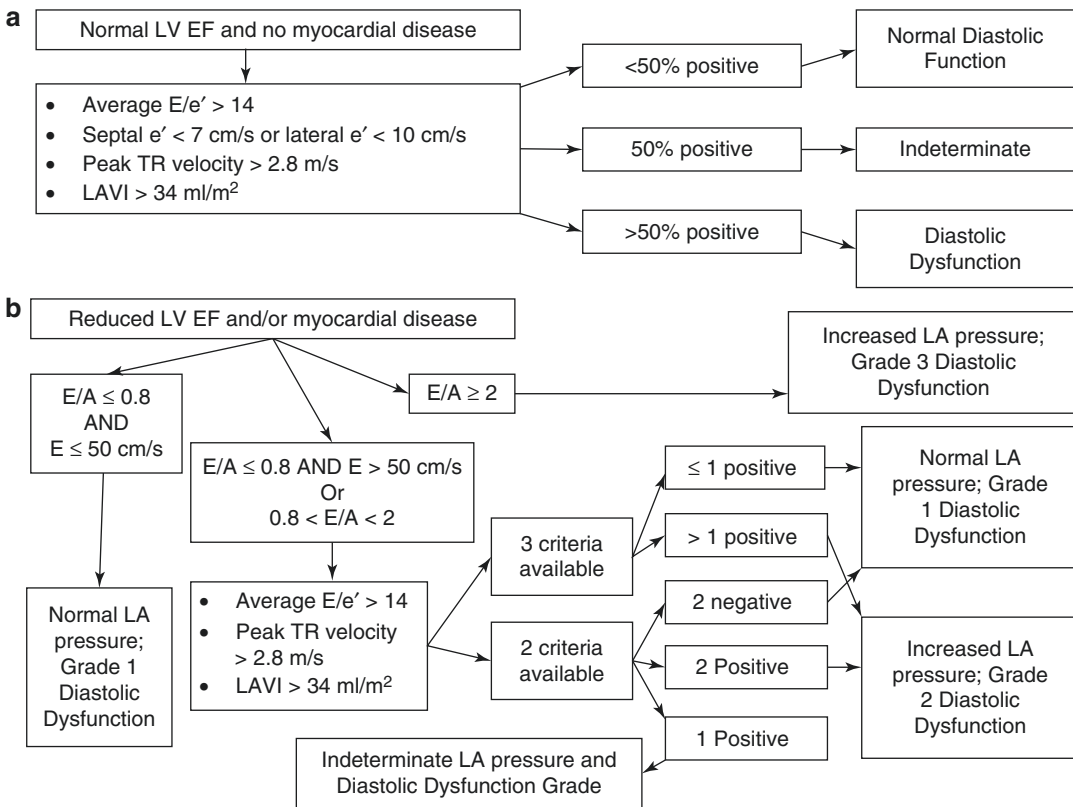


Fig. 6.19 Algorithms for assessment of left atrial pressure and diastolic function. **(a)** Algorithm for assessment of diastolic function in patients without myocardial disease and with a normal LV EF. **(b)** Algorithm for assessment of left atrial pressure and diastolic dysfunction grade

in patients with a reduced LV EF and/or myocardial disease. *LV EF* left ventricular ejection fraction, *TR* tricuspid regurgitation, *LAVI* left atrial volume index, *LA* left atrial. Adapted from Nagueh et al. [10]

across valves, and the degree of regurgitation of valves. To understand how this quantification works, a basic understanding of the principles of flow is necessary. In the following sections, basic principles of flow will be reviewed. These basic principles will be elaborated upon further in upcoming chapters on valvular heart disease.

The Bernoulli Equation

A simplified version of the Bernoulli equation is frequently utilized in echocardiography to calculate the peak pressure gradient across an orifice (such as a stenotic or regurgitant heart valve) from

a velocity measurement. The simplified Bernoulli equation defines the pressure difference between two locations by the following equation where P is pressure difference and v is velocity:

$$P = 4v^2$$

The velocity, v , is assessed by CW Doppler. For example, to calculate a peak gradient across a stenotic heart valve the peak velocity across that valve obtained by CW Doppler is used in the simplified Bernoulli equation [13].

The Continuity Equation

The continuity equation is based on the principle that in a closed circuit, the flow through two separate points must be equal. Flow is

calculated by the following equation where Q is flow, A is cross-sectional area, and v is velocity:

$$Q = A \times v$$

Since the velocity of blood flow changes throughout the cardiac cycle, stroke volume (SV) is frequently used in the continuity equation. The SV is the volume of blood to pass through the heart during systole and is typically measured at the level of the LVOT [13]. It is calculated from the following formula where A is the cross-sectional area and VTI is the velocity time integral:

$$SV = A \times VTI$$

The VTI is measured by tracing the outer shell of a PW or CW Doppler signal. The cardiac output (CO) can next be calculated by the following formula where HR is the heart rate in beats per minute:

$$CO = SV \times HR$$

The continuity equation states that SV_1 and SV_2 must be equal where SV_1 is the stroke volume at point A and SV_2 is the stroke volume at point B and points A and B are locations in a closed circuit. Therefore:

$$SV_1 = SV_2$$

$$A_1 \times VTI_1 = A_2 \times VTI_2$$

For example, the continuity equation can be used to calculate the area of the aortic valve (AV) in aortic stenosis by calculating the LVOT cross sectional area, the LVOT VTI, and the AV VTI and solving for the AV area. In the equation below A_1 and VTI_1 are LVOT measurements and A_2 and VTI_2 represent the aortic valve:

$$A_2 = (A_1 \times VTI_1) / VTI_2$$

The LVOT is presumed to be a circular structure for this measurement and its cross-sectional

area is calculated by the following formula where D is the diameter of the LVOT:

$$A = D^2 (\pi / 4)$$

The LVOT VTI is measured from a PW Doppler signal taken at the same level as the measurement of the LVOT diameter. The AV VTI is measured from a CW Doppler signal across the AV.

Limitations of Measurements and the Need for Quality Control

Quantitative echocardiographic measurements have several general limitations which can be minimized by careful optimization of the echocardiographic image prior to making measurements and by attention to detail when measurements are performed. Measurements of LV size and function by 2D are limited by the ability to accurately define endocardial borders and by assumptions they make about LV geometry and function. When adequate images can be obtained, 3D measurements of LV size and function are generally preferred because they are not limited by geometric assumptions. However, 3D measurements are limited by image quality and are not feasible for all patients. Doppler measurements of velocity are limited by the ability to align the Doppler beam parallel to blood flow or tissue motion. Further details of the limitations of specific measurements and common pitfalls to be avoided when making measurements can be found in the sections of this chapter specific to a given measurement.

Quality control in an echo laboratory is essential to maintain a high standard of practice. Quality control encompasses multiple domains including patient selection, performance of the exam, interpretation of the exam, and timely reporting of exam results which have been addressed in detail by the European Society of Echocardiography [14]. Specifically as relates to echocardiographic measurements, periodic assessment of the accuracy of echocardiographic measurements when compared with those obtained by other imaging techniques and periodic assessment of intra- and inter-observer variability in measurements are recommended. Additionally, maintaining echo lab

accreditation, following societal guidelines for echocardiographic measurements, and participation in continuing medical education by sonographers and physicians are all important aspects of quality control [14].

Conclusion

Echocardiographic measurements are widely relied upon for assessment of cardiac structure and function. In many instances, such as in heart failure or valvular heart disease, they have a significant impact on clinical decision making in patient care. Therefore, it is imperative that they are as accurate as possible. Obtaining accurate echocardiographic measurements requires careful attention to detail when optimizing the echocardiographic image and when performing measurements on that image. It also requires a thorough understanding of the strengths and limitation of each measurement, so that measurements are only performed when they are expected to be accurate and so that when there is a choice between several different methods for making a quantitative assessment, the optimal method for a given patient is selected.

References

- Lang RM, Badano LP, Mor-Avi V, Afilalo J, Armstrong A, Ernande L, et al. Recommendations for cardiac chamber quantification by echocardiography in adults: an update from the American Society of Echocardiography and the European Association of Cardiovascular Imaging. *J Am Soc Echocardiogr*. 2015;28:1–39 e14.
- Lang RM, Bierig M, Devereux RB, Flachskampf FA, Foster E, Pellikka PA, et al. Recommendations for chamber quantification: a report from the American Society of Echocardiography's guidelines and standards committee and the chamber quantification writing group, developed in conjunction with the European Association of Echocardiography, a branch of the European Society of Cardiology. *J Am Soc Echocardiogr*. 2005;18:1440–63.
- Mulvagh SL, Rakowski H, Vannan MA, Abdelmoneim SS, Becher H, Bierig SM, et al. American Society of Echocardiography consensus statement on the clinical applications of ultrasonic contrast agents in echocardiography. *J Am Soc Echocardiogr*. 2008;21:1179–1201; quiz 1281.
- Dorosz JL, Lezotte DC, Weitzenkamp DA, Allen LA, Salcedo EE. Performance of 3-dimensional echocardiography in measuring left ventricular volumes and ejection fraction: a systematic review and meta-analysis. *J Am Coll Cardiol*. 2012;59:1799–808.
- Oh JK, Seward JB, Tajik AJ. *The echo manual*. Philadelphia: Lippincott Williams & Wilkins; 2006. p. 130–46.
- Baumgartner H, Hung J, Bermejo J, Chambers JB, Evangelista A, Griffin BP, Iung B, Otto CM, Pellikka PA, Quinones M. Echocardiographic assessment of valve stenosis: EAE/ASE recommendations for clinical practice. *Eur J Echocardiogr*. 2009;10:1–25.
- Rudski LG, Lai WW, Afilalo J, Hua L, Handschumacher MD, Chandrasekaran K, et al. Guidelines for the echocardiographic assessment of the right heart in adults: a report from the American Society of Echocardiography endorsed by the European Association of Echocardiography, a registered branch of the European Society of Cardiology, and the Canadian Society of Echocardiography. *J Am Soc Echocardiogr*. 2010;23:685–713; quiz 786–688.
- Nagueh SF, Appleton CP, Gillebert TC, Marino PN, Oh JK, Smiseth OA, et al. Recommendations for the evaluation of left ventricular diastolic function by echocardiography. *J Am Soc Echocardiogr*. 2009;22:107–33.
- Hurrell DG, Nishimura RA, Ilstrup DM, Appleton CP. Utility of preload alteration in assessment of left ventricular filling pressure by Doppler echocardiography: a simultaneous catheterization and doppler echocardiographic study. *J Am Coll Cardiol*. 1997;30:459–67.
- Nagueh SF, Smiseth OA, Appleton CP, Byrd BF III, Dokainish H, Edvardsen T, et al. Recommendations for the evaluation of left ventricular diastolic function by echocardiography: an update from the American Society of Echocardiography and the European Association of Cardiovascular Imaging. *J Am Soc Echocardiogr*. 2016;29:277–314.
- Prioli A, Marino P, Lanzoni L, Zardini P. Increasing degrees of left ventricular filling impairment modulate left atrial function in humans. *Am J Cardiol*. 1998;82:756–61.
- Klein AL, Tajik AJ. Doppler assessment of pulmonary venous flow in healthy subjects and in patients with heart disease. *J Am Soc Echocardiogr*. 1991;4:379–92.
- Quinones MA, Otto CM, Stoddard M, Waggoner A, Zoghbi WA. Recommendations for quantification of doppler echocardiography: a report from the doppler quantification task force of the nomenclature and standards committee of the american society of echocardiography. *J Am Soc Echocardiogr*. 2002;15:167–84.
- Popescu BA, Andrade MJ, Badano LP, Fox KF, Flachskampf FA, Lancellotti P, et al. European Association of Echocardiography recommendations for training, competence, and quality improvement in echocardiography. *Eur J Echocardiogr*. 2009;10:893–905.

Myocardial Deformation Imaging

7

Alaa Mabrouk Salem Omar
and Partho P. Sengupta

Global and regional assessment of myocardial functions represents the most frequent indication for an echocardiography. Parameters such as fractional shortening, ejection fraction (EF), etc., have been developed to assess global myocardial contractile function. Regional functional assessment is also important particularly in the context of coronary heart disease management. LV function assessments still remain largely dependent on two-dimensional (2D) echocardiography either quantitatively by the biplane method of discs used to calculate LV ejection fraction (EF), or qualitatively using visual assessment of EF and regional wall motion. However, the inherent subjectivity in visual assessment of EF and the inconsistencies in manual estimation using the biplane Simpson's method could potentially lead to inconsistent therapeutic decisions [1, 2]. Moreover, these methods are influenced by the loading conditions, thus do not really represent true reference measures of myocardial contractility.

Myocardial deformation imaging represents a novel and more accurate technique for the assess-

ment of regional and global myocardial functions. The concept of deformation imaging relies upon the characteristic orientation of myocardial fibers and the resultant mechanical properties.

Anatomical Basis and Basic Measurements

Myocardial fibers are a three-dimensional continuum that change orientation gradually from a subendocardial right-handed helix with positive angles, to a subepicardial left-handed helix with negative angles (Fig. 7.1). Because of this unique fiber arrangement, the LV undergoes complex multi-dimensional deformation in the longitudinal, radial and circumferential directions. During contraction, myocardial deformation is in the form of shortening in the longitudinal and circumferential directions and thickening in the radial direction (Fig. 7.2). Moreover, as a result of their anatomical arrangement and the fixed pericardial space, myofibers also slide over each other creating shear deformation. Shear deformation can occur in the circumferential-radial, longitudinal-radial, and circumferential-longitudinal planes [3]. The largest shear deformation occurs in the circumferential-longitudinal plane and is visually identified as LV twist which resembles the wringing of a cloth to squeeze out water (Fig. 7.2b). In the subepicardium, this twist aids contraction in the principal fiber direction. In the subendocardium, the torque enhances shortening in the

A. M. S. Omar
Icahn School of Medicine at Mount Sinai, Division of
Cardiology, New York, NY, USA

BronxCare Hospital Center, Department of Internal
Medicine, Bronx, NY, USA

P. P. Sengupta (✉)
Section of Cardiology, West Virginia University
Health Sciences Center, Morgantown, WV, USA
e-mail: partho.sengupta@hsc.wvu.edu

Fig. 7.1 Myocardial fibers arrangement. (a) The sub-endocardial fibers (inner) are arranged as a right handed helix, and the sub-epicardial fibers (outer) are arranged as a left handed helix. (b) Blunt dissection tissue specimen showing the right handed positive angle the subendocardial myofibers, (c) blunt dissection tissue specimen showing the left handed negative angle the subepicardial myofibers From [3] with permission

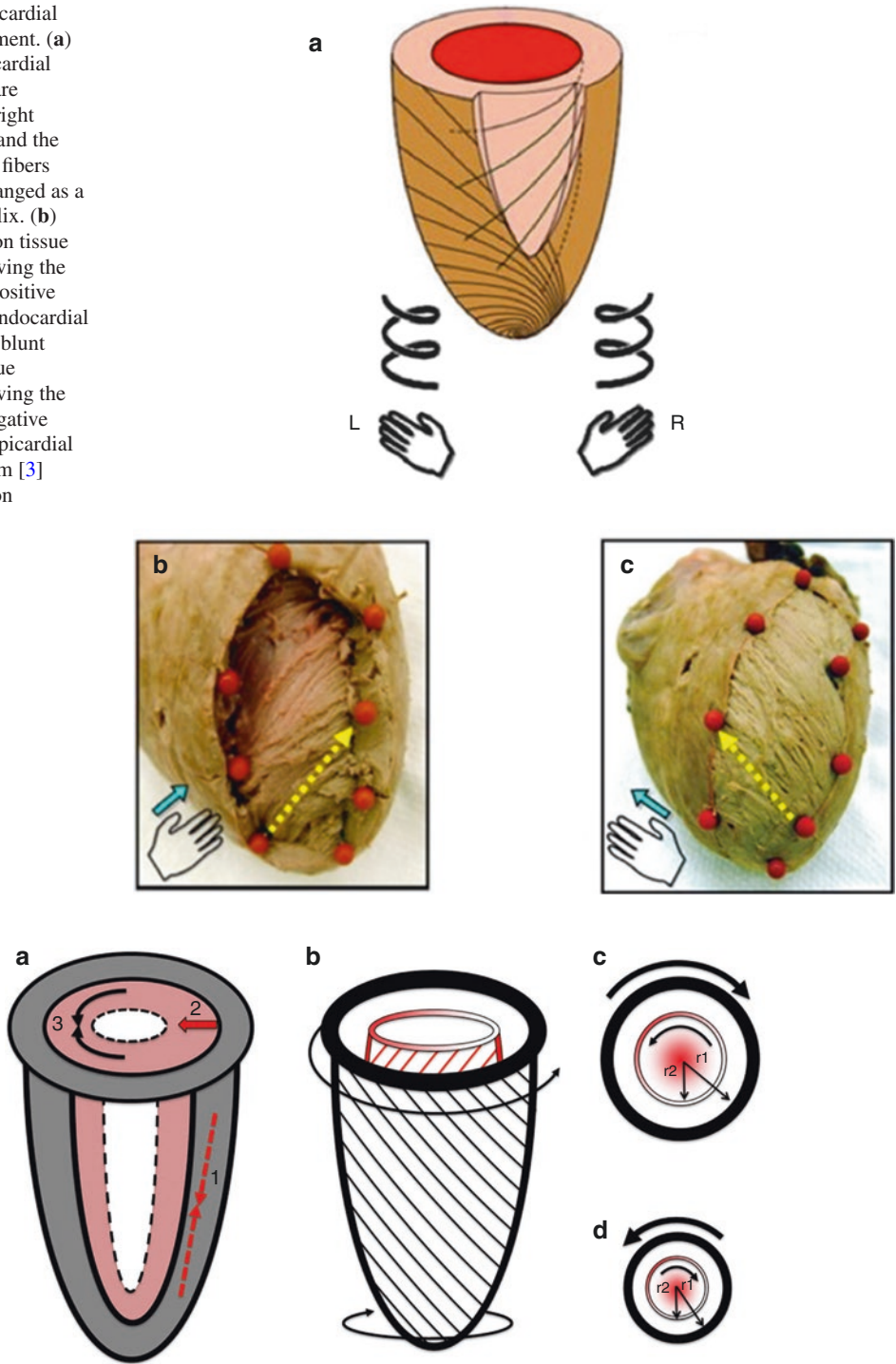


Fig. 7.2 Myocardial deformation in different directions. (a) LV deforms in the form of longitudinal and circumferential directions and thickening in the radial direction. (b) In addition, LV rotates basally in the clockwise direction and apically in the counter clock wise direction causing

LV twist. (c, d) The fiber direction of endocardial and epicardial layers cause them to rotate in different directions, however because the radius of the epicardial helix (r_1) is bigger than that of the endocardial layer (r_2) rotation of the LV follows the epicardial fibers

circumferential direction causing more radial thickening than what would be expected from contraction alone. Moreover, in the subendocardium, this torque causes fiber rearrangement such that subendocardial fibers are sheared toward the LV cavity for LV wall thickening, whereas the LV base is pulled toward the apex, shortening the longitudinal axis of the LV [4].

Thus, the outcome of this complex deformation is that contraction of the subendocardial fibers is more associated with longitudinal shortening. On the other hand, contraction of the subepicardial fibers is more associated with circumferential shortening. Radial thickening represents the sum of deformations of both the subepicardial and subendocardial deformations in the radial directions. Finally, despite that both layers contribute to rotational mechanics, directions of rotation of the LV base and apex follow those of the subepicardial layer because of the larger radius of rotation.

In summary:

The LV exhibits three-dimensional (3D) LV deformation for which:

1. *Longitudinal and circumferential shortening and radial thickening, in addition to shearing in the circumferential-radial, longitudinal-radial, and circumferential-longitudinal planes, represent deformation.*
2. *The circumferential-longitudinal shear deformation is identified as LV rotational mechanics (LV twist).*
3. *Endocardial fibers are more associated with longitudinal mechanics, while epicardial fibers are more associated with circumferential mechanics. Radial deformations represent the sum of subendocardial and subepicardial deformations in the radial direction. Despite that both layers contribute to LV rotational mechanics, the directions of rotation follow those of the epicardial layer because of the larger radius.*

Deformation Parameters

Several parameters can be used to describe myocardial motion and deformation in all directions and can potentially assess global and regional

myocardial function (Table 7.1). These parameters include measurements of displacement, velocity, strain, strain rate, rotation and torsion.

If a moving object changes its position overtime however all its parts move in the same velocity, the object is said to have undergone “displacement”. If, however, different parts of the object move but with different velocities, the object changes shape and is said to have undergone “deformation.”

Thus, parameters available for assessment of myocardial mechanics should be classified into two distinct categories; first, parameters that can assess myocardial wall motion (displacement and velocity); and, second, parameters that can assess myocardial wall deformation (strain, strain rate, and torsion) [3–11]. Unlike displacement and velocity, strain and strain rate have the advantage of being able to characterize regional myocardial function independent of translational motion, and to differentiate between active and passive myocardial tissue movements.

Velocity and Displacement

By definition, displacement is the vector difference between the starting and the ending positions of a moving object. This object in echocardiography would be the myocardial region of interest (ROI). Velocity, on the other hand, is the rate at which displacement changes with time. Displacement (in centimeters or millimeters) is used to describe how far a myocardial segment moves from an initial point in a certain direction and velocity (in cm/s) is used to describe how fast the myocardium moves in that particular direction.

During systole, ventricular myocardium travels towards apex, thus systolic LV velocities are positive. On the other hand, during diastole the myocardial returns back to its initial position, thus velocities are negative.

Myocardial velocities and displacement can also be measured for the left atrium (LA), but because LV phases are opposite to those of the LV, their values are opposite to those of the LV.

In order to record velocities with high temporal resolution, especially in fast occurring phases of the cardiac cycle, high frame rates of recording is needed. Pulsed tissue Doppler offers the highest temporal resolution suitable for recording veloci-

Table 7.1 Different echocardiographic measurements used to assess myocardial deformation

	Definition	Parameters
Displacement (cm)	Distance of a myocardial segment from its initial position	Longitudinal displacement Radial displacement Circumferential displacement
Velocity (cm/s)	Velocity of displacement (displacement/time)	Longitudinal velocity Radial velocity Circumferential velocity
Strain (%)	Change in length of an object within a certain direction relative to its baseline length (L_0-L_1/L_0)	Global longitudinal strain (GLS) Global radial strain (GRS) Global circumferential strain (GCS)
Strain rate (s^{-1})	The speed of deformation (i.e. strain)	Peak systolic global longitudinal strain rate (GLS- R_s) Early diastolic global longitudinal strain rate (GLS- R_E) Late diastolic global longitudinal strain rate (GLS- R_A) Peak systolic global radial strain rate (GRS- R_s) Early diastolic global radial strain rate (GRS- R_E) Late diastolic global radial strain rate (GRS- R_A) Peak systolic global circumferential strain rate (GCS- R_s) Early diastolic global circumferential strain rate (GCS- R_E) Late diastolic global circumferential strain rate (GCS- R_A)
Rotation	Outcome of contraction of the helically arranged myocardial fibers causing counter-clockwise rotation of the apex and clockwise rotation of the base as viewed from the apex	Peak systolic apical rotation (apical-R) Peak systolic basal rotation (basal-R) LV twist (LVT) LV torsion (LV- <i>tor</i>) Percentage of LV untwist at mitral valve opening (%LV-UT-MVO) LV untwist rate (LV-UTR) Time to peak untwist (TTP-UT)

ties at the mitral annulus, and color tissue Doppler usually offers relatively lower frame rates, however, offers the option of recording myocardial, rather than mitral annular, velocities.

strain, however, the most used in echocardiography is the Lagrangian strain (S_L) equation in which the end-systolic length of a myocardial segment (L) is compared to the initial length [the end-diastolic length (L_0)], and is defined as:

$$S_L = \frac{L - L_0}{L_0} \times 100(\%)$$

Strain and Strain Rate

Strain

The term “strain” is usually used in physics to describe “stretching” of a segment. In echocardiography strain is used to describe “deformation” of myocardial segments [12]. The knowledge of tissue motion allows computing the tissue strain that measures the effective local tissue deformation. Different equations can be used to calculate

Strain can be computed taking a tissue segment of length L along any specified direction. When this segment is taken along the longitudinal direction it gives the *longitudinal* strain or *circumferential* strain when it is taken along the circumference, or it is the *radial* strain when the length is taken over the thickness.

When a myocardial segment gets smaller (contracting) strain has negative values, while when a myocardial segment becomes longer (e.g. stretching or thickening) strain has positive values. Because the left ventricle shortens longitudinally and circumferentially and thickens radially, peak LV systolic longitudinal and circumferential strains are negative while radial strain is positive. For example, if the initial segment length is 10 mm and it shortens longitudinally to 8 mm, the longitudinal strain is -20% .

Strain Rate

As velocity is for displacement, strain rate (SR) is the rate at which strain changes over time, and can be calculated from Lagrangian strain follows:

$$SR_L = \frac{dS}{dt} = \frac{1}{L_0} \frac{dL}{dt} (s^{-1})$$

Because strain rate reflects the instantaneous change in strain over time, irrespective of the starting point, Lagrangian strain-rate, which involves measurements at initial length (L_0), is not commonly used. Instead, a physically congruous equation for strain rate (natural strain-rate, or SR_N) is used:

$$SR_N = \frac{1}{L} \frac{dL}{dt} (s^{-1});$$

where L is the rate of shortening relative to the actual length of the tissue, independently from its original length.

We can summarize then that Lagrangian strain (S_L) and natural strain rate (SR_N) are the most frequently used parameters in assessment of cardiac mechanics.

LV Rotation and Twist

Another characteristic deformation of the left ventricle is torsion or twist results from LV apical and basal opposite rotatory movement that resembles the wringing of a towel to squeeze out water. The structural mechanism of LV twist lies in the counter-directional subendocardial right-handed and subepicardial left-handed helical arrangement of myocardial fibers that result in sliding of the sheets of fibers over one-another causing shear deformation (Fig. 7.3) [3]. Shear deformation in the circumferential-longitudinal plane and is called as LV twist.

Because of its geometrical helical shape, the contraction of the subepicardial fibers would rotate the apex counterclockwise and the base clockwise (Fig. 7.2), whereas contraction of sub-

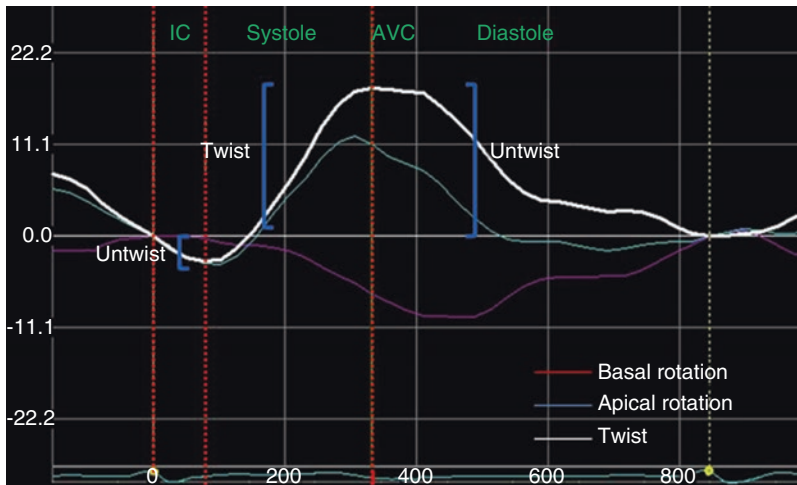


Fig. 7.3 LV rotation mechanical events during the cardiac cycle. During isovolumic contraction (IC), the LV exhibits brief untwist (clockwise rotation of the apex and counterclockwise rotation of the base) which is followed by twist during ejection (counterclockwise rotation of the

apex and clockwise rotation of the base). This is followed by the recoil, i.e. untwist (clockwise rotation of the apex and counterclockwise rotation of the base) that starts in IVR and continues into early diastole

endocardial fibers would rotate the apex and base in exactly the opposite directions. The reason these opposing forces do not cancel out is due to the greater rotational radius of the outer epicardial layer which exerts a larger lever arm force and therefore, dominates the overall direction of rotation (Fig. 7.2c, d).

During isovolumic contraction (IC), the LV exhibits brief untwist (clockwise rotation of the apex and counterclockwise rotation of the base) which is followed by twist during ejection (counterclockwise rotation of the apex and clockwise rotation of the base). This is followed by the recoil, i.e. untwist (clockwise rotation of the apex and counterclockwise rotation of the base) that starts in IVR and continues into early diastole (Fig. 7.3) [4].

Terminologies and definitions commonly used for describing the features of LV twist mechanics are shown in Table 7.1. Importantly, it is not uncommon to use the terms torsion and twist interchangeably to describe LV rotational mechanics, despite that they have different definitions. LV *twist* (expressed in degrees or radians) refers to the absolute difference in the magnitude of apical and basal rotation, and LV *torsion* (in degrees or radians per centimeter) refers to the normalized twist, where the twist angle is divided by the distance between the cross-sectional planes of the LV at the base and apex.

Echocardiographic Assessment of Myocardial Deformation

Echocardiographic deformation imaging was first introduced as a post-processing feature of tissue Doppler imaging (TDI) with velocity data converted to strain and strain rate. Strain imaging information has more recently also been derived from tissue tracking technologies that can be applied to cardiac magnetic resonance and echocardiography. Echocardiographic tissue tracking relies on the computer processing of speckle tracking. Table 7.2 summarizes advantages and

Table 7.2 Advantages and disadvantages of the different echocardiographic methods used for tissue tracking

	Advantages	Disadvantages
TDI	<ul style="list-style-type: none">– Very high frame rates– Good in the assessment of longitudinal velocities	<ul style="list-style-type: none">– Extremely angle independent– Not suitable for assessment of deformation in the circumferential and radial directions as well as rotations
2D-STE	<ul style="list-style-type: none">– Less angle independent– Easy and handy bedside tool	<ul style="list-style-type: none">– Quality of tracking is better in proximal than distal speckles– Through plane motion– Inability of simultaneous assessment of deformations in all directions– Depends on ultrasound quality
3D-STE	<ul style="list-style-type: none">– Simultaneous assessment of all direction– More speckles in the pyramidal sample	<ul style="list-style-type: none">– Limited spatiotemporal resolution– Depends on ultrasound quality– Relative complexity of offline image processing

limitations of different echocardiographic methods that can be used for deformation images.

Tissue Doppler Deformation Imaging

Spectral pulsed tissue Doppler as well as color tissue Doppler can be used as tools for myocardial tissue tracking to assess segmental and global myocardial velocities and deformation (Figs. 7.4 and 7.5).

The greatest advantage of tissue Doppler imaging is the high recording frame-rates which makes tissue Doppler currently still the echocardiographic method capable of studying myocardial deformation with the highest possible temporal resolution. TDI of the mitral annular (Fig. 7.4) has been, and still is, used as a method of assessment of the overall longitudinal LV functions.

Fig. 7.4 Spectral tissue Doppler imaging (TDI) of the septal mitral annulus

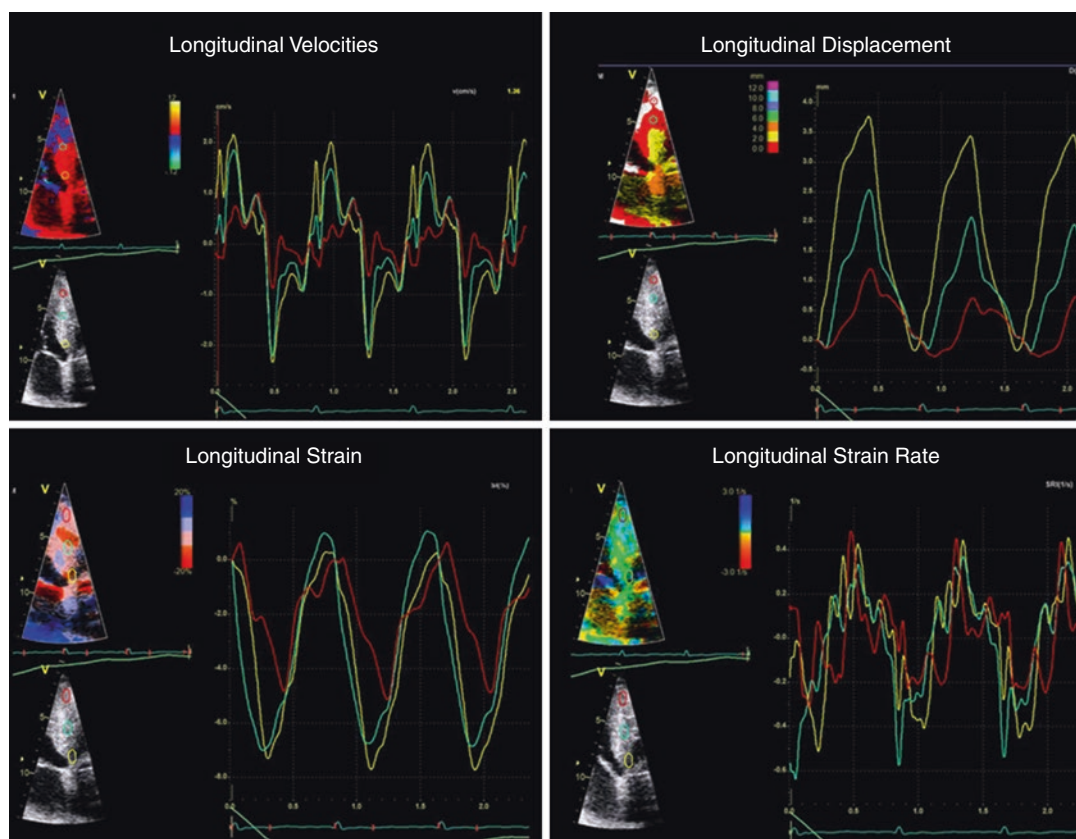
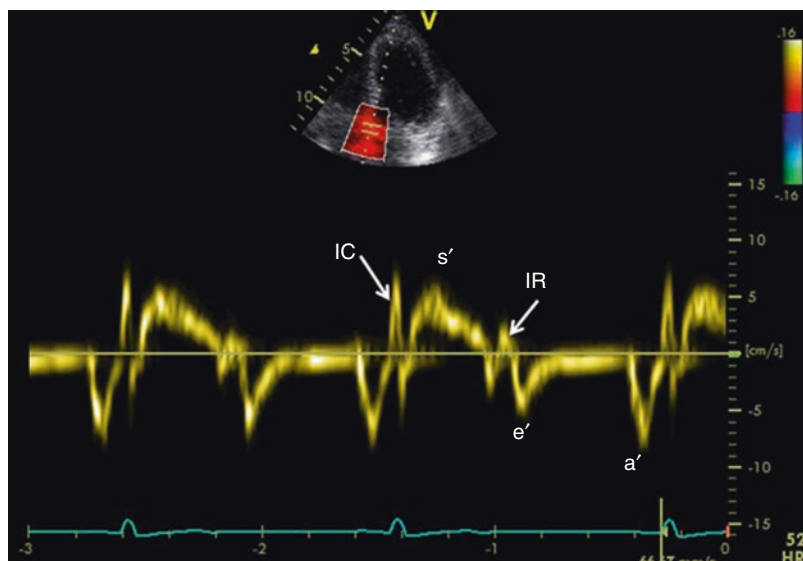


Fig. 7.5 The use of color color tissue Doppler imaging (TDI) to derive LV longitudinal deformations (velocities, displacement, strain, and strain rate) in apical 4-chamber view

On the other hand, color tissue Doppler imaging can assess segmental as well as global assessments of all myocardial deformation parameters.

In addition to myocardial velocity and displacement, the first description of echocardiographic strain was derived from TDI velocity data using the Doppler equation. Strain rate also could be calculated using color TDI velocity data using the equation ($SR = V1 - V2/L$), where SR is the strain rate, V1 is the velocity at point 1, V2 is the velocity at point 2, and L = length of the ROI between (distance between the points where V1 and V2 were measured, and is usually set by default to 10 mm).

Precautions While Acquiring TDI

Spectral Pulsed TDI

1. ROI size and position should be set to remain inside the myocardium throughout the cardiac cycle.
2. Scale and baseline and sweep speed should be adjusted so that the signal fills most of the display while taking into consideration the heart rate.
3. Gain should be decreased to values that produce an almost black background with least possible noise.
4. The interrogation must be aligned with the direction of the motion to be interrogated with an angle $<15^\circ$, to decrease velocity underestimation.

Color TDI

1. High frame rates are usually required (>100 frames/s). Thus, depth and sector width should be adjusted to desired area while maximizing the frame rate.
2. Separate acquisitions should be made for each wall from slightly different transducer positions to allow the motion direction to be as parallel and as aligned as possible with the ultrasound beam.
3. Changing the transducer position while recording should be avoided because it creates reverberation artifacts.
4. The velocity scale should be set to a range that avoids aliasing in any region of the myocardium.

5. All efforts must be made to acquire images with similar heart rate.

Strengths of TDI

Because of the high recording frame rate, spectral pulsed TDI has the advantage of online measurements of velocities and time intervals with excellent temporal resolution. The use of such velocities has a proven clinical value especially in the assessment of conditions such as ischemia and diastolic function.

Pitfalls of TDI

1. As with all other Doppler methods, TDI is significantly angle dependent. Thus, can produce significant underestimation of velocities. The significant angle-dependency of TDI made it only useful for measurements of mechanics in the longitudinal direction, while it was not considered useful in assessment of the other components of myocardial deformation.
2. Color Doppler-derived strain and SR are noisy thus, even with expertise and high levels of training interpretation of curves can be significantly time consuming and exhausting.
3. TDI-derived velocities can be affected by cardiac translational motion and movement of adjacent structures and by respiratory variation movements

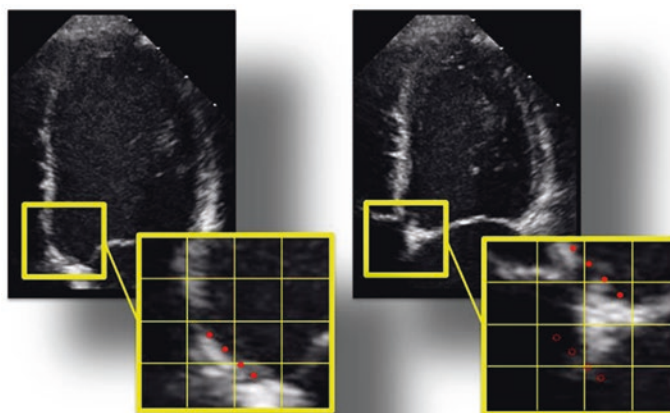
Accordingly, color tissue Doppler is currently not a preferable method of deformation imaging. Other echocardiographic tissue tracking echocardiographic methods like STE are less-angle dependent and can track myocardial segments in all directions.

In Summary

Spectral and color TDI have the highest recording frame rates among all methods of deformation imaging.

1. *TDI mitral annulus is currently effectively used for assessment of LV ischemia and diastolic dysfunction.*
2. *Color TDI can be used for segmental assessments of the LV as well as RV and LA deformation.*
3. *However, TDI is significantly angle dependent, thus can only be used for the assessment in the longitudinal direction.*

Fig. 7.6 Tissue tracking by assessment of patterns along a line. Speckles in the basal septal border of the LV were tracked from end-diastole to end-systole (red solid dots in the left panel, and red empty dots on the right panel) and can be seen to have shifted position upward and towards the cavity (red solid dots on the right panel)



4. *The angle dependency, in addition to the high noise to signal ratio and the great effect of translation motion and respiration made TDI the least popular method that can be used for assessment of segmental and global myocardial deformation.*

Tissue Tracking Deformation Imaging

Studying myocardial deformation is currently possible by tissue tracking technology, which is feasible using echocardiography and cardiac magnetic resonance imaging (CMR). However, the lower temporal resolution of CMR, in addition to its higher cost, and contraindication of magnetism in patients with pacemaker and intra-cardiac defibrillator implantations, give advantages for echocardiography over CMR as a simple handy tool for tissue tracking.

Tissue tracking refers to methods of identifying a pattern along a line or in a region of interest (ROI) on a specific image and recognizing the same pattern within subsequent images or frames (Fig. 7.6).

The definition of ROI in this context is very important. A complete myocardial ROI (Fig. 7.7) is the part of the myocardium defined at the end-diastole by the endocardial border as its inner con-

tour and the epicardial border as its outer contour. Myocardium in-between is defined by an axis between both borders, i.e. the middle ROI axis.

Both the endocardial and epicardial contours can be either manually user-identified or automatically tracked with the possibility to edit them manually, if needed.

Different generations of the software appear to have different ROI defaults. Some software versions use the border detection (Fig. 7.8a) and others use full thickness assessments (Fig. 7.8b). Software versions that depend on border detection are capable of endocardial and epicardial contouring. Because the inclusion of pericardium within the ROI may result in reduction of measured strains, epicardial border is usually not drawn, thus the measurements typically refer to the single endocardial border.

Software versions that depend on the assessment of the full thickness of the myocardial wall usually do so by averaging measurements obtained over the full myocardial thickness which are typically represented with the mid-wall line as a reference of full wall thickness (Fig. 7.8b).

Finally, tissue tracking application is possible using two-dimensional speckle tracking (2D-STE) and three-dimensional speckle tracking (3D-STE) (see below).

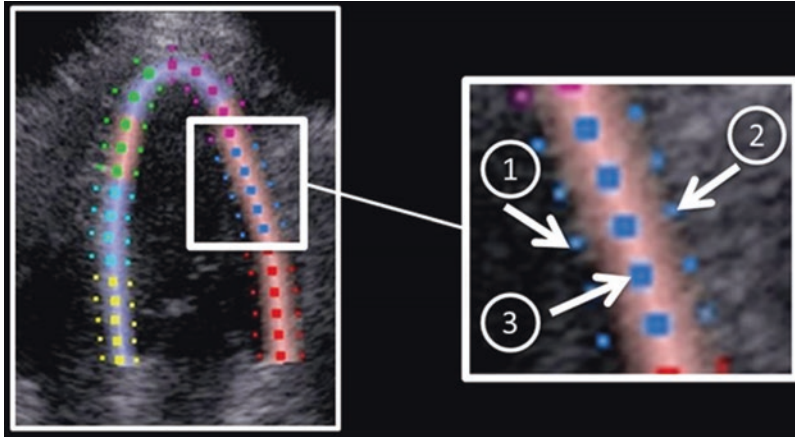


Fig. 7.7 Boundaries of a region of interest (ROI) used for speckle tracking. On left panel, the whole LV is shown after manual speckle tracking, on the right panels, the inner boundary represents the endocardial border (arrow

1), the outer boundary represents the epicardial border (arrow 2), and the myocardium in-between is represented by a middle line (arrow 3)

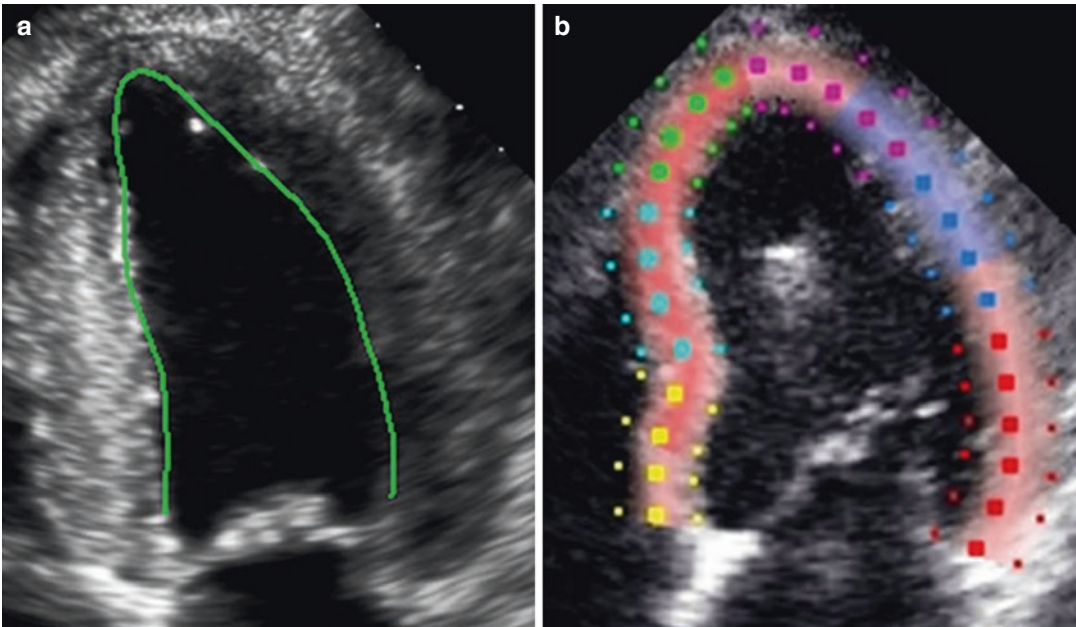


Fig. 7.8 Examples of methods used for tissue tracking. (a) Endocardial border tracking, (b) full thickness tracking

In summary:

Tissue tracking detects a pattern in a ROI in a specific frame and tracks in subsequent frames

1. A complete myocardial ROI is composed of endocardial border as its inner contour, epicardial border as its outer contour and axis between both borders defining the myocardium.

2. Some software versions derive deformation parameters by tracking the endocardial border and others average values for the whole myocardial thickness by tracking the mid-wall line
3. Tissue tracking application is feasible for both 2D and 3D images.

Two-Dimensional Speckle Tracking Echocardiography

In 2004, a tissue tracking echocardiographic application that can be used to assess myocardial mechanics was introduced and was called speckle-tracking echocardiography (STE). 2D-STE is a gray-scale based technique which is angle-independent and hence permits more comprehensive assessment of myocardial deformation. STE depends on the

anisotropic acoustic properties of the myocardium, which is caused by the presence of myocardial patterns of constructive-destructive interferences that are seen in the image as granular noise of bright and dark dots, or the so called speckle noise. Speckles are stable acoustic markers that can be tracked by STE software on a frame-by-frame basis in different directions (Fig. 7.9) and can be used to generate strain and strain rate curves (Fig. 7.10).

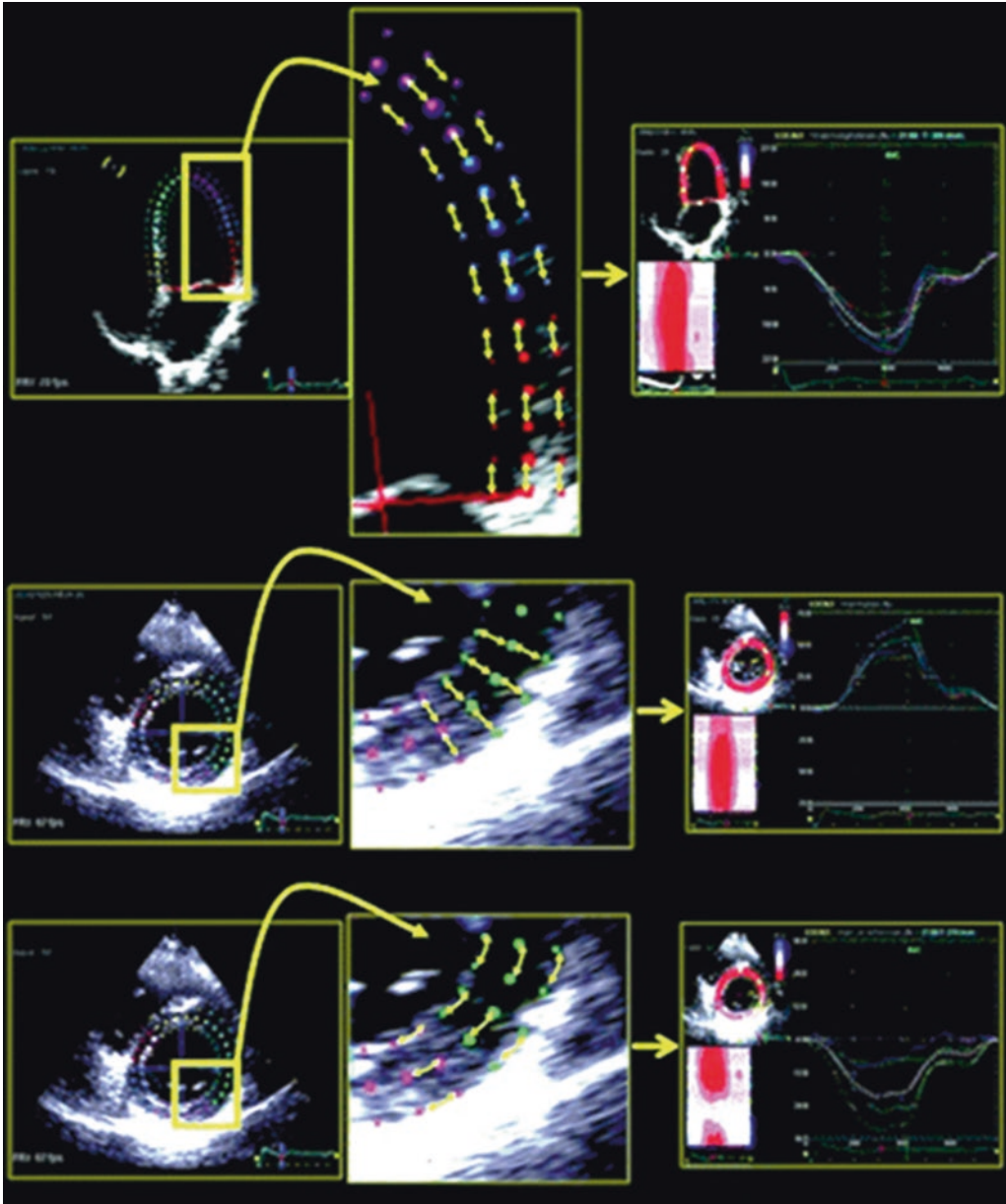


Fig. 7.9 Representation of the use of 2D-STE in the tracking of speckles in different directions to derive strain curves. From [13]; with permission

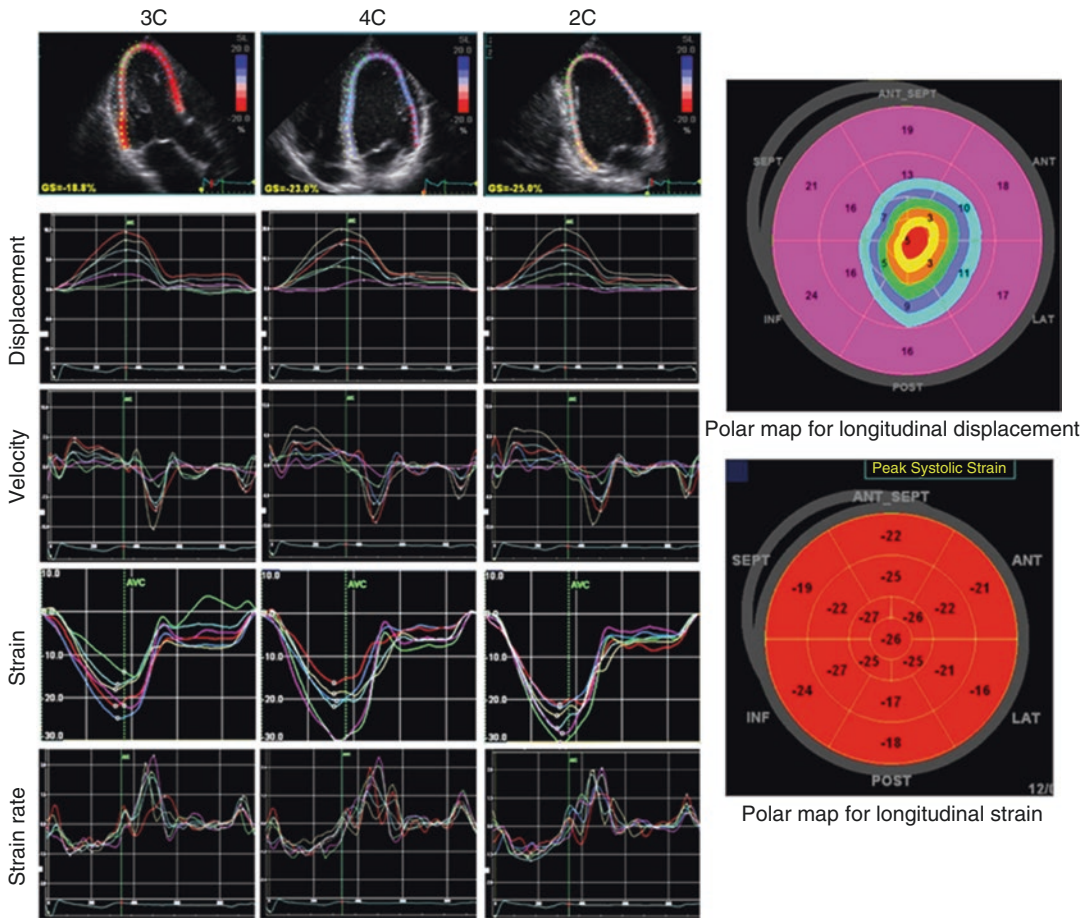


Fig. 7.10 The use of 2D-STE to derive LV longitudinal deformations (velocities, displacement, strain, and strain rate) in apical; 4-chamber view

Precautions in 2D STE Image Acquisition

1. Image acquisition should be done with frame rates between 50 and 80 frames/s. Higher frame rates might be needed in case of tachycardia.
2. If values are to be averaged from different views, all tracked views must have the same frame rate.
3. Extra care should be paid to avoid apical 4-chamber and short axis views foreshortening. This is because inaccuracies in longitudinal strain measurements arise from apical 4-chamber foreshortening and rotational mechanics variables are seriously affected by foreshortening of the apical short axis level.
4. Sector depth and width should be adjusted so that the whole LV is included with least possible, if any, outside the ROI.

5. Artifacts that resemble speckle patterns should be avoided because they will influence the quality of tracking.
6. Similarly, the short-axis cuts of the left ventricle should be circular shaped to assess the deformation in the anatomically correct circumferential and radial directions.

Advantages and Strengths

1. 2D-STE is relatively cheap and readily available at the bedside
2. Compared to TDI, 2D-STE is relatively an angle independent method capable of characterizing myocardial deformations.
3. Image acquisition with appropriate resolution and sufficient frame rate allows tracking of the motion of the speckles throughout the cardiac cycle to derive deformation parameters (Table 7.2).

While TDI is limited to the measuring deformation in relation to the probe, 2D-STE allows measurement in all directions including of circumferential and radial components irrespective of the direction of the beam.

Potential Pitfalls and Technical Considerations

1. 2D-STE is greatly dependent on the image quality, making it difficult in instances of poor echogenic windows, ultrasound dropouts and reverberations.
2. Through plane motion is the out-of-plane motion of speckles that particularly occurs at the short axis when the base descends toward the apex in systole (Fig. 7.11). Through plane motion is a particular disadvantage, because, even with the best image quality, 2D-STE is unable to track speckles that fall out of plane in subsequent tracking frames.
3. In addition, because the quality is worse in the distal parts of the ultrasound sector, speckles that are proximally located produce better tracking quality [5].
4. Despite that compared to TDI, STE is less affected by the angle or the ultrasound beam, 2D-STE is not completely angle independent.

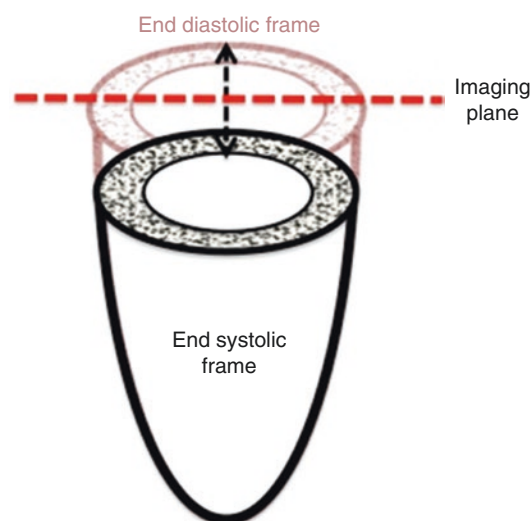
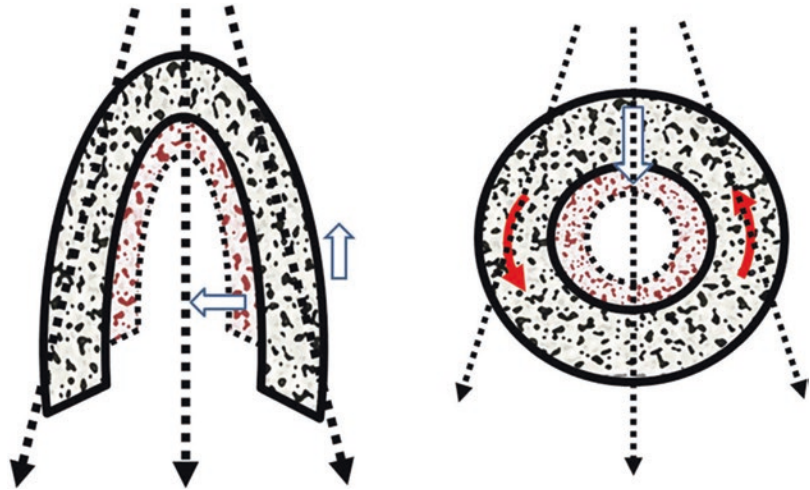


Fig. 7.11 Through-plane-motion. During systole, the basal short axis plane moves apically away from the imaging plane, thus speckles in that plane are not available anymore for tracking

This is because ultrasound images normally have better resolution along the ultrasound beam compared with the perpendicular direction. Thus, speckles are clearer and easier to track in views where their movement is recorded parallel to the insonation angle. Therefore, apical views are more suitable for tracking speckles in the longitudinal direction than the radial direction, while parasternal short axis views are suitable for tracking speckles in the radial as well as the circumferential direction (Fig. 7.12).

5. Selection of frame rates sufficient for tracking usually represents a tradeoff in the clinical settings where increasing the sector width for better spatial resolution will be accompanied with a decrease in frame rates. Moreover, under-sampling at the usual acquisition frame rates is common in patients with tachycardia, and when assessment is required for events occurring in fast phases like isovolumic contraction and relaxation [5].
6. When using STE to measure LV twist, image quality of basal LV short-axis recordings can be a limitation. This is due in part to acoustic problems related to the depth of the basal part of the ventricle and to the wide sector angle that is necessary to visualize the entire LV base.
7. Furthermore, Because LV rotation increases toward the apex, it is important to standardize the apical short-axis view. Apical plane should be captured in as distal plane as possible where a circular apical short-axis can be seen with little or no RV in plane.
8. Global strain might be inaccurate if too many segmental strain values are discarded because of suboptimal tracking.
9. A significant limitation of the current implementation of 2D STE is the differences between hardware and software vendors which creates large variability both for methods of measurements and normal values. The American Society of Echocardiography (ASE) and European Association of Echocardiography (EAE), and the industry have initiated a task force that aims at standardization of the use of 2D-STE deformation imaging among vendors and users.

Fig. 7.12 Effect of insonation angle on myocardial deformation assessment by 2D-STE. Apical views are more suitable for tracking speckles in the longitudinal direction than the radial direction, while parasternal short axis views are suitable for tracking speckles in the radial as well as the circumferential direction



In summary:

Anisotropic acoustic properties of the myocardium create white speckles on black background that can be tracked using 2D-STE.

1. *Advantages: Cheap, available at bedside, angle independent relative to tissue Doppler, can track myocardial deformation in all directions*
2. *Limitations: Dependent on imaging quality, inaccuracies with through plane motion, worse tracking in distal speckles compared to proximal ones, lower frame rates are associated with poorer tracking*

3D Speckle Tracking Echocardiography

With the advancements in matrix-array ultrasound transducers, STE became also possible using three-dimensional echocardiographic techniques (3D-STE). In “full-volume” mode, multiple wedge-shaped sub-volumes are acquired over consecutive cardiac cycles during a single breath hold and reconstructed into one pyramidal volume sample. Within the full volume pyramidal sample, the thicker sector of image acquisition allows for capturing more speckles in the 3D image. Pyramidal data sets are processed using semi-automated 3D STE software, which allows for automatic tracking of the endocardial and epicardial borders after anatomical correction and identification of the apical views. The semiautomatic nature of the software allows for subsequent manual adjustment to

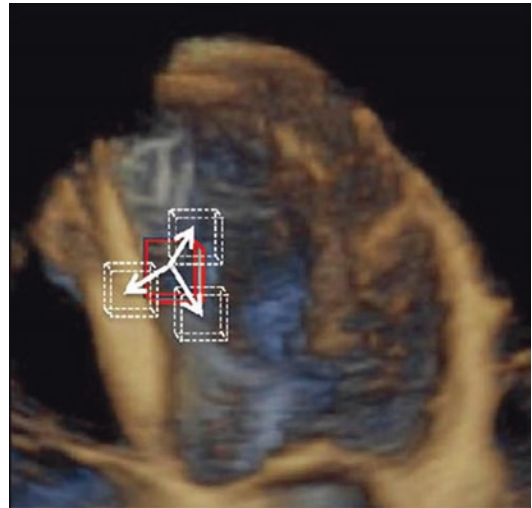


Fig. 7.13 3D full volume image representing the possible directions that can be simultaneously assessed using 3D-STE. From [14]; with permission

the tracked borders if the original boarder detection was suboptimal. Speckles are then tracked in the 3D space throughout the cardiac cycle and regional and global deformation parameters can be calculated similar to 2D-STE.

Unlike 2D-STE, speckles can be tracked simultaneously in all directions to derive all deformation parameters, alleviating the effect of through plane motion and allowing for assessment of speckles blinded to 2D-STE planes (Fig. 7.13).

Potential Pitfalls and Technical Considerations

The major limitations of 3D STE can be listed as follows:

1. 3D-STE assessments are still controversial because of the known limited spatiotemporal resolution. This is because the failure of including the whole LV in the full pyramidal volume has a detrimental effect on temporal resolution. In addition, the need for recording multiple cardiac cycles usually comes on the expense on the frame rate. It is likely, however, that 3D data sets will be acquired in a single-beat mode, allowing imaging at sufficiently high frame rates and thus increasing the 3D-STE resolution.
2. As with 2D-STE, dependency on image quality is a major issue.
3. Low spatial-temporal resolution affects the frame-to-frame tracking ability causing sub-optimal myocardial tracking.
4. Although this methodology has been validated against sonomicrometry and CMR, there is no true noninvasive “gold standard” to validate the use of 3D-STE in humans. Thus, the accuracy and the clinical value of this new technology in a wide variety of clinical scenarios is still questionable

In Summary

1. *3D-STE is feasible and carries the advantage of being able to detect more speckles and, unlike 2D-STE, track them in all directions in the same time alleviating the through plane motion disadvantage of 2D-STE.*
2. *3D-STE, however, suffers great spatiotemporal resolution limitation and validation of values produced is still questionable because there is no real gold standard to compare to. Finally, 3D-STE is still subjected to several 2D disadvantages like the dependence on frame rates and image quality.*

Timing of Mechanical Events

The selection of a reference points in time that represents different mechanical events in the car-

diac cycle is crucial for measurements. End-diastole, characterized by the closure of the mitral valve, is commonly used to delineate the beginning of the cardiac cycle. Marking the frame that precedes mitral valve closure as the beginning of the cardiac cycle is usually used for this purpose. Alternatively, the beginning of the QRS complex or the peak of the R-wave in the ECG can be used as surrogate time markers; however, they may be suboptimal under certain circumstances e.g. conduction disturbances.

Another important time point in the cardiac cycle is the end systole. End-systole coincides with aortic valve closure (AVC), which can be visualized in the parasternal or apical long-axis view. This specific time point usually guides specific measurements being measured during the cardiac cycle. For instance, LV strain is usually measured at ventricular end systole (End-systolic strain). It should be however mentioned that peak systolic strain sometimes occurs in early systole especially in situations where there is regional dysfunction. Moreover, the peak global strain may coincide with AVC, or it may appear after aortic valve closure. In the latter case, it is usually described as ‘post-systolic shortening’.

Segmental vs. Global Strain

Strain values in a specific direction can be expressed in a segmental fashion follows the same geographical assumptions of the 17-myocardial segments used for wall motion score index. Strain then can be averaged to represent strain values for each coronary artery territory, or more commonly, the average of all segmental values of strain in a specific direction represent the global strain, i.e. *global longitudinal strain* is the average of the longitudinal strain values of all segments in apical views, *global circumferential strain* and *global radial strain* are the average of the circumferential and radial strain values, respectively, of all segments in parasternal short axis views.

In a similar fashion, rotation can also be expressed in a segmental fashion in both the basal

and apical short axis views. The average of the segments at the basal level will represent the overall basal rotation and the average at the apical level will represent the overall apical rotation. These values will then be used to calculate twist and torsion.

Principal Strain

Principal strain (PS) is the local magnitude and direction of the outcome of shortening and lengthening deformations (Fig. 7.14). PS is widely applied in structural engineering however is still a new concept in the field of biology and more specifically myocardial mechanics that can simultaneously assess deformations in all directions and thus may simplify the assessment of tissue deformation by circumventing the need for multidirectional strain assessments which usually needs several studies in different 2D-echocardiographic views. The use of 3D-technology for tissue tracking makes it possible to study and assess PS.

Deformation Imaging in Other Cardiac Chambers

Right Ventricle

Because of the complex geometry and because of having heavily trabeculated inner wall contour, the right ventricular (RV) function assessment is usually challenging.

Compared to the LV, the major contributor to overall RV performance is longitudinal shortening of the RV free wall and the interventricular septum.

A simple quantitative approach to assess longitudinal RV function is the measurement of the tricuspid annular plane systolic excursion (TAPSE; Fig. 7.15), which estimates the level of the systolic excursion of the lateral tricuspid valve annulus toward the apex in the four-chamber view. Tricuspid annular plane systolic excursion has demonstrated an excellent correlation

with radionuclide ventriculography-derived RV EF and has proven to be a strong predictor of prognosis in heart failure. Nevertheless, it can be angle dependent especially in the settings of enlarged RV where it might lead to great inaccuracies.

Tissue Doppler Imaging Derived Velocities

TDI and STE both provide indices of RV function. Spectral TDI measurement of the tricuspid annular velocities and color Doppler assessment of myocardial velocities from apical 4-chamber view can be used in the assessment of RV systolic and diastolic longitudinal functions. Tricuspid annular velocities (Fig. 7.16) are used as a correlate of RV function, because longitudinal displacement of the RV base accounts for the greater proportion of total RV volume change in comparison with radial shortening in normal ventricles.

TDI-derived systolic velocities can be used to assess RV systolic function. Normal systolic velocity by pulsed TDI is >12 cm/s. Isovolumic contraction velocity and acceleration can also be used for the assessment of RV systolic function with the advantage of being less load dependent.

In addition, peak early and late diastolic velocity can also be measured, allowing a similar evaluation of RV diastolic function and right atrial (RA) pressure to that used for the LV and LA, by using the ratio between pulsed Doppler derived trans-tricuspid early diastolic velocity (RV-E) to TDI-derived lateral tricuspid annulus early diastolic velocity (RV-e'), i.e. $RV-E/e'$.

Assessment of RV Deformation

Strain and strain rate can be measured to assess RV functions using color TDI, 2D-STE and 3D-STE (Figs. 7.16 and 7.17). Both methods were found comparable. Again, because RV function is mainly due to longitudinal shortening, TDI and STE can be used to measure RV longitudinal strain and strain rate.



Fig. 7.14 Color-coded LV end-systolic still frames and the corresponding Bull's Eye Maps for 3D-STE-derived area tracking in; (a) a patient with DCM; and (b) a normal subject. From [14]; with permission

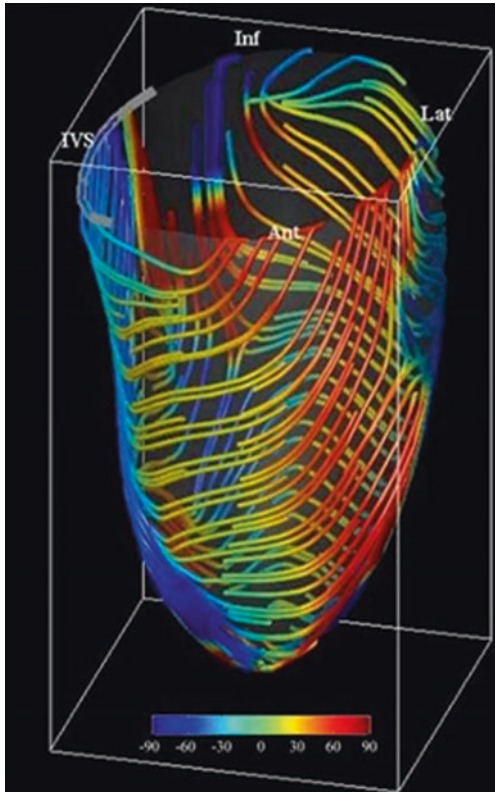


Fig. 7.15 Average diastolic fiber strain (derived from principal strain, which simultaneously integrates myocardial deformations in all directions, including LV twist) reconstructed from 3-dimensional speckle-tracking endocardial surface strain. Strain lines are colored by their angles represented by the color bar on the bottom. From [15]; with permission

Using 2D-STE, strain and strain rate values can be derived from tracking of both the RV free wall and the LV septum or from tracking only the RV free wall. Because RV free wall measurements were found to be of more prognostic value, they are used more often (Fig. 7.17) [6].

It is to be noted that, because of the complex geometry of the RV, strain and strain rate values of the RV, in contrast to the LV, are less homogenous and have reverse base-to-apex gradient, with values reaching their highest in the apical segments.

In patients with RV disease or dysfunction, peak systolic strain and SR are significantly reduced and delayed compared with individuals with normal RV function.

Left Atrium

The four basic mechanical functions by which the left atrium (LA) contributes to LV filling are the reservoir, conduit, active contractile pump and suction force functions. While invasive assessments of LA functions represent the gold standard, non-invasive assessment of the LA function is feasible using 2-D echocardiography of LA volumes, and by Doppler indices using trans-mitral flow (e.g. E/A, E-wave deceleration time and E/e' ratios) and by pulmonary venous flow (e.g. S/D ratio and D-wave deceleration time).

However, underestimation of LA volume due to foreshortened 2D echocardiographic images is common while Doppler assessment is an indirect method of LA function and pressure that is also limited in a lot of situations.

Alternatively, the non-invasive global LA function and regional LA wall deformation are currently feasible using TDI, 2D-STE (Fig. 7.18) and 3D-STE. LA volume curves during one cardiac cycle can also be obtained using 2D-STE. Thus, 2D-STE provides several LA mechanical indices that can be used in the assessment of regional and global LA function.

It is to be noticed, however, that because LA and LV events fall out of phase, i.e. LA systolic events occur during LV diastole and vice versa, LA strain and strain rate values are usually opposite to those expected for the LV. For example, normal LA longitudinal strain would be positive in value during LV end systole, in contrast to the negative LV values that would be obtained in the same time point.

Two different modalities have been proposed to quantify atrial deformation by STE

- 12 segments method:
 - Six segments from each of the apical 4- and 2-chamber
 - QRS onset is taken as the reference time point so that a positive peak atrial longitudinal strain will be measured representing atrial reservoir function (Fig. 7.19a).

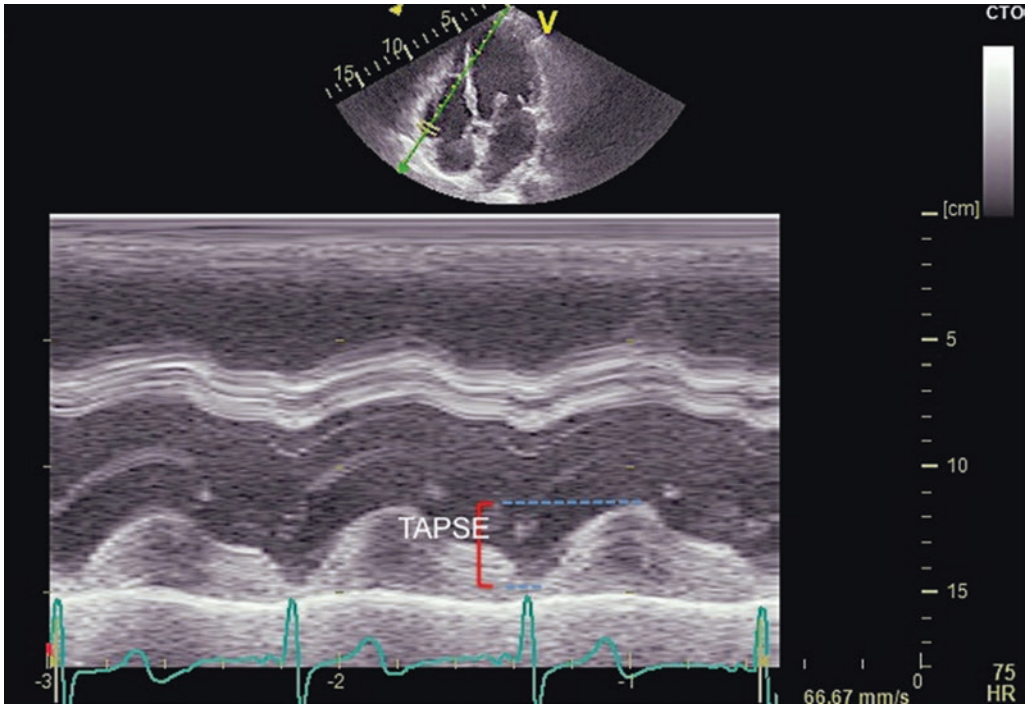
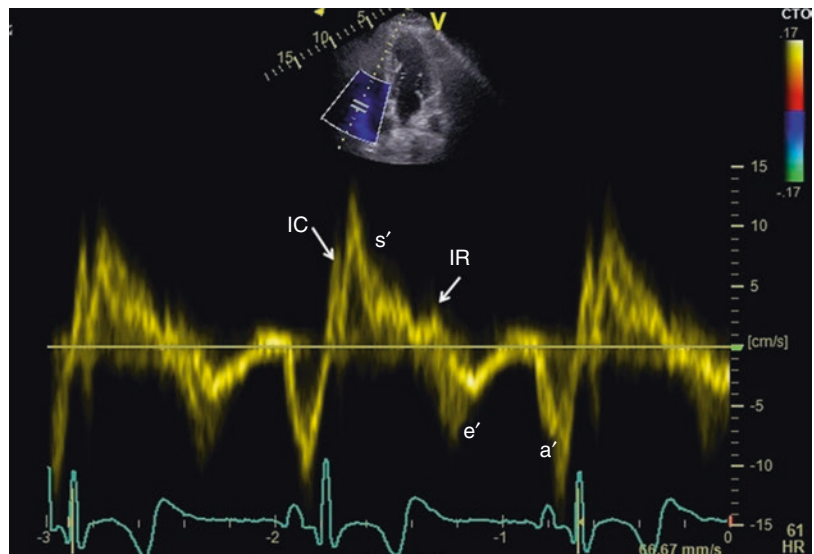


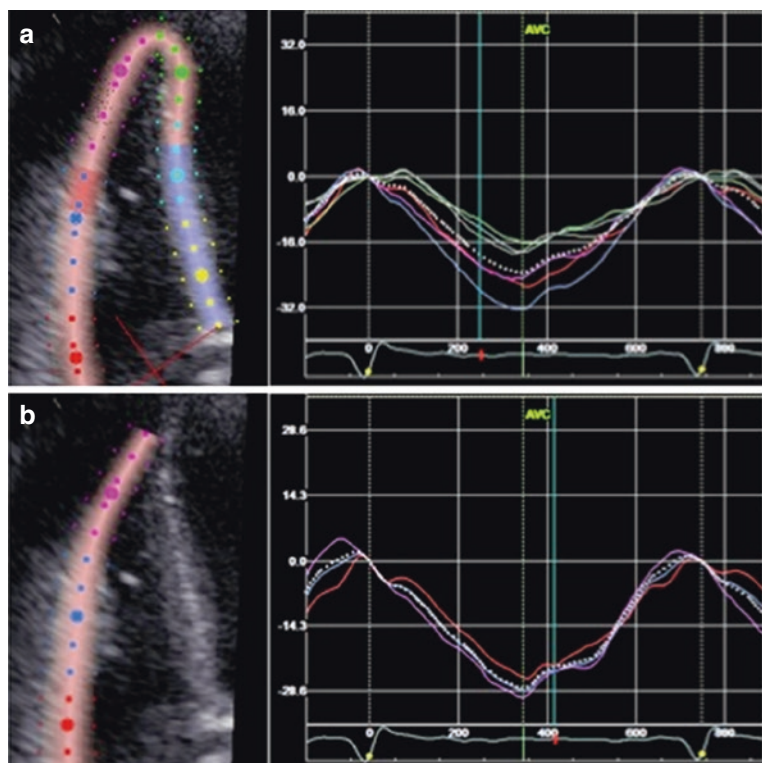
Fig. 7.16 Measurement of tricuspid annular plane systolic excursion (TAPSE)

Fig. 7.17 Spectral tissue Doppler imaging (TDI) of the tricuspid annulus



- 15 segments method:
 - Similar to the 12 segment method in addition to three posterior wall segments from the apical 3-chamber view
 - P wave is taken as the reference point. As such, the positive peak atrial strain (corresponding to LA conduit function) is preceded with a negative peak atrial longitudinal strain (corresponding to atrial systole) (Fig. 7.19b).

Fig. 7.18 2D-STE of the RV, (a) speckle tracking of the septum and the free wall with the resultant longitudinal strain curves of 6 segments, (b) speckle tracking of the free wall with the resultant longitudinal strain curves of 3 segments



The high feasibility of LA strain measurements with either TDI or STE makes it a very promising tool in the assessment of LA functions in different clinical scenarios. However, difficulties in tracking still may arise especially in instances with dilated pulmonary veins or with large LA appendage which affect the accuracies of the LA strain imaging.

Right Atrium

2D-STE and TDI can be potentially used to assess RA functions. Some early trials to study normal values of RA strain were done, however more validation is needed. Recent studies have suggested that the use of RA strain can be useful in some disease states.

The greatest challenge facing RA is probably that it is the cardiac chamber that has the thinnest wall, making it difficult to be adequately tracked.

Normal Values and Variability

The most recent guidelines for chamber quantification recommend the use of LV-GLS and RV-GLS in the assessment of LV and RV functions [6]. A review of major reports showed that LV-GLS measured by different vendors had a relatively wide range of normal cut-off values (-17.3 to -21.5%) [6]. As for the RV-GLS, Pooled data from single center studies suggested that normal RV-GLS derived from the free wall should be more negative than -20% [6]. A recent meta-analysis showed that normal values of global circumferential strain (GCS) ranged between -20.9 and -27.8% , and global radial strain (GRS) ranged between 35.1 and 59.0% , with mean values of -23.3 , and 47.3% , respectively [7].

This wide range of normal values is mainly because strain values are currently calculated using different vendors' software, which differs according to the definition being used for

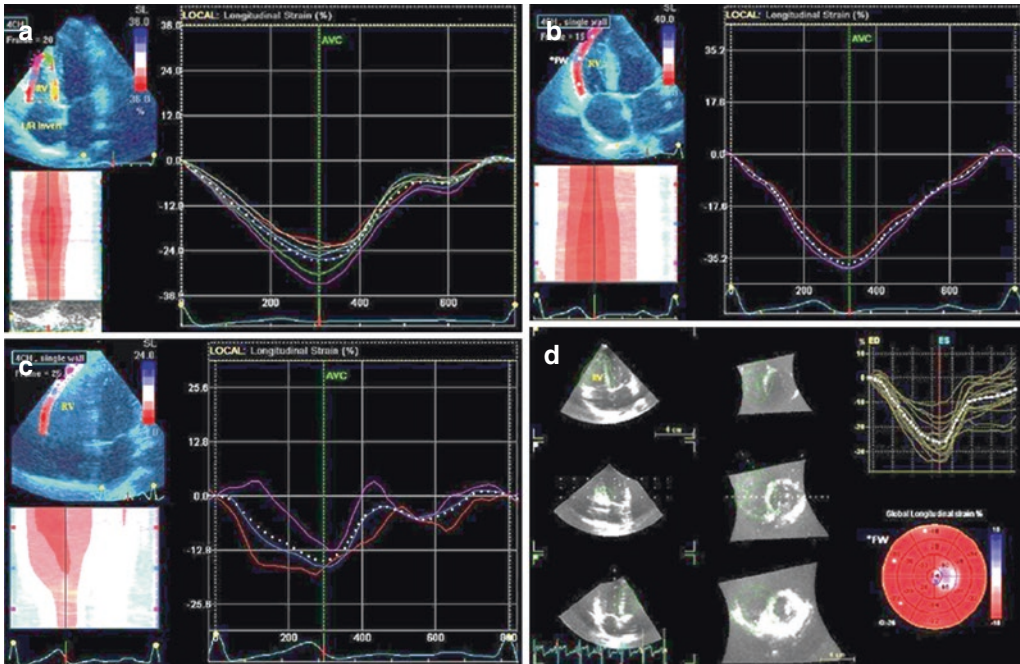


Fig. 7.19 Representative 2D and 3D RV strain images in normal controls and PH patients. (a) 2D-STE showing global and regional RV longitudinal strain in a normal subject. (b) 2D-STE showing global and regional free-

wall RV longitudinal strain in a normal subject. (c) Decrease of RV-GLS in a patient with chronic PH. (d) 3D-STE of the RV multi-plane view in a normal subject. From 16; with permission

measurement (endocardial, midwall or epicardial) [8]. Other sources of variability include that strain calculations are limited by the image quality and are load and age dependent.

In case of LV rotational mechanics, a standardized method of LV apical short axis acquisition adds is lacking thus adds another source for variability. Moreover, age-specific normal ranges of LV twist (LVT) and untwist and LA strain, thus far, have been derived from small studies. Also, Despite so, LV-GLS is still the least variable deformation parameter, and because of its great clinical benefit, the guidelines still encourage the use of GLS and suggest that peak systolic LV-GLS in a healthy individual should be observed at approximately -20% , with the following precautions:

1. Lower values should be expected in males and with increasing age [6].

2. Serial measurements in an individual patient should always be carried out using the same vendor machine and software [6].

While LV-GLS and RV-GLS are currently recommended to be used in the clinical settings, GCS, GRS, LV rotational mechanics, and LA strain remain as deformation parameters with potential clinical value awaiting accuracy validation.

Clinical Applications

Deformation imaging can be used currently to assess variety of diseases. The following are examples of clinical situations where assessment of myocardial deformation is of value (Table 7.3).

Table 7.3 Myocardial deformation in different cardiovascular diseases

	GLS	GRS	GCS	LV-T	LV-UTR
Cardiac risk factor induced subclinical myocardial dysfunction	↓	↓	Normal or ↑	Normal or ↑	Normal or ↓
Ischemic heart disease (IHD)	↓	↓	Normal or ↑	Normal or ↑	Delayed/ may ↓
Dilated cardiomyopathy (DCM)	↓	↓	↓	↓	↓
LV noncompaction	↓	↓	↓	Absent	Absent
Hypertrophic cardiomyopathy (HCM)	↓	↓	Normal or ↑	Normal or ↑	Delayed/ may ↓
Restrictive cardiomyopathy (RCM)	↓	↓	↓	↓	↓
Constrictive pericarditis (CP)	Normal	Normal	↓	↓	↓
Aortic stenosis (AS)	↓	↓	Normal or ↑	Normal or ↑	Delayed/ may ↓
Mitral regurgitation (MR)	↓	↓	Normal or ↑	Normal or ↑	Delayed/ may ↓
Heart failure preserved ejection fraction (HFPEF)	↓	↓	Normal or ↑	Normal or ↑	Normal or ↓
Heart failure reduced ejection fraction (HFREF)	↓	↓	↓	↓	↓

Subclinical Myocardial Dysfunction

In longstanding risk factors such as hypertension, diabetes mellitus and hyperlipidemia [9–11] the microscopic structures of the myofibers is altered due to micro-vascular ischemia, intra-myocardial fibrosis, or collagen degradation products accumulation, resulting in subclinical myocardial dysfunction which usually starts in the endocardial layer. The endocardial dysfunction causes depression in GLS and GRS values, and the relative sparing of the epicardial layer to normal or even compensatory exaggeration in GCS and LV twist, while untwist is usually delayed [12].

Coronary Heart Disease

In patients suffering from coronary artery disease (CAD) and myocardial infarction (MI), STE can be used to assess global and segmental myocardial function. GLS is usually reduced in CAD and usually correlates positively with systolic function. Moreover, the augmentation of GLS after dobutamine stress echocardiography suggests myocardial viability.

Segmental longitudinal strain assessment can also be used to identify ischemic territories [17], myocardial scarring [18], to estimate infarct size, and to identify viable myocardial

segments during low-dose dobutamine echocardiography [19].

In addition, ischemic and scarred segments also have depressed and delayed peaking of systolic circumferential, and radial strain and strain rate [20]. LV-twist may be preserved in patients with normal EF who have subendocardial ischemia which cause unopposed epicardial fibers, while it is depressed with low EF and in transmural ischemia [4]. On the other hand, untwist is usually delayed and depressed.

Dilated Cardiomyopathy (DCM)

The significant myocardial remodeling that occurs in DCM is usually accompanied by loss of myocardial mechanics in all directions, an effect that was shown to be related to the severity of LV systolic dysfunction. GLS in these patients is of particular prognostic value and can be used to assess response to therapy, predict the occurrence of major cardiovascular events and the need for intervention [21]. An increase in GLS after cardiac resynchronization therapy (CRT) can be used to predict responders and depressed levels of GLS. In terminal patients requiring cardiac transplantation is predictive of graft rejection [22, 23].

In addition to the abnormal strain values in patients with DCM, the increased sphericity of the LV apex affects the overall rotational mechanics and is usually accompanied by significant decrease in apical rotation and overall LV twist.

Hypertrophic Cardiomyopathy (HCM)

In patients with HCM, endocardial dysfunction leads to a prominent decrease in GLS and GRS, and because of the epicardial layer thickening, these patients usually have increased LVT and normal GCS with delayed LV untwist [24]. GLS can be effectively used to differentiate pathological from physiological hypertrophy of trained athletes. Surgical myomectomy was found to normalize GCS and LVT in these patients [25].

Constrictive Pericarditis (CP) vs. Restrictive Cardiomyopathy (RCM)

STE can help differentiate CP and RCM, two conditions that involve diastolic dysfunction with different mechanisms. RCM is usually associated with endocardial dysfunction that causes depression in GLS and GRS with relatively spared epicardial fibers, thus the preserved GCS and LVT. On the other hand, in CP the subepicardial fibers affection with relative sparing of subendocardial fibers leads to preserved GLS and GRS, while GCS and LVT are usually depressed (Fig. 7.20) [26].

Valvular Heart Disease

In patients with aortic stenosis (AS) and preserved ejection fraction, the subendocardial ischemia resulting from the pressure-overload causes attenuation of GLS with relative preservation or increase in LVT [27]. Treatment of AS by surgical or trans-catheter aortic valve replacement (TAVR) cause normalization of all LV mechanics [27, 28].

In patients with mitral regurgitation (MR) and normal EF depression in GLS, GCS, and GRS are usually associated with the insidious myocardial dysfunction [29], while LVT might be preserved until the development of evident systolic failure [30]. In MR patients undergoing mitral

valve repair, pre-procedural GLS predicts post-procedural EF reduction [31].

Myocardial Mechanics in Heart Failure

Early in the course of heart failure, symptoms can develop despite normal ejection fraction, or the so-called heart failure with preserved ejection fraction (HFpEF). STE based studies have shown that a decreased GLS can be used as a marker of insidious systolic function in those patients and is associated with higher levels of pro-BNP levels and worse diastolic function [32]. Exercise is usually associated with further depression of GLS and provocation of symptoms in these patients. Endocardial dysfunction early in the course of heart failure is the underlying mechanism for the abnormal longitudinal function. The reason why EF is preserved in these patients is that GCS and LVT usually increase to compensate for the decreased GLS. With the progression of the underlying pathology and the appearance of evident LV systolic dysfunction in the form of reduced ejection fraction (HFrEF), GLS further decrease LVT and GCS fail to compensate, thus myocardial pump failure occurs leading to LV dilatation (Fig. 7.21) [33, 34].

Clinical Applications in Other Chambers

The Right Ventricle

Patients with RV dysfunction due to a variety of causes were found to depressed RV strain and strain rate values. Examples for that would be pulmonary hypertension, in amyloidosis, systemic sclerosis, congenital heart diseases, and arrhythmogenic RV cardiomyopathy. RV strain was found to be a sensitive marker that is useful as an early indicator of RV dysfunction in patients who still have normal right sided pressures. (Figs. 7.22, 7.23, and 7.24).

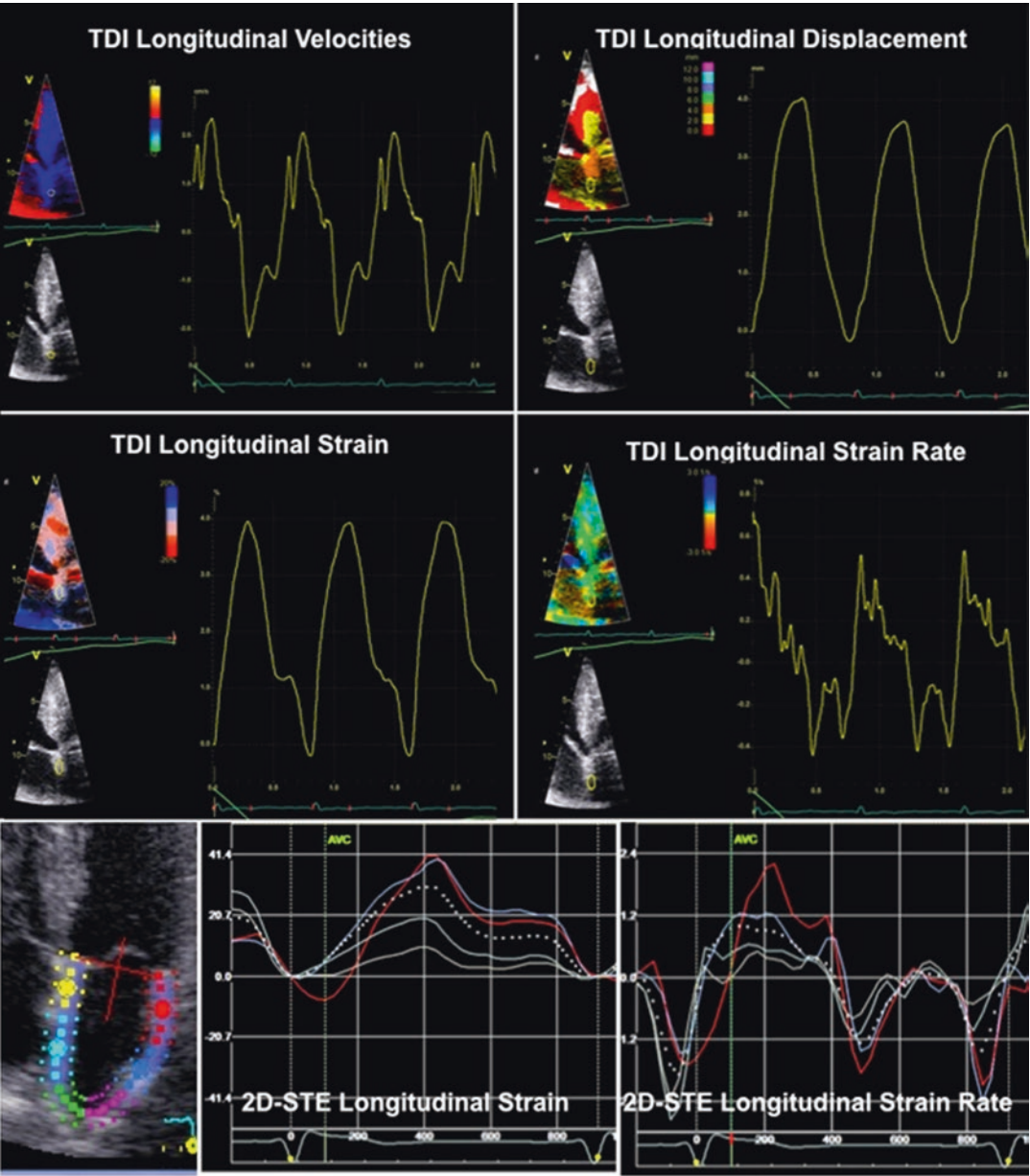


Fig. 7.20 The use of 2D-STE to derive LA longitudinal deformations (velocities, displacement, strain, and strain rate) in apical; 4-chamber view by color TDI (upper 4 panels) and 2D-STE, lower 2 panels

The Left Atrium

In ASD patients treated with atrial septal occluder devices, LA strain and strain rate are reduced compared with control subjects. LA strain and strain rate and velocities are also reduced in patients undergone successful cardioversion or

catheter ablation for atrial fibrillation. Conversely, LA strain was shown to be increased in patients with mitral regurgitation.

Regional heterogeneity of LA strain and strain values has been reported in healthy subjects, with the highest value in the inferior wall

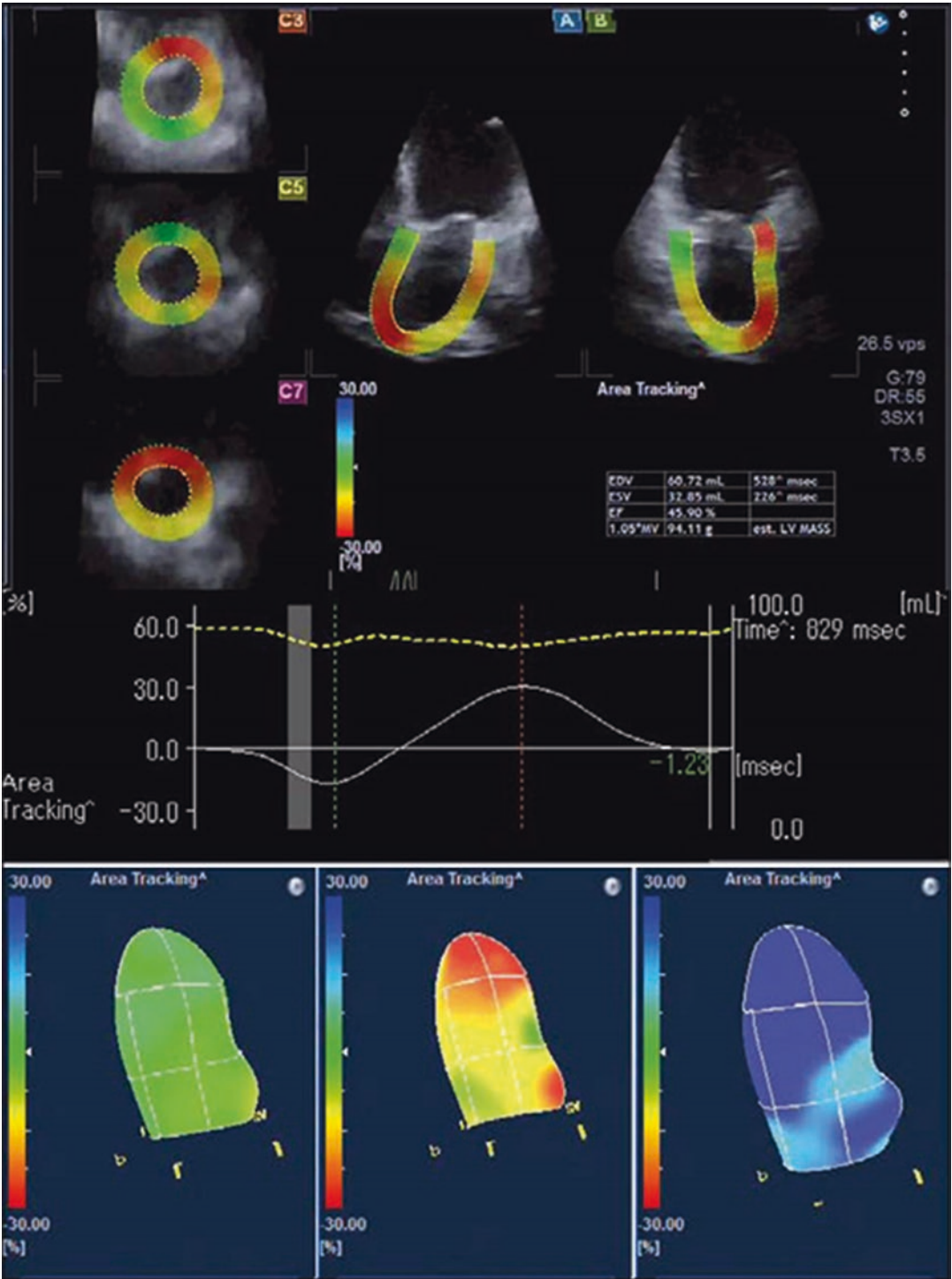


Fig. 7.21 3D-STE Left atrial tracking images in a 45-year-old man with paroxysmal atrial fibrillation. From 35; with permission

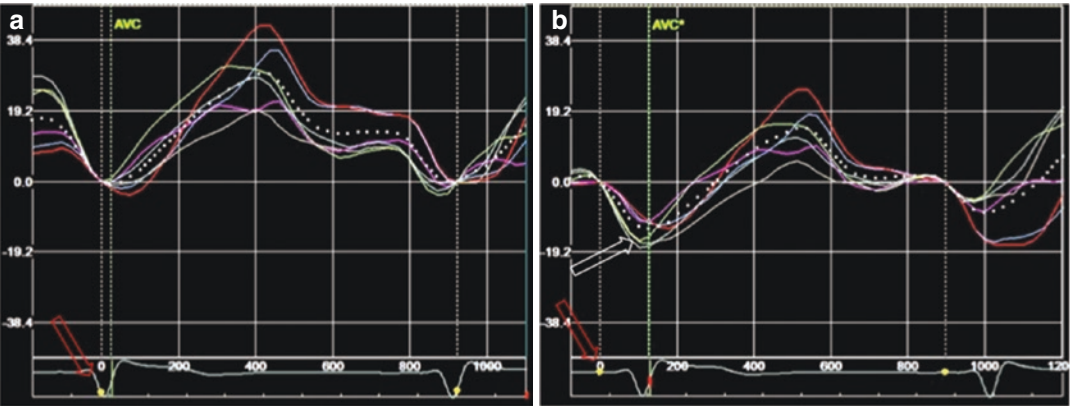
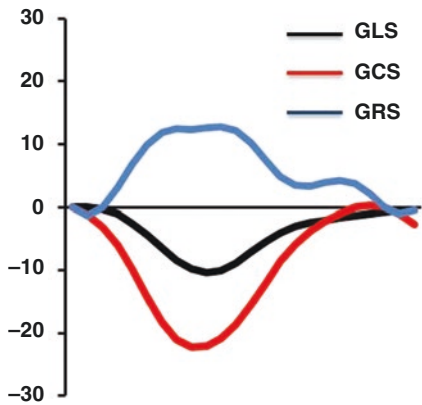


Fig. 7.22 Different methods used for assessment of LA strain and strain rate using 2D-STE (a) QRS onset as a reference point thus measuring the positive peak left atrial (LA) longitudinal strain, and (b) P wave as the reference

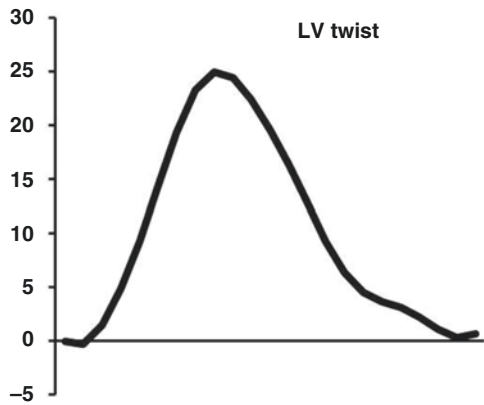
point allowing the measurement of a first negative peak LA longitudinal strain (LA systole), of a second positive peak LA strain (LA conduit function), and of their sum

RCM

a

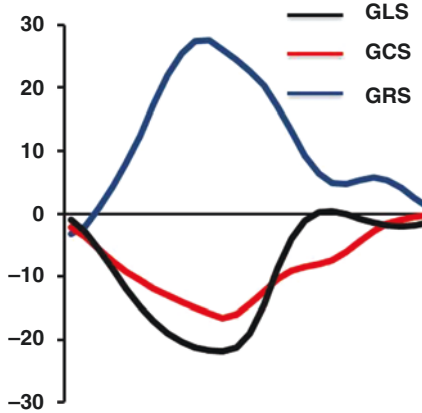


b

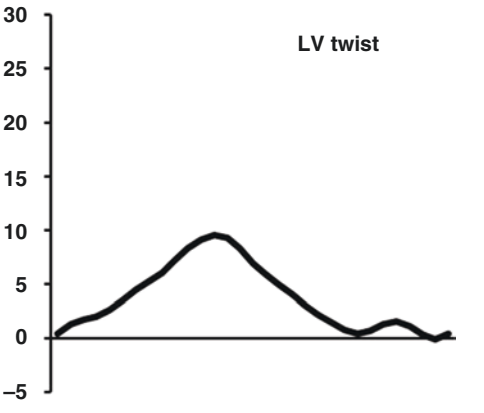


CP

c



d



HFpEF

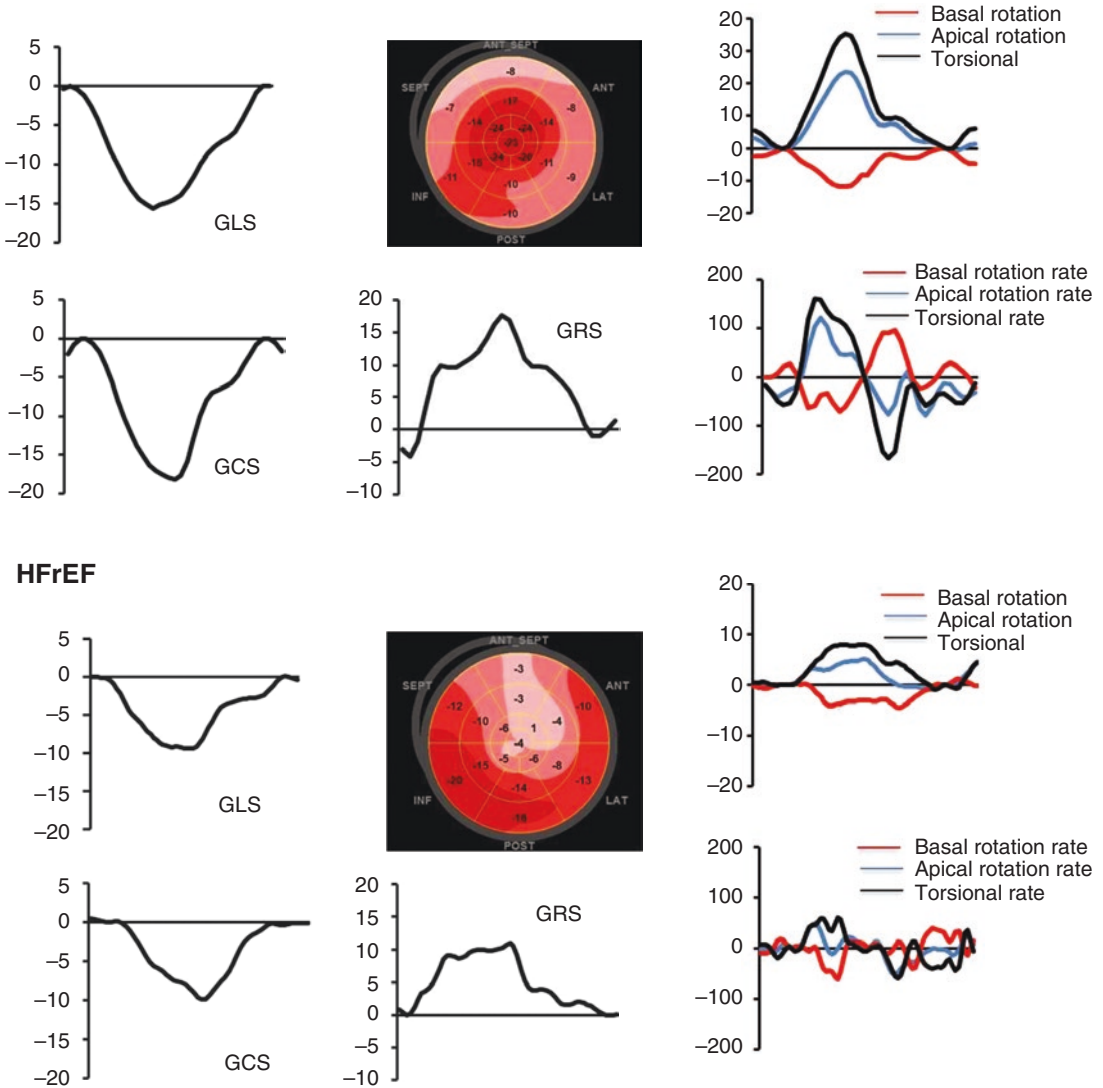


Fig. 7.24 2D-STE in heart failure with preserved EF (HFpEF) and heart failure with reduced ejection fraction (HFrEF). In HFpEF, GLS and GRS are depressed due to

the endocardial dysfunction. However, this is compensated by LV twist and GCS. In HFrEF, compensation is lost and mechanics are significantly depressed in all directions

Fig. 7.23 The use of 2D-STE to differentiate restrictive cardiomyopathy (RCM) from constrictive pericarditis (CP). (a) RCM is usually associated with endocardial dysfunction that causes depression in GLS and GRS with rela-

tively spared epicardial fibers, thus the preserved GCS and LVT. (b) In CP the subepicardial fibers affection with relative sparing of subendocardial fibers leads to preserved GLS and GRS, while GCS and LVT are usually depressed

in comparison with mid and superior LA segments. LA inferior wall is one of the best predictors of sinus rhythm maintenance after atrial fibrillation cardioversion and that LA strain is more improved at lateral wall in CRT responders.

References

- Barbosa D, Heyde B, Dietenbeck T, Houle H, Friboulet D, Bernard O, D'hooge J. Quantification of left ventricular volume and global function using a fast automated segmentation tool: validation in a clinical setting. *Int J Cardiovasc Imaging*. 2013;29:309–16.
- Cannesson M, Tanabe M, Suffoletto MS, McNamara DM, Madan S, Lacomis JM, Gorcsan J 3rd. A novel two-dimensional echocardiographic image analysis system using artificial intelligence-learned pattern recognition for rapid automated ejection fraction. *J Am Coll Cardiol*. 2007;49:217–26.
- Sengupta PP, Krishnamoorthy VK, Korinek J, Narula J, Vannan MA, Lester SJ, et al. Left ventricular form and function revisited: applied translational science to cardiovascular ultrasound imaging. *J Am Soc Echocardiogr*. 2007;20:539–51.
- Sengupta PP, Tajik AJ, Chandrasekaran K, Khandheria BK. Twist mechanics of the left ventricle: principles and application. *JACC Cardiovasc Imaging*. 2008;1:366–76.
- Voigt JU, Pedrizzetti G, Lysyansky P, Marwick TH, Houle H, Baumann R, et al. Definitions for a common standard for 2D speckle tracking echocardiography: consensus document of the EACVI/ASE/Industry Task Force to standardize deformation imaging. *Eur Heart J Cardiovasc Imaging*. 2015;16:1–11.
- Lang RM, Badano LP, Mor-Avi V, Afilalo J, Armstrong A, Ernande L, et al. Recommendations for cardiac chamber quantification by echocardiography in adults: an update from the American Society of Echocardiography and the European Association of Cardiovascular Imaging. *J Am Soc Echocardiogr*. 2015;28:1–39 e14.
- Yingchoncharoen T, Agarwal S, Popovic ZB, Marwick TH. Normal ranges of left ventricular strain: a meta-analysis. *J Am Soc Echocardiogr*. 2013;26:185–91.
- Nagata Y, Takeuchi M, Mizukoshi K, et al. Intervendor variability of two-dimensional strain using vendor-specific and vendor-independent software. *J Am Soc Echocardiogr*. 2015;28:630–41.
- Jellis C, Martin J, Narula J, Marwick TH. Assessment of nonischemic myocardial fibrosis. *J Am Coll Cardiol*. 2010;56:89–97.
- Crendal E, Walther G, Vinet A, Dutheil F, Naughton G, Lesourd B, et al. Myocardial deformation and twist mechanics in adults with metabolic syndrome: impact of cumulative metabolic burden. *Obesity (Silver Spring)*. 2013;21:E679–86.
- Maharaj N, Khandheria BK, Libhaber E, Govender S, Duarte R, Peters F, Essop MR. Relationship between left ventricular twist and circulating biomarkers of collagen turnover in hypertensive patients with heart failure. *J Am Soc Echocardiogr*. 2014;27:1064–71.
- Sengupta PP, Narula J. Reclassifying heart failure: predominantly subendocardial, subepicardial, and transmural. *Heart Fail Clin*. 2008;4:379–82.
- Mondillo S, Galderisi M, Mele D, Cameli M, Lomoriello VS, Zacà V, et al. Speckle-tracking echocardiography: a new technique for assessing myocardial function. *J Ultrasound Med*. 2011;30(1):71–83.
- Urbano-Moral JA, Patel AR, Maron MS, Arias-Godinez JA, Pandian NG, et al. Three-dimensional speckle-tracking echocardiography: methodological aspects and clinical potential. *Echocardiography*. 2012;29(8):997–1010.
- Omar AM, Vallabhajosyula S, Sengupta PP. Left ventricular twist and torsion: research observations and clinical applications. *Circ Cardiovasc Imaging*. 2015;8(6):e003029.
- Vitarelli A, Mangieri E, Terzano C, Gaudio C, Salsano F, Rosato E, et al. Three-dimensional echocardiography and 2D-3D speckle-tracking Imaging in chronic pulmonary hypertension: diagnostic accuracy in detecting hemodynamic signs of right ventricular (RV) failure. *J Am Heart Assoc*. 2015;4(3):e001584. <https://doi.org/10.1161/JAHA.114.001584>.
- Dandel M, Hetzer R. Echocardiographic strain and strain rate imaging—clinical applications. *Int J Cardiol*. 2009;132:11–24.
- Asanuma T, Uranishi A, Masuda K, Ishikura F, Beppu S, Nakatani S. Assessment of myocardial ischemic memory using persistence of post-systolic thickening after recovery from ischemia. *JACC Cardiovasc Imaging*. 2009;2:1253–61.
- Ng AC, Sitges M, Pham PN, Tran da T, Delgado V, Bertini M, et al. Incremental value of 2-dimensional speckle tracking strain imaging to wall motion analysis for detection of coronary artery disease in patients undergoing dobutamine stress echocardiography. *Am Heart J*. 2009;158:836–44.
- Shimoni S, Gendelman G, Ayzenberg O, Smirin N, Lysyansky P, Edri O, et al. Differential effects of coronary artery stenosis on myocardial function: the value of myocardial strain analysis for the detection of coronary artery disease. *J Am Soc Echocardiogr*. 2011;24(7):748–57.
- Nahum J, Bensaid A, Dussault C, Macron L, Clémence D, Bouhemad B, et al. Impact of longitudinal myocardial deformation on the prognosis of chronic heart failure patients. *Circ Cardiovasc Imaging*. 2010;3:249–56.
- Clemmensen TS, Logstrup BB, Eiskjaer H, Poulsen SH. Changes in longitudinal myocardial deformation during acute cardiac rejection: the clinical role of two-dimensional speckle-tracking echocardiography. *J Am Soc Echocardiogr*. 2015;28:330–9.
- Bernard A, Donal E, Leclercq C, Schnell F, Fournet M, Reynaud A, et al. Impact of cardiac resynchronization therapy on left ventricular mechanics: under-

- standing the response through a new quantitative approach based on longitudinal strain integrals. *J Am Soc Echocardiogr.* 2015;28:700–8.
24. Geyer H, Caracciolo G, Abe H, Wilansky S, Carerj S, Gentile F, et al. Assessment of myocardial mechanics using speckle tracking echocardiography: fundamentals and clinical applications. *J Am Soc Echocardiogr.* 2010;23:351–69; quiz 453–5.
 25. Moravsky G, Bruchal-Garbicz B, Jamorski M, Ralph-Edwards A, Gruner C, Williams L, et al. Myocardial mechanical remodeling after septal myectomy for severe obstructive hypertrophic cardiomyopathy. *J Am Soc Echocardiogr.* 2013;26:893–900.
 26. Sengupta PP, Krishnamoorthy VK, Abhayaratna WP, Korinek J, Belohlavek M, Sundt TM 3rd, et al. Disparate patterns of left ventricular mechanics differentiate constrictive pericarditis from restrictive cardiomyopathy. *JACC Cardiovasc Imaging.* 2008;1:29–38.
 27. Carasso S, Cohen O, Mutlak D, Adler Z, Lessick J, Aronson D, et al. Relation of myocardial mechanics in severe aortic stenosis to left ventricular ejection fraction and response to aortic valve replacement. *Am J Cardiol.* 2011;107:1052–7.
 28. Poulin F, Carasso S, Horlick EM, Rakowski H, Lim KD, Finn H, et al. Recovery of left ventricular mechanics after transcatheter aortic valve implantation: effects of baseline ventricular function and postprocedural aortic regurgitation. *J Am Soc Echocardiogr.* 2014;27:1133–42.
 29. Kim MS, Kim YJ, Kim HK, Han JY, Chun HG, Kim HC, et al. Evaluation of left ventricular short- and long-axis function in severe mitral regurgitation using 2-dimensional strain echocardiography. *Am Heart J.* 2009;157:345–51.
 30. Zito C, Carerj S, Todaro MC, Cusmà-Piccione M, Caprino A, Di Bella G, et al. Myocardial deformation and rotational profiles in mitral valve prolapse. *Am J Cardiol.* 2013;112:984–90.
 31. Pandis D, Sengupta PP, Castillo JG, Caracciolo G, Fischer GW, Narula J, et al. Assessment of longitudinal myocardial mechanics in patients with degenerative mitral valve regurgitation predicts postoperative worsening of left ventricular systolic function. *J Am Soc Echocardiogr.* 2014;27:627–38.
 32. Kraigher-Krainer E, Shah AM, Gupta DK, Santos A, Claggett B, Pieske B, et al. Impaired systolic function by strain imaging in heart failure with preserved ejection fraction. *J Am Coll Cardiol.* 2014;63:447–56.
 33. Partridge JB, Smerup MH, Petersen SE, Niederer PF, Anderson RH. Linking left ventricular function and mural architecture: what does the clinician need to know? *Heart.* 2014;100:1289–98.
 34. Claus P, Omar AM, Pedrizzetti G, Sengupta PP, Nagel E. Tissue tracking technology for assessing cardiac mechanics: principles, normal values, and clinical applications. *JACC Cardiovasc Imaging.* 2015;8:1444–60. <https://doi.org/10.1016/j.jcmg.2015.11.001>.
 35. Seo Y, Ishizu T, Atsumi A, Kawamura R, Aonuma K. Three-dimensional speckle tracking echocardiography: a promising tool for cardiac functional analysis. *Circ J.* 2014;78(6):1290–301. <https://doi.org/10.1253/circj.CJ-14-0360>.

Transesophageal Echocardiography: Principles and Application

8

Partho P. Sengupta and Bijoy K. Khandheria

Transesophageal echocardiography (TEE) involves ultrasound imaging of cardiovascular system from the confines of the gastro-esophageal tract. This helps reduce signal attenuation and permits the use of higher ultrasound frequencies, thereby providing an enhanced spatial resolution.

TEE for recording continuous wave Doppler velocities of cardiac flow was first described by Side and Josling [1]. Subsequently, the first transesophageal M-mode echocardiogram was reported by Frazin et al. [2], while Hisanaga et al. illustrated the use of cross-sectional real time imaging using a scanning device that consisted of a rotating single element in an oil-filled balloon mounted at the tip of the gastroscope [3]. One year after their first report, Hisanaga et al. also described a linear mechanical scanner that was suitable for transesophageal echocardiographic studies but its applications were limited due to rigidity of the mechanical sector scanning device. The initial acceptance of TEE was offset by the logistic difficulties of introducing rigid endo-

scopes. In 1982, Jacques Souquet produced the first mono- and multiplane electronic phased-array probes. The ensuing technological developments that facilitated the transition of TEE to its present clinical status included the introduction of flexible endoscope, miniaturization and improvements in transducer designs, serial improvement in scanning capabilities from monoplane, biplane to multiplane views and the addition of spectral and color Doppler imaging. TEE is currently used in approximately 5–10% of patients being evaluated in the cardiovascular ultrasound imaging and hemodynamic laboratory (Table 8.1).

Patient Preparation and Instrumentation

TEE can be performed as an outpatient or inpatient procedure. Fasting based on conscious sedation guidelines, an intravenous access, careful history to rule out presence of laryngeal or gastroesophageal diseases and removal of dentures are prerequisites.

- Absolute contraindications to TEE include esophageal stricture, diverticulum, tumor and recent esophageal or gastric surgery.
- Topical spray, intravenous sedation, a drying agent to minimize oral secretion and use of appropriate lubrication are helpful. Although the risk of bacterial endocarditis is extremely low and routine

P. P. Sengupta (✉)
Section of Cardiology, West Virginia University
Health Sciences Center, Morgantown, WV, USA
e-mail: partho.sengupta@hsc.wvu.edu

B. K. Khandheria
University of Wisconsin School of Health,
Milwaukee, WI, USA

Echocardiography, Aurora Health Care,
Milwaukee, WI, USA

Global Health, Milwaukee, WI, USA

Table 8.1 Transesophageal echocardiography cross sections

Window (depth from incisors)	Cross section (panel in Fig. 8.3)	Multipane angle range	Structures imaged
Upper esophageal (20–25 cm)	Aortic arch long axis (s)	0°	Aortic arch, left brachio v
	Aortic arch short axis (t)	90°	Aortic arch, PA, PV, left brachio v
Mid esophageal (30–40 cm)	Four-chamber (a)	0–20°	LV, LA, RV, RA, MV, TV, IAS
	Mitral commissural (g)	60–70°	MV, LV, LA
	Two-chamber (b)	80–100°	LV, LA, LAA, MV, CS
	Long axis (c)	120–160°	LV, LA, AV, LVOT, MV, asc aorta
	RV inflow-outflow (m)	60–90°	RV, RA, TV, RVOT, PV, PA
	AV short axis (h)	30–60°	AV, IAS, coronary ostia, LVOT, PV
	AV long axis (i)	120–160°	AV, LVOT, prox asc aorta, right PA
	Bicaval (l)	80–110°	RA, SVC, IVC, IAS, LA
	Asc aortic short axis (o)	0–60°	Asc aorta, SVC, PA, right PA
	Asc aortic long axis (p)	100–150°	Asc aorta, right PA
	Desc aorta short axis (q)	0°	Desc thoracic aorta, left pleural space
	Desc aorta long axis (r)	90–110°	Desc thoracic aorta, left pleural space
Transgastric (40–45 cm)	Basal short axis (f)	0–20°	LV, MV, RV, TV
	Mid short axis (d)	0–20°	LV, RV, pap mm
	Two-chamber (e)	80–100°	LV, MV, chordae, pap mm, CS, LA
	Long axis (j)	90–120°	LVOT, AV, MV
	RV inflow (n)	100–120°	RV, TV, RA, TV chordae, pap mm
Deep transgastric (45–50 cm)	Long axis (k)	0–20° (anteflexion)	LVOT, AV, asc aorta, arch

Reproduced with permission from the recommendations of American Society of Echocardiography [24]

Brachio v Brachiocephalic vein, *PA* pulmonary artery, *PV* pulmonic valve, *LV* left ventricle, *LA* left atrium, *RV* right ventricle, *RA* right atrium, *MV* mitral valve, *TV* tricuspid valve, *IAS* interatrial septum, *LAA* left atrial appendage, *CS* coronary sinus, *AV* aortic valve, *LVOT* left ventricular outflow tract, *prox proximal*, *RVOT* right ventricular outflow tract, *SVC* superior vena cava, *IVC* inferior vena cava, *RPA* right pulmonary artery, *asc* ascending, *desc* descending, *pap mm* papillary muscles

antibiotic prophylaxis before TEE is not advocated, occasionally, some high-risk patients such as those with prosthetic valves, multivalvular involvement or those with a past history of infective endocarditis, may require antibiotic prophylaxis. However, there is no sufficient scientific evidence that even this is necessary and the practice largely depends on local protocols.

- Before the introduction of the scope into the esophagus, the array is rotated to 0° to place the transducer into a conventional transverse plane. A bite guard is used always unless the patient is edentulous. Placing the imaging surface facing the tongue directs the ultrasound beam towards the anterior chest wall while the transducer is in the esophagus. The tip of the transducer is advanced into the esophagus gently without force and stopped if any resistance is encountered. After moving the trans-

ducer into the desired location, the probe is manipulated to orient the imaging planes for obtaining the desired cross-sectional images. The multipane TEE transducer consists of a single array of crystals that can be electronically and mechanically rotated in an arc of 180° (Figs. 8.1, 8.2, 8.3, and 8.4). Scanning along desired planes are obtained by observing the images develop as the probe is manipulated, rather than by relying on the depth markers on the probe or the angle icon. There are individual variations in the anatomic relationship of the esophagus to the heart; in some patients, the esophagus lies adjacent to the lateral portion of the atrioventricular groove, whereas in others it is positioned directly posterior to the left atrium. This relationship is taken into consideration when developing each desired cross-sectional views.

Fig. 8.1 Multiplane transesophageal echocardiographic views (0, 45, 90 and 135°) obtained from mid-esophagus. (RA right atrium, RAA right atrial appendage, TV tricuspid valve, RV right ventricle, LA left atrium, LV left ventricle, LVO left ventricle outflow, Asc Ao, ascending aorta, MPA main pulmonary artery, R, L and N right, left and non-coronary aortic sinus)

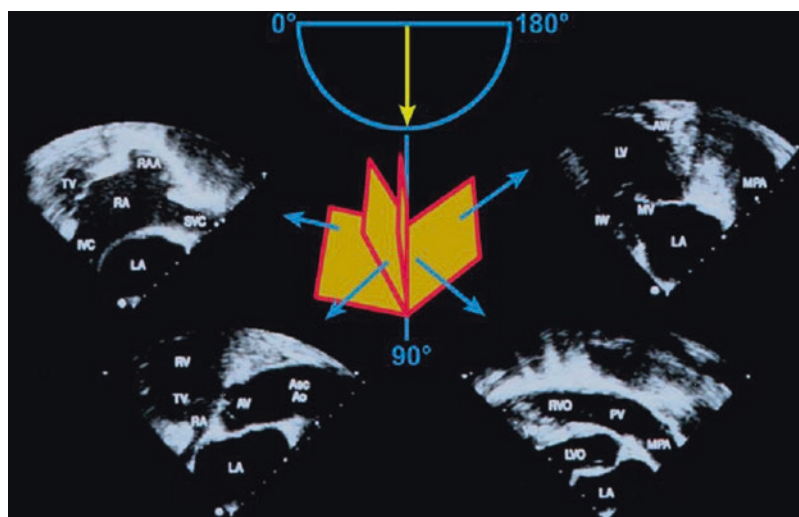
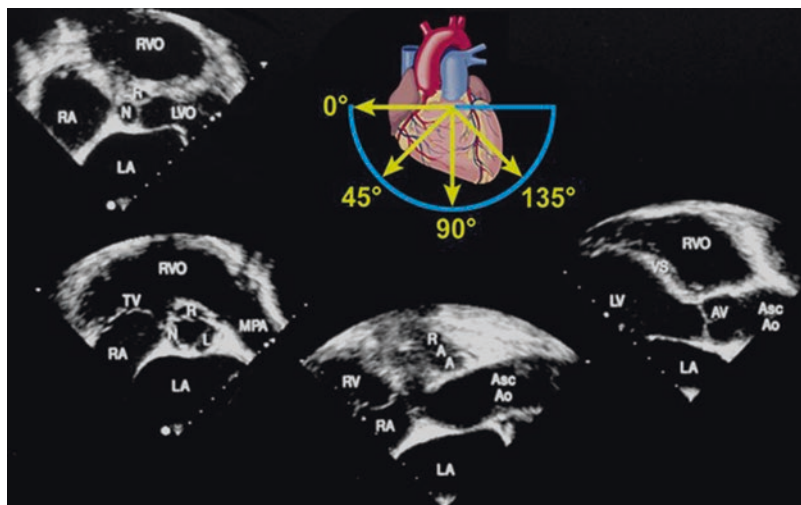


Fig. 8.2 Series of longitudinal views obtained with tip of transducer in midesophagus. The shaft of the scope is rotated to patients's left for obtaining optimal image of the mitral valve (MV) and the left ventricular (LV) inflow views. Sequence of longitudinal views is obtained by pro-

gressively rotating the shaft of scope to the patients's right. (RA right atrium, RAA right atrial appendage, TV tricuspid valve, RV right ventricle, LA left atrium, LV left ventricle, MV mitral valve, MPA main pulmonary artery, SVC superior vena cava, IVC Inferior vena cava)

- Although each of the views represents echocardiographic image in cross-section, moving the probes through the entire extent of a structure permits a rapid three-dimensional evaluation of cardiac structures. Although the TEE study needs to examine all the regions of the heart and great vessels, examination can be initially targeted for resolving the primary issue for which TEE is

being performed. Almost all views obtained by surface echocardiography can be duplicated by TEE.

Left Ventricle

From the mid esophagus, LV can be visualized by positioning the transducer posterior to the LA.

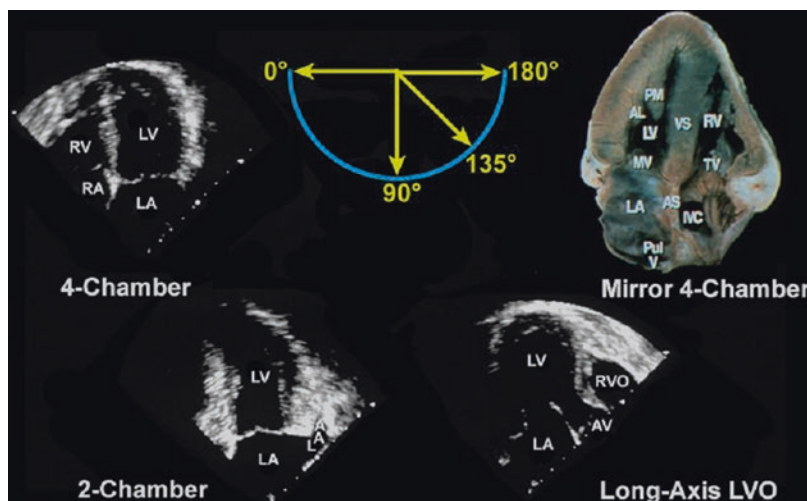
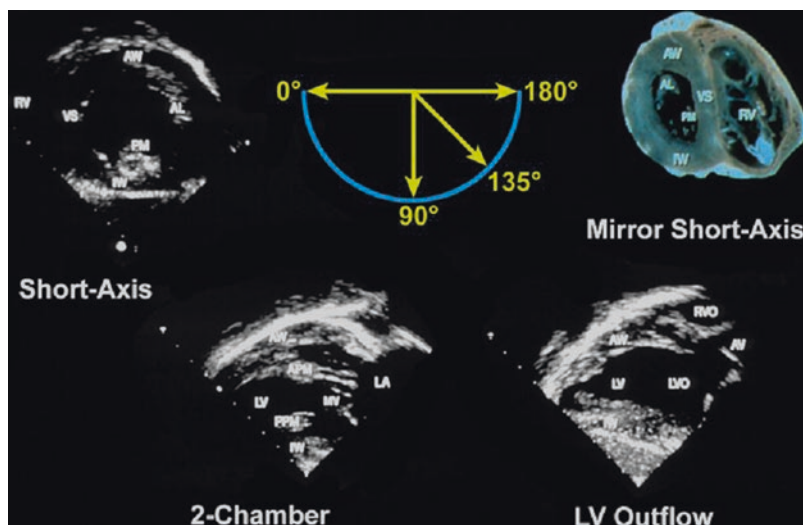


Fig. 8.3 Series of multiplane apical long-axis TEE views obtained by rotating the probe through 0, 90, 135 and 180°. The two-chamber view is comparable to midesophageal two-chamber view but with the transducer retroflexed and cardiac apex displayed upward. Long-axis

view is comparable to mid-esophageal long-axis view of left ventricular outflow but with transducer retroflexed and cardiac apex displayed upward. (*Pul V* pulmonary vein, *VS* ventricular septum, *PM* papillary muscle, *LV* left ventricle, *MV* mitral valve, *TV* tricuspid valve)

Fig. 8.4 Series of multiplane trans-gastric views. With tip of transducer in a stable transgastric position, the probe is rotated to obtain an array of short and long axis views. (*AW* anterior wall, *IW* inferior wall, *VS* ventricular septum, *AL* antero-lateral papillary muscle, *PM* postero-medial papillary muscle, *RVO* right ventricular outflow, *LA* left atrium, *LV* left ventricle, *LVO* left ventricle outflow, *VS* ventricular septum)



0–20°

The four-chamber view is obtained by rotating the multiplane angle from 0 to 10–20°.

80–100°

Mid esophageal two-chamber view is developed by rotating the angle by 80–100°. Internal landmarks consist of the left atrial appendage and coronary sinus.

120–160°

For obtaining the long axis view, the angle is further rotated between 120° and 160°. Here the LV outflow and the ascending aorta can well be visualized.

Transgastric Views

The transgastric views of the LV are acquired by advancing the probe into the stomach and

anteflexing the tip. The short axis view appears at 0° , whereas the long axis view appears at 90° . The transgastric short axis view of the LV at the level of mid segment is used for assessing LV chamber size, wall thickness and chamber functions.

Mitral Valve

The mitral valve (Fig. 8.5) is examined on TEE by using the four mid-esophageal and two transgastric views. The transmitral flow velocity profile is examined using spectral pulsed wave Doppler (PWD) to evaluate LV diastolic function in the mid esophageal four-chamber or mid esophageal long axis view by placing the sample volume between the tips of the open mitral leaflets.

0–20°

The mitral valve leaflets in this view are visualized along the 4-C chamber view. The posterior mitral leaflet P1 is to the right of the image display, and the anterior mitral leaflet A3 is to the left.

60–70°

Further rotation of the imaging plane aligns it parallel to the line that intersects the two commissures of the mitral valve. Leaflet A2 is seen in the middle while leaflets P1 and P3 are seen on the right and left sides respectively.

80–100°

This results in midesophageal two-chamber view in which leaflet P3 is displayed to the left and the leaflet A1 is on the right.

120–160°

This forms the midesophageal long axis view in which the posterior mitral leaflet P2 is to the left of the display and the anterior leaflet A2 is to the right.

The Transgastric

The transgastric basal short axis view provides a short axis view of the MV and is generally obtained at a multiplane angle of 0° . The transgastric two-chamber view are useful for examining the chordae tendinae, which lie perpendicular to the ultrasound beam in this view.

Aortic Valve

Mid-Esophagus

Once the aortic valve is viewed during in its short axis from the transducer positioned in the mid-esophagus, the angle is further rotated to approximately 30° – 60° until a symmetrical image of all three cusps come into view.

120–130°

The long axis view is the best for assessing the size of the aortic root by measuring the diameters

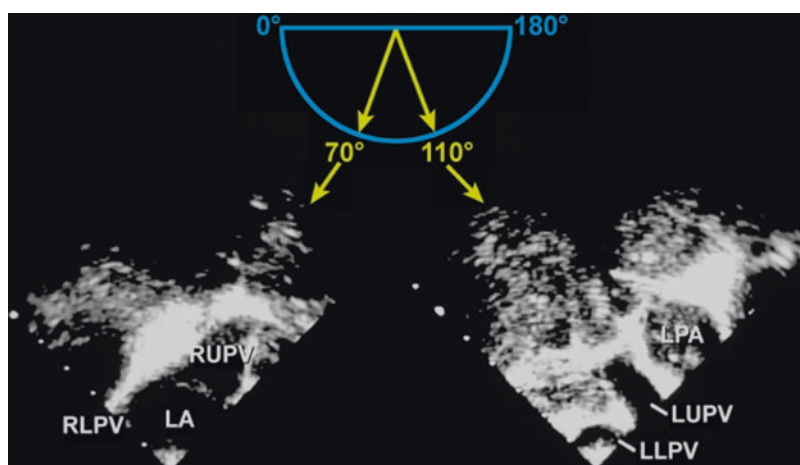


Fig. 8.5 Transesophageal planes for the assessment of the mitral valve

of the AV annulus, sinuses of Valsalva, sinotubular junction, and proximal ascending aorta.

The Transgastric Views

Detailed evaluation of the valve anatomy is difficult in these views because the LV outflow tract and aortic valve are located in the far field. Thus these views are primarily reserved for directing Doppler beam parallel to flow through the aortic valve, which is not possible from the mid esophageal window. The transgastric long axis view is developed by rotating the multiplane angle to 90–120°. For developing the deep transgastric view, the probe is advanced deep into stomach and flexed, turned, rotated and advanced gradually with trial and error for developing an optimum view.

Left Atrium

Examination of the left atrium (LA) is initiated with the mid esophageal four-chamber view. From midesophageal four chamber view, the multiplane angle is rotated through 90° for obtaining orthogonal view of the LA. In each of the views the entire chamber and its contents can be examined by panning the probe from top to bottom or by turning the

probe from side to side. In the four-chamber view, the left atrial appendage (LAA) can be seen to open near the superior and lateral aspect of LA. The left upper pulmonary vein (LUPV) enters the LA just lateral to the LAA.

The left lower pulmonary vein (LLPV) enters the LA just below the LUPV and is then identified by turning the transducer slightly farther to the left and advancing 1–2 cm (Fig. 8.6).

In the four-chamber view, the right upper pulmonary vein (RUPV) is imaged by turning the probe to the right at the level of the LAA. Like the LUPV, the RUPV can be seen entering the LA in an anterior to posterior direction. The right lower pulmonary vein, which enters the LA nearly at a right angle to the Doppler beam, can be identified by turning the probe slightly to right and advancing the probe by 1–2 cm.

90°

The interatrial septum (IAS) is examined at the mid esophageal level by moving the probe slightly to the right of midline and advancing and withdrawing the probe through its entire superior-inferior extent. From the mid esophageal four-chamber view, the multiplane angle is rotated forward to approximately 90. The LAA is seen as an out-pouching of the lateral, superior aspect of the

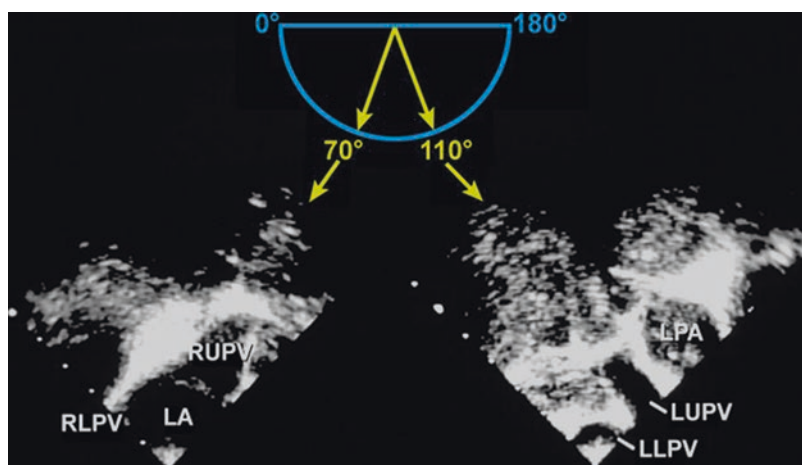


Fig. 8.6 Simultaneous TEE visualization of upper and lower pulmonary veins. For imaging of the right pulmonary veins (left panel), the angle is maintained at 70–80° in mid-esophagus and rotated rightwards, whereas for imaging the left pulmonary veins (right panel), the angle

is rotated at 100–110° and the scope is rotated to left. (RUPV right upper pulmonary vein, RLPV right lower pulmonary vein, LUPV left upper pulmonary vein, LLPV left lower pulmonary vein)

LA. From there, the LUPV is identified by turning the probe slightly farther to the left.

80–110°

The bicaval view is developed from the mid esophageal two-chamber view by turning the probe to the right and rotating the multiplane angle forward between 80° and 110° until both the superior vena cava (SVC) and the inferior vena cava (IVC) come into view.

Right Ventricle

The examination of the right ventricle (RV) begins at the mid esophageal four-chamber view.

60–90°

The RV inflow-outflow view can be developed by rotating the multiplane angle forward between 60° and 90° keeping the TV visible until the right ventricular outflow track opens up and the pulmonary valve (PV) and main pulmonary artery (PA) come into view.

The Transgastric

RV inflow view can be developed further by turning the probe to the right until the RV cavity is located in the center of the display and the multiplane angle is rotated forward between 100° and 120° until the apex of the RV appears in the left side of the display. This cross-section provides good views of the inferior (diaphragmatic) portion of the RV free wall.

Tricuspid Valve

The tricuspid valve can be visualized in the mid esophageal four-chamber view.

The multiplane angle can be further rotated to develop the mid esophageal RV inflow-outflow view and these views are repeated with color flow Doppler to detect flow abnormalities of the TV.

The transgastric views of the TV are obtained by advancing the probe into the stomach and developing the transgastric RV inflow view. A short axis view of the TV can be developed by

withdrawing the probe slightly toward the base of the heart until the tricuspid annulus is in the center of the display and rotating the multiplane angle backwards to approximately 30°.

Right Atrium

The examination of the RA is initiated from the mid esophageal *four-chamber view* followed by the mid esophageal *bicaval view* developed by rotating the multiplane angle between 80° and 110°. This view also provides good images of the right atrial appendage that emanates from the superior, anterior aspect of the RA.

Pulmonary Artery

The mid esophageal short axis view at the level of the aortic valve provides a view of the pulmonary veins and the main pulmonary artery (PA).

0°

The multiplane angle is rotated back toward 0° and the probe is anteflexed or withdrawn slightly to display the bifurcation of the main PA with the right PA at the top of the display coursing off to the patient's right. The left PA arches over the left mainstem bronchus after bifurcating from the main PA and is difficult to visualize with TEE due to the intervening airway.

The mid esophageal RV inflow-outflow view displays the pulmonary veins in long-axis and is useful for detecting pulmonic regurgitation by color flow Doppler. The main PA and the pulmonary veins can also be seen in the upper esophageal aortic arch short axis view.

Thoracic Aorta

Mid esophageal views can be used for assessing the ascending aorta in its short axis view by adjusting the angle until the vessel appears circular, usually between 0° and 60°. The probe can be advanced or withdrawn for examining different levels of the aorta.

100–150°

The multiplane angle can be rotated between 100° and 150° to develop the mid esophageal ascending aortic long axis view in which the anterior and posterior walls of the aorta appear parallel to one another.

Descending Aorta

TEE examination of the descending thoracic aorta is accomplished by turning the probe to the left from the mid esophageal four-chamber view for displaying the descending aortic short axis view.

The aortic arch is imaged with the multiplane angle at 0° by withdrawing the probe while maintaining an image of the descending thoracic aorta until the upper esophageal window is reached. The multiplane angle is rotated to 90° to develop the upper esophageal aortic arch short axis view, and the probe is turned to the right to move the imaging plane proximally through the arch and to the left to move distally.

Clinical Applications

Infective Endocarditis

TEE is superior to transthoracic echocardiography for better delineation of the shape and size of vegetations and for assessing the structural complications such as myocardial abscess, fistulas, mycotic aneurysms, valvular aneurysms or perforations, flail leaflets or prosthetic valve dehiscence [4, 5]. TEE is also superior than transthoracic echocardiograms TEE has a higher sensitivity (76–100%) and specificity (94%) than transthoracic echocardiography for diagnosing perivalvular extension of infection [6]. The cost-effectiveness and incremental utility of TEE when used in conjunction with the clinical information is particularly higher in patients who have an intermediate clinical likelihood of infective endocarditis [7]. A negative TEE in a patient with suspected infective endocarditis virtually rules out an infection of the native valve, except in very early phases of the disease when vegetations may not be detected. When

clinical suspicion of infective endocarditis is high and results from TEE are negative, a repeat TEE is warranted within 7–10 days, which may demonstrate previously undetected vegetations or abscess.

Evaluation of Prosthetic Valves

TEE is the procedure of choice for detecting abnormalities of mitral valve prostheses (perivalvular regurgitations, cusp abnormalities in tissue prosthesis, embolic events, patient-prosthesis mismatch and malfunction of repaired valves and implanted rings) (Fig. 8.3) [8]. The aortic valve lies in a plane perpendicular with the esophagus, with a flow that has an asymmetric profile, therefore assessment of a prosthetic aortic valve by TEE may be more challenging. However, TEE is useful in detecting abnormalities of aortic valve prosthesis, particularly those related to periprosthetic tissue. A deep trans-gastric view is required for assessing the gradient across the prosthesis and for better assessment of prosthetic aortic valve regurgitation.

TEE is also useful in diagnosing prosthetic valve thrombosis and for assessing success of thrombolytic therapy. TEE allows a close examination of the sewing ring and the occluder, thus helping differentiate pannus from a thrombus and for establishing the mechanism of an incomplete occluder opening. TEE is also useful in providing a high resolution assessment of valves in tricuspid and pulmonic positions.

Cardioembolic Strokes

The likelihood of identifying a potential cardiac source of emboli depends on how thoroughly a patient is evaluated. TEE has a higher accuracy in identifying abnormal lesions in patients with cardio-embolic strokes [9]. These include abnormalities of the left and right atrium and appendages, intra-atrial septum, patent foramen ovale, atrial septal aneurysm, vegetations, spontaneous contrast, left ventricular clots and various cardiac masses.

The diagnostic yield of TEE for a cardiac source of emboli in a group of patients presenting with unexplained stroke or transient ischemic attacks is high with a potential lesions identified in over 50% of the studies. However, one third of patients who have a cardio-embolic stroke also have concomitant cerebral or vascular atherosclerosis, which can confound the diagnosis. Moreover, no absolute clinical or laboratory gold standard exists for diagnosing a potentially cardio-embolic lesion; hence risk stratification schemes have been suggested based upon strength of the association of a given lesion with ischemic strokes.

Atrial Fibrillation

Atrial arrhythmias predispose to emboli formation. A sustained impairment or transient stunning results in poor emptying and enlargement of left atrium and left atrial appendage, leading consequently to stasis and thrombus formation. Transient paroxysms of atrial fibrillation may lead to thrombus formation in the left atrium. Left atrial thrombus may be detected in the presence of sinus rhythm [10]. Conversely, the lack of visualization of appendage thrombi on TEE after stroke does not exclude the appendage as the embolic source. In absence of well formed thrombi, a dense spontaneous contrast has been shown to be a strong predictor of ischemic strokes. An annual thromboembolic event rate of 12% has been observed in patients with spontaneous echo contrast compared to 3% in patients without it [11].

In patients with atrial fibrillation, clinical and echocardiographic markers of thromboembolism are helpful for risk stratification and include a history of hypertension, a previous thrombo-embolic event, and heart failure. Echocardiographic risk factors include left ventricular systolic function, left ventricular hypertrophy, left atrial enlargement and spontaneous echocardiographic contrast. The absolute risk of stroke in atrial fibrillation shows marked variation with age and coexisting cardiovascular diseases, ranging from 2 to 18% per year depending on the investigated

patient population [12]. Short term anticoagulation combined with TEE before cardioversion has been suggested to be an effective alternative to 3–4 weeks of empiric anticoagulation before cardioversion [13]. Economic analysis of TEE – facilitated acute cardioversion has been shown to result in higher initial treatment costs but a lower subsequent outcome-associated costs, resulting in no significant cost difference between the two strategies [14].

Aortic Diseases

Transesophageal examination is extremely valuable for managing patients with aortic diseases (aortic dissections, intramural injury, and aortic trauma) [15]. In a comparative imaging of multi-lane TEE with spiral CT and MR imaging, the sensitivity and specificity of TEE for diagnosing aortic dissections has been reported as 98% and 95% respectively [16]. However care needs to be taken to differentiate reverberation artifacts. Conversely false-negatives may occur when small dissections are located within upper ascending aorta or proximal aortic arch. The reverberation artifacts may be differentiated using M-mode echocardiography. The chief advantage of TEE in imaging aortic dissections is that it provides diagnostic information faster than other modalities and, the only modality which can be used intra-operatively during surgery. TEE has also been found useful in screening patients with suspected aortic trauma and for diagnosing acute aortic intramural hematomas.

There may be an association between large atheromas in the ascending aorta and the aortic arch and an increased risk of cerebral embolic events in patients older than 60 years. Morphologic features such as atheroma protrusion and ulceration have been shown to carry significantly higher risk of embolic events, particularly after cardiopulmonary bypass or following invasive procedures such as cardiac catheterization or intra-aortic balloon placement. Although TEE has been used to assess atheromas and their morphologies, it is not clear whether atheroma thickness is directly related to the

mechanism of stroke or represents a marker for other conditions. In a recent study, the association between previous ischemic strokes, transient ischemic episodes and aortic atherosclerosis was found to be insignificant once age and gender related adjustments were made [17]. The overall importance of aortic atherosclerosis in the pathogenesis of cerebrovascular accidents is thus not clear and needs to be correlated with associated risk factors such as hypertension, coagulation and lipid disorders.

Cardiac Masses

TEE is superior to transthoracic echocardiography in delineating cardiac masses and masses adjacent to the heart, such as in the pulmonary arteries and mediastinum. It is particularly useful for differentiating structural features such as site of attachment, consistency as in cystic versus solid, and infiltration into surrounding structures, that are useful for differentiating thrombi and benign from malignant neoplasms. TEE is particularly advantageous in detecting masses posterior to mechanical devices or in left atrial appendages. TEE is also useful in detection of thrombi lying in the proximal portion of the pulmonary arteries [18].

Congenital Heart Diseases and Intracardiac Shunts

Transesophageal echocardiography is superior to routine surface echocardiography for the evaluation of specific cardiac defects, such as certain types of atrial septal defects, anomalous pulmonary venous connections, and complex cardiac malformations. The technique is particularly useful in atrial septal defects. Sinus venosus defects and anomalous pulmonary vein drainage are detected more easily by TEE as compared to transthoracic echocardiography because of the proximity of the transducer to the atrial septum.

TEE is recommended in any patient with an unexplained dilatation of the right side of the

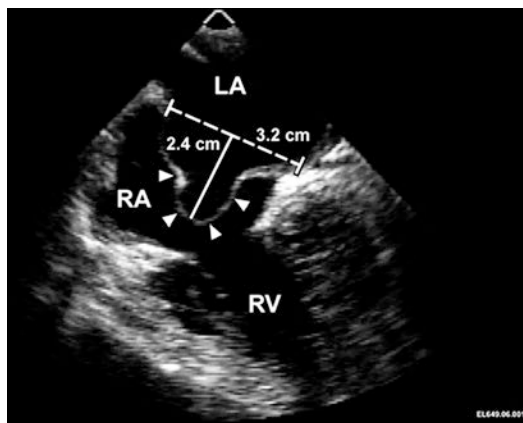


Fig. 8.7 Transesophageal echocardiography for delineating atrial septal aneurysm (arrows)

heart for ruling out a sinus venosus atrial septal defect and associated pulmonary venous abnormalities [19].

TEE is also useful for visualizing the margins of an atrial septal defect for defining candidates who may benefit from non-surgical device closure of the defect (Fig. 8.7).

TEE has been used for detecting shunt flow across foramen ovale in adults. Patent foramen ovale (PFO) and stroke remains a subject of intense investigation with no clear answers. Patent foramen may also be associated with atrial septal aneurysms and presence of both these lesions have been also been implicated in recurrent embolic strokes [20]. Administration of intravenous contrast is important for defining patency at rest. A right to left shunting of three or more contrast bubbles during normal breathing is diagnostic for presence of a PFO. The sensitivity of an intravenous injection of contrast in detecting a PFO improves threefolds if an injection is given through the femoral vein in contrary to antecubital vein.

Critically Ill Patients

The limited acoustic windows in critically ill patients make TEE an attractive alternative to transthoracic echocardiography. In addition to the usual indications for TEE (suspected

endocarditis, source of embolus, and suspected aortic dissection), there are several indications that are unique to critical care patients. These include:

1. Assessment of unexplained hypotension,
2. Suspected massive pulmonary embolism,
3. Unexplained hypoxemia, and
4. Complications of cardiothoracic surgery.

Unlike transthoracic echocardiography, TEE can visualize emboli lodged in the proximal pulmonary arteries. The right pulmonary artery can be observed for most of its course; however, the left pulmonary artery rarely can be observed beyond its first 2 cm.

Less common indications for TEE in the critical care unit include continuous hemodynamic monitoring, evaluation of potential transplant donors, and guidance of central-line placement. The recent development of transnasal TEE probes may allow for monitoring in the awake patient. The potential benefits of the transnasal probe include less risk for esophageal trauma in patients with varices or coagulopathies and less need for sedation in those with compromised respiratory or hemodynamic status.

Perioperative and TEE During Procedures

TEE is valuable in the perioperative period and can provide incremental information for either changing the pre-operative plan or prompting immediate revision of hemodynamically significant residual defects.

Intraoperative TEE is extremely useful in patients undergoing valve repairs, replacements and reoperative surgeries. In patients undergoing mitral valve repairs, TEE is extremely useful for the surgeons in making a decision about the choice of the surgical procedure which may include chordal shortening, chordal transfer, artificial chords, posterior leaflet sliding technique, anterior leaflet resection or placement of annulra ring. Routine intraoperative echocardiography has also been found to be cost-effective in children undergoing cardiac surgery for congenital heart lesions [21].

Transeophageal echocardiography also plays a role in the interventional laboratory for percutaneous interventions such as transcatheter closure of atrial septal defects (Fig. 8.8) and ventricular septal defects. It is used before the procedure for identifying the defect, excluding multiple defects,

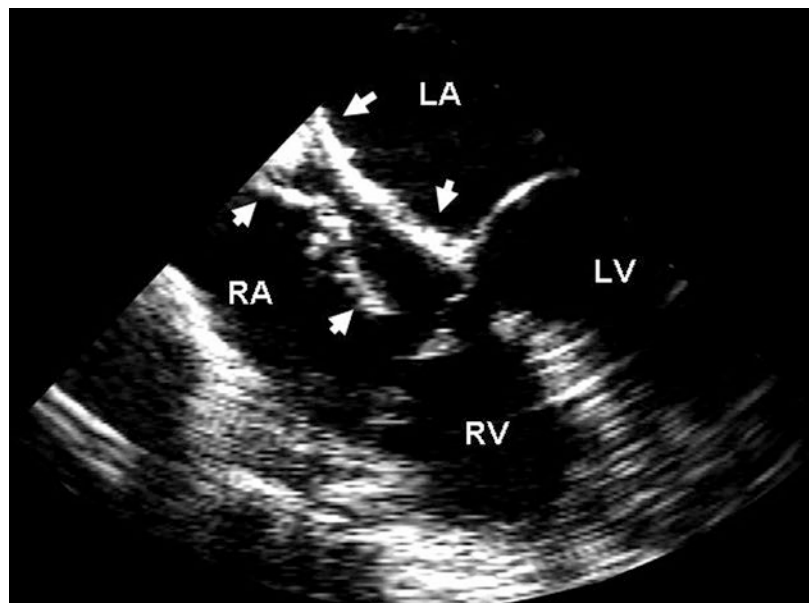


Fig. 8.8 Amplatzer device (arrows) positioned across an atrial septal defect

measuring the adequacy of the rim of the interatrial septum and its distance from the pulmonary vein and the mitral valve and superior vena cava, balloon sizing of the stretched diameter, and for proper placement of the occluder. TEE is also used as an important imaging modality for blade atrial septostomy and closure of baffle fenestrations following total caval pulmonary connection and closure of baffle leak following the Mustard or Senning surgeries.

Other interventional procedures where TEE is useful include balloon mitral valvuloplasty, non-surgical reduction of ventricular septum in patients with hypertrophic cardiomyopathy and trans-septal catheterization for placement of catheter during radiofrequency ablation of cardiac arrhythmias.

TEE also plays an important role in patients with heart failure undergoing implantation of left ventricular assist devices for selecting the type of the assist device necessary (right versus left or biventricular), optimization of device performance, the evaluation of hypoxemia and the determination of patients' ability to be weaned from the mechanical device [22, 23]. A correct positioning of canula under TEE guidance optimizes the LV filling, besides intraoperative recognition of right ventricular failure,

which can decrease pump flow due to inadequate left sided filling.

Pitfalls

TEE needs expertise for avoiding potential erroneous diagnosis resulting from misinterpretation of normal and abnormal anatomy.

- *Air* within the esophagus and stomach, or an air-filled trachea and bronchi intervening between probe and cardiac structures can consistently produce artifacts or interfere with certain tomographic views.
- *Reverberation signals* or ghost shadows are common and result from impedance mismatch resulting in linear artifacts most commonly seen in the upper ascending and mid-descending aorta. Imaging of the upper ascending aorta with the horizontal plane is limited by a blind spot caused by interposed bronchus between the esophagus and upper ascending aorta (Fig. 8.9).
- *Normal anatomy* may be interpreted abnormal. These include muscular trabeculations in the atrial appendage mistaken as mass or thrombus, the terminal portion of the partition

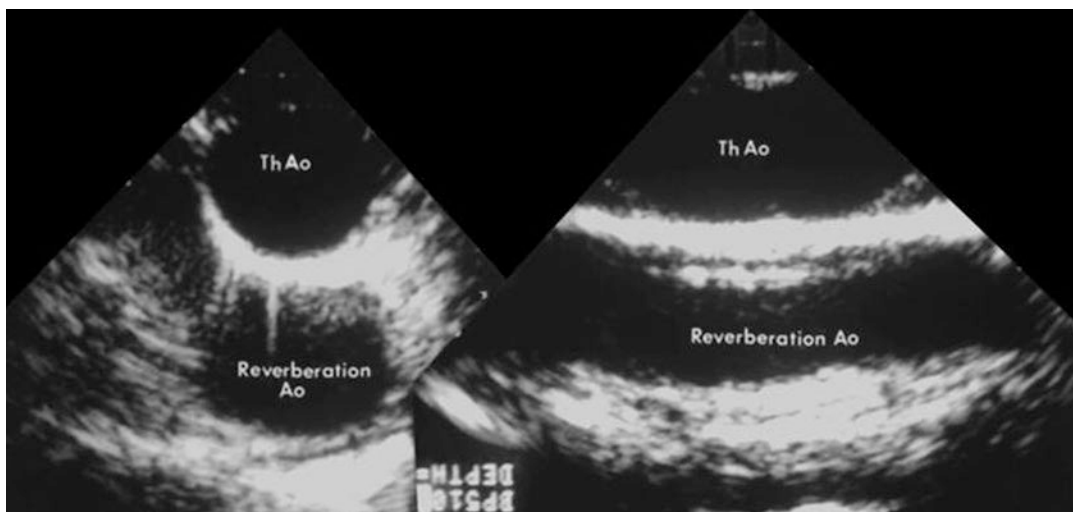


Fig. 8.9 Reverberation artifacts in descending thoracic aorta

between the left atrial appendage and left upper pulmonary vein appearing as a globular mass, fat laden fossa ovalis (Fig. 8.10) or lipomatous hypertrophy of the atrial septum interpreted as a mass (Fig. 8.11) and surgical sutures appearing filamentous or pedunculated and interpreted as mass or vegetations.

- “Echo-free spaces”: Certain normal structures generate echo-free spaces and may be

incorrectly interpreted as cysts or abscesses. These include the transverse and the oblique sinus.

- *Other difficulties* that may be encountered during TEE include the adequate visualization and quantification of aortic valve regurgitation, aortic valve and pulmonary valve gradient estimation and non-foreshortened visualization of the left ventricular apex.

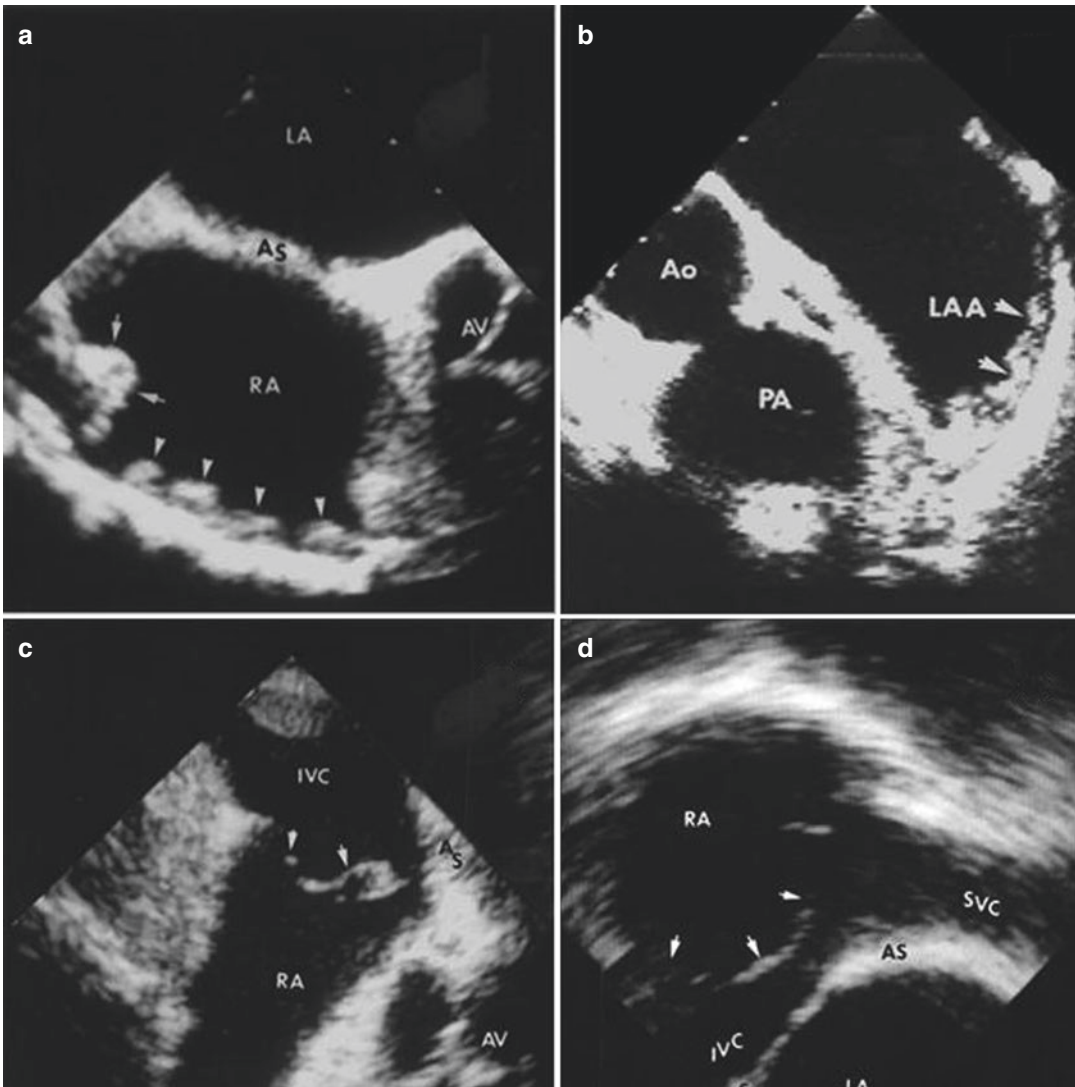


Fig. 8.10 Panel **a** and **b** show the appearance of pectinate muscle in right and left atrial appendage respectively which may be confused as thrombi. Panel **c** and **d** show

the appearance of Eustachian valve in the right atrium which may be interpreted as an abnormal structure

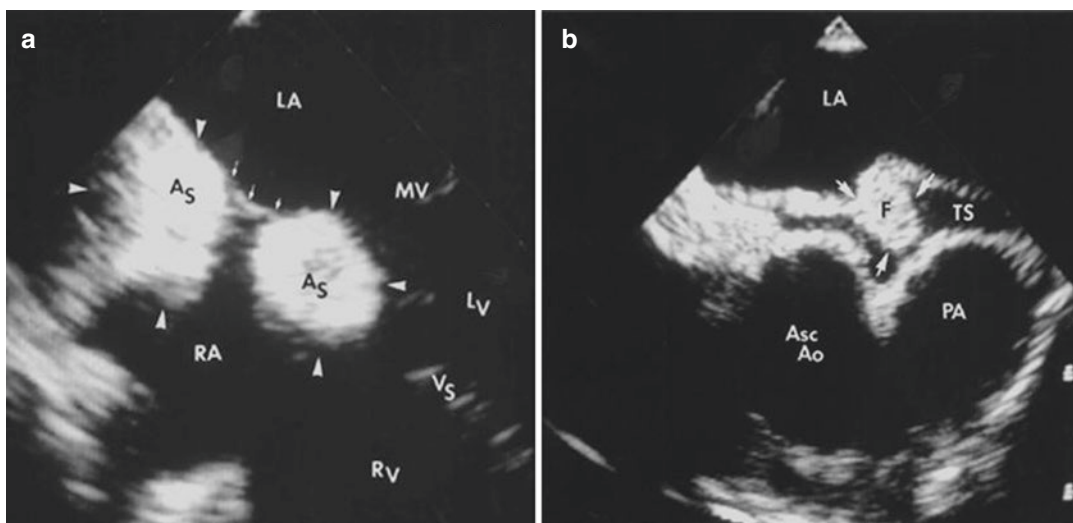


Fig. 8.11 Diagnostic pitfalls during TEE. Lipomatous inter-atrial septum (panel **a**), the membrane of the fossa ovalis is spared while the remaining septum is thickened

- Finally, ultrasound transducers generate heat. During prolonged monitoring, the device may be required to be shut down periodically to allow cooling.

Complications

Procedural risks are low in trained hands. However, they need to be explained clearly to the patient. These include transient throat pain, laryngospasm, aspiration, hypotension, hypertension, tachycardia, mucosal bleeding, esophageal rupture and rare risk of death. Benzocaine topical spray can cause toxic methemoglobinemia. The treatment is administration of methylene blue in addition to supportive measures. Being semi-invasive, appropriate training requirements are needed and have been laid down by both, the American Society of Echocardiography [24] and the British Society of Echocardiography.

Conclusions

Easy applicability, lower costs, portability, and instantaneous availability of test results have made TEE a valuable imaging modality in clinical cardiology. The utility of TEE in visualizing

resulting in a dumbbell mass like appearance. Panel (**b**) shows normal appearance of the transverse sinus which appears as an echo free space

cardiovascular structures and its incremental value over transthoracic echocardiography have been well established. Future miniaturization of the TEE transducer design is likely to improve application in a wider sub-group of patients including premature infants, children, pregnant women, and patients with hemodynamic instability. A smaller probe design would help minimize discomfort from longer monitoring of cardiovascular hemodynamics and therapy.

TEE provides high quality two dimensional images, which therefore provide a basis for 3-D reconstructions. Since the atrial cavities lie close to esophagus, TEE is likely to be useful for 3-D imaging of regurgitation jets, particularly those with eccentric orifices and orientations. Real time 3-D imaging would also facilitate accurate monitoring of catheter based techniques, radiofrequency ablations and for intraoperative monitoring of surgical techniques that require appreciation of complex geometries like the valves and the subvalvular apparatus.

References

1. Side CD, Gosling RG. Non-surgical assessment of cardiac function. *Nature*. 1971;232:335–6.
2. Frazin L, Talano JV, Stephanides L, et al. Esophageal echocardiography. *Circulation*. 1976;54:102–8.

3. Hisanaga KHA, Nagata K, Yoshida S. A new transesophageal real time two dimensional echocardiographic system using a flexible tube and its clinical application. *Proc Jpn Soc Ultrason Med.* 1977;32:43–4.
4. Seward JB, Khandheria BK, Freeman WK, et al. Multiplane transesophageal echocardiography: image orientation, examination technique, anatomic correlations, and clinical applications. *Mayo Clin Proc.* 1993;68:523–51.
5. Pearlman AS, Gardin JM, Martin RP, et al. Guidelines for physician training in transesophageal echocardiography: recommendations of the American Society of Echocardiography Committee for physician training in echocardiography. *J Am Soc Echocardiogr.* 1992;5:187–94.
6. Vilacosta I, Graupner C, San Roman JA, et al. Risk of embolization after institution of antibiotic therapy for infective endocarditis. *J Am Coll Cardiol.* 2002;39:1489–95.
7. Bayer AS, Bolger AF, Taubert KA, et al. Diagnosis and management of infective endocarditis and its complications. *Circulation.* 1998;98:2936–48.
8. Heidenreich PA, Masoudi FA, Maini B, et al. Echocardiography in patients with suspected endocarditis: a cost-effectiveness analysis. *Am J Med.* 1999;107:198–208.
9. Khandheria BK, Seward JB, Oh JK, et al. Value and limitations of transesophageal echocardiography in assessment of mitral valve prostheses. *Circulation.* 1991;83:1956–68.
10. Palazzuoli A, Ricci D, Lenzi C, et al. Transesophageal echocardiography for identifying potential cardiac sources of embolism in patients with stroke. *Neurol Sci.* 2000;21:195–202.
11. Agmon Y, Khandheria BK, Gentile F, et al. Clinical and echocardiographic characteristics of patients with left atrial thrombus and sinus rhythm: experience in 20 643 consecutive transesophageal echocardiographic examinations. *Circulation.* 2002;105:27–31.
12. Leung DY, Black IW, Cranney GB, et al. Prognostic implications of left atrial spontaneous echo contrast in nonvalvular atrial fibrillation. *J Am Coll Cardiol.* 1994;24:755–62.
13. Kamp O, Verhorst PM, Welling RC, et al. Importance of left atrial appendage flow as a predictor of thromboembolic events in patients with atrial fibrillation. *Eur Heart J.* 1999;20:979–85.
14. Klein AL, Grimm RA, Murray RD, et al. Use of transesophageal echocardiography to guide cardioversion in patients with atrial fibrillation. *N Engl J Med.* 2001;344:1411–20.
15. Klein AL, Murray RD, Becker ER, et al. Economic analysis of a transesophageal echocardiography-guided approach to cardioversion of patients with atrial fibrillation: the ACUTE economic data at eight weeks. *J Am Coll Cardiol.* 2004;43:1217–24.
16. Smith MD, Cassidy JM, Souther S, et al. Transesophageal echocardiography in the diagnosis of traumatic rupture of the aorta. *N Engl J Med.* 1995;332:356–62.
17. Keren A, Kim CB, Hu BS, et al. Accuracy of biplane and multiplane transesophageal echocardiography in diagnosis of typical acute aortic dissection and intramural hematoma. *J Am Coll Cardiol.* 1996;28:627–36.
18. Agmon Y, Khandheria BK, Meissner I, et al. Relation of coronary artery disease and cerebrovascular disease with atherosclerosis of the thoracic aorta in the general population. *Am J Cardiol.* 2002;89:262–7.
19. Russo A, De Luca M, Vigna C, et al. Central pulmonary artery lesions in chronic obstructive pulmonary disease: a transesophageal echocardiography study. *Circulation.* 1999;100:1808–15.
20. Pascoe RD, Oh JK, Warnes CA, et al. Diagnosis of sinus venosus atrial septal defect with transesophageal echocardiography. *Circulation.* 1996;94:1049–55.
21. Mas JL, Arquiza C, Lamy C, et al. Recurrent cerebrovascular events associated with patent foramen ovale, atrial septal aneurysm, or both. *N Engl J Med.* 2001;345:1740–6.
22. Randolph GR, Hagler DJ, Connolly HM, et al. Intraoperative transesophageal echocardiography during surgery for congenital heart defects. *J Thorac Cardiovasc Surg.* 2002;124:1176–82.
23. Scalia GM, McCarthy PM, Savage RM, et al. Clinical utility of echocardiography in the management of implantable ventricular assist devices. *J Am Soc Echocardiogr.* 2000;13:754–63.
24. Shanewise JS, Cheung AT, Aronson S, Stewart WJ, et al. ASE/SCA guidelines for performing a comprehensive intraoperative multiplane transesophageal echocardiography examination: recommendations of the American Society of Echocardiography Council for intraoperative echocardiography and the Society of Cardiovascular Anesthesiologists Task Force for certification in perioperative transesophageal echocardiography. *J Am Soc Echocardiogr.* 1999;12:884–900.

Part II

Valvular Heart Disease

Aortic Pathology

9

Richard A. E. Wheeler

Anatomy of the Aortic Valve and Aortic Root

When assessing any patient with aortic valvular disease it is essential to understand the basic anatomy of the valve and integral to this approach is an appreciation of the surrounding aorta which together with the leaflets forms a functional unit. This is particularly important when considering the different causes of aortic regurgitation. The aortic root describes the aortic valve from its location at the left ventricular outlet to the sinotubular junction [1]. The aortic sinuses are formed from the three bulges within the root with two being named according to the location of the left and right coronary arteries and the third logically called the non-coronary sinus. The coronary arteries arise close to the level of the sinotubular junction. The right coronary sinus is the largest including its height with the left coronary sinus being the smallest. This leads to a slight tilt to the plane of the sinotubular junction in relation to the plane at the base of the sinuses. The aortic sinuses are at their largest in diastole facilitating coronary blood flow in diastole.

The leaflets are then named accordingly and are attached to the aortic root in a semilunar

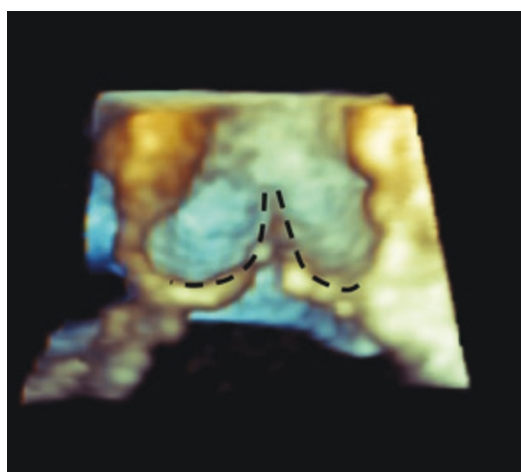


Fig. 9.1 3D transoesophageal echo of the aortic root demonstrating the arrangement of the leaflets (dashed lines) and aortic sinuses

fashion (Fig. 9.1). This anatomical arrangement explains why the aortic valve does not have a true fibrous annulus, although we often refer to the measurement at the hinge points of the leaflets in that way for clinical reasons when assessing valve size. The normal aortic valve (AV) has an area of approximately 3.0–4.0 cm² (Fig. 9.2).

Aortic Stenosis

The accurate assessment of aortic stenosis (AS) is a core component of adult echocardiography given the frequency of this condition and the

R. A. E. Wheeler
Department of Cardiology, University Hospital
of Wales, Cardiff, UK
e-mail: Richard.Wheeler@wales.nhs.uk

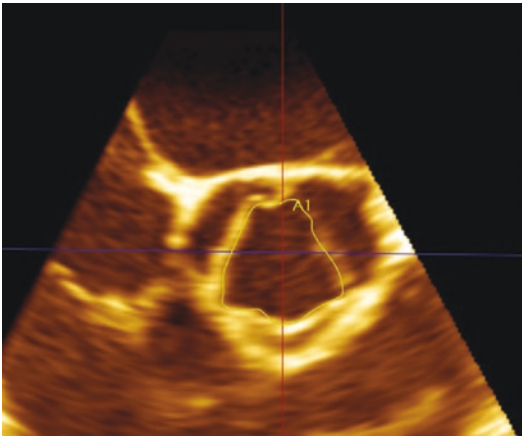


Fig. 9.2 3D transoesophageal echo in short axis showing a normal aortic valve in mid systole fully open. The planimetry measured 3.1 cm²

significant mortality and morbidity with which it is associated. In Western populations approximately one quarter of the people over 65 have a degree of valve thickening with 3% over 75 having severe stenosis [2]. The commonest cause of AS is acquired due to age related degenerative disease characterised by calcification of a previously normal trileaflet valve (Table 9.1, Fig. 9.3). This process is slow taking place over many years and in its early stages is often referred to as aortic

Table 9.1 Causes of aortic stenosis

Degenerative calcific
Bicuspid
Rheumatic
Congenital

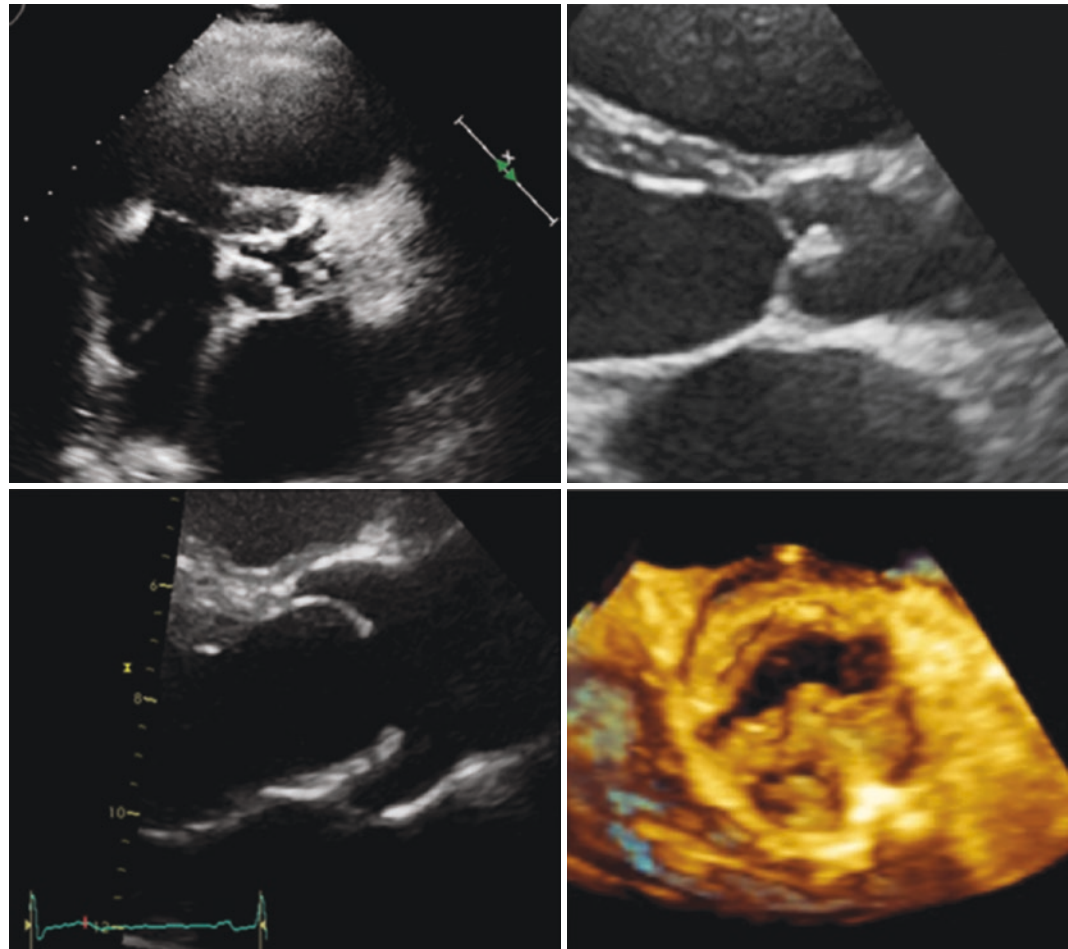


Fig. 9.3 Parasternal short axis of a degenerative aortic valve with moderate stenosis (top left).Parasternal long axis view of a rheumatic aortic valve with characteristic thickening at the leaflet tips (top right). Parasternal long

axis view of a bicuspid valve with characteristic doming of the leaflets in systole (bottom left). Transoesophageal echo 3D short axis of a bicuspid valve with mild stenosis (bottom right)

sclerosis with valve thickening starting at the base of the leaflets but with no haemodynamic stenosis. Bicuspid valves have a prevalence of between 0.5 and 2% within the population and are another very important group of patients with AS [3]. The associated aortopathy with this condition and the higher risk of aortic dissection demands a particularly thorough approach. Rheumatic AS is now a much smaller group in the West but remains important on a worldwide basis. It is important to differentiate rheumatic disease as the pathology causing stenosis is fundamentally different with leaflet thickening and commissural fusion. True congenital AS often involves a unicuspid valve but is usually diagnosed in childhood and is most often the remit of paediatric cardiology.

Pathophysiology

The fundamental principle is of chronic pressure overload with increased left ventricular (LV) systolic blood pressure, increased myocardial mass and prolonged ejection time. LV function is maintained by the gradual development of compensatory concentric left ventricular hypertrophy (LVH). This leads to an increased myocardial oxygen demand which in turn promotes a detrimental effect on global LV function. Eventually with the onset of LV dilatation the ejection fraction falls and there is an increase in LV filling pressure which is also translated to increased pulmonary pressures [4]. Most patients are symptomatic at this late stage in the disease and it is well established that the onset of symptoms represents an ominous course in terms of increased mortality and sudden cardiac death. The long latent phase prior to this period is one of the key reasons why thorough clinical and echo assessment is so important.

With this knowledge it therefore follows that the key areas of echo assessment are:

- Aortic valve structure and morphology with two dimensional (2D) echo.
- Quantification of the degree of stenosis.
- LV function including wall thickness.
- Coexisting valve disease.
- Right heart evaluation, particularly pulmonary artery pressure.

Echo Assessment of Aortic Stenosis

Morphology

The first part of any valve assessment starts with structure and morphology with 2D echo. (For the majority of cases this can be achieved with transthoracic echo [TTE] but where imaging is suboptimal then transoesophageal echo [TOE] may be very helpful.) This allows us to determine whether the AV is trileaflet or bicuspid and also to discern the level of obstruction i.e. valvar, sub-valvar or supra-valvar. The parasternal long and short axis projections are the standard views to obtain these data. Particular emphasis must be placed on leaflet thickening and the presence and location of calcification. With degenerative disease this usually starts at the base of the leaflets. It is helpful to describe leaflet thickening using a semi-quantitative gradation of mild, moderate or severe. The presence of calcification is important as this has implication for adverse outcome [5] and potentially for surgical technique at the time of valve replacement, if the changes are extensive. Remember that the hallmark for detecting calcification on echo is the presence of dropout distally.

Measuring the diameter of the left ventricular outflow tract (LVOT) is performed from these parasternal long axis views. 2D zoom is preferable to maximise accuracy. This is a hugely important measurement as we shall see in the next section covering quantification of AS and the continuity equation. Ideally the measurement should be at the same point as where the PW doppler signal is obtained during the apical 5 chamber analysis, and certainly within 1 cm of the hinge points of the aortic leaflets (Fig. 9.4). Measurement of the aortic annulus is subtly different but has received increased attention and description in recent years due to the growth of transcatheter aortic valve implantation (TAVI). The aortic annulus is measured from the hinge points of the leaflets from inner edge to inner edge in mid systole [6]. This is often a difficult measurement due to protruding calcium and thickening into the lumen which should not be included as this would lead to significant underestimation of the diameter (Fig. 9.5). It is well described that the LVOT and aortic annulus

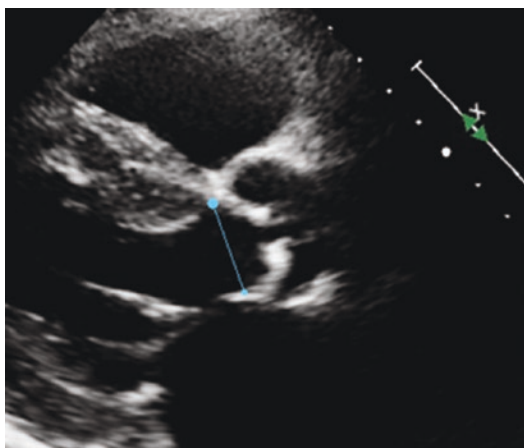


Fig. 9.4 Parasternal long axis view showing measurement of the LVOT diameter taken in mid systole

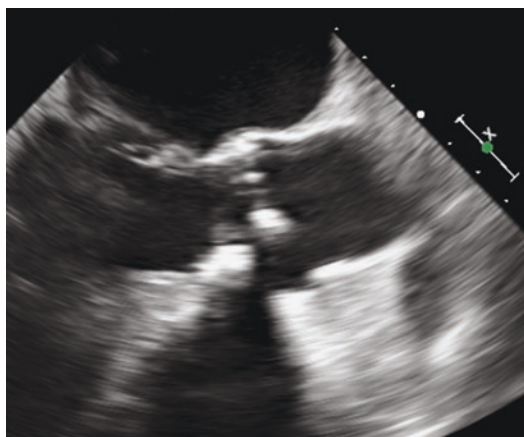


Fig. 9.5 Transoesophageal long axis view showing a challenging image to measure due to calcification extending into the LVOT

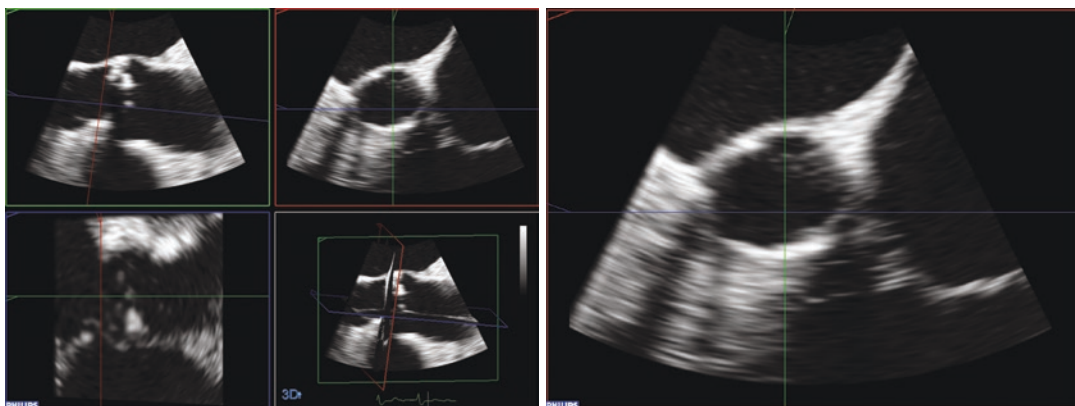


Fig. 9.6 Reconstructed 3D TOE image showing the oval shape of the LVOT (right)

may be elliptical in shape and this is one of the limitations of a one dimensional measurement in the parasternal projection. 3D echo, particularly on TOE, can help to improve the accuracy by assessing the orthogonal plane or the area (Fig. 9.6).

A thorough assessment of the aortic root and ascending aorta is mandatory in all patients with aortic valve disease and will be covered later in the chapter.

Leaflet mobility must also be described and indeed this can often give important clues as to the type of valve. For example, with a bicuspid valve the leaflets may be seen to dome in systole. Young adults may have significant stenosis of a bicuspid valve without calcification. This can be easily overlooked in the short axis projection if

images are taken below the leaflet tips giving the impression of non-severe stenosis. There may also be an eccentric closure line when viewed in the long axis projection. In older patients, extensive leaflet thickening and calcification within a bicuspid valve can make it very difficult to distinguish from a degenerative trileaflet valve.

Bicuspid valves most often result from fusion of the right and left coronary cusps (80%), with the next most common type showing fusion of the right and non-coronary cusps (20%). Fusion of the non and left coronary cusps is rare. When viewing a bicuspid valve in the closed position (diastole) it may appear to be trileaflet if there is raphe present. For this reason it may be more accurate to make the diagnosis in systole trying to observe an elliptical orifice and only two commissures.

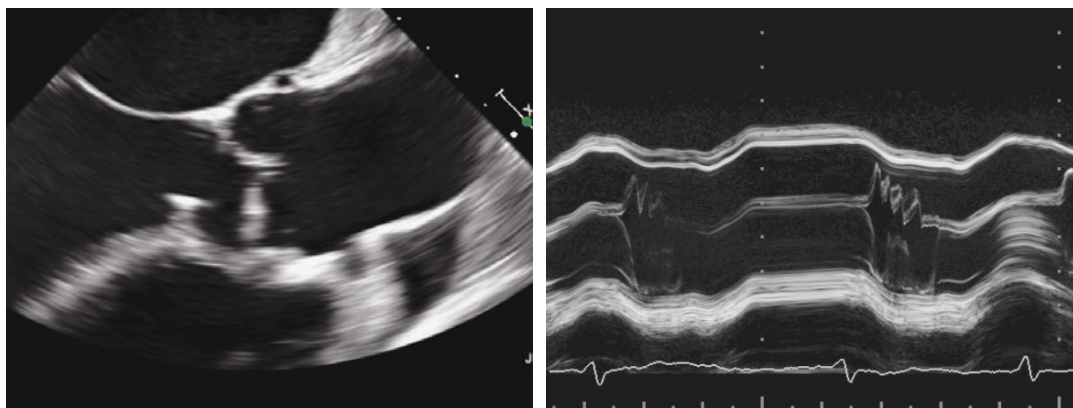


Fig. 9.7 TOE long axis image of a subaortic membrane causing mild subvalvar stenosis. The image on the right is the corresponding M-mode showing fluttering of the aortic leaflets due to the turbulent flow

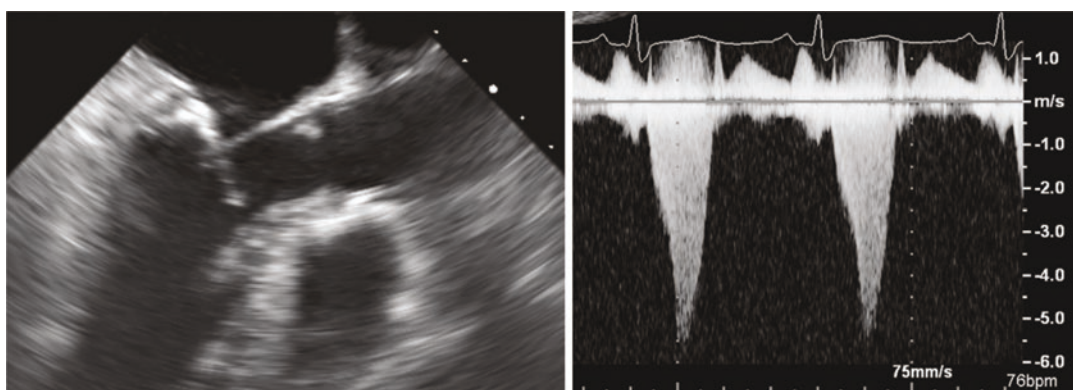


Fig. 9.8 On the left is a TOE long axis view of a patient with mild septal hypertrophy but marked systolic anterior motion of the mitral valve and dynamic LVOT obstruction.

The CW Doppler signal is shown on the right with the characteristic dynamic waveform

Rheumatic valves are characterised by commissural fusion and leaflet thickening which is particularly prominent at the tips and along the edges of the leaflets. This may lead to a more triangular shaped orifice. The mitral valve is frequently involved in the rheumatic process and therefore there will often be clues to the underlying aetiology from analysis of the other valves.

Defining the level of obstruction is always important in patients with a suspicion of AS or being referred on the basis of a systolic murmur. Most experienced sonographers tend to stick to a sequence of 2D, colour flow, pulsed wave (PW) and continuous wave Doppler (CW) imaging in order to minimise the chances of missing such pathologies. In subvalvar stenosis there may be an

obvious anatomical abnormality such as marked septal hypertrophy or the presence of a sub-aortic membrane (Fig. 9.7). Sometimes the septal hypertrophy is relatively mild but with coexistent systolic anterior motion of the mitral valve causing subvalvar obstruction (Fig. 9.8). Colour Doppler will define in more detail where any turbulence might start from. Initial parasternal views will then be followed by the apical 5 chamber view in order to perform full spectral Doppler analysis. Subvalvar obstruction due to LVH may be dynamic with a characteristic late peaking velocity on CW Doppler. This particular waveform is often seen in patients with hypertrophic cardiomyopathy but is not pathognomonic of the condition. The same type of waveform due to outflow tract obstruction can be seen under certain

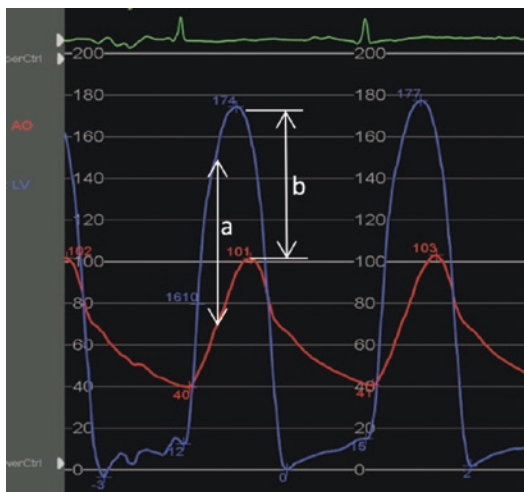


Fig. 9.9 Catheter lab data showing simultaneous measurement of LV and aortic pressures in a patient with severe aortic stenosis undergoing TAVI. Measurement a shows the peak instantaneous gradient which is usually higher than the ‘peak to peak’ (b)

physiological conditions such as underfilling and tachycardia. This is actually a common finding in more elderly patients undergoing major surgery or with intercurrent critical illness with these adverse loading conditions. A diagnostic echo on intensive care under such circumstances can greatly help the management of a patient to guide correction of these parameters e.g. adequate filling, avoiding inotropes and controlling heart rate.

Quantification of Stenosis

The quantification of aortic stenosis follows on in a logical way after the initial assessment of structure and morphology and is crucial to the clinical management of the patient. It is well established that the non-invasive quantification of aortic stenosis with echocardiography can be used in preference to invasive catheter based measurements. There are however, fundamental differences in these measurements with echo measuring a peak instantaneous gradient rather than a ‘peak to peak’ gradient. Peak instantaneous measurements are higher than ‘peak to peak’ and occur at an earlier point in systole (Fig. 9.9). The key measurements include the peak aortic velocity, the mean gradient and the aortic valve area by the continuity equation. The ratio of the peak aortic

velocity to the LVOT velocity can also be useful in certain circumstances.

Key measurements for the quantification of aortic stenosis

- Peak transaortic velocity
- Mean transaortic gradient
- Aortic valve area by the continuity equation
- Ratio of the peak to LVOT velocity

The peak transaortic pressure gradient is calculated from the peak velocity according to the simplified Bernoulli equation which assumes that the velocity proximal to the valve is low enough to be ignored i.e. <1 m/s:

$$\Delta P = 4V^2$$

If velocities within the LVOT exceed approximately 1.5 m/s then this should be taken into account as follows:

$$\Delta P = 4(V_{\max}^2 - V_{\text{LVOT}}^2)$$

Mean gradients are measured by tracing around the outside of the CW Doppler waveform. This is effectively the same as averaging all the peak instantaneous gradients throughout systole. Most clinical situations utilise peak gradients from echo but there are a number of situations where mean gradients can be helpful including the assessment of prosthetic valves.

These measurements are taken from the apical 5 chamber view using continuous wave Doppler. Pulse wave Doppler is used for the LVOT velocities. Every effort should be made to ensure parallel alignment of the Doppler beam with the direction of blood flow as deviation from this angle of insonation will lead to underestimation of velocities. This can be achieved by good positioning of the patient but also considering alternative echo windows such as right parasternal and the suprasternal notch using the non-imaging transducer (pencil probe). It is inadvisable to use angle correction algorithms which some manufacturers have developed. When trying to obtain the perfect apical 5 chamber view it may be necessary to move the transducer more laterally in order to achieve the best alignment (Fig. 9.10).



Fig. 9.10 Trying to achieve a good quality apical 5 chamber image for CW Doppler of the transaortic gradient is often facilitated by moving the transducer further around into the axilla (right). This allows excellent align-

ment to the direction of blood flow as compared to a more medial position (left) which often leads to underestimation of the peak aortic velocity

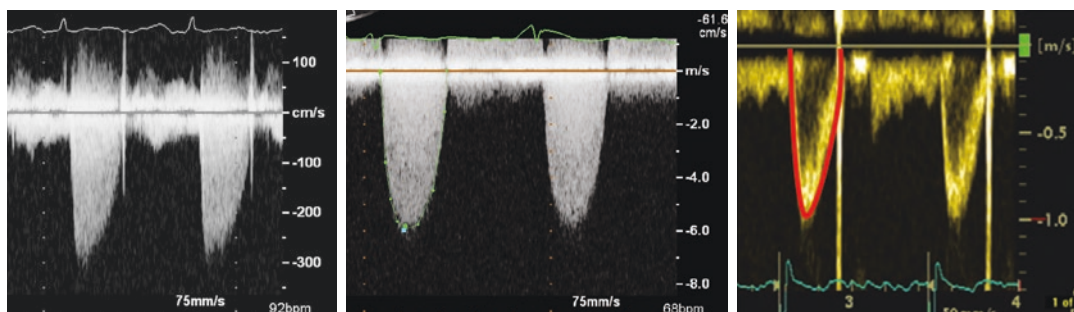


Fig. 9.11 CW Doppler showing an example of moderate aortic stenosis with a triangular shaped profile (left) as compared to a patient with critical stenosis with a gradual

upslope and extremely high peak velocities (middle). The image on the right shows a PW Doppler signal with an example of how to measure the VTI

Spectral Doppler should always be guided by colour flow imaging to be sure as to where you are recording data. This is particularly important if there is a parallel jet of mitral or tricuspid regurgitation in close proximity which may be erroneously recorded.

When recording spectral Doppler, the display should be optimised including the gain, velocity scale and sweep speed to allow the most accurate off line analysis. When recording PW Doppler for LVOT velocities the wall filters may need to be reduced to make sure there is no gap in data near the baseline. It is important to record up to five beats, particularly in atrial fibrillation, to allow mean calculations.

The peak velocity is usually the most important component of the CW Doppler signal through the aortic valve but there are other key

points. The shape of the tracing can help in the determining the severity of disease. For example, in critical aortic stenosis there will be a more gradual upslope of the tracing with the maximum velocity occurring later in systole. This is the Doppler correlate of a slow rising pulse on clinical examination (Fig. 9.11). In moderate aortic stenosis there is often a very brisk upstroke with the peak velocity occurring early in systole. We have already seen the characteristic shape of the CW Doppler with dynamic LVOT obstruction as distinct from fixed valvar stenosis.

It is crucial to understand that pressure gradients and hence transaortic velocity depends on the volume of flow across the valve and therefore there are a number of conditions which will influence these data. The commonest clinical example is from impaired LV function which will lower

transaortic gradients producing the pathophysiology of low flow/low gradient aortic stenosis which will be covered separately. Significant mitral regurgitation may also reduce transaortic flow which can lead to underestimation of gradients. The reverse is true for aortic regurgitation which increases stroke volume and therefore may lead to overestimation of the degree of aortic stenosis.

Continuity Equation

The aortic valve area (AVA) can be calculated using the continuity equation which uses the principle that the stroke volume proximal to the valve within the LVOT is the same as the stroke volume at the point of stenosis. The equation requires three components:

- LVOT diameter
- LVOT velocity time integral
- Peak aortic velocity time integral

The stroke volume within the LVOT can be calculated by multiplying the cross sectional area (CSA) by the velocity time integral (VTI). It therefore follows that the continuity equation can be written:

$$AVA \times VTI_{AV} = CSA_{LVOT} \times VTI_{LVOT}$$

One of the key advantages of the continuity equation is that it is less flow dependent than relying on peak gradients. However, great care needs to be taken in measuring each of these components. We have already described the measurement of the LVOT diameter in the previous section. The LVOT VTI is taken with PW Doppler from the apical 5 chamber or apical 3 chamber views. It is important to have a smooth outline and a distinct peak which allows tracing of the modal velocity (Fig. 9.11).

Pitfalls of the Continuity Equation

It can be seen from the equation that by using cross sectional areas the measurements of the LVOT diameter are squared. This helps to explain why errors in LVOT diameter are often the biggest source of discrepancy when calculating AVA. Previous studies should always be looked at when patients attend for serial monitoring in clinic. This helps to define which acoustic window will

give the optimal views and indeed whether previous measurements were accurate. LVOT diameters do not change significantly over time. If there is particular difficulty making this measurement from TTE then one should consider the use of transoesophageal echo. The continuity equation assumes a circular LVOT area and it is increasingly recognised that many patients have an elliptical shape. This may be another reason to consider TOE (including 3D) in order to assess in more detail.

Using the velocity ratio between the LVOT and the transaortic measurements can be an additional tool in the quantification of aortic stenosis. This can be done either with peak velocities or with the respective VTIs. A normal valve has a ratio of 1 whilst severe stenosis will be present when the ratio is 0.25 or less. This parameter is often known as the dimensionless index.

The final point relates to the fact that when using the continuity equation we are measuring effective orifice area (EOA) rather than anatomical areas which tend to be slightly larger. However, this rarely makes any important difference in terms of clinical management. Anatomical AVA can be measured using planimetry in a short axis projection. Whilst this measurement may be less flow dependent, it is often inaccurate due to difficulty in defining the precise edge of the leaflets even when TOE is used.

Clinical Decision Making in Aortic Stenosis

For many patients the interpretation of the data listed in Table 9.2 will be straight forward with little controversy as to how to manage the patient. However, there are a number of more challenging scenarios which warrant further explanation. The surgical management of patients with significant aortic stenosis can be guided by a logical step-wise approach as seen in Fig. 9.12.

Low Flow/Low Gradient Aortic Stenosis with Impaired LV Function

If LV function is impaired then the peak and mean gradients across the aortic valve will be

Table 9.2 Quantification of aortic stenosis

	Mild	Moderate	Severe
Peak aortic velocity (m/s)	2.6–2.9	3.0–4.0	>4.0
Mean gradient (mmHg)	<20	20–40	>40
AVA (cm ²)	>1.5	1.0–1.5	<1.0
Indexed AVA (cm ² /m ²)	>0.85	0.6–0.85	<0.6
Dimensionless index			<0.25

Note that indexed measurements need to be interpreted with caution with more obese patients as AVA does not increase with body weight per se

reduced. This is defined within a scenario where LV ejection fraction is <50%, a mean gradient <40 mmHg and a calculated AVA by the continuity equation <1.0 cm² [7]. One of the key learning points here is to first be aware that the patient can still have severe aortic stenosis despite these lower than expected numbers. Dobutamine stress echo may be useful in such patients to distinguish true severe aortic stenosis with contractile reserve from moderate aortic stenosis but impaired LV function. This is of great importance for clinical management as patients with poor contractile reserve have high operative mortality for aortic valve replacement. Dobutamine stress echo should be performed with caution given the risks of arrhythmias. True severe aortic stenosis can be defined as a mean gradient >40 mmHg at any point during the infusion or EOA <1.2 cm². Contractile reserve is most reliably assessed by an increase in the LVOT VTI of >20%.

Low Flow/Low Gradient Aortic Stenosis with Preserved LV Function

A typical example of this situation is where we encounter a peak velocity of <4 m/s but a calculated AVA by the continuity equation of <1.0 cm². This can occur for a number of reasons and has received more attention in recent years due to recognition of the problem in our growing cohort of more elderly patients. If the LV is anatomically small e.g. in a patient with reduced body surface area (BSA) the stroke volume may be low but with a normal ejection fraction. Another contributor to a small LV might be significant concentric LVH. The reduced stroke volume leads

to reduced transaortic flow and hence reduced gradients. The LVOT VTI may provide the first clue to reduced stroke volume with measurements <15 cm. Several other coexisting pathologies will also contribute to this phenomenon e.g. severe diastolic dysfunction, mitral regurgitation, mitral stenosis, right heart dysfunction and tricuspid regurgitation. Increased afterload can also reduce peak aortic gradients which again may be commonly found in elderly hypertensive patients. This can be calculated using Valvulo-arterial impedance but this is not a widely used parameter.

Mixed Aortic Valve Disease

In patients with coexistent aortic regurgitation the stroke volume may be increased leading to higher than expected peak and mean gradients across the aortic valve. This may give a dataset of a peak gradient >4 m/s but with an EOA of >1.0 cm². The interpretation of this situation is helped by careful assessment of valve morphology to define the dominant haemodynamic lesion and also studying the shape of the CW Doppler which may have the characteristic early peaking triangular profile in moderate aortic stenosis.

Aortic Regurgitation

Aortic regurgitation (AR) shares many of the key themes of aortic stenosis being a common valve lesion and with echocardiography remaining the key imaging tool for diagnosis and quantification. The list of possible causes of this condition are diverse and often dictates that the clinician has a good understanding of coexistent medical problems which can be intimately related (Table 9.3).

Pathophysiology

Aortic regurgitation is characterised by volume overload with the inevitable consequences to LV size and function. The precise changes that occur depend very much on the particular aetiology as AR can develop acutely in conditions

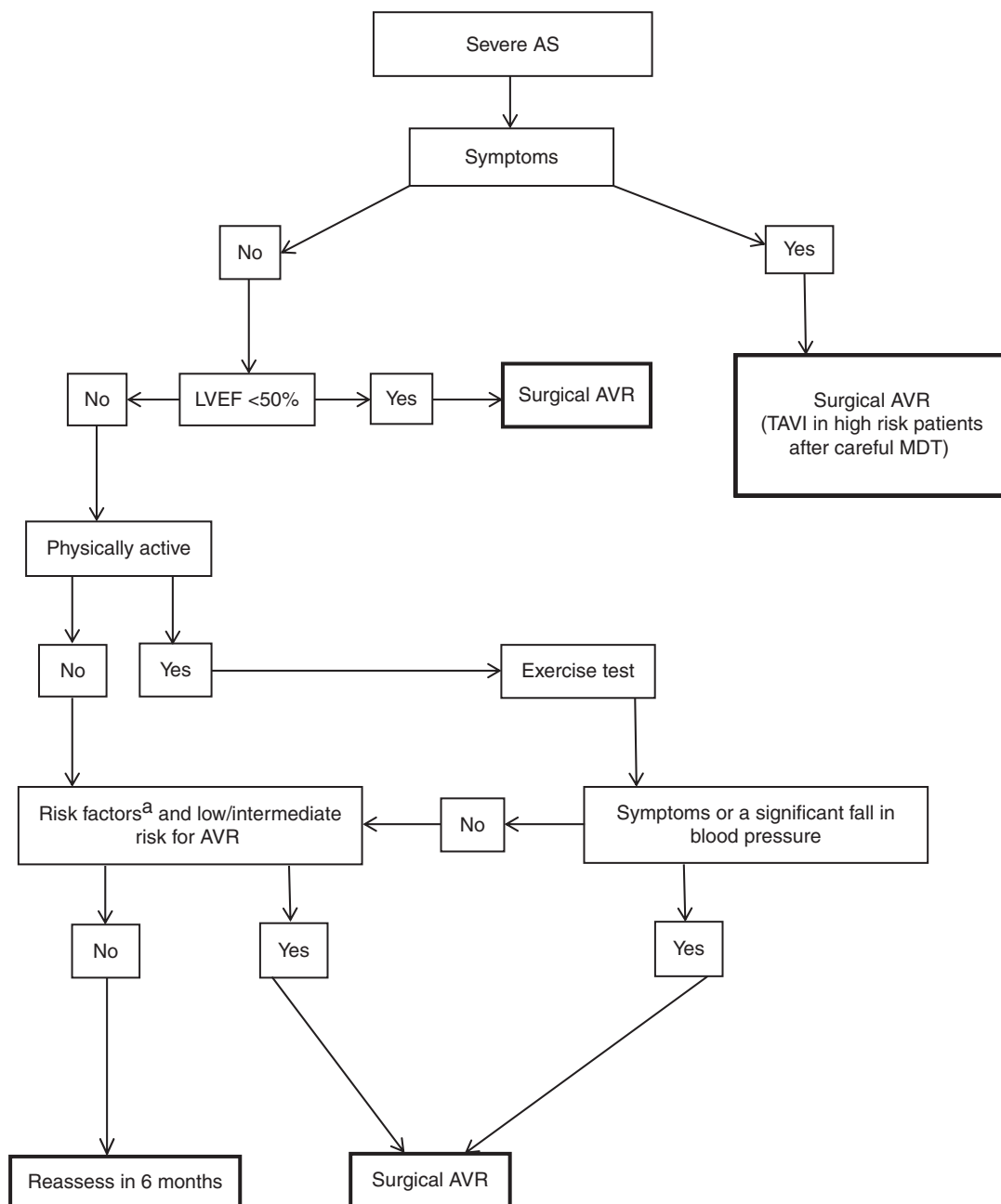


Fig. 9.12 Surgical management of aortic stenosis. ^a Risk factors include peak velocity >5.5 m/s, severe valve calcification and progression of peak gradient ≥ 0.3 m/s per year. Adapted from [7]

such as infective endocarditis or dissection. In the chronic state, there is progressive dilatation of the LV with compensatory LV hypertrophy to maintain cardiac output. Unlike in mitral regurgitation where the LV may be considered to be ‘off loaded’, AR leads to a chronic increase in

afterload which further contributes to LV hypertrophy and eventually irreversible dysfunction. This is one of the reasons why detailed assessment of LV function is so important in the assessment of patients with AR as this is often the main factor which dictates the timing of aortic valve

Table 9.3 Causes of aortic regurgitation

Disease of the leaflets	Disease of the aortic root
Degenerative	Idiopathic root dilatation
Bicuspid	Hypertension
Rheumatic	Aortoannular ectasia
Infective endocarditis	Aortic dissection
Myxomatous disease	Marfan's syndrome
Congenital—unicuspid/ quadricuspid	Loeys-Dietz syndrome
Reiter's syndrome	Ehlers-Danlos syndrome
Aortic cusp prolapse with VSD	Osteogenesis imperfecta
Anorectic drugs	Syphilitic aortitis
Trauma	

replacement if there is progressive dilatation or evidence of impaired systolic function.

Echo Assessment of Aortic Regurgitation

Morphology

As described for aortic stenosis, the starting point of echo assessment is 2D imaging of the valve to identify the anatomy and to decide on aetiology. Given the list of possible causes listed above one can easily appreciate that careful analysis of the aortic root is equally important to leaflet pathology. Dilatation of the aortic root, for example in Marfan's syndrome will lead to malcoaptation of the leaflets (even if they are morphologically normal) with resultant aortic regurgitation. Measurements of the aorta should include the sinuses of Valsalva, the sinotubular junction and the ascending aorta which are all taken in diastole (see section on the aorta). If the ascending aorta is not well seen then alternative modalities should be used such as TOE or CT/MRI.

Degenerative disease may give rise to a mixed picture of aortic stenosis and regurgitation. Bicuspid valve disease is often in association with dilatation of the ascending aorta and therefore particular care should be taken to image as much of the thoracic aorta as possible. The ascending aorta can be well seen from a parasternal view but in a higher ribspace. Identification of mobile masses and destruction of the aortic leaflets will help to confirm a clinical diagnosis of endocarditis which may have been suspected due to sepsis and a diastolic murmur of AR.

In some patients with AR there can be additional data obtained from views of the mitral valve with reduced opening of the anterior leaflet. M-mode can also help to assess high frequency fluttering of the anterior leaflet which is the basis of the Austin-Flint murmur by auscultation.

Quantification of Aortic Regurgitation

Colour Doppler

Colour flow Doppler is frequently the most important component when analysing AR and follows on immediately after 2D imaging. Multiple views should be obtained to define the jet including parasternal long and short axis, apical 5 and apical 3 chamber. Care should be taken to ensure that the correct colour scale and gain settings are used. The three main parts of the AR jet are the flow convergence zone, the vena contracta and the turbulent jet within the LV (Fig. 9.13). Colour Doppler semi-quantitation of aortic regurgitation is shown in Table 9.4.

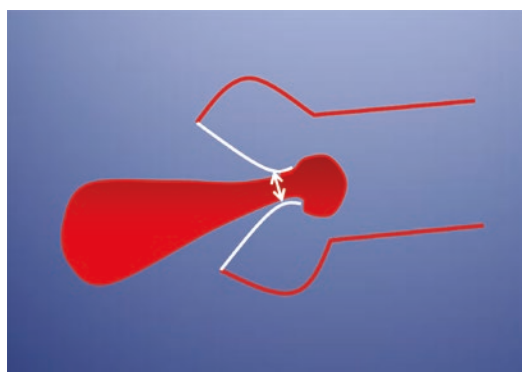


Fig. 9.13 Schematic representation of a regurgitant jet showing the flow convergence zone, vena contracta (white arrow) and the turbulent jet

Table 9.4 Quantitative analysis of aortic regurgitation

	Severe AR
Jet width/LVOT diameter	$\geq 65\%$
Vena contracta	>6 mm
Pressure half time	<200 ms
Regurgitant volume	>60 ml
Regurgitant fraction	$\geq 50\%$
EROA	≥ 0.3 cm ²

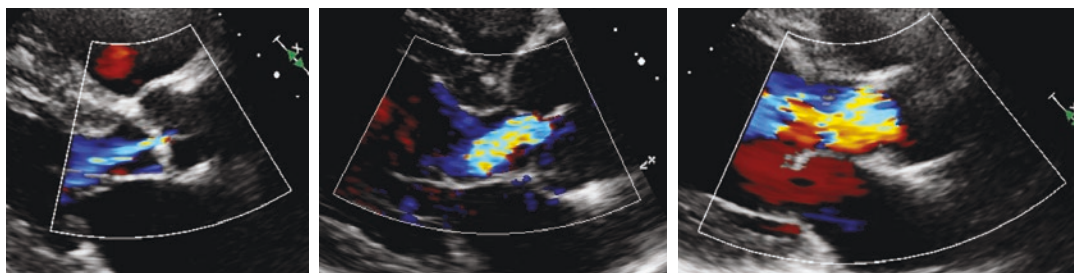


Fig. 9.14 Parasternal long axis views of three patients displaying mild, moderate and severe aortic regurgitation based on the width of the jet within the LVOT

Size of the Regurgitant Jet

Whilst this is often the easiest technique to visualise the AR jet it has limited use in quantification. Measurement of the jet area is not recommended as it can be influenced by loading conditions and will often be underestimated in the presence of eccentric flow. The width of the jet within the LVOT can be measured as a proportion of the total width of the LVOT (Fig. 9.14). A jet width ratio >65% is regarded as severe AR but this can be difficult to measure with eccentric jets.

Vena Contracta

The vena contracta is the narrowest part of the jet as measured on colour Doppler, downstream of the regurgitant orifice. This is slightly smaller than the anatomical orifice but this is rarely of any clinical consequence. The advantages of this parameter is that it is relatively independent of flow rate and is technically less demanding than other techniques. The vena contracta is best imaged in a zoomed parasternal long axis view and may require angulation of the transducer to a slightly off axis plane. >6 mm defines severe AR whilst <3 mm would be mild. Given the small numbers involved, one can see that very careful measurement is required in order to avoid large percentage errors which might lead to misdiagnosis of AR. Problems also arise when there are multiple jets or when the shape of the orifice is non-circular. TOE may allow more accurate measurements and there may be an emerging role for 3D analysis of the actual shape of the regurgitant orifice although there is not enough data at the moment to support its use in clinical practice.

Flow Convergence and PISA

The proximal isovelocity surface area (PISA) or flow convergence technique allows quantification of the degree of AR in a similar method used in mitral regurgitation. This is a difficult technique in AR and is often improved by the use of TOE to visualise the flow convergence zone in more detail. Zoomed images are used with the Nyquist limit reduced to optimise the hemispheric convergence zone and the colour scale adjusted towards the direction of the jet. By the principle of conservation of mass the flow rate at the PISA is equal to the flow rate at the regurgitant orifice.

$$\text{Flow rate} = 2\pi r^2 \times V_{\text{aliasing}}$$

Continuous wave Doppler is then used to record the regurgitant jet to allow measurement of the peak velocity and the velocity time integral. The effective orifice area (EROA) can be calculated by dividing the flow rate by the peak velocity.

$$\text{EROA} = \text{Flow rate} / V_{\text{max}}$$

Regurgitant volume (RV) can be calculated as follows:

$$\text{RV} = \text{EROA} \times \text{VTI}_{\text{AR}}$$

Quantification of Flow

It is possible to calculate the AR regurgitant volume by measuring total stroke volume at the LVOT and subtracting the mitral inflow stroke volume. This is a relatively simple principle but is prone to

error due to the number of calculations and geometric assumptions involved. Stroke volume (SV) at the LVOT is calculated in the usual way by measuring the diameter of the LVOT to calculate cross sectional area (CSA) and the velocity time integral (VTI) of flow using pulsed wave Doppler.

$$SV_{LVOT} = CSA \times VTI_{LVOT}$$

In the absence of mitral regurgitation, the mitral valve annulus is then measured in the apical 4 chamber view to obtain the cross-sectional area which is then multiplied by the VTI of mitral inflow taken at the level of the annulus rather than at the leaflet tips.

$$SV_{mitral} = CSA \times VTI_{mitral}$$

Regurgitant volume and regurgitant fraction can then be calculated. These measurements should be done regularly in the echo lab if a high standard of accuracy and reproducibility is to be achieved.

Continuous Wave Doppler

Good quality spectral Doppler analysis of the AR jet is mandatory and of course follows on after colour Doppler imaging. This is usually performed from the apical 5 chamber view but other views may be suitable if the angle of insonation is appropriate. The density of the CW signal can be used to

comment on severity but this is only a qualitative estimate. The bulk of the analysis is from the rate of deceleration (pressure half time) of the AR slope. As the degree of AR increases the deceleration time shortens as LV end diastolic pressure increases. A pressure half time of <200 ms is strongly suggestive of severe AR (Fig. 9.15). Pressure half time will be affected by LV and aortic compliance and of course will be very dependent on good alignment of the Doppler beam.

Flow Reversal in the Thoracic/Abdominal Aorta

In severe AR it may be possible to detect flow reversal in the descending thoracic aorta and/or the abdominal aorta. This is the echo correlate of DeRosier's sign during clinical examination. A small amount of flow reversal during early diastole in the descending thoracic aorta is normal. The key feature to demonstrate in severe AR is holodiastolic flow reversal (Fig. 9.16).

Clinical Decision Making in Aortic Regurgitation

Most patients with acute severe AR e.g. infective endocarditis or aortic dissection will be symptomatic and require urgent consideration of

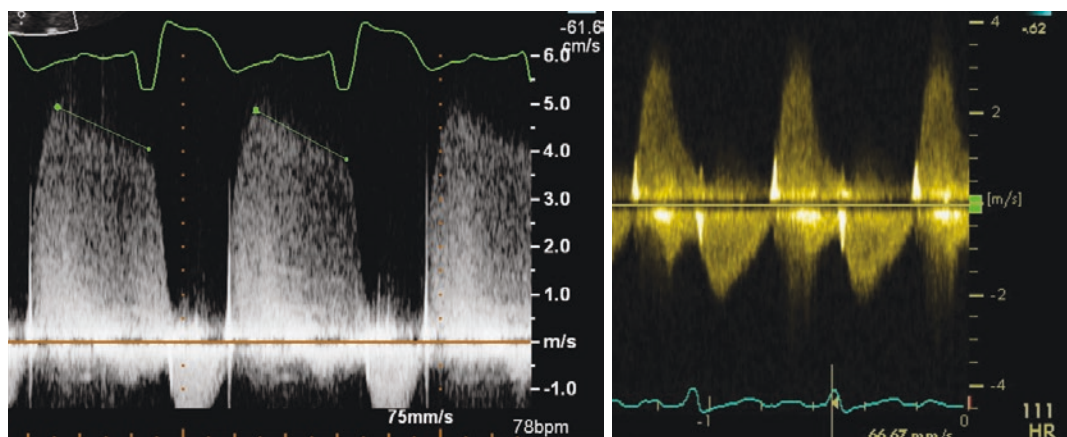


Fig. 9.15 CW Doppler from the apical 5 chamber view comparing mild AR with severe AR. The pressure half time in the first case (left) was >500 ms indicated by the

gradual slope. The CW trace in the severe AR case (right) is very steep and nearly reaches the baseline with a pressure half time of <200 ms

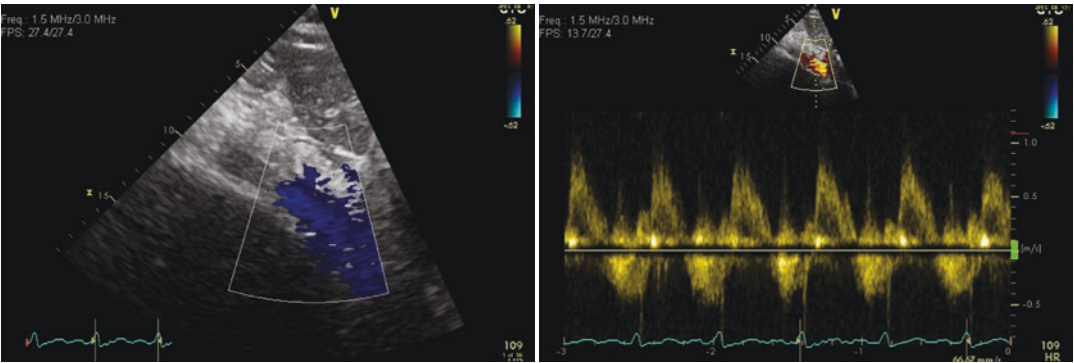


Fig. 9.16 Diastolic flow reversal in the abdominal aorta taken from the subcostal window. Note the holodiastolic flow reversal on PW doppler (below the line)

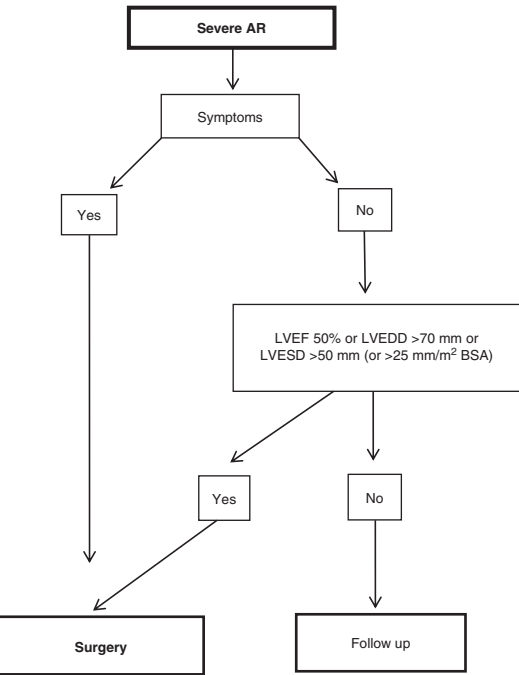


Fig. 9.17 Surgical management of aortic regurgitation. Adapted from [7]

surgery. The decision for surgery in chronic severe AR is more challenging and will take into account the presence of symptoms, LV function and the size of the aortic root/ascending aorta (Fig. 9.17).



Fig. 9.18 Large vegetations on the aortic valve prolapsing into the LVOT

Masses on the Aortic Valve

The commonest cause of a mass present on the aortic leaflets would be a vegetation in the context of infective endocarditis. This is often more clearly seen with TOE (Fig. 9.18) and will be covered in more detail in the chapter on endocarditis. Rarely one will see tumours attached to the leaflets and these can be benign such as a fibroelastoma (Fig. 9.19). These may be asymptomatic but can also be a cardiac source of embolism forming the substrate for accumulation of platelet and fibrin material.

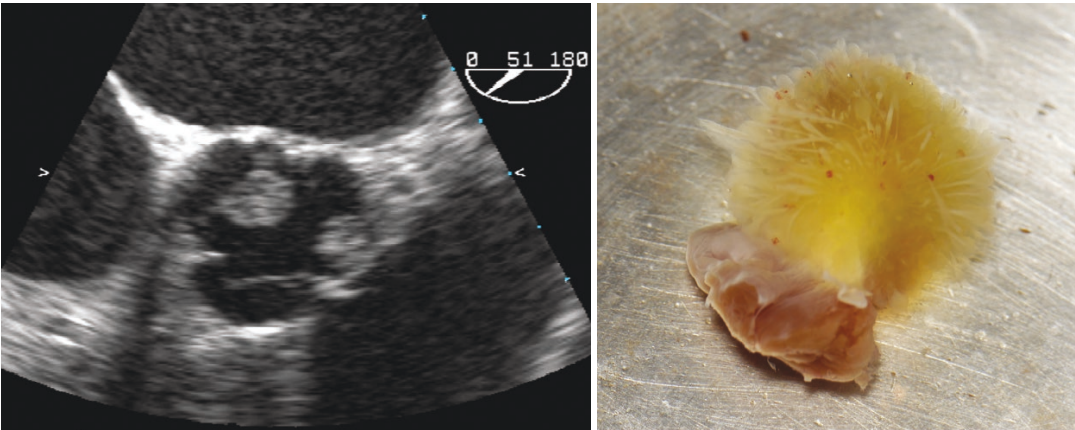


Fig. 9.19 Intraoperative TOE of a patient with multiple fibroelastomas within the heart. Two were attached to the non and left coronary leaflets. The actual structure of

these tumours is better understood when seen suspended in fluid—characteristic sea anemone

Table 9.5 Indications for surgery on aneurysms of the aortic root and ascending aorta

Underlying pathology	Measurement of the aorta (mm)
Normal aortic valve/no known connective tissue disease	≥55
Bicuspid aortic valve	
Normal valve and no risk factors ^a	≥55
Normal valve with risk factors	≥50
Abnormal valve requiring replacement	≥45
Marfan’s	
Normal aortic valve and no risk factors ^b	≥50
Risk factors present	≥45

Adapted from Erbel et al. [8]

^aRisk factors in the context of a bicuspid aortic valve include coarctation, systemic hypertension, family history of dissection or an increase in aortic dimensions by >3 mm/year

^bRisk factors in the context of Marfan’s syndrome include family history of dissection, severe aortic or mitral regurgitation, increase in aortic dimensions by >3 mm/year or a plan for pregnancy

Echo Assessment of the Aorta

Disease of the thoracic aorta often occurs in association with aortic valve disease. The decision to consider cardiac surgery may depend entirely on the assessment of aortic dimensions (Table 9.5) and therefore a thorough interrogation of the thoracic aorta is very important. There are a number

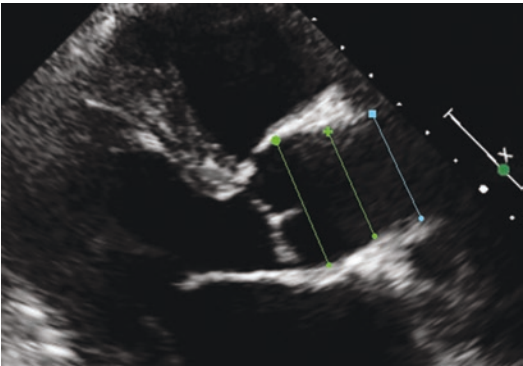


Fig. 9.20 Parasternal long axis view showing positions for the standard measurement of the aortic sinuses, sinotubular junction and ascending aorta in diastole aiming to keep the measurement planes perpendicular to the long axis of the aorta (white dashed line)

of other conditions affecting the aorta which we will also cover in this section.

TTE allows multiple acoustic windows looking at the aortic root, ascending, arch and the proximal abdominal aorta. TOE gives a more complete analysis of the thoracic aorta but there is a small blindspot in the high ascending aorta due to interposition of the right main bronchus. This is rarely of any clinical significance but needs to be appreciated. The standard assessment of the aortic root and ascending aorta is performed from the parasternal views on TTE (Fig. 9.20) and requires measurements at four points—the annulus, sinuses of Valsalva, sinotubular junction

and the ascending aorta. The annulus is measured in mid-systole from inner edge to inner edge, but the other three are made at end-diastole using the leading edge to leading edge convention [6]. The ascending aorta is often seen more clearly from a higher parasternal window. It is important that aortic dimensions are indexed for body surface area and this is particularly important in children with the use of Z-scores. As the aortic root enlarges the margin between the sinotubular junction and ascending aorta often becomes less distinct—so called effacement (Fig. 9.21).

Bicuspid Valve Disease

Patients with bicuspid valve disease frequently have aortic dilatation and have a significantly higher risk of aortic dissection. This risk of aortic dilatation is independent of the haemodynamic lesion of the valve and therefore the term ‘post

stenotic dilatation’ has the potential to mislead. The commonest site of dilatation is in the ascending aorta (Fig. 9.22). If this is not well seen on TTE then it is essential to consider alternative imaging either with TOE or CT/MRI. Careful assessment should also be made for coarctation which is associated with bicuspid valve disease. The suprasternal window can often provide excellent 2D views and quantification of stenosis using CW Doppler (Fig. 9.23).

Marfan's Syndrome

Marfan's syndrome is an autosomal dominant condition and is the most common inherited connective tissue disorder. The mutations affect the gene encoding fibrillin which is an essential gly-

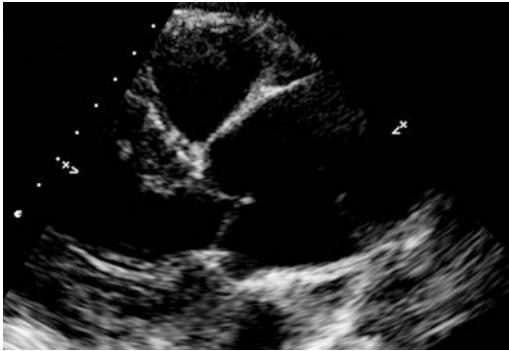


Fig. 9.21 Dilated aortic root and ascending aorta with effacement of the sinotubular junction

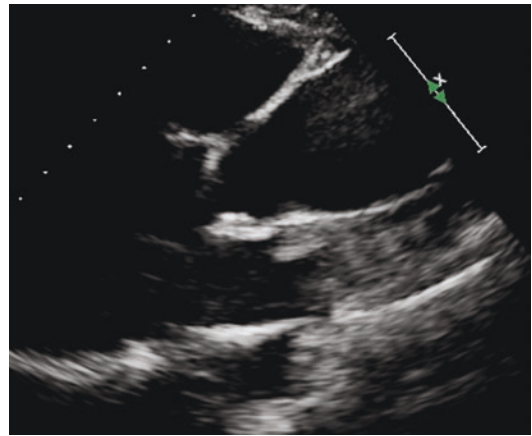


Fig. 9.22 Patient with a bicuspid aortic valve with classical dilatation of the ascending aorta seen in the parasternal long axis view on TTE

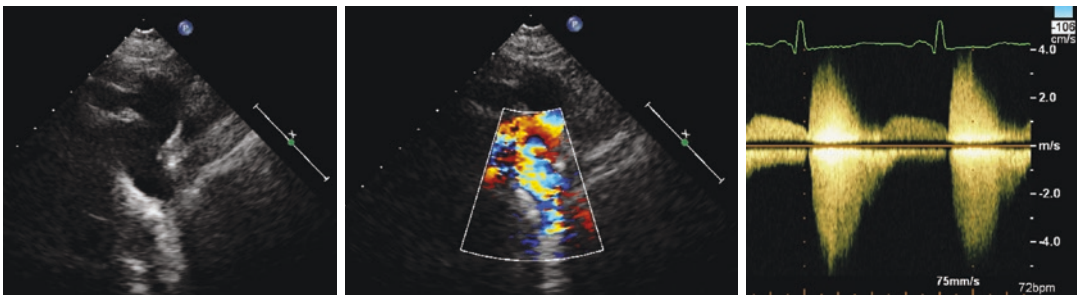


Fig. 9.23 Suprasternal views of a patient with an aortic coarctation showing narrowing of the aortic isthmus with turbulent colour flow Doppler and high velocity flow into the descending thoracic aorta

coprotein involved in the structure but also cell signalling pathways within connective tissue. Patients tend to have a typical phenotype with tall stature, long limbs and arachnodactyly. The most important clinical manifestations tend to affect the aorta and heart valves with a significant risk of aortic dissection. The aortic root is the most common section of aorta affected and is the focus of cardiac imaging in such patients.

Loeys-Dietz Syndrome

Loeys-Dietz syndrome is also an autosomal dominant connective tissue disorder but was first described only in 2005 [9]. The condition is characterised by a combination of extreme arterial tortuosity and aneurysms affecting any part of the arterial tree, hypertelorism (wide set eyes) and a bifid uvula. Aortic enlargement occurs commonly but the rate of progression and the incidence of dissection and rupture is substantially higher than compared to Marfan's syndrome. Given this aggressive course there have been recommendations to consider prophylactic aortic surgery at much lower dimensions (≥ 42 mm) but more evidence is likely to be required. Patients may require total aortic replacement in some cases due to progressive dilatation or from dissection (Fig. 9.24).

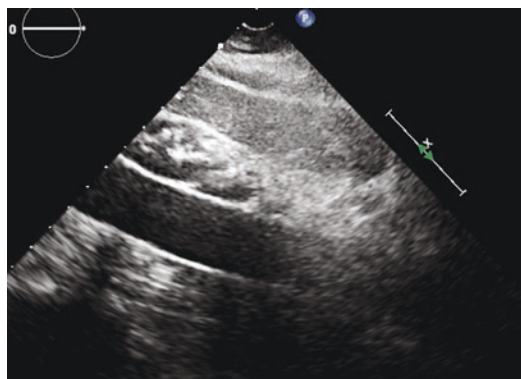


Fig. 9.24 Subcostal views showing a patient with Loeys-Dietz syndrome who has had replacement of the entire thoracoabdominal aorta due to dissection and progressive dilatation



Fig. 9.25 Parasternal long axis view showing an acute Type A dissection with a dilated aortic root and the dissection flap (arrowed) extending into the ascending aorta

Acute Aortic Syndromes

Patients with acute aortic syndromes can present with aortic dissection, intramural haematoma or with an atherosclerotic ulcer. Clinical presentations can be very similar and therefore accurate and early diagnosis with imaging is essential. Surgical intervention is often required and mortality is high if left untreated.

Aortic Dissection

Aortic dissection is usually categorised as Type A or Type B depending on involvement of the ascending aorta/aortic root. This division is extremely helpful in that Type A dissection almost always requires emergency surgical cor-

rection. Good clinical acumen is required in order to identify patients who attend the emergency department with a possible dissection but this is hugely supported by early cardiac imaging. TTE has an obvious advantage being a bedside test and will have a high sensitivity in detecting a dissection flap. If images are suboptimal or if the clinical suspicion remains high then it is mandatory to obtain further imaging either with CT/MRI or in selected cases TOE.

The hallmark of identifying aortic dissection on echo is identification of a flap (Fig. 9.25). This can often be highly mobile and must be

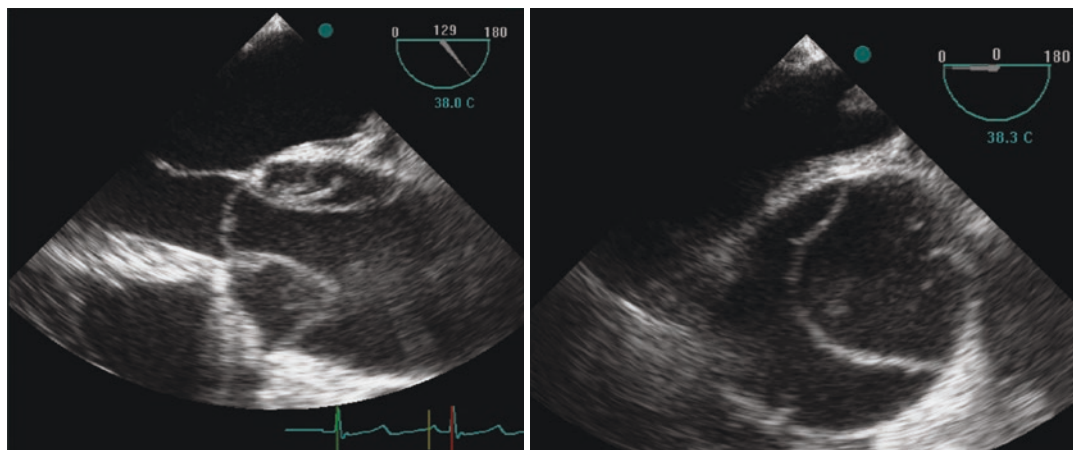


Fig. 9.26 TOE of acute Type A aortic dissection with the flap prolapsing through the aortic valve acting as a conduit for severe aortic regurgitation (left). Short axis view of the

ascending aorta demonstrating the true lumen which expands in systole (right)

distinguished carefully from artefact such as reverberation or side lobe artefact. In Type A dissection the flap may involve the aortic root and disrupt the aortic valve leading to severe AR. Other mechanisms of aortic regurgitation include pre-existing valve disease, aortic dilatation or prolapse of the flap through the orifice of the valve acting as a conduit for AR (Fig. 9.26). There may be obvious signs of pre-existing disease e.g. bicuspid valve, which could be the key risk factor in that particular patient. There will often be an acute on chronic enlargement of the aorta given the weakening produced by the acute dissection. The presence of pericardial effusion is an ominous sign in a patient with a suspected aortic syndrome and should always be taken seriously. The pericardium inserts several centimetres up the ascending aorta and therefore bleeding can occur directly into this space in Type A dissection.

A patient with an acute aortic syndrome may be acutely unwell and one of the challenges of bedside TTE is to acquire views from all the available acoustic windows including suprasternal and subcostal views. The use of CT/MRI and TOE will be dictated by local availability and expertise but the key message is that any delay in cardiac imaging should be minimised. For example, a patient with clear evidence of Type A dissection on TTE may need to proceed directly to cardiac theatre with no further investigations pro-

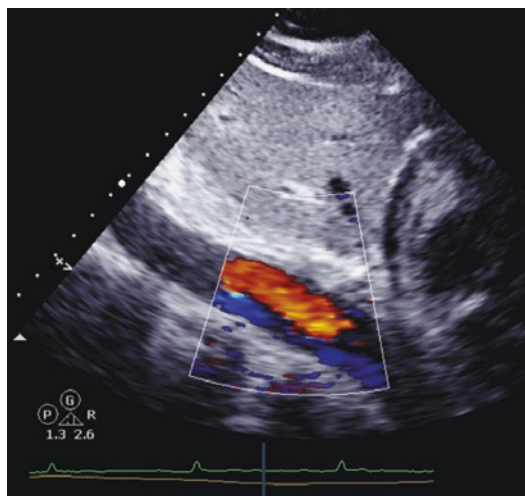


Fig. 9.27 Subcostal views show differential flow within a Type B aortic dissection

vided full discussion has taken place with the surgical team.

Type B aortic dissection is often more difficult to diagnose on clinical assessment and may not be easily seen on TTE. However, full use of the subcostal and suprasternal window may be able to identify a flap in some cases (Fig. 9.27).

Intramural Haematoma

In some patients with an acute aortic syndrome there is a bleed into the wall of the aorta without

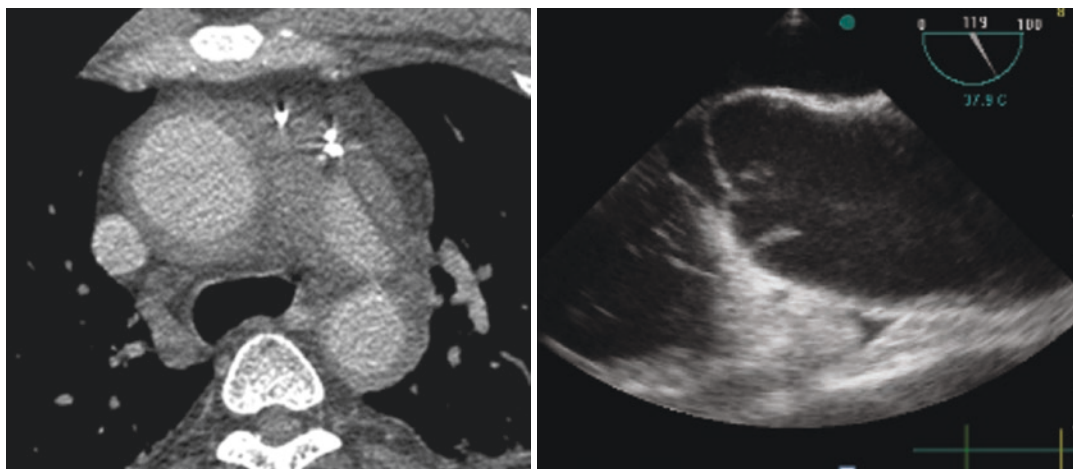


Fig. 9.28 A patient with intramural haematoma demonstrated on CT with thickening of the aortic wall which was difficult to see on echo but the TOE images also detected a dissection flap in the root close to the aortic leaflets

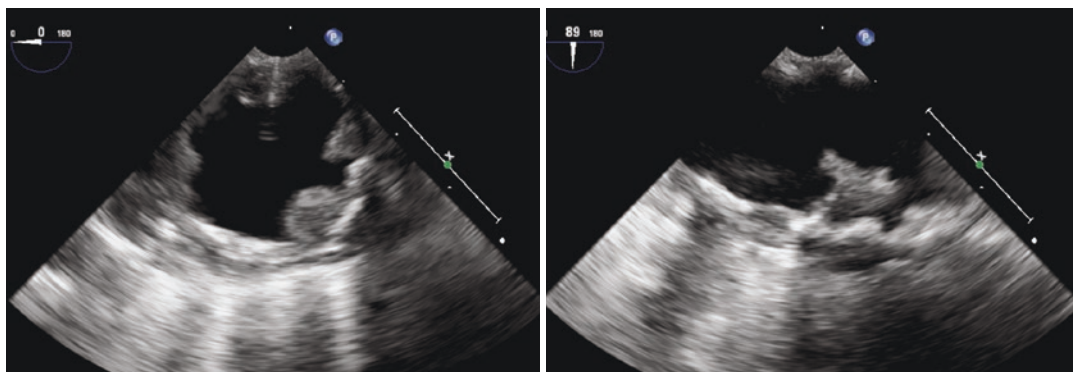


Fig. 9.29 TOE images showing extensive protruding atheroma in the proximal descending thoracic aorta and also the distal arch

an intimal tear. This may present in the exact same way as a classical dissection with typical chest and back pain but is slightly more challenging to see with imaging—both echo and CT/MRI. One of the key features to identify is thickening of the aortic wall (Fig. 9.28).

Penetrating Atherosclerotic Ulcer

This is the third lesion which falls within the spectrum of acute aortic syndromes but is less common. This tends to occur in older hypertensive males. The ulcerated atherosclerotic lesion traverses through the intima into the media and in its early stages may be asymptomatic. TOE may demonstrate extensive atheromatous disease in

the thoracic aorta which can also be the substrate for embolic stroke (Fig. 9.29). However, with disease progression of a penetrating ulcer there is a risk of dissection or even rupture.

Sinus of Valsalva Aneurysms

Sinus of Valsalva aneurysms (SVAs) are rare with an incidence of approximately 0.1%. They occur due to abnormalities in the elastic and muscular tissue in the media of the aortic wall. They are usually congenital in origin but can also be acquired in the context of infective endocarditis. There are often other associated cardiac defects such as ventricular septal defect or aortic regurgitation. They are more

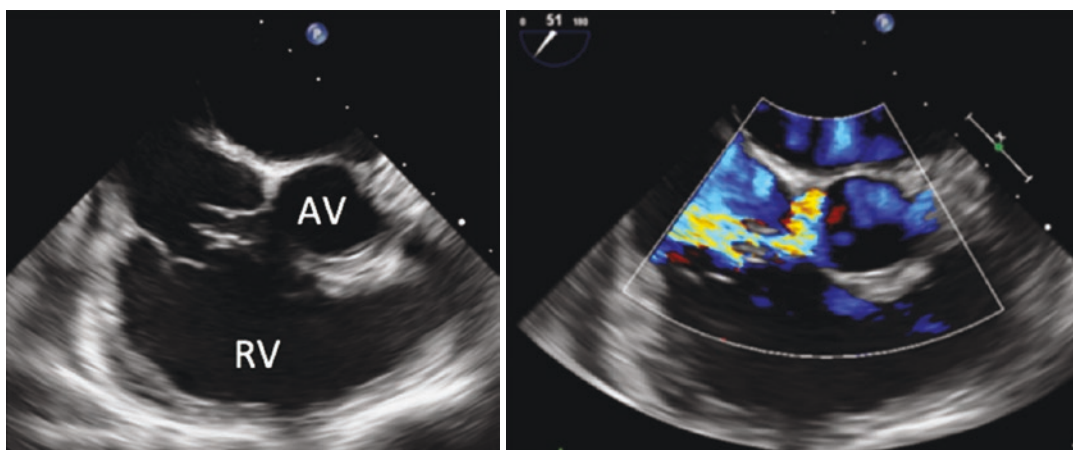


Fig. 9.30 Short axis view on TOE (left) showing the 'wind sock' structure extending from the non-coronary sinus into the right atrium. (RV – right ventricle, AV – aortic valve).

Colour Doppler from the same view (right) showing the large shunt from aorta to right atrium

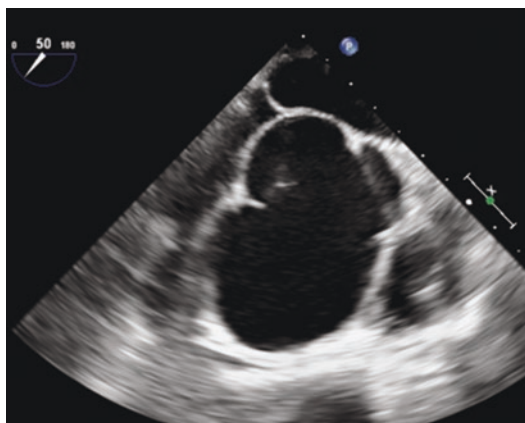


Fig. 9.31 TOE short axis view showing a sinus of Valsalva aneurysm involving the right coronary sinus and leading to a degree of obstruction of the right ventricular outflow tract

common in males and in the Asian population. They can arise from any of the coronary sinuses but the right coronary sinus is by far the most common—65–86%. The non-coronary sinus is affected in 10–30% and the left coronary sinus in 2–5% of cases. Involvement of more than one sinus is also described in case reports. The commonest complication of SVA is rupture into another cardiac chamber and this is usually the right atrium or right ventricle (Fig. 9.30). Other complications are determined by the anatomy of the aneurysm e.g. right ventricular outflow tract

obstruction (Fig. 9.31). Chest pain and shortness of breath are the most frequent presenting symptoms. Patients may be asymptomatic in the presence of an unruptured SVA and the diagnosis may be found as an incidental finding during echocardiography or cross-sectional imaging for another reason.

Take Home Message/Conclusion

The accurate echocardiographic assessment of aortic valve disease is at the core of contemporary cardiology and is an essential skill for all clinicians involved. Aortic stenosis is common and there is an increasing focus on the concept of flow measurement, indexed for body surface area, in order to identify the different pathophysiologies that may occur. The thoracic aorta can be comprehensively assessed from TTE and TOE. Early and accurate bedside diagnosis can greatly improve patient outcomes in a number of life threatening conditions.

References

1. Ho SY. Structure and anatomy of the aortic root. *Eur J Echocardiogr.* 2009;10(1):i3–10. <https://doi.org/10.1093/ejehocardi/jen243>. Review.
2. Chambers JB. Aortic stenosis. *Eur J Echocardiogr.* 2009;10(1):i11–9. <https://doi.org/10.1093/ejehocardi/jen240>. Review.

3. Schaefer BM, Lewin MB, Stout KK, Gill E, Prueitt A, Byers PH, Otto CM. The bicuspid aortic valve: an integrated phenotypic classification of leaflet morphology and aortic root shape. *Heart*. 2008;94(12):1634–8.
4. Spaccarotella C, Mongiardo A, Indolfi C. Pathophysiology of aortic stenosis and approach to treatment with percutaneous valve implantation. *Circ J*. 2011;75(1):11–9.
5. Rosenhek R, Binder T, Porenta G, Lang I, Christ G, Schemper M, et al. Predictors of outcome in severe, asymptomatic aortic stenosis. *N Engl J Med*. 2000;343:611–7.
6. Lang RM, Badano LP, Mor-Avi V, Afilalo J, Armstrong A, Ernande L, et al. Recommendations for cardiac chamber quantification by echocardiography in adults: an update from the American Society of Echocardiography and the European Association of Cardiovascular Imaging. *J Am Soc Echocardiogr*. 2015;28(1):1–39.
7. Baumgartner H, Falk V, Bax JJ, De Bonis M, Hamm C, Holm PJ, Iung B, Lancellotti P, Lansac E, Rodriguez Muñoz D, Rosenhek R, Sjögren J, Tornos Mas P, Vahanian A, Walther T, Wendler O, Windecker S, Zamorano JL; ESC Scientific Document Group. 2017 ESC/EACTS Guidelines for the management of valvular heart disease. *Eur Heart J*. 2017;38(36):2739–91.
8. Erbel R, Aboyans V, Boileau C, Bossone E, Bartolomeo RD, Eggebrecht H, et al. 2014 ESC guidelines on the diagnosis and treatment of aortic diseases: document covering acute and chronic aortic diseases of the thoracic and abdominal aorta of the adult. The task force for the diagnosis and treatment of aortic diseases of the European Society of Cardiology (ESC). *Eur Heart J*. 2014;35(41):2873–926.
9. Loeys BL, Schwarze U, Holm T, Callewaert BL, Thomas GH, Pannu H, et al. Aneurysm syndromes caused by mutations in the TGF-beta receptor. *N Engl J Med*. 2006;355:788–98.

Recommended Reading

- Baumgartner H, Hung J, Bermejo J, Chambers JB, Evangelista A, Griffin BP, Iung B, Otto CM, Pellikka PA, Quiñones M, American Society of Echocardiography, European Association of Echocardiography. Echocardiographic assessment of valve stenosis: EAE/ASE recommendations for clinical practice. *J Am Soc Echocardiogr*. 2009;22(1):1–23.
- Lancellotti P, Tribouilloy C, Hagendorff A, Moura L, Popescu BA, Agricola E, European Association of Echocardiography, et al. European Association of Echocardiography recommendations for the assessment of valvular regurgitation. Part 1: aortic and pulmonary regurgitation (native valve disease). *Eur J Echocardiogr*. 2010;11(3):223–44.
- Lindroos M, Kupari M, Heikkala J, Tilvis R. Prevalence of aortic valve abnormalities in the elderly: an echocardiographic study of a random population sample. *J Am Coll Cardiol*. 1993;21:1220–5.
- Nishimura RA, Grantham JA, Connolly HM, et al. Low-output, low-gradient aortic stenosis in patients with depressed left ventricular systolic function: the clinical utility of the dobutamine challenge in the catheterization laboratory. *Circulation*. 2002;106:809–13.
- Stewart BF, Siscovick D, Lind BK, Gardin JM, Gottdiener JS, Smith VE, et al. Clinical factors associated with calcific aortic valve disease: cardiovascular health study. *J Am Coll Cardiol*. 1997;29:630–4.

Joseph Kisslo, J. Daniel Rivera, David Adams,
Burkhard G. Mackenson, Alicia Armour,
Ashlee Davis, Joshua Lander,
and Donald D. Glower

Cardiac Anatomic Relationships

Parasternal Long Axis

Examination of the heart by ultrasound begins with a parasternal long-axis. Figure 10.1 shows an anatomic section of the ventricular (LV) long axis from the aortic root (right side) to the left ventricular apex (left side). The right ventricle is seen anteriorly (upwards) on the figure as it wraps around the left ventricle. Note that the papillary muscles of the left ventricle emerge from the ventricular free wall (arrow) and give rise to the chordae tendineae of the two mitral valve leaflets.

The longer anterior mitral valve leaflet is easily seen and connects right to the aorta directly with the posterior aortic (Ao) wall and aortic valve. Thus, there is what is called “mitral and aortic continuity” in the left heart. The posterior

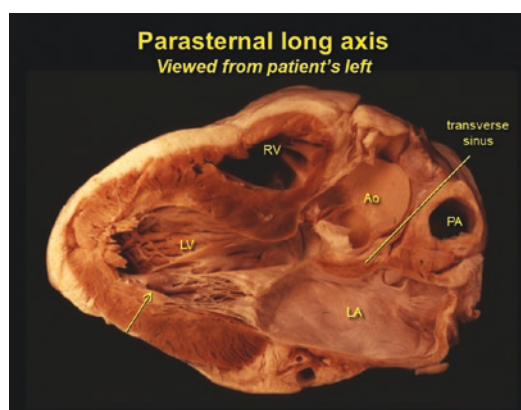


Fig. 10.1 Anatomic section cut along a typical parasternal long axis used in two-dimensional echocardiography. The arrow points to the base of the papillary muscles emerging from the left ventricular free wall. *LV* left ventricle, *RV* right ventricle, *LA* left atrium, *Ao* aorta, *PA* main branch of the pulmonary artery. Modified from Kisslo, Leech & Adams: *Essentials of Echocardiography*

J. Kisslo (✉)
Division of Cardiology, Duke University Medical
Center, Durham, NC, USA
e-mail: joseph.kisslo@duke.edu

J. Daniel Rivera · D. Adams · A. Armour · A. Davis
J. Lander
Cardiac Diagnostic Unit, Duke University Health
Center, Durham, NC, USA

B. G. Mackenson
Department of Anesthesia, University of Washington,
Seattle, WA, USA

D. D. Glower
Department of Surgery, Duke University Medical
Center, Durham, NC, USA

mitral valve leaflet is seen attached to the mitral annulus along the posterior ventricular free wall. Therefore the posterior mitral leaflet is the mural leaflet. The left atrium (LA) is posterior to the aorta and one of the main pulmonary artery (PA) branches sits posterior to the aorta and just above to the left atrium. Many observers imagine that the left atrial anterior wall and posterior aortic wall are one. That is, however, not true as there is a pericardial sinus, the transverse sinus, that is between the aorta and the left atrium. This transverse sinus will prove to be an important space for surgical approaches to the atrium in the oper-

ating room. The circumflex coronary artery and the larger coronary sinus are seen in the posterior atrio-ventricular groove (not marked).

Selected diastolic and systolic frames from an actual echocardiogram are seen in Fig. 10.2. A large right ventricular trabeculation is seen in the diastolic frame (left panel). In diastole, the aortic valve is in the closed position and the mitral valve is open. The anterior mitral valve leaflet is again noted to be the longest in comparison to the posterior (mural) leaflet and is contiguous with the posterior aortic wall demonstrating mitral-aortic continuity. The right hand panel shows the same heart in systole with the closed mitral valve and the open aortic valve. The pulmonary artery main branch (PA) is seen above the left atrium and posterior to the aorta, as in the previous figure. In most patients this is the right main stem pulmonary artery branch. Behind the left atrium is the descending aorta (desc Ao). Note that the size of the left atrium (LA) is approximately the diameter of a normal aorta. When looking at an echo-

cardiogram, observers need a quick approximation of sizes and this is a handy relationship to keep in mind. Of course, if both the aorta and left atrium are dilated, this approximation estimate can be misleading.

Selected diastolic and systolic frames in Fig. 10.3 show a somewhat thicker left ventricle (LV hypertrophy) with a slightly enlarged left atrium. Again, only a portion of the right ventricle is visualized as it wraps around the left. The posterior mitral valve leaflet is attendant to the posterior wall and is easily identified by its attachment only to the wall. The anterior mitral leaflet is again identified by its connection to the posterior wall of the aorta. We emphasize these attachments as they become particularly important for recognition of the two mitral leaflets from the various two and three-dimensional echocardiographic presentations.

Similar selected frames are seen in Fig. 10.4, this time with a remarkably dilated left atrium that is much bigger than the normal aorta. There

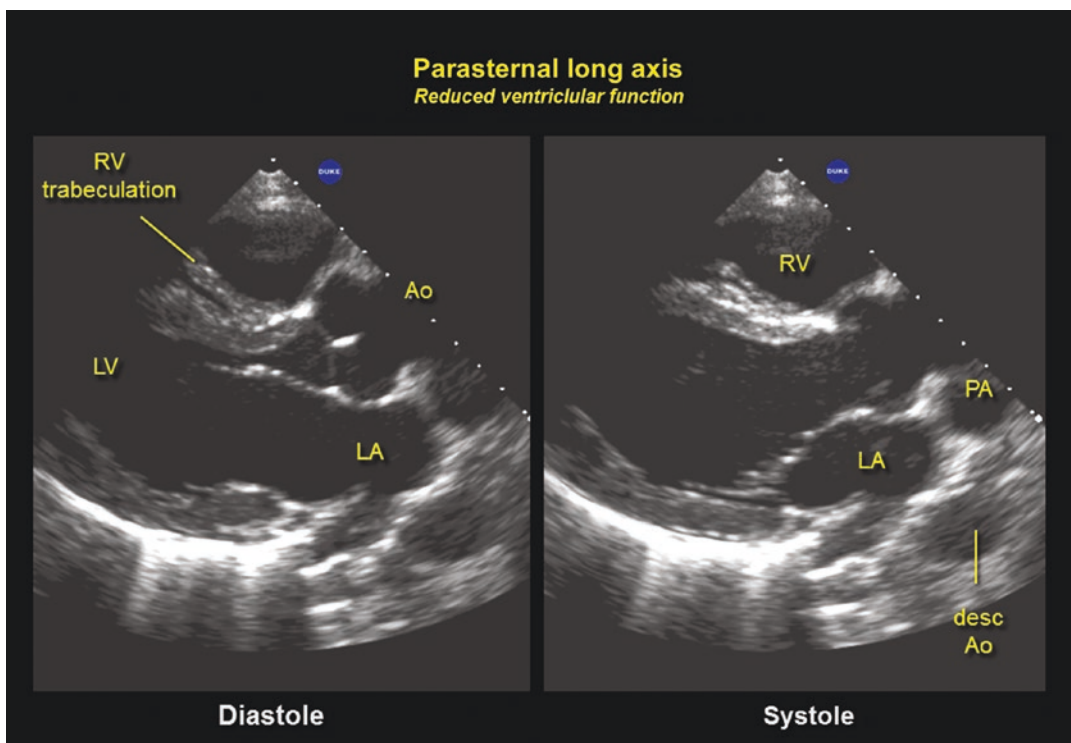


Fig. 10.2 Parasternal long axis from a patient with a normal size left atrium. Note one of the main pulmonary artery branches (PA) on the top of the left atrium (LA). Compare this with Fig. 7.1

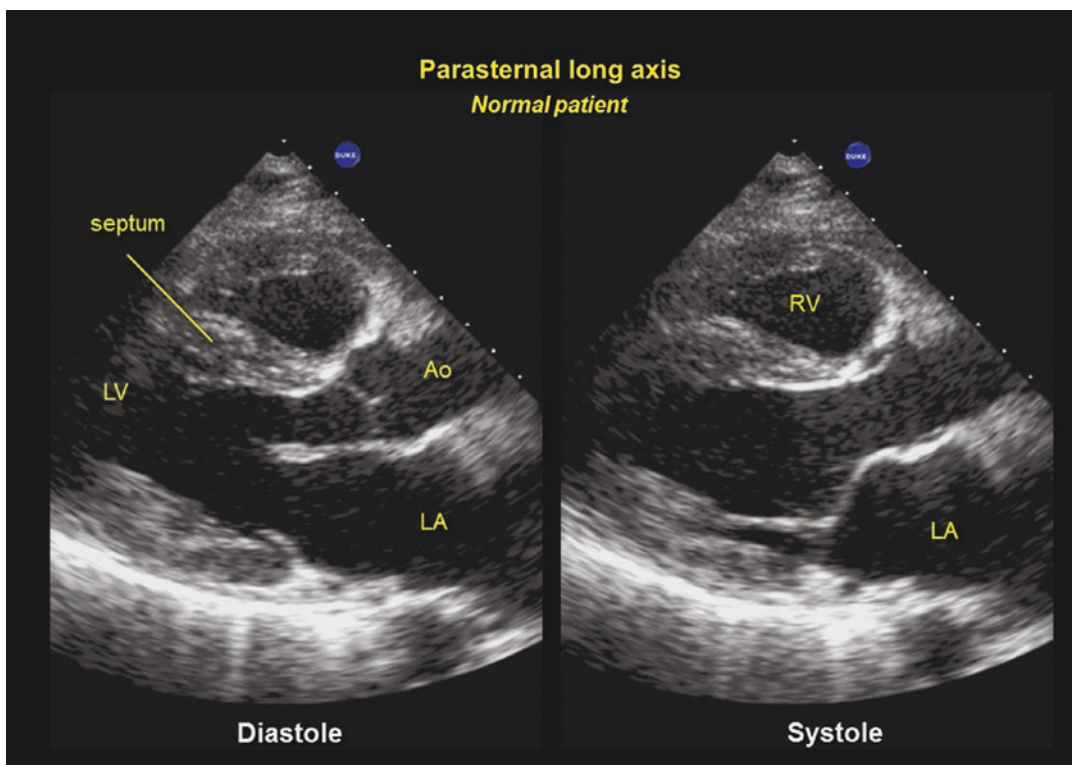


Fig. 10.3 Parasternal two-dimensional echocardiographic images in diastole and systole from a normal patient demonstrating mitral valve echocardiographic

anatomy. Note that the anterior mitral leaflet is longer than the posterior mitral leaflet

is also a dilated left ventricle as well as the atrium in this 50 y.o. patient with a severe dilated cardiomyopathy. A portion of the descending aorta (desc Ao) is seen right posterior to the heart. Note in the systolic frame (right panel) the mitral valve leaflets are again identified by their various attachments. The anterior mitral leaflet is attached to the posterior aortic wall while the posterior mitral leaflet is attached to the ventricular wall itself. Because of this attachment of the anterior mitral leaflet to the aorta, some people call it the “aortic” mitral leaflet. This nomenclature is rarely used, but is wholly descriptive of the attachment. The “mural” leaflet is short, but is easily seen attached to the posterior left ventricular wall at the mitral annulus.

There are numerous small biologic variations in the shape and configuration of cardiac structures, but the relationships pointed out to this point are rather consistent from heart to heart in individuals with normal cardiac relationships.

The anatomic section seen in Fig. 10.5 shows the long axis of a left ventricle as viewed from the patient’s left hand side from the free wall looking medially. The interior surface of the left ventricular wall is, therefore, the interventricular septum. The face of the intraventricular septum is smooth just underneath the aortic valve, but becomes hyper-trabeculated towards the ventricular apex. Again, chordae tendineae can be seen arising from a portion of the papillary muscle on the inferior side of the ventricle that rests upon the diaphragm. This particular specimen has a uniquely good picture of the coronary sinus as it wraps in the left-sided atrio-ventricular groove. The transverse sinus of the pericardium is well seen as it separates the aorta and the left atrium. The transverse sinus is rarely differentiated by echocardiography techniques because it is usually collapsed and not filled with fluid. Note that the transverse sinus is not recognizable in Figs. 10.2, 10.3, and 10.4.

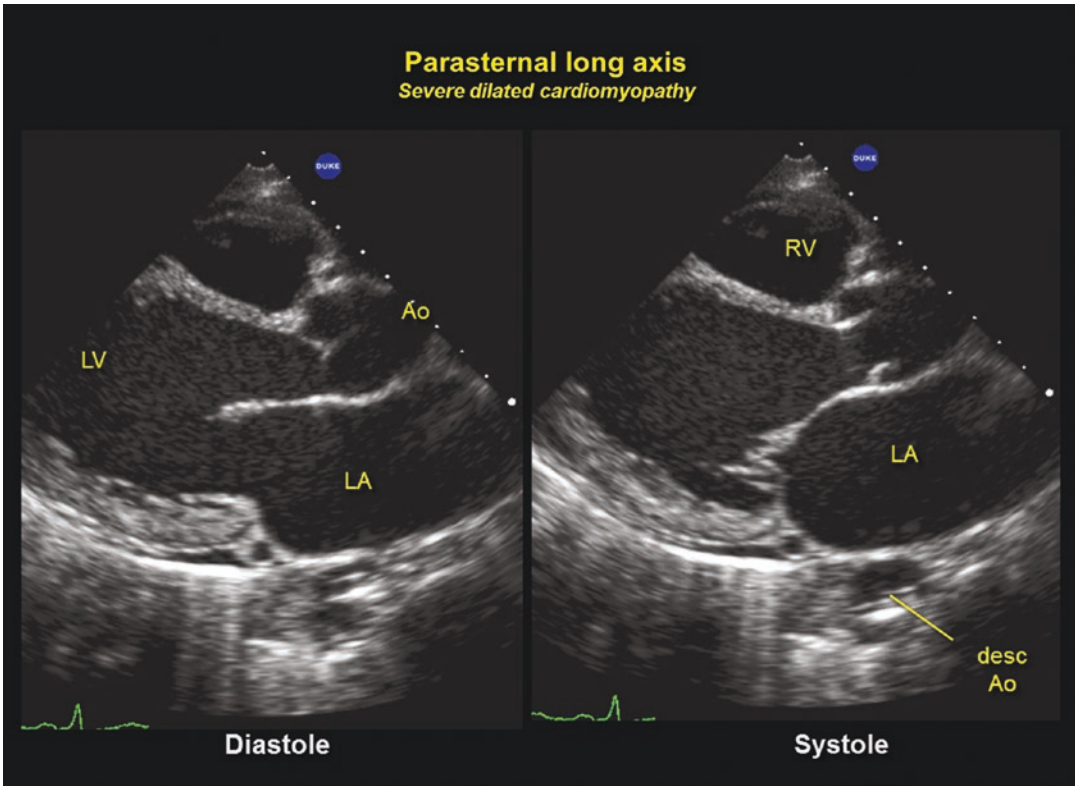


Fig. 10.4 Parasternal two-dimensional echocardiographic images in diastole and systole from a patient with a dilated cardiomyopathy, including a dilated left atrium. Note the mitral-aortic continuity. *desc Ao* descending aorta

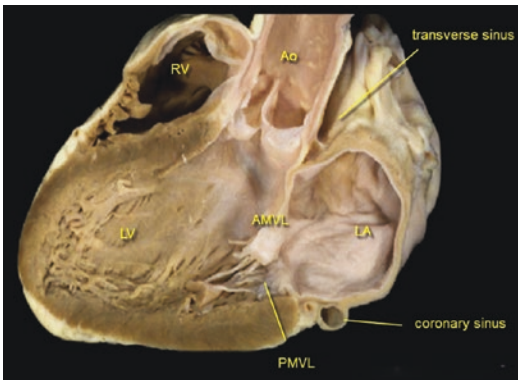


Fig. 10.5 Long axis cut anatomic cut specimen along the plane of the long axis used for two-dimensional echocardiography. Note the chordae tendineae inserting into the tips of the mitral leaflet tips. A large coronary sinus is easily seen adjacent to a smaller circumflex coronary artery in the posterior atrio-ventricular groove. *PMVL* posterior mitral valve leaflet. Courtesy R.H. Anderson, MD. Modified from Kisslo: Thinking in 3D

Three-dimensional echocardiographic sections that appear in Fig. 10.6 show the transverse sinus to be poorly identified. However, one can see the anatomic structures of the face of the interatrial septum inside of the left atrium (LA). The diastolic frame shows the mitral valve structures in the open position and the aortic valve in its closed position.

The right hand panel of Fig. 10.6 shows the mitral valve in its closed position. A set of primary chordae tendineae (1°) are seen attaching to the tip of the posterior mitral valve leaflet from the tip of the papillary muscle. Secondary (2°) chordae tendineae are seen going to the backside of the anterior mitral leaflet along the left ventricular outflow tract. Such secondary chordae can also be seen from papillary heads to the underside of the posterior mitral leaflet, between the leaflet and ventricular wall.

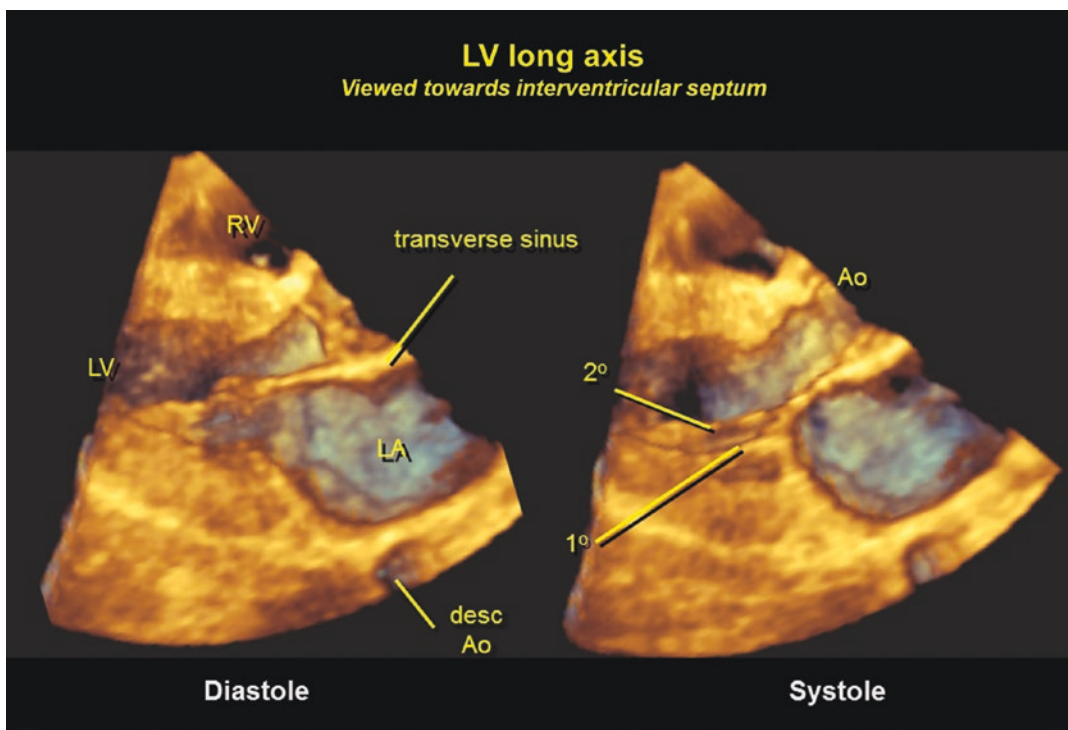


Fig. 10.6 Parasternal long axis perspective from a three-dimensional echocardiogram viewed from the left ventricular free wall. The descending aorta is seen behind the

heart. 1° primary chordae tendineae, 2° secondary chordae tendineae

These secondary chordae become very important when severe mitral regurgitation is encountered due to broken mitral chordae and surgical repair is contemplated. If chordae are intact on a leaflet opposite to the leaflet with broken chords, a chordal transfer may be done if appropriate to the repair procedure. In any event, the composite of the mitral valve in long axis contains recognition of the two mitral leaflets, their rough proportions and details of their attachments.

A view from the other side of the left ventricle is seen in the anatomic section in Fig. 10.7 where the viewer is looking at the free wall as the interior left ventricular surface. Here, the perspective is that from the intraventricular septum towards the posterior and anterior left ventricular walls. The infero-medial papillary muscle is seen along the inferior aspect of the left ventricle while the antero-lateral papillary is

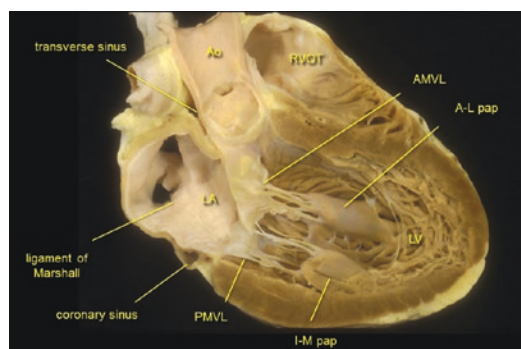


Fig. 10.7 Half of the human left ventricle anatomic specimen cut along the parasternal long axis of the left ventricle. The half shown is opposite to those shown in Figs. 10.1 and 10.5. Here the LV perspective is viewed from the ventricular septum towards the free wall and includes lateral portions of the left atrium discussed in the text. AMVL anterior mitral valve leaflet, A-L pap antero-lateral papillary, I-M pap infero-medial papillary. Courtesy S.Y. Ho, MD. Modified from Kisslo: Thinking in 3D

seen in its mid-ventricular position, entirely on the free wall. The various chordae tendineae appear to spring from the tips of the papillary muscles in a vast array and connect to the various mitral leaflet edges as primary chordae tendineae. The attachments of the mitral leaflets are as previously described, the anterior mitral valve leaflet (AMVL) to the posterior aortic wall and aorta and the posterior mitral valve leaflet (PMVL) to the free wall. These attachments will come in handy when trying to differentiate the various leaflets of the mitral valve apparatus in free space.

Just above the mitral annulus in the left atrium in Fig. 10.7 are other important structures. Two large ostia of the two left pulmonary veins are seen in the superior portions of the left atrial wall. Between two prominent ostia and the mitral valve apparatus is the ligament of Marshall. This ligament is important because it is the site of interest for (RF) ablation for atrial arrhythmias. The left

atrial appendage os is then situated between the Ligament of Marshall and the mitral annulus, but is poorly seen in this anatomic specimen.

A similar view, using three-dimensional echo, is seen in Fig. 10.8. The dark shadows of the orifices of the pulmonary veins are seen posteriorly, just behind the ligament of Marshall. Further anterior to the Ligament of Marshall is the os of the left atrial appendage. Other structures such as the aortic valve and mitral valve are easily identified. Note the locations of the papillary muscles within the left ventricle.

Further details of this area within the lateral wall of the left atrium are detailed in Fig. 10.9. Note the left upper pulmonary vein (LUPV) and the relationships of these pulmonary veins to the Ligament of Marshall, the os of the left atrial appendage, the mitral annulus and the mitral leaflets. Real-time, three-dimensional echocardiography clearly shows these relationships that are difficult to appreciate by two-dimensional

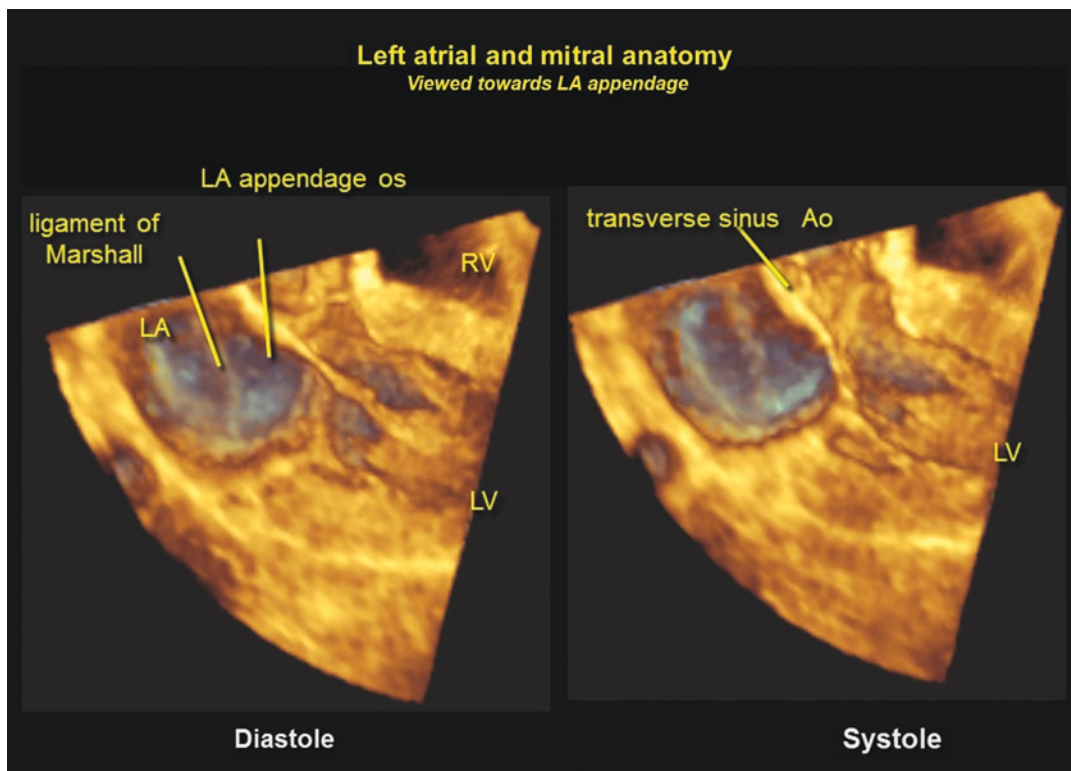


Fig. 10.8 Three-dimensional echocardiogram of the heart from a similar perspective of the cut section seen in the previous figure. Pulmonary atrial veins, ligament of Marshall and the os of the atrial appendage are seen

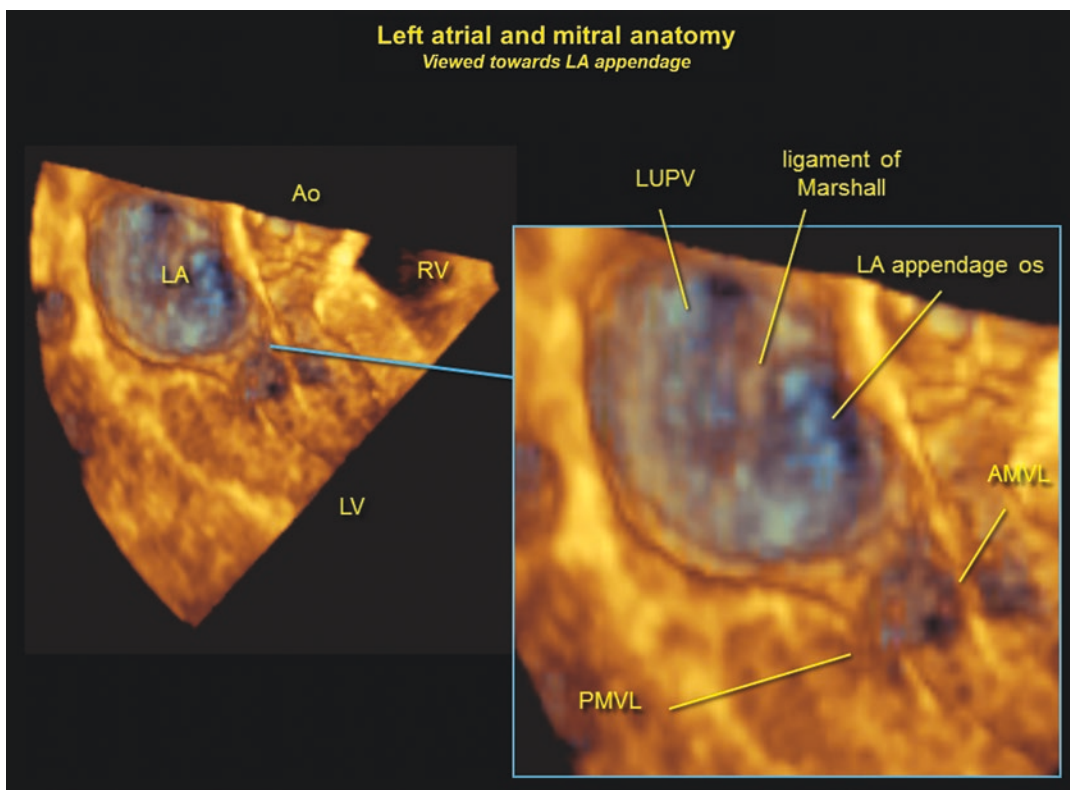


Fig. 10.9 Details of the paired images presented in the previous Figure. Detailed images of the left atrial anatomy are possible using three dimensional echocardiography. LUPV left upper pulmonary vein

echocardiography alone. Such relationships are impossible to recognize by M-mode echo as it lacks spatial information in anything beyond depth.

Parasternal Short Axis

With three-dimensional echo, almost any orientation is permissible as it is like holding the heart in ones' hand and rotating the heart into any position. Conventional two-dimensional echocardiography views the heart from its apex towards the base. The left hand panel of Fig. 10.10 shows a cut short axis section at the level of the mitral valve leaflet tips looking upwards toward the cardiac base. The right hand panel shows a similar section at the level through the papillary muscles. In both panels, the right ventricle is seen to wrap around the left. The interventricular septum is easily identified between the two ventricles. The

remaining portions of the left ventricular wall that do not comprise the septum may be referred to as the free wall.

The clinical relationships to learn are those of the papillary muscles and the mitral valve commissures. Note the infero-medial papillary (inferior pap) sits at the junction of the septal and free walls at approximately eight o'clock on the ventricular short axis (right panel). This location at the junction of the septal and free walls is critical to identifying this given papillary. In contrast, the antero-lateral papillary (anterior pap) is located only on the ventricular free wall surface, attached only to the free wall. Look back at Fig. 10.7 to see these relationships in the specimen cut along the opposing ventricular long axis.

By comparing the left and right hand panels of Fig. 10.10, one can appreciate the location of the inferior mitral commissure to the infero-medial papillary. This commissure is properly called the

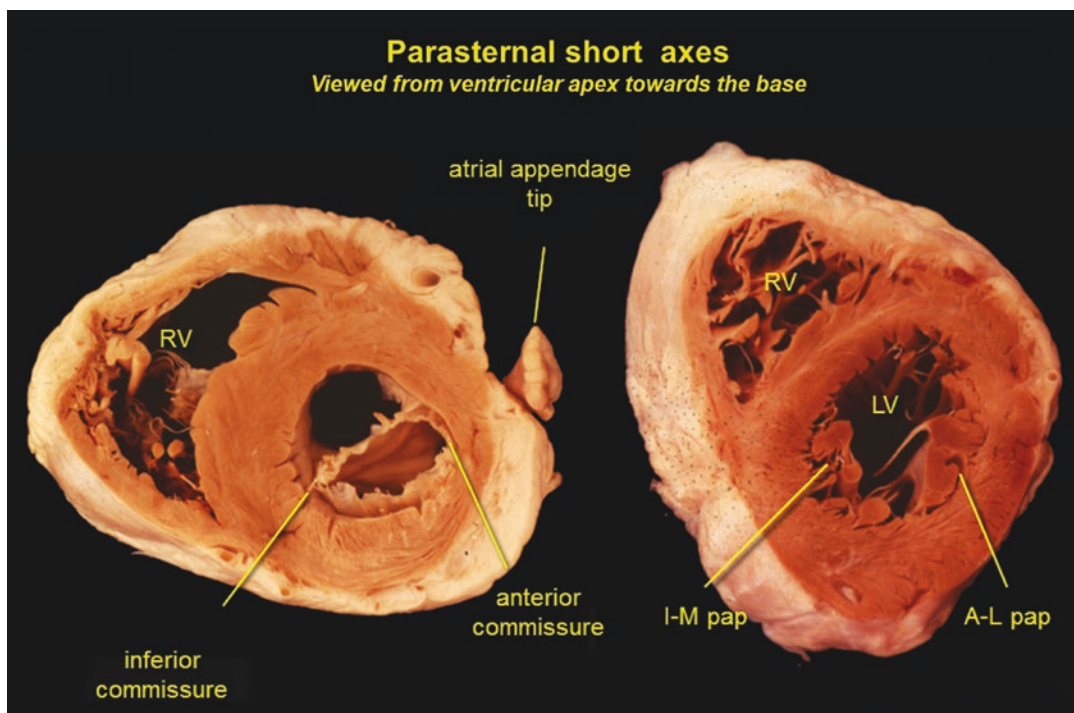


Fig. 10.10 Parasternal short axes obtained from the chest wall in the short axis view of the mitral leaflet tips and papillary bases seen by two-dimensional echocardiogra-

phy. Modified from Kisslo, Leech & Adams: Essentials of Echocardiography

infero-medial commissure, but this chapter will use “inferior” for short. Likewise, note the location of the antero-lateral papillary and its relationship to the anterior commissure. Similarly, we will use the word “anterior” for antero-lateral commissure and papillary. Of further critical note is the position of the left atrial appendage tip as it peeks out over the ventricular free wall border in the left panel of Fig. 10.10. It can easily be appreciated how a surgeon could incise the left atrial appendage tip and inserted a finger over the mitral annulus in the left atrium and into the anterior commissure to perform a mitral commissurotomy for rheumatic mitral stenosis.

These critical relationships are further documented in the series of two-dimensional echocardiograms seen in Figs. 10.11 and 10.12. In Fig. 10.11 the mitral orifice is seen in the open position in a patient with a dilated cardiomyopathy. The positions of the commissures are identified on this echocardiogram obtained from the chest wall. The mitral valve is seen in

the open position in diastole in the left hand panel and in the closed position in systole in the right hand panel. The left atrial appendage tip is identified as it peeks over the left ventricular brim. The left atrial appendage tip is not easily identified in most echocardiograms from the chest wall, but can be appreciated in easy to image patients and the operator knows specifically where to point the transducer array.

The locations of the papillary muscles in the mid ventricular region are seen in Fig. 10.12 when the interrogating plane is angle a bit towards the LV apex from the plane noted in the previous figure. Again, the inferior papillary is adjacent to the junction of the intraventricular septum and the free wall. The anterior papillary sits on the free wall entirely. These are easily identified both in diastole and systole. The size of both papillary heads are roughly symmetric. But sweeping the transducer in the chest wall position from base towards apex, the relationships between papillaries and commissures can be better appreciated.

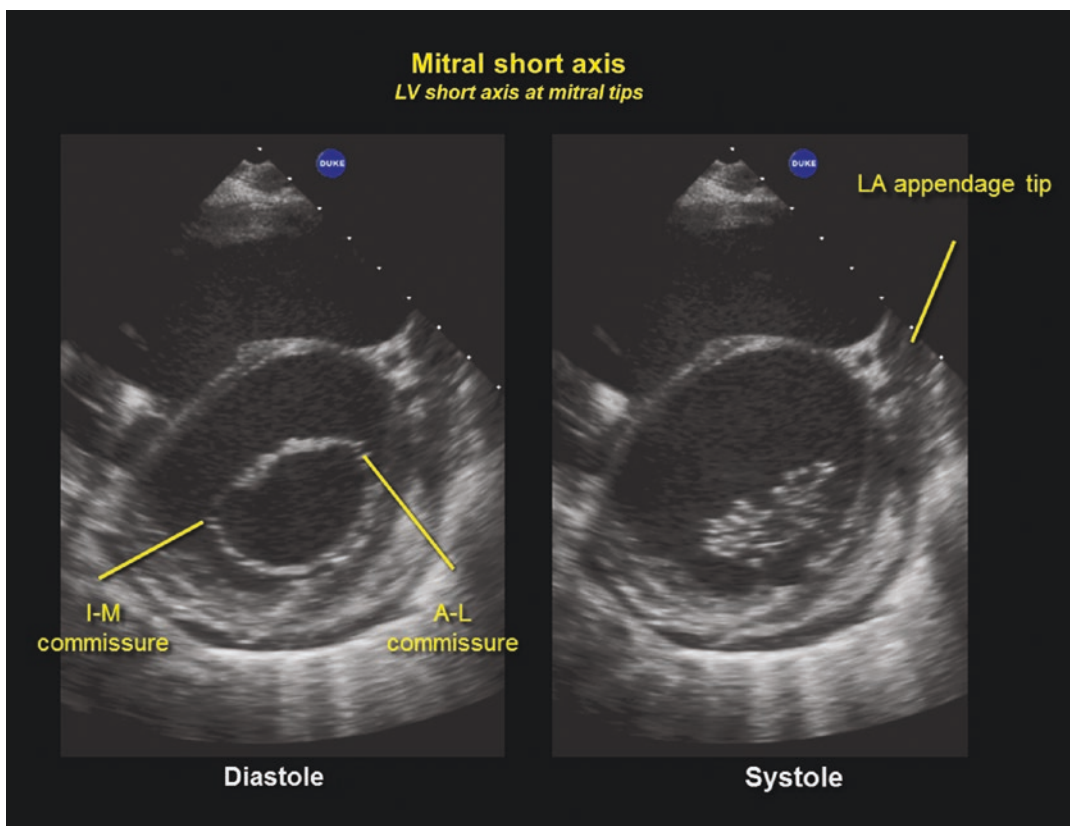


Fig. 10.11 Parasternal short axis echo view from the chest wall at the level of the papillary tips in a patient with a dilated cardiomyopathy

The anterolateral muscle bundle of the left ventricle (Bundle of Moutaerdt) resides along the anterior endocardial wall (Fig. 10.13). This muscle bundle is present in over 40% of normal individuals and is frequently mistaken for an accessory papillary muscle. When left ventricular hypertrophy is present (as in hypertension, aortic stenosis or hypertrophic cardiomyopathy, the anterolateral muscle bundle can be quite prominent).

Apical Views

Another critical view for the evaluation of mitral anatomy is the apical four chamber. Traditionally, echocardiography orients this view with the apex of the left ventricle towards the top of the sector arch as visualized in the left hand panel of the

Fig. 10.14. Both ventricles are seen juxtaposed and separated by the intraventricular septum. The interatrial septum is seen between both atria. The arrow points towards yet another septum, the common septum shared by the left ventricle and the right atrium that is called the atrio-ventricular septum. Thus, there are really three septa to the heart, not just two. Of other note is the fact that the mitral valve apparatus is farther away from the ventricular apex than the tricuspid apparatus. Note the position of these two atrio-ventricular (AV) valves in this left panel. The chordae tendineae supporting the mitral valve emerge from the papillary muscles attached to the ventricular free wall surfaces. In contradistinction, the tricuspid valve apparatus, nearer to the apex, is supported by chordae tendineae both from the free wall and the interventricular septum. Accordingly, mitral and tricuspid valves

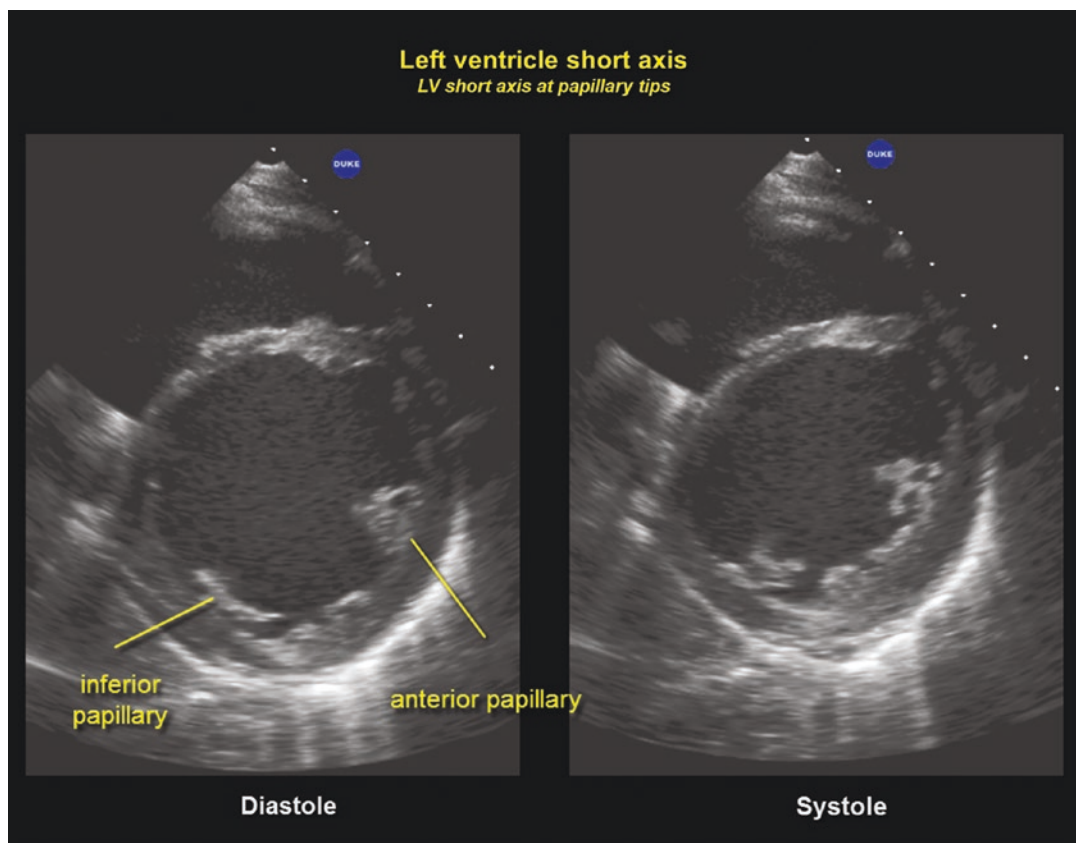


Fig. 10.12 Parasternal short axis echo view from the chest wall at the level of the papillary bases in a patient with a dilated cardiomyopathy

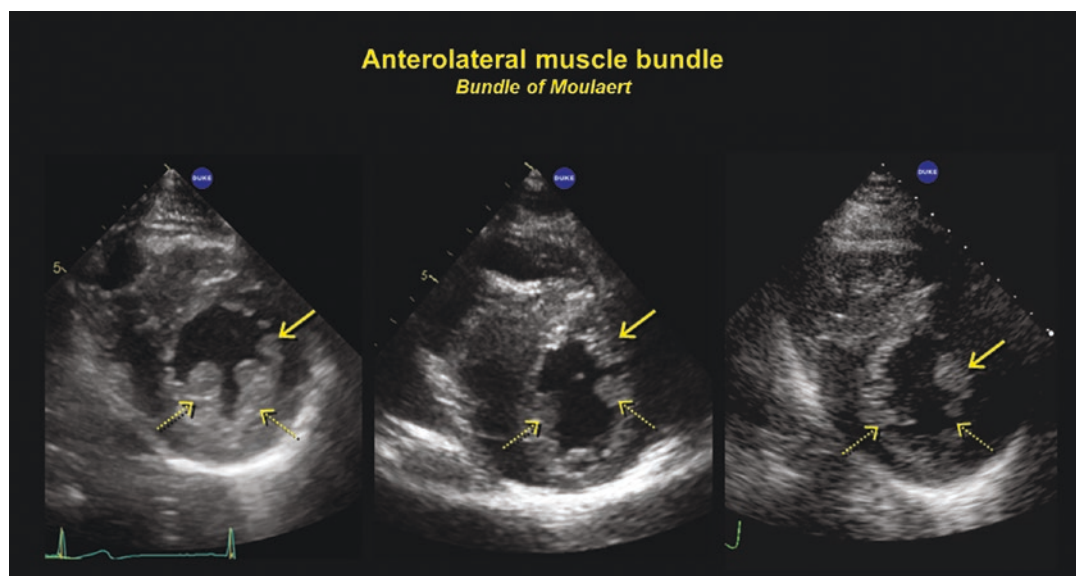


Fig. 10.13 The anterolateral muscle bundle of the left ventricle (Bundle of Moulardt) resides along the anterior endocardial wall and is present in over 40% of normal individuals and is frequently mistaken for an accessory

papillary muscle. Solid arrows point to the Bundle of Moulardt while the dotted arrows point to the papillary muscles. In cases of left ventricular hypertrophy, the Bundle of Moulardt can be quite large

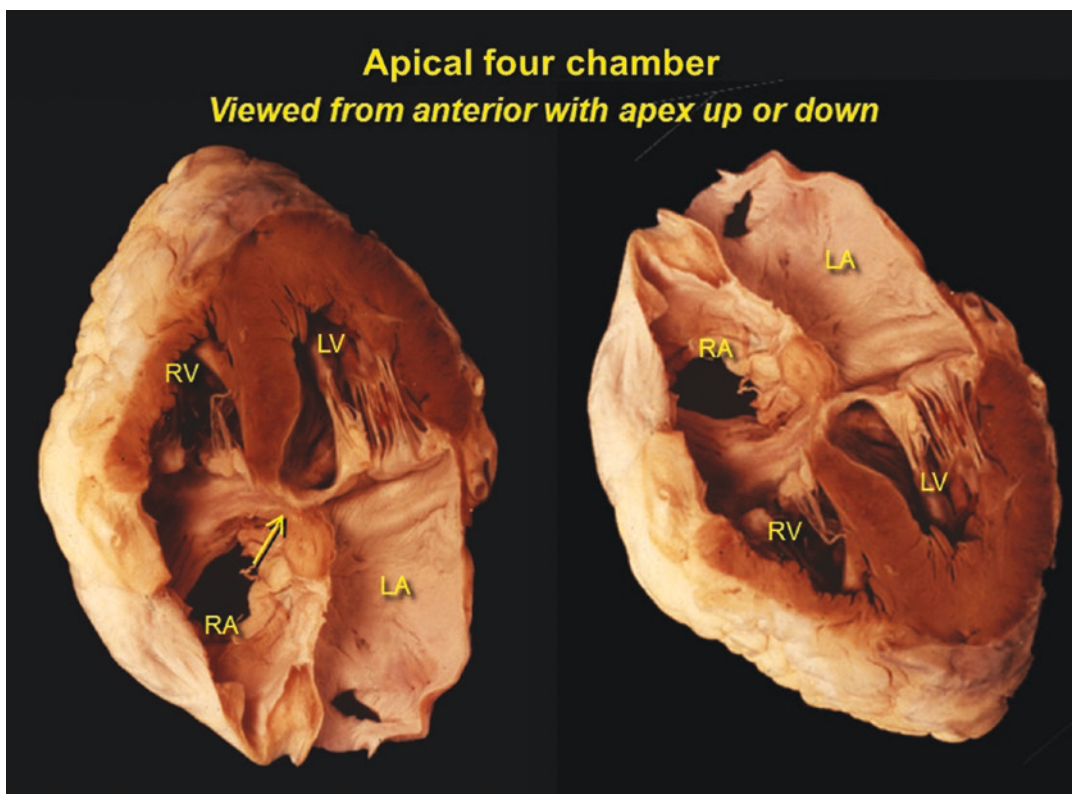


Fig. 10.14 Anatomic cut sections representing the echocardiographic apical four chamber view. The arrow points to the atrio-ventricular septum. Modified from Kisslo, Leech & Adams: Essentials of Echocardiography

can be differentiated by their position in relationship to the cardiac apex and their attachments to ventricular walls.

The other presentation sometime used for the apical four chamber view is with the cardiac apex in the down position. This, so called, “anatomic presentation” is much preferred by pediatric cardiologists and others users because one can easily visualize and remember the position of the heart in the intact human. We think the apex in the down position helps all users of echocardiography to remember anatomic relationships. In addition, it corresponds to presentations of the heart in X-ray, EKG, CT and other imaging techniques. Of course, relationships between chambers and valves are unaltered no matter what the presentation used for imaging. Users of three-dimensional echocardiography will profit greatly by orienting their apical four chamber views with the apex down in two-dimensional echocardiography and

then creating the three dimensional images from that point.

An actual echocardiogram of an apical four-chamber view of the left ventricle is seen in Fig. 10.15. Both left and right ventricles (LV and RV) and atria (LA and RA) are identified. The atrio-ventricular valves are seen to open and close. Again, note that the atrio-ventricular septum is indicated by the arrow in both the diastolic (left) and systolic (right) still frames. The tricuspid valve is located closest to the ventricular apex while the mitral valve is the farthest away. An examiner should always note the presence of three septa in the heart. This very short atrio-ventricular septum is altered in such defects AV canal defects.

A similar view can be obtained with the transducer positioned in the subcostal area and the interrogating array pointed in the same plane, but from a different transducer position. The transducer is then directed superiorly and a similar four-chamber view can be obtained (Fig. 10.16).

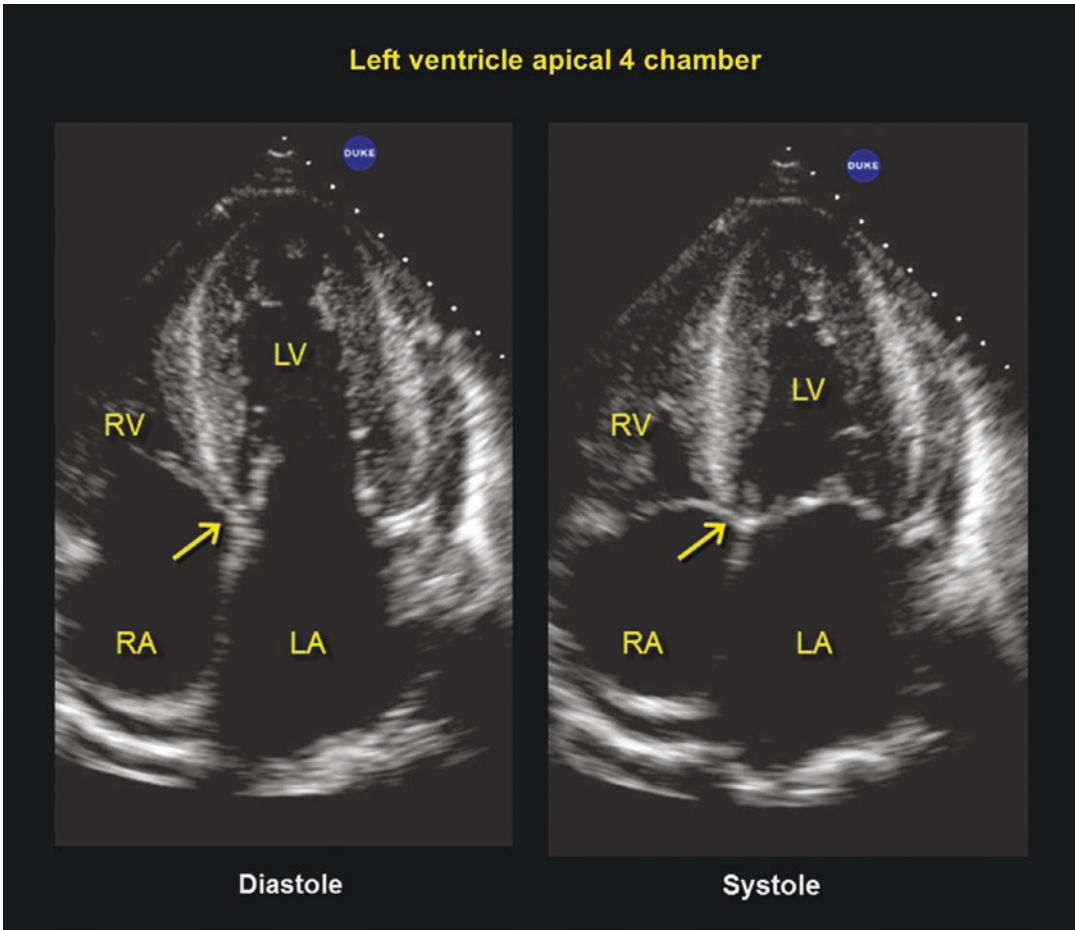


Fig. 10.15 Two dimensional echocardiographic images in diastole and systole oriented in the apical four chamber view for comparison. The arrow points to the atrio-ventricular septum

The arrow points again to the atrio-ventricular septum.

An actual two-dimensional echocardiogram from a patient with an enlarged left ventricle and a very enlarged left atrium is seen in Fig. 10.17 from the subcostal transducer position. Here the interatrial septum is seen to bulge from the left atrium to the right atrium. The highly reflective targets near the apex of this sector arch are from reflections from the liver tissue. The mitral valve is seen in the closed position. Because the mitral valve apparatus is far away from the transducer the resolution of the details of chordal structures are not as well seen in this view.

One of the more remarkable views of the left ventricle and mitral valve are seen from three-

dimensional echocardiography in this so-called, frontal long-axis view (Fig. 10.18). Here, the orientation of the apex is toward the bottom in a more anatomic presentation, with the aorta and the cardiac base oriented towards the top of the figure. Thus, the length of the left ventricle is seen from base to apex while viewing the back of the heart and the papillary muscles relationships to the mitral valve. On both sides are the papillary structures with chordal attachments toward the face of the anterior mitral valve leaflet (AMVL). Here the anterior mitral valve leaflet is seen on *enface* as it moves forward and back toward and away from the viewer when imaged in real-time. Remember that the right ventricle is anterior to the left ventricle and curves around

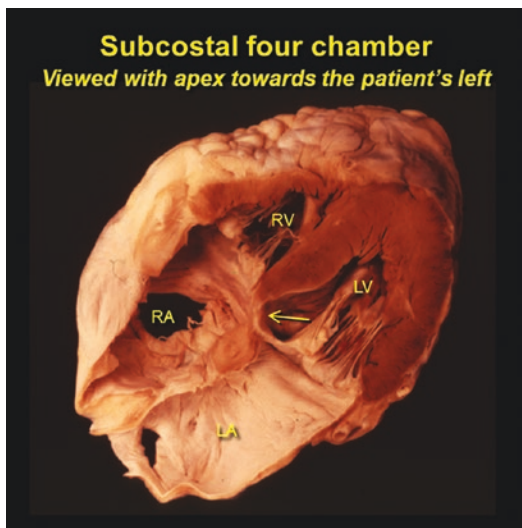


Fig. 10.16 Anatomic cut section along the orientation of the subcostal view from chest wall echocardiography. Modified from Kisslo, Leech & Adams: Essentials of Echocardiography



Fig. 10.17 Two-dimensional echocardiogram from the subcostal view. Compare to Fig. 10.15

the left ventricle. Here, the right ventricle and most of the interventricular septum is cut away, but the the right ventricular inlet (RV inlet in the upper left) in the upper left and the right ventricular outlet (RV outlet in the upper right) remain. The actual body of the right ventricle is in the

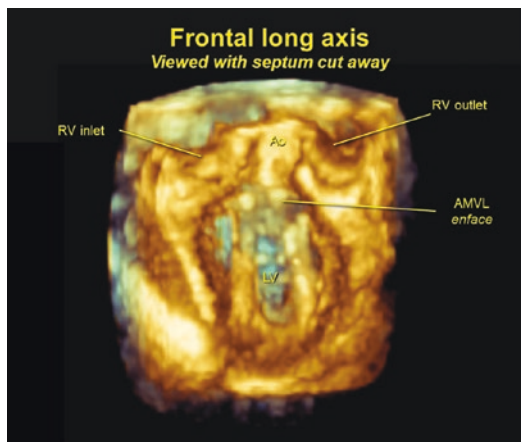


Fig. 10.18 Frontal long axis by three-dimensional echocardiography with the base at the top and left ventricular apex oriented towards the bottom. Using this view, the relation of the papillary muscles to the mitral valve are easily identified.

portion that is cut away. Of particular note in this view is that the papillary muscles are in a vertical position and well within the lateral limits of the mitral valve annulus. The papillary to the left is the infero-medial and the papillary to the right is the antero-lateral. For best understanding of all these spatial relationships, review all of the anatomic figures from Fig. 10.1 to Fig. 10.18.

The Surgical View

An additional view remains and is termed the surgical view. Until the advent of three dimensional echo, such a presentation of surfaces that are routinely encountered by surgeons in the operating room was not possible. Using three-dimensional echo, one can record an entire volume of three-dimensional data, then crop the image to view various internal cardiac structures. Three-dimensional images viewed in this chapter are the result of such acquisition techniques and cropping.

One of the best views for the communication of information concerning the mitral valve is this surgical view. When surgeons approach the mitral valve they generally do so from the left atrial approach but cutting into the roof of the atrium in the transverse sinus or some other approach to view

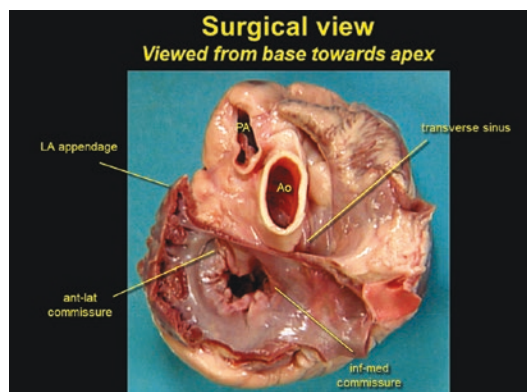


Fig. 10.19 Anatomic specimen of a porcine heart showing the typical surgical approach. The anterior commissure is oriented towards the left atrial appendage. Modified from Kisslo: Thinking in 3D

directly into the mitral valve orifice. Figure 10.19 shows a section from a porcine heart specimen in a surgical view. The pulmonary artery is seen arising anterior to the aorta and the left atrium is behind the aorta and separated from it by the transverse sinus. Note the location of the left atrial appendage to the left and its relationship to the antero-lateral commissure. The infero-medial commissure is seen on the opposite side of the mitral orifice, towards the interatrial septum. Multiple scallops are seen along the posterior mitral valve leaflet.

The observer of this view should be impressed that the anterior mitral valve leaflet comprises of approximately 40% of the mitral valve annular structure. The remainder (60%) is taken up by the posterior, or mural, leaflet. Accordingly, the normal anterior mitral leaflet is the longest in length, but the narrowest around the annulus. The opposite is true of the posterior (or mural) mitral leaflet (shortest in length but widest around the annulus).

This surgeon's view is seen in the human specimen in Fig. 10.20. The pulmonary artery courses from the right to the left, anterior to the aorta (top of the picture). Note the coronary arteries emerging from the aorta at approximately 10 o'clock (left main) and 3 (right coronary) o'clock along the aortic circumference. The transverse sinus then separates the aorta from the posterior atrial structures. The left atrium and its appendage are directly behind the aorta.

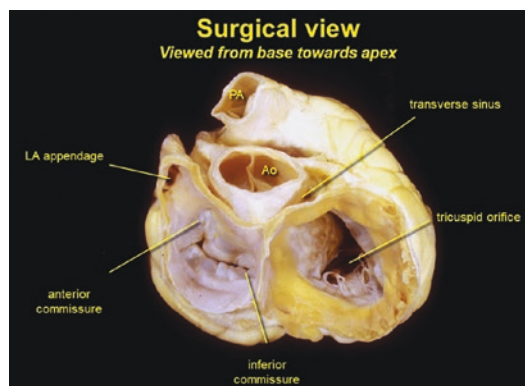


Fig. 10.20 Anatomic human specimen oriented into the surgical view. For details see text. Courtesy S.Y. Ho, MD. Modified from Kisslo: Thinking in 3D

The most critical relationship is that of the anterior commissure to the atrial appendage. When the atria is opened, one looks for the os of the left atrial appendage and the commissure just below the os indicates the antero-lateral mitral commissure.

In this specimen, structures from the tricuspid orifice are also seen. The two circles of the mitral and tricuspid annuli have the aorta wedged posterior between them. This is a normal relationship in a properly septated atrio-ventricular valve assembly. In AV Canal defects (atrio-ventricular septal defects) there is a common mitral-tricuspid orifice and the aorta is markedly anteriorly displaced.

These remarkable relationships may also be visualized by three-dimensional echocardiography. Figure 10.21 shows such a still-frame captured during isometric contraction with the pulmonic, aortic and mitral and tricuspid valves in the closed positions. The interatrial septum is seen between the two atrio-ventricular valves. Such a view is not possible by conventional two-dimensional echocardiography.

Such relationships are further enhanced by studying Fig. 10.22, similar to the previous two previous views. The pulmonary artery and aortic relationships are as previously noted. The transverse sinus is shown to separate the aorta from both the left atrium and right atrium. In addition, both atrial appendages are seen to curl anteriorly around the great vessels. Once again,



Fig. 10.21 Three dimensional echocardiographic cut section showing the orientation of the mitral, aortic and tricuspid valves

the anterior commissure points towards the os of the left atrial appendage and the inferior commissure is seen at the opposite side. In addition, the coronary sinus emerges from the right atrium and circles clockwise around the mitral valve annulus.

This coronary sinus can also be identified by three-dimensional echocardiography. This is demonstrated in Fig. 10.22 and again in Fig. 10.23 where the coronary sinus is easily seen to emerge from the right atrium and circle in the same clockwise pattern around the mitral valve annulus. This is an extraordinary image of the relationship of the coronary sinus to the mitral annulus. While the left atrial appendage itself is not seen in this view, one can see a defect in the annulus where the os is usually located adjacent to the anterior commissure.

Since a variety of electrophysiology procedures involve the insertion of catheters into the coronary sinus. The identification of this structure is of growing importance. As well, there are a number of forthcoming devices under investigation which may be inserted into the coronary sinus for reconfiguration of the mitral valve annulus in the setting of severe mitral regurgitation. Thus, routine visualization of the coronary sinus will become imperative over time as these techniques demand guidance by echocardiographic approaches.

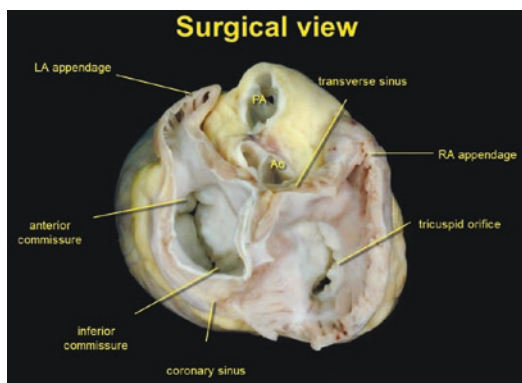


Fig. 10.22 Anatomic human specimen, cut and oriented into the surgical view. Note the anterior commissure orientation towards the left atrial appendage. Courtesy R.H. Anderson, MD. Modified from Kisslo: Thinking in 3D

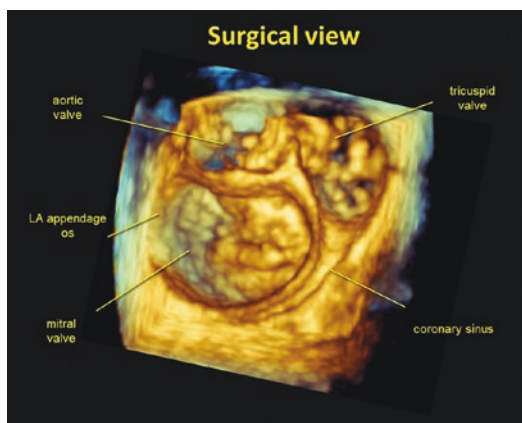


Fig. 10.23 Three-dimensional echocardiographic still-frame in systole of the surgical view of the mitral valve. The annulus is cropped to reveal the coronary sinus emerging connecting to the posterior portion of the right atrium. Note how the coronary sinus encircles the mitral annulus

Further examination of structures above and below the mitral apparatus are seen in Fig. 10.24. Here a long axis section is shown in the left hand panel of the left atrium and left ventricle. The ligament of Marshall is identified in this same individual as seen in Figs. 10.8 and 10.9. Note that there is a slight downwards tilting of the left ventricular apex so that this patient is imaged in a more anatomically correct position. The rotation of the left panel clearly shows secondary chordae tendinae to

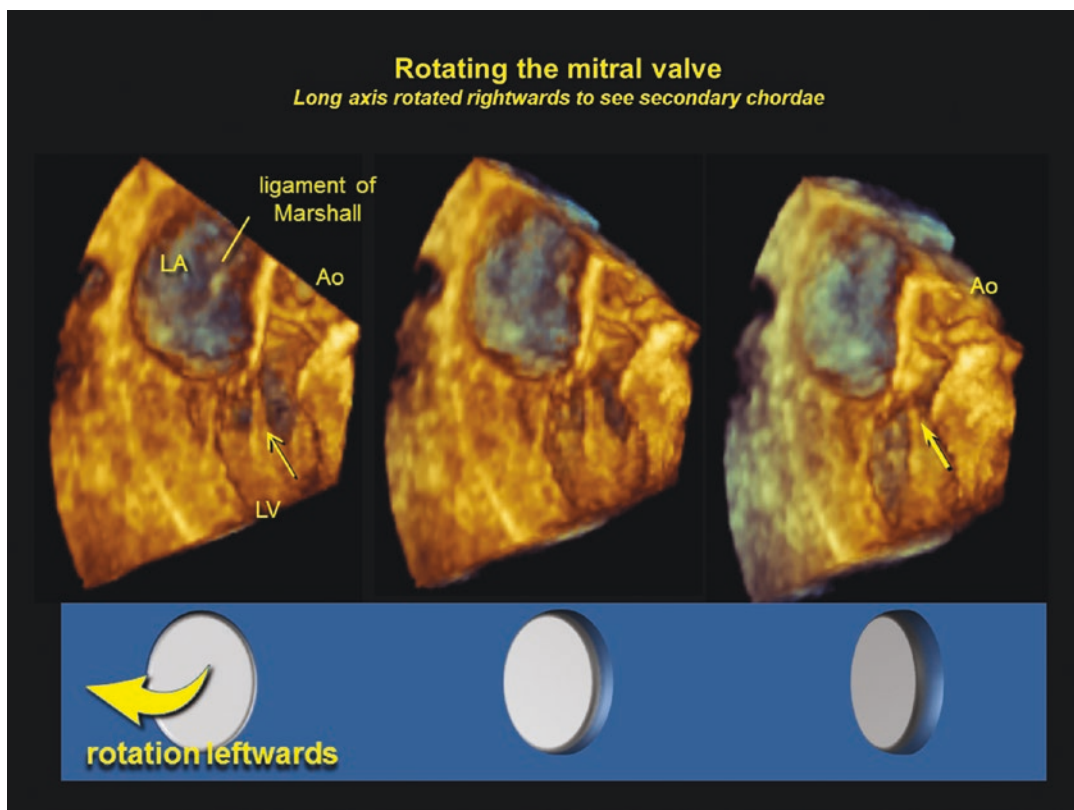


Fig. 10.24 Three-dimensional echocardiographic still frame of the long axis of the left ventricle showing the left atrium, mitral valve and left ventricle from the septal side

towards the LA and LV lateral walls. The arrow points toward secondary chordae as the image is rotated

the anterior side of the closed anterior mitral valve leaflet. This section is taken from isometric contraction so that both the aortic and mitral valves are closed. As the heart is progressively tilted toward the left and the back wall of the left atrium is seen the supporting chordal structures can easily be identified.

Functional Mitral Valve Anatomy

Functional Anatomic Segments

With the advent of mitral valve repair, it became necessary for cardiac surgeons to precisely identify the location of mitral regurgitation. The most popular anatomic descriptive system is the functional classification of Carpentier. This classifica-

tion recognizes three major regions of the posterior mitral valve leaflet; P_1 , P_2 , and P_3 as seen in Fig. 10.25 with a schematic diagram in the left panel. This nomenclature system begins at the antero-lateral commissure and extends clockwise to the posterior medial commissure. Using the traditional chest wall echo orientation, the numbering would begin (right panel Fig. 10.25) at the right side of the image (left atrial appendage) and circle clockwise. No matter the orientation, or view, one needs to identify the left atrial appendage location in order to properly assign these regions.

Figure 10.26 shows a short axis or mitral apparatus near the mid portions of the mitral valve leaflets from the chest wall in a patient with prominent posterior leaflet scallops. This patient has a very large P_2 scallop and the remaining P_1 and P_3

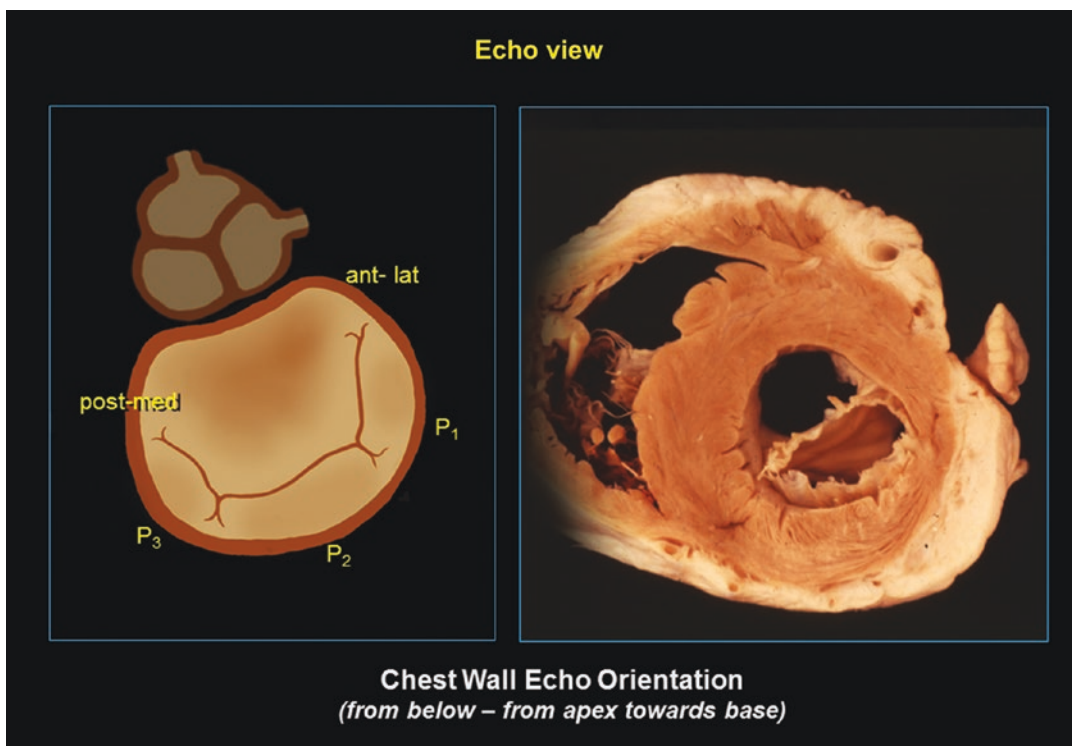


Fig. 10.25 Schematic and anatomic sections demonstrating the posterior mitral leaflet segments from the standard chest wall two-dimensional orientation (from below)

regions are easily seen. In this individual both commissural areas are also easily identified in this mid-diastolic frame. The orientation is from the standard chest wall short axis configuration.

Functional Nomenclature in Other Views

The proper orientation for the surgical view may be somewhat confusing at first. The chest wall echo visualizes structures from below (left hand panel Fig. 10.26) and the surgical view is from above (right hand panel Fig. 10.27). In these two different orientations, the image seen in the left hand panel is simply flipped over like turning a playing card from the chest echo orientation to the surgical orientation. To facilitate understanding of this view reversal, one may look at the palm of their right hand. This can be imagined as viewing the mitral apparatus from below (with your

thumb as the left atrial appendage). Then, simply turn your hand over and look at its back-side. Using this orientation, your thumb is at the left, the equivalent of surgical orientation (right hand panel Fig. 10.27).

Given this turning from one side to the other, the labels identifying the various commissures and posterior valve leaflet scallops are also reversed from one view to the other in Fig. 10.27. Also note the orientation of the aortic valve and the various coronary ostia as views are flipped. Because the views are reversed, the right coronary artery still emerges most anteriorly. The chest wall echo visualizes the ostium of the left coronary artery at approximately three o'clock on the aortic valve circumference. In the surgical view, surgeons will locate the left coronary artery at approximately 9 o'clock on the aortic circumference.

The opposing segments of the anterior mitral valve leaflet are also identified (Fig. 10.28). Since the os of the left atrial appendage is at the upper

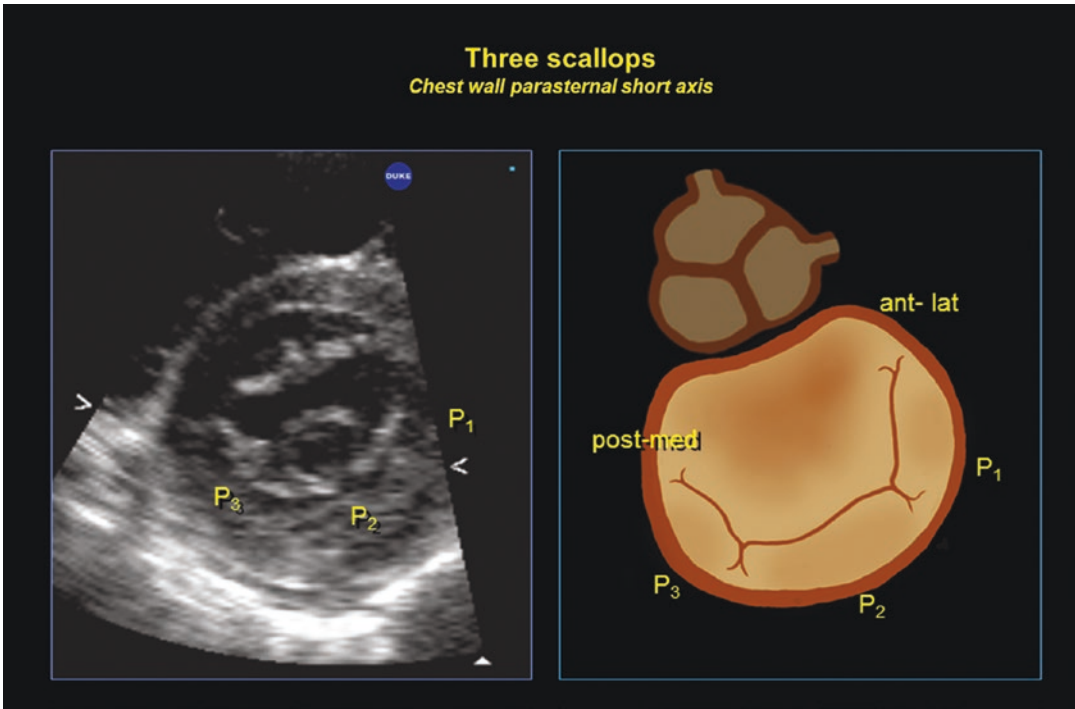


Fig. 10.26 Still frame mid-diastolic short axis of an echocardiogram showing the three scallops of the posterior mitral leaflet and accompanying schematic diagram.

The anterior commissure is at the right when oriented from the two-dimensional echo standard from below

left of the mitral apparatus in the surgical orientation, the nomenclature begins at the atrial appendage and moves counter clockwise in the surgical presentation. Therefore, the A₁ segment opposes the P₁ segment and so forth.

Figure 10.29 shows an actual three-dimensional echocardiogram presented from the transesophageal approach and oriented in the surgical view in a patient with prominent posterior leaflet scallops. Both the antero-lateral and posterior-medial commissures are crisply identified in the left sided diastolic panel. In systole (right hand panel) the various opposing segments are seen. This patient has a somewhat prominent P₂ segment that makes identification of this scallop most easy in both diastole and systole. In reality, the various mitral valve scallops may be comprised of several smaller scallops and in normal individuals are much less clearly differentiated.

Compare the images seen in Fig. 10.29 with those seen in Figs. 10.19 , 10.20, 10.21, 10.22

and 10.23. Surgeons have little choice in orienting the human mitral valve since standard surgical approaches dictate that valve replacement and/or repair be performed from the atrial perspective. Therefore, it is imperative that echocardiographers learn to reorient their images as to provide surgeons with the appropriate view.

These orientations may be even more complicated when one takes into consideration standard chest wall echo presentations from those seen by standard transesophageal two-dimensional echo presentations (Fig. 10.30). Since the transducer is behind the heart in the transesophageal (TEE) two-dimensional approach, the mitral valve is actually flipped from front to back. The aortic position is, obviously, reversed. Again, the easiest way to identify these structures is to locate both the aorta and the left atrial appendage, and this gives location to the antero-lateral commissure and the assignment of all the attendant segments.

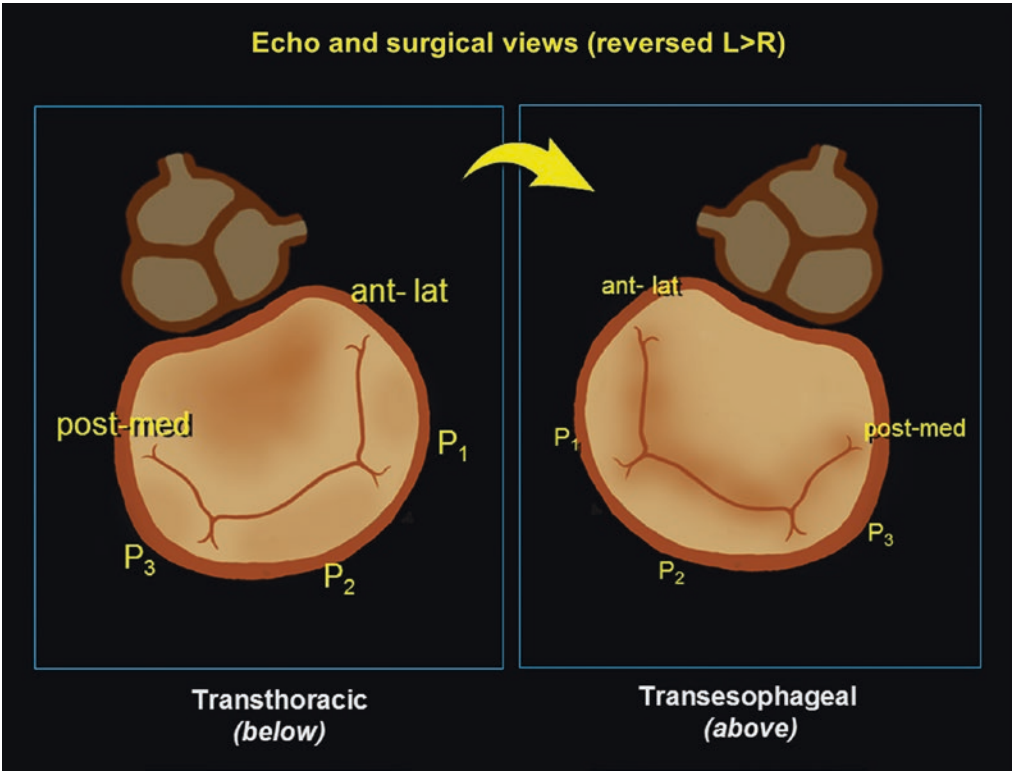


Fig. 10.27 Schematic comparison of the orientations of echocardiographic images from the standard short axis of the mitral valve from the chest wall compared to that visualized by surgeons in the operating room. See text discussion

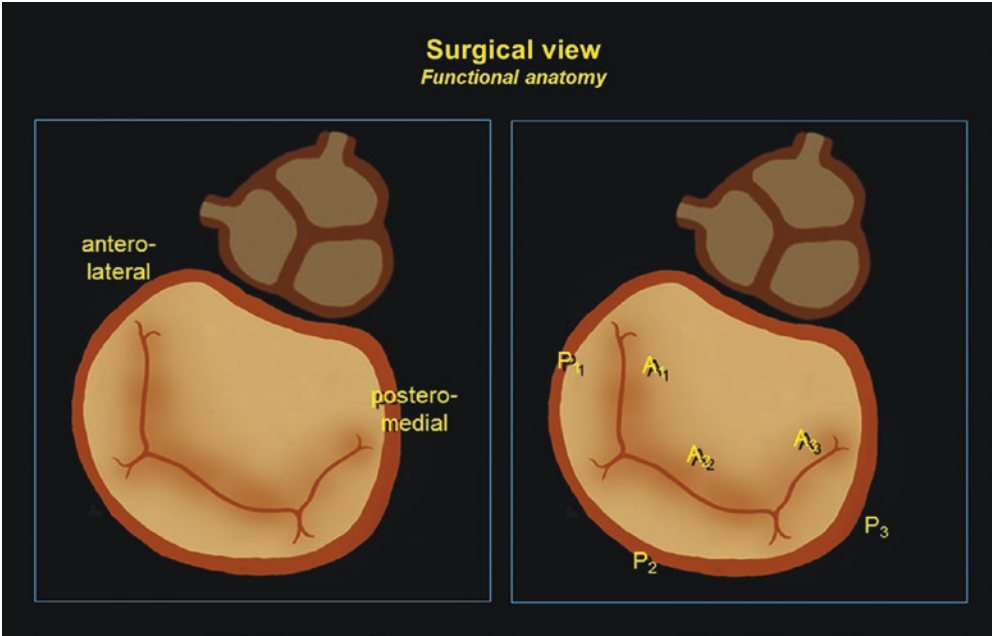


Fig. 10.28 Functional anatomy of the mitral valve presented in the surgical view. The segment numbering starts at the antero-lateral commissure

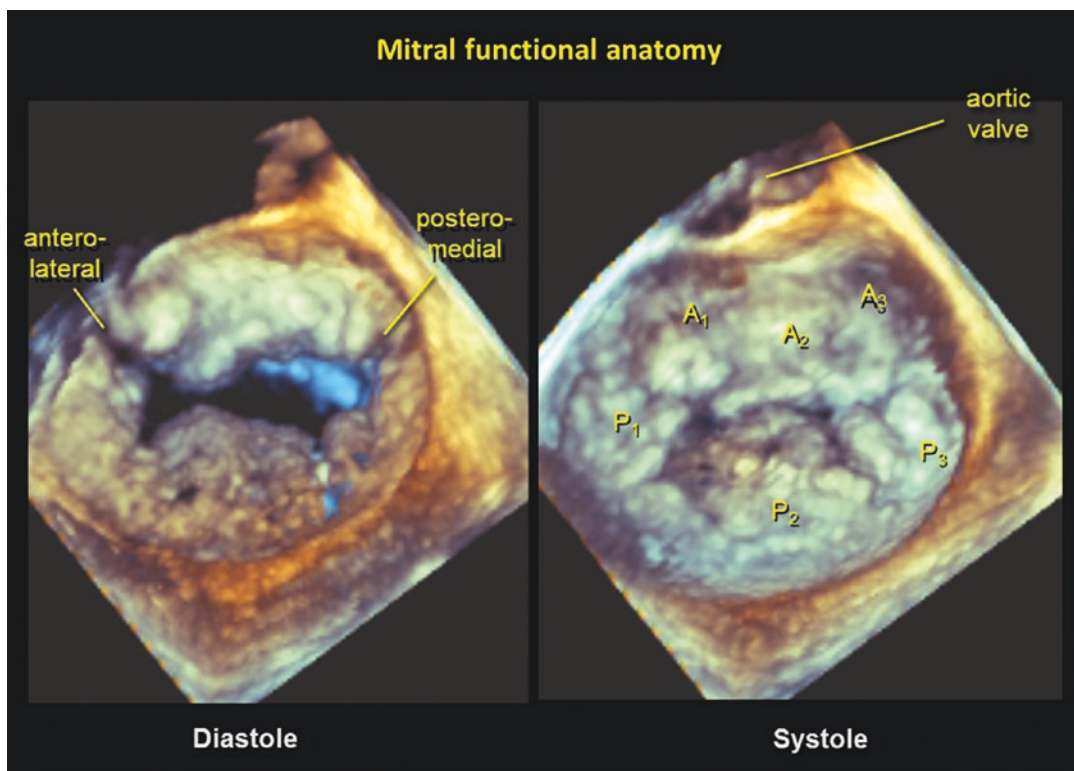


Fig. 10.29 Paired diastolic and systolic three-dimensional views from the surgical view (atrium down towards the ventricle). The various leaflet segments are labeled. The aortic valve is anterior

As A-mode echo moved into M-mode, then two-dimensional echo emerged and now we are at the advent of three-dimensional echo, there are multiple, infinite and potentially confusing orientations that resulted. It is expected that most examiners will orient images anatomically as time moves forward so that images will be consistent from technique to technique. Old image orientations, like old imaging methods, take long to change and even longer to die from common use. Remembering where the left coronary, atrial appendage and papillary muscles are helps to orient the anatomically normal mitral valve in any view.

The schematic drawing shown in Fig. 10.31 diagrams the mitral annulus cut at the antero-lateral commissure and the mitral leaflets opened to reveal the entire mitral circumference. Doing this reveals the entire array of the various segments to be unfolded in a straight line. Note that since the cut occurred at the antero-lateral commissure the P_1 segment is located at the far right in this diagram. It is important to also see that

chordal attachments arising from each of the papillary head go to both of the leaflets. In this case, the centrally diagrammed postero-medial papillary gives chordal structures to both to the anterior and posterior leaflet segments. The same is true for the antero-medial papillary (but not diagrammed).

Such a cut was actually made in a porcine heart and is demonstrated in Fig. 10.32 with the leaflets splayed out along a straight line. Both anterior and posterior mitral leaflets are identified and chordal structures can be seen to support both of the leaflets from any one papillary. In this, a thumb is located in the lower right position. This marks the antero-lateral commissure and where the anterior papillary was divided to open the entire array of leaflets, scallops, chordal structures and papillaries. The infero-medial papillary is located centrally. Note that the delicate attachment of the chordae tendinae is they arise from the papillary heads and then to join the tips of the primary chordal insertions in the leaflet tips. Secondary chords are not visualized in this

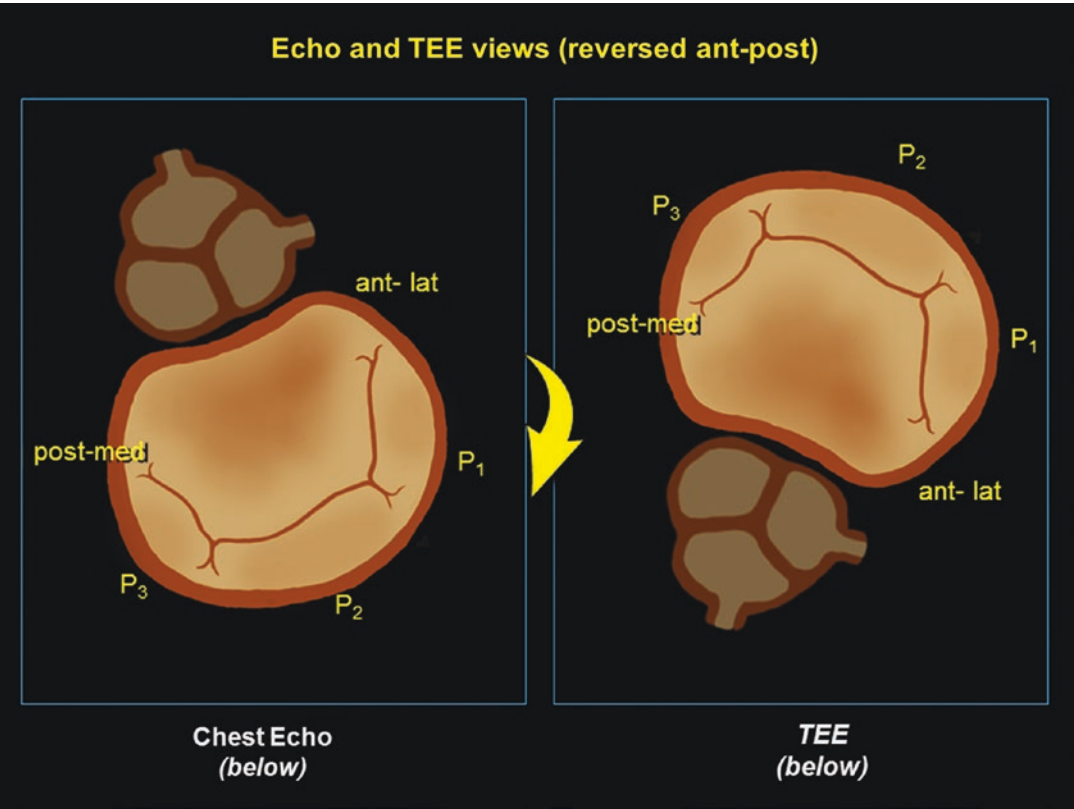


Fig. 10.30 Comparison of schematic diagrams of the orientation of standard chest wall echocardiograms of the mitral valve with those during transesophageal echocardiography

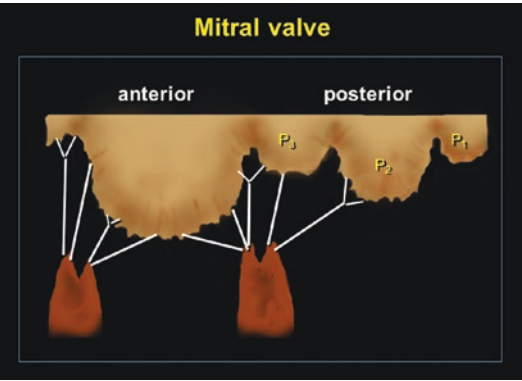


Fig. 10.31 Schematic diagram of the mitral valve, cut at the antero-lateral commissure and then laid flat. The anterior leaflet is the longest from top-bottom, but only occupies about 40% of the annulus

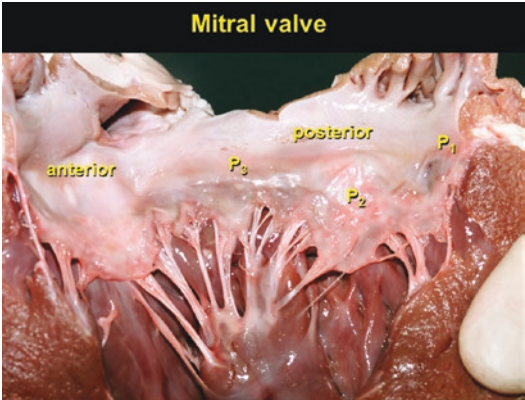


Fig. 10.32 The porcine mitral valve, cut at the antero-lateral commissure as in the previous figure. The large papillary muscle at the center is the infero-medial. This demonstrates how each papillary muscle gives rise to chordae tendineae to both leaflets. Modified from kisslo: Thinking in 3D

image because they go to the backside of the leaflets.

In summary, it is important to recognize where mitral valve leaflets are attached in order to identify which is the anterior or posterior leaflet. The

anterior is attached to the aorta in an otherwise normal individual while the posterior is attached to the ventricular wall (the “mural” leaflet). Keeping this in mind will always allow an

examiner to differentiate these leaflets. As well, the anterior mitral leaflet is the longest in comparison to the posterior leaflet. However, the anterior leaflet takes up only 40% of the mitral valve annulus.

Remember that the left atrial appendage marks the antero-lateral commissure, no matter the view or technique. On the ventricular side of the antero-lateral commissure is the antero-lateral papillary muscle, attached to the free wall of the left ventricle. The postero-lateral commissure has the postero-lateral papillary just below it in the ventricle. If one looks at the mid portion of the anterior mitral leaflet in Figs. 10.19, 10.20, 10.21, 10.22, and 10.23 as well as the schematic diagrams in Figs. 10.25, 10.26, 10.27, 10.28, 10.29, and 10.30, one can appreciate that the mid portion of the anterior leaflet is just behind the aorta. Given this anatomic orientation of the aorta to the anterior mitral valve leaflet, one might expect a “cleft” (seen in AV Canal defects) to go directly toward the aorta. As will be seen near the end of this chapter (see Figs. 10.146 and 10.147), such a cleft does not go in this direction, because there is a significant rotation of the entire mitral valve apparatus in AV canal defect patients. Rather, such a cleft goes towards the interventricular septum.

Mitral Valve Spatial Movement and Flow Profiles

Cyclical Mitral Valve Movement

The first recognition of mitral valve movement came from the M-mode echocardiogram. Here, a single line of information is directed from the chest wall toward the mitral valve apparatus as seen in Fig. 10.33. The diagram of the left ventricle is in the parasternal long-axis orientation with apex at the left and aorta to the right. The chest wall is at the top. Most examiners will easily recognize the rapid to and fro movement of the mitral valve by any examination technique whether it be M-mode, two-dimensional, or three-dimensional echocardiography.

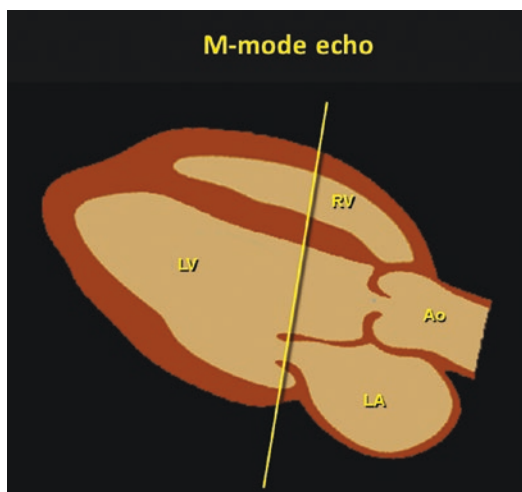
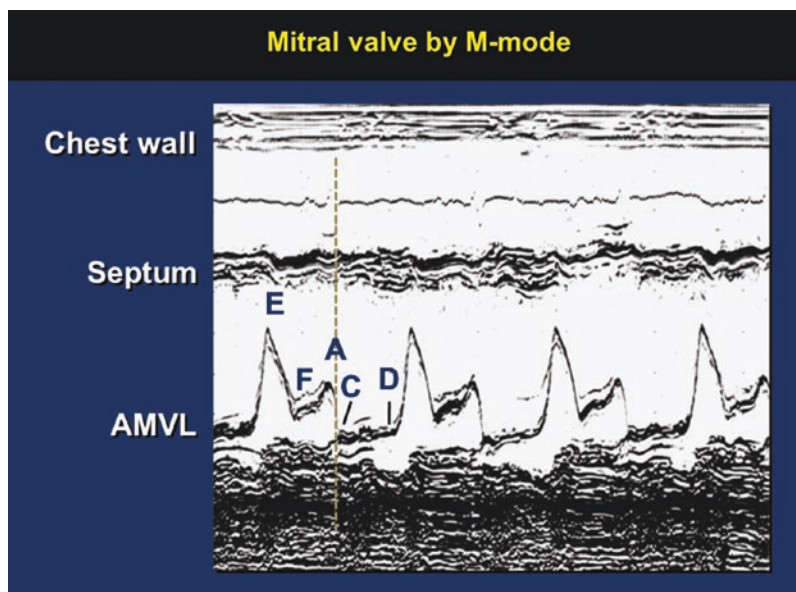


Fig. 10.33 Schematic diagram of the path of a single M-mode beam, directed posteriorly from the chest wall to intercept both leaflets of the mitral valve

Figure 10.34 shows a typical M-mode echocardiogram of both the anterior and posterior mitral valve leaflets as they move to and fro between diastole and systole. Because the anterior leaflet is the longest, its motion is the greatest in comparison to the posterior leaflet, which is hardly seen during this examination. In fact, the posterior leaflet appears almost buried on the posterior ventricular wall. The mitral valve first opens and moves anteriorly to its E point, the point of maximum excursion. This corresponds to the rapid inflow of blood during the rapid filling period of diastole. The valve leaflet then drifts posterior to its F point where it lingers during mid-diastole, in the period known as diastasis (where little flow occurs). With atrial contraction, there is a slight anterior movement to the A point. This is followed by systolic closure to the C point following the QRS complex of the EKG (vertical –line). At the C point, the anterior and posterior valve leaflets meet and then drift slightly anterior to the D point during ventricular systole as it is carried with the anteriorly moving left ventricular and aortic supporting structures. Then in diastole, the process repeats itself over and over in a cyclical fashion. As such, the normal M-mode appearance of the mitral valve is a passive envelope of flow.

Fig. 10.34 M-mode echocardiogram of the normal mitral valve showing wide excursion of the anterior mitral leaflet (AMVL) in diastole



During this cycle, the aorta moves anterior in systole and posteriorly in diastole. The mitral annulus itself moves toward the ventricular apex as the left ventricle shortens and contracts.

Given that a patient is in normal sinus rhythm, the patterns of E and A excursions are usually seen in most normal mitral valve leaflet M-mode examinations if the leaflets are pliable and free of intrinsic disease. Of course, best imaging of a mitral valve is obtained when the interrogating sound beam is perpendicular to the mitral valve apparatus itself (a specular orientation). This is generally done from the anterior third through fifth intercostals spaces with the beam directed posterior to encounter the anterior mitral leaflet.

Since the normal mitral valve leaflet is a passive envelope of flow, the mitral valve flow profiles by either pulsed or continuous wave Doppler show a marked resemblance to movements detected by M-mode (Fig. 10.35). Note that the E and A points are identified in the M-mode, pulsed-wave and continuous wave recordings of mitral valve movement and flow.

The best Doppler recordings are detected from the ventricular apex, parallel to flow. Using this apical approach for Doppler interrogation, a small degree of retrograde flow oppo-

site to the diastolic flow can be seen in systole. Some of this low velocity flow away from the transducer represents flow out of the left ventricle during mechanical systole that is caught between the leaflets as they close. This is called "backflow".

Normal Doppler Mitral Profiles

Cyclical flow through the normal mitral valve orifice is shown in Fig. 10.36 (top panel). Note the relationship of diastolic flow to the EKG. Flow into the left atrium through a pulmonary vein is also shown in the lower panel in this figure. There is filling of the left atrium from the pulmonary vein during the entirety of the cardiac cycle, one being predominantly in diastole (D wave) and the other predominantly in systole (S wave). The general contour of flow through the mitral orifice itself is as previously indicated and forms the E point (occurring with the D point of flow from pulmonary vein D point in diastole). As the mitral valve is *opened*, the atrium serves as a simple conduit of flow from pulmonary vein through the left atrium and into the left ventricle. When the mitral valve is closed, flow continues from the pulmonary vein (S wave) into the left

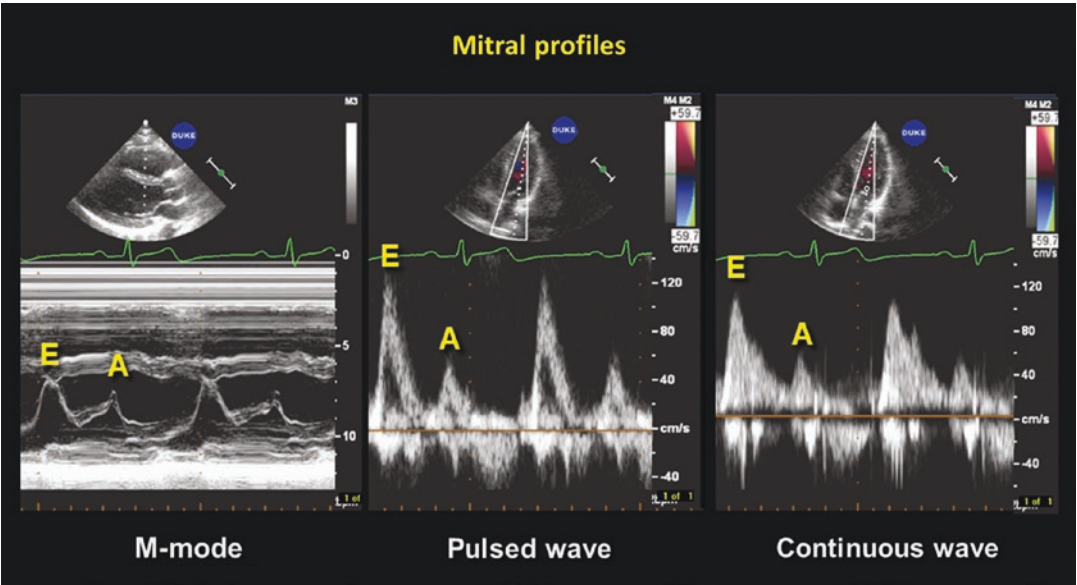


Fig. 10.35 Movement profiles of the mitral valve by M-mode (left panel), pulsed wave Doppler (middle panel) and continuous wave Doppler (right panel). All show the greatest degree of movement or flow with passive ventricular filling in the first one-third of diastole

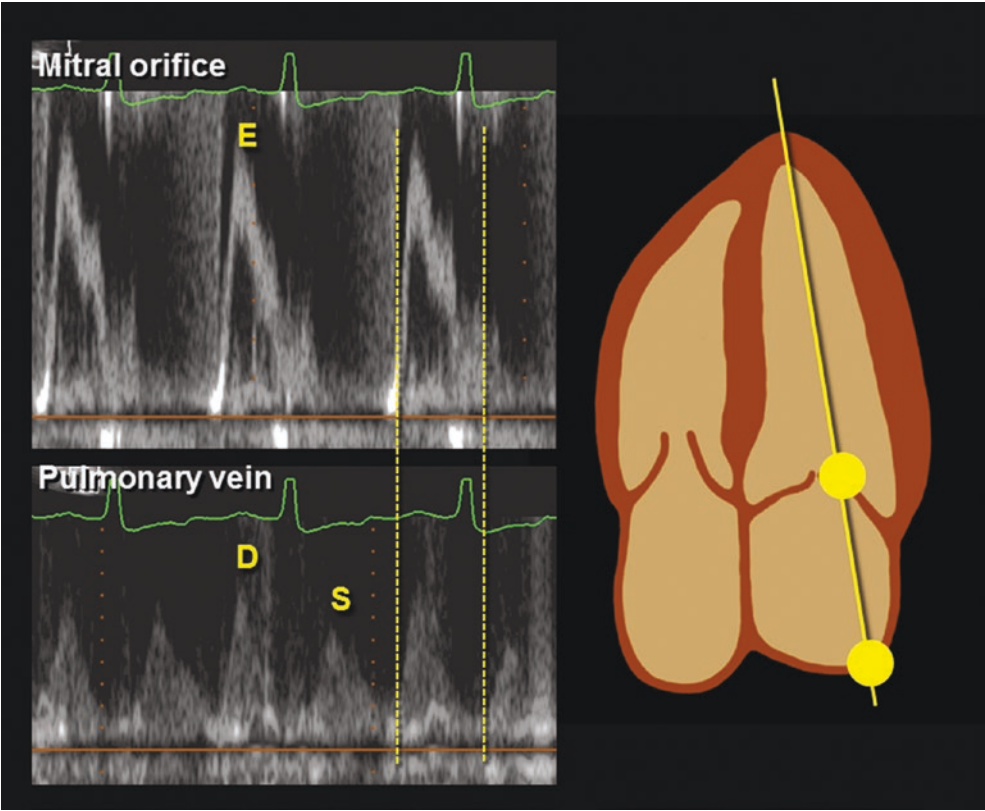


Fig. 10.36 Comparison of pulsed Doppler spectral flow profiles at the level of the mitral orifice (top panel) and pulmonary vein (bottom panel). Note how the diastolic flow profiles are similar in diastole as the atrium serves as a conduit with flow from lungs through the atrium to the ventricle. In systole, the normal antegrade mitral flow stops but the pulmonary venous flow continues to fill the atrium (now acting as a reservoir)

atrium and the atrium functions as a reservoir (S wave lower panel of Fig. 10.36). When pressure rises in the left atrium due to mitral regurgitation or high left ventricular filling pressures, this antegrade flow during systole is frequently suppressed. Most initial students of echocardiography do not realize that flow continues into the heart during the entirety of the cardiac cycle in normal patients. The normal ventricle will fill during diastole but the normal atrium fills during both diastole *and* systole.

Continuous wave Doppler interrogation of abnormal mitral flows includes mitral stenosis and mitral regurgitation (Fig. 10.37). Mitral stenosis is a diastolic event (note the EKG in the upper panel) where there is spectral broadening and a slow diastolic descent. Note that the peak

velocity in mitral stenosis is between 2.0 and 3.0 m/s. In mitral regurgitation (lower panel) there is a high velocity flow away from the transducer in systole. This high velocity flow goes from a very high pressure chamber (left ventricle) to a low pressure chamber (left atrium). In this setting of mitral regurgitation there is an increased systolic flow approaching 4–5 m/s retrograde into the left atrium from the left ventricle depending upon the various pressures. In these examples (dashed horizontal lines) the diastolic stenotic flow approaches 2.4 m/s while the systolic regurgitant flow is slightly over 4 m/s. Note that the scale on the right side shifts from cm/s to m/s between the two interrogations. These continuous wave Doppler tracings are not from the same patient.

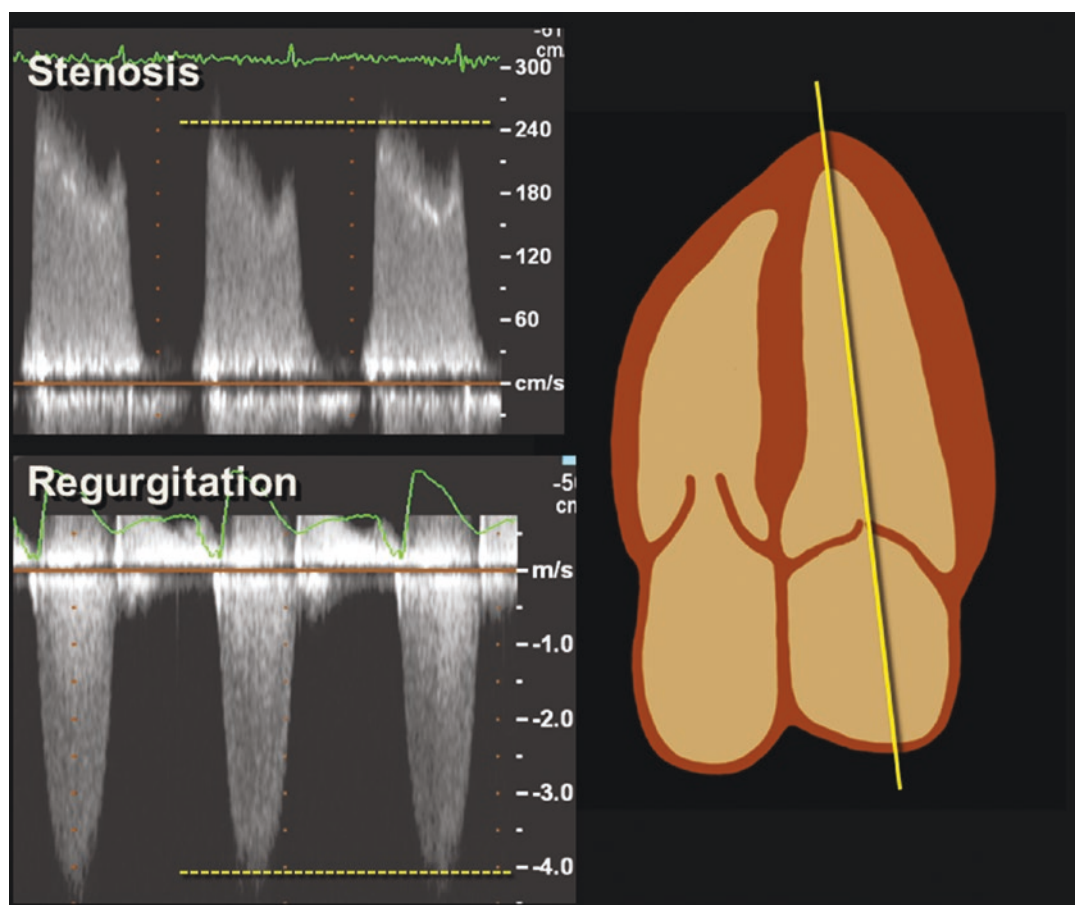


Fig. 10.37 Typical abnormal continuous wave flow profiles in mitral stenosis (top panel) and mitral regurgitation (bottom panel)

Comprehensive Evaluation of Mitral Regurgitation

Mitral regurgitant jets have four basic components by color flow Doppler. Comprehensive evaluation of the mitral valve requires that one examine at all four components of the jet when evaluating color flow images for mitral regurgitation (Fig. 10.38). As flow converges in the left ventricle in systole just proximal to the regurgitant orifice it forms into a three-dimensional volume of flow convergence. Here, flow begins to accelerate in velocity. It then narrows into the fastest velocity of a regurgitant jet where the flow accelerates through the actual regurgitant orifice itself. Then, as the flow jet emerges from the regurgitant orifice into the left atrium the jet splays out into a large area of turbulence, much like water going over the precipice of the waterfall into the waterfall itself. This third area of turbulence is the first thing a viewer recognizes when viewing a regurgitant jet in the left atrium. The fourth, and last, effect is the downstream effect of suppression or reversal of systolic flow into the left atrium in systole through a pulmonary vein (Fig. 10.39).

Of course, various quantitative indices can be applied to these different areas recognized in the two-dimensional color flow image. The area of flow convergence can be described in what is known as the PISA (proximal isovelocity surface area) for the derivation of effective regurgitant

orifice area (EROA) (Fig. 10.40). As the jet then passes through the area of flow acceleration (the jet orifice) the flow will increase somewhat in velocity (in the vena contracta) and the diameter of this flow acceleration can be measured. The most obvious area is that of the flow disturbance within the left atrium itself. Beginners in echocardiography will be most attracted to this area, but it is the least reliable in the various descriptive indices now described for the severity of mitral regurgitation. Lastly, there is the effect seen downstream from the regurgitation when there is pulmonary venous flow suppression or actual reversal of pulmonary venous inflow during systole. When such suppression or reversal is noted, the regurgitant jet is likely severe.

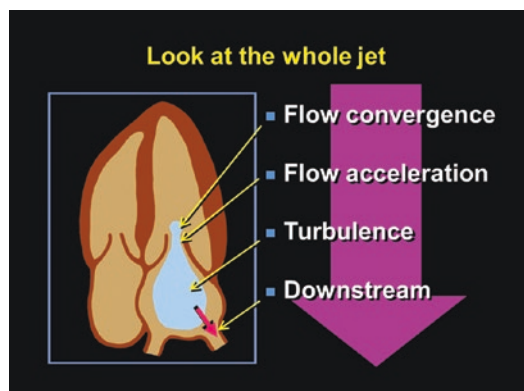


Fig. 10.39 Schematic diagram of the four areas of interest in a comprehensive evaluation of mitral regurgitation by color flow Doppler

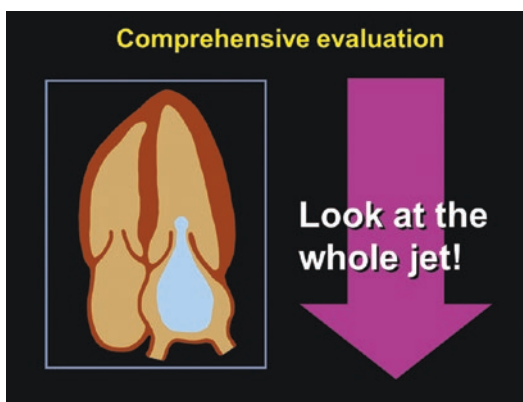


Fig. 10.38 Schematic diagram of the comprehensive color evaluation of mitral regurgitation

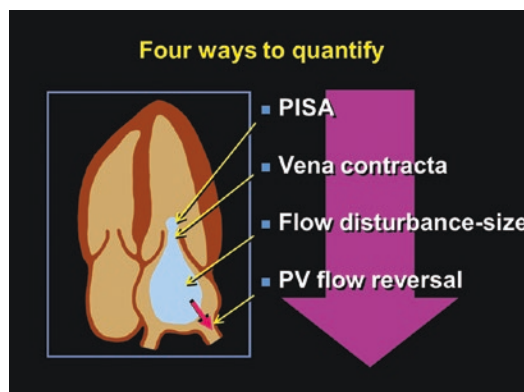


Fig. 10.40 Schematic diagram of the four ways to quantify the color flow Doppler of mitral regurgitation

Of course, as the jet increases in size, one may expect a larger PISA, vena contracta, area of flow disturbance (jet size) and either a decrease in systolic venous flow or reversal itself (Fig. 10.41).

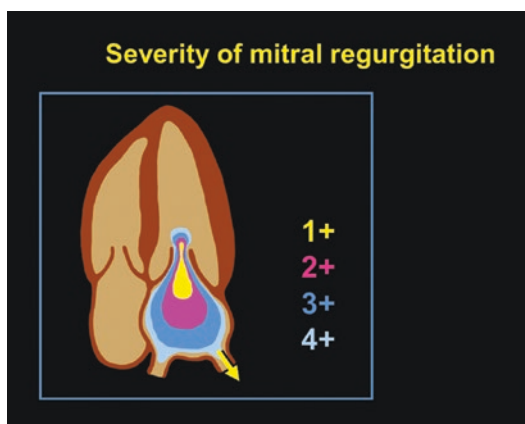


Fig. 10.41 Schematic summary of the degrees of severity of color flow Doppler in mitral regurgitation. As the severity increases, so do the sizes of all components

Flow is actually quite organized as it moves into the area of flow acceleration (PISA) and into the vena contracta (flow acceleration). The flow into the atrium is, however, quite disorganized and turbulent at it emerges from the regurgitant orifice. The area of the jet in the left atrium is therefore subject to many factors. One major factor is the size of the atrium. Imagine a jet made up of 50 cc being received in a very large left atrium as opposed to the same volume jet being received in a small left atrium. The dispersal of forces and the size and pressure of the receiving chamber can all, therefore, effect the size of this jet, and thus render it unreliable. Given these observations, however, note the examples of mild and severe mitral regurgitation noted from the chest wall apical four chamber approach in Fig. 10.42. In each case, note the size of the flow convergence (PISA), flow acceleration (jet diameter at the vena contracta), size of the jet in the left atrium as well as the presence of flow reversal in

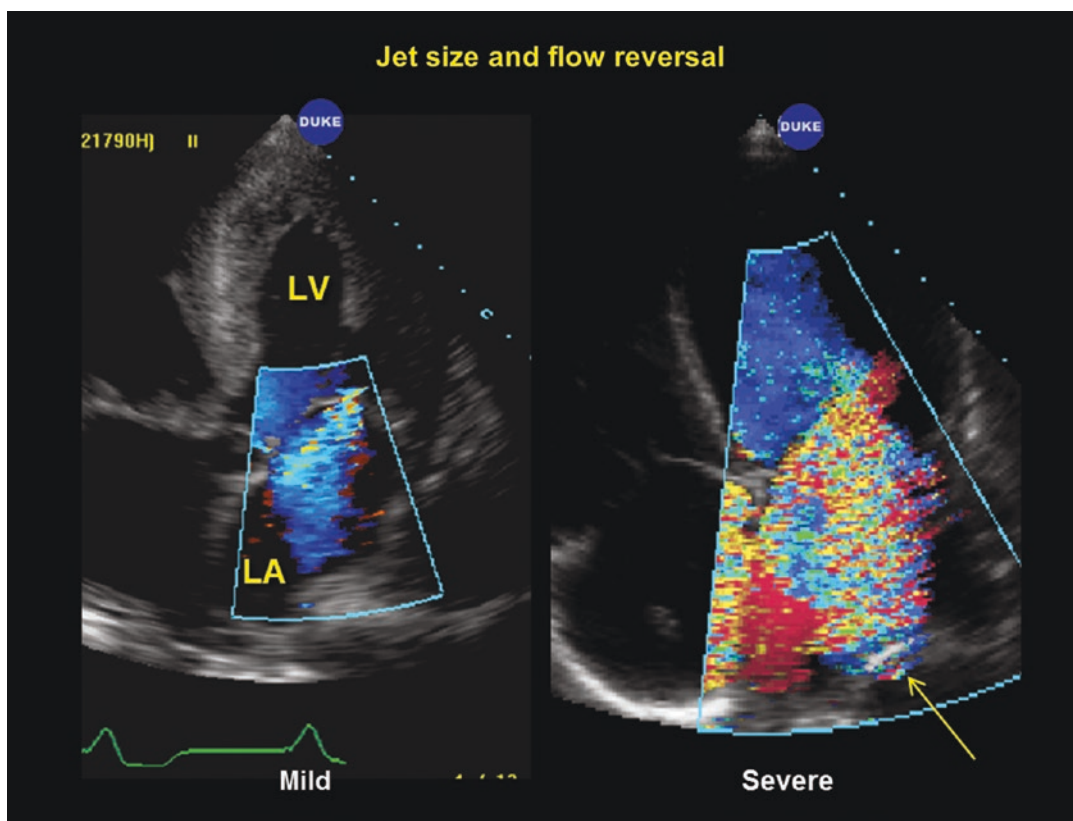


Fig. 10.42 Apical four chamber views from two different patients, one with mild and the other severe mitral regurgitation

the pulmonary vein. The right panel (arrow) shows such actual reversal compatible with severe mitral regurgitation. Always look at all four components of mitral regurgitation when evaluating severity.

As previously mentioned, the size of the jet may be the least reliable quantitative index of these various descriptors. This is in part because the regurgitant flow into the chamber is affected by the constraints induced of the blood that is residual within the left atrium during systole. As well, attenuation of the ultrasound signal may artifactually and significantly reduce the size of the jet. Various individuals have try to relate the size of the left atrium in relationship to the size of the regurgitant jet, but with little absolute reliability. Jets also have duration and such duration must subjectively, or objectively, be taken into account when assessing regurgitant jet severity.

Another notable example of the unreliability of jet size is the so-called Coanda effect (Fig. 10.43). In this case, the regurgitant jet is directed from the valve orifice directly adjacent the atrial wall where it curls around the left atrium. This is sometimes informally referred to as a “wall hugger” jet and can occur along any of the atrial walls. When this occurs, most subjective analytic schemes increase the severity of mitral regurgitation one grade higher than would be estimated by the size of the jet alone. In the example shown in Fig. 10.43 (arrow) one

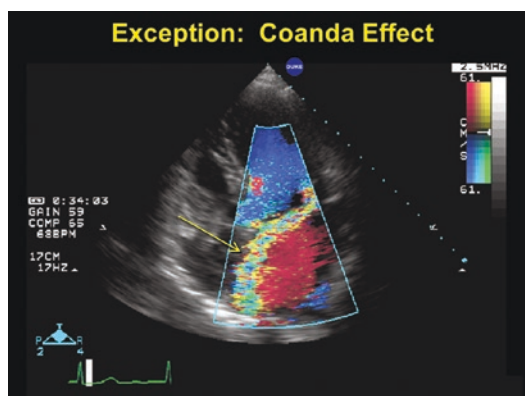


Fig. 10.43 The Coanda effect is present when a regurgitant jet is directed against a wall. Note the large zone of convergence

can appreciate a larger zone of convergence and flow acceleration than would normally be likely from a jet of this modest size. This phenomenon results from rather complex dispersions of kinetic energy and is beyond the scope of discussion in this basic chapter.

Calculations of Jet Severity

It is common in many laboratories to assign values for the calculations of the severity of mitral regurgitation on the basis of PISA, and subsequently effective regurgitant orifice area (*EROA*). This is performed by a series of maneuvers described elsewhere in this book. The method is dependent on the assumption that the isovelocity shell revealed by a color baseline shift is a perfectly symmetric hemisphere. The larger the PISA, the larger the regurgitant jet. Calculation of jet diameter through the vena contracta suffers from a similar limitation as it also assumes a symmetric flow acceleration area.. Both are demonstrated Fig. 10.44. Larger areas and diameters imply larger jets, but neither is precise measure of mitral regurgitation. Despite all these limitations, one measurement or estimation can be used to verify another and a comprehensive review can result in a very useful clinical estimate of severity of mitral regurgitation. Values

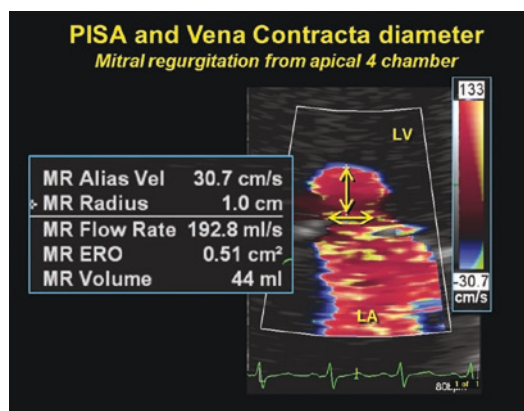


Fig. 10.44 Flow through the zone of convergence (vertical arrow) and zone of flow acceleration through the regurgitant orifice (horizontal arrow) is generally organized and can be quantified

Table 10.1 Vena contracta diameter and effective regurgitant orifice area

	Severity of mitral regurgitation		
	Mild	Moderate	Severe
Vena contracta width (cm)	<0.3	0.3–0.69	≥0.7
EROA (cm ²)	<0.20	0.20–0.39	≥0.40

for vena contracta diameter and EROA are seen in Table 10.1. Mention of PISA and EROA should not be construed as endorsement of these measures in routine practice. Such estimates are based on the assumption that the mitral valve regurgitant orifice is perfectly symmetric, which continued use of three-dimensional color flow echo is proving is not the case. Such an assumption explains the differences between the ERO method and other measures of severity encountered in clinical practice.

Mitral Timing Relationships

Spectral Doppler indices of the severity of mitral regurgitation also exists. They are dependent of an understanding of the various pressure relations that exist in left sided heart contraction and relaxation. Figure 10.45 shows the timing relationships of left sided pressures in the Aorta (Ao), left ventricle (LV) and the left atrium (LA). As the pressure rises in the left ventricle during mechanical systole, it exceeds that of the left atrium and mitral valve closes. This initiates a period of rising left ventricular pressure with no movement of blood that precedes the opening of the aortic valve. This interval is known as the period of isovolumic contraction. The term “isovolumic”, of course, means that there is no volume change prior to aortic valve opening.

As the pressure in the left ventricle exceeds that in the aorta the aortic valve opens, mechanical systole ensues and blood is ejected until the left ventricular pressure drops below that of the aorta. When aortic pressure drops, the aortic valve shuts. Isovolumic relaxation then ensues as the ventricular pressure falls until mitral valve opening. Diastole then begins. Note the

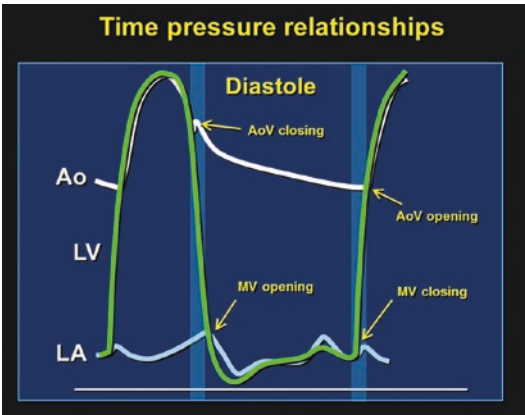


Fig. 10.45 Schematic diagram of the relationship between left atrial, left ventricular and aortic pressures during the cardiac cycle. The light blue areas represent the periods of isovolumic relaxation and isovolumic contraction

light blue interval areas indicated in Fig. 10.45 of the isovolumic relaxation period at the end of systole and then the isovolumic contraction period at the beginning of systole in the subsequent beat.

Relationships of Spectral Doppler

Of course, aortic stenosis (AS) and mitral regurgitation (MR) are both systolic events. As well, aortic regurgitation (AR) and mitral stenosis (MS) are both diastolic events. Because of the proximity of the aortic to the mitral valve, these various regurgitations and stenoses may be confused for one another. These complex timings in relationship to aortic and mitral stenotic and regurgitant flows are illustrated in Fig. 10.46 where mitral regurgitation and mitral stenosis are illustrated in orange and aortic stenosis and aortic regurgitation are illustrated in green. The various valve left-sided valve openings and closings are indicated with the blue shaded areas denoting isovolumic relaxation and contraction (identified in the previous figure) added. Figures 10.45 and 10.46 should be carefully correlated.

At first, it may appear that the spectral profile of aortic stenosis resemble mitral insufficiency

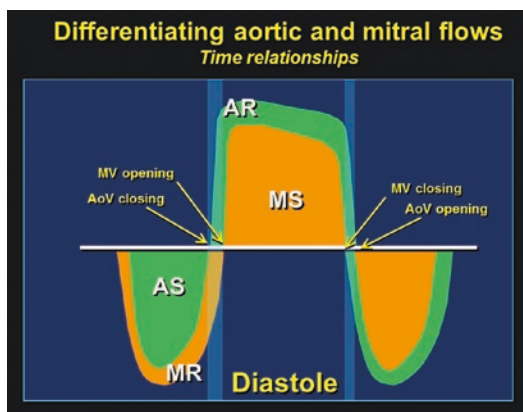


Fig. 10.46 Schematic diagram showing the timing relationships of abnormal flows through the left-sided heart valves. Aortic stenosis and mitral regurgitation are systolic events and may be confused with one another. Aortic regurgitation and mitral stenosis are diastolic events and may also be confused. The light blue areas represent the periods of isovolumic relaxation and isovolumic contraction

and those of aortic insufficiency resemble mitral stenosis. These various disease profiles may be differentiated by a knowledge of the various timing relationships of left-sided valvular opening and closings. Figure 10.47 shows the relationships between these various normal spectral velocities. The duration of mitral insufficiency is generally longer than that of mitral stenosis, in part, because the time from mitral valve closing to mitral valve opening is longer than from aortic valve opening to closing. Similarly, the aortic closing to aortic opening is longer than from mitral opening to closing.

The problem of recording flow across the mitral and aortic valves simultaneously (Fig. 10.48) results partly from the fact that the ultrasound beam width in spectral Doppler is large enough to detect more than one jet at the same time. Failure to appreciate the phenomenon

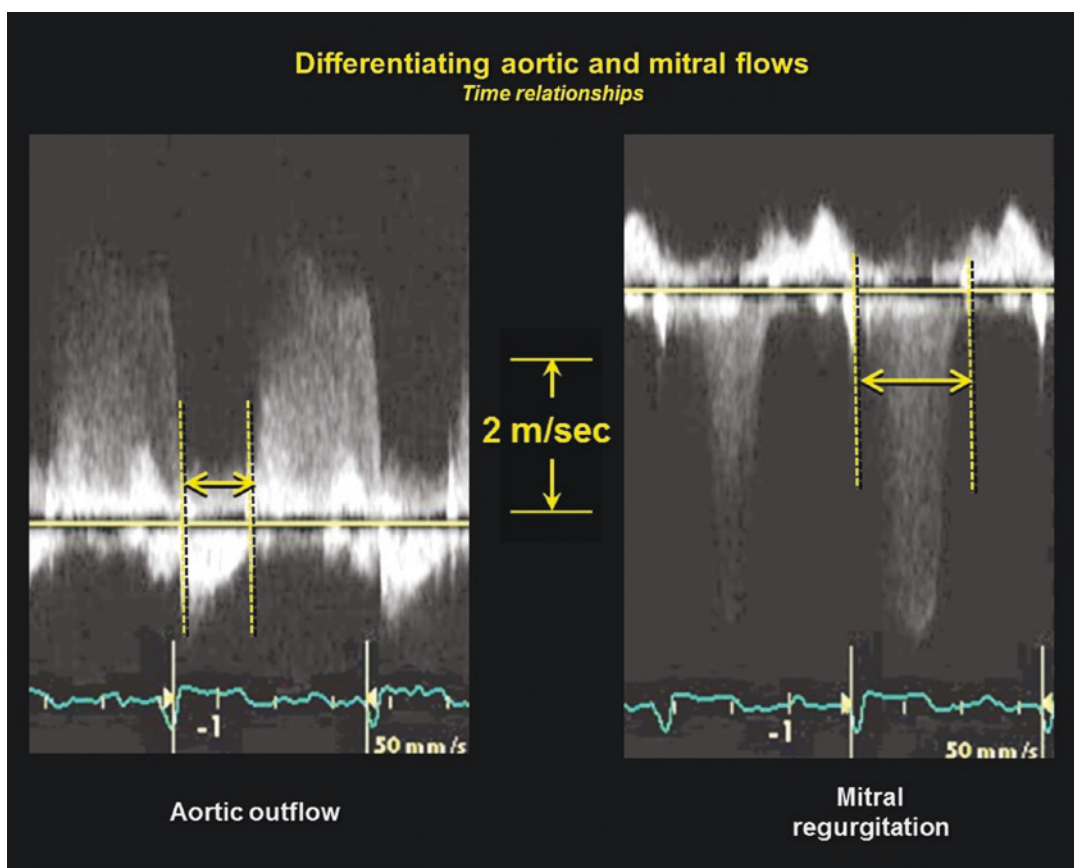


Fig. 10.47 Continuous wave Doppler recordings through the aortic outflow (left panel) and mitral inflow (right panel) to differentiate systolic aortic flow from mitral

regurgitant flow durations. Mitral flow duration in a normal is longer than aortic flow duration

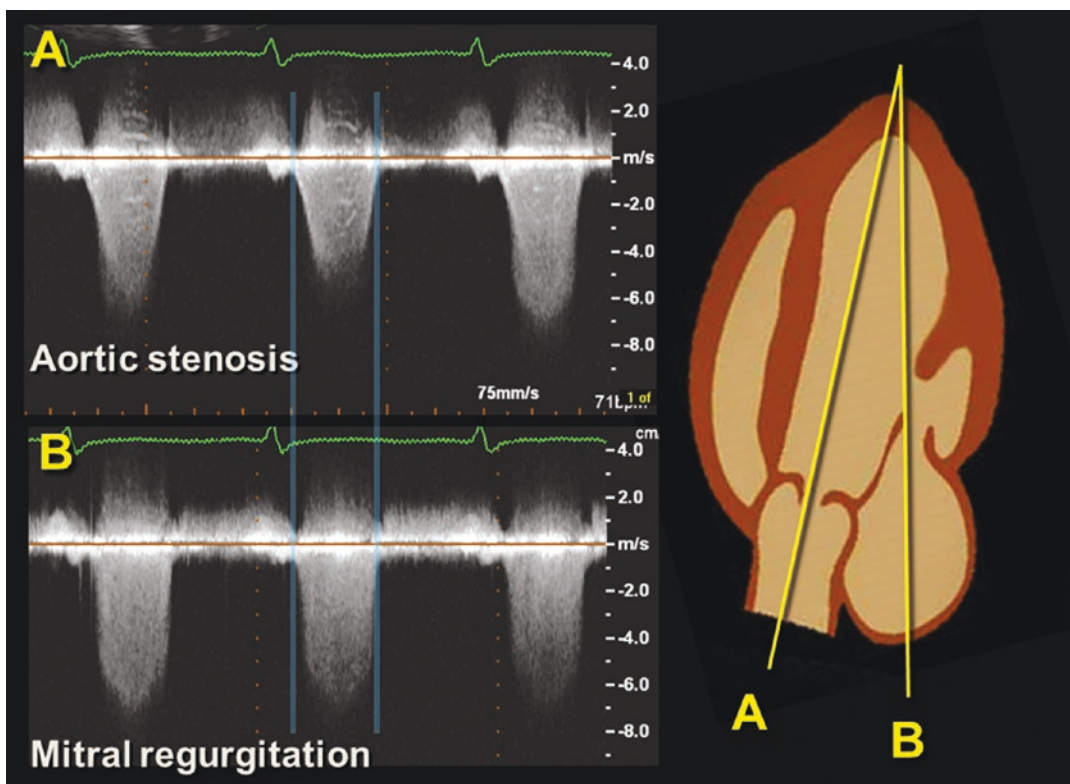


Fig. 10.48 Continuous wave Doppler recordings from a patient with aortic stenosis (top panel) and mitral regurgitation (bottom panel). The light blue areas represent the periods of isovolumic relaxation and isovolumic contraction

of jet width may lead the unwary beginner to diagnose mitral stenosis, for example, when only aortic regurgitation is present.

Using these principles, spectral aortic and mitral flows may be differentiated using spectral Doppler tracings of mitral flow. Note in Fig. 10.47 that the duration of aortic outflow is quite a bit shorter than the duration of mitral regurgitation in this patient and then compare these observations to Fig. 10.46. While the velocity of mitral regurgitation in this individual is considerably higher than the normal aortic velocity seen in the left panel, aortic flow may be confused with mitral regurgitation in a patient where aortic stenosis and mitral regurgitation coexist. They can be differentiated by their location and duration.

This phenomenon is somewhat better illustrated in Fig. 10.48 where an elevated systolic velocity jet from aortic stenosis is seen in the top panel and coexistent mitral regurgitation is indicated in the

bottom panel, also having elevated velocity. In this setting, one could easily confuse the continuous Doppler of aortic stenosis with that of mitral regurgitation or vice-versa. The duration of the more severe mitral regurgitation may also be reduced because the mitral regurgitation encroaches into the period of isovolumic relaxation.

Similar problems could exist between aortic regurgitation and mitral stenosis, both diastolic events. The top panel of Fig. 10.49 shows aortic regurgitation and the bottom panels show the delayed diastolic descent of mitral stenosis. Again, identification of the various isometric periods will help somewhat in differentiating these flows.

The clinical difficulty in differentiating left sided systolic jets is particularly highlighted in cases of hypertrophic cardiomyopathy where left ventricular outflow tract (LVOT) obstruction commonly coexists with mitral regurgitation (Figs. 10.50, 10.51, and 10.52). Such a patient is illustrated in Fig. 10.50 where the systolic

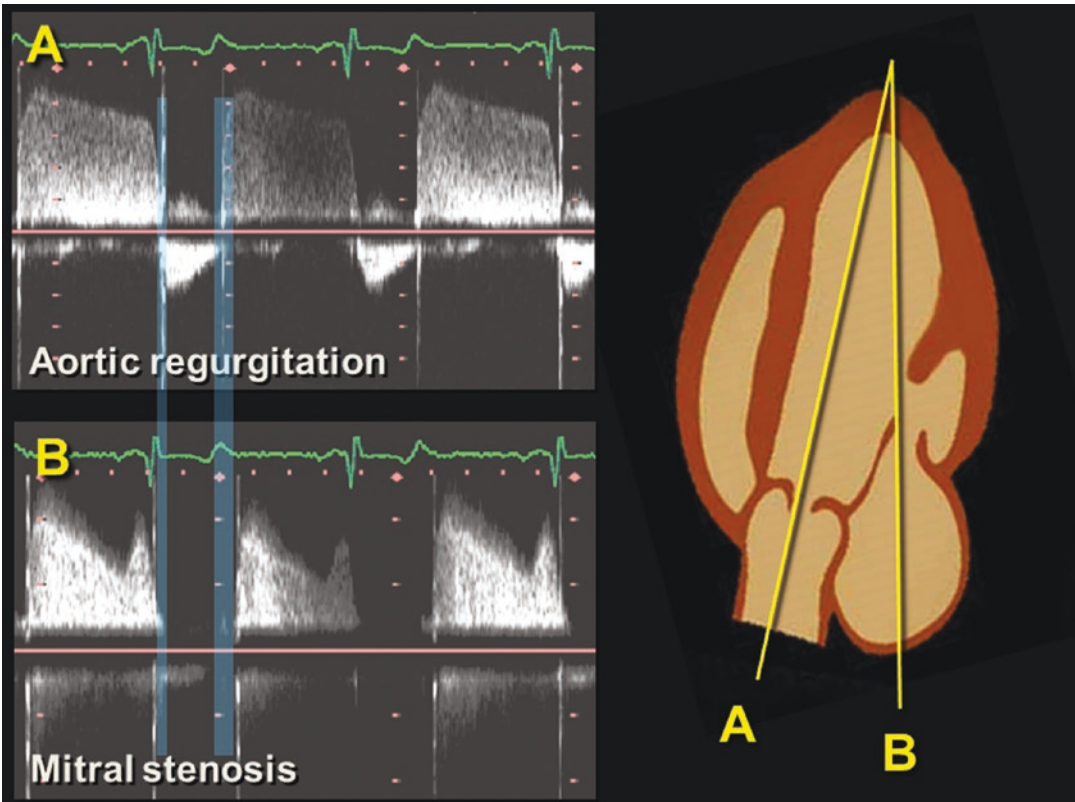


Fig. 10.49 Continuous wave Doppler recordings from a patient with aortic regurgitation (top panel) and mitral stenosis (bottom panel). The light blue areas represent the periods of isovolumic relaxation and isovolumic contraction

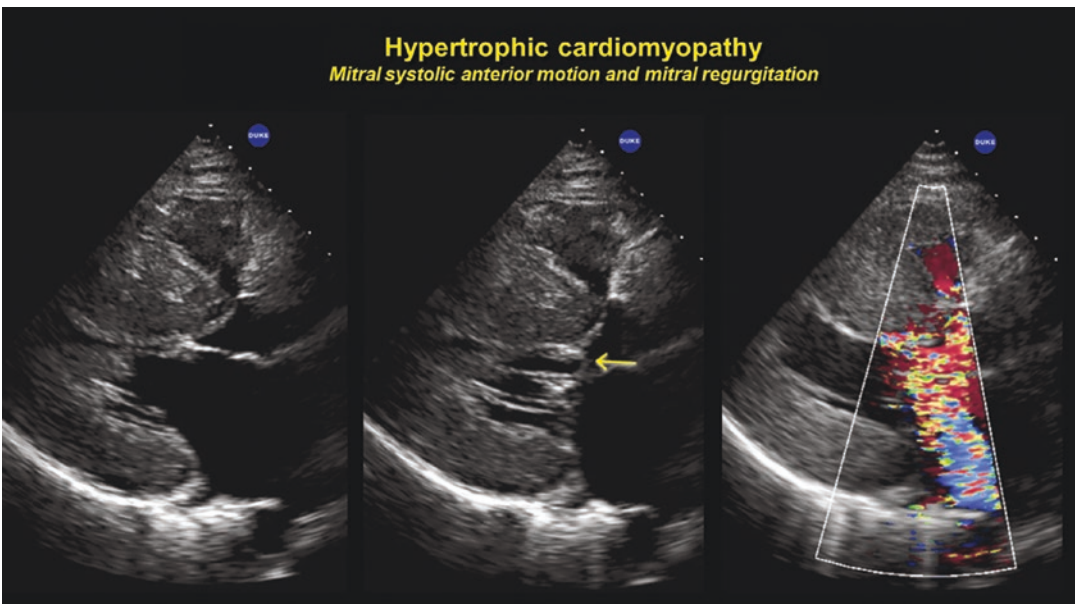


Fig. 10.50 Two-dimensional echocardiograms from a patient with hypertrophic cardiomyopathy. The left panel shows a diastolic parasternal long axis view with the mitral leaflets open. The middle panel show a systolic frame with the mitral leaflets closed and the presence of systolic anterior motion (SAM) of the anterior mitral leaflet (arrow) resulting in systolic turbulence in the LVOT and mitral regurgitation by color flow (right panel)

Fig. 10.51 The situation encountered in the patient in Fig. 10.50 may result in the appearance of multiple velocity jets by continuous wave Doppler, due to its lack of spatial discrimination (arrows)

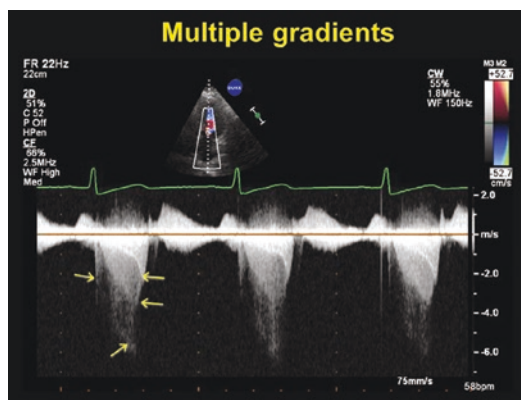
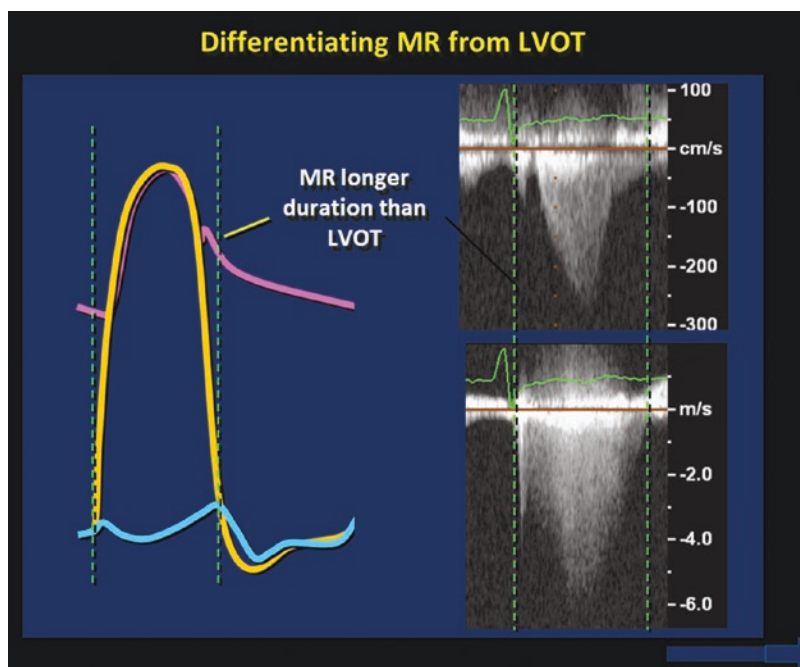


Fig. 10.52 In these types of patients the jets may be differentiated (Fig. 10.50) when the principle of jet duration is applied. The mitral regurgitant jet is longer in duration (bottom panel) than the LVOT jet (top panel)



anterior motion of the mitral apparatus (arrow) is present and systolic turbulences is seen in both the LVOT and left atrium (right panel). The spectral Doppler tracing from this patient in Fig. 10.51 shows the presence of multiple jets (multiple arrows). In these types of patients the jets may be differentiated (Fig. 10.52) when the principle of jet duration is applied. The mitral regurgitant jet is longer in duration (bottom panel) than the LVOT jet (top panel).

Use of Color Flow Doppler Controls

Mitral regurgitation during systole can be seen by color flow Doppler in the left atrium in systole using color flow Doppler (Fig. 10.53). Note that there is an area of color mosaic in the left atrium this patient examined in the parasternal long axis from the chest wall. The patient has a dilated cardiomyopathy so the left ventricle and left atrium are both dilated.

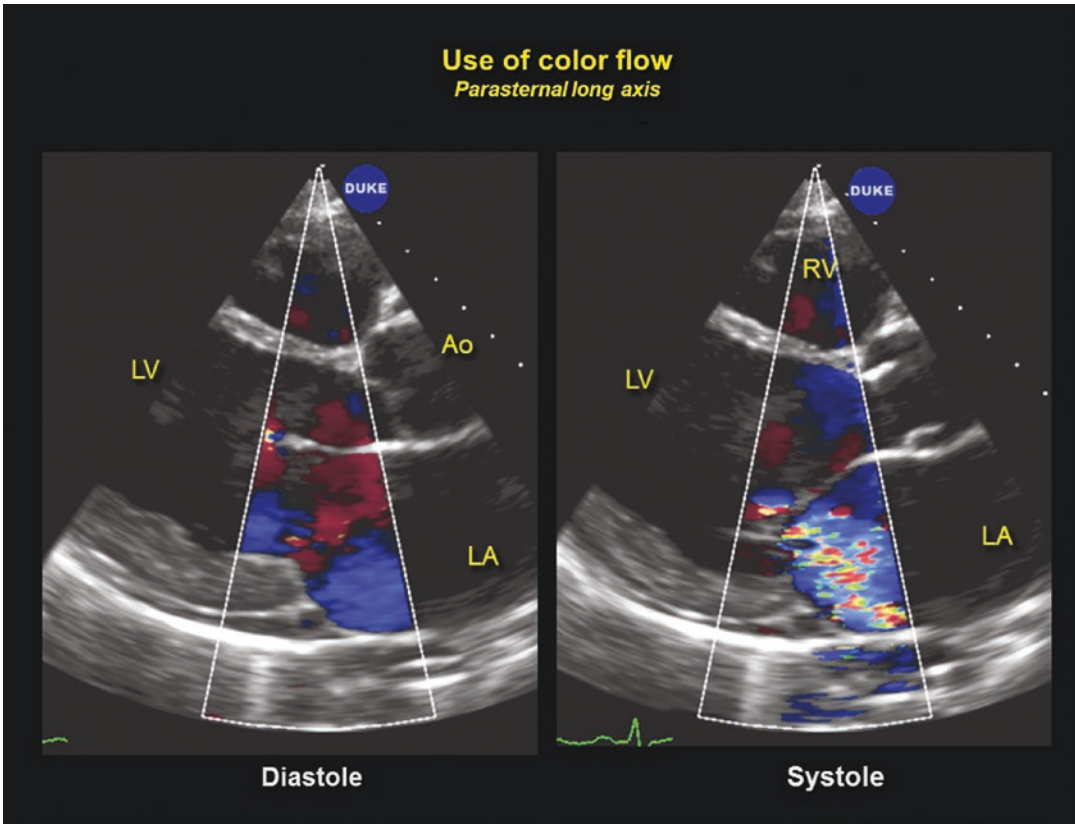


Fig. 10.53 Diastolic and systolic still frames from a parasternal long axis of the left ventricle in mild mitral regurgitation

One *serious problem* for color flow Doppler is the fact that improper use of the color controls can result in the marked increase in jet size (Fig. 10.54). In this example, a subject with known trivial mitral regurgitation (left panel) can demonstrate an area of more sizable regurgitation (right panel) when the improper settings are employed. Multiple factors can control this creation of a spuriously sized jet and profoundly affect the estimation of jet severity.

Use of Color Gain

The first, and most obvious, control is that of overall color gain. Figure 10.55 shows a left

panel where normal color gain is demonstrated. The right panel shows a remarkable increase in the overall color gain resulting in a somewhat larger jet when color gain is increased. Both of these images were obtained during the isometric contraction period with both the mitral and aortic valves in the closed positions.

Further evidence of the effect of variable color Doppler gain is noted in Fig. 10.56. Here, there is low color gain in the left panel followed by correct gain in the middle panel and obvious, excessive color Doppler gain the right panel. Excessive color gain is characterized by the sparkling appearance of a variety of pixels seen in the right color image. The hallmark of correct gain

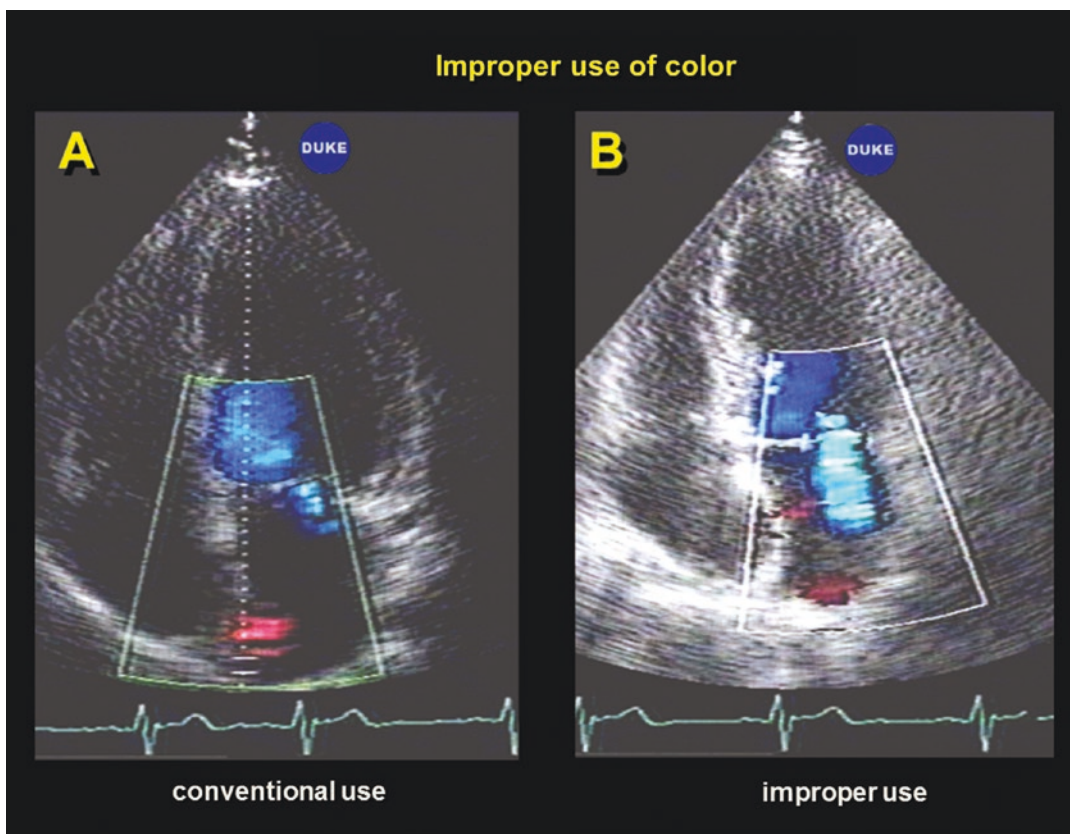


Fig. 10.54 Apical four chamber views from the same volunteer showing that improper use of the color flow controls may artifactually increase the size of a regurgitant jet

(middle panel) is the detection of some low velocity flow in the left ventricular outflow tract as well as lower velocity flows seen surrounding the turbulent jet. The lower velocity flows surrounding the turbulent jet reflect the movement of red cells already present in the left atrium that are engaged by the regurgitation. This phenomenon is known as the “entrainment”.

These observations of improper use of color gain are not machine manufacturer specific even though various different machines may display color flow somewhat differently. The effect of overall increases in color gain is shown in an alternate manufacturer’s device seen in Fig. 10.57. Here the three panels show an obvious increase in the size of the color flow jet of

mitral regurgitation encountered as the color gain is increased from settings of 12 to 24. Numbers displayed on devices for gain are all relative and have no specific meaning except that one gain is higher than another. It should be noted that the individual demonstrated here is the same individual seen in Fig. 10.56. These different machines may display the color noise encountered by remarkably excessive color gain in different ways but excess color gain will always result in a bigger jet. Figure 10.58 shows evidence of color noise in the apex of the left ventricle in an apical four chamber view that renders the color flow image almost uninterpretable. Note the sparkling of tissue noise at the ventricular apex in this view.

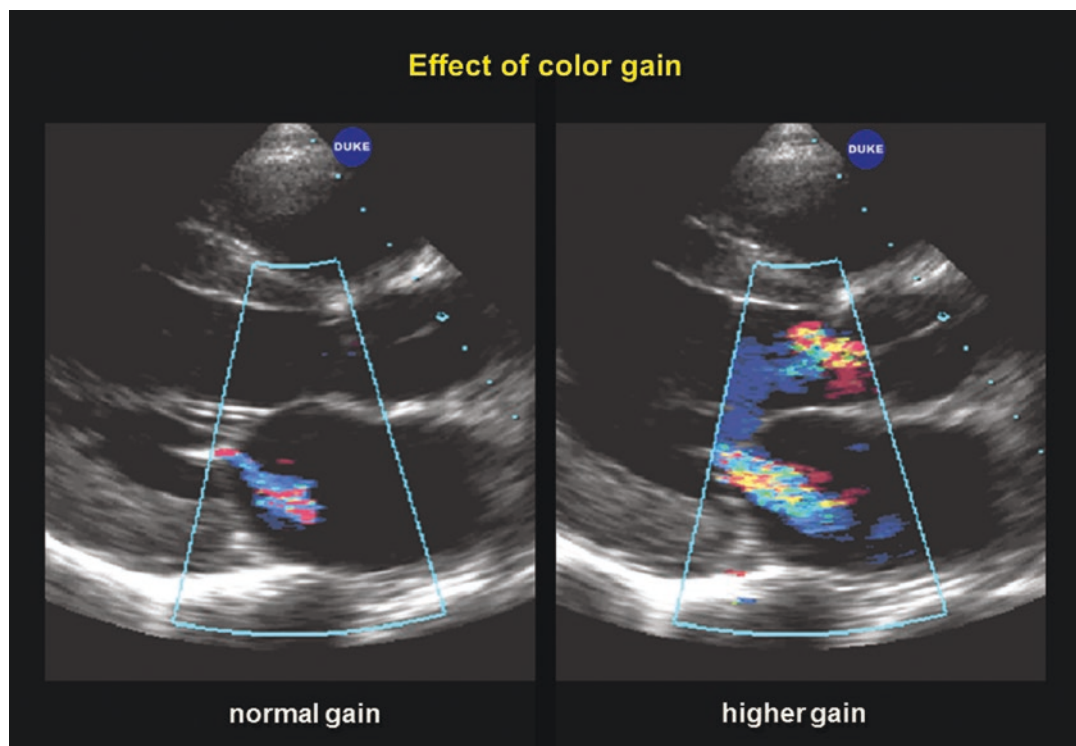


Fig. 10.55 Parasternal long axis from a patient with a centrally directed small degree of mitral regurgitation that increased in size with an increase in color gain

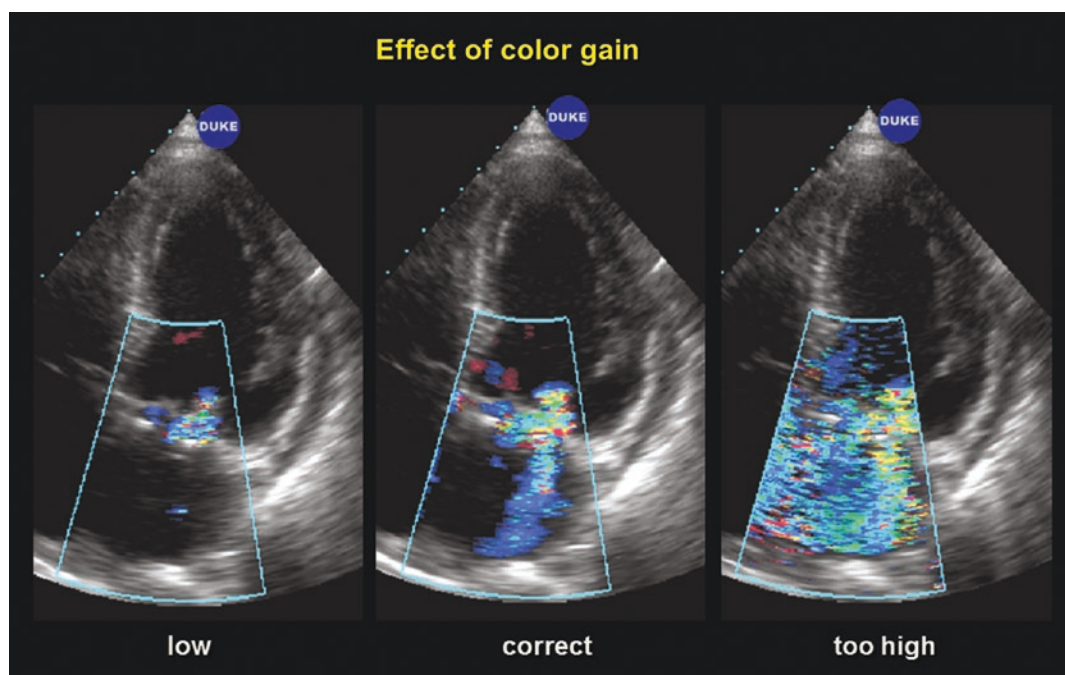


Fig. 10.56 Three panels from the apical four-chamber view in a subject with trivial mitral regurgitation where there is low, correct and excessively high color gain. The

excessive color gain floods the image with sparkling in the low velocity color

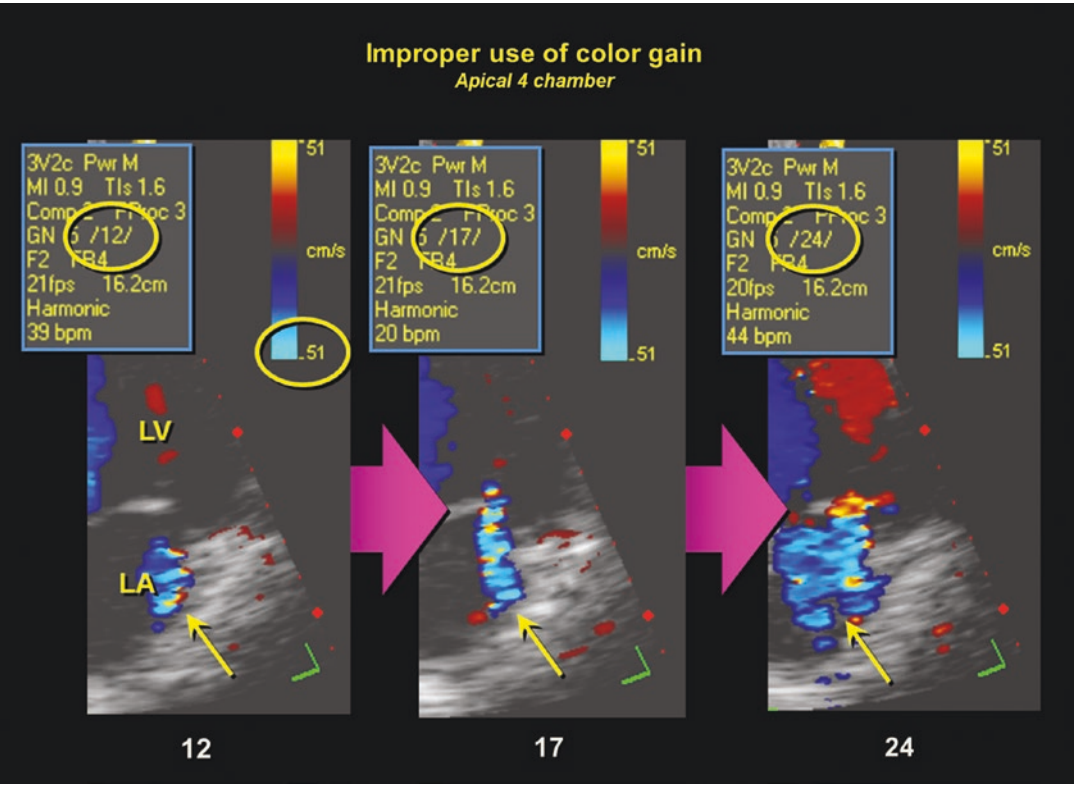


Fig. 10.57 Three panels from a subject with trivial mitral regurgitation from the apical four-chamber view showing artifactual increase in jet size with increase in color flow gain. This is the same patient as in Fig. 10.56

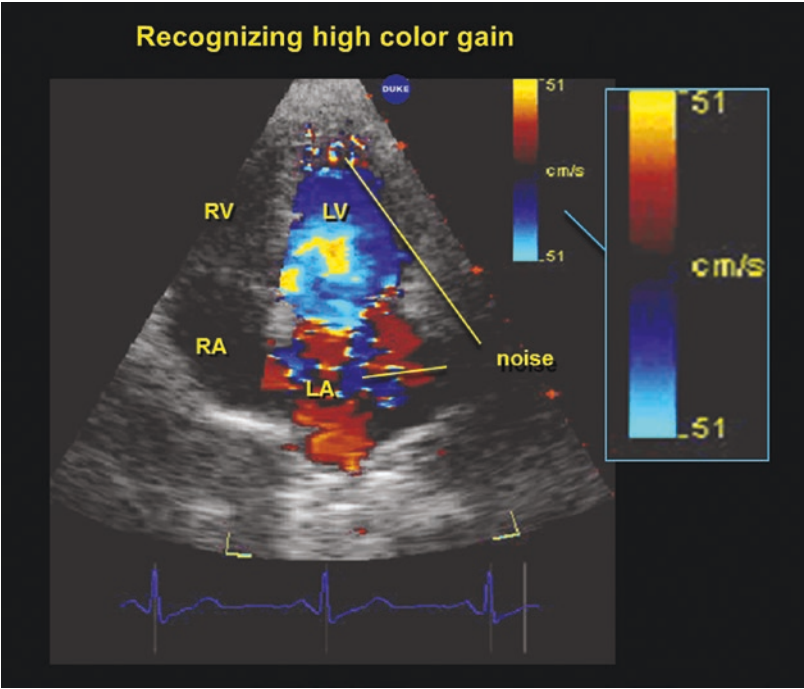


Fig. 10.58 Apical four chamber view with markedly excessive color gain that renders the color flow unintelligible. Note the excess color gain makes the tissue around the apex sparkle

Altered Nyquist (or Scale Factor)

Another major factor that can significantly alter the size of the color jet is Nyquist shift. With lowering of the Nyquist (color scale factor) progressively lower velocities will be displayed with increased brightness, artifactually increasing jet size. Most international standards for the display of color flow images of mitral regurgitation from the apical four chamber view recommend scale factor (Nyquist settings) in the 60 cm/s range (0.60 m/s). Figure 10.59 shows a remarkable increase in the size of a color flow jet from a Nyquist setting of 78 cm/s down to 49 cm/s. All other factors were held the same during this demonstration of this phenomenon in an otherwise normal individual.

Effect of Frame Rate and Persistence

Figure 10.60 shows the effect of decreased frame rate when a moving jet is encountered. The left two panels evidence of a moving jet at 25 frames per second as it moves from frame to frame in time. On the right is the same individual encountered at a slower frame rate where the two jets are “added” into a single frame, obscuring dynamics and artifactually increasing jet size. Obviously, the maximum temporal sampling that is possible will provide a truer depiction of dynamic jet size. One should absolutely avoid widening the color flow sector arc, thus slowing frame rate and obscuring flow dynamics.

Similarly, color frames obtained over a period of time could potentially be added to one another in any given display using a control

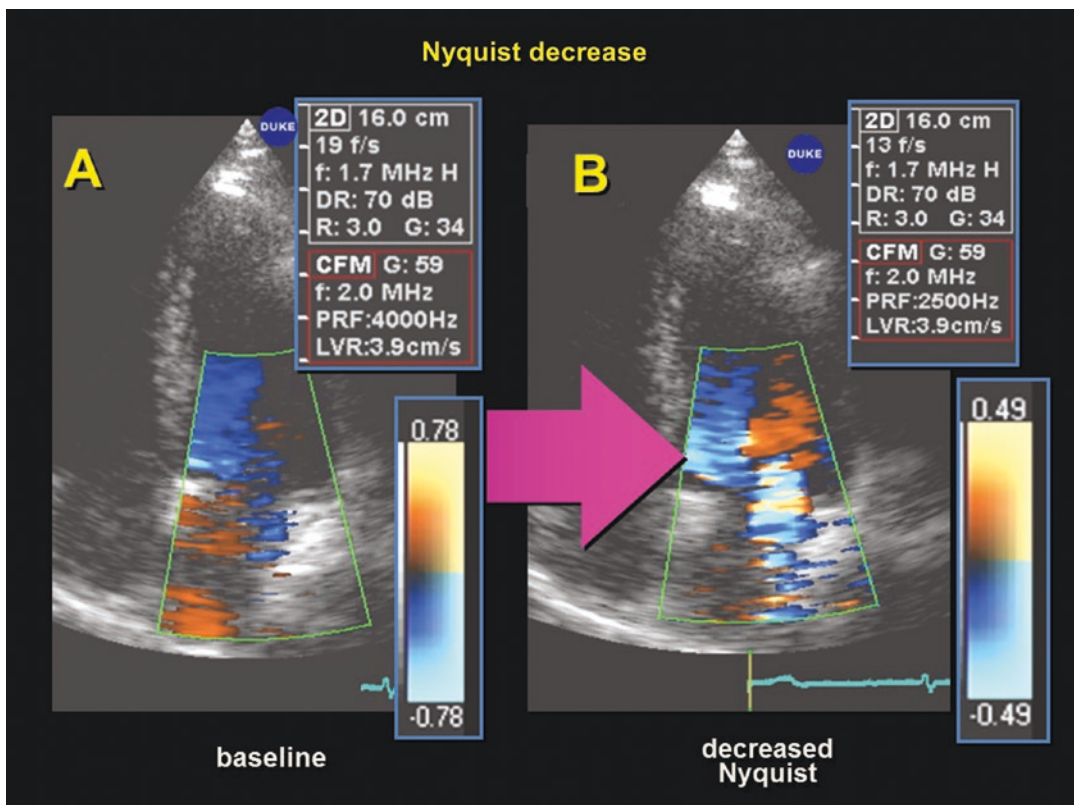


Fig. 10.59 Effect of the decrease in Nyquist limit (scale factor or PRF) as the jet size is markedly increased. For mitral regurgitation, Nyquist limits should be set at about 60 cm/s

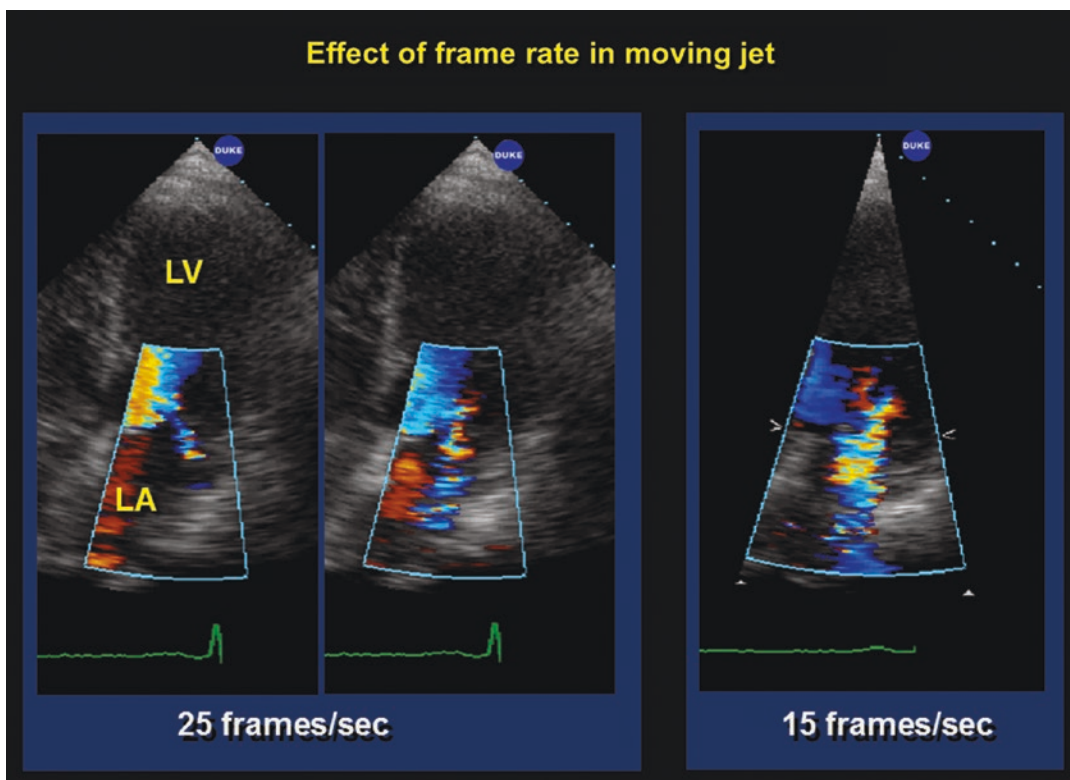


Fig. 10.60 Low frame rates may also increase the size of a mitral regurgitant jet

called persistence. Figure 10.61 demonstrates the addition of multiple frames in a moving image so that the net effect is to markedly increase jet size. All other factors are held constant, including the Nyquist limit, as indicated in the inset boxes that reflect system settings. Neither two-dimensional echo image nor color persistence should be used in echocardiography. The heart moves much too rapidly to make these controls be of any use in the examination of cardiac structures. *Never use persistence any time* when examining a heart as things move.

Excess Image Gain

There is also the possibility of decreasing jet size by certain setting factors. This decrease in jet size is demonstrated in Fig. 10.62. Here, excess image gain alone is added to the system settings from the properly obtained image in the

left hand panel. The added image gain encroaches on pixels occupied by color and the color is eliminated as an image display can provide a picture of either black and white anatomic information or color flow information, but not both at the same time. Note the image gain increase on the right has increased low amplitude image noise into the picture that causes a haze within the cardiac chambers, displacing low velocity flow, previously detected in the image on the left. Excess image gain, as well as color gain should be avoided in the conduct of any color flow examination. Beginners with echocardiography will encounter this problem frequently as the use of excess image gain is frequently used to acquire anatomic targets when skill sets for transducer angulation and proper aiming are lacking. This sets up a cycle of increased image gain followed by increased color gain until a terribly distorted image of anatomy and flow is encountered.

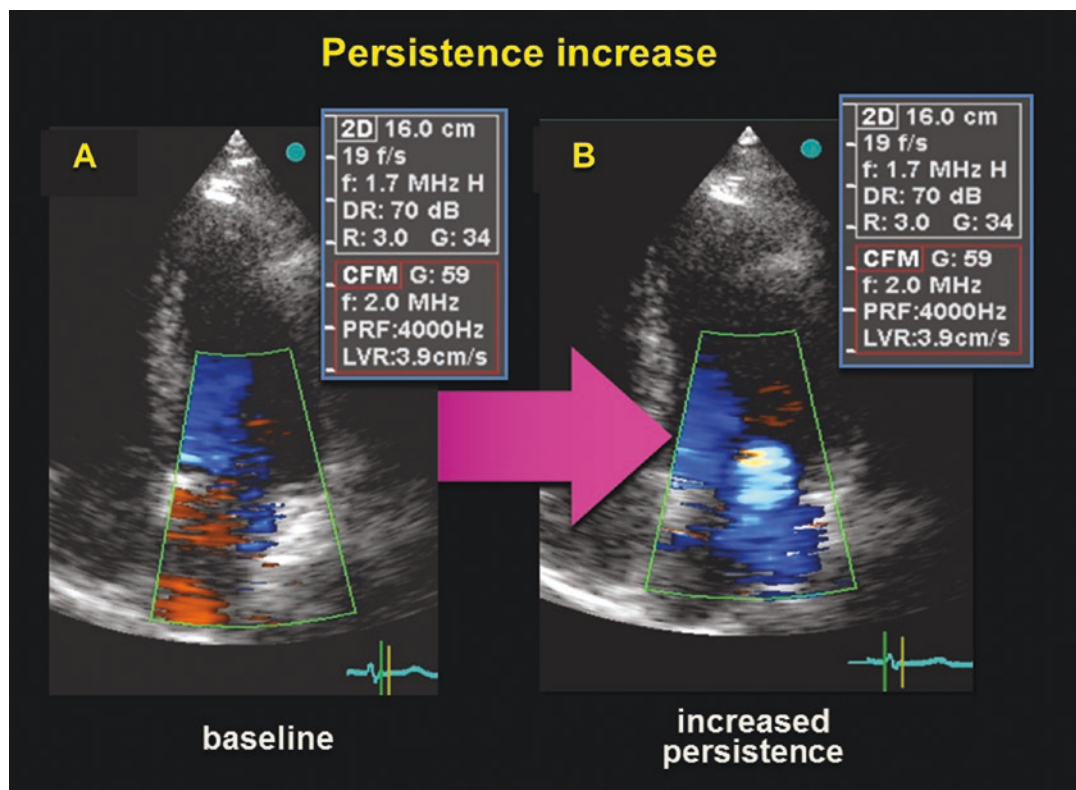


Fig. 10.61 Image persistence may also increase the size of a jet and have no place in echocardiography for examination of the rapidly moving heart

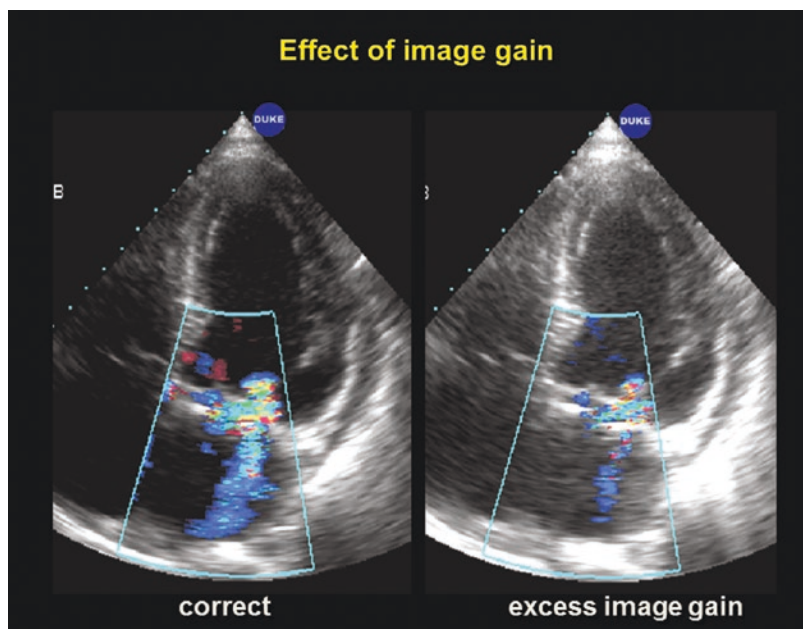


Fig. 10.62 Excess image gain may suppress the color as black and white anatomic information competes with color flow information for display in any given pixel

System Setting Variability in Jet Size

These and other factors can increase the size of a color flow jet. Figure 10.63 shows the addition of multiple factors to move a rather negligible jet seen in Panel 1 into a somewhat sizable jet seen in Panel 7. The various steps along the way can be seen to increase the jet size in progressive steps from left to right, each at the same point in the cardiac cycle, just with different settings.

Such manipulated settings can be obtained with any color flow machine. Figure 10.60 demonstrates such manipulations with an alternate device in the same individual depicted in Fig. 10.64. The major factors that exist in such manipulation are the increase in color gain, together with the decrease in Nyquist settings, but other less obvious factors can be added to distort image reliability of size, and thus, estimation of severity. Both excessive color gain and low Nyquist should always be avoided. Likewise, these manipulations should be recognized by any interpreter of color flow information.

Jet Duration

The simple size of a jet in a still frame follow image can never be accurately relied upon as an absolute indicator of jet severity by itself. Size and jet duration must be taken together. It is well known that mitral regurgitation is classically described as a holosystolic jet by physical examination. Figure 10.65 shows successive new acoustic frames from the four chamber chest wall approach in an individual with trivial mitral regurgitation. Note that the jet size remains small throughout the most of systole (solid arrows). Systolic frames are indicated with S and the last frame of the previously diastole and first frame of the next diastole are depicted by D. Figure 10.66 shows an ever increasing large jet in a patient with more significant mitral regurgitation (solid arrows).

When the mitral valve shuts in early systole, and before the aortic valve opens, the left ventricle is contracting prior to ventricular ejection (isometric/isovolumic contraction).

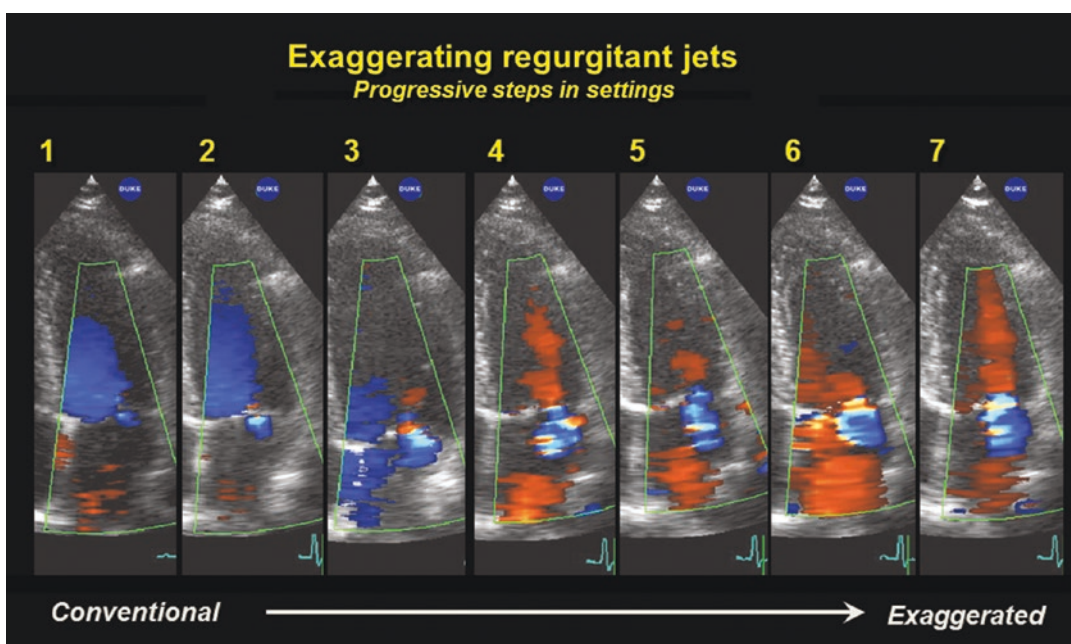


Fig. 10.63 Between Panels 1 and 7, several color flow settings are changed to artifactually increase the size of this trivial mitral regurgitant jet. The various steps along

the way can be seen to increase the jet size in progressive steps from left to right, each at the same point in the cardiac cycle, just with different settings

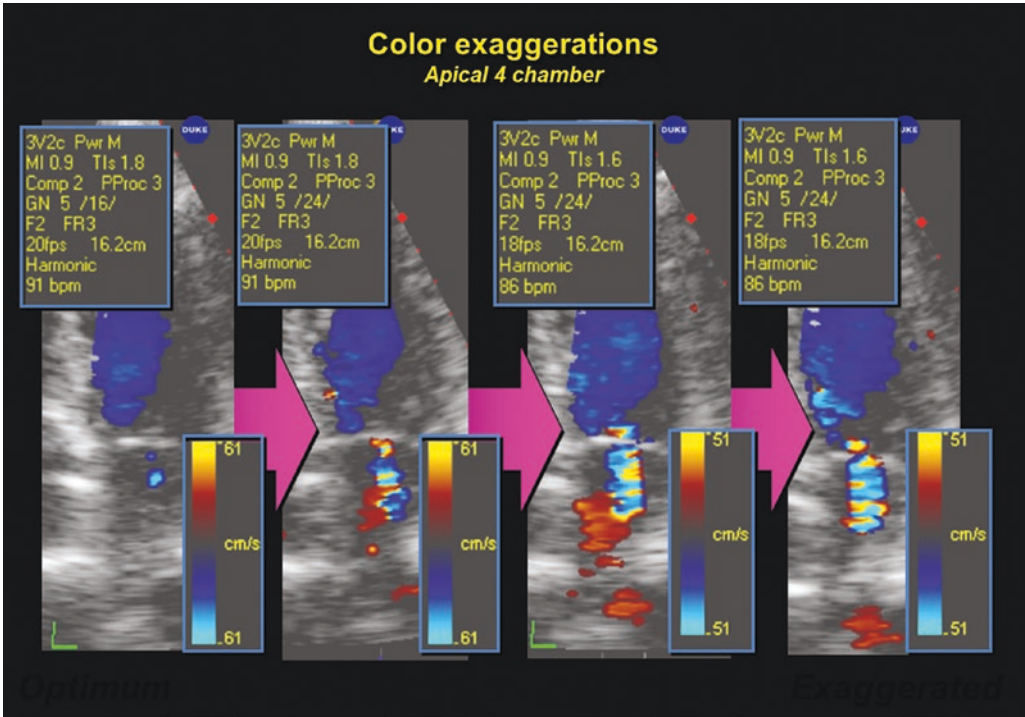


Fig. 10.64 The size of the trivial mitral regurgitant jet is again increased in this image from the apical four-chamber view by use of improper settings. The machine used here

is different from that seen in the previous figure. Improper use of color gain and Nyquist are the main problems

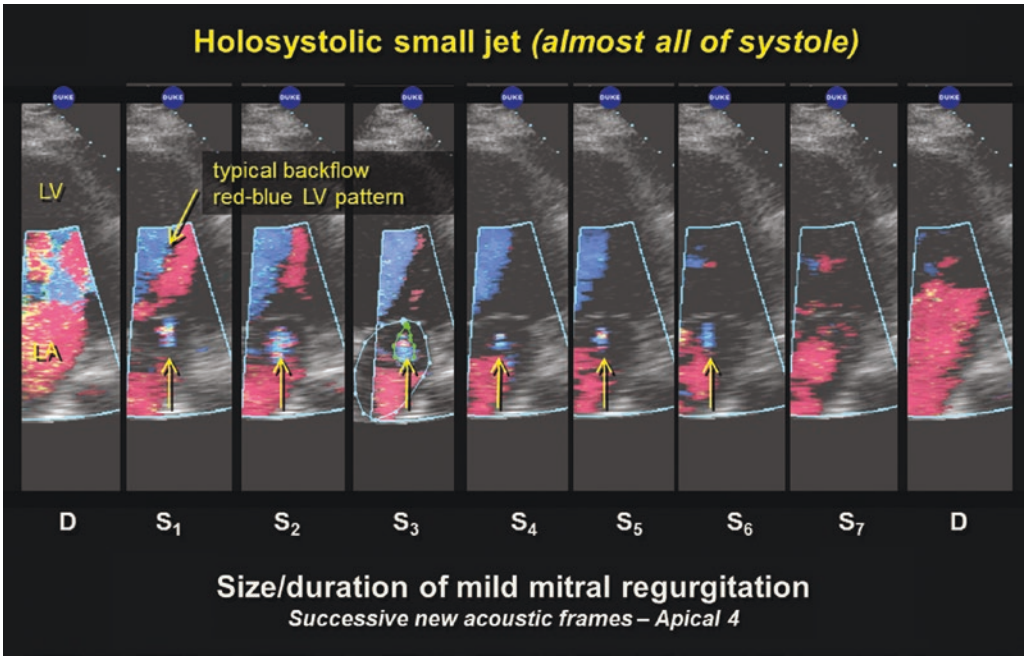


Fig. 10.65 Successive new acoustic frames from a volunteer with mild mitral regurgitation. The last frame of diastole (D) is followed by successive systolic frames and finishes with the first diastolic frame (D) of the next dia-

stolic cycle. The solid arrow shows the duration of the minimal mitral regurgitation throughout all but one systolic frame. Jets have duration as well as size

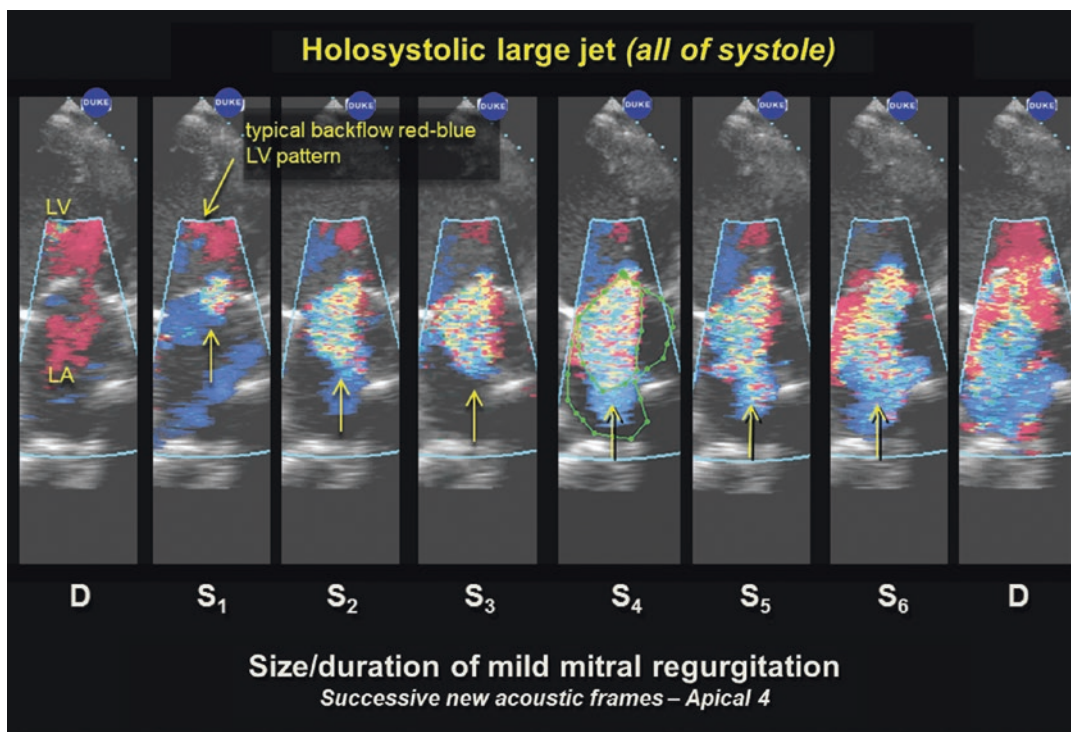


Fig. 10.66 Successive new acoustic frames from a volunteer with severe mitral regurgitation. The solid arrows show the jet to grow in size and last throughout systole. All jets have duration as well as size

Some blood is trapped (entrained) in the closing mitral orifice and when the leaflets shut there usually is some movement of blood posteriorly into the left atrium that accompanies the closing velocity of the leaflets. This phenomenon is known as “backflow”, but may also be termed by the words “closing velocity”, “mitral flash”, entrainment or other such terms. This is found in almost all individuals and if further demonstrated in Fig. 10.67 (dashed arrow). This phenomenonism, therefore, characterized by a frame detected in early systole as well as a quite typical back flow, red-blue pattern of systolic flow within the left ventricle. One would be markedly mistaken if the backflow determined in frame S₂ in Fig. 10.68 was taken as mitral regurgitation. The turbulent flow noted in this acoustic frame is entirely compatible the backflow phenomenon and there is no evidence of regurgitation seen in any other systolic frame.

Hints from Spectral Doppler

There are other spectral Doppler findings which may assist an examiner in determining the severity of regurgitation. Figure 10.69 shows a continuous wave spectral Doppler tracing from an individual with mild regurgitation (patient CG, left panel) compared to a patient with more significant regurgitation (patient LR, right panel). The method for determining the severity of mitral regurgitation using spectral Doppler relies on the subtle comparison of diastolic flow (seen above the baseline) to the regurgitant systolic flow seen below the baseline in brightness. Simply expressed, the brightness of any Doppler signal reflects the number of red blood cells moving through a Doppler sample if spectral Doppler gain settings are properly set. The left hand panel of Fig. 10.69 shows a remarkably bright antegrade signal in diastole when compared to the much less bright regurgitant flow signal (dashed arrow).

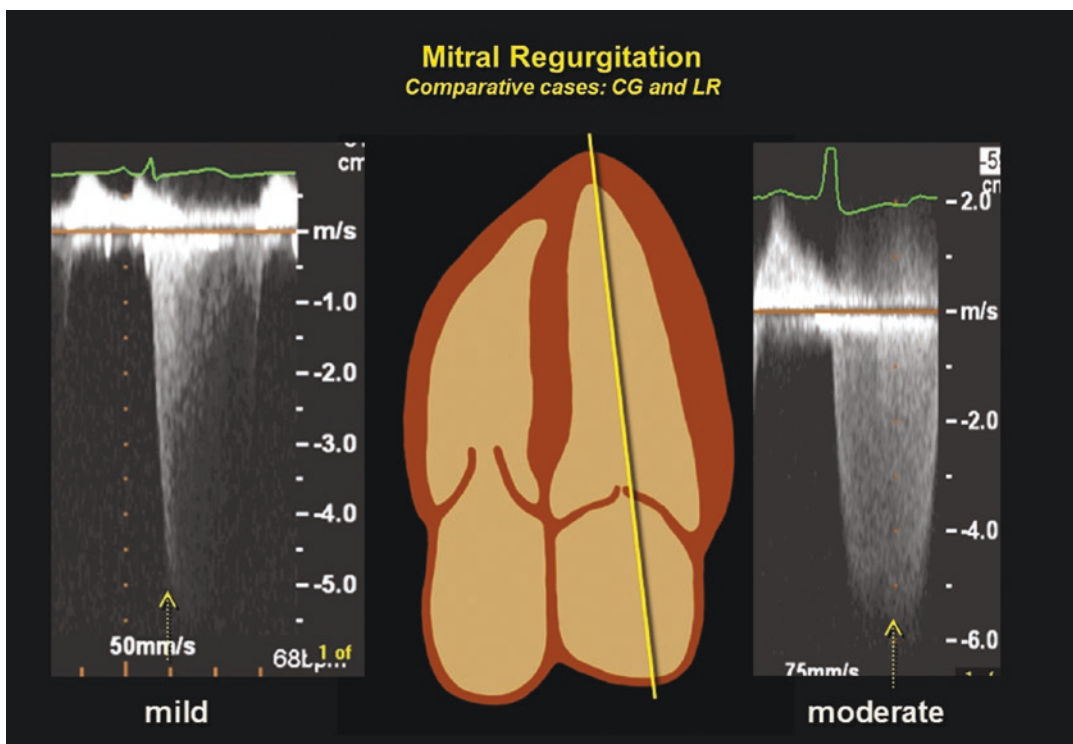


Fig. 10.69 Two contrasting continuous wave recordings of mild and more severe mitral regurgitation from two different patients. One can also use the intensities of the Doppler recordings to indicate severity of regurgitation. See text

patient depicted on the right, in comparison to the patient on the left.

Given all these expressed limitations, it should not be interpreted that Doppler and/or echo methods yield unreliable results. Rather, these methods turn out to be additive as a user of these techniques learns to apply proper control settings and then use the comprehensive characteristics of color flow and spectral Doppler to render a reliable estimate of severity of mitral regurgitation. No single factor should ever be used and jet duration should always be taken into account.

In addition, it is recommended that a beginner always try to avoid the use of hyphenated degrees of mitral regurgitation, such as “mild-moderate” or “moderate-severe”. While it is accepted that such borderline degrees may actually occur a simple grading system of none, trivial, mild, moderate and severe is preferred (or 0, 1+, 2+, 3+ and 4+). When intermediate hyphenated

degrees are avoided, the interpreter is forced to check all the factors in arriving at a conclusion. Echocardiography takes discipline to use every tool available to achieve a reliable clinical diagnosis.

Mitral Stenosis

In examining the disorders that induce abnormal mitral valve flow and function, mitral stenosis first comes into attention. In fact, one of the first applications for the diagnostic use of echocardiography was for the detection and assessment of severity of mitral stenosis. Rheumatic mitral stenosis is manifest by thickening of the mitral valve leaflet tips. Figure 10.71 shows a pathologic specimen of rheumatic mitral stenosis with the irregular orifice that results from this chronic inflammatory process. Not only are the leaflet tips thickened but the commissures become fused

Fig. 10.70 Parasternal long axis color flow systolic still frame images from the same patients shown in the previous figure

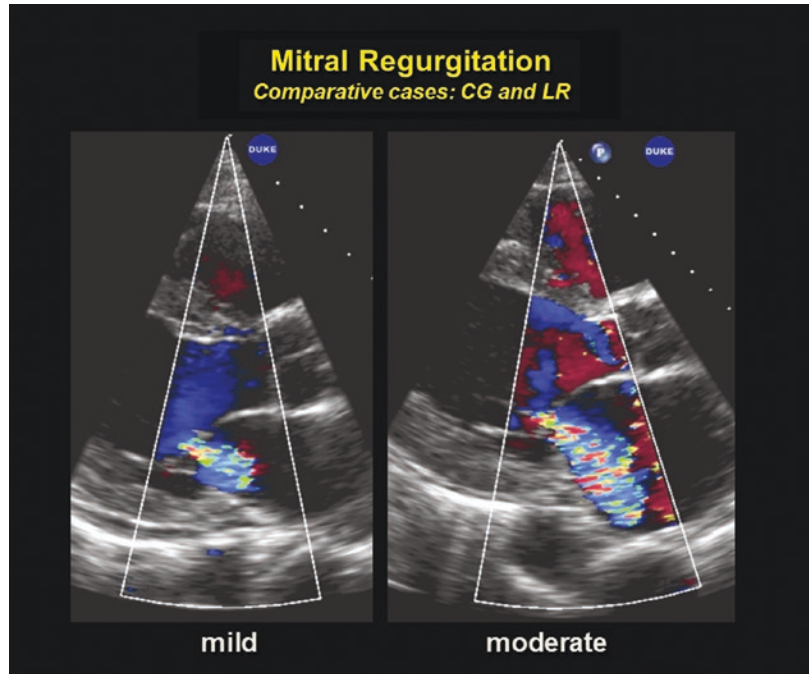


Fig. 10.71 Anatomic pathologic specimen of a rheumatic mitral valve. There is thickening of leaflet tips and commissural fusion (arrows). Modified from Kisslo, Leach & Adams: Essentials of Echocardiography

(arrows). Contrast this image viewed from the atrium down toward the mitral valve orifice with other pathologic specimens in Figs. 10.19, 10.20, 10.21, and 10.22.

Also contrast the appearance of a normal M-mode echocardiogram shown in Fig. 10.72

(left panel) with that of mitral stenosis (right panel). The M-mode movement of the tip of a normal mitral valve leaflet shows broad excursion and rapid deceleration during the period of passive ventricular filling from the E to F slope. In mitral stenosis, there is remarkable thickening of the mitral valve leaflet with significant restriction of the E to F slope. During the early days of echocardiography the determination of the rate of E to F slope was used for the estimation of the severity of mitral stenosis. This has long been abandoned and is no longer in common clinical use because it could detect severe mitral stenosis but could not differentiate moderate from mild stenosis. For all clinical purposes, measurement of E-F slope by M-mode has no clinical application.

Most recently, real-time three dimensional echocardiography has been used to inspect the mitral orifice, either from the chest wall or transesophageal approach. These methods began in this institution and the first clinical images were introduced from humans in 1993 [1]. Figure 10.73 shows a contemporary still frame three-dimensional echocardiographic images in

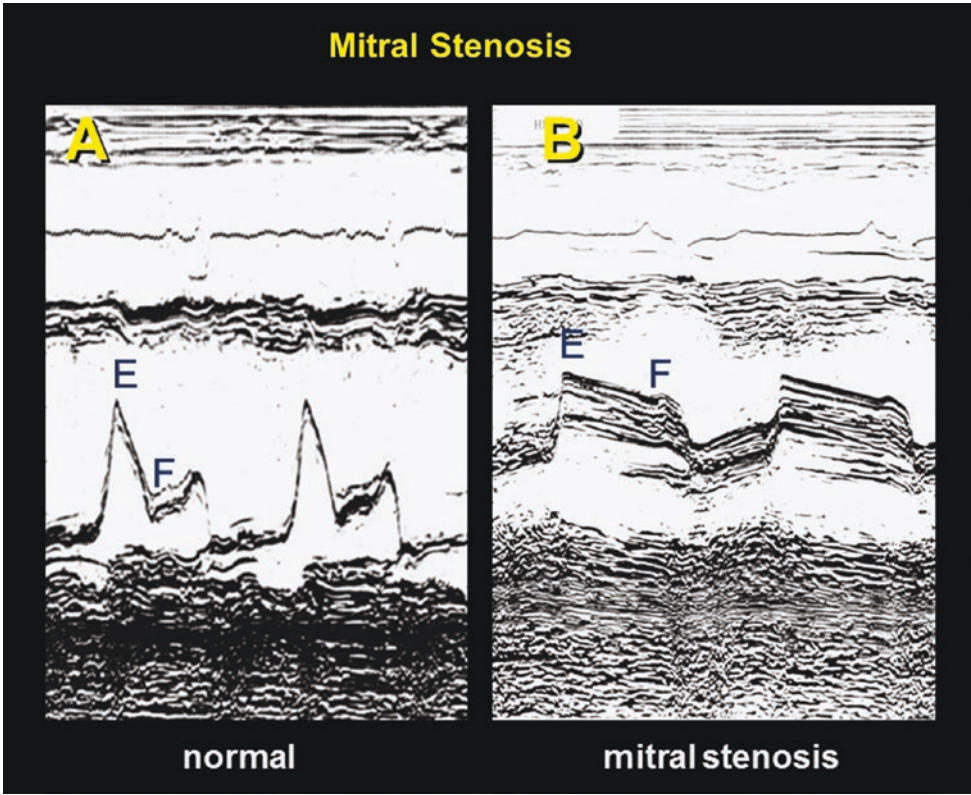


Fig. 10.72 Comparison of M-mode echo recordings from a normal mitral valve and one with mitral stenosis

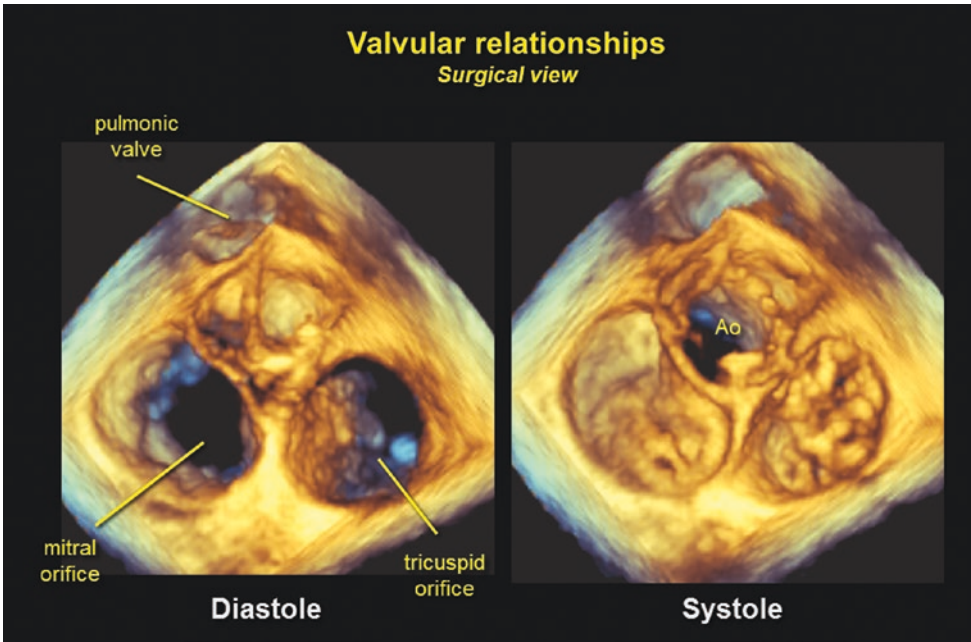


Fig. 10.73 Relationships of the mitral, aortic and tricuspid valves from the surgical view in a three-dimensional echocardiogram in diastole (left) and systole (right)

diastole (left panel) and systole (right panel) from an individual with no evidence of rheumatic mitral valve disease using transesophageal echocardiography and displayed in the surgical view. The mitral and tricuspid orifices are clearly visualized. The aorta is positioned as previously described anteriorly between the two atrial-ventricular valve openings. Valve leaflets are easily identified and both A-V orifices open widely.

Contrast the findings in Fig. 10.74 (mitral stenosis) with those of Fig. 10.73 (no mitral stenosis). In Fig. 10.74 the open mitral orifice in a patient with moderate restriction of diastolic opening is seen from the three-dimensional echocardiographic approach obtained from the chest wall. The mitral valve is viewed from the left ventricular perspective up towards the left atrium in the left panel and shows marked thickening of the leaflet tips together with commissural fusion. In the right panel, the same mitral orifice is visualized from the atrial side toward the ventricle. The left atrial appendage is clearly seen and is dilated. The commissural fusion is again readily noted.

In severe mitral stenosis, the mitral valve opening is even more severely restricted. The more restricted rheumatic mitral valve orifice is seen in Fig. 10.75 from the left ventricular perspective toward the atrium (left panel) and the left atrial side toward the ventricle (right panel). Here there is even more severe leaflet tip thickening and remarkable commissural fusion than noted in the previous figure.

A more troublesome expression of rheumatic mitral valve disease is demonstrated in Fig. 10.76 where both left and right panels are viewed from the left atrium toward the ventricle. The mitral orifice is severely restricted as seen in previous examples. However, in this patient, there is remarkable thickening of the annulus that can be seen to extend far into the commissures, rendering successful mitral commissurotomy unlikely (arrow). One can also easily appreciate the marked dilation of the left atrial appendage in this patient, together with large trabeculation at the appendage tip which appears to divide the atrial appendage in two.

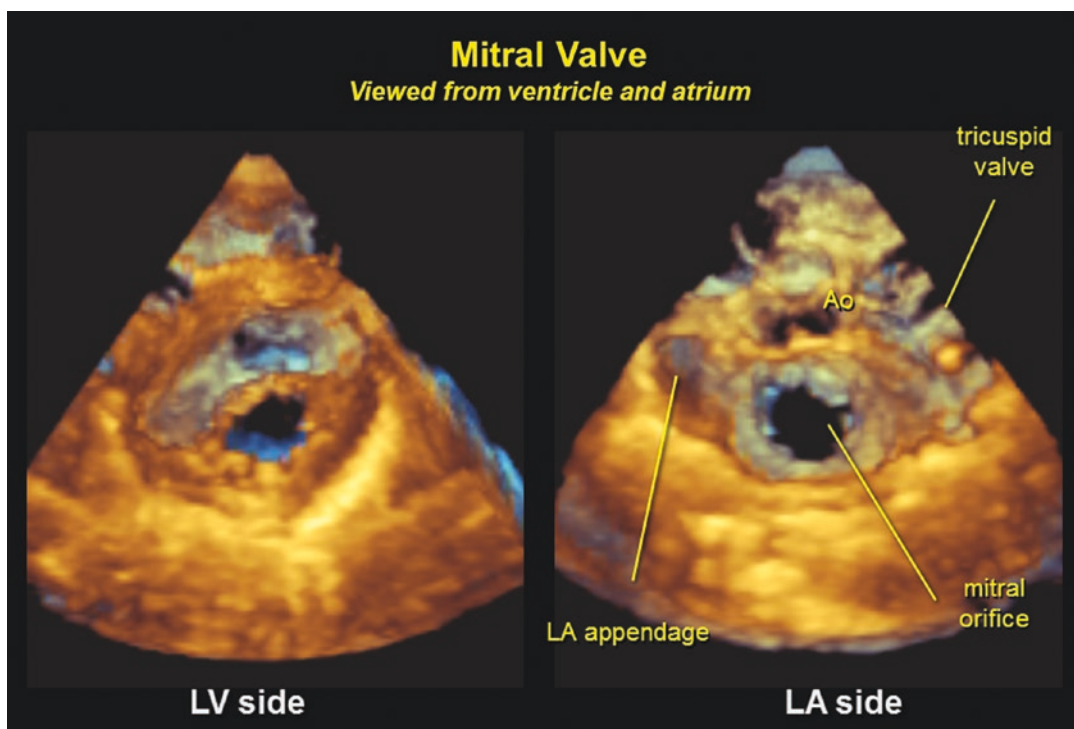


Fig. 10.74 Three-dimensional echocardiographic still frames showing a stenotic mitral valve orifice from the ventricular (left) and atrial (right) perspectives. There is leaflet tip thickening and commissural fusion

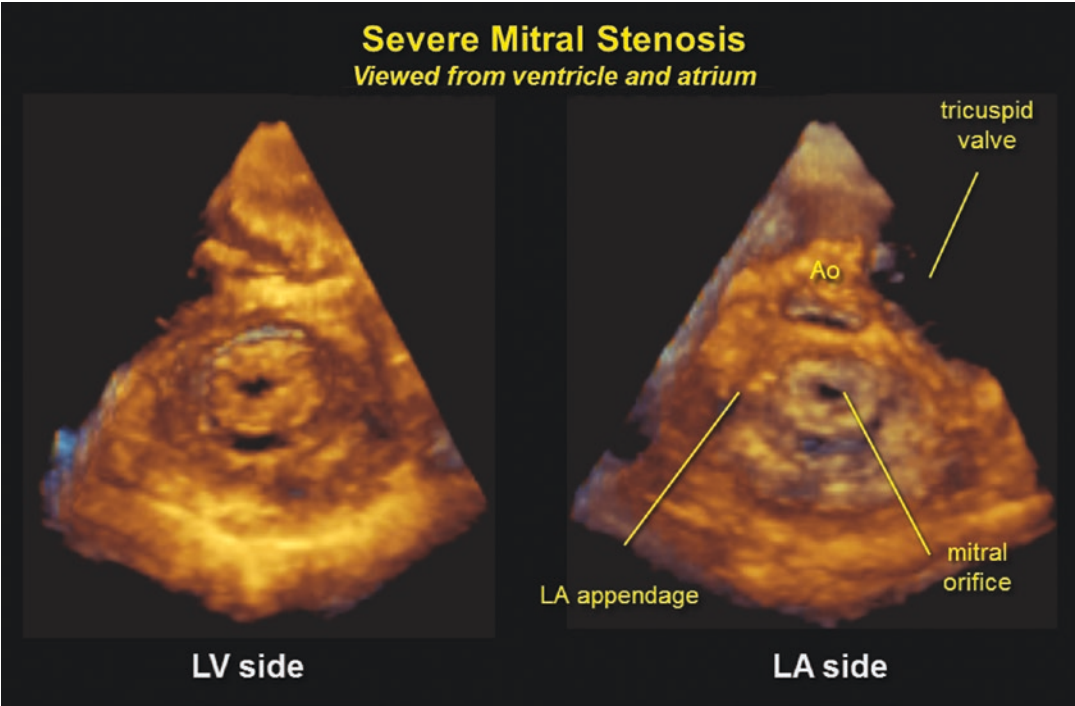


Fig. 10.75 Three-dimensional echocardiographic still frames showing a severely stenotic mitral valve orifice from the ventricular (left) and atrial (right) perspectives.

There is even more leaflet tip thickening and commissural fusion than in the similar views in the previous figure

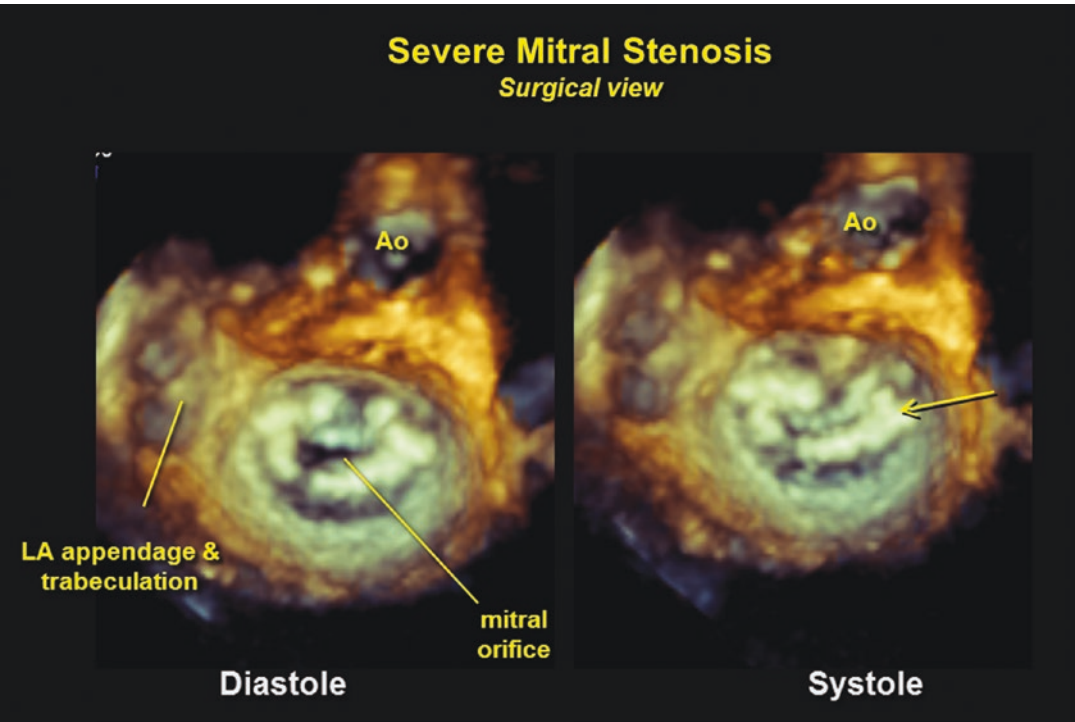


Fig. 10.76 Surgical view of a three-dimensional echocardiogram in mitral stenosis. In this patient, there is marked annular and suprannular thickening and fibrosis (arrows)

Indeed, this patient underwent mitral valve replacement due to the marked annular and commissural thickening.

Despite the advent of three-dimensional echocardiography, two-dimensional echocardiography still plays a very significant role. The pattern of diastolic movement of the anterior mitral valve leaflet seen in Fig. 10.77 is characteristic of rheumatic mitral stenosis. The leaflet tip is restricted and bends toward the restricted posterior mitral leaflet in diastole because of leaflet tip attachment and commissural fusion. This pattern results in a very narrow orifice. The body of the anterior mitral leaflet (arrow) is usually, however, frequently spared in this disorder except in its most severe forms. The left atrium is significantly enlarged in both systole and diastole. Note the mitral

valve closing patterns in systole. This opening pattern of the mitral valve apparatus in diastole is sometimes referred to as “diastolic doming”, as the mitral valve leaflets form a dome-like structure from atrium towards ventricle during ventricular filling. What is most significant is to recognize the attachment of leaflet tips and to recognize that rheumatic involvement of the mitral valve is manifest by disease at the leaflet tips and commissures, frequently sparing the body of anterior mitral valve leaflet (Fig. 10.78).

Because of this leaflet tip restriction, systolic closure is impaired and rheumatic mitral regurgitation can consequently result (Fig. 10.75). Again, the left atrium is seen to be massively dilated in this individual with several mitral stenosis. When mitral stenosis is severe and mitral

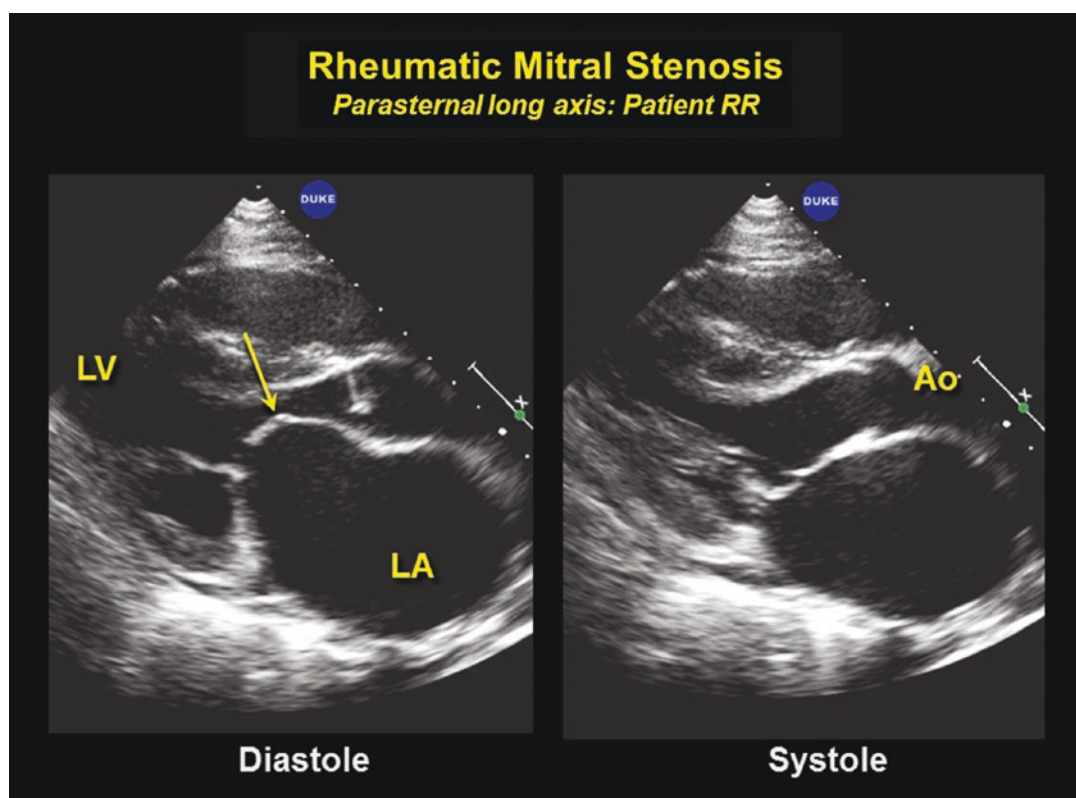


Fig. 10.77 Two-dimensional echocardiographic parasternal long axis view of rheumatic mitral stenosis showing tethering of the anterior mitral valve leaflet tip. The

body of the leaflets remain mobile (arrow) in all but the most severe disease. Rheumatic mitral valve disease is a disease of leaflet tips

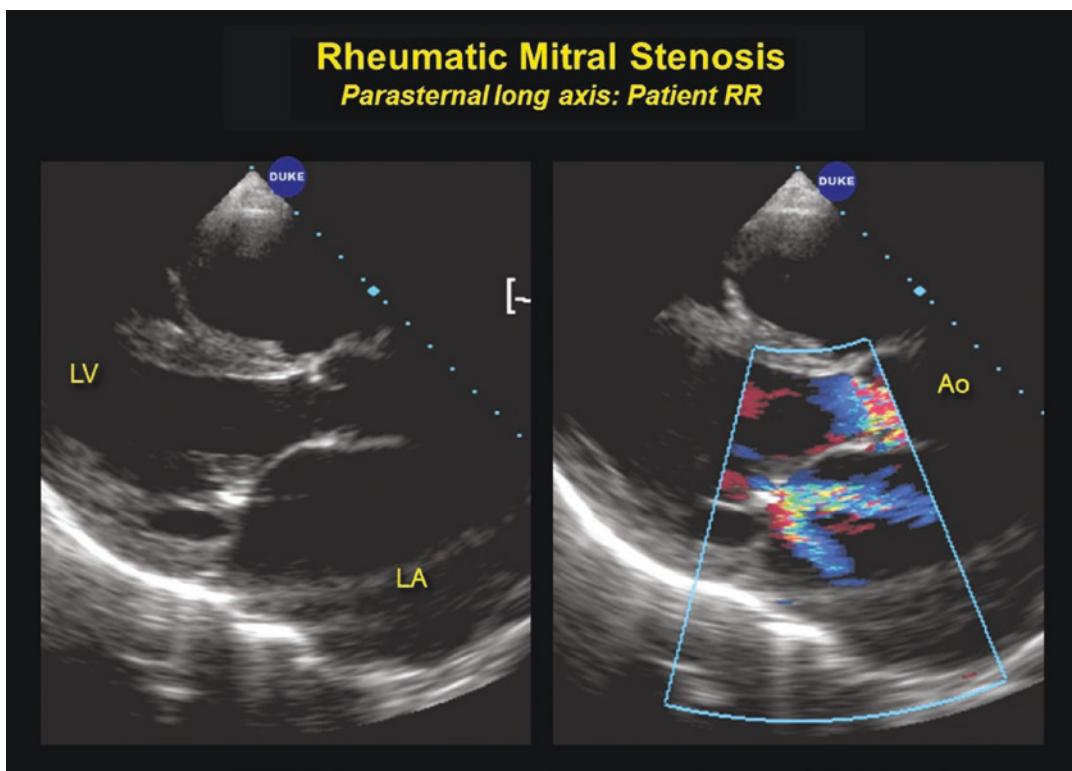


Fig. 10.78 Two-dimensional echocardiographic parasternal long axis view of rheumatic mitral stenosis. The color flow image at the right shows mitral regurgitation

regurgitation is significant, mitral commissurotomy is not performed either by balloon (at catheterization) or surgically. Rather, the mitral valve is replaced. Open mitral valve repair with this combination of findings has had only variable results.

Doppler patterns of normal and mitral stenosis can also be differentiated. In panel A of Fig. 10.79, the normal antegrade mitral Doppler flow is seen. There is a narrow Doppler spectrum of velocities and a rapid E–F slope with easily recognized preservation of the A wave, following atrial contraction. Panel B shows the typical pattern of mitral valve obstruction with marked delay in the degradation of the E–F slope and significant spectral broadening. Spectral broadening refers to the presence of multiple velocities in the recording at any one point in time.

Planimetry of the Mitral Orifice

Since the mitral orifice may be directly visualized by two-dimensional echocardiography with proper transducer angulation, this is an ideal technique for determining the cross-sectional area of the mitral valve. Figure 10.80 contrasts mitral valve opening during diastole in an individual with no mitral stenosis (left panel) with that in an individual with severe mitral stenosis (right panel). Most echocardiographic systems will provide a method for easy planimetry of these valve orifices.

Figure 10.81 contrasts two patients with mitral stenosis. One if moderate (left panel) and one is severe (right panel) [2]. Proper detection of a rheumatic valve orifice by two-dimensional echocardiography requires some operator experience to adjust the plane of examination directly

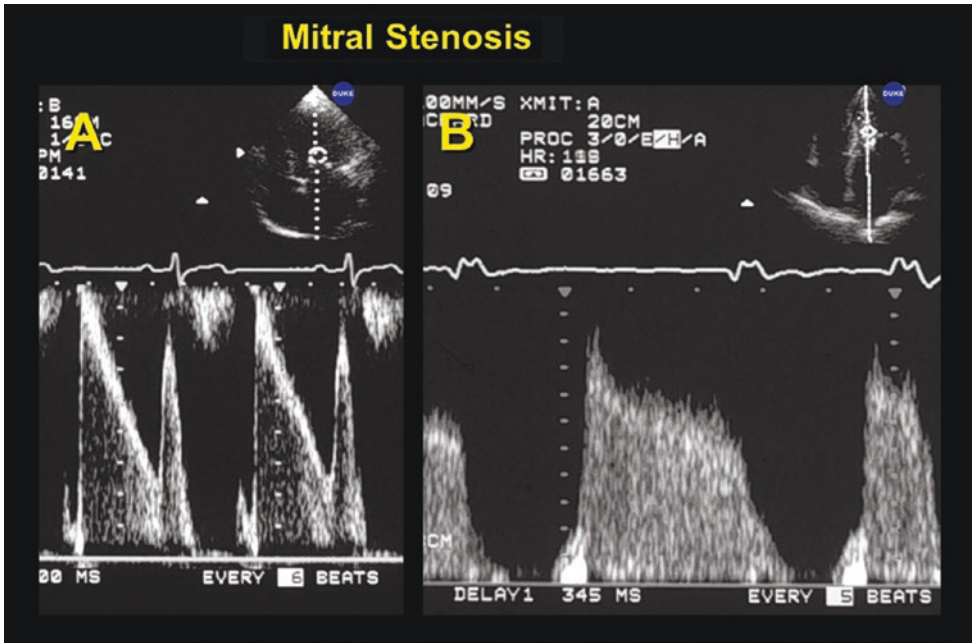


Fig. 10.79 Spectral Doppler recordings from the apex showing normal mitral diastolic flow compared to mitral stenosis. In mitral stenosis there is spectral broadening and a slow diastolic flow decay

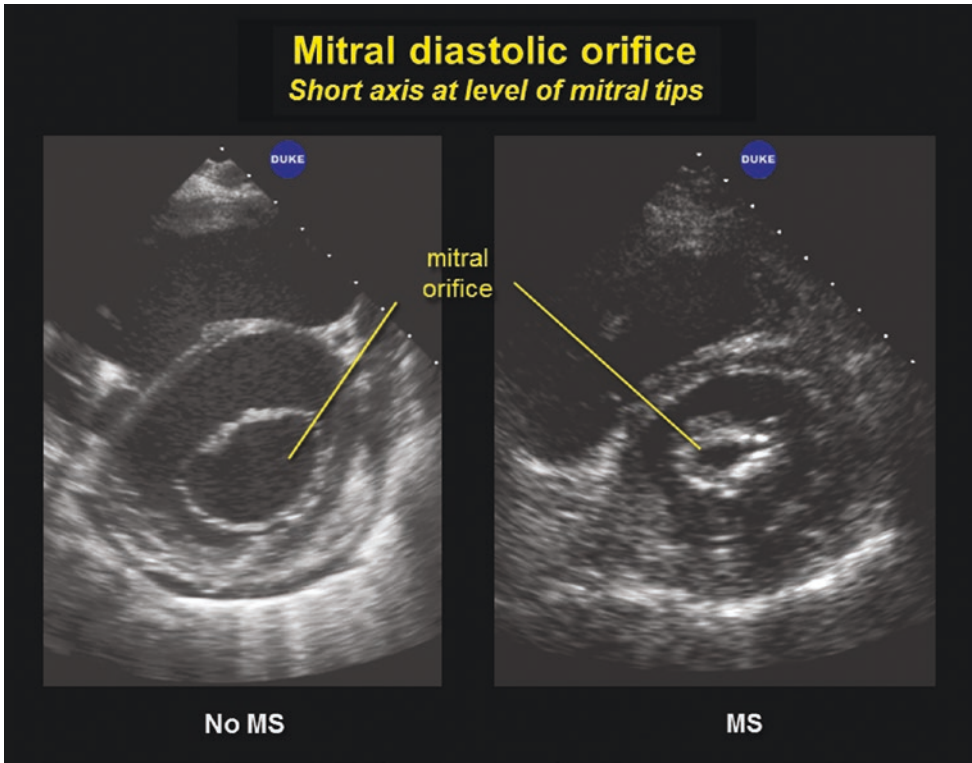


Fig. 10.80 Parasternal two-dimensional short axis still frames comparing mitral diastolic orifice area in a patient with no mitral stenosis (left) to one with a restricted orifice of mitral stenosis (right)

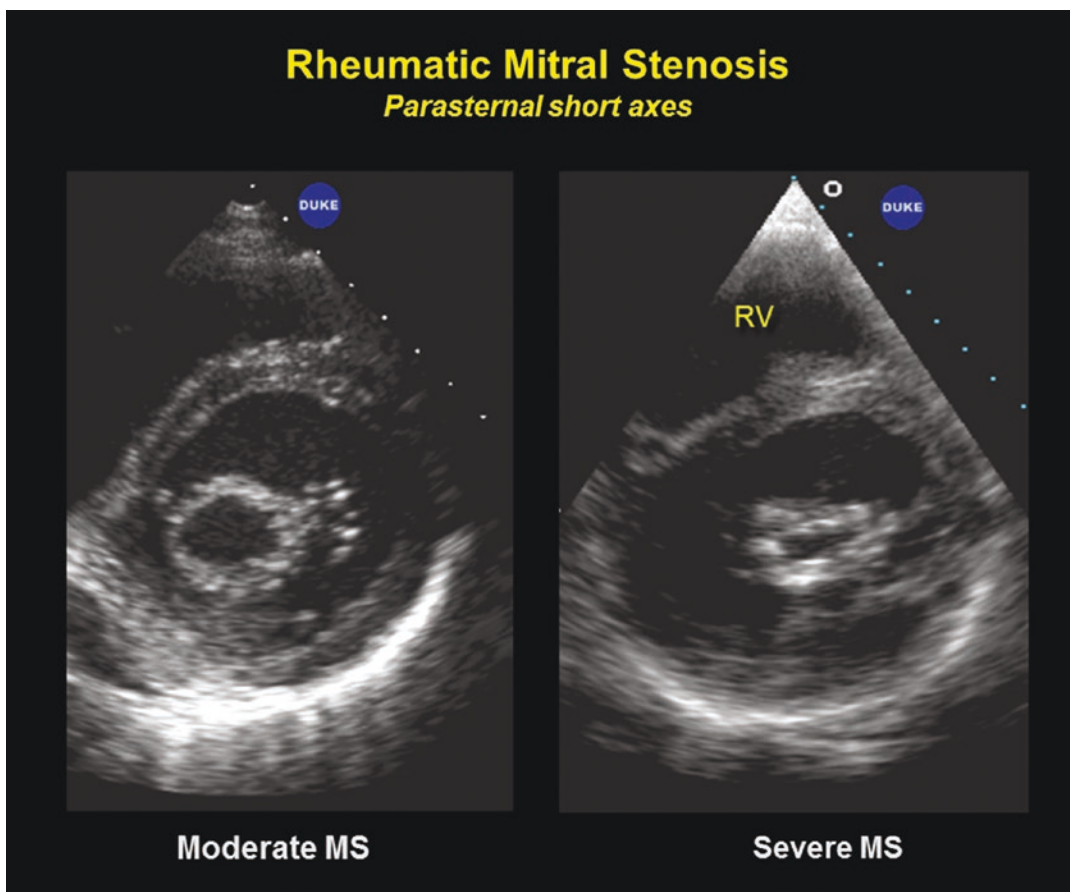


Fig. 10.81 Parasternal two-dimensional diastolic short axis still frames from a patient with moderate (left) mitral stenosis compared to one with severe mitral stenosis (right)

through the leaflet tips. If diagonally oriented through the body of the anterior mitral leaflet to the tip of the posterior leaflet, the orifice will appear artifactually large due to angulation. Proper assessment also requires that the image gain be properly set lest the orifice be depicted as too small by excess image gain.

Using proper technique, it is long been accepted that two-dimensional echocardiography can reliably demonstrate mitral valve leaflet tip cross-sectional area. Various mitral valve orifices are demonstrated in Fig. 10.82 with comparative echocardiographic and catheterization determined mitral valve orifice area [2]. The correlation of echo and catheterization valve areas is shown in Fig. 10.83 from an

early paper where this capability was demonstrated ($r = -0.93$). Of course, consistent methods can be used in any one center that lead to measurement consistencies. Such correlations are generally not as effective following mitral commissurotomy.

Results of such correlations from a multi-center study involving the Balloon Valvuloplasty Registry showed much wider variation when two-dimensional echo determined valve area and catheterization valve area were compared (Fig. 10.84) [3]. While this correlation is less than ideal it does reflect the variations that might occur from institution to institution and as hemodynamic situations may vary between echocardiographic and hemodynamic assessments.

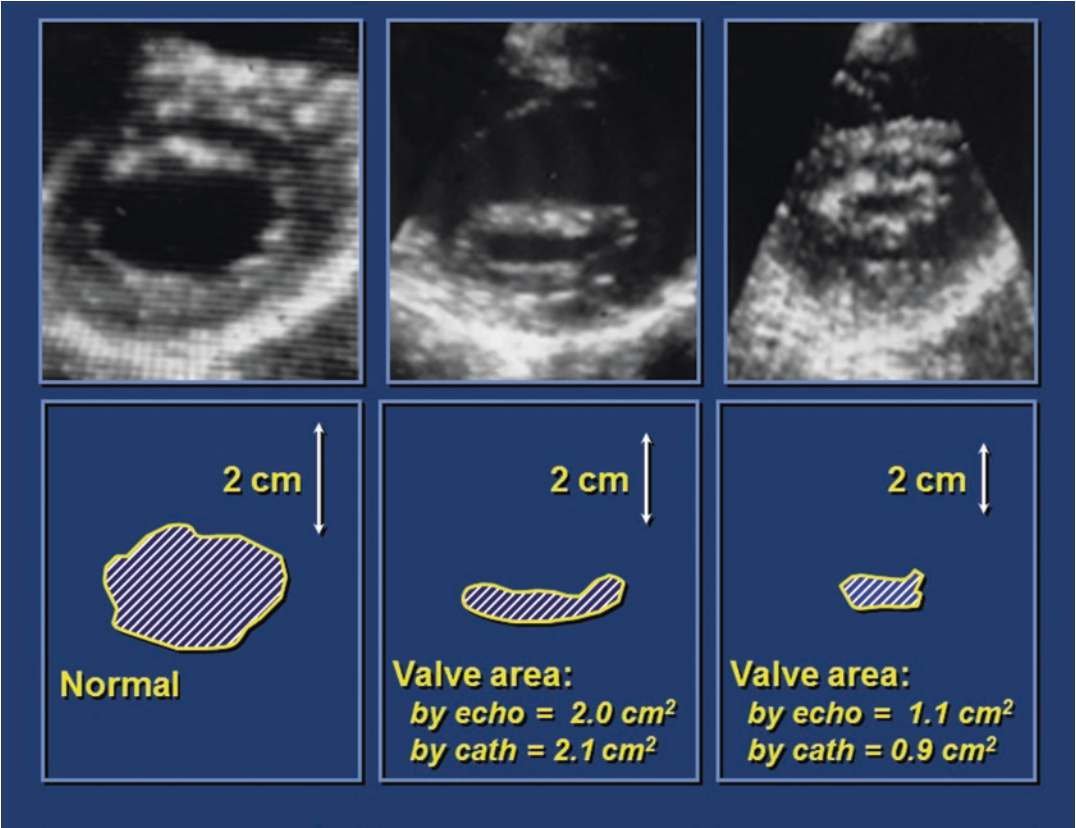


Fig. 10.82 Compared diastolic orifice measurements showing progressively smaller mitral orifice size with more severe mitral stenosis. Redrawn after Nichol et al. [4]. Redrawn after: Nichol, et al: Circulation, 55:1977

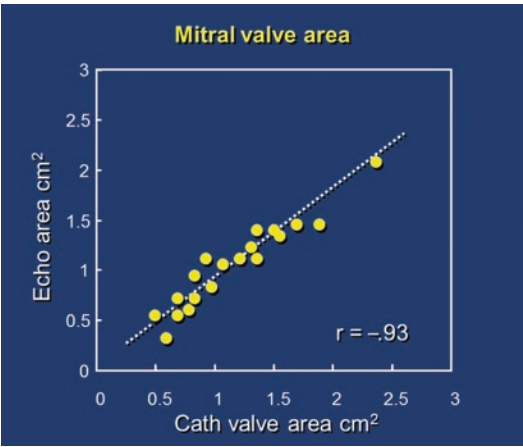


Fig. 10.83 Comparison of echo calculated valve area from catheterization calculated valve area. Redrawn after Nichol et al. [4]. Redrawn after: Nichol, et al: Circulation, 55:1977

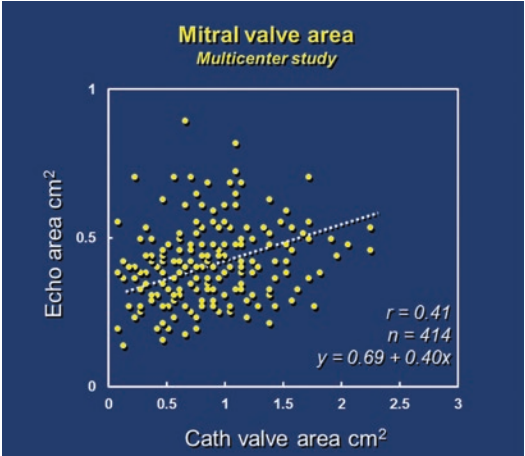


Fig. 10.84 Comparison of echo calculated valve area from catheterization calculated valve area from a large multicenter study. Redrawn after Kisslo [3]. Redrawn after Kisslo, J.: JACC, 11:114A, 1989

Mean Mitral Gradient by Doppler

Another method for determining severity of mitral stenosis by Doppler is the measurement of mean mitral gradient. When using this method, the Doppler continuous wave transducer is placed at the ventricular apex and angled through the mitral orifice in diastole. The resulting diastolic flow signal is then traced within the software package of the ultrasound machine to determine the mean mitral gradient according to the method described by Hatle (Fig. 10.85) [1]. Figure 10.86 shows the correlations from this approach for determination of mean mitral gradient when measurements are made by Doppler and by hemodynamics simultaneously in a single institution. The correlations are excellent.

Variations are, however, encountered when measurements are made by multiple institutions and determined non simultaneously with catheterization. These variations are seen in Fig. 10.87 from the multicenter study previously mentioned.

Pressure Half-Time Mitral Valve Area

There is another method for determination of mitral valve area using the degradation of the gradient in mitral stenosis by Doppler echocardiography referred to the pressure half-time method. This method is dependent on determining the time interval that it takes for the mitral gradient to drop to half its initial value.

Figure 10.88 shows how the pressure half-time is measured. The starting point is the time of peak velocity (Point 1), which in this example is approximately 2.4 m/s. This corresponds to a peak pressure gradient of approximately 24 mmHg by the modified Bernoulli eq. A line along the diastolic descent of the mitral valve spectrum is then drawn (Step 2). The point is then found along this line where the pressure is then dropped to one-half of its initial value (to Point 3). This point is rapidly determined by dividing the initial velocity by the 1.4 (which is the square root of 2). In this case $2.4/1.4 = \text{equals } 1.71 \text{ m/s}$. Thus, when the velocity falls to 1.71 m/s the pres-

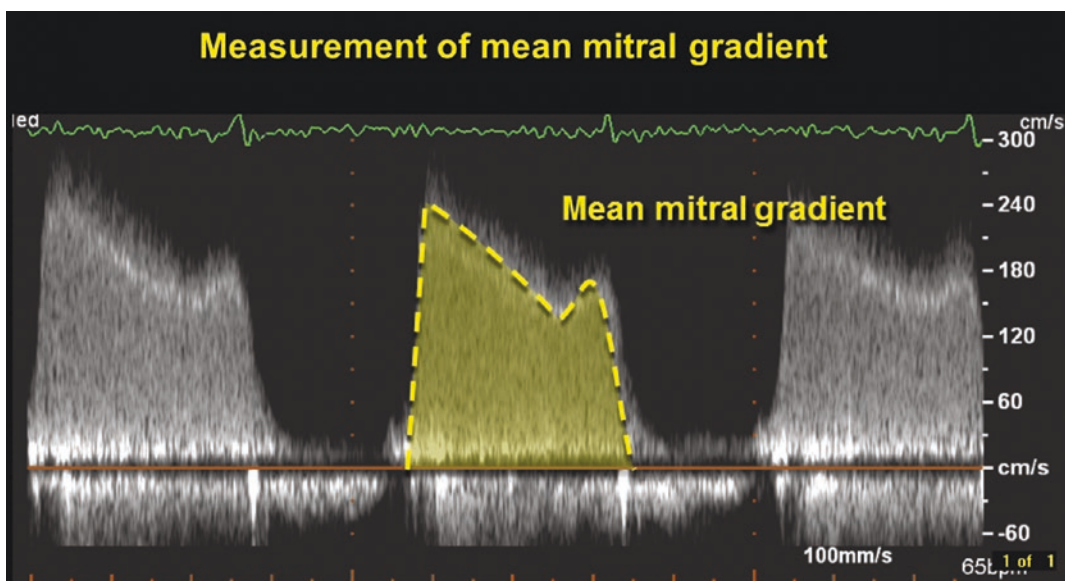


Fig. 10.85 Measurement of mean mitral gradient

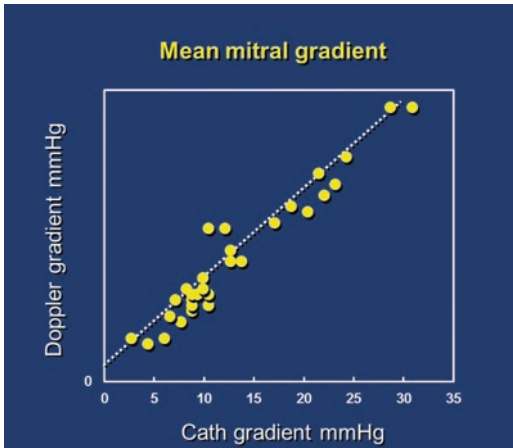


Fig. 10.86 Mean mitral gradient by Doppler compared to simultaneous measurement of mean mitral gradient at catheterization. Redrawn after Hatle and Angelsen [1]. Redrawn after Hatle, L. et al: Doppler Ultrasound in Cardiology. Lea & Febiger. 1985

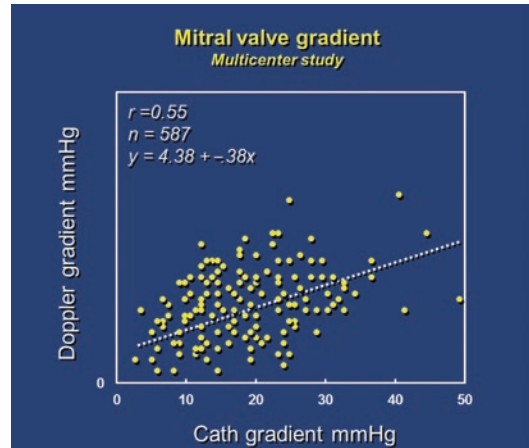


Fig. 10.87 Comparison Doppler calculated mean mitral gradient to non-simultaneous catheterization measured mean mitral gradient from a large multicenter study. Redrawn after Kisslo [3]. Redrawn after Kisslo, J.: JACC 11:114A, 1989

sure is at one-half of its initial value seen at Point 1. The pressure half-time is simply the time interval between Point 1 and Point 3, in this case approximately 250 ms (Interval 4).

Subsequently, Hatle and Angelsen [1] found the pressure half-time could be used to estimate mitral valve area from an empirical formula shown in the bottom of Fig. 10.88. In this series of 20 patients, they found a stronger correlation between this Doppler-derived estimate and catheterization-derived mitral valve area (Fig. 10.89), again a single institution. Once again, however, when these quantitative manipulations are applied to larger populations in a multicenter study, these correlations are less exact (Fig. 10.90).

The advantage of all these quantitative approaches is that a clinician is not dependent on any single measurement for the assessment of the severity of mitral stenosis. Rather, one can implement all methods and then implement a conclusion that is most consistent with the quantitative and subjective findings. In severe mitral stenosis, the left atrium is dilated and right ventricular pressures are elevated (through determination of peak right ventricular systolic pressure from tricuspid regurgitation).

Beginners in echocardiography sometimes think that a single measure can determine the severity of the disorder alone. It is the clinical decision making process, all factors must be

taken into account and then a decision as to severity of stenosis rendered. Observers should take into account other factors such as left atrial size and right ventricular pressure when applying the terms mild, moderate or severe to rheumatic mitral stenosis by echocardiography. Measures should correlate to a reasonable degree or the observer has made some error with the measurement that is in conflict with others.

Echocardiography is not alone in this need for proper clinical decision making processes. A clinician would not apply the diagnosis of diabetes to a single measurement of blood sugar of 140 mg/100 ml. Rather, proper clinical practice is to perform other tests, such as blood sugar determination in a fasting condition and a glucose tolerance testing or other procedure to ensure the reliability of a diagnosis is not dependent on one measurement alone. Echocardiography is no different and still remains the most readily available and best non-invasive or invasive method for determination of the severity of mitral stenosis or insufficiency.

Wide variations of measurements are not unique to indices of the mitral valve in large multicenter studies as seen in the Balloon Valvuloplasty Registry data for aortic valve indices shown in Fig. 10.91. Left panel illustrates variation of mean aortic gradient and right panel variations in aortic valve area by the continuity

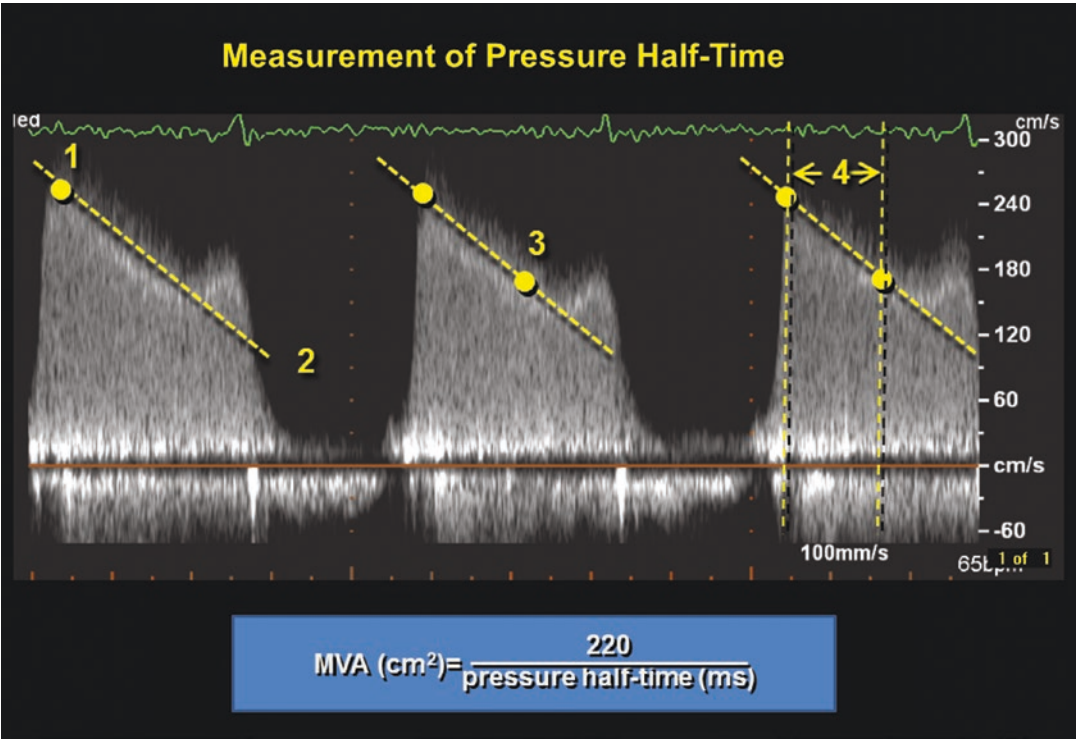


Fig. 10.88 Steps in the calculation of mitral valve area by pressure half-time

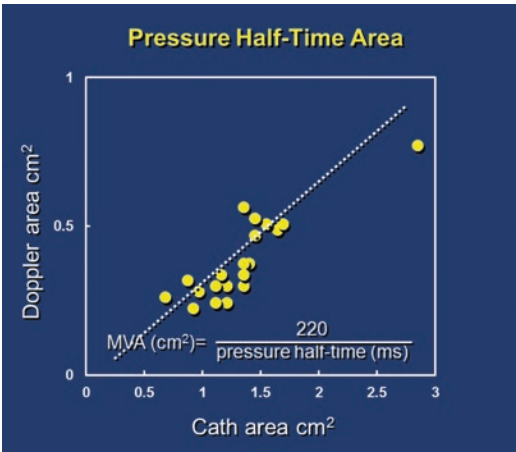


Fig. 10.89 Comparison of mitral valve area calculated from pressure half-time to that calculated at cardiac catheterization. Redrawn after Hatle [1]. Redrawn after Hatle, L. et al: Doppler Ultrasound in Cardiology. Lea & Febiger. 1985

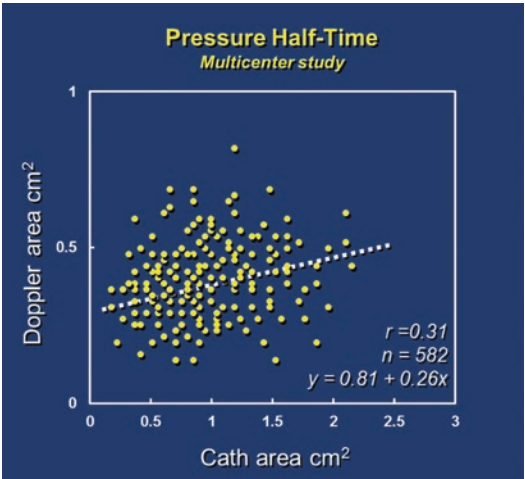


Fig. 10.90 Comparison of mitral valve area calculated from pressure half-time to that calculated at cardiac catheterization from a large multicenter study. Redrawn after Kisslo [3]. Redrawn after Kisslo, J.: JACC 11:114A, 1989

equation seen in the Balloon Valvuloplasty Registry. Echo flow measures are just derivatives of Doppler detected flow information. It is imperative for any and every lab to institute a

Continuing Quality Improvement process in their laboratories to evaluate their proficiency and accuracy of quantitative valvular measurement indices.

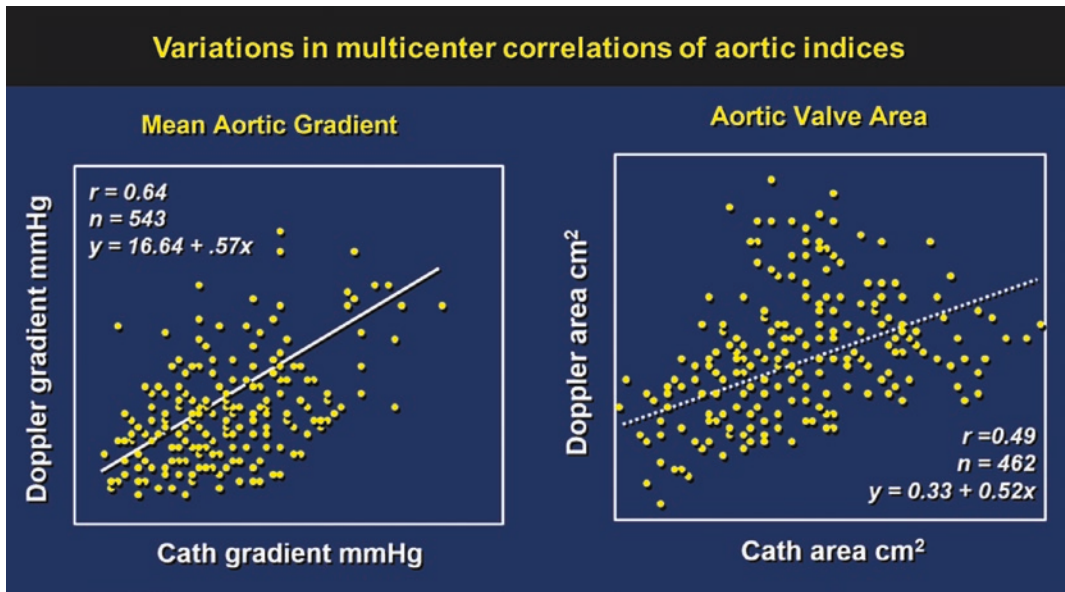


Fig. 10.91 Wide variations of measurements are not unique to indices of the mitral valve in large multicenter studies. Left panel illustrates variation of mean aortic gradient and right panel variations in aortic valve area by the

continuity equation seen in the Balloon Valvuloplasty Registry. Echo flow measures are just derivatives of Doppler detected flow information. Redrawn after Kisslo [3]. Redrawn after Kisslo, J.: JACC 11:114A, 1989

Mitral Prolapse

The combination of echocardiographic imaging methods for determination of mitral valve anatomy together with Doppler assessment of the location and severity of mitral regurgitation is now the principle method for evaluation of mitral degenerative disorders such as mitral valve prolapse. Almost two thirds of mitral regurgitation is due to such disorders and these techniques have found immense value in planning surgical procedures as well as evaluating the results of these procedures.

The M-mode echocardiogram in Fig. 10.92 shows the classic appearance of mitral prolapse using this one-dimensional technique. There is a posterior bowing of the mitral valve apparatus in late systole (arrow). Depending on the angulation of a single beam used in M-mode, there are multiple sources for error. In addition, there is no guarantee that the entire mitral valve can be interrogated by a single beam except in the hands of a few experts. Accordingly, the application of M-mode in this

disorder lost favor with the advent of two-dimensional echocardiography.

Figure 10.93 shows three dimensional views from the patient's left side of mitral valve prolapse. Left panel is in diastole. Middle panel is in systole where posterior prolapse is seen. The right panel shows the same prolapse, slightly rotated. There is systolic anterior motion of the tips of the mitral valve abutting the interventricular septum due to the redundant leaflet tip in the middle and right panels. The arrow points to the membranous portion of the interventricular septum which is frequently seen as a hole due to 'drop out of target information' (left and right panels).

Figure 10.94 demonstrates an angled surgical view of diastole (left panel) and systole (right panel) of the mitral valve in the same patient as in Fig. 10.93. The arrow points to predominant prolapse of the P₁ portion of the P₂ segment of the posterior leaflet. Slight prolapse of the anterior leaflet is also seen.

Quantitative measures may be applied to mitral valve closure by three-dimensional echocardiography. Figure 10.95 shows computerized

Fig. 10.92 The classic appearance of mitral valve prolapse by M-mode echo. There is a mid-late systolic posterior motion of the mitral valve (arrow)

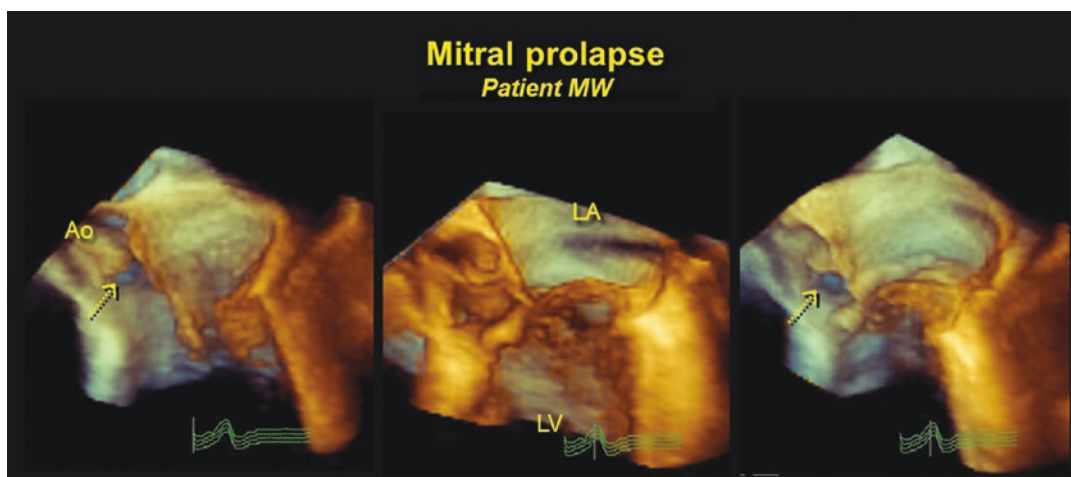
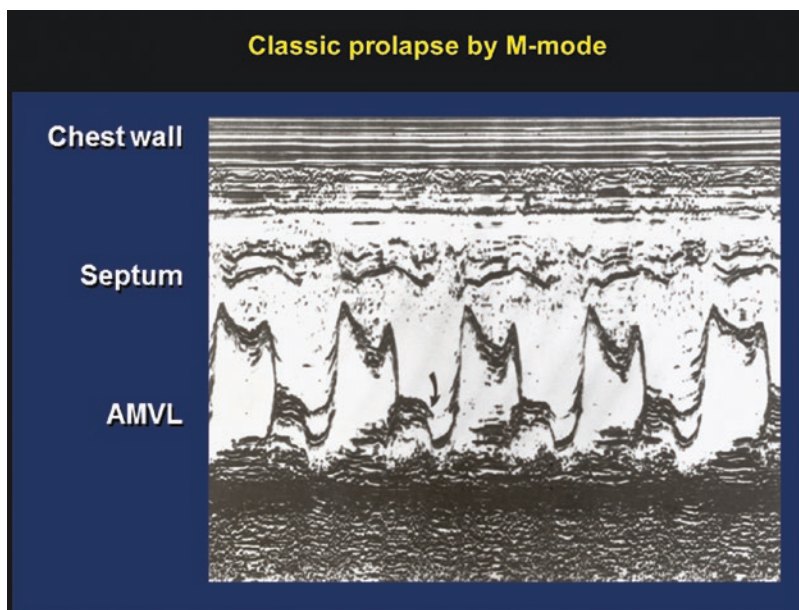


Fig. 10.93 Three dimensional views from a patient's left side of mitral valve prolapse. Left panel is in diastole. Middle panel is in systole where posterior prolapse is seen. The right panel shows the same prolapse, slightly rotated. There is systolic anterior motion of the tips of the

mitral valve abutting the interventricular septum due to the redundant leaflet tip in the middle and right panels. The arrow points to the membranous portion of the interventricular septum which is frequently seen as a hole due to 'drop out of target information' (left and right panels)

contouring of leaflet surfaces of the three-dimensional echocardiogram from the same patient as in Figs. 10.93 and 10.94 (left panel). Note the contours drawn of each leaflet (middle column) and the myriad of quantitative indices that may be calculated (right panel). While such indices have been found helpful in mitral valve repairs, they are, not yet, used commonly.

Functional Classification of Mitral Regurgitation

Mitral valve prolapse is included in the currently applied descriptions of the functional classification of the etiology of mitral regurgitation. Because most mitral regurgitation can be surgically managed by valve repair, rather than

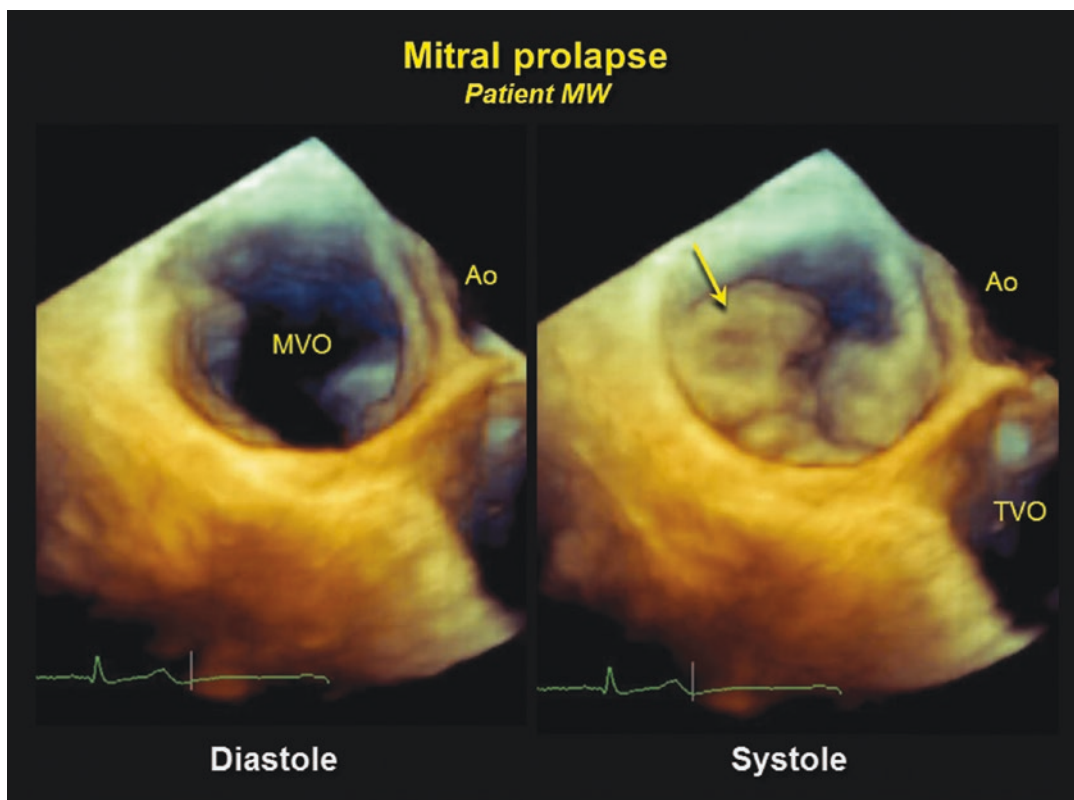


Fig. 10.94 Angled surgical view of diastole (left panel) and systole (right panel) of the mitral valve in the same patient as in Figs. 10.93 and 10.95. The arrow points to

predominant prolapse of the P_1 portion of the P_2 segment of the posterior leaflet. Slight prolapse of the anterior leaflet is also seen

replacement, this classification is now widely used.

Currently, the functional classification of mitral regurgitation is described as consisting of three basic types. Normal mitral valve coaptation occurs with the tips of the mitral leaflets located well into the left ventricle in systole, far from the mitral valve annulus (Fig. 10.96). This level of coaptation provides adequate surfaces for coaptation of both leaflets to prevent significant regurgitant flow into the atrium in systole.

In Type I mitral regurgitation there the mitral annulus is stretched, usually due to dilatation of the left ventricle as seen with dilated cardiomyopathy. When the annulus dilates, the leaflets are stretched and there is a resultant failure of the leaflets to coapt except at the very leaflet tips, if at all. Accordingly, there is little leaflet surface to impede regurgitation. This Type I will be discussed later in the section on congestive heart failure. Surgical correction of this type of mitral regurgitation

involves the placement of a mitral valve ring to bring the leaflet tips down into the left ventricle.

Type II is usually due to abnormalities we commonly describe as mitral valve prolapse where there is a mal-apposition of leaflet tips. This could occur in the anterior, or posterior mitral valve leaflet tips where coaptation of one or both leaflets approaches the mitral annulus. Given this mal-apposition, the leaflet tips do not align and mitral regurgitation results. Surgical repair of this type of mitral regurgitation is based upon removal (by quadrilateral resection of a prolapsing P_2 segment) or alignment of prolapsing leaflet tips by chordal transfer, chordal shortening or other alignment techniques.

Type III mitral regurgitation is due to a specific restriction of a valve leaflet or leaflets. Type IIIa is found in patients with rheumatic mitral stenosis where there is significant diastolic and systolic restriction of the posterior mitral leaflet. Type IIIa uncommonly results in surgical repair.

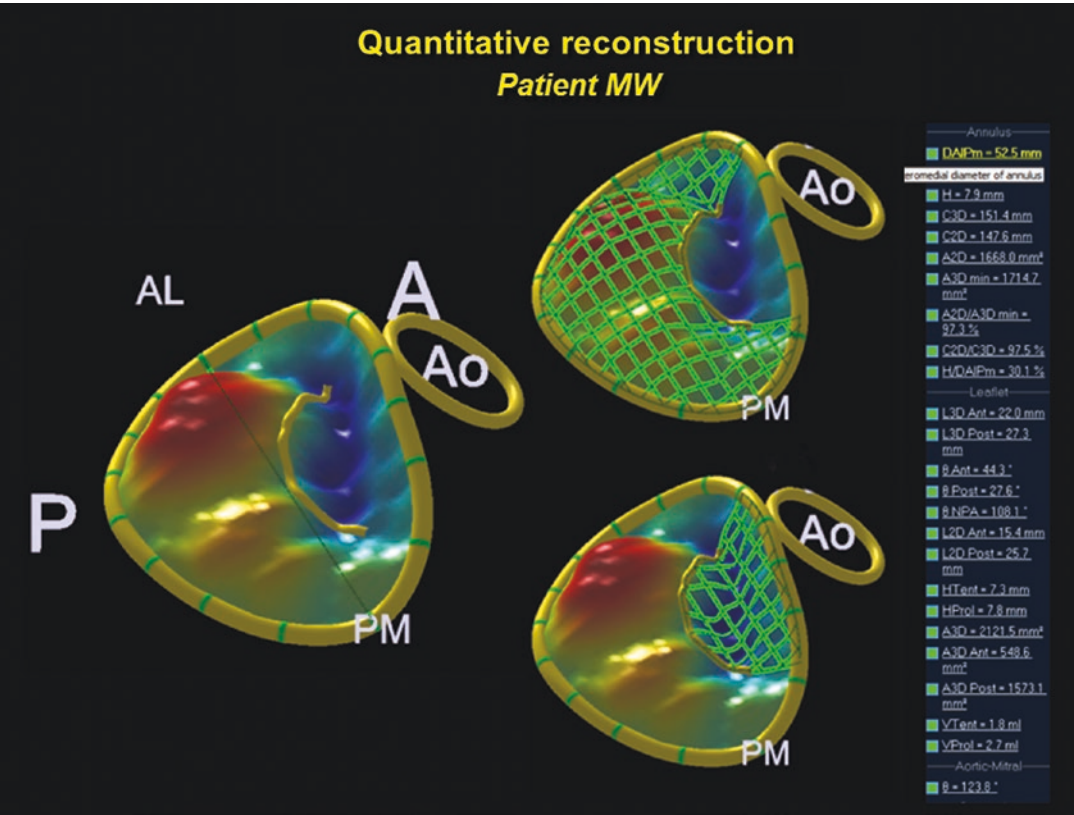


Fig. 10.95 Quantitative measures may be applied to mitral valve closure by three-dimensional echocardiography. Left panel shows computerized contouring of leaflet surfaces of the three-dimensional echocardiogram from the same patient as in Figs. 10.93 and 10.94 (left panel) in the same

orientation. Note the grid like contours drawn of each leaflet (middle column) and these myriad of quantitative indices that may be calculated (right panel). While such detailed indices have been found helpful in mitral valve repairs, they are, not in common use on a widespread basis



Fig. 10.96 The functional classification of mitral regurgitation. For details, see text

Type IIIb is a bit different and is found in individuals with underlying wall motion abnormalities due to ischemic heart disease. In this setting, there is posterior wall motion abnormalities where there is stretching of the mitral valve apparatus that result in abnormalities of valve movement. Type IIIb is surgically treated by the placement of the smallest mitral ring available to not only approximate the leaflet, but to remodel the proximal ventricle to allow the posterior leaflet chordae to approximate those of the anterior leaflet.

Typical Type II, P2 Leaflet Prolapse

Figure 10.97 shows a two-dimensional echocardiogram in the parasternal long axis from the

chest wall in a 58 y.o. patient with Type II valve leaflet motion. Prolapse of both the anterior and posterior mitral valve leaflets (arrows) is seen as both leaflets billow back into the left atrium in systole. This movement of both leaflets into the atrium in systole is better appreciated in Fig. 10.98 by three-dimensional echocardiography from the transesophageal approach. In this series of systolic still images, the mitral apparatus is viewed from a posterior perspective as both leaflets emerge just over the mitral annulus in systole (left panel). The middle and right panels show the appearance of these leaflets as the mitral valve annulus is tilted into the more recognizable surgical view. All three panels were obtained during peak systole as both the anterior and posterior leaflets are billow upwards into the atrium (arrows). The schematic discs below show the

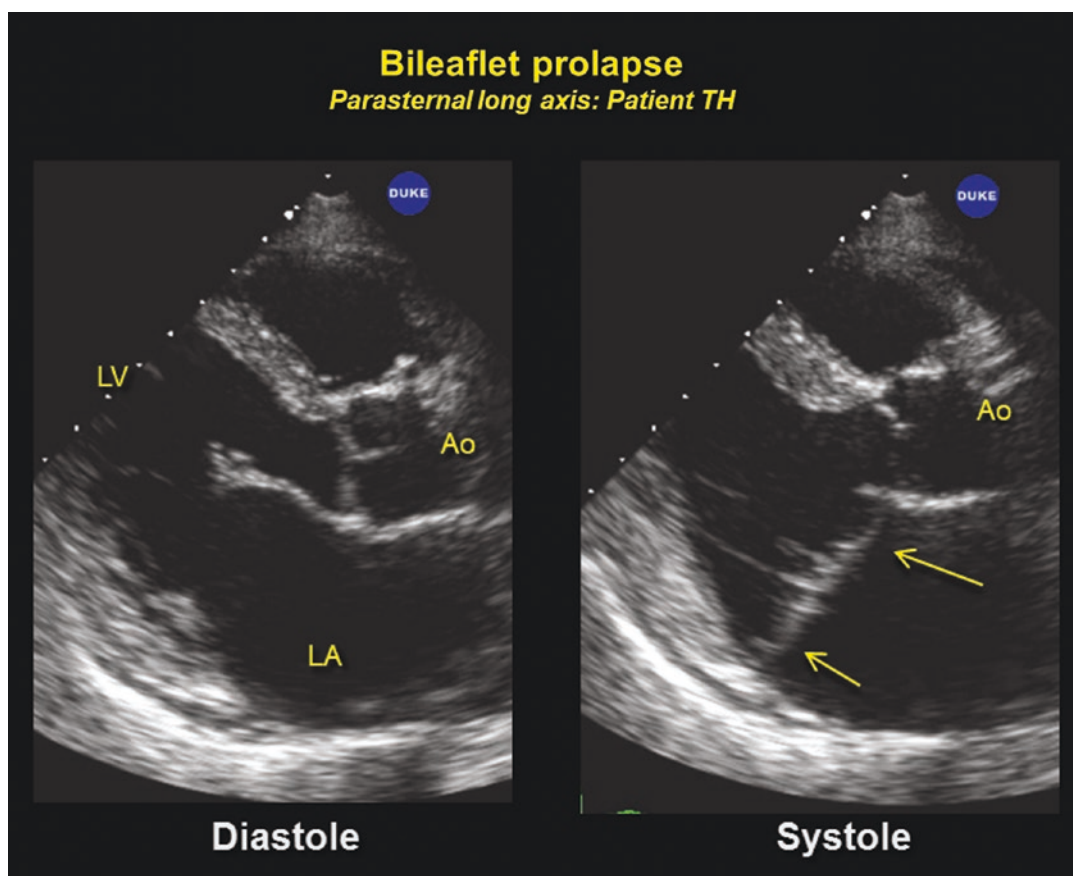


Fig. 10.97 Parasternal long axis two-dimensional echocardiographic still frames showing marked prolapse of the A₂ and P₂ scallops

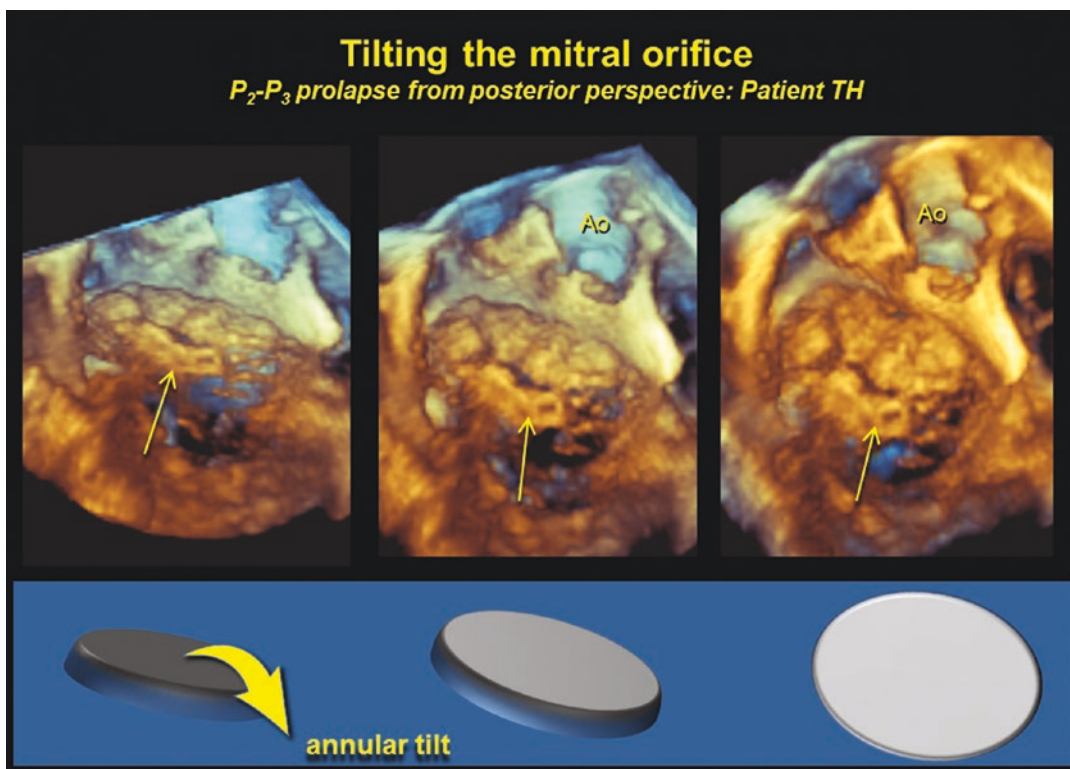


Fig. 10.98 Three-dimensional echo view of the same mitral prolapse seen in the previous figure

tilting of the still frame as the full extent of these leaflets are viewed from the atrium.

Evaluation of leaflet motion can actually be assisted by inspection of color flow patterns during systole. In the vast majority of instances, the direction of any given regurgitant jet is opposite the leaflet that prolapses. Figure 10.99 shows an apical four-chamber view in a patient with posterior mitral leaflet prolapse (left panel). The right panel shows the regurgitant jet clearly opposite the prolapse as it is directed toward the atrial septum, then posteriorly into the atrium (arrows). Most mitral regurgitation that comes to surgical repair is anteriorly directed, indicating that most Type II mitral regurgitation is due to posterior leaflet prolapse.

A schematic diagram of P₂ prolapse is shown in Fig. 10.100 from a parasternal long axis (left panel) and the surgical view right panel. Segments A₂ and P₂ are encountered in the two-dimensional echocardiographic long axis view.

From these schematic diagrams, one can appreciate how mitral regurgitation from Type II, P₂ prolapse would therefore be direct anteriorly along the backside of the anterior mitral valve leaflet toward the anterior aspects of the left atrial wall.

Actual three-dimensional echocardiographic images from a systolic frame of significant P₂ leaflet chordal thickening and flail is demonstrated in Fig. 10.101. The massively fibrotic chordal structures can be seen (arrow) to prolapse into the left atrium during systole. The annulus is again tilted as indicated in the discs in the blue bar below. Here, body of the posterior leaflet does not seem to prolapse as much as its thickened tip and remarkable chordal structures.

Contrast the previous three-dimensional figure with that shown in Fig. 10.102. Here there is massive P₂ bulging with obvious chordal flail in this tilting systolic still frame. The annulus is

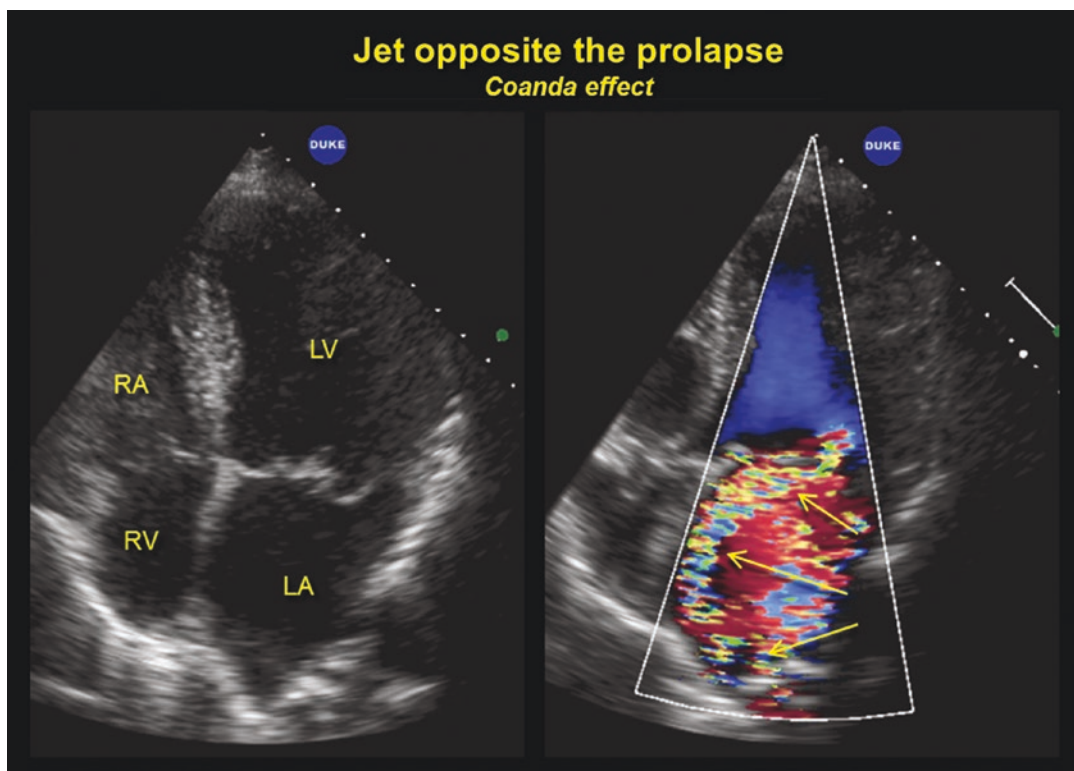


Fig. 10.99 Apical four-chamber view of mitral regurgitation directed against the atrial septum. The jet direction is opposite the prolapsing leaflet

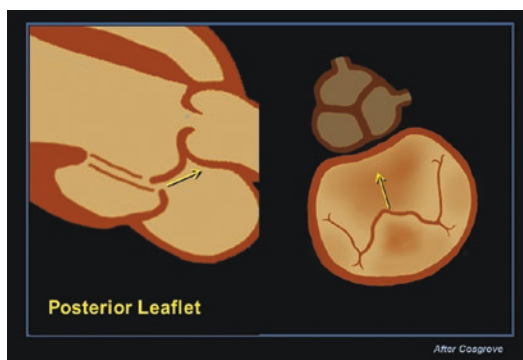


Fig. 10.100 Schematic representation of prolapse of the P₂ segment

rotated from side to side in the still frame to allow examination of the full extent of the mitral valve prolapse and chordal flail by the three-dimensional echocardiography still-frames.

The mitral valve apparatus can also be viewed from below from the left ventricular perspective towards the mitral valve apparatus and into the aortic outflow tract (Fig. 10.103). The upwards doming of the P₂ segment can be visualized from this perspective and then revealed further by tilting the heart forward. As the still frame images are tilted anteriorly the gaping orifice of the P₂ segment can be seen (right hand panel).

An actual surgical photograph of this mitral valve prolapsing segment is shown in Fig. 10.104. The dilated body of the P₂ segment is easily identified as are the broken chordae tendinea. This patient underwent a quadrilateral resection of the P₂ segment and the placement of a ring during mitral valve repair. In a quadrilateral resection, the P₂ segment is excised and the adjacent P₁ and P₃ segments are sutured together

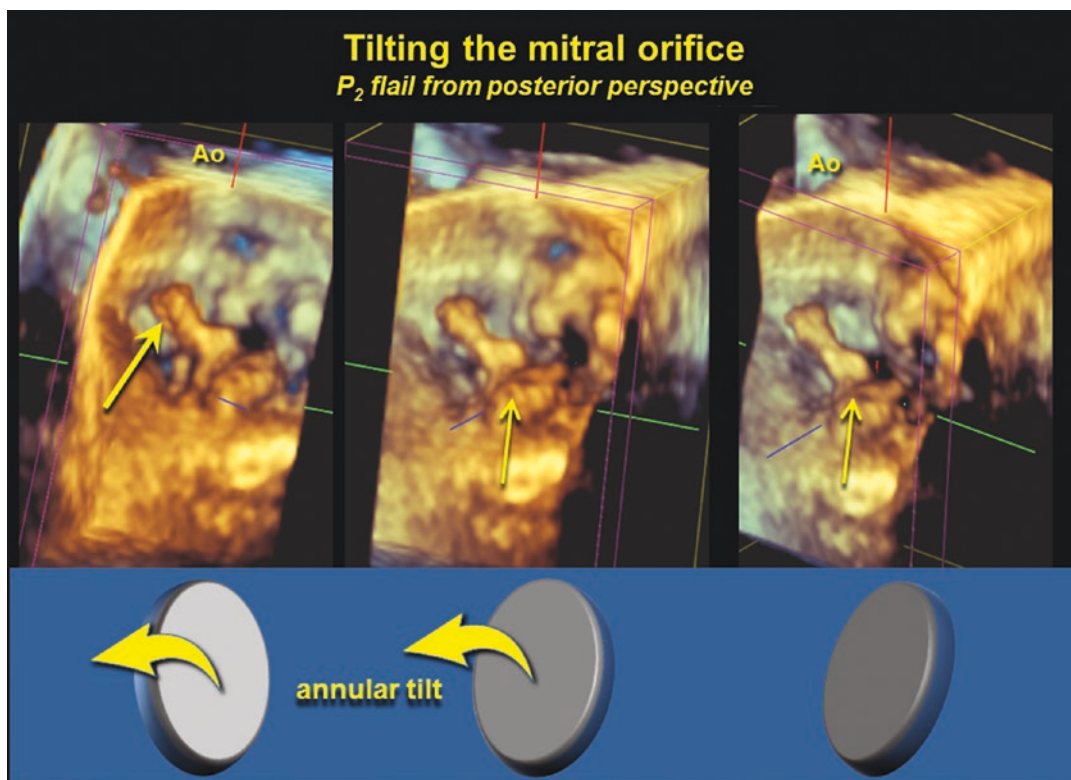


Fig. 10.101 Three-dimensional echo systolic frames from the surgical view in a patient with marked flail of thickened structures from the P₂ segment

and a mitral ring is put into place to stabilize the mitral apparatus. Residual of this approximation of the P₁ and P₃ segments is seen at the arrow in Fig. 10.105.

Figure 10.106 shows an M-mode echocardiogram from another patient with similar P₂ prolapse. The dashed arrow points to the prolapsing segment in the M-mode that markedly resembles the M-mode tracing seen previously in Fig. 10.92. The solid arrow in the two-dimensional parasternal long axis of the inset echocardiogram above shows the P₂ prolapse quite clearly. Two-dimensional echocardiography shows more spatial information than M-mode and is currently the standard for evaluation of mitral prolapse, either from the chest wall or transesophageal approaches.

The transesophageal echocardiogram from this patient also demonstrated the P₂ leaflet prolapse

and further indicated that there was flail of the P₂ leaflet tip (Fig. 10.107). There is no need for a diagnostic transesophageal echo in mitral valve prolapse if the chest wall echocardiogram is of superior quality, except in the setting of possible/probable/definite mitral valve repair. However, few older patients have such high quality images and clinicians must resort to the transesophageal approach for more detailed leaflet analysis.

In this case, the three-dimensional echo from the esophagus revealed even more information as the prolapse was seen to extend from the P₂ segment into the P₃ segment. Figure 10.108 shows the mitral apparatus viewed in three-dimensions from the posterior perspective and the mitral annulus is rotated into the surgical view. The marked billowing of the P₂ segment with flail of the leaflet tip is easily seen as is billowing of the P₃ segment. A more detailed

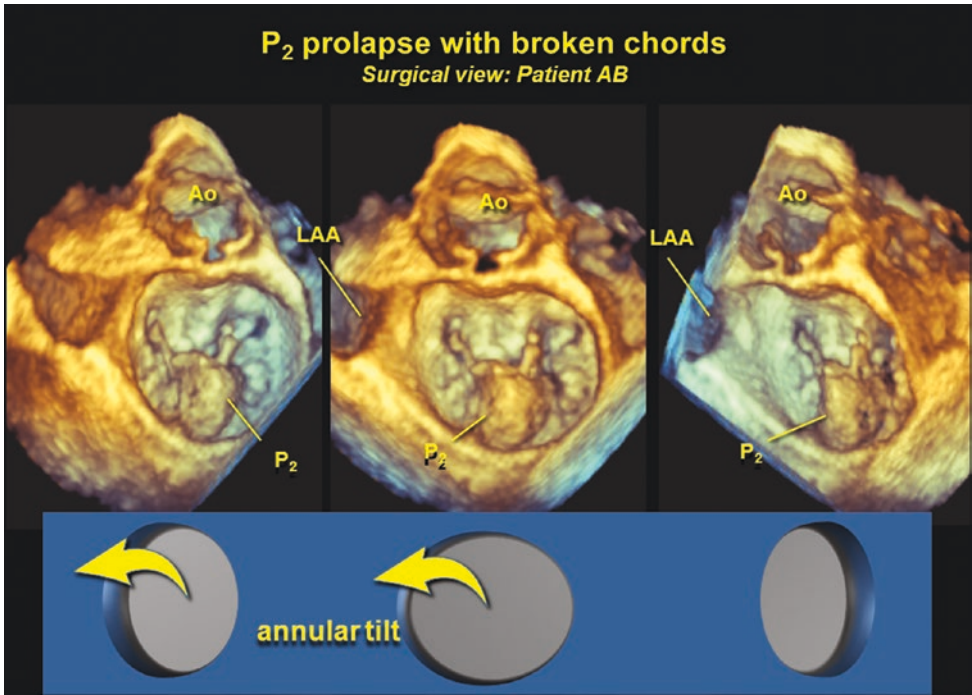


Fig. 10.102 Three-dimensional echo systolic frames from the surgical view in a patient with P₂ prolapse and broken chords to the P₂ segment

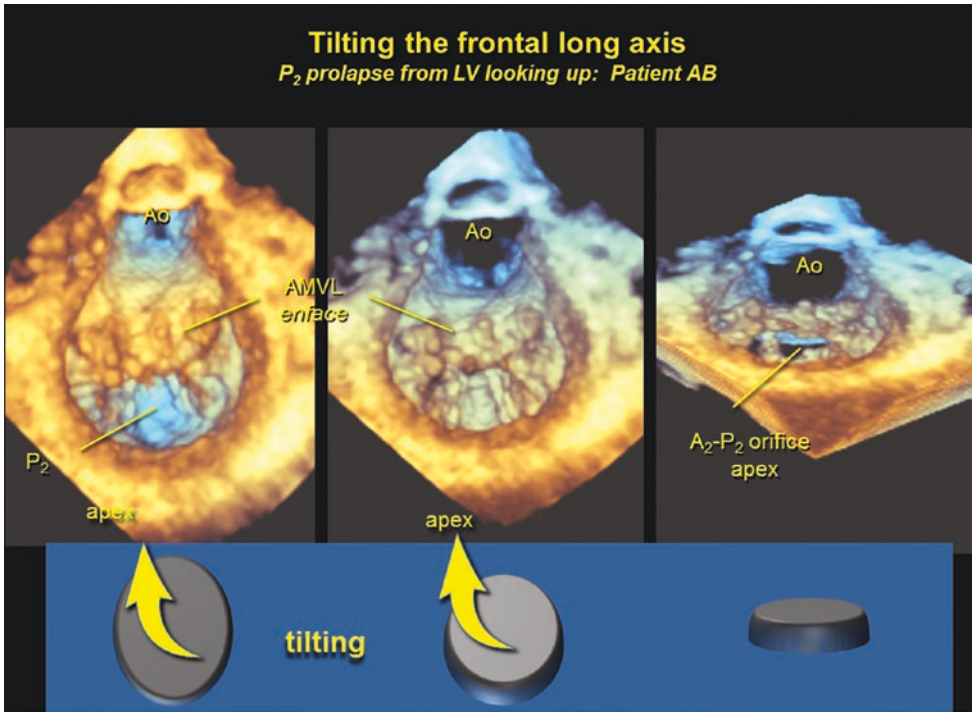


Fig. 10.103 Three-dimensional echo systolic frames of the mitral apparatus viewed from the left ventricle towards the atrium in the same patient with P₂ prolapse as in the previous figure. When tilted downwards, failure of coaptation between A₂ and P₂ is seen

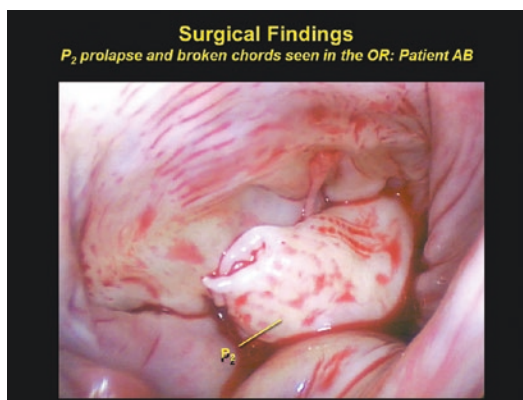


Fig. 10.104 The findings of P₂ mitral prolapse with broken chordae seen at surgery from the same patient seen in the previous two figures

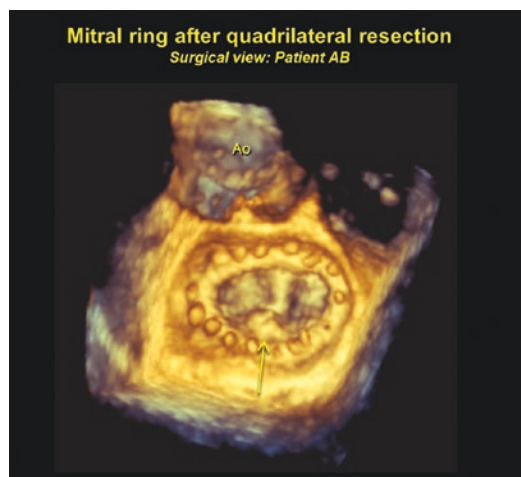


Fig. 10.105 This patient underwent mitral repair with a quadrilateral resection of P₂ and placement of a mitral ring

Fig. 10.106 M-mode and two-dimensional echocardiogram showing P₂ prolapse

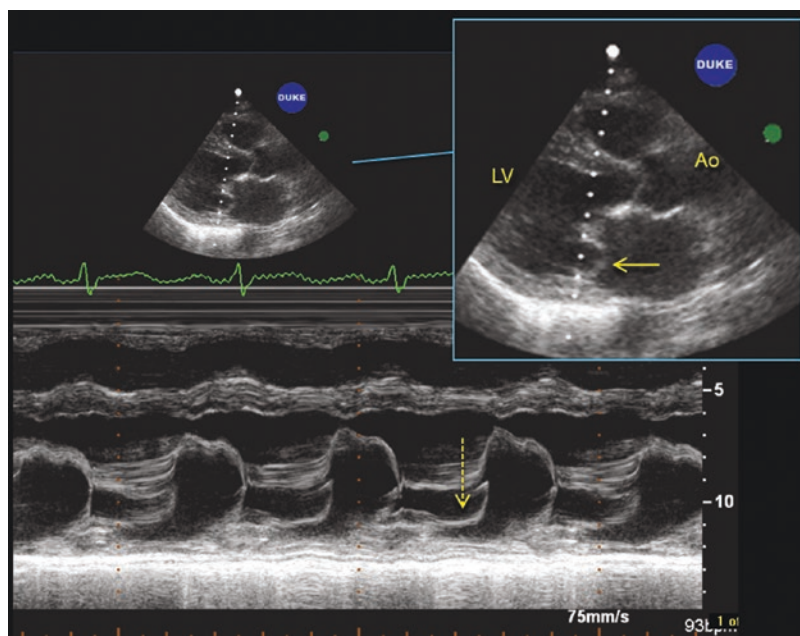


image set is seen in Fig. 10.109 where these distortions of the P₂–P₃ segments have resulted in failure to coapt between the A₁–P₁ segments, rendering the valve an unlikely candidate for repair.

Repair of the mitral valve was attempted, but failed, and the surgical procedure resulted in the placement of a bi-leaflet prosthetic valve seen in

Fig. 10.110. After weaning from cardiopulmonary bypass, the bi-leaflet prostheses is visualized by three-dimensional transesophageal echocardiography in Fig. 10.111. The two prosthetic leaflets are open in diastole (left panel) revealing the three diastolic flow orifices typical of these bileaflet valves. The leaflets are seen in the closed position in the panel on the right.

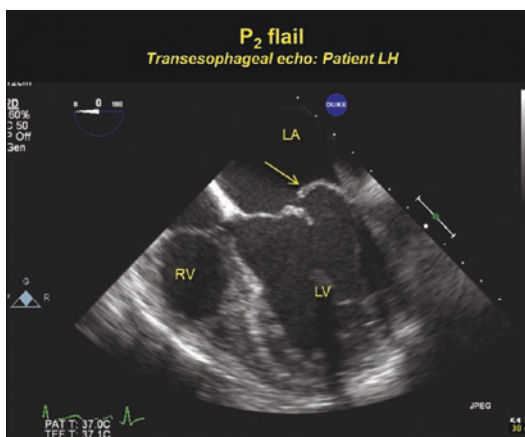


Fig. 10.107 The transesophageal echo showed flail at the tip of the P₂ segment from the patient seen in the previous figure

Typical Type II, A₂ Leaflet Prolapse

The anatomic features of prolapse in any mitral valve segment can be visualized by two- or three-dimensional echocardiography. Schematic demonstration of anterior leaflet prolapse of an A₂ segment is shown in Fig. 10.112. When prolapse of this segment is encountered the direction of the mitral regurgitant jet is markedly posterior (Fig. 10.113). In this figure, a massive A₂ prolapse is identified (left panel arrow). The color flow Doppler frame in the right panel (arrow) shows massive mitral regurgitation opposite the leaflet segment prolapse and directed posteriorly. Occasionally, callus-like patches may be seen

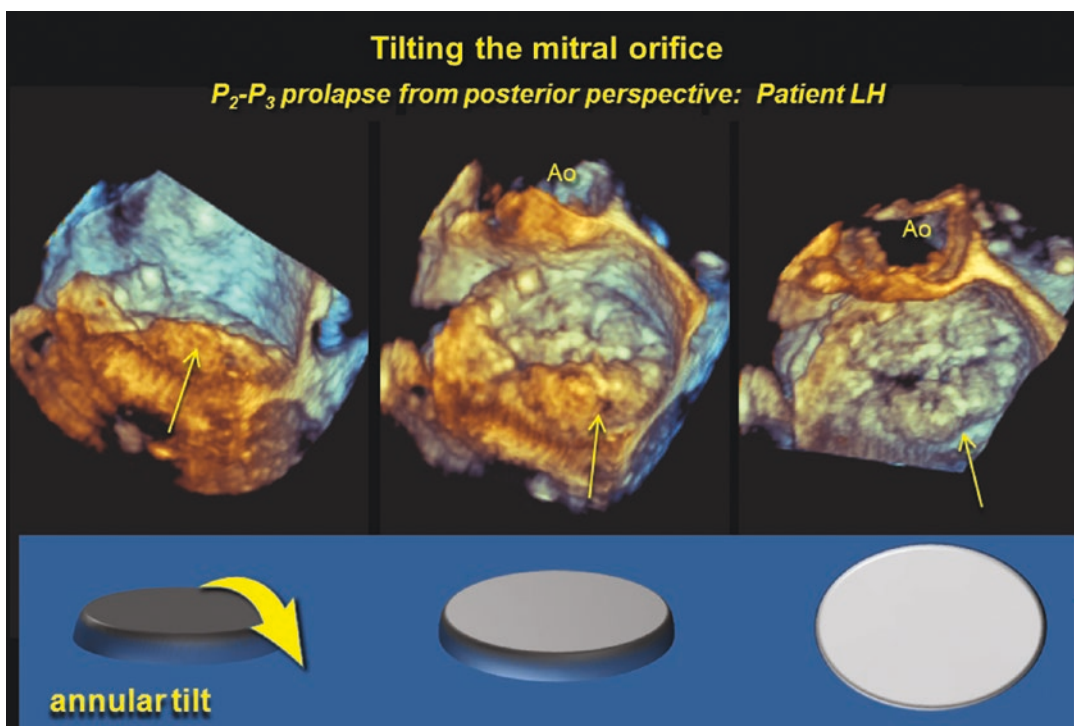


Fig. 10.108 A three-dimensional echocardiogram displayed in the surgeon's view also shows flail extending into the P₃ segment. In addition, there was no coaptation

between the P₁ and A₁ segments that confounded surgical repair. This is the same patient seen in the two previous figures

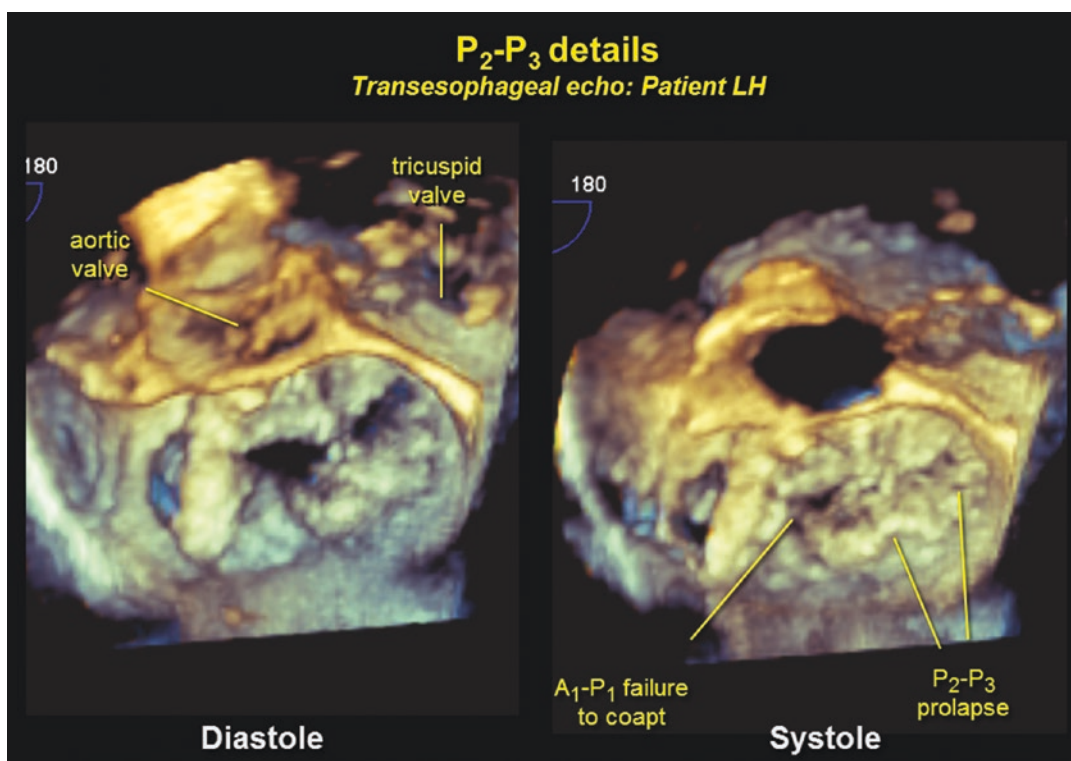


Fig. 10.109 Closer look at the surgeon's view in this patient showing the P₂ and P₃ flail with failure to coapt between the P₁ A₁ segments



Fig. 10.110 Repair was attempted by failed and the mitral valve was replaced using a bi-leaflet mechanical prosthesis

on the atrial walls at the impact site of mitral regurgitant jets and are known as McCallum's patches.

The three-dimensional echocardiogram of this patient is seen in Fig. 10.114 where the massively domed A₂ segment is revealed as it prolapses back into the mitral orifice in this surgical view. The annulus is again rotated side to side in this systolic still-frame to allow further examination. In real-time, an examiner would perform these rotations as mitral valve apparatus moves with the cardiac cycle to examine the mitral valve in all spatial conditions.

The surgical findings from a patient with a similar problem of A₂ prolapse is demonstrated Fig. 10.115. In this individual, the A₂ prolapse is

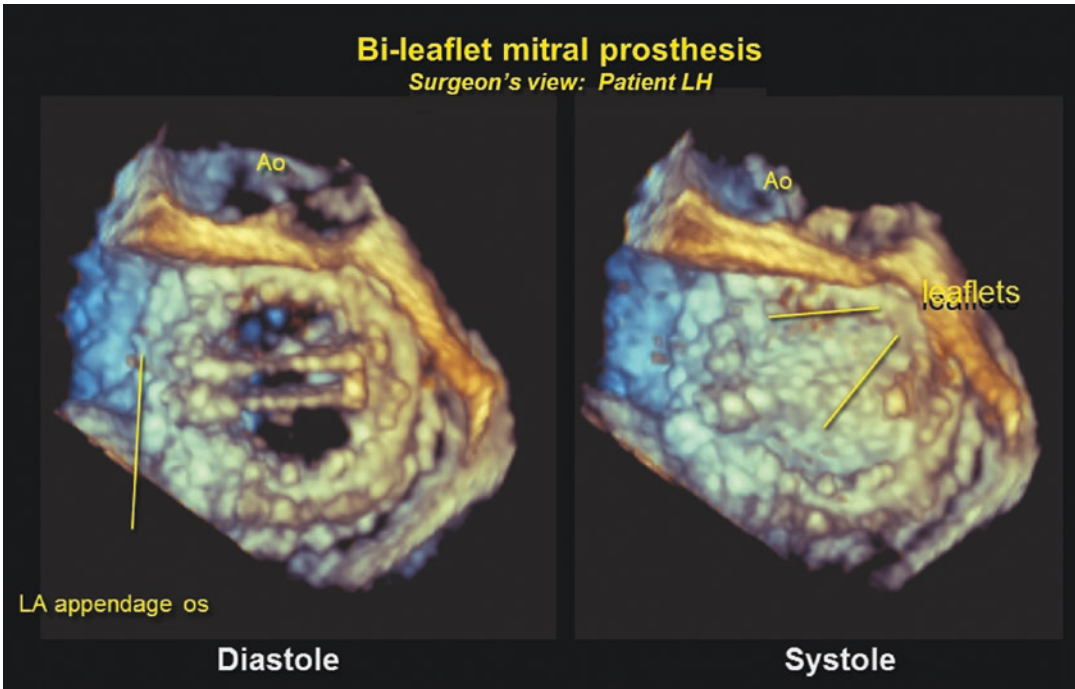


Fig. 10.111 Three-dimensional echo of the mechanical prosthesis seen in the previous figure

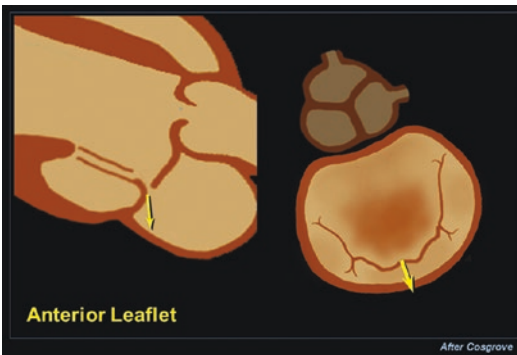


Fig. 10.112 Schematic representation of prolapse of the A₂ segment

not as severe as is seen in the patient in the previous Fig. 10.114 but, nevertheless, demonstrates the problem and appearance of this type of prolapse at surgery. This patient underwent successful mitral valve repair that included plastic procedures to the A₂ chordal segments and placement of a mitral valve ring.

Visualization of Other Mitral Procedures

Three-dimensional echocardiography can be used for visualization of a variety of prosthetic valves. A mitral bioprosthesis is seen from the left ventricular perspective (looking towards the mitral orifice and left ventricular outflow tract) in Fig. 10.116. The three supporting stents are readily identified, as are the closed valve leaflets in systole. The valve orifice is tilted anteriorly to offer slightly different perspective of the three-dimensional prosthetic valve.

Another surgical technique with growing use is the placement of a surgical stitch between the A₂ and P₂ segments. While this results in a small degree of obstruction at the level of the mitral orifice, there is usually plenty of room to accommodate such a stitch when prolapsing mitral leaflets are encountered. This is commonly called the Alfieri Stitch and can reduce the surgical pump times.

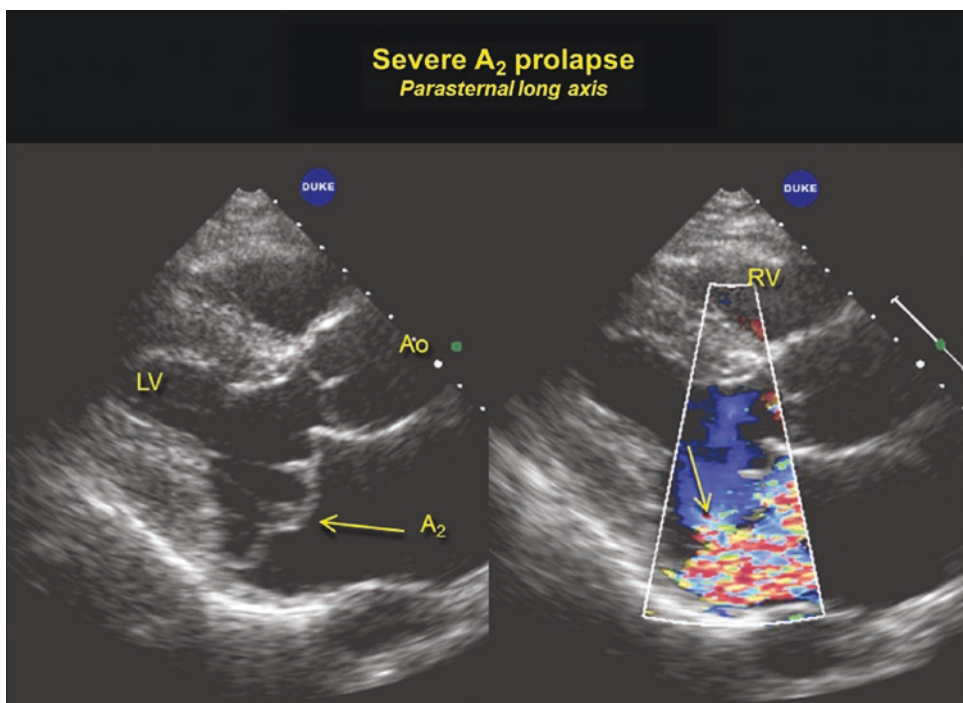


Fig. 10.113 Parasternal long axis of the mitral valve in a patient with huge A₂ segment prolapse (arrow left panel). The mitral regurgitation is directed posteriorly (arrow, right panel)

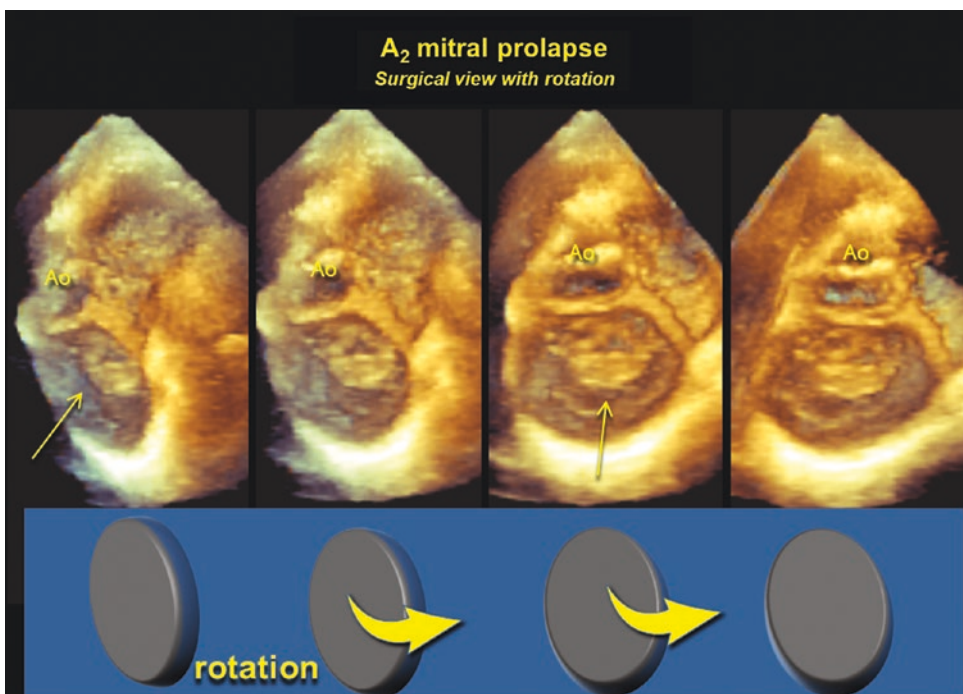


Fig. 10.114 Three-dimensional systolic still frame from the patient seen in the previous figure in the surgical view. There is huge doming of the A₂ segment (arrow)



Fig. 10.115 Surgical photograph of the mitral valve from a patient with similar A₂ prolapse

Such a stitch is shown in Fig. 10.117 where the two residual mitral orifices are readily demonstrated.

At the time of preparation of this chapter, there is also growing interest and experience in the catheterization-based insertion of mitral valve clips for the repair of A₂–P₂ mitral prolapse and its consequent regurgitation. Figure 10.118 shows the rotation of a mitral valve annulus when the such a clip is introduced from the left atrial side (via a catheter across the interatrial septum) and then through the mitral valve orifice. In this figure, the clip is in the open position. The mitral orifice is in the surgical view and is tilted from a slightly posterior perspective directly into the mitral orifice in the right panel.

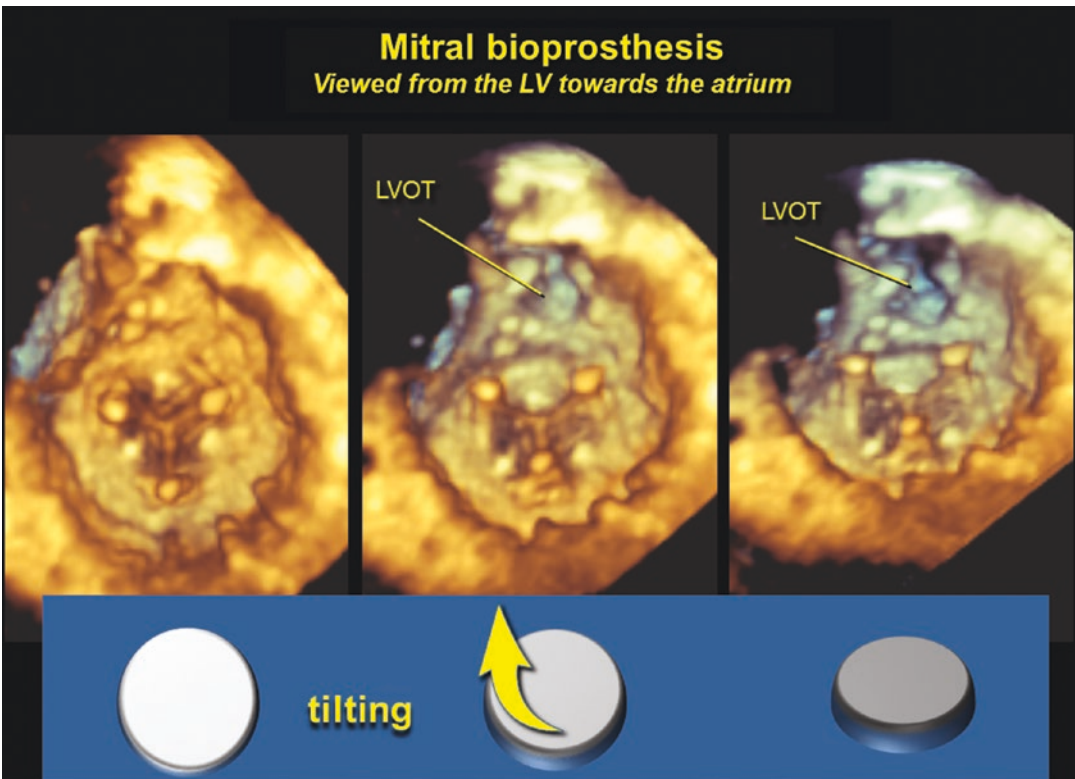


Fig. 10.116 Porcine bioprosthesis depicted in place from the left ventricular perspective, up into the mitral orifice. The stents of the prosthesis are easily recognized

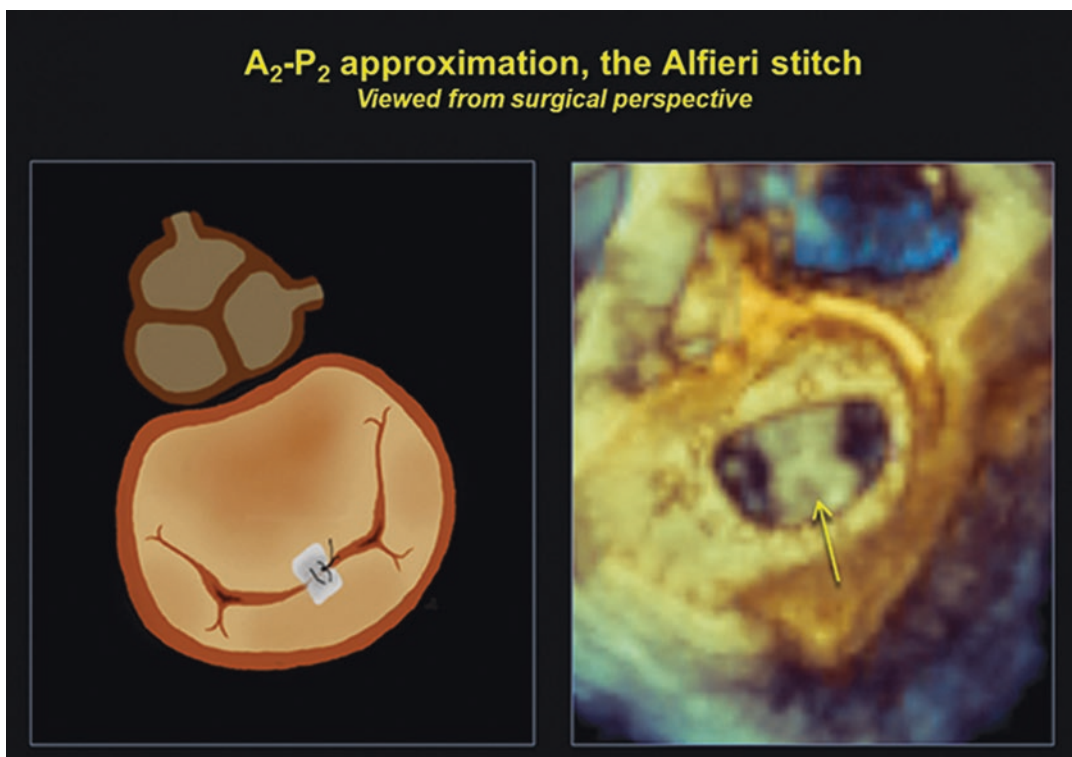


Fig. 10.117 Sometimes it is beneficial for the surgeon to suture the A₂ and P₂ segments, the Alfieri stitch. The characteristic post stitch three-dimensional image is seen on the right with the joined in the center, creating two

diastolic orifices. A mitral prosthetic ring is also in place. The arrow points to the surgical approximation (right panel)

As the clip is introduced in the heart, the clip is in the closed position as it is advanced towards the mitral valve orifice and the prolapsing leaflet segments (Fig. 10.119, left panel) and then opened as it approaches the actual orifice (Fig. 10.119, middle panel). The device is then progressively inserted through the mitral valve orifice and then rotated so that the open clip can engage both the A₂ and P₂ segments (Fig. 10.119, right panel). As the open clip is then pulled backwards, it can then grasp the A₂ and P₂ segments as it is then closed. The catheter is then disengaged from the stable clip, leaving the mitral orifice with a double-opening, markedly resembling the Alfieri stitch (A₂-P₂ surgical approximation).

Mitral Regurgitation and Congestive Heart Failure

As any examiner with echocardiography knows, mitral regurgitation is frequently associated with congestive heart failure. This is usually Type I mitral valve regurgitation that results from dilatation of the mitral valve annulus. Figure 10.120 shows parasternal short axis of mitral valve in the closed position in systole, extending from commissure to commissure. When the mitral valve coaptation points are examined in this view with color flow Doppler, one can appreciate mitral regurgitation along the entire coaptation line (right panel Fig. 10.120). If surgical intervention is neces-

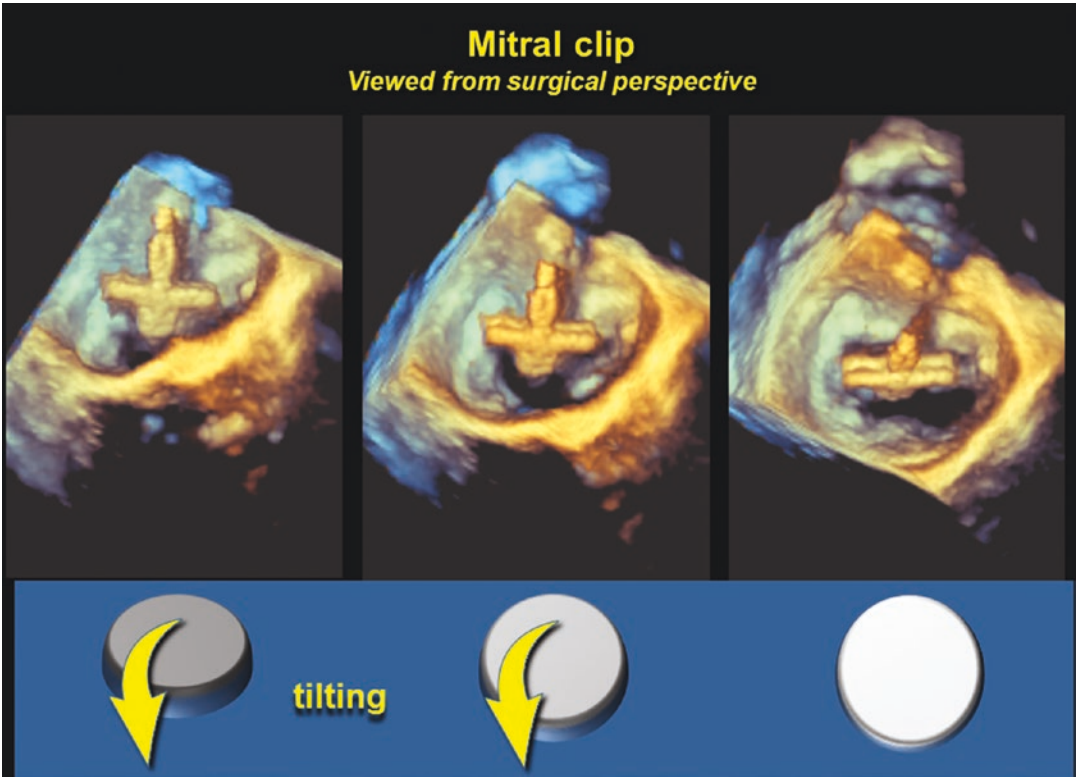


Fig. 10.118 A catheter based mitral clip is seen above the mitral orifice in a three-dimensional still frame of an open mitral valve in diastole. For details, see text

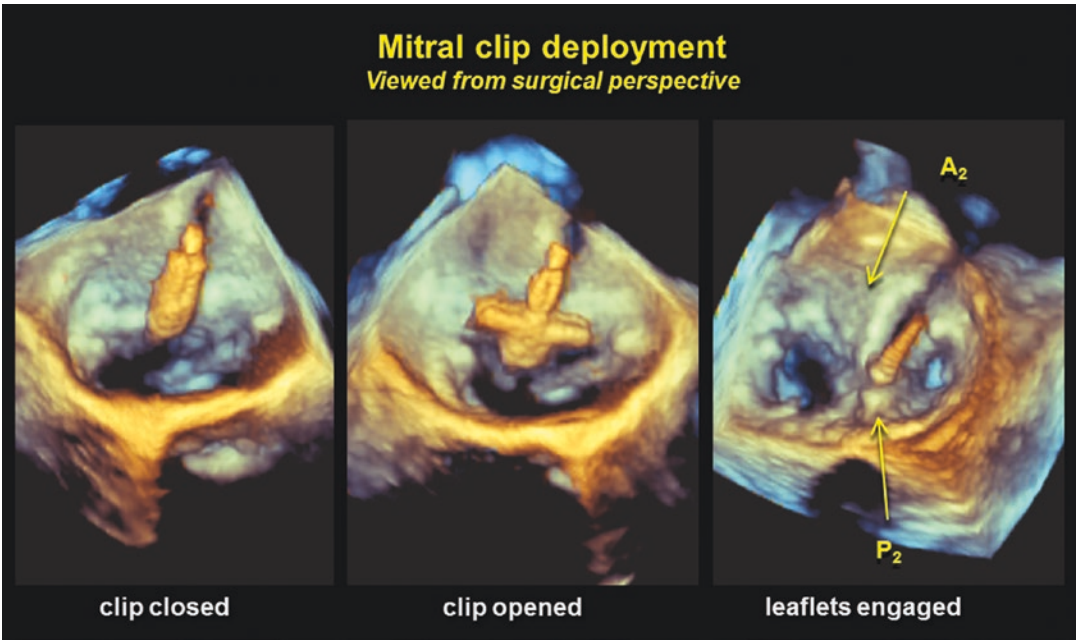


Fig. 10.119 The clip is closed (left panel), then opened (center panel) then is pushed through the mitral orifice to engage the A₂ and P₂ segments. For details, see text

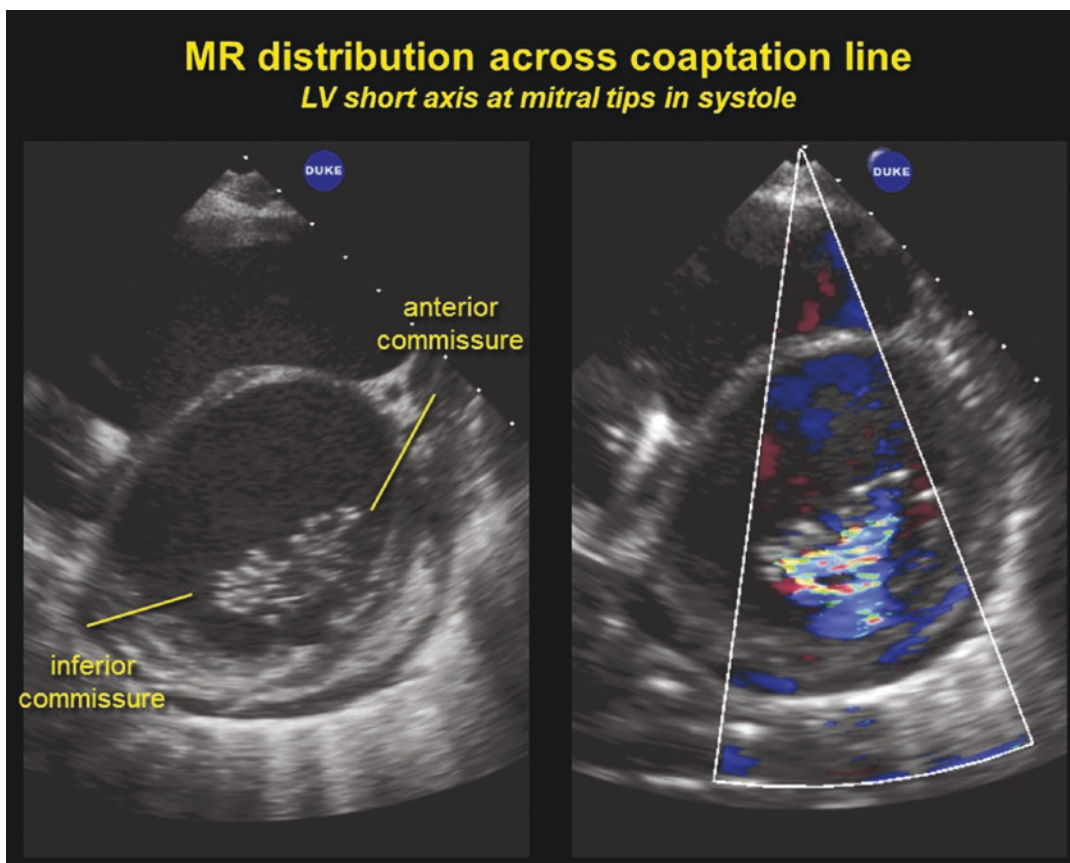


Fig. 10.120 Short axis parasternal view of a closed mitral orifice in a patient with a dilated cardiomyopathy and mitral regurgitation. Using color flow, the mitral regurgitation can be seen along the entire mitral coaptation line (right panel)

sary in this disorder, a mitral ring is usually put in place to bring the leaflet tips downwards into the left ventricle to allow the leaflets to coapt properly.

The three dimensional echocardiogram shown in Fig. 10.121 shows the left ventricle in two individuals from the left ventricular frontal long axis three-dimensional view. The anterior mitral leaflet is seen *enface* and compares the orientation of the papillary muscles in each of these patients. The left panel shows the orientation of the papillary muscles in a patient with mild mitral regurgitation. The papillary muscles are aligned vertically and are within the

mitral annulus. Compare the orientation of these papillary muscles to those seen in the right panel from a patient with a dilated cardiomyopathy and more severe mitral regurgitation. In the right panel, the papillary muscles are seen to be laterally displaced and are pointed more medially. Also compare these images to that seen in Fig. 10.18 taken from a normal individual in a similar frontal long axis view. Thus, mitral valve coaptation is not only a leaflet phenomenon, but is dependent upon the orientation of supporting structures such as the papillary muscles and their relationship to the entire mitral valve apparatus.

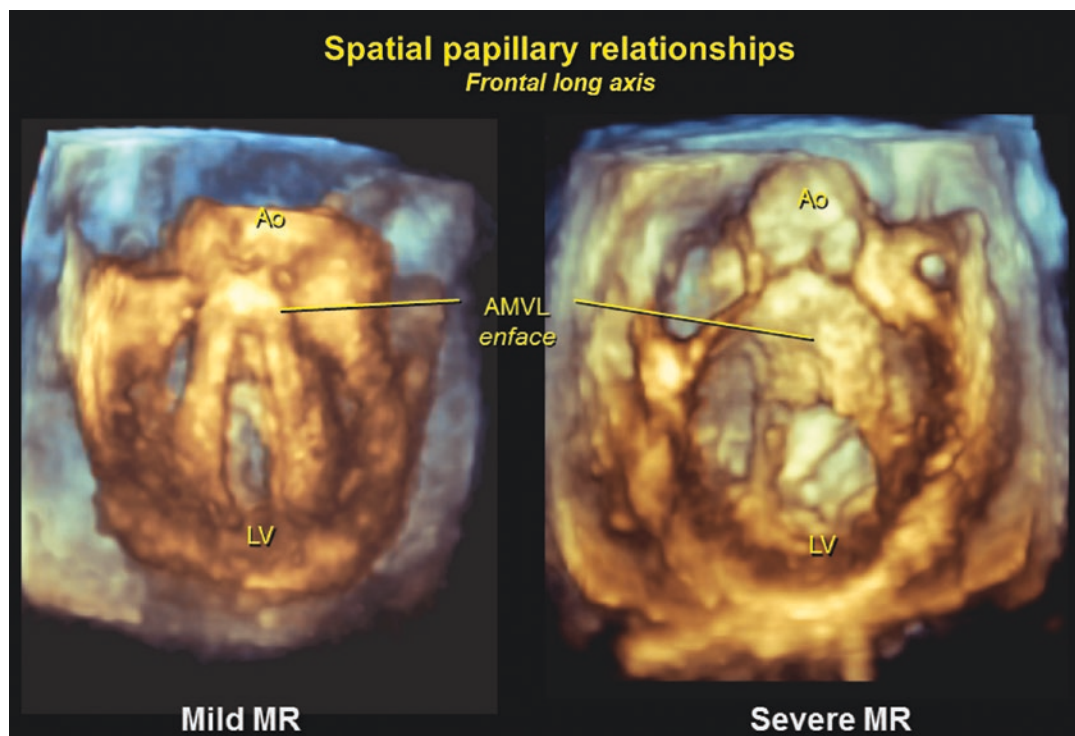


Fig. 10.121 Frontal long axes from base (towards figure top) down towards apex (bottom of figure) of the left ventricles of two patient. Note the orientation of the papillary muscles vertically in the left panel and compare this to the

positions of the papillaries in the image in the right panel from a patient with dilated cardiomyopathy. For details, see text

Mitral Annular Calcification/Fibrosis

Calcification and/or fibrosis of the mitral valve annulus is a common finding in elderly patients. Such a finding is manifest by two-dimensional echocardiography as a bright spot in the posterior mitral valve annulus (MAC = mitral annular calcification). Because of the marked reflectivity of significant calcification and/or fibrosis, sound waves do not usually penetrate such a structure and a shadow can be seen posterior to the abnormal annulus. Such mitral valve annular calcification is usually quite bright and the shadow is the hallmark that this is a calcific structure. Note that echocardiography is not a technique that can differentiate tissues. Calcification can only be inferred by shadowing seen from structures in the far field. Most echocardiographers mistakenly believe that bright targets equal calcifica-

tion, which is not true. It is best to use the joint term “calcification and/or fibrosis” to not fall into the mistaken trap that brightness equals fibrosis.

Such mitral valve annular calcification can be much larger, particularly in patients with chronic renal failure. Mitral annular calcification is also seen in patients with hypertrophic cardiomyopathy. A chest wall echocardiogram from a patient with renal failure is seen in Fig. 10.122 in the parasternal long axis view. The images are of high quality and the bright target of the annular calcification (MAC) reveals an ultrasonic shadow extending posteriorly from the MAC.

A parasternal long axis image from an elderly patient demonstrates a large annular calcification from the chest wall parasternal long axis view in the left panel of Fig. 10.123. The patient also had

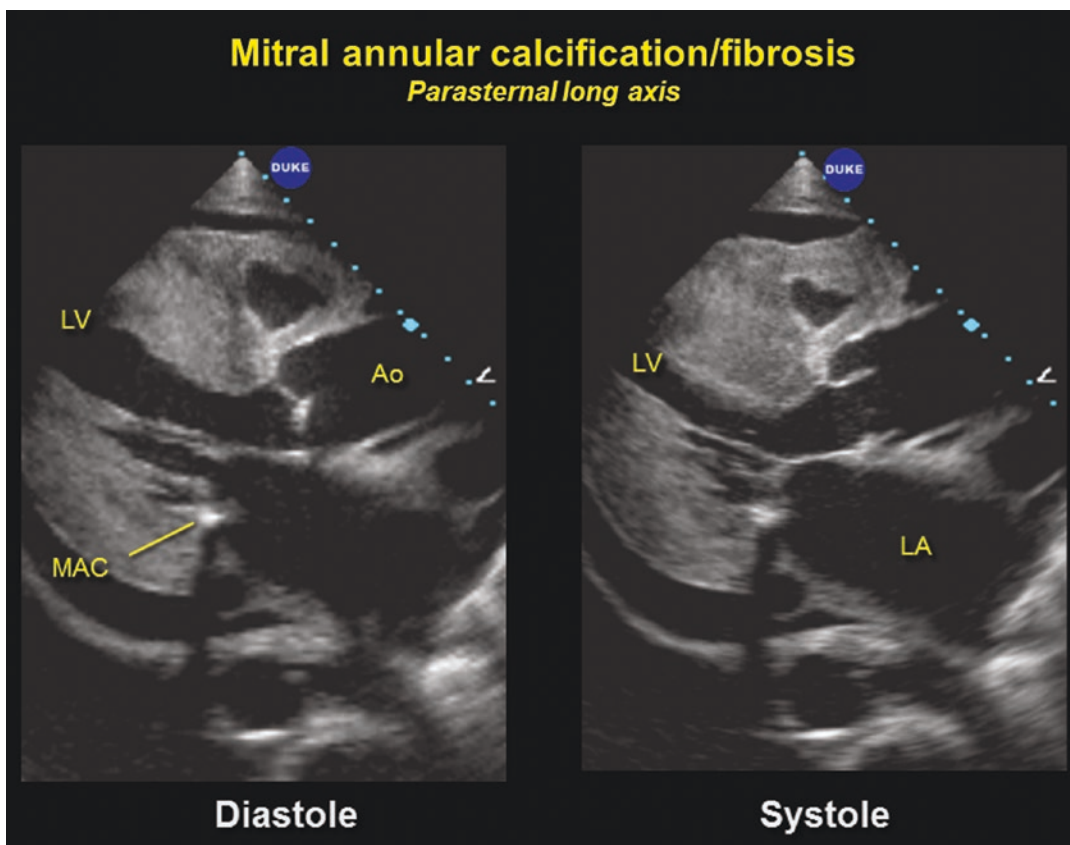


Fig. 10.122 Parasternal long axis from a patient with renal failure and mitral annular calcification (arrow). Note the shadowing from the MAC. Echocardiography is not a

tissue characterization technique. If there is no shadowing, calcification cannot be inferred

chronic obstructive lung disease and the quality of the chest wall image is suboptimal. The transesophageal echocardiogram of this patient is seen in the right hand panel where the annular thickening can be easily differentiated from surrounding mitral structures. From the chest wall, no shadowing can be seen, thus calcification cannot be inferred. By TEE, shadowing is seen.

The three-dimensional echocardiogram from the patient seen in the previous figure is demonstrated in Fig. 10.124. The massive annular fibrosis/calcification is seen just posterior to the mitral orifice in the open position in diastole and the closed position in systole. It is necessary to use two-dimensional echocardiography to differentiate this three-dimensional appearance from that of mitral valve prolapse.

Infective Vegetative Endocarditis

The appearance of mitral valve vegetations is dramatic when using any echocardiographic technique. These mass lesions are seen to oscillate rather rapidly and are usually attached to the flow surfaces of cardiac valvular structures. The M-mode echocardiogram in Fig. 10.125 shows the typical rapidly oscillating masses encountered in endocarditis and is seen just anterior to the mitral valve apparatus (arrow). While this oscillation resulted from an aortic valve vegetation that prolapsed into the left ventricular outflow tract during diastole, such oscillations are typical of vegetations from any leaflet. This given lesion resulted in massive aortic regurgitation and preclosure of the mitral

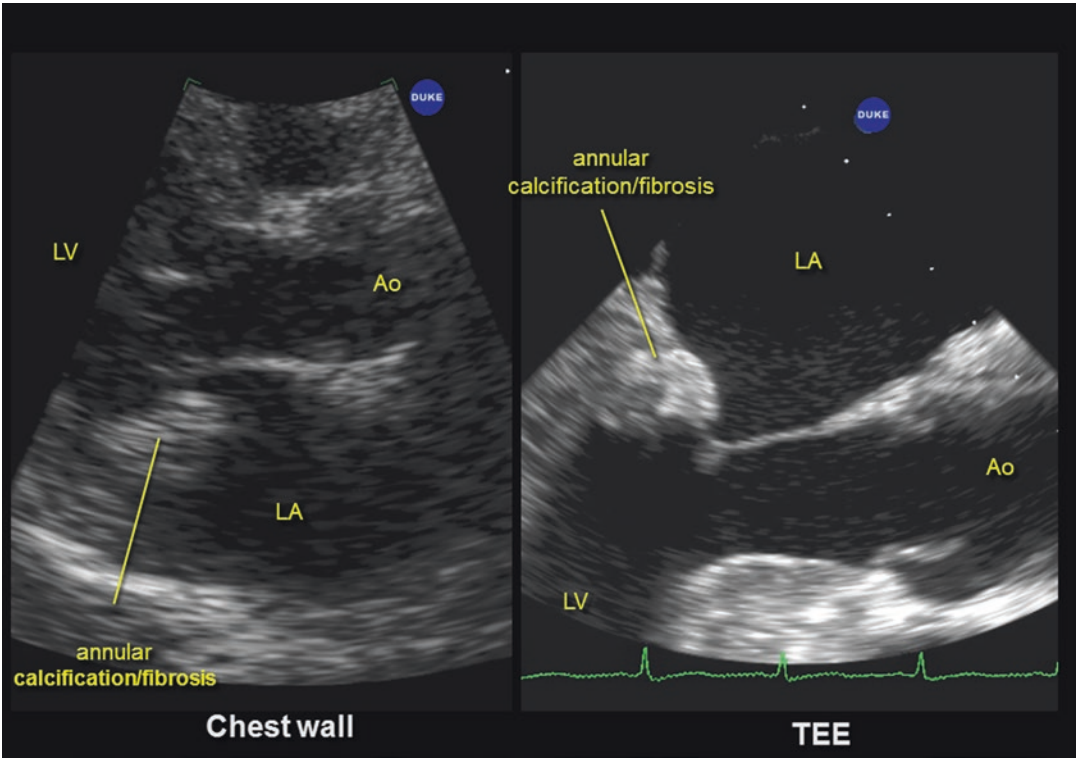


Fig. 10.123 Chest wall and transesophageal echo still frames from a patient with mitral valve fibrosis/calcification. Since there no shadowing, calcification cannot be inferred

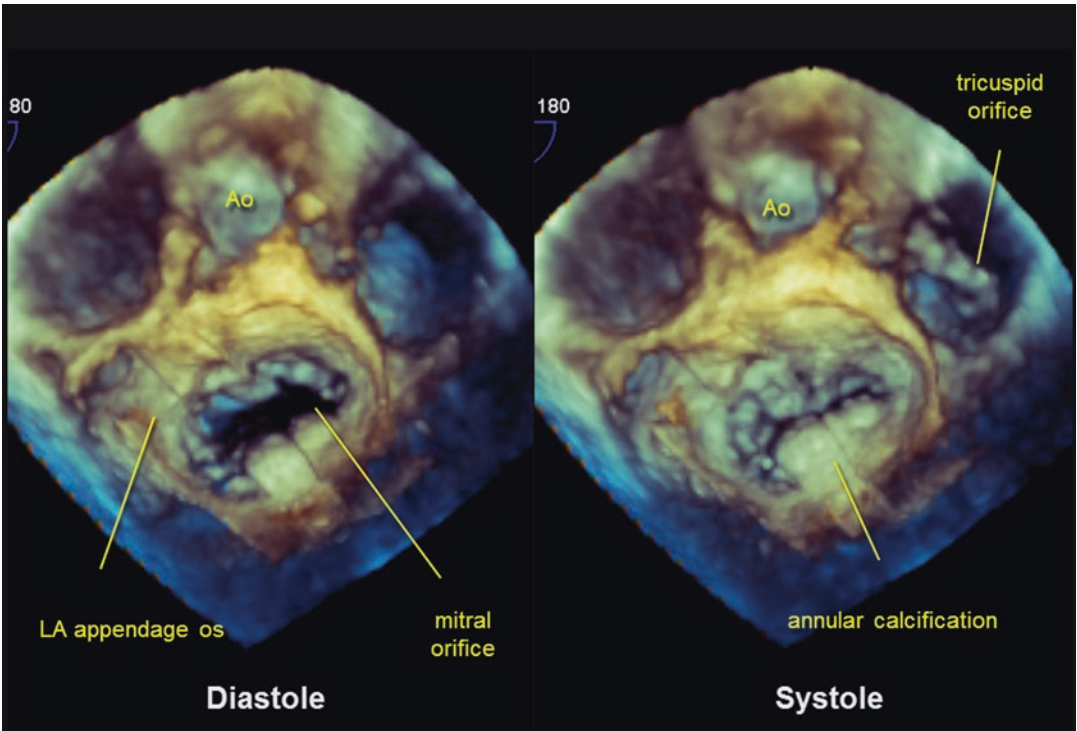


Fig. 10.124 Three-dimensional image of the mitral orifice in the surgeons view in a patients with mitral annular calci-fication. Without two-dimensional echo, it is difficult to differentiate mitral annular calcification from prolapse by 3D

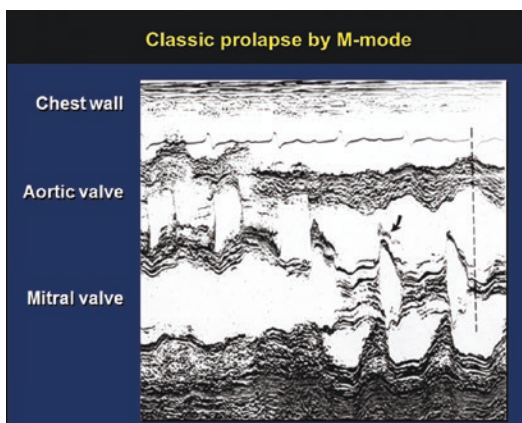


Fig. 10.125 M-mode echocardiogram from a patient with vegetative endocarditis. The rapidly oscillating mass lesion (arrow) is seen just anterior to the mitral valve. This vegetation was on the aortic valve and resulted in severe aortic regurgitation, causing premature closure of the mitral apparatus (dashed line) because of the high end-diastolic pressures

valve apparatus (vertical line) prior to the QRS complex of the EKG. Such mitral preclosure is a generally ominous sign in aortic regurgitation as it results from the high late diastolic pressures that prematurely close the mitral valve in late diastole. The role of echocardiography and vegetative endocarditis is discussed fully elsewhere in this volume.

These oscillating masses can be viewed on the mitral apparatus by two-dimensional echocardiography as shown in Fig. 10.126. Here, a single oscillating mass can be appreciated by two-dimensional echocardiography only in the moving picture, not the still picture as depicted. It does, however, result in a posteriorly directed mitral regurgitant jet that is seen in the right hand panel. This lesion was also attendant to a small number of ruptured chordae tendineae causing mild mitral prolapse of the A₂ segment.

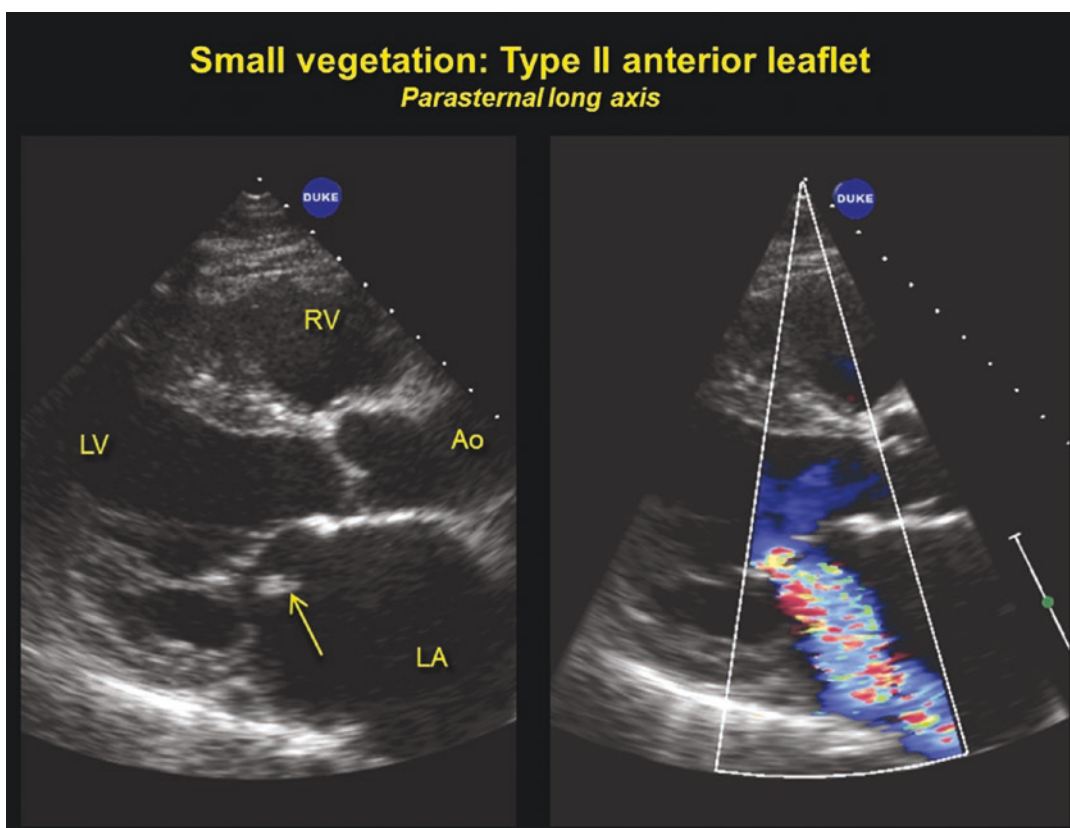


Fig. 10.126 Parasternal long axis from a patient with a small mitral vegetation (arrow). This resulted in the mitral insufficiency seen in the color flow in the right panel

A two-dimensional echocardiogram from another patient with a small oscillating vegetative mass is seen in Fig. 10.127. This lesion was attendant to the P₂ segment and is denoted by the arrow. Immediately after initial detection and blood culture, but in the absence of any untoward hemodynamic complications, the patient suffered a stroke and the follow up echocardiogram showed disappearance of this vegetative mass (right hand panel).

These lesions may be attendant with all degrees of mitral regurgitation. Figure 10.128 shows mitral regurgitation using three-dimensional echocardiography and color flow Doppler. There is a perforation of the A₂ segment at its midpoint. The rotation is turned side to side to show the extent of this small perforation. In this patient, the area of perforation was surgically

debrided and the anterior mitral valve leaflet was patched.

Vegetations come in all varieties and locations along the lines of mitral valvular flow (usually on the atrial side). Occasionally, there may be huge vegetative masses attendant to vegetative endocarditis. Figure 10.129 shows a massive vegetation invading the anterior mitral valve leaflet and extending into the left ventricular outflow tract both in diastole and systole (dashed arrow) in a patient with chronic renal failure, diabetes and peripheral vascular disease. Another large mass can be seen at the tip of the anterior mitral valve leaflet and extends into the ventricle in diastole and then back into the atrium in systole (solid arrow).

Of interest, if this patient's echocardiogram 4 years prior to the onset of the episode of endo-

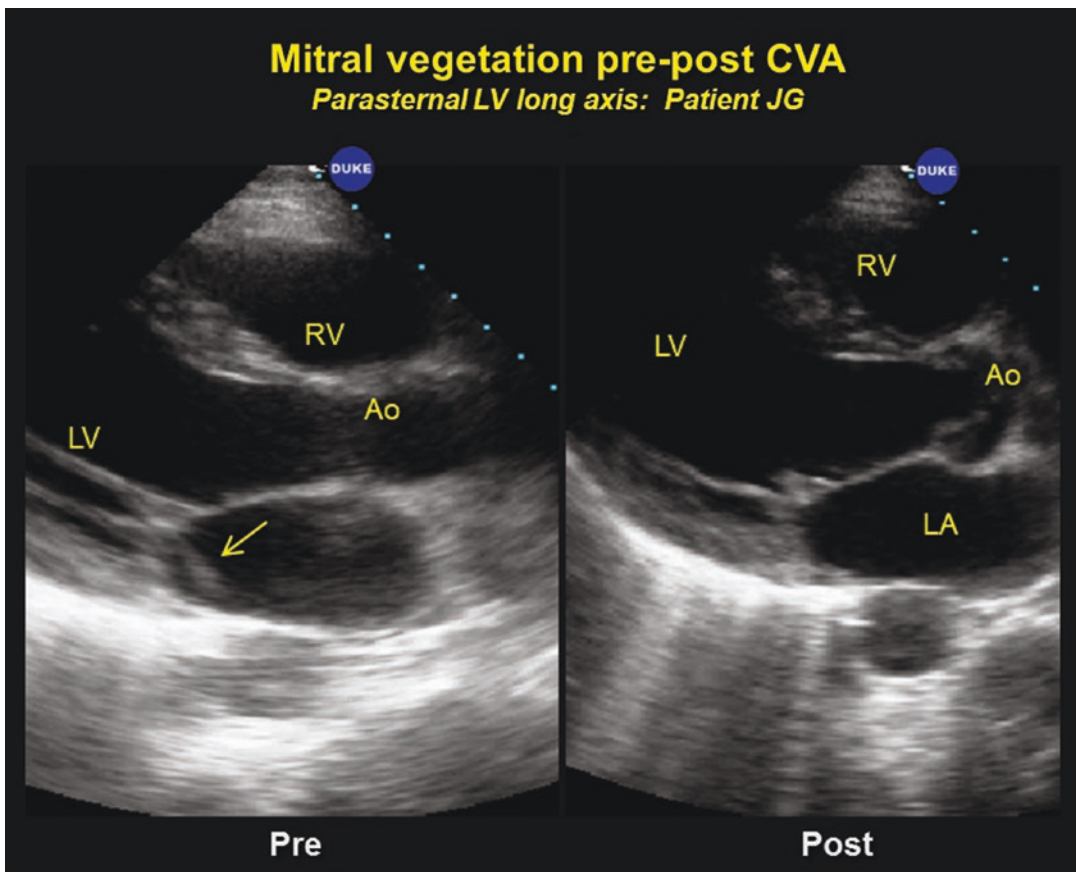


Fig. 10.127 Another small vegetation on the mitral apparatus is seen on the left panel (arrow). After blood cultures the patient sustained a stroke and the vegetation was no longer seen

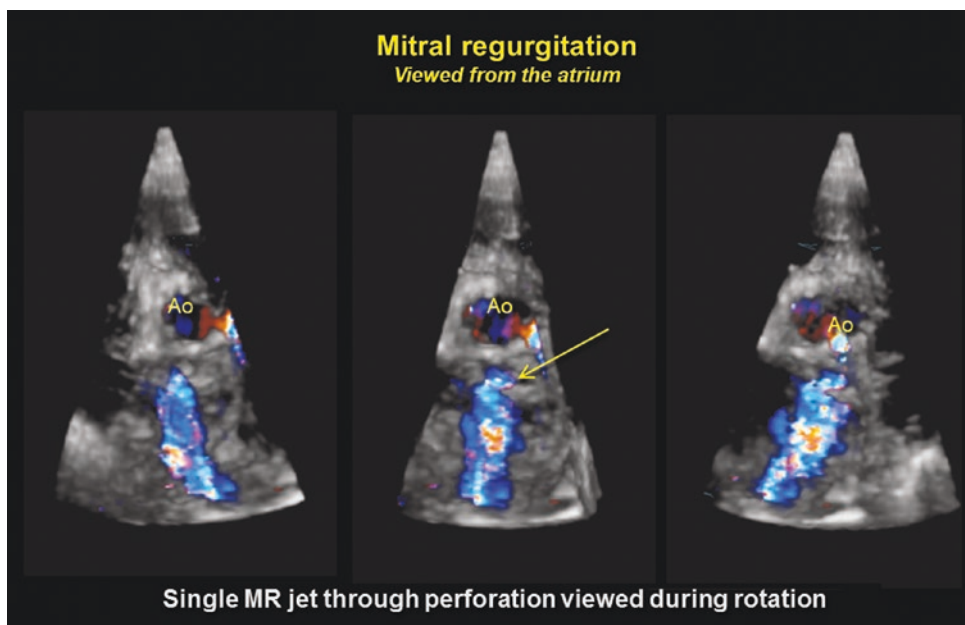


Fig. 10.128 Mitral regurgitation seen in the surgeon's view from the chest wall in a three dimensional echo. The regurgitation originates through a small perforation in the mid portion of the anterior mitral leaflet (arrow)

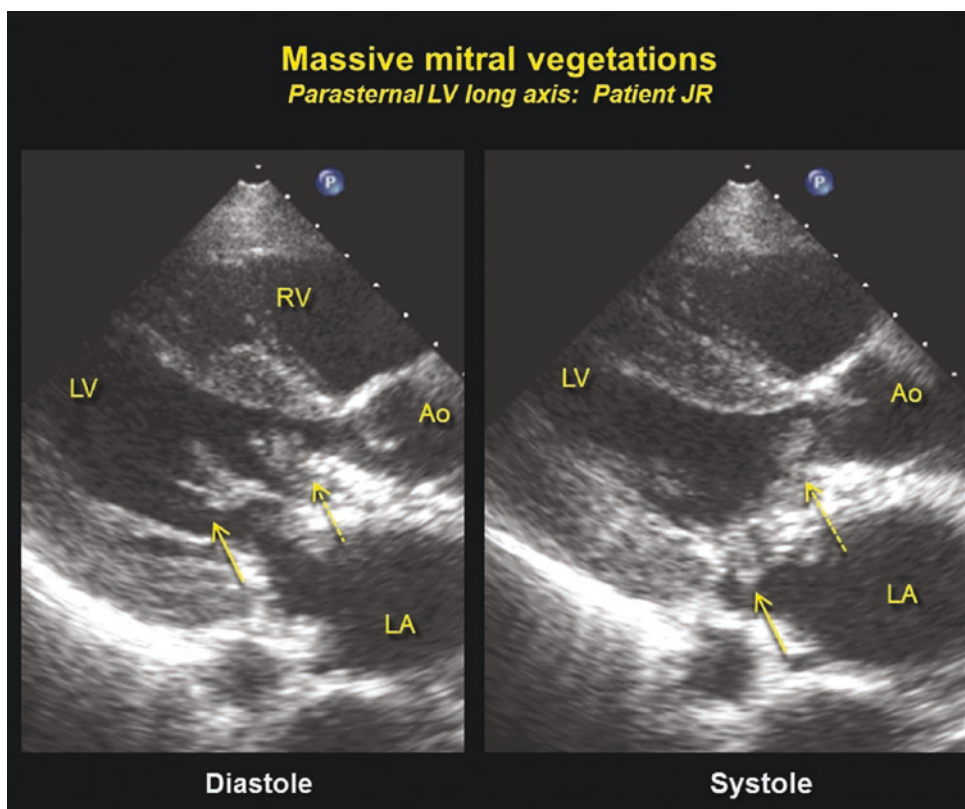


Fig. 10.129 Large vegetative masses invading the anterior mitral leaflet. Portions of the mass partially obstruct the LV outflow tract in systole (right panel) while another part prolapses into the left atrium (arrow)

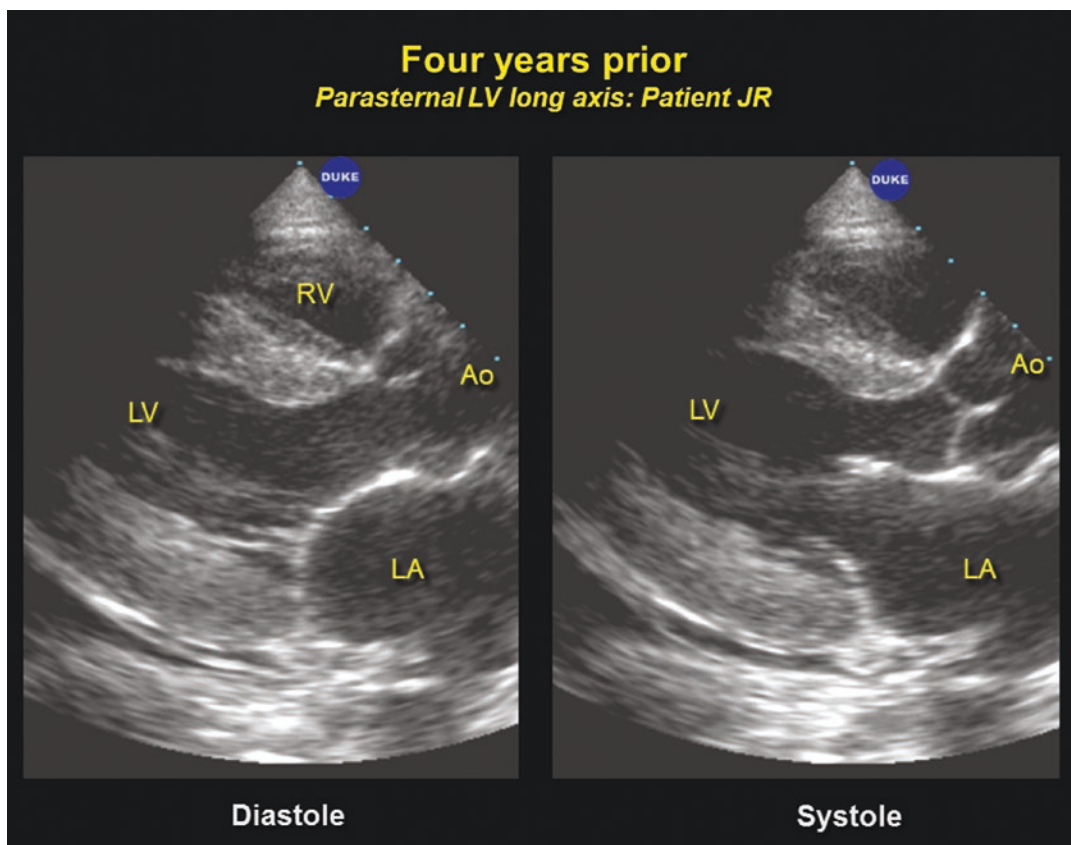


Fig. 10.130 Echocardiogram performed 4 years earlier on the patient seen in Fig. 10.121. No vegetative masses were seen then

carditis showed no evidence of infection and was performed during another episode of infection that did not result in endocarditis. While left ventricular hypertrophy and mild pericardial effusion is identified, no vegetative masses are seen (Fig. 10.130). This vegetation seen 4 years later in Fig. 10.129 was extensive and its invasion of the mitral leaflet dramatic. The overall medical condition of the patient precluded attempts at surgical correction and the patient later died of overwhelming sepsis.

When surgical intervention is entertained, transesophageal and three-dimensional echocardiography are indicated. Figure 10.131 shows a transesophageal echocardiogram from a patient with a large vegetative mass along the posterior mitral valve leaflet. The three-dimensional echocardiogram conducted during mitral valve repair of this same patient is seen with this large mass

located primarily on the P₂ segment (Fig. 10.132). The mitral annulus is again rotated from side to side and then tilted. Visualizing the full extent of the mass with three-dimensional echocardiography surgical repair can be readily facilitated and more and more three-dimensional studies are being conducted for decision making concerning mitral valve repair.

Left Atrial Myxoma

The most dramatic entity seen by echocardiography is the presence of a left atrial myxoma. Here, this benign tumor of the left atrium is seen to move through the mitral valve orifice in diastole (Fig. 10.133) with the cardiac cycle. This patient was a 55 year old female suffering from progressive shortness of breath. Left atrial myxomata are

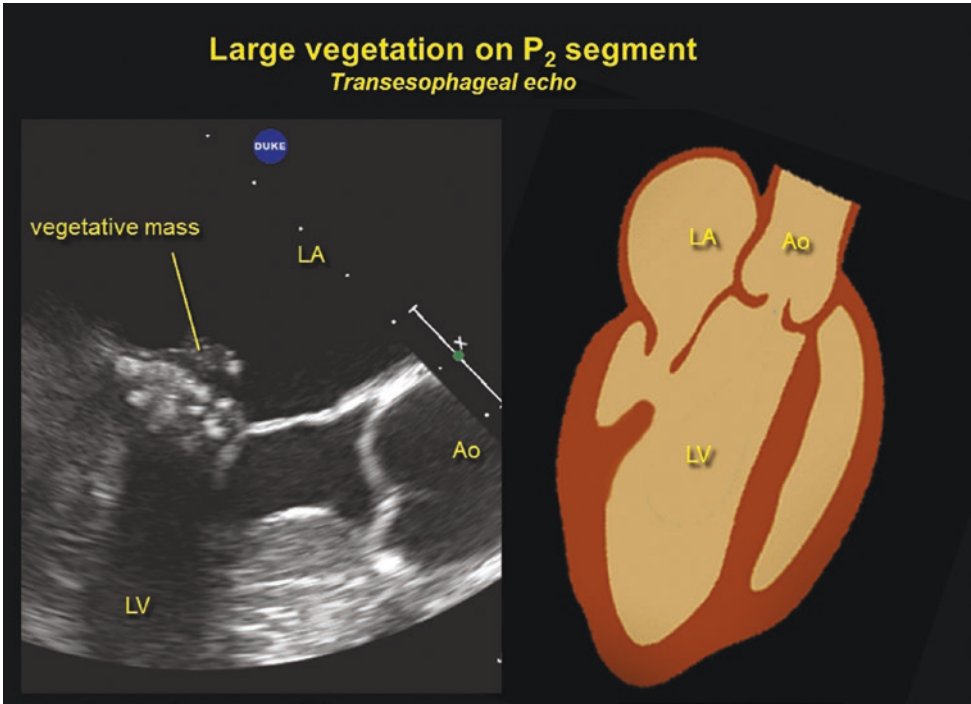


Fig. 10.131 Transesophageal echo with a cluster of vegetations seen along the P₂ segment in a patient with endocarditis

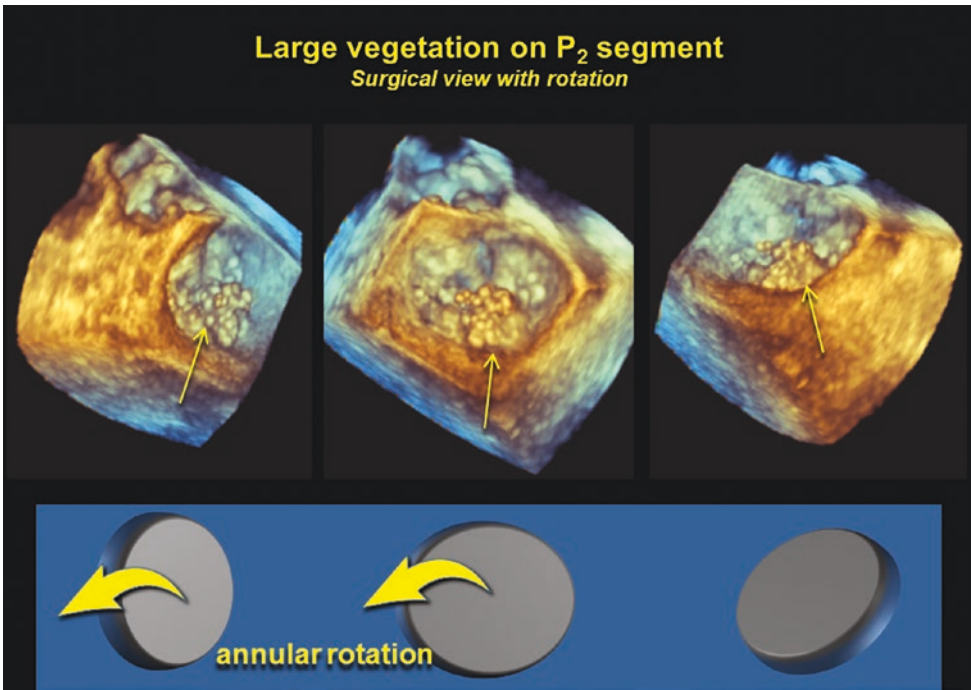


Fig. 10.132 Three-dimensional echo in the surgical view showing the sessile cluster of vegetations residing over the P₂ segment

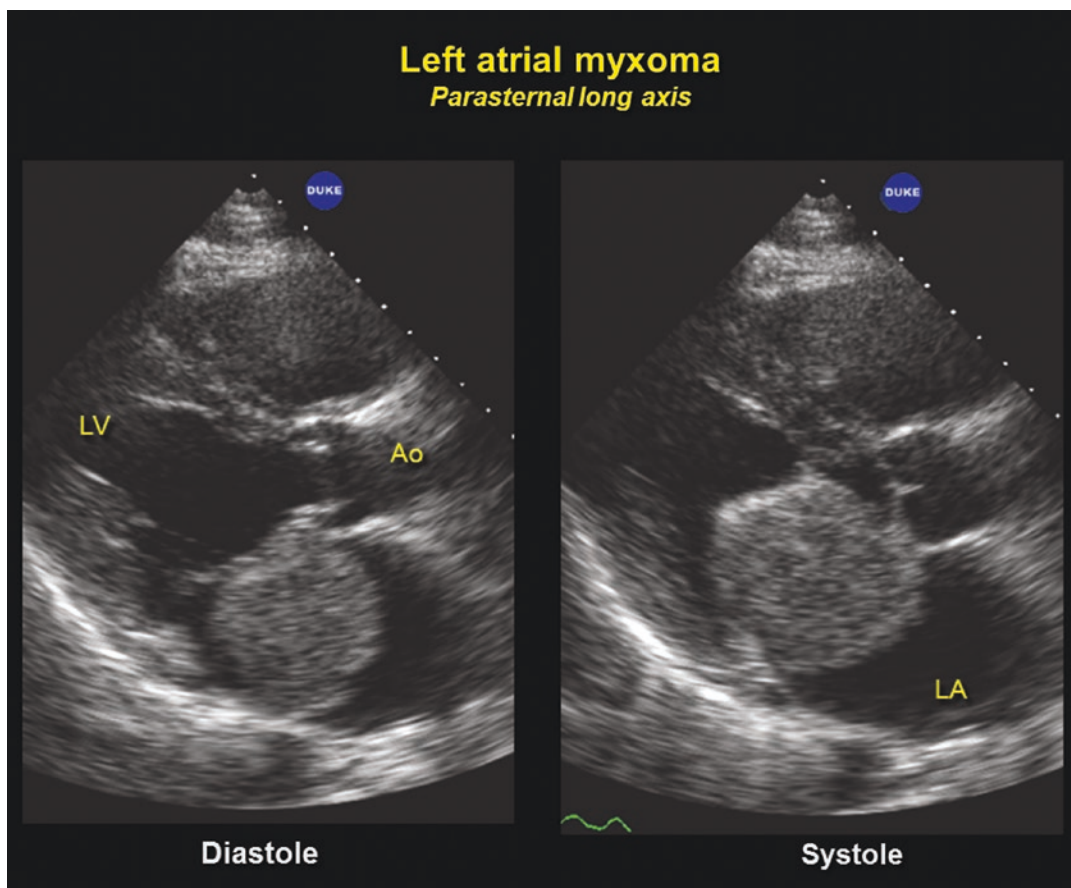


Fig. 10.133 Typical parasternal long axis of a left atrial myxoma, prolapsing into the mitral orifice in diastole

found in predominantly female patients over the age of 50.

Such tumors are not, however, restricted to older female patients. The parasternal echocardiogram from another patient with a massive left atrial myxoma is seen in Fig. 10.134 and is from a 17 year old male, also suffering from progressive shortness of breath. The two-dimensional echocardiogram in this picture shows the mitral valve in the open position and the massive tumor prolapsing towards the left ventricle in diastole. The M-mode echocardiogram on the right shows the mitral valve to open in early diastole, rapidly followed by the tumor an instant later (arrow). This movement has been well-correlated with the “tumor-plop” heard on auscultation in patients with this disorder. Figure 10.135 shows this large

tumor in the left atrium in systole (Panel A) and then progressively moving through the mitral valve annulus in diastole (through Panel D). Such movements are incredibly dramatic and this series of still frames is nowhere near as impressive as viewing the tumor movement in real-time. The diastolic movements depicted, however, readily demonstrate the physiologic problem encountered in these patients with occlusion of the mitral valve orifice and symptoms of shortness of breath. Note that this tumor is not homogeneous. Panel A shows an area of necrosis within the tumor.

While a large myxoma is responsible for multiple color artifacts seen when using color flow imaging, the mitral valve should be carefully examined for the presence of mitral regurgitation

Fig. 10.134 Parasternal long axis of a myxoma in a young male. The M-mode echo shows movement of the tumor mass into the mitral inflow just after mitral valve opening (arrow)

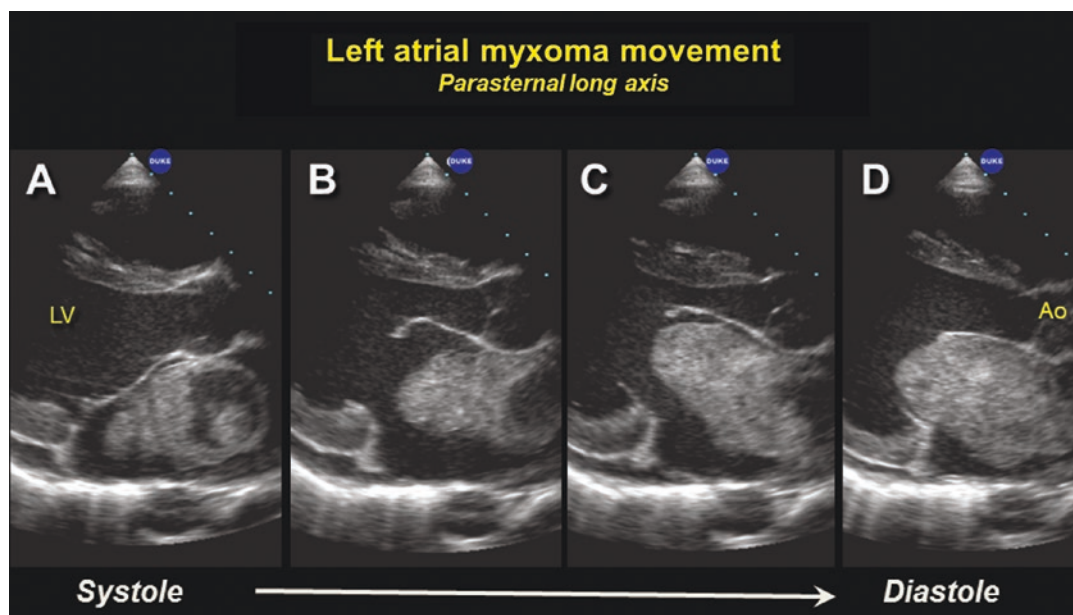
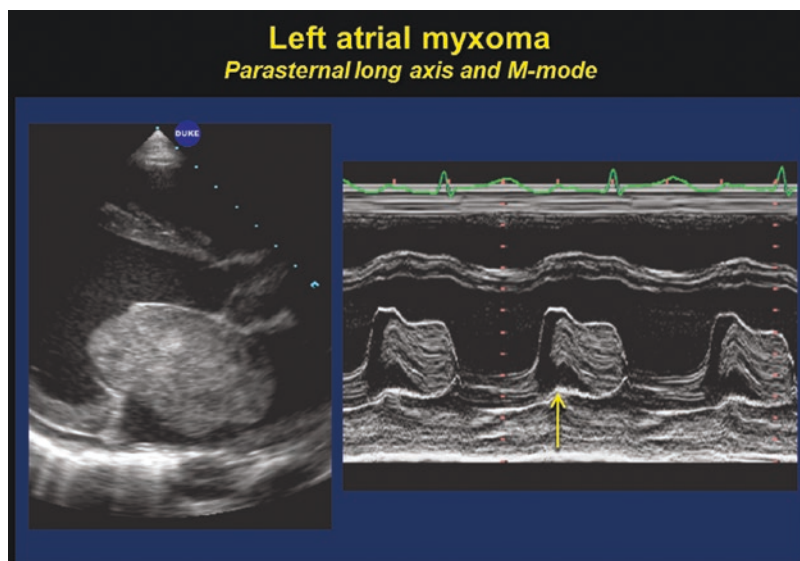


Fig. 10.135 Serial diastolic frames showing prolapse of this massive tumor into the mitral orifice

(right hand panel, Fig. 10.136). This patient's massive mitral regurgitation was caused by distortion of the mitral valve apparatus due to the tumor and completely disappeared following surgical resection. In fact, attendant mitral regurgitation in patients with atrial myxoma rarely need surgical repair as the regurgitation usually disappears with tumor removal.

An examiner using echocardiography should not be distracted by the appearance of the tumor itself. One of the most important things that echocardiography can contribute is to determine the location of attachment of these large tumors. It is now well accepted that the point of attachment must be completely surgically excised to eliminate recurrence. Figure 10.137

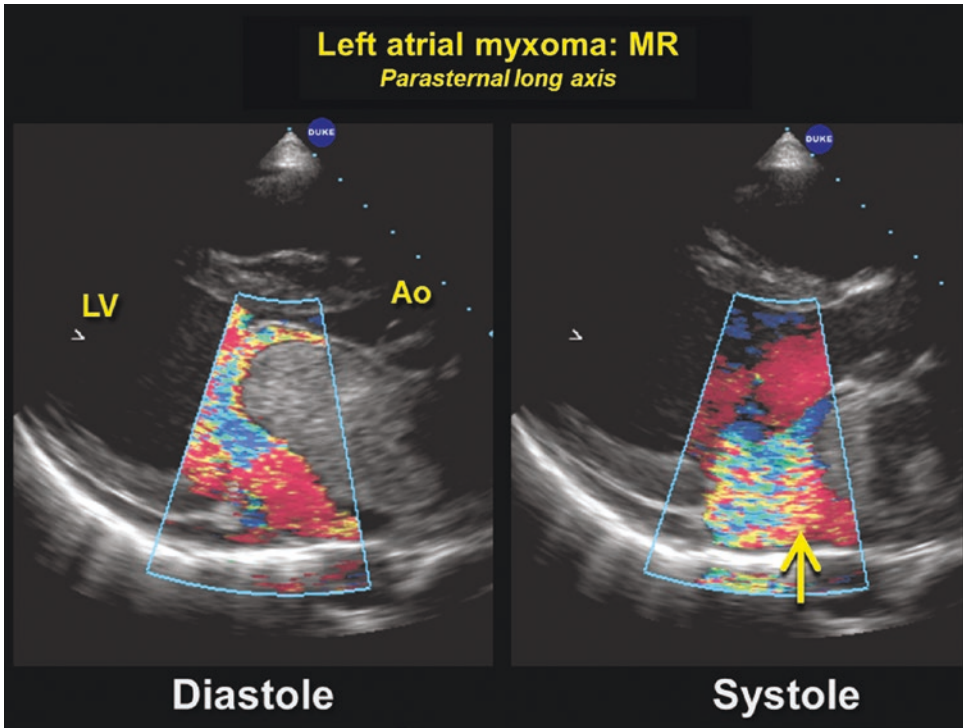


Fig. 10.136 Mitral regurgitation (right panel, arrow) often results from left atrial myxoma, but frequently resolves after surgical removal

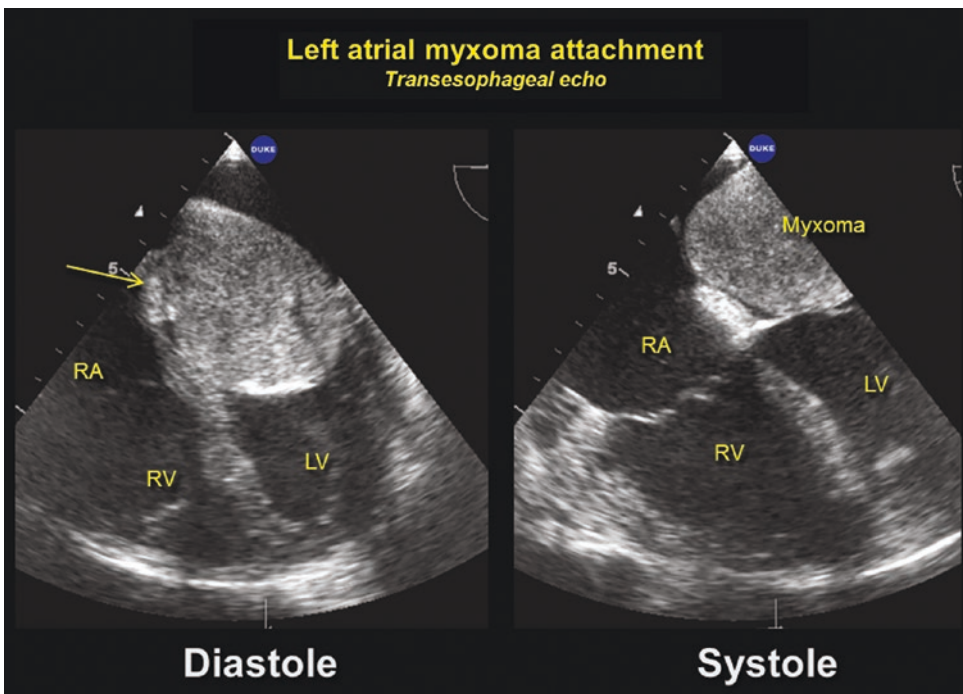


Fig. 10.137 Transesophageal echo showing the point of attachment of a myxoma on the atrial septum in the fossa ovalis. It is important to find the point of attachment to aid in directing the approach for surgical removal of the mass

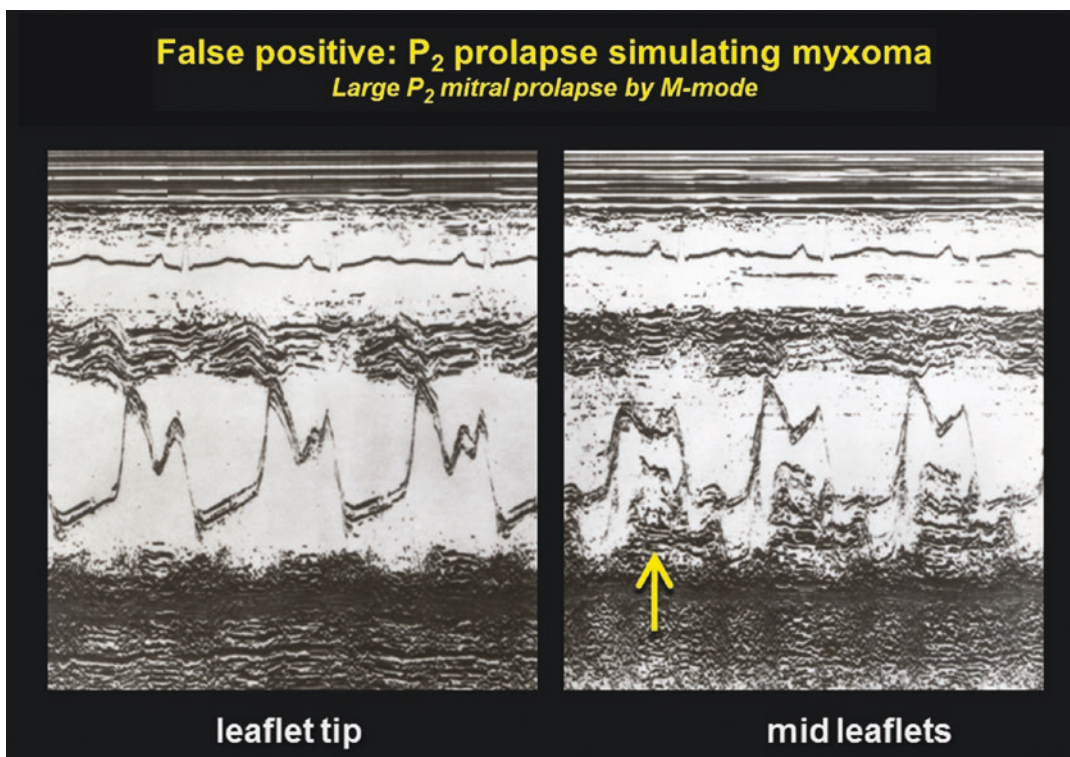


Fig. 10.138 A large P_2 segment prolapsing down into the mitral orifice may simulate left atrial myxoma (right panel, arrow)

shows the point of attachment of this tumor to be the mid atrial septum. This is the same patient depicted in long axis in Fig. 10.134. Most atrial myxomata will be attached along the atrial septum and the atrial septum is, therefore, removed with the tumor at the time of surgery. The atrial septum is then patched. Wherever the tumor is located, the point of attachment to the heart should never be missed by echocardiography as it can determine the best approach for surgical resection.

A left atrial myxoma may be simulated by mitral prolapse with M-mode echocardiography. One important factor to recognize is that a large P_2 segment of mitral valve prolapse may simulate a left atrial myxoma attached along the posterior left atrial surface. Figure 10.138 shows a normal mitral valve at the leaflet tip by M-mode. When the transducer is angled somewhat more cephalad it encounters the large P_2 segment prolapsing

down into the mitral valve orifice. Thus, prolapse is both a systolic and diastolic phenomenon. Two-dimensional echocardiography can readily differentiate these entities. While M-mode echocardiography is hardly ever, if ever, performed as a stand alone procedure over the recent decade, this example serves to help understand spatial movement of cardiac structures. In our laboratory, M-mode echocardiography is rarely, if ever, performed.

Figure 10.139 shows a left ventricular, rather than, left atrial myxoma using M-mode echocardiography. The myxoma was located on the septal surface of the left ventricular outflow tract and appeared to represent a massive structure anterior to the moving mitral valve (arrow). While such confusions exist with M-mode echocardiography, two-dimensional echocardiography can readily differentiate the location of these tumors.

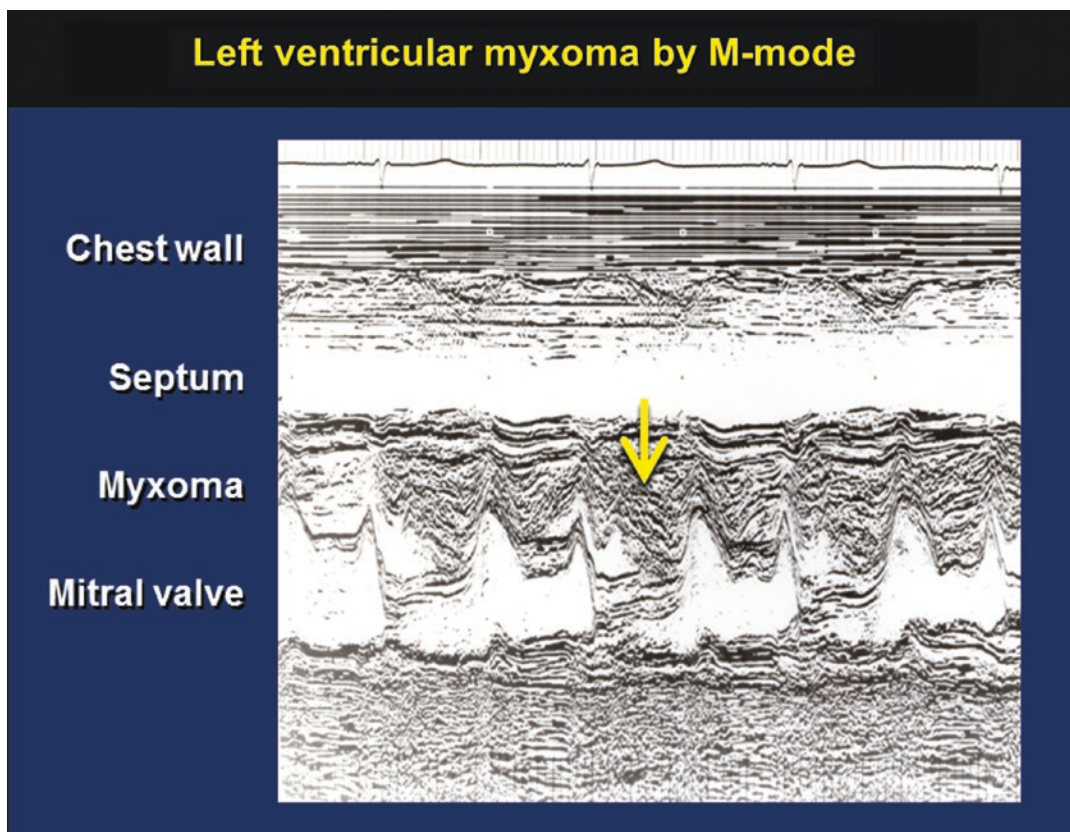


Fig. 10.139 M-mode echocardiogram of a left ventricular myxoma that obliterated the left ventricular outflow tract (arrow)

Congenital Anomalies of the Mitral Valve

There are multiple congenital anomalies of the mitral valve and only few can be discussed in the context of this chapter. One interesting anomaly is shown in Fig. 10.140, where a congenital double orifice mitral valve is shown. Movement of the mitral apparatus may resemble that of mitral stenosis in this entity with restriction of the valve leaflet tip in the parasternal long axis. In the short axis view, these patients are sometimes misdiagnosed as having mitral stenosis. If the restriction to flow in diastole is minimum, there may be no symptoms associated with this disorder. However, more commonly, there are symptoms due to mitral valve leaflet obstruction and they are progressive shortness of breath.

Figure 10.141 shows another patient with such a double orifice of congenital origin. Again, the anterior mitral valve leaflet tip is bowed slightly posteriorly in diastole and the typical double orifice is easily recognized. When the transducer is moved to the apical four chamber view, the double orifice can again be noted (left hand panel Fig. 10.142). When color flow is then utilized the double orifice can readily be identified (right hand panel). Even more rare is the presence of a triple orifice mitral valve. Two-dimensional echocardiogram from the chest wall is identified in such a patient in Fig. 10.143 where a parasternal long axis (left panel) and short axis (right panel) are shown. Reconstruction of the mitral valve with a triple orifice mitral valve is impossible at the present time and this patient had to undergo mitral valve replacement consequent to significant symptoms due to mitral restriction.

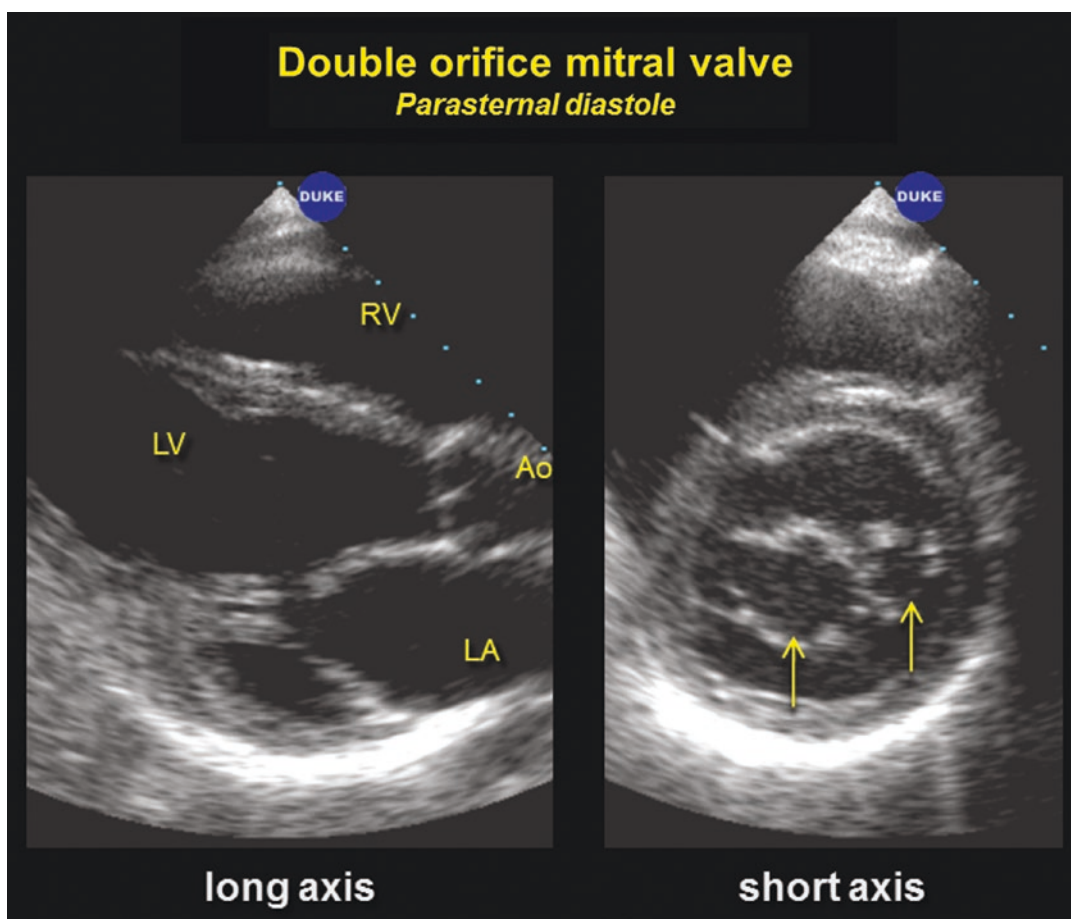


Fig. 10.140 Parasternal long and short axis from a patient with a double orifice mitral valve (arrows, right panel)

Figure 10.144 demonstrates an entity where an incorrect diagnosis of mitral valve orifice would be rendered and results from mitral prolapse. The left hand panel shows a patient with typical P_2 mitral valve prolapse seen in the parasternal long axis (arrow). The orthogonal short axis (right panel) shows diastolic frame through the body of the large P_2 segment simulating a multiple orifice mitral valve. Obviously, the parasternal long axis in this entity would help differentiate these two entities (Fig. 10.145).

Another false positive for double mitral orifice of the congenital variety is that acquired by patients undergoing the Alfieri stitch procedure. The left hand panel of Fig. 10.146 from a patient with surgically prove double orifice mitral valve while the right hand panel shows a patient after

the Alfieri stitch. While the two show a double mitral orifice, one is congenital and the other is obviously surgically acquired. An adequate patient history and physical examination should show evidence of previous surgical intervention and further help differentiate these entities.

Patients with other congenital lesions of the mitral valve may present simulating mitral stenosis. What one such entity is an arcade lesion that is manifest by marked thickening of the posterior leaflet and very poor differentiation of the chordal structures. A patient with this entity is shown in Fig. 10.146. These patients may be easily confused with those of rheumatic mitral stenosis. They are, however, exceedingly rare.

A much more common abnormality of the mitral valve is found in patients with atrio-

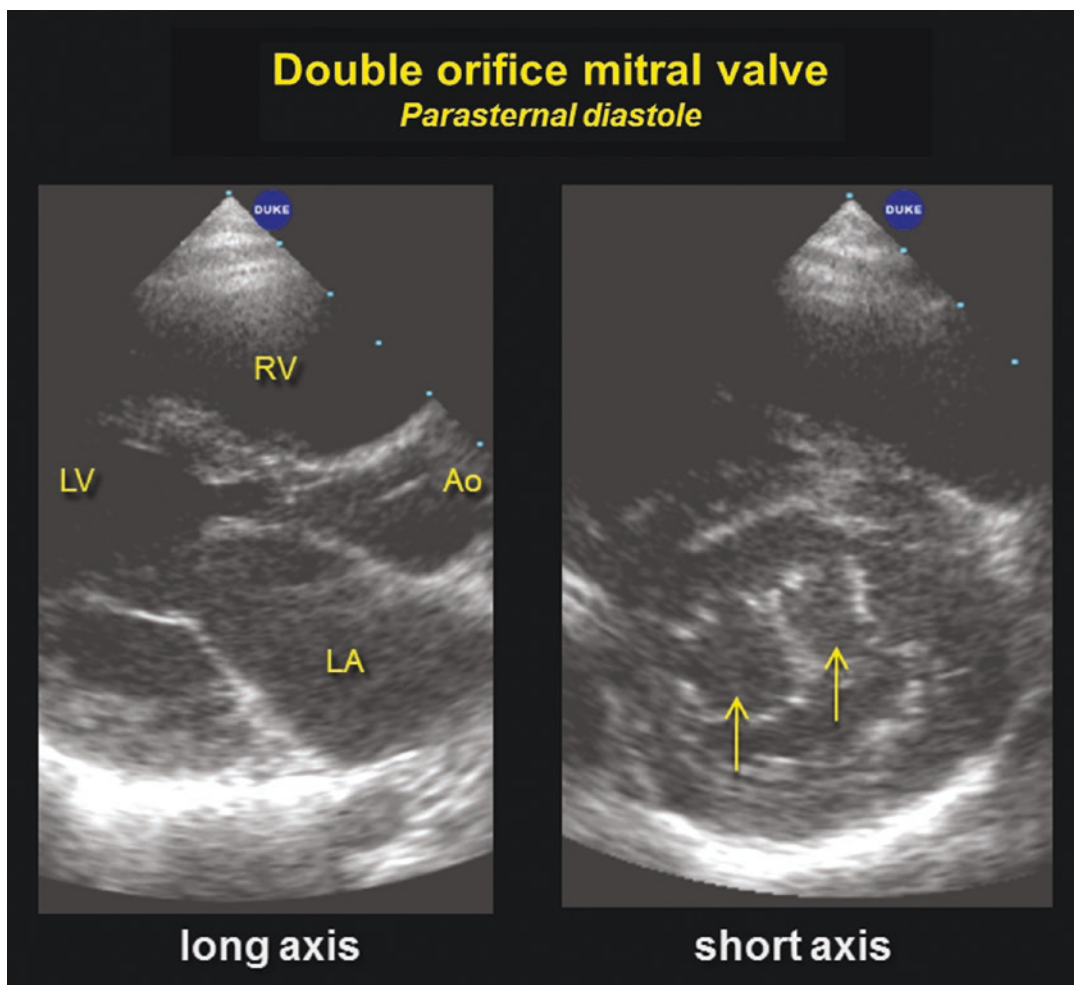


Fig. 10.141 Parasternal long and short axis from yet another patient with a double orifice mitral valve (arrows, right panel)

ventricular septal defects. In this disorder, there is a huge congenital rotation of the entire mitral apparatus and malformation of the mitral and tricuspid apparatus. There may be a so-called “cleft” of the anterior mitral valve leaflet (Fig. 10.147). With an AV Canal defect, the “cleft” is really due to a trileaflet left-sided AV valve. This “cleft” is typically angled toward the intra-ventricular septum and may result in attendant mitral regurgitation. Of course, other findings of atrio-ventricular septal defect (AV canal defect) are usually seen.

Transesophageal echocardiography can dramatically reveal the mitral “cleft”

(Fig. 10.148). Note that the cleft is, indeed, directed toward the interventricular septum and the tricuspid orifice due to the rotation of the entire mitral apparatus in atrio-septal defects. If the apparatus was normally positioned, the “cleft” would go into the aortic valve, which it does not. While difficult to first appreciate, the left sided AV valve apparatus in a patient with an atrio-septal defect is normally three leaflets. For this reason, simple surgical closure of the “cleft” is approached cautiously and repair should only be entertained by experienced surgical hands (Figs. 10.149 and 10.150).

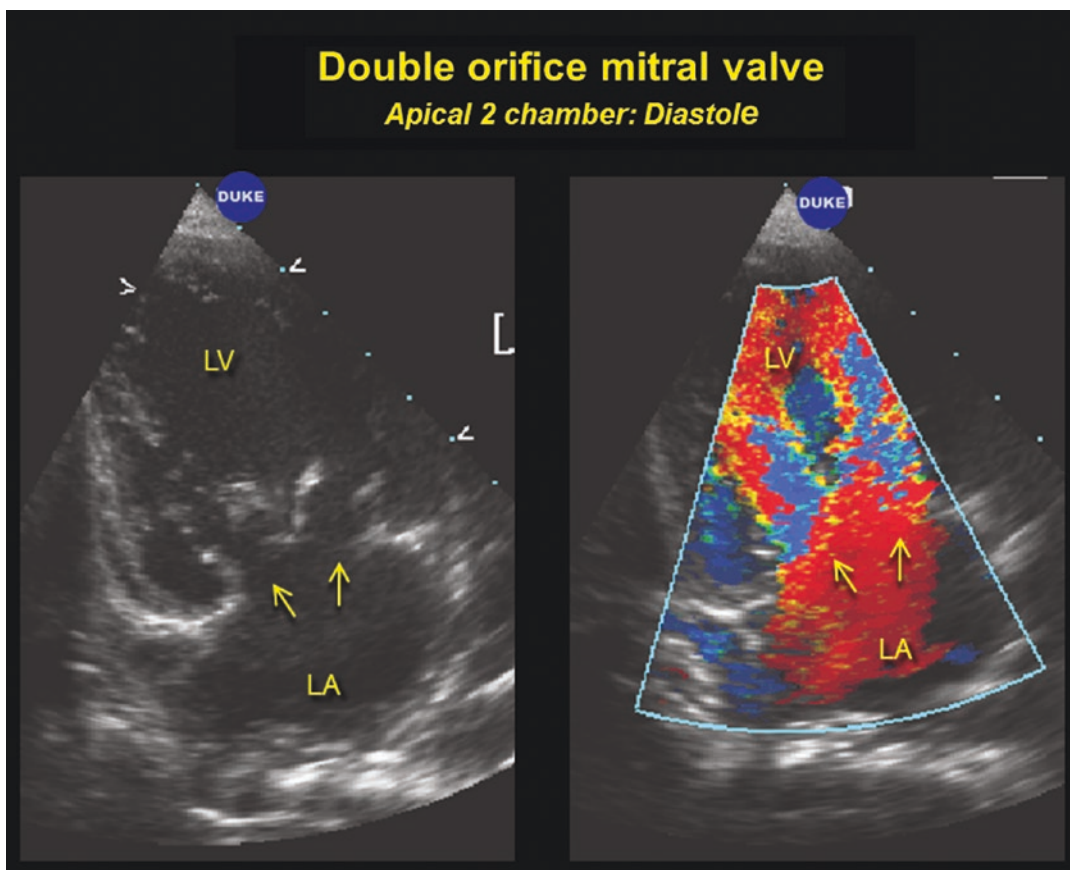


Fig. 10.142 Both orifices of the valve seen in the previous figure can be visualized from the apex. Two LV inlet flow jets can be seen

One of the more profound anomalies of the mitral valve is that seen in hypoplastic left heart syndrome. Figure 10.140 shows a parasternal long axis from an infant with hypoplastic left heart syndrome with marked dysplasia of the mitral and aortic apparatus and a rather diminutive left ventricle. These patients are, obviously, not encountered in the adult population.

Another congenital heart lesion that could present with symptoms of marked mitral valve obstruction is that of cor triatriatum. While the symptoms may be that of mitral stenosis the movements of the mitral valve leaflet are usually quite normal. However, (Fig. 10.141) a membrane is seen across the atrium just superior to the mitral valve annulus. The obstruction is at the level of this membrane. The figure shows such a

membrane demonstrated from the apical four chamber in an image obtained from the chest wall or from an attendant transesophageal echocardiogram. Simple surgical removal of this membrane results in a profound alleviation of symptoms.

An annulo-leaflet mitral band is seen by transesophageal echocardiography (left panel) of Fig. 10.151. These bands go from a leaflet to the annulus, in this case from the anterior leaflet to the posterior portions of the mitral annulus. The same patient and problem is depicted in the right panel. Most do not require surgical resection. This anomaly was found in a patient undergoing routine transesophageal echo prior to left atrial ablation due consequent to atrial fibrillation.

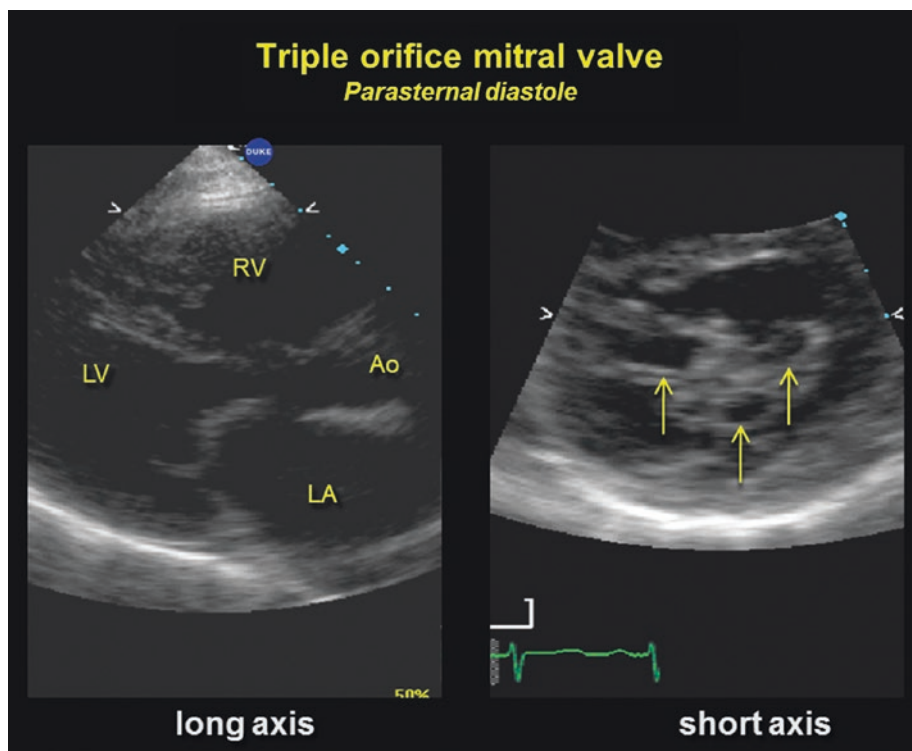


Fig. 10.143 While exceedingly rare, a triple orifice mitral valve can also be detected (arrows, right panel)

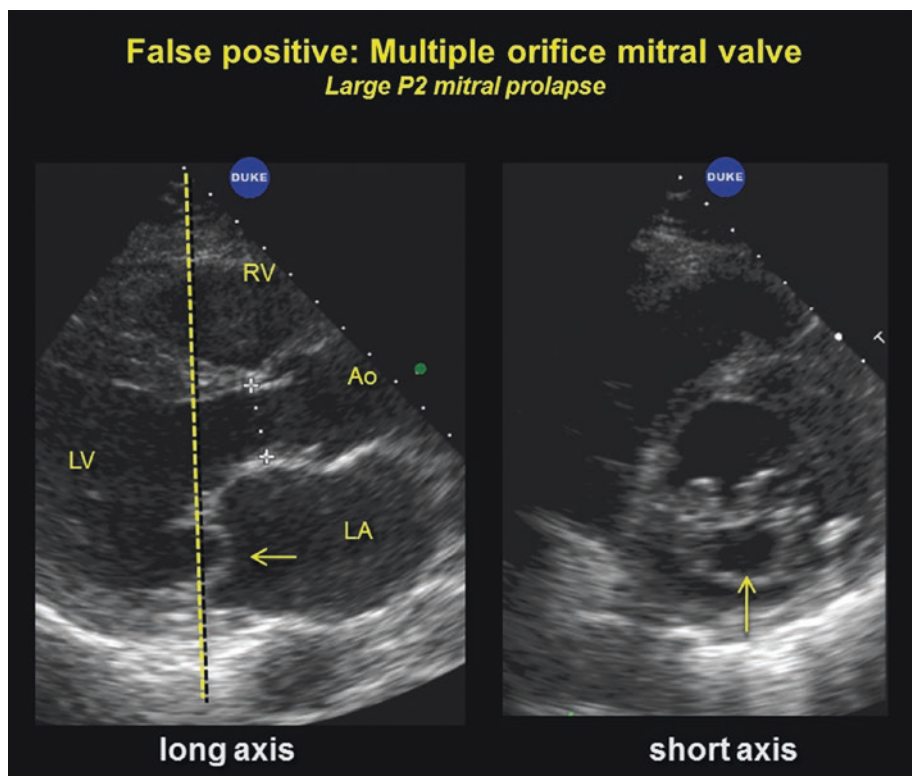


Fig. 10.144 One false positive for a multiple orifice mitral valve is seen where the “dome” of the prolapsing P₂ segment simulates a triple orifice valve in systole (arrow, right panel)

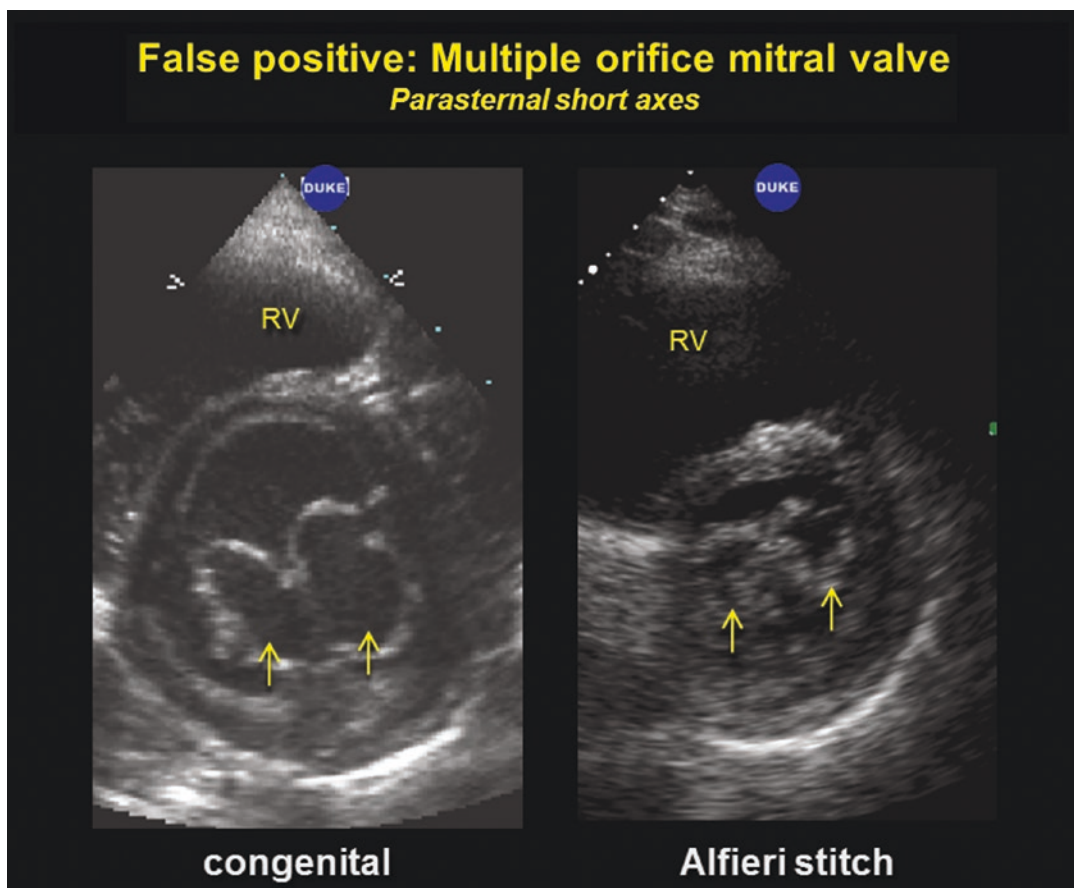


Fig. 10.145 Another false positive for a congenital double orifice mitral valve is in patients with history of Alfieri stitch. An adequate history will obviate this problem

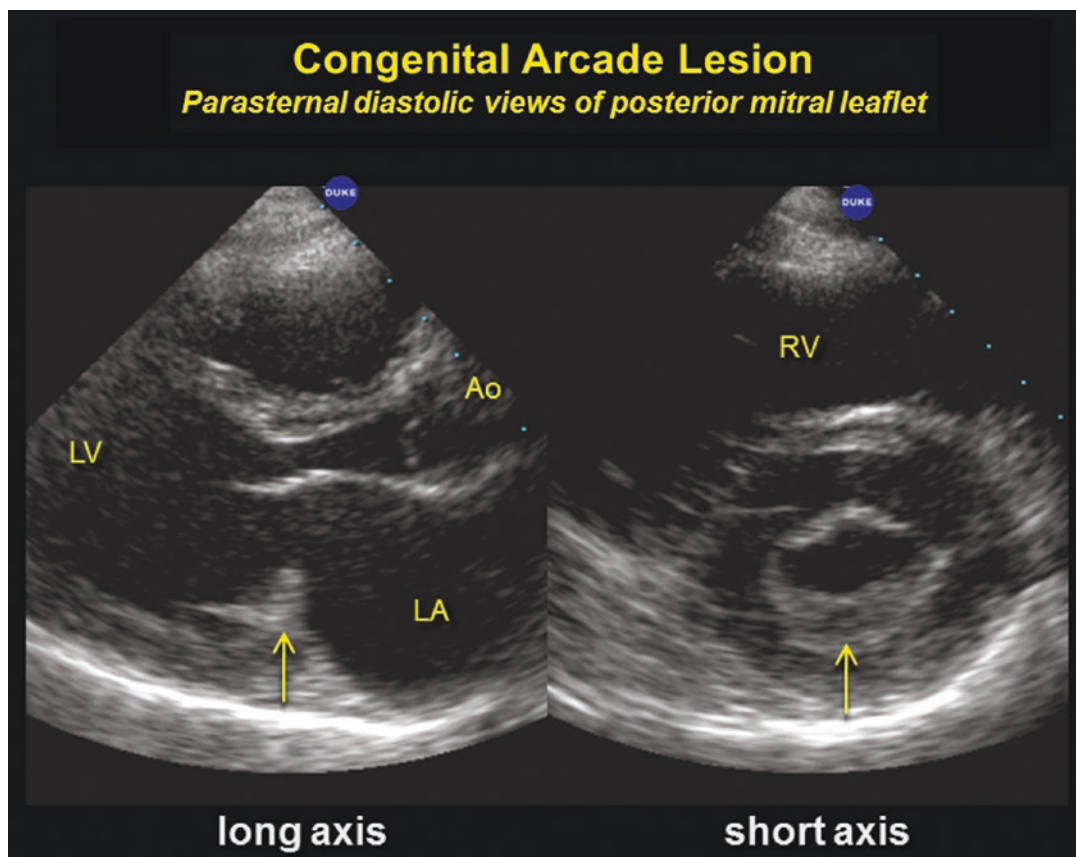


Fig. 10.146 Arcade lesion of the mitral valve in an adult patient. For details, see text

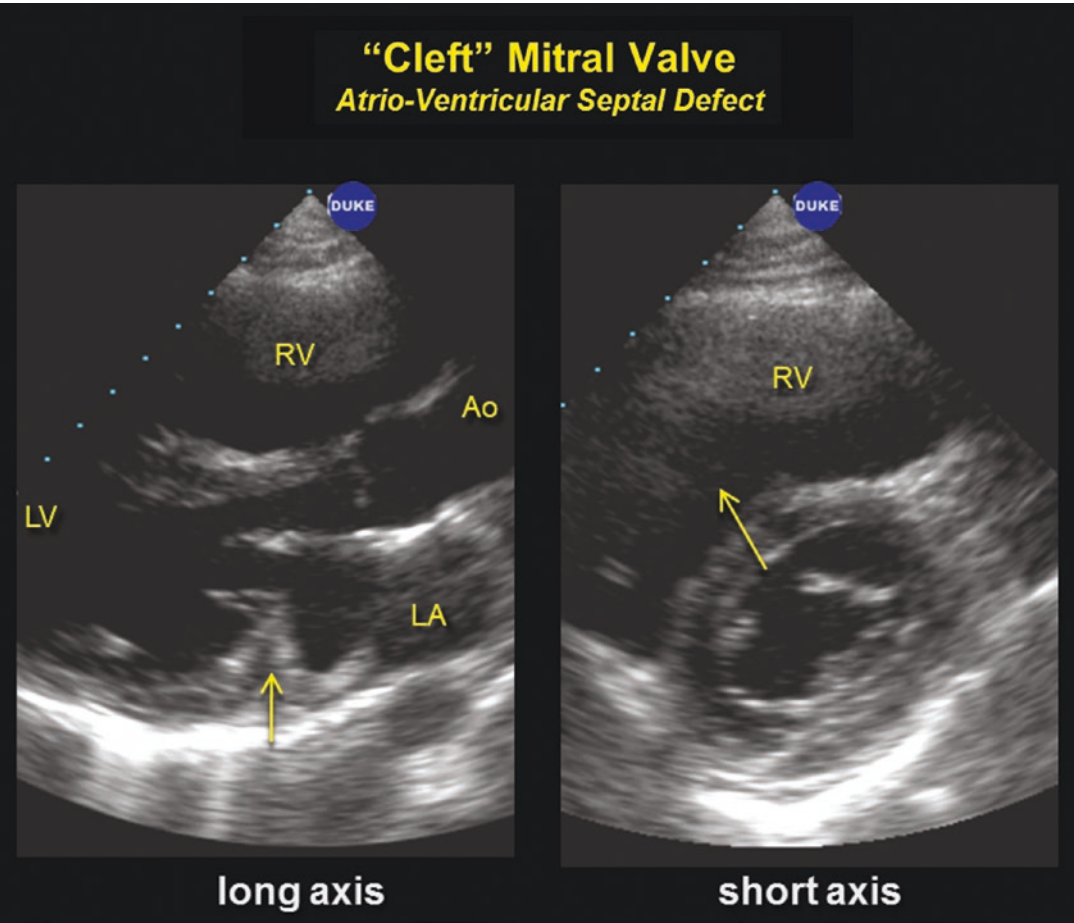


Fig. 10.147 Parasternal long axis from a patient with an AV Canal defect (atrio-ventricular septal defect) with mal-alignment of the mitral and aortic valves (left panel).

The so called “cleft” in this disorder seems to be aimed at the interventricular septum (right panel, arrow)

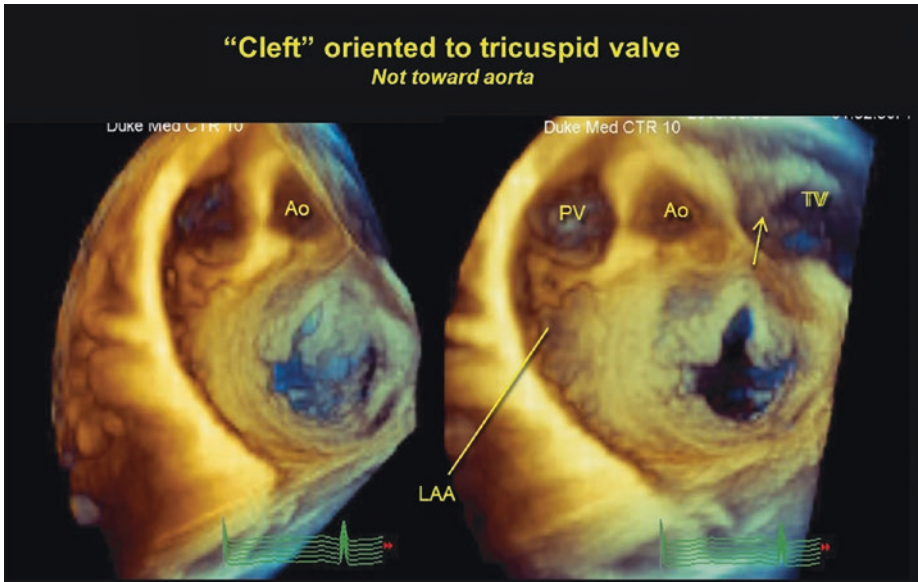


Fig. 10.148 Three-dimensional echocardiogram from a patient with an atrio-septal defect and so called “cleft” mitral leaflet. Note that the cleft is, indeed, directed toward the interventricular septum and the tricuspid orifice due to the rotation of the entire mitral apparatus in atrio-septal defects. If the apparatus was normally posi-

tioned, the “cleft” would go into the aortic valve, which it does not. While difficult to first appreciate, the left sided AV valve apparatus in a patient with an atrio-septal defect is normally three leaflets. For this reason, simple surgical closure of the “cleft” is approached cautiously and repair should only be entertained by experienced surgical hands

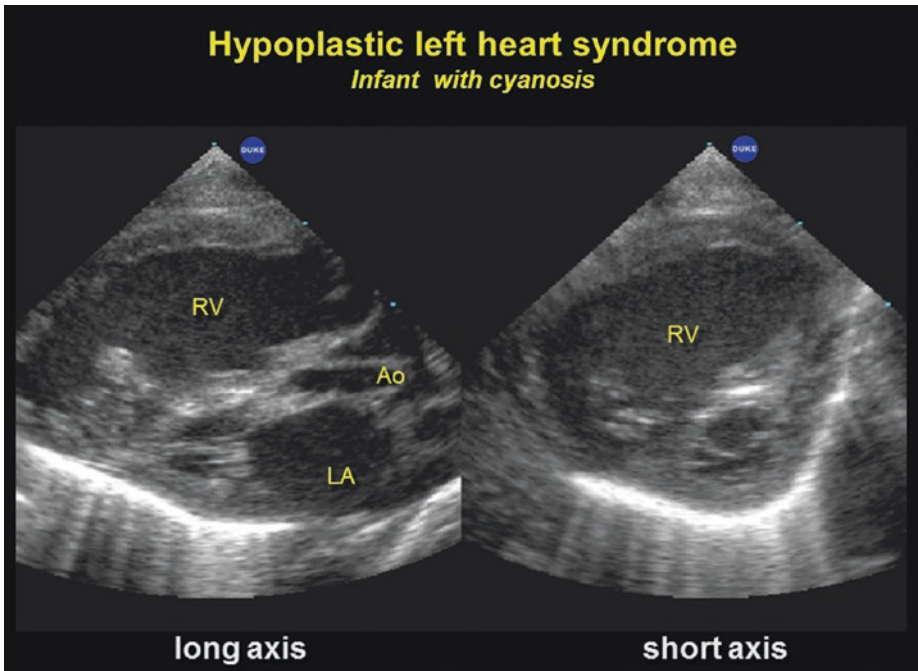


Fig. 10.149 Hypoplastic left heart syndrome in an infant. The mitral and aortic valves and left ventricle are dysplastic and diminutive

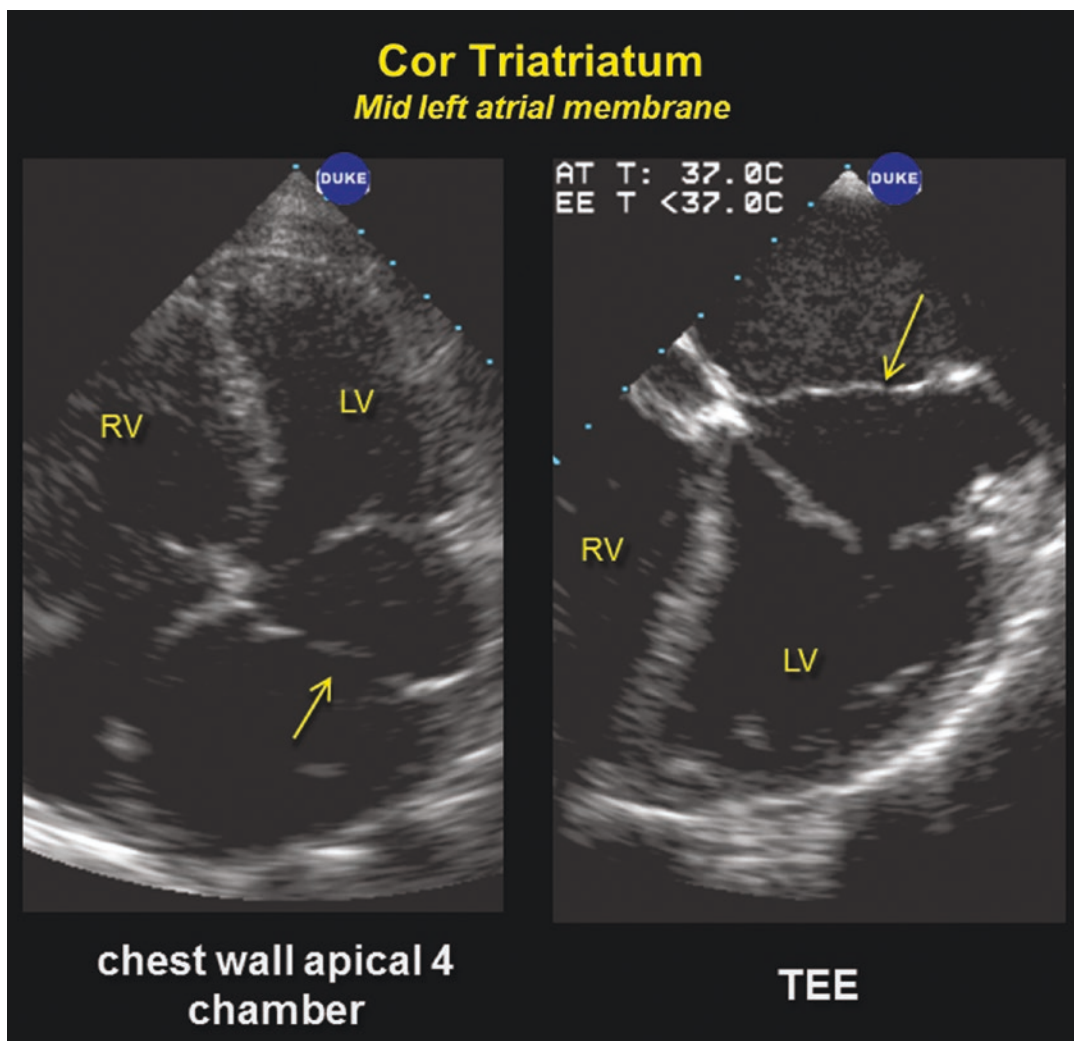


Fig. 10.150 A membrane of cor triatriatum is seen in the apical four chamber view (arrow, left panel) and the trans-esophageal (right panel)

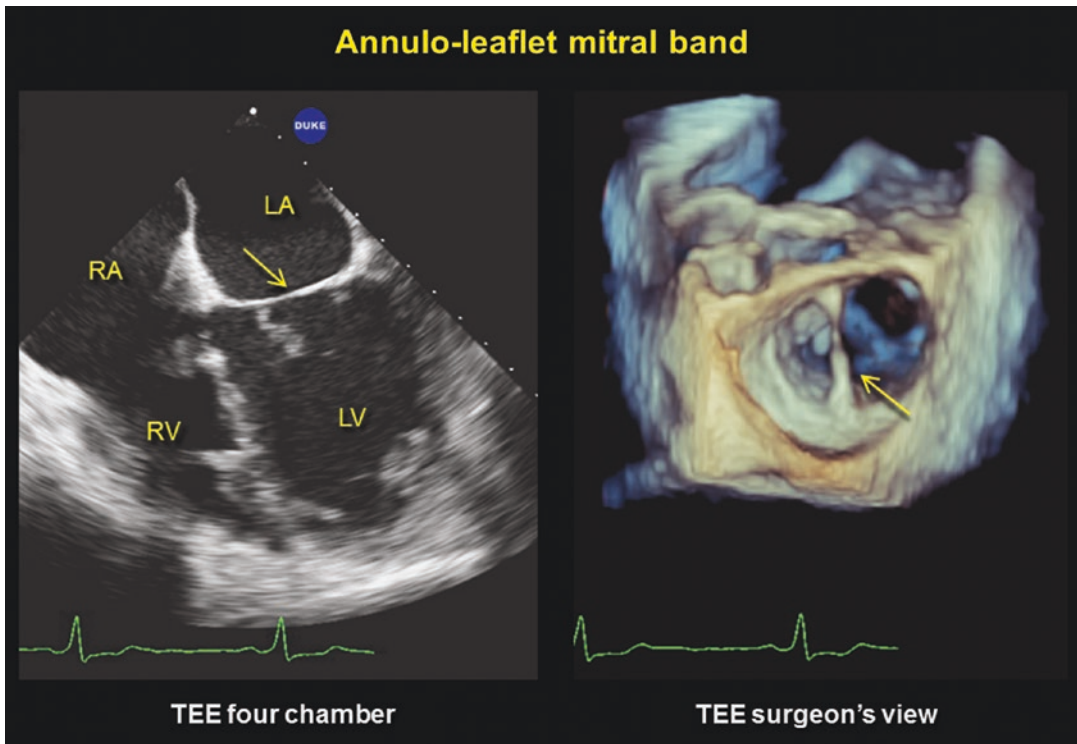


Fig. 10.151 An annulo-leaflet mitral band is seen by transesophageal echocardiography (left panel). These bands go from a leaflet to the annulus. The same patient

and problem is depicted in the right panel. Most do not require surgical resection

Recommended Reading

1. Hatle L, Angelsen B. Doppler ultrasound in cardiology. 2nd ed. Philadelphia: Lea and Febiger; 1985.
2. Kisslo J, Smith SW, von Ramm OT. Real-time, three-dimensional echocardiography: a beginning. In: Chambers J, Monaghan MJ, editors. Echocardiography: an international review. New York: Oxford University Press; 1993. p. 96–101.
3. Kisslo J. NHLBI balloon valvuloplasty registry: Doppler-echo evaluation of mitral stenosis pre- and post-balloon valvuloplasty (Abstr). J Am Coll Cardiol. 1989;13:114A.
4. Nichol PM, Gilbert BW, Kisslo JA. Two-dimensional echocardiographic assessment of mitral stenosis. Circulation. 1977;55:120–8.

Tricuspid and Pulmonary Valve Disease

11

Anne Bernard and Patrizio Lancellotti

Introduction

Right-sided valves diseases are less frequent than left-sided valves diseases. Even if they are better tolerated, severe right-sided valves diseases are associated with poor prognosis and should be carefully assessed. Echocardiography is the primary imaging modality for initial and longitudinal evaluation of these patients. However due to the complexity of right-sided valves anatomy and function, evaluation is mostly based on qualitative assessment. Echocardiography also plays a major role in the assessment of tricuspid regurgitation severity that is required before mitral valve surgery.

In this chapter, we will present an overview of diseases that affect the tricuspid and pulmonary valves, discuss 2D and 3D echocardiographic methods that allow their precise description, and

highlight how to assess the severity of valvular regurgitation and stenosis.

Tricuspid valve

The tricuspid valve (TV) apparatus includes leaflets, chordae, papillary muscles, and annulus. It is placed in a slightly more apical position than the mitral valve. The TV is classically described as having three leaflets of unequal size (septal, anterior and posterior). However there might be some variability from two to four leaflets. The septal and the anterior leaflets are larger than the posterior leaflet: the anterior leaflet is usually the largest and extends from the infundibula region anteriorly to the inferolateral wall posteriorly; the septal leaflet extends from the interventricular septum to the posterior ventricular border; the posterior leaflet attaches along the posterior margin of the annulus from the septum to the inferolateral wall. There are three papillary muscles that contribute chordae to the leaflets (anterior, posterior and septal) [1]. Each leaflet has chordal attachments to one or more papillary muscles. The TV has the largest area of all the valves, estimated at 6–7 cm². The annulus is elliptical saddle-shaped and becomes more circular when dilated. The annulus expands in diastoles and constricts in mid-systole. The proper function of TV requires the coordination of right ventricle (RV), right atrium (RA), papillary muscles,

A. Bernard (✉)

Cardiology Department, University of Tours,
Tours, France

EA 4245 Transplantation Immunité et Inflammation,
University of Tours, Tours, France
e-mail: anne.bernard@univ-tours.fr

P. Lancellotti (✉)

University of Liège Hospital, GIGA Cardiovascular
Sciences, Department of Cardiology, CHU Sart
Tilman, Liège, Belgium

Gruppo Villa Maria Care and Research, Anthea,
Bari, Italy
e-mail: plancellotti@chu.ulg.ac.be

chordae, and both interatrial and interventricular septae.

Several views are required to evaluate TV during a 2D echocardiographic study. 2D transthoracic echocardiography (TTE) standard views to assess TV are:

- parasternal RV inflow view with inferomedial angulation and slight clockwise rotation of the probe: (anterior and posterior leaflets) (Fig. 11.1);
- parasternal short-axis view at the aortic valve level (anterior leaflet attached to RV free wall and the other adjacent to the aorta is either the septal or the posterior leaflet);
- apical four-chamber view (septal and anterior) (Fig. 11.1);
- subcostal view (four chamber similar to apical view and short-axis similar to parasternal short-axis view).

Transoesophageal echocardiography (TOE) is advised in case of poor acoustic windows or sub-optimal TTE images. It is of particular interest for the diagnosis of venous catheters and lead infection when endocarditis is suspected. Standard TOE views (Fig. 11.2) to assess TV are:

- four-chamber view (standard) at mid oesophageal level 0–20°. The anterior and septal leaflets are seen;
- at mid-oesophageal level 30–80° with clockwise rotation of the probe to the right, the short-axis view becomes visible. The posterior leaflet is seen to the left and the anterior or septal leaflet to the right of the image. This view also allows the visualization of RVOT, the pulmonary valve and the pulmonary artery;
- between 80 and 120° with lateral flexion (RV two-chamber view), anterior and posterior leaflets;
- at 120°, rightward rotation of the probe shaft yields the long-axis RV inflow view (anterior and posterior leaflets).

Real-time 3D echocardiography can be used as an additive approach [2]. It provides an “en face” view of the TV, allowing the visualization of the three leaflets that is challenging with 2D echocardiography (Fig. 11.3). 3D TTE views to assess TV can be obtained from the apical and/or parasternal short-axis view. There is no standard view for the assessment of TV with 3D TOE but it can be obtained from mid-level at 0–20° [3].

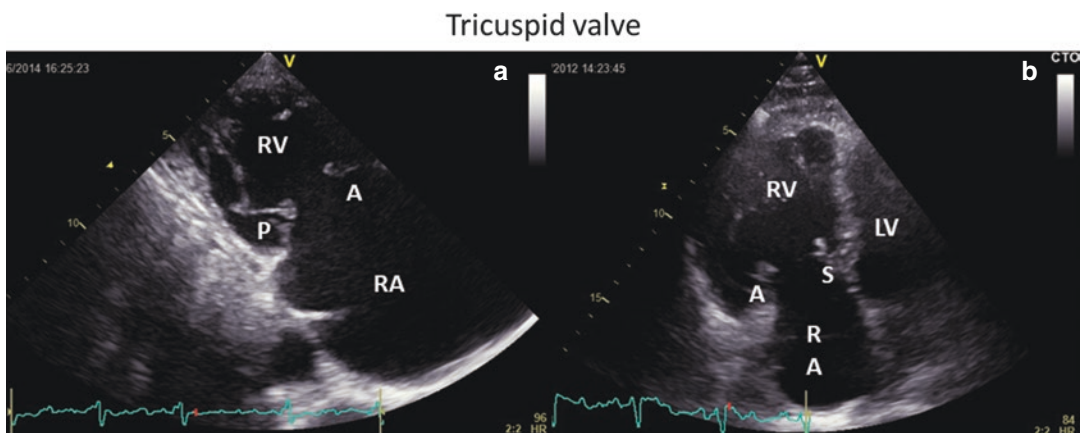


Fig. 11.1 Tricuspid valve. Standard TTE views. A, Right ventricular inflow view (S, septal; A, anterior leaflets). B, Apical four-chamber view (S, septal; A, anterior leaflets). Example of a severely dilated RV due to severe TR

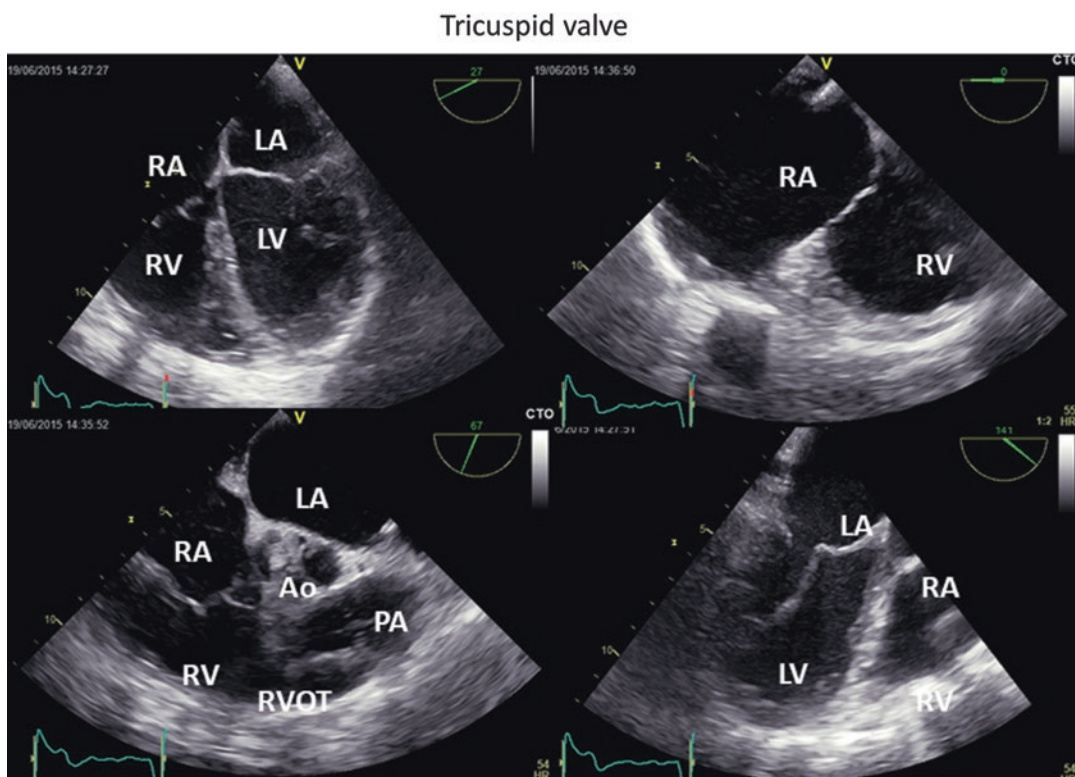


Fig. 11.2 Standard TOE views of the tricuspid valve

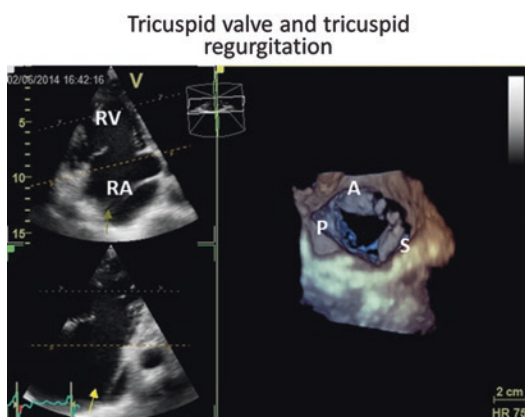


Fig. 11.3 Tricuspid valve and tricuspid regurgitation. Three-dimensional transthoracic echocardiography of the tricuspid valve (view from right atrium): coaptation defect due to severe tricuspid annulus dilatation; the three tricuspid cusps are well seen

Specific 3D analysis with zoom particularly may be required because the three leaflets and commissures are not at the same level.

Tricuspid Regurgitation

Mild tricuspid regurgitation (TR) is frequently encountered in the normal disease-free individual. The prevalence could reach 65–75% [4]. In this case, valve leaflets are normal and the RV is not dilated. Peak systolic velocities are between 1.7 and 2.3 m/s.

Pathological TR is most often secondary, rather than due to a primary valve lesion. It has been now clearly demonstrated that severe TR is associated with poor prognosis. TR is associated with less survival, worse functional capacity and increased surgical risk.

Etiology: Functional or secondary TR

About 80% of cases of TR are secondary. Impaired valve coaptation is related to tricuspid annular dilatation, papillary muscle displacement and leaflet tethering in the setting of RV remodeling due to pressure and/or volume overload. Most often secondary TR is caused by left-sided heart valve diseases, pulmonary hypertension, congenital heart defects, and cardiomyopathy.

Primary TR

Primary TR may be caused by **congenital disease** such as Ebstein's anomaly [5]. It is characterized by an exaggerated apical displacement of the insertion of the septal and posterior leaflets of the TV compared to the septal insertion of the mitral valve (usually greater than 11 mm).

Rheumatic involvement of the TV is less common than that of left-sided valves. Regurgitation is a consequence of deformity, shortening and retraction of one or more leaflets of the TV as well as shortening and fusion of the chordae tendineae and papillary muscles. **TV prolapse** is generally associated with mitral valve prolapse and is defined as a mid-systole posterior leaflet displacement beyond the annular plane. It most often involves the septal and anterior tricuspid leaflets. The most common phenotype of tricuspid prolapse is diffuse myxomatous degeneration (Barlow's disease). It is generally associated with left-sided valve disease. In the **carcinoid disease**, the valve appears thickened, fibrotic with markedly restricted motion during cardiac cycle. 2D/3D echo shows ineffective leaflet coaptation and lacks of commissural fusion (Fig. 11.4).

Other causes of TR include infective endocarditis, radiation, endomyocardial fibrosis and blunt chest wall trauma. Iatrogenic damages can also induce TR: cardiac surgery, biopsies and intra-annular RV pacemaker or implantable cardioverter-defibrillator leads (Fig. 11.5).

Assessment of Severity

TV morphology analysis to determine the precise mechanism of TR is mandatory. Like for

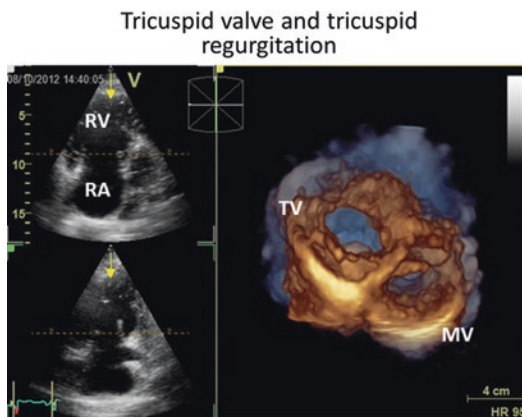


Fig. 11.4 Three-dimensional TTE of the tricuspid valve: carcinoid disease with rigidity of all tricuspid cusps (view from the right ventricle)

the mitral valve, the Carpentier's classification is the most common used: type I: leaflet perforation (infective endocarditis) or more frequently by annular dilatation; type II: prolapse of one or more leaflets; and type III: restricted motion as the consequence of rheumatic disease, significant calcifications, toxic valvulopathy, secondary TR. A flail TV is specific for significant TR (Table 11.1).

Tricuspid annulus diameter is a main part of the echocardiographic examination [6]. It is assessed in the apical four-chamber view as the lateral inner edge to septal inner edge by 2D and even better by 3D echocardiography [7]. Normal TV annulus diameter is 28 ± 5 mm. Significant tricuspid annular dilatation is defined by a diastolic diameter of >21 mm/m² (>40 mm). These reference measures are currently used to propose TV repair at the time of left-sided valve surgery [8]. In secondary TR, the severity of tricuspid leaflet restriction should also be assessed. A coaptation distance >8 mm characterizes patients with significant tethering (distance between the tricuspid annular plane and the point of coaptation in mid-systole from the apical four-chamber view) [9]. A tenting area >1 cm² has been shown to be associated with severe TR [10].

Colour Doppler is used for diagnosing TR and helps in the screening of mild vs. severe TR. Larger

Tricuspid valve and tricuspid regurgitation

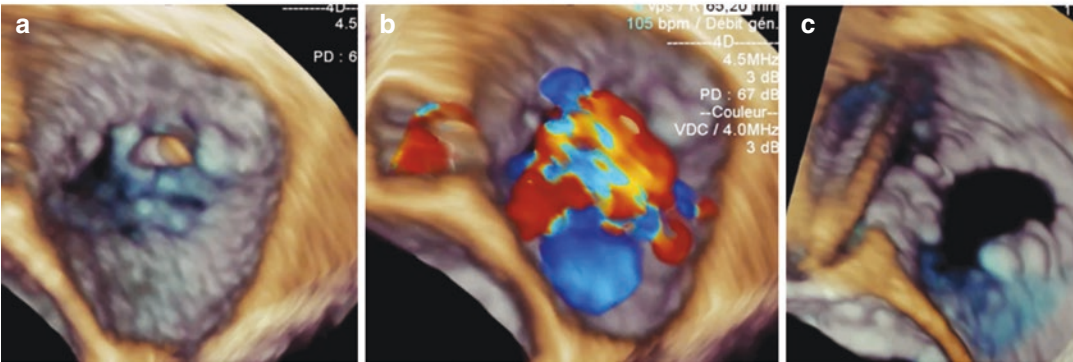


Fig. 11.5 Three-dimensional TTE of the tricuspid valve (view from right atrium). (a) Coaptation defect due to cardioverter-defibrillator lead. (b) Three-dimensional colour Doppler showing severe tricuspid degurgitation. (c) After tricuspid annuloplasty

Table 11.1 Valve anatomy, valve hemodynamics and hemodynamic consequences of severe tricuspid regurgitation and severe tricuspid stenosis adapted from EACVI Recommendations and 2014 ACC/AHA guidelines [8, 11]

Definition	Valve anatomy	Valve hemodynamics	Hemodynamic consequences
Severe TR	<i>Primary</i> Flail or grossly distorted leaflets <i>Secondary</i> Severe annular dilatation (>40 mm or 21 mm/m ²)	<ul style="list-style-type: none">• Central jet area >10 cm²• Vena contracta width >0.7 cm• CW jet density and contour: dense, triangular with early peak• PISA radius >9 mm• EROA ≥40 mm² and regurgitant volume ≥45 mL• Hepatic vein flow: systolic reversal	<ul style="list-style-type: none">• RV/RA/IVC dilated with decreased IVC respirophasic variation• Elevated RA pressure• Diastolic interventricular septal flattening• Reduced RV systolic function
Severe TS	<ul style="list-style-type: none">• Thickened, distorted, calcified leaflets	<ul style="list-style-type: none">• T1/2 ≥190 ms• Mean diastolic gradient ≥5 mmHg• Valve area ≤1.0 cm²	<ul style="list-style-type: none">• RA/IVC enlargement

RA right atrium, RV right ventricle, IVC inferior vena cava, TR tricuspid regurgitation, TS tricuspid stenosis, CW continuous wave

colour jets that extend deep into the right atrium represent more TR than small thin jets that appear just beyond the tricuspid leaflets (Fig. 11.6).

Vena contracta width allows a semi-quantitative assessment of TR. It is imaged in the apical four-chamber view using the same settings as for mitral regurgitation. A vena contracta ≥7 mm is in favour of severe TR [11]. 3D echo allows measurement of vena contracta area without any erroneous geometric assumptions.

However its use is limited in routine practice at the moment.

The continuous wave (CW) Doppler of TR jet analyses signal intensity and shape. A dense signal with a full envelope indicates more severe TR than a faint signal. In case of right atrial pressure elevation, the envelope may be truncated with a triangular contour and an early peak velocity. In severe TR, peak velocity is most often <2 m/s (Fig. 11.7).

Tricuspid valve and tricuspid regurgitation

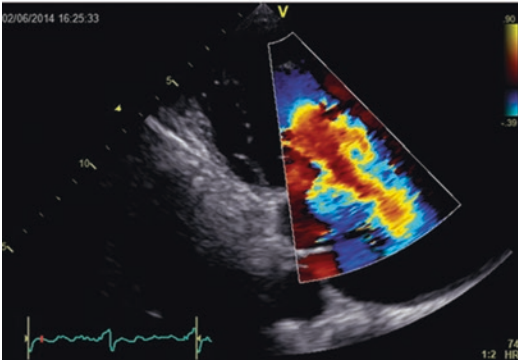


Fig. 11.6 Colour Doppler, RV inflow view; severe tricuspid regurgitation

Tricuspid valve and tricuspid regurgitation

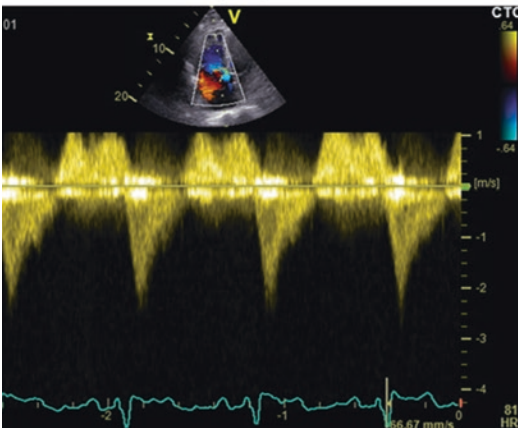


Fig. 11.7 Continuous wave Doppler of a severe tricuspid regurgitation: triangular and dense signal with an early peak velocity of 2 m/s

The flow convergence method has been validated in small studies to quantify the TR severity. The apical four-chamber view and the parasternal long- and short-axis views are classically recommended for optimal visualization of the PISA. The Nyquist limit is lowered to ~15–40 cm/s. The PISA radius is measured at mid-systole using the first aliasing. A TR PISA radius >9 mm at a Nyquist limit of 28 cm/s indi-

Tricuspid valve and tricuspid regurgitation

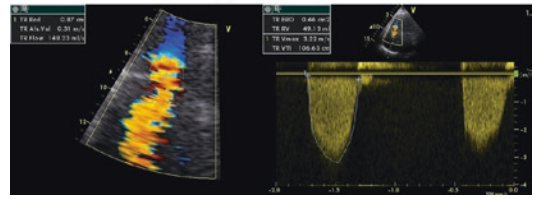


Fig. 11.8 PISA method for quantification of a severe tricuspid regurgitation

cates severe TR whereas a radius <5 mm suggests mild TR [12]. An EROA ≥ 40 mm² or a regurgitant volume of ≥ 45 mL indicates severe TR [8] (Fig. 11.8). This method is less accurate in eccentric jets. The 3D echo measurement obtained from regurgitant colour jet such as vena contracta, jet area and jet volume has been described but values are not well established yet (Fig. 11.9).

Pulsed wave (PW) Doppler analyses of the antegrade velocity of tricuspid inflow obtained at the tricuspid leaflet tips. A peak E velocity ≥ 1 m/s suggests severe TR.

PW Doppler evaluation of hepatic venous flow pattern is another aid for grading TR. The systolic hepatic flow reversal is specific for severe TR (Fig. 11.10). It represents the strongest additional parameter for evaluating the severity of TR.

Consequences of TR are RA and RV dilatation (Fig. 11.11), a dilated and pulsatile inferior vena cava and hepatic vein, a dilated coronary sinus and systolic bowing of the interatrial septum toward the LA. Right heart dilatation is not significant of severe TR but its absence suggests milder degree of TR. A rapid anterior motion of the interventricular septum at the onset of systole (paradoxical ventricular septal motion) represents a qualitative sign of RV volume overload due to severe TR (Fig. 11.12). Evaluation of the RV dimensions and function should be conducted, despite existing limitations of current indices of RV function [6]. Chronic TR may cause progressive RV dysfunction. TAPSE and systolic tissue Doppler velocity are good

Tricuspid valve and tricuspid regurgitation

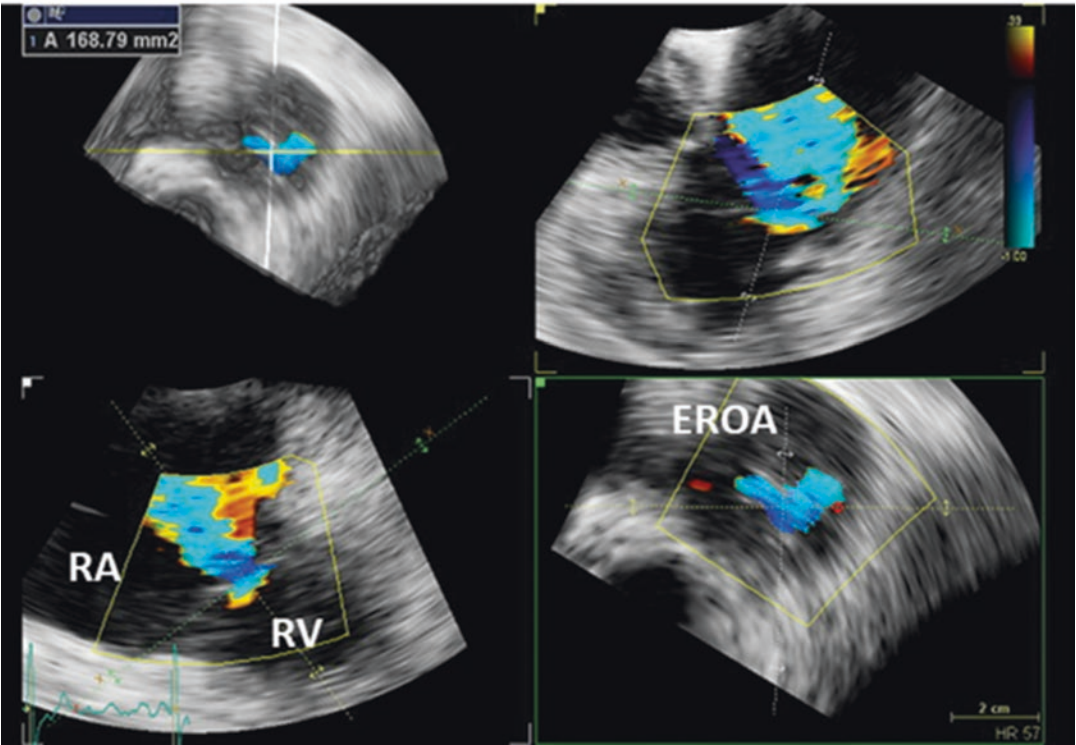


Fig. 11.9 Quantification of a severe tricuspid regurgitation with 3D TTE

Tricuspid valve and tricuspid regurgitation

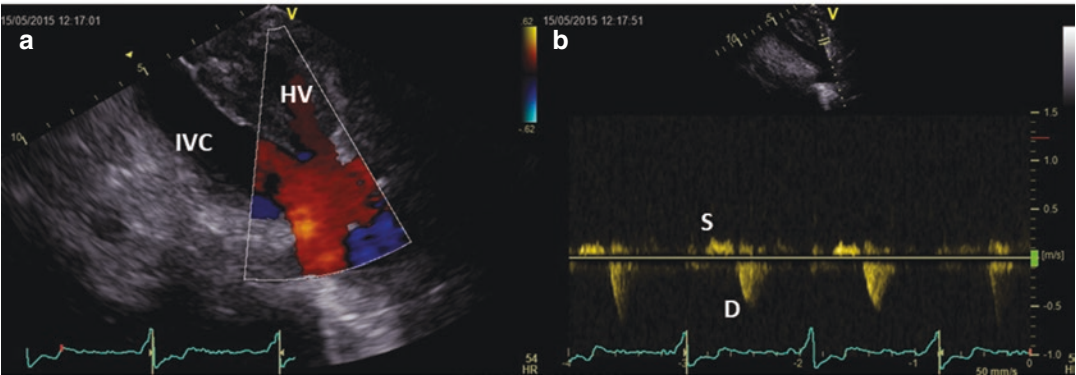


Fig. 11.10 Plethoric inferior vena cava and hepatic veins. Systolic flow reversal. (a) Colour Doppler (subcostal view). (b) Pulsed wave Doppler

Tricuspid valve and tricuspid regurgitation

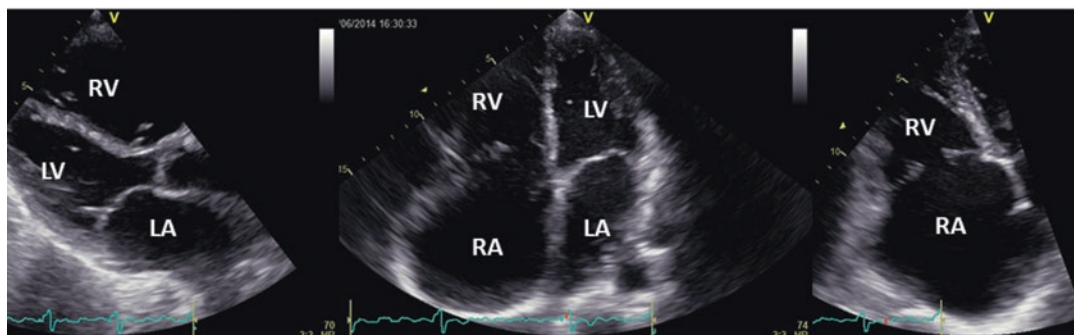


Fig. 11.11 Right ventricular dilatation (left, parasternal long axis view; middle, apical four-chamber view) and right atrium dilatation (right, apical four-chamber view, zoom)

Tricuspid valve and tricuspid regurgitation

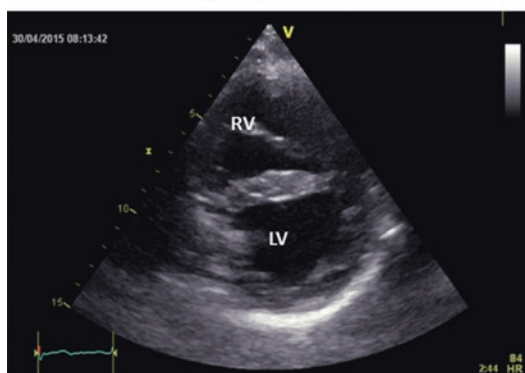


Fig. 11.12 Paradoxical ventricular septal motion at the onset of systole suggesting RV volume overload due to TR (parasternal long-axis view)

parameters to assess RV function but are less accurate in patients with severe TR. A TAPSE <15 mm and a systolic tissue Doppler velocity measured at the lateral tricuspid annulus <11 cm/s are considered as significantly reduced [8].

Pulmonary artery pressure is assessed by calculating the RV to RA pressure gradient using the modified Bernoulli eq. (CW Doppler TR jet) and then adding an assumed RA pressure.

Echocardiographic assessment of TR includes integration of data from 2D/3D imaging of the valve, right heart chambers, septal motion and inferior vena cava as well as Doppler measures of

regurgitant severity (Table 11.1). TTE examination for TR should also characterize any associated left-sided heart disease. LV function should be assessed as well.

Tricuspid Stenosis

Etiology and Mechanisms

Tricuspid stenosis (TS) is the less frequent valve disease among all valve diseases. Rheumatic heart disease is the commonest cause (90%) and is usually associated with mitral and/or aortic valve involvement that often dominates the presentation. Other causes of TS are carcinoid syndrome (always combined with TR, which is commonly predominant), obstruction by RA myxoma and rare congenital malformations.

Most commonly, TS is accompanied by regurgitation so that the higher flows through the valve further increase the transvalvular gradient and contribute to a greater elevation of right atrial pressures.

Assessment of Severity

Qualitative evaluation requires the assessment of the anatomy of the valve (Table 11.1). Commissural fusion, the anatomy of the valve and its subvalvular apparatus are the most important determinants of valvuloplasty [6]. The leaflets appear thickened, distorted, calcified and with restricted motion secondary to commissural

fusion, leading to a relatively fixed orifice. Diastolic doming of the leaflets is typical of rheumatic cause. Chordae are short and are thickened. In carcinoid syndrome, the leaflets are severely immobile. Colour Doppler shows narrowing of the diastolic inflow jet, higher velocities that produce mosaic colour dispersion and associated valve regurgitation.

Quantitative assessment is partly based on the transtransvalvular peak and mean diastolic pressure gradients measured by CW Doppler. A mean diastolic gradient ≥ 5 mmHg at a heart rate of 70 beats per minute is considered indicative of clinically significant TS [13]. However the transtricuspid diastolic gradient is highly variable and is affected by heart rate, forward flow and phases of the respiratory cycle and should be interpreted carefully. Pressure half time allows evaluation of TV area by the formula: $TV \text{ area} = 190/PHT$. $T \frac{1}{2} \geq 190$ ms is in favour of severe TS.

Planimetry of the TV area is the best evaluation but is difficult with 2D echo mainly due to inadequate cut planes. 3D TTE measurement of TV area is feasible. The cut plane needs to be modified, as the three commissures are not at the same cut planes. A normal TV area is of 4.8 ± 1.6 cm². A valve area ≤ 1.0 cm² signifies severe TS. The same can be obtained by real-time 3D TOE.

Indirect findings of significant TS are RA enlargement and inferior vena cava enlargement. RV size and function are preserved.

Pulmonary Valve

The pulmonary valve (PV) is a three-leaflet structure, anatomically similar to the aortic valve (2 posteriors: right and left, and one anterior) but positioned more superior, leftward and anterior. PV is thinner than aortic valve because of the lower pressures in the right than in the left heart system. PV diseases also involve the pulmonary artery (PA) and right ventricular outflow tract (RVOT). Echocardiography plays a major role in the assessment and management of PV stenosis and regurgitation. However evaluation of the PV anatomy is more difficult than for other valves (limited by poor acoustic access).

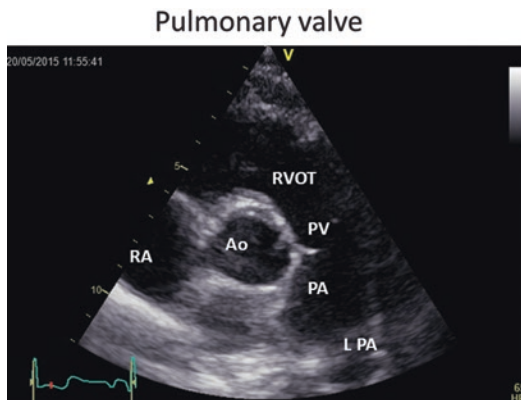


Fig. 11.13 Pulmonary valve. Parasternal short-axis view of the pulmonary valve (RA right atrium, RVOT right ventricle outflow tract, PV pulmonary valve, PA pulmonary artery, LPA left pulmonary artery, Ao, aorta)

2D TTE standard views used to assess PV are:

- parasternal short axis view at the aortic valve level where the bifurcation of the PA is also visualized (Fig. 11.13);
- parasternal long-axis projection of the RVOT and PV, obtained by rotating the transducer approximately 90° with angulation toward the right shoulder;
- apical 5-chamber view, through clockwise angulation of transducer to bring in the RVOT;
- subcostal short-axis view with anterior angulation.

The role of TOE is limited since the PV is more difficult to image (far from the probe). 2D TOE views used to assess PV are:

- high oesophageal position at 0-degree rotation with a long-axis view of the PA from the valve plane to its bifurcation which allows imaging of RVOT;
- short-axis view at mid-oesophageal level 30–80° with clockwise rotation to the right, which allows visualization of the anterior and posterior cusps.

Real-time 3D echocardiography is feasible in 95% of patients. 3D TTE allows the assessment of RVOT and PV annulus (shape and size) [14].

Pulmonary stenosis

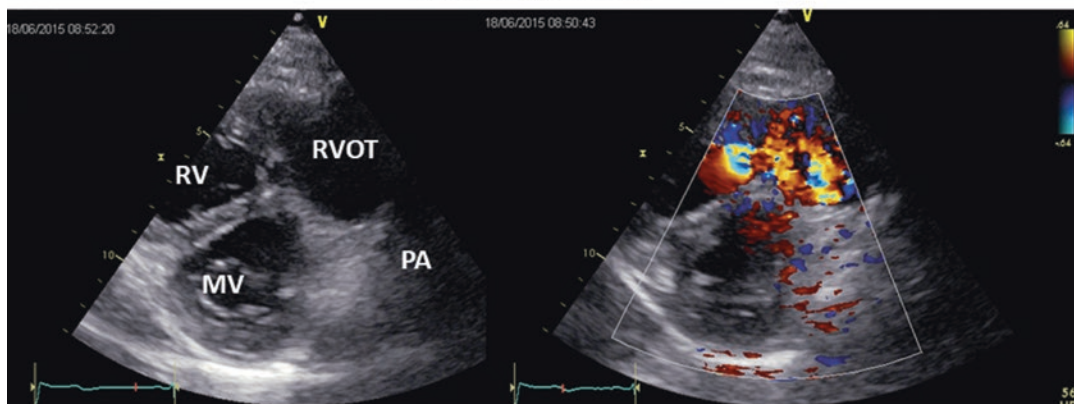


Fig. 11.14 Pulmonary stenosis. Subvalvular pulmonary stenosis due to RVOT obstruction secondary to development of midcavity muscle bundles due to congenital

ventricular septal defect. On the left, gray-scale parasternal short-axis view; on the right, colour Doppler showing flow acceleration

Full assessment of PV cusps and commissures could be obtained by 3D TOE.

Pulmonary Stenosis

Etiology and Mechanisms

Pulmonary stenosis (PS) is a frequent congenital anomaly accounting for 8% of all congenital heart disease. It is most often isolated but may be integrated in complex syndromes such as tetralogy of Fallot. When isolated, PS may be valvular (80–90%), sub or supra-ventricular [15].

PS might also be an acquired disease. Rheumatic affection is rare and usually associated with other valves involvement. Carcinoid syndrome results in shortening and thickening of the PV leaflet, similar to the involvement of the TV (combined stenosis and regurgitation with usually predominant regurgitation). Extrinsic obstruction of the PV may be produced by cardiac tumours or by aneurysm of the sinus of Valsalva.

Three morphologic types of valvular stenosis may be identified: a typical form with a dome-shaped valve with commissural fusion; dysplastic valves without commissural fusion and unicuspid or bicuspid valve [16].

Subvalvular stenosis can be encountered in congenital diseases. Congenital ventricular septal defect may be associated with RVOT obstruction

secondary to development of obstructive midcavitary muscle bundles (double chamber RV) (Fig. 11.14).

Assessment of Severity

Qualitative evaluation of PV requires analysis of valve anatomy with the number of cusps, which may be difficult in adult patients: unicuspid, bicuspid or dysplastic valves. Rigidity of the cusps (fibrosis or calcification) and commissural fusion are also analysed (Fig. 11.15) [13]. A systolic dome-shaped valve is typical of PS (Fig. 11.16). Annulus and RVOT diameters are measured during early ejection phase from short axis or from right ventricular outflow view. By color Doppler, there is evidence of PS as accelerated flow beyond the stenotic PV. With increasing severity, the flow is directed more toward the left PA. PW Doppler reveals increased systolic velocity and helps to localize the stenosis level (valvular, subvalvular or supra-ventricular). A velocity curve with a late systolic peak is mostly associated with a dynamic infundibular obstruction (Fig. 11.17).

Quantitative assessment is mainly based on the transpulmonary pressure gradient measured by CW Doppler (Fig. 11.18) [13]. A maximal gradient greater than 64 mmHg ($V_{max} > 4$ m/s, which corresponds to a PV area < 1 cm²/m²) denotes severe PS [11] (Table 11.2). Generally a peak transvalvular gradient less than 36 mmHg is

considered to be a mild lesion. If there is concomitant significant pulmonary regurgitation (PR), maximal gradient may overestimate the severity of stenosis. The calculation of PV area using continuity equation is not routinely used. Multiplane views from 3D TOE allow the measurement of the actual valve area.

Indirect findings associated with PS should be assessed such as RV hypertrophy (>5 mm) and/or dilatation, RA enlargement and post-stenotic PA dilatation (normal value <25 mm) (Fig. 11.19). RV

hypertrophy can manifest as dynamic infundibular obstruction. PA systolic pressure is determined as RV systolic pressure—PV pressure gradient.

Therapeutic Guidance

Echocardiography has a significant role in timing and identifying candidates for balloon valvulotomy. The size of the pulmonary annulus should be defined in order to define the optimal balloon size for successful dilatation of the valve. Indications for a balloon valvulotomy include patients with-

Pulmonary stenosis

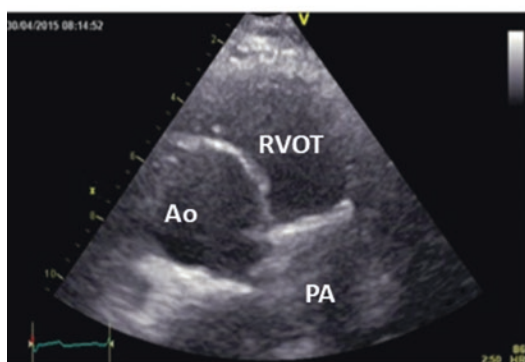


Fig. 11.15 Isolated pulmonary valve stenosis: calcification of the pulmonary cusps with commissural fusion; typical systolic dome-shaped valve

Pulmonary stenosis

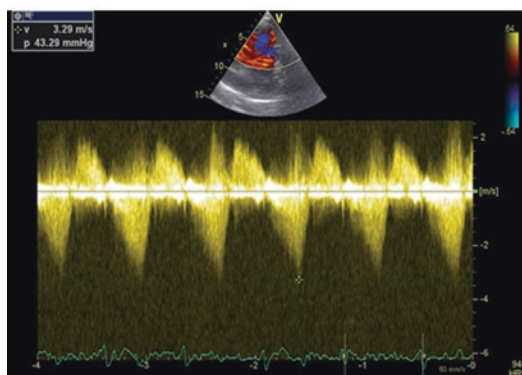


Fig. 11.17 Pulmonary stenosis CW Doppler demonstrating a mild to moderate pulmonary stenosis with a late systolic peak suggesting a dynamic infundibular obstruction

Pulmonary stenosis

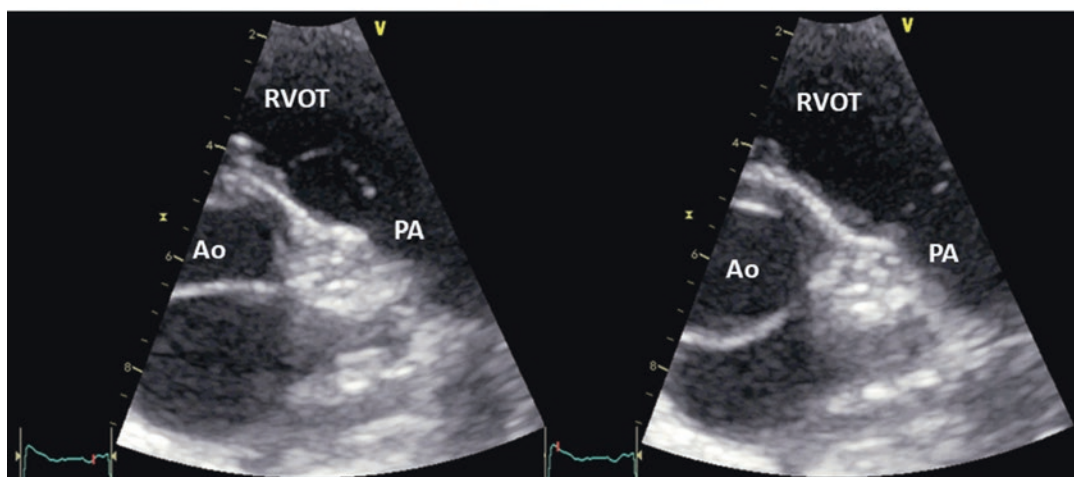


Fig. 11.16 Congenital isolated pulmonary valve stenosis with mild systolic dome-shaped valve. Left, diastole; right, systole

Pulmonary stenosis

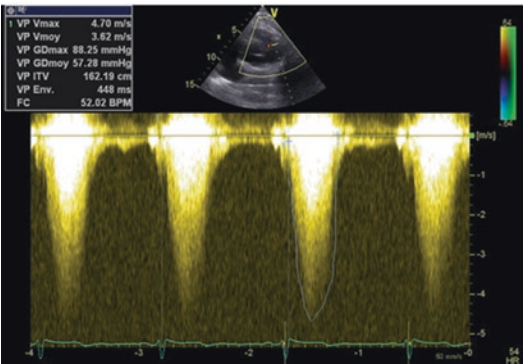


Fig. 11.18 Severe pulmonary stenosis continuous wave Doppler demonstrating a peak gradient of 88 mmHg

out symptoms and peak gradient >60 mmHg and a dome-shaped valve; patients with symptoms and peak gradient >50 mmHg and a dome-shaped valve [17]. Patients should be referred for surgery if hypoplastic annulus or severe regurgitation or sub or supra valvular stenosis.

Pulmonary Regurgitation

Etiology

Mild PR has been reported in 40–78% with normal PV. Acquired mild-to-moderate PR is most often seen in patients with pulmonary hyperten-

Table 11.2 Valve anatomy, valve hemodynamics and hemodynamic consequences of severe pulmonary regurgitation and severe pulmonary stenosis adapted from EACVI Recommendations and 2014 ACC/AHA guidelines [11, 19]

Definition	Valve anatomy	Valve hemodynamics	Hemodynamic consequences
Severe PR	Distorted or absent leaflets, annular dilatation	<ul style="list-style-type: none">• Colour jet fills RVOT• CW jet density and contour: dense laminar flow with steep deceleration slope; may terminate abruptly	<ul style="list-style-type: none">• Paradoxical septal motion (volume overload pattern)• RV enlargement
Severe PS	<ul style="list-style-type: none">• Thickened, distorted, possibly calcified leaflets with systolic doming and/or reduced excursion• Other anatomic abnormalities may be present, such as narrowed RVOT	<ul style="list-style-type: none">• Vmax >4 m/s; peak instantaneous gradient >64 mmHg	<ul style="list-style-type: none">• RV hypertrophy• possible RV, RA enlargement• Post-stenotic enlargement of main PA

RA right atrium, RVOT right ventricular outflow tract, RV right ventricle, PA pulmonary artery, PR pulmonary regurgitation, PS pulmonary stenosis, CW continuous wave

Pulmonary stenosis

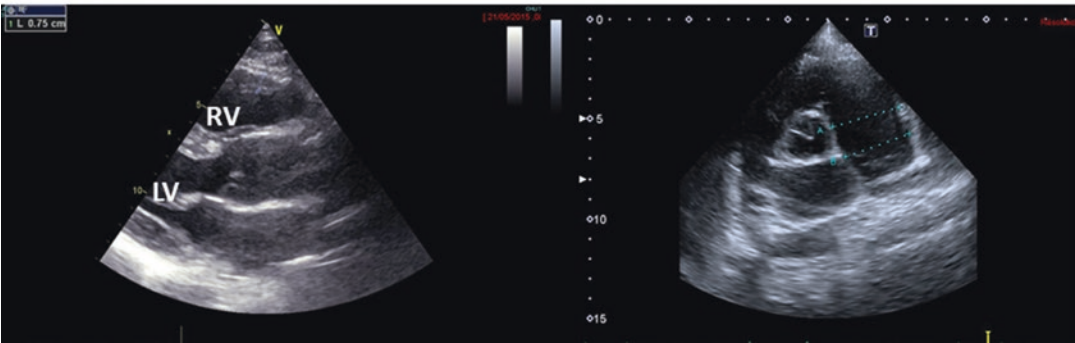


Fig. 11.19 Indirect findings with pulmonary stenosis. On the left, right ventricular hypertrophy (7 mm) visualized on a parasternal long-axis view; on the right, poststenotic PA dilatation (34 mm)

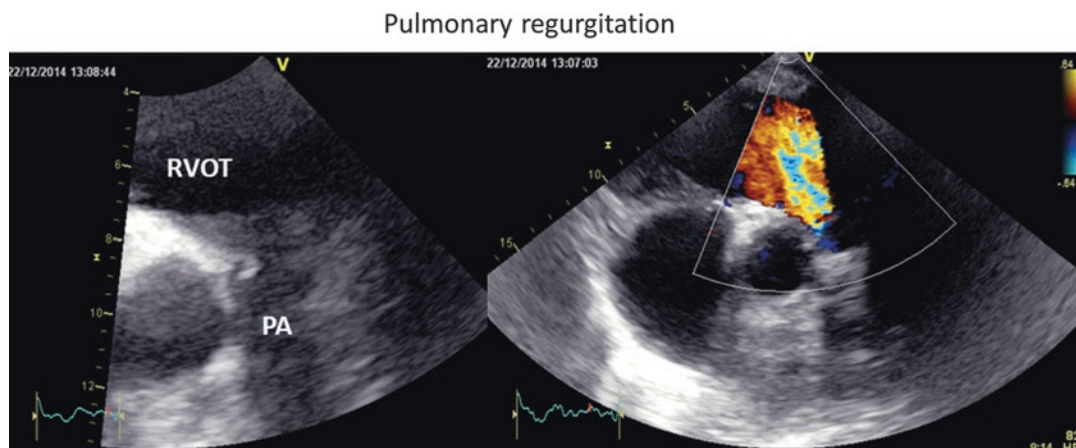


Fig. 11.20 Pulmonary regurgitation. Carcinoid heart disease of the pulmonary valve: on the left, parasternal short-axis view showing rigidity and fibrosis of one of the

cusps; on the right, colour Doppler showing moderate to severe pulmonary regurgitation

sion with dilatation of the PA. Severe PR is uncommon and usually observed in patients with anatomic abnormalities of the valve (quadricuspid or bicuspid valves, hypoplasia) or post-repair of tetralogy of Fallot [18]. Other causes include infectious endocarditis, carcinoid syndrome (Fig. 11.20) and rheumatic heart disease.

Assessment of Severity

Qualitative evaluation of PR [19] looks for anomalies of cusp number, valve motion (doming or prolapse) or structure (absent PV, hypoplasia) (Table 11.2). Color Doppler reveals a diastolic jet in the RVOT, beginning at the PV and directed towards the RV (Fig. 11.21). In severe PR, diastolic flow reversal may be seen in the PA. Severe PR has a longer duration of flow (holodiastolic) and a wider jet as the regurgitant jet crosses the PV than physiologic PR. When equalization of diastolic PA and right ventricular pressures occurs early in diastole, the colour jet can be brief and inaccurate. The density of the CW signal and the deceleration slope provide a qualitative measure of regurgitation (Fig. 11.22). The assessment of PR severity is usually estimated by the diameter of the jet at its origin [20]. The maximum colour jet diameter (width) is measured in diastole immediately below the PV (at the junction of the RVOT and pulmonary annulus) in the parasternal short-axis view or from the subcostal view. Although

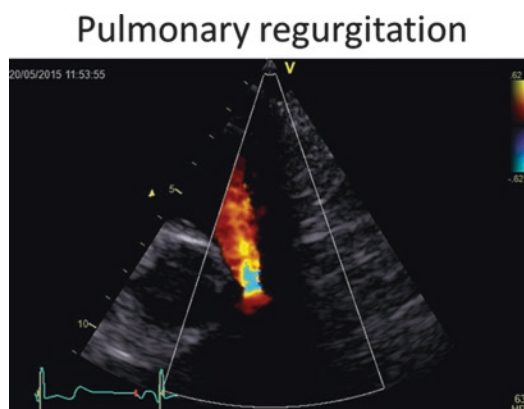


Fig. 11.21 Example of a moderate pulmonary regurgitation

this measurement suffers from a high inter-observer variability, a jet width that occupies >65% of the RV outflow tract width measured in the same frame is in favour of severe PR.

A semi-quantitative evaluation of PR can be provided by measurement of vena contracta width. Although the vena contracta width is probably a more accurate method than the jet width to evaluate PR severity by colour Doppler, it lacks validation studies. The 3D vena contracta is correlated with the 2D vena contracta and could provide more quantitative assessment of PR [21].

Quantitative evaluation of PR severity has been less validated and there is no clinically

Pulmonary regurgitation

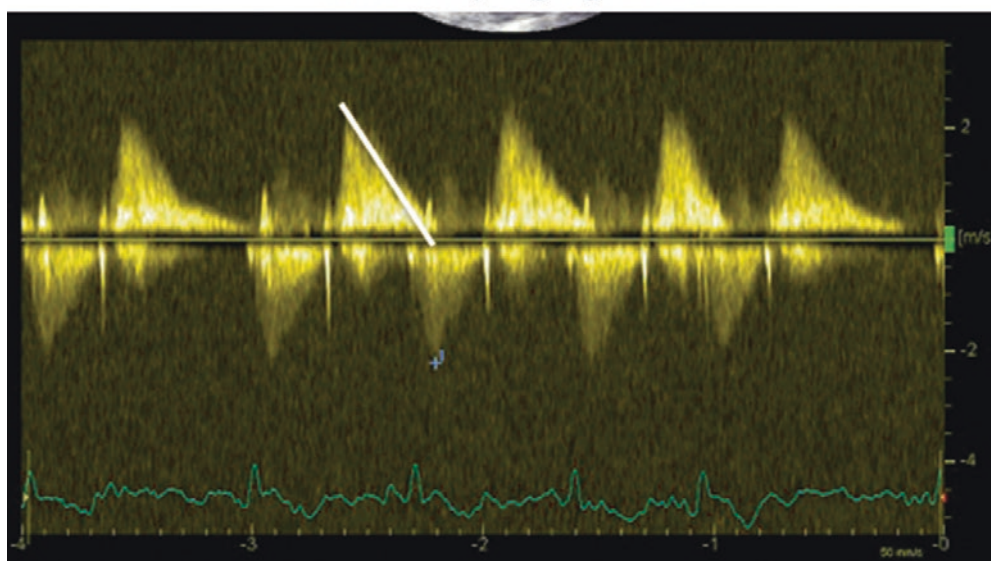


Fig. 11.22 Continuous wave Doppler of a severe pulmonary regurgitation demonstrating a steep deceleration slope

accepted method of quantifying PR using CW Doppler (Table 11.2).

Evaluation of the consequences of PR requires evaluation of the size and function of RV. Evidence of RV dilatation is however not specific for severe PR. Nevertheless, its absence suggests milder degree of PR.

References

1. Lamers WH, Virágh S, Wessels A, Moorman AF, Anderson RH. Formation of the tricuspid valve in the human heart. *Circulation*. 1995;91:111–21.
2. Anwar AM, Geleijnse ML, Soliman OII, McGhie JS, Frowijn R, Nemes A, van den Bosch AE, Galema TW, Cate Ten FJ. Assessment of normal tricuspid valve anatomy in adults by real-time three-dimensional echocardiography. *Int J Cardiovasc Imaging*. 2007;23:717–24.
3. Badano LP, Agricola E, Pérez de Isla L, Gianfagna P, Zamorano JL. Evaluation of the tricuspid valve morphology and function by transthoracic real-time three-dimensional echocardiography. *Eur J Echocardiogr*. 2009;10:477–84.
4. Shiran A, Sagie A. Tricuspid regurgitation in mitral valve disease incidence, prognostic implications, mechanism, and management. *J Am Coll Cardiol*. 2009;53:401–8.
5. Baumgartner H, Bonhoeffer P, De Groot NMS, de Haan F, Deanfield JE, Galie N, Gatzoulis MA, Gohlke-Baerwolf C, Kaemmerer H, Kilner P, Meijboom F, Mulder BJM, Oechslin E, Oliver JM, Serraf A, Szatmari A, Thaulow E, Vouhe PR, Walma E. ESC guidelines for the management of grown-up congenital heart disease (new version 2010): the Task Force on the Management of Grown-up Congenital Heart Disease of the European Society of Cardiology (ESC). *Eur Heart J*. 2010;31:2915–57.
6. Vahanian A, Alfieri O, Andreotti F, Antunes MJ, Baron-Esquivias G, Baumgartner H, Borger MA, Carrel TP, De Bonis M, Evangelista A, Falk V, Jung B, Lancellotti P, Pierard L, Price S, Schafers HJ, Schuler G, Stepinska J, Swedberg K, Takkenberg J, O'Connell Von UO, Windecker S, Zamorano JL, Zembala M. Guidelines on the Management of Valvular Heart Disease (version 2012): The Joint Task Force on the Management of Valvular Heart Disease of the European Society of Cardiology (ESC) and the European Association for Cardio-Thoracic Surgery (EACTS). *Eur Heart J*. 2012;33:2451–96.
7. Kwan J, Kim G-C, Jeon M-J, Kim D-H, Shiota T, Thomas JD, Park K-S, Lee W-H. 3D geometry of a normal tricuspid annulus during systole: a comparison study with the mitral annulus using real-time 3D echocardiography. *Eur J Echocardiogr*. 2007;8: 375–83.
8. Lancellotti P, Moura L, Pierard LA, Agricola E, Popescu BA, Tribouilloy C, Hagendorff A, Monin JL, Badano L, Zamorano JL. European Association of echocardiography recommendations for the assessment of valvular regurgitation. Part 2: mitral and

- tricuspid regurgitation (native valve disease). *Eur J Echocardiogr.* 2010;11:307–32.
9. Fukuda S, Gillinov AM, McCarthy PM, Stewart WJ, Song J-M, Kihara T, Daimon M, Shin M-S, Thomas JD, Shiota T. Determinants of recurrent or residual functional tricuspid regurgitation after tricuspid annuloplasty. *Circulation.* 2006;114:1582–7.
 10. Kim H-K, Kim Y-J, Park J-S, Kim KH, Kim K-B, Ahn H, Sohn D-W, Oh B-H, Park Y-B, Choi Y-S. Determinants of the severity of functional tricuspid regurgitation. *Am J Cardiol.* 2006;98:236–42.
 11. Nishimura RA, Otto CM, Bonow RO, Carabello BA, Erwin JP, Guyton RA, O’Gara PT, Ruiz CE, Skubas NJ, Sorajja P, Sundt TM, Thomas JD. 2014 AHA/ACC guideline for the management of patients with valvular heart disease. *J Am Coll Cardiol.* 2014;63:e57–e185.
 12. Tribouilloy CM, Enriquez-Sarano M, Capps MA, Bailey KR, Tajik AJ. Contrasting effect of similar effective regurgitant orifice area in mitral and tricuspid regurgitation: a quantitative Doppler echocardiographic study. *J Am Soc Echocardiogr.* 2002;15:958–65.
 13. Baumgartner H, Hung J, Bermejo J, Chambers JB, Evangelista A, Griffin BP, Iung B, Otto CM, Pellikka PA, Quiñones M. Echocardiographic assessment of valve stenosis: EAE/ASE recommendations for clinical practice. *Eur J Echocardiogr.* 2009;10:1–25.
 14. Anwar AM, Soliman O, van den Bosch AE, McGhie JS, Geleijnse ML, Cate Ten FJ, Meijboom FJ. Assessment of pulmonary valve and right ventricular outflow tract with real-time three-dimensional echocardiography. *Int J Cardiovasc Imaging.* 2007;23:167–75.
 15. Cuypers JAAE, Witsenburg M, van der Linde D, Roos-Hesselink JW. Pulmonary stenosis: update on diagnosis and therapeutic options. *Heart.* 2013;99:339–47.
 16. Vida VL, Angelini A, Guariento A, Frescura C, Fedrigo M, Padalino M, Sanders SP, Thiene G, Stellin G. Preserving the pulmonary valve during early repair of tetralogy of Fallot: anatomic substrates and surgical strategies. *J Thorac Cardiovasc Surg.* 2015;149:1358–1363.e1.
 17. Warnes CA, Williams RG, Bashore TM, Child JS, Connolly HM, Dearani JA, del Nido P, Fasules JW, Graham TP, Hijazi ZM, Hunt SA, King ME, Landzberg MJ, Miner PD, Radford MJ, Walsh EP, Webb GD. ACC/AHA 2008 Guidelines for the Management of Adults with Congenital Heart Disease: A Report of the American College of Cardiology/American Heart Association Task Force on Practice Guidelines (writing committee to develop guidelines on the management of adults with congenital heart disease). *Circulation.* 2008;118:e714–833.
 18. Bouzas B, Kilner PJ, Gatzoulis MA. Pulmonary regurgitation: not a benign lesion. *Eur Heart J.* 2005;26:433–9.
 19. Lancellotti P, Tribouilloy C, Hagendorff A, Moura L, Popescu BA, Agricola E, Monin JL, Pierard LA, Badano L, Zamorano JL, on behalf of the European Association of Echocardiography, Document Reviewers, Sicari R, Vahanian A, Roelandt JRTC. European Association of echocardiography recommendations for the assessment of valvular regurgitation. Part 1: aortic and pulmonary regurgitation (native valve disease). *Eur J Echocardiogr.* 2010;11:223–44.
 20. Williams RV, Minich LL, Shaddy RE, Pagotto LT, Tani LY. Comparison of Doppler echocardiography with angiography for determining the severity of pulmonary regurgitation. *Am J Cardiol.* 2002;89:1438–41.
 21. Pothineni KR, Nanda NC, Burri MV, Bell WC, Post JD. Live/real time three-dimensional transthoracic echocardiographic description of chordoma metastatic to the heart. *Echocardiography.* 2008;25:440–2.

The Role of Stress in Valvular Heart Disease

12

Luc A. Pierard

Introduction

Echocardiography is the cornerstone for evaluation of valvular disease. The majority of recommendations for valve interventions are based on the presence of symptoms, valvular severity and haemodynamics assessed at rest. However, valve diseases have a dynamic component with changes influenced by patient's heart rate, blood pressure, loading conditions and ventricular-arterial coupling. Imaging at rest could miss subclinical myocardial dysfunction. Exercise testing can evaluate valve disease during conditions which correspond to patient's daily activities. Stress imaging can identify haemodynamic changes induced by exercise or pharmacological agents.

Indications for Stress Testing

Stress testing should be considered in the presence of discrepancy between patient's symptoms and valvular severity: presence of symptoms but non-severe disease or absence of symptoms in the presence of severe disease. Exercise testing should be preferred over pharmacological stress. The prevalence of valve disease increases largely

with age, especially in the elderly patients. Symptomatic status can be difficult to insure because many patients reduce their activities progressively to avoid symptoms and may sometimes deny their symptoms. In addition, it is frequently difficult to ascertain that developing symptoms are related to valve disease, especially in the presence of co-morbidities such as coronary artery disease, systemic or pulmonary hypertension or chronic obstructive pulmonary disease. Therefore, stress imaging, in particular exercise echocardiography provides Doppler information, exercise-induced changes in aortic stenosis (AS) and mitral stenosis (MS), the dynamic condition of mitral regurgitation (MR), changes in systolic pulmonary arterial pressure, left ventricular (LV) filling pressure and LV function. There are contraindications to exercise testing: when valve intervention is recommended (symptomatic severe AS or MS), uncontrolled arrhythmias, systemic hypertension and inability to perform an adequate exercise.

Stress Protocols

Exercise testing should be performed under closed supervision. Symptom-limited test is desirable obtaining $\geq 85\%$ of predicted heart rate if possible. The patients should be tested without withdrawal of usual medications. Exercise echocardiography should be performed by an

L. A. Pierard
Cardiology Services, Domaine Universitaire
du Sart Tilman, Liege, Belgium
e-mail: lpierard@chu.ulg.ac.be

experienced cardiologist or sonographer. Semi-supine bicycle exercise testing is preferable to treadmill exercise because the latter technique allows imaging only during the recovery period [1]. Semi-supine exercise on a dedicated tilting table permits continuous monitoring and measurements at each state, including peak stress. The work load should be adapted for the individual patient: initially at 50 W with an increase of 25 W every 2 min when LV function is preserved; starting at 25 W with a 10 W increase every 2 min in elderly patients or in patients with decreased LV function. Criteria for stopping the test include: development of symptoms (significant dyspnea, chest pain, dizziness or syncope); decrease in systolic blood pressure, significant atrial or ventricular arrhythmias and ≥ 2 mm ST segment depression [2]. The relevant test parameters differ for every valvular disease. Table 12.1 presents parameters and indications for interventions according to valvular heart disease.

Aortic Stenosis

AS is the most prevalent valve disease in Europe [3].

Exercise Testing

Patients have a long latent asymptomatic period in which the risk of sudden cardiac death is low, lower than that of aortic valve replacement (AVR). Severe AS is defined by peak aortic velocity ≥ 4 m/sec, mean pressure gradient ≥ 40 mmHg and aortic valve area ≤ 1.0 cm² or ≥ 0.6 cm²/m². AVR is indicated in symptomatic patients and in patients with LV ejection fraction(EF) <50% (class I recommendation). Symptoms can be reported spontaneously by the patient or can develop during exercise testing. Exercise testing without imaging is useful to unmask symptoms in “pseudo-asymptomatic” patients. Up to one third of patients who claimed to be asymptomatic develop symptoms with exercise testing [4]. Dizziness is the most frequent symptom during exercise in the upright position (treadmill test). A

Table 12.1 Exercise stress echocardiography protocols according to valvular heart disease

	Aortic stenosis	Mitral stenosis	Mitral regurgitation
Baseline	Comprehensive resting echocardiography		
25 W	Mean aortic gradient	Mean mitral gradient	PISA radius
	Aortic valve area		CW MR jet
			EROA, RVol
	SPAP	SPAP	CW TR jet
	TR jet velocity	TR jet velocity	SPAP
	E/e' ratio		
Each 25 W increment and at peak	Symptoms	Symptoms	Symptoms
	Mean aortic gradient	Mean mitral gradient	EROA, RVol
	Aortic valve area		
	SPAP	SPAP	SPAP
	TR jet velocity		
	GLS		GLS
	LV function: 2-dimension grey-scale images in 4, 2 and 3 chamber views (>60 FPS)		

CW continuous wave Doppler, EROA effective regurgitant orifice area, FPS frame per second, GLS Global longitudinal strain, LV left ventricle, MR mitral regurgitation, PISA proximal isovelocity surface area, PW pulsed-wave Doppler, RVol Regurgitant volume, SPAP systolic pulmonary artery pressure, TR tricuspid regurgitation

negative exercise test supports watchful waiting strategy, because the negative predictive value is very high. In contrast, the positive predictive value is good only in patients <70-years-old and physically active but much lower in patients >70-years-old [4]. Although the occurrence of symptoms is the most powerful parameter to stratify patient's risk, other parameters have also prognostic value: inadequate increase in systolic blood pressure (<20 mmHg increase or decrease) and complex ventricular arrhythmias. During treadmill test, dizziness has the highest positive predictive value for the development of symptoms during the following year. In contrast, ST-depression (>2 mm, horizontal or down sloping), does not improve the predictive value, and

cannot reliably identify concomitant coronary artery disease. New parameters can predict long-term mortality: metabolic equivalent (METs) $<85\%$ -predicted METs [5] and post-exercise slow heart rate recovery (decrease in heart rate from peak to 1 min post-exercise).

Of note, exercise testing is safe in asymptomatic or event pseudo-asymptomatic patients with AS. Even if some studies have found exercise testing safe in patients with class II NYHA, exercise testing remains contra-indicated in symptomatic patients (class III recommendation in both European and American guidelines).

Exercise Echocardiography (Fig. 12.1)

Angina, dizziness or syncope during exercise can usually be linked to valve disease. In semi-supine position, the most frequent symptom is dyspnea. The occurrence of rapidly reversible dyspnea at high workload should not be considered as pathological especially in old patients. In contrast, dyspnea developing in the early stages of exercise should be considered pathological, but this is a non-specific symptom that could develop in deconditioned patients or patients with co-morbidities.

Mean Gradient

Exercise-induced increase in mean pressure gradient is associated with an increased risk of cardiac events. exercise-induced increase in mean pressure gradient $>18\text{--}20$ mmHg has been shown to be independently associated with a large increase in risk [6, 7]. Such an increase in pressure gradient during exercise can reflect the presence of a more severe AS and a rigid, non-compliant aortic valve.

Changes in LV Function

The following parameters of LV function can be useful to stratify risk: decrease or small increase in LVEF during exercise, LV global longitudinal strain (GLS) with 2D speckle tracking method

increasing $<1.4\%$ during exercise [8–10]. A reduction of LV contractile reserve in basal segments may be more specific. Although the guidelines suggest assessing changes in LV function with exercise, there are no precise cut-off values. Indeed, parameters may fall within the range for test-retest variability. LV longitudinal strain has not yet been validated against patient outcome but can predict maximal exercise capacity in terms of peak oxygen consumption.

Systolic Pulmonary Artery Pressure

Pulmonary hypertension at rest (SPAP >50 mmHg) is associated with poor prognosis and higher mortality rate after AVR. However, pulmonary hypertension at rest is rare in asymptomatic patients. In contrast, exercise pulmonary hypertension (SPAP >60 mmHg) may develop in more than one half of asymptomatic patients and seems to be independently associated with an increased risk of cardiac events [11].

Impact on Management

No randomized trial has been yet conducted with patients with asymptomatic severe AS. Table 12.2 presents the current guidelines in this setting.

Low Flow/Low Gradient AS

Patients with severe AS can have low gradient despite reduced aortic valve area as a result of low forward stroke volume. This condition can be associated with reduced LVEF ($<40\%$) or preserved LV ejection fraction (so called paradoxical low-flow severe AS).

Low-flow/low-gradient AS with reduced LV ejection fraction is defined as aortic valve area <1.0 cm² or >0.6 cm²/m², low pressure gradient ($<30\text{--}40$ mmHg), low LVEF ($<40\%$) and low flow (stroke volume index <35 ml/m²) [12, 13]. Two different conditions need to be identified: true severe AS related to fixed severe AS with afterload mismatch and concomitant myocardial

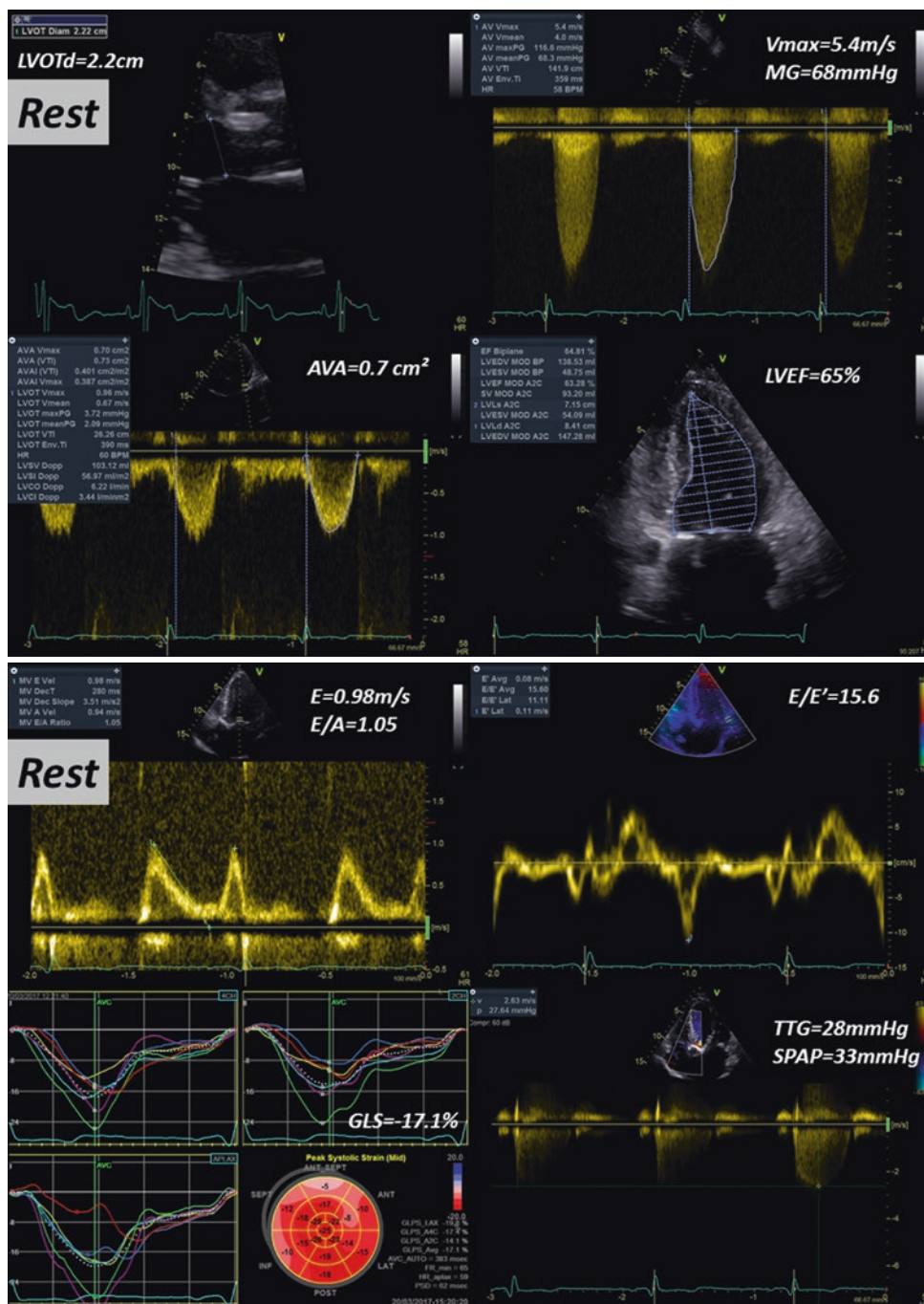


Fig. 12.1 Panel a. Asymptomatic patient with severe aortic stenosis (AS). Rest echocardiography identifies a transvalvular peak velocity (Vmax) of 5.4 m/s, an aortic valve area (AVA) by the continuity equation of 0.7 cm², indicating severe AS. The left ventricular ejection fraction (LVEF) is preserved, 65% by Simpson's biplane rule. LVOTD-left ventricular outflow tract diameter; Vmax-maximal transaortic velocity; MG-mean transaortic pressure gradient. Panel b. Rest echocardiographic evaluation pleads for elevated left ventricular (LV) filling pressures

with an E/e' ratio >15. However, the transtricuspid systolic pressure gradient (TTG) is low, pleading for a low likelihood of pulmonary hypertension at rest (estimated systolic pulmonary artery pressure SPAP = 33 mmHg). The global longitudinal strain (GLS) is low in this patient. Panel c. At low level exercise, the MG increases of only 8 mmHg, but the patient develops rapidly exercise induced pulmonary hypertension, SPAP = 78 mmHg. Moreover, the GLS at low level exercise is reduced as compared to rest, while there is no increase in LVEF with exercise

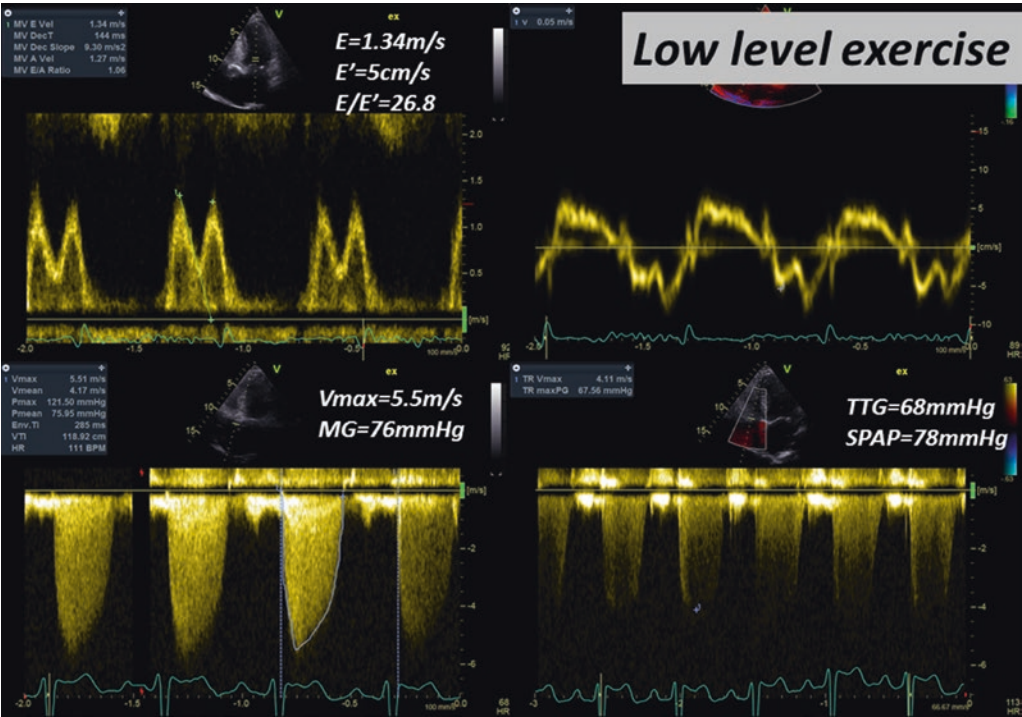


Fig. 12.1 (continued)

Table 12.2 Suggested predictors of outcome with exercise testing and imaging in severe valve disease

Aortic stenosis	– Contra-indicated in symptomatic patients
	– Symptoms related to valve disease
	– <85% predicted METs
	– Increase in mean gradient ≥ 18 –20 mmHg
	– Decrease in LVEF
	– Small change in LV GLS <1.4%
Primary MR	– Pulmonary hypertension (SPAP >60 mmHg)
	– Symptoms related to valve disease
	– <100% predicted METs
	– Abnormal HRR (<18% beat drop in HR at 1 min post exercise)
	– Increase in EROA >10 mm ²
	– Increase in RVol >15 ml
	– PHT (SPAP >50 mmHg)
	– RV dysfunction (TAPSE <19 mm)
Secondary MR	– Increase of LV GLS <2%
	– Dyspnea
	– Increase in EROA >13 mm ²
	– PHT (SPAP >60 mmHg)

METs metabolic equivalents, *GLS*; *LVEF* left ventricular ejection fraction, *Global longitudinal strain*, *HRR* heart rate reduction, *EROA* effective regurgitant orifice area, *RVol* Regurgitant volume, *SPAP* systolic pulmonary artery pressure, *PHT* pulmonary hypertension

contractile dysfunction vs pseudo-severe AS corresponding to non-severe AS and cardiomyopathy. According to guidelines, Dobutamine stress echocardiography should be considered for this purpose [14]. A low-dose protocol is recommended: gradual increment of Dobutamine (5 $\mu\text{g/kg/min}$) at least 5 min interval up to a maximum dose of 20 $\mu\text{g/kg/min}$. True severe AS in the presence of flow reserve is defined as an increase in mean gradient to >40 mmHg (ACC/AHA guidelines), and small (<0.3 cm²) increase in aortic valve area [12]. Flow reserve is defined by >20% increase of stroke volume with Dobutamine. Patients with true AS and flow reserve will benefit the most from aortic valve intervention [15]. Pseudo-severe AS is identified by significant increase in aortic valve area (≥ 0.3 cm²) and a mean pressure gradient <40 mmHg. These patients must be treated with heart failure therapy. A third condition is possible: absence of flow reserve. The distinction between true and pseudo-severe AS is of course difficult in the absence of contractile reserve. AVR may be considered (class IIb) but with an increased risk of early post-operative mortality

and a good long-term survival in the patients who can be discharged from the hospital. In the absence of flow reserve, other imaging modalities are indicated, especially calcium score using computed tomography [16, 17]. As the increase in transvalvular flow differs from patient to patient, an interesting parameter is the projected aortic valve area (AVA) [18]. It consists on the evaluation of AVA at a mean transvalvular flow rate (Q) of 250 ml/s. The equation is: $AVA_{proj} = (AVA_{peak} - AVA_{rest}) / (Q_{peak} - Q_{rest}) \times (250 - Q_{rest}) + AVA_{rest}$. Q is obtained by dividing stroke volume (in ml) by LV ejection time at rest and at peak Dobutamine, respectively. An AVA_{proj} is severe when $\leq 1.0 \text{ cm}^2$.

Low Flow/Low Gradient AS with Preserved LV Ejection Fraction

This condition is defined by LVEF $\geq 50\%$, stroke volume index $\leq 35 \text{ ml/m}^2$, mean pressure gradient $< 40 \text{ mmHg}$ and AVA $< 1 \text{ cm}^2$ [19]. It is essential to confirm carefully that AS is severe. Indeed, in the continuity equation, LV outflow tract is considered to be circular, although it is frequently elliptic, leading to an underestimated stroke volume. The role of stress testing and imaging remains limited [20]. A vasodilatory stress catheterization using nitroprusside could be used. Exercise echocardiogram could theoretically be useful, but the patients who could undergo an intervention need to be symptomatic, according to ESC/EACTS and AHA/ACC guidelines [12, 13].

Aortic Regurgitation

Exercise testing is useful to unmask symptoms and to assess functional capacity.

In contrast, exercise echocardiography is not routinely recommended in patients with aortic regurgitation (AR). Heart rate increase reduces diastolic time and thus regurgitant volume. LVEF measurement during exercise is probably less

interesting than the assessment of LV longitudinal function using time Doppler imaging and preferably 2Dstrain imaging [21]. No cut-off value has yet been validated in this setting. Practically, the assessment of contractile reserve may be useful in patients with borderline value of LVEF and/or systolic dimension.

Mitral Stenosis

The ESC/EACTS and ACC/AHA guidelines indicate that stress echocardiography is useful in patients who present a discrepancy between severity of MS at rest and symptoms in two conditions: the patients with mild MS but limiting dyspnea and asymptomatic patients with moderate to severe MS for unmasking symptoms [12, 13].

Exercise stress is more physiologic and preferable in patients who can exercise. Dobutamine stress echocardiography can also be performed and is safe and feasible. Whatever the need of stress, medical therapy should not be withdrawn, especially β -blocking agents.

Exercise capacity needs to be evaluated. Transmitral and tricuspid velocities are recorded to estimate transmitral mean gradient changes and SPAP.

With Dobutamine, a cut-off value of mean pressure gradient of 18 mmHg allows a good prediction of further events [22]. With exercise, it is not only the magnitude of increase in mean pressure gradient and SPAP but the rapidity of such an increase. For exercise, the cut-off value of SPAP is of 60 mmHg. This value is frequently obtained in elderly patients at peak exercise. It is important to measure exercise-induced changes at each stage of exercise and rather than to only compare rest to peak exercise values [23] (Fig. 12.2).

Atrioventricular compliance is calculated as follows: AV compliance (ml/mmHg) = $1270 / (MVA [\text{cm}^2] / E\text{-wave downslope} [\text{cm/s}])$ [24]. AV compliance is considered to be low when $\leq 4 \text{ ml/mmHg}$.

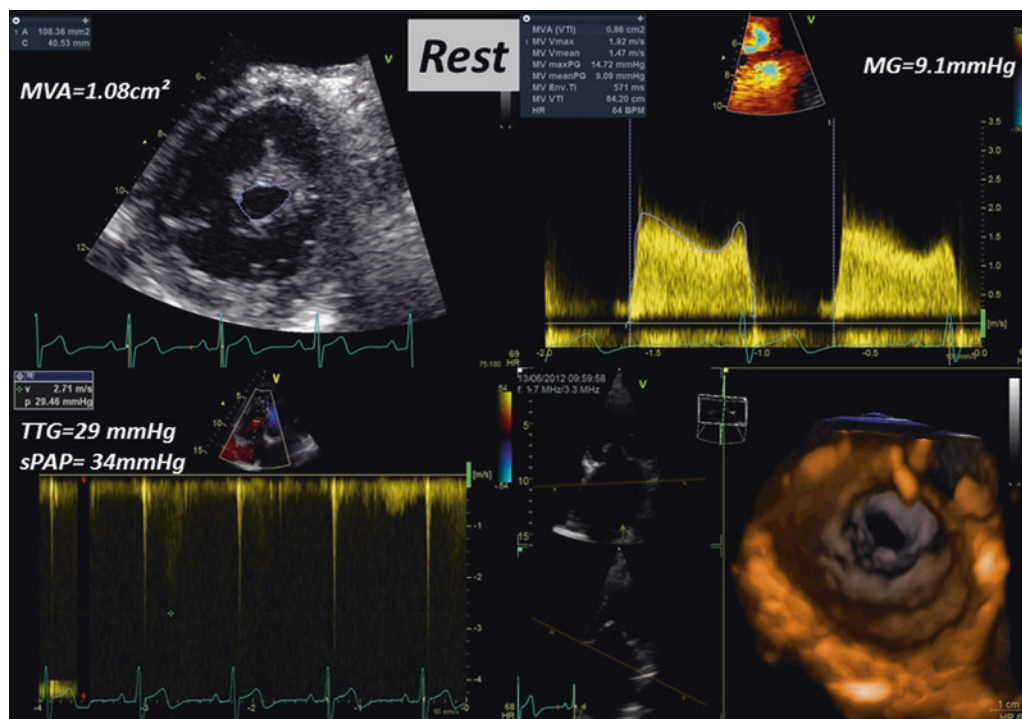


Fig. 12.2 Panel a. Asymptomatic young patient (36 years old) with moderate mitral stenosis of rheumatic etiology. Rapidly during exercise the patient develops an increase of transmitral pressure gradient up to 20.5 mmHg accompa-

nied by a significant increase in systolic pulmonary artery pressure. *MVA* mitral valve area by planimetry, *MG* transmitral diastolic pressure gradient, *HR* heart rate, *TTG* tricuspid pressure gradient, *sPAP* systolic pulmonary pressure

Mitral Regurgitation

Primary Mitral Regurgitation

Primary organic MR is usually well tolerated even when it is severe. The hemodynamic consequences of severe primary MR are LV remodeling, pulmonary hypertension and atrial fibrillation. The indications of MVR are the presence of symptoms (class I), LV dilatation: end-systolic diameter ≥ 40 mm in the ACC/AHA guidelines [12] or ≥ 45 mm for ESC/EACTS guidelines (class I) or LVEF $\leq 60\%$ [13].

Primary MR is a dynamic condition. Exercise testing can identify patients with symptoms out of proportion with MR severity at rest. Reduced exercise capacity is associated with a guarded prognosis, regardless of resting MR severity [25].

According the American and European guidelines, exercise echocardiography on a dedicated table should be used to evaluate changes in MR severity, SPAP and right ventricular function. Exercise-induced changes in MR are not related to the severity of MR at rest. A significant increase in MR severity is defined as an increase of ERO ≥ 10 mm² and RVol ≥ 15 ml [26]. Such changes are correlated with exercise-induced pulmonary hypertension. While pulmonary hypertension at rest is unfrequent in asymptomatic patients, exercise-induced pulmonary hypertension, defined as SPAS >60 mmHg is much more frequently observed and is associated with reduced event-free survival [27]. RV function during exercise can be assessed using tricuspid annular plane systolic excursion (TAPSE). Exercise-induced RV dysfunction is identified when TAPSE is <19 mm [28].

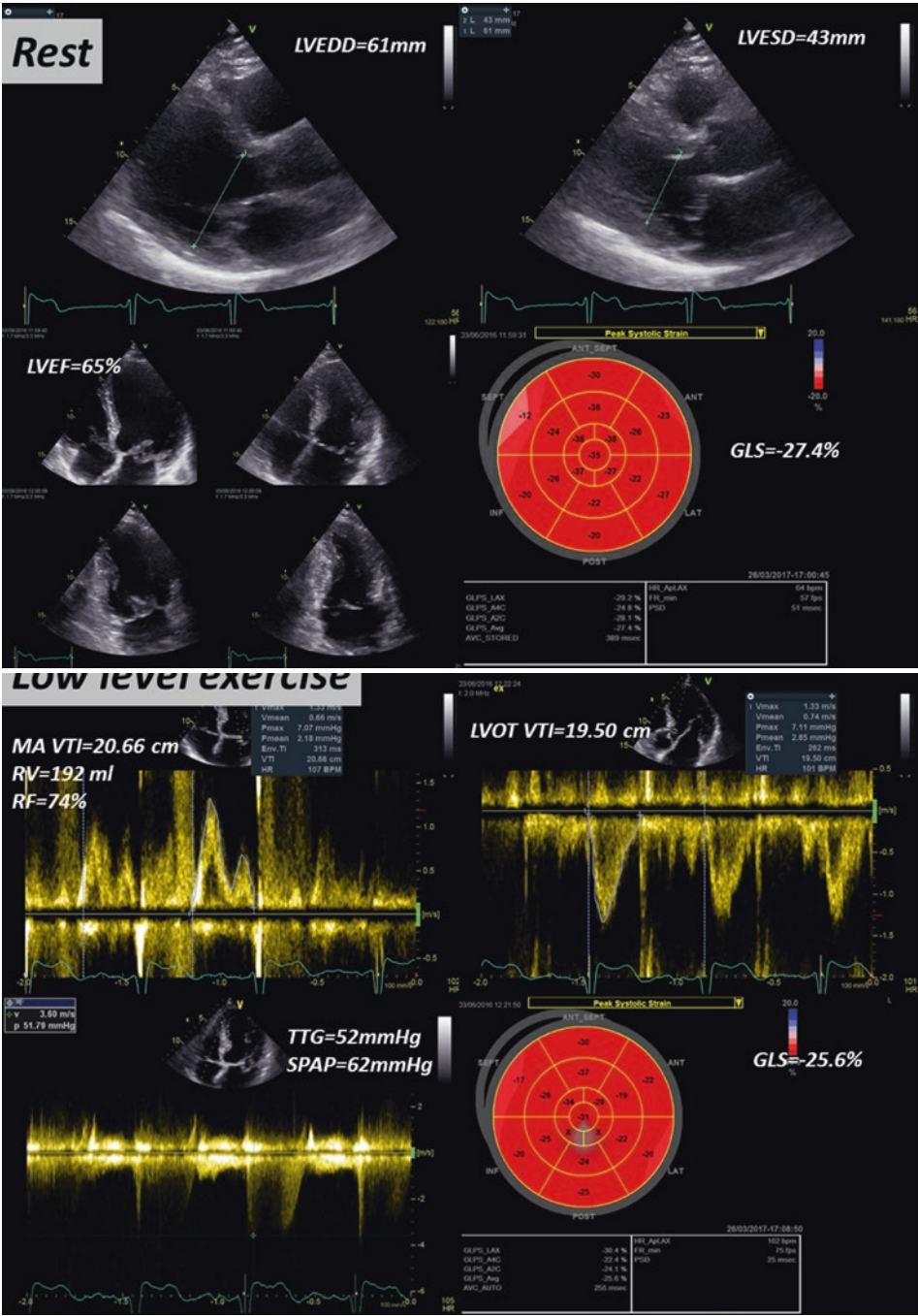


Fig. 12.3 Panel a. Asymptomatic patient with severe organic mitral regurgitation (MR) due to a prolapse of the posterior mitral valve leaflet. The left ventricular end-diastolic diameter (LVEDD) is enlarged, as well as the end-systolic diameter (LVESD = 43 mm), the left ventricular ejection fraction is preserved (LVEF = 65%), as well as the GLS = -27.4%. The PISA method and the Doppler volumetric method indicate severe MR. Panel b. During low level exercise, there is a rapid increase in pulmonary artery pressure (SPAP = 62 mmHg) and a decrease

in LV longitudinal function, as assessed by GLS (GLS = -25.6%), both predictors of worse outcome in an asymptomatic patient with severe MR. *EROA* effective regurgitant orifice area by PISA method, *RV* regurgitant volume, *PISA-RV* regurgitant volume by PISA method, *E* transmitral early diastolic velocity, *MA* mitral annulus, *VTI* velocity time integral, *TTG* transtricuspid systolic pressure gradient, *SPAP* systolic pulmonary artery pressure, *LVOTd* left ventricular outflow tract diameter

Contractile Reserve

Identify subclinical LV dysfunction is important as absence of contractile reserve with exercise predicts worse post-operative LV function. Absence of contractile reserve can be defined as <4% increase in LVEF [29] or exercise-induced increase <2% of global longitudinal strain (GLS). This parameter appears to be more reliable, as increased LVEF can be related to exercise-induced increase in MR severity [30] (Fig. 12.3).

Impact on Management

In asymptomatic patients with severe primary MR and LVEF the ESC/EACTS guidelines in 2012 indicate that surgery may be considered in patients with SPAP ≥ 60 mmHg as a class IIb recommendation (This has been taken out in the 2017 Guidelines). Exercise echocardiography can stratify risk and prognosis. Reduced exercise capacity (<100% predicted METs), abnormal heart rate response (<18 beat drop in heart rate at 1 min post-exercise) [31], significant exercise-induced increase in MR, patients without LV contractile reserve can be integrated in the decision making. Such patients could be submitted to early mitral valve repair (MVR) in high-volume surgical centers.

Secondary Mitral Regurgitation

Secondary MR is not a valve disease but represents the consequences of LV dilatation and dysfunction. It is a complication of dilated cardiomyopathy and more frequently coronary artery disease, in patients with prior myocardial infarction, especially frequent after posterior myocardial infarction. Mitral valvular deformation results from apical and posterior displacement of one or both papillary muscles which increase tethering forces and lead to incomplete mitral valve closure [32]. Tethering forces can be estimated by tenting area or tenting volume and apical displacement of the coaptation point.

Indication for Stress Testing

The 2014 ACC/AHA guideline do not make a recommendation for stress testing in patients

with secondary MR. the 2012 ESC/EACTS guidelines indicate that stress testing is useful in patients with mild MR undergoing elective coronary artery bypass grafting and in patients with unexplained dyspnea out of proportion with MR severity at rest, patients with acute pulmonary edema without an obvious cause and for risk stratification of mortality and heart failure [13, 33, 34]. In the 2017 Guidelines, combined surgery is no longer recommended in patients with moderate secondary MR submitted to surgical revascularization. Dobutamine stress echocardiography can evaluate myocardial viability and/or inducible ischemia. However, exercise echocardiography is better suited to evaluate the dynamic component of secondary MR.

Changes in MR Severity

In patients with ischemic MR, there is no relationship between the severity of MR at rest and the exercise induced increase or decrease of MR. Exercise-induced increase in ERO ≥ 13 mm² is associated with increased mortality and hospitalization for acute heart failure [35, 36]. It is frequently accompanied by pulmonary hypertension. Technically, assessing pulmonary hypertension from peak tricuspid regurgitation velocity is easier than measurement of dynamic increase in MR severity which can be reproducible only in experienced hands (Fig. 12.4).

Management

Both American and European guidelines recommend combined mitral valve surgery in patients undergoing surgical revascularization who have severe secondary MR. A randomized trial has shown no difference between MV repair and MV replacement [37]. In addition, another trial in patients with only moderate secondary MR did not show a benefit from combined surgery as compared to revascularization alone [38]. Although there is no precise recommendation in the official guidelines [39], exercise echocardiography can identify patient who could be submitted to combined surgery: patients with severe dyspnea during

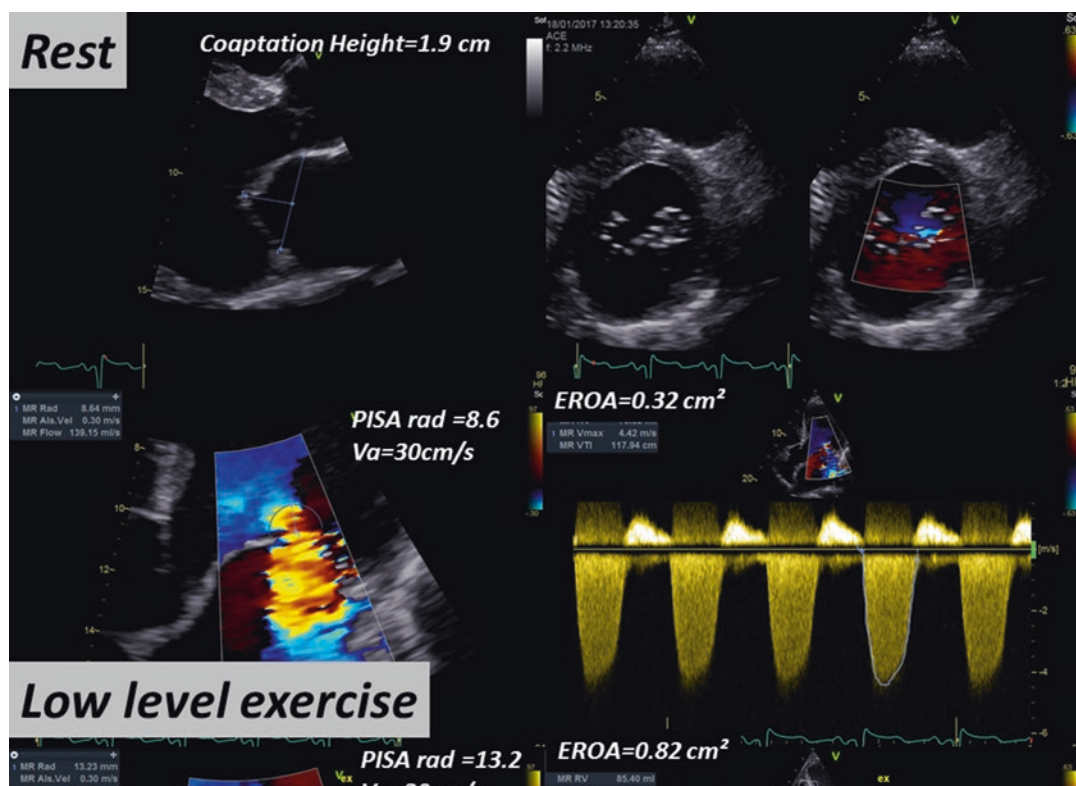


Fig. 12.4 Patient with severe ischemic mitral regurgitation at rest with severe deformation of the mitral valve apparatus. There is already pulmonary hypertension present at rest. After a low workload of 35 W, the patient develops an increase in mitral regurgitation severity

accompanied by a significant increase in pulmonary artery pressure. *PISA rad* proximal isovelocity surface area radius, *Va* aliasing velocities, *EROA* effective regurgitant orifice area, *TTE* transtricuspid pressure gradient, *sPAP* systolic pulmonary pressure

exercise associated with a large increase in MR severity and the development of significant pulmonary hypertension.

management based on stress imaging is associated with improved outcomes.

Conclusion

Most recommendations for valve intervention are still based on presence of symptoms related to valve disease and LV consequences at rest. Stress testing is indicated in the presence of discrepancies between clinical symptoms and severity of valve disease. Exercise imaging can provide, in addition of inducible symptoms, the dynamic components of valve disease and their consequences on LV function and pulmonary circulation. Large registries and preferably randomized clinical trials are required to indicate that clinical

References

1. Pellikka PA, Nagueh SF, Elhendy AA, Kuehl CA, Sawada SG, American Society of Echocardiography. American Society of Echocardiography recommendations for performance, interpretation, and application of stress echocardiography. *J Am Soc Echocardiogr*. 2007;20(9):1021–41.
2. Lancellotti P, Magne J, Pierard LA. The role of stress testing in evaluation of asymptomatic patients with aortic stenosis. *Curr Opin Cardiol*. 2013;28(5):531–9.
3. Iung B, Baron G, Butchart EG, Delahaye F, Gohlke-Barwolf C, Levang OW, Tornos P, Vanoverschelde JL, Vermeer F, Boersma E, Ravaud P, Vahanian A. A prospective survey of patients with valvular heart disease in Europe: The Euro Heart Survey on Valvular Heart Disease. *Eur Heart J*. 2003;24(13):1231–43.

4. Das P, Rimington H, Chambers J. Exercise testing to stratify risk in aortic stenosis. *Eur Heart J*. 2005;26(13):1309–13.
5. Masri A, Goodman AL, Barr T, Grimm RA, Sabik JF, Gillinov AM, Rodriguez LL, Svensson LG, Griffin BP, Desai MY. Predictors of long-term outcomes in asymptomatic patients with severe aortic stenosis and preserved left ventricular systolic function undergoing exercise echocardiography. *Circ Cardiovasc Imaging*. 2016;9(7).
6. Lancellotti P, Lebois F, Simon M, Tombeux C, Chauvel C, Pierard LA. Prognostic importance of quantitative exercise Doppler echocardiography in asymptomatic valvular aortic stenosis. *Circulation*. 2005;112(9 Suppl):I377–82.
7. Marechaux S, Hachicha Z, Bellouin A, Dumesnil JG, Meimoun P, Pasquet A, Bergeron S, Arsenault M, Le Tourneau T, Ennezat PV, Pibarot P. Usefulness of exercise-stress echocardiography for risk stratification of true asymptomatic patients with aortic valve stenosis. *Eur Heart J*. 2010;31(11):1390–7.
8. Leurent G, Donal E, de Place C, Chabanne C, Gervais R, Fougere C, le Helloco A, Daubert JC, Mabo P, Laurent M. Argument for a Doppler echocardiography during exercise in assessing asymptomatic patients with severe aortic stenosis. *Eur J Echocardiogr*. 2009;10(1):69–73.
9. Lancellotti P, Karsera D, Tumminello G, Lebois F, Pierard LA. Determinants of an abnormal response to exercise in patients with asymptomatic valvular aortic stenosis. *Eur J Echocardiogr*. 2008;9(3):338–43.
10. Donal E, Thebault C, O'Connor K, Veillard D, Rosca M, Pierard L, Lancellotti P. Impact of aortic stenosis on longitudinal myocardial deformation during exercise. *Eur J Echocardiogr*. 2011;12(3):235–41.
11. Lancellotti P, Magne J, Donal E, O'Connor K, Dulgheru R, Rosca M, Pierard LA. Determinants and prognostic significance of exercise pulmonary hypertension in asymptomatic severe aortic stenosis. *Circulation*. 2012;126(7):851–9.
12. Nishimura RA, Otto CM, Bonow RO, Carabello BA, Erwin JP 3rd, Guyton RA, O'Gara PT, Ruiz CE, Skubas NJ, Sorajja P, Sundt TM 3rd, Thomas JD, Members AATF. 2014 AHA/ACC guideline for the management of patients with valvular heart disease: executive summary: a report of the American College of Cardiology/American Heart Association Task Force on Practice Guidelines. *Circulation*. 2014;129(23):2440–92.
13. Joint Task Force on the Management of Valvular Heart Disease of the European Society of C, European Association for Cardio-Thoracic S, Vahanian A, Alfieri O, Andreotti F, Antunes MJ, Baron-Esquivias G, Baumgartner H, Borger MA, Carrel TP, De Bonis M, Evangelista A, Falk V, Jung B, Lancellotti P, Pierard L, Price S, Schafers HJ, Schuler G, Stepinska J, Swedberg K, Takkenberg J, Von Oppell UO, Windecker S, Zamorano JL, Zembala M. Guidelines on the management of valvular heart disease (version 2012). *Eur Heart J*. 2012;33(19):2451–96.
14. Monin JL, Monchi M, Gest V, Duval-Moulin AM, Dubois-Rande JL, Gueret P. Aortic stenosis with severe left ventricular dysfunction and low trans-valvular pressure gradients: risk stratification by low-dose dobutamine echocardiography. *J Am Coll Cardiol*. 2001;37(8):2101–7.
15. Monin JL, Quere JP, Monchi M, Petit H, Baleynaud S, Chauvel C, Pop C, Ohlmann P, Lelguen C, Dehant P, Tribouilloy C, Gueret P. Low-gradient aortic stenosis: operative risk stratification and predictors for long-term outcome: a multicenter study using dobutamine stress hemodynamics. *Circulation*. 2003;108(3):319–24.
16. Cuffe C, Serfaty JM, Cimadevilla C, Laissy JP, Himbert D, Tubach F, Duval X, Jung B, Enriquez-Sarano M, Vahanian A, Messika-Zeitoun D. Measurement of aortic valve calcification using multislice computed tomography: correlation with haemodynamic severity of aortic stenosis and clinical implication for patients with low ejection fraction. *Heart*. 2011;97(9):721–6.
17. Clavel MA, Messika-Zeitoun D, Pibarot P, Aggarwal SR, Malouf J, Araoz PA, Michelena HI, Cuffe C, Larose E, Capoulade R, Vahanian A, Enriquez-Sarano M. The complex nature of discordant severe calcified aortic valve disease grading: new insights from combined Doppler echocardiographic and computed tomographic study. *J Am Coll Cardiol*. 2013;62(24):2329–38.
18. Clavel MA, Burwash IG, Mundigler G, Dumesnil JG, Baumgartner H, Bergler-Klein J, Senechal M, Mathieu P, Couture C, Beanlands R, Pibarot P. Validation of conventional and simplified methods to calculate projected valve area at normal flow rate in patients with low flow, low gradient aortic stenosis: the multicenter TOPAS (True or Pseudo Severe Aortic Stenosis) study. *J Am Soc Echocardiogr*. 2010;23(4):380–6.
19. Hachicha Z, Dumesnil JG, Bogaty P, Pibarot P. Paradoxical low-flow, low-gradient severe aortic stenosis despite preserved ejection fraction is associated with higher afterload and reduced survival. *Circulation*. 2007;115(22):2856–64.
20. Clavel MA, Ennezat PV, Marechaux S, Dumesnil JG, Capoulade R, Hachicha Z, Mathieu P, Bellouin A, Bergeron S, Meimoun P, Arsenault M, Le Tourneau T, Pasquet A, Couture C, Pibarot P. Stress echocardiography to assess stenosis severity and predict outcome in patients with paradoxical low-flow, low-gradient aortic stenosis and preserved LVEF. *JACC Cardiovasc Imaging*. 2013;6(2):175–83.
21. Wahi S, Haluska B, Pasquet A, Case C, Rimmerman CM, Marwick TH. Exercise echocardiography predicts development of left ventricular dysfunction in medically and surgically treated patients with asymptomatic severe aortic regurgitation. *Heart*. 2000;84(6):606–14.
22. Reis G, Motta MS, Barbosa MM, Esteves WA, Souza SF, Bocchi EA. Dobutamine stress echocardiography for noninvasive assessment and risk stratification of patients with rheumatic mitral stenosis. *J Am Coll Cardiol*. 2004;43(3):393–401.

23. Brochet E, Detaint D, Fondard O, Tazi-Mezalek A, Messika-Zeitoun D, Iung B, Vahanian A. Early hemodynamic changes versus peak values: what is more useful to predict occurrence of dyspnea during stress echocardiography in patients with asymptomatic mitral stenosis? *J Am Soc Echocardiogr*. 2011;24(4):392–8.
24. Schwammenthal E, Vered Z, Agranat O, Kaplinsky E, Rabinowitz B, Feinberg MS. Impact of atrioventricular compliance on pulmonary artery pressure in mitral stenosis: an exercise echocardiographic study. *Circulation*. 2000;102(19):2378–84.
25. Messika-Zeitoun D, Johnson BD, Nkomo V, Avierinos JF, Allison TG, Scott C, Tajik AJ, Enriquez-Sarano M. Cardiopulmonary exercise testing determination of functional capacity in mitral regurgitation: physiologic and outcome implications. *J Am Coll Cardiol*. 2006;47(12):2521–7.
26. Magne J, Lancellotti P, Pierard LA. Exercise-induced changes in degenerative mitral regurgitation. *J Am Coll Cardiol*. 2010;56(4):300–9.
27. Magne J, Lancellotti P, Pierard LA. Exercise pulmonary hypertension in asymptomatic degenerative mitral regurgitation. *Circulation*. 2010;122(1):33–41.
28. Kusunose K, Popovic ZB, Motoki H, Marwick TH. Prognostic significance of exercise-induced right ventricular dysfunction in asymptomatic degenerative mitral regurgitation. *Circ Cardiovasc Imaging*. 2013;6(2):167–76.
29. Lee R, Haluska B, Leung DY, Case C, Mundy J, Marwick TH. Functional and prognostic implications of left ventricular contractile reserve in patients with asymptomatic severe mitral regurgitation. *Heart*. 2005;91(11):1407–12.
30. Magne J, Mahjoub H, Dulgheru R, Pibarot P, Pierard LA, Lancellotti P. Left ventricular contractile reserve in asymptomatic primary mitral regurgitation. *Eur Heart J*. 2014;35(24):1608–16.
31. Naji P, Griffin BP, Asfahan F, Barr T, Rodriguez LL, Grimm R, Agarwal S, Stewart WJ, Mihaljevic T, Gillinov AM, Desai MY. Predictors of long-term outcomes in patients with significant myxomatous mitral regurgitation undergoing exercise echocardiography. *Circulation*. 2014;129(12):1310–9.
32. Lancellotti P, Marwick T, Pierard LA. How to manage ischaemic mitral regurgitation. *Heart*. 2008;94(11):1497–502.
33. Grigioni F, Enriquez-Sarano M, Zehr KJ, Bailey KR, Tajik AJ. Ischemic mitral regurgitation: long-term outcome and prognostic implications with quantitative Doppler assessment. *Circulation*. 2001;103(13):1759–64.
34. Pierard LA, Lancellotti P. The role of ischemic mitral regurgitation in the pathogenesis of acute pulmonary edema. *N Engl J Med*. 2004;351(16):1627–34.
35. Lancellotti P, Lebrun F, Pierard LA. Determinants of exercise-induced changes in mitral regurgitation in patients with coronary artery disease and left ventricular dysfunction. *J Am Coll Cardiol*. 2003;42(11):1921–8.
36. Lancellotti P, Gerard PL, Pierard LA. Long-term outcome of patients with heart failure and dynamic functional mitral regurgitation. *Eur Heart J*. 2005;26(15):1528–32.
37. Acker MA, Parides MK, Perrault LP, Moskowitz AJ, Gelijns AC, Voisine P, Smith PK, Hung JW, Blackstone EH, Puskas JD, Argenziano M, Gammie JS, Mack M, Ascheim DD, Bagiella E, Moquete EG, Ferguson TB, Horvath KA, Geller NL, Miller MA, Woo YJ, D'Alessandro DA, Ailawadi G, Dagenais F, Gardner TJ, O'Gara PT, Michler RE, Kron IL, CTSN. Mitral-valve repair versus replacement for severe ischemic mitral regurgitation. *N Engl J Med*. 2014;370(1):23–32.
38. Michler RE, Smith PK, Parides MK, Ailawadi G, Thourani V, Moskowitz AJ, Acker MA, Hung JW, Chang HL, Perrault LP, Gillinov AM, Argenziano M, Bagiella E, Overbey JR, Moquete EG, Gupta LN, Miller MA, Taddei-Peters WC, Jeffries N, Weisel RD, Rose EA, Gammie JS, DeRose JJ Jr, Puskas JD, Dagenais F, Burks SG, El-Hamamsy I, Milano CA, Atluri P, Voisine P, O'Gara PT, Gelijns AC, CTSN. Two-year outcomes of surgical treatment of moderate ischemic mitral regurgitation. *N Engl J Med*. 2016;374(20):1932–41.
39. Baumgartner H, Falk V, Bax JJ et al. *Eur Heart J* 2017;38:2739–91.

Replacement Heart Valves

13

John Chambers

Introduction

Approximately 500,000 heart valve replacement operations are performed each year worldwide. Although a definitive treatment for many types of native valve disease, replacement valves have their own natural history which is distinct from that of a normal native valve. Echocardiography is the gold-standard for assessing normal function and detecting and quantifying complications. This chapter will describe:

- The types of replacement valve and their normal appearance
- Complications of replacement valves and how they affect the echocardiogram
- Assessing forward flow and how to differentiate normal flow, patient-prosthesis mismatch and pathological obstruction
- Differentiating normal and pathological regurgitation
- Endocarditis

Types of Replacement Valve and Normal Appearance

Assessing replacement valves on echocardiography is harder and more time-consuming than for native valves. Shielding from the ultrasound beam by mechanical parts can obscure vegetations or a regurgitant jet. Blooming or reverberation artifacts can cause overdiagnosis of abnormal masses or of calcification. It is necessary to use off-axis as well as conventional cuts. If intermittent sticking of a leaflet is suspected from the history or examination it may be necessary to sustain a view for several minutes.

Echocardiography can detect the broad types of replacement valve. The implantation card given to the patient or the surgical notes are needed to supply the design and size of the valve, both of which are needed for interpreting hemodynamic function. The main types are divided broadly into mechanical (Table 13.1) and biological (Table 13.2) which includes an important relatively new class of transcatheter valve.

Mechanical Valves

A mechanical valve consists of an occluder (leaflet, tilting disc or ball) inside a valve housing and attached to a sewing ring (Fig. 13.1). These structures are usually visible on echocardiography and are more obvious in the mitral position (*see*

J. Chambers
Cardiothoracic Department, St Thomas' Hospital,
London, UK
e-mail: john.chambers@gstt.nhs.uk

Table 13.1 Designs of biological replacement heart valve

Type	Example designs
Stented xenograft	
Porcine	Medtronic: Mosaic Hancock standard and Hancock II (Medtronic) Carpentier-Edwards standard and suprannaur St Jude medical Bior, Bioimplant, Epic AorTech Aspire Labcor Carbomedics Synergy
Pericardial	Sorin—Mitroflow, Pericarbon MORE* Baxter—Perimount St Jude—Biocor pericardia, Trifecta Labcor pericardial
Stentless	
Porcine	St Jude Medical Toronto* Medtronic Freestyle Cryolife-Obrien* Cryolife-Ross Stentless porcine pulmonary Edwards Prima Plus AorTech Aspire St Jude Biocor, Quattro stentless mitral Labcor Shelhigh Skeletorized Super-Stentless aortic porcine and pulmonic
Pericardial	Sorin Pericarbon SOLO 3F-SAVR
Autograft (Ross Operation)	As whole root or subcoronary implantation
Homograft	Usually aortic, occasionally pulmonary
Sutureless	Sorin—Perceval Edwards—Intuity ATS Medical—3F Enable Arbor surgical technologies—Trilogy
Transcatheter	Edwards Lifesciences—SAPIEN Medtronic—CoreValve St Jude—Portico Jena

*Indicates withdrawn

Appendix). For a valve in the aortic position it may be difficult to image a cage which is usually seen best in an apical long-axis view. The most commonly implanted mechanical valve is now the bileaflet mechanical valve (Fig. 13.1d). The various designs differ in the composition and purity of the pyrolytic carbon, in the shape and opening angle of the leaflets, the design of the pivots, size and shape of the housing and the

Table 13.2 Designs of mechanical replacement heart valve

Design	Types
Bileaflet mechanical replacement valves	<ul style="list-style-type: none"> • St Jude medical: standard, HP, Masters and Regent • Carbomedics: standard, reduced cuff, Optiform, Orbis and supra-annular (Top Hat). Carboseal includes a woven aortic graft • Edwards Tekna • Sorin Bicarbon • Edwards Mira • ATS • On-X • Medtronic Advantage • Jyros
Tilting disc	<ul style="list-style-type: none"> • Bjork-Shiley monostrut^a • Sorin Monoleaflet Allcarbon • Medtronic-Hall • Omnicarbon • Ultracor
Caged-ball	<ul style="list-style-type: none"> • Starr-Edwards • Smeloff-Cutter

^aIndicates withdrawn from sale

design of the sewing ring. The St Jude Medical valve has a deep housing with pivots contained on flanges which can be imaged echocardiography. The Carbomedics has a shorter housing allowing the leaflet tips to be imaged clearly. The On-X has a long, flared housing and this is also obvious at echocardiography.

There should be no abnormal extrinsic masses attached to the valve although stitches may be seen and thin fibrinous strands are normal. It is normal to see echoes resembling bubbles in the left ventricle in the presence of a replacement mitral valve. These occur with all designs but are most frequent with bileaflet mechanical valves. They are caused by aggregation of red cells as a result of high stresses at the edge of the leaflet as it closes (Fig. 13.1).

Biological Valves

Most biological replacement valves are stented xenografts (Table 13.1) (Fig. 13.2). The stent is a plastic or wire structure covered in fabric with the cusps of the valve placed inside and a sewing ring



Fig. 13.1 Images of replacement heart valves. Stented biological valves (a) Magna-Ease (bovine pericardial), (b) Epic (porcine). Stentless biological valve (c) Medtronic Freestyle.

Bileaflet mechanical mitral valve (d) OnX, (e) Master HP. Single tilting disc (f) Medtronic-Hall. Transcatheter (g) Edwards SAPIEN, (h) Medtronic Corevalve

attached outside. The valve cusps usually consist of pericardium or a porcine aortic valve.

A stentless heterograft valve usually consists of a preparation of porcine aorta (Fig. 13.1c). The aorta may be relatively long or may be

sculpted to fit under the coronary arteries. Some are tricomposite and one is made out of bovine pericardium. It was hoped that these valves would be better than stented valves in terms of hemodynamics, durability and complication



Fig. 13.1 (continued)

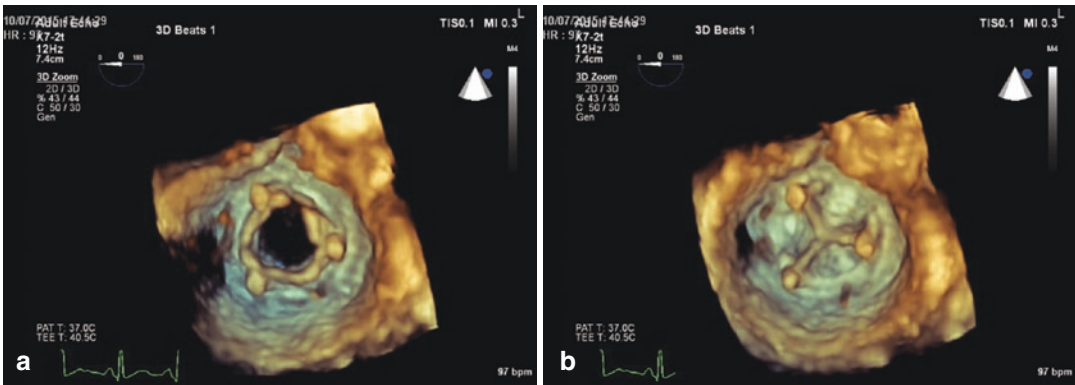


Fig. 13.2 Normal biological mitral valve. This is a 3D TEE image showing the valve from the LV view open (a) and closed (b)

rates. This has largely not been borne out and some have now been withdrawn. When newly implanted, stentless valves may be surrounded by oedema and haematoma. This ultimately resolves over 3–6 months and is associated with a rise in effective orifice area and a fall in trans-aortic pressure difference. After this it may be difficult to appreciate that the valve is replaced and not native.

Homograft valves consist of human aortic or occasionally pulmonary valves which are usually

cryopreserved and usually left unstented. They have good durability if harvested early after death and do not need anticoagulation. For this reason they may be used as an alternative to a mechanical valve in the young. They may also be used for choice in the presence of endocarditis since they allow wide clearance of infection with replacement of the aortic root and valve and the possibility of using the attached flap of donor mitral leaflet to repair perforations in the base of the recipient's anterior mitral leaflet.

The Ross Procedure consists of substituting the patient's own pulmonary valve for the diseased aortic valve. Usually a homograft is then implanted in the pulmonary position. The rationale for such a complex procedure is that a living valve with good durability is placed in the important aortic side while the replacement valve is placed in the low pressure right side. The procedure has a relatively high early complication rate but good long-term results. There is evidence that the autograft grows which is particularly important for avoiding repeated surgery in children. It may also be relatively resistant of infection. When performing echocardiography it is important to remember to assess the homograft as well as the autograft.

Transcatheter valves (Fig. 13.1g and h) are composed of pericardial leaflets mounted in a metallic stent which is either self-expandable (CoreValve) or inflated using a balloon (SAPIEN). On echocardiography these valves resemble conventional stented xenografts but are more likely to have regurgitation through or around the valve.

Complications and How They May Affect the Echocardiogram

There is no ideal replacement valve and all can have complications which may show on echocardiography as an abnormal appearance with evidence of regurgitation or stenosis. Patients usually present with breathlessness and the challenge for the echocardiographer is to differentiate various problems which may coexist (Table 13.3):

- Malfunction of the replacement valve including patient-prosthesis mismatch
- LV dysfunction (including coronary disease—causing wall motion abnormalities on exercise)
- New problems with other valves
- RV dysfunction and pulmonary hypertension
- Pericardial effusion

3.1 Primary failure means deterioration of the valve without secondary infection or other cause. It is almost exclusively a problem of the biological valves and occurs more quickly for the mitral than the aortic position. The survival to 10 years is about 70% in the aortic and 60% in the mitral position. Durability is worse in the younger patient (aged under 60 years for the aortic and under 65 years for the mitral position). It may also be worsened by hypertension, renal failure or diabetes. Leaflet escape has occurred for a small number of types of mechanical valve notably the Bjork-Shiley Convexo-Concave. The most reliable signs of early failure are cusp thickness with new transprosthetic regurgitation which give a warning to follow the patient frequently to plan elective surgery. A proportion of biological valves develop sudden catastrophic failure as a result of an early tear or abrasion extending.

3.2 Thrombosis is relatively uncommon in biological valves and in mechanical valves in the aortic position. It occurs at a rate of about 0.1–0.2% p.a. in mechanical valve in the mitral position and more frequently in the tricuspid position.

3.3. Thromboembolism is probably related more to patient factors such as age, cardiac

Table 13.3 Complications of replacement heart valves

Complication	Mechanical	Biological	Echocardiographic effect
Primary failure	–	+++	Thickened cusps with regurgitation >> stenosis
Thrombosis	+++	+	Obstruction
Thromboembolism	+++	++	Nil
Endocarditis	++	++	Vegetations, abscess, dehiscence
Pannus	+	+	Obstruction of closure or opening of leaflet. May be intermittent
Dehiscence	++	++	Paraprosthetic regurgitation
Bleeding	+++	+	Nil

Redrawn from Rimington H and Chambers JB. Echocardiography: a guide to reporting and interpreting. 3rd Ed Taylor and Francis

rhythm, left ventricular function and atrial size than to the replacement valve. It occurs at a rate of 1–4% p.a. in mechanical and 1–2% p.a. in biological valves and is more common for valves in the mitral than the aortic position.

3.4 Pannus is overgrowth of endothelium which covers the valve and interferes with the opening of the occluder. It is mainly a problem of mechanical valves. Usually it leads to obstruction, but may occasionally hold a valve open and cause regurgitation. It may also induce secondary thrombosis or thromboembolism.

3.5 Endocarditis occurs in approximately 3% of patients in the first year then about 0.5–1% per year thereafter. It is similar in frequency in mechanical and biological valves although possibly less common in mechanical valves in the mitral position. The stentless valves (autograft, homograft and stentless heterografts) are perceived to be relatively resistant to infection although this remains unproved.

3.6 Dehiscence is the opening of a gap outside the sewing ring leading to paraprosthetic regurgitation. This may occur at the time of surgery as a result of technique or poor tissues as a result of heavy calcification, endocarditis or abnormalities of collagen e.g. Marfan Syndrome. It is more likely in valves with relatively thin sewing rings and less likely in valves with bulky sewing rings (e.g. Starr-Edwards). It may occur late as a result of endocarditis, but also on occasions with disintegration of the sewing ring and degeneration of the patient annulus.

3.7 Mild hemolysis occurs in almost all mechanical valves, but is usually compensated. The blood lactate dehydrogenase and bilirubin levels are high and the haptoglobin level low, but the haemoglobin level normal. Anemia occasionally occurs in the presence of an aggravating cause such as iron deficiency, but otherwise suggests the presence of a paraprosthetic leak. This is often small and clinically occult. It may only be detected by transoesophageal echocardiography.

3.8 Bleeding is included as a valve related complication because warfarin is essential for

mechanical valves and so cannot be dissociated from the valve itself. It occurs at a rate of about 2% p.a. in mechanical valves, 1% p.a. for biological mitral valves and 0.5% p.a. for biological aortic valves.

Forward Flow. Is There Obstruction?

Aortic Position

Measurements should be taken over one to three cycles in sinus rhythm but usually 5 in atrial fibrillation. The minimum dataset for Doppler-derived measurements (Table 13.4) is peak velocity, derived mean pressure difference and effective orifice area by the continuity equation. The mean pressure difference is important

Table 13.4 Minimum dataset for the echocardiography of replacement valves

Full minimum standard study in all cases including LV and RV and other valves	
<i>Forward flow through the replacement valve</i>	
Aortic position	Peak velocity, derived mean pressure difference and effective orifice area by the continuity equation
Pulmonary position	Peak velocity, derived mean pressure difference
Mitral position	Peak velocity, derived mean pressure difference
Tricuspid position	Peak velocity, derived mean pressure difference and pressure half-time
<i>Other parts of the heart</i>	
Replacement valve regurgitation	Site—through or paraprosthetic Grade
LV	Size and function (a hyperdynamic LV a useful indirect sign of severe mitral regurgitation)
Right heart	RV size and function, estimated PA systolic pressure (pulmonary hypertension may be a sign of mitral dysfunction)
Aorta	Most likely to continue to dilate of diameter >41 mm at the time of surgery
Other valves	

because it is calculated using the whole waveform and better reflects function than using the peak velocity alone. Because of the flow dependence of velocity and pressure difference, effective area by the continuity equation (EOA) should be calculated routinely from the formula:

$$EOA = CSA \times VTI_1 / VTI_2$$

where CSA is left ventricular outflow cross-sectional area in cm² calculated from the diameter assuming circular cross-section; VTI₁ is subaortic velocity integral in cm and VTI₂ is aortic velocity integral in cm.

Errors arise if the peak velocity is used in place of the velocity integral and it is not valid to substitute the labelled size of the replacement valve for the left ventricular outflow tract diameter because this may differ widely from its true size. For serial studies it is reasonable to use the ratio of the velocity integrals since this avoids measuring the left ventricular outflow tract diameter.

Apparently high velocities are common in normally-functioning but small prostheses in the aortic position and effective orifice areas considered severely stenotic for a native valve may be normal. You need to differentiate:

- Normal function of a small e.g. size 19 or 21 valve
- Patient prosthesis mismatch
- Pathological obstruction

The key is the appearance and movement of the cusp or occluder. The valve is pathological if these are thickened or immobile and the diagnosis is confirmed if the Doppler measurements are outside the normal range for the size and types of valve (Table 13.5; Appendix). The cusps may not always be visible transthoracically. TEE is then indicated but may still not image the cusp or occluder so it may be easier to use fluoroscopy for mechanical valves and CT for biological valves. There are a number of indicators of pathology (Table 13.6).

By contrast in both normal function and patient-prosthesis mismatch the valve moves normally and the Doppler measurements are within the normal range. The difference is that in patient-prosthesis mismatch the valve is too small for the patient's size and this is detected by indexing for BSA (Table 13.7). Up to 70% of replacement aortic valves have a degree of patient-prosthesis mismatch which is severe in 10%. This is most important in the perioperative period in the presence of significant LV systolic impairment. Early mortality is then

Table 13.5 Diagnosis of high velocities

Diagnosis	Appearance of cusp	Movement of cusp or occluder	Doppler in normal range	EOAi
Normal function	Normal	Normal	Yes	>0.85
Patient-prosthesis mismatch	Normal	Normal	Yes	<0.85
Pathological	Thickened	Reduced	No	<0.85

Table 13.6 Features suggesting replacement aortic malfunction

Abnormal thickening and/or reduced movement of cusp or occluder
Failure of colour flow to fill in the orifice in at least two views
Vmax, gradient or EOA outside normal range for size and design
Increase in gradient by >25% from previous studies
In the absence of serial studies suspicious if:
• V max >4.0 m/s
• Mean pressure difference >35 mmHg
• EOA <0.8 cm ²
• Acceleration time >100 ms

Table 13.7 Thresholds for patient-prosthesis mismatch in replacement aortic and mitral valves

	Mild ^a	Moderate	Severe
Aortic (cm ² /m ²)	>0.85	0.60–0.85	<0.60
Mitral (cm ² /m ²)	>1.2	0.9–1.2	≤0.9

^aAll replacement valves are small compared to a normal native valve so mild patient-prosthesis is normal

increased massively by a factor over 50 times compared with if there is no patient-prosthesis mismatch. Thereafter it may reduce the regression of LV hypertrophy and contribute to late clinical events, but becomes particularly important if it contributes to exertional symptoms. The echocardiographer has to provide the information to decide whether the patient may benefit from redo surgery to implant a larger valve sometimes with the use of techniques to enlarge the aortic root. It is far better to avoid patient-prosthesis mismatch than to deal with it after surgery and the echocardiographer can warn that the annulus is unusually small for the size of patient. There are charts available to help the surgeon implant a replacement valve of suitable size (Fig. 13.3).

Mitral Position

The minimum dataset is peak velocity, mean pressure difference and pressure half-time.

The Hatle formula ($220/\text{pressure half-time}$) cannot be used to estimate orifice area in normal replacement valves and is only valid for moderate or severe stenosis with orifice area $<1.5 \text{ cm}^2$. For valve areas above this, the pressure half-time reflects atrial and left ventricular compliance characteristics and loading conditions.

Heavily calcified cusps and reduced occluder motion are the most reliable signs of obstruction and the cusps or occluder are usually imaged more easily than in the aortic position. In a bileaflet mechanical valve, partial obstruction may be obvious when one leaflet clearly moves less than the other. Even if image quality is suboptimal, colour mapping can identify obstruction by showing a narrowed, high velocity inflow jet with

‘wrap-around’ aliasing (Fig. 13.4) although transoesophageal imaging may sometimes be necessary to confirm this. In a stenotic stented biological valve, the jet can be narrow at the level of the immobile cusps, but can expand rapidly to fill the orifice towards the tips of the stents. It is therefore easy to miss the abnormality. Severe impairment of left ventricular function may also cause reduced valve opening, but this will be associated with a thin, low-velocity inflow signal on colour mapping.

The colour signal can be unreliable in the presence of severely disturbed flow especially when associated with mobile thrombus or vegetations. These can cause artefacts making the colour signal spuriously broad and identified by dark areas mixed with the colour.

Quantitative Doppler confirms the diagnosis if the pressure half-time is markedly prolonged usually to $>200 \text{ ms}$ with an elevated peak velocity usually $>2.5 \text{ m/s}$ and mean pressure difference $>10 \text{ mmHg}$. Indirect signs, including a rising pulmonary artery pressure or a slow-filling left ventricle may occasionally help.

Patient-prosthesis mismatch occurs as commonly in the mitral as in the aortic position. It may contribute to a failure in the pulmonary artery pressure to fall after valve surgery (Table 13.8).

Pulmonary Position

The minimum dataset is peak velocity and mean gradient. Effective orifice area can be measured but little normal data are available. Signs suggesting obstruction are given in Table 13.9.

Tricuspid Position

The minimum dataset is peak velocity, mean pressure difference and pressure half-time. The pressure half-time is even more variable on the right than on the left side of the heart. There are few normal ranges because few valves are implanted. Obstruction may be suggested first by

		EOAi by prosthesis size (mm)				
Prosthesis size (mm)	19	21	23	25	27	29
Average EOA (cm ²)	1.1	1.3	1.5	1.8	2.3	2.7
BSA (m ²)						
0.6	1.83	2.17	2.50	3.00	3.83	4.50
0.7	1.57	1.86	2.14	2.57	3.29	3.86
0.8	1.38	1.63	1.88	2.25	3.38	3.38
0.9	1.22	1.44	1.67	2.00	2.56	3.00
1	1.10	1.30	1.50	1.80	2.30	2.70
1.1	1.00	1.18	1.36	1.64	2.09	2.45
1.2	0.92	1.08	1.25	1.50	1.92	2.25
1.3	0.85	1.00	1.15	1.38	1.77	2.08
1.4	0.79	0.93	1.07	1.29	1.64	1.93
1.5	0.73	0.87	1.00	1.20	1.53	1.80
1.6	0.49	0.88	0.88	0.88	1.88	1.69
1.7	0.65	0.76	0.88	1.06	1.35	1.59
1.8	0.61	0.72	0.83	1.00	1.28	1.50
1.9	0.58	0.68	0.79	0.95	1.21	1.42
2	0.55	0.65	0.75	0.90	1.15	1.35
2.1	0.52	0.62	0.71	0.86	1.10	1.29
2.2	0.50	0.59	0.68	0.82	1.05	1.23
2.3	0.48	0.57	0.65	0.78	1.00	1.17
2.4	0.46	0.54	0.63	0.75	0.96	1.13
2.5	0.44	0.52	0.60	0.72	0.92	1.08

Fig. 13.3 Chart for predicting patient-prosthesis mismatch. The chart gives the projected indexed effective orifice area (EOAi) for each level of patient's body surface area (BSA; left side) and size (top of chart) of a given model of prosthesis (hypothetical model in this example). Green cells indicate that the projected EOAi is >0.85 cm²/

m², yellow cells indicate borderline values, and red cells indicate a risk of mismatch. *Reproduced with permission from Pibarot P and Dumesnil J. Patient-prosthesis mismatch: definition, clinical impact and prevention. Heart 2006;92:1022–9*

reduced cusp or occluder motion or a narrowed colour signal (Table 13.10). Often the indirect signs are useful since the right atrium and inferior vena cava can be imaged in most patients even if parasternal and apical views are poor. An engorged, unreactive inferior vena cava with a dilated right atrium and small right ventricle all suggest tricuspid obstruction. A transtricuspid peak velocity >1.6 m/s in the absence of significant tricuspid regurgitation is also suggestive.

The pressure half-time is variable and not helpful unless markedly prolonged, >230 ms.

Cause of Obstruction

Although obstruction may often be detected transthoracically and primary failure in a biological replacement valve is usually obvious, a TEE is usually necessary to confirm obstruction

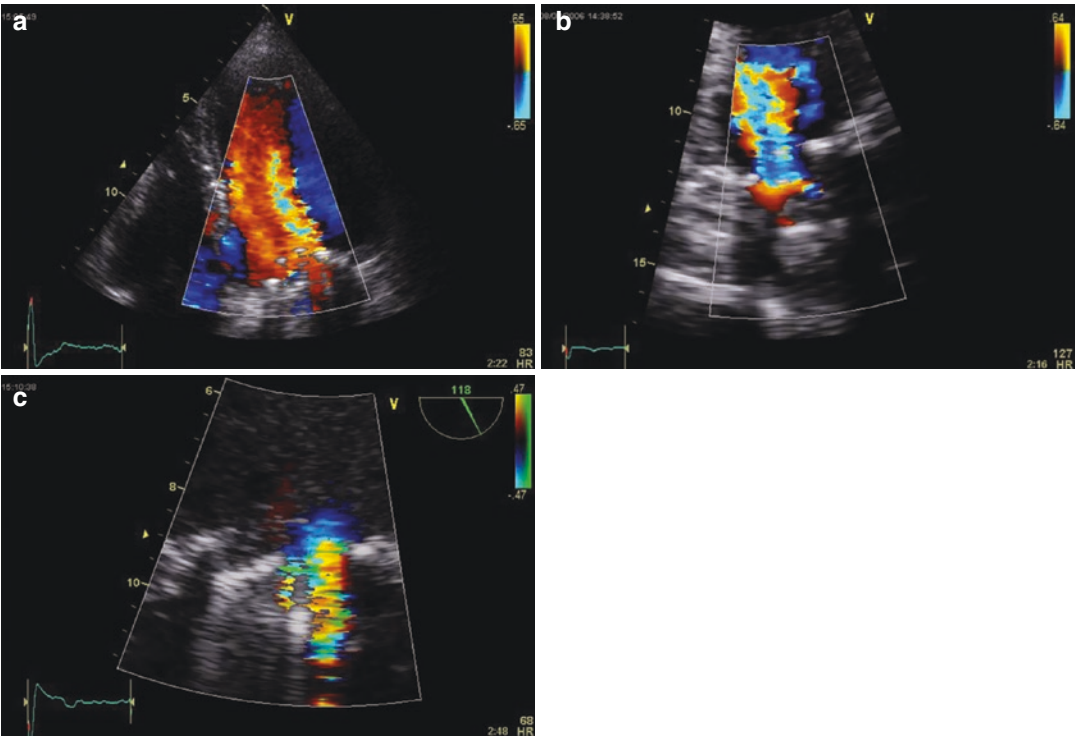


Fig. 13.4 Obstructed bileaflet mechanical valve. These are apical 4-chamber transthoracic image with colour Doppler showing a normal valve (a) and an obstructed

valve (b) with a narrowed colour inflow signal and aliasing. The confirmatory TEE is shown in (c)

Table 13.8 Features suggesting obstruction of replacement mitral valve

Thickened and immobile cusps or occluder
Narrowed colour inflow
Pressure half-time >200 ms with V max ≥ 2.5 m/s
Change in measurements by > about 25% from previous study
Increase in pulmonary artery pressure
EOA <1.0 cm ²
$VTI_{mv}/VTI_{LVOT} > 2.5$

Table 13.9 Features suggesting pulmonary obstruction

Cusp thickening or immobility
Narrowing of colour flow
Peak velocity above 2 m/s for homograft and 3 m/s for all other valve types (suspicious, not diagnostic)
Increase in peak velocity on serial studies (more reliable)
Impaired right ventricular function

Table 13.10 Features suggesting obstruction of a replacement tricuspid valve

Thickened and immobile cusps or occluder
Narrowed colour inflow
Dilated IVC or right atrium
Peak velocity >1.6 m/s (in the absence of severe tricuspid regurgitation)
Mean gradient >6 mmHg
Pressure half-time >230 ms

in mechanical valves and to elucidate the underlying cause:

- Thrombus
- Pannus
- Vegetation
- Mechanical effects (e.g. flail chord or severe subaortic septal bulge)

Thrombus and also vegetations are associated with low density echoes, while pannus is typically highly echogenic (Fig. 13.5). A thrombus is usually larger than pannus and more likely to extend into the left atrium and the appendage. However minor pannus may be overlain by thrombus so conclusive differentiation may not be possible. The clinical history may also be useful. A shorter duration of symptoms and inadequate anticoagulation suggests thrombus rather than pannus. Onset of symptoms less than a month from surgery predict thrombus as a period of 6 months or more is usually necessary for pannus formation. Pannus may be difficult to detect on echocardiography even using TEE. CT may then be useful.

Guidelines for the management of left sided valve thrombosis recommend transesophageal echocardiography to visualize abnormal leaflet motion and to image the size and mobility of thrombus in relation to the valve and the left atrium. Thrombolysis is recommended for (a) tricuspid thrombosis, (b) for left-sided thrombosis if surgery is contra-indicated or (c) failure of intravenous heparin in patients in any group

with a small clot and/or who are in functional class I and II.

Regurgitation

Does the Valve Rock?

This suggests dehiscence and is proved by overlaying color Doppler and demonstrating a paraprosthetic regurgitant jet. Usually rocking in the aortic position implies a large dehiscence, about 30% of the sewing ring. In the mitral position if the surgeon has retained the posterior leaflet there may be rocking without dehiscence

Where Is the Regurgitation on Colour Mapping?

Minor regurgitation is normal in virtually all mechanical valves (Fig. 13.6). Early valves had a closing volume as the leaflet closed followed by true regurgitation around the occluder. For the Starr-Edwards, there is a small closing volume

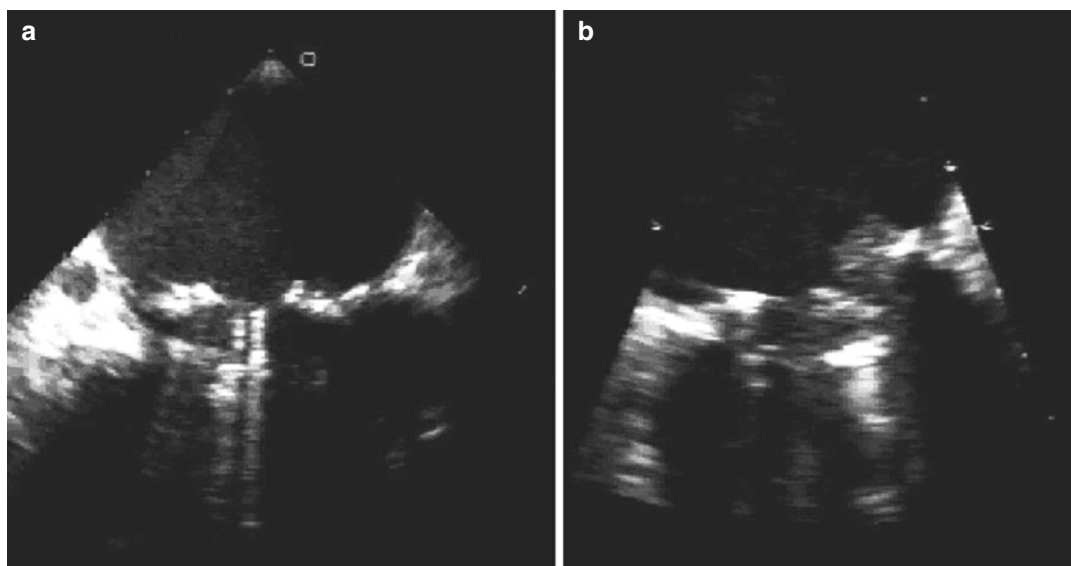
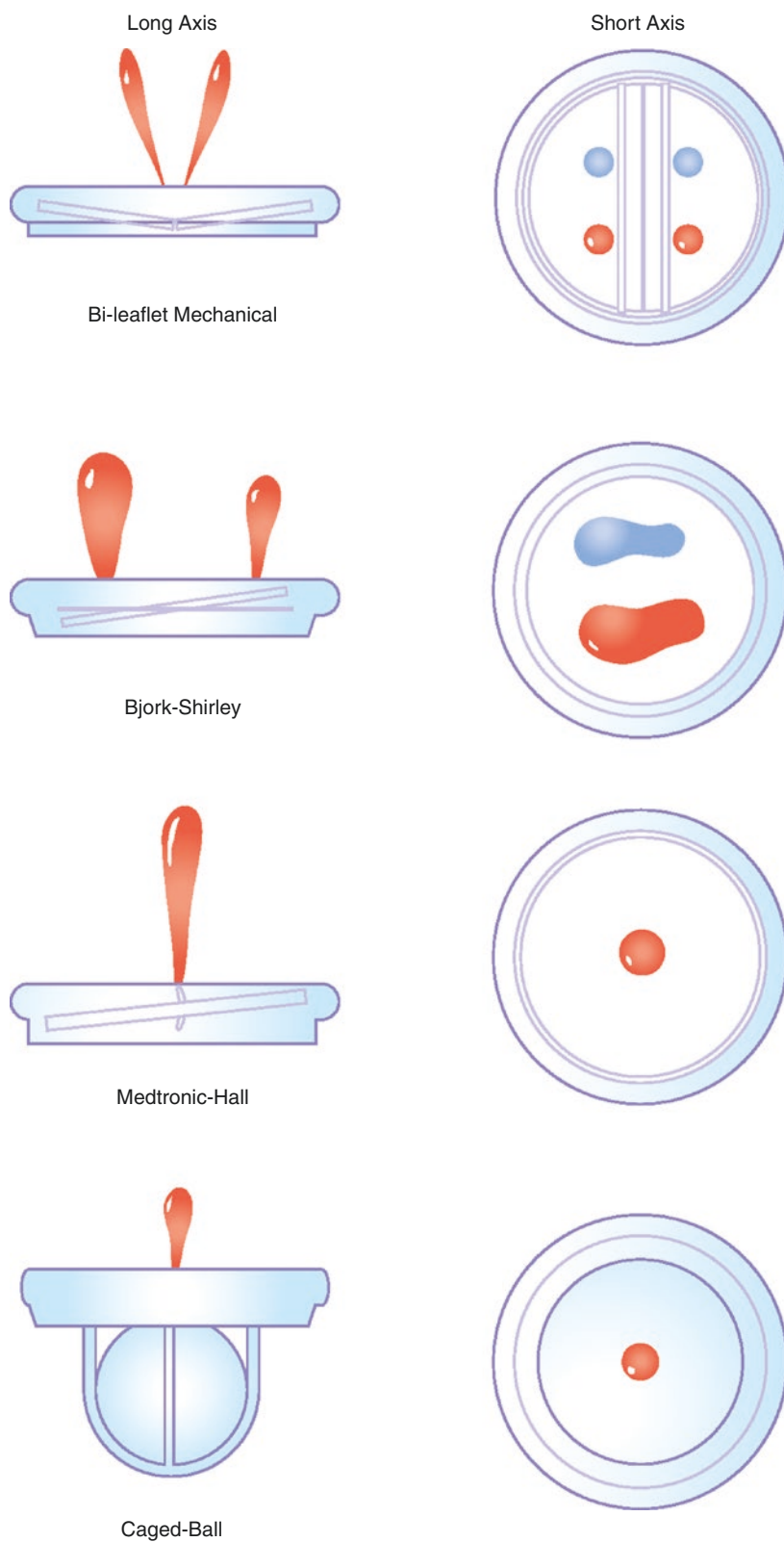


Fig. 13.5 Causes of obstruction. Pannus is more echodense (a). Thrombus is relatively large and of low echo density (b)

Fig. 13.6 Patterns of normal regurgitation. Reproduced from H Rimington and J Chambers. *Echocardiography: a practical guide for reporting and interpretation*. Taylor and Francis



and usually little or no true regurgitation. The single tilting disk valves have both types of regurgitation, but the pattern may vary. The Bjork-Shiley valve has a minor and major jet from the two orifices while the Medtronic-Hall valve has a single large jet through a central hole in the disk.

The bileaflet valves have continuous leakage through the pivotal points where the lugs of the leaflets are held in the housing. These are thought to prevent the formation of thrombus at sites of stasis and are called 'washing jets'. These can look large, up to 5 cm long and 1 cm wide. They are usually found in formation, two from each pivotal point giving a characteristic appearance on imaging in a plane just below the valve. Sometimes these single pivotal washing jets divide into two or three separate 'plumes' and in some valve designs such as the St Jude Medical there may be a jet around the edge of one or other leaflet. The jets are invariably low in momentum so that they are homogenous in colour with aliasing confined to the base of the jet.

Regurgitation through the valve is also increasingly reported in normal biological valves. This is mainly because echocardiography machines are becoming increasingly sensitive. Stentless valves including homografts and autografts are more likely than the stented valves to have minor regurgitant jets, usually at the point of apposition of all three cusps or at one or more commissure. In stented valves, the regurgitation is usually at the point of apposition of the cusps.

Transcatheter valves commonly leak through and around the valve. Even small paraprothetic regurgitation is associated with a poorer outcome although the explanation of this is not known.

However, in a biological valve, a broad jet, particularly if it is bigger than on previous studies, is a sign of primary failure or endocarditis (Fig. 13.7). Large transprosthetic jets are uncommon in mechanical valves, but can occur if the leaflet is held open by thrombus or a vegetation.

Paraprothetic leaks have their origin outside the sewing ring and can usually be detected trans-thoracically (Fig. 13.8) even in the mitral position (Fig. 13.9). Although the mechanical parts of the valve shield the interatrial part of the jet from

ultrasound, a significant jet has a neck and an intraventricular portion of flow acceleration. Even these are occasionally invisible for posterior paraprothetic regurgitation in the mitral position. However, the majority of paraprothetic leaks occur at the mitral-aortic fibrosa. It may sometimes be difficult to differentiate a paraprothetic jet from an asymmetric jet through the valve especially those beginning at the base of cusps or at a commissure and TEE is then indicated. 3D TEE is essential to measure the size of the dehiscence to determine whether percutaneous closure is feasible.

Paraprothetic leaks are pathological by definition but may not be of clinical significance. Small paraprothetic leaks are more common in valves with thin sewing rings or patients with poor tissue for example as a result of endocarditis or Marfan syndrome.

Quantification

Broadly, the same methods can be used as for native regurgitation.

However, assessing the height of an aortic jet relative to the left ventricular outflow tract diameter may be difficult if it is eccentric and care must be taken to measure the diameter of the jet perpendicular to its axis. Multiple small normal transprosthetic jets cannot be quantified accurately, but this is not necessary in clinical practice. For paraprothetic jets, the proportion of the circumference of the sewing ring occupied by the jet gives an approximate guide to severity: mild (<10%), moderate (10–25%), severe (>25%).

Because of shielding, it may be difficult to quantify a jet in the mitral position using TTE. However, the likelihood of severe regurgitation can be judged by indirect signs predominantly overactivity of the left ventricle or occasionally a rise in pulmonary artery pressure compared with an earlier study. TEE is always necessary to quantify the jet definitively and a precise measurement of the length of the sewing ring affected and of the maximum gap during rocking can be produced. This is essential for planning percutaneous closure.

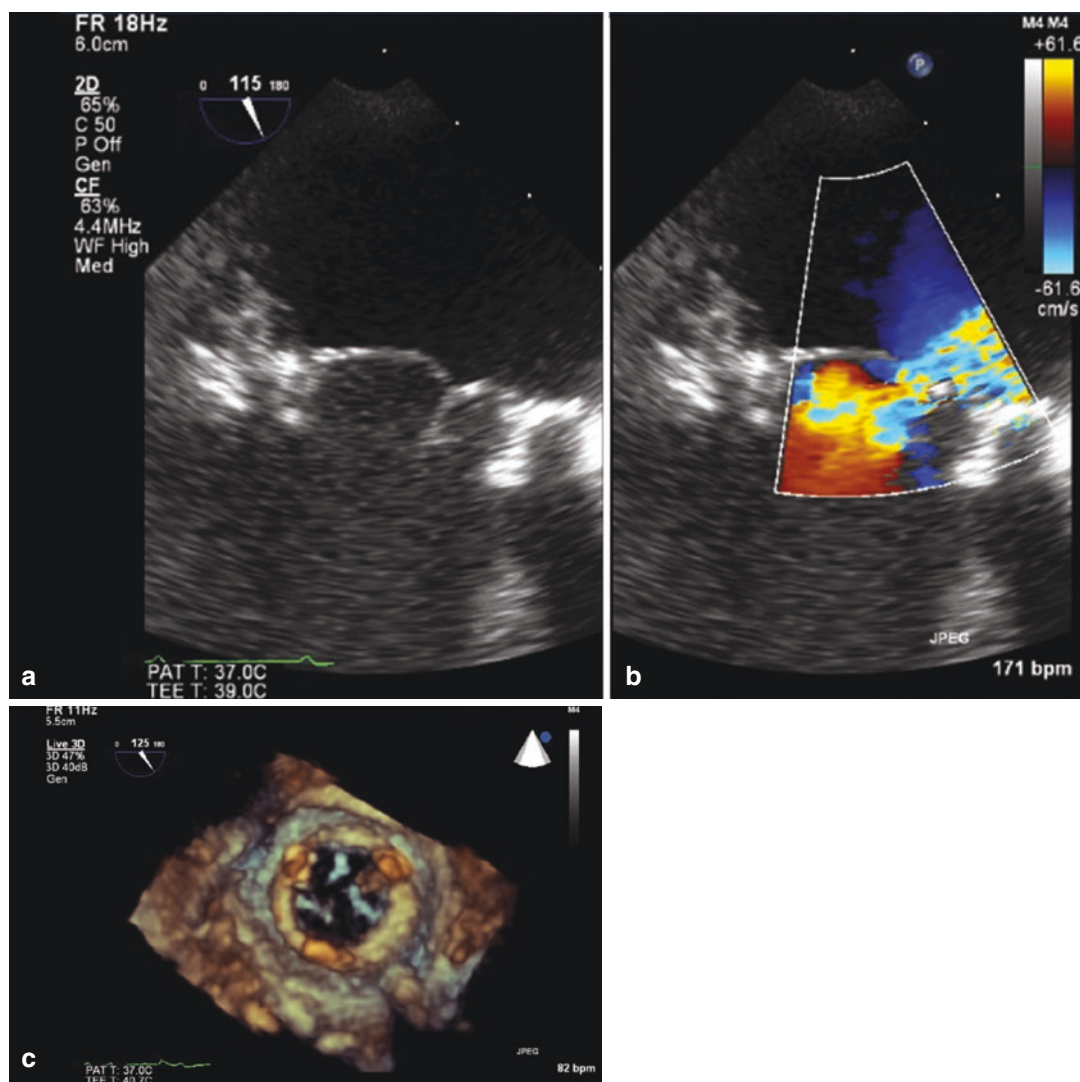


Fig. 13.7 Primary failure of a biological mitral valve. The 2D TEE (a) shows prolapse with a broad jet of regurgitation on color mapping (b). The 3D image (c) shows better that all three cusps are disrupted

Fig. 13.8 Paraprosthetic aortic regurgitation. Transthoracic parasternal long-axis (a) and short-axis (b) views are shown

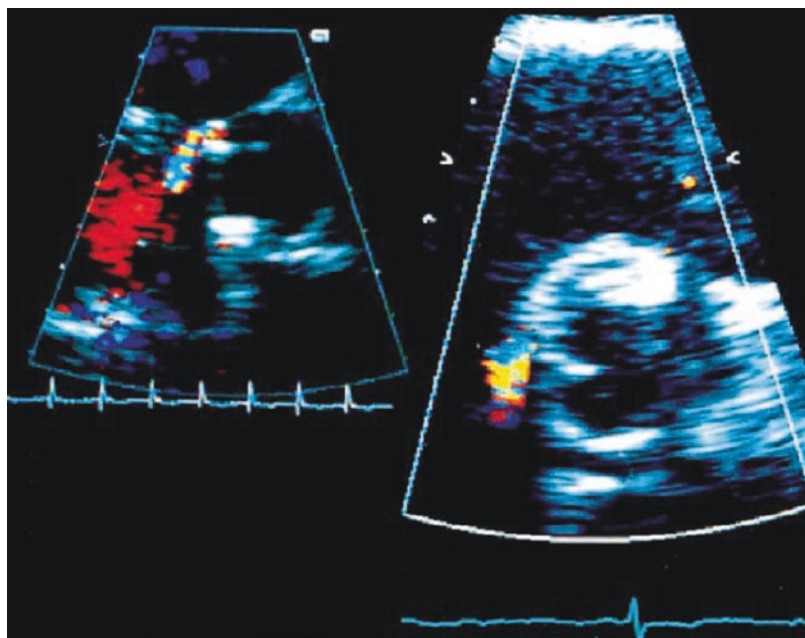
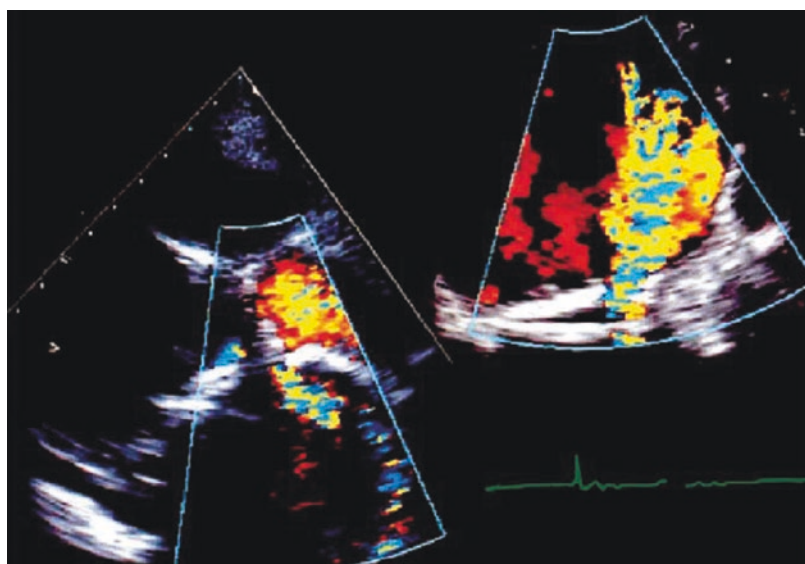


Fig. 13.9 Paraprosthetic mitral regurgitation. Although the interatrial portion of the jet is incompletely seen on transthoracic imaging (a) because of shielding, the neck and interventricular flow acceleration are usually visible. The interatrial jet is more easily imaged on TEE (b)



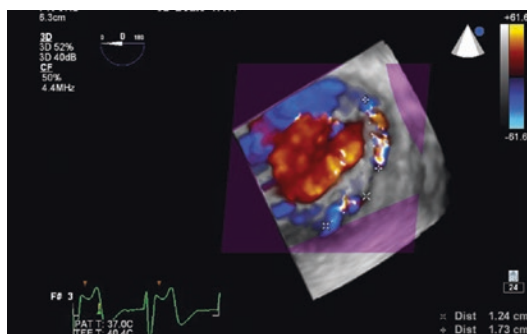


Fig. 13.10 Vegetations on a bileaflet mechanical valve

Endocarditis

Vegetations and local complications (dehiscence, abscess, perforation, fistula) may be obvious even on transthoracic echocardiography especially if the valve is biological. However if the valve is mechanical, VEGETATIONS are often difficult to detect transthoracically and TEE is then necessary (Fig. 13.10).

However the echocardiogram must never be interpreted outside the clinical context. It is never possible to differentiate vegetations from a segment of disrupted cusp. Nor is it possible to differentiate generalised valve thickening as a result of infection from primary failure even on TEE. Similarly, normal swelling and haematoma around a recently-implanted stentless valve cannot be differentiated from an abscess.

Timing of Echocardiography

Preoperative

As well as the full assessment of the native valve disease and the rest of the heart echocardiography may be needed:

TAVI Echocardiography is essential for planning a TAVI procedure. The aortic annulus diameter to plan the feasibility and size of TAVI. A dilated aorta may preclude some devices. A large subaortic bulge may suggest a Corevalve rather

Ross

than SAPIEN. A small LV cavity precludes an apical approach

The pulmonary valve needs to be normal and the pulmonary and aortic annulus of similar size. A Ross procedure is not advisable if the aortic annulus is large, above 27 mm, since this may be associated with progressive dilatation of the autograft.

Homograft

The aortic annulus size gives a guide to size of the graft to be ordered

Perioperative Intraoperative echocardiography is not essential for the routine implantation of all valves but must be considered:

- If there is an associated mitral valve repair
- In endocarditis to check for an aortic root abscess or involvement of other valves
- To confirm annulus and sinotubular junction diameters when implanting a stentless valve
- To assess competency of a Ross or stentless valve after surgery

In the immediate postoperative period, echocardiography may be needed for assessing left ventricular function, detecting pericardial effusions and assessing loading conditions. Severe left ventricular hypertrophy usually with outflow obstruction after valve replacement for severe aortic stenosis may cause left ventricular failure and hypotension. These may be treated according to protocol with inotropic agents and diuretics which exacerbate the situation. The diagnosis is made on echocardiography and the treatment is withdrawal of inotropes, the use of drugs to slow the heart and improve LV filling and the gradual withdrawal of diuretics.

Postoperative A study should be performed in the early postoperative period to act as a baseline. Every valve is different and this study acts as a 'finger-print' against which to compare future studies. For example there may be mild paraprosthesis regurgitation. If the patient presents later with fever, the finding of a paraprosthesis jet might be a

Table 13.11 Timing of echocardiography

Time	Function or indication
Preoperative	Assessing the index valve disease and the rest of the heart Sizing a homograft or TAVI Assessing suitability for a Ross procedure
Perioperative	Detecting leaks TAVI
Early	Baseline function
Routine	For biological valves annually from 7 years from implantation
Additional	On the clinical suspicion of dysfunction Symptom, Murmur, hemolysis

sign of endocarditis if it is new, but not if it has already been documented. The timing of the baseline study depends on circumstances. Ideally it should be at the first postoperative visit usually after 4 to 6 weeks when the chest wound has healed, chest wall edema has resolved and left ventricular function has recovered. However if the patient is being transferred and may not return, it may be best to perform the study before hospital discharge.

Later after surgery routine echocardiography is not necessary if the patient is well and the examination normal. A study is needed if malfunction is suspected (Table 13.11). For biological valves it may be reasonable to study annually beyond about 5 years after surgery for mitral valves and 7 years for aortic valves because of the known failure rate. The rationale is to detect failure early to allow careful follow-up and planning of elective surgery with acceptable surgical risk.

When Is TEE Necessary?

TEE is necessary more frequently than with native valves especially for replacement valves in the mitral position because of the problem of shielding (Table 13.12):

- When endocarditis is suspected particularly for mechanical valves. However vegetations and complications may be obvious transthoracically and anterior aortic root abscesses are better seen transthoracically than transoesophageally. If the transthoracic study is diagnostic, it is only necessary to have a transoesophageal

Table 13.12 Indications for TEE

Endocarditis clinically likely
Obstruction suggested by TTE to: <ul style="list-style-type: none"> – image leaflets or – detect thrombus, pannus or vegetations
To image leaflet opening to differentiate patient prosthesis mismatch from pathological obstruction in an aortic valve replacement
Haemolysis (small regurgitant jet often not detected on TTE)
Symptomatic patient and suboptimal TTE imaging
Paraprothetic mitral regurgitation: <ul style="list-style-type: none"> • To quantify jets of uncertain severity • To assess size of dehiscence before percutaneous closure
Thromboembolism despite therapeutic INR (to detect pannus or thrombus)
Before and during transcatheter valve implantation

- study if surgery is being discussed in order to check the other valves and to look for an abscess. This can be performed perioperatively.
- Despite a normal transthoracic study, if valve dysfunction is suspected from the presence of an abnormal murmur, breathlessness, or hemolysis
 - The grade of mitral regurgitation is uncertain on transthoracic examination
 - Thromboembolism recurs despite adequate anticoagulation since this suggests the presence of vegetation or alternatively of pannus acting as a nidus for thrombus formation
 - Obstruction of a mechanical valve to differentiate thrombosis from the other causes and to decide whether surgery or thrombolysis should be considered
 - During transcatheter interventions including valve implantations and closure of paraprothetic regurgitation

Conclusions

Echocardiography of replacement heart valves is more demanding than for native valves. There are some key points:

- Almost all replacement valves are obstructive compared to normal native valves. The differentiation between normal and pathological obstruction may be difficult

- Quantitative Doppler should always be interpreted in the clinical context; normal ranges vary with design, position and size
- Velocities are flow dependent; always calculate effective orifice area for valves in the aortic position
- The pressure half-time method for calculating effective orifice area is not valid in normal replacement mitral valves
- Transvalvar regurgitation is normal in almost all mechanical valves and many biological valves
- Transthoracic and transoesophageal echocardiography are complimentary and neither should not be considered in isolation

Appendix: Normal Ranges for Replacement Heart Valves: Mean (Standard Deviation)

Aortic Position

	Vmax (m/s)	Mean ΔP (mmHg)	EOA (cm ²)
1a. Biological			
<i>Homograft</i>			
22 mm	1.7 (0.3)	5.8 (3.2)	2.0 (0.6)
26 mm	1.4 (0.6)	6.8 (2.9)	2.4 (0.7)
<i>Porcine</i>			
Carpentier-Edwards			
21 mm	2.8 (0.5)		1.2 (0.2)
23 mm	2.8 (0.7)		1.1 (0.2)
25 mm	2.6 (0.6)		1.2 (0.3)
27 mm	2.5 (0.5)		1.3 (0.3)
29 mm	2.4 (0.4)		1.4 (0.1)
Intact			
21 mm	1.0 (0.1)	19.3 (7.4)	1.5 (0.3)
23 mm	1.3 (0.1)	18.8 (6.1)	1.6 (0.3)
25 mm	1.4 (0.2)	18.8 (8.0)	1.9 (0.3)
27 mm		15.0 (3.7)	
Hancock			
23 mm		12.0 (2.0)	
25 mm	2.4 (0.4)	11.0 (2.0)	
27 mm	2.4 (0.4)	10.0 (3.0.)	
<i>Bovine Pericardial</i>			
Labcor-Santiago			
19 mm		10.1(3.1)	1.3 (0.1)
21 mm		8.2 (4.5)	1.3 (0.1)
23 mm		7.8 (2.9)	1.8 (0.2)
25 mm		6.8(2.0)	2.1 (0.3)

	Vmax (m/s)	Mean ΔP (mmHg)	EOA (cm ²)
1b Single tilting disk			
Bjork-Shiley			
21 mm	3.0 (0.9)		1.1 (0.3)
23 mm	2.4 (0.5)	14 (7.0)	1.3 (0.3)
25 mm	2.1 (0.5)	13.0 (5.0)	1.4 (0.4)
27 mm	2.0 (0.3)	10.0 (2.0)	1.6 (0.3)
Medtronic Hall			
21 mm		13.0 (4.0)	1.4 (0.1)
23 mm	2.3 (0.9)		
25 mm	2.1 (0.3)		
Omnicarbon			
21 mm	3.0 (0.3)	20.0 (5.0)	
23 mm	2.7 (0.3)	18.0 (5.0)	
25 mm	2.5 (0.3)	15.0 (4.0)	
27 mm	2.1 (0.2)	12.0 (2.0)	
1c. Bileaflet mechanical			
St Jude			
19 mm	3.0 (0.6)	19.4 (7.2)	1.0 (0.3)
21 mm	2.6 (0.3)	14.8 (4.3)	1.3 (0.2)
23 mm	2.5 (0.5)	13.5 (5.9)	1.3 (0.3)
25 mm	2.4 (0.5)	12.2 (5.9)	1.8 (0.4)
27 mm	2.2 (0.5)	11.0 (5.0)	2.4 (0.6)
29 mm	2.0 (0.1)	7.0 (1.0)	2.7 (0.3)
Carbomedics			
19 mm	3.2 (0.4)	19.3 (8.5)	0.9 (0.3)
21 mm	2.5 (0.5)	13.7 (5.5)	1.3 (0.4)
23 mm	2.4 (0.4)	11.0 (4.6)	1.6 (0.4)
25 mm	2.3 (0.3)	9.1 (3.5)	1.8 (0.4)
27 mm	2.1 (0.4)	7.9 (3.4)	2.2 (0.6)
29 mm	1.8 (0.4)	5.6 (3.0)	3.2 (1.6)
1d. Ball and cage			
<i>Caged-ball</i>			
Starr-Edwards			
23 mm	3.4 (0.6)		1.1 (0.2)
24 mm	3.6 (0.5)		1.1 (0.3)
26 mm	3.0 (0.2)		

Mitral Position

	Vmax (m/s)	Mean ΔP (mmHg)	PHT (ms)
2a. Porcine			
Carpentier-Edwards			
27 mm		6.0 (2.0)	95 (12)
29 mm	1.5 (0.3)	4.7 (2.0)	110 (30)
31 mm	1.5 (0.3)	4.5 (2.0)	102 (34)
33 mm	1.4 (0.2)	5.4 (4.0)	94 (26)
Intact			
25 mm		7.8 (2.4)	
27 mm		5.4 (1.5)	

	Vmax (m/s)	Mean ΔP (mmHg)	PHT (ms)
Hancock			
29 mm		2.0 (0.7)	
31 mm		4.9 (1.7)	
33 mm		5.0 (2.0)	
	Vmax (m/s)	Mean ΔP (mmHg)	PHT (m/s)
2b. Bovine Pericardial			
Labcor-Santiago			
27 mm		2.8 (1.5)	85 (18)
29 mm		3.0 (1.3)	80 (34)
	Vmax (m/s)	Mean ΔP (mmHg)	PHT (ms)
2c. Single tilting disc			
Bjork-Shiley			
25 mm	1.6 (0.3)		
27 mm	1.5 (0.2)	2.7 (0.8)	94 (31)
29 mm	1.4 (0.4)	2.0 (0.1)	85 (22)
31 mm	1.5 (0.3)	3.4 (2.2)	81 (20)
33 mm	1.3 (0.6)		75 (25)
Medtronic-Hall			
29 mm	1.6 (0.1)		69 (15)
31 mm	1.5 (0.1)		77 (17)
Omnicarbon			
25 mm		6.0 (2.0)	
27 mm		6.0 (2.0)	
29 mm		5.0 (2.0)	
31 mm		6.0 (2.0)	
	Vmax (m/s)	Mean ΔP (mmHg)	PHT (ms)
2d. Bileaflet mechanical			
St Jude			
27 mm	1.6 (0.3)	5.0 (2.0)	
29 mm	1.6 (0.3)	4.5 (2.4)	81 (9)
31 mm	1.7 (0.4)	5.2 (3.0)	84 (12)
Carbomedics			
25 mm	1.6 (0.2)	4.3 (0.7)	92 (20)
27 mm	1.6 (0.3)	3.7 (1.5)	91 (24)
29 mm	1.8 (0.3)	3.7 (1.3)	79 (11)
31 mm	1.6 (0.4)	3.3 (1.1)	92 (20)
33 mm	1.4 (0.3)	3.4 (1.5)	79 (18)
Edwards-Duromedics			
27 mm	1.9 (0.3)		105 (14)
29 mm	1.8 (0.2)		89 (18)

	Vmax (m/s)	Mean ΔP (mmHg)	PHT (ms)
31 mm	1.7 (0.3)		99 (18)
	Vmax (m/s)	Mean ΔP (mmHg)	PHT (ms)
2e. Caged ball			
Starr-Edwards			
28 mm	1.8 (0.2)		130 (25)
30 mm	1.8 (0.2)		100 (40)
32 mm	1.9 (0.4)		125 (60)

Recommended Reading

- Grunkemeier GL, Li H-H, Naftel DC, Starr A, Rahimtoola SH. Long-term performance of heart valve prostheses. *Curr Probl Cardiol.* 2000;25:73–156.
- Jamieson WR. Update on technologies for cardiac valvular replacement, transcatheter innovations, and reconstructive surgery. *Surg Technol Int.* 2010;20:255–81.
- Nishimura RA, Otto CM, Bonow RO, Carabello BA, Erwin JP, Guyton RA, et al. AHA/ACC Guideline for the management of patients with valvular heart disease. *J Am Coll Cardiol.* 2014. <https://doi.org/10.1016/j.jacc.2014.02.536>.
- Pibarot P, Dumesnil JG. Valve prosthesis-patient mismatch, 1978 to 2011: from original concept to compelling evidence. *J Am Coll Cardiol.* 2012;60:1136–9.
- Rahimtoola SH. Choice of prosthetic heart valve in adults. *J Am Coll Cardiol.* 2010;55:2413–26.
- Vahanian A, Alfieri O, Andreotti F, Antunes MJ, Baron-Esquivias G, Baumgartner H, et al. Guidelines on the management of valvular heart disease (version 2012). *Eur Heart J.* 2012;33:2451–96.
- Zamorano JL, Badano LP, Bruce C, et al. EAE/ASE recommendations for the use of echocardiography in new transcatheter interventions for valvular heart disease. *JASE.* 2011;24:937–65. and *Europ Heart J* 2011;32:2189–2214.
- Zoghbi WA, Chambers JB, Dumesnil JG, Foster E, Gottdiener JS, Grayburn PA, Khandheria BK, Levine RA, Marx GR, Miller FA, Nakatani S, Quinones MA, Rakowski H, Rodriguez LL, Swaminathan M, Waggoner AD, Weissman NJ, Zabalgoitia M. American Society of Echocardiography recommendations for evaluation of prosthetic valves with two-dimensional and Doppler echocardiography. *J Am Soc Echo.* 2009;22:975–1014.

Infective Endocarditis

14

Trine K. Lauridsen, Joseph Kisslo,
and Anna Lisa Crowley

Infective endocarditis (IE) is an infection of the endocardial lining of the heart, the heart valves, intracardiac devices or prosthetic valves. The infection is mainly localized on the valvular structures, generally on the flow side of the valves or at locations with endocardial damage. Figure 14.1 shows a pathologic section of aortic valve leaflets, each with a rim of shaggy looking vegetative masses. Note these are on the flow side of the aortic leaflets and not inside the aortic valve cusps.

Over time the clinical presentation of IE has changed markedly. Today the disease mainly affects the elderly population with severe comorbidities. Many patients specifically have pre-existing cardiac disease. The incidence of infectious endocarditis (IE) is 5–10 per 100,000 in industrial countries and the complication rate is high with a 1-year mortality of 20–40% despite advanced antibiotic treatment and improved surgical techniques. The problem is further complicated by the continuing emergence of antibiotic resistant organisms.



Fig. 14.1 Pathologic necropsy specimen of the array of aortic valve leaflets; from a patient who died of sepsis. The three aortic leaflets are seen. The brownish discolored masses are vegetations due to infectious endocarditis (arrows). The dashed arrow points to the ostium of the right coronary artery, near the top of the right coronary sinus of Valsalva. Note that coronary arteries emerge from higher than the leaflet tips, quite near the sino-tubular junction in most people. The right panel shows an elongated vegetation (arrow) capable of prolapsing down into the left ventricular outflow tract in diastole, that would create a similar echo appearance to those from the patients in Figs. 14.3 and 14.5

In the era before echocardiography, IE was diagnosed clinically by the onset of a new cardiac murmur, fever, and a constellation of hemorrhagic or immunologic physical findings the skin. Figure 14.2 shows the hands of a patient with IE where multiple Osler nodes and a single hemorrhagic Janeway lesion are seen. Both Osler nodes and Janeway lesions are part of the hemorrhagic/

T. K. Lauridsen
Department of Cardiology, Copenhagen University
Hospital Glostrup, Glostrup, Denmark
J. Kisslo (✉) · A. L. Crowley
Division of Cardiology, Duke University Medical
Center, Durham, NC, USA
e-mail: joseph.kisslo@duke.edu

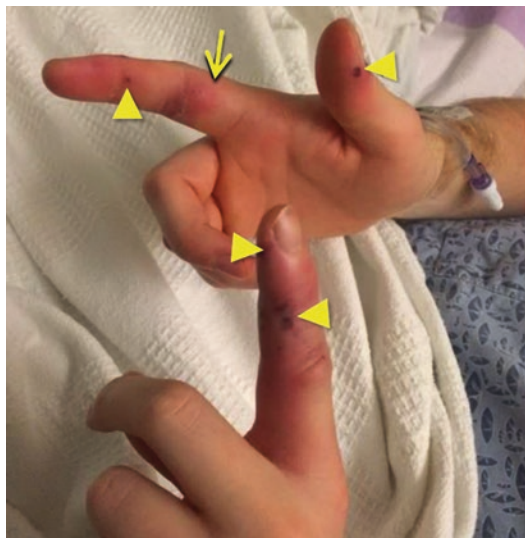


Fig. 14.2 A patient with *S. aureus* infective endocarditis demonstrating multiple immunologic Osler nodes (arrowheads) and a hemorrhagic Janeway lesion (arrow)

immunologic cutaneous manifestations of IE that are sometimes encountered in patients with this disorder.

With the introduction of echocardiography, these cardiac vegetative masses became visible in vivo by transthoracic echocardiography and by 1968, M-mode established a role in the evaluation of patients with suspected endocarditis. Figure 14.3 shows a typical M-mode recording of aortic endocarditis where the interrogating beam is swept from the aortic and aortic valve (left side of the image) through the left ventricular outflow tract and mitral valve (mid portion of the image) and then into the left ventricle (right portion of the image). The arrow points to an oscillating mass seen in the outflow tract in diastole, typical of a vegetative mass lesion from the aortic valve. M-mode, however, lacked readily identifiable spatial information.

By the 1980s two-dimensional echocardiography was widely available and assumed the principle role for detecting infectious endocarditis mass lesions. Figure 14.4 shows an early two-dimensional echocardiogram from a patient with a vegetative lesion on the atrial (flow) side of the anterior mitral valve leaflet. The remain-

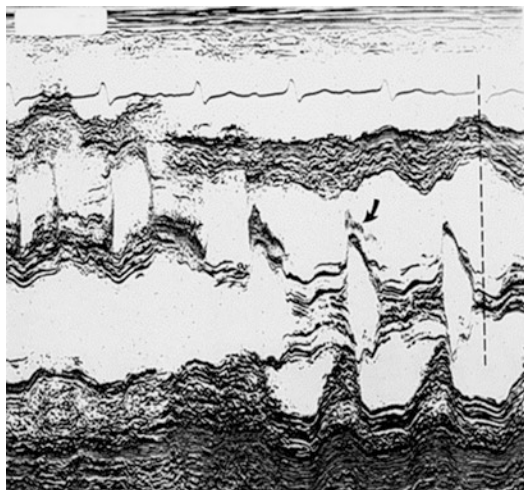


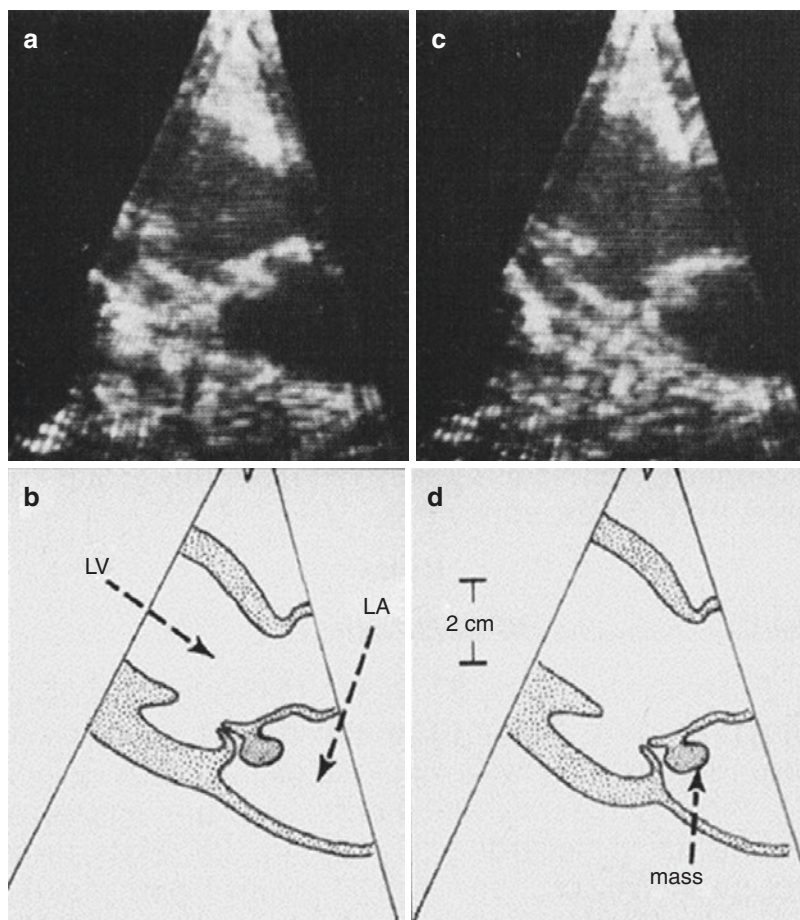
Fig. 14.3 M-mode sweep from the aortic valve (image left) through the left ventricular outflow tract (mid image) and into the left ventricle (image right) taken in the early 1970s from a patient with aortic valve endocarditis. Note the oscillating mass (arrow) typical of vegetative masses just anterior to the mitral leaflet seen in diastole as it prolapsed down into the left ventricular outflow tract, oscillating in the aortic regurgitant jet. This patient's vegetation on the left coronary cusp was not unlike that seen in Fig. 14.1 and by two-dimensional echo in Fig. 14.5. In systole, the mass was thrown into the proximal aorta. The vertical line demonstrates mitral valve pre-closure due to severe aortic insufficiency

der of echo images in this chapter are from more contemporary echocardiography devices that show considerable improvement in image quality.

Figure 14.5 shows apical three-chamber views from a patient very similar to those seen in Figs. 14.1 and 14.3, with a vegetative mass lesion on the left coronary cusp that prolapses down into the left ventricular outflow tract in diastole (arrow). With the progression in echocardiographic image quality, Doppler, and other advanced echocardiographic techniques, echocardiography has been used to study IE in large patient populations.

The necropsy specimen in Fig. 14.6 demonstrates a very large aortic valve vegetation. This specimen serves as a reminder that these vegetations are comprised of a variety of fibrin, thrombus, and debris. It is no wonder that embolic stroke is high on the list of complications of IE.

Fig. 14.4 Very early (1980) two-dimensional echocardiogram in the parasternal long axis of a patient with clinical evidence of infection and positive blood cultures for *S. viridans*. A vegetative mass is attached to the atrial (flow) surface of the anterior mitral valve leaflet. Images have markedly improved since the beginning of two-dimensional echocardiography. From Stewart et al.; with permission



Echocardiography for the Diagnosis of IE

The diagnosis of IE was first postulated in 1885 by the famed Canadian clinician William Osler during his Gulstonian Lecture at the Royal College of Physicians in London. Since then, several sets of criteria for the diagnosis of IE evolved over the decades. Even though bacteriologic typing and immunologic evaluation techniques improved, the heart valves could not be directly inspected except at autopsy or surgery.

The von Reyn criteria criteria brought together major and minor clinical, bacteriologic serologic and histopathologic findings that formed the basis for the diagnosis of IE from the 1980s to the year 2000. These criteria classified patients with suspected IE in four categories: definite, proba-

ble, or possible IE as well as rejected. The von Reyn criteria did not, however, include echocardiographic findings and suffered from the fact that most patients were classified in the probable or possible categories, leading to continuing patient management uncertainties.

During the mid 1990s, echocardiographic findings were included into a new set of diagnostic criteria by physicians at Duke University, known as the Duke Criteria. By including echocardiographic information and eliminating the “probable” category, markedly fewer patients ended up in the uncertain middle categories (Fig. 14.7). This system markedly simplified patient management decisions. These Duke criteria for IE were modified in 2000 (Table 14.1) and now serve as the principle diagnostic criteria for establishing the clinical diagnosis of IE. Originally intended as a tool for epidemio-

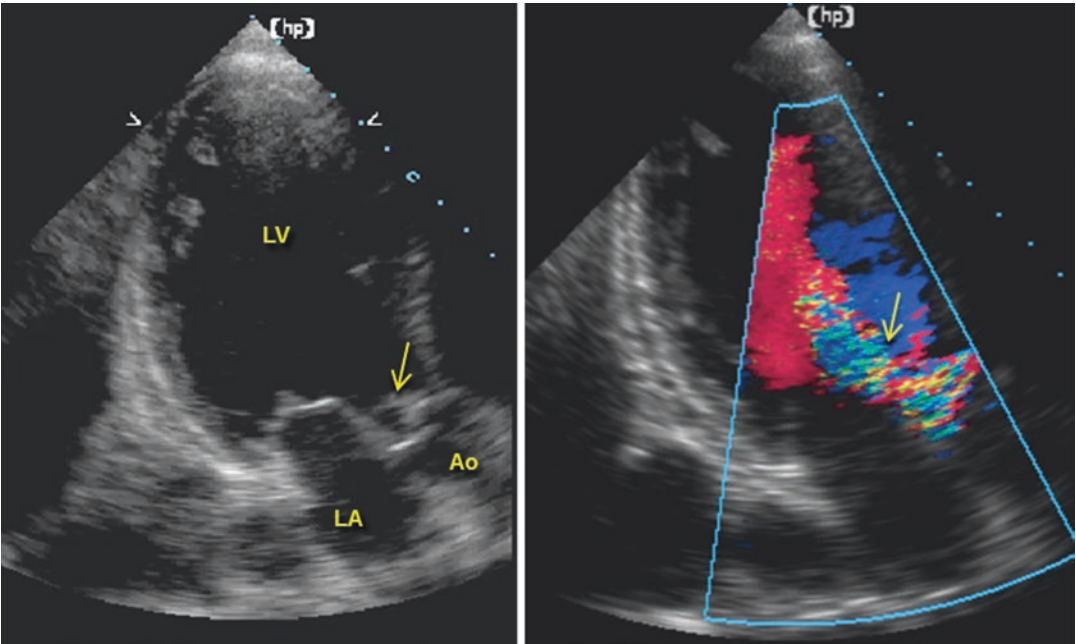


Fig. 14.5 Apical three-chamber still frames in diastole of a patient with typical aortic valve endocarditis. A vegetative mass lesion can be seen below the aortic valve (arrow, left panel). The endocarditis resulted in a turbulent jet of

aortic insufficiency (arrow, Right panel). While not from the same patients seen in Figs. 14.1 and 14.3, this vegetative lesion was similarly located on the left coronary cusp



Fig. 14.6 Necropsy specimen of another patient who died of aortic endocarditis, stroke and sepsis. This massive vegetation is comprised of fibrin, vegetative matter and debris that nearly occluded the left ventricular outflow tract

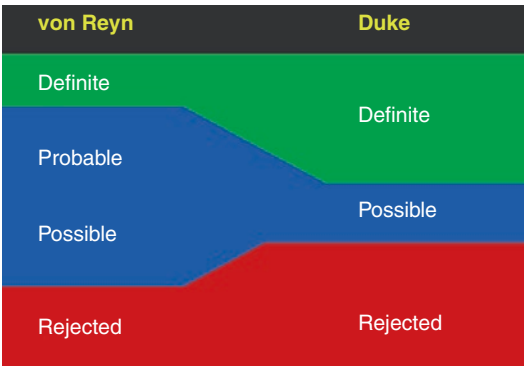


Fig. 14.7 Illustrative diagram of how the Duke Criteria for the diagnosis of IE changed clinical classification of patients with suspected IE by including echocardiographic criteria

logical research, the major and minor criteria of the Duke system established a three tiered classification system: definite IE, possible IE, or rejected IE (Table 14.2). These modified Duke criteria are now accepted worldwide and are included in diagnostic and treatment guidelines

for patients with suspected IE of major societies such as the American Heart Association (AHA), American College of Cardiology (ACC) and the European Society of Cardiology (ESC).

Key diagnostic echocardiographic findings in IE are the presence of a vegetation, abscess,

Table 14.1 Diagnosis of infective endocarditis by the modified Duke criteria

Modified Duke criteria: diagnosis of infective endocarditis ^a
Major criteria
<i>Blood culture positive for IE</i>
<ul style="list-style-type: none"> • Typical microorganisms consistent with IE from 2 separate blood cultures: <i>Viridans streptococci, Streptococcus bovis, HACEK group, Staphylococcus aureus; or community-acquired enterococci, in the absence of a primary focus; or</i> • Microorganisms consistent with IE from persistently positive blood cultures, defined as follows: <i>At least 2 positive cultures of blood samples drawn >12 h apart; or</i> <i>All of 3 or a majority of 4 separate cultures of blood (with first and last sample drawn at least 1 h apart)</i> <i>Single positive blood culture for Coxiella burnetii or antiphase I IgG antibody titer >1:800</i>
<i>Evidence of endocardial involvement</i>
<ul style="list-style-type: none"> • Echocardiogram positive for IE (TEE recommended in patients with prosthetic valves, rated at least “possible IE” by clinical criteria, or complicated IE [paravalvular abscess]; TTE as first test in other patients), defined as follows: <i>Oscillating intracardiac mass on valve or supporting structures, in the path of regurgitant jets, or on implanted material in the absence of an alternative anatomic explanation; or</i> <i>Abscess; or</i> <i>New partial dehiscence of prosthetic valve</i> • New valvular regurgitation (worsening or changing of pre-existing murmur not sufficient)
Minor criteria
<ul style="list-style-type: none"> • Predisposition, predisposing heart condition or injection drug use • Fever, temperature >38°C • Vascular phenomena, major arterial emboli, septic pulmonary infarcts, mycotic aneurysm, intracranial hemorrhage, conjunctival hemorrhages, and Janeway’s lesions • Immunologic phenomena: Glomerulonephritis, Osler’s nodes, Roth’s spots, and rheumatoid factor • Microbiological evidence: Positive blood culture but does not meet a major criterion as noted above or serological evidence of active infection with organism consistent with IE • Echocardiographic minor criteria eliminated

^aData from Li et al.**Table 14.2** Definition of infective endocarditis by pathological and clinical criteria

Modified Duke criteria: Definition of infective endocarditis ^a
Definite infective endocarditis
<i>Pathologic criteria</i>
1. Microorganisms demonstrated by culture or histologic examination of a vegetation, a vegetation that has embolized, or an intracardiac abscess specimen; or pathologic lesions; vegetation or intracardiac abscess confirmed by histologic examination
2. Showing active endocarditis
<i>Clinical criteria</i>
1. Two major criteria; or
2. One major criterion and three minor criteria; or
3. Five minor criteria
Possible infective endocarditis
1. One major criterion and one minor criterion; or
2. Three minor criteria
Rejected
1. Firm alternate diagnosis explaining evidence of infective endocarditis; or
2. Resolution of infective endocarditis syndrome with antibiotic therapy for <4 days; or
3. No pathologic evidence of infective endocarditis at surgery or autopsy, with antibiotic therapy for <4 days; or
4. Does not meet criteria for possible infective endocarditis, as above.

^aData from Li et al.

valvular dehiscence and new valvular regurgitation. A vegetation is defined as an irregularly shaped oscillating echogenic mass adherent to, yet distinct from, cardiac surfaces including valve structures, myocardium, and intra-cardiac devices. When evaluating echocardiograms for prosthetic valve endocarditis, echocardiographic variables of main interest are new or worsening paravalvular regurgitation, valvular dehiscence and paravalvular complications such as abscess and pseudoaneurysm, which are often surgical emergencies.

Table 14.3 enumerates several key characteristics important for understanding echocardiographic manifestations of IE. The body of this chapter will roughly group patients with these manifestations in order to understand how echocardiography images are interpreted. In each case, two major Duke Criteria were used to establish the diagnosis of IE, namely the presence of a vegetation (or other qualifying echo manifestation) and the presence of appropriate positive blood cultures).

Vegetations

Figure 14.8 shows parasternal long axis and aortic short axis views of a patient with an obvious aortic valve vegetation (arrow). Echo suffers from the fact that not all patients make

images as good as those demonstrated in this figure. Older patients, those with lung disease, or large body habitus, make suboptimal images from the chest wall and transesophageal echo must be employed for more precise echo evaluation.

A 70-year old male with a history of prostate cancer presented to the emergency room with intermittent fever over 4 weeks. He was admitted to the hospital with a urinary tract infection and treated with IV Ciprofloxacin. Four blood cultures grew *enterococcus faecalis*. After admission he developed progressive dyspnea and hypotension following the onset of an early diastolic decrescendo murmur of aortic insufficiency. Transesophageal echo (Fig. 14.9, left panel) demonstrated a 15 mm definite oscillating mass lesion (compatible with a vegetation) on the non-coronary aortic cusp with partial destruction of the valve and severe aortic regurgitation (Fig. 14.9, right panel). The patient was referred for bioprosthetic aortic valve replacement (AHA Guidelines indication for early valve surgery, Class IIa, Level of Evidence B). In this case, the presence of the vegetation represented a major criterion that, in association with the positive blood cultures, assured the diagnosis of endocarditis.

Figure 14.10 shows echo images from another patient with fever and sepsis. The left panel does not reveal abnormalities. By sweeping the trans-

Table 14.3 Echo characteristics of endocarditis

Lesion	Description
Vegetation	Irregularly shaped, discrete echogenic mass adherent to, yet distinct from cardiac surface
	Oscillation of mass is supportive, but not mandatory
Abscess	Thickened area or mass within the myocardium or annular region
	Appearance is non-homogeneous with both echogenic and echolucent characteristics
	Evidence of flow within the area is supportive, but not mandatory
Aneurysm	Echolucent space bounded by thin tissue
Fistula	Connection between two distinct cardiac blood spaces through nonanatomical channel
Leaflet perforation	Defect in body of myocardial valve leaflet with evidence of flow through the defect
Valvular dehiscence	Rocking motion of prosthetic valve with excursion >15° in at least one direction

Adapted from Sachdev et al.

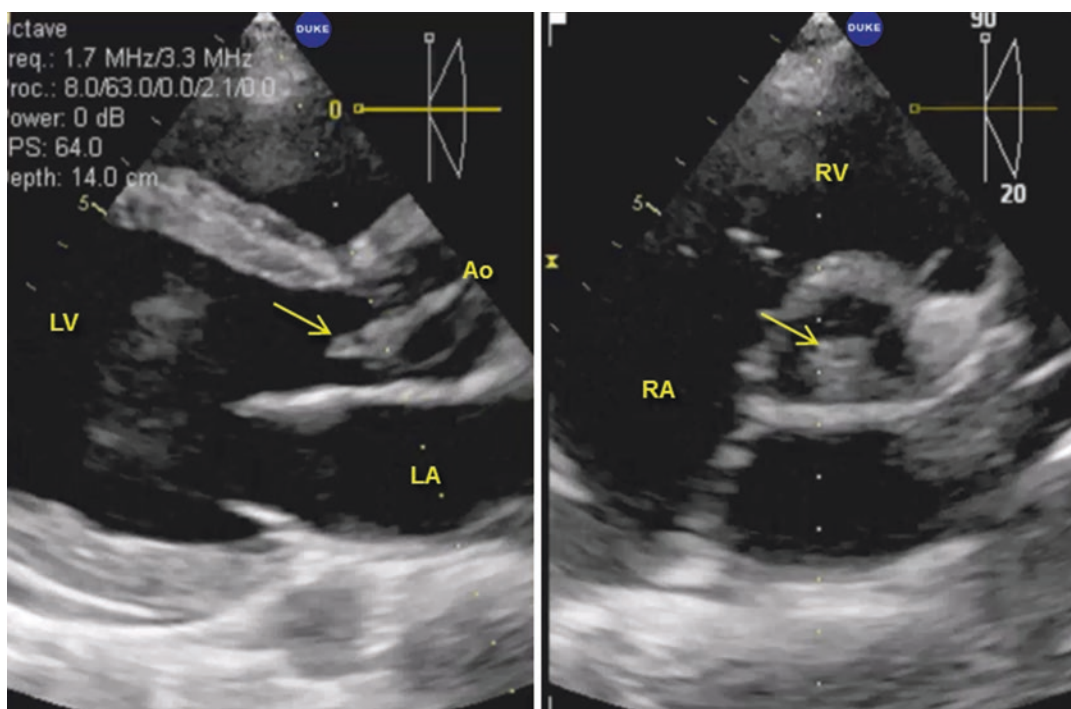


Fig. 14.8 Biplane two-dimensional echocardiograms from a patient with IE in the parasternal long axis (left panel) and aortic short axis (right panel). An aortic mass is seen in both views. Image quality in this patient is quite good

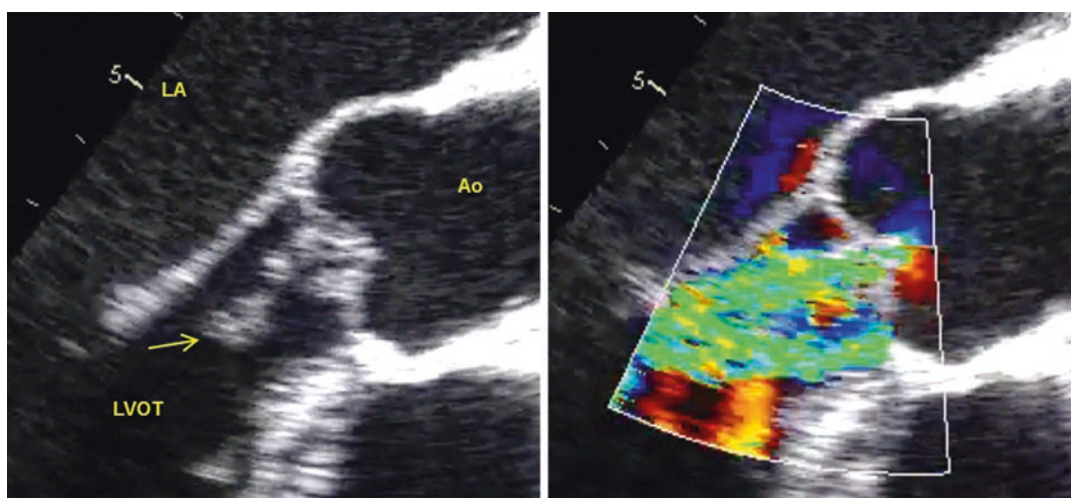


Fig. 14.9 Transesophageal echo views of the left ventricular outflow tract. A 15 mm oscillating mass lesion is seen prolapsing down into the left ventricular outflow tract in diastole (left panel, arrow). The right panel shows severe aortic regurgitation emanating from two regurgi-

tant orifices: one is at the central point of coaptation of the aortic valve leaflets and the other along the aortic wall adjacent to where the right coronary leaflet joins the interventricular septum. For details, see text

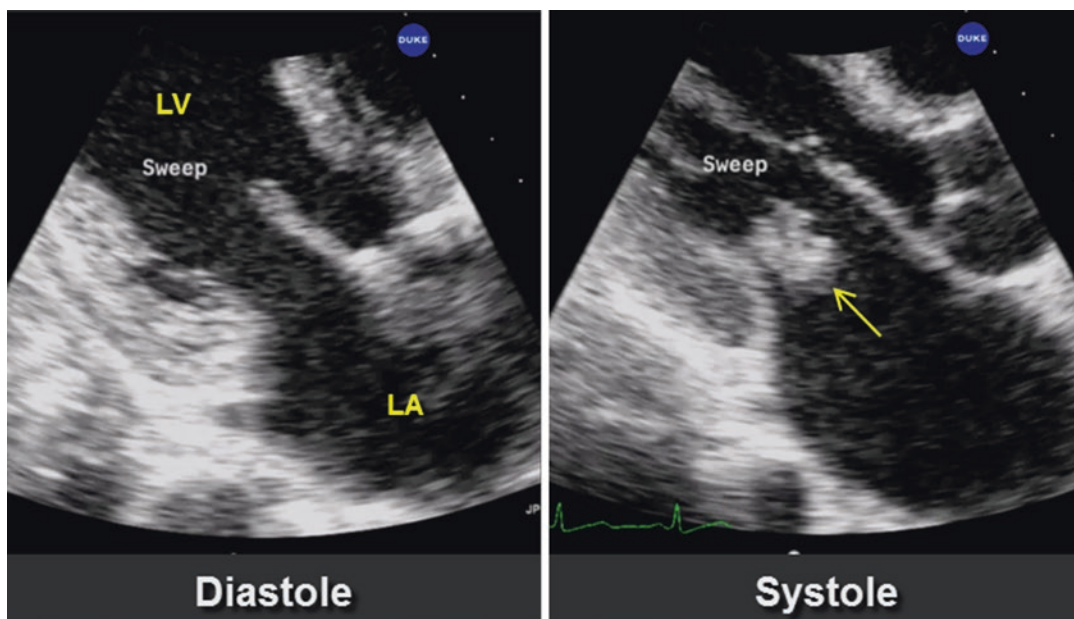


Fig. 14.10 Parasternal long axis zoom frames from a patient with mitral valve endocarditis. Both frames are diastolic but the sequence points out that the examiner must have to manipulate the transducer across all structures as the vegetations may not be detected in standard

views. In this case, the transducer was manually swept from left to right and back in the long axis window to completely examine the aortic and mitral valves in the long axis

ducer beam from side to side, a large vegetation was detected at a slight off-angle (right panel). When examining cardiac valves by echo, the examiner must sweep side to side or up and down to completely examine all of the anatomic valve structures.

Vegetations can change over time. The patient in Fig. 14.11 presented in a similar fashion and a thin, linear vegetation was noted (left panel). The patient was not extremely toxic. Appropriate antibiotics were begun and the patient defervesced. A few days into treatment, the patient experienced a right middle cerebral artery stroke. Repeat echo (right panel) showed that the vegetation was no longer present. In this case, the vegetation likely embolized.

The patient in Fig. 14.12 was being followed for chronic renal failure and malignant hypertension. This echo shows left ventricular hypertrophy and a small pericardial effusion, but no evidence of mass lesions. The patient was also a main-line drug addict, dependent on opiates. One month after this index echo, the patient pre-

sented with high fever and positive blood cultures. Note in the echocardiogram (Fig. 14.13) at the time of presentation there are multiple elongated vegetations on the mitral valve in both diastole (filling mitral inflow) and systole (with vegetations thrown into the left ventricular out-flow tract).

Another patient is shown in Figs. 14.14, 14.15 and 14.16 who was being followed for mitral valve prolapse. Parasternal long axes echoes in Fig. 14.14 show the patient a few months prior to admission with typical systolic findings of prolapse but without evidence of mass lesions. Like most of the other patients, this individual presented with fever, lassitude, laboratory evidence of infection and positive blood cultures. Repeat echocardiogram showed a large irregular mitral mass, compatible with a vegetation, given the clinical presentation (Fig. 14.15). A three-dimensional echo (Fig. 14.16) showed multiple, large, irregular vegetative mass lesions on the mitral valve.

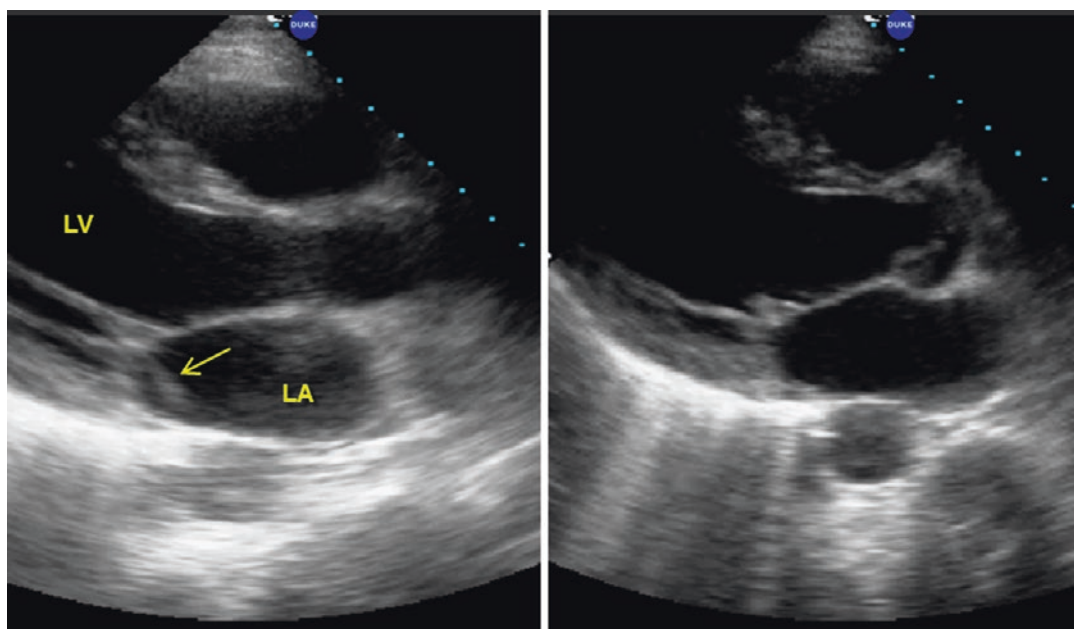


Fig. 14.11 Vegetations can change. These parasternal long axes were taken from a patient with *S. aureus* bacteremia. The left panel shows an elongated vegetative mass

attached to the mitral valve (arrow). The patient had a septic stroke and repeat echo (right panel) showed that the vegetation was no longer detectable

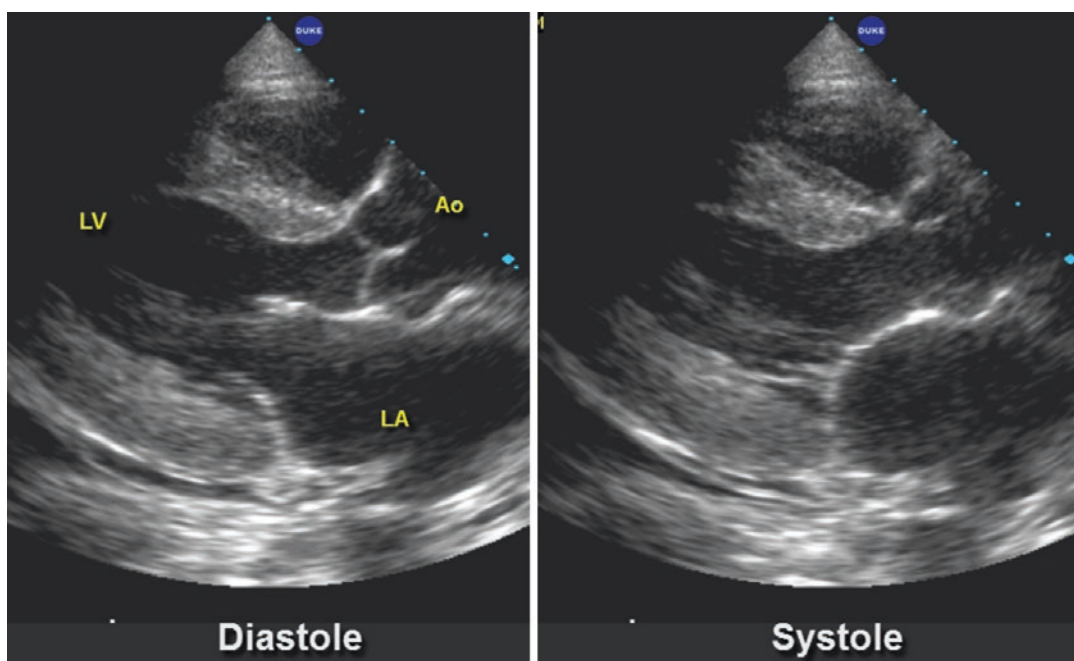


Fig. 14.12 Parasternal long axes in diastole (left panel) and systole (right panel) in a patient being followed for chronic renal failure and malignant hypertension. Despite

her physical problems she was also a main-line drug addict. No vegetative masses are seen. This is the same patient as in the following figure

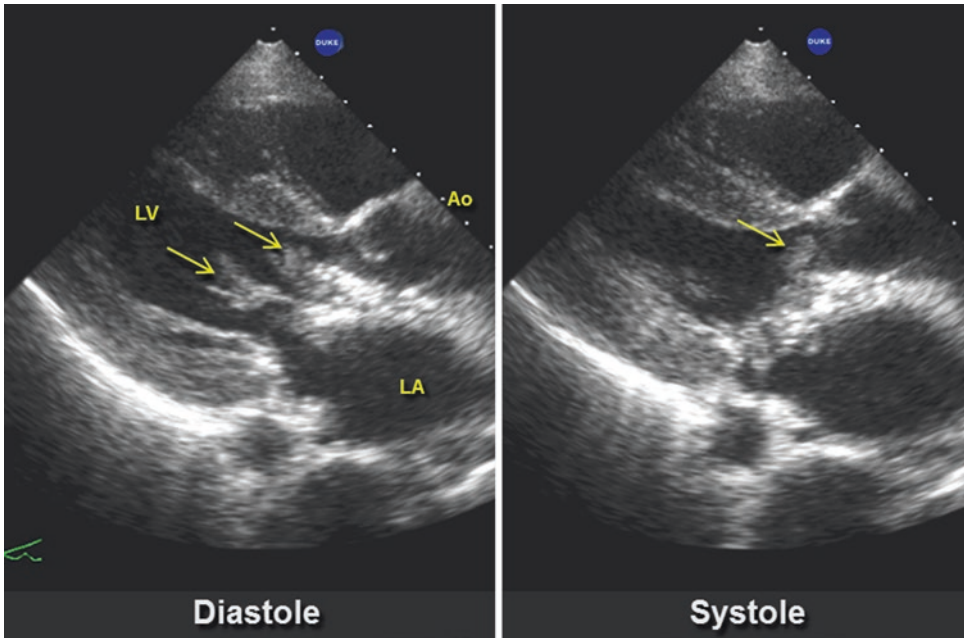


Fig. 14.13 Parasternal long axes in diastole (left panel) and systole (right panel) from the same patient as in the previous figure after contracting IE. Multiple massive vegetations are seen in the mitral orifice in diastole and

then some are thrown in to the left ventricular outflow tract in systole (arrows). Despite treatment, the patient died

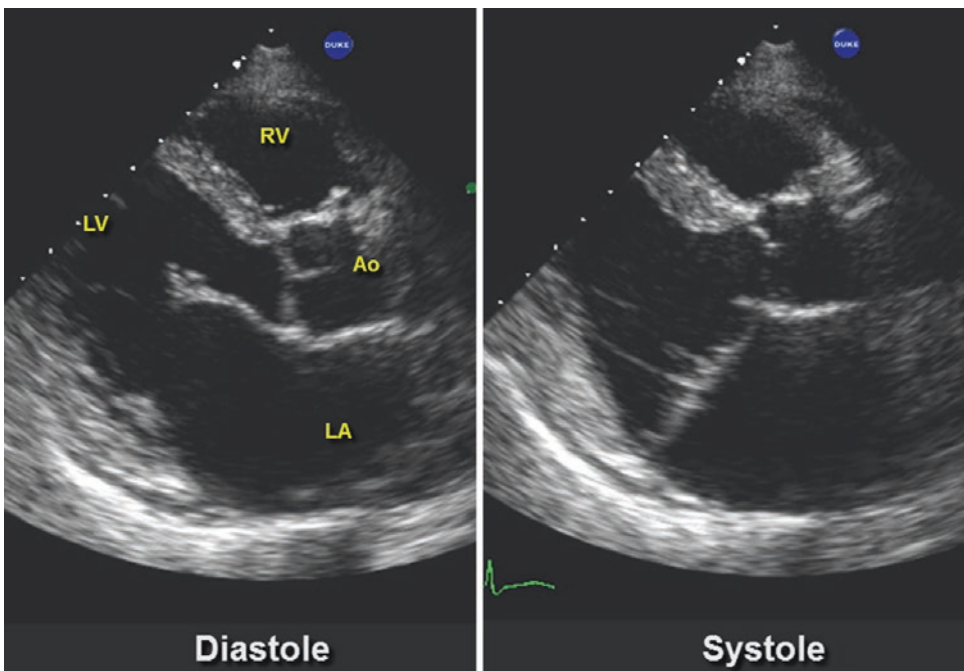


Fig. 14.14 Parasternal long axis of a patient with mitral prolapse. The mitral valve is open in diastole (left panel) and closed in systole (right panel) with leaflets prolapsing

into the left atrium. Left atrial enlargement is present and no mass lesions are seen. This patient is also depicted in the next two figures

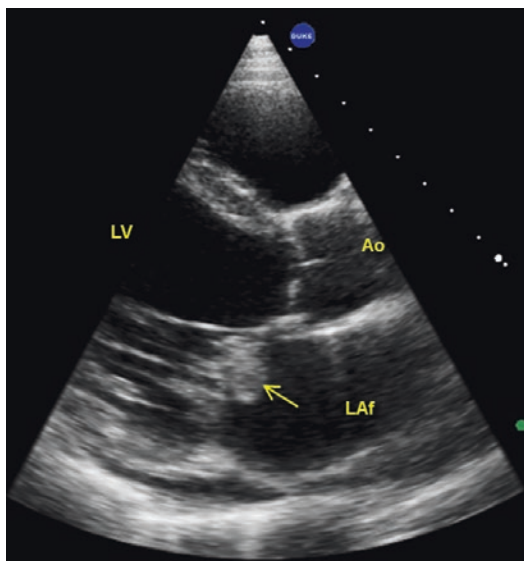


Fig. 14.15 Parasternal long axis of the left ventricle in the same patient with mitral prolapse after the patient presented with septicemia and fever. A large, multi-lobulated mass lesion is now seen on the mitral valve, typical of IE. This is the same patient as in the previous and following figures

New Valvular or Paravalvular Regurgitation

Of course, the examination of a patient with suspected IE also includes examination for valvular regurgitation. The patient in Fig. 14.17 was followed for dilated cardiomyopathy and mild regurgitation for several years. After experiencing progressive, but rapid onset of shortness of breath combined with fevers, the patient presented for evaluation. The echocardiogram showed presence of vegetations on both the aortic valve (top row) and mitral valve (bottom row) together with associated severe aortic and massive mitral regurgitations of new onset.

A 60-year old woman with a history of diabetes was admitted to a tertiary center with *S. aureus* bacteremia. Two years earlier she was treated for IE and underwent a mechanical mitral valve replacement due to acute bacterial valvular destruction causing severe mitral regurgitation and heart failure. During the month prior to the current admission, she developed the recurrent

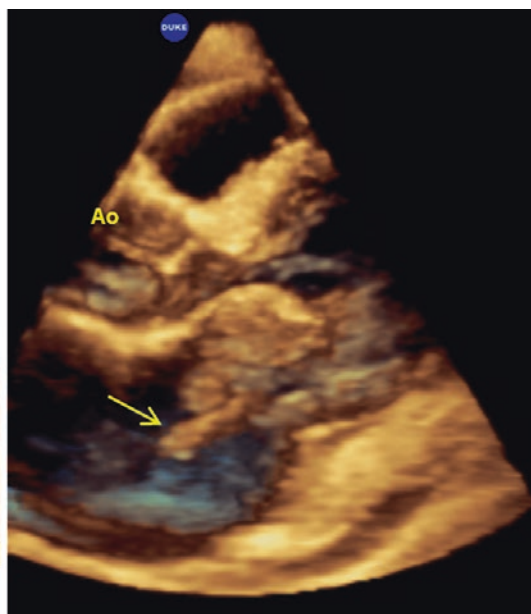
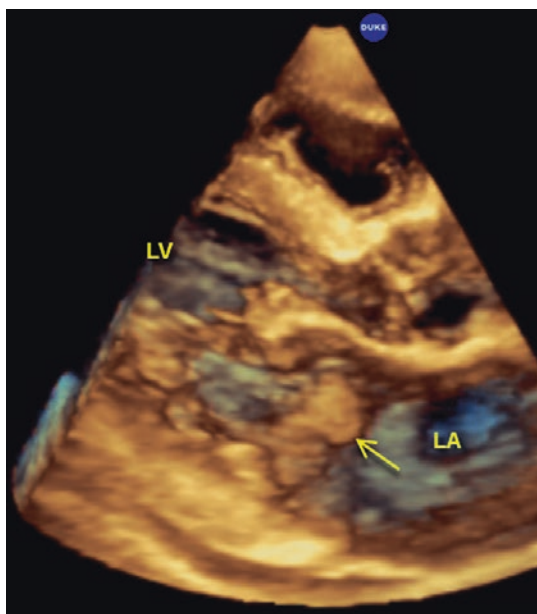


Fig. 14.16 Three-dimensional echo cut in the long axis in the same patient depicted in the previous two figures, after the patient contracted IE. The heart (from a single three-dimensional acquisition) is cut in the long axis in diastole with one half rotated left (facing the interventric-

ular septum), and the other half rotated right (facing the anterior left ventricular wall.). The multi-lobulated mass lesion of the mitral valve is much larger and polymorphous than originally thought by two-dimensional echo)

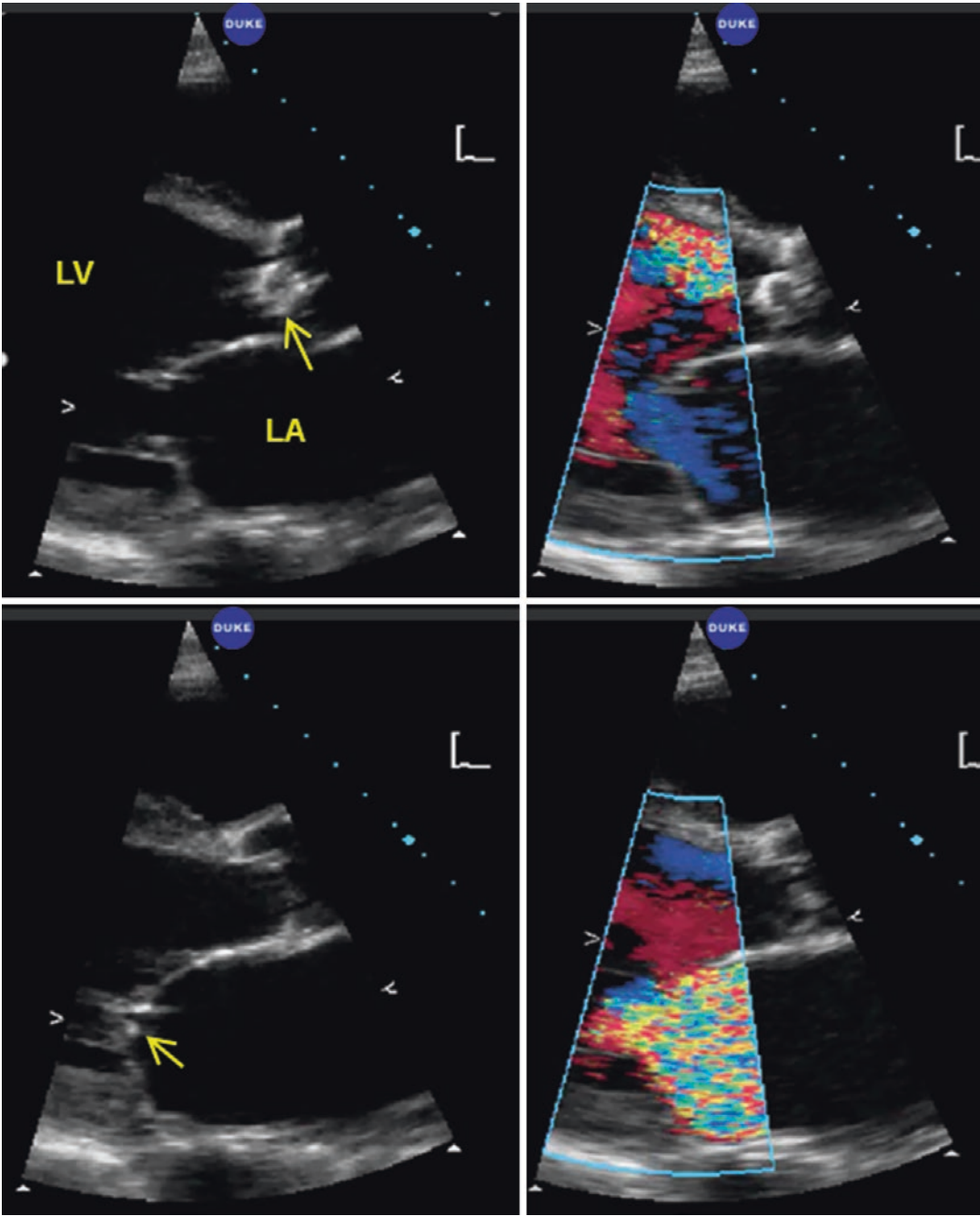


Fig. 14.17 Paired parasternal long axes in diastole (top row) and systole (bottom row) in a patient with a large mass lesion on the aortic valve (arrow top left) and a tiny vegetation (bright dot, arrow, lower left). Aortic insufficiency is severe (upper right) as is mitral regurgitation (lower right)

S. aureus bacteremia secondary to a diabetic foot ulcer (Fig. 14.18) leading to high fever, chills and shortness of breath. TEE images of the mitral valve showed a new severe paravalvular mitral regurgitant leak (Fig. 14.8). Once treated with antibiotics, the patient underwent another mitral valve replacement. In this case, the presence of the new mitral prosthetic paravalvular regurgitant jet represented a major criterion that, in association with the positive blood cultures, assured the diagnosis of endocarditis and subsequent treatment plan.

The presence of new paravalvular regurgitation in patients with prosthetic valves is a near certain sign for IE and constitutes a major echo criteria in the Duke system (as seen in the patient in Figs. 14.18 and 14.19). The sudden onset of native valvular regurgitation, however, is not as



Fig. 14.18 Photograph of a 1.0 × 1.5 cm large non-healing ulceration. Samples from surrounding skin and wound cultures grew *S. aureus*

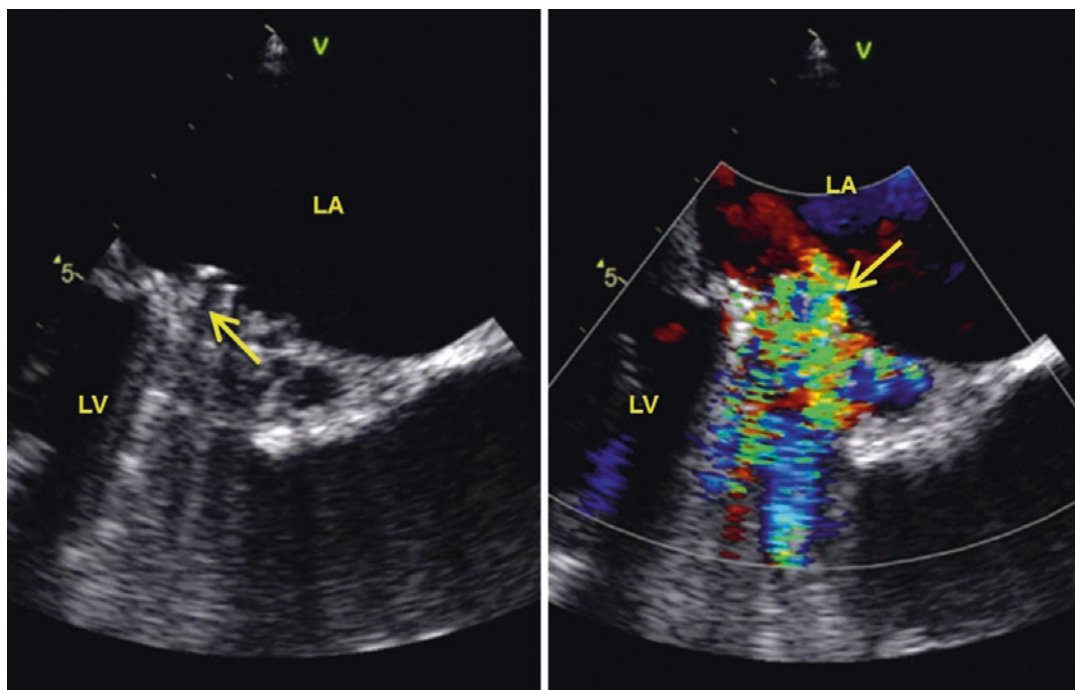


Fig. 14.19 TEE of the mitral valve shows an open double leaflet mechanical mitral valve (arrow). The acoustic shadow and reverberations from the prosthetic valve in

distance obscure visibility on the other side of the valve away from the transducer (left panel). The right panel shows a jet (arrow) due to a paravalvular leak

pathognomonic (as in the patient in Fig. 14.17) as there are a host of other reasons that could account for these findings. In this patient, the presence of vegetations assured the qualification for one major criterion.

Intracardiac Device IE

A 55-year old male with known ischemic cardiomyopathy and previous placement of a primary prophylactic ICD was admitted to the hospital with severe chest pain. Thoracic contrast CT revealed a Type B aortic dissection and the patient was referred for subacute surgery with insertion of a percutaneous stent in the descending aorta (Fig. 14.20). Six months later, the patient was readmitted with chest pain and high fever. Blood cultures revealed coagulase negative staphylococci (CoNS) in 5 of 6 samples. TEE shows an 8 mm oscillating vegetation/thrombotic formation on the ICD lead in the right ventricle (Fig. 14.21). An 18F-FDG PET/CT confirmed the presence of an IE infection on the ICD

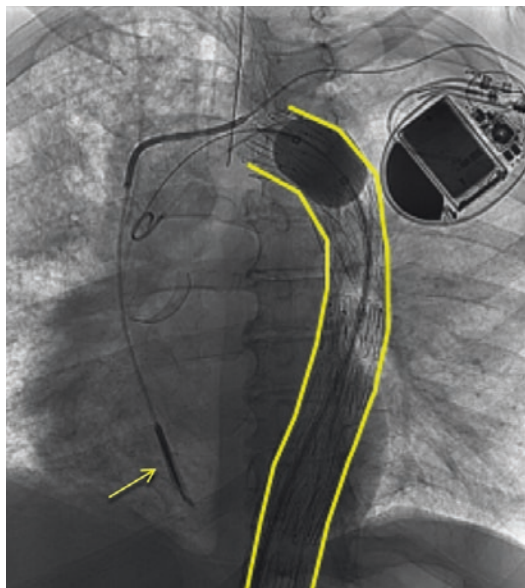


Fig. 14.20 Fluoroscopy of the chest during placement of a thoracic endovascular aortic repair (TEVAR) of the descending and abdominal aorta. Note the defibrillator in the subclavicular area of the patient's left chest and the CD lead in the right ventricle (yellow arrow). Also, note the balloon in the aorta near the transverse arch used for deploying one of the TEVAR devices

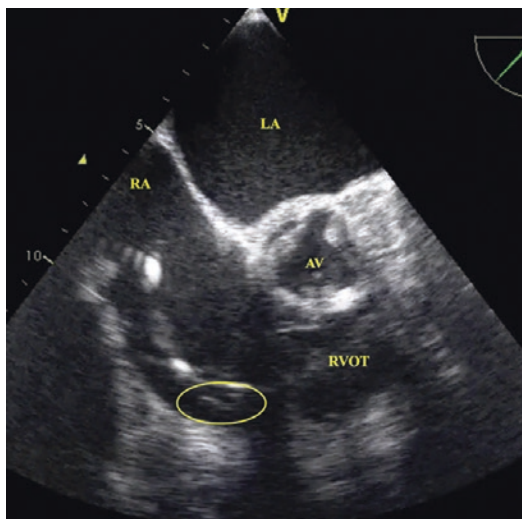


Fig. 14.21 TEE shows an oscillating 8 mm large vegetation on the ICD lead located in the right ventricle In the patient in the previous figure

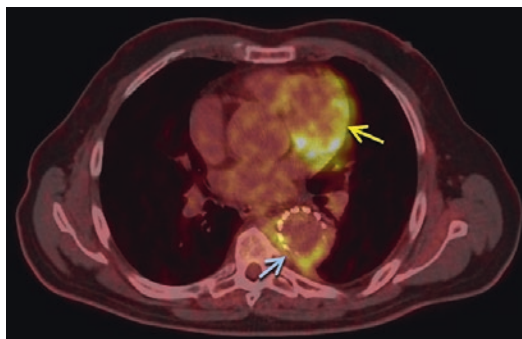


Fig. 14.22 PET/CT reveals infection in close relation to the TEVAR implant (blue arrow) in the descending aorta. The image brightness at the ends of both arrows confirms the infection on the TEVAR implant and at the ICD lead in the right ventricle (yellow arrow)

(Fig. 14.22, blue arrow) and revealed another infection on the thoracic stent (Fig. 14.22, yellow arrow). In accordance with AHA guidelines the ICD system was removed and the patient treated with 6 weeks of intravenous antibiotics followed by a 3 months oral antibiotic regimen for the Thoracic Endovascular Aortic Repair (TEVAR) device infection. In this case, the presence of the oscillating mass on the ICD represented a major criterion that, in association with the positive blood cultures, assured the diagnosis of endocarditis and subsequent treatment plan.

Mass lesions on catheter based systems can be troublesome diagnostically. Given the positive blood cultures in the previous patient this mass was presumed to be a vegetation. It should be noted, however, that there is little information on the prevalence of mass lesions on indwelling catheters in patients who have no symptoms of IE and who have negative blood cultures. Practical experience with echo shows that oscillating small

masses are not uncommon on indwelling lines in asymptomatic patients.

The patient in Figs. 14.23 and 14.24 underwent mitral valve repair, including valve ring, several years before clinical presentation suspicious for IE. The TEE images showed a large mass lesion prolapsing into the left atrium through the repaired mitral valve by two-dimensional echo. The three-dimensional TEE echo study is most

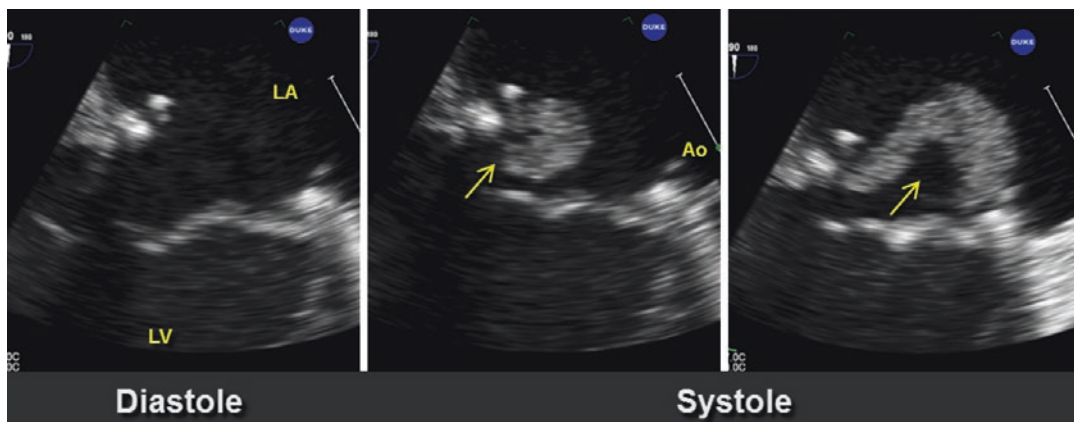


Fig. 14.23 Transesophageal two-dimensional zoom views through a patient who previously underwent a mitral valve repair and placement of a mitral ring and 2 years later presents with fever and positive blood cultures for *S. aureus*. Left panel shows diastole with no evidence of a vegetation as it was down into the left ventricle. The

middle panel shows a massive vegetation starting to move into the mitral orifice and then bulge into the left atrium (arrow). The right panel shows the dramatic appearance of the whole vegetation (arrow) revealing that the vegetation was attached at two points on each side of the mitral ring. This is the same patient as in the following figure

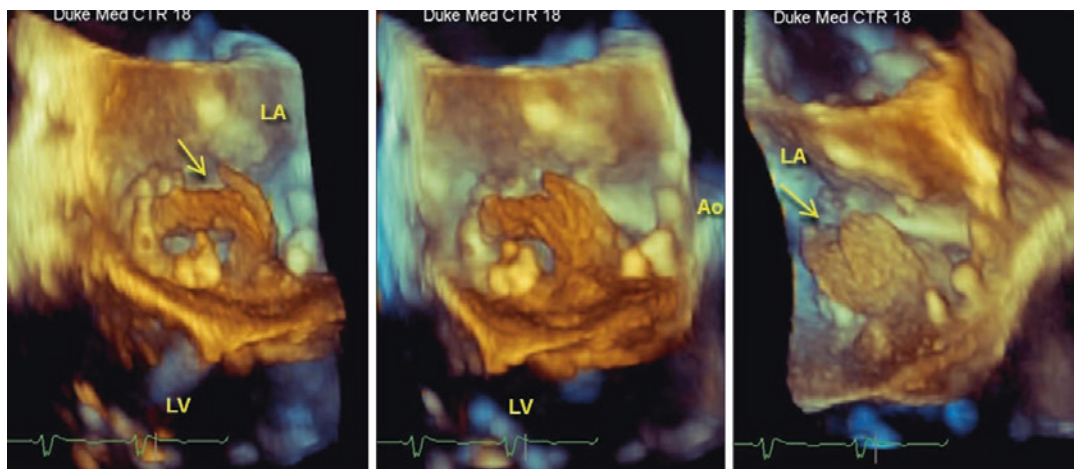


Fig. 14.24 Three-dimensional transesophageal echocardiographic still frames from the same patient as seen in the previous figure as the massive, polymorphous vegetation (arrows) bulges upwards into the left atrium. Note the

various projections of the massive vegetation. The three panels are from slightly different tilts and rotations in the surgeon's view

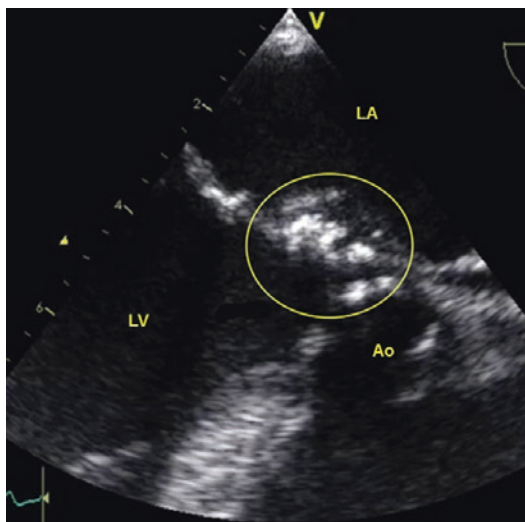


Fig. 14.25 An abscess is defined as a thickened area or mass within the myocardium or annular region with a non-homogeneous echogenic or echolucent appearance. This figure displays a long axis TEE view with an abscess in a typical area between the anterior mitral leaflet and LVOT. The patient underwent subacute aortic root surgery with insertion of an aortic root bioprosthesis

dramatic showing the massive vegetation spanning from one side of the valve ring to the other as it prolapses into the left atrium.

Abscess

An abscess is a thickened area or mass within the myocardium or annular region with a non-homogeneous echogenic or echolucent appearance. Figure 14.25 displays a long axis TEE view with an abscess in a typical area between the anterior mitral leaflet and LVOT. The patient underwent subacute aortic root surgery with insertion of an aortic root bioprosthesis.

Another patient is shown in Fig. 14.26 where a cluster of vegetations is seen in the short and long axis using the TEE approach. Note the bulging space between the aorta and the left atrium which represents an abscess of the aortic valve that penetrated posteriorly.

Figure 14.27 shows a necropsy specimen of a human heart that has been sectioned in half in the fashion of a parasternal long axis (or apical three-chamber) view. Note that the posterior wall of the aorta does not share a common wall with the left

atrium. Rather, there is a space between the two structures (arrows) that is the transverse sinus of the pericardium. Aortic abscesses tend to burrow posteriorly as there is available space, tissue and normal pericardial fluid to serve as a culture medium. Anterior to the aorta, the right ventricular outflow tract and pulmonary artery are densely adhered to the aorta, providing little opportunity for abscess to form.

The tangential TEE short axis of the aorta in Fig. 14.28 shows another patient with an aortic abscess into the transverse sinus. When abscesses are located in this position, surgical correction invariably requires aortic root replacement.

Aneurysm and Pseudoaneurysm

A rare complication of endocarditis is an aneurysm or pseudoaneurysm of tissue between the aortic and mitral valve referred to by some as the mitral aortic intervalvular fibrosa (MAIVF). In this context, the tissue is actually not fibrous or dense, rather it is soft and is referred to by others as the aorto-mitral curtain. The tissue is relatively avascular and is the weakest segment of the aortic ring, prone to infection and trauma. The TEE image in Fig. 14.29 demonstrates the characteristic dynamic expansion during early systole and collapse in diastole of a pseudoaneurysm. There is cyclical expansion and retraction in this abnormality and the right hand panel shows communication with the left ventricular outflow tract. Differentiation from an abscess is nearly impossible by echo alone and it remains a tissue diagnosis. Both are treated the same way by surgical replacement of the aortic root.

Fistula

A fistula is a communication between two neighboring cavities through a perforation. Figure 14.30 displays a long axis TEE view of the aortic valve with color Doppler showing a communication between LVOT/base of the aortic root and the left atrium. The patient had severe aortic and mitral IE complicated by heart failure and was referred to acute cardiac surgery, but went into cardiac arrest without the ability to resuscitate.

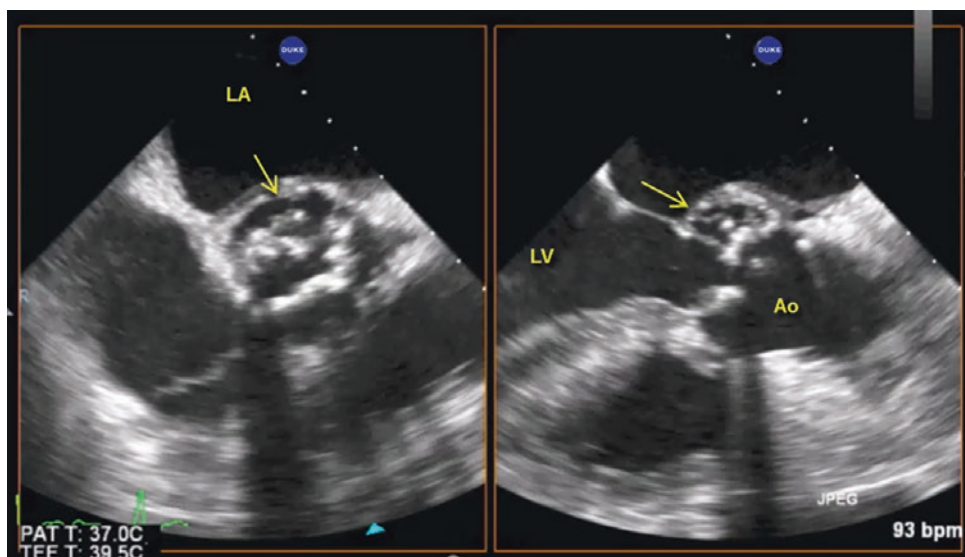


Fig. 14.26 Abscesses of the aortic valve frequently occur posteriorly by the infection eroding posteriorly into the transverse sinus of the pericardium (the space between the aorta and the left atrial anterior wall). The left panel shows a TEE short axis view of the aorta with the abscess in this

location (arrow) along with multiple vegetations on the aortic valve leaflets. The right panel is a TEE view of the LV long axis showing the area of the abscess (arrow) between the displaced aortic valve and base of the mitral valve

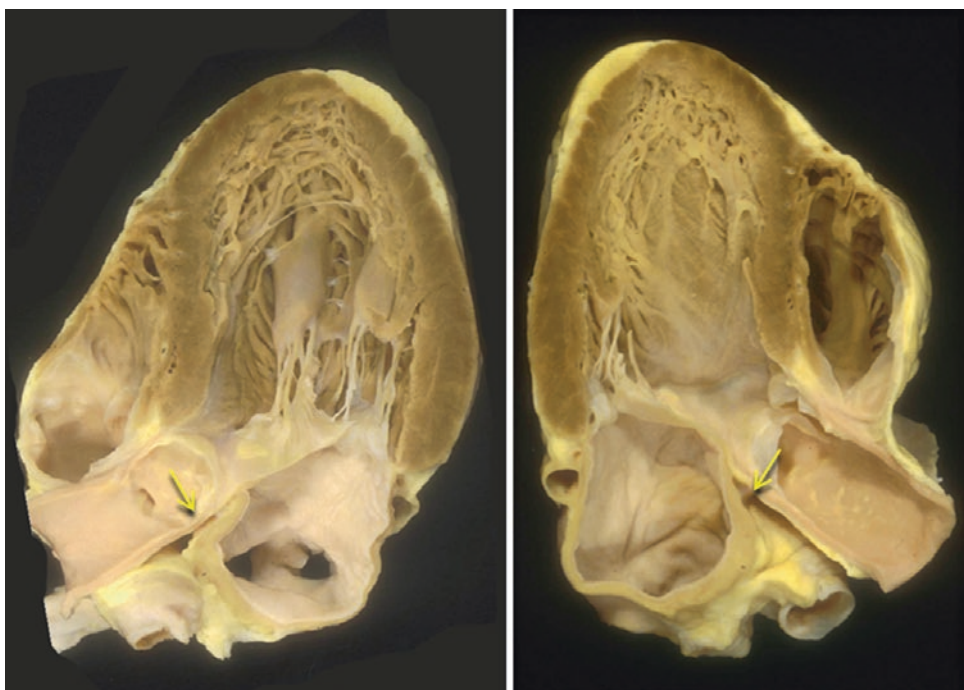


Fig. 14.27 Necropsy section of a human heart in the long axis of the left ventricle each half unfolded to the sides, like opening a book. The arrows point to the transverse sinus that separates the aorta and left atrium. Aortic abscesses usually go posteriorly into/around the trans-

verse sinus rather than anteriorly. Anterior to the aorta and aortic valve are the right ventricular outflow tract and pulmonary artery that are adherent, leaving little room for abscess formation. *Photographs courtesy of Yen Ho, MD*

A much clearer example of a fistula is seen in Fig. 14.31. Usually, when a fistula occurs there are elements of abscess, paravalvular regurgitation and other pathologic characteristics of IE involved so that the diagnostic line are blurred. In

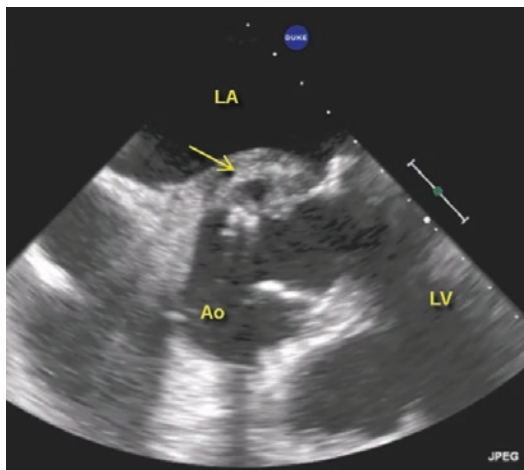


Fig. 14.28 TEE angulated view showing an abscess (arrow) of the aortic valve into the transverse sinus

this patient, who had a previous St. Jude valve mitral replacement. The mechanical prosthesis is in the open position in the left panel. In the two sequential systolic frames (middle and right panels) the infection has obviously burrowed around the prosthetic sewing ring and the systole flow regurgitates back into the left atrium through the fistula. Such fistulas require surgical correction.

Native Valve Perforation

Definition of a perforation is evidence of blood flow through a cardiac structure at a point that does not include the valve orifice. Figure 14.32 displays a long axis TEE view with color Doppler with perforations of the mitral valve. Several regurgitant jets are seen through perforations in both the anterior and posterior leaflets. The patient underwent subacute cardiac surgery with mitral valve repair.

Another patient with a perforation of a native valve is seen in Fig. 14.33. This patient underwent a previous mitral valve repair with placement of a mitral ring. In this case, multiple

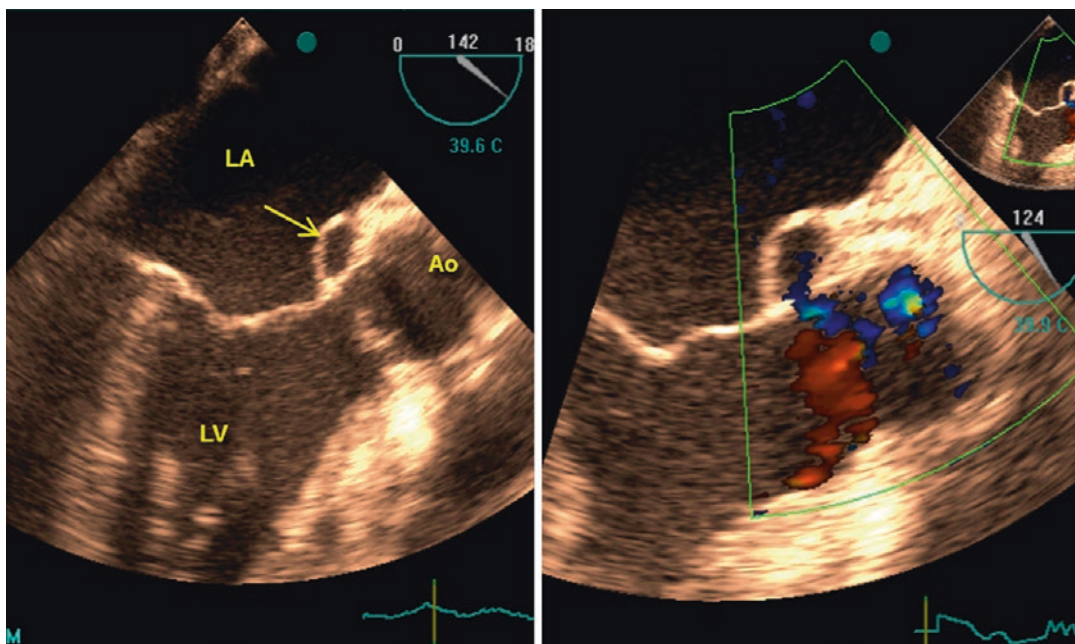


Fig. 14.29 An uncommon complication of endocarditis is a pseudoaneurysm in the area of cardiac valves. The TEE image in the left panel demonstrates the characteristic dynamic expansion during early systole (right panel)

and decreased size in diastole (left panel). The right panel demonstrates communication with the LV outflow tract. Differentiation from an abscess by echo alone is impossible

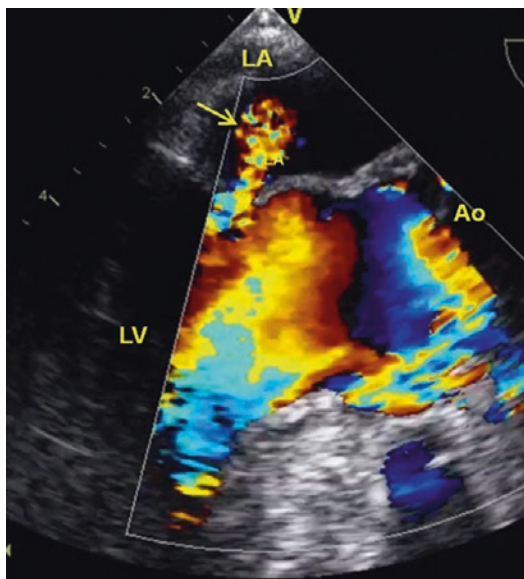


Fig. 14.30 A fistula is defined as a communication between two neighboring cavities through a perforation. This TEE view of the aortic valve during systole shows a flow jet between the VOT/base of the aortic root and the left atrium. The patient had severe aortic and mitral IE complicated by heart failure and was referred to acute cardiac surgery, but went into cardiac arrest without the ability to resuscitate

vegetations are seen (left panel). The perforation is seen with color Doppler through the base of the anterior mitral valve leaflet, just inside the mitral ring.

Prosthetic Valve Dehiscence

New valvular dehiscence of a prosthetic valve is pathognomonic for IE in the setting of other major criteria for endocarditis. Vegetations do not need to be present. Figure 14.34 shows a long axis TEE view of a prosthetic aortic valve with a 25 degree rocking motion between the valve and the aortic root from early (left panel) to late (right panel) in systole. Color Doppler demonstrates severe paravalvular regurgitation (C).

Sensitivity and Specificity of TTE and TEE in IE

The sensitivity for diagnosing vegetations in native valves is 70% for TTE and >95% for TEE. For diagnosis of vegetations in prosthetic valves the numbers are significantly lower with only 50% sensitivity for TTE and 90% for

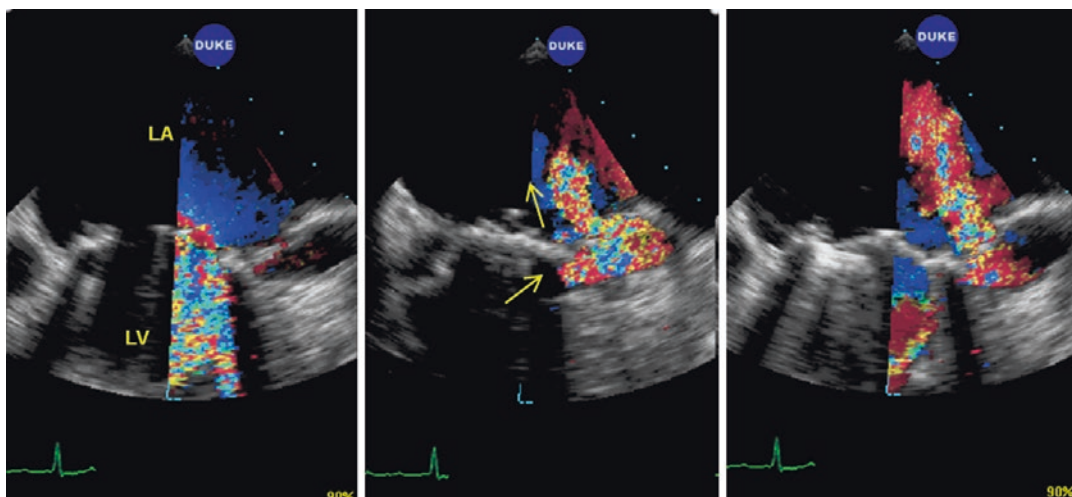


Fig. 14.31 Sequential TEE long axis views through a double disc mechanical valve in a patient with fever and positive blood cultures. The left panel shows turbulence through the orifice of the valve in diastole. A large cavity is seen to the right of the valve that represents a valve ring abscess with fistula formation into an abscess cavity from the left ventricle in early systole

(horizontal arrow, middle panel) the leads to the emptying of the fistula into the left atrium (vertical arrow, middle panel). The right panel is from a bit later in systole that clearly shows the double disc valve closed. The entire constellation of findings results in a paravalvular regurgitant leak

TEE. Identification of vegetations is difficult in the presence of pre-existing valvular lesions such as calcified lesions or mitral valve prolapse. Similarly, the acoustic shadow of a prosthetic valve may induce reverberation artifacts resulting

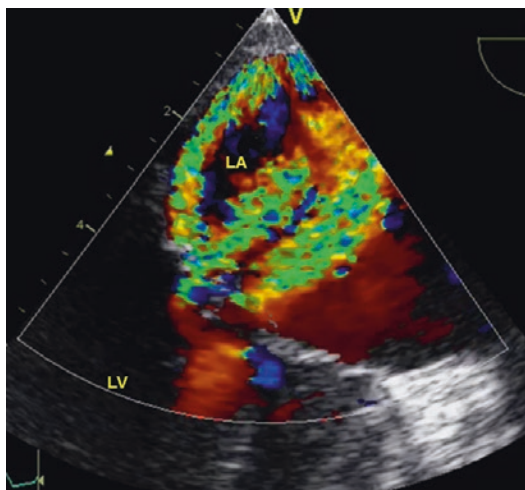


Fig. 14.32 Definition of a perforation is evidence of blood flow through a cardiac structure at a point that does not include the valve orifice. This TEE displays a long axis TEE view with color Doppler with perforations of the mitral valve. Several regurgitant jets are seen through perforations in both the anterior and posterior leaflets. The patient underwent subacute cardiac surgery with mitral valve repair

in false negative echocardiograms. Further, the diagnosis is challenging in case of small vegetations (<5 mm), recent embolization of the vegetation, and in nonvegetant IE. Accordingly, valvular perforation, mitral lesions and aneurysms are best assessed using TEE. However, TTE plays a central role in early diagnosis of both native and prosthetic IE to evaluate the haemodynamic consequences of valvular dysfunction, measurement of pulmonary artery pressure, detection of pericardial effusion and assessment and monitoring of left ventricular systolic function.

TEE is superior to TTE in detecting paravalvular complications of IE. The sensitivity of TTE for detecting an abscess is less than 50%, whereas TEE markedly improves the sensitivity for defining paravalvular complications of IE (75–100%) while preserving excellent specificity (95%) and positive and negative predictive values (88% and 87%, respectively). When combined with color Doppler techniques, TEE is superior to TTE for revealing the distinctive flow patterns of fistulas and pseudoaneurysms and to rule out communications from unruptured abscess cavities. Thus, TEE is recommended for the initial assessment of patients suspected of having paravalvular complications to IE.

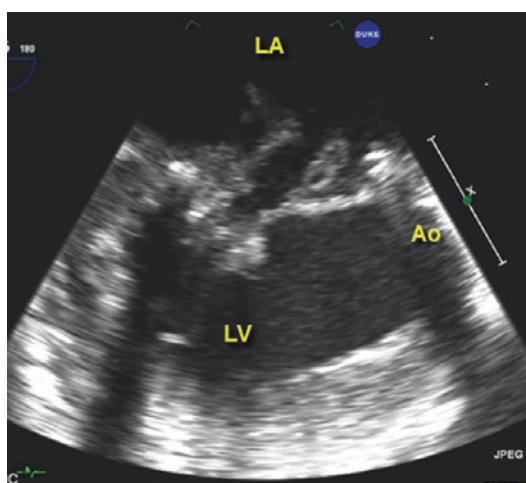
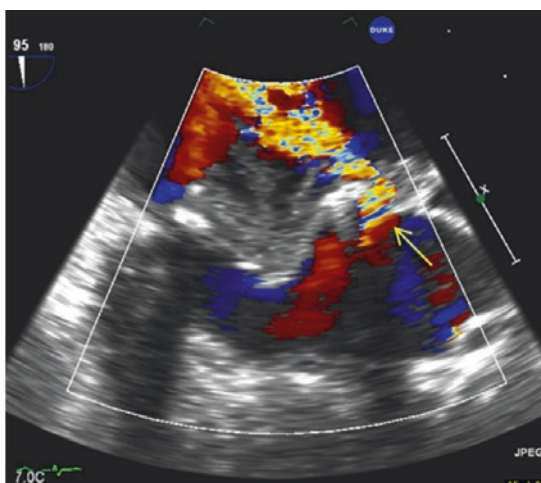


Fig. 14.33 TEE still frames through a native mitral valve on a patient who underwent a previous mitral valve repair with a mitral ring. Multiple vegetations are seen in the left



panel, prolapsing into the left atrium in systole. The right panel shows a perforation (arrow) through the native mitral ring near the prosthetic mitral valve ring

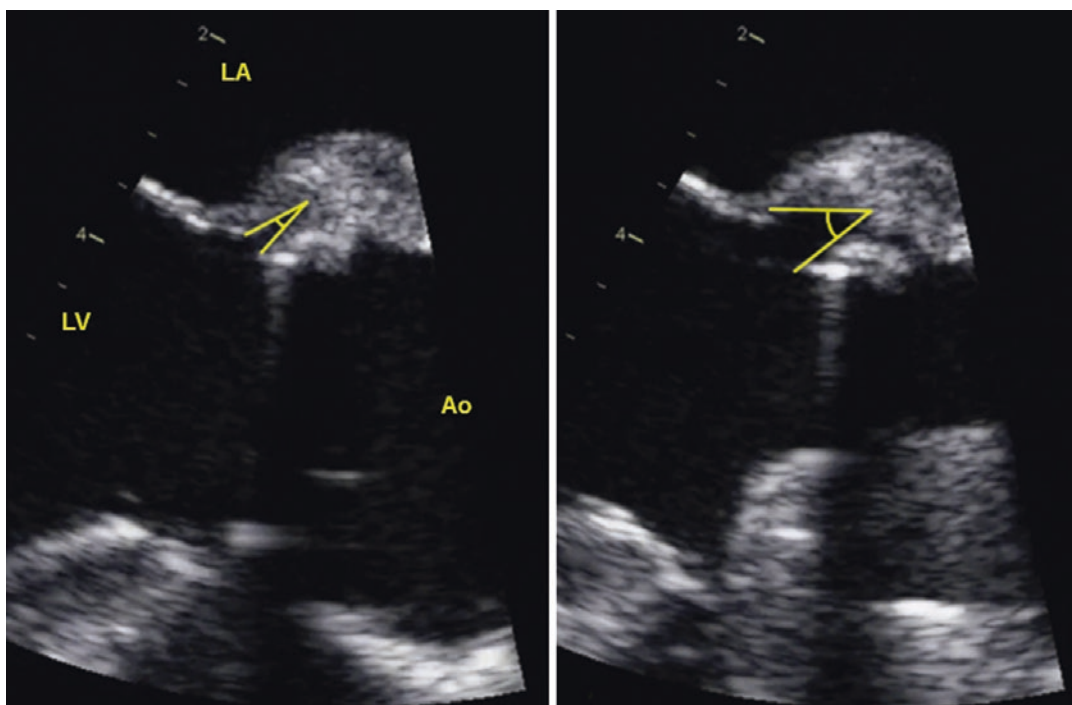


Fig. 14.34 New valvular dehiscence of a prosthetic valve is pathognomonic for IE. Dehiscence is defined as paravalvular regurgitation by echocardiography, with or without rocking motion of the prosthesis. These zoomed long axis TEE views of a prosthetic aortic valve with a 25

degree rocking motion between the valve and the aortic root from early (left panel) to late (right panel) systole. Color Doppler demonstrated severe paravalvular regurgitation

Guideline Recommended Algorithms for Using Echo to Diagnose IE

In the European guidelines, TTE is recommended initially in suspected IE followed by TEE in all cases except low clinical suspicion of IE (Fig. 14.35). Interestingly, the American Heart Association guidelines do not recommend TEE in patients with a positive TTE if no high risk echocardiographic features are present (Fig. 14.36). Further, the AHA guidelines divide patients into low, moderate or high clinical suspicion of IE, whereas the ESC guidelines only use existing or no-existing clinical suspicion. In both guidelines, repeat echocardiogram is recommended if the initial echocardiogram was negative but a high clinical suspicion of IE remains.

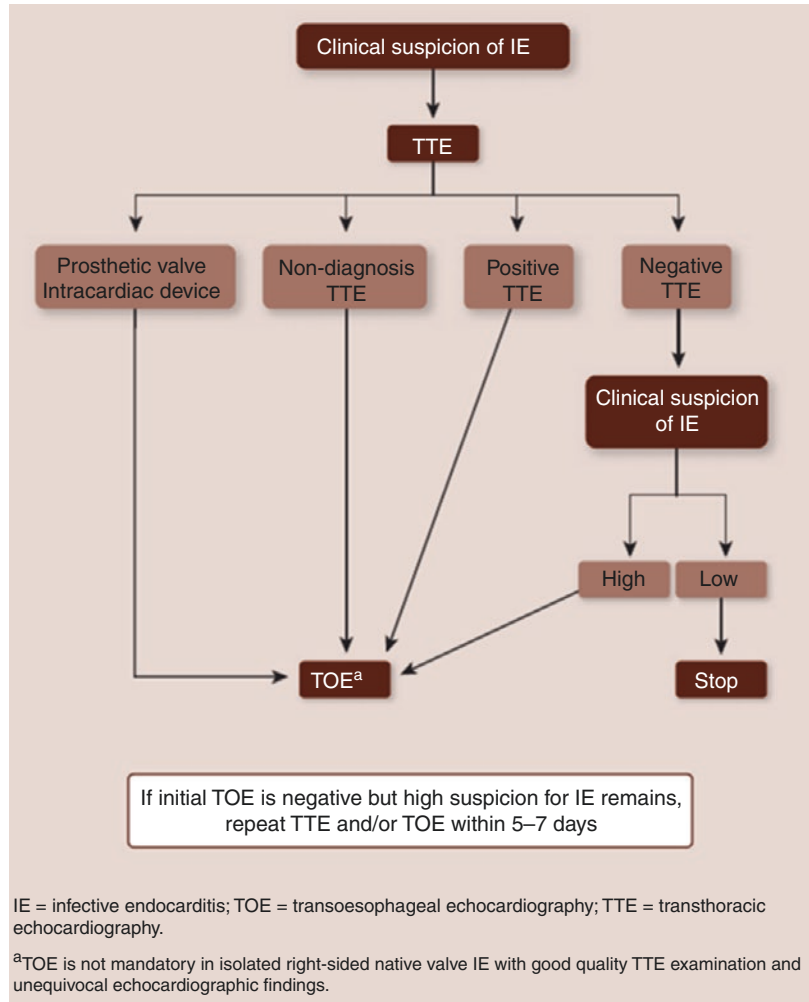
There is little data concerning the changes in vegetation size over time. What data that does exist indicates that vegetations in successfully

treated patients remain the same size or may actually increase in size slightly over time.

Echocardiographic Diagnostic Agreement in Evaluation of IE

Comparing the accuracy of echocardiographic interpretations to a gold standard of pathology is only possible in examination of IE patients that undergo surgery or autopsy. In the absence of these gold standards, echocardiographic reproducibility for the diagnostic assessment of IE can be examined. A recent study from the International Collaboration of Endocarditis (ICE) found that agreement in the assessment of echocardiographic variables associated with diagnosis and complications of IE is moderate to excellent, with highest agreement for LVEF, aortic abscess and the presence and location of vegetations.

Fig. 14.35 ESC recommendations for the Indications for echocardiography in suspected infective endocarditis



Lowest agreement was in assessing vegetation mobility. The Interobserver agreement for diagnostic variables is substantial to excellent for both TTE and TEE (Table 14.4).

Echocardiography for the Prognosis of IE

Echocardiographic markers have been studied with regard to predicting outcome in left-sided IE with conflicting results. For example, large or

highly mobile vegetations have been studied as potential risk factors for embolic events and mortality. Yet, studies regarding vegetation size report discordant results. Large, prospective studies have found that vegetation size was an independent predictor of embolic events and mortality, while others found that vegetation size was independently associated with embolic events, but not mortality.

Echocardiographic predictors of mortality have been studied in a large international prospective cohort from the International

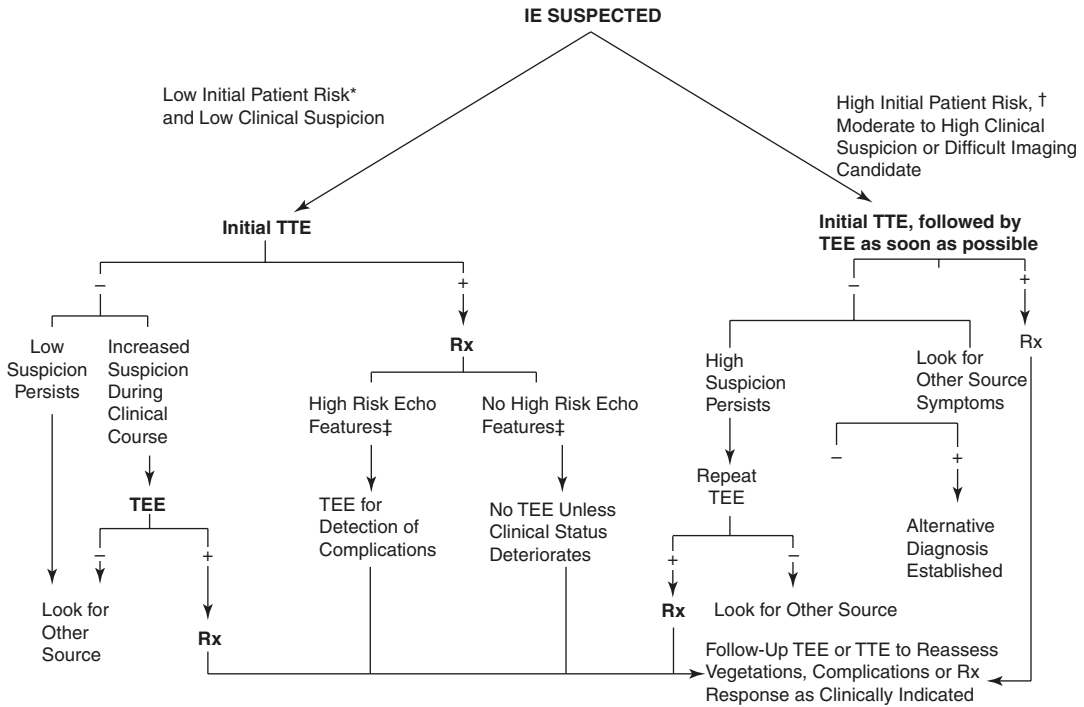


Fig. 14.36 AHA recommendations for the Indications for echocardiography in suspected infective endocarditis. Rx indicates prescription. †High initial patient risks include prosthetic heart valves, many congenital heart diseases, previous endocarditis, new murmur, heart failure,

or other stigmata of endocarditis. ‡High-risk echocardiographic features include large or mobile vegetations, valvular insufficiency, suggestion of perivalvular extension, or secondary ventricular dysfunction

Collaboration on Endocarditis. For *S. aureus* left-sided IE, specific predictors of in-hospital mortality are presence of an abscess or impaired systolic function (LVEF <40%). Similarly, heart failure as a complication to IE is the main cause of mortality in IE.

Note that premature closure of the mitral valve (Fig. 14.3) denotes severe aortic regurgitation with equilibration of left ventricular end diastolic pressure with aortic diastolic pressure. These patients usually are in severe acute heart failure.

Identification of echocardiographic predictors of outcome that can be revealed at time of diagnosis can add valuable information, not only for diagnosis and extent of cardiac complications, but also for early patient risk strati-

fication and referral for surgery. The indications for surgery in patients with IE are broadly expressed as: (1) Intractable heart failure, (2) Continued positive blood cultures and (3) Repeated embolization. Most patients presented in this chapter were managed surgically due to items 1 and 2 in combination with knowledge of modern surgical techniques. Repeated embolization is often confounded by the fact that patients who have experienced hemorrhagic strokes (instead of ischemic strokes) have an exceedingly high mortality at cardiopulmonary bypass. If such is the case, surgery must be delayed until the hemorrhagic stroke has healed to avoid the serious complications of complete anticoagulation necessary for cardiac surgery.

Table 14.4 Inter-observer agreement stratified by echo type: TTE or TEE

	Transthoracic echo K _{weighted} (95% CI) n = 47	Transesophageal echo K _{weighted} (95% CI) n = 63
Vegetation present		
Mitral	0.79 (0.71,0.98)	0.95 (0.90,0.99)
Aortic	0.91 (0.80,1.00)	0.89 (0.80,0.99)
Tricuspid	0.96 (0.92,1.00)	0.89 (0.78,1.00)
Device	0.66 (0.03,1.00)	1.00
Valvular regurgitation		
Mitral	0.75 (0.62,0.87)	0.89 (0.83,0.95)
Aortic n	0.84 (0.73,0.96)	0.93 (0.88,0.97)
Tricuspid	0.61 (0.35,0.86)	0.68 (0.49,0.88)
Complication		
Perforation mitral	0.45 (0.01,0.90)	0.94 (0.82,1.00)
Perforation aortic	0.79 (0.39,1.00)	1.00
Abscess mitral	0.37 (0.00,0.93)	1.00
Abscess aortic	0.79 (0.39,1.00)	0.80 (0.61,0.99)
Vegetation characteristics		
Mobility	0.58 (0.21,0.95)	0.72 (0.55,0.89)
Size	0.74 (0.57,0.90)	0.74 (0.57,0.90)

Summary Points

- The incidence of IE is increasing and the complications and mortality remain high despite advanced antibiotic and surgical therapies.
- Echocardiography plays a key role in diagnosing endocarditis in the modified Duke criteria.
- The sensitivity and specificity of transthoracic and transesophageal echocardiography for diagnosing IE and complications vary depending on modality and the presence of native or prosthetic material.
- European and American societies have published guidelines with recommended diagnostic algorithms for the use of echocardiography in patients suspected of having IE.
- Some echocardiographic variables have been identified as prognostically important which can help risk stratify patients at the time of diagnosis for early antibiotic and/or surgical therapies.

Suggested Readings

1. Holland TL, Baddour LM, Bayer AS, Hoen B, Miro JM, Fowler VG Jr. Infective endocarditis. *Nat Rev Dis Primers*. 2016;2:16059. <https://doi.org/10.1038/nrdp.2016.59>.
2. Cahill TJ, Prendergast BD. Infective endocarditis. *Lancet*. 2016;387(10021):882–93. [https://doi.org/10.1016/S0140-6736\(15\)00067-7](https://doi.org/10.1016/S0140-6736(15)00067-7). Epub 2015 Sep 1. Review.
3. Baddour LM, Wilson WR, Bayer AS, Fowler VG Jr, Tleyjeh IM, Rybak MJ, et al. American Heart Association Committee: infective endocarditis in adults: diagnosis, antimicrobial therapy, and management of complications: a scientific statement for healthcare professionals from the American Heart Association. *Circulation*. 2015;132(15):1435–86.
4. Habib G, Lancellotti P, Antunes MJ, Bongiorni MG, Casalta JP, Del Zotti F, et al. 2015 ESC guidelines for the management of infective endocarditis: the task force for the management of infective endocarditis of the European Society of Cardiology (ESC). Endorsed by: European Association for Cardio-Thoracic Surgery (EACTS), the European Association of Nuclear Medicine (EANM). *Eur Heart J*. 2015;36(44):3075–128.
5. Li JS, Sexton DJ, Mick N, Nettles R, Fowler VG Jr, Ryan T, et al. Proposed modifications to the Duke criteria for the diagnosis of infective endocarditis. *Clin Infect Dis*. 2000;30:633–8.
6. Habib G, Badano L, Tribouilloy C, Vilacosta I, Zamorano JL, Galderisi M, et al. Recommendations for the practice of echocardiography in infective endocarditis. *Eur J Echocardiogr*. 2010;11:202–19.
7. Reynolds HR, Jagen MA, Tunick PA, Kronzon I. Sensitivity of transthoracic versus transesophageal echocardiography for the detection of native valve vegetations in the modern era. *J Am Soc Echocardiogr*. 2003;16:67–70.
8. Mugge A, Daniel WG, Frank G, Lichtlen PR. Echocardiography in infective endocarditis: reassessment of prognostic implications of vegetation size determined by the transthoracic and the transesophageal approach. *J Am Coll Cardiol*. 1989;14:631–8.
9. Daniel WG, Mügge A, Martin RP, Lindert O, Hausmann D, Nonnast-Daniel B, et al. Improvement in the diagnosis of abscesses associated with endocarditis by transesophageal echocardiography. *N Engl J Med*. 1991;324:795–800.
10. Lauridsen TK, Selton-Suty C, Tong S, Afonso L, Cecchi E, Park L, et al. Echocardiographic agreement in the diagnostic evaluation for infective endocarditis. *Int J Cardiovasc Imaging*. 2016;32(7):1041–51.
11. Thuny F, Di Salvo G, Belliard O, Avierinos JF, Pergola V, Rosenberg V, et al. Risk of embolism and death in infective endocarditis: prognostic value of

- echocardiography: a prospective multicenter study. *Circulation*. 2005;112(1):69–75. Epub 2005 Jun 27. Erratum in: *Circulation*. 2005 Aug 30;112(9).
12. Lauridsen TK, Park L, Tong SY, Selton-Suty C, Peterson G, Cecchi E, et al. Echocardiographic findings predict in-hospital and 1-year mortality in left-sided native valve *Staphylococcus aureus* endocarditis: analysis from the international collaboration on endocarditis-prospective Echo cohort study. *Circ Cardiovasc Imaging*. 2015;8(7):e003397.
 13. Kiefer T, Park L, Tribouilloy C, Cortes C, Casillo R, Chu V, et al. Association between valvular surgery and mortality among patients with infective endocarditis complicated by heart failure. *JAMA*. 2011;306(20):2239–4.
 14. Stewart JA, Silimperi D, Harris P, Wise NK, Fraker TD, Kisslo JA. Echocardiographic documentation of vegetative lesions in infective endocarditis: clinical implications. *Circulation*. 1980;61:374–80.
 15. Sachdev M, Peterson GE, Jollis JG. Imaging techniques for diagnosis of infective endocarditis. *Cardiol Clin*. 2003;21:185–95.

Part III

Assessing the Right Ventricle

Assessing the Right Ventricle

15

Vasileios Kamperidis, Petros Nihoyannopoulos,
Jeroen J. Bax, and Victoria Delgado

Right Ventricle Anatomy and Function

The RV is the most anterior cardiac chamber located immediately behind the sternum. The complex shape of the RV, triangular in the long-axis (frontal view) and crescental in the short-axis (cross section) following the curvature of the interventricular septum, challenges its analysis with 2D imaging. However, the RV has several anatomical landmarks and segments with specific functions that facilitate its evaluation. In contrast to the left ventricle, the RV is characterized by coarse trabeculae, moderator band and a discontinuity between the inlet and the outflow valves (Fig. 15.1) [1]. In addition, the implantation of the septal leaflet of the tricuspid valve is more apical in comparison to the insertion point of the anterior mitral leaflet. These are important ana-

tomical landmarks that permit the identification of the RV in congenital heart diseases.

Functionally, the RV can be divided into three parts: the inflow region, the trabeculated apical myocardium and the outflow region or infundibulum. The inflow region extends from the atrio-ventricular junction demarked by the hinge lines of the tricuspid valve leaflets to the insertion of the papillary muscles into the ventricular walls. The trabeculated apical segment is defined by the insertion of the papillary muscles and moderator band and the true RV apex. The moderator band carries a fascicle of the right bundle branch of the conduction system. The septal aspect of the RV contains the septomarginal trabeculation which consists of an anterior and posterior arm demarcating the ventriculo-infundibular fold (Fig. 15.2). This ventriculo-infundibular fold separates the tricuspid and the pulmonary valves forming the supraventricular crest. Superiorly, the fold continues with the muscular part of the outflow region or subpulmonary infundibulum ending in the pulmonary valve. The arterial supply of the RV is most frequently provided by the right coronary artery and its acute marginal branches. The free lateral and anterior walls are supplied by these branches. The posterior descending coronary artery supplies the inferior wall and its septal branches supply the posterior interventricular septum. The left anterior descending coronary artery supplies the moderator band through the first septal branch and part

V. Kamperidis

Department of Cardiology, Leiden University
Medical Center, Leiden, The Netherlands

Department of Cardiology, AHEPA University
Hospital, Thessaloniki, Greece

P. Nihoyannopoulos

Imperial College London, Hammersmith Hospital,
London, UK
e-mail: petros@imperial.ac.uk

J. J. Bax · V. Delgado (✉)

Department of Cardiology, Leiden University
Medical Center, Leiden, The Netherlands
e-mail: v.delgado@lumc.nl

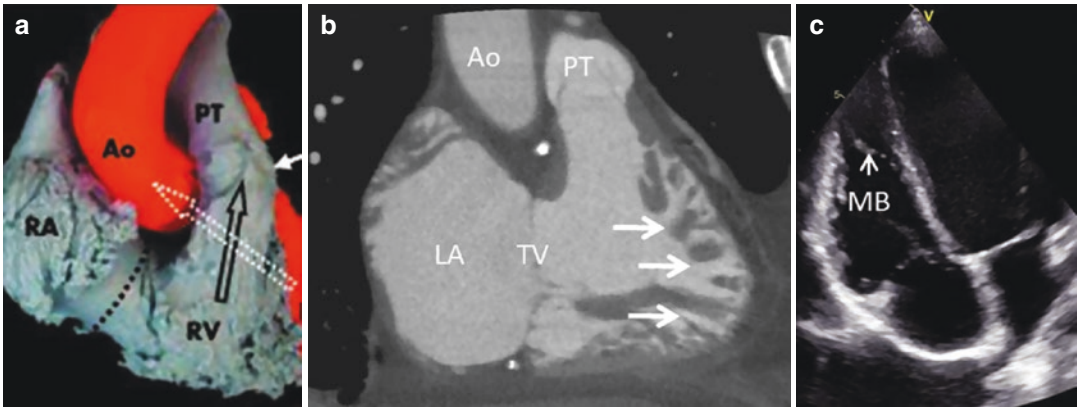


Fig. 15.1 Anatomical characteristics of the right ventricle. Panel **a** shows endocast of a normal heart with right heart chambers coloured blue and left heart chambers coloured red. Anteriorly viewed, the characteristic cross-over arrangement of the left and right ventricular outflows can be appreciated (crossing arrows) with the pulmonary artery being the most anterior structure (white arrow). Reproduced with permission from Ho et al. [1] On panel

b, the oblique sagittal view of the right ventricle shows the characteristic trabecularization of the apical unit (white arrows). On echocardiography, (panel **c**), the moderator band (MB) can be visualized in the apical 4-chamber view focused on the right ventricle (arrow). *Ao* aorta, *LA* left atrium, *MB* moderator band, *PT* pulmonary tract, *RA* right atrium, *RV* right ventricle, *TV* tricuspid valve

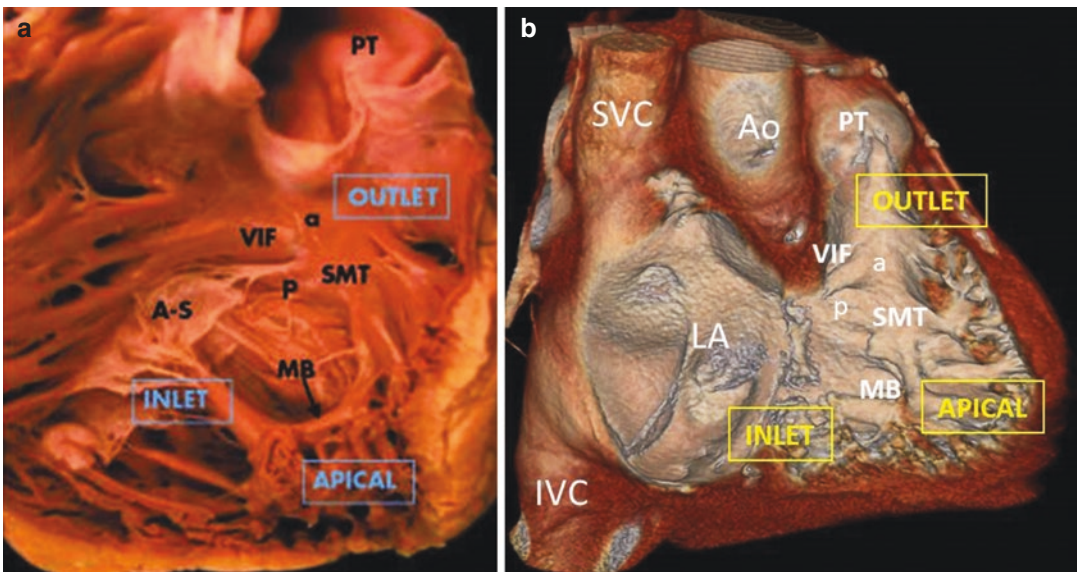


Fig. 15.2 Anatomical characteristics of the septal aspect of the right ventricle. Several structures can be differentiated in the septal aspect of the right ventricle (panel **a**): the septomarginal trabeculation (SMT) with its anterior (a) and posterior (p) arms embracing the ventriculo-infundibular fold (VIF) and the moderator band (MB) crossing the

ventricular cavity as a distinct bundle. Reproduced with permission from Ho et al. [1] On 3-dimensional volume rendering of the right ventricle, the same anatomical structures can be appreciated (panel **b**). *Ao* aorta, *IVC* inferior vena cava, *LA* left atrium, *SVC* superior vena cava, *PT* pulmonary tract

of the RV apex whereas the conus branch supplies the infundibulum.

The characteristic disposition of the muscular fibres of the RV, mostly oriented obliquely in the inlet region and circumconal in the infundibu-

lum, leads to a peristaltic contraction pattern that starts in the inlet region and ends in the infundibulum [2]. The normal thickness of the RV wall is 3–5 mm. Although the RV will provide the same stroke volume as the left ventricle, this will

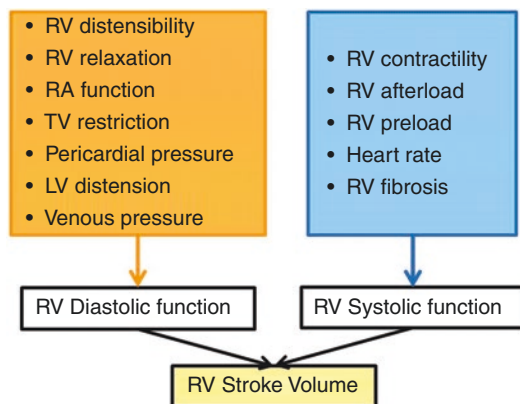


Fig. 15.3 Factors influencing the right ventricular function. *LV* left ventricular, *RA* right atrium, *RV* right ventricle

be accomplished by a reduced afterload [3]. Other factors that influence the RV function are summarized in Fig. 15.3. Myocardial contractility, RV preload, heart rate, pericardial pressure, RA function and LV distension are important determinants of the RV performance. How the RV can adapt to disease in order to maintain the stroke volume depends on the type and severity of the RV myocardial injury, time course of the disease (acute versus chronic) and onset of the disease (newborn, pediatric or adulthood) [4].

Assessment of RV Dimensions

In assessing the RV dimensions and function with 2D transthoracic or transesophageal echocardiography, multiple acoustic windows and views are needed. In addition, right atrial size and inferior vena cava diameter and collapsibility should be integrated in the assessment of RV dimensions and function (*see* Chap. 27) [5].

The RV should be imaged from the conventional and focused apical 4-chamber views, left parasternal long- and short-axis views, left parasternal RV inflow and subcostal views when using transthoracic echocardiography. Furthermore, by tilting the probe on the apical 5-chamber views, the most anterior and posterior sections of the RV can be assessed having as anatomical landmarks the moderator band and the coronary sinus, respectively (Fig. 15.4). On transesophageal echocardiography,

mid-esophageal 4-chamber and the RV inflow-outflow views and the transgastric short- and long-axis views complete the study of the RV (Fig. 15.5).

The normal dimensions of the RV have been recently updated in the American Society of Echocardiography guidelines (endorsed by the European Association of Echocardiography and the Canadian Society of Echocardiography) [5]. From current literature reporting values of RV dimensions in normal individuals without any history of heart disease, a meta-analysis was performed to obtain the pooled estimates of the mean, lower and upper reference values and their respective 95% confidence intervals (Table 15.1). However, the reference values for body mass index, gender and ethnicity categories could not be derived since patient-level data were not available. RV wall thickness, linear dimensions of the several functional parts of the RV and RV areas can be obtained from 2D transthoracic echocardiography. RV volumes are better measured from 3D transthoracic echocardiographic data. Regarding the assessment of RV size and function with transesophageal echocardiography, there are inadequate data to define specific recommendations and therefore, the present section will focus on transthoracic echocardiographic assessment [6].

RV Wall Thickness and Linear Dimensions

RV free wall thickness can be measured at end-diastole from M-mode or 2D recordings from the subcostal view (Fig. 15.6). Optimization of the endocardial border definition by decreasing the depth, and if image quality permits, and using fundamental imaging is important to accurately measure the RV free wall thickness. Trabeculations and papillary muscle should be excluded from the measurement. Abnormal RV wall thickness is defined by >5 mm thickness measured on parasternal long-axis or subcostal views. Increased RV free wall thickness usually results from RV pressure overload (pulmonary hypertension) [7–9] but can be also observed in physiological conditions such as elite athletes [10]. RV thickness has been independently associated with prognosis of patients with heart failure and pulmonary hypertension [9, 11].

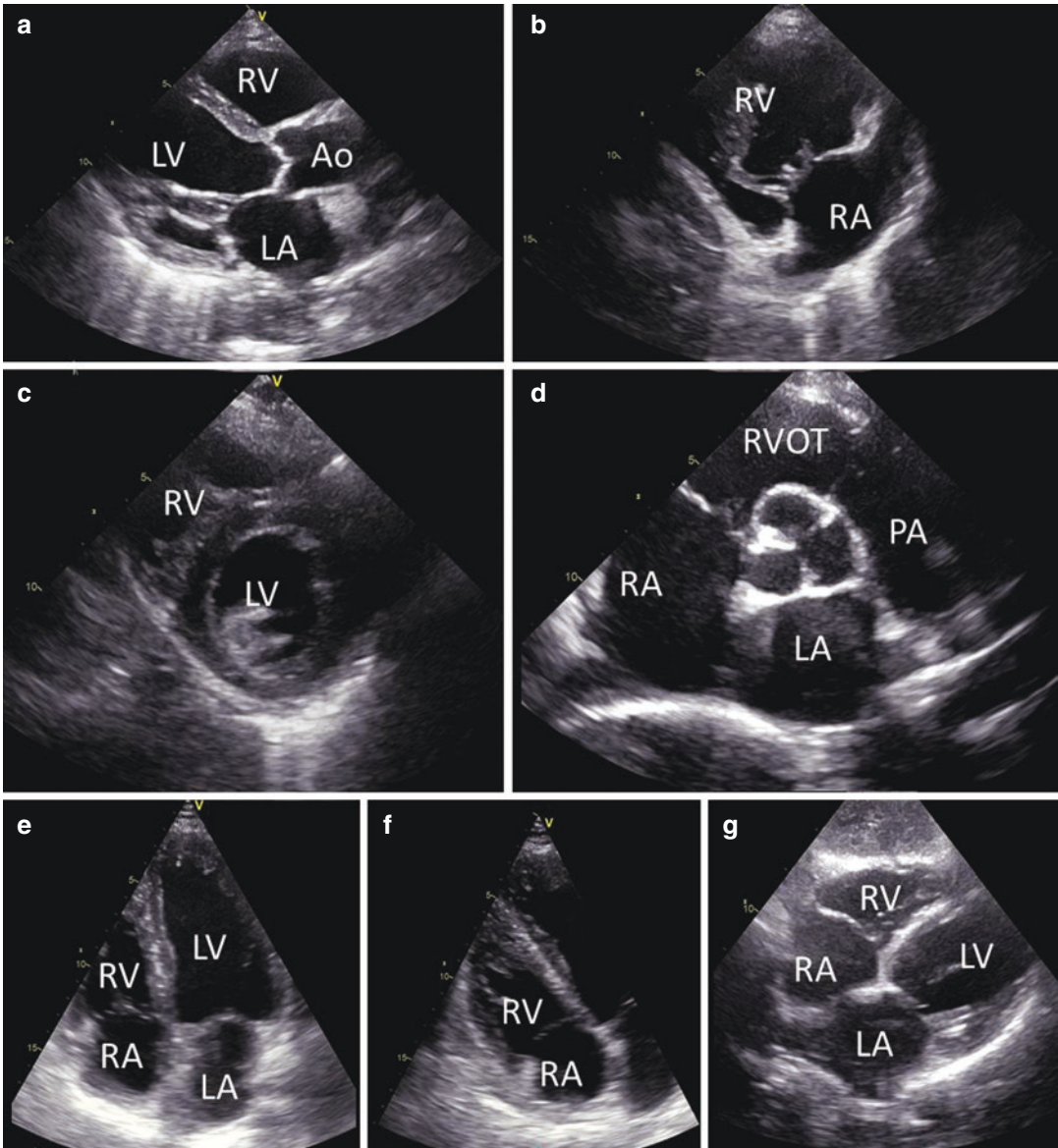


Fig. 15.4 Transthoracic echocardiographic assessment of the right ventricle. Conventional transthoracic echocardiographic acquisitions of the right ventricle (RV) include the parasternal long-axis view (panel **a**), imaging the RV anterior wall, the parasternal long-axis view of the RV inflow (panel **b**) to visualize the inferior and anterior walls, the parasternal short-axis view at mid-ventricular level (panel **c**), showing the inferior lateral and anterior

walls, and aortic valve level (panel **d**), to visualize the right ventricular outflow tract (RVOT), the apical 4-chamber view (panel **e**) and focused apical RV view (panel **f**) and the subcostal view (panel **g**). *Ao* aorta, *LA* left atrium, *LV* left ventricle, *PA* pulmonary artery, *RA* right atrium, *RV* right ventricle, *RVOT* right ventricular outflow tract

End-diastolic RV linear dimensions measured with 2D transthoracic echocardiography include the basal and mid cavity RV diameter and RV longitudinal diameter obtained on focused apical

4-chamber views and the proximal diameter of the RVOT measured on the parasternal long-axis or short-axis views and the distal diameter of the RVOT measured below the pulmonary valve in

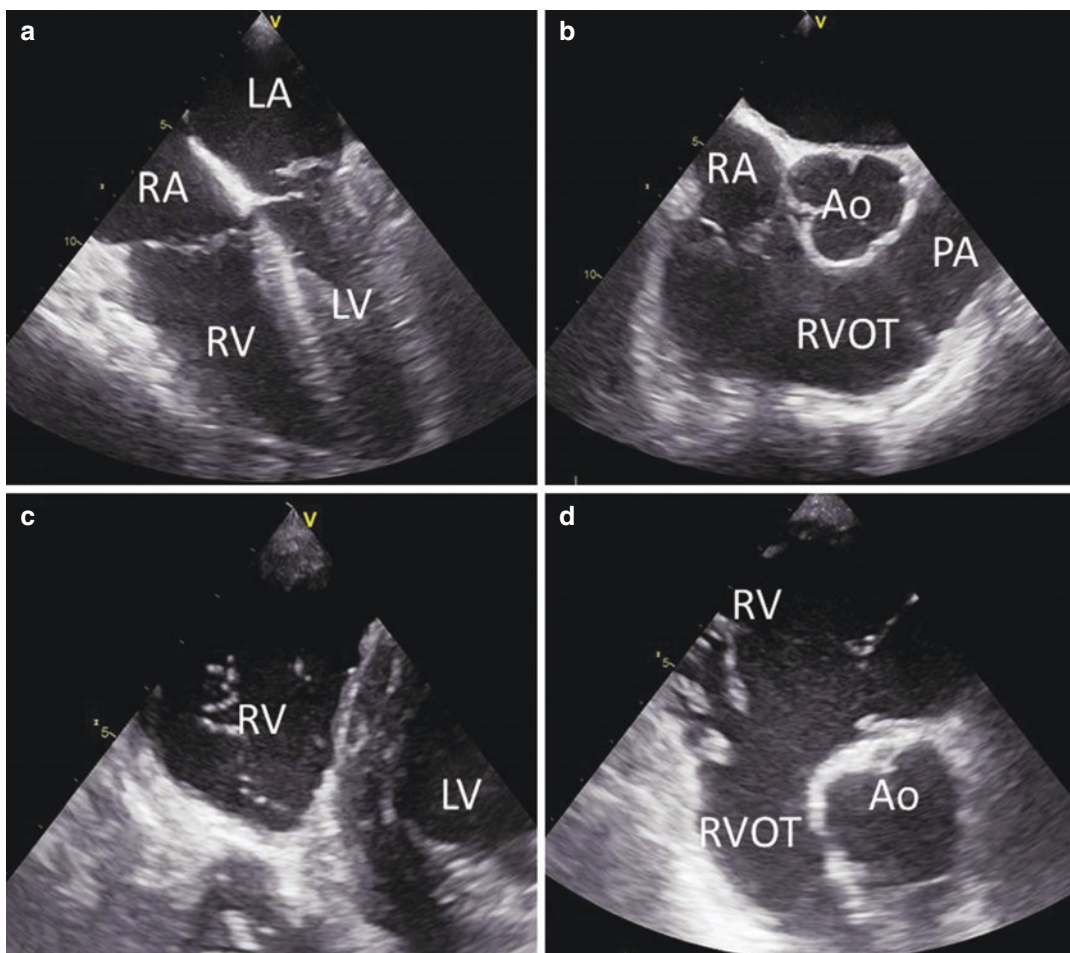


Fig. 15.5 Transesophageal echocardiographic assessment of the right ventricle. The mid-esophageal 4 chamber view at 0° (panel **a**), the right ventricular inflow-outflow view (at 30–60°, panel **b**) and the transgastric short- (panel **c**) and long-axis (panel **d**) views should be acquired when

assessing the right ventricular function with transesophageal echocardiography. *Ao* aorta, *LA* left atrium, *LV* left ventricle, *PA* pulmonary artery, *RA* right atrium, *RV* right ventricle, *RVOT* right ventricular outflow tract

the parasternal short-axis view (Fig. 15.7). In addition, from the focused apical 4-chamber view, the RV end-diastolic and end-systolic areas can be obtained. The RV focused apical 4-chamber view enhances the imaging of the RV lateral wall with the transducer properly positioned on the cardiac apex with the plane through the left ventricle in the center of the cavity avoiding visualization of the left ventricular outflow tract or the coronary sinus (which would lead to foreshortened views of the RV) [5]. In normal individuals, the RV end-diastolic area is approximately two thirds of that of the left ven-

tricle. In response to pressure or volume overload the RV responds with dilatation of the cavity and specific change in the geometry: while pressure overload is characterized by encroachment of the septum into the left ventricular cavity along the entire cardiac cycle, in volume overload the leftward deviation of the septum occurs during the diastole whereas during systole, the normal transeptal pressure gradient is maintained and the septum keeps the normal shape and position [12]. Other cardiomyopathies may result in different patterns of RV dilatation. For example, in RV arrhythmogenic dysplasia, thinning of the RV

Table 15.1 Normative values for RV dimensions on 2-dimensional echocardiography

Variable	Abnormal	Studies	No	Lower reference value (95% CI)	Mean (95% CI)	Upper reference value (95% CI)
RV wall thickness (mm)	>5	4	180	4 (3–4)	5 (4–5)	5 (5–6)
RV basal diameter (mm)	>42	10	376	24 (21–27)	33 (31–35)	42 (39–45)
RV mid cavity diameter (mm)	>35	12	400	20 (15–25)	28 (23–33)	35 (30–41)
RV longitudinal diameter (mm)	>86	12	359	58 (50–61)	71 (67–75)	86 (80–91)
RVOT PLAX diameter (mm)	>33	12	405	18 (15–20)	25 (23–27)	33 (30–35)
RVOT proximal diameter (mm)	>35	5	193	21 (18–25)	28 (27–30)	35 (31–39)
RVOT distal diameter (mm)	>27	4	159	17 (12–22)	22 (17–26)	27 (22–32)
RV end-diastolic area (cm ²)	>25	20	623	10 (8–12)	18 (16–19)	25 (24–27)
RV end-systolic area (cm ²)	>14	16	508	4 (2–5)	9 (8–10)	14 (13–15)
RV end-diastolic volume index (mL/m ²)	>80	3	152	44 (32–55)	62 (50–73)	80 (68–91)
RV end-systolic volume index (mL/m ²)	>46	1	91	19 (17–21)	33 (31–34)	46 (44–49)

CI confidence interval, PLAX parasternal long-axis, RV right ventricle, RVOT right ventricular outflow tract

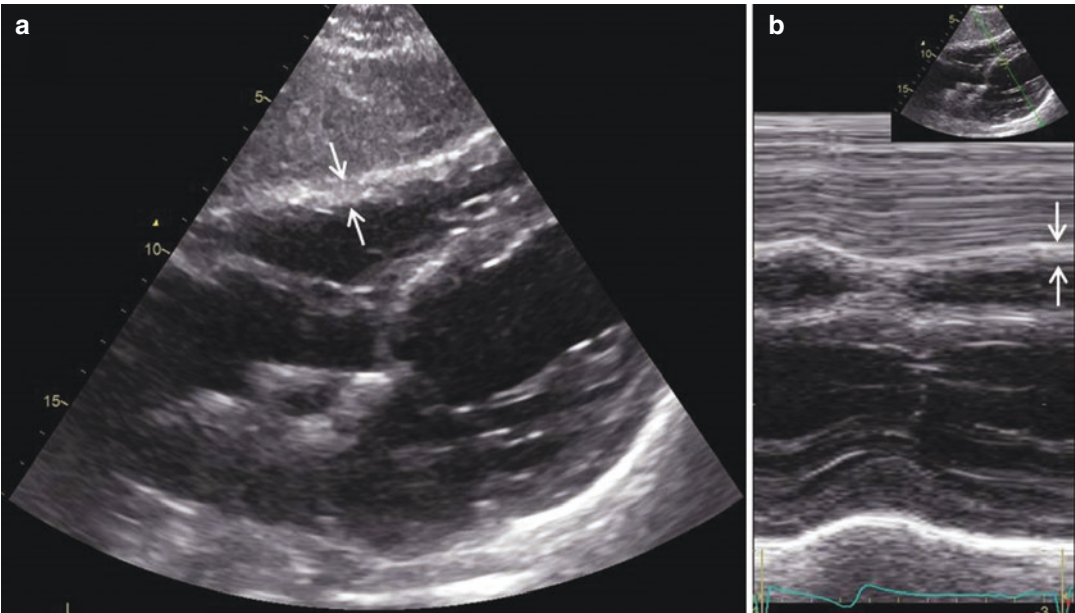


Fig. 15.6 Measurement of the right ventricular wall thickness. From the subcostal view, the linear dimension of the right ventricular wall thickness on bidimensional mode (panel **a**) or M-mode (panel **b**)

free wall, aneurysms near the apex and dilatation of the RVOT are characteristic depending on the extension of the disease [13]. Several studies have demonstrated the prognostic value of several dimensions of the RV in several diseases [11, 14, 15]. In patients with idiopathic pulmonary

arterial hypertension, a RV diameter measured on the parasternal long-axis view >36.5 mm was associated with increased all-cause mortality at follow-up [11]. In patients with chronic pulmonary disease, end-diastolic RV dimension was independently associated with increased risk of

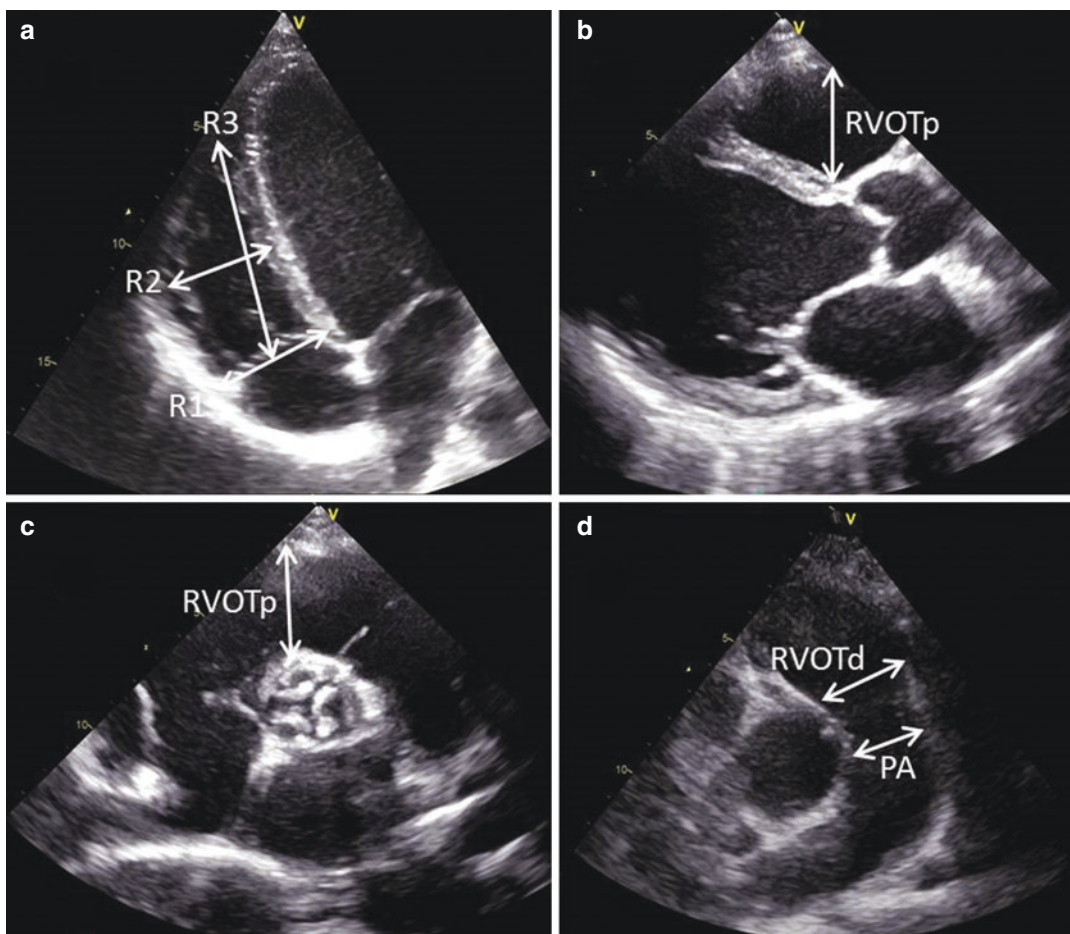


Fig. 15.7 Linear dimensions of the right ventricle. From the focused apical 4-chamber view the basal (R1), mid-cavity (R2) and longitudinal (R3) diameters of the right ventricle can be measured (panel **a**). The proximal part of the right ventricular outflow tract (RVOTp) can be mea-

sured on the parasternal long-axis view (panel **b**) or the short-axis view (panel **c**) above the aortic valve. The distal part of the RVOT (RVOTd) can be measured on the focused view of the pulmonary artery (PA) (panel **d**)

all-cause mortality (hazard ratio 1.27, $p = 0.0032$) [15]. In patients undergoing tricuspid annuloplasty, larger end-diastolic mid-cavity diameter was associated with worse prognosis [14].

RV Volume Assessment

Two-dimensional echocardiographic assessment of RV volumes can be performed by using the area-length and disk summation methods applied to the focused apical 4-chamber view. Both methods are based on important geometrical assumptions and exclude the RVOT resulting in significant underestimation of RV volumes when compared with 3D imaging techniques (echocar-

diography or magnetic resonance imaging). Accordingly, assessment of RV volumes and the derivation of RV ejection fraction with 2D echocardiography is not recommended.

3D Echocardiography

Assessment of RV volumes with 3D echocardiography has been one of the major breakthroughs of the last decades. Data showing the accuracy of 3D echocardiographic methodologies to assess RV volumes, in comparison with magnetic resonance imaging as reference standard, are accumulating (Table 15.2) [16–30]. From the RV focused apical 4-chamber view, the 3D dataset of the RV full

Table 15.2 Comparison of 3D echocardiography RV volumes and ejection fraction with MRI derived values

Study (year)	No.	Underlying pathology	RT3DE method	CMR method	RVEDV R (Bias and 2SD)	RVESV R (Bias and 2SD)	RVEF R (Bias and 2SD)
Prakasa et al. [16] (2006)	58	40% ARVD	2 orthogonal apical planes	SAX slices	0.50 (−15.9 ± 17.8 mL)	0.72 (−6.8 ± 8.9 mL)	0.88 (−1 ± 8%)
Nesser et al. [17] (2006)	20	30% CAD 30% healthy	SAX slices	SAX slices	0.85 (−1.6 ± 18.2 mL)	0.86 (0.1 ± 13.4 mL)	0.86 (−2 ± 9.4%)
Jenkins et al. [18] (2007)	50	RV wall motion abnormalities	12 apical planes	SAX slices	0.60 (−3 ± 10 mL)	0.55 (−4 ± 7 mL)	0.72 (2 ± 4%)
Niemann et al. [19] (2007)	30	53% CHD	3 orthogonal planes	3 orthogonal planes	0.99 (0.91 ± 4.5 mL)	0.98 (0.71 ± 6.1 mL)	0.97 (0.16 ± 12.5%)
Gopal et al. [20] (2007)	71	Healthy	3 orthogonal planes	SAX slices	0.8 (−16 ± 17.8 mL)	0.8 (−8.3 ± 11.4 mL)	0.7 (−1.7 ± 10.2)
Lu et al. [21] (2008)	17	Healthy	3 orthogonal planes	SAX slices	0.98 (−7.0 ± 9.0 mL)	0.96 (−3.2 ± 7.1 mL)	0.89 (0.3 ± 4.1%)
Iriart et al. [22] (2009)	37	59% CHD	3 orthogonal planes	SAX slices	0.93 (−18.7 ± 20.6 mL)	0.92 (−9.1 ± 15.3 mL)	0.73 (−0.2 ± 5.5%)
Khoo et al. [23] (2009)	28	CHD	3 orthogonal planes	3 orthogonal planes	0.89 (−21.6 ± 13 mL)	0.88 (−15.2 ± 22 mL)	0.83 (−2.6 ± 6.0%)
Sugeng et al. [24] (2010)	28	25% pulmonary hypertension	3 orthogonal planes	3 orthogonal planes	0.87 (−14 ± 73 mL)	0.89 (−9 ± 53 mL)	0.87 (−2 ± 12%)
Grapsa et al. [25] (2010)	60	Pulmonary hypertension	SAX slices	SAX slices	0.74 (−3.7 ± 28.7 mL)	0.75 (−0.02 ± 24.4 mL)	0.66 (−4 ± 15.8)
Leibundgut et al. [26] (2010)	100	25% myocarditis 13% ARVD	3 orthogonal planes	SAX slices	0.84 (−10.2 ± 21.2 mL)	0.83 (−4.5 ± 14.5 mL)	0.72 (−0.4 ± 7.5%)
Van der Zwaan et al. [27] (2011)	120	74% CHD	3 orthogonal planes	SAX slices	0.97 (−17 ± 36 mL)	0.96 (−3 ± 29 mL)	0.71 (−3 ± 13%)
Dragulescu et al. [28] (2012)	36	c-ToF	3 orthogonal planes	SAX slices	0.98 (−18.2 ± 17.8 mL)	0.98 (−9.1 ± 16.2 mL)	0.85 (−1.1 ± 4.8%)
Zhang et al. [29] (2013)	61	27% healthy	3 orthogonal planes	SAX slices	0.97 (−2.2 ± 15.1 mL)	0.96 (−2.6 ± 15.8 mL)	0.71 (−0.86 ± 16.0%)
Kim et al. [30] (2015)	27	63% ICM	3 orthogonal planes	SAX slices	0.90 (−14 ± 23 mL)	0.89 (−6 ± 21 mL)	0.77 (−3 ± 9%)

ARVD arrhythmogenic right ventricular dysplasia, CAD coronary artery disease, CHD congenital heart disease, CMR cardiac magnetic resonance, c-ToF corrected tetralogy of Fallot, ICM ischemic heart disease, No number of patients, RVEDV right ventricular end-diastolic volume, RVEF right ventricular ejection fraction, RVESV right ventricular end-systolic volume, RT3DE real-time 3-dimensional echocardiography, SAX short-axis, SD standard deviation

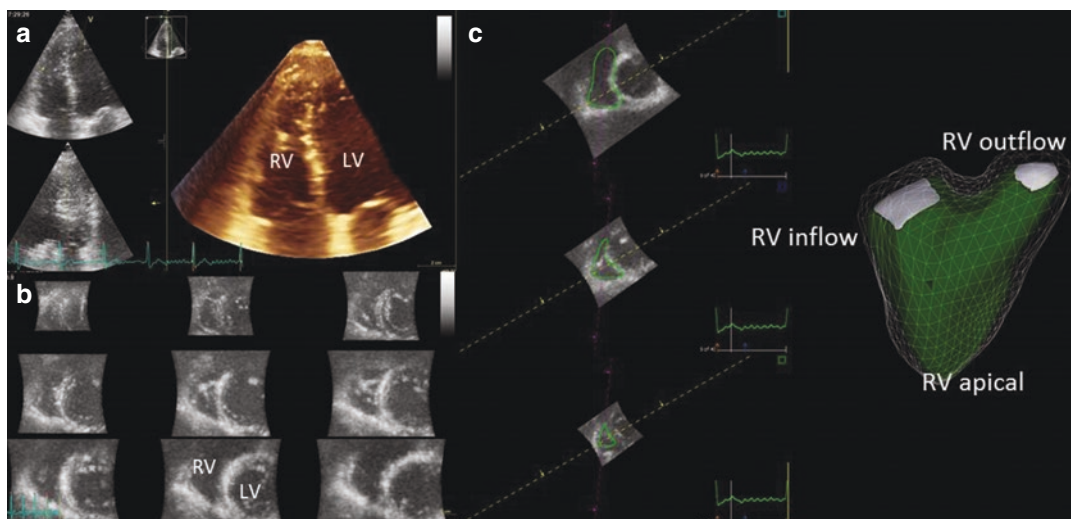


Fig. 15.8 Assessment of right ventricular volumes and function with 3-dimensional transthoracic echocardiography. From a focused apical view of the right ventricle (panel **a**), visualizing simultaneously two orthogonal planes (the 4-chamber view in the left upper corner and the apical right ventricular outflow tract view in the left bottom corner) and the 3-dimensional full-volume

cropped. To ensure inclusion of the right ventricular walls into the full-volume, visualization of nine slices (from the base until the apex) is helpful (panel **b**). Finally, postprocessing the 3-dimensional full-volume dataset with dedicated software permits quantification of right ventricular volumes and ejection fraction (panel **c**). *LV* left ventricle, *RV* right ventricle

volume is acquired using ECG-gating along 4–7 consecutive beats. Sequential pyramidal subvolumes of the RV are acquired and stitched to form the full volume (Fig. 15.8). Therefore, regular heart rhythm and 4–7 s of breath hold are needed to reduce at minimum the stitching artefacts. One of the largest series defining the reference values for 3D echocardiographic RV volumes included 507 healthy volunteers (260 women; 45 ± 16 years old; range 18–90 years) [31]. The analysis was feasible in 94% of individuals. The study showed that 3D echocardiographic RV volumes are strongly influenced by age and anthropometric parameters.

Assessment of RV Function

When assessing the RV function with echocardiography, several methods can be used. These can be grouped in volumetric and non-volumetric methods. Volumetric methods include RV area fractional change (FAC) and RV ejection fraction. Non-volumetric methods include RV dp/dt , myocardial performance index and strain indices derived from 3D speckle tracking echocardiogra-

phy, which provide a global assessment of RV function, and tricuspid annulus plane systolic excursion (TAPSE), tissue Doppler imaging derived velocities and longitudinal strain and strain indices derived from 2D speckle tracking echocardiography, which provide a regional assessment RV function. The reference values for each functional parameter are provided in Table 15.3. More recently, data on RV global function assessed with 3D speckle tracking echocardiography are accumulating and will be discussed in this section.

RV Fractional Area Change and Ejection Fraction

From the apical 4-chamber view of the RV on 2D transthoracic echocardiography, the RV FAC is calculated as the difference between the end-diastolic and end-systolic RV areas divided by the end-diastolic RV area and expressed as percentage. Care must be taken to properly align the probe and obtain the plane that transects the RV in the longitudinal axis avoiding foreshortening. A RV FAC value $\geq 35\%$ defines normal RV systolic function. Several studies have demonstrated the prognostic value of RV fractional area change

Table 15.3 Normative values of right ventricular systolic function

Variable	Abnormal	Studies	No	Lower reference value (95% CI)	Mean (95% CI)	Upper reference value (95% CI)
Fractional area change (%)	<35	36	1276	35 (32–38)	49 (47–51)	63 (60–65)
RV ejection fraction (%)	<44	12	596	44 (38–50)	58 (53–63)	71 (66–77)
TAPSE (mm)	<16	46	2320	16 (15–18)	23 (22–24)	30 (29–31)
Myocardial performance index						
Pulsed wave Doppler	>0.4	17	686	0.15 (0.10–0.20)	0.28 (0.24–0.32)	0.40 (0.35–0.45)
Tissue Doppler imaging	>0.55	8	590	0.24 (0.16–0.32)	0.39 (0.34–0.45)	0.55 (0.47–0.63)
TDI-S' (cm/s)						
Pulsed wave	<10	43	2139	10 (9–11)	15 (14–15)	19 (18–20)
Color-coded	<6	5	281	6 (5–7)	10 (9–10)	14 (12–15)

CI confidence interval, RV right ventricle, TAPSE tricuspid annulus plane systolic excursion, TDI tissue Doppler imaging

in several clinical scenarios: heart failure, pulmonary arterial hypertension, arrhythmogenic RV dysplasia, myocardial infarction and valvular heart disease [32–36]. One of the limitations of this method is that does not include the RVOT, which plays an important role in the global function of the RV contributing with 15% of the total RV ejection fraction [37–39].

Two-dimensional RV ejection fraction is derived from subtracting the end-systolic volume from the end-diastolic volume and dividing by end-diastolic volume. It is also expressed as percentage. Calculation of RV volumes has been described above. However, due to the complex 3D shape of the RV and the numerous geometric assumptions needed to calculate 2D RV ejection fraction, current guidelines do not recommend its use in routine clinical practice [5]. Recent advances on knowledge-based reconstruction, a hybrid approach that combines conventional 2D echocardiographic data and reference library of RV shapes to reconstruct a 3D RV volume, has shown superior test-retest reproducibility to quantify RV volumes compared with conventional 2D echocardiographic assessed of RV areas [40, 41]. The technology behind knowledge-based reconstruction has been previously described [40, 41], and consists of a magnetic localizer attached to the transthoracic probe and connected to a dedicated console, from which a mechanical arm with a magnetic field generator hangs over the

patient. The magnetic localizer detects orthogonal magnetic fields from the generator so that the transthoracic probe is localized in the 3D space and the point of any 2D acquisition (Fig. 15.9). Conventional parasternal long-axis view, short-axis views at the papillary muscle and apical levels, parasternal RV inflow and parasternal RVOT including the pulmonary valve hinge points and the infundibulum views, apical 4-chamber and off-axis RV apical views are acquired during a 2-second period and transferred to and digitized at 30f/s in a dedicated 2D knowledge-based reconstruction console. Off-line, several anatomical RV landmarks are plotted at end-systole and end-diastole with their respective 3D spatial coordinates and the algorithm interpolates between the plotted points using as reference a catalogue of RV shapes obtained from magnetic resonance imaging from patients. Using this technique, Knight and coworkers showed a good agreement between 2D knowledge-based reconstruction and magnetic resonance imaging for the measurement of RV end-diastolic volume (3.5 ± 25.0 mL), end-systolic volume (0.9 ± 19.9 mL) and ejection fraction ($0.4 \pm 10.2\%$) and no significant inter- and intra-observer test-retest differences [41].

However, 3D transthoracic echocardiography is currently being regularly used in routine clinical practice. Post-processing software permits assessment of RV volumes and ejection fraction including all the functional segments of the

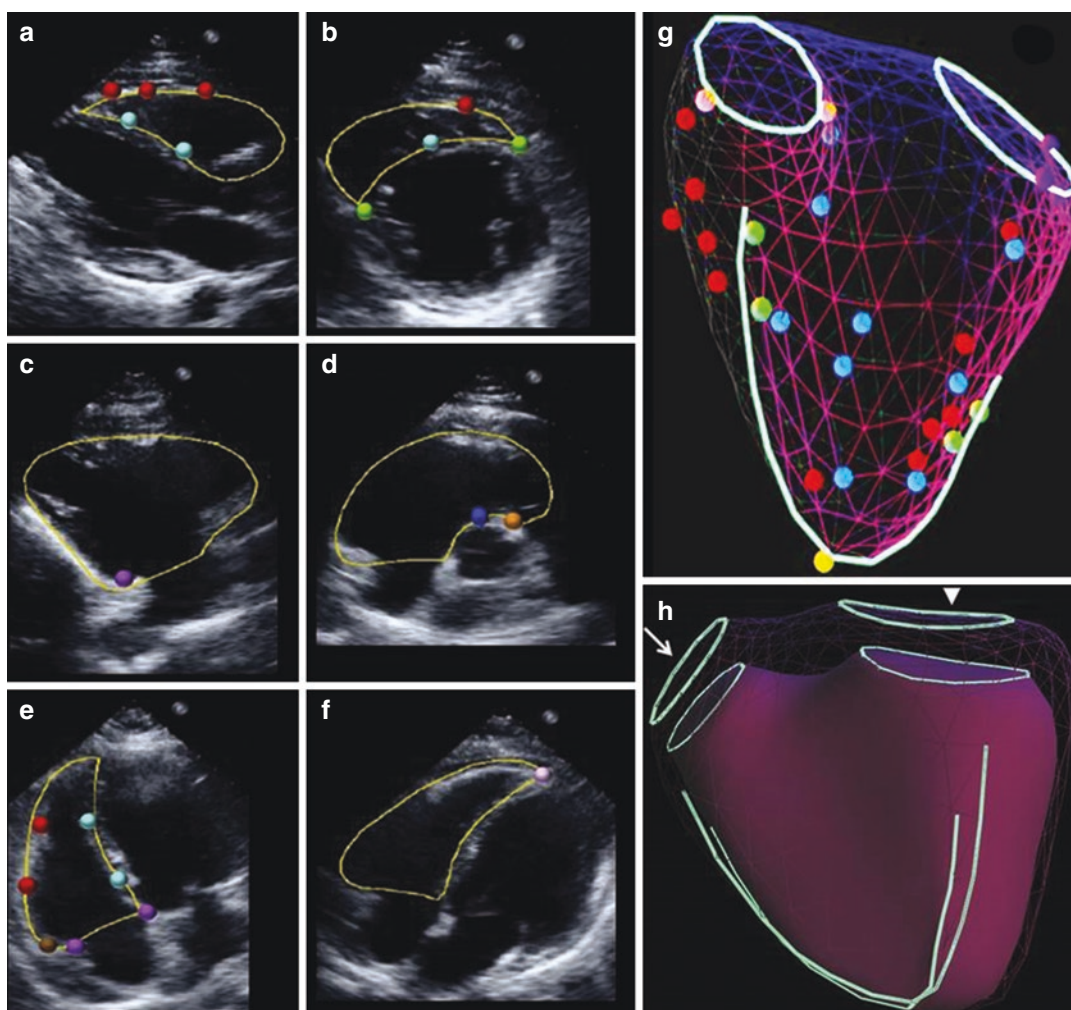


Fig. 15.9 Use of knowledge-based reconstruction for 3-dimensional modelling of the right ventricle from 2-dimensional transthoracic echocardiographic data. Panels **a–f** show the several views of the right ventricle obtained with 2-dimensional transthoracic echocardiography. The several anatomical landmarks are marked

with color-coded points that will be used to reconstruct the 3-dimensional model (panel **g**) and the nested view of the model at end-diastole and end-systole (panel **h**). The arrowheads indicate the pulmonary artery (left) and the inflow of the right ventricle (right). Reproduced with permission from Bhawe et al. [40]

RV. As mentioned above, RV ejection fraction can be calculated by subtracting 3D end-systolic volume from end-diastolic volume divided by end-diastolic volume (Table 15.2).

Non-Invasive Assessment of RV dp/dt

This parameter of global RV systolic function and contractility is based on the pressure raised in the RV. From the continuous wave Doppler spectral signal of the tricuspid regurgitant jet, the time required for the tricuspid regurgitant jet to

increase in velocity from 1 to 2 m/s is calculated which represents 12 mmHg increase by using the simplified Bernoulli equation (Fig. 15.10). This pressure increase is divided by the time (in seconds) leading to the RV dp/dt (mmHg/s). In contrast to the left ventricle, RV dp/dt has been scarcely used in clinical practice and there are no data in healthy individuals. In patients without proper continuous wave Doppler signal of the tricuspid regurgitant jet, this parameter cannot be assessed.

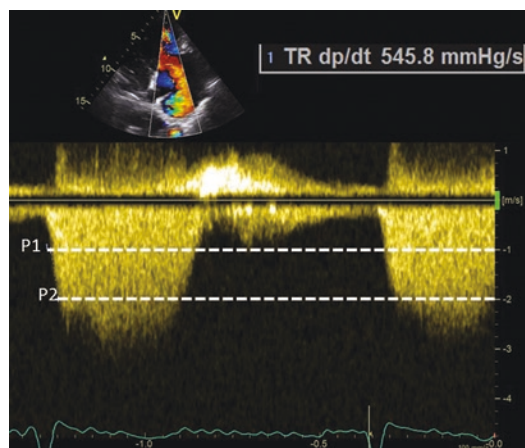


Fig. 15.10 Calculation of dP/dt as a global measure of right ventricular systolic function. From the continuous wave Doppler of the tricuspid regurgitant jet, the pressure at 1 m/s and at 2 m/s is calculated and corrected for the time the right ventricle needs to increase the pressure. In this example, the value of dP/dt indicates preserved global systolic function

Myocardial Performance Index This non-volumetric global parameter of systolic and diastolic RV function, also known as Tei index [42], is defined as the ratio between the RV isovolumic time and the ejection time (Fig. 15.11). The isovolumic time is calculated by summing the isovolumic relaxation and contraction times measured on pulsed wave Doppler spectral signal of the tricuspid inflow from the end of the A wave until the onset of the E wave. The ejection time is estimated from pulsed wave Doppler of the RV outflow from the onset of the flow until the end of the flow. This approach needs two different acquisitions and cardiac beats leading to significant beat to beat variability measurements in patients with irregular heart rate (atrial fibrillation). This limitation can be overcome by using pulsed wave or color-coded tissue Doppler imaging measurements where the isovolumic and ejection times are measured within the same cardiac cycle (Fig. 15.11). Other limitations of this RV functional parameter include its load dependency, particularly when right atrial pressure is increased. In this situation, the right atrial and ventricular pressures equate rapidly resulting in shortened isovolumic relaxation time and reduced myocardial performance index. Using

the pulsed wave Doppler approach, the upper reference limit of the Tei index is 0.40, whereas using pulsed tissue Doppler imaging the threshold is 0.55. The higher the value is, the worse the RV performance is.

This parameter has been evaluated to monitor the response to treatment in patients with chronic thromboembolic pulmonary hypertension, idiopathic pulmonary arterial hypertension and patients with acute decompensated heart failure for example [43–45]. In 93 patients with chronic thromboembolic pulmonary hypertension undergoing pulmonary thromboendarterectomy, RV Tei index decreased from 0.52 ± 0.19 to 0.33 ± 0.10 ($p < 0.001$) [45]. RV Tei index was significantly correlated with pulmonary vascular resistances before and after the procedure indicating that RV Tei index may be a valuable non-invasive parameter to monitor the disease severity. In addition, the prognostic implications of this parameter have been evaluated in several studies including patients with heart failure, cardiomyopathies (Chagas disease) and chronic pulmonary disease [15, 46–48].

Tricuspid Annular Plane Systolic Excursion (TAPSE)

One of the most frequently used parameters of regional RV function is the TAPSE index. From the apical 4-chamber view, placing the M-mode cursor through the lateral tricuspid annulus and aligning it along the longitudinal movement, the TAPSE index is measured as the distance of the systolic excursion of the RV annulus along its longitudinal plane (Fig. 15.12). This parameter has been correlated with global measures of RV systolic function (radionuclide ventriculography, biplane Simpson RV ejection fraction and fractional area change) [49–51]. Numerous studies totalling >2000 healthy controls have provided the reference normal values of this parameter. The lower reference value is 16 mm.

The prognostic value of TAPSE has been demonstrated in several populations (pulmonary hypertension, heart failure, aortic stenosis, arrhythmogenic RV dysplasia) [32, 52–55]. However, TAPSE has all the limitations of a regional measure of systolic function which includes its inaccuracy to assess RV systolic

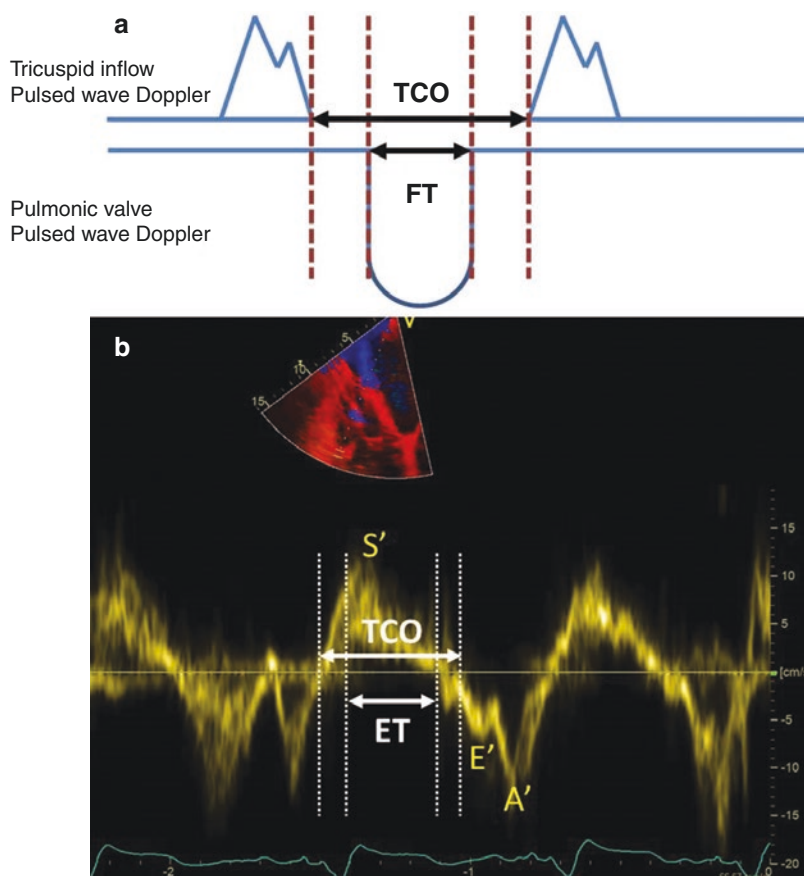


Fig. 15.11 Quantification of right ventricular myocardial performance index. Panel **a** illustrates the measurement of the right ventricular myocardial performance index from pulsed wave Doppler recordings of the tricuspid inflow and pulmonic outflow. The tricuspid valve closure opening time (TCO) is measured from the end of the A-wave until the onset of the E-wave of the following cardiac cycle. The ejection time is measured from the onset until the end of the pulmonic flow. The difference between TCO and ET corrected for the ET yields the myocardial performance index $[(TCO-ET)/ET]$. This measurement can be performed within the same acquisition by using

pulsed-wave tissue Doppler imaging (panel **b**). From the spectral signal obtained at the lateral part of the tricuspid annulus, the isovolumic contraction wave is identified (a positive wave before the systolic peak velocity, S') and its onset and end are defined by the dotted lines. The isovolumic time is recognised by the presence of a negative wave before the early diastolic velocity (E') and the onset and end are defined by the dotted lines. The TCO time is measure from the onset of the isovolumic contraction until the end of the isovolumic relaxation. The ET is measured between the end of the isovolumic contraction and the onset of the isovolumic relaxation

function if regional wall motion abnormalities are present and the assumption that the displacement of the lateral annulus of the RV represents the function of the entire RV. In addition, TAPSE may be affected by loading conditions. To overcome these limitations, Guazzi et al. evaluated the ratio between TAPSE and pulmonary artery systolic pressure as an index of the RV length-force relationship [56]. Heart failure patients with a TAPSE/pulmonary arterial sys-

tolic pressure ≤ 0.35 mm/mmHg had significantly worse survival compared with patients with a ratio >0.35 mm/mmHg (hazard ratio 10.3, 95% confidence interval 5.4–19.8; $p < 0.001$).

Tissue Doppler Velocity Imaging

Measurement of myocardial velocities with tissue Doppler imaging is another method to assess RV systolic function. Based on pulsed wave or color-coded tissue Doppler imaging, the systolic

Fig. 15.12 Tricuspid annulus plane systolic excursion (TAPSE) measurement. Aligning the M-mode cursor along the longitudinal movement of the lateral annulus of the tricuspid valve, the systolic excursion of the tricuspid annulus plane can be measured (arrow)

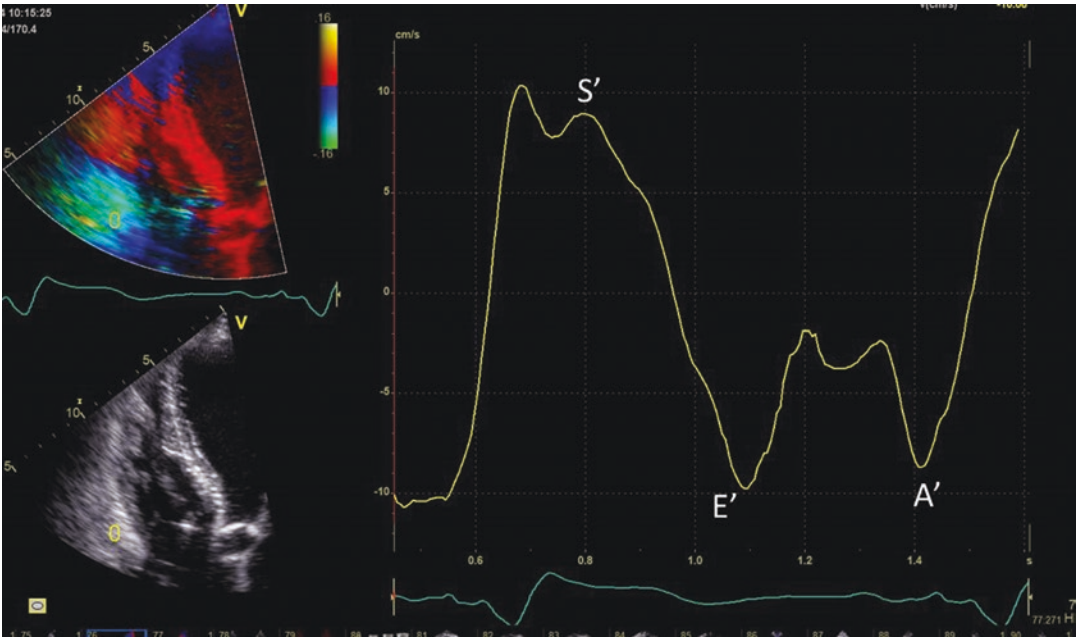
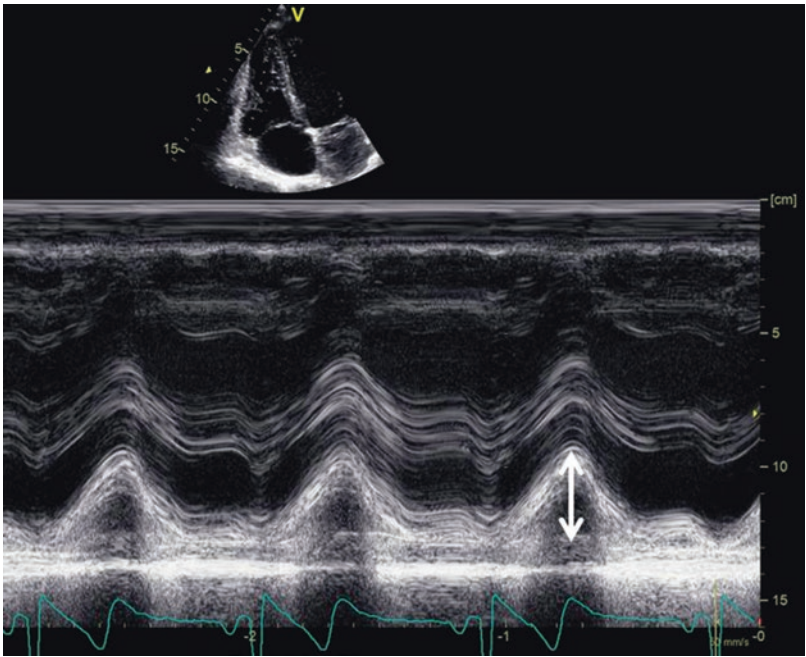


Fig. 15.13 Tissue Doppler velocity imaging of the right ventricle. On color-coded tissue Doppler velocity imaging of the right ventricle, the sample volume is placed at the basal segment of the right ventricular free wall. The time-

velocity curves are displayed, recognizing the positive systolic peak velocity (S') and the early (E') and late (A') diastolic peak velocities

velocity of the lateral tricuspid annulus and the basal RV free wall can be measured. The sample volume and cursor are aligned along the ultrasound beam and the spectral signal can be

obtained live (with pulsed wave tissue Doppler imaging) or off line (with color-coded tissue Doppler imaging) where several velocities can be identified (Fig. 15.13): by determining the

tricuspid and pulmonary valves opening and closing times (on pulsed wave Doppler of the RV inflow and outflow), the first positive velocity that appears after tricuspid valve closure and before pulmonary valve opening represents the isovolumic contraction and it is followed by a larger positive velocity, named S' , which defines RV systolic function; after pulmonary valve closure and before tricuspid valve opening, the first negative velocity represents the isovolumic relaxation and it is followed by an early (E') and late (A') negative diastolic velocities. This pattern should be recognized when evaluating RV systolic function with this methodology. With color-coded tissue Doppler imaging, the velocity values are usually smaller than those obtained with pulsed wave Doppler tissue imaging since the former uses encoded data which represent mean values. To obtain accurate and reproducible values, care must be taken to properly align the ultrasound beam with the longitudinal movement of the RV free wall since as any Doppler technique, tissue Doppler imaging is angle-dependent. The lower reference values of S' measured

with pulsed wave and color-coded tissue Doppler imaging are 10 cm/s and 6 cm/s respectively [5].

Several studies have demonstrated the prognostic value of RV tissue Doppler derived systolic velocity in various clinical situations (myocardial infarction, heart failure, pulmonary hypertension secondary to connective tissue diseases) [57–59].

Assessment of RV Systolic Function with Strain Imaging

Strain imaging measures the percentage of deformation of a myocardial segment relative to its original length or thickness. Strain rate measures the rate of deformation of the myocardial segment over time and has been considered closer reflector of myocardial contractility. From color-coded tissue Doppler imaging derived strain, longitudinal strain and strain rate of the basal and mid-level of the RV free wall visualized on the apical 4-chamber view can be measured (Fig. 15.14). Because its angle-dependency, reproducible assessment of strain/strain rate of the apical segment or other types of deformation (radial/circumferential) with tissue

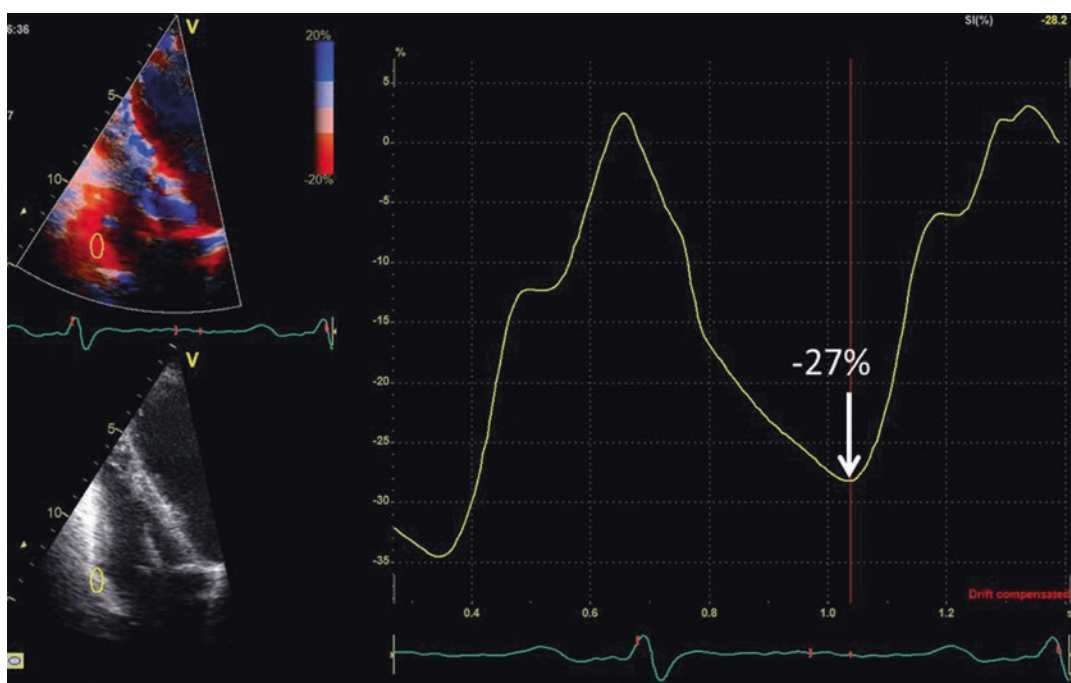


Fig. 15.14 Tissue Doppler derived strain imaging of the right ventricle. The time-strain curve of the basal segment of the right ventricular free wall is displayed. From the

focused apical 4-chamber view, longitudinal strain is measured. This example shows preserved right ventricular systolic function

Doppler imaging is less feasible. Recommendations for color-coded tissue Doppler imaging data acquisition and subsequent strain analysis include: appropriate alignment of the ultrasound beam along the direction of deformation with $<10\text{--}15^\circ$ of off-axis, acquisition of three consecutive beats during breath-holding and narrow imaging sector to allow high frame rate (ideally ≥ 150 f/s).

In contrast to myocardial velocities which are influenced by myocardial tethering, myocardial strain assesses the active deformation of a myocardial segment and can differentiate between scar and viable myocardium. Normative data are not available and the provided mean values in healthy populations have large standard deviations which preclude recommendations for reference limits. Nevertheless, the clinical value of RV color-coded tissue Doppler derived longitudinal strain has been largely demonstrated in several clinical scenarios [60–62]. In patients with pulmonary arterial hypertension, Borges et al. demonstrated that vasodilator therapy was associated with significant improvements in RV longitudinal strain (from -10.1 ± 6.3 to $-14.1 \pm 75\%$, $p = 0.021$) [62]. In patients with familial amyloidotic polyneuropathy, tissue Doppler derived RV longitudinal strain could identify subclinical RV dysfunction before overt morphologic and echocardiographic abnormalities were present [61].

Two-dimensional strain imaging permits assessment of regional and global multidirectional strain (longitudinal, radial and circumferential) and in the last decade the use of speckle tracking echocardiography has provided a large body of evidence showing the clinical value of this imaging technique to assess regional and global RV systolic function. In contrast to tissue Doppler derived strain imaging, speckle tracking echocardiography is angle independent. However, the frame rate of the data where the algorithm is applied is usually lower challenging the measurement at high heart rates. From the apical 4-chamber view, the RV myocardium is included in a region of interest manually or semiautomatically traced. There is currently no consensus whether the interventricular septum should be included in the region of interest or only the RV free wall [63]. The algorithm tracks frame to frame the

speckles (natural acoustic markers) equally distributed within the myocardium along the cardiac cycle and provides the time-strain curves in two orthogonal directions (longitudinal shortening and transversal thickening) (Fig. 15.15).

Normal values have not been established so far and the reported values in the literature are derived from small populations of healthy volunteers. The clinical and prognostic value of longitudinal RV strain has been demonstrated in different populations (pulmonary hypertension, acute myocardial infarction, heart failure) [34, 64–66].

3D Strain Imaging

Due to the 3D complex of the RV, the use of recently developed 3D speckle tracking strain imaging may overcome some of the limitations of 2D speckle tracking echocardiography. From a 3D full volume dataset of the RV, the multiplanar reformations are aligned to visualize the endocardial and epicardial borders of the RV displaying two orthogonal apical views and three short-axis views. The outflow part of the RV is excluded from the analysis. The endocardial border is delineated at an end-diastolic frame and the epicardial border is semiautomatically detected allowing further manual adjustment to the wall thickness. The speckles within the myocardium are tracked frame to frame along the cardiac cycle and the time-strain curves are plotted along with a polar map or 3D volume rendering of the RV with the regional strain values (Fig. 15.16). Longitudinal, circumferential and radial strain can be derived. In addition, global area strain can be obtained representing the percentage of change of longitudinal strain relative to circumferential strain. These 3D strain parameters have correlated with 3D RV volumes and ejection fraction and RV systolic pressures in patients with pulmonary hypertension [67, 68]. In addition, the prognostic value of these parameters was demonstrated in 97 patients with pulmonary hypertension [68]. Patients with a global area strain $>-24.7\%$, circumferential strain $>-9.9\%$ and longitudinal strain $>-16.1\%$ had significantly worse prognosis compared with patients with more preserved values [68]. Three-

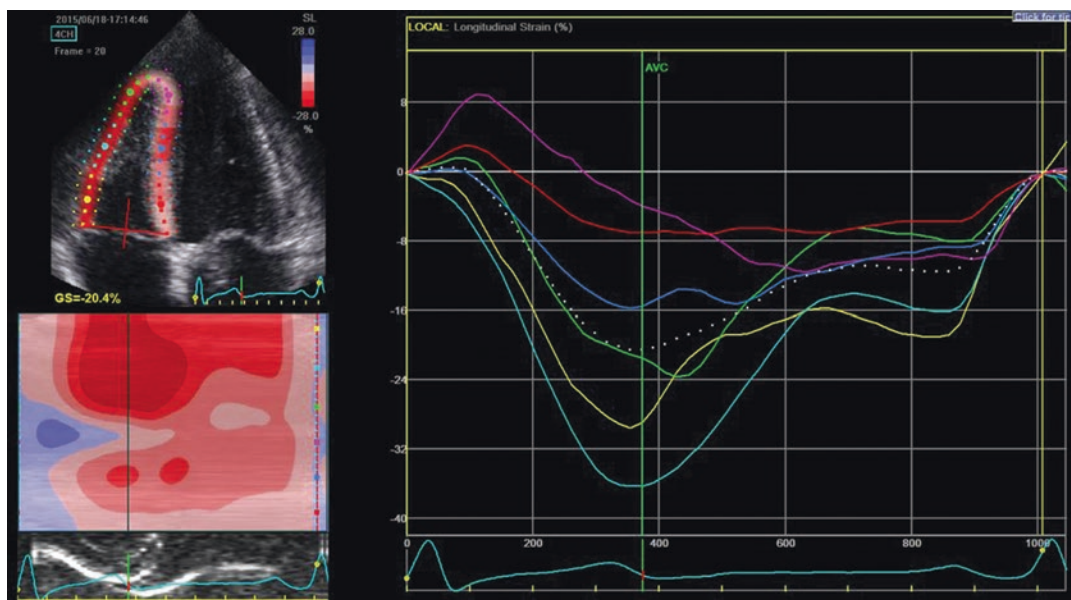


Fig. 15.15 Two-dimensional speckle tracking echocardiography longitudinal strain of the right ventricle. The region of interest including the free wall and septum of the right ventricle is displayed. The time-strain curves of the

six right ventricular segments and the global value (white dotted curve) show the longitudinal deformation pattern of the right ventricle. The peak value is -20.4%

dimensional radial strain was not significantly associated with outcome. These initial investigations need further validation in larger populations. One of the limitations of this technique in patients with dilated RV is the relatively low feasibility (around 85%) since the entire RV volume cannot be included in the imaging sector. In addition, the optimal frame rate for 3D speckle tracking analysis has to be established.

Assessment of RV and Pulmonary Circulation Hemodynamics

Estimation of RV systolic pressures and systolic, diastolic and mean pulmonary arterial pressure complete the assessment of the RV. Pulmonary vascular resistances can be also estimated with Doppler echocardiographic techniques but are not implemented in routine clinical practice.

RV systolic pressures are estimated combining peak tricuspid regurgitant jet velocity and right atrial pressure. Applying the simplified Bernoulli equation, the transtricuspid pressure gradient can be estimated from the peak tricuspid

regurgitant jet velocity on continuous wave Doppler recordings (Fig. 15.17). The right atrial pressure is estimated from the inferior vena cava diameter and collapsibility (*see* Chap. 27). The sum of the trans-tricuspid gradient and the right atrial pressure yield the RV systolic pressures. An accurate measurement of the peak tricuspid regurgitant jet velocity requires appropriate alignment of the cursor through the jet since as any Doppler technique, it is angle dependent and may result in underestimation. Therefore, imaging of the tricuspid regurgitant jet from different echocardiographic views should be performed to obtain the best alignment. A value of ≤ 36 mmHg defines normal RV systolic pressures. Above 40 mmHg, current European Society of Cardiology/American College of cardiology Foundation/American Heart Association guidelines on management of pulmonary hypertension recommend further evaluation with invasive assessment [69, 70].

In the absence of stenosis of the pulmonary valve or increased gradient across the RVOT, the RV systolic pressure is an estimate of the systolic pulmonary pressure. Diastolic pulmonary arterial

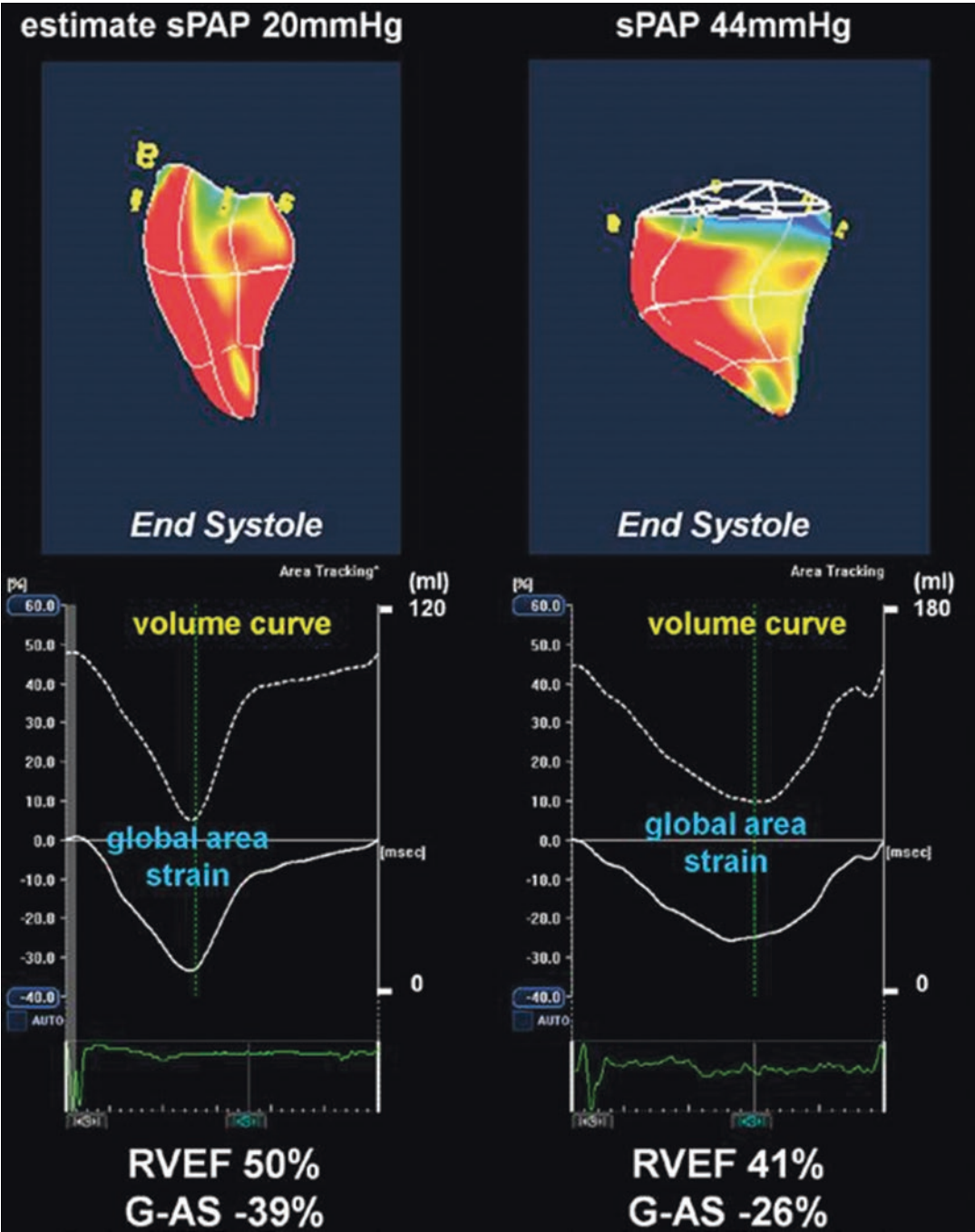


Fig. 15.16 Right ventricular 3-dimensional speckle tracking echocardiography. The 3-dimensional wall motion tracking images and the volume and global area strain curves are displayed for a healthy control and for a patient with pulmonary hypertension. The patient with

pulmonary hypertension shows lower right ventricular ejection fraction and global area strain compared with the healthy control. Reproduced with permission from Ryo et al. [67]

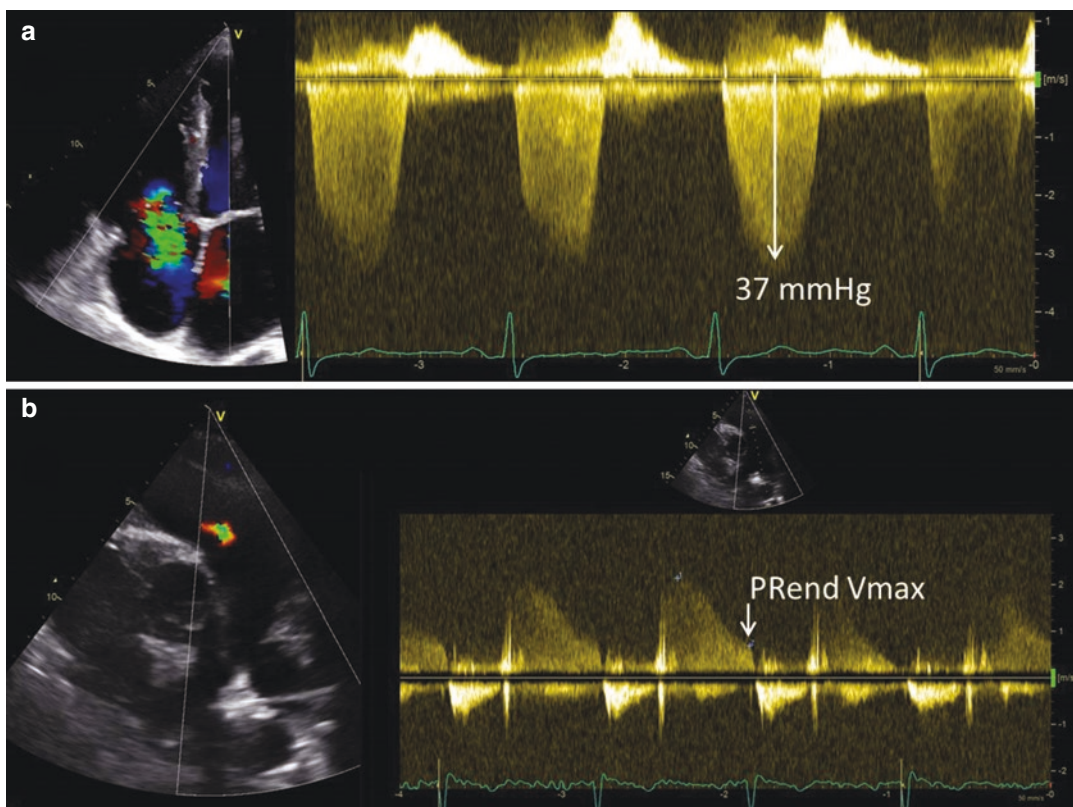


Fig. 15.17 Estimation of right ventricular systolic pressures and diastolic pulmonary arterial pressure. From the spectral signal on continuous wave Doppler of the tricuspid regurgitant jet, the peak velocity can be measured and, with the modified Bernoulli equation, the pressure gradient can be calculated (panel **a**). By adding the right atrial pressure, the right ventricular systolic pressures can be

estimated. The diastolic pulmonary arterial pressure is estimated from the continuous wave Doppler of the pulmonary regurgitant jet measuring the velocity at end-diastole (panel **b**). After applying the modified Bernoulli equation, the right atrial pressure value is added yielding the diastolic pulmonary pressure

pressure is estimated from the pulmonary regurgitant jet envelope on continuous wave Doppler (Fig. 15.17). The end-diastolic jet velocity is measured and by applying the simplified Bernoulli equation and summing the right atrial pressure, the diastolic pulmonary arterial pressure is obtained. The mean pulmonary arterial pressure can be calculated as 1/3 of the systolic pressure plus 2/3 of the diastolic pressure. It can be also estimated by measuring the acceleration time on pulsed wave Doppler recordings of the RV ejection flow and using the formula: $79 - (0.45 \times \text{acceleration time})$ [71]. Other groups have developed similar formulae to estimate mean arterial pres-

sure. In general, the shorter the acceleration time is, the greater the pulmonary vascular resistance and the mean pulmonary arterial pressure are.

Finally, to differentiate between true elevated pulmonary pressures (due to pulmonary vascular disease) and high flow status, estimation of pulmonary vascular resistance may be useful. By calculating the ratio of peak tricuspid regurgitation jet velocity (m/s) to the RVOT velocity-time integral (cm) the pulmonary vascular resistance can be calculated. However, in patients with high pulmonary vascular resistance measured invasively, this method is not accurate.

Diastolic RV Function

In contrast to the left ventricle, assessment of RV diastolic function has not attracted much attention and is usually limited to the assessment of RV systolic pressures, right atrial size and diameter and collapsibility of the inferior vena cava. From pulsed wave Doppler recordings of the transtricuspid inflow, the RV diastolic function can be assessed similarly to the left ventricle: the peak early (E) and late (A) diastolic velocities and the deceleration time of the E wave can be measured. In addition, from pulsed wave tissue Doppler imaging, the diastolic velocities of the tricuspid annulus (E' and A') and the isovolumic relaxation time can be measured. Subsequently the E/E' ratio can be calculated as a measure of RV filling pressures. An E/A ratio <0.8 suggests the presence of impaired relaxation, whereas an E/A ratio between 0.8 and 2.1 with an E/E' ratio >6 or predominant diastolic flow in the hepatic veins suggest pseudonormal filling pattern and an E/A ratio >2.1 with a deceleration time of the E wave <120 ms and late diastolic antegrade flow in the pulmonary artery indicate restrictive filling pattern [5]. In clinical practice, assessment of RV diastolic function is recommended for early detection of subclinical RV dysfunction and for risk stratification of patients with known RV failure [72].

Conclusion

Assessment of RV dimensions and function is an integral part of the routine echocardiogram since it has important clinical and prognostic implications. Recent advances in 3D echocardiography have overcome some of the limitations of 2D echocardiography to comprehensively assess the 3D shape of the RV and have provided powerful prognostic tools to manage patients with cardiac and extracardiac diseases. Tissue Doppler imaging and 2D strain imaging have provided additional RV functional information that permits early detection of subclinical disease and has incremental prognostic value over known clinical and echocardiographic parameters. Finally, hemodynamic assessment of the RV and evaluation of RV diastolic function complete the evaluation.

References

1. Ho SY, Nihoyannopoulos P. Anatomy, echocardiography, and normal right ventricular dimensions. *Heart*. 2006;92(Suppl 1):I2–13.
2. Sheehan F, Redington A. The right ventricle: anatomy, physiology and clinical imaging. *Heart*. 2008;94(11):1510–5.
3. Chin KM, Coghlan G. Characterizing the right ventricle: advancing our knowledge. *Am J Cardiol*. 2012;110(6 Suppl):3S–8S.
4. Haddad F, Hunt SA, Rosenthal DN, Murphy DJ. Right ventricular function in cardiovascular disease, part I: anatomy, physiology, aging, and functional assessment of the right ventricle. *Circulation*. 2008;117(11):1436–48.
5. Rudski LG, Lai WW, Afilalo J, Hua L, Handschumacher MD, Chandrasekaran K, et al. Guidelines for the echocardiographic assessment of the right heart in adults: a report from the American Society of Echocardiography endorsed by the European Association of Echocardiography, a registered branch of the European Society of Cardiology, and the Canadian Society of Echocardiography. *J Am Soc Echocardiogr*. 2010;23(7):685–713.
6. Hahn RT, Abraham T, Adams MS, Bruce CJ, Glas KE, Lang RM, et al. Guidelines for performing a comprehensive transesophageal echocardiographic examination: recommendations from the American Society of Echocardiography and the society of cardiovascular anesthesiologists. *J Am Soc Echocardiogr*. 2013;26(9):921–64.
7. Quaife RA, Chen MY, Lynch D, Badesch DB, Groves BM, Wolfel E, et al. Importance of right ventricular end-systolic regional wall stress in idiopathic pulmonary arterial hypertension: a new method for estimation of right ventricular wall stress. *Eur J Med Res*. 2006;11(5):214–20.
8. Hilde JM, Skjorten I, Grotta OJ, Hansteen V, Melsom MN, Hisdal J, et al. Right ventricular dysfunction and remodeling in chronic obstructive pulmonary disease without pulmonary hypertension. *J Am Coll Cardiol*. 2013;62(12):1103–11.
9. Burke MA, Katz DH, Beussink L, Selvaraj S, Gupta DK, Fox J, et al. Prognostic importance of pathophysiologic markers in patients with heart failure and preserved ejection fraction. *Circ Heart Fail*. 2014;7(2):288–99.
10. Zaidi A, Ghani S, Sheikh N, Gati S, Bastiaenen R, Madden B, et al. Clinical significance of electrocardiographic right ventricular hypertrophy in athletes: comparison with arrhythmogenic right ventricular cardiomyopathy and pulmonary hypertension. *Eur Heart J*. 2013;34(47):3649–56.
11. Ghio S, Pazzano AS, Klersy C, Scelsi L, Raineri C, Camporotondo R, et al. Clinical and prognostic relevance of echocardiographic evaluation of right ventricular geometry in patients with idiopathic pulmonary arterial hypertension. *Am J Cardiol*. 2011;107(4):628–32.

12. Louie EK, Rich S, Levitsky S, Brundage BH. Doppler echocardiographic demonstration of the differential effects of right ventricular pressure and volume overload on left ventricular geometry and filling. *J Am Coll Cardiol.* 1992;19(1):84–90.
13. Te Riele AS, Tandri H, Sanborn DM, Bluemke DA. Noninvasive multimodality imaging in ARVD/C. *JACC Cardiovasc Imaging.* 2015;8(5):597–611.
14. Yiu KH, Wong A, Pu L, Chiang MF, Sit KY, Chan D, et al. Prognostic value of preoperative right ventricular geometry and tricuspid valve tethering area in patients undergoing tricuspid annuloplasty. *Circulation.* 2014;129(1):87–92.
15. Burgess MI, Mogulkoc N, Bright-Thomas RJ, Bishop P, Egan JJ, Ray SG. Comparison of echocardiographic markers of right ventricular function in determining prognosis in chronic pulmonary disease. *J Am Soc Echocardiogr.* 2002;15(6):633–9.
16. Prakasa KR, Dalal D, Wang J, Bomma C, Tandri H, Dong J, et al. Feasibility and variability of three dimensional echocardiography in arrhythmogenic right ventricular dysplasia/cardiomyopathy. *Am J Cardiol.* 2006;97(5):703–9.
17. Nesser HJ, Tkalec W, Patel AR, Masani ND, Niel J, Markt B, et al. Quantitation of right ventricular volumes and ejection fraction by three-dimensional echocardiography in patients: comparison with magnetic resonance imaging and radionuclide ventriculography. *Echocardiography.* 2006;23(8):666–80.
18. Jenkins C, Chan J, Bricknell K, Strudwick M, Marwick TH. Reproducibility of right ventricular volumes and ejection fraction using real-time three-dimensional echocardiography: comparison with cardiac MRI. *Chest.* 2007;131(6):1844–51.
19. Niemann PS, Pinho L, Balbach T, Galuschky C, Blankenhagen M, Silberbach M, et al. Anatomically oriented right ventricular volume measurements with dynamic three-dimensional echocardiography validated by 3-tesla magnetic resonance imaging. *J Am Coll Cardiol.* 2007;50(17):1668–76.
20. Gopal AS, Chukwu EO, Iwuchukwu CJ, Katz AS, Toole RS, Schapiro W, et al. Normal values of right ventricular size and function by real-time 3-dimensional echocardiography: comparison with cardiac magnetic resonance imaging. *J Am Soc Echocardiogr.* 2007;20(5):445–55.
21. Lu X, Nadvoretzkiy V, Bu L, Stolpen A, Ayres N, Pignatelli RH, et al. Accuracy and reproducibility of real-time three-dimensional echocardiography for assessment of right ventricular volumes and ejection fraction in children. *J Am Soc Echocardiogr.* 2008;21(1):84–9.
22. Iriart X, Montaudon M, Lafitte S, Chabaneix J, Reant P, Balbach T, et al. Right ventricle three-dimensional echography in corrected tetralogy of Fallot: accuracy and variability. *Eur J Echocardiogr.* 2009;10(6):784–92.
23. Khoo NS, Young A, Occleshaw C, Cowan B, Zeng IS, Gentles TL. Assessments of right ventricular volume and function using three-dimensional echocardiography in older children and adults with congenital heart disease: comparison with cardiac magnetic resonance imaging. *J Am Soc Echocardiogr.* 2009;22(11):1279–88.
24. Sugeng L, Mor-Avi V, Weinert L, Niel J, Ebner C, Steringer-Mascherbauer R, et al. Multimodality comparison of quantitative volumetric analysis of the right ventricle. *JACC Cardiovasc Imaging.* 2010;3(1):10–8.
25. Grapsa J, O'Regan DP, Pavlopoulos H, Durighel G, Dawson D, Nihoyannopoulos P. Right ventricular remodelling in pulmonary arterial hypertension with three-dimensional echocardiography: comparison with cardiac magnetic resonance imaging. *Eur J Echocardiogr.* 2010;11(1):64–73.
26. Leibundgut G, Rohner A, Grize L, Bernheim A, Kessel-Schaefer A, Bremerich J, et al. Dynamic assessment of right ventricular volumes and function by real-time three-dimensional echocardiography: a comparison study with magnetic resonance imaging in 100 adult patients. *J Am Soc Echocardiogr.* 2010 Feb;23(2):116–26.
27. Van Der Zwaan HB, Geleijnse ML, Mcghe JS, Boersma E, Helbing WA, Meijboom FJ, et al. Right ventricular quantification in clinical practice: two-dimensional Vs. three-dimensional echocardiography compared with cardiac magnetic resonance imaging. *Eur J Echocardiogr.* 2011;12(9):656–64.
28. Dragulescu A, Grosse-Wortmann L, Fackoury C, Mertens L. Echocardiographic assessment of right ventricular volumes: a comparison of different techniques in children after surgical repair of tetralogy of Fallot. *Eur Heart J Cardiovasc Imaging.* 2012;13(7):596–604.
29. Zhang QB, Sun JP, Gao RF, Lee AP, Feng YL, Liu XR, et al. Feasibility of single-beat full-volume capture real-time three-dimensional echocardiography for quantification of right ventricular volume: validation by cardiac magnetic resonance imaging. *Int J Cardiol.* 2013;168(4):3991–5.
30. Kim J, Cohen SB, Atalay MK, Maslow AD, Poppas A. Quantitative assessment of right ventricular volumes and ejection fraction in patients with left ventricular systolic dysfunction by real time three-dimensional echocardiography versus cardiac magnetic resonance imaging. *Echocardiography.* 2015;32(5):805–12.
31. Maffessanti F, Muraru D, Esposito R, Gripari P, Ermacora D, Santoro C, et al. Age-, body size-, and sex-specific reference values for right ventricular volumes and ejection fraction by three-dimensional echocardiography: a multicenter echocardiographic study in 507 healthy volunteers. *Circ Cardiovasc Imaging.* 2013;6(5):700–10.
32. Saguner AM, Vecchiati A, Baldinger SH, Rueger S, Medeiros-Domingo A, Mueller-Burri AS, et al. Different prognostic value of functional right ventricular parameters in arrhythmogenic right ventricular cardiomyopathy/dysplasia. *Circ Cardiovasc Imaging.* 2014;7(2):230–9.

33. Kammerlander AA, Marzluf BA, Graf A, Bachmann A, Kocher A, Bonderman D, et al. Right ventricular dysfunction, but not tricuspid regurgitation, is associated with outcome late after left heart valve procedure. *J Am Coll Cardiol*. 2014;64(24):2633–42.
34. Fine NM, Chen L, Bastiansen PM, Frantz RP, Pellikka PA, Oh JK, et al. Outcome prediction by quantitative right ventricular function assessment in 575 subjects evaluated for pulmonary hypertension. *Circ Cardiovasc Imaging*. 2013;6(5):711–21.
35. Skali H, Zornoff LA, Pfeffer MA, Arnold MO, Lamas GA, Moye LA, et al. Prognostic use of echocardiography 1 year after a myocardial infarction. *Am Heart J*. 2005;150(4):743–9.
36. Campbell P, Takeuchi M, Bourgoun M, Shah A, Foster E, Brown MW, et al. Right ventricular function, pulmonary pressure estimation, and clinical outcomes in cardiac resynchronization therapy. *Circ Heart Fail*. 2013;6(3):435–42.
37. Van Der Hulst AE, Roest AA, Delgado V, Holman ER, De RA, Blom NA, et al. Relationship between temporal sequence of right ventricular deformation and right ventricular performance in patients with corrected tetralogy of Fallot. *Heart*. 2011;97(3):231–6.
38. Lindqvist P, Henein M, Kazzam E. Right ventricular outflow-tract fractional shortening: an applicable measure of right ventricular systolic function. *Eur J Echocardiogr*. 2003;4(1):29–35.
39. Geva T, Powell AJ, Crawford EC, Chung T, Colan SD. Evaluation of regional differences in right ventricular systolic function by acoustic quantification echocardiography and cine magnetic resonance imaging. *Circulation*. 1998;98(4):339–45.
40. Bhawe NM, Patel AR, Weinert L, Yamat M, Freed BH, Mor-Avi V, et al. Three-dimensional modeling of the right ventricle from two-dimensional transthoracic echocardiographic images: utility of knowledge-based reconstruction in pulmonary arterial hypertension. *J Am Soc Echocardiogr*. 2013;26(8):860–7.
41. Knight DS, Schwaiger JP, Krupickova S, Davar J, Muthurangu V, Coghlan JG. Accuracy and test-retest reproducibility of two-dimensional knowledge-based volumetric reconstruction of the right ventricle in pulmonary hypertension. *J Am Soc Echocardiogr*. 2015.
42. Kim WH, Otsuji Y, Seward JB, Tei C. Estimation of left ventricular function in right ventricular volume and pressure overload. Detection of early left ventricular dysfunction by Tei index. *Jpn Heart J*. 1999;40(2):145–54.
43. Verhaert D, Mullens W, Borowski A, Popovic ZB, Curtin RJ, Thomas JD, et al. Right ventricular response to intensive medical therapy in advanced decompensated heart failure. *Circ Heart Fail*. 2010;3(3):340–6.
44. Chen SL, Zhang FF, Xu J, Xie DJ, Zhou L, Nguyen T, et al. Pulmonary artery denervation to treat pulmonary arterial hypertension: the single-center, prospective, first-in-man PADN-I study (first-in-man pulmonary artery denervation for treatment of pulmonary artery hypertension). *J Am Coll Cardiol*. 2013;62(12):1092–100.
45. Blanchard DG, Malouf PJ, Gurudevan SV, Auger WR, Madani MM, Thistlethwaite P, et al. Utility of right ventricular Tei index in the noninvasive evaluation of chronic thromboembolic pulmonary hypertension before and after pulmonary thromboendarterectomy. *JACC Cardiovasc Imaging*. 2009;2(2):143–9.
46. Nunes MC, Rocha MO, Ribeiro AL, Colosimo EA, Rezende RA, Carmo GA, et al. Right ventricular dysfunction is an independent predictor of survival in patients with dilated chronic Chagas' cardiomyopathy. *Int J Cardiol*. 2008;127(3):372–9.
47. Vizzardi E, D'Aloia A, Bordonali T, Bugatti S, Piovanelli B, Bonadei I, et al. Long-term prognostic value of the right ventricular myocardial performance index compared to other indexes of right ventricular function in patients with moderate chronic heart failure. *Echocardiography*. 2012;29(7):773–8.
48. Meluzin J, Spinarova L, Hude P, Krejci J, Kincl V, Panovsky R, et al. Prognostic importance of various echocardiographic right ventricular functional parameters in patients with symptomatic heart failure. *J Am Soc Echocardiogr*. 2005;18(5):435–44.
49. Miller D, Farah MG, Liner A, Fox K, Schluchter M, Hoit BD. The relation between quantitative right ventricular ejection fraction and indices of tricuspid annular motion and myocardial performance. *J Am Soc Echocardiogr*. 2004;17(5):443–7.
50. Lopez-Candales A, Dohi K, Rajagopalan N, Edelman K, Gulyasy B, Bazaz R. Defining normal variables of right ventricular size and function in pulmonary hypertension: an echocardiographic study. *Postgrad Med J*. 2008;84(987):40–5.
51. Kaul S, Tei C, Hopkins JM, Shah PM. Assessment of right ventricular function using two-dimensional echocardiography. *Am Heart J*. 1984;107(3):526–31.
52. Galli E, Guirette Y, Feneon D, Daudin M, Fournet M, Leguerrier A, et al. Prevalence and prognostic value of right ventricular dysfunction in severe aortic stenosis. *Eur Heart J Cardiovasc Imaging*. 2015;16(5):531–8.
53. Leong DP, Hoke U, Delgado V, Auger D, Witkowski T, Thijssen J, et al. Right ventricular function and survival following cardiac resynchronisation therapy. *Heart*. 2013;99(10):722–8.
54. Forfia PR, Fisher MR, Mathai SC, Houstens-Harris T, Hemnes AR, Borlaug BA, et al. Tricuspid annular displacement predicts survival in pulmonary hypertension. *Am J Respir Crit Care Med*. 2006;174(9):1034–41.
55. Ghio S, Klersy C, Magrini G, D'Armini AM, Scelsi L, Raineri C, et al. Prognostic relevance of the echocardiographic assessment of right ventricular function in patients with idiopathic pulmonary arterial hypertension. *Int J Cardiol*. 2010;140(3):272–8.
56. Guazzi M, Bandera F, Pelissero G, Castelvécchio S, Menicanti L, Ghio S, et al. Tricuspid annular plane systolic excursion and pulmonary arterial systolic pressure relationship in heart failure: an index of right ventricular contractile function and prognosis. *Am J Physiol Heart Circ Physiol*. 2013;305(9):H1373–81.

57. Hsiao SH, Lee CY, Chang SM, Lin SK, Liu CP. Right heart function in scleroderma: insights from myocardial Doppler tissue imaging. *J Am Soc Echocardiogr.* 2006;19(5):507–14.
58. Bistola V, Parissis JT, Paraskevaidis I, Panou F, Nikolaou M, Ikonomidis I, et al. Prognostic value of tissue Doppler right ventricular systolic and diastolic function indexes combined with plasma B-type natriuretic peptide in patients with advanced heart failure secondary to ischemic or idiopathic dilated cardiomyopathy. *Am J Cardiol.* 2010;105(2):249–54.
59. Dokainish H, Zoghbi WA, Ambriz E, Lakkis NM, Quinones MA, Nagueh SF. Comparative cost-effectiveness of B-type natriuretic peptide and echocardiography for predicting outcome in patients with congestive heart failure. *Am J Cardiol.* 2006;97(3):400–3.
60. Kjaergaard J, Hastrup SJ, Sogaard P, Chen X, Bay NH, Kober L, et al. Advanced quantitative echocardiography in arrhythmogenic right ventricular cardiomyopathy. *J Am Soc Echocardiogr.* 2007;20(1):27–35.
61. Lindqvist P, Olofsson BO, Backman C, Suhr O, Waldenstrom A. Pulsed tissue Doppler and strain imaging discloses early signs of infiltrative cardiac disease: a study on patients with familial amyloidotic polyneuropathy. *Eur J Echocardiogr.* 2006;7(1):22–30.
62. Borges AC, Knebel F, Eddicks S, Panda A, Schattke S, Witt C, et al. Right ventricular function assessed by two-dimensional strain and tissue Doppler echocardiography in patients with pulmonary arterial hypertension and effect of vasodilator therapy. *Am J Cardiol.* 2006;98(4):530–4.
63. Mor-Avi V, Lang RM, Badano LP, Belohlavek M, Cardim NM, Derumeaux G, et al. Current and evolving echocardiographic techniques for the quantitative evaluation of cardiac mechanics: ASE/EAE consensus statement on methodology and indications endorsed by the Japanese society of echocardiography. *Eur J Echocardiogr.* 2011;12(3):167–205.
64. Sade LE, Ozin B, Atar I, Demir O, Demirtas S, Muderrisoglu H. Right ventricular function is a determinant of long-term survival after cardiac resynchronization therapy. *J Am Soc Echocardiogr.* 2013;26(7):706–13.
65. Antoni ML, Scherptong RW, Atary JZ, Boersma E, Holman ER, Van Der Wall EE, et al. Prognostic value of right ventricular function in patients after acute myocardial infarction treated with primary percutaneous coronary intervention. *Circ Cardiovasc Imaging.* 2010;3(3):264–71.
66. Haack ML, Scherptong RW, Marsan NA, Holman ER, Schalij MJ, Bax JJ, et al. Prognostic value of right ventricular longitudinal peak systolic strain in patients with pulmonary hypertension. *Circ Cardiovasc Imaging.* 2012;5(5):628–36.
67. Ryo K, Goda A, Onishi T, Delgado-Montero A, Tayal B, Champion HC, et al. Characterization of right ventricular remodeling in pulmonary hypertension associated with patient outcomes by 3-dimensional wall motion tracking echocardiography. *Circ Cardiovasc Imaging.* 2015;8(6):41–51.
68. Smith BC, Dobson G, Dawson D, Charalampopoulos A, Grapsa J, Nihoyannopoulos P. Three-dimensional speckle tracking of the right ventricle: toward optimal quantification of right ventricular dysfunction in pulmonary hypertension. *J Am Coll Cardiol.* 2014;64(1):41–51.
69. McLaughlin VV, Archer SL, Badesch DB, Barst RJ, Farber HW, Lindner JR, et al. ACCF/AHA 2009 expert consensus document on pulmonary hypertension: a report of the American College of cardiology Foundation Task force on expert consensus documents and the American Heart Association: developed in collaboration with the American College of Chest Physicians, American Thoracic Society, Inc., and the Pulmonary Hypertension Association. *Circulation.* 2009;119(16):2250–94.
70. Galie N, Hoeper MM, Humbert M, Torbicki A, Vachiery JL, Barbera JA, et al. Guidelines for the diagnosis and treatment of pulmonary hypertension: the task force for the diagnosis and treatment of pulmonary hypertension of the European Society of Cardiology (ESC) and the European Respiratory Society (ERS), endorsed by the international society of heart and lung transplantation (ISHLT). *Eur Heart J.* 2009;30(20):2493–537.
71. Kitabatake A, Inoue M, Asao M, Masuyama T, Tanouchi J, Morita T, et al. Noninvasive evaluation of pulmonary hypertension by a pulsed Doppler technique. *Circulation.* 1983;68(2):302–9.
72. Sallach JA, Tang WH, Borowski AG, Tong W, Porter T, Martin MG, et al. Right atrial volume index in chronic systolic heart failure and prognosis. *JACC Cardiovasc Imaging.* 2009;2(5):527–34.

Julia Grapsa

Right Ventricle Anatomy

The right ventricle (RV) has a complex anatomy: it is the most anteriorly positioned cardiac chamber, directly behind the sternum and it marks the inferior border of the heart. It is anatomically subdivided into three components: the inflow tract (sinus), which includes the tricuspid valve (TV), the outflow tract (infundibulum or conus) which represents the smooth outflow region, separated from the inflow tract by crista supraventricularis and the highly trabeculated apical portion [1–5].

In contrast to the near conical shape of the left ventricle (LV), RV is more triangular in shape and it curves over the LV. In cross section the normal cavity appears crescentic. Thus, the curvature of the ventricular septum places the RV outflow tract antero-cephalad to that of the LV resulting in a characteristic “cross-over” relationship between right and left ventricular outflow tracts [4–6].

The RV wall is significantly thinner (<5 mm thick) than LV wall. That is the reason that RV remodels easier when compared to the LV, in pressure and volume overload. Furthermore, differently from the LV, the myocytes within the RV are longitudinally orientated in the subendocardium and circumferentially orientated in the thin subepicardial layer. Accordingly, its contraction

pattern consists of a longitudinal, a circumferential and an inward contraction and the longitudinal one is the major contributor to the overall RV performance [3–6].

Echocardiography with deformation imaging has already demonstrated that the RV contracts with an initial contraction of the free wall towards the septum and a longitudinal contraction of the base towards the apex. The contribution of the septum is significant and it bulges into the RV cavity due to the LV contraction.

Two-dimensional echocardiographic examination of the RV cavity is difficult, due to the complex shape of the cavity and the heavy trabeculation which makes mapping of endocardium and epicardium rather difficult. That is the main reason why care should be taken when assessing the RV and usually the imaging assessment is a multimodality approach, including three-dimensional echocardiography or even cardiac magnetic resonance [5–7].

Right Atrial Anatomy

The right atrium (RA) is divided into two distinct parts: the thin sinus venosus posteriorly and the auricle or RA appendage, anteriorly. The sinus venosus is attached medially to the left atrium and postero-laterally to the crista terminalis. It includes the venous part (insertion of the inferior and superior vena cava), the vestibulum, and the

J. Grapsa
Imperial College of London, London, UK

atrial septum. RA appendage merges posterolaterally from the crista terminalis and overlies the aortic root [8].

Crista terminalis extends from the superior vena cava to the inferior vena cava. Posteriorly to the tricuspid valve, at its most superior edge is the orifice of the coronary sinus. Thebesian valve is often seen at the opening of the coronary sinus.

The fossa ovalis, thin membrane between the right and left atria, lies at the middle portion of right atrium posterior wall, at the lower part of the septum, above and to the left of the orifice of the inferior vena cava. The Eustachian valve (inferior vena caval valve) is a semilunar, extension of the inferior vena cava, with wide variability in length and shape. In the fetus this valve serves to direct the blood from the inferior vena cava, through the foramen ovale, into the left atrium. The Chiari's network is a congenital remnant of the right valve of the sinus venosus [8].

Physiology

Right Ventricular Physiology

A number of anatomical and physiological features of the RV and its response to PH are important when assessing it using echocardiography [3–7]. Certain anatomical features in particular make it difficult to examine the RV in detail, especially when using two-dimensional (2D) echocardiography. In particular, identifying the borders of the RV can be difficult because of the heavily trabeculated myocardium, while the available image windows can be limited because of the retrosternal position. In contrast to the LV and the systemic circulation, the pulmonary vascular bed is a low-resistance system in healthy individuals. The RV is more compliant than the LV and adapts better to volume loading than to pressure loading. The LV and RV do not function independently of one another as the mechanics of one ventricle will impact on the other (ventricular interdependence) and this process is mediated by the interventricular sep-

tum. Ventricular septal geometry and motion are largely determined by the difference in pressure across the ventricular septum. Under normal circumstances, the higher pressures in the LV cavity mean the interventricular septum bows into the lower pressure RV cavity (Fig. 16.1). In patients with pulmonary hypertension pressure in the RV increases causing the septum to flatten in systole as the pressures in both ventricles begin to converge [8–11]. Eventually, when the RV becomes severely pressure loaded, the septum may even bulge into the LV cavity. These changes also impact on both LV systolic and diastolic function. Another change seen in the RV in pulmonary hypertension is ventricular remodeling, which is a result of chronic progressive pressure loading. This is initially in the form of hypertrophy and later as dilation. The remodeling results in progressive contractile impairment, low cardiac output and, eventually, RV failure [10, 11] (Fig. 16.2).

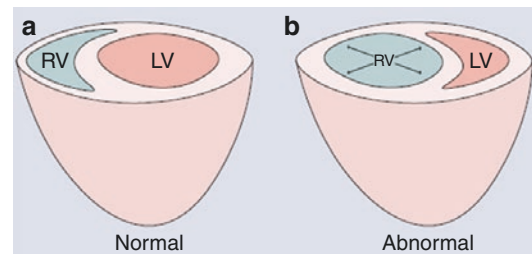


Fig. 16.1 (a) Normal right ventricle. (b) Pressure and volume overload of the right ventricle. Changes in pulmonary hypertension

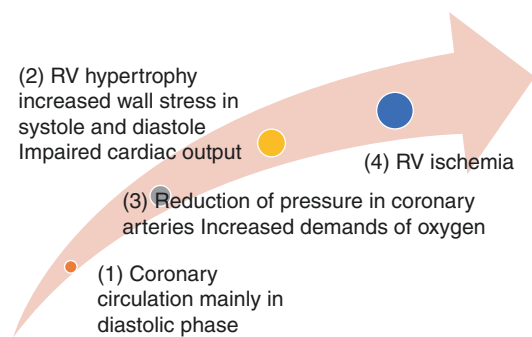


Fig. 16.2 Right ventricular physiology changes in pulmonary hypertension

Right Atrial Physiology

The RA acts as a reservoir for systemic venous return through the superior vena cava, inferior vena cava and the smaller caliber coronary sinus that drains blood from the coronary system. The filling pattern is divided into three distinct phases: a dominant systolic phase, a diastolic phase, followed by a third short atrial contraction phase with small reversal (upstream) flow from the RA into the systemic veins. During diastole the tricuspid valve opens, and blood from the RA is drained into the RV in two distinct phases (early and late diastolic filling, respectively). The first phase is passive with pressure gradient-derived flow, followed by active atrial contraction. The RA pressure varies significantly with the respiratory cycle and is usually between 3 and 8 mmHg [8, 9].

The RA increases in size and volume in response to prolonged increase in pressure and/or volume loads (as in pulmonary hypertension and significant tricuspid valve regurgitation, respectively). The RA also enlarges in response to chronic atrial fibrillation. The increase of RA size and volume has prognostic value in assessing right (and left) heart diseases [11, 12].

Changes in Pulmonary Hypertension

Septal geometry and motion is largely influenced by the ventricular pressure difference. Under normal circumstances, the considerably higher pressures in the left ventricular cavity render it circular in cross-section and the septum bows in to the RV. Pressure-loading of the RV resulting from increased pulmonary artery pressure, causes the septum to flatten in systole as the right and left ventricular pressures begin to converge and when the RV becomes severely pressure loaded, the septum may even bulge in to the left ventricular cavity. In a volume-loaded RV with diastolic dysfunction and high end-diastolic pressures, the septum will flatten in diastole. These changes will impact on both left ventricular systolic and diastolic function [13, 14].

In acute pressure-loading, such as pulmonary embolic disease, the RV will dilate and its free wall will become hypokinetic, but chronic progressive pressure-loading, as in pulmonary hypertension, will lead to RV remodeling, notably hypertrophy. The process is not like the physiological hypertrophy of an athlete's heart, but will also result in myocardial fibrosis, inflammation, myocyte apoptosis and necrosis (forms of cell death) and abnormal contractile function. RV systolic and diastolic function will therefore deteriorate and it is thought these parameters determine exercise capacity, symptoms and prognosis. The assessment of RV function is therefore a key component of the assessment of a patient with pulmonary hypertension. RV dilatation leads to tricuspid annular dilatation, often resulting in significant tricuspid regurgitation. When this is coupled with already-present systolic dysfunction and increased afterload, this will further reduce 'forward' stroke volume in to the pulmonary circulation and resultant cardiac output. The additional volume-loading as a consequence of this will further impair RV diastolic function, increase RV end-diastolic pressure and displacement of the interventricular septum [15, 16].

How to Perform Two-Dimensional Echocardiography in Patients with Pulmonary Hypertension

The most important advice is to perform the whole echocardiographic protocol and never omit views because they might be crucial in identifying the underlying cause of pulmonary hypertension (for example LV diastolic dysfunction).

Dedicated Views for Patients with Pulmonary Hypertension

Parasternal Long Axis View of RV Inflow Tract

In pulmonary hypertension, RV apex is hypertrophied and the cavity is dilated. The assessment of RV systolic function is best performed in this view [16]. The papillary muscles of the

RV are usually hypertrophied and they are easily distinguished. Typically, there are two principal papillary muscles (anterior and posterior) with a smaller supracristal (or conus) papillary muscle. In this view the tricuspid annulus can be imaged and its diameter measured. The normal range is between 1.3 and 2.8 cm in systole. Two of the three tricuspid valve leaflets are seen: the anterior and septal leaflets. Assessment of tricuspid leaflet mobility and systolic apposition is important for the exclusion of any primary cause of tricuspid valve disease such as rheumatic fever (with involvement of mitral valve in most of the cases), carcinoid, sarcoidosis or endocarditis. In secondary tricuspid insufficiency due to RV dilatation, the leaflets are normal with reduced apposition secondary to tricuspid annular dilatation.

Parasternal Long Axis View of the RV Outflow Tract

The normal RV outflow tract dimension is 1.8–3.4 cm in diastole. The determination of the dilatation of pulmonary artery is important for the diagnosis of pulmonary hypertension. The normal diameter of main pulmonary artery is 0.9–2.9 cm (corrected to height) and normal annulus diameter is 1–2.2 cm [19].

Short Axis at the Level of Left Ventricular Papillary Muscles

The RV in pulmonary hypertension is often dilated and hypertrophied, such that it compresses the LV, giving it a characteristic D-shaped appearance in systole. Normally, the LV appears circular in shape, both in systole and diastole. When the RV is pressure-loaded, the ventricular septum deforms and may even curve towards the LV cavity. This distortion may be quantified by the LV eccentricity index which is described later [16, 19].

Apical Four-Chamber View

Normally, the RV appears triangular in shape and about the one-third the size of the LV. The apex of the RV is located closer to the base of the heart than that of the LV. However, in pul-

monary hypertension, the cavity is dilated and hypertrophied to an extent depending on the degree of pressure and volume loading. The normal wall thickness for the RV (measured at the lateral free wall) is 0.2–0.5 cm (0.2 ± 0.05 cm/m² indexed to body surface area).

When measuring the area of the RV and the right atrium, normal values are as following: RV end-diastole 20.1 ± 4 cm², RV end-systole: 10.9 ± 2.9 cm² and right atrium in end-systole 13.5 ± 2 cm² [6, 9, 10].

In pulmonary hypertensive patients, RV free wall is the first to become hypertrophied (in parallel with the apex), demonstrate systolic dysfunction and lower tissue myocardial velocities. Modalities such as tissue Doppler imaging, which measure these velocities, tend to predict systolic and diastolic dysfunction of the RV free wall [14–16]. The apex is frequently hypertrophied and akinetic. Careful examination of the RV apex, using zoom and focus modalities, should be performed, to exclude a thrombus or an apical mass [10].

The hypertrophic moderator band often is seen traversing the RV near the apex. Considerable individual variability in the shape and wall motion of the RV, particularly at the apex, is seen in healthy individuals, so caution is needed in diagnosing an abnormal RV from any single tomographic view.

Subcostal View

The subcostal view allows the assessment of RV dysfunction and thickness of RV walls, in patients with difficult parasternal or apical windows [17–19]. By rotating the transducer inferiorly from the subcostal four-chamber view, a long-axis of the inferior vena cava is obtained as it enters the right atrium. The size of the proximal 2–3 cm of the inferior vena cava at rest and changes in size with respiration are used to estimate right atrial pressure. The hepatic veins (especially the central hepatic vein) are helpful in assessing right atrial pressure and for recording right atrial Doppler filling patterns. The proximal abdominal aorta is imaged in long axis medial to the inferior vena cava [19].

RV Pressure Versus Volume-Loading

RV volume overload, results from an atrial septal defect, partial abnormal pulmonary venous drainage, tricuspid or pulmonary insufficiency, causes an increase in RV end-systolic and end-diastolic volumes with normal RV ejection fraction. In RV pressure overload the RV dilates with the ventricular septum “pushing” to the left during systole. An inverse relationship between RV ejection fraction and afterload develops (pulmonary artery pressure or pulmonary vascular resistance). RV pressure overload distorts both LV systolic and diastolic geometry due to the interventricular dependence. Chronic RV pressure overload causes distortion of the geometrical shape and LV physiology resulting in significant degree of LV diastolic dysfunction and eventually—at end stages of pulmonary hypertension—of LV systolic dysfunction (Fig. 16.3). The effect on the LV is the reduction of LV ejection fraction, stroke volume, end-diastolic and end-systolic volume, as well as prolongation of the LV isovolumic

relaxation time. The different effects of volume versus pressure-loading of the RV on the LV are best illustrated by the LV eccentricity index [19].

Qualitative Assessment of The RV

Dilatation

Normally the RV is 1/3 of the size of the LV in the parasternal long axis view. One of the first changes in the RV in response to the increased preload and afterload is dilatation, which progresses with worsening PH.

Hypertrophy

In the face of chronically elevated RV afterload, the RV walls become hypertrophied. One of the first anatomical elements to do so is the moderator band, which in normal subjects it is thin and sometimes difficult to see.

Measurements	Volume loading	Pressure loading	Pressure and volume loading
Dilatation	↑↑	↑	↑↑
Hypertrophy	↑	↑↑	↑↑
Contractility	↓ or ↔	↓↓	↓↓
Tricuspid annular dilatation	↑↑	↑	↑↑
Tricuspid regurgitant jet (volume)	↑↑	↑	↑↑
TAPSE	↔ or ↑	↓	↓ or ↔
LV eccentricity index at end-systole	↔	↑	↑
LV eccentricity index at end-diastole	↑	↔	↑

Fig. 16.3 Pressure versus volume right ventricular overload: the changes in echocardiographic indices

Contractility

In PH, RV impairment is global: this is in contrast to other conditions affecting the RV, such as RV infarction or arrhythmogenic RV cardiomyopathy, where there will be regional wall motion abnormalities [19, 23].

Measurements

Right Atrial Pressure

From the subcostal view, measurement of the diameter of the inferior vena cava at end-expiration and during an inspiratory manoeuvre provides an estimate of right atrial (RA) pressure [22]. A normal diameter of the inferior vena cava (1.2–2.3 cm) and the segment adjacent to the right atrium collapses by at least 50% with respiration, will simply normal right atrial pressure. Failure for the inferior vena cava to collapse with respiration and/or dilation of the inferior vena cava and hepatic veins is associated with higher right atrial pressures.

RV Systolic Pressure (Tricuspid Regurgitant Velocity)

Tricuspid regurgitant velocity is derived from the application of continuous wave Doppler along the tricuspid regurgitant jet, from apical four chamber projections or from the parasternal RV inflow view, if the regurgitant jet is eccentric [2, 6, 19–22]. The peak velocity reflects the RV to right atrial pressure difference, ΔP , and in the absence of pulmonary stenosis, the RV systolic pressure (RVSP) is assumed to equal pulmonary artery systolic pressure (PASP), and is calculated through the Bernoulli Equation:

$$PASP = RVSP = 4(VTR)^2 + RAP$$

(VTR: tricuspid regurgitant velocity, RAP: right atrial pressure)

Note that in cases of severe free-flow tricuspid regurgitation, the Bernoulli equation is not valid.

Pulmonary Artery Mean and Diastolic Pressure

As with the tricuspid regurgitant jet, the Bernoulli Equation can be applied to calculate pulmonary arterial end-diastolic pressure (PEDP) (6):

$$PEDP = 4(VED)^2 + RAP$$

(VED: end-diastolic pulmonary regurgitant velocity)

Mean pulmonary artery pressure, may also be derived from the pulmonary regurgitant velocity:

$$\text{Mean PAP} = 4(PR\ VBD)^2 + RAP$$

(VBD: beginning of diastole pulmonary regurgitant velocity)

RV Outflow Tract Acceleration Time

RV outflow tract acceleration time is the time in milliseconds from the beginning of the pulmonary ejection until the maximum of the systolic velocity. It is measured by pulsed-wave Doppler with the sample volume positioned at the centre of the pulmonary artery, ideally at the annulus, in the parasternal short-axis view (Fig. 16.4). In normal people, the acceleration time exceeds 140 ms and it shortens in PH. A value below 105 ms is suggestive of PH. This measurement is particularly important when the peak tricuspid regurgitant jet is not visible [21].

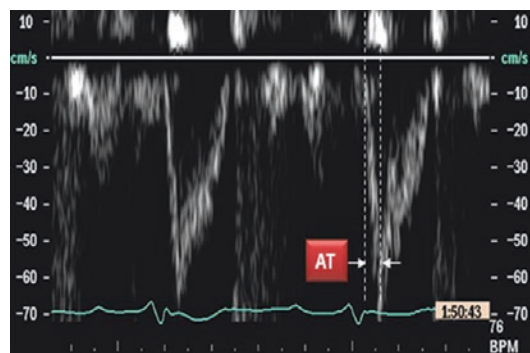


Fig. 16.4 Right ventricular outflow tract acceleration time is measured by pulsed-wave Doppler with the sample volume positioned at the centre of the pulmonary artery, ideally at the annulus, in the parasternal short-axis view

Measurement of Right Atrial Volume Index

The measurement of RA volume index is usually performed from the apical four-chamber view or from the subcostal view [23–26]. Atrial volume is measured at end-systole, where the maximum atrial volume can be obtained.

The single plane area-length method is used and RA volume is measured using the area and the long axis length of the atrium (Fig. 16.5):

$$\text{RA volume index} = (0.85 A^2 / L) / \text{BSA}$$

[A: area of atrium in any view (cm²), L: long axis length of atrium (cm), BSA: body surface area]. The normal right atrial volume when indexed for body surface area is 34 mL/m² for men and 27 mL/m² for women). Right atrial volume may also be measured with three-dimensional echocardiography as per the Simpson's rule and the reconstruction via short axis disks from the base of the right atrium towards the tricuspid annulus (Fig. 16.5).

RV Fractional Area Change

RV fractional area change (FAC) is calculated as follows [24, 25]:

$$\text{RV FAC}(\%) = (\text{AED} - \text{AES}) / \text{AED}$$

Where AED is end-diastolic area and AES is end-systolic area, measured from the apical four-chamber view.

Left Ventricular Eccentricity Index

Eccentricity index is measured by the parasternal short-axis at the level of LV papillary muscles. It is measured as the ratio of the minor axis of the LV parallel to the septum, divided to minor-axis perpendicular to the septum. The index is measured in end-diastole and end-systole. In a purely pressure-loaded RV, there is flattening of the interventricular septum in end-systole, which results in increased end-systolic LV eccentricity index. In pure volume-loading, the eccentricity index will be increased in end-diastole [23, 31, 32] (Fig. 16.6).

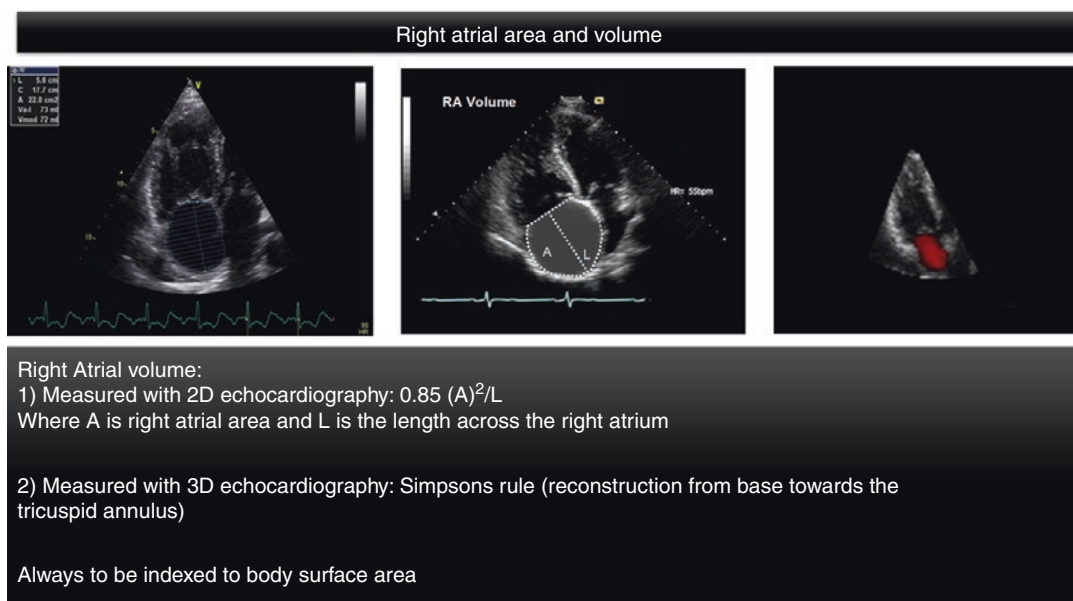


Fig. 16.5 Assessment of right atrial area and volume

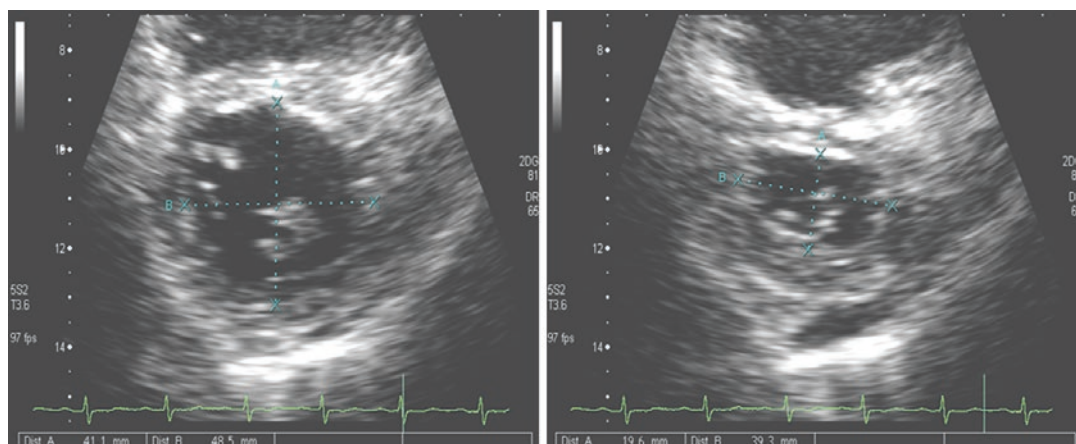


Fig. 16.6 Eccentricity index of the left ventricle. It is measured as the ratio of the minor axis of the LV parallel to the septum, divided to minor axis perpendicular to the septum. The index is measured in end-diastole and end-systole

Tissue Doppler Imaging

Two Types of Tissue Doppler Imaging Can Be Applied on the Assessment of the RV

- Pulsed mode tissue Doppler imaging: Peak velocities and the acceleration and deceleration of structures can be measured. A pulsed-wave Doppler sampling gate of 2–4 mm and a sweep of 100–150 mm/s are used.
- Conventional colour Doppler mapping: Measurements are made from the apical four-chamber view, with the patient holding their breath in end-expiration.

RV Diastolic Dysfunction

Diastolic dysfunction comprises:

- poor relaxation
- decreased compliance (change in unit volume per unit pressure)

Diastolic function of the RV can be assessed with many parameters, and those useful in PH include [27–30]:

Isovolumic relaxation time when prolonged, it indicates poor myocardial relaxation. A normal isovolumic relaxation time is 75 ± 12 ms. With

abnormal relaxation, the value is usually in excess of 110 ms. However, when restriction is present with high right atrial pressures, isovolumic relaxation time will fall below normal to durations less than 60 ms.

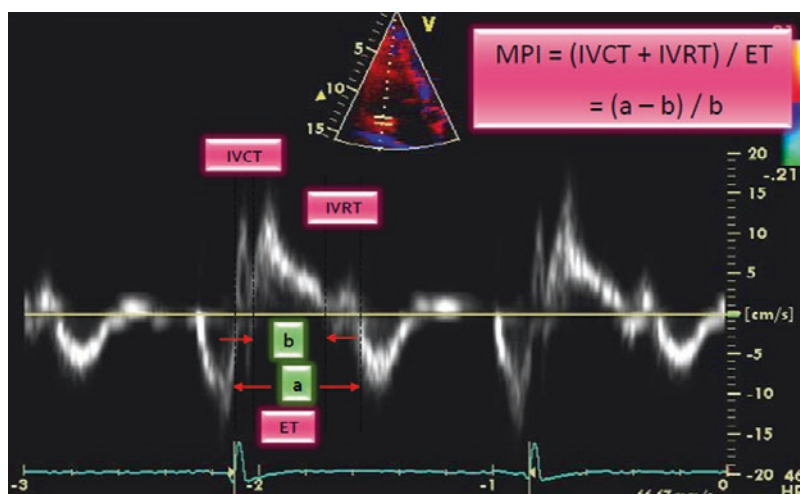
Tricuspid Inflow (E Wave Deceleration)

Deceleration of inflow of the E wave is measured by deceleration time, which shortens with decreasing RV compliance. Deceleration time is complex, as higher RA pressures also shorten it. A normal deceleration time is 198 ± 23 ms; values over 240 ms indicate impaired relaxation, and under 160 ms suggest restriction.

Myocardial Performance Index of the RV

Myocardial performance index, also known as Tei Index, combines a combination of systolic and diastolic measurements (Fig. 16.7). The normal range for RV myocardial performance index is 0.28–0.32 [28, 29]. It is relatively unaffected by heart rate, loading conditions or the presence and the severity of tricuspid regurgitation. In patients with idiopathic pulmonary arterial hypertension, the index correlates with symptoms and values above 0.88 predict poor survival [34].

Fig. 16.7 Measurement of right ventricular myocardial performance index with tissue Doppler imaging



S' Wave Velocity

The patient has to be in sinus rhythm and the velocities are indexed to the heart rate. The S' wave velocity is normally greater than 12 cm/s, and we consider a cut-off value of 11.5 cm/s, below which RV myocardial function may be impaired [29, 30].

Tricuspid Annular Plane Systolic Excursion

Tricuspid annular plane systolic excursion is the reflection of the movement the base to apex shortening of the RV in systole (longitudinal function) [17, 18]. During ventricular systole, long axis shortening is created by motion of both atrioventricular valve annulae toward the cardiac apex. Because the septal attachment of the tricuspid annulus is relatively fixed, the majority of tricuspid annular motion occurs in its lateral aspect.

The measurement of tricuspid annular plane systolic excursion is derived from the apical four chamber view. Special care has to be taken for the whole RV to be included in the view with no dropout in the endocardial outline along the interventricular septum and RV free wall. The width of sector should be limited onto the RV free wall, and the M-mode cursor should be positioned on the lateral portion of the tricuspid annulus, measuring in control sweep mode [33, 34].

Maximal tricuspid annular plane systolic excursion is defined by the total excursion of the tricuspid annulus from its highest position after

atrial ascent to the peak descent during ventricular systole. Earlier studies using two-dimensional echocardiography showed that in the normal RV this value exceeds 16 mm. Using M-mode the normal range is higher (24.9 ± 3.5 mm); 25.4 ± 4.9 mm and a value of 20.1 mm has been shown to be a useful cut-off in identifying PH [19, 34, 35].

Advanced RV Imaging

Real-Time Three-Dimensional Echocardiography

Two-dimensional echocardiography has been established as the most widely applied imaging tool in clinical cardiology practice. Its application helps in morphological and functional assessment of cardiac chambers and valves. The advancement in technology of echocardiographic machines and its software analysis minimized many difficulties and limitations. However, two dimensional applications still carry some limitations. It requires mental conceptualization of a series of multiple orthogonal planer or tomographic images into an imaginary multidimensional reconstruction for better understanding of complex intracardiac structures and their spatial relation with surroundings. Many of two dimensional formula used for volume quantification and ejection fraction calculation especially for

LV are based on geometric assumption that may not be true providing varied results in the setting of chamber dilatation or distortion and in the presence of regional wall motion abnormalities.

Three-dimensional echocardiography has developed the last 15 years and provides more accurate assessment of ventricular volume, mass and function as well as a more complete view of the valves. The third-generation echocardiographic machines with the developed matrix array transducer which consists approximately 3000 firing elements, have improved the contrast resolution and penetration. With this transducer, the entire heart image could be obtained by a pyramidal full-volume acquisition of four cardiac cycles. The development in software made the data off-line analysis faster and easier.

The new modality of real time three-dimensional echocardiography (3DE) seems to offer the ability to improve and expand the diagnostic capabilities of cardiac ultrasound. The development of 3DE systems circumvents many of the disadvantages of reconstructive methods from two dimensional images. It has been widely applied to the LV with great results and a significant degree of accuracy and repro-

ducibility. Most studies that have applied 3D echocardiographic techniques to the RV have involved primarily rotational or freehand scanning methods: most of these series demonstrated improved accuracy of RV function assessment. Furthermore, several studies have compared 3DE with cardiac magnetic resonance imaging (CMR), demonstrating excellent agreement between the two modalities and good intra and inter-observer reproducibility of both [36–38, 41].

Protocol

The patient is placed at a left decubitus position, as in two-dimensional echocardiography and with the use of a different transducer (central X4 transducer, frequency of 3- to 4-MHz, volumetric frame rate 16–24 frame/s, imaging depth 6–16 cm, rotation speed 6 Hz and pulse length 2.5 cycles) than the one used for conventional echocardiography, the apical four chambers view is captured. The patient must hold his breath for seconds so that the view to be captured properly (Fig. 16.8) [40–42].

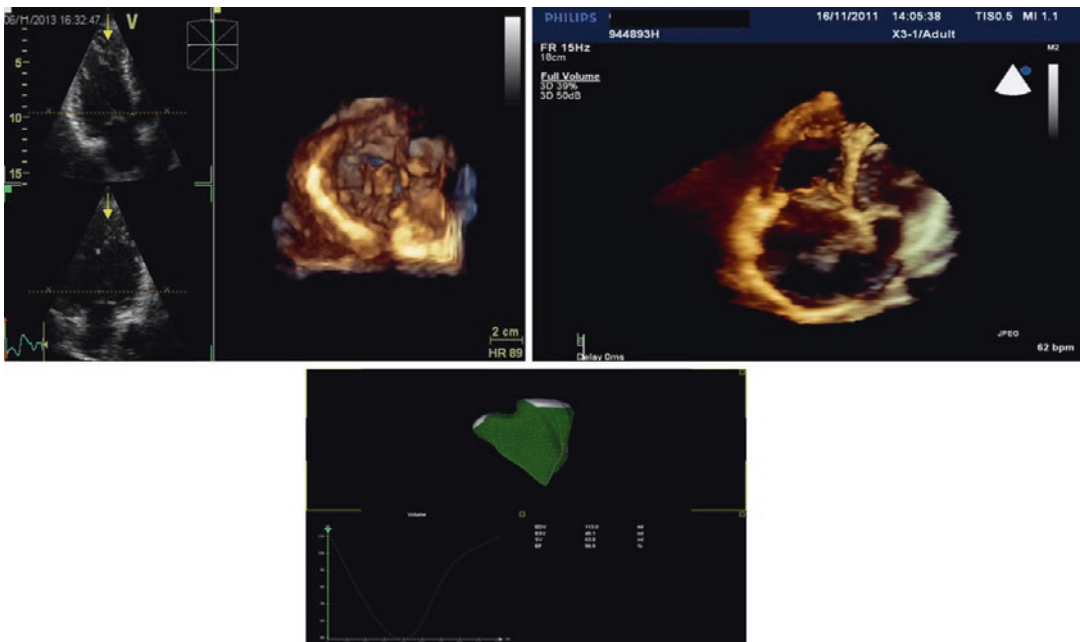


Fig. 16.8 Three-dimensional echocardiography of the right ventricle

Using sequential long axis planes of the RV, volumetric data sets were regenerated within offline analysis system (4D analysis, TomTec, Munich, Germany) permitting endocardial contours delineation. End-diastole phase was defined as the peak of the R wave of the QRS complex and end-systole as the first frame before opening of the tricuspid valve. RV volumes were calculated by manual tracing along the endocardial contours in sequential long axis planes of the ventricle, from ventral to dorsal at 7 mm intervals. Note that when delineating the endocardium, interventricular septum should be included as 1/3 for the normal and 2/3 for the hypertrophied RV. Furthermore, trabeculations should be included in the blood pool. Simpson's rule was employed to calculate values for epicardial and endocardial borders. This allowed calculation of end-diastolic volume, end-systolic volume, stroke volume, ejection fraction and RV mass.

3DE allows quantitative measurements of RV mass without the need to rely on geometric assumptions. Using the same full-volume 3D data set of RV volume calculation, it is possible to identify epicardial boundaries of the RV wall. The latter is used to calculate an epicardial cast of the RV at end-diastole. The volume of this cast is then subtracted from the epicardial cast and the volume of RV myocardium is obtained. By multiplying myocardial volume by the specific density of myocardial muscle (1.05 g/mL), RV mass derives [38, 41, 42].

Several parameters are estimated such as RV long and short axis in end-diastole, RA long and short axis in end-systole and RA volume, the thickness of lateral free wall through RV short axis (RV wall hypertrophy is defined when the thickness is bigger than 5 mm), tricuspid annular diameter in end-diastole and end-systole and the tethering area between the annulus and the leaflets. In addition, 3DE is useful for the assessment of the tricuspid valve in detail, such as in the case of a tricuspid valve cyst or prolapse [41].

Speckle Tracking: Strain

The speckle pattern is used to track myocardial motion and strain rate is based on the Lagrangian formula which was used to describe systolic deformation.

Speckle tracking has been validated by ultrasonomicrometry in the longitudinal direction and rotation. It has been widely applied to the LV and recently has been introduced for the assessment of the RV in PH. Its advantage is that it is angle-independent and that it can track in two or even three dimensions. Drop-outs and reverberations affect tracking as well as too low or high frame rate. Speckle tracking is frame rate sensitive that is why an adjustment of the frame rate between 50 and 80 frames per second is the best possible.

Protocol

Standard greyscale 2D images are acquired in the 2- and 4-chamber apical views as well as the parasternal short axis views at the level of the papillary muscles. Special care is taken to avoid oblique views from the mid-level short axis images and to obtain images with the most circular geometry possible. All images are recorded with a frame rate of at least 50 fps (50–80 fps) to allow for reliable operation of the software (Fig. 16.9a). From an end-systolic single frame, a region of interest is traced on the endocardial cavity interface by a point-and-click approach. Then an automated tracking algorithm follows the endocardium from this single frame throughout the cardiac cycle. All myocardial regions are included. The acoustic markers which are called speckles equally distribute in the region of interest and can follow the entire cardiac cycle. The distance between the speckles is measured as a function of time, and parameters of myocardial deformation are calculated. The RV myocardium is divided into six segments and displayed into six segmental time-strain curves for radial, circumferential and longitudinal strain.

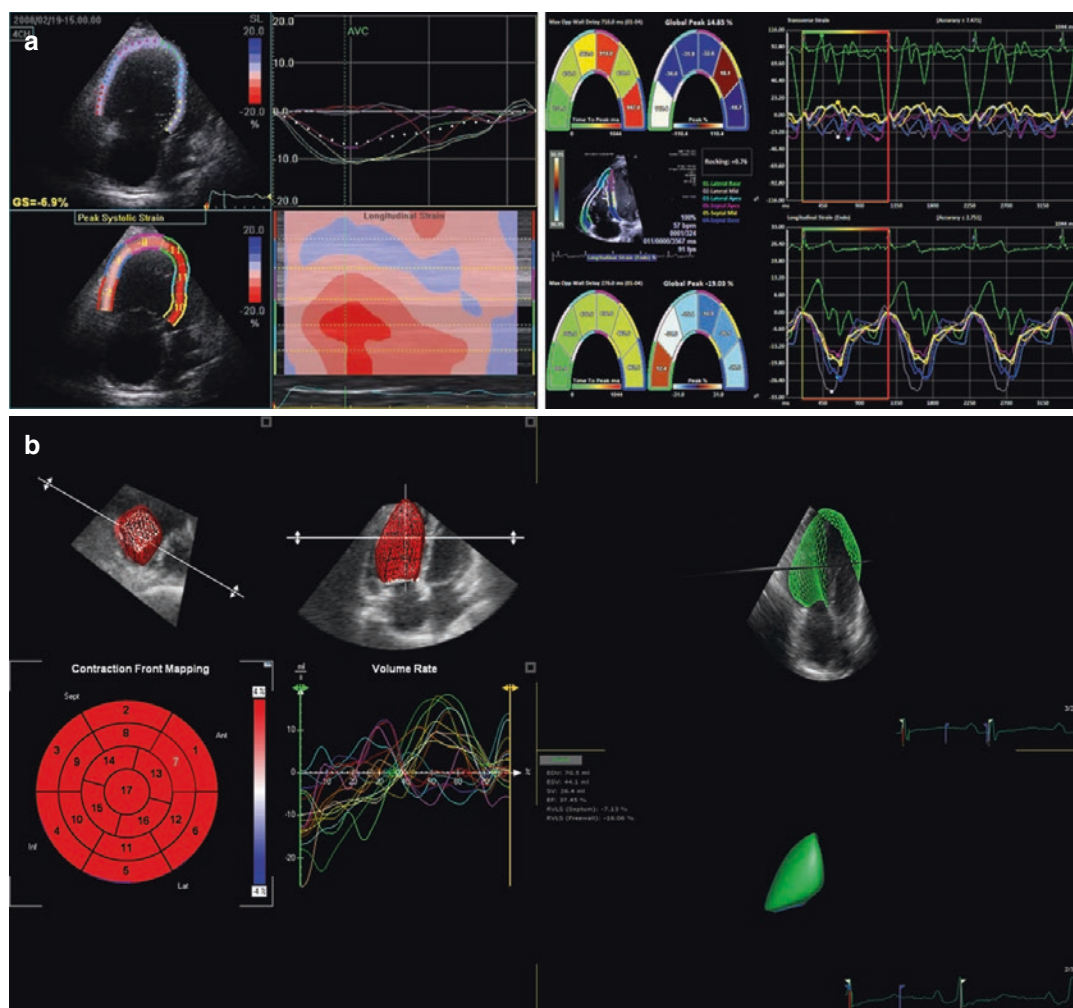


Fig. 16.9 Two-dimensional (a) and three-dimensional (b) speckle tracking of the right ventricle

Two-Dimensional Speckle Tracking Echocardiography

The main advantages of speckle tracking echocardiography are that this technique uses conventional grey scale images and is relatively angle independent, and therefore it circumvents some of the limitations inherent to TDI. RV myocardial longitudinal strain and strain rate are parameters that are independent of ejection fraction and allow quantification of regional myocardial deformation. The images must be obtained at frame rates higher than 60 frames/s and only one cardiac cycle is required. Measurements of strain and strain rate have shown significant RV myocardial abnormalities in patients with amyloidosis, pulmonary hypertension, atrial septum

defects and arrhythmogenic RV cardiomyopathy. The view of choice is the focused RV apical four-chamber view. There is no consensus on which method, full RV myocardium (i.e. including interventricular septum too) or RV free wall only of generating strain measurements is more accurate and correlates best prognosis. Also, there is still a lack of data for normal values of RV strain measurements in adults. A strong correlation between longitudinal strain of different RV segments and RV global function has been demonstrated when patients with RV dysfunction were compared to healthy volunteers. In patients with chronic left heart failure referred for heart transplantation RV longitudinal strain is a strong predictor of outcome.

Multiple studies have shown the prognostic role of speckle tracking echocardiography in patients with pulmonary artery hypertension and that the RV free wall longitudinal strain has been an independent predictor of various RV parameters, including mean pulmonary artery pressure.

3D Speckle Tracking

The complex geometry of the RV is ideally displayed using a 3D imaging modality. However, further investigation and reliable validation are required for assessing RV myocardial deformation with 3D speckle tracking (Fig. 16.9b) [37, 39]. The ratio of longitudinal to circumferential strain is called area strain and has proven significant correlation with functional parameters such as the walking capacity of pulmonary hypertensive patients [39].

Furthermore, RV global longitudinal strain should be separated from RV free wall strain in order to avoid the bias from the interventricular dependency [39].

Effect of Heart Rate and Body Surface Area

Most indices of function are unaffected by heart rate, yet some require correction when heart rate exceeds 100 or drops below 70. These are RV outflow tract acceleration time, myocardial performance index, S' wave velocity and isovolumic relaxation time. In order to index to heart rate, the measurement should be multiplied by 75/heart rate, e.g.:

$$\begin{aligned} &\text{RV outflow tract acceleration time (indexed to heart rate)} \\ &= \text{RV outflow tract acceleration time} \times 75 / \text{heart rate} \end{aligned}$$

When indexing measurements for body surface area (BSA), they should be divided by the BSA (Dupois & Dupois), where:

$$\begin{aligned} \text{BSA} &= 0.007184 \times \text{weight (kg)}^{0.425} \\ &\quad \times \text{height (cm)}^{0.725} \end{aligned}$$

For the normal man, BSA is 1.9 m² and for the normal woman, BSA is 1.6 m².

Stroke Volume, Cardiac Output and Pulmonary Vascular Resistance

Echocardiography uses the combination of two dimensional and pulsed-wave Doppler imaging to measure cardiac output. Stroke volume can be derived from the product of the velocity time integral of the Doppler profile and the cross-sectional area of the LV outflow tract. Cardiac output is the product of stroke volume and heart rate [19].

$$\begin{aligned} \text{Stroke volume} &= \text{velocity time integral (LV outflow tract)} \\ &\quad \times \text{cross-sectional area (LV outflow tract)} \end{aligned}$$

$$\text{Cardiac output} = \text{stroke volume} \times \text{heart rate}$$

Similarly, RV stroke volume and cardiac output can be measured from the proximal RV outflow tract, just within the pulmonary valve from the parasternal short-axis view.

In order to calculate pulmonary vascular resistance, continuous-wave Doppler is used to determine the peak tricuspid regurgitant velocity as described above: the highest velocity is used. In patients with atrial fibrillation, the average of five measurements should be taken.

$$\begin{aligned} \text{Pulmonary vascular resistance (Wood units)} &= 10 \times \left(\frac{\text{peak tricuspid regurgitant velocity}}{\text{velocity time integral RV outflow tract}} \right) \\ &\quad + 0.16 \end{aligned}$$

This measurement has been shown to correlate well with pulmonary vascular resistance measured at cardiac catheterisation over a range of right and left atrial pressures. A value of peak tricuspid regurgitant velocity/velocity time integral RV outflow tract less than 0.2 has 94% sensitivity for a pulmonary vascular resistance of less than 2 Wood Units at catheterisation. As the definition of pulmonary arterial hypertension includes a pulmonary vascular resistance greater than 3 Wood Units, a value of peak tricuspid regurgitant velocity/velocity time integral RV outflow tract less than 0.2 will exclude most cases of pulmonary arterial hypertension. While measures of stroke volume, cardiac output and pulmonary vascular resistance are readily measurable at echocardiography and correlate with right and left heart function and the underlying pulmonary vascular resistance, these measurements are not considered core to the protocol and are thus not mandatory measurements. The value of serial measurements in the follow-up of PH has not been validated.

Outcomes in Pulmonary Hypertension

The primary abnormality in PH is increased afterload on the RV due to elevated pulmonary vascular resistance caused by remodelling of the resistance pulmonary arteries. It is possible that the RV itself is predisposed to abnormal remodelling due to the same genetic abnormalities underlying vascular remodelling, but this is highly speculative. Nonetheless, it is clear from many studies that it is cardiac function which determines prognosis and exercise capacity. In particular, it is worth noting that pulmonary arterial pressure by itself does not correlate at all well with exercise capacity or prognosis [19, 42]. This is made abundantly obvious from the fact that pulmonary arterial pressure will fall with advancing RV failure. As RV failure progresses, cardiac output falls and right atrial pressure rises. Values from cardiac catheterisation associated with poor prognosis are:

- Cardiac index <2.1 L/min/m²
- Right atrial pressure >10 mmHg
- Mixed venous oxygen saturation $<63\%$

(low values indicate increased oxygen extraction due to lower cardiac output)

In line with these measurements, echocardiographic follow-up studies have shown increased right atrial size to be associated with poor prognosis. Persistently high right atrial pressure may lead to the development of a pericardial effusion, which is a powerful predictor of mortality.

Other echocardiographic features that have been shown to correlate with survival include markers of myocardial function such as myocardial performance index, RV fractional area change and tricuspid annular plane systolic excursion. A cut-off value of greater than 0.88 for myocardial performance index and less than 15 mm for tricuspid annular plane systolic excursion have been particularly associated with poor prognosis. Increases in LV eccentricity index at end-diastole have also been shown in several studies to be associated with worse outcomes, indicating the adverse impact of LV compression. Patients with values above 1.7 have a significantly higher risk of dying. While it may be important to use cut-off values from echocardiography to risk-stratify patients, there are many other powerful clinical indicators of severity, such as functional class, hemodynamics and exercise capacity. Nonetheless, there are problems with using these measures in following the clinical course of patients or response to therapy. Hemodynamics can only be obtained by invasive means; functional class is a crude assessment for only small to moderate change; and exercise capacity can be influenced by many other factors.

Implementation of The Current Guidelines in Echocardiographic Assessment for Pulmonary Hypertension

Two-dimensional, Doppler and contrast examinations can be used to identify congenital heart disease. High pulmonary blood flow found on pulsed wave Doppler in the absence of a detectable shunt or significant dilatation of proximal pulmonary artery despite only moderate pulmonary hypertension may warrant transoesophageal

examination with contrast or cardiac magnetic resonance imaging to exclude sinus venosus atrial septal defect and/or anomalous pulmonary venous return.

Right atrial area greater than 26 cm² and the presence of pericardial effusion may indicate high risk patients with pulmonary hypertension. However, it should be mentioned that sole echocardiographic markers may not indicate pulmonary hypertension or become prognostic. The multi-indiced approach for right heart assessment is the one preferred. Furthermore, RV speckle tracking is a promising imaging modality.

In cases of suspicion of left ventricular diastolic dysfunction, Doppler echocardiographic signs should be assessed even if their reliability is considered low. Right heart catheterisation should be considered when the diagnosis remains uncertain after non-invasive investigations.

The practical clinical value of exercise Doppler echocardiography in the identification of cases with pulmonary hypertension limited to exercise is uncertain because of the lack of validated criteria and prospective confirmatory data.

References

- McQuillan BM, Picard MH, Leavitt M, et al. Clinical correlates and reference intervals for pulmonary artery systolic pressure among echocardiographically normal subjects. *Circulation*. 2001;104:2797–802.
- Galie N, et al. The task force for the diagnosis and treatment of pulmonary hypertension for the European Society of Cardiology (ESC) and the European Respiratory Society (ERS), endorsed by the International Society of Heart and Lung Transplantation (ISHLT). *Eur Heart J*. 2009;30:2493–537.
- Haddad F, Hunt SA, Rosenthal DN, et al. Right ventricular function in cardiovascular disease, part I: anatomy, physiology, aging, and functional assessment of the right ventricle. *Circulation*. 2008;117:1436–48.
- Haddad F, Doyle R, Murphy DJ, et al. Right ventricular function in cardiovascular disease, part II: pathophysiology, clinical importance, and management of right ventricular failure. *Circulation*. 2008;117:1717–31.
- Ho SY, Nihoyannopoulos P. Anatomy, echocardiography, and normal right ventricular dimensions. *Heart*. 2006;92(Suppl 1):i2–13.
- Badano LP, Ginchina C, Easaw J, Muraru D, Grillo MT, Lancellotti P, Pinamonti B, Coghlan G, Marra MP, Popescu BA, De Vita S. Right ventricle in pulmonary arterial hypertension: haemodynamics, structural changes, imaging, and proposal of a study protocol aimed to assess remodelling and treatment effects. *Eur J Echocardiogr*. 2010;11(1):27–37.
- Cameli M, Khayyal M, Marino F, Augustine D, Forshaw T, Mondillo S, Stankovic I, Surkova E, Timeshova T, Vasco N, Badano L, Grapsa J. Club 35 EACVI web spotlight: comments on right ventricle assessment in the new echocardiography recommendations. *Eur Heart J Cardiovasc Imaging*. 2015;16(11):1185–6.
- Faletta FF, Muzzarelli S, Dequarti MC, Murzilli R, Bellu R, Ho SY. Imaging-based right-atrial anatomy by computed tomography, magnetic resonance imaging, and three-dimensional transoesophageal echocardiography: correlations with anatomic specimens. *Eur Heart J Cardiovasc Imaging*. 2013 Dec;14(12):1123–31.
- Garbi M, Habib G, Plein S, Neglia D, Kitsiou A, Donal E, Pinto F, Bax J, Achenbach S, Popescu BA, Edvardsen T, Badano LP, Stefanidis A, Bucciarelli-Ducci C, Derumeaux G, Luis Zamorano J, Lüscher TF, Maurer G, Lancellotti P. Appropriateness criteria for cardiovascular imaging use in clinical practice: a position statement of the ESC/EACVI taskforce. *Eur Heart J Cardiovasc Imaging*. 2014 May;15(5):477–82.
- Foale R, Nihoyannopoulos P, McKenna W, et al. Echocardiographic measurement of the normal adult right ventricle. *Br Heart J*. 1986;56:33–44.
- Consensus statement on the management of pulmonary hypertension in clinical practice in the UK and Ireland. *Heart*. 2008;94(Suppl 1):i1–i41.
- Consensus statement on the management of pulmonary hypertension in clinical practice in the UK and Ireland. *Thorax*. 2008;63(Suppl 2):ii1–ii41.
- Yoshida K, Yoshikawa J, Shakudo M, et al. Color Doppler evaluation of valvular regurgitation in normal subjects. *Circulation*. 1988;78:840–7.
- Kitabatake A, Inoue M, Asao M, et al. Noninvasive evaluation of pulmonary hypertension by a pulsed Doppler technique. *Circulation*. 1983;68:302–9.
- Lang RM, Bierig M, Devereux RB, et al. Recommendations for chamber quantification: a report from the American Society of Echocardiography's Guidelines and standards committee and the chamber quantification writing group, developed in conjunction with the European Association of Echocardiography, a branch of the European Society of Cardiology. *J Am Soc Echocardiogr*. 2005;18:1440–63.
- Maeba H, Nakatani S, Sugawara M, et al. Different time course of changes in tricuspid regurgitant pressure gradient and pulmonary artery flow acceleration after pulmonary thromboendarterectomy: implications for discordant recovery of pulmonary artery pressure and compliance. *Circ J*. 2007;71:1771–5.
- Forfi PR, Fisher MR, Mathai SC, et al. Tricuspid annular displacement predicts survival in pulmonary hypertension. *Am J Respir Crit Care Med*. 2006;174:1034–41.
- Kaul S, Tei C, Hopkins JM, et al. Assessment of right ventricular function using two-dimensional echocardiography. *Am Heart J*. 1984;107:526–31.

19. Howard LS, Grapsa J, Dawson D, Bellamy M, Chambers JB, Masani ND, Nihoyannopoulos P, Simon R, Gibbs J. Echocardiographic assessment of pulmonary hypertension: standard operating procedure. *Eur Respir Rev*. 2012;21(125):239–48.
20. Lee CY, Chang SM, Hsiao SH, et al. Right heart function and scleroderma: insights from tricuspid annular plane systolic excursion. *Echocardiography*. 2007;24:118–25.
21. Olson JM, Samad BA, Alam M. Prognostic value of pulse-wave tissue Doppler parameters in patients with systolic heart failure. *Am J Cardiol*. 2008;102:722–5.
22. Abbas A, Lester S, Moreno FC, et al. Noninvasive assessment of right atrial pressure using Doppler tissue imaging. *J Am Soc Echocardiogr*. 2004;17:1155–60.
23. Santamore WP, Dell'Italia LJ. Ventricular interdependence: significant left ventricular contributions to right ventricular systolic function. *Prog Cardiovasc Dis*. 1998;40:289–308.
24. Stein PD, Sabbah HN, Anbe DT, et al. Performance of the failing and nonfailing right ventricle of patients with pulmonary hypertension. *Am J Cardiol*. 1979;44:1050–5.
25. Schnittger I, Gordon EP, Fitzgerald PJ, et al. Standardized intracardiac measurements of two dimensional echocardiography. *J Am Coll Cardiol*. 1983;2:934–8.
26. Wang Y, Gutman JM, Heilbron D, et al. Atrial volume in a normal adult population by two-dimensional echocardiography. *Chest*. 1984;86:595–601.
27. Dujardin KS, Tei C, yeo TC, et al. Prognostic value of a Doppler index combining systolic and diastolic performance in idiopathic-dilated cardiomyopathy. *Am J Cardiol*. 1998;82:1071–6.
28. Tei C, Dujardin KS, Hodge DO, et al. Doppler echocardiographic index for assessment of global right ventricular function. *J Am Soc Echocardiogr*. 1996;9:838–47.
29. Yeo TC, Dujardin KS, Tei C, et al. Value of a Doppler derived index combining systolic and diastolic time intervals in predicting outcome in primary pulmonary hypertension. *Am J Cardiol*. 1998;81:1157–61.
30. Alam M, Wardell J, Andersson E, et al. Characteristics of mitral and tricuspid annular velocities determined by pulsed wave Doppler tissue imaging in healthy subjects. *J Am Soc Echocardiogr*. 1999;12:618–28.
31. Feneley M, Gavaghan T. Paradoxical and pseudo-paradoxical interventricular septal motion in patients with right ventricular volume overload. *Circulation*. 1986;74:230–8.
32. Ryan T, Petrovic O, Dillon JC, et al. An echocardiographic index for separation of right ventricular volume and pressure overload. *J Am Coll Cardiol*. 1985;5:918–27.
33. Hammarstrom E, Wranne B, Pinto FJ, et al. Tricuspid annular motion. *J Am Soc Echocardiogr*. 1991;4:131–9.
34. Lopez-Candales A, Dohi K, Rajagopalan N, et al. Defining normal variables of right ventricular size and function in pulmonary hypertension: an echocardiographic study. *Postgrad Med J*. 2008;84:40–5.
35. Anavekar NS, Skali H, Bourgoun M, et al. Usefulness of right ventricular fractional area change to predict death, heart failure, and stroke following myocardial infarction (from the VALIANT ECHO study). *Am J Cardiol*. 2008;101:607–12.
36. Tadic M. Multimodality evaluation of the right ventricle: an updated review. *Clin Cardiol*. 2015;38(12):770–6.
37. Ryo K, Goda A, Onishi T, Delgado-Montero A, Tayal B, Champion HC, Simon MA, Mathier MA, Gladwin MT, Gorcsan J 3rd. Characterization of right ventricular remodeling in pulmonary hypertension associated with patient outcomes by 3-dimensional wall motion tracking echocardiography. *Circ Cardiovasc Imaging*. 2015;8(6)
38. Blanchard DG, DeMaria AN. Right ventricular 3-dimensional strain in pulmonary hypertension: the quest to see the future. *J Am Coll Cardiol*. 2014;64(1):52–3.
39. Smith BC, Dobson G, Dawson D, Charalampopoulos A, Grapsa J, Nihoyannopoulos P. Three-dimensional speckle tracking of the right ventricle: toward optimal quantification of right ventricular dysfunction in pulmonary hypertension. *J Am Coll Cardiol*. 2014;64(1):41–51.
40. Wang J, Prakasa K, Bomma C, et al. Comparison of novel echocardiographic parameters of right ventricular function with ejection fraction by cardiac magnetic resonance. *J Am Soc Echocardiogr*. 2007;20:1058–64.
41. Grapsa J, Gibbs JS, Dawson D, Watson G, Patni R, Athanasiou T, Punjabi PP, Howard LS, Nihoyannopoulos P. Morphologic and functional remodeling of the right ventricle in pulmonary hypertension by real time three dimensional echocardiography. *Am J Cardiol*. 2012;109(6):906–13.
42. Grapsa J, O'Regan DP, Pavlopoulos H, Durighel G, Dawson D, Nihoyannopoulos P. Right ventricular remodelling in pulmonary arterial hypertension with three-dimensional echocardiography: comparison with cardiac magnetic resonance imaging. *Eur J Echocardiogr*. 2010 Jan;11(1):64–73.

Introduction

Pulmonary embolism (PE) is a common condition with an incidence exceeding 1 in 1000 and a mortality rate of >15% in the first 3 months after diagnosis [1]. It has a wide clinical spectrum ranging from asymptomatic, small PE to large, life-threatening causing haemodynamic instability and cardiogenic shock. Early diagnosis is therefore essential so early treatment can be instituted. PE may be separated in acute PE often presenting in the emergency department with acute onset of chest pain and the differential diagnosis from myocardial infarction is often challenging. Chronic PE in the other hand may be a more long-standing condition leading to breathlessness and right heart failure. The differential diagnosis from other causes of breathlessness and heart failure may be difficult.

PE may escape prompt diagnosis since the clinical signs and symptoms such as breathlessness, chest pain, fever, haemoptysis or syncope are non-specific [2]. A high index of clinical suspicion is therefore essential. When the clinical

presentation raises the suspicion of PE in an individual patient, it should prompt further objective testing. The ECG and chest x-ray may rapidly identify alternative diagnoses, especially myocardial infarction and chest infection, respectively. Arterial blood gas measurements have proved disappointing. Normal values of the alveolar-arterial oxygen gradient do not exclude acute PE [3], while hypoxemia discriminates poorly between those who do and do not have acute PE [4]. Prompt and accurate diagnosis of PE is facilitated by careful clinical evaluation that assesses the probability of PE and makes appropriate use of the plasma D-dimer ELISA and chest CT scanning [5]. Echocardiography, and more recently pocket-size echocardiography, used in the emergency department may help in the prompt diagnosis of PE by detecting right ventricular overload or detecting any other abnormality such as valve disease, aortic dissection, left ventricular failure or a regional wall motion abnormality that can divert the attention away from PE, even in the hands of junior doctors [6], while awaiting for the biomarkers to come back from the lab.

Predisposing conditions for developing venous thrombosis include vascular endothelial damage, blood hypercoagulability and blood flow stasis. The most common reversible risk factors for PE however are obesity and cigarette smoking, an increasing pandemic in our society. Public awareness with PE has centered on long-haul air travel,

D. Dawson
Department of Echocardiography, Imperial College
Healthcare NHS Trust, Hammersmith Hospital,
London, UK

P. Nihoyannopoulos (✉)
Imperial College London, NHLI, Hammersmith
Hospital, London, UK
e-mail: petros@imperial.ac.uk

a rare cause of venous thromboembolism [7]. PE also occurs in the context of illness attributable to surgery, trauma, immobilization, cancer [8], oral contraceptives [9] pregnancy, and postmenopausal hormone replacement therapy [10] but also blood stasis from immobility, polycythemia (hyperviscosity) or chronic right heart failure.

Pathophysiology

Acute PE interferes with both the circulation and gas exchange. Right ventricular (RV) failure due to pressure overload is considered the primary cause of death in severe PE [11]. The haemodynamic response to PE is related to the size and the location of the embolus. The abrupt increase in pulmonary vascular resistance results in RV dilatation, which alters the contractile properties of the RV myocardium via the Frank-Starling mechanism. The increase in RV pressure and volume leads to an increase in wall tension and myocyte stretch, free wall hypokinesis, tricuspid annular dilatation and secondary tricuspid regurgitation. The reduced forward RV stroke volume raises RV diastolic and right atrial (RA) pressure and compromises left ventricular (LV) filling. The development of significant tricuspid regurgitation will further reduce forward RV output and LV filling. RV pressure overload and prolonged RV contraction, which extends into early LV diastole, causes leftward bulging of the ventricular septum and distortion of the LV chamber geometry, reducing LV distensibility and further impairing LV filling while neurohumoral activation leads to inotropic and chronotropic stimulation and increased right ventricular oxygen demand and right ventricular ischaemia [12]. This will result in reduced contractility and eventually right ventricular output, reduced left ventricular preload and drop in systemic blood pressure and eventually cardiogenic shock. Figure 17.1 shows the cascade of the key factors contributing to haemodynamic collapse in acute pulmonary embolism.

The haemodynamic consequences of PE become evident when the pulmonary arterial bed becomes occluded by more than 30%. Mechanical obstruction of the pulmonary circulation, hypox-

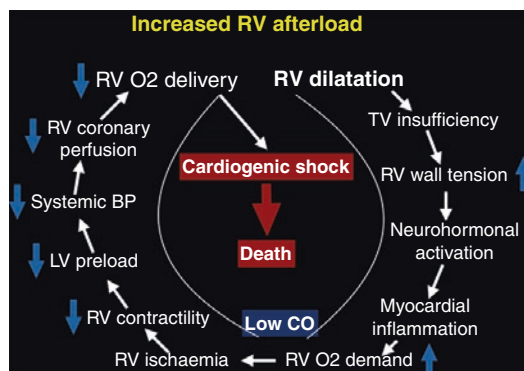


Fig. 17.1 Pathophysiologic mechanisms of acute pulmonary embolization leading to haemodynamic collapse. *BP* blood pressure, *CO* cardiac output, *LV* left ventricular, *RV* right ventricular, *TV* tricuspid valve

emia and further pulmonary vasoconstriction, caused by platelet released chemical mediators from the thrombus, increase vascular resistance and right ventricular afterload.

The normal right ventricle (RV) is thin walled and compliant, filling at low pressure and ejecting against low vascular resistance. The ventricle accepts a wide range of filling volumes with small changes in filling pressure (preload), whilst poorly tolerating sudden increases in afterload. The normal RV is unable to acutely generate a mean pulmonary artery pressure greater than 40 mmHg.

If the abrupt increase in afterload, following PE, cannot be tolerated by the RV, then acute RV failure may result leading to electromechanical dissociation or systemic hypotension progressing to shock and death.

PE can affect both pulmonary circulation and gas exchange in the lungs. Occlusion of the pulmonary arterial bed from large or multiple emboli causes an increase in pulmonary vascular resistance and alveolar dead space.

In the lungs, ventilated alveoli distal to the occlusion are not perfused resulting in ventilation perfusion mismatch, hypoxemia (decreased arterial PO_2) and decreased surfactant production, which may result in adhesive atelectasis (lung tissue collapse). Compensatory hyperventilation may trigger further secondary bronchoconstriction and pulmonary vasoconstriction.

Recurrent pulmonary emboli and/or progressing RV dysfunction may result in developing

systemic hypotension and shock in a initially stable patient.

The acute formation of thrombus by activation of coagulation mechanisms is associated with simultaneous fibrinolysis activation. In PE the process of fibrinolysis is however ineffective. Fibrinolysis causes plasmin to breakdown clot fibrin and release D-dimer [13]. Plasma D-dimer levels therefore become elevated but this is not specific to VTE and also occurs in a variety of other conditions including inflammation, infection, aortic dissection and cancer.

Classification of Pulmonary Embolism

The clinical classification of acute PE severity is based on early mortality risk with the critical factor for prognosis being the haemodynamic effect of the PE, rather than the anatomic distribution and size of the pulmonary thromboemboli. Terminology of classification varies between North American and European with divisions of either acute massive, acute sub-massive and acute small PE or high, intermediate and low risk of PE related to early death, respectively [14].

Acute massive or high-risk PE is characterised by haemodynamic instability with persistent hypotension and cardiogenic shock and carries a mortality risk of greater than 15%. Acute sub-massive or intermediate risk PE is characterised by haemodynamic stability but evidence of RV dysfunction and or myocardial injury and carries a mortality risk of between 3 and 15%. Acute small or low risk PE is associated with a less than 1% mortality risk.

Diagnosis of Pulmonary Embolism

Due to the non-specific clinical presentation of PE, diagnosis is challenging. Clinical signs, symptoms, patient risk factors, laboratory tests and appropriate imaging modalities guide the assessment of likelihood of PE in an individual patient. Symptoms include dyspnoea, chest pain, haemoptysis and syncope. Signs include those of DVT (with unilateral leg swelling and/or pain),

Table 17.1 Symptoms and signs of pulmonary embolism

Symptoms	Signs
Dyspnoea	Tachypnoea ($\geq 20/\text{min}$)
Chest pain (pleuritic)	Tachycardia ($>100/\text{min}$)
Chest pain (substernal)	Signs of DVT
Cough	Fever ($>38.5^{\circ}\text{C}$)
Haemoptysis	Cyanosis
Syncope	

tachypnoea, tachycardia, hypotension and cyanosis (Table 17.1).

Chest X-ray findings such as plate like atelectasis, pleural effusion and elevated hemidiaphragm are non-specific. However, chest X-ray, may be useful in excluding other conditions such as pneumothorax, pneumonia and rib fracture [15].

Electrocardiographic (ECG) changes are also usually non-specific. The ECG may show sinus tachycardia or signs of RV strain, including right axis deviation, complete or incomplete right bundle branch block, T-wave inversion in anterior precordial leads and an S wave in lead I and Q wave and T-wave inversion in lead III, or it may suggest an alternative diagnosis such as myocardial infraction or pericarditis [16].

Blood gas analysis typically shows arterial hypoxaemia and hypocapnea (respiratory alkalosis) in acute PE patients. However, the absence of hypoxemia does not exclude PE.

An elevated D-dimer plasma level, although a sensitive indicator of acute VTE is not specific. A normal plasma level however suggests that an acute PE or DVT is highly unlikely.

Circulating troponin and plasma natriuretic peptides levels are both useful prognostic biomarkers in acute PE. Increased myocardial stretch, from RV overload, leads to the release of natriuretic peptides and myocardial cell damage releases troponin. Elevated levels of theses biomarkers therefore suggest right ventricular dysfunction and myocardial damage respectively and differentiate between low and intermediate risk in acute PE.

Pulmonary angiography has been generally superseded by less invasive multi-detector computer tomographic (MDCT) angiography, because of its imaging quality and its ability to visualise the pulmonary vasculature at least to the segmental level [17]. Ventilation-perfusion (V/Q) lung scanning using is useful in patients

with suspected PE where MDCT is contraindicated such as in patients with major renal impairment, anaphylaxis to intravenous contrast, or pregnancy. Perfusion scans are combined with ventilation studies for which multiple tracers such as xenon (Xe)-522 133 gas, Tc-99m-labeled aerosols, or Tc-99m-labeled carbon microparticles (Technegas) can be used. The purpose of the ventilation scan is to increase specificity: in acute PE, ventilation is expected to be normal in hypoperfused segments (mismatch) [18].

Pulmonary angiography has remained the gold standard for the diagnosis or exclusion of PE for many years, but is rarely performed now as less-invasive CT angiography offers similar diagnostic accuracy [19]. Pulmonary angiography is more often used to guide percutaneous catheter-directed treatment of acute PE.

Echocardiography in Acute Pulmonary Embolism

In the first instance it is important that the echocardiographer is well trained in echocardiography and preferably being accredited so that he/she is familiar with all projections and in particularly those specific to the right heart, which is challenging to image. One of the commonest mistakes is to misinterpret a normal right heart structure with an abnormality. The normal right heart structures that will need to be identified first before making a pathological diagnosis are:

- The moderator band
- The Eustachian valve
- The Chiari complex

Direct visualisation of right heart thrombus using echocardiography is uncommon, with thrombus seen in less than 4% of suspected PE patients and therefore its main role in these patients is in identifying the indirect signs of acute pressure overload. RV dysfunction as detected on echocardiography occurs in at least 25% of patients with PE.

- In haemodynamically unstable patients with shock or hypotension immediate bed-side

echocardiography is useful for the differential diagnosis excluding pericardial tamponade, aortic dissection, acute coronary syndrome, ventricular septal rupture or acute valvular dysfunction, but also detecting evidence of RV dysfunction and raised pulmonary pressure as well as the possible visualisation of right heart thrombi. Unequivocal signs of RV pressure overload and dysfunction in a haemodynamically compromised patient with suspected PE justify emergency revascularization treatment for PE [20].

- In haemodynamically stable patients with diagnosed PE, echocardiographic assessment of RV morphology and function may assist in risk stratification, differentiating between those at low or intermediate mortality risk [20].

Perhaps the greatest contribution of echocardiography however is the ruling out of any echocardiographic signs of RV overload or dysfunction, which practically exclude PE as the cause of haemodynamic instability (Tables 17.2 and 17.3).

Table 17.2 Echocardiographic findings in patients with acute pulmonary embolism

• Right ventricular dilatation and hypokinesia
• Ventricular Septal flattening in systole suggestive RV pressure overload
• Direct visualisation of thrombus in the pulmonary arteries or thrombus in transit through the atrial septum
• Elevated pulmonary pressures measured by the maximal TR velocity jet (usually >3 m/s)

Table 17.3 Echocardiographic criteria for diagnosis of pulmonary embolism

• RV dilatation
– Increased RV/LVEDD ratio
• RV impairment (depressed contractility)
– McConnell sign
• RV pressure overload
• Raised pulmonary systolic pressure
– Increased TR velocity
– Decreased pulmonary acceleration time
• Disturbed RV ejection pattern
– 60/60 sign
• Impaired myocardial performance
– RV MPI and V index

Detection of Thrombus in the Pulmonary Arteries or in Transit: Across the Atrial Septum

The direct visualisation of mobile thrombi within the right heart is rare but highly diagnostic when detected and is associated with increased mortality. With transthoracic echocardiography (TTE) thrombus is seen most commonly in patients with suspected PE within the proximal inferior vena cava (IVC) or right atrium and appear as mobile, often worm-like masses, which if unattached appear to swirl around within the associated chamber, usually in the atria. In Fig. 17.2 a long thrombus originating from the inferior vena cava is clearly visualised while in Fig. 17.3 a large thrombus in the right atrium is seen. Imaging of the proximal IVC, right heart chambers, pulmonary trunk and proximal branches is possible with TTE utilising parasternal, apical and subcostal acoustic windows. In Fig. 17.4, a thrombus in the main pulmonary artery is clearly visualised.

Using a combination of apical and parasternal projection of the right ventricle, it is possible to identify fragments or even a long worm-like highly mobile thrombus as it crosses the atria septum via a patent foramen ovalae (Fig. 17.5). These thrombi are called thrombi-in-transit as they are literally “caught” as they cross the atrial septum. These thrombi are rare to visualise but when seen, they form the most solid evidence of the culprit for pulmonary embolisation. Bubble study with bolus IV injection of agitated saline

may detect reverse shunting across a PFO and identifies suspected PE patients with an increased risk of paradoxical embolism.

Transoesophageal echocardiography (TOE) may be useful in the detection of emboli in the central pulmonary arteries particularly in haemodynamically unstable patients in an intensive care setting. Thrombi appear as echogenic masses with distinct borders protruding into the lumen of the artery. Identifying disturbed colour Doppler flow around the thrombus and visualisation of it in multiple planes reduces the misinterpretation of artefact. TOE imaging allows visualisation of the right

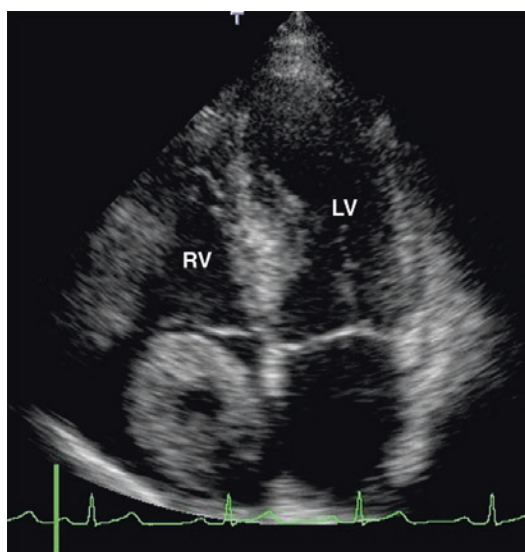


Fig. 17.3 Apical four-chamber projection showing a large thrombus in the right atrium. *LV* Left ventricle, *PV* right ventricle

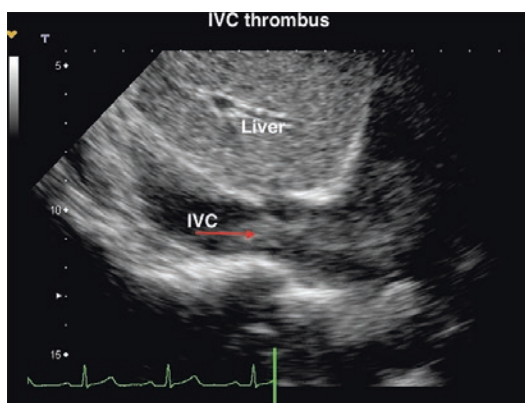


Fig. 17.2 Subcostal projection showing a large thrombus originating from the IVC and protruding into the RA. *IVC* Inferior vena cava, *RA* Right atrium

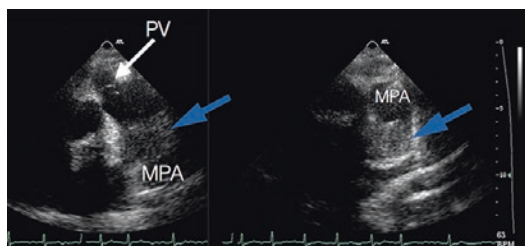


Fig. 17.4 Pulmonary artery views demonstrating a large proximal thrombus in the main pulmonary artery (arrow). On the left, the main pulmonary artery is clearly seen with the thrombus sitting before the bifurcation of the pulmonary arteries (left). On the right, a modified view focusing on the thrombus. *MPA* Main pulmonary artery, *PV* Pulmonary valve

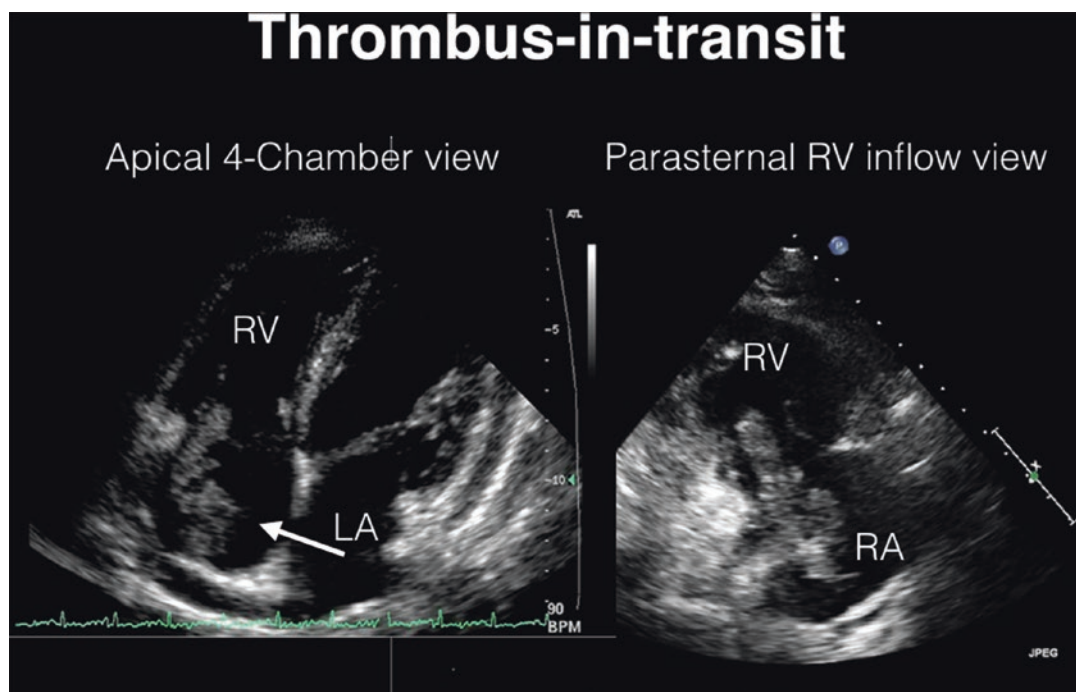


Fig. 17.5 Thrombus-in-transit. On the left, apical four-chamber projection demonstrating a worm-like highly mobile thrombus in the right atrium. On the right, a right ventricular inflow view from the same patient showing the

thrombus into the right atrium but also protruding through the tricuspid valve into the right ventricle. The arrow showing the passage through the atrial septum. *LA* Left atrium, *RA* Right atrium, *RV* Right ventricle

heart utilising mid-oesophageal four-chamber (0°), mid-oesophageal RV inflow-outflow (60°) and mid-oesophageal bicaval (110°) views. Imaging the main pulmonary trunk and right branch is achieved from the mid-oesophageal AV view (0°) with anteflexion and the upper-oesophageal AV view (0°). Visualisation of the proximal left branch is more difficult due to acoustic shadowing from the left main bronchus. Crucially, using TOE the entirety of the atrial septum can be evaluated for the presence of a patent foramen ovalae (PFO) and possible lodged thrombus.

Detection of RV Dysfunction

Acute PE may lead to RV pressure overload and dysfunction. TTE findings include:

- RV dilatation
- Free-wall hypokinesis
- paradoxical interventricular septal motion
- tricuspid regurgitation

- raised pulmonary pressure
- dilated non-collapsing inferior vena cava
- LV diastolic abnormalities

However, these signs are non-specific and may be present with concomitant cardiac or respiratory disease.

Dilatation of the RV is commonly judged by comparison with the LV size either qualitatively or as a ratio of basal dimension (RV:LV) from the parasternal long-axis view (Fig. 17.6). However, due to the complex geometry of the RV, no single echocardiographic measurement provides reliable assessment regarding size function so that the RV should be imaged from multiple acoustic windows. Other causes of RV dilatation include chronic pulmonary hypertension, congestive heart failure, chronic tricuspid regurgitation, atrial septal defect, RV infarction and cardiomyopathy.

With an abrupt increase in RV afterload and wall stress, following acute PE, reduced myocardial contraction or hypokinesis of the RV free wall may be seen on echocardiography. This is

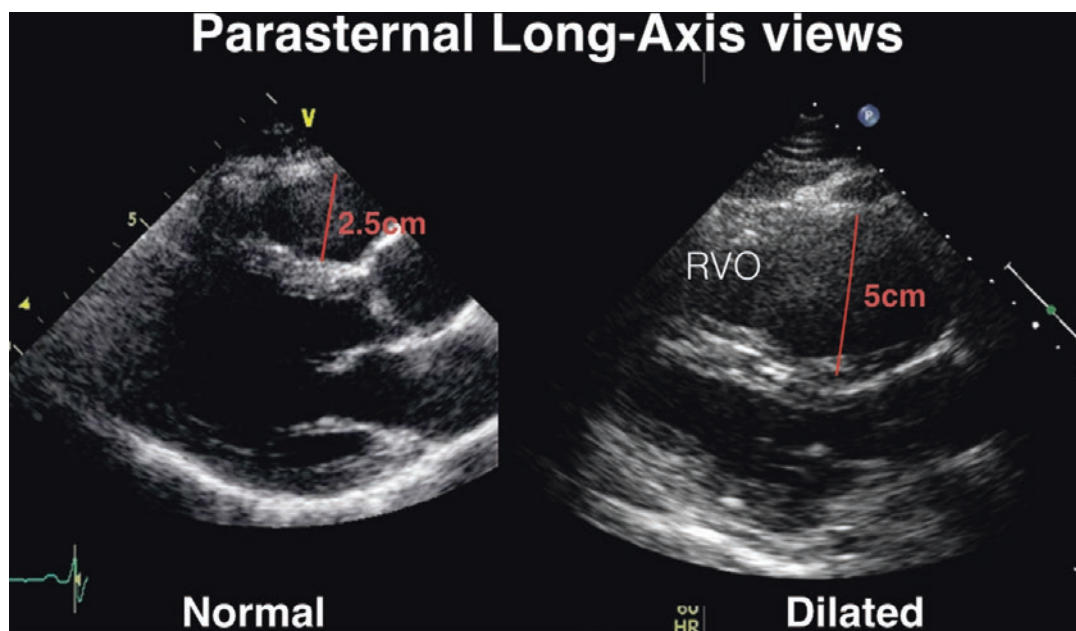


Fig. 17.6 Parasternal long-axis projection from a normal individual (left) demonstrating the normal 1/3 to 2/3 relationship between the right and left ventricles respectively. In this instance the RV outflow track measures 2.5 cm. On

the right, the RV is clearly dilated at 5 cm and obviously larger than the LV. LV Left ventricle, RV right ventricle, RVO right ventricular outflow track

clearly identified by the reduced fractional area change (FAC) evaluated from apical four-chamber projections. It has been found to be an independent predictor of heart failure, sudden death, stroke, and/or mortality in studies of patients after pulmonary embolism [21].

A distinctive pattern of mid free wall hypokinesis with a normal or hyperdynamic RV apex, the McConnell sign, has been described in patients with PE (Fig. 17.7), but this wall motion pattern is not specific and has also been seen in patients with RV infarction.

Recent studies looking at regional and global RV peak longitudinal systolic strain using 2D speckle tracking echocardiography [22, 23], in the apical four chamber view, the strain values are reduced in stable normotensive PE patients (Fig. 17.8). This pattern was noted in all segments of the RV free wall, with highly significant differences among the basal, mid, and apical segments. Speckle tracking may be useful in providing a quantitative method of detecting RV dysfunction and in differentiating stable PE patients between intermediate and low risk. Although both RVFWS and FAC were helpful for detecting the acuity of

RV pressure overload, RVFWS was more reproducible [22]. Finally, the addition of RVFWS provided incremental value to clinical and traditional echocardiographic variables. However, out-of-plane motion remains a potential limitation of two-dimensional segmental strain, which may be overcome by three-dimensional imaging [24].

Tricuspid annular plane systolic excursion (TAPSE) is also useful in differentiating normotensive PE patients between low and intermediate risk categories. With a TAPSE <16 cm patients are at intermediate risk. TAPSE is an expression of longitudinal RV systolic function and is measured from the M-mode tracing of the lateral tricuspid annulus of the RV from the apical four-chamber view (Fig. 17.9). TAPSE represents longitudinal function of the right ventricle. The greater the descent of the base of the RV free wall in systole, the better the RV systolic function.

Dilatation and loss of inspiratory collapse of the IVC may also result from RV dysfunction and the raised right heart filling pressure. Subcostal views are best utilised to image the IVC and observe its size and collapsibility (Fig. 17.10). Importantly, RA pressure is usually estimated by

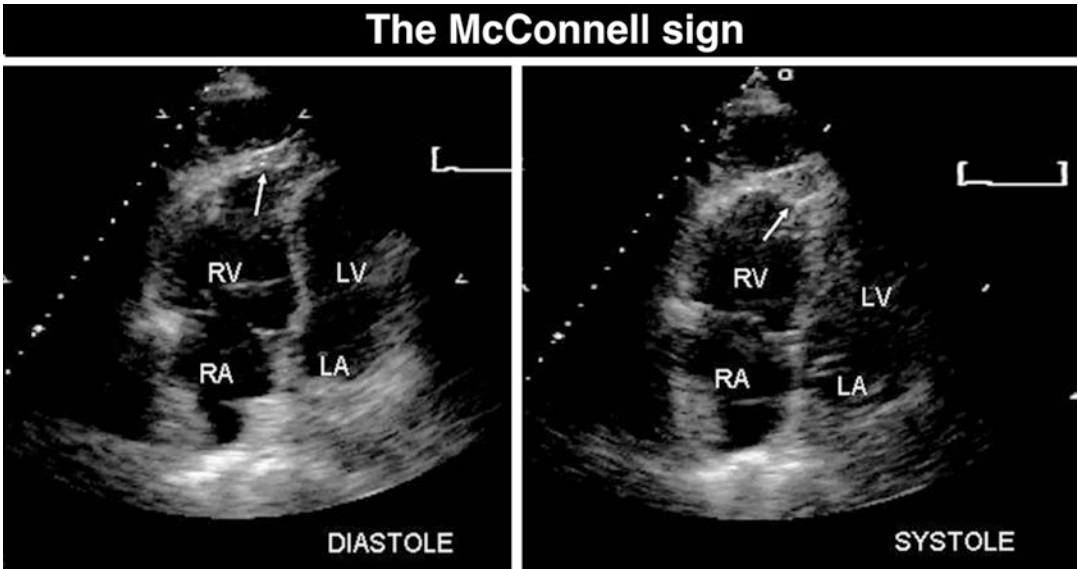


Fig. 17.7 The McConnell sign characterised by a dilated RV with free wall hypokinesia in contrast with the preserved apical contraction. On the left, diastolic frame showing the full expansion of the apex and on the right the apex is coming in the cavity

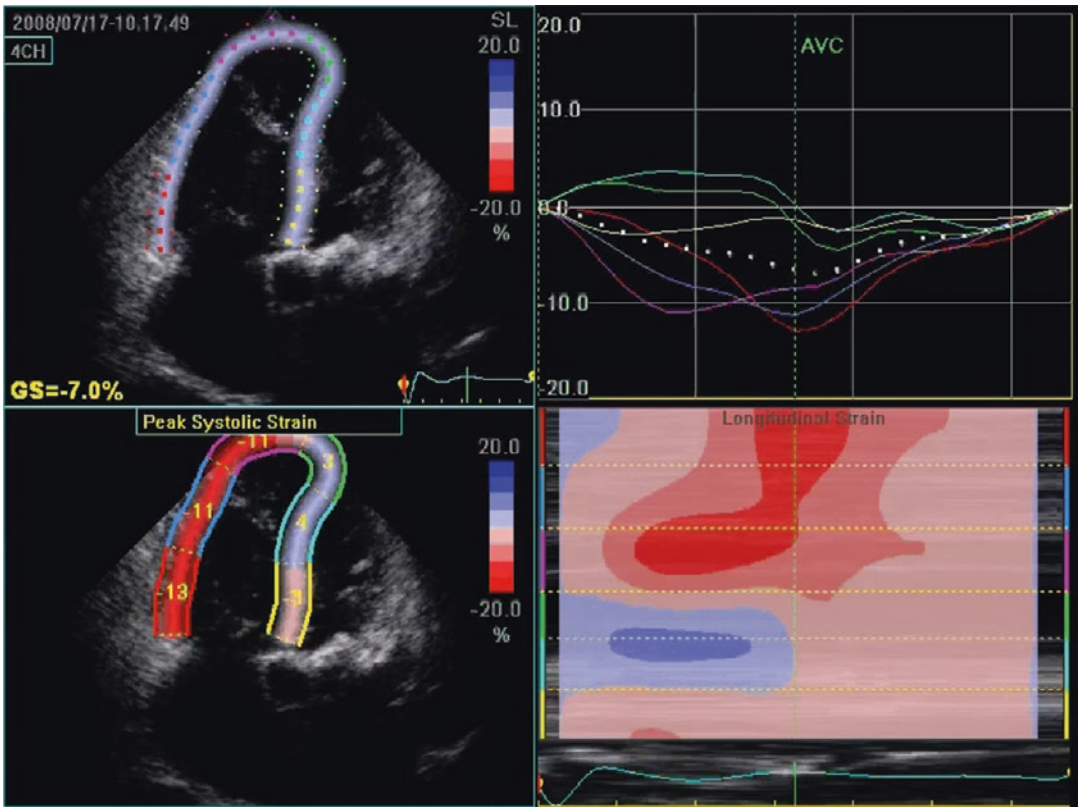


Fig. 17.8 This figure shows two dimensional speckle tracking values of the RV from a patient with recent pulmonary embolism and elevated pulmonary arterial pressures. Note that all speckle tracking values are reduced from base to apex

IVC diameter and the presence of inspiratory collapse. As RA pressure increases, this is transmitted to the IVC, resulting in reduced collapse with inspiration and IVC dilatation.

Leftward shift of the interventricular septum (IVS) may result from RV pressure overload. The parasternal short axis view, at mid-ventricular level or the apical four-chamber view, allows assessment of IVS flattening or bulging toward the LV (Fig. 17.11).

Evaluation of RV Systolic Pressures

Elevated pulmonary systolic pressure as a result of increased pulmonary vascular resis-

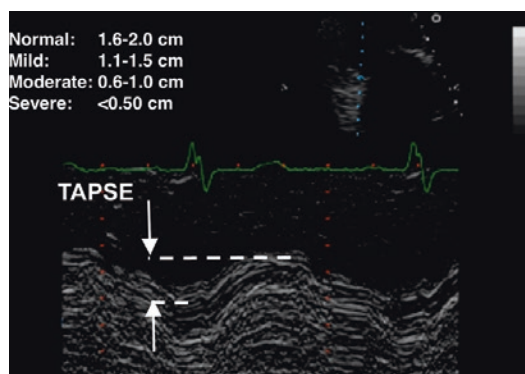


Fig. 17.9 From apical four-chamber projections, the systolic movement of the base of the RV free wall can be recorded and provides one of the most obvious movements on normal echocardiography. In case of elevated RV systolic pressures, this is progressively reduced

tance and RV afterload may be estimated by measuring the peak tricuspid regurgitant (TR) jet velocity with continuous wave Doppler and using the modified Bernoulli Equation and addition of the estimated RA pressure. A peak TR velocity greater than 2.6 m/s indicates elevated pulmonary pressure (Fig. 17.12). The inability of the normal RV to generate pressure above 60 mmHg following acute afterload increase, suggests that a peak TR velocity greater than 3.7 m/s in acute PE patients may be consistent with pre-existing cardiopulmonary disease, especially in the presence of increased RV wall thickness (>0.5 cm).

Proximal obstruction of the pulmonary arterial bed by thromboemboli and the early return of the reflected systolic pressure wave interfere with early RV ejection and result in shortened acceleration time (AT) and mid-systolic deceleration or early 'notching' in the pulsed wave (PW) Doppler tracing from the RV outflow tract (Fig. 17.13). An RV outflow tract AT less than 90 ms suggests elevated pulmonary pressure. This may be particularly useful in patients without measurable TR velocity so that an AT<90 ms may be suggestive of elevated RV systolic pressures.

The combined findings of reduced RV outflow tract AT less than 60 ms and TR pressure gradient above 30 mmHg but less than 60 mmHg, form the '60/60 sign', which has been found to have good specificity in acute PE patients (Fig. 17.14).

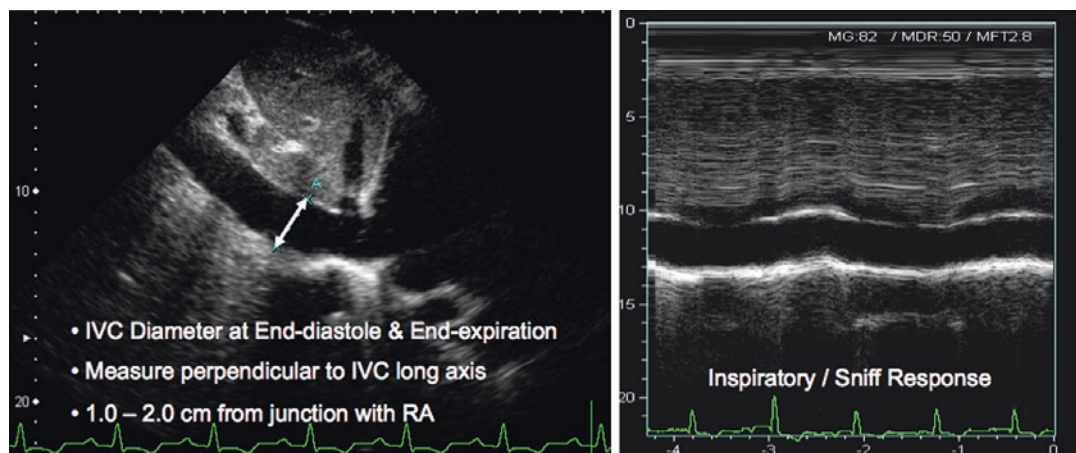


Fig. 17.10 From subcostal projections the IVC can easily be identified with estimates of RA pressures (left). The lack of collapsibility during a sniff (right) it indicated elevated RA pressures

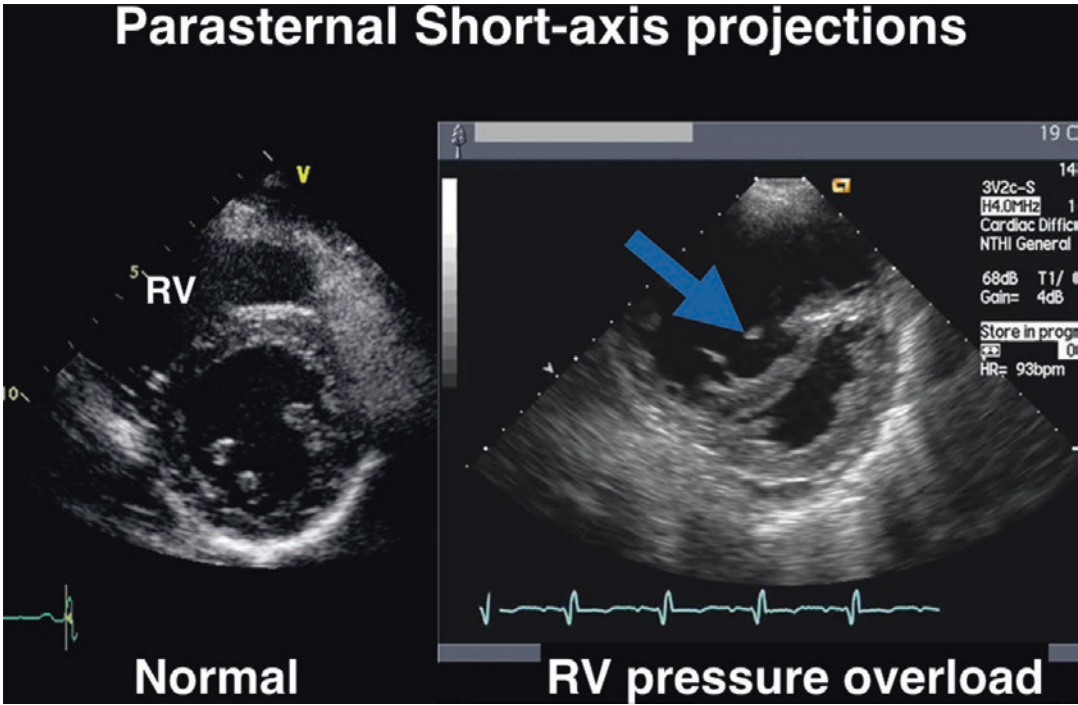


Fig. 17.11 Parasternal short-axis view demonstrating a perfect circular expansion in systole from a normal individual (left) but in a patient with markedly elevated RV

systolic pressures, there is a marked D-shape deformation of the septum suggestive of RV pressure overload

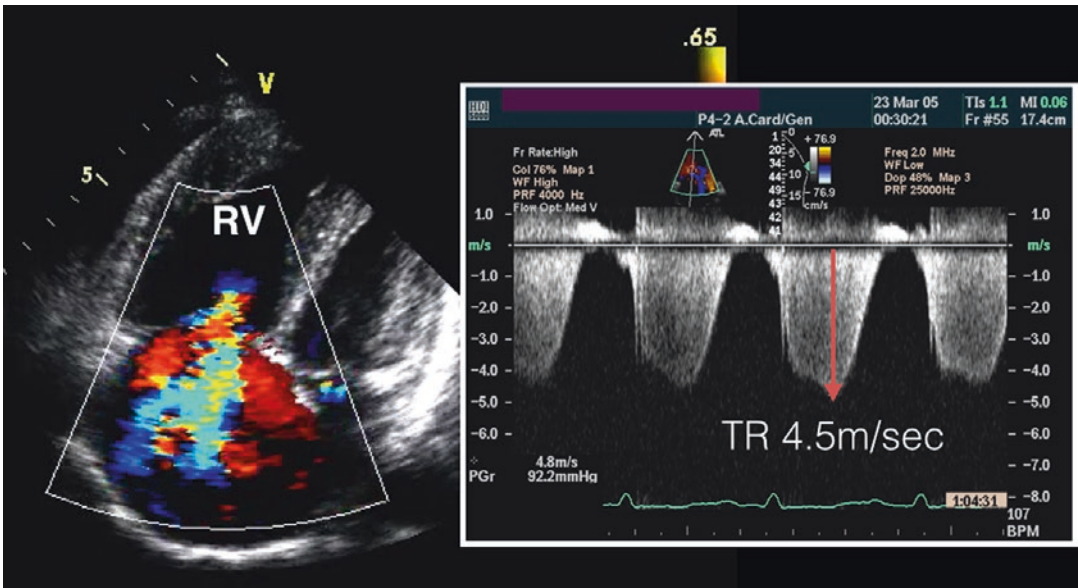


Fig. 17.12 Four-chamber view (left) with significant tricuspid regurgitation. On the right, using continuous wave Doppler the maximal TR velocity can be measured. In this

patient, the velocity is 4.5 m/s suggestive of markedly elevated RV systolic pressures. *TR* Tricuspid regurgitation, *RV* Right ventricle

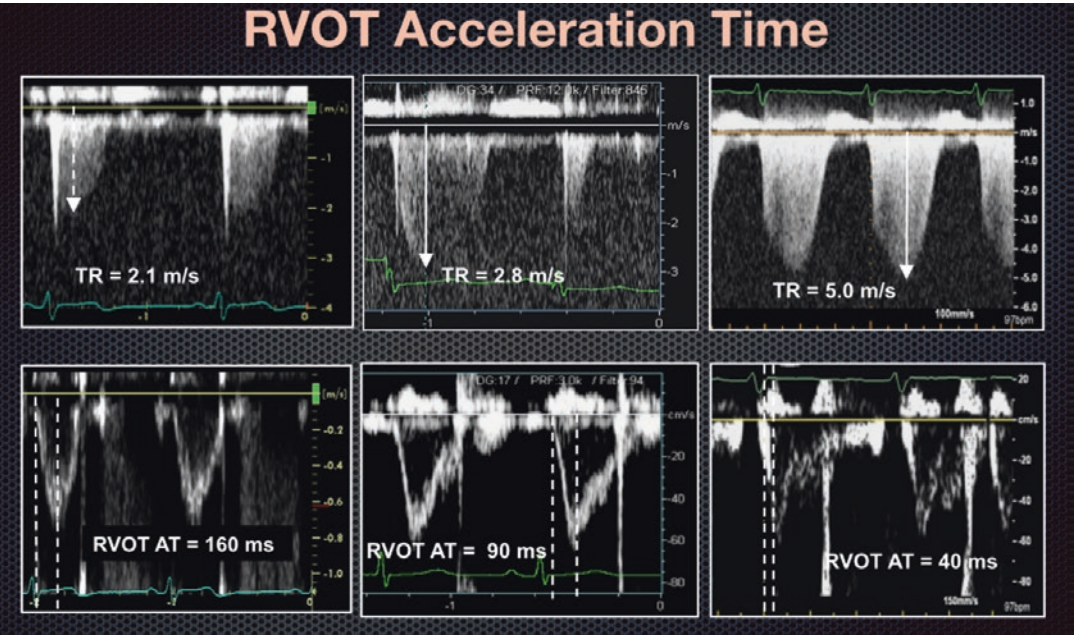


Fig. 17.13 Pulsed wave Doppler from the RV outflow track from three different patients demonstrating the acceleration time in relation to the maximal TR jet velocity. Note that as the TR velocity is higher, the AT becomes

shorter. *AT* Acceleration time (msec), *RV* Right ventricle, *RVOT* Right ventricular outflow track, *TR* Tricuspid regurgitation

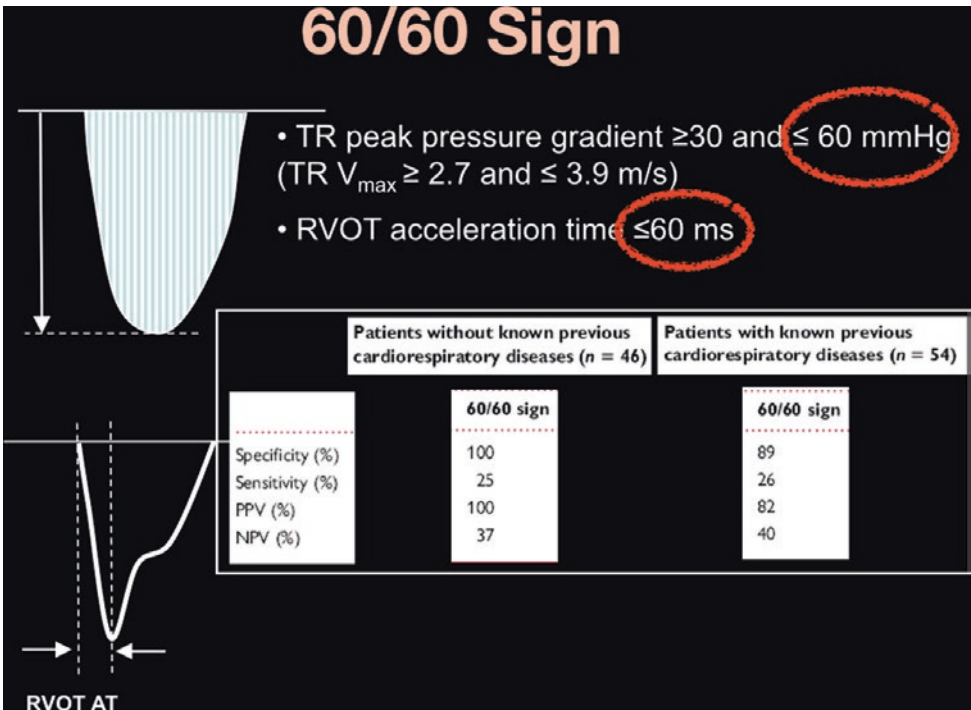


Fig. 17.14 The calculation of the 60/60 sign is the combination of an $AT < 60$ ms and a maximal RV pressure gradient between 30 and 60 mmHg. *AT* Acceleration time

(msec), *RVOT* Right ventricular outflow track, *TR* Tricuspid regurgitation

Management of Patients with Pulmonary Embolism

Echocardiography is very useful for identifying patients with pulmonary embolism who may have a poor prognosis and may facilitate a change in management by identifying those at high risk who might otherwise escape early detection. It is simple to repeat and assess RV function during treatment. It can also help assessing whether thrombus is sufficiently central to warrant potential surgical embolectomy. Meta-analyses have shown that RV dysfunction detected by echocardiography is associated with an elevated risk of short-term mortality in patients without haemodynamic instability, but its overall positive predictive value is low [25, 26]. Finally, echocardiography can be used to assess whether a selected intervention such as thrombolysis is improving right ventricular function and diminishing elevated pulmonary artery pressures.

Conclusion

PE is a common and potentially serious condition if not diagnosed and treated promptly. Due to its non-specific clinical presentation diagnosis is challenging and immediate patient management is based on early mortality risk and an important determinate is the presence of RV dysfunction. Although Echocardiography has limited value as a diagnostic test in PE patients based on directly imaging thromboemboli in the right heart and pulmonary arteries, it is useful in differential diagnosis and in the immediate detection of RV dysfunction in shocked or hypotensive high risk patients and in the differentiation of stable patients with confirmed PE in to intermediate and low risk categories.

Individual signs of RV dysfunction on echocardiograph: RV dilatation, free wall hypokinesia, paradoxical interventricular septal motion, raised pulmonary pressure or disturbed RV ejection pattern, are either non-specific or have limited sensitivity, especially in patients with

concomitant cardiac or respiratory disease. However accumulative echocardiography signs reduce the risk of false diagnosis.

References

1. Goldhaber SZ, Visani L, De Rosa M. Acute pulmonary embolism: clinical outcomes in the international cooperative pulmonary embolism registry (ICOPER). *Lancet*. 1999;353:1386–9.
2. Pollack CV, Schreiber D, Goldhaber SZ, Slattery D, Fanikos J, O'Neil BJ, Thompson JR, Hiestand B, Briesse BA, Pendleton RC, Miller CD, Kline JA. Clinical characteristics, management, and outcomes of patients diagnosed with acute pulmonary embolism in the emergency department: initial report of EMPEROR (Multicenter emergency medicine pulmonary embolism in the real world registry). *J Am Coll Cardiol*. 2011;57(6):700–6.
3. Stein PD, Goldhaber SZ, Henry JW. Alveolar-arterial oxygen gradient in the assessment of acute pulmonary embolism. *Chest*. 1995;107:139–43.
4. Stein PD, Goldhaber SZ, Henry JW, et al. Arterial blood gas analysis in the assessment of suspected acute pulmonary embolism. *Chest*. 1996;109:78–81.
5. British Thoracic Society Standards of Care Committee Pulmonary Embolism Guideline Development Group. British Thoracic Society guidelines for the management of suspected acute pulmonary embolism. *Thorax*. 2003;58:470–83.
6. Panoulas VF, Daigeler A-L, Malaweera ASN, Lota AS, Baskaran D, Rahman S, Nihoyannopoulos P. Pocket-size hand-held cardiac ultrasound as an adjunct to clinical examination in the hands of medical students and junior doctors. *Eur Heart J Cardiovasc Imaging*. 2013;14:323–30.
7. Lapostolle F, Surget V, Borron SW, et al. Severe pulmonary embolism associated with air travel. *N Engl J Med*. 2001;345:779–83.
8. Schulman S, Lindmarker P. Incidence of cancer after prophylaxis with warfarin against recurrent venous thromboembolism: duration of anticoagulation trial. *N Engl J Med*. 2000;342:1953–8.
9. Vandenbroucke JP, Rosing J, Bloemenkamp KW, et al. Oral contraceptives and the risk of venous thrombosis. *N Engl J Med*. 2001;344:1527–35.
10. Rossouw JE, Anderson GL, Prentice RL, et al. Risks and benefits of estrogen plus progestin in healthy postmenopausal women: principal results from the Women's health initiative randomized controlled trial. *JAMA*. 2002;288:321–33.
11. Wood KE. Major pulmonary embolism: review of a pathophysiologic approach to the golden hour of hemodynamically significant pulmonary embolism. *Chest*. 2002;121:877–905.

12. Molloy WD, Lee KY, Girling L, Schick U, Prewitt RM. Treatment of shock in a canine model of pulmonary embolism. *Am Rev Respir Dis*. 1984;130(5):870–4.
13. Goldhaber SZ, Elliott DG. Acute pulmonary embolism: part I: epidemiology, pathophysiology, and diagnosis. *Circulation*. 2003;108:2728–9.
14. Konstantinides SV, Torbicki A, Agnelli G, Danchin N, Fitzmaurice D, Galié N, et al. ESC guidelines on the diagnosis and management of acute pulmonary embolism. *Eur Heart J*. 2014;35:3033–80.
15. Elliott CG, Goldhaber SZ, Visani L, DeRosa M. Chest radiographs in acute pulmonary 2165 embolism. Results from the international cooperative pulmonary embolism registry. *Chest* 2166. 2000;118(1):33–8.
16. Geibel A, Zehender M, Kasper W, Olschewski M, Klima C, Konstantinides SV. Prognostic value of the ECG on admission in patients with acute major pulmonary embolism. *Eur Respir J*. 2005;25(5):843–8.
17. Ghaye B, Szapiro D, Mastora I, Delannoy V, Duhamel A, Remy J, Remy-Jardin M. 2300 Peripheral pulmonary arteries: how far in the lung does multi-detector row spiral CT allow 2301 analysis? *Radiology*. 2001;219(3):629–36.
18. Alderson PO. Scintigraphic evaluation of pulmonary embolism. *Eur J Nucl Med*. 1987;13(2346 Suppl):S6–10.
19. van Beek EJ, Reekers JA, Batchelor DA, Brandjes DP, Buller HR. Feasibility, safety and 2395 clinical utility of angiography in patients with suspected pulmonary embolism. *Eur Radiol* 2396. 1996;6(4):415–9.
20. Kucher N, Luder CM, Dornhofer T, Windecker S, Meier B, Hess OM. Novel management 2455 strategy for patients with suspected pulmonary embolism. *Eur Heart J*. 2003;24(4):366–76.
21. Nass N, McConnell MV, Goldhaber SZ, Chyu S, Solomon SD. Recovery of regional right ventricular function after thrombolysis for pulmonary embolism. *Am J Cardiol*. 1999;83:804–6.
22. Vitarelli A, Barillà F, Capotosto L, D'Angeli I, Truscelli G, De Maio M, Ashurov R. Right ventricular function in acute pulmonary embolism: a combined assessment by three-dimensional and speckle-tracking echocardiography. *J Am Soc Echocardiogr*. 2014;27(3):329–38. <https://doi.org/10.1016/j.echo.2013.11.013>.
23. Wright L, Dwyer N, Power J, Kritharides L, Celermajer D, Marwick TH. Right ventricular systolic function responses to acute and chronic pulmonary hypertension: assessment with myocardial deformation. *J Am Soc Echocardiogr*. 2016;29(3):259–66. <https://doi.org/10.1016/j.echo.2015.11.010>.
24. Smith BC, Dobson G, Dawson D, Charalampopoulos A, Grapsa J, Nihoyannopoulos P. Three-dimensional speckle tracking of the right ventricle: toward optimal quantification of right ventricular dysfunction in pulmonary hypertension. *J Am Coll Cardiol*. 2014;64:41–51.
25. Coutance G, Cauderlier E, Ehtisham J, Hamon M, Hamon M. The prognostic value of markers of right ventricular dysfunction in pulmonary embolism: a meta-analysis. *Crit Care*. 2011;15(2):R103.
26. Sanchez O, Trinquart L, Colombet I, Durieux P, Huisman MV, Chatellier G, Meyer G. Prognostic value of right ventricular dysfunction in patients with haemodynamically stable pulmonary embolism: a systematic review. *Eur Heart J*. 2008;29(12):1569–77.

Part IV

Pericardial Disease

Pericardial Effusion, Tamponade, and Constrictive Pericarditis

18

Terrence D. Welch and Jae K. Oh

Introduction

Clinical syndromes involving the pericardium are relatively few in number but have many causes and a wide range of clinical manifestations. Diagnosis may be challenging and should include a careful history and physical examination, electrocardiogram, chest radiograph, appropriate laboratory assessment, and cardiac imaging. Echocardiographic evaluation is recommended as the first-line imaging test for all patients with suspected pericardial disease, and is often supplemented by cross-sectional imaging with computed tomography and magnetic resonance [1–3]. Pericardial effusion and tamponade, constrictive pericarditis, and acute pericarditis are the most frequently encountered and clinically important entities. Less common pericardial abnormalities include congenital absence of the pericardium, pericardial cysts, and pericardial tumors.

T. D. Welch

Section of Cardiology, Dartmouth-Hitchcock Medical Center, Geisel School of Medicine at Dartmouth, Hanover, NH, USA

J. K. Oh (✉)

Division of Cardiovascular Diseases, Mayo Clinic, Rochester, MN, USA
e-mail: oh.jae@mayo.edu

Pericardial Anatomy and Function

The pericardium consists of a serous membrane and a fibrous sac (Fig. 18.1). The serous membrane covers the surface of the heart and proximal great vessels, where it is called the visceral pericardium. The serous membrane then folds back to line the inside of the fibrous sac, and together these two layers are called the parietal pericardium. The space between the two layers normally contains 25–50 mL of fluid, which is secreted by the visceral pericardium, and has a pressure equal to intrapleural pressure. The pericardium may serve as a barrier against infection, provide lubrication to reduce friction between the heart and contiguous structures, and ensure a relatively stable position of the heart in the thorax [4]. Because it is relatively inelastic, the pericardium does have the potential to influence cardiac hemodynamics and function. It limits acute distention of the heart and contributes to diastolic interaction between the two ventricles, such that the filling of one ventricle affects the filling dynamics of the other. This ventricular interdependence becomes exaggerated in the setting of compressive pericardial disease (tamponade or constriction).

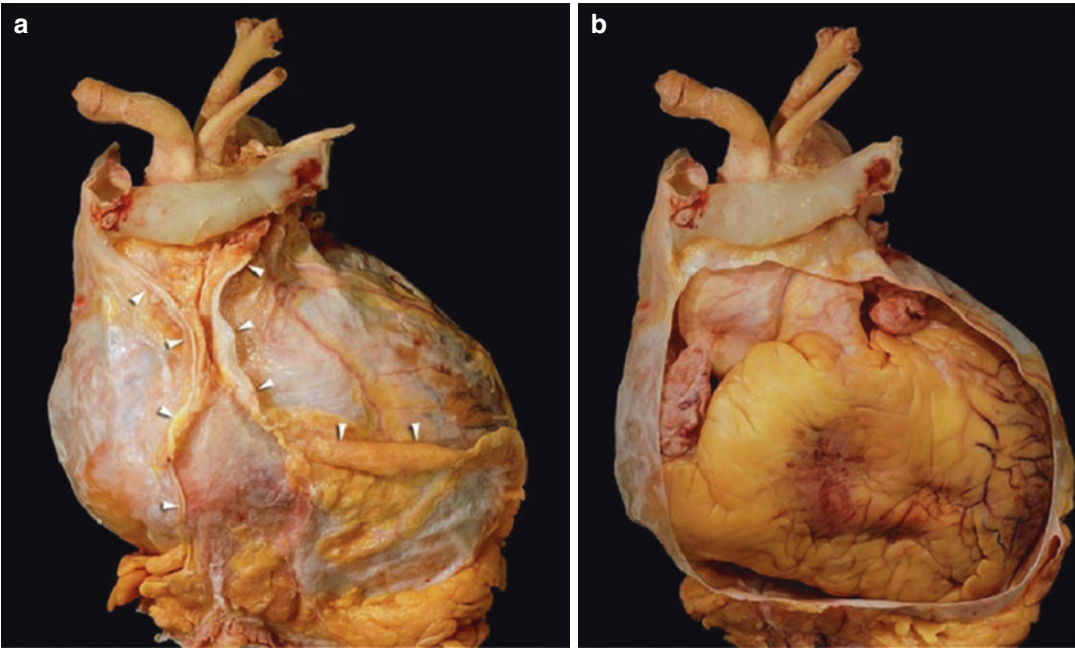


Fig. 18.1 (a) Anterior view of the intact pericardial sac. The attachment of the fibrous pericardium to the diaphragm is seen at the bottom, with abundant epi-pericardial fat. The mediastinal pleura invests the lateral portions of the fibrous pericardium, with anterior reflections indicated by the white arrowheads. (b) The pericar-

dial sac has been opened anteriorly to show the heart and great vessels in anatomic position. The proximal portions of the great vessels are intrapericardial, with fusion of the adventitia of the great vessels with the fibrous pericardium. (From Klein et al. [3]; with permission)

Pericardial Effusion

When the amount of fluid or blood in the pericardial space exceeds approximately 50 mL, an effusion becomes evident on the echocardiogram as an echolucent space that persists throughout the cardiac cycle [3]. The fluid may be circumferential or loculated, with characteristics ranging from transudative to exudative, serosanguinous, or even frankly bloody, depending on the etiology.

Etiology

Excess pericardial fluid may accumulate due to any disease that affects the pericardium. Common causes include malignancy, postpericardiotomy syndrome after cardiothoracic surgery, and perforation of the heart from invasive procedures. These and other causes of pericardial effusions are listed in Table 18.1. Many effusions remain “idiopathic” despite thorough investigations.

Table 18.1 Etiologies of pericardial effusion

Malignancy
Postoperative (postpericardiotomy)
Cardiac puncture from invasive procedures (electrophysiology studies, cardiac catheterization, pacemaker/ICD implantation)
Ischemic heart disease related (postinfarct as in Dressler’s syndrome; myocardial rupture)
Infectious
Immune/connective tissue diseases (lupus; rheumatoid arthritis; vasculitides)
Idiopathic
Renal failure
Drug-related and anticoagulants
Postradiation
Chest trauma
Hypothyroidism
Amyloidosis

Clinical Features

A pericardial effusion may be asymptomatic and incidentally discovered with echocardiography or a cross-sectional imaging study, such

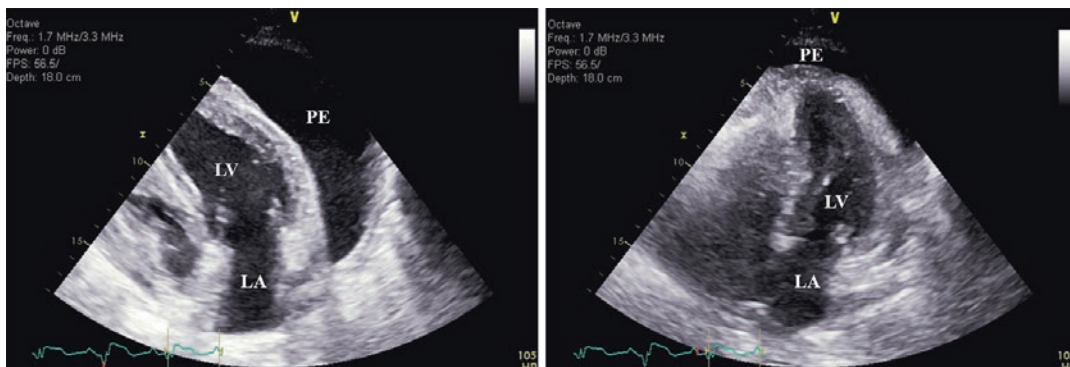


Fig. 18.2 Apical 4-chamber view demonstrating a large circumferential pericardial effusion. There is a characteristic “swinging” motion of the heart in the pericardial

space. Both images are captured at end-diastole. *LV* left ventricle, *LA* left atrium, *PE* pericardial effusion

as a computed tomography scan. In other cases, patients may present with symptoms related to the underlying cause. For example, acute pericarditis causes chest pain and is sometimes accompanied by a pericardial effusion. In other cases, patients may present with symptoms related to hemodynamic compromise caused by the effusion.

Echocardiographic Features

Echocardiography allows qualitative assessment of the amount and location of pericardial fluid, as well as hemodynamic assessment. By convention, pericardial effusions are described as small (<1 cm rim of fluid at end-diastole), moderate (1–2 cm rim of fluid at end-diastole), or large (>2 cm rim of fluid at end-diastole) [3]. Additional categories of trivial (<0.5 cm rim of fluid at end-diastole) and very large (>2.5 cm rim of fluid at end-diastole) may be used. The fluid may be visible in a circumferential space around the heart or, less commonly, may be loculated and visible only in some echocardiographic views. When the pericardial effusion is massive, the heart may have a characteristic “swinging” motion in the pericardial cavity, which is responsible for the electrocardiographic finding of “electrical alternans” (Fig. 18.2).

Blood clots typically appear as echo-bright coagulum in the pericardial space (Fig. 18.3) and are generally found after cardiac surgery or as a complication of an invasive cardiac procedure,

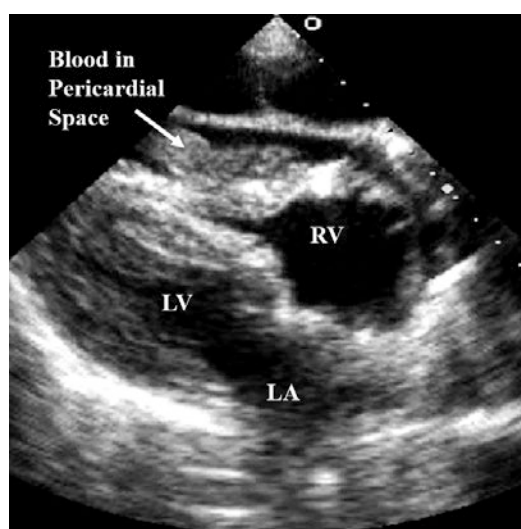


Fig. 18.3 Echo-bright coagulum is seen in the pericardial space adjacent to the right ventricle. *LV* left ventricle, *LA* left atrium, *RV* right ventricle

myocardial infarction, or aortic dissection. Local or widespread compression of the cardiac chambers may ensue, leading to life-threatening tamponade. A focal hematoma or loculated effusion may be difficult to detect by standard transthoracic imaging and may require trans-esophageal echocardiography or cross-sectional imaging for diagnosis [3, 5–7].

A pericardial effusion must be distinguished from an epicardial fat pad or pleural effusion, both of which may occasionally mimic a pericardial effusion. An epicardial fat pad is likely to be most prominent anteriorly, and will have an

echo-bright appearance consistent with tissue instead of the echo-free appearance consistent with a transudative effusion. In contrast to a pleural effusion, a pericardial effusion is most often circumferential and is located anterior to the descending thoracic aorta. A pleural effusion is located posterior to the descending thoracic aorta.

Cardiac Tamponade

Cardiac tamponade is a potentially life-threatening form of heart failure that occurs when cardiac filling is impaired due to excess pericardial fluid under pressure. Tamponade is best viewed as a spectrum of hemodynamic abnormalities rather than as a diagnosis that is either present or not present. The echocardiogram helps define a patient's position on that spectrum.

The rapidity with which the effusion accumulates determines how much fluid is necessary to cause tamponade. Modest effusions that have accumulated acutely may cause tamponade, as in the case of hemorrhagic effusions caused by cardiac perforation. In these situations, the rapid accumulation of a small amount of excess fluid inside a relatively inelastic pericardium leads to increased pericardial pressure and hemodynamic collapse that may be life-threatening if not promptly treated. In more chronic disease states, large pericardial effusions (up to 2 L) may develop without significant hemodynamic compromise because the pericardium is allowed to "stretch" [8].

The following echocardiographic findings help determine the extent of hemodynamic derangement related to a pericardial effusion and should be considered in the context of bedside clinical assessment.

Cardiac Chamber Collapse

Cardiac chamber collapse occurs when pericardial pressure exceeds the pressure within the chamber. This is typically a phasic phenomenon, reflecting the dynamic changes in transmural pressure (intracardiac pressure minus pericardial pressure) throughout the cardiac cycle. The right heart chambers are most commonly affected. Because pressure within the right atrium is lowest throughout the cardiac cycle, this chamber tends to be affected first and is therefore considered a highly sensitive finding for tamponade

[9–11]. Right atrial collapse occurs at the end of ventricular diastole (Fig. 18.4) and may persist into ventricular systole. Brief collapse may occur in the absence of clinical tamponade, but collapse that persists for at least one-third of the cardiac cycle has been shown to be a highly sensitive (94%) and specific (100%) finding for tamponade [11]. This finding may be absent when right atrial hypertension coexists with tamponade.

Right ventricular collapse requires higher pericardial pressure than right atrial collapse, and therefore right ventricular collapse is considered a less sensitive but more specific sign of tamponade [9, 12–14]. Right ventricular collapse occurs in early diastole (Figs. 18.5 and 18.6). As with right atrial collapse, this finding may be absent despite the presence of tamponade if right heart

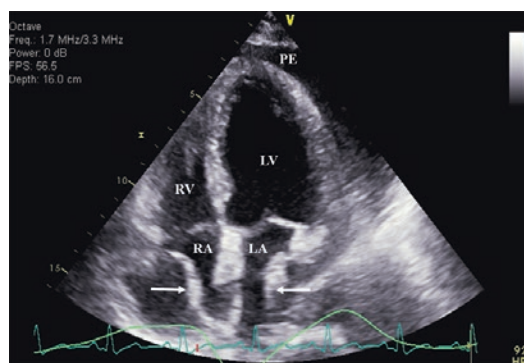


Fig. 18.4 Tamponade with right atrial and left atrial compression (arrows) extending into ventricular systole. LV left ventricle, RV right ventricle, LA left atrium, RA right atrium, PE pericardial effusion

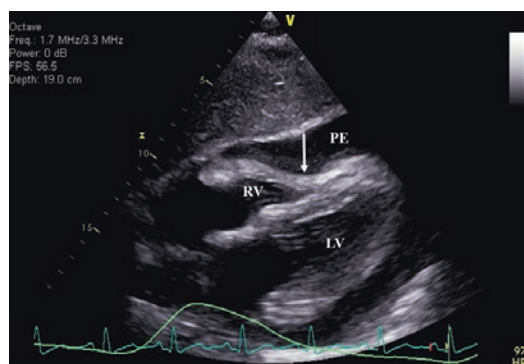


Fig. 18.5 Tamponade with right ventricular compression (arrow) in ventricular diastole. LV left ventricle, RV right ventricle, PE pericardial effusion

Fig. 18.7 Tamponade with ventricular septal shift toward the LV during inspiration (annotated arrow) by M-mode assessment (parasternal short-axis imaging). This finding indicates enhanced ventricular interaction. *LV* left ventricle, *RV* right ventricle, *PE* pericardial effusion

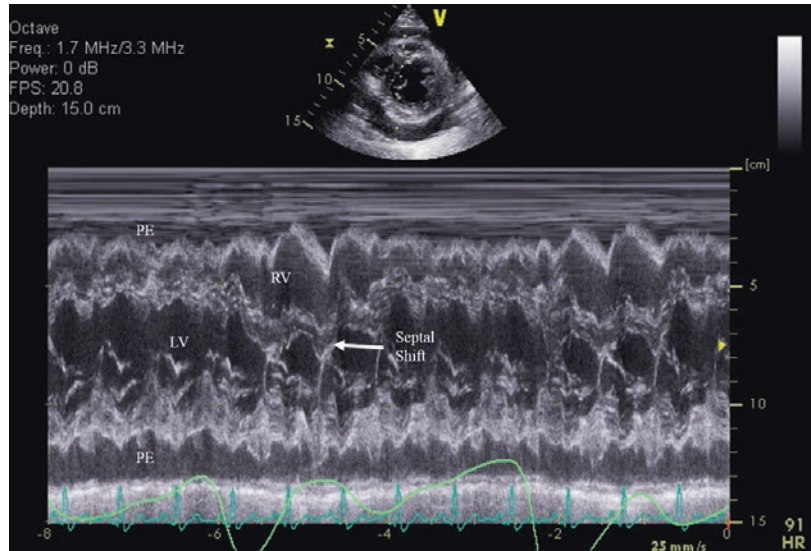
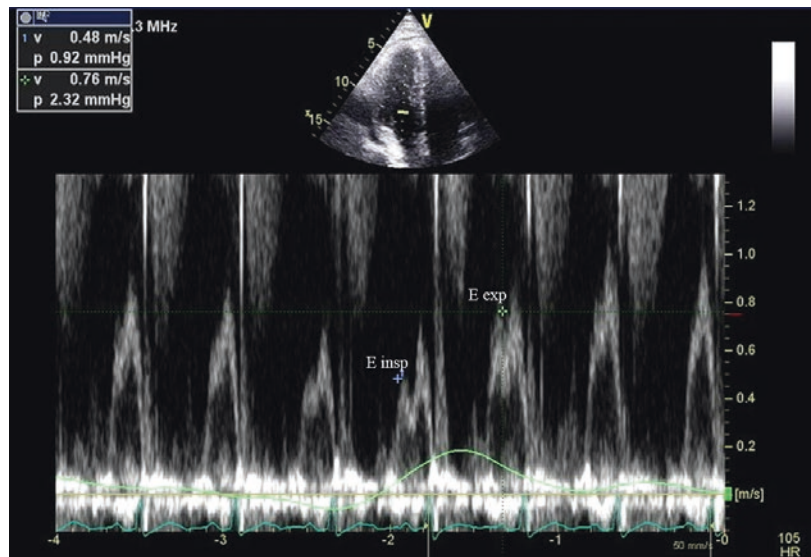


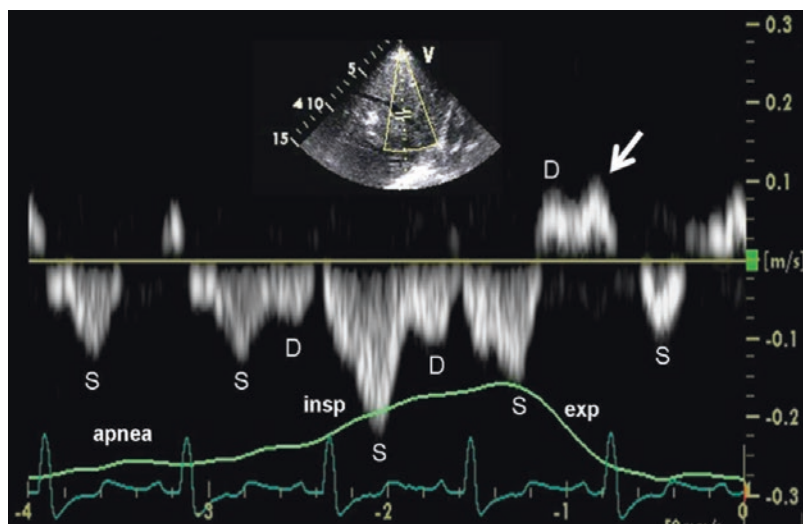
Fig. 18.8 Tamponade with >30% change in mitral E velocity during the respiratory cycle (apical 4-chamber view in Mayo Clinic format). *E insp* E velocity during inspiration, *E exp* E velocity during expiration



Doppler findings are probably most sensitive for detection of hemodynamic effect from a pericardial effusion, being present in many cases before a clinical diagnosis of tamponade is present [21–23]. Reduced left-heart filling during inspiration leads to a decrease in the early diastolic (E) velocity across the mitral valve (Fig. 18.8); the velocity then increases again during expiration. There is typically a greater than 30% change in mitral E velocity during the respiratory cycle, calculated as follows: [(expiratory

velocity—inspiratory velocity)/expiratory velocity $\times 100$] [3, 21, 22]. Mitral E velocity variation should be present even when diastolic filling predominantly occurs with atrial contraction (with A wave velocity greater than E wave velocity), as is sometimes the case in tamponade. The pulmonary vein Doppler profile will also demonstrate an inspiratory decrease in left-heart filling. Reciprocal changes occur at the tricuspid valve, with typically a >60% change in tricuspid E velocity (inspiration greater than expiration)

Fig. 18.9 Hepatic venous Doppler profile in tamponade. During apnea, forward flow (below the baseline) occurs only in systole (S). With inspiration (insp), systolic forward flow increases and diastolic (D) forward flow appears. With the first beat of expiration (exp), diastolic flow reversal occurs (arrow). From Klein et al. [3]; with permission



during the respiratory cycle [3, 21]. The hepatic veins typically show predominantly systolic forward flow that increases with inspiration and decreases with expiration, with marked reduction and often reversal of diastolic flow during expiration (Fig. 18.9) [21, 22]. Similar findings occur in the superior vena cava Doppler profile. Characteristic venous Doppler has been shown to have high positive and negative predictive value for a diagnosis of tamponade, but may not be obtainable in up to one-third of patients [12].

The diagnostic test performance characteristics of 2-D and Doppler findings were evaluated in a prospective study of 110 patients with moderate-to-large effusions, 38 of whom had a clinical diagnosis of cardiac tamponade. The presence of any chamber collapse had the highest sensitivity (90%), while the combination of right atrial and ventricular collapse plus abnormal hepatic venous flow had the highest specificity (98%) [12].

Echocardiographically Guided Pericardiocentesis

The most effective, and potentially life-saving, treatment for cardiac tamponade is expeditious removal of the pericardial fluid. When performed “blindly,” percutaneous pericardiocentesis has been reported to be unsuccessful in up to 14% of cases, with a 4% rate of death and 11% rate of

hemopericardium [24]. Two-dimensional echocardiography can guide pericardiocentesis by locating the optimal site for needle entry and has accordingly made the procedure more effective and dramatically safer. In the largest published series from the Mayo Clinic, 1127 pericardiocenteses were performed over 21 years with a procedural success rate of 97% and a major complication rate of 1.2% [25]. The reported major complications in this series were: death (1 patient), cardiac laceration (5), vessel laceration (1), pneumothorax (5), infection (1) and sustained ventricular tachycardia (1). Echocardiographic guidance for percutaneous pericardiocentesis is therefore recommended whenever possible [26].

Relative contraindications to percutaneous pericardiocentesis include aortic dissection, penetrating thoracic trauma, or myocardial rupture, as these cases should be managed with emergent surgery [1, 26, 27]. The procedure is also relatively contraindicated in the setting of a severe coagulopathy. Surgical intervention is not always required for tamponade caused by cardiac perforation during a diagnostic or therapeutic cardiac procedure. In another large series from the Mayo Clinic, 82% of these cases were handled definitively with percutaneous pericardiocentesis alone [28].

The procedural steps for performing percutaneous pericardiocentesis have been well-described [29, 30] and demonstrated on an online

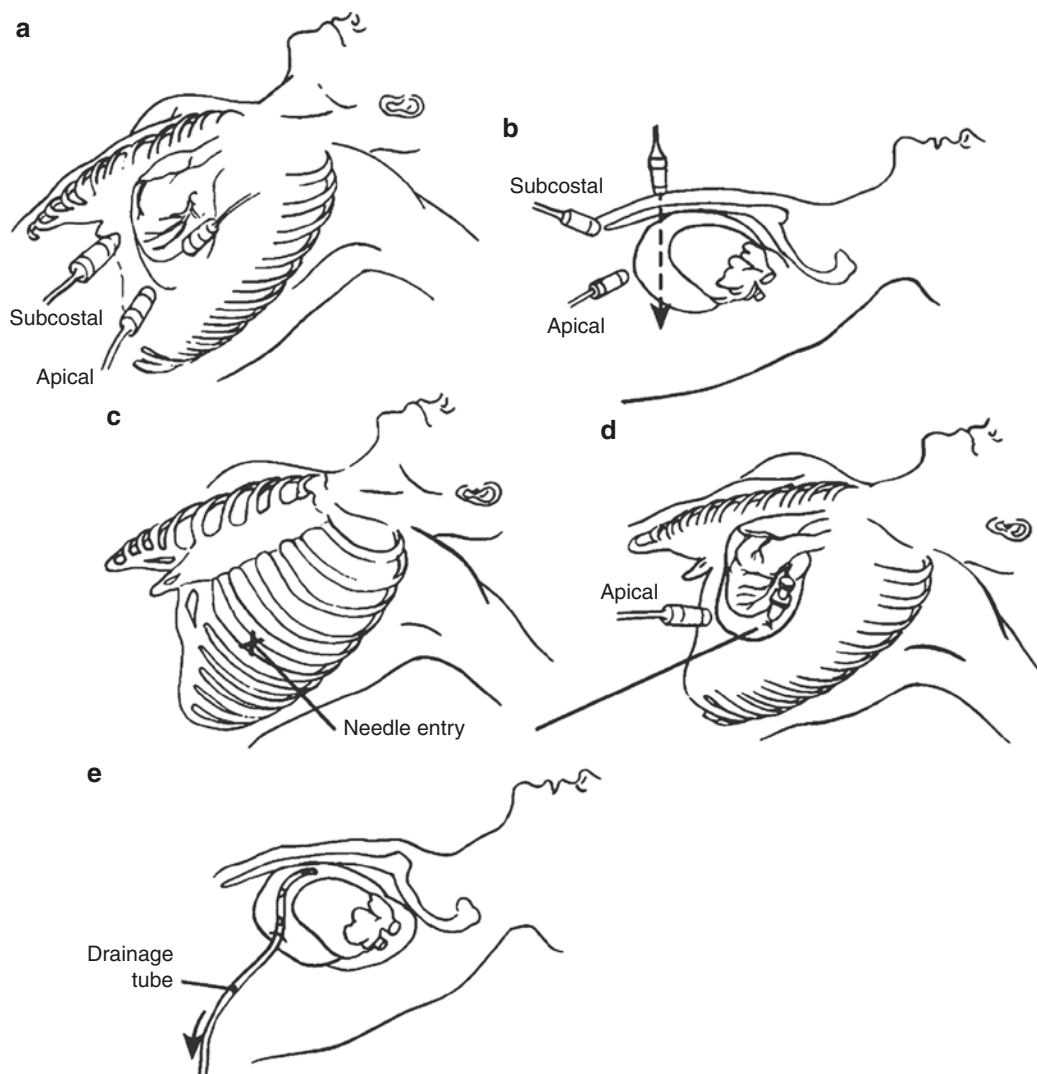


Fig. 18.10 Echocardiographically guided pericardiocentesis: ideal site for needle entry by echocardiographic guidance. Procedural steps are listed below. Step 1. Locate an area on the chest or subcostal region from which the largest amount of pericardial effusion can be visualized, and mark it (**a–c**). Step 2. Determine the depth of effusion from the marked position and the optimal angulation. Step 3. After sterile preparation and local anesthesia, perform pericardiocentesis (**d**). Step 4. When in doubt about the location of the needle, inject agitated saline through the needle and image it from a remote site to locate the bub-

bles. Step 5. Monitor the completeness of the pericardiocentesis with repeat echocardiography. Step 6. Place a 6F or 7F pigtail catheter in the pericardial space to minimize reaccumulation of fluid (**e**). Step 7. Drain any residual fluid or fluid that has reaccumulated via the pigtail catheter every 4–6 h. If after 2–3 days pericardial fluid has not reaccumulated, as seen echocardiographically, the pigtail catheter may be removed. From Oh JK, Seward JB, Tajik AJ. *The Echo Manual*. 3rd ed. PA: Lippincott William & Wilkins, 2007, p 296. With permission of Mayo Foundation

video [26]. Figure 18.10 details the approach used at the Mayo Clinic. The most commonly selected location for needle entry is the parasternal area [25]. If this location is used, care must be taken to ensure that the puncture site avoids the

course of the internal mammary artery (3–5 cm from the parasternal border) [3]. The position of the needle can be evaluated by administration of agitated saline contrast while imaging. Under most circumstances, a pig-tail (6 or 7 French)

catheter is introduced and left in the pericardial sac for several days with intermittent drainage (every 4–6 h). This practice has reduced the rate of recurrent effusion, such that sclerosing agents and surgical management are now uncommonly required.

Constrictive Pericarditis

Constrictive pericarditis is characterized by restricted ventricular filling due to an inelastic pericardium. This treatable cause of heart failure may be difficult to distinguish from other disorders such as restrictive cardiomyopathy. Diagnosis requires understanding of its unique pathophysiology and meticulous diagnostic testing, including echocardiography and sometimes hemodynamic catheterization, computed tomography (CT), or cardiac magnetic resonance imaging (cMRI).

Etiologies

Although tuberculosis remains the dominant cause of constrictive pericarditis in parts of the world with high prevalence of human immunodeficiency virus [31], it is now rare elsewhere. Most cases of constrictive pericarditis encountered in North American and European practice are now thought to be idiopathic or due to prior cardiac surgery, prior acute pericarditis, or prior radiation therapy [32–35]. Less common causes include rheumatologic disease, infection, trauma, and malignancy (Table 18.2).

Pathology and Pathophysiology

The pericardium is typically thickened and calcified, although has been reported to be normal in thickness in up to 18% of cases [36]. Inflammation may be present, particularly in subacute cases. In chronic constriction, the pericardium is usually calcified and fibrotic, with scarring that may involve the epicardium.

The constrictive pericardium limits cardiac volume and restricts filling, leading to elevation and equalization of pressures in all cardiac chambers. High atrial driving pressures cause rapid early diastolic filling of the ventricles, which

Table 18.2 Causes of constrictive pericarditis

Postoperative
Idiopathic
Postacute pericarditis of any cause
Radiation induced
Uremia
Connective tissue disease (systemic lupus erythematosus, scleroderma, rheumatoid arthritis)
Post-trauma
Drugs (cainamide, hydralazine, methysergide)
Neoplastic pericardial disease (melanoma, mesothelioma)
Tuberculosis, fungal infections (histoplasmosis, coccidiomycosis), parasitic infections
Postmyocardial infarct
Post-Dressler syndrome
Postpurulent pericarditis
Pulmonary asbestosis

stops abruptly once ventricular volume reaches the limit imposed by the constrictive pericardium. Cardiac output decreases and venous pressure increases.

Because ventricular expansion is limited by the pericardium, the right and left sides of the heart compete with each other for space. This “enhanced ventricular interaction,” or filling of one side at the expense of the other, becomes especially evident during the respiratory cycle because the constrictive pericardium “insulates” the cardiac chambers from the normal changes in intrathoracic pressure. In other words, intracardiac and intrathoracic pressures become relatively “dissociated.” During inspiration, intrathoracic and pulmonary venous pressures decrease, while the pressures in the left heart chambers decrease to a lesser extent, if at all. The gradient for left-heart filling is therefore reduced, which causes preload and subsequent stroke volume to decrease. Reduced left ventricular diastolic volume causes a shift in the position of the interventricular septum to the left and allows for augmented right ventricular filling. These changes reverse during expiration. Recognition of this unique pathophysiology, as originally described by Hatle et al. [37], is the basis for the modern approach to the echocardiographic diagnosis of constrictive pericarditis.

Clinical Features

The majority of patients present in heart failure, with dyspnea on exertion and edema being the most commonly reported symptoms [32]. The physical examination typically reveals signs of elevated venous pressure. Nearly all patients will have elevated jugular venous pressure, with a steep, deep y descent that reflects the early rapid filling of the right ventricle. There may be an inspiratory rise in the jugular venous pressure (Kussmaul's sign). An early diastolic sound, termed a pericardial knock, may be heard, signifying the abrupt cessation of filling as ventricular expansion reaches the limit imposed by the constrictive pericardium. Hepatomegaly and ascites may be detected. Respiratory variation in systolic blood pressure (pulsus paradoxus) may occur because of the previously described dissociation of intrathoracic and intracardiac pressures and enhanced ventricular interaction.

The symptoms of constriction may significantly improve or even resolve with pericardiectomy. In contrast, there is no long-term effective treatment for restrictive cardiomyopathy, which causes a very similar clinical presentation.

Echocardiographic Findings

Echocardiography is indicated for all patients suspected of having heart failure or pericardial disease [2, 38], and is therefore typically the initial diagnostic test performed. A standard echocardiogram will allow exclusion of other causes of heart failure and may provide clues to the diagnosis of constrictive pericarditis. However, in most cases it will be necessary to perform a “constriction protocol” echocardiogram with simultaneous recording of respiration to more accurately identify features of constriction and rule out a restrictive cardiomyopathy. Although the underlying pathologic cause of constriction is different from that of cardiac tamponade, the respiration-related changes in right- and left-sided cardiac filling are similar in the two conditions.

Dissociation of Intrathoracic and Intracardiac Pressures and Enhanced Ventricular Interaction

Evaluation of ventricular septal motion along with the mitral and hepatic vein Doppler pro-

files allows identification of the unique pathophysiologic mechanisms that underlie constrictive pericarditis [37, 39, 40]. As previously discussed, respiratory variation in left-sided cardiac filling occurs because the heart is “insulated” in the abnormal pericardium. Inspiration reduces intrathoracic pressure more than intracardiac pressure and therefore reduces the pressure gradient for filling of the left heart. The trans-mitral early (E) diastolic velocities (Fig. 18.11) decrease immediately after the onset of inspiration. The mitral E velocity on the first beat of expiration is compared with the first beat of inspiration and the percent change is calculated using the following formula: [(expiratory velocity—inspiratory velocity)/expiratory velocity $\times 100$] [3]. Using this formula, mitral E velocity variation has been reported to be in the range of 15–35% in constriction [37, 39–41]. The pulmonary vein forward velocity in diastole will change in a similar manner during the respiratory cycle [41, 42].

Reduced left ventricular filling causes the interventricular septum to shift toward the left ventricle (Fig. 18.12). Expiration restores the pressure gradient for filling of the left heart, such that trans-mitral velocities increase and the interventricular septum shifts back toward the right ventricle. This respiratory ventricular septal shift should be distinguished from a beat-to-beat oscillatory movement of the septum that might be best

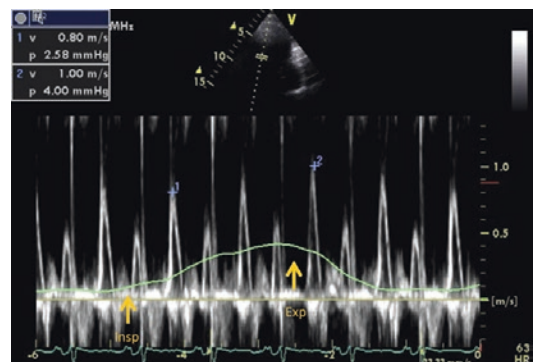


Fig. 18.11 Pulsed-wave Doppler recording (apical window in Mayo Clinic format) at the level of the open mitral leaflet tips in a patient with constrictive pericarditis. Note inspiratory decrease and expiratory increase in early (E) inflow velocity. *Insp* inspiration, *Exp* expiration. From Welch et al. [40]; with permission

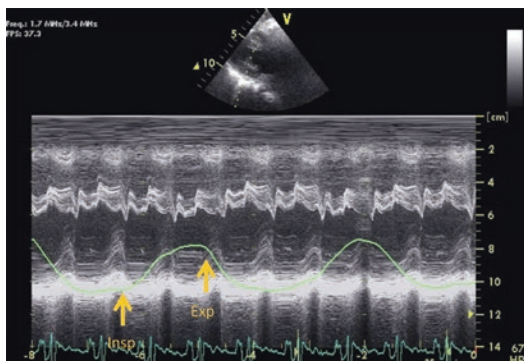


Fig. 18.12 Mid-ventricular septal M-mode recording (parasternal long axis) in a patient with constrictive pericarditis. Note leftward ventricular septal shift in inspiration. Also evident is a beat-to-beat septal diastolic “shudder.” *Insp* inspiration, *Exp* expiration. Used with permission from Welch et al. [40]; with permission

termed a septal “shudder.” The septal shudder likely relates to enhanced ventricular interaction on a millisecond scale, which may arise from slight differences in timing of tricuspid and mitral valve opening and right and left atrial contraction [43–45]. The septal shudder is probably less clinically useful than the respiration-related septal shift, as a septal shudder will be difficult to distinguish from other relatively common beat-to-beat septal abnormalities (e.g. due to conduction abnormalities and the post-cardiac-surgical state).

Abnormal filling of the right heart during expiration is manifested by reduced diastolic forward velocities and exaggerated late-diastolic reversals in the hepatic vein Doppler profile (Fig. 18.13). Trans-tricuspid diastolic velocities will change analogously, with increased velocities during inspiration and decreased velocities during expiration; reported percent changes have ranged from 48 to 55% [37, 39].

Respiratory variation in filling velocities can also occur in other conditions such as chronic obstructive lung disease, asthma, right ventricular infarction, severe sleep apnea, and pulmonary embolism. These other conditions can usually be recognized by their other clinical and 2-D echocardiographic features, but obstructive lung disease may be best differentiated with the use of the superior vena cava Doppler profile. In obstructive lung disease, respiratory variation in

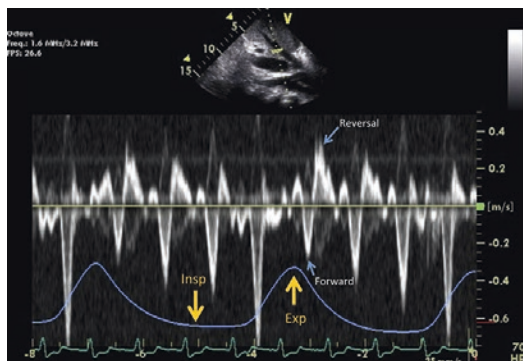


Fig. 18.13 Pulsed-wave Doppler recording (subcostal window) within the hepatic vein in a patient with constrictive pericarditis. Note prominent diastolic flow reversals in expiration, with the diastolic reversal ratio defined as reversal velocity divided by forward velocity (~ 0.35 m/s reversal velocity divided by ~ 0.30 cm/s forward flow velocity yields a diastolic reversal ratio of 1.2). *Insp* inspiration, *Exp* expiration. Used with permission from Welch et al. [40]; with permission

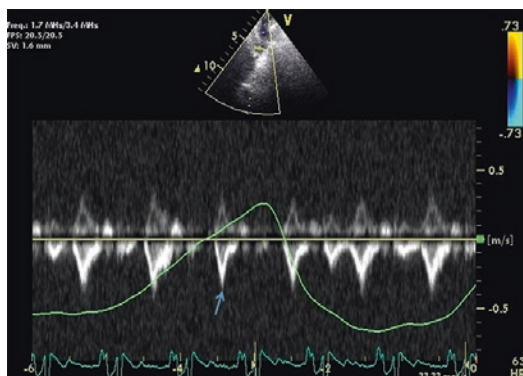


Fig. 18.14 Pulsed-wave Doppler recording (right supraclavicular window) within the superior vena cava in a patient with constrictive pericarditis. Note that during inspiration the velocity of blood flow (marked by arrow) toward the right atrium does not increase, but rather decreases mildly, consistent with a Kussmaul’s sign

Doppler velocities is caused by markedly negative intrathoracic pressure during inspiration, not all of which can be transmitted to the cardiac chambers. Flow from the superior vena cava into the right atrium increases substantially, and forward velocities in the superior vena cava may change more than 35% [46]. In contrast, inspiratory forward flow velocities in the superior vena cava do not increase significantly and may even decrease in constrictive pericarditis (Fig. 18.14).

Diastolic Assessment in Constriction

In addition to revealing characteristic respiratory variation in right- and left-sided cardiac filling in constriction, Doppler echocardiography allows identification of unique myocardial relaxation properties. The early diastolic mitral annular tissue velocity (e') is a measure of diastolic relaxation and would therefore be expected to be reduced in heart failure due to myocardial disease, but not in constrictive pericarditis in its pure form. Preserved or even elevated e' velocities have been documented in constriction and provide an important means of differentiating constriction from restriction [40, 47, 48]. Comparison of the medial and lateral mitral annular e' velocities may also help in diagnosing constriction. Rather than the usual pattern of the lateral e' being higher than the medial e' , the medial e' velocity is often higher in constriction (Fig. 18.15). This finding has been termed “annulus reversus” and is likely due to tethering of the lateral myocardium by the constrictive pericardium, with “compensation” by the medial annulus [49].

Filling pressures are usually elevated in constriction, and the ratio of early (E) to late (A) trans-mitral filling velocities is therefore typically pseudo-normal or restrictive ($E/A > 0.8$, and usually significantly higher) [39, 40, 50]. The ratio of E to e' is lower than expected because of the preserved or even elevated e' that is uniquely found in constriction. This approximately inverse relationship between E/e' and

left-sided filling pressure in constriction has been termed “annulus paradoxus” [51].

Strain Imaging in Constriction

Abnormal contraction and relaxation patterns may be further defined with speckle-tracking strain imaging. In constriction, circumferential systolic strain, torsion, and early diastolic untwisting have been shown to be reduced, while global longitudinal systolic strain tends to be preserved [52]. Further analysis of regional longitudinal systolic strain patterns has shown that lateral strain is reduced compared to septal strain in constriction (Fig. 18.16), and that this abnormality improved after pericardiectomy [53]. Myocardial strain imaging therefore appears to be an important addition to a “constriction-protocol” echocardiogram.

Other Echocardiographic Findings in Constriction

Plethora of the inferior vena cava (maximum diameter >2.1 and/or $<50\%$ collapse with inspiration) is present in nearly all patients with constrictive pericarditis and might be considered a prerequisite, assuming that the patient is not hypovolemic [40]. Other findings may include deformation of the cardiac contour, tethering of the right ventricular free wall at its interface with the diaphragm and liver, thickening of the pericardium, and flattening of the posterior left ventricular wall during diastole.

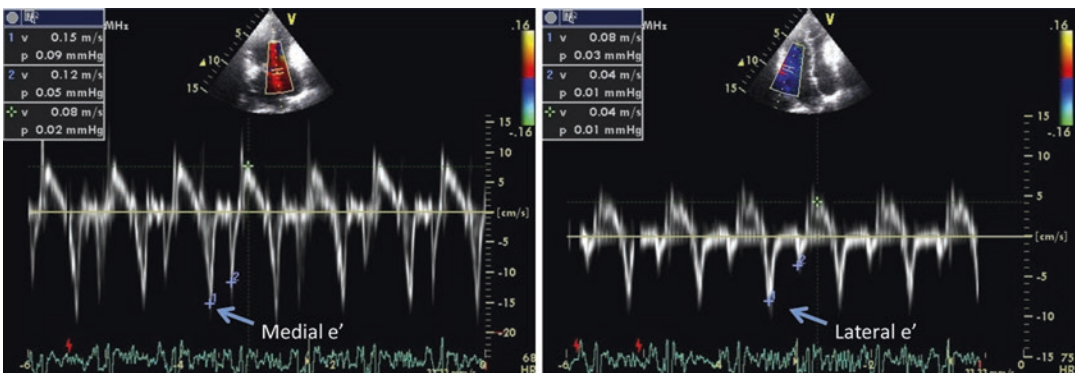


Fig. 18.15 Medial (left) and lateral (right) mitral annular tissue Doppler recording (apical window in Mayo Clinic format) in a patient with constrictive pericarditis. Note

normal to increased early relaxation velocity (e'), with medial velocity greater than lateral (“annulus reversus”). From Welch et al. [40]; with permission

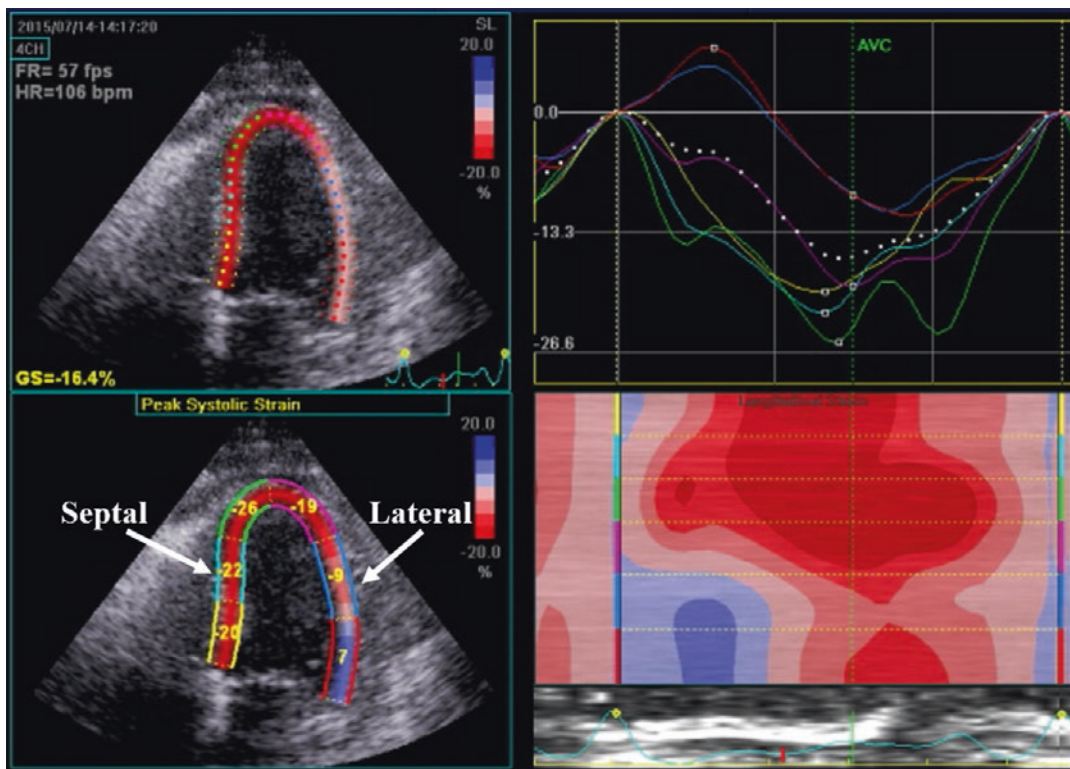


Fig. 18.16 Apical 4-chamber view showing longitudinal systolic strain (speckle-tracking) in a patient with constrictive pericarditis. Lateral strain is prominently reduced

compared to septal strain, because of the tethering effects of the diseased pericardium

Differentiating Constriction from Restriction: Mayo Clinic Diagnostic Criteria

The clinical manifestations of constriction and restriction are similar, despite these conditions having distinctly different pathophysiologic mechanisms. Both are caused primarily by diastolic filling abnormalities, and global systolic function as judged by ejection fraction is generally preserved. However, the diastolic filling impairment arises from noncompliant ventricular myocardium in restriction and from inelastic pericardium in constriction. This fundamental difference yields distinct echocardiographic findings.

The two-dimensional echocardiographic assessment of cardiac morphology is generally insufficient for diagnosis. Thickening of the pericardium may be evident in constriction. Greater

enlargement of the left atrium and increased ventricular wall thickness may be evident in restriction. The inferior vena cava is plethoric in both disorders.

Assessment of respiration-related changes in filling dynamics and myocardial relaxation properties provides the key to distinguishing constriction from restriction. In a study of 130 patients with surgically confirmed constrictive pericarditis compared with 36 patients with restriction or severe tricuspid regurgitation, the following five findings were found to be associated with a diagnosis of constriction: presence of ventricular septal shift, variation in mitral inflow velocities (≥ 10 – 15% , depending on method of calculation), preservation of medial e' velocity (≥ 9 cm/s), medial $e' >$ lateral e' (ratio ≥ 0.91), and exaggerated hepatic vein diastolic reversals in expiration (defined by the ratio of reversal velocity to forward velocity, ≥ 0.79 ; see Fig. 18.13) [40]. Test

Table 18.3 Test performance characteristics for the diagnosis of surgically-confirmed constrictive pericarditis

Variable	Sensitivity (%)	Specificity (%)	Positive predictive value (%)	Negative predictive value (%)
#1 Ventricular Septal shift	93	69	92	74
#2 Change in mitral E vel. $\geq 14.6\%$ ^a	84	73	92	55
#3 Medial e' velocity ≥ 9 cm/s	83	81	94	57
#4 Medial e'/Lateral e' ≥ 0.91	75	85	95	50
#5 HV ratio in expiration ≥ 0.79	76	88	96	49

Cutpoints for continuous variables were selected from ROC analysis: ventricular septal shift, medial e' velocity (≥ 9 cm/s), and HV diastolic reversal/velocity in expiration (≥ 0.79) HV hepatic vein

^aUsing [(expiratory velocity—inspiratory velocity)/inspiratory velocity $\times 100$]; value will be slightly lower if the currently recommended [(expiratory velocity—inspiratory velocity)/expiratory velocity $\times 100$] is used

performance characteristics are summarized in Table 18.3. With the exception of variation in mitral inflow velocities, these findings remained discriminatory even in the subset of patients with atrial fibrillation or flutter. In multivariable analysis, only ventricular septal shift, preserved or increased medial e', and exaggerated hepatic vein diastolic flow reversals in expiration were independently associated with the diagnosis of constrictive pericarditis. The finding of ventricular septal shift along with either of the other two findings yielded the optimal combination of sensitivity (87%) and specificity (91%).

Based on the preceding findings, the Mayo Clinic Echocardiographic Diagnostic Criteria for Constrictive Pericarditis were established. In patients with heart failure and preserved ejection fraction, a mitral inflow E/A ratio >1 and plethoric inferior vena cava are pre-requisites for constrictive pericarditis or restrictive cardiomyopathy. The presence of a respiration-related ventricular septal shift along with septal mitral annulus e' velocity >8 cm/sec and significant expiratory diastolic flow reversal in the hepatic vein Doppler profile is diagnostic or strongly suggestive of constrictive pericarditis. Mitral e' velocity may be lower than 8 cm/sec if there is concomitant myocardial disease, as may occur after radiation therapy.

Restrictive cardiomyopathy is typically characterized by a restrictive mitral inflow pattern,

exaggerated inspiratory (rather than expiratory) hepatic vein diastolic flow reversals, and low medial e' velocity. Respiration-related ventricular septal shift and variation in mitral inflow velocities are typically absent.

If the diagnosis remains uncertain after careful clinical evaluation and a constriction-protocol echocardiogram, additional investigation should be conducted and may include hemodynamic catheterization, computed tomography, and/or magnetic resonance imaging.

Effusive-Constrictive Disease and Transient Pericardial Constriction

Effusive-constrictive pericarditis occurs when pericardial fluid accumulates between the layers of a constrictive pericardium. After removal of pericardial fluid, constrictive hemodynamics persist [54, 55]. Some patients develop effusive-constrictive disease as part of a subacute, inflammatory pericardial process that may be “transient” and respond to anti-inflammatory therapy. Correctly identifying which patients have transient constriction is best accomplished through assessment of inflammatory markers and cardiac magnetic resonance imaging [56]. The degree of late-gadolinium enhancement of the pericardium (Fig. 18.17) suggests the extent of inflammation and therefore the potential for reversibility.

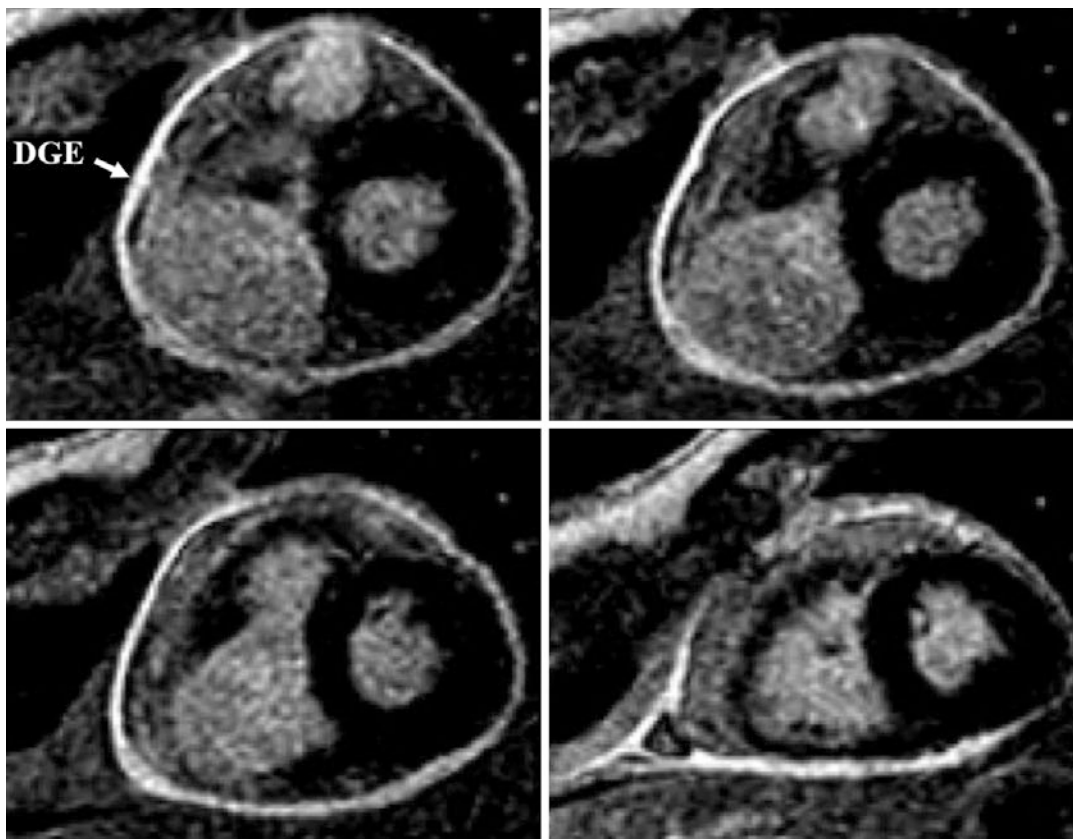


Fig. 18.17 Delayed gadolinium enhancement (annotated arrow) of the circumferential pericardium on cardiac magnetic resonance imaging in a patient with constrictive

pericarditis. This finding suggests significant inflammation of the pericardium that may respond to anti-inflammatory therapy

Congenital Absence of the Pericardium

Rarely, the pericardium may be congenitally absent. A partial defect may be present, most commonly involving the left side of the pericardium, or the pericardium may be completely absent [57]. Up to 30% of patients with congenitally absent pericardium have associated congenital cardiac defects, including atrial septal defect, bicuspid aortic valve, patent ductus arteriosus, and tetralogy of Fallot [58]. Patients may be asymptomatic or present with paroxysmal stabbing chest discomfort. In rare situations, portions of the heart may herniate through a partial pericardial defect, leading to acute complications including ST-elevation

myocardial infarction and even sudden death due to cardiac strangulation [57, 59]. Surgical treatment is necessary for patients with cardiac herniation through partial defects.

The frontal chest radiograph may provide clues to the diagnosis of congenitally absent pericardium. A complete left-sided defect is associated with leftward shift of the cardiac silhouette, straightening and elongation of the left heart border, obscuration of the right heart border by the spine, and radiolucent bands of lung tissue between the aortic knob and main pulmonary artery [57].

Echocardiographic imaging is abnormal in a number of respects. The heart is usually shifted

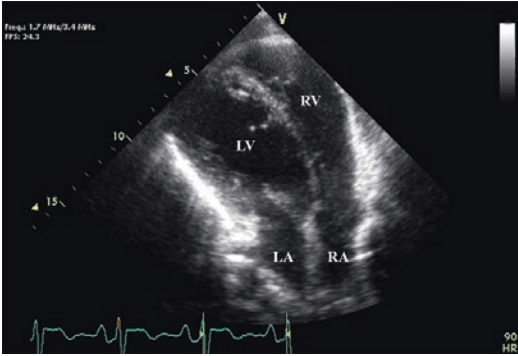


Fig. 18.18 Congenital absence of the left pericardium (apical 4-chamber view in Mayo Clinic format). The heart is shifted to the left in the thorax, with a “teardrop” configuration. *LV* left ventricle, *LA* left atrium, *RV* right ventricle, *RA* right atrium

to the left in the thorax and has a “teardrop configuration,” with elongation of the atria and bulbous-appearing ventricles (Fig. 18.18) [58]. Other reported echocardiographic abnormalities include altered imaging windows (higher and more lateral), cardiac hypermobility, paradoxical or flat ventricular septal systolic motion, and abnormal swinging of the heart [60].

Both cardiac computed tomography and magnetic resonance imaging will typically show insertion of lung tissue between the great arteries or between the base of the heart and the diaphragm with absence of the left pericardium, and into both atrioventricular grooves with complete absence of the pericardium (Fig. 18.19) [57].

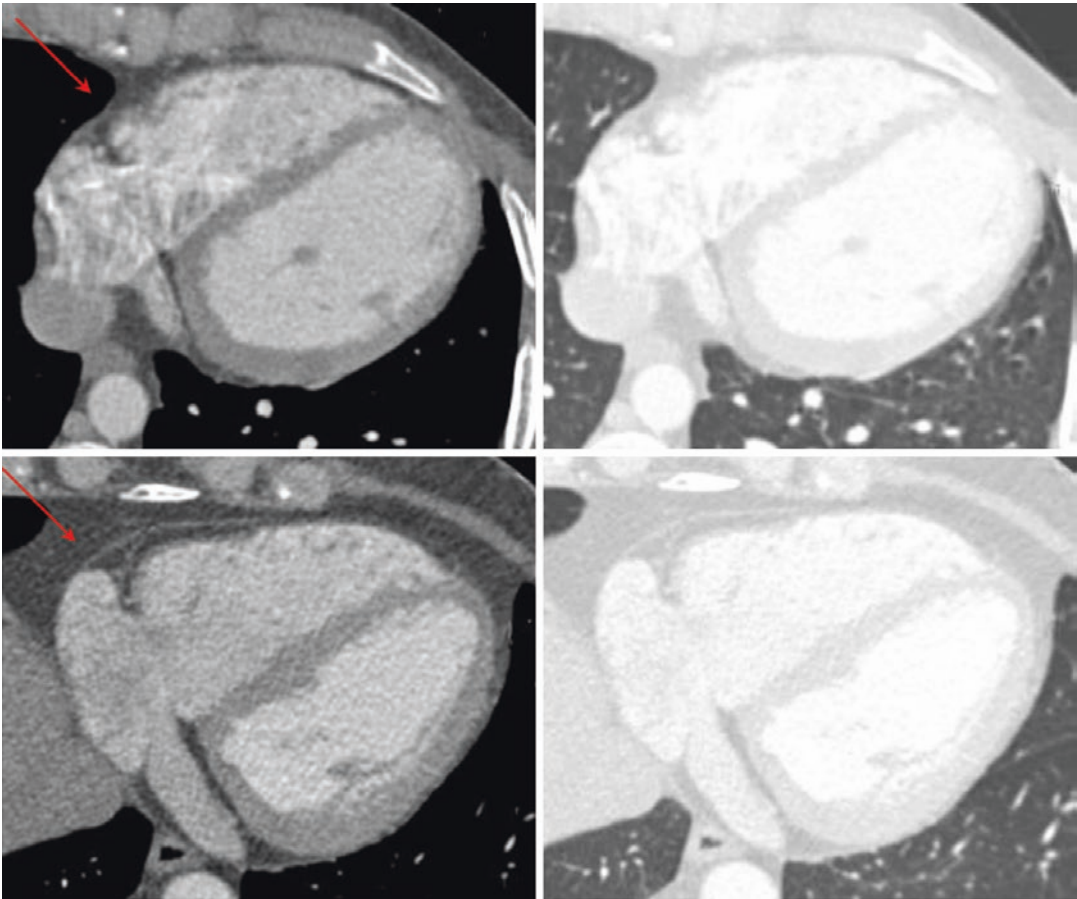


Fig. 18.19 Axial computed tomography images in patients with congenitally absent pericardium (top left and right panels), compared to a patient with normal pericardium (bottom left and right panels). Note insertion of lung

tissue into the right (red arrow) and left atrioventricular grooves when the pericardium is absent; this finding is not seen in the presence of normal pericardium. From Klein et al. [3]; with permission

Pericardial Cyst

A pericardial cyst is considered a benign entity and is usually incidentally found on imaging. Although usually found at the right costophrenic angle, it may also occur at the left costophrenic angle or elsewhere [61]. Echocardiographic imaging typically reveals a round or oval echolucent space surrounded by a wall, adjacent to the heart (Fig. 18.20) [62]. Cardiac computed tomography and magnetic resonance imaging (Fig. 18.21) offer superior tissue characterization. The cyst typically appears as a well-circumscribed, smooth-walled structure with non-enhancing fluid contents [3]. Clinical com-

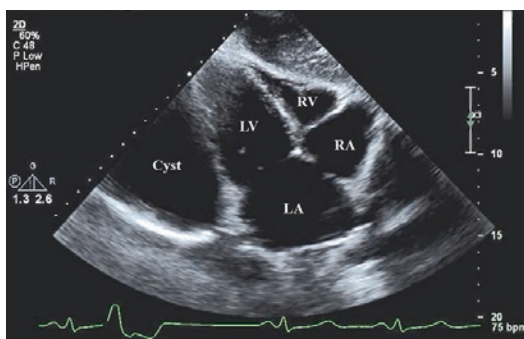


Fig. 18.20 Pericardial cyst (subcostal view). The cyst is found at the left costophrenic angle. LV left ventricle, RV right ventricle, LA left atrium, RA right atrium

plications appear to be rare, and therapy is not required in an asymptomatic patient. There are, however, isolated reports of acute complications such as tamponade and erosion into adjacent structures [61].

Pericardial Tumors

Pericardial tumors may be divided into primary (benign and malignant) and metastatic. Primary tumors are rare and typically benign, with examples including teratoma, lipoma, fibroma, hemangioma, and lymphangioma [3]. They may grow to impinge upon the cardiac or mediastinal contents, and are typically surgically excised for histopathologic diagnosis and relief of symptoms. The most common primary malignant tumors of the pericardium are malignant mesothelioma and angiosarcoma [3]. These may cause symptoms related to myocardial invasion, pericardial effusion with tamponade, and constrictive pericarditis. Treatment options are typically limited and prognosis is poor. The vast majority of tumors involving the pericardium are malignant and metastatic (Fig. 18.22), most commonly from mesothelioma and carcinoma of the lung, ovary, stomach, and prostate [63]. These pericardial tumors may cause pericarditis and effusion leading to pericardial tamponade.



Fig. 18.21 Anterior pericardial cyst (arrows) as seen by cardiac magnetic resonance imaging. (a) T1W axial image showing hypointensity in the loculated fluid, consistent with a cyst containing simple fluid. (b) T1W sagit-

tal image after administration of gadolinium shows that the cyst is non-enhancing. From Klein et al. [3]; with permission



Fig. 18.22 Subcostal view showing a diffusely thickened, nodular (arrow) visceral pericardial surface, consistent with tumor mass. A pericardial effusion is also present. From Klein et al. [3]; with permission

Treatment may sometimes require a palliative pericardial window in addition to therapy for the underlying cancer. The prognosis associated with metastatic disease of the pericardium is generally very poor.

Conclusion

Echocardiography is the initial diagnostic modality of choice for pericardial disease, given that it provides a non-invasive, bedside assessment of both anatomy and pathophysiology. A comprehensive echocardiogram will identify the size and location of a pericardial effusion, assess the hemodynamic impact of the effusion, and guide percutaneous drainage when necessary. Constrictive pericarditis may be suggested or even diagnosed with echocardiography, particularly when the study is tailored to include investigation for the unique hemodynamic features of constriction.

References

1. Maisch B, Seferovic PM, Ristic AD, et al. Guidelines on the diagnosis and management of pericardial diseases executive summary; The task force on the diagnosis and management of pericardial diseases of the European society of cardiology. *Eur Heart J*. 2004;25(7):587–610.
2. Douglas PS, Garcia MJ, Haines DE, et al. ACCF/AHA/ASNC/HFSA/HRS/SCAI/SCCM/

SCCT/SCMR 2011 Appropriate Use Criteria for Echocardiography. A Report of the American College of Cardiology Foundation Appropriate Use Criteria Task Force, American Society of Echocardiography, American Heart Association, American Society of Nuclear Cardiology, Heart Failure Society of America, Heart Rhythm Society, Society for Cardiovascular Angiography and Interventions, Society of Critical Care Medicine, Society of Cardiovascular Computed Tomography, and Society for Cardiovascular Magnetic Resonance Endorsed by the American College of Chest Physicians. *J Am Coll Cardiol*. 2011;57(9):1126–66.

3. Klein AL, Abbata S, Agler DA, et al. American society of echocardiography clinical recommendations for multimodality cardiovascular imaging of patients with pericardial disease: endorsed by the society for cardiovascular magnetic resonance and society of cardiovascular computed tomography. *J Am Soc Echocardiogr*. 2013;26(9):965–1012.e1015.
4. Spodick DH. The normal and diseased pericardium: current concepts of pericardial physiology, diagnosis and treatment. *J Am Coll Cardiol*. 1983;1(1):240–51.
5. Kocher GS, Jacobs LE, Kotler MN. Right atrial compression in postoperative cardiac patients - detection by transesophageal echocardiography. *J Am Coll Cardiol*. 1990;16(2):511–6.
6. Brooker RF, Farah MG. Postoperative left atrial compression diagnosed by transesophageal echocardiography. *J Cardiothor Vasc Anesth*. 1995;9(3):304–7.
7. Duvernoy O, Larsson SG, Persson K, Thuren J, Wikstrom G. Pericardial-effusion and pericardial compartments after open-heart-surgery - an analysis by computed-tomography and echocardiography. *Acta Radiol*. 1990;31(1):41–6.
8. Spodick DH. Acute cardiac tamponade. *N Engl J Med*. 2003;349(7):684–90.
9. Singh S, Wann LS, Schuchard GH, et al. Right ventricular and right atrial collapse in patients with cardiac-tamponade - a combined echocardiographic and hemodynamic-study. *Circulation*. 1984;70(6):966–71.
10. Kronzon I, Cohen ML, Winer HE. Diastolic atrial compression - a sensitive echocardiographic sign of cardiac-tamponade. *J Am Coll Cardiol*. 1983;2(4):770–5.
11. Gillam LD, Guyer DE, Gibson TC, King ME, Marshall JE, Weyman AE. Hydrodynamic compression of the right atrium: a new echocardiographic sign of cardiac tamponade. *Circulation*. 1983;68(2):294–301.
12. Merce J, Sagrista-Sauleda J, Permanyer-Miralda G, Evangelista A, Soler-Soler J. Correlation between clinical and Doppler echocardiographic findings in patients with moderate and large pericardial effusion: implications for the diagnosis of cardiac tamponade. *Am Heart J*. 1999;138(4 Pt 1):759–64.
13. Armstrong WF, Schilt BF, Helper DJ, Dillon JC, Feigenbaum H. Diastolic collapse of the right ventricle with cardiac-tamponade - an echocardiographic study. *Circulation*. 1982;65(7):1491–6.

14. Himelman RB, Kircher B, Rockey DC, Schiller NB. Inferior vena cava plethora with blunted respiratory response: a sensitive echocardiographic sign of cardiac tamponade. *J Am Coll Cardiol.* 1988;12(6):1470–7.
15. Fusman B, Schwinger ME, Charney R, Ausubel K, Cohen MV. Isolated collapse of left-sided heart chambers in cardiac tamponade: demonstration by two-dimensional echocardiography. *Am Heart J.* 1991;121(2 Pt 1):613–6.
16. Chuttani K, Tischler MD, Pandian NG, Lee RT, Mohanty PK. Diagnosis of cardiac-tamponade after cardiac-surgery - relative value of clinical, echocardiographic, and hemodynamic signs. *Am Heart J.* 1994;127(4):913–8.
17. Chuttani K, Pandian NG, Mohanty PK, et al. Left-ventricular diastolic collapse - an echocardiographic sign of regional cardiac-tamponade. *Circulation.* 1991;83(6):1999–2006.
18. McGregor M. Current concepts: pulsus paradoxus. *N Engl J Med.* 1979;301(9):480–2.
19. Shabetai R, Fowler NO, Fenton JC, Masangka M. Pulsus paradoxus. *J Clin Invest.* 1965;44(11):1882.
20. Reddy PS, Curtiss EI, Otoole JD, Shaver JA. Cardiac-tamponade - hemodynamic observations in man. *Circulation.* 1978;58(2):265–72.
21. Appleton CP, Hatle LK, Popp RL. Cardiac tamponade and pericardial effusion: respiratory variation in transvalvular flow velocities studied by Doppler echocardiography. *J Am Coll Cardiol.* 1988;11(5):1020–30.
22. Burstow DJ, Oh JK, Bailey KR, Seward JB, Tajik AJ. Cardiac tamponade: characteristic Doppler observations. *Mayo Clin Proc.* 1989;64(3):312–24.
23. Leeman DE, Levine MJ, Come PC. Doppler echocardiography in cardiac-tamponade - exaggerated respiratory variation in transvalvular blood-flow velocity integrals. *J Am Coll Cardiol.* 1988;11(3):572–8.
24. Krikorian JG, Hancock EW. Pericardiocentesis. *Am J Med.* 1978;65(5):808–14.
25. Tsang TS, Enriquez-Sarano M, Freeman WK, et al. Consecutive 1127 therapeutic echocardiographically guided pericardiocenteses: clinical profile, practice patterns, and outcomes spanning 21 years. *Mayo Clin Proc.* 2002;77(5):429–36.
26. Fitch MT, Nicks BA, Pariyadath M, McGinnis HD, Manthey DE. Emergency pericardiocentesis. *New Engl J Med.* 2012;366(12):E17–U19.
27. Isselbacher EM, Cigarroa JE, Eagle KA. Cardiac-tamponade complicating proximal aortic dissection - is pericardiocentesis harmful. *Circulation.* 1994;90(5):2375–8.
28. Tsang TSM, Freeman WK, Barnes ME, Reeder GS, Packer DL, Seward JB. Rescue echocardiographically guided pericardiocentesis for cardiac perforation complicating catheter-based procedures - The Mayo Clinic experience. *J Am Coll Cardiol.* 1998;32(5):1345–50.
29. Salem K, Mulji A, Lonn E. Echocardiographically guided pericardiocentesis - the gold standard for the management of pericardial effusion and cardiac tamponade. *Can J Cardiol.* 1999;15(11):1251–5.
30. Tsang TSM, Freeman WK, Sinak LJ, Seward JB. Echocardiographically guided pericardiocentesis: evolution and state-of-the-art technique. *Mayo Clin Proc.* 1998;73(7):647–52.
31. Mutyaba AK, Balkaran S, Cloete R, et al. Constrictive pericarditis requiring pericardiectomy at Groote Schuur Hospital, Cape Town, South Africa: causes and perioperative outcomes in the HIV era (1990–2012). *J Thorac Cardiovasc Surg.* 2014;148(6):3058–65.e1.
32. Ling LH, Oh JK, Schaff HV, et al. Constrictive pericarditis in the modern era: evolving clinical spectrum and impact on outcome after pericardiectomy. *Circulation.* 1999;100(13):1380–6.
33. Bertog SC, Thambidorai SK, Parakh K, et al. Constrictive pericarditis: etiology and cause-specific survival after pericardiectomy. *J Am Coll Cardiol.* 2004;43(8):1445–52.
34. Szabo G, Schmack B, Bulut C, et al. Constrictive pericarditis: risks, aetiologies and outcomes after total pericardiectomy: 24 years of experience. *Eur J Cardiothorac Surg.* 2013;44(6):1023–8; discussion 1028.
35. George TJ, Arnaoutakis GJ, Beaty CA, Kilic A, Baumgartner WA, Conte JV. Contemporary etiologies, risk factors, and outcomes after pericardiectomy. *Ann Thorac Surg.* 2012;94(2):445–51.
36. Talreja DR, Edwards WD, Danielson GK, et al. Constrictive pericarditis in 26 patients with histologically normal pericardial thickness. *Circulation.* 2003;108(15):1852–7.
37. Hatle LK, Appleton CP, Popp RL. Differentiation of constrictive pericarditis and restrictive cardiomyopathy by Doppler echocardiography. *Circulation.* 1989;79(2):357–70.
38. Hunt SA, Abraham WT, Chin MH, et al. 2009 focused update incorporated into the ACC/AHA 2005 guidelines for the Diagnosis and Management of Heart Failure in Adults: a report of the American College of Cardiology Foundation/American Heart Association Task Force on Practice Guidelines: developed in collaboration with the International Society for Heart and Lung Transplantation. *Circulation.* 2009;119(14):e391–479.
39. Oh JK, Hatle LK, Seward JB, et al. Diagnostic role of Doppler echocardiography in constrictive pericarditis. *J Am Coll Cardiol.* 1994;23(1):154–62.
40. Welch TD, Ling LH, Espinosa RE, et al. Echocardiographic diagnosis of constrictive pericarditis: Mayo Clinic criteria. *Circ Cardiovasc Imaging.* 2014;7(3):526–34.
41. Rajagopalan N, Garcia MJ, Rodriguez L, et al. Comparison of new Doppler echocardiographic methods to differentiate constrictive pericardial heart disease and restrictive cardiomyopathy. *Am J Cardiol.* 2001;87(1):86–94.
42. Klein AL, Cohen GI, Pietrolungo JF, et al. Differentiation of constrictive pericarditis from restrictive cardiomyopathy by Doppler transesophageal echocardiographic measurements of respiratory variations in pulmonary venous flow. *J Am Coll Cardiol.* 1993;22(7):1935–43.

43. Himelman RB, Lee E, Schiller NB. Septal bounce, vena cava plethora, and pericardial adhesion: informative two-dimensional echocardiographic signs in the diagnosis of pericardial constriction. *J Am Soc Echocardiogr*. 1988;1(5):333–40.
44. Coylewright M, Welch TD, Nishimura RA. Mechanism of septal bounce in constrictive pericarditis: a simultaneous cardiac catheterisation and echocardiographic study. *Heart*. 2013;99(18):1376.
45. Tei C, Child JS, Tanaka H, Shah PM. Atrial systolic notch on the interventricular septal echogram: an echocardiographic sign of constrictive pericarditis. *J Am Coll Cardiol*. 1983;1(3):907–12.
46. Boonyaratavej S, Oh JK, Tajik AJ, Appleton CP, Seward JB. Comparison of mitral inflow and superior vena cava Doppler velocities in chronic obstructive pulmonary disease and constrictive pericarditis. *J Am Coll Cardiol*. 1998;32(7):2043–8.
47. Garcia MJ, Rodriguez L, Ares M, Griffin BP, Thomas JD, Klein AL. Differentiation of constrictive pericarditis from restrictive cardiomyopathy: assessment of left ventricular diastolic velocities in longitudinal axis by Doppler tissue imaging. *J Am Coll Cardiol*. 1996;27(1):108–14.
48. Ha JW, Ommen SR, Tajik AJ, et al. Differentiation of constrictive pericarditis from restrictive cardiomyopathy using mitral annular velocity by tissue Doppler echocardiography. *Am J Cardiol*. 2004;94(3):316–9.
49. Reuss CS, Wilansky SM, Lester SJ, et al. Using mitral ‘annulus reversus’ to diagnose constrictive pericarditis. *Eur J Echocardiogr*. 2009;10(3):372–5.
50. Syed FF, Schaff HV, Oh JK. Constrictive pericarditis—a curable diastolic heart failure. *Nat Rev Cardiol*. 2014;11(9):530–44.
51. Ha JW, Oh JK, Ling LH, Nishimura RA, Seward JB, Tajik AJ. Annulus paradoxus: transmitral flow velocity to mitral annular velocity ratio is inversely proportional to pulmonary capillary wedge pressure in patients with constrictive pericarditis. *Circulation*. 2001;104(9):976–8.
52. Sengupta PP, Krishnamoorthy VK, Abhayaratna WP, et al. Disparate patterns of left ventricular mechanics differentiate constrictive pericarditis from restrictive cardiomyopathy. *JACC Cardiovasc Imaging*. 2008;1(1):29–38.
53. Kusunose K, Dahiya A, Popovic ZB, et al. Biventricular mechanics in constrictive pericarditis comparison with restrictive cardiomyopathy and impact of pericardiectomy. *Circ Cardiovasc Imaging*. 2013;6(3):399–406.
54. Hancock EW. Subacute effusive-constrictive pericarditis. *Circulation*. 1971;43(2):183–92.
55. Sagrista-Sauleda J, Angel J, Sanchez A, Permanyer-Miralda G, Soler-Soler J. Effusive-constrictive pericarditis. *New Engl J Med*. 2004;350(5):469–75.
56. Feng D, Glockner J, Kim K, et al. Cardiac magnetic resonance imaging pericardial late gadolinium enhancement and elevated inflammatory markers can predict the reversibility of constrictive pericarditis after antiinflammatory medical therapy: a pilot study. *Circulation*. 2011;124(17):1830–7.
57. Shah AB, Kronzon I. Congenital defects of the pericardium: a review. *Eur Heart J Cardiovasc Imaging*. 2015;16(8):821–7.
58. Abbas AE, Appleton CP, Liu PT, Sweeney JP. Congenital absence of the pericardium: case presentation and review of literature. *Int J Cardiol*. 2005;98(1):21–5.
59. Wilson SR, Kronzon I, Machnicki SC, Ruiz CE. A constrained heart: a case of sudden onset unrelenting chest pain. *Circulation*. 2014;130(18):1625–31.
60. Connolly HM, Click RL, Schattenberg TT, Seward JB, Tajik AJ. Congenital absence of the pericardium: echocardiography as a diagnostic tool. *J Am Soc Echocardiogr*. 1995;8(1):87–92.
61. Patel J, Park C, Michaels J, Rosen S, Kort S. Pericardial cyst: case reports and a literature review. *Echocardiography*. 2004;21(3):269–72.
62. Pezzano A, Belloni A, Faletra F, Binaghi G, Colli A, Rovelli F. Value of two-dimensional echocardiography in the diagnosis of pericardial cysts. *Eur Heart J*. 1983;4(4):238–46.
63. Bussani R, De-Giorgio F, Abbate A, Silvestri F. Cardiac metastases. *J Clin Pathol*. 2007;60(1):27–34.

Part V

Ischemic Disease

Coronary Artery Disease: Assessing Regional Wall Motion

19

Paramjit Jeetley, Rajdeep S. Khattar,
and Roxy Senior

Introduction

The assessment of left ventricular systolic function and particularly regional wall motion has become increasingly important in determining the severity and prognosis of coronary artery disease (CAD). Echocardiography, with its high spatial and temporal resolution, is an ideally suited non-invasive method of assessing such changes in wall motion. In the acute situation, the ability to detect these changes can be very useful in the early detection of myocardial ischemia, even preceding ECG changes and symptoms. Equally in patients presenting acutely with chest pain, with inconclusive ECGs, normal regional wall motion may help to exclude underlying myocardial ischaemia.

In patients presenting with a prior history of CAD, the presence of regional wall motion abnormalities (RWMA) and associated left ventricular wall thinning can give valuable information regarding the site and severity of previous myocardial damage and the extent of subsequent adverse remodelling. Re-evaluation of these patients following medical therapy or revascu-

larisation allows any change in left ventricular function and geometry to be fully assessed.

Enhancements in ultrasound technology, particularly the routine incorporation of harmonic imaging, have helped to improve the reliability of regional wall motion assessment. The use of intravenous ultrasound contrast agents to improve left ventricular opacification (LVO) has also improved the reproducibility of regional wall motion analysis. Other echocardiographic imaging modalities including automated endocardial border detection using integrated back scatter, tissue Doppler and 2D speckle tracking imaging of myocardial displacement, velocity, strain and strain rate, and real time 3D echocardiography are being developed for a more detailed assessment of global and regional myocardial function.

Regional Wall Motion Abnormality: How Does It Occur?

There is a well-established relationship between regional coronary blood flow and contractile function in the corresponding myocardial territory. In patients with normal coronary arteries, coronary perfusion is maintained even when the oxygen demands of the tissue are increased. For example, during exercise there is an increase in myocardial blood flow which maintains appropriate tissue oxygenation and normal regional wall motion.

P. Jeetley
Department of Cardiovascular Medicine, Northwick
Park Hospital and Institute for Medical Research,
Middlesex, UK

R. S. Khattar · R. Senior (✉)
Royal Brompton Hospital and Imperial College,
London, UK

In patients with coronary artery disease, regional blood flow at rest remains normal leading to preserved coronary perfusion, despite sometimes quite severe stenosis of the supplying artery. This is achieved by compensatory vasodilation of the arterioles which maintains resting myocardial blood flow (MBF) until stenosis severity exceeds 90% (although the presence of collaterals may maintain normal MBF even in this situation). As a result, in patients with significant coronary artery disease and no previous myocardial infarction, regional wall motion tends to be entirely normal at rest. However, if oxygen demand of the subtended myocardium is increased, for example during exercise, since the vasodilator response is already near maximal, there is an inability to further increase coronary perfusion to that area. This leads to a reduction in contractile function of the affected myocardium leading to a regional wall motion abnormality. Importantly, regional wall motion abnormalities occur early in the “ischaemic cascade” preceding ECG changes and symptoms (Fig. 19.1). When the oxygen demands of the myocardium are subsequently reduced and returned to baseline, there is resolution of myocardial ischemia and wall motion returns to normal.

Acute coronary artery occlusion as seen in acute myocardial infarction (AMI) leads to a rapid reduction in resting myocardial blood flow and hence cessation of muscular contraction in the area supplied, leading to a reduction in global and regional left ventricular function. Relief of the occlusion, either spontaneously or by pharmacological or interventional treatment, can lead

to recovery of regional wall motion, but this is dependent on the duration of coronary artery occlusion and the extent of myocardial necrosis that has occurred as a result. The degree and duration of myocardial ischaemia determines the severity of the regional wall motion abnormality from mild hypokinesis to complete akinesis of the affected myocardial region. In certain instances of severe reversible ischaemia, wall motion may not return to normal for several hours after the acute episode due to myocardial stunning.

In chronic coronary artery disease, gradual and progressive reduction in myocardial blood flow due to the progression of CAD may result in down regulation of myocardial contractile function with preserved metabolic activity. This disease state is known as hibernating myocardium such that when myocardial blood flow is restored by revascularisation, contractile function gradually returns to normal within a few weeks. Diminished contractile function in chronic CAD may also occur due to myocardial stunning due to repeated ischaemic episodes. These ischaemic episodes may occur either at rest (vasospasm) or during increased myocardial oxygen demand such as exercise.

Wall Motion Versus Systolic Wall Thickening for the Assessment of CAD

There are some limitations to using wall motion as the sole criterion for myocardial ischaemia. The movement of any given segment of the ventricle is influenced by the adjacent muscle to which it is attached. For example, in a chamber with a dyskinetic ischaemic segment, some of the adjacent normal tissue may appear hypokinetic because its motion may be influenced by pulling forces from the adjacent affected myocardium. The reverse phenomenon can also occur. If vigorously contracting normal muscle is next to an ischaemic area, the hyperdynamic segment may pull the ischaemic muscle towards the cavity, which may mask the abnormally perfused area. In general, the assessment of regional wall

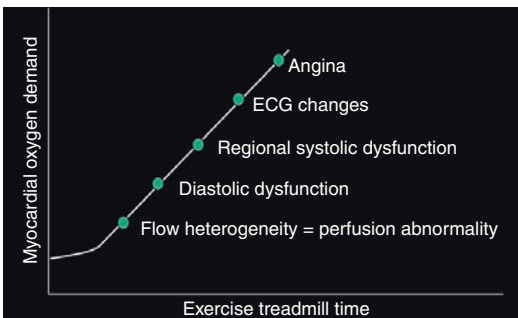


Fig. 19.1 Diagram of ischemic cascade

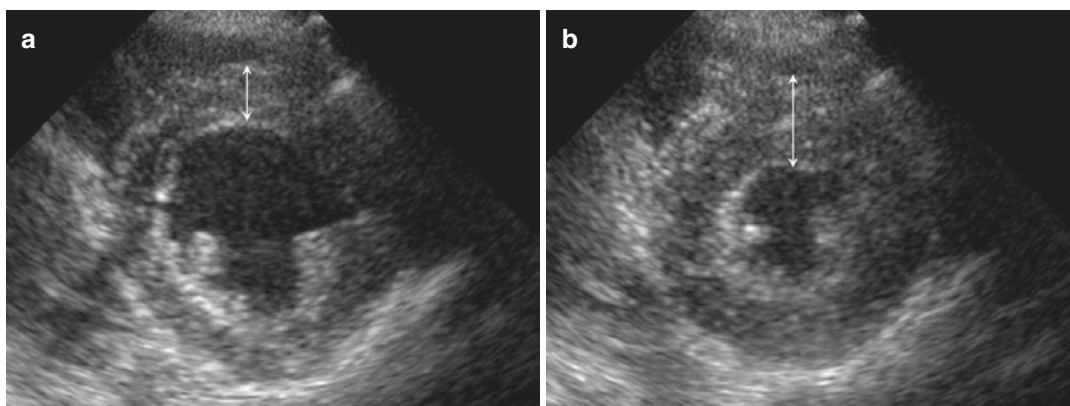


Fig. 19.2 PSAX views in diastole (a) and systole (b) demonstrating systolic wall thickening

motion tends to overestimate the extent of myocardial ischemia.

A more specific manifestation of myocardial ischaemia is a reduction of systolic wall thickening, rather than motion. Normal myocardial muscle increases in thickness during systole (Fig. 19.2). During ischaemia there is a reduction or absence of systolic wall thickening. Indeed, there may also be systolic thinning during acute ischaemia, with greater wall thickening in diastole compared to systole (Fig. 19.3). It has been shown that the extent and severity of wall thickening abnormality is superior to that of wall motion abnormality evaluation for predicting outcome after (AMI) [1].

Situations in which wall motion may be abnormal with preserved wall thickening include left bundle branch block (LBBB), Wolf-Parkinson-White syndrome and ventricular paced rhythm. The presence of preserved systolic wall thickening in these conditions infers that the wall motion abnormalities are not due to underlying CAD.

Basic Anatomy and Echocardiographic Findings

Three major epicardial coronary arteries and their branches provide blood to different regions of the heart. Although there are small variations between individuals, the pattern of this supply remains broadly the same. The left main coronary artery arises from the left sinus of Valsalva

and divides into two branches: the left anterior descending artery (LAD) and the left circumflex artery (LCx). The LAD runs down the interventricular groove and supplies the anterior wall (via its diagonal branches), anterior septum and apex of the heart. The left circumflex artery runs laterally down the atrioventricular groove where, together with its obtuse marginal branches, it supplies the lateral wall. The right coronary artery (RCA) originates from the right sinus of Valsalva and runs infero-medially down the atrioventricular groove. Its branch, the posterior descending artery (PDA), supplies the inferior wall and the inferior septum. About 80% of patients have a dominant right coronary artery; the remaining 20% are left dominant with the posterior descending artery arising from the left circumflex artery (Figs. 19.4 and 19.5). The posterior wall can be supplied either by the posterolateral branches of the RCA or from obtuse marginal branches of the LCx. Equally, there is significant variation of the blood supply to the apex where both the LAD and the PDA may contribute to areas of the apex.

Several models have been used to divide the left ventricular myocardium into segments in order that regional wall motion can be accurately described and quantified. The LV myocardium may be divided into three sections: base, mid-section and apex. Each section is then divided into segments that correspond to areas in the LV wall. The most recent recommendations from

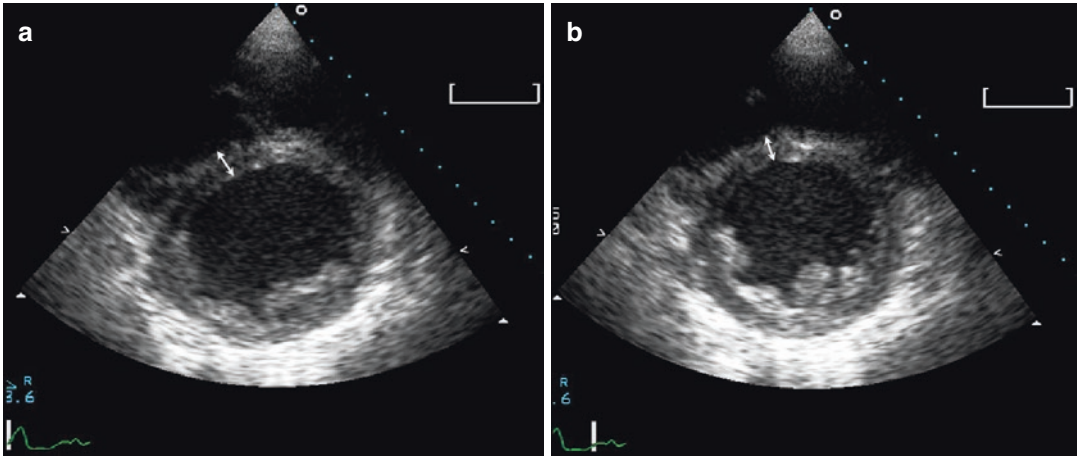


Fig. 19.3 PSAX views of (a) diastole and (b) systole showing absent wall thickening in a patient with acute myocardial infarction (AMI)

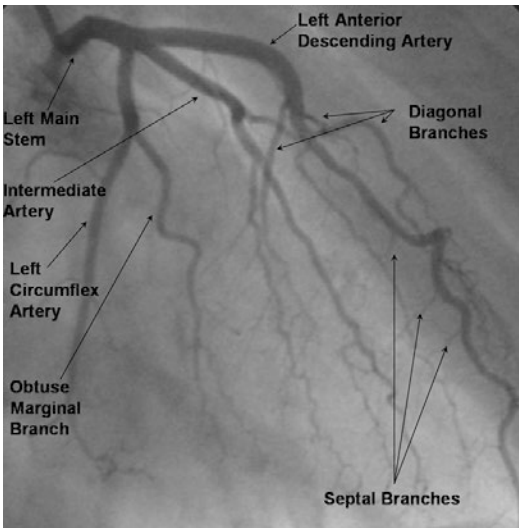


Fig. 19.4 Coronary angiogram showing left coronary system and branches

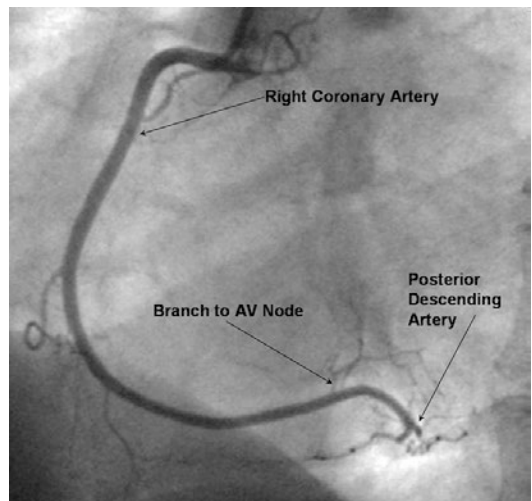


Fig. 19.5 Coronary angiogram showing right coronary system and branches

the American College of Cardiology (ACC) and American Heart Association (AHA) [2] are to use a 17-segment model (Fig. 19.6). This divides the base and mid-ventricular cavity into six segments each, with the apex having four segments and a fifth very distal apical “cap” which is best assessed in the apical 2- and 4- chamber views. Commonly a “bulls-eye” plot (Fig. 19.7) of all of these segments is used to note the individual segment scores, with the basal segments on the outside, followed by the mid-cavity and then the

apex. This allows clear visualization of regional wall motion on a single format with a broad indication of the vascular supply (Fig. 19.8).

The location of regional wall motion abnormalities correspond to the coronary artery territories as follows:

LAD: Usually affects the anterior septum, anterior wall and the anterior apex. Depending on the individual, the diagonal branches may also supply parts of the lateral wall. If the vessel is large, the inferior and posterior aspects of

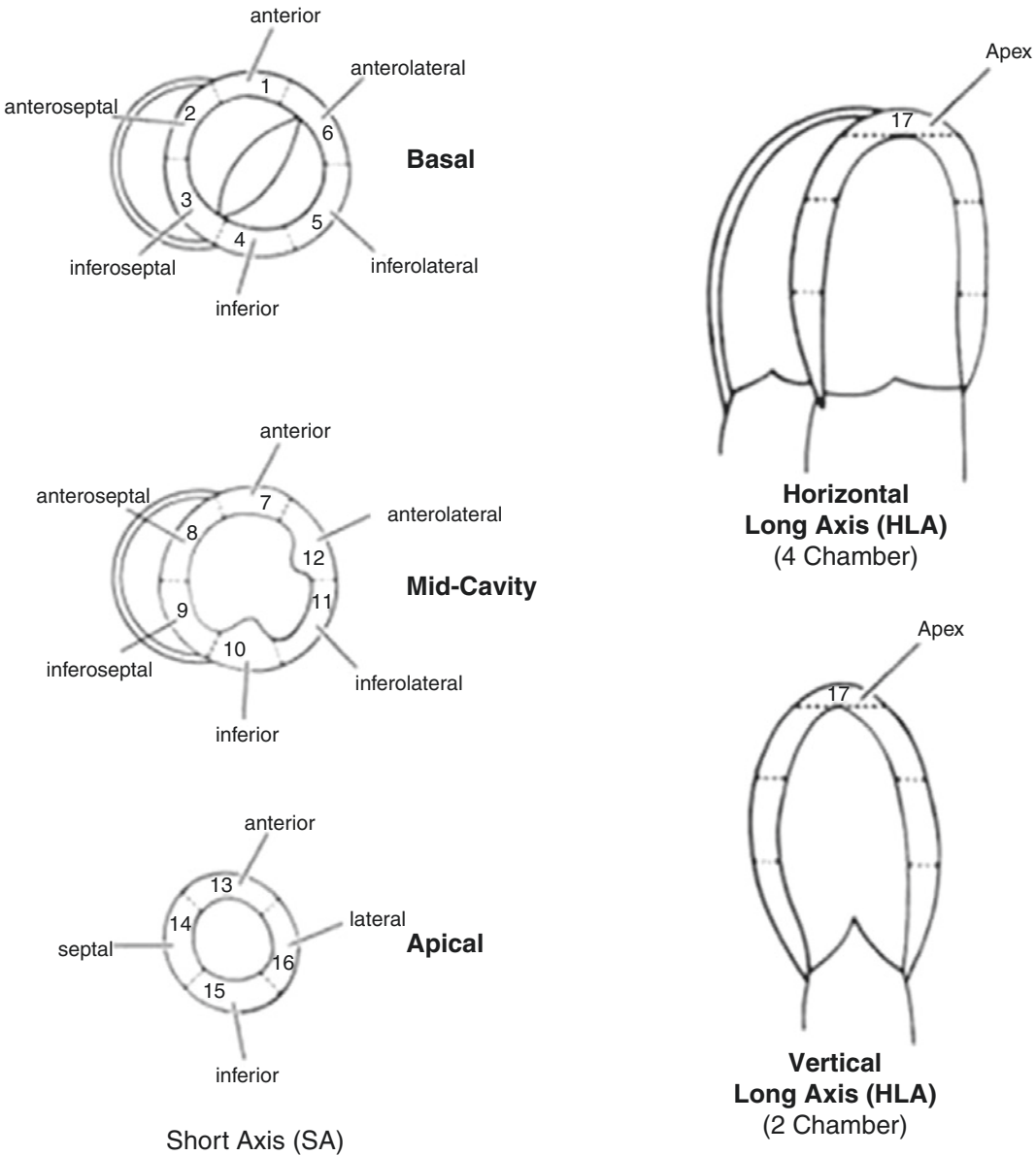


Fig. 19.6 Diagram representing the PSAX, apical 4- chamber and apical 2-chamber views of the ACC/AHA recommended 17 segment left ventricular model [2]

the apex may also be supplied. Occlusion of the distal LAD commonly only affects apical segments; mid vessel lesions affect both apex and mid-cavity segments, and proximal occlusion leads to reduction in wall motion along the whole of the anterior wall and septum. Occlusion of the first diagonal branch of the

LAD commonly causes an anterior or antero-lateral wall motion abnormality.
LCx: Disease in this artery tends to affect the lateral and posterior walls of the left ventricle. Individual variations in coronary anatomy make precise localisation of lesions in this territory difficult because of the overlap with

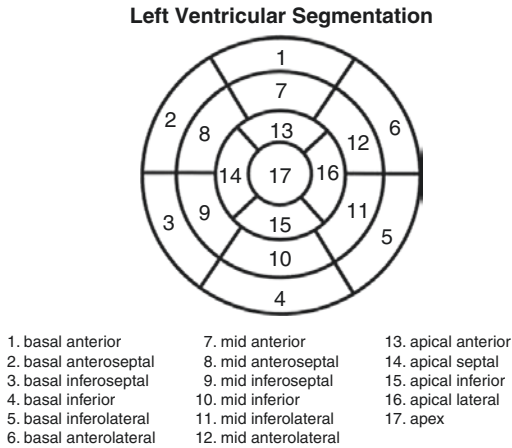


Fig. 19.7 ACC/AHA recommended “bulls-eye” plot of the 17 segment model [2]

other arteries. Nevertheless, as posterior wall ischemia is difficult to identify by ECG, the detection of regional wall motion abnormality in this area improves the detection of CAD, most often due to pathology of the LCx artery.

RCA: The posterior descending branch of the right coronary artery supplies the inferior septum and inferior wall of the left ventricle. Wall motion abnormalities in these areas strongly suggest RCA involvement. Depending on the dominance of the vessel, inferior regions of the apex may also be affected.

Clearly individual differences in coronary anatomy affect the areas of wall motion abnormality ascribed to a given coronary artery territory. This is particularly true of the territories supplied by the right coronary artery and the left circumflex artery where there can be considerable overlap in the areas of myocardium supplied. It can be helpful, therefore, to divide the regions of abnormality into the anterior circulation (consisting of those affected by the left anterior descending artery and its branches) and posterior circulation (right coronary and circumflex lesions).

Collateral vessel formation in cases of chronic occlusion and ischaemia as well as previous coronary artery by-pass surgery, affect the accuracy of localizing CAD by regional wall motion analysis. In general, however, the site of regional wall

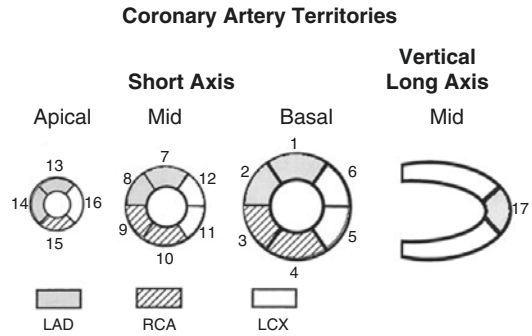


Fig. 19.8 ACC/AHA 17 segment model with corresponding coronary arteries. LAD left anterior descending, RCA right coronary artery, LCX left circumflex artery [2]

motion abnormalities correlates reasonably well with the location of disease in the coronary arteries and can serve as a guide for further management.

Regional Wall Motion Analysis

A comprehensive assessment of left ventricular wall motion by echocardiography is made using the standard apical 4-, 2-, and 3-chamber views along with the parasternal long axis and short axis views. This allows complete visualisation of all left ventricular walls, and hence all three vascular territories. Clear visualisation of the endocardial border is crucial for the proper assessment of regional wall motion. The best way to assess wall motion in each of these views is to consider a series of point targets along the endocardial border and the epicardium. As normal contraction occurs, the endocardium moves inwards (endocardial excursion) with left ventricular cavity shrinkage (area shrinkage). There is a reduction in the cavity perimeter (perimeter shrinkage) and the distance between the endocardium and epicardium increases (wall thickness). In patients with ischaemia, there is a reduction in the degree of endocardial excursion and a decrease in the amplitude of wall thickening. This can be seen clearly when compared to adjacent, normally contracting areas of myocardium. Of the two parameters, the degree of endocardial thickening is the most reproducible and reliable method of

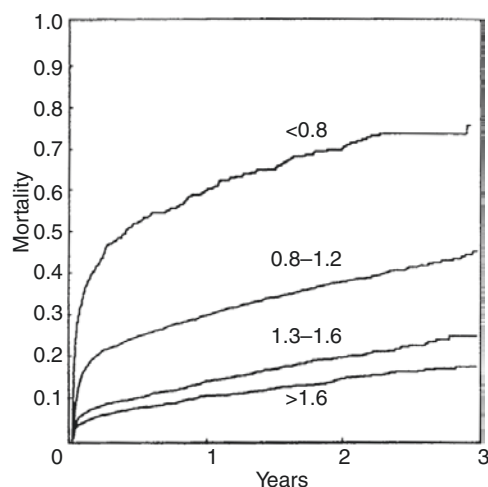


Fig. 19.9 Graph demonstrating relationship between mortality and WMSI (wall motion score index) over time [3]

wall motion assessment. It is important to take into account translational and rotational motion of the left ventricle which may give one a false impression of preserved wall motion. The absence of endocardial excursion effectively rules out any significant wall thickening.

Following image interpretation, regional wall motion can be scored according to a 4-point semi-quantitative scale using the 17 segment LV model. Each segment can be ascribed a score whereby normal wall thickening = 1, hypokinesia = 2, akinesia = 3 and dyskinesia = 4. A wall motion score index can be derived by adding the scores of each individual segment and dividing by the total number of segments assessed. In those with normal wall motion at rest, the wall motion score index with stress, can be used to give an indication of the extent and severity of ischemia. The wall motion score index has been shown to be an important prognostic indicator in patients with CAD (Fig. 19.9) [3, 4].

Acute ST-Elevation Myocardial Infarction

Acute myocardial infarction (AMI) occurs when there is acute occlusion of an epicardial coronary artery, leading to myocardial necrosis. The usual

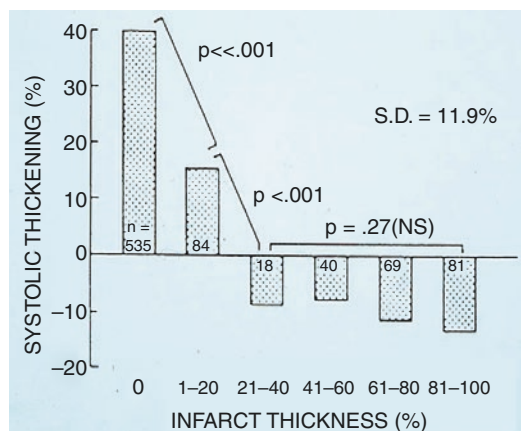


Fig. 19.10 Graph demonstrating the relationship between the transmural extension of infarction and regional wall thickening [5]

cause for this is rupture of an atherosclerotic plaque leading to thrombus formation. There is subsequent occlusion of the artery by the thrombus leading to a rapid decrease in perfusion to the region of myocardium supplied by that artery. Continued ischemia to that area leads to myocardial necrosis and permanent loss of contractile function.

Current treatments for AMI focus primarily on percutaneous coronary intervention and adjunctive anti-platelet therapy to secure patency of the infarct-related artery. The purpose of these treatments is to reduce the time of coronary occlusion, re-establish normal coronary perfusion and thereby reduce the degree of myocardial necrosis. It is well known that the degree of myocardial damage seen after infarction is directly related to the duration of artery occlusion supplying that area, the extent of the myocardium at risk and the degree of collateral circulation. It is also well recognised that the area of the myocardium most vulnerable to ischaemia is the sub-endocardial layer, and that the sub-endocardium contributes to 85% of left ventricular wall thickening (Fig. 19.10). When the area of myocardial necrosis extends beyond the sub-endocardial region, involving the full thickness of the left ventricular wall, this may lead to severe abnormalities in left ventricular geometry, size and function.

Echocardiographic Assessment in Acute ST-Elevation Myocardial Infarction

Since both myocardial ischaemia and infarction produce regional wall motion abnormalities, it is not possible to differentiate between them in patients presenting acutely with chest pain. However, the absence of regional wall motion abnormality on echocardiography may be help to exclude significant underlying coronary artery disease in patients presenting with chest pain and equivocal ECG changes.

After myocardial infarction, early assessment of patients can give useful information on the site and extent of wall motion abnormality, together with a response to any therapy given. Assessment of regional wall motion allows localisation of the infarct related artery. An occlusion of the LAD commonly leads to anterior septal, anterior wall and apical akinesia. The anterior septum can be visualised in the parasternal long and short axis views, as well as the apical 3 and 5-chamber views (Fig. 19.11). Anterior wall ischaemia is best shown in the parasternal short axis and apical 2-chamber views. Left circumflex stenosis often involves the lateral and posterior left ventricular walls. Identification of a posterior wall motion abnormality (using the apical 3-chamber and parasternal long axis views) may be helpful in the acute setting, as 12-lead ECG diagnosis of a posterior myocardial

infarct is often missed. Right coronary artery occlusion involves the inferior wall and inferior septum. This is clearly seen in the apical 2-chamber view (Fig. 19.12). The right coronary artery also commonly supplies the right ventricle, the function of which may become impaired. This may be important in the acute management of patients so assessment in the apical 4-chamber view may be important to assess the degree of right ventricular hypokinesia.

The presence of a wall motion abnormality following acute ischaemia may be due to myocardial infarction, stunning, hibernation or a combination of pathologies. Following an acute MI, the extent and severity of wall motion abnormality is an important predictor of outcome. Around 4–6 weeks after myocardial infarction, areas of transmural infarction become thinned and akinetic, or even dyskinetic. They may also become more echogenic when visualised with ultrasound (Fig. 19.13). Due to the sheer and pressure changes that occur in the LV, these abnormalities can change the shape and size of the ventricle (remodelling), representing the final sequelae of the infarction process.

Areas that remain severely hypokinetic or akinetic, but do not demonstrate any other changes may be stunned or hibernating. Myocardial hibernation occurs when there is prolonged wall motion abnormality due to repetitive stunning. To distinguish necrotic from viable myocardium (stunned or hibernating),

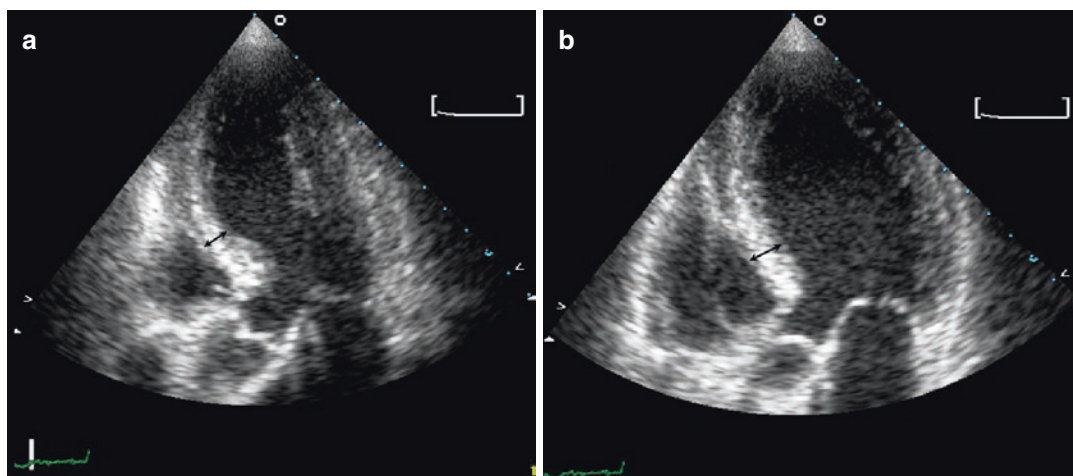


Fig. 19.11 Apical 5 chamber view (aorta seen) showing lack of wall thickening in systole (a) and (b) diastole in a patient with antero-septal infarction

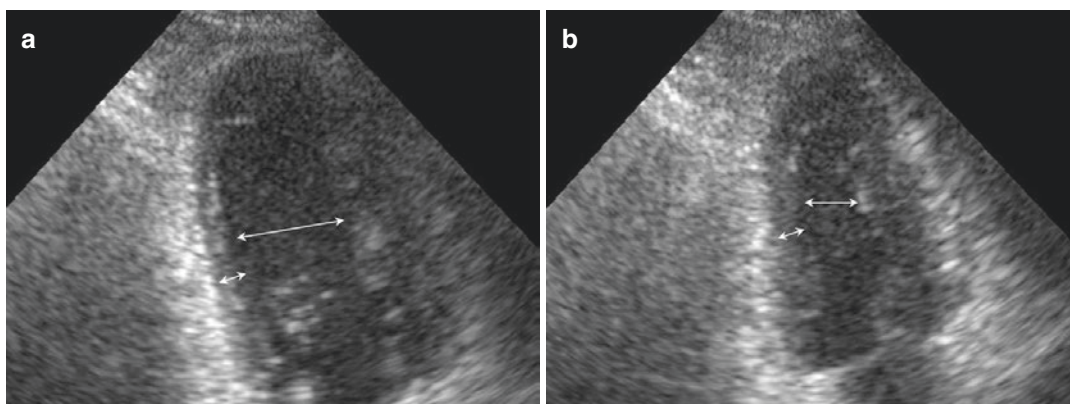


Fig. 19.12 A case of inferior wall infarction. Apical 2 chamber view showing lack of wall thickening from diastole (a) to systole (b)

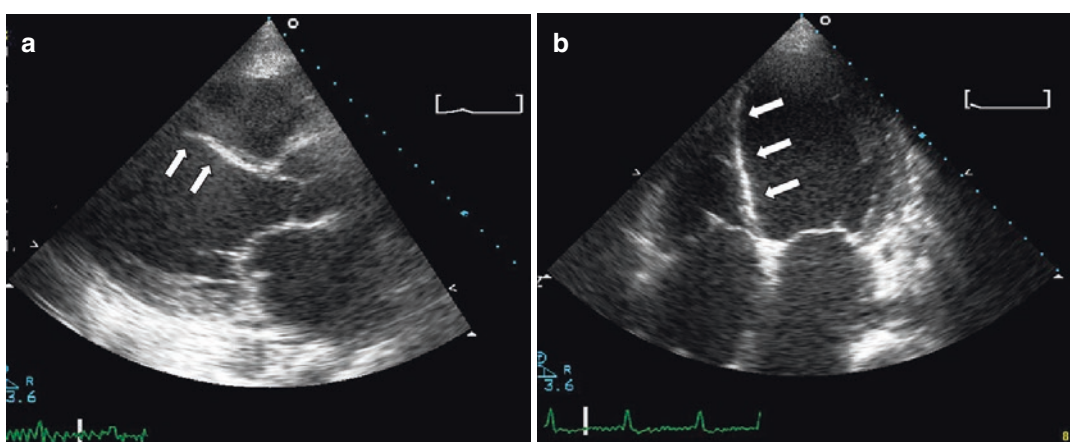


Fig. 19.13 A patient with thinning and scarring of the septum seen in parasternal long axis view (a) and the apical 4 chamber view (b) following LAD infarction

techniques assessing contractile reserve (dobutamine stress echocardiography), microvascular integrity (myocardial contrast echocardiography) or myocyte metabolism (radionuclide techniques) are useful. If these studies do not demonstrate significant myocardial necrosis, these areas are considered viable and contractile function in these segments is likely to improve after revascularisation.

Non-ST Elevation Acute Coronary Syndromes

Non-ST elevation acute coronary syndromes consist of unstable angina and Non-ST elevation myocardial infarction. In a similar manner to

ST-elevation myocardial infarction, atherosclerotic plaque rupture leads to thrombus formation and causes acute coronary occlusion. However, this occlusion tends to be incomplete or transient often due to a combination of coronary vasospasm and spontaneous downstream embolization of thrombus, causing small areas of myocardial damage, detectable by a rise in highly sensitive troponin assays. The duration of ischemia and degree of myocardial damage is much less than in acute ST-elevation myocardial infarction leading to less extensive and milder regional wall motion abnormalities which may be transient in nature. Consequently, echocardiographic assessment should be performed early after the onset of symptoms. Normal wall motion in a patient who is pain free with a normal ECG,

does not exclude an acute coronary syndrome. However, the absence of regional wall motion abnormality during symptoms excludes significant underlying coronary artery disease.

In the context of an acute coronary syndrome, mild regional wall motion abnormality suggests only a small amount of sub-endocardial myocardial damage. More severe hypokinesia may reflect more prolonged ischaemia leading to significant myocardial damage, or a degree of myocardial stunning overlying a small area of infarction. Echocardiographic assessment of regional wall motion, may overestimate the area of jeopardized myocardium as normal adjacent myocardium may become hypokinetic due to local tethering forces from the affected wall.

Improving Endocardial Definition

As already stated, clear visualisation of the ventricular walls and in particular the endocardial border is vital to the assessment of regional wall motion. Around 15% of patients have poor endocardial definition on conventional echocardiography. This may be due to a variety of reasons including large body habitus, lung disease, poor echo windows or distorted architecture of the left ventricle. A number of new methods have been developed to help overcome these limitations and improve endocardial border definition.

Harmonic Imaging

Conventional (or fundamental) echocardiography uses a transducer to emit and receive ultrasound waves at one frequency. However, not all signals reflected back from myocardial tissue are of the original frequency; some may be twice or even three times the emitted frequency. These are known as harmonic frequencies. Harmonic imaging uses broad band transducers that are capable of receiving reflected signals of twice or three times the original frequency and thus improve image quality. The technique was originally developed for better visualisation of microbubbles in contrast studies. However, myocardial tissue was also found to emit harmonic frequencies providing superior image quality during standard trans-thoracic echocardiography. The use of harmonic imaging is now standard practice allowing clearer definition of the endocardial border and reducing the number of spurious echoes within the LV cavity (Fig. 19.14) [6].

Left Ventricular Opacification Using Contrast Agents

Despite the use of harmonic imaging, there are still patients in whom endocardial definition may remain a problem. This may be overcome by the use of intravenous ultrasound contrast agents. These agents consist of gas filled microbubbles in

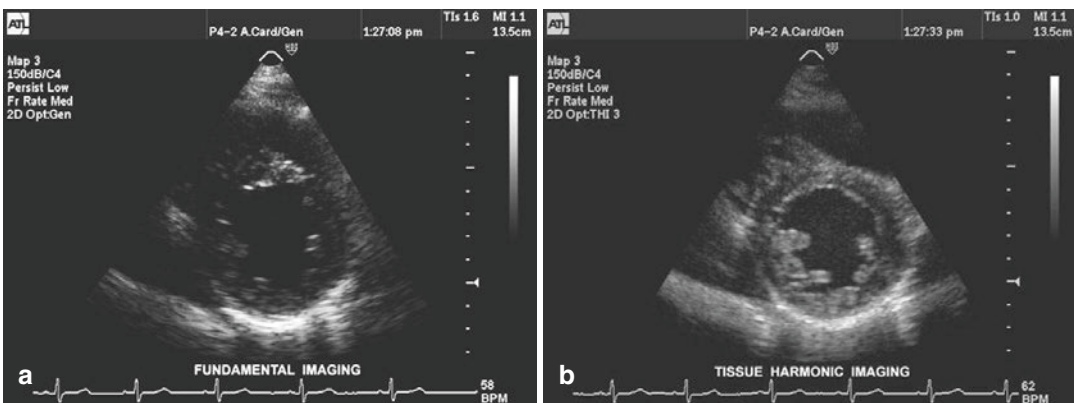


Fig. 19.14 Image showing PSAX in fundamental and harmonic imaging showing improved endocardial definition

a protein shell, which reflect ultrasound, generate harmonic back-scatter and enhance ultrasound information. The development of microbubbles, that can be injected intravenously and remain stable through the pulmonary circulation into the LV cavity, has been a major advance in contrast imaging. A single, slow bolus injection is usually enough to image the left ventricle in the standard apical and parasternal views. The microbubbles are eliminated from the body within a few minutes via the reticuloendothelial system, with the gas escaping from the lungs. Opacification of the left ventricle (Fig. 19.15) has been shown to sig-

nificantly improve endocardial border delineation in a number of studies, and is now being used in patients with poor images in both resting and stress echocardiography. The use of intravenous contrast for LV opacification (LVO) has improved reader confidence and reduced inter- and intra-observer variability in the interpretation of regional wall motion abnormalities. Newer techniques such as power modulation and power pulse inversion are now being used to better detect microbubbles at lower powers and in real time, allowing clear visualisation of the endocardial border.

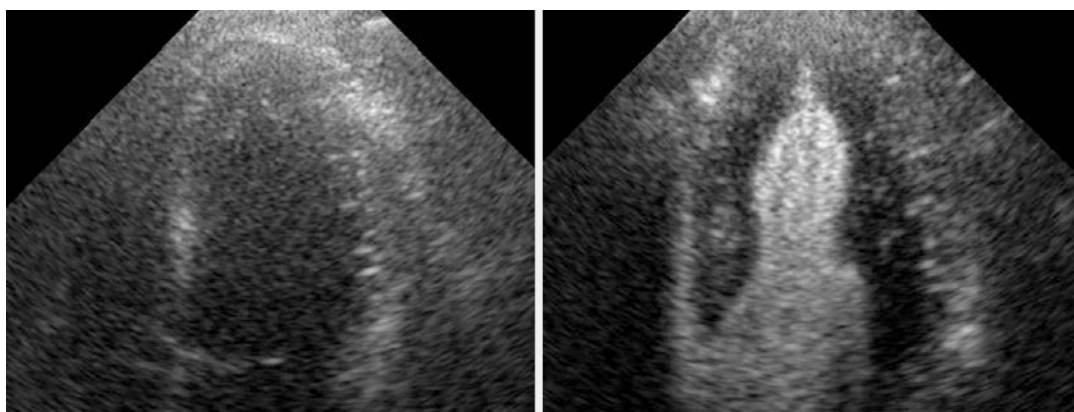


Fig. 19.15 Image with poor endocardial definition before and after LV opacification with contrast

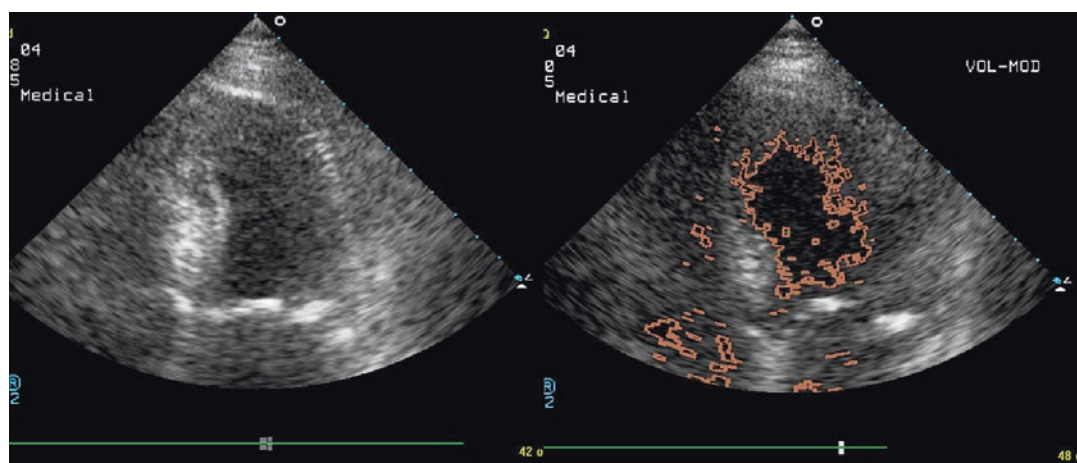


Fig. 19.16 Apical 4 chamber view with and without automated border tracking

Automated Endocardial Border Tracking

Analysis of regional wall motion using two-dimensional echocardiography tends to be subjective, qualitative and dependent on the experience of the observer. Alternative, more objective methods have therefore been sought and one such technique is the automated detection of endocardial borders [7]. This was originally tried by manually tracing the borders, but was found to be time-consuming, complicated and could only be performed off-line. Newer developments have been used to automate this procedure using the difference between the ultrasound backscatter emitted from the endocardium and blood in the LV cavity. When an image is acquired, the backscatter information along the scan line is analysed and each pixel classified as either blood or tissue. There is sufficient difference between the energy returned from the blood in the LV (low) and the endocardium (high) for this distinction to be made. Once this interface has been established along the whole of the endocardium, it can be tracked. Each pixel is colour coded and is superimposed onto the 2-dimensional image. The construction is then integrated with the original scan image and can be performed on-line. This leads to real-time

tracking of the endocardial border which is continually updated frame-by-frame (Fig. 19.16).

Colour coded endocardial tracking (Colour Kinesis and A-SMA) is an extension of this automated process (Fig. 19.17). Once the endocardial border has been defined on the basis of the backscatter from the blood and tissue, the inward (systolic) and outward (diastolic) movement is colour-coded. Each pixel is given a specific colour dependent on the direction of movement which is then compared to the previous frame so that an accurate measurement of systolic function and regional motion is possible. The colour overlays are superimposed onto the grey scale images which are updated on a frame by frame basis. This allows real time assessment of systolic function and regional wall motion using a visual colour scale (Fig. 19.17).

The main limitation of automated endocardial border tracking is that its success depends on good image quality. The acquisition of poor images leads to poor tracking of the endocardial border which in turn leads to poor colour-coded tracking images. The use of contrast agents to improve endocardial definition for automated tracking systems was previously not possible due to the imaging modalities available. Newer techniques such as power modulation have improved this situation with improved contrast specific imaging

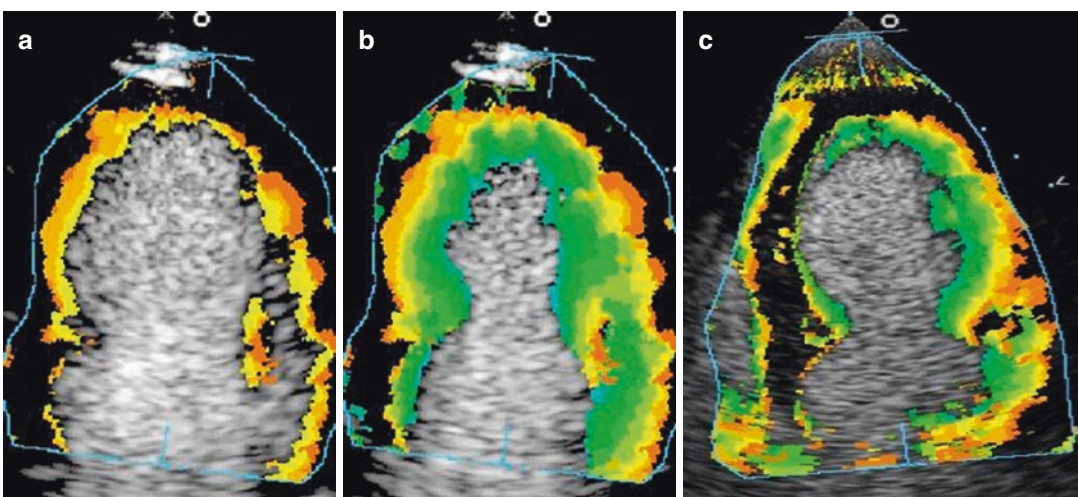


Fig. 19.17 Demonstration of colour kinesis in the apical 4-chamber for automated endocardial tracking. At end-diastole (a) a thin rim of colour delineates the endocardium. (b) There is progressive change in colour depicting

increasing wall thickening (c) lack of change in colour during systole depicting lack of wall thickening with normal change in colour in the lateral wall

modalities. The principle of detecting the energy difference between the blood-tissue interface remains, but the energy given out by the microbubbles causing LV opacification is far greater than that given out by the endocardium. The interface therefore remains well defined and colour-coded endocardial tracking can be achieved. The benefits of such a technique are not only the clearer visualisation of the endocardium, but also the potential for quantifying the degree of movement.

Three-Dimensional Echocardiography

A potential limitation of two-dimensional echocardiography relates to foreshortening of the apical views and therefore inadequate visualization

of the true apex. This has been overcome by 3-D echocardiography which captures the entire volume of the LV during image acquisition. Advances in computer and transducer technologies now allow real-time 3-D imaging of the heart without the need for intensive off-line post-processing manoeuvres. Three-dimensional echocardiographic images may be acquired in real-time by the acquisition of multiple pyramidal data sets per second in a single cardiac cycle. This allows simultaneous imaging of all segments of the left ventricle. These images may be displayed as volume rendered, surface rendered, wire-framed or 2D tomographic slices (Fig. 19.18). The latter allows assessment of wall thickening in each segment of the LV particularly the apex in a very reliable manner.

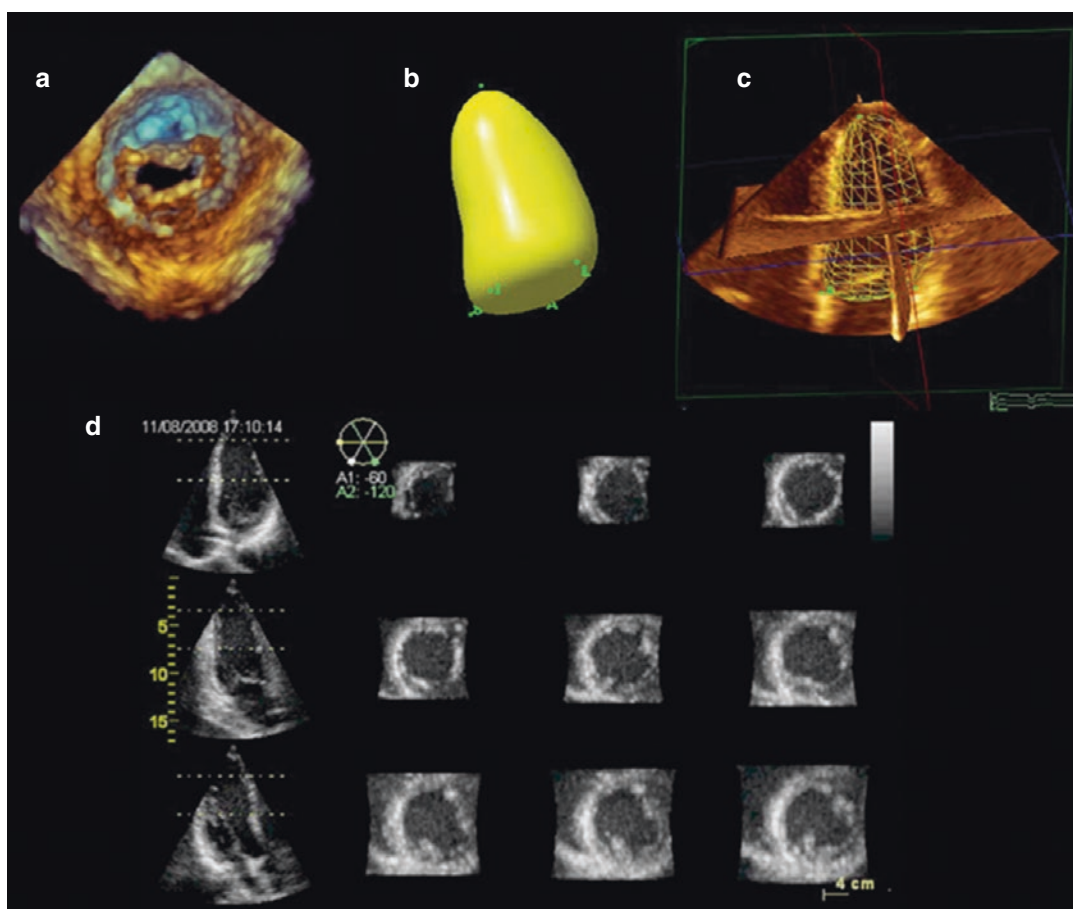


Fig. 19.18 Three-dimensional echocardiographic images presented in four broad categories: (a) volume rendered, (b) surface rendered, (c) wireframed and (d) 2D tomographic slices [8]

The feasibility of 3-D echocardiography is improving, but is limited by the need for high image quality and good operator experience. Further enhancements in temporal and spatial resolution, and data manipulation will be needed in the future to improve the utility of the technique. The use of ultrasound contrast agents in 3D evaluation may further improve assessment of regional wall motion in patients with reduced image quality. However, the feasibility of contrast imaging with 3-D echocardiography needs to be demonstrated.

**Tissue Doppler Imaging
of Myocardial Velocities**

Tissue Doppler imaging (TDI) allows the measurement of high amplitude, low frequency Doppler signals arising from the myocardium

and mitral annulus. A pulsed wave Doppler sample volume is placed within an area of the myocardium or the annulus and the systolic and diastolic velocities at that point are then displayed (Fig. 19.19). Virtually any area of the myocardium can be interrogated in this manner allowing the quantitative assessment of regional systolic function by measuring the S wave peak velocity. Myocardial velocities in the longitudinal direction can be derived from apical views and in the radial direction from short-axis views. The technique may show changes in regional function that are not revealed by global LVEF measurements. However, myocardial velocity measurements are affected by translational movement and tethering, making it difficult to discriminate akinetic segments that are pulled, from actively contracting segments. In addition, velocities are not uniformly distributed across the myo-



Fig. 19.19 Normal pattern of tissue Doppler derived myocardial systolic (S' wave), early diastolic (E' wave) and late diastolic (A' wave) velocities from the medial aspect of the mitral annulus

cardium, decreasing from base to apex, making it difficult to establish reference values. For these reasons, the technique is not an integral part of standard clinical practice for regional wall motion assessment.

Assessment of Myocardial Strain

Myocardial deformation imaging may overcome some of the limitations of velocity measurements. The LV myocardial architecture is such that the mid-myocardium consists of transverse fibres, the sub-endocardial layers have a right-handed helical arrangement and the sub-epicardial layers have an opposite helical arrangement. This structure broadly determines the components of myocardial deformation such that the sub-endocardial region contributes mainly to the longitudinal function of the LV, whereas the midwall and sub-epicardium contributes predominantly to rotational motion. Strain and strain rate measurements represent the magnitude and rate of change of myocardial fibre length which is an energy requiring process in both systole and diastole. Reductions in strain and strain rate are seen early in the development of many pathophysiologic states including myocardial ischemia.

Colour-coded TDI data allow simultaneous measurements of myocardial velocities from the entire myocardium. These data can be extrapolated to obtain displacement, strain and strain rate measurements. Tissue Doppler data are readily available and allow online measurements of velocities and time intervals with high temporal resolution. However, the technique is limited by angle dependency, and strain and strain rate measurements with TDI require training and experience for proper interpretation and recognition of artifacts.

Two-dimensional speckle tracking echocardiography is a new method for assessing myocardial deformation that may overcome some

of the limitations of TDI. The technique allows myocardial motion to be analysed from frame to frame by tracking natural acoustic markers, referred to as speckles, generated from interactions between ultrasound and myocardium within a defined region of interest. By analysing and tracking the motion of speckles from standard apical and short-axis views, deformation may be quantified along the longitudinal, radial and circumferential axes independent of angulation. Moreover, the technique does not require high frame rate images and can be performed by dedicated software on normal 2D pictures. The data are analysed off-line by manual definition of the region of interest and automated tracking of the myocardium. Strain and strain rate values can be obtained for a single myocardial segment or provide a global measure as the average of all segments of the LV (Fig. 19.20). The same segments may also be evaluated along the radial and circumferential axes. As the sub-endocardial layer mainly contributes to longitudinal function and is the most vulnerable to an ischaemic insult, reduced longitudinal strain may be noted in affected myocardial segments and areas of infarction. Despite potentially useful applications, strain measurements are not yet incorporated into routine clinical assessment of regional myocardial function. Speckle tracking echocardiography relies on good image quality and the assumption that a given speckle can be tracked from one frame to the next, which may not be the case when excessive cardiac motion occurs. 3D speckle tracking echocardiography offers advantages of overcoming foreshortening, the ability to measure a greater number of myocardial segments and reduced examination time. However, 3D techniques are highly dependent on image quality, use lower frame rates and require rigorous validation. Most importantly, there are as yet unresolved differences in inter-vendor strain measurements that limit the widespread applicability of the technique.

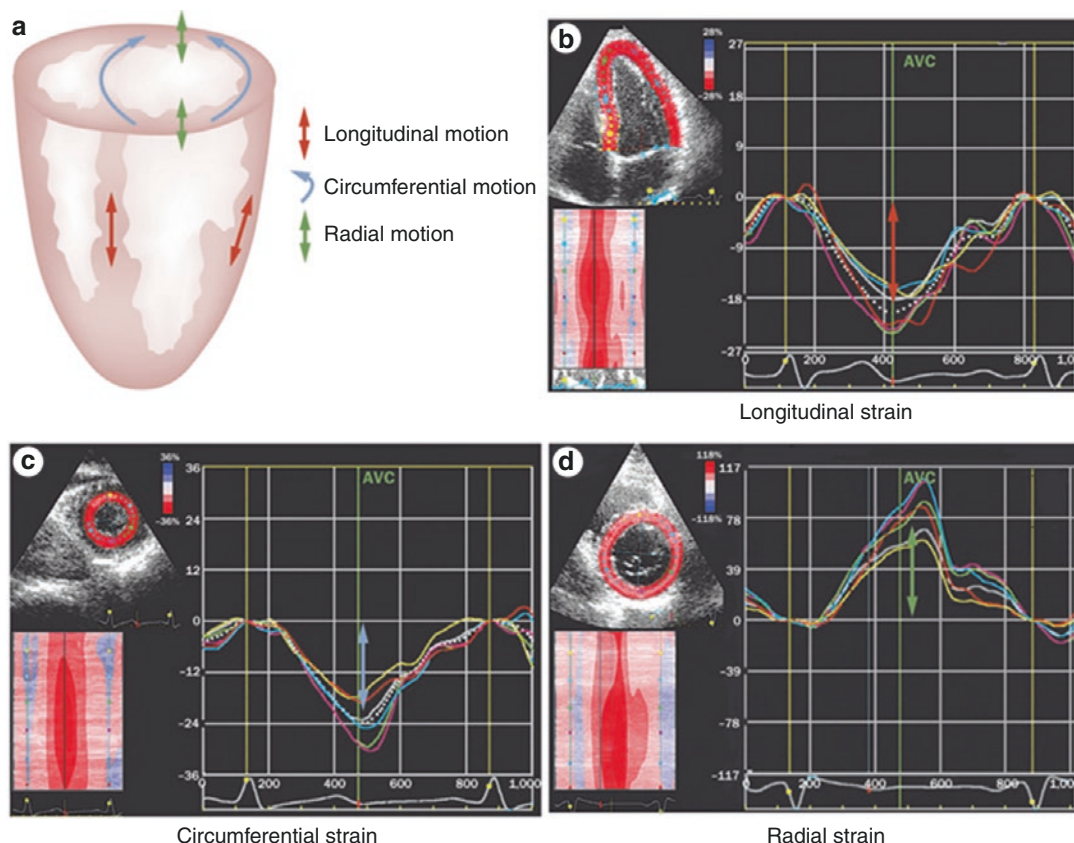


Fig. 19.20 Two-dimensional speckle tracking strain of the left ventricular myocardium. Arrows denote the direction of movements (a). Myocardial fiber shortening in longitudinal (b) and circumferential directions (c) during systole represents negative strain, whereas thickening and

lengthening in the radial direction represents positive strain. Arrows in (b–d) represent mean strain values in these directions. AVC aortic valve closure. (Ref: [9] Ozkan A, Kapadia S, Tuzcu M et al. *Nature Reviews Cardiology* 8, 494–501); with permission

References

1. Senior R, Basu S, Khattar R, Lahiri A. Independent prognostic value of the extent and severity of systolic wall thickening abnormality at infarct site after thrombolytic therapy. *Am Heart J*. 1998;135:1093–8.
2. Cerqueira MD, Weissman NJ, Dilsizian V, Jacobs AK, Kaul S, Laskey WK, Pennell DJ, Rumberger JA, Ryan T, Verani MS. Standardized myocardial segmentation and nomenclature for tomographic imaging of the heart: a statement for healthcare professionals from the Cardiac Imaging Committee of the Council on Clinical Cardiology of the American Heart Association. *Circulation*. 2002;105:539–42.
3. Kober L, Torp-Pederson C, Carlsen J, Videbaek R, Egelblad H. An echocardiographic method for selecting high risk patients shortly after acute myocardial infarction for inclusion in multicentre studies (as used in TRACE study) TRAndalopril Cardiac Evaluation. *Eur Heart J*. 1994;15:1616–20.
4. Kjoller E, Kober L, Jorgenson S, Torp-Pederson C. Long term prognostic importance of hyperkinesia following acute myocardial infarction. TRACE study group. TRAndalopril Cardiac Evaluation. *Am J Cardiol*. 1999;83:655–9.
5. Leibernann AN, Weiss JL, Jugdutt BI, et al. Two-dimensional echocardiography and infarct size: relationship of regional wall motion and thickening to the extent of myocardial infarction in the dog. *Circulation*. 1981;63:739–46.
6. Swinburn JM, Stubbs P, Soman P, Collinson P, Lahiri A, Senior R. Independent value of tissue harmonic echocardiography for risk stratification in patients with non-ST-segment elevation acute chest pain. *J Am Soc Echocardiogr*. 2002;15:1031–7.
7. Platts DG, Monaghan MJ. Colour encoded endocardial tracking: the current state of play. *Eur J Echocardiogr*. 2003;4:6–16.
8. Mor-Avi V, Sugeng L, Lang RM. Real time 3-dimensional echocardiography: an integral component of the echocardiographic examination in adult patients? *Circulation*. 2009;119:314–29.
9. Ozkan A, et al. Assessment of left ventricular function in aortic stenosis. *Nat Rev Cardiol*. 2011;8:494–501.

Echocardiography for Assessing Acute Myocardial Infarction and Complications

20

Otto Kamp

Introduction

According to the sequence of the ischemic cascade, regional contractile dysfunction precedes both electrocardiographic changes and symptoms during myocardial ischemia (Fig. 20.1). Thus, due to the suboptimal performance of the electrocardiogram to reliably detect or exclude acute coronary syndromes, including myocardial infarction (MI), evaluation of regional contractile function using echocardiography in patients with acute chest pain is clinically relevant. Echocardiography is portable, non-invasive, easily repeatable, efficacious, low-cost, and

widely available, rendering it uniquely suited for emergency medicine use. The visual analysis of segmental wall motion is the hallmark for the diagnosis. Furthermore, Doppler echocardiography can be useful for assessing the location and extent of MI, in diagnosing silent complications as left ventricular thrombus, left ventricular (pseudo) aneurysm and mechanical complications after MI. It also provides prognostic information that is important for risk stratification. Stress echocardiography can be applied in the emergency room for diagnosis of acute coronary syndromes and also for risk stratification after MI. Finally, three-dimensional echocardiography combined with speckle tracking is more sensitive than two-dimensional echocardiography for the evaluation of wall motion.

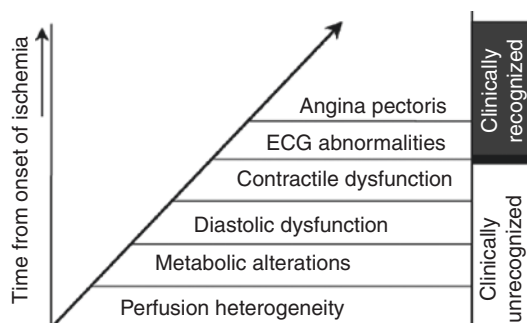


Fig. 20.1 The ischemic cascade: contractile dysfunction precedes electrocardiographic changes and symptoms as manifestation of myocardial ischemia

O. Kamp
Department of Cardiology, VU University Medical Center, Amsterdam, The Netherlands
e-mail: o.kamp@vumc.nl

Acute Chest Pain

The Problem

Acute non-traumatic chest pain is one of the most common symptoms for which patients seek emergency medical consultation, comprising up to 15% of total patient volume in emergency departments. In the USA, an estimated eight million annual visits for chest pain to the emergency department typically result in hospital admissions for further evaluation in approximately 70% of such patients. It is among the

Table 20.1 Chest pain in the emergency room

<i>Cardiac</i>
Myocardial ischemia or infarction
Aortic dissection
Pericarditis
<i>Pulmonary</i>
Pulmonary embolism
Other causes of pulmonary hypertension
<i>Chest wall trauma</i>
Myocardial or pericardial contusion
Traumatic valve and aortic injury
<i>Noncardiac chest pain</i>
Gastrointestinal
Musculoskeletal

more challenging and complex symptoms, as the diagnoses for patients with chest pain range from minor disease processes, such as costochondritis or oesophageal spasm, to life-threatening conditions as acute MI, pulmonary embolism, or aortic dissection (Table 20.1). Furthermore, up to three fourths of the admissions for presumed acute coronary syndromes prove to be incorrect, while anywhere between 2 and 8% of patients with acute cardiac ischemia or MI are erroneously discharged from the emergency department, with an increased associated short-term mortality rate ranging from 10 to 26%. Although relatively small, the incidence of failure to admit this patient category with a life-threatening condition is important as it may result in potentially serious and preventable morbidity and mortality in tens of thousands of patients.

Medicolegal Implications

There are also medico-legal implications, as the failure to diagnose acute coronary syndromes or MI accounts for the single greatest cause of dollars lost in malpractice lawsuits in emergency medicine in the USA. Although currently mainly an issue in the United States, juridification of medicine is increasing rapidly elsewhere, and implications on the practice of emergency medicine may be equally profound. Consequently, focusing on patient welfare and medico-legal implications of failure to detect acute coronary

syndromes alike, results in the liberal admission policy as is traditionally applied in patients with chest pain syndromes. However, as the current era of managed care and health care reform requires cost-containment, and as a result of the increasing awareness that an overly defensive medical system with its unnecessary admissions and procedures constitutes a form of iatrogenous morbidity per se, impetus is added to the development of more efficient approaches to manage this particular group of patients.

Work-Up in Acute Chest Pain Syndromes

The aim of the initial triage of patients presenting with acute chest pain would be to differentiate acute coronary syndromes as the underlying cause from other potentially serious conditions, particularly aortic dissection and pulmonary embolism, or less serious conditions (Table 20.1). The short-term risk of death or life-threatening complications should be established readily in patients with suspected acute coronary syndromes in order to ensure rapid initiation of most appropriate treatment while patients who are at very low likelihood of having an adverse outcome related to acute coronary syndromes may thus be safely discharged for outpatient follow-up.

Typically, history taking, the clinical examination and ECG are important when performing the initial triage in acute chest pain patients. It is increasingly recognized that a number of specific patient groups typically present with atypical symptoms of myocardial ischemia, such as women, diabetics, and the elderly. Physical examination is often normal at presentation, while the initial 12-lead electrocardiogram is critically important. Patients with acute chest pain and ST-segment deviation of more than 0.1 mV in two or more contiguous leads or left bundle branch block not known to be old, are suspected to have transmural ischemia or MI and are thus at high risk for short-term major adverse cardiac events. Patients classified as having an acute coronary syndrome with ST-elevation, should

undergo urgent revascularization (PCI) unless contra-indicated.

The presence of ST-segment depression of more than 0.1 mV raises the suspicion of myocardial ischemia and identifies patients suffering from an acute coronary syndrome with an associated intermediate-to-high risk. Emergency revascularization is generally considered not to be an option in these patients, while admission to hospital is indicated, preferably in a cardiac care surroundings and subsequent delayed revascularization.

The majority of cases, however, present with normal electrocardiograms or non-specific ECG changes, and it is these patients that pose the greatest diagnostic dilemma for triage.

As a second step to further stratify these low-to-intermediate risk patients, methods to detect biochemical evidence of irreversible myocardial injury are commonly applied. However, no serum biochemical marker reliably identifies or excludes unstable angina, troponin negative, at any time after symptom onset. Thus, the traditional 'rule out acute MI' approach by serial enzyme testing alone may deprive many patients with acute coronary syndromes of early therapy to prevent progression to MI and death.

Although serial ECG or continuous ST-segment monitoring is of proven benefit, early non-invasive evaluation of myocardial ischemia by echocardiography may be of particular value.

Diagnosis of Myocardial Infarction

The diagnosis of an acute MI is based upon history, 12-lead ECG and serologic markers such as creatine kinase and cardiac troponins. Cardiac imaging and in this scenario echocardiography has been used for early identification of acute coronary syndromes or MI patients whose presenting symptom is acute chest pain, as well as to evaluate prognosis in this population.

Myocardial ischemia produces regional wall motion abnormalities. The presence of regional dyssynergy can predict an acute MI or myocardial ischaemia with a high sensitivity and moderate specificity. It is difficult however to distinguish

between infarction (necrosis, irreversible) and ischaemia (reversible) or stunning (contractile dysfunction after temporary flow/oxygen disturbance). Other conditions however may also produce regional wall motion abnormalities, such as prior MI, focal myocarditis, prior cardiac surgery, right ventricular volume overload, left bundle branch block and ventricular pre-excitation. With transient coronary artery occlusion during percutaneous coronary interventions, within 20 s wall motion abnormalities are observed prior to onset of ECG changes or symptoms, the so-called ischemic cascade (Fig. 20.1).

In the setting of an acute MI, patients with multivessel coronary disease usually show more extensive regional asynergy than patients with single-vessel disease. Thus, there is a clear diagnostic yield of echocardiography over the use of conventional clinical and ECG criteria. The extent of regional asynergy is also predictive for in-hospital complications in patients with MI.

As summarized in Table 20.2, with the exception of two small-sized studies performed in a very low risk population, the large majority of studies indicates that echocardiography may indeed be of substantial benefit in the evaluation of patients with acute non-traumatic chest pain. Practically, in the absence of wall motion abnormality, a MI or an acute ischaemic syndrome can be ruled out. Although the number of patients with falsely negative studies may be of some concern, such patients typically have a low complication rate, while the accuracy of echocardiography may be significantly enhanced when imaging is performed during or shortly after resolution of symptoms.

Although clinically of less concern, the number of falsely positive studies may be reduced when a simple comparison with an earlier echo study is possible.

In order that echocardiography be most useful for diagnosis and early risk stratification of patients with acute coronary syndromes, it would need to be available immediately in the emergency department as the sensitivity to detect transient wall motion abnormalities is in its highest during or shortly after acute ischemia.

Table 20.2 Studies evaluating the use of echocardiography to predict presence of acute myocardial infarction or acute coronary syndrome in patients with acute chest pain

Authors	Year	No. of adequate studies	Clinical criterion	Echocardiographic criterion	Sensitivity (%)	Specificity (%)	PPV (%)	NPV (%)	(+)LR	(-)LR
Horowitz et al.	1982	65	AMI	RWMA	94	84	86	93	5.9	14
			CAD		94	93	94	93	13.4	15.5
Loh et al.	1982	30	AMI	Severe hypokinesis	83	100	100	90	4	5.9
				Mild hypokinesis	83	72	67	90	3.0	4.2
Oh et al.	1985	26	AMI	RWMA	71	100	100	90	4	3.4
Sasaki et al.	1986	46	AMI	RWMA	93	87	78	96	7.2	12.4
			CAD		74	96	94	79	18.5	3.7
Peels et al.	1990	43	AMI	RWMA	92	53	46	94	2.0	6.6
			ACS/CAD		88	78	85	82	4.0	6.5
Sabia et al.	1991	169	AMI	RWMA	93	57	31	98	2.2	8.1
Gibler et al.	1995	901	Cardiac disease	RWMA	47	99	32	99	47	1.9
Izumi et al.	1995	74	AMI	RWMA	97	–	–	–	–	–
Kontos et al.	1998	260	AMI	RWMA/EF <40%	96	70	23	99	3.2	17.5
			AMI/PCI		91	75	44	98	3.6	8.3
Kontos et al.	1998	185	AMI	RWMA/EF <40%	100	82	16	100	5.6	4
			AMI/PCI/CAD		85	85	32	99	5.7	5.7
Mohler et al.	1998	92	AMI	nRWMA	83	84	56	95	5.2	4.9
			ACS		49	100	100	57	4	2.0
Luotolahti et al.	1999	81	ACS	RWMA	97	50	95	67	1.9	16.7
Kontos et al.	2002	149	AMI	RWMA/EF <40%	91	–	–	–	–	–
Swinburn et al.	2002	80	AMI	RWMA	92	47	23	97	1.7	5.8
Pooled data		996	AMI	RWMA	91	72	39	98	3.3	8.0
		726	ACS		83	81	70	90	4.4	4.8

The magnitude of the likelihood ratios represents the predictive rule-in (*positive* likelihood ratio) or rule-out (*negative* likelihood ratio) power of a test. Likelihood ratios are largely independent of the severity or the prevalence of disease in the index population. As opposed to sensitivity, specificity, and predictive values, and may thus represent pre-dictive power more adequately

Technology to provide transtelephone interpretation of digital images is available, and may significantly aid in realizing the optimal deployment of the technique. Although preliminary evidence suggests substantial cost saving potential, a formal study of the economics of incorporating echocardiography into routine evaluation of chest pain patients in the emergency department, or of basing triage decision on its results, has yet to be materialised.

Extent of Myocardial Infarction

Several investigators have addressed the ability of early echocardiography to provide prognostic information on intermediate or long-term follow-up in patients with acute coronary syndromes. Largely, these studies rely on the assessment of the number of affected segments or a

wall motion score index, rather than on the presence of regional dysfunction alone. The number of affected myocardial segments may be more closely related to the degree of left ventricular dysfunction, a major determinant of mortality and morbidity in patients with acute coronary syndromes. Echocardiography may be of particular benefit to identify patients who are at high risk:

- In non ST-segment elevation MI and in non Q-wave MI, presence or absence of segmental contractile dysfunction in 3 or more segments on the first day of the event added significantly to the predictive power of routinely available parameters to identify patients at high risk for predicting in-hospital major adverse cardiac events.
- In patients with acute chest pain and a non ST-segment elevation MI, echocardiography on admission could predict the risk of adverse events at 30 days (death, MI, revascularization), while the predictive power of wall motion abnormalities was better than that of clinical data, ECG, or baseline troponin measurements.
- In summary, echocardiography provides incremental prognostic information in patients presenting with acute chest pain syndromes. Specifically, the cardiac event rate does not only vary according to the presence or absence of left ventricular dysfunction but it also differs between the severity of contractile dysfunction.

Stress Echocardiography in The Emergency Room

Stress echocardiography has been proposed for additional risk stratification of patients with normal early resting echocardiograms, or after an short observation period during which myocardial injury markers prove negative. It may be of particular benefit in patients with acute coronary syndromes who do not show any resting wall motion abnormality as a result of the transient nature of ischemia-induced regional dysfunction, whose ischemic burden is below the detection threshold of echocardiography,

or, in situations where there is pre-existing wall motion abnormalities.

- Using dobutamine stress echocardiography, 72% of patients without ischemic changes on the ECG that would otherwise have been admitted to hospital could be discharged on average several hours after presentation when troponins are negative and the dobutamine stress is normal. In an other study, patients with acute chest pain, non-diagnostic ECG and normal biochemical markers underwent simultaneous stress ECG- and echocardiography. A normal echocardiographic study was associated with an event-free 12-month survival in 100% of patients, while prognostic power of stress echocardiography was superior than that of stress ECG.
- Dobutamine stress echocardiography was applied to risk stratify patients with similar clinical characteristics after a mean observation period of 3 h. In contrast to the earlier studies, patients were at relatively high risk, as evidenced by 45% of positive studies. At multivariate analysis, the only independent predictor of adverse cardiac events during 6-month follow-up was new or worsening wall motion abnormalities on the stress echocardiogram.
- A predischARGE dobutamine stress echocardiogram has also important independent prognostic value in low-risk, troponin negative, chest pain patients. It should be recognized, that in this clinical setting the incremental yield of stress echocardiography over standard stress ECG remains yet to be determined.
- Although stress echocardiography provides an attractive alternative for functional testing in patients who are unable to perform physical exercise, who have abnormal baseline ECG, or who belong to a population where false positive rates for stress electrocardiography testing is relatively high.

Pitfalls

Stress echocardiography may not easily distinguish wall motion abnormalities due to

reversible ischemia or acute MI from those that result from previous MI and scar. The observation that scarred segments may be characterized by increased echodensity in conjunction with a reduced diastolic thickness of 5 mm or less, may be helpful to better discriminate acute ischemic dysfunction from scar (Fig. 20.2). Also, a relatively small MI with only non-transmural involvement may not readily be detected by echocardiography.

A good echocardiographic window is critical for reliable and accurate evaluation of segmental contractile function. Intravenous contrast echocardiography may be of particular benefit for use in patients with acute chest pain (Fig. 20.3). Reliable endocardial border detection is the

conditio sine qua non for the evaluation of segmental contractile function, but may be impaired in up to 10–15% of investigations.

Both at rest and during stress, an intravenous injection of contrast improved endocardial border definition in up to 96% of cases, which translates to a significant increase in diagnostic accuracy, as intra- and interobserver variability are reduced, not merely between expert readers, but also between assessments by novices' compared with those made by experts. Therefore, contrast is indicated if 2 or more segments out of 17 segments can not be visualized.

Myocardial Contrast Echocardiography

Myocardial contrast echocardiography permits real-time bedside evaluation of myocardial perfusion as well as contractile function following intravenous injection of microbubbles. Identifying absence of a perfusion defect in conjunction with normal ventricular function, virtually excludes acute ischemia in a symptomatic patient evaluated for acute chest pain. Finding however a defect in a patient without a history of acute MI confirms its presence. In an established acute MI, the size of the defect reflects the myocardial area-at-risk and may help choosing the optimal therapeutic option.

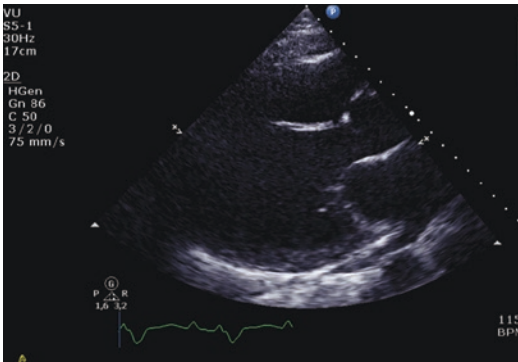


Fig. 20.2 Scar tissue in old anterior MI, LV dilatation and septal wall thinning

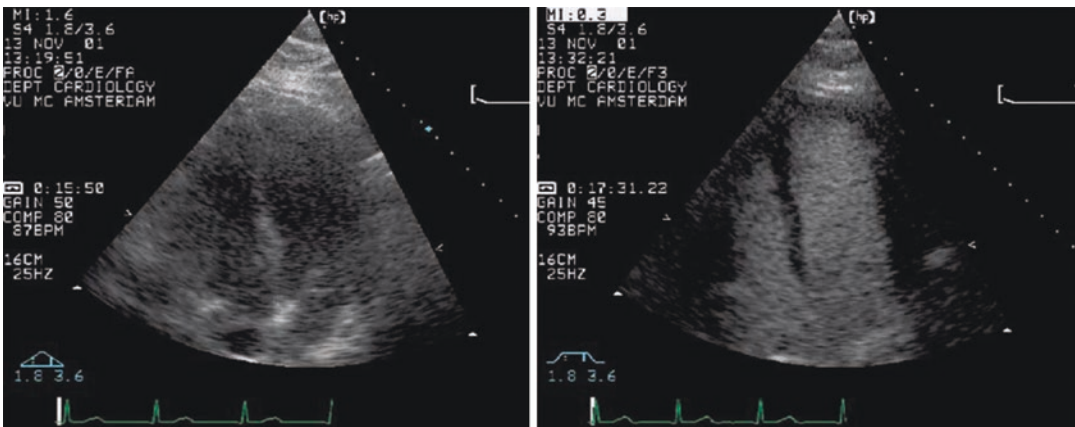


Fig. 20.3 Improved endocardial border detection using contrast agents

Risk Stratification

Following initial triage on basis of clinical and ECG parameters, there is an increasing evidence of the ability of two-dimensional echocardiography to accurately diagnose and risk stratify patient with acute chest pain. Echocardiography can detect early, before biochemical marker analysis become available, and more accurately patients with at low risk as the absence of segmental contractile dysfunction is an indicator against MI. It is likely that the accuracy of echocardiography in general and in the identification of acute coronary syndromes in particular, improves significantly in the presence of symptoms.

As tertiary triage following exclusion of irreversible damage by biochemical marker analysis, stress echocardiography is a powerful tool offering significant additional diagnostic and prognostic information.

Apart from acute myocardial ischemia, echocardiography reliably identify the presence or absence of most of the major non-ischemic cardiovascular causes of acute chest pain, e.g. aortic dissection or pulmonary embolism.

Availability and Trained Staff

However, optimal use of the technique in the emergency department requires dedicated and trained sonographers, high-quality equipment, around the clock availability of both image acquisition and interpretation services, and, importantly, realistic and thorough knowledge on the performance of echocardiography in this specific setting. We would advocate the use of contrast to further enhance echocardiography’s diagnostic accuracy and efficiency, both at rest and during stress.

Prognosis After Myocardial Infarction

Outcome after acute MI is related to the severity of left ventricular dysfunction, the presence or absence of residual myocardial ischemia and the

Table 20.3 Factors influencing prognosis of patients after acute MI

Age	Myocardial viability
Sex residual/recurrent ischemia	Residual/recurrent ischemia
Hypertension extent of CAD	Extent of CAD
Diabetes ventricular arrhythmias	Ventricular arrhythmias
Previous MI status of infarct-related artery	Status of infarct-related artery
LV function	
LV size	

occurrence of cardiac arrhythmias (Table 20.3). Using clinical characteristics and various techniques, patients with acute MI can be stratified into low or high-risk for subsequent morbidity and mortality. Two-dimensional and Doppler echocardiography has been shown to be useful and can easily be performed over time or during changes with treatment. It assists in the determination of prognosis based upon assessment of infarct size (regional left ventricular function), infarct expansion (global left ventricular function) and left ventricular diastolic function. Furthermore, inducible myocardial ischemia can be assessed by stress echocardiography, whereas low-dose dobutamine echocardiography can be used to detect myocardial viability.

Regional Left Ventricular Function

In the acute phase, MI is a regional disease leading to segmental wall motion abnormalities in the region served by the occluded coronary artery, and this regional left ventricular dysfunction can be detected by two-dimensional echocardiography. Using the standard parasternal and apical windows, the left ventricular can be imaged and divided into multiple segments for wall motion analysis. The number of segments into which the ventricle can be divided differs between publications, but the American Society of Echocardiography has recommended 16 segments (Fig. 20.4). Recently, a 17 segments division has been proposed for all imaging modalities, identifying the top of the apex as a separate segment. Each segment is assigned

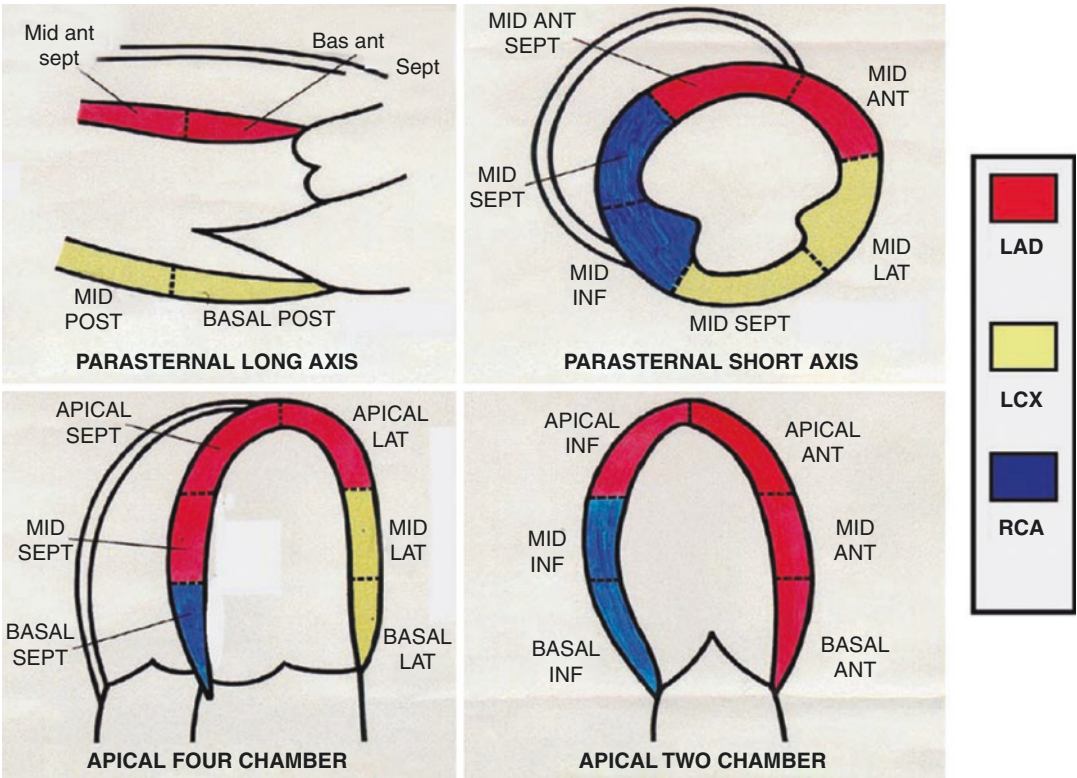


Fig. 20.4 The segmental division of the left ventricle as recommended by the American Society of Echocardiography

a numerical value based on the degree of wall motion abnormality, e.g. normal contracting segment (=1); segment with hypokinesis (=2); akinesis (=3); dyskinesis (=4) or aneurysmatic deformed (=5). A compensatory hyperkinetic segment is frequently scored as 0 (Table 20.4). Analysis is not only performed by degree of endocardial motion but more specifically by degree of myocardial thickening: thickening of more than 5 mm is normal contraction, between 2 and 5 mm is hypokinesis, less than 2 mm thickening is akinesis, and no thickening and outward motion is dyskinesis. Frequently, the interface between contracting and non-contracting tissue forms a visually distinctive pattern, the so-called “hinge point”. A wall motion score (WMS) index is calculated by summing up the scores for each segment and dividing by the number of segments analysed. This semi-quantitative analysis has been shown to correlate well with clinical status and ejection fraction and can identify high-risk patients (Table 20.5). There is a reasonable

Table 20.4 Regional wall motion score index

Each wall region (segment) is assigned a number, based upon its motion:	
0	= Hyperkinetic
1	= Normal
2	= Hypokinetic
3	= Akinetic
4	= Dyskinetic
5	= Aneurysmatic
1½	= Mildly hypokinetic
2½	= Severely hypokinetic
$WMSI = \frac{\text{sum of all segments}}{\text{no. of segments scored}}$	

relationship between myocardial segments and their supplying epicardial coronary artery. For example, the anterosseptum is almost always perfused by the left anterior descending artery and the inferior wall is mostly supplied by the right coronary artery. The lateral wall by the circumflex artery.

Table 20.5 Regional wall motion score index related to left ventricular function and ejection fraction

Regional wall motion score index and ejection fraction	
WMSI: 1	Normal LV function (EF > 60%)
WMSI: 1–1.5	Mildly depressed LV function
WMSI: 1.5–2	Moderately depressed LV function (EF 30–45%)
WMSI: >2	Severely depressed LV function (EF < 30%)

Pre-Thrombolytic Period

In the pre-thrombolytic period, patients with a high WMS (index) at admission had a higher rate of in-hospital mortality (27–40%) or serious in-hospital complications (death, shock, heart failure and arrhythmias; 68–94%) than patients with limited dysfunction of the left ventricular (2–7% and 7–18%, respectively). Also 1-year mortality was significantly higher in patients with a poor WMS at admission or predischARGE compared with patients with a good WMS (44–63% vs 0–13%). WMS index was an independent predictor of in-hospital and 1-year mortality, when compared with clinical variables.

Thrombolytic and Primary PCI Era

In the thrombolytic and primary PCI era, WMS (index) remains predictive of mortality and other serious cardiac events. In 6676 patients with acute MI it was shown that WMS index had prognostic importance for up to ≥5 years, both in patients treated with thrombolytic therapy and in patients not receiving this treatment (TRACE study). When compared with clinical variables or exercise test results, WMS index is the most powerful independent predictor. However, compared to WMS index during low- or peak dose dobutamine stress echocardiography, resting WMS index has less predictive value.

Studies have shown that regional left ventricular function may change over time after acute MI. Again in the TRACE study, repeated echo examination of left ventricular function during the first year has independent prognostic value

concerning death and worsening of heart failure. In that study, a decrease of 0.1 U of WMS index in patients with reduced systolic function, was indicative of an increase in the risk of death of 24–37%, which stresses the importance of serial evaluations.

Compensatory Hyperkinesia and Remote Asynergy (Remodelling)

For the evaluation of the left ventricular remodeling after acute MI, attention needs to be drawn also to the non-infarcted area. Both compensatory hyperkinesia and remote asynergy, however, have important prognostic implications. Compensatory hyperkinesia, defined as increased contractility of the non-infarct zone, occurs in a significant proportion of patients with AMI. It is more common in the acute phase and reduced by the use of β-blockade. Compensatory hyperkinesia occurs more frequently in patients with one vessel disease; absence of hyperkinesia is associated with a higher WMS and subsequent higher cardiac mortality. Hyperkinesia has been shown to have additional prognostic value to WMS index concerning long-term mortality in the TRACE study.

Remote Asynergy

Remote asynergy, defined as asynergy not directly adjacent to the infarcted area, occurs in approximately 20% of patients with AMI. Whereas hyperkinesia is more common in patients with one vessel disease, remote asynergy is predictive of multivessel disease. Remote asynergy is, like multivessel disease, related to recurrent ischemic events and higher cardiac mortality.

Global Left Ventricular Function

The WMS index is not only predictive of mortality and other serious cardiac events, but also related to infarct expansion and left ventricular

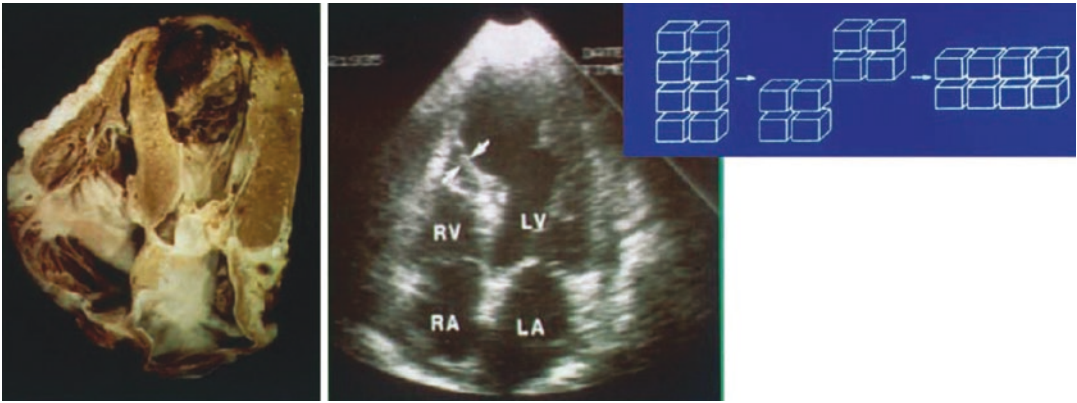


Fig. 20.5 Infarct expansion is caused by rearrangement of myocytes in the infarct zone

remodeling (Fig. 20.5). Several investigations have shown that the extent of left ventricular dysfunction is independently associated with progressive left ventricular dilatation. In 233 patients with a first anterior MI, treated with thrombolysis and with an acute WMS index >2 , an increase left ventricular volume indexes in the first 3 months was observed, whereas patients with a WMS index ≥ 2 did not have left ventricular remodeling.

Infarct Expansion

Infarct expansion is an important and early complication of acute MI that can be readily detected by two-dimensional echocardiography. It refers to an alteration in regional ventricular topography due to lengthening and thinning of the infarcted segment and results in left ventricular dilatation with global distortion of left ventricular shape. Infarct expansion is generally seen in patients with large, transmural, anterior MI, and is accompanied by increased mortality independent of left ventricular function.

Global Left Ventricular Shape

Global left ventricular shape is also important. Systematic quantitative assessment of left

ventricular shape, apart from left ventricular volume and function, have been attempted only recently. Two methods used to assess left ventricular shape after AMI:

1. the length/width ratio: the ratio of the ventricular long-axis length to left ventricular diameter,
2. the sphericity index: volume observed/volume of sphere using long axis as diameter.

The shape of the normal left ventricular is referred to as ellipsoid. Left ventricular shape tends to become abnormally wide (spherical) in left ventricular dilatation (Fig. 20.6). A more pronounced shape distortion has been associated with increased left ventricular volumes, decreased ejection fraction and more extensive wall motion abnormalities. After anterior MI, the degree of left ventricular sphericity correlates with exercise capacity: those with the highest sphericity index had the lowest exercise capacity and the highest heart failure score (Fig. 20.7). In patients with idiopathic dilated cardiomyopathy, a more spherical left ventricular has been associated with poor survival. Finally, it has been shown that increased left ventricular sphericity is the primary factor in the etiology of mitral regurgitation rather than mitral annular dilatation or left ventricular enlargement.

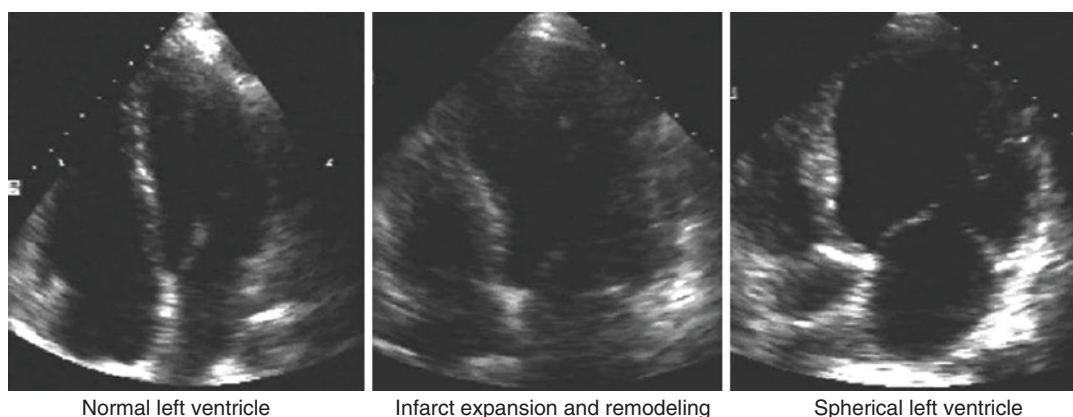


Fig. 20.6 Left ventricular shape changes in left ventricular dilatation

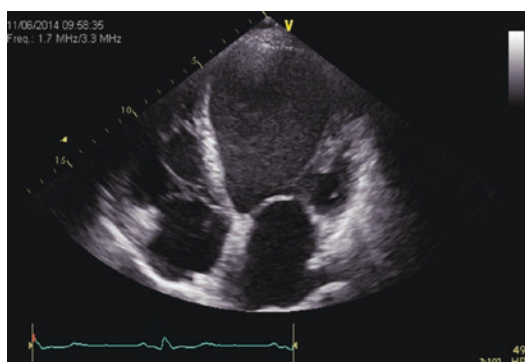


Fig. 20.7 Old anterior MI, global LV dilatation

Quantitating Left Ventricular Function

Left ventricular remodeling after AMI, resulting in dilatation of the left ventricle, is a progressive process beginning in the early phase and continuing for months and years. Our knowledge about the mechanisms and temporal sequence of left ventricular remodeling have been mainly derived from quantitative two-dimensional echocardiographic evaluation (Fig. 20.8). Previous investigations have identified left ventricular function, anterior infarct location, and the patency status of the infarct-related artery as the most important independent predictors of remodeling. Furthermore, serial quantitative echocardiography has been used in

several large, multicenter clinical trials (GISSI-1 to 3, SAVE, CONSENSUS-II) to demonstrate the beneficial effect of thrombolysis and angiotensin-converting enzyme inhibitors on left ventricular remodeling after AMI.

Progressive increase in left ventricular size is associated with deterioration in left ventricular function and increased mortality. It has been shown that left ventricular end-systolic volume is the primary predictor of mortality after AMI and the SAVE and GISSI-2 and 3 trials proved that quantitative echo measurements are the most powerful independent predictors of adverse cardiovascular events. Changes in left ventricular size and ejection fraction provide additional prognostic information, just like the additional value of changes in regional left ventricular function. In hospital survivors of acute MI treated with primary angioplasty for 5.3 years subsequent analysis showed that ejection fraction at 6 months and improvement in ejection fraction (from baseline to 6 months) were more important predictors of mortality than ejection fraction at the acute phase. Also in the V-HeFT trials, change in ejection fraction of $>5\%$ from baseline to 6 months and 1 year was the strongest predictor of mortality, even after adjustment for baseline ejection fraction. Regarding ejection fraction, the relation with mortality has been described as a hyperbolic curve with an upturn in mortality occurring at ejection fraction values of less than 40%. In the steep segment of the curve, a reduction of 10 points in ejection

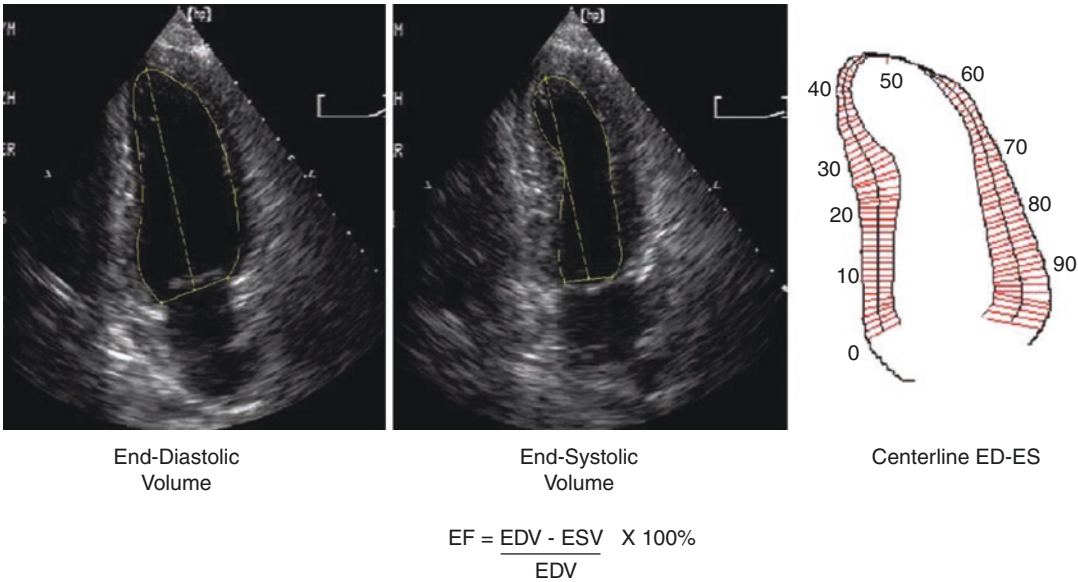


Fig. 20.8 Quantitative 2-D echocardiographic evaluation of volumes and ejection fraction

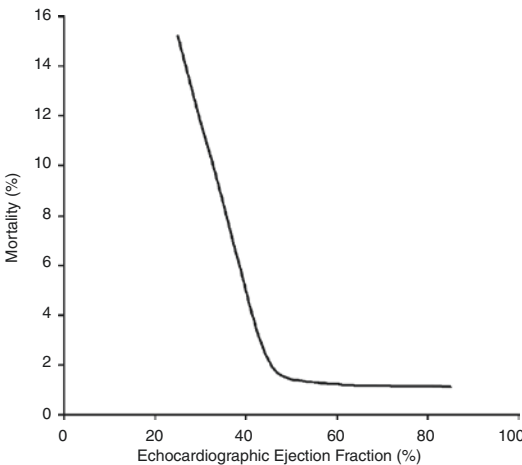


Fig. 20.9 Relation between mortality and ejection fraction (GISSI-2 trial)

fraction (from 30 to 20%) results in an upturn in mortality from 8 to 16%. In the flat part of the curve, the same reduction in ejection fraction (from 60 to 50%) leads to a non-significant increase in mortality from 1 to 1.5% (Fig. 20.9). With the help of the biplane method of Simpson (summed disks-method) in two perpendicular apical views, usually the AP4CH and AP2CH, endocardial contours can be traced during systole and diastole for EF and volumes. Trabeculae and papillary muscles are not included in the contour tracings and con-

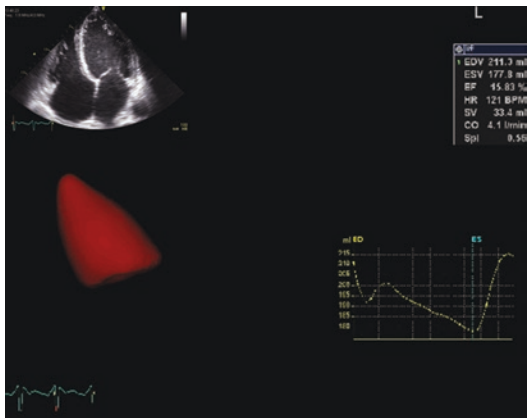


Fig. 20.10 Apical view: 3D assessment of LV function, EF 16%

sidered part of the LV cavity. More recently, 3D echocardiography is used for LV chamber quantification, without assumptions on geometry and avoiding foreshortening (Fig. 20.10). This allows for a higher accuracy and reproducibility than 2D chamber quantification.

Ischemic Mitral Regurgitation

Mitral regurgitation occurs frequently after myocardial infarction. If a papillary muscle is included in the infarcted area, this can result in

papillary dysfunction, unable to shorten during systole and thus with elongation leading to a prolaps of the mitral valve. It can exist temporary in the setting of reversible ischemia. Prolaps due to myocardial infarction is not seen often, because wall motion abnormalities reduces left ventricular inward motion and retract the valve. Wall motion abnormalities in the area of a papillary muscle group and left ventricular dilatation most frequently causes retraction of the valvular leaflet, with incomplete coaptation and a jet direction in the same direction as the retracted leaflet. In presence of global LV dilatation both leaflets malcoaptate, the closing point is displaced towards the apex. This are the so-called incomplete closure and tenting. Color Doppler echocardiography can be used to assess presence and severity of mitral regurgitation in patients with (acute) MI (Fig. 20.11). Significant mitral regurgitation—

moderate (grade 2) or severe (grades 3 and 4), graded according to the method of Helmcke et al.,—has been found in 3–21% of patients following acute MI. The incidence and severity of mitral regurgitation changes during follow-up, with the highest incidence on the 7th day. Most studies have demonstrated a relation between mitral regurgitation and inferoposterior infarct location, while others found either no influence of infarct location or an increased incidence in anterior infarctions. Significant mitral regurgitation has been correlated to female gender, older age and previous MI. Furthermore, abnormalities of left ventricular shape—more spherical ventricles—and inferoposterolateral wall motion abnormalities have been found to be independent predictors of mitral regurgitation.

Mechanisms

- The most dramatic aetiology results from frank rupture of a part or the papillary muscle. The incidence of this complication is reported to be only 1%. The infarction is usually posterior and is often small and localized; ejection fraction is frequently maintained. There is a high prevalence of one-vessel disease and occluded infarct-related arteries.
- Another form of ischemic mitral regurgitation results from papillary muscle dysfunction. The pathogenesis of this form of mitral regurgitation is unclear. Small changes in the spatial relation of the papillary muscles and the mitral valve leaflets and ventricular annulus (due to regional wall motion abnormalities and left ventricular shape changes) may produce incomplete mitral leaflet closure, resulting in eccentric mitral regurgitation. This mechanism is more common in inferoposterior MIs, possibly because the blood supply to the posterior papillary muscle is provided by 1 rather than by 2 coronary vessels, as in the anterior papillary muscle.
- The third category consists of patients with multiple MIs or anterior aneurysms with low ejection fractions. The regurgitation results from the central area of the mitral valve and is secondary to generalized ventricular and

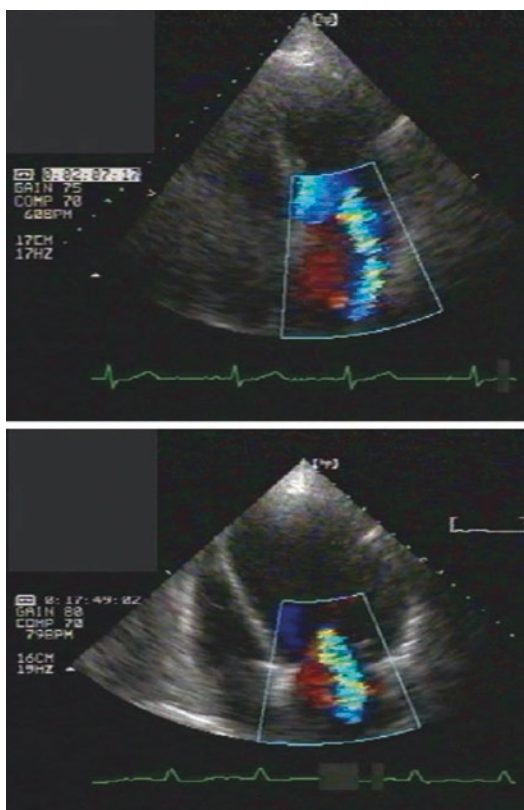


Fig. 20.11 Color Doppler evaluation of mitral regurgitation and mechanism of ischemic mitral regurgitation: papillary muscle rupture; papillary muscle dysfunction; mitral annular dilatation/generalized dilatation

annular dilatation. Presence of mitral regurgitation on catheterization or Doppler echocardiography has been related to higher cardiovascular mortality and severe congestive heart failure. In patients studied with Doppler echocardiography within 48 h after acute MI, the 1-year mortality was 48% in patients with mitral regurgitation, and 11% in those without. In other studies, mitral regurgitation was found to be an independent predictor of cardiovascular mortality.

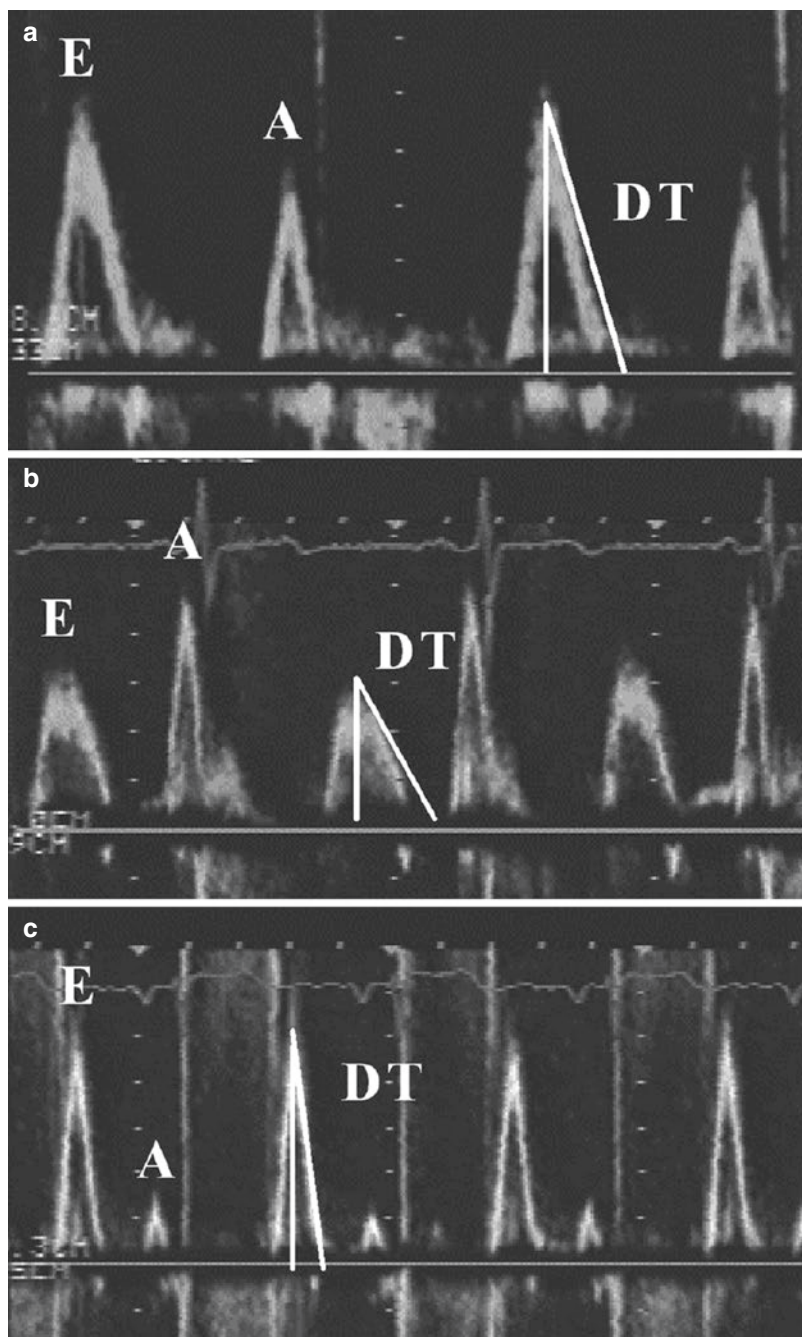
Left Ventricular Diastolic Function

Pulsed Doppler echocardiography is useful for assessment of left ventricular diastolic properties. Three distinct abnormal mitral inflow patterns have been described and correlated with hemodynamic findings.

- One pattern, characterized by a low E wave, a high A wave, a low E/A ratio and a prolonged E deceleration time (Fig. 20.12b), is thought to be the consequence of impaired relaxation in the presence of normal left ventricular filling pressures. It has been described in normal aging, left ventricular hypertrophy and acute ischemia.
- The opposite pattern, characterized by high E waves, low A waves, high E/A ratio and short E deceleration time (Fig. 20.12c), is associated with high left ventricular filling pressure and increased chamber stiffness and is observed in advanced cardiac disease. The short deceleration time suggest an early equalization of pressures in the left atrium and the left ventricular.
- The third pattern is essentially a normal pattern that has been referred to as “pseudonormal” (Fig. 20.12a). This pattern may represent a transitional state between impaired relaxation and restrictive patterns in patients with left ventricular systolic dysfunction.
- The ratio of E and e' (E/e') provides another indication of LV filling pressures. The measurements are most frequently obtained from the AP4CH avoiding an angle more than 20° between annulus motion and the cursor. A E/e' of 15 or higher is indicative for elevated LV filling pressure. However, this measurement is not reliable in patients with significant annulus calcification, mitral regurgitation and after mitral surgery.

Several investigators have studied the left ventricular filling patterns in patients with AMI. An abnormal relaxation pattern has been shown to be more common in patients with small infarctions. In contrast, patients with large infarctions exhibit often a “pseudonormalized” or even restrictive pattern within the first week. It has been demonstrated that this pattern frequently changes over time becoming less restrictive pattern, maybe as result of left ventricular remodeling. Patients with anterior MI treated with primary angioplasty and a restrictive filling pattern at day 3 (defined as E deceleration time ≤ 130 ms) had progressive increases in left ventricular volume indexes at 6 months, in contrast to patients with nonrestrictive filling. E deceleration time was the most powerful predictor of left ventricular dilatation. Limited studies have assessed the relation between left ventricular filling patterns and prognosis after AMI. In patients examined with serial Doppler echocardiography on days 1, 3, 7 and 3 months after AMI, left ventricular filling patterns were related to clinical follow-up for 32 ± 17 months. The survival rate at

Fig. 20.12 Mitral inflow patterns after myocardial infarction. (a) Normal or pseudonormal inflow pattern. (b) Impaired relaxation pattern. (c) Restrictive pattern



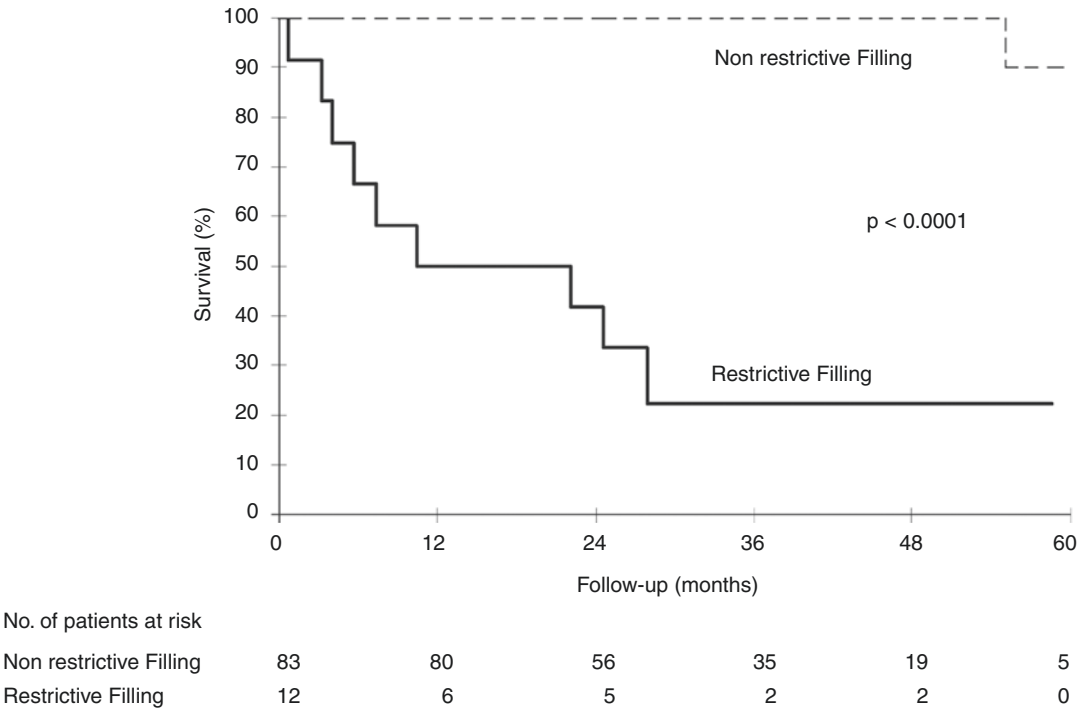


Fig. 20.13 Left ventricular filling and cardiac survival

1 year was 100% in patients without restrictive filling and 50% in those with restrictive filling (Fig. 20.13). Left ventricular filling pattern was the most powerful independent predictor of cardiac death and adds significant prognostic information to indicators of systolic dysfunction (ejection fraction and end-systolic volume). Others also found that restrictive filling was an independent predictor of cardiac death. Finally, it has been demonstrated that the presence of restrictive filling is an independent predictor of heart failure after AMI. An explanation for this observation may be the markedly elevated filling pressure often found in those patients. Also, a strong relation between restrictive filling and elevated pulmonary wedge pressure in post MI patients with left ventricular systolic dysfunction was observed. An E/A ratio >2 was associated with pulmonary capillary wedge pressure ≥ 20 mm Hg in 96% of patients, whereas E deceleration time provides an accurate estimate of left ventricular filling pressure in patients with a “normal” E/A ratio.

Left Ventricular Spatial Flow Pattern

Color Doppler echocardiography and pulsed wave Doppler flow mapping can be used to assess the flow patterns in the left ventricle.

Normal left ventricular flow is characterized by:

1. simultaneous onset of blood motion at the mitral valve and the apical level.
2. a discontinued Doppler signal along the lateral wall (a diastolic positive wave, followed by a negative wave during systole) and inter-ventricular septum (an early diastolic positive wave, followed by a negative wave at late diastole and systole).

Abnormal flow patterns can be recognized:

1. Apical rotating flow and vortex ring formation characterized by systolic persistence of red near the lateral wall. On pulsed Doppler, there is a continuously positive flow signal near the lateral wall and a continuously negative signal near the septum.

2. Vortex ring formation is characterized by central red flanked on both sides by blue during diastole. On pulsed wave Doppler this pattern is characterized by an apparent delay in onset of blood motion at the apical level compared with the mitral valve; in addition, a higher flow velocity compared with normal is found at the apex.

The presence of an abnormal flow pattern after AMI is highly associated with left ventricular thrombus formation. In patients with acute MI, flow patterns were examined within 24 h, after 6 weeks and 3 months. None of the patients with a normal left ventricular flow pattern at the first examination developed a thrombus, versus 40% of patients with an abnormal flow pattern. Furthermore, an abnormal left ventricular flow pattern has been shown to be an independent predictor of thrombus formation.

Mechanical Complications: Ventricular Septal Rupture, Papillary Muscle Rupture, Free Wall Rupture

In the presence of a chronic existence of a myocardial rupture with pericardial adhesions, a pseudo aneurysm develops (Fig. 20.14) (Table 20.6). The wall of the aneurysm exist only of peri-

cardium. The thin wall is prone to rupture, and may lead to acute mortality. A special type is the sacular pseudo aneurysm. This is a diverticle-like expansion of the pericardium in the presence of a small myocardial rupture. Accurate diagnosis of a pseudo aneurysm is critical important, because it allows the patient to be operated upon. Discrimination of a true aneurysm can be difficult. In this respect contrast echocardiography can be helpful.

A true aneurysm is formed after a large myocardial infarction with a thin and fibrotic wall, and bulges outwards (Fig. 20.15). There is a diastolic abnormal bulging contour, and a systolic dyskinetic motion. The wall of a true aneurysm exists from thin and fibrotic myocardium and not only form pericardium. The risk of rupture is small in contrast to the pseudo aneurysm. Distinction between the two types can be made by the size of the opening; this is wide for true aneurysms and small for pseudo aneurysms. Color Doppler and contrast can be helpful.

Pericardial effusion is not only observed after a free LV wall rupture (Fig. 20.16), but also as an aspecific reaction to a transmural infarction. The patient may have chest discomfort and signs of pericarditis on ECG. Tamponade is infrequently seen in these patients.

Mitral regurgitation can be caused by an infarcted papillary muscle rupture (Fig. 20.17). If a small part of the head of the muscle is ruptured, this can be

Fig. 20.14 AP4CH:
Apical located pseudo
aneurysm with thrombus

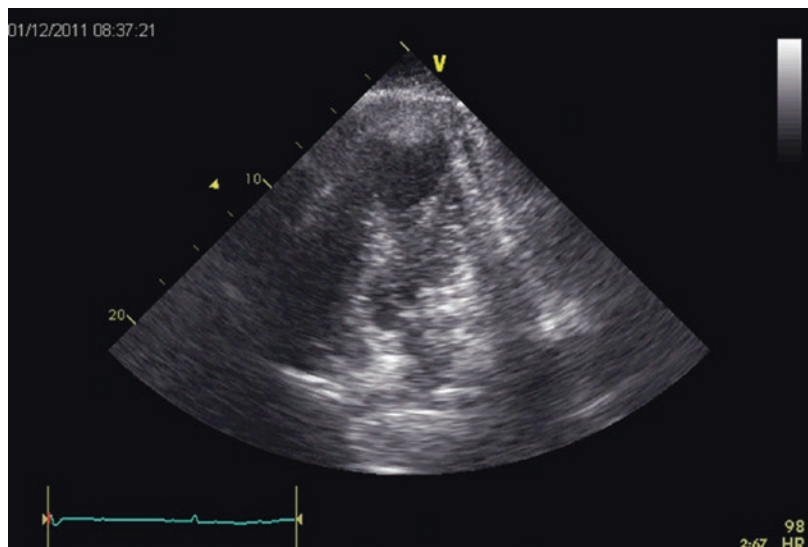


Table 20.6 Complications after myocardial infarction

Silent
– Thrombus left ventricle
– Pseudo aneurysm
– True aneurysm
– Pericardial effusion
– Mitral regurgitation (due to LV dilatation)
Mechanical
– Mitral regurgitation (due to papillary muscle dysfunction, EMA's, papillary muscle rupture)
– Ventricular septal defect
– Free LV wall rupture

hardly distinguished from a chordal rupture. If the entire papillary muscle ruptures, this occurs most frequently several days after the myocardial infarction. Most frequently, it is a relatively small myocardial infarction, and sometimes not recognized earlier. Due to the severe mitral regurgitation, pulmonary congestion occurs, whilst the cardiac output reduces. The patient is acutely severe dyspnoeic and hypotensive. The mitral regurgitation murmur is not audible due to the large regurgitation orifice and the small pressure differences between left

Fig. 20.15 AP2CH: true basal inferoseptal aneurysm (A)

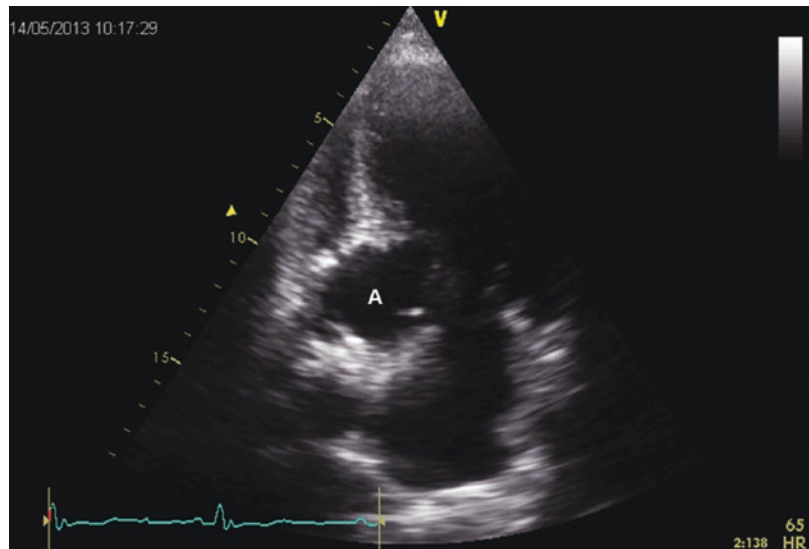
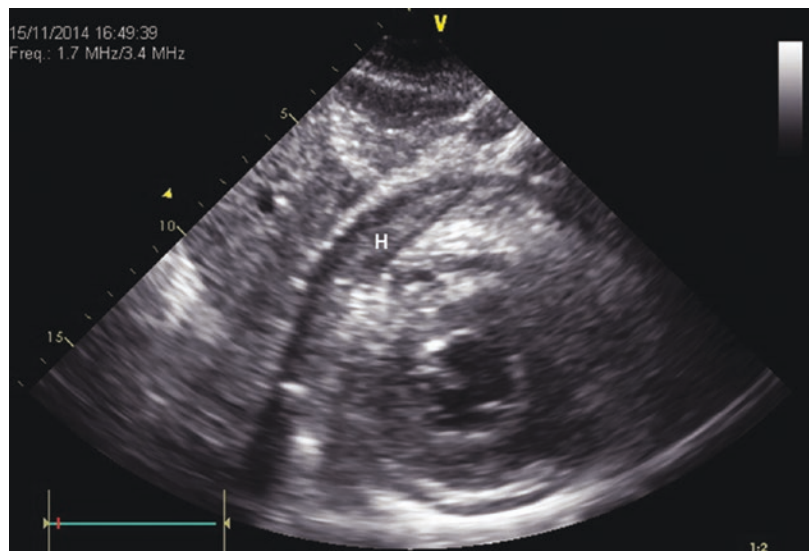


Fig. 20.16 Free wall rupture, tamponade and intrapericardial haematoma (H)



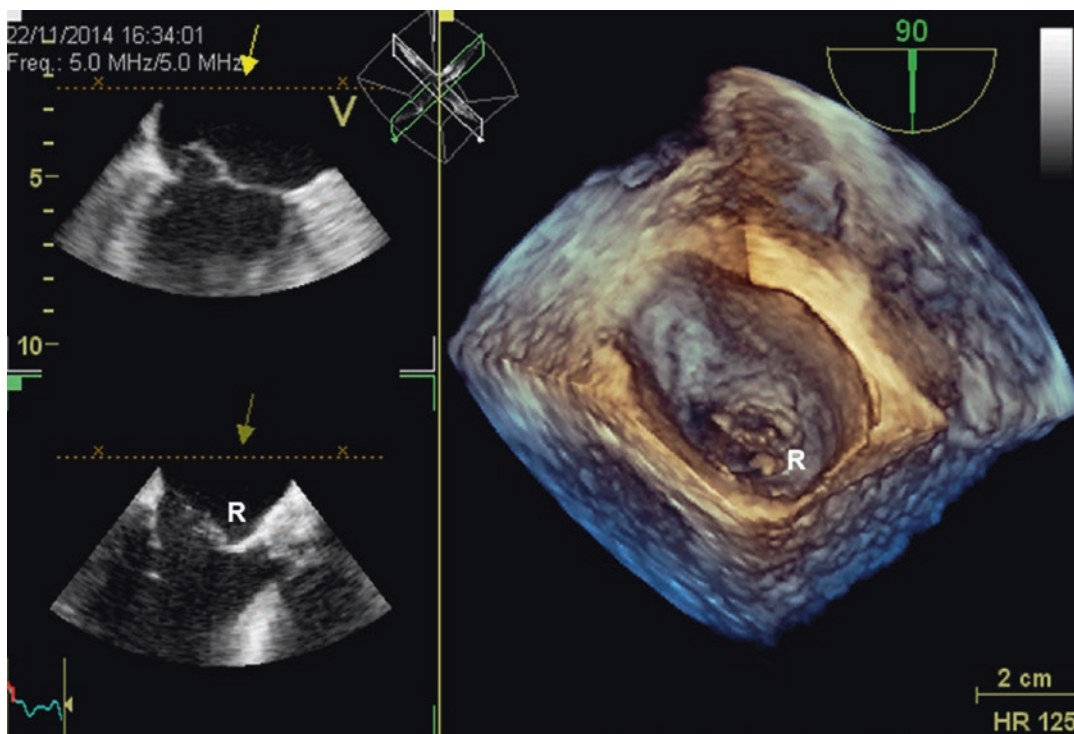


Fig. 20.17 TEE and 3D: papillary muscle rupture (R)

ventricle and left atrium. A transoesophageal echocardiogram should be performed unless diagnosis can be made by transthoracic echocardiography.

A ventricular septal rupture can develop due to necrosis of the intraventricular septum (Fig. 20.18). By physical exam a holosystolic murmur can be observed. Frequently, a small or moderate size myocardial infarction is present. The patient is often critical ill. The shunt provides acute volume overload of the pulmonary circulation and the left ventricle. Diagnosis can be obtained by color Doppler by demonstrating flow from the left ventricle through the septum and into the right ventricle (image). A hyperdynamic left ventricle except the infarcted area can be seen. The right ventricular peak pressure should be determined because volume overload of the shunt can lead to pulmonary hypertension.

Not only the septum can rupture, but also the free left ventricular wall. Very frequently the patient dies due to tamponade. Sometimes the patient survives due to resistance to flow because of pericardial adhesions or thrombus at the site of rupture. This can be recognized by

local or global pericardial effusion and an akinetic area in the free wall of the left ventricle, while diagnosis is confirmed by two-dimensional images or color Doppler flow through the rupture.

Silent Complications: Left Ventricular Thrombi, Aneurysm, Pseudoaneurysm

A left ventricular thrombus is mostly found in the setting of a transmural MI with a clear akinetic or dyskinetic state of the infarcted wall segment where the regional bloodflow is low (Fig. 20.19). This can occur in a true or pseudo aneurysm, infarcted wall segment, most frequently in the apex. Disability or even mortality after acute MI may be the result of a left ventricular thrombus and subsequent embolization. In the GISSI-III study, the incidence was approximately 12% in anterior MI's, mostly observed in the left ventricular apex, and 2% in MI at other sites. Most thrombi occur within the first 2 weeks after acute MI and are easily detected by

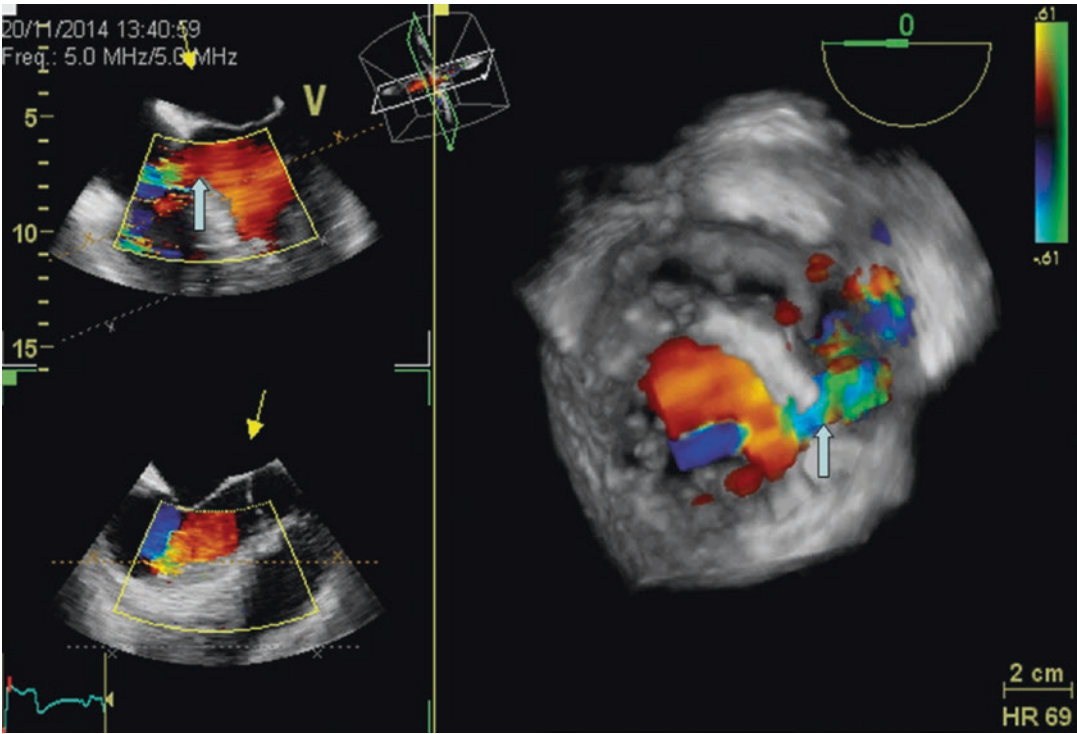
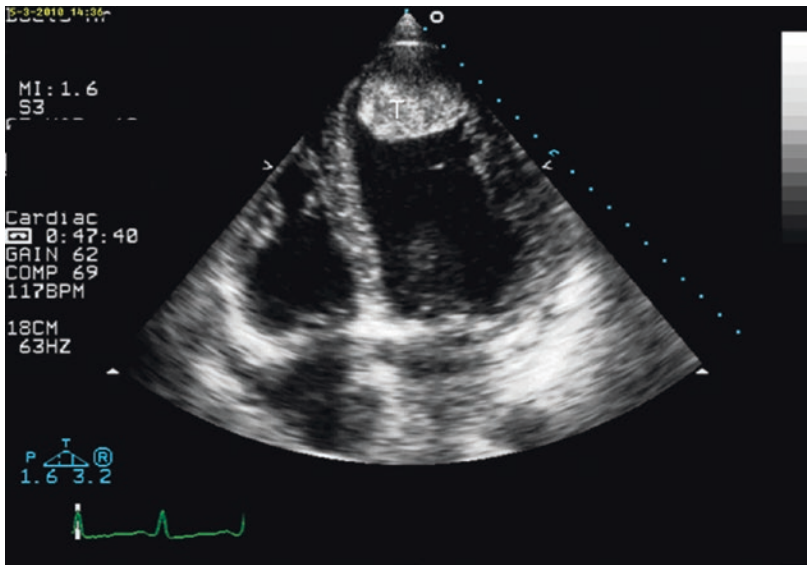


Fig. 20.18 3D TEE image of ventricular septal rupture () with color Doppler

Fig. 20.19 AP4CH:
Severe LV dysfunction
and protruding apical
thrombus (T)



two-dimensional echocardiography with a sensitivity of almost 95% and a specificity of 90%. Oral anticoagulation (warfarin, coumarin) is the treatment of choice to prevent embolic events. Mobile

and protruding thrombi and adjacent hyperkinesia are markers of high risk of systemic embolization. It can be difficult to discriminate a small apical thrombus from a normal trabeculae in the apical

area due to nearfield transducer artefacts. Use of a high frequency transducer and correct position of the focal zone can be helpful or additional contrast echocardiography. A thrombus is recognized as a mass by demarcation with color Doppler or contrast. The disappearance or reduction in size of left ventricular thrombi during anticoagulation therapy can be observed by serial two-dimensional echocardiography in approximately half of the patients during 1-year follow-up. Resolution was more likely to occur in patients without apical dyskinesia.

Myocardial Viability

Low-dose dobutamine echocardiography is one of the available techniques for determining the presence of viable myocardium (Fig. 20.20).

The response of myocardial segments that are dysfunctional at rest to low-dose dobutamine predicts recovery of regional function after acute MI with sensitivities and specificities ranging from 66 to 100% and from 68 to 94%, respectively (Tables 20.7 and 20.8). Several studies have evaluated the prognostic implications of myocardial viability in patients with AMI and in patients with recent or previous MI. The presence of myocardial viability in the Echo Dobutamine International Cooperative (EDIC) Study in 778 patients early after acute MI was associated with an increased incidence of unstable angina. Others also demonstrated that presence of viable myocardium independently predicts ischemic events. Myocardial viability was the single best predictor of cardiac events (mainly unstable angina and revascularization procedures) in patients with

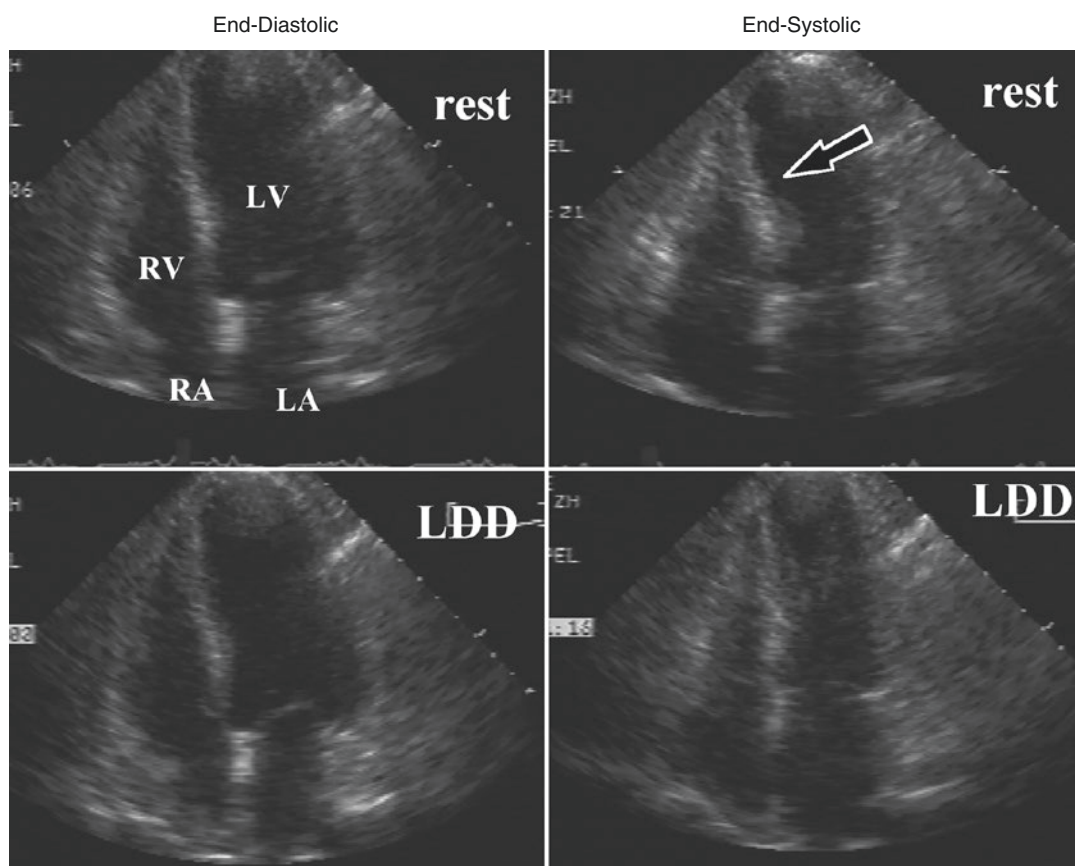


Fig. 20.20 End diastolic and end systolic still frames of an apical four-chamber view at rest and during low-dose dobutamine infusion. Note the presence of myocardial

viability in the middle and apical segment of the infero-septal wall (arrow)

Table 20.7 Sensitivities and specificities of low-dose dobutamine echocardiography to detect functional recovery after acute MI

Authors	Patients (n)	Follow-up echo (mo)	Sensitivity (%)	Specificity (%)
Pierard	17	9	100	70
Smart	63	1	86	90
Previtali	59	2	79	68
Salustri	57	3	66	94
Watada	21	1	83	86
Leclercq	40	2	82	83
Smart	11.5	1–2	86	83

Table 20.8 Appropriate use of echocardiography in (suspected) chest pain/myocardial infarction

• Acute chest pain with suspected MI and nondiagnostic ECG when a resting echocardiogram can be performed during pain
• Hypotension or hemodynamic instability of uncertain or suspected cardiac etiology
• Evaluation of a patient without chest pain but with other features of an ischemic cause or laboratory markers indicative of ongoing MI
• Suspected complication of MI, including but not limited to acute mitral regurgitation, ventricular septal defect, free wall rupture or tamponade, shock, right ventricular involvement, heart failure or thrombus
• Initial evaluation of ventricular function following ACS/MI
• Re-evaluation of ventricular function following ACS/MI during recovery phase when results will guide therapy
• Selective use of contrast when 2 or more LV segments are not seen
• Viability assessment with dobutamine stress in known moderate to severe LV dysfunction after MI

previous MI. The presence of myocardial viability independently predicted recurrent ischemia in patients early after acute MI.

The prognostic impact of viability on cardiac mortality remains unresolved. Myocardial viability did not predict cardiac death, which predominantly correlated with age and ejection fraction in some studies. Ejection fraction, but not myocardial viability, was significantly associated with the occurrence of cardiac death in some studies. Only in patients with an ejection fraction lower than 35%, cardiac death occurred less frequently in patients with viability who underwent revascularization. In these patients with reduced ejection fraction, absence of viability predicted a high mortality rate.

Similar conflicting results have been found early after acute MI. In patients with left ventricular systolic dysfunction and with myocardial viability, the presence of left ventricular dysfunction was predictive for hard cardiac events. In other studies, hard events were not predicted by the presence of myocardial viability and thus myocardial viability did not have independent

prognostic value. Prospective studies on the impact of myocardial viability in patients' outcome however are lacking. Until that time, the presence of myocardial viability is currently a strong indicator for revascularization.

Residual Myocardial Ischemia

Stress echocardiography in patients after MI can be safely performed predischarge with use of exercise-related or pharmacologically induced stress, including dobutamine and dipyridamole. It is based on the principle that stress-induced ischemia result in new or worsening wall motion abnormalities that can be detected by two-dimensional echocardiography. During the last 10 years, digital technologies have rendered stress echocardiography more feasible. A single cardiac cycle can be stored before, during and after stress, and replayed indefinitely. Each loop can be reviewed in synchrony, side by side with other loops, through which the comparison of different conditions is made easier.

Exercise echocardiography has been used to evaluate patients after acute MI. The occurrence of new or worsening wall motion abnormalities predicted the development of future cardiac events, with a sensitivity ranging from 63 to 80% and a specificity of 78 to 95%. However, major limitations of these studies are the relatively small sample size and the inclusion of soft and subjective endpoints, such as unstable angina and revascularization procedures, in order to document prognostic power.

High dose dobutamine echocardiography has been found very useful for risk stratification after acute MI. Two-dimensional echocardiography is performed during infusion of dobutamine up to 40 $\mu\text{g/kg/min}$, and if necessary, with addition of atropine. The contractile response of stunned myocardium to high dose dobutamine is variable, depending on the infarct-related artery stenosis. When there is a flow limiting stenosis, a biphasic response can be found (improvement at low dose followed by worsening at high dose), while, when there is no flow limiting stenosis, the improvement of stunned myocardium continues throughout the infusion. In this way, dobutamine echocardiography is able to predict the presence of a severe residual stenosis of the infarct-related artery and can identify high-risk patients who benefit most from revascularization procedures.

Moreover, dobutamine echocardiography is able to elucidate transient wall motion abnormalities in the remote area. The occurrence of remote asynergy during stress testing has shown to be correlated with multivessel coronary artery disease and is predictive of future ischemic events.

The prognostic impact of inducible ischemia by high dose dobutamine after acute MI have been extensively studied. Several studies have evaluated the event rate of both hard and spontaneous cardiac events in patients with a negative versus a positive dobutamine stress echocardiogram. The risk of cardiac death doubles if the test is positive. Positivity of dobutamine stress echocardiography is an independent predictor of hard cardiac events (death and non-fatal reinfarction) and all cardiac events (death, non-fatal reinfarction and unstable angina). Wall motion

score index at peak dose dobutamine, reflecting the extent of MI and ischemia, is found to be an independent predictor of cardiac death.

Dipyridamole echocardiography can also be used to evaluate myocardial viability, residual ischemia and prognosis after AMI.

Future Developments

Three-dimensional echocardiography may become the ultimate diagnostic modality because it can display the left ventricle, its size, shape and abnormalities in motion from any perspective. With the use of the real-time 3D modality with a matrix transducer, the echo examination will become more standardised and less operator dependent. Cardiac cross-sections that are difficult or impossible to obtain from the regular precordial studies can be computed from the data set in any desired plane (anyplane echocardiography). The images needed for diagnosis are only part of the total three-dimensional data set and left ventricular function in patients with coronary artery disease can be visually assessed and quantified. Specifically, true volumes of aneurysmal left ventricles can be assessed without geometric assumptions rather than using one or two orthogonal planes. The echo examination itself will be easier and quicker, but more time will be needed for subsequent wall motion analysis at a viewing station and for left ventricular volume calculations.

Clinical Recommendations and Implications

The goal of risk stratification after acute MI is to identify patients whose outcomes can be improved through specific medical interventions. Patients with the highest risk for cardiac death or recurrent ischemic events benefit most from aggressive medical therapy and/or revascularization procedures. In times of evidence-based and cost-effective management, the selection of a test that provides the most useful diagnostic and prognostic information is of paramount

importance. In this regard, echocardiography has proven its value. Patients who have nearly normal left ventricular function have a very low risk for death and may therefore be candidates for early discharge from the hospital.

Predischarge or early postdischarge stress testing should be used for further risk stratification within this group of patients. Only in patients who cannot exercise or whose baseline ECG precludes accurate interpretation of exercise-induced ischemia, pharmacologically induced stress echocardiography should be performed. The incremental value of additional echocardiography in all patients has not been shown to be worth the increased costs.

Routine reevaluation by echocardiography in the absence of any change in clinical status is not recommended. In the evaluation of systemic hypotension and/or a suspected mechanical complication of MI, echocardiography is of utmost importance to differentiate between low output due to poor left ventricular function, decreased preload, peripheral vasodilatation or cardiac tam-

ponade or mechanical complications as ventricular septal rupture, papillary muscle rupture and free wall rupture. This will be discussed in more detail in a later chapter.

Patients with moderate to severe systolic dysfunction are at higher risk for cardiac death, heart failure and left ventricular dilatation. Pulsed wave Doppler of left ventricular filling should be assessed, because presence of restrictive left ventricular filling identifies patients at very high risk of cardiac death. Assessment of myocardial viability and presence and extent of ischemia could be useful to define the potential efficacy of revascularization procedures.

Finally, serial echocardiography is recommended in patients with moderate to severe left ventricular dysfunction to assess changes in regional and global systolic function and left ventricular volumes, since these changes have independent prognostic value and can be used to guide therapy. Serial echocardiography is also recommended in patients with left ventricular thrombi.

Thomas H. Marwick

Pathophysiology

The underlying principle of stress echocardiography is that ischemic tissue (and in non-ischemic disease, other types of pathologic tissue) is unable to augment function during stress. Moreover, the extent of coronary disease determines the extent and severity of ischemia, which in turn determines the time-course and spatial distribution of abnormal wall motion. Therefore, inducible wall motion abnormalities may be subtle (or even absent) if the stenosis is moderate, or distal, or if the level of stress is inadequate.

The implications of these pathophysiological considerations are that:

- (a) the nature of stress is selected to maximize the development of ischemia,
- (b) acquisition needs to be optimized to pick up potentially transient wall motion abnormalities,
- (c) diagnostic criteria should incorporate markers of subtle ischemic changes.

Stress Testing

Preparations

Preparation for stress testing are well known and should be little influenced by adding echocardiography, with the exception of leaving imaging windows clear of electrodes. Anti-ischemic therapy is usually stopped before diagnostic but not for prognostic studies. The evidence supporting the practical aspects of performing this test have been well reviewed in current guidelines, and the following section seeks to provide practical guidance [1].

Selection of Stress Method

Stress echocardiography may be performed with exercise and non-exercise stressors, although the use of echo contrast agents may make insertion of an intravenous line important for both techniques. The selection of either stress protocol should be tailored to each patient, and in the opinion of this author, an effective stress echo laboratory should offer both exercise and pharmacologic modalities.

Patients who are unable to exercise maximally (who account for up to 40% of patients requiring functional testing) require a non-exercise stress, of which there are four categories—exercise simulating agents (e.g. dobutamine),

T. H. Marwick
Baker Heart and Diabetes Institute,
Melbourne, VIC, Australia
e-mail: tom.marwick@baker.edu.au

vasodilators (dipyridamole, adenosine), pacing stress and agents with specific indications such as ergonovine, cold pressor and mental stress. The latter two categories will not be discussed further.

In patients who are able to exercise maximally, either treadmill or bicycle exercise (upright or supine) may be used. The latter may not offer as potent a stress as does maximal exercise on the treadmill, but compensates for this by permitting peak imaging, which is sometimes of interest in identifying the time of onset of ischemia, and avoiding the problem of rapid resolution of ischemia. The overall accuracies of treadmill and bicycle stress are similar, the bicycle being more sensitive and less specific.

The selection is driven by local preference and expertise. Finally, while exercise echo tests are equipment intensive (treadmill or ergometer, stress ECG computer, and echocardiography machine), they usually require only two persons (supervising physician or exercise physiologist and sonographer). In contrast, most sites involve three staff for pharmacologic stress—the additional person being a nurse to supervise the infusion. Due to both this reason, and because of the duration of these protocols, pharmacologic stress is not performed in some laboratories.

Which Stressor?

- *1. Exercise stress:* Exercise testing is preferable to pharmacologic stress if the patient is able to exercise, to allow symptoms to be better correlated with workload, obtain prognostically important hemodynamic and exercise capacity data, and stress the heart more vigorously, which optimizes test sensitivity.
- Imaging can be performed before and immediately after treadmill exercise, upright or supine bicycle ergometry. Careful consideration should be given to logistic details, especially regarding rapid acquisition of post-exercise images, which should start within 10–20 s of the end of exercise and be finished within 60–90 s. The advantage of supine bicycle ergometry is that imaging can be performed throughout the stress test.

Pharmacological Stress The issue of which pharmacological stressor is most feasible and accurate has been hotly debated! Early animal work using quantitative two-dimensional echocardiography and microspheres showed that dobutamine was more effective in inducing myocardial dysfunction but produced smaller blood flow heterogeneity for similar coronary lesions. In contrast, dipyridamole induced large differences in regional subendocardial perfusion, but regional myocardial dysfunction was only observed when an absolute decrease in subendocardial blood flow was present. Subsequent clinical studies suggested that vasodilator stress echo was less sensitive, probably because the agents are not very potent stressors from the standpoint of inducing ischemia by increasing oxygen demand. As a consequence, “third generation” protocols have been developed that incorporate an agent to increase cardiac workload (e.g. atropine and dobutamine), and these new protocols have analogous results to those obtained with dobutamine and atropine. Indeed, the development of myocardial contrast echocardiography is leading to new interest and application of vasodilator stress echocardiography because its intense coronary hyperemia allows detection of perfusion heterogeneity. Specific indications for pharmacologic stress are listed in Table 21.1.

Dobutamine is by far the most widely used pharmacologic stress, and is suitable for most

Table 21.1 Indications for pharmacologic rather than exercise stress

	Clinical situation
Inability to exercise maximally	Vascular disease Chronic lung disease Neurologic/orthopedic problems Poor functional capacity (advanced age)
Specific indications	Myocardial viability (dobutamine or dipyridamole) Detection of coronary spasm (ergonovine)
Interpretation	Resting wall motion abnormalities
Application of new technologies	Myocardial contrast echocardiography Myocardial tissue Doppler/strain

patients, although it is contraindicated in patients with severe hypertension and serious arrhythmias. Dobutamine is usually administered incrementally in 3 min stages, starting at 5 mcg/kg/min, and increasing to 40 mcg/kg/min stages, with atropine being added (if not contraindicated) if the test is negative at peak dose.

The end-points of the test are:

- completion of the protocol,
- development of severe ischemia,
- intolerable symptoms
- development of side-effects, including arrhythmias, hypotension (symptomatic or to <100 mmHg) or hypertension (>220/120).

Over two-thirds of patients attain peak dose or achieve an ischemic end-point. Usually, stopping the drug is sufficient for the treatment of side-effects but sometimes beta blockers are required. Serious events (defined as those necessitating hospital admission) occur in 1 to 3:1000 patients. Nonetheless, while side-effects may concern the physician performing the test and compromise its sensitivity (see below), major complications are exceedingly rare.

One advantage of on-line echocardiographic imaging is that the extent and severity of ischemia may be better appreciated than they might with the electrocardiogram alone, or with pre- and post-stress imaging alone. This may permit termination of the stress before severe left ventricular dysfunction develops or prevent a premature termination without any objective evidence of ischemia.

Coronary vasodilator stress is used as the stressor of choice in some parts of Europe.

The two vasodilator stressors used are dipyridamole and adenosine.

- (a) *Dipyridamole* exerts its effects indirectly, by increasing endogenous adenosine levels by reducing cellular re-uptake and metabolism. Dipyridamole induces ischemia by causing coronary “steal” that effectively shunts blood from the territory of a stenosis by allowing it to run off into non-stenosed territories. The preparation of the

test is similar to the other stressors, although an important difference is that coffee, tea and cola drinks should be avoided for a day before the examination, because the xanthines contained in these agents antagonize the effects of dipyridamole on adenosine metabolism as well as competitively inhibiting adenosine activity. Dipyridamole is administered intravenously at a rate of 0.56 mg/kg/min over 4 min, followed 2 min later by an additional 0.28 mg/kg/min over 2 min infusion if the initial response is negative and there have been no major side-effects. Aminophylline 240 mg iv should be available for immediate use in case of an adverse dipyridamole-related event.

- (b) *Adenosine* acts directly and rapidly on vascular smooth muscle, and is usually used with an incremental dose schedule; the most widely used dose for echocardiography is 140 mg/kg/min injected over a period of 6 min. Imaging is performed continuously throughout the infusion. **Side-effects:** Dipyridamole and adenosine have a similar side-effect profile. The high-dose dipyridamole protocol induces minor side-effects in about two-thirds of patients, but these rarely prevent completion of the study. Aminophylline usually provides rapid relief. The side-effects of adenosine are brief, but more intense and frequent than those of dipyridamole; side-effects prevent about a third of patients from completion of high-dose protocols. The symptoms are similar to those with dipyridamole stress, although chest discomfort and dyspnea are more frequent. Cessation of the infusion is usually the only treatment required for side-effects because of the very short duration of action. Serious side-effects are very rare but include severe myocardial ischemia and infarction, bronchospasm, and complete heart block.

Dipyridamole and adenosine stress are contraindicated in patients with untreated atrio-ventricular block, and bronchospastic disorders (asthma).

Acquisition

Equipment

Harmonic Imaging

The development of tissue harmonic imaging has had a major influence on image quality; its benefits on reproducibility and feasibility have made the technique indispensable for stress echocardiography. Lateral gain correction may also improve visualization of the lateral wall. Despite these developments, 2D image quality remains a problem in some patients, with failure to image >1 segment in 30% of patients (especially in the anterior and lateral walls), and some significant

impairment in visualization in 10–15%. Unless severe, incomplete visualization does not so much jeopardize accuracy in experienced laboratories, but it does compromise the acquisition of clinically important information about the nature and extent of ischemia.

Contrast Imaging

The use of left heart contrast agents has become a practical solution for this problem, improving image quality, increasing the confidence level of readers, reducing downstream costs and improving accuracy for stress echocardiography (Fig. 21.1). However, we favor judicious and selective use of contrast in com-

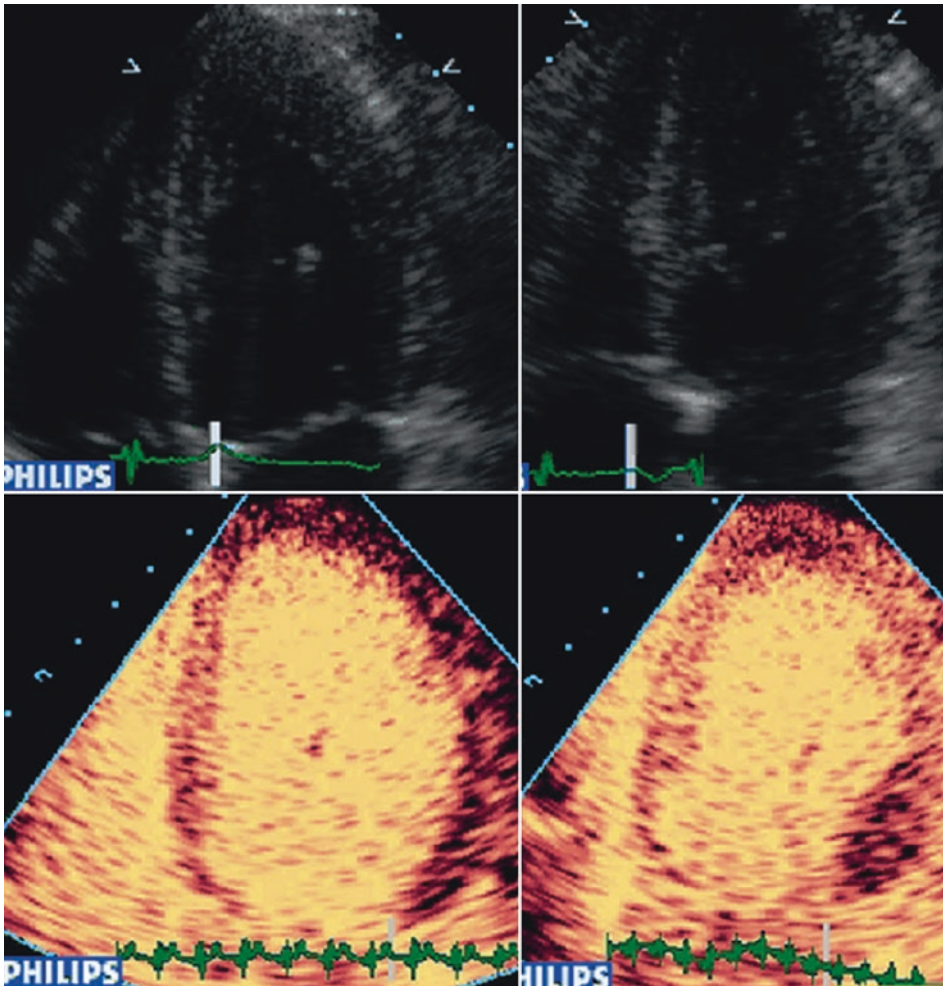


Fig. 21.1 Use of a left heart contrast agent to improve LV opacification. Upper right and left images show rest and stress images respectively, illustrating poor visualization of the lateral wall. Lower images have been obtained after

injection of Definity, including a flash for bubble destruction to facilitate assessment of myocardial perfusion. Printed images are end-systolic freeze-frames

bination with stress echocardiography—potential problems include shadowing, emphasis of the endocardial border rather than thickening, and cost.

Image Acquisition

Digital Image Acquisition

Multiple views have to be recorded to ensure visualisation of LV segments supplied by each of the three major coronary distributions. Typically, four views are sufficient (Fig. 21.2). The parasternal long- and short-axis as well as apical four- and two-chamber views. Subcostal or additional short-axis views can be substituted when necessary or when more appropriate visualisation of specific anatomy. For the majority of examinations, 50 ms intervals are sufficient for capture and playback.

Stress echo studies should be reviewed in side-by-side (rest-stress) format. Continuous digital capture of multiple cycles is valuable to examine off-axis images, the ability to see different walls in different parts of the respiratory cycle, and avoidance of sampling artifacts. A study from the Mayo

Clinic showed an alteration of interpretation from side-by-side review by review of continuous images (using video recording, which is has now been superceded), in 40% of segments, and this altered the final diagnosis in 14% of patients.

Attention to Detail

The successful performance of stress echocardiography is based upon meticulous attention to practical issues.

1. *Avoid excessive gain settings* (Fig. 21.3), as this may obscure endocardial detail. The depth and zoom window must be altered to optimize image size and definition.
2. *Same myocardial regions*: The acquired views must be of the same regions of myocardium throughout the test, so that the window and view must be the same (Fig. 21.4).
3. *True 2-chamber view*: Particular attention should be paid to acquisition of a true apical 2-chamber view (anterior and inferior walls) rather than an apical long-axis view (anteroseptal and posterior walls), as this may be the only view of the right coronary artery territory.

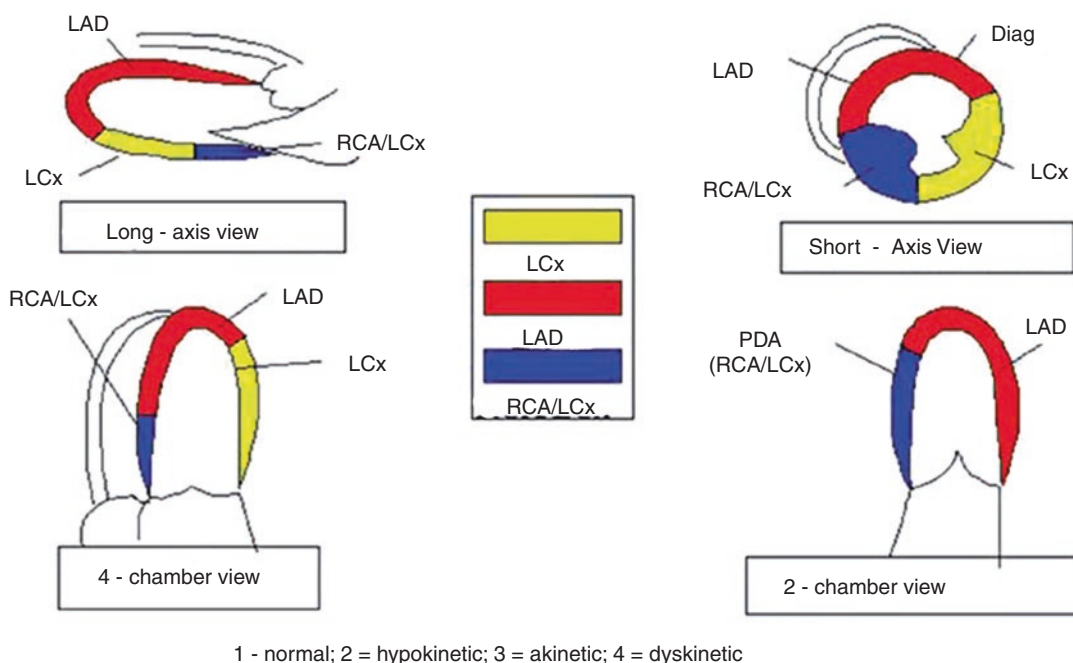


Fig. 21.2 The four typical views needed for to be recorded and attribution to coronary vascular territories together with the wall motion scoring system

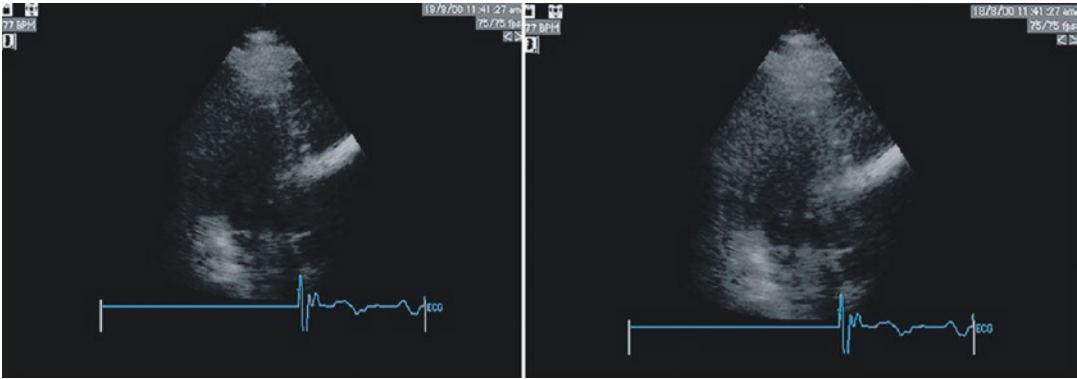


Fig. 21.3 Use of excessive gain settings. The response to suboptimal images is often to increase gain settings (right panel). This is often counter-productive, increasing near-field artifact and reducing endocardial resolution

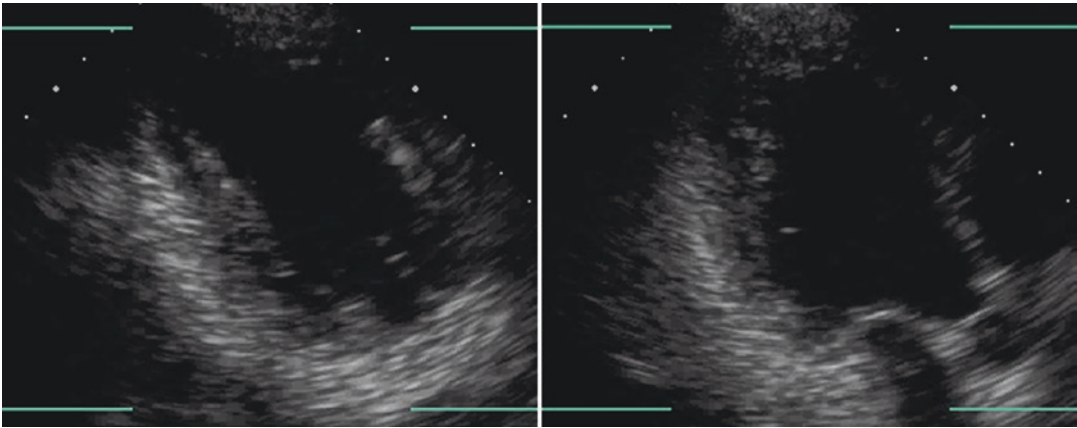


Fig. 21.4 Importance of maintaining the same imaging plane for comparison of pre- and post-stress images. Failure to provide a true apical two chamber view may preclude visualization of the right coronary territory

4. *ECG signal.* Care must be taken to optimize the ECG signal and avoid sampling extrasystolic cycles. Errors with ECG triggering may make the digital cine-loops useless, so

The Roadmap

1. *The initial imaging step* in a stress echo exam should be a truncated standard echo-Doppler examination, including a brief M-mode, transmitral pulsed-wave Doppler and color examination. A complete echocardiogram

is often not possible for logistic reasons, so if an unexpected finding is identified, we reschedule the patient to return for a more complete study.

2. *Images should comprise apical, parasternal and/or subcostal views* before, during and after stress. The sequence for post-stress images is best varied with the clinical setting. Because early post-stress imaging time is particularly valuable, and the apex is the most common site of a wall motion abnor-

malinity, we perform apical views first. If resting dysfunction is already identified in one view, it is usually preferable to start with another view.

3. *Optimizing endocardial definition* and avoidance of foreshortening the left ventricular cavity are critical, but in other respects, the principles of 2D imaging for stress echocardiography are a little different from normal. Images may be enhanced by asking the patient to exhale, although sometimes the window is improved by partial inspiration, especially in the apical 2-chamber view. Contact between the heart and chest wall may be improved by using a cut-out bed, which allows room for the transducer when the patient lies as far as possible onto the left side (for supine imaging) or by leaning forward on the bicycle (for upright imaging). Views are modified to attend more to the myocardium than to the valves (e.g. long axis parasternal images are often obtained through a lower window).
4. *During exercise echo*, image quality and speed of acquisition need to be balanced, because of the potentially rapid resolution of ischemia.
5. *Remember that* a complete set of imperfect but “readable” images in the first minute may prove more useful than perfect views obtained over several minutes.
6. *Use of Doppler*: Although stress echocardiography is typically performed with 2D-echocardiography, stress Doppler studies have been reported for the evaluation of both systolic and diastolic function, valvular heart disease, and coronary flow reserve (using signals from the left anterior descending and other vessels) [2]. Their application to assessment of systolic function—previously constrained by measurement error in volumetric calculations—may be facilitated with the use of strain imaging. More favorable results have been obtained for evaluation of diastolic

parameters, although these may be influenced by pathologies other than ischemia. Nonetheless, the evaluation of filling pressure with stress (calculated by transmitral flow and tissue velocity) may become an interesting application of stress echocardiography.

7. *Color-flow Doppler* may be used to identify stress-induced mitral regurgitation.

Interpretation

Semi-Quantitative Interpretation

The qualitative comparison of regional function at rest and stress is the basis of the clinical interpretation of stress echocardiography. Many stress echocardiographers still divide the left ventricle into 16 segments (septal, lateral, anterior and inferior at the apex, with these segments as well as anteroseptal, and posterior segments at the base and mid-papillary muscle level), but the “official” 17 segment model includes an apical cap that is often not seen by echo. Some quantitative algorithms use 18 segments (3 in each view). Each segment is scored as normal, hypokinetic or dyskinetic (Fig. 21.2). By averaging the scores of individual segments, a “score index” may be obtained, which gives a semi-quantitative index of global systolic function [3].

Rules for Qualitative Interpretation

The following rules for qualitative interpretation were devised by a group of expert centres [4].

Rule 1: Minor degrees of hypokinesia are not identified as ischemia (especially if only apparent at peak, and not post-exercise).

Rule 2: Abnormalities are corroborated whenever possible with another view.

Rule 3: Segments are not identified as abnormal if they do not make sense in terms of

coronary territories (e.g. isolated mid-septal abnormalities).

Rule 4: Isolated basal inferior or basal septal segments are not identified as abnormal in the absence of an abnormal neighboring segment.

Rule 5: Read with multiple observers whenever possible, and to blind the interpretation to all other data.

Structured Review

Use the digital side-by-side images as the primary data, supported by video images to examine non-standard views, and to check M-mode and Doppler.

Technical review: check that images are triggered correctly and the pre-, peak and post-stress views are comparable.

Brief review of the whole study: checking if wall motion is normal at rest, then to see if there are obvious changes in cavity size (suggesting multivessel disease) or cavity shape.

Segmental analysis comparing regional function in each of the 16 segments at rest and stress. Function is compared both by examining the continuous cine-loop and then frame-by-frame, using the digital images and paying particular attention to contraction during the first part of systole (especially if there is excessive rotational or translational movement).

Regional scoring: For regional wall motion scoring, the distinction of severe hypokinesia from akinesia may be helped by assessment of endocardial excursion <5 mm and <2 mm, respectively. However, the timing of movement and thickening rather than excursion are important parameters; regions which fail to thicken or which move only in late systole (after movement of the adjacent myocardium), may be moving passively, and should be considered as akinetic irrespective of endocardial excursion. In Table 21.2 we describe the “do and don’ts” of stress echo.

The Report

The schema for interpretation of rest and stress regional wall motion abnormalities is summarized in Table 21.3.

1. Resting wall motion abnormalities are usually characterized as infarcted, but mild hypokinesia should be interpreted with caution, as it can be a normal variant.
2. Some segments considered to be infarcted using these criteria (maybe as many as 50%) are viable. The evaluation of wall thickness (Fig. 21.4) is a good resting marker of non-viable tissue (<6 mm), although myocardium of normal thickness does not exclude recent or non-transmural infarction.
3. Other resting markers of viability include preservation of cyclic variation of integrated backscatter, strain, and preservation of perfusion (Fig. 21.5).
4. Augmentation of segmental function with low-dose dobutamine stress may also identify viable tissue (Fig. 21.6).

Table 21.2 “Do and don’ts” of stress echo

Do	Don’t
Look at the left ventricle (not left atrium)	Over-gain (especially in near-field)
Ensure pre- and post-views are same	Foreshorten the LV cavity
Acquire in inspiration or exhalation	Sacrifice speed for perfection
Optimize positioning	
Sample plenty of cycles	

Table 21.3 Interpretation of exercise and pharmacologic stress echocardiography

Nature of tissue	Resting function	Low-dose	Peak/post-stress function
Normal	Normal	Normal	Hyperkinetic
Ischemic	Normal	Normal (except with severe CAD)	Reduction vs. rest Reduction vs. adjacent Delayed contraction
Viable, non-ischemic	Rest WMA	Improvement	Sustained improvement
Viable, ischemic	Rest WMA	Improvement	Reduction (compared with low-dose)
Infarction	Rest WMA	No change	No change



Fig. 21.5 Significance of wall thinning. The posterior wall is thinned, and would be very unlikely to show contractile reserve with dobutamine, or recover after revascularization

Defining an Ischemic Response

Myocardial ischemia is characterized by the development of:

1. New or worsening regional dysfunction. The normal response to either exercise or dobutamine stress is to increase myocardial thickening (the most reliable parameter). The speed of contraction (arguably the most sensitive parameter), and the endocardial excursion (probably the most widely used parameter).
2. Failure to augment function has been reported in normal segments, so the previous characterization of this tissue as ischemic appears to be wrong. One exception to the use of worsening

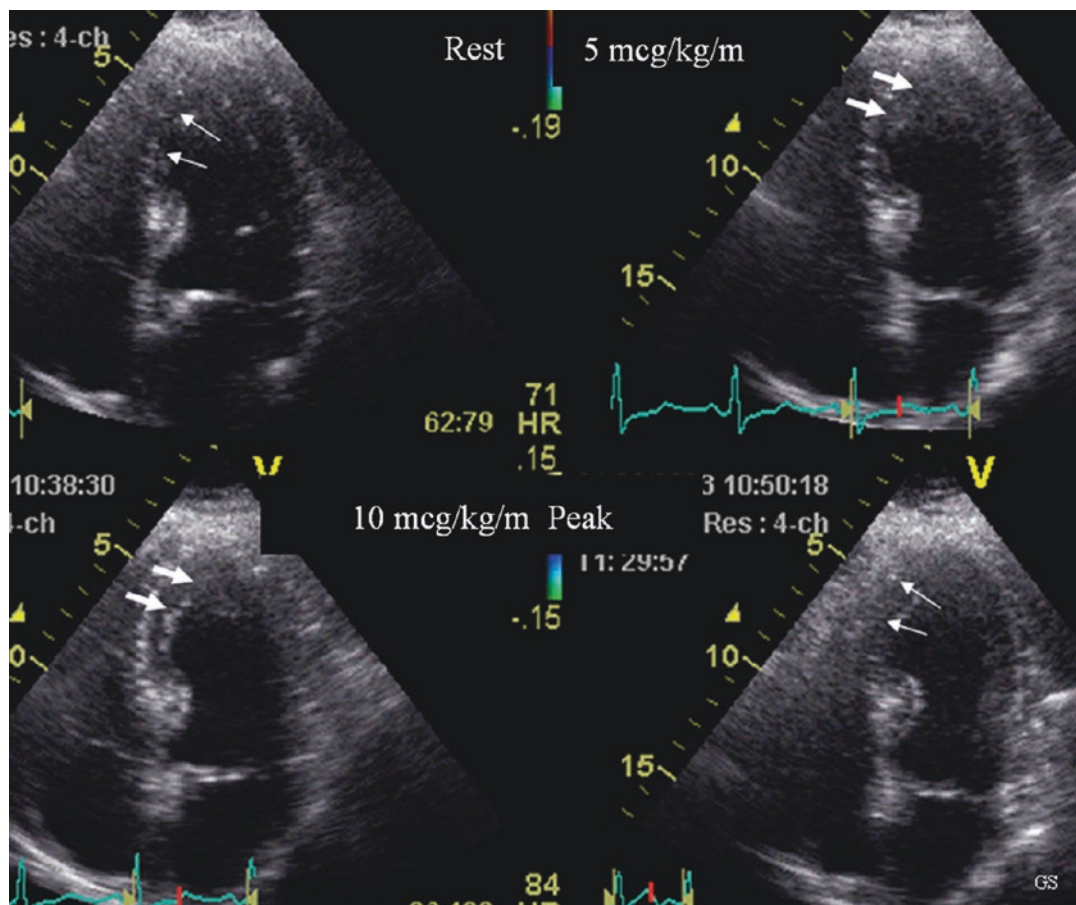


Fig. 21.6 Detection of myocardial viability with dobutamine stress echocardiography. The resting image shows an apical septal wall motion abnormality, which improves at 5 and 10 mcg/kg/min of dobutamine and deteriorates at

peak (a biphasic response). Printed images are end-systolic freeze-frames and arrows identify new wall motion abnormalities

function as a marker of ischemia is the response of akinetic segments during bicycle or dobutamine echocardiography—we do not classify a further deterioration of function as ischemia, as increased loading may be responsible for such a response.

3. The changes in end-systolic ventricular shape are an often-neglected but quite accurate guide to the development of ischemia (Figs. 21.7 and 21.8).

The Magnitude of Ischemia

The extent of coronary disease may be inferred from the site of abnormal wall motion, the number of abnormal segments, severity (segmental wall motion score), time of onset and offset of ischemia, and the effect of ischemia on global left ventricular function. The contents of a stress echo report are summarized in Table 21.4.

Pitfalls in the Standard Performance of Stress Echocardiography

Failure to recognize abnormal wall motion when angiographically-significant coronary disease is present may be caused by:

- angiographic features,
- patient characteristics,
- inadequate stress, or
- imaging and interpretation issues.

False positive results: (i.e. an apparent wall motion abnormality without significant coronary stenosis) are most frequently due to interpretation errors.

- False positive results may occur due to over-interpretation—especially of basal wall motion abnormalities.
- Sometimes, inducible dysfunction is apparent rather than real—for example, peri-infarct zones may be tethered by the akinetic infarcted segment and consequently fail to improve segment and consequently fail to improve function with stress, or even appear dyskinetic if the infarct bulges during stress.
- False positive scans may be induced by an abnormal activation sequence (pacing, left bundle branch block), abnormal septal motion (prior cardiac surgery or RV volume overload) and heterogeneity related to cardiomyopathy and aortic regurgitation.

While many of these false positives are avoidable with adequate training, some situations (e.g.

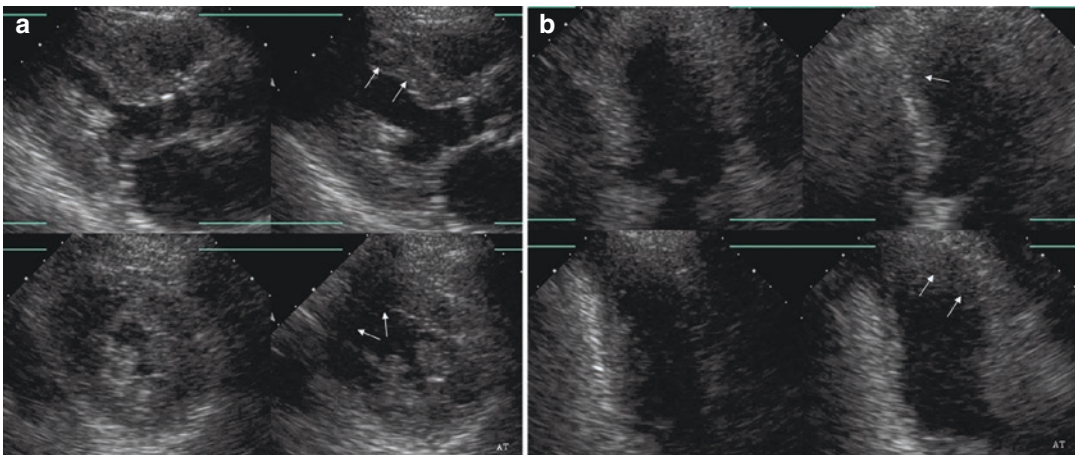


Fig. 21.7 (a) Detection of left anterior descending ischemia at exercise echo. This is a good case to emphasize the importance of putting the involved segments into a pattern—here involving anteroseptum, apex and anterior wall. Resting images are shown on the left and post-exercise images on the right. Printed images are end-systolic freeze-frames and arrows identify new wall motion abnormalities. (b) Detection of left anterior descending ischemia at exercise echo. This is a good case to emphasize the importance of putting the involved segments into a pattern—here involving anteroseptum, apex and anterior wall. Resting images are shown on the left and post-exercise images on the right. Printed images are end-systolic freeze-frames and arrows identify new wall motion abnormalities

emia at exercise echo. This is a good case to emphasize the importance of putting the involved segments into a pattern—here involving anteroseptum, apex and anterior wall. Resting images are shown on the left and post-exercise images on the right. Printed images are end-systolic freeze-frames and arrows identify new wall motion abnormalities

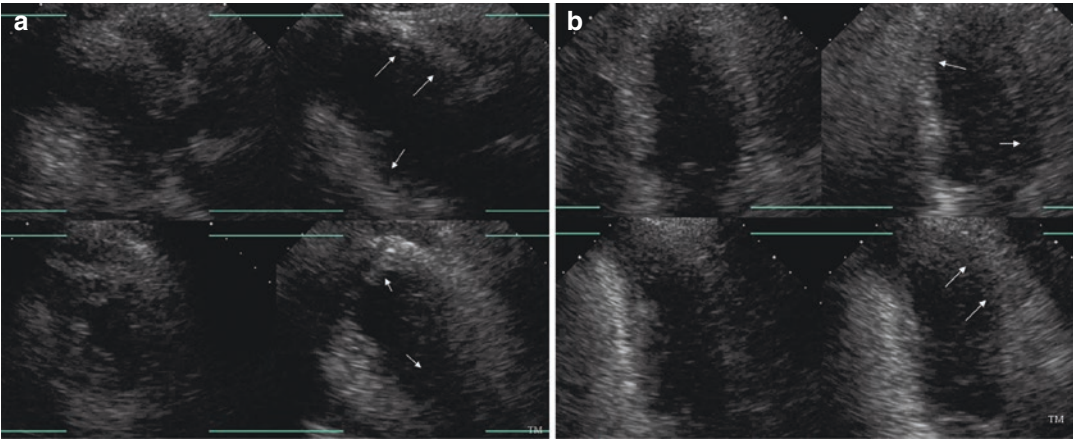


Fig. 21.8 (a) Detection of multivessel ischemia at exercise echo. In addition to left anterior descending wall motion abnormalities in the septum and anteroseptum, there is LV cavity enlargement and posterolateral wall motion abnormalities are also detected. This is a good case to emphasize that every segment must be systematically compared—even when the test is clearly abnormal, and especially if there is LV cavity enlargement. Resting images are shown on the left and post-exercise images on the right. Printed images are end-systolic freeze-frames and arrows identify new wall motion abnormalities. (b)

Detection of multivessel ischemia at exercise echo. In addition to left anterior descending wall motion abnormalities in the septum and anteroseptum, there is LV cavity enlargement and posterolateral wall motion abnormalities are also detected. This is a good case to emphasize that every segment must be systematically compared—even when the test is clearly abnormal, and especially if there is LV cavity enlargement. Resting images are shown on the left and post-exercise images on the right. Printed images are end-systolic freeze-frames and arrows identify new wall motion abnormalities

Table 21.4 Contents of a stress echo report

Heading	Detail
Resting images	LV size and global function Resting wall motion abnormalities (including score) Other problems that may account for symptoms (e.g. valvular)
Stress response	Limiting symptoms, side-effects Angina and ST segment responses Hemodynamic response (including adequacy of heart rate) Exercise capacity
Stress images	LV size and global function Segmental function—presence, site, extent and severity of abnormal function, time of onset and duration after stress Wall motion score
Conclusion	Presence and extent of infarction and viability (if resting function is abnormal) Exercise/dobutamine stress response (non-echo aspects) Response based on subjective analysis, wall motion score and/or ejection fraction

patients with prior coronary bypass surgery, left bundle branch block, extensive wall motion abnormalities or in the presence of suboptimal images) are difficult even for experts.

- One important category that can be relied on to annoy angiographers is the “false positive” angiogram, whereby coronary disease is identified on the basis of a moderate (e.g. 50 or 60%) stenosis that is actually not flow-limiting, even during hyperemia. The arbitrary selection of >50% diameter stenosis to identify “significant” disease is because this approximates a level below which lesions do not limit flow under conditions of peak vasodilation, but it should be recognized that the 50–70% range includes many stenoses which are physiologically non-significant.
- Even allowing for discrepancies between anatomical stenosis severity and physiological sequelae, there are other fundamental problems in defining the accuracy of non-invasive tests from the coronary arteriogram, including observer variability and problems posed by assessment of eccentric stenoses, and poor correlation between the anatomic severity of stenoses and their effects on flow.
- Newer invasive measures of coronary stenosis severity such as coronary flow reserve and myocardial fractional flow reserve offer both a physiologic index that addresses the anatomy

vs physiology dichotomy as well as the problems of subjectivity. Patients with a FFR <0.75 can be expected to have unequivocal evidence of reversible myocardial ischemia on noninvasive testing, and this approach is the best solution if there is concern about a negative stress echo in the setting of an apparently abnormal angiogram.

- Erroneous results may be due to inadequate equipment or insufficient training. Technically difficult studies due to poor image quality remain a problem, even in the era of harmonic imaging and echo contrast. The greatest potential pitfalls relate to the interpretation of studies.

False negative results may occur due to failure to appreciate the subtle manifestations of ischemia (hypokinesis, tardokinesis).

- Patient factors may limit the ability to induce ischemia.
- Anti-anginal therapy may prevent the identification of ischemia, and therefore, *diagnostic* testing should be performed after interruption of therapy—especially beta blockers. The implications of ongoing therapy for *prognostic* testing are less clear—sometimes the assumption is made that events are less likely if the heart is protected from ischemia, but an important role of prognostic testing of patients with suspected disease is simply to allocate low risk to those without disease, and this process is compromised by testing on therapy.
- The use of an inappropriate stressor may contribute to false negative results. A negative test due to inability to exercise maximally or tolerate maximal pharmacologic stress should be identified as non-diagnostic. Even if maximal, pharmacologic stress is less potent than exercise, and inadequate stress may fail to induce ischemia. A useful aphorism is that if the patient is able to exercise maximally, exercise stress is the better choice—because of the

greater workload, the information derived from exercise capacity and the more reliable ST segment response.

- Extreme hemodynamic changes may influence wall motion. Severe stress-induced hypertension may magnify the development of regional wall motion abnormalities and actually cause wall motion abnormalities in the absence of coronary disease, and in contrast, reduction of LV volumes (e.g. “cavity obliteration” with peak doses of dobutamine) may hide wall motion abnormalities due to milder coronary disease.

Quantitative Interpretation

The problem: Subjectivity is the bane of stress echocardiography. Without special training, competent readers of transthoracic echo have an accuracy of approximately 60–70%. Picano [5] reported that 100 supervised studies were required to bring the accuracy of “novices” experienced in echocardiography to the level of “experts”. As importantly, pattern recognition skills attenuate when they are not used and limited data suggest that accuracy is related to reading volume (Fig. 21.9).

Subjective analysis leads groups of readers to have different reading styles, which leads to variations between expert centers. The first study of this topic [6] showed the major causes of discordant interpretation were milder degrees of coronary disease, and especially suboptimal image quality. A re-examination of the same topic over 7 years later showed improvement in concordance related to improved image quality due to harmonic imaging, side-by-side review, and standard reading criteria [4].

The solution to subjective interpretation may be the adoption of quantitative approaches to the evaluation of left ventricular wall motion—if not as a substitute, then as a guide to standard wall motion analysis.

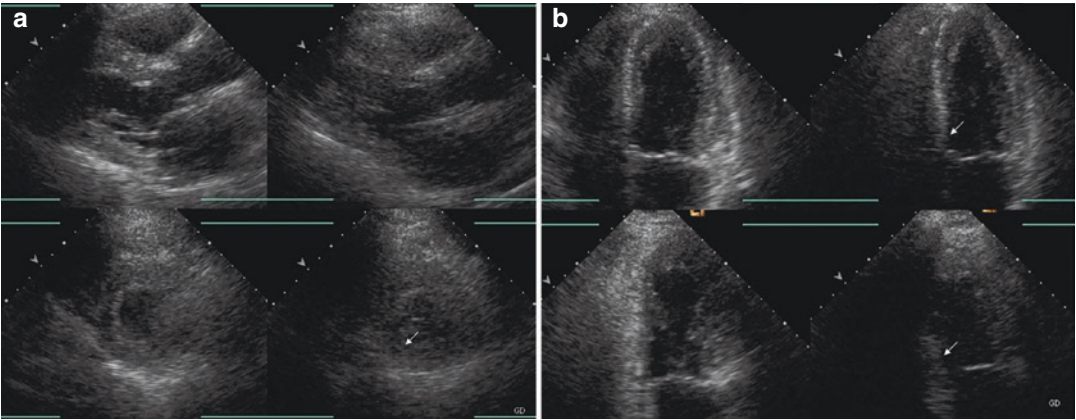


Fig. 21.9 (a) Difficulties posed by interpretation of the inferior wall. Apical 2-chamber views show a shape change in the inferior wall. This is a good case to emphasize that the basal inferior should only be identified as abnormal in the presence of an adjacent abnormal segment—here the basal septum and the mid-inferior are both implicated. Resting images are shown on the left and post-exercise images on the right. Printed images are end-systolic freeze-frames and arrows identify new wall motion abnormalities. (b) Difficulties posed by interpreta-

tion of the inferior wall. Apical 2-chamber views show a shape change in the inferior wall. This is a good case to emphasize that the basal inferior should only be identified as abnormal in the presence of an adjacent abnormal segment—here the basal septum and the mid-inferior are both implicated. Resting images are shown on the left and post-exercise images on the right. Printed images are end-systolic freeze-frames and arrows identify new wall motion abnormalities

1. Global systolic function may be quantified by tracing endocardial contours in systole and diastole in order to obtain ventricular volumes and ejection fraction. However, global indices are relatively insensitive to mild ischemia (because of compensation by non-ischemic walls), and are non-specific for coronary disease. Nonetheless, this approach is useful in some situations (e.g. assessment of contractile reserve in valvular disease and viability), and may be strengthened by the application of three-dimensional echocardiography.
2. The simplest approach to quantifying regional function is the application of a semi-quantitative wall motion score, although these do not truly measure function independent of the observer.
3. True quantitation of regional function may be performed from M-mode, two-dimensional or Doppler methods, some of which are in the realm of “new technologies” (Table 21.5).

Table 21.5 Application of new technology to stress echo interpretation

Category	Specific tests	Status
Radial motion	Color kinesis	Improves accuracy of novice readers Image quality-dependent, ?best with contrast
	Center-line	Image quality-dependent
	Strain etc.	May be possible with speckle tracking
Longitudinal motion	Tissue Doppler	Improves accuracy of novice readers Limited by translational motion
	Strain rate and strain	Promising but still under-developed

- Generally, these can be categorized into approaches that
- (a) track endocardial radial motion, and
 - (b) those that measure longitudinal shortening.
4. The approach which is most analogous with standard visual assessment is the measure-

ment of radial thickening or endocardial excursion. Although assessment of thickening is independent of tethering, translation or rotation, its feasibility is limited by problems of not only tracking the endocardium but also the epicardial border.

5. Although the measurement of endocardial excursion using the center-line method is supported by evidence, the steps for this procedure—tracing and superimposition of systolic and diastolic images, drawing of a center-line midway between these profiles, arrangements of chord perpendicular to the centerline, and measurement of chord lengths, normalized for body size and the diastolic perimeter length—are too onerous for practice. Recent image processing advances have enabled automated contour-detection and correction of translational movement by use of the apex and mitral valve plane as a frame of reference. A similar method used automated tracking of the myocardial border, using the difference in backscatter between the myocardium and blood pool. These techniques may provide a guide to less experienced readers, but are limited by image quality (which limits the ability to trace the endocardial border), compensation for rotational or translational movement of the heart (both fixed and floating frames of reference have potential problems—failure to correct for such movement may cause false positives, but their correction may hinder the detection of milder abnormalities), and selection of appropriate systolic and diastolic frames.
6. Tissue Doppler imaging measures the velocity of myocardial movement within a sample volume relative to the transducer, using the same principles as the use of Doppler for measurement of blood flow, but with manipulation of the controls to include high amplitude, low velocity signals. This technique is especially valuable for quantification of longitudinal (base-apex) function. Although tissue Doppler based techniques have more favorable signal-

noise ratios than edge-detection methods, these methods have important limitations—in particular, the apex cannot be assessed adequately as it is fixed and velocities are low. Problems posed by tethering and translation have been addressed by the development of strain rate and strain imaging, which examine a velocity gradient between adjacent sample volumes.

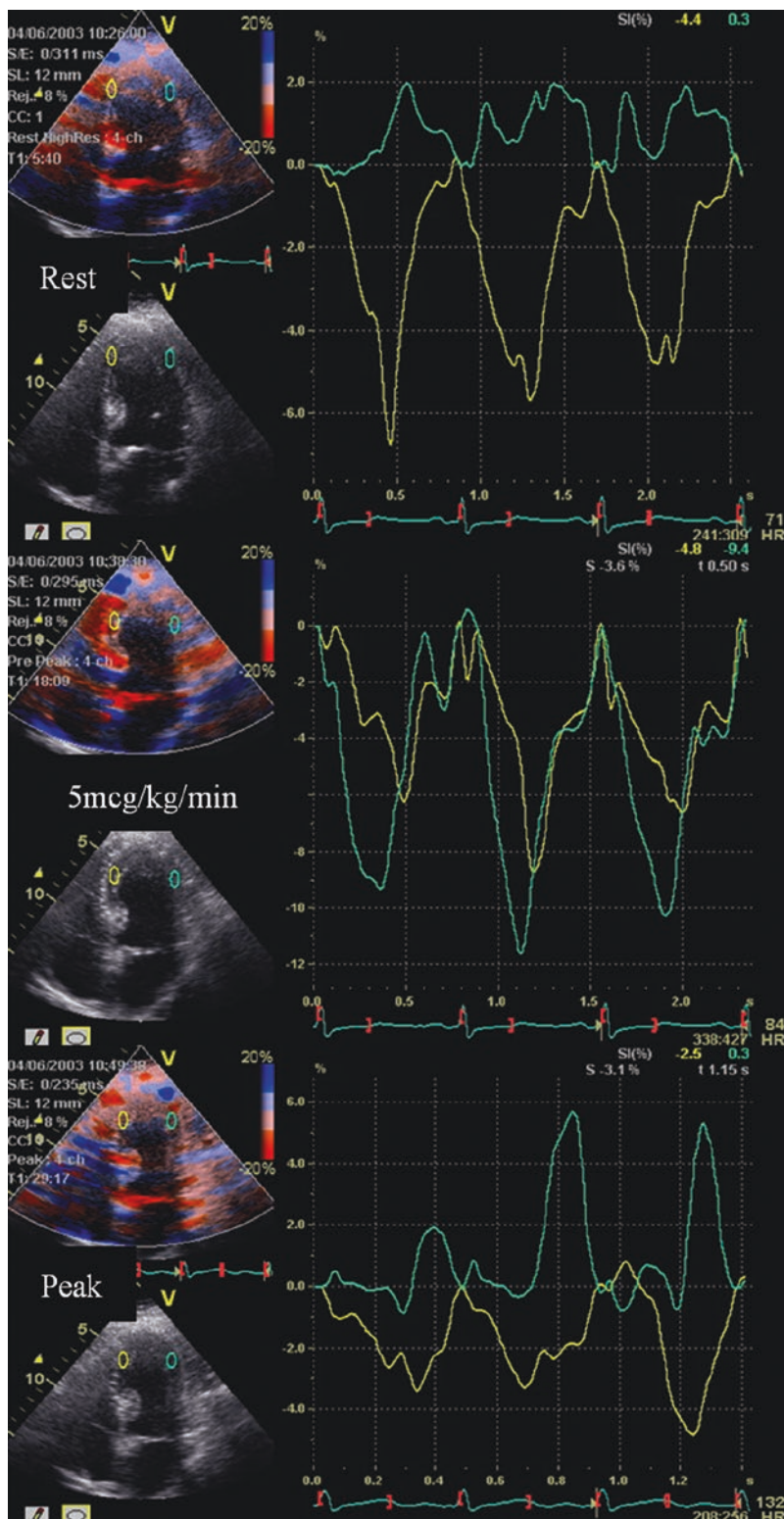
7. Strain (Figs. 21.10 and 21.11). Clinical studies with strain techniques have also produced favorable results [7], but have still not been incorporated into standard practice. Part of the problem is that tissue velocity-based strain was susceptible to angulation issues, but the speckle-tracking approach has relatively low temporal resolution, and may be limited by signal quality problems imposed by hyperventilation and motion. An interesting approach is to use the phenomenon of “ischemic memory” to diagnose ischemia after exercise [8].

The need for a reliable quantitative approach remains one of the greatest challenges of stress echocardiography. The reality is that quantitative stress echo remains a research rather than a clinical tool.

Accuracy

The calculation of sensitivity, specificity and diagnostic accuracy is based on comparison of a non-invasive technique with a gold standard—generally coronary angiography [1]. However, the measurement of sensitivity and specificity do not address the efficacy of stress echocardiography for addressing several important questions, including the ability to identify ischemia and viability in the post-infarction patient, the recognition of multivessel disease as such, and the ability to identify ischemia within a particular territory.

Fig. 21.10 Application of strain imaging to the identification of viability in a patient with resting apical wall motion abnormalities. The apical septal wave-forms are shown in yellow and the apical lateral in blue. Strain is reduced in the septum at rest and the lateral is actually lengthening (positive wave). Low-dose dobutamine causes reversal of the lateral wall, which now shortens, compared to little change in the septum. At peak, the lateral deteriorates and again lengthens—signifying a biphasic response



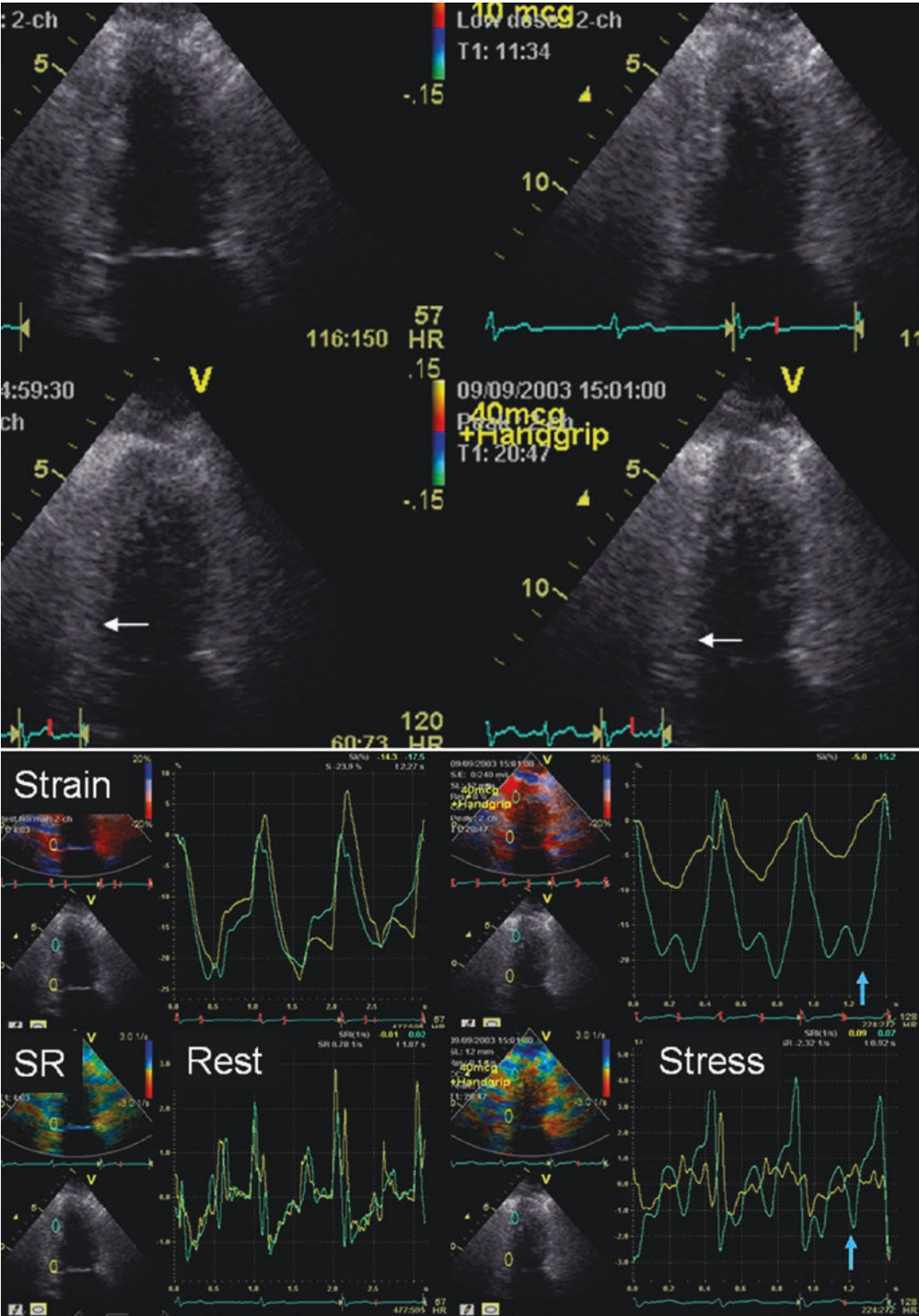


Fig. 21.11 Application of strain and strain-rate imaging to the identification of ischemia in the inferior wall. The basal inferior wave-forms are shown in yellow and the apical in blue. Wave-forms are normal in both at rest. At

peak dobutamine, strain decreased and SR fails to increase in the basal inferior, and milder ischemia in the apex is evidenced by the development of post-systolic thickening (blue arrows)

The reported accuracy of stress echocardiography is influenced by several technical and clinical aspects. The contributions of impaired image quality, submaximal stress, and the limitations of coronary angiography have been alluded to above.

Clinical Factors Influencing Accuracy

Referral bias may influence accuracy if a particular subgroup are over-represented and especially if a subgroup are referred preferentially to angiography (post-test referral bias) [9]. Studies showing the latter produce a characteristic pattern of high sensitivity (patients with a positive test proceed to angiography) and low specificity (the only patients with a normal angiogram are those with a false positive result). Even when care is taken to avoid influencing the performance of angiography, study designs comparing the findings of stress echocardiography with coronary anatomy are necessarily biased towards a group with severe enough coronary disease to warrant angiography.

For similar reasons, over-representation of patients with more extensive CAD or prior infarction tends to inflate sensitivity. Patients with multivessel disease or tight stenoses are likely to have a more extensive area of abnormal wall motion and conversely, small risk areas in patients with mild or single vessel disease may not be identified, leading to lower sensitivity in this situation. Indeed, single vessel and mild coronary

disease are the main angiographic predictors of false negative results [10]. Fortunately, the outcome of patients is more governed by functional evidence of ischemia than coronary anatomy, and patients with “false negative” stress echocardiograms have a benign prognosis. In the post-infarct patient, the diagnosis of coronary disease is already established.

Accuracy of Stress Echocardiography

The accuracy of different stress echocardiography techniques is summarized in Fig. 21.12. Generally, sensitivities are in the 80–85% range, with specificities in the 85% range [1]. Exercise echo is the more sensitive and dipyridamole echo the most specific—reflecting the more potent stress with exercise but the possibility of artifact due to image quality issues.

The ability to recognize multivessel disease, identify extent of disease, differentiate performance in each location, and discriminate ischemia from scar are important parameters that are not expressed by sensitivity and specificity. The presence of multivessel disease makes it easier to identify that disease is present, but this high sensitivity for detection of disease hides a quite limited ability to recognize that more than one vessel is involved, apart from in patients with previous myocardial infarction—where multivessel disease is implied by a new wall motion abnormality, separate from the infarct zone. Thus, the ability to recognize multivessel disease with prior

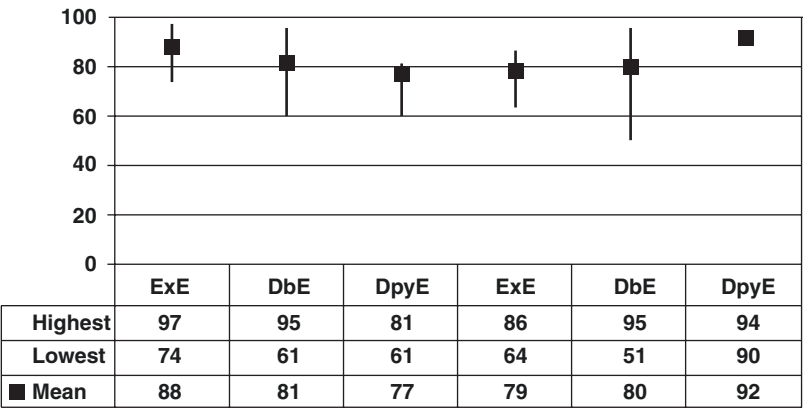


Fig. 21.12 Accuracy of different approaches for diagnosis of CAD with stress echocardiography. Reproduced with permission from Marwick [13]

infarction is >80%, while it is only 50% in those without prior infarction. Clues to the presence of multivessel disease are left ventricular cavity enlargement and reduction of ejection fraction (but this is rare with dobutamine stress), the combination of a positive stress echo with ST segment changes of >0.2 mV, earlier onset of ischemia (i.e. at lower levels of exercise or lower dose of pharmacologic stress, or low heart-rate and rate-pressure product).

Exercise vs Pharmacologic Stress

There is no choice but to use pharmacologic stress in patients who can only exercise submaximally, but its use is more controversial in patients who could otherwise exercise. While this approach makes the acquisition easier, it makes the interpretation more difficult because the workload on the heart is less and therefore extent of ischemia is less. Comparative studies between dipyridamole and exercise stress (in patients able to exercise) have shown higher feasibility for the drug, with varying sensitivity and specificity, although the general consensus is that exercise is more sensitive and less specific. The same conclusions have been made with comparison of dobutamine and exercise stress.

Selection of the Optimal Pharmacologic Stress

The choice of stressor is simple in some subgroups of patients who cannot exercise, who have specific contraindications to one or other stressor. Patients with hypertension or arrhythmias should undergo a vasodilator rather than an inotropic stress, and patients with bronchospasm or conduction disorders should be submitted for dobutamine testing. In the majority of patients, who lack these contraindications, comparisons between dobutamine and dipyridamole have shown similar accuracy, although dobutamine is more sensitive for single-vessel disease and dipyridamole is more specific.

Comparison with Other Approaches

Comparison with the Exercise ECG

Although the exercise ECG is the simplest and most widely used test for non-invasive detection of coronary disease, its dependence upon adequate stress and an interpretable ECG limit its feasibility to <50% of patient warranting functional testing for CAD. The sensitivity and specificity of the exercise ECG vary widely, with mean values of $68 \pm 16\%$ and $77 \pm 17\%$, respectively. Of course, the exercise test offers much more than just the ST segment response, and various scores that include not only the ST data, but also correction for heart rate, or a combination with exercise capacity and hemodynamics have improved the accuracy of the test.

In direct comparisons between exercise echo and conventional exercise ECG, the imaging test gave better sensitivity and specificity, as well obtaining otherwise inaccessible data such as the site of disease. Limited data with exercise scores show these to be better than the ST analysis alone, but still inferior to stress echo.

Difficult Subgroups for Standard Exercise Testing (LBBB, LVH, Women)

Circumflex artery: Imaging techniques certainly offer diagnostic information in the right coronary and left circumflex territories, and are therefore superior to the ECG, which is non-diagnostic.

Left Bundle Branch Block: The problems arise in the LAD territory, where left bundle branch block is a difficult situation for all non-invasive techniques, because this conduction disturbance may influence both perfusion and function in the absence of CAD. The sensitivity of stress echocardiography in the anterior circulation depends on the ability to interpret thickening rather than wall motion and to visualize the distal anterior wall in the 2-chamber view. The general consensus is that vasodilator stress SPECT is more feasible than stress echocardiography.

LV hypertrophy is an important cause of false positive ST segment responses at stress testing, even if the ST segment appears to be interpretable. While left ventricular hypertrophy has been associated with false positive SPECT imaging, it has not been shown to influence the accuracy of stress echocardiography. The only exception are patients with concentric remodelling, in whom transmural wall stress is low and therefore ischemia may not be provoked, even in the presence of CAD.

Women: Although the standard stress test is still useful in women—especially if the ECG is combined with functional capacity—the ST response in women has a lower accuracy than in men. Myocardial perfusion imaging may be used to circumvent this problem, although it is not without problems, related to the smaller female heart and breast attenuation problems. The accuracy of stress echocardiography is not compromised in women, and the results are superior to those of the exercise ECG, even after correction for referral bias.

Clinical Implications of Superiority of Exercise Echo vs Exercise ECG

Stress echocardiography is the functional test of choice in patients who are unable to exercise and those with an uninterpretable ECG, or when management questions are poorly answered by the exercise ECG alone—for example, when the site of ischemia or the presence of multivessel disease requires definition. To this could be added subgroups of patients where the stress ECG has been shown to be inferior to stress echo—e.g. patients with LVH and hypertension. The wider use of stress echo as an alternative to stress ECG testing is not supported by guidelines of appropriate use criteria [11].

Comparison with Other Stress-Imaging Approaches

The examination of myocardial function and perfusion at rest and after stress is now possi-

ble with both nuclear cardiology and magnetic resonance imaging, but still rarely assessed with contrast stress echocardiography. Perfusion imaging identifies the presence of coronary disease on the basis of stress-induced perfusion heterogeneity—which may not necessarily parallel the presence of myocardial ischemia. This occurs earlier in the ischemic cascade, and therefore inherently more sensitive than awaiting the development of inducible wall motion abnormalities, as well as being less likely to be influenced by anti-anginal drug therapy, which prevents the development of ischemia.

The indications for perfusion scintigraphy, stress MRI and stress echocardiography are similar;

- (1) Diagnosis of coronary artery disease in patients unsuitable for routine exercise testing or in patients with an intermediate risk of disease,
- (2) Assessment of the physiologic significance of known coronary stenosis,
- (3) Assessment of prognosis, as determined from the quantity of infarcted tissue, and the amount of ischemic tissue,
- (4) Follow-up after intervention.

The advantages and disadvantages of myocardial perfusion scintigraphy and stress echocardiography are summarized in Table 21.5. Despite the favorable record of the nuclear techniques and the benefit of more automated interpretation, they have disadvantages with respect to cost (of imaging equipment, isotopes and disposables), patient convenience (although this is less problematic than in the thallium era) and availability. Stress echocardiography does not share these technical problems and can offer real-time imaging of the heart (possibly enhancing safety and enabling visualization of the time-course of ischemia), but is technically more difficult. Perfusion assessment using magnetic resonance imaging is very accurate, but remains constrained by access to the technique and cost.

Accuracy of Stress Echocardiography vs Perfusion Scintigraphy

The sensitivity and specificity of SPECT are respectively quoted to be about 90% and 70%, comparing with 80 and 85% by stress echocardiography. The use of receiver operator characteristic curves to correct for the inevitable variations between studies showed similar levels of accuracy—with SPECT being more sensitive, but less specific than echocardiography [12]. These findings have been supported by head-to-head comparisons between the techniques using exercise or dobutamine stress. The results with vasodilator stress show less sensitivity for echocardiography.

As mentioned above, there are many clinical settings where the parameters of sensitivity and specificity are insufficient for comparison of the tests. Patients after myocardial infarction are one such example, as sensitivity and specificity do not discriminate between the diagnoses of scar and ischemia. However, differences between the tests certainly occur in this respect—the concordance between echocardiography and perfusion scintigraphy with respect to the identification of normal, ischemic or infarcted myocardium is between 70 and 80%. In the situation that exercise echo identifies scar by within segments identified as ischemic by SPECT, the segments are often found to be viable. Generally, this may be avoided by the use of dobutamine (which permits recognition of a biphasic response).

When to Choose Stress Echocardiography vs Scintigraphy (and Vice Versa)

Much has been written about the comparison between stress echocardiography and scintigraphy. However for both techniques, local expertise remains the most important issue. However, once this condition is fulfilled, we believe that the selection of one or other test should be tailored to the clinical circumstances as follows [13]:

Perfusion imaging may be more useful in;

- (1) Post-infarction patients. Scintigraphy is more able to identify combinations of ischemia and infarction, is accurate for the detection of viable myocardium (although dobutamine echocardiography is useful in this respect), and lacks the problem of peri-infarct tethering seen with echocardiography.
- (2) Patients requiring vasodilator stress (those unable to exercise and also unable to undergo dobutamine testing). Only perfusion imaging is recommended for diagnostic purposes, as vasodilator echocardiography is insensitive, particularly for single vessel disease.
- (3) Patients with poor echocardiographic windows (though these individuals are difficult to predict without performing resting imaging, and the window may paradoxically improve with post-exercise hyperventilation).

Echocardiography is more useful in;

- (1) Those with left ventricular hypertrophy and left bundle branch block. Stress echocardiography appears to be more specific than perfusion scintigraphy in these situations (though these data await confirmation).
- (2) Patients in whom safety is a major concern (potentially unstable or severely ischemic). Using echocardiography, ischemia may be observed “on-line” and the appropriate action taken.
- (3) Studies being performed to assess the adequacy of therapy (as echocardiography visualizes ischemia) rather than perfusion heterogeneity.
- (4) Patients with a suspicion of significant valvular or pericardial components to their presentation.
- (5) Women. The use of nuclear perfusion imaging in women has some important limitations, including breast attenuation artifacts and ability to resolve ischemia in the small female heart. There have been no direct comparisons, but in a meta-analysis, both sensitivity and specificity were less with nuclear than echo imaging.

- (6) Left ventricular hypertrophy. In contrast to the favorable results with echocardiography in LVH, perfusion scintigraphy in patients with LV hypertrophy often shows both false negatives (reduction of hyperemia in normal segments, suboptimal stress) and false positives (non-uniform reduction of perfusion reserve due to LVH). Direct comparison of stress echo with myocardial perfusion scintigraphy in hypertensive patients showed that the specificity of echocardiography was significantly greater than that of scintigraphy.

Stress Echocardiography vs Magnetic Resonance Imaging

Magnetic resonance imaging may be used to assess wall motion at rest and stress, perfusion and viability. As the image quality is uniformly high, this technique may offer a quantitative solution to regional LV function assessment, and the first reports of such an approach are now 20 years old. Strain imaging is also feasible. To date, however, neither are part of the standard array of stress-imaging techniques that are routinely performed.

Most of the comparative studies between dobutamine MRI and dobutamine echocardiography have focused on the assessment of myocardial viability. In an original study of >200 patients, both tests were unable to evaluate 18 patients (9%)—due to poor image quality at echocardiography and due to claustrophobia and obesity with MRI. The sensitivity of dobutamine echocardiography and MRI were 74% and 86% respectively, with specificities of 70% and 86%, but these differences were no significant when poor-quality echo studies were excluded.

Stress Echocardiography vs Coronary CT

The role of stress echocardiography in comparison with coronary computed tomography angiography (CTA) is both complementary and competitive. Both diagnostic and prognostic

studies have shown that coronary CTA as a particularly high native predictive value. Apart from patients with calcified vessels and uncontrolled atrial fibrillation, both of which provide difficult technical challenges, the main reservation about coronary CTA is that anatomic evidence of coronary disease may be coincidental rather than because of symptoms. Without a functional corollary, the identification of coronary stenoses may provoke revascularisations which are not indicated. The solution to this problem will be found in the development of coronary flow reserve, computed from flow mechanics.

Coronary CTA has been shown to be very effective in urgent evaluation of patients presenting with chest pain. In patients with chest pain in non-urgent settings, the current role of coronary CTA is controversial. In the UK, the National Institute of Clinical Excellence has proposed coronary CTA as the first test in the evaluation of patients in the setting (<https://www.nice.org.uk/guidance/cg95/chapter/recommendations-for-research>). If such a policy is adopted, it will be important to distinguish patients with known coronary disease, where a functional test remains appropriate, as well as individuals with positive CTA findings and atypical symptoms, where the association may not be causative. Indeed, some jurisdictions have found that the introduction of coronary CTA has increased costs, as the utilization of functional testing has increased.

Echocardiographic Determination of Myocardial Viability

Definition and Clinical Relevance

The most widespread definition of viable myocardium is that it is dysfunctional tissue following infarction, that is potentially recoverable following myocardial revascularization. This clearly has limitations—first, it is a retrospective diagnosis after treatment, second, not all live tissue is able to recover function (due for example to adjacent fibrosis), third, it does not specify a time following revascularization (some tissue may take >6 months to recover) and fourth, it

ascribes disproportionate importance on the sub-endocardium (which is the main contributor to resting function).

Reversible LV dysfunction may occur in the context of ischemic, stunned and hibernating myocardium. Myocardial “stunning” (dysfunction despite normalization of coronary perfusion) is a state of contraction-perfusion mismatch that is usually associated with acute episodes—for example after successful reperfusion therapy of myocardial infarction. Longer-term dysfunction in viable tissue has been ascribed to chronic reduction of flow, which is often termed “hibernation”, is usually ascribed to a match between contraction and perfusion, but may frequently be due to recurrent stunning. Eventually, this tissue develops progressive structural damage and behaves more like hibernating myocardium; increasing fibrosis is associated with loss of contractile reserve, less tracer uptake and less thickening after revascularization.

This topic is important clinically because the entity of viable myocardium is common—40–50% of regions showing Q waves or dysfunction after infarction are not irreversibly damaged and may be improved after revascularization. This tissue may have an important influence on clinical decision-making in patients with severe LV dysfunction, where the risks and costs of surgery should be balanced by the likelihood of functional recovery and prognostic benefit. The identification of viable tissue in patients with heart failure may also be another indication for viability testing. Ischemic cardiomyopathy accounts for 50% of patients on heart transplant lists, and observational studies show that revascularization of appropriately selected patients is associated with a survival comparable to transplantation. However, the widespread testing of patients with heart failure for viable myocardium remains of unproven value.

Use of Echocardiographic Techniques to Predict Functional Recovery

The echocardiographic assessment of viability is often considered to relate to contractile reserve.

However, a spectrum of information may be obtained from resting echocardiography (wall motion, wall thinning and LV volumes), dobutamine or dipyridamole stress (ischemia and contractile reserve), contrast echocardiography (perfusion), and new technologies (strain imaging).

The echocardiographic hallmarks of scar tissue are that it is thinned and dense. This is meaningful in relation to the likelihood of functional recovery. A wall thickness >0.6 cm has a sensitivity of 94% and specificity of 48% for recovery of function. The nature of wall motion is sometimes considered to be a simple clue to identification of viability on the resting echo. While there can be no thickening without live tissue, the specificity of this finding is limited because this tissue (e.g. in a nontransmural MI) may not be able to improve function due to tethering. Paradoxically, akinetic tissue that is all viable may recover more than hypokinetic tissue that is partly alive and partly infarcted. Finally, ventricles with extensive scar, severe LV dilatation or a restricted filling pattern are less likely to significantly improve ejection fraction after revascularization.

Augmentation of regional function with low dose dobutamine (5–10 mcg/kg/min) or dipyridamole identifies the possibility of viability, but as discussed above, the reliability of this signal depends on what happens next. Continued augmentation up until peak dose may indicate a patent infarct-related artery or well collateralized tissue, but may also be seen in a non-transmural infarction. The development of ischemia at high heart-rates (i.e. a “biphasic response”) denotes a stenosed infarct related artery, and is a reliable predictor of functional recovery after revascularization. The determinants of the viability responses to stress include the amount of viable tissue, the degree of residual stenosis, the extent and magnitude of collaterals, the size of the risk area, tethering, and the presence of drug therapy [14]. Impairment of coronary flow reserve is important in the development of ischemia, and therefore the biphasic response discussed above, but some preservation of flow reserve is critical to permit augmentation of function in response to low dose dobutamine. These issues, as well as

differences in populations and techniques, lead to some variation in the recorded accuracy of stress echocardiography for prediction of viability, but most studies are in the range of 76–87% for sensitivity and 82–92% for specificity.

The use of stress echo to predict functional recovery may be associated with some false negative and false positive results in addition to the usual causes mentioned in relation to predicting angiographic CAD. Viable tissue that has extensive ultrastructural damage may take time to recover both metabolism and function, so “false positive” findings may relate to early performance of the post-revascularization scan. Similarly, revascularization that does not lead to functional recovery at rest may improve contractile reserve or function at peak stress.

Another disadvantage of using regional recovery as the gold standard of viability is that doctors and patients seek revascularization for overall rather than regional benefits. Although reduced LV function has problems as a marker of functional impairment among different patients with heart failure, it is a predictor of adverse outcome, and an improvement could reasonably be expected to translate into prognostic benefit. The results of dobutamine echo have been shown to predict a meaningful (e.g. 5%) improvement in ejection fraction, either by stipulating the extent of biphasic segments (e.g. >4 of 16 segments) or a >5% improvement of ejection fraction at low dose—both offer a sensitivity and specificity of >80% for predicting improvement in ejection fraction. Similarly, the likelihood of remodeling is reduced in the presence of revascularized viable myocardium. The other factors that influence the likelihood of recovery—including the number of thinned and akinetic segments, deceleration time and ventricular volumes—have been discussed above.

The problem with using ejection fraction as the marker of global recovery is that this parameter does not correlate well with functional class. A few studies have compared functional class before and after revascularization of viable tissue, and show that the extent of viability may indeed translate into an improvement of functional capacity. Interestingly, the presence of

viable myocardium by low dose DbE also predicts the improvement in functional capacity after moderate exercise training.

Finally, the final important global parameter is prognosis. Interestingly, observational studies of all modalities for the diagnosis of viability have shown that the presence of viable myocardium is an adverse factor if this tissue is left non-revascularized [15]. Moreover, revascularization of viable myocardium was found to reduce this risk—a reduction that is greatest in patients with severely reduced LV function and more extensive viability. However, an imaging substudy of the only randomized trial of viability in patients with coronary artery disease and left ventricular dysfunction (STICH) showed that viable myocardium was associated with survival, but with no difference in outcome between CABG and medical therapy [16].

Comparison with Other Approaches for the Detection of Myocardial Viability

There are four alternative techniques to contractile reserve for the assessment of myocardial viability; metabolic approaches (SPECT or PET), cell membrane integrity (thallium) perfusion assessment (SPECT or contrast echo), and assessment of the extent of scar (contrast enhanced MRI). The different modalities that assess these parameters have been compared in a meta-analysis, summarized in Fig. 21.13.

Viable myocardium may be identified by the presence of metabolically active cells within a dysfunctional area. The commonest approach involves the identification of a mismatch between uptake of radiolabelled glucose (FDG—a marker of metabolic activity) and reduced myocardial perfusion. The usual imaging technique is positron emission tomography (PET), but modifications can be made to visualize this tracer with SPECT. FDG imaging is highly sensitive but somewhat non-specific for prediction of functional recovery, probably because relatively small islands of viable tissue may not be able to contribute to functional recovery if they are splinted

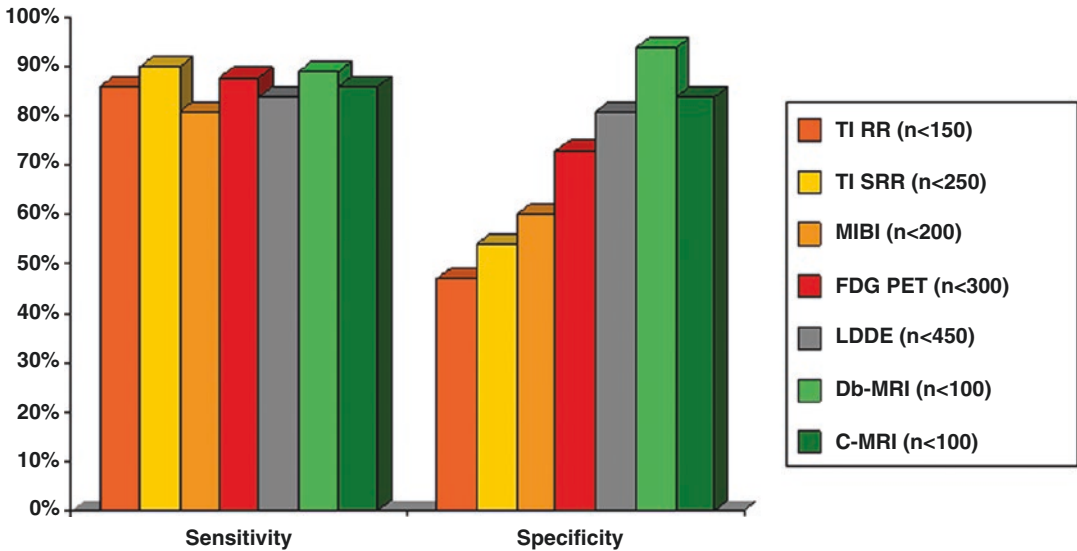


Fig. 21.13 Accuracy of different approaches for diagnosis of viability (modified from Bax [19])

by adjacent scar tissue. Failure of the technique to gain wide acceptance probably reflects the difficulty and inconvenience of obtaining FDG, which has a short half-life. Unfortunately, there are very few comparative data between dobutamine echo and FDG-PET imaging. In one early study, concordance between the two techniques for prediction of recovery was 79%, but PET overestimated the likelihood of recovery.

The concentration of cationic tracers within the cell is against an electrochemical gradient, so membrane integrity is necessary for their concentration within the cell. This process underlies delayed uptake of thallium within perfusion defects. Combination with stress has provided a technique that is sensitive for ischemia and correlates well with position emission tomography for the prediction of functional recovery after revascularization. Likewise, this technique is very sensitive, although the specificity is suboptimal, with several series showing specificities in the range of 50%. Several head-to-head studies have compared thallium SPECT and dobutamine echo, and these show a reproducible pattern of higher specificity of dobutamine echo, but higher sensitivity for thallium imaging. In part, the greater specificity of dobutamine echo is an artifact of

functional recovery being highly dependent on the integrity of the subendocardium, while thallium uptake may occur in isolated islands of viable myocardium intermixed with scar, which may be unable to recover function after revascularization because of tethering by adjacent scar.

Myocardial perfusion may now be measured with SPECT, myocardial contrast echo (MCE) or newer techniques including MRI and ultrafast CT. SPECT assessment of perfusion alone is a marker of viability to the extent that non-viable tissue generally has low flow; recovery is unlikely after revascularization if tracer activity is <60% of maximum. MCE is a marker of intact microvasculature; segments with reduced function that show no opacification with MCE are very unlikely to recover (high sensitivity), but those with opacification may or may not recover. The degree of improvement may be predicted from the degree of the contrast effect. Scoring walls from 0 (no contrast), to 0.5 (partial contrast), to 1 (maximal contrast), the same group was able to predict no improvement in segments without a contrast response, intermediate levels of improvement in those with a patchy response, had substantial improvement in those with diffuse opacification of the segment. These data were gathered using

coronary injection of microbubbles, and whether intravenous injection can be applied for the same purpose remains to be proven.

MRI is able to provide contractile reserve and perfusion information, but its unique aspect relates to the ability to identify the extent of scar, reflecting the concentration of gadolinium within infarcted regions, the phenomenon of hyperenhancement. In follow-up studies after revascularization, the likelihood of recovery in groups with no hyperenhancement, hyperenhancement involving <50% of the myocardium, and hyperenhancement in >50% of the wall have been shown to be respectively 78%, 53%, and 8%.

Conclusion

The number of possible tests for the identification of viability is bewildering. In general terms, the most appropriate test for patients after myocardial infarction is one that is able to detect heterozonal ischemia, peri-infarct ischemia and viable myocardium. The following guidelines have previously been proposed [13];

- (1) The “local” best test should be chosen; both nuclear and echocardiographic techniques effectively identify regional and global functional recovery, as well as identifying patients at risk of major events
- (2) There may be some benefit in using resting thallium or sestamibi imaging to define viability in the unstable patient
- (3) Perfusion-based studies (SPECT or contrast echo) are sensitive and best used when the clinician has a high level of preparedness to proceed to revascularization.

Perhaps the most important message, however, is to keep the presence and extent of viability in the context of a number of other clinical and angiographic parameters that determine the results of revascularization—including angina, ventricular size, infarct size, co-morbid diseases of the LV, adequacy of adequate target vessels for bypass and collateral vessels.

Prognostic Value of Stress Echocardiography

The main determinants of risk in patients with coronary artery disease are the severity of LV dysfunction and the extent of myocardial ischemia. The standard approach to gathering these data for clinical decision-making is based upon the extent of coronary disease and severity of LV dysfunction at coronary angiography and left ventriculography—the detection of three-vessel or left main coronary disease identifies subgroups with 5 year mortalities of 15% or 43%. Nonetheless, the reason why the number of stenosed coronary vessels carry prognostic significance is because this is a marker of the extent of myocardial ischemia, which may be identified by stress echo or other non-invasive techniques. Especially in those who have limited symptoms or who are controlled on medical therapy, a valuable use of stress echo is therefore in the risk stratification of patients: intervention cannot be justified on prognostic grounds if the expected mortality is <1% per year [17]. For example, in chronic stable angina, the overall risk of a major event is 4%. Clinical data (pertaining to age, the severity of angina, a history of diabetes, hypertension or prior infarction, and resting ST segment depression) may be used to identify subgroups at higher and lower risk, and stress testing may be used to further sub-stratify the groups.

Significance of a Negative Stress Echocardiogram

Patients with normal exercise or pharmacologic stress echocardiograms have a benign prognosis over several years of follow-up. The yearly mortality of these patients is <1%, confirming that their prognosis could not be improved by intervention. As always, no finding in isolation is reliable, and some patients with a negative stress echo have a higher risk of cardiac events. There are three major groups; first, those at higher risk on clinical grounds (older patients and those with

diabetes mellitus or left ventricular hypertrophy), those in whom the negative test result is obtained at submaximal exercise (<85% age-predicted maximum heart-rate or <6 METS—reflecting that the heart was insufficiently stressed to become ischemic), and those in whom a wall motion abnormality may have been missed (e.g. patients having angina in the absence of identifiable wall motion abnormalities). A points score has been created to identify the likelihood of a stress echo result producing a misleading prognosis.

Significance of a Positive Stress Echocardiogram

Both death and cardiac events are predicted by the presence of ischemia, scar, or both at either exercise or dobutamine echocardiography. These echo data are both independent predictors of outcome and also incremental to other data. Nonetheless, the overall event rate in the presence of a positive test is <20%, and therefore positive results need to be sub-stratified on the basis of clinical risk, extent and severity of ischemia and the extent of infarction, ischemic threshold and the remainder of the stress testing data. Most important in this respect is the Duke treadmill score; the prognostic value of echo data is limited in patients with low risk and high risk scores, but intermediate risk patients, who account for 40–50% of patients in most series, may be substratified by stress-imaging studies. In these patients, those with a negative or weakly positive test can be managed medically, while those with wall motion abnormalities in multiple vascular territories have an event rate similar to the high risk patients and justify further investigation and intervention.

Prognostic Assessment After Myocardial Infarction

Although the interventional treatment of infarction has become progressively more aggressive in the acute stage or in patients with unstable coronary syndromes, there is currently no

consensus regarding the superiority of an angiographic or a non-invasive approach in the stable post-infarction patient. Despite a frequent desire to define the coronary anatomy, this is not a powerful predictor of outcome (apart from in the highest risk patients such as 3-vessel or left main disease) and provides only inferential information about the extent of ischemic burden or residual viable myocardium. The alternative is a stepwise approach, whereby the two goals of non-invasive testing are the identification of patients at low risk for recurrent events (a group in whom further testing is unnecessary), and the recognition of patients who are at high risk for recurrent cardiac events (in whom intervention should be focused with the goal of avoiding these events) [13].

This predictive process is based upon not just non-invasive but also demographic, clinical and anatomic features:

- (1) baseline demographic and clinical variables such as advanced age, female sex, prior medical history, including previous MI, and the presence of cardiovascular risk factors, particularly diabetes and hypertension;
- (2) clinical variables early in the course of the MI, such as tachycardia, hypotension, Killip class, site (anterior vs. other), type (Q wave vs. non-Q wave) and size of infarction, and ventricular arrhythmias;
- (3) functional indices including resting left ventricular function, exercise capacity, and the presence of spontaneous or inducible ischemia; and
- (4) severity of coronary disease determined at angiography.

Both the extent of left ventricular damage (on the resting images) and the extent of jeopardized myocardium (on stress images), may be obtained by stress echocardiography. The selection of exercise echocardiography allows the detection of echocardiographic evidence of ischemia to complement prognostic information obtained from resting functional indices (e.g. ejection fraction), together with exercise capacity and ST segment analyses, and exercise testing is useful in reassuring patients about their ability to resume

usual activities after myocardial infarction. However, pharmacologic stress techniques have been more extensively studied in the post-infarction population, because tests can be performed earlier and offer viability data. In the landmark Echo Persantine Italian Co-operative (EPIC) multicenter study of 925 patients, the mortality of patients with a negative study was only 2%, compared with only 7% of subjects with a positive test result at low dose. Likewise, the Echo Dobutamine International Co-operative (EDIC) study showed that cardiac death and major events were independently predicted by peak wall motion score index.

Non-invasive prognostic evaluation has become less common in the era of modern acute revascularization practice, although it remains pertinent in patients presenting late. In this setting, the relative roles of the stress echocardiogram and exercise ECG in the post-infarct patient are disputed. Some authors argue that because the negative predictive value of ExECG for mortality is comparable to that of a negative dipyridamole echo (2% vs 1.6%), the standard stress test should be the initial step, with stress echocardiography used for risk stratification of positive stress tests. Others (including this author) favor replacing the exercise test because of its lower feasibility, limited prognostic power and inability to identify the culprit vessel as well as viability.

Prediction of Peri-Operative Cardiac Risk in Patients Undergoing Major Non-cardiac Surgery

The increasing prevalence of cardiac problems and the aging of the population have led cardiac complications of surgery to become a major cause of peri-operative mortality and morbidity. Symptomatic patients require evaluation on their own merits. As in other situations of risk evaluation, the first step should be a clinical evaluation of risk level—based on the nature of surgery and the cardiac history. Although very helpful for identifying risk, it should be recognized that the peri-operative use of stress echocardiography is a common source of inappropriate use [11]. Patients undergoing minor surgery or without clinical markers of risk (angina, past infarction, heart failure, diabetes, renal impairment, advanced age) are unlikely to have a cardiac complication and do not require stress echocardiography. In those that require stress echo, the predictive value of a negative test is >95%, implying that an at-risk patient with a negative test does not require further investigation. As in other situations, the degree of risk associated with a positive test should be sub-stratified on the basis of clinical risk status and ischemic threshold (Fig. 21.14).

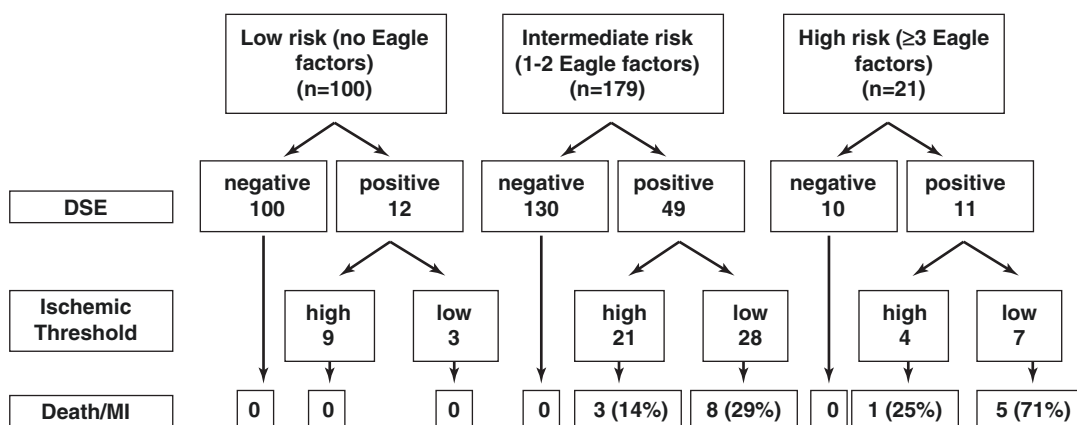


Fig. 21.14 Step-wise approach to risk stratification of patients undergoing vascular surgery (adapted from Poldermans et al. [20]). Patients with low clinical risk (i.e. no Eagle factors) have a low prevalence of ischemia and none in this study had events. Those at intermediate and

high risk with a negative scan have a low risk of events. Those with positive tests may be sub-stratified based on the number of risk factors and ischemic threshold into groups having risks of from 14 to 71%

Use of Stress Echocardiography in Non-coronary Heart Disease

The findings of resting echocardiography may not explain the occurrence of exertional symptoms in patients with not only coronary but also non-coronary heart disease. In these situations, exercise echocardiography testing is the most physiologic means of gathering these data.

Stress Echo in Valvular Heart Disease

Assessment during stress may elucidate the cause of symptoms in patients with marked symptoms but only apparently moderate stenosis, or those with intermittent symptoms (e.g. ischemic mitral regurgitation or intermittent valve prolapse).

The principal indications for stress echo in aortic stenosis are asymptomatic individuals with severe stenosis and those with low gradients. The former may simply reflect inactivity, and a simple stress test (with careful monitoring) may be sufficient to quantify the real exercise capacity and symptom status. The second situation is perhaps more difficult—such patients have thickened aortic valves with severe left ventricular dysfunction, and it is unclear whether reduced valve excursion reflects reduced LV ejection or reduced function is due to severe aortic stenosis [18]. The resting aortic valve area is of value; a valve area of $<0.6 \text{ cm}^2$, typically associated with a mean gradient of $>30 \text{ mmHg}$ usually signifies significant aortic stenosis. However, if the distinction is unclear, the response to low doses of dobutamine may elucidate the mechanism. First, failure to improve LV function with dobutamine portends an adverse outcome. If the LV improves, an increment of gradient and fixed valve area suggests the underlying cause to be aortic stenosis. Improvement of valve area suggests that the valve is opening more because the ventricle is now pushing harder—although whether such individuals should forego surgery is debated, it is

less likely to have a favorable effect than in the patients with a gradient response.

Exercise echocardiography may be of benefit in patients with apparently mild mitral stenosis at rest, who exhibit significant exertional symptoms. When this is performed, the most important parameter is tricuspid regurgitant severity and velocity, with some additional information from the increase in mitral gradient during exercise testing.

In healthy patients with an obviously repairable mitral valve, early operation is probably the most reliable means of avoiding the development of LV dysfunction. Likewise, asymptomatic patients who are suitable for surgery should clearly proceed if the preoperative ejection fraction is $<55\%$, as a delay will risk a further deterioration of post-operative function. However, in patients where the valve is non-repairable or may not be repairable, or when there is concurrent disease that would increase the risk of surgery, further evaluation of risk and benefit may be of value. The rationale behind the use of stress echocardiography for assessment of regurgitant valve lesions is to examine LV contractile reserve. This may facilitate the early detection of LV decompensation and justify intervention before either symptoms or overt LV dysfunction are apparent. Indeed, the most accurate variables for prediction of post-operative LV dysfunction are exercise end-systolic volume index $>27 \text{ ml/m}^2$, ejection fraction $<68\%$, or change of ejection fraction with exercise $<5\%$. The identification of preserved contractile reserve has been associated with favorable outcome in both aortic and mitral regurgitation.

Conclusions

Stress echocardiography now has an established role as an accurate and cost-effective approach to the diagnosis and risk assessment of CAD, viability and non-coronary heart disease. The lack of automation and the need for training remain its greatest challenges.

References

1. Sicari R, Nihoyannopoulos P, Evangelista A, et al. Stress echocardiography expert consensus statement: European Association of Echocardiography (EAE) (a registered branch of the ESC). *Eur J Echocardiogr*. 2008;9:415–37.
2. Rigo F, Cortigiani L, Pasanisi E, et al. The additional prognostic value of coronary flow reserve on left anterior descending artery in patients with negative stress echo by wall motion criteria. A Transthoracic Vasodilator Stress Echocardiography Study. *Am Heart J*. 2006;151:124–30.
3. Nishimura RA, Reeder GS, Miller FA, et al. Prognostic value of predischARGE 2-dimensional echocardiogram after acute myocardial infarction. *Am J Cardiol*. 1984;53:429–32.
4. Hoffmann R, Lethen H, Marwick T, et al. Standardized guidelines for the interpretation of dobutamine echocardiography reduce interinstitutional variance in interpretation. *Am J Cardiol*. 1998;82:1520–4.
5. Picano E, Lattanzi F, Orlandini A, Marini C, L'Abbate A. Stress echocardiography and the human factor: the importance of being expert. *J Am Coll Cardiol*. 1991;17:666–9.
6. Hoffmann R, Lethen H, Marwick T, et al. Analysis of interinstitutional observer agreement in interpretation of dobutamine stress echocardiograms. *J Am Coll Cardiol*. 1996;27:330–6.
7. Voigt JU, Exner B, Schmiedehausen K, et al. Strain-rate imaging during dobutamine stress echocardiography provides objective evidence of inducible ischemia. *Circulation*. 2003;107:2120–6.
8. Ishii K, Suyama T, Imai M, et al. Abnormal regional left ventricular systolic and diastolic function in patients with coronary artery disease undergoing percutaneous coronary intervention: clinical significance of post-ischemic diastolic stunning. *J Am Coll Cardiol*. 2009;54:1589–97.
9. Detrano R, Lyons KP, Marcondes G, Abbassi N, Froelicher VF, Janosi A. Methodologic problems in exercise testing research. Are we solving them? [Review]. *Arch Intern Med*. 1988;148:1289–95.
10. Armstrong WF, O'Donnell J, Dillon JC, McHenry PL, Morris SN. Complementary value of two-dimensional exercise echocardiography to routine treadmill exercise testing. *Ann Intern Med*. 1986;105:829–35.
11. Wolk MJ, Bailey SR, Doherty JU, et al. ACCF/AHA/ASE/ASNC/HFSA/HRS/SCAI/SCCT/SCMR/STS 2013 multimodality appropriate use criteria for the detection and risk assessment of stable ischemic heart disease: a report of the American College of Cardiology Foundation Appropriate Use Criteria Task Force, American Heart Association, American Society of Echocardiography, American Society of Nuclear Cardiology, Heart Failure Society of America, Heart Rhythm Society, Society for Cardiovascular Angiography and Interventions, Society of Cardiovascular Computed Tomography, Society for Cardiovascular Magnetic Resonance, and Society of Thoracic Surgeons. *J Am Coll Cardiol*. 2014;63:380–406.
12. Fleischmann KE, Hunink MG, Kuntz KM, Douglas PS. Exercise echocardiography or exercise SPECT imaging? A meta-analysis of diagnostic test performance. *JAMA*. 1998;280:913–20.
13. Marwick TH. Stress echocardiography: its role in the diagnosis and evaluation of coronary artery disease. 2nd ed. Boston: Kluwer Academic Publishers; 2003.
14. Kaul S. Response of dysfunctional myocardium to dobutamine. “The eyes see what the mind knows”. *J Am Coll Cardiol*. 1996;27:1608–11.
15. Allman KC, Shaw LJ, Hachamovitch R, Udelson JE. Myocardial viability testing and impact of revascularization on prognosis in patients with coronary artery disease and left ventricular dysfunction: a meta-analysis. *J Am Coll Cardiol*. 2002;39:1151–8.
16. Bonow RO, Maurer G, Lee KL, et al. Myocardial viability and survival in ischemic left ventricular dysfunction. *N Engl J Med*. 2011;364:1617–25.
17. Gibbons RJ, Chatterjee K, Daley J, et al. ACC/AHA/ACP-ASIM guidelines for the management of patients with chronic stable angina: a report of the American College of Cardiology/American Heart Association Task Force on Practice Guidelines (Committee on Management of Patients with Chronic Stable Angina). *J Am Coll Cardiol*. 1999;33:2092–197.
18. Nishimura RA, Carabello BA, Faxon DP, et al. ACC/AHA 2008 guideline update on valvular heart disease: focused update on infective endocarditis: a report of the American College of Cardiology/American Heart Association Task Force on Practice Guidelines: endorsed by the Society of Cardiovascular Anesthesiologists, Society for Cardiovascular Angiography and Interventions, and Society of Thoracic Surgeons. *Circulation*. 2008;118:887–96.
19. Bax JJ. *J Am Coll Cardiol*. 1995.
20. Poldermans D, Arnesen M, Fioretti PM, et al. Improved cardiac risk stratification in major vascular surgery with dobutamine-atropine stress echocardiography. *J Am Coll Cardiol*. 1995;26:648–53.

Assessing Myocardial Viability: Principles and the Role of Echocardiography

22

Agnès Pasquet, Bernhard Gerber,
and Jean-Louis J. Vanoverschelde

Introduction

Heart failure is a leading cause of healthcare expenditures, hospitalization, and mortality in developed countries. With the aging of the population and increasing prevalence of chronic diseases, such as hypertension, diabetes mellitus, and obesity, the current heart failure epidemic will significantly worsen in the near future.

During the last decades, progress in pharmacologic and non-pharmacologic treatments have contributed to improve prognosis of patient with heart failure. Nevertheless, results obtained could be considered as insufficient and dysfunctional myocardium represent a privileged target for other therapeutic options. Because coronary artery remains one of the main causes of heart failure, myocardial revascularization seems to be a logic treatment for such patients.

As a result of improved anaesthetic, surgical, and myocardial protection techniques, the surgical risks of performing coronary artery bypass graft (CABG) in these patients have decreased significantly in recent years, to less than 6%. Myocardial revascularization has subsequently become a valid treatment option in selected patients with observed survival benefits compared to medical therapy, and in some cases, improvement in heart failure symptoms and functional status.

From the mid-1980s, the concept of hibernating of viable myocardium has emerged to characterize chronically dysfunctional myocardium able of functional recovery after revascularization. Observational studies have suggested that patients with ischemic left ventricular dysfunction and a significant amount of viable myocardium identified by various non-invasive imaging modalities could benefit from myocardial revascularization. Suggested benefit were not only on global and regional left ventricular function but also on heart failure symptoms and most important on survival. Unfortunately, the recent STICH trial raise some question about the usefulness of detection of myocardial viability.

It is the purpose of this chapter to review the actual understanding of the pathophysiology of chronically dysfunctional but viable myocardium and its implications for detection of myocardial viability using echocardiography but also to discuss the clinical role of myocardial viability at present time.

A. Pasquet (✉) · B. Gerber · J.-L. J. Vanoverschelde
Division of Cardiology, Cliniques Universitaires St
Luc, Brussels, Belgium

Pole of Cardiovascular Research (CARD), Institut de
Recherche Expérimentale et Clinique, Division of
Cardiology, Department of Cardiovascular Diseases,
Cliniques Universitaires St. Luc Université
Catholique, Brussels, Belgium
e-mail: agnes.pasquet@uclouvain.be

Historical Perspective

The spectrum of left ventricular (LV) dysfunction caused by atherosclerotic coronary artery disease has expanded over the last quarter of the twentieth century. Traditionally, it was assumed that heart failure arose from either reversible ischemia (anginal equivalent) or irreversible myocardial infarction. Insights gained from more recent functional, metabolic and morphological studies have led to the concept of dysfunctional but viable myocardium (stunned and hibernating) and to that of ventricular remodelling.

The term “myocardial hibernation” was proposed in the mid-1980s by Rahimtoola to describe a state of diminished resting ventricular function in the setting of coronary artery disease. He proposed that myocardial hibernation develops as a protective mechanism wherein persistent myocardial hypoperfusion in the absence of myocardial necrosis leads to downregulation of myocardial contractility. Ross subsequently coined the term “perfusion-contraction matching” to characterize the adaptive response of the hibernating myocardium to diminished perfusion. The concept of evaluating perfusion and contraction simultaneously to characterize the mechanisms underlying contractile dysfunction has fostered considerable research interests and stimulated the use of perfusion imaging, not only to address basic pathophysiological mechanisms but also to detect viable myocardium clinically in coronary patients.

Pathophysiology

Observations in Humans with Chronic Reversible Ischemic Dysfunction

Perfusion: Contraction Matching

Assessment of perfusion-contraction matching in patients with chronic LV ischemic dysfunction requires the ability to measure regional myocardial blood flow in absolute terms and to correlate these findings with data on regional myocardial function, acquired simultaneously. Until recently, this has only become possible using positron emission tomography (PET) with either ^{13}N -ammonia or ^{15}O -water as flow tracers. PET is a truly quantitative method allowing computation

of quantitative estimates of regional transmural myocardial perfusion.

Resting PET flow measurements obtained in chronically dysfunctional but viable myocardium are summarized in Fig. 22.1. Based on the results of these studies, it appears that the transmural blood flow to dysfunctional but viable segments is remarkably variable, about one half of the segments showing reduced perfusion, as predicted by Rahimtoola, whereas the other half displays only minor and often no reduction in transmural myocardial blood flow.

Recent development of cardiac magnetic resonance (CMR) imaging allows to further characterize myocardial blood flow in the different myocardial layers. Using CMR, Selvanayagam demonstrated that sub endocardial myocardial blood flow was reduced at rest in patients with hibernating myocardium when compared with myocardium without significant coronary artery in the same patient. He also demonstrated that after revascularization the subendocardial myocardial blood flow was normalized when the function improves.

Myocardial Flow Reserve

Irrespective of resting flow, perfusion reserve mainly represented by the coronary flow reserve is always reduced in dysfunctional but viable myocardium, albeit more severely in segments with low rest perfusion than in those with normal rest perfusion. The severity of coronary flow reserve reduction directly impacts on the ability of dysfunctional but viable myocardium to improve in contraction upon inotropic stimulation, as this requires increases myocardial blood flow and oxygen consumption (*vide infra*).

Inotropic Reserve

In patients, dysfunctional but viable myocardium often has the capacity to improve function when challenged by an inotropic stimulus, such as post-extrasystolic potentiation or the infusion of catecholamines. However, the response of viable segments to these stimuli greatly varies from segment to segment as well as with the intensity and the duration of stimulation.

Most viable segments exhibit a biphasic response when challenged by increasing levels of inotropic stimulation. At low

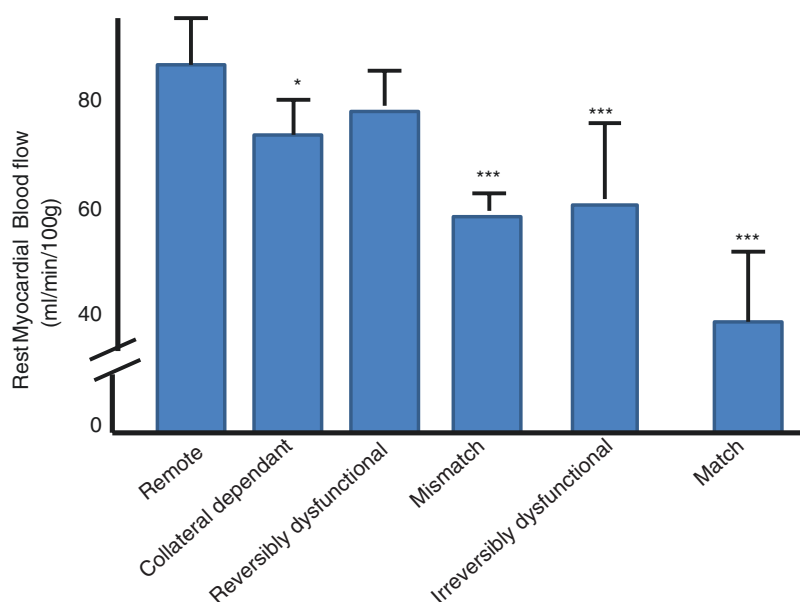


Fig. 22.1 Bar graph of rest myocardial blood flow (MBF) measured with ^{13}N -ammonia or ^{15}O -water in remote, non-infarcted collateral-dependent, reversibly dysfunctional, irreversibly dysfunctional, PET flow-metabolism mismatch and PET flow-metabolism match segments of

patients with chronic left ventricular ischemic dysfunction. * $p < 0.05$, *** $p < 0.001$ vs. remote segments. Adapted from Vanoverschelde J-L and Melin JA. The pathophysiology of myocardial hibernation. Current controversies and future directions. *Prog Cardiovasc Dis* 2001;43:387–398

levels, and provided that sufficient residual flow reserve is present (vide infra), systolic wall thickening usually increases and starts earlier in systole. At higher levels, when the increased in demand cannot be matched anymore by a further increase in myocardial blood flow because of the underlying coronary disease, systolic function deteriorates back and can even become worse than at baseline. The observation of this peculiar biphasic pattern is extremely important to rule out other causes of regional dysfunction such as the presence of a subendocardial scar or the overall process of remodeling that accompanies left ventricular dilatation. In contrast to truly viable segments, segments affected by one of these two entities indeed usually display a sustained contractile response at both low and high levels of inotropic stimulation.

It is important to mention that not every viable segment improves functionally during inotropic stimulation, and that about 25% of “metabolically” viable segments, i.e. those with preserved energy metabolism, exhibit no response whatsoever to an inotropic challenge. Compared to viable segments with recruitable inotropic reserve,

those lacking contractile reserve usually have a lower resting myocardial blood flow and take up more glucose under fasting conditions than normal segments or viable segments with recruitable inotropic reserve, a finding which is consistent with either ongoing or impending myocardial ischemia, and thus with a severely blunted myocardial flow reserve. This hypothesis is further supported by the results of several animal and human studies that have shown that improvements in mechanical function during inotropic stimulation are always attended by similar directional changes in myocardial blood flow and oxygen consumption. This implies that sufficient residual flow reserve must be present for the expression of a positive contractile response during inotropic stimulation.

There certainly are other factors that contribute to the lack of inotropic reserve in otherwise viable myocardium. Preliminary data indeed suggest that the severity of the structural changes affecting the cardiomyocytes may also impact on the ability of viable myocardium to respond to an inotropic stimulus. In a recent study, the likelihood of a positive inotropic response to dobutamine was indeed found to be inversely

proportional to the mass of residual myocytes showing severe myofibrillar loss. There is also evidence that downregulation of β -adrenoreceptors in viable segments contributes to decrease to likelihood to unmask residual inotropic reserve.

Structural Modifications

Besides the changes in resting myocardial blood flow and flow reserve, several structural alterations that affect the microcirculation, the cardiomyocytes and the extracellular matrix have described in dysfunctional but viable segments. Most of the available information on these structural changes has been gathered from studies in which human myocardial biopsy specimens were harvested at the time of bypass surgery.

Microcirculation

In general, histological analysis of human dysfunctional myocardium has demonstrated that the microvasculature was better preserved in the segments that will ultimately improve function after revascularization than in those that will not (Fig. 22.2). This is particularly true for the capil-

laries whose density and cross sectional area are usually within the normal range in reversibly dysfunctional segments. By contrast, there is a much greater heterogeneity among the segments that eventually do not recover function after revascularization, approximately half of them showing significant capillary rarefaction whereas the other half show no or minimal changes. As expected, the major determinant of capillary density appears to be the severity of interstitial fibrosis.

Myocyte Alterations

The primary alterations include depletion of contractile elements. In some cells, this is limited to the vicinity of the nucleus, whereas in others it is very extended, leaving only few or no sarcomeres at the cell periphery. Myofibrillar loss is not accompanied by major cell volume changes, which is clearly different from atrophic degeneration. The space previously occupied by the myofilaments is filled with an amorphous, strongly PAS-positive material, typical of glycogen (Fig. 22.3). At the ultrastructural level, adaptive rather than degenerative ischemic changes are

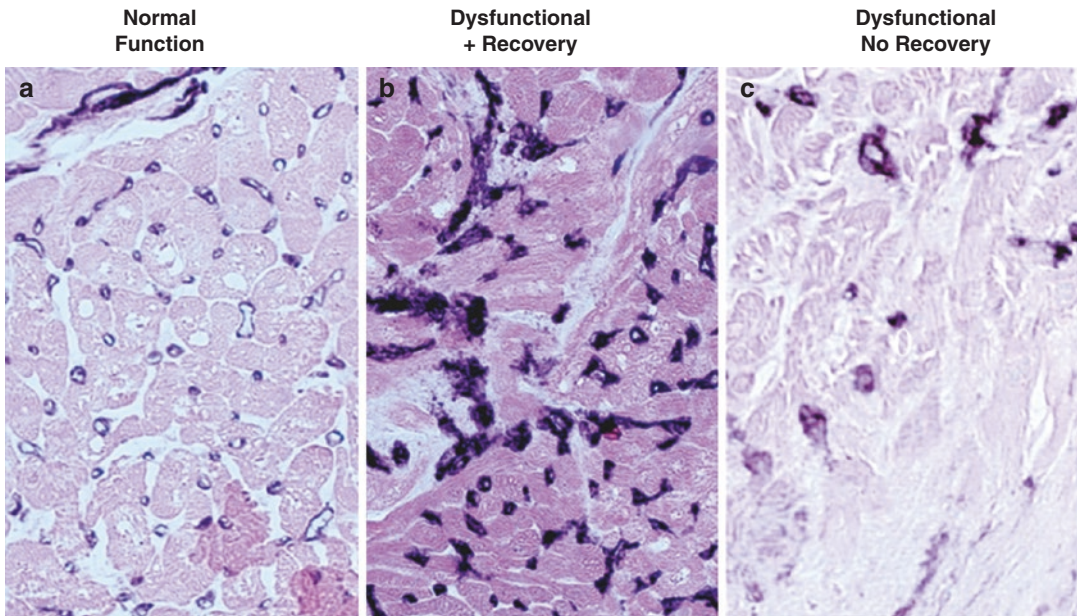


Fig. 22.2 Biopsy specimens from three different segments with CD31 staining. (a) In a segment with normal resting function, the microcirculation is preserved. (b) In a dysfunctional segment that improved after revascularization, the microvascular density is normal. (c) Low capillary density and significant fibrosis are seen in a dysfunctional seg-

ment that did not recover function. Reproduced with permission from Shimoni et al. Microvascular structural correlates of myocardial contrast echocardiography in patients with coronary artery disease and left ventricular dysfunction. Implications for the assessment of myocardial hibernation. *Circulation*. 2002;106:950–956

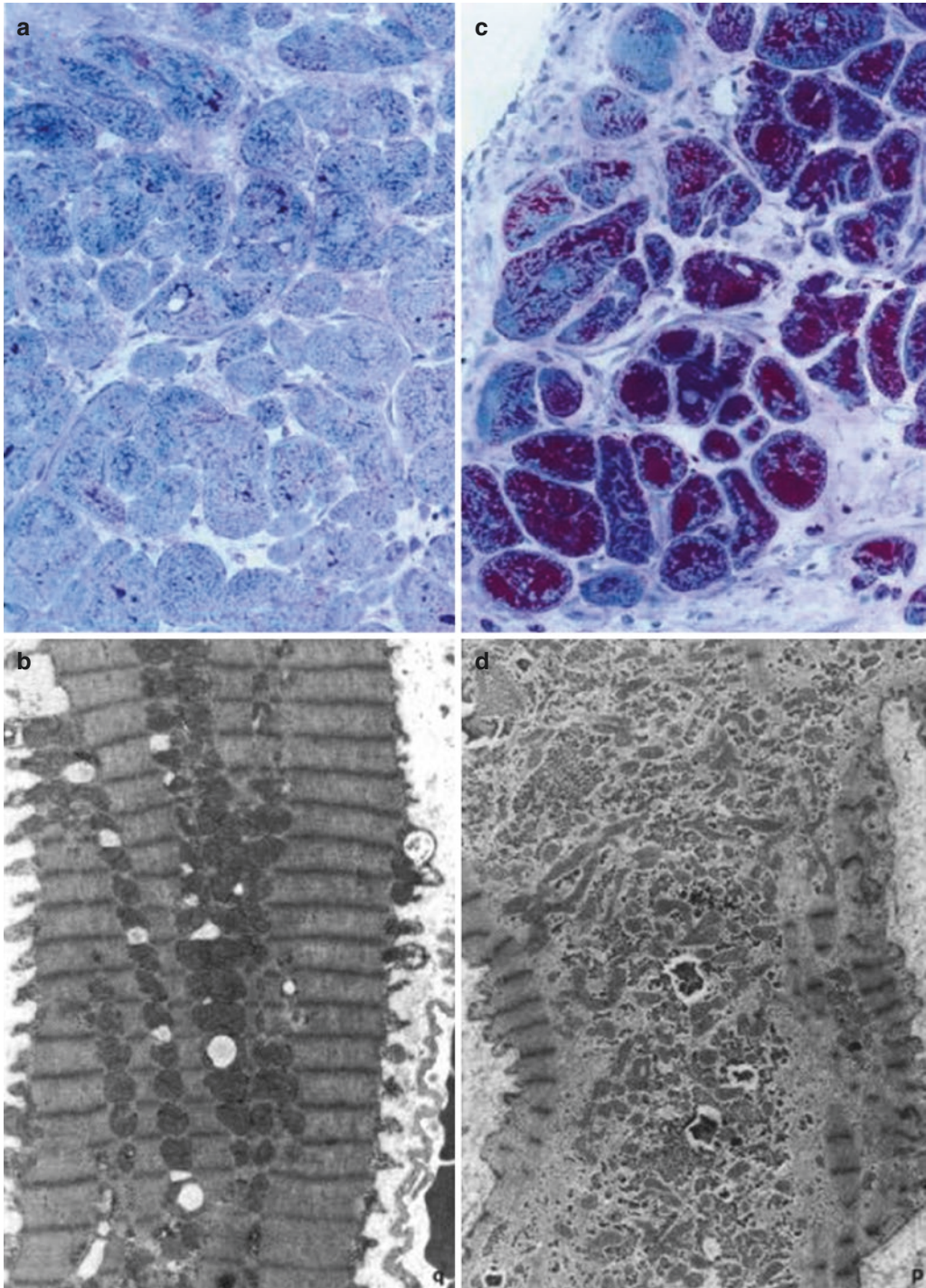


Fig. 22.3 (a) Light micrograph of myocardium showing normal cardiomyocytes with virtually no glycogen (PAS staining in red). (b) Transmission electron micrograph of a normal cardiac myocyte. (c) Representative light micrograph of a biopsy sample of human hibernating myocardium. Cardiac myocytes are depleted of their contractile material and filled with glycogen (PAS positive staining).

(d) Representative transmission electron micrograph of a hibernating cardiomyocyte. The myolytic cytoplasm is devoid of sarcomeres and filled with glycogen. Magnification: (a, c) $\times 320$; (b) $\times 7100$; (d) $\times 7500$. Reproduced with permission from Vanoverschelde J-L et al. Chronic myocardial hibernation in humans. From bedside to bench. *Circulation* 1997;95:1961–1971

observed. The mitochondria are increased in number and display alterations in size and shape. They are unevenly distributed within the cytoplasm. Most appear doughnut-shaped and show loss of contact sites between inner and outer mitochondrial membranes or decreased numbers of cristae. The nuclear alterations range from irregular tortuous nuclear outlines, with even distribution of heterochromatin over the nucleoplasm, to chromatin clumping near the nuclear membrane and throughout the whole nucleoplasm. Loss of sarcoplasmic reticulum, T-tubules and sarcomeres but increased endoplasmic reticulum provides additional support for an adaptive phenomenon.

Molecular Mechanism

Reductions in the protein and mRNA content of myosin the contractile protein, the thin filament complex actin, α -actin, desmin, and titin have been found in dysfunctional myocardium and the distribution of titin within the cardiomyocyte is altered. Consistent with depressed contractility, a reduction in phosphorylation of myosin regulatory light chain 2 and cardiac troponin I was observed in mouse model of myocardial dysfunction in which chronic ischemia was induced by vascular endothelial growth factor (VEGF) sequestration. Because phosphorylation of myosin regulatory light chain 2 is critical for cardiac muscle contraction, dephosphorylation of this protein may be a potential mechanism that significantly limits contractility in the failing heart.

Cytoskeletal proteins such as desmin, tubulin and vinculin are disorganized. The expression of connexin-43, a major gap junction protein, and that of nuclear A-type lamins are also reduced. These findings suggest that structural disassembly and altered regulation of myofilament proteins contribute to cardiac dysfunction.

Beside alteration in contractile proteins, molecular change in dysfunctional myocardium include depression of energy metabolism and mitochondrial function, disruption of calcium signaling and sensitivity, and induction of a distinct subset of cardioprotective genes.

Maintenance of calcium handling is essential for myocyte contraction. Disruption of proteins mediating calcium flux is associated with reduced

contractile force. Both Ca^{2+} influx and free intracellular Ca^{2+} concentration were reduced in ischemic dysfunctional myocardium, consistent with an excitation–contraction coupling defect.

From a biochemical point of view, tissue content of ATP, total adenine nucleotides and phosphocreatine usual remain nearly normal, and mitochondrial function, as reflected by the ADP/ATP and PCr/ATP ratios, also remains nearly intact. Nevertheless, there is a switch of preferred substrate from fatty acids to glucose in dysfunctional myocardium. This was demonstrated non-invasively in human patients PET with fluorine-18 labeled deoxyglucose (18F-FDG) and this provides the rationale for using radionuclide myocardial perfusion imaging with glucose analogs, such as 18F-FDG, to differentiate dysfunctional viable myocardium from nonviable myocardium.

“Adult” cardiomyocytes have reduced capacity for regeneration, and several cardiac pathology will induce cell death. Thus, the ability of cardiomyocytes to survive cytotoxic insults as ischemia; is indispensable for maintenance of the heart’s health. New studies using genomic and proteomic approaches were performed to identify additional stress–response and cytoprotective genes in dysfunctional myocardium. These genes included a powerful suppressor of caspases, inhibitor of apoptosis, stress–response genes HSP27 and HSP70, as well as a novel growth-promoting H11 kinase (H11K). The findings were further validated in human heart failure with PET-confirmed dysfunctionnal cardiac segments. Both, mRNA and protein levels of inhibitor of apoptosis, HSP70 and H11K were significantly upregulated in dysfunctionnal human myocardium, compared with the remote normal tissue. Although the role of inhibitor of apoptosis and HSP27/HSP70 in preservation of cell viability was previously established, the function of H11K in dysfunctional myocardium remains unknown. It has been suggested that H11K may promote myocyte viability through an increase in glucose uptake.

Extracellular Matrix

The interstitial alterations consist in increased amounts of collagen (type I and III) and fibronectine deposition. Within the widened interstitium are variable numbers of fibroblasts and macrophages,

and scant increased amounts of elastic fibers. Importantly, acute ischemic changes such as endothelial swelling of the microvasculature are absent. Given their severity, the structural changes that affect dysfunctional but viable myocardium impact on its ability to respond to an inotropic stimulus and on the speed at which it may or may not recover after revascularization. Not surprisingly, segments with less fibrosis or with less severe cardiomyocyte alteration and remodelling are more likely to improve function following the administration of dobutamine or after revascularization.

Recent studies have suggested that the structural changes occurring in hibernating myocardium are the consequence of a dedifferentiation process. The hibernating cardiomyocytes indeed show many features of neonatal cardiomyocytes, including (1) depletion of contractile filaments, (2) presence of rough sarcoplasmic reticulum, (3) accumulation of glycogen, (4) occurrence of irregularly shaped nuclei with peculiar distribution of chromatin, (5) loss of organized sarcoplasmic reticulum, (6) lack of T-tubules, and (7) vesiculization of the sarcolemma. Not all the characteristics of the altered cardiomyocytes resemble those of embryonic cells, however. For instance, the remaining sarcomeres in the altered cells often retain their orderly arrangement at the cell periphery, while they are randomly distributed in embryonic cells. Also, the amount of glycogen seen in altered cardiomyocytes far exceeds that reported in the embryo. The hypothesis of dedifferentiation is further substantiated by immunohistological studies showing that hibernating cardiomyocytes re-express contractile proteins that are specific to the fetal heart, such as the α -smooth muscle actin, while at the same time, they exhibit the same organization of structural proteins like titin as developing cardiomyocytes. In addition, cardiotin, a recently described high molecular weight protein absent in fetal cells, is also absent from the altered cells. These findings reinforce the thesis that hibernating cardiomyocytes undergo partial dedifferentiation.

Animal models have also improved our understanding of the morphological alterations seen in reversible ischemic dysfunction. Several studies have indeed indicated that myofibrillar disassembly, myofibrillar loss and increased glycogen

content develop rapidly after a critical limitation in flow reserve. Interestingly, these changes seem to take place similarly in dysfunctional and in normally perfused remote regions of the dysfunctional hearts. Similar changes in cardiomyocyte morphology and signs of dedifferentiation were detected in other models of cardiac dysfunction, including chronic atrial fibrillation, 33 infarct border zone, and in explanted hearts from patients with heart failure. Thus, the pathological changes described in humans with chronic but reversible dysfunction do not appear to reflect the chronicity of LV dysfunction nor do they appear to arise as a direct consequence of ischemia. The fact that myolysis occurs globally in ischemic cardiomyopathy raises the possibility that these morphological changes reflect a response to chronic elevations in preload or stretch.

Insights Gained from Animal Models of Chronic Reversible Ischemic Dysfunction

In acute experimental coronary occlusion in animal models, it had been demonstrated that reduction in transmyocardial blood flow will affect more subendocardial region than subepicardial region. Only a 20% reduction in subendocardial blood flow may induce a severe regional dysfunction with only a minor reduction of the transmyocardial blood flow.

Chronic coronary stenosis and progressive ameroid occlusion models have shed a new light on both the mechanisms and the temporal progression of reversible ischemic dysfunction. During the first weeks after the onset of dysfunction, endocardial blood flow has consistently found to be either normal or only marginally decreased. At that time, chronic myocardial stunning is thus the most likely mechanism for the observed dysfunction, an hypothesis which is further supported by the strong relation between the reduction in subendocardial flow reserve and the severity of dysfunction. With time and probably also increases in the physiological significance of the underlying coronary narrowings, some of the dysfunctional segments, which appeared "chronically stunned" on early examination, eventually

become underperfused. It is noteworthy that the transition from chronic stunning to chronic hibernation only occurs for threshold reductions in myocardial flow reserve. The critical nature of coronary flow reserve reduction required to produce hibernating myocardium likely explains why not all studies have demonstrated a progression to hibernating myocardium distal to a chronic stenosis. For example, circumflex ameroid models (rapidly progressing stenoses) in dogs usually display normal resting perfusion, with a well-developed collateral circulation, yet hibernating myocardium can develop when source collateral flow is limited. The experimental data thus suggest that chronic reversible myocardial ischemic dysfunction is a complex, progressive and dynamic phenomenon, that is initiated by repeated episodes of ischemia, and in which resting perfusion, although initially preserved, may subsequently become reduced, probably in response to the decrease in myocyte energy demand. Indeed, the persistence of some degree of flow reserve, even when resting myocardial blood flow is

reduced suggests that the reduction in rest flow is somehow secondary to that in resting contractile function, and could serve as a way to increase residual myocardial perfusion reserve.

The Physiological Spectrum of Myocardial Viability

Initially, it was thought that myocardial ischemia resulted in either irreversible myocardial necrosis (i.e., myocardial infarction) or complete and rapid recovery of myocyte function (i.e., typical angina). However, it is now clear that ischemia produces a continuum of myocardial adaptive responses (Fig. 22.4). Altogether, the currently available data thus suggest that a spectrum of myocardial dysfunction exists in patients with coronary disease (Table 22.1). The initial stages of dysfunction most likely correspond to chronic stunning and are characterized by normal resting perfusion but reduced flow reserve, mild myocyte alterations,

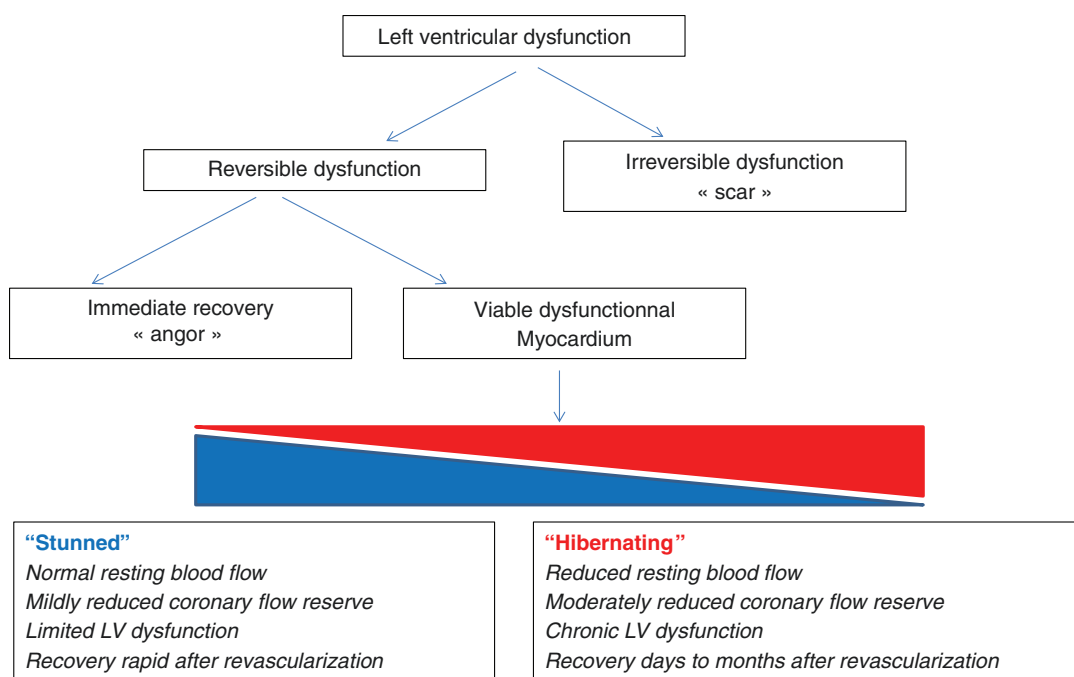


Fig. 22.4 Schematic representation of myocardial states present in left ventricular dysfunction and the continuum of different states of viable myocardium

Table 22.1 The patterns of chronic ischemic dysfunction

	Rest flow	Flow reserve	Inotropic reserve	Metabolism	Structural changes	Reversibility
Chronic stunning	↔	↓	Yes	↔	No	Yes
Transition phase	↔	↓	Yes	↔	Mild dedifferentiation	Yes
Chronic hibernation	↓	↓↓	May be absent	↔	More severe dedifferentiation/fibrosis	Delayed/incomplete
Infarction	↓	↓↓	No	↓	Fibrosis	No
Remodeling	↔	↔	May be absent	↔	Fibrosis	No

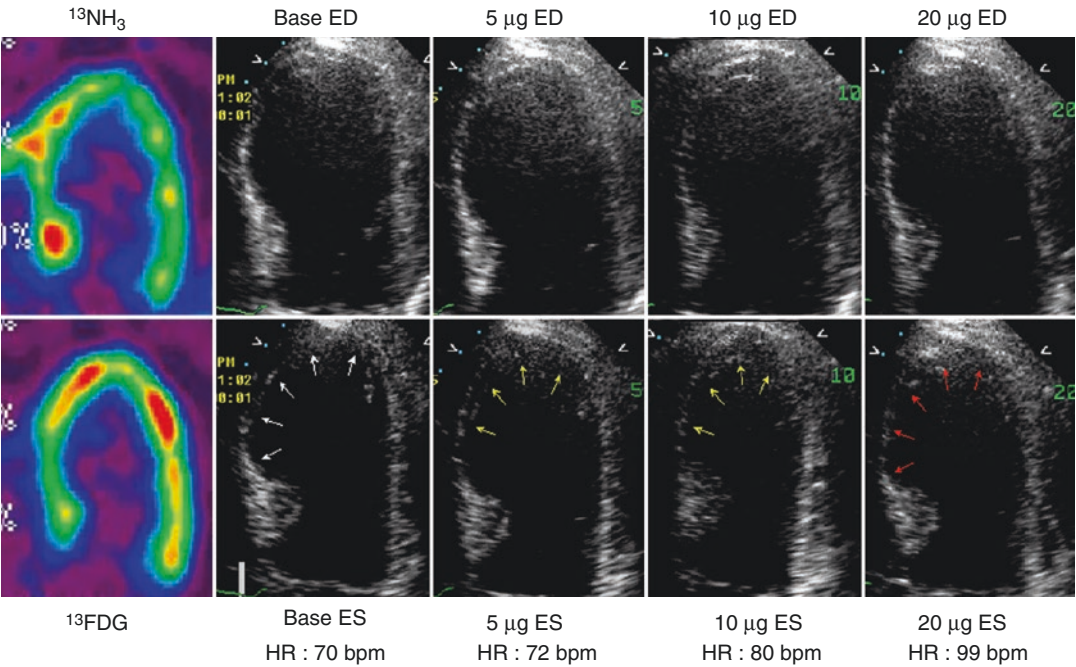


Fig. 22.5 Inotropic response to dobutamine in dysfunctional segments (white arrows) with normal rest flow ($^{13}\text{NH}_3$) and FDG uptake (^{18}FDG). The upper row shows images obtained from the apical 4-chamber view in end-diastole at baseline and during the infusion of 5, 10 and 20 $\mu\text{g kg}^{-1} \text{min}^{-1}$ of dobutamine. The lower row shows the corresponding end-systolic

images. The yellows arrows indicate segments improving function, whereas red arrows indicate deteriorating segments. The sequence illustrates a typical biphasic response in the distal septum and the apex. Since blood flow and FDG uptake are normal in these segments, this is an example of chronically stunned myocardium

maintained membrane integrity (allowing the transport of cations and metabolic fuels), preserved capacity to respond to an inotropic stimulus and no or little tissue fibrosis (Fig. 22.5). Following revascularization, functional recovery is likely to be rapid and complete. At the opposite, more advanced stages of dysfunction are probably associated with reduced rest per-

fusion, increased tissue fibrosis, perhaps more severe myocyte remodeling and a decreased ability to respond to inotropic stimuli. Nonetheless, membrane function and energy metabolism long remain preserved (Figs. 22.6 and 22.7). Following revascularization, functional recovery, if any, is usually quite delayed and in the end mostly incomplete.

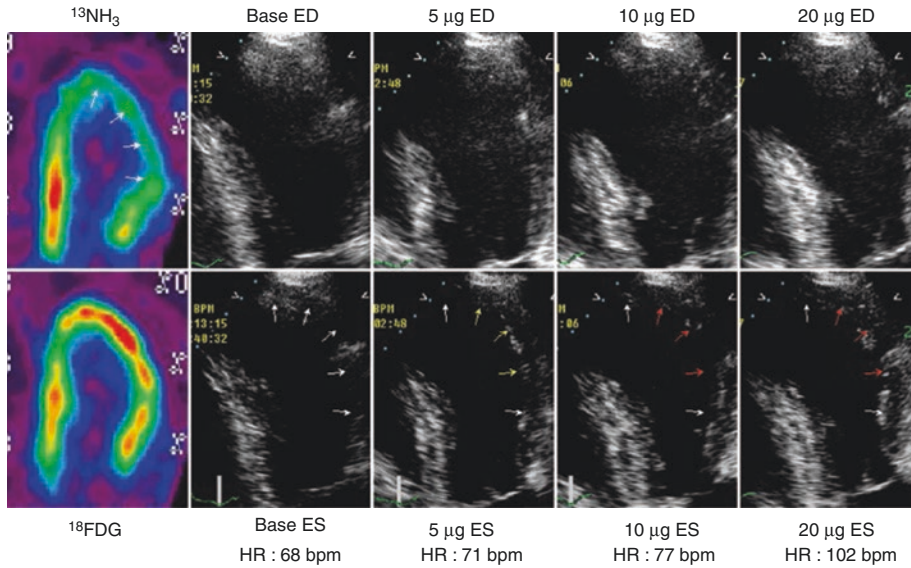


Fig. 22.6 Inotropic response to dobutamine in dysfunctional segments (white arrows) with mildly reduced rest flow ($^{13}\text{NH}_3$) and a normal FDG uptake (^{18}FDG). The upper row shows images obtained from the apical 2-chamber view in end-diastole at baseline and during the infusion of 5, 10 and 20 $\mu\text{g kg}^{-1} \text{min}^{-1}$ of dobutamine. The lower row shows the corresponding end-systolic images.

The yellow arrows indicate segments improving function, whereas red arrows indicate deteriorating segments. The sequence illustrates a very transient biphasic response in the mid anterior segment, followed by immediate deterioration at low heart rate. Since blood flow was slightly reduced and FDG uptake was normal in that segment, this is an example of mildly hibernating myocardium.

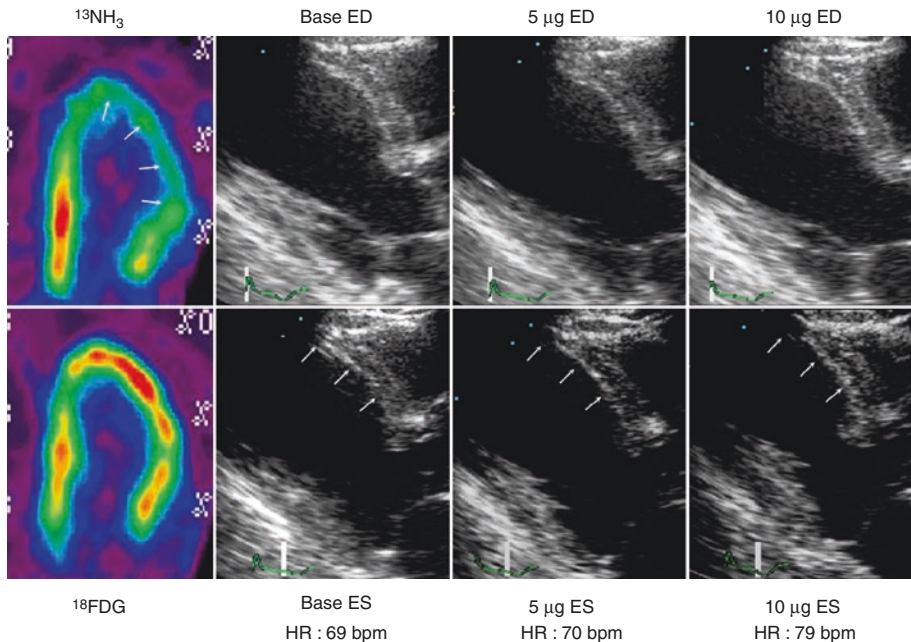


Fig. 22.7 Inotropic response to dobutamine in dysfunctional segments (white arrows) with moderately reduced rest flow ($^{13}\text{NH}_3$) and a normal FDG uptake (^{18}FDG). The upper row shows images obtained from the parasternal long-axis view in end-diastole at baseline and during the infusion of 5 and 10 $\mu\text{g kg}^{-1} \text{min}^{-1}$ of dobutamine. The lower row shows the corresponding end-systolic images.

The sequence illustrates the absence of inotropic reserve in the anteroseptal segment. Since blood flow was definitively reduced and FDG uptake was normal in that segment, this is an example of severely hibernating myocardium.

Implications for the Clinical Identification of Viable Myocardium

Our current understanding of the pathophysiology of myocardial viability allows to formulate some basic principles on which our clinical assessment can be based. They are summarized in Table 22.2.

1. The most important determinant of the return of resting contractile function following revascularization is the severity of the underlying tissue fibrosis, whether interstitial or infarct-related. Accordingly, tissue characterization methods using CMR gadolinium late enhancement technique, specifically assess the presence and the extend of tissue fibrosis. Contrary, the mass of residual viable could be highlighted by technique such as thallium and metabolic imaging.
2. The second most important determinant of functional recovery is the severity of the structural abnormalities affecting the cardiomyocytes. When present, these structural alterations usually indicate a severe and long lasting process. Reversibility, if any, will probably be incomplete and quite delayed. From an imaging point of view, the segments presenting with these alteration are quite easy to identify. Indeed, as any viable segment, they usually retain the ability to accumulate thallium or FDG. However, in contrast to viable segments lacking these alterations, they most often fail to respond to an inotropic stimulus.
3. Viable segments display a variety of perfusion patterns. During the early stages of the

disease, rest flow is usually normal and perfusion reserve is reduced. The observation of a normal rest perfusion, by SPECT, PET, CMR or myocardial contrast echocardiography thus constitutes a strong argument in favor of myocardial viability. However, in the absence of flow reserve measurements, it may be quite difficult to make the distinction between viable and remodeled myocardium. The mere presence of a normal rest flow is thus not sufficient to positively establish the diagnosis of myocardial viability. Similarly, a mildly reduced rest perfusion does not exclude the presence of residual viable myocardium. At the later stages of the disease, rest flow may indeed become slightly reduced. However, severe reductions in rest flow are not compatible with the presence of viable myocardium (Fig. 22.8). As viable segments with reduced rest flow rarely exhibit residual inotropic reserve, their identification probably requires some form of metabolic imaging.

Based on these observations, the following working hypothesis can be proposed:

- when flow, metabolic, tissue characterization and inotropic reserve imaging concur on the presence of residual viable myocardium, the likelihood of tissue fibrosis and myocyte structural alterations is small and the likelihood of functional recovery after successful revascularization is high;
- when flow, metabolic, tissue characterisation and inotropic reserve imaging concur on the lack of residual viable myocardium, severe tissue fibrosis is probably present and revascularization is not likely to bring in any significant functional benefit or prognostic advantage;
- when metabolic imaging suggests the presence of viable myocardium but flow and/or inotropic reserve imaging does not, or tissue characterization show a significant amount of fibrosis, significant myocyte alterations, exhausted flow reserve or a combination of these factors are likely present. The recovery of resting contractile function following revascularization is uncertain, and,

Table 22.2 Main characteristics of viable myocardium

• Mainly non-infarcted
• Sufficient resting perfusion to
– Non-infarcted provide metabolic fuels
– Allow washout of metabolic byproducts
• Maintained membrane integrity to
– Generate transmembrane ionic gradients
– Transport energy providing substrates
• Preserved metabolic machinery for glucose, fatty acid and O ₂ consumption
• Recrutable inotropic reserve

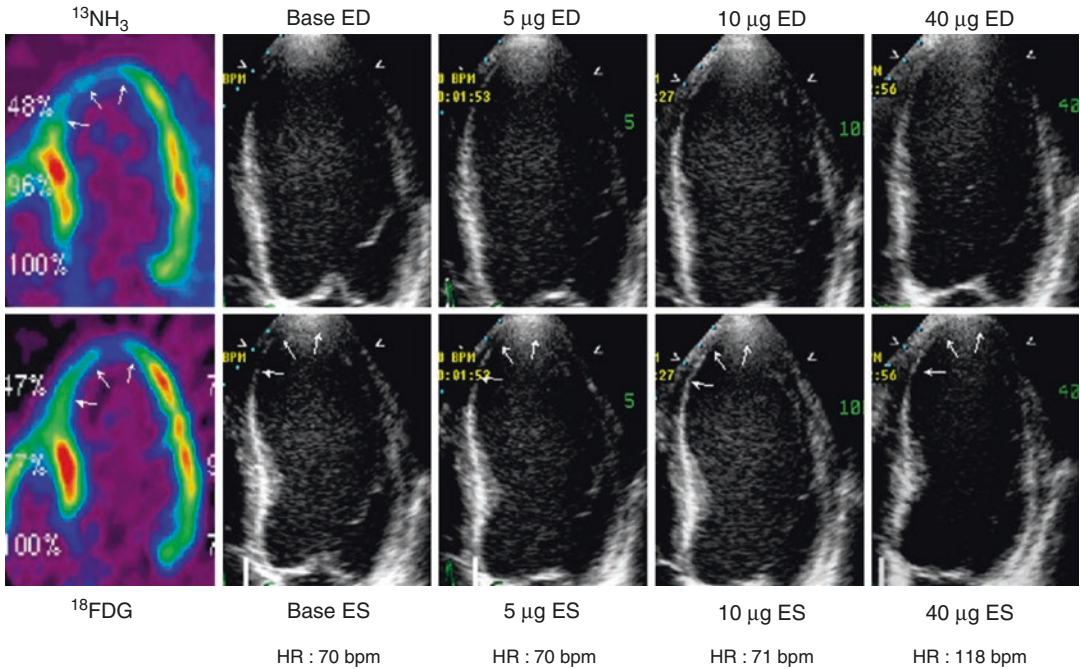


Fig. 22.8 Inotropic response to dobutamine in dysfunctional segments (white arrows) with severely reduced rest flow ($^{13}\text{NH}_3$) and FDG uptake (^{18}FDG). The upper row shows images obtained from the apical 4-chamber view in end-diastole at baseline and during the infusion of 5, 10

and $40 \mu\text{g kg}^{-1} \text{min}^{-1}$ of dobutamine. The lower row shows the corresponding end-systolic images. The absence of inotropic reserve in the distal septum. Since blood flow and FDG uptake were both reduced in that segment, this is an example of irreversibly infarcted myocardium

unfortunately, largely unpredictable. Based on previous studies, this particular viability pattern probably occurs in about 20–45% of “metabolically” viable segments and contribute to both the low specificity of the metabolic imaging approaches and the low sensitivity of the methods based on inotropic reserve.

Role of Echocardiography

Echocardiography is probably the most versatile cardiac imaging modality in our diagnostic armamentarium. In many aspects, it is essential to the identification of myocardial viability. First, it readily identifies the core of the problem, i.e. the presence of regional wall motion abnormalities. It also allows to assess their

severity, both qualitatively and quantitatively. Second, it allows for the initial characterization of the dysfunctional segments, both in terms of residual wall thickness and tissue reflectivity. Segments thinner than 5 mm in diastole are frequently nonviable and those containing bright linear echoes, particularly in the subendocardium are likely to be highly fibrotic. Third, when combined with the use of ultrasonic contrast agents, echocardiography permits the assessment and the quantification of myocardial blood flow, both at rest and during hyperemia. Fourth, when performed during an inotropic challenge, such as the infusion of increasing doses of dobutamine, it allows for the evaluation of the presence of recruitable inotropic reserve. And last but not least, it certainly is the most frequently used technique to assess functional recovery after revascularization.

Rest Echocardiography

Diastolic wall thickness measured during resting echocardiography provides some information on the relative amounts of myocardial tissue versus fibrotic scar tissue within a particular myocardial segment. In a recent study, in which the assessment of diastolic wall thickness was made using 2-dimensional and M mode measurements, a diastolic wall thickness > 5 mm had a sensitivity of 100% but a specificity of only 28% for predicting recovery of contractility at 1 year following surgical revascularization. Reduced wall thickness, however, had a very high negative predictive value (97–100%), suggesting that if the diastolic wall thickness is < 5 mm, additional testing and revascularization may not be indicated. The appeal of this method is obvious, as rest echocardiography is readily available and relatively inexpensive when compared with alternative techniques of assessing myocardial viability. However, it is limited by its poor specificity and the variability in the image quality which affects the accuracy and reproducibility of wall thickness measurements, as well as by the relatively small number of segments exhibiting reduced thickness (< 15 –20%). Yet, the high negative predictive value of a thinned segment confirms the long-standing clinical impression regarding the poor likelihood of recovery of contractility in scarred and thinned walls.

Left ventricular remodeling plays also an important role for prediction of functional recovery. Multiple scarred territories can lead to left ventricular dilatation. Very dilated left ventricle (end diastolic volume greater than twice the upper limit of normal) is unlikely to demonstrate significant global functional recovery, in other word improvement in ejection fraction. And we know that ejection fraction is one of the major determinant of survival in heart failure patient. Classical 2-dimensional echocardiography is certainly not the best tools to assess left ventricular volume and gold stan-

dard remains CMR but this is the most widely available tools.

Ultrasonic tissue characterization is another approach that can define the physical state of the myocardium and can therefore complement the assessment of LV function and chamber dimensions by rest 2-dimensional echocardiography. The baseline assumption underlying the use of ultrasonic tissue characterization is that pathological changes affecting the myocardium, including ischemia, result in alterations of its fundamental physical properties that can be detected using ultrasonic integrated backscatter imaging. Experimental studies have indicated that physiologic myocardial contraction and relaxation were paralleled by a cardiac cycle-dependent variation of integrated backscatter that reflects regional, intramural contractile performance. Cyclic variations of the backscatter signal are blunted during experimental myocardial ischemia and recover more quickly than does systolic wall thickening with reperfusion. Studies in humans with reperfused myocardial infarction have shown that assessment of cardiac cycle-dependent variations of integrated backscatter allowed accurate delineation of reversible (stunning) from irreversible (infarction) tissue injury, thus providing a potentially useful adjunct for the noninvasive evaluation of regional contractile function and for the detection of potentially viable myocardium. Similar findings were recently made in patients with chronic left ventricular dysfunction (Fig. 22.9). In one study, the persistence of cardiac cycle-dependent variation of integrated backscatter was found to closely correlate with the presence of recruitable inotropic reserve. Assessment of ultrasonic tissue characterization may thus provide a simple measure of intramural contractile function which is relatively independent of resting wall motion or thickening and which parallels contractile reserve. The main disadvantage of this approach, however, is its dependence on fiber orientation and the need to acquire the data in segments that oriented perpendicularly to the ultrasound beam.

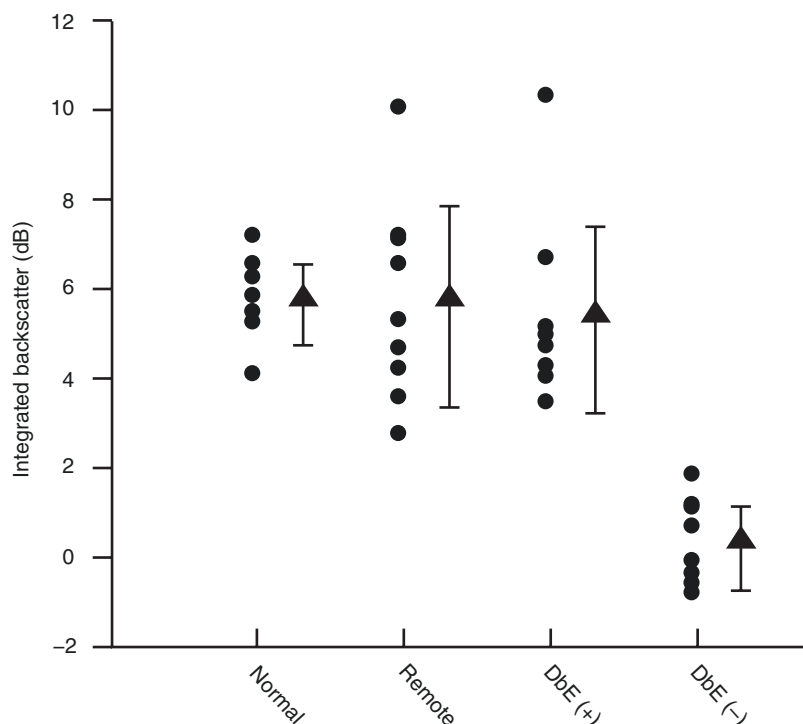


Fig. 22.9 Individual values of cardiac cycle-dependent variations of integrated backscatter among the control segments, the remote normally contracting segments, the dysfunctional segments showing improvement with inotropic stimulation (DbE+) and those with persistent dys-

function (DbE-). Reproduced with permission from Pasquet A et al. Relation of ultrasonic tissue characterization with integrated backscatter to recruitable inotropic reserve in chronic left ventricular ischemic dysfunction. *Am J Cardiol* 1998;81:68-74

Myocardial Contrast Echocardiography

Myocardial contrast echocardiography (MCE) allows for the evaluation of regional myocardial perfusion and segmental wall motion. Actually, the technique involves intravenous injection of an ultrasound contrast agent, which consists of microbubbles approximately the size of a red blood cell.

First, MCE was used for left ventricle opacification, allowing an easier detection of endocardial border and assessment of segmental wall motion contraction. MCE will also facilitate calculation of left ventricular volume and ejection fraction.

The main interest of MCE is that these microbubbles are able to pass into the microcirculation and can be detected by echocardiography as opacification of myocardial tissue. The basic pathophysiological premise

behind MCE is that viable myocardium has an intact microcirculation, whereas infarcted, non-viable tissue loses this microvasculature. Therefore, MCE provides a direct evaluation of vascular integrity and an indirect estimate of cellular integrity. Earlier investigators used the intracoronary route for contrast administration. In both the immediate post infarction setting or in patients with chronic dysfunction, MCE predicted recovery of LV function after revascularization with a high sensitivity (85-94%) and a lower specificity (43-65%). From these initial studies, MCE appeared to have similar test properties as other methods that assess myocardial perfusion, such as thallium scintigraphy. However, it has the added advantage of providing additional information regarding wall contractility and motion.

Thanks to the development of new ultrasonic contrast agents that can cross capillaries and

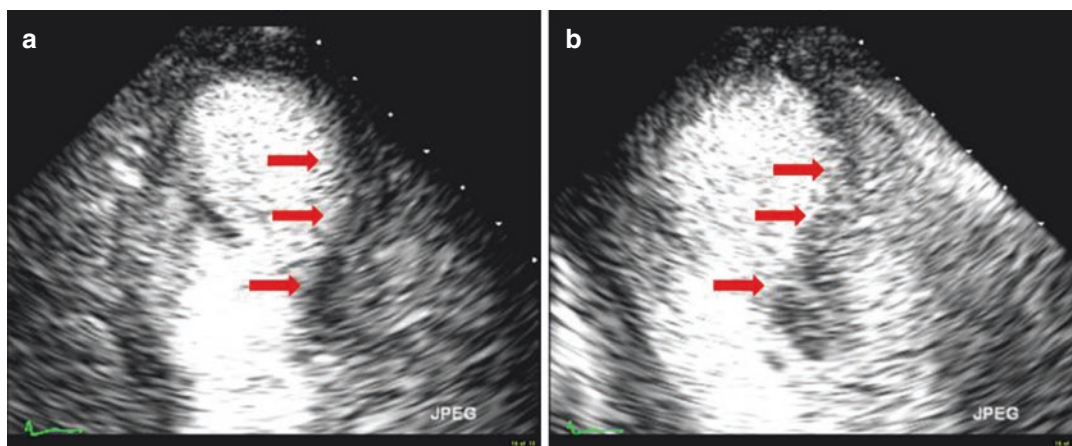


Fig. 22.10 Left panel. 3-chamber view showing an akinetic antero-septal and apex wall (a) with absent contrast opacification; 6 months later after revascularisation

(b) contrast opacification is present in the antero-septal wall and partly in the apex, antero-septal wall function was improved after revascularisation

therefore could be injected intravenously, and the introduction of newer contrast imaging modalities, such as power pulse inversion and power modulation, that greatly reduce the destruction of the microbubbles by ultrasound, interest in MCE to assess myocardial viability has grown even further. By allowing essential parameters of the microcirculatory function, such as myocardial blood flow and blood volume, to be measured, MCE indeed offers the unique opportunity to directly assess the microcirculation of the dysfunctional segments and hence the likelihood of their recovery. As expected, measures of myocardial blood volume with MCE have been found to correlate with microvascular density and capillary area and inversely with collagen content. They can therefore be used to differentiate viable from non viable segments (Fig. 22.10). Measures of myocardial blood velocity and flow have also been shown to bear an inverse correlation with collagen content. Yet, their relationship with microvascular density appears to be somewhat more complex. When microvascular density is reduced, myocardial blood flow and velocity have usually been found to be reduced in proportion. By contrast, when the microvascular density is preserved, myocardial blood flow and velocity can either be normal or reduced. Thus, in the presence of normal values for myocardial blood volume, MCE parameters of myocardial blood flow

and velocity may help differentiate chronically stunned from truly hibernating myocardium. Accordingly, assessment of microcirculatory function with MCE allows to predict functional recovery. More than ten studies have reported sensitivities ranging from 62% to 92% and specificity somewhat lower from 67% to 87% but better than with thallium imaging. Nonetheless, this technique remains technically challenging and may be difficult to use in some myocardial segments due to shadowing and attenuation.

Stress Echocardiography

The demonstration of contractile reserve using various provocative stimuli such as post-extra-systolic potentiation, nitroglycerin, coronary vasodilators (e.g., dipyridamole), arterial vasodilators (e.g., levosimendan), inotropes (e.g., isoprenaline, adrenaline, dopamine or dobutamine) infusion and low level exercise can be studied with echocardiography. Dobutamine stress echocardiography (DSE) is the most accepted and widely available of these techniques. Its diagnostic and prognostic value has been well documented in the detection of myocardial viability.

Dobutamine is a synthetic catecholamine that stimulates primarily β_1 -adrenergic receptors with minimal β_2 and α_1 effects. At low doses

(<10 $\mu\text{g kg}^{-1} \text{min}^{-1}$), it demonstrates a relatively more potent inotropic effect than chronotropic effect, allowing stimulation of myocardial contractility before significant increases in heart rate, and presumably ischaemia, occur. At higher doses, both inotropic and chronotropic stimulation occur, resulting in increased cardiac output, myocardial oxygen consumption, and ischaemia in myocardial regions subtended by significantly stenosed coronary arteries.

The protocol in most stress echocardiography laboratories uses dobutamine infusion at two low-dose stages (5 and 10 $\mu\text{g kg}^{-1} \text{min}^{-1}$), with each stage lasting 3 min. Some advocate utilizing an even lower starting dose of 2.5 $\mu\text{g kg}^{-1} \text{min}^{-1}$ because in patients with critical coronary stenosis, myocardial ischaemia may be precipitated even with doses as low as 5 $\mu\text{g kg}^{-1} \text{min}^{-1}$ in the other hand, the widespread use of long acting beta blockers for heart failure may move the low-dose threshold toward 20 $\mu\text{g kg}^{-1} \text{min}^{-1}$. Thereafter, the dose is increased in 10 $\mu\text{g kg}^{-1} \text{min}^{-1}$ increments to a maximum dose of 50 $\mu\text{g kg}^{-1} \text{min}^{-1}$. Atropine may be given if the target heart rate is not achieved with standard dobutamine doses. The test is terminated when the patient achieves 85% of the age predicted maximum heart rate or clinical or echocardiographic evidence of ischaemia occurs.

Most viable segments will demonstrate improvement of contractility at doses of 10 $\mu\text{g kg}^{-1} \text{min}^{-1}$ or less. The benefit of proceeding to higher doses of dobutamine, even if contractile reserve is demonstrated at lower doses, is to observe a 'biphasic response'. In the presence of significant coronary stenosis, an initial improvement in systolic wall thickening may occur at low doses of dobutamine, representing the region's contractile reserve as previously stated. However, as oxygen consumption increases as contractility and heart rate rise, the flow-limiting stenotic vessel is unable to keep up with the oxygen demand, and the ensuing ischemia leads to hypokinesis of the affected wall segment. This biphasic response demonstrates two critical components to the definition of myocardial viability, namely viability itself and flow limitation. It is therefore not surprising that the biphasic response has the best pre-

dictive value of all the possible responses to dobutamine in determining improvement in LV function following revascularization. In a recent study, <15% of myocardial segments demonstrating either no change or sustained improvement with low and high dose dobutamine had functional recovery with revascularization, while 72% of segments with a biphasic response recovered function. Accordingly, the combined low and high dose approach in all patients who do not have contraindications should be recommended.

The cumulative sensitivity, specificity and predictive value of DSE based on a recent meta-analysis were 81%, 86% and 83%, respectively. Although generally good, these sensitivities and specificities imply that there were a significant number of false positive findings (i.e. demonstration of contractile reserve without significant functional recovery on revascularization) as well as false negative ones (i.e. functional recovery without evidence of contractile reserve). The former may be partially explained by tethering of non-viable segments to adjacent viable ones, leading to the illusion of improved function. Additionally, the presence of non-transmural infarction, where a segment of myocardium consists of an admixture of viable tissue and necrotic scar, can lead to this result. If the proportion of scar is relatively large, or the viable portion already has normal blood flow, then revascularization would not be expected to lead to functional improvement. Of course, if revascularization is incomplete, an otherwise viable segment may remain dysfunctional. Finally, functional recovery may occur more slowly than allowed for by the follow-up periods in these studies.

The observation of improved LV function despite a 'negative' DSE may be explained by the fact that the myocardial flow reserve in these regions may be so low that any increase in oxygen demand, even in viable segments, leads to ischemia. Additionally, the ultrastructural changes occurring in viable myocardium discussed earlier may be so profound that contraction is not possible until sustained restoration of blood flow has taken place.

DSE also emerges as a tool to predict prognosis in patients with chronic left ventricular

dysfunction. Several studies have now demonstrated that long-term survival is significantly better among patients with echocardiographic evidence of myocardial viability who had been revascularized than in those with either viable myocardium treated medically, nonviable myocardium undergoing revascularization or nonviable myocardium treated medically. These data lend further support to the use of dobutamine echocardiography for assessment of myocardial viability, as this technique not only allows accurate identification of which patient will improve regional and global left ventricular function after coronary revascularization, but also may indicate those most likely to benefit with respect to prognosis.

As with most imaging techniques, patient factors can limit image quality in DSE, which can adversely affect accuracy. Obesity and lung disease, for example, may lead to poor acoustic windows in approximately 10% of patients. Harmonic imaging and ultrasound contrast agents have been used to enhance endocardial border detection, as well as transoesophageal imaging. Given that the interpretation of contractile function is subjective, improved image quality can reduce interreader variability.

One additional limitation of stress echocardiography, is that interpretation of wall motion change is limited by subjectivity and requires some training. Myocardial deformation will be impaired in the proportion of the extent of the fibrosis. Thus myocardial deformation measurement by echo using strain, strain rate or speckle tracking could be useful to quantify response to dobutamine. Strain rate at Low dose dobutamine correlates with the presence of myocardial viability evidenced by PET FDG imaging, with an optimal cut-point for this purpose being a strain-rate increment of $>0.23/s$. A strain-rate increment of $>0.25/s$ also predicts functional recovery after revascularization (sensitivity 80%, specificity 75%).

Finally, DSE has been compared with other methods for evaluating myocardial viability, such as single photon emission computed tomography (SPECT) positron emission tomography (PET) and cardiac magnetic resonance (CMR), in many studies and reviews. Schinkel et al. pooled data from all published studies reporting the sensitivity

or specificity of nuclear techniques and/or DSE in predicting functional recovery after revascularization. DSE had a slightly lower sensitivity (80%) compared with SPECT, PET and CMR (83-92-84%), but a significantly greater specificity (78% for DSE versus 54-63-63% for SPECT, PET and CMR), positive predictive value are similar for all the modalities (75% for DSE, 74% for PET, 74% for SPECT and 72% for CMR).

Real Time 3D Echocardiography

With the arrival of real time probes and technical improvement, 3-dimensional echocardiography (3D echo) has emerged as a new and useful echocardiography tools.

The first advantage of 3D echo is to permits more accurate volume and function measurements without needing to make any geometric assumptions, which is desirable if the LV has been involved in multiple previous myocardial infarctions. Ejection fraction measured by 3D echo correlated well with CMR measurement considered as the gold standard for LV function assessment. Volumes are underestimated by 3D echo in comparison with CMR but this is mainly due to difference in calculation method (inclusion or not of myocardial trabeculations, level of mitral annulus...). MCE could also be one useful adjunct to 3D echo in case of patient with poor echogenicity.

We have already explained the importance of fibrosis to explain the lack of recovery of some dysfunctional segment. Infarct scars are usually imaged by delayed-enhanced cardiac magnetic resonance (DE-cMR). 3D echo with MCE could also be used for detection and quantification of myocardial scars. We already know that myocardial scar reflect ultrasound more effectively than normal myocardium. Modification of echo settings and use of MCE allows to better visualize scar. The highest contrast-to-noise ratio was obtained with second-harmonic imaging (1.6/3.2 MHz), at a mechanical index of 0.5, in the presence of contrast. Using this modality, 3D-echo allows identifying myocardial scars with good sensitivity and specificity compared with

DE-cMR (respectively 78% and 99% on segmental basis, 96% and 90%, on per patient basis) also allows for a reasonably accurate quantification of scar tissue (mass and transmural extent). Results are nonetheless better in the inferior/posterior walls than in the anterior/lateral walls.

In the future, 3D strain could certainly add some value for help in recognition of viable myocardium.

Clinical Role of Myocardial Viability Nowadays

Numerous study encompassing viability testing have been published unfortunately most of these studies are single center studies and observational. In addition differences in definition of viability, cutoffs for clinical endpoints, and differences in inclusion criteria results in challenges in their applicability to clinical practice.

Nevertheless, two important initial concepts have surfaced. First, in patients with ischemic cardiomyopathy and viability noted on noninvasive testing, medical treatment alone is associated with worse outcomes, and conversely, those patients with viability detected by noninvasive testing, including SPECT, FDG-PET, CMR and echocardiography, demonstrate significantly improved survival with revascularization compared with medical therapy alone.

Recently, a few prospective trial regarding clinical role of myocardial viability have been published.

The CHRISTMAS (Carvedilol Hibernation Reversible Ischemia Trial: Marker of Success) trial was a double-blind, randomized trial of medical therapy in chronic LV dysfunction. This trial assessed the efficacy of carvedilol treatment in patients with hibernation or ischemia using both nuclear and echocardiographic techniques to identify the presence and extent of hibernation. The study found that the volume of myocardium affected by hibernation, ischemia, or both is an important determinant of the improvement of LV function (as assessed by LVEF) with carvedilol treatment, with little or no increase in LVEF in the absence of viability.

The PARR-2 study was designed to assess the effectiveness of FDG-PET–assisted management in patients with severe LV dysfunction and suspected CAD compared with standard of care. The study failed to demonstrate a significant reduction in cardiac events with FDG-PET–directed therapy compared with the standard of care. Several specificity of this study need to be noted. First the standard of care arm could include one other viability testing and secondly an important proportion (25%) of the FDG-PET were managed at the discretion of the referring cardiologist and not according to the image recommendation. A substudy of PARR-2 demonstrated that in patient with more than 7% of the LV with viability, revascularization improve a composite endpoint (cardiac death, myocardial infarction and hospital admission) at 1 year.

STICH (Surgical Treatment for Ischemic Heart Failure) was designed to examine the outcomes of patients with CAD and LV dysfunction randomized either to OMT alone or OMT plus CABG surgery. A substudy of the STICH investigation sought to examine the role of myocardial viability in identifying patients who might have a survival benefit with surgical revascularization. The performance of a viability test was let to the choice of the cardiologist. Only 601 patients of the initially 1212 patients included in the STICH trial were included in this substudy. Dobutamine stress echocardiography of SPECT were used for viability assessment and classified using a binary approach (presence of 11 or more viable segments for SPECT and five or more viable segments for Dobutamine). Among the enrolled patients, 487 patients were found with and 114 without substantial viable myocardium. Rough analysis, suggested that the presence of substantial myocardial viability improve the long term survival with 63% survival of patients with viability versus 49% survival of patients without viability. Nevertheless, after adjustment for baseline variables, this significance was lost. Additionally, there was no demonstrable relationship between the viability information, treatment allocation, or patient outcome, and this was true regardless of whether patients were grouped according to

intention-to-treat analysis or according to the treatment actually received.

Do the results of the STICH trial suggest that testing for myocardial viability testing is useless and should be abandoned?

The results of this trial are controversial mainly due to limitations and methodological concerns and remain a source of vigorous debate. Several limitations of this trial need to be mentioned. First this substudy is non randomized. Less than one half of the patients enrolled in the initial study were included in this substudy and the selection of the patients for viability testing was performed at clinician discretion. So a bias in recruitment or patient selection could not be excluded. Baseline characteristics in patients with and without viability shows significant difference. Viability was considered as a binary response and threshold retained were controversial. Presence of inducible ischemia was not consistently addressed or reported. Groups are unbalanced with a smaller sample size for the group with non viable myocardium. Moreover, clinicians were not blinded to the results of viability testing.

Finally, the question of “myocardial viability” is not so simple that “dead or alive!”. Other parameters need also to be considered: end diastolic volume and ejection fraction, presence of large amounts of scar tissue or of myocardial ischemia are strong determinant of outcome. Therefore revascularization may offer some potential benefit as reduction of inducible ischemia, effect on ventricular remodeling, reduction of ventricular arrhythmias.

Conclusions

Over the past three decades, much has been learned about the mechanisms underlying myocardial viability in patients with coronary artery disease. Reasonable evidence from over 100 nonrandomized studies of more than 3000 patients with viability testing in the last two decades has consistently demonstrated its usefulness. Revascularization of chronically but reversibly dysfunctional myocardium has progressively emerged as a potential alternative in

the treatment of heart failure secondary to coronary artery disease as it seems to be able to improve regional and global left ventricular function, to decrease heart failure symptoms and to improve long-term survival. The recent studies have highlighted the complexity of decision making in patients with left ventricular dysfunction. Because of their limitation, these studies does not support sufficient grounds for abandoning the logical concept of viability. These trails have also generated new questions regarding patients selection for revascularization including the extent of viable myocardium, the role residual ischemia, the impact of LV remodeling, the complex interaction of viability and scar, some procedural issues as possibility or not to perform complete revascularization and presence of comorbidities. So presence of myocardial viability is still a clinical question nowadays. But perhaps not in all patients with LV dysfunction. It will be specially useful to predict response to revascularization in selected patients (as example in patients with higher surgical risk or to determine the amount of viable myocardium in patient with severely depressed left ventricular function...). Viable myocardium is also a marker of prognosis. Same if we could argue that multimodality imaging with certainly have an interest in this setting. Among the several techniques that are available for identifying viable myocardium, echocardiography appears to be particularly well suited, first because is wide availability, low cost, and radiation free and secondly as it allows to investigate two main features of myocardial viability, i.e. maintained resting perfusion and residual inotropic reserve.

Suggested Reading

1. Vanoverschelde J-LJ, Wijns W, Depré C, Essamri B, Heyndrickx G, Borgers M, Bol A, Melin JA. Mechanisms of chronic regional postischemic dysfunction in humans: new insights from the study of non-infarcted collateral dependent myocardium. *Circulation*. 1993;87:1513–23.
2. Vanoverschelde J-LJ, Wijns W, Borgers M, Heyndrickx G, Depré C, Flameng W, Melin JA. Chronic myocardial hibernation in humans. From bedside to bench. *Circulation*. 1997;95:1961–71.

3. Ross J Jr. Myocardial perfusion-contraction matching. Implications for coronary heart disease and hibernation. *Circulation*. 1991;83:1076–83.
4. Cauty JR, Fallavollita JA. Resting myocardial flow in hibernating myocardium: validating animal models of human pathophysiology. *Am J Physiol*. 1999;277:H417–22.
5. Borgers M, Thoné F, Wouters L, Ausma J, Shivalkar B, Flameng W. Structural correlates of regional myocardial dysfunction in patients with critical coronary artery stenosis: chronic hibernation? *Cardiovasc Pathol*. 1993;2:237–45.
6. Bax JJ, Wijns W, Cornel JH, Visser FC, Boersma E, Fioretti PM. Accuracy of currently available techniques for prediction of functional recovery after revascularization in patients with left ventricular dysfunction due to chronic coronary artery disease. *J Am Coll Cardiol*. 1997;30:1451–60.
7. Selvanayagam JB, Jerosch-Herold M, Porto I, et al. Resting myocardial blood flow is impaired in hibernating myocardium: a magnetic resonance study of quantitative perfusion assessment. *Circulation*. 2005;112:3289–96.
8. Rahimtoola SH, Dilsizian V, Kramer Ch M, Marwick TH, Vanoverschelde J-LJ, from picture to practice paradigms. Chronic ischemic left ventricular dysfunction: from pathophysiology to imaging and its integration into clinical practice. *JACC Cardiovasc Imaging*. 2008;1:536–55.
9. Bayeva M, Sawicki KT, Bultler J, Gheorghiade M, Ardehali H. Molecular and cellular basis of viable dysfunctional myocardium. *Circ Heart Fail*. 2014;7:680–91.
10. Schinkel AFL, Bax JJ, Poldermans D, Elhendy A, Ferrari R, Rahimtoola SH. Hibernating myocardium: diagnosis and patient outcomes. *Curr Probl Cardiol*. 2007;32:375–410.
11. Anavekar N, Chareonthaitawee P, Narula J, Gersh B. Revascularization in patients with severe left ventricular dysfunction. Is the assessment of viability still viable? *J Am Coll Cardiol*. 2016;67:2874–87.
12. Montant P, Chenot F, Goffinet C, Poncelet A, Vancraeynest D, Pasquet A, Gerber BL, Vanoverschelde J-LJ. Detection and quantification of myocardial scars by contrast-enhanced 3D echocardiography. *Circ Cardiovasc Imaging*. 2010;3:415–23.
13. Allman KC, Shaw LJ, Hachamovitch R, Udelson JE. Myocardial viability testing and impact of revascularization on prognosis in patients with coronary artery disease and left ventricular dysfunction: a metaanalysis. *J Am Coll Cardiol*. 2002;39:1151–8.
14. Cleland JGF, Pennell DJ, Ray SG, CHRISTMAS (Carvedilol Hibernating Reversible Ischaemia Trial: Marker of Success) Investigators, et al. Myocardial viability as a determinant of the ejection fraction response to carvedilol in patients with heart failure (CHRISTMAS trial): randomized controlled trial. *Lancet*. 2003;362:14–21.
15. Beanlands RSB, Nichol G, Huszti E, PARR-2 Investigators, et al. F-18-fluorodeoxyglucose positron emission tomography imaging-assisted management of patients with severe left ventricular dysfunction and suspected coronary disease: a randomized, controlled trial (PARR-2). *J Am Coll Cardiol*. 2007;50:2002–12.
16. D'Egidio G, Nichol G, Williams KA, PARR-2 Investigators, et al. Increasing benefit from revascularization is associated with increasing amounts of myocardial hibernation: a substudy of the PARR-2 trial. *J Am Coll Cardiol Img*. 2009;2:1060–8.
17. Bonow RO, Maurer G, Lee KL, STICH Trial Investigators, et al. Myocardial viability and survival in ischemic left ventricular dysfunction. *N Engl J Med*. 2011;364:1617–25.

Introduction

The use of contrast in echocardiography is not new. In 1968 Gramiak and Shah were the first who described use of saline as a contrast agent in an M-Mode study of aortic root in patients undergoing ascending aortography. They had noted a cloud of echo at the tip of cardiac catheters following intra cardiac injection of different substances including saline. This was attributed to mini bubble formation resulting from rapid injection. They credited Claude Joyner for the idea, who had used saline as contrast agent in anatomical identification of the mitral valve echo [1]. The technique of injecting agitated saline containing very small air bubbles is still used regularly and has become a standard method for identifying shunts through a patent foramen ovale or small atrial septal defects.

This chapter describes the basic physics of interaction between contrast microbubbles and ultrasound. It explains how that interaction can be utilised to provide sensitive contrast detection so that the technique can be used in a variety of different clinical settings.

Basic Principles

Types of Contrast Agent

In order to provide efficient ultrasound backscatter, ultrasound contrast agents must contain microbubbles with a very different acoustic density to the surrounding medium (blood). Hand agitated saline is basically small bubbles of air suspended in saline. They, however, dissolve in blood quickly and are visible by echocardiography only for few seconds following a venous injection. They are not designed to survive trans pulmonary passage and are not able to opacify the left side of the heart, thus the presence of saline bubbles within the left heart, suggests an intra-cardiac shunt with a right to left component or an arterio-venous malformation when they appear in the left side after three cardiac cycles. It was only found empirically that saline microbubble stability could be improved by mixing it with small amount of blood. This can be explained by red cell surfactant forming a core around the saline microbubble. Although this effect was known for many years, it was only in late 1980s that commercial ultrasound contrast agents were marketed [2].

Commercially produced agents are specifically designed to cross the lungs, opacify the left heart and possibly the myocardium. These demands place a number of constraints upon the design of ultrasound contrast agents. In order to survive trans pulmonary passage, they must be

M. Eskandari (✉) · M. J. Monaghan
Department of Cardiology, King's College Hospital,
London, UK
e-mail: mehdi.eskandari@nhs.net

physiologically inert, have a size comparable to red blood cells and the contained gas within the contrast microspheres must be prevented from dissolving in blood. This objective can be achieved by either using a thick microbubble shell to prevent diffusion (first generation microbubbles), or a high molecular weight gas, which is not soluble in blood (second generation microbubbles). Therefore, contrast agents containing air or nitrogen, which are highly soluble in blood, require a thick, impermeable shell; whereas agents with a thin shell require a high molecular weight gas such as sulphur hexafluoride or perfluorocarbon (Fig. 23.1 and Table 23.1). Alunex, the first commercial ultrasound contrast agent that was approved for human use in 1994, is an example of an air bubble protected by solid shell (albumin).

Contrast Microbubble Response to Ultrasound

Microbubbles can act as a resonant system. Figure 23.2 illustrates the formula that describes

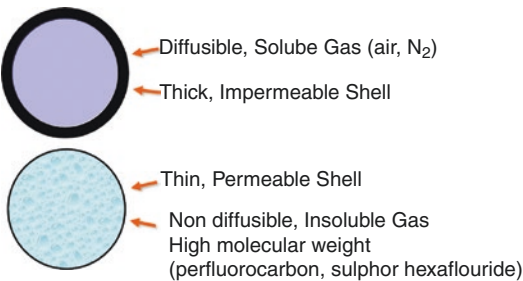


Fig. 23.1 In order to survive transpulmonary passage and persist in the circulation, the gas within contrast agents must be prevented from diffusing into blood. This is achieved either by using a thick, impermeable shell or by using a high molecular weight, insoluble gas

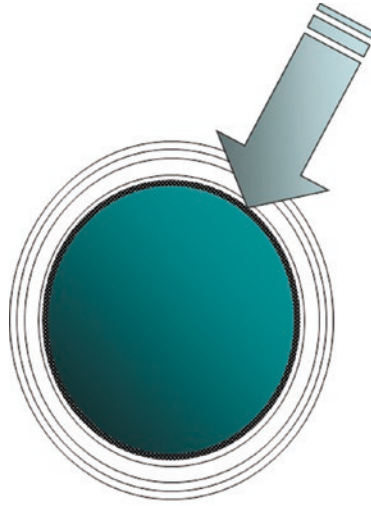
the resonant frequency of a free gas bubble. As previously stated, the contrast microbubbles must have a size not greater than red blood cells so that they behave physiologically within the microcirculation. In practice, this means that the modal diameter is approximately 4 μ . Using a diameter of 4 μ and standard values for the other parameters described in Fig. 23.2 the resonant frequency is approximately 2 MHz. This frequency very conveniently falls within the bandwidth of ultrasound frequencies used in echocardiography and essentially means that contrast microbubbles will resonate within the ultrasound field.

Figure 23.3 demonstrates the very important ratio between the incident or transmitted ultrasound energy and the backscattered or reflected energy. Although this ratio is described by a very complex formula, with a number of important components, the most important factor determining the magnitude of the backscattered signal is the bubble size. The backscatter of a bubble is related to sixth power of its radius thus even a small decrease in size results in a large reduction in backscatter signal [3]. This explains why first generation air-filled microbubbles were not as strong backscatters as second generation. Because of oxygen and nitrogen leak, air-filled microbubbles reduce in size rapidly resulting in significant loss of backscatter power. Using a diameter of 4 μ and standard values for the other parameters described in Fig. 23.3, the difference in backscattered ultrasound intensity between a typical ultrasound contrast agent and blood is approximately 100 million. Although this difference is extremely large and therefore contrast microbubbles are very powerful scatterers of ultrasound, in practice there are a number of important factors which limit the ability of an

Table 23.1 Commercially available ultrasound contrast agents [2, 10]

Agent	Bubble size (μ)	Gas	Shell	Approved
Optison	3–4.5	Perfluorocarbon (C3F8)	Human albumin	EU, USA
Sono Vue	2–8	Sulphur hexafluoride (SF6)	Phospholipids	Europe, China, S Korea, India, Hong Kong, Singapore
Definity	1.1–3.3	Perfluorocarbon (C3F8)	Phospholipids	Worldwide
Sonazoid	3	Perfluorobutane (C4F10)	Phospholipids	Japan

Fig. 23.2 Formula describing the resonant frequency of a free gas bubble. Using standard parameters and a bubble radius of $2\ \mu$ (diameter of $4\ \mu$), the resonant frequency is approximately 2 MHz. This conveniently falls within the bandwidth of diagnostic ultrasound



$$fr = \frac{1}{2\pi R} \sqrt{\frac{3\Psi P}{\rho}}$$

fr = resonant frequency

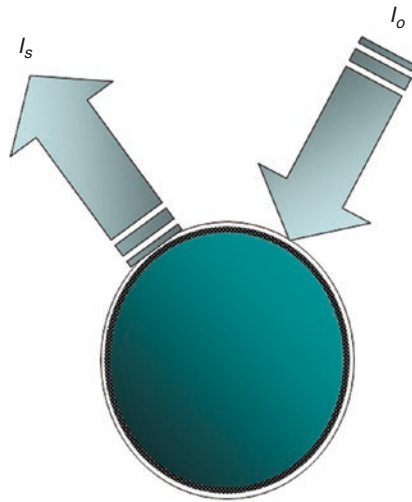
R = bubble radius

P = Pressure

Ψ = heat capacity

ρ = density of medium

Fig. 23.3 Formula describing the ratio between incident and backscattered ultrasound intensity from a free gas bubble. One of the most important components is the bubble size. The magnitude of the backscattered signal intensity is proportional to the sixth power of the radius



$$\frac{I_s}{I_o} = \frac{1}{9} nV \frac{k^4 R^6 (\Psi_k + \Psi_p)^2}{r^2}$$

I_s = backscattered intensity

I_o = incident intensity

n = density of scatterers

V = occupied volume

k = wave number

R = particle radius

Ψ_k = compressibility term

Ψ_p = density term

r = distance

ultrasound scanner to image contrast microbubbles efficiently. For example, at normal diagnostic ultrasound intensities, most contrast microspheres will fracture, implode and be destroyed. This gives rise to a swirling appearance of contrast within the cardiac chambers as blood containing destroyed contrast mixes with undestroyed contrast. This is most apparent near the left ventricular apex, when an apical imaging window is used, because the ultrasound intensity is at its greatest in the near field.

The proportional blood volume within the myocardium is significantly lower than within the ventricular cavities. The blood also moves much slower within the myocardium, therefore a far lower concentration of contrast microbubbles are exposed to ultrasound for a longer time than within the ventricles which makes them more likely to be destroyed. Furthermore, the backscattered signal from myocardial tissue is significantly higher than that from blood. All these factors mean that myocardial perfusion studies

are technically more challenging than left ventricular opacification (LVO) studies as it's much more difficult to detect and image contrast microbubbles within the myocardium than within the left ventricle. One potential solution to this problem may be to administer a larger volume of contrast so that the concentration of microbubbles within the blood, and hence the myocardium, is increased. However, if the microbubble concentration is increased, this results in attenuation of the ultrasound signal as the microbubbles form an impenetrable barrier to ultrasound transmission. This phenomenon is frequently seen within the right ventricular cavity where the microbubble concentration is higher before transpulmonary passage. However, it can also be visualised in the left ventricle as the delivered contrast volume is increased.

So far we know that contrast microbubbles resonate within a diagnostic ultrasound field. Another very important feature of microbubbles is their compressibility. This means that they contract and expand (oscillate) in response to positive and negative pressure phases of ultrasound frequencies. The behaviour of a gas microbubble oscillation varies with the amount of negative phase pressure within the ultrasound field, expressed by mechanical index (MI), an indication of transmitted ultrasound power. The mechanical index is defined as dividing peak negative pressure by square root of ultrasound frequency [4]. At very low MI <0.1 microbubbles oscillate in a linear fashion (equal contraction and expansion) producing backscatter mainly within the range of transmitted ultrasound frequency (fundamental frequency) and therefore will not be distinguishable from surrounding tissue signals [5]. The main difference in acoustic property between contrast microbubbles and tissue is at MI >0.1 , where microbubbles, unlike tissue, will oscillate in a non-linear fashion within ultrasound field (Fig. 23.4). This means that the magnitude of compression and rarefaction are not the same with each oscillation. Therefore, in addition to backscatter within fundamental frequency, microbubbles start producing backscattered signals with lesser amplitude at harmonic frequencies. For example, a microbubble interro-

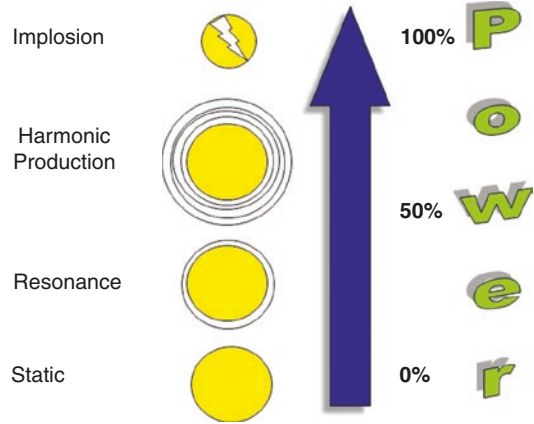


Fig. 23.4 As incident ultrasound power increases, the microbubble will resonate, generate harmonics and finally implode, releasing the encapsulated gas which quickly dissolves

gated by a 2 MHz transducer will reflect 2 MHz signals (fundamental) and 4 MHz (second harmonic—twice the transmitted fundamental frequency) backscatter signals and so forth.

At high MI, which is used in conventional 2D echocardiography, most contrast microspheres will fracture, implode and be destroyed. However, upon microbubble destruction, a high amplitude backscatter signal will be produced which although transient (dependent how quickly the gas microbubble will be disappeared) is rich in harmonics (second, third and so forth) and can be utilised for myocardial perfusion studies. Of note, at high MI tissue also produces harmonic signals, which needs to be suppressed. When low MI is used (<0.4), microbubbles will not explode, however the reflected second harmonic signals are weak and more difficult to detect. Furthermore, at low MI tissue usually will not reflect harmonic signals, which is an advantage.

In summary, two important features of contrast microbubbles that make them suitable for contrast echocardiography are first that they are resonant with frequencies within the range of diagnostic ultrasound and second their high compressibility (oscillation) in comparison with surrounding tissue and blood. Although conventional ultrasound imaging modalities can demonstrate opacification of cardiac cavities, however to reliably detect contrast microbubbles within the

myocardium in order to evaluate myocardial perfusion, it is clear that alternative ultrasound imaging techniques need to be utilised. The non-linear, resonant response of microbubbles within an ultrasound field is utilised in different contrast imaging techniques to enhance the backscatter signal and suppress signal tissue resulting in significant increase in contrast to tissue signal ratio. This although very important for evaluating myocardial perfusion, is also useful for enhancing endocardial border detection in LVO.

Contrast Imaging Techniques

Contrast specific imaging technologies conveniently separate themselves into methods that rely on or cause microbubble destruction and those techniques that aim to preserve the microbubbles—non-destructive imaging. Table 23.2 illustrates some of the currently available contrast specific imaging techniques.

Destructive Imaging Techniques

Destructive imaging techniques use an MI >1.0, whereas non-destructive techniques use an MI <0.4 in order to limit contrast destruction. As explained, at higher MI the non-linear resonance of contrast microbubbles within the ultrasound field results in a strong generation of harmonic signals upon the destruction of the microbubble. Typically these harmonics will occur at multiples of the transmitted frequency (second, third, and

so forth), with the strongest response occurring at the second harmonic. There is also a tissue signal at the second harmonic frequency but fortunately it is lower in amplitude than the contrast signal. So if the frequency receive filters on the scanner are set to only receive the second harmonic frequency, then the contrast signal amplitude will be greater than that of the tissue. Therefore, the important contrast to tissue signal ratio is increased. Although destructive techniques are sensitive for microbubble detection, they have to be used in an intermittent imaging mode. This is because during real time imaging there is no chance that capillary network will be filled with microbubbles. This was first observed by Porter who noted that triggered imaging allows time for contrast microbubbles to replenish the myocardium following each destructive frame [4]. In practice, this means that a frame is acquired every 1, 2, 3 or up to 10 cardiac cycles (triggered to ECG). Intermittent or triggered imaging can be used with both harmonic and power Doppler systems.

Second Harmonic Imaging

With each pulse, backscatter signals rich in harmonics are returned to the transducer, filtered out from fundamental and tissue harmonics, they provide static images of myocardial perfusion. Furthermore, with incremental increase in the triggering intervals, the rate of contrast replenishment over time can be assessed both qualitatively and quantitatively. To improve the qualitative assessment of myocardial perfusion, myocardial signals can be digitally subtracted and microbubbles signal can be enhanced by colour coding techniques although the process is time consuming (Fig. 23.5) [5, 6].

Ultra Harmonics

It was previously explained that at higher MI tissue also produces harmonics of lower amplitude. However this happens primarily at the second harmonic. At higher harmonics, the tissue signal will be negligible but there will still be a contrast signal. These techniques essentially rely upon receiving selected higher frequencies. However, the received contrast signal amplitude is still very

Table 23.2 Destructive and non-destructive contrast specific imaging modalities

<i>Destructive contrast imaging techniques (high MI)</i>
Second harmonic imaging
Ultraharmonics
Pulse inversion
Harmonic power Doppler
<i>Non-destructive contrast imaging techniques (low MI)</i>
Power modulation
Power pulse inversion
Cadence contrast imaging
Contrast pulse sequencing

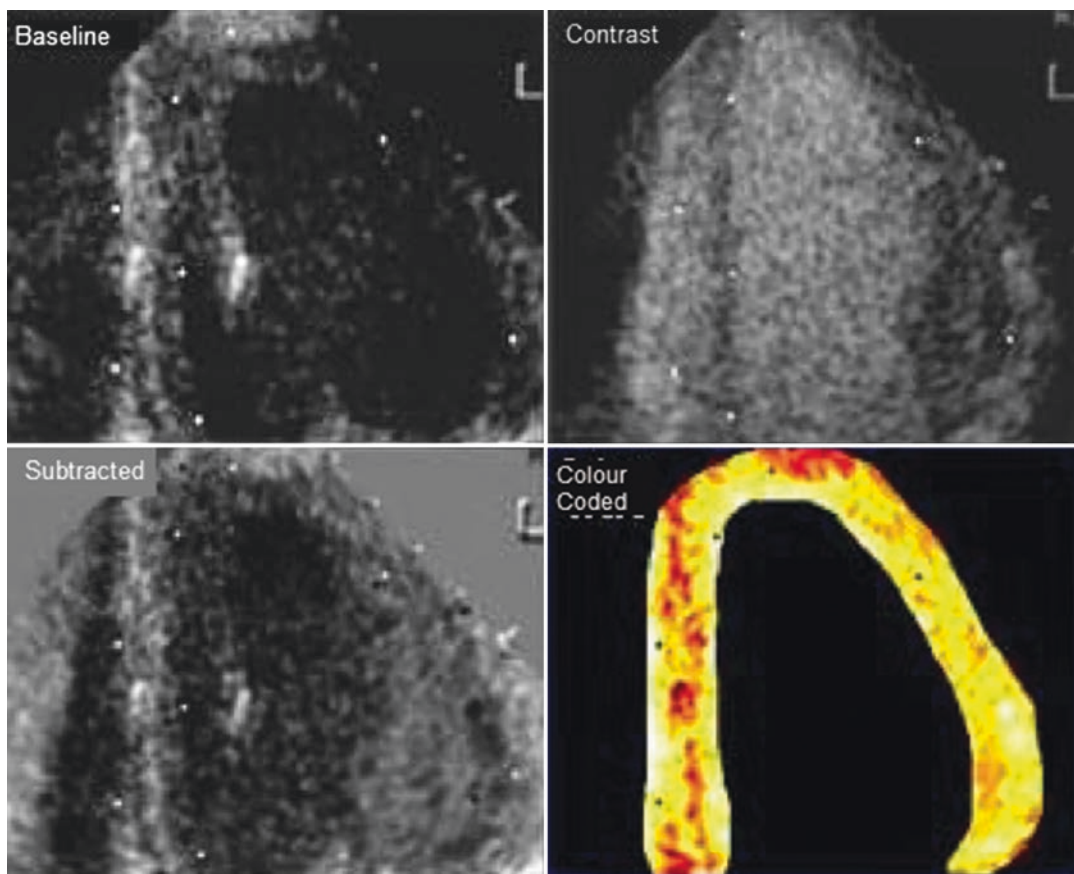


Fig. 23.5 Triggered second harmonic imaging with subtraction and colour coding. Modified from Moir and Marwick [6]

small at these higher harmonics—making them susceptible to noise and artefacts. In addition, specially constructed broad-bandwidth transducers have to be utilised to detect these higher harmonics.

Contrast harmonic imaging is currently rarely used in isolation in contrast echocardiography. Harmonic power Doppler and pulse inversion are other high MI techniques in that they actually measure the change in backscattered signal from one pulse to another.

Harmonic Power Doppler

This technique is very similar to that utilised in conventional colour flow Doppler—essentially a moving target indicator. Using this technique, two pulses are sent down the same scan line shortly after each other. A Reflected signal is

derived from both microbubbles and myocardium with the first pulse. However, when a second pulse is transmitted down the same scan line, shortly after first one, the reflected signal is generated only from myocardium as the first pulse has already destroyed the microbubble. The detected frequency shift from the pair of the reflected signals will be shown as colour on the corresponding segment of myocardium (representing the presence of contrast and hence perfusion). The Saturation of the colour represents the amplitude of the frequency shift. It is important to note that this technique in fact does not measure microbubbles movement in circulation but their destruction. If there are no microbubbles in the myocardium (no perfusion), there won't be a shift in reflected frequency between two pulses (both coming from myocardium) and thus no

colour will be displayed (perfusion defect). The major limitation of this technique is myocardial tissue motion artefact. In a segment of myocardium with no perfusion and hence no contrast, there still may be a reflected signal because of myocardial tissue motion which can cause frequency shift and falsely interpreted as contrast destruction (hence interpreted as presence of perfusion, false negative test). A potential solution can be increasing Doppler frequency to reduce the time between two pulses to minimise the artefact from myocardial tissue movement. However this could result in false positive results. We know that it takes time for the microbubbles to disappear from circulation. If the pulses are too close to each other, the second pulse might detect the residual contrast and not myocardium only, masking the expected frequency shift which would be consistent with no contrast destruction (hence interpreted as no perfusion, false-positive result) [6].

Pulse Inversion Doppler

This technique is very similar to harmonic power Doppler but utilises two pulses, which are 180° out of phase with each other. The two pulses are sent down the same scan line in rapid succession (if there is positive pressure in the first pulse, there will be a negative pressure in the second pulse). The reflected signals from myocardial tissue will be linear and therefore the two signals will cancel each other out on the beam former and no echo signal will be formed. We know the contrast microbubbles however respond in a non-linear fashion and cannot cancel each other out. The difference in the backscattered signal again indicates the presence of contrast in myocardium reflecting myocardial perfusion. Harmonic imaging uses narrow bandwidth to separate harmonic from fundamental frequencies. This technique avoids the band limitation since it's not based on filtering the fundamental signals but subtracting them, allowing use of broader transmit and receive bandwidth resulting in improving resolution and higher sensitivity to contrast [4]. As explained before, myocardial tissue can also produce non-linear signals, which could be a limitation to this technique. Since pulse inversion

Doppler uses two pulses form each image line, any motion in between these pulses can result in incomplete removal of tissue signal. Since this technique is a grayscale mode, the motion artefact can be simply decreased by brightening the grayscale image [4].

The strength of destructive techniques is their sensitivity because microbubbles produce strong backscatter signals upon destruction. The bubble destruction; however, means that intermittent imaging is required which is more difficult to use and is challenging to maintain the same view between triggers, in addition, wall motion cannot be simultaneously seen.

Non-destructive Imaging Techniques

Inability to simultaneously assess myocardial wall motion with destructive techniques is considered by many to be an important disadvantage. In order to provide wall motion information, the frame rate needs to be increased from one frame every few cardiac cycles, to a minimum of 20 frames a second. If the frame rate is to be increased without causing bubble destruction then the MI needs to be decreased significantly—usually <0.4 . A low MI will minimise microbubble destruction and will generate only a very weak but stable non-linear backscattered signal. Therefore, more sensitive contrast detection methods have to be used, which at the same time will suppress the tissue signal. Furthermore, myocardial tissue will not generate non-linear signals at low MI, which is another advantage of non-destructive techniques. Low MI methods are called real-time because microbubbles are not destroyed and the higher frame rates allow evaluation of wall motion and perfusion simultaneously.

Essentially these techniques work on similar principles. They all send multiple, low amplitude pulses down each scan line. Each pulse varies from the preceding one in amplitude, phase or a combination of both. Different manufacturers use one or more of these techniques for their real-time methods and some of the proprietary names for these techniques are listed in Table 23.2.

Power Modulation

Figures 23.6 and 23.7 illustrate the basic principles utilised in this technique, which is one of the low MI real-time methods. With this methodology, multiple pulses are transmitted down each scan line, however each alternate pulse is of 50% amplitude. The ultrasound scanner doubles the received signals from the 50% amplitude pulses and then subtracts that from the received signal from the 100% amplitude pulses. This means that in theory backscattered signals from a linear reflector such as myocardial tissue should cancel each other out, thereby suppressing the myocardial signal. Whereas contrast microbubbles are non-linear reflectors and so the doubled backscatter signal from the 50% amplitude pulse does not cancel the signal created by the 100% amplitude pulse. The remaining signal indicates the presence of contrast within the scan plane, which signifies myocardial perfusion. In theory and usually also in practice, the only image signals seen when utilising low MI non-destructive real-

time imaging are those derived from contrast microbubbles and tissue signals are completely suppressed resulting in high sensitivity but reduced spatial resolution.

Power Pulse Inversion

This technique uses a combination of pulse inversion (alternating polarity) and power Doppler concept. The power Doppler will use the frequency shift to detect presence of contrast in myocardium and the pulse inversion helps to overcome artifact from myocardial motion. This technique benefits from high resolution but is limited by attenuation, especially in basal segments.

As previously mentioned, the great advantage of this type of contrast imaging technique is that it potentially permits evaluation of both left ventricular wall motion with excellent endocardial definition and myocardial perfusion through evaluation of myocardial blood volume. At low contrast microbubble concentrations, there may

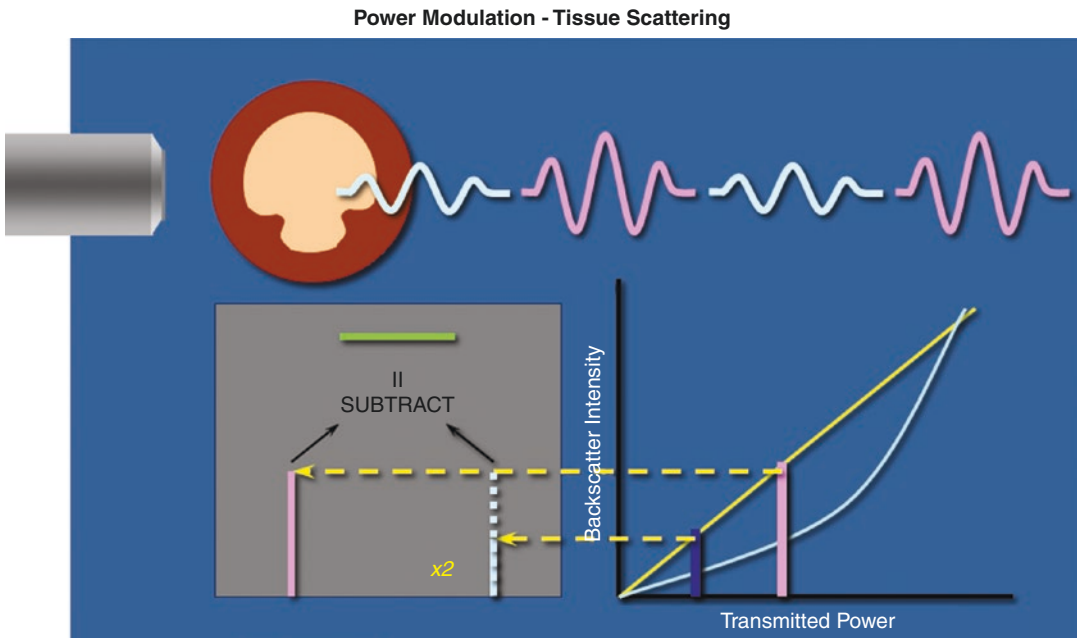


Fig. 23.6 Power modulation uses varying amplitude ultrasound pulses where alternate pulses are 50% in amplitude of the preceding one. When scattering occurs from a linear tissue reflector, the 50% amplitude pulse creates a 50% amplitude backscattered signal. This received

signal is doubled in amplitude and then subtracted from the signal received from a full amplitude pulse. This effectively means that the backscattered signals from linear reflectors such as myocardial tissue cancel each other out, suppressing the tissue signal

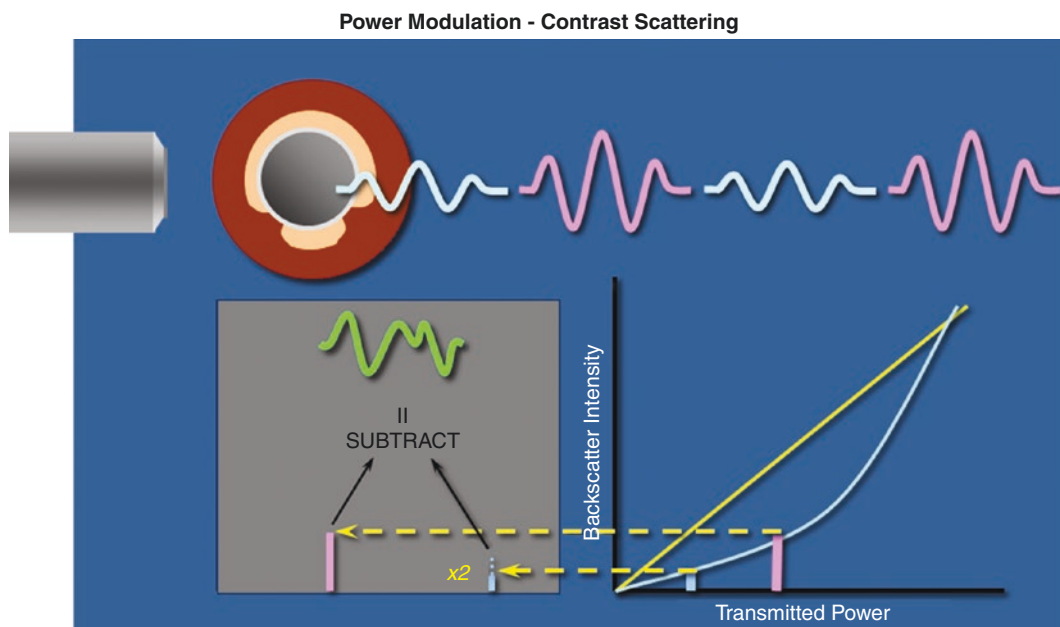


Fig. 23.7 Contrast microbubbles are non-linear scatterers, therefore the backscattered signals from the doubled 50% amplitude pulses and the full amplitude pulses do not

cancel each other out when subtracted. This leaves a signal representing the presence of contrast

be insufficient contrast within the myocardium to cause any enhancement and the only contrast that can be seen is within the LV cavity. Since the myocardium will be black and the cavity bright, this results in excellent endocardial definition. Therefore when performing LVO studies it's sensible to reduce the MI to <0.4 . Frame rates of >25 Hz can be achieved and this is quite satisfactory for assessment of LV wall motion during stress echocardiography. As the contrast microbubble concentration is increased in the blood, either by increasing the bolus volume or infusion rate, then sufficient microbubbles will appear within the myocardium to cause myocardial enhancement. The myocardial contrast signal intensity is directly proportional to the number of microbubbles within a unit volume of myocardium and this equates to the myocardial blood volume. In order to assess myocardial blood flow velocity, a series of high MI pulses are transmitted to cause microbubble destruction. The rate of replenishment, reflecting blood velocity, then can be assessed both qualitatively and quantitatively. Multiplying contrast intensity

by velocity reflects myocardial blood flow (see myocardial perfusion).

Contrast Administration: Bolus or Infusion?

Generally speaking, most commercially available contrast agents can be administered either using bolus or infusion administration methods. Bolus injections are usually considered satisfactory for LVO studies. They have the advantage of being easy and quick to set up and usually result in less contrast usage. The recommended doses are 0.5 ml of diluted Definity (one vial-1.5 ml in 8.5 ml of saline), 0.3 ml of non-diluted Optison (3 ml vial) followed by 3–5 ml of saline flush over 10 s [7] and 0.3 ml of non-diluted SonoVue followed by 1–2 ml of saline flush [8]. Effective opacification varies with the type of ultrasound contrast agents and the amount of bolus. Repeat boluses can be administered if needed.

As shown in Fig. 23.8, bolus injections result in a shorter time period during which the contrast

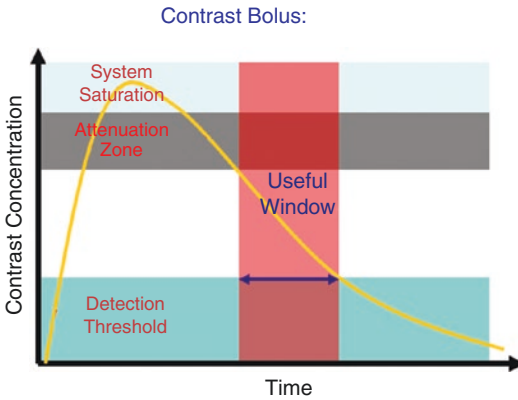


Fig. 23.8 During a bolus contrast injection, there is a limited time window on the decay part of the concentration curve where the contrast concentration is below the attenuation level but above the detection threshold

signal intensity is at an appropriate level without significant attenuation. Since the contrast concentration is constantly changing during a bolus injection it is not possible to quantify myocardial blood flow as described later. However, relatively under-perfused myocardial segments can often be appreciated for a transient period during the decay phase of the bolus.

The microbubbles used in most commercial contrast agents usually settle out quite rapidly and rise to the top of the solution in which they are suspended. This means that it is necessary to constantly agitate the syringe containing the contrast (by shaking or rubbing the vial) to keep the microbubbles suspended. During an infusion this is even more difficult. Some infusion pumps have been developed which help to keep the contrast suspended by constantly rotating the syringe containing the microbubbles.

The main advantage of contrast infusion is that the infusion rate can be precisely adjusted so that the contrast concentration falls between the detection threshold and attenuation zones, allowing for a long useful imaging time window, as illustrated in Fig. 23.9. Once set up, an infusion requires less operator intervention and could reduce the number of operators required for a contrast study. Infusions can be used for both LVO and perfusion studies. If quantification of myocardial blood flow is to be performed (as described later) then a constant contrast infusion is mandatory.

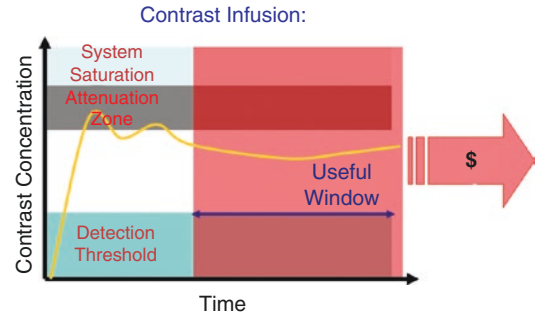


Fig. 23.9 With a constant infusion of contrast, the infusion rate can be adjusted so that contrast concentration is at a level which is above the detection threshold but below the attenuation level. This results in a prolonged imaging window but results in higher contrast usage and increased associated costs

Recommendation for Clinical Use

Contrast echocardiography has been shown to improve diagnostic accuracy in a wide range of clinical settings, has prognostic implications, improves patient outcome and is considered a marker of quality control in echocardiography. Table 23.3 summarises common clinical indications for contrast echocardiography [7, 9, 10].

Global and Regional Left Ventricle Function

Assessment of left ventricular (LV) function is the most common reason for performing an echocardiogram in the adult patient population. LV ejection fraction (LVEF) remains a strong diagnostic tool with prognostic value in prediction of adverse outcomes in patients with heart failure, after myocardial infarction and revascularization [9]. In order to improve accuracy and reduce variability, quantitative assessment of LV volumes and EF is a recommended method in major society guidelines [11]. Despite technological improvement such as second harmonic imaging and higher frequency transducers, suboptimal imaging can be faced in 10–15% of echocardiography studies [12]. Inadequate image quality can arise in patients who have a poor imaging window because of lung/rib artefacts, severe obesity

Table 23.3 Clinical indications for contrast echocardiography

1. Cardiac structures
(a) Quantification of left ventricular volumes and ejection fraction, assessment of regional wall motion abnormality at rest
• Improvement in endocardial border delineation in difficult to image patients (difficulty in visualizing more than two segments) (ASE, EACVI) ^a
• To increase accuracy and reproducibility in all patients (ASE, EACVI)
• To increase reader confidence in all patients (ASE, EACVI)
(b) Left ventricular structure abnormalities when non-enhanced images are suboptimal (ASE, EACVI)
• Left ventricular apical thrombus
• Apical hypertrophic cardiomyopathy
• Left ventricular non-compaction ^b
• Complications of myocardial infarction: Left ventricular rupture, aneurysm and pseudoaneurysm,
(c) Cardiac masses, thrombus (ASE, EACVI)
(d) Extra cardiac anatomy including aortic dissection and femoral pseudo aneurysm (ASE)
(e) Improvement in right ventricle visualisation (ASE)
(f) Stress induced (takotsubo) cardiomyopathy (ASE) ^c
(g) Enhancement of Doppler signals for evaluation of valvular disease/diastolic function (ASE)
2. Stress echocardiography in difficult to image patients
3. Myocardial Perfusion Imaging (Not approved by FDA)
(a) Detection of coronary artery disease (EACVI)
(b) Detection of acute coronary syndrome in patients presented to emergency department with chest pain (EACVI)
(c) Detection of myocardial variability (including patients with ST elevation myocardial infarction) (EACVI)
(d) Assessment of coronary flow reserve (EACVI)
(e) Low MI real time perfusion imaging in assessment of patients with chest pain in emergency department or during stress echocardiography when contrast is needed due to difficult imaging (ASE)

ASE American Society of Echocardiography, EACVI European Association of Cardiovascular Imaging

^aMandated by Intersocietal Accreditation Commission (IAC) Echocardiography for lab accreditation

^bWhen Left ventricular non-compaction is suspected an intermediate MI setting of 0.3–0.5 is recommended for better delineation of trabeculations [7]

^cIn addition to Left ventricular opacification for better delineation of endocardial border to characterize the takotsubo pattern, delayed but present perfusion may help exclude epicardial coronary artery disease

or chronic lung disease. Although, automatic endocardial border detection systems have the potential to improve quantitative analysis by removing the need for manual tracing of the LV border, these systems are also limited by poor image quality. If the endocardium is poorly defined, then the software will have as much difficulty following the endocardial boundary as will the human eye. LVO is therefore recommended when two or more contiguous segments are not seen on non-contrast images to improve endocardial border delineation for better assessment of global and regional LV function [9]. The Impact of contrast echocardiography on patient management and resource utilisation is even more pronounced in critically ill and ventilated patients when technical difficulties result in around 30% uninterpretable studies [12]. It is

really only the advent of contrast that has made it possible to quantify regional LV function in a wide variety of patients, including those with poor echocardiography windows and therefore when contrast is used less than 5% of transthoracic echocardiography studies should be identified as un-interpretable [12].

It's important to note that non-contrast echocardiography, regardless of the image quality, underestimates ejection fraction by 3–6% and LV volumes by 30–40% [13]. It is inherent to significant variability—reported as high as 14% [14] and has limited reproducibility. This can have diagnostic and prognostic implication. A typical example would be eligibility for device therapy in heart failure when accurate quantification of LVEF is crucial. Serial assessment of LV function in valvular heart disease or in

patients undergoing cardio toxic chemotherapy is another important example. LVO helps to reduce underestimation of LV volumes, improves accuracy and reproducibility and increases reader's confidence and makes echocardiography perfectly suited for quantification of LVEF in serial studies in a wide range of cardiovascular conditions.

Optimal Imaging Techniques in LVO

Conventional second harmonic imaging can be used for LVO studies. It filters out reflected fundamental signals and improves LVO image quality. However, the high MI used in standard echocardiography, destroys microbubbles resulting in swirling appearance especially in apex. We also know that at high MI, myocardial tissue also produces second harmonic signals, which makes it even more difficult to determine the endocardial boundary. Low MI setting (<0.4 —a very low MI <0.2 in modern scanners); therefore, can be used in LVO to minimise tissue harmonics. The absence of contrast destruction allows much better visualisation of the left ventricular apex than when conventional high MI second harmonic imaging is used with contrast. In addition, the receive filters on the ultrasound system need to be adjusted to ensure exclusion of the tissue fundamental signal. In lower contrast volumes, there may be insufficient contrast within the myocardium to cause any enhancement and the only contrast that can be seen is within the LV cavity. Since the myocardium will be black and the cavity bright, this results in excellent endocardial definition. Therefore, if second harmonic imaging is to be used in LVO, it is sensible to reduce the MI <0.4 (preferably 0.1 – 0.2) to limit the tissue signal and contrast destruction. Most modern echo systems have a manufacturer's pre-set which automatically selects a relatively low MI and optimises the machine setting to improve contrast enhancement. If the pre-set is available, it is recommended.

It should be noted while apical imaging is greatly enhanced with LVO, parasternal views

may initially deteriorate because as described earlier high concentration of contrast in right ventricle before trans pulmonary passage works as a barrier to ultrasound transmission and causes attenuation. For this reason a contrast study should start with apical views. Activate the contrast pre-set as previously discussed. Adjusting the time-gain compensation (TGC) is very important and requires considerable experience to obtain very low background noise (from myocardium and blood) and homogenous image. Move the focal position to mitral valve level and reduce the sector width until a frame rate >25 Hz is obtained. Bolus injections of contrast (followed by saline flush) or an infusion may be used for this type of study. If inadequate contrast opacification is obtained then a larger bolus volume or higher infusion rate should be tried. If attenuation occurs (because of higher contrast concentration) and far field objects are obscured, then reduce the bolus volume or infusion rate. If the basal segments are not visualised because of attenuation a foreshortened apical view may help to resolve this. Alternatively, or in addition, a few frames (5–10) at high MI (impulse or flash function) will destroy contrast within the LV cavity and myocardium, reducing attenuation and improving endocardial definition. It should go without saying that the basic rules of ensuring precisely defined scan planes, avoiding foreshortened views and careful tracing of the endocardial border still apply, as they do in noncontrast studies. An example of a contrast LV opacification study is shown in Fig. 23.10. This study was performed in an intensive care patient where the only other way of assessing left ventricular function satisfactorily would have been to perform a transoesophageal echocardiogram.

Recently, some manufacturers have adapted their automatic endocardial border detection systems to work with contrast, so that the LV cavity is recognised as having a bright, high intensity signal from contrast, whereas the myocardium is recognised as being dark. The high contrast change from the bright cavity to dark myocardium provides an easy boundary for the software to follow and LV volumes can be calculated on a

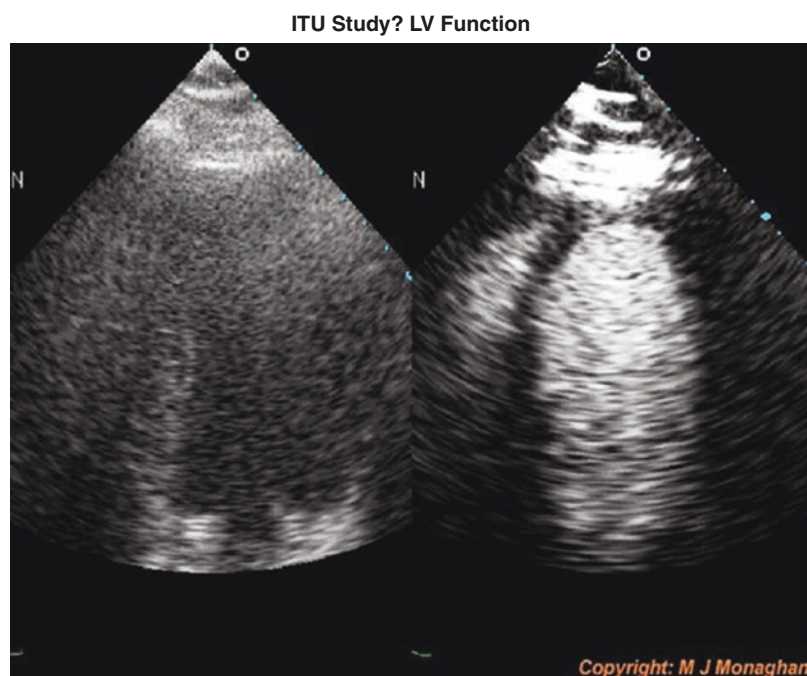


Fig. 23.10 Apical 4 chamber view using tissue harmonic imaging (on left) in an intensive care unit patient with very poor imaging windows. The patient had been recovering slowly post cardiac surgery and the request was to assess LV function. Image quality was so poor that no comment could be confidently made about LV function. Before proceeding to perform a transoesophageal echo a

contrast study was performed (right frame). Evaluation of the LV endocardial border was significantly enhanced, especially at the apex and the lateral wall, allowing an accurate assessment of LV function without needing to proceed to a transoesophageal echo. The improvement in image quality was even more evident on real-time images than on these still frames

frame by frame basis, which is impractical during manual tracing. This allows calculation of more sophisticated parameters of LV function and application to a wider patient population, including those with suboptimal windows. An example of this technology is shown in Fig. 23.11. Similar technology can also be used to study regional left ventricular function as shown in Fig. 23.12. Here, the automatic boundary detection system again detects the border between the contrast filled cavity and the dark myocardium. As the border moves in during systole, a coloured band is overlaid on the image every 35 or 40 ms. Thicker bands represent more excursion of the endocardium whereas very thin bands represent akinetic or hypokinetic segments. These images can be segmented and the regional contraction (fractional area change) calculated and compared for all segments.

Left Ventricular Structure Abnormalities

Left Ventricular Apical Thrombus

Transthoracic echocardiography is the standard imaging modality for detection of LV thrombus with specificity and sensitivity of 95% and 86% respectively [15]. However in patients with suboptimal echo windows, assessment of LV for thrombus can be challenging; missing a thrombus especially if it's small or laminar or mistaking an artefact for thrombus. The LV apex is the most common site for thrombus formation and it can be the most difficult area to visualise because of near field artefacts especially if the image is foreshortened. Standard echocardiography techniques to help clarify the diagnosis include avoiding foreshortening, identification

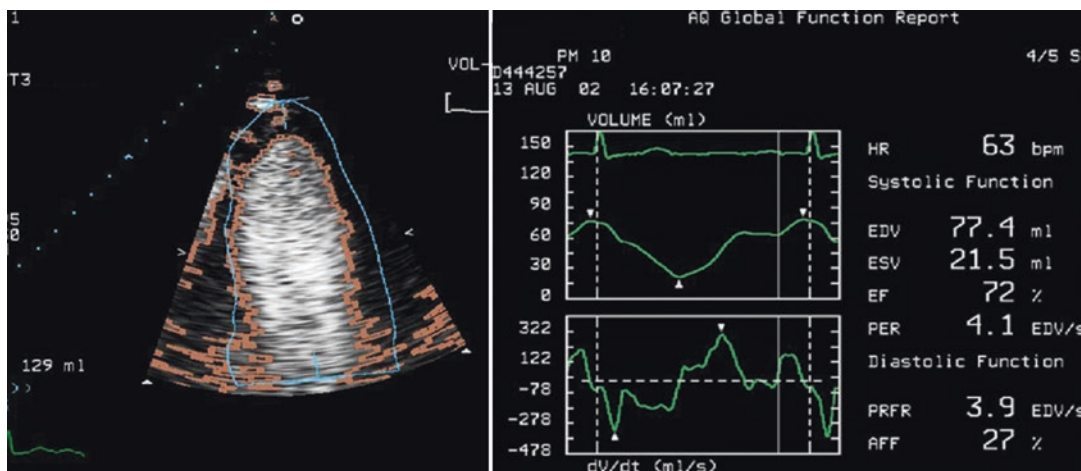


Fig. 23.11 Evaluation of global left ventricular function during a continuous contrast infusion of Sonovue and using the Contrast CK software from Philips Medical Systems. The left frame shows a bright contrast filled LV cavity and a dark myocardium. The LV endocardium is tracked (orange) on a frame by frame basis and LV volume

within the blue region of interest is calculated using the method of discs. In the right hand frame a graph displaying LV volume changes during one cardiac cycle and the first derivative (dV/dt) is seen. Automatically generated calculations such as end-diastolic and end-systolic volumes together with ejection fraction etc. are also displayed

of associated wall motion abnormality, use of higher imaging frequencies with harmonics, adjustment of the focal point to the depth of interest and use of colour flow Doppler with a low velocity scale (low PRF) to see if there is flow across the area of the image where thrombus is being questioned.

In a substantial number of patients, these techniques will still leave the question of possible LV thrombus unresolved and contrast can be extremely useful. Again, low MI real-time imaging should be used, if available. The contrast will improve apex visualisation, which would help to avoid foreshortening. Thrombus will appear as a dark filling defect adjacent to the akinetic myocardium. An example of an apical LV thrombus that could not be satisfactorily delineated using conventional echo techniques is shown in Fig. 23.13. Simultaneous use of flash destruction/reperfusion with high MI can be also helpful to demonstrate perfusion defect in the adjacent myocardium as substrate for thrombus formation. It also differentiates thrombus from vascularised tumour, which is further discussed in the next section.

Intracardiac Masses

Transthoracic echocardiography has a sensitivity of 93% for diagnosing intracardiac masses [16]. More rarely, intracardiac masses may represent tumours. Malignant tumours are usually located in right side of the heart and they include intra-mural or a combination of the intramural and intracavitary masses. Extension to vena caval or pulmonary veins is another feature suggestive of a malignant mass [17]. Conventional 2D echocardiography poses a challenge for tissue characterisation and differentiation of thrombus from tumours. Contrast echocardiography and perfusion imaging, could be used in assessing vascularity of the cardiac masses which can be helpful in differentiating malignant (with neo-vascularization-most commonly sarcoma) or vascularized tumours (e.g. cavernous haemangioma) from thrombus (avascular) or stromal tumours (myxoma, lipoma and fibroma which have sparse vascularity or are completely avascular) [16, 17]. Here again, a real time low MI is used. Gain and compression setting should be optimised for visualisation of the mass perfusion (typically within the range of 40–80%) with the focus set at the level of

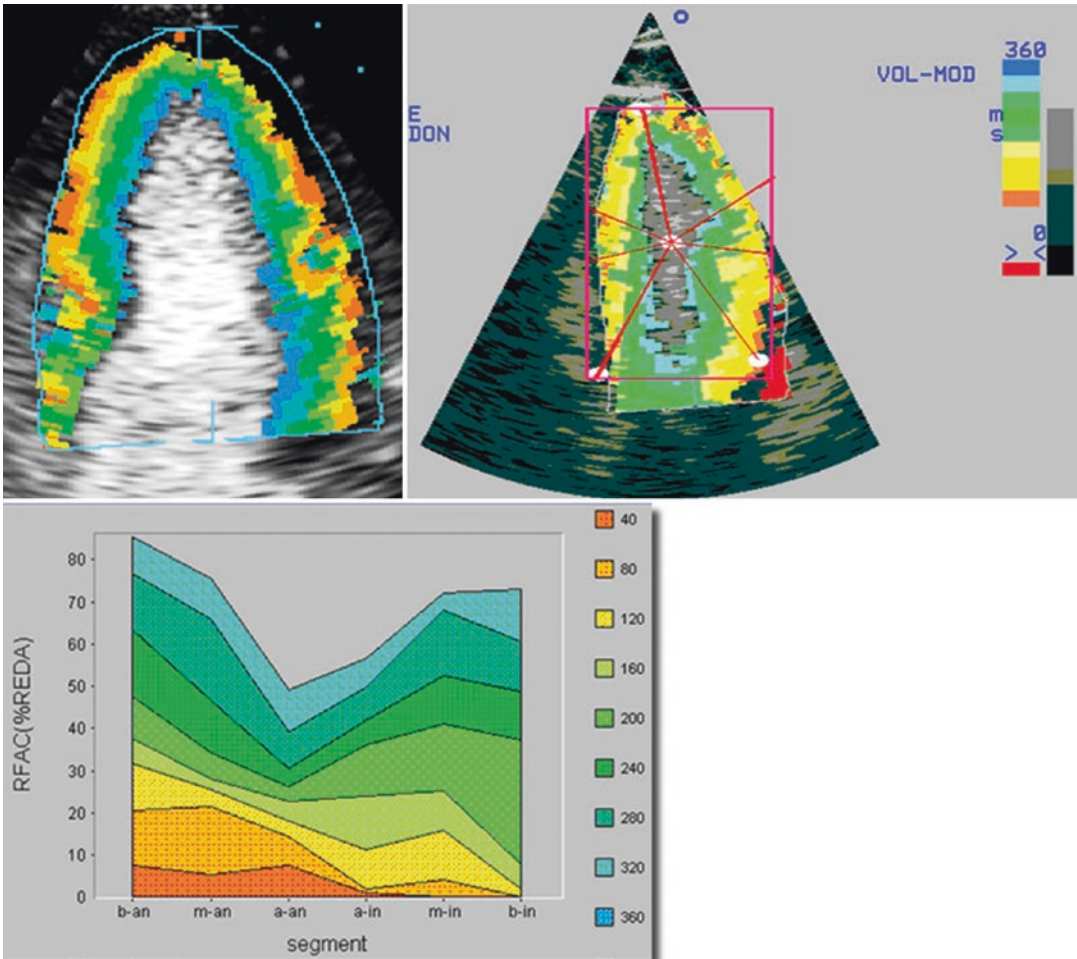


Fig. 23.12 Quantitative Contrast Colour Kinesis (Philips Medical Systems) images showing an apical 4 chamber view at the top left with contrast in the LV cavity and coloured bands overlaid on the image representing systolic excursion of the endocardium. Thicker colour bands represent more systolic excursion of the corresponding segments. The scan plane has been semi-automatically

segmented into six segments (top right) and the fractional area change calculated in each segment. The fractional area changes for all six segments are plotted in the bottom diagram and allow comparison of contraction between segments. In this example, the apical segments show reduced fractional area change

the mass. Once the mass is demonstrated by opacifying the relevant cardiac chamber with contrast, an impulse of high MI >1 is transmitted using at least for four frames (up to ten if needed) to destroy microbubbles within the mass. This prevents “false-positive perfusion” resulting from saturation artifact due to high gain settings, which may provide the same appearance [16, 18]. The replenished mass with contrast can be compared against an area of interest in adjacent perfused myocardium qualitatively or quantitatively using dedicated software

assessing mean pixels intensity. The software assesses both the degree of replenishment and the rate at which this happens. Typically myocardial tissue is highly vascular showing more replenishment than avascular thrombus or poorly vascularised stromal tumour. On the contrary, a malignant tumour contains highly concentrated dilated vessels and hence the replenishment rate will be faster than myocardium. A malignant tumour will be opacified with contrast (higher pixel density than adjusted myocardium) whereas thrombus will not [18].

Post Anterior MI, for CABG, ?Thrombus

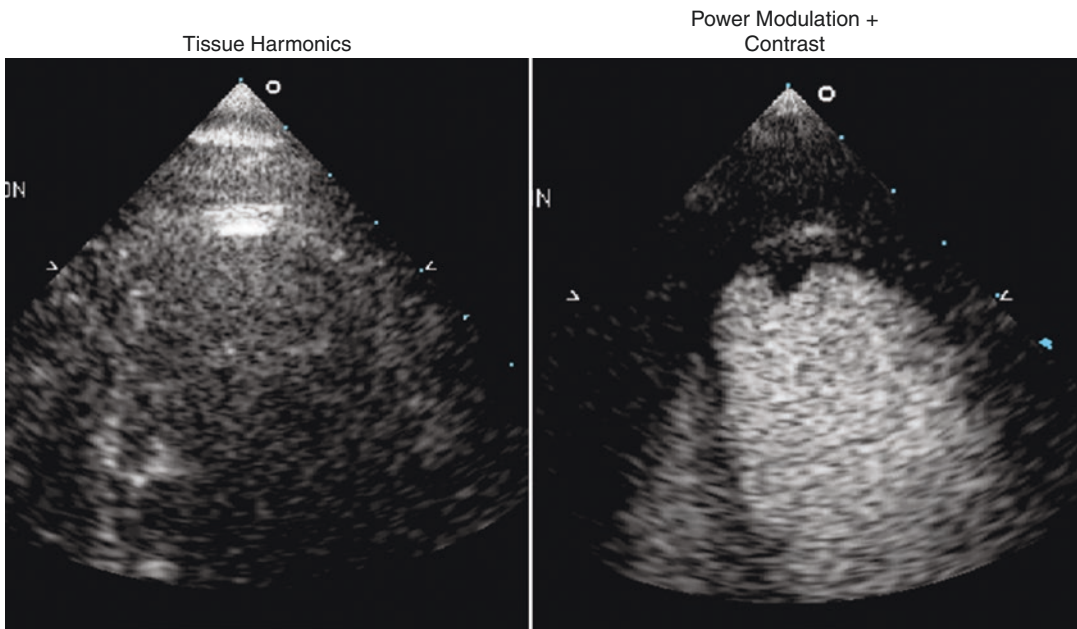


Fig. 23.13 Zoomed apical 4 chamber views in a patient who had had an anterior infarct and a conventional echocardiogram (left) suggestive of a large apical thrombus. A contrast study using Power Modulation demonstrates that

the structure previously thought to represent a thrombus is probably a false tendon. However, there is a small filling defect at the apex which was subsequently confirmed at surgery to represent a small thrombus

Enhancement of Doppler Signals

Modern echocardiographic imaging systems have extremely sensitive Doppler processing and the need for enhancement is limited. However, enhancement can be performed using contrast microbubbles. Even after the microbubbles have collapsed and only shell fragments are left in the circulation, considerable spectral Doppler enhancement occurs. This means that contrast enhanced Doppler recordings can be performed at the end of a conventional contrast LVO or perfusion study, when there is no visible contrast left in the cavities. Shell fragments will still be circulating and these act as excellent Doppler scatterers. An example of spectral Doppler enhancement using contrast is seen in Fig. 23.14. In this case, considerable enhancement of the continuous wave Doppler signal from mitral and tricuspid regurgitation is seen. In addition, pulsed wave analysis of pulmonary vein flow is also improved.

Stress Echocardiography

Although stress echocardiography has a high sensitivity and specificity for the detection of coronary disease and evaluating myocardial viability, it is the most demanding and difficult echo technique to perform and interpret. This is because image quality can often be very poor at peak stress, irrespective of whether pharmacological or exercise stress has been performed, resulting in as high as 30% studies being reported as non-diagnostic. This can increase inter-observer variability and low reproducibility [9]. High image quality with excellent endocardial definition therefore is essential for the performance and analysis of stress echo studies. It is important to be able to visualise all myocardial segments and detect subtle wall motion or thickening abnormalities. For these reasons, the aforementioned benefits of contrast echocardiography in improving endocardial border delineation has been translated into stress echo-

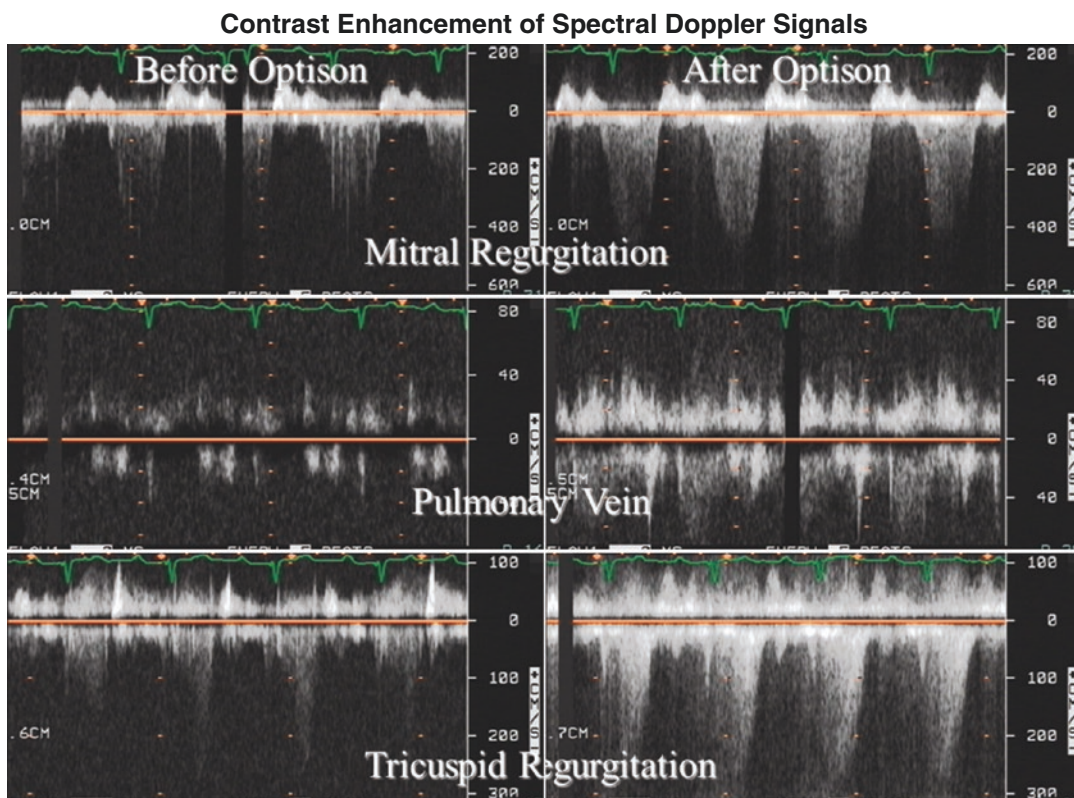


Fig. 23.14 Enhancement of spectral Doppler recordings using the Contrast agent Optison. This was obtained at the end of a conventional LVO contrast study when very little

contrast was visible, however the Contrast shell fragments still generate a strong Doppler signal and show enhanced visualisation of mitral, tricuspid and pulmonary vein flow

cardiography and contrast agents have become an almost mandatory component of most stress echocardiography laboratories. Contrast stress echocardiography has been shown to improve accuracy, reproducibility and reader confidence for both experienced and inexperienced readers [9]. When contrast is used, less than 10% of stress echo studies should be reported as non-diagnostic [19]. Although the greatest benefit is seen with poor baseline images, it's also important to note that it is very difficult to predict, based upon the baseline images, how much image quality will deteriorate (because of tachycardia and hyperventilation) by the time peak stress is achieved and it can be very difficult to compare non-contrast baseline images with contrast enhanced peak stress images. Therefore, we advocate the use of contrast in virtually all stress cases.

It is very easy to incorporate contrast into a standard stress protocol, especially when pharmacological stress is being performed and an IV line is already in place. If a 3-way tap is connected to the end of venous cannula then the contrast should not be administered through the side arm or the top port of the cannula. This is to minimise contrast destruction by avoiding the shear forces associated with a 90° turn. We prefer to use a Y connector with a narrow bore connection for the contrast to avoid microbubbles settling out, which can happen in a 3-way tap. Contrast infusion pumps usually have narrow bore connection tubing for the same reason and this should always be used.

For the reasons previously mentioned, low MI real-time imaging is the preferred contrast imaging modality to use. Apical destruction of contrast at high MI can really limit the detection of

localised apical wall motion abnormalities, limiting the sensitivity of the test. Low MI imaging minimises this problem and provides excellent endocardial delineation because of lack of back-scatters derived from myocardial tissue. Since low MI real-time techniques often have lower frame rates, it will usually be necessary to reduce the sector width by 20–30° in order to ensure that the frame rate is greater than 25 Hz. It is obviously very important at high heart rates to maintain a reasonable imaging frame rate and this is one of the limitations of low MI techniques. Nevertheless, unless the LV cavity is very large it is usually possible to reduce the sector width enough to get an adequate frame rate. Contrast can be administered via bolus injections if necessary. However, as described previously, contrast infusion does confer several advantages and can reduce the number of personnel required in the stress echocardiography lab. As explained earlier, at lower doses of contrast there won't be sufficient microbubbles to reach the myocardium and only the LV cavity is filled with contrast resulting in excellent endocardial delineation (myocardium will look black and LV cavity bright). Increasing

contrast volume will enhance myocardium, which allows assessment of myocardial perfusion.

Figure 23.15 illustrates a suggested protocol for using contrast during dobutamine stress echocardiography. This can be adapted for either bolus injections or infusions. Bolus injections are usually performed approximately 20–30 s before images are acquired. Whereas infusions take a little longer to reach a steady state and 45 s lead-in is usually necessary. The infusion can and should be discontinued between imaging stages, in fact once the apical views have been obtained there will be sufficient contrast left in the circulation to allow parasternal images to be obtained. As shown in the protocol, it is preferably to collect apical images first and then the parasternal images so that the contrast level has fallen and the chances of attenuation by high volume of contrast in right ventricle minimised. Contrast attenuation is less of a problem with low MI imaging techniques. Figure 23.16 illustrates contrast enhanced parasternal short axis images with minimal attenuation. However, it is prudent to try and modify the imaging window to avoid the right ventricle as much as possible in order to minimise attenuation

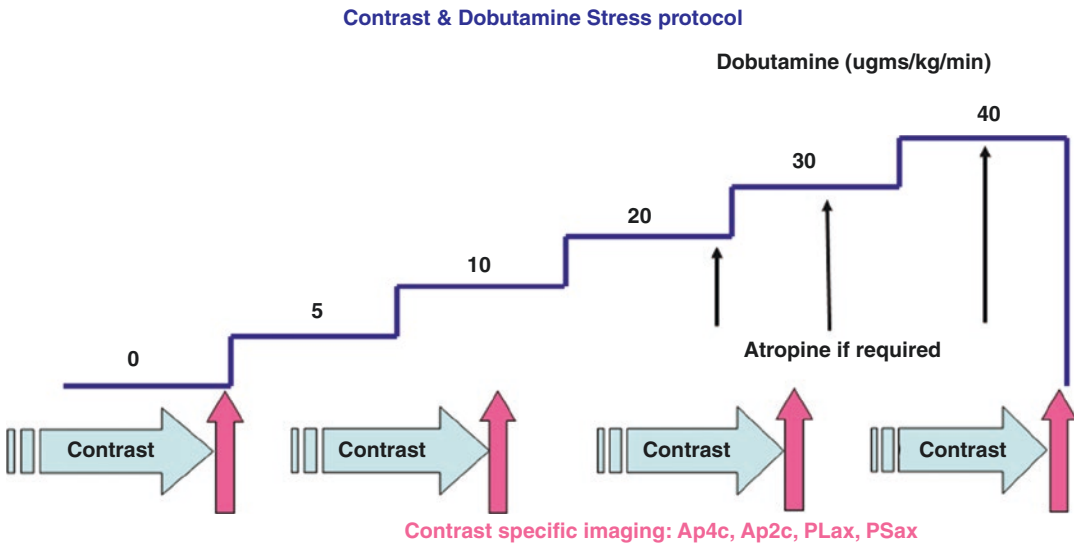


Fig. 23.15 Suggested protocol for combining contrast with a dobutamine stress echo protocol. Imaging is performed at baseline, low dose, intermediate dose and at peak. Imaging sequence commences with apical views to minimise the effects of attenuation. Contrast bolus injections

are administered approximately 30 s before each imaging acquisition sequence and repeated if necessary. Infusions would need to be re-started approximately 45 s before imaging and can be stopped after apical views have been obtained

induced by high volume of contrast in right ventricle. If parasternal windows are unobtainable because of attenuation or other reasons, then the apical 3-chamber view may be substituted for the parasternal long axis and the short axis omitted since all segments will be seen in other views.

As previously described for resting LV opacification studies, the contrast bolus dose or infusion rate should be adjusted so that attenuation is minimised and far field structures are clearly seen. During the peak of a bolus, some attenuation is inevitable and it is important to wait until the optimal part of the decay curve before acquiring images (Fig. 23.8). A transient reduction in contrast concentration can be achieved by using the “flash” or “impulse” function which will destroy contrast, especially in the myocardium (thus the myocardium will look much darker),

and this usually creates excellent endocardial definition in the few beats following destruction.

This section has concentrated on the use of contrast for improving endocardial definition during stress echocardiography studies. This along with LVO currently represents the major licensed application for contrast agents and is undoubtedly the appropriate starting point for introducing contrast into the echo lab. In the next section, the use of contrast is extended into the evaluation of myocardial perfusion.

Myocardial Perfusion

In order to understand myocardial perfusion imaging, it's crucial to understand myocardial blood supply and perfusion. Coronary blood cir-

Low MI Contrast Imaging DSE–Parasternal Views

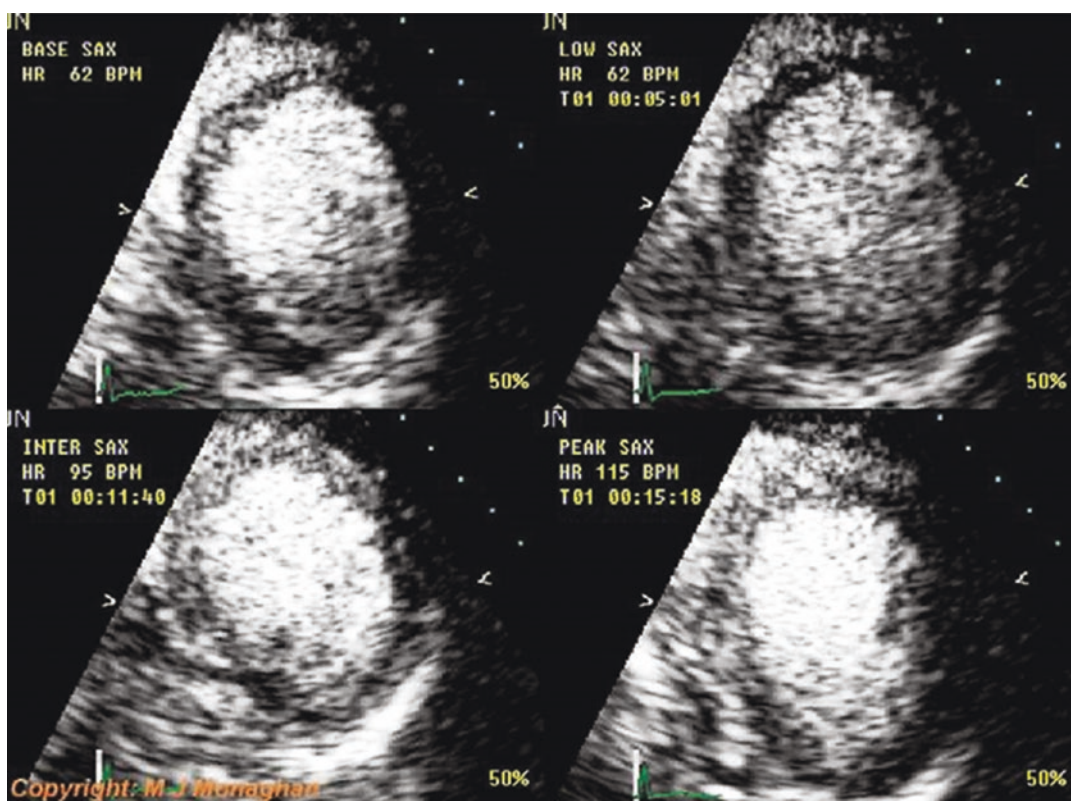


Fig. 23.16 Using low MI imaging, contrast attenuation is minimised and so parasternal views (as shown here) can usually be used. Good endocardial definition is seen at all

stages of dobutamine stress and some myocardial enhancement is also evident, allowing appreciation of myocardial thickness

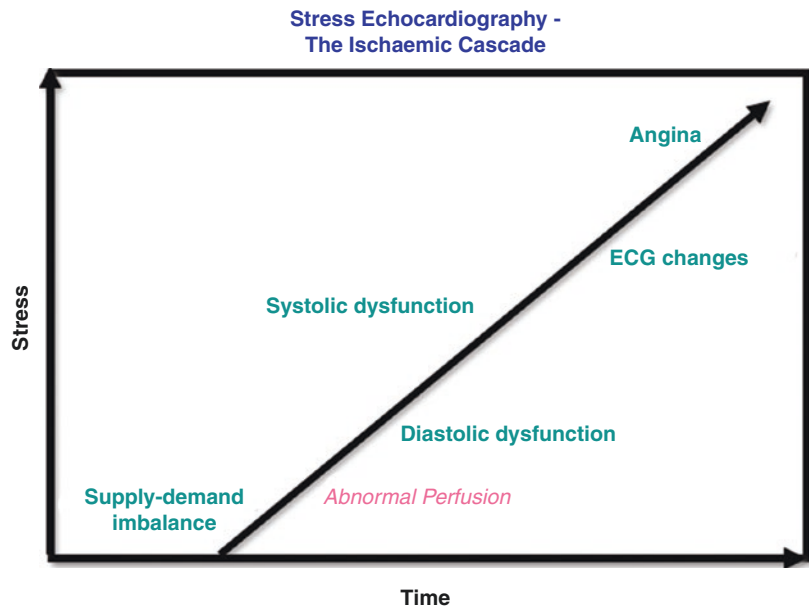
culuation consists of arteries, arterioles, capillary network, venules, and veins. The epicardial coronary arteries branch into myocardium in a perpendicular way, forming several levels of branches to smallest arterioles that feed the capillary network. Myocardial tissue resides a third of coronary circulation within itself, called myocardial blood volume, of which close to 90% is in the capillary network. Capillaries have an average diameter of 6.3μ and traverse the length of myocyte with a mean functional length of 0.5–1 mm [20]. During contrast injection/infusion the entire myocardial capillary network can be filled with microbubbles. The intensity of backscattered ultrasound (i.e. video intensity) from a unit volume of myocardium is then directly proportional to the number of scattering interfaces within that volume of myocardium. As discussed in contrast imaging techniques, most contrast specific imaging modalities suppress tissue signals so that the backscattered ultrasound signal intensity is mainly due to the number of contrast microbubbles within the unit volume of myocardium. Since, unlike nuclear agents, microbubbles are pure intravascular tracer the number of microbubbles, and hence backscattered signal intensity, is proportional to the blood volume within the myocardium being imaged. It means any alteration in microbubble backscatter

intensity must reflect change in myocardial blood volume. The rate of contrast replenishment and enhancement in intensity after microbubble destruction, which reflects the velocity, can also be assessed. Therefore, myocardial contrast echocardiography (MCE) has the ability to demonstrate both myocardial blood volume and velocity on a regional basis. The combination of these two parameters represents myocardial blood flow.

Detection of Coronary Artery Disease: Stress Myocardial Contrast Echocardiography (MCE)

The classical ischaemic cascade, as illustrated in Fig. 23.17, demonstrates that one of the first indicators of an imbalance between myocardial oxygen demand and supply is a reduction in myocardial perfusion. Since we know that these occur early in the ischaemic cascade, they should be more sensitive markers than regional wall motion/thickening abnormalities, chest pain and ECG changes [21]. Therefore, MCE has the potential to facilitate evaluation of myocardial perfusion. The delay in contrast appearance (decreased velocity) and reduction in contrast intensity (reduced myocardial blood volume) forms the basis of detection of ischaemia by MCE.

Fig. 23.17 The classical ischaemic cascade demonstrating the sequence of events that occur during stress induced ischaemia. Abnormalities in myocardial perfusion occur earlier than mechanical or ECG changes. Therefore, methods which are able to detect stress induced perfusion abnormalities should have good sensitivity for diagnosing reversible ischaemia



Impairment in sub-endocardium myocardial blood flow is responsible for myocardial dysfunction in a variety of cardiac diseases including ischaemic heart disease, hypertensive heart disease and small vessel disease. It's farthest part of myocardium from epicardial coronary arteries and is compressed by both LV cavity and the rest of myocardium during cardiac contraction. The better resolution of MCE compared to SPECT provides the ability to assess subendocardial perfusion in clinical settings [22]. When ischaemia is only limited to the sub-endocardium, it is also difficult to diagnose it with other forms of stress echocardiography. The recruitment of subepicardial contraction by dobutamine may mask the subendocardial ischaemia resulting in false negative results. Therefore, MCE improves the diagnostic sensitivity for detection of reversible ischaemia over and above that already established for conventional stress echocardiography. Since stress MCE can be used in combination with conventional stress echocardiography techniques and can provide enhanced wall motion plus perfusion data, it also increases our diagnostic confidence. This is particularly helpful when wall motion findings are equivocal or subtle. Presence of perfusion defect in such cases confirms the presence of wall motion abnormality.

Up to 80% of circulating oxygen is consumed by myocardial cells (this is 25% for the rest of the body) and therefore any increase in demand must be dealt with by an increase in coronary blood flow which can be up to fourfold to sixfold (coronary flow reserve). To match myocardial oxygen demand in various situations, arterioles and/or capillary network play a crucial role in maintaining adequate myocardial perfusion despite variation in flow and pressure. Arterioles afford their autoregulatory role through vasodilation whilst capillaries lack smooth muscles and achieve their role by recruitment of new vessels. Both mechanisms result in reducing the resistance downstream to coronary stenosis. It has been shown that coronary stenosis up to 45% does not cause significant decrease in blood flow. At rest and in the presence of non-critical coronary stenosis (<85–90%), despite reduction in blood flow beyond the stenotic

lesion, arteriolar vasodilation and capillary network recruitment mechanisms maintain adequate myocardial perfusion. It's however during stress that already exhausted autoregulatory mechanisms won't be able to match myocardial oxygen demand. Coronary stenosis must exceed 85–90% to cause decrease in myocardial perfusion at rest despite autoregulation. Assessment of critical stenosis (>90%) at rest is often difficult and complex owing to presence of collaterals which can contribute to maintaining coronary blood flow [6].

An important variable in the methodology for stress MCE then is the choice of stress agent. *Exercise* increases coronary blood flow through endothelial mediated mechanisms to meet increase in myocardial oxygen demand and although it is preferred choice in stress echocardiography [23], exercise stress MCE can be challenging because of increased respiratory effort at peak exercise. Other choices are a positive inotrope agent such as dobutamine or inducing maximal hyperaemia by coronary vasodilators such as adenosine and dipyridamole. The ultimate result in all methods would be an increase in coronary blood flow.

The inotropes work by increasing myocardial oxygen demand (similar to exercise) and this in turn causes an increase in myocardial blood flow. However, in myocardial segments supplied by stenosed vessel, flow is unable to increase. In the presence of exhausted arteriolar vasodilation and, in order to maintain adequate hydrostatic pressure across perfusion bed, part of capillary network collapses which is so-called "capillary de-recruitment". This means that myocardial blood volume effectively decreases in these segments and therefore, the backscatter contrast signal intensity decreases as explained previously. Capillary de-recruitment will be reversed upon stopping stress, which explains reversible perfusion defect on MCE.

Coronary vasodilators work by using the "coronary steal" phenomenon. Myocardial blood flow increases substantially in perfusion beds supplied by coronary vessels with normal flow reserve and no flow limiting lesions. However, in coronary arteries with flow limiting lesions

(>45%) a further drop in flow occurs beyond the lesion that is proportional to the degree of stenosis. This causes deviation of blood flow towards normal perfusion territories. To deal with reduced perfusion pressure in ischaemic territories, capillary de-recruitment occurs to maintain hydrostatic pressure across the capillary network at cost of reduction in myocardial blood volume (and hence reduced contrast signal intensity). Vasodilator stress MCE is an attractive option due to rather short test time (around 15–20 min) however it lacks wall motion assessment. In real world practice MCE during dobutamine stress echocardiography is the most commonly used modality.

Exercise stress MCE is more challenging due to increased respiratory rate and the brief period that images should be taken—usually less than 90 s. However, it has been shown that MCE can be incorporated in exercise stress echocardiography in routine clinical setting [24] and improves wall motion analysis sensitivity [5].

Although it is sometimes useful to record baseline myocardial contrast studies at rest, As explained earlier we know that even in the presence of an epicardial coronary stenosis <85–90%, owing to arteriolar vasodilatory effect, resting myocardial perfusion will be normal. Therefore, if resting wall motion and thickening is normal in an individual segment, one can usually assume that perfusion will be normal and a contrast study at this point may be superfluous. If myocardial contrast opacification is absent in a normally contracting segment at rest then this represents an artefact due to attenuation or inadequate gain/ultrasound penetration. During stress, we would expect changes in perfusion to be evident before wall motion abnormalities. Therefore, the stress MCE images can be taken, if required, at a sub-maximal stage. This technique can be utilised successfully during conventional dobutamine stress echo. Dobutamine act as a vasodilator in low doses and therefore resulting hyperaemia may be able to detect perfusion defects before maximal dose of dobutamine induces demand ischaemia. The fact that this methodology can be used during dobutamine stress echocardiography further underlines

it's suitability as a starting point for performing these types of studies.

It was explained previously that that myocardial blood flow is directly proportional to the product of blood volume and velocity. Both these parameters can be readily evaluated and appreciated during stress MCE, using a variety of techniques with contrast bolus or infusion.

Contrast Bolus

A linear relationship between microbubble concentration and signal intensity is necessary in MCE. At a certain level echocardiography scanners reach a saturation point where no longer contrast video intensity is proportional to myocardial blood volume. This becomes especially important in bolus injection of contrast in which transient high contrast concentration can be reached even in regions with low myocardial blood flow [5]. As explained before, it's only during the decay portion of the contrast bolus (Fig. 23.8) that contrast concentration in the myocardium falls through the critical level, where it is possible to differentiate ischaemia-induced differences in myocardial blood volume (Fig. 23.18). This is usually visualised initially in the sub-endocardium as a dark rim, whilst the subepicardium remains bright. As the contrast concentration decays further, the entire transmural extent of the myocardium becomes dark. Spatial variations in contrast enhancement during the bolus decay phase are critical aids to recognising ischaemic segments. A homogeneous, transmural decay in contrast intensity (mirrored in other segments at the same image depth) simply represents contrast decay. Whereas, heterogeneous opacification and especially a dark sub-endocardium rim is highly suggestive of stress induced ischaemia. Myocardial segments that remain unopacified during the entire contrast administration usually represent infarcted and irreversibly ischaemic tissue especially if a significant resting wall motion abnormality is present. With the bolus injection, the myocardial contrast intensity, as we know, is a reflection of myocardial blood volume. Note that the estimate of myocardial blood flow cannot be calculated from bolus injection because the mean transit time of contrast cannot be obtained [5].

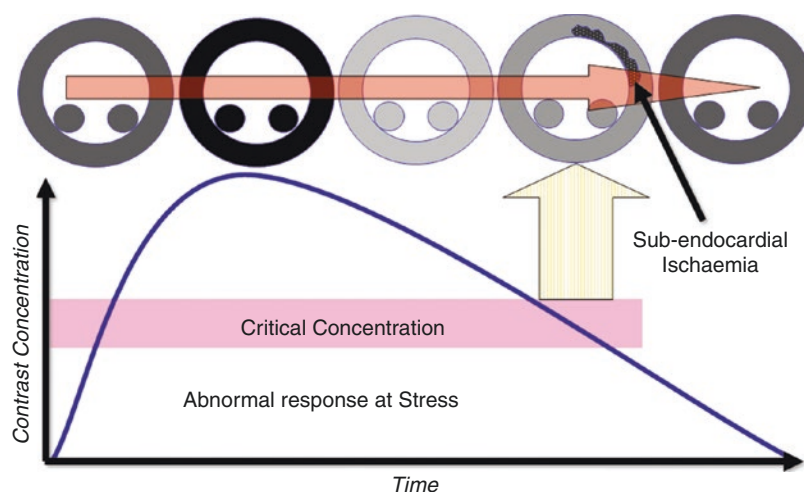


Fig. 23.18 Diagram illustrating the principle of using bolus injections during stress myocardial contrast echocardiography. During the wash-out phase of the bolus, the contrast concentration falls through a critical level where it is possible to visualise spatial differences in myocardial blood volume secondary to ischaemia. During the peak of

the bolus, the myocardium is saturated with contrast and during the tail, the contrast concentration is insufficient to cause myocardial opacification. The available imaging time window, during which the critical concentration occurs, is fairly short

Contrast Infusion

As explained before, contrast infusion can be precisely adjusted so that the contrast concentration falls between the detection threshold and attenuation zones, allowing for a long useful imaging time window, as illustrated in Fig. 23.9. This is a practical advantage compared to bolus injection where attenuation artefact due to high microbubble concentration in LV cavity occurs.

Low MI MCE

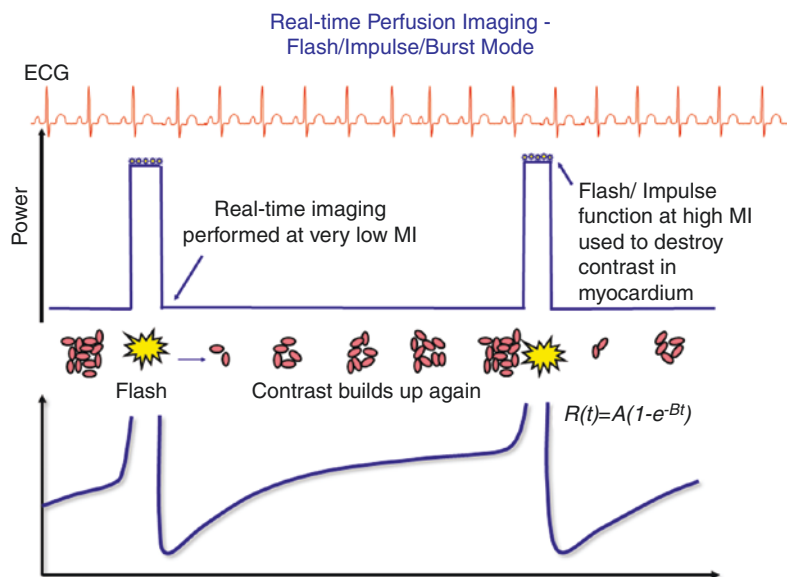
As previously discussed, real-time low MI imaging techniques provide excellent endocardial definition at adequate frame rates. Myocardial perfusion information can also be simultaneously obtained and is therefore incremental to the wall motion data. This methodology provides an excellent starting point for performing stress MCE studies. As explained before, the non-destructive low MI imaging methodology typically uses an output MI of <0.4 to avoid microbubble destruction (see contrast imaging techniques). If a few frames (usually 5–10) of high output power are fired using the “impulse”, “burst” or “flash” function, then contrast microspheres will be destroyed. This usually results in

the myocardial contrast effect disappearing, whereas the left ventricular cavity remains bright because the contrast concentration is significantly greater in the cavity. The wash-in of contrast into the myocardium, following destruction can then be observed to assess myocardial blood flow. Careful adjustment of contrast infusion rate and machine settings is critical to ensure that complete contrast destruction in the myocardium occurs without significant cavity destruction.

Off-line analysis of the images allows for quantitative assessment of myocardial blood flow. A region of interest is positioned within individual myocardial segments. The contrast signal intensity can then be plotted as a reperfusion curve, as illustrated in Fig. 23.19. The slope of the curve is proportional to blood flow velocity and the peak or plateau to blood volume. The product of both parameters (the slope time plateau) is proportional to myocardial blood flow, which will be reduced in ischaemic zones. A comparison before and after stress (especially vasodilator) will permit an assessment of coronary blood flow reserve.

However, a semi-quantitative approach can also be taken by direct observation of the number

Fig. 23.19 Diagram illustrating the basic principles of low MI real-time perfusion imaging with flash/impulse contrast destruction. Following the destruction frames, contrast re-perfuses into the myocardium. A the plateau portion of the re-perfusion curve and is proportional to myocardial blood volume. B the initial slope of the curve and is proportional to blood flow velocity. $R(t)$ is proportional to myocardial blood flow



of cardiac cycles taken for an individual segment to reperfuse. We know that contrast microbubble velocity in myocardium is 1 mm/s. Given an ultrasound elevation beam of 5 mm, it would take up to 5 s (or in another word five beats assuming a heart rate of 60 at rest) for myocardium to be homogenously opacified. Delayed reperfusion (>4–5 cycles at rest), especially in the sub-endocardium, is highly suggestive of ischaemia. During stress, increased myocardial blood flow (fourfold to sixfold) should mean that an individual segment will reperfuse more quickly than at rest after bubble destruction and this should occur within 1 s (2–3 cardiac cycles) at peak stress (assuming heart rate 140).

There is a naturally occurring cyclic variation in the myocardial contrast effect and this, together with segmental motion, can make interpretation of these images in a real-time mode difficult. Therefore, it is often easier to use a triggered capture mode on the ultrasound system, so that only end-systolic or end-diastolic frames are stored. Subsequent analysis of these frames, without the confounding effects of cyclic intensity variations and wall motion, is often easier. Again this methodology can be used with both inotropic or vasodilator stress, as previously outlined. In practice, it is most commonly utilised with vasodilator stress since it is perfusion alone, rather than per-

fusion and wall motion data that are being analysed. However, in Fig. 23.20 the use of this technique during dobutamine stress, demonstrating both perfusion and wall motion abnormalities is seen.

High MI MCE

As previously mentioned, destructive imaging techniques use high MI to destroy contrast microspheres within the myocardium (see contrast imaging techniques). Due to contrast destruction, these methods are utilised with intermittent imaging to allow myocardial replenishment after each bubble destruction and therefore no wall motion data is available. By varying the triggering interval from one frame every cardiac cycle to up to one frame every 10 cycles, it's possible to obtain data on myocardial blood flow. The longer the triggering intervals are set, the more microbubbles replenish the capillaries (and hence higher signal intensity) until finally a plateau phase is reached. It is important to step through an acquisition sequence where the triggering interval is varied and increased in a stepwise fashion. Software on some ultrasound systems permits the creation of a triggering sequence, which simplifies and standardises image acquisition. During long triggering intervals it can be difficult to maintain a constant scan plane (e.g. for 4–5 s), since the echocardiog-

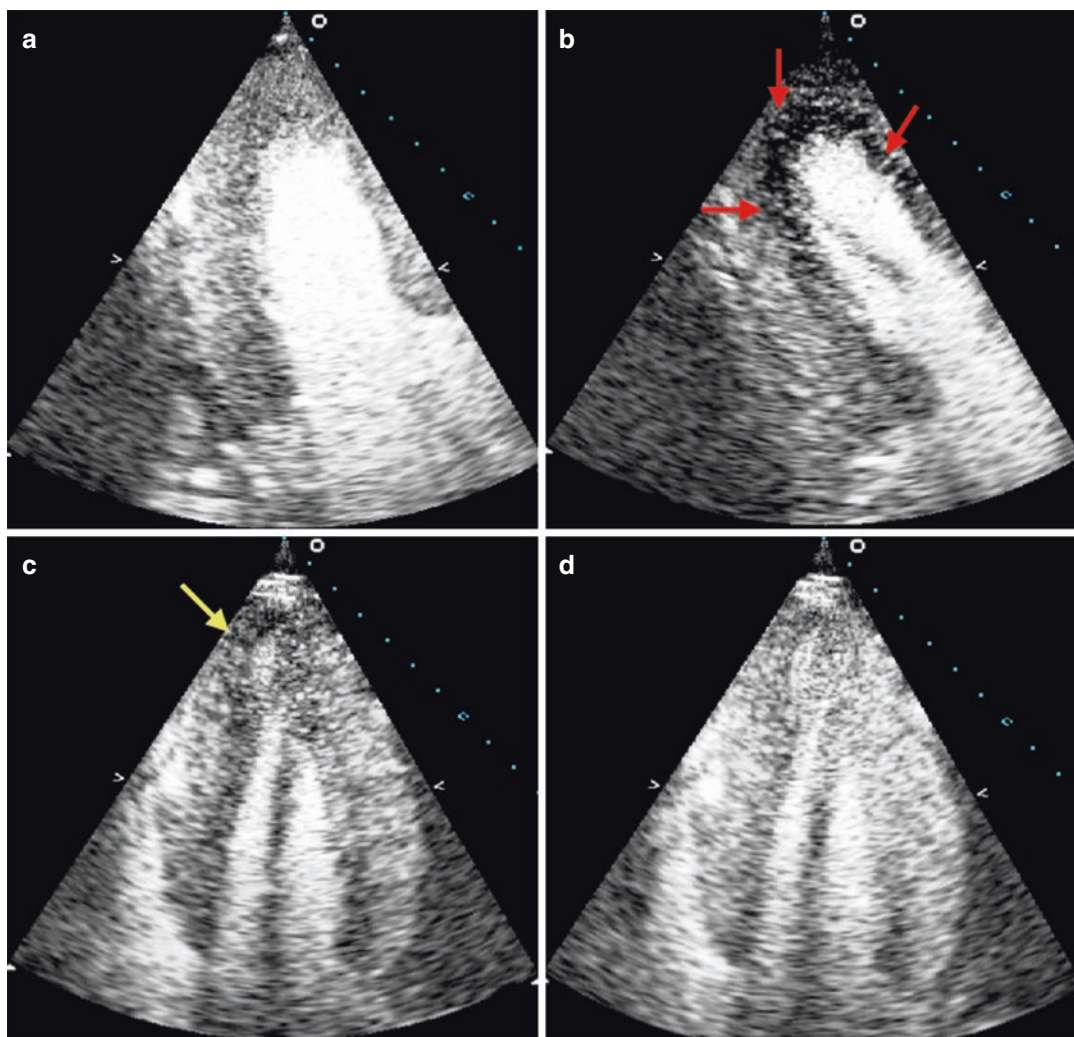


Fig. 23.20 Contrast destruction-reperfusion study during dobutamine stress echo in a patient with 70% lesion at mid portion of the left anterior descending artery and severely diseased right coronary artery with a 90% lesion. Panels (a) and (b) are end-systolic apical two chamber views at rest three beats post destruction (a) and at peak stress one beat post destruction (b). A significant subendocardial defect is seen in the anterior, apical and inferior

walls (red arrows). Panels (c) and (d) are both apical 4 chamber views at peak stress. Panel (c) is one beat post destruction and shows an apical and septal subendocardial defect (yellow arrow). It also demonstrates an aneurysmal “pouching” of the apex which was even more evident on real-time images. Panel (d) is three beats post destruction and the subendocardial defects have filled in although the apical shape distortion is still evident

rapher has no moving landmarks. It is possible on some ultrasound systems to utilise low MI real-time imaging (“monitoring mode”) between the high MI destructive frames and this certainly makes performing intermittent imaging much easier. The other important issue during this type of stress MCE imaging is to decide which part of the cardiac cycle should be used for the trigger acqui-

sition point. Although there is no absolute rule, end-systole is most commonly utilised because the myocardium is thicker, the left ventricular cavity is small and contrast attenuation is limited. Setting up the instrument controls for this type of imaging requires considerable experience in order to avoid artefacts caused by wall motion, contrast attenuation or incomplete contrast destruction.

Since myocardial blood flow increases during stress we would expect that reperfusion would occur with shorter trigger intervals than at baseline. For example, during vasodilator stress using either dipyridamole or adenosine, the normal coronary flow reserve response results in blood flow increasing by a factor of four. Therefore, at rest it may take a trigger interval of four cardiac cycles for an individual segment to perfuse. Whereas, under maximum coronary vasodilation, reperfusion should occur in one cycle. So we can compare baseline images with a trigger interval of four cycles to stress images acquired with a one-cycle interval.

Although this form of stress MCE is usually performed with vasodilator stress, it can also be utilised with inotropic stress. As previously mentioned, coronary physiology dictates that during stress induced ischaemia, relative reductions in myocardial blood volume, secondary to capillary de-recruitment, will result in slower reperfusion into ischaemic territories. Therefore, at short triggering intervals during stress, a perfusion defect may be visualised. Increased wall motion, due to the inotropic effect, may result in more wall motion artefacts when this type of stress is used. Consequently, harmonic power Doppler is more commonly used in combination with vasodilator stress.

Accuracy

Accuracy of stress MCE against other modalities has been extensively studied. Studies comparing MCE against coronary angiography have shown a sensitivity and specificity of 83% and 80% respectively [10]. A meta-analysis of eight studies comparing sensitivity and specificity of MCE and SPECT/dobutamine stress echocardiography against coronary angiography as gold standard revealed a higher sensitivity favouring MCE [25]. In another study, comparing MCE against cardiac MRI yielded sensitivity and specificity of 85% and 74%. Two more recent large multicentre studies however showed some conflicting results [26]. Using coronary angiography as gold standard for detecting epicardial vessel with more than 70% stenosis, although MCE sensitivity was

higher comparing to SPECT, specificity was lower which could be accounted for by the presence of microvascular ischaemia [27].

Evaluation of Patients with Suspected Acute Coronary Syndrome

Owing to its ability as a bedside diagnostic test, MCE can play a unique role in assessing patients with chest pain presenting to emergency department. It can be used to rule out acute coronary syndrome for early discharge. A negative stress MCE predicts excellent outcome in 1 year [10].

Management of Acute Myocardial Infarction

One of the earliest clinical applications of MCE was in patients with acute myocardial infarction (AMI), when the aim of treatment must be to salvage as much myocardium as possible using some form of reperfusion therapy. It is important to know if patency has been restored to the infarct related artery and if microvascular perfusion has been achieved. Resting MCE can be used for assessment of ultimate infarct size at the time of AMI and also assessment of reperfusion success following thrombolysis which could help determine if rescue percutaneous coronary intervention (PCI) is needed [28]. The demonstration of microvascular perfusion implies microvascular integrity and hence myocardial viability [29] and therefore resting MCE can also be used to assess residual myocardial ischaemia following acute AMI. MCE also offers incremental prognostic information and is a strong independent predictor of outcomes and LV reverse remodelling [30–32].

It's sensible to perform a MCE study 90 min after thrombolysis to assess the infarct zone and to decide whether rescue PCI is needed or not [10]. In Fig. 23.21 an Apical 4 chamber power modulation contrast perfusion image is seen in a patient with an acute anterior myocardial infarction treated with thrombolysis. The apical area shows almost transmural perfusion defect

Acute anterior MI, 99% LAD lesion

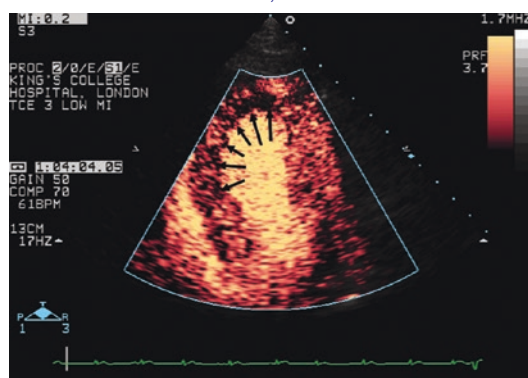


Fig. 23.21 Apical 4 chamber power modulation contrast perfusion image in a patient with an acute anterior myocardial infarction treated with thrombolysis. At the apex a perfusion defect is seen which is almost completely transmural (no-reflow). Whereas the septum demonstrates patchy perfusion and a subendocardial rim of poor perfusion (low-reflow). The patient proceeded acutely to angiography and stenting of a 99% left anterior descending artery lesion

whereas the septum demonstrates patchy perfusion and a subendocardial rim of poor perfusion. The image was obtained >10 beats following destruction and we can see a fairly large perfusion defect that has clearly failed to replenish. We know therefore that there is an extensive area of myocardium at jeopardy, which is unsupported by collaterals. The near transmural extent of the apical defect implies that thrombolysis might have failed to achieve infarct related artery patency (the perfusion defect following successful reperfusion would no longer remain transmural and the perfusion defect would be smaller because of post ischaemic hyperaemia). The patient proceeded acutely to angiography and stenting of a 99% left anterior descending artery lesion. However, it's important to note that in some cases, despite restoration of coronary artery patency either by thrombolysis or PCI, prolonged ischaemia may cause sustained microvascular damage and absence of microvascular perfusion which denotes loss of myocardial cells and necrosis. This is known as the low-reflow or no-reflow syndrome, first introduced by Kolner et al. on animal model in 1974. Ito demonstrated in 1992 that in 25% of their patients with myocardial infarction and no myocardial contrast opacifica-

tion, despite a patent infarct related artery, regional and global LV function were worse at 1 month follow-up, compared to those showing opacification in the infarct bed [30].

To assess residual ischaemia in AMI treated with thrombolysis or PCI, it is sensible to wait at least 48 h before performing resting MCE and 5 days to perform vasodilator MCE. This is because firstly post-ischaemic hyperaemia may result in underestimating the infarct size and secondly post ischemic flow has a dynamic nature and the extent of no reflow phenomenon could change over time [28]. It also may be reasonable to also perform a dobutamine stress if contrast opacification is not seen. Those with persistent no reflow 3–5 days after revascularisation would have an unfavourable prognosis and should have aggressive medical treatment with close follow up [10].

Assessment of collateral flow, as a marker of preservation of viability in untreated recent acute myocardial infarction with an occluded vessel, was another indication of MCE in early years. In the presence of adequate collateral flow, although the subtended region will be replenished with microbubbles, this would be slower owing to slower flow. Sabia et al. showed that adequate collateral flow can maintain myocardial viability and restoring antegrade flow as late as 5 weeks after AMI can improve regional wall motion abnormality [33]. However, regions that do not replenish within 10–15 cardiac cycles have markedly reduced perfusion and unlikely to show improvement in function with revascularisation [28].

Myocardial Viability Studies

As previously explained, the presence of contrast opacification of the myocardium implies an intact coronary microvasculature. Intact coronary microvasculature is a prerequisite for maintaining myocardial viability. When viable myocardium is not present, the microcirculation collapses and therefore contrast opacification will be reduced, patchy or absent. In another word there is an inverse relationship between contrast density and

Contrast and DSE - VE Viability Study

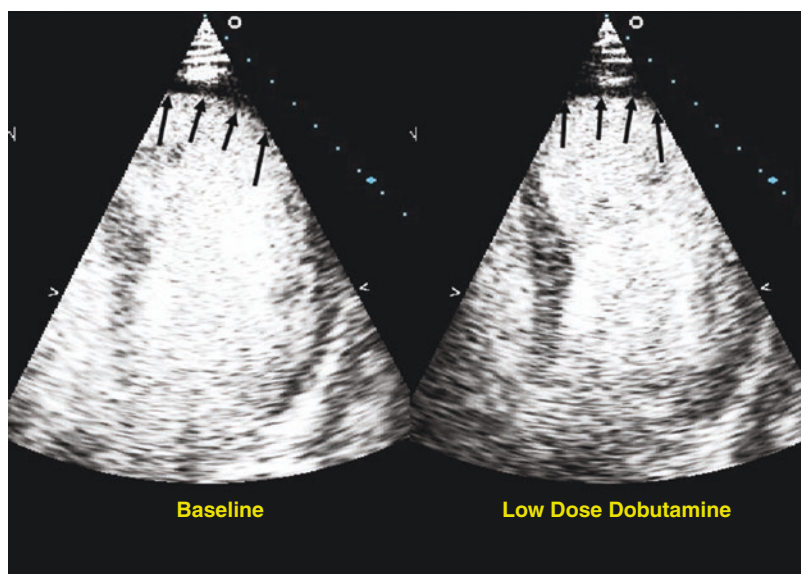


Fig. 23.22 End-systolic parasternal long axis view Apical 4 chamber views at rest (left) and during low dose (20ug/kg/min) dobutamine stress (right) in a patient with extensive anterior myocardial infarction. Simultaneous low-MI contrast perfusion imaging has been performed and demonstrates no contrast opacification in the apical

segments but relatively good opacification of the septum and lateral wall. This implies lack of microvascular integrity in the apical myocardium and this same territory also failed to demonstrate any contractile reserve during low dose dobutamine

collagen content. It's important to note that viability can be maintained in hypokinetic, akinetic and dyskinetic segments in the form of stunned or hibernating myocardium. Stunned myocardium usually follows acute ischaemia (even after reperfusion) and resolves spontaneously whereas hibernating myocardium is associated with coronary artery disease and improves after revascularization [6]. Both qualitative and quantitative stress MCE has been shown to have comparable accuracy to SPECT and dobutamine stress echocardiography for predicting functional recovery in coronary artery disease. An analysis of 20 studies including 738 patients to assess accuracy of MCE in predicting viability yielded sensitivity and specificity of 85% and 70% respectively. In one study specificity of stress MCE was higher than the other two techniques—where MCE-derived myocardial blood flow could detect viability in segments without contractile reserve on dobutamine stress echo study [5].

It's important to note that myocardial blood flow velocities may be very low in akinetic but

viable myocardial segments, therefore it may take >10 beats post destruction for a segment to re-opacify with contrast following destruction. So one should wait for between 10 and 15 beats before making a judgement on microvascular integrity in studying viability in patients with coronary artery disease.

An example of a patient with no opacification in the infarct bed is shown in Fig. 23.22. The lack of microvascular integrity in this thin infarct bed implies no myocardial viability. A low-dose dobutamine study confirmed lack of contractile reserve in the same area and revascularisation of an occluded left anterior descending lesion was not attempted. In Fig. 23.23, late opacification of the distal akinetic septum was seen in this patient with previous antero-septal infarction. Follow-up echo studies post revascularisation demonstrated a significant improvement in wall motion. Although this patient also had a low dose dobutamine stress echo to demonstrate contractile reserve, the demonstration of viability by contrast really made this superfluous.

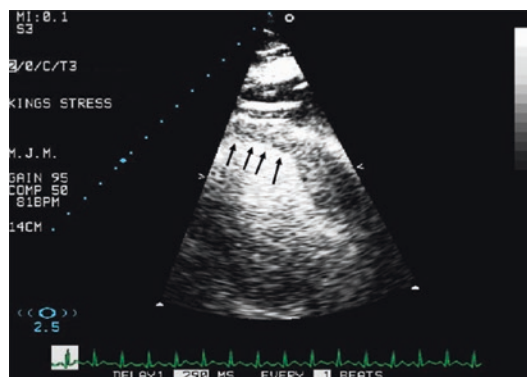


Fig. 23.23 End-systolic parasternal long axis view during low-MI contrast perfusion imaging in a patient with an antero-septal infarct. The distal septum is thin compared to the basal septum and it was akinetic however it did opacify late with contrast, implying microvascular integrity. Furthermore, subsequent low dose dobutamine stress study demonstrated contractile reserve in this territory. PCI was performed to a high grade proximal left anterior descending artery lesion and a follow-up echocardiogram at 2 months demonstrated only minor antero-apical hypokinesia

Stress MCE can also be used to differentiate the ischaemic versus non-ischaemic cause of heart failure, when history and presentation is not suggestive of the former [34] and in presence of CAD, it can answer the important question of viability.

Cost, accessibility, spatial resolution, lack of ionising radiation and the fact that MCE is a bedside technique confers many advantages over more traditional methods of detecting coronary artery disease and assessing viability. There is a wealth of data supporting the diagnostic and prognostic utility of MCE. Stress MCE has been recommended in European guidelines in assessment of stable coronary artery disease [35] however, its clinical uptake remains as low as 10% in United Kingdom [36]. As described earlier more recent inconsistent reports of sensitivity and specificity of MCE to identify coronary artery disease has prevented this technique overcoming the complex regulatory body rules such as US Food and Drug Administration (FDA) for approval and its use remains off label in North America. Further work on the contrast microbubbles, integration of quantitative wall motion analysis into MCE and adjustment of microbubble

infusion based on weight and opacification, is needed [26].

Safety of Ultrasound Contrast Agents

In October 2007, FDA issued a box warning for ultrasound contrast agents, which resulted in multiple contraindications including unstable patients such as those with respiratory failure, worsening heart failure, unstable angina and acute myocardial infarction as well as severe pulmonary hypertension. This was following a report of four deaths and a number of cardiorespiratory adverse incidents, which had occurred during or after administration of contrast agents [37]. Subsequent studies in response to FDA warning showed no causal relationship between the reported adverse events and contrast use. In fact mortality in critically ill patients who had undergone contrast injection was lower in a large registry [38]. It's likely that the majority of reported advert events resulting in the FDA warning were due to the underlying serious disease than the contrast [37]. There is also sufficient evidence that supports the safety of ultrasound contrast agents in pulmonary hypertension patients [39, 40]. Although a 'black box' warning still exists, aforementioned contraindications no longer apply [41]. The risk of ultrasound contrast agents seems small, and considerably less than the risk of inadequate cardiac function assessment from failure to use contrast agents in critically ill patients [12]. However one small but serious adverse effect i.e. anaphylactic shock remains of concern. The risk has been reported as low as 1:10,000 and been attributed to direct activation of complements [41]. When detected and treated promptly the overall anaphylaxis prognosis is good however a significant portion of cases undergoing ultrasound contrast study are those with underlying severe cardiopulmonary disease which puts them at higher risk. Therefore, the individuals involved in ultrasound contrast studies should have formal training in detecting and treatment of anaphylactic reaction. Resuscitation equipment and drugs including allergy kit should

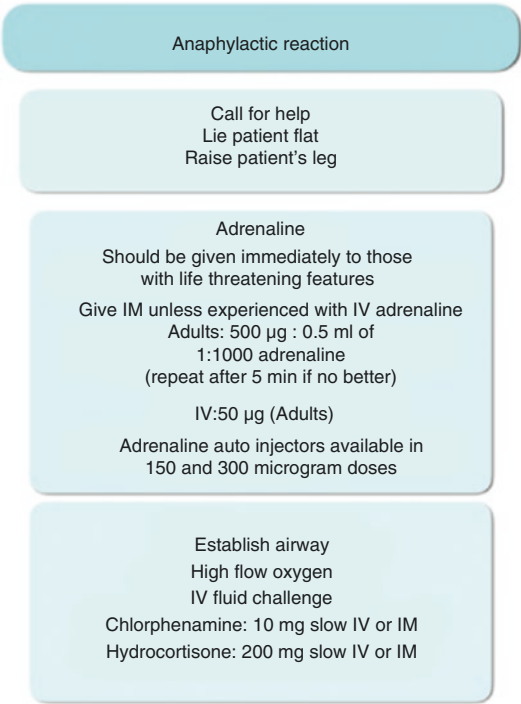


Fig. 23.24 Suggested algorithm for treatment of anaphylactic reaction, modified from Resuscitation Council UK guideline

be available for immediate use and should be checked regularly (Fig. 23.24).

Whilst presence of right to left shunt remains a contraindication by FDA, large reviews have failed to show the link between ultrasound contrast agents and embolization. Since the prevalence of PFO can be as high as 35%, use of ultrasound contrast agents in small PFO (with small right to left shunt) is not contraindicated in major society guidelines [7].

A list of common minor side effects of different contrast agents is summarised in Table 23.4.

Future of Contrast Echocardiography

Therapeutic Applications and Molecular Imaging

An interesting and very promising use of ultrasound contrast agents appear to be in the area of

Table 23.4 Most frequent minor side effects of ultrasound contrast agents in clinical trials [10]

Agent	Side effects
Optison	Headache (5.4%), nausea and/or vomiting (4.3%), warm sensation or flushing (3.6%), dizziness (2.5%)
Sonovue	Headache (2.1%), nausea (1.3%), chest pain (1.3%), taste perversion (0.9%), hyperglycaemia (0.6%), injection site reaction (0.6%), paresthesia (0.6%), vasodilation (0.6%), injection site pain (0.5%)
Definity	Headache (2.3%), flushing (1.1%), back pain (1.2%), Nausea (1.0%)
Sonazoid	Headache (1%), diarrhea (1%)

drug delivery or molecular imaging. When a contrast microbubble is destroyed by ultrasound it appears that extreme shear forces are created around the bubble. These shear forces may open up pores in the vessel endothelium and/or cell membrane. If a drug is attached to the bubble by binding, electrostatic charge or by incorporating it within the bubble structure then it has been shown bubble disruption significantly enhances transfection of the carried material into the vessel wall or cell matrix. This has the potential of allowing high concentration local delivery of drugs or genes to a specific area of interest in an organ, without exposing the whole body to potentially toxic levels of the material. Contrast microbubbles can be designed to have a critical fragility so that they can be visualised in the circulation at a low MI or certain imaging frequency without destruction. Then they can be destroyed/disrupted at a desired location by applying one or more focussed ultrasound beams, which have a power or frequency designed to exceed the bubble fragility limit.

Sonothrombolysis

Contrast microbubbles have been used to enhance the delivery of thrombolytic agents to occlusive clot in embolic stroke. The technique has been shown to be superior in more complete recanalization in a number of clinical studies. To minimise operator dependency, an operator independent 2 MHz trans cranial Doppler device is under investigation at the time of writing [42].

Molecular Imaging

This will need microbubbles that are designed specifically such that they carry ligands. These ligands can bind to specific sites on the vessel wall, to unregulated receptors on endothelial cells and to atherosclerotic plaques [2]. Potential applications of this technology include cancer treatment, stem cell treatment and angiogenesis, ischaemia, reperfusion injury, transplant rejection and inflammatory diseases. There are commercially available targeted contrast agents however studies in these areas are in preclinical setting.

3D Contrast Studies

Real time 3D echocardiography offers significant advantages in the analysis of the left ventricular volumes, ejection fraction, regional wall motion and shape over conventional 2D echo techniques. However, 3D echocardiography suffers from the same degradations in image quality that beset 2D echocardiography. In particular, lung and rib artefacts can significantly degrade endocardial definition on 3D studies. Contrast agents can improve 3D image quality and endocardial definition to the same extent that they improve 2D images. However, since “whole volume” 3D images are usually acquired over several cardiac cycles, it is preferable to use a contrast infusion rather than a bolus.

Real time 3D echocardiography has been used as a useful technique during stress echocardiography as it offers full volume image acquisition in one or two transducer position and overcomes LV foreshortening. It is currently used as an adjunctive technique to 2D stress echocardiography, however with ongoing advances in 3D echocardiography, there is the potential for the technique to become an independent and superior modality to 2D stress echocardiography. Again contrast is proving to be an invaluable tool to enhance analysis of wall motion and thickening during these studies.

Preliminary attempts to demonstrate myocardial perfusion using real-time 3D echo have been extremely encouraging, although this remains a research technique at the time of writing. The

potential of being able to calculate precisely, in 3D, infarct size and the volume of ischaemic myocardium etc. is very exciting [43]. Several ultrasound system vendors have incorporated contrast specific imaging modalities, as previously described, into their 3D imaging systems. However, one of the current main limiting factors is the frame (volume) rate, which is low compared to 2D imaging. It is likely that that this limitation will be overcome in the future.

Conclusion

Contrast echocardiography has proved itself an invaluable technique for the enhancement of endocardial borders in patients with suboptimal images and during stress studies. It has also been shown, in several studies, to reduce the need for further investigations in patients with poor echo windows and therefore is highly cost-effective. In addition, the delineation of intra-cardiac masses and the enhancement of cardiac Doppler signals are also proving important applications, although not as widely used. However, the major clinical utility of ultrasound contrast agents in the heart is in the evaluation of myocardial perfusion. Whether used for demonstrating reversible ischaemia, myocardial viability or following acute myocardial infarction, contrast agents can significantly enhance diagnosis at the bedside, and positively influence patient management.

References

1. Gramiak R, Shah PM. Echocardiography of the aortic root. *Invest Radiol.* 1968;3(5):356–66.
2. Faez T, Emmer M, Kooiman K, Versluis M, van der Steen A, de Jong N. 20 years of ultrasound contrast agent modeling. *IEEE Trans Ultrason Ferroelectr Freq Control.* 2013;60(1):7–20.
3. Wei K, Jayaweera AR, Firoozan S, Linka A, Skyba DM, Kaul S. Quantification of myocardial blood flow with ultrasound-induced destruction of microbubbles administered as a constant venous infusion. *Circulation.* 1998;97(5):473–83.
4. Powers J, Porter TR, Wilson S, Averkiou M, Skyba D, Bruce M. Ultrasound contrast imaging. *Medicamundi.* 2000;44(2):28–36.

5. Porter TR, Xie F. Myocardial perfusion imaging with contrast ultrasound. *JACC Cardiovasc Imaging*. 2010;3(2):176–87.
6. Moir S, Marwick TH. Combination of contrast with stress echocardiography: a practical guide to methods and interpretation. *Cardiovasc Ultrasound*. 2004;2:15.
7. Porter TR, Abdelmoneim S, Belcik JT, McCulloch ML, Mulvagh SL, Olson JJ, et al. Guidelines for the cardiac sonographer in the performance of contrast echocardiography: a focused update from the American Society of Echocardiography. *J Am Soc Echocardiogr*. 2014;27(8):797–810.
8. EACVI Toolboxes, European Association of Cardiovascular Imaging: European Society of Cardiology. [cited 2016]. Available from: <https://www.escardio.org/Guidelines-&-Education/Practice-tools/EACVI-toolboxes/Contrast-Echo/Sonovue-contrast-agent>.
9. Mulvagh SL, Rakowski H, Vannan MA, Abdelmoneim SS, Becher H, Bierig SM, et al. American Society of Echocardiography consensus statement on the clinical applications of ultrasonic contrast agents in echocardiography. *J Am Soc Echocardiogr*. 2008;21(11):1179–201.
10. Senior R, Becher H, Monaghan M, Agati L, Zamorano J, Vanoverschelde JL, et al. Contrast echocardiography: evidence-based recommendations by European Association of Echocardiography. *Eur J Echocardiogr*. 2009;10(2):194–212.
11. Picard MH, Adams D, Bierig SM, Dent JM, Douglas PS, Gillam LD, et al. American Society of Echocardiography recommendations for quality echocardiography laboratory operations. *J Am Soc Echocardiogr*. 2011;24(1):1–10.
12. Kurt M, Shaikh KA, Peterson L, Kurrelmeyer KM, Shah G, Nagueh SF, et al. Impact of contrast echocardiography on evaluation of ventricular function and clinical management in a large prospective cohort. *J Am Coll Cardiol*. 2009;53(9):802–10.
13. Marwick TH, Narula J. Contrast echocardiography: over-achievement in research, under-achievement in practice? *JACC Cardiovasc Imaging*. 2010;3(2):224–5.
14. Johri AM, Picard MH, Newell J, Marshall JE, King ME, Hung J. Can a teaching intervention reduce interobserver variability in LVEF assessment: a quality control exercise in the echocardiography lab. *JACC Cardiovasc Imaging*. 2011;4(8):821–9.
15. Stratton JR, Lighty GW Jr, Pearlman AS, Ritchie JL. Detection of left ventricular thrombus by two-dimensional echocardiography: sensitivity, specificity, and causes of uncertainty. *Circulation*. 1982;66(1):156–66.
16. Kirkpatrick JN, Wong T, Bednarz JE, Spencer KT, Sugeng L, Ward RP, et al. Differential diagnosis of cardiac masses using contrast echocardiographic perfusion imaging. *J Am Coll Cardiol*. 2004;43(8):1412–9.
17. Lepper W, Shivalkar B, Rinkevich D, Belcik T, Wei K. Assessment of the vascularity of a left ventricular mass using myocardial contrast echocardiography. *J Am Soc Echocardiogr*. 2002;15(11):1419–22.
18. Mansencal N, Revault-d'Allonnes L, Pelage JP, Farcot JC, Lacombe P, Dubourg O. Usefulness of contrast echocardiography for assessment of intracardiac masses. *Arch Cardiovasc Dis*. 2009;102(3):177–83.
19. Plana JC, Mikati IA, Dokainish H, Lakkis N, Abukhalil J, Davis R, et al. A randomized cross-over study for evaluation of the effect of image optimization with contrast on the diagnostic accuracy of dobutamine echocardiography in coronary artery disease: the OPTIMIZE trial. *JACC Cardiovasc Imaging*. 2008;1(2):145–52.
20. Bednarz J, Waggoner A, Moos S, Witt SA, McCulloch M, Sisk E, et al. Myocardial contrast echocardiography: a series on contrast echocardiography, article 5. *J Am Soc Echocardiogr*. 2002;15(10):1111–9.
21. Leong-Poi H, Rim SJ, Le DE, Fisher NG, Wei K, Kaul S. Perfusion versus function: the ischemic cascade in demand ischemia: implications of single-vessel versus multivessel stenosis. *Circulation*. 2002;105(8):987–92.
22. Marwick TH. Assessment of subendocardial function with myocardial contrast echocardiography. *JACC Cardiovasc Imaging*. 2008;1(3):279–81.
23. Salerno M, Beller GA. Noninvasive assessment of myocardial perfusion. *Circ Cardiovasc Imaging*. 2009;2(5):412–24.
24. Shah BN, Gonzalez-Gonzalez AM, Drakopoulou M, Chahal NS, Bhattacharyya S, Li W, et al. The incremental prognostic value of the incorporation of myocardial perfusion assessment into clinical testing with stress echocardiography study. *J Am Soc Echocardiogr*. 2015;28(11):1358–65.
25. Dijkman PA, Senior R, Becher H, Porter TR, Wei K, Visser CA, et al. Myocardial contrast echocardiography evolving as a clinically feasible technique for accurate, rapid, and safe assessment of myocardial perfusion: the evidence so far. *J Am Coll Cardiol*. 2006;48(11):2168–77.
26. Thomas JD. Myocardial contrast echocardiography perfusion imaging: still waiting after all these years. *J Am Coll Cardiol*. 2013;62(15):1362–4.
27. Senior R, Moreo A, Gaibazzi N, Agati L, Tiemann K, Shivalkar B, et al. Comparison of sulfur hexafluoride microbubble (SonoVue)-enhanced myocardial contrast echocardiography with gated single-photon emission computed tomography for detection of significant coronary artery disease: a large European multicenter study. *J Am Coll Cardiol*. 2013;62(15):1353–61.
28. Hayat SA, Senior R. Myocardial contrast echocardiography in ST elevation myocardial infarction: ready for prime time? *Eur Heart J*. 2008;29(3):299–314.
29. Ragosta M, Camarano G, Kaul S, Powers ER, Sarembock IJ, Gimple LW. Microvascular integrity indicates myocellular viability in patients with recent myocardial infarction. New insights using myocardial contrast echocardiography. *Circulation*. 1994;89(6):2562–9.
30. Ito H, Tomooka T, Sakai N, Yu H, Higashino Y, Fujii K, et al. Lack of myocardial perfusion immediately after successful thrombolysis. A predictor of

- poor recovery of left ventricular function in anterior myocardial infarction. *Circulation*. 1992;85(5):1699–705.
31. Jain M, Upadaya S, Zarich SW. Serial evaluation of microcirculatory dysfunction in patients with Takotsubo cardiomyopathy by myocardial contrast echocardiography. *Clin Cardiol*. 2013;36(9):531–4.
 32. Khumri TM, Nayyar S, Idupulapati M, Magalski A, Stoner CN, Kusnetzky LL, et al. Usefulness of myocardial contrast echocardiography in predicting late mortality in patients with anterior wall acute myocardial infarction. *Am J Cardiol*. 2006;98(9):1150–5.
 33. Sabia PJ, Powers ER, Ragosta M, Sarembock IJ, Burwell LR, Kaul S. An association between collateral blood flow and myocardial viability in patients with recent myocardial infarction. *N Engl J Med*. 1992;327(26):1825–31.
 34. Senior R, Janardhanan R, Jeetley P, Burden L. Myocardial contrast echocardiography for distinguishing ischemic from nonischemic first-onset acute heart failure: insights into the mechanism of acute heart failure. *Circulation*. 2005;112(11):1587–93.
 35. Task Force M, Montalescot G, Sechtem U, Achenbach S, Andreotti F, Arden C, et al. 2013 ESC guidelines on the management of stable coronary artery disease: the task force on the management of stable coronary artery disease of the European Society of Cardiology. *Eur Heart J*. 2013;34(38):2949–3003.
 36. Bhattacharyya S, Chehab O, Khattar R, Lloyd G, Senior R. British Society of E. Stress echocardiography in clinical practice: a United Kingdom National Health Service Survey on behalf of the British Society of Echocardiography. *Eur Heart J Cardiovasc Imaging*. 2014;15(2):158–63.
 37. Main ML, Goldman JH, Grayburn PA. Thinking outside the “box”—the ultrasound contrast controversy. *J Am Coll Cardiol*. 2007;50(25):2434–7.
 38. Main ML, Hibberd MG, Ryan A, Lowe TJ, Miller P, Bhat G. Acute mortality in critically ill patients undergoing echocardiography with or without an ultrasound contrast agent. *JACC Cardiovasc Imaging*. 2014;7(1):40–8.
 39. Main ML, Grayburn PA, Lang RM, Goldman JH, Gibson CM, Sherwin P, et al. Effect of Optison on pulmonary artery systolic pressure and pulmonary vascular resistance. *Am J Cardiol*. 2013;112(10):1657–61.
 40. Wever-Pinzon O, Suma V, Ahuja A, Romero J, Sareen N, Henry SA, et al. Safety of echocardiographic contrast in hospitalized patients with pulmonary hypertension: a multi-center study. *Eur Heart J Cardiovasc Imaging*. 2012;13(10):857–62.
 41. Main ML. Contrast echocardiography: safety in numbers. *Cardiology*. 2012;122(4):248–50.
 42. Tsvigoulis G, Alleman J, Katsanos AH, Barreto AD, Kohrmann M, Schellinger PD, et al. Comparative efficacy of different acute reperfusion therapies for acute ischemic stroke: a comprehensive benefit-risk analysis of clinical trials. *Brain Behav*. 2014;4(6):789–97.
 43. Bhan A, Kapetanakis S, Rana BS, Ho E, Wilson K, Pearson P, et al. Real-time three-dimensional myocardial contrast echocardiography: is it clinically feasible? *Eur J Echocardiogr*. 2008;9(6):761–5.

Part VI

Cardiomyopathy and Heart Failure

The Cardiomyopathies

24

Petros Nihoyannopoulos and Perry Elliott

Introduction

Cardiomyopathies are a diverse group of conditions characterised by structural and functional abnormalities of the heart muscle that are unexplained by coronary artery disease, hypertension or valve disease [1]. They are grouped into morphological and functional phenotypes, each of which can be caused by genetic and non-genetic mechanisms (Table 24.1). Most genetic cardiomyopathies are monogenic disorders (i.e. the genetic mutation is sufficient to cause disease), but they can appear sporadic when a mutation has arisen de novo. Non-familial or non-genetic cardiomyopathies are subdivided into idiopathic (no identifiable cause) and acquired disorders in which ventricular dysfunction is a complication of a disorder unrelated to a primary disturbance of cardiomyocyte function. Examples of the latter include cardiac amyloidosis, haemochromatosis and myocarditis. By convention, left ventricular dysfunction caused by coronary artery disease,

hypertension, valve disease and congenital heart disease is excluded from the term cardiomyopathy, although they can coexist.

Hypertrophic Cardiomyopathy

Definitions

Hypertrophic cardiomyopathy (HCM) is a clinical diagnosis based on the demonstration of increased left ventricular wall thickness unexplained solely by abnormal cardiac loading conditions [1, 2] (Fig. 24.1). In most adolescents and adults, HCM is an autosomal dominant trait caused by mutations in cardiac sarcomere protein genes [2, 3]. In less than 10% of infants and children and a smaller proportion of adults, HCM is caused by inborn errors of metabolism, neuromuscular disorders and malformation syndromes [2–4].

Pathology

The gross pathology of HCM is characterised by ventricular hypertrophy involving predominantly the left ventricle, but also the right ventricle in a significant number of patients (Fig. 24.2) [5, 6]. The hypertrophy can be either asymmetrical, that is, a difference in maximal thickness of ventricular septum and posterior wall, or concentric equally involving the entire left ventricle, or

P. Nihoyannopoulos (✉)
Imperial College London, Hammersmith Hospital,
London, UK
e-mail: petros@imperial.ac.uk

P. Elliott
University College London, London, UK
UCL Institute of Cardiovascular Science,
London, UK

Barts Heart Centre, St. Bartholomew's Hospital,
London, UK

Table 24.1 Examples of different diseases that cause cardiomyopathies^a

	HCM	DCM	ARVC	RCM	UNCLASSIFIED
Familial	<p><i>Familial, unknown gene</i></p> <p><i>Sarcomeric protein disease</i></p> <ul style="list-style-type: none"> • β myosin heavy chain Cardiac myosin binding protein C Cardiac troponin I Troponin-T α-tropomyosin Essential myosin light chain Regulatory myosin light chain Cardiac actin α-myosin heavy chain Titin Troponin C <p><i>Glycogen storage disease</i></p> <p>(e.g. GSD II (Pompe's disease); GSD III (Forbes' disease), AMP kinase (WPW, HCM, conduction disease))</p> <p><i>Lysosomal storage diseases</i></p> <p>(e.g. Anderson-Fabry disease, Hurler's syndrome)</p> <p><i>Disorders of fatty acid metabolism</i></p> <p><i>Carnitine deficiency</i></p> <p><i>Phosphorylase B kinase deficiency</i></p> <p><i>Mitochondrial cytopathies</i></p> <p>(e.g. MELAS, MERFF, LHON)</p> <p><i>Syndromic HCM</i></p> <ul style="list-style-type: none"> • Noonan's syndrome • LEOPARD syndrome • Friedrich's ataxia • Beckwith-Wiedemann syndrome • Swyer's syndrome (pure gonadal dysgenesis) <p><i>Other:</i></p> <ul style="list-style-type: none"> • Muscle LIM protein • Phospholamban promoter • Familial amyloid 	<p><i>Familial, unknown gene</i></p> <p><i>Sarcomeric protein mutations</i></p> <p>(see HCM)</p> <p>Z band:</p> <p>Cypher/Zasp</p> <p>Muscle LIM protein</p> <p>TCAP</p> <p><i>Cytoskeletal genes:</i></p> <ul style="list-style-type: none"> • Dystrophin • Desmin • Metavinculin • Sarcoglycan complex • CRYAB • Epicardin <p><i>Nuclear membrane</i></p> <ul style="list-style-type: none"> • Lamin A/C • Emerin <p><i>Intercalated disc protein mutations</i></p> <p>(see ARVC)</p> <p><i>Mitochondrial cytopathy</i></p>	<p><i>Familial, unknown gene</i></p> <p><i>Intercalated disc protein mutations</i></p> <ul style="list-style-type: none"> • Plakoglobin • Desmoplakin • Plakophilin 2 • Desmoglein 2 • Desmocollin 2 <p><i>Cardiac ryanodine receptor (RyR2)</i></p> <p><i>Transforming growth factor-β3 (TGFβ3)</i></p>	<p><i>Familial, unknown gene</i></p> <p><i>Sarcomeric protein mutations:</i></p> <ul style="list-style-type: none"> • Troponin I (RCM \pm HCM) • Essential light chain of myosin • Locus 10q23.3 <p><i>Familial amyloidosis</i></p> <ul style="list-style-type: none"> • Transthyretin (RCM + neuropathy) • Apolipoprotein (RCM + nephropathy) <p><i>Desminopathy</i></p> <p><i>Pseuxanthoma elasticum</i></p> <p><i>Haemochromatosis</i></p> <p><i>Anderson-Fabry disease</i></p> <p><i>Glycogen storage disease</i></p> <p><i>Endomyocardial fibrosis (familial)</i></p> <ul style="list-style-type: none"> • (Fusion FIP1-like-1/PDGFRα genes) 	<p><i>Left ventricular non-compaction:</i></p> <ul style="list-style-type: none"> • Barth syndrome • Lamin A/C • ZASP • α-dystrobrevin

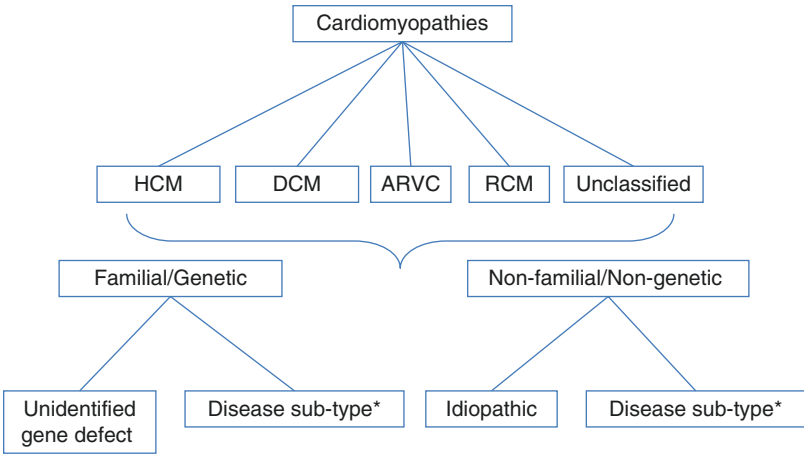
Table 24.1 (continued)

	HCM	DCM	ARVC	RCM	UNCLASSIFIED
Non-Familial	<i>Obesity</i> <i>Infants of diabetic mothers</i> <i>Athletic training</i> <i>Amyloid (AL/prealbumin)</i>	<i>Myocarditis (infective/toxic/immune)</i> <i>Kawasaki disease</i> <i>Eosinophilic (Churg Strauss syndrome)</i> <i>Viral persistence</i> <i>Drugs</i> <i>Pregnancy</i> <i>Endocrine</i> <i>Nutritional—</i> Thiamine, carnitine, selenium, hypophosphataemia, hypocalcaemia. <i>Alcohol</i> <i>Tachycardiomyopathy</i>	Inflammation?	<i>Amyloid (AL/prealbumin)</i> <i>Scleroderma</i> <i>Endomyocardial fibrosis</i> <ul style="list-style-type: none"> • Hypereosinophilic syndrome • Idiopathic • Chromosomal cause • Drugs: (serotonin, methysergide, ergotamine, mercurial agents, busulfan) <i>Carcinoid heart disease</i> <i>Metastatic cancers</i> <i>Radiation</i> <i>Drugs: Anthracyclines</i>	<i>Tako Tsubo Cardiomyopathy</i>

^aData from Elliott et al. [1]

ARVC arrhythmogenic right ventricular cardiomyopathy, DCM dilated cardiomyopathy, HCM hypertrophic cardiomyopathy, RCM restrictive cardiomyopathy

Fig. 24.1 Classification of cardiomyopathies



distal, affecting predominantly the cardiac apex (Fig. 24.3). The hypertrophy frequently becomes manifest during puberty, although some rare cases of HCM are seen in infancy.

The papillary muscles are often displaced anteriorly and may have abnormal insertion into the mitral valve. There is often an area of endocardial fibrosis on the septum beneath the aortic

valve caused by repeated contact with the anterior leaflet of mitral valve. The mitral valve itself is often structurally abnormal with an elongated anterior mitral valve leaflet.

Histologically, familial HCM is characterised by a triad of myocyte hypertrophy, myocyte disarray (disorganisation of the myocardium with adjacent myocytes aligned obliquely or



Fig. 24.2 Gross pathology of a patient with hypertrophic cardiomyopathy. Notice the marked amount of hypertrophy involving the entire heart

perpendicular to each other) and interstitial fibrosis [5, 6]. Although myocyte disarray occurs in many diseases, extensive disarray (more than 10% of the ventricular myocardium) is generally considered to be a highly specific marker for HCM. Small intramural coronary arteries are often dysplastic and narrowed due to thickening caused by smooth muscle cell medial wall hyperplasia (Fig. 24.4). When HCM is caused by an underlying systemic disorder, other features such as glycogen storage or amyloid infiltration will be evident.

Pathophysiology

The functional abnormalities seen in HCM include a high ejection fraction of 80–100% caused by the small left ventricular cavity. The



Fig. 24.3 Cross sectional section from a patient with hypertrophic cardiomyopathy demonstrating the amount of fibrosis (white areas in the middle of the myocardium)

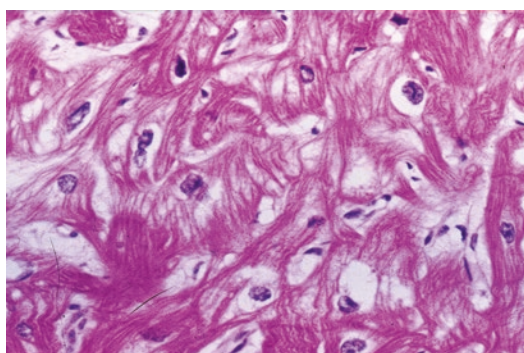


Fig. 24.4 Histology of the myocardium demonstrating the amount of abnormal fiber arrangement

powerful radial contraction and complete emptying of the ventricle often occurs in association with intraventricular pressure gradients [7, 8]. When the gradient is subaortic it occurs in association with a systolic anterior movement of the mitral valve. Gradients may be persistent (gradient at rest), labile (spontaneously variable), or appear only on provocation (latent). Although initially HCM was thought to be mainly a disorder of left ventricular systolic function, it is now widely appreciated that the main problem is in diastole with abnormal passive and active phase of diastole. Myocardial hypertrophy and fibrosis contribute to impaired passive filling of the ventricles.

Diagnosis

The diagnosis is based on the presence of left ventricular wall thickness ≥ 15 mm (at end-diastole) in ≥ 1 LV myocardial segments unexplained solely by abnormal cardiac loading conditions [2].

Symptoms of dyspnoea, chest pain, dizziness or syncope can lead to a discovery of HCM but they are present in only half of all patients. In the remainder, particularly in children and adolescents, the diagnosis is made as the result of family screening or following the discovery of a murmur or electrocardiographic evidence of left ventricular hypertrophy. When present, symptoms are typically variable and often exacerbated by exercise, large meals or alcohol.

In patients with left ventricular outflow obstruction, clinical examination often reveals an ejection systolic murmur and a pansystolic murmur of mitral regurgitation that increase with reducing LV load (Valsalva, standing from squat). In patients with rare phenocopies, various non-cardiac abnormalities can suggest a specific cause [9]. Specific features to note in the family history include sudden cardiac death (SCD), unexplained heart failure, cardiac transplantation, pacemaker and implantable cardiac defibrillator (ICD) implants, and evidence for systemic disease (stroke at a young age, skeletal muscle weakness, renal dysfunction, etc.).

The ECG abnormal in most patients and is often the first investigation that leads to a suspicion of HCM because it shows left ventricular hypertrophy (Fig. 24.5). Abnormal QRS axis and deep Q or inverted T waves in the setting of ventricular hypertrophy are strongly suggestive of HCM.

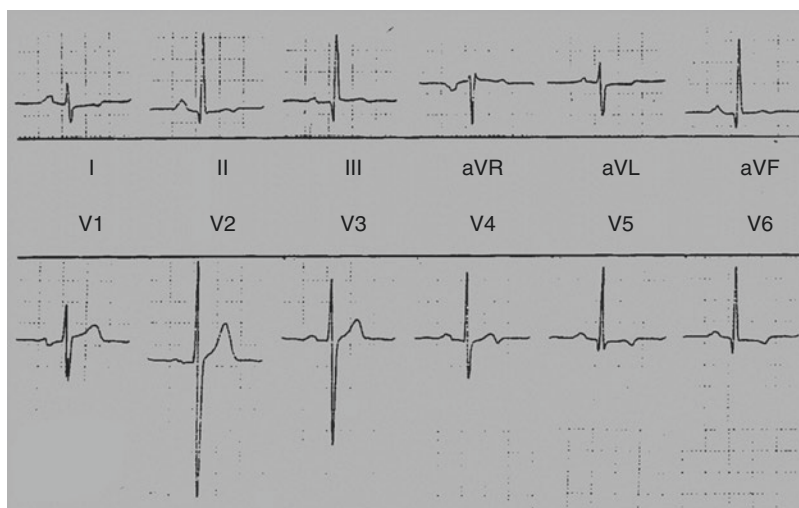
The Role of Echocardiography

The diagnosis of HCM requires the demonstration of left ventricular hypertrophy. Echocardiography however should play a supportive role to the clinical diagnosis of HCM, as the diagnosis of the condition is clinical and requires the systematic search for causes of left ventricular hypertrophy.

The original M-mode recording techniques were invaluable in describing the early diagnostic criteria for HCM. Those were:

1. the presence of asymmetric hypertrophy of the ventricular septum (ASH), defined as the ratio of septal and posterior left ventricular wall thickness at end-diastole been equal or greater than 1.3 cm.
2. the systolic anterior motion of the mitral valve (SAM)
3. the premature, mid-systolic closure of the aortic valve in the presence of a small and vigorously contracting left ventricle (Fig. 24.6).

Fig. 24.5 A typical electrocardiogram from a hypertrophic cardiomyopathy patient demonstrating voltage criteria for ventricular hypertrophy, mainly in the septal leads, Q-waves inferiorly as well as abnormal repolarisation



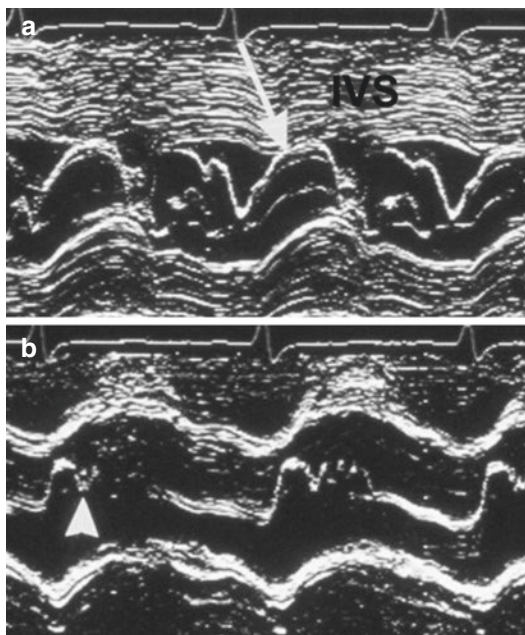


Fig. 24.6 A representative M-mode echocardiogram from a patient with hypertrophic cardiomyopathy highlighting the four main echocardiographic features of the condition. (a) mid-systolic closure of the aortic valve (arrowhead), (b) systolic anterior motion of the mitral valve (arrow) and asymmetric left ventricular hypertrophy together with a small, vigorously contracting left ventricle

An inherent disadvantage of M-mode echocardiography is that only a small portion of the left ventricle can be examined at a time with a single ultrasound beam, usually passing through the anterior septum and posterior wall. Patients with HCM however, may show a wide distribution of hypertrophy.

Two-dimensional echocardiography shows anatomic sections of the heart so that the true size and shape of the valves and cavities can be appreciated. ASH, SAM and mid-systolic closure of the aortic valve are not pathognomonic of HCM, as each one can also occur in a variety of other conditions with no common pathophysiologic mechanism. The presence of ASH is no longer a prerequisite for the diagnosis of HCM. Conditions such as systemic hypertension, athlete's heart or even aortic stenosis can cause the ventricular septum to appear thicker than the left ventricular free wall and conversely, in many patients with HCM the septum

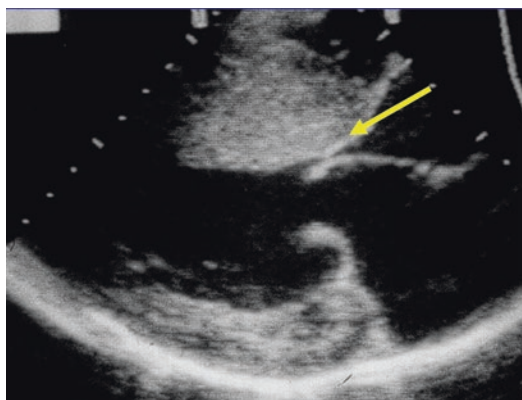


Fig. 24.7 Two-dimensional echocardiogram of the parasternal long-axis view of the left ventricle in diastole showing marked ventricular septal hypertrophy, small end-diastolic dimensions (41 mm). Note that the mitral valve is impinging the ventricular septum (arrow). At the point of contact with the ventricular septum the anterior mitral leaflet and the endocardial surface of the septum are more echogenic implying fibrosis

and the free wall may be of similar thickness (concentric hypertrophy).

The parasternal long-axis view is important in the visualisation of the ventricular septum, the left ventricular outflow tract and the mitral valve and its subvalvular apparatus (Fig. 24.7). It is the view of choice for the visualisation of S.A.M. of the mitral valve and mid-systolic closure of the aortic valve. It is important to obtain simultaneous M-mode and two-dimensional echocardiographic recordings of the mitral and aortic valve motion since M-mode provides a better temporal resolution and two-dimensional echocardiography better spatial resolution. High frequency phenomena, such as S.A.M. and mid-systolic closure of the aortic valve, can then be better appreciated and analysed. Left ventricular measurements can also be obtained from the parasternal long-axis view under simultaneous two-dimensional echocardiographic control to ensure that the M-mode beam line transects the left ventricle perpendicularly.

Parasternal short axis-view is useful to localize and describe the extent of ventricular hypertrophy (Fig. 24.8). Serial parasternal short-axis views are crucial for the definition of the extent and shape of left ventricular hypertrophy. They provide the opportunity to

determine whether segmental hypertrophy exists in other areas of the left ventricle, such as the posterior septum, anterolateral free wall and posterolateral free wall. The cross-sectional view at the left ventricular base, shows the mitral valve in the left ventricular cavity. The mid-portion shows the two papillary muscles; the postero-medial to the left and the



Fig. 24.8 Short-axis parasternal view of a HCM patient with marked septal hypertrophy and normal posterior wall at mid-ventricular level

antero-lateral to the right of the image. The cross-sectional view of the apex shows the left ventricle in circular orientation.

From these serial short axis views the left ventricle can be divided into four segments at mitral and papillary muscle level and two at the apex, so that the anterior, lateral inferior and posterior septal walls can be measured (Fig. 24.9). Thus, by combining the parasternal long- and short-axis views, the left ventricular walls can be examined comprehensively and the localisation and extent of ventricular hypertrophy can be fully described. Echocardiographic imaging of the right ventricle is also important, as approximately one third of patients with HCM may have right ventricular hypertrophy.

Echocardiographically, HCM is a condition characterised by:

1. *hypertrophy of all (concentric) or portion of the walls of the left ventricle, that is, ventricular septum (asymmetric), or apex (distal);*
2. *dilated left atrium*
3. *small, non-dilated ventricles*

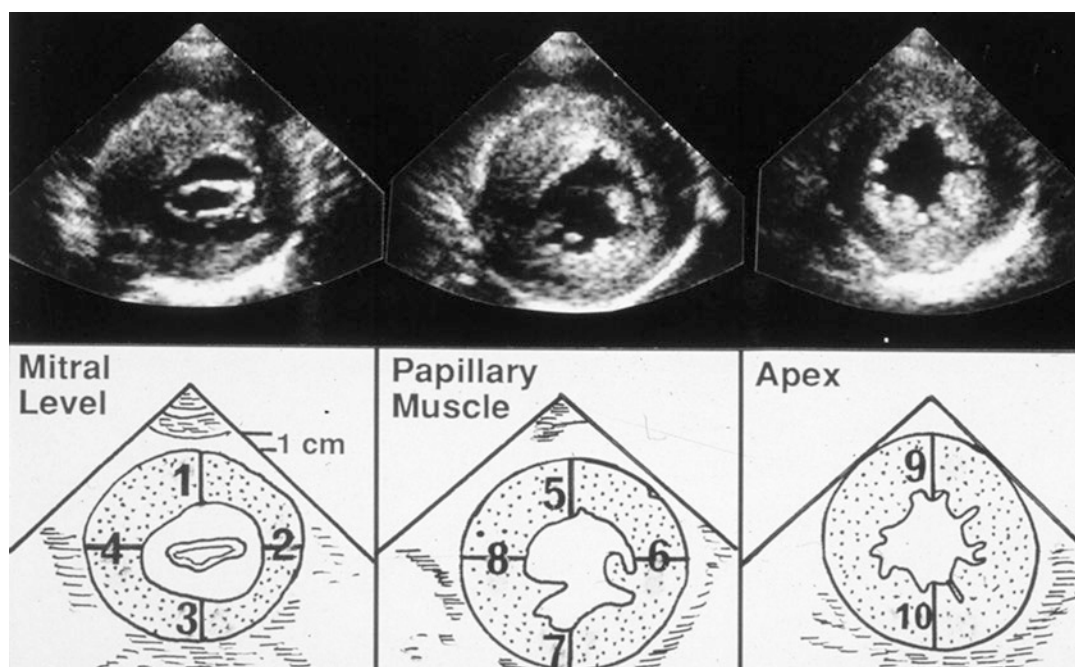


Fig. 24.9 Serial short-axis, cross-sectional views of the left ventricle at mitral valve, papillary muscles level and apex, demonstrating the segments of myocardial wall measured routinely in patients with hypertrophic cardiomyopathy

4. *absence of any other cardiac or systemic condition that increases left ventricular afterload sufficiently to cause hypertrophy (aortic stenosis-valvular subvalvular; supra-valvular; coarctation, systemic hypertension, renal failure)*
5. *normal or super-normal ejection fraction in the absence of other hyperdynamic states (fever, pregnancy, hyperthyroidism).*

Associated findings such as SAM or mid-systolic closure of the aortic valve should not be considered diagnostic. When all the echocardiographic features are present, together with the suggestive clinical picture, a firm diagnosis of HCM can be made. When however only a number of these findings is present, the diagnosis can only be made after exclusion of other causes of ventricular hypertrophy.

Patterns of LV Hypertrophy

Asymmetric septal hypertrophy (ASH) is the most frequent form of left ventricular hypertrophy and has been regarded as the hallmark of HCM. Although this hypertrophy usually involves the basal anterior septum to a variable extent and severity, it may also involve the apical, mid or posterior septum in isolation. ASH may be confined to the most proximal septum as a discrete “tumour-like” swelling in an otherwise normal ventricular septum. Variation in ventricular hypertrophy in HCM emphasizes the need of obtaining serial parasternal short axis cuts at multiple levels along the left ventricle, so that the complete distribution of the ventricular hypertrophy can be ascertained. Using this, now well standardised approach, Shapiro and McKenna [10] defined three patterns of left ventricular hypertrophy; asymmetric left ventricular hypertrophy encountered in 55% of their patients, symmetric in 31% and distal in the remaining 14%. Although ASH has been commonly defined as a septum to posterior wall ratio of 1.3:1, the same authors proposed a ratio of 1.5:1 in defining ASH which increased the sensitivity and specificity of this echocardiographic finding for the diagnosis of patients with HCM.

Frequently, wall thickness is strikingly heterogeneous and contiguous segments of the left ven-

tricle may differ greatly in thickness. Maron et al. [11] described a large variability of distribution of left ventricular hypertrophy, grouped in four basic categories of ventricular hypertrophy.

- Type I was described as hypertrophy confined in the anterior portion of the ventricular septum and was encountered in 10% of their patients.
- Type II described as hypertrophy involving both the anterior and posterior segments of ventricular septum and was seen in 20% of their patients.
- Type III was the most frequently encountered distribution of ventricular hypertrophy seen in 52% of their patients and it involved both the ventricular septum and left ventricular free wall (Fig. 24.10).
- Type IV left ventricular hypertrophy was encountered in 18% of their patients in whom it involved the posterior septum, lateral wall or the apical regions, all inaccessible to the M mode echocardiographic beam (Fig. 24.11). Thus, in this type of hypertrophy, the anterior wall and ventricular septum and the inferior wall were free of hypertrophy and the diagnosis of HCM would be missed should two-dimensional echocardiography not been performed with careful scrutiny of these areas.



Fig. 24.10 Parasternal short-axis view from a patient with type III distribution of ventricular hypertrophy. Note the extensive septal and anterior free wall hypertrophy

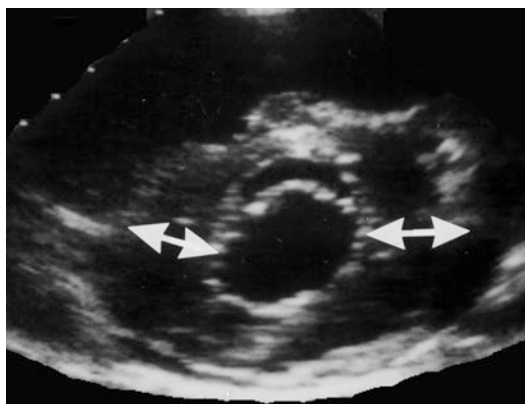


Fig. 24.11 Parasternal short-axis view of the left ventricle at mitral valve level demonstrating a very eccentric form of ventricular hypertrophy (Type IV). Here the lateral wall and posterior septum are markedly hypertrophied (25 and 20 mm respectively), whereas the anterior and posterior walls are normal

Patients with widespread hypertrophy involving most of the ventricular septum as well as portions of the left ventricular free wall (type III) had greater prevalence of functional limitations than did patients with the three other morphologic types combined.

Concentric or symmetrical left ventricular hypertrophy is also frequently seen in patients with HCM and when this occurs, the echocardiographic differentiation from secondary causes of left ventricular hypertrophy such as systemic hypertension, or the “athletes heart”, may be difficult (Fig. 24.12).

Predominantly distal (apical) distribution of left ventricular hypertrophy is also found in a substantial number of patients (Fig. 24.13). This type was initially described in Japanese patients with giant negative T-waves on the ECG while ventricular hypertrophy was confined to the left ventricular apex. These patients were only mildly symptomatic and have a good prognosis. Based primarily on angiographic studies, as many as 25% of Japanese patients with HCM have been reported to have hypertrophy confined to the true left ventricular apex. This distribution of hypertrophy characteristically creates a spade-like deformity of the left ventricular cavity during diastole and this is well seen by two-dimensional echocardiography from the apical four-chamber projection.

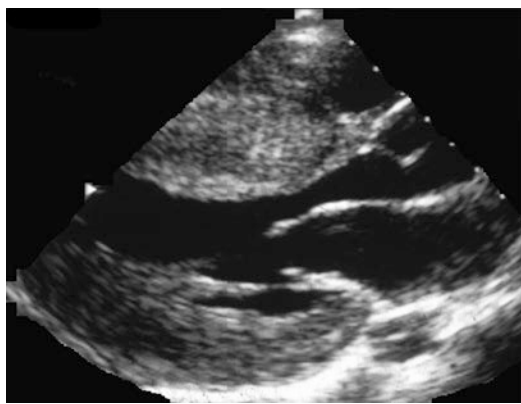


Fig. 24.12 Parasternal long-axis view from a patient with HCM of the concentric type. Note that both the septum and the posterior wall are of similar thickness

The right ventricle can also be involved in patients with HCM. Using standardised views across the right ventricular inflow tract, right ventricular outflow tract and apical and subcostal views, the right ventricle can be imaged in its integrity. As many as 40% of patients with hypertrophic cardiomyopathy may also have right ventricular hypertrophy to a variable degree.

HCM can be seen with increasing frequency in the elderly. However, only a limited number of patients have the ‘classical’ clinical and echocardiographic features with left ventricular outflow tract gradient. Most often such patients are discovered incidentally when undergoing investigations of coronary artery disease and yet others have been hypertensives. These elderly patients with septal hypertrophy often have mitral annular calcification (Fig. 24.14) and an angulated (sigmoid) septum (Fig. 24.15). These patients generally have no evidence of family history and it can be argued whether this patient group really represents the same disease.

Diagnostic Difficulties

No single diagnostic technique is sufficient to cover the entire spectrum of the disease and all the clinical, electrocardiographic and echocardiographic data are required to diagnose HCM. Table 24.2 lists some of the possible causes for misdiagnosing HCM.

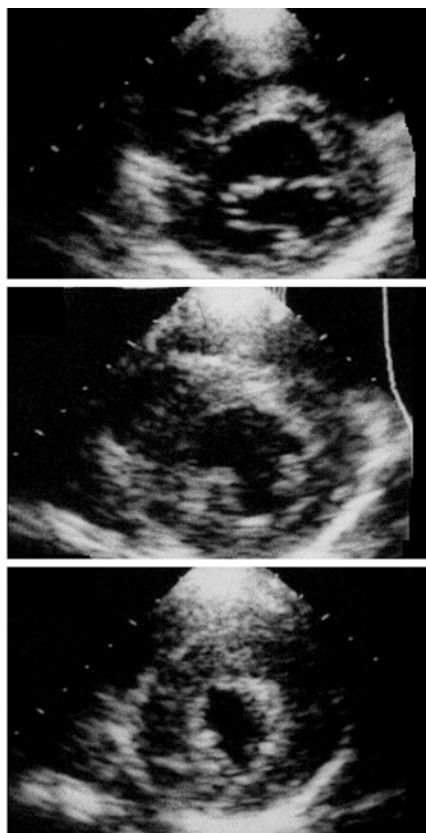


Fig. 24.13 Parasternal long-axis and serial parasternal short-axis views of the left ventricle from a patient with hypertrophic cardiomyopathy of the apical type. Note that the wall thickness is normal at the base (upper panel),

marginally thickened (13 mm) at papillary muscle level (middle panel) and clearly hypertrophied (22 mm) at the apex

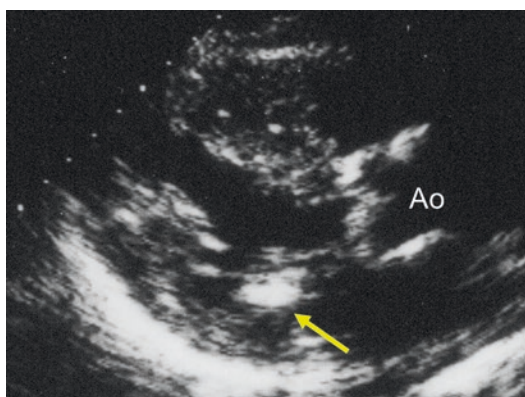


Fig. 24.14 Parasternal long-axis view from an 80 year old patient with chest pain. Notice the mild septal hypertrophy (13 mm) with normal LV cavity and normal size LA. There is extensive mitral annular calcification noted posteriorly (arrow)

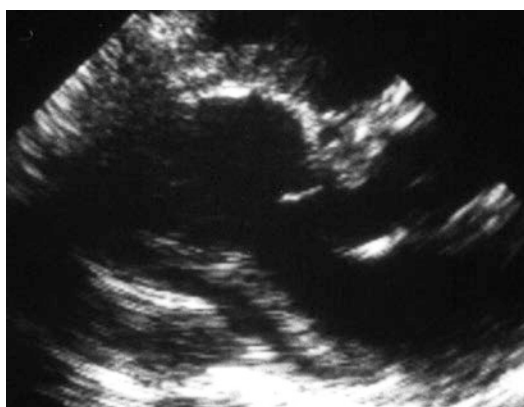


Fig. 24.15 Parasternal long-axis view from an 81 year old patient with a markedly angulated ventricular septum. Note that the very proximal portion of the septum is sharply angled towards the LV outflow which risks to be mis-interpreted with HCM

Mild or Absent Ventricular Hypertrophy

It is important to investigate suspected cases of HCM in order to exclude the diagnosis, particularly in high-risk families. Within families with HCM, up to one third of adults carrying a sarcomere gene protein mutation do not express LV hypertrophy, but it may appear later in the adult age [2, 3]. A 13 mm threshold for LVWT is advised for familial screening in first degree relatives [2] but should be interpreted in the light of other suggestive features such as ECG abnor-

malities and other subtle preclinical features including abnormal tissue Doppler and strain, incomplete SAM, elongation of the mitral valve leaflets, abnormal papillary muscles and LV crypts. If genetic screening is not performed in relatives or if the causative mutation is unknown, ECG and echocardiography should be repeated in first degree relatives every 6–12 months if there are non-diagnostic abnormalities and every 1–2 years between 10–20 years of age and 2–5 years in adults if ECG and echocardiography are normal. Figure 24.16 is from a patient with normal echocardiogram yet the ECG is clearly abnormal. This patient had a troponin T mutation.

Table 24.2 Possible causes of misdiagnosis of HCM

• Tangential image (poor technique)
• Left ventricular pseudotendons
• Right ventricular moderator band
• Sigmoid septum (angled septum)
• ASH in the presence of aortic stenosis or systemic hypertension particularly in the presence of inferior myocardial infarction
• High level of athletic training (?)
• Specific heart muscle diseases

Left Ventricular False Tendons (Fig. 24.17)

These are fibrous bands within the normal left ventricle running parallel to the ventricular septum. Echocardiographically, they appear as linear echoes within the LV cavity, which run parallel with the endocardial surface of the septum. When grey scale gain control is incorrectly set, they

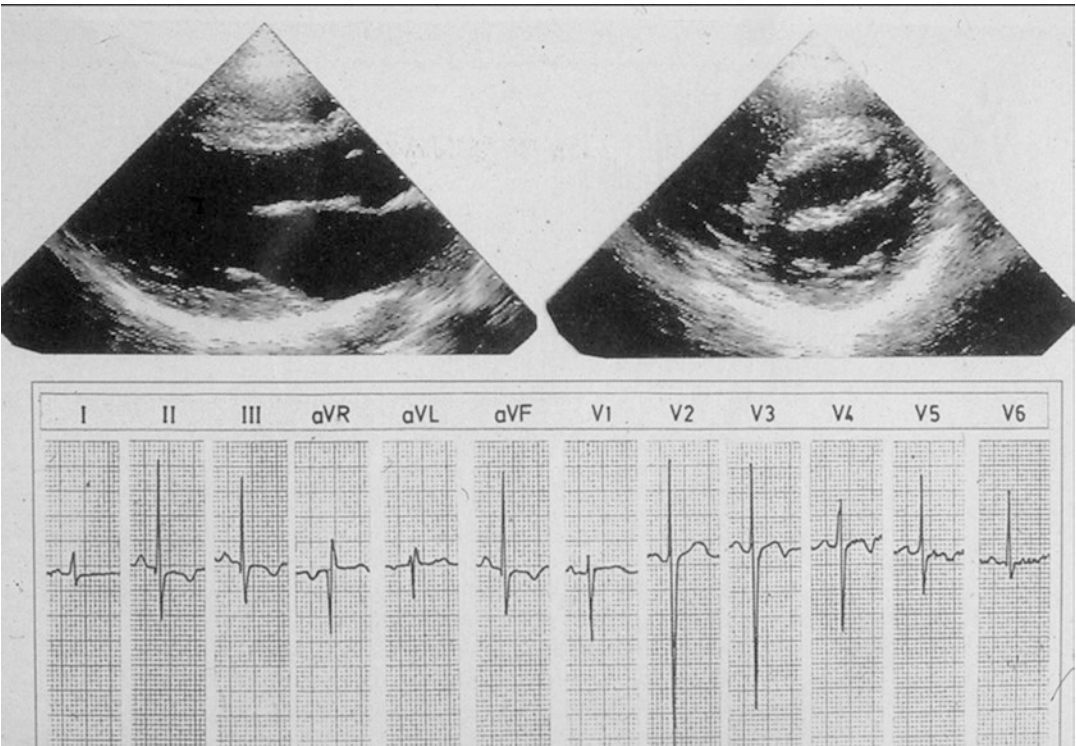


Fig. 24.16 Parasternal projections from a patient with Troponin T mutation. Notice the normal echocardiogram with a markedly abnormal ECG (Produced with permission from Heart)

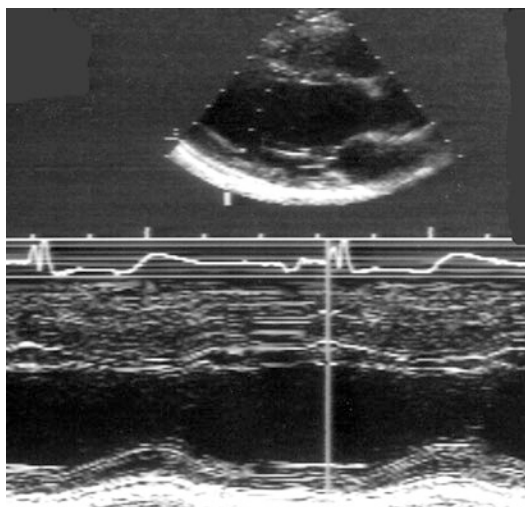


Fig. 24.17 Parasternal long-axis (top) and respective M-mode echocardiogram from a normal individual. Notice the bright linear echoes running in parallel to the ventricular septum that can potentially be included in the measurement of the septal wall thickness

may give the impression of increased myocardial thickness. The differential diagnosis can be made from short axis projections where the tendons are cut cross-sectionally and therefore the septal thickness can better be appreciated.

Right Ventricular Moderator

Band (Fig. 24.18)

This is a band of muscle that joins the right ventricular inflow to the outflow tract. It is a normal cardiac structure invariably present in all patients and it is used to characterise the right ventricle. As with the false tendons, when gain setting are inappropriately set, the space between moderator band and ventricular septum may not be apparent, thus including the moderator band with the septal wall measurements.

Angulated (Sigmoid) Septum (Fig. 24.15)

One should be aware of the possible false diagnosis of asymmetrical septal hypertrophy, when acute angulations of the ventricular septum occurs (sigmoid septum). In the elderly population the ventricular septum tends to continue from the anterior aortic wall in an acute angle, so that it easily gives the false impression of a localised subaortic septal thickening viewed from left

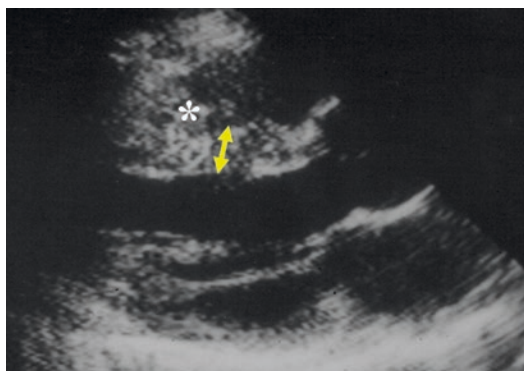


Fig. 24.18 Patients with mild right ventricular pressure overload demonstrating RV hypertrophy and a prominent moderator band (asterisk)

parasternal projections. Such angulation appears to form a localised septal thickening at the proximal portion of the anterior septum, particularly when the M-mode beam transects the septum at this level and can easily be mis-interpreted as ASH and thus HCM. Left ventricular wall thickening, small outflow tract dimensions and a small incomplete SAM, may complete the illusion of HCM.

Oblique (Tangential) Measurements

These include mis-interpretations of normal variants of left ventricular shape, or can be due to oblique longitudinal sections of the left ventricle (off-axis views) and the presence of other causes leading to ventricular hypertrophy.

Congenital Heart Disease (Fig. 24.18)

ASH is relatively common in infants with congenital heart disease. The overall prevalence of disproportionate septal hypertrophy in one study was 10% and was exceeding 20% in patients with pulmonary stenosis or pulmonary hypertension.

Thinning of the Posterior Wall (Myocardial Infarction)

ASH may occur in conditions causing thinning or thickening of the left ventricular posterior wall relative to the septum. This abnormal septum to posterior wall thickness ratio is commonly encountered in coronary artery disease

patients either because of segmental hypertrophy of the septum i.e. secondary to systemic hypertension or, more commonly, as a result of transmural myocardial infarction of the posterior wall, causing thinning which produces an abnormal ratio even in the presence of normal septal thickness.

Concentric Hypertrophy

Concentric hypertrophy is the predominant pattern in left ventricular hypertrophy caused by increased afterload and in patients with myocardial infiltration and intramyocardial storage disease.

The elevated ejection fraction however seen in HCM together with an ECG, should, in the majority of cases, differentiate patients with HCM from those with cardiac infiltration where ventricular contraction is often depressed. There is a subset of patients with small left ventricular cavity, moderate left ventricular hypertrophy and hyperdynamic systolic function secondary to long-standing systemic hypertension. These patients are usually elderly and may exhibit a systolic anterior motion of the mitral valve, an outflow tract gradient and impaired diastolic function. In practice, the diagnosis of HCM should not be made in these patients because the hypertrophy is secondary to a known aetiology. It is conceivable however, to have a common disease such as systemic hypertension in association with a rare cardiac condition such as hypertrophic cardiomyopathy, in which case the differential diagnosis is extremely difficult clinically and should be avoided. Perhaps future genetic markers may be able to differentiate the two conditions.

Cardiac Amyloidosis

Cardiac amyloidosis may occasionally prove difficult to differentiate from HCM patients with concentric hypertrophy, particularly at an early stage of the disease. Both may show a similar degree of concentric left and right ventricular hypertrophy and the described “sparkling” myocardial texture lacks specificity for cardiac amyloidosis. The depressed systolic function in cardiac amyloidosis usually contrasts well with the usual vigorous ventricular contraction seen

in HCM. The thickened valves and atrial septum (with amyloid infiltration) may on occasions be of some help in the differential diagnosis. A low voltage electrocardiogram in patients with cardiac amyloidosis will add to the differential diagnosis but cardiac biopsy will conclusively differentiate the two conditions.

Hypertrophy in Athletes

Another occasional diagnostic difficulty occurs in some athletes who may present symmetric or even asymmetric left ventricular hypertrophy. Ventricular hypertrophy may represent either a physiologic adaptation with more hypertrophy than usual or abnormal hypertrophy because of underlying HCM, putting the patient at risk for sudden death. Regular intake of anabolic steroids, combined with intense isometric exercise may lead to a further increase in left ventricular wall thickness in relation to internal ventricular dimensions overshadowing an underlying primary myocardial disorder.

The discrimination between HCM and physiologic adaptation may lie in cavity dimensions rather than in the wall thickness, whether asymmetric or not (Table 24.3). In HCM, the cavity dimensions tend to be at the lower end of the normal spectrum, whereas the athlete is vagotonic with resting bradycardia and the ventricular dimensions at the upper normal limits or above while LA size is increased. It is exceedingly rare for athletes of any sort to have a wall thickness greater than 13 mm. In practical terms, the combination of a wall thickness of >13 mm together with a LA size >41 mm should effectively rule out the diagnosis of athlete’s heart.

Table 24.3 Differentiation between patients with HCM and athletes

Parameters	HCM	Athletes
Wall thickness (mm)	≥13	<13
LVEDd (mm)	≤50	>50
LA (mm)	≥41	<40
E (cm/s)	Reduced	Increased
A (cm/s)	Increased	Reduced
E/A	>1	<1
Deceleration time (ms)	Increased	Reduced
IVRT (ms)	Increased	Reduced

The Mitral Apparatus

The mitral apparatus is visualised in its integrity from parasternal and apical long-axis as well as parasternal short-axis projections and these represent the optimal views for the visualisation and assessment of systolic anterior motion of the mitral valve (S.A.M.).

Controversy still exists as to the mechanisms of SAM. There are three dominant hypotheses evoking the mechanisms of SAM:

1. a Venturi effect resulting in the mitral valve cusp to be aspirated into the relatively low pressure chamber by the high velocity of blood flow through the left ventricular outflow tract
2. abnormal mitral valve cusp apposition at the onset of systole in association with a small left ventricular cavity
3. secondary to an abnormal positioning of the papillary muscles which are displaced forward and medially during systole in association with a small left ventricular cavity.

SAM is associated with the presence of left ventricular outflow tract gradient measured at cardiac catheterisation. The presence of SAM is not pathognomonic of HCM. This systolic anterior motion of the mitral valve can also occur whenever there is a small, hypertrophied left ventricle in association with a hyperdynamic ejection as well as in patients who are hypovolaemic and/or dehydrated. SAM is also common in elderly patients with an angulated septum or hypertensive heart, especially when preload and afterload have been reduced by diuretics. Similarly, the absence of SAM does not necessarily preclude the diagnosis of HCM.

The Aortic Valve

Early closure of the aortic valve was one of the earliest echocardiographic features in HCM and usually concurs with the presence of SAM and a subaortic gradient. It has been thought to occur when the left ventricular outflow tract gradient peaks in mid-to-late systole, causing the aortic valve cusps to come together during this time, not because there is a significant amount of blood left

in the ventricle unable to be ejected, but rather because there is not enough blood left in the ventricle to be ejected during the later part of systole. Like SAM, mid-systolic closure of the aortic valve is non-specific and may be seen in other conditions such as discrete subaortic stenosis as well as in any hyperdynamic left ventricle.

Patients with HCM can have mild aortic incompetence. This may be the result of some degree of annular distortion without annular dilatation. This may arise from the asymmetrical septal hypertrophy, which causes the ejection flow to be directed eccentrically against the aortic valve. The constant impact of the high velocity blood flow with the aortic valve would produce a wear and tear of the cusps leading to aortic regurgitation. The minor valvular degeneration may become the site of vegetations during bacteraemia.

Doppler Echocardiography

The addition of Doppler techniques to two-dimensional echocardiography provides comprehensive haemodynamic assessment in HCM patients. Pulsed wave Doppler is particularly useful in the assessment of the left ventricular filling characteristics. Systolic events are predominantly characterised by the presence of increased intra-ventricular velocities and the presence or absence of gradient. Continuous-wave Doppler is a reliable method for measuring the peak systolic pressure drop (gradient) across the left ventricular outflow tract using the simplified Bernoulli equation ($P = 4V^2$). Colour flow imaging complements the anatomic information obtained by two-dimensional echocardiography by demonstrating the pattern of progressive intraventricular flow systolic acceleration and the location of aliasing and/or the presence of outflow tract turbulence.

Diastolic Events

The basic functional disorder in HCM occurs during diastole with impaired relaxation, filling and compliance of the ventricles. Far from being uniform, myocardial dysfunction is patchy and

irregular depending upon the extent and distribution hypertrophy, myocyte disarray and fibrosis.

Early studies using M-mode echocardiography demonstrated that the rates of filling and relaxation of the left ventricle are abnormal in patients with hypertrophic cardiomyopathy. Doppler echocardiographic recordings are easier to obtain in nearly all patients and provide a good overall estimate of diastolic filling abnormalities of the left ventricle.

Diastolic velocity waveforms are recorded with pulse wave Doppler by positioning the sample volume at the tips of the mitral valve during diastole. There are several patterns of left ventricular diastolic filling in a variety of different cardiac disease dependent upon the interrelation of left ventricular relaxation, left atrial pressure and intrinsic left ventricular chamber stiffness. In HCM patients, the period during which the heart is isovolumic is often prolonged, left ventricular filling is slow and the proportion of filling volume resulting from atrial systole may be increased. These pathophysiologic changes are reflected in the pulsed Doppler recording of the trans-mitral waveform. Impaired ventricular relaxation results in prolonged isovolumic relaxation time, slower early ventricular filling ("E" wave) and a compensatory exaggerated atrial systolic filling ("A" wave), in patients who have normal left atrial pressure, so that the ratio E/A is reduced (Fig. 24.19). In more severe cases, with increased left atrial pressure (>15 mmHg), the extent of rapid filling is increased with a consequent reduction of the atrial contribution, giving the impression of normal left ventricular filling (pseudonormalised). Normalisation of the diastolic filling pattern in HCM can also happen in the presence of significant mitral regurgitation. More advanced still, with decreased compliance and high left ventricular filling pressures, there is accelerated rapid early filling and normal or reduced late filling similar to patients with restrictive physiology. Often, no correlation can be found between symptoms (predominantly breathlessness) and Doppler diastolic indices as a number of symptomatic patients may have "normalised" diastolic indices [12]. A much better correlation could be found between patient's professed symptomatic status and maximal oxygen consumption

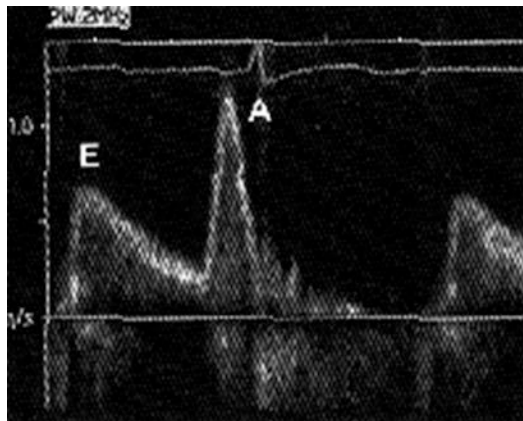


Fig. 24.19 A typical transmitral velocity profile from a patients with HCM. Note the reduced E-wave velocity with prolonged deceleration time and a compensatory increase of the A-wave (impaired relaxation). This is the earliest diastolic abnormality that occurs in such patients and may not be associated with breathlessness

and anaerobic threshold during cardiopulmonary exercise testing.

While sensitive, Doppler diastolic parameters lack specificity since they may be influenced by multiple factors, including the intrinsic properties of the cardiac muscle and loading conditions of the heart as well as heart rate and patient age. Although heart rate and arterial pressure have important influences on left ventricular diastolic filling, it is the interplay between left atrial pressure on mitral valve opening, mitral regurgitation, left ventricular relaxation, chamber stiffness that determine the rate and extent of early and late diastolic filling.

Colour flow imaging can distinguish the high pre-systolic inflow velocity (A wave) from the lower velocity of the early diastolic filling flow (E wave) by the increased brightness of the red-orange colour occurring in late diastole, which also often aliases. Since patients with HCM usually have small left ventricular cavity dimensions, the higher velocity in late diastole may be seen into the left ventricular cavity and even on occasions reaching the cardiac apex.

Systolic Events

The systolic events in patients with HCM may be categorized into two main groups. First, those

occurring in the left ventricular cavity and out-flow tract and secondly the presence of mitral regurgitation.

Intraventricular Flow Velocity

Doppler echocardiography is used to measure blood flow velocities within the heart, particularly for calculating pressure gradients across stenotic valves. This method is also valid for calculating the dynamic gradient across the left ventricular outflow tract in patients with HCM. In contrast with fixed obstruction, the flow velocity profile in patients with HCM, as obtained with continuous wave Doppler, presents a slow and gradual increase which only reaches maximal velocity late in systole changing the overall shape of the flow velocity (Fig. 24.20). If there is no high velocity in the left ventricular outflow tract at rest, the late-peaking velocity contour may be brought out in some patients with provocative manoeuvres following amyl nitrate inhalation, or during a Valsalva manoeuvre. The velocity contour reflects both the timing and the magnitude of the pressure drop across the left ventricular outflow tract.

Colour-flow imaging can identify the uniformity or the non-uniformity of the intraventricular flow. In the normal individuals from the apical four-chamber and two-chamber projections, the ventricular flow coded in blue (blood flow directed away from the transducer) progressively

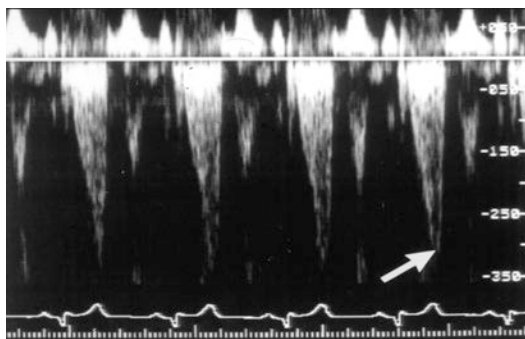


Fig. 24.20 Continuous wave Doppler directed across the left ventricular outflow tract showing the characteristic delayed systolic peak (arrow) of the velocity waveform. In this patient the peak velocity was 3.2 m/s reflecting a pressure gradient of 42 mmHg

becomes brighter as it moves from the apex towards the left ventricular outflow tract. At this position, it will alias and the flow map demonstrates a central red zone (colour reversal) immediately below the aortic valve. In patients with HCM, the intraventricular colour-flow map during systole is characterised by a non-homogeneous blue colour with a lighter hue compared with normals and typically aliases at mid-ventricular level, at the level of the hypertrophied papillary muscles or at the level of the mitral valve.

When SAM occurs, the systolic flow at this level becomes turbulent with a “mosaic” colour pattern (Fig. 24.21). When the flow crosses the aortic valve into the ascending aorta it becomes laminar again with homogenous red colour, as seen from the suprasternal window (flow moving towards the transducer).

With the superimposition of colour-coded blood flow on M-mode echocardiograms, an improved timing of the intraventricular systolic events can be obtained. This provides higher temporal resolution and a wider range of velocities displayed in colour so that an accurate analysis of timing and direction of the blood flow can be performed. High velocity turbulent flow usually occurs at the time when the mitral valve leaflets impinge on the ventricular septum during systole. When it then reaches the outflow tract, it encounters the anteriorly positioned mitral leaflets (SAM) and loses its laminar characteristics to become turbulent with the typical mosaic pattern (green-yellow) on colour flow imaging. At this level further flow acceleration occurs reaching velocities as high as 5–6 m/s (Fig. 24.22).

Occasionally, in some patients with HCM, turbulent flow can be seen in the middle of the left ventricle or even at the apex caused by obstruction at mid-ventricular level (Fig. 24.23).

Mitral Regurgitation

Mitral regurgitation is a well recognised component of the complex pathophysiology encountered in patients with HCM. It is usually associated with the SAM of the mitral valve and the development of an intraventricular gradient. Patients who do not present with SAM of the mitral valve rarely present with mitral regurgitation.

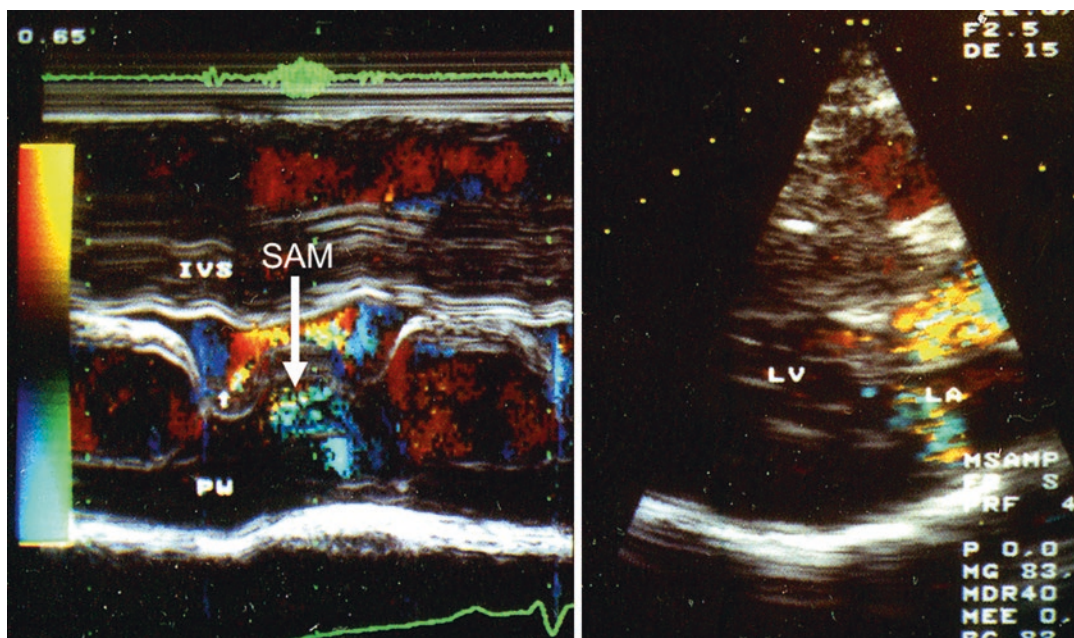


Fig. 24.21 Colour flow Doppler superimposed to M-mode echocardiography (left) and long-axis parasternal view from a HCM patient. Note that the mitral regurgitation on the M-mode begins before the SAM-septal

contact, while the mitral regurgitation begins in mid-systole. On the right, the mitral regurgitant jet is directed posteriorly into the left atrium while the left ventricular outflow gradient directed anteriorly towards the aorta



Fig. 24.22 Colour flow Doppler in a representative hypertrophic cardiomyopathy patient. From the apex, high velocity systolic flow is apparent away from the transducer (light blue), passing from the middle of the left ventricle where in aliases into red colour. When blood flow reaches the subaortic area, it becomes turbulent (green-yellow colour) suggesting the presence of an outflow gradient

Colour flow imaging can detect the presence of mitral regurgitation with high sensitivity and specificity. The most useful transducer locations are generally the apical four-chamber and two-chamber projections, but also the parasternal long and short axis may be very useful in detecting jets directed posteriorly (Fig. 24.21). Mitral regurgitation in patients with HCM is noted as a mosaic pattern (turbulent flow) present in the left atrium during systole. When the jet is directed anteriorly it may easily be confused with the turbulent jet of the left ventricular outflow tract. With continuous wave Doppler alone it can be very difficult to separate these two high velocity jets and a great deal of expertise is required in both the recording and the interpretation. The shape of the two systolic flows is typically different. The left ventricular outflow tract velocity has the characteristic scimitar or dagger shape late peaking contour, as opposed to the more symmetrical velocity curve of mitral regurgitation.

With colour flow imaging the left ventricular outflow tract flow velocity and mitral regurgitant jet can readily be distinguished and allow for a

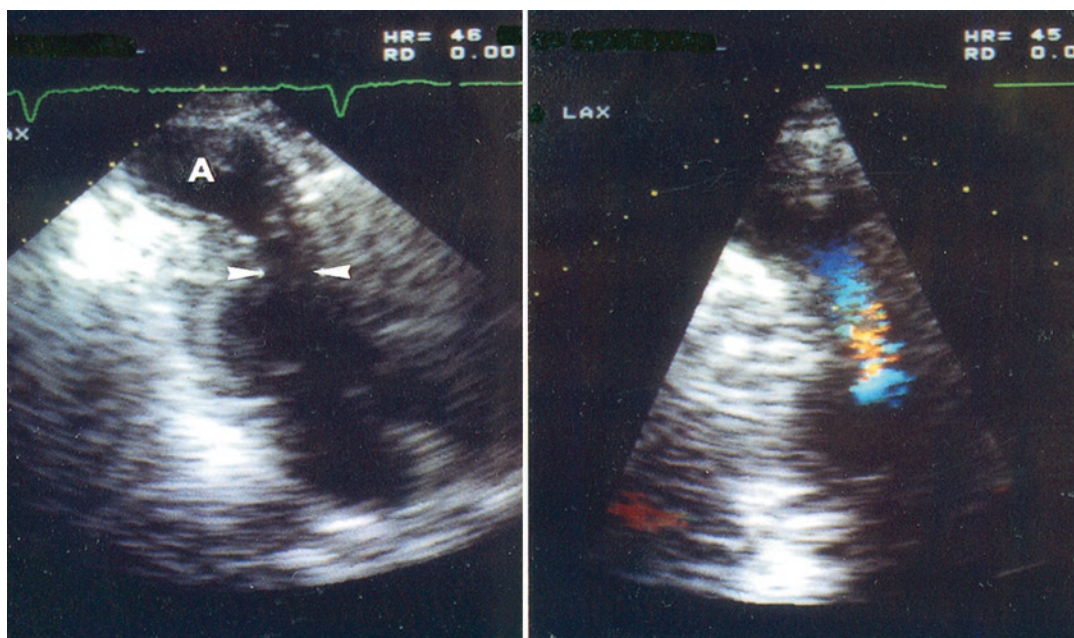


Fig. 24.23 Apical long-axis view with colour flow mapping in a hypertrophic cardiomyopathy patient with mid-ventricular gradient. Note on the left the narrowing of the

left ventricular cavity in its middle portion (arrowheads) and on the right, the turbulent flow originating at that level

better alignment of the continuous wave Doppler beam and LV outflow tract velocity.

The exact mechanism of mitral regurgitation in patients with HCM remains controversial and perhaps more than just one mechanism is involved. It is possible that an “eject, obstruct, leak” sequence occurs during which mitral regurgitation results from left ventricular outflow tract “obstruction”. Mitral regurgitation however is usually the result of contortion of the mitral apparatus, which begins in early systole. This is supported by the Doppler studies showing that mitral regurgitation begins early, before the occurrence of systolic anterior motion to septal contact. The onset of mitral regurgitation occurs less than 100 ms after the electrocardiographic R wave, whereas the onset of systolic anterior motion of the mitral valve follows that. As systole progresses there is a further decrease in left ventricular systolic dimensions and mitral valve distortion following the anterior mitral leaflet-septal contact. This would therefore result in an increased amount of mitral regurgitation occurring later in systole.

A third cause of mitral regurgitation is mitral annular calcification. This pattern, as mentioned earlier on, is particularly encountered in the older patients with HCM. Finally, mitral regurgitation can also result from structural mitral valve disease or papillary muscle displacement. When an additional structural abnormality of the valve is present, then the mitral regurgitant jet is often directed centrally into the left atrium. Transoesophageal echocardiography may be important here to make the precise diagnosis particularly if a surgical procedure such as myectomy is planned, so that the mitral valve may also need to be intervened upon.

The Role of Tissue Doppler Imaging

Assessment of LV function in patients with cardiomyopathies is routinely performed using cross sectional echocardiography. Being predominantly semi-quantitative, relying on visual assessment of LV function, two-dimensional echocardiography poses a significant limitation to the assessment of both regional as well

as global ventricular function. Volume changes such as ejection fraction, end-systolic and end-diastolic volumes are also load dependent and less sensitive to subtle changes over time. Tissue Doppler provides a robust, objective method of assessing ventricular function. By inverting the amplitude and frequency filters, tissue Doppler can measure the lower velocities originating from myocardial motion and filter out the higher blood pool velocities in an inverse fashion of the traditional Doppler recordings.

Tissue Doppler imaging may be used in three different ways:

1. Pulsed wave recordings of the mitral annular velocities from up to six annular positions (four-chamber, two-chamber and three-chamber projections)
2. Pulsed TDI from selected myocardial regions (basal, middle and distal regions)
3. Colour TDI from two-dimensional recordings of the myocardium.

Assessment of the myocardium produces three types of measurement either longitudinally or radially. These include velocity differences between two selected myocardial points of interest, as well as myocardial deformation indices, such as myocardial strain and strain rate. Myocardial strain reflects the deformation of tissue in response to an applied force. The first temporal derivative of strain is strain rate and represents the velocity change in myocardial fibre length over time. Recent software advances permit real-time strain and strain rate determination and regional strain rates between the epicardium and endocardium representing the myocardial velocity gradient, which correlates with regional ventricular contractility. HCM is characterised by impaired myocardial deformation in hypertrophic segments caused by myocyte disarray and myocardial fibrosis. TDI offers a unique modality that can monitor the presence and potential change of myocardial contractility over time.

TDI can be applied in five ways to assess the ventricle in hypertrophic cardiomyopathy patients:

1. Assess mitral annular velocities (systolic, diastolic or both)

2. Assess longitudinal function of the proximal and mid LV (velocities and strain and strain rate)
3. Assess radial LV function (myocardial velocity gradients or strain rate)
4. Assess diastolic function and filling LV pressures
5. Differentiation from athlete's heart

Mitral Annular Velocities (Fig. 24.24)

A number of studies have used TDI of mitral annular velocities for the early detection of mutation carriers, even when myocardial wall thickness was normal. Systolic (Sa) and early diastolic (Ea) PW velocities at the mitral annulus are lower in mutation carriers [13].

- A lateral Sa > 13 cm/s had a sensitivity of 100% and a specificity of 93% for differentiating the mutation positives without hypertrophy from controls and a lateral Ea < 14 cm/s had a 100% sensitivity and 90% specificity.

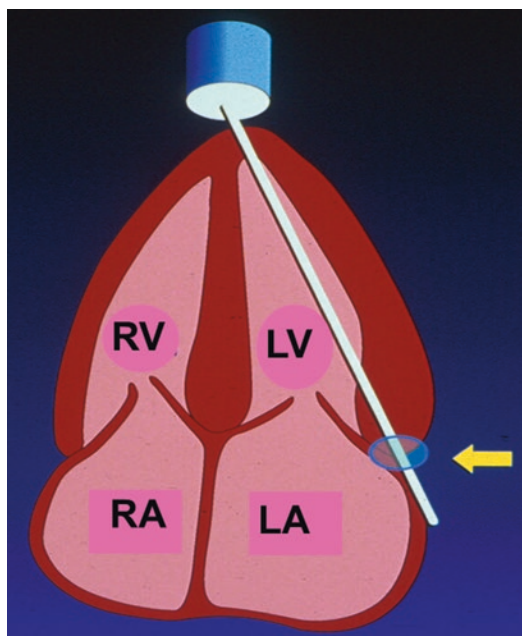


Fig. 24.24 Apical four-chamber projection demonstrating the Pulsed Wave sample volume positioned at the lateral corner of the mitral annulus (arrow)

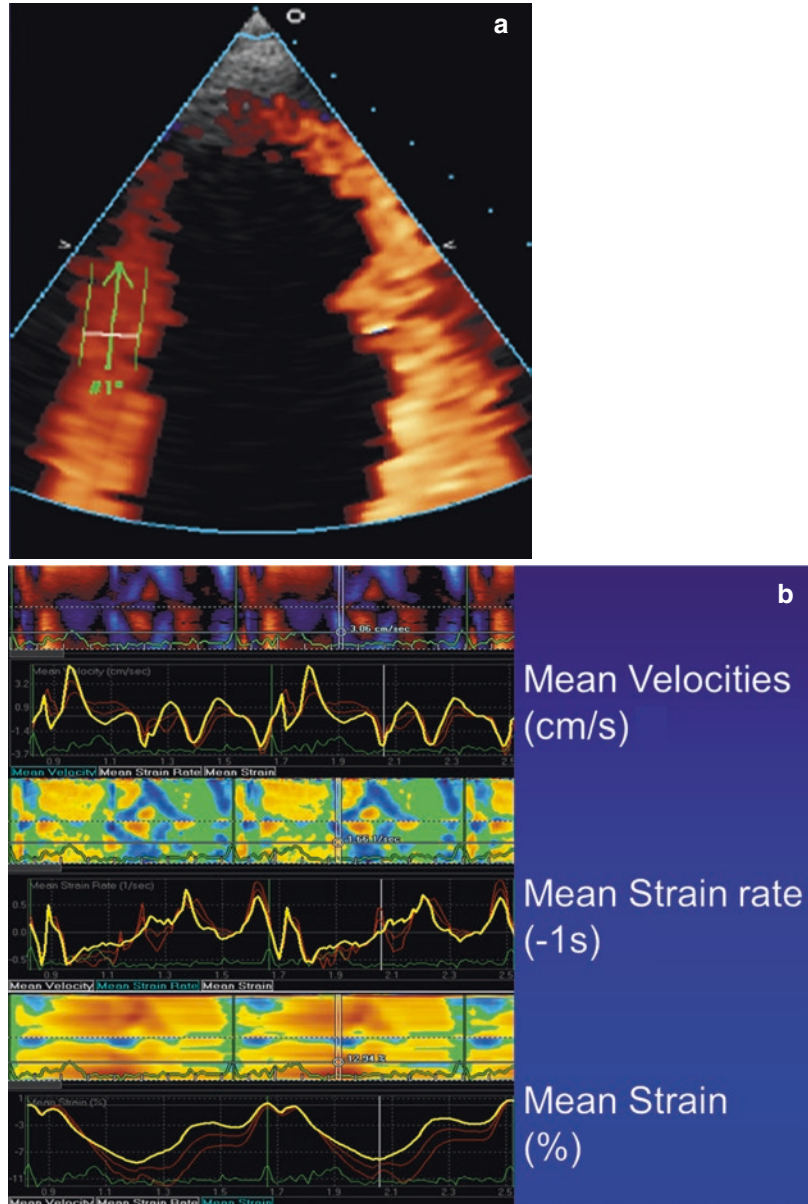
- A septal $Sa < 12$ cm/s and $Ea < 13$ cm/s both had a 100% sensitivity and 90% specificity.
- Although significant overlap exists between controls and cardiomyopathy patients, these studies indicate that TDI can provide an easy and complementary role in the diagnosis of hypertrophic cardiomyopathy patients. Importantly, it raises the possibility in identifying pre-clinical cases of cardiomyopathy patients.

Assessing Longitudinal Function

(Fig. 24.25)

From apical projections, longitudinal function of the LV can be assessed by specifically interrogating a myocardial region of interest (Fig. 24.25a). Three main parameters may be measured; tissue velocities (cm/s), strain rate (-1 s) and strain (%) (Fig. 24.25b). Tissue velocity measurements may not differentiate tissue movement due to active contraction from passive motion that results either

Fig. 24.25 (a) Apical four-chamber projection from a cardiomyopathy patient demonstrating the interrogation of the myocardial region of interest in the proximal (basal) septum. (b) Same patient with the three main tissue Doppler parameters of myocardial velocities and deformation. One systolic and two diastolic waveforms are identified each time and measured



from translational motion of the whole heart or from a “tethering” of normal surrounding tissue on a segment of disease myocardium. Strain and strain rate on the other hand are minimally affected by passive motion and therefore are expected to be more sensitive readings of myocardial function.

Assessing Radial LV Function

Left ventricular radial myocardial function may be assessed from parasternal long- or short-axis projections using colour TDI. This is visually appealing and easily applicable technique, which discloses differential velocities between the sub-endocardium and sub-epicardium. Normally, a higher velocity of shortening and relaxation are observed in the endocardium compared to the epicardium and this can be quantified as a myocardial velocity gradi-

ent (MVG). The myocardial velocity gradient across the septum or the posterior wall may be measured throughout the cardiac cycle. As with the longitudinal function, one systolic (S) and two diastolic (early and late) waveforms can be measured. MVG are typically reduced in HCM patient and this reduction is grater with a greater amount of hypertrophy. The amount of MVG reduction is also proportional to the degree of hypertrophy (Fig. 24.26).

Assess Diastolic Function and LV Filling Pressures (Fig. 24.27)

The ratio between early trans-mitral diastolic velocity and mitral annular velocity (E_m/E_a), either from the septal or lateral annular corners, often known as the E_m/E_a index, has been used as a robust predictor of LV filling pressures. In

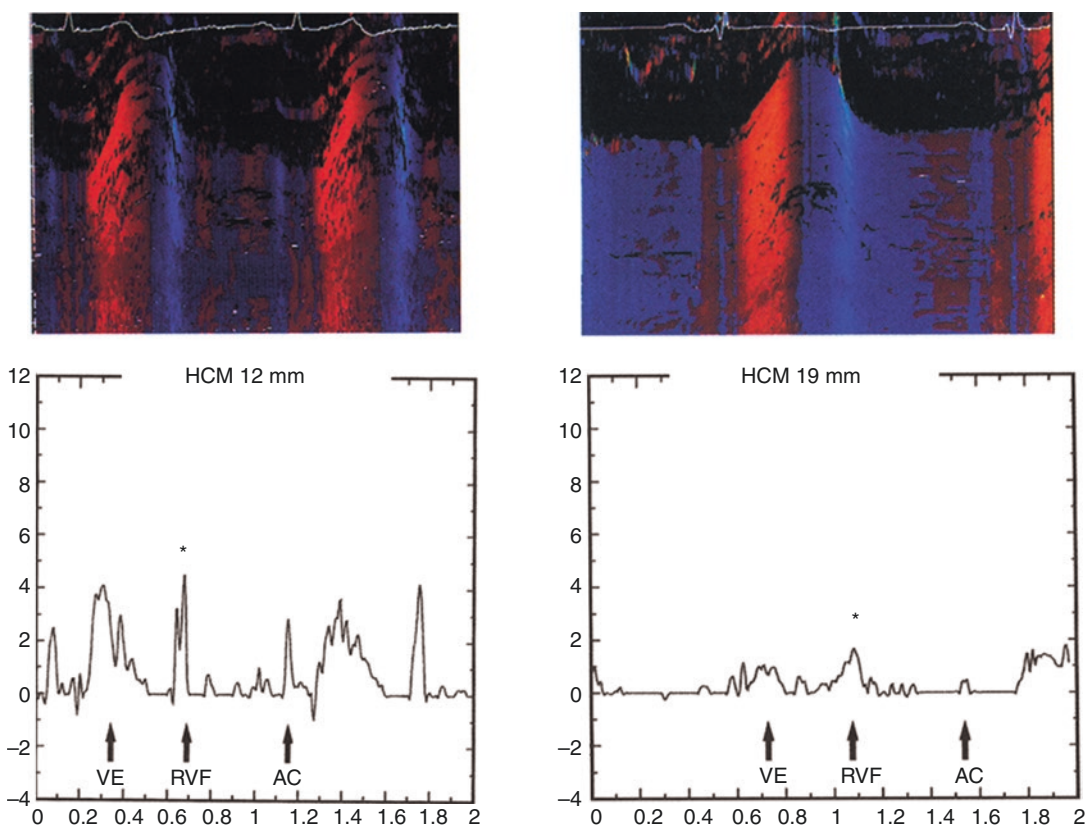
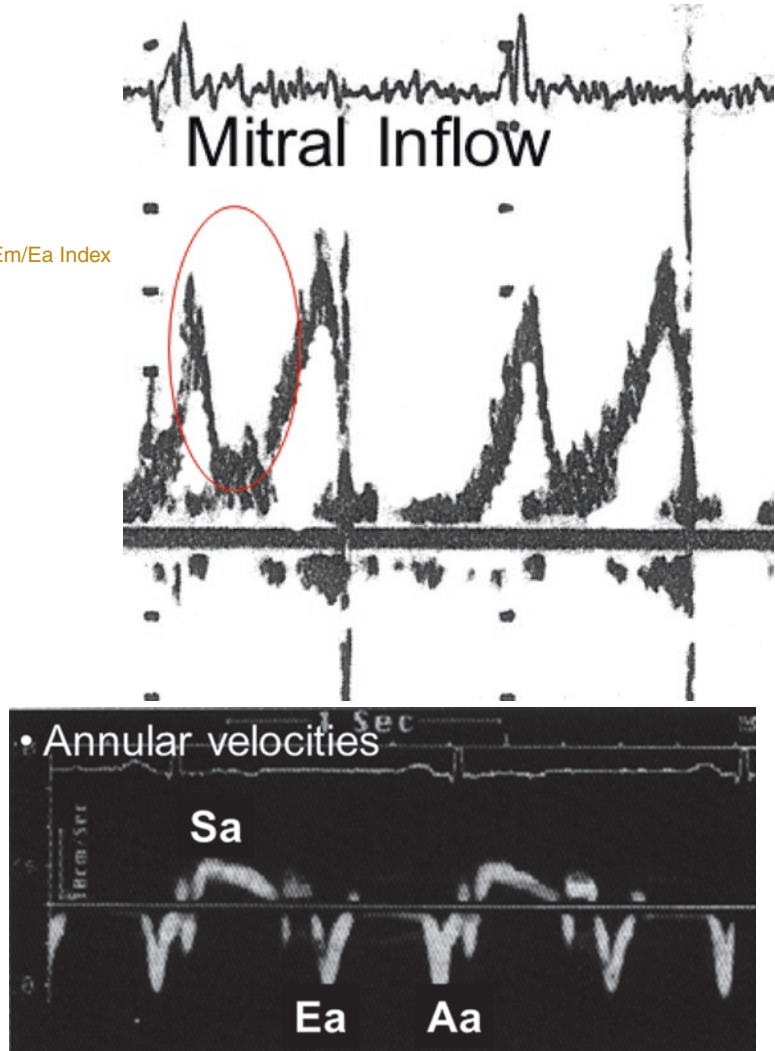


Fig. 24.26 Myocardial velocity gradient (MVG) in hypertrophic cardiomyopathy. From parasternal short-axis projections, the MVG of the posterior wall can be measured. Note that the grater the hypertrophy, the grater

the reduction of MVG, particularly those of the systolic gradient (VE) and the early diastolic gradient corresponding to the rapid ventricular filling (RVF)

Fig. 24.27 The early mitral Em to annular Ea Index of assessing diastolic filling pressures. Annular velocities may be measured from both lateral and septal annular positions

• Em/Ea Index



patients with a positive genotype for hypertrophic cardiomyopathy a $Em/Ea > 8$ cm/s can be predictive of HCM even when filling pressures are normal.

Differentiation from Athlete's Heart

The distinction of physiologic versus pathologic LV hypertrophy is often difficult and may be crucial for the individual's career as a professional athlete. While two-dimensional echocardiography is helpful (see above) TDI can aid differential diagnosis. While in physiologic hypertrophy both, systolic and diastolic velocities and MVG are high, often higher than in normals, in pathologic hypertrophy (HCM), these velocities are reduced (Fig. 24.28). The accuracy in separat-

ing HCM from athletes is high when the systolic MVG is ≤ 7 (sensitivity 96% and specificity 95%) [14].

Predictors of Prognosis

Hypertrophic cardiomyopathy (HCM) is a complex and variable clinical phenotype but the disease usually progresses slowly with many years of stable or minor symptoms and is compatible with a normal life expectancy [2]. Sudden cardiac death (SCD) can occur at any age but recent cohort studies show that heart failure and stroke related deaths are increasingly important causes of morbidity and mortality in the long-term [2, 15].

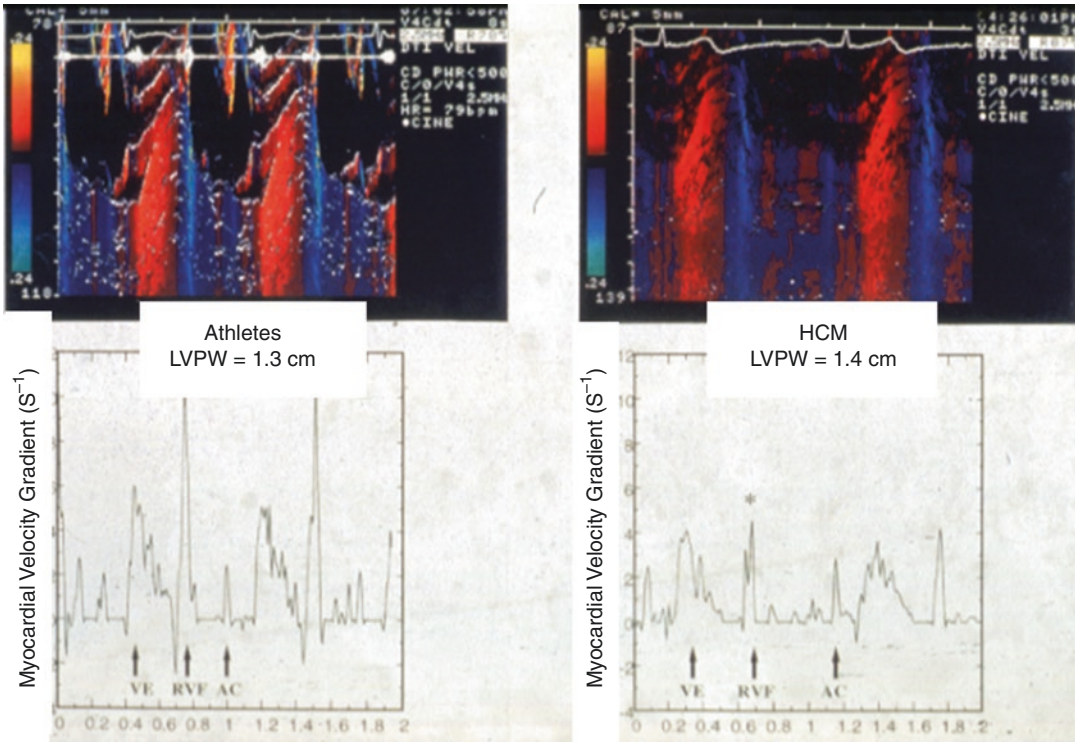


Fig. 24.28 Myocardial velocity gradients from an athlete (left) and a patient with hypertrophic cardiomyopathy (right). Notice that despite similar amounts of hypertro-

phy, the HCM patient presents with lower rapid filling (early diastolic) velocity gradient

Echocardiography has a central role in the prediction of all adverse events.

Sudden cardiac death is a rare event, occurring in less than 1% of patients per year. Current ESC guidelines recommend a recently validated model—HCM Risk-SCD—for the estimation of 5 year risk to guide decisions on ICD implantation [2, 15]. The score incorporates several variables derived from echocardiographic evaluation; specifically, maximum LV wall thickness, left atrial dimension and LV outflow tract gradient.

The clinical profile of advanced heart failure in HCM varies between patients. In some, it is associated with diastolic dysfunction with preserved ejection fraction and small LV size; in others, symptoms are caused by systolic left ventricular dysfunction [2]. Echocardiography thus has an important role in defining the cause of heart failure and determining management. In the early stages of the disease, conventional non-invasive indices of cardiac performance are within the normal range but as the

disease progresses, there is a deterioration in LV diastolic and systolic function associated with either mild-to-moderate LV dilation, decreased LV wall thickness and reduced LV ejection fraction (sometimes referred to as the ‘burnt-out’ phase) or severe LV diastolic dysfunction and severe atrial dilation (‘restrictive’ phenotype).

Atrial fibrillation and thromboembolism are common complications of HCM and are associated with reduced survival. LA size is one of the most important risk factors for AF and stroke and should be monitored closely in patients during follow-up [16].

Dilated Cardiomyopathy

Idiopathic Dilated Cardiomyopathy

Dilated cardiomyopathy (DCM) is characterized by LV dilatation and LV systolic impairment in

the absence of abnormal loading conditions (e.g. hypertension, valve disease, congenital heart disease) or coronary artery disease sufficient to cause global systolic dysfunction [1]. Right ventricular dilatation and dysfunction may also be present and there are overlapping phenotypes between DCM, ARVC with left ventricular involvement and LV non-compaction [17]. The prevalence of DCM is conservatively estimated at 1 in 2500 adults.

Without genetic testing and familial evaluation, DCM appears to be idiopathic in many individuals, but 35–40% of consecutive patients have an identifiable genetic mutation [3]. Familial screening often reveals mild LV dysfunction or dilatation in relatives. Other causes of DCM include toxin exposure, neuromuscular disorders, inborn errors of metabolism and malformation syndromes.

Familial/Genetic DCM

A number of genetic mutations can cause DCM most of which are transmitted as an autosomal dominant trait. Many genes are implicated including those coding proteins of the cardiac sarcomere, nuclear envelope, cytoskeleton, mitochondria and calcium transporters [18]. X-linked inheritance accounts for between 2 and 5% of familial cases of DCM and is mostly associated with Duchenne, Becker and Emery-Dreifuss muscular dystrophies. Isolated X-linked DCM, also caused by mutations in the dystrophin gene, is characterized by raised serum creatine kinase, but no clinical features of muscular dystrophy. Female carriers of dystrophin mutations can develop DCM later in life, usually in their 50s.

The Role of Echocardiography

Echocardiography can quickly establish the diagnosis of left ventricular systolic dysfunction by demonstrating ventricular enlargement as well as ventricular systolic dysfunction (Fig. 24.29). This typically involves all LV segments and often it involves both the left and the right ventricles. Often however, the left ventricular dimensions

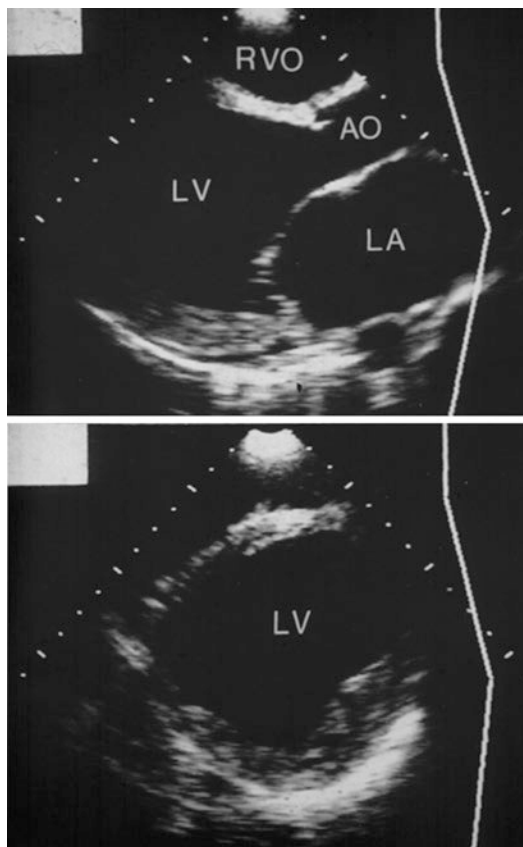


Fig. 24.29 Parasternal long-axis (top) and short-axis (bottom) from a patient with dilated cardiomyopathy. Note the marked dilatation of the left ventricle

remain normal and the only abnormality may be diffuse ventricular dysfunction alone. This may well represent a milder form or an earlier stage of cardiomyopathy. Regular follow up with repeat echocardiographic examinations is used to monitor changes of ventricular dimensions and function.

Particular attention should be made to measure the ventricular dimensions perpendicular the ventricular walls as it is possible to overestimate the chamber dimensions when the ventricle is measured obliquely. In the authors' experience, this oblique measurements is the single, most common aetiology of false diagnoses of dilated cardiomyopathy (Fig. 24.30).

Patients with ischaemic heart failure and dilated cardiomyopathy may present with similar symptoms and is crucial to separate the two conditions as treatment is very different. This is difficult to

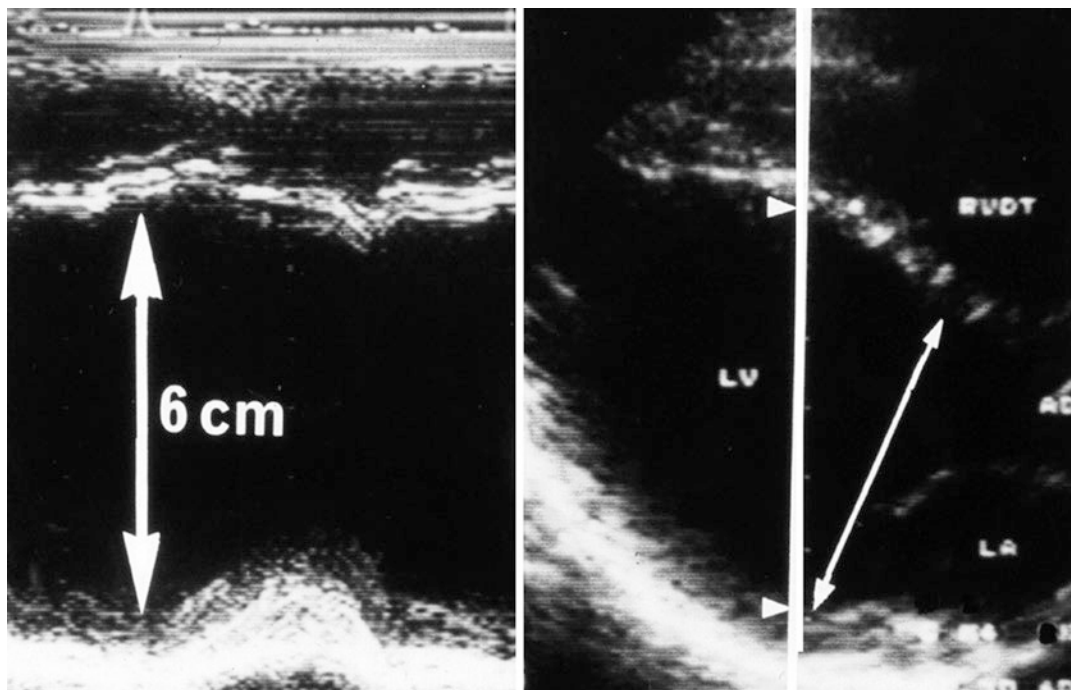


Fig. 24.30 Parasternal long-axis projection from a normal individual who was mis-diagnosed as having dilated cardiomyopathy because of the oblique M-mode mea-

surements of the ventricular cavity. Note that when the ventricle was measured perpendicularly, the size and function was normal

achieve with echocardiography alone. There are however some clues that when present, could help to make a differential diagnosis. Typically, patients with coronary heart failure have dilated ventricles with regional wall motion abnormalities as oppose to DCM where the dilatation and the ventricular dysfunction is more global. If there is an apical aneurysm this may be easily identified and suggest the diagnosis of coronary artery disease. The right ventricle is not often involved in coronary artery disease while in DCM it is frequently affected. Occasionally, the myocardium may be thin and echogenic in case of an old myocardial infarction which will imply scar tissue. Coronary artery disease patients tend to be older than 40 years of age while DCM patients are younger.

Doppler Echocardiography

Mitral Regurgitation

Left ventricular dilatation will lead to mitral annular enlargement, which will cause the mitral

leaflets not to appose properly and consequently lead to functional mitral regurgitation. This can be visualized with colour Doppler and quantified. While in some occasions the causal link between mitral regurgitation and dilated ventricle may be difficult to establish, the association of a globally hypokinetic LV with mitral regurgitation points to primary myocardial disease. Rarely the mitral regurgitation is severe in dilated cardiomyopathies and when this happens then it is more difficult to rule out mitral regurgitation as the prime culprit of LV dysfunction. When the mitral valve however is entirely structurally normal with normal leaflet texture and no prolapse, this should point out to a myocardial disease (or indeed ischaemic aetiology) as the cause of mitral regurgitation.

Estimate of LV Pressures

With the use of continuous wave Doppler, an estimate of intraventricular pressures could be ascertained and in particular the right ventricular pressures. In the presence of mild tricuspid regurgitation, the maximal velocity gradient will cor-

respond to the pressure gradient between RV and RA. Adding the level of the jugular venous pressure to the pressure gradient provides an estimate of RV pressure. When the JVP is not visible, then arbitrarily we add 10 mmHg to the pressure gradient assuming that this reflects the normal RA pressure.

With pulse-wave Doppler the assessment of diastolic LV function can be ascertained and an estimation of LV filling pressures performed. As in patients with hypertrophic cardiomyopathy, trans-mitral velocity profiles may be used to obtain longitudinal follow-up data on disease progression. The mitral inflow velocity signals accurately reflect pressure differences between the left atrium and left ventricle. Abnormally slow LV relaxation, with low LA pressure, gives rise to a pattern of slow acceleration of mitral flow in early diastole (E wave) with concomitant and probably compensatory increase in flow velocity with atrial contraction (A wave). At the opposite end of the spectrum are patients with stiff LV giving rise to a very high early velocity (E wave) across the mitral valve with rapid equalization of atrial and ventricular pressures, which represent the dip-and-plateau pressure contour at cardiac catheterization. This pattern usually is accompanied by a diminutive A wave during atrial filling. Between these two ends of the spectrum is the normal filling pattern with the early filling velocity somewhat larger than the atrial flow velocity.

Intracardiac Flow and Risk of Embolisation

The reduced systolic ventricular function and chamber dilatation produce a fairly characteristic intracavitary flow pattern, commonly seen in patients with dilated, poorly contracting ventricles. Swirling of the intracardiac flow can often be spontaneously visualized at the cardiac apex reflecting the high intracavitary filling pressures and the decreased flow velocity profile, predisposing factors for thrombus formation. With colour flow imaging the pattern of intraventricular flow velocity profile can be characterized and predict those patients in which regional stasis occur. From apical four-chamber projections, a series of short boluses of flow can be visualized during

diastole, giving the appearance of “puffs of smoke”. Because of low output state, the velocity of flow is low so that the usual colour flow map of intraventricular inflow is shown by the darker shades of red. During systole, the left ventricular outflow tract will also exhibit low velocities with absence of aliasing indicative of low output.

Ventricular dilatation with diffuse hypokinesia in patients with dilated cardiomyopathy, together with the low intraventricular velocities, constitutes a major risk for the development of intraventricular thrombi with the risk of systemic embolisation. Echocardiography can readily identify the presence of an intraventricular thrombus and lead to prompt anticoagulant treatment. Thrombi are usually attached at the apex (Fig. 24.31) and may be laminar or protruding with a narrow point of attachment on the endocardial surface.

Tissue Doppler Imaging

Tissue Doppler may be used to detect regional or global myocardial dysfunction, particularly in patients with normal chamber dimensions. One particular application is in patients who have been

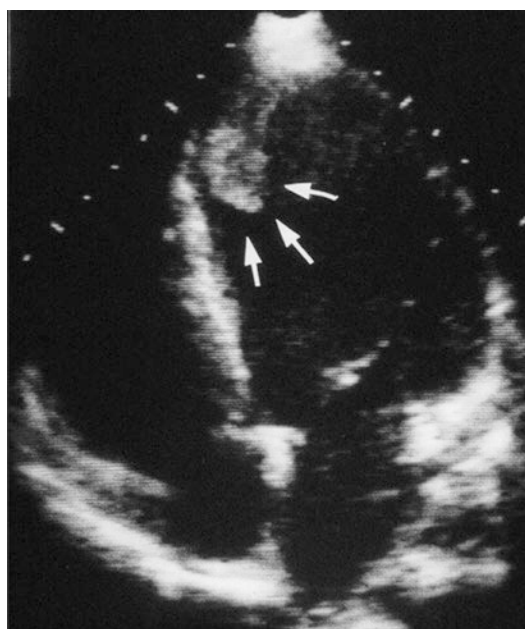


Fig. 24.31 Apical four-chamber view from a patient with dilated cardiomyopathy. Note the presence of an apical thrombus. The patient was not receiving anticoagulation

identified suffering from a genetic condition, which may lead to left ventricular dysfunction and dilatation such as patients with Duchenne muscular dystrophy in whom it might be useful to detect early left ventricular dysfunction, prior to any clinical manifestation of heart failure. This may have therapeutic implications such that an early treatment might prevent left ventricular remodeling.

Tissue Doppler may be used by measuring mitral annular velocities as well as myocardial velocity gradients or left ventricular strain and strain rate. Mean tissue Doppler velocities and radial strain rate of the LV posterior wall at peak systole and early diastole may be reduced while conventional echocardiography may be normal.

The early diastolic mitral annular velocity (E_m) is a good indicator of diastolic function. At ≥ 10 cm/s, diastolic function is usually normal, but at ≤ 8 cm/s it will imply diastolic dysfunction.

A more precise way to establish early ventricular dysfunction and predict elevation of LV filling pressures is by using the ratio of early transmitral diastolic velocity (E wave) over the early mitral annular velocity (E_m). *A $E/E_m > 10$ will imply elevated filling pressures with high sensitivity and specificity.*

Family Screening

Family screening is important and echocardiography is ideally suited for this. Large series of asymptomatic relatives have shown that 29% of relatives had abnormal echocardiograms. The majority of affected relatives are asymptomatic and cannot be identified by relying on history alone. Echocardiography therefore plays an important role for the early recognition of affected family members, which may promote the early institution of treatment in an attempt to prevent ventricular remodelling.

Myocarditis

Myocarditis is a challenging diagnosis due to its variable clinical presentation [19]. Its incidence is also difficult to determine as endomyocardial biopsy (EMB), the diagnostic gold standard, is used infrequently. In patients presenting with

mild symptoms and minimal ventricular dysfunction, myocarditis often resolves spontaneously without specific treatment but up to 30% of patients with biopsy-proven myocarditis can progress to DCM. Prognosis in myocarditis varies according to the underlying aetiology. The European Society of Cardiology Working Group on Myocardial and Pericardial Diseases have recently proposed diagnostic criteria for clinically suspected myocarditis. Myocarditis is defined as inflammatory disease of the myocardium defined by established histological, immunological and immunohistochemical criteria. The term inflammatory cardiomyopathy is defined as myocarditis in association with cardiac dysfunction. The histological diagnosis of myocarditis includes different forms, classified according to the type of inflammatory cell infiltrate: lymphocytic, eosinophilic, polymorphic, giant cell myocarditis and cardiac sarcoidosis.

Clinical presentation of myocarditis ranges from mild symptoms of chest pain and palpitation associated with transient ECG changes to life-threatening cardiogenic shock and ventricular arrhythmia. It affects individuals of all ages, although it is most frequent in the young. In all cases of suspected myocarditis, it is important to exclude coronary artery disease and other cardiovascular and extra-cardiac non-inflammatory diseases that could explain the clinical presentation.

Global ventricular dysfunction, regional wall motion abnormalities, and diastolic dysfunction with preserved ejection fraction may occur in myocarditis [20, 21]. Histologically proven myocarditis may resemble dilated, hypertrophic and restrictive cardiomyopathy and can mimic ischaemic heart disease. Fulminant myocarditis often presents with a non-dilated, thickened and hypocontractile left ventricle as the intense inflammatory response results in interstitial oedema and loss of ventricular contractility. Non-invasive imaging including echocardiography, cardiac magnetic resonance and nuclear imaging provide complementary diagnostic information. Echocardiography helps to rule out non-inflammatory cardiac disease such as valve disease and is useful in monitoring changes in cardiac chamber size, wall thickness, ventricular function and pericardial effusions.

Cardiac Toxins

A variety of substances can affect the heart leading to dilated cardiomyopathy. Perhaps the commonest toxin is alcohol. Macrocytosis is a useful indicator of chronically high alcohol consumption even in the absence of abnormal liver function. A raised gamma-glutamyltransferase (gamma GT) may be an indicator of only recent rather than long-term alcohol intake, whereas raised levels of other liver enzymes may be due to a chronic alcohol hepatitis.

There is an individual susceptibility to the adverse effects of alcohol on the myocardium, which may well be genetically predisposed. The heart is typically markedly dilated with global ventricular dysfunction but it may show dramatic improvement after a patient has stopped drinking. Figure 24.32 is from a patient with alcohol induce dilated cardiomyopathy. The heart is markedly dilated and shows diffuse hypokinesia as demonstrated by the simultaneous M-mode echocardiogram.

Anthracyclines given as doxorubicin have important toxic subcellular effects that can eventually lead to intracellular calcium overload and depressed cardiac function. The echocardiographic findings are again those similar to dilated cardiomyopathy with global ventricular dysfunction. As in all dilated cardiomyopathies, it is important to look for the presence in LV thrombus as those patients with dilated ventricles may be prone to thromboembolism.

Cardiomyopathy Associated with Pregnancy and Parturition

Peripartum cardiomyopathy typically occurs during the third trimester of pregnancy or during the first 6 months postpartum without obvious cause and without prior evidence of heart disease. Because it is rare, the literature is limited and filled with anecdotal cases and heterogeneous material. Heart failure with peripheral oedema and ventricular dilatation may be sudden and catastrophic or more insidious. An immunological interaction between mother and fetus can be postulated. This may be responsible for “myocarditis” frequently found on biopsy with interstitial and perivascular lymphocytic infiltration in the presence of myocyte necrosis with or without fibrosis.

The echocardiographic findings are usually those of a non-dilated left ventricle with global hypokinesia (increased end-systolic dimensions), similar to myocarditis (Fig. 24.33). Occasionally, the differential diagnosis with viral myocarditis is difficult and should rely mainly on clinical grounds. It is important to look for LV thrombus as this will carry a high risk for embolisation and anticoagulation may be needed. When LV dysfunction is discovered in the context of arrhythmias and congestive cardiac failure during the third trimester or immediately post delivery, the diagnosis is straight forward. Careful follow-up is mandatory as the disease can deteriorate rap-

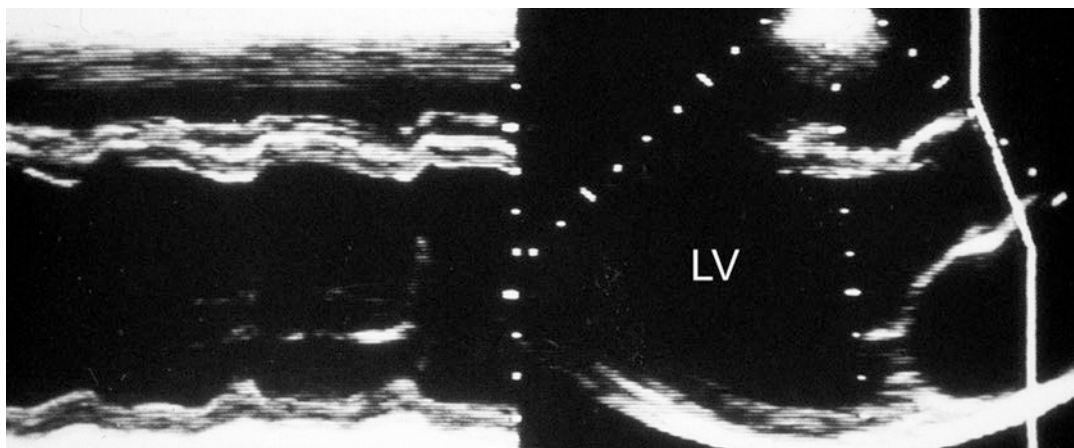


Fig. 24.32 M-mode echocardiogram (left) and parasternal long-axis view from a patient with marked alcohol consumption and heart failure. The echocardiographic pattern is that of dilated cardiomyopathy with reduced contraction

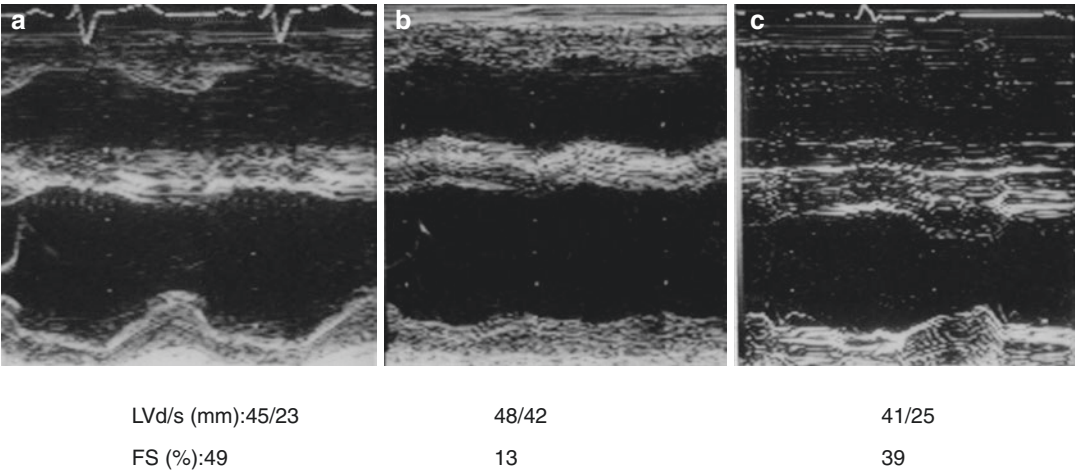


Fig. 24.33 Serial M-mode tracing from a patient with peripartum cardiomyopathy. (a) Before pregnancy, (b) Three days after delivery of a healthy baby and (c) One

year later. (b) The patient was extremely ill and was considered for cardiac transplantation. (c) The patient had completely recovered

idly with ventricular dilatation and further ventricular dysfunction or can improve from severe hypokinesia to mild ventricular dysfunction and reduced ventricular size to complete recovery.

Typically, peripartum cardiomyopathy can evolve in three ways of approximately equal thirds: 30% of patients may return to normal in up to a year post-delivery, 30% may deteriorate and evolve in to dilated cardiomyopathy and 30% may remain unchanged. The remaining 10% of patients may be in any intermediate stage. Persisting cardiomegaly at 6 months is usually associated with high mortality and the women may be candidates for cardiac transplantation.

Isolated Left Ventricular Non-compaction

Left ventricular noncompaction of the myocardium (LVNC) is characterised by prominent trabeculations and deep intertrabecular recesses in association with a thin compacted epicardial muscle layer. In some patients, it is associated with left ventricular dilatation and systolic dysfunction [1, 22].

LVNC can occur in an isolated form but is more commonly associated with other congenital cardiac disorders or hypertrophic and dilated cardiomyopathy. The prevalence of LVNC, esti-

mated from retrospective studies, ranges from 4.5 to 26 per 10,000 adult patients referred for echocardiography. Many patients are completely asymptomatic, but some present with congestive heart failure, thromboembolism and arrhythmias including sudden cardiac death.

LVNC is best viewed as a developmental abnormality. During early embryogenesis ventricular trabeculations develop in the distal left ventricle soon after looping and serves primarily as a means to increase myocardial oxygenation in the absence of effective coronary circulation. At the same time when ventricular septation occurs, the trabeculae start to condense (compact) in their portions adjacent to the outer myocardium adding to its overall ventricular thickness. At 6 weeks of development, fine trabeculae that may be present. At 12 weeks, the trabeculae begin to coalesce at a time when ventricular septation is completed. In the early fetal period the compact layer forms most of the myocardial mass. Failure for the left ventricle to condense (become compacted) may result to the isolated left ventricular non-compaction.

Familial disease is reported in 18–50% of adults with isolated LVNC, mostly with an autosomal dominant mode of inheritance. Numerous mutations in genes encoding sarcomere proteins have been reported including MYH7, ACTC1, TNNT2, TNNI3, MYL2 and MYL3.

The diagnosis is made by echocardiography in the vast majority of patients by the combination of the clinical picture of breathlessness or palpitations and the echocardiographic appearance of coarsely trabeculated left ventricle, often distally, presenting with a degree of subendocardial recesses (Fig. 24.34). The affected ventricle appears as two layers; a compact (solid) epicardial layer and an endocardial layer consisting of prominent trabecular meshwork and deep inter-trabecular spaces/recesses. This is best visualized in apical four-chamber projections and parasternal short axis views.

Restrictive Cardiomyopathy

Restrictive cardiomyopathy is defined by a pattern of ventricular filling in which small increases in ventricular volume causes a steep rise in ventricular pressure due to increased myocardial stiffness [1]. For many years, there has been confusion regarding this terminology as “restrictive physiology” occurs in different pathologies, including HCM and DCM. To promote consistent terminology, current ESC rec-

ommendations suggest that the term RCM should only be used when the characteristic physiology occurs in patients with a normal ventricular wall thickness and volume. Restrictive cardiomyopathy is caused by several conditions, including infiltrative and storage disorders and endomyocardial disease. In adults, RCM is often caused by cardiac amyloidosis, while in the tropics, endomyocardial fibrosis is the commonest cause [23].

Types of Restrictive Cardiomyopathies

Cardiac Amyloidosis

The diagnostic criteria of restrictive cardiomyopathy depend a lot upon the underlying condition. In cardiac amyloidosis, interstitial infiltration of the atria and ventricles lends the cardiac chambers a firm rubbery consistency.

Systemic amyloidosis is a disorder of protein metabolism in which characteristic abnormal extracellular protein material is deposited in organs and tissues. It causes considerable morbidity and is usually fatal. The heart is often involved in light chain amyloid and congestive heart failure

Isolated Left Ventricular Non-compaction

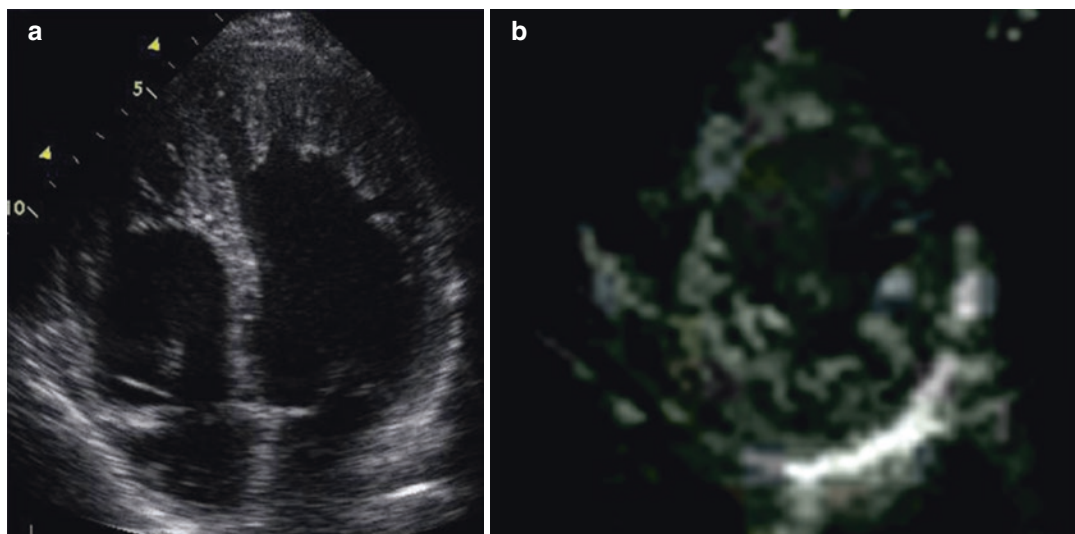


Fig. 24.34 Isolated Left Ventricular Non-compaction. On the left, parasternal short-axis view at distal LV showing the unusually coarsely trabeculated LV. On the right,

apical four-chamber from the same patient clearly demonstrating the deep recesses seen at the apex. We are grateful to Dr. Perry Elliott for providing this picture

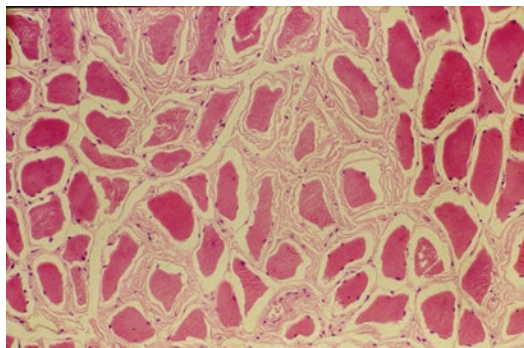


Fig. 24.35 Amyloid deposition among normal myocytes. Note that the myocardial fibers (here cut cross-sectionally) are normally arranged. The amyloid protein is infiltrated in the interstitial tissue among myocytes

is one of the dominant clinical manifestations (Fig. 24.35). The advent of modern echocardiography has greatly contributed to the ante mortem recognition of amyloid infiltration of the heart.

Not every form of amyloidosis involves the heart. AL amyloidosis involves the heart in 90% of the cases and commonly presents as heart failure while AA amyloidosis (reactive) only rarely affects the heart and when it does, it causes less functional impairment than in AL amyloidosis. Amyloid deposition begins in focal sub-endocardial accumulations and within the myocardium between the muscle fibres. Expansion of these myocardial deposits eventually causes pressure atrophy and separation of myocardial fibres. This mechanism is responsible for the marked thickening of the left and right ventricular walls, normal or decreased LV cavity size, reduced LV diastolic and systolic function. The walls of intramural coronary arteries as well as the conductive system are infiltrated and this accounts for the electrocardiographic abnormalities seen in some patients. The endocardium is also involved and may be associated with overlying thrombus. It also causes focal or diffuse valvular thickening but clinical valvular dysfunction is uncommon. Finally, the small amyloid heart may be surrounded by a large pericardial effusion.

The echocardiographic findings suggestive of amyloid infiltration of the heart, which although non-specific when taken individually, they are highly suggestive in combination, consisting

of thickened RV and LV walls with granular sparkling (ground glass appearance), normal or small LV cavity and enlarged atria (Fig. 24.36). Depressed myocardial contraction and relaxation is also characteristic of amyloid heart disease and this finding may greatly facilitate the differential diagnosis with hypertrophic cardiomyopathy (Fig. 24.37). Figure 24.38 is from a patient with AL amyloidosis with marked wall thickening and an abnormal diastolic function. Note that the transmitral velocities exhibit a “restrictive filling pattern” with absent late diastolic filling suggestive of elevated filling pressures. Involvement of the heart valves and atrial septum which appear homogeneously thickened without altering the valves motion may also be present. An other important characteristic of patients with amyloid heart disease is the preservation of apical contractility compared with the rest of the myocardium. This apical “sparing” can best be appreciated using global longitudinal strain where by apical strains are higher than the rest of myocardium.

Endomyocardial Fibrosis and Eosinophilic Cardiomyopathy (Löffler's Endocarditis)

Restrictive ventricular physiology can be caused by endocardial fibrosis, fibroelastosis and thrombosis. These disorders are sub-classified according to the presence of eosinophilia into endomyocardial diseases with hypereosinophilia (or hypereosinophilic syndromes (HES)) and endomyocardial disease without hypereosinophilia (e.g. endomyocardial fibrosis). Parasitic infection, drugs such as methysergide, inflammatory and nutritional factors are implicated in acquired forms of endomyocardial fibrosis.

In the acute hypereosinophilic variant—Löffler's endocarditis—there is an acute inflammatory process with myocardial tissue infiltration involves one or both ventricular apices, the chordae tendinae and the ventricular inflow tracts. This results in mitral and tricuspid regurgitation and impaired diastolic filling. Endomyocardial fibrosis is endemic in tropical and subtropical parts of Africa, India, Asia, and South and Central America, and may account for up to 25% of cardiac-related deaths in equatorial Africa. It is rare

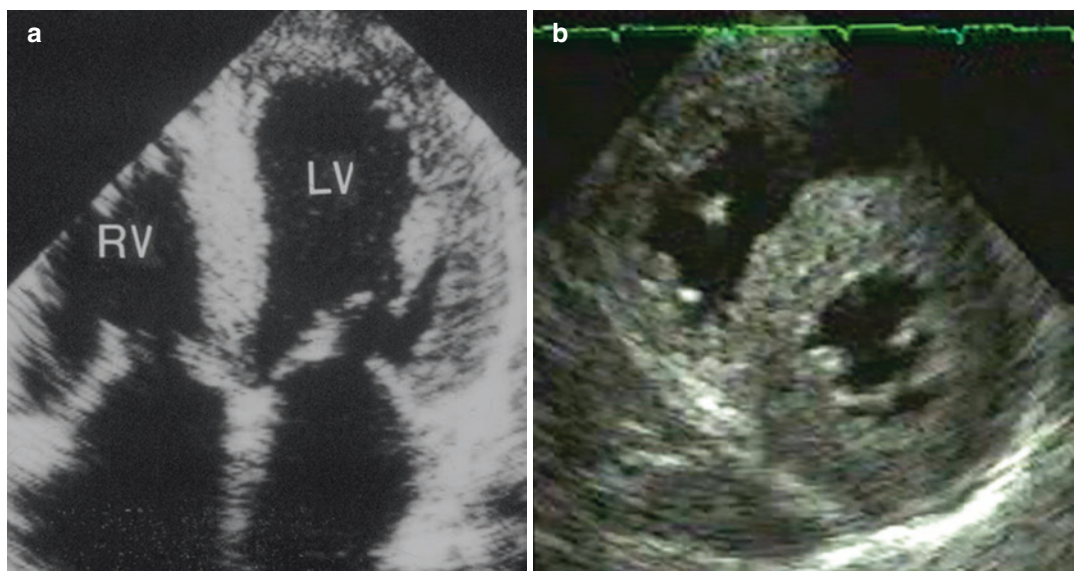


Fig. 24.36 Systemic amyloidosis. Apical four-chamber view (a) and short-axis (b) demonstrating marked wall thickness (15 mm) concentrically. Note the homogeneous

texture of both ventricles and the thickening of the mitral and tricuspid leaflets. The right ventricle is also thickened

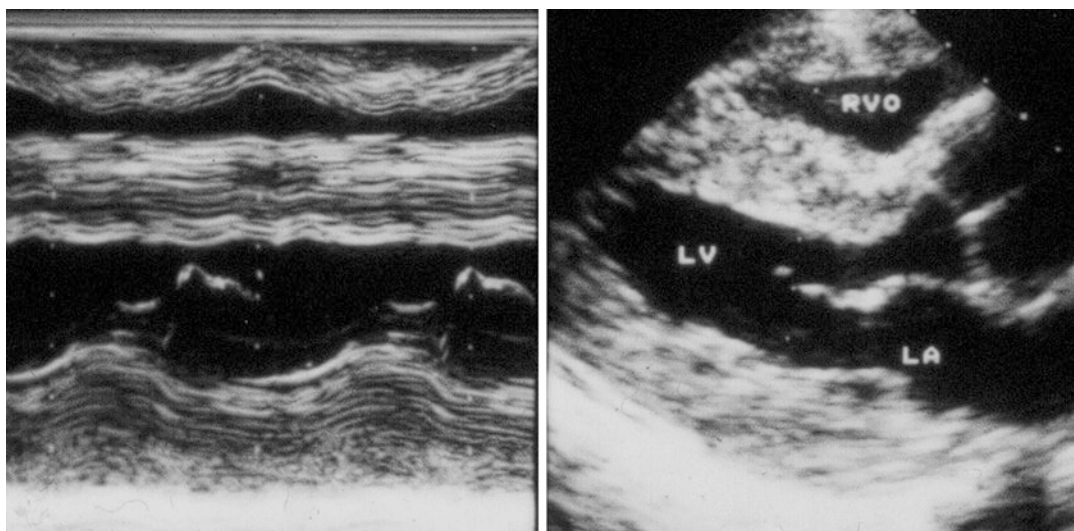


Fig. 24.37 Parasternal long-axis from a patient with cardiac amyloidosis with the corresponding M-mode echocardiogram to demonstrate the reduced left ventricular function. Note again the markedly thickened RV free wall

outside the tropics. Adolescents and young adults are most frequently affected. Disease onset is usually insidious, with progressive biventricular failure and a poor prognosis. Typically, fibrous endocardial lesions in the right and/or left ventricular inflow tract cause atrioventricular valve incompetence.

Echocardiography The echocardiographic characteristics of hypereosinophilic syndrome are typical and pathognomonic. There is extensive LV and RV thrombus usually packing the ventricular apices (Fig. 24.39). This is frequently called the “box-glove” sign because of the left ventricular resemblance of a box glove. The ventricular

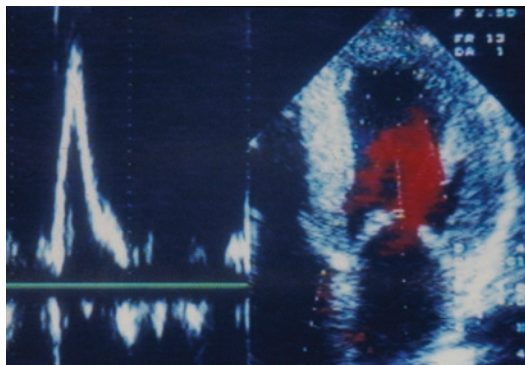


Fig. 24.38 Amyloid heart disease. Pulsed wave Doppler from the mitral valve demonstrating a “restrictive pattern” with absent late diastolic filling of the transmitral velocity suggesting of markedly impaired left ventricular diastolic function with elevated filling pressures

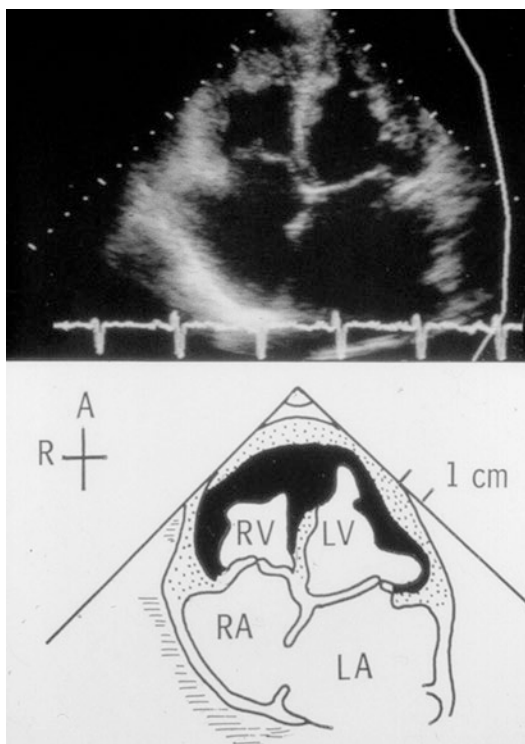


Fig. 24.39 Apical four-chamber view from a patient with endomyocardial fibrosis. Note the packing of the left and right ventricular apex and the marked dilatation of the atria

systolic function is usually preserved but there is restriction to ventricular filling manifested by an early diastolic halt on the M-mode echocardiogram (Fig. 24.40). With high-resolution two-dimen-

sional echocardiography, a distinct high intensity linear echo is identified covering the endocardial surface of the left and the right ventricles. This localized echo-dense area corresponds to areas of fibrosis extending from the apex to the basis of the ventricles and the papillary muscles (Fig. 24.41a). Cardiac Magnetic resonance imaging can also demonstrate the presence of intraventricular thrombus as well as the amount and extent of endocardial fibrosis (Fig. 24.41b). Often this material extends to the ventricular inflow track and involves the mitral or tricuspid chords and leaflets leading to significant valvular regurgitation (Fig. 24.42). Bi-atrial enlargement is also found in the majority of these patients as a result of the restrictive ventricular filling imposed by the non-compliant ventricle. The extent of valvular involvement however can better be appreciated with echocardiography.

Idiopathic Restrictive Cardiomyopathy

Many cases of RCM in adults, and the majority in children, are idiopathic. Familial disease is described in approximately 30% of patients with idiopathic restrictive cardiomyopathy [24, 25] and mutations in cardiac sarcomere protein genes particularly troponin I but also cardiac troponin T, α -cardiac actin and β -myosin heavy chain are the commonest genetic cause. Mutations in the gene encoding desmin (an intermediate filament protein with key structural and functional roles within skeletal and cardiac myocyte myofibrils) cause RCM associated with skeletal myopathy and cardiac conduction system abnormalities.

Patients are typically in class III or IV of the NYHA classification for heart failure at presentation, the atria are usually disproportionately dilated compared to the normal or near-normal ventricular size, the left ventricle has normal or near normal ejection fraction in the absence of hypertrophy. Histology is normally non specific and can show normal findings or non-specific degenerative changes, including myocyte hypertrophy and mild to severe interstitial fibrosis. Some myocardial disarray can also be present and when this occurs, genetic forms should be considered [25].

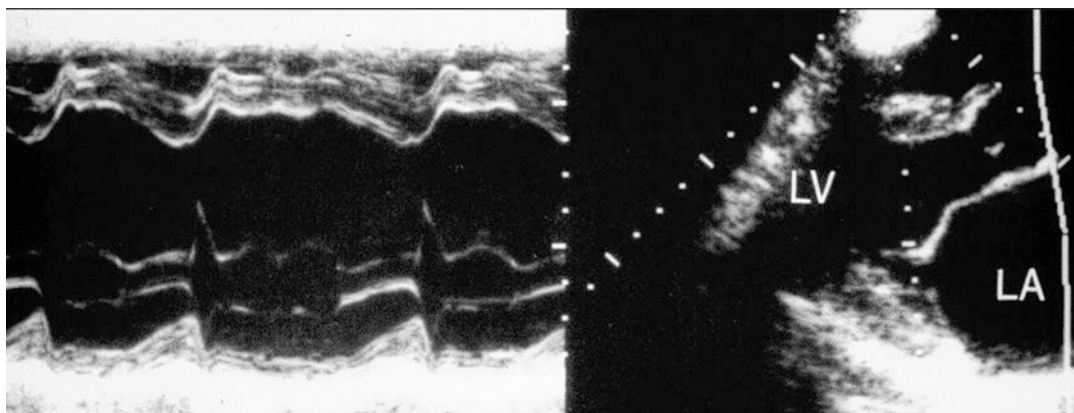


Fig. 24.40 M-mode and two-dimensional echocardiography from the same patient with endomyocardial fibrosis as in Fig. 24.31 demonstrating the abnormal diastolic left ventricular filling. During diastole, the left ventricle fills

rapidly in early diastole and then remains unchanged during the rest of diastole. Note that the systolic function is preserved

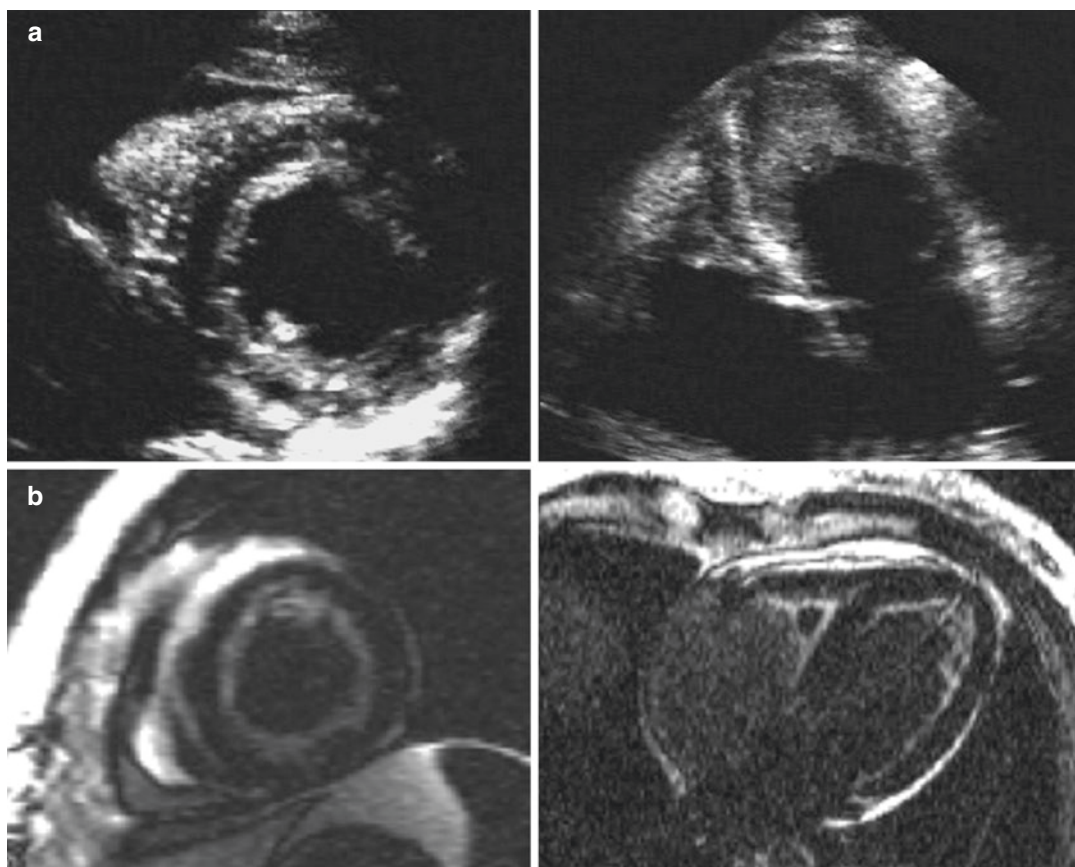


Fig. 24.41 (a) Parasternal short axis (left) and four-chamber (right) views from a patient with hypereosinophilic syndrome. Notice the bright endocardial echoes surrounding the cavity suggestive of fibrosis. In the apical four-chamber view, a typical “boxing-glove” appearance of the left ventricle with the apical thrombus packing the

apex of both, the left and the right ventricles. (b) Cardiac Magnetic Resonance Imaging with corresponding images from the same patient as in Fig. 24.33a showing again the extent of endocardial fibrosis (short axis and four chamber)

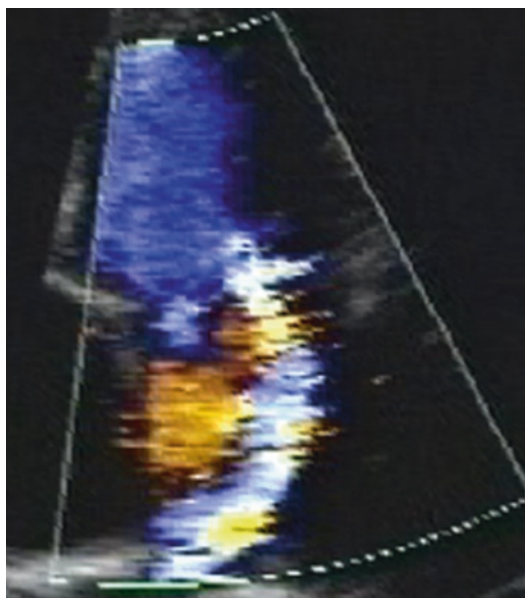


Fig. 24.42 Colour Doppler imaging showing the extent of mitral regurgitation. Calculated regurgitant volume 35 ml (moderate)

Restrictive Physiology

Increased ventricular filling pressures with the typical dip-and-plateau pattern are the haemodynamic hallmarks of restrictive cardiomyopathies, whatever the aetiology. Atrial pressures usually exceed 15 mmHg, right atrial pressure is required to be more than 7 mmHg and pulmonary capillary wedge pressure is required to be more than 12 mmHg [26]. In contrast with the equal left- and right-sided diastolic pressures in constrictive pericarditis, diastolic pressures are separable by more than 5 mmHg in restrictive cardiomyopathy due to unequal involvement and compliance of the two ventricles. However, this separation is not seen at baseline in restrictive cardiomyopathy and it is often not demonstrable despite provocative tests such as volume loading, leg rising, exercise or pharmacological interventions. Even the dip-and-plateau may be absent in restrictive cardiomyopathies.

Patients with restrictive cardiomyopathy either due to cardiac amyloidosis or endomyocardial fibrosis show ventricular filling abnormalities along the spectrum from a more advanced traditional restrictive pattern to a milder abnor-

mal relaxation with long isovolumic relaxation time (IVRT), reduced rate of acceleration to the low early peak velocity (E-wave), slow deceleration rate and relatively high atrial wave.

Distinction Between Restrictive Cardiomyopathy and Constrictive Pericarditis

Restrictive cardiomyopathy presents a clinical and haemodynamic picture that is usually indistinguishable from constrictive pericarditis. The differential diagnosis is crucial as constrictive pericarditis is curable whereas restrictive cardiomyopathy is not. Endomyocardial biopsy is useful in revealing the presence of myocardial disease. In addition to echocardiography, computed tomography and cardiac magnetic resonance imaging can be used to define pericardial thickness with or without the presence of calcification. Most common causes of constrictive pericarditis used to be tuberculosis, followed by idiopathic (viral), and following open heart surgery, radiation therapy and uremia. Now however the commonest cause is after open-heart surgery followed by radiation therapy and uraemia and these conditions rarely lead to calcification so that imaging techniques alone may not be sufficient to cover the entire spectrum of pericardial constriction. Consequently, when pericardial thickening is present, the diagnosis is relatively straight forward but when this is not the case, dynamic Doppler echocardiography during the respiratory cycle will play a crucial role in the differential diagnosis.

Normally there is interdependence between the RV and LV during respiration as the pericardium transmits the intrathoracic pressures to the intrapericardial and intracardiac chambers. During inspiration, there is a drop in intrathoracic pressures which will be transmitted to the intracardiac chambers with a parallel reduction of pulmonary capillary and left ventricular diastolic pressures, keeping the transmitral and trans-tricuspid diastolic gradients virtually unchanged (<20%), an increase of venous return and a slight increase in RV size. In constrictive pericarditis

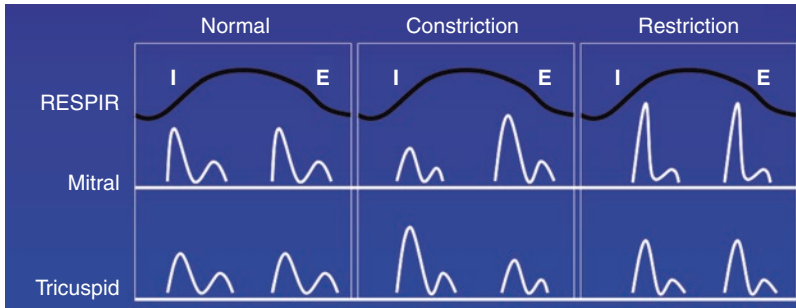


Fig. 24.43 Diagrammatic representation of the transmitral early (E wave) and late (A-wave) velocities during diastole throughout the respiratory cycle. Note the dynamic differences between restrictive cardiomyopathy and constrictive pericarditis during inspiration and expira-

tion. In constrictive pericarditis, the transmitral velocities are reduced while the tricuspid velocities are increased in deep inspiration, while the opposite happens during expiration. In restrictive cardiomyopathy there is little respiratory variation

because of the pericardial shell, the drop in intrathoracic pressures will not be transmitted to the intracardiac pressures so that the systemic venous and RA pressures do not fall during inspiration and the transmitral gradient will be reduced as oppose to the trans-tricuspid gradient which will be increased. Consequently, during inspiration the transmitral velocities will be reduced (E wave) and tricuspid velocities increased (E wave) in constrictive pericarditis while in restrictive cardiomyopathy will remain unchanged [27] (Fig. 24.43).

Arrhythmogenic Right Ventricular Cardiomyopathy (ARVC)

Definitions and Pathophysiology

Arrhythmogenic right ventricular cardiomyopathy—or arrhythmogenic cardiomyopathy—is a primary heart muscle disorder affecting 1 in every 1000–5000 adults and constitutes one of the major causes of sudden cardiac death (SCD) in young athletes. Early symptoms include palpitations, syncope and sudden cardiac death and at later stages patients may develop heart failure. Clinically, it is characterised by right and/or left ventricular wall motion abnormalities and dilatation and for much if its course is ventricular arrhythmias. It usually manifests between the second and fourth decade of life and is more

prevalent and severe in individuals engaged in athletic activity [28].

Histologically, the disease is characterised by fibrofatty replacement of myocardial tissue. Lesions initially affect the subepicardial layers of the myocardial wall and extend towards the endocardium as the disease progresses. ARVC was originally considered to affect the right ventricle exclusively, but it is known now to be a biventricular disease. ARVC is familial in about 60% of cases and is mostly inherited in an autosomal dominant trait except for a few rare autosomal recessive forms including Naxos disease. Most causative mutations occur in genes encoding for desmosomal proteins (plakoglobin, desmocollin-2, plakophilin-2, desmoplakin and desmoglein-2).

Criteria for Diagnosis of ARVC

Diagnosis of ARVC is challenging compared to other cardiomyopathies as there is no gold standard clinical test. Task force criteria have been developed by a group of experts and were revised in 2010 to improve specificity and sensitivity [29]. The new criteria include quantitative parameters defined by comparison with normal subject data. A definite diagnosis of ARVC is achieved when two major, or one major and two minor, or four minor criteria from different categories are met (Table 24.4) [30].

Table 24.4 Criteria for the diagnosis of ARVC

1. Global or regional dysfunction and structural alterations		
Major	By 2D echo	Regional RV akinesia, dyskinesia, or aneurysm and one of the following (end diastole): <ul style="list-style-type: none">• PLAX RVOT ≥ 32 mm (corrected for body size [PLAX/BSA] ≥ 19 mm/m²)• PSAX RVOT ≥ 36 mm (corrected for body size [PSAX/BSA] ≥ 21 mm/m²)• Or fractional area change $\leq 33\%$
	By CMR	Regional RV akinesia or dyskinesia or dyssynchronous RV contraction and one of the following: <ul style="list-style-type: none">• Ratio of RV end-diastolic volume to BSA ≥ 110 mL/m² (male) or ≥ 100 mL/m² (female)• Or RV ejection fraction $\leq 40\%$
	By RV angiography	Regional RV akinesia, dyskinesia, or aneurysm
Minor	By 2D echo	Regional RV akinesia or dyskinesia and one of the following (end diastole): <ul style="list-style-type: none">• PLAX RVOT ≥ 29 to <32 mm (corrected for body size [PLAX/BSA] ≥ 16 to <19 mm/m²)• PSAX RVOT ≥ 32 to <36 mm (corrected for body size [PSAX/BSA] ≥ 18 to <21 mm/m²)• Or fractional area change $>33\%$ to $\leq 40\%$
	By CMR	Regional RV akinesia or dyskinesia or dyssynchronous RV contraction and one of the following: <ul style="list-style-type: none">• Ratio of RV end-diastolic volume to BSA ≥ 100 to <110 mL/m² (male) or ≥ 90 to <100 mL/m² (female)• Or RV ejection fraction $>40\%$ to $\leq 45\%$
2. Tissue characterization of wall		
Major	Fibrofatty replacement of myocardium on endomyocardial biopsy	
	Residual myocytes $<60\%$ by morphometric analysis (or $<50\%$ if estimated), with fibrous replacement of the RV free wall myocardium in ≥ 1 sample, with or without fatty replacement of tissue on endomyocardial biopsy	
Minor	Residual myocytes $<60\%$ by morphometric analysis (or $<50\%$ if estimated), with fibrous replacement of the RV free wall myocardium in ≥ 1 sample, with or without fatty replacement of tissue on endomyocardial biopsy	
3. Repolarization abnormalities		
Major	• Inverted T waves in right precordial leads (V1, V2, and V3) or beyond in individuals >14 years of age (in the absence of complete right bundle-branch block QRS ≥ 120 ms)	
Minor	• Inverted T waves in leads V1 and V2 in individuals >14 years of age (in the absence of complete right bundle-branch block) or in V4, V5, or V6	
	• Inverted T waves in leads V1, V2, V3, and V4 in individuals >14 years of age in the presence of complete right bundle-branch block	
4. Depolarization/conduction abnormalities		
Major	• Epsilon wave (reproducible low-amplitude signals between end of QRS complex to onset of the T wave) in the right precordial leads (V1 to V3)	
Minor	• Late potentials by SAECG in ≥ 1 of 3 parameters in the absence of a QRS duration of ≥ 110 ms on the standard ECG	
	Filtered QRS duration (fQRS) ≥ 114 ms	
	Duration of terminal QRS <40 μ V (low-amplitude signal duration) ≥ 38 ms	
	Root-mean-square voltage of terminal 40 ms ≤ 20 μ V	
	• Terminal activation duration of QRS ≥ 55 ms measured from the nadir of the S wave to the end of the QRS, including R', in V1, V2, or V3, in the absence of complete right bundle-branch block	

(continued)

Table 24.4 (continued)

<i>5. Arrhythmias</i>	
Major	<ul style="list-style-type: none">• Nonsustained or sustained ventricular tachycardia of left bundle-branch morphology with superior axis (negative or indeterminate QRS in leads II, III, and aVF and positive in lead aVL)
Minor	<ul style="list-style-type: none">• Nonsustained or sustained ventricular tachycardia of RV outflow configuration, left bundle-branch block morphology with inferior axis (positive QRS in leads II, III, and aVF and negative in lead aVL) or of unknown axis• >500 ventricular extrasystoles per 24 h (Holter)
<i>6. Family history</i>	
Major	<ul style="list-style-type: none">• ARVC confirmed in a first-degree relative who meets current task force criteria• ARVC confirmed pathologically at autopsy or surgery in a first-degree relative• Identification of a pathogenic mutation categorized as associated or probably associated with ARVC in the patient under evaluation
Minor	<ul style="list-style-type: none">• History of ARVC in a first-degree relative in whom it is not possible or practical to determine whether the family member meets current task force criteria
	<ul style="list-style-type: none">• Premature sudden death (35 years of age) due to suspected ARVC in a first-degree relative
	<ul style="list-style-type: none">• ARVC confirmed pathologically or by current task force criteria in second-degree relative

(2010 Revised Task Force Criteria for arrhythmogenic cardiomyopathy) Two major, or one major and two minor, or four minor criteria: definite diagnosis of AC. One major and one minor, or three minor criteria: borderline diagnosis; One major, or two minor criteria from different categories: possible diagnosis

Echocardiographic Characteristics

Echocardiography is the diagnostic test of choice but this needs to be performed comprehensively following standardized protocols for the detailed imaging of the right ventricle [16]. As ARVC affects primarily the right ventricle, it is important to perform all right ventricular views, which include the RV inflow and outflow views. The typical presentation will be that of a young patient with ventricular arrhythmias. This patient will be referred for an echocardiographic examination, which should be conducted in an expert department to look for subtle RV abnormalities.

The earliest abnormalities that can be detected may be focal areas of myocardial dysfunction, which may involve the RV inflow, apex and/or the RV outflow tract. These areas however may easily be missed or not interpreted as pathological as there may well be considered as normal variants of the RV function. Figure 24.44 shows a discrete aneurysm of the RV apex seen from the apical four-chamber view. Here, particular attention was made to visualize the entire right ventricle at

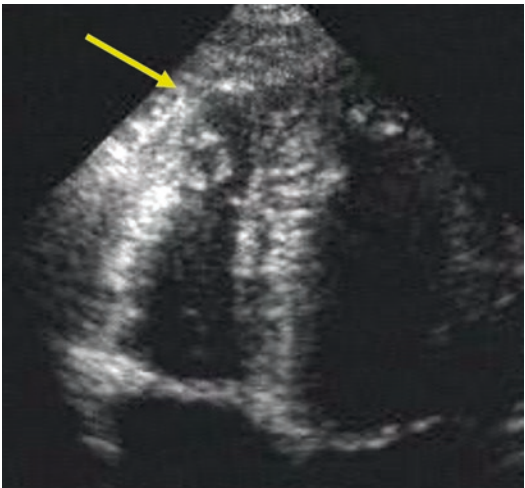


Fig. 24.44 Apical four-chamber view from a patient with ARVC. Notice that in this view, particular attention was made to visualize the entire RV. Only then, the discrete aneurys at the apex was visualized (arrow)

the expense of the left, which is not always performed in routine echocardiography.

The more obvious and pathognomonic abnormalities are those of localized aneurismal regions of the *triangle of dysplasia* in the form of end-sys-

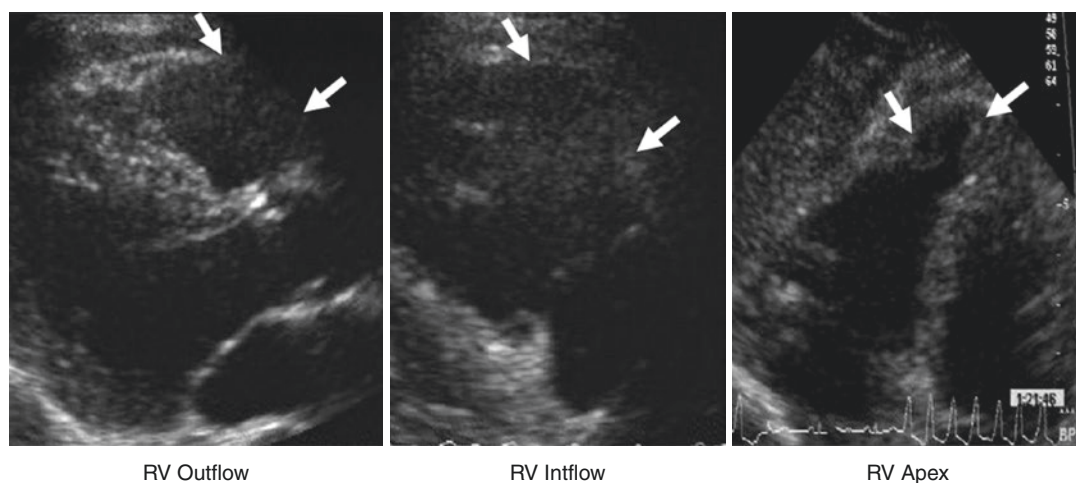


Fig. 24.45 Successive echocardiographic views from a patient with Arrhythmogenic RV cardiomyopathy to illustrate the *triangle of dysplasia*. On the left panel, there is a localized akinetic area in the outflow tract seen from parasternal long-axis view (arrows). In the middle panel,

the RV inflow track view with a localized akinetic region in the free wall (arrows). On the right panel, apical four-chamber projection demonstrating an apical aneurysm on the RV (arrows)

tolic bulges (Fig. 24.45). As long as the RV inflow and outflow tract projections are carefully recorded, missing those regional dyskinetic regions is difficult. It is possible that in one patient such abnormalities are seen in more than one region.

In a more advanced stage of ARVC, extended areas of RV free wall may become thin and akinetic which together with RV dilatation, will form the typical pattern of AVC (Fig. 24.46). The diagnosis here is difficult to miss. Ultimately, the whole of the RV will be dilated and hypokinetic.

Lastly, in the most severe and advanced cases, the LV will become involved and could mimic that of non-specific dilated cardiomyopathy. Global RV dysfunction is most common in patients with cardiac arrest, although this is not necessary true in patients with first presentation. Functional and structural worsening of RV performance may be the major risk factor for cardiac arrest in ARVC patients.



Fig. 24.46 Apical four-chamber view from a patient with a severe form of ARVC. In contrast with the patient in Fig. 24.42 where the aneurysm was very localised, here the entire RV is dilated and poorly contracting

Conclusion

While it is convenient to classify cardiomyopathies in four major groups, there is an overlap between the anatomic and functional characteristics in many instances. As the genetic demystification of the cardiomyopathies continues, the boundaries of the various types of cardiomyopathies may better be determined. Until that time, we should continue to categorizing our patients in the four groups and echocardiography is currently the best imaging modality to do so. Cardiomyopathies have a familial nature and it is important to screen family members, as often the diagnosis may be more revealing once the family screening has been completed and again, the role of echocardiography here is pivotal. As the causes and pathophysiology of cardiomyopathies are better understood, it may be argued that in future, the term “idiopathic” may no longer be sustainable.

References

1. Elliott P, Andersson B, Arbustini E, Bilinska Z, Cecchi F, Charron P, Dubourg O, Kühl U, Maisch B, McKenna WJ, Monserrat L, Pankuweit S, Rapezzi C, Seferovic P, Tavazzi L, Keren A. Classification of the cardiomyopathies: a position statement from the European Society of Cardiology Working Group on myocardial and pericardial diseases. *Eur Heart J*. 2008;29(2):270–6.
2. Elliott RM, Anastasakis A, Borger MA, Borggreve M, Cecchi F, Charron P, Hagege AA, Lafont A, Limongelli G, Mahrholdt H, McKenna WJ, Mogensen J, Nihoyannopoulos P, Nistri S, Pieper PG, Pieske B, Rapezzi C, Rutten FH, Tillmanns C, Watkins H. 2014 European Society of Cardiology Guidelines on diagnosis and management of hypertrophic cardiomyopathy. *Eur Heart J*. 2014;35:3733–2779.
3. Charron P, Arad M, Arbustini E, Basso C, Bilinska Z, Elliott P, Helio T, Keren A, McKenna WJ, Monserrat L, Pankuweit S, Perrot A, Rapezzi C, Ristic A, Seggewiss H, van LI, Tavazzi L. Genetic counselling and testing in cardiomyopathies: a position statement of the European Society of Cardiology Working Group on myocardial and pericardial diseases. *Eur Heart J*. 2010;31:2715–26.
4. Nugent AW, Daubeney PE, Chondros P, Carlin JB, Cheung M, Wilkinson LC, Davis AM, Kahler SG, Chow CW, Wilkinson JL, et al. The epidemiology of childhood cardiomyopathy in Australia. *N Engl J Med*. 2003;348:1639–46.
5. Hughes SE, McKenna WJ. New insights into the pathology of inherited cardiomyopathy. *Heart*. 2005;91:257–64.
6. Davies MJ, McKenna WJ. Hypertrophic cardiomyopathy – pathology and pathogenesis. *Histopathology*. 1995;26:493–500.
7. Wigle ED, Sasson Z, Henderson MA, Ruddy TD, Fulop J, Rakowski H, Williams WG. Hypertrophic cardiomyopathy. The importance of the site and the extent of hypertrophy. A review. *Prog Cardiovasc Dis*. 1985;28:1–83.
8. Maron MS, Olivetto I, Zenovich AG, Link MS, Pandian NG, Kuvin JT, Nistri S, Cecchi F, Udelson JE, Maron BJ. Hypertrophic cardiomyopathy is predominantly a disease of left ventricular outflow tract obstruction. *Circulation*. 2006;114:2232–9.
9. Rapezzi C, Arbustini E, Caforio AL, Charron P, Gimeno-Blanes J, Heliö T, Linhart A, Mogensen J, Pinto Y, Ristic A, Seggewiss H, Sinagra G, Tavazzi L, Elliott PM. Diagnostic work-up in cardiomyopathies: bridging the gap between clinical phenotypes and final diagnosis. A position statement from the ESC working group on myocardial and pericardial diseases. *Eur Heart J*. 2013;34(19):1448–58.
10. Shapiro LM, McKenna WJ. Distribution of left ventricular hypertrophy in hypertrophic cardiomyopathy: a two-dimensional echocardiographic study. *J Am Coll Cardiol*. 1983;2:437.
11. Maron BJ, Gottdiener JS, Epstein SE. Patterns and significance of distribution of left ventricular hypertrophy in hypertrophic cardiomyopathy. A wide angle, two-dimensional echocardiographic study of 125 patients. *Am J Cardiol*. 1981;48:418–28.
12. Nihoyannopoulos P, Karatasakis G, Frenneaux M, McKenna WJ, Oakley CM. Diastolic function in hypertrophic cardiomyopathy; relation to exercise capacity. *J Am Coll Cardiol*. 1992;19:536–40.
13. Nagueh SF, Bachinski LL, Meyer D, Hill R, Zoghbi WA, Tam JW, Quinones MA, Roberts R, Marian AJ. Tissue Doppler imaging consistently detects myocardial abnormalities in patients with hypertrophic cardiomyopathy and provides novel means for an early diagnosis before and independently of hypertrophy. *Circulation*. 2001;104:128–30.
14. Palka P, Lange A, Fleming AD, Donnelly JE, Dutka DP, Starkey IR, Shaw TR, Sutherland GR, Fox KA. Differences in myocardial velocity gradient measured throughout the cardiac cycle in patients with hypertrophic cardiomyopathy, athletes and patients with left ventricular hypertrophy due to hypertension. *J Am Coll Cardiol*. 1997;30(3):760–8.
15. O'Mahony C, Jichi F, Pavlou M, Monserrat L, Anastasakis A, Rapezzi C, Biagini E, Gimeno JR, Limongelli G, McKenna WJ, Omar RZ, Elliott PM, Hypertrophic Cardiomyopathy Outcomes Investigators. A novel clinical risk prediction model for sudden cardiac death in hypertrophic cardiomyopathy (HCM risk-SCD). *Eur Heart J*. 2014;35(30):2010–20.
16. Guttman OP, Pavlou M, O'Mahony C, Monserrat L, Anastasakis A, Rapezzi C, Biagini E, Gimeno

- JR, Limongelli G, Garcia-Pavia P, McKenna WJ, Omar RZ, Elliott PM. Hypertrophic Cardiomyopathy Outcomes Investigators. Prediction of thromboembolic risk in patients with hypertrophic cardiomyopathy (HCM risk-CVA). *Eur J Heart Fail*. 2015;17:837–45.
17. Pinto YM, Elliott PM, Arbustini E, Adler Y, Anastakis A, Böhm M, Duboc D, Gimeno J, de Groote P, Imazio M, Heymans S, Klingel K, Komajda M, Limongelli G, Linhart A, Mogensen J, Moon J, Pieper PG, Seferovic PM, Schueler S, Zamorano JL, Caforio AL, Charron P. Proposal for a revised definition of dilated cardiomyopathy, hypokinetic non-dilated cardiomyopathy, and its implications for clinical practice: a position statement of the ESC working group on myocardial and pericardial diseases. *Eur Heart J*. 2016;37(23):1850–8.
18. McNally EM, Golbus JR, Puckelwartz MJ. Genetic mutations and mechanisms in dilated cardiomyopathy. *J Clin Invest*. 2013;123(1):19–26.
19. Caforio AL, Pankuweit S, Arbustini E, Basso C, Gimeno-Blanes J, Felix SB, Fu M, Heliö T, Heymans S, Jahns R, Klingel K, Linhart A, Maisch B, McKenna W, Mogensen J, Pinto YM, Ristic A, Schultheiss HP, Seggewiss H, Tavazzi L, Thiene G, Yilmaz A, Charron P, Elliott PM, European Society of Cardiology Working Group on Myocardial and Pericardial Diseases. Current state of knowledge on aetiology, diagnosis, management, and therapy of myocarditis: a position statement of the European Society of Cardiology Working Group on myocardial and pericardial diseases. *Eur Heart J*. 2013;34(33):2636–48. 2648a-2648d.
20. Felker GM, Boehmer JP, Hruban RH, Hutchins GM, Kasper EK, Baughman KL, Hare JM. Echocardiographic findings in fulminant and acute myocarditis. *J Am Coll Cardiol*. 2000;36:227–32.
21. Pinamonti B, Alberti E, Cigalotto A, Dreas L, Salvi A, Silvestri F, Camerini F. Echocardiographic findings in myocarditis. *Am J Cardiol*. 1988;62:285–91.
22. Towbin JA, Lorts A, Jefferies JL. Left ventricular non-compaction cardiomyopathy. *Lancet*. 2015;386:813–25.
23. Kushwaha SS, Fallon JT, Fuster V. Restrictive cardiomyopathy. *N Engl J Med*. 1997;336:267–76.
24. Denfield SW, Rosenthal G, Gajarski RJ, Bricker JT, Schowengerdt KO, Price JK, Towbin JA. Restrictive cardiomyopathies in childhood. Etiologies and natural history. *Tex Heart Inst J*. 1997;24:38–44.
25. Mogensen J, Kubo T, Duque M, Uribe W, Shaw A, Murphy R, Gimeno JR, Elliott P, McKenna WJ. Idiopathic restrictive cardiomyopathy is part of the clinical expression of cardiac troponin I mutations. *J Clin Invest*. 2003;111:209–16.
26. Shebatai R. Pathophysiology and differential diagnosis of restrictive cardiomyopathy. *Cardiovasc Clin*. 1988;19:123–32.
27. Hatle LK, Appleton CP, Popp RL. Differentiation between constrictive pericarditis and restrictive cardiomyopathy by Doppler echocardiography. *Circulation*. 1989;79:357–70.
28. Basso C, Corrado D, Marcus FI, Nava A, Thiene G. Arrhythmogenic right ventricular cardiomyopathy. *Lancet*. 2009;373(9671):1289–300.
29. Marcus FI, McKenna WJ, Sherrill D, et al. Diagnosis of arrhythmogenic right ventricular cardiomyopathy/dysplasia: proposed modification of the task force criteria. *Eur Heart J*. 2010;31(7):806–14.
30. Foale RA, Nihoyannopoulos P, McKenna WJ, Kleinebenne A, Nadazdin A, Rowland E, Smith G. The echocardiographic measurements of the normal adult right ventricle. *Br Heart J*. 1986;56:33.

Manish Bansal, Partho P. Sengupta,
and Bijoy K. Khandheria

Heart failure is referred to a constellation of clinical signs and symptoms that results from either an inadequate ‘forward’ cardiac output (e.g. fatigue, cardiac cachexia, hypotension) or ‘backward’ circulatory congestion (e.g. dyspnea, hepatomegaly and ascites, dependent edema). It is estimated that nearly five million Americans suffer from heart failure, with an incidence approaching 10 per 1000 population among persons older than 65 years of age [1]. Heart failure accounts for nearly 20% of all hospital admissions among persons older than 65 years. The overall risk of death is approximately 5–10% per year, although an untreated patient with severe left ventricular (LV) dysfunction has a 1-year survival of only 50% [2, 3]. The term ‘LV dysfunction’, is used clinically in recognition of the fact that an abnormal myocardial function, either systolic, diastolic or mixed, underlies the clinical syndrome of heart

failure and determines the clinical pattern of presentation. Other factors playing vital roles include age, sex, underlying etiology and the pattern of neuro-hormonal mechanisms that attempt to counterbalance the hemodynamic effects of a compromised heart muscle function. In absence of a reversible etiology, these homeostatic changes, however, initiate a vicious cycle in which the chamber progressively dilates, hypertrophies, and becomes spherical—a process referred to as ‘remodeling’. Echocardiography, by virtue of its ability to provide simultaneous structural and functional assessment, plays a pivotal role in establishing the pattern and magnitude of myocardial dysfunction. Further, being user friendly, cost-effective and readily available, the use of echocardiography has grown widely in recent years for risk stratification of heart failure in patients with either symptomatic or sub-clinical forms of LV dysfunction and for serial tracking of responses following initiation of therapeutic strategies for halting or reversing cardiac remodeling.

M. Bansal
Medanta – The Medicity, Gurgaon, Haryana, India

P. P. Sengupta (✉)
Section of Cardiology, West Virginia University
Health Sciences Center, Morgantown, WV, USA
e-mail: partho.sengupta@hsc.wvu.edu

B. K. Khandheria
University of Wisconsin School of Health,
Milwaukee, WI, USA

Echocardiography, Aurora Health Care, Milwaukee,
WI, USA

Global Health, Milwaukee, WI, USA

Clinical Staging and Etiology of Heart Failure: Role of Echocardiography

The current American College of Cardiology/American Heart Association practice guidelines for heart failure divide the disorder into four stages (Table 25.1), two of which (stages A and B) are in asymptomatic individuals [4].

Echocardiography plays a key role in clinical staging of heart failure and differentiating reversible from non-reversible causes of LV dysfunction. Coronary artery disease is the underlying cause of heart failure in approximately two thirds of the patients (Fig. 25.1). Systolic dysfunction results from myocardium that is either viable or irreversibly damaged. Identification of dysfunctional myocardium with preserved viability presents an excellent opportunity to ameliorate heart failure

by revascularization. Echocardiography, by demonstrating regional motion abnormalities, permits recognition of ischemic etiology of heart failure. Further, dobutamine stress echocardiography or myocardial contrast echocardiography provide useful estimate of the extent of viable myocardial and coronary microcirculatory reserve. Similarly, the patients with non-ischemic causes of systolic dysfunction may also have either an identifiable etiology (e.g. hypertension, valvular heart disease, myocardial infiltration, myocarditis or pericardial diseases, Figs. 25.2, 25.3, 25.4, and 25.5) or may have no discernable cause (e.g. idiopathic dilated cardiomyopathy). Echocardiography is pivotal in the diagnosis and management of several of these conditions such as valvular heart diseases, cardiomyopathies and pericardial diseases. Even in idiopathic dilated cardiomyopathy, echocardiography may be helpful in selection of therapeutic interventions. For example, dobutamine stress echocardiography is useful in these patients for identifying those who would benefit with beta blockade. Improvement in myocardial contractility with dobutamine has been shown to predict the extent of improvement in systolic ventricular

Table 25.1 Clinical stages of heart failure

Stage	Description
Stage A	Patients at a high risk for developing heart failure but has no structural disorder of the heart
Stage B	Patient with structural disorder of heart but who has never developed symptoms of heart failure
Stage C	Patient with past or current symptoms of heart failure with underlying structural heart disease
Stage D	Patient with end-stage disease requiring specialized treatment strategies as mechanical circulatory support, continuous inotropic infusions, cardiac transplantation, or hospice care

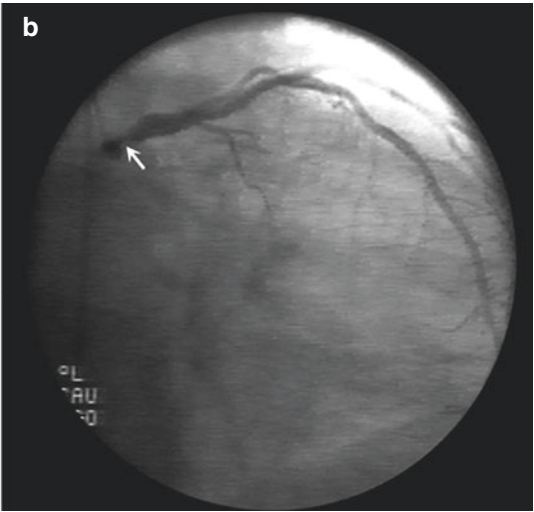
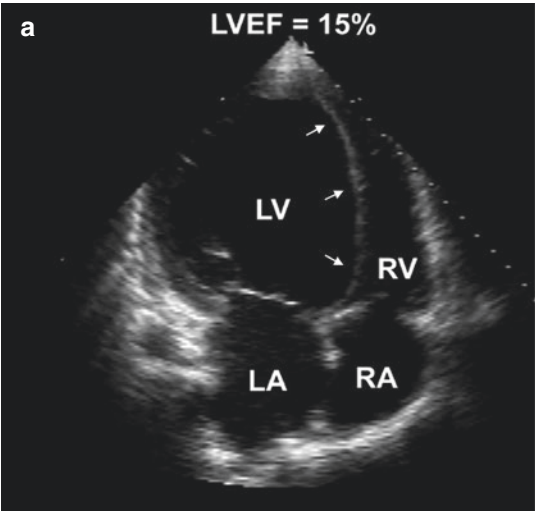


Fig. 25.1 Coronary artery disease is an underlying etiological factor in about two-third patients with heart failure. The picture shows echo in a patient with ischemic cardiomyopathy (a). Note the thinned out and scarred

inter-ventricular septum (arrows). Coronary angiogram (b) showed a tight stenosis of the left main coronary artery (arrow). LA left atrium, LV left ventricle, RA right atrium, RV right ventricle

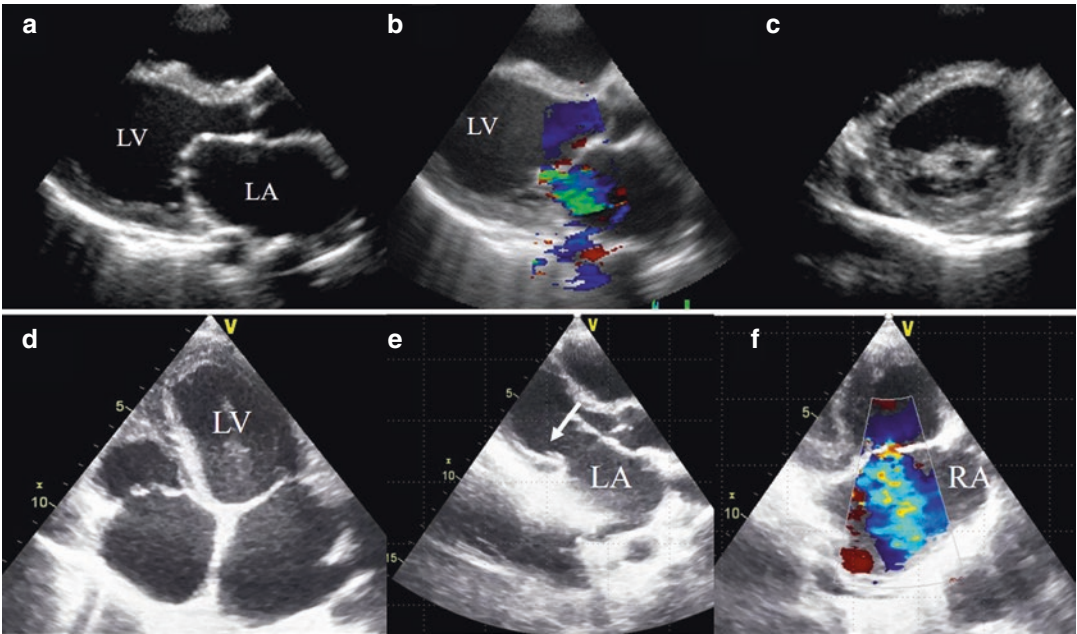


Fig. 25.2 Echocardiography is a versatile tool for identifying cardiac structural disorders in patients with heart failure. Panel **a–c** show echocardiographic findings in a patient with rheumatic mitral valve disease with severe left ventricular systolic dysfunction resulting from an underlying rheumatic carditis. Panel **d–f** show echocardiographic findings in a patient with heart failure resulting

from a severe endomyocardial fibrosis. Note the obliterated left ventricular apex due to formation of mural thrombi (**d**), tethering of posterior mitral leaflet (arrow, **e**) and tricuspid regurgitation due to severe pulmonary hypertension (**f**). *LA* left atrium, *LV* left ventricle, *RA* right atrium

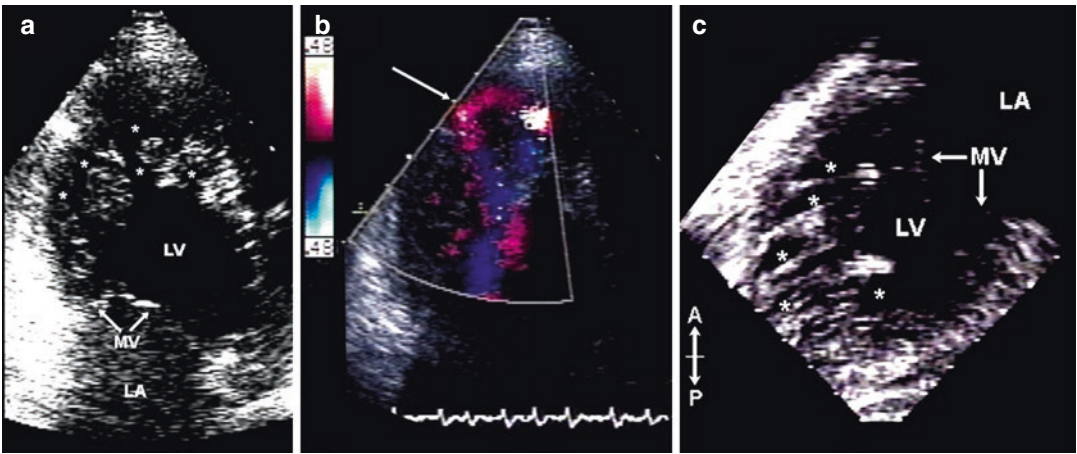


Fig. 25.3 Picture of an adult patient with non-compaction of left ventricle. Note the multiple intra-trabecular sinoids identified on transthoracic (**a**) and trans-esophageal echocardiography (**c**) which communicate with left ven-

tricular cavity (free color flow, **b**). Non-compacted left ventricle is a relatively recent echocardiographic recognition of heart failure in children and adults. *LA* left atrium, *LV* left ventricle, *MV* mitral valve

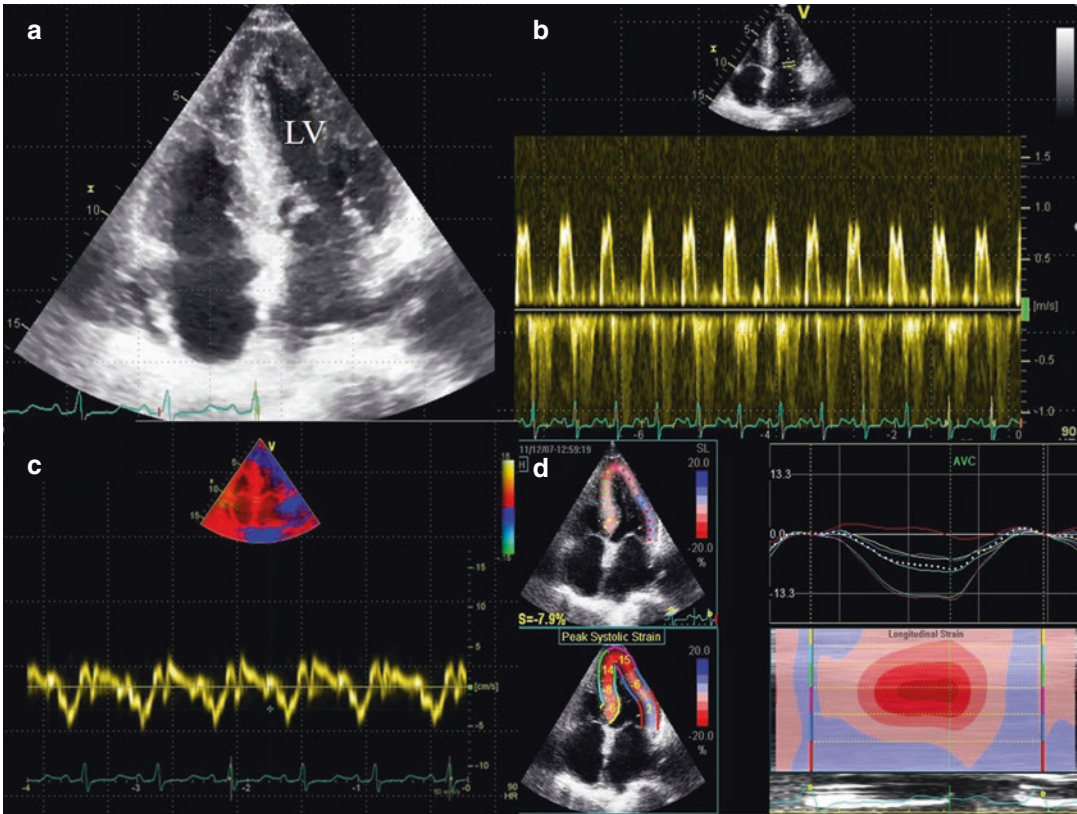


Fig. 25.4 Heart failure due to an advanced cardiac amyloid disease. Note the apical 4-chamber view with thickened myocardium (a). Mitral inflow velocities (b),

reduced mitral annular velocities (c), and markedly reduced left ventricular longitudinal strain with apical sparing (d). LV left ventricle

function following the use of beta-blockers [5]. The role of echocardiography in patients undergoing cardiac resynchronization therapy (CRT) has been a topic of intense exploration and is discussed in detail in another chapter in this book.

Depending on the predominant underlying mechanism, heart failure can also be classified as heart failure with preserved ejection fraction (EF; LVEF $\geq 50\%$), heart failure with mid-range EF (LVEF 40–49%) and heart failure with reduced EF (LVEF $<40\%$). Needless to mention, echocardiography is central to this classification of heart failure.

Quantification of LV Systolic Dysfunction

LV systolic dysfunction is generally defined as an EF less than 50% and occurs in 50–60% patients

with heart failure. The differentiation of normal from reduced LV systolic performance has therapeutic and prognostic implications [4, 6, 7]. In a recent population based survey of middle aged to elderly adults without previous myocardial infarction or evidence of coronary artery disease, reduced EF by echocardiography ($<40\%$) was associated with a 35% risk for cardiovascular death and 12% risk for all-cause mortality. Segmental and global LV dysfunction were associated with 3.3-fold and 3.8-fold higher rates of cardiovascular death, respectively [7]. LVEF is traditionally computed from echocardiography by using systolic and diastolic volumes obtained from biplane planimetry of paired orthogonal long-axis apical views. However, at vast majority of the centers, LVEF is usually mentioned as a descriptive grade of function, using subjective visual assessment by the echocardiographer. While in general, quantitative techniques provide

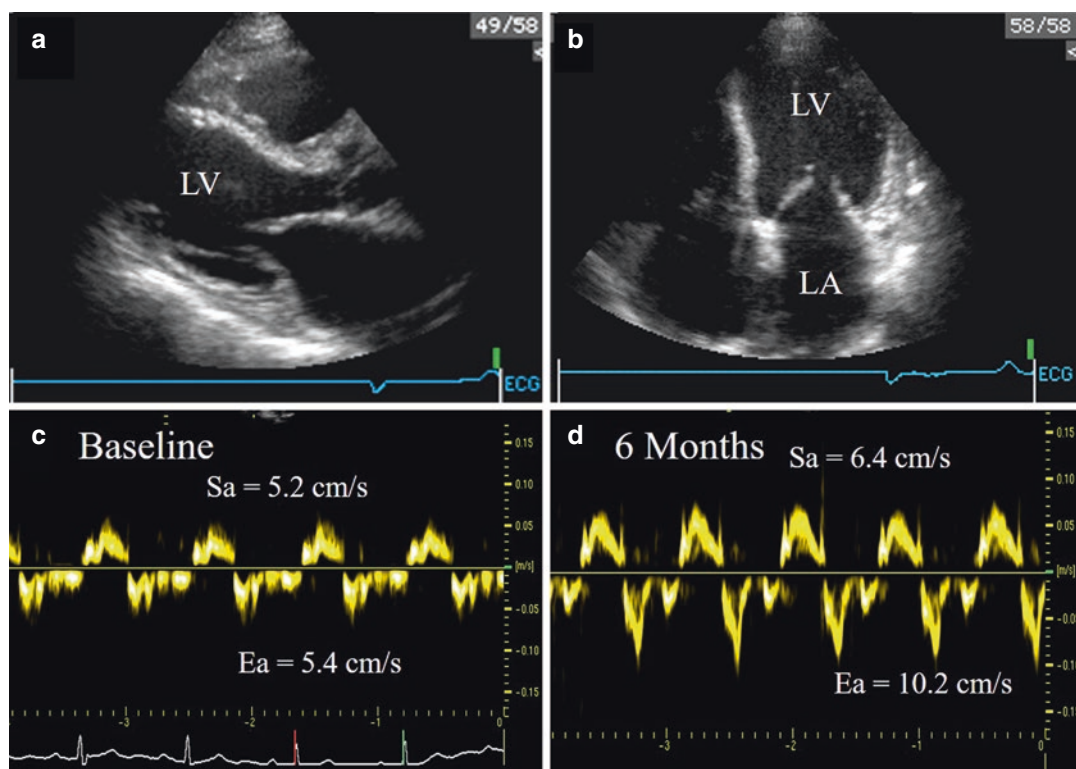


Fig. 25.5 Spontaneous improvement of left ventricular systolic dysfunction in a patient with myocarditis. Mitral annular velocities from interventricular septum showed

significant improvement within 6 months. *Ea* early diastolic mitral annular velocity, *Sa* peak systolic mitral annular velocity, *LA* left atrium, *LV* left ventricle

more accurate thresholding, grading based on visual eyeballing, when used by experienced readers, has not been found to be inferior to other reference methods. When available, three-dimensional (3D) echocardiography provides more accurate assessment of LV volumes and EF than two-dimensional (2D) echocardiography and is the modality of choice for this purpose [8]. However, compared with 2D, 3D echocardiography has greater dependence on gray-scale image quality and generally has lower temporal resolution, unless multi-beat acquisition is performed which often introduces stitch artifacts.

Other echocardiographic variables that have been alternatively used for grading LV systolic function include fractional shortening and wall motion index or score. Doppler echocardiography provides useful noninvasive estimation of LV stroke volume and cardiac output. Spectral velocity recordings in patients with valvular regurgitation can also be used for estimating chamber

pressures and dp/dt (rate of change of pressure over time). The current recommendation of the American society of echocardiography advocates routine measurement of LV EF, diastolic volume, mass and wall motion score using the 16- or 17-segment LV model [8]. Assuming that the purpose of echocardiography is to establish whether or not LVEF is in the range of less than 40%, a value of <30% by Simpson's rule, or >1.7 by wall motion index, can be assumed to qualify as systolic dysfunction. Similarly, a value of >50% or <1.0 can reliably be assumed to quantify a normal systolic function [9].

Quantification of Diastolic Dysfunction

Although majority of the patients with systolic dysfunction have some degree of diastolic dysfunction, population based studies have

highlighted that 40–50% of individuals with overt features of heart failure may have apparently normal LV systolic function (EF more than 50%), also referred to as diastolic heart failure [10, 11], or more appropriately, heart failure with preserved EF. Recent reports highlight a high prevalence of pre-clinical isolated diastolic dysfunction in population who subsequently suffer a marked increase in all-cause mortality, independent of age, sex and EF [12]. Thus, quantification of an abnormal LV diastolic function is equally important in patients who exhibit symptoms of heart failure as well as those in whom diastolic dysfunction is clinically silent. Although clinical

diagnosis of heart failure with normal EF effectively identifies those with abnormal diastolic function, an objective measurement of diastolic function is desirable for grading the pattern of dysfunction since it helps in determining the underlying mechanisms and choice of therapeutic intervention (Fig. 25.6).

Echocardiographic Indices for Assessing LV Diastolic Function

Mitral Inflow Velocities

LV relaxation is an energy dependent process that begins during the ejection phase of systole and

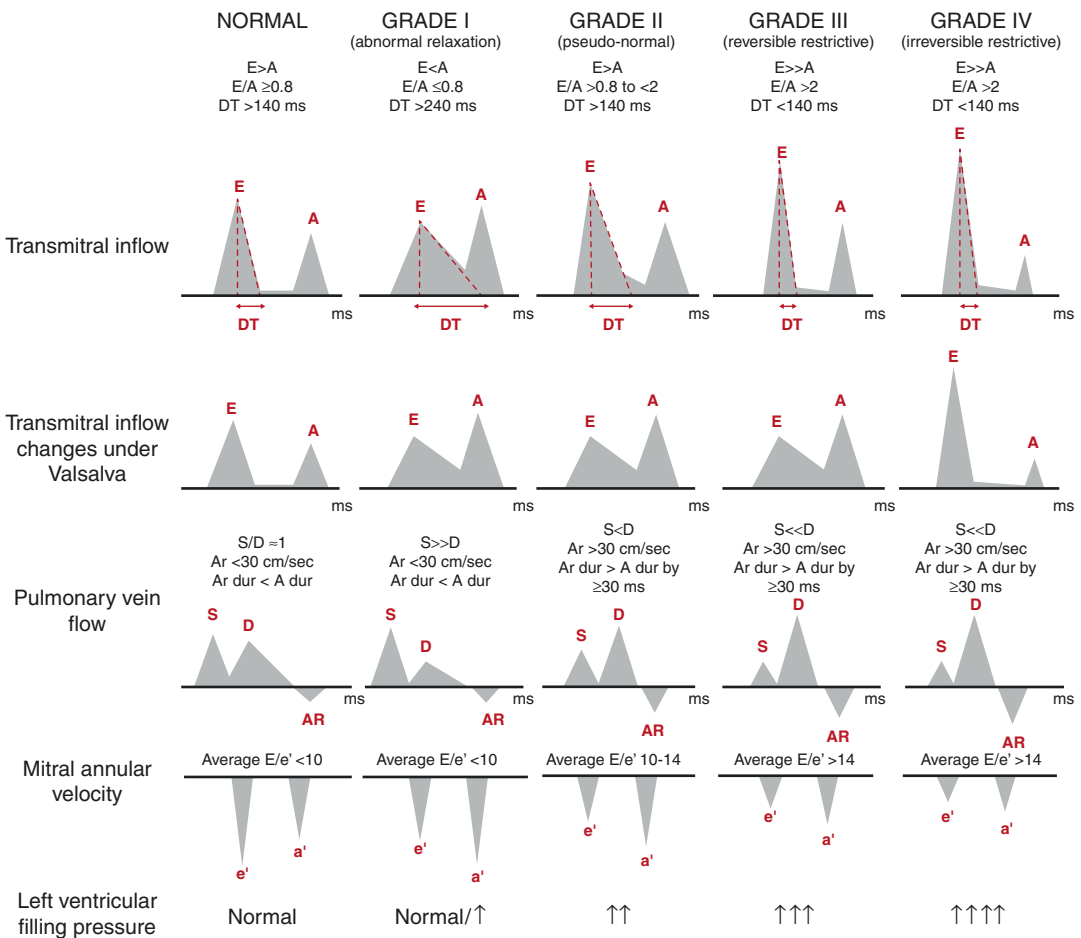


Fig. 25.6 Echocardiographic evaluation of left ventricular diastolic dysfunction. A mitral inflow late diastolic velocity, e' mitral annular late diastolic velocity, Ar pulmonary venous atrial reversal wave, D pulmonary venous

diastolic velocity, DT deceleration time of mitral E velocity, E mitral inflow early diastolic velocity, e' mitral annular early diastolic velocity, S pulmonary venous systolic velocity. Adapted from Duarte and Fernandez [94]

continues through the isovolumic relaxation and the rapid filling phases. During exercise the rate and the extent of LV relaxation increases proportionately and is crucial for continued normal pattern of LV filling despite shortening of diastolic filling period. This acceleration in LV relaxation during exercise is mediated by an enhanced sympathetic tone and is markedly blunted in heart failure. The left atrial to LV gradient and left atrial pressure during early diastolic filling therefore rises during exercise in patients with heart failure causing symptoms of shortness of breath. When more advanced, the diastolic filling abnormalities become apparent even at rest.

In a normal heart, a rapid flow velocity during early inflow occurs following mitral valve opening (E wave) followed by deceleration of flow during diastasis. Atrial contraction at the end of diastole results in a second wave (A wave). The initial abnormality of diastolic function is characterized by a decrease in mitral E velocity and prolongation of deceleration time and a tall A wave causing a reduced E/A ratio (abnormal relaxation or grade I or mild diastolic dysfunction). With progression of disease and further decline of active myocardial relaxation, filling of the left ventricle becomes increasingly dependent on the left atrial contraction and an increasing left atrial pressure. An increased mean left atrial pressure “pseudonormalises” the flow from the left atrium to left ventricle, with increasing velocity of E wave and shortening of the deceleration time, resembling a normal state (pseudonormal or moderate or grade II diastolic dysfunction). In the latter stages, LV chamber compliance is severely impaired so that a rising left atrial pressure causes rapid early mitral inflow (higher E velocity) with rapid equilibration of left atrial and LV pressures causing early truncation of the E wave (very short deceleration time), with very little contribution to filling from atrial contraction (small A wave) (restrictive or severe or grade III–IV diastolic dysfunction). In the initial stages (grade III), the filling pressures can be lowered to reverse the restrictive pattern to lower grades of diastolic dysfunction, but in the later stages, the restrictive pattern persists

despite manipulation of filling pressure indicating an irreversible stage of diastolic dysfunction (grade IV).

Although mitral inflow velocities and E/A ratio have been shown to predict LV filling pressures and determine prognosis, they have some limitations. The prediction of LV filling pressures is accurate only in patients with concomitant systolic dysfunction, whereas patients with normal systolic function show a wide scatter. The distinction between normal versus pseudonormal filling is difficult and other parameters are needed for differentiation. Preload modification, using glyceryl trinitrate or the Valsalva maneuver, are useful means of unmasking elevated filling pressures. However, this may not always be practical in clinical practice and some patients may not be able to perform an adequate Valsalva maneuver [13, 14].

Pulmonary Venous Doppler Velocities

Pulmonary venous flow (systolic versus diastolic predominance) has been used for predicting left atrial pressure in selected patients. The comparison of the duration of flow at atrial contraction across the mitral valve (mitral inflow) with the duration of flow-reversal into the pulmonary veins can be used for estimating the LV end diastolic pressure. In presence of normal left atrial pressure, systolic flow is dominant, and the systolic filling fraction is usually greater than 60%. There is a small reverse component following the diastolic wave, reflecting atrial contraction. This back flow occurs because of lack of valves at the pulmonary vein-atrial junction. With rising filling pressures, a worsening relative compliance of the left ventricle compared with the pulmonary venous circuit is observed. Transmitral flow at atrial contraction is shortened while retrograde flow into low resistance pulmonary venous circuit becomes more marked and continues for a longer duration. If the duration of atrial reversal flow in the pulmonary vein exceeds by more than 30 ms the duration of flow across the mitral valve, raised LV end diastolic pressure can be diagnosed with high specificity. Thus, the use of pulmonary venous flow is useful for distinguishing a normal transmitral filling pattern from pseudonormalization. However,

the major limitation in the use of the pulmonary venous signals is that these signals are often difficult to obtain and interpret.

Mitral Annular Velocities

The velocity of the mitral annulus represents velocity of changes in LV long-axis dimensions. In normal LV relaxation after systole, the peak mitral annular early-diastolic velocity (E') recorded by tissue Doppler imaging precedes the peak early passive diastolic transmitral flow (E) recorded by conventional pulsed-wave Doppler ultrasound. In situations where this relaxation is impaired, E' follows E . Apart from timing, the magnitude of E' has also been proposed to represent the intrinsic speed of myocardial relaxation and has a modest correlation with the time constant of relaxation. It is therefore used for differentiating between the effects of “suction” versus “transmitral pushing” when the left atrial pressure is high. In the initial stages of diastolic dysfunction, the relaxation velocity (E') decreases and remains reduced throughout the remaining stages of impaired diastole. A combination of mitral inflow velocities with the mitral annular velocity into a ratio (E/E') has been shown to provide superior prediction of LV filling pressure. This can be used for resolving normal from pseudonormal filling since patients with diastolic dysfunction and apparently normal mitral inflow pattern exhibit a reduced mitral annular velocity (E') and an elevated E/E' ratio. If E/E' is >15 (using medial E'), LV filling pressure is raised, and when E/E' is <8 filling pressure is low. However, between 8 and 15 there is considerable variability in filling pressure [13, 14].

Flow Propagation

Color Doppler M-mode provides a unique window into the fluid dynamics of flow across the mitral valve. The speed of propagation (slope of the first aliasing velocity at the leading edge of the E-wave) is enhanced with rapid relaxation and LV suction. With normal LV diastolic filling, rapid relaxation generates a dynamic pressure gradient, from base towards LV apex. During early diastolic filling, peak LV filling therefore rapidly propagates sequentially from mitral orifice towards apex. In contrast, filling related to left atrial contraction does not pass the mid portion of left ventricle.

With onset of diastolic dysfunction, a blunting of early-diastolic flow propagation is seen, however propagation velocity does not pseudonormalize. Color M-mode flow propagation can be combined in a ratio with the mitral E velocity to provide a load-adjusted parameter (E/V_p) which strongly correlates with filling pressures. The chief limitations of this tool are lack of consensus on technique and theoretical concerns that this will be invalid in small LV cavities [15, 16].

Other Doppler Variables in Hemodynamic Assessment

Doppler velocity tracings can also be used for calculating systolic and diastolic time intervals and have been shown to be closely linked with overall LV performance. Combined Doppler myocardial performance index [(isovolumic contraction time + isovolumic relaxation time)/ejection time] has been shown to have significant correlation with LV end-diastolic pressure and is a sensitive indicator of overall cardiac dysfunction in patients with mild-moderate congestive heart failure [17]. Other applications of Doppler in patients with heart failure include use of continuous wave Doppler for estimating pulmonary artery pressures from spectral tracings of tricuspid and pulmonary regurgitation. Besides Doppler, a simple 2D inspection of the inferior vena cava during subcostal imaging for its size and collapsibility with deep inspiration provides a useful estimate of the right atrial filling pressure.

Integrating Different Measures of LV Diastolic Function

A major limitation of the echocardiographic assessment of LV diastolic function is that the different Doppler indices are often not concordant with each other in the same patient. Also, there is considerable overlap between values in healthy individuals and those with diastolic dysfunction, which further complicates the assessment. To overcome these challenges, the American Society of Echocardiography has recommended an algorithm for assessment of LV diastolic function in patients with reduced LVEF or those with preserved LVEF but with a myocardial disease (Fig. 25.7) [18]. The algorithm takes in to consideration the following key variables—mitral inflow

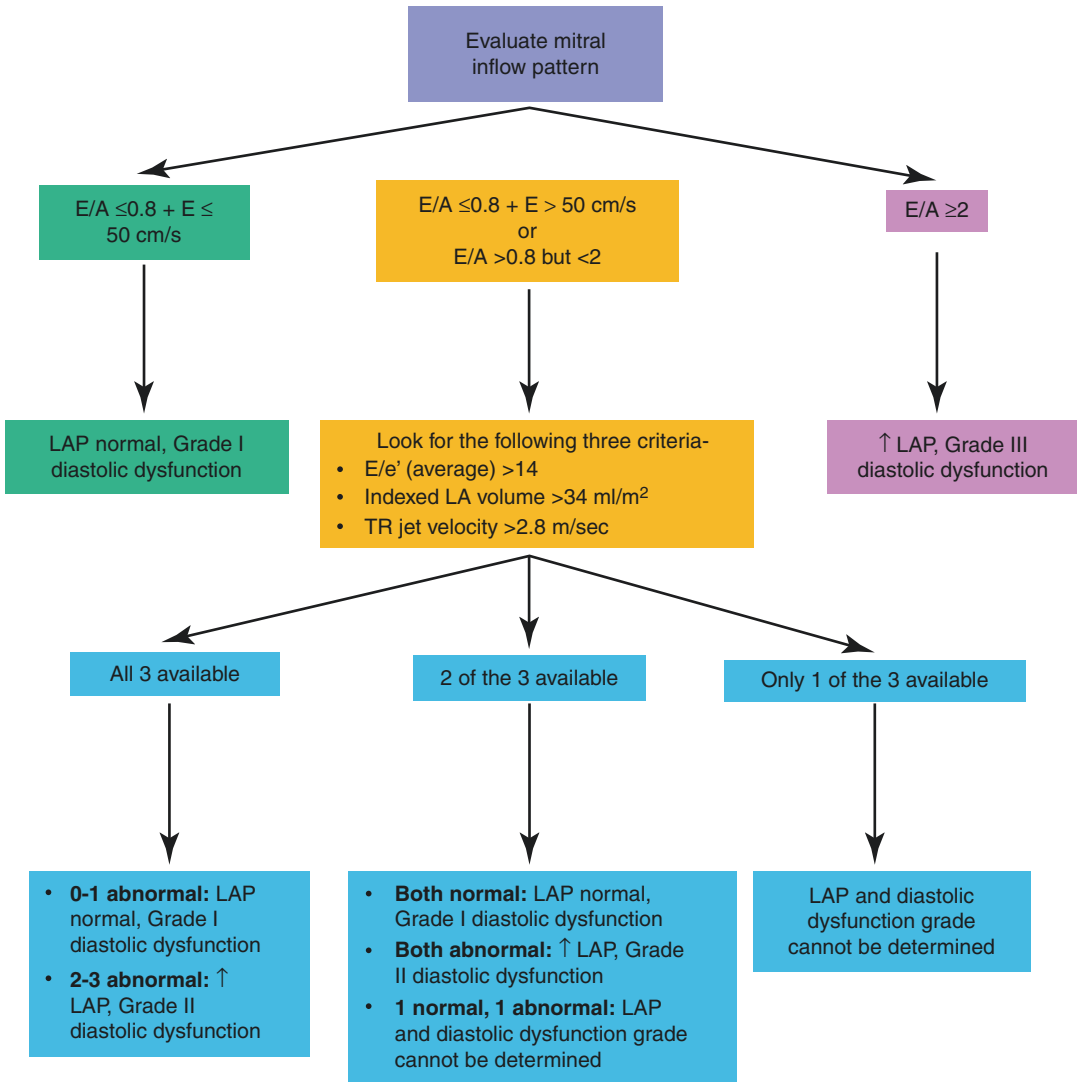


Fig. 25.7 Algorithm for echocardiographic estimation of left atrial pressure and grading left ventricular diastolic function in patients with myocardial disease (modified from: Nagueh et al. [18]). *A* mitral inflow late diastolic

velocity, *E* mitral inflow early diastolic velocity, *e'* mitral annular early diastolic velocity, *LA* left atrial, *LAP* left atrial pressure, *TR* tricuspid regurgitation

velocities, mitral *E/e'*, peak velocity of tricuspid regurgitation jet, and indexed left atrial volume.

Role of Myocardial Mechanics in Evaluation of Heart Failure Patients

Although LVEF is an extensively validated measure of LV systolic function, it has certain limitations. The foremost limitation is that LVEF is an

oversimplified, global index of LV contractile function and is therefore unable to characterize the complex multidimensional deformation of the left ventricle during the cardiac cycle. Additionally, being a global measure, LVEF is insensitive to subtle impairment in LV contractile function occurring during the early stages of diseases. Myocardial deformation imaging overcomes these limitations inherent in LVEF and has provided great insights in to the development and progression of heart failure.

LV myocardium is composed of muscle layers with helically arranged myofibers. Because of the helical arrangement, longitudinal contraction of the muscle fibers results in 3D deformation of the left ventricle, characterized by shortening in longitudinal and circumferential directions, thickening in radial direction and rotation and twist along the long-axis. Speckle-tracking echocardiography (STE), a gray-scale based technique, permits comprehensive assessment of LV myocardial deformation. Using STE, these different components of LV deformation can be measured as longitudinal strain, circumferential strain, radial strain, apical and basal rotation and twist, respectively [19].

Although the different layers of LV myocardium functionally behave as a continuum, the long-axis shortening is governed predominantly by the subendocardial fibers due to their more parallel alignment with the LV long-axis. In contrast, the sub-epicardial layers determine predominantly the circumferential shortening and the rotation of the left ventricle. Thus, depending on the muscle layer involved in the disease process, distinct patterns of LV contractile dysfunction can emerge, resulting in distinct heart failure phenotypes as described below (Fig. 25.8) [20].

Heart Failure with Predominant Longitudinal Dysfunction

Since most of the myocardial diseases initially involve the subendocardial layer, longitudinal strain is the first one to get compromised. The LVEF however remains preserved due to the relatively unopposed contractile response of the sub-epicardial layers [21]. As a result, LV circumferential strain and twist are normal or may even be exaggerated at this stage [22, 23]. LV diastolic function however is compromised because even mild impairment of subendocardial function may lead to significant slowing of the LV relaxation [24]. These patients usually present with heart failure with preserved EF (Fig. 25.9).

Heart Failure with Predominant Circumferential Dysfunction

When there is predominant involvement of the subepicardial layers, it leads to impairment of

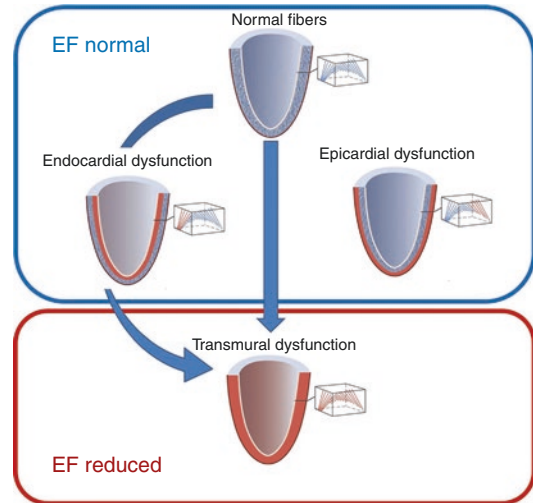


Fig. 25.8 Classification of heart failure based on myocardial mechanics. Selective impairment of only endocardial or epicardial layer results in predominant longitudinal or circumferential dysfunction, respectively, manifesting as heart failure with preserved ejection fraction. Progressive transmurular affection causes exhaustion of the compensatory mechanisms and development of dilated myocardial chambers and reduction of ejection fraction (reproduced from: Omar et al. [20]); with permission. *EF* ejection fraction

circumferential and twist mechanics of the left ventricle but the LVEF remains relatively preserved due to compensatory augmentation of subendocardial contraction [25]. LV diastolic function is impaired even in these patients as normal LV twist-untwist is important for early diastolic suction. Thus, these patients also present with heart failure with preserved EF. This pattern of LV myocardial dysfunction is typically seen in pericardial diseases that tend to involve the heart from outside (Fig. 25.10).

Heart Failure with Transmurular Dysfunction (Longitudinal and Circumferential Dysfunction)

Transmurular involvement of the LV myocardium results in simultaneous impairment of LV longitudinal and circumferential mechanics leading to a fall in LVEF and LV dilatation [21, 26]. These patients typically present with heart failure with reduced EF. Such transmurular involvement of the left ventricle can occur either due to acute transmurular injury, as in ST-segment elevation

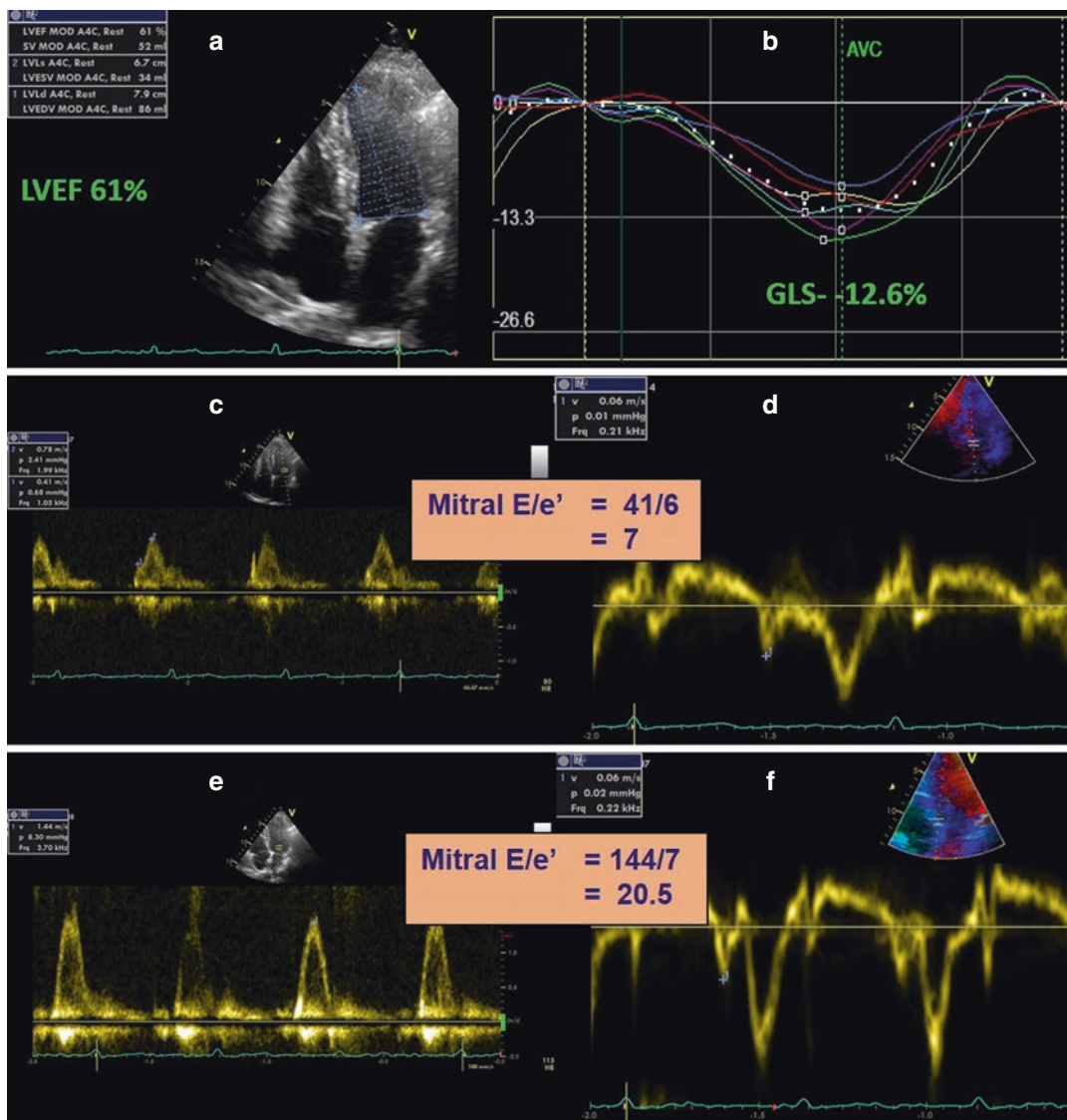


Fig. 25.9 A patient with previous coronary angioplasty presented with significant exertion dyspnea. His left ventricular ejection fraction was normal (a) but global longitudinal strain was significantly reduced (b). Exercise stress did not reveal any significant inducible wall motion abnormality. However, his left ventricular filling pressure

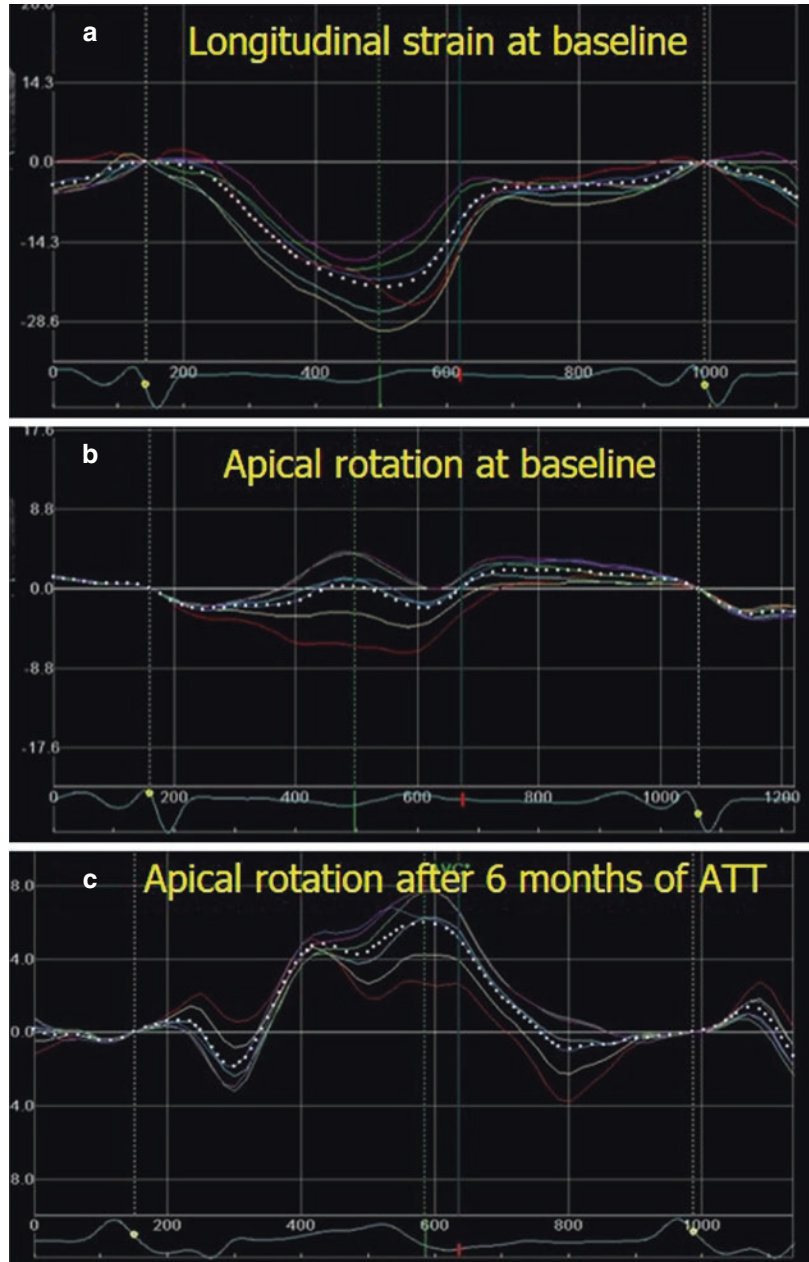
which was normal at rest (c, d) rose sharply on exercise (e, f), thus consistent with a diagnosis of heart failure with preserved ejection fraction. *E* mitral inflow early diastolic velocity, *e'* mitral annular early diastolic velocity, *GLS* global longitudinal strain, *LVEF* left ventricular ejection fraction

myocardial infarction, or due to gradual extension of the disease process from the subendocardial or subepicardial regions.

Interestingly, molecular changes in the LV myocardium have been shown to mimic the layer-specific myocardial dysfunction as described above. For example, a significant reduction in

beta-adrenergic receptors density in the subendocardial layers has been demonstrated in heart failure patients. The receptor density is restored by treatment with beta-blockers with a concomitant improvement in LV long-axis function [27, 28]. A similar association has been reported between the functioning of myocyte calcium handling

Fig. 25.10 Relatively preserved longitudinal strain (a) but markedly impaired apical rotation (b) in a patient with chronic constricted pericarditis. (c) The apical rotation recovered completely after 6-months of antitubercular treatment (modified from: Bansal et al. [93]). ATT antitubercular therapy



apparatus and myocardial mechanics in patients with end-stage dilated cardiomyopathy [29].

Apart from heart failure phenotyping, myocardial deformation imaging also has considerable prognostic value. Several studies have shown that in patients with reduced LVEF, global longitudinal strain (GLS), the average longitudinal

strain of all LV myocardial segments, is an independent predictor of all-cause mortality and the risk for heart failure-related hospitalization [30, 31]. In these patients, reduced GLS provides incremental value when added to LVEF and clinical variables. Further, in ischemic LV systolic dysfunction, myocardial deformation imaging

helps in predicting the risk of LV negative remodeling and the likelihood of segmental and global functional recovery [31–36]. It is also helpful in assessment of mechanical dyssynchrony which again is a predictor of all-cause mortality or heart failure hospitalization [37]. Even in patients with preserved LVEF, GLS provides prognostically relevant information. For example, in the TOPCAT (Treatment of Preserved Cardiac Function Heart Failure With an Aldosterone Antagonist) trial, impaired GLS was found to be the most important echocardiographic predictor of cardiovascular death or HF [38]. Similar incremental value of GLS has been demonstrated in several other conditions that manifest as heart failure with preserved EF [39, 40].

STE also permits quantification of left atrial and right ventricular (RV) contractile function, which has so far been difficult using the traditional approaches. Clinical utility of such information in heart failure patients is currently being defined [20].

Echocardiography for Guiding Management Strategies in Heart Failure

Echocardiography in Critical Care Units

In the evaluation of a patient who is in heart failure and is hypotensive, it is often required to establish the volume status, especially if the patient is mechanically ventilated. A simple visual inspection for the LV contractility by either transthoracic or transesophageal echocardiography is immensely useful in these situations and a practical tool that allows rapid discrimination between depressed myocardial function and hypovolemia as the causative factor. Similarly diagnosing pulmonary embolism, extent of functional mitral regurgitation, presence of LV clots, extent of RV dysfunction, status of intracardiac hemodynamics are important for deciding management strategies in these patients and can be readily obtained from echocardiography.

Therapeutic and Surgical Interventions

Patients with exertional symptoms and an abnormal relaxation or pseudonormal relaxation pattern with preserved atrial filling benefit from agents that slow the heart rate and allow more time for diastolic filling, whereas those with restrictive pattern benefit most with diuretic therapy. The patients with documented systolic dysfunction need treatment with angiotensin converting enzyme inhibitors, beta blockade, digoxin and diuretics [4, 6, 41]. Among those with ischemic cardiomyopathy, recognition of the patients who may benefit from coronary revascularization can be accomplished by combining information about the extent and the location of wall motion abnormalities and intracardiac hemodynamics with results of stress echocardiography. If a patient is undergoing coronary artery bypass surgery and also has secondary mitral regurgitation, the need to intervene on mitral valve depends on accurate assessment of regurgitation severity. The decision about the need for mitral valve surgery should ideally be made pre-operatively as mitral regurgitation severity often decreases under the influence of general anesthesia which often poses a therapeutic dilemma [42, 43]. Echocardiography also facilitates percutaneous or surgical management of various other potentially reversible causes of heart failure such as severe aortic stenosis, primary severe mitral regurgitation, severe aortic regurgitation, constrictive pericarditis, etc. CRT is an established treatment for patients with symptomatic heart failure due to significant LV systolic dysfunction with ECG evidence of intraventricular conduction defect. Although echocardiography is not routinely employed for selection of patients undergoing CRT, it may still be useful for this purpose. Additionally, echocardiography may be helpful in selection of optimum site for LV lead placement, optimization of CRT device settings and follow-up of patients undergoing CRT. These issues are discussed in greater detail in the chapter on CRT.

End-stage heart disease with advanced heart failure is the primary indication for LV assist

device (LVAD) insertion and/or cardiac transplant. Echocardiography plays a pivotal role in guiding these advanced heart failure therapies as discussed below [44, 45].

Mechanical Circulatory Support with Ventricular Assist Devices

The development of LVADs has been a remarkable technical innovation that has significantly improved survival of patients with advanced heart failure, who often have no other lifesaving therapeutic option. Although originally developed for use as a 'bridge-to-transplantation', further technical refinements have seen LVADs emerge as a viable alternative to transplant for patients who are not suitable for cardiac transplantation [46, 47]. Accordingly, LVADs are now increasingly used as 'destination therapy'. Virtually all LVADs implanted today are continuous flow devices with HeartMate II (HM-II, Thoratec Corporation, Pleasanton, CA) and HVAD (HeartWare International, Inc., Framingham, MA) being the two most common variants. Echocardiography is critical at every stage of management in patients undergoing LVAD implantation.

Pre-procedure Evaluation

A comprehensive echocardiographic examination is essential in all patients being considered for LVAD implantation. Transthoracic echocardiography (TTE) is the initial modality used, but TEE may be needed in critically ill, ventilated patients in whom transthoracic acoustic window may not be adequate. A TEE is also often needed to exclude certain specific abnormalities [such as intracardiac clot, patent foramen ovale (PFO), etc.] for which TTE may not be sufficiently accurate.

The echocardiographic examination should include all parameters that would be relevant in any patient with heart failure, but in addition, there are certain specific 'red-flag' findings that need careful attention [44]

- **LV size and systolic function:** Accurate assessment of LV size is essential, as it serves as the baseline for subsequent monitoring and

decision-making following LVAD implantation. Additionally, a small LV size poses a risk for adverse outcomes after the device implantation [48]. LV end-diastolic internal dimension obtained from the parasternal long-axis view is the most reproducible and the useful parameter for this purpose. Estimation of LV end-diastolic volume, although desirable, is difficult to perform, particularly during the post-operative period. For the same reason, estimation of LVEF using the modified Simpson's method is also challenging and linear-methods are often used. In patients with suboptimal endocardial border delineation, use of ultrasound contrast is strongly recommended.

- **LV thrombus, apical aneurysms, trabeculae:** Morphological abnormalities involving LV apex interfere with insertion of and normal functioning of the LVAD inflow cannula. Additionally, the presence of LV thrombus also poses a risk for embolic complication.
- **RV dysfunction:** The implantation of an LVAD results in sudden volume overload on the right ventricle, which can unmask or worsen pre-existing RV systolic dysfunction. This complication is known to occur in roughly 13–44% of the patients undergoing LVAD implantation and is associated with significant morbidity and mortality [49, 50]. Preemptive implantation of a biventricular assist device instead of an LVAD is preferable in patients at risk for developing RV failure. Therefore, pre-operative prediction of post-operative RV failure is crucial. Several different risk scores combining clinical, biochemical, echocardiographic and cardiac catheterization data have been developed for this purpose, but with variable predictive accuracy [49–53]. Among echocardiographic parameters, tricuspid regurgitation duration and severity [48, 54], an RV: LV end-diastolic diameter ratio of >0.75 [55], reduced RV longitudinal strain (less negative than 9.6%) [56] and altered ventricular septal geometry [57] have been shown to predict post-operative RV failure but no single parameter has been found to be accurate enough.

- Intracardiac shunt: LV unloading with LVAD lowers side left side intracardiac pressures resulting in right to left shunting across an untreated interatrial or interventricular communication. This leads to significant systemic hypoxemia and increases the risk for paradoxical embolism. Therefore, any intracardiac communication needs to be meticulously looked for and closed at the time of LVAD implantation [58]. Injection of agitated saline combined with Valsalva maneuver is mandatory to exclude a shunt at atrial level [44].
- Valve stenosis: Moderate or severe mitral stenosis, if present, needs to be corrected before LVAD implantation to ensure unimpeded blood flow to the LVAD. Similarly, more than mild tricuspid or pulmonary stenoses are also not desirable. In contrast, aortic stenosis of any severity per se does not pose any problem during LVAD support but a patent aortic valve serves as an important safety mechanism in the event of severe pump failure. Therefore, severe aortic stenosis may warrant surgical correction prior to LVAD implantation. When assessing valve stenosis severity, it must be remembered that transvalvular gradients are generally underestimated due to reduced cardiac output [44].
- Valvular regurgitations: The presence of aortic regurgitation (AR) leads to a wasteful recirculation of blood within the aorta-left ventricle-LVAD circuit. Hence, more than mild AR must be surgically corrected at the time of LVAD implantation [58]. The AR severity is however often underestimated due to altered loading conditions and tachycardia and needs very careful assessment [44]. Compared with AR, mitral regurgitation generally improves with LVAD insertion as the LV is unloaded and usually poses no serious problems. Presence of moderate pulmonary or tricuspid regurgitation signify high risk for post-operative RV failure and are unfavorable findings.
- Prosthetic heart valves: A mechanical valve in aortic position is at significantly elevated risk of valve thrombosis once LVAD is implanted because the blood flow through the aortic

valve is markedly reduced. Hence, a mechanical aortic valve should be replaced with a tissue valve at the time of LVAD implantation.

- Aortic diseases: Since LVAD outflow cannula is inserted in to the ascending aorta, diseases such as ascending aortic aneurysm, aortic dissection or coarctation pose serious threats during the intraoperative period and therefore, need to be diagnosed pre-operatively.
- Infective endocarditis: Active infective endocarditis is an absolute contraindication for LVAD implantation. Hence, any echocardiographic finding suggestive of infective endocarditis warrants thorough evaluation.

Peri-Implantation TEE

All pre-operative findings need to be confirmed once again just prior to LVAD implantation, to ensure that no significant finding was missed earlier and that there has not been any significant interval change.

Air entrainment is an inevitable complication during insertion of LVAD inflow cannula and requires meticulous de-airing prior to coming off cardiopulmonary bypass. TEE guidance is essential to facilitate this. Right coronary artery is the most common site for air embolism due to its anterior location [58]. Hence, acute RV systolic dysfunction immediately after coming off cardiopulmonary bypass should alert the surgical team about the possibility of air embolism.

Once LVAD is activated, immediate echocardiographic monitoring is needed to optimize the pump speed, ensure proper positioning of and flow through inflow and outflow cannula and to exclude any immediate complications. When performing echocardiography in a patient on LVAD support, all the images should always be annotated with the device name and the pump speed.

- Pump speed: Activation of the LVAD results in unloading of the left ventricle leading to deviation of interventricular septum towards left side and reduced forward flow through the aortic valve. Both these features help in optimizing the pump speed [44]. At optimum pump speed, the septum is generally shifted slightly leftwards.

Excessive leftward deviation indicates too high pump speed or markedly elevated RV pressure, whereas rightward deviation suggests a too-low pump speed. Similarly, depending on native LV contractile function and the LVAD speed, aortic valve can be opening intermittently, opening constantly or not opening at all. The pump speed can be set as per the institutional protocol to allow either intermittent opening of the aortic valve or no opening at all.

- Inflow and outflow cannula (Fig. 25.11): The position of the inflow and outflow cannula needs to be ascertained and any visible obstruction needs to be excluded. Excessive

angulation of the inflow cannula towards the ventricular septum should be avoided. Doppler interrogation of the flow in to the inflow cannula is feasible only with HM II and not with HVAD due to the characteristic Doppler artifact produced by the intrapericardial location of its impeller housing. In case of HM II, the flow should be laminar with peak velocities typically <1.5 m/s. The outflow cannula can be seen entering the ascending aorta though its anterior wall. The flow is again laminar with peak velocity usually <2 m/s [44].

- Immediate post-operative complications: Several important complications may arise

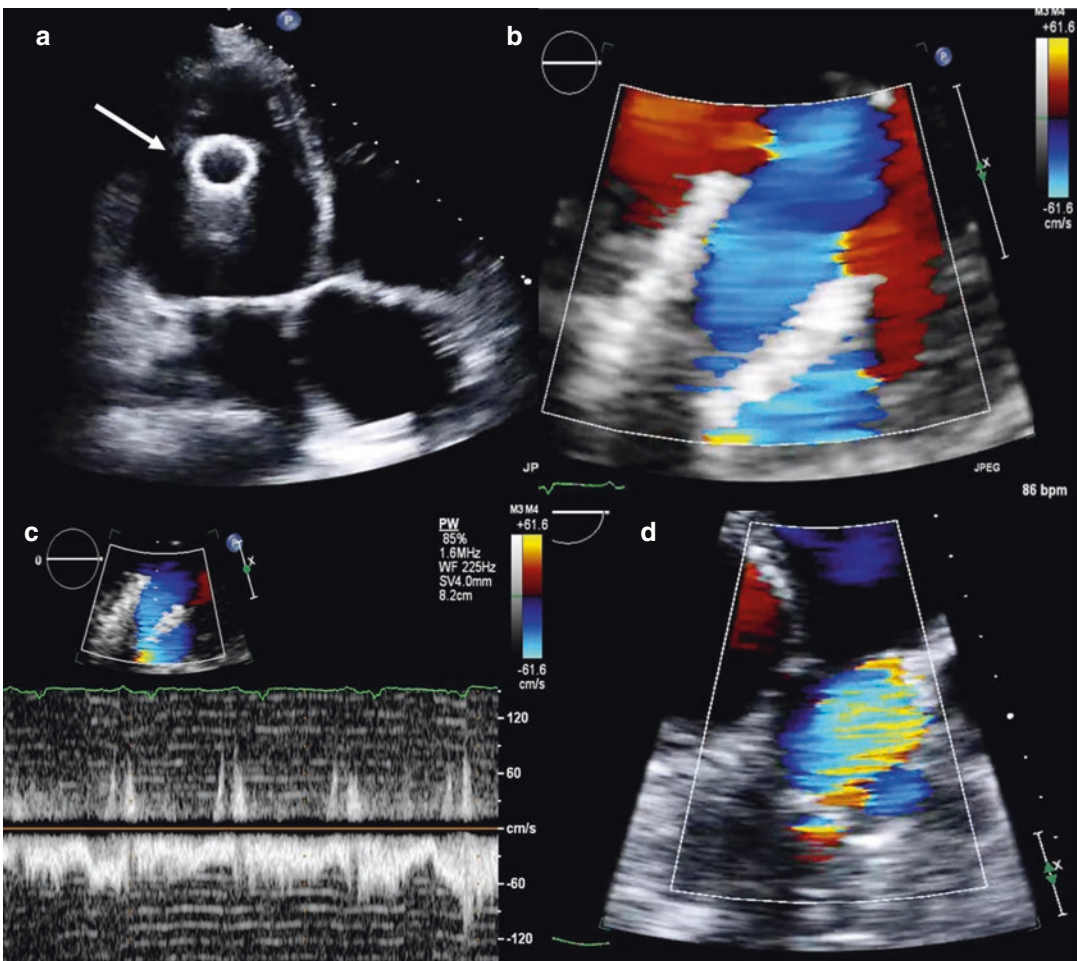


Fig. 25.11 Echocardiographic images from a patient on HeartMate II left ventricular assist device. (a)–(c) Inflow cannula is seen at the left ventricular apex with laminar

flow pattern and the flow velocities well within the normal range; (d) outflow cannula in the ascending aorta with flow striking the closed aortic valve

during the immediate/early post-operative period after LVAD implantation. RV systolic dysfunction, AR and right to left shunting through a PFO, which were not apparent earlier, may suddenly appear due to the alterations in intracardiac hemodynamics. Depending on the pump-speed and native LV contractility, the AR may be predominantly diastolic, nearly continuous, or continuous. The accurate assessment of AR severity is challenging but a vena contracta width of ≥ 0.3 cm or a jet width/LV outflow tract width of $>46\%$ at a Nyquist limit of 50–60 cm/s generally indicate at least moderate AR [44]. Pericardial collection with or without tamponade is another important complication during the early post-operative period.

Post-implantation Follow-Up

Following LVAD implantation and initial device optimization, further repeat echocardiographic studies may be needed during the hospital stay depending on the clinical course of the patient. In clinically stable patients, routine surveillance echocardiography is usually performed at the time of discharge, at 1 month, 3 months, 6 months and every 6 months thereafter [44]. Additional, ‘out-of-protocol’ studies may be needed from time to time for troubleshooting any acute issues.

During surveillance echocardiograms, a comprehensive echocardiogram is performed first, followed by evaluation of specific, device-related findings [44]. The extent of LV unloading needs to be ascertained and inflow and outflow cannula flow is checked. Complications such as AR, RV systolic dysfunction, intracardiac thrombus formation, should also be looked for. If the hemodynamics are not within the desirable limits, optimization of the pump speed may be needed. This is performed by step-wise increasing or decreasing the pump speed while monitoring for aortic valve opening, ventricular septal position, tricuspid regurgitation severity, flow through the inflow and outflow cannula and evidence of any suction event. Pump speed optimization is a very specialized procedure, requires considerable expertise, and therefore, should be performed

only in the presence of a sufficiently trained member of the LVAD team [44].

Echocardiography is also the first step in the evaluation of the patients who present with either worsening heart failure or because of any device-related alarms. Meticulous echocardiographic examination is required to ascertain the cause of the alarm. The common causes of low-flow alarm include LVAD suction event, inflow or outflow obstruction/kinking, hypovolemia, RV failure, tamponade, arrhythmias, significantly increased blood pressure, etc. Conversely, the high-flow/high-power alarm is usually due to impeller thrombosis/pump malfunction, systemic vasodilatation as in sepsis, or AR. A systematic echocardiographic examination would permit recognition of the cause of the alarm in most of the cases [44].

Role in Patients Undergoing Cardiac Transplantation

Compared with the patients receiving an LVAD, the role of echocardiography is less critical in those undergoing cardiac transplant. The preoperative echocardiography work-up of a prospective cardiac transplant recipient is less elaborate, and even after the transplant, echocardiography mainly has supplementary role.

Pre-operative Evaluation of the Donor

Excluding any significant cardiac disease in the donor is of utmost significance. Mild global LV systolic dysfunction is common in brain-dead patients who are being considered as potential donors. An LVEF $\geq 45\%$ without inotropic support is considered acceptable [59]. The presence of regional wall motion abnormalities suggestive of coronary artery disease would generally exclude the patient as a potential donor. However, in brain-dead patients, regional wall motion abnormalities may also occur because of myocardial contusion, traumatic brain injury, etc. [60]. Accurate differentiation of these conditions from coronary artery disease may be challenging. Most other structural lesions, when more than mild, would also exclude the patient as a cardiac donor.

Pre-operative Evaluation of the Transplant Recipient

Extensive pre-operative echocardiographic evaluation of a cardiac transplant recipient is not required as the native heart will be removed during the transplant procedure. However, there are certain specific findings that merit attention. The presence of significantly elevated pulmonary vascular resistance with elevated pulmonary pressures portends greater risk for post-operative right heart failure. In such cases, the surgical and intensive care team must be prepared for a period of hemodynamic instability following the transplant surgery. The hemodynamic compromise is greatest during the immediate post-operative period and depending on the reversibility of pulmonary hypertension, RV dysfunction may or may not improve with time.

Presence of intracardiac clots and aortic atheromas are other important findings that need to be carefully looked for because they may result in embolic complications during the surgery if proper care is not taken.

Post-operative Evaluation of the Recipient

TEE evaluation is required during the transplant procedure to ensure adequacy of de-airing procedure, to assess immediate post-operative cardiac function, and to facilitate hemodynamic management during the peri-operative period. TEE helps in optimizing hemodynamics by permitting simultaneous assessment of RV volume status and its response to inotropes and pulmonary vasodilator therapy.

In unstable patients, frequent echocardiographic examinations may be needed during the immediate/early post-transplant period to look for the graft function and to rule out any surgical complications such as pericardial tamponade. Once the patient is stabilized, a repeat study should be performed at the time of discharge and subsequently at least every 3 months during the first year and at least every 6 months thereafter [45]. Apart from these routine echocardiograms, additional studies would be needed whenever any cardiac dysfunction is suspected.

The main objectives of follow-up echocardiograms in cardiac transplant recipients are to

assess the graft function and to permit timely recognition of post-transplant complications, namely acute or chronic graft rejection, cardiac allograft vasculopathy (CAV) and early or late graft failure due to any other cause. However, it should be noted that endomyocardial biopsy is the recommended technique for detection of graft rejection whereas coronary angiography is the preferred modality for diagnosing CAV. Nonetheless, echocardiography remains an important modality because of its ease of application and its ability to permit comprehensive cardiac assessment.

Echocardiographic imaging in cardiac transplant recipients is usually challenging due to several reasons [45]. The altered position and orientation of the donor heart as compared to the native heart necessitate the use of unconventional imaging views for adequate visualization. The presence of tachycardia, myocardial edema, altered atrial dynamics, use of drugs such as inotropes and immunosuppressive therapy and various post-operative complications interfere with accurate assessment of cardiac function. Furthermore, the interpretation of echocardiographic findings is also difficult because not only the values of most of the echocardiographic parameters differ substantially from the accepted normal ranges, there is considerable heterogeneity among the transplant recipients themselves. It is advised that a comprehensive echocardiographic study should be performed at approximately 6-months follow up which then serves as a good baseline reference for subsequent comparisons [45].

Several echocardiographic abnormalities are encountered in cardiac transplant patients during the immediate/early post-operative period [45]. LV wall thickness is usually increased due to myocardial edema and inflammation [61]. Paradoxical septal motion is common with LVEF being in the normal/low normal range [62]. Abnormalities of LV diastolic function are also common with altered mitral E/A ratio, reduced E wave deceleration time and reduced E' velocity [61, 63]. Pulmonary pressures are elevated and variable degree of acute RV dilatation and dysfunction with tricuspid regurgitation occur almost

invariably due to sudden exposure of 'untrained' right ventricle to increased afterload [64, 65]. Pericardial effusions are seen in almost two-thirds of all patients [66]. Most of these abnormalities gradually subside over the next few days/weeks but may not return to 'normal' levels. Six months is a reasonable time-frame for this functional recovery to take place, unless interrupted by some complications [45].

Acute graft rejection is usually accompanied by a repeat deterioration in many of the parameters described above [45, 66–73]. However, while worsening of these parameters may indicate the possibility of graft rejection, none of the echocardiographic abnormalities per se is sufficiently accurate to diagnose graft rejection reliably. A combination of multiple echocardiographic parameters though may help [45]. In general, greater is the number of abnormal findings, more is the risk of graft dysfunction and worse is the prognosis. More importantly, an unchanged echocardiogram from the previous baseline has very high negative predictive value for graft rejection and is thus useful for excluding ongoing rejection [45].

Given the ability of myocardial strain imaging to detect subclinical LV systolic dysfunction, several studies have explored utility of strain measurement for early recognition of impending rejection [74–77]. GLS is generally reduced during the immediate post-transplant period and recovers with time [78]. Sudden drop in GLS may indicate graft rejection but the results have been inconsistent [74, 75]. However, persistently reduced GLS has been shown to be associated with worse prognosis and higher risk of death in transplant recipients [78]. Several other strain measurements have also been evaluated for prediction of graft rejection [76, 77].

While coronary angiography is the recommended modality for diagnosing CAV, stress echocardiography is a useful adjunctive modality, particularly in patients with renal dysfunction in whom coronary angiography needs to be avoided. Dobutamine is the preferred stressor patients because the denervated heart is unable to respond adequately to exercise stress. Dobutamine echocardiography has a sensitivity

of 70–80% and specificity of 80–90% for detection of significant CAV [45, 79–81]. The addition of strain imaging and myocardial contrast perfusion imaging to dobutamine echocardiography improve its diagnostic accuracy for detection of CAV [82–84]. Besides its role in diagnosing CAV, dobutamine echocardiography also has considerable prognostic value. A negative dobutamine stress test is associated with low risk of major adverse cardiac events at 1-year [81] whereas a positive stress test has been shown to be an independent predictor of cardiac events or death at 4-years [85].

Echocardiography and Heart Failure Screening

The progressive nature of heart failure has generated recent interests in its detection in early pre-clinical stages. In a recent large community-based study, 3% of overall population had asymptomatic left ventricular dysfunction (EF < 50%). During a mean follow up of 12 years, 26% of these patients developed congestive heart failure. Although the rates of heart failure and death in individuals with subclinical dysfunction were two to fourfold higher than those with normal LV function, the median survival free of heart failure was 10 years suggesting a window for early identification and intervention [86]. Randomized controlled clinical trials have established that therapy in these patients can delay or prevent onset of congestive heart failure. The advent of STE, as discussed above, has enhanced our ability to detect subclinical LV systolic dysfunction, even before it becomes apparent as reduction in LVEF, with potential therapeutic implications. Echocardiography therefore is likely to play a vital role as a screening tool for primary and secondary prevention of heart failure in community-based interventions. However, the major limitation in its use for mass screening is its cost. Recent advances in ultrasound technology have resulted in miniaturization of the echocardiography systems with development of portable ultrasound machines [87]. Preliminary reports of its use for heart failure screening in

community has found an acceptable accuracy for detecting LV systolic dysfunction, hypertrophy and valvular regurgitation [88–90].

Summary and Future Directions

During the last three decades, echocardiography has emerged as an important clinical tool for providing reliable diagnostic and prognostic information in patients with heart failure. With recent emergence of quantitative parameters in Doppler-ultrasound and development of novel strategies for halting or reversing cardiac remodeling, application of echocardiography as a noninvasive tool for identifying systolic and diastolic dysfunction has shown remarkable growth in clinical practice. However, with wider utilization, standardization of variables and protocols for measuring LV systolic and diastolic function would be needed. LVEF has consistently been shown in clinical trials to predict risk of mortality, with patients with lower LVEF having higher mortality. However, with 40–50% of patients in recent heart failure trials having normal LVEF, it may be required to develop a global parameter that would closely reflect the remodeling process and the functional aberrations in heart failure. Recently developed 2D and 3D measures of LV geometry and function appear particularly attractive in this regard, but would need careful validation in larger trials. The current clinical utilization of Doppler for assessment of diastolic dysfunction is also highly variable between and within echocardiographic laboratories and merits standardization. Further, an appropriate variable or a combination of variables whose recognition and modulation could prevent the progression of diastolic heart failure would be required to be identified [14]. While the recognition and treatment of asymptomatic LV systolic dysfunction has been shown to halt progression of heart failure, the benefits of identification of subclinical diastolic dysfunction by echocardiography and its intervention also remain to be addressed in future trials. The ongoing advances in the field of cognitive computing with incorporation of machine learning for echocardiographic interpretation appear to be promising developments [91, 92]. The use of

machine-learning algorithms allows integration of vast amount of echocardiographic data which can help in rapid, automated and accurate detection of cardiac structural and functional abnormalities. Such an approach has particular application in heart failure evaluation wherein early and accurate recognition of subtle harbingers of subsequent heart failure may be critical.

References

1. Mosterd A, Hoes AW. Clinical epidemiology of heart failure. *Heart*. 2007;93:1137–46.
2. Dhir M, Nagueh SF. Echocardiography and prognosis of heart failure. *Curr Opin Cardiol*. 2002;17:253–6.
3. Jessup M, Brozena S. Heart failure. *N Engl J Med*. 2003;348:2007–18.
4. Yancy CW, Jessup M, Bozkurt B, et al. 2013 ACCF/AHA guideline for the management of heart failure: a report of the American College of Cardiology Foundation/American Heart Association Task Force on Practice Guidelines. *J Am Coll Cardiol*. 2013;62:e147–239.
5. Eichhorn EJ, Grayburn PA, Mayer SA, et al. Myocardial contractile reserve by dobutamine stress echocardiography predicts improvement in ejection fraction with beta-blockade in patients with heart failure: the Beta-Blocker Evaluation of Survival Trial (BEST). *Circulation*. 2003;108:2336–41.
6. Ponikowski P, Voors AA, Anker SD, et al. 2016 ESC Guidelines for the diagnosis and treatment of acute and chronic heart failure: The Task Force for the diagnosis and treatment of acute and chronic heart failure of the European Society of Cardiology (ESC) Developed with the special contribution of the Heart Failure Association (HFA) of the ESC. *Eur Heart J*. 2016;37:2129–200.
7. Devereux RB, Roman MJ, Palmieri V, et al. Prognostic implications of ejection fraction from linear echocardiographic dimensions: the Strong Heart Study. *Am Heart J*. 2003;146:527–34.
8. Lang RM, Badano LP, Mor-Avi V, et al. Recommendations for cardiac chamber quantification by echocardiography in adults: an update from the American Society of Echocardiography and the European Association of Cardiovascular Imaging. *J Am Soc Echocardiogr*. 2015;28:1–39 e14.
9. McGowan JH, Cleland JG. Reliability of reporting left ventricular systolic function by echocardiography: a systematic review of 3 methods. *Am Heart J*. 2003;146:388–97.
10. Owan TE, Hodge DO, Herges RM, Jacobsen SJ, Roger VL, Redfield MM. Trends in prevalence and outcome of heart failure with preserved ejection fraction. *N Engl J Med*. 2006;355:251–9.

11. Vasan RS. Diastolic heart failure. *BMJ*. 2003;327:1181–2.
12. Redfield MM, Jacobsen SJ, Burnett JC Jr, Mahoney DW, Bailey KR, Rodeheffer RJ. Burden of systolic and diastolic ventricular dysfunction in the community: appreciating the scope of the heart failure epidemic. *JAMA*. 2003;289:194–202.
13. Naqvi TZ. Diastolic function assessment incorporating new techniques in Doppler echocardiography. *Rev Cardiovasc Med*. 2003;4:81–99.
14. Ommen SR, Nishimura RA. A clinical approach to the assessment of left ventricular diastolic function by Doppler echocardiography: update 2003. *Heart*. 2003;89(Suppl 3):iii18–23.
15. Garcia MJ, Ares MA, Asher C, Rodriguez L, Vandervoort P, Thomas JD. An index of early left ventricular filling that combined with pulsed Doppler peak E velocity may estimate capillary wedge pressure. *J Am Coll Cardiol*. 1997;29:448–54.
16. Vitarelli A, Gheorghiane M. Transthoracic and transesophageal echocardiography in the hemodynamic assessment of patients with congestive heart failure. *Am J Cardiol*. 2000;86:36G–40G.
17. Bruch C, Schmermund A, Marin D, et al. Tei-index in patients with mild-to-moderate congestive heart failure. *Eur Heart J*. 2000;21:1888–95.
18. Nagueh SF, Smiseth OA, Appleton CP, et al. Recommendations for the evaluation of left ventricular diastolic function by echocardiography: an update from the American Society of Echocardiography and the European Association of Cardiovascular Imaging. *J Am Soc Echocardiogr*. 2016;29:277–314.
19. Mor-Avi V, Lang RM, Badano LP, et al. Current and evolving echocardiographic techniques for the quantitative evaluation of cardiac mechanics: ASE/EAE consensus statement on methodology and indications endorsed by the Japanese Society of Echocardiography. *J Am Soc Echocardiogr*. 2011;24:277–313.
20. Omar AM, Bansal M, Sengupta PP. Advances in echocardiographic imaging in heart failure with reduced and preserved ejection fraction. *Circ Res*. 2016;119:357–74.
21. Claus P, Omar AM, Pedrizzetti G, Sengupta PP, Nagel E. Tissue tracking technology for assessing cardiac mechanics: principles, normal values, and clinical applications. *JACC Cardiovasc Imaging*. 2015;8:1444–60.
22. Meimoun P, Elmekies F, Benali T, et al. Assessment of left ventricular twist mechanics by two-dimensional strain in severe aortic stenosis with preserved ejection fraction. *Ann Cardiol Angeiol (Paris)*. 2011;60:259–66.
23. Kraigher-Krainer E, Shah AM, Gupta DK, et al. Impaired systolic function by strain imaging in heart failure with preserved ejection fraction. *J Am Coll Cardiol*. 2014;63:447–56.
24. Vinereanu D, Nicolaidis E, Tweddel AC, Fraser AG. “Pure” diastolic dysfunction is associated with long-axis systolic dysfunction. Implications for the diagnosis and classification of heart failure. *Eur J Heart Fail*. 2005;7:820–8.
25. Sengupta PP, Krishnamoorthy VK, Abhayaratna WP, et al. Disparate patterns of left ventricular mechanics differentiate constrictive pericarditis from restrictive cardiomyopathy. *JACC Cardiovasc Imaging*. 2008;1:29–38.
26. Sengupta PP, Narula J. Reclassifying heart failure: predominantly subendocardial, subepicardial, and transmural. *Heart Fail Clin*. 2008;4:379–82.
27. Beau SL, Tolley TK, Saffitz JE. Heterogeneous transmural distribution of beta-adrenergic receptor subtypes in failing human hearts. *Circulation*. 1993;88:2501–9.
28. Gruner Svealv B, Tang MS, Waagstein F, Andersson B. Pronounced improvement in systolic and diastolic ventricular long axis function after treatment with metoprolol. *Eur J Heart Fail*. 2007;9:678–83.
29. Cordero-Reyes AM, Youker K, Estep JD, Torre-Amione G, Nagueh SF. Molecular and cellular correlates of cardiac function in end-stage DCM: a study using speckle tracking echocardiography. *JACC Cardiovasc Imaging*. 2014;7:441–52.
30. Sengelov M, Jorgensen PG, Jensen JS, et al. Global longitudinal strain is a superior predictor of all-cause mortality in heart failure with reduced ejection fraction. *JACC Cardiovasc Imaging*. 2015;8:1351–9.
31. Hung CL, Verma A, Uno H, et al. Longitudinal and circumferential strain rate, left ventricular remodeling, and prognosis after myocardial infarction. *J Am Coll Cardiol*. 2010;56(22):1812.
32. Abate E, Hoogslag GE, Antoni ML, et al. Value of three-dimensional speckle-tracking longitudinal strain for predicting improvement of left ventricular function after acute myocardial infarction. *Am J Cardiol*. 2012;110(7):961.
33. Bochenek T, Wita K, Tabor Z, et al. Value of speckle-tracking echocardiography for prediction of left ventricular remodeling in patients with ST-elevation myocardial infarction treated by primary percutaneous intervention. *J Am Soc Echocardiogr*. 2011;24:1342–8.
34. Altiok E, Tiemann S, Becker M, et al. Myocardial deformation imaging by two-dimensional speckle-tracking echocardiography for prediction of global and segmental functional changes after acute myocardial infarction: a comparison with late gadolinium enhancement cardiac magnetic resonance. *J Am Soc Echocardiogr*. 2014;27:249–57.
35. Iwahashi N, Gohbara M, Kataoka S, et al. Global longitudinal strain by 3d speckle tracking after ST-elevation myocardial infarction is useful for predicting left ventricular remodeling: comparison with Tc99m-Sestamibi. *J Am Coll Cardiol*. 2015;65:A1228.
36. Altiok E, Becker M, Zwicker C, et al. Layer-specific analysis of myocardial deformation with 2d speckle-tracking echocardiography for prediction of functional recovery in acute myocardial infarction. *J Am Coll Cardiol*. 2012;59:E1142.
37. Shin SH, Hung CL, Uno H, et al. Mechanical dyssynchrony after myocardial infarction in patients with

- left ventricular dysfunction, heart failure, or both. *Circulation*. 2010;121:1096–103.
38. Shah AM, Claggett B, Sweitzer NK, et al. Prognostic importance of impaired systolic function in heart failure with preserved ejection fraction and the impact of spironolactone. *Circulation*. 2015;132:402–14.
 39. Herrmann S, Bijmens B, Stork S, et al. Using simple imaging markers to predict prognosis in patients with aortic valve stenosis and unacceptable high risk for operation. *Am J Cardiol*. 2013;112:1819–27.
 40. Galli E, Lancellotti P, Sengupta PP, Donal E. LV mechanics in mitral and aortic valve diseases: value of functional assessment beyond ejection fraction. *JACC Cardiovasc Imaging*. 2014;7:1151–66.
 41. Lainchbury JG, Redfield MM. Doppler echocardiographic-guided diagnosis and therapy of heart failure. *Curr Cardiol Rep*. 1999;1:55–66.
 42. Gisbert A, Souliere V, Denault AY, et al. Dynamic quantitative echocardiographic evaluation of mitral regurgitation in the operating department. *J Am Soc Echocardiogr*. 2006;19:140–6.
 43. Lancellotti P, Tribouilloy C, Hagendorff A, et al. Recommendations for the echocardiographic assessment of native valvular regurgitation: an executive summary from the European Association of Cardiovascular Imaging. *Eur Heart J Cardiovasc Imaging*. 2013;14:611–44.
 44. Stainback RF, Estep JD, Agler DA, et al. Echocardiography in the management of patients with left ventricular assist devices: recommendations from the American Society of Echocardiography. *J Am Soc Echocardiogr*. 2015;28:853–909.
 45. Badano LP, Miglioranza MH, Edvardsen T, et al. European Association of Cardiovascular Imaging/ Cardiovascular Imaging Department of the Brazilian Society of Cardiology recommendations for the use of cardiac imaging to assess and follow patients after heart transplantation. *Eur Heart J Cardiovasc Imaging*. 2015;16:919–48.
 46. McMurray JJ, Adamopoulos S, Anker SD, et al. ESC Guidelines for the diagnosis and treatment of acute and chronic heart failure 2012: The Task Force for the Diagnosis and Treatment of Acute and Chronic Heart Failure 2012 of the European Society of Cardiology. Developed in collaboration with the Heart Failure Association (HFA) of the ESC. *Eur Heart J*. 2012;33:1787–847.
 47. Peura JL, Colvin-Adams M, Francis GS, et al. Recommendations for the use of mechanical circulatory support: device strategies and patient selection: a scientific statement from the American Heart Association. *Circulation*. 2012;126:2648–67.
 48. Topilsky Y, Oh JK, Shah DK, et al. Echocardiographic predictors of adverse outcomes after continuous left ventricular assist device implantation. *JACC Cardiovasc Imaging*. 2011;4:211–22.
 49. Matthews JC, Koelling TM, Pagani FD, Aaronson KD. The right ventricular failure risk score a pre-operative tool for assessing the risk of right ventricular failure in left ventricular assist device candidates. *J Am Coll Cardiol*. 2008;51:2163–72.
 50. Kormos RL, Teuteberg JJ, Pagani FD, et al. Right ventricular failure in patients with the HeartMate II continuous-flow left ventricular assist device: incidence, risk factors, and effect on outcomes. *J Thorac Cardiovasc Surg*. 2010;139:1316–24.
 51. Dang NC, Topkara VK, Mercado M, et al. Right heart failure after left ventricular assist device implantation in patients with chronic congestive heart failure. *J Heart Lung Transplant*. 2006;25:1–6.
 52. Santambrogio L, Bianchi T, Fuardo M, et al. Right ventricular failure after left ventricular assist device insertion: preoperative risk factors. *Interact Cardiovasc Thorac Surg*. 2006;5:379–82.
 53. Atluri P, Goldstone AB, Fairman AS, et al. Predicting right ventricular failure in the modern, continuous flow left ventricular assist device era. *Ann Thorac Surg*. 2013;96:857–63; discussion 863–4.
 54. Potapov EV, Stepanenko A, Dandel M, et al. Tricuspid incompetence and geometry of the right ventricle as predictors of right ventricular function after implantation of a left ventricular assist device. *J Heart Lung Transplant*. 2008;27:1275–81.
 55. Vivo RP, Cordero-Reyes AM, Qamar U, et al. Increased right-to-left ventricle diameter ratio is a strong predictor of right ventricular failure after left ventricular assist device. *J Heart Lung Transplant*. 2013;32:792–9.
 56. Grant AD, Smedira NG, Starling RC, Marwick TH. Independent and incremental role of quantitative right ventricular evaluation for the prediction of right ventricular failure after left ventricular assist device implantation. *J Am Coll Cardiol*. 2012;60:521–8.
 57. Park CS, Akhabue E, Bansal M, et al. Dynamic changes in LV radius as a marker of septal configuration for predicting RV failure following LVAD implantation. *JACC Cardiovasc Imaging*. 2016;10(5):598–9.
 58. Feldman D, Pamboukian SV, Teuteberg JJ, et al. The 2013 International Society for Heart and Lung Transplantation Guidelines for mechanical circulatory support: executive summary. *J Heart Lung Transplant*. 2013;32:157–87.
 59. Lima B, Rajagopal K, Petersen RP, et al. Marginal cardiac allografts do not have increased primary graft dysfunction in alternate list transplantation. *Circulation*. 2006;114:127–32.
 60. Seiler C, Laske A, Gallino A, Turina M, Jenni R. Echocardiographic evaluation of left ventricular wall motion before and after heart transplantation. *J Heart Lung Transplant*. 1992;11:867–74.
 61. Goland S, Siegel RJ, Burton K, et al. Changes in left and right ventricular function of donor hearts during the first year after heart transplantation. *Heart*. 2011;97:1681–6.
 62. Gorcsan J 3rd, Snow FR, Paulsen W, Arrowood JA, Thompson JA, Nixon JV. Echocardiographic profile of the transplanted human heart in clinically well recipients. *J Heart Lung Transplant*. 1992;11:80–9.

63. Valantine HA, Appleton CP, Hatle LK, et al. A hemodynamic and Doppler echocardiographic study of ventricular function in long-term cardiac allograft recipients. Etiology and prognosis of restrictive-constrictive physiology. *Circulation*. 1989;79:66–75.
64. Stehlik J, Edwards LB, Kucheryavaya AY, et al. The Registry of the International Society for Heart and Lung Transplantation: twenty-seventh official adult heart transplant report—2010. *J Heart Lung Transplant*. 2010;29:1089–103.
65. Leeman M, Van Cutsem M, Vachieri JL, Antoine M, Leclerc JL. Determinants of right ventricular failure after heart transplantation. *Acta Cardiol*. 1996;51:441–9.
66. Sun JP, Abdalla IA, Asher CR, et al. Non-invasive evaluation of orthotopic heart transplant rejection by echocardiography. *J Heart Lung Transplant*. 2005;24:160–5.
67. Sagar KB, Hastillo A, Wolfgang TC, Lower RR, Hess ML. Left ventricular mass by M-mode echocardiography in cardiac transplant patients with acute rejection. *Circulation*. 1981;64:II217–20.
68. Valantine HA, Yeoh TK, Gibbons R, et al. Sensitivity and specificity of diastolic indexes for rejection surveillance: temporal correlation with endomyocardial biopsy. *J Heart Lung Transplant*. 1991;10:757–65.
69. Dandel M, Hummel M, Muller J, et al. Reliability of tissue Doppler wall motion monitoring after heart transplantation for replacement of invasive routine screenings by optimally timed cardiac biopsies and catheterizations. *Circulation*. 2001;104:II84–91.
70. Puleo JA, Aranda JM, Weston MW, et al. Noninvasive detection of allograft rejection in heart transplant recipients by use of Doppler tissue imaging. *J Heart Lung Transplant*. 1998;17:176–84.
71. Mankad S, Murali S, Kormos RL, Mandarino WA, Gorcsan J 3rd. Evaluation of the potential role of color-coded tissue Doppler echocardiography in the detection of allograft rejection in heart transplant recipients. *Am Heart J*. 1999;138:721–30.
72. Haddad F, Fisher P, Pham M, et al. Right ventricular dysfunction predicts poor outcome following hemodynamically compromising rejection. *J Heart Lung Transplant*. 2009;28:312–9.
73. Ciliberto GR, Anjos MC, Gronda E, et al. Significance of pericardial effusion after heart transplantation. *Am J Cardiol*. 1995;76:297–300.
74. Sarvari SI, Gjesdal O, Gude E, et al. Early postoperative left ventricular function by echocardiographic strain is a predictor of 1-year mortality in heart transplant recipients. *J Am Soc Echocardiogr*. 2012;25:1007–14.
75. Kato TS, Oda N, Hashimura K, et al. Strain rate imaging would predict sub-clinical acute rejection in heart transplant recipients. *Eur J Cardiothorac Surg*. 2010;37:1104–10.
76. Marciniak A, Eroglu E, Marciniak M, et al. The potential clinical role of ultrasonic strain and strain rate imaging in diagnosing acute rejection after heart transplantation. *Eur J Echocardiogr*. 2007;8:213–21.
77. Roshanali F, Mandegar MH, Bagheri J, et al. Echo rejection score: new echocardiographic approach to diagnosis of heart transplant rejection. *Eur J Cardiothorac Surg*. 2010;38:176–80.
78. Eleid MF, Caracciolo G, Cho EJ, et al. Natural history of left ventricular mechanics in transplanted hearts relationships with clinical variables and genetic expression profiles of allograft rejection. *JACC Cardiovasc Imaging*. 2010;3:989–1000.
79. Derumeaux G, Redonnet M, Mouton-Schleifer D, VACOMED Research Group, et al. Dobutamine stress echocardiography in orthotopic heart transplant recipients. *J Am Coll Cardiol*. 1995;25:1665–72.
80. Spes CH, Mudra H, Schnaack SD, et al. Dobutamine stress echocardiography for noninvasive diagnosis of cardiac allograft vasculopathy: a comparison with angiography and intravascular ultrasound. *Am J Cardiol*. 1996;78:168–74.
81. Spes CH, Klauss V, Mudra H, et al. Diagnostic and prognostic value of serial dobutamine stress echocardiography for noninvasive assessment of cardiac allograft vasculopathy: a comparison with coronary angiography and intravascular ultrasound. *Circulation*. 1999;100:509–15.
82. Eroglu E, D'Hooge J, Sutherland GR, et al. Quantitative dobutamine stress echocardiography for the early detection of cardiac allograft vasculopathy in heart transplant recipients. *Heart*. 2008;94:e3.
83. Rodrigues AC, Bacal F, Medeiros CC, et al. Noninvasive detection of coronary allograft vasculopathy by myocardial contrast echocardiography. *J Am Soc Echocardiogr*. 2005;18:116–21.
84. Hacker M, Hoyer HX, Uebleis C, et al. Quantitative assessment of cardiac allograft vasculopathy by real-time myocardial contrast echocardiography: a comparison with conventional echocardiographic analyses and [Tc99m]-sestamibi SPECT. *Eur J Echocardiogr*. 2008;9:494–500.
85. Bacal F, Moreira L, Souza G, et al. Dobutamine stress echocardiography predicts cardiac events or death in asymptomatic patients long-term after heart transplantation: 4-year prospective evaluation. *J Heart Lung Transplant*. 2004;23:1238–44.
86. Wang TJ, Evans JC, Benjamin EJ, Levy D, LeRoy EC, Vasan RS. Natural history of asymptomatic left ventricular systolic dysfunction in the community. *Circulation*. 2003;108:977–82.
87. Seraphim A, Paschou SA, Grapsa J, Nihoyannopoulos P. Pocket-sized echocardiography devices: one stop shop service? *J Cardiovasc Ultrasound*. 2016;24:1–6.
88. Senior R, Galasko G, McMurray JV, Mayet J. Screening for left ventricular dysfunction in the community: role of hand held echocardiography and brain natriuretic peptides. *Heart*. 2003;89(Suppl 3):iii24–8.
89. Prinz C, Voigt JU. Diagnostic accuracy of a hand-held ultrasound scanner in routine patients referred for echocardiography. *J Am Soc Echocardiogr*. 2011;24:111–6.

90. Fukuda S, Shimada K, Kawasaki T, et al. Pocket-sized transthoracic echocardiography device for the measurement of cardiac chamber size and function. *Circ J*. 2009;73(6):1092.
91. Sengupta PP, Huang YM, Bansal M, et al. Cognitive machine-learning algorithm for cardiac imaging: a pilot study for differentiating constrictive pericarditis from restrictive cardiomyopathy. *Circ Cardiovasc Imaging*. 2016;9:e004330.
92. Narula S, Shameer K, Salem Omar AM, Dudley JT, Sengupta PP. Machine-learning algorithms to automate morphological and functional assessments in 2D echocardiography. *J Am Coll Cardiol*. 2016;68:2287–95.
93. Bansal M, Mehrotra R, Kasliwal RR. Loss of left ventricular torsion as the predominant mechanism of left ventricular systolic dysfunction in a patient with tubercular cardiomyopathy. *Echocardiography*. 2012;29:E221–5.
94. Duarte R, Fernandez G. Assessment of left ventricular diastolic function by MR: why, how and when. *Insights Imaging*. 2010;1:183–92.

Echocardiography in Cardiac Resynchronization Therapy

26

Ulas Höke, Jeroen J. Bax, Nina Ajmone Marsan,
and Victoria Delgado

Introduction

Cardiac resynchronization therapy (CRT) is an established therapy for heart failure patients with depressed left ventricular ejection fraction (LVEF) <35%, prolonged QRS >120 ms and mild-to-severe heart failure (HF) symptoms despite optimal pharmacological therapy [1]. Improvements in clinical symptoms, left ventricular (LV) function and mitral regurgitation as well as significant reductions in all-cause and cardiac mortality rates and heart failure rehospitalizations have been reported [2–8]. However, between 30% and 40% of patients do not improve after CRT and the reasons for these relatively high non-response rates to CRT remain still unclear [9, 10].

LV dyssynchrony is an independent determinant of response to CRT [11, 12]. However, definition of LV dyssynchrony is still highly debated. Recent guidelines have included QRS morphology as a criterion for CRT indication [1]. Based on previous studies, patients with left bundle branch block (LBBB) QRS morphology have benefited of CRT at larger extent than patients with right bundle branch block morphology [3, 8, 12, 13]. However, among patients with LBBB QRS morphology, LV activation may change considerably [14]. The

presence of fixed or functional lines of block as assessed with 3-dimensional LV mapping may lead to distinct patterns of LV dyssynchrony that may also influence response to CRT [14]. Non-invasive imaging techniques permit characterization of LV activation pattern and quantification of LV dyssynchrony in heart failure patients with wide QRS and have provided several indices of LV dyssynchrony to predict response to CRT. The Predictors of Response to CRT (PROSPECT) trial was the first multicenter prospective trial to explore the role several echocardiographic dyssynchrony parameters to predict response to CRT [15]. With 498 enrolled patients, the trial demonstrated the modest accuracy of a dozen of echocardiographic LV dyssynchrony parameters to predict response to CRT [15]. However, the observational study design, the inclusion of patients with LVEF>35% or LV end-diastolic dimensions <65 mm, and technical related issues (different vendors, poor acoustic window) may have had significant impact on the results. Furthermore, several pathophysiological factors, such as myocardial scar and LV lead position were not considered in the interpretation of the results of the PROSPECT trial [16]. Subsequent studies have in fact shown that an integrative approach, including assessment of LV dyssynchrony, site of latest activation and presence of transmural scar at the segments targeted by the LV or amount of myocardial scar, may provide a more accurate selection of patients that will benefit from CRT [17–19].

U. Höke · J. J. Bax (✉) · N. Ajmone Marsan · V. Delgado
Department of Cardiology, Leiden University
Medical Center, Leiden, The Netherlands
e-mail: j.j.bax@lumc.nl

Two-dimensional and 3-dimensional echocardiographic deformation imaging, cardiac magnetic resonance (CMR) and nuclear imaging are valuable tools to assess all these pathophysiological determinants of response to CRT. Furthermore, fusion imaging of positron emission tomography (PET) and computed tomography or CMR and fluoroscopy have permitted accurate visualization of cardiac vein anatomy overlaid on myocardial scar tissue providing an accurate guidance for LV lead delivery [20, 21].

Furthermore, after CRT implantation, the role of optimization of the device settings to improve clinical outcomes remains debatable [22]. Several echocardiographic approaches have been evaluated to optimize CRT settings.

The present chapter reviews the role of echocardiography to select heart failure patients who are candidate for CRT and the latest advances achieved after PROSPECT trial on multimodality imaging.

LV Dyssynchrony Assessment

Previous meta-analysis pooling data of more than 5000 heart failure patients included in CRT randomized controlled trials has shown that patients with a QRS duration ≥ 150 ms clearly benefit from CRT, whereas this benefit is more questioned in patients with a QRS duration between 120 and 149 ms [23]. Furthermore, the sub-analysis of the MADIT-CRT trial showed that the outcomes were significantly superior in patients treated with CRT who had LBBB QRS morphology than patients with other types of intraventricular conduction defects [12]. Accordingly, current European Society of Cardiology guidelines for diagnosis and management of heart failure patients have modified the inclusion criteria for CRT indication [1]. One quarter of heart failure patients have LBBB QRS morphology [24]. The delayed activation of the left ventricle due to LBBB is characterized by contraction of the interventricular septum against a lateral wall that is passively stretched and followed by late contraction of the lateral wall against the stretched interventricular septum leading to inefficient LV

global contraction. However, this mechanical pattern may change depending on the LV substrate (i.e. areas of scar) and the effect of CRT may vary accordingly [14].

Several imaging techniques have provided multiple LV dyssynchrony indices that try to characterize the LV mechanical activation dispersion and to predict response to CRT. Table 26.1 summarizes the echocardiographic LV dyssynchrony parameters that were evaluated in the PROSPECT trial [15]. Although the results of the PROSPECT trial showed a modest accuracy of a dozen of M-mode and Doppler echocardiography and tissue Doppler imaging derived LV dyssynchrony parameters to predict response to CRT [15], subsequent analyses have shown that the presence of significant LV dyssynchrony assessed with tissue Doppler imaging for example is associated with increased likelihood of response to CRT and improved outcome [11, 25]. Therefore, analysis of LV dyssynchrony with imaging techniques provides incremental information in the selection of patients for CRT implantation.

However, in the last years the focus has been shifted towards evaluation of active mechanical deformation with speckle tracking echocardiography or tagged-CMR and towards global evaluation with 3-dimensional imaging techniques to characterize LV mechanical dispersion or dyssynchrony.

2D Speckle Tracking Echocardiography

Two-dimensional speckle tracking echocardiography analyzes multidirectional active myocardial deformation by tracking frame to frame the movement of the speckles (natural acoustic markers equally distributed within the myocardium) along the cardiac cycle. Applied to the LV short-axis view, LV dyssynchrony is frequently measured as the time difference between peak radial strain of the (antero)septal and (postero) lateral walls (Fig. 26.1) [26]. A time difference ≥ 130 ms has demonstrated to predict response to CRT with relative high accuracy

Table 26.1 Echocardiographic parameters of cardiac dyssynchrony evaluated in the PROSPECT trial

Echocardiographic parameter	Echocardiographic technique	Description of the method	Cut-off value of LV dyssynchrony
Septal-to-posterior wall motion delay	M-mode	Time difference between the inward motion of the septum and the posterior wall measured on parasternal long-axis view of the LV	≥ 130 ms
Interventricular mechanical dyssynchrony	Pulsed wave Doppler	Time difference between the onset of the pulmonary flow and the aortic flow measured on parasternal short-axis view at the level of the aortic valve and LV apical long-axis view, respectively	≥ 40 ms
LV filling time/RR interval	Pulsed wave Doppler	Duration of LV filling time measured on pulsed wave Doppler recordings of the mitral inflow (from onset of E wave to end of A wave) corrected for the RR interval	$\leq 40\%$
LV pre-ejection interval	Pulsed wave Doppler	Time interval between the beginning of the QRS and the onset of the LV ejection measured on LV apical long-axis view	≥ 140 ms
Left lateral wall contraction	M-mode Pulsed wave Doppler	Presence of overlap between the end of the lateral wall contraction (on M-mode recordings) and onset of LV filling (on pulsed wave Doppler recordings of the mitral inflow)	Any overlap
Ts-(lateral-septal)	TDI	Time delay between the peak systolic velocity of the basal septal and lateral walls measured on the LV apical 4-chamber view	≥ 60 ms
Ts-SD	TDI	Standard deviation of time from onset of QRS to peak systolic velocity of 12 LV segments (6 basal and 6 mid-ventricular)	≥ 32 ms
Peak velocity difference	TDI	Maximal time delay between the earliest and the latest peak systolic velocity of 6 LV basal segments	≥ 110 ms
Delayed longitudinal contraction	TDI Strain rate imaging	Number of LV basal segments with delayed longitudinal contraction with a systolic contraction component in early diastole on TDI and confirmed with strain rate imaging	≥ 2 basal segments
Ts-peak displacement	TDI	Maximal time delay between peak systolic displacement of 4 segments	\geq Median
Ts-peak (basal)	TDI	Maximal time delay between peak systolic velocities of 6 LV basal segments	\geq Median
Ts-onset (basal)	TDI	Maximal difference of time to onset of systolic velocity of 6 LV basal segments	\geq Median

A late diastolic velocity, E early diastolic velocity, LV, left ventricular, TDI tissue Doppler imaging, Ts time to

(83% sensitivity and 80% specificity) and has been independently associated with improved outcome after CRT implantation [11, 27]. Furthermore, the assessment of LV mechanical dispersion with longitudinal strain speckle tracking echocardiography has also demonstrated good accuracy to predict response to CRT [28]. By calculating the standard deviation of the difference between peak and end-systolic longitudinal strain of 16 LV segments (in the apical 4-, 2- and 3-chamber views), Lim and coworkers

derived the strain dyssynchrony index, an index that combines activation time and myocardial contractile reserve (Fig. 26.1) [28]. A cut-off value of strain dyssynchrony index $\geq 25\%$ had a high accuracy to predict significant LV reverse remodeling after CRT (area under the curve: 0.94). Unlike tissue Doppler imaging techniques, the measurement of myocardial deformation with speckle tracking echocardiography is not influenced by the insonation angle of the ultrasound beam. However, some 2-dimensional speckle

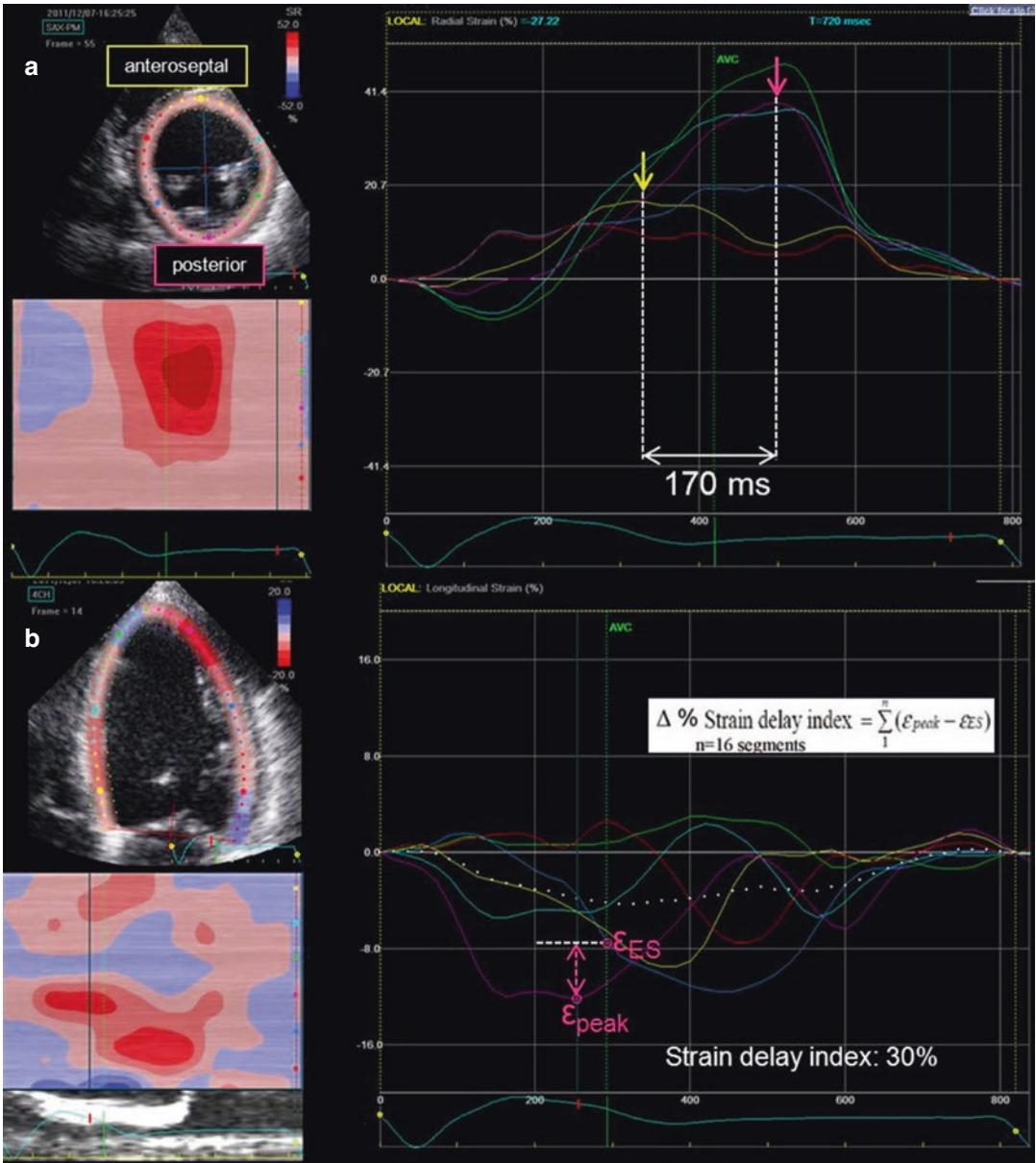


Fig. 26.1 Assessment of LV dyssynchrony with 2-dimensional speckle tracking echocardiography. Panel (a) shows an example of a patient with significant LV dyssynchrony as assessed with radial strain. The time difference between peak radial strain of the anteroseptal and posterior segments is 170 ms. Panel (b) shows the mea-

surement of strain delay index based on longitudinal strain. This index evaluates the time difference and longitudinal strain magnitude between peak and end-systolic longitudinal strain of 16 segments. In this example, strain delay index indicates significant dyssynchrony (>25%). *ES* end-systolic

tracking echocardiography derived LV dyssynchrony parameters do not provide information on the global LV mechanical activation pattern and some parameters are computed based on the acquisition of several views during different car-

diac cycles, introducing a potential beat-to-beat variability in its calculation [29]. In this regard, the development of 3-dimensional imaging techniques has enabled the assessment of global LV mechanical dyssynchrony.

3-Dimensional Echocardiographic Techniques

One of the first LV dyssynchrony indices based on real-time 3-dimensional echocardiography was the systolic dyssynchrony index (Fig. 26.2). From a LV 3-dimensional full volume, the LV endocardial border is manually or semiautomated defined (depending on the post-processing software) at end-systole and end-diastole and a mathematical 3-dimensional model of the left ventricle is derived. This model is subsequently divided into 16 or 17 segments and the LV mechanical dyssynchrony is quantified by calculating the standard deviation of time to minimum regional volume of 16 or 17 LV subvolumes. A recent meta-analysis pooling data from 600 heart failure patients undergoing CRT implantation demonstrated a good accuracy of real-time 3-dimensional echocardiography to predict response to CRT [30]. A weighted mean systolic dyssynchrony index of 9.8% predicted response to CRT with a sensitivity of 93% and a specificity of 75% [30].

Furthermore, from triplane LV echocardiographic data, tissue Doppler imaging can be applied and LV dyssynchrony can be calculated as the standard deviation of time to peak velocity of 12 basal and mid ventricular segments [31]. Particularly, tissue synchronization imaging has provided a rapid and intuitive visualization of LV mechanical dyssynchrony providing color-coded polar map plots of the left ventricular activation. The earliest activated segments are color-coded in green whereas the latest activated segments are color-coded in orange (Fig. 26.2). Using this methodology, van de Veire et al. demonstrated that a standard deviation of time to peak systolic velocities ≥ 33 ms predicted response to CRT with 90% and 83% sensitivity and specificity, respectively [31].

Finally, the recent developed 3-dimensional speckle tracking has also permitted quantification of LV dyssynchrony. Unlike 2-dimensional speckle tracking echocardiography, 3-dimensional speckle tracking echocardiography permits analysis of myocardial deformation of the true full LV volume avoiding foreshortened images and it is not affected by the out-of-plane

motion of the speckles. From a 3-dimensional LV full volume, the endocardial borders are manually traced and the software displays a region of interest including the myocardial wall and tracks the speckles along the cardiac cycle. Longitudinal, circumferential and radial strains are then calculated. In heart failure patients undergoing CRT implantation, the role of 3-dimensional speckle tracking to characterize LV dyssynchrony and predict response to CRT has been tested [32, 33]. LV dyssynchrony can be calculated as the standard deviation of time to peak strain for 16 LV segments. In a series of 54 heart failure patients treated with CRT, 3-dimensional speckle tracking demonstrated a larger LV dyssynchrony compared with healthy volunteers (124 ± 48 ms vs. 28 ± 11 ms, respectively; $p < 0.001$) [32]. Furthermore, the software provides an index of global LV performance (area strain) computing LV shortening in two directions (longitudinal and circumferential) and LV dyssynchrony (calculated as the standard deviation of time to peak strain of 16 segments) (Fig. 26.2). The accuracy of this 3-dimensional speckle tracking derived parameter to predict response to CRT has been recently tested in 14 heart failure patients [34]. A cutoff value of $\geq 3.8\%$ predicted response to CRT with a sensitivity of 78% and specificity of 100% [34]. However, the low temporal resolution of 3-dimensional speckle tracking may be an important limitation in LV dyssynchrony assessment. Therefore, the results of published studies reporting the accuracy of this technique to predict response to CRT should be taken with caution since the proposed cut-off values of the LV dyssynchrony indices.

Magnetic Resonance Imaging

CMR is a valuable 3-dimensional imaging technique to characterize LV dyssynchrony. Using steady-state free-precession sequence, a stack of short-axis slices covering the entire left ventricle are acquired and the LV mechanical dyssynchrony can be analyzed by evaluating the regional radial wall motion. The standard deviation of the phase shift of the maximum radial

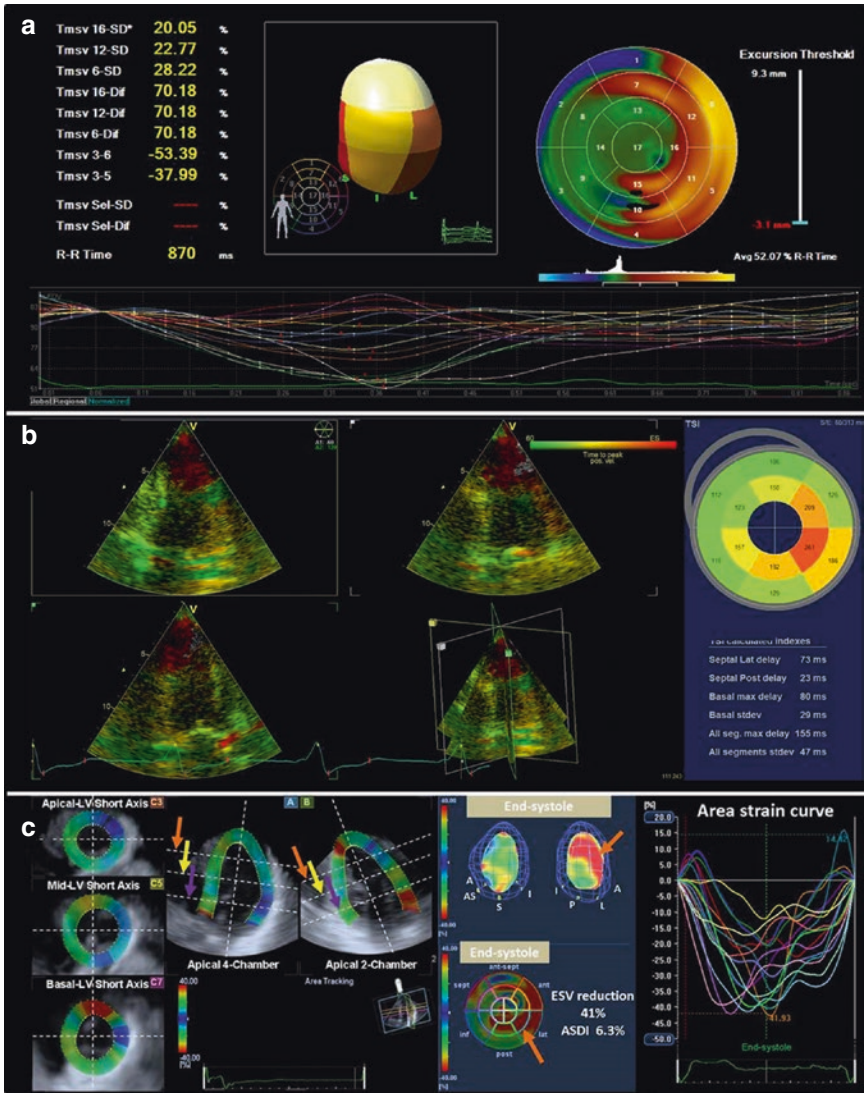


Fig. 26.2 Three-dimensional echocardiographic techniques to evaluate LV dyssynchrony. Panel (a): LV dyssynchrony can be quantified from 3-dimensional full-volume datasets of the left ventricle by measuring the systolic dyssynchrony index (standard deviation of time to minimum systolic volume of 16 subvolumes [Tmsv16-SD]). The LV mechanical dispersion can be also visualized on color-coded polar maps, with the earliest activated regions coded in blue and the latest activated areas coded in orange-red. In this example, the patient shows significant LV dyssynchrony (Tmsv16-SD 20.05%) and the lateral and posterior LV regions as the most delayed activated areas. The time-volume curves of the 16 regional subvolumes are plotted in a graph providing also a visual estimation of LV dyssynchrony. Panel (b): Assessment of LV dyssynchrony with triplane tissue synchronization imaging. The polar map shows the time to peak systolic velocity of 12 basal and midventricular LV

segments. LV dyssynchrony is calculated as the standard deviation of time to peak systolic velocity of the 12 segments. In this example, there is significant LV dyssynchrony (standard deviation: 47 ms) and the mid posterolateral segment is the most delayed activated area. Panel (c): With 3-dimensional speckle tracking, area strain index is derived by computing LV shortening in two directions (longitudinal and circumferential) and LV dyssynchrony (calculated as the standard deviation of time to peak strain of 16 segments). In this example, after defining the region of interest, the software derives 3-dimensional model of the left ventricle providing the value of area strain index (6.3%). This 3-dimensional model permits visualization of the latest activated areas (coded in red). The time to area strain curves for the 16 segments can be visually assessed in a graph. Adapted from Tatsumi et al. [34]

wall motion of all LV segments provides the LV dyssynchrony index known as CMR-tissue synchronization index (Fig. 26.3). Using this technique, Chalil et al. demonstrated that CMR-tissue synchronization index was independently associated with long-term outcome of heart failure patients treated with CRT [35]. Patients with a CMR-tissue synchronization index ≥ 110 ms had fivefold increased mortality risk compared with patients with a CMR-tissue synchronization index < 110 ms [35]. Therefore, this CMR-derived LV dyssynchrony parameter may be of importance in the patient selection for CRT. In addition, tagged CMR permits assessment of longitudinal and circumferential strain in 3 dimensions and provides data on LV mechanical activation that is operator independent [17]. Particularly, the measurement of LV mechanical dyssynchrony has been largely based on circumferential strain data provided by tagged-CMR. Applying harmonic phase

method to LV short-axis tagged slices, circumferential strain is assessed and time to peak circumferential strain is measured to provide the LV mechanical index, the so-called circumferential uniformity ratio estimate (CURE) (Fig. 26.3) [17]. This LV dyssynchrony index ranges from 0 (pure dyssynchrony) to 1 (perfect synchronous). In 20 patients undergoing CRT implantation, Bilchick et al. demonstrated that a CURE index < 0.75 had 90% accuracy to predict response to CRT (positive predictive value: 87% and negative predictive value: 100%) [17].

Nuclear Imaging

Finally, LV dyssynchrony can be also assessed with nuclear imaging techniques. Quantitative ECG-gated single photon emission computed tomography (SPECT) characterizes LV dyssyn-

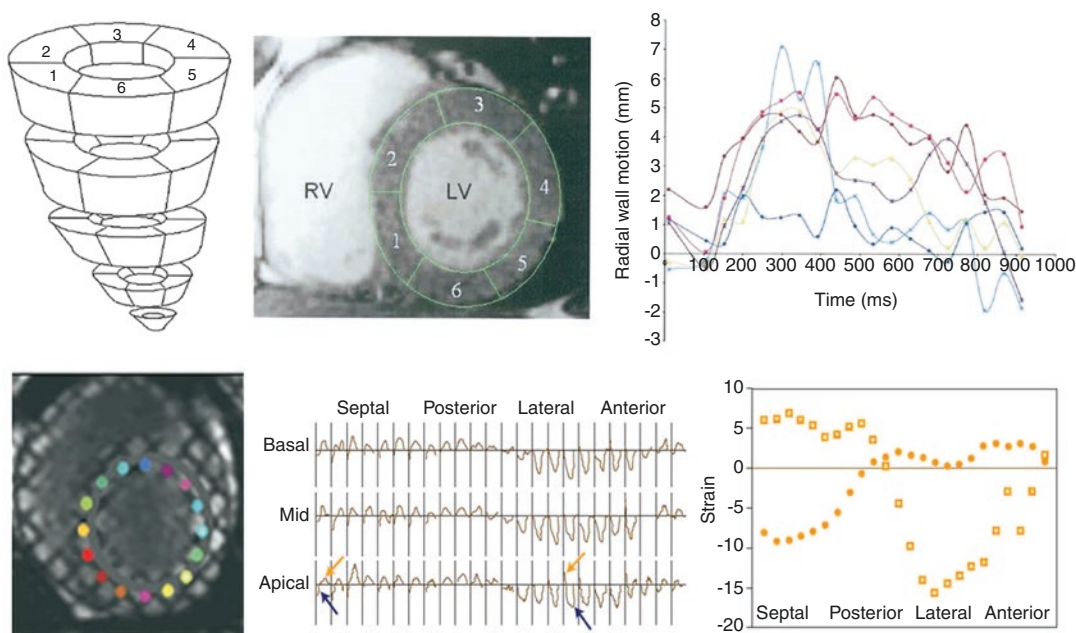


Fig. 26.3 LV dyssynchrony assessment with cardiac magnetic resonance. Panel (a): Assessment of LV dyssynchrony with CMR based on evaluation of regional radial wall motion. From steady-state free-precession sequence, a stack of short-axis slices covering the entire left ventricle are acquired. The time to segmental radial wall motion can be displayed in a graph. The standard deviation of the phase shift of the maximum radial wall motion of all LV segments provides the LV dyssynchrony index known as

CMR-tissue synchronization index. Panel (b): With tagged-CMR, circumferential strain can be measured at 12 LV segments (septal, posterior, lateral and anterior at pical, mid and basal levels of the left ventricle). Time to peak circumferential strain is measured providing the circumferential uniformity ratio estimate (CURE) index. This index ranges from 0 (dyssynchronous) to 1 (synchronous). Reproduced with permission from Chalil et al. [35] and Bilchick et al. [17]

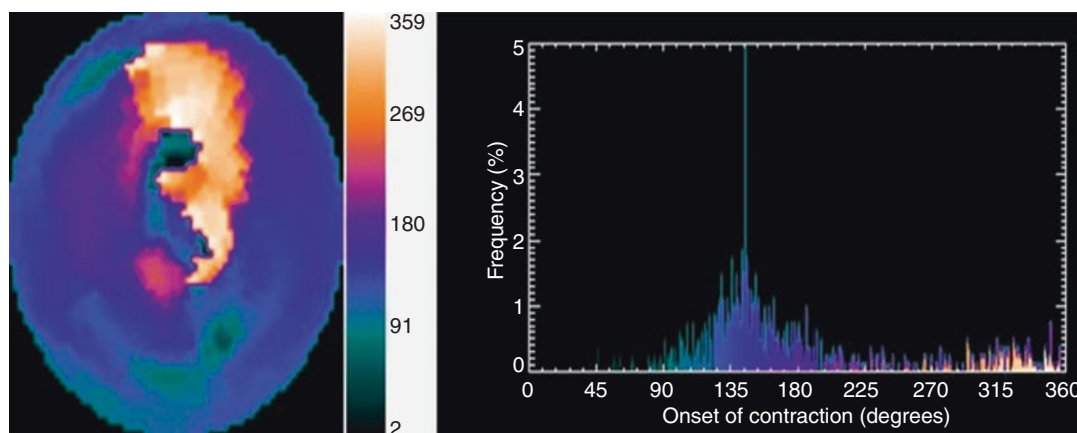


Fig. 26.4 Assessment of LV dyssynchrony with gated myocardial perfusion SPECT. Example of a heart failure patient with LV dyssynchrony as assessed with gated

myocardial perfusion SPECT. The polar map shows the heterogeneous phase angle distribution whereas the histogram shows a broad peaked histogram

chrony by calculating the phase angle of multiple LV samples and providing the phase angle distribution in a polar map or a histogram (Fig. 26.4). The bandwidth and the phase standard deviation are the LV dyssynchrony parameters. The proposed optimal cut-off value of the histogram bandwidth to predict response to CRT was 72.5° (sensitivity 83% and specificity 81%) whereas a phase standard deviation $\geq 19.6^\circ$ predicted response to CRT with a sensitivity and specificity of 83% and 81%, respectively [36].

As many non-randomized single center trials published prior to the PROSPECT trial, the evidence provided by these new studies using novel technologies demonstrates and confirms that assessment of LV dyssynchrony plays an important role in selecting heart failure patients for CRT. However, subsequent studies following the PROSPECT trial have included in their analyses other pathophysiological factors that may influence the response to CRT such as myocardial scar or LV lead position and that were not evaluated in the PROSPECT trial.

LV Lead Position: Site of Latest Activation

Cannulation of the coronary sinus and placement of an LV lead in a suitable tributary that permits a stable position, avoids phrenic nerve stimula-

tion and reduces LV dyssynchrony (as assessed with significant shortening of the QRS duration or with imaging techniques) is the most crucial aspect of CRT implantation. Lateral or posterolateral veins are the preferred locations for LV lead placement. However, several observational studies and two randomized trials have demonstrated that location of the LV pacing lead at the area of latest mechanical activation is associated with superior CRT outcomes [18, 37–39]. Assessment of the latest activated region of the left ventricle can be performed with echocardiographic and CMR techniques. Several echocardiographic techniques such as triplane tissue synchronization imaging, 3D speckle tracking or 3D echocardiography have demonstrated to accurately localize the site of latest activation. Two-dimensional speckle tracking echocardiography may be the imaging technique providing the largest evidence on the relevance of evaluating the site of latest activation and the impact of a concordant LV lead position [18, 37, 39]. With this technique, the latest activated areas are identified on the time-radial strain graphs as the segments with the most delayed peak radial strain. The first randomized trial evaluating the effect of LV lead position (coincident or not with the site of latest activation) on response to CRT and long-term outcome was the TARGET (Targeted Left Ventricular Lead Placement to Guide Cardiac

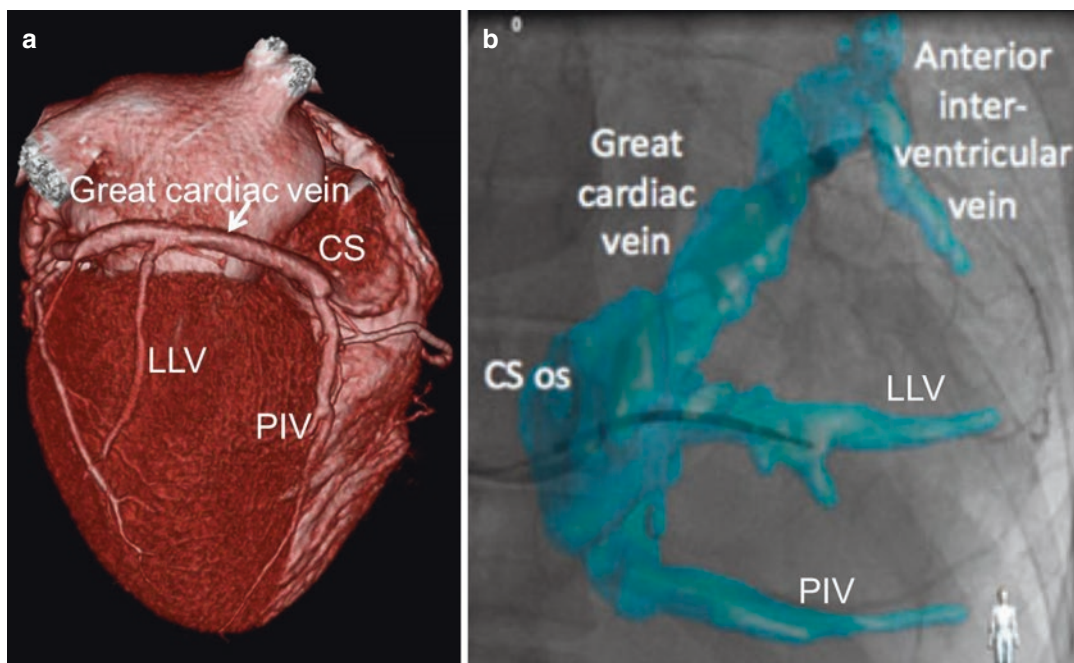


Fig. 26.5 Evaluation of coronary venous anatomy with MDCT and CMR. Prior to CRT implantation, MDCT permits accurate assessment of venous coronary anatomy. The example shows the posterior interventricular vein and the left lateral vein as tributaries of the coronary sinus (panel (a)). With CMR the coronary venous anatomy can

be also evaluated and the data can be merged with real-time fluoroscopy permitting accurate guidance of LV lead positioning (panel (b)). Reprinted with permission from Duckett et al. [20]. CS coronary sinus, LLV left lateral vein, PIV posterior interventricular vein

Resynchronization Therapy) trial [37]. A total of 220 patients treated with CRT were randomized to LV lead positioning according to 2-dimensional speckle tracking analysis results (concordant with the latest activated segments) or to conventional LV lead placement. At 6 months follow-up, the response rate to CRT ($\geq 15\%$ reduction in LV end-systolic volume) was significantly higher among patients with an LV lead coincident with the site of latest activation than in patients in whom the LV lead was placed conventionally (70% vs. 55%, $p = 0.031$). In addition, patients with an LV lead position concordant with the site of latest activation showed superior long-term outcome than patients with a discordant LV lead position (10% vs. 21% cumulative incidence of combined endpoint of HF hospitalizations or all-cause mortality; $p < 0.001$) [37].

Furthermore, noninvasive assessment of coronary venous anatomy may be helpful to plan the implantation strategy. In ischemic heart failure

patients, particularly, the presence of a suitable lateral or posterolateral vein is less frequent and may challenge the LV lead positioning [40]. MDCT and CMR permit accurate non-invasive assessment of the coronary sinus and tributaries (Fig. 26.5). Evaluation of the coronary venous anatomy prior to CRT implantation has been associated with reduced procedural times, use of contrast volume and fluoroscopy times [41]. Furthermore, MDCT or CMR data can be integrated with fluoroscopy and provide an optimal guidance for LV lead positioning (Fig. 26.5).

Myocardial Scar

Coronary artery disease is the leading cause of heart failure. A subanalysis of the CARE-HF trial showed that patients with ischemic heart failure benefited from CRT at a lesser extent than patients with non-ischemic heart failure [42].

Similarly, a population-based study including almost 15,000 patients treated with CRT demonstrated that ischemic etiology was one of the strongest prognostic factors [9]. Observational studies have shown that placing the LV lead on an area of transmural myocardial scar is associated with high likelihood of non-response to CRT [18, 19]. In addition to the location of transmural scar, the extent or burden of myocardial scar has an important influence on the effects of CRT [43–45].

Delayed contrast-enhanced CMR and radionuclide myocardial perfusion imaging are considered the gold standard for assessment of myocardial scar (Fig. 26.6). Delayed contrast-enhanced CMR has higher spatial resolution than nuclear imaging techniques and permits exact visualization of the transmural extent of myocardial scar. With this technique, Leyva et al. demonstrated that patients with an LV lead placed at myocardial areas with transmural scar had six-fold higher risk of cardiovascular death than patients without transmural scar (hazard ratio; 6.34, 95% confidence interval 3.64–11.0, $p < 0.0001$) [19]. Furthermore, using radionu-

clide myocardial perfusion imaging two large studies have demonstrated that global myocardial scar burden has an independent influence on long-term outcome of patients treated with CRT [43, 45]. In 213 heart failure patients treated with CRT who underwent pre-procedural PET ($n = 46$) or SPECT ($n = 167$) myocardial perfusion imaging, Xu et al. showed that an extent of myocardial scar $>22\%$ together with an age < 70 years were associated with superior long-term survival after CRT [45]. In addition, Adelstein et al. quantified myocardial scar burden with rest-redistribution ^{201}Tl -SPECT in 190 ischemic heart failure patients treated with CRT [43]. A summed rest score ≥ 27 identified patients with large myocardial scar burden. Patients with a summed rest score < 27 showed larger LV reverse remodeling and improvement in LVEF and had twofold higher survival free from cardiac transplant or LV assist device implantation as compared with patients with a summed rest score ≥ 27 [43].

Assessment of myocardial viability and scar with echocardiographic techniques is also feasible. Particularly, speckle tracking echocardiographic techniques have been validated against

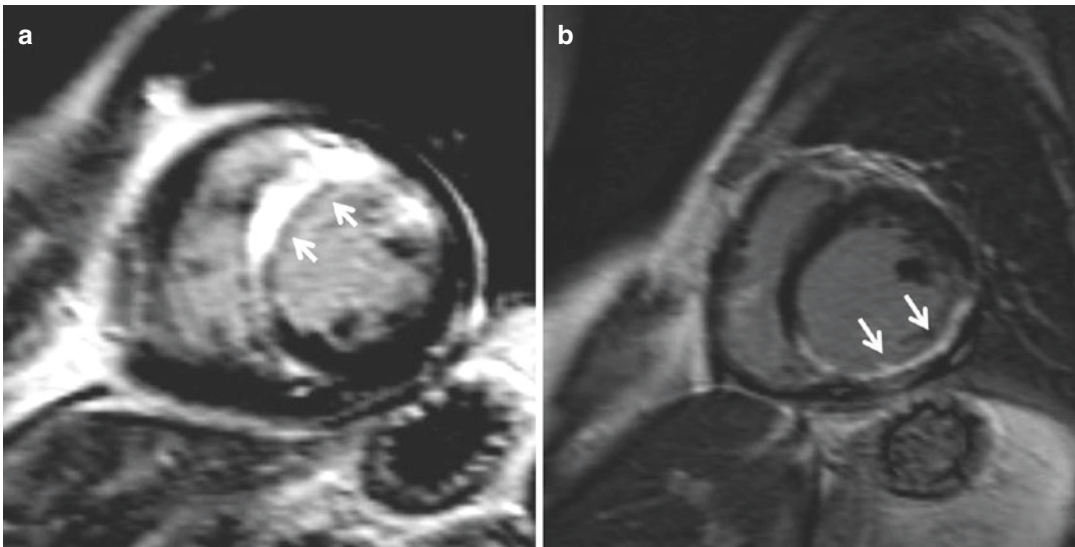


Fig. 26.6 Evaluation of location and extent of myocardial scar. Panel (a) shows the example of a patient with transmural myocardial scar on delayed contrast-enhanced cardiac magnetic resonance in the septum and anteroseptum of the left ventricle (arrows). Panel (b) shows the

example of a patient with transmural scar in the inferoseptum and posterolateral regions (arrows). The position of the left ventricular lead in an area with transmural scar may lead to non-response to cardiac resynchronization therapy

contrast-enhanced CMR to identify transmural myocardial scar [46]. Using speckle tracking radial strain echocardiography, a value of peak radial strain $<16.5\%$ has been proposed to identify regions of transmural myocardial scar [46]. In 397 ischemic heart failure patients the presence of transmural scar as assessed with speckle tracking radial strain echocardiography at the area targeted by the LV lead was independently associated with poor outcome [18]. The addition of myocardial scar in the segment targeted by the LV lead had incremental prognostic value over LV dyssynchrony, LV lead position and other well-known clinical prognostic markers [18].

This evidence suggests that integration of several pathophysiological determinants of CRT efficacy may be more important in patient selection rather than relying on one single selection criterion.

CRT Optimization

Simultaneous right and left ventricular pacing with a sensed atrioventricular (AV) delay programmed at 110–120 ms is the most common mode of CRT pacing [47]. However, these empirically programmed settings may not provide optimal LV filling or result in the most synchronous LV contraction in every patient. Previous study has shown that non-optimal AV delay was the cause of non-response to CRT in 45% of heart failure patients whereas suboptimal interventricular (VV) delay was less frequently the cause of suboptimal clinical response [48]. Optimization of CRT settings aims at achieving 100% biventricular pacing, maximum contribution of the left atrial contraction to the LV filling and at eliminating residual LV dyssynchrony. However, randomized and non-randomized trials evaluating the effects of AV and/or VV delay optimization on clinical outcomes have shown controversial results. Recent meta-analysis pooling data of 4356 patients treated with CRT showed no differences in clinical or echocardiographic outcomes between patients who underwent AV and/or VV delay optimization and patients with empirically programmed settings [22]. The lack of standardized methodologies to

optimize the CRT device and the inclusion of heterogeneous populations in clinical trials (responders and non-responders to CRT) may explain the controversial results of CRT optimization across the different studies. Several echocardiographic methods have been largely used for CRT optimization (Table 26.2) [49].

Heart failure patients may have a conduction delay between the atrium and the ventricle (too long AV delay) leading to a short LV filling time. On echocardiography, this situation is recognized by a fusion of the early (E) and late (A) wave velocities on pulsed wave Doppler recordings of the transmitral inflow. In addition, diastolic mitral regurgitation can be observed if the pressures in the LV exceed the pressures of the left atrium before the LV contraction starts, leading to a further reduced LV preload and stroke volume. By shortening the AV delay, the E and A waves separate thereby increasing the LV filling time and leading to higher preload of the LV (Fig. 26.7). Optimization of the AV delay seeks for the shortest AV delay without truncation of the A wave. Table 26.2 summarizes the different echocardiographic methods to optimize the AV delay. Among them, the iterative method is the most frequently used. This method is based on pulsed wave Doppler recordings of the mitral inflow. From a long AV delay, the pulsed wave Doppler of the mitral inflow is recorded, and subsequently the AV delay is shortened in 20 ms steps until the A wave is truncated by the LV contraction on the spectral Doppler signal. Then, the AV delay is lengthened by steps of 10 ms until obtaining the optimal LV filling time. This method was used in the SMART-AV trial [50].

Optimization of the VV delay may help to improve the response of patients with a non-optimal LV lead position. Residual LV dyssynchrony or more pronounced LV dyssynchrony after CRT implantation may occur leading to suboptimal clinical outcomes. By adjusting further the VV delay, a more physiological activation of the LV may be achieved. Several echocardiographic methods have been proposed to optimize the VV delay and are based on assessment of surrogates of stroke volume or assessment of mechanical dyssynchrony (Table 26.2).

Table 26.2 Echocardiographic methods for CRT optimization

	Target mechanism	Echocardiographic method	Description
AV optimization	Optimization of LV diastolic filling	Iterative method	On pulsed wave Doppler recordings of the mitral inflow, the LV filling time is measured at different AV delays (from long to short at 20 ms steps). The shortest AV delay without truncation of the A wave if the optimal AV delay
		Ritter's method	On pulsed wave Doppler recordings of the mitral inflow obtained at two extreme AV delays (AV_{long} and AV_{short}), the time between the QRS complex onset to the completion of the A wave is measured. The optimal AV delay is calculated based on the formula: $AV_{short} + [(AV_{long} + Q_{Along}) - (AV_{short} + Q_{Ashort})]$
		Mitral inflow VTI	Measurement of the VTI of the transmitral inflow on pulsed wave Doppler recordings. The optimal AV delay provides the largest VTI
		Meluzin's method	On pulsed wave Doppler recordings of the transmitral inflow, a long AV delay is set. The time between the end of the A wave and the onset of mitral regurgitation spectral signal is measured (t1). The difference between long AV delay and t1 yields the optimal AV delay
	Optimization of LV systolic function	LV dP/dt	In patients with mitral regurgitation, the time needed to raise the pressure from 4 to 36 mmHg is measured on continuous wave Doppler recordings. The optimal AV delay is given by the shortest time
		LVOT VTI	On pulsed wave Doppler recordings of the LV outflow, the velocity time integral of the LVOT flow is measured and the stroke volume derived. The optimal AV delay provides the largest stroke volume
		Myocardial performance index	Measured on pulsed wave Doppler of the transmitral inflow and LVOT or on pulsed wave TDI, the sum of isovolumic contraction and relaxation times divided by the ejection time provides the myocardial performance index. The optimal AV delay yields the lowest myocardial performance index
VV optimization	Optimization of LV systolic function	LVOT VTI	On pulsed wave Doppler recordings of the LV outflow, the velocity time integral of the LVOT flow is measured and the stroke volume derived. The optimal VV delay provides the largest stroke volume
	Optimization of LV mechanical dyssynchrony	Interventricular mechanical dyssynchrony	Time difference between the onset of the pulmonary flow and the aortic flow measured on parasternal short-axis view at the level of the aortic valve and LV apical long-axis view, respectively. The optimal VV delay yields the shortest interventricular mechanical dyssynchrony
		Ts-peak and Ts-SD	On TDI, the time delay between the peak systolic velocity of the basal septal and lateral walls measured on the LV apical 4-chamber view or the standard deviation of time from onset of QRS to peak systolic velocity of 12 LV segments (6 basal and 6 mid-ventricular) are measured. The optimal VV delay provides the shortest time delay or lowest standard deviation
		Real-time 3D echocardiography	From 3D full volume datasets of the LV, the standard deviation of time from onset of QRS to minimum volume of 16–17 segments is measured. The optimal VV delay provides the lowest standard deviation

3D 3-dimensional, AV atrioventricular, LV left ventricular, LVOT left ventricular outflow tract, SD standard deviation, TDI tissue Doppler imaging, Ts time to, VTI velocity time integral, VV interventricular

From pulsed wave Doppler recordings of the LV outflow, the stroke volume can be calculated by measuring the velocity time integral of the spectral signal. Using this method, the effect of several VV delay configurations on stroke volume can be assessed. Stroke volume is assessed during RV pre-stimulation (from +60 to +20 ms), simultaneous stimulation (0 ms) and LV pre-stimulation (from -20 to -60 ms). The VV delay that yields the largest velocity time integral and stroke volume would be considered the optimal delay. In addition, other studies have shown the value of tissue Doppler imaging to assess LV dyssynchrony across the several VV delay settings [49, 51, 52].

Future Steps: Imaging Integration

Technological advances have permitted integration or fusion of imaging techniques to provide information on several pathophysiological factors that may influence CRT response. One of the first experiences evaluating LV dyssynchrony and LV lead position in relation to areas of myocardial scar used 3-dimensional imaging fusion with ^{18}F -FDG-PET/CT [21]. In 14 candidates for CRT, LV dyssynchrony was assessed with LV phase analysis of data obtained with ECG-gated PET [21]. Histogram bandwidth, phase angle standard deviation and global phase entropy (reflecting uniformity of movement) were provided. In addition, myocardial scar was detected from LV ^{18}F -FDG polar maps normalized to the highest glucose uptake. Areas with <50% uptake

identified non-viable areas (myocardial scar). Finally, integrating ^{18}F -FDG-PET and low-dose CT images, the LV lead tip was localized and assigned to viable or nonviable (scar) myocardium (Fig. 26.7). Responders to CRT showed more LV dyssynchronous contraction, less burden of myocardial scar and less frequently LV leads were placed in areas with nonviable myocardium [21]. In addition, Duckett et al. demonstrated the usefulness of integrating MDCT or delayed contrast-enhanced CMR with fluoroscopy to guide CRT implantation [20]. Specific post-processing softwares permit segmentation of the coronary venous anatomy and myocardial scar from delayed contrast-enhanced CMR data and overlay these data onto real-time fluoroscopy providing further guidance to CRT implantation [20]. In addition, Doring et al. showed the value of integrating LV mechanical activation data obtained with 3D transesophageal echocardiography with 3D data of the coronary sinus and venous tributaries obtained with rotational angiography (Fig. 26.8). The sites of latest activation are color-coded in red while the earliest activated segments are color-coded in blue. By interpolating the 3D model of the cardiac venous anatomy and the LV 3D activation map, the position of the LV lead can be guided to target the site of latest activation [52]. Recently, the role of fusion imaging on CRT optimization has also been evaluated. The polar maps of LV activation obtained with 3D real-time transesophageal echocardiography are fused with 3D models of the venous anatomy and position of the LV lead obtained with rotational angiography. In patients with suboptimal

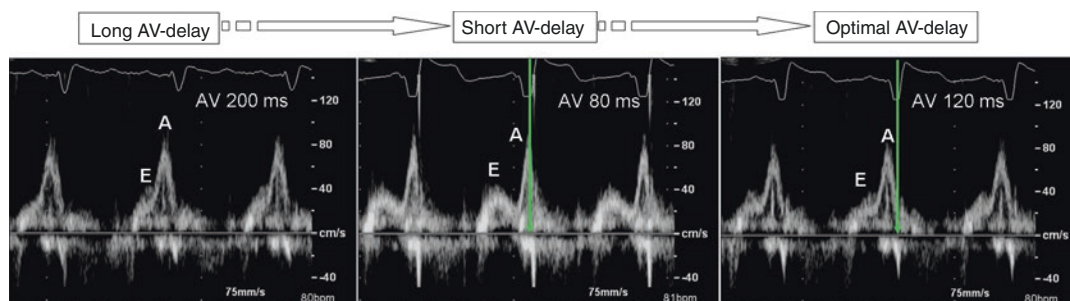


Fig. 26.7 Optimization of the atrioventricular delay following the iterative method. From a long atrioventricular (AV) delay, where the early (E) and late (A) diastolic waves are fused, the AV delay is shortened by 20 ms steps

until the A wave is truncated. From that time, the AV delay is lengthened to obtain the shortest AV delay without truncation of the A wave. Reproduced with permission from Bertini et al. [49]

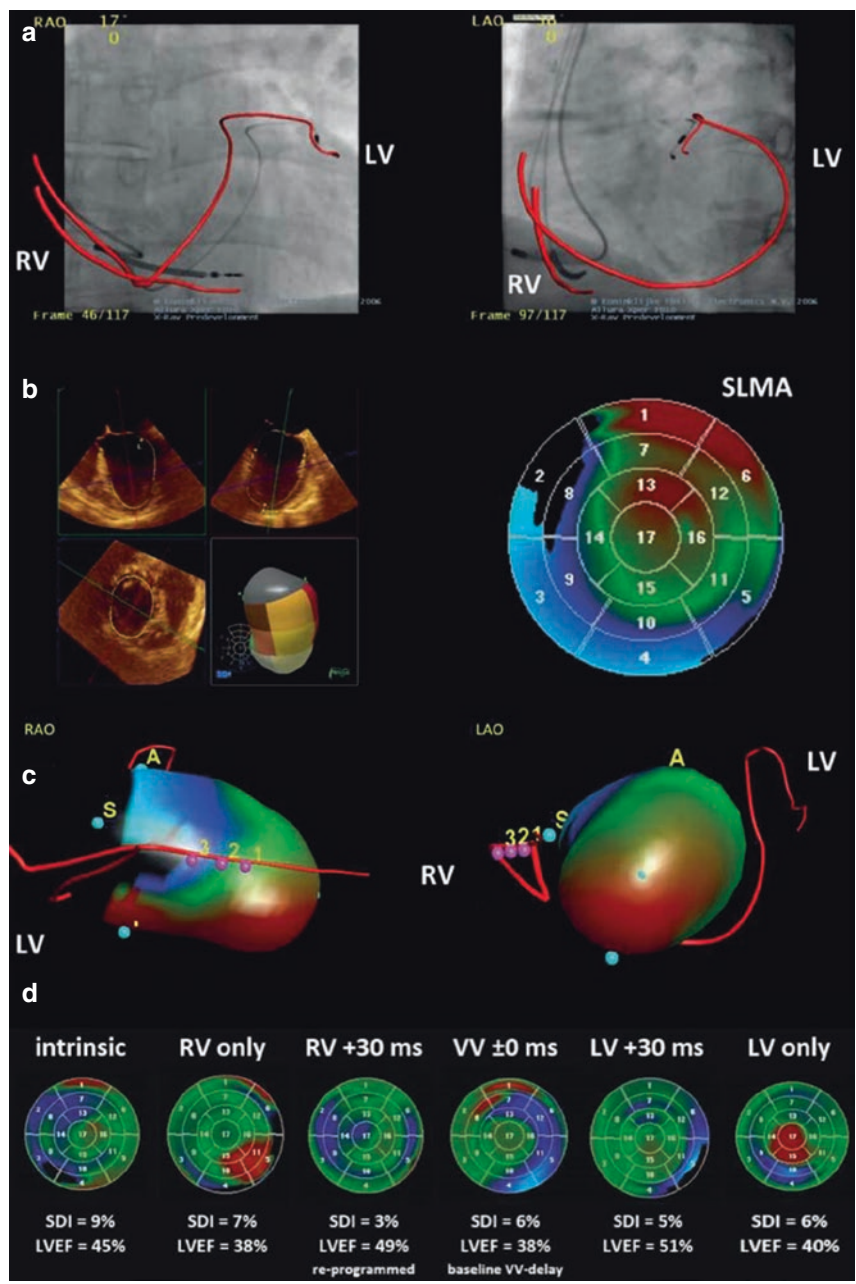


Fig. 26.8 Fusion imaging in cardiac resynchronization therapy. Panel (a): On fluoroscopic rotation scan, the course of the right and left ventricular leads is registered. The right anterior oblique (RAO) and left anterior oblique (LAO) views are shown. Panel (b): Reconstruction of the 3-dimensional (3D) left ventricular (LV) model obtained with transesophageal echocardiography. The polar map with the time to minimum regional volume is provided. Panel (c): The 3D LV model with the time to minimum regional volume for all LV segments is displayed and fused with the angiographic rotation scan data indicating the position of the LV lead relative to the site of latest

activation (color-coded in red). Panel (d): several VV delays are tested and the standard deviation of time from onset of QRS to minimum volume of 16–17 segments is measured (SDI). The optimal VV delay provides the lowest SDI and highest LV ejection fraction (LVEF). In this example, 30 ms pre-stimulation of the LV may be the preferred VV delay. Reproduced with permission from Nitsche et al. [53]. LAO left anterior oblique, LV left ventricle, RAO right anterior oblique, RV right ventricle, SDI standard deviation of time to minimum regional volume, SLMA site of latest mechanical activation, VV interventricular

position of the LV lead (not coinciding with the site of latest activation), changes in the polar maps across the several VV delay settings can be evaluated and the VV delay that leads to the more synchronous activation can be selected (Fig. 26.8) [53]. These new areas of research on image integration may in the future contribute to improved patient selection for CRT.

Conclusions

Cardiac resynchronization therapy is one of the main therapeutic breakthroughs in heart failure of the last decades. Published data has demonstrated 60–70% efficacy of this therapy in improving LV function, inducing LV remodeling and improving long-term outcome of heart failure patients. However, the associated costs and risks demand an accurate selection of heart failure patients to maximize the results. The PROSPECT trials showed us that single evaluation of LV dyssynchrony may not be sufficient to identify the patients who will benefit from CRT. Many observational studies have demonstrated that LV dyssynchrony, LV lead position and location and extent of myocardial scar are independent determinants of response to CRT and need to be evaluated prior to CRT implantation. Currently, echocardiography, with a high availability and cost-effectiveness, is the method of choice to evaluate most of the pathophysiological determinants of response to CRT. Particularly, speckle tracking echocardiography has been demonstrated to be a valuable tool to assess LV dyssynchrony, site of latest activation and myocardial scar. However, assessment of myocardial scar may be preferably performed with delayed contrast-enhanced CMR or radionuclide imaging techniques. In this regard, CMR is a comprehensive imaging tool to assess LV dyssynchrony, location and extent of myocardial scar and coronary venous anatomy. Furthermore, optimization of CRT device settings in patients with suboptimal response may be guided by echocardiographic techniques. Although the results of several trials have shown inconclusive, current recommendations consider

optimization of CRT device with echocardiography as a bailout methodology to improve the outcomes of heart failure patients with minimal improvement in symptoms after device implantation. Finally, post-processing imaging tools permit overlay of segmented CMR 3-dimensional datasets on real-time fluoroscopy, facilitating implantation and optimization of CRT devices. However, the availability is limited and in patients with pacemaker devices or with severe renal dysfunction the use of this technique may be contraindicated. Additional randomized studies selecting candidates for CRT based on current recommendations, taking these pathophysiological factors into account, may further establish the role of imaging techniques in patient selection for CRT.

References

1. McMurray JJ, Adamopoulos S, Anker SD, Auricchio A, Bohm M, Dickstein K, et al. ESC guidelines for the diagnosis and treatment of acute and chronic heart failure 2012: the task force for the diagnosis and treatment of acute and chronic heart failure 2012 of the European Society of Cardiology. Developed in collaboration with the heart failure association (HFA) of the ESC. *Eur Heart J*. 2012;33(14):1787–847.
2. Abraham WT, Hayes DL. Cardiac resynchronization therapy for heart failure. *Circulation*. 2003;108(21):2596–603.
3. Bristow MR, Saxon LA, Boehmer J, Krueger S, Kass DA, De MT, et al. Cardiac-resynchronization therapy with or without an implantable defibrillator in advanced chronic heart failure. *N Engl J Med*. 2004;350(21):2140–50.
4. Cleland JG, Daubert JC, Erdmann E, Freemantle N, Gras D, Kappenberger L, et al. The effect of cardiac resynchronization on morbidity and mortality in heart failure. *N Engl J Med*. 2005;352(15):1539–49.
5. Daubert C, Gold MR, Abraham WT, Ghio S, Hassager C, Goode G, et al. Prevention of disease progression by cardiac resynchronization therapy in patients with asymptomatic or mildly symptomatic left ventricular dysfunction: insights from the European cohort of the REVERSE (resynchronization reverses Remodeling in systolic left ventricular dysfunction) trial. *J Am Coll Cardiol*. 2009;54(20):1837–46.
6. Linde C, Abraham WT, Gold MR, St John SM, Ghio S, Daubert C. Randomized trial of cardiac resynchronization in mildly symptomatic heart failure patients and in asymptomatic patients with left ventricular dysfunction and previous heart failure symptoms. *J Am Coll Cardiol*. 2008;52(23):1834–43.

7. Moss AJ, Hall WJ, Cannom DS, Klein H, Brown MW, Daubert JP, et al. Cardiac-resynchronization therapy for the prevention of heart-failure events. *N Engl J Med*. 2009;361(14):1329–38.
8. Tang AS, Wells GA, Talajic M, Arnold MO, Sheldon R, Connolly S, et al. Cardiac-resynchronization therapy for mild-to-moderate heart failure. *N Engl J Med*. 2010;363(25):2385–95.
9. Bilchick KC, Kamath S, DiMarco JP, Stukenborg GJ. Bundle-branch block morphology and other predictors of outcome after cardiac resynchronization therapy in Medicare patients. *Circulation*. 2010;122(20):2022–30.
10. Delgado V, Bax JJ. Assessment of systolic dyssynchrony for cardiac resynchronization therapy is clinically useful. *Circulation*. 2011;123(6):640–55.
11. Gorgsan J III, Oyenuga O, Habib PJ, Tanaka H, Adelstein EC, Hara H, et al. Relationship of echocardiographic dyssynchrony to long-term survival after cardiac resynchronization therapy. *Circulation*. 2010;122(19):1910–8.
12. Zareba W, Klein H, Cygankiewicz I, Hall WJ, McNitt S, Brown M, et al. Effectiveness of cardiac resynchronization therapy by QRS morphology in the Multicenter automatic defibrillator implantation trial-cardiac resynchronization therapy (MADIT-CRT). *Circulation*. 2011;123(10):1061–72.
13. Gervais R, Leclercq C, Shankar A, Jacobs S, Eiskjaer H, Johannessen A, et al. Surface electrocardiogram to predict outcome in candidates for cardiac resynchronization therapy: a sub-analysis of the CARE-HF trial. *Eur J Heart Fail*. 2009;11(7):699–705.
14. Auricchio A, Fantoni C, Regoli F, Carbucicchio C, Goette A, Geller C, et al. Characterization of left ventricular activation in patients with heart failure and left bundle-branch block. *Circulation*. 2004;109(9):1133–9.
15. Chung ES, Leon AR, Tavazzi L, Sun JP, Nihoyannopoulos P, Merlino J, et al. Results of the predictors of response to CRT (PROSPECT) trial. *Circulation*. 2008;117(20):2608–16.
16. Bax JJ, Gorgsan J III. Echocardiography and non-invasive imaging in cardiac resynchronization therapy: results of the PROSPECT (predictors of response to cardiac resynchronization therapy) study in perspective. *J Am Coll Cardiol*. 2009;53(21):1933–43.
17. Bilchick KC, Dimaano V, Wu KC, Helm RH, Weiss RG, Lima JA, et al. Cardiac magnetic resonance assessment of dyssynchrony and myocardial scar predicts function class improvement following cardiac resynchronization therapy. *JACC Cardiovasc Imaging*. 2008;1(5):561–8.
18. Delgado V, Van Bommel RJ, Bertini M, Borleffs CJ, Marsan NA, Arnold CT, et al. Relative merits of left ventricular dyssynchrony, left ventricular lead position, and myocardial scar to predict long-term survival of ischemic heart failure patients undergoing cardiac resynchronization therapy. *Circulation*. 2011;123(1):70–8.
19. Leyva F, Foley PW, Chalil S, Ratib K, Smith RE, Prinzen F, et al. Cardiac resynchronization therapy guided by late gadolinium-enhancement cardiovascular magnetic resonance. *J Cardiovasc Magn Reson*. 2011;13:29.
20. Duckett SG, Ginks MR, Knowles BR, Ma Y, Shetty A, Bostock J, et al. Advanced image fusion to overlay coronary sinus anatomy with real-time fluoroscopy to facilitate left ventricular lead implantation in CRT. *Pacing Clin Electrophysiol*. 2011;34(2):226–34.
21. Uebleis C, Ulbrich M, Tegtmeyer R, Schuessler F, Haserueck N, Siebermair J, et al. Electrocardiogram-gated 18F-FDG PET/CT hybrid imaging in patients with unsatisfactory response to cardiac resynchronization therapy: initial clinical results. *J Nucl Med*. 2011;52(1):67–71.
22. Auger D, Hoke U, Bax JJ, Boersma E, Delgado V. Effect of atrioventricular and ventriculoventricular delay optimization on clinical and echocardiographic outcomes of patients treated with cardiac resynchronization therapy: a meta-analysis. *Am Heart J*. 2013;166(1):20–9.
23. Sipahi I, Carrigan TP, Rowland DY, Stambler BS, Fang JC. Impact of QRS duration on clinical event reduction with cardiac resynchronization therapy: meta-analysis of randomized controlled trials. *Arch Intern Med*. 2011;171(16):1454–62.
24. Baldasseroni S, Opasich C, Gorini M, Lucci D, Marchionni N, Marini M, et al. Left bundle-branch block is associated with increased 1-year sudden and total mortality rate in 5517 outpatients with congestive heart failure: a report from the Italian network on congestive heart failure. *Am Heart J*. 2002;143(3):398–405.
25. Shanks M, Delgado V, Ng AC, Auger D, Mooyaart EA, Bertini M, et al. Clinical and echocardiographic predictors of nonresponse to cardiac resynchronization therapy. *Am Heart J*. 2011;161(3):552–7.
26. Suffoletto MS, Dohi K, Cannesson M, Saba S, Gorgsan J III. Novel speckle-tracking radial strain from routine black-and-white echocardiographic images to quantify dyssynchrony and predict response to cardiac resynchronization therapy. *Circulation*. 2006;113(7):960–8.
27. Delgado V, Ypenburg C, Van Bommel RJ, Tops LF, Mollema SA, Marsan NA, et al. Assessment of left ventricular dyssynchrony by speckle tracking strain imaging. Comparison between longitudinal, circumferential, and radial strain in cardiac resynchronization therapy. *J Am Coll Cardiol*. 2008;51(20):1944–52.
28. Lim P, Buakhamsri A, Popovic ZB, Greenberg NL, Patel D, Thomas JD, et al. Longitudinal strain delay index by speckle tracking imaging: a new marker of response to cardiac resynchronization therapy. *Circulation*. 2008;118(11):1130–7.
29. Mor-Avi V, Lang RM, Badano LP, Belohlavek M, Cardim NM, Derumeaux G, et al. Current and evolving echocardiographic techniques for the quantitative evaluation of cardiac mechanics: ASE/EAE consensus statement on methodology and indications endorsed

- by the Japanese Society of Echocardiography. *J Am Soc Echocardiogr*. 2011;24(3):277–313.
30. Kleijn SA, Aly MF, Knol DL, Terwee CB, Jansma EP, Abd El-Hady YA, et al. A meta-analysis of left ventricular dyssynchrony assessment and prediction of response to cardiac resynchronization therapy by three-dimensional echocardiography. *Eur Heart J Cardiovasc Imaging*. 2012;13(9):763–75.
 31. van de Veire NR, Bleeker GB, De SJ, Ypenburg C, Holman ER, van der Wall EE, et al. Tissue synchronisation imaging accurately measures left ventricular dyssynchrony and predicts response to cardiac resynchronisation therapy. *Heart*. 2007;93(9):1034–9.
 32. Tanaka H, Hara H, Saba S, Gorcsan J III. Usefulness of three-dimensional speckle tracking strain to quantify dyssynchrony and the site of latest mechanical activation. *Am J Cardiol*. 2010;105(2):235–42.
 33. Thebault C, Donal E, Bernard A, Moreau O, Schnell F, Mabo P, et al. Real-time three-dimensional speckle tracking echocardiography: a novel technique to quantify global left ventricular mechanical dyssynchrony. *Eur J Echocardiogr*. 2011;12(1):26–32.
 34. Tatsumi K, Tanaka H, Tsuji T, Kaneko A, Ryo K, Yamawaki K, et al. Strain dyssynchrony index determined by three-dimensional speckle area tracking can predict response to cardiac resynchronization therapy. *Cardiovasc Ultrasound*. 2011;9:11.
 35. Chalil S, Stegmann B, Muhyaldeen S, Khadjooi K, Smith RE, Jordan PJ, et al. Intraventricular dyssynchrony predicts mortality and morbidity after cardiac resynchronization therapy: a study using cardiovascular magnetic resonance tissue synchronization imaging. *J Am Coll Cardiol*. 2007;50(3):243–52.
 36. Boogers MM, Van Kriekinge SD, Henneman MM, Ypenburg C, Van Bommel RJ, Boersma E, et al. Quantitative gated SPECT-derived phase analysis on gated myocardial perfusion SPECT detects left ventricular Dyssynchrony and predicts response to cardiac resynchronization therapy. *J Nucl Med*. 2009;50(5):718–25.
 37. Khan FZ, Virdee MS, Palmer CR, Pugh PJ, O'Halloran D, Elsik M, et al. Targeted left ventricular lead placement to guide cardiac resynchronization therapy: the TARGET study: a randomized, controlled trial. *J Am Coll Cardiol*. 2012;59(17):1509–18.
 38. Saba S, Marek J, Schwartzman D, Jain S, Adelstein E, White P, et al. Echocardiography-guided left ventricular lead placement for cardiac resynchronization therapy: results of the speckle tracking assisted resynchronization therapy for electrode region (STARTER) trial. *Circ Heart Fail*. 2013;6(3):8.
 39. Ypenburg C, Van Bommel RJ, Delgado V, Mollema SA, Bleeker GB, Boersma E, et al. Optimal left ventricular lead position predicts reverse remodeling and survival after cardiac resynchronization therapy. *J Am Coll Cardiol*. 2008;52(17):1402–9.
 40. van de Veire NR, Schuijf JD, De SJ, Devos D, Bleeker GB, de RA, et al. Non-invasive visualization of the cardiac venous system in coronary artery disease patients using 64-slice computed tomography. *J Am Coll Cardiol*. 2006;48(9):1832–8.
 41. Girskey MJ, Shinbane JS, Ahmadi N, Mao S, Flores F, Budoff MJ. Prospective randomized trial of venous cardiac computed tomographic angiography for facilitation of cardiac resynchronization therapy. *Pacing Clin Electrophysiol*. 2010;33(10):1182–7.
 42. Wikstrom G, Blomstrom-Lundqvist C, Andren B, Lonnnerholm S, Blomstrom P, Freemantle N, et al. The effects of aetiology on outcome in patients treated with cardiac resynchronization therapy in the CARE-HF trial. *Eur Heart J*. 2009;30(7):782–8.
 43. Adelstein EC, Tanaka H, Soman P, Miske G, Haberman SC, Saba SF, et al. Impact of scar burden by single-photon emission computed tomography myocardial perfusion imaging on patient outcomes following cardiac resynchronization therapy. *Eur Heart J*. 2011;32(1):93–103.
 44. Marsan NA, Westenberg JJ, Ypenburg C, Van Bommel RJ, Roes S, Delgado V, et al. Magnetic resonance imaging and response to cardiac resynchronization therapy: relative merits of left ventricular dyssynchrony and scar tissue. *Eur Heart J*. 2009;30(19):2360–7.
 45. Xu YZ, Cha YM, Feng D, Powell BD, Wiste HJ, Hua W, et al. Impact of myocardial scarring on outcomes of cardiac resynchronization therapy: extent or location? *J Nucl Med*. 2012;53(1):47–54.
 46. Becker M, Hoffmann R, Kuhl HP, Grawe H, Katoh M, Kramann R, et al. Analysis of myocardial deformation based on ultrasonic pixel tracking to determine transmural strain in chronic myocardial infarction. *Eur Heart J*. 2006;27(21):2560–6.
 47. Brignole M, Auricchio A, Baron-Esquivias G, Bordachar P, Boriani G, Breithardt OA, et al. 2013 ESC guidelines on cardiac pacing and cardiac resynchronization therapy: the task force on cardiac pacing and resynchronization therapy of the European Society of Cardiology (ESC). Developed in collaboration with the European heart rhythm association (EHRA). *Eur Heart J*. 2013;34:24.
 48. Mullens W, Grimm RA, Verga T, Dressing T, Starling RC, Wilkoff BL, et al. Insights from a cardiac resynchronization optimization clinic as part of a heart failure disease management program. *J Am Coll Cardiol*. 2009;53(9):765–73.
 49. Bertini M, Delgado V, Bax JJ, van de Veire NR. Why, how and when do we need to optimize the setting of cardiac resynchronization therapy? *Europace*. 2009;11(Suppl 5):v46–57.
 50. Ellenbogen KA, Gold MR, Meyer TE, Fernandez LI, Mittal S, Waggoner AD, et al. Primary results from the SmartDelay determined AV optimization: a comparison to other AV delay methods used in cardiac resynchronization therapy (SMART-AV) trial: a randomized trial comparing empirical,

- echocardiography-guided, and algorithmic atrio-ventricular delay programming in cardiac resynchronization therapy. *Circulation*. 2010;122(25):2660–8.
51. Vidal B, Sitges M, Marigliano A, Delgado V, Diaz-Infante E, Azqueta M, et al. Optimizing the programming of cardiac resynchronization therapy devices in patients with heart failure and left bundle branch block. *Am J Cardiol*. 2007;100(6):1002–6.
52. Doring M, Braunschweig F, Eitel C, Gaspar T, Wetzel U, Nitsche B, et al. Individually tailored left ventricular lead placement: lessons from multimodality integration between three-dimensional echocardiography and coronary sinus angiogram. *Europace*. 2013;15(5):718–27.
53. Nitsche B, Eitel C, Bode K, Wetzel U, Richter S, Doring M, et al. Left ventricular wall motion analysis to guide management of CRT non-responders. *Europace*. 2015;17(5):778–86.

Assessing Atrial Function

27

Melissa Leung, Jeroen J. Bax,
Nina Ajmone Marsan, and Victoria Delgado

The atria are thin walled chambers that play an important role in ventricular filling. This function can be divided into several phases: (1) a reservoir phase for pulmonary vein flow return during ventricular systole, (2) a conduit phase for blood transiting the pulmonary veins to the left ventricle (LV) (for the left atrium (LA)) and for blood transiting the superior and inferior vena cava to the right ventricle (for the right atrium (RA)) during early ventricular diastole, and (3) an active contractile phase that augments ventricular filling in late ventricular diastole [1].

Assessment of atrial dimensions and function has important clinical and prognostic implications. A large body of evidence demonstrates that echocardiographic assessment of LA size is important to predict adverse cardiovascular outcomes in myocardial infarction, atrial fibrillation (AF), stroke, hypertension, hypertrophic cardiomyopathy, mitral regurgitation. Furthermore, LA enlargement is a biomarker of both the severity and chronicity of diastolic dysfunction and magnitude of LA pressure elevation. Initial M-mode and 2-dimensional (2D)

linear measurements have progressed to area and then volumetric measurements, followed by 3-dimensional (3D) measurements, providing superior assessment of structural and functional mechanics. Advancement in cardiac computed tomography (CT), and cardiac magnetic resonance imaging (CMR) have further made possible validation of these aforementioned echocardiographic techniques, and consequently, a better understanding of their limitations. Functional assessment of the LA by means of phasic volumetric assessment, spectral Doppler, and advanced imaging techniques such as tissue Doppler and strain imaging have demonstrated increasing prognostic importance in a variety of cardiovascular conditions.

Although the RA has not raised as much attention as the LA, there is now growing data on reference values for RA size and function, and its importance in pulmonary hypertension has been established [2, 3].

This chapter outlines the currently accepted methods for assessment of atrial size and function using both 2D and 3D techniques, and its prognostic implications.

M. Leung
Department of Cardiology, Liverpool Hospital,
University of New South Wales, Sydney, NSW, Australia

Department of Cardiology, Leiden University
Medical Center, Leiden, The Netherlands

J. J. Bax · N. Ajmone Marsan · V. Delgado (✉)
Department of Cardiology, Leiden University
Medical Center, Leiden, The Netherlands
e-mail: V.Delgado@lumc.nl

The Left Atrium

Anatomy

The LA is the most posteriorly situated of all the cardiac chambers. It lies anterior to the descending

thoracic aorta, tracheal bifurcation, and oesophagus from which it is separated by the fibrous pericardium. The transverse pericardial sinus lies anterior to the left atrium, and in front of the sinus lies the root of the aorta. The LA begins at the junction of the four pulmonary veins, which enter from its posterior aspect, and terminate at the fibrous ring that marks the atrioventricular junction at the mitral valve orifice. The LA has five muscular walls: superior (which lies in close proximity to the bifurcation of the pulmonary trunk and the right pulmonary artery), posterior, left lateral, septal, and anterior (situated behind the aortic root). The LA appendage opens from its anterolateral aspect as a finger-like pouch extending from the os. The coronary sinus runs along the posteroinferior region of the LA, within the epicardium of the atrioventricular groove (Fig. 27.1). Knowledge of the anatomy of the LA is integral to accurate assessment of its structural and functional mechanics.

Assessment of Left Atrial Size

Two-dimensional echocardiography is the most widely used method to assess LA dimensions (Table 27.1). However, the complex 3D geometry of the LA challenges the assessment of its

dimensions with 2D techniques. Three-dimensional echocardiography, CT and CMR can better characterize the 3D geometry of the LA and are therefore considered methods of reference.

Two-Dimensional Measurements

Linear Measurements

Traditional measurement of anteroposterior LA dimensions is typically performed on transthoracic parasternal long-axis views, using either M-mode (Fig. 27.2a) or 2D images (Fig. 27.2b). The American Society of Echocardiography (ASE) and the European Association of Cardiovascular Imaging (EACVI) recommended normal reference ranges for men are 3.0–4.0 cm, and for women are 2.7–3.8 cm [4]. The anteroposterior diameter has been extensively used and has been shown to provide prognostic information in a number of conditions. In the Framingham Heart Study, the age-adjusted risk of stroke increased with each 10 mm increment in LA dimension by 2.2-fold in men, and 2.0-fold in women [5], whilst in a separate Framingham cohort of patients aged 59–90 years of age, each 5 mm increment of LA dimension increased the hazard ratio (HR) for non-rheumatic atrial fibrillation by 1.39 (95%

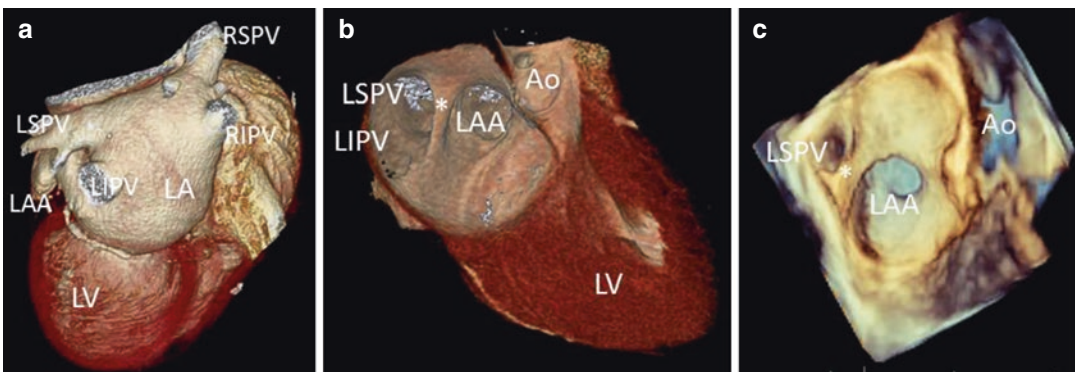


Fig. 27.1 3D reconstructions of the heart. From a postero-inferior computed tomographic (CT) projection (panel a), the left superior (LSPV), left inferior (LIPV), right superior (RSPV), and right inferior pulmonary veins (RIPV) can be seen entering the LA. The LA appendage (LAA) and left circumflex artery are also clearly demonstrated. Panel b is a fly-through CT projection, showing

the left lateral aspect of the LA. The separation of the LAA from the LSPV and LIPV posteriorly by the ridge (asterisk); and the aorta (Ao), anteriorly are important structures in transcatheter and electrophysiological procedures. Similar anatomical structures are also be demonstrated in the transoesophageal echocardiographic image in panel c

Table 27.1 Recommendations for the echocardiographic assessment of LA size

LA parameter	Normal values	Advantages	Disadvantages
<i>2D measurements</i>			
Linear dimension (Anteroposterior diameter)	Normal reference ranges for men: 3.0–4.0 cm, and for women: 2.7–3.8 cm [4]	<ul style="list-style-type: none"> • Simple to measure • Reproducible • Prognostic value in stroke, non-valvular AF, risk of cardiovascular death 	<ul style="list-style-type: none"> • Single dimension only • Insensitive to changes in LA size • Accuracy of M-mode measurement is limited by the insonant angle of the ultrasound beam
Area	The upper reference limit for LA area is 21.9 cm ² [37]	<ul style="list-style-type: none"> • Better representation of true LA size than anteroposterior diameter alone 	<ul style="list-style-type: none"> • Dedicated maximized apical 4-chamber image recommended to avoid LA foreshortening
Biplane volume (Recommended technique)	Upper reference limit for indexed LA volume is 34 ml/m ² [4]	<ul style="list-style-type: none"> • Relies on fewer geometric assumptions • More sensitive and accurate measure of asymmetric remodeling and changes in LA size • More robust predictor of cardiovascular events than anteroposterior diameter or area • Prognostic value in mitral regurgitation; acute myocardial infarction; non-valvular AF; stroke, cardiovascular death, and heart failure in patients in sinus rhythm; and dilated cardiomyopathy 	<ul style="list-style-type: none"> • Dedicated maximized apical 4- and 2-chamber images recommended • Still underestimates LA volume because of foreshortening of images • Limited by the assumption of spherical geometry of the LA
<i>3D measurements</i>			
Volume	Normal reference values for 3D maximum LA volumes are 15–42 ml/m ² in men, and 15–39 ml/m ² in women [16]	<ul style="list-style-type: none"> • Improved diagnostic accuracy and reproducibility compared with 2D volumes • No geometric assumptions about LA geometry • Prognostic value in severe LV dysfunction, and predictor of adverse cardiovascular events in normals • Stronger correlation with cardiovascular events compared to 2D volumes 	<ul style="list-style-type: none"> • Lack of standardised methodology • Limited information on normal reference values • Lower temporal resolution • Requires patient cooperation for breath hold image acquisition • Image quality required to provide good anatomical assessment on 3D echocardiography is contingent on having a good acoustic window

confidence interval [CI] 1.14–1.68) [6]. LA diameter was correlated with the risk of cardiovascular death in a population based study of 5888 elderly subjects, and in 830 Finnish men; however after adjusting for traditional clinical risk factors and left ventricular mass, respectively, were no longer significant predictors [7, 8]. This may be related to the fact that LA dilatation occurs in both the

supero-inferior direction, as well as the medio-lateral direction, and may be hampered in the anteroposterior direction by the aortic root, anteriorly, and oesophagus, descending aorta and trachea posteriorly. Furthermore, the accuracy of the anteroposterior diameter is limited by the insonant angle of the ultrasound beam. Therefore, measurement of the anteroposterior dimension is

likely to be insensitive to changes in LA size and should be used in conjunction with other measures.

LA Area

The maximum LA area may be planimetered in the apical 4- and 2-chamber views at the end of LV systole, just before the mitral valve opens, taking care to exclude the confluences of the pulmonary veins, the LA appendage, and the area under the mitral valve annulus (Fig. 27.2c). Given that the long-axis of the LV and LA are in different planes, dedicated apical images should be taken to ensure the maximal short- and long-axis dimensions [4]. However, given the practical similarities with measuring LA volume and its concomitant extensive literature on prognostic value, the use of LA area for sizing is of limited utility and no longer recommended.

LA Volume

LA volume is the currently recommended method for assessing LA size [4]. The measurement of LA volume relies on fewer geometric assumptions, provides a more sensitive and accurate measure of changes in LA size, and has a stronger association with outcomes in cardiac patients compared to anteroposterior diameter and LA area [9–11].

There are a number of methods to measure LA volume including the ellipsoid method and the modified Simpson's biplane method of discs (Fig. 27.3). Due to the relative inaccuracies of the three linear measurements used to calculate volume in the ellipsoid method, the biplane method is preferred. As with LA area measurements, the importance of maximizing the short- and long-axis dimensions is underscored. The biplane method has demonstrated a close correlation with LA vol-

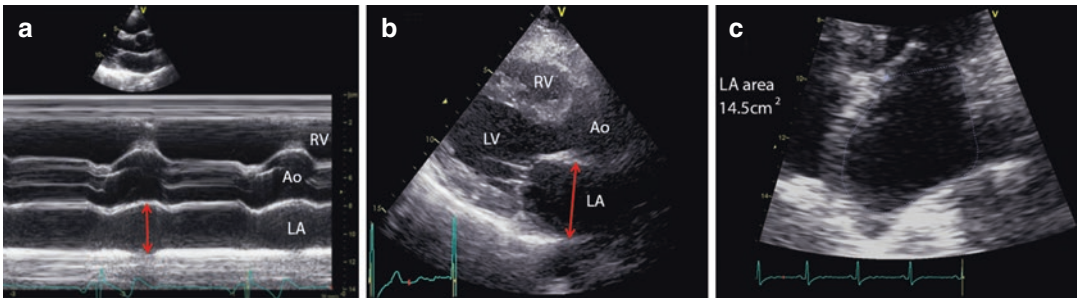


Fig. 27.2 LA anteroposterior diameter measured in the parasternal long axis view by M-mode (panel a) and 2D images (panel b). The measurement is performed at end-systole when LA volume is largest. A zoomed image

ensuring maximal short- and long-axis dimensions of the LA is shown in panel c. The blood-tissue interface is planimetered, taking care to exclude the pulmonary veins and the area under the mitral valve

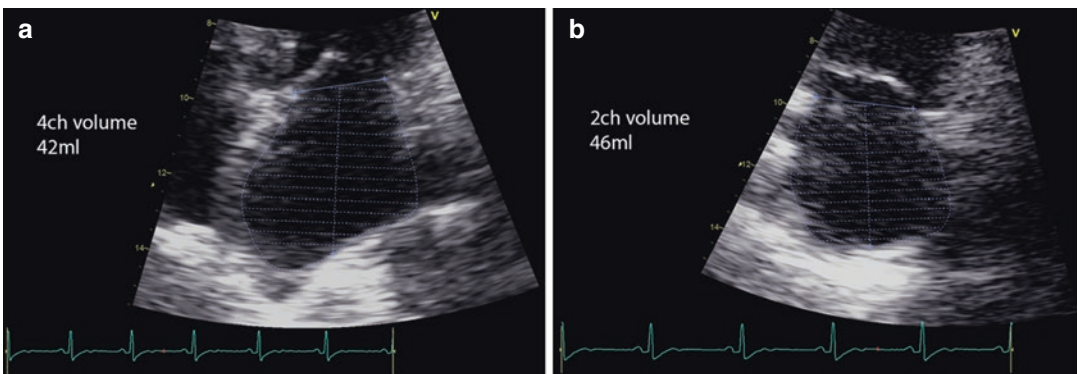


Fig. 27.3 LA volume measurement using a Simpson's biplane approach in the apical 4- (panel a) and 2-chamber (panel b) views, tracing the blood tissue interface and avoiding the pulmonary veins and LA appendage

ume calculated by 3D echocardiography, computed tomography (CT), as well as cardiac magnetic resonance imaging (CMR). The upper reference limit for indexed LA volume is 34 ml/m².

The prognostic significance of LA volume has been shown in a number of different cardiovascular conditions. In a study of 492 patients with organic mitral regurgitation in sinus rhythm, an indexed LA volume at diagnosis of ≥ 60 ml/m² had increased mortality (HR: 2.8 [95% CI: 1.2–6.5], $p = 0.016$) and cardiac events (HR: 5.2 [95% CI: 2.6–10.9], $p < 0.0001$) with medical management compared with patients with LA index < 40 ml/m² [12]. Mitral surgery in these patients markedly improved outcome and restored life expectancy; following surgery patients with LA index ≥ 60 ml/m² versus < 60 ml/m² did not incur excess mortality or cardiac events (both $p > 0.30$). Following acute myocardial infarction, an indexed LA volume > 32 ml/m² was a powerful marker for increased all-cause mortality, independent of clinical data and other echocardiographic measures of LV systolic and diastolic function [13, 14]. A large LA volume has been independently associated with a higher risk of non-valvular AF in studies of elderly and hypertrophic cardiomyopathy patients. However, a subsequent cross-sectional study of individuals ≥ 45 years of age showed that despite indexed LA volume and diastolic dysfunction being univariate predictors of all-cause mortality, after controlling for diastolic dysfunction, LA volume was no longer an independent predictor of mortality [15]. It is likely that this relationship is due to the effects of diastolic dysfunction rather than the LA volume having an independent prognostic value, per se. In addition, LA volume has been associated with the risk of stroke, cardiovascular death and heart failure in patients with sinus rhythm. Additionally, in patients with dilated cardiomyopathy, increasing LA volumes have been independently associated with poorer survival after correcting for left ventricular end-systolic volumes, diastolic dysfunction, and mitral regurgitation.

Despite the strong outcome data on 2D LA volume measurements, this technique still underestimates LA volume because of foreshortening of images. Furthermore, this method is still lim-

ited by the assumption of spherical geometry of the LA, whereas the shape of the LA often changes as it enlarges.

Three-Dimensional Measurements

The limitations associated with 2D assessment of LA size, including reproducibility and maximisation of LA size by imaging plane, and geometric assumptions have been overcome by 3D echocardiography. RT3DE measurement of LA volumes have been validated against CT and CMR and have improved diagnostic accuracy and reproducibility compared with 2D volumes. The LA volumes measured on 3D echocardiography are generally larger than those measured using the 2D method. Normal reference values for 3D maximum LA volumes reported in a recent study by Aune et al. are 15–42 ml/m² in men, and 15–39 ml/m² in women [16].

Real-time 3D echocardiography (RT3DE) using a second-generation matrix array transducer is a rapid method for LA assessment using the apical transthoracic approach. There are three main methods by which atrial assessment can be made (Fig. 27.4): 3D guided biplane, narrow angle, and full-volume dataset acquisition [17]. Data are acquired in the apical view with the image aligned to obtain optimal border delineation of the LA in the far field. Three-dimensional guided biplane analysis (Fig. 27.4a) uses the RT3DE dataset to identify anatomically correct and non-foreshortened apical 4- and 2-chamber views of the LA. Following this, the biplane method of discs may then be used to calculate LA volumes. Although this method uses 3D data to optimize the acquisition of 2D images, it improves the accuracy of maximizing LA volumes. However, this method is still subject to geometric assumptions and may still underestimate LA size (depending on the plane of LA enlargement). The narrow angle acquisition mode (live-3D) displays a narrow angle pyramidal volume of $30^\circ \times 60^\circ$ and allows real-time 3D imaging without the need for ECG gating. The 3D data acquired with this mode is characterized by high temporal and spatial resolution

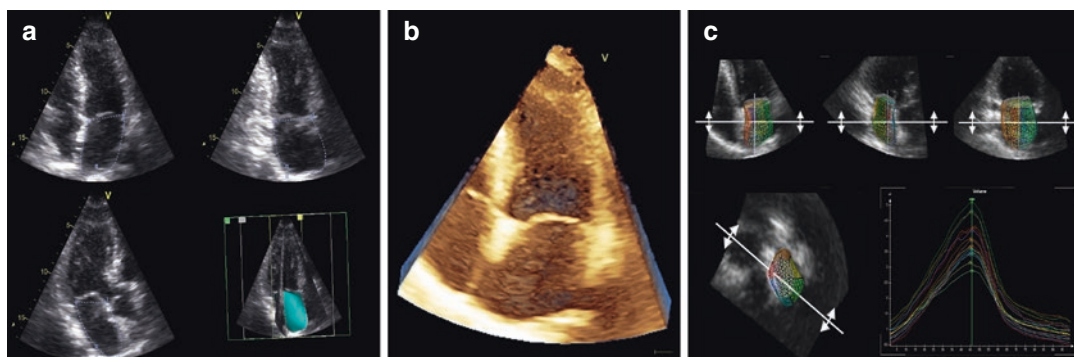


Fig. 27.4 RT3DE measurements of LA volume. 3D-guided triplane images may be used to obtain improved anatomical alignment of the apical 4-, 2-, and 3-chamber views (panel **a**). The blood tissue interface may be then traced to obtain maximum and minimum LA volumes, as well as ejection fraction. Live-3D may also be used to

measure LA size (panel **b**). Using full-volume multi-beat reconstructions (panel **c**), the 3D longitudinal and transverse axes may be aligned at the geometric centre of the LA. After marking the mitral annulus and dome in each view, semi-automatic endocardial border tracing allows tracking of LA volumes at any phase of the cardiac cycle

(Fig. 27.4b). The full-volume dataset (Fig. 27.4c) allows inclusion of a larger cardiac volume within the pyramidal scan of $90^\circ \times 90^\circ$, and is gated to the electrocardiogram (ECG). This mode is acquired by merging or stitching narrower scans over 4–5 consecutive heartbeats providing high temporal resolution but relatively lower spatial resolution compared with live-3D or 3D zoom acquisition modes. The 3D zoom mode displays a smaller magnified pyramidal volume limited to the LA providing high spatial resolution data but with lower temporal resolution compared with multi-beat full-volume acquisition mode. To post-process and analyze the data, the 3D longitudinal axis and LA axis is aligned in parallel with the transverse axis placed at the level of the geometric centre of the LA and the LA volume is then derived from semi-automatic endocardial border tracing by marking the dome of the superior aspect of the atrium lying opposite the annulus and four mitral annular points (anterior, inferior, septal and lateral) (Fig. 27.4c).

Three-dimensional LA volume has been demonstrated to be independently associated with cardiac death and heart failure hospitalisation in a study of 108 patients with severe left ventricular dysfunction and in sinus rhythm (HR 1.06, $p < 0.001$) [18]. Additionally, patients with a 3D LA volume < 100 ml were found to

have a significantly higher 1-year event-free survival than those with LA volume ≥ 100 ml (80 ± 7 vs $48 \pm 10\%$, $p < 0.001$). Caselli et al. examined 2D and 3D LA volumes in 178 outpatients referred for echocardiography and followed them for a median of 45 months [19]. On univariate analysis, LA maximum and minimum volumes were associated with cardiovascular events (HR: 1.055; CI: 1.031–1.080 and HR: 1.049; CI: 1.028–1.070, respectively; $p < 0.001$ for both). By multivariate analysis, 3D echocardiography derived LA minimum volume was identified as the best independent predictor of adverse cardiovascular events (HR: 1.217; CI: 1.075–1.378; $p = 0.002$). Furthermore, 3D volumes showed a stronger correlation with cardiovascular events compared to 2D volumes, suggesting an incremental benefit of risk assessment using RT3DE.

Despite the advantages of 3D echocardiography, a lack of standardised methodology as well as limited information on normal reference values limit this technique at the present time. Additionally, the image quality required to provide good anatomical assessment on 3D echocardiography is contingent on having a good acoustic window. Unlike the LV, the LA is in the far field in the apical views further limiting the reliability of the echocardiographic measurements.

Assessment of Left Atrial Function

There are a number of methods available for the assessment of LA function, including the measurement of phasic volumes, spectral Doppler indices, as well as tissue Doppler velocities and strain.

Left Atrial Phasic Volumes

LA function may be represented by three phasic volumes: the passive emptying volume, conduit volume, and active emptying (booster pump) volume. *LA reservoir function* is determined by atrial compliance, atrial relaxation and contractility, and LV systolic function and end-systolic volume. It is calculated as the difference between the maximum LA volume at LV end-systole (before mitral valve opens), and the minimum volume at LV end-diastole (when mitral valve closes). *LA conduit function* is the volume of blood that passes from the pulmonary veins through the LA and into the left ventricle while the mitral valve is open and is influenced by atrial compliance as well as LV relaxation and compliance. It is calculated as total LV stroke volume minus total LA stroke volume. *LA booster pump function* represents the volume of blood that is actively propelled into the left ventricle by active contraction of the LA, and is influ-

enced by the degree of venous return, LV end-diastolic pressures, and LV systolic reserve. It is calculated as the LA volume prior to atrial systole (LA volume just prior to the p-wave on the ECG) minus the minimum LA volume at LV end-diastole (Fig. 27.5). These functions can be calculated from LA volumes obtained with 2D or 3D echocardiography, as described above.

The predictive value of LA reservoir function has been shown in 574 adults without prior arrhythmia followed-up for a mean of 1.9 ± 1.2 years [20]. Subjects with new AF or atrial flutter had lower LA reservoir function (as measured by total LA emptying fraction) and higher maximum LA volumes. The age adjusted risk of AF or atrial flutter was highest for subjects with concomitant LA emptying fractions <49% and maximum LA volume >38 ml/m² (HR 9.3, $p = 0.003$). A reduced LA reservoir function was found to markedly increase the risk of new onset AF or atrial flutter, independent of maximum LA volume, LV function, and clinical risk factors.

Spectral Doppler Indices

Transmitral and Pulmonary Venous Flow

Spectral Doppler waveforms obtained from pulmonary venous flow (representing LA filling)

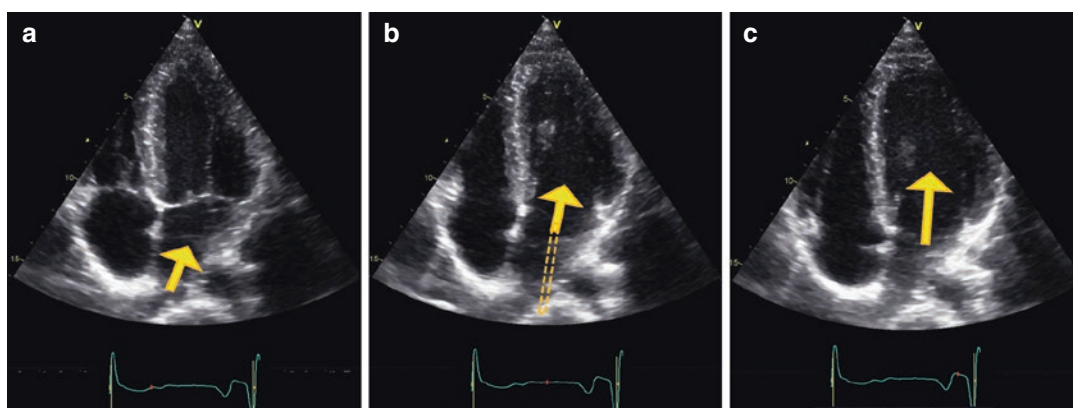


Fig. 27.5 LA phasic function. Panel **a**: LA reservoir function represents the maximal LA volume at LV end-systole. Panel **b**: LA conduit function representing the volume of blood that passes from the pulmonary veins

through the LA and into the left ventricle while the mitral valve is open. Panel **c**: LA booster pump function representing the volume of blood that is actively propelled into the left ventricle by active contraction of the LA

and transmitral inflow (representing LA emptying) provide readily available and easy-to-interpret information about LA mechanical function. LA reservoir function is reflected by the pulmonary venous systolic (S) flow velocity. LA conduit function is reflected in the peak transmitral early (E wave) velocity, the ratio of the peak E and late (A) velocities, as well as the pulmonary venous diastolic (D) flow velocity. The relative contribution of LA booster pump function is assessed by the velocity time integral (VTI) of the A wave; the atrial filling fraction, the ratio of the mitral A wave VTI to the total diastolic transmitral flow ($A_{VTI}/[E_{VTI} + A_{VTI}]$); as well as the magnitude and duration of the pulmonary venous atrial reversal flow (Fig. 27.6).

Atrial Ejection Force

Atrial ejection force, the force exerted by the LA to propel blood forwards into the left ventricle during atrial systole, may also be used to assess LA mechanical function as well as LV diastolic function. Atrial ejection force may be calculated as the product of the mass and acceleration of blood ejected from the LA during LA systole, where mass may be further defined as the product of the density of blood ($\rho = 1.06 \text{ g/cm}^3$) and volume of blood passing through the mitral orifice:

$$\text{LA ejection force} = 0.5 \times 1.06 \text{ g/cm}^3 \times \text{mitral annulus area} \times (\text{peak A-velocity})^2$$

The mitral annulus area is measured in the apical 4 chamber view, and is assumed to be circular. The peak A velocity is obtained with the sample volume at the mitral annulus.

LA ejection force has been used as a marker of recovery after successful cardioversion whereby ejection force was depressed immediately after cardioversion, and progressive improvement was demonstrated over successive weeks in patients who maintained sinus rhythm. In this setting, a higher atrial ejection force was associated with a more marked reduction in LA size after restoration of sinus rhythm. The Strong Heart Study examined a population-based sample of middle-aged and elderly adults with a high prevalence of hypertension and diabetes and without prevalent cardiovascular disease [21]. LA ejection force

was associated with geometric changes of the heart (higher LV dimensions, LV mass, stroke volume, and cardiac output (all $p < 0.01$)) and with increased rate of combined fatal and nonfatal cardiovascular events ($HR = 1.033$, 95% $CI = 1.005\text{--}1.061$; $p = 0.021$), independently of demographic characteristics, risk factors, LV geometry, and transmitral diastolic pattern.

There are a number of factors that limit the utility and measurement of spectral Doppler traces. Interpretation is limited in the setting of sinus tachycardia, arrhythmias such as AF, high-quality pulmonary venous Doppler traces, and conduction system disease. Furthermore, the measurements of mitral annular diameter and peak transmitral A velocity are not performed simultaneously; Doppler indices are highly load dependent and may be influenced by changes in LV diastolic function, age, mitral valve disease, or abnormal haemodynamics, thus limiting the accuracy of these measurements.

Tissue Doppler Velocities and Myocardial Deformation Imaging

Tissue Doppler Imaging

Tissue Doppler imaging (TDI) is a preload-independent measure of the systolic and diastolic intrinsic low myocardial velocities in the longitudinal plane. Pulsed-wave TDI requires real time data acquisition, and has high temporal resolution. Colour-coded TDI generates a spatial map of myocardial velocities, measuring the modal velocity, and has comparatively lower temporal resolution. Offline analysis of colour-coded TDI traces provide simultaneous information about the global or segmental function of any region of the LA in the same imaging view. Using pulsed-wave or colour-coded TDI, the peak velocity at the mitral annulus in late diastole due to atrial contraction (a' or A_m velocity) provides an easily obtainable measure of global LA function. There is no significant difference between the basal lateral and basal septal a' velocities, and this measure correlates well with peak A velocity, atrial fraction and atrial ejection force [1]. Three peak tissue velocities can be identified from the time-velocity curves: systolic velocity (s') which

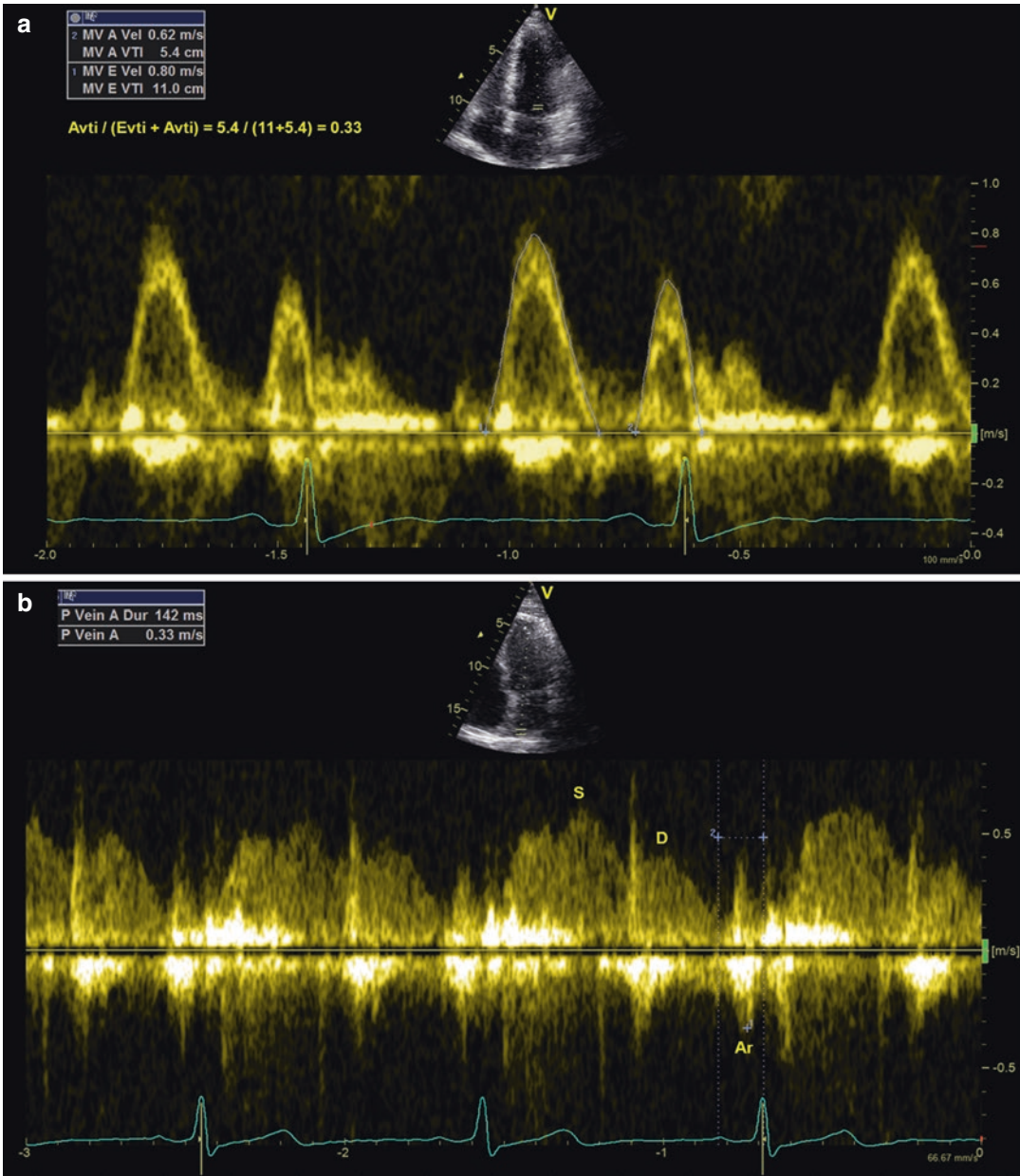


Fig. 27.6 Assessment of atrial function by transmitral and pulmonary inflow spectral Doppler tracings. The relative contribution of LA booster pump function is assessed by the ratio of the mitral A wave VTI to the total diastolic

transmitral flow ($A_{VTI} / [E_{VTI} + A_{VTI}]$; panel **a**); as well as the magnitude and duration of the pulmonary venous atrial reversal flow (panel **b**)

reflects LA reservoir function, early diastolic velocity (e') which reflects conduit function, and late diastolic velocity (a') which reflects booster pump function (Fig. 27.7).

Segmental atrial function can be evaluated using colour-coded TDI. The atria may be divided

into 2 basal, 2 mid-atrial, and 2 annular segments in both the apical 4- and 2-chamber views. A decreasing gradient of atrial contraction velocity from annulus to base has been demonstrated, and normal values have been reported. Akin to other Doppler techniques, TDI is limited by its angle

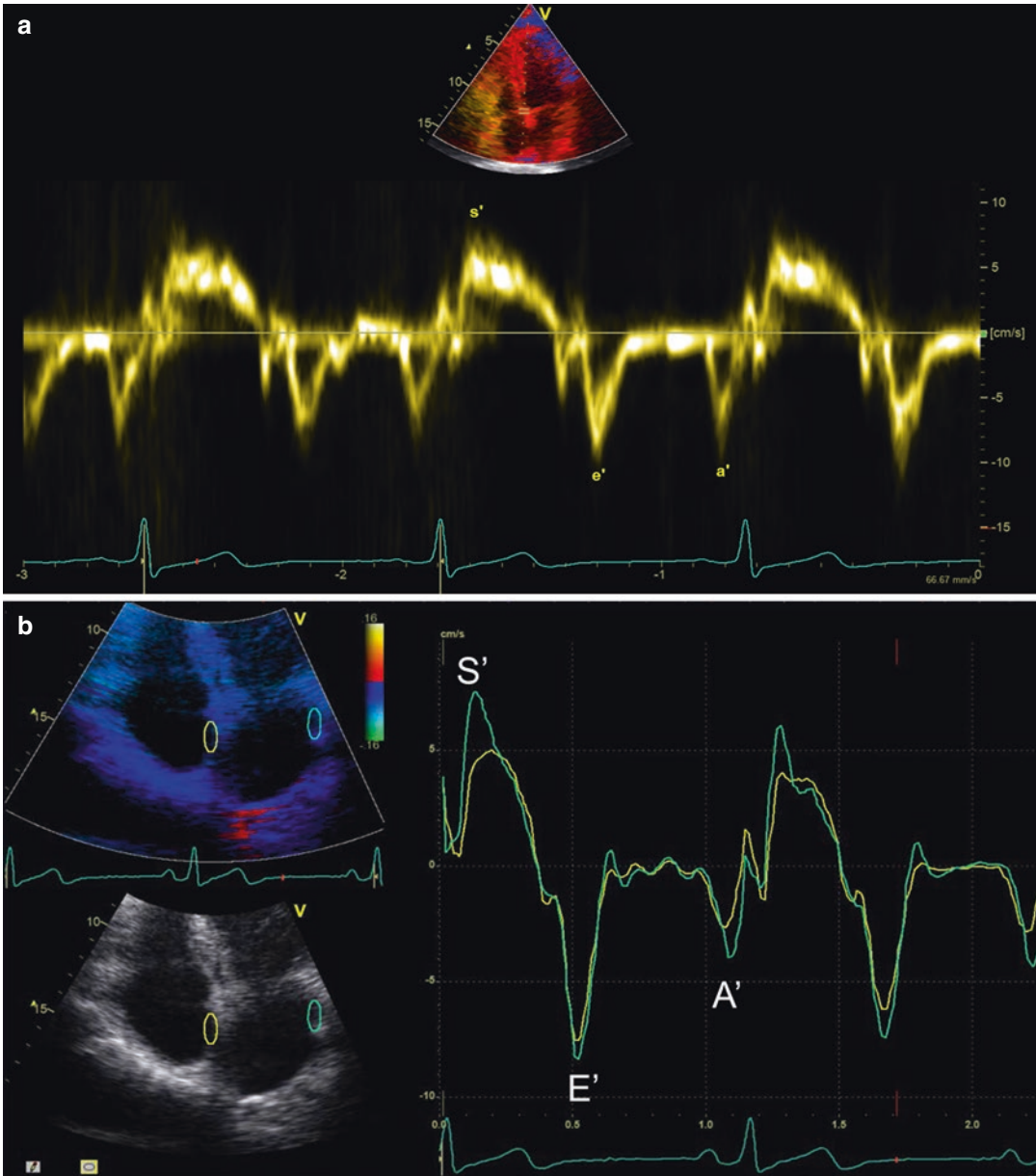


Fig. 27.7 Pulse wave and colour tissue Doppler. Panel **a** demonstrates pulse wave tissue Doppler obtained at the mitral valve septal annulus. Three peak tissue velocities can be identified from the time-velocity curves: systolic velocity (s') which reflects LA reservoir function, early

diastolic velocity (e') which reflects conduit function, and late diastolic velocity (a') which reflects booster pump function. Panel **b** demonstrates assessment of LA function using colour tissue Doppler at the mid-septal and mid-lateral walls in the apical 4-chamber view

dependency, effects of tethering from neighbouring myocardium and cardiac motion.

The prognostic value of TDI velocities incremental to clinical and other echocardiographic parameters has been demonstrated. Wang et al. studied 353 subjects with cardiac disease versus

165 normal controls followed up over a 2-year period and found that an a' velocity of >7 cm/s compared with ≤ 4 cm/s predicted cardiac death with a hazard ratio of 11.53, whereas an a' velocity between 4 and 7 cm/s predicted death with a hazard ratio of 4.28 [22]. Yamamoto et al.

followed 96 patients over 29 months and found that a late diastolic mitral annular velocity ≤ 5 cm/s independently predicted worse cardiac mortality or heart failure hospitalization [23].

Myocardial Deformation Imaging

Strain and strain rate (SR) imaging examine the magnitude and the instantaneous rate by which myocardial deformation occurs during the cardiac cycle. Negative strain indicates myocardial shortening or contraction, whilst positive strain represents lengthening. Global and regional LA strain and strain rate may be assessed using either TDI velocities or applied to grey-scale 2D images using software such as 2D speckle tracking or velocity vector imaging. SR is derived from the colour-coded TDI map of myocardial velocities for the myocardial region of interest, and strain is calculated by integrating the SR data with respect to time. 2D speckle tracking involves the frame-by-frame tracking of unique acoustic backscatter fingerprints of the atrial wall that are generated due to the reflected ultrasound beam with myocardial tissue. The displacement of this acoustic fingerprint between two pixels represents myo-

cardial deformation and is independent of the angle of insonation. Good image quality and frame rates of 50–70 Hz are required for accurate tracking. The main advantages of this technique are the angle independency and site specificity, making strain measurements in walls not parallel to the ultrasound beam more reliable than colour-coded TDI derived strain. The thin-walled atria, lack of contiguous atrial wall due to the LA appendage and pulmonary vein insertions, and far-field location of the LA on transthoracic echocardiograms are the main challenges to speckle tracking of the LA. Currently, LA analysis requires application of software analysis packages which are designed and validated for the LV.

When assessing LA deformation, the zero baseline or reference point on the ECG is important. If ventricular end-diastole (QRS onset) is chosen as the reference point, the peak positive longitudinal strain (ϵ_s) corresponds to atrial reservoir function, whilst the strain during early and late diastole (ϵ_e and ϵ_a , respectively) correspond to the conduit and booster pump function (Fig. 27.8). If atrial end-diastole (P-wave onset)

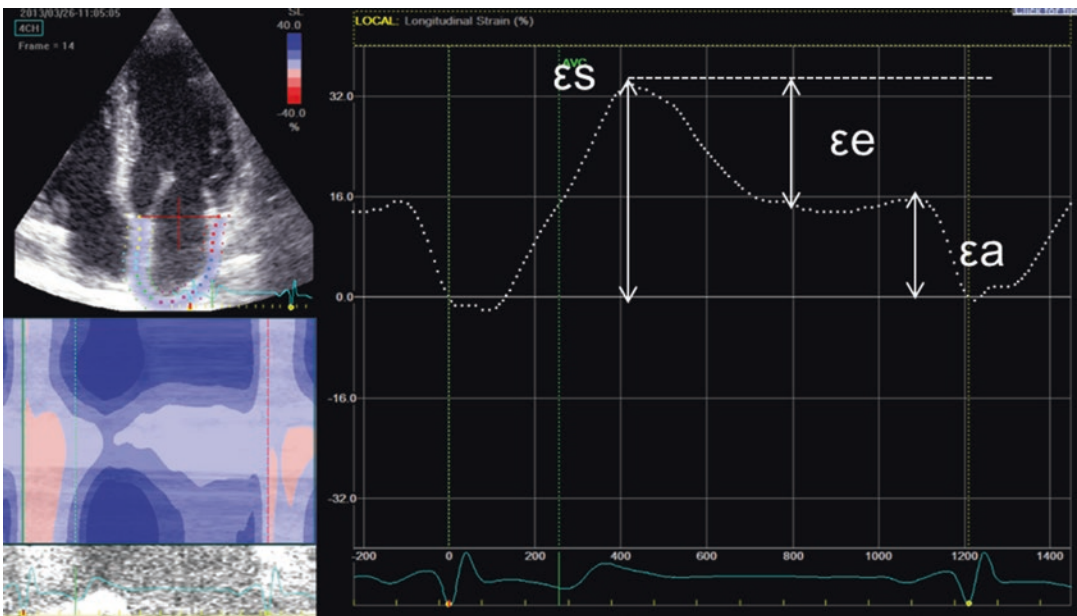
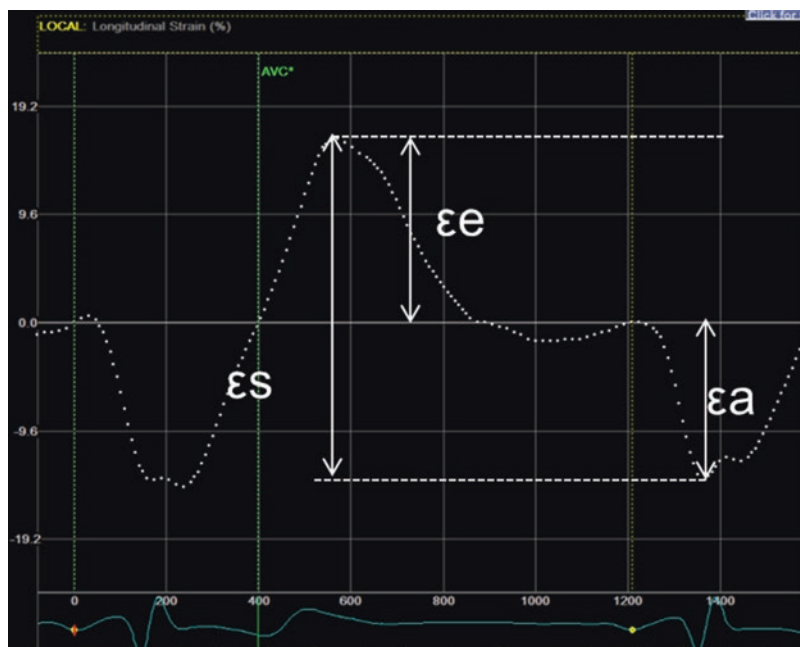


Fig. 27.8 Assessment of LA strain referenced to the QRS-wave onset of the ECG. Here, the strain curve is positive throughout the cardiac cycle. The peak positive longitudinal strain (ϵ_s) corresponds to atrial reservoir

function, whilst the strain during early and late diastole (ϵ_e and ϵ_a , respectively) correspond to the conduit and booster pump function

Fig. 27.9 LA strain assessment referenced to the P-wave onset of the ECG. The first negative peak (ϵ_a) represents the LA booster pump function, the positive peak (ϵ_e) represents the conduit function, and the summation of ϵ_a and ϵ_e (ϵ_s) represent the reservoir function when the LA fills from the minimum LA volume to the maximum LA volume



is chosen as the reference point, the first negative peak (ϵ_a) represents the LA booster pump function, the positive peak (ϵ_e) represents the conduit function, and the summation of ϵ_a and ϵ_e (ϵ_s) represent the reservoir function when the LA fills from the minimum LA volume to the maximum LA volume (Fig. 27.9). Regardless of which reference point is used, the SR in ventricular systole (SR-S), early (SR-E) and late diastole (SR-A) reflect reservoir, conduit, and booster pump functions. Normal values of 2D speckle tracking strain have been reported for strain measured in 12 segments in the apical 4- and 2-chamber views referent to QRS onset where the mean ϵ_s of 60 healthy individuals was $42.2 \pm 6.1\%$.

LA strain has been associated with ultrastructural changes of the LA wall. A reduced LA strain has been shown to correlate with LA wall fibrosis on CMR in patients with AF, as well as fibrosis determined histologically in patients with mitral valve disease. In addition, the prognostic importance of the separate evaluation of LA phasic function using strain and SR imaging has been demonstrated. Reduced LA strain correlated with CHADS2 score [24] and stroke in patients with persistent AF. In patients undergoing catheter ablation for AF, LA reservoir function (ϵ_s , SR-S)

is a predictor for the maintenance of sinus rhythm [25], and is an independent predictor of LA reverse remodelling (odds ratio: 1.813; 95% confidence interval: 1.102–2.982; $p = 0.019$) [26]. In patients with ST-segment elevation myocardial infarction treated with primary percutaneous coronary intervention, LA strain was independently associated with the composite endpoint of all-cause mortality, reinfarction and hospitalization for heart failure after adjusting for clinical and echocardiographic parameters (HR 0.94, CI 0.89–0.99, $p = 0.02$) [27]. Additionally, LA strain provided a small incremental value to LA maximal volume and traditional risk factors for the prediction of adverse outcome with an increase in the model global χ^2 from 40.2 to 43.1 ($p = 0.03$). In patients with severe organic mitral regurgitation, LA reservoir strain $\leq 24\%$ was associated with guideline-based criteria for mitral valve surgery and provided incremental risk stratification to established indications for mitral valve surgery for worse postoperative survival [28].

Despite its clinical utility, 2D LA deformation imaging is limited in its ability to account for the 3D contraction and shortening which may account for the disappearance of speckles from 2D images due to through-plane cardiac motion

and the complexities in LA geometry. This has been addressed by recent studies utilizing 3D speckle tracking echocardiography (3DSTE) in LA assessment [29, 30]. 3DSTE enables the analysis of longitudinal and circumferential strain from the same 3D dataset, in addition to measurement of LA global area strain (Global area strain = longitudinal strain \times circumferential strain) [30]. The feasibility and reproducibility of LA strain using 2D compared with 3DSTE was examined by Mochizuki et al. and was found to have smaller interobserver and intraobserver variability attributed to the higher degree of automation of the 3D software. Furthermore, LA longitudinal strain values determined by 3DSTE were 22% lower than by the corresponding 2D approach, which was purported to be due to the out-of-plane movement of speckles on 2D STE, and is concordant with differences reported for LV strain. However, it is important to highlight that specific speckle tracking software designed for the LA is currently not available, and the application of software for LV analysis has not been validated in this regard.

The Right Atrium

Although the importance of the LA in cardiovascular disease has become increasingly recognized and research on this chamber has dominated attention in the last decade, very little echocardiographic research has evaluated structural and functional aspects of the right atrium (RA). Most studies on the right heart have focused on assessment of mean RA pressure and pulmonary hypertension [31–36]. In certain pathophysiologic states, the right heart is a critical factor determining the outcomes of patients: pulmonary hypertension, certain types of intracardiac shunts, patients with congenital heart disease, and patients with various pulmonary conditions. The unusual geometry of the right heart, and the absence of a convenient orthogonal view of the right atrium in particular, poses significant challenges in its characterization, and is the principal reason that has hampered research advances into methods of assessment.

Anatomy

The right atrium (RA) is a thin ovoid structure that lies slightly anteriorly and to the right of the left atrium. The RA begins at the junction of the superior and inferior vena cava, and coronary sinus, which enter from its posterior aspect, and terminate at the fibrous ring that marks the atrio-ventricular junction at the tricuspid valve orifice. The fibromuscular Eustachian valve, which usually regresses during embryological development, may be present adjacent to the inferior vena cava. The Chiari network is a delicate membranous structure that arises near the orifice of the inferior vena cava and serves as the valve of the coronary sinus. The ostium of the coronary sinus is located medial to the Eustachian valve, and is guarded by a flap of thin fibrous tissue called the Thebesian valve. The crista terminalis extends from the superior vena cava, inferiorly, to separate the venous inflow portion of the right atrium from the right atrial appendage. The fossa ovalis is an important anatomic landmark on the atrial septum to identify when performing transseptal punctures for left-sided catheter based procedures, and varies from heart to heart. These structures can be identified with 3D transesophageal echocardiography and are relevant during electrophysiological and transcatheter procedures (Fig. 27.10).

Assessment of Right Atrial Size

Measurement of the RA is most commonly performed in the apical 4-chamber view.

Linear Measurements Using 2D transthoracic images, the major long-axis distance of the RA may be measured in the apical 4-chamber view at the end of ventricular systole, from the center of the tricuspid annulus to the center of the superior RA wall, parallel to the interatrial septum. The RA minor distance is defined from the midlevel of the RA free wall to the interatrial septum, perpendicular to the long-axis (Fig. 27.11). RA size is gender dependent and normal values have recently been established based on three cohorts of more than

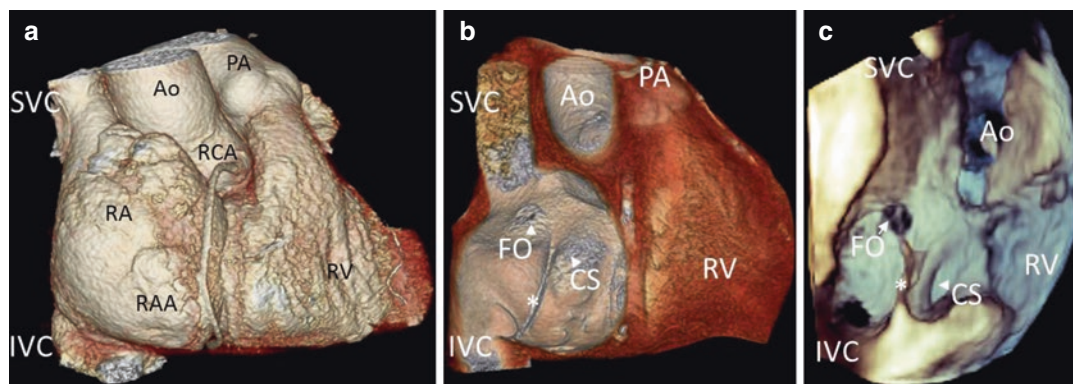
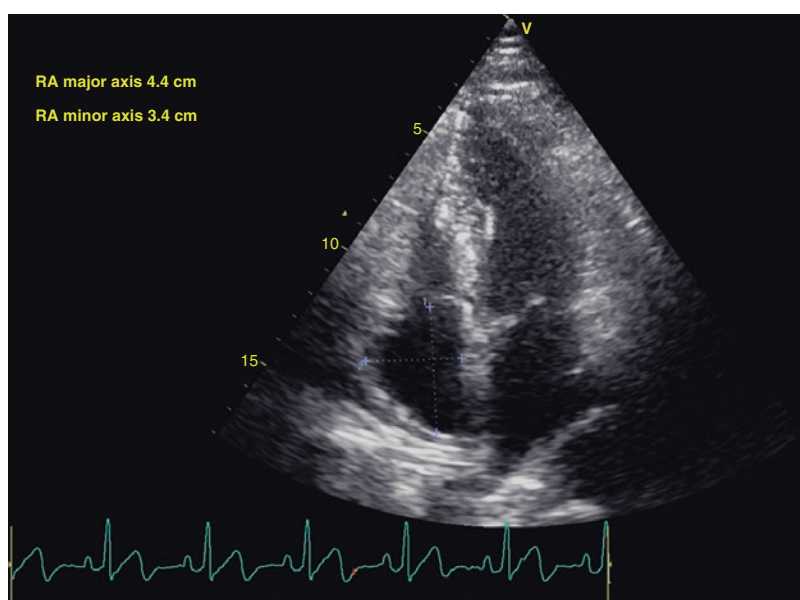


Fig. 27.10 CT (panels **a** and **b**) and 3D transoesophageal echocardiographic (panel **c**) reconstructions of the RA demonstrating important anatomical landmarks for trans-

catheter and electrophysiological procedures. *FO* foramen ovale, *SVC* superior vena cava, *CS* coronary sinus, *PA* pulmonary artery, *RAA* right atrial appendage

Fig. 27.11 The RA major and minor axis is measured in the apical 4-chamber view at the end of ventricular systole, from the center of the tricuspid annulus to the center of the superior RA wall, parallel to the interatrial septum. The RA minor distance is measured at the mid-level of the RA free wall to the interatrial septum, perpendicular to the long-axis



2400 patients [37–39]. The normal range for indexed RA minor axis dimension in both men and women is 1.9 ± 0.3 cm/m². The normal range for major axis dimension in women is 2.5 ± 0.3 cm/m², and in men is 2.4 ± 0.3 cm/m². Although easy to obtain, the RA linear measurements are unidimensional only, and make assumptions that RA enlargement is symmetrical (Table 27.2).

RA Area RA area may be planimetered in the apical 4-chamber view at end-systole, in the frame just prior to tricuspid valve opening by measuring along the blood-tissue interface

from septal to lateral annulus, taking care to exclude the area under the tricuspid valve annulus, superior and inferior vena cavae and RA appendage (Fig. 27.12a). The upper reference limit for RA area is 18 cm² [40]. RA area has been shown to be a predictor of outcome in primary pulmonary hypertension and chronic heart failure [3, 41, 42]. Although previously recommended for assessment of RA size, area measurements are also limited by assumptions of chamber symmetry and have now been replaced by RA volume measurements as the recommended technique [4].

Table 27.2 Recommendations for the echocardiographic assessment of RA size

RA parameter	Normal values	Advantages	Disadvantages
<i>2D measurements</i>			
Linear dimension	Normal range for indexed RA minor axis dimension in both men and women is 1.9 ± 0.3 cm/m ² Normal range for major axis dimension in women is 2.5 ± 0.3 cm/m ² , and in men is 2.4 ± 0.3 cm/m ²	<ul style="list-style-type: none"> • Simple to measure • Established normal values 	<ul style="list-style-type: none"> • Single dimension only • Dependent on scan plane • Based on assumptions that RA enlargement is symmetrical
Area	The upper reference limit for RA area is 18 cm ² [40]	<ul style="list-style-type: none"> • Better representation of true RA size than linear dimensions • Established normal values • Prognostic value in pulmonary hypertension and chronic heart failure 	<ul style="list-style-type: none"> • Dedicated maximized apical 4-chamber image recommended to avoid RA foreshortening • Dependent on scan plane
Single plane volume (Recommended technique)	Normal ranges are 25 ± 7 ml/m ² in men, and 21 ± 6 ml/m ² in women [4]	<ul style="list-style-type: none"> • Relies on fewer geometric assumptions • Reproducible • More sensitive and accurate measure RA size compared to linear measurements • Prognostic value in systolic heart failure, and predicting AF recurrence following electrical cardioversion 	<ul style="list-style-type: none"> • Dedicated maximized apical 4-chamber images recommended • Still underestimates RA volume because of foreshortening of images and single plane approach • Limited by the assumption of spherical geometry of the RA
<i>3D measurements</i>			
Volume	The upper and lower reference ranges for indexed 3D RA volumes are 47 ml/m ² and 20 ml/m ² , respectively [16]	<ul style="list-style-type: none"> • Improved diagnostic accuracy and reproducibility compared with 2D volumes • No geometric assumptions about RA geometry 	<ul style="list-style-type: none"> • Lack of standardised methodology • Limited information on normal reference values • Lower temporal resolution • Requires patient cooperation for breath hold image acquisition • Image quality required to provide good anatomical assessment on 3D echocardiography is contingent on having a good acoustic window • Limited information on prognostic significance

RA Volume *2D volume assessment:* 2D measurements are performed in a dedicated apical 4-chamber view, tracing the blood-tissue interface using a similar technique to area measurements (Fig. 27.12b). Since there is no standard

orthogonal view of the RA to perform biplane calculation, single plane area-length or disc summation approaches are recommended [4]. Normal ranges for 2D RA volume are based on two recent large datasets [37, 39] and are larger in men

(25 ± 7 ml/m²) compared with women (21 ± 6 ml/m²) [4]. 2D measured RA volumes have been shown to be smaller than those measured with CMR [43], yet still accurate and reproducible ($r = 0.98$, bias -5.15 ml/m², limits of agreement ± 10.1 ml/m²) [44].

2D RA volume is also positively correlated with the occurrence of atrial fibrillation and flutter as well as the degree of pulmonary hypertension in patients with congenital heart disease, and respiratory disease. In patients with chronic systolic heart failure, increasing indexed RA volume has been associated with worsening right ventricular systolic function, LV ejection fraction, LV diastolic function and low functional capac-

ity, and was an independent predictor of death, transplant or heart failure hospitalization [3]. In a study of 95 patients, indexed RA volume was recently shown to be superior to indexed LA volume in the prediction of AF recurrence after electrical cardioversion [45].

3D volume assessment: A limited number of recent studies have demonstrated the feasibility of RT3DE evaluation of RA volume and its superiority over 2DE measurements [46]. The measurement of RA volume using pyramidal full-volume datasets is performed by using a deformable shell model and apply two points to identify the tricuspid annulus in the two apical views, and one point to identify the centre of the posterior wall (Fig. 27.13). Following this, man-

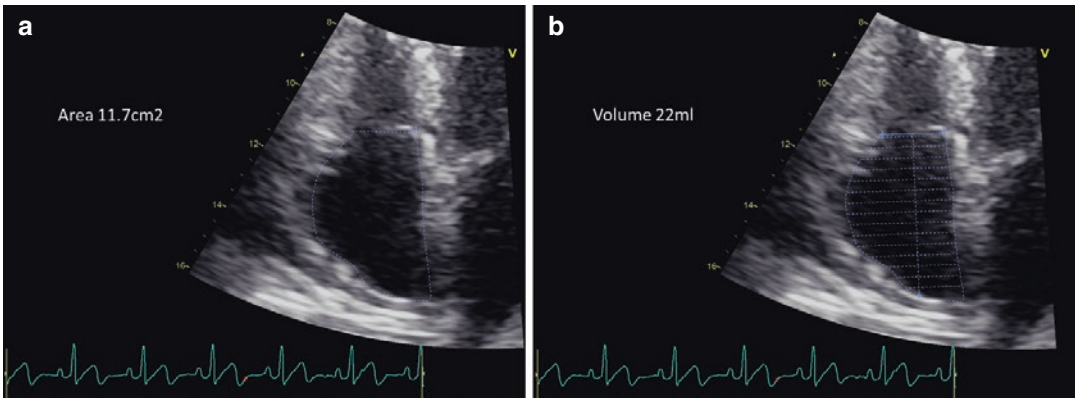


Fig. 27.12 A dedicated apical 4-chamber view at end-systole may be used to planimeter the RA along the blood-tissue interface from septal to lateral annulus (panel a).

However, 2D Simpson's single plane assessment of RA volume (panel b) provides improved accuracy for RA size assessment

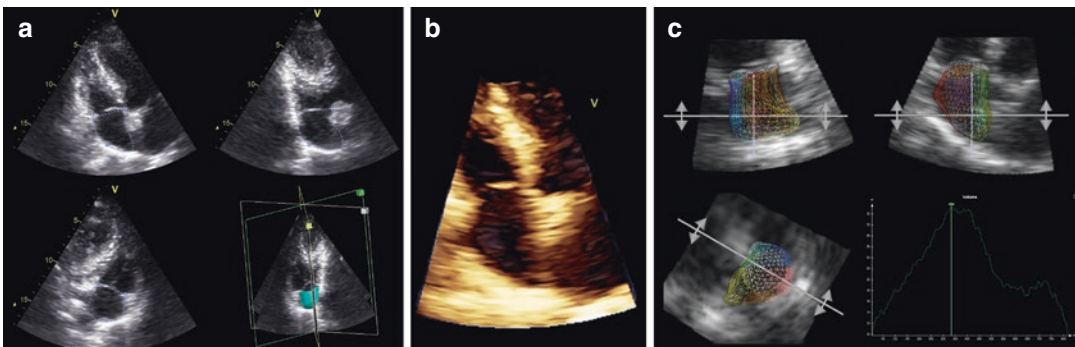


Fig. 27.13 RT3DE guided triplane (panel a) and live-3D (panel b) analysis of RA volume. Full-volume multi-beat reconstructions may be measured in orthogonal views to

obtain RA volumes throughout the cardiac cycle (panel c) and ejection fraction

ual adjustments may be made to exclude the RA appendage and vena cavae from the cavity volume to finally obtain maximum and minimum volumes and ejection fraction. The upper and lower reference ranges reported by Aune et al. for indexed 3D RA volumes are 47 ml/m² and 20 ml/m², respectively [16]. Validation of 3D RA volumes with CMR have shown good correlation ($r = 0.91$) with a small bias (12.06 ml) and narrow limits of agreement (25.56 ml), and showed better correlation with CMR volumes than 2D volumes in this regard [39].

Assessment of Right Atrial Function

RA Phasic Volumes The determinants and calculation of RA reservoir, conduit, and booster pump functions are similar to that of the LA. RA phasic function examined in a small healthy population demonstrated a reduction passive emptying fraction in those aged ≥ 60 years ($46.0 \pm 23.3\%$ vs. $59.9 \pm 15.4\%$, $p = 0.011$) and a larger active emptying volume (7.0 ± 3.5 vs. 4.9 ± 2.5 ml/m², $p = 0.013$) and fraction ($54.0 \pm 23.3\%$ vs. $40.1 \pm 15.4\%$, $p = 0.011$) compared to those aged < 60 years (similar to changes seen with aging in the LA) [47]. In the study by Willens et al., a separate group of 33 patients with pulmonary arterial hypertension and 33 matched controls, similarly showed that patients with pulmonary arterial hypertension had larger RA volumes, systolic filling volume (18.3 ± 6.9 vs. 12.3 ± 4.9 ml/m², $p < 0.001$) and active emptying volume and fraction (11.2 ± 6.9 vs. 5.4 ± 3.0 ml/m², $p < 0.001$; 60.7 ± 29.9 vs. $44.9 \pm 19.0\%$, $p = 0.017$) and smaller passive emptying fraction ($39.3 \pm 29.9\%$ vs. $55.1 \pm 19.0\%$, $p = 0.017$) compared to controls [47].

Tissue Doppler and Speckle Tracking Imaging Limited studies have utilized TDI and speckle tracking imaging in the assessment of RA function, and thus the role of these techniques in the assessment of RA deformation dynamics has yet to be established. The feasibility and reproducibility of RA function assessment, as

well as normal values by speckle tracking have been reported by two laboratories [39, 48]. Reference values for RA function using 2DST are age-specific [39]. D'Andrea et al. performed 2DST of the RA free wall on 130 patients with dilated cardiomyopathy before and 6 months after cardiac resynchronization therapy, and found that patients who responded to cardiac resynchronization therapy (defined as a reduction in LV end systolic volume of 15%) had smaller indexed RA area (19.7 ± 5.5 cm²/m in non-responders vs. 13.2 ± 4.4 cm²/m in responders; $p < 0.001$) and higher RA strain ($24.3 \pm 10.2\%$ in non-responders vs. $40.2 \pm 8.9\%$ in responders; $p < 0.001$) [49]. No studies examining RA function using advanced imaging techniques and cardiovascular outcomes have been performed to date.

Measurement of RA Pressures

RA pressure estimation provides an estimation of intravascular volume and is an integral component in haemodynamic assessments and estimation of pulmonary artery pressures. The normal range for RA pressure is between 1 and 7 mmHg. The gold standard for the evaluation of RA pressure is invasive monitoring using a central venous catheter, however inherent risks and invasiveness make this impractical for routine use. Although the clinical estimation of RA pressures is performed by examining jugular venous pulsations, technical difficulties such as a short neck, prior neck surgery or obesity may pose significant challenges to this. 2D echo and Doppler assessment of the inferior vena cava (IVC), superior vena cava, and hepatic vein indices of size and flow, Doppler systemic venous flow, tricuspid valve inflow, tricuspid annulus tissue Doppler, and RA dimensions form part of the noninvasive evaluation of RA pressures.

The echocardiographic estimation of RA pressures is most commonly performed by the diameter of the IVC, and its respiro-phasic variation [34]. Increasing RA pressures are transmitted to the IVC, which causes dilatation of the IVC and reduced collapsibility upon inspiration (negative

intrathoracic pressure). Imaging of the IVC in its long axis is best performed in the subcostal view, with the maximal diameter measured in end-expiration, 1–2 cm from the junction of the RA and IVC (Fig. 27.14). The collapsibility of the IVC should also be assessed during quiet respiration, and also with a sniff, whilst ensuring that the diameter change does not represent movement of the IVC into another plane. Table 27.3 summarizes the 2010 American Society of Echocardiography guidelines for the echocardiographic assessment of the RA pressures [40].

It should be noted that RA pressure estimation by IVC collapse cannot be reliably used in

patients receiving mechanical ventilation. In the absence of this, an IVC diameter <12 mm provides reasonable correlation with RA pressures <10 mmHg, whilst a small and collapsed IVC suggests hypovolaemia [50].

Increased RA pressures have prognostic implications for both morbidity and mortality. In patients with heart failure followed for a mean of 32 months, an elevated jugular venous pressure was associated with an increased risk of hospitalization for heart failure (relative risk, 1.32; 95% confidence interval, 1.08–1.62; $p < 0.01$), death or hospitalization for heart failure (relative risk, 1.30; 95% confidence interval, 1.11–1.53; $p < 0.005$), and death from pump failure (relative risk, 1.37; 95% confidence interval, 1.07–1.75; $p < 0.05$) [51]. Elevated RA pressure has been similarly shown to strongly reduce survival in dilated cardiomyopathy [52], patients awaiting cardiac transplantation [53], and in a broad spectrum of patients with cardiovascular disease [54]. These studies highlight the importance of accurate assessment of RA pressure in the haemodynamic profiling and management of patients, as well as outcomes [55, 56].

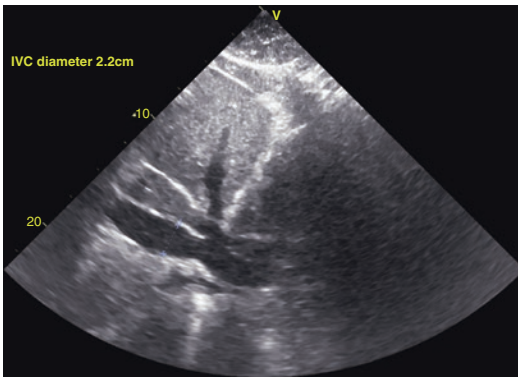


Fig. 27.14 The IVC and hepatic vein may be seen in this subcostal view. The maximal IVC diameter is measured in end-expiration, approximately 1–2 cm from the junction of the RA and IVC. Collapsibility of the IVC with respiration should also be assessed to determine RA pressures

Table 27.3 American Society of Echocardiography guidelines for the echocardiographic assessment of the RA pressures [40]

IVC diameter	Interpretation
<2.1 cm that collapses >50% with a sniff	Normal RA pressure of 3 mmHg (range, 0–5 mmHg)
>2.1 cm that collapses <50% with a sniff	High RA pressure of 15 mmHg (range, 10–20 mmHg)
Indeterminate cases in which the IVC diameter and collapse fall in between the abovementioned criteria	An intermediate value of 8 mmHg (range, 5–10 mmHg) may be used, and secondary indices of elevated RA pressure should be integrated

Summary and Recommendations

This chapter covers the recommendations for assessment of LA and RA structure and function by echocardiography. Echocardiography remains the imaging modality of choice for LA and RA assessment due to its widespread availability and lack of radiation. Assessment of LA size should be performed using biplane LA volumes where there is robust evidence on clinical implications. The assessment of LA function is an emerging field with several methods available for the assessment of LA function, including phasic volumes, spectral Doppler indices, as well as tissue Doppler velocities and strain. Unlike LA size assessment, these techniques have not yet been adopted into clinical practice. In the era of LA interventions such as radiofrequency catheter ablation, further research using advanced techniques to assess the effect of these interventions on LA function, subsequent effects

on cardiovascular outcomes, and the implications of this on management decisions is of much interest. Refinement of advanced LA imaging in other cardiovascular disease states may provide new parameters with incremental prognostic information over existing techniques to improve patient management.

RA structural assessment is recommended using a single plane area-length volume or disc summation approach. Normal reference values have now been incorporated into guidelines. Assessment of RA size has shown promise in atrial fibrillation, heart failure, pulmonary hypertension and congenital heart disease. There are now growing data on reference values for 3D RA volumes, and RA function. Limited studies have utilized tissue Doppler and speckle tracking imaging in the assessment of RA function, and thus the role of these techniques in the assessment of RA deformation dynamics is yet to be established. Furthermore, no studies examining RA function using advanced imaging techniques and cardiovascular outcomes have been performed to date, however this represents an evolving area.

References

1. Leung DY, Boyd A, Ng AA, Chi C, Thomas L. Echocardiographic evaluation of left atrial size and function: current understanding, pathophysiologic correlates, and prognostic implications. *Am Heart J*. 2008;156(6):1056–64.
2. Cioffi G, de Simone G, Mureddu G, Tarantini L, Stefenelli C. Right atrial size and function in patients with pulmonary hypertension associated with disorders of respiratory system or hypoxemia. *Eur J Echocardiogr*. 2007;8(5):322–31.
3. Sallach JA, Tang WW, Borowski AG, Tong W, Porter T, Martin MG, Jasper SE, Shrestha K, Troughton RW, Klein AL. Right atrial volume index in chronic systolic heart failure and prognosis. *JACC Cardiovasc Imaging*. 2009;2(5):527–34.
4. Lang RM, Badano LP, Mor-Avi V, Afilalo J, Armstrong A, Ernande L, Flachskampf FA, Foster E, Goldstein SA, Kuznetsova T. Recommendations for cardiac chamber quantification by echocardiography in adults: an update from the American Society of Echocardiography and the European Association of Cardiovascular Imaging. *J Am Soc Echocardiogr*. 2015;28(1):1–39. e14.
5. Benjamin EJ, D'Agostino RB, Belanger AJ, Wolf PA, Levy D. Left atrial size and the risk of stroke and death The Framingham Heart Study. *Circulation*. 1995;92(4):835–41.
6. Vaziri SM, Larson MG, Benjamin EJ, Levy D. Echocardiographic predictors of nonrheumatic atrial fibrillation. The Framingham Heart Study. *Circulation*. 1994;89(2):724–30.
7. Gardin JM, McClelland R, Kitzman D, Lima JA, Bommer W, Klopfenstein HS, Wong ND, Smith V-E, Gottdiener J. M-mode echocardiographic predictors of six-to seven-year incidence of coronary heart disease, stroke, congestive heart failure, and mortality in an elderly cohort (the Cardiovascular Health Study). *Am J Cardiol*. 2001;87(9):1051–7.
8. Laukkanen JA, Kurl S, Eränen J, Huttunen M, Salonen JT. Left atrium size and the risk of cardiovascular death in middle-aged men. *Arch Intern Med*. 2005;165(15):1788–93.
9. Tsang TS, Abhayaratna WP, Barnes ME, Miyasaka Y, Gersh BJ, Bailey KR, Cha SS, Seward JB. Prediction of cardiovascular outcomes with left atrial size: is volume superior to area or diameter? *J Am Coll Cardiol*. 2006;47(5):1018–23.
10. Tsang TS, Barnes ME, Bailey KR, Leibson CL, Montgomery SC, Takemoto Y, Diamond PM, Marra MA, Gersh BJ, Wiebers DO. Left atrial volume: important risk marker of incident atrial fibrillation in 1655 older men and women. In: *Mayo Clinic proceedings*, vol. 5. Rochester: Elsevier; 2001. p. 467–75.
11. Pritchett AM, Jacobsen SJ, Mahoney DW, Rodeheffer RJ, Bailey KR, Redfield MM. Left atrial volume as an index of left atrial size: a population-based study. *J Am Coll Cardiol*. 2003;41(6):1036–43.
12. Le Tourneau T, Messika-Zeitoun D, Russo A, Detaint D, Topilsky Y, Mahoney DW, Suri R, Enriquez-Sarano M. Impact of left atrial volume on clinical outcome in organic mitral regurgitation. *J Am Coll Cardiol*. 2010;56(7):570–8.
13. Møller JE, Hillis GS, Oh JK, Seward JB, Reeder GS, Wright RS, Park SW, Bailey KR, Pellikka PA. Left atrial volume a powerful predictor of survival after acute myocardial infarction. *Circulation*. 2003;107(17):2207–12.
14. Beinart R, Boyko V, Schwammenthal E, Kuperstein R, Sagie A, Hod H, Matetzky S, Behar S, Eldar M, Feinberg MS. Long-term prognostic significance of left atrial volume in acute myocardial infarction. *J Am Coll Cardiol*. 2004;44(2):327–34.
15. Pritchett AM, Mahoney DW, Jacobsen SJ, Rodeheffer RJ, Karon BL, Redfield MM. Diastolic dysfunction and left atrial volume: a population-based study. *J Am Coll Cardiol*. 2005;45(1):87–92.
16. Aune E, Baekkevar M, Roislien J, Rodevand O, Otterstad JE. Normal reference ranges for left and right atrial volume indexes and ejection fractions obtained with real-time three-dimensional echocardiography. *Eur J Echocardiogr*. 2009;10(6):738–44.
17. Hung J, Lang R, Flachskampf F, Shernan SK, McCulloch ML, Adams DB, Thomas J, Vannan M,

- Ryan T. 3D echocardiography: a review of the current status and future directions. *J Am Soc Echocardiogr.* 2007;20(3):213–33.
18. Suh I-W, Song J-M, Lee E-Y, Kang S-H, Kim M-J, Kim J-J, Kang D-H, Song J-K. Left atrial volume measured by real-time 3-dimensional echocardiography predicts clinical outcomes in patients with severe left ventricular dysfunction and in sinus rhythm. *J Am Soc Echocardiogr.* 2008;21(5):439–45.
19. Caselli S, Canali E, Foschi ML, Santini D, Di Angelantonio E, Pandian NG, De Castro S. Long-term prognostic significance of three-dimensional echocardiographic parameters of the left ventricle and left atrium. *Eur J Echocardiogr.* 2010;11(3):250–6.
20. Abhayaratna WP, Fatema K, Barnes ME, Seward JB, Gersh BJ, Bailey KR, Casaclang-Verzosa G, Tsang TS. Left atrial reservoir function as a potent marker for first atrial fibrillation or flutter in persons ≥ 65 years of age. *Am J Cardiol.* 2008;101(11):1626–9.
21. Chinali M, de Simone G, Roman MJ, Bella JN, Liu JE, Lee ET, Best LG, Howard BV, Devereux RB. Left atrial systolic force and cardiovascular outcome: The Strong Heart Study. *Am J Hypertens.* 2005;18(12):1570–6.
22. Wang M, Yip GW, Wang AY, Zhang Y, Ho PY, Tse MK, Lam PK, Sanderson JE. Peak early diastolic mitral annulus velocity by tissue Doppler imaging adds independent and incremental prognostic value. *J Am Coll Cardiol.* 2003;41(5):820–6.
23. Yamamoto T, Oki T, Yamada H, Tanaka H, Ishimoto T, Wakatsuki T, Tabata T, Ito S. Prognostic value of the atrial systolic mitral annular motion velocity in patients with left ventricular systolic dysfunction. *J Am Soc Echocardiogr.* 2003;16(4):333–9.
24. Saha SK, Anderson PL, Caracciolo G, Kiotsekoglou A, Wilansky S, Govind S, Mori N, Sengupta PP. Global left atrial strain correlates with CHADS 2 risk score in patients with atrial fibrillation. *J Am Soc Echocardiogr.* 2011;24(5):506–12.
25. Schneider C, Malisius R, Krause K, Lampe F, Bahlmann E, Boczor S, Antz M, Ernst S, Kuck K-H. Strain rate imaging for functional quantification of the left atrium: atrial deformation predicts the maintenance of sinus rhythm after catheter ablation of atrial fibrillation. *Eur Heart J.* 2008;29(11):1397–409.
26. Tops LF, Delgado V, Bertini M, Marsan NA, Den Uijl DW, Trines SA, Zeppenfeld K, Holman E, Schalij MJ, Bax JJ. Left atrial strain predicts reverse remodeling after catheter ablation for atrial fibrillation. *J Am Coll Cardiol.* 2011;57(3):324–31.
27. Antoni ML, ten Brinke EA, Atary JZ, Marsan NA, Holman ER, Schalij MJ, Bax JJ, Delgado V. Left atrial strain is related to adverse events in patients after acute myocardial infarction treated with primary percutaneous coronary intervention. *Heart.* 2011;97(16):1332–7.
28. Debonnaire P, Leong DP, Witkowski TG, Al Amri I, Joyce E, Katsanos S, Schalij MJ, Bax JJ, Delgado V, Marsan NA. Left atrial function by two-dimensional speckle-tracking echocardiography in patients with severe organic mitral regurgitation: association with guidelines-based surgical indication and postoperative (long-term) survival. *J Am Soc Echocardiogr.* 2013;26(9):1053–62.
29. Mor-Avi V, Lang RM, Badano LP, Belohlavek M, Cardim NM, Derumeaux G, Galderisi M, Marwick T, Nagueh SF, Sengupta PP. Current and evolving echocardiographic techniques for the quantitative evaluation of cardiac mechanics: ASE/EAE consensus statement on methodology and indications endorsed by the Japanese Society of Echocardiography. *Eur J Echocardiogr.* 2011;12(3):167–205.
30. Mochizuki A, Yuda S, Oi Y, Kawamukai M, Nishida J, Kouzu H, Muranaka A, Kokubu N, Shimoshige S, Hashimoto A. Assessment of left atrial deformation and synchrony by three-dimensional speckle-tracking echocardiography: comparative studies in healthy subjects and patients with atrial fibrillation. *J Am Soc Echocardiogr.* 2013;26(2):165–74.
31. Brennan JM, Blair JE, Goonewardena S, Ronan A, Shah D, Vasaiwala S, Kirkpatrick JN, Spencer KT. Reappraisal of the use of inferior vena cava for estimating right atrial pressure. *J Am Soc Echocardiogr.* 2007;20(7):857–61.
32. Gullace G, Savoia M. Echocardiographic assessment of the inferior vena cava wall motion for studies of right heart dynamics and function. *Clin Cardiol.* 1984;7(7):393–404.
33. Kircher BJ, Himelman RB, Schiller NB. Noninvasive estimation of right atrial pressure from the inspiratory collapse of the inferior vena cava. *Am J Cardiol.* 1990;66(4):493–6.
34. Moreno FL, Hagan AD, Holmen JR, Pryor TA, Strickland RD, Castle CH. Evaluation of size and dynamics of the inferior vena cava as an index of right-sided cardiac function. *Am J Cardiol.* 1984;53(4):579–85.
35. Nagueh SF, Kopelen HA, Zoghbi WA. Relation of mean right atrial pressure to echocardiographic and Doppler parameters of right atrial and right ventricular function. *Circulation.* 1996;93(6):1160–9.
36. Ommen SR, Nishimura RA, Hurrell DG, Klarich KW. Assessment of right atrial pressure with 2-dimensional and Doppler echocardiography: a simultaneous catheterization and echocardiographic study. In: Mayo Clinic proceedings, vol. 1. Rochester: Elsevier; 2000. p. 24–9.
37. Kou S, Caballero L, Dulgheru R, Voilliot D, De Sousa C, Kacharava G, Athanassopoulos GD, Barone D, Baroni M, Cardim N. Echocardiographic reference ranges for normal cardiac chamber size: results from the NORRE study. *Eur Heart J Cardiovasc Imaging.* 2014;15(6):680–90.
38. D'Oronzio U, Senn O, Biaggi P, Gruner C, Jenni R, Tanner FC, Greutmann M. Right heart assessment by echocardiography: gender and body size matters. *J Am Soc Echocardiogr.* 2012;25(12):1251–8.
39. Peluso D, Badano LP, Muraru D, Dal Bianco L, Cucchini U, Kocabay G, Kovács A, Casablanca S, Illiceto S. Right atrial size and function assessed

- with three-dimensional and speckle-tracking echocardiography in 200 healthy volunteers. *Eur Heart J Cardiovasc Imaging*. 2013;14(11):1106–14.
40. Rudski LG, Lai WW, Afilalo J, Hua L, Handschumacher MD, Chandrasekaran K, Solomon SD, Louie EK, Schiller NB. Guidelines for the echocardiographic assessment of the right heart in adults: a report from the American Society of Echocardiography: endorsed by the European Association of Echocardiography, a registered branch of the European Society of Cardiology, and the Canadian Society of Echocardiography. *J Am Soc Echocardiogr*. 2010;23(7):685–713.
 41. Raymond RJ, Hinderliter AL, Willis PW, Ralph D, Caldwell EJ, Williams W, Ettinger NA, Hill NS, Summer WR, de Boisblanc B. Echocardiographic predictors of adverse outcomes in primary pulmonary hypertension. *J Am Coll Cardiol*. 2002;39(7):1214–9.
 42. Bustamante-Labarta M, Perrone S, de la Fuente RL, Stutzbach P, de la Hoz RP, Torino A, Favaloro R. Right atrial size and tricuspid regurgitation severity predict mortality or transplantation in primary pulmonary hypertension. *J Am Soc Echocardiogr*. 2002;15(10):1160–4.
 43. Whitlock M, Garg A, Gelow J, Jacobson T, Broberg C. Comparison of left and right atrial volume by echocardiography versus cardiac magnetic resonance imaging using the area-length method. *Am J Cardiol*. 2010;106(9):1345–50.
 44. Ebtia M, Murphy D, Gin K, Lee PK, Jue J, Nair P, Mayo J, Barnes ME, Thompson DJS, Tsang TSM. Best method for right atrial volume assessment by two-dimensional echocardiography: validation with magnetic resonance imaging. *Echocardiography*. 2015;32:734–9. <https://doi.org/10.1111/echo.12735>.
 45. Luong C, Thompson DJ, Bennett M, Gin K, Jue J, Barnes ME, Colley P, Tsang TS. Right atrial volume is superior to left atrial volume for prediction of atrial fibrillation recurrence after direct current cardioversion. *Can J Cardiol*. 2015;31(1):29–35.
 46. Muller H, Burri H, Lerch R. Evaluation of right atrial size in patients with atrial arrhythmias: comparison of 2D versus real time 3D echocardiography. *Echocardiography*. 2008;25(6):617–23.
 47. Willens HJ, Fertel DP, Qin J, Labrador E, Lowery MH. Effects of age and pulmonary arterial hypertension on the different phases of right atrial function. *Int J Cardiovasc Imaging*. 2008;24(7):703–10.
 48. Padeletti M, Cameli M, Lisi M, Malandrino A, Zacà V, Mondillo S. Reference values of right atrial longitudinal strain imaging by two-dimensional speckle tracking. *Echocardiography*. 2012;29(2):147–52.
 49. D'Andrea A, Scarafile R, Riegler L, Salerno G, Gravino R, Cocchia R, Castaldo F, Allocca F, Limongelli G, Di Salvo G. Right atrial size and deformation in patients with dilated cardiomyopathy undergoing cardiac resynchronization therapy. *Eur J Heart Fail*. 2009;11(12):1169–77.
 50. Jue J, Chung W, Schiller NB. Does inferior vena cava size predict right atrial pressures in patients receiving mechanical ventilation? *J Am Soc Echocardiogr*. 1992;5(6):613–9.
 51. Drazner MH, Rame JE, Stevenson LW, Dries DL. Prognostic importance of elevated jugular venous pressure and a third heart sound in patients with heart failure. *N Engl J Med*. 2001;345(8):574–81.
 52. Unverferth DV, Magorien RD, Moeschberger ML, Baker PB, Fettes JK, Leier CV. Factors influencing the one-year mortality of dilated cardiomyopathy. *Am J Cardiol*. 1984;54(1):147–52.
 53. Morley D, Brozena SC. Assessing risk by hemodynamic profile in patients awaiting cardiac transplantation. *Am J Cardiol*. 1994;73(5):379–83.
 54. Damman K, van Deursen VM, Navis G, Voors AA, van Veldhuisen DJ, Hillege HL. Increased central venous pressure is associated with impaired renal function and mortality in a broad spectrum of patients with cardiovascular disease. *J Am Coll Cardiol*. 2009;53(7):582–8.
 55. Dellinger RP, Levy M, Carlet J, Bion J, Parker M, Jaeschke R, Reinhart K, Angus D, Brun-Buisson C, Beale R, Calandra T, Dhainaut J-F, Gerlach H, Harvey M, Marini J, Marshall J, Ranieri M, Ramsay G, Sevransky J, Thompson BT, Townsend S, Vender J, Zimmerman J, Vincent J-L. Surviving sepsis campaign: international guidelines for management of severe sepsis and septic shock: 2008. *Intensive Care Med*. 2008;34(1):17–60.
 56. Michard F, Teboul J-L. Predicting fluid responsiveness in ICU patients: a critical analysis of the evidence. *Chest*. 2002;121(6):2000–8.

Part VII

Masses, Emboli and Trauma

Echocardiography is the most common method for the detection of cardiac masses. Masses can be described as *intracavitary* (within chambers but floating within the chambers, or great vessels, and attached to chamber walls, valves or great vessels) or *intramural* (located within the muscular structure of the walls). Intracavitary masses can be firmly and broadly attached to walls and are referred to as having a *sessile attachment*. Alternatively, intracavitary masses may be attached to walls or valves by a long, or short, stalk (or pedicle or peduncle) and are referred to as *pedunculated*. Sessile masses move with the cardiac motion, but they move in synchrony with the attached structure. Pedunculated masses are hypermobile and generally oscillate if the stalk is long enough.

Etiologies of such masses are varied and may be due to tumors (benign or malignant), thrombi (ventricular or atrial), infection (bacterial or fungal), trauma and a host of other serious and less serious reasons. As will be seen, normal structures or artifacts may be interpreted as abnormal masses by the less experienced interpreter.

J. Kisslo (✉)

Division of Cardiology, Duke University Medical Center, Durham, NC, USA
e-mail: joseph.kisslo@duke.edu

P. Barker

Department of Pediatrics, Division of Pediatric Cardiology, Duke University Medical Center, Durham, NC, USA

The Importance of Clinical Context

Pre-echocardiographic clinical suspicion for the presence of intracardiac masses is variable but depends entirely on clinical context of patient clinical presentation. For example, when a patient presents following a stroke, but with atrial fibrillation, one logically suspects the presence of a left atrial (LA) thrombus. On the other hand, when a patient presents with a stroke, but with normal sinus rhythm and the presence of evidence of myocardial infarct by EKG, the pre-exam clinical suspicion for a left ventricular (LV) mural thrombus rises. It could be that when another patient presents with a stroke, but with evidence of fever and positive blood cultures, suspicion for bacterial endocarditis increases, and an intracardiac vegetation(s) becomes the primary suspicion.

Clinical context and associated findings, therefore determine pre-test clinical suspicion for the presence of masses and help direct the echocardiographic examination. In many cases, however, there is no index of suspicion and masses are detected that lead to remarkable clinical surprise. As is well known, other than the “tumor plop” in patients with atrial myxomas, there are few physical findings on examination of the heart specific for cardiac masses.

As will be seen, many cardiac masses look alike. Determination of the etiology of masses is usually by knowledge of the frequency of the

occurrence of such masses. For example, large masses in the left atrium are usually left atrial myxomas. Otherwise, absolute determination of the etiology of cardiac masses must await pathologic (gross or microscopic) examination.

It is important to finally note, that to detect a mass requires that the echo examiner point the interrogating probe at the mass. While an initially overly simplistic principle, it must be constantly emphasized that, “if you don’t point at it, you can’t see it!”

Echocardiography in Comparison to Other Cardiac Imaging Modalities

Because echocardiographic frame rates are high, such rapid motions as found in pedunculated masses can be detected by echocardiography but they may not be visible with other techniques such as MRI or CT. MRI or CT images are built over multiple cardiac cycles and presented at ~15–20 frames per second (FPS or fps). Echo images are derived over a single cardiac cycle (generally 30–60 frames per second or higher) (in what is called real-time). At 30 fps the duration of an acoustic frame is 33 ms. At 60 fps, the duration of an acoustic frame is ~17.5 ms.

Since ultrasound imaging does depend upon rapid sound transmission and reflection sequences, then moving the ultrasound beam, it is more precisely “relatively” real time. Whatever the case, ultrasound achieves far more rapid image acquisition than competitive imaging methods and are temporally coherent. Newer echo machines capable of 300–2000 fps and are incipient to the clinical marketplace. MRI and CT methods have some temporal incoherency.

Ultrasound techniques are performed using a hand held transducer and, therefore, the field of view is dependent on the examiner actually pointing at a given target. CT and MRI techniques have wide fields of view in comparison. Resolution (as defined by the ability to separate two targets in space) of an ultrasound image is uniform in depth (determined by transducer frequency) but is variable laterally (due to various

physical factors concerning variable beam width). CT and MRI images have uniform resolution in depth (range) and laterally (azimuthally).

Context for Assigning a Diagnosis Reemphasized

The assignment of a specific etiology of a cardiac mass depends primarily on clinical context. For example, when a rapidly moving small mass is seen on a cardiac valve, the origin is likely endocarditis if the patient presents with signs of an infection. Without evidence of infection, that same appearing mass becomes more likely due to tumor (such as a fibroelastoma). Thus, proper interpretation of an echocardiogram requires some knowledge of clinical context. An echo cannot tissue differentiate and an actual tissue diagnosis is not possible until an actual tissue diagnosis is obtained at surgery or autopsy. Cardiac ultrasound only provides brightness (amplitude) information.

Continued experience with any imaging method improves the predictive accuracy of any interpreter of cardiac images, but at the same time should prompt that interpreter to exercise prudent caution. Common experience also indicates that presumptions may occasionally be incorrect. Some of the biggest surprises occur when beginners assume they know enough to precisely tell what type of mass is present on the basis of an image alone. For example, it is never surprising when those with vast clinical experience interpreting echo images are less prone to assign a specific tumor type in comparison to those with less experience. It is always best to look at two or three other things in clinical context or specific characteristics of masses, rather than just look at the mass alone.

These multiple limitations, notwithstanding, echocardiography has great use and remains the primary method for detection of intracardiac masses in modern care of patients with cardiac disease. While this chapter is intended for those initially learning about cardiac ultrasound, there are parts that go into remarkable detail and are wholly appropriate for those currently practicing echocardiography.

Thrombi

The most common cardiac masses are thrombi (most frequently in the left atrium in the setting of atrial fibrillation and left ventricle in the setting of anterior wall myocardial infarction). Less commonly, thrombi may be found in any cardiac chamber or great vessel.

Left Ventricular Thrombus

Left ventricular mural thrombi are most commonly found at the left ventricular apex and occur invariably in the setting of myocardial infarction, usually an anterior wall infarction in the distribution of the left anterior descending coronary (LAD) artery. Figure 28.1 shows an apical four-chamber view in a patient following an LAD infarction where a circular apical mural thrombus is easily noted. A normal left ventricular apex is quite thin normally so apical thinning is not of diagnostic help.

Following a myocardial infarction, subendocardial hemorrhage and surrounding chamber stasis combine to create a thrombus. Thrombi are

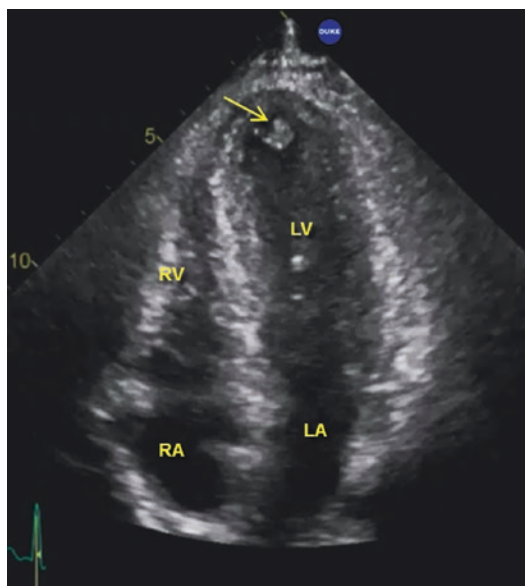


Fig. 28.1 Apical four-chamber view in a patient post anterior myocardial infarction. A circular thrombus is seen at the apex

significantly less common in the setting of inferior wall infarction as the right coronary artery feeds much less of the left ventricle and rarely feeds the ventricular apex.

Left ventricular mural thrombi are usually not detected in the first hours or days following an anterior infarction, most likely because the fresh thrombus does not have a significant acoustic impedance difference from blood (rendering the very fresh thrombus acoustically invisible). When a thrombus is detected, however, it is difficult to tell by echo whether it is relatively new or old by echo characteristics alone.

Thrombi may come in all sizes and shapes. Figure 28.2 shows three different apical views from another patient following an anterior wall myocardial infarction. Note the amorphous shape of this giant layered mural thrombus. While this thrombus is large, it is important to angle the transducer back and forth from the apical window to be sure that the apex is completely interrogated.

Thrombi are not always single. Figure 28.3 shows apical views from yet another patient following an anterior wall myocardial infarction where multiple apical mural thrombi are noted (left panel). The corresponding left ventricular angiogram (right panel) also shows these multiple apical mural thrombi.

One factor that helps differentiate a mural thrombus from other masses (such as left ventricular myxoma) is the presence of an underlying wall motion abnormality. While spontaneous thrombi may occur outside the setting of acute infarction, they are exceedingly rare.

Images of the left ventricle are frequently suboptimal in older patients, particularly those who are obese and or who have chronic lung disease render the images suboptimal. It is now invariably accepted that specialized ultrasound contrast materials may be used for left ventricular chamber delineation. Such contrast materials and administration techniques are discussed in the chapter on contrast.

Figure 28.4 is from a patient following an anterior wall infarction where a few targets are seen at the apex that only suggest the presence of a thrombus. Administration of contrast material clearly delineates the large, solitary thrombus.

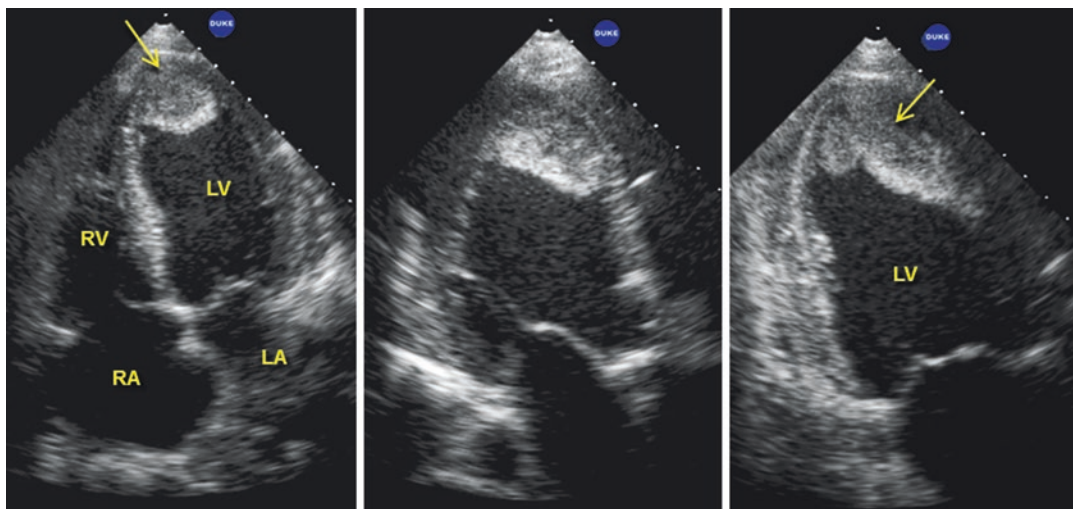


Fig. 28.2 Apical four (left panel), three (middle panel) and two-chamber (right panel) views in a patient post anterior myocardial infarction. The apical thrombus is

clearly seen and is amorphous in shape. Compare to the circular thrombus seen in the previous figure

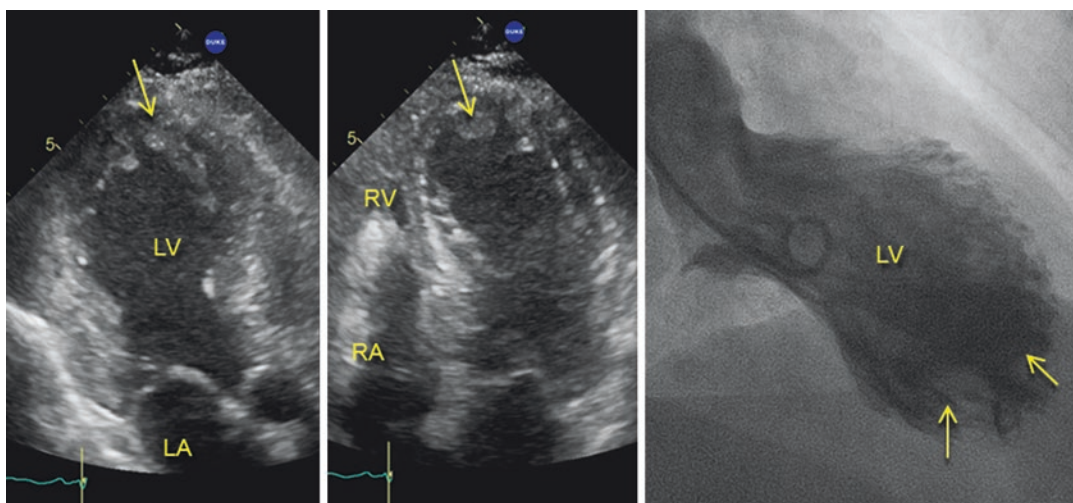


Fig. 28.3 Apical three- (left panel) and four-chamber (middle panel) views of another patient following an anterior wall myocardial infarction. Multiple thrombi are seen

at the apex (arrows). The right panel shows the left ventricular angiogram with the negative contrast of the multiple thrombi visible (arrows)

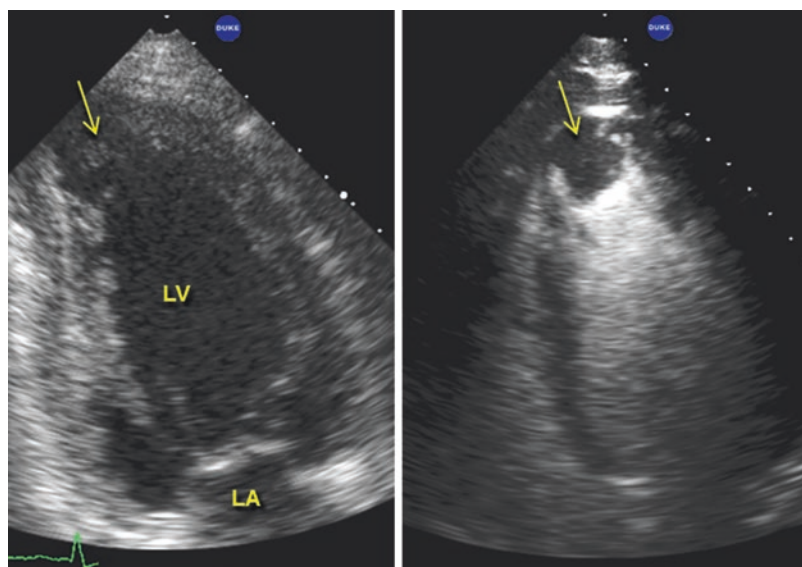
The presence of a thrombus, of course, leads to the increased possibility of embolization and stroke. There was an old clinical dictum in the days prior to echocardiography: If a patient presents with a stroke, an ECG should be obtained to look for a myocardial infarction.

Whether an echocardiogram should be ordered in all patients following myocardial infarction is

debatable and readers are directed to current clinical practice guidelines in this regard. Likewise, current guidelines determine best practices regarding routine anticoagulation of patients after anterior wall infarctions.

The absence of a thrombus by echo, particularly in the very early hours or days after infarction, does not exclude its presence. Sometimes

Fig. 28.4 Apical two-chamber views in a patient following an anterior myocardial infarction. The left panel is without contrast and an apical mass is suspected, but cannot be confirmed. Following administration of contrast, an apical mural thrombus is obvious



the thrombi are exceedingly small. When apical views are used, it should be remembered that some echocardiographic systems have somewhat diminished near field target acquisition. This situation can be partially overcome by using a higher frequency echo transducer at shallow image depths (which maximizes near field resolution, alters echo pulse characteristics and modifies other image characteristics).

Sometimes small thrombi are difficult to detect or differentiate from trabeculations near the ventricular apex. For reasons that are unknown, clinical experience shows that chronically dilated left ventricles tend to be hypertrabeculated at the ventricular apex making detection of small thrombi among the trabeculations most difficult.

It is always best to interrogate the ventricular apex with the highest frequency probe possible. In our experience, there has never been a single ultrasound probe built by any manufacturer that is ideal for all purposes in an adult echo or pediatric echo lab. Adult echo labs ideally should have two transducers for routine use: one ~2.5–3.5 MHz for general purposes and one ~5–7.5 MHz for special instances of near field imaging.

Modern transducers are all broadband and cannot be fully described by center frequency

alone. Single transducer solutions should be approached with caution despite the desire of echo users to want a single transducer solution for every purpose or manufacturers to market such transducers under the presumption that one probe could actually solve all problems. This single transducer solution is further complicated when single transducers for both two- and three dimensional echocardiography are encountered. While transducer technology has improved remarkably, it is not yet at the point where one transducer does everything with the highest clinical qualities of resolution and target acquisition to cover all situations. Our echo laboratory does not embrace single transducer solutions.

Echo imaging by the transesophageal approach is usually not productive in identifying apical LV thrombi. From this approach, the LV apex is far distant from the transducer (15 cm or greater). TEE examinations are performed using a small aperture, high frequency transducer making the LV apex difficult to see due to far field signal attenuation and marked beam spread. It is far better to go to a chest wall examination with a high frequency transducer at the apex or contrast imaging rather than perform an unwarranted and more costly TEE examination for an apical mural thrombus.

Blunt cardiac trauma may also precipitate thrombosis on a cardiac wall. In this case, such thrombi are known to resolve quickly, sometimes within days. Use of such anticoagulant therapies mentioned above are usually contraindicated in the setting of trauma because of bleeding risks and/or extending tissue damage.

While it is logically undesirable to have a mural thrombus, surgical extraction of a mural thrombus is rarely performed. Whether anticoagulation or thrombolysis is employed is dependent on the patient and clinical circumstances as well as current clinical guidelines.

Left Atrial Thrombi

Patients with atrial fibrillation or, less commonly, other atrial tachycardias provide an infrequent, but certainly not uncommon setting for thrombosis within the left atrial appendage. Such thrombi are usually at the apex of the left atrial appendage and best noted by transesophageal echocardiography. Figure 28.5 shows left atrial appendage thrombi in three different patients. In one (left panel), the thrombus is circular. In another (middle panel) the thrombus is layered at the apex of

the appendage. In the third (right panel) there is a large thrombus with central areas of cavitation. Why right atrial appendage thrombi are so uncommon is not understood.

Figure 28.6 shows the varied appearance of an appendage thrombus with slight transducer angulation. Administration of echo contrast is also useful in situations where it is uncertain whether a thrombus is present or not. It is important to remember that the atrial appendage edge is not a perfect circular orifice or conical tip. The appendage tip is rather a linear structure, complicated by pectinate muscles (*see* Fig. 28.43, right panel, later in this chapter) so small thrombi may be most difficult to detect. Occasionally, the normal pectinate muscles seen at the tips of the atrial appendages are incorrectly identified as small thrombi, particularly in dilated atrial appendages due to chronic atrial fibrillation.

TEE examination is not without artifact and other interpretive problems that may mistakenly identify the presence of a thrombus. The Ligament of Marshall is the bright angular target between the left atrial appendage and left upper pulmonary vein (LUPV) seen in Figs. 28.5 and 28.6. In the early days of echo, this structure was originally called the “Coumadin Ridge” (implying it

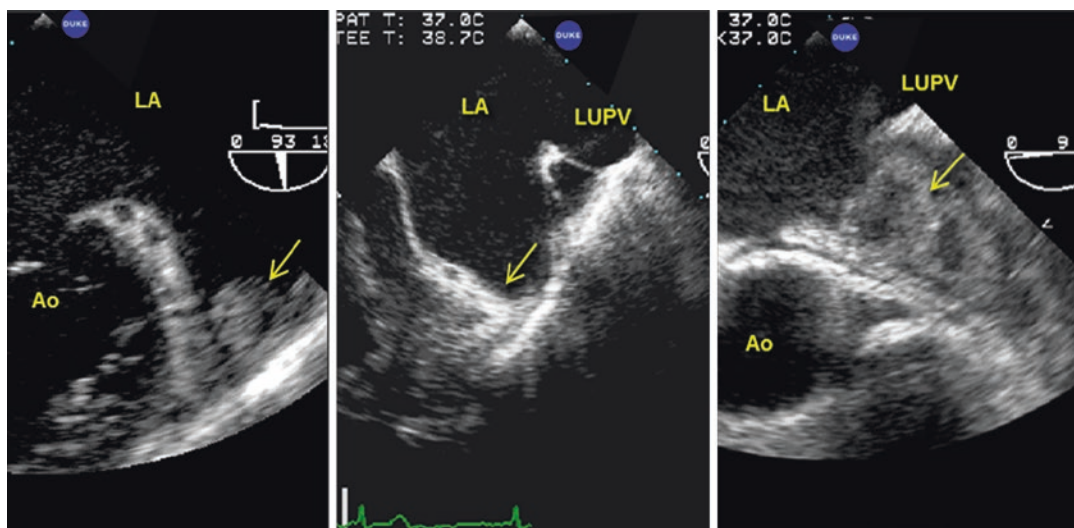


Fig. 28.5 Three examples of left atrial appendage thrombi obtained by transesophageal echo in patients with atrial fibrillation. Left panel shows a circular thrombus. Middle panel shows a layered thrombus at the tip of the

appendage. The right panel shows a thrombus almost filling the entire appendage. Determining a left atrial appendage thrombus is sometimes confounded by difficulties imposed by artifact(s)

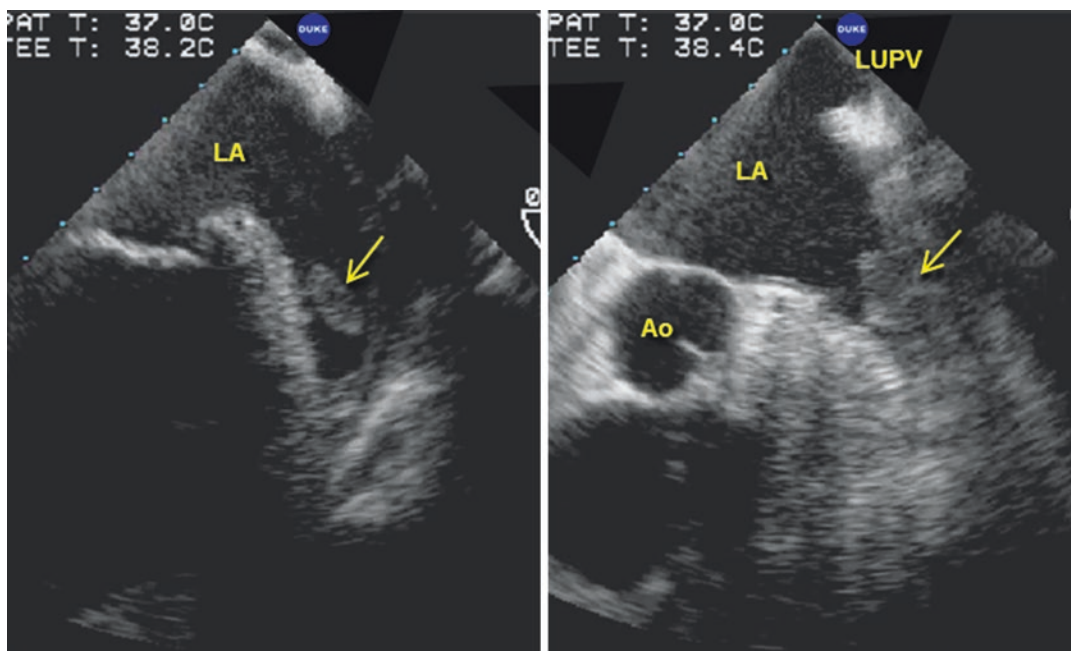


Fig. 28.6 Transesophageal echo views of a patient with atrial fibrillation. Slight alteration of the probe position demonstrated more of the thrombus (right panel)

could be misinterpreted as a thrombus and, thus, incorrectly prompt anticoagulation therapy). The ligament carries some of the internodal conduction pathways through the atrium to the atrioventricular node and is a common site for radiofrequency (RF) ablation during left atrial ablation procedures.

Occasionally, a side lobe artifact (a type of ultrasound artifact due to highly reflective targets) originates from the Ligament of Marshall or posterior aortic root that is mistakenly interpreted as a thrombus. Side lobes can be recognized as liner targets emanating laterally in the sector arc but are without discrete edges. As well, side lobes tend to appear to go through actual anatomic targets. Angulation of the TEE probe may change the brightness of the side lobe by changing the angle of incidence to the culprit bright target.

The phenomenon of a “smoke” appearance to blood flow in low flow situations confounds the identification of left atrial appendage thrombus. Such smoke originates from the acoustic speckle reflected from blood components and is present in all blood flow situations, given the perfect

acoustic sampling rate along with the perfect velocity of movement of the blood.

The size and position of speckle can be altered by changing the factors just mentioned making spontaneous smoke-like appearance of blood more, or less, apparent. With newer, more advanced imaging systems, smoke is more and more frequently encountered and its presence does not indicate the presence of a thrombus. When encountered, an operator should change the transducer frequency (possible with broad band transducers), change depth (which changes pulse repletion frequency) or speeding up or slowing flow with the cardiac cycle or exercising the patient to increase blood velocity. If these actions do not eliminate the smoke, echo contrast should be employed.

Details of the role of echocardiography in the management of patients with atrial fibrillation where atrial ablation or cardioversion is anticipated are discussed elsewhere in this book. Likewise, management of patients who experience cerebral or systemic embolization due to suspected or proven intracardiac thrombus are discussed in the chapter concerning the source of an embolus.

Common Tumors

Like elsewhere in the body, tumors of the heart may be benign or malignant and also either primary or secondary. Myxoma is the most frequent primary cardiac tumor in adults, commonly occurring in the left atrium, attached to the atrial septum by a variable stalk and are intracavitary. Rhabdomyoma is the most commonly occurring tumor in children and are intramyocardial (intramural) and frequently multiple. Papillary fibroelastoma is another tumor that is usually attached on, or near, cardiac valves, suspended from a long stalk. All are benign, but managed differently.

Myxoma

There is hardly a more dramatic than the presence of a cardiac myxoma. Figure 28.7 shows the typical appearance of a left atrial myxoma. In systole, the myxoma is in the left atrial cavity. In diastole, the tumor typically prolapses into the mitral orifice.

These tumors may occur anywhere in the heart but are typically found in the left atrium, attached to the interatrial septum. Figure 28.8 shows the tumor of the patient in Fig. 28.7 along with the line derived M-mode recording of the

mitral valve (right panel). The tumor is seen to move rapidly into the mitral orifice in the M-mode shortly after the mitral valve opens (arrow, right panel). Such rapid dropping of the tumor into the mitral orifice is accompanied by a low frequency heart sound known as the “tumor plop” that occurs shortly after the second heart sound.

Figure 28.9 shows the sequential motion of an atrial myxoma as it moves through its rather dramatic path into and out of the mitral orifice. In systole, these tumors are invariably associated with mitral regurgitation (Fig. 28.10).

Due to the propensity of these tumors to grow large (obstructing flow) and/or to embolize portions of the tumor, they are almost always surgically removed. It is most important for an echo examiner to identify the point of tumor attachment. Figure 28.11 (right panel) shows the anchor point of this tumor to be on the floor of the oval fossa (fossa ovalis), the most typical point of attachment. Knowing the point of attachment indicates the surgical approach (through the left atrium or right atrium in this case).

When removed, a large portion of the attachment point is typically removed to prevent the tumor from re-growing. If the tumor and its attachment anchor point are both removed, the patient prognosis is excellent. When attached to the atrial septum, one approach is to enter the

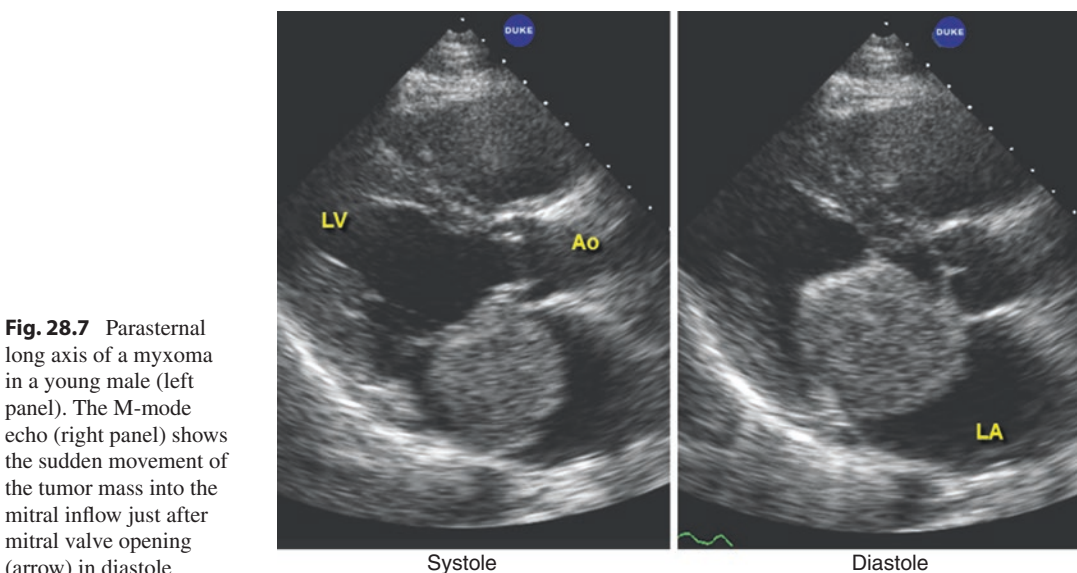


Fig. 28.7 Parasternal long axis of a myxoma in a young male (left panel). The M-mode echo (right panel) shows the sudden movement of the tumor mass into the mitral inflow just after mitral valve opening (arrow) in diastole

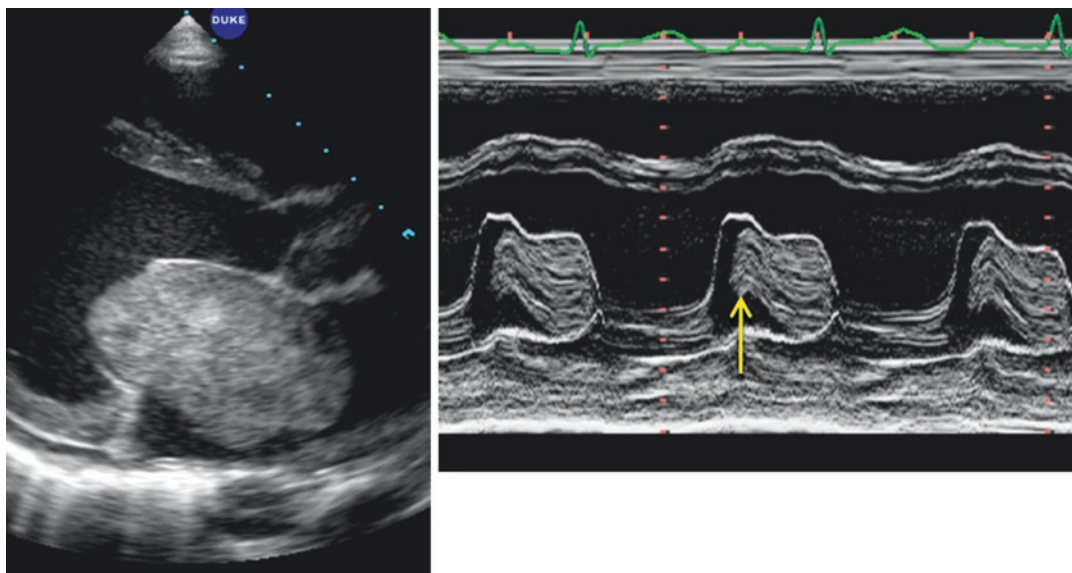


Fig. 28.8 Left panel is a parasternal long axis of the patient seen in the previous figure. The right panel shows a line derived M-mode of the tumor as it moves into place

after the mitral valve opens (arrow). This delayed, but rapid motion of the tumor into the mitral orifice correlates with the sound of the: “tumor plop” by auscultation

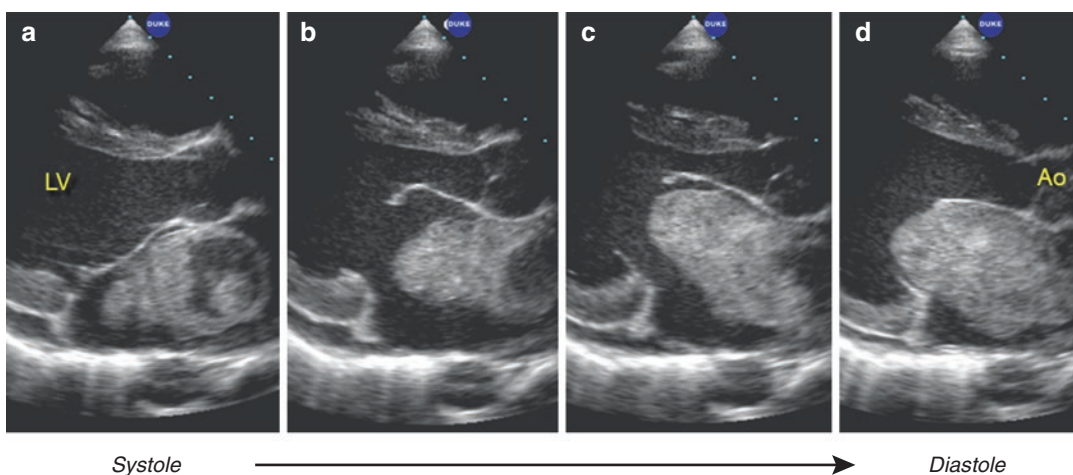


Fig. 28.9 Serial diastolic frames depicting typical two-dimensional movement of a massive myxoma as it moves sequentially into the mitral orifice. *LV* Left Ventricle, *Ao* Aorta

right atrium, do an encircling removal of the attachment point of the atrial septum and deliver the tumor through the newly created atrial septal defect. The atrial septum is then patched.

Figure 28.12 shows a patient with a much broader point of attachments. Figure 28.13 shows yet another presentation with evidence of protrusion of the tumor through the foramen ovale.

Careful examination of the point of attachment always helps surgical planning.

Figure 28.14 demonstrates how a myxoma could create an interatrial shunt as it distorts the floor of the oval fossa when it prolapses into the mitral orifice.

Diagnosis of a left atrial myxoma is generally done with echocardiography and patients do not

Fig. 28.10 Mitral regurgitation (right panel, arrow) often results from left atrial myxoma, but frequently resolves after surgical removal

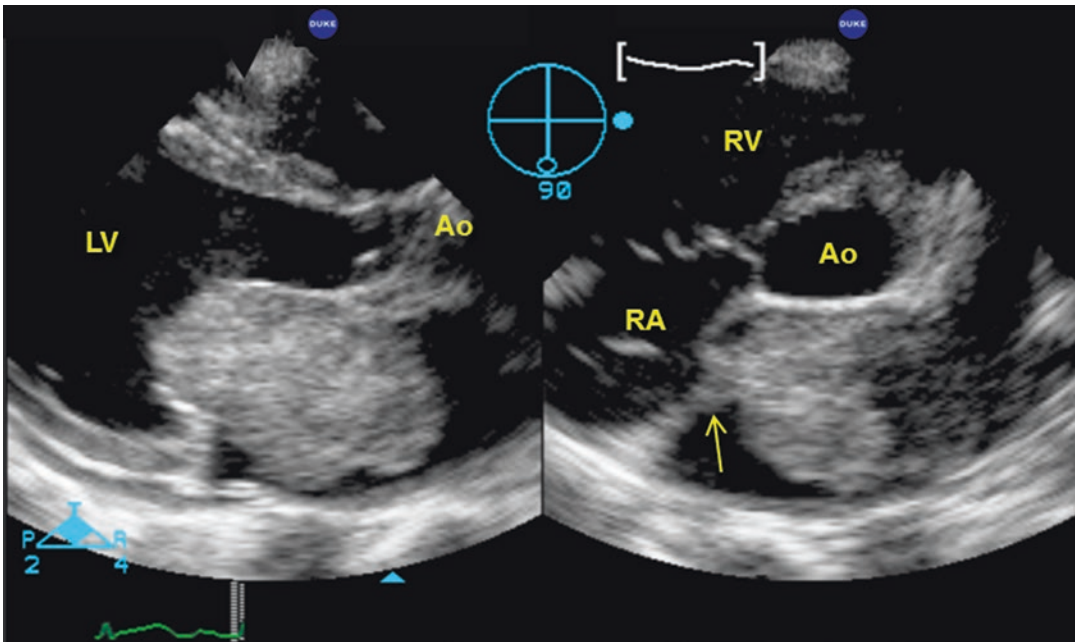
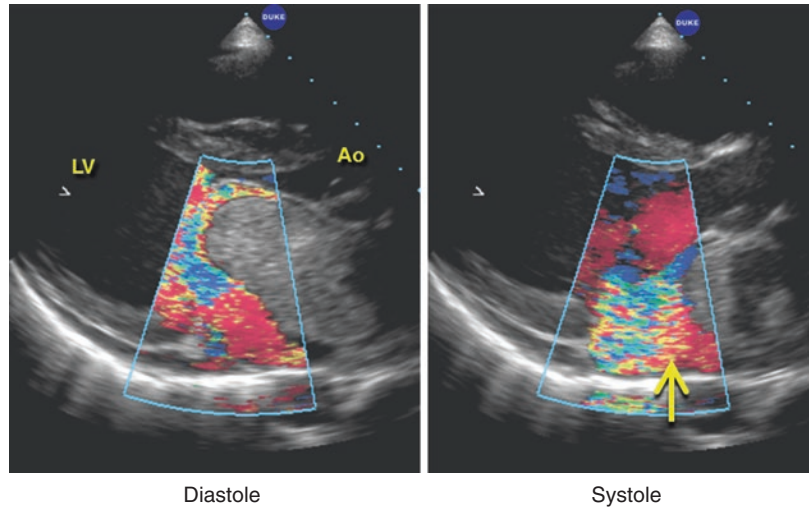


Fig. 28.11 It is most important to detect the origin site of intracavitary tumors of the heart in anticipation of surgical planning for removal. Left panel shows a parasternal long axis of a myxoma prolapsing into the mitral orifice. The right panel shows a parasternal short axis at the level of

the aorta with the tumor origin site located in the middle of the atrial septum. Here, the tumor seems to tug at the atrial septum in diastole and the tumor stalk is about 1–1.5 cm wide. Most left atrial myxomas are anchored at the floor of the oval fossa

require cardiac catheterization or angiography. With the advent of MRI, there is sometimes redundant testing performed. If a myxoma is found by echo or by MRI, the other test is invariably not required and serves only to drive up health care cost.

In the past, when only M-mode echo was available, severe prolapse of the posterior mitral leaflet with marked enlargement of the P2 segment simulated a left atrial myxoma (Fig. 28.15) as the interrogating beam was moved from leaflet tip in a superior direction. With two-dimensional

Fig. 28.12 Transesophageal echo showing the point of attachment of a myxoma on the atrial septum in the fossa ovalis, in this case about 1.5 cm wide. It is important to find the point of attachment to aid in directing the approach for surgical removal of the mass

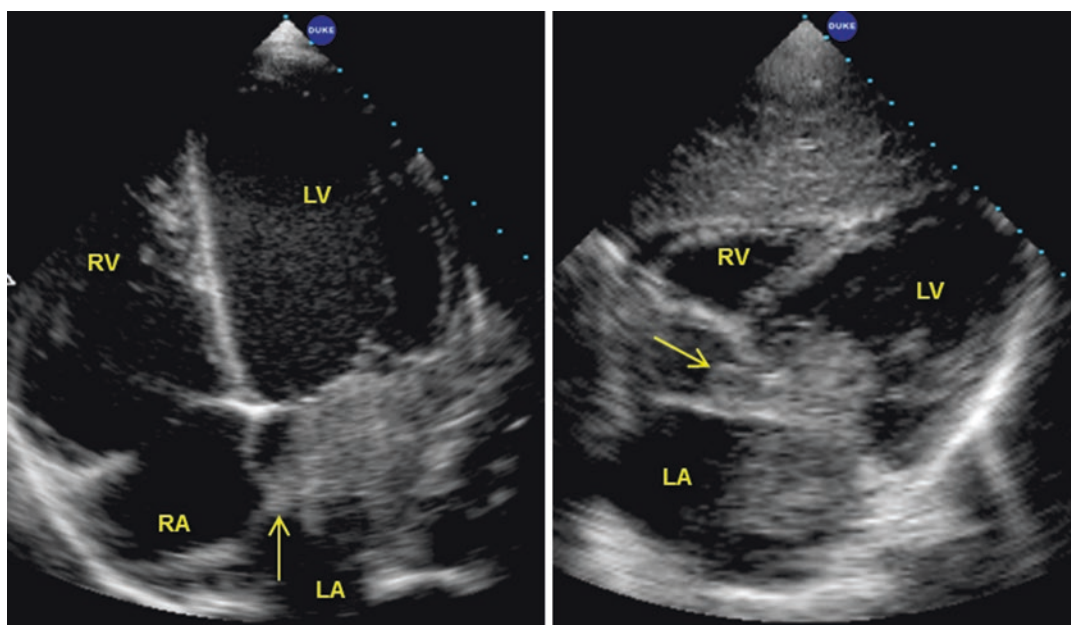
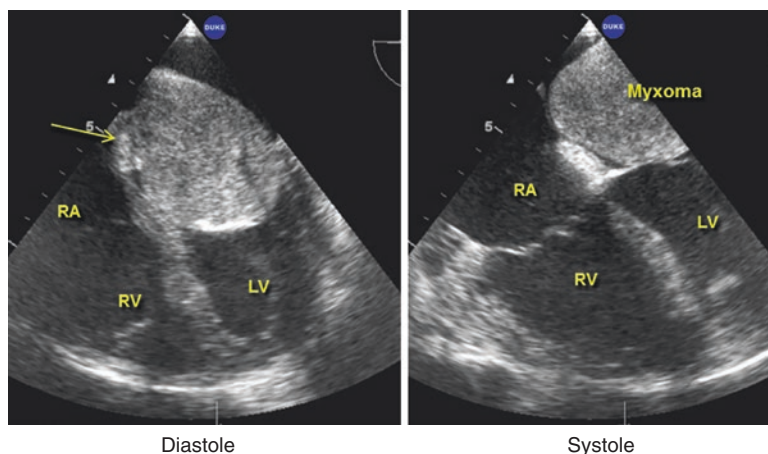


Fig. 28.13 The left panel shows an apical four-chamber view of the anchor point of an atrial myxoma in the same patient as seen in Fig. 28.5 (arrow). Slight inferior angulation of the interrogating probe demonstrates a portion of the tumor protruding through the foramen ovale, thus revealing the fact that the tumor is actually biatrial. It is

not uncommon for a typical left atrial myxoma (anchored at the fossa ovalis) to protrude into the right atrium. Some protrusions may be larger than the protrusion in this case. It is important to carefully examine the point of tumor attachment to reveal all the details necessary for surgical planning

echo, M-mode is no longer required except for historical or illustrative purposes.

Atrial myxomas are not always attached to the mid portion of the atrial septum. Figure 28.16 shows a polymorphous myxoma with a broad attachment located more posteriorly in the atrium by transesophageal echo. Removal of this myx-

oma required reconstruction of the intersection of the posterior limbus of the atrial septum as it joined the posterior atrial wall.

Figures 28.17, 28.18, and 28.19 show the surgical specimens of myxomas from six different patients that demonstrate the variable appearance of these tumors. The specimens in Fig. 28.17 are

Fig. 28.14 Transesophageal echocardiogram views of a left atrial myxoma showing a central core of liquefaction. The left panel shows the tumor in systole while the right panel reveals the point of attachment (solid arrow) in diastole. When the tumor prolapses into the mitral orifice, it tugs on the atrial septum causing a small diastolic shunt (dashed arrow) from left to right

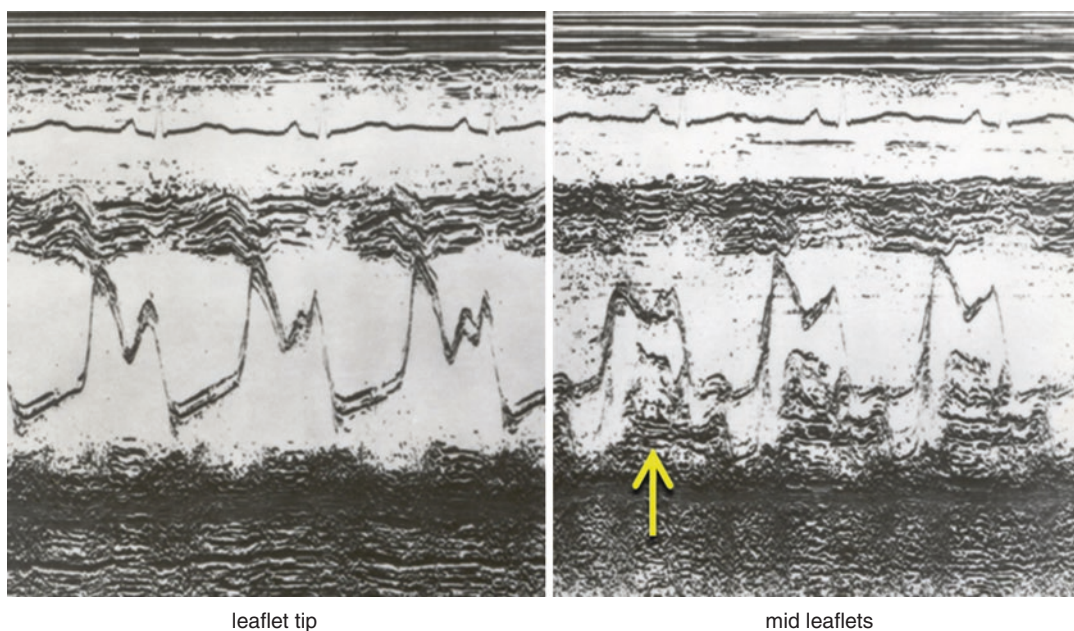
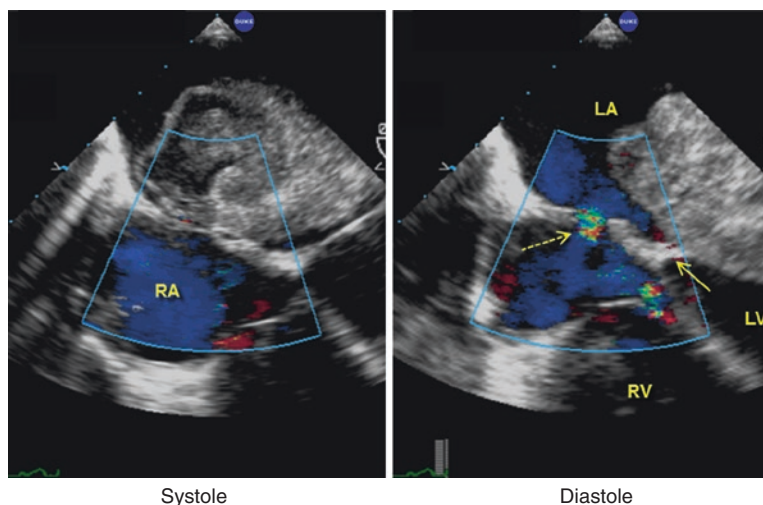


Fig. 28.15 The left panel is an M-mode of a normal mitral valve. The right panel shows an M-mode from patient with mitral prolapse. A large P2 segment can prolapse down into the mitral orifice and may simulate a left atrial myxoma (right panel, arrow). M-mode, with its lim-

ited field of view may lead to such diagnostic errors. It is usually easy to tell the difference between mitral prolapse and left atrial myxoma by two-dimensional echocardiography. See the Chap. 10 on mitral valve disease

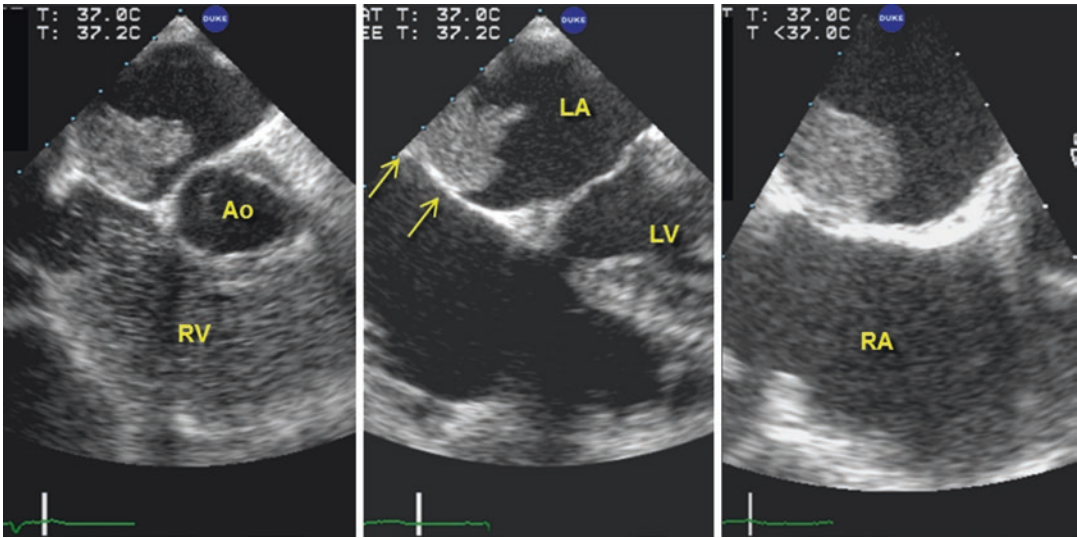


Fig. 28.16 Not all left atrial myxomas are anchored at the ovale fossa. This figure depicts the amorphous character of some myxomas in these transesophageal echo images at different points in the cardiac cycle in a patient with a left atrial myxoma anchored quite posteriorly. Note

the broad point of attachment (middle panel, arrows) at the junction in the posterior limbus of the atrial septum as it joins the posterior atrial wall. This tumor required some reconstruction of the atrial wall and atrial septum at surgery for complete tumor removal

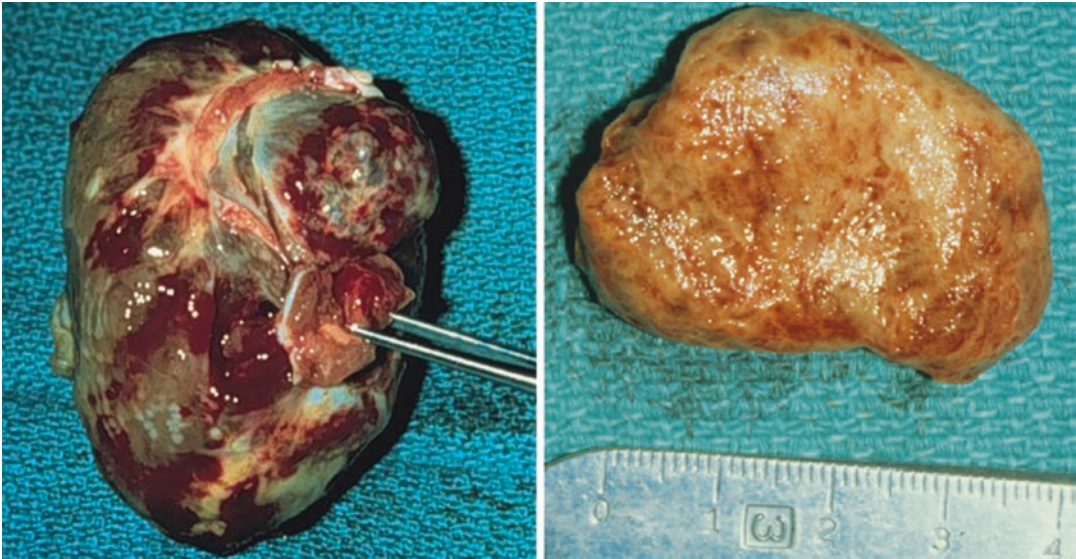


Fig. 28.17 Anatomic specimens of two atrial myxomas. Together with the subsequent two figures, these show the various anatomic appearances of myxomas. The left panel shows a well-encapsulated tumor with a portion protruding through the oval fossa. A thin portion of the atrial sep-

tum is seen surrounding the portion that protruded in the right atrium. The right panel shows another left atrial myxoma where the tumor surface looks less well encapsulated



Fig. 28.18 Another anatomic specimen is seen that has been sectioned in half showing a heterogeneous tumor interior (top panel). Yet another specimen of another tumor shows the friable nature and danger of embolization in some intracardiac tumors

well encapsulated while those in Fig. 28.18 are varied. The tumor shown in the lower panel of Fig. 28.18 was friable and likely prone to embolization. The tumors in Fig. 28.19 have irregular surfaces and varied tumor stalks.

Myxomas can occur in any chamber, great vessel or valve. Figure 28.20 demonstrates an M-mode of a giant left ventricular myxoma that had a broad attachment point on the posterior surface of the interventricular septum. This patient suffered from extreme impairment of flow with near total occlusion of the left ventricular outflow tract.

Figure 28.21 is a parasternal long axis from a patient where an oscillating mass was detected near the ventricular apex. The tumor was removed through an apical ventriculotomy. When myxomas are found in any location other than the left atrium, it is best to also examine all first degree relatives of the patient because of the familial nature of these type of myxomas.

Rhabdomyoma

Rhabdomyomas are tumors of the cardiac muscle and are, thus, almost always intramural and in the



Fig. 28.19 These two additional surgical specimens of atrial myxomas show more gelatinous appearances, with multiple small lobules

Fig. 28.20 Myxomas can rarely be located anywhere in the heart, in any chamber or great vessel or on any valve. This M-mode shows the appearance of a tumor from a patient with a left ventricular myxoma attached to the posterior surface of the interventricular septum that obliterated the left ventricular outflow tract (arrow) in systole

Chest wall
Septum
Myxoma
Mitral valve

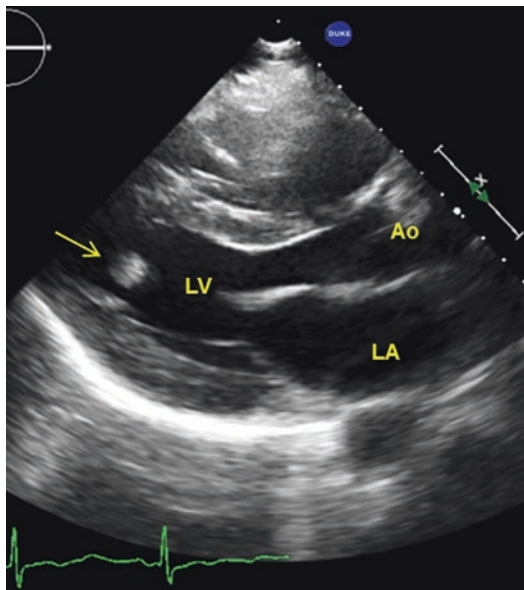
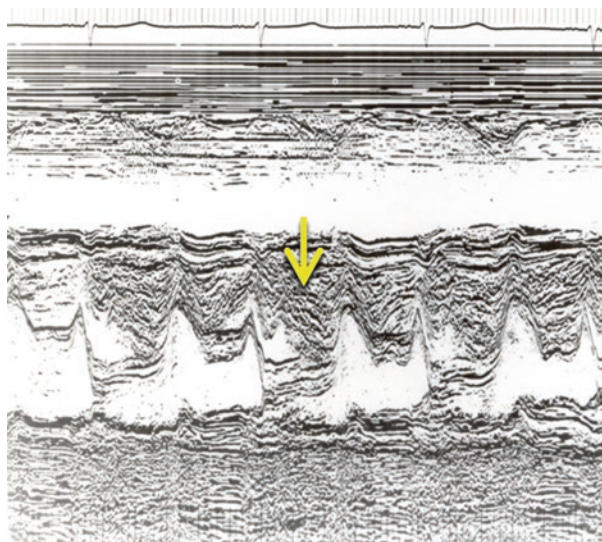


Fig. 28.21 Parasternal long axis from a patient with a small left ventricular myxoma (arrow), located near the ventricular apex

walls of the ventricles, rather than the atria. They are the most common tumors in children and are almost always multiple. They are rarely removed as they commonly regress over time and removal/resection would cause destruction of adjoining cardiac muscle. Figure 28.22 shows large tumors

in the walls of the interventricular septum in a neonate (left panel) that regressed by age five (right panel).

The images in the neonate in Fig. 28.23 are striking because of the multiplicity of tumors, particularly the massive tumor in the interventricular septum (middle panel). A three-dimensional image, accompanied by biplane images of this septal tumor appear in Fig. 28.24. Three-dimensional echo is usually minimally helpful except in sizing these intramyocardial tumors. Of interest is the ability to detect these tumors and watch their growth in utero as noted in Fig. 28.25. Here the tumors were detected on an initial routine prenatal ultrasound examination and were small and limited in number (at 20 weeks gestation). By 38 weeks gestation, the tumors grew in size. While post-natal tumor regression is variable, these tumors are usually gone by teen years and are very rarely detected by adult years.

Papillary Fibroelastoma

Papillary fibroelastomas are usually up to 2 cm in size and attached on or near the cardiac valves (left sided) by means of a long, thin stalk. These

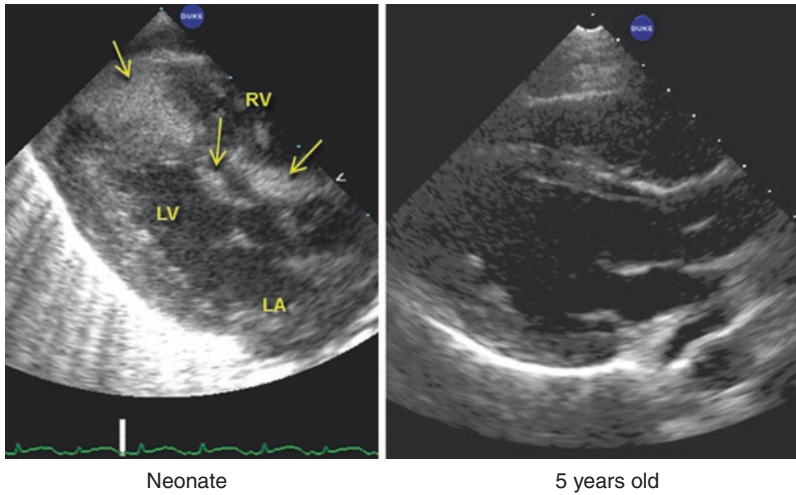


Fig. 28.22 The most common tumor in children is a rhabdomyoma. These are invariably multiple and tend to regress in size over time. The left panel shows a parasternal long axis from a neonate that shows multiple tumors within the interventricular septum (arrows). Multiple

other large intramyocardial tumors were located in other walls and chamber. The right panel shows a parasternal long axis of the same patient at age 5. The tumor masses have regressed

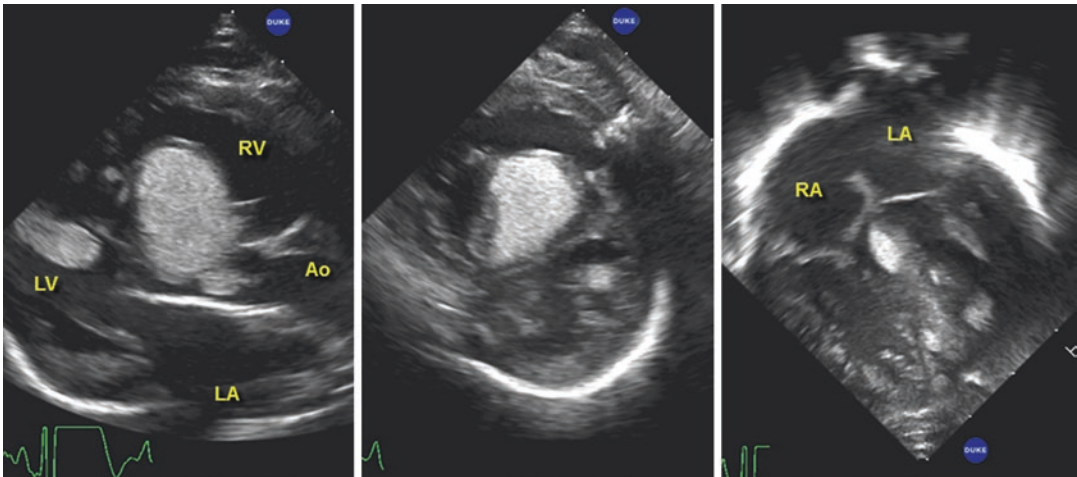


Fig. 28.23 Parasternal long axis (left panel), short axis (middle panel) and apical four chamber (right panel) from a neonate born with multiple rhabdomyomas of the inter-

ventricular septum, left and right ventricles, almost two numerous to count. These tumors were detected and followed by fetal echo prior to birth

tumors are quite reflective as they are comprised of dense tissue and they are highly mobile because of their long stalks.

Figure 28.26 shows a mobile mass on the underside of the posterior mitral leaflet from the apical

four-chamber view. Figure 28.27 is a three-dimensional echo of an aortic valve papillary fibroelastoma that was attached to an aortic valve leaflet. Figure 28.28 is an autopsy specimen from another patient, similar to the one in Fig. 28.27, showing

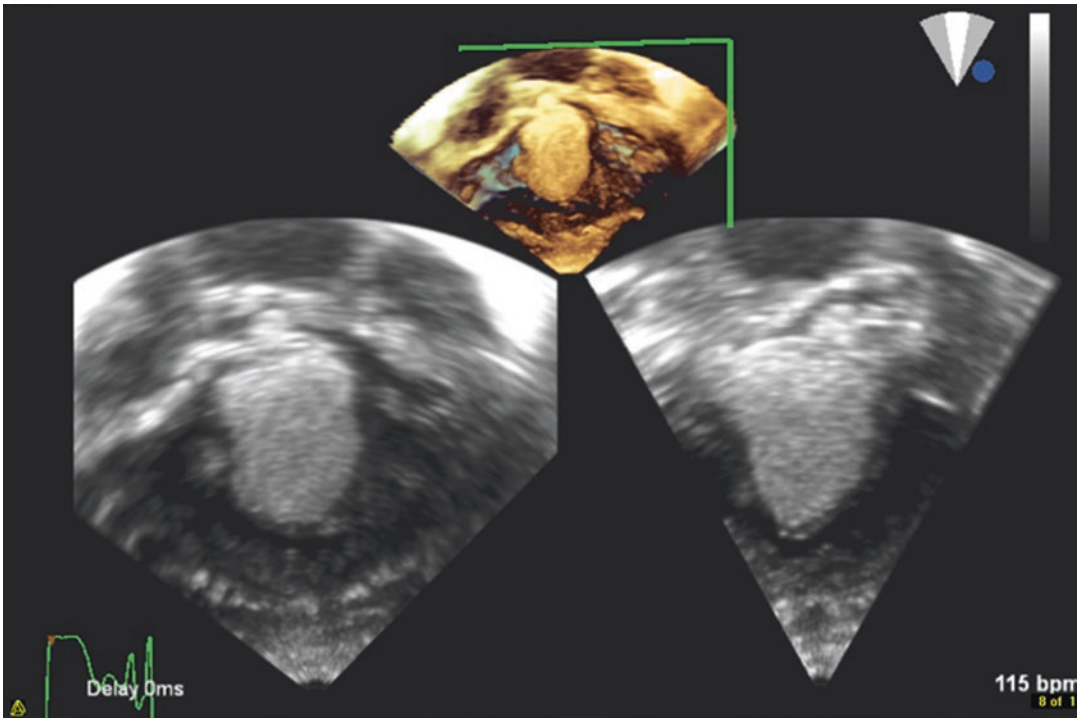


Fig. 28.24 Three-dimensional echo and two orthogonal B-scans of the largest interventricular septal tumor seen in the patient depicted in the middle panel of the previous figure

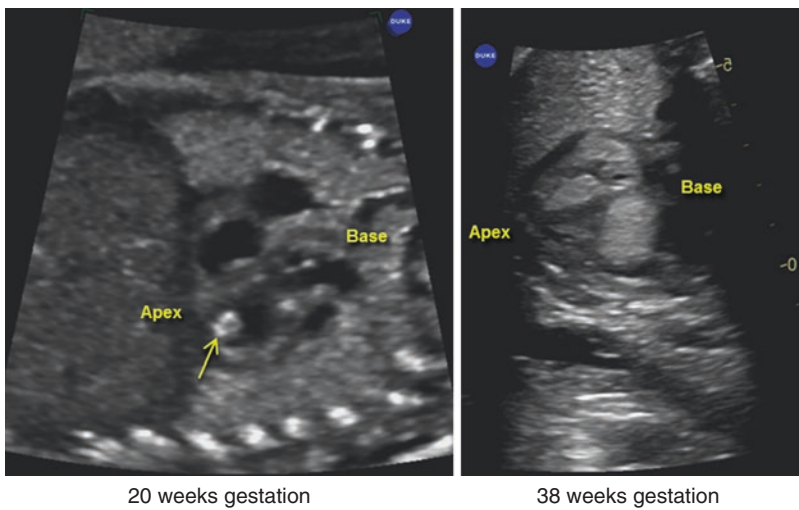


Fig. 28.25 Fetal scans of the patient seen in the previous two figures. The left panel is a five chamber variant view of the fetal heart in-utero view showing a large tumor near the left ventricular apex taken at 20 weeks gestation. The right panel shows a similar view at 38 weeks that demon-

strates multiple vary large tumor masses, clearly changed from 20 weeks. For continuity and clarity, the right panel has be flipped horizontally to match the orientation in the left panel

Fig. 28.26 Apical four-chamber views in diastole (left panel) and systole (right panel) from a patient with a papillary fibroelastoma attached to a secondary chorda tendinea, underneath the P2 segment of the posterior mitral leaflet (arrows). The mass was hypermobile

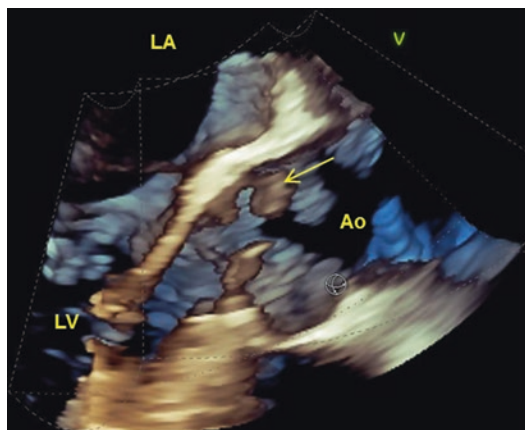
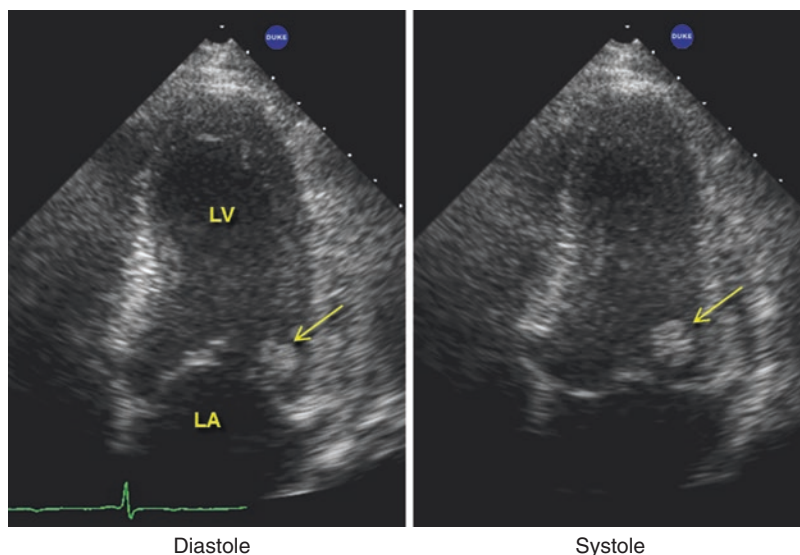


Fig. 28.27 Three-dimensional transesophageal echocardiograms of the left ventricular outflow tract and proximal aorta from a patient with a papillary fibroelastoma of the base of an aortic valve leaflet (arrow). *Image courtesy of General Electric Ultrasound*

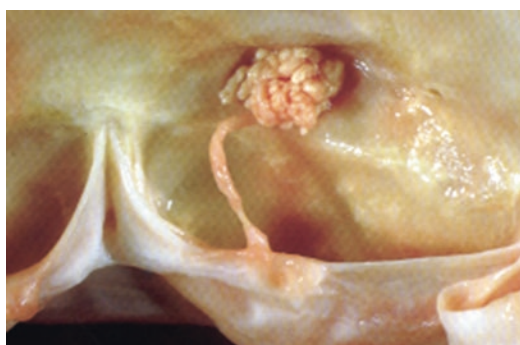


Fig. 28.28 Pathologic specimen of a typical cardiac papillary fibroelastoma. Here the tumor is attached near the Node of Arantii of the right coronary cusp of a patient with intermittent angina. Note the tumor is on a long stalk and occludes the ostium of the right coronary artery. When attached to the aortic valve, these tumors may occlude coronary inflow. *Image courtesy of Robert H. Anderson, MD and Anton Becker, MD*

the long tumor stalk. In this case the tumor occluded the orifice of the right coronary artery.

Transesophageal views from another patient with a papillary fibroelastoma are seen in Fig. 28.29. In this case, the tumor was attached to a mitral chord and it was seen to move well into the left ventricular outflow tract in systole.

Like myxomas and rhabdomyomas, the diagnosis of a papillary elastoma is made presumptively by the enumerated characteristics typical of the detected masses. These elastomas are most commonly removed because of a possibility of embolization or occlusion of coronary flow (when attached to the aortic valve). Until removal

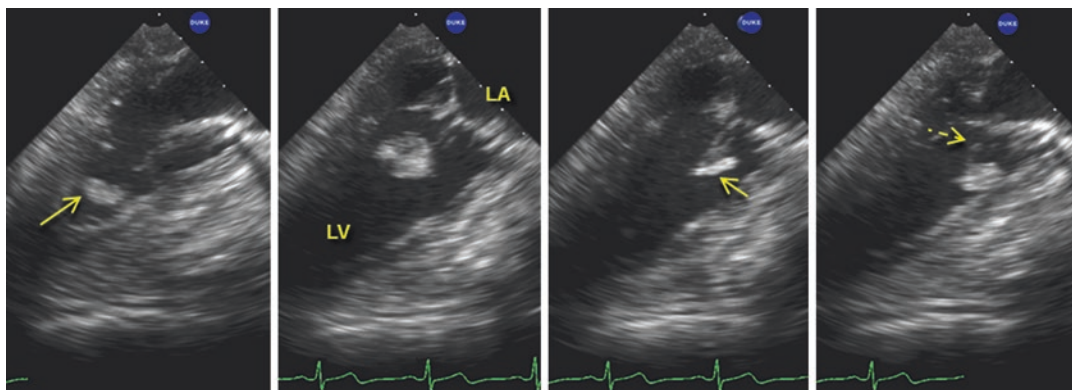


Fig. 28.29 Serial transesophageal three-chamber views of the left ventricular outflow tract of a patient with a hypermobile papillary fibroelastoma. In diastole (left panel) the tumor is seen in the left ventricle (arrow) while in systole (third panel) the tumor is thrown into the left

ventricular outflow tract (arrow). One frame in late systole shows the tumor attachment on a stalk (dashed arrow, right panel) from the underside of the anterior mitral leaflet. Significant angulation from standard views had to be made to align with the path of the rapidly moving tumor

and microscopic examination, however, diagnostic certainty is not possible.

Bacterial Endocarditis and Non-bacterial Endocarditis

Bacterial or fungal endocarditis is more common than tumors of the heart, and is dealt with in detail in the chapter concerning endocarditis. Infection(s) of heart valves leads to the formation of mass lesions on the valves or other endocardial surfaces known as vegetations.

Bacterial Endocarditis

This topic is covered elsewhere in this book but it is appropriate, however, to provide a single example of bacterial endocarditis as part of the current discussion. Figure 28.30 shows a transesophageal echocardiogram from a patient who presented with fever and positive blood cultures for *S. aureus*. An oscillating mass was detected just above the P2 segment of the posterior mitral leaflet (Fig. 28.30, arrow).

Three dimensional transesophageal echo showed an irregular mass lesion just where P2 joins the posterior mitral annulus (Figs. 28.31 and 28.32). The mass appears quite sessile and has an irregular surface, but needed further differentiation from other causes for mass lesion.

In patients who are clinically infected, the first diagnostic possibility becomes endocarditis. In this patient, the distal portions of P2 were unaffected and the surface of the mass was coarsely irregular and unlike that seen in isolated P2 prolapse (see Chap. 10 on the mitral valve). Myxoma is another possibility but the point of attachment is most unusual and the base of the current lesion is broad, both making myxoma unlikely. Spontaneous thrombus in this area is also possible but such thrombi on the mitral apparatus have only been reported in mitral prolapse, and they are exceedingly rare.

Once again, it is clinical context that usually helps narrow diagnostic possibilities. In this patient, the presence of fever and positive blood cultures makes the diagnosis of vegetative endocarditis most likely. Without fever and the positive blood cultures, the diagnosis of atypical atrial myxoma would rise on the diagnostic possibility list.

Fig. 28.30 Transesophageal view in a three-chamber view from a patient with fever that demonstrates a vegetative mass above a prosthetic mitral ring

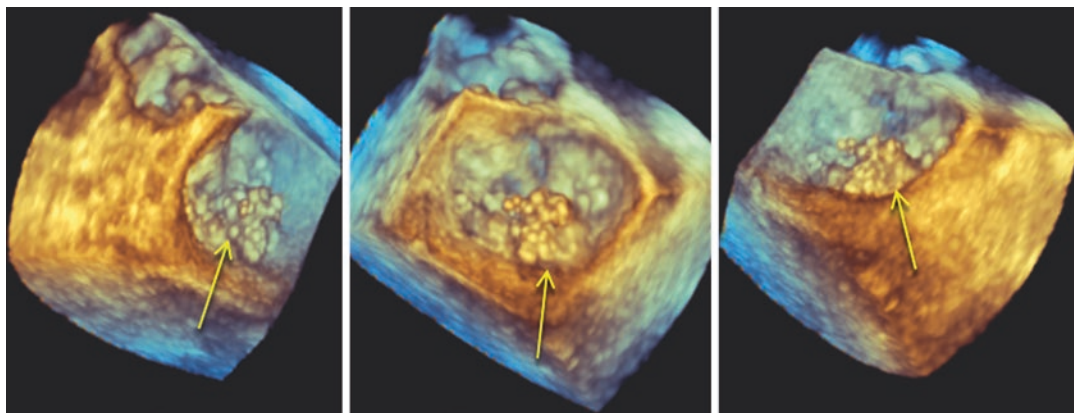
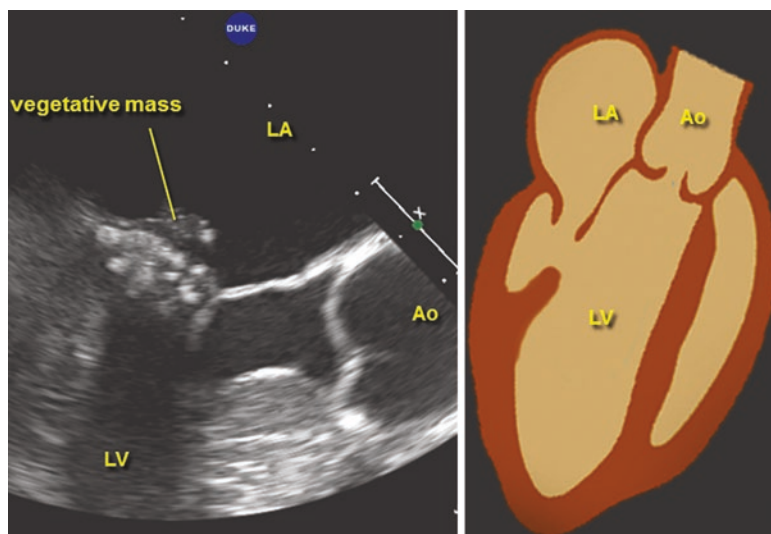


Fig. 28.31 Three-dimensional echo in the surgical view showing the sessile cluster of vegetations residing over the P2 segment from various angles. The arrows point to

the vegetation. Bacterial vegetations are common etiologies for intracardiac masses

Non-bacterial Thrombotic Endocarditis

It is possible to encounter oscillating mass lesions on valves or endocardial surfaces that are neither tumor, nor vegetation, nor other readily explainable entity. Figure 28.33 shows an uncommon three-dimensional echocardiographic view of the right atrium, with the anterior right atrial wall and appendage removed to reveal the superior vena cava on top and the inferior vena cava on the

bottom. Looking into the right atrium the interatrial septum is seen, and the oval fossa is clearly bulging (due to mitral regurgitation in this patient).

A small oscillating mass lesion is noted (arrow) on the superior limbus of the atrial septum, just above the oval fossa. This patient recently underwent a right and left cardiac catheterization. Most likely, the right sided catheter scratched the atrial septum, producing a small thrombus or bit of fibrous material.

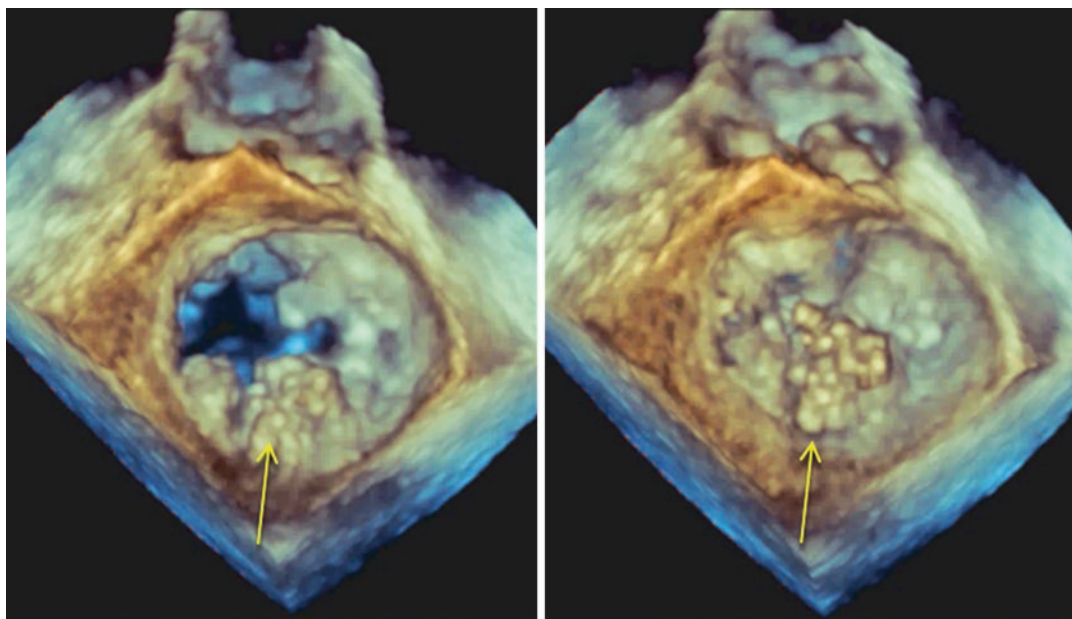


Fig. 28.32 Three-dimensional echo in the surgical view showing the sessile vegetation cluster in the same patient in the previous two figures. The multi-lobulated vegetative mass is easily seen. The arrows point to the vegetation

Non-bacterial thrombotic endocarditis (NBTE) is a term that is loosely associated with little oscillating mass lesions that look like they are endocarditis, but there is no evidence of infection. These could be old, spontaneously healed bacterial endocarditis or they could be due to trauma or other inflammatory reason where the endocardial surface is disrupted and small thrombotic/fibrotic lesions appear in the process of healing.

This scenario recalls the experimental rabbit model for the creation of endocarditis by Durack [1] where he scratched the atrial endocardial surface of rabbits with catheters, creating small lesions. He then injected active bacterial cultures of that then latched onto the small tears and thrombi, and created an active bacterial endocarditis lesion at the point of trauma of the atrial wall.

When such lesions appear in the right heart in the setting where interruption of the endocardial surface by a catheter (transient or indwelling) as seen in the patient in Fig. 28.33, we refer to these lesions informally as “Durack” lesions. NBTE

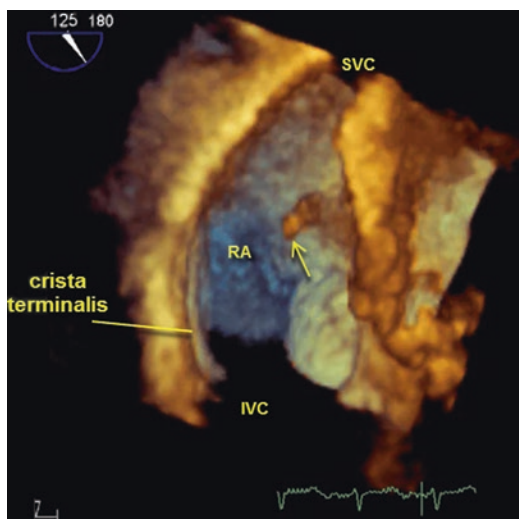


Fig. 28.33 Three-dimensional frontal view of the right atrium. Note the superior and inferior venae cavae and the position of the crista terminalis. The arrow points to an oscillating mass adherent to the superior limb of the atrial septum, just above a bulging floor of the oval fossa. The patient recently had a right sided cardiac catheterization where the atrial septum was likely scratched resulting in a localized thrombus

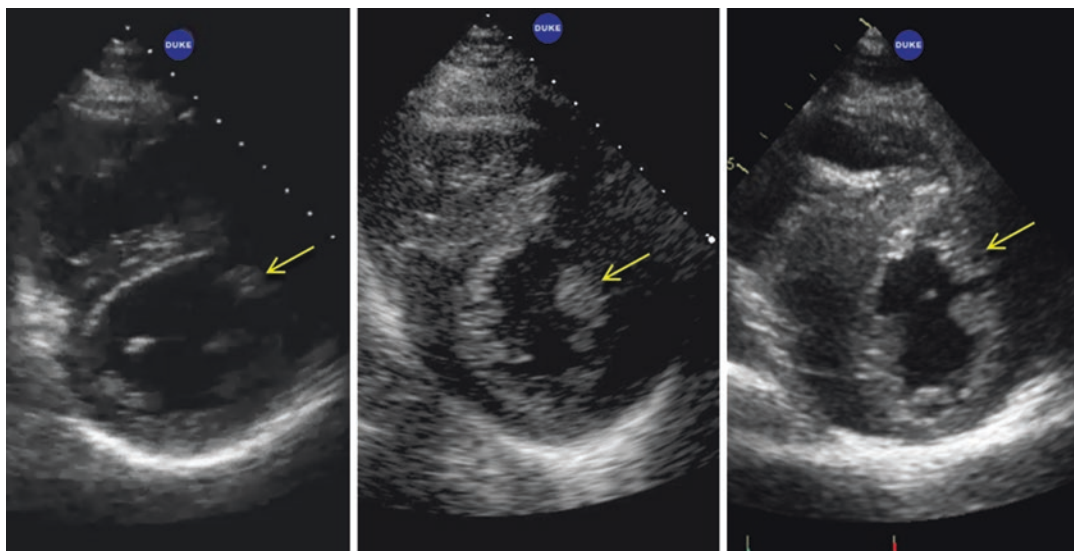


Fig. 28.34 In about 40% of normal patients, the anterolateral muscle bundle of the left ventricle is prominent (Bundle of Moulaert) and has been mistaken as an endocardial tumor or accessory papillary muscle when prominent. This bundle is located anterior to the antero-lateral papillary muscle and runs longitudinally in the left

ventricle. This bundle is shown in three different patients (arrows) and it becomes particularly prominent in patients with left ventricular outflow tract obstruction. The patients in the middle and right panels have hypertrophic cardiomyopathy

might also be a proper term in this context. Some oscillating mass lesions defy easy diagnostic classification.

Normal Anatomy Sometimes Confused with Masses

There is a longitudinal muscle bundle usually seen in the short axis view of the left ventricle by echo (Fig. 28.34). This muscle bundle is just anterior to the antero-lateral papillary muscle of the left ventricle and is known as the antero-lateral muscle bundle described by Moulaert [2]. It can be quite prominent, particularly in patients with left ventricular outflow tract obstruction (Fig. 28.35). In rare cases where this bundle is prominent an inexperienced echocardiographer may also incorrectly identify this structure as an accessory papillary muscle. However, it has no chordal connections to the mitral valve leaflets. In our laboratories, it is referred to as the Bundle of Moulaert.

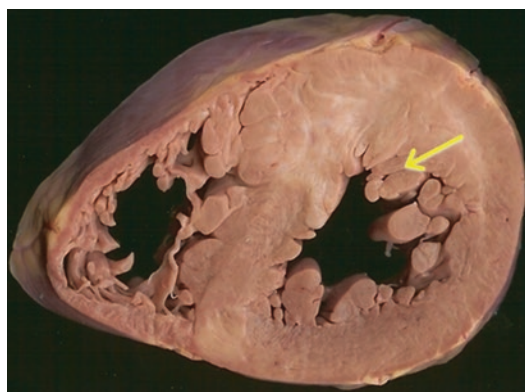


Fig. 28.35 Pathologic specimen showing the anterolateral muscle bundle (Bundle of Moulaert) from a patient with HOCM. Modified after Choudhury, L. et al. *J Am Coll Cardiol* 2002;40:2156–2164

Central Tendon of the Diaphragm

We have encountered another problem with inexperienced readers as some identify the occasionally seen posterior compression of the IVC as it enters the right atrium to be due to

adjacent tumor (Fig. 28.36). This compression is more prominent in some people more than others. While tumor is possible, this posterior compression is most commonly caused by the central tendon of the diaphragm wrapping around the inferior vena cava. Figure 28.37 depicts the diaphragmatic openings and shows this tendinous structure snarling the vena cava from behind.

Ruptured Papillary Muscle

While particularly less common in the days of angioplasty and coated stents, a ruptured papillary muscle will present as a mass lesion attached to the mitral leaflet. Figure 28.38 shows serial apical four chamber views where the papillary head is seen approximating its original position adjacent to the stump of the original papillary muscle (left and middle panels) in diastole. In systole, the ruptured papillary head was thrown into the left atrium (right panel). This lesion was

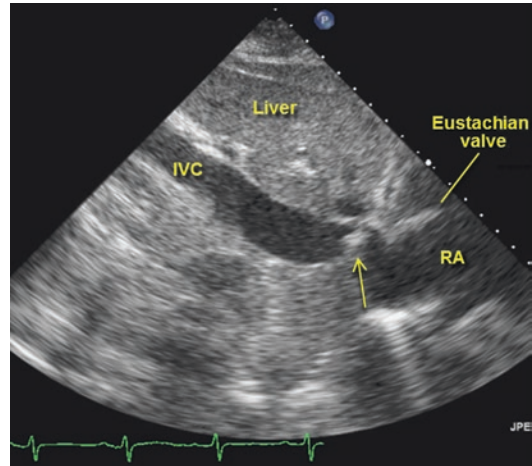


Fig. 28.36 Long axis of the inferior vena cava below the diaphragm. At this point the liver is both anterior and posterior (caudate lobe of the liver). The central tendon of the diaphragm (arrow) is normally seen to impinge in the posterior aspect of the IVC (see next figure). This is a normal finding in some people that may be mistaken due to an external IVC mass. The Eustachian Valve (valve of the inferior vena cava) is seen anterior to the entrance of the IVC into the right atrium

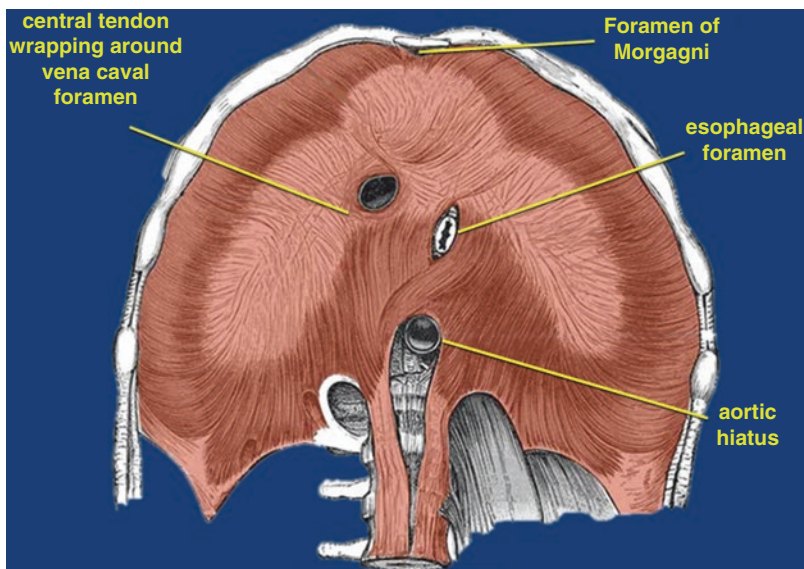


Fig. 28.37 The anatomy of the diaphragm pictured from below (looking up into the diaphragmatic dome) depicting the various passages of anatomic structures from the thoracic to the abdominal cavity. The opening (foramen or hiatus) through the diaphragm that allows the vena cava to pass through from the thoracic cavity to the abdominal cavity is surrounded by a muscular/tendinous structure

known as the central tendon. The central tendon may look to impinge on the vena cava as seen in the previous figure. This is a normal finding. *Image is modified from Gray, H and Goss, C: Anatomy of the Human Body. Lea & Febiger. Philadelphia, 1963 and subsequently copied and modified by teachmeanatomy.com*

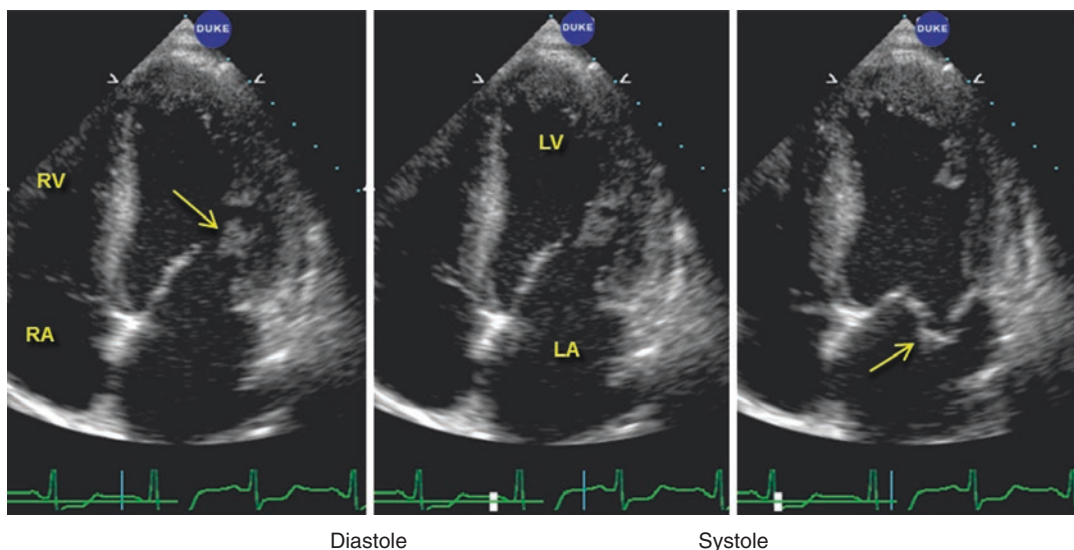


Fig. 28.38 Sequential apical four-chamber views from a patient with a ruptured papillary muscle (arrows). The left and middle panels show the ruptured papillary head just

approximating the basal portions of the papillary muscle in diastole. In systole, the papillary head is thrown into the left atrium leaving its basilar stump

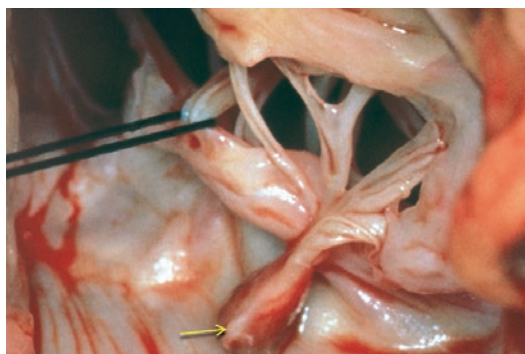


Fig. 28.39 Surgical image from a patient with a ruptured papillary muscle (arrow) undergoing mitral valve repair. Image courtesy of Toby Cosgrove, MD

associated with severe mitral regurgitation and the patient underwent emergency mitral valve repair re-implanting the ruptured papillary head into the left ventricular wall.

Figure 28.39 is a surgical view of a very similar patient. The mitral orifice is seen and the ruptured papillary head is pulled out of the mitral orifice and brought into the surgical field. The three dimensional echocardiogram in the surgeon's view of yet a third. Quite similar, patient is shown in Fig. 28.40. The left panel shows the mitral valve open in diastole while the systolic

view (right panel) shows the papillary head as it is thrown into the left atrium. These latter two patients also underwent similar surgical repair, rather than valve replacement. Based on the echo alone, these can resemble endocarditis. The clinical setting of a recent myocardial infarction, abrupt onset of heart failure and mitral regurgitation and the appearance of the papillary head approaching its stump confirms the diagnosis. The fact that none of these patients showed signs of clinical infection was also helpful.

Inverted Atrial Appendage

One curious abnormality that can present as a mass lesion in the left atrium is inversion of the left atrial appendage. Such an abnormality can be spontaneous or iatrogenic, inadvertently occurring during manipulation of the heart during cardiac surgery. Figure 28.41 demonstrates a transesophageal echo during cardiac surgery where a mass suddenly appeared in the left atrium (arrow). A transesophageal three-dimensional echo in the surgeon's view demonstrated the same mass lesion emerging from the os (mouth or orifice) of the atrial appendage (Fig. 28.42).

The surgeon easily pulled the beating, but inverted atrial appendage out of the left atrium

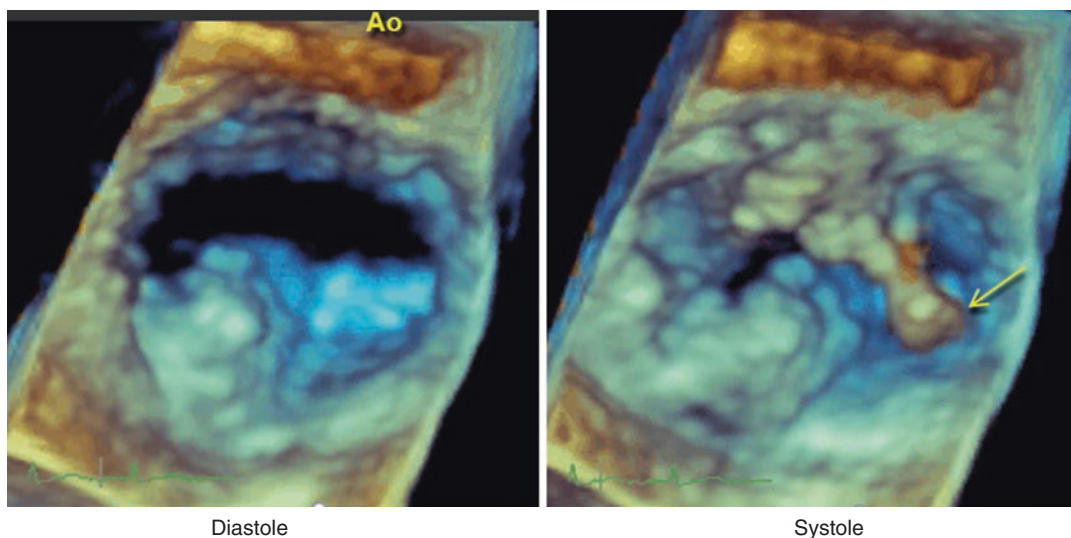


Fig. 28.40 Three-dimensional echocardiogram from yet another patient with a ruptured papillary muscle head. The left panel shows the mitral valve open in diastole from the surgical perspective. The right panel is the same valve in

systole with the papillary head (arrow) thrown into the left atrium. Although from different patients, note the similarities to the previous two figures

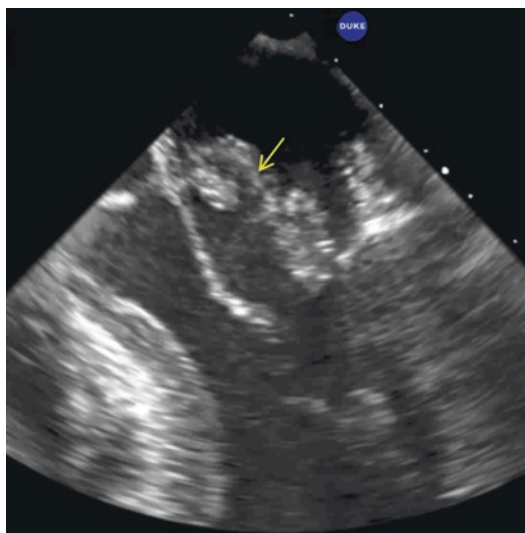


Fig. 28.41 Transesophageal echocardiographic still frame in the three-chamber view showing a large linear mass in the left atrium (arrow)

where a normally appearing appendage was seen (Fig. 28.43, left panel). The right panel of Fig. 28.43 shows a pathologic specimen of a human heart where the atria have been cut away revealing the mitral and tricuspid valves and both

atrial appendages. We have encountered such instances in ambulatory patients.

Also note the pectinate muscles at the tips of the atrial appendages, and how these normal structures can be incorrectly identified as left atrial thrombi, particularly in patients with dilated atrial appendages due to chronic atrial fibrillation.

Residual Anatomy After Mitral Valve Repair/Replacement

There are many techniques and combinations of techniques used in mitral valve repair or replacement. Knowing some of these techniques is helpful in sorting out mass lesions identified after cardiac valve surgery. Leaflet plications or residual pledgeted materials can simulate mass lesions.

One such patient is encountered in Fig. 28.44 where a preoperative transesophageal echocardiogram shows clear Carpentier Type 2, P2 prolapse (see mitral Chap. 10). Due to accompanying severe mitral regurgitation, the patient underwent mitral valve replacement with a double disc leaflet prosthesis.

Figure 28.45 shows the post operative surgical view of the same patient where a mass lesion was

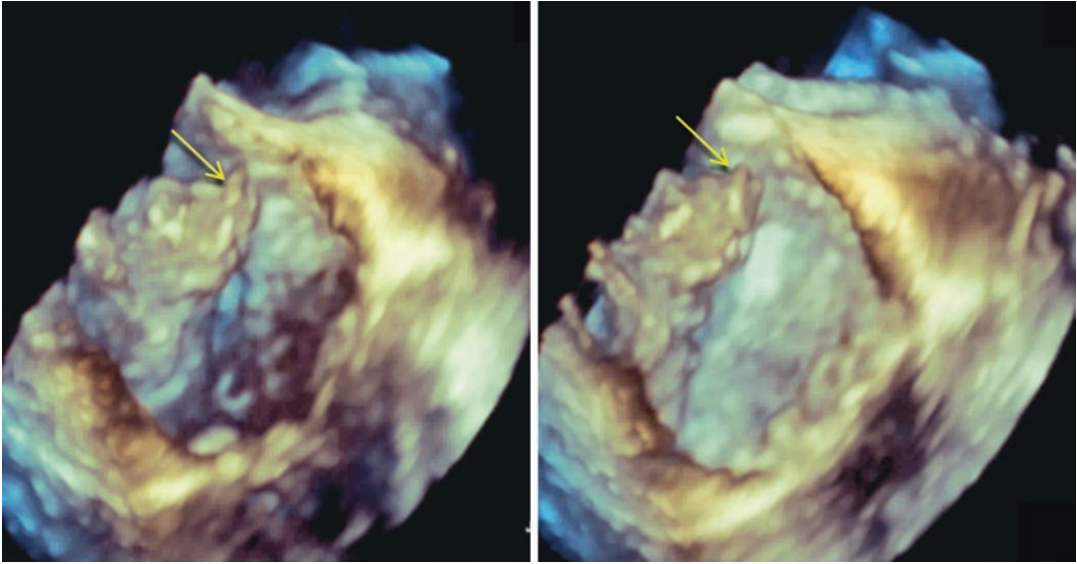


Fig. 28.42 Three dimensional transesophageal echocardiographic still frames in diastole (left panel) and systole (right panel) correlating to the mass (arrows) seen in the previous figure. The mass originates from the os of the

atrial appendage and it resembles the form and structure of the atrial appendage and was due to an inversion of the atrial appendage into the left atrium

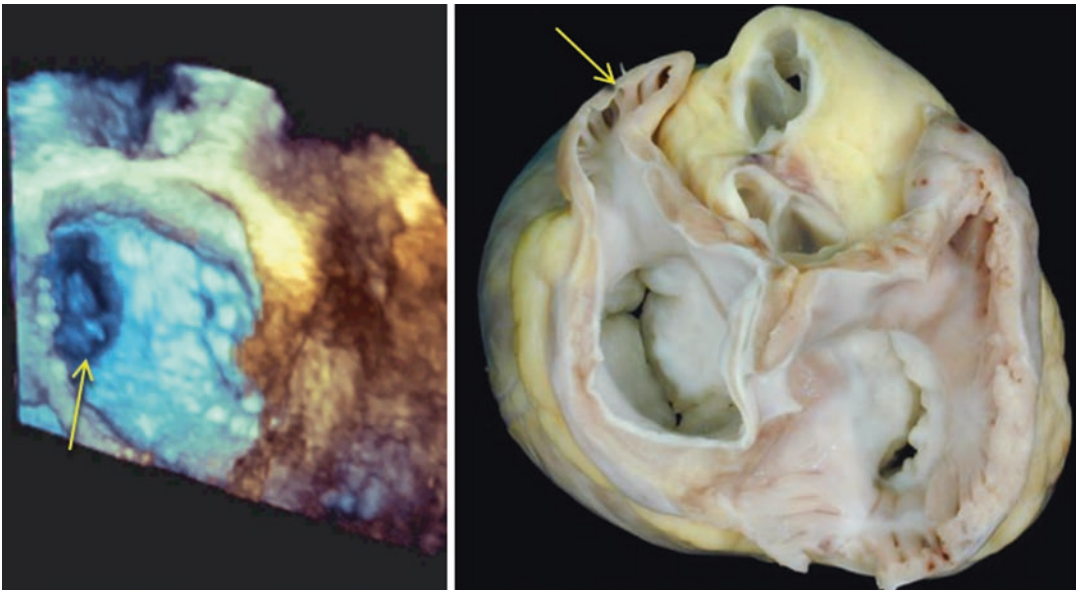


Fig. 28.43 Three dimensional transesophageal echocardiographic still frame (left panel) from the same patient seen in the two previous figures once the atrial appendage reverted to its normal external position. The arrow in the left panel points to the open os of the appendage and appears normal. The right panel shows a pathologic cut specimen through the base of a heart. Showing the posi-

tion of the mitral and the tricuspid valves. The arrow points to the tip of the left atrial appendage. Note the striated pectinate muscles at the tip of the atrial appendage that may resemble thrombi unless the normal presence and location of these muscles is known. *Right image courtesy of R.H. Anderson, MD*

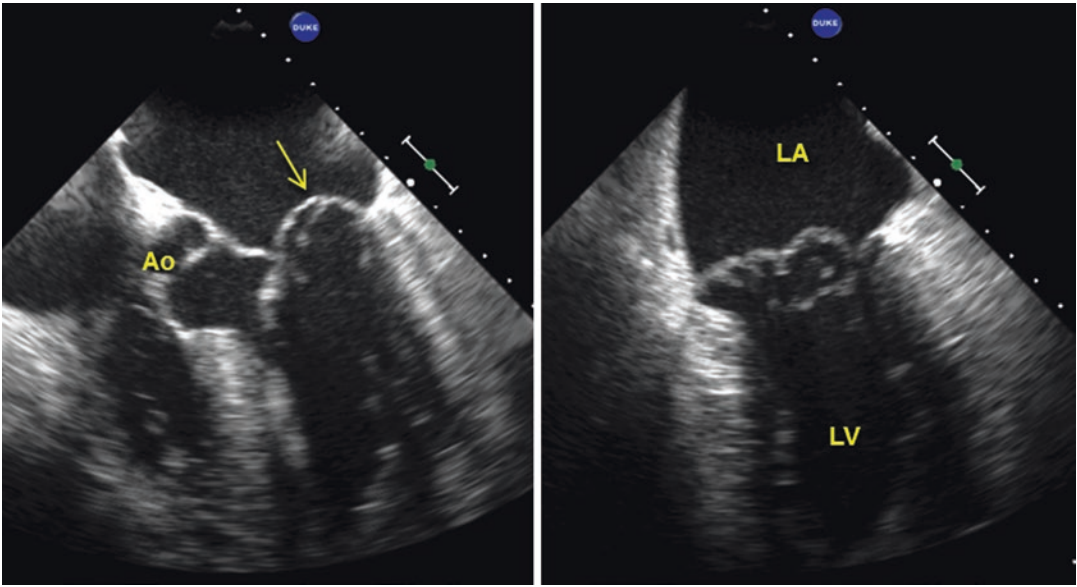


Fig. 28.44 Transesophageal echocardiograms in the three-chamber (left panel) and two-chamber (right panel) views showing obvious prolapse (arrow) of the P2 segment. The images were obtained prior to mitral valve replacement

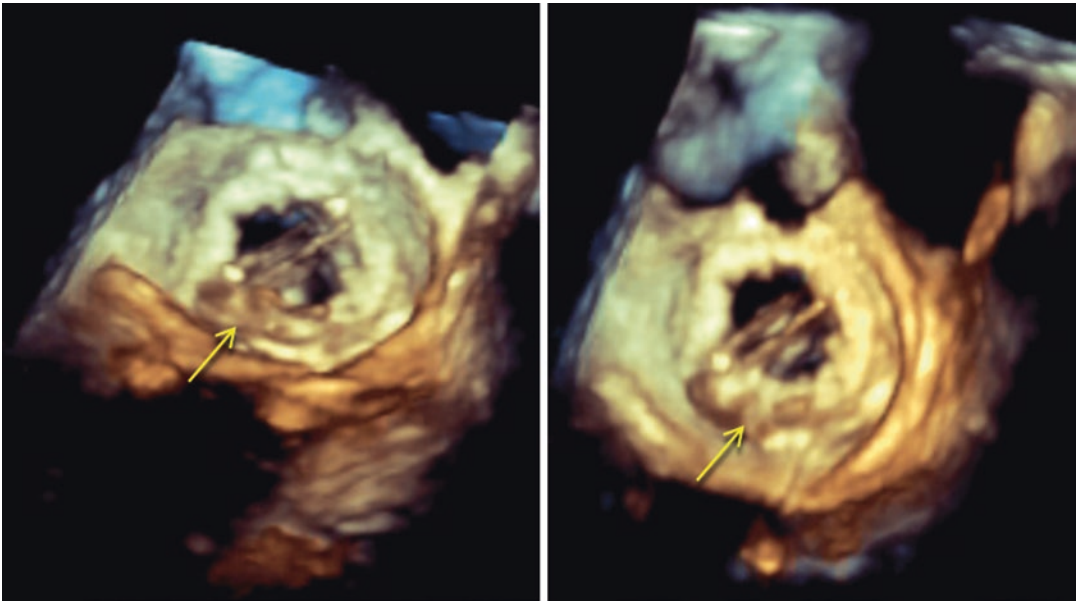


Fig. 28.45 Transesophageal three-dimensional images following replacement of the mitral valve in the patient from the previous figure. The bi-leaflet mitral prosthesis is seen in position and the arrow points to a mass lesion (left

panel). With slight tilting of the image, the mass is seen in the right panel (arrow). In this case, the posterior mitral leaflet and cords were preserved and the leaflet body gathered into the left atrium before the prosthesis was inserted

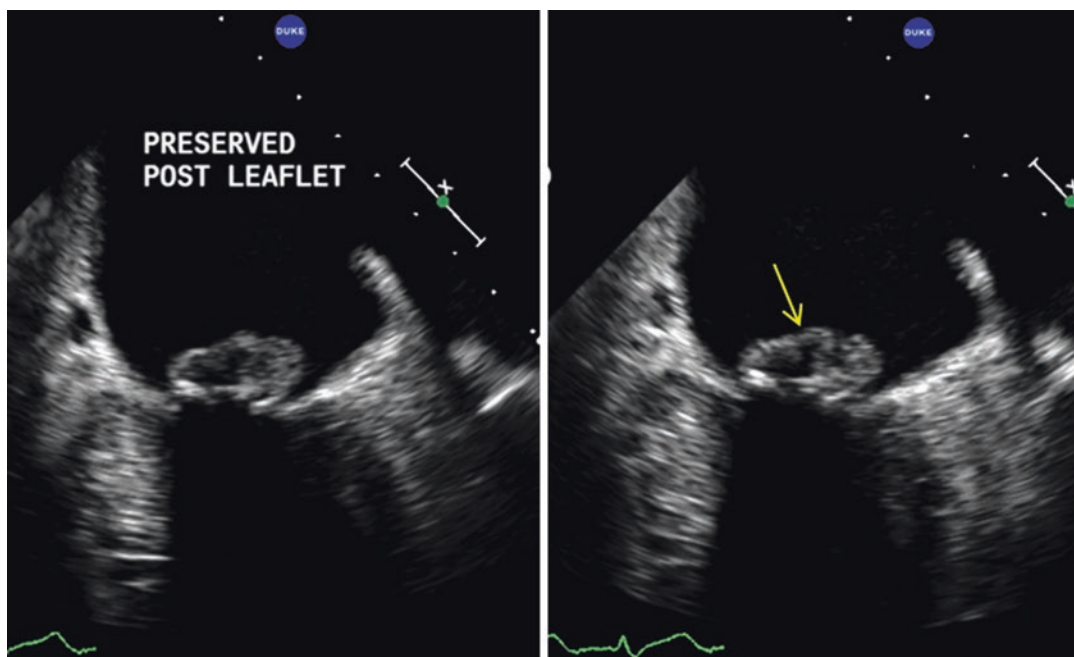


Fig. 28.46 Transesophageal echocardiogram showing the posterior leaflet gathered above the mitral prosthetic ring

noted along the posterior portion of the prosthetic valve ring. In this patient, the large prolapsing posterior leaflet was gathered and pulled into the left atrium to preserving the posterior leaflet chordae, which enhances post operative ventricular function. Then the valve prosthesis was put into place, leaving the retained posterior leaflet as the mass.

Had this patient appeared post operatively with a fever and/or positive blood culture this mass could easily have been interpreted as a vegetative lesion. The anesthesiologist who performed the echocardiogram in the operating room, however, left documentation as to the origin of the mass lesion on the screen (Fig. 28.46).

Artifact

There are multiple artifacts that can confound the certain diagnosis of the presence of an intracardiac mass and lead to incorrect interpretation. The patient seen in Fig. 28.47 was a 67 y.o. male with a previous history of anterior wall infarction and heart failure who was having transient neurological events. The apical four-chamber view demonstrated a suspicious mass lesion along the hypokinetic interventricular septum that was ini-

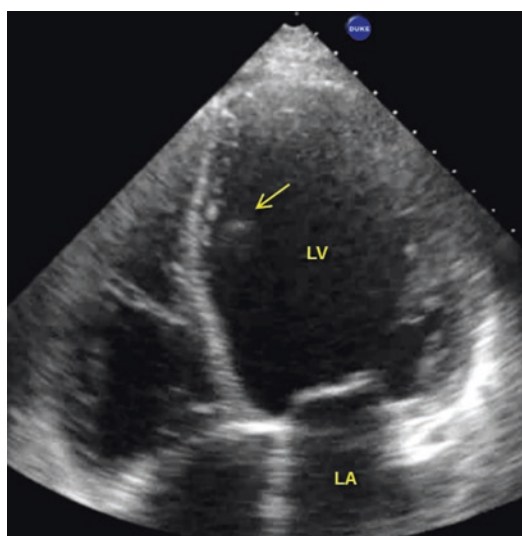


Fig. 28.47 This apical four-chamber view demonstrated a suspicious mass lesion along the hypokinetic interventricular septum (arrow) in this 67 y.o. male with a previous history of anterior wall infarction and heart failure who was having transient neurological events. Is this real or an artifact?

tially incorrectly diagnosed as an intraventricular thrombus (arrow).

Fig. 28.48 It's an artifact. The left hand panel shows the suspicious mass lesion positioned at 8.4 cm from the transducer face. As soon as the color is turned on, the suspected lesion moves to 6.4 cm (right hand panel) proving that it was only a reverberant artifact and not a real target. For details, see text

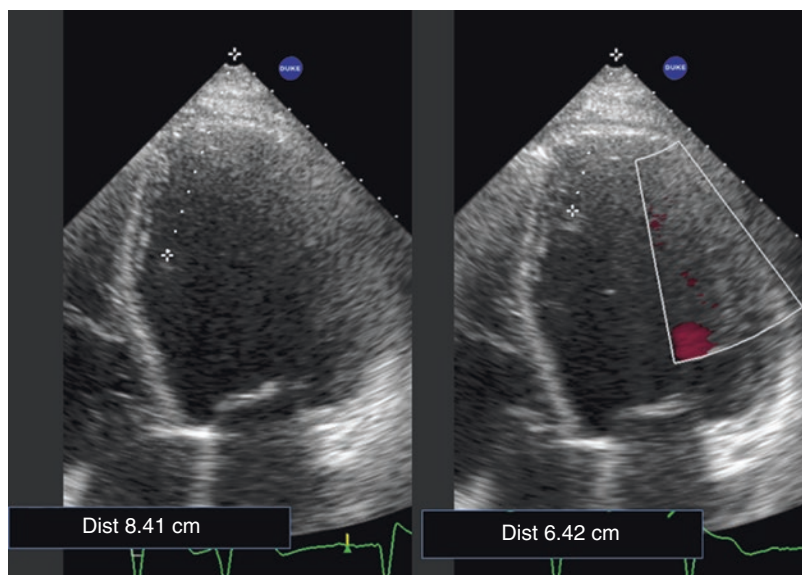
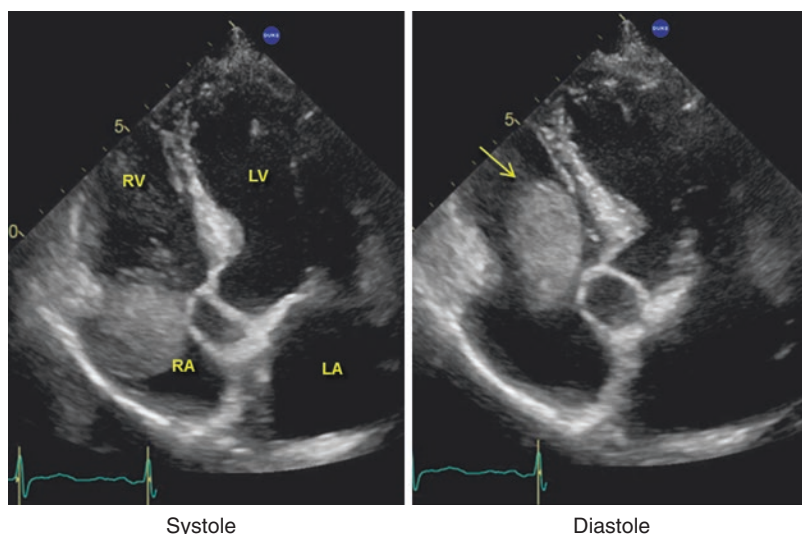


Fig. 28.49 Systolic (left panel) and diastolic (right panel) images from a patient with a large mass lesion of the right atrium. The mass protrudes into the orifice of the tricuspid valve in diastole (arrow) and resembles a myxoma



The left hand panel showed the suspicious mass lesion positioned at 8.4 cm from the transducer face. As soon as the color was turned on, the suspected lesion moved to 6.4 cm (right hand panel) from the transducer face. The movement of the target in space confirmed it as a reverberant artifact and not a real target. When color is turned on, system prf (pulse repetition frequency) changes resulting in the movement of the artifact from one place to another. As previously mentioned, changing depth or transducer frequency

may also move, or eliminate, artifacts. Changing scan depths in this patient also moved the position of the confounding artifact (Fig. 28.48).

Other Cardiac Tumors and Masses

Multiple other different cardiac tumors can affect the heart and many of them may initially resemble myxomas. Figure 28.49 shows a large right atrial mass prolapsing into the tricuspid orifice in

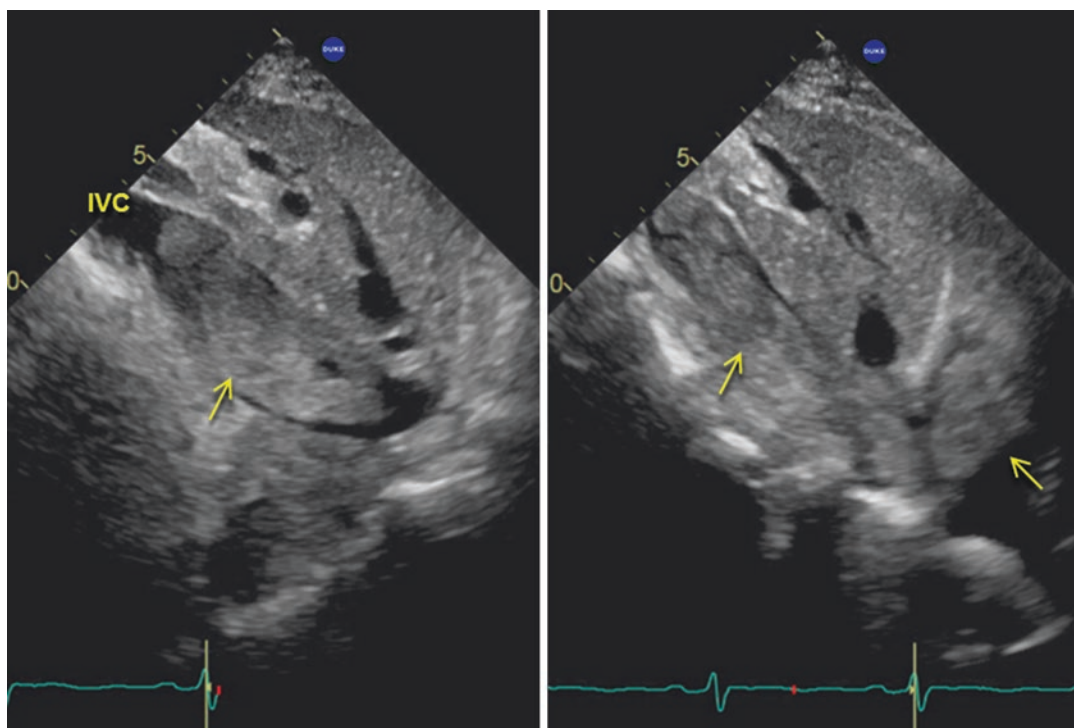


Fig. 28.50 Long axis views of the inferior vena cava in the same patient pictured in the previous figure. The mass is seen to be originating in the inferior vena cava well below the diaphragm. Slight probe angulation (right panel) showed the mass filling the inferior vena cava

(left arrow) and extending into the right atrium (right arrow). These are the typical findings in a renal cell carcinoma and demonstrate why the venae cavae must be examined for the origin site of all right sided large mass lesions

diastole. The anchor point was, however, not readily identified in the atrium.

When the transducer was positioned in the long axis of the inferior vena cava, the mass was seen to fill the proximal IVC and then continue into the right atrium (Fig. 28.50). Such presentation of a right sided cardiac tumor originating in the abdomen and extending into the heart are typical of renal cell carcinomas. Compare these images to the normal IVC seen in Fig. 28.36. This propensity of renal cell carcinomas to grow into the IVC is characteristic of these tumors.

This possibility emphasizes the need for complete echo examinations. Further, Intracavitary mass lesions should always be traced more proximally in the blood flow to make sure the anchor point of the tumor is always identified.

Sometimes the intracavitary masses look almost identical to myxomas and an initial impression of the mass being a myxoma may be statistically valid, but not always correct. The

right atrial mass lesion noted in Fig. 28.51 is shown in the right ventricular inlet view. When a biplane examination was done, the tumor was seen to be biatrial and extend through the interatrial septum (Fig. 28.52). Note, however, there is a break in the posterior pericardial right atrial border just posterior to the left hand arrow in the right panel of Fig. 28.52. Coronary angiograms showed the blood supply of the mass to be from both coronaries (Fig. 28.53). Other imaging studies showed this to be a ganglioma mass tumor extending from the central nervous system posterior to the heart, through the right atrial wall and into the cardiac chambers. When anything is unusual, additional imaging techniques can be helpful. The break in the posterior right atrial wall in this case was of significant importance.

Another complex case is seen in Fig. 28.54 where multiple large cystic masses from the right atrium prolapse through the tricuspid valve in diastole. These cystic masses were anchored to

the tip of a Denver shunt emptying into the right atrium. Denver shunts are used to drain excess intraabdominal fluid to the right atrium. In this case, the shunt was placed to manage chylous ascites. The MRI in Fig. 28.55 shows the masses,

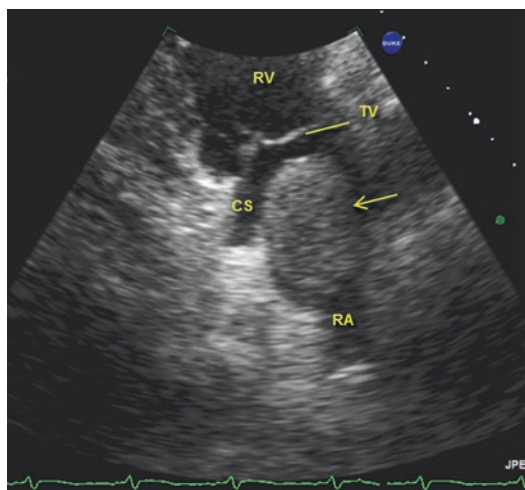


Fig. 28.51 Chest wall right ventricular inlet view from a patient with a large atrial mass resembling a myxoma. The mass was not in the inferior vena cava and did not prolapse through the tricuspid valve in diastole. CS is coronary sinus

but was not helpful in supplying additional data in this patient. The mass was determined to be a chyloma that had formed at the shunt tip.

Figure 28.56 is from a patient in his mid-50s who was physically wasted and debilitated. The echo showed a large cystic mass in the interventricular septum by chest wall (left panel) and transesophageal echo (right panel). As a late teenager, the patient was a shepherd in north-west Africa. With a rapid, but directed detailed evaluation for infection, the immunoassays confirmed the suspected diagnosis of echinococcosis as the likely origin of the cyst. The cystic mass was surgically debried and appropriate chemotherapy administered.

Other cardiac tumors can be lymphomas, melanomas (intracavitary and intramural), angiosarcomas or others. Common things are common but continued experience indicates that it is prudent to expect an unpredicted tissue result. The diagnostic term, “-oma” (without specifying the type) is a somewhat humorous way of referring to tumor masses that will invariably be correct, while emphasizing that surprises are always possible!

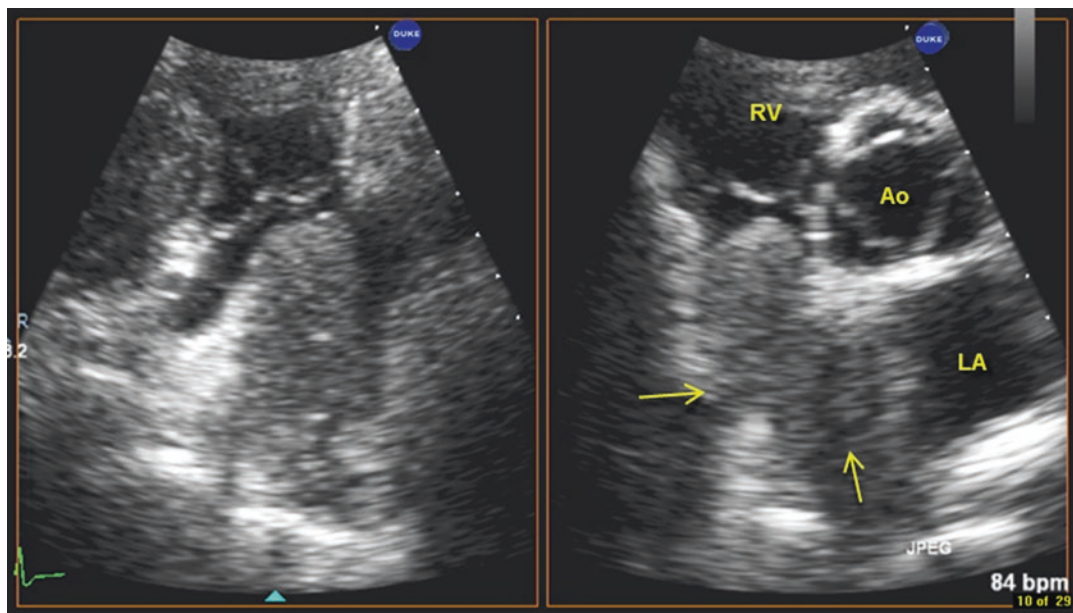
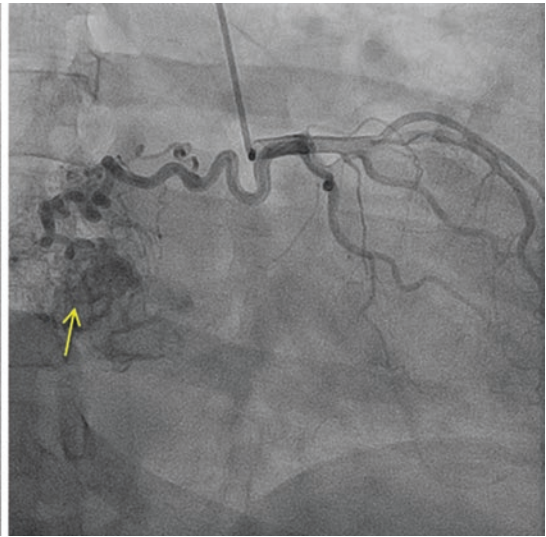


Fig. 28.52 Biplane views of the same mass in the previous figure where the right panel shows the mass extend through the atrial septum into in both atria. Despite its

similarity to an atrial myxoma, it was proven to be a ganglioma at surgery



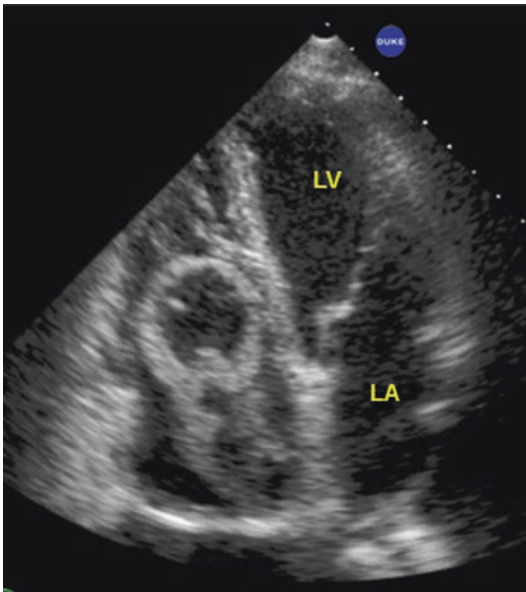
RCA



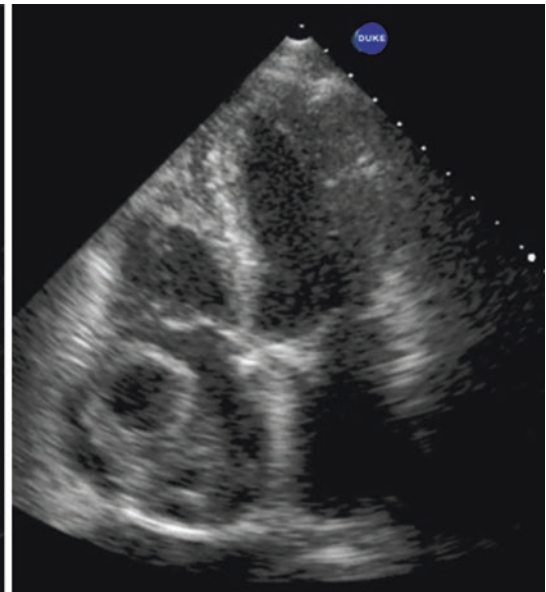
LCA

Fig. 28.53 Coronary angiograms from the patient with the ganglioma showing the abnormal large vessels leading to a tumor blush (arrows) that demonstrated the blood

supply of the tumor mass. *RCA* right coronary artery, *LCA* left coronary artery



Diastole



Systole

Fig. 28.54 Large mobile cystic masses in the right atrium in diastole (left panel) and systole (right panel) in a patient with a Denver shunt. The masses originated at the

tip of the Denver catheter. This cystic structure was determined to be a chyloma at surgery

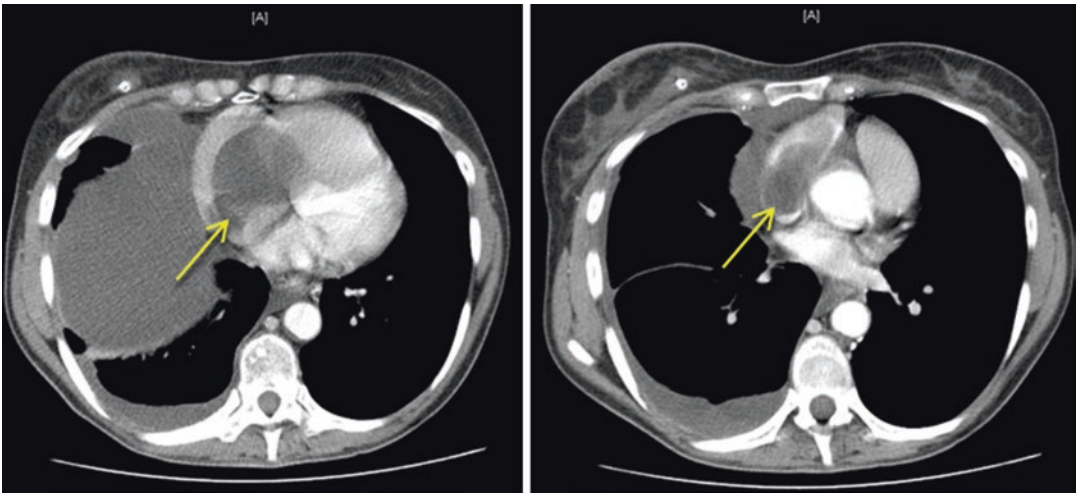


Fig. 28.55 MRI short axes demonstrating the outline of the chyloma (arrows) in the right atrium seen in the previous patient

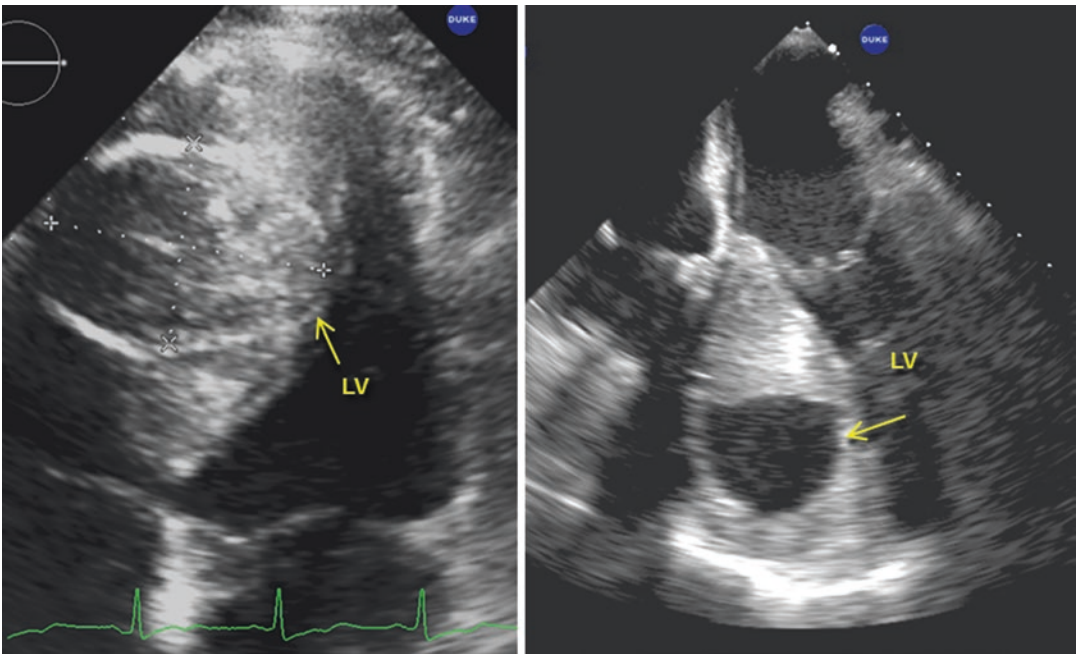


Fig. 28.56 The apical four chamber view in the left panel shows an oval, cystic mass in the mid interventricular septum measuring about $3.5 \times \sim 6$ cm taken from a 53 y.o. man with chronic wasting and debilitation. The transesophageal four-chamber view in the right panel more

precisely delineates the cystic structure. The difference appearance was due to different transducer angulations. This was later shown to be an echinococcal cyst that underwent surgical drainage and reconstruction

References

1. Durack DT, Beeson PB. Experimental bacterial endocarditis. I. Colonization of a sterile vegetation. *Br J Exp Pathol.* 1972;53:44–9.
2. Moulaert AJ, Oppenheimer-Dekker AJ. Anterolateral muscle bundle of the left ventricle, bulboventricular flange and subaortic stenosis. *Am J Cardiol.* 1976;37:78–81.

Ayan R. Patel, Anthony Caffarelli,
and Natesa G. Pandian

With the advent of multiplane transesophageal imaging, echocardiography provides excellent visualization of the thoracic aorta in the majority of patients. While computed tomography (CT) and cardiac magnetic resonance (CMR) are robust tools that portray the aortic anatomy in detail, the ease, versatility and bed-side ability of echocardiography for imaging the heart and aorta have made this modality the primary tool for noninvasive evaluation of cardiac diseases. Using a combination of right and left parasternal, suprasternal, and subcostal views, significant portions of the thoracic aorta may be visualized by transthoracic imaging. However, the sensitivity of transthoracic imaging for the detection of aortic dissection, intramural hematoma, and atheroma has been limited, making transesophageal imaging the optimal modality for patients in whom these conditions are suspected. Epicardial scanning may also be useful as an adjunct for imaging in the intraoperative setting.

Transthoracic Imaging

In patients with adequate transthoracic windows, transthoracic echocardiography can provide important diagnostic information in patients with suspected aortic disease.

- *Parasternal views:* The aortic valve, aortic root, and ascending aorta can be visualized from the right parasternal view and from a left parasternal view that is optimized for visualization of the aorta (Fig. 29.1a, b). In addition, a transverse view of the descending aorta can be obtained from the left parasternal view. Measurement of the aortic annulus, sinus of Valsalva and ascending aortic diameters can be obtained from the transthoracic parasternal views in most patients. Measurements of the aortic annulus should be made in mid-systole, while measurements of the aortic root (Sinus of Valsalva, sinotubular junction, and ascending aorta) should be made at end-diastole. Measurements of the aortic root should be made perpendicular to the axis of the aorta, and the largest diameter from the right coronary sinus of Valsalva to the posterior sinus of Valsalva should be obtained [1]. If the aorta is dilated above this level, the maximum diameter of the aorta should be measured and the site of measurement should be recorded and indicated in the report. In patients with dissection of the ascending aorta, a dissection flap may be visualized from the parasternal

A. R. Patel
Cardiovascular Imaging and Hemodynamic
Laboratory, Tufts Medical Center, Boston, MA, USA

A. Caffarelli
Hoag Hospital, Heart and Vascular Institute,
Newport Beach, CA, USA

N. G. Pandian (✉)
Cardiovascular Imaging and Hemodynamic
Laboratory, Tufts Medical Center, Boston, MA, USA

Hoag Hospital, Heart and Vascular Institute,
Newport Beach, CA, USA
e-mail: natesa.pandian@hoag.org

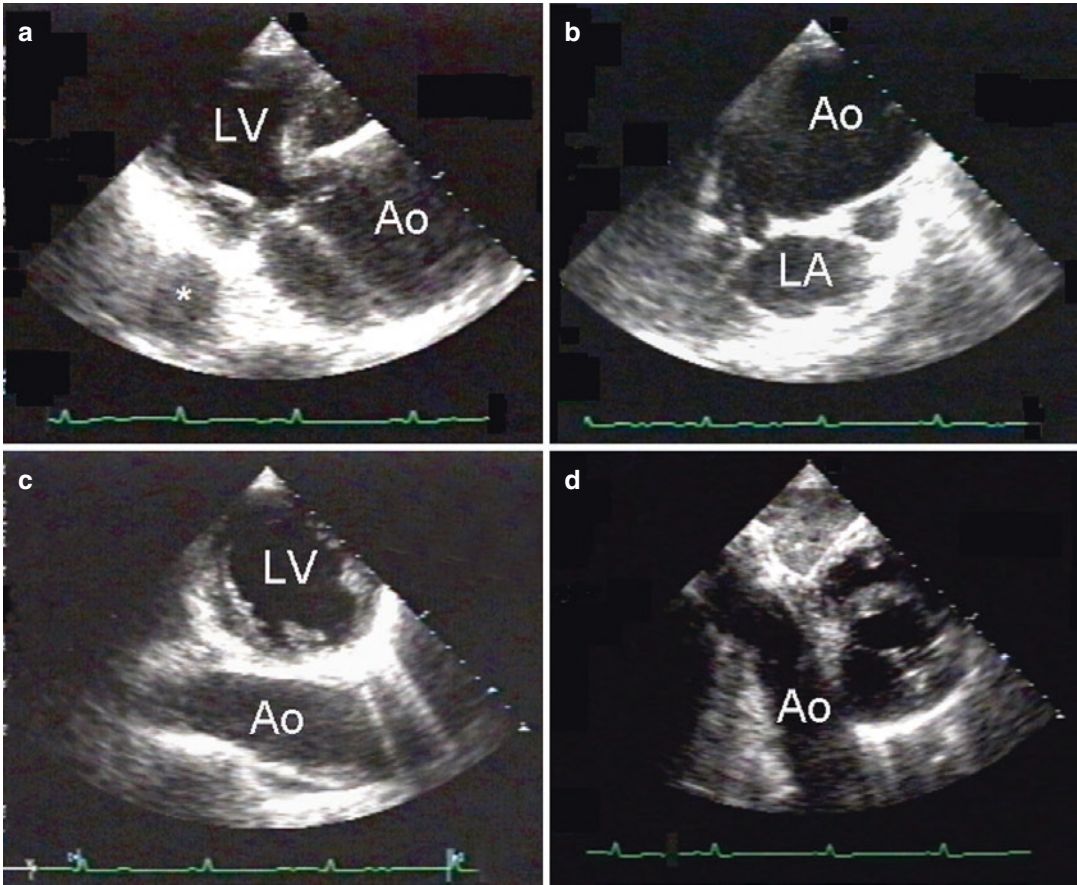


Fig. 29.1 Transthoracic imaging in a patient with an ascending aortic aneurysm and dilated descending aorta. (a) modified left parasternal longitudinal view of the ascending aorta (transverse view of the descending aorta is marked with asterisk); (b) right parasternal view of the ascending aorta; (c) parasternal short-axis view of the descending aorta; (d) subcostal view of the descending aorta. *Ao* aorta, *LA* left atrium, *LV* left ventricle

is marked with asterisk); (b) right parasternal view of the ascending aorta; (c) parasternal short-axis view of the descending aorta; (d) subcostal view of the descending aorta. *Ao* aorta, *LA* left atrium, *LV* left ventricle

views in patients with good transthoracic windows. The presence of other abnormalities such as aortic insufficiency or a pericardial effusion may provide indirect evidence of a possible dissection. Longitudinal views of the thoracic descending aorta may be obtained from the parasternal short axis view and subcostal windows (Fig. 29.1c, d).

- *The suprasternal view* allows visualization of the aortic arch and proximal thoracic descending aorta. From this view, pathology such as aortic atheroma or dissection flaps may be seen in some patients (Fig. 29.2). The suprasternal view is also useful for evaluation of

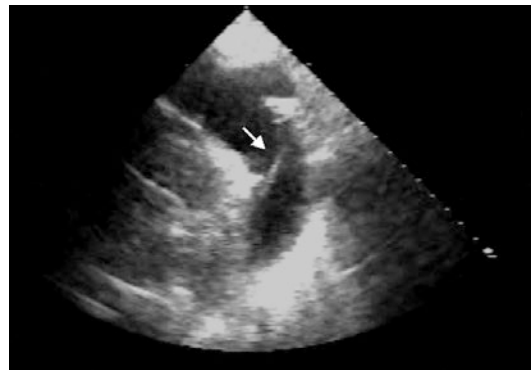


Fig. 29.2 Transthoracic imaging in the suprasternal view demonstrating a dissection flap (arrow) in the proximal descending thoracic aorta

aortic coarctation, in which narrowing of the aorta may be visualized; complementary use of Doppler imaging provides evidence of a gradient across the area of stenosis.

Transesophageal Imaging

- Ascending aorta:** Transesophageal imaging of the ascending aorta is predominantly obtained at the mid-esophageal level. The short axis view of the aorta is usually obtained between 30 and 60°. Various levels of the aorta may then be imaged by withdrawing and advancing the probe. A long axis view of the ascending aorta is obtained by rotating the angle to between 100 and 150°. From this view, the aortic annulus, sinuses of Valsalva, sinotubular junction, and proximal ascending aorta are visible. Further withdrawal of the probe at 90–100° orientation permits visualization of the more superior aspects of the ascending aorta in most patients. However, a portion of the distal ascending aorta is typically not visualized due to the intervening

trachea, and supplemental transthoracic supra-sternal imaging should be utilized in patients with suspected aortic disease in order to fully visualize the ascending aorta. In adults, the aortic annulus is often elliptical rather than circular, with a smaller diameter in the sagittal plane (standard two-dimensional echocardiographic long-axis view), and a larger diameter in the coronal plane [2]. Three-dimensional echocardiography (3DE) is therefore an attractive additional tool. By aligning multiple reconstruction planes in 3DE, the precise size and geometry of the aortic ring and root can be obtained. The 3DE derived aortic ring area has been found to correlate well with computed tomography derived measurements as well as with intra-operative anatomic measurements. From 3DE image sets, measurements not easily available in 2D imaging, such as aortic annular area, leaflet length and inter-commissural distances, are derived. These assessments have implications in surgical valve repair and in choosing the valve type and size for transcatheter aortic valve implantation (Fig. 29.3).

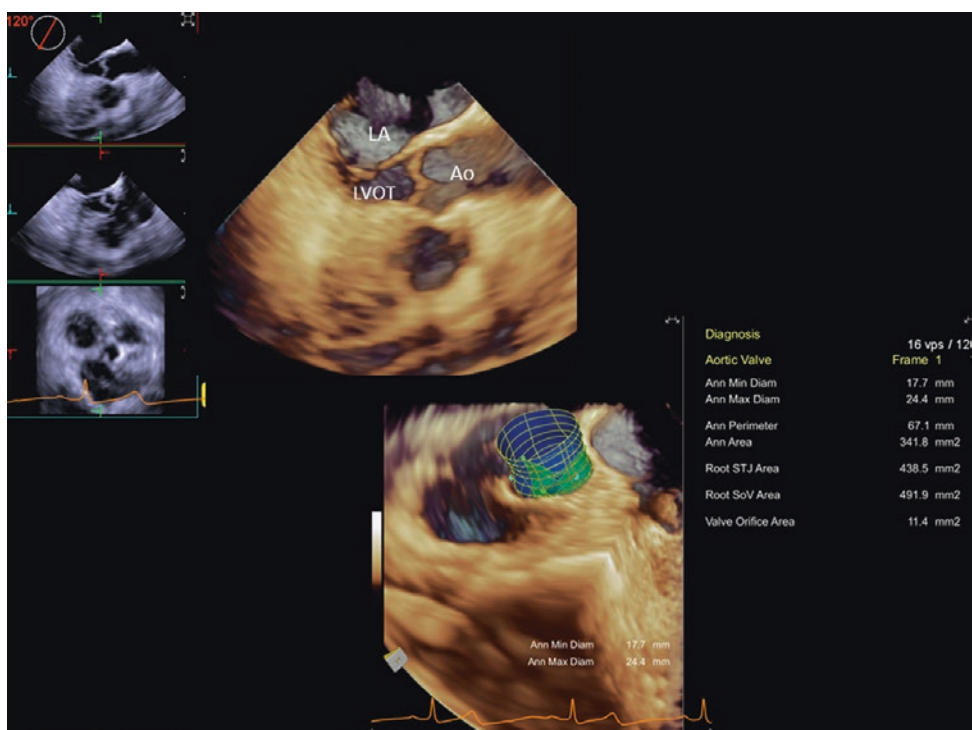


Fig. 29.3 Three-dimensional transesophageal echocardiographic assessment of aortic annular size. The aortic annular size is obtained at the aortic valve cusp hinge-

points. The aortic annular area and maximum and minimum aortic annular diameters can be obtained

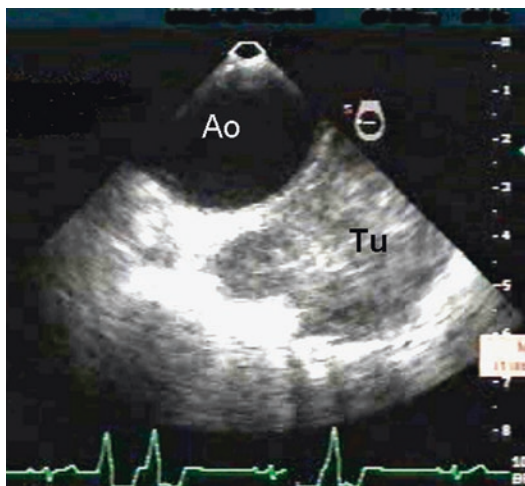


Fig. 29.4 Transesophageal echo transverse image of the descending aorta in a patient with an adjacent mediastinal tumor. *Ao* aorta, *Tu* tumor

- *The descending thoracic aorta:* is visualized by rotating the probe counter-clockwise, until a circular cross-sectional view of the aorta is obtained. Figure 29.4 demonstrates a transverse view of the descending aorta by transesophageal echo, in a patient with a mediastinal tumor. As the probe is withdrawn, more proximal aspects of the descending aorta are visualized. With further withdrawal of the probe, the aortic arch may be seen. Turning the probe clockwise allows visualization of the more proximal portion of the aortic arch. In some patients, the origin of the left subclavian and left carotid arteries may also be seen by withdrawal of the probe from the aortic arch level.

Aortic Aneurysm

Definition

Aneurysms are defined as localized dilatation of the aorta (Fig. 29.1), typically at least 50% enlarged compared to normal diameter [3]. Normal aortic diameter values are shown in Table 29.1 [2, 4, 5]. Aortic diameter normally increases with age, usually expanding by 1–2 mm over a 10-year period [6].

Etiologies

Underlying conditions that cause degeneration of the medial layer of the aortic wall predispose to the development of aneurysms. The major causes of such degenerative changes include hypertension, atherosclerosis, post-stenotic dilation, and inherited connective tissue disorders (such as Marfan, vascular Ehlers-Danlos, Loeys-Dietz, or familial thoracic aneurysm syndromes). Bicuspid aortic valve and aortic coarctation are hereditary conditions that are associated with an increased prevalence of aortic aneurysm. Rarely, aortic dilatation may occur due to inflammatory vasculitis, such as Takayasu's disease, Giant Cell arteritis, or infectious causes, such as *Staphylococcus aureus*, *Salmonella*, and treponemal aortitis. Localized forms of aneurysm include sinus of Valsalva aneurysms (Fig. 29.5), which may rupture into the right heart or interventricular septum, and annuloectasia, which involves dilatation of the aortic annulus and root.

Pseudoaneurysms

Pseudoaneurysms are characterized by partial disruption of the aortic wall, and are contained by the adventitia and some of the medial layer. Pseudoaneurysms may occur due to hemorrhage of a penetrating aortic ulcer, infection, or trauma.

Aortic Rupture

Aortic rupture is the most common cause of death associated with aortic aneurysms. It has been observed that aneurysms that are 6 cm or greater in diameter have a five-fold increase in risk of rupture, and that aneurysms that are 5–6 cm in diameter have a more rapid growth rate than smaller aneurysms. For this reason, aortic root replacement for degenerative aortic aneurysms should be considered when aortic root diameter reaches 5.5 cm. In patients with Marfan syndrome and a thoracic aortic aneurysm, elective root replacement is recommended when the aortic root diameter is ≥ 5 cm or if rapid aneurysm

Table 29.1 Normal values of aortic root dimensions in adults

Aortic root	Absolute values (cm)		Indexed values (cm/m ²)	
	Men	Women	Men	Women
Annulus	2.6 ± 0.3	2.3 ± 0.2	1.3 ± 0.1	1.3 ± 0.1
Sinus of Valvalva	3.4 ± 0.3	3.0 ± 0.3	1.7 ± 0.2	1.8 ± 0.2
Sinotubular junction	2.9 ± 0.3	2.6 ± 0.3	1.5 ± 0.2	1.5 ± 0.2
Proximal ascending aorta	3.0 ± 0.4	2.7 ± 0.4	1.5 ± 0.2	1.6 ± 0.3

Adapted from Roman et al. [4] and Hiratzka et al. [5]. Reprinted from: J Am Soc Echocardiogr, vol 28(1); Lang RM, Badano L, Mor-Avi V et al., Recommendations for Cardiac Chamber Quantification by Echocardiography in Adults: An Update from the American Society of Echocardiography and the European Association of Cardiovascular Imaging, pages 1–39.e14, Copyright 2015, with permission from the American Society of Echocardiography (Elsevier) [2]

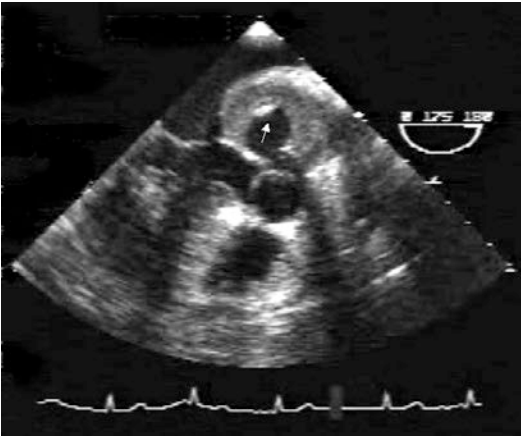


Fig. 29.5 Transesophageal echo image of a thrombosed Sinus of Valsalva aneurysm (arrow)

growth is present; in women with Marfan syndrome who are planning a pregnancy, aortic root replacement may be considered when the diameter exceeds 4 cm [3, 6]. Loeys-Dietz syndrome has a particularly aggressive course, and it is recommended that elective aneurysm repair be considered in affected individuals with aortic root diameter ≥ 4.2 cm [5]. In individuals with bicuspid aortic valve (BAV) associated aortopathy, progressive aortic dilatation is associated with an increased risk of aortic dissection and/or rupture; an increase of ≥ 0.5 cm per year is a risk factor for these complications. After initial diagnosis of aortic dilatation in patients with BAV, follow-up imaging should be obtained at 6 months; if the ascending aorta and aortic root diameters are stable and are < 4.5 cm, and if there is no patient history or family history of aortic dissection, surveillance can be performed annually; otherwise, surveillance should be performed every 6 months

[1]. Surgical intervention is indicated for asymptomatic patients with BAV associated aortic aneurysm when the aortic root or ascending aorta diameter is ≥ 5.5 cm. In patients who are undergoing aortic valve replacement, it is reasonable to proceed with surgical intervention for the aorta if the ascending aorta or aortic root diameter is > 4.5 cm. It is also reasonable to proceed with surgical intervention in BAV patients with aortic diameters of ≥ 5 cm if other risk factors for aortic dissection (such as family history or rapid aortic expansion) are present or if the patient is a low risk surgical candidate and the surgery will be performed in an experienced center. In patients with short stature, indexed aortic diameter of ≥ 2.5 cm/m² may be a better predictor of risk than absolute diameter [29].

Imaging

In most cases, aortic root aneurysms can be adequately visualized with transthoracic echocardiography; in patients with known aneurysms, serial evaluation should be performed to assess for increase in aneurysmal size. Transesophageal echocardiography will help to define the shape and the extent of the aneurysm as well as the descending thoracic aorta.

Aortic Dissection

Aortic dissection involving the ascending aorta is associated with an extremely high mortality, if untreated, and prompt diagnosis is therefore crucial. The reported incidence of aortic dissection

is approximately 2000 new cases annually in the United States. There is a 1–2% mortality associated with each passing hour after the development of an acute ascending aortic dissection, reaching nearly 30% at 48 h [7].

Imaging

The primary imaging modalities for diagnosing acute aortic dissection are transesophageal echocardiography and computed axial tomography (CT). Magnetic resonance imaging provides excellent sensitivity and specificity for identifying thoracic aortic disease and may be useful in some patients, but is generally impractical in an unstable setting. Invasive aortography has largely been replaced by noninvasive imaging techniques for the diagnosis of aortic dissection. Transthoracic echocardiography may detect dissection in some patients, but has a lower sensitivity than transesophageal echocardiography. Transesophageal echocardiography has the advantage of being a versatile, relatively noninvasive technique that can be performed rapidly at the bedside.

The reported sensitivities and specificities for detection of aortic dissection are 77–80% and 93–96%, respectively, for transthoracic echocardiography, and 88–98% and 90–95% for transesophageal echocardiography [5]. CT scan has very high diagnostic accuracy for aortic dissection, particularly with newer generation electrocardiographically gated multidetector scanners. In ambiguous cases, use of more than one imaging modality may be necessary.

Pathophysiology

The aortic wall is composed of three layers: the outer tunica adventitia, the inner layer of the tunica intima, and the intervening tunica media. The tunica adventitia contains elastic tissue and the vasa vasorum, whereas the tunica media is composed of collagen, elastin, and extracellular matrix proteoglycans. A layer of vascular endothelium comprises the tunica intima. The pres-

ence of elastin provides the normal aorta with the ability to withstand pulsatile flow without rupturing. However, abnormalities in the structure of the aortic wall can result in an increased susceptibility to dissection or rupture. With increasing age, the amount of elastin in the aortic media decreases and the amount of collagen increases, thereby increasing vascular stiffness. In addition, dilation of the aorta can result in increased susceptibility to dissection. Increases in wall stress are primarily experienced by the media, and can result from increased aortic radius and increased radial pressure within the vessel. Conversely, wall stress is inversely related to vessel wall thickness. Subsequently, a dilated and thin-walled aorta is subject to increased stress forces. The aortic intimal layer is exposed to shear forces within the vessel, which can also contribute to the development of dissection. An increase in these stress forces can result in separation of the intimal and medial layers of the aorta. The tear is propagated by shear forces further separating the layers of aortic wall.

Etiologies

Etiologies for the development of aortic dissection are shown in Table 29.2. Hypertension is a common risk factor for the development of aortic dissection, and a history of atherosclerosis is also highly prevalent in patients with acute aortic syndromes. Patients with connective tissue disorders, such as Marfan Syndrome, Vascular Ehlers-Danlos Syndrome (Type IV), bicuspid aortic valve, Loeys-Dietz syndrome, annuloaortic ectasia, and familial thoracic aneurysm syndromes are at increased risk for the development of aortic dissection. In patients who were aged <40 years in the International Registry of Aortic Dissection (IRAD), inherited genetic syndromes affecting the aorta and prior aortic surgery were important risk factors for aortic dissection [8].

1. *Marfan Syndrome.* Marfan syndrome is associated with a deficiency of the glycoprotein fibrillin, owing to a fibrillin-1 gene mutation, leading to a loss of elastic tissue and deposi-

Table 29.2 Risk factors for aortic dissection

Hypertension
Connective tissue disorders
Marfan syndrome
Ehlers-Danlos syndrome
Loeys-Dietz syndrome
Annuloaortic ectasia/familial aortic dissection
Bicuspid aortic valve
Aortic coarctation
Turner's syndrome (especially in association with hypertension, bicuspid aortic valve, or coarctation)
Vasculitis
Takayasu's arteritis
Giant cell arteritis
Behçet's disease
Infectious aortitis
Blunt trauma
Rapid deceleration injury
Surgical manipulation
Cardiac surgery
Cardiac catheterization/intervention
Intra-aortic balloon pump
Cocaine use
High intensity weight-lifting/strenuous resistance training
Pregnancy (possible risk factor)

tion of mucopolysaccharide substances in the aortic media. In patients with Marfan Syndrome, aortic dilation predominantly involves the aortic root.

2. *Vascular Ehlers-Danlos Syndrome (Type IV)* is associated with a Type III collagen defect and subsequent structural abnormalities of the aortic wall. Arterial dissection or rupture can involve thoracic as well as abdominal arterial vessels.
3. *Loeys-Dietz Syndrome* is associated with mutations in transforming growth factor beta type I or type II (TGFB1 and TGFB2). Vascular tortuosity may be seen in the head and neck vessels, although other vessels may be involved. Patients commonly develop aortic root aneurysms, but can also develop more widespread aneurysms in the vasculature.
4. *Familial Thoracic Aneurysm and Dissection.* Familial thoracic aortic aneurysm includes patients with genetically-based thoracic aortic aneurysm or dissection who family history of thoracic aortic pathology in the absence of

other connective tissue disease syndromes. A number of genetic mutations have been associated with this syndrome, including TGFB2, ACTA 2, and MYH 11. It has been observed that these patients develop thoracic aortic aneurysms at a younger age than patients with sporadic aortic disease [5].

These syndromes are associated with abnormalities in the composition of the aortic media which result in an increased vulnerability to dissection. Factors associated with increased risk of dissection in patients with Marfan syndrome include advanced age, male gender, and aortic root size greater than 60 mm, rate of increase of the aortic diameter, pregnancy, and family history of aortic dissection, [6, 8–10]. The 2010 ACCF/AHA thoracic aortic disease guidelines recommend that an echocardiogram be performed at the time of diagnosis of Marfan syndrome and at 6 months, with annual imaging thereafter if the aortic diameter is stable [5]. In individuals with Marfan syndrome and an aortic diameter ≥ 4.5 cm or with significant increase in aortic diameter, more frequent surveillance is recommended. In patients with Loeys-Dietz syndrome or other genetic mutation associated with thoracic aortic disease, complete aortic imaging is recommended at initial diagnosis and follow-up [5].

5. *Systemic hypertension:* Other conditions which result in disruption of the aortic intima and media can also lead to aneurysmal dilation, increased wall stress, and increased susceptibility to dissection (Table 29.2). Hypertension is associated with degenerative changes in the aortic media. Increased blood pressure and these pathologic changes in the media can result in aortic dilatation and increased susceptibility to dissection in patients with hypertension.
6. *Vasculitis:* In patients with vasculitis, structural changes in the aortic media may weaken the aortic wall.
7. *Thoracic trauma,* or iatrogenic injury is another potential cause of aortic dissection. Iatrogenic injury may occur during cardiac surgery, or due to percutaneous intravascular catheter procedures.

8. *Pregnancy*: The association between pregnancy and aortic dissection remains controversial. Some authors have reported an increased risk of aortic dissection in pregnant women; however, whether this association is independent of other risk factors (such as hypertension or underlying aortic connective tissue disorders) is not well understood.

Classification

One of the key aspects in the evaluation of dissection is identification of the extent of dissection, which has critical implications for prognosis and management. Dissections involving the ascending aorta have an extremely high mortality rate and require immediate surgery. The Stanford and DeBakey classification systems are commonly used to describe the extent of dissection (Fig. 29.6). The Stanford system divides dissections into two forms: Type A, involving the ascending aorta; and Type B which does not involve the ascending aorta. The DeBakey system of classification divides dissections into Type I (involvement of ascending aorta and extending distally to the arch or descending aorta), Type II (limited to ascending aorta), and Type III (descending aorta).

Clinical Presentation

Common presenting symptoms for patients with Type A dissections include chest pain, back pain, abdominal pain, syncope, and stroke [7]. Patients may also present with heart failure (due to aortic insufficiency or cardiac tamponade), pulse defi-

cits, murmur of aortic insufficiency, cardiogenic shock, renal failure, or evidence of bowel or limb ischemia. The electrocardiogram is usually non-specific, but may occasionally demonstrate ischemia, if the coronaries arteries are involved.

In patients with Type A dissection, medical therapy should be commenced immediately, and emergent surgery to replace the ascending aorta (with possible aortic valve replacement, if the aortic valve is involved) is indicated. Thoracic aortic dissections which do not involve the ascending aorta are generally managed medically, if the patient is asymptomatic. The mainstay of medical therapy is blood pressure control and reduction of arterial shear stress with intravenous beta-blockade. Nitroprusside, as a second line agent, is often also used to control blood pressure in the acute setting. Indications for surgical intervention in patients with Type B dissection include persistent pain, persistent hypotension, evidence of malperfusion such as limb, bowel ischemia, or paraplegia, false lumen expansion, or impending rupture.

Echocardiographic Findings

Using multiple imaging planes, including parasternal and suprasternal imaging, transthoracic echocardiography can identify an aortic intimal flap in some cases. The finding of an otherwise unexplained pericardial effusion, dilated ascending aorta, or acute aortic insufficiency on transthoracic imaging should also heighten the suspicion for a possible dissection. However, the sensitivity of transthoracic echocardiography for the identification of aortic pathology is limited, and transesophageal imaging is required in many cases. Transesophageal echocardiography can be performed rapidly at the bedside, and provides high-resolution images of the thoracic descending aorta, aortic arch, and most of the ascending aorta. The potential disadvantages of transesophageal echocardiography are that it is semi-invasive and often requires some sedation. In addition, some branch vessels may not be visualized. A small portion of the distal ascending aorta is not visualized by transesophageal echo-

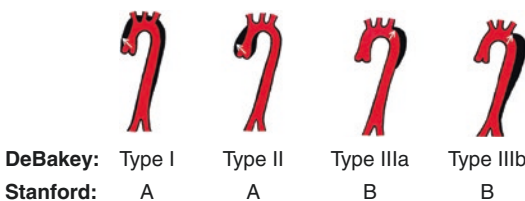


Fig. 29.6 Schematic of the commonly-used DeBakey and Stanford classification systems

cardiography, due to the intervening air-filled trachea. However, dissection limited to only this portion of the distal ascending aorta is uncommon. Supplemental imaging with transthoracic echocardiography in the suprasternal view may be useful to further evaluate the distal ascending aorta and proximal arch.

The Intimal Flap

The classic finding in aortic dissection is an intimal flap, which may be visualized in the longitudinal and short axis views (Fig. 29.7). Reverberations may occasionally create linear artifacts that resemble an intimal flap; imaging in multiple planes should therefore be employed to avoid making a false positive diagnosis. In addition, the use of color Doppler imaging is helpful for distinguishing an intimal flap (which may be associated with abnormal color flow patterns) from artifact. The entry site of the dissection can

often be identified. The dissection most commonly propagates distally, although it may occasionally extend proximally in the aorta, known as retrograde dissection. The dissection flap separates the lumen of the aorta into true and false lumens (Fig. 29.8).

False Lumen

Echocardiographic findings in patients with aortic dissection may include thrombus or spontaneous echocardiographic contrast in the false lumen of the aorta. In some cases, the false lumen may be completely thrombosed. Color Doppler imaging is also helpful in identifying the true and false lumens (Fig. 29.9), as well for differentiating true dissection from artifact.

Coronary Arteries

Echocardiography is also useful in identifying the sequelae of aortic dissection. Extension of the

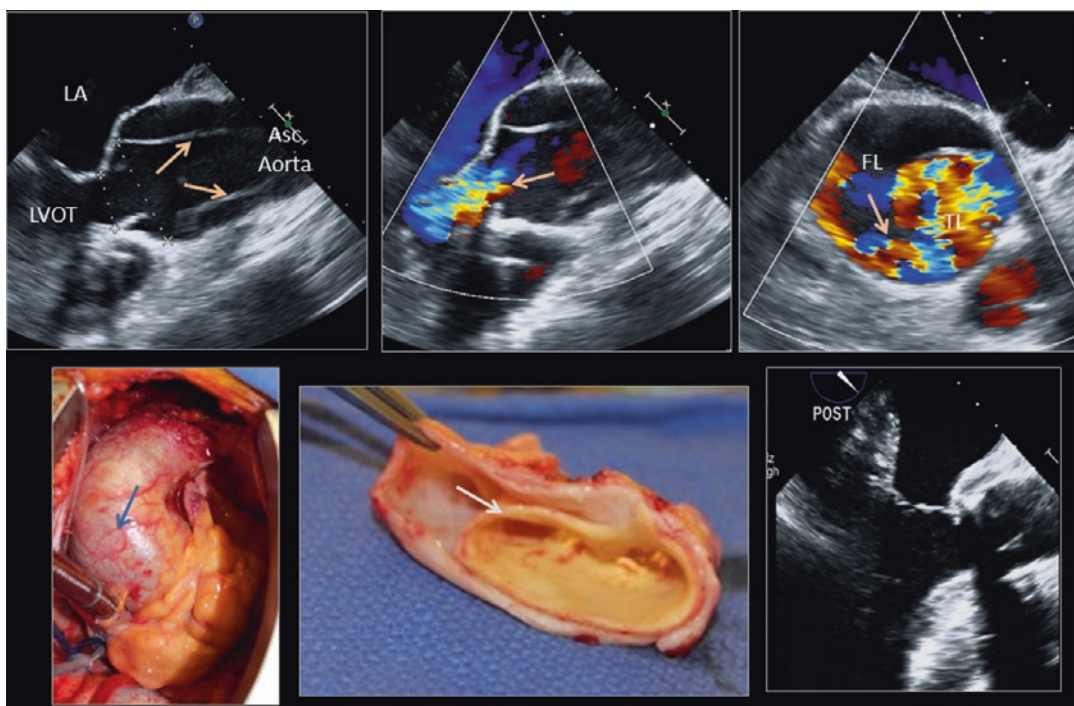


Fig. 29.7 Images from a patient with ascending aortic dissection. Top left: The longitudinal view depicts the intimal flap (arrows) that originates in the aortic root; the aortic ring is of normal size but aorta is dilated immediately above the ring level; Top middle: Severe aortic regurgitation is noted (arrow); Top right: Color Doppler shows the true lumen with flow and the arrow points to the entry site;

Bottom left: Intraoperative photo shows blueish coloration (arrow) all along one side of the dilated aorta, depicting the zone of false lumen; Bottom middle: Arrow points to the large intimal flap in this resected aortic segment. Bottom right: Post-operative image displays the repaired aorta with a prosthetic valve. *LA* left atrium, *LVOT* left ventricular outflow tract

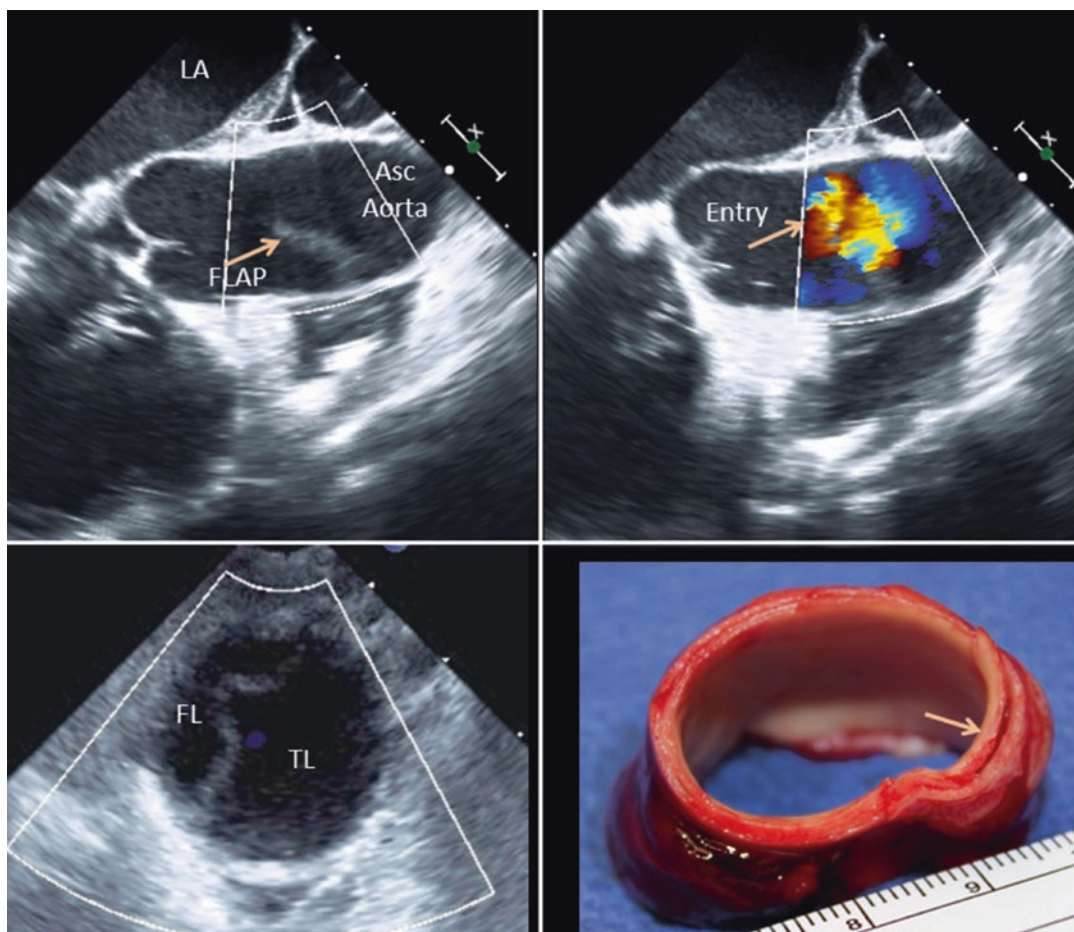


Fig. 29.8 Top left: Longitudinal image of the ascending aorta shows the intimal flap (arrow); Top right: Color flow imaging depicts the entry site (arrow); Bottom left: Image of the descending aorta reveals the dissection extending

into portion of the aorta as well. *TL* true lumen, *FL* false lumen; Bottom right: The intimal flap and extensive dissection is seen in this resected ascending aorta

dissection into the coronary arteries may be visualized, and the presence of a wall motion abnormality may indicate possible ischemia and coronary involvement.

Aortic Regurgitation

Other cardiac complications which may be identified by echocardiography include aortic insufficiency (Fig. 29.10).

Pericardial Effusion

This is an important echocardiographic finding which may imply some partial aortic wall rupture and the development of cardiac tamponade.

Surgery

Even after surgical repair, patients with a history of aortic dissection may develop rupture of an aneurysm or dissection at a remote site. In view of the high mortality associated with rupture or dissection, routine periodic follow-up of post-operative patients with imaging studies is recommended [5].

Intramural Hematoma

Intramural hematoma is a variant of aortic dissection that has been increasingly recognized due to improvements in aortic imaging. Its distinguishing

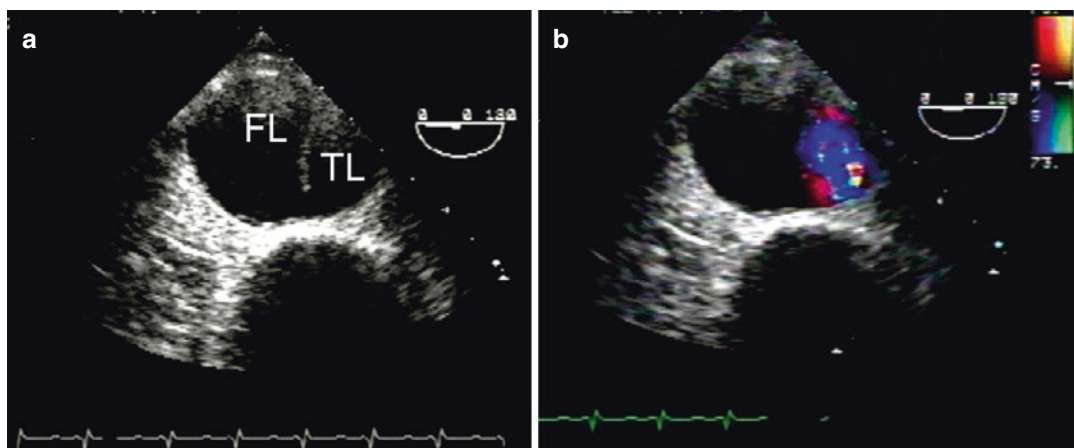


Fig. 29.9 Transesophageal echo image of a descending aortic dissection in a patient with Marfan's syndrome. (a) Two-dimensional imaging demonstrates the true lumen (TL), which is smaller than the false lumen (FL); (b) Color Doppler demonstrates flow in the true lumen

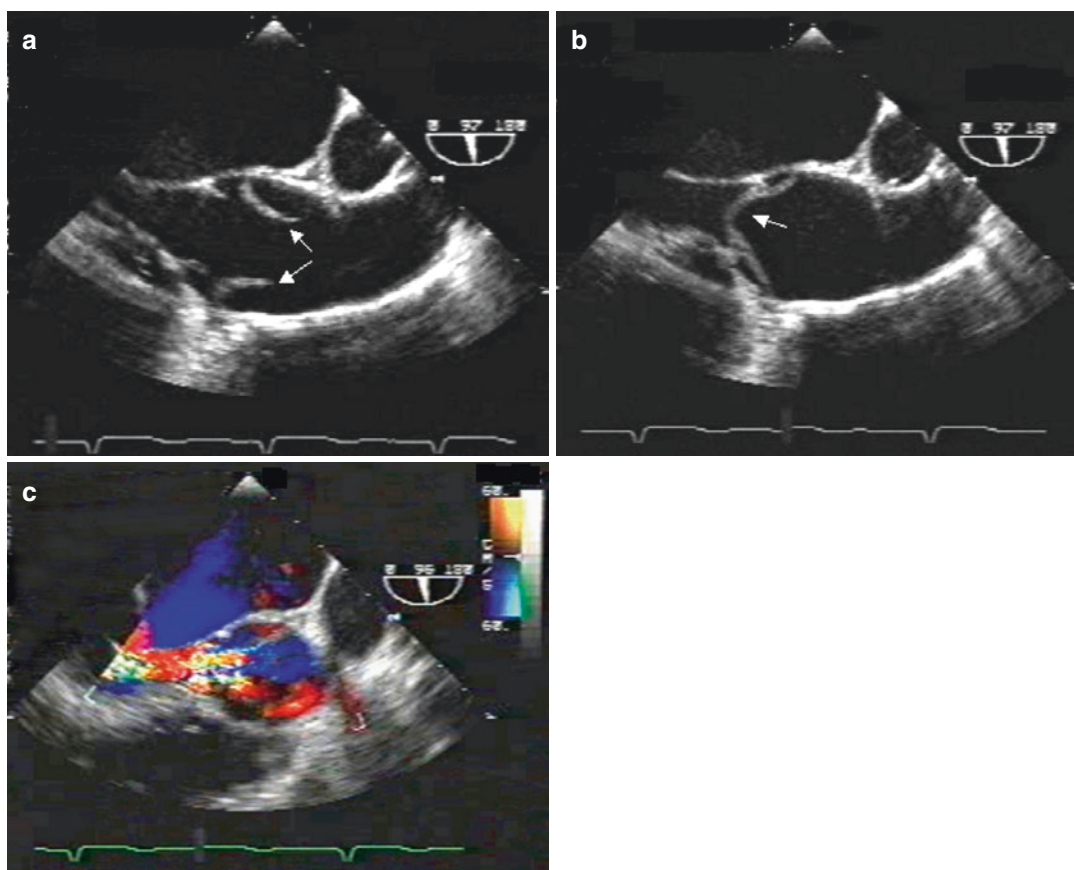


Fig. 29.10 Transesophageal echo long-axis image of an ascending aortic dissection, with intimal flap (arrows) prolapsing into the aortic valve; (a) systolic image; (b) diastolic image; (c) Color Doppler demonstrates severe aortic insufficiency

feature is the lack of an intimal tear. Studies report that 13–29% of aortic dissections are intramural hematomas [11]. Intramural hematoma may occur via several mechanisms. Rupture of the vasa vasorum, with hemorrhage into the media of the aortic wall is one potential mechanism for the development of intramural hematoma. The presence of underlying medial degeneration may predispose to the development of hemorrhage. Another potential mechanism is rupture of atherosclerotic plaque or penetrating aortic ulcer, which can also lead to hemorrhage into the aortic media. Finally, blunt trauma to the aorta may be associated with the development of intramural hematoma.

Imaging

Since no intimal flap or false lumen is present, intramural hematoma may not be apparent on angiography. With echocardiography, the distinct features of intramural hematoma include the absence of an intimal flap, and crescentic or circular thickening of the aortic wall (>0.7 cm) [10] (Figs. 29.11 and 29.12). The major challenge in the diagnosis of intramural hematoma is distinguishing it from atherosclerotic plaque. The echocardiographic features of these two entities are summarized in Table 29.3. Central displacement of the intimal layer is seen in

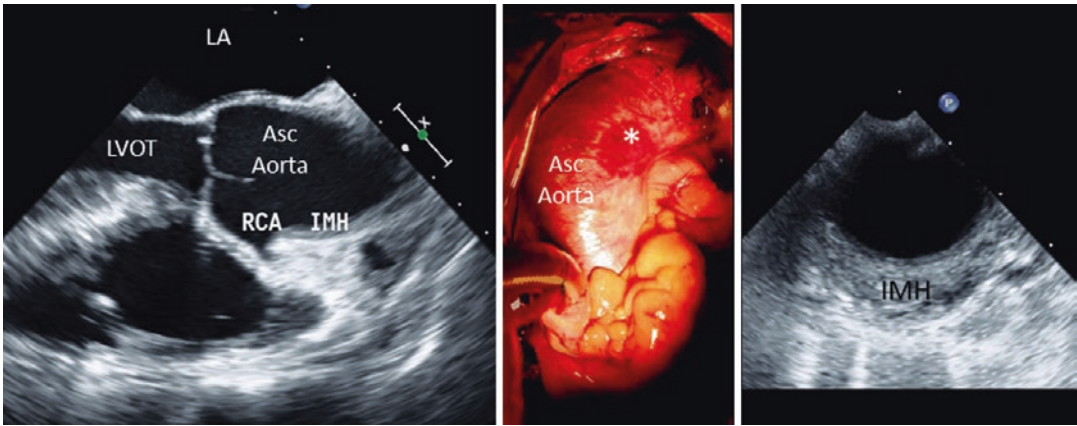


Fig. 29.11 Long axis (left panel) and short axis (right panel) transesophageal echo views of an intramural hematoma, showing central displacement of the intimal layer. The intraoperative photograph of the ascending aorta

shows a site of intramural bleeding (center panel). Asc ascending, IMH intramural hematoma, LVOT left ventricular outflow tract, RCA right coronary artery

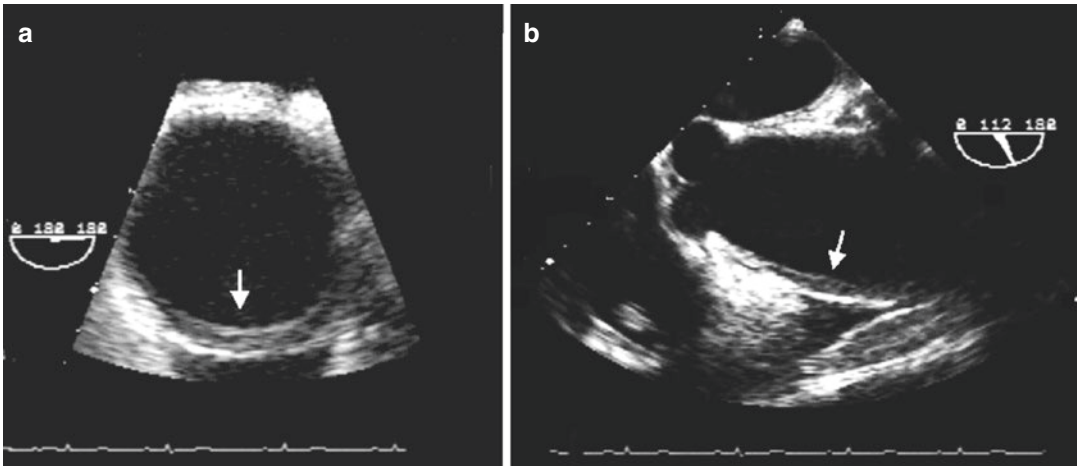


Fig. 29.12 Short axis (a) and long axis (b) transesophageal echo images of intramural hematoma (arrow) in the ascending aorta. The luminal surface has a smooth surface, and the area of hematoma appears relatively hypochoic

Table 29.3 Echocardiographic characteristics of intramural hematoma versus atherosclerotic plaque

	Intramural hematoma	Atherosclerotic plaque
Intraluminal surface	Usually smooth	Usually irregular
Echodensity	Hypoechoic	Hyperechoic
Intimal layer	Inwardly displaced	Nondisplaced
Extent of aortic involvement	Usually localized	Usually diffuse
Pericardial effusion	May be present	—

intramural hematoma. Compared to atherosclerotic plaque, the area of the hematoma frequently appears relatively homogenous and hypoechoic. In addition, the luminal wall in intramural hematoma is usually relatively smooth, compared with the irregular surface typically seen in patients with significant atherosclerotic plaque [12].

Clinical Significance

Initial observations have reported that the prognosis and mortality rates for intramural hematoma are similar to those for classic aortic dissection. However, subsequent data suggest that intramural hematoma may have a more favorable prognosis than classic Type a dissection [12]. Patients with intramural hematoma may progress to dissection with an intimal tear or even frank rupture due to destabilization of the aortic wall; therefore, generally speaking, the management of intramural hematoma remains similar to that of classic dissections (i.e.- surgery for ascending aortic involvement, and medical therapy for stable patients without ascending aortic involvement).

Penetrating Aortic Ulcers

Pathophysiology

Penetrating atherosclerotic ulcer is a distinct pathologic entity that can lead to disruption of the

aortic wall. Patients with atherosclerotic disease often have superficial ulcerations of atherosclerotic plaque, which are usually confined to the intima. However, in some cases, the ulcer may penetrate through the internal elastic lamina and into the media. Subsequent hemorrhage into and beyond the medial layer of the aorta can lead to intramural hematoma, pseudoaneurysm formation, or frank rupture. Occasionally, penetrating atherosclerotic ulcers may lead to a limited dissection. Penetrating ulcers are usually associated with extensive atherosclerotic disease, and unlike classic dissection, more commonly occur in the descending thoracic aorta.

Clinical Significance

Penetrating ulcers typically occur in elderly, hypertensive patients. The majority of patients present with symptoms of chest or back pain. Treatment with antihypertensive therapy should be instituted immediately. Patients with symptomatic penetrating ulcers of the ascending aorta or arch are considered high-risk for rupture, and early surgery has been recommended [13]. Penetrating ulcers of the descending aorta may be managed conservatively in stable patients. However, surgical intervention is indicated if complications such as persistent pain, hemodynamic instability, pseudoaneurysm, pericardial effusion, bloody pleural effusion, or expanding intramural hematoma ensue [13].

Imaging

Penetrating aortic ulcers may be identified by transesophageal echocardiography, CT scan, magnetic resonance imaging, or aortography; however, the findings may be subtle. On transesophageal echocardiography, atherosclerotic plaque, crater-like ulcerations (Fig. 29.13) and asymmetric thickening of the aortic wall may be seen [14]. Patients who are managed nonoperatively should have serial follow-up imaging studies to identify the development of complications.

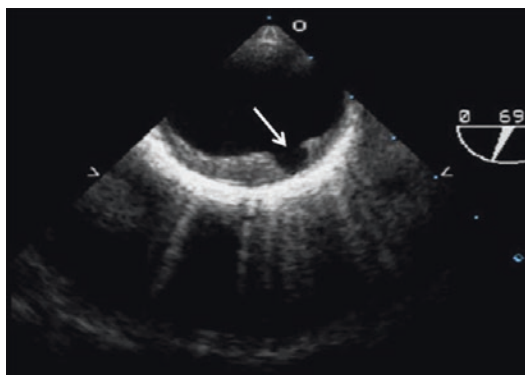


Fig. 29.13 Transesophageal echo image of a penetrating atherosclerotic ulcer (arrow). Reprinted from: *J Am Soc Echocardiogr*; vol 28(2); Goldstein SA, Evangelista A, Abbara S et al., *Multimodality Imaging of Diseases of the Thoracic Aorta in Adults: From the American Society of Echocardiography and the European Association of Cardiovascular Imaging*; pages 119–82; Copyright 2015, with permission from the American Society of Echocardiography (Elsevier) [1]

Aortic Trauma

Pathophysiology

Aortic trauma usually occurs as the result of a horizontal deceleration injury, such as in motor vehicle accidents, or vertical deceleration injury, such as falling from a height. The site most vulnerable to deceleration injury is the aortic isthmus, at the junction of the aortic arch and descending aorta, which is tethered by the ligamentum arteriosum. Other points which are susceptible to aortic trauma are the ascending aorta above the sinus of Valsalva, the origin of the innominate artery, and at the level of the diaphragmatic hiatus [15, 16]. Traumatic injury to the aorta is associated with a high mortality rate, with only 20% of patients surviving to reach the hospital [17]. Of patients that survive, many sustain an aortic rupture that is contained by the adventitial layer, i.e. an aortic pseudoaneurysm.

Imaging

Although angiography has been considered the standard imaging modality for detection of aortic trauma, it carries the risk of exacerbation

of vascular trauma, and requires transport of a potentially unstable patient. Computed tomography outlines the aorta and its pathology nicely. However sick patients with acute aortic syndromes are often not stable enough to undergo computed tomography. Transesophageal echocardiography has the advantage of providing rapid imaging at the bedside, but cannot be performed in patients with severe facial injury or cervical spine injury. In addition, injuries involving the distal ascending aorta or great vessels may not be detected, and other imaging modalities may be required in some cases.

In patients with traumatic blunt aortic injury, subadventitial aortic rupture may be seen by transesophageal echocardiography as a thick and irregular flap in the aortic lumen, due to deep laceration of the intimal and medial layers of the aorta [18]. The orientation of the flap is often perpendicular to the longitudinal axis of the aorta. In the case of less extensive lacerations, an intimal flap may occur; this may appear similar to a classic dissection, or may be a free flap without the presence of a false lumen. Other findings include pseudoaneurysm, fusiform dilation of the aorta, intramural hematoma, intraluminal thrombus, or aortic luminal obstruction (“pseudo-coarctation”). The presence of increased distance between the esophageal probe and the aorta (>1 cm) suggests the presence of a mediastinal hematoma, and may be indirect evidence of aortic trauma [4, 18].

Aortic Atheromatous Disease

Pathophysiology

Aortic atheromatous disease has been increasingly recognized as an important cause of stroke, particularly in elderly patients. In patients with stroke, the prevalence of aortic atheroma is as high as that of carotid artery disease or atrial fibrillation [6]. The prevalence of aortic atheroma in patients with an embolic event has ranged from 21% to 27%. Recognized risk factors for the development of atheromatous disease include advanced age, hypertension, hypercholesterolemia, diabetes, metabolic syndrome, and smoking.

Classification

Morphologic features of aortic plaque which are associated with an increased risk of embolization include increased plaque size, presence of ulcerations, and presence of mobile components [19, 20]. Atheroma is defined as intimal thickening ≥ 2 mm, with irregularity. Most early studies have defined significant atheroma as lesions having a thickness of ≥ 5 mm. However, the French Study of Aortic Plaques in Stroke Group observed that a plaque thickness of ≥ 4 mm confers a significantly increased risk of an embolic event, compared to plaques < 4 mm [21]. Various degrees of aortic atheroma, as seen on transesophageal imaging, are shown in Fig. 29.14. Imaging from

a patient with mobile Grade 5 atherosclerotic plaque is seen in Fig. 29.15, and an example of severe aortic plaque with ulceration is shown in Fig. 29.16.

Clinical Significance

It has been observed that the mobile components seen on atherosclerotic plaque are usually thrombi. Embolic events due to aortic atheroma may occur spontaneously, or subsequent to procedures such as cardiac catheterization, intra-aortic balloon pump, or cardiac surgery. In some cases, embolization may occur due to atheroembolic syndrome, but it is believed that thrombi

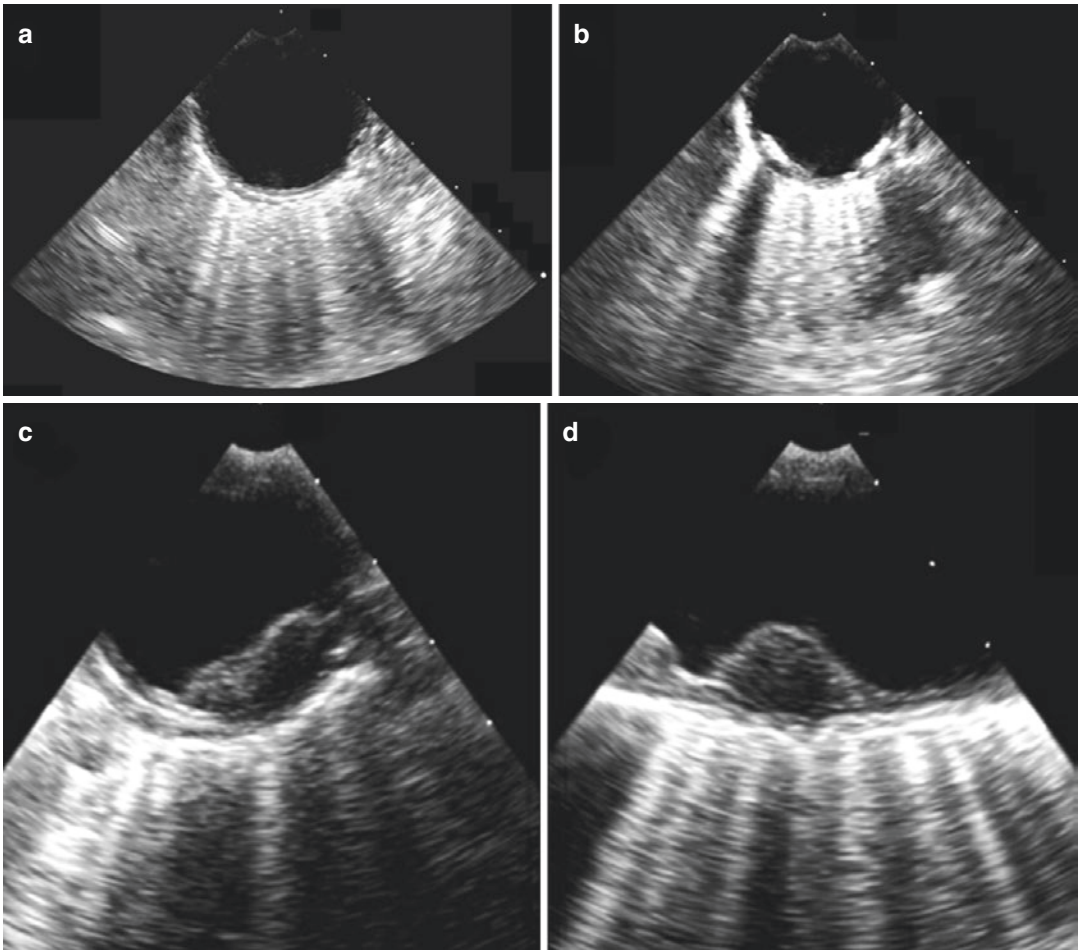


Fig. 29.14 Transesophageal imaging demonstrating varying morphologies of atherosclerotic plaque. (a) Normal descending aorta; (b) Moderate plaque in the

descending aorta; (c) Longitudinal view of the descending aorta in a patient with severe protruding atheroma; (d) Transverse view in the same patient as shown in (c)

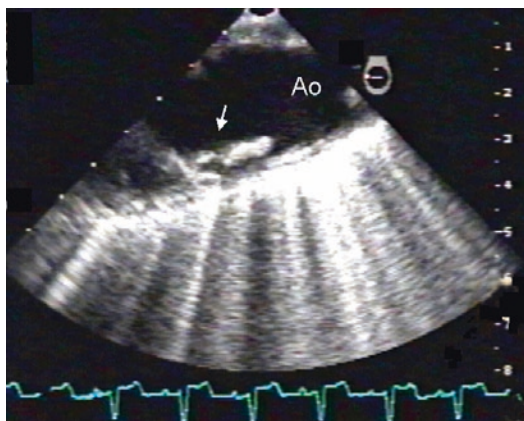


Fig. 29.15 Transesophageal echo image of the aortic arch in a patient with protruding and mobile atheroma (arrow). Ao aorta

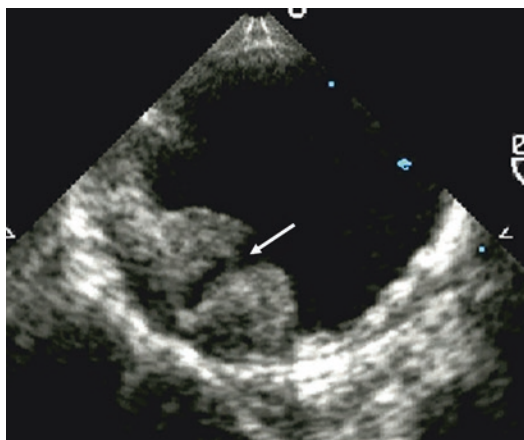


Fig. 29.16 Transesophageal echo image in a patients with an ulcerated atherosclerotic plaque (arrow) in the descending aorta

are responsible for most embolic events. Despite this, the role of anticoagulation in these patients has not been clearly established. Aortic atherosclerosis is a coronary heart disease equivalent and secondary prevention strategies, such as lipid-lowering therapy, are indicated. Antiplatelet therapy for prevention of cardiovascular events should also be considered. Available data indicate that dual-antiplatelet therapy does not confer added benefit over monotherapy for prevention of vascular events [22–24]. The use of hydroxyethyl glutaryl coenzyme A (HMG-CoA) reductase inhibitors in patients with aortic atheroma has been shown to be associated with a reduction in stroke [25]. HMG-CoA reductase inhibitors reduce low-density lipoprotein cholesterol levels and may thereby stabilize atherosclerotic plaque. In addition, anti-thrombotic actions of statins have also been described, which may have salutary effects on the development of plaque thrombosis.

Imaging

Transesophageal echocardiography is the primary modality used to detect aortic atheroma. There is some evidence that epicardial imaging may provide an even higher sensitivity for detection of atheromatous lesions, and can be a useful adjunct in the intra-operative setting

[26]. The clinical utility of aortic plaque imaging has primarily been in patients who have sustained an unexplained stroke, and in patients who are undergoing cardiac surgery. Among patients undergoing cardiac surgery, elderly patients who have mobile lesions are at particularly high risk for embolic events. In a study of patients aged >65 years old who were undergoing cardiac surgery, 18% of subjects were found to have protruding atheroma on intra-operative transesophageal echo. Almost half of those with protruding atheroma also had mobile components, and there was a 25% incidence of stroke in these patients (compared with 2% in others) [20]. Intraoperative embolization may occur due to cross-clamping of the aorta, “sand-blasting” effect from cannula flow, or manipulation of the aorta during surgery.

There is some evidence that modification of surgical techniques (such as alteration of the cannulation site, or use of off-pump coronary artery bypass graft surgery) in high-risk patients may decrease the incidence of peri-operative embolic strokes [20, 27]. However, even with these measures, the stroke rate in high-risk patients appears to be higher than the general population. Given the potentially devastating consequences of peri-operative stroke, identification of the location and extent of atheromatous disease is important for planning the optimal surgical approach.

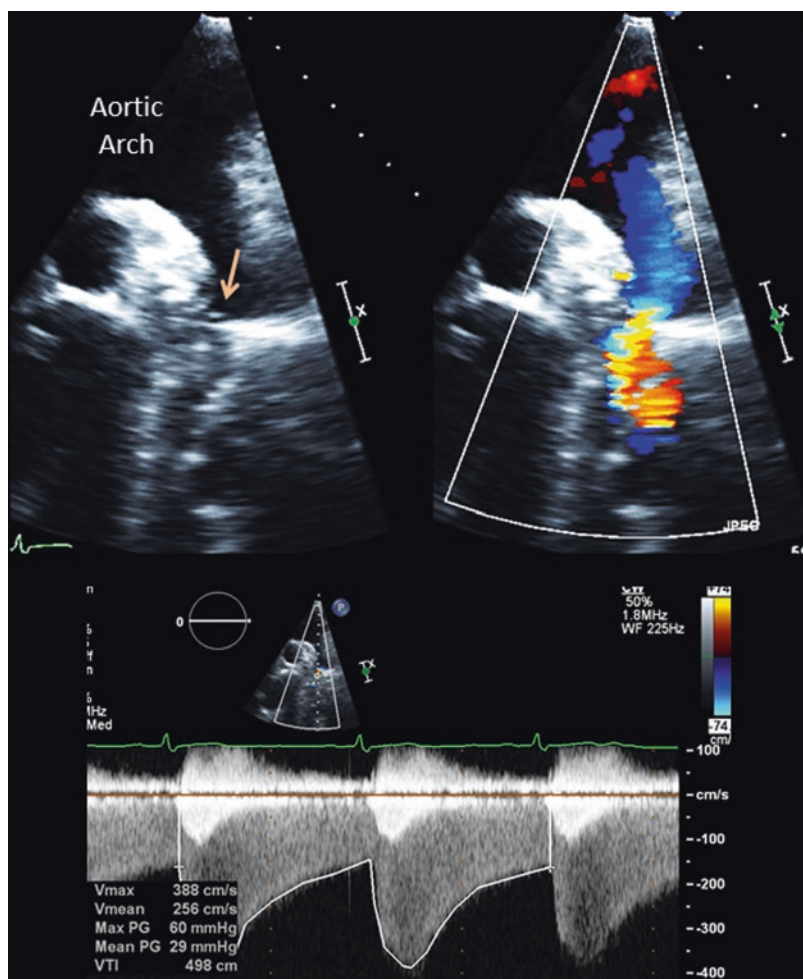
Palpation of the aorta during surgery is a relatively insensitive technique [28], and fails to identify the majority of atheromatous lesions seen on transesophageal echo. Thus, use of aortic imaging is an important peri-operative tool to identify patients at high-risk.

Aortic Coarctation

Coarctation of the aorta is a congenital disorder with the main feature of narrowing or constriction of an aortic segment in the descending thoracic aorta, either at post-ductal (seen usually in adults) and preductal (infantile) location. Depending on the severity of aortic narrowing, the blood pressure is increased to varying

degrees causing increased afterload to the left ventricle. The development of collateral vessels may compensate to certain extent but severe coarctation eventually leads to left heart failure and other hypertension-related complications. 2D echo imaging from a suprasternal location depicts the presence, location and morphology of coarctation. Pulsed Doppler, with the sample volume moved in a graded manner in the descending aorta demonstrates sudden increase in velocity and aliasing at the site of coarctation and color Doppler depicts the flow turbulence. Continuous wave Doppler interrogation of the descending aortic lumen captures the increased systolic velocity from which pressure gradients can be derived (Fig. 29.17). In severe coarctation, the pressure gradient is also

Fig. 29.17 Suprasternal recordings in a patient with aortic coarctation depicts the anatomic narrowing (arrow in top left) and turbulent flow (top right). Continuous wave Doppler (bottom panel) demonstrates a significant gradient both in diastole and systole



noted in diastole. Generally a peak gradient of 20 mmHg or more is considered significant and directs the need for intervention. Other factors such as symptoms, degree of proximal hypertension, and associated lesions influence the type and timing of percutaneous or surgical intervention.

Conclusion

Echocardiography has proven to be a valuable tool in the evaluation of aortic disorders. Transthoracic echocardiography is often the initial method in non-acute aortic syndromes. It is useful for follow-up of aortic dilatation and aortic coarctation. In acute aortic syndromes, transesophageal imaging is critical to detect and describe the underlying problems such as aortic dissection, intramural hematoma, and symptomatic penetrating ulcer, and their complications. Intraoperative transesophageal echocardiography guides operative planning and aids in the evaluation of the surgical efficacy and complications. Evaluation with computed tomography or magnetic resonance imaging can be helpful in patients in whom transthoracic and transesophageal echocardiography proves to be technically difficult or insufficient.

References

- Goldstein SA, Evangelista A, Abbata S, Arai A, Asch FA, Badano L, Bolen MA, Connolly HM, Cuellar-Calabria H, Czerny M, Devereux RB, Erbel RA, Fattori R, Isselbacher EM, Lindsay JM, McCulloch M, Michelena HI, Nienaber CA, Oh JK, Pepi M, Taylor AJ, Weinsaft JW, Zamorano JL. Multimodality imaging of diseases of the thoracic aorta in adults: from the American Society of Echocardiography and the European Association of Cardiovascular Imaging Endorsed by the Society of Cardiovascular Computed Tomography and Society for cardiovascular magnetic resonance. *J Am Soc Echocardiogr*. 2015;28:119–82.
- Lang RM, Badano LP, Mor-Avi V, Afzalilo J, Armstrong A, Ernande L, Flachskampf FA, Foster E, Goldstein SA, Kuznetsova T, Lancellotti P, Muraro D, Picard MH, Rietzschel ER, Rudski L, Spencer KT, Tsang W, Voight J. Recommendations for cardiac chamber quantification by echocardiography in adults: an update from the American Society of Echocardiography and the European Association of Cardiovascular Imaging. *J Am Soc Echocardiogr*. 2015;28:1–39.e14.
- Kouchoukos NT, Dougenis D. Medical progress: surgery of the thoracic aorta. *N Engl J Med*. 1997;336:1876–88.
- Roman MJ, Rosen SE, Kramer-Fox R, Devereux RB. Prognostic significance of the pattern of aortic root dilation in Marfan syndrome. *J Am Coll Cardiol*. 1993;22:1470–6.
- Hiratzka LF, Bakris GL, Beckman JA, Bersin RM, Carr VF, Casey DE Jr, Eagle KA, Hermann LK, Isselbacher EM, Kazerooni EA, Kouchoukos NT, Lytle BW, Milewicz DM, Reich DL, Sen S, Shinn JA, Svensson LG, Williams DM. 2010 ACCF/AHA/AATS/ACR/ASA/SCA/SCAI/SIR/STS/SVM Guidelines for the diagnosis and management of patients with thoracic aortic disease: a report of the American College of Cardiology Foundation/American Heart Association Task Force on Practice Guidelines, American Association for Thoracic Surgery, American College of Radiology, American Stroke Association, Society of Cardiovascular Anesthesiologists, Society for Cardiovascular Angiography and Interventions, Society of Interventional Radiology, Society of Thoracic Surgeons, and Society for Vascular Medicine. *Circulation*. 2010;121:e266–369.
- Erbel R. Diseases of the thoracic aorta. *Heart*. 2001;86:227–34.
- Tsai TT, Nienaber CA, Eagle KA. Acute aortic syndromes. *Circulation*. 2005;112:3802–13.
- Januzzi JL, Isselbacher EM, Fattori R, Cooper JV, Smith DE, Fang J, Eagle KA, Mehta RH, Nienaber CA, Pape LA, International Registry of Aortic Dissection (IRAD). Characterizing the young patient with aortic dissection: results from the International Registry of Aortic Dissection (IRAD). *J Am Coll Cardiol*. 2004;43(4):665.
- Leggett ME, Unger TA, O'Sullivan CK, Zwink TR, Bennett RL, Byers PH, Otto CM. Aortic root complications in Marfan's syndrome: identification of a lower risk group. *Heart*. 1996;75:389–95.
- Gott VL, Pyeritz RE, Magovern GJ, Cameron DE, McKusick VA. Surgical treatment of aneurysms of the ascending aorta in the Marfan syndrome. *N Engl J Med*. 1986;314:1070–4.
- Mohr-Kahaly S. Aortic intramural hematoma: from observation to therapeutic strategies. *J Am Coll Cardiol*. 2001;37:1611–3.
- Sawhney N, DeMaria AN, Blanchard DG. Aortic intramural hematoma: an increasingly recognized and potentially fatal entity. *Chest*. 2001;120:1340–6.
- Troxler M, Mavor AID, Homer-Vanniasinkam S. Penetrating atherosclerotic ulcers of the aorta. *Br J Surg*. 2001;88:1169–77.
- Blanchard DG, Kimura BJ, Dittich HC, DeMaria AN. Transesophageal echocardiography of the aorta. *JAMA*. 1994;272:546–51.
- Vlahakes GJ, Warren RL. Traumatic rupture of the aorta. *New Engl J Med*. 1995;332:389–90.

16. Pretre R, Chilcott M. Current concepts: blunt trauma to the heart and great vessels. *New Engl J Med*. 1997;336:626–32.
17. Willens HJ, Kessler KM. Transesophageal echocardiography in the diagnosis of diseases of the thoracic aorta: part II- atherosclerotic and traumatic diseases of the aorta. *Chest*. 2000;117:233–43.
18. Goarin JP, Catoire P, Jacquens Y, Saada M, Riou B, Bonnet F, Coriat P. Use of transesophageal echocardiography for the diagnosis of traumatic aortic injury. *Chest*. 1997;112:71–80.
19. Montgomery DH, Ververis JJ, McGorisk G, Frohwein S, Martin RP, Taylor WR. Natural history of severe atheromatous disease of the thoracic aorta: a transesophageal echocardiographic study. *J Am Coll Cardiol*. 1997;29:95–101.
20. Katz ES, Tunick PA, Rusinek H, Ribakove G, Spencer FC, Kronzon I. Protruding aortic atheroma predict stroke in elderly patients undergoing cardiopulmonary bypass: experience with intraoperative transesophageal echocardiography. *J Am Coll Cardiol*. 1992;20:70–7.
21. Amarenco P, Cohen A, Tzourio C, Bertrand B, Hommel M, Bessou G, Chaneul C, Touboul P-J, Bousseau M-G. Atherosclerotic disease of the aortic arch and the risk of ischemic stroke. *N Engl J Med*. 1994;331:1474–9.
22. Diener HC, Bogousslavsky J, Brass LM, Cimminiello C, Csiba L, Kaste M, Leys D, Matias-Guiu J, Rupprecht HJ, MATCH investigators. Aspirin and clopidogrel compared with clopidogrel alone after recent ischaemic stroke or transient ischaemic attack in high-risk patients (MATCH): randomised, double-blind, placebo-controlled trial. *Lancet*. 2004;364(9431):331.
23. Bhatt DL, Fox KA, Hacke W, Berger PB, Black HR, Boden WE, Cacoub P, Cohen EA, Creager MA, Easton JD, Flather MD, Haffner SM, Hamm CW, Hankey GJ, Johnston SC, Mak KH, Mas JL, Montalescot G, Pearson TA, Steg PG, Steinhubl SR, Weber MA, Brennan DM, Fabry-Ribaud L, Booth J, Topol EJ. CHARISMA Investigators: clopidogrel and aspirin versus aspirin alone for the prevention of atherothrombotic events. *N Engl J Med*. 2006;354(16):1706.
24. SPS3 Investigators, Benavente OR, Hart RG, McClure LA, Szychowski JM, Coffey CS, Pearce LA. Effects of clopidogrel added to aspirin in patients with recent lacunar stroke. *N Engl J Med*. 2012;367(9):817–25.
25. Tunick PA, Nayar AC, Goodkin GM, Mirchandani S, Franciscone S, Rosenzweig BP, Freedberg RS, Katz ES, Applebaum RM, Kronzon I. Effect of treatment on the incidence of stroke and other emboli in 519 patients with severe thoracic aortic plaque. *Am J Cardiol*. 2002;90:1320.
26. Wilson MJ, Boyd SY, Lisagor PG, Rubal BJ, Cohen DJ. Ascending aortic atheroma assessed intraoperatively by epiaortic and transesophageal echocardiography. *Ann Thorac Surg*. 2000;70:25–30.
27. Sharony R, Bizakis CS, Kanchuger M, Galloway AC, Saunders PC, Applebaum R, Schwartz CF, Ribakone GH, Culliford AT, Baumann FG, Kronzon I, Colvin SB, Grossi EA. Off-pump coronary artery bypass grafting reduces mortality and stroke in patients with atheromatous aortas: a case control study. *Circulation*. 2003;108(Suppl II):II-15–20.
28. Joffe II, Jacobs LE, Lampert C, Owen AA, Ioli AW, Kotler MN. Role of echocardiography in perioperative management of patients undergoing open heart surgery. *Am Heart J*. 1996;131:162–76.
29. Hiratzka LF, Nishimura RA, Bonow RO et al. Surgery for Aortic Dilatation in Patients With Bicuspid Aortic Valves. *Circulation* 2016;133(7):680–6.



Source of Embolus

30

Wissam Alajaji, Hussain Isma'eel, Patrick J. Nash,
Ronan J. Curtin, and Allan L. Klein

Introduction

Acute organ or limb ischemia due to arterial obstruction is typically due to one of two pathogenic processes: acute thrombotic occlusion on a substrate of significant local arterial disease or an embolism from the heart or proximal diseased large vessels (most commonly the thoracic aorta). The proportion of acute ischemic events that are embolic in etiology depend on a number of factors including the age of the subject, the likelihood of intrinsic vascular disease, and the vascular bed affected. Investigation after such an event is focused on defining the underlying process responsible for the event, with the primary aim being to prevent further potentially more devastating events. Echocardiography is the primary investigative tool for evaluating for a potential source of embolism. For the remainder of this discussion, intra-cardiac and thoracic aor-

tic sources of emboli will be collectively labeled as “cardiovascular emboli,” emphasizing that not all potential sources of emboli lie within the heart. This chapter initially focuses on defining the role of echocardiography in assessing for potential cardiovascular sources of embolus, including the indications for echocardiography, which is the optimal modality (transesophageal or transthoracic), and how to perform a comprehensive echocardiographic study. The remainder of the chapter discusses individual potential sources (both probable and possible sources), reviewing the evidence for the association between each potential source and embolic events, characteristic echocardiographic features, how to evaluate for it comprehensively with echocardiography, and current treatment strategies.

Epidemiology

Stroke is among the most common and devastating clinical consequences of cardiovascular emboli. In 2009, the age-standardized death rate attributable to all CVDs was 237.1 per 100,000, with death rates attributable to stroke, HDs, and other cardiovascular causes being 38.9, 116.1, and 81.0 per 100,000, respectively. Furthermore, data from NHANES 2009–2010 reveal that overall, 7.2% of Americans self-reported having some type of CVD including 3.2% with coronary heart disease (CHD), 2.7% with stroke and 2.0% with

W. Alajaji (✉)
Department of Cardiovascular Medicine, Akron City
Hospital-Summa Health System, Akron, OH, USA

H. Isma'eel
Department of Cardiology, American University of
Beirut, Beirut, Lebanon

P. J. Nash
Department of Cardiology, University Hospital
Galway, Galway, Ireland

R. J. Curtin · A. L. Klein
Department of Cardiovascular Medicine, Cleveland
Clinic Foundation, Cleveland, OH, USA

congestive heart failure (CHF). Currently about 20% of acute neurological events are suggested to be attributable to cardiovascular emboli. A further 40% are classified as “cryptogenic,” though there are increasing data suggesting associations with possible cardiovascular sources of emboli in these. For young people with acute ischemic strokes (~4 5 years), the proportion that are due to cardiovascular emboli is significantly higher (>50%), as a potential embolic source is more likely to be the only identifiable cause. This is in contrast to older patients who are more likely to have identifiable coexisting intrinsic cerebrovascular disease. It is also possible that for some patients, the entire source of the embolus may have embolized, creating a false-negative echocardiographic study, underestimating the true proportion of patients who have a cardiovascular source of embolus.

Potential Cardiovascular Sources of Embolus

The literature documenting the relationships between potential cardiovascular embolic sources is limited by the fact that a large proportion of current evidence is based on nonrandomized case control series and not prospective studies. Potential sources of emboli within the cardiovascular system are best divided into two groups based on the level of current available evidence: probable or possible sources (Table 30.1). The majority are due to embolism of intra-cardiac thrombus, which in more than half of all cases is located within the left atrium (LA), primarily within the left atrial appendage (LAA). Atrial fibrillation and rheumatic mitral valve disease (primarily mitral stenosis) are the most common predisposing factors. Left ventricular (LV) thrombus, usually in the setting of a severe apical wall motion abnormality (akinesia or aneurysm), is the second most common potential source of embolism (25%). Large vegetations and left-sided tumors (myxoma or papillary fibroelastoma) are much rarer findings. Thoracic atheroma is increasingly being identified and linked to embolic events. The association is greatest for “complex” plaque (i.e. >4 mm thick, or peduncu-

Table 30.1 Potential cardiovascular sources of embolus

Probable sources	Predisposing condition
Left atrial (appendage) thrombus	Atrial fibrillation; rheumatic mitral valve disease; severe LV dysfunction
Left ventricular thrombus	Previous MI (esp. anterior, with apical aneurysm); dilated cardiomyopathy
Vegetations ≥10 mm	Mitral and/or aortic valve
Cardiac tumors	Myxoma; papillary fibroelastoma
Complex aortic atheroma	
Prosthetic valves	Mitral or aortic
Possible sources	Predisposing condition
Patent foramen ovale	Atrial septal aneurysm
Spontaneous echo contrast	Atrial fibrillation; rheumatic mitral valve disease; severe LV dysfunction
Vegetations <10 mm	Mitral and/or aortic valve
Valvular strands/ Lamb1’s excrescences	Mitral or aortic
Atrial septal defect	
Mitral annular calcification	

Adapted from Chen EW, Redberg RF. Echocardiographic evaluation of the patient with a systemic embolic event. In: Otto CM, ed. *The Practice of Clinical Echocardiography*. 2nd ed. Philadelphia. PA: WB Saunders, 2002, p 807
LV left ventricular, MI myocardial infarction

lated and mobile lesions). An acute ischemic event in a patient with a prosthetic mechanical valve is cardioembolic until proven otherwise. Other echocardiographic findings are listed as possible sources as the level of evidence is less robust. A patent foramen ovale (PFO) has been associated with increased risk of ischemic stroke, especially in younger people, though it is such a common finding in the general population (20–25%) that determination of definite cause and effect is difficult. The combination of an atrial septal aneurysm (ASA) and a PFO is associated with a several fold increase in risk of stroke compared to a PFO alone. Other findings where possible associations with embolic events have been suggested include LA spontaneous echo contrast (SEC), valvular strands, mitral annular calcification, mitral valve prolapse, and smaller vegetations (Fig. 30.1, Table 30.2).

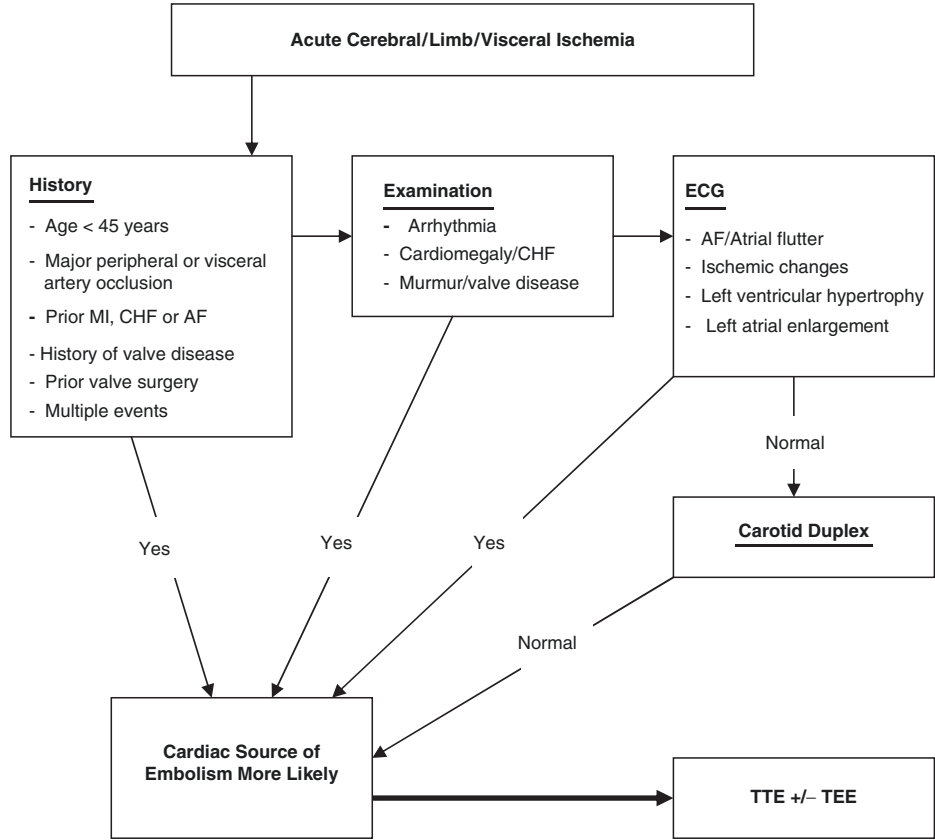


Fig. 30.1 Investigation algorithm for a potential source of embolus: (*MI* myocardial infarction, *CHF* congestive heart failure, *AF* atrial fibrillation, *ECG* electrocardiogram, *TTE* transthoracic echocardiography, *TEE* transesophageal echocardiography)

Table 30.2 Recommendations for echocardiography in patients with neurological events or other vascular occlusive events (AHA/ACC/ASE 2003 guideline update for the clinical application of echocardiography)

<i>Class I</i>
Patients of any age with abrupt occlusion of a major peripheral or visceral artery
Younger patients (typically <45 years) with cerebrovascular events
Older patients (typically >45 years) with neurological events without evidence of cerebrovascular disease or other obvious cause
Patients for whom a clinical therapeutic decision (e.g., anticoagulation) will depend on the results of echocardiography
<i>Class IIa</i>
Patients with suspicion of embolic disease and with cerebrovascular disease of questionable significance
<i>Class IIb</i>
Patients with neurological events and intrinsic cerebrovascular disease of a nature sufficient to cause the clinical event
<i>Class III</i>
Patients for whom the results of echocardiography will not impact a decision to institute anticoagulant therapy or otherwise alter the approach to diagnosis or treatment

Adapted from: Cheitlin MD, Armstrong WF, Aurigemma GP, Beller GA, Bierman FZ, Davis JL, Douglas PS, Faxon DP, Gillam LD, Kimball TR, Kussmaul WG, Pearlman AS, Philbrick JT, Rakowski H, Thys DM. ACC/AHA/ASE 2003 guideline update for the clinical application of echocardiography: a report of the American College of Cardiology/American Heart Association Task Force on Practice Guidelines (ACC/AHA/ASE Committee to Update the 1997 Guidelines for the Clinical Applications of Echocardiography). 2003. American College of Cardiology Web Site. Available at <<http://www.acc.org/qualityandscience/clinical/guidelines/echo/index.pdf>>

Transthoracic vs. Transesophageal Echocardiography

The sensitivity of transthoracic echocardiography (TTE) for detection of potential sources of embolus is low, as the most common potential causes are not well visualized by TTE. In the absence of clinical cardiac disease, the diagnostic yield is as low as 1%, increasing to 15% with clinical cardiac abnormalities. Its primary use is for assessing LV global and regional systolic function and apical LV thrombus.

Assessment of the inter-atrial septum and the thoracic aorta. Overall TEE identifies significantly more potential sources of embolus than TTE (39–57% vs. 15–19%). Evaluation for a potential source of embolus is now the leading clinical indication for TEE in most laboratories (26% in one registry series). The use of contrast might enhance the yield of TEE for detection of LAA thrombi and the benefit was maximized when studies were limited by the presence of spontaneous echo contrast, or when there was poor LAA emptying velocity. Furthermore, contrast can often help distinguish severe spontaneous echo contrast sludge and required to optimally visualize the LA and in thrombus in particular the posterior-lying LAA (the most common location of thrombus). However, it is probably best to consider the two modalities as complementary rather than mutually exclusive (Table 30.3).

Table 30.3 Role of transthoracic and transesophageal echocardiography for detection of potential sources of embolus

Possible source of embolus	Transthoracic echo	Transesophageal echo
LA mural thrombus/ SEC	+	+++
LAA thrombus/SEC	–	+++
LAA filling velocity	–	+++
Valve strands	+	+++
Vegetations	+	+++
Papillary fibroelastoma	+	+++
LV aneurysm	+++	+
LV apical thrombus	++	+
Patent foramen ovale	– ++ (bubble)	+++
Atrial septal aneurysm	++	+++
Thoracic aortic atheroma	–	+++

– not seen, + poor, ++ intermediate, +++ excellent, LA left atrium, LAA left atrial appendage, LV left ventricle

Table 30.4 Comprehensive TEE examination for potential source of embolus

<i>Midesophageal view at 0–15° rotation</i>
Retroflex transducer to open a four-chamber view for initial assessment of the LA and mitral valve
Zoom in on the mitral valve and LA and examine in detail for any abnormalities
Slightly anteflex and/or withdraw the probe slightly to visualize the LAA (arises from anterolateral aspect of the LA near the lateral aspect of the mitral ring and left upper pulmonary vein)
<i>Midesophageal 45–90°</i>
Further views of the LA and LAA (usually best view to visualize the LAA)
Doppler LAA flow—1 cm into the LAA from its junction with the main LA cavity
Clockwise rotation will give short-axis view of the aortic valve (strands, vegetations)
Visualize the interatrial septum in the near field—interrogate with color Doppler (Nyquist <40 cm/s)
<i>Midesophageal 120°</i>
Further views of the LA and mitral valve and long-axis view of the aortic valve and aortic root
Slight clockwise rotation of the transducer will give a short-axis view of the LAA
Further clockwise rotation of transducer will give bicaval view—optimal view of the interatrial septum
Give agitated saline—to evaluate for right-to-left shunt at baseline and after Valsalva (ask patient to cough)
From the long-axis view of the aortic valve—bring angle back to ~100° and withdraw transducer to focus on the tubular ascending aorta
<i>Transgastric view</i>
Short- and long-axis views of the LV for LV function
Thoracic aorta
Begin in transgastric view at 0° (short axis of thoracic aorta)—decrease depth to maximize aorta
Withdraw transducer slowly—if any abnormality, visualize in long- and short-axis views (0° and 180°)
At ~20 cm from incisors the distal aortic arch will come into view—rotate 20° and turn clockwise to open the long-axis view of the aortic arch

Thrombus in the LV is best visualized by TTE, while most other potential sources are better seen by TEE. A comprehensive approach to TEE for evaluation of possible sources of embolus is outlined in (Table 30.4).

Left Atrium Anatomy

The LA is located posteriorly within the heart, in close proximity to the esophagus and therefore

is best visualized by TEE. From an embolic perspective, most interest focuses on the LAA. This is a blind-ended sac located along the antero-superior aspect of the LA and connected to the rest of the LA by a relatively narrow isthmus. It is a remnant of the original embryonic LA and its exact physiologic role remains unclear. A number of anatomic features are important to be aware of when evaluating it by TEE (Figs. 30.2, 30.3, 30.4, and 30.5).

1. Its size varies widely (length between 16 and 51 mm, diameter: 5–40 mm). A very “small” appendage, often gives rise to concerns that a

much larger appendage with laminated thrombus is being overlooked.

2. It typically has a twisted long axis, requiring multiple planes to visualize it comprehensively.
3. Typically it is multilobed (≥ 2 lobes in 80%). Therefore, it is essential to comprehensively evaluate for any additional lobes that may not be immediately apparent (Fig. 30.3).
4. In contrast to the rest of the LA, its walls are trabeculated, with parallel ridges of muscle giving it a comb-like appearance (pectinate muscles) (Fig. 30.5). These may be mistaken for thrombus or conversely small thrombi

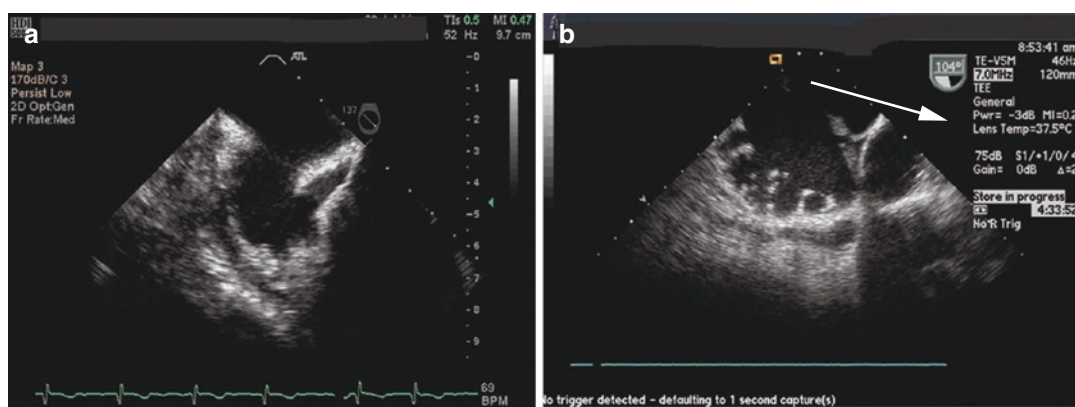


Fig. 30.2 TEE view (100–120°) of the LAA. (a) shows a bilobed appendage. (b) demonstrates prominent normal pectinate ridges (arrow), which may be confused for possible thrombus 6

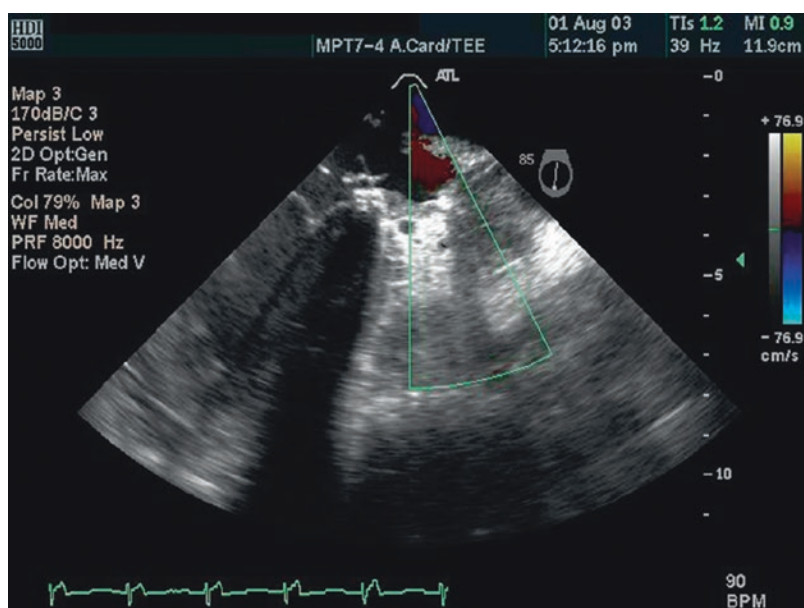


Fig. 30.3 TEE view at 85° showing that the LAA has been surgically removed

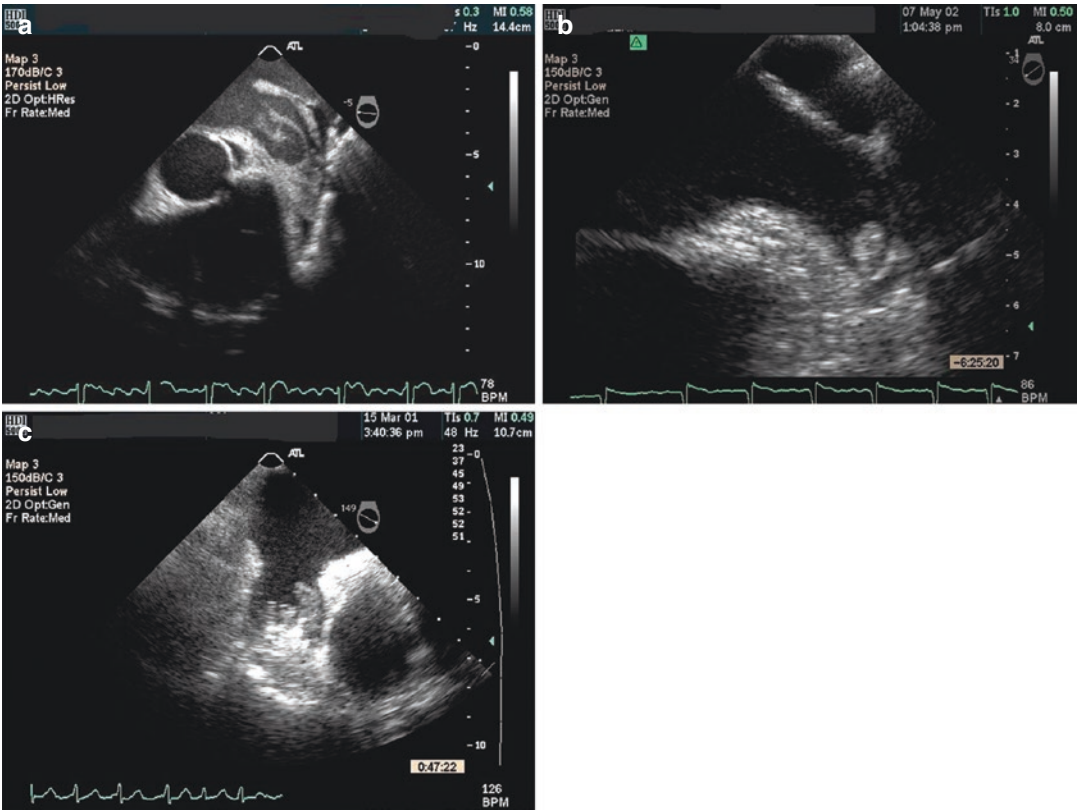


Fig. 30.4 LAA thrombus—(a) shows laminated thrombus in the LAA apex with spontaneous echo contrast in the rest of the LAA. (b) shows a small focal protuberant mass typical of thrombus. (c) shows a LAA full of thrombus

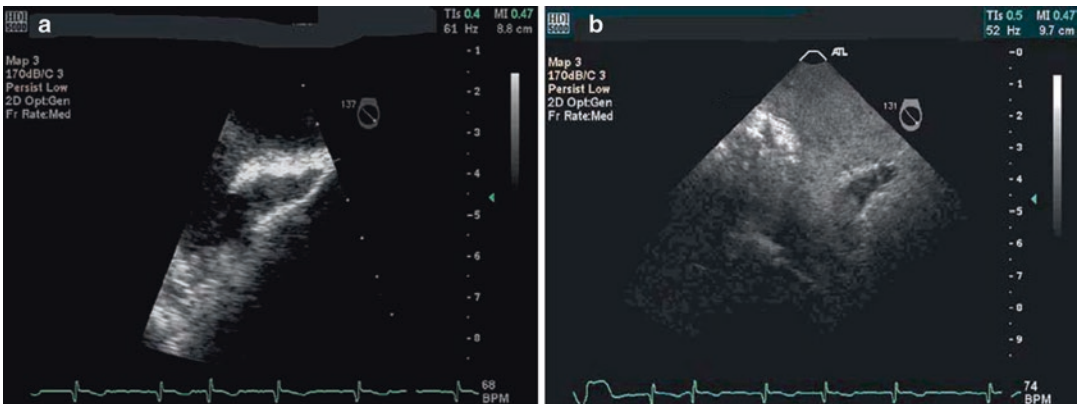


Fig. 30.5 Intravenous microbubble contrast clarifies possible LAA thrombus. (a) shows some haziness in the LAA, which raises a suspicion of possible thrombus. (b) The

image was obtained after contrast demonstrating a filling defect, highly suggestive of thrombus the arrow should be removed from figure b

between these ridges may be over-looked. A thrombus typically appears as a more solitary protrusion into the LAA cavity and may have independent motion (Fig. 30.6). Figure 30.7 demonstrates left atrial strain.

Left Atrial Appendage Doppler

Late diastolic positive forward flow wave (out of the appendage—toward the TEE probe), associated with LA contraction, (after the electrocar-

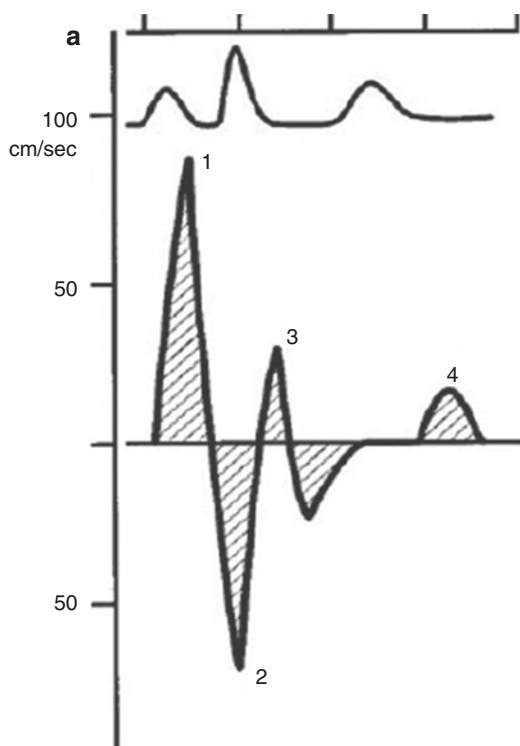


Fig. 30.6 Normal Doppler appearance of LAA flow. From: Agmon Y, Khandheria BK, Gentile F, Seward JB. *J Am Coll Card*. 1999;34:1867–77. Copyright 1999 with permission from Elsevier

diographic P wave, normal peak velocity >50 cm/s), and followed by an early negative systolic wave. The remaining Doppler pattern typically consists of at least two low-amplitude alternating waves with the final forward wave (positive wave) representing LAA outflow associated with early passive filling of the LV (correlated with the mitral inflow E wave). In atrial fibrillation the flow pattern changes, though active flow is still commonly seen with alternating positive and negative “fibrillatory” waves (Fig. 30.8), typically with lower flow velocities than those seen in sinus rhythm.

Echocardiographic Assessment of the Left Atrium (Figs. 30.2, 30.3, 30.4, 30.5, 30.6, 30.8, and 30.9)

Only limited information about the LA can be obtained by TTE. Left atrial size (either by internal dimension, area, or volume) can usually be

satisfactorily obtained. The presence of left atrial enlargement (transverse diameter for the parasternal long-axis view >4.0 cm) or rheumatic mitral stenosis in a patient with a history of cerebral/systemic embolism, especially with atrial fibrillation, increases the likelihood of LAA thrombus. Recently, assessing left atrial strain using angle independent speckle tracking echocardiography is becoming more available. Using this technique left atrial mechanics during the various phases of the left atrial filling-emptying cycle can be assessed (left atrial strain figure). Patients with high left atrial fibrosis burden are expected to have abnormal mechanics, therefore would be at higher risk of recurrence of atrial fibrillation after catheter ablation of atrial fibrillation. Emerging studies are supporting this hypothesis with global left atrial strain $>23.2\%$ predicting sinus rhythm maintenance after pulmonary vein isolation. How left atrial strain is going to be incorporated into daily clinical practice is subject to future prospective studies.

Mural LA thrombus (if extensive enough) can be visualized by TTE (sensitivity of 25–57%, specificity of 63–83%). However most LA thrombus occurs in the LAA, and this is rarely satisfactorily seen by TTE (sensitivity of 0–16%). TEE is, therefore, the imaging modality of choice for accurate and comprehensive assessment of the LA for thrombus.

With TEE, the LA is in near field and the transducer should be adjusted to the highest frequency (typically 7 MHz) for optimal imaging, with the image depth adjusted to approximately 10 cm to maximize the LA size in the display. It is important to adjust all imaging parameters to avoid misinterpreting near-field artifacts. Starting at the midesophageal view (0° of rotation), the probe should be gently advanced and withdrawn a few centimeters to image the inferior and superior aspects of the LA and inspected in multiple angles of rotation, to prevent overlooking mural thrombus, especially along the posterior wall (Fig. 30.10). The LAA is located near the antero-superior aspect of the mitral valve annulus, and at 0° of rotation usually requires the probe to be withdrawn a little, where it typically has a triangular appearance, separated from the left upper pulmonary vein by a ridge of tissue called the limbus. Once located, it should be closely exam-

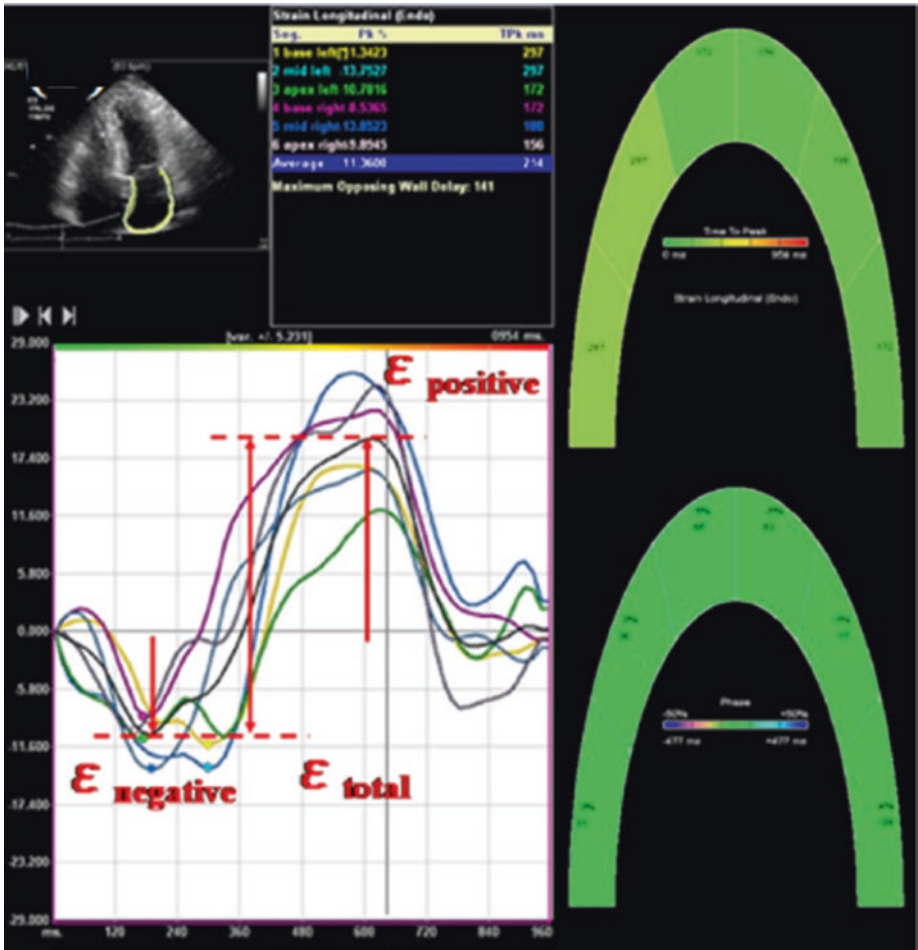


Fig. 30.7 Left atrial strain: using P wave onset as zero strain time point, the average left atrial strain goes negative during atrial contraction to reach Peak Negative, then

starts to increase in systole during atrial filling phase to reach Peak Positive. Global left atrial strain is Peak Positive – Peak Negative

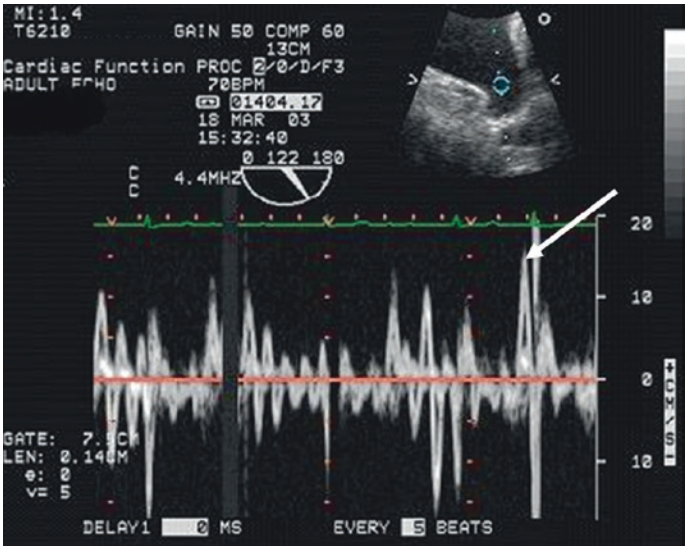


Fig. 30.8 LAA Doppler flow in a patient with atrial fibrillation. Peak emptying velocities (*highlighted*) are markedly reduced (<20 cm/s)

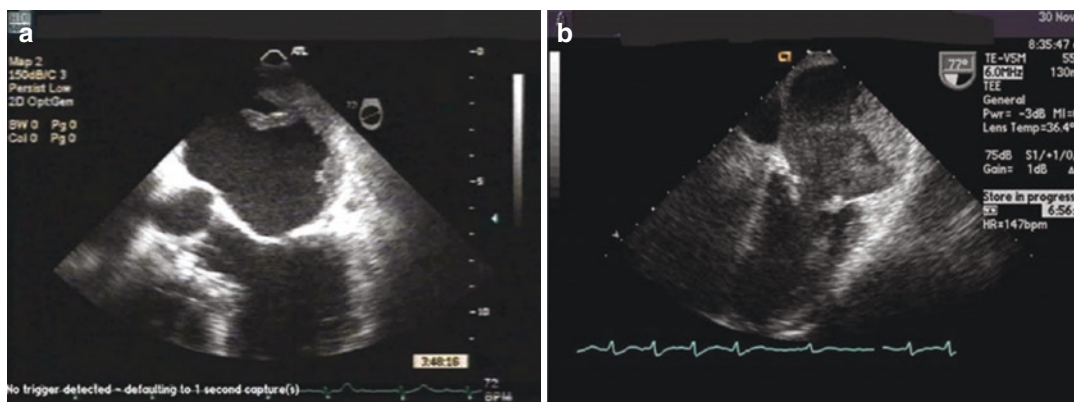


Fig. 30.9 Two examples of LA mural thrombus. Image (a) shows mobile pedunculated mural thrombus along the posterior wall of the LA. Image (b) shows thrombus along the lateral wall of the LA in a patient with mitral stenosis

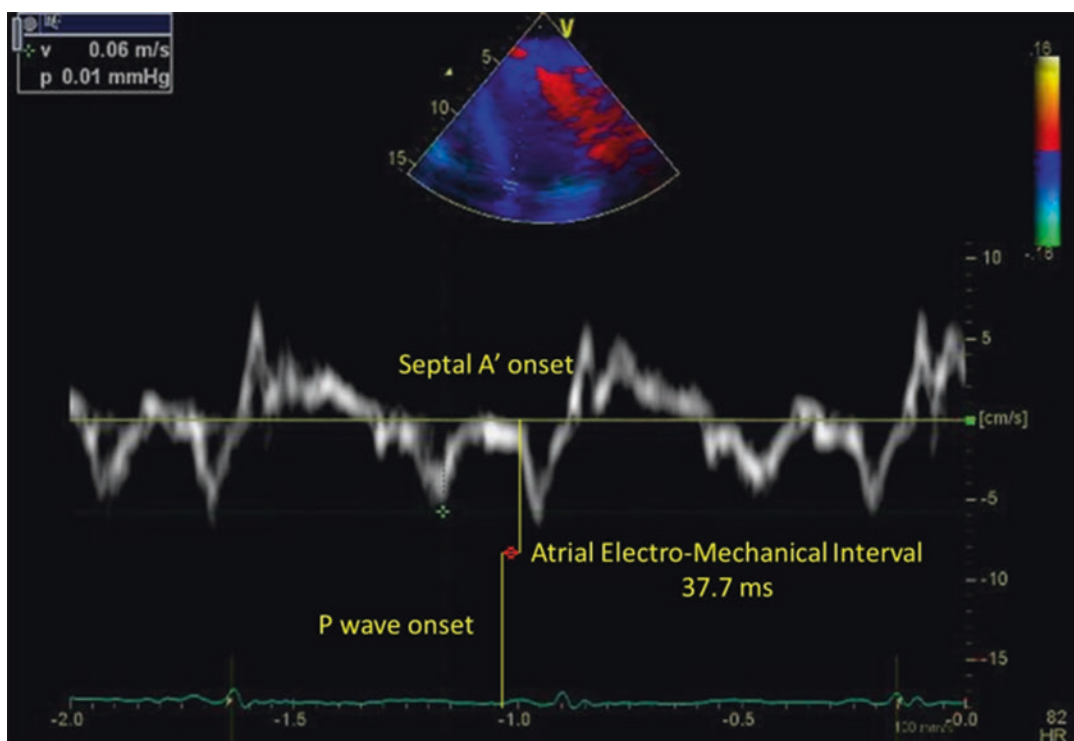


Fig. 30.10 Tissue Doppler wave form with the red horizontal line between the two yellow vertical lines delineating the AEMI

ined in multiple imaging planes, including 45°, 90°, and 120° views. Long-axis views of the LAA are obtained between 0° and 90°, with the orthogonal short-axis views typically best seen at ≥120° (Figs. 30.2, 30.3, and 30.4). Pulsed-wave Doppler of LAA flow is often best obtained at 90–120° views, as it can usually be optimally aligned with LAA outflow in this view. Thrombi may be very small and any possible thrombus

should be imaged in at least two orthogonal planes (Fig. 30.4). If there is persistent concern about possible thrombus in the LAA, use of a contrast agent (Optison™ or Imagent™ or Definity™—albumin or synthetic microbubbles, that cross the pulmonary vasculature and opacify the left heart) can help to clarify its presence/absence (Fig. 30.5). Increasingly the LAA is being ligated or stapled during cardiac surgery,

especially if the patient has a history of atrial fibrillation (Fig. 30.3). Though still in its typical location, no flow should persist across its isthmus with the main LA cavity when interrogated with color-flow Doppler. Residual flow implies a residual channel and potential for LAA thrombus to embolize. With some surgical procedures it has been standard to remove the entire LAA (historical closed mitral valvotomy, Maze procedures), and confusion can arise about the presence or absence of the LAA if the exact operative procedure is unclear. Recently, a number of potential percutaneous devices to occlude the LAA have been developed. The WATCHMAN Device was shown in the PROTECT-AF and ASAP studies to be a good alternative for patients who cannot take anticoagulation. Inserting this device requires good planning for proper sizing of the device relative to the orifice of the LAA. This can be done with TEE and CT. The different shape of the LAA orifice challenges the success of this procedure. On the other hand, the LARIAT procedure is more complex with the need for reaching the LAA percutaneously and also localizing it through the pericardium. Once the localizing tools meet, this is used to insert a device that seals the LAA from the pericardial side. Naturally this procedure has different complications related to the pericardial approach.

Left Atrial Thrombus (Figs. 30.4, 30.5 and 30.9)

Thrombus in the LA can be sessile or pedunculated, fixed or mobile, and typically appears as an irregularly shaped, gray, echodense intracavitary mass that is acoustically distinct from the LA endocardium. It is commonly associated with spontaneous echo contrast (SEC) (Fig. 30.4). Atrial fibrillation is the usual predisposing factor for LA thrombus and in particular LAA thrombus, though 5–10% of all thrombi occur in patients in sinus rhythm without significant mitral valve disease, often in the setting of severe LV dysfunction. The prevalence of LA thrombus in patients with atrial fibrillation of >48 h duration (who were not anticoagulated) has been reported as between 8 and 15%, almost all occurring within the LAA. A comprehensive TEE examination in

experienced hands can usually detect LA thrombus with a sensitivity and specificity approaching 95–100%. Patients in atrial flutter, despite having more organized LA contraction compared to those with atrial fibrillation, can have evidence of LAA dysfunction (lower Doppler velocities) and LAA thrombus may still occur.

Factors Associated with Left Atrial Thromboembolism in Atrial Fibrillation

A number of significant independent clinical predictors of stroke in patients with AF have been identified, including increasing age, female sex, hypertension, prior cerebrovascular event, LV dysfunction, diabetes mellitus, and coronary artery disease with a protective effect from mitral regurgitation. In addition, a number of echocardiographic factors have been identified that are associated with LA thrombus formation and thromboembolism.

1. LAA Size: The larger the LAA, the more likely it will contain thrombus
2. LAA Doppler flow pattern (Fig. 30.6): Peak emptying LAA velocities represent LAA function and lower velocities are associated with more severe LAA dysfunction. Low velocities (<20 cm/s) correlate strongly with the presence of LA thrombus and SEC. Low Doppler velocities can help with the evaluation of unclear LAA masses, increasing the likelihood that these represent LA thrombus. The risk of stroke for patients in atrial fibrillation is increased for those with reduced LAA velocities and is more than four times greater for patients with peak velocities <20 cm/s.
3. Presence of SEC (Fig. 30.4a): SEC or “smoke” representing local blood stasis is associated with an increased incidence of thrombus formation and thromboembolism. Increasingly severe qualitative ten gradations of SEC (from mild intermittent SEC to a severe semiturbid appearance –“sludge”) are associated with incremental increases in thromboembolic risk.
4. Comorbidities CHADS₂ and CHADS₂ + Vasc: CHADS₂ (CHF, HTN, DM, Age > 75 , stroke/

TIA) is the acronym to present the co-morbidities associated with increased risk of stroke where each condition scores as 1 except stroke/TIA scores as 2. A more recently introduced scoring system -CHADS₂-VASC score—further reclassified low CHADS₂ 0–1 population into CHADS₂-VASC ≥ 2 in 74% of cases. The annual incidence of SSE in CHADS₂-VASC score of 1 and ≥ 2 was 0.9% and 2.1% respectively. Moreover, analysis of the ROCKET AF data revealed that renal dysfunction has additive value for stroke risk and systemic embolism in patients with non-valvular atrial fibrillation. Furthermore, recent data showed that LVEF < 20% is associated with LA or LAA sludge or thrombus- a surrogate of stroke. Therefore, considering extending CHADS₂ score to R(2)CHADS(2) index to include kidney function, and studying the incremental clinical benefit achieved from further splitting LV function are ideas for consideration. Interestingly, this co-morbidities score seems to function in predicting stroke in non-atrial fibrillation such as the population with pacemaker devices.

5. Atrial electromechanical interval (AEMI) > 82 m-s (Fig. 30.10): AEMI is the interval between the onset of P-Wave on Surface ECG and the onset of MV septal A' in TDI. The AEMI predicted a higher risk subpopulation among a low CHADS₂ risk group who are not otherwise candidates for anticoagulation. Among patients with paroxysmal atrial fibrillation and CHADS₂ score 0–1, those with AEMI of >82 ms had significantly higher rates of cardioembolism 48% vs. 15%, $P < 0.05$. Furthermore, the longer the AEMI duration, the higher the degree of atrial fibrosis, remodeling and size.
6. Size and mobility of LAA thrombus: Larger (>1.5 cm), pedunculated and mobile thrombi are associated with a higher risk of systemic embolism.
7. Presence of complex aortic atheroma: The coexistence of complex aortic atheroma (>4.0 mm thick, pedunculated, mobile) is associated with a greater risk of stroke in patients in atrial fibrillation. The exact mechanism underlying this relationship remains unclear as it applies also to plaque in the descending aorta and therefore is not entirely related to atheromatous emboli. It is suggested that it is a surrogate for a greater total vascular disease burden.
8. Evidence of LAA thrombus, SEC, or a peak emptying velocity <20 cm/s are associated with an annual 7.5% risk of stroke. The combination of one of the above LAA findings and complex aortic atheroma increases the annual rate to ~20%. If neither of these TEE findings is present, the annual stroke risk is 1.2%. TEE also has an important role in evaluating patients prior to DC cardioversion. A TEE-guided approach as shown in the ACUTE trial (early cardioversion in the absence of LA clot) was associated with a quicker achievement of sinus rhythm, reduced major and minor bleeding rates, similar likelihood of maintaining sinus rhythm, and similar embolic rates when compared to the traditional conservative route of anticoagulation for 4 weeks prior to cardioversion. Of note, the use of low molecular weight heparin (LMWH) was found to be as safe as unfractionated heparin based approach for anticoagulation with shorter length of stay with LMWH.

Left Atrial Spontaneous Echo Contrast

The term “spontaneous echo contrast” (SEC) or “smoke” has been coined for the TEE appearance of swirling “smoke-like” echodensity within the heart, most commonly within the LA and in particular the LAA (Figs. 30.4a and 30.11). SEC can be appreciated by TTE but is much better seen by TEE. It is a marker of stasis, reflecting low flow states and probably reflecting aggregation of blood cells at low shear rates. SEC is also a likely precursor of thrombus. It is the most common TEE finding among patients referred for evaluation of a possible cardiac source of embolism, especially those with atrial fibrillation or left atrial enlargement. SEC is best appreciated with higher gain settings and can be differentiated from background “noise” by its swirling motion. Its dependence on transducer settings makes it difficult to quantify; however, it can be generally graded into mild or severe groups. The term “LAA sludge” (Fig. 30.4) has

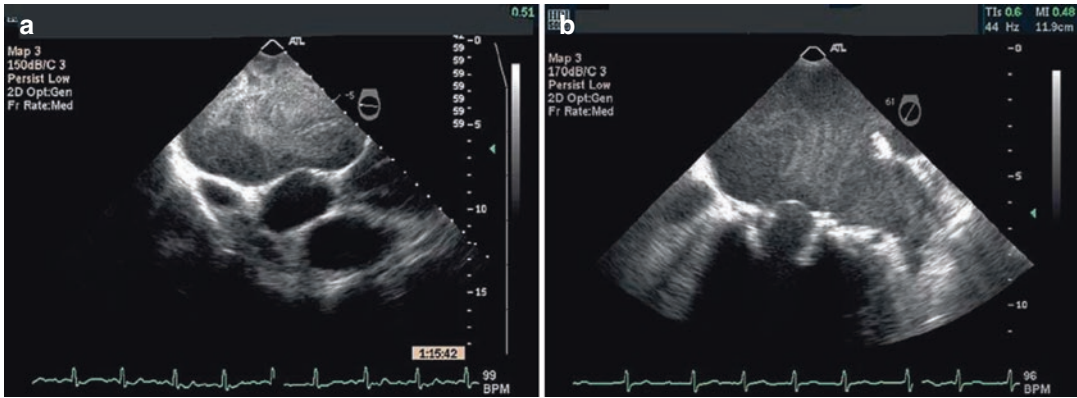


Fig. 30.11 Two examples typical of spontaneous echo contrast (SEC) or “smoke” in the LA

been coined for severe viscid SEC, without clear thrombus formation, though often differentiation between these is difficult. It is regarded as representing a stage further along the continuum toward thrombus formation and has been suggested to have greater prognostic significance than SEC. Recent data has shown that LAA sludge is independently associated with subsequent thromboembolic events and all-cause mortality in patients with AF.

Spontaneous Echo Contrast and Thromboembolism

There is a strong association between SEC and LA thrombus. The presence of SEC is an independent predictor of thromboembolic risk; and in patients with atrial fibrillation, it is associated with an increase in the embolic rate from 3 to 12% per year. Mitral regurgitation is associated with reduced frequency of SEC, as presumably the regurgitation “washes” out the LA preventing stasis. It is much less commonly seen in patients in sinus rhythm (2% in one large series, all of whom had LA enlargement) than those with atrial fibrillation (20% prevalence in one series), but it is still associated with a higher incidence of stroke. Currently, there is no consensus on treatment of SEC in the absence of definite LA thrombus or atrial fibrillation, though its presence mandates a comprehensive examination of the LA for possible thrombus.

Left Atrial Tumors

Primary cardiac tumors are rare with a prevalence of 0.002–0.03% at autopsy, with myxomas accounting for up to 50% of all primary tumors and more than 80% of LA tumors. Metastatic tumors rarely extend into the LA and can simulate an atrial myxoma. LA myxomas are the usual tumors associated with embolic events though any left-sided tumor can cause embolic complications either due to embolism of tumor fragments itself or embolization of fragments of thrombus that form on the tumor surface.

Left Atrial Myxoma

These benign tumors occur more frequently in women, with a mean age of presentation of 56 years. Morphologically they appear as a gelatinous friable mass that most commonly arises on a stalk from the interatrial septum in the region of the fossa ovalis. They vary in size but are often not detected until they become very large, by which time they may prolapse through the mitral valve during diastole (Fig. 30.12). From an echocardiographic point of view, they typically appears as a mobile, well-circumscribed, nonhomogenous mass that may contain cyst-like structures and/or areas of calcification. Usually they can be identified by TTE; however, TEE is often required to comprehensively visualize the tumor and help plan the surgical approach. It is important to exclude the presence of multiple masses, confirm

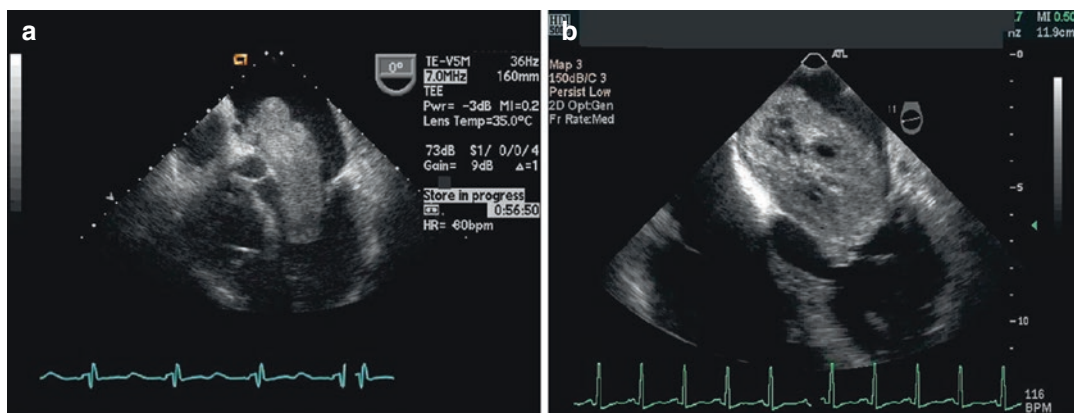


Fig. 30.12 LA myxoma—the upper image shows a large tumor that appears to be attached to the interatrial septum, prolapsing through the mitral valve during diastole. The

lower image shows a large tumor with some cystic features prolapsing through the mitral valve

the point of attachment, and ensure that the mitral valve appears normal. This should be distinguished from a large LA thrombus, though these typically are attached to the posterior wall and produce a layered appearance. From a clinical perspective, an embolic event (often multiple territories) is the initial presentation in up to one-third of patients. Other presentations include symptoms associated with mitral valve obstruction or systemic constitutional symptoms (fever, weight loss). Once identified, a myxoma should be surgically removed. Long-term outlook is excellent, though 5% may recur, especially in those patients with the familial form.

Left Ventricular Thrombus

Thrombus in the LV usually occurs in the setting of marked regional systolic dysfunction post-acute myocardial infarction (AMI), typically after large anteroapical infarcts, especially if there is evidence of LV aneurysm formation. Though less common, thrombus can also form (typically at the apex) in those with a dilated cardiomyopathy and severe global LV systolic dysfunction. Modern reports suggest that LV thrombus develops in about 5% of patients with AMI (~12% in those with anterior wall infarcts) who receive thrombolysis, an incidence that is significantly lower than in the pre-thrombolytic era (~20%). Most LV thrombi develop within the

first 2 weeks post AMI (mean of 9.5 days). Those who develop thrombus early (within 48–72 h of infarction) have a very poor prognosis, dying from complications related to the size of their infarct and not embolic complications. Stasis in large areas of infarction and possibly endocardial inflammation during the acute phase of infarction providing a thrombogenic surface are suggested as the primary pathophysiologic factors.

Echocardiographic Identification

LV thrombus is better seen by TTE than TEE (Fig. 30.13). High sensitivity (95%) and specificity (90%) of TTE for LV thrombus have been reported in the past; however, more recent studies suggest a sensitivity of less than 50% when compared to contrast-enhanced MRI and/or surgical confirmation. TEE is not the test of choice as it is usually difficult to visualize the true apex, making exclusion of apical thrombus difficult. Typically LV thrombus appears as a distinct echodensity in the LV apex, which is seen throughout the cardiac cycle in at least two different echocardiographic views. It may have an irregular surface and may be sessile or pedunculated, mobile, or is mandatory to adequately visualize the LV apex in all patients with anteroapical LV dysfunction to prevent missing small thrombi that may not appear in all views. Using modern multifrequency transducers, the apical regional should be magnified, the frequency

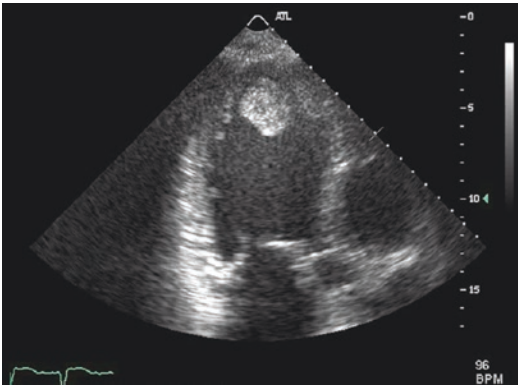


Fig. 30.13 Apical three-chamber view demonstrating a large left ventricular apical mass suggestive of thrombus

maximized to optimize resolution in the near field, and the focus adjusted toward the LV apex. If there is uncertainty about an LV apical thrombus, filling the area with color Doppler signals of low velocity (reduce the Nyquist limit) will enable color interrogation of the LV apex and can help to better define if there is an apical filling (flow) defect. Also, intravenous contrast agents can and should be utilized to opacify the LV apex and confirm any apical filling abnormality if there is uncertainty. Data has shown that with contrast stromal tumors and thrombi appear hypo-enhanced, whereas malignant and vascular tumors are hyper-enhanced compared to adjacent myocardium.

Risk of Embolization

The risk of systemic embolization from an LV thrombus is reportedly as high as 10%. The risk is greatest in the first 3 months post infarction, after which time the thrombus becomes organized and is less likely to embolize. Older age, lower ejection fraction, and absence of anti-thrombotic agents or anticoagulation are independently associated with increased embolic risk and stroke. Also larger, protruding, mobile thrombi are more likely to embolize. The presence of contiguous zones of akinesia and hyperkinesia is suggested to increase the risk of embolus. These patients with LV systolic dysfunction, irrespective of whether they are in sinus rhythm or atrial fibrillation, are also at increased risk for LAA thrombus formation. All patients with LV thrombus should be anticoagulated for at

least 3 months and up to 1 year. Currently both European and American consensus guidelines do not advocate routine anticoagulation for patients (whether ischemic or nonischemic) with severe LV dysfunction unless there is echocardiographic evidence of LV thrombus, a history of atrial fibrillation, or other indication for anticoagulation.

Valvular Vegetations

Vegetations due to infective endocarditis are potentially important sources of embolism. Typically the patient has a history of recurrent fever and constitutional symptoms and a possible precipitant (recent dental or other invasive procedure). The primary identification of vegetations during evaluation for a potential source of embolus is unusual, as clinically the diagnosis is usually suspected. Therefore, a large proportion of vegetations are identified before major embolic complications occur.

Echocardiographic Features

Vegetations have a number of typical echocardiographic features and the diagnosis can usually be made with a relatively high degree of certainty by echocardiography in combination with the clinical scenario (Fig. 30.14). They appear less reflective (gray) compared to normal valve tissue and are located upstream of the valve in the line of the jet of regurgitation (atrial surface of the mitral valve and ventricular surface of the aortic cusps). Typically they appear lobulated with irregular, poorly defined borders and have chaotic motion, in contrast to other valvular masses (fibroelastomas, etc.), which tend to be more highly reflective, with well-defined borders and less chaotic motion. Thin stringy valvular attachments, with a narrow base, are more likely to be noninfectious fibrinous strands than vegetations. Features that help to discriminate vegetations from other masses include the presence of leaflet destruction, valve regurgitation, and abscess or fistula formation. The sensitivity of TTE for detecting features of endocarditis is reported to be between 44 and 60%, compared to a sensitivity of 88 and 100% for TEE. Small vegetations (<3.0 mm) are typically not seen by transthoracic imaging. Infection on prosthetic valves can

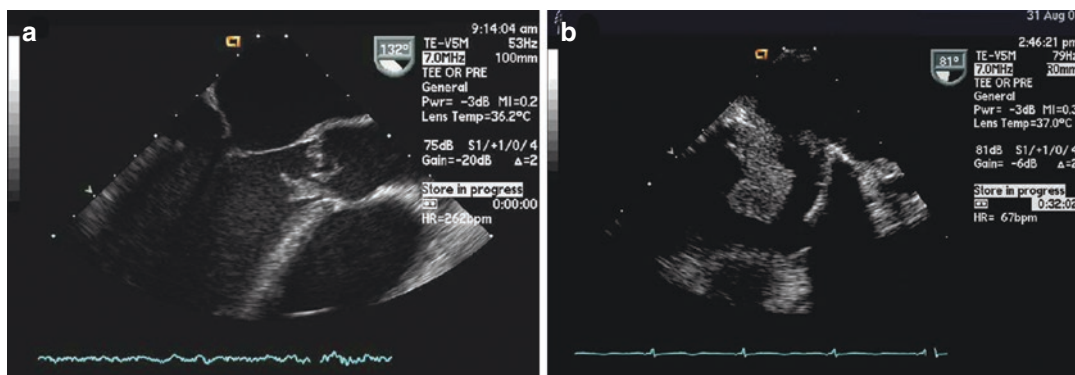


Fig. 30.14 Image (a) shows a vegetation on the right coronary cusp, prolapsing into the LV. Image (b) shows a large vegetation on the posterior leaflet of the mitral valve prolapsing into the LV during diastole

be even more difficult to detect by TTE. Specificity for either modality is high (>90%), though with the superior resolution of TEE, the increased sensitivity may occur at the expense of a slightly reduced specificity (potential to label small benign fibrinous strands on native and prosthetic valves, or nonsignificant mobile suture material on prosthetic valves as small vegetations).

Factors Associated with Vegetation Embolism

The risk of embolization associated with vegetations varies widely (17–50%). Factors associated with embolic risk include vegetation size, mobility, and temporal changes in vegetation size. The most significant echocardiographic feature that is predictive of embolic risk is vegetation size. Vegetations >10 mm have a significantly higher incidence of embolic events compared to smaller vegetations (47% vs. 19%). Enlarging or unchanged vegetations after 4–8 weeks of therapy are associated with an increased incidence of embolic events (45% vs. 17%). Vegetations in the mitral position appear to have a greater embolic risk. Certain organisms are associated with larger vegetations including *Staphylococcus aureus* and the HACEK group of organisms. Despite adequate antibiotic therapy, vegetations may become organized and persist, and these residual lesions are much less likely to embolize.

Historical data suggested that vegetation size can change rapidly with treatment, and in the

absence of other indications for surgery (severe valvular destruction, abscess or fistula formation) a prudent strategy was to treat with appropriate antimicrobials and reassess with repeat TEE in 1–2 weeks. However, recent evidence found that early (within 48 h) surgery as compared to conventional treatment for infective endocarditis carries significantly less embolic events, 3% vs. 23% respectively (hazard ratio, 0.10; 95% confidence interval [CI], 0.01–0.82; $P = 0.03$). There was no significant difference in all-cause mortality at 6 months in the early-surgery and conventional-treatment groups (3% and 5%, respectively; hazard ratio, 0.51; 95% CI, 0.05–5.66; $P = 0.59$). The rate of the composite end point of death from any cause, embolic events, or recurrence of infective endocarditis at 6 months was 3% in the early-surgery group and 28% in the conventional-treatment group (hazard ratio, 0.08; 95% CI, 0.01–0.65; $P = 0.02$).

Prosthetic Valves

An embolic event in a patient with a prosthetic valve is presumed related to the prosthesis until proven otherwise. The source of embolus can be valve thrombosis, valvular vegetations, or left atrial thrombus (with a mitral prosthesis). In one series of patients, with prosthetic valves undergoing TEE for investigation of a potential source of embolus, thrombus was detected on the valve in ~25%. For mechanical prostheses, the overall rate of thromboembolism is 0.7–1% per patient year for those treated with anticoagulation—a much lower rate (4% per patient year) than those without

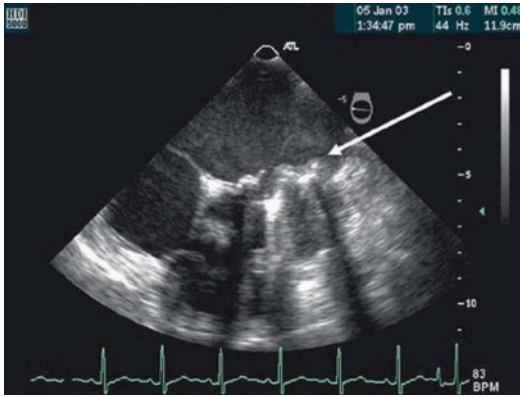


Fig. 30.15 Bileaflet mechanical mitral valve (St. Jude) with fixation of the lateral leaflet secondary to thrombus (arrow) and SEC in the LA cavity

any anticoagulation. The relative risk of embolism is higher with mitral valve prostheses than aortic prostheses, most likely related to the lower flow velocities across the mitral valve. TEE is the investigation of choice for assessing prosthetic mechanical valves. Due to acoustic shadowing, the LA cannot be satisfactorily seen by TTE, and aortic prostheses are typically better seen with TEE. Vegetations or thrombus on these valves can appear similar, though vegetations are typically associated with constitutional symptoms and possible perivalvular regurgitation or partial valve dehiscence. Thrombus typically occurs in the scenario of inadequate anticoagulation. Typically thrombus is mobile, on the valve occluder and valve ring, is associated with SEC, and may cause valve obstruction with elevated Doppler gradients (Fig. 30.15). Treatment of mechanical valve thrombus depends on its severity and hemodynamic consequences. Those with evidence of valve obstruction are usually hemodynamically compromised and traditionally have required urgent surgery. Thrombolysis is now emerging as an effective alternative. For those without evidence of significant obstruction, aggressive and fastidious anticoagulation is warranted.

Fibrinous Strands/Lambl's Excrescences

The literature concerning these two terms is somewhat confusing and they are sometimes



Fig. 30.16 Fibrinous strand on the right coronary cusp of the aortic valve (Lambl's excrescences)

used interchangeably. Though the term “Lambl's excrescences” is usually only applied to those on the aortic valve, there is no evidence to suggest that mitral “fibrinous strands” are different. These strands are thin (up to 1.5 mm in width), elongated (up to 10 mm in length), frequently multiple, and located on the leaflet's line of closure, on the atrial side of the mitral valve, and on the ventricular side of the aortic valve (Fig. 30.16). Histologically they consist of a core of connective tissue with collagen and elastic fibrils or of an acellular hyaline material covered by endothelium. They have also been identified on prosthetic valves. They are equally frequent in both genders and all age groups, which negates against them being primarily a “degenerative” phenomenon. They are very common (~40% prevalence), with the mitral valve being a more common location than the aortic valve. The role of these valve strands in cardiac embolism is unclear. Initial retrospective studies suggested a relationship. However, more recent data have failed to show any association with embolic events and they do not appear to change over time. Therefore, based on current evidence, they are not thought to represent a significant embolic source and do not warrant treatment.

Papillary Fibroelastoma

These rare benign tumors are the most common type of valve tumor. They are more commonly seen on the aortic valve than the mitral valve but may arise from anywhere on the endocardium. From an echocardiographic perspective, they typically are small (<20 mm diameter), round, or

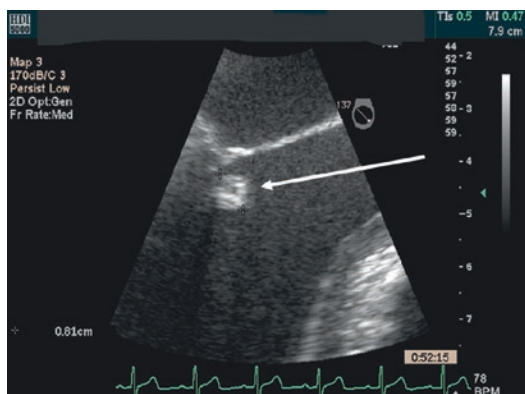


Fig. 30.17 Papillary fibroelastoma on the anterior leaflet of the mitral valve

oval in shape with well-demarcated borders, have a homogenous texture, and are more echodense than thrombus (Fig. 30.17). Typically, they are single with more than half having a stalk and being mobile. They are most commonly seen on the aortic aspect of the aortic valve cusps or the atrial aspect of the mitral valve leaflets. Many are detected incidentally. Typically they do not cause valvular dysfunction.

In the largest series reported, followed up for a mean of almost 2 years, there was a 6.6% incidence of neurologic events. The presence of a stalk (and hence tumor mobility) is reported to be a predictor of embolic risk. It is unclear whether embolic complications are due to thrombus forming on these tumors or embolization of fragments of the tumor itself. Current treatment of these tumors remains unclear. No data exist for the efficacy of anticoagulation or antiplatelet therapy, though treatment with aspirin appears sensible. Asymptomatic patients with small nonmobile tumors can be observed. It is unclear if large mobile tumors in asymptomatic people should be removed. In the setting of an embolic event, surgery is generally recommended.

Mitral Stenosis

Rheumatic mitral stenosis is typically associated with marked LA enlargement, atrial fibrillation, high risk of LA thrombus formation, and systemic embolization (20% lifetime incidence). These patients can have very large amounts of thrombus within the LA. Embolization can occur

despite the presence of sinus rhythm and appears to be unrelated to the severity of the stenosis. The primary risk factors identified for thromboembolism are age and the presence of atrial fibrillation. Currently anticoagulation is indicated for all who have atrial fibrillation, a history of a systemic embolism, or echocardiographic evidence of LA thrombus (ACC/AHA Guidelines 2006). Anticoagulation of patients on the basis of severity of mitral stenosis, severe LA enlargement (LA diameter > 5.5 cm), or the presence of spontaneous echo contrast remains controversial. Early intervention in MS might be more protective rather than delayed intervention, in order to reduce the risk of embolic events. In a non-randomized retrospective analysis study, early percutaneous mitral commissurotomy as opposed to conventional management in asymptomatic moderate mitral stenosis showed that during a median follow-up of 8.3 years, there were three cardiovascular deaths and five cerebral infarctions in the PMC group ($n = 106$) compared with 16 cardiovascular deaths, 112/138 respectively.

Mitral Annular Calcification

Mitral annular calcification (MAC) is one of the most common valve abnormalities detected by echocardiography in elderly patients who are referred for a cardiac source of embolism. It is easily seen by TTE (with TEE tending to underestimate the degree of calcification). MAC is defined by increased echodensity of the mitral annulus, most common posteriorly, but may extend around the entire annulus, giving the appearance of a calcified ring like at the base of the mitral valve. It is found predominantly in elderly women (48% prevalence in a series—mean age of 81 years) and is associated with obesity, systolic hypertension, aging, aortic stenosis, and renal failure. A number of retrospective studies have suggested that MAC is a risk factor for stroke, postulating that it may serve as a nidus for thrombus formation. However, in recent studies MAC was also found to be strongly associated with carotid and complex aortic atheroma. It therefore remains controversial whether MAC is an independent risk factor for stroke or just a marker of increased risk.

Mitral Valve Prolapse

It has been suggested that the redundant leaflets associated with myxomatous mitral valve prolapse (MVP) may act as a nidus for thrombus. Older studies showed a relationship between mitral valve prolapse and stroke, particularly in young patients. However the data from more recent studies have been conflicting. The largest prospective study of MVP and stroke (777 patients) demonstrated an overall twofold increased risk of ischemic stroke. Independent risk factors for ischemic stroke in this population of patients with MVP were older age, mitral leaflet thickening, subsequent development of atrial fibrillation, and need for cardiac surgery. Currently, guidelines (ACC/AHA 2006) update advise that primary prevention of stroke with aspirin may be considered for patients in sinus rhythm with evidence of high-risk MVP (leaflet thickening >5 mm and/or leaflet redundancy). In addition, secondary prevention of stroke with warfarin may be considered for patients with evidence of high-risk MVP, but without standard indications for anticoagulation such as atrial fibrillation or LA thrombus.

Mechanical Valves and Cardio-Embolic Events

Mechanical valves have been in use for more than 30 years so far. These valves initially were more thrombogenic, such as the ball in cage valve, as opposed to the newer heart valves that are available nowadays. The older valve related events almost made these valves replace disease by another. With the advancement of technology, the risk of valve related embolic events has become less nowadays, however, embolic events are still existing and did not become zero so far. Therefore, careful anticoagulation strategies balance and allow less occurrence of thrombotic and or bleeding events which can sometimes be catastrophic. Hence, Self-testing of INR in patients with mechanical heart valve was studied and did significantly reduce the bleeding complications, however, the cost of the device and kit is still major drawback making the device less affordable to the majority of patients [1]. Also, the risk

of thrombotic complication has long been known to be related valve position. Mitral valve carries the higher risk followed by aortic, followed by right sided valves. Recently, lower dose warfarin with target INR 1.5–2 was tested against conventional 2–3 post mechanical aortic valve replacement [2]. The mean INR was 2.50 ± 0.63 for the control and 1.89 ± 0.49 for the test groups ($P < 0.0001$). The test group experienced significantly lower major (1.48% vs 3.26%/pt-yr; $P = 0.047$) and minor (1.32% vs 3.41%/pt-yr; $P = 0.021$) bleeding rates. The incidence of stroke, transient ischemic attack, total neurologic events, and all-cause mortality were similar between the two groups. Moreover, there is evidence that using a no anticoagulation strategy postoperatively in mitral valve repair and bioprosthetic replacement does not increase the risk of stroke or mortality [3]. Thirty-day mortality in patients discharged from the index hospitalization was 1.2% and was similar for the two groups ($P = 0.99$). Four ischemic perioperative strokes were detected; three in the warfarin group and one in the no warfarin group ($P = 0.99$). Bleeding complications were comparable between the two groups ($P = 0.72$). In a multivariate analysis, warfarin was not related to mortality. Moreover, when thrombotic valves events happen, it seems to be already late for prevention of embolic events. Recent data suggest that there is a high prevalence of silent brain infarction in patients presenting with mechanical heart valve thrombosis [4]. Silent brain infarction was present in 27 of 72 patients (37.5%; 95% confidence interval [CI] 27.2, 49.1). The study found that, most patients with SBI (57; 82.6%) had sub-therapeutic anticoagulation at presentation and Atrial fibrillation were strongly associated with the presence of SBI (odds ratio [OR] 5.60; 95% CI 1.32, 23.87; $p = 0.02$).

Patent Foramen Ovale and Atrial Septal Aneurysm

Anatomy

During fetal development, the interatrial septum develops from the fusion of the residual septum primum (lower portion) and the septum secun-

dum (upper portion). Normally the septum secundum overlies the septum primum on the left creating a flap, leaving a patent channel between both atria in utero. This serves as a conduit for the flow of oxygenated blood from the right atrium to the LA, bypassing the high-resistance unoxygenated lungs. After birth, with inflation of the lungs, right atrial pressure drops below LA pressure, causing the two layers of this flap to oppose each other and they typically fuse, closing over this connection (foramen ovale). However, in up to 25% of the population, these two flaps do not fuse completely resulting in a persistent PFO. Typically there is little flow across the residual PFO and any spontaneous flow is typically from left to right as the LA pressure is higher. However, if right atrial pressure exceeds LA pressure either transiently (with Valsalva or other such maneuvers) or more chronically (pulmonary thromboembolic disease), flow can be directed from right to left, with the potential that right-sided venous thromboembolism can cross into the arterial circulation and result in systemic emboli. An atrial septal aneurysm (ASA) is defined as a bulging of the interatrial septum in its midportion (fossa ovalis). The differentiation between a normal mobile septum and an ASA is arbitrary. The most commonly used definition for an ASA is if the sum of the maximum excursions of the midpoint of the aneurysm in both directions from the midline is ≥ 15 mm. The prevalence of a PFO decreases with increasing age (34% in the first three decades, decreasing to 20% in the ninth decade). An ASA is much less frequent, occurring in 1–2% of the general population. Though when it is present, there is a very high prevalence of having an associated PFO (56–77%).

Echocardiography signals giving a false impression of a defect. If optimal subcostal images are possible, a better alignment (the interatrial septum lies perpendicular to the imaging plane) provides for more optimal assessment. Often in this view with color Doppler, a PFO can be suggested by the appearance of a narrow jet of left-to-right flow. Assessment of right-to-left shunting is achieved by injecting agitated saline into an antecubital vein to opacify the right atrium and documenting the appearance of bub-

bles within the LA within 3–5 cardiac cycles, either spontaneously or during a Valsalva maneuver (transient increases in right atrial pressure). Late (>5 beats) appearance of bubbles within the LA.

Transesophageal echocardiography is the imaging modality of choice for evaluating for a PFO (Fig. 30.18). Its presence can often be suggested by TTE; however, the interatrial septum is in the “far field” and in the apical four-chamber view it lies parallel to the ultrasound beam. Therefore there is often “drop-out” of the echo may be due to intrapulmonary shunting and does not necessarily imply flow across the interatrial septum. Agitated saline is created by mixing 8–9 ml of sterile saline with 1 ml of air in a 10-ml syringe, followed by repeated rapid injection to and from another syringe connected via a three-way stopcock until the mixture appears cloudy. Addition of approximately 1 ml of blood (withdrawn prior to injection) improves its contrast potential. TEE is more sensitive for the detection of a PFO than TTE (22% vs. 8%, in one series). By TEE, the interatrial septum lies in the “near field” and can be evaluated with superior resolution in multiple planes. Typically a PFO appears like a flap, near the inferior aspect of the interatrial septum, though color-Doppler interrogation of the septum is necessary to confirm its presence. Flow across a PFO is typically minimal and of low velocity; therefore, the color-aliasing velocity (Nyquist limit) should be reduced, to enable detection of lower velocity signals. Confirmation of right-to-left shunting (which is of most interest in the setting of its systemic embolic potential) requires right-sided contrast (agitated saline). Typically a PFO appears much smaller when measured by echocardiography than when it is sized with a balloon across it, emphasizing that it can stretch and potentially accommodate the passage of a much larger thrombus across it than would be appreciated visually. The size of right-to-left shunting across a PFO is graded arbitrarily based on the number of bubbles seen crossing, with <10 bubbles considered a trivial shunt, ≥ 10 bubbles a small shunt and intense opacification of the LA suggesting a large shunt. An ASA can be seen by TEE or TTE but is more optimally seen by TEE (Fig. 30.19). In one series, 27% of ASA

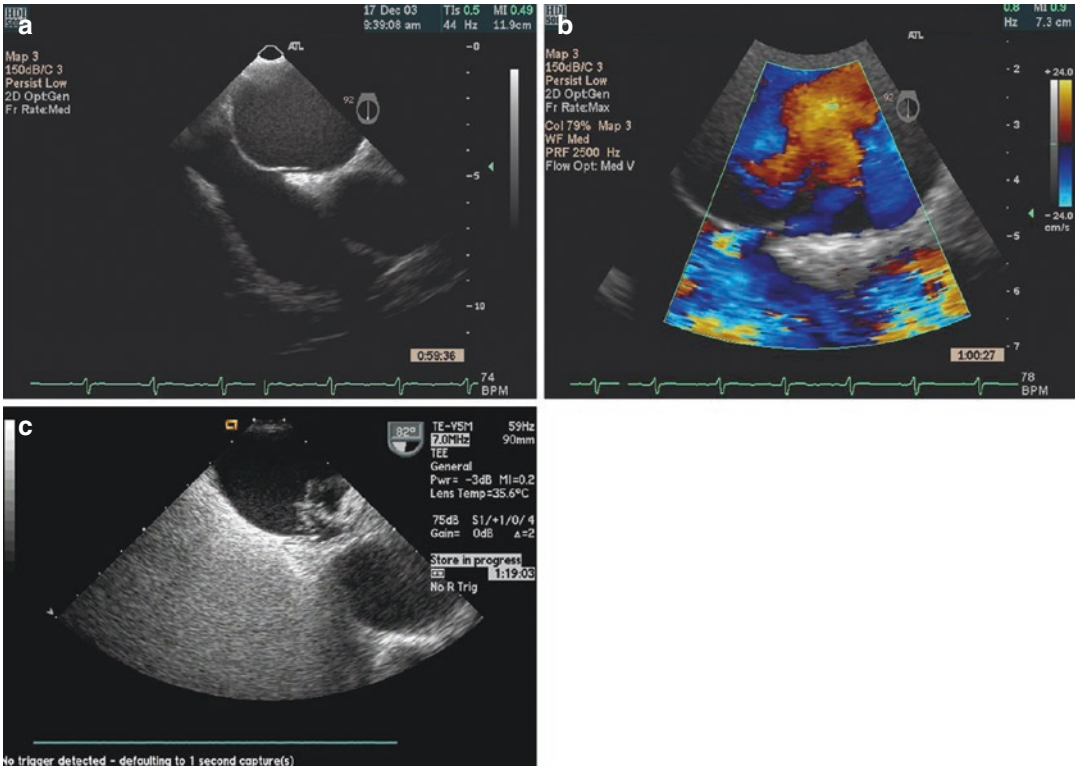


Fig. 30.18 Patent foramen ovale (PFO): the 2-D TEE image shows the typical appearance of a PFO, which was confirmed by color Doppler (left-to-right shunt) and bubble injection (right-to-left shunt) Complex aortic ather-

oma: Image (a) demonstrates severe sessile atheroma in the descending aorta. Image (b) shows a focal pedunculated atheromatous lesion in the thoracic aorta. Image (c) shows diffuse severe complex atheroma

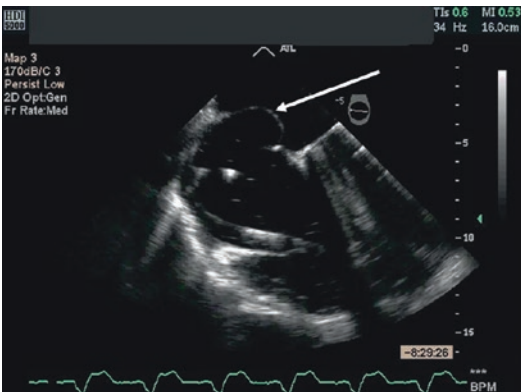


Fig. 30.19 An atrial septal aneurysm (white arrow) with bulging of the septum into the LA

noted by TEE were not detected by TTE. By TTE, it is best appreciated in the four-chamber apical or subcostal views. By TEE, it can be seen in multiple views with the bicaval view (at $\sim 90^\circ$) probably being best.

Potential Mechanisms of Stroke

A number of potential mechanisms underlying stroke in patients with a PFO have been proposed, highlighting the persistent confusion surrounding this relationship.

1. Paradoxical embolism of a right-sided clot:

This remains the primary putative mechanism of stroke in these patients. There are anecdotal case reports of thrombus caught in transit across a PFO. In order for an embolism to cross the PFO, the embolism has to occur at the same time as there is increased right atrial pressures, either transiently (Valsalva) or more persistently (elevated right-sided pressures). One series of younger patients with stroke reported no difference in the frequency of a Valsalva provoking activity at the time of the stroke between those with and those without a PFO. Although one study found evidence of

deep venous thrombosis (DVT) in 57% of patients with arterial embolism and a PFO, the rate in several other studies was much lower (4–10%). Overall, despite the appealing hypothesis of paradoxical embolism, evidence remains scanty.

2. Thrombosis in situ:

There are some anecdotal reports of small amounts of thrombus being identified in PFOs of patients with strokes and also within ASA, suggesting that local thrombus formation may be an alternative hypothesis.

3. Coexistence of atrial arrhythmias: Some data suggest a potential role of transient atrial arrhythmias in thrombosis formation in patients with a PFO

Association of PFO with Embolic Events

A PFO is a common finding and confirming a cause and effect with embolic events has proven difficult. Most data have come from retrospective case control studies. The original study suggested that a PFO was present in 40% of young (<55 years) people with TIA and was significantly associated with a PFO (odds ratio = 3.1) and an ASA (odds ratio = 6.1). The combination of a PFO plus ASA was associated with much higher rate of stroke (odds ratio = 15.6). These associations were not found in older patients. One recently published, prospective study followed up 585 randomly sampled community residents 45 years or older for a median of 5.1 years. 140 (24.3%) had a PFO and 11 (1.9%) an ASA by TEE. There was no association between PFO and stroke (hazard ratio: 1.46, 95% confidence interval: 0.74–2.88, $p = 0.28$). However there was a trend toward a link between ASA and cerebrovascular events (hazard ratio: 3.72, 95% confidence interval: 0.88–15.71, $p = 0.074$). The risk of recurrent cerebrovascular events in patients with cryptogenic stroke and PFO ranges from 1.5 to 12% per year, depending on the study population. Although one study has

shown a significantly higher risk of recurrent stroke in patients with PFO and ASA (4-year recurrence rate: 15.2% vs. 2.3% for PFO alone and 4.2% for neither), other studies have not replicated these findings.

A number of factors have been suggested to be associated with increased risk:

1. PFO size—the larger the PFO, the stronger the association
2. Right-to-left shunting—More shunting is associated with higher risk, especially right-to-left shunting without provocation.
3. Presence of an ASA/increased mobility of the septum—This may be due to the mechanical effect of it acting like a wind sail to direct flow from the inferior vena cava to the PFO.
4. PFO with a “tunnel” like appearance
5. Documented deep venous thrombosis stroke, and 54% of those with a cryptogenic stroke, compared to 10% in a control group. In a meta-analysis of nine studies in patients <55 years, the rate of stroke

Treatment

There is no evidence to suggest that any treatment is warranted if a PFO or ASA is identified in an asymptomatic patient. Furthermore, therapeutic choices in patients who present with a cryptogenic stroke and an atrial septal abnormality are limited. In a prospective study of aspirin therapy in 581 patients with cryptogenic stroke the risk of recurrent stroke at 4 years was 2.3% in patients with PFO alone, 15.2% in patients with both PFO and ASA, 0% in patients with ASA alone, and 4.2% among patients without an atrial septal abnormality. Only one study has prospectively compared therapy with aspirin to warfarin in patients with cryptogenic stroke and PFO. In the PICCS study (PFO in cryptogenic stroke), patients were randomized to warfarin (INR: 1.4–2.8) or aspirin 325 mg daily. In the subset of 98 patients with cryptogenic stroke and PFO there was no significant difference in the 2-year recurrent stroke and death rate between the two treatment arms (17.9% vs. 9.5%, respectively; $p = 0.28$). On the other hand, surgical closure of a PFO is

achieved either by simple suture closure or patch occlusion. Several small series of surgical closure have been reported with varying rates of recurrent stroke (4–20%). Because of the morbidity and mortality of cardiac surgery, isolated surgical closure of a PFO has more or less been supplanted by percutaneous closure. Several devices have been developed for percutaneous PFO closure, and earlier case series showed rates of recurrent stroke of 0–5% following device implantation. Major complications appear to occur at a rate of 1–3% (device embolization, thrombosis, infection, fracture, CVA, pulmonary embolism, arrhythmia, transfusion). Only the Amplatzer™ and Cardioseal™ devices have received approval for the treatment of PFO through a Humanitarian Device Exemption from the U.S. Food and Drug Administration (FDA). The labeling of these devices restricts their use to patients with PFO and cryptogenic stroke who have failed conventional drug therapy. More recently, three prospective randomized trials (CLOSURE I, PC and RESPECT) failed to show decreased rate of recurrent CVA with PFO closure. Only in the RESPECT

trial did a subgroup analysis show that patients with atrial septal aneurysm and substantial shunt gained benefit from PFO closure. Furthermore, a meta-analysis incorporating all these results suggested increased risk from PFO closure and found no benefit. This leaves very limited place for PFO closure, and in 2012 the American College of Chest Physicians Antithrombotic Therapy and Prevention of Thrombosis Panel recommended PFO closure (grade 2C) in cases of recurrent cryptogenic stroke through aspirin therapy and cryptogenic stroke in the setting of both PFO and DVT. Of note, these guidelines were published before the results of the three clinical trials were out and could possibly change once revisited.

Thoracic Aortic Atheroma

Atheroma in the thoracic aorta is not adequately visualized by TTE; thus, TEE is the imaging modality of choice (Fig. 30.20). It is usually divided into three portions: ascending portion, aortic arch, and descending aorta. From a cerebral

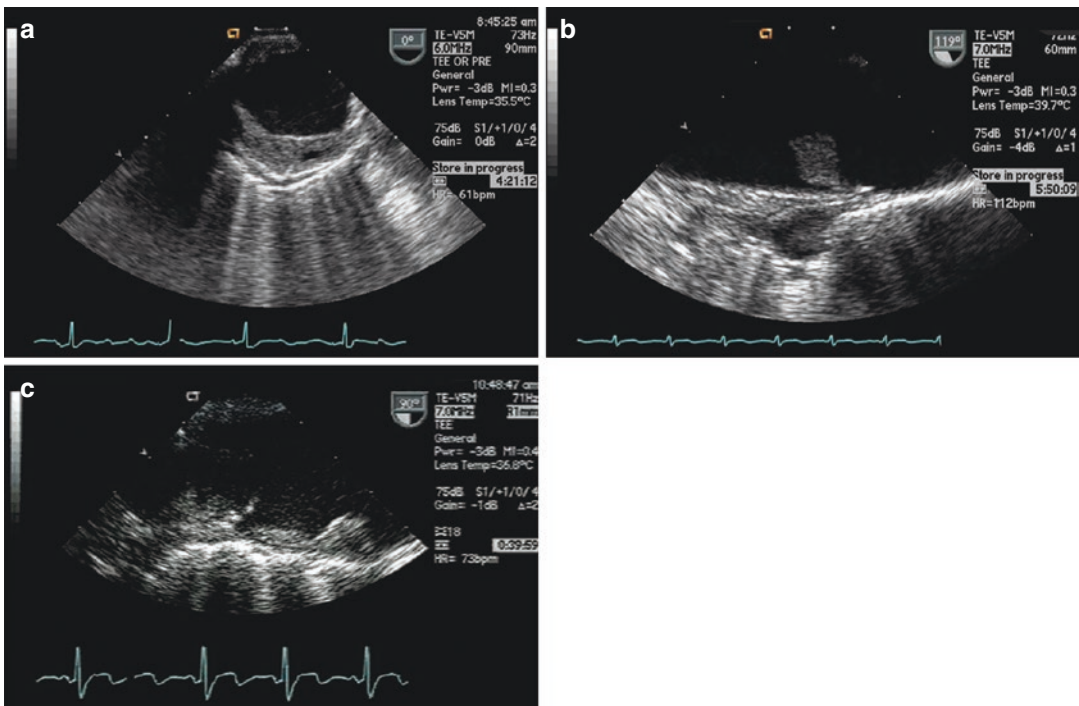


Fig. 30.20 Complex aortic atheroma: the upper image demonstrates severe sessile atheroma in the descending aorta. The middle image shows a focal pedunculated ath-

eromatous lesion in the thoracic aorta. The lower image shows diffuse severe complex atheroma

embolic risk, it is the ascending thoracic aorta and the aortic arch proximal to the origin of the left common carotid that are of most interest. With TEE, the aortic root is best seen in the long-axis view of the aortic valve ($\sim 120^\circ$). Slight withdrawal of the transducer with a reduction in the angle of rotation (~ 90 – 100°) will give satisfactory long-axis visualization of the tubular ascending aorta. There is an echocardiographic blind spot at the junction of the upper ascending aorta and aortic arch due to the interposition of the left main bronchus. Visualization of the descending aorta begins in the transgastric view with posterior.

Echocardiographic Assessment

Atherosclerotic changes in the thoracic aorta are increasingly being recognized as a potentially important source of embolus. It is common with a reported rotation of the probe shaft to bring the descending thoracic aorta into the imaging window. The descending aorta lies behind and very close to the upper portion of the stomach and the esophagus, and the depth of the imaging plane should be adjusted to magnify the aorta.

The probe is gradually withdrawn to visualize the entire thoracic descending aorta, which at 0° of rotation appears in its short axis. Any abnormality should be evaluated in its short and long axes with imaging at 0° and 90° of rotation, respectively. As the probe is withdrawn to about 20 cm from the incisors, the aortic arch will begin to appear. This is best visualized by rotating the probe anteriorly to open out a long-axis view of the aorta and visualize the origin of the great vessels. Visualization of the aortic arch is generally kept until the end of the study as many patients experience reflex gagging with the probe in this position and find it the most uncomfortable part of the study necessitating its removal. Ultrasound cannot differentiate the vessel intimal layer from the media but does detect a change between the media and the bright adventitia. Therefore, for quantification purposes, it is standard to measure the thickness to the level of the bright adventitia and label this as the “plaque” thickness. Traditionally aortic atheroma has been graded using a scoring system of I–IV, though it is probably better to measure the depth of the plaque and describe its characteristics (presence of areas

of ulceration, calcification, sessile vs. pedunculated, and/or degree of plaque mobility). In histologic comparison, TEE showed good correlation in the separation of normal and minimal intimal thickening from more complex atheromas (93% agreement) with 100% agreement in the detection of mobile thrombus.

Association of Thoracic Aortic Atheroma and Stroke

Observational case-control series have shown a significantly higher prevalence of complex atheroma (mobile or ulcerated plaque and plaque >4 mm thick) in patients with a stroke (21–27%) compared to controls (4–13%). In prospective studies, the incidence of stroke at 1 year in patients with protruding atheroma was 12%, with an incidence for all embolic events of 33%. The combination of atrial fibrillation and complex aortic plaque is associated with a higher risk of stroke (12–20% at 1 year) compared to a stroke risk of 1–2% for those with atrial fibrillation without significant aortic plaque. Regardless of anticoagulation or aspirin, this is further evidence to suggest the independent significant embolic potential associated with aortic atheroma. The prevalence of stroke or other embolic events appears to be influenced by plaque morphology. Plaque size (depth), plaque calcification, and plaque mobility are all important features. Increased plaque thickness is associated with a higher risk of stroke with a cut-off of ≥ 4 mm in particular associated with a significantly higher risk of stroke. The significance of visible plaque ulceration is unclear with the available data suggesting that ulceration in thinner plaques is associated with increased risk, while this relationship is not significant in thicker (>4 mm) plaques. The presence of calcification within plaques is associated with a reduced risk of embolic events, a feature likely explained by the fact that calcification most likely represents the presence of more chronic fibrotic, less lipid-laden plaques. Mobile components to aortic atheroma are also associated with increased embolic risk with echopathologic correlation suggesting that these mobile elements are thrombus. Based on current evidence, it appears that most embolic events related to aortic atherosclerosis

are secondary to embolization of thrombus that formed on these atherosclerotic lesions.

Emboli During Aortic Manipulation

There is a risk of emboli with aortic manipulation during cardiac surgery or during left heart catheterization. Embolic complications are rare during cardiac catheterization (0.5% rate of stroke). However, when embolic complications do occur, aortic atheroma is a common association. Reported rates of embolic complications during cardiac surgery involving cardiopulmonary bypass are of the range of 2–7%. Those with aortic atheroma >5 mm on TEE have significantly higher risk of intraoperative stroke. Intraoperative TEE or epicardial echocardiography is used to assess the aorta to help risk stratify these patients and locate a safe point for cannula insertion and crossclamping.

Epicardial echocardiography uses a high-frequency small-sized (transthoracic) transducer covered with a sterile sheath, placed directly on the aorta to visualize the ascending aorta and aortic arch with excellent resolution. A “stand-off” (a saline filled glove) can increase the distance between the transducer and the aorta enabling satisfactory visualization of the anterior wall that may be difficult to see (too close) with the transducer placed directly on the aorta.

Management of Patients with Aortic Atheroma

No consensus exists as to optimal management of patients with complex aortic atheroma. Use of antithrombotic agents and/or anticoagulants appears logical in view of the pivotal role of thrombus in embolic events. Aspirin therapy is generally given for all patients with significant atherosclerotic disease. HMGCo-A reductase inhibitors (statins), with their documented benefits in people with atherosclerosis, are usually also considered. A reduction in the incidence of stroke has been documented for hyperlipidemic patients and also in those with more “normal” cholesterol levels. Despite the fact that anticoagulant therapy has not been prospectively assessed for patients with aortic atheroma, observational

data suggest that it is probably beneficial. Thrombectomy and endarterectomy of complex aortic arch atheroma may be considered for good surgical candidates with recurrent embolic events despite optimal medical therapy. However this approach is associated with a high rate of neurological and vascular complications.

Overall Approach to Evaluation

A cardiovascular source of embolus is increasingly being identified when investigating patients with acute cerebral, peripheral, or visceral ischemia. Most reports have focused on sources of embolus in patients with a stroke. As outlined, the level of evidence demonstrating conclusive cause and effect is limited, and these potential sources are best described as “associations” rather than conclusive causes. It is important to thoroughly evaluate patients for all potential sources, and it is not exceptional to find more than one potential source in a patient, especially as the prevalence of many of these factors increases with advancing age. Additionally, both carotid disease and thoracic atheroma are manifestations of the same disease process, and it is not surprising that patients with significant carotid atherosclerosis have a higher prevalence of aortic arch atherosclerosis than those without carotid disease. Therefore, evaluation of the aorta may be warranted, especially if the neurologic event is contralateral to carotid stenosis or if carotid disease is associated with peripheral or visceral emboli.

Impact of Echocardiography on Patient Management

Once the acute phase of a neurological event has occurred, the primary aim is to identify any potentially treatable sources and prevent recurrent, potentially fatal events. Data suggest recurrence rates for all stroke subtypes of 9.4% per year and 10% for cryptogenic stroke. TEE has been reported as being useful in risk stratifying patients post stroke. One series of patients, who were followed for 2 years and stratified into low

and high risk (based on the presence of at least one likely or possible risk factor for embolism at TEE), showed that those in the low-risk group had significantly better survival (92% vs. 63%, $p = 0.04$). In the STEPS study (242 patients followed after TEE for unexplained stroke) TEE, by demonstrating aortic atheroma and LV dilatation, identified subgroups at high risk of recurrent stroke if treated with aspirin alone, suggesting a potential role for TEE to help guide therapy and influence outcome after an index cerebral event. However, prospective studies are needed to determine whether identification of predictors of stroke recurrence can be translated into improved patient outcome.

Intervention Related Cardio-Embolic Events

With the extended use of interventions in the management of cardiovascular diseases, there have been observations of adverse effects such as iatrogenic strokes and systemic embolization. Coronary angiography, one of the most widely used procedures, along with percutaneous revascularization has revolutionized the treatment of CAD. However, when strokes complicate these procedures, it negates the benefits derived from it, and precipitates harm. Potential causes of the unwanted iatrogenic embolic events are failure of proper flush, improper connections, or incomplete bubble emptying. Using certain techniques might help reduce this risk. Researchers showed that flushing the catheters in the descending aorta then advancing it to aortic root did significantly reduce the incidence of microembolisation in comparison to the standard catheter preparation in the ascending aorta. Also, minimizing the number of catheter maneuvers carries a significantly lower risk of brain microembolisation. Furthermore, left radial access was found to have less risk of brain embolization than right radial. This finding was mostly related to the less number of catheter maneuvers needed from left radial approach. Moreover, the technology advancements allowed the introduction of new procedures into the world of cardiovascular disease management. One of these complex procedures is percutaneous transcatheter aortic valve

insertion (TAVI), which has become the procedure of choice for high surgical risk aortic stenosis patients. TAVI has been shown to be associated with an increased risk of vascular embolic events (30-day stroke rate ranges from 2 to 5%). Similarly, atrial fibrillation ablation is being done more frequently nowadays. Many observational studies found silent strokes secondary to these procedures. Therefore, weighing the risk of vascular events associated with these interventions it is expected that with technology advancement, increased expertise, and careful patient selection these procedures ought to become more safer overtime. An example of a technology modification to reduce stroke is the introduction of circular MER catheter in AF ablation.

Newer Oral Anticoagulation Therapy (NOAC)

The recent introduction of the new oral anticoagulant (NOAC) therapies provided more options for patients with non-valvular atrial fibrillation. The major advantages of NOAC are that these agents do not require monitoring, have fast onset of action, and reduced significantly the risk of intracranial bleeding when compared to oral vitamin K antagonist (VKA). The major disadvantages of these agents are that their use is contraindicated in the presence of severe renal failure and lack of an antidote to reverse their effect when needed. Please refer to Table 30.5 for the characteristics of the various agents and the evidence of their use in patients with atrial fibrillation (Fig. 30.21). In addition to using NOAC as chronic replacement of VKA, recently the XVeRT Trial found that oral rivaroxaban can be safely used as a possible alternative to VKA therapy for preventing thromboembolic events in patients undergoing elective cardioversion.

Extending the use of NOAC for mechanical heart valves has been attempted. The trial Dabigatran versus Warfarin in Patients with Mechanical Heart Valves was terminated prematurely after the enrollment of 252 patients because of an excess of thromboembolic and bleeding events among patients in the dabigatran group. Similarly, the RE-ALIGN trial was terminated

Table 30.5 NOAC vs. warfarin or aspirin data in atrial fibrillation related cardioembolic risk

Anticoagulant/aspirin	Mechanism	Efficacy	Bleeding	
			Intracranial	Major
Apixaban 5 mg/BID ^a	Anti-factor Xa	1.6% per year	0.26% per year	1.4% per year
Dabigatran 150 mg/BID ^b	Anti-thrombin pro-drug	1.11% per year	0.10% per year*	3.11% per year*
Rivaroxaban 20 mg/day ^c	Anti-factor Xa	1.7% per year	0.5% per year	
Vitamin K antagonist	Anti-factors II, VII, IX, X, protein C&S	1.69% per year 2.2% per year	0.38% per year Approximately 0.7% per year	3.36% per year
Aspirin	Cox 1 & 2 inhibitor	3.7% per year	0.31% per year	1.2% per year

^aStuart J. Connolly et al. AVERROES Trial. N Engl J Med 2011; 364:806–817 March 3, 2011. Statistically significant reduction in the risk of intracranial hemorrhage

^bStuart J. Connolly et al. RE-LY Trial. N Engl J Med 2009; 361:1139–1151 September 17, 2009. *Statistically significant reduction in ischemic stroke as compared to warfarin group 1.69% per year, also, significantly less risk of ICH when compared to warfarin 0.38%

^cManesh R. Patel et al. ROCKET AF. N Engl J Med 2011; 365:883–891 September 8, 2011. Approximately non-inferior to warfarin P < 0.001, non-superior P = 0.12. Significant reduction in the risk of intracranial hemorrhage

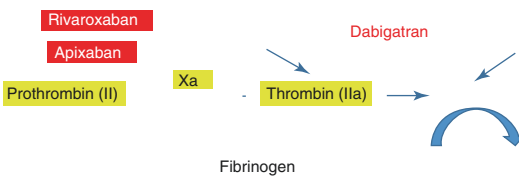


Fig. 30.21 Common pathway of coagulation cascade

early on due to higher thrombotic complications in patients with mechanical heart valves and receiving dabigatran as compared to those treated with warfarin. Thus, so far the data does not support the use of NOAC therapy in patients with mechanical heart valves.

References

1. Thrombosis Res. 2014;133(2):149–153.
2. J Thoracic Cardiovasc Surg. 2014;147(4):1202–1210. discussion 1210–1.
3. Eur J Cardio-Thoracic Surg. 2013;44(1):24–31.
4. Am J Cardiovasc Drugs. 2012;12(5):345–8.
5. Cappato R, Ezekowitz MD, Klein AL, Camm AJ, Ma CS, Le Heuzey JY, Talajic M, Scanavacca M, Vardas PE, Kirchhof P, Hemmrich M, Lanius V, Meng IL, Wildgoose P, van Eickels M, Hohnloser SH. X-VerT investigators. Eur Heart J. 2014a;35(47):3346–55. <https://doi.org/10.1093/eurheartj/ehu367>. Epub 2014 Sep 2.
6. Cheitlin MD, Armstrong WF, Aurigemma GP, et al. ACC/AHA/ASE 2003 guideline update for the clinical application of echocardiography—summary article: a report of the American College of Cardiology/American Heart Association task force on practice guidelines (ACC/AHA/ASE Committee to update the 1997 guidelines for the clinical application of echocardiography). J Am Coll Cardiol. 2003;42:954–70.
7. Donal E, Yamada H, Leclercq C, Herpin D. The left atrial appendage, a small blind ended structure: a review of its echocardiographic evaluation and its clinical role. Chest. 2005;128:1853–62.
8. Goldman ME, Croft LB. Echocardiography in search of a cardioembolic source. Curr Probl Cardiol. 2002;27:342–58.
9. Homma S, Sacco RL. Patent foramen ovale and stroke. Circulation. 2005;112:1063–72.
10. Homma S, Sacco RL, Di Tullio MR, Sciacca RR, Mohn JP, PICSS Investigators. Effect of medical treatment in stroke patients with patent foramen ovale. Circulation. 2002;105:2625–31.
11. Macleod MR, Amarenco P, Davis SM, Donnan GA. Atheroma of the aortic arch: an important and poorly recognized factor in the etiology of stroke. Lancet Neurol. 2004;3:408–14.
12. Udell JA, et al. Patent foramen ovale closure vs medical therapy for stroke prevention: meta-analysis of randomized trials and review of heterogeneity in meta-analyses. Can J Cardiol. 2014;30(10):1216–24.
13. Cappato R, et al. Rivaroxaban vs. vitamin K antagonists for cardioversion in atrial fibrillation. Eur Heart J. 2014;35(47):3346–55.

Part VIII

Congenital Heart Disease

Congenital Heart Disease: Simple Lesions

31

Maria Boutsikou, George Giannakoulas,
Michael A. Gatzoulis, and Wei Li

Introduction

Congenital heart malformations affect nearly 0.8% of live births and include a broad spectrum of clinical entities varying from simple lesions to very complex ones incompatible with life. Adults with congenital heart disease have either history of reparative operation in childhood or have remained asymptomatic until adulthood [1]. Echocardiography remains one of the most valuable imaging tools for the diagnosis and follow-up of patients with congenital heart disease [2]. Transthoracic 2D echocardiography (2D TTE) and Color Doppler are imaging modalities capa-

ble to set the diagnosis in the vast majority of congenital abnormalities.

Transoesophageal echocardiography (TOE) is extensively used for [3]:

- diagnosis
 - In cases of non-diagnostic TTE in suspected cases of congenital malformations
 - In patients with history of congenital heart disease and suspected infective endocarditis, prosthetic valves or cardiac arrhythmias prior to cardioversion
- perioperative guidance (assisting therapeutic decisions and monitor perioperative complications).
- TOE guided percutaneous interventions (mainly ASD and VSD transcatheter closure).

In addition, advanced echocardiographic modalities such as 3D TTE or TOE permit image acquisition and presentation of cardiac structures in three spatial dimensions. Three-dimensional echo imaging plays an important role in pre-surgical planning, guidance of catheter intervention and functional assessment of the heart [4].

The congenital heart defects discussed in this chapter are common, straightforward lesions with a structural abnormality causing hemodynamic problems, including intracardiac communications, valvular lesions as well as simple great vessel malformations.

M. Boutsikou (✉)
The Royal Brompton Hospital, Adult Congenital
Heart Centre and Centre for Pulmonary
Hypertension, London, UK
e-mail: M.Boutsikou@rbht.nhs.uk

G. Giannakoulas
Aristotle University of Thessaloniki, AHEPA
Hospital, Cardiology Department,
Thessaloniki, Greece

M. A. Gatzoulis
Adult Congenital Heart Center and Center for
Pulmonary Hypertension, Royal Brompton Hospital,
National Heart and Lung Institute, Imperial College,
London, UK

W. Li
Adult Congenital Heart Disease Echocardiography,
Adult Congenital Heart Centre and Centre for
Pulmonary Hypertension, Royal Brompton Hospital
and the National Heart and Lung Institute, Imperial
College, London, UK

Atrial Septal Defect

Anatomy and Physiology

Atrial septal defects (ASD) are direct communications permitting blood flow between the atria. They consist the third more common form of congenital heart defects and may present either as an isolated lesion or as a part of a more complex cardiac malformation [5].

The types of ASDs are named after their location in the interatrial septum.

- Secundum (foramen ovale) ASD (70–75% of cases) is located within fossa ovalis. Its size varies from few millimeters to 3 cm or even more in the setting of a stretched atrial septum due to biatrial dilatation, while its shape may present from elliptical to circular shape. They are usually isolated lesions but they may also be present as part of complex congenital heart disease or in genetic syndromes such as Holt-Oram, Noonan syndrome or trisomy 21. Majority of secundum ASD cases are often amenable to percutaneous transcatheter closure.
- Primum ASD (15–20% of cases) involves the lower (primum) portion of the atrial septum near the crux of the heart and may be seen as an isolated defect or in form of atrioventricular septal defect. Surgery is the only therapeutic option.
- Sinus venosus ASD (5–10% of cases) is further classified into superior sinus venosus defect, which is located in the superior portion of the atrial septum near the superior vena cava (SVC) and inferior sinus venosus defect (<1%) which is located near the inferior vena cava (IVC). Superior sinus venosus defects are usually associated with anomalous return of the right upper pulmonary vein to right atrium (RA)/SVC junction.
- Coronary sinus septal defect or “unroofed” coronary sinus (<1%) is characterized by partial or complete lack of separation of the coronary sinus from the left atrium (LA) allowing the right and left atria to communicate through the defect and the coronary sinus orifice. Partial or complete anomalous pulmonary

vein return to the as well as persistent left SVC may coexist (Raghib syndrome) [6].

- Common atrium is the rarest form of ASD, characterized by absence of all components of the atrial septum. Common atrium is usually seen in heterotaxy syndromes, coexisting with more complex lesions.

These defects produce a left-to-right atrial shunt, which eventually causes enlargement of right cardiac chambers. Patients with small to moderate shunts can be usually asymptomatic. Dyspnea, fatigue, atrial arrhythmias and congestive heart failure occur in larger shunts. The development of pulmonary hypertension although rare in patients with ASD, may complicate the natural history of the disease and should be sought during an extensive echocardiographic evaluation. Most individuals with an ASD are identified and repaired in childhood.

Echocardiographic Evaluation

2D Transthoracic Echocardiography (TTE)

On 2D TTE ASDs are depicted as echo dropouts with well-defined edges in the atrial septum. The goals of the echocardiographic assessment in patients with ASD are

- Determination of
 - The anatomic location of the septal defect
 - Its size and shape
- Identification of associated lesions
- Determination of
 - The degree and direction of shunting
- Evaluation of the hemodynamic significance of the shunt.

The best views to reveal an ASD in TTE are:

- The subcostal 4-chamber view, in which the echo beam is kept perpendicular to the atrial septum, is considered to be ideal for imaging the interatrial septum, especially in patients with poor parasternal echo windows (Fig. 31.1). It is the preferred view for the mea-

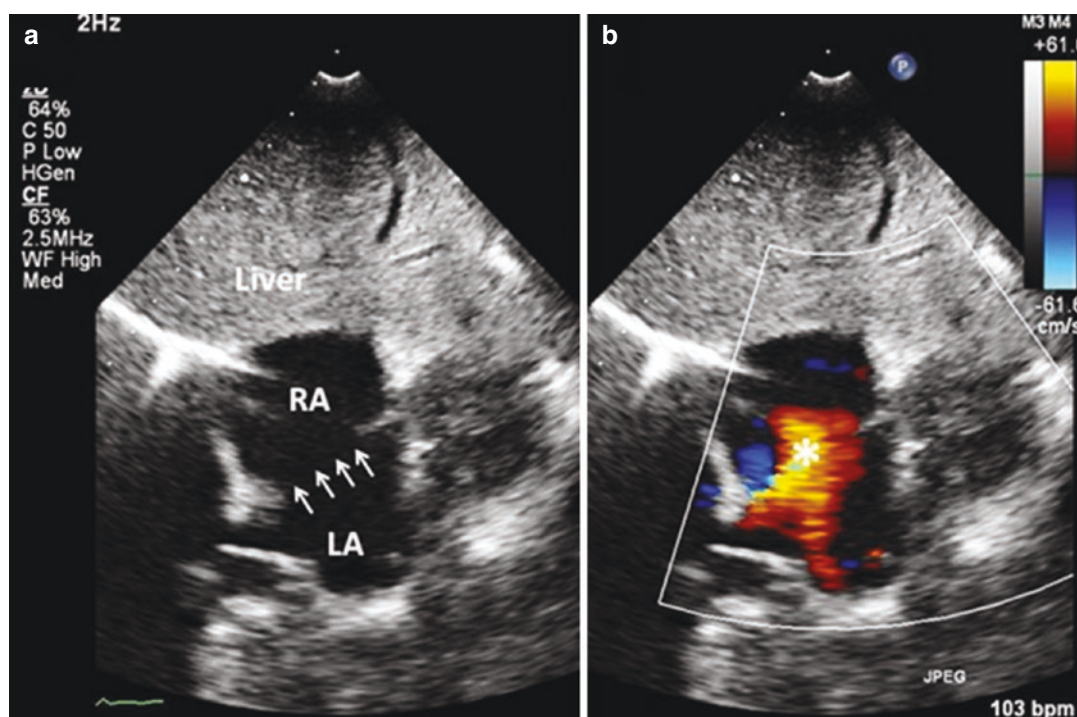


Fig. 31.1 (a) 2D TTE Subcostal 4 chamber view showing a large secundum ASD (arrows). (b) Color Doppler image shows a broad flow jet directed towards the right atrium (L->R shunt)(asterisk)

surement of the diameter of secundum ASD, while the evaluation of the rim from the defect to the right pulmonary veins can also be made from this view. Subcostal short view is very useful in demonstrating SVC type ASD.

- The left and right parasternal short axis views may sometimes generate clear images for sinus venosus defects as the atrial septum is visualized posterior to the aortic root running in an anterior–posterior orientation. These views may not be suitable for the determination of the size of the ASD due to the parallel ultrasound beam orientation to the atrial septum, but are ideal for the evaluation of both the aortic and the posterior rims.
- The apical 4-chamber and especially a modified view, obtained by moving the probe towards the sternum up to the point where the atrial septum is seen almost perpendicular to the beam and then by angulating it anteriorly, may be helpful in obtaining the optimal view of the atrial septum (Fig. 31.2). Classical apical 4-chamber view is used for the evaluation of the hemodynamic consequences of the ASD

and for the estimation of RV pressure, but its use is not recommended for the determination of the size of an ASD, as the parallel alignment of the atrial septum to the ultrasound beam can lead to an overestimation of its size.

For the extended evaluation of interatrial septum, multiple views should be used to evaluate the size, shape and location of the ASD as well as for the determination of its relationship with adjacent structures such as the venae cavae, the pulmonary veins, the atrioventricular valves and the coronary sinus [7]. Secundum ASDs are usually visualized in the mid-portion of the interven-tricular septum, while primum ASDs are located next to the annuli of atrioventricular valves. Direct imaging of the other types of ASD by 2D TTE can be very challenging, as sinus venosus ASDs are located in the drainage of either superior or inferior vena cava, while coronary sinus ASD is seen in the orifice of the coronary sinus to the left atrium. When the defects are not adequately visualized, injection of agitated saline through a peripheral vein could assist in their

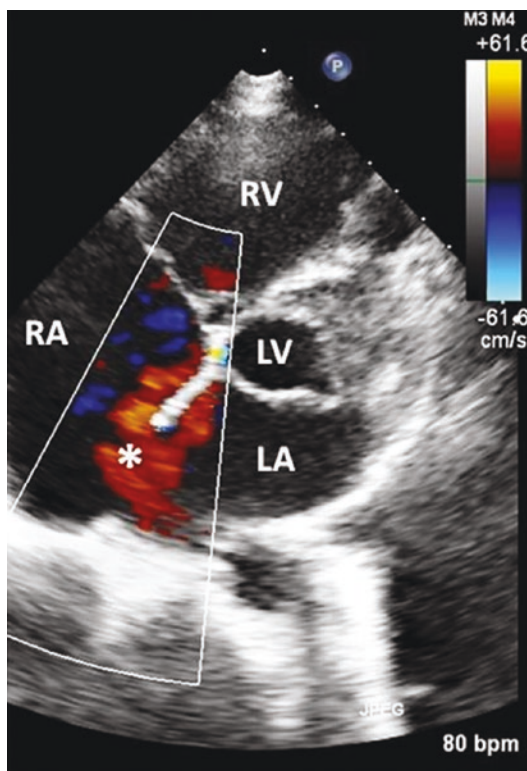


Fig. 31.2 Modified apical 4 chamber view from TTE. Color Doppler demonstrates the left to right flow through a large secundum ASD

diagnosis, as well as in the assessment of residual shunts after transcatheter closure. In this case, microbubbles pass within three to five cardiac cycles from the right to the left atrium through the interatrial septal defect. Even in the context of predominant left to right shunt, there is a period of transient right to left shunting during which contrast passes into the left atrium [8]. Additionally, contrast echocardiography could lead to the diagnosis of coronary sinus septal defect and persistent left superior vena cava, since contrast may appear initially in the left and then in the right atrium when saline contrast is injected into left arm [9].

ASDs are not always round in shape, as shape changes during cardiac cycle even in the same patient. A precise measurement of both the dimensions of the defect and the adjacent rims is essential for the estimation of feasibility for percutaneous transcatheter closure. As the size of an ASD varies

during the cardiac cycle, it is best to measure its maximum dimension during atrial diastole.

The extensive echocardiographic study of an ASD patient should also include the evaluation of all cardiac chambers and pulmonary artery [7]. Potential signs of hemodynamically significant ASD that should always prompt a search for a defect are dilated right heart chambers and diastolic flattening of the interventricular septum (IVS). Extension of IVS flattening to the systolic phase of the cardiac cycle is an index of right ventricular pressure overload and is a typical sign of pulmonary hypertension.

The direction of the flow across the interatrial septum can be seen on color Doppler. Since the pressure gradient between the atria is small, the flow is usually left to right, its velocity is low (usually less than 1–1.5 m/s) and occurs in late ventricular systole and early diastole. The use of pulse wave spectral Doppler can help in the detection of bidirectional shunts. Calculation of shunt ratio is usually not necessary. Right ventricular enlargement indicates a hemodynamically significant shunt, being present when the output of the right heart exceeds the one produced by the left by 50% ($Q_p/Q_s \geq 1.5$).

Right ventricular peak systolic pressure is essential information to obtain as part of the examination, even in patients with no clear marks of hemodynamic significant shunts. The best tricuspid regurgitant Doppler signal should be sought from multiple views. By applying the modified Bernoulli equation to the peak velocity of the tricuspid regurgitation jet, the pressure gradient between the right ventricle and right atria is obtained. Adding on an estimated or measured mean right atrial pressure to this pressure gradient gives the estimate of right ventricular systolic pressure in mmHg [$RV \text{ systolic pressure (mmHg)} = 4 \times TR \text{ velocity (m/s)}^2 + RA \text{ pressure (mmHg)}$].

Transoesophageal Echocardiography (TOE)

Transoesophageal echo is a very useful imaging tool [3]:

- In cases with right sided volume overload with neither evident ASD nor other identifiable cause of volume overload.
- For optimal visualization and characterization of ASDs in patients with poor TTE acoustic windows.
- For evaluation of the presence of sinus venous defects (Fig. 31.3) with or without partial anomalous pulmonary vein drainage (more often right upper pulmonary vein).
- For determining the mode of treatment (suitability for percutaneous closure). In this case TOE is used to assess the diameter of the defect as well as the rims of the septum surrounding the ASD (Fig. 31.4). All rims should be measured in mutiplane views.
- For intraprocedural guidance in cases of percutaneous or surgical closure of the defects and for early detection of complications, such as cardiac perforations, device embolization or malposition, thrombus formation, pericardial effusion, residual postoperative defects etc.

Midoesophageal (ME) bicaval, modified ME aortic valve short axis view, ME 4-chamber view and ME 2-chamber view are the best views to demonstrate ASDs. In all cases, multiple views should be used for the precise evaluation of the size and shape of the ASD, the rims and the surrounding structures. Special attention should be paid to the determination of the relationship of the ASD with the venae cavae, the pulmonary veins, the coronary sinus and the atrioventricular valves.

3D Echocardiography

Apical 4-chamber view, right parasternal and subcostal views are the best views for the demonstration of ASDs using 3D TTE. In selected patients it can be used instead of 2D TOE for the assessment of the dimensions and the location of the ASDs as well as their spatial relations with the adjacent atrial structures [10].

Real-time 3D TOE using live 3D and 3D zoom or 3D full-volume mode are the imaging of choice in assessing size, location and feasibility of device closure of ASD. 3D TOE images of en face right

atrial and left atrial views and transgastric bicaval sagittal views acquired with the 3D zoom and live 3D modes should be used routinely. 3D TOE can provide accurate measurements of the size of the ASD and the surrounding structures during transcatheter closure (Fig. 31.5) and intraoperatively and is especially useful in the case of multiple defects (Fig. 31.6). It can also be very useful in recognizing periprocedural complications, such as residual shunts, device malposition or fractures [11]. 3D TOE has shown that all types of ASDs, except sinus venosus ones, have significant size variation over the cardiac cycle [12].

Cautions

- Normal anatomic variants are important to recognize in order to avoid pitfalls. These include atrial septal aneurysm, Eustachian valve (associated with the entrance of the IVC into the right atrium) and Chiari network (a strand-like structure that extends from the orifices of the SVC and IVC).
- Dropout of echo signal from the foramen ovale occurs when the echo beam is parallel to the inter-atrial septum in the apical 4-chamber view. This gives the false appearance of a septal defect. This is avoided by trying to direct the beam perpendicular to the septum as in the subcostal view and also by combining visualisation of colour flow across the defect with the dropout in 2D echocardiography caused by the ASD.
- The imaging and recognition of an ASD may be proved difficult in the presence of Eisenmenger syndrome. Atrial tachycardia and RV dydfunction where low velocity bidirectional flow on both sides of the septum may mask the defect and give the impression of an intact septum.

Ventricular Septal Defect

Anatomy and Physiology

Ventricular septal defects (VSD) represent the most common form of congenital heart diseases,

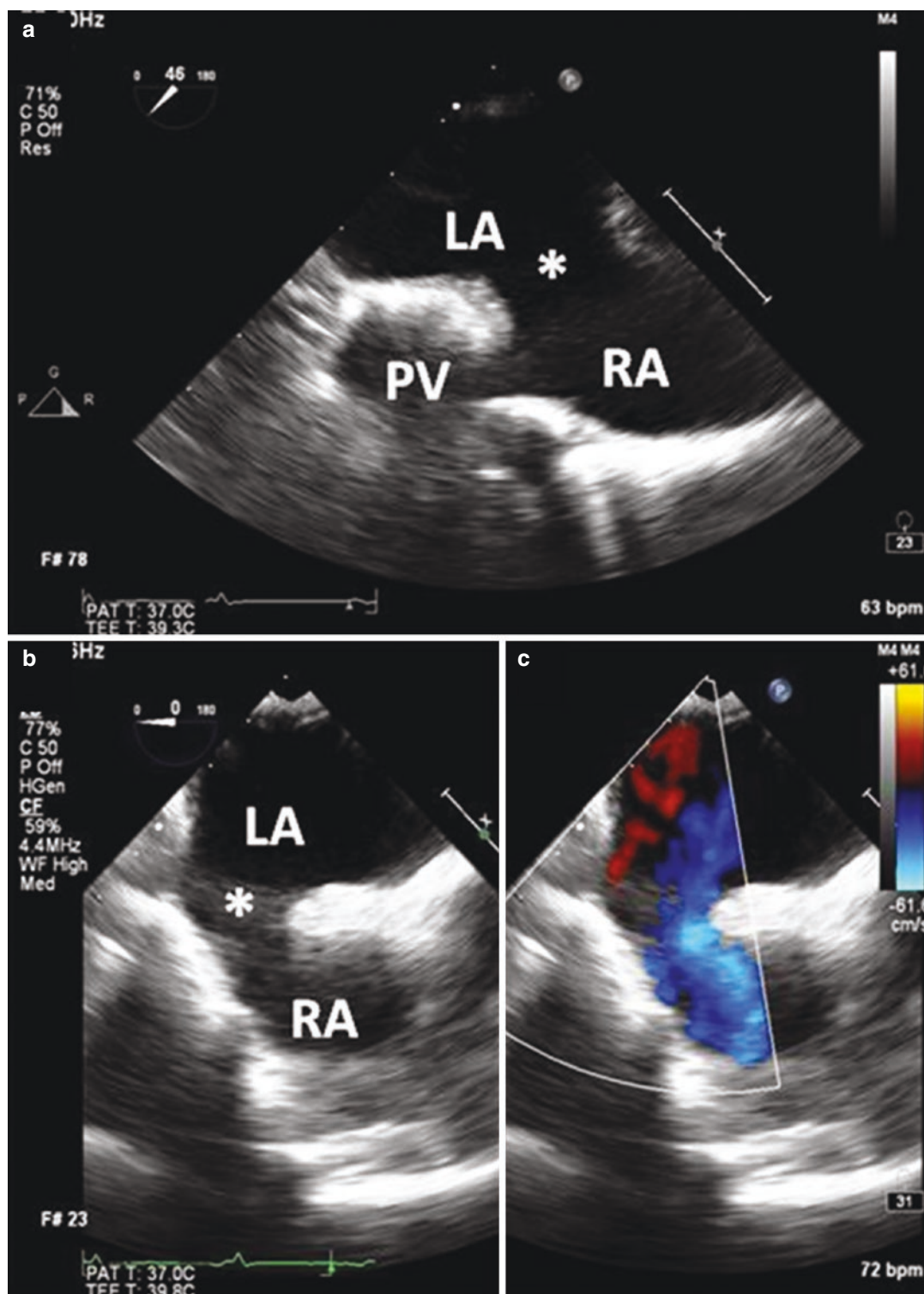


Fig. 31.3 TOE mid-oesophageal view. (a) SVC type Sinus venosus ASD (asterisk) with anomalous pulmonary vein drainage to the right atrium. (b) TOE of mid-oesophageal

view at 0° from same patient showing communication of left and right atria through a sinus venosus ASD (asterisk). (c) Color Doppler showing the interatrial flow

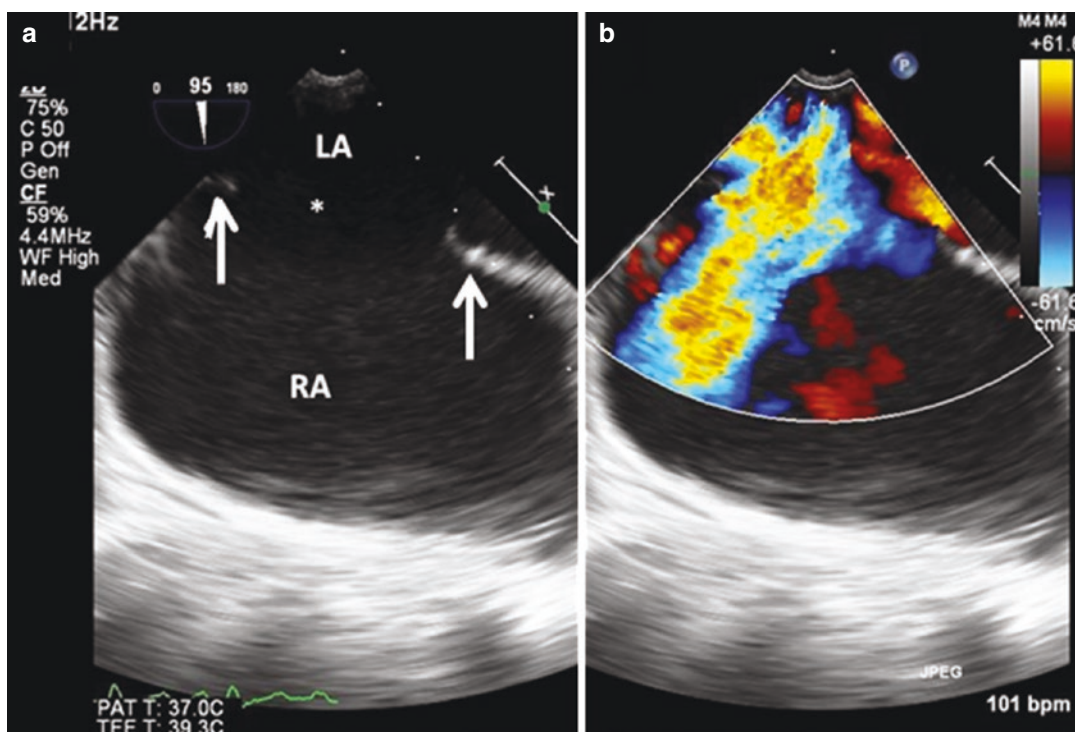


Fig. 31.4 TOE mid-oesophageal cava view. (a) Large secundum type ASD (asterisk). Arrows point the superior and posterior rims of the ASD. (b) Color Doppler shows a broad flow jet directed towards the right atrium

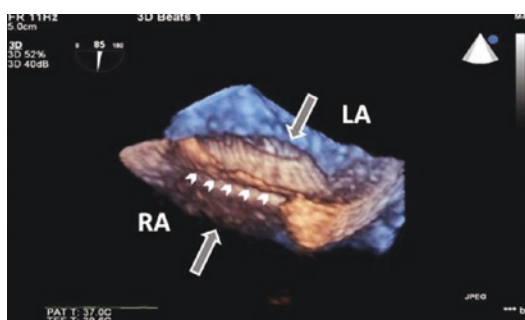


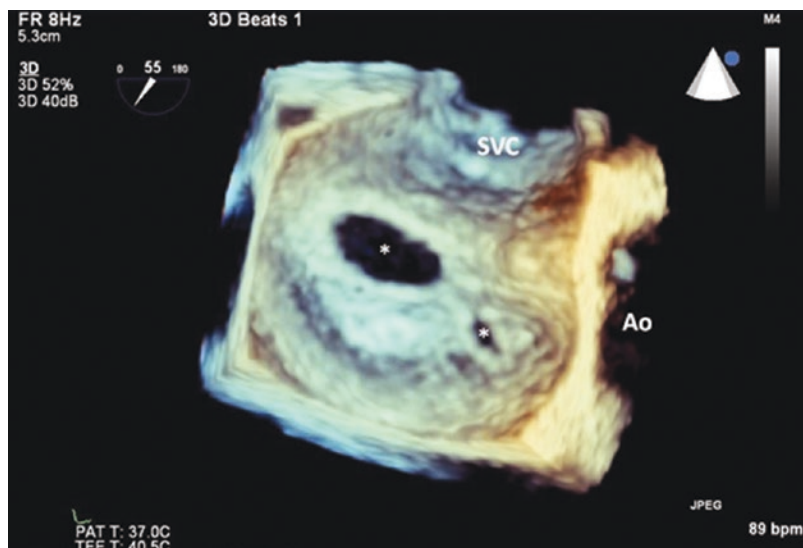
Fig. 31.5 3D TOE. Large arrows point the position of interatrial communication. Small white arrows show the transcatheter closure device

affecting almost 4 in 1000 live infants and accounting for almost 40% of all congenital cardiac malformations. The interventricular septum has a membranous and muscular portion. The membranous septum is thin and relatively small, roughly 5 mm in diameter. It is bordered by the aortic valve superiorly at the junction of the right and non-coronary cusps and by the muscular septum inferi-

orly. The muscular component comprises the majority of the septum and is divided into inlet, outlet and trabecular portion. VSDs are classified according to their location within the septum or at its margins [13]. The most common locations are:

- Perimembranous defect (70–80% of cases), bordered by membranous septum and fibrous tissue comprising the junction between valvar leaflets and atrial fibrous body. According to their location, they are further described as subtricuspid or subaortic VSDs as they open close to the atrioventricular or the semilunar valve respectively.
- Muscular defects (20% of cases) occur anywhere within the trabecular portion of the septum and may be isolated defects, multiple (Swiss-cheese septum) or coexist with perimembranous or juxta-arterial defects. They are exclusively surrounded by muscular rims and can open into the ventricular inlet, outlet or apex.

Fig. 31.6 3D TOE. Asterisks show two secundum atrial septal defects



- Doubly committed juxta-arterial defect (5–8% of cases). It is characterized by fibrous continuity between the leaflets of the pulmonary and the aortic valves or presence of a common arterial valve. The right cusp of the aortic valve may herniate into the defect creating progressive aortic regurgitation.

The anatomic distinction of a VSD plays a significant clinical role, in regards to the possibilities of spontaneous closure, the need for surgical closure and the surgical approach, the possible involvement of the conduction system or the coexistence of associated lesions.

According to their hemodynamic significance, VSDs are further characterized as:

- Restrictive, usually the defect is small and there is significant interventricular pressure gradient. The shunt is usually small ($Q_p/Q_s < 1.5$) and with no significant hemodynamic burden.
- Non-restrictive, the shunt is large ($Q_p/Q_s > 2.5$) and the defect causes a significant left ventricular (LV) volume overload, dilatation of left heart chambers, pulmonary hypertension and finally the development of Eisenmenger physiology with elevated pulmonary vascular resistance and bidirectional shunting.

VSDs can present as isolated lesions. However, they can also be part of more complex cardiac malformations such as tetralogy of Fallot, congenitally corrected transposition of the great arteries, anomalies involving the left or the right ventricular outflow tract, coarctation of the aorta and interrupted aortic arch and univentricular hearts [1].

Echocardiographic Evaluation

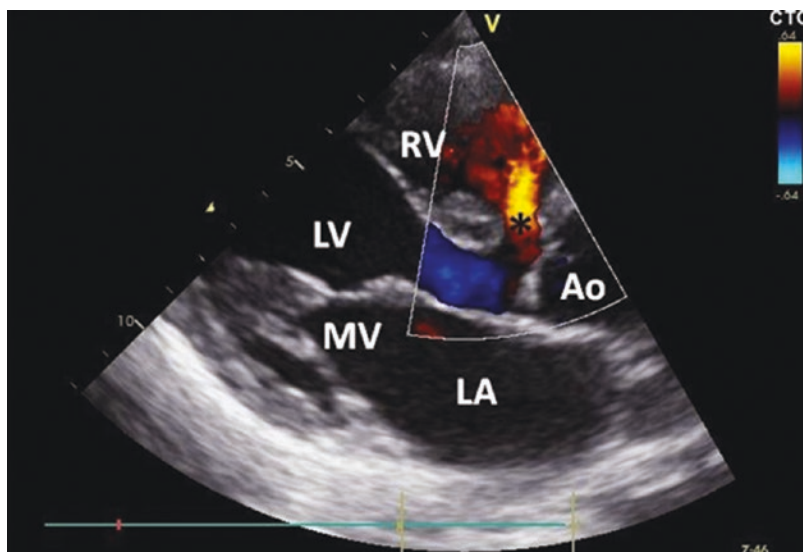
2D Transthoracic Echocardiography

Transthoracic echocardiography is the mainstay of modern diagnosis of VSDs.

The goals of echocardiographic evaluation of a VSD are:

- Determination of
 - the anatomic location within the septum and in relation with tricuspid, aortic and pulmonary valves
 - the size of the defect
- Characterization of
 - the size, direction and hemodynamic significance of the shunt
 - LV dimensions
 - Dilatation or hypertrophy of the right ventricle
 - Biventricular function
 - Increased pulmonary artery pressures

Fig. 31.7 TTE of parasternal long axis view. Color Doppler shows the perimembranous VSD flow with left to right shunt (asterisks)



- Identification of associated lesions (e.g. aortic regurgitation, coarctation of the aorta, more complex congenital heart disease).

Interventricular septum should be imaged from several planes in order to provide a precise diagnosis. The best views to accomplish this are:

- the parasternal long axis view, from which, with a minimal medial angulation, the illustration of the perimembranous VSD is ideal. This is seen at the level of the aortic valve, where the defect can be demonstrated inferiorly to the right coronary cusp of the aortic valve and next to the septal leaflet of the tricuspid valve (Fig. 31.7). Prolapse of the right coronary cusp into subaortic VSD is well seen.
- the parasternal short axis view is ideal for the illustration of VSD location. From this view, perimembranous sub-tricuspid VSDs are seen between 9 o' clock and 11 o' clock position. A juxta-arterial VSD is seen between 12 o' clock and the hinge of the pulmonary artery. A perimembranous subaortic VSD will be located between 11 and 12 o' clock. Inlet VSDs are better seen from parasternal short axis view at the level of the mitral valve. Muscular VSDs may be located anywhere within the trabecular septum, requiring careful screening at different levels from basal to apical segments.

- the apical 4 chamber view, where by tilting the echo beam inferiorly an inlet VSD can be better viewed between the atrioventricular valves. In this view, muscular VSDs can also be viewed more apically [8].

As in ASDs, a VSD should not be considered as being a round deficit of the interventricular septum. Its shape is often complex and may be obscured during systole due to myocardial contraction. It can literally be located anywhere in the interventricular septum, vary in size, and be single or multiple, isolated or as a part of a more complex congenital heart defect [13]. Perimembranous defects should be sought medially to the interventricular septum, close to the septal leaflet of the tricuspid valve (Fig. 31.8). Doubly committed defects are situated anteriorly and more to the left of the aortic annulus and are further classified as being above (located leftward to the midline and adjacent to the pulmonary valve) or below (located to the right of the midline) the crista supraventricularis. An inlet VSD is located posteriorly toward the crux of the heart. In the presence of an uncomplicated inlet VSD, tricuspid valve is normally placed apically compared to mitral valve. An atrioventricular septal defect should be sought, in cases where both atrioventricular valves are located at the same level. Muscular VSDs may appear as

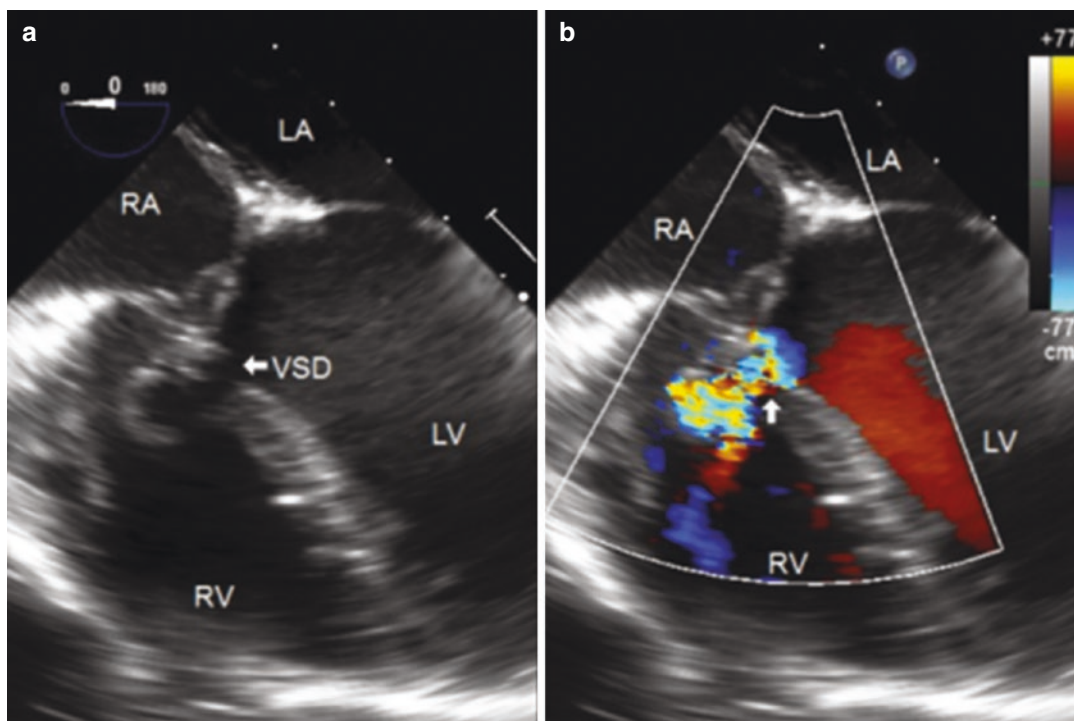


Fig. 31.8 2D TOE from mid-oesophageal four chamber view. Arrow points a perimembranous VSD

narrow channels crossing the muscular septum, with the orifice of the one side being displaced from the orifice of the other side of the septum, giving the impression of an irregular tunnel.

Given the complexity in the anatomy of the interventricular septum, the simultaneous use of both 2D and color Doppler echocardiography proved useful especially for detecting small defects. After identifying the jet, the Doppler beam should be placed in parallel to the blood flow, in order to obtain a reliable velocity signal. The modified Bernoulli equation is used to calculate the interventricular pressure difference, to obtain an estimate of RV and PA systolic pressure (in the absence of pulmonary stenosis). In restrictive VSDs, the blood flow from the left to the right ventricle is recorded as a high velocity turbulent systolic jet crossing the ventricular septum suggesting normal pulmonary vascular resistance. Flow across the defect may continue into diastole as LV diastolic pressure usually exceeds RV diastolic pressure. When diastolic left to right shunting velocity exceeds 1 m/s, this suggests left

ventricular diastolic dysfunction and elevated end-diastolic pressure. Nonrestrictive VSDs are characterized by smaller interventricular pressure gradient and thus by lower velocity jet. With larger defects and elevated pulmonary artery systolic pressure, jet velocity is lower, but pulmonary vascular resistance may still be normal or only mildly elevated. In cases with elevated RV systolic pressure and pulmonary vascular resistance, bidirectional or net right-to-left flow may occur across the VSD indicating obstructive pulmonary vascular disease (Eisenmenger physiology).

The hemodynamic burden of VSD may lead to serious complications. Left ventricular volume overload, resulting from a large defect, leads to left heart enlargement and even to left ventricular failure, especially in patients with large nonrestrictive defects. Left atrial and ventricular enlargement are usually present when the left-to-right shunt volume exceeds 50% of systemic flow ($Q_p/Q_s \geq 1.5$). In clinical suspicion of endocarditis, vegetations can be identified on both the aortic and the tricuspid valves or the membranous septal aneurysm.

3D Echocardiography

With 3D TTE the size, the location and the spatial relation of the VSD with the adjacent structures can be assessed more precisely. Apical four chamber view with narrow angle and zoomed acquisitions is the best view to visualize the interventricular septum. En face view of the defect obtained by 3D TTE, can contribute to the choice of the best therapeutic approach whether this is surgical or percutaneous closure.

Moreover 3D TOE, can be a valuable tool intraoperatively assisting on the optimal sizing and positioning of the closure materials. En-face presentation of the ventricular septum from both RV and LV can be achieved from a four chamber view using live 3D or full volume acquisition (Figs. 31.9 and 31.10). After device deployment, live 3D with color flow Doppler is optimal for assessing the result.

Cautions

- Trabecular defects are the more difficult to detect with 2D echocardiography. They are often serpiginous and right and left ventricular sites may not be in the same plane. In cases of a distorted right aortic

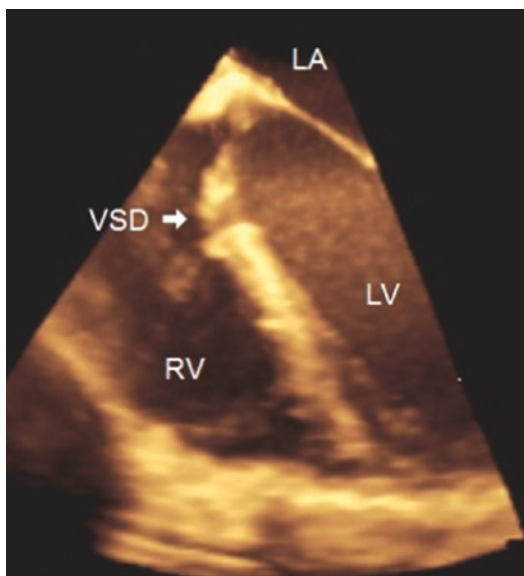


Fig. 31.9 3D TOE from mid-esophageal four chamber view showing a small muscular VSD (white arrow)

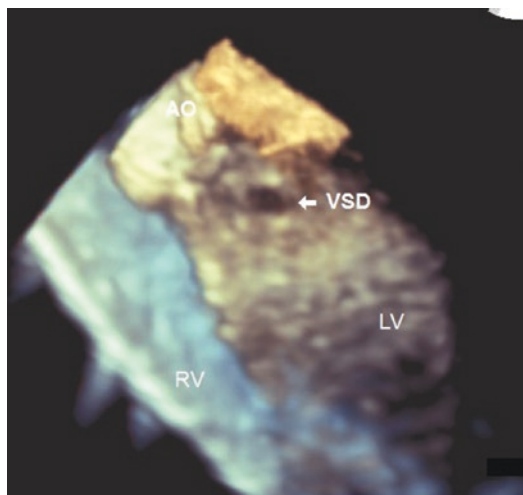


Fig. 31.10 3D TOE from same patient as in Fig 31.9. En face view of the small muscular VSD from LV side (white arrow)

cuspid that prolapses into the VSD, the defect itself may not be visible. The use of color Doppler (turbulent flow) may help to detect the defect.

- Measurement of peak VSD velocity can be problematic if the jet is deflected by the tricuspid valve, septal aneurysm or muscle bundle. The true interventricular pressure gradient may be underestimated if the echo beam is not parallel to the VSD jet.
- The estimate of the right ventricular pressure from the VSD velocity must correlate with that determined by the tricuspid regurgitation velocity. Any significant disparity needs to be resolved. The jet lesion produced by the VSD in the same area with tricuspid regurgitation jet usually causes overestimation of right ventricular pressure and in this case other signs of elevated pulmonary vascular resistance should be sought.
- In cases of large inlet VSDs, care should be taken in order for them not to be misdiagnosed as double-inlet left ventricle.
- In small perimembranous and outlet VSDs, low-velocity diastolic shunt flow may precede the high-velocity systolic jet, presumably owing to slight differences in late interventricular diastolic pressures. This diastolic flow

is sometimes mistaken for aortic regurgitation or another aortic lesion, such as a sinus of Valsalva fistula or coronary artery fistula.

Atrioventricular (AV) Septal Defect

Anatomy and Physiology

Division of the common A-V canal occurs by fusion of the superior and inferior endocardial cushions. Failure of this affects the structures derived from endocardial cushion tissue to varying degree [1].

A complete AV septal defect consists of

- Ostium primum ASD
- VSD of the inlet septum
- Common five leaflet valve with an anterior bridging leaflet, a posterior bridging leaflet, a left mural leaflet, a right mural leaflet, and a right antero-superior leaflet. This valve is all at the same level within the ASD and VSD. The AV valve is usually equally committed to both ventricles, but may be primarily committed to one ventricle. Further description of the AV valve is based on the extent and location of attachments of the anterior bridging leaflet. The following Rastelli classification is useful for the decision of the most suitable surgical intervention [11].
 - Type A. Tethered by chordae to the crest of the ventricular septum
 - Type B. Attached to an anomalous papillary muscle in the RV
 - Type C. Free floating (no chordal attachments)

A partial AV septal defect (ostium primum ASD) consists of

- An AV valve divided into right and left sided orifices by a band of tissue connecting the superior and posterior bridging leaflets. In this case, the AV valve is displaced downward (but both sides still at the same level) into the ven-

tricle and anchored to the crest of the septum eliminating the VSD component

- Tri-leaflet left atrioventricular valve
- A small, restrictive VSD may be present

Echocardiographic Evaluation

The goals of the examination are to

- Define the components of the AV septal defect
- Define the morphology (single orifice or two separate orifices) and chordal attachments of the leaflets of the AV valve
- Estimate size and function of the right and left ventricles
- Determine the extent of the ASD and VSD and the extent of shunting.

2D Transthoracic Echocardiography (TTE)

The best views are the apical and subcostal 4 chamber and the parasternal long and short axis views [8]. The apical and subcostal 4-chamber views are best for evaluation of the inlet portion of the heart. They show the ASD and VSD well (Fig. 31.11). In some instances, the VSD may be closed by chordae attachments or tricuspid valve tissue. The parasternal short axis view is helpful to determine whether one or two orifices are present and how well they line up with the ventricles. If two orifices are present, the left AV valve is usually composed of three leaflets; superior bridging leaflet, inferior bridging leaflet and mural leaflet. This is seen best by watching the motion of the anterior leaflet that separates in the middle as the valve opens in diastole. Addition of color will show the location of the regurgitant jet originating from closure line between superior and inferior bridging leaflets.

Doppler is helpful to define the types of intracardiac shunting present and the degree of AV valve regurgitation. The precise hemodynamics vary depending on the shunt.

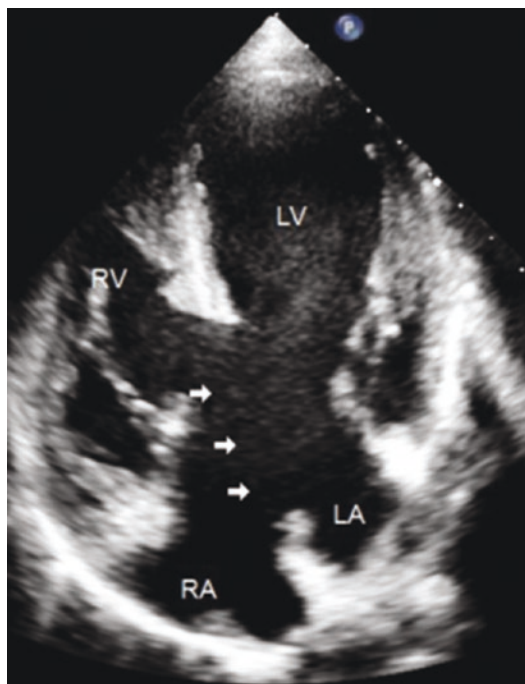


Fig. 31.11 TTE 2D apical 4 Chamber view. Arrows point the AVSD (ASD and VSD) with a common atrioventricular valve. *S* superior bridging leaflet, *I* inferior bridging leaflet, *M* mural leaflet

- Predominate shunting at the atrial level produces the finding typical of an ASD
- Shunting at both atrial and ventricular level occurs with complete AV septal defect. The risk of this physiology is early development of irreversible pulmonary vascular disease unless the pulmonary circulation is protected by RVOT obstruction.
- Significant AV valve regurgitation
- It is also important to evaluate both ventricular outflow tracts for obstruction. This can be due to a muscular obstruction or chordae crossing the outflow tract and inserting into the septum, especially from the left side.

Transesophageal Echocardiography (TOE)

TOE is useful in providing detailed assessment of atrioventricular valve morphology and function.

3D Echocardiography

3D TTE with en face view as well as with the ability of image acquisition from different angles can provide more detailed information regarding the size of the atrioventricular defect, the surrounding structures and the atrioventricular valve (Fig. 31.12) [11]. Specifically, 3D TEE

- Provides detailed imaging of the five leaflets of the atrioventricular valve and especially of the anterior bridging valve. This information is important for the categorization of AVSD into the three Rastelli types.
- Provides information on the morphology of the five leaflets of atrioventricular valve.
- As with 2D TTE colour Doppler is useful in assessment of the severity of the AV valve regurgitation.

Cautions

Because of the broad spectrum of anomalies that may be present, a thorough echocardiographic evaluation by a sonographer familiar with defects is essential.

- Assessment of systolic pulmonary artery pressure from the tricuspid regurgitation can be a problem. Using VSD shunt velocity may provide a more accurate estimation.
- LV to RA shunt is common. Caution should be taken to differentiate it from tricuspid regurgitation.

Patent Ductus Arteriosus

Anatomy and Physiology

Ductus arteriosus is a blood vessel connecting the pulmonary artery bifurcation, at the origin of the left pulmonary artery to the inner curvature of the aorta opposite to the left subclavian artery. The pulmonary orifice is usually smaller than the

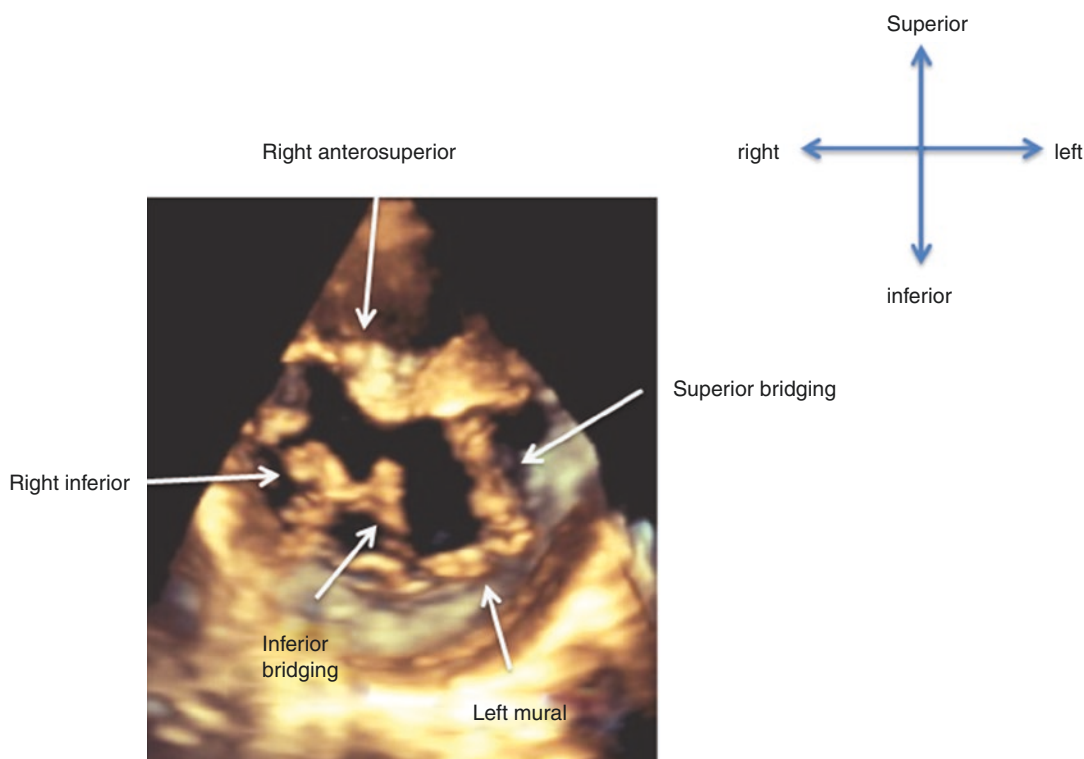


Fig. 31.12 3D TTE. En face view of the common atrioventricular valve in a patient with AVSD

aortic end, thus, creating a funnel shape. While essential in the fetus for the bypass of the pulmonary circulation, the ductus normally closes once flow through the lungs is established shortly after birth. Patent ductus arteriosus (PDA) accounts for 5–10% of all congenital malformations and is more common in premature infants.

A PDA can be short, long, straight or tortuous in shape, making complete visualization difficult. The consequences of the left-to-right shunt from a PDA depend upon its size and the pulmonary vascular resistance. As with a VSD, the degree of enlargement of the left atrium and left ventricle is a useful marker of the magnitude of the shunt. Trivial shunts may be asymptomatic, detected only when a murmur is heard, or noted incidentally on echocardiography performed for another indication. Medium shunts result in heart failure due to volume overload of the left heart, while large PDAs usually result in increased pulmonary vascular resistance. If uncorrected, pulmonary arterial hypertension

develops and the shunt becomes bidirectional with cyanosis of the lower, but not the upper extremities (differential cyanosis).

Echocardiographic Evaluation

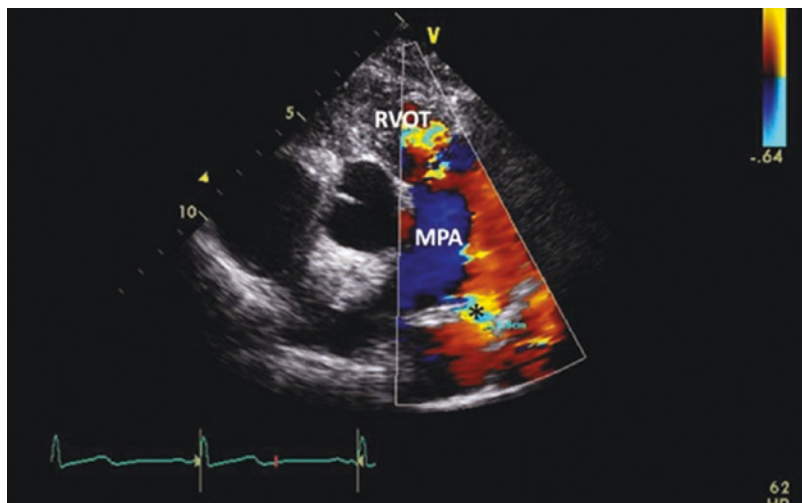
2D Transthoracic Echocardiography

Although 2D imaging of a PDA is easy in neonates and small children, its exposure may be proved difficult in adults. The goals of the echocardiographic evaluation of an adult patient with a PDA are:

- Identification of
 - the size of the ductus
 - the shape of the ductus
- Quantification of its hemodynamic significance
 - LA and LV dimensions
 - LV function
- Establishment of RV and PA systolic pressure

The best 2D views to visualize a PDA are [14]:

Fig. 31.13 TTE parasternal short axis view- Color Doppler. Asterisk shows PDA with antegrade flow from the descending aorta to the main pulmonary artery



- High-left parasternal view directed towards the PA bifurcation. In this view, the main pulmonary artery appears to be divided in three instead of the normal two branches, with the third branch being the PDA. By rotating the beam clockwise, the entire length of the ductus may be depicted.
- suprasternal notch focusing on the descending aorta opposite to the left subclavian and swinging toward the left pulmonary artery. In this view, PDA is visualized as a narrow channel.

The diagnosis of a PDA is made more easily with Doppler than 2D imaging of the duct (Fig. 31.13). Turbulent flow in the main pulmonary artery that persists throughout the cardiac cycle is an important clue for the presence of a PDA. Despite the fact that the flow through the ductus in the pulmonary artery is continuous, it is usually visualized as a diastolic red jet, because its systolic component is mixed with the normal systolic flow of the vessel. Flow within the duct should also be evaluated.

Most commonly, a high velocity flow from left-to-right reaching a peak in late systole is present. From the suprasternal view, holodiastolic flow reversal from the descending aorta into the duct can also be recorded. In patients with elevated pulmonary vascular resistance and pulmonary hypertension, the PDA shunt may be difficult to be distinguished as its velocity decreases due to decreased pressure difference.

The pressure gradient calculation using Doppler velocity across the duct or tricuspid regurgitation provides information about right ventricular and pulmonary arterial systolic pressure. In most instances, pulmonary arterial systolic pressure is normal or only slightly increased. Rarely, a bidirectional shunt is present, characterized by a right-to-left shunt in early diastole followed by left-to-right flow in late systole and diastole. This indicates significantly elevated pulmonary vascular resistance and Eisenmenger physiology.

Left heart dimensions and systolic function should also be evaluated in patients with PDA. Although in cases with small PDA the hemodynamic burden is not significant and normal size and function of left heart is the usual finding, in those with larger defects the echocardiographic study may reveal enlargement of left ventricle and atrium with impaired left ventricular systolic function and pulmonary hypertension. Other associated defects such as VSD, coarctation of the aorta, etc., should also be sought. The pulmonary artery may appear dilated, aneurismal or calcified, especially in older adults. In adult patients with pulmonary hypertension and Eisenmenger physiology the duct is often difficult to be identified by color Doppler. Indirect elements such as right heart enlargement, flattening of the interventricular septum towards left ventricle and a systolic notch in the M-mode of

the pulmonary valve may be seen. Other imaging modalities such as CT or CMR should be used to confirm the diagnosis.

Transoesophageal Echocardiography (TOE)

The therapy of choice in patients with PDA today is its transcatheter closure with the use of different types of devices, for reducing the risk of developing pulmonary hypertension or endocarditis. As in ASD closure, TOE plays a significant role in periprocedural guidance, providing useful information on the anatomic details of the ductus. The best view to visualize PDA is at 135°, in which the ductus is located between the left pulmonary artery and the aorta. The use of TOE has markedly reduced the fluoroscopic periprocedural time. TOE is also used for the immediate post-closure evaluation of patients with PDA playing a significant role in the verification of the proper placement of the device, which should be seen between the bifurcation of the pulmonary artery and the inferior margin of the aorta as well as in the identification of possible residual shunts.

3D Echocardiography

3D TTE can provide more accurate information than 2D TTE regarding the diameter, the length of the duct and the anatomical type of the duct. The best view to acquire images of the duct is from the parasternal notch position [15]. Additionally, it can provide a complementary analysis of left atrial and ventricular dimensions and volumes.

3D TOE can also be used during surgery or percutaneous closure in order to assess the optimal device position, the presence of residual shunts through the duct or the probable obstruction of the left pulmonary artery after the placement of the closure device.

Cautions

- Low velocity retrograde flow in late systole secondary to swirling flow within an enlarged PA should not be mistaken for ductal flow.
- Continuous flow into the PA is also seen with a coronary artery fistula, an anomalous coronary artery or an aortopulmonary window. These

are rare congenital abnormalities that should not be confused with a PDA.

- The pandiastolic flow reversal in the descending aorta due to antegrade flow into the ductus in diastole, recorded from the suprasternal view, should not be confused with the diastolic flow reversal due to aortic regurgitation.

Pulmonary Stenosis (PS)

Anatomy and Physiology

Pulmonary stenosis can be valvular, subvalvular (infundibular), or supra-valvular. This section will focus on valvular stenosis.

Valvular pulmonary stenosis is present in approximately 7–10% of the patients with congenital heart disease [1]. Is usually an isolated lesion but sometimes is related to other cardiac abnormalities such as ASDs, congenitally corrected transposition of the great arteries, tetralogy of Fallot or chromosomal disorders such as Noonan Syndrome and Williams Syndrome.

In valvar pulmonary stenosis, usually three leaflets are present, but with thickened and fused commissures and a reduced orifice. Unicuspid or bicuspid valves are uncommon.

Echocardiographic Evaluation

The goals of the examination are to

- Characterize the anatomy of the valve
- Define the site and severity of the stenosis
- Determine consequences of stenosis on the RV

2D Transthoracic Echocardiography

Best views include the parasternal short and long axis and subcostal of the RV [8]. The 2-D images show thickened pulmonary valve cusps, restricted systolic motion, and doming in systole.

The main PA is often dilated (post-stenotic dilatation), but the extent of dilation does not correlate with the severity of stenosis.

The severity of the obstruction is determined by measuring the peak Doppler velocity across the pulmonary valve. Multiple transducer positions should be checked to be certain to obtain the highest velocity. The pressure gradient is calculated using the modified Bernoulli equation. The instantaneous pressure gradient by Doppler echo correlates well with the peak-to-peak gradient obtained at catheterization. The degree of stenosis is judged mild when the peak instantaneous gradient is less than 40 mmHg, moderate when gradient is between 40 and 70 mmHg and severe when gradient is >70 mmHg. Valvuloplasty or surgery is usually considered with gradients above 50 mmHg. With at least moderate obstruction, right ventricular hypertrophy, particularly of the infundibulum, may be present. When mild stenosis is present, progression is rare; however, moderate to severe stenosis usually progresses.

3D Echocardiography

Pulmonary valve is difficult to be adequately visualized by 2D echocardiography in adults. 3D TTE echocardiography provides useful information on pulmonary valve morphology as it can provide en-face view of the valve. Parasternal right ventricular outflow tract view with and without color using narrow angle and zoomed acquisitions is the best view to visualize the pulmonary valve [10]. 3D TEE may assist intraoperatively in accurate evaluation and monitoring of the valve repair.

Cautions

- The pressure gradient is flow dependent and may not always be a reliable indicator of severity of stenosis. This is the case when flow across the valve is reduced secondary to poor RV systolic function or when flow is increased due to insufficiency of the pulmonary valve.
- A large left-to-right shunt can cause increased velocity across the pulmonary valve when no stenosis of the valve is present. If increased flow is due to a shunt, the RVOT and PA velocities are both increased. In contrast, in pulmonary stenosis, the RVOT velocity should be normal while the PA velocity is increased.

Aortic Stenosis

Anatomy and Physiology

Sites of obstruction in the aortic valve region include the valve (71%), the subvalvular region (23%), and the supra-annular region (6%). This section will focus on valvular aortic stenosis.

Valvular abnormalities include

- Bicuspid valve (most common)
- Unicuspid valve
- Acommissural (diaphragmatic) valve
- Three-leaflet valve with fusion along the commissures (uncommon)
- Quadrate-leaflet valve (extremely rare).

Aortic stenosis may be present at birth (usually acommissural or unicuspid valves) or a congenitally abnormal valve becomes stenotic over time.

Other associated congenital abnormalities can be present in approximately one third of the patients with bicuspid aortic valve. These include the coarctation of aorta, subvalvular aortic stenosis, parachute mitral valve, interatrial or interventricular communications, Ebstein anomaly and hypoplastic left heart syndrome [1].

Dilatation of aortic root and ascending aorta is more common in patients with a bicuspid aortic valve even if the valve itself is functionally normal and it usually progresses with age. Aortic dissection and rupture may occur earlier and more often in patients with bicuspid aortic valve compared to the general population.

Echocardiographic Evaluation

The goals of the examination are to

- Characterize the anatomy of the valve
- Determine the severity of the stenosis
- Evaluate the effect of the stenosis on the LV
- Identify associated anomalies

2D Transthoracic Echocardiography

Views to interrogate the aortic valve include the parasternal short and long and apical and subcostal 4-chamber. 2-D images easily define the abnormalities of the valve. The parasternal short axis is best for defining the leaflet morphology while the long axis is best for valve motion during systole.

- In the short axis view, a true bicuspid valve doesn't show the usual "Y" pattern of the normal three-leaflet valve, but has two leaflets of relatively equal size, a straight closure line in diastole and a non-circular orifice in systole.
- A three-leaflet valve with fused commissures has the "Y" pattern, but the commissures are very much thickened with varying degrees of leaflet fusion.
- A unicommissural valve is seen in infants and children. It has a single commissure along half the diameter of the orifice and in systole a circular orifice that is eccentrically positioned.

To be certain to obtain the highest Doppler velocity, the valve is imaged in multiple views including the apical, suprasternal, right parasternal and subcostal. The following methods are used to determine the severity of the stenosis and the need for intervention: peak aortic jet velocity, mean pressure gradient, and valve area. Inherent differences exist between the methods. Whichever one is used needs to be integrated with clinical information.

Severe aortic stenosis is characterized by the following

- Peak aortic jet velocity > 4.0 m/s
- Mean systolic gradient > 40 mmHg
- Aortic Valve Area < 1.0 cm²

Aortic valve area can be calculated using the continuity equation. While this is the standard method used in adults with aortic valve disease, this method has not been well studied in infants and children.

Transesophageal Echocardiography (TOE)

TOE provides detailed information

- On the morphology and anatomy of the aortic valve.
- The degree and the location of the calcification of the valve can be also evaluated.
- Accurate assessment of the dimension of the aortic annulus
- Detailed evaluation of the dimensions of the aortic root and the ascending aorta

The annulus diameter, sub-valve stenosis and supra-valve stenosis can be best assessed at the mid—oesophagus level with 120° rotation (Fig. 31.14). A short axis view of the aortic valve can be obtained by rotation of the image plane about 45°.

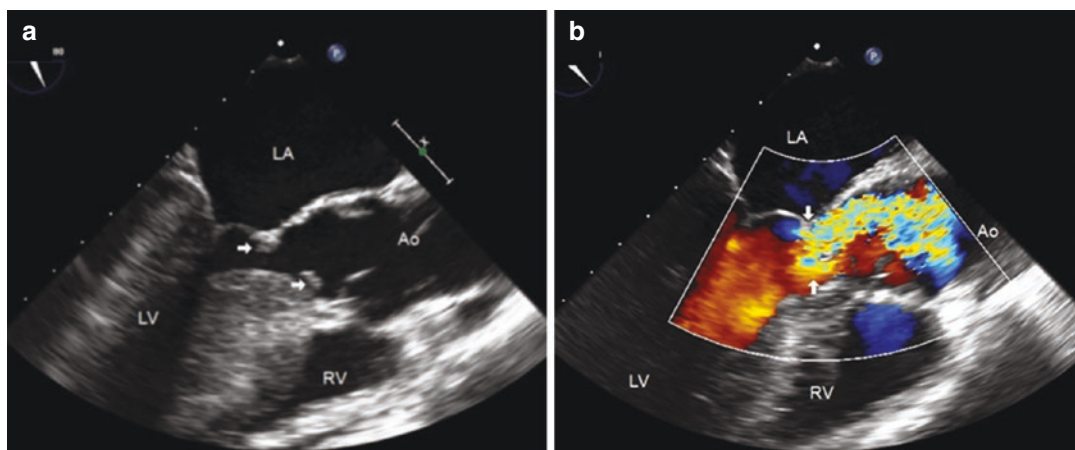


Fig. 31.14 TOE 2D mid-oesophageal left ventricular outflow tract view from a patient with subaortic stenosis. (a) Arrows point the presence of a fibromuscular ridge just

below the aortic valve. (b) Color flow Doppler showing flow acceleration at the subaortic level (white arrows)

3D Echocardiography

Parasternal long or short axis, narrow angle and zoomed acquisitions with or without color are the best views to evaluate the severity of aortic stenosis [10]. 3D TTE enables detailed visualization of the aortic valve leaflets. It can reveal redundancy of the aortic valve leaflets or identify quadricuspid aortic valves. It can also visualize in detail the entire aortic arch. 3D TEE provide with more accurate assessment of valve morphology, the size of the aortic annulus and the adjacent anatomic structures (Figs. 31.15 and 31.16).

Cautions

- In infants, critical aortic stenosis with severe LV dysfunction must be separated from a primary abnormality of LV function. A hypertrophied LV due to critical AS must be separated from a hypoplastic LV. A normal appearing aortic valve and normal Doppler velocity across the valve make these two alternatives more likely.
- Proper alignment with the jet is imperative to avoid underestimating the gradient.
- The gradient is affected by volume of flow so that LV dysfunction and low cardiac output give a lower gradient while aortic insufficiency increases the gradient.

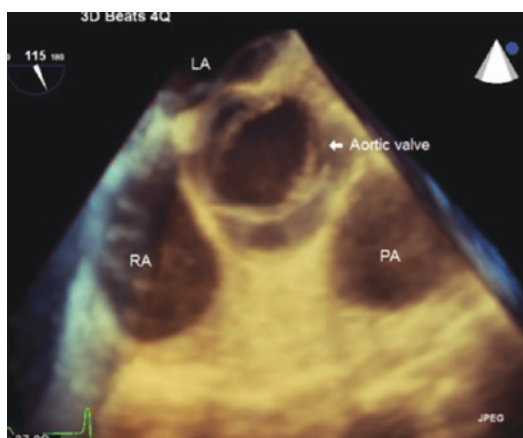


Fig. 31.15 3D TOE mid-oesophageal short axis view from a patient with bicuspid aortic valve. Enface view of the valve leaflet demonstrating bicuspid aortic valve

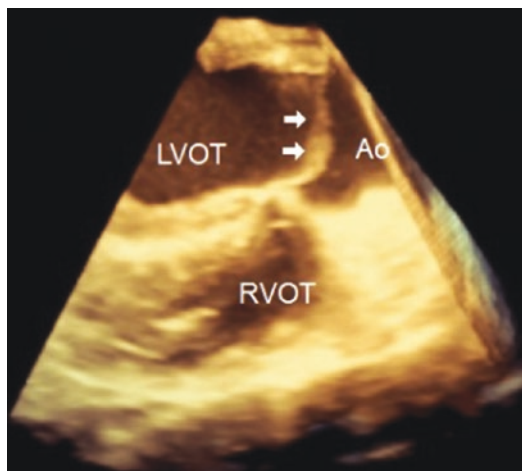


Fig. 31.16 3D TOE mid-oesophageal left ventricular outflow tract view from patient with bicuspid aortic valve showing slightly thickened and doming bicuspid aortic valve (white arrows)

Coarctation of the Aorta

Anatomy and Physiology

Coarctation of the aorta (AoCoA) is the fifth most common congenital heart defect presenting in approximately 5–8% of live births with congenital heart disease and is more common in males [16]. It is almost always located opposite to the ductus arteriosus or ligamentous arteriosum and appears as a shelf-like narrowing of the aortic lumen just below the left subclavian artery. The degree, the extent and the morphology of the narrowing varies from a discrete point to a tubular hypoplasia of the aorta.

AoCoA can be either an isolated defect, or part of a more complex congenital defect. This lesion has high incidence (> of 50%) of associated cardiac abnormalities including aortic hypoplasia, abnormal aortic valve, ventricular septal defect or patent ductus arteriosus, mitral valve anomalies or as part of transposition of the great arteries and double outlet right ventricle (Taussig-Bing anomaly). Bicuspid aortic valve is the most common association. Aortic atresia and interrupted aortic arch are severe but uncommon variations.

The diagnosis of AoCoA may escape attention in childhood, and adults with undiagnosed disease may present with systemic arterial hypertension

and difference in blood pressure between upper and lower extremities, heart failure, aortic rupture and endocarditis.

Echocardiographic Evaluation

2D Transthoracic Echocardiography

As in the majority of cardiac malformations, imaging of AoCoA is easier in children than in adults. The best 2D views to visualize an AoCoA are:

- the suprasternal and the right parasternal window, in which the arch and the descending aorta are best viewed.
- the long axis view of the aortic arch, in which the aortic arch and the branchiocephalic vessels are identified and the coarctation is visualized as a narrowing of the aortic lumen beyond the left subclavian artery.

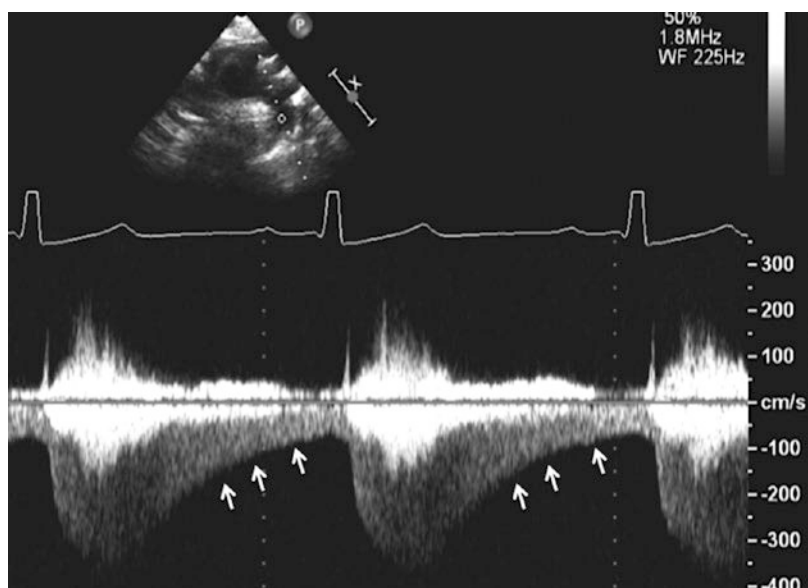
The echocardiographic study should concentrate on the assessment of obstruction or aortic dilatation at the coarctation site and on the evaluation of aortic valve function [16]. It is important to identify the presence of post-stenotic aortic dilation as well as other concomitant cardiac malformations.

The goals of echocardiographic evaluation of coarctation of the aorta are:

- Identification of all the great vessels
- Evaluation of the size of the proximal aorta
- Determination of
 - the site of narrowing in the descending aorta
 - its distance from the orifice of the left subclavian artery
 - presence of aneurysm in AoCoA proximity
- Assessment of the dimension and function of the left ventricle
- Evaluation of the aortic valve
 - assessment of morphology (number of cusps, presence of raphe)
 - identification of possible regurgitation and quantification of its severity
- Evaluation of the degree of obstruction by the Doppler flow pattern
- Patency of the duct

Color Doppler is useful to locate the site of turbulence and the continuous wave beam should be directed to this region. The typical pattern for significant obstruction is increased systolic velocity with continuous forward flow throughout diastole (diastolic tail) (Fig. 31.17). In cases

Fig. 31.17 Spectral CW Doppler through coarctation of aorta in descending aorta shows the increased peak systolic flow velocity with antegrade diastolic flow (white arrow) so called diastolic tail



with less severe obstruction the signal may be of high velocity but restricted to the systole. Doppler gradients from the peak systolic velocity alone tend to overestimate the catheter-measured gradient. A better correlation has been shown when the velocity proximal to the coarctation (V_1) is included in the expanded Bernoulli equation $\Delta P = 4 (V_2^2 - V_1^2)$. Recognition of Doppler flow patterns in the abdominal aorta is proved useful in the detection of upstream obstruction. Patients with significant AoCoA, the abdominal aortic flow profile is characterized by a delay in the systolic upstroke, turbulence in systole, and variable degrees of diastolic antegrade flow [17].

In patients with repaired AoCoA, residual or recurrent stenosis as well as aneurysms in the area of previous repair site or in the ascending aorta should be sought [16].

Transoesophageal Echocardiography (TOE)

Given that in most adult patients the direct imaging of the anatomy of the aortic arch and descending aorta is limited, other imaging techniques may be used for the assessment of the AoCoA. TOE is an imaging modality that may recognize both the site and the configuration of the obstruction. Quantification of the luminal narrowing is achieved in a short axis view of the aorta, in which the area of narrowing and turbulence is apparent as the probe is moved up or down, while the long axis view will show the narrow segment. The disadvantages of imaging modality include the difficulty in obtaining the Doppler gradients, as the narrowed area usually lies perpendicular to the interrogating Doppler beam, as well as the inadequate visualization of the branch vessels and the collaterals.

3D Echocardiography

3D TTE can also provide information on the extracardiac vascular landmarks. Suprasternal notch position with wide angle is the best view to visualize the aortic arch and the descending aorta [15]. Having the ability to take views from different angles 3D TTE can help to an echocardiographic “reconstruction” of the coarctation site.

Cautions

- A long, narrowed segment of the aorta without discrete obstruction causes acceleration of flow, giving an increased peak velocity suggestive of obstruction. The lack of diastolic forward flow, however, helps to distinguish this flow acceleration from true obstruction.
- In patients with uncorrected coarctation, the direction of the jet may be very eccentric. This can lead to underestimation of the severity of the obstruction due to misalignment of the jet direction and the ultrasound beam.
- Left-to-right run off of flow through a patent ductus arteriosus or by a net of well-developed collaterals may reduce the velocity through the coarctation, leading to an underestimation of the pressure gradient.
- With aortic atresia or interruption, the large duct supplying the descending aorta must not be mistaken as the aortic arch. This can be avoided by identifying the origination of the arch vessels.
- In patients with severe coarctation or interrupted aorta, there will not be an increased velocity if descending aorta is supplied by an unrestrictive patent ductus.
- Tangential imaging plane through the aorta may give the impression of lumen narrowing.
- False positive diagnosis for AoCoA may be encountered in high output states (e.g. significant aortic regurgitation) and in patients with stenosis at the origin of the left subclavian artery.

Ebstein Anomaly of the Tricuspid Valve

Anatomy and Physiology

Ebstein anomaly is present in approximately 1% of patients with congenital heart malformations [1]. The lesion is characterized by apical (downward) displacement of septal and posterior leaflets of the tricuspid valve into the RV chamber. The anterior leaflet is tethered to the RV free wall and may have restricted movement or be a large sail-like leaflet that can obstruct the RV outflow

tract. This abnormal tricuspid valve is variably regurgitant and occasionally stenotic. Various anatomic abnormalities concerning the right heart chambers may be present in patients with Ebstein anomaly;

- Adherence of tricuspid leaflets to the underlying myocardium.
- A portion of the proximal right ventricle is incorporated into the RA (atrialized RV). Dilatation of the atrialized portion of the right ventricle.
- Tethering of the anterior leaflet to the RV free wall

The functional RV maybe hypoplastic with impaired systolic function. A PFO or ASD are frequently present and results in cyanosis. WPW syndrome is associated with this anomaly (10–15% of cases), predisposing to tachyarrhythmias. Variation in the severity of the valvular abnormalities results in a wide spectrum of symptoms from critically ill to an incidental finding in an asymptomatic individual.

Echocardiographic Evaluation

Goals are to

- Define severity of apical displacement of the septal and posterior leaflets from the anatomic annulus and the size and tethering of the anterior leaflet
- Determine degree of regurgitation
- Quantify adequacy of RV size and systolic function
- Establish presence of ASD/PFO

TTE Echocardiography

The best views for evaluating the TV include the apical 4-chamber view, parasternal RV inflow view and the subcostal coronal view [8]. There is no uncertainty in making the diagnosis in moderate to severe cases, but milder forms can be problematic.

Since the tricuspid valve is normally more apically positioned than the mitral valve, accepted criteria for abnormal apical displacement of the TV is more than 8 mm/m² (or > 20 mm in adults) from the mitral valve insertion in the apical 4 chamber view.

Doppler provides an estimate of the severity of regurgitation and presence of stenosis. The subcostal view enables interrogation of the inter-atrial septum to look for a PFO or ASD. If unclear, the rapid IV injection of agitated blood-saline mixture can be used to determine if right to left shunting is present.

3D Echocardiography

The apical four chamber view and the parasternal right ventricular inflow view, with narrow angle and zoomed acquisitions with or without color, are the best views to visualize the tricuspid valve (Fig. 31.18). 3D TTE can assist the evaluation of patients for surgical repair. It is very useful in evaluating the degree of tethered and non tethered areas of the three tricuspid valve leaflets (Fig. 31.19). 3D Color Doppler can provide very efficient quantitative information on tricuspid regurgitation since it can evaluate accurately the size and the shape of vena contracta.

In symptomatic individuals, surgical repair of the valve is possible if the anterior leaflet is of sufficient size and mobility to create a monocuspid valve and if the RV is of sufficient size and with adequate function after plication of the atrialized portion of the RV. If repair is not possible, the preferred replacement valve is a stented allograft or heterograft. A Fontan repair is done with severe RV dysfunction or hypoplasia.

Cautions

- The fibrous annulus of the tricuspid valve should not be mistaken for valve tissue
- RV tissue bands should be distinguished from displaced valve tissue
- Myxomatous disease of the TV should be distinguished from a large sail-like anterior leaflet.

Fig. 31.18 3D TTE of patient with Ebstein anomaly of tricuspid valve. Apical 4 chamber view. Apical displacement of the septal leaflet of tricuspid valve with abnormal chordae tethering of anterior leaflet and large atrialised portion of the RV

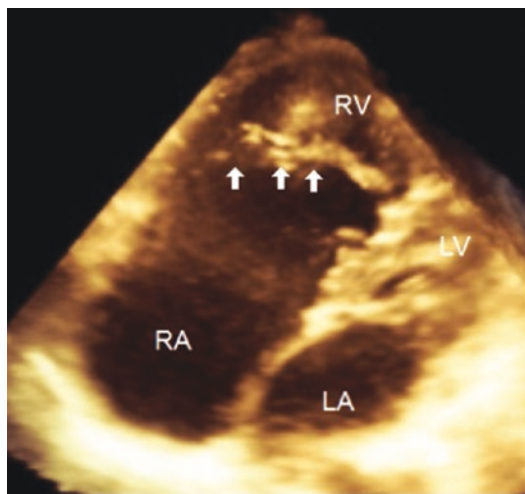
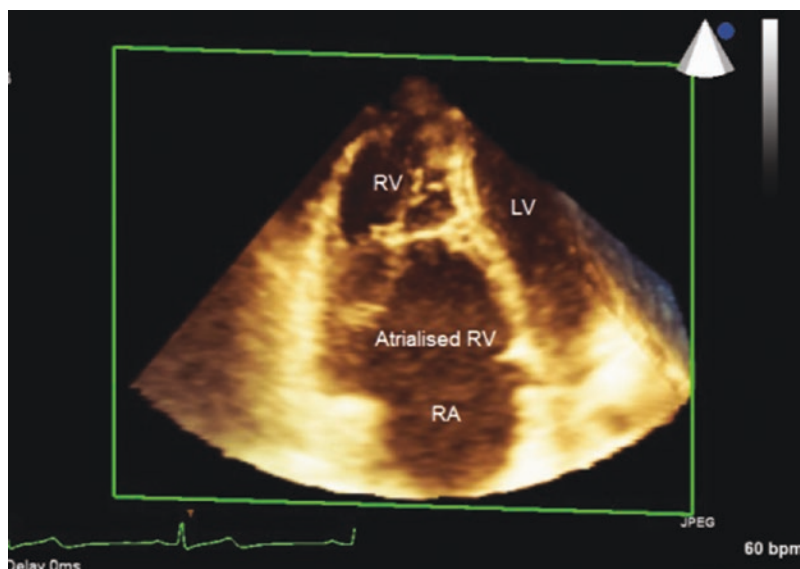


Fig. 31.19 3D TTE of Modified apical 4 chamber view of patient with Ebstein anomaly. White arrows show the enlarged and sail-like anterior leaflet with abnormal distal attachment

Conclusion

The population of adult patients with congenital heart diseases (CHD) increases constantly, thanks to the significant evolution of surgical

and interventional techniques and improvement in early diagnosis and medical management. Echocardiography is one of the most valuable imaging tools for the initial diagnosis and long term follow up of patients with CHD due to its wide availability in Cardiology departments and is easily applied in across all patient care settings. It provides significant anatomic information leading to the initial diagnosis, the haemodynamic effect of the lesions and its utility extends to follow up of this group of patients.

Echocardiographic examination of patients with congenital heart lesions requires intricate knowledge of the anatomy and physiology of the normal heart and its congenital defects. 2D imaging using multiple views including non-standard imaging planes and the use of Doppler imaging provides invaluable information on the anatomy and physiology of the lesions. Advanced imaging modalities such as 3D TTE and 3D TOE contribute to a better understanding of the congenital lesions as well as the adjacent anatomic structures, providing incremental benefit for pre-operative planning or guidance during percutaneous or surgical interventions.

References

1. Gatzoulis MA, Webb GD, Daubeney PEF. Diagnosis and management of adult congenital heart disease. 2nd ed. Amsterdam: Elsevier Saunders; 2011. p. 2–4.
2. Babu-Narayan SV, Giannakoulas G, Valente AM, Li W, Gatzoulis MA. Imaging of congenital heart disease in adults. *Eur Heart J*. 2015;37(15):1182–95. <https://doi.org/10.1093/eurheartj/ehv519>.
3. Flachskampf FA, Wouters PF, Edvardsen T, et al. Recommendations for transoesophageal echocardiography: EACVI update 2014. *Eur Heart J Cardiovasc Imaging*. 2014;15:353–65.
4. Simpson J, Lopez L, Acar P, et al. Three-dimensional echocardiography in congenital heart disease: an expert consensus document from the European Association of Cardiovascular Imaging and the American Society of Echocardiography. *Eur Heart J Cardiovasc Imaging*. 2016;17(10):1071–97.
5. Geva T, Martins JD, Wald RM. Atrial septal defects. *Lancet*. 2014;383:1921–32.
6. Moorman AFM, van den Hoff MJB, de Jong F, et al. Myocardialization: a novel mechanism of cardiac septation. In: Clark EB, Nakazawa M, Takao A, editors. Etiology and morphogenesis of congenital heart disease: twenty years of progress in genetics and developmental biology. Armonk: Futura; 2000. p. 131–5.
7. Silvestry FE, Cohen MS, Armsby LB, et al. Guidelines for the echocardiographic assessment of atrial septal defect and patent foramen ovale: from the American Society of Echocardiography and Society for Cardiac Angiography and Interventions. *J Am Soc Echocardiogr*. 2015;28:910–58.
8. Otto CM. Textbook of clinical echocardiography. 5th ed. Amsterdam: Elsevier Saunders; 2013.
9. Porter TR, Abdelmoneim S, Belcik JT, et al. Guidelines for the cardiac sonographer in the performance of contrast echocardiography: a focused update from the American Society of Echocardiography. *J Am Soc Echocardiogr*. 2014;27:797–810.
10. Lang RM, Badano LP, Tsang W, et al. EAE/ASE recommendations for image acquisition and display using three-dimensional echocardiography. *J Am Soc Echocardiogr*. 2012;25:3–46.
11. Bleich S, Nanda NC, Hage FG. The incremental value of three-dimensional transthoracic echocardiography in adult congenital heart disease. *Echocardiography*. 2013;30:483–94.
12. Roberson DA, Cui W, Patel D, et al. Three-dimensional transesophageal echocardiography of atrial septal defect: a qualitative and quantitative anatomic study. *J Am Soc Echocardiogr*. 2011;24:600–10.
13. Penny DJ, Vick GW III. Ventricular septal defect. *Lancet*. 2011;377:1103–12.
14. Chugh R, Salem MM. Echocardiography for patent ductus arteriosus including closure in adults. *Echocardiography*. 2015;32:125–39.
15. Yang HS, Bansal RC, Mookadam F, Khandheria BK, Tajik AJ, Chandrasekaran K. Practical guide for three-dimensional transthoracic echocardiography using a fully sampled matrix array transducer. *J Am Soc Echocardiogr*. 2008;21:979–89.
16. Baumgartner H, Bonhoeffer P, De Groot NMS, et al. ESC guidelines for the management of grown-up congenital heart disease (new version 2010). *Eur Heart J*. 2010;31:2915–57.
17. Sanders SP, MacPherson D, Yeager SB. Temporal flow velocity profile in the descending aorta in coarctation. *J Am Coll Cardiol*. 1986;7:603–9.

Assessing the Patient with Congenital Heart Disease

32

John M. Simpson and Karolina Hall

Background

The echocardiographic assessment of the patient with congenital heart disease (CHD) has many similarities, but also some important differences from the patient with acquired disease. This chapter addresses the approach to the echocardiographic examination, the nomenclature used to describe CHD and examples of unrepaired and repaired congenital heart defects. It is not possible to cover all forms of CHD but the key features of some of the commoner types of defect are addressed as well as the approach for echocardiographic surveillance following repair. The major focus of this chapter is on echocardiography as this is the dominant modality used during clinical review but the importance of other modalities such as magnetic resonance imaging (MRI) or Computed Tomography (CT) will be discussed where relevant. Multimodality imaging has become the norm in the assessment of the patient with CHD particularly for surgical planning, follow-up after surgery and in older patients with suboptimal acoustic windows [1, 2].

Electronic Supplementary Material The online version of this chapter (https://doi.org/10.1007/978-3-319-71617-6_32) contains supplementary material, which is available to authorized users.

J. M. Simpson (✉) · K. Hall
Department of Congenital Heart Disease, Evelina
London Children's Hospital, London, UK
e-mail: john.simpson@gstt.nhs.uk

Sequential Segmental Approach to Description of Anatomy

The most important premise underpinning the echocardiographic examination of CHD is that cardiac situs, position of the heart and cardiac connections may all be abnormal and these need to be visualised in a systematic manner. The way in which this is described is referred to as “sequential segmental analysis” [3]. This approach subdivides the connections of the heart into a number of “building blocks” consisting of the venous drainage to the atriums, the connection of the atriums to the ventricular mass and the connection of the ventricles to the great arteries. The great arteries are determined by their characteristics i.e. the aorta gives rise to the coronary arteries and head/neck vessels and the pulmonary artery bifurcates to supply each lung. Crucially, the naming of cardiac structures does not relate to their position in the body but to their characteristic morphology. Cardiac situs relates primarily to atrial arrangement. The most consistent feature identifying the left and right atriums is the morphology of the atrial appendages. The left atrial appendage has a narrow base and the pectinate muscles are confined to the appendage itself so that the vestibule of the atrium itself is smooth. In contrast, the right atrial appendage has a broad base and the pectinate muscles extend into the vestibule of the right atrium (Fig. 32.1a, b). Similarly, the right and left ventricles are not

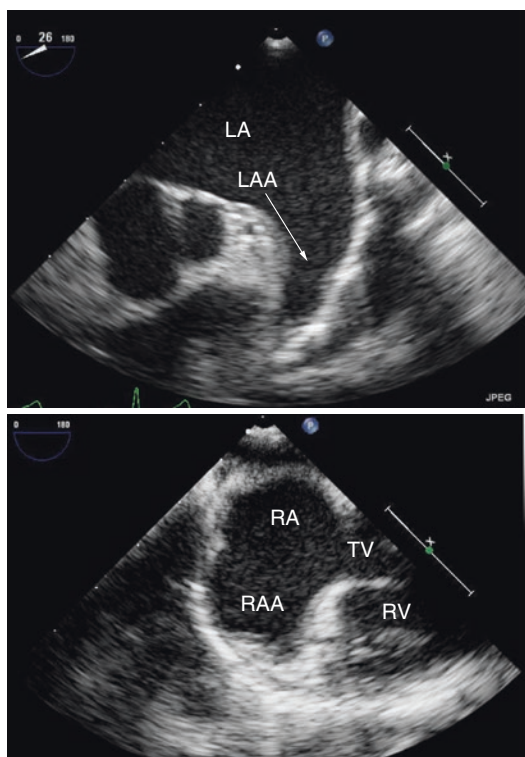


Fig. 32.1 Atrial appendages. A transoesophageal echocardiogram showing: (a) the left atrial appendage which has a finger-like shape. (b) the right atrial appendage which has a typical triangular shape and a broad base. (See Video 32.1a, b). Abbreviations: LA left atrium, RA right atrium, LAA left atrial appendage, RAA right atrial appendage, TV tricuspid valve, RV right ventricle

defined by their position but by their morphology. The left ventricle has a smooth surface due to fine trabeculations and has an atrioventricular valve of mitral type i.e. bileaflet, which has no septal attachments. The mitral valve is inserted further from the apex of the ventricle than the tricuspid valve, thus there is “differential insertion” of the atrioventricular valves into the ventricular septum. The morphological right ventricle has a coarsely trabeculated endocardial surface with a moderator band towards the apex. The tricuspid valve has chordal attachments to the ventricular septum in contrast to the mitral valve. A summary of the characteristic features of different cardiac structures, based on morphology is shown in Table 32.1. If the morphologic left atrium is

connected to the morphologic left ventricle then the connection is described as concordant, but if it is connected to the morphologic right ventricle the connection is described as discordant. The same approach is adopted to describe the connection of the right atrium to the ventricular mass. Absent right or left atrioventricular connections and double inlet ventricles are also covered within this system of nomenclature, which makes no embryological assumptions.

A similar logic is used to describe the connection of the ventricles to the great arteries. If the left ventricle connects to the aorta this is described as concordant and if it connects to the pulmonary artery this is described as discordant. It should be emphasised that the connection of the great arteries is not defined by their relationship to each other, but by the connection to the ventricle. In some situations a great artery may arise above a ventricular septal defect with a degree of override so that there may be difficulty in determining from which ventricle a great artery arises. In this setting, the usual approach is to adopt a “50% rule” meaning that if a great artery is deemed to be more than 50% committed to one ventricle it is defined as arising from that ventricle. It does not matter if the aortic or pulmonary valve is stenotic with respect to its commitment to either ventricle. The situation is more complex if there is atresia of either the aortic or pulmonary valve. The optimal description in this setting is to describe the origin of the patent great artery e.g. aorta arises from left ventricle with pulmonary atresia. This approach avoids any confusion of trying to “connect” an atretic vessel to either ventricle.

One of the problems with using appendage morphology to determine the atrial arrangement is that it can be extremely difficult to visualise the atrial appendages by transthoracic echocardiography. If transoesophageal echocardiography is used, the atrial appendages are far more clearly visualised (Fig. 32.1a, b). In practice, and particularly if TOE is not being undertaken the arrangement of the atrial appendages is inferred from the arrangement of the abdominal vessels. This is an important concept which

Table 32.1 Table describing the characteristic features of the atria, ventricles and great arteries which may be used to assist in description of congenital heart lesions

<i>Atrium</i>	<i>Appendage</i>	<i>Pectinate muscles</i>		
Left atrium	Narrow based	Confined to appendage		
Right atrium	Broad based	Extend to vestibule		
<i>Ventricle</i>	<i>AV valve</i>	<i>Septal attachment</i>	<i>Insertion</i>	<i>Myocardium</i>
Left ventricle	Mitral type	No	MV further from apex than TV	Smooth
Right ventricle	Tricuspid	Yes		Trabeculated Moderator band
<i>Great arteries</i>				
Aorta	Gives rise to head and neck vessels and coronary arteries			
Pulmonary Artery	Gives rise to branch pulmonary arteries			

is usually, but not invariably correct. Thus, if the aorta descends to the left of the spine and the inferior vena cava is anterior and rightward then this is a strong indicator that there is usual atrial arrangement (Fig. 32.2a). Similarly if the aorta descends to the right and the inferior vena cava is anterior and leftward, this would be consistent with mirror image atrial arrangement (Fig. 32.2b). In rare instances, there is neither usual atrial arrangement nor mirror image. This is variably described in the literature as laterality disturbance, isomerism, visceral heterotaxy or polysplenia/asplenia syndrome [4]. It is important for the echocardiographer to recognise this group of lesions because there are characteristic associated cardiovascular abnormalities which are summarised in Table 32.2. The terminology used at these authors' institution is to describe these as disturbances of laterality characterised by isomerism of the left atrial appendage or right atrial appendage.

Echocardiographic Approach

Having understood the principles of nomenclature of the different parts of the heart and the conventions related to connections, the echocardiographer requires a consistent systematic approach to assess all of the cardiac connections.

Subcostal Short Axis View of the Abdominal Vessels

The starting point of every transthoracic congenital echocardiographic examination is a short axis view just below the level of the diaphragm. This is used to determine the position of the inferior vena cava and the descending aorta which, as outlined above, is used as a surrogate for the atrial arrangement. Normally, the inferior vena cava lies anterior and to the right of the aorta which in turn descends to the left of the spine and this is taken to infer usual atrial arrangement. Different permutations of the abdominal vessels and the implication of these findings are shown in Fig. 32.2a–d. The drainage of the inferior vena cava to the right atrium is confirmed in a long axis view as well as the position and pulsatility of the descending aorta (Fig. 32.3a–c).

Whilst remaining in a subcostal projection, the next step is to scan cranially simply to determine whether the apex of the heart is pointed to the left, to the right or directly anterior (Fig. 32.4a, b). Terms such as dextrocardia, dextroposition, dextroversion and mesocardia should be avoided as they are confusing and a simple statement of apex left, right or directly anterior is preferred as this is simple to understand and unambiguous. In smaller and younger patients, the atrial septum and pulmonary veins may be clearly seen in a subcostal view as can the connection of the superior and

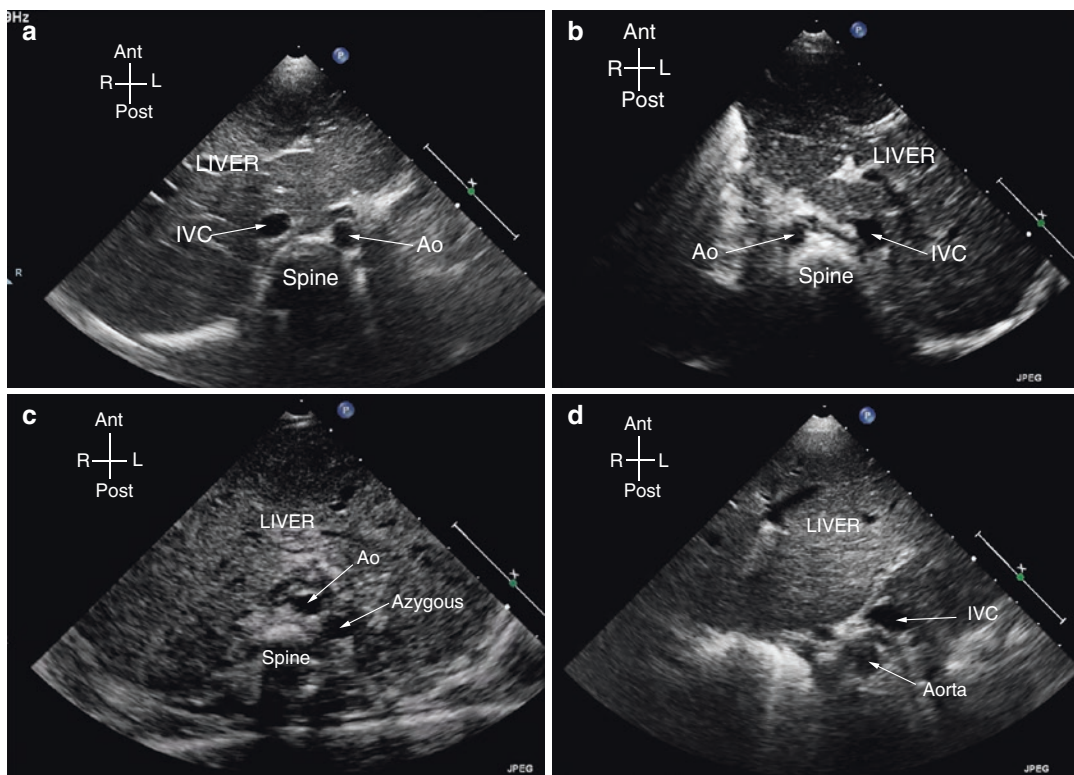


Fig. 32.2 Arrangement of the abdominal vessels. Short axis views of the abdominal vessels by transthoracic echocardiography are used in clinical practice to infer cardiac situs. (a) Usual arrangement of the abdominal vessels. The liver is seen to the right. The aorta descends to the left of the spine and the inferior vena cava is more anterior and rightwards. (b) Mirror image atrial arrangement. The liver is on the left. The aorta descends to the right of the spine and the inferior vena cava is anterior and to the left. (c) Interruption of the inferior vena cava. Interruption of the

inferior vena cava is frequently associated with isomerism of the left atrial appendages. In this image the IVC is interrupted with azygous continuation posterior and to the left of the descending aorta. (d) Isomerism of the right atrial appendages. This short axis view of the abdominal vessels shows a midline liver. The aorta descends to the left of the spine with the IVC almost directly anterior also on the left side of the spine. See Video 32.2a–d. Abbreviations: IVC inferior vena cava, Ao aorta, Azygous Azygous vein

inferior vena cava to the right atrium. The normal connection of the SVC to the right atrium is shown in the figure, but this becomes progressively more difficult as patients become older and larger. Examples of normal and abnormal pulmonary venous drainage are shown in Fig. 32.5a, b. A widely applied view for checking the drainage of all pulmonary veins is the “crab” view which is a suprasternal coronal view of the back of the left atrium. This latter view is best deferred until suprasternal views of the systemic veins and aortic arch are being obtained. Paediatric echocardiography guidelines describe an approach to defining all major cardiac connections from a sub-costal view [5] but this becomes progressively

more difficult to achieve in practice in older children, adolescents and adults due to the poor acoustic access. Alternative views are equally valid including modified four chamber views, suprasternal acoustic windows and modified parasternal views.

The next informative view is the apical four chamber view. The sonographic window will vary according to the position of the apex but the transducer should never be left/right inverted to produce an image more akin to normal regardless of the position of the cardiac apex. From the apical four chamber view, the pulmonary veins should be visualised draining to the left atrium. By sweeping inferiorly, the inferior vena cava can

Table 32.2 Characteristic features of cases of laterality disturbance. The individual features are variable and may not be present in all cases

	Isomerism of the left atrial appendages	Isomerism of the right atrial appendages
<i>Inferior vena cava</i>	Interrupted with azygous continuation above diaphragm	Inferior vena cava and aorta on same side (left or right)
<i>Superior vena cava</i>	Single or bilateral	Single or bilateral
<i>Pulmonary veins</i>	Symmetrical with 2 veins draining to each atrium	Anomalous pulmonary venous drainage
<i>Atrioventricular conduction</i>	Sinus rhythm, slow sinus or heart block	Usually normal
<i>Intracardiac abnormality</i>	Variable from normal to severely abnormal	Atrioventricular septal defect Pulmonary stenosis / atresia
<i>Gastrointestinal</i>	Malrotation of the bowel	Malrotation of the bowel
<i>Spleen</i>	Polysplenia	Asplenia

be confirmed to be draining to the right atrium. The four chamber view is critical for assessing the atrioventricular connections. Specific note should be made of the morphological features of the atriums and the corresponding ventricles. There should be differential insertion of the atrioventricular valves (Fig. 32.6a, b). Where there are discordant atrioventricular connections there is reversal of the normal offsetting of the atrioventricular valves (Fig. 32.7). However, other abnormalities of the connections between the atriums and ventricles may be found including absence of the right atrioventricular valve, absence of the left atrioventricular valve, double inlet ventricle (where both atrioventricular valves are committed to the same ventricle) and a common atrioventricular valve. The features of the atrioventricular septal defect are shown in Fig. 32.8a–d. Even in the context of concordant atrioventricular connections, the morphology of the atrioventricular valve may be abnormal. The left atrioventricular valve is well seen on a short axis view and anomalies such as a double orifice mitral valve may be appreciated with this approach (Fig. 32.9).

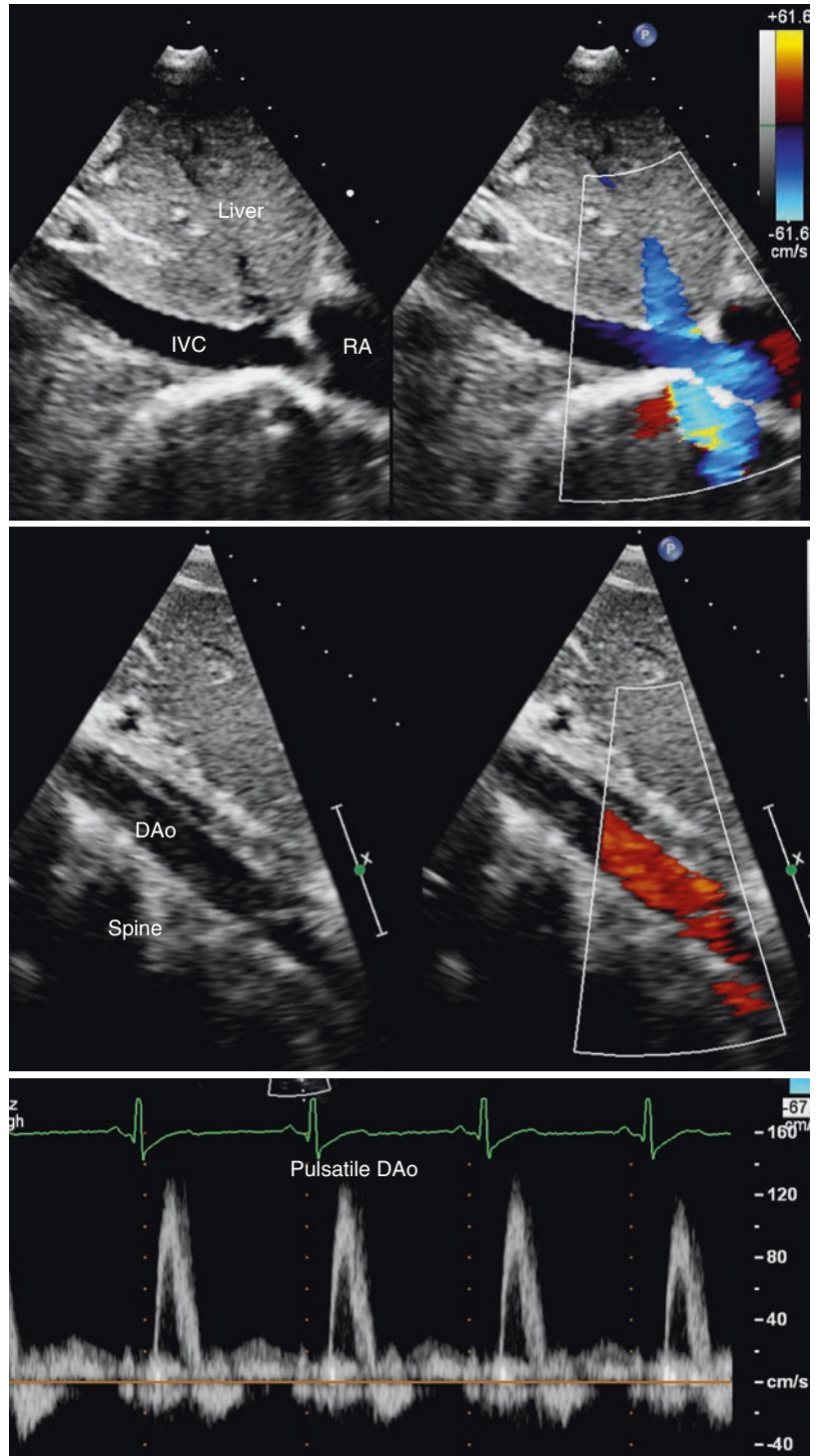
The ability to visualise valves using 3D echocardiography means provides both a depth of field and also the ability to achieve novel sonographic planes, for example visualisation of a parachute mitral valve (Fig. 32.10a, b) [6]. Congenital abnormalities of the tricuspid valve are interrogated using multiple planes including the four chamber view, short axis views and by the application of 3D echocardiography. In Ebstein anomaly there is apical displacement of the septal and inferior leaflets of the tricuspid valve as well as abnormal rotation of the valvar attachments. The application of 2D and 3D echocardiography to visualise the anatomy is illustrated in Fig. 32.11a–d.

Even where the connections between the atriums and ventricles are concordant, the size of the ventricles may be similar i.e. balanced, or one ventricle may be substantially larger than the other i.e. unbalanced. It is extremely rare for there to be truly a “single ventricle”. It is much more common that there is one large ventricle and a second ventricle which is much smaller. In terms of patient management, for patients in whom a biventricular repair may not be feasible, the circulation may be described as “functionally single ventricle” to emphasise the physiology whilst acknowledging that there is not truly only a single ventricle.

Assessment of the Outflow Tracts

The outflow tracts are assessed from a combination of views including angled apical, long axis, short axis and subcostal projections. From the four chamber view it is usually possible to angle the transducer cranially or to rotate the transducer to visualise the outflow tracts. From the apical views, only the very proximal portion of each great artery can be visualised to that their branching pattern is not usually able to be visualised except in infants and children. Short axis views are used in sonographic sweeps from the apex of the ventricles to the great arteries to determine the relative position of cardiac structures, including the great arteries. The characteristic branching of the pulmonary artery and origin of the coronary arteries from the aorta are visualised in the short axis as well as the morphology of the aortic

Fig. 32.3 Sagittal cut of abdominal vessels. (a) Normal IVC to RA drainage. Sagittal cut of the IVC draining to the RA through the liver. This view is performed to complement short axis views of the abdominal situs to check the relative position of the abdominal vessels and their connection to the heart. (b) Normal pulsatile abdominal Aorta. Sagittal cut of the abdominal aorta along the left of spine. This view demonstrates the pulsatile nature of a normal aorta upstream from this point. (c) Pulsed Wave Doppler of this vessel confirms that the abdominal aorta has normal pulsatility. Note that the angle of insonation must be maintained to as close to 0 as possible to obtain a truly representative waveform. See Video 32.3a–c. Abbreviations: IVC inferior vena cava, RA right atrium, Ao Aorta



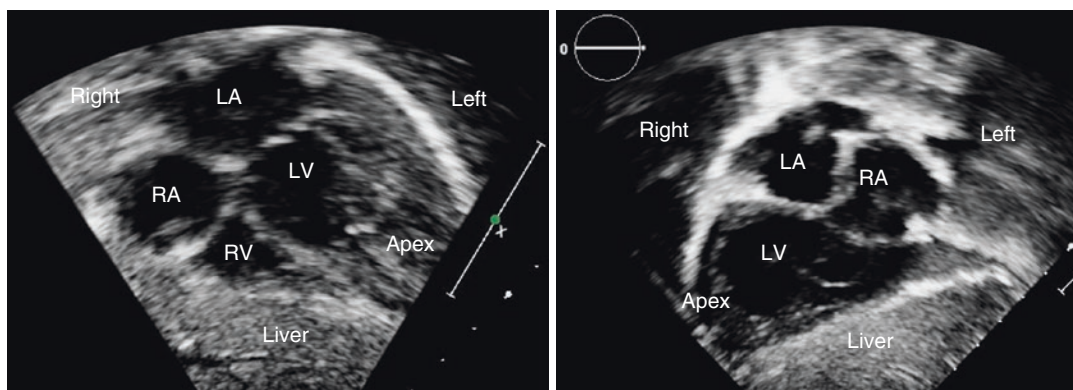


Fig. 32.4 Position of the cardiac apex from subcostal view. The subcostal view provides an ideal projection to determine the position of the apex of the heart whether this is to the left (a), right (b) or anterior. If the subcostal views are inadequate then the position of the apex can be

determined by sweeping the probe from left to right across the thorax to find the true apical four chamber view. Abbreviations: LA left atrium, RA right atrium, LV left ventricle, RV right ventricle

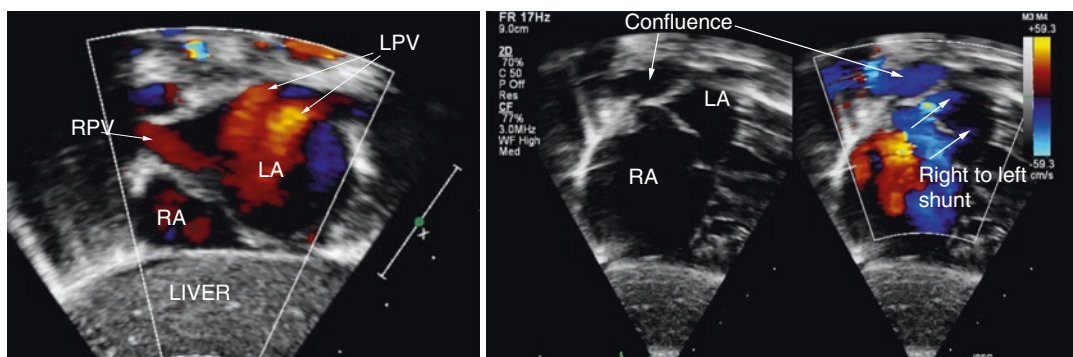


Fig. 32.5 Subcostal view of the pulmonary veins. The pulmonary venous drainage can be visualised in smaller patients from a subcostal projection. (a) Pulmonary veins draining to the LA. (b) Total anomalous pulmonary venous drainage. The pulmonary veins drain to a confluence behind the left atrium. In this example, the veins

drain superiorly to the innominate vein and back to the RA (not shown). Flow into the LA is maintained by right to left shunting of blood across the atrial septum (arrows). See Video 32.4a, b. Abbreviations: LPV left pulmonary veins, RPV right pulmonary veins, LA left atrium, RA right atrium

valve. In the normal heart, the pulmonary artery wraps around the aorta with the pulmonary valve anterior and to the left of the aorta (Fig. 32.12a). However, in some classic lesions, notably transposition of the great arteries the short axis view shows both the aortic valve and pulmonary valve in an enface orientation due to their abnormal parallel orientation (Fig. 32.12b). Parasternal long axis views are used in the assessment of the

congenital patient and can demonstrate lesions such as transposition of the great arteries (Fig. 32.13). When utilising the parasternal long axis view, the branching pattern of the great arteries is not clearly seen and a classic error if applying this view in isolation is to assume that the vessel leaving the left ventricle is the aorta. Furthermore, if the orientation of the heart is abnormal, for example with the apex to the right,

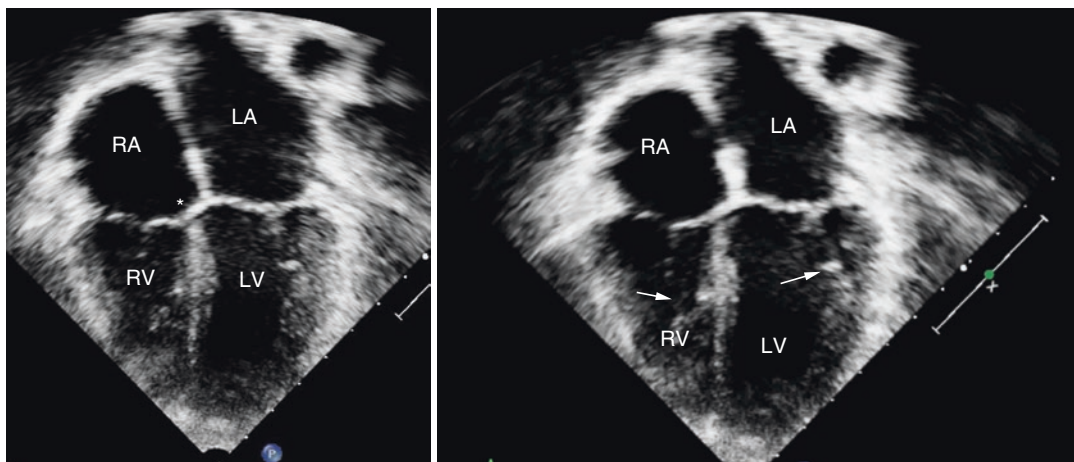


Fig. 32.6 Apical four chamber view demonstrating normal offset of the mitral and tricuspid valves. (a) Note that the MV is inserted further from the cardiac apex than the TV; the differential insertion is marked with an asterisk (*). (b) Note the attachments of the MV and TV. The attachments of the MV are to the free wall of the LV

whereas the TV has septal attachments. The attachments are shown by the arrows and the differential insertion of the atrioventricular valves is shown by the asterisk (*). See Video 32.5. Abbreviations: RA right atrium, LA left atrium, RV right ventricle, LV left ventricle, MV mitral valve, TV tricuspid valve

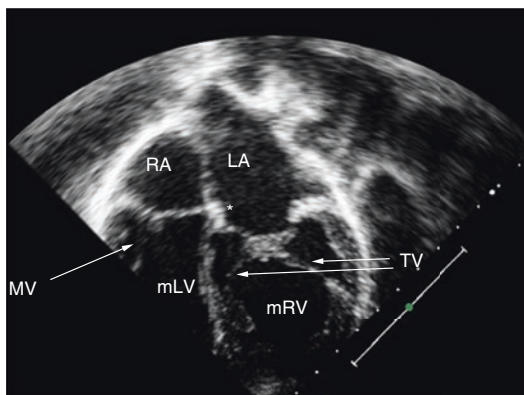


Fig. 32.7 Discordant atrioventricular connections. Apical four chamber view of the heart with discordant atrioventricular connections. The LA connects to a morphological RV via the TV which has septal attachments (arrowed). The RA connects to a morphological LV through the MV which only has attachments to the free wall of the morphological LV. There is reversal of the normal pattern of offsetting of the attachment of the atrioventricular valves to the ventricular septum (*). See Video 32.6. Abbreviations: RA right atrium, LA left atrium, MV mitral valve, TV tricuspid valve, mLV morphological left ventricle, mRV morphological right ventricle

the transducer will require to be rotated to show a true long axis projection. Thus it is preferable to determine the position of the apex using a four chamber view before proceeding to the long axis

projection. A further sonographic projection which is far more extensively used in congenital practice than elsewhere is the “ductal cut” which is used to profile the length of the arterial duct. This is obtained from a high left parasternal position with the ultrasound transducer in a vertical position (Fig. 32.14). This projection is normally superior to the short axis projection to confirm patency of the arterial duct because it avoids superimposition of the arterial duct on the left pulmonary artery.

The suprasternal projections are obtained as the last part of the echocardiographic examination particularly in younger patients. From the suprasternal projection, the ascending aorta, aortic arch, superior vena cava, branch pulmonary arteries and pulmonary veins can be imaged. The left or right sidedness of the aortic arch is determined by the branching pattern of the aortic arch. In a left aortic arch the first vessel to arise is the innominate artery which courses superiorly and rightwards to branch into the right carotid and right subclavian artery (Fig. 32.15a). A right aortic arch gives rise to a left sided innominate artery which passes superiorly and leftwards bifurcating into the left carotid and left subclavian artery (Fig. 32.15b). If visualisation of the branching

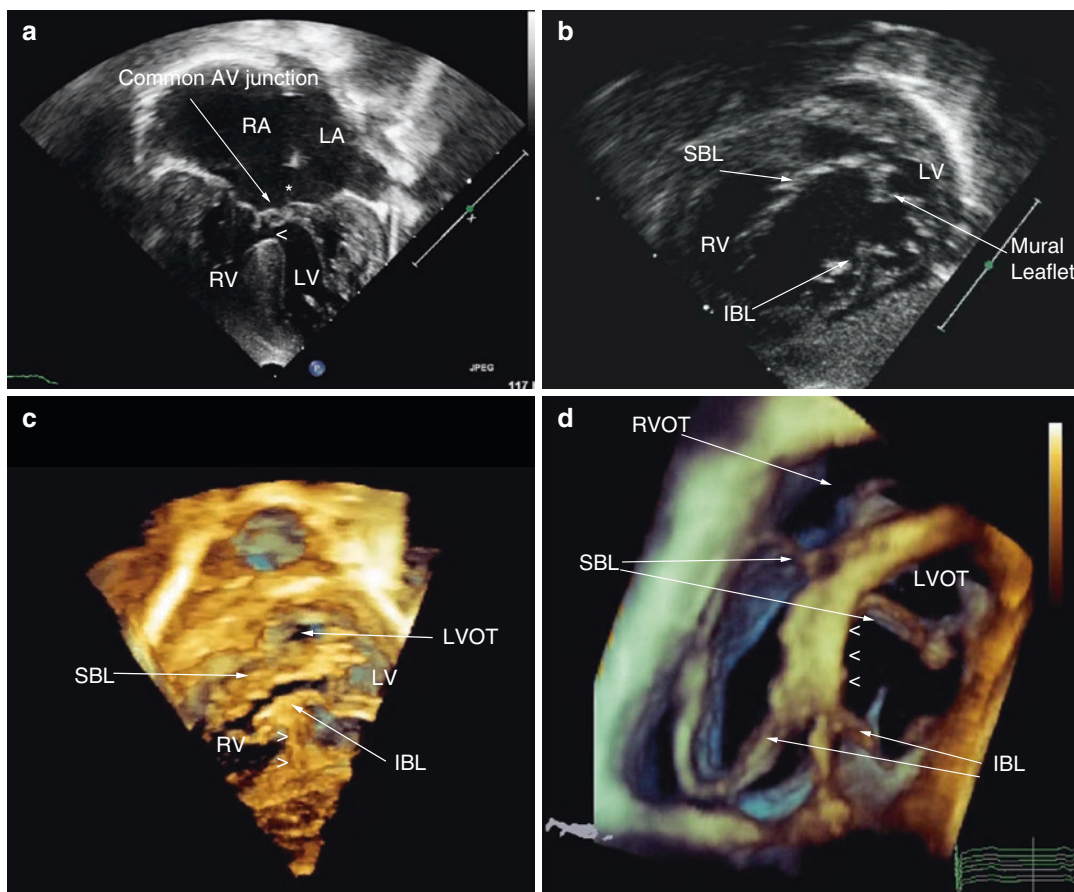


Fig. 32.8 Atrioventricular septal defect. (a) Apical four chamber view of a complete AVSD. The atrial (*) and ventricular () components of the defect are indicated. The common atrioventricular valve bridges between the left and right ventricles. (b) Subcostal view of the defect showing the common atrioventricular junction with inferior and superior bridging leaflets as well as the left sided mural leaflet. (c) Three-dimensional echocardiogram of an AVSD. The valve is visualised *en face* from the ven-

tricular apex. The depth of field shows the entirety of the superior and inferior bridging leaflets. (d) 3D transesophageal echocardiogram of an atrioventricular septal defect projected from the ventricular aspect. See also Video 32.7a–d. Abbreviations: RA right atrium, LA left atrium, RV right ventricle, LV left ventricle, SBL superior bridging leaflet, IBL inferior bridging leaflet, LVOT left ventricular outflow tract, RVOT right ventricular outflow tract

pattern is technically difficult the relationship of the aortic arch to the trachea is also helpful—a left aortic arch passes to the left of the trachea and vice versa.

From a suprasternal coronal plane the superior vena cava, transverse aortic arch and right pulmonary artery can be visualised. This view can also be used to visualise all four pulmonary veins as they drain to the left atrium. This latter view has been termed the “crab view” and allows visualisation of a vertical vein in the context of supracardiac total anomalous pulmonary venous drainage (Fig. 32.16a, b).

Use of Z-Scores in Growing Patients

In fully grown adult patients, assessment of the size of a cardiac structure and classification as normal or abnormal is typically done by reference to a “normal range” of values for any given feature, for example, size of the aortic valve annulus. The vast majority of primary surgical repairs of congenital heart lesions are performed in childhood and in decision-making, the size of cardiac structures may be critically important. In this setting, it is quite impossible to use a single set of normal ranges because the normal range itself will be

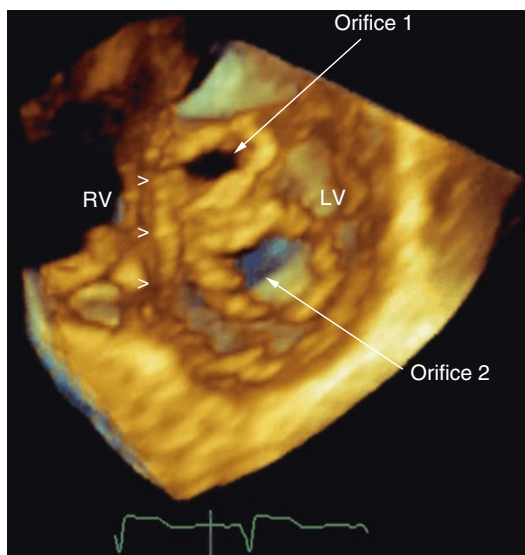


Fig. 32.9 Double orifice mitral valve. Three-dimensional projection of a double-orifice mitral valve seen from the apex of the LV. The separate orifices can be clearly visualised, aided by the depth of field of the technique. The ventricular septum is marked by the open headed arrows. See Video 32.8. Abbreviations: *LV* left ventricle, *RV* right ventricle

influenced by the size of the patient. Thus, the description of normality of size of different cardiac structures cannot be done by using a single normal range. The approach to this difficulty is to measure the size of different cardiac variables in large numbers of patients of different size, permitting the creation of graphs which include size-specific mean values and standard deviations. Z-scores refer to how many standard deviations above or below a size-specific mean value a given patient lies. A positive value means that a measurement lies above the mean and a negative value that the measurement is below the mean. This approach facilitates sequential measurements in growing patients and comparison between groups of patients of different size. Although this approach has been predominantly applied in children, it is now being used in adolescence through to adulthood [7]. An example is shown in Table 32.3 and a more detailed description of the approach has been published [8].

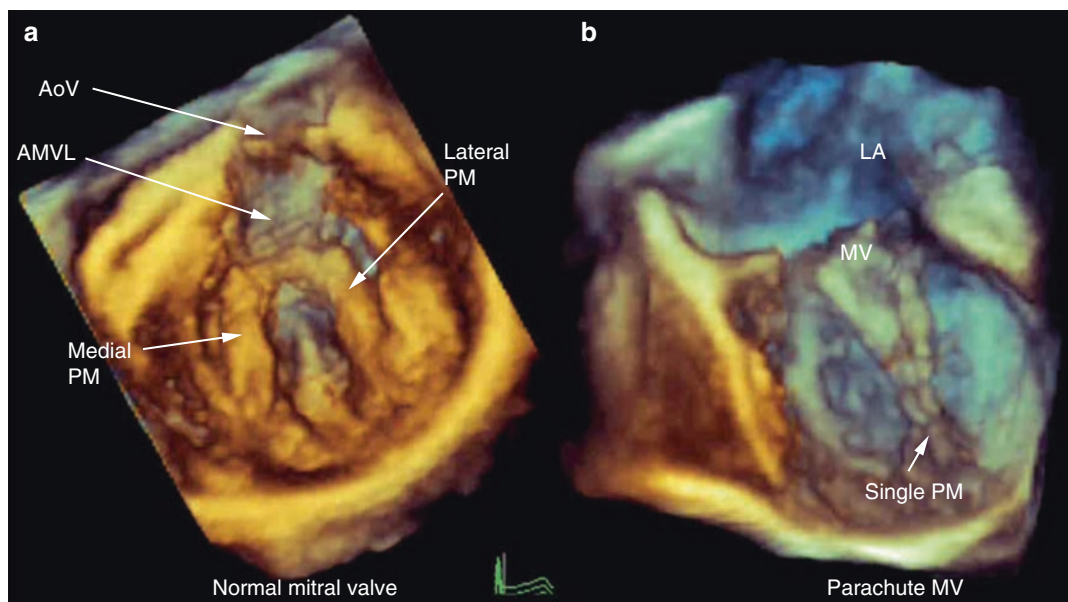


Fig. 32.10 Normal and parachute mitral valves. 3D echocardiography is ideal for the assessment of congenitally abnormal atrioventricular valves. These 3D images are projected *en face* to the AMVL to show the chordal support. (a) This image shows a normal MV with two

well-spaced papillary muscles supporting the chordal apparatus. (b) This image shows a single papillary muscle which receives chords from the lateral and medial aspects of the MV. Abbreviations: *AMVL* anterior mitral valve leaflet, *AoV* aortic valve, *PM* papillary muscle

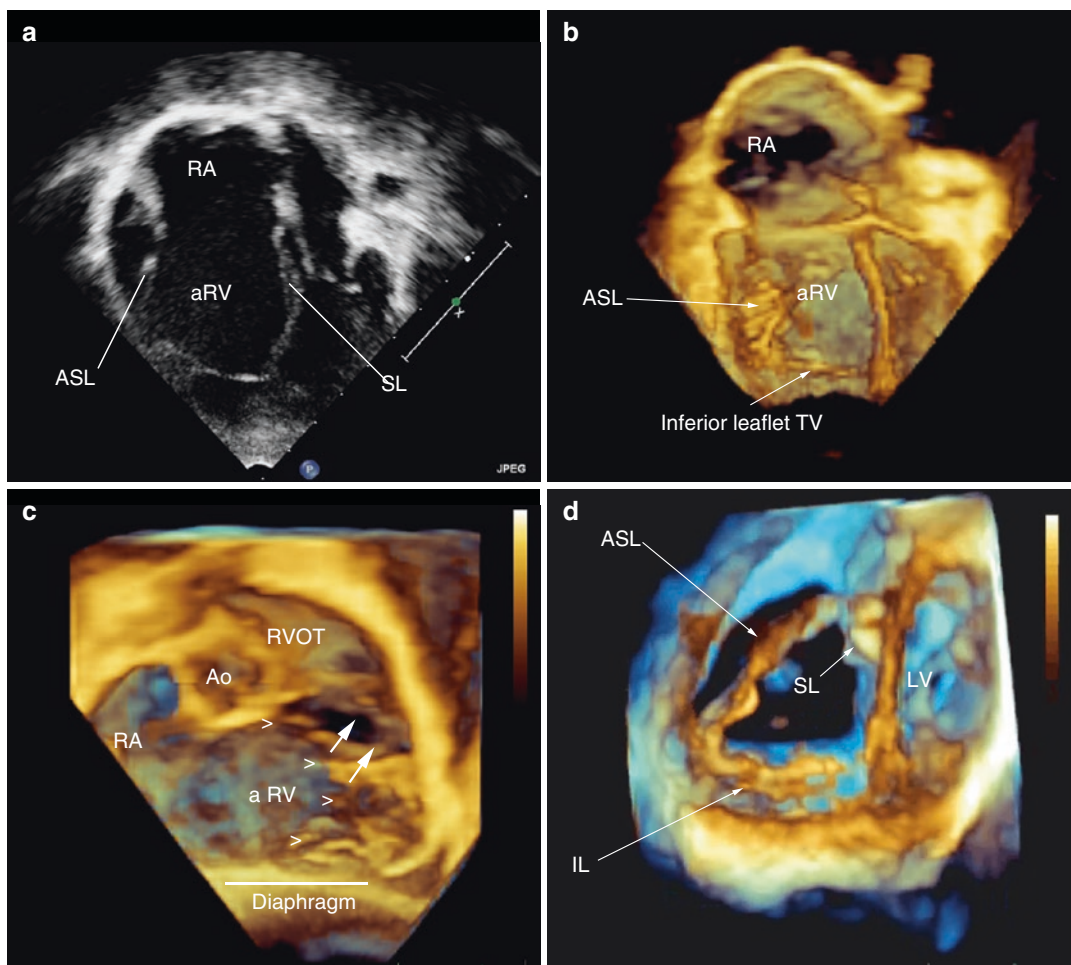


Fig. 32.11 Ebstein's anomaly of the tricuspid valve. (a) Apical four chamber view of Ebstein's malformation of the TV. The septal leaflet of the TV is displaced apically, so the normal pattern of differential insertion of the mitral and tricuspid valves is completely lost. The "atrialised" portion of the right ventricle is shown. (b) Three-dimensional projection of the apical four chamber view of Ebstein's anomaly. Note the apical displacement of the inferior TV leaflet and the long sail-like anterosuperior leaflet. (c) Subcostal oblique three-dimensional echocardiographic view of the

TV in Ebstein's anomaly. The TV is displaced towards the RV apex () but is also rotated superiorly towards the RVOT (arrows). (d) Three-dimensional echocardiographic view of the TV in Ebstein's anomaly. Three-dimensional short-axis projection *en face* to the orifice of the TV. The depth of field allows visualisation of the anterosuperior, hypoplastic septal and inferior leaflets of the TV. See Video 32.9a–c. Abbreviations: RA right atrium, aRV atrialised portion of right ventricle, TV tricuspid valve, SL septal leaflet, ASL anterosuperior leaflet, IL inferior leaflet

Specific Cardiac Lesions

Some cardiac lesions merit particular consideration because of the implications for long term follow up and echocardiographic review. These lesions are important because they are some of the commoner forms of congenital

heart disease for which long term survival is now the norm and for which sequential echocardiographic review is essential to detect longer term complications. For all the lesions discussed, echocardiography is not the sole imaging modality used and a multimodality approach is employed.

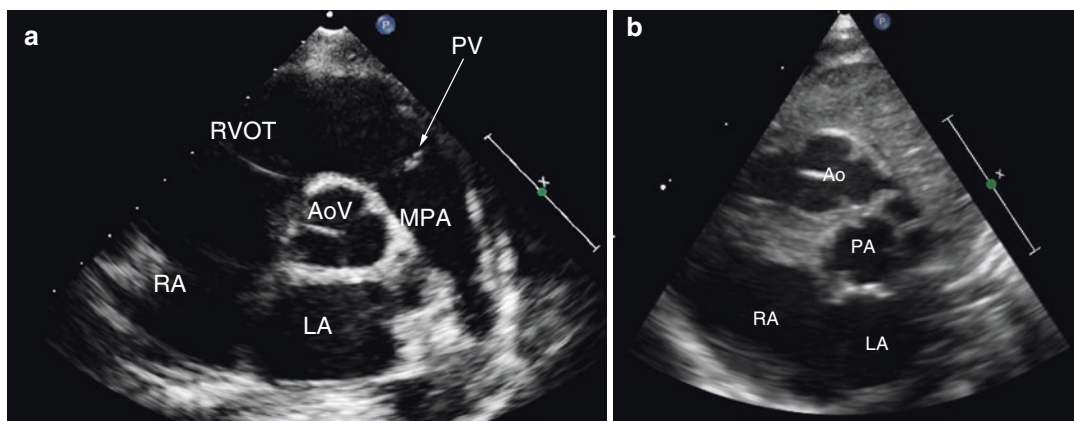
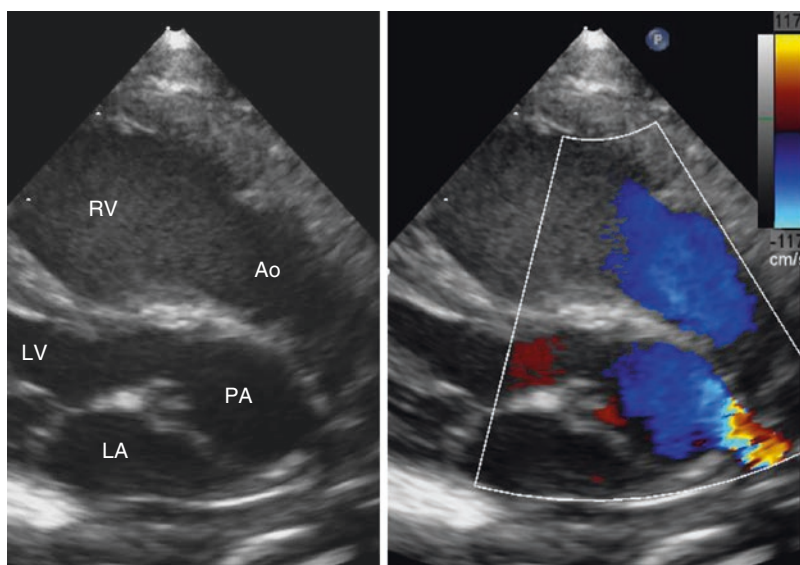


Fig. 32.12 Parasternal short axis view of the normal heart and transposition of the great arteries. (a) In the normal heart the RVOT wraps around the aorta which is seen in short axis. (b) In transposition of the great arteries, the aorta and pulmonary artery lie in a more parallel arrangement than normal, so that a parasternal short axis view can

show the cross-section of both the aorta and pulmonary valves in a single sonographic cut. See Video 32.10. Abbreviations: RA right atrium, LA left atrium, RVOT right ventricular outflow tract, PV pulmonary valve, MPA main pulmonary artery, Ao aorta, PA pulmonary artery

Fig. 32.13 Parasternal long axis view of simple transposition of the great arteries. The great arteries run parallel to each other with the aorta anterior to the pulmonary artery. See Video 32.11. Abbreviations: LA left atrium, LV left ventricle, PA pulmonary artery, RV right ventricle, Ao aorta



Tetralogy of Fallot

Tetralogy of Fallot is one of the more common forms of cyanotic congenital heart disease with an incidence of 0.4 per thousand liveborn infants. This condition has several characteristic features including overriding of the aorta, antero-superior deviation of the outlet septum accompanied by a variable degree of muscular subpulmonary and / or pulmonary valve stenosis. Figure 32.17a–c show the characteristic echocardiographic

appearances of the condition. A rapid checklist for the important pre-operative echocardiographic features is shown in Table 32.4. Tetralogy of Fallot may coexist with an atrioventricular septal defect which can be excluded by four chamber and short-axis imaging of the atrioventricular junction. In most cases, the VSD will be perimembranous, characterised by continuity of the tricuspid and aortic valve. More rarely, the VSD may be doubly committed, characterised by fibrous continuity of the aortic and pulmonary

Fig. 32.14 Ductal Cut.

A high sagittal view under the left mid-clavicle to demonstrate the proximal main pulmonary artery and the distal aortic arch, joined by a patent arterial duct, visible here as a red flare on colour Doppler. See Video 32.12. Abbreviations: *PA* pulmonary artery, *PDA* patent ductus arteriosus, *dAo* distal Aorta

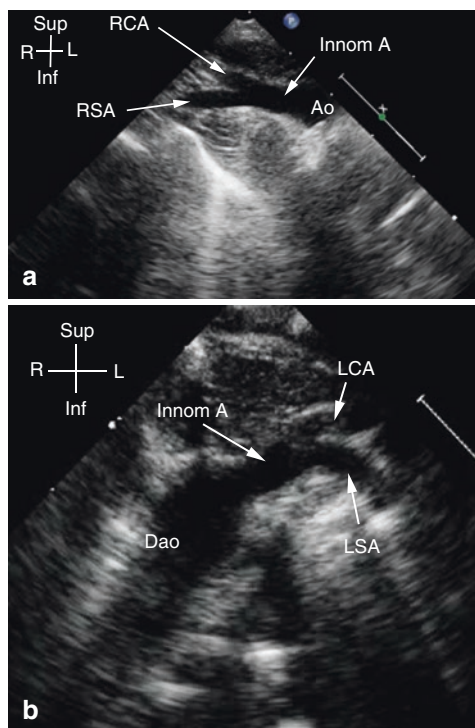
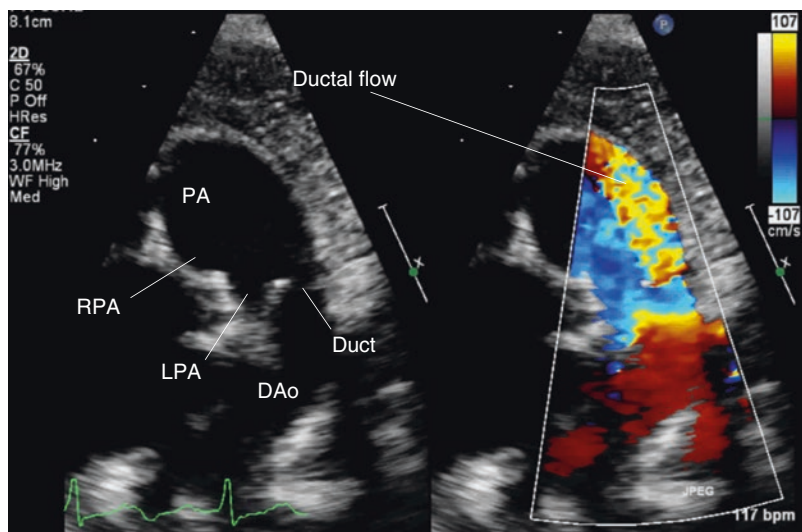


Fig. 32.15 Suprasternal coronal view of the branching pattern of the aortic arch. (a) In a left sided aortic arch the first branch is the innominate artery which heads to the right side and bifurcates into the right carotid and right subclavian arteries. (b) In a right sided aortic arch, there is usually mirror image branching so that the first vessel heads to the left as is a left sided innominate artery which bifurcates into the left carotid and left subclavian arteries. Abbreviations: *RCA* right carotid artery, *RSA* right subclavian artery, *LCA* left carotid artery, *LSA* left subclavian artery, *Innom A* innominate artery, *Ao* aorta. See Video 32.13a, b

valves. In the latter case, the infundibular septum will be absent and some would not apply a diagnostic label of tetralogy of Fallot at all. The “commitment” of the aorta to the left or right ventricle depends on whether the aorta is judged to arise more or less than 50% from the left or right ventricle. This is assessed either in a long axis view or by sonographic sweep from the great arteries to the ventricles in a short axis view. The anatomy of the right ventricular outflow tract is crucial in planning the surgical repair. This should include assessment of the severity of subpulmonary stenosis and pulmonary valve stenosis which can be differentiated by the characteristic shapes of the Doppler trace. The dynamic, muscular subpulmonary obstruction has a late increase in velocity, in contrast to the more symmetrical valvar trace. The pulmonary valve and branch pulmonary artery size should be measured and z-scores calculated. In some cases, the pulmonary valve is tethered severely leading to supravulvar pulmonary stenosis. The angle of the branch pulmonary arteries to the main pulmonary artery should be noted. The left pulmonary artery may take an acute angle from the main pulmonary artery leading to significant kinking of the vessel and reduction of flow. An assessment of these variables will inform whether surgical resection of the subpulmonary stenosis coupled with pulmonary valvotomy or dilation of the pulmonary artery will be sufficient to relieve right ventricular outflow tract obstruction or whether a

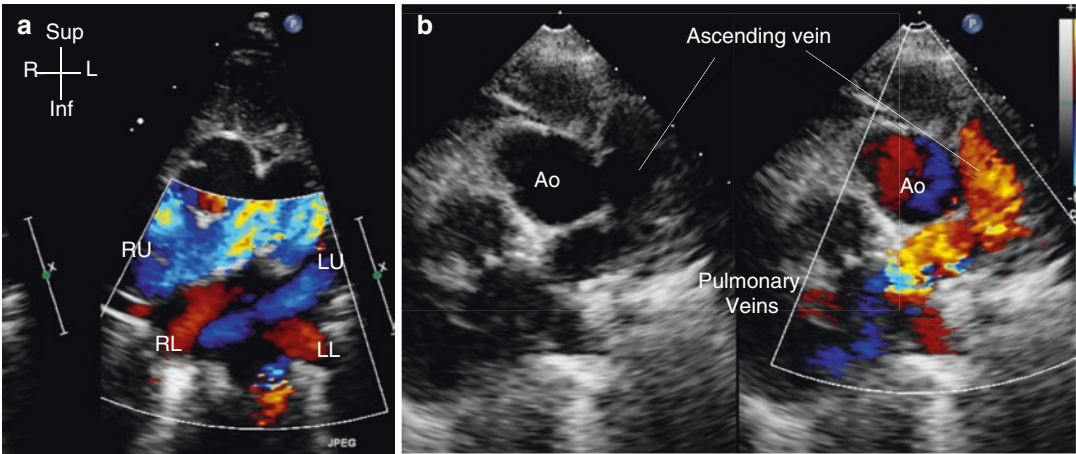


Fig. 32.16 Suprasternal coronal view of the pulmonary venous drainage and supracardiac total anomalous pulmonary venous drainage. (a) This view permits visualisation of all four pulmonary veins to the left atrium. (b) Suprasternal coronal ‘crab’ view of the pulmonary veins but with supracardiac total anomalous pulmonary venous

drainage via an ascending vein (red on colour Doppler) that drains into the innominate vein. See Video 32.14a, b. Abbreviations: RU right upper pulmonary vein, RL right lower pulmonary vein, LU left upper pulmonary vein, LL left lower pulmonary vein, PVC pulmonary venous confluence, AscV ascending vein, Ao Aorta, PA pulmonary artery

Table 32.3 Example of aortic root Z-scores for a patient followed through adolescence into young adulthood

Female patient age (years)	Patient BSA(m2)	Aortic root dimension (mm)	Z-score
15	1.5	28	+0.32
18	1.6	33	+1.96
21	1.7	35	+2.43
24	1.8	37	+2.9

Z-scores permit comparison of values, taking account of factors which may impact normal ranges such as age, sex and size. The Z-score indicates how many standard deviations above or below the mean a particular measurement lies

transannular patch will be required. If the latter is required, then significant pulmonary valve regurgitation will invariably be present postoperatively with implications for pulmonary valve replacement during later life. The coronary artery anatomy is important, especially if a transannular patch is going to be performed. It is essential to exclude the presence of a coronary artery crossing anterior to the right ventricular outflow tract. This is best by sweeping anteriorly from a short axis view of the great arteries. Most commonly, this results from the left anterior descending coronary artery arising from the right coronary artery or the presence of dual left anterior

descending coronary arteries but other variants occur more rarely.

Surgical repair is now typically undertaken in infancy and involves closure of the ventricular septal defect and relief of right ventricular outflow tract obstruction (Fig. 32.18a–e). In some cases relief of right ventricular outflow tract obstruction can be achieved by resection of subpulmonary myocardium without surgery on the pulmonary valve itself (valve sparing). In the majority of cases, however, the surgeon will also have to enlarge the pulmonary valve annulus by the use of a transannular patch. This leads to pulmonary valve regurgitation which is a central consideration in postoperative follow-up. In modern practice, surgical mortality is small and the infant will require review through childhood and adult life. An echocardiography checklist in the follow-up of operated tetralogy of Fallot is shown in Table 32.5. It should be emphasised that the imaging approach to such patients is multimodality, making extensive use of MRI and CT in particular [9].

During repair of tetralogy of Fallot, the ventricular septal defect is closed using an angled patch which both closes the VSD and baffles blood from the left ventricle to the aorta. Any residual

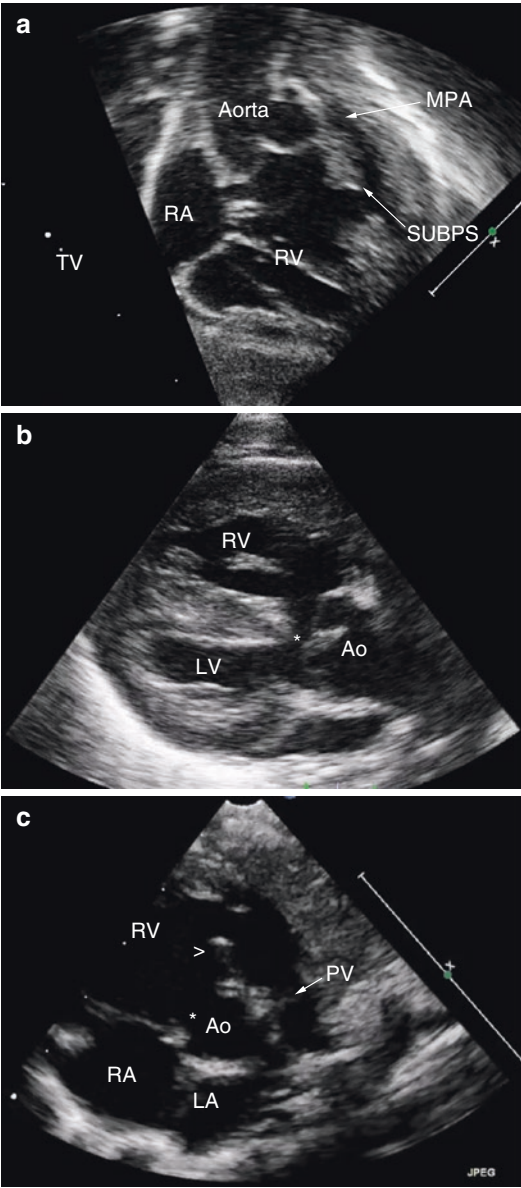


Fig. 32.17 Tetralogy of Fallot—preoperative findings. (a) Subcostal oblique view of tetralogy of Fallot. The aorta is much larger than the pulmonary artery and there is muscular subpulmonary obstruction due to antero-superior deviation of the outlet septum. (b) Parasternal long axis view demonstrating a ventricular septal defect (*) and aortic override typical of Tetralogy of Fallot. (c) Parasternal short-axis view demonstrating the large perimembranous ventricular septal defect (*), the anterosuperior deviation of the infundibular septum (>), the consequent infundibular stenosis and the hypoplastic pulmonary valve typical of Tetralogy of Fallot. See Video 32.15a–c. Abbreviations: RA right atrium, LA left atrium, RV right ventricle, LV left ventricle, Ao aorta, PV pulmonary valve, MPA main pulmonary artery, SubPS Subpulmonary stenosis

Table 32.4 Preoperative checklist for tetralogy of Fallot

Feature	Considerations
<i>Atrioventricular connection</i>	Concordant atrioventricular connections Exclude atrioventricular septal defect Exclude straddling mitral or tricuspid valve
<i>Ventricular septal defect</i>	Position e.g. perimembranous Exclude additional defects
<i>Aorta</i>	Commitment to left or right ventricle Left (70%) or right sided (30%) aortic arch Patency of arterial duct
<i>Right ventricular outflow tract</i>	Subpulmonary stenosis Pulmonary valve size and Doppler gradient Supravalvar pulmonary valve stenosis Size of branch pulmonary arteries
<i>Coronary arteries</i>	Exclude coronary artery crossing anterior to the right ventricular outflow tract

VSDs should be confirmed to be restrictive by the presence of a high velocity jet (>4 m/s) from left to right and the absence of volume loading of the ventricles. Dilation of the aortic root is well-recognised as a long term complication. The size of the aortic root and aortic valve annulus should be measured and the severity of aortic valve regurgitation should be estimated. The aorta is of above average size even prior to repair and so a z-score of aortic size greater than zero is invariable. The rate of growth of the aorta should be tracked both by absolute measurement and with the use of z-scores as outlined above. The risk of aortic dissection appears low even where the aortic root is significantly dilated and in the vast majority of patients aortic valve regurgitation is either absent or mild. Echocardiographic estimation of the severity of pulmonary regurgitation is difficult in the patient with repaired tetralogy of Fallot. In practice, the width of the colour flow regurgitant jet is compared to the pulmonary valve annulus dimension (>0.7 is severe), the shape of the pulmonary regurgitant jet on Doppler (a deceleration time of <100 ms is severe), pulsatility of the branch pulmonary arteries and reversal of blood flow in dias-

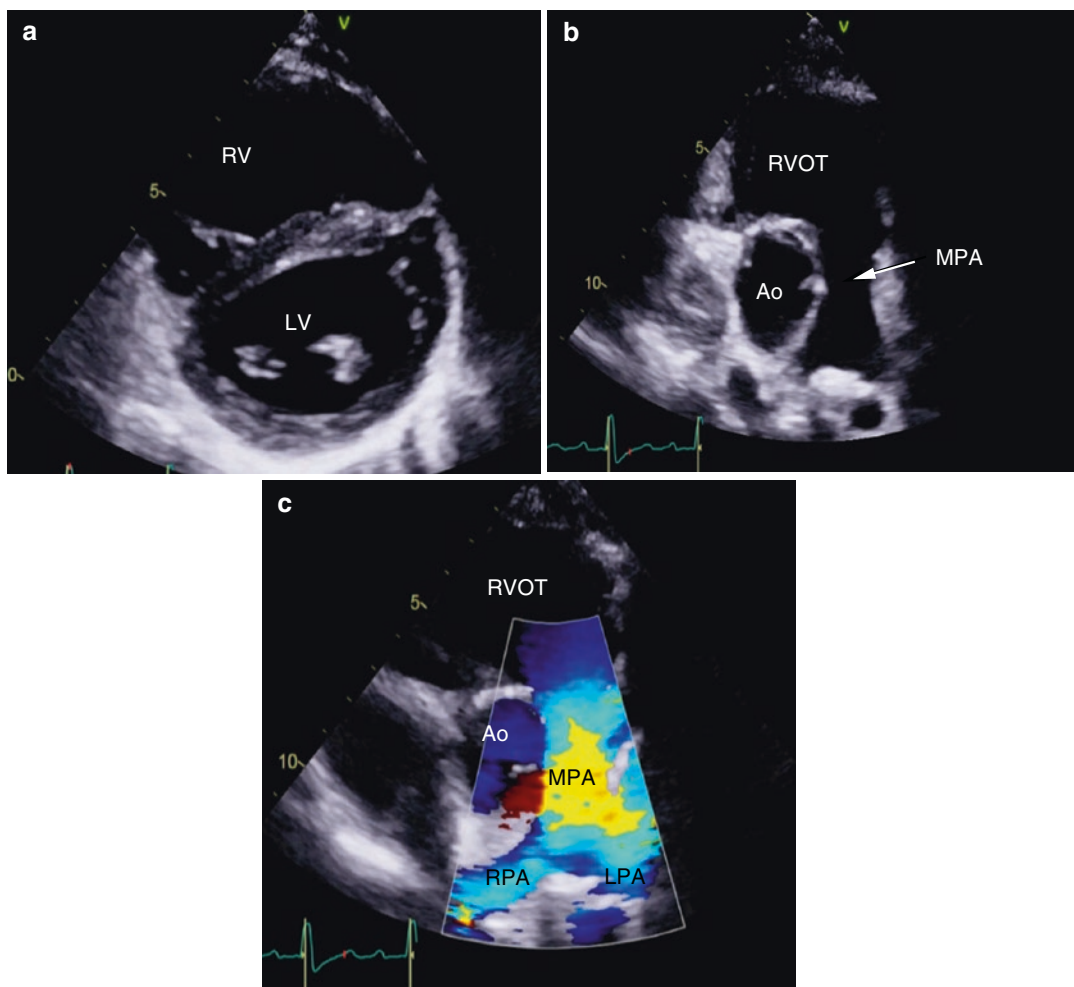


Fig. 32.18 Postoperative evaluation in tetralogy of Fallot. (a) Short axis view of the left and right ventricles demonstrating volume loading of RV and flattening of the ventricular septum. (b) Short axis view of the RVOT demonstrating dilation. (c) Colour flow Doppler showing reversal of blood flow in the main pulmonary artery and branch pulmonary arteries during diastole. Retrograde flow in the branch pulmonary arteries confirms significant pulmonary regurgitation. (d) Doppler trace of antegrade and retrograde flow in the pulmonary artery. The retrograde flow velocity has a rapid rate of

decline (line) and returns to baseline early in diastole confirming significant pulmonary regurgitation. (e) MRI of the branch pulmonary arteries in tetralogy of Fallot demonstrating “kinking” of the proximal LPA. This projection is from behind the pulmonary arteries looking anterior. The origin of the LPA is stenosed and superior to the origin of the RPA. Abbreviations: RV right ventricle, LV left ventricle, RVOT right ventricular outflow tract, MPA main pulmonary artery, LPA left pulmonary artery, RPA right pulmonary artery, Ao aorta

tole in the branch pulmonary arteries are all employed (Fig. 32.18c, d). Echocardiographic assessment of RV volume and function is very challenging in the patient with repaired tetralogy of Fallot. The standard approach for assessment of the size of the right ventricle should be adopted as previously described [10]. However, current 2D echocardiographic techniques do not permit quantification of the pulmonary regurgitant fraction nor

accurate determination of right ventricular volume. Semi-automated 3D echocardiography provides an alternative means of measuring the volume and ejection fraction of the right ventricle, but tends to produce lower volumes than MRI, particularly when the RV is dilated, so 3D echocardiographic measurements and MRI cannot be used interchangeably. Thus, imaging of the postoperative patient with tetralogy of Fallot does not

Table 32.5 Postoperative echocardiography checklist for tetralogy of Fallot

Feature	Considerations
<i>Ventricular septum</i>	Residual ventricular septal defect
<i>Aorta</i>	Aortic root dilation Aortic valve regurgitation
<i>Right ventricle</i>	Size and function of the right ventricle Size: 2D, 3D echo Function: 2D FAC, 2D strain, 3DEF, TDI, TAPSE Tricuspid valve regurgitation severity and velocity Exclusion of residual RVOT obstruction at subvalvar, pulmonary valve and supra-valvar level Doppler—PW / CW / CFM Exclusion of aneurysm of RVOT Pulmonary regurgitation Doppler—PW/CW/CFM Size / obstruction of branch pulmonary arteries Doppler—PW/CW/CFM
<i>Left ventricle</i>	Size and function of the left ventricle 2D, M-mode (if no paradoxical septal motion) 2D strain, TDI, PV flow pattern, MV inflow
<i>Coronary arteries</i>	Anatomy of coronary arteries prior to surgical or transcatheter pulmonary valve implantation

This table is a brief checklist of the important considerations in follow-up of the patient with operated tetralogy of Fallot

FAC fractional area change, *EF* ejection fraction, *TDI* tissue Doppler imaging, *PW* pulsed wave Doppler, *CW* continuous wave Doppler, *CFM* colour flow Doppler mapping, *RVOT* right ventricular outflow tract, *PV* pulmonary valve, *MV* mitral valve, *TAPSE* tricuspid annulus plane systolic excursion, *2D* two dimensional, *3D* three dimensional

rest solely with echocardiography. MRI is used extensively to quantify the size and function of the right ventricle, to quantify pulmonary valve regurgitation and imaging of the right ventricular outflow tract, branch pulmonary arteries and coronary arteries. MRI also has the potential to detect myocardial scar by the use of late gadolinium enhancement. This informs decision-making related to insertion of a competent pulmonary valve either by surgery or using a catheter approach. There is considerable debate about the criteria for surgical or catheter implantation of a competent pulmonary valve. Once the RV end-diastolic volume exceeds 150 ml/m² end-systolic volume exceeds 85 ml/m²

or RVEF is less than 45% then pulmonary valve replacement would at least be considered in most units.

Transposition of the Great Arteries

In transposition of the great arteries (TGA), the aorta arises entirely or predominantly from the morphologic RV and the pulmonary artery arises entirely or predominantly from the LV. This group of conditions may have associated lesions including VSD, pulmonary valve stenosis and coarctation of the aorta. In “simple” TGA there are no such associated lesions and in the immediate postnatal period survival depends on mixing of oxygenated and deoxygenated blood by maintaining fetal shunts such as patency of the arterial duct by administration of prostaglandin E or patency of the foramen ovale by balloon atrial septostomy. An echocardiographic checklist for the assessment of the preoperative patient with transposition of the great arteries is shown in Table 32.6. The surgical management of

Table 32.6 Preoperative checklist for transposition of the great arteries

Feature	Considerations
<i>Ventricles</i>	Relative size Presence and location of ventricular septal defect(s)
<i>Atrioventricular valves</i>	Concordant/discordant connection Straddling/override of mitral or tricuspid valve Cleft mitral valve Exclude valvar attachments into outflow tracts
<i>Great arteries</i>	Commitment of aorta and pulmonary valve to ventricles Relative position and of aortic/pulmonary valves Morphology of aortic and pulmonary valves + Doppler assessment for stenosis Exclude sub-pulmonary stenosis, pulmonary stenosis Exclude subaortic obstruction / aortic valve obstruction / coarctation of the aorta Patency of arterial duct
<i>Coronary arteries</i>	Define coronary artery arrangement in particular to exclude single coronary artery or intramural course

simple TGA has been revolutionised by the introduction of the arterial switch operation (ASO). Integral parts of the ASO include transection of the aorta which is relocated to the pulmonary arterial position and vice versa. The great arteries are transected above their respective valves and the coronary arteries are transferred on “buttons” of aortic tissue to the pulmonary artery which functions as the “neo-aorta”. Following surgery, the branch PAs leftwards or rightwards anterior to the ascending aorta (Le Compte manoeuvre) (Fig. 32.19a). Longer term considerations for echocardiographic follow-up include assessment of global and regional ventricular function of the LV in view of the reimplantation of the coronary arteries. Branch pulmonary artery stenosis, particularly on the left is a well-recognised complication following surgery and should be assessed during review. Imaging of the branch pulmonary arteries is readily achieved in younger patients using a modified high short axis view but this becomes progressively more difficult in older patients. Suprasternal views with leftward or rightward tilt may assist visualisation of the branch PA anatomy and Doppler assessment in older patients. Measurement of the aortic valve annulus, root and ascending aortic dimension is important because progressive dilation in this area is becoming increasingly recognised. Aortic valve regurgitation is usually mild and central but can become more severe as the annulus dilates (Fig. 32.19b, c). Although aortic root dilation is relatively frequent, this does not tend to change rapidly and the majority of patients have not required surgical reintervention to date. Table 32.7 describes the important echocardiographic considerations during follow-up. This situation is evolving as many of the initial survivors of arterial switch surgery are only now reaching middle adult life. As patients become older, CT or MRI is increasingly used to evaluate the coronary arteries, ventricular function, the aorta and branch pulmonary arteries (Fig. 32.19d).

Follow-Up After Atrial Redirection Procedures (Senning or Mustard Procedures)

The arterial switch operation was only introduced in the 1980s and prior to that time patients

were managed by surgical redirection of the systemic and pulmonary venous drainage. The Senning operation uses atrial tissue to baffle SVC and IVC blood to the left ventricle which remains connected to the pulmonary artery and the pulmonary venous return drains to the morphologic right ventricle which remains the systemic ventricle. An alternative approach was the Mustard operation which used either synthetic or pericardial baffles to achieve the same effect. Thus, for either of these approaches, the flow of blood is “physiologically” corrected but the morphologic RV supports the systemic arterial circulation and the morphologic LV supports the pulmonary circulation (Fig. 32.20a–d). The late complications of this repair include obstruction to either the systemic or pulmonary venous pathways, right ventricular failure or arrhythmias.

The Fontan Circulation

For many congenital heart lesions it may be impossible to divide the heart into separate pulmonary and systemic circulations. This may be due to imbalance of ventricular size, abnormal atrioventricular connections or the arrangement of the great arteries precluding a biventricular repair. Thus, the cardiac morphology of the patient with a functionally single ventricle circulation is heterogeneous. The long term surgical strategy in this patient group is to connect the systemic veins directly to the pulmonary arteries (total cavopulmonary connection (TCPC)), so that the pulmonary circulation is supplied under passive venous pressure. The blood returning into the atriums is pumped by the ventricle(s) into the systemic arterial circulation to perfuse the tissues. The venous return from the tissues flows into the superior and inferior vena cava which in turn drain into the pulmonary arterial circulation (Figs. 32.21a, b and 32.22a–c). Thus, the systemic and pulmonary arterial circulations are in series with no subpulmonary ventricle. The creation of a total cavopulmonary connection is normally staged by the initial connection of the superior vena cava to the pulmonary arteries (Hemifontan operation or Glenn shunt). There is variability in the surgical technique to complete

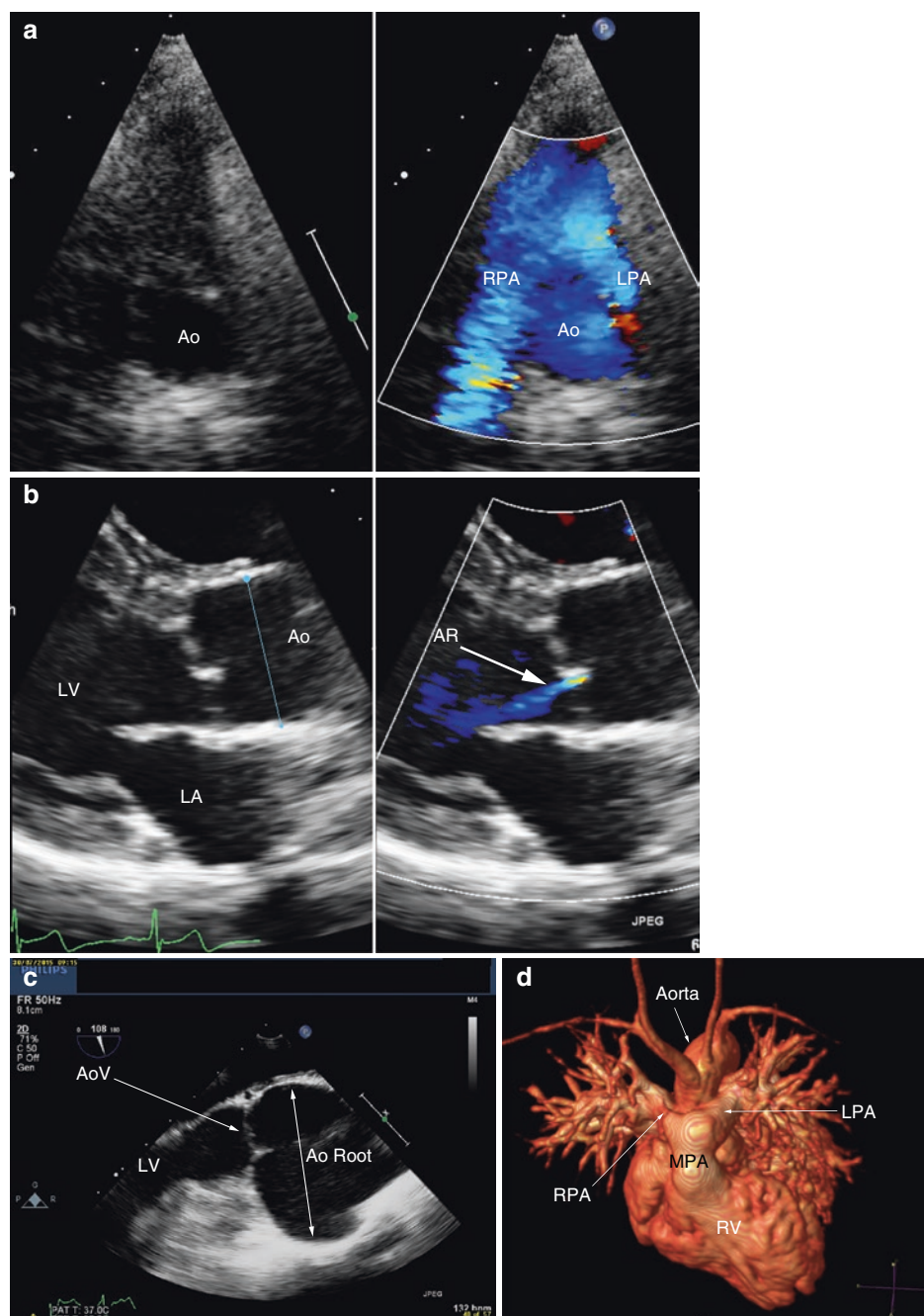


Fig. 32.19 Transposition of the great arteries following the arterial switch operation. (a) High parasternal short-axis showing the branch pulmonary arteries positioned anteriorly to the aorta following the Lecompte Manoeuvre during the arterial switch operation. In larger patients it becomes difficult to see the branch pulmonary arteries which are better appreciated with the use of colour flow Doppler. (b) Parasternal long axis view of adolescent patient following an arterial switch operation. There is mild central aortic regurgitation. The aortic annulus is dilated as is the aortic root (38 mm, marked by calipers)

with loss of the normal anatomy of the sinotubular junction. (c) Transoesophageal echocardiogram demonstrating aortic root dilation following the arterial switch operation. (d) MRI of the branch pulmonary arteries following an arterial switch operation. The branch pulmonary arteries both pass in front of the ascending aorta following the Le Compte manoeuvre during the arterial switch operation. See Video 32.16a, b. Abbreviations: RA right atrium, LA left atrium, RPA right pulmonary artery, LPA left pulmonary artery, LV left ventricle, AR aortic valve regurgitation

Table 32.7 Postoperative checklist for transposition of the great arteries

Feature	Considerations
<i>Ventricular septal defect</i>	Residual ventricular septal defect
<i>Aorta</i>	Aortic root dilation Aortic valve regurgitation Supravalvar aortic stenosis Residual obstruction of aortic arch
<i>Great arteries</i>	Exclusion of residual LVOT obstruction at subvalvar, aortic valve or supravalvar level Doppler—PW / CW / CFM Exclusion of residual RVOT obstruction at subvalvar, pulmonary valve and supravalvar stenosis Doppler—PW / CW / CFM Exclusion of branch pulmonary artery stenosis
<i>Ventricular function</i>	Assessment of size and function of the left ventricle Exclusion of regional wall motion abnormalities

Postoperative checklist

LVOT left ventricular outflow tract, *PW* pulsed wave Doppler, *CW* continuous wave Doppler, *CFM* colour flow mapping on Doppler

the TCPC which has evolved with surgical era. The initial approach was to connect the right atrial appendage directly to the pulmonary arteries (atriopulmonary Fontan) but this means of connection was far less efficient in terms of preservation of kinetic energy of the blood than current approaches. The most commonly used current techniques involve insertion of an artificial conduit to connect the inferior vena cava to the pulmonary arteries (extra-cardiac conduit) or creation of a tunnel within the right atrium (lateral tunnel) to permit blood from the inferior vena to flow to the lungs. In many instances a small hole (“fenestration”) is created between the systemic venous pathway and the atrium to maintain preload to the ventricle at the expense of a mild degree of systemic arterial desaturation. The exact approach varies largely by institutional preference (Figs. 32.21a, b and 32.22a–c). The resting cardiac output following a TCPC is around 70% of normal and there is a subnormal

capacity to increase cardiac output in response to physiological demand such as exercise. Given the “low flow” state in the systemic veins and the pulmonary circulation, patients with a TCPC are normally maintained on aspirin or warfarin to reduce the tendency to clot formation, in Fontan pathways, atrial appendages or other blind ending stumps which may result from surgical intervention. Due to the underlying cardiac lesion, loading conditions and multiple surgeries, this group of patients is at high risk of atrial and ventricular arrhythmias, further increasing the risk of clot formation.

The Fontan circulation poses major challenges in terms of the means of echocardiographic assessment, particularly with respect to assessment of ventricular function. Other modalities such as MRI, CT and cardiac catheterisation complement echocardiography in this group of patients [11]. The underlying anatomy is extremely variable so that the systemic ventricle may be of left ventricular, right ventricular or indeterminate type. Loading conditions are abnormal with preload derived from the pulmonary venous return to the heart supplemented in some cases by aortopulmonary collateral flow or flow through the fenestration in the Fontan circuit. Resting cardiac output in the Fontan circulation is reduced to around 70% of normal, which leads to neurohormonal activation, increasing ventricular afterload. Prior to Glenn anastomosis, the heart may be volume loaded due to the presence of a systemic to pulmonary artery shunt or pulmonary artery band in the context of obstructed and unprotected pulmonary blood flow, respectively.

Following the TCPC, the reduced venous return to the ventricle means that the ventricle is “preload-starved” compared to the normal circulation. Prior to echocardiographic evaluation of the patient with the Fontan circulation there are several key facts which the echocardiographer needs to establish. Firstly, the native cardiac lesion should be known, for example tricuspid atresia, hypoplastic left heart syndrome or double

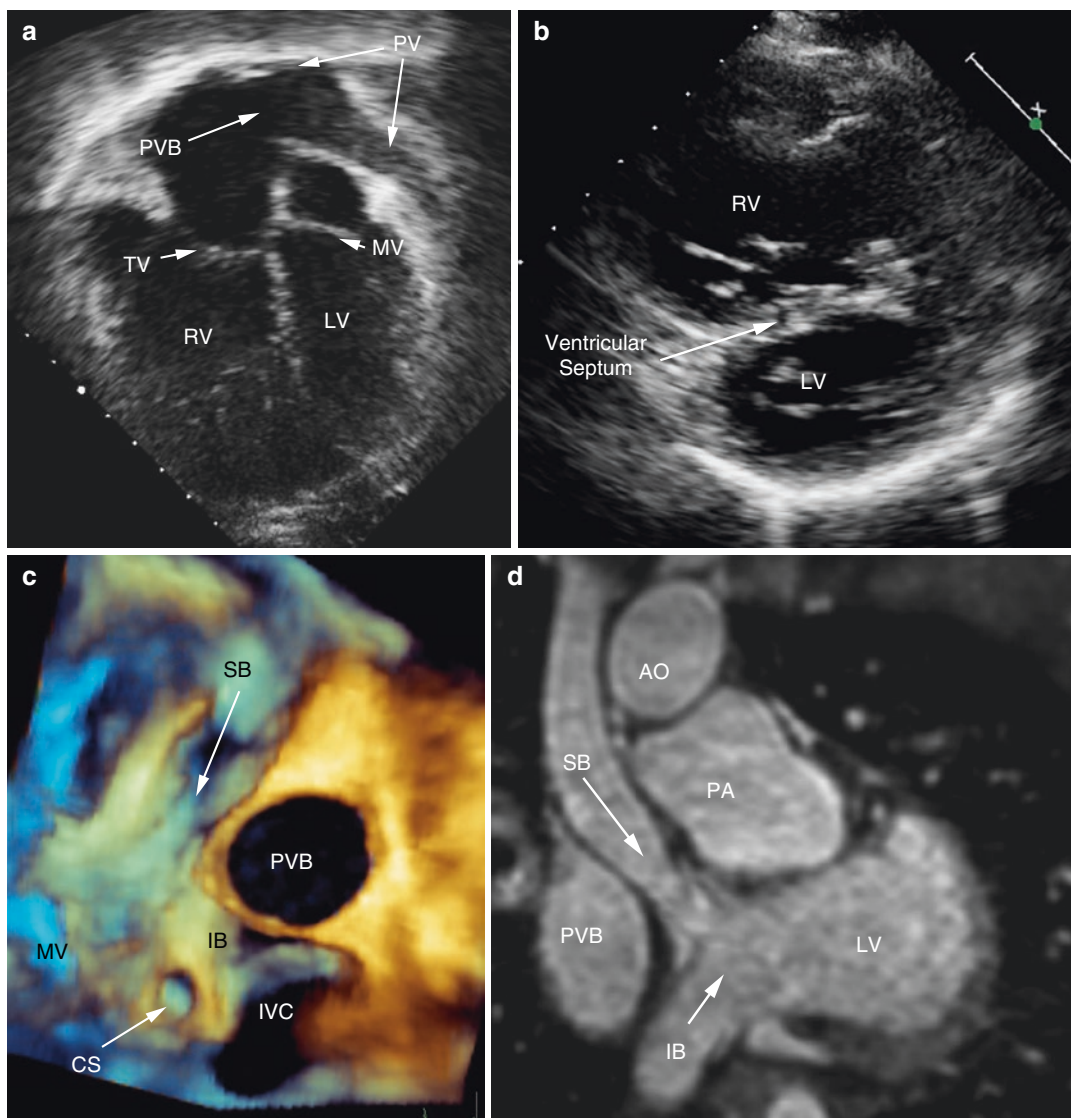


Fig. 32.20 Transposition of the great arteries treated by redirection of atrial flow (Senning operation). **(a)** Apical four chamber view showing the pulmonary veins being diverted through the pulmonary venous baffle towards the tricuspid valve and systemic RV. The RV is larger than the LV, the opposite of the normal appearance. **(b)** Short axis view showing the large RV and flattened ventricular septum following the Senning operation. The RV is at systemic pressure and the LV at lower (pulmonary artery) pressure, accounting for the flattening of the ventricular septum. **(c)** Three-dimensional transoesophageal echocardiogram showing the systemic venous baffles viewed from the left side. The superior baffle is seen passing

obliquely inferior to divert superior vena caval flow to the MV. The inferior baffle diverts blood from the inferior vena cava obliquely and superiorly to the MV. The position of the coronary sinus and the pulmonary venous baffle is also appreciated. **(d)** MRI of the superior and inferior venous baffles taking blood to the LV. This imaging is unconstrained by acoustic windows. See Video 32.17a–c. Abbreviations: *SB* superior baffle, *IB* inferior baffle, *PVB* pulmonary venous baffle, *IVC* inferior vena cava, *CS* coronary sinus, *MV* mitral valve, *TV* tricuspid valve, *LV* left ventricle, *RV* right ventricle, *PV* pulmonary veins, *PA* pulmonary artery, *Ao* aorta

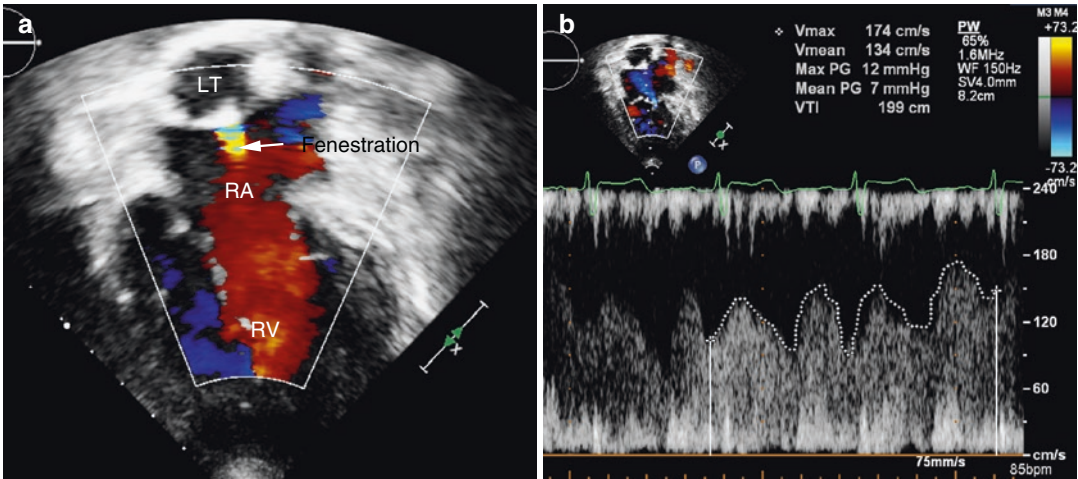


Fig. 32.21 Hypoplastic left heart syndrome following completion of total cavopulmonary connection. **(a)** Apical four chamber view showing features of hypoplastic left heart syndrome; no LV is seen. The flow through the TV into the RV is shown in red. The lateral tunnel is seen in short axis within the RA. Aliased flow is seen in the fenestration in the lateral tunnel, allowing some blood to flow from the lateral tunnel into the RA. This maintains pre-

load to the ventricle at the price of a modest degree of desaturation. **(b)** Doppler interrogation of the fenestration flow. The flow is phasic from the lateral tunnel to the RA. Tracing the velocity profile permits estimation of the mean pressure gradient which approximates the transpulmonary pressure gradient. This is normally around 4–8 mm Hg. Abbreviations: LT lateral tunnel, RA right atrium, RV right ventricle

inlet left ventricle. Secondly, the echocardiographer needs to understand the procedures which the patient has undergone and the exact surgical approach taken to complete the Fontan circulation. Thirdly, the underlying cardiac rhythm should be known as this impacts the interpretation of Doppler assessment. Fourthly, the echocardiographer has to understand the necessary preconditions for the Fontan circulation to function effectively. These preconditions include adequate systolic and diastolic function to permit low ventricular filling pressures, low pulmonary vascular resistance, absence of obstruction at any location in the circulation and optimal function of the atrioventricular and arterial valves.

At a practical level, there are several key issues which need to be addressed by the echocardiographer. A checklist for the assessment of the Fontan patient is shown in Table 32.8.

The key themes which the echocardiographer needs address can be summarised as follows.

1. Obstruction of the Fontan circuit

Obstruction at any site in the Fontan circulation is poorly tolerated. The outflow tracts, aortic arch, systemic veins, branch pulmonary arteries and pulmonary veins require careful assessment by 2D, colour flow and Doppler to exclude stenosis. With regard to the systemic veins, pulsed Doppler assessment can be useful to detect occult obstruction. Normally, there is phasic flow in the systemic veins with increased flow velocity with inspiration as decreased intrathoracic pressure encourages venous return but in the presence of distal obstruction the flow becomes less phasic with little or no respiratory variation. Doppler interrogation of flow across the Fontan fenestration typically gives a mean gradient of 4–8 mmHg, providing a surrogate for the transpulmonary pressure gradient. An increased in the mean gradient can indicate obstruction within the Fontan circuit. The systemic and pulmonary

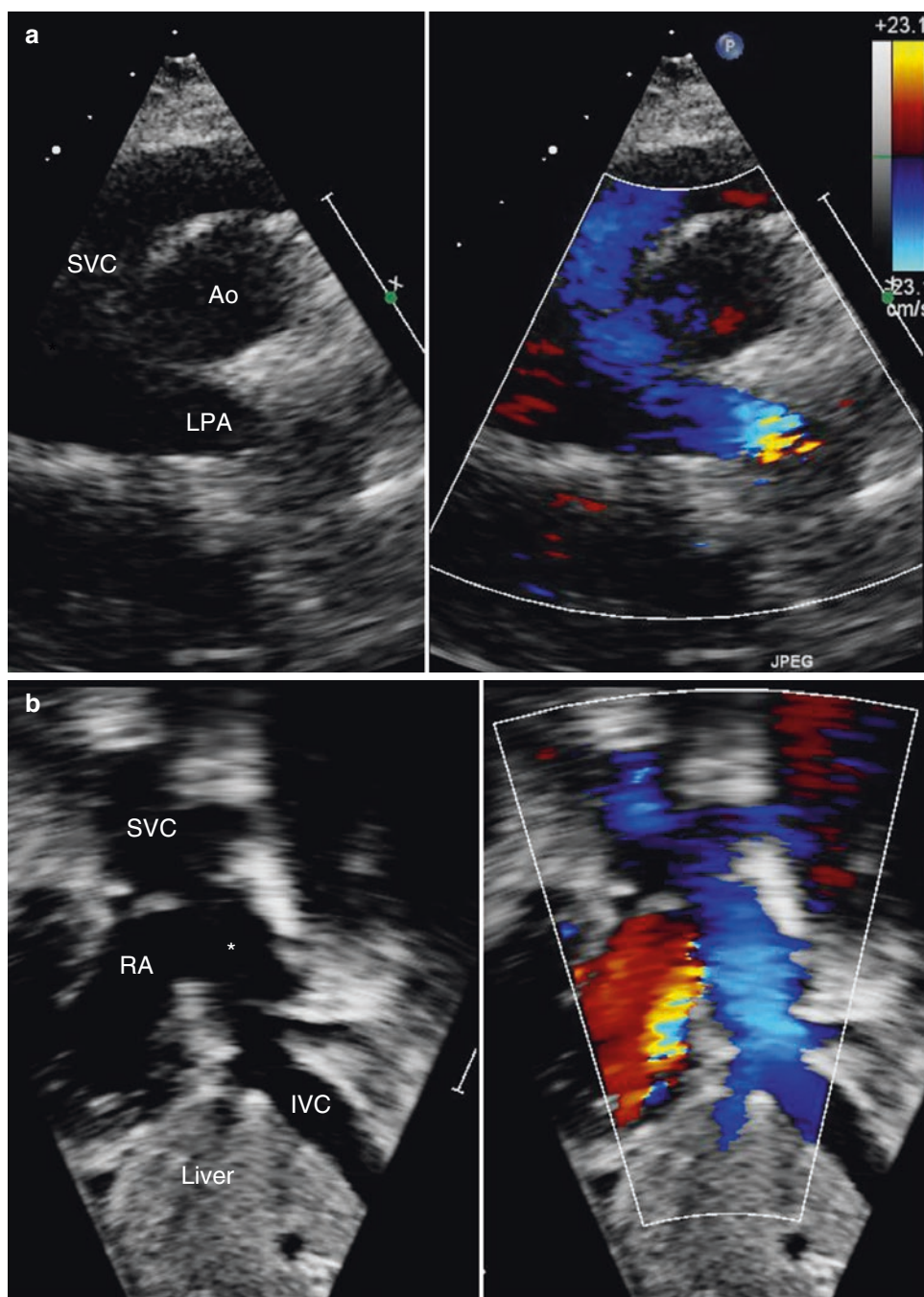


Fig. 32.22 The anastomosis of the systemic veins to the pulmonary arteries can be visualised both on echocardiography and by MRI, particularly when echocardiographic imaging is technically difficult. (a) Suprasternal short-axis view of the superior anastomosis (*) in the Fontan circulation, connecting the SVC with the pulmonary arteries. (b) Subcostal sagittal view of the inferior limb of the total cavopulmonary connection. The flow from the IVC through the

lateral tunnel (*) can be visualised right up to the point where the SVC joins the pulmonary arteries. (c) Gadolinium enhanced MRI image of the total cavopulmonary connection. The “full picture” of the anatomy can be seen including the distal pulmonary arteries which is not accessible by echocardiography. See Video 32.19a–c. Abbreviations: *Ao* Aorta, *LPA* left pulmonary artery, *SVC* superior vena cava, *RPA* right pulmonary artery

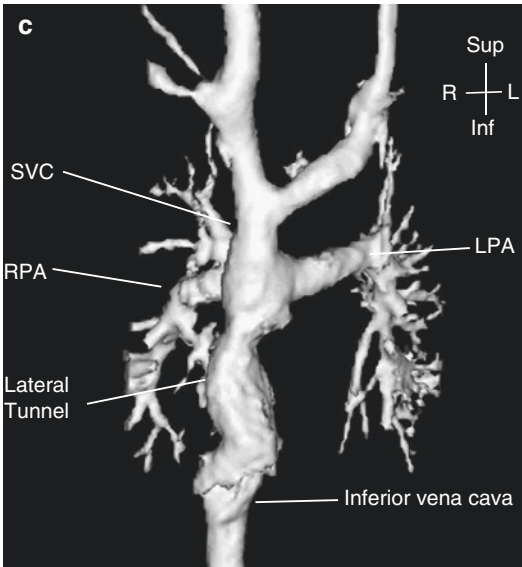


Fig. 32.22 (continued)

venous circulations are technically difficult by transthoracic echocardiography and extensive use is made of MRI, CT and transoesophageal echocardiography to detect occult obstruction.

2. Valvar regurgitation

Atrioventricular valve regurgitation adversely affects Fontan circulatory physiology by increasing atrial pressure, impacting on pulmonary venous return to the heart and reducing the efficiency of the ventricle. Quantitative assessment of atrioventricular valve regurgitation is difficult by echocardiography, particularly given the diverse morphology of the AV valves in this group of patients. Use of techniques such as PISA or direct 3D measurement of the effective regurgitant orifice area have not been validated in patients with the Fontan circulation. For serial assessments, similar ultrasound settings should ideally be used so that trends can be observed for an individual patients. Worsening AV valve regurgitation can be a marker of deteriorating ventricular function which needs to be considered in the overall assessment of the patient. MRI may be used to quantify regurgitant fraction of the valve as well if there is doubt as to the severity.

Table 32.8 Echocardiographic assessment of the functionally single ventricle circulation

Feature	Considerations
<i>Inferior vena cava</i>	Dilation / collapsibility Hepatic vein Doppler Spontaneous echo contrast PW Doppler assessment of respiratory variation of flow
<i>Lateral tunnel and extracardiac connection</i>	2D imaging Colour and PW assessment Check for pleural/pericardial effusion in perioperative period
<i>Ventricular function</i>	Subjective assessment of ventricular function Objective assessment of ventricular function <ul style="list-style-type: none">– MAPSE / TAPSE– Fractional area change– 2D strain– 3D volume where geometry permits– Tissue Doppler imaging– Doppler of AV inflow patterns
<i>Atrioventricular valve regurgitation</i>	Subjective assessment of AV valve regurgitation on colour flow Doppler Doppler interrogation of AV regurgitation (dP/dt) Effective regurgitant orifice area
<i>Outflow tract obstruction</i>	Doppler interrogation of the outflow tracts and aortic arch to exclude obstruction
<i>Superior vena cava and pulmonary artery flow</i>	2D visualisation of SVC to pulmonary artery connection Colour flow Doppler and PW Doppler assessment of SVC and branch pulmonary artery flow Assessment of respiratory variation to flow

AV Aortic valve, 2D two dimensional, CFM colour flow mapping by Doppler, PW pulse wave Doppler, CW continuous wave Doppler, TAPSE tricuspid annulus plane systolic excursion, MAPSE mitral annulus plane systolic excursion, TDI tissue Doppler imaging, 3D three dimensional, SVC superior vena cava

3. Ventricular function

Objective assessment of ventricular function in the patient with a Fontan circulation is a complex issue [12]. There is heterogeneity of ventricular morphology and abnormal loading conditions which change through stages of surgical pallia-

tion. Furthermore, there is a fundamental problem of comparison of functional parameters to a valid “normal” reference range. For example tissue Doppler, TAPSE or strain normal values from a normal subpulmonary right ventricle cannot reasonably be compared to a systemic right ventricle in the setting of single ventricle physiology. At these authors’ unit we use fractional area change of ventricles or 2D strain to assess systolic function as these have had the best correlation with MRI-derived EF and appear superior to subjective assessment of ventricular function [13, 14]. There are attractions of using a semi-automated 3D echocardiographic approach to estimate ventricular volumes and EF but the agreement with MRI derived data appears suboptimal at present. Although systolic ventricular dysfunction is a recognised risk factor early in the stages of surgery, diastolic dysfunction plays a major role in longer term failure of the Fontan circulation. This finding is likely to be multifactorial related to abnormal ventricular morphology, abnormal and changing loading conditions, multiple surgeries and myocardial fibrosis and scar formation. Non-invasive surrogates of filling pressures e.g. E/e' ratio have not proven sufficiently robust to avoid invasive assessment by cardiac catheterisation in the context of the failing Fontan. The accepted gradation of diastolic dysfunction in the normal heart has traditionally ranged from normal through impaired relaxation, pseudonormalisation and restriction. This categorisation is based on increased left atrial pressure as a consequence of diastolic dysfunction. Although this has been applied to the Fontan circulation, there is little validation of its use in the Fontan context where the lack of preload contrasts with the situation of the diastolic dysfunction in the normally connected heart. Thus, in practice, institutions will typically decide which echocardiographic parameters to track in a particular group of patients and assess changes longitudinally rather than against a “normal” reference range. It should be emphasised that many echocardiographic measures of systolic or diastolic have not been extensively validated against other techniques such as MRI nor has echocardiographic estimation of filling pressures or diastolic function by comparison with invasive methods.

4. Echocardiographic signs of “Fontan Failure”

The echocardiographer should be alert to hard evidence of significant dysfunction of the Fontan circulation. The particular signs include dilation of the inferior vena cava with little change during a “sniff” test. The presence of spontaneous contrast in the IVC should also be of concern. The presence of ascites and pleural effusions suggest elevation of venous pressure. If there is increased regurgitation of the systemic AV valve(s) this should be regarded as a potential marker of deteriorating ventricular function, which may not be reflected in measures of deformation such as 2D strain. Any new clot formation within the atrium, ventricle or Fontan pathway should be regarded a marker of dysfunction of the Fontan circulation. The echocardiographer should be alert to new tachyarrhythmias such as atrial flutter as this may be evidence on 2D or M-mode assessment of wall motion even when it is less apparent on the ECG. The onset of tachyarrhythmias dramatically reduces the efficiency of the Fontan circulation and should be treated promptly. Imaging of the Fontan circulation is multimodality with MRI in particular assuming a crucial role in the assessment of the Fontan patient. MRI is unconstrained by acoustic windows and can assess systemic, pulmonary and arterial components of the circulation. Ventricular volumes, EF and AV valve regurgitation can be quantified without geometric constraint. Furthermore, veno-venous and arterio-venous collateral flow can be measured, myocardial fibrosis identified and recently intraventricular and intraluminal flow patterns can be visualised by the use of 4D flow techniques [11].

References

1. Orwat S, Diller G-P, Baumgartner H. Imaging of congenital heart disease in adults: choice of modalities. *Eur Heart J Cardiovasc Imaging*. 2014;15:6–17.
2. Babu-Narayan SV, Giannakoulas G, Valente AM, Li W, Gatzoulis MA. Imaging of congenital heart disease in adults. *Eur Heart J*. 2016;37:1182–95.
3. Anderson RH. How should we optimally describe complex congenitally malformed hearts? *Ann Thorac Surg*. 1996;62:710–6.
4. Anderson RH, Sarwark AE, Spicer DE, Backer CL. Exercises in anatomy: cardiac isomerism.

- Multimed Man Cardiothorac Surg. 2014;2014. <https://doi.org/10.1093/mmcts/mmu027>.
5. Lai WW, Geva T, Shirali GS, Frommelt PC, Humes RA, Brook MM, et al. Guidelines and standards for performance of a pediatric echocardiogram: a report from the task force of the pediatric Council of the American Society of echocardiography. *J Am Soc Echocardiogr*. 2006;19:1413–30.
 6. Rice K, Simpson J. Three-dimensional echocardiography of congenital abnormalities of the left atrioventricular valve. *Echo Res Pract*. 2015;2:R13–24.
 7. Devereux RB, de Simone G, Arnett DK, Best LG, Boerwinkle E, Howard BV, et al. Normal limits in relation to age, body size and gender of two-dimensional echocardiographic aortic root dimensions in persons ≥ 15 years of age. *Am J Cardiol*. 2012;110:1189–94.
 8. Chubb H, Simpson JM. The use of Z-scores in paediatric cardiology. *Ann Pediatr Cardiol*. 2012;5:179–84.
 9. Valente AM, Cook S, Festa P, Ko HH, Krishnamurthy R, Taylor AM, et al. Multimodality imaging guidelines for patients with repaired tetralogy of fallot: a report from the american society of echocardiography: developed in collaboration with the society for cardiovascular magnetic resonance and the society for pediatric radiol. *J Am Soc Echocardiogr*. 2014;27:111–41.
 10. Rudski LG, Lai WW, Afilalo J, Hua L, Handschumacher MD, Chandrasekaran K, et al. Guidelines for the echocardiographic assessment of the right heart in adults: a report from the American Society of Echocardiography endorsed by the European Association of Echocardiography, a registered branch of the European Society of Cardiology, and the Canadian Society of Echocardiography. *J Am Soc Echocardiogr*. 2010;23:685–713. quiz 786–8
 11. Kutty S, Rathod RH, Danford DA, Celermajer DS. Role of imaging in the evaluation of single ventricle with the Fontan palliation. *Heart*. 2016;102:174–83.
 12. Burchill LJ, Mertens L, Broberg CS. Imaging for the assessment of heart failure in congenital heart disease: ventricular function and beyond. *Heart Fail Clin*. 2014;10:9–22.
 13. Ruotsalainen H, Bellsham-Revell H, Bell A, Pihkala J, Ojala T, Simpson J. Right ventricular systolic function in hypoplastic left heart syndrome: a comparison of velocity vector imaging and magnetic resonance imaging. *Eur Heart J Cardiovasc Imaging*. 2015;17(6):687–92.
 14. Bell A, Rawlins D, Bellsham-Revell H, Miller O, Razavi R, Simpson J. Assessment of right ventricular volumes in hypoplastic left heart syndrome by real-time three-dimensional echocardiography: comparison with cardiac magnetic resonance imaging. *Eur Heart J Cardiovasc Imaging*. 2014;15:257–66.

Assessing the Adult with Congenital Heart Disease

33

Maria Boutsikou, Michael A. Gatzoulis, and Wei Li

Introduction

Adults with congenital heart disease (ACHD) represent a unique growing patient population. A few decades ago, many patients born with congenital heart disorders were unable to survive into adulthood. However, the continuous progress in diagnostic techniques, the advances in cardiac surgery and the evolution of new therapeutic options such as catheter interventions have altered the natural history of these disorders and improved the quality of life and the survival prospects of these patients.

The spectrum of congenital heart lesions varies extensively among the adult population. The

majority of these patients have been diagnosed in infancy or childhood and have undergone palliative and/or reparative surgery; despite ongoing advances in cardiac surgery and intervention, residual anatomic and haemodynamic abnormalities are, nevertheless common amongst them. Heart failure, arrhythmias and premature cardiac death are relatively common late ACHD complications of patients with ACHD thus, clearly need lifelong follow up in specialized centers. Imaging and in particular echocardiography plays a significant role not only in the initial diagnosis but also for longitudinal follow up of these patients. It is widely used to

- Establish the anatomic diagnosis
- Assess the effect of surgical repair or interventions
- Identify acquired or residual lesions
- Assess valvular, atrial and ventricular function
- Guide transcatheter interventions and assess the result
- Monitor the intra- and postoperative status
- Guide pacing optimization

This chapter focuses on the echocardiographic evaluation of complex congenital heart malformations; with a focus on initial diagnosis, post-operative evaluation and identification of complications.

M. Boutsikou
Adult Congenital Heart Disease, The Royal Brompton Hospital, Adult Congenital Heart Centre and Centre for Pulmonary Hypertension, London, UK

M. A. Gatzoulis
Adult Congenital Heart Center and Center for Pulmonary Hypertension, Royal Brompton Hospital, National Heart and Lung Institute, Imperial College, London, UK

W. Li (✉)
Adult Congenital Heart Disease Echocardiography, Adult Congenital Heart Centre and Centre for Pulmonary Hypertension, Royal Brompton Hospital and the National Heart and Lung Institute, London, UK
e-mail: W.Li@rbht.nhs.uk

Segmental Analysis

Echocardiography is an invaluable imaging modality for the diagnosis and follow up of the patients with congenital heart disease. However, the great variety and the complexity of congenital cardiac abnormalities make the study of these patients quite challenging. In order to make a clear and complete diagnosis we must employ sequential segmental analysis. Analyze heart sequentially, creates an important checklist that will eliminate any oversight. Sequential segmental approach is particularly helpful in describing complex congenital abnormalities where abnormal connections and relationship of chambers often coexist. We will briefly present, herewith the steps of segmental analysis and how they should be applied using transthoracic echocardiography (TTE):

- Determination of the thoraco-abdominal situs
- Determination of atrial situs
- Determination of the cardiac and apex position
- Analysis of atrioventricular connections
- Ventriculoarterial connection
- Associated malformations and function of segments

In congenital heart disease there are multiple different combinations. Normality has to be proven. Cardiac chambers and great arteries should be recognized by their specific morphology not by their position.

Determining the thoraco-abdominal status prior to intracardiac anatomy analysis is useful for the determination of atrial arrangement. Chest X-ray is also useful for the determination of thoraco-abdominal situs. In cases of normal atrial arrangement (situs solitus) the right main bronchus is short and lies over the right pulmonary artery (PA) while the left main bronchus is longer with subarterial course (under the left PA). Consequently, the left PA lies superiorly to the right in the posterior to anterior projection. Additionally, the right lung is bilobed and the left is trilobed. Furthermore, the liver is right sided while the stomach and spleen are left sided. Situs

inversus is characterized by mirror image bronchial, pulmonary and abdominal anatomic arrangement. The presence of bilateral left or right bronchial and lung morphology and incomplete lateralization of abdominal organs with a midline position of liver and stomach is characterized as isomerism (left or right, respectively).

Determination of atrial situs: When there is normal anatomic arrangement of atria (atrial situs solitus), the morphological right atrium is on the right and the morphological left atrium on the left. In the vast majority of cases normal cardiac situs follows normal abdominal situs. Although left and right atrium have distinct morphologic features in their appendages and pectinate muscles, these are often difficult to be identified on the TTE imaging in adult patients. Thus the relative position of the great vessels seen from the subcostal view in TTE is used to infer the cardiac atrial arrangement. When there is usual atrial arrangement (or situs solitus), aorta lies on the left side of the spine and IVC on the right. In cases of atrial situs inversus there is a mirror anatomical image, where right atrium is on the left side and the left atrium on the right side. In the subcostal view, the aorta lies on the right side of the spine and the IVC on the left. In cases of left atrial isomerism there are two atria with the morphologic characteristics of the left atrium. In the subcostal view, the aorta and the IVC are on the same side of the spine and the aorta is posteriorly to the IVC. When right atrial isomerism is present, the atria have the morphologic characteristics of the right atrium. In the subcostal view both the great vessels are on one side of the spine and the IVC is posteriorly to the aorta.

Determination of the cardiac position: Firstly, the position of the heart within the thorax should be determined. Position of the heart in the left hemithorax, the right hemithorax or in the midline defines levocardia, dextrocardia and mesocardia respectively. The orientation of the cardiac apex may be different from the position of the heart within the thorax. In TTE, cardiac position could be determined from the subcostal view.

Identification of ventricular morphology and topology: The identification of the distinct morphologic features of each ventricle is very

important in the segmental analysis. Parasternal, apical and subcostal views are required for this part of the analysis.

Cardiac morphology: The presence of trabeculated endocardial surface, the moderator band, the chordal attachments of the tricuspid valve to the trabeculated septal surface and the presence of a trileaflet valve more apically inserted than mitral valve are the main morphologic features of the right ventricle in the normal setting. The main morphologic features of the left ventricle are the smooth endocardial surface, the presence of two papillary muscles without chordal attachments to the septum and the fibrous continuity of the aortic valve with a two leaflet atrioventricular valve, more basally displaced than the right atrioventricular valve.

Ventricular topology: describes the special relationship of the two ventricles. The first step to determine the ventricular topology is to identify the morphologic right ventricle. If hypothetically, after placing the palmar surface of the right hand on the septal surface of the morphologic right ventricle with the wrist on the cardiac apex, the thumb is in the inlet and the other fingers on the right ventricular outlet, then there is right-hand topology which is considered the normal pattern. Similarly, if the palmar surface of the left hand can be placed on the septal surface of the right ventricle in the same way then it is described as left.

Analysis of atrioventricular valve morphology and relationships: Atrioventricular relationships are determined by the type of connections between the atria and the ventricles. Parasternal, apical and subcostal views could be useful for this part of the analysis. Biventricular atrioventricular connections are present when there are two ventricles present and each atrium connects to its own morphologic ventricle. If the morphologic right atrium is connected to the morphologic right ventricle and the morphologic left atrium is connected to the morphologic left ventricle then there is atrioventricular concordance. If the morphologic right atrium is connected to the morphologic left ventricle and the morphologic left atrium is connected to the morphologic right ventricle then there is atrioventricular discordance. In case of the presence of univentricu-

lar physiology with a dominant and a rudimentary ventricle or rarely with a solitary of indeterminate ventricle there are three types of atrioventricular relationships: double inlet, absent left or absent right atrioventricular connection.

Ventriculo-arterial relationships: For the determination of the ventriculoarterial relation it is important to identify the morphology of the ventricles (described above) and the great arteries. Aorta is an arching vessel, which normally gives origin to the coronary arteries and the head and neck vessels, while PA bifurcates to the left and right pulmonary arteries. In the normal ventriculoarterial arrangement (concordant), the morphologic left ventricle gives rise to the aorta and the morphologic right ventricle gives rise to the PA. The pulmonary valve lies anteriorly and to the left of the aorta. The right PA courses posteriorly to the aorta. Parasternal, apical and subcostal and suprasternal views are useful for this part of the analysis.

In D-type ventriculo arterial discordance (D-transposition of the great arteries) the morphologic LV gives rise to the PA and the morphologic right ventricle gives rise to the aorta but the ventricles remain in their normal positions.

In L-type ventriculo arterial discordance (mainly seen in Congenitally Corrected Transposition of the great arteries- ccTGA) the morphologic LV gives rise to the PA and the morphologic right ventricle gives rise to the aorta but atrio-ventricular discordance is present and the RV lies to the left of the LV.

There are cases when more than 50% of both great arteries exit from one ventricle (either left or right); the respective anatomic malformations are called double outlet left or right ventricle.

The final category of ventriculoarterial relationship is single outlet from the ventricular mass. This includes solitary arterial trunk with either aortic atresia (hypoplastic left heart syndrome) or pulmonary atresia and common arterial trunk (common arterial valve and direct supply of the coronary, systemic and pulmonary arteries).

Associated anomalies: every echocardiographic study should be completed with the recognition and description of any associated cardiac anomalies.

Tetralogy of Fallot

Anatomy and Physiology

Tetralogy of Fallot (TOF) is the most common cyanotic congenital heart malformation, accounting for almost 10% of all congenital heart defects [1]. In anatomic terms, the malformation is composed of four constant features: right ventricular outflow tract (RVOT) stenosis, ventricular septal defect (VSD), right ventricular (RV) hypertrophy, large aorta, overriding the septum (biventricular origin of the aortic valve leaflets).

Although these anatomic characteristics are always present in patients with TOF, the severity of subpulmonary/infundibular stenosis varies as does the degree of RV hypertrophy. The spectrum of clinical presentation of patients with TOF varies therefore, between patients with good pulmonary blood flow (pink tetralogy) to the other extreme of patients with pulmonary atresia, presenting with profound cyanosis when the PDA closes. The pulmonary valve is usually dysplastic but not often the main cause of obstruction [1]. Pulmonary branch stenosis or PA hypoplasia has been reported in 50% of the cases [1] (Fig. 33.1).

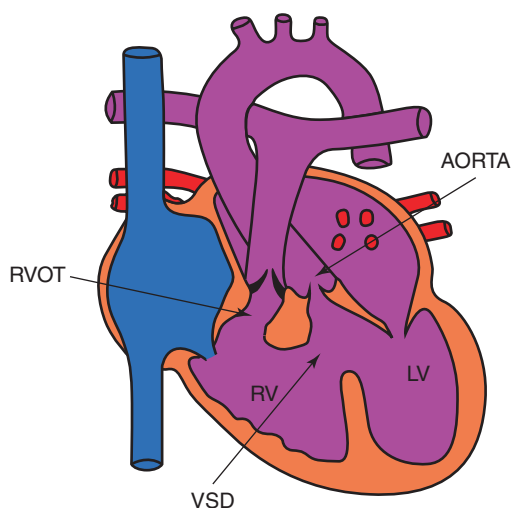


Fig. 33.1 Schematic diagram of the anatomy of tetralogy of Fallot. The presence of ventricular septal defect with overriding aorta, permits mixing of oxygenated and not oxygenated blood. RV right ventricle, LV left ventricle, VSD ventricular septal defect

Associated Lesions

Common associated lesions found in patients with TOF are patent foramen ovale (PFO), atrial septal defect (ASD), atrioventricular septal defect (AVSD), right aortic arch and coronary anomalies. Occasionally, one of the two pulmonary arteries may be absent (usually the left). In 15% of patients with TOF, a depletion of chromosome 22q11 exists, also known as Di George syndrome which is characterized among others, by cardiac anomalies, facial abnormalities, thymic hypoplasia, learning difficulties, mental disorders and early onset of psychiatric disease [1].

Transthoracic Echocardiography (TTE) in Unoperated Patients

Unoperated patients: the goals of echocardiographic assessment are:

- *Sequential segment analysis* to determine cardiac position and situs (subcostal long axis view), pulmonary and systemic venous connections to the atria (subcostal short axis view, apical four chamber view).
- *Atrioventricular (AV) valve morphology and function* (subcostal short axis view, parasternal long axis view—RV inflow view, apical four chamber view, apical two chamber and apical three chamber view).
- *Assessment of VSD, aortic override and aortic valve.* Direction of shunt and maximum velocity through the VSD, by continuous wave (CW) Doppler 2D, color flow Doppler, spectral Doppler in parasternal long axis view, parasternal short axis view, apical four and five chamber views. Aortic valve morphology and function (parasternal long axis view, parasternal short axis view, apical five chamber view)
- *Assessment of the site and the degree of RVOT obstruction.* Color Doppler and pulse wave (PW) Doppler could be applied sequentially to assess the level of obstruction, while CW Doppler is applied for the evaluation of the severity of obstruction. Parasternal long axis

(RV outflow view) and parasternal short axis view are the best for RVOT obstruction evaluation

- *Assessment of pulmonary valve abnormalities and coexistence of PA stenosis.* Assessment of pulmonary valve function and of pulmonary branch stenosis. RVSP is estimated from TR velocity with CW Doppler (parasternal long axis—RV inflow view, parasternal short axis view and apical four chamber view).
- *Determination of aortic arch sidedness and the presence of aortopulmonary collaterals* (suprasternal view)
- *Assessment of coronary artery anomalies* (parasternal short axis view, modified apical four chamber view angulated anteriorly)
- *Assessment of associated abnormalities.* Including patent ductus arteriosus (PDA) with CW Doppler (parasternal short axis, supra-sternal view).

Surgical Therapy

Most patients with TOF present during infancy. Surgery is the treatment for patients with TOF, and most patients have undergone at least one palliative or reparative operation in the past.

Palliative Procedures

Prior to surgical repair or in cases where repair is not feasible, a number of palliative procedures could take place in patients with TOF. They aim to increase PA blood flow:

- *Blalock–Taussig shunt (BT shunt):* classic, subclavian artery to PA anastomosis or modified, placement of interposition graft between subclavian artery and ipsilateral PA.
- *Waterston shunt:* Ascending aorta to main or right PA anastomosis (side to side)
- *Potts shunt:* Descending aorta to left PA anastomosis (side to side)
- *Brock procedure:* Infundibular resection or closed pulmonary valvotomy
- *Relief of RVOT obstruction* (without closure of the VSD).

Residual lesions and/or complications after palliative procedures: Palliative shunts especially Waterston and Potts shunt may lead to pulmonary hypertension while BT shunts and Potts anastomosis may result in branch PA stenosis. Patient with Brock procedure will still have the original anatomical abnormality but less severe RVOT obstruction and variable degrees of pulmonary regurgitation.

Transthoracic Echocardiography (TTE) After Palliative Procedures

The goals of echocardiographic assessment should focus on the investigation of the possible post-operative residual haemodynamic lesions, complications and ventricular function.

- *Assessment of patency of BT shunts:* The shunts can usually be visualized from supra-sternal view. Aliased color Doppler flow helps in identify the position of shunt. Flow through the shunt should be high velocity (>4 m/s) continuous throughout systole and diastole with characteristic sawtooth Doppler spectral pattern, consistent with the continuous aortic to pulmonary pressure gradient present. Reduced flow velocity often suggests increase in PA pressure. Shunt stenosis can be challenging. Narrow jet on color flow is suggestive of shunt stenosis. Doppler velocity can often underestimate the pressure gradient as the modified Bernoulli equation is invalid in assessing long segmental narrowing. Other imaging modalities (CMR or CT) can be helpful in identify shunt narrowing. Pulmonary hypertension is not uncommon in patients after a Waterston or Potts shunt. These two shunts are more or less abandoned as palliation.

Surgical Repair

Surgical repair includes VSD closure and relief of the RVOT obstruction. The latter may include resection of the infundibular muscle, combined with a of RVOT or transannular patch. In cases of

dysplastic or restrictive pulmonary valve, pulmonary valvotomy or pulmonary valve replacement maybe involved. In patients with extreme pulmonary stenosis (PS) (pulmonary atresia) repair includes an RV to PA conduit. Surgical repair also includes the correction of concomitant anomalies such as the augmentation of stenotic pulmonary arteries, the closure of PFOs and ASDs if they are present. In modern era, most adult patients with diagnosis of TOF will have had surgical repair during infancy or early childhood although there can very occasionally be adults survive with palliative procedures or without any intervention.

The most common residual anatomic and haemodynamic abnormalities after reparative surgery are:

- Pulmonary regurgitation
- Residual or recurrent RVOT obstruction or branch pulmonary stenosis
- Akinetic and aneurysmal RVOT
- RV dilatation and dysfunction
- Tricuspid regurgitation
- Residual VSD and/or ASD
- Aortic dilatation and aortic regurgitation
- Left ventricular (LV) dysfunction

Transthoracic Echocardiography (TTE)

- *Pulmonary regurgitation (PR):* PR is an important residual hemodynamic lesion commonly seen in adults with repaired TOF. It may result in right ventricular volume overloading, dilatation and dysfunction. PR can be visualized by color Doppler imaging from the parasternal long axis (RV outflow) view and parasternal short axis view. Severe PR can be quantified by color Doppler PR width >0.98 cm and diastolic flow reversal in the main or branch PAs). CW and PW Doppler signal could contribute to the estimation of PR severity; dense spectral CW Doppler signal and early termination of PR Doppler signal (PR index <0.77) are indicative of significant pulmonary regurgitation. PR jet width/pulmonary annulus ratio cutoff of >0.7 also identifies patients with severe PR. A pressure half-time <100 ms has good sensitivity and specificity for severe PR. It should be noted that both pulmonary regurgitation duration and PR pressure half time can be shortened by increased RV end-diastolic pressure. Therefore in patient with high RV end-diastolic pressure, PR can be overestimated using PR index and pressure half time. Main PA diameter is measured at its midpoint during systole and the branch PAs are measured at the level of origin. Color flow imaging and CW Doppler in PA branches could be used to assess pulmonary branch stenosis. (parasternal long axis RV outflow view, parasternal short axis view, suprasternal view).
- *Residual RVOT lesions:* Residual RVOT obstruction can be present at any level. From parasternal and sub costal long axis and short axis view, RVOT can be visualized on 2D. Color, PW and CW Doppler is helpful to identify the site of obstruction either at infundibular, pulmonary valve or supra-avalvar level. The infundibular stenosis usually has a late peaking of Doppler signal while valve or supra-valvar pulmonary stenosis has mid systolic peaking. The grading for the severity of obstruction should be similar to that used for assessment of simple pulmonary stenosis
- *Aneurysmal dilatation and akinetic RV anterior wall* are commonly seen in patients with repaired TOF especially when a transannular patch was used. If present, it contributes to overall RV dilatation and dysfunction. The dimension of aneurysm and length of akinetic wall should be measure from parasternal or subcostal long and short axis view.
- *Main PA and proximal branch PAs.* From standard parasternal short axis view or high left and right parasternal window and suprasternal view main PA and proximal left and right pulmonary arteries can be assessed. Color, pulse wave and continuous wave Doppler should be used to estimate any pulmonary valvular abnormalities and branch stenosis.
- *Tricuspid valve anatomy and function:* Tricuspid valve dysfunction, mainly regurgi-

tation is usually functional, secondary to RV dilatation or maybe organic related to VSD closure. Color Doppler in the latter demonstrates that TR jet originates from the VSD patch and the septal attachment of tricuspid valve. Valve prolapsing due to chordae rupture or previous infective endocarditis and damaged valve due to pacemaker or defibrillator occasionally may be present.

- *Assessment of RV size:* RV dilatation and dysfunction are common in repaired TOF. RV dimension should be assessed from multiple echo views. Dilatation of RV outflow area and/or aneurysmal formation is often the early presentation which contributes to the overall increase in RV volume and should be measured from parasternal or sub-costal long and short axis views. RV inflow dimensions are measured from focused RV apical four-chamber view with both crux and the apex visible to avoid foreshortening. A diameter >4.2 cm at base and >3.5 cm at the mid cavity level indicate RV dilatation.
- *Assessment of RV function:* RV systolic function can be assessed by RV fractional area change (FAC), tricuspid annular plane systolic excursion (TAPSE) and Tissue Doppler velocity of tricuspid annulus. The inlet part of RV function is often maintained at the early stage of disease. It is the aneurysmal akinetic RVOT often resulting in overall reduced RV ejection fraction measured by CMR. Therefore, nongeometric parameters such as myocardial acceleration during isovolumic contraction, myocardial performance index (Tei index), and total isovolumic time maybe more accurate in reflecting true RV function. Echocardiographic assessment of myocardial deformation using 2D speckle-tracking is less angle dependent and has been shown to provide prognostic value in patient with pulmonary hypertension, should be routinely applied to this group of patients. Assessment of RV diastolic dysfunction need to combine the Doppler profile in MPA (antegrade flow during atrial systole, 'a' wave), right atrial dilatation, flow reversal in hepatic vein and IVC dilatation and non-collapsing [2]. Doppler

indices of tricuspid valve inflow are not always reliable for assessment of RV diastolic function.

- *Right atrium:* RA area can be measured by 2D echocardiography from apical four chamber view. Area >18 cm² suggests RA dilatation.
- *LV size and function.* LV dimension, regional and global function should be routinely assessed. Several studies have shown that LV dysfunction is an important prognostic marker for premature death in TOF.
- *Aortic root and ascending aorta dilatation.* From parasternal long axis view, aortic root diameter at three levels (hinge point, sinus level and sino-tubular junction) and proximal ascending aorta can be made using 2D imaging during mid to late systole (maximal expansion).
- *Presence and severity of aortic regurgitation* can be assessed using color and CW Doppler (parasternal long axis and apical five chamber views).
- *Residual shunts.* Residual VSD commonly located at the superior end of the patch can be identified using 2D and color Doppler flow mapping from multiple planes. Using the continuous Doppler flow velocity across the VSD right ventricular systolic pressure can be assessed.

$$\text{RV systolic pressure} = \text{BP} - 4 \times V_{\text{max}}^2$$

(maximum velocity across VSD).

Residual ASD or presence of PFO can also be identified using Color Doppler.

Transesophageal (TOE)/Three Dimensional (3D) Echocardiography

TOE could be used preoperatively for the assessment of the size of VSD, the level and severity of RVOT obstruction, the presence of additional lesions. Additionally it is a useful tool intraoperatively for the assessment of hemodynamically significant lesions that could affect the postoperative clinical course and the result of surgical repair.

Three-dimensional TTE could provide more precise assessment of the size of the VSD and its relation with the surrounding structures. Additionally, 3D echocardiography could be very useful in the assessment of RV volume and pulmonary regurgitation [3] and help for identification of high risk patients who qualify for closer follow up or intervention [4].

Transposition of the Great Arteries (D-TGA)

Anatomy and Physiology

Transposition of the great arteries (TGA) is a congenital cardiac anomaly characterized by atrioventricular concordance and ventriculoarterial discordance. In patients with TGA the aorta arises from the RV and the PA from the LV while the atria are normally positioned in relation to the ventricles. TGA accounts for 5–10% of all CHD and is the second most common cyanotic lesion after TOF [5, 6] (Fig. 33.2).

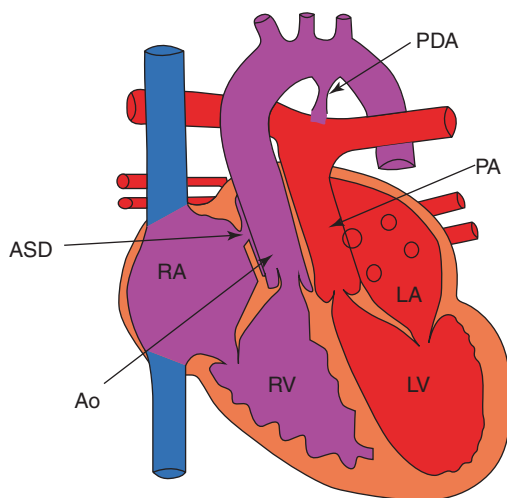


Fig. 33.2 Schematic diagram of the transposition of the great arteries. There is atrioventricular concordance but ventriculoarterial discordance. The presence of VSD or ASD allows mixing of circulations and survival at birth. *AO* aorta, *PA* pulmonary artery, *RA* right atrium, *RV* right ventricle, *LV* left ventricle, *LA* left atrium, *ASD* atrial septal defect, *PDA* patent ductus arteriosus

Associated Lesions

- VSD is one of the most common associated lesions, present in approximately half of the patients with TGA. Perimembranous VSDs are the most frequent, present in one third of the cases [6].
- LVOT obstruction (subpulmonary or pulmonary stenosis)
- Coronary artery anomalies with the most frequent one being the anomalous origin of the circumflex artery from the right coronary artery (18% of the cases) [6].
- PFOs, ASD, PDA and persistent left superior vena cava (SVC), partial or total anomalous pulmonary vein drainage, anomalies of AV valves and anomalies of the great arteries (e.g. coarctation of aorta, interrupted aortic arch, hypoplastic aortic arch).

Patient born with simple transposition of great arteries cannot survive without additional lesions. Communication between systemic and pulmonary circulation at any level can help to mix blood and increase the oxygen saturation in the systemic circulation and hence improve survival.

Echocardiographic Assessment of Unrepaired Cases

- *Assessment of cardiac position and situs* (subcostal long axis view, color Doppler)
- *PV and systemic venous connection to the atria* (subcostal short axis view, apical four chamber view, color Doppler)
- *AV valve morphology and function* (subcostal short axis view, parasternal long axis view—RV inflow view, apical four chamber view, apical two chamber and apical three chamber view, color Doppler, CW and PW Doppler)
- *Identification of the morphologic characteristics of each ventricle*. Confirm that the morphological RV is on the right side and the morphological LV on the left in patients with usual atrial arrangement. Assessment of ventricular size and function. Identification of regional wall motion abnormalities (paraster-

nal short and long axis, apical views four chamber, five chamber and three chamber view)).

- *Determination of ventriculoarterial connections.* The great vessels are parallel with the aorta arising from the RV and lying anteriorly to the PA. The latter arises from the LV and courses posteriorly to the aorta. The pulmonary bifurcation and originating coronary artery aids the identification of the two vessels (parasternal long axis view, parasternal short axis view, apical five chamber view).
- *Assessment of morphology and function of semilunar valves* (2D, color and spectral Doppler in parasternal long and short axis, and apical five and three chamber views).
- *Identification of VSDs.* Assessment of size and location. Acquisition of peak velocity and instantaneous peak gradient across the VSD (2D, color and CW Doppler in parasternal long axis view, parasternal short axis view, apical four and five chamber view)
- *Assessment of the site and the degree of LVOT obstruction* (parasternal long axis view, parasternal short axis view, apical four chamber view with color and spectral Doppler)
- *Assessment of PA stenosis if present* (2D, color Doppler, CW Doppler in parasternal long axis view—RV outflow view, parasternal short axis view, suprasternal view).
- *Determination of aortic arch sidedness and the presence of other associated anomalies such as CoA, PDA* (color Doppler and CW Doppler for the assessment of velocities across the CoA and PDA in suprasternal view)
- *Assessment of coronary artery anomalies* (parasternal short axis view, modified apical four chamber view angulated anteriorly, color Doppler). The identification of coronary artery anatomy is one of the most challenging parts of the echocardiographic assessment of patients with TGA. Careful 2D imaging with use of optimized settings is important. Careful inspection of the area between the semilunar valves in parasternal short axis when possible may reveal a double border of the posterior aortic root which is evidence of coronary artery passing between the aortic and pulmonary roots.

Interventional Therapy

Palliative Procedures

Balloon atrial septostomy (Rashkind procedure): Creation of an artificial communication between the atria in order to allow mixing of the arterial and venous blood in infants with TGA and intact ventricular septum.

Surgical Repairs

Atrial Switch Operation (Mustard OR Senning)

Restoration of the physiologic circulation by redirection of the venous return to the contralateral ventricle whereas the RV remains the systemic ventricle. Thus, during these procedures, baffles are used for the redirection of systemic venous blood from the IVC and SVC to the LV and through the pulmonary valve to the PA; subsequently oxygenated blood from the pulmonary veins (PV) is redirected to the systemic RV by travelling through what is outside the baffle but within the remainder of the common atrium (the atrial septum is excised) and through the aortic valve to the aorta. In the Mustard procedure the baffle is constructed with pericardial tissue within the atria, while in Senning procedure the atrial septal and free wall flaps are used for the construction of the baffles.

The most common post-operative complications, usually late, in patients who have undergone atrial switch operation include:

- Systemic RV dysfunction and progressive tricuspid regurgitation (TR)
- Baffle leaks or obstruction.
- Pulmonary arterial hypertension
- LVOT obstruction
- Atrial arrhythmias
- Sudden cardiac death

Transthoracic Echocardiography for Patients After Atrial Switch Operation

Additionally to the basic echocardiographic evaluation presented previously, the following issues should be addressed in patients post atrial switch operation.

- *Assessment of pulmonary and systemic venous pathways.* Identification of baffle leak or obstruction. Venous pathway can be identified from parasternal long axis view with anterior angulation, parasternal short axis view, apical and sub-costal views. Calcified baffle with narrow pathway on 2D and turbulent flow on color Doppler mapping usually indicate venous pathway obstruction. When there is mild obstruction, flow velocity across the pathway increases ($V_{\max} > 1.6$ m/s) but still pulsatile. With severe obstruction, flow becomes continuous but flow velocity is not necessarily high. Azygous dilatation with increased flow towards lower body often is an indirect sign of SVC pathway obstruction.

Small baffles leak are common in patients post Mustard or Senning operation. Using color Doppler the shunt through the leak can be identified. Using mixed blood and saline contrast injection through the peripheral vein is helpful to identify the baffle leak. The other helpful indirect sign of significant baffle leak is LV volume overloading, presenting as normal sized instead of compressed banana shaped LV, provided there is no LV hypertension to account for it.

- *Assessment of systemic RV systolic function and evaluation of TR.* Accurate assessment of systemic RV function is challenging. FAC, TAPSE, Tai index, tissue Doppler imaging (TDI) and isovolumic myocardial acceleration of the RV free wall and longitudinal strain using 2D speckle tracking all can be used in assessing RV function.
- *Organic tricuspid valve regurgitation* from abnormal prolapsing leaflet or damaged valve due to surgical closure of VSD or endocarditis can be seen in some patients. More common is functional tricuspid regurgitation due to annular dilatation and ventricular dysfunction. Color Doppler and spectral Doppler are used for the estimation of TR severity in the parasternal long axis (RV inflow) view, parasternal short axis and apical four chamber view.
- *Assessment of LV function and LVOT obstruction.* In patients with TGA, LV cavity size is

small and wraps around the systemic RV (banana shape). LV appears equal in size with the systemic RV in the parasternal short axis view in cases of LV pressure or volume overload. Variable degree of LVOT obstruction can be seen. Obstruction (sub-pulmonary stenosis) can be due to muscular-fibrosis ridge or ring.

- *Pulmonary hypertension.* Due to the morphological LV supporting the pulmonary circulation, increased PA pressure can be well compensated for very long period. LV dilatation and dysfunction only develop at late stage of disease. Mitral regurgitation is very rarely seen during the compensated period. Therefore, increase in PA pressure is often missed. Recording pulmonary regurgitation velocity even with trivial to mild degree of regurgitation often provides estimation of mean PA pressure. Normal shaped LV without any source of volume overload can be an indirect sign for increase in PA pressure.

Arterial Switch Operation

This type of anatomic repair has replaced the atrial switch operation and became the procedure of choice in the 1980s following its original description in 1976. It is performed early in life and includes switch of the aorta and the coronary arteries from the systemic RV and of the PA from the LV and reattachment of both great arteries to the appropriate ventricles. The coronary arteries are reimplanted into the neo-aorta. With this procedure the ventriculo-arterial concordance is normalized. Often, during the arterial switch operation the PA is brought anteriorly by a maneuver called LeCompte. The most common complications after the arterial switch operation include:

- Pulmonary stenosis (PS) (most frequently at the level of anastomosis)
- Neo-aortic root dilatation with aortic regurgitation
- Coronary ostia stenosis and biventricular dysfunction
- Pulmonary hypertension

Echocardiographic Evaluation After Arterial Switch Operation

- **RVOT and PAs:** RVOT stenosis is the most common reason for late reoperation after the arterial switch operation. Stenosis can be at any level but most commonly at the suture line of the neo- pulmonary artery. Main PA and pulmonary branches after the LeCompte maneuver can be difficult to visualize by conventional 2D echo view. A high parasternal short axis view or suprasternal view in some cases can demonstrate the PA bifurcation with the proximal course of the branches. Peak velocities in the distal PA <2 m/s are considered within normal limits. Trivial supralvalvar pulmonary stenosis with peak flow velocity between 2 and 2.5 m/s is very common. Peak flow velocity in distal PA ≥ 4 m/s would suggest significant stenosis. But if the stenosis involves a long narrow segment, then the gradient can be underestimated using the Bernoulli equation. In some cases, apical five chamber view with further anterior angulation or sub-costal oblique sagittal view can demonstrate better the anastomosis between the main PA and proximal branches. A high parasternal long-axis view can demonstrate the RVOT from the RV to the main PA (sometimes even to the bifurcation) anterior to the ascending aorta. From this view sub-valvar PS and pulmonary valve function can be assessed. Severity of pulmonary regurgitation can be assessed using the same parameters as described in assessment of repaired TOF [6].
- **Neo-aortic root and valve:** Neo-aortic root dilatation and aortic valve regurgitation is a late complication of arterial switch operation. Aortic root diameter can be measured from parasternal long axis views at three levels during systole. Aortic valve regurgitation, if present, should be assessed from parasternal long and short axis views and apical five-chamber and three-chamber views. Severity of aortic regurgitation can be graded based on the diameter of the jet's vena contracta, end-diastolic velocity of aortic regurgitation and the degree of diastolic

retrograde flow in the descending and abdominal aorta. LV dilatation and active contraction is often the sign of significant aortic regurgitation

- **Assessment of biventricular size and function.** Abnormal coronary artery anatomy and surgical coronary artery translocation are the substrates for myocardial ischemia after arterial switch operation. Many patients with arterial switch repair have a low normal LV ejection fraction. All known parameters for assessing LV and RV function should be employed in these patients. Dobutamine and exercise stress echo is helpful in identifying inducible myocardial ischemia and reduced contractile reserve in patients with significant coronary artery lesions.
- **Pulmonary hypertension.** Late-onset of pulmonary hypertension is a rare but important complication. Tricuspid and pulmonary regurgitation velocities can be used for estimating PA pressure. When working out pressure gradients, coexist PS should be taking into account. Right ventricular hypertrophy in the absence of RVOT obstruction may be an indirect sign of pulmonary hypertension.

Rastelli Operation

It is usually performed in TGA patients with large subaortic VSD and PS. The operation includes placement of a patch to establish communication between the LV and the aorta through the VSD; oversewn the pulmonary valve then connect the RV to the PA with a valved conduit. Thus, the physiologic circulation is restored since the oxygenated blood is directed through the baffle to the aorta and the venous blood from the RV through the conduit to the PA. The most common complications after Rastelli operation include:

- Conduit degeneration resulting in stenosis and/or regurgitation
- Secondary RV dilatation and dysfunction, TR
- Obstruction of the LV to aorta pathway
- Aortic regurgitation
- LV dysfunction
- Residual VSD

Echocardiographic Evaluation After the Rastelli Operation

- *Evaluation of the RV-PA pathway:* RV-PA conduit degeneration and stenosis are inevitable late after repair. The surgically placed RV-PA conduit is often antero superiorly located. Therefore high parasternal or suprasternal views are helpful in identifying and assessing the conduit and valve function. Bright calcifications on 2D are often a clue for conduit location. Color Doppler is particularly helpful to identify flow through the conduit and to guide interrogation by spectral Doppler. CW Doppler probe (pencil probe) is useful in detecting the highest flow velocity through the conduit and the proximal branch PAs. Conduit stenosis is often at multiple levels and involves long segments, gradient can, therefore be underestimated with the modified Bernoulli equation. Estimation of PA systolic pressure is based on the peak gradient across the conduit and the tricuspid regurgitation velocity. When there is a residual VSD, flow velocity across it can also assist with RV systolic pressure estimation.
- *Evaluation of LV to aorta pathway.* Obstruction at LV to aorta pathway can easily be overlooked or underestimated due to the respective angulation. Nonstandard transducer position and modified apical views can help in detecting the highest flow velocity across the LVOT and aorta. Aortic regurgitation is one of the late complications and should be assessed in the same way as in isolated aortic regurgitation.
- *Detection of residual VSDs.* Residual VSD often seen at the border of the VSD patch. VSD patch dehiscence can also be seen in patients long after repair and after infective endocarditis. This will result in acute increase in shunt volume across the residual VSDs (2D, color Doppler and CW Doppler in order to obtain peak velocity across residual VSD in the subcostal, parasternal long and short axis views).

Transesophageal (TOE)/Three Dimensional (3D) Echocardiography

TOE is not widely used for the diagnosis of TGA but is a valuable tool for the intra and postoperative evaluation of these patients. It is useful in

- Visualization of the great vessels and the presence of PDA
- Assessment of baffle leak or obstruction in TGA patients post atrial switch operation. In many cases the TTE windows are very poor, thus TOE could evaluate the presence of these complications. Additionally, exclusion of the presence of thrombi in the atria and baffles prior to cardioversion in cases of atrial arrhythmias.

In patients undergoing arterial switch operation TOE may be used intraoperatively for assessing regional wall motion abnormalities, visualization of reimplantation of coronary arteries' sites, and the presence of residual VSD. Additionally, in cases with poor TTE windows, TOE could be used for the assessment of aortic and pulmonary supravulvar anastomoses and for evaluation of PA and branch stenosis after the LeCompte maneuver.

Three D echocardiography offers better visualization of the valves especially the tricuspid valve which is often dysfunctional in patients with TGA. All the tricuspid valve leaflets can be clearly visualized. Quantification of the severity of regurgitation, identification of leaflet defects, sizing of the area of non coaptation and assessment of valve prolapse are some of the advantages with 3D TTE assessment [7]. Additionally, it offers more detailed assessment of outflow tract obstruction and visualization of the pulmonary valve. Three D TTE can be valuable in the identification of atrial baffle obstructions, which are important but difficult to assess by conventional 2D TTE [8].

Dobutamine Stress Echocardiography/Contrast Echocardiography

Dobutamine stress is useful for assessing ventricular contractile reserve, exclusion of ischemia in TGA patients after arterial switch operation and for assessing further dynamic LV and RV outflow tract obstruction. Furthermore, injection of agitated saline through a peripheral vein could be helpful for the detection of baffle leaks in patients with poor echocardiographic windows.

Congenitally Corrected Transposition of the Great Arteries (L-TGA/ccTGA)

Anatomy and Physiology

Congenitally corrected transposition of the great arteries (ccTGA) is a congenital cardiac anomaly characterized by atrioventricular and ventriculoarterial discordance. It is a rare congenital malformation accounting for 0.5% of all types of CHD. In patients with ccTGA the right atrium receives systemic venous blood from the IVC and the SVC. The right atrium is connected through the AV valve (in this case the mitral valve) to the morphological LV. The venous blood enters the LV and through the pulmonary valve is delivered to the PAs. The oxygenated blood enters through the pulmonary veins to the morphological left atrium and then through the AV valve (in this case the tricuspid valve) to the morphological RV. The aorta arises from the RV and delivers the oxygenated blood to the body. Ventricular loop is abnormal with a morphologic LV being on the right and aligned with the morphologic RV and the latter being on the left. It is also called L-transposition because the morphological RV is in the levoposition. The great ves-

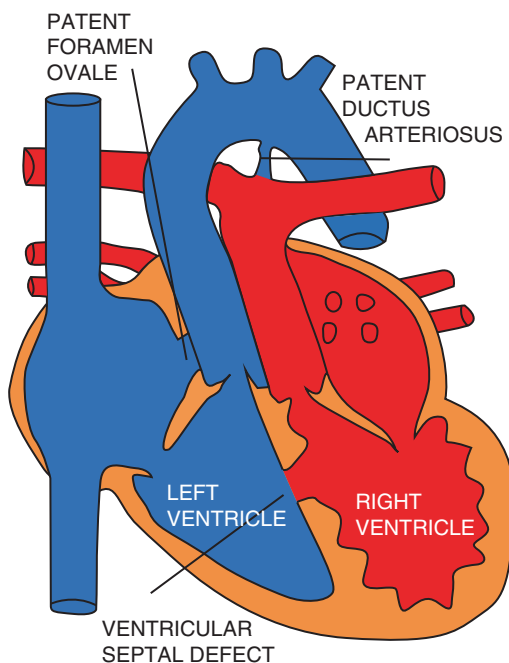


Fig. 33.3 Schematic diagram of the congenitally corrected transposition of great arteries. There is both atrioventricular and ventriculoarterial discordance. The systemic circulation is supported by the right ventricle

sels are also abnormally oriented with the aorta being usually anterior and to the left of the PA. In very rare cases, there will be abnormal atrial arrangement (mirror image), morphological RA is on the left connect to morphological LV and give rise to aorta. Morphological LA is on the right connect to morphological RV and give rise to PA (Fig. 33.3).

Associated Lesions

More than 90% of the patients with ccTGA have associated cardiac anomalies] [9–12].

- About 20% of patients with ccTGA have dextrocardia [6], while 5% of the patients present with atrial situs inversus [7]

- VSD is one of the most common associated lesions, present in approximately 60-80% of the patients with ccTGA (mostly perimembranous VSDs) [6].
- LVOT obstruction (subvalvar and/or valvar) is present in 50% of cases. The subvalvar stenosis can be fibromuscular ridge or ring, or fibrous tissue tags originating from any of the valves near outflow tract. Occasionally, LVOT obstruction is caused by the large aneurysmal membranous septum. LVOT obstruction is commonly associated with a VSD and tricuspid valve abnormalities.
- Tricuspid valve anomalies are very common occurring in approximately 90% of the cases. The malformation of the tricuspid valve varies including Ebstein malformation, thickening of the tricuspid valve leaflets, straddling valve [6].
- Other associated anomalies include mitral valve abnormalities (cleft mitral valve, straddling valve), ASD, coarctation of aorta (CoA), coronary artery anomalies. Complete heart block (acquired) is also associated with this anomaly.

Transthoracic Echocardiography (Unrepaired Cases)

- *Assessment of cardiac position and atrial situs.* Subcostal imaging facilitates detection of atrial situs and position of the cardiac position and apex and thus determines the presence or absence of dextrocardia or mesocardia. Abdominal and atrial sidedness is usually concordant (70% of cases). Sub-costal cross-sectional view can demonstrate the position of the great vessels, whereas color and pulse wave Doppler can help differentiate abdominal aorta from IVC. At this section, abdominal aorta has flow towards the transducer, therefore red on color Doppler whereas flow in IVC is away from transducer, therefore is blue. On pulse wave Doppler, abdominal aortic flow is pulsatile during systole with peak flow velocity about 1 m/s, whereas IVC flow typically has S and D wave with much lower velocity.
- *Ventricular morphology and atrioventricular connection* can be best determined from apical four chamber views. RV and LV can be differentiated by their intrinsic characteristic morphological features. The RV is usually guarded by tricuspid valve which has septal attachments and apical displacement as compared to mitral valve. This can be easily identified.
- *AV valve morphology and function.* Abnormality of the systemic AV valve is very common. Apical four chamber view is ideally suited to describe the morphology of the AV valves. From this view, septal leaflet of systemic AV valve is often seen more displaced towards apex resembling that of Ebstein malformation of the tricuspid valve. But it is different from the typical right sided Ebstein's anomaly with no large sail like anterior leaflet and no rotational displacement of septal and posterior leaflets. In rare cases quadra-cuspid systemic AV valve can be seen from short axis views. Straddling of the AV valves in the presence of a VSD can also be present and it may preclude surgical repair. Haemodynamics of both AV valves can be assessed from apical four chamber views with color, pulse wave and continuous wave Doppler. Parasternal long and short axis views and sometimes subcostal views should also be used together with color and Doppler for the assessment of valve function.
- *Determination of ventriculoarterial connection.* The connection of the ventricles with the great arteries can be identified best in an anterior position of the transducer and a modified apical five chamber view, PA is recognized by its bifurcation and aorta usually has coronary arteries arising from its root. The great vessels are parallel to each other, with the aorta arising from the RV and lying anteriorly and leftward to the PA. The latter arises from the LV and courses posteriorly and rightward to the aorta. A high parasternal short-axis view may show the abnormal arterial relationship. In patients with ccTGA, it may be challenging to obtain a standard parasternal long axis view and the diagnosis should be considered if this is the case.
- *Identification of VSDs.* Orientation of the interventricular septum can be demonstrated from parasternal short axis view. From this view, perimembranous VSD can be assessed for its size and

direction of shunting by 2D and Color Doppler. Peak flow velocity should be obtained by continuous wave Doppler and pressure difference between systemic RV and pulmonary LV can be calculated. When VSD is adjacent to the subpulmonary region and there is co-existence of sub valvar and valvar pulmonary stenosis, peak flow velocity across VSD can easily be mixed with the flow velocity from the valvar and subvalvar PS. Careful recording of the mitral valve regurgitation can help in accurately calculating the pulmonary LV systolic and PA pressure.

- *Assessment of the site and the degree of LVOT obstruction.* LVOT obstruction can occur at valvar and/or subvalvar level. Isolated valvar pulmonary stenosis is less common than combined subvalvar and valvar obstruction. LVOT obstruction can be identified from modified apical five-chamber views. 2D image can help to identify the morphology and level of obstruction. Color and Doppler can assess the severity of obstruction by detecting peak flow velocity and calculate the gradient. When the obstruction originates from multiple levels, it is difficult to determine the severity of obstruction at each level. But multi-layered Doppler profile often results from different flow velocities hence suggesting obstruction at different levels. Often modified parasternal and subcostal views can also provide images for the LVOT morphology but it may still be challenging to align the ultrasound beam parallel to the direction of blood flow. After identifying the site of obstruction, using blind continuous wave Doppler probe usually can detect the peak flow velocity across the obstruction.
- *Determination of aortic arch sidedness and the presence of other associated anomalies* such as CoA, PDA, aortic arch obstruction and persistence of left superior vena cava. (Color and CW Doppler for the assessment of velocities across the CoA, aortic arch obstruction and PDA in suprasternal views).
- *Assessing ventricular function.* Accurate assessment of systemic RV function is challenging by echocardiography. Standard methods of Echo assessment of morphological LV cannot be applied to the morphological RV. Ventricular systolic dysfunction by ejection

fraction tends to be underestimated especially when severe tricuspid regurgitation co-exists. FAC, TAPSE, myocardial performance index (Tai index), tissue Doppler imaging (TDI) and isovolumic myocardial acceleration of the RV free wall and myocardial deformation could be used in assessing RV function.

Surgical Therapies

Palliative Surgery and Physiologic Repair

PA banding has been done early in life for patients with large VSD without pulmonary stenosis. Patients with severe PS may receive arterial shunts. Physiologic repair usually includes VSD closure, and placement of LV to PA conduit for LVOT obstruction.

Double Switch Operation

Combination of atrial switch (Mustard or Senning) and arterial switch operation which restores the physiologic circulation by redirection of the venous return to the contralateral ventricle via atrial baffles and the arterial switch operation which offers anatomic correction of the ventriculoarterial continuity constitutes what we call anatomic repair.

Echocardiographic Assessment in Patients After Surgical Repair

Additionally to the basic echocardiographic evaluation presented herewith, the following issues should be addressed in patients postoperatively.

- Assessment of RV and AV valve function
- Identification of baffle leak/obstruction after atrial switch and arterial switch or Rastelli operation.
- Assessment of LV function after PA banding.

Transesophageal (TOE)/Three Dimensional (3D) Echocardiography

Transesophageal echocardiography may be used in patients with suboptimal echocardiographic windows to

- Exclude thrombus formation in atrial appendages prior to cardioversion in patients with supraventricular tachycardia.
- Describe in detail the morphology of the AV valves
- Assessment of LVOT obstruction
- The presence and the position of ASD
- Assessment of baffle leak or obstruction in ccTGA patients post double switch operation.

In patients undergoing surgical repair, TOE could be used intraoperatively for evaluation of prosthetic valve function, detection of residual atrial or ventricular septal defect or for monitoring PA banding.

Ebstein Anomaly of the Tricuspid Valve

Anatomy and Physiology

Ebstein anomaly is present in approximately 1% of patients with congenital heart malformations [13]. It is a myopathy of the right ventricle and is characterized by: embryonic failure of delamination of the septal, inferior and anterior leaflets of the tricuspid valve (TV) resulting in adherence of the leaflets to the underlying right ventricular myocardium; apical displacement of the tricuspid leaflets' annular hinge points (septal > inferior > anterior) with an anteroapical shift in the functional TV orifice toward the RVOT; dilatation of the atrialized portion of the RV; anterior leaflet fenestrations, redundancy or tethering and muscularization; and dilatation of the anatomic TV annulus.

Associated Anomalies

The most commonly associated cardiac defects include atrial septal defect or patent foramen ovale (~80–90%) and RVOT obstruction that can occur secondary to structural abnormalities (pulmonary valve stenosis or pulmonary atresia), branch PA stenosis or patent ductus arteriosus. Bicuspid aortic valve and myocardial non-

compaction have also been reported in Ebstein anomaly.

Arrhythmias are common and include accessory conduction pathways (Wolff–Parkinson–White syndrome) in 15–20% and atrial fibrillation or flutter that occur with increasing frequency with advancing age; 30–40% of affected patients will develop atrial tachyarrhythmias by 50 years of age.

Echocardiographic Evaluation in Unrepaired Cases

Two-dimensional echocardiography is the diagnostic test of choice. The following are the features:

- *Apical displacement of the septal and/or posterior leaflets of the tricuspid valve into the RV chamber.* This is best demonstrated from apical four-chamber view (for septal leaflet) and parasternal long axis RV inflow view. The normal distance between the septal hinge points of the tricuspid and mitral valve is less than 0.8 cm/m². A value >0.8 cm/m² is a diagnostic feature of Ebstein anomaly [13] along with evidence of failure of delamination with points of tethering between the leaflets and underlying myocardium. (Fig. 33.4)

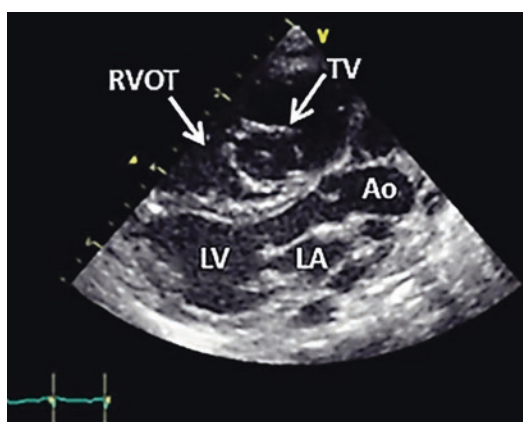


Fig. 33.4 2D echocardiography, parasternal long axis view showing displacement and rotation of the tricuspid valve towards the RVOT in a case of Ebstein anomaly. RVOT: Right ventricular outflow tract. AO aorta, LA left atrium, LV left ventricle, TV tricuspid valve

- *Elongated, redundant and/or sail-like anterior leaflet with abnormal chordae tethering to the apex or RV free wall.* This can also be demonstrated from parasternal RV inflow or apical four chamber views.
- *Variable degree of atrialised portion of the right ventricle with dilatation and thinning of the wall.* Dilatation of the right atrioventricular junction.
- *The orifice of TV is displaced and rotated towards the RVOT (in some cases):* The orifice of the TV, when opening into the RVOT, can be seen from the parasternal long axis and apical five chamber views. From the apical four chamber view, the tethered anterior leaflet and fail to delaminated septal leaflet can be visualized. However, the coaption of the valve leaflets and the valve orifice cannot be demonstrated (Fig. 33.4).
- *Tricuspid valve regurgitation and stenosis.* Most adults have moderate to severe tricuspid regurgitation with multiple or single large regurgitation jets. In severe cases, color flow map may not show regurgitation jet clearly due to low pressure difference between RV and RA and to large amount of regurgitation. Severity of tricuspid valve regurgitation is better demonstrated by pulsed wave or continuous wave Doppler profile of low velocity laminar flow or triangular shaped Doppler trace. This is because of near equal RV and RA pressure from severe tricuspid regurgitation. Tricuspid stenosis is rarely seen in unrepaired Ebstein anomaly (Fig. 33.5).
- *Anatomic severity* can be assessed by the Celemajer index [14]. This index calculated from the chamber area ratio in apical four chamber view at end-diastole, using $(RA + \text{atrialised RV}) / (RV + LA + LV)$. A ratio ≥ 1 in conjunction with cyanosis has been associated with reduced exercise tolerance in adult patients (Fig. 33.6).
- *Assessment of ventricular function.* Accurate assessment of RV function is challenging in Ebstein anomaly. A thin walled right ventricle often presents as hyperdynamic due to the presence of severe tricuspid regurgitation. TAPSE usually has high normal or above nor-

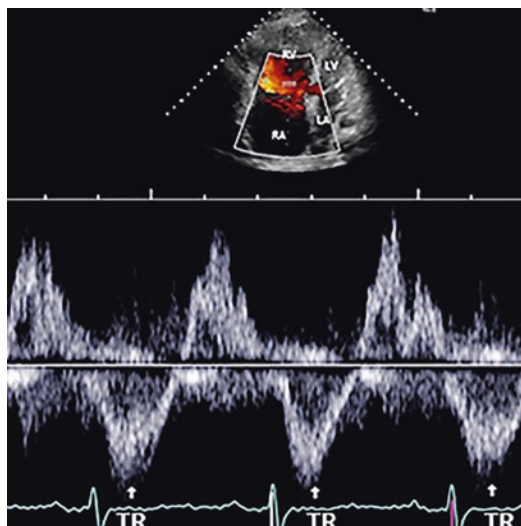


Fig. 33.5 Pulse wave Doppler; early peaking and triangular shape of TR retrograde velocity signal consistent with severe tricuspid regurgitation. TR tricuspid regurgitation

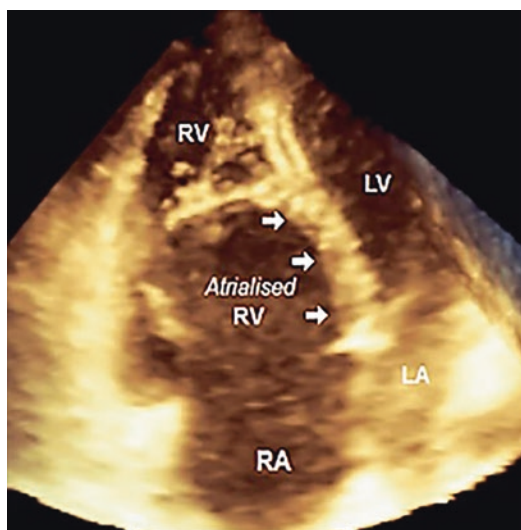


Fig. 33.6 3D echocardiography, apical four chamber view showing marked apical displacement of the septal tricuspid leaflet in a patient with Ebstein anomaly. RA right atrium, RV right ventricle, LV left ventricle, LA left atrium

mal values. FAC and Tei index have been recommended for assessment of RV function in Ebstein anomaly. LV function can be assessed using conventional parameters. Mild degree of LV dysfunction is common. The segment of

intra-ventricular septum along the atrialised RV is often very thin hypokinetic and paradoxical (bulging to the left during systole). In some cases, this can result in left ventricular outflow tract obstruction especially post tricuspid valve repair or replacement surgery.

- *Associated lesions:* PFO or ASD are very common. The flow through the defect is often right to left. In adult patients, modified parasternal four chamber views (from parasternal short axis views moving the transducer down near the lower part of sternum) are best to identify an ASD or PFO. Subcostal view, if obtainable, can also demonstrate atrial communications.
- 3D echocardiography has been used as an adjunct for additional information on TV anatomy-leaflets, subvalvar apparatus and as a pre-operative tool.

Surgical Valve Repair or Replacement

In symptomatic individuals, surgical repair of the valve is possible if the anterior leaflet is of sufficient size and mobility to create a mono-cuspid valve and the RV of sufficient size and reasonably preserved function. Numerous tricuspid repair techniques exist; results are variable. The cone reconstruction can achieve nearly anatomic restoration of TV anatomy and has shown to have better long term results [15].

If repair is not possible, the preferred replacement valve is stented tissue prosthesis. An additional bidirectional cavopulmonary shunt may be an option to consider for patients with severe RV dysfunction or RV hypoplasia. Percutaneous TV implantation has been attempted successfully for patients with previous tissue valve replacement.

Echocardiographic Evaluation After TV Repair and Replacement

- *Evaluation of TV function.* Thickening of valve leaflets and limited excursion are signs

of valve degenerative change. Color and Doppler can be used to assess valve stenosis and regurgitation. Early valve degeneration has been seen and may occur even months after valve repair or replacement.

- *Assess biventricular size and function, bi-atrial dimensions.*
- *Detect complications after surgery* such as LVOT obstruction, peri valvular leak and exclusion of pericardial effusion.

Transesophageal (TOE)/Three Dimensional (3D) Echocardiography

TOE is very helpful intraoperatively in:

- Evaluating residual TV regurgitation/stenosis after repair.
- Assessing of the integrity of repair and of concomitant anomalies (ASD)
- Evaluating of right coronary artery territory after RV plication
- Excluding iatrogenic VSDs

With 3D echocardiography, the apical four chamber and the parasternal RV outflow views, using narrow angle and zoomed acquisitions (with or without color), are the best views to visualize the TV. Three D TTE can assist the evaluation of patients for surgical repair; it is particularly helpful in evaluating the degree of tethered and non-tethered areas of the three TV leaflets. Three D Color Doppler can also provide reliable quantitative information on tricuspid regurgitation since it can evaluate accurately the size and the shape of vena contracta.

Specific tips:

- The fibrous annulus of the TV should not be mistaken for valve tissue
- RV tissue bands should be distinguished from displaced valve tissue
- Myxomatous disease of the TV should be distinguished from a large sail-like anterior leaflet.

Univentricular Heart

The definition of univentricular heart includes a group of congenital malformations with the presence of a single dominant functional ventricle (either left or right morphology) which connects to both atria either with two atrioventricular valves (double inlet) or only one valve (atretic or absent other valve). In most cases, there is also a small second ventricular chamber, but it lacks of its inlet or outlet component therefore is incomplete and rudimentary. Very rarely, there is univentricular connection to a solitary ventricle. There are also cases of very large VSDs or of straddling AV valve where ventricular septation is not feasible; these cases are also called univentricular hearts although they have a biventricular atrioventricular connection and adequate sized two ventricles [6, 13]. Cases of univentricular hearts represent approximately 1–2% of all CHD [16].

Anatomy and Physiology

The complexity of anatomy of this group of lesions underscores the importance of detailed systematic segmental analysis. The atrial anatomical arrangement could be situs solitus, situs inversus or ambiguous in cases of left or right isomerism.

AV connection types include double inlet left or right ventricle (DILV or DIRV, respectively), absent left or right AV connection (tricuspid or mitral atresia) or complete and unbalanced AVSD. The AV valves may be overriding the septum, which means the valve annulus can be attached to either side of the septum. In double inlet ventricle, one AV valve enters into the ventricle and less than 50% of the other valve annulus is committed to the contralateral ventricle. Straddling of the AV valve occurs when a feature of the AV valve apparatus (papillary muscle or chordae) is overarching and attaching to contralateral ventricle through the VSD.

Ventricular morphology could be determined according to the anatomic characteristics pre-

sented earlier in this chapter. According to them, the ventricles could be recognized as morphologically right or left or indeterminate. Ventricular topology should also be determined as described earlier in the segmental analysis section of the present chapter. Ventriculoarterial connections can be concordant, discordant (TGA type), double outlet when both great vessels arise from one ventricle and single outlet in cases of common arterial trunk or aortic/pulmonary atresia.

Associated Lesions

Various degrees of sub-valvar, valvar and supra-valvar PS are commonly seen in natural survivors of adult patients with univentricular heart. Stenosis can be progressive and some patients born with severe PS may develop pulmonary atresia with time. Progressive PS is associated with worsening in cyanosis. Pulmonary atresia or diminished blood flow across the stenosed pulmonary valve often concur with palliative procedures undertaken to enhance blood flow such as Blalock-Tausig or central arterial shunts. Aortic valve stenosis or atresia and CoA may be present. In adult patients, aortic root and ascending aorta dilatation are more common than aortic stenosis. As a consequence, progressive aortic valve regurgitation can develop and some patients come to require surgical AVR. Anomalies of the pulmonary or systemic venous return can also be present, especially in cases of atrial isomerism. VSDs and ASDs are common, of variable size and location. In some patients, the VSD may be non-restrictive in infancy but become restrictive with significant gradient, across it after PA banding and/or a Fontan type repair. This can limit blood flow into the aorta in the setting of double inlet ventricle or tricuspid atresia with VA discordance and haemodynamically resembles sub-aortic stenosis. Restrictive ASD can also be haemodynamically important in the setting of mitral atresia when pulmonary venous flow needs to pass through the ASD into the RA and then to the ventricle.

Echocardiographic Evaluation in Unrepaired Cases

Complete segmental analysis should be carefully followed. The examination should start from subcostal views, followed by the apical, parasternal, high parasternal and suprasternal views. Nonstandard views can be helpful in identifying specific anatomical issues, whereas continuous wave Doppler with the pencil probe can be used to optimize the angle of interrogation of the Doppler beam:

- *Assessment of cardiac position, direction of cardiac apex, abdominal and atrial situs.* This can be carried out from subcostal short and long axis views. Use 2D echo to identify the cardiac location and apex direction and color flow map and Doppler to differentiate the abdominal aorta from IVC hepatic vein or azygous vein.
- *PV and systemic venous connections to the atria* can be defined from same subcostal, suprasternal and parasternal views. Other abnormalities in systemic venous return, like interruption of the inferior caval vein with azygous continuation should not be missed.
- *AV connection and AV valve morphology and function* are best visualized from apical four-chamber views. In univentricular hearts, there are three possible connections: Double inlet, absent or atresia of one of the inlets or a common AV valve.
- *Double inlet ventricle:* is defined as more than 50% of both AV valves connected to one ventricle. From apical four chamber view, two or common AV valves can be seen entering the single ventricle. Parasternal short axis views can also demonstrate two AV valves opening into one ventricle. Overriding and straddling atrioventricular valves are best seen at apical four chamber views. In some hearts, two AV valves may not be at the same plane, one is more anterior than the other, the probe at apical four-chamber view need to be tilted anteriorly or posteriorly to identify them. Straddling sometimes can be seen from parasternal short axis view at VSD level when straddled chordae are seen across the VSD inserting into the other side of septum. There may be various malformations of the AV valves. Stenosis of one AV valve due to valvular or annular calcification has been seen in relatively older patients. When the atrial septum is intact or a restrictive atrial communication is present, AV valve stenosis is apparent by color and spectral Doppler assessment. In the presence of nonrestrictive atrial communication, flow can be distributed more through the non-stenotic valve. Therefore the color and Doppler flow profile across the stenosed AV valve may not reflect accurately the degree of stenosis. In such circumstances, the assessment of AV valve stenosis relies mainly on 2D imaging. AV valve regurgitation can be assessed in the same way as assessing MV or TV function.
- *Atrioventricular valve atresia (Absent left or right AV connection):* can be due to atrioventricular valve atresia either tricuspid or mitral, produced by an imperforate valve, or complete absence of the atrioventricular connection. When there is an imperforate valve, 2D echo from apical four chamber view usually shows thin membranous structure at either MV or TV position; this membranous structure is doming into ventricle during atrial systole. In hearts with absent AV connection, there is usually a thick band of bright, echogenic border at the atrioventricular groove (Fig. 33.6).
- *Ventricular morphology and function.* Most hearts with univentricular atrioventricular connection have two ventricles – one big (main) and one small (rudimentary). Ventricular morphology can often be difficult to identify by 2D echo. But the relative position of the rudimentary ventricle to the dominant ventricle often helps in determining ventricular morphology. Usually, superior either left or rightward subarterial outlet chamber is a morphological RV while LV lies inferoposteriorly. The superior and posterior relation of the two ventricles can be assessed from parasternal long and short axis views and apical four and five chamber views; the later are best to demonstrate rudimentary chambers

located on the left or right side of the main ventricle. When the dominant ventricle is left, the ventricular septum is usually anterior-superiorly located and can be seen in either the long or short axis view. When the septum is located posteriorly and inferiorly, then the dominant ventricle is of right morphology. Although the majority of univentricular hearts have two ventricles, in rare cases, there is only one ventricle, described as solitary and indeterminate.

- *Quantitative assessment of ventricular function* is challenging in univentricular hearts. There is a relatively small number of patients, given the variation of the anatomic spectrum, therefore there is no normal reference values. In general, biplane Simpson's method can be applied for the morphological LV to calculate ejection fraction (EF) and fractional area change (FAC) better for the RV. Both EF and FAC are useful parameters for the follow-up of patients as interval changes are important. M-mode and TDI recording of long axis function (both left and right side recordings) can also be applied. Two-dimensional echocardiography can assess regional wall motion abnormalities, which is common in univentricular hearts. Three-dimensional echocardiography may provide better and more accurate values for ventricular volumes systolic function and asynchrony.
- *Ventricular arterial (VA) connection.* There can be various types of ventriculo-arterial connection, but most frequent pattern with heart of double inlet to a dominant left ventricle is discordant ventricular – arterial connections. When there is double inlet left ventricle, rudimentary right-sided RV with concordant ventricular-arterial connection, this is called the Holms heart.

In patients with either tricuspid or mitral atresia, ventricular arterial connection can be concordant or discordant with variable degrees of pulmonary stenosis.

Levels of pulmonary stenosis can be demonstrated by 2D imaging from parasternal long axis, short axis and apical five-chamber views.

In cases of dominant LV and VA discordance, PA identified by its bifurcation is posterior to the aorta at parasternal long axis views, and either to the left or right of the aorta at short axis views. From apical views, PA is first seen when scanning from four to five chamber views. Severity of PS can be assessed by continuous wave Doppler as for simple PS. Peak flow velocity more than 4 m/s across sub-valvar, valvar and supra-valvar PS is considered important. If PS peak flow velocity is ≤ 4 m/s, and the VSD not restrictive, then there is a risk of increased PA pressures. If there is no PS and with a non-restrictive VSD patients are likely to have developed pulmonary arterial hypertension and Eisenmenger physiology.

- *Bicuspid aortic valve with aortic regurgitation* has been seen in patients with univentricular hearts. More common is aortic regurgitation subsequent to aortic root dilatation. Aortic root and proximal ascending aortic dimensions can be measured from parasternal long axis views. A diameter more than 3.8 cm is considered abnormal.
- *Assessment of size and location of the VSD.* VSDs can be single or multiple and are identified from parasternal long axis, short axis and apical views. Restrictive VSDs in the setting of single LV with VA concordance can result in reduced pulmonary blood flow but prevent the development of pulmonary hypertension. In VA discordance, restrictive VSD leads to in effect sub-aortic stenosis.
- *Assessment of associated abnormalities:* ASD, persistent left SVC.
- *Determination of aortic arch sidedness and the presence of PDA* (suprasternal view, color Doppler and CW Doppler for the assessment of velocities across the CoA and PDA)

Surgical Interventions

Atrial septectomy: This is done in the setting of stenosis or atresia of one of the two AV valves with intact atrial septum or a restrictive atrial communication.

Arterial shunt: including Blalock-Taussig shunt and central shunt (as previously described) to augment pulmonary blood flow in patients with pulmonary stenosis or atresia.

PA banding: PA banding is performed in infancy to reduce pulmonary blood flow and prevent the development of pulmonary arterial hypertension. Most patients will end up with a Fontan type operation. But there are still adults, who have had PA banding as their definitive palliation.

Glenn operation: Palliative operation which includes anastomosis of the SVC to the ipsilateral PA to increase the pulmonary blood flow and their oxygen saturations.

- *Classical Glenn:* End to end anastomosis of the SVC to the distal right PA, performed via a right thoracotomy. Acquired arteriovenous pulmonary malformations and systemic arterial desaturation are common late post Glenn complications.
- *Bidirectional Glenn:* End to side anastomosis of the SVC to the PA.

Fontan Operation: This procedure is aiming to redirect the systemic venous blood from SVC and IVC to the PA directly (TCPC) as via the right atrium and thus separate the two circulations and oxygenated blood from de-oxygenated blood (Fig. 33.7). It is a radical concept that palliates patients with univentricular hearts, albeit there is no ventricle supporting the pulmonary circulation. There are different modifications of the Fontan procedure;

- *Atriopulmonary Fontan (AP Fontan):* Non valved connection between the right atrium (RA) and the PA
- *Classical Fontan:* Connection between RA and PA with a valved conduit
- *Fenestrated Fontan:* Artificial fenestration of the interatrial patch or baffle to create a pressure relief atrial valve allowing for a right to left shunt. This allows low pressures in the systemic venous circulation and maintenance of blood flow in the systemic circulation, albeit at the expense of cyanosis.

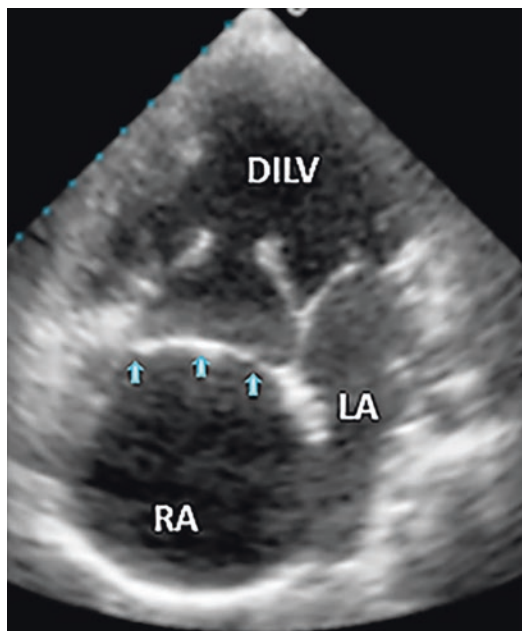


Fig. 33.7 2D echocardiography, apical four chamber view; post Fontan; arrow point to the Patch above right AV valve

- *Total cavopulmonary connection (TCPC):* Using either intra-atrial or extracardiac tunnel directing blood flow from the IVC to the lower portion of the right PA. SVC is anastomosed to the right PA usually as bidirectional Glenn anastomosis.
- *RA-RV Fontan (Bjork modification):* The RA is connected to the RV with a valved conduit in patients with mild/moderate RV hypoplasia.

The most common complications after Fontan operation are:

- Fontan or TCPC pathway obstruction and thrombus formation. This may be at different levels of anastomosis including the atriopulmonary connection, the lateral tunnel, the SVC, and/or stenosis secondary to thrombus formation in the RA.
- PV obstruction caused by severe RA dilatation (right pulmonary vein obstruction) in patients with atriopulmonary Fontan or coronary sinus dilatation (left pulmonary vein obstruction).

- Restrictive VSD. In the setting of VA discordance, restrictive VSD may lead to subaortic stenosis.
- AV valve dysfunction (usually regurgitation).
- Ventricular dysfunction
- Formation of venous- venous collaterals leading to cyanosis.

Echocardiographic Evaluation

- *Post PA Banding.* Banding can be seen in parasternal long axis and apical five chamber views whereas PA is best seen in long axis views. Banding normally located above pulmonary valve just before the bifurcation. Effective banding should have high flow velocity across it. The gradient calculated using peak flow velocity and Bernoulli equation should be compared with systemic blood pressure to rule out pulmonary hypertension. When patients develop pulmonary hypertension as results of pulmonary emboli or pulmonary venous hypertension, the peak flow velocity across the banding may be lower. The band sometimes migrates distally into pulmonary branches resulting in unilateral pulmonary stenosis; PA hypertension can develop in the contralateral lung.
- *Post Glenn Procedure:* Glenn anastomosis can be evaluated from high parasternal or suprasternal short axis view using color and Doppler. The flow into the Glenn anastomosis should be of low velocity, laminar with phasic respiratory variation. Low scale (lowering the Nyquist limit) color Doppler should be used. Turbulent flow on color flow mapping and continuous flow on pulse wave Doppler often suggest stenosis. The stenosis of Glenn anastomosis can be difficult to detect, as the flow velocity is normally low. Reduced flow to PA on color Doppler and increased redirected flow to lower body via dilated azygous vein are often indirect sign of Glenn stenosis. When there is significant forward flow from PA, systolic reverse flow often can be recorded at the SVC PA anastomosis or in the branch PA. This phenomenon is known as competitive to PA flow.
- *Post Fontan Procedure:* In patients with TCPC, the SVC to PA anastomosis should be assessed as described above. IVC to PA conduit can usually be seen from sub-costal long axis views and modified parasternal views (from apical four chamber views moving the transducer closer to the sternum). At this modified parasternal view, IVC to PA conduit (intra-cardiac or extra-cardiac) is often visualized from its short axis view as a circle on 2D image. When rotating the probe clockwise and sometimes move the probe up towards a short axis location, the conduit can be seen on its long axis view. The anastomosis at both IVC end and PA end can be visualized. Using low scaled color flow map and pulsed wave Doppler the flow through the IVC to PA can be assessed. Normally there is low velocity flow in the Fontan circulation with respiratory variation. Small flow reversals could be evident in patients after TCPC conversion. Evidence of obstruction and presence of thrombi should always be investigated using 2D color and spectral Doppler. Intracardiac baffle leaks, patency and size of atrial fenestrations can be detected using color flow Doppler. Doppler flow velocity recorded from the baffle leak or fenestration is very useful and it can help in estimation of the transpulmonary pressure gradient (Fig. 33.8). In atrio-pulmonary Fontan, the RA to pulmonary anastomosis is best visualized from parasternal short axis views when the main PA and bifurcation are shown on 2D echo images; with slight anterior angulation the anastomosis sometimes can be seen between the RA and MPA close to the RPA. Low scale color Doppler mapping can show the laminar flow in non-obstructed cases. When there is narrowing or obstruction, color Doppler will show turbulent flow and pulsed wave Doppler profile will be low velocity but continuous flow without respiratory variation. RA and TCPC pathways should be carefully assessed looking for thrombus.
- *Exclusion of pulmonary vein obstruction and sufficient atrial communication:* All four pulmonary veins should be identified. High

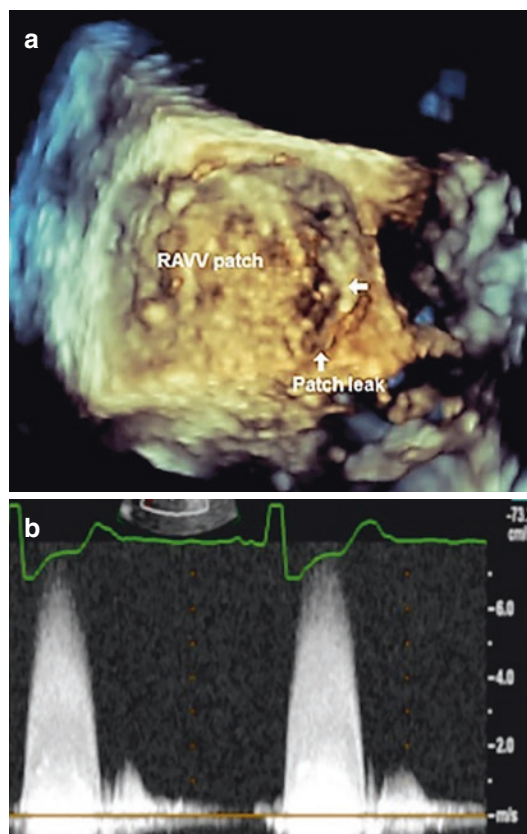


Fig. 33.8 Patch leak in a patient with DILV after Fontan operation. (a) Colour flow 2D imaging, (b) 3D echocardiography. Arrow points the colour jet from main LV to right atrium through the right AV valve patch. RA right atrium, LA left atrium, MLV morphologic left ventricle

velocities or loss of phasic variation is suggestive of obstruction. In AP Fontan, right sided pulmonary venous obstruction can be seen as the result of a severely dilated RA. In patients with TCPC, pulmonary venous obstruction may be the result of inappropriate baffle creation, especially in patients with anomalous pulmonary venous drainage. In some patients, pulmonary venous obstruction develops after device closure of fenestration. Pulmonary venous obstruction is best demonstrated from apical four chamber views. Color Doppler can demonstrate flow acceleration, whereas pulsed wave Doppler shows increased flow velocity (>1.6 m/s).

- **AV valve function.** AV valve regurgitation is more common than stenosis after the Fontan

repair. Severity of regurgitation can be quantified in the same way as with concordant, biventricular circulations. Even moderate AV valve regurgitation can have significant haemodynamic effects on the Fontan circulation, especially when ventricular dysfunction is also present.

- **VSD.** Restrictive VSD will have similar haemodynamic effects with sub-aortic stenosis in patients with double inlet LV or tricuspid atresia and VA discordance. It is an important residual or acquired haemodynamic lesion and a substrate for sudden cardiac death. VSD size can be assessed from parasternal long, short axis views and apical four or five chamber views. When the VSD dimension is less than aortic root hinge diameter, there is a risk that the VSD may be restrictive. Doppler flow velocity across the VSD of more than 2 m/s would suggest possible restriction. Left ventricular hypertrophy is also indirect sign of significant obstruction. Exercise echo may be helpful in assessing the degree of subaortic stenosis.
- **Ventricular size, hypertrophy and function** should also be assessed as mentioned earlier. After the Fontan type of repair, ventricular dimensions should be within normal limit. Increased ventricular size can be the result of myocardial dysfunction or excess volume from aortopulmonary shunts or valvular regurgitation. The diastolic function is difficult to assess due to abnormal AV valve anatomy and abnormal pulmonary venous flow.
- **Aortic arch to exclude re-coarctation and to detect aorto-pulmonary collaterals.**
- **Residual antegrade flow from the ventricle to the PA and exclusion of the presence of thrombus in the PA stump** (2D, color flow Doppler from the parasternal long, short axis view, subcostal view, five chamber apical view).
- **Evaluation of aortic or neo-aortic root dilatation and aortic valve regurgitation.**

In summary, Fontan type circulation should be a silent circulation; any turbulent flow is abnormal and should be thoroughly assessed for its hemodynamic effects.

Transesophageal (TOE)/Three Dimensional (3D) Echocardiography

TOE may provide a better image of Fontan circulation in patients with poor echocardiographic windows and exclude obstruction, intracardiac baffle leaks, patency and size of interatrial fenestration and presence of thrombi [17]. Three dimension TTE may be useful in more precise evaluation of ventricular volumes and assessment of ventricular systolic function.

References

1. Babu-Narayan S, Gatzoulis MA. Tetralogy of Fallot. In: Diagnosis and management of adult congenital heart disease. 2nd ed. Philadelphia: Elsevier; 2011. p. 316–27.
2. Gatzoulis MA, Clark AL, Cullen S, Newman CG, Redington AN. Right ventricular diastolic function 15 to 35 years after repair of tetralogy of Fallot. Restrictive physiology predicts superior exercise performance. *Circulation*. 1995;91(6):1775–81.
3. Pothineni KR, Wells BJ, Hsiung MC, et al. Live/real time three-dimensional transthoracic echocardiographic assessment of pulmonary regurgitation. *Echocardiography*. 2008;25:911–7.
4. Bleich S, Nanda NC, Hage FG. The incremental value of three-dimensional transthoracic echocardiography in adult congenital heart disease. *Echocardiography*. 2013;30:483–94.
5. Mertens LL, Otto Vogt M, Marek J, Cohen MS. Transposition of the great arteries. In: *Echocardiography in pediatric and congenital heart disease*. 2nd ed. Philadelphia: Wiley; 2012. p. 398–416.
6. Tay Lik Wui T, Yip JW, Li W. *Echocardiography*. In: *Diagnosis and management of adult congenital heart disease*. 2nd ed. Philadelphia: Elsevier; 2011. p. 28–43.
7. Enar S, Singh P, Douglas C, et al. Live/real time three-dimensional transthoracic echocardiographic assessment of transposition of the great arteries in the adult. *Echocardiography*. 2009;26:1095–104.
8. Ahmed S, Nekkanti R, Nanda NC, et al. Three-dimensional transesophageal echocardiographic demonstration of intraatrial baffle obstruction. *Echocardiography*. 2003;20:683–6.
9. Van Praagh R, Plett JA, Van Praagh S. Single ventricle. Pathology, embryology, terminology and classification. *Herz*. 1979;4:113–50.
10. Oechslin E. Physiologically “corrected” transposition of the great arteries. In: *Echocardiography in pediatric and congenital heart disease*. 2nd ed. Philadelphia: Wiley; 2012. p. 439–55.
11. Choueiter NF, Choy RM. Echocardiographic imaging of single-ventricle lesions. In: *Echocardiography in congenital heart disease*. Philadelphia: Elsevier; 2011. p. 132–44.
12. Weigel TJ, Driscoll DJ, Michels VV. Occurrence of congenital heart defects in siblings of patients with univentricular heart and tricuspid atresia. *Am J Cardiol*. 1989;64:768–71.
13. Gatzoulis MA, Webb GD, Daubeney PEF. *Diagnosis and management of adult congenital heart disease*. 2nd ed. Philadelphia: Elsevier; 2011.
14. Celermajer DS, Bull C, Till JA, Cullen S, Vassilikos VP, Sullivan ID, Allan L, Nihoyannopoulos P, Somerville J, Deanfield JE. Ebstein’s anomaly: presentation and outcome from fetus to adult. *J Am Coll Cardiol*. 1994;23(1):170–6.
15. Anderson HN, Dearani JA, Said SM, Norris MD, Pundi KN, Miller AR, Cetta ML, Eidem BW, O’Leary PW, Cetta F. Cone reconstruction in children with Ebstein anomaly: the Mayo Clinic experience. *Congenit Heart Dis*. 2014;9(3):266–71.
16. Shiina A, Seward JB, Edwards WD, et al. Two-dimensional echocardiographic spectrum of Ebstein’s anomaly: detailed anatomic assessment. *J Am Coll Cardiol*. 1984;3:356–70.
17. Lang RM, Badano LP, Tsang W, Adams DH, Agricola E, Buck T, et al. American Society of Echocardiography; European Association of Echocardiography/EAE/ASE recommendations for image acquisition and display using three-dimensional echocardiography. *J Am Soc Echocardiogr*. 2012;25(1):3–46.

Part IX

Strain

Strain Basics and Global Longitudinal Strain

34

Joseph Kisslo, Daniel Forsha,
Minna Moreira Dias Romano,
Fawaz Abdulaziz M. Alenezi, Kasper Emerek,
Zainab Samad, and Niels Risum

Measurement of myocardial global longitudinal strain (GLS) is no longer a research tool. Rather, GLS is now used for risk assessment and management of patients with a wide variety of clinical disorders. GLS is clearly a useful supplement to routine quantitative analysis of left ventricular performance along with ejection fraction and left ventricular diameters.

Utility of Global Longitudinal Strain

Here are the conclusions to this chapter, right in the beginning. GLS is now a standard in the care of patients with cardiovascular disease. GLS can be used to follow improvement or deterioration as

well as prediction of outcome in a wide variety of disorders.

Cardiac valvular disease including: mitral regurgitation, aortic regurgitation, aortic stenosis, infective endocarditis and other valvular clinical conditions.

Ischemic heart disease including: post myocardial infarction, post coronary bypass and other revascularization and ischemic disorders.

Heart failure of all causes including: conduction disorders, ischemic and non-ischemic cardiomyopathies, infiltrative cardiomyopathies, hypertrophic cardiomyopathies and other heart failure disorders.

Congenital heart disease including: heart failure, valvular and conduction abnormalities as listed above. There is less data on patients with congenital structural disease.

Thus, begins the need to know about strain in general and GLS. In that learning endeavor, beginning users meet obstacles, just like the experts. When different analytic software is used, numbers for GLS differ. The overwhelming majority of studies that attest to the utility of GLS, all have in common one thing; one type of image system and analytic software was used for each study and data from analytic software from multiple studies were not mixed.

This chapter is not a review chapter. This is a chapter of learning. The previous two paragraphs provide the necessary data review to stimulate interest, and have cause to understand what strain

J. Kisslo (✉) · F. A. M. Alenezi · Z. Samad
Division of Cardiology, Duke University Medical Center,
Durham, NC, USA
e-mail: joseph.kisslo@duke.edu

D. Forsha
Pediatric Cardiology, Children's Mercy Hospital,
Kansas City, MO, USA

M. M. D. Romano
Cardiology Center, Medical School of Ribeirão Preto,
University of São Paulo, São Paulo, Brazil

K. Emerek
Department of Clinical Medicine, Aalborg University,
Aalborg, Denmark

N. Risum
Division of Cardiology, Rigshospitalet, Copenhagen,
Denmark

is and how it works. This chapter will leave the reader with the idea that, for GLS to be useful in following patients with cardiovascular disease, users should use one way of calculating GLS at the present time. Heart disease is chronic, and standardized methods are necessary to provide useful quantitative data over time.

Strain, as we know it today, is seemingly rather simple to understand. Expressed in the most basic form, strain is just the percent change in distance (length) between two targets from one baseline condition (example diastole) to another (example systole).

Learning about strain begins with the enticement that strain looks directly at myocardial contractility. The literature is filled with papers lauding the utility of GLS in ischemic, valvular and congenital heart disease. These factors give the easy impression that GLS is an almost perfect measure and that echocardiography is just the perfect tool to supply such a measure. Indeed, there is a certain romance with strain over the last 5–6 years as it has come into more common use. But like any romance, problems occur. This chapter begins with simplicity, then takes the reader on a difficult journey, finally ending with simplicity.

Clinical Use of Strain

When initially learning about strain, a beginner becomes overwhelmed with the different types of strain: longitudinal, circumferential, radial, and transverse. Then the concept of strain rate is introduced, a student then becomes completely overwhelmed. Being discouraged, strain can then become just a computer screen full of wiggling lines, complex displays and arrays of numbers that are so numerous that a user is both dazzled and confused. What's worse is when a user tries to correlate numbers resulting from different ultrasound machines from different vendors in multi-vendor laboratories.

Simplifying the Process

This chapter, and the succeeding two chapters, are a trilogy that attempts to simplify the pro-

cess of initial learning about how strain is calculated, what components of strain are useful, how to use strain in certain situations and, provides a firm basis about the pitfalls of strain. Of all the types of strain, it is longitudinal strain that has found the most clinical acceptance. Accordingly, the focus will be on longitudinal strain and not all the others. This chapter will not overwhelm the reader with columns of numbers and reviews of previous studies. Rather, it will simply construct a story of about GLS. A normal value of GLS is, by the way, from -15% to 20 or -25% . Numbers that are deeply negative are good. Numbers that approach zero (less negative are bad).

It may seem that this chapter will spend much time explaining how strain is derived. Practical experience teaching students of global longitudinal strain shows that as soon as a student encounters varying numbers for GLS, discouragement rapidly ensues. This is known, but shouldn't impede learning to reduce the variables that can be encountered. Then GLS can be usefully employed.

Global vs Regional Strain

"Global" strain refers to data derived from the whole left ventricle. Global strain assessment from longitudinal strains measured from three apical views produces a number called global longitudinal strain (GLS). Strain measures are taken from a multitude of myocardial segments, then generally averaged to produce the GLS number of percent change. It is the summation of the regional strains. GLS is measured every day on every patient possible in the Duke Echo Laboratory.

"Regional" strains result from series of speckle calculation from certain myocardial segments. Regional strains can provide quantitative and timing information, and some examples of the use of regional strains will be presented at the end of this chapter. Much more detailed information on regional strains are found in the next two chapters. As a preview of these chapters, clinical experience in the Duke Echo Laboratory indicates that the strength of regional strains lies in

the relationships of movement of one myocardial wall compared to another, and not currently in the timing and quantitative data.

Strain

Figure 34.1 explains that strain is simply a measure in change in length. The left panel shows the starting length to be short (blue bar) and then getting longer (blue + red bar). In this case the length doubles. When this occurs, the starting length (L_0) adds the red length, and the strain is +100% (expressed as a positive since it lengthens). The right panel shows the starting length to be long (blue + red bar) that then gets shorter (blue bar). In this diagrammatic case, it shortens by half. When this occurs, the starting length (L_0) loses the red length and the strain is -50% (expressed as a negative since it shortens).

The schematic in Fig. 34.2 extends this concept by explaining two major different ways to consider strain. Not everything is simple as first thought in Fig. 34.1 as there is more than one way to calculate strain. Following the heart, frame by frame, perhaps 60 frames over one heartbeat (if there were 60 frames per second at a heart rate of 60), and as targets move in and out of view, it may not be possible to have the same target seen in the beginning, still seen in the end. The left panel is Lagrangian strain (S_L) and represents the method in the previous figure as it

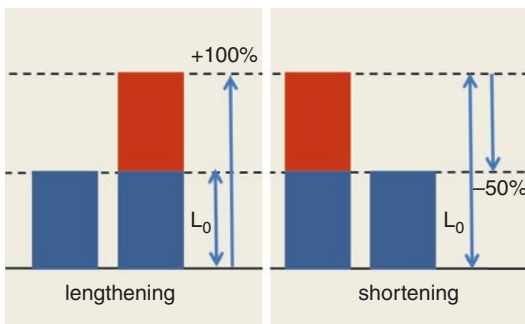


Fig. 34.1 Strain just measures a change. The objects in this picture change. The left panel shows a positive change (adding the red bar) while the right panel shows a negative change. Most longitudinal strains are negative because the ventricle sortens in systole

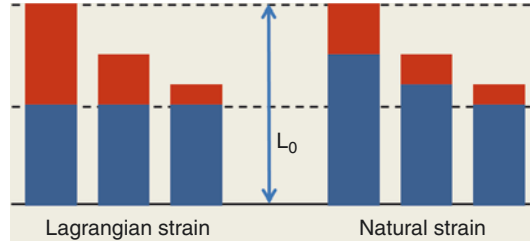


Fig. 34.2 This schematic shows there is more than one way to calculate strain. Following the heart, frame by frame, perhaps 60 frames over one heartbeat (if there were 60 frames per second at a heart rate of 60) and as targets move in and out of view it may not be possible to have the same target seen in the beginning, still seen in the end. The left panel is Lagrangian strain (S_L) and represents the method in the previous figure as it assumes one could detect a starting and ending length of the same object. The right panel demonstrates what is called Natural strain (S_N). This method takes into account that the same object may not be able to be tracked from beginning to end of a cardiac cycle. Natural strain relates the instantaneous length change to the variable instantaneous length at every measurement period sampling period. This measurement depends on the constantly changing lengths and while it is much more difficult to understand than Lagrangian strain the learning message is that the heart constantly moves and special math may be needed to calculate strain. A beginner should not labor over trying to understand the calculation of Natural strain except to know it is more complex than Lagrangian strain and it is used in many echo speckle tracked systems. *Modified from Voigt, E, et al.: J Am Soc Echocardiogr. 2015;28:183–193*

assumes one could detect a starting and ending length of the same object. The right panel demonstrates Natural strain (S_N). This method takes into account that the same object may not be able to be tracked from beginning to end of a cardiac cycle. Natural strain relates the instantaneous length change to the variable instantaneous length at every measurement period sampling period. This measurement depends on the constantly changing lengths, and while it is much more difficult to understand than Lagrangian strain, the learning message is that the heart constantly moves and special math may be needed to calculate strain. Strain is updated beat to beat. A beginner should not labor over trying to understand the calculation of Natural strain except to know it is more complex than Lagrangian strain, and it is used in many echo speckle tracked systems.

$$\text{Strain} = \frac{L_1 - L_0}{L_0} = \frac{\Delta L}{L_0} = \%$$

L = instantaneous length
 L_0 = original length
 ΔL = change in length

Fig. 34.3 The basic formula for strain is shown. This basic formula for strain is easily recognized as the same formula for ejection fraction, but substitutes length for volume. If this was just end-diastolic and end systolic length, it would apply to Lagrangian strain. If each of the lengths were, however, instantaneous (performed serially from frame to frame) it would be Natural strain. Manufacturers of ultrasound equipment generally do not reveal what kind of strain they are calculating. It can be assumed, however, that when speckle tracked strain is employed, it can be it is likely Natural strain for reasons discussed in later figures

The basic formula for strain is shown in Fig. 34.3. This basic formula for strain is easily recognized as the same formula format for ejection fraction, but substitutes length for volume. If this was just end-diastolic and end systolic length, it would apply to Lagrangian strain. If each of the lengths were, however, instantaneous (performed serially from frame to frame) it would be Natural strain. Manufacturers of ultrasound equipment generally do not reveal what kind of strain they are calculating. It can be assumed, however, that when speckle tracked strain is employed, it can be it is likely Natural strain for reasons discussed in later figures.

One of the variables between machines, therefore, is the methods used to calculate the strain. Different machines may calculate strain differently.

Speckle Tracking

Ultrasound machines transmit and receive ultrasound with complex electronics called beamformers. Beamformers are, in part, what determine the quality of the image along with

patient variables, system settings and what transducer is used. All ultrasound machines use different beamformers and processing techniques. Transducers are specific to ultrasound manufacturers and further vary with frequency, aperture size, and other factors. The point here is that images vary for multiple reasons, before any speckle detection system is applied.

Speckle is anything (Fig. 34.4) in the ultrasound image: real anatomic targets, noise or artifact. Speckle is, therefore, just white dots on a black background, the acoustic signature of whatever you are looking at. Speckle tracking is a self-descriptive word. Speckle tracking is a method is to follow the speckle in an ultrasound image. The left panel demonstrates a parasternal long axis from a patient with a highly reflective myocardium due to amyloidosis. The myocardium is filled with target speckle information. The right panel is the same image, but with all the extraneous targets outside the left ventricular myocardium digitally covered leaving an area of interest. The arrows point to the fact there is speckle within the area of interest of all sizes and shapes. These are the speckles that are followed over time.

Look carefully at the size and shape of the speckle within the myocardial walls in Fig. 34.5. The left panel shows the short axis of the left ventricle emphasizing that speckle is the acoustic signature that is displayed in the ultrasound picture. Speckle varies in size and shape depending on where it is in the image. Speckle from real targets gets larger in the far field (deeper into the tissues) because of ultrasound beam spread. While the quality of this image is good, speckle can be from real anatomic targets, noise, and artifact. The ultrasound machine places regions of interest in the field to apply complex mathematic methods to detect and follow the speckle over time. Also note that while heart muscle is relatively uniform, the speckle in the septum looks smaller in size than the speckle in the posterior LV wall (arrows).

An anatomic specimen of a real human heart cut in the apical four chamber view is shown in Fig. 34.6. The boxes simulate regions of interest (ROI). The three panels demonstrate That there are differences in the tissues within the boxes.

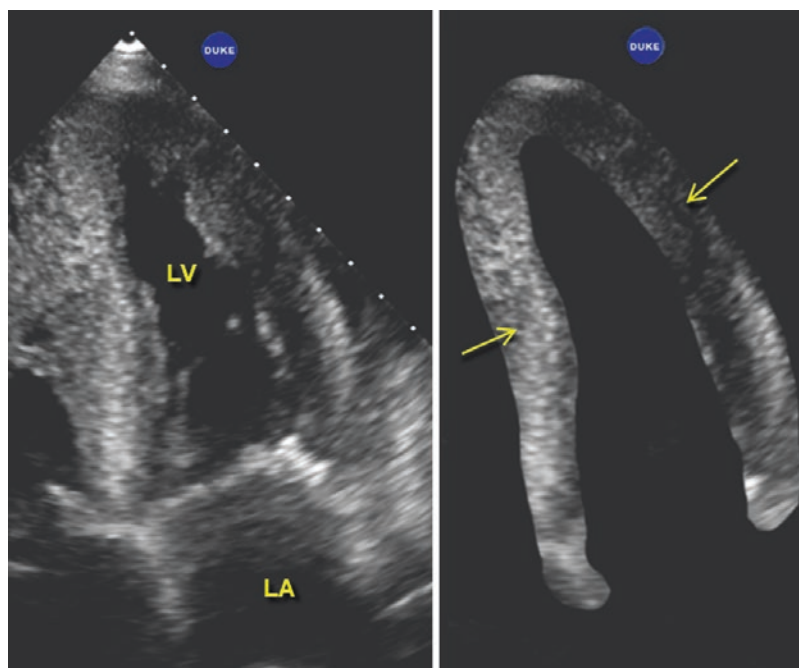


Fig. 34.4 Speckle is anything in the ultrasound image: real anatomic targets, noise or artifact. Speckle is, therefore, just white dots on a black background, the acoustic signature of whatever you're looking at. Speckle tracking is a self-descriptive word. Speckle tracking is a method to follow the speckle in an ultrasound image. The left panel demonstrates a parasternal long axis from a patient with a highly reflective myocardium due to amyloidosis.

The myocardium is filled with target speckle information. The right panel is the same image, but with all the extraneous targets outside the left ventricular myocardium digitally taken covered leaving an area of interest. The arrows point to the fact there is speckle within the area of interest of all sizes and shapes. These are the speckles that are followed over time

Below is a simulated strain curve that begins at the zero point in diastole. The curve dips low, approaching -20% in systole as the targets are tracked together as the ventricle shortens in systole. The targets return to the original position in diastole and the strain line returns to zero.

Complex mathematics is used to detect and follow speckle and speckle patterns. Figure 34.7 depicts but one formula of the many that are possible for this purpose.

Figure 34.8 shows an interventricular septum from the apical four chamber view in the same patient as Fig. 34.4. Speckles get brighter and darker, and come and go as the heart rotates and contracts. These are sequential frames of a thickened interventricular septum. Only 12 of 60 frames are shown. The bright dot seen near the top in the purple circles moves out after four

frames. The linear row of speckles within the first three frames then disappear while the horizontal speckle in the blue circles lasts six frame and the bright speckle lasts for nine frames. Hearts rotate in and out of plane.

Note the red circles in the third frame from the right. As the linear target wanes in the blue circle in the preceding frame a ROI would do a search and may pick the linear target in the either the bottom or the top red circles, rendering spurious results. Natural strain methods are likely used in this patient to trend the direction and amplitude of speckles and employ the complex mathematics to keep up with these differing sizes and shapes and their appearance and disappearance. The detection algorithms can't possibly apply to all circumstances. Even given these conditions, speckle detection is usually successful.

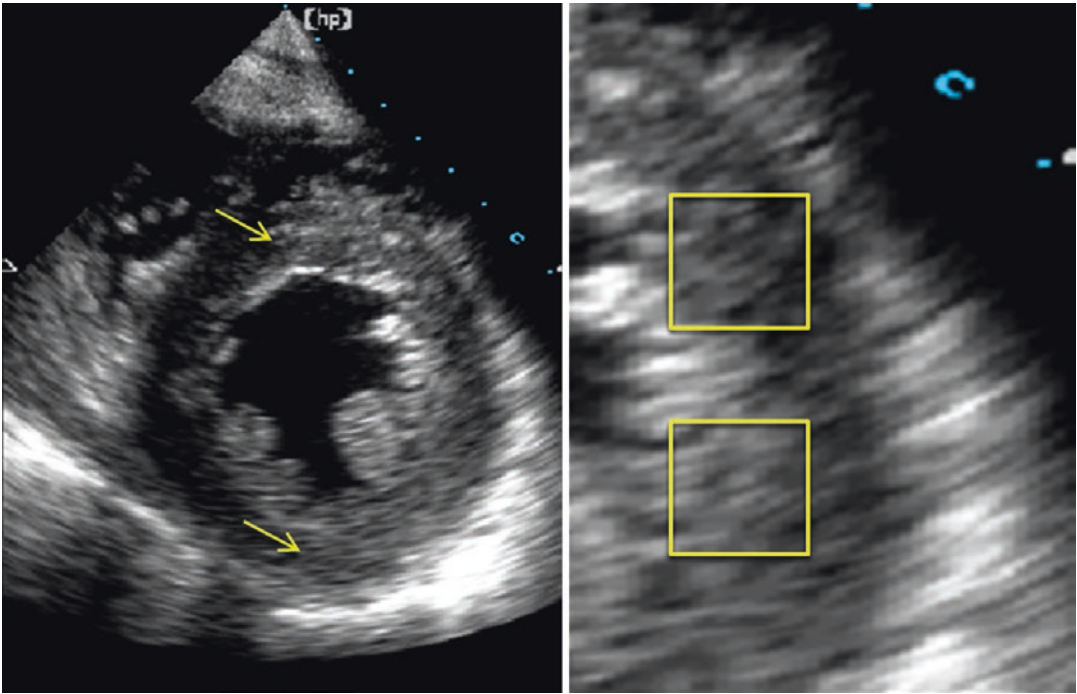


Fig. 34.5 Left panel shows the short axis of the left ventricle emphasizing that speckle is the acoustic signature that is displayed in the ultrasound picture. While the quality of this image is good, speckle can be from real anatomic targets, noise and artifact. The ultrasound machine

places regions of interest in the field to apply complex mathematic methods to detect and follow the speckle over time. Also note that while heart muscle is relatively uniform, the speckle in the septum looks smaller in size than the speckle in the posterior LV wall (arrows)

The Case for Longitudinal Strain

There is no question that longitudinal strain is the most reproducible and has enjoyed the paramount position amongst the different types of strain. Figure 34.9 emphasizes that longitudinal strain is recorded from the ventricular apex. In this case, systole causes a negative deflection of the strain curves. Both radial and circumferential strains are recorded from ventricular short axes at every level, but the usual standard is from the left ventricular short axis view at the papillary tips. While not depicted here, circumferential strains are normally negative deflections of the strain curves, while radial strains are positive deflections (as speckle pairs move together in systole in this view). Strain rates can also be measured from any of these approaches.

Some readers will find it discomforting that this chapter dispenses with examples of circumferential and radial strains and strain rate. These

alternates to longitudinal strain, however, can be distracting to those initially acquiring understanding and elementary skills in using speckle tracked strain. It is best to acquire some mastery of longitudinal strain. In the Duke clinical echo laboratory, only longitudinal strains are used.

Longitudinal Strain and Regions

The important usual display components are fourfold in Fig. 34.10, and may be different for different manufacturers as there are no common display standards at the present time. First, there is a cartoon showing where the regions of interest have been applied (upper left). Ventricular walls are divided into six segments per two-dimensional view, each represented by a different color. Second, the tracings from the six different segments are displayed in a time-interval histogram. The color of each segmental line in the graphic

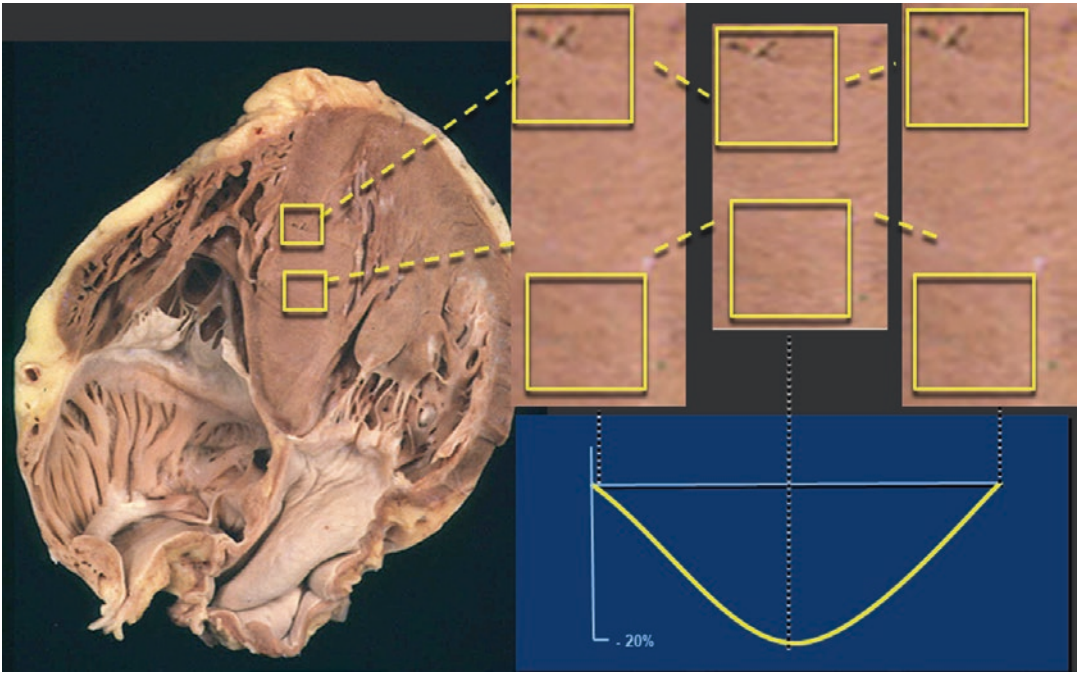


Fig. 34.6 Anatomic specimen of a human heart cut in the apical four chamber view. The boxes simulate areas of interest (ROI). The three panels demonstrate that there are differences in the tissues within the boxes. Below is a simulated strain curve that begins at the zero point in diastole.

tole. The curve dips low, approaching -20% in systole as the target are tracked together as the ventricle shortens in systole. The targets return to the original position in diastole and the strain line returns to zero. *Anatomic section courtesy of R.H. Anderson, MD*

Sum of the Absolute Differences

$$SAD = \sum_{i=0}^{M-1} \sum_{j=0}^{N-1} |I_{ij} - T_{ij}|$$

Fig. 34.7 Complex mathematics is used to detect and follow the speckle. There are multiple mathematic models that can be used

display corresponds to the same color in the ROI cartoon. Third, there is a vertical line marked AVC which indicates where aortic valve closure occurs. In longitudinal strains, the nadir of all the walls is usually seen at, or around, aortic valve closure. Note that the dashed white line in the center of all the multicolored lines is the mean value of the six lines. Fourth, an ECG display (in this case at the image bottom) to relate timing in

the strain curves to the ECG signal. The yellow dot indicated the point where the analysis begins. The large colored tracing on the left is a linear M-mode of tracing throughout the cardiac cycle. Beginners are encouraged to ignore this portion of the display.

In Fig. 34.10 the regional strain curves start at the zero point (yellow dot on the ECG). All strain must start at zero to establish the initial length from which strain is measured. As systole proceeds, the strain curves are roughly parallel as speckles move closer to each other as systole proceeds. All the curves peak roughly at the same time at, or near, aortic valve closure. Aortic valve closure is usually obtained from the spectral Doppler tracing from the aortic valve.

From aortic valve closure, diastolic filling begins. As the speckles move apart during diastole, the curves eventually return to the zero point at end-diastole. End-diastole conveniently occurs precisely with all the lines coming together

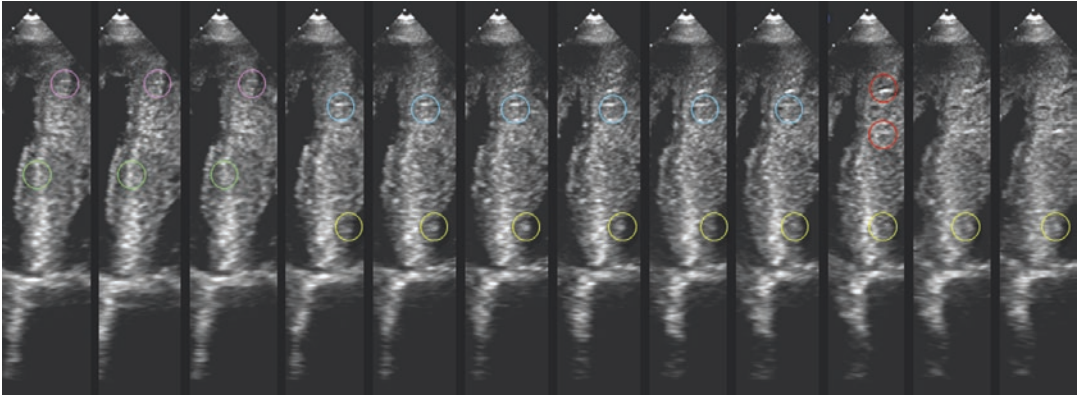


Fig. 34.8 Speckles get brighter and darker and come and go as the heart rotates and contracts. These are sequential frames of a thickened interventricular septum. Only 12 of 60 frames are shown. The bright dot seen near the top in the purple circles moves out after four frames. The linear row of speckles within the first three frames (green circles) then disappear while the horizontal speckle in the blue circles last six frame and the bright speckle lasts for

nine frames. Hearts rotate in and out of plane. Note the red circles in the third frame from the right. As the linear target wanes in the blue circle in the preceding frame a ROI would do a search and may pick the linear target in the either the bottom or the top red circles, rendering spurious results. Natural strain methods are likely used in this patient to trend the direction and amplitude of speckle

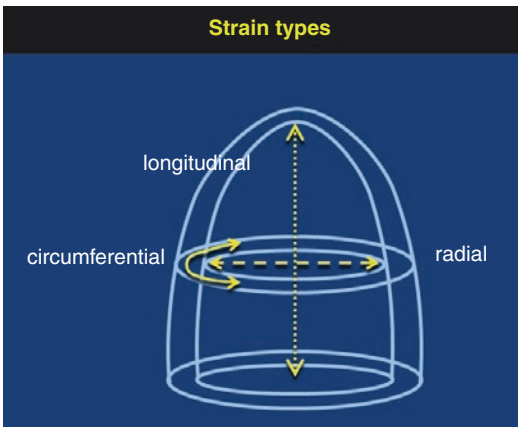


Fig. 34.9 Three types of strain. Longitudinal strains are obtained from the ventricular apex and cause negative deflections in the strain curves in systole. Longitudinal strains are obtained from the apical views. Circumferential strains are those obtained from the ventricular short axis view and are also negative in systole. Short axis views also provide images for determining radial strains. Radial strains are normally positive in systole as speckle movement occurs towards the center of the ventricle. Strain rates from any of these views are also possible. This chapter deals only with longitudinal strains

exactly at zero. In reality, end diastole may be at different strain values for each segment. Most manufacturers progressively force the lines back to zero electronically.

In Fig. 34.10, the yellow line represents the proximal septum (in the four chamber view) and the red line is from the opposite basal lateral wall. Figure 34.11 schematically represents the six segment model and corresponding colors of the six regions in the apical four chamber view. Yellow = basal septum; cyan = mid-septum; green = distal septum; purple = distal lateral wall; blue = mid-lateral wall and red = basal lateral wall. These color segments correspond to the strain lines. Unfortunately, not all manufacturers adhere to the same color display convention.

The advantage of global longitudinal strain is that it is calculated as an average of an average of an average, and small errors can be averaged out. First regions are determined, and regional strains are derived from the average of the many, many speckles found in each segment. Then the global strain for any view is the average of all six segments (averaged again). Then the global longitudinal strain is determined by averaging all three views yet again (for the third time). Global strains are, therefore rather robust (no matter how they are calculated) because of the abundance of numbers used in the final determination. This gives global longitudinal strain less variability than chamber diameters or volumes. Another advantage is, other than the user applying the

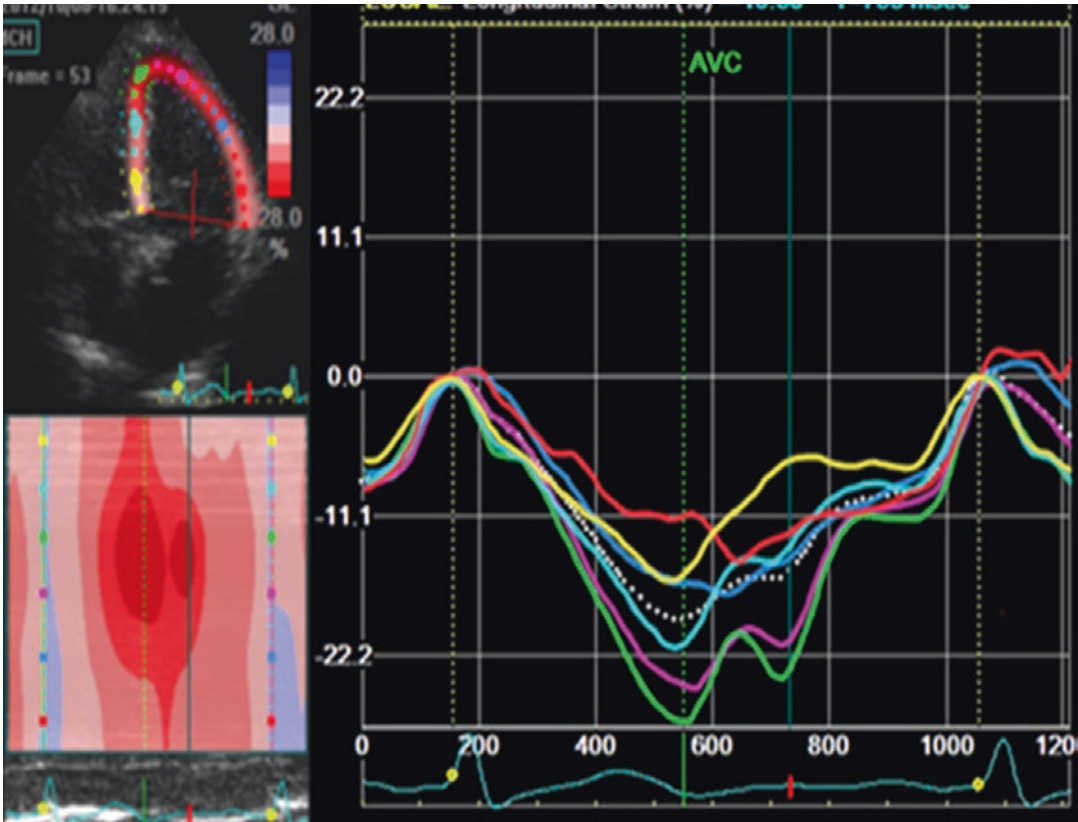


Fig. 34.10 Typical display of longitudinal strain curves in a normal individual. The important usual display components are fourfold in and may be different for different manufacturers as there are no common display standards at the present time. First, there is a cartoon showing where the regions or interest have been applied (upper left). Ventricular walls are divided into six segments per two-dimensional view, each represented by a different color. Second, the tracings from the six different segments are displayed in a time-interval histogram. The color of each segmental line in the graphic display corresponds to the same color in the ROI cartoon. Third, there is a vertical

line marked AVC which indicates where aortic valve closure occurs. In longitudinal strains, the nadir of all the walls is usually seen at, or around, aortic valve closure. Note that the dashed white line in the center of all the multicolored lines is the mean value of the six lines. Fourth, an ECG display (in this case at the image bottom) to relate timing in the strain curves to the ECG signal. The yellow dot indicated the point where the analysis begins. The large colored tracing on the left is a linear M-mode of tracing throughout the cardiac cycle. Beginners are encouraged to ignore this portion of the display

region of interest, the process is automated for any manufacturer consequently reducing user error.

There is an additional method to make strain calculations more reproducible. Despite the user's impression that strain is determined from delineated regions, such may not actually be the case for some manufacturers systems (Fig. 34.12). Regions may overlap, extending beyond their borders. This technique has the added advantage, including even more speckle determinations, making the ultimate calculations more robust.

The strains in Fig. 34.13 were obtained from a two-chamber view in another normal individual. The colors here apply to different walls than seen in the four-chamber view as the colors remain fixed in relation to the screen even though the echo views can be altered behind the region of interest. With this manufacturer, the yellow, cyan and green are on the left and the purple, blue and red are on screen right. The global strain for this view is -20.8% , which is normal.

The various colored lines are almost completely synchronous in this example, peaking at

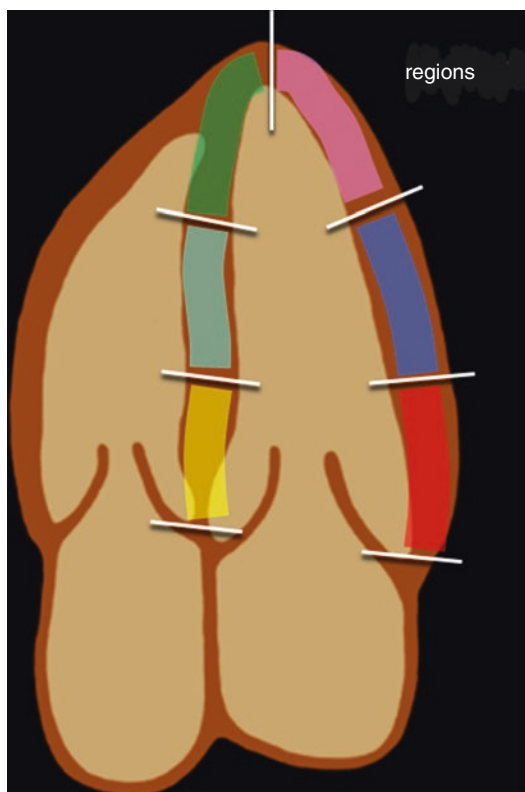


Fig. 34.11 Schematic diagram showing the apical four-chamber view divided up into six segments and colors applied to each segment. From the apical four chamber view. Yellow = basal septum; cyan = mid-septum; green = distal septum; purple = distal lateral wall; blue = mid-lateral wall and red = basal lateral wall. These color segments correspond to the strain lines. Unfortunately, not all manufacturers adhere to the same color display convention. Strain calculations result from measurements taken from many speckles with a segment and then are averaged to produce an average strain for that segment. The global strain is an average of the average of all six segments for any view and then, again, averaged for all three apical views

aortic valve closure. Note the white squares on the various strain lines indicating where the peak strains were determined. All are at the nadir of the curves at, or before, aortic valve closure. Here, the colored M-mode is large and displays the various colored segments over time, left to right. In this convention, as strains become more negative, below zero, the M-mode becomes more red. If segments move positive, the M-mode would be blue. Here, the ECG is at the bottom of the right hand panels. The white moving target in

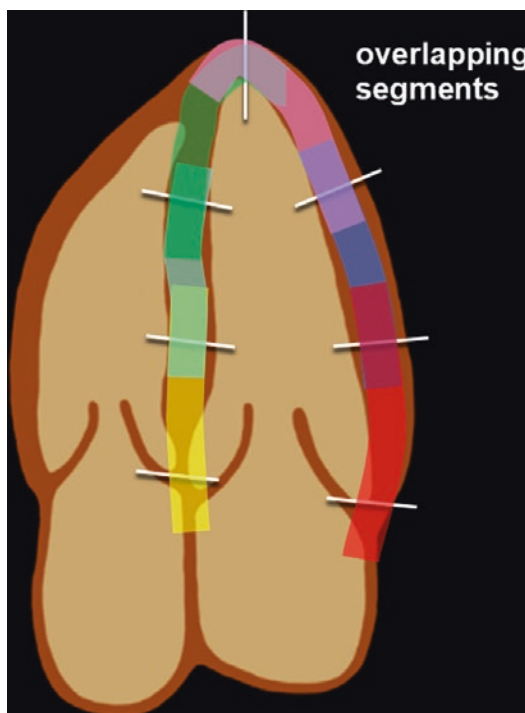


Fig. 34.12 There is an additional method to make strain calculations more reproducible. Despite the user's impression that strain is determined from delineated regions, such may not actually be the case for some manufacturers systems. Regions may overlap, extending beyond their borders. This technique has the added advantage including even more speckle determinations, making the ultimate calculations more robust

back of the ECG is a derived M-mode of the mitral valve. Beginners should avoid concern about the colored M-mode.

Figure 34.14 shows two strain recordings from the apical four-chamber view from a normal individual from different manufacturers. Unfortunately, there is no agreement among manufacturers as to standard displays and/or standard color assignments to the various segments. Beginners will have to note color designations in manufacturer's literature.

Not Just Regions, but Lines and Thicknesses

Strain may be calculated along lines or thicknesses. Strain can be determined along the

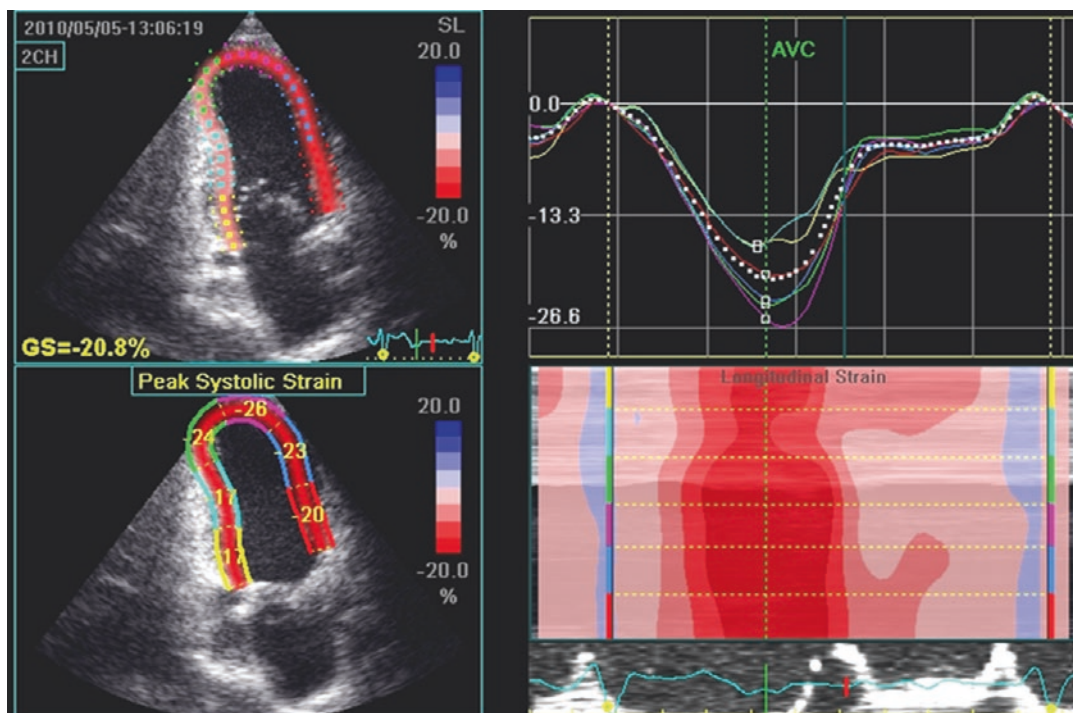


Fig. 34.13 This strain recording is from a two-chamber view in another normal individual. The colors here apply to different walls than seen in the four-chamber view as the colors remain fixed in relation to the screen even though the echo views can be altered behind the region of interest. With this manufacturer, the yellow, cyan and green are on the left and the purple, blue and red are on screen right. The various colored lines are almost completely synchronous in this example, peaking at aortic valve closure. Note the white squares on the various strain lines indicating where the peak strains were determined.

All are at the nadir of the curves at, or before, aortic valve closure. Here, the colored M-mode is large and displays the various colored segments over time, left to right. In this convention, as strains become more negative, below zero, the M-mode becomes more red. If segments move positive, the M-mode would be blue. Here, the ECG is at the bottom of the right hand panels. The white moving target in back of the ECG is a derived M-mode of the mitral valve. Beginners should avoid concern about the colored M-mode. The global strain for this view is -20.8% , which is normal

endocardial, mid-myocardial or epicardial surfaces (Fig. 34.15). Users should be aware that mid-myocardial to some manufacturers means full thickness. Strain values can vary depending upon what line is chosen. The two most common are the mid-myocardial (line or full thickness), and endocardial line. Users should be aware of how their system is set up, particularly making sure that machines are measuring speckles from the same place when machine to machine comparisons are done. The actual lines are not as precise as might be indicated from this schematic diagram and depend upon the size of the search area of each ROI. Users cannot generally access or adjust the size of the ROI's in machines.

Displays do not generally allow the user to see the paths of moving speckles. When seen, however, it is most interesting to follow the complex paths of speckles throughout the cardiac cycle (Fig. 34.16).

Users should keep in mind that when a left ventricle shortens in its longitudinal direction, shortening is not equally distributed (Fig. 34.17). When the heart moves between diastole to systole, the left ventricle shortens in its long axis (solid arrow) about 15–25%. Whereas the apex usually contributes little to ventricular shortening, the base is usually quite active, contributing to most of the shortening.

This same concept is illustrated using the three-dimensional echo LV volume renditions of a normal left ventricle (Fig. 34.18). The horizon-

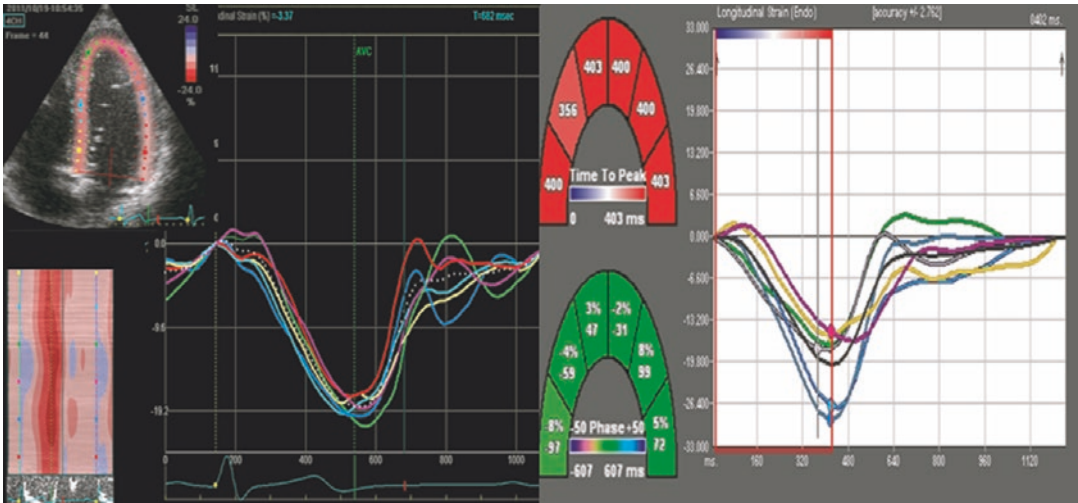


Fig. 34.14 These are two strain recordings from the apical four-chamber view from a normal individual by two manufacturers systems. The interfaces are different and colors are different. Unfortunately, there is no agreement

among manufacturers as to standard displays and/or standard color assignments to the various segments. Beginners will have to note color designations in manufacturers literature

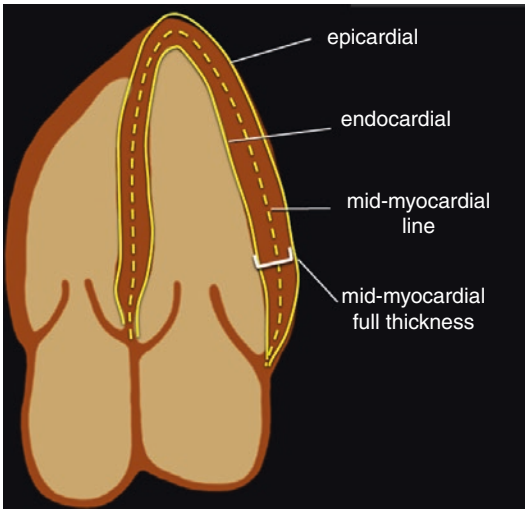


Fig. 34.15 Strain may be calculated along lines or thicknesses. Strain can be determined along the endocardial, mid-myocardial or epicardial surfaces. Users should be aware that mid-myocardial to some manufacturers means full thickness. Strain values can vary depending upon what line is chosen. The two most common are the mid-myocardial (line or full thickness) and endocardial line. Users should be aware of how their system is set up, particularly making sure that machines are measuring speckles from the same place when machine to machine comparisons are done. The actual lines are not as precise as might be indicated from this schematic diagram and depend upon the size of the search area of each ROI. Users cannot generally access or adjust the size of the ROI's in machines

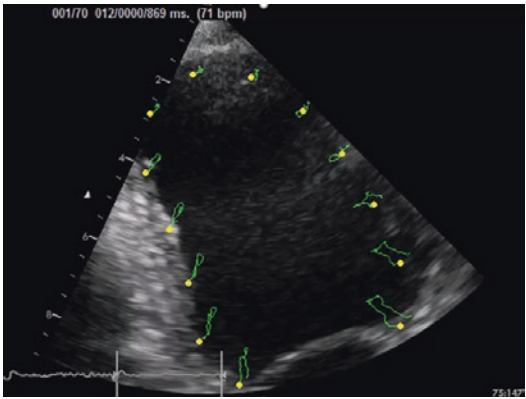


Fig. 34.16 This interesting display shows the paths traversed by given speckles followed in one manufacturer's system. Motion is never only in one direction

tal dashed lines are the starting points of the apex and base in diastole. In systole, the apex moves a little, but the base contributes most to longitudinal shortening. (solid arrow).

While the apex moves little in normal heart, its strain may still be in the -15 to 20% range. This represents a little mind-twisting exercise that is solved by remembering that strain is percent movement. If something moves from 2 mm length to 1 mm, its strain would be -50% . Strain is a relative number and is not absolute displacement.

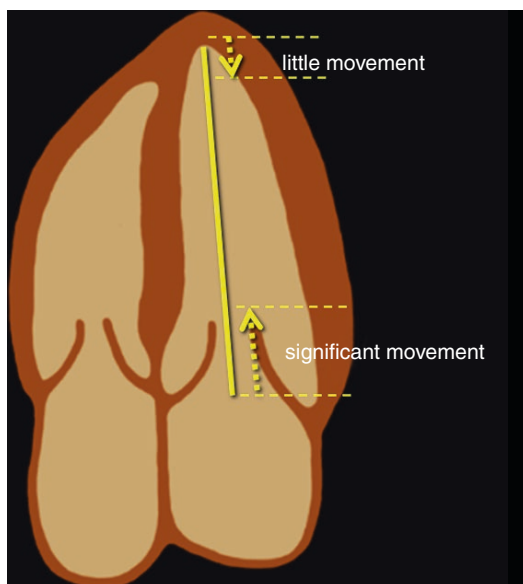


Fig. 34.17 When the heart moves, between diastole to systole, the left ventricle shortens in its long axis (solid arrow) about 15–25%. Whereas the apex usually contributes little to ventricular shortening, the base is usually quite active, contributing to most of the shortening

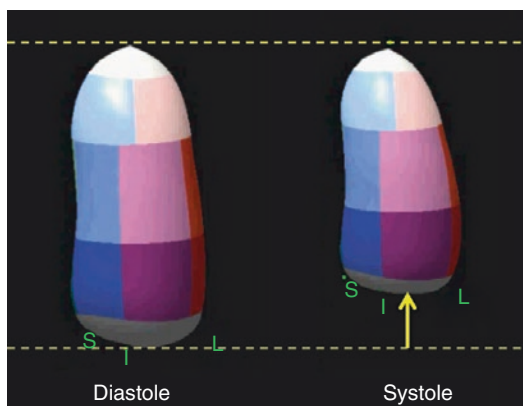


Fig. 34.18 Another depiction of longitudinal left ventricular shortening based on three-dimensional echo LV volume renditions of a normal left ventricle. The horizontal dashed lines are the starting points of the apex and base in diastole. In systole, the apex moves a little but the base contributes most to longitudinal shortening. (solid arrow)

Timing: Frame Rate and When in the Cycle to Measure

Ultrasound machines scan at roughly 30–60 frames per second. If too few frames per second

are obtained, then the full extent of cardiac motion might not be able to be detected. If too many frames per second are obtained, it might be that algorithms cannot detect the small changes that occur from frame to frame. Currently, it is recommended that images are obtained at 30–60 frames per second. Some systems allow 30 fps and others require approximately 60 fps or they will not allow strain to be calculated. For beginners, the frames per second usually appears on the image display in Hertz (Hz).

Given adequate fps an ultrasound system can generate longitudinal strain curves for the three apical views (Fig. 34.19). This is the display of strain curves from all three views in a normal individual. Note that most lines are roughly timed the same, with nadirs (white squares) at, or before, aortic valve closure (peak systolic strain). The display at the lower right is a target diagram summarizing the various values of peak strain (the maximum, found anywhere on the curves) without regard to systole or diastole. In this normal individual, differences may not be that great. Thus, it is important to consider not only where the strain number is obtained in the myocardium, but when.

Figure 34.20 demonstrates how to understand timing issues. If a maximum and minimum length are determined, it is important to know when these measures are obtained in the cardiac cycle. Different timings result in different numbers. There is peak systolic strain, which is the peak strain prior to, or at, aortic valve closure (yellow squares). There is also end systolic strain, which is the strain precisely at aortic valve closure (green squares). Frequently peak systolic and end systolic strain occur at the same time. Peak strain is when the strain is measured any peak time during the cardiac cycle (red squares) and could occur in diastole in late contracting segments (lower left panel). It is important to know when your system is measuring strain.

Raw or DICOM

Most on-cart strain calculation systems use “raw” ultrasound images. Such images are referred to as

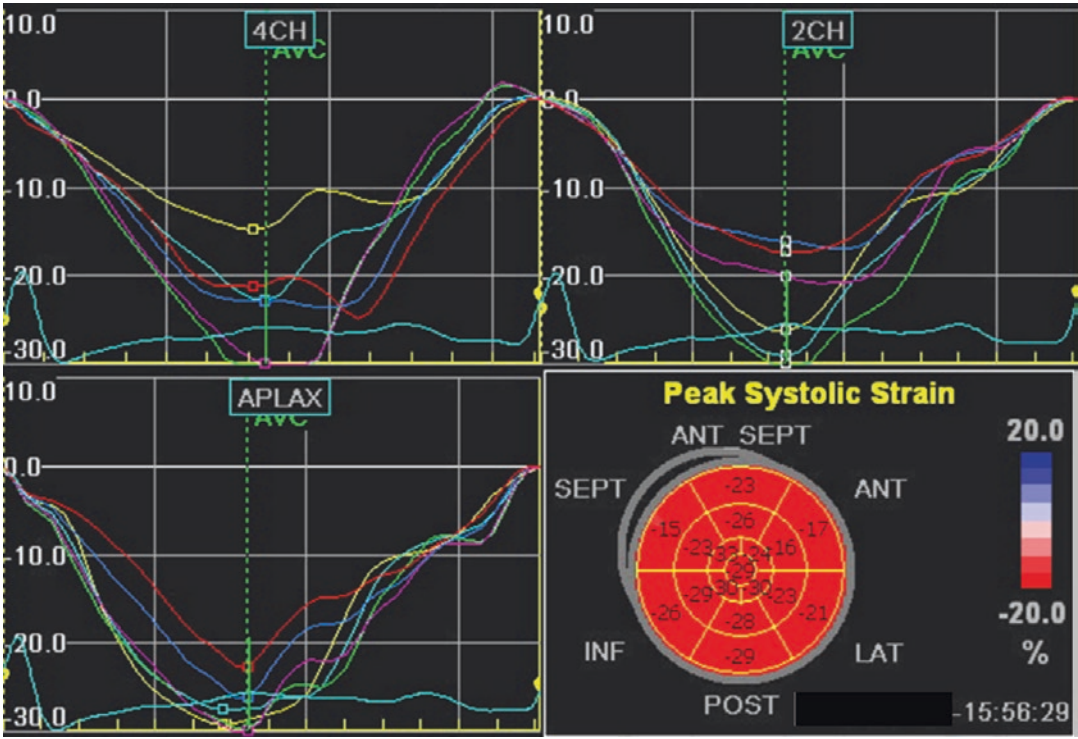
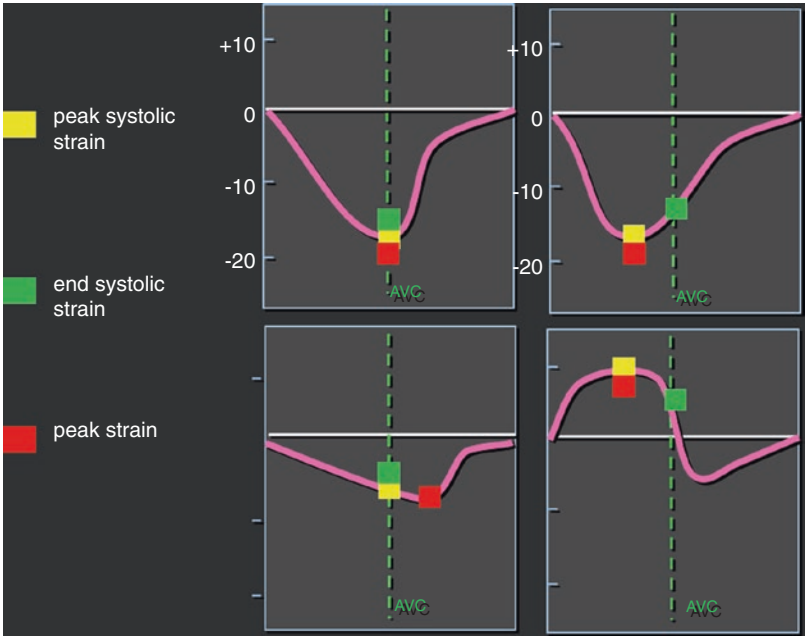


Fig. 34.19 This is the display of strain curves from all three views in a normal individual. Note that most lines are roughly timed the same, with nadirs (white squares) at, or before, aortic valve closure (peak systolic strain).

The display at the lower right is a target diagram summarizing the various values of peak strain. (the maximum, found anywhere on the curves without regard to systole or diastole)

Fig. 34.20 There is peak systolic strain, which is the peak strain prior to, or at, aortic valve closure (yellow squares). There is also end systolic strain, which is the peak strain precisely at aortic valve closure (green squares). Many times peak systolic and end systolic strain occur at the same time. Peak strain is when the strain is measured any peak time during the cardiac cycle (red squares) and could occur in diastole. In late contracting segments (lower left panel). It is important to know when your system is measuring strain



raw as they contain the highest ultrasound target amplitude data possible because they are without significant temporal or spatial processing. These images require large digital storage space and they can only be viewed by equipment or playback systems from the same manufacturer of the acquisition equipment. In raw images, the fps displayed in playback are the same as the fps at which they were obtained. Analysis can then be performed at “acquisition rates”.

Once images are saved in a DICOM format, there is considerable temporal and spatial processing that is performed in order to reduce digital storage requirements and allow images to be viewed across multiple viewing platforms. These images require only modest digital storage space in comparison to raw. A user should know if their system export settings compress the number of fps. For example, images obtained at 60 fps might only be exported from the machine at 30 fps.

One manufacturer’s analytic software for raw image analysis cannot analyze another’s raw images strain data because the software vendor specific. Vendor neutral software is available in the marketplace for analysis of DICOM images across platforms. Multivendor echo image acquisition equipment laboratories may be handicapped in providing as consistent analytic methodology as possible without vendor neutral analytic systems.

Numbers

To this point a reader may be thoroughly discouraged that strain determination has so many problems that it is unusable. Variable it is, but unusable it is definitely not. Here is a summary list of factors considered so far.

Speckle: Speckle is the acoustic signature of tissue and includes anatomic targets, noise and artifact. Speckle does not result from the myocardium alone.

Ultrasound machine: Different beamformers and transducers make different sizes and shapes of speckle.

Calculating strain: There are different types of strain, Lagrangian and Natural. Different math is used in different circumstances.

Strain algorithms: Multiple methods exist for detecting speckle and measuring its movement. A user doesn’t know which algorithms a machine uses and, likely, could never understand them anyway.

Position in the image: Strain can be calculated along various lines or thicknesses of muscle:

Endocardial, mid-muscular, epicardial or full thickness mid muscular.

Timing in the image: Different peak strains can be calculated depending on timing in the cardiac cycle: peak, peak systolic or end-systolic.

Type of strain: Longitudinal strains seem to work, but problems exist with circumferential and radial. Understanding strain rate is difficult for most people.

Understanding all these problems won’t help a user produce a strain number if only one machine is used and one method is adhered to. The problems occur in multivendor labs when users are trying to follow a patient over time with different machines. Is also possible that internal system settings are changed from time to time by users or defaults are changed with system upgrades. There is no gold standard that exists for strain as exists for measurement of diameter or volume. One machine or approach cannot be calibrated against another. Strain is simply “strain”, a number that is calculated. One can see, however, how important it is to know a bit about how that number is generated.

Comparisons

There many machine to machine comparisons and inter-and inter-observer studies published. All indicate that if proper controls are in place and machine settings are approximated as best as can be done, then strain numbers have tolerable variability. The numbers produced are not the same, but they are close.

One such small study was performed in our laboratory between vendor specific image acqui-

sition systems (GE and Philips), and vendor specific (GE) and vendor neutral (TomTec) analytic software. Images were analyzed at 30 and 60 fps. Comparisons for longitudinal strain had clinically acceptable inter- and intra-observer variabilities (Fig. 34.21). Radial and transverse strain comparisons were unacceptable.

The reading list at the end of this chapter contains very useful comparative information for a larger and more complete study between vendors.

Resolution Affects Strain

Ultrasound images do not have uniform resolution. This is most readily seen in any image of a liver (Fig. 34.22). With minor exceptions, the liver is homogeneous organ anatomically. However, when examining the speckle size and shape the deeper into the tissue, the farther out one looks along the arrow, the wider the speckles becomes.

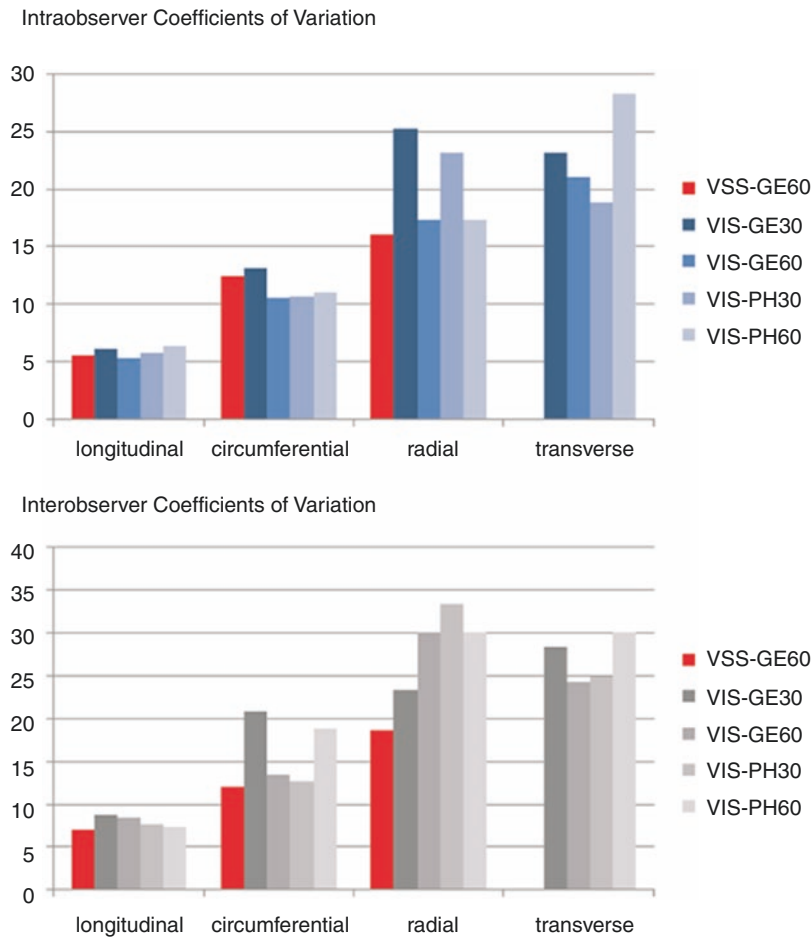


Fig. 34.21 Intra- and interobserver reproducibility. Coefficients of variation for analysis of longitudinal, radial, circumferential and transverse strain. VSS-GE60, GE Images at acquisition frame rate (≈ 60 fps) analyzed by vendor specific software (EchoPAC). VIS-GE30, GE images at 30 fps analyzed by vendor independent software (TomTec). VIS-GE60, GE Images at acquisition frame rate (≈ 60 fps) analyzed by vendor independent

software. VIS-PH30, Phillips images at 30 fps analyzed by vendor independent software. VIS-PH60, Phillips images at acquisition frame rate (≈ 60 fps) analyzed by vendor independent software. Comparisons for longitudinal strain had clinically acceptable inter- and intra-observer variabilities. Radial and transverse strain comparisons were unacceptable, VIS vendor independent software, VSS vendor specific software

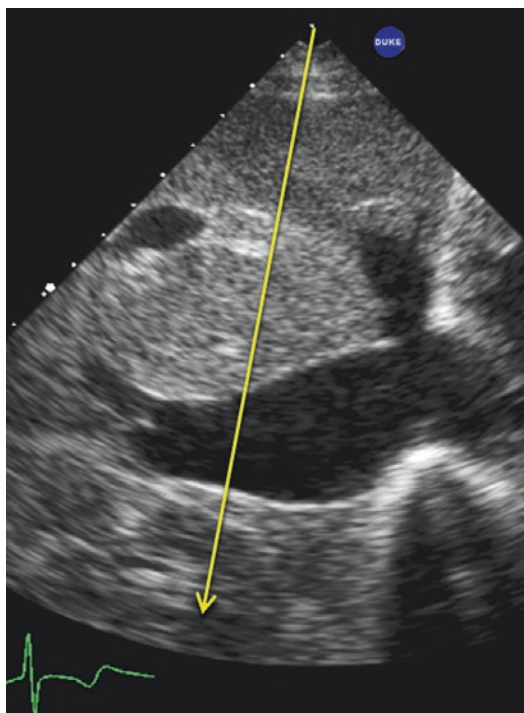


Fig. 34.22 The liver shows non-uniform speckle for an organ that is, for the most part, uniform in tissue structure. Look at the speckle size increasing the farther one goes into tissue along the arrow

Such problems with varying speckle size are also seen in the heart. Figure 34.23 is in the parasternal long in a patient with left ventricular hypertrophy where the speckle is easily seen. Little noise is present. Compare the speckle size in the near (arrow in the septum) vs the laterally smeared and larger speckle in the far field (arrow in the posterior wall).

Ultrasound has uniform resolution in range (depth) so that speckles are more uniform in that dimension. Range resolution is determined by wavelength (frequency) of the transducer. Speckles, however, are wider and wider the farther one looks from the transducer due to beam spread (Fraunhofer effect). One of the likely reasons that longitudinal strain seems to work better may be due to the more uniform resolution along the direction of ventricular movement.

A schematic diagram of the short axis of the left ventricle is shown in Fig. 34.24. The resolution

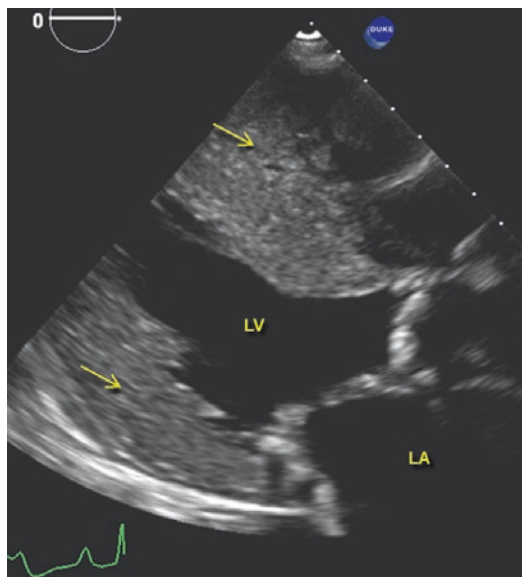


Fig. 34.23 This imaging phenomenon is also seen in the heart with the speckle size in the septum (arrow) more narrow than the speckle size in the posterior wall (arrow). Targets in the far field tend to smear laterally due to beam width reducing lateral (azimuthal) resolution in the far field. For details, see text

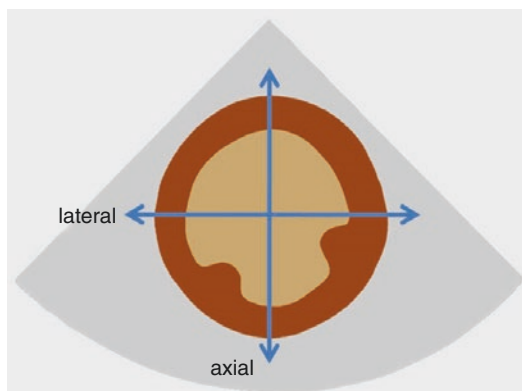


Fig. 34.24 A schematic diagram of the short axis of the left ventricle. The resolution in the axial beam encountering the anterior septum and the postero-lateral wall takes advantage of good resolution in that dimension for targets moving front to back. Lateral resolution is, however, impaired with lateral smearing of reflectors in the side walls. This lateral smearing likely makes the side-to-side movement of speckle in this dimension during systole much more difficult to detect because of overlap of targets from one time to another

in the axial beam encountering the anterior septum and the postero-lateral wall takes advantage of good resolution in that dimension for targets moving front to back. Lateral resolution is, however, impaired with lateral smearing of reflectors in the side walls. This lateral smearing likely makes the side-to-side movement of speckle in this dimension during systole much more difficult to detect because of overlap of targets from one time to another. The algorithms that detect strain in ROI's front and back are likely the same but the imaging circumstances are different.

Functional Patterns

Resolution along the ultrasound beam is then well suited for evaluation of movement in the axial (depth or range) dimension. Any given regional segment can have multiple strain functional patterns. Functional patterns are assessed by the whether the peak strain is normal, low (closer to zero) or paradoxical (high). Normal strains (global or regional in any segment) are about -15 to -20% and all peak roughly at the same time (about at the point of aortic valve closure).

Three major functional patterns are noted in Fig. 34.25. Hypocontractile segmental strain values are reduced, with values considerably below normal (closer to zero). Non-functional segments have no contraction or demonstrate a holosystolic bulge during systole. Non-functional segments may be due to scar, ischemia or other reason why segments do not contract. Other patterns may exist, beginners are urged to look for these patterns.

Examples of patients with functional abnormalities are shown in Fig. 34.26, each with strain curves taken from the apical four-chamber view. Contrast these strain curves with the normal patients seen in Figs. 34.10, 34.14, 34.15, and 34.16. The patient in the left panel shows markedly reduced strain curves (near zero) with a global longitudinal strain of -3.8% . Walls are timed rather uniformly (arrow). The patient has a diffuse cardiomyopathy. The patient in the right panel shows marked holosystolic bulging (arrow) of the red and blue walls, the infarction area. Note the walls opposite the infarct are normal.

Figure 34.27 shows a strain set from another patient with a myocardial infarction, this one localized to a small area of the posterior wall. V Note the holosystolic bulging (yellow curve,

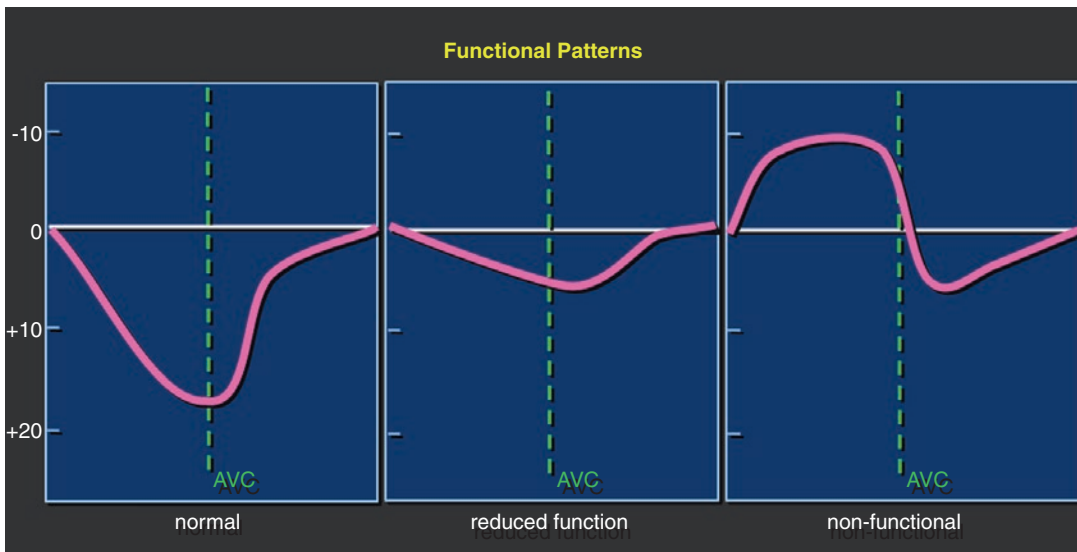


Fig. 34.25 Three major functional patterns schematically drawn. Hypocontractile segmental strain values are reduced, with values considerably below normal (closer to zero). Non-functional segments have no contraction or

demonstrate a holosystolic bulge during systole). Non-functional segments may be due to scar, ischemia or other reason why segments do not contract. Other patterns may exist, beginners are urged to look for these patterns

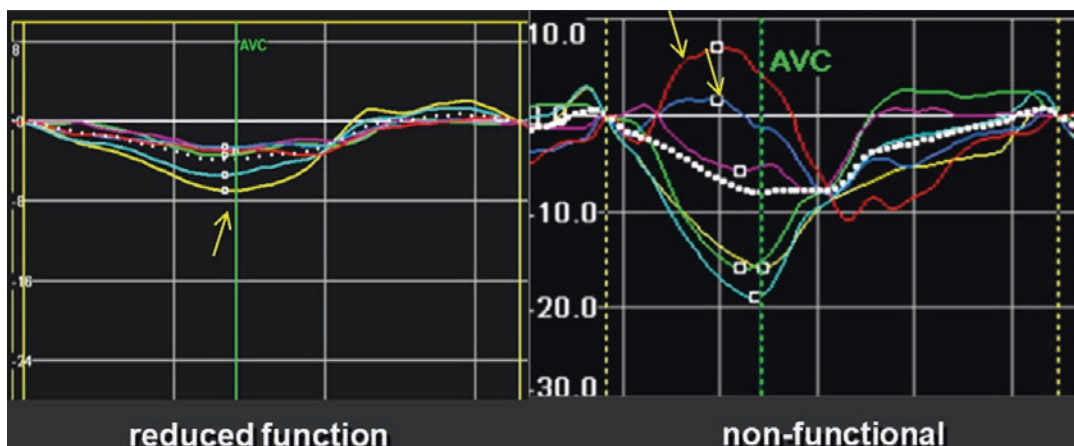


Fig. 34.26 Examples of patients with functional abnormalities, each with strain curves taken from the apical four chamber view. Contrast these strain curves with the normal patients seen in Figs. 34.10, 34.13, 34.14, and 34.19. The patient in the left panel shows markedly reduced strain curves (near zero) with a global longitudinal strain of -3.8% . Walls are, however, timed rather uni-

formly (arrow). The patient has a diffuse cardiomyopathy. The patient in the right panel shows marked holosystolic bulging (arrow) of the red and blue walls, which are the apical and mid-lateral walls. The GLS is about -9% . And is reduced. This patient has a transmural infarction in the area of the holosystolic bulging. Note the walls opposite the infarct are normal

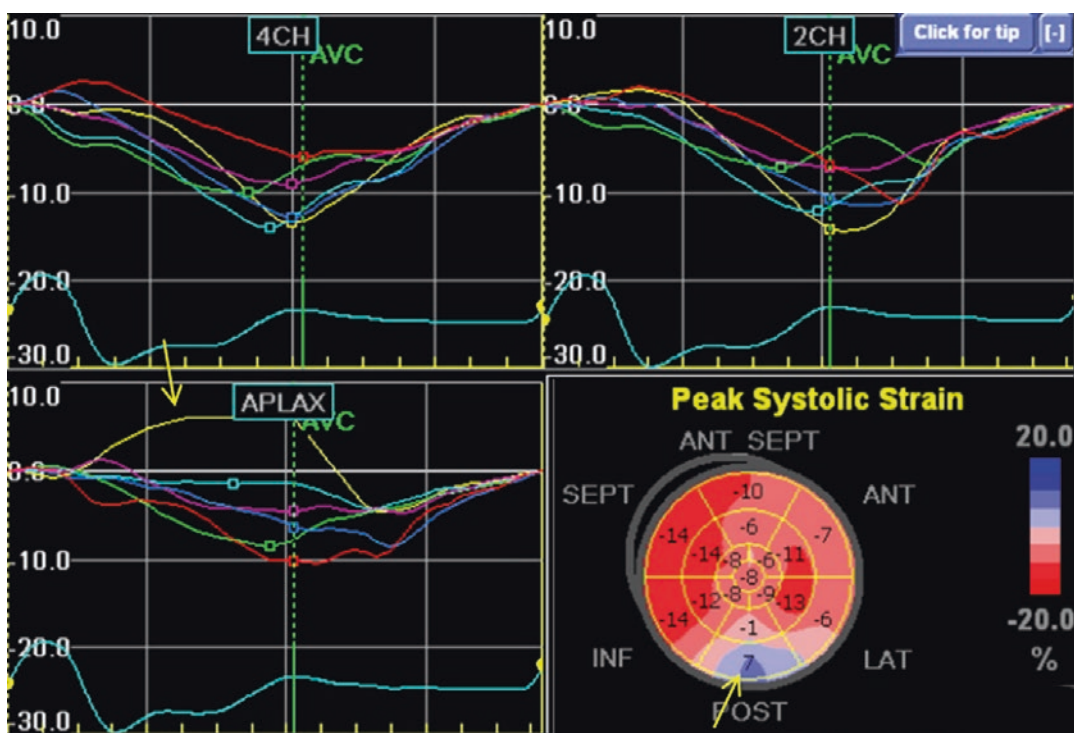


Fig. 34.27 Strains from three apical views from a patient with a localized posterior wall infarction. Note the bulging (yellow curve, arrow) in the apical long axis

which corresponds to the positive strains (blue patch) seen in the target display (lower right, arrow). Contrast this set of strains with the set in the normal in Fig. 34.19

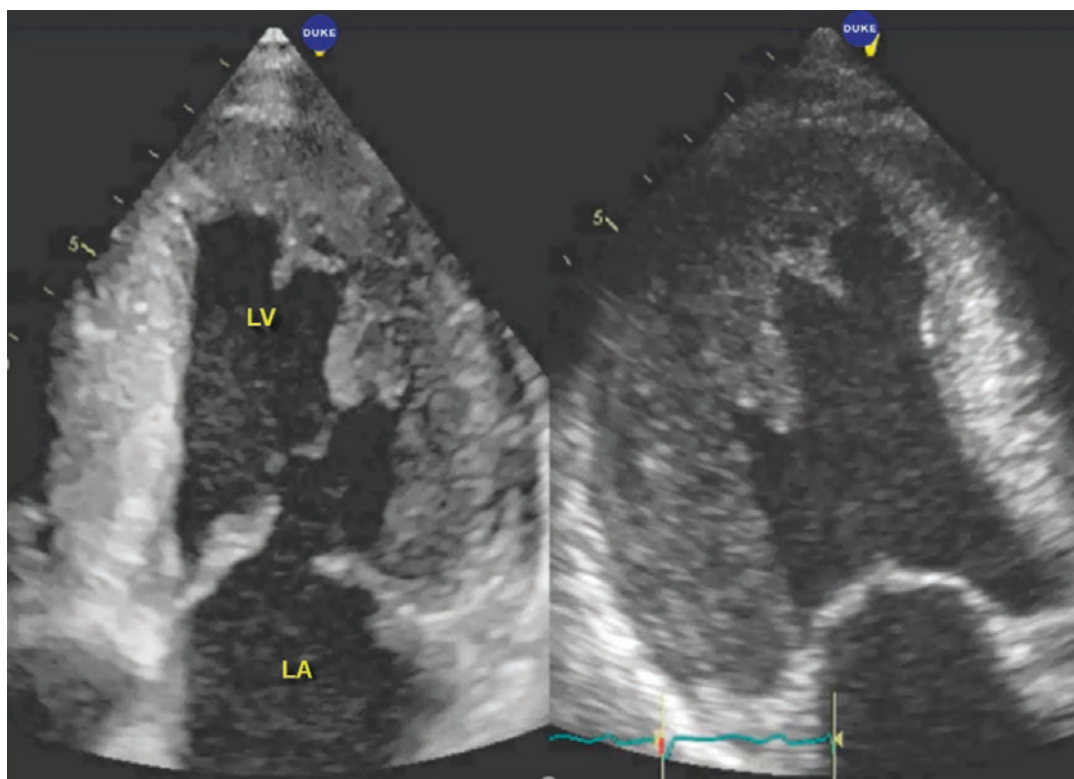


Fig. 34.28 Apical four and two chamber views from a patient with amyloidosis and subjective overall ventricular hypocontractility. The strains from this patient are shown in the next figure

arrow) in the apical long axis which corresponds to the positive strains (blue patch) seen in the target display (lower right, arrow). Contrast this set of strains with the set in the normal in Fig. 34.19.

Amyloidosis, rather characteristically, shows diffuse hypocontractility except for the apex (Fig. 34.28). Figure 34.29 shows apical four and two chamber views from a patient with amyloidosis and subjective overall ventricular hypocontractility. The strains from this patient are shown in the next figure.

This composite of the strains from the three apical views of the patient in the previous figure with amyloidosis. The strains show the characteristic hypocontractility of all the segments with an unusual preservation of the apex (arrows). This apical preservation is a special finding in patients with amyloid heart disease. Not the red in the middle of the target display. The GLS is -7% .

Apical two chamber view and strains from a patient with Chagas Disease showing preserved strains are presented in Fig. 34.30. As preview of

the next chapter, note the timing abnormality of the posterior wall. (arrow). Despite the fact that LV movement looked normal by echo, this revealed a marked conduction delay. These stains were performed with another analytic system so the designated wall colors are different than other Figures in this Chapter. It is of interest, however, that all the various strains, endocardial and epicardial from this system are shown in the lower left.

Length of Line

After wrestling with the concepts of this chapter, it will come as a welcome relief to know that there is growing traction to the concept of strain calculation from changes in the length of an endocardial line (Fig. 34.31). In this approach the endocardium is detected, just like most ultrasound systems do with some reproducibility for calculation of ejection fraction. Instead of calculating a volume, the system simply determines

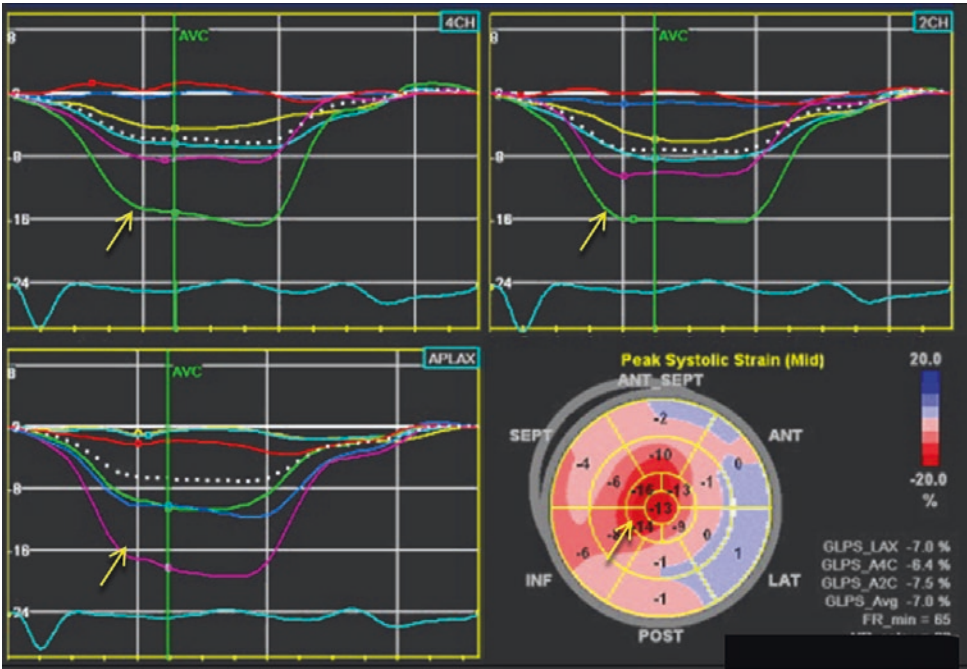


Fig. 34.29 This composite of the strains from the three apical views of the patient in the previous figure with amyloidosis. The strains show the characteristic hypocontractility of all the segments with an unusual preservation

of the apex (arrows). This apical preservation is a special finding in patients with amyloid heart disease. Not the red in the middle of the target display. The GLS is -7%

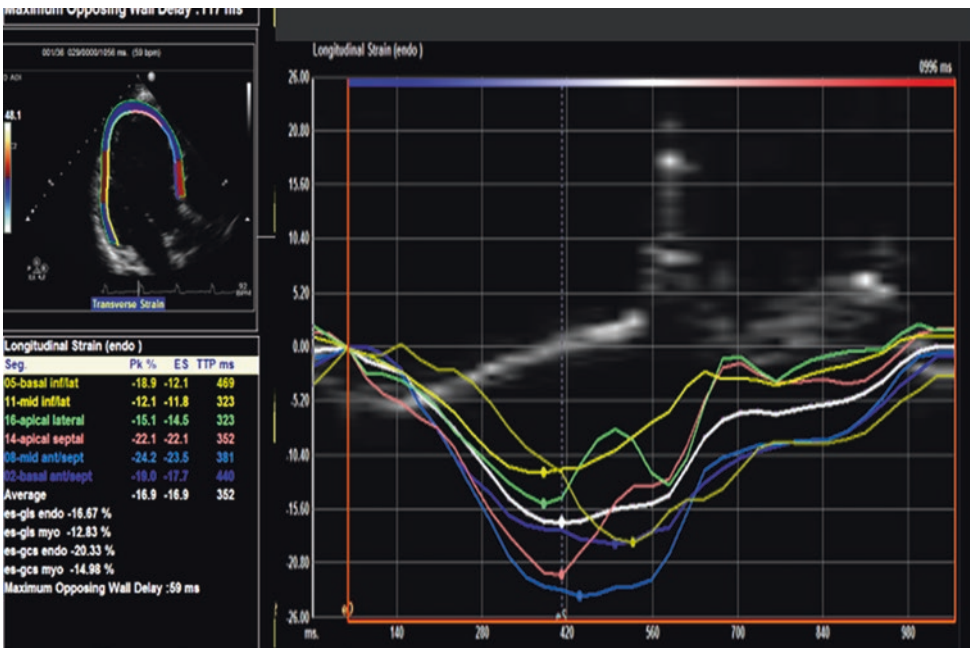


Fig. 34.30 Apical two chamber view and strains from a patient with Chagas Disease showing preserved strains. As preview of the next chapter, note the timing abnormality of the posterior wall. (arrow). Despite the fact that LV movement looked normal by echo, this revealed a marked

conduction delay. These stains were performed with another analytic system so the designated wall colors are different than other Figures in this Chapter. It is of interest, however, that all the various strains, endocardial and epicardial from this system are shown in the lower left

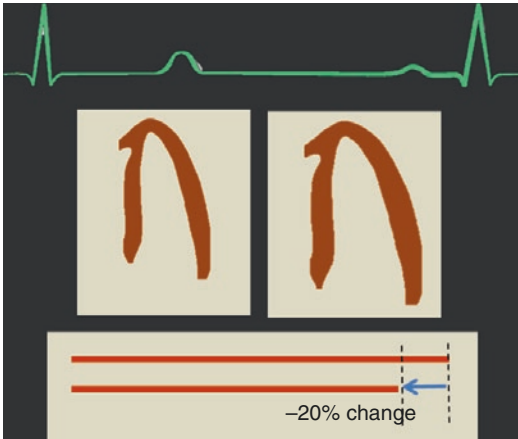


Fig. 34.31 The length of line concept for the determination of GLS has an appeal as it avoids all the difficulties of speckle tracking mentioned in this chapter. In this approach the endocardium is detected, just like most ultrasound systems do with some reproducibility for calculation of ejection fraction. The length of the endocardium is detected in diastole and compared to the length detected in systole. Then by Lagrangian strain, a simple GLS is calculated by length of line change. In this example, the GLS is -20% . *Modified after TomTec*

the length of the endocardial line in diastole and compared to the length detected in systole. Then by Lagrangian strain, a simple GLS is calculated by length of line change. In this example, the GLS is -20% . It's just like measuring with a string and holding the string up against a ruler.

Time will tell whether this simplistic method finds validation and acceptance in avoiding the variabilities between systems introduced by complex speckle tracing methodologies. Speckle tracing is used to find the endocardial line, but after that it is simple strain.

In the meantime, the only way seeming practical to find consistency in the calculation of strain by speckle tracking is to simply do it one way if vendor specific approaches are used. If this latter is used over the simplistic approach, then mastery of this chapter is recommended.

Suggested Reading

- Farsalinos KE, et al. Head-to-head comparison of longitudinal strain measurements among nine different vendors: the EACVI/ASE intervendor comparison study. *J Am Soc Echocardiogr.* 2015;28:1171–81.
- Risum N, et al. Variability of global left ventricular deformation analysis using vendor dependent and independent 2D speckle tracking software in adults. *J Am Soc Echocardiogr.* 2012;25:1195–203.
- Voigt E, et al. Definitions for a common standard for 2D speckle tracing echocardiography. *J Am Soc Echocardiogr.* 2015;28:183–93.



Regional Strain: The Physiology of Dyssynchrony

35

Niels Risum, Daniel Forsha, Kasper Emerek,
Peter Sogaard, and Joseph Kisslo

There are two major functional applications for speckle tracked strain used in the study of cardiac function: global and regional. This chapter is about regional functional strain assessment. The basics of ultrasound speckle tracking and strain are discussed in detail elsewhere in this volume and this current chapter assumes a familiarity with these principles.

Strain applications evolved from sonomicrometry techniques first reported in 1956 (Fig. 35.1) by Robert Rushmer and Dean Franklin, physiologists at the University of Washington. A brief review of the past will put the present use of strain into context.

Sonomicrometry used *through* transmission ultrasound where two tiny ultrasound crystals (attached to wires) were inserted onto, or into, ani-

mal myocardium so the ultrasound emitted from the transmitting crystal could pass to the receiving crystal. Of interest, Inge Edler and Helmuth Hertz in Sweden were almost concurrently first using chest wall *reflected* ultrasound to look at cardiac anatomy and disease in intact human beings.

Both techniques were suited to measure the changing distances between cardiac structures. Chest wall echo, however, was impeded by significant signal attenuation and distortions of image quality due to bone, lungs, and other factors. Sonomicrometry had no such impediment but did require an open chest model. Sonomicrometry then made rapid advancements in the study of regional cardiac muscle function. The tiny crystals became smaller and smaller and could be inserted into regions of the myocardium of experimental animals. Strain (% change in distance between the crystals) was then born as a descriptor of cardiac movement, frequently in combination with hemodynamic pressure measurement. Over the ensuing two to three decades, sonomicrometry methods played a critical role in establishing the fundamentals of cardiac physiologic principles used today.

Chest wall reflected echo, on the other hand, evolved more slowly. It took time to recognize and differentiate cardiac anatomic structures and subsequently establish scanning methodology, all the while limited by variable image quality. Creating reasonable images through the chest was much more difficult than simply sending ultrasound pulses from one sonomicrometer to another.

N. Risum

Division of Cardiology, Rigshospitalet, Copenhagen, Denmark

D. Forsha

Pediatric Cardiology, Children's Mercy Hospital, Kansas City, MO, USA

K. Emerek

Department of Clinical Medicine, Aalborg University, Aalborg, Denmark

P. Sogaard

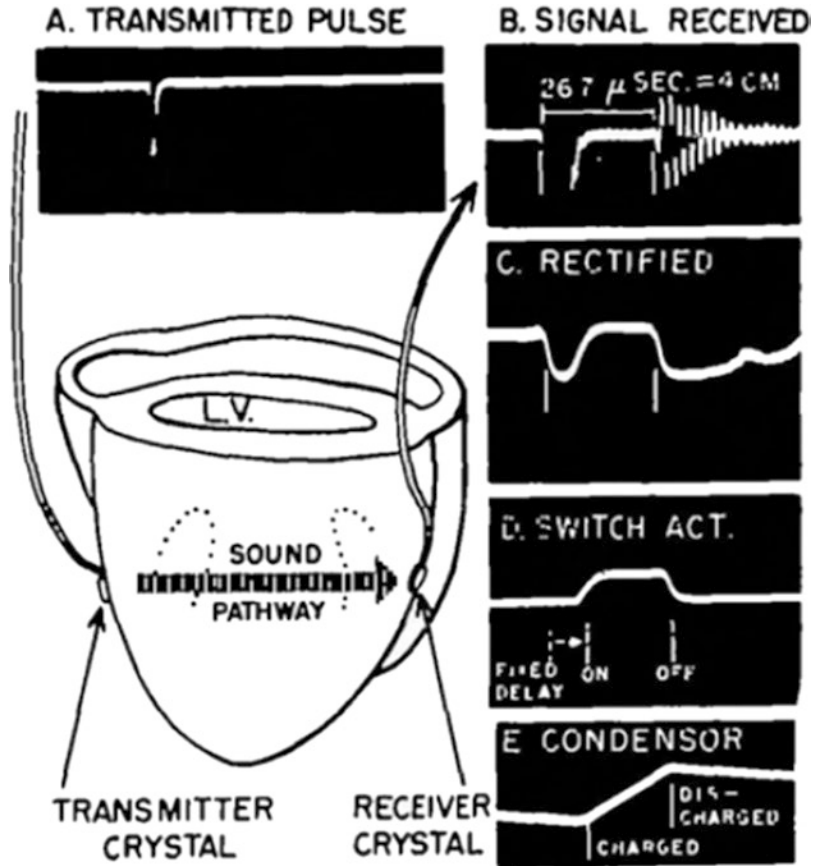
Department of Cardiology, Aalborg University, Aalborg, Denmark

J. Kisslo (✉)

Division of Cardiology, Duke University Medical Center, Durham, NC, USA

e-mail: joseph.kisslo@duke.edu

Fig. 35.1 Sono-micrometry was first used in 1956 by Rushmer to study the movements of the animal heart with ultrasound. Tiny ultrasound crystals were inserted onto the myocardium, one a transmitter and the other a receiver. This was not reflected ultrasound, but rather was through transmission ultrasound. Reproduced with permission of the American Heart Association: Rushmer. RF, Franklin DL, Ellis RM: Left ventricular dimensions recorded by sonocardiometry. *Circ Res* 4:684, 1956



Progressively, technology advanced and chest wall images were of acceptable quality in enough people to begin evaluation of cardiac function with clinical echocardiography. Of interest is that chest wall echo took the basic strain formula and adapted it to changes in LV diameter (shortening fraction) and volume (ejection fraction). All echocardiographers are familiar with this mathematic process.

By the 1990s, the surge in sonomicrometry based study waned. When talking with those who were a part of the experimental sonomicrometry/strain generation of investigators, all recall their excitement with strain, but they also lament their frustrations.

First, strain was only a one dimensional measure. The percent change between two points in space just couldn't capture all the necessary parameters of the complex movements of the heart as it twisted and turned, moving in and out,

side to side, and up and down with each cardiac cycle. Physiologic questions became more and more complex, and point-to-point through transmission ultrasound could not look in all dimensions simultaneously.

Second, many recognized that strain only described shortening in one sampling region and along one line. It became apparent that function in one region of the heart depended on another region, or regions, to more adequately describe function. Spatial relationships were important to understand regional function. An ultrasound pulse from one set of crystals would interfere with the pulse from another so the use of multiple sets of sonomicrometry pairs was not possible.

Most importantly, they realized that strain was but one number that needed to be combined instantaneously with other measures such as pressures and time to provide answers to rapidly

evolving more and more detailed questions. Strain was not the perfect answer and, in any event, it was foolish to think that complex cardiac function could be expressed by a single measure.

Overall, they realized that cardiac function could not be summarized in one number as the heart was a complex unit of interacting relationships. Strain was not perfect and multiple limitations forced investigators to limit expectations.

Imaging capabilities through the chest wall progressively improved with each new generation of echo machines. Techniques for signal processing evolved and processing hardware provided speeds that were, heretofore, unimaginable. Accordingly, the allure of strain has returned. To understand the use of strain for assessing regional myocardial function, the lessons of the past and the limitations of strain discussed in the chapter on global strain must be kept in mind.

This Chapter

All lamentations aside, speckle tracked strain determined from the chest wall helps us to understand more and more aspects of cardiac physiology. This chapter will seem unusual to some as it will not call upon endless quantitative indices to bring basic understanding to regional strains. Little will be mentioned of measurement of precise time to peak strain or precise determination of the value of peak strain in regions. Rather, it will feature relationships of movement between heart walls as revealed by patterns of motion and timing. Calculating numbers is for research while beginning to understand patterns brings awareness and enlightenment as to what is possible.

Pattern analysis can be divided into two major categories: functional and timing. Functional patterns refer to whether a wall strain is normal, reduced function or non functional. Timing patterns refer to general patterns of timing: normal timing, “classic” dyssynchrony timing or heterogeneous (or other) timing. Patterns provide a rough structure to begin to learn how to read regional strain images.

Functional Patterns

A review of the functional patterns discussed in the chapter on global strain is appropriate. Figure 35.2 shows multicolored regional longitudinal strain curves from an apical four-chamber view in a normal individual. All the walls move mostly synchronously, not in perfect alignment, but close. Coincident with the onset of the QRS in the ECG, all the walls show slight positive strain as the ventricle builds pressure in response to isovolumic contraction. Since strains very early in systole do show some minimum stretch, something must be moving so “isovolumic,” rather than “isometric” may be a better word to understand this critical time period after the mitral valve shuts and pressure builds before the aortic valve opens.

As will be seen, placing the starting point for measuring strain at the onset of the QRS is critical for evaluating some abnormal regional strain patterns. Most analytic software systems automatically select the peak of the QRS as the starting point for strain analysis. Not all strain analytic software allow a user to move the starting point to the onset of the QRS, but they should. When the QRS is wide, it could be that dyssynchronous opposite wall movement occurs before the peak of the R wave and if the peak of the R wave is chosen as the start point, critical pattern information is obscured. Routinely starting at QRS onset is highly recommended as a matter of routine.

All the walls then contract and peak almost simultaneously until the vertical green line of aortic valve closure (AVC). AVC is another critical timing point as it is the descriptor that marks end-systole when using strain. AVC can be placed by a user from the spectral Doppler recording of aortic valve flow. As the ventricle fills in diastole, the speckle stretches, rapidly in the beginning of diastole (with rapid ventricular filling, the rapid filling wave-RFW) and then more slowly (with slow ventricular filling, the slow filling wave-SFW) until atrial contraction (A wave) where the walls stretch.

Resolution along the ultrasound beam is then well suited for evaluation of movement in the axial

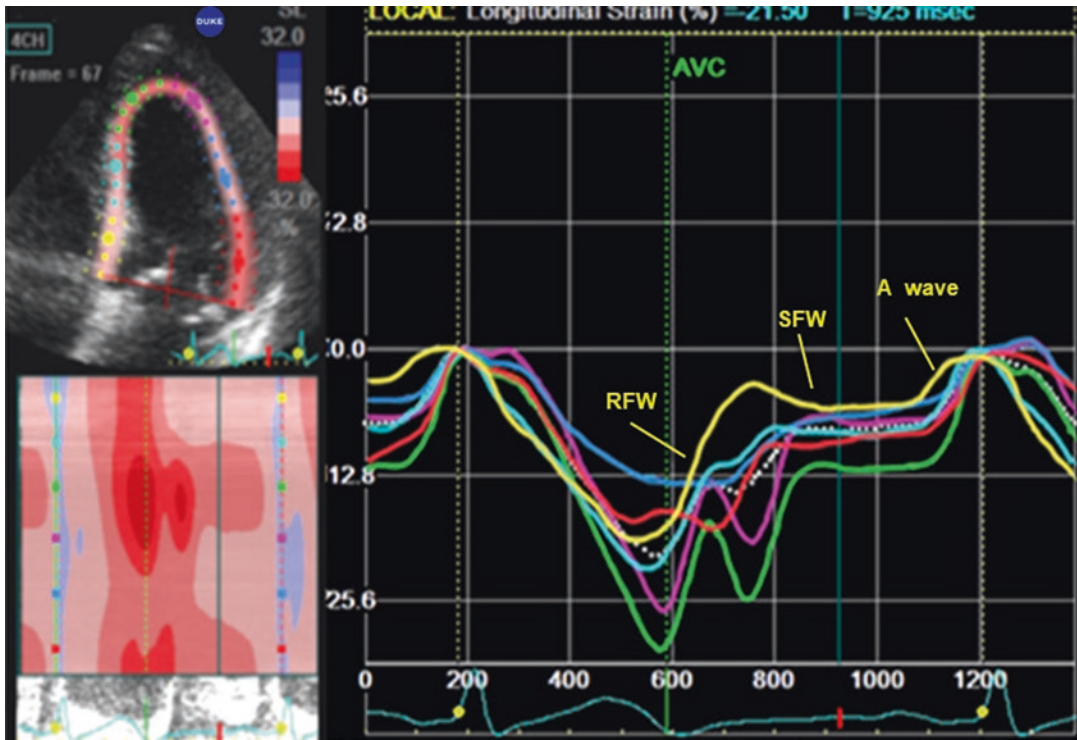


Fig. 35.2 Apical four-chamber view with strains from a normal individual. All the strain curves are negative and have their nadir at, or about, aortic valve closure in this normal tracing. GLS (dashed white line) is about -21%

(depth or range) dimension in the apical views so longitudinal strain is used for regional pattern analysis. Any given regional segment can have multiple strain functional patterns. Functional patterns are assessed by the whether the peak strain is normal, low (closer to zero) or paradoxical (high). Normal strains (global or regional in any segment) are about -15 to -20% and all peak roughly at the same time (about at the point of aortic valve closure).

Three major functional patterns are noted in Fig. 35.3. While no scale values are shown in these schematics, the normal strain in the left panel has a nadir at about -15% . The reduced function strains in the middle panel have values considerably below normal (closer to zero), perhaps about -6% . Non-functional segments have no systolic contraction and characteristically demonstrate a holosystolic bulge during systole. These non-functional segments may be due to scar, ischemia, hibernation, stunning or other reason. While other patterns certainly exist, beginners are urged to look for these three major patterns.

Examples of patients with the three main patterns are seen in Fig. 35.4 and all are taken from the apical four chamber view. Contrast the abnormal strain curves (middle and right panels) with the normal (left panel). The patient in the middle panel shows markedly reduced strain curves (arrow, closer to zero) with a global longitudinal strain of -3.8% . Walls are timed rather uniformly (arrow) in this patient with a diffuse cardiomyopathy. The patient in the right panel shows marked holosystolic bulging (arrow) of the red and blue walls, the infarction area. Note the walls opposite the infarction are normal. The red and blue bulging strains are the basal and mid-lateral walls. The GLS of the bulging walls cancel out the GLS of the well contracting walls. If the regional strain patterns were not examined and interpreted, a clinician who only looked at the low calculated GLS would get the idea that the entire left ventricle has poor function. GLS alone is an imperfect number.

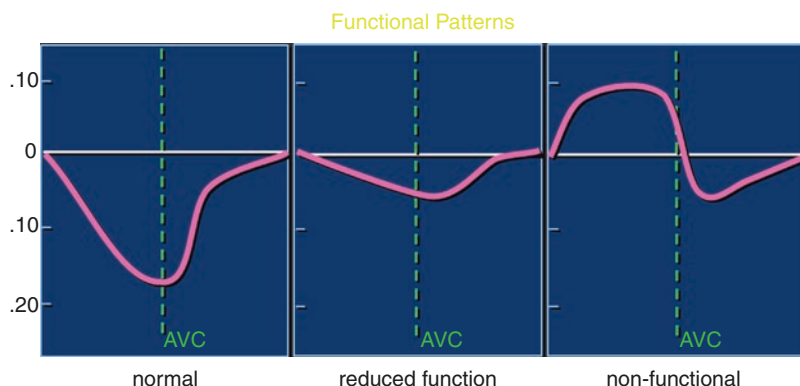


Fig. 35.3 Three major functional patterns schematically drawn. Hypocontractile segmental strain values are reduced, with values considerably below normal (closer to zero). Non-functional segments have no contraction or

demonstrate a holosystolic bulge during systole). Non-functional segments may be due to scar, ischemia or other reason why segments do not contract. Other patterns may exist, but beginners are urged to look for these patterns

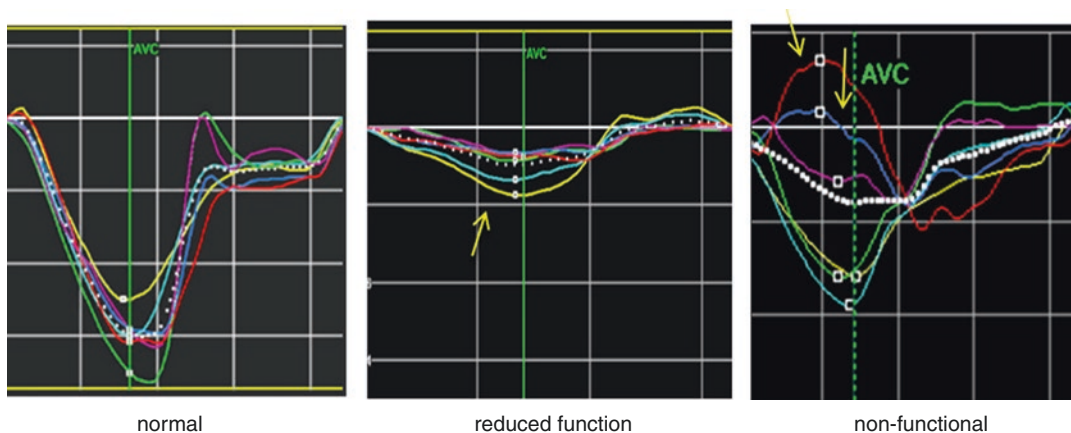


Fig. 35.4 Examples of patients with functional abnormalities, each with strain curves taken from the apical four chamber view. Contrast these strain curves with the normal patients. The patient in the left panel shows markedly reduced strain curves (near zero) with a global longitudinal strain of -3.8% . Walls are, however, timed rather uniformly (arrow). The patient has a diffuse cardiomyopa-

thy. The patient in the right panel shows marked holosystolic bulging (arrow) of the red and blue walls, which are the apical and mid-lateral walls. The GLS is about -9% . And is reduced. This patient has a transmural infarction in the area of the holosystolic bulging. Note the walls opposite the infarct are normal

The three view strain set in Fig. 35.5 is from a patient with mitral insufficiency. The strain curves in the left hand panels (apical four and three chamber views are normal) loosely resemble each other in amplitude and timing. The upper right panel is from the apical two chamber view and shows bulging red walls in the red, blue and purple curves with early systolic stretching (called pre contraction stretch or pre-stretch) and two of the curves (red and blue) have late peak-

ing after AVC. This pattern is abnormal, but only in the two-chamber view. This pattern comes close to a classic dyssynchronous pattern (see later pattern descriptions) but does not fulfill all criteria. For now, it is important to just recognize it as abnormal. When all walls bulge in early systole as noted in the lower left panel, this is normal and excused as due to isovolumic contraction.

Contrast the generally normal patterns in Fig. 35.5 with the strain curves from a patient

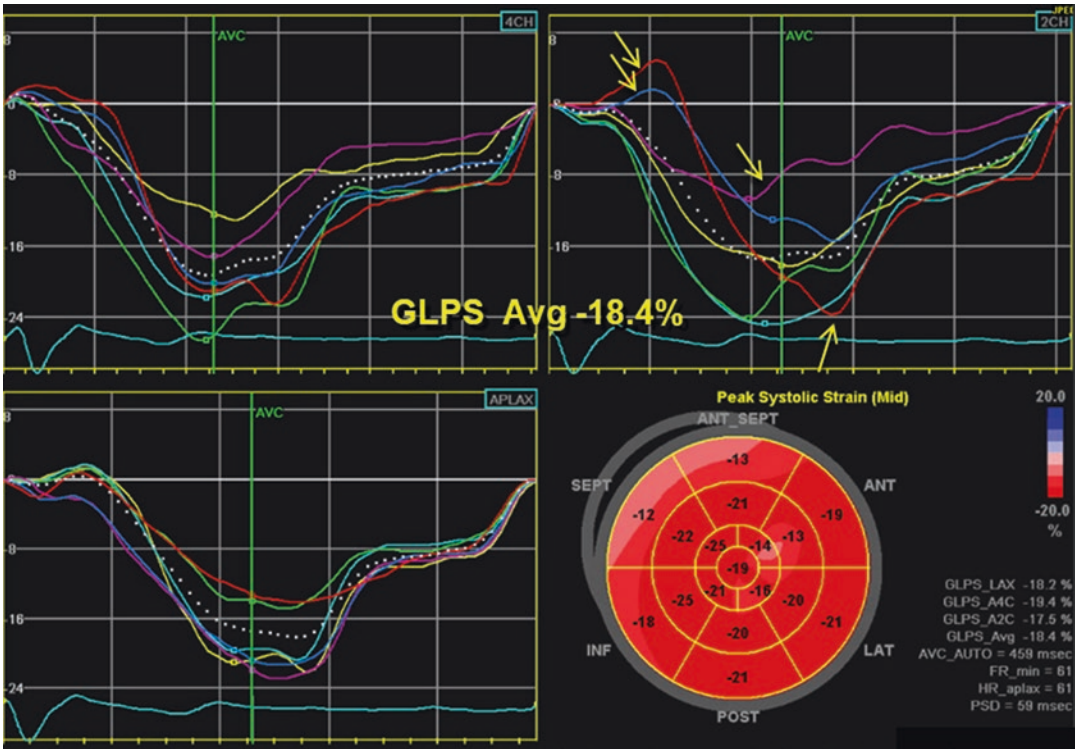


Fig. 35.5 The three view strain set is from a patient with mitral insufficiency. The strain curves in the left hand panels (apical four and three chamber views are normal) loosely resemble each other in amplitude and timing. The upper right panel is from the apical two chamber view and shows bulging red walls in the red, blue and purple curves

with early systolic stretching (called pre contraction stretch or pre-stretch), and two of the curves (red and blue) have late peaking after AVC. This pattern is abnormal, but only in the two-chamber view. This pattern comes close to a classic dyssynchronous pattern (see later pattern descriptions) but does not fulfill all criteria

with a diffuse ischemic cardiomyopathy seen in Fig. 35.6. The GLS is reduced. Note the individual view GLS values in the lower right corner. The apical four chamber curves (upper left) have uniform reduced function. The curves in the lower left (apical three chamber view) show a peculiar criss-crossing pattern (arrow) that cancel each other mathematically and render a view GLS of zero (dashed arrow lower right). GLS is just mathematics, and strange results like this can occur. One normally contracting segment is seen preserved in the yellow curve (basal lateral inferior wall in this two-chamber view). The darker red segments in the lower right reflect this normal contraction. Mixed patterns are possible.

Figure 35.7 shows parasternal long axis and apical four-chamber views from a patient with diffuse dilatation of the LV and an apical thrombus originally thought to be a non-ischemic

cardiomyopathy with thrombus. The arrow refers to the myocardial segment referred to in Fig. 35.9.

The schematic demonstrating the six wall segments of the apical four-chamber view show the colors attributed to each wall in this analytic system (Fig. 35.8). This serves as a reminder of the importance of knowing the color coding system for each analysis software. When manufacturers provide the option to use this color scheme it is most helpful to interpreters. Two of the three major ultrasound manufacturers have this option. The colors originate from a very early machine that had the ability to analyze strains. Thusly, this is a legacy color coding system.

The strain set in Fig. 35.9 is from the same patient shown in Fig. 35.7, and shows diffuse hypocontractility except for a localized non-functional segment in the posterior wall (arrow, apical long axis) representing a localized myocar-

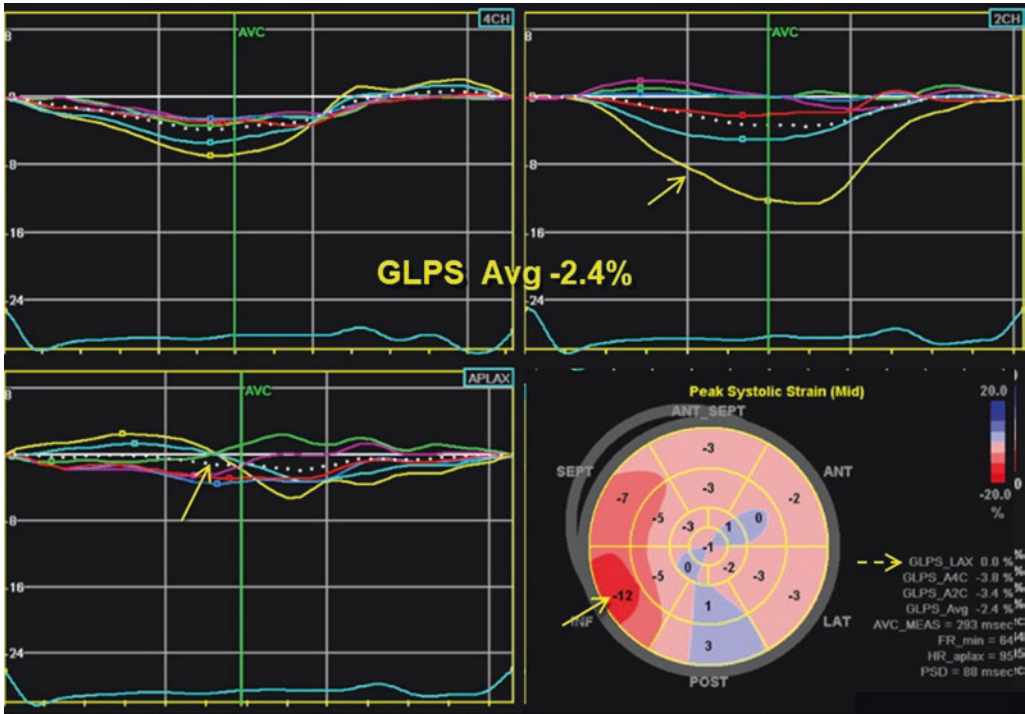


Fig. 35.6 The GLS is reduced in this strain set from a patient with a diffuse ischemic cardiomyopathy. Note the individual view GLS values in the lower right corner. The apical four chamber curves (upper left) have uniform reduced function. The curves in the lower left (apical three chamber view) show a peculiar criss-crossing pattern (arrow) that cancel each other mathematically and render

a view GLS of zero (dashed arrow lower right). GLS is just mathematics and strange results like this can occur. One normally contracting segment is seen preserved in the yellow curve (basal lateral inferior wall in this two-chamber view). The darker red segments in the lower right reflect this normal contraction. Mixed patterns are possible

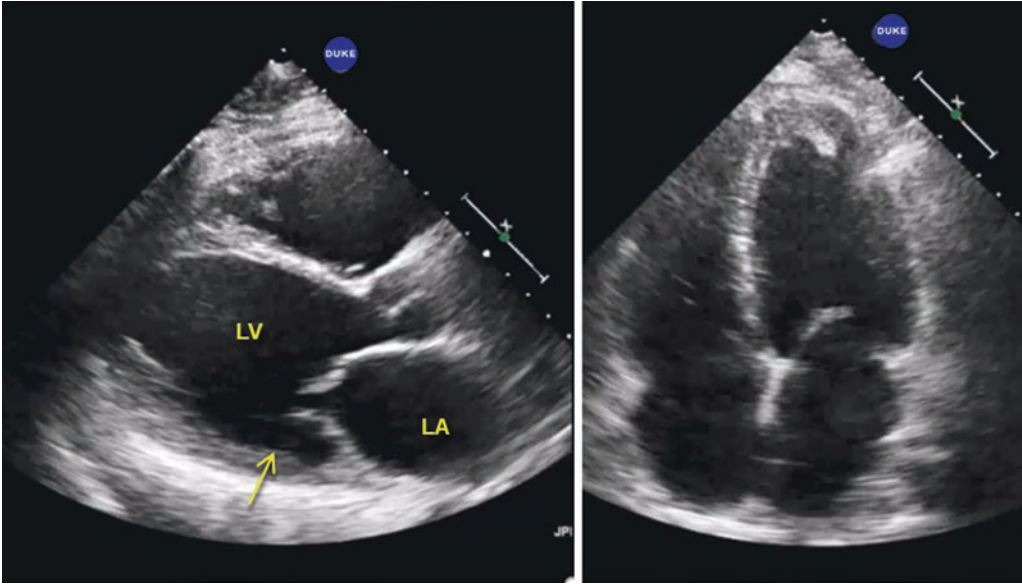


Fig. 35.7 Parasternal long axis and apical four-chamber views from a patient with diffuse dilatation of the LV and an apical thrombus originally thought to be a non-isch-

emic cardiomyopathy with thrombus. The arrow refers to the myocardial segment referred to in Fig. 35.9

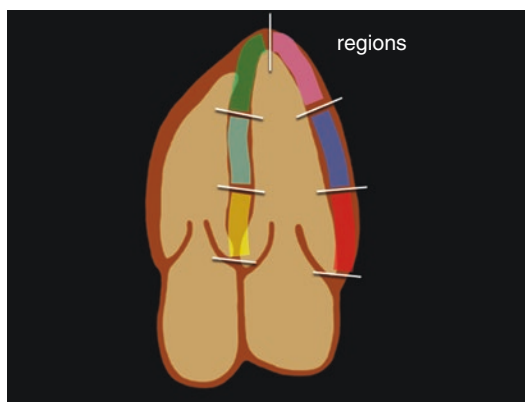


Fig. 35.8 Schematic diagram showing the apical four chamber view divided up into six segments and colors applied to each segment. Yellow = basal septum; cyan = mid-septum; green = distal septum; purple = distal lateral wall; blue = mid-lateral wall and red = basal lateral wall. These color segments correspond to the strain lines. Unfortunately, not all manufacturers adhere to the same color display convention. Strain calculations result from measurements taken from many speckles with a segment and which are averaged to produce an average strain for that segment. The global strain is an average of the average of all six segments for any view and then, again, averaged for all three apical views

dial infarction. Note the holosystolic bulging (yellow curve, arrow) in the apical long axis which corresponds to the positive strains (blue patch) seen in the target display (lower right, arrow) as well as the arrow in Fig. 35.5. Contrast this set of strains with the set in the normal in Fig. 35.5.

Other Functional Patterns

Amyloidosis, rather characteristically, shows diffuse hypocontractility except for the apex. Figure 35.10 shows apical four and two chamber views from a patient with amyloidosis and subjective overall ventricular hypocontractility. The strains from this patient are shown in the next figure.

Figure 35.11 is the composite of the strains from the three apical views of the patient with amyloidosis in the previous figure. The strains show the characteristic hypocontractility of all the segments with an unusual preservation of the apical segments (arrows). This apical preservation is a special finding in patients with amyloid

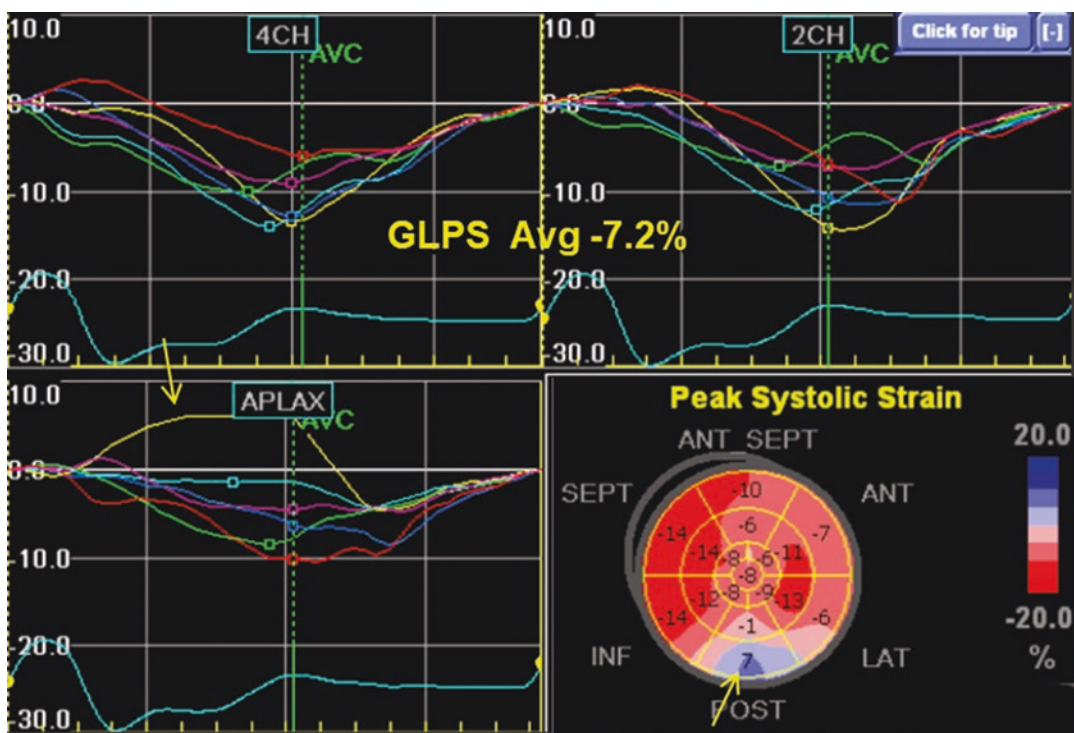


Fig. 35.9 Strains from three apical view is from a patient with a localized posterior wall infarction. Note the bulging (yellow curve, arrow) in the apical long axis which

corresponds to the positive strains (blue patch) seen in the target display (lower right, arrow). Contrast this set of strains with the set in the normal in Fig. 35.5

Fig. 35.10 Apical four and two chamber views from a patient with amyloidosis and subjective overall ventricular hypocontractility. The strains from this patient are shown in the next Figure

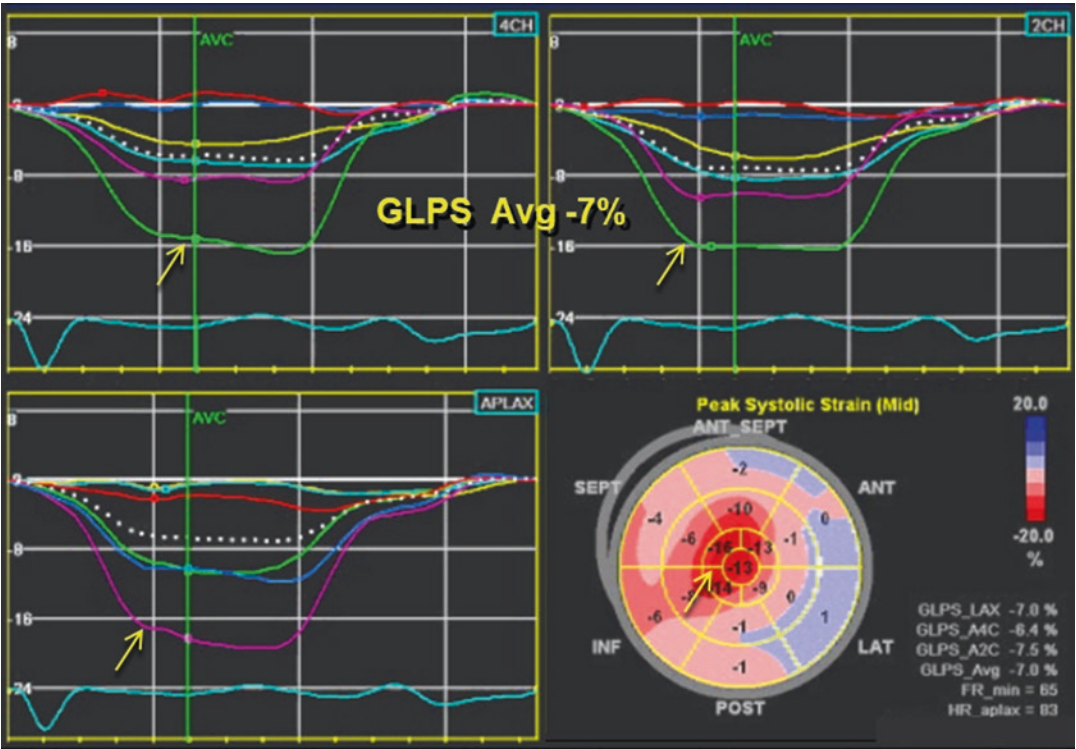
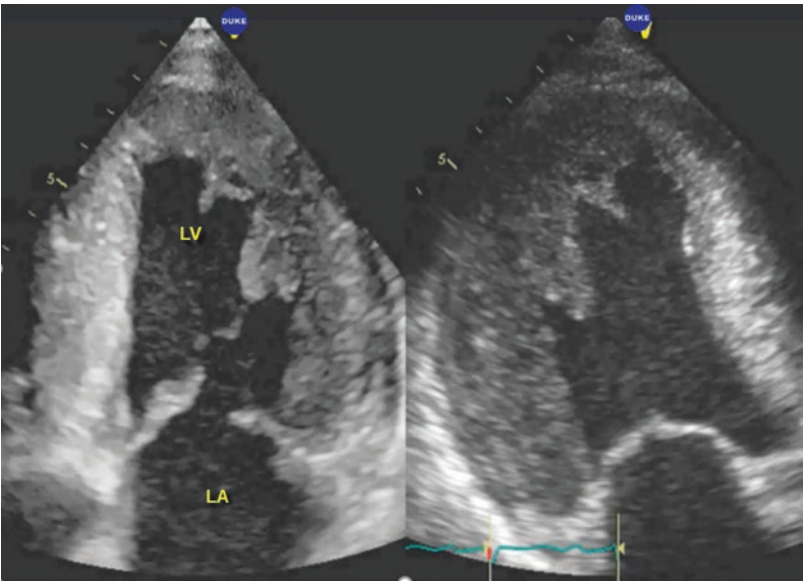


Fig. 35.11 This composite of the strains from the three apical views of the patient in the previous figure with amyloidosis. The strains show the characteristic hypocontractility of all the segments with an unusual preservation of

the apex (arrows). This apical preservation is a special finding in patients with amyloid heart disease. Not the red in the middle of the target display. The GLS is -7%

heart disease. Note the red in the middle of the target display. The GLS is -7% .

Other disorders such as Chagas Disease can manifest a host of regional patterns from normal

to reduced function to non-functional. Due to the common presence of left bundle branch block or right bundle branch block with left anterior fascicular block, abnormal timing patterns are also

possible. Interpretation of specific patterns in Chagas Disease presents a daunting regional interpretive task. Common experience in the Duke Echo laboratory with Chagasic patients indicates that characteristic patterns will, in time, be described.

Timing Patterns

Abnormal timing patterns generally reflect abnormalities in the electrical conducting system. When a heart beats, electrical excitation precedes mechanical contraction. Cardiac electrical activity has been the purview of electrophysiologists while mechanical activity has been the purview of echocardiographers and other cardiac imaging specialists. It is no secret that neither of these subspecialties of cardiology knows much about the fund of knowledge of the other except for basic generalities. This section on timing abnormalities also serves as a primer of the anatomy of the conducting system as well as an introduction to the physiologic relationships between electrical and mechanical activity of the heart. This information is important in order to understand the mechanical physiology of left bundle branch block (LBBB), the most common of the conduction timing abnormalities encountered.

Further, this section is about electrical activation and contraction coupling, and is not about measurements of timing (example, time to peak), nor calculation of peak strain values. Rather, it is about learning functional relationships and interdependencies between electrical and mechanical activities. This section on LBBB mechanical physiology is not meant to reprise, nor contradict anything else in this volume.

LBBB and Dyssynchrony, an Example of Timing Abnormalities

A third of patients who receive a cardiac resynchronization (CRT)-device for heart failure due to LBBB fail to respond, emphasizing the need for further improvement of current selection cri-

teria. Although response to CRT is multifactorial, correction of mechanical dyssynchrony induced by LBBB has a key role. Echocardiography is the most commonly applied technique to assess mechanical dyssynchrony prior to CRT and several studies have documented its value in prediction of response. Others have argued that certain echo methods are too difficult to perform, and need further refinement in order to be of use in routine clinical practice.

Current criteria for placement of a CRT device is primarily placed on the presence of symptoms of Class II (or greater) heart failure, low ejection fraction, and LBBB QRS-morphology with a QRS duration of greater than 140 ms (normal ~80 ms). Many more patients have LBBB than become symptomatic enough to qualify for CRT intervention attesting to the fact that cardiac performance is varied in these patients.

CRT is a therapy that alters mechanical timing relationships. Because so many LBBB patients exist without need for CRT, it is most likely that there are many who do not have significantly altered mechanical impairment. Further, mechanical dyssynchrony due to true abnormal activation like LBBB is different from mechanical dyssynchrony because of heterogeneities in contraction that results from LVH, scar, or other reasons that increase cardiac size. The larger the heart the longer it takes for the electricity to travel through the myocardium.

It may be that many of the echo techniques and indices applied to date do not reliably reflect the underlying mechanical activation delay likely necessary for CRT to be effective. For example, although a time-to-peak delay may reflect abnormal electrical activation it can also represent heterogeneity in contraction force and duration. Thus, there is a continuing need to understand the mechanisms of dyssynchrony and improve on methods to identify dyssynchrony amenable to CRT. If we understand the physiology of LBBB we could potentially understand which LBBB patients should be paced so that symptoms never occur or even understand which other regional heterogeneities (but without LBBB) are amenable to new therapies.

The Anatomy of the Specialized Conducting System

Figure 35.12 shows a schematic diagram of the cardiac electrical conduction system (yellow lines) superimposed on a pathologic section of an actual heart in an attempt to simulate the major pathways of electrical conduction through the ventricles. These relevant pathways begin at the large yellow oval which represents the atrioventricular (AV node). The AV node is located just above the tricuspid valve in the posterior right atrial wall in the center of the Triangle of Koch (Triangle of Koch not pictured). From there the electrical pathway emerges in a common bundle (the Bundle of HIS) whereupon it splits into two, one being the right bundle and the other being the left bundle. Readers are referred to any standard textbook of cardiac anatomy or electrocardiography for details.

The right bundle runs superficially down the subepicardial regions of the septal surface of the interventricular septum, and then its fibers spread across the septo-marginal trabeculation (also known as the moderator band) to the anterior portions of the right ventricle. Some fibers run

down to the RV apex before fanning out to portions of the anterior right ventricular wall.

After the right bundle splits from the HIS bundle, the left bundle goes through the membranous septum emerging just on the subendocardial surface of the left side of the interventricular septum, very close to the aortic valve leaflets and splits into two, one being the anterior fascicle, and the other being the posterior fascicle. In this schematic overlay, the anterior fascicle (long yellow line) traverses toward the base of the antero-lateral papillary. The inferior fascicle dives posteriorly toward the base of the infero-medial papillary (not seen in this illustration as it is behind the antero-lateral papillary).

Figure 35.13 shows a fixed pathologic specimen of another human heart where the subendocardial common left bundle emerges from the membranous septum splits into the anterior and posterior fascicles, seen as two lighter than wide linear streaks in this specimen. The infero-medial papillary muscle is pictured.

Occasionally, the left bundle splits into three fascicles, anterior, middle and inferior. Figure 35.14 is an opened fresh porcine heart to

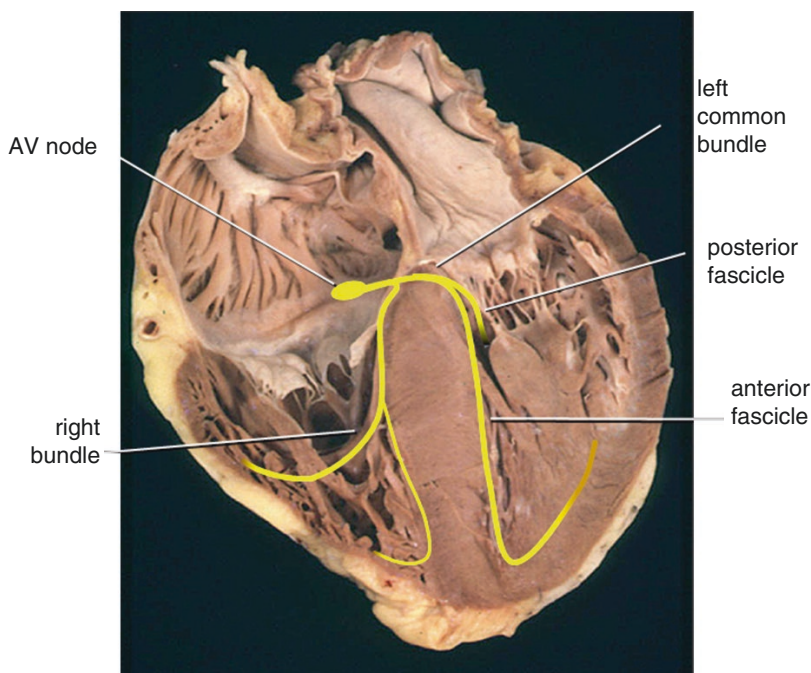


Fig. 35.12 Schematic diagram of the conducting system from the atrioventricular node into left and right bundles to the myocardium. For details see text. *Photograph courtesy of R.H. Anderson, MD*

Fig. 35.13 Anatomic section of the left ventricle showing the membranous septum, and the left common bundle bifurcating into the anterior and posterior fascicles. The fascicles are insulated at this level. *Photograph courtesy of R.H. Anderson, MD*

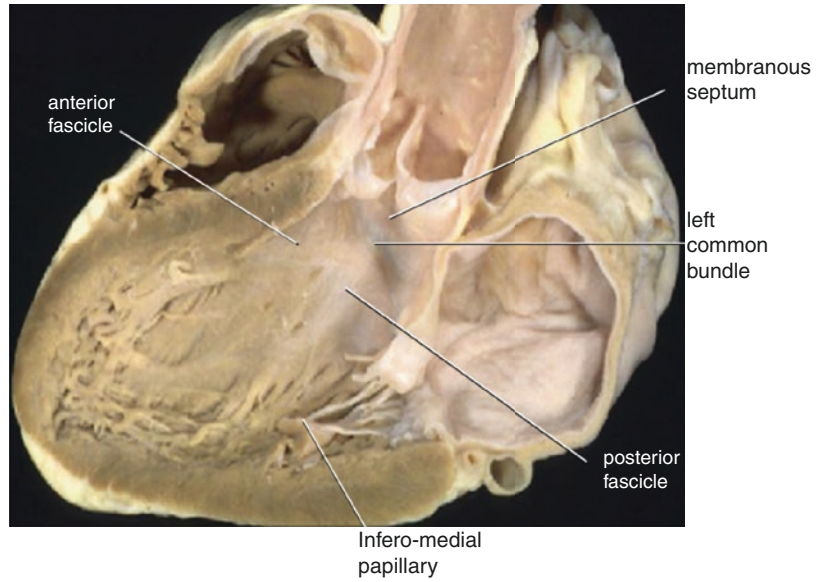
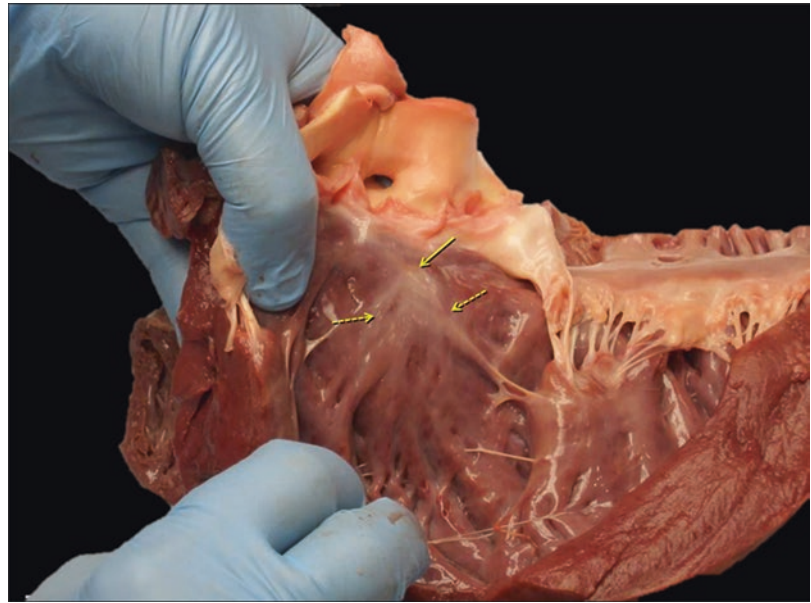


Fig. 35.14 Opened fresh porcine heart to view the wide left bundle that splits into two fascicles, anterior and posterior (arrows) with the anterior fascicle giving off a third, middle fascicle just after the bifurcation of the left bundle



view the wide left bundle that splits into two fascicles, anterior and posterior (arrows) with the anterior fascicle giving off a third, middle fascicle just after the bifurcation of the left bundle.

Figure 35.15 is a three-dimensional echo showing the same anatomy of the left ventricle. The membranous septum is seen just under the aortic valve, in the aortic interleaflet triangle between the right and non-coronary leaflets. By

three-dimensional echo, the membranous septum invariably appears as a hole in the septum rather than as a membrane, most likely due to ultrasound drop-out.

The Sequence of Electrical Activation-Contraction Coupling

The sequence of electrical activation and contraction (and activation-contraction coupling) is

important for understanding timing patterns. Figure 35.16 is a diagrammatic representation of the electrical cascade from the sino-atrial node (SA) to the point of muscle contraction. The proximal ventricular conducting system then leads distally to thin filaments known as Purkinje fibers. These Purkinje fibers then distribute the electrical impulses to the ventricular muscle where they ultimately jump from myocardial cell to cell in the final distribution sequence.

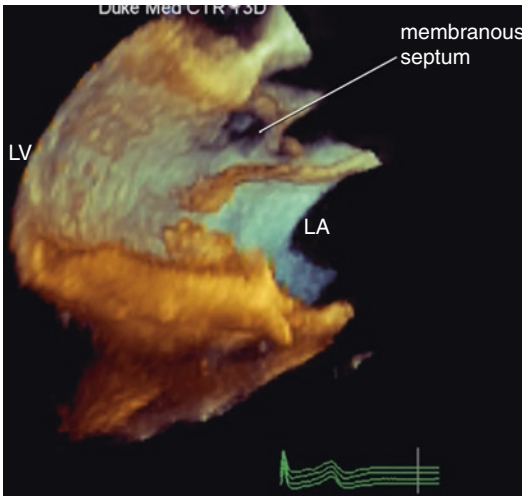
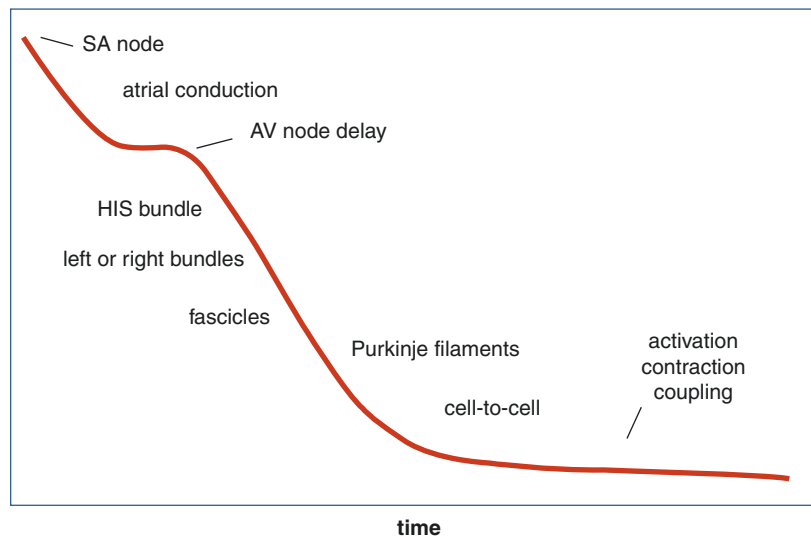


Fig. 35.15 Three-dimensional echo in the same orientation as the anatomic specimens as Figs. 35.13 and 35.14

Even though this electrical system has proximal pathways, the left ventricle first contracts distally because the proximal specialized conducting system is insulated in the main bundles, not allowing electricity to escape until about two-thirds of the way down the ventricular septum. If the insulation was not present, the ventricular muscle would contract proximally first, forcing blood in two directions, both towards the ventricular apex and out the aorta, which, of course, does not happen. If no insulation was present, then early proximal septal contraction would also lead to potential ventricular outflow obstruction.

Emerging from the insulated pathways distally, the first areas to contract in the left ventricle are near the bases of the papillary muscles and in the right ventricle on the anterior free wall near the termination of the septal-marginal trabeculation. In a normal adult, this transit of electricity from the AV node all the way around to the most distal portions of the ventricle takes about 60–90 m (the normal width of the QRS complex on ECG). The electrical signal first moves very quickly through the proximal (insulated) portions of the specialized conducting system. As the electricity is distributed onwards into the Purkinje fibers it begins to slow. When finally jumping from myocardial cell-to-cell in the distal stages of the conduction system, the electricity slows until it reaches all portions of the ventricular

Fig. 35.16 Diagrammatic representation of the cascade of electrical activity from SA node to muscle and activation-contraction coupling. The more steep the slope, the faster the conduction speed. Cell-to-cell conduction is slow



myocardium. Muscle cells near the proximal, well insulated, specialized conducting system do finally receive the electrical signals, but do so in a retrograde fashion, cell-to-cell, from the distal exit points.

In this context, the distribution of electricity can be roughly compared to the common example we all experience with automobile traffic. When travelling along a super highway, traffic can move very fast but cannot exit except on designated off-ramps. When exiting the off ramps, traffic begins to slow. Then it slows even more when traffic enters city streets and travels block to block.

When the electricity finally arrives, myocardial cells then contract, providing that there are no problems with the contracting mechanism. This point is known as the electrical activation-contraction coupling point for the purposes of this discussion. Obviously, as noted in the previous chapter, there could be reduced contraction or non-function (due to fibrosis/ischemia/other reason).

Timing Patterns

Types of Timing Patterns

There are two major timing patterns of note beyond normal that are schematically drawn in Fig. 35.17. The heterogeneous pattern is when none of the peak strains come close to systolic peaking at the same time (middle panel, Fig. 35.17). The peaks are widely dispersed. This type of pattern is commonly seen in patients with

dilated cardiomyopathy and invariably reveals a diffuse reduction of segmental peak strain values below -10% .

The second pattern is the classic pattern. It is classic for LBBB because it follows the contraction sequence seen in LBBB (right panel, Fig. 35.17). Here the basal septum is drawn in yellow and the basal lateral wall is drawn in red, the color convention in this chapter (apical four-chamber view). Following the physiologic progression of the electrical signal in LBBB and subsequent contraction, the classic pattern reveals the septum to contract first (as it receives the electrical signal without impedance). Given the LBBB, it takes considerably longer for the electrical signal to get to the lateral wall. The electrical signal arrives late at the lateral wall because the activating signal jumps slowly cell to cell as the left bundle, fascicles and left sided Purkinje fibers are blocked so the red wall stretches. When the lateral (red tracing) finally contracts it terminates septal contraction and then peaks after AVC. This results in the classic appearance of early opposing septal contraction and lateral bulging, followed by lateral contraction and termination of septal contraction with the lateral wall peaking after AVC. Note the obvious criss-cross of the yellow (septal) and red (lateral) strain curves.

Figure 35.18 shows actual strain curves from a patient with a predominantly heterogeneous pattern (left panel) and another with an obvious classic LBBB pattern (right panel). The yellow arrow points to the early (normal) septal contraction while the blue arrow points to the reciprocal stretching (or bulging) of the opposing

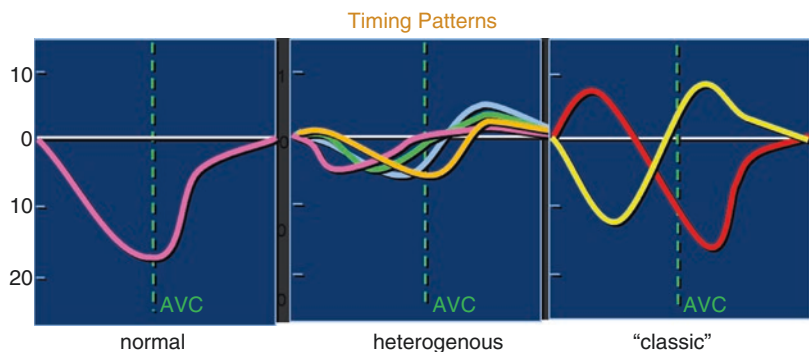


Fig. 35.17 Diagrammatic representation of three major timing patterns. For details see text

Timing Patterns

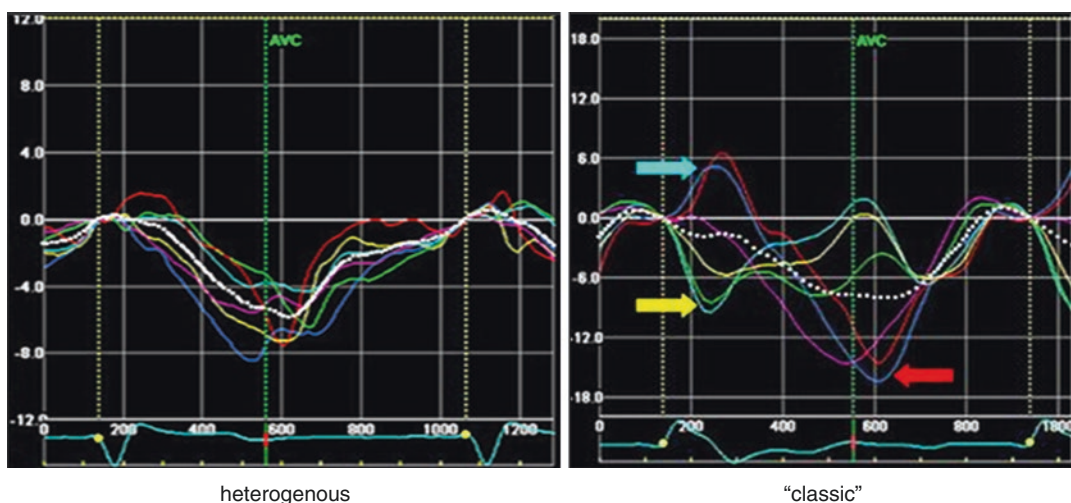


Fig. 35.18 Two major abnormal regional timing patterns. Note the ECG at the bottom of the panels. Analysis was begun with a zero point of timing (ECG yellow dot) at the beginning of the QRS. The left panel shows the heterogeneous pattern, frequently found in patients with dilated cardiomyopathy. Note that peak contraction is dispersed and peak strains are reduced (towards zero) at about -5% . All walls are a contractile jumble of peaks. Even if CRT is instituted, clinical improvement is unlikely. The right panel shows the classic pattern of treatable left

bundle branch block. The classic pattern consists of opposing wall motions. Note the septum (yellow and green lines) contract in early systole (yellow arrow) while the opposite lateral wall (red and blue lines) bulges (blue arrow). When the lateral wall finally receives the electrical signal, the lateral wall then contracts, peaking after aortic valve closure (red arrow). Recognizing the classic pattern requires opposing wall motions followed by late contraction of the early bulging segments

lateral wall. When the lateral walls finally receive the electrical signal, they contract quite forcefully, terminating septal contraction and then peaking late (red arrow).

Thus, the appearance is of two opposing walls (or sets of walls) going in opposite directions. The septum contracts and the lateral wall bulges. The lateral wall is dependent on cell-to-cell pathway for the command electrical signal to arrive, and it begins its contraction late. Since the free lateral wall is such a great mass, when it finally does contract, its contraction overwhelms the septum and seemingly terminates septal contraction. This stretching is also called “pre-stretch”. In LBBB this pattern is most commonly seen in the apical four-chamber view.

The apical strain set in Fig. 35.19 shows a heterogeneous pattern in the upper left panel (apical four-chamber view). Other views are mostly heterogeneous. Only walls with the strict criteria for the classic pattern are referred to as having the

classic pattern. If criteria are partially fulfilled, they can be called heterogeneous. For purposes of this discussion, if strain curves do not fit any given major pattern, they could be classified as “other”.

Figure 35.20 details a schematic diagram of a classic pattern and further identifies three components of the pattern used in defining the strict criteria for the classic pattern, thought to comprise true LBBB. These include: (1) early contraction of at least one basal or mid-ventricular segment in the septal or antero-septal wall, and early stretching in at least one basal or mid-ventricular segment in the opposing wall, (2) the early peak contraction that occurred in the first 70% of the systolic ejection phase, and (3) the early stretching wall showed peak contraction after AVC (holosystolic stretching segments do not fulfill the criteria). All three criteria are required to be deemed classical.

A classical pattern pre-CRT is shown in Fig. 35.21 (left panel) and one day after CRT (right

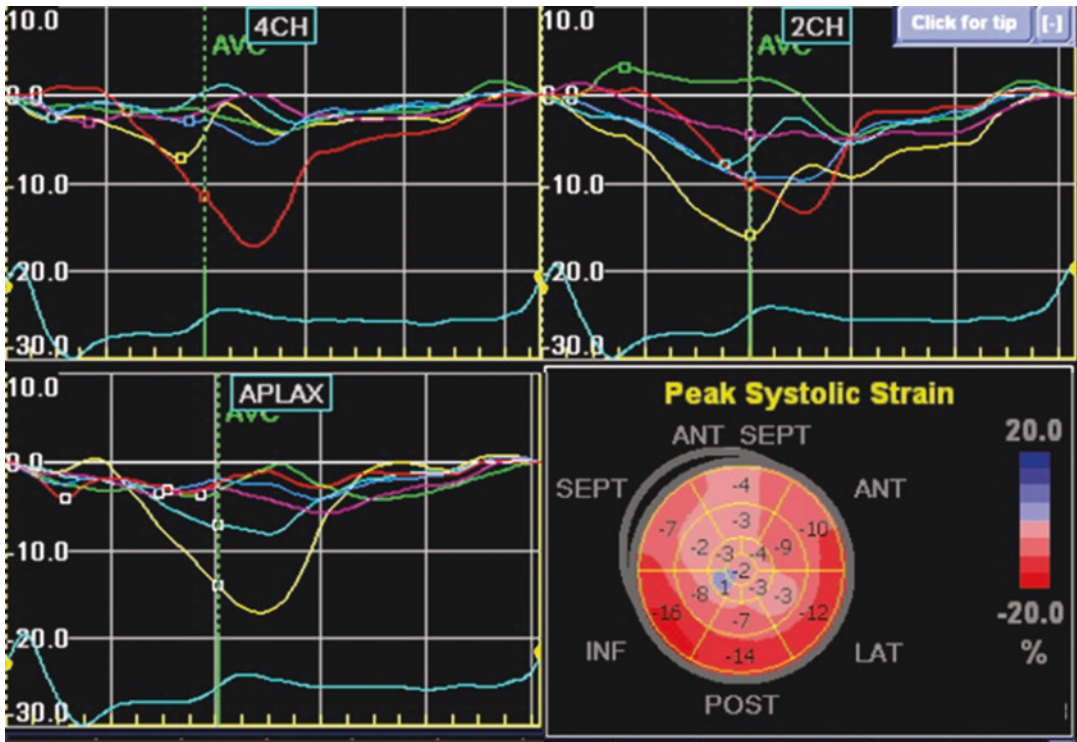


Fig. 35.19 A heterogeneous pattern in the upper left panel (apical four-chamber view) from a patient with heart failure. Other views are mostly heterogeneous. Only walls

with the strict criteria for the classic pattern are referred to as having the classic pattern. If criteria are partially fulfilled, they can be called heterogeneous or “other”

panel) where the opposing wall contractile patterns are neutralized. The presence of a classical pattern is 95% sensitive and 91% specific for response as tested in a single and multicenter experience and far exceeds the predictive ability of time-to-peak methods. Response, of course, is not determined by resolution of the classical strain pattern, but rather is defined as a reduction in LV end systolic volume of $\geq 15\%$ at 6 months. Symptomatic improvement occurs in 75% of patients treated with CRT who have the classic pattern.

Time-to-peak parameters can be seen in patients with the heterogeneous pattern. Time-to-peak approaches are conceptually limited by reflecting global changes in myocardial function without providing information of the nature of wall deformation throughout the heart cycle. Significant time-to peak delays can be caused by delays in activation but can also be due to regional variations in contractile force and duration, in which case the role for CRT is not clear. The results of studies into the classical pattern suggest that patients with mechanical delays due to heterogeneities in contractile properties, in the

absence of a classical pattern, are unlikely to respond. In fact, they rarely do.

The utility of the classic pattern is shown in Figs. 35.22 and 35.23. Figure 35.22 demonstrates Kaplan–Meier curves showing freedom from death, LVAD or heart transplant after CRT in relation to the presence of a LBBB contraction pattern assessed by 2D strain echocardiography. Figure 35.23 demonstrates Kaplan–Meier curves showing freedom from death, LVAD or heart transplant after CRT. Patients were subdivided by baseline QRS duration and the presence of LBBB contraction pattern. It appears that the presence of a classic pattern CRT has importance over QRS duration alone in predicting outcome.

In the presence of a classical pattern, waiting too long prior to CRT sometimes does not produce a favorable response. Figure 35.24 shows strain in the apical four-chamber view in a 47 year old male who, despite having a classic pattern (arrows) for well over 8 years did not receive CRT. Over that period of time, he was lost to follow-up at an outside institution but then returned with a much more dilated and hypocontractile left

ventricle in late Class III congestive heart failure. Listed for heart transplantation, a CRT was placed as a last measure without response. He was successfully transplanted.

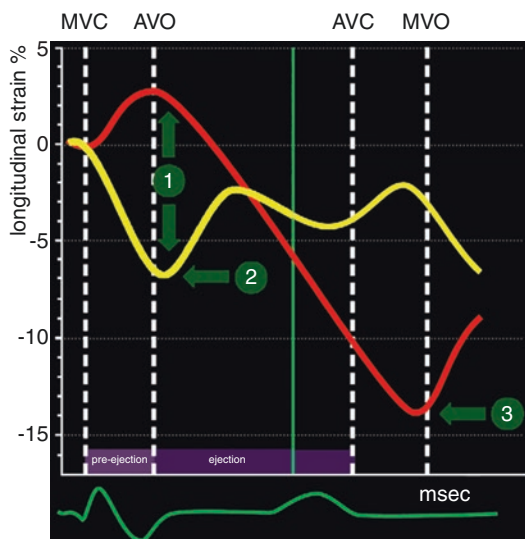


Fig. 35.20 All three criteria must be fulfilled: (1): Early contraction of at least one basal or mid-ventricular segment in the septal or antero-septal wall (green curve) and early stretching in at least 1 basal or mid-ventricular segment in the opposing wall (dark blue curve), (2) Early peak contraction does not exceed 70% of the ejection phase (red vertical line). In case of double peaks the first peak is considered and (3) The early stretching wall shows peak contraction after AVC. AVC aortic valve closure, AVO aortic valve opening, MVC mitral valve closure, MVO mitral valve opening. Reprinted with permission from Risum et al. [4]

Remember not all early segmental bulging is the classic pattern. Figure 35.25 shows apical four chamber strains from a normal individual. Note the early bulging of many segments compatible with isovolumic contraction. No late peaking segments are noted. Bulging from isovolumic contraction is common and should not be confused with the bulging of the classical pattern.

Regional Strain Pattern Correlations to ECG

If LBBB is the culprit in activation delay-induced heart failure, then a more specific electrical activation pattern should be present by ECG, and the typical mechanical pattern should be detectable by echo in the same patient. In fact, some correlations between strain and the 12 lead ECG do exist and provide a preliminary view of specifically defined electrophysiologic and echocardiographic determined activation-mechanical relationships.

LBBB by Strict ECG Criteria

The classic criteria for correctable mechanical dyssynchrony are described earlier in this chapter. It is important to note that there are also relatively new 12 ECG criteria for LBBB. These strict criteria for LBBB are defined as QRS duration

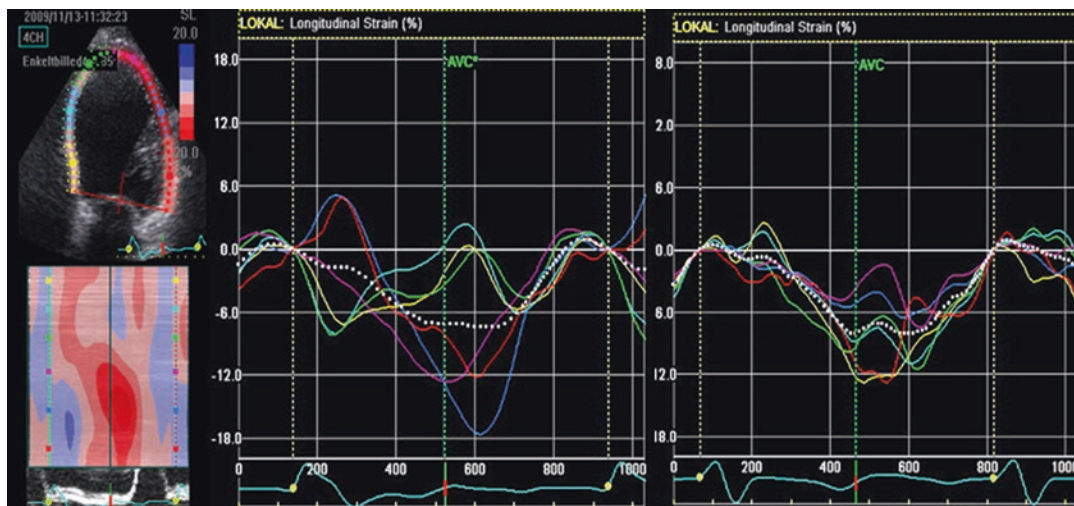


Fig. 35.21 Pre and post CRT apical four chamber strains from a patient with LBBB. The panel on the left shows a classical pattern that was not seen after CRT

Fig. 35.22 Kaplan–Meier curves showing freedom from death, LVAD or heart transplant after CRT in relation to the presence of a LBBB contraction pattern assessed by 2D strain echocardiography. Reprinted with permission from Risum et al. [4]

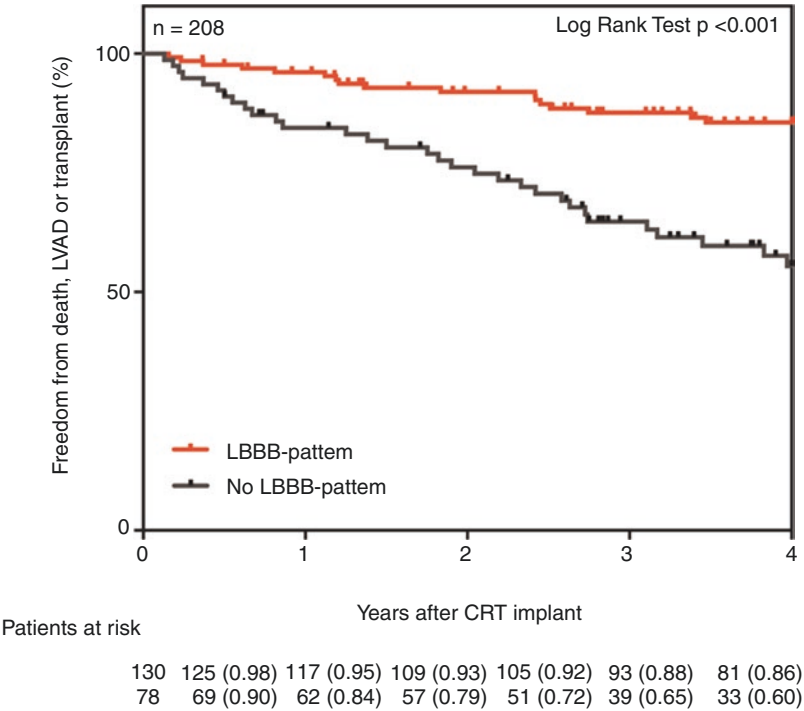
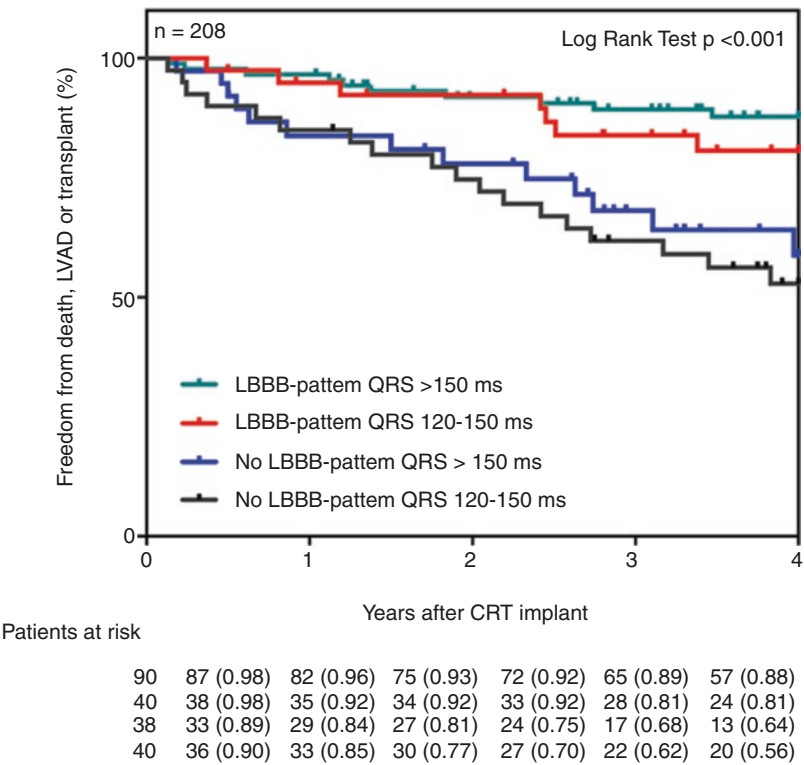


Fig. 35.23 Kaplan–Meier curves showing freedom from death, LVAD or heart transplant after CRT. Patients were subdivided by baseline QRS duration and the presence of LBBB contraction pattern. Reprinted with permission from Risum et al. [4]



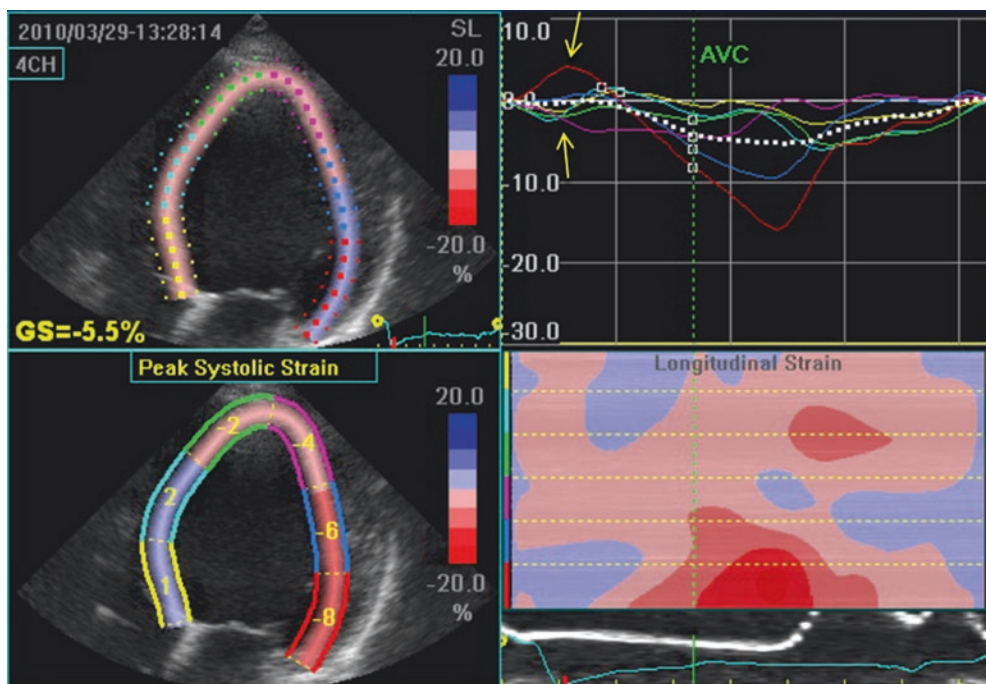


Fig. 35.24 Strains in the apical four-chamber view in a 47 year old male who, despite having a classic pattern (arrows) for well over 8 years, did not receive CRT. Over that period of time, he was lost to follow-up returned with

a much more dilated and hypocontractile left ventricle in late Class III congestive heart failure. Listed for heart transplantation, a CRT was placed as a last measure without response. He was successfully transplanted

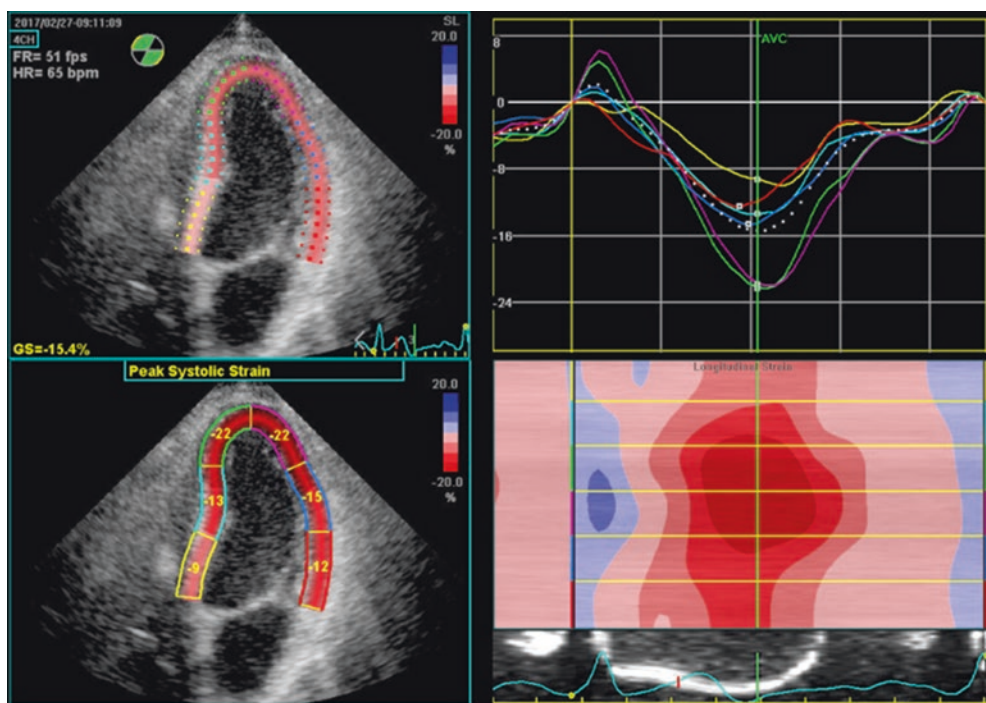
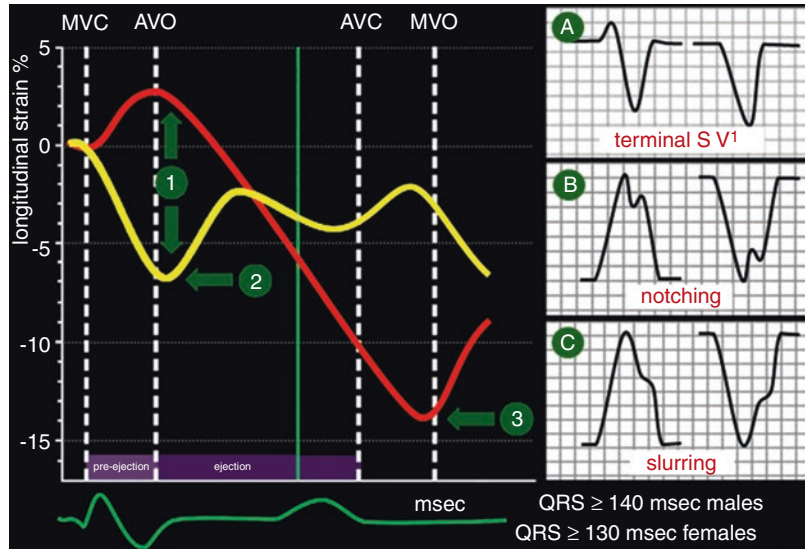


Fig. 35.25 Apical four chamber strains from a normal individual. Note the early bulging of many segments compatible with isovolumic contraction. No late peaking seg-

ments are noted. Bulging from isovolumic contraction is common and should not be confused with the bulging of the classical pattern

Fig. 35.26 Reprise of the strain criteria for strict LBBB and summary of the strict criteria for ECG. Reprinted with permission from Risum et al. [3]



≥ 140 ms (men) or ≥ 130 ms (women) and QS or RS in leads V_1 and V_2 , and mid-QRS slurring or notching in ≥ 2 contiguous leads of V_1 , V_2 , V_5 , V_6 , I and a VL. Figure 35.26 Reprises the classic pattern of LBBB by strain along with a summary of the strict criteria for ECG determined LBBB.

Figure 35.27 shows apical four chamber strains in two patients with strict criteria LBBB by ECG but different contraction patterns. Upper panel: A characteristic LBBB opposing classic strain pattern is seen including (1) early peak contraction in the septal wall with (yellow arrow), (2) early pre-stretch in the lateral wall (blue arrow), (3) late lateral peak contraction (red arrow). Lower panel B: Segments show a synchronous contraction timed at aortic valve closure (blue arrow) despite the widened QRS by ECG. The strain curves are enhanced for purposes of clarity. While correlations are not perfect, there is a very strong correlation of strict criteria for LBBB by ECG, and strict criteria for classical strain pattern of LBBB.

Interpretation of Regional Strains

There is enough substrate in this chapter to provide a reasonable basis for beginning to interpret regional strain patterns. This chapter, together with the chapter on global strain and the chapter on strain in congenital heart disease provides of trilogy for understanding the basics of strain. These supply a modestly experienced echo person with the tools to pick out certain basic patterns and have a vision of the use of strain In clinical practice. Strain has taken a considerably journey since the days of Rushmer and Franklin. It is most likely that echo based strain techniques will also be combined with pressure to provide even more information about cardiac function.

By looking at patterns, one begins to construct an idea of how the ventricle contracts in three dimensions. The “new” strain has arrived and, even without numbers, is finding its role in patient care.

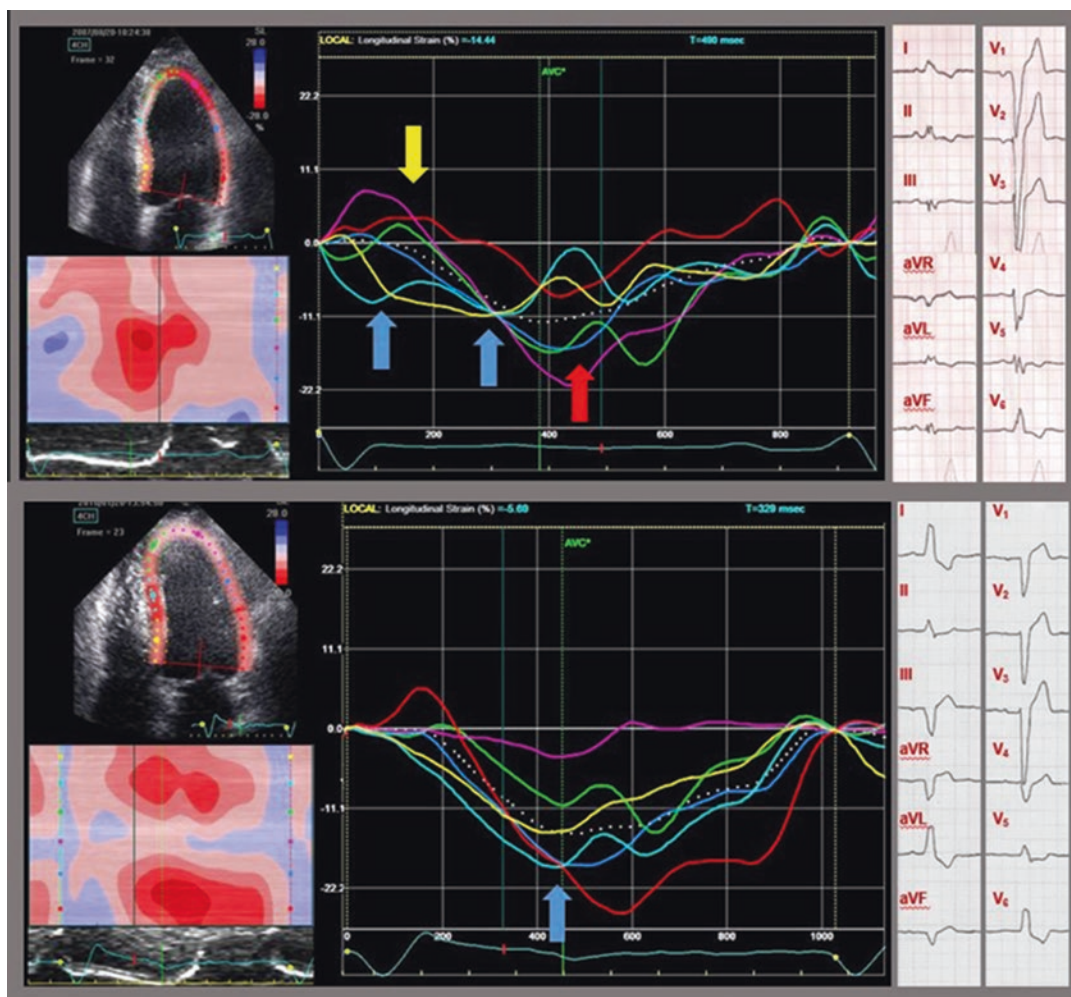


Fig. 35.27 Apical four chamber strains in two patients with strict criteria LBBB by ECG but different contraction patterns. Upper panel: A characteristic LBBB opposing classic strain pattern is seen including (1) early peak contraction in the septal wall with (yellow arrow), (2) early prestretch in the lateral wall (blue arrow), (3) late lateral peak contraction (red arrow). Lower panel B: Segments show a synchronous contraction timed at aortic valve clo-

sure. (blue arrow) despite the widened QRS by ECG. The strain curves are enhanced for purposes of clarity. While correlations are not perfect, there is a very strong correlation of strict criteria for LBBB by ECG and strict criteria for classical strain pattern of LBBB. The strain curves are enhanced for purposes of clarity. Reprinted with permission from Risum et al. [4]

Reading List

1. Rushmer RF, Franklin DL, Ellis RM. Left ventricular dimensions recorded by sonocardiometry. *Circ Res*. 1956;4:684.
2. Risum N, Jons C, Olsen NT, Fritz Hansen T, Bruun NE, Hojgaard MV, Valeur N, Kronborg MB, Kisslo J, Sogaard P. Simple regional strain analysis to predict response to cardiac resynchronization therapy: rationale, initial results and advantages. *Am Heart J*. 2012;163:697–704.
3. Risum N, Strauss D, Sogaard P, Loring Z, Hansen TF, Bruun NE, Wagner G, Kisslo J. Left bundle-branch block: the relationship between electrocardiogram electrical activation and echocardiography mechanical contraction. *Am Heart J*. 2013;166:340–8.
4. Risum N, Tayal B, Fritz-Hansen T, Bruun NE, Jensen MT, Lauridsen TK, Saba S, Kisslo J, Gorcsan J III, Sogaard P. Identification of true left bundle branch block contraction by strain echocardiography is additive to electrocardiography in prediction of long-term outcome after cardiac resynchronization therapy. *J Am Coll Cardiol*. 2015;66(6):631–41.
5. Klein MR, Sundh FM, Simlund J, Harrison JK, Jackson KP, Hughes GC, Wagner GS, Risum N, Sogaard P, Strauss DG, Kisslo J. Immediate mechanical effect of acute left bundle branch block. *J Electrocardiol*. 2015;48:643–51.

Strain in Complex Congenital Heart Disease in Infants and Children

36

Daniel Forsha, Joseph Kisslo, Niels Risum,
and Piers Barker

Varying degrees of heart failure is common in infants with complex single ventricular heart disease. Sometimes the heart failure is progressive without a clear etiology and unresponsive to intense pharmacotherapy creating a critical management dilemma. These infants typically share a common history of repeated and lengthy intensive care unit (ICU) admissions and they often require temporizing measures of extracorporeal membrane oxygenation (ECMO), or ventricular assist device (VAD) before progressing to cardiac transplantation or death.

It is well established that mechanical dyssynchrony can cause heart failure in adults with left bundle branch block (LBBB), that is responsive to cardiac resynchronization therapy (CRT). Echocardiography has played a controversial role in identifying patients who have mechanical dyssynchrony and are responsive to CRT. Many

echocardiographic dyssynchrony criteria do not improve on an electrocardiogram (ECG) for prediction of CRT response.

However, a recently described “classic” pattern uses regional pattern analysis on speckle tracking strain analysis (Fig. 36.1) with an excellent CRT response predictive profile. This pattern identifies the opposing wall physiology consistent with activation delays causing mechanical dyssynchrony that should respond to CRT.

While CRT is efficacious in some single ventricle patients, no reports exist that guide the pediatric cardiologist in the interpretation of mechanical dyssynchrony and distinguish between the different causes. CRT in this population is complicated by the degree of anatomic variability, small patient size, and difficulty in properly placing epicardial leads due to the pericardial adhesions from multiple surgeries; CRT candidates must be chosen carefully. This chapter discusses three complex infants with an acute prolongation of their QRS duration followed by rapidly progressive, refractory heart failure. In each, speckle tracking strain analysis was used to differentiate the “classic” pattern of dyssynchrony demonstrating the physiology of activation delay induced heart failure (ADI-HF) from mechanical dyssynchrony caused by other etiologies. Raised awareness of ADI-HF in the failing single ventricle may stimulate further study into its frequency, natural history, and the effectiveness of early CRT. In addition, these cases call for

D. Forsha
Pediatric Cardiology, Children’s Mercy Hospital,
Kansas City, MO, USA

J. Kisslo (✉)
Division of Cardiology, Duke University Medical
Center, Durham, NC, USA
e-mail: joseph.kisslo@duke.edu

N. Risum
Division of Cardiology, Rigshospitalet, Copenhagen,
Denmark

P. Barker
Department of Pediatrics, Division of Pediatric Cardiology,
Duke University Medical Center, Durham, NC, USA

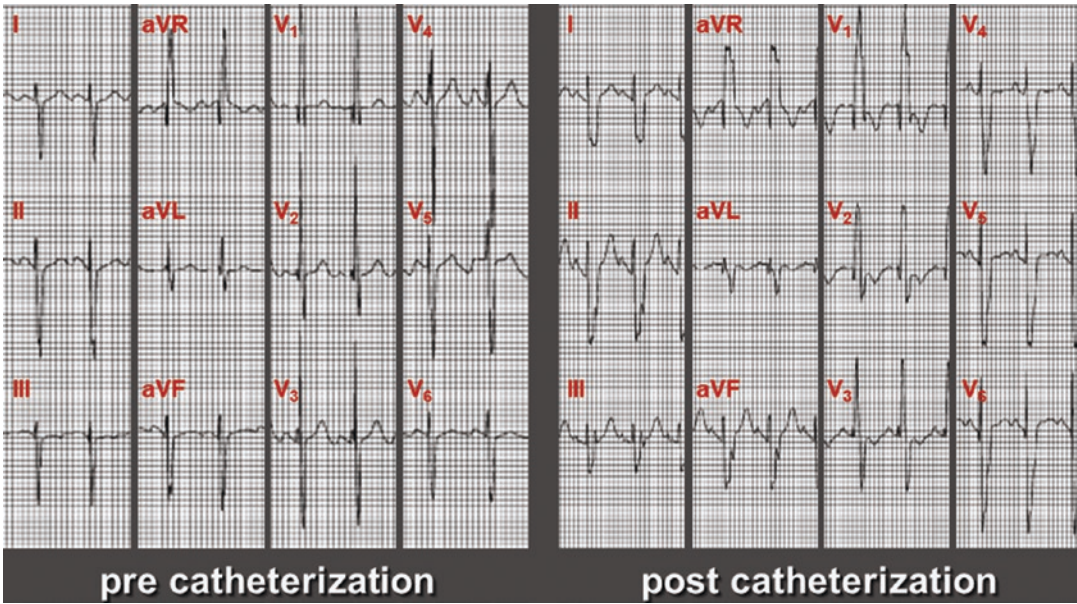


Fig. 36.1 ECG pre and post cardiac catheterization showing the development of a significant cardiac activation delay post catheterization

innovative design and development of new pacing lead systems particularly suited to infants and children.

Cases

The following selected cases will illustrate how use of the functional and timing patterns described elsewhere in this volume may be used in small children with complex congenital heart disease.

Case 1

The patient was a full term (2.8 kg) female with an unbalanced, right dominant AV septal defect with mild regurgitation, mildly hypoplastic left ventricle (LV), double outlet RV, severe pulmonary valve stenosis. Post-natally, she was clinically stable with low-normal bi-ventricular systolic function, a normal QRS duration and oxygen saturations between 80 and 95% on room air. She did not require medical support and was discharged to home.

Her condition was unchanged at her routine pre-Glenn cardiac catheterization, which confirmed her normal pre-Glenn hemodynamics.

However, during the procedure, the QRS duration prolonged acutely into a permanent RBBB pattern (Fig. 36.1). In the following month, she developed symptomatic heart failure with moderately decreased ventricular systolic function. With the etiology of her heart failure unrecognized at that time, she proceeded to a bidirectional Glenn procedure. Her intraoperative course was uncomplicated, but she had a prolonged convalescence with persistently diminished function and eventual discharge on multiple heart failure medications.

Ventricular function progressively worsened and the dyskinetic septal motion prompted a prospective dyssynchrony echocardiogram. Strain analysis using regional pattern analysis met criteria for the “classic” pattern with early LV wall contraction and late RV freewall contraction following early stretch (Fig. 36.2). Multiple time to peak (TTP) strain indices were also positive with a maximal opposing wall delay of 203 ms (adult CRT response threshold ≥ 130 ms¹⁰) and standard deviation of the time to peak of all segments of 84 ms (adult CRT response threshold ≥ 60 ms¹⁰). Due to the prolonged systolic duration, diastolic filling was also significantly abnormal. Retrospective strain analysis was performed on images obtained pre- and post-RBBB onset (Fig. 36.3) by means of the TomTec analysis software. The differences are

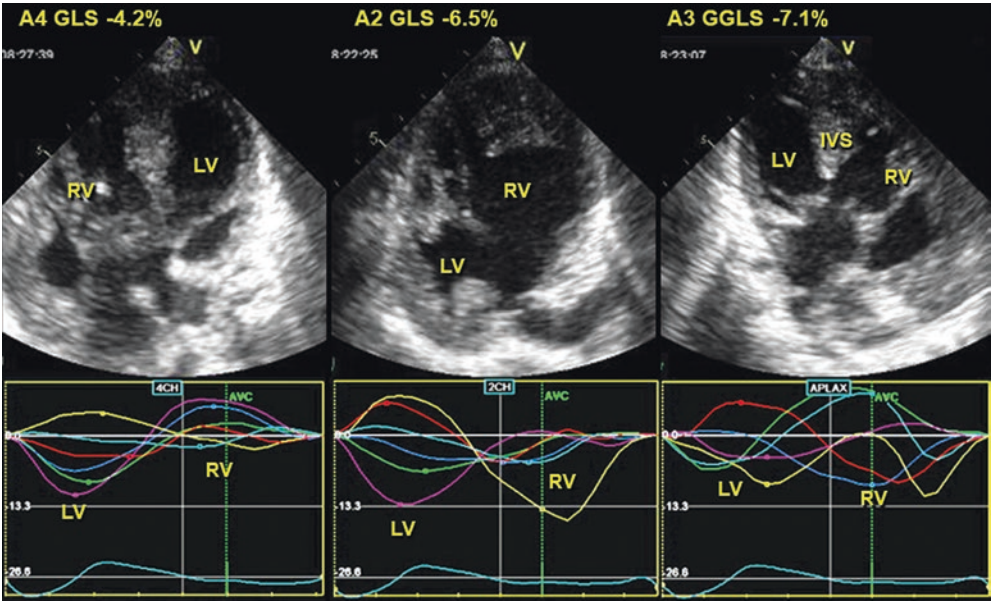


Fig. 36.2 Strain analysis of comprehensive multi-apical views of Case 1. Imaging planes are equivalent to the 3 LV apical views (transducer notch at 3, 1, and 11 o'clock). The lower panels show strain analysis tracking the entirety of the LV and RV freewall and excluding the diminutive

ventricular septum. Global peak systolic strain is severely diminished. All criteria for the “classic” pattern are met in each view. Aortic valve closure (AVC) is shown by a green vertical line. Intraventricular septum (IVS)

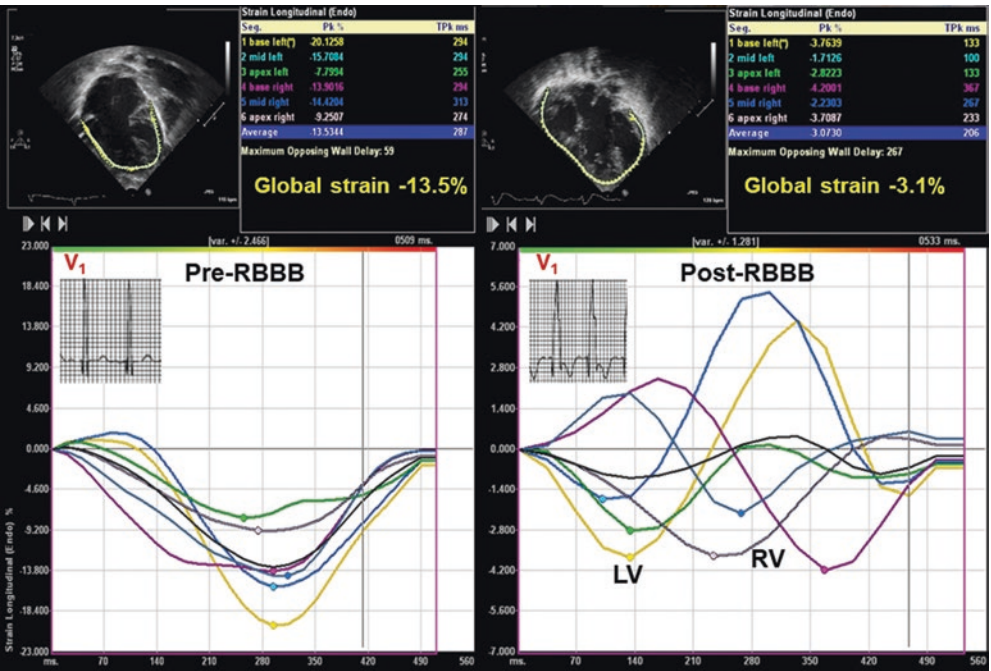


Fig. 36.3 Two-dimensional strain analysis tracking the biventricular freewall on pre-BBB four-chamber apical view and post-RBBB view. The pre-RBBB strain curves demonstrate low-normal to mildly diminished global peak systolic strain and a synchronous contraction pattern. The ECG V1 lead (inset) shows a top-normal QRS duration

(84 ms). The post-RBBB curves show severely diminished global peak systolic strain and a “classic” pattern of dyssynchrony with early LV freewall contraction and late RV free wall contraction. The 2D image shows dramatic remodeling of the RV and the V1 lead shows prolongation of the QRS duration (136 ms) into a RBBB pattern

dramatic with pre-RBBB synchrony and post-RBBB analysis.

One week prior to a scheduled placement of a biventricular epicardial pacing system, she was admitted to the ICU, rapidly progressed to ECMO deployment, and was listed for transplant. A VAD was placed and insertion of epicardial biventricular temporary pacing leads was not feasible at that time due to repeated ventricular tachyarrhythmias while dissecting to the identified LV lead placement position. Support was withdrawn leading to patient demise after development of a severe intracranial hemorrhage.

Case 2

The next infant was a full term (2.6 kg) male with hypoplastic left heart variant with moderate mitral and aortic stenosis and a mild-moderately hypoplastic left ventricle and normal RV normal function with an intact septum and mild tricuspid

regurgitation (TR), a hypoplastic aortic arch and a narrow QRS duration (60 ms).

A Norwood procedure with a Sano shunt was performed with no obvious complications. However, 1 week later, an ECG showed prolongation of the QRS duration (94 ms) with RBBB morphology. He was discharged to home with low-normal bi-ventricular systolic function. In the months leading up to the Glenn procedure, his RV systolic function became mildly diminished with a subtle dyskinetic wall motion.

The post-Glenn echo showed moderately decreased RV systolic function with an exaggerated paradoxical wall motion and moderate TR. A prospective dyssynchrony study demonstrated early septal/LV contraction and late RV freewall contraction meeting “classic” pattern criteria (Fig. 36.4). TTP indices also met thresholds for CRT. Retrospective strain analysis again demonstrated a transition between a relatively synchronous contraction pre-RBBB and a dyssynchronous post-RBBB with significant dysfunction. Due to

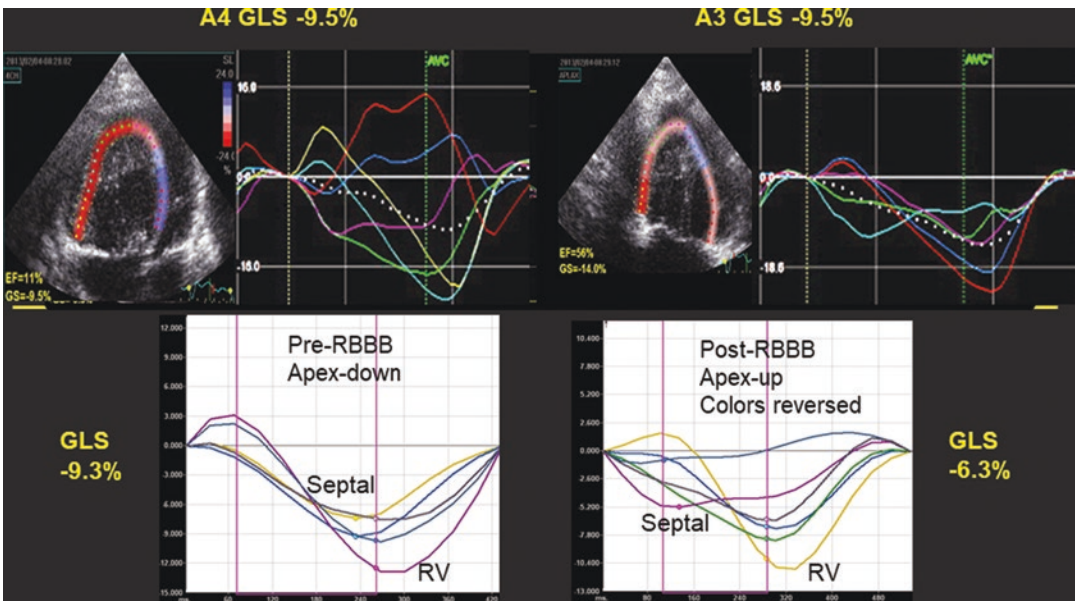


Fig. 36.4 Strain analysis of Case 2 illustrating the “classic” pattern with early septal and late RV freewall contraction in the setting of mild-moderately diminished systolic function. The two chamber equivalent view was of insufficient quality for strain analysis. Alternate system strain analysis (lower) utilized four-chamber equivalent views and shows a nearly synchronous pattern on a pre-Norwood

echocardiogram (pre-RBBB) with only small activation delays existed between the septum and the RV freewall as the septum is peaking very near end-systole. The post-RBBB strain curves (post-Glenn echocardiogram) demonstrate a decline in peak strain and development of a “classic” pattern. Vertical lines identify aortic valve opening (AVO) and closure (AVC)

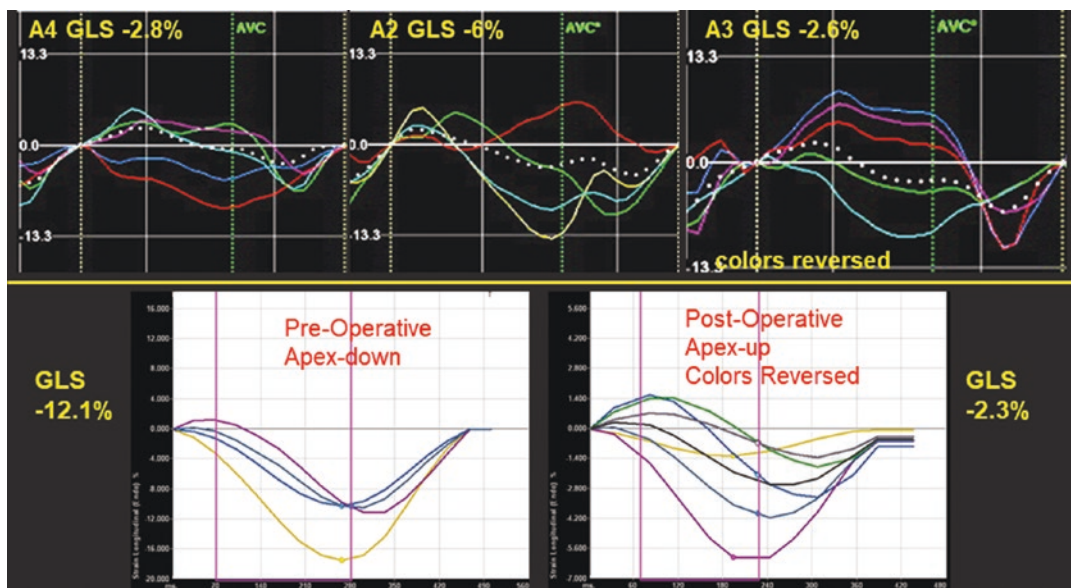


Fig. 36.5 Strain analysis of Case 3 (upper) illustrating holo-systolic stretch of the septal and apical segments seen best in the 4- and 3-chamber equivalent views compatible with non-functioning segments. Alternate system strain analysis confirms synchronous contraction pre-operatively (apical segments were excluded for poor tracking) and similar strain analysis curves to the original

system analysis post-operatively. The post-operative mid-septal (cyan) and apical (green/white) segments stretch almost completely through systole, which is mildly different from the complete holo-systolic stretch seen in the original analysis, likely due to increased temporal and spatial averaging. Vertical lines demonstrate AVO and AVC

his poorly compensated ADI-HF, 2 months later, he went to the OR for redo sternotomy and placement of three epicardial leads to his right atrium and LV and RV lateral basal walls.

Case 3

This infant had a two ventricle repair and a different etiology of ventricular dysfunction but is included to show how strain analysis can distinguish between etiologies. This full term female (2.7 kg) had membranous pulmonary atresia with ventricular septal defect (VSD) and aorto-pulmonary collaterals. She was discharged home after placement of a central shunt with low-normal biventricular systolic function, and normal QRS duration (56 ms).

She remained stable, and was subsequently admitted for unifocalization, RV to pulmonary artery conduit, and fenestrated VSD closure. Intra-operative monitoring showed prolongation of the QRS duration (114 ms) with moderately dimin-

ished LV function and a newly dyskinetic septum. A prospective dyssynchrony study demonstrated holosystolic stretch in the septal/apical segments with diastolic rebound consistent with a septal infarct that did not meet criteria for the “classic” pattern. Retrospective strain analysis showed near holo-systolic stretch of non-functional segments in apical and septal segments that was not present pre-operatively (Fig. 36.5). This holosystolic stretch is characteristic of non-functional segments. Magnetic resonance imaging confirmed an infarct to the LAD territory. One year later, she had not been discharged, and was in palliative care status.

Complex Strain Analysis in Children with Complex Disease

These cases clearly demonstrate the utility of strain analysis in single ventricle patients in two infants after acute onset BBB. The “classic” pattern differentiated ADI-HF from a septal infarct in an infant with a complex two ventricle repair.

In the ADI-HF cases, ventricular dysfunction closely followed the acute onset of the RBBB and development of mechanical dyssynchrony. The fact that problems with cardiac conduction system delays can lead to ADI-HF appears to be an under-recognized entity in this population.

Challenges and Opportunities Using Strain Analysis in the Congenital Population

In the first two cases, delayed diagnosis of ADI-HF led to missed opportunities to insert epicardial multisite pacing leads during the Glenn procedure. The delayed recognition was due to the novelty of utilizing strain technology in complex anatomy infants as well as the complexity of the underlying anatomy with multiple potential causes for functional decline. When Case 1 was first analyzed with 2DSE, the LV and RV were analyzed separately using the small ventricular septum as the opposing wall. Using this methodology, there was intra-ventricular synchrony with inter-ventricular dyssynchrony noted that is not highly predictive of CRT response. In retrospective, it does not make physiologic sense to analyze a single ventricle with minimal ventricular septum in that manner, but that was amongst the first complex infants that we analyzed with 2DSE. This led to a 1 month delay in diagnosing ADI-HF and her eventual decompensation preceded the planned CRT procedure. This led to an alternate plan of simultaneous VAD and CRT, which to our knowledge, has not been published in the literature. However, there is a case report of an adult with cardiomyopathy who underwent CRT while on ECMO support followed rapidly by discontinuation of ECMO and significant functional recovery. Another report detailed an infant with LBBB and cardiomyopathy bridged to a CRT device with a VAD with complete recovery.

Taken together, this information suggests that CRT options should not be dismissed if a patient requires mechanical support. Recognition of ADI-HF in case 2 occurred earlier, but not prior to his Glenn procedure. While RV dysfunction was

only mild pre-Glenn, we would have considered prophylactic epicardial multi-site lead placement at the time of Glenn in this patient. The timing of his exaggeration of his dyssynchronous motion and worsening of this RV function occurring post-Glenn, even though he developed the RBBB at time of Norwood, will require more research. Re-opening his chest for lead placement is currently under consideration. Unfortunately, large trials in this population are lacking to confirm that CRT works in these patients.

Several multi-center studies have shown that various types of congenital heart disease (systemic LV, systemic RV, and single ventricle) identified as dyssynchronous by non-standardized assessments respond to CRT. Unfortunately, the total number of single ventricle patients in all these trials was 24 and many of these were older children and teens post-Fontan; they had a 60% CRT response rate as seen by an improvement in systemic ventricular ejection fraction. The significant responder rate creates optimism around use of CRT in this population, especially considering the various non-specific criteria used to identify dyssynchronous patients in these studies.

Questions remain including proper lead placement locations in various types of congenital heart disease and proper dyssynchrony criteria. A plethora of dyssynchrony criteria exist in the literature. Most offer no additional CRT predictive power over a simple QRS duration [6], which typically has a CRT response rate between 60 and 70%. Many of them identify regional wall motion abnormalities that can be caused by scar, regional fibrosis, and altered loading conditions and lead to dyskinetic contraction patterns and time to peak strain delays in patients who are unlikely to respond to the electrical therapy of CRT. When trying to define dyssynchronous patients caused by an underlying conduction system insult, as diagnosed by the “classic” pattern, that are most likely to respond to the electrical therapy of biventricular pacing, we prefer the term ADI-HF.

The criteria for the “classic” pattern identify opposing wall physiology resulting specifically from an activation delay such as BBB. This pattern is highly predictive of CRT response (>90% sensitivity and specificity) in adults with LBBB

cardiomyopathy. An independent group reported that CRT response rates varied in sub-groups divided by different types of strain patterns with the best responding sub-groups demonstrating strain patterns similar to the “classic” pattern. While studies describing the predictive characteristics of the “classic” pattern in congenital heart disease are pending, the underlying opposing wall physiology caused by activation delays should follow the same guiding principles. We believe that a strain methodology using pattern analysis to identify ADI-HF will decrease the non-responder rate in all populations and that it will lead to better outcomes in properly identified failing single ventricles.

Prospective Strain Analysis Methodology

Our methodology for image acquisition for all prospectively obtained strain studies utilizes multi-planar apical imaging. This imaging is standard of care in LV imaging, and has been recently described in the RV as it was utilized with the children described in this chapter. Due to the potential for regional heterogeneities in function and timing in this type of patient, a comprehensive approach, such as this, should be standardized. Studies in adults with LBBB as well as transposition patients with systemic RVs have identified ADI-HF patients in whom the “classic” pattern would

have been missed if only the 4-chamber view had been analyzed.

These cases indicate that complex strain analysis can be used in small children with complex congenital heart disease and open the door to new avenues of thought concerning the origin and treatment of heart failure in children.

Suggested Reading

- Forsha D, Risum N, Smith PB, Samad Z, Kanter RJ, Barker P, Kisslo J. A novel, comprehensive RV strain analysis: frequently encountered ventricular activation abnormalities in the systemic right ventricle. In: American Heart Association scientific sessions 2012. Los Angeles, CA: Circulation; 2012. p. 11371.
- Forsha D, Risum N, Smith PB, Kropf A, Rajagopal S, Samad Z, Kanter RJ, Barker P, Kisslo J. A novel comprehensive RV strain analysis: echocardiographic approach to define a normal adult population. In: American Heart Association scientific sessions 2012. Los Angeles, CA: Circulation; 2012. p. A9974.
- Leenders GE, Lumens J, Cramer MJ, De Boeck BW, Doevendans PA, Delhaas T, et al. Septal deformation patterns delineate mechanical dyssynchrony and regional differences in contractility: analysis of patient data using a computer model. *Circ Heart Fail*. 2012;5:87–96.
- Risum N, Ali S, Olsen NT, Jons C, Khouri MG, Lauridsen TK, et al. Variability of global left ventricular deformation analysis using vendor dependent and independent two-dimensional speckle-tracking software in adults. *J Am Soc Echocardiogr*. 2012;25:1195–203.
- Risum N, Jons C, Olsen NT, Fritz-Hansen T, Bruun NE, Hojgaard MV, et al. Simple regional strain pattern analysis to predict response to cardiac resynchronization therapy: rationale, initial results, and advantages. *Am Heart J*. 2012;163:697–704.

Part X

Special Applications

Introduction

The benefits of exercise on the cardiovascular system are well established, however very occasionally a young athlete may die from a quiescent cardiac abnormality. Although the incidence of sudden death in athletes is low, the visibility afforded by such catastrophes, particularly when a high profile athlete is involved, has a major impact on the nation and calls for initiatives to identify young athletes who may be at risk. Over the past three decades an increasing number of sporting organisations have implemented mandatory cardiac evaluations, which include echocardiography. An appreciation of the structural adaptations to intensive exercise is important to reduce false positive rates because absolute cardiac dimensions in athletes often exceed predicted upper limits for the relatively sedentary population and may overlap with those observed in patients with primary cardiomyopathies. The differentiation between physiological cardiac

enlargement and cardiomyopathy is crucial but may be challenging in some instances.

Cardiac Adaptation to Intensive Exercise

The term “athlete” is used to describe an individual who is proficient in sport and other forms of physical exercise. In the evaluation of any athlete it is useful to consider the impact of the type, the dose, and the duration of exercise on the heart and cardiovascular system.

Of critical importance is the appreciation of the type of sport or sports that the athlete is engaged in. By convention, sports are broadly divided into low, moderate or high intensity and classified into two categories, notably dynamic and static [1] (Fig. 37.1).

The purpose of this classification is to highlight different haemodynamic effects imposed on the cardiovascular system by dynamic training, as compared to static training. Dynamic training is also sometimes referred to as endurance or isotonic training and typical examples include long-distance running, cycling, swimming and rowing. Physical activity of a dynamic nature results in increased maximum oxygen consumption, cardiac output, stroke volume and systolic blood pressure with an associated fall in peripheral vascular resistance and heart rate. The overall effect on cardiovascular physiology is an increase in

A. D'Silva
St. George's University of London, St. George's
University Hospital NHS Foundation Trust,
London, UK
e-mail: adsilva@doctors.org.uk

S. Sharma (✉)
Department of Cardiovascular and Cell Sciences,
St. George's University of London, London, UK
e-mail: sasharma@sgul.ac.uk

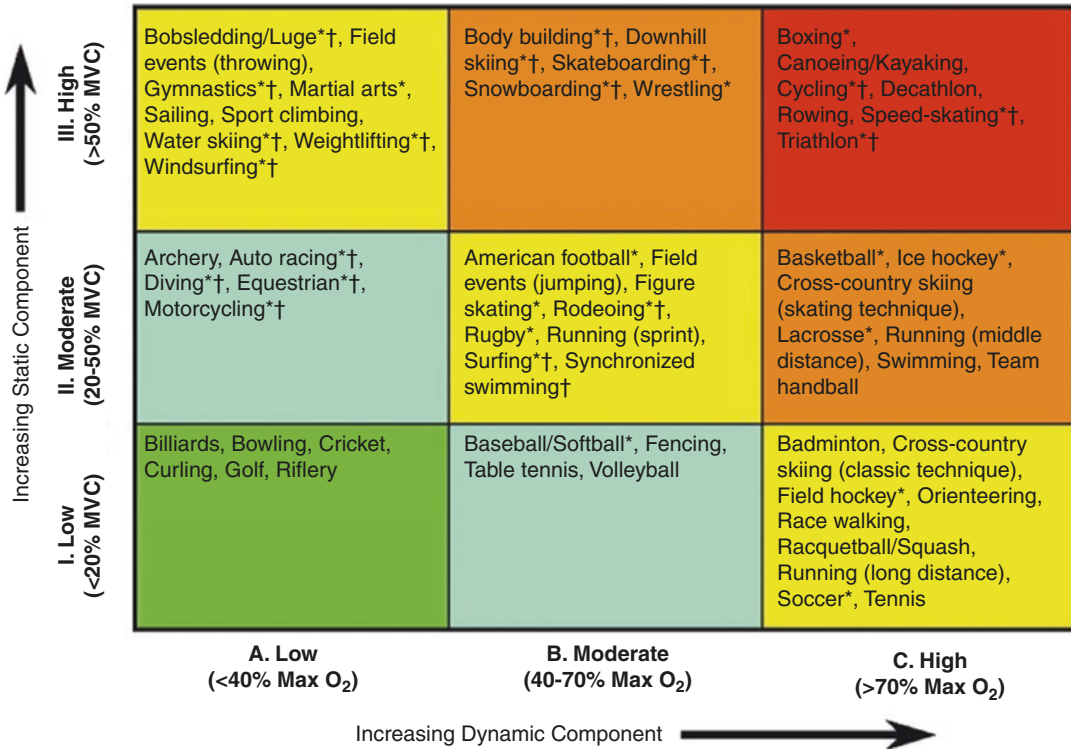


Fig. 37.1 Sports classification based on peak static and dynamic components achieved during competition. The lowest total cardiovascular demands (cardiac output and blood pressure) are shown in green and the highest in red.

Max O₂ maximal oxygen uptake, *MVC* maximal voluntary contraction. *Danger of bodily collision. †Increased risk if syncope occurs (adapted from Mitchell et al. in the report of the 36th Bethesda Conference) [1]

cardiac preload but a reduction in afterload, which generates a predominantly volume-loaded left ventricle (LV).

Static training, by comparison, is also sometimes referred to as strength or isometric training with typical examples being weightlifting, wrestling and throwing heavy objects. Physical activity of this nature results in only a mild increase in oxygen consumption and cardiac output but substantial increases in blood pressure, even exceeding 400 mmHg for brief periods, increased peripheral vascular resistance and heart rate. The effect on physiology is proportionally higher afterload, resulting in a pressure-loaded LV. In reality, most athletic disciplines combine dynamic and static modes of physical conditioning in variable proportions.

Cardiac Dimensions in Athletes

As a group, when compared with sedentary controls, athletes have a slightly increased septal and posterior wall thickness on echocardiography, in the order of 15–20%. Even with this increase, most athletes will exhibit absolute LV wall thickness measurements of 7–12 mm, which are within normal limits for the general population. The LV cavity in athletes tends to be approximately 10% greater than that of non-athletes and here the absolute value frequently approaches 54 mm, which is considered the upper limit of normal for men and exceeds that for women in the general population [2]. Similarly the right ventricle is increased by 10% and both the RV outflow tract dimensions and the RV internal

Cardiac Adaptation to Exercise – The Athlete's Heart

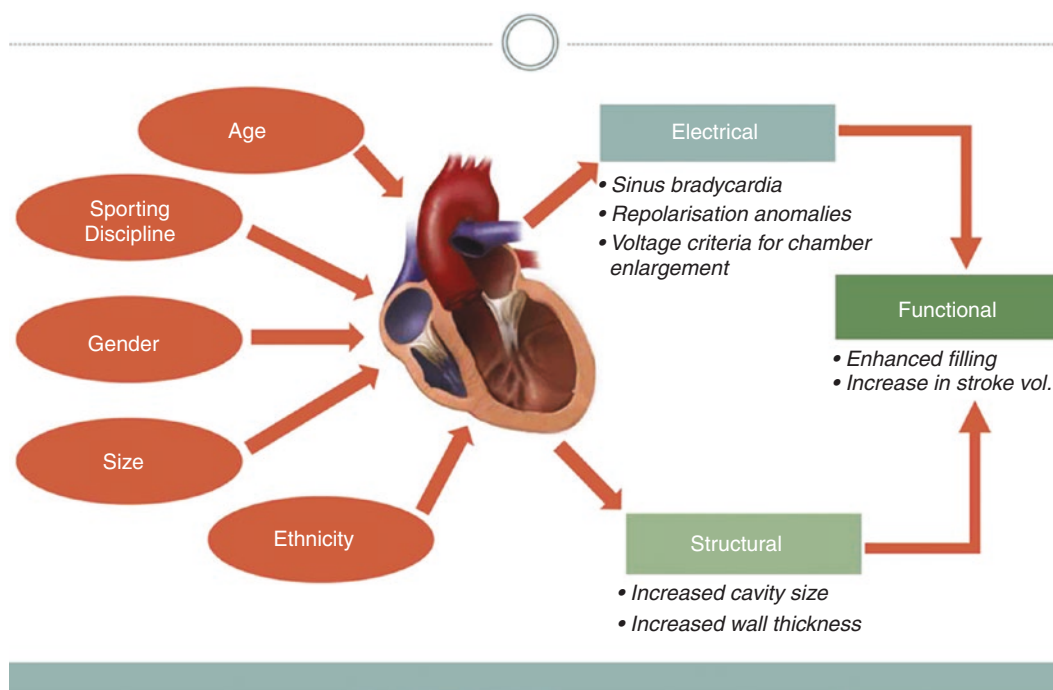


Fig. 37.2 Determinants of cardiac dimensions and physiological adaptation in the athlete's heart

diameters often exceed predicted upper limits for the general population [3–5].

In any individual athlete, the magnitude of increase in these echocardiographic parameters is governed by several factors, which include age, gender, ethnicity, body size and type of sport (Fig. 37.2).

With respect to the type of sport, athletes participating in static or power sports, such as weightlifting, acquire a pressure-loaded LV, which results in mild left ventricular hypertrophy (LVH) and very small increases in cavity size. The LV mass to cavity ratio is >2 and this pattern of left ventricular hypertrophy (LVH) is termed concentric LVH (Fig. 37.3).

Athletes participating in dynamic or endurance sports such as running, cycling and rowing, have to generate large cardiac outputs for several hours at a time and are faced with a large preload and volume-loaded LV. Such individuals develop a large LV cavity. The LV also hypertrophies to

maintain wall tension. The overall LV mass is increased but the LV mass to LV cavity ratio is <2 ; this pattern of LVH is termed eccentric hypertrophy [6] (Fig. 37.3). Indeed, endurance athletes have the biggest LV cavities and the thickest hearts. When comparing LV wall thickness and cavity size across various sports, wrestling, a power sport, results in a greater increase in wall thickness but a lesser increase in cavity size, nevertheless LV wall thickness measurements rarely exceed 12 mm. Long-distance runners and cyclists by comparison, develop large LV cavities and wall thickness measurements [7] (Fig. 37.4). As a rule, the greatest cardiac dimensions are usually detected in adult males with a large body surface area of around 2 m^2 who participate in endurance sports, such as rowing, canoeing, long-distance running, cycling and swimming.

Forty-five percent of athletes will have an LV cavity size $\geq 55 \text{ mm}$. In any given sporting

Fig. 37.3 Diagram of LV remodeling pattern based on LVH and LV mass-cavity ratio. Reproduced with permission from Rodriguez et al. [6]

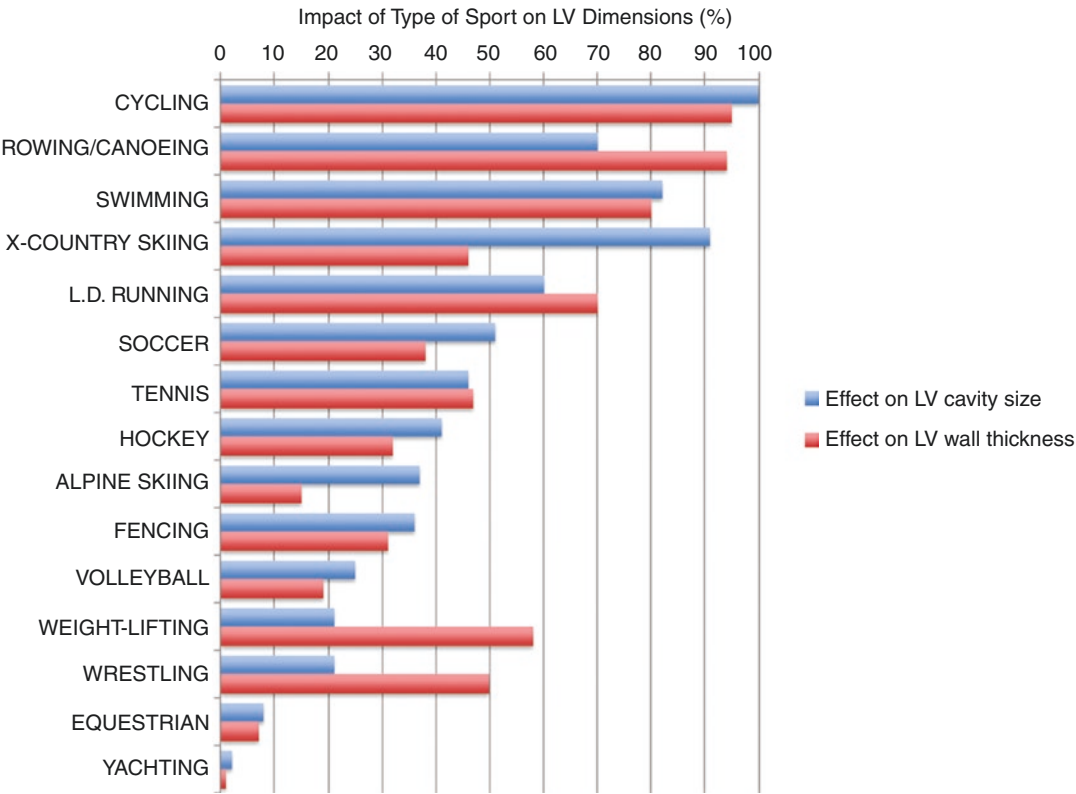
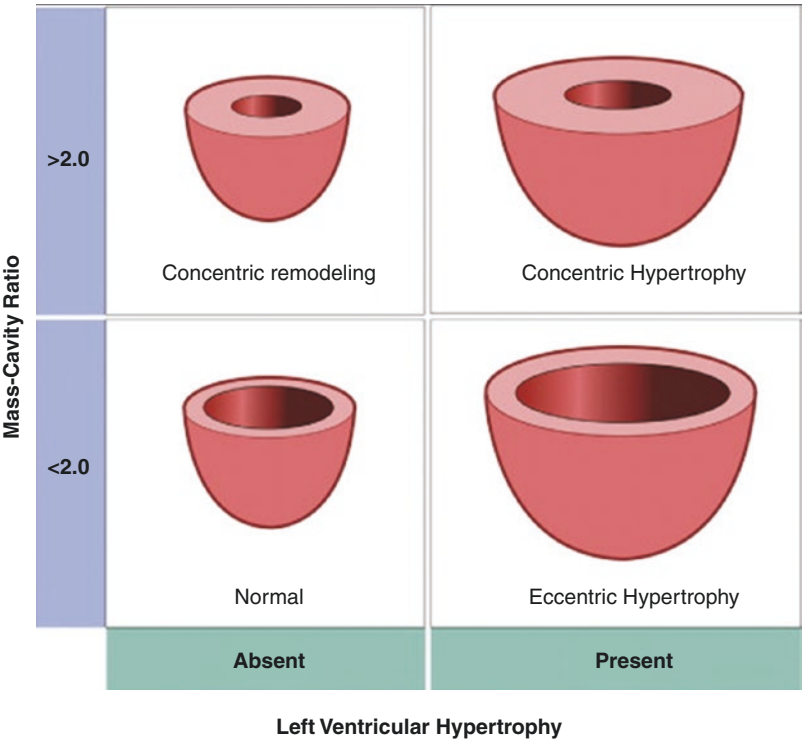


Fig. 37.4 Effect of specific sport on LV cavity size and LV wall thickness. Reproduced with permission from Maron and Pelliccia [7]

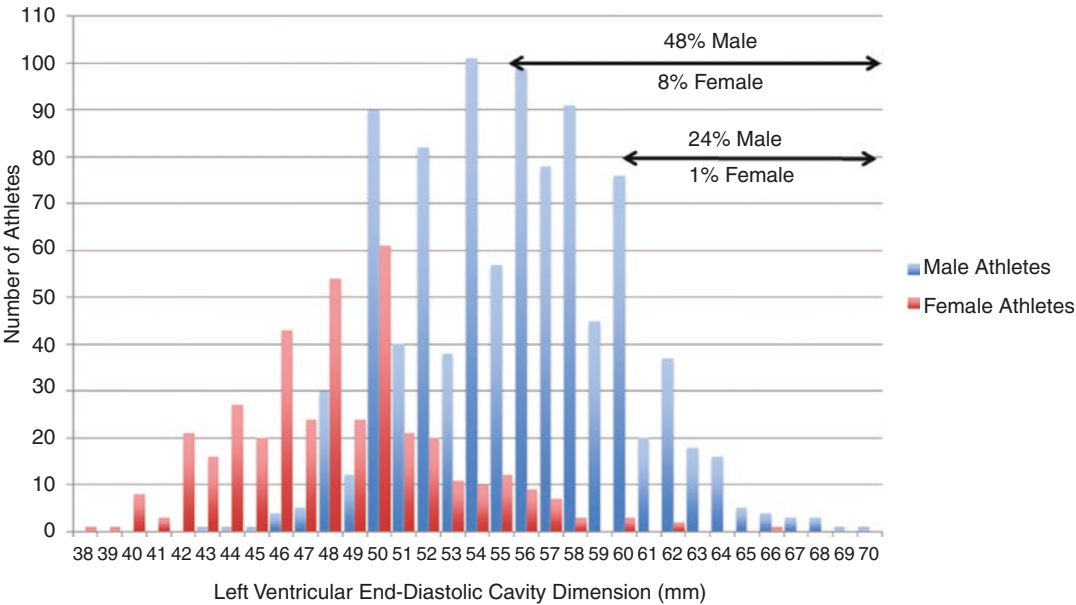


Fig. 37.5 Distribution of end-diastolic left ventricular cavity size in 957 male and 352 female elite athletes. Redrawn from Pellicia et al. [8]. ©1999 American College of Physicians. All rights reserved

Table 37.1 Echocardiographic upper reference limits (two standard deviations above the cohort mean) for cardiac dimensions in athletes according to ethnicity, age and gender

Ethnicity	Age	Gender	LVEDD (mm)	LVWT (mm)	RVOT1 (mm)	RVD1 (mm)
White	Adult	Male	≤64	≤12	≤43	≤55
		Female	≤57	≤11	≤40	≤49
	Adolescent (14–18)	Male	≤58	≤12	–	–
		Female	≤54	≤11	–	–
Black	Adult	Male	≤62	≤15	≤43	≤55
		Female	≤56	≤12	≤40	≤49
	Adolescent (14–18)	Male	≤62	≤14	–	–
		Female	≤57	≤11	–	–

Reproduced with permission from Sharma et al. [9]

discipline, female athletes have smaller cardiac dimensions compared with males, which may be due to a variety of factors including smaller size, lower mean body mass and possibly exercising at lower intensity levels. Comparing gender, 48% of male athletes have a LV cavity >55 mm, compared with only 8% of female athletes. Indeed, 24% of male athletes have an LV cavity size ≥60 mm, which can be consistent with dilated cardiomyopathy (DCM), compared to only 1% of female athletes [8] (Fig. 37.5).

In general, absolute values for cavity dimensions exceeding upper limits should not be of concern, unless the athlete is symptomatic, has a

family history of cardiomyopathy or if systolic or diastolic function are impaired.

The physiological upper limits of cardiac dimensions in athletes in relation to age, sex and ethnicity are provided in Table 37.1 [9, 10].

Diagnostic Difficulties

Athlete's Heart versus Hypertrophic Cardiomyopathy (HCM)

The vast majority of athletes show LV wall thickness measurements that fall within the normal range for the general population (<12 mm).

However, an important minority, notably male endurance athletes and some athletes of African or Afro-Caribbean origin who engage in high dynamic sports exhibit wall thickness measurements between 13 and 16 mm, that overlaps with morphologically mild HCM [9]. Most individuals with HCM cannot compete in sports at a national level because the combination of LVH, impaired myocardial relaxation, myocardial fibrosis and small vessel disease is not conducive to the augmentation of stroke volume and generating large increases in cardiac output for sustained periods. The majority of people with HCM have a wall thickness of 20 mm or more, a small LV cavity size and impaired diastolic function. However, it is important to appreciate the heterogeneity of this condition and there are some affected individuals with only mild LVH and seemingly normal diastolic function who can compete in high level sport, particularly skill sports of a start-stop nature such as football, basketball and baseball.

Multi-faceted Assessment

When faced with a male athlete with a LV wall thickness of 13–16 mm who falls into the grey zone between physiological LVH and HCM, the distinction between the two entities requires the cardiologist to use multiple sources of information from the history, the demographics of the athlete, the electrocardiogram (ECG), the echocardiogram, exercise testing, cardiac magnetic resonance imaging (CMR) and the evaluation of first-degree relatives with potential additional information provided by genetic tests.

History and Demographics

Most athletes are asymptomatic, however, chest pain, breathlessness that is out of proportion to effort or greater than one's peers, palpitation, exertional dizziness and syncope are ominous features. The athlete who expresses symptoms and has LVH requires full assessment exploring the possibility of underlying pathology. Similarly, a sinister family history should arouse suspicion. This may include cardiomyopathy, premature sudden death or other more subtle suggestions of serious pathology associated

with ventricular arrhythmias culminating in unexplained drowning, road traffic accidents and seizure disorders.

Demographic data should be taken into consideration, as physiological LVH is only seen in adult male athletes with a large body surface area, participating in dynamic sports. A LV wall thickness of >12 mm in female athletes and small white athletes aged <16 years old should be viewed with suspicion and considered as pathological LVH. Black ethnicity deserves additional consideration because both adults and adolescents can develop physiological LVH.

The Echocardiogram

Echocardiography is a fundamental tool in the assessment of an athlete with LVH. The echocardiogram provides information relating to the magnitude of LVH, the pattern of LVH, and the relative increase in LV wall thickness compared to the LV cavity. The echocardiogram is also used to detect and quantify LV outflow obstruction including intracavity gradients, measure diastolic function and longitudinal systolic function. Finally, the echocardiogram plays an important role in risk stratification in HCM.

Magnitude of Left Ventricular Hypertrophy

With respect to the magnitude of LVH, 1.5–3% of white athletes have a LV wall thickness of >12 mm but never more than 16 mm [11–13]. By contrast, 13–18% of black athletes have an LV wall thickness of >12 mm but again, not more than 16 mm [12]. Therefore, irrespective of ethnicity, a LV wall thickness of 16 mm or more in an athlete indicates pathology.

When considering gender, white female athletes do not develop a LV wall thickness exceeding 11 mm. By comparison, 3% of black female athletes have LV wall thickness >11 mm but never more than 13 mm [14] (Fig. 37.6).

White athletes in the adolescent age group, 14–18 years, very rarely exhibit LVH > 12 mm (0.6%) and when it has been detected, it is always in individuals aged ≥16 years old with adult body dimensions. 7% of adolescent black athletes have

a LV wall thickness ≥ 12 mm but never more than 15 mm [15]. LVH in black adolescent athletes is recorded from the age of 15 years onwards. As such, it is possible to find a LV wall

thickness of 14–15 mm in young black football players of 15 or 16 years of age, without any other indicative features of cardiac pathology (Fig. 37.7).

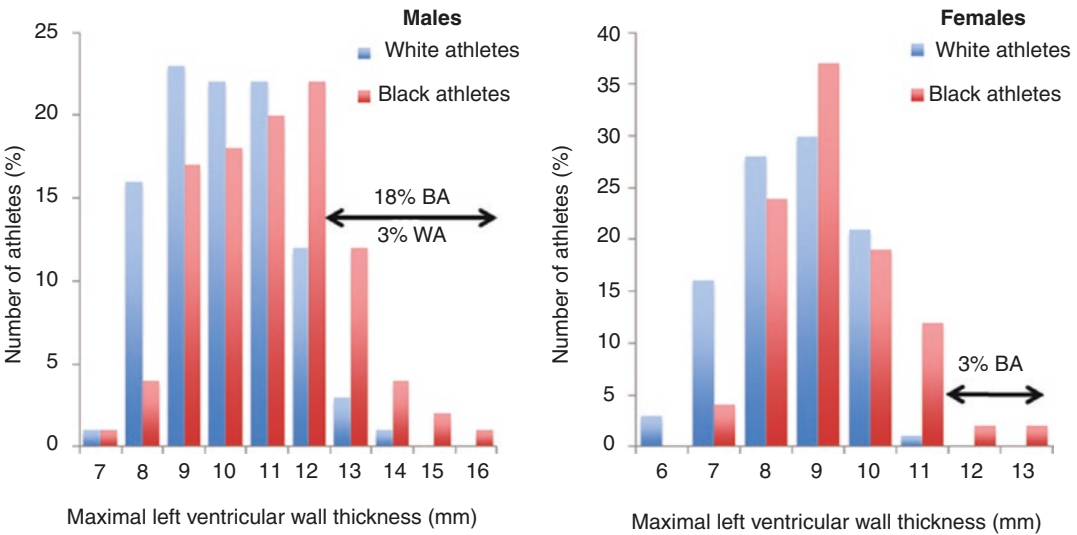


Fig. 37.6 Comparison of maximal left ventricular wall thickness (mm) in male athletes and female athletes of black and white ethnicity. BA black athletes, WA white

athletes. Reproduced with permission from Basavarajaiah et al. [12], Rawlins et al. [14] and Papadakis et al. [13]

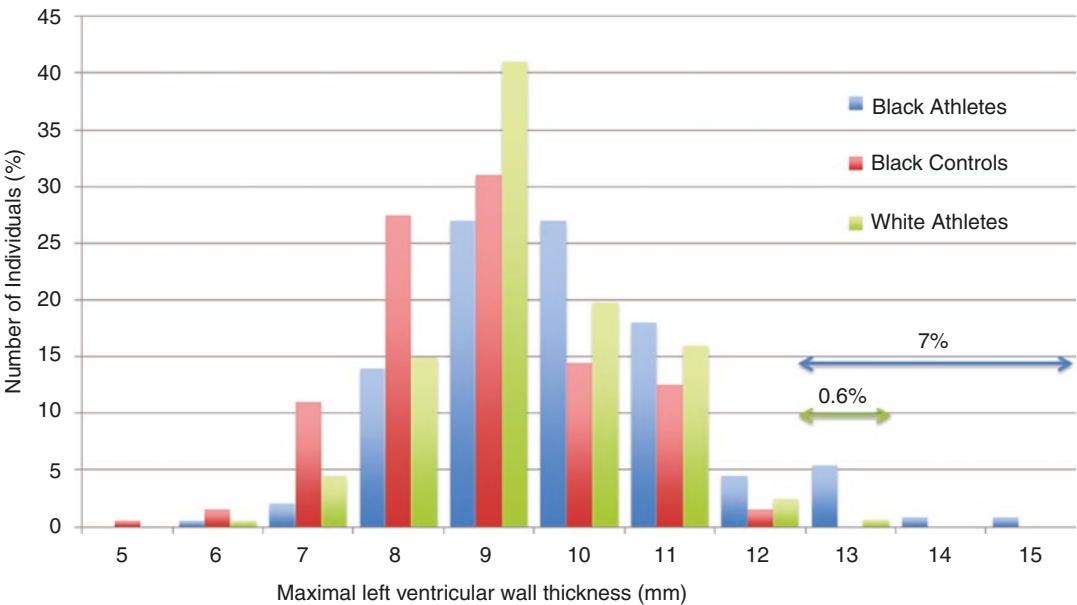


Fig. 37.7 Left ventricular wall thickness measurements in black and white adolescent athletes. Reproduced with permission from Sheikh et al. [15]

Pattern of Left Ventricular Hypertrophy

Hypertrophic cardiomyopathy is a morphologically heterogeneous disease and almost any pattern of LVH is possible. The most common pattern is asymmetrical septal hypertrophy in approximately 60% of cases where the septal to posterior wall ratio is $>1.3:1$. Almost 10% of patients show LVH confined to the left ventricular apex. In contrast, athletes with physiological LVH have a very smooth, uniform pattern of hypertrophy that does not differ by >2 mm between adjacent cardiac segments (Fig. 37.8). Therefore, the presence of asymmetrical septal hypertrophy or other non-homogeneous patterns of LVH are indicative of HCM and warrant further assessment. In our experience of assessing over 100 young athletes with HCM, we have observed that most have asymmetrical septal hypertrophy or LVH confined to the apex. Only

14% show homogeneous patterns of left ventricular hypertrophy with LV wall thickness measurements of 13–16 mm [16]. In such athletes further information from the echocardiogram may facilitate differentiation from physiological LVH.

Left Ventricular Hypertrophy Relative to Left Ventricular Cavity Size

Arguably, the most useful echocardiographic observation to differentiate physiological LVH from HCM is the proportion of the LV wall thickness relative to the LV cavity size. In general, athletes with physiological LVH exhibit an enlarged LV cavity size >54 mm [11, 16, 17]. A large LV cavity size with normal indices of function may be reassuring in the athlete with LVH as this is more likely to represent physiology than pathology. However, our experience of assessing

Pattern of Left Ventricular Hypertrophy in HCM

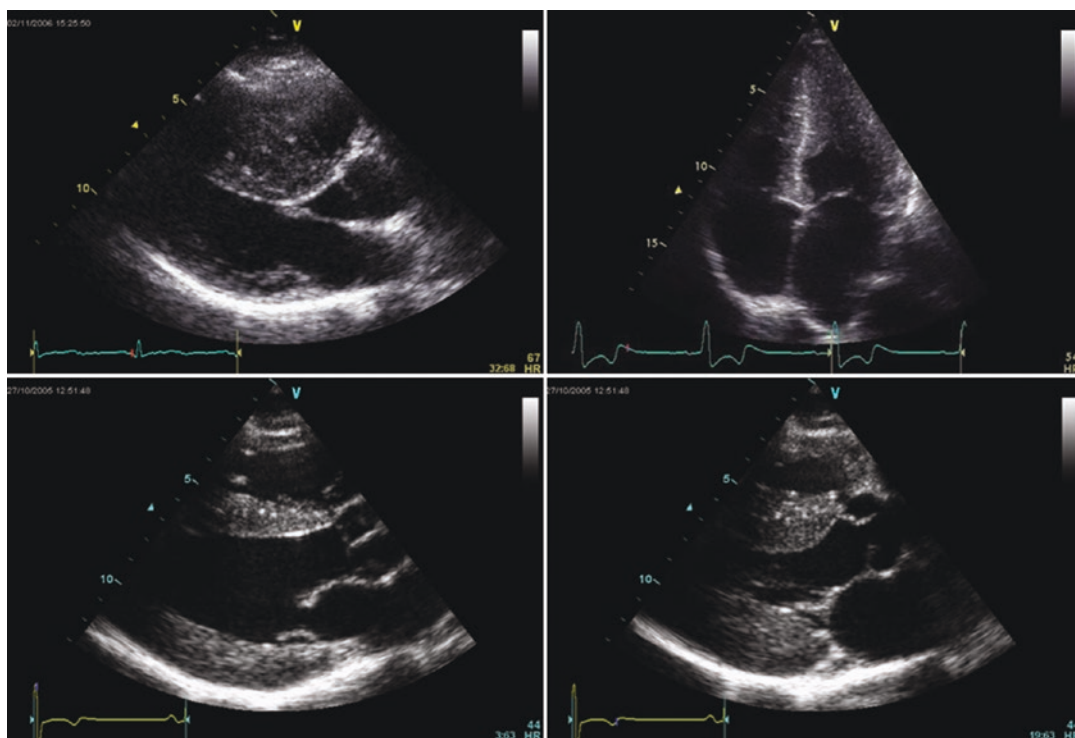


Fig. 37.8 Patterns of hypertrophy in HCM. Clockwise from top left; Asymmetrical septal hypertrophy, apical hypertrophy, symmetrical/concentric hypertrophy with systole and diastole shown

athletes with HCM shows that although a LV cavity >54 mm is a good discriminator and supports physiological LVH, 3% of athletes with HCM shows a combination of mild concentric LVH (13–16 mm) and a LV cavity >54 mm [16]. The h/R ratio is a useful objective measure of this relationship, where h is the sum of the LV septal and posterior wall thickness in diastole, and R is the LV end-diastolic cavity dimension (Fig. 37.9). An athlete with an h/R ratio of >0.5 should be considered to have pathological LVH.

Left Ventricle Outflow Tract Obstruction

Dynamic LV outflow tract obstruction is not seen in athletes. Athletes normally have enlarged left ventricular outflow tracts, rather than narrowed, and do not exhibit hyperdynamic left ventricular contraction, which are both required for systolic

anterior motion of the mitral valve that results in mechanical left ventricular outflow tract obstruction. The presence of systolic anterior motion of the mitral valve leaflet and dynamic LV outflow obstruction in an athlete with LVH is indicative of HCM.

Diastolic Function

Athletes show normal or supranormal indices of diastolic function whereas abnormal myocardial relaxation is considered the hallmark of HCM. As with all other aspects of the disease, the myocardial filling pattern ranges from normal in some individuals to severely impaired in others. Various parameters of diastolic function can be helpful in distinguishing between physiological LVH and HCM including LV inflow velocities, E wave deceleration times, isovolumetric relaxation times, tissue Doppler e' , E/e' ratio and pulmonary

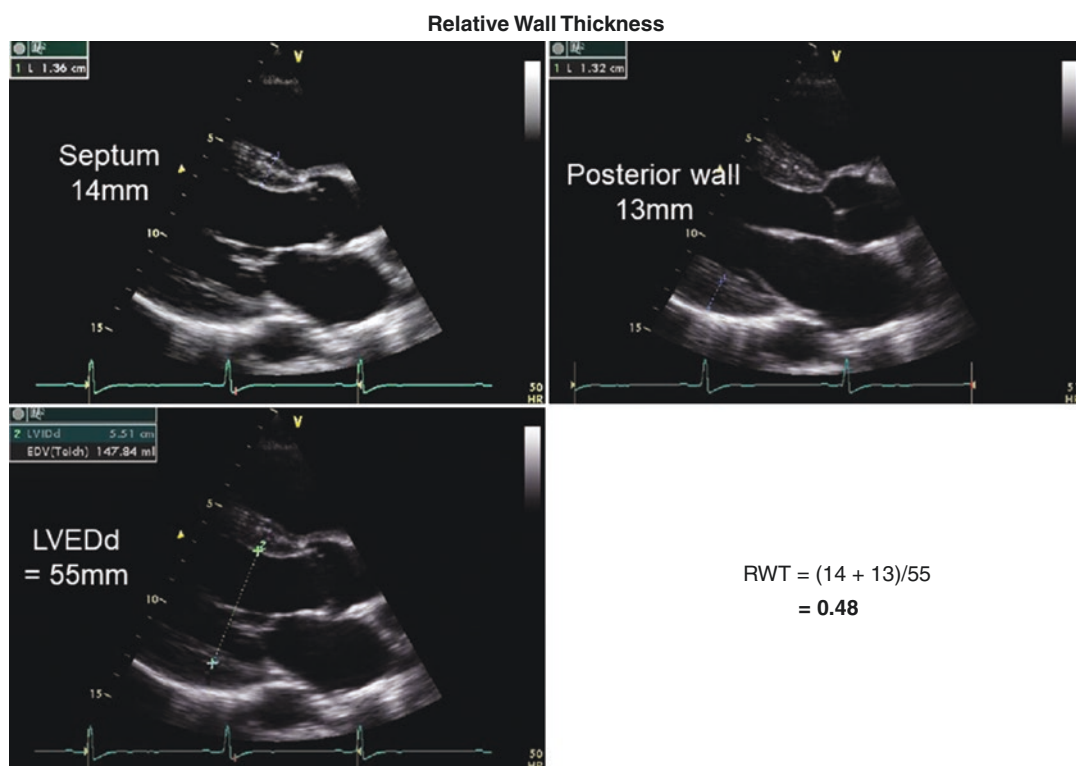


Fig. 37.9 Calculation of the h/R ratio in an athlete with physiological LVH. Measurements of LV wall thickness and cavity size in diastole are given

vein Doppler (Table 37.2). Athletes reveal normal mitral valve filling patterns and have normal E:A ratios. Using pulsed wave tissue Doppler to assess the lateral LV annulus, athletes have normal or high e' values, usually well in excess of 10 cm/s. An E/ e' ratio of less than 8 is also suggestive of physiology (Fig. 37.10). Measurements taken adjacent to the medial mitral valve annulus appear to be less reproducible in observing this useful echocardiographic finding. It is important to

emphasize that whilst all of these parameters are useful in the diagnosis of HCM in large cohort studies, their absence does not reliably exclude HCM in athletic individuals. Indeed our experience suggests that most athletes (90%) with definite HCM have a lateral $e' > 9$ cm/s and 92% have an E/ $e' < 12$ [16].

Systolic Function

Athletes have normal systolic function and some endurance athletes may show a borderline low ejection fraction due to a large LV cavity and resting bradycardia. In contrast, individuals with HCM have a mathematically high ejection fraction and fractional shortening because they generally have a small LV cavity. However, when assessing systolic annular (S_a) velocities on pulsed wave tissue Doppler, most patients with HCM have low velocities below 10 cm/s. Athletes register much higher values, usually well above 10 cm/s. Tissue Doppler longitudinal strain studies reveal that athletes with physiological LVH show normal, homogenous patterns of strain, whereas patients with HCM have low and

Table 37.2 Indices of diastolic function in athletes with physiological LVH as compared to patients with HCM

Diastolic function in HCM		
	Physiological LVH	HCM
E wave	Increased/Normal	Decreased
A wave	Normal	Increased
E/A ratio	>1	≤1
Deceleration time	Normal	Increased
IVRT	Normal	Increased
e'	>9	≤9
E/ e'	<8	≥12
Pulmonary vein	S/D > 1	S/D < 1

HCM hypertrophic cardiomyopathy, IVRT isovolumetric relaxation time, LVH left ventricular hypertrophy

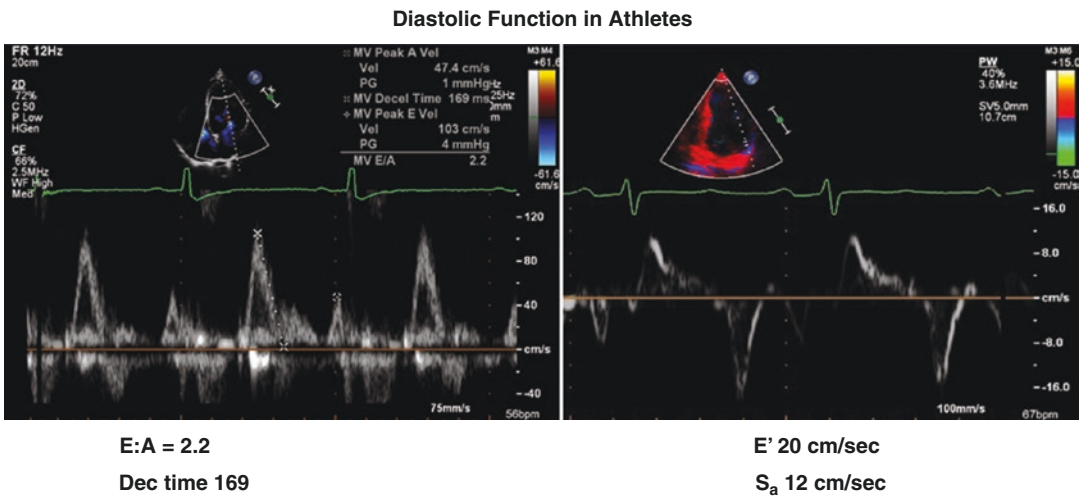


Fig. 37.10 An example of pulsed wave trans-mitral Doppler and pulsed wave tissue Doppler imaging assessing the lateral LV annulus of an athlete. S_a systolic annular velocity

Table 37.3 Indices of systolic function in athletes with physiological LVH as compared to patients with HCM

Systolic function in HCM		
	Physiological LVH	HCM
EF	Normal/decreased	Increased/normal
FS	Normal/decreased	Increased/normal
S _a	>10 cm/s	≤10 cm/s
TDI longitudinal strain	Normal/homogenous	Low/heterogenous (<−10%)
STI	Normal	Attenuated

EF ejection fraction, FS fractional shortening, HCM hypertrophic cardiomyopathy, LVH left ventricular hypertrophy, S_a systolic annular velocity, TDI tissue Doppler imaging, STI speckle tracking imaging

heterogenous strain patterns (Table 37.3). A study of 15 HCM patients, 20 athletes and 18 healthy controls, has shown that a global longitudinal strain of <−10% is suggestive of HCM, with a 95% diagnostic specificity [18].

Repeat Assessment After Detraining

In some instances the differentiation between physiological LVH and HCM cannot be resolved after echocardiography, for example, an athlete with a mildly abnormal ECG, LV wall thickness of 13 mm, LV end-diastolic cavity dimension of 50 mm and normal systolic and diastolic function. In this situation, detraining may facilitate the differentiation on the understanding that an athlete with physiological LVH will demonstrate regression of LVH after a 6-week period of detraining, whereas an athlete with HCM will show very small reductions in LV wall thickness. Unsurprisingly, most athletes are resistant to detraining as this costs fitness and team selection and therefore despite its clinical utility, detraining is not always possible if the athlete is not willing to comply.

The Electrocardiogram

In many instances additional information from ancillary investigations such as the electrocardio-

gram (ECG) may provide important information for the clinical diagnosis. Whilst it is common to observe large QRS complexes in both athletes and individuals with HCM, athletes usually show isolated voltage increases for LVH that are not accompanied by other markers of pathological LVH such as ST-segment depression or T wave inversion in the lateral leads. Although T wave inversion in leads V₁–V₄ is a normal variant in black athletes (Fig. 37.11), the presence of lateral T wave inversion always requires comprehensive testing even if the echocardiogram is normal. Furthermore, pathological q waves (q/S > 0.25) are not a feature of the athlete's ECG.

In contrast, patients with HCM, including athletes affected with the condition, frequently show ST segment depression and deep T wave inversion in the lateral leads (>80%) and a third show pathological q waves. Deep T wave inversion in the mid and lateral precordial leads (V₃–V₆) (Fig. 37.12) is highly suggestive of apical HCM but may be associated with a normal echocardiographic appearance. Contrast echocardiography is particularly useful for making the diagnosis in the echocardiography laboratory in such cases. CMR permits better visualization of the apex and anterolateral LV wall and provides a unique advantage in the identification of myocardial fibrosis, often allowing it to be diagnostic in apical HCM (Fig. 37.13). Indeed CMR is the investigation of choice for athletes with unexplained T wave inversion following echocardiography [19].

The Role of Cardiopulmonary Exercise Testing

As individuals with HCM do not augment stroke volume very well, they usually do not achieve very high peak VO₂ values on cardiopulmonary exercise testing. A peak VO₂ of 50 ml/min/kg or more than 120% of that predicted for age, gender and size predicts physiological over pathological LVH [20] (Fig. 37.14).

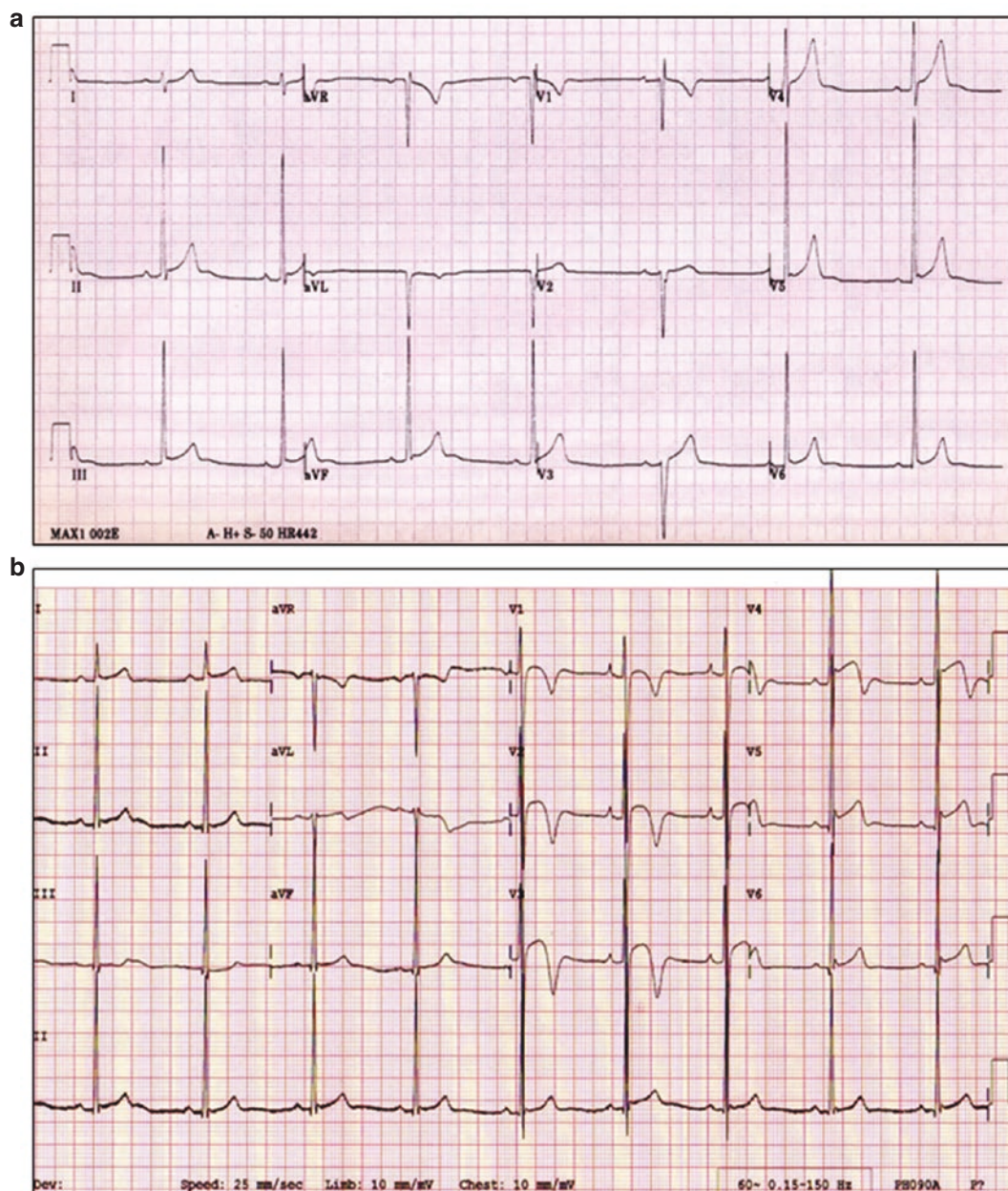


Fig. 37.11 (a) A normal athlete's electrocardiogram showing isolated increases in QRS voltages in the left precordial leads (V₅ and V₆) without ST segment depression

or T wave inversion. (b) An electrocardiogram from a healthy black athlete with deep T wave inversion in leads V₁-V₄ and preceding convex ST segment elevation

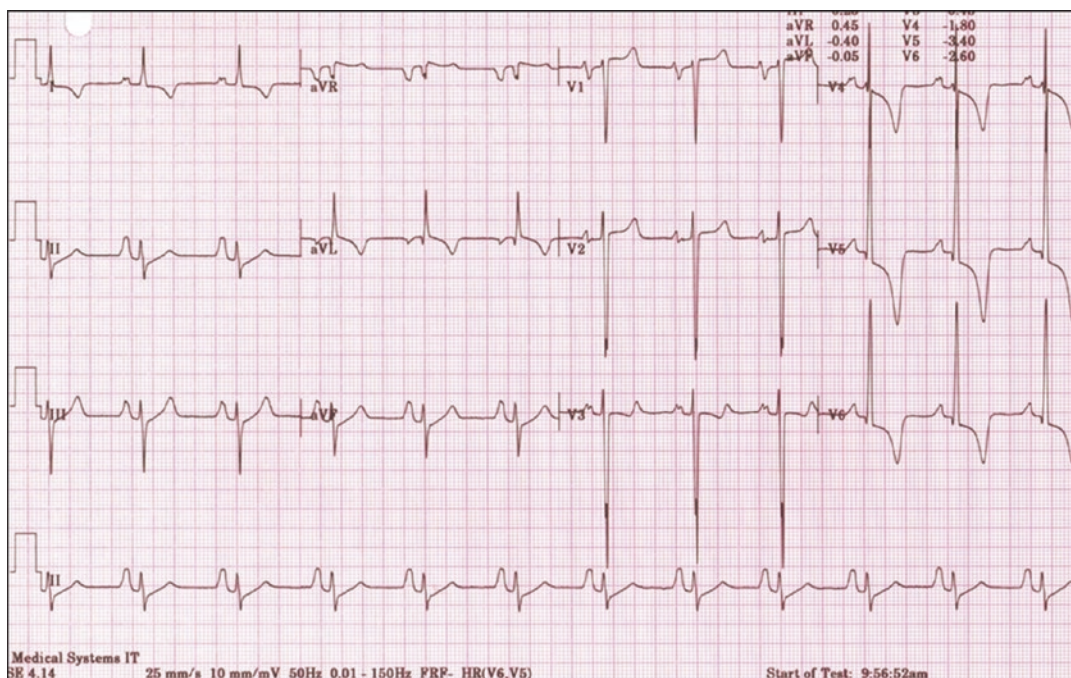


Fig. 37.12 An abnormal electrocardiogram from a patient with apical HCM, showing deep T wave inversion from the mid precordial to lateral leads with increases in QRS voltages and ST segment depression in the left precordial leads



Fig. 37.13 Apical hypertrophic cardiomyopathy on cardiac magnetic resonance imaging. Steady-State Free Precession (SSFP) Cine four chamber view

Athlete's Heart versus Dilated Cardiomyopathy (DCM)

Some athletes exhibit marked increases in LV cavity dimensions and low calculated ejection fractions, which raises suspicion of DCM. This scenario is not uncommon in endurance athletes. In a study of 216 Tour de France cyclists, 147 (51%) had LV cavities >60 mm and 12% had ejection fractions of less than 50%. In this situation the Simpson's formula to assess LV performance can result in the false interpretation that LV function is impaired by not appreciating the specific loading conditions of the athlete's heart. In other words, an athlete with a big ventricle and low peripheral vascular resistance, who is resting, does not require much LV wall systolic

Fig. 37.14 Algorithm summarizing how to distinguish between physiological left ventricular hypertrophy of the athlete's heart and hypertrophic cardiomyopathy. *HCM* hypertrophic cardiomyopathy, *LA* left atrium, *LV* left ventricle, *LVH* left ventricular hypertrophy

Bizarre patterns of hypertrophy

LA > 50 mm

LV outflow tract obstruction

Impaired diastolic function

ST depression/Deep T wave inversion

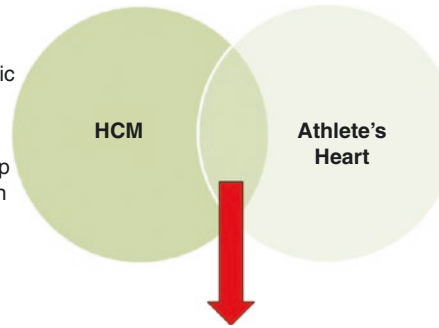
Impaired LV function

Female gender

Peak $\text{VO}_2 > 50$ ml/kg/min

Myocardial fibrosis

Athlete's Heart or HCM



LV cavity > 54 mm

h/R ratio < 0.5

Isolated Sokolow-Lyon LVH

Absence of HCM in first degree relatives

Regression of LVH with detraining

LVH 13-16 mm

excursion to achieve an adequate cardiac output. Although there are few studies investigating methods for differentiating physiological increases in LV cavity size with low basal ejection fraction from DCM, there is information to suggest that a dramatic improvement in parameters of systolic LV function at exercise echocardiography would be consistent with athlete's heart [21]. Measurements of ejection fraction at peak exercise, or pulsed wave tissue Doppler e' and systolic annular velocity should increase to well within expected normal ranges. In fact, an athlete with a large LV cavity dimension usually predicts a high peak oxygen consumption and such individuals frequently reveal a peak oxygen consumption of >50 ml/min/kg.

By comparison, an athlete with DCM may be symptomatic with breathlessness and exercise intolerance. On the resting echocardiogram, pulsed wave tissue Doppler will demonstrate a low e' velocity and a low systolic annular velocity of <9 cm/s. Utilising exercise cardiac imaging, an increase in LV ejection fraction of $\geq 10\%$ from resting baseline favours a physiologically dilated, athletic ventricle. Increases of LV ejection fraction of $<10\%$, inability to augment ejection fraction during exercise or a decrease from baseline are all suggestive of DCM, with increasing likelihood in the latter [22]. A lower than pre-

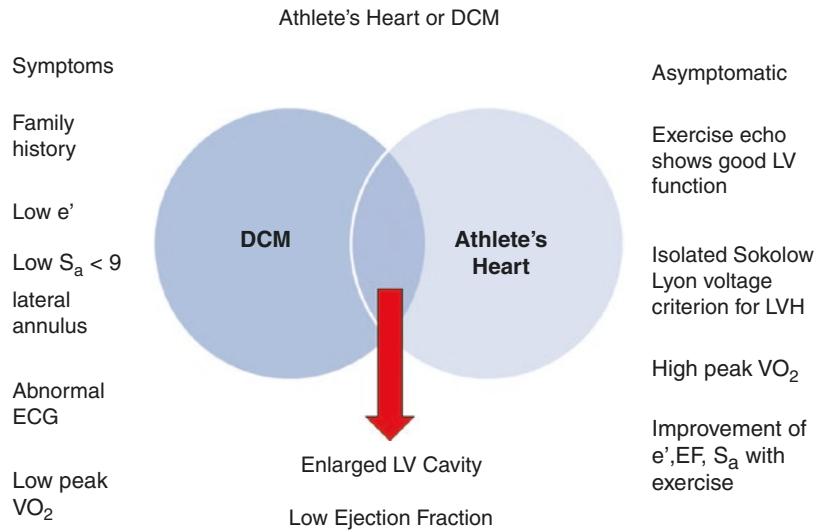
dicted peak VO_2 , an abnormal ECG, and evidence of myocardial fibrosis on CMR would support pathology (Fig. 37.15).

Athlete's Heart versus Arrhythmogenic Right Ventricular Cardiomyopathy (ARVC)

The right ventricle (RV) is occasionally referred to as the "forgotten chamber". This is certainly not due to its lack of importance in cardiovascular physiology but to the poverty of tools that exist to describe right ventricular structure and function. The assessment of the RV may be challenging using echocardiography as it is incompletely visualized in any 2-dimensional window due to its crescentic shape. However, the assessment of the RV of an athlete is essential considering that the RV sustains a greater magnitude of haemodynamic stress than the LV during exercise [23] and that ARVC is a recognized cause of sudden death in young athletes.

As with the LV, the RV in athletes is also increased in size compared with non-athletes. A significant proportion of athletes reveal a RV cavity dimension exceeding upper limits for the general and relatively sedentary population. Among endurance athletes, 40% have a

Fig. 37.15 Algorithm summarizing how to distinguish between physiological left ventricular dilatation of the athlete's heart and dilated cardiomyopathy. *ECG* electrocardiogram, *EF* ejection fraction, *LV* left ventricle, *LVH* left ventricular hypertrophy, *Sa* systolic annular velocity



right ventricular outflow tract diameter exceeding upper limits of normal according to the American Society of Echocardiography [24] and 57% have an enlarged right ventricular inflow tract diameter [4].

ARVC cannot be diagnosed using a solitary investigation and requires the integration of multiple sources of information to satisfy Task Force criteria [25]. The major echocardiographic criterion for ARVC is regional RV akinesia, dyskinesia or aneurysm, plus at least one of the following; a RVOT measurement taken from the parasternal long axis view of >32 mm, or taken from the parasternal short axis view of >36 mm, or a fractional area change of $<33\%$ [25]. When applying these cut off values to athletes, a large proportion of athletes fall into the grey zone between physiological RV enlargement and ARVC. A large study evaluating 300 black athletes and 375 white athletes participating in 25 sporting disciplines showed that RV enlargement considered significant in the Task Force criteria for ARVC was frequently observed in athletes of both ethnicities (45.0% black athletes and 58.5% white athletes) [3] (Fig. 37.16). A slightly low RV fractional area change can be explained by the fact that an enlarged right ventricle does not have to pump in dynamic fashion at rest in athletes. Therefore, a dilated RV with borderline low RV fractional area change (31–40%) should not raise alarm in

an asymptomatic athlete in the absence of a family history of ARVC [26].

Echocardiographic Parameters for the Differentiation of Physiological Right Ventricle Enlargement from ARVC

In contrast to individuals with ARVC, athletes exhibit a symmetrically enlarged LV (Fig. 37.17). A RV basal dimension (RVD1) to LV end-diastolic diameter of ≤ 0.9 is suggestive of physiological RV enlargement [26].

Athletes have normal indices of RV systolic function including a high tricuspid annular peak systolic excursion (TAPSE) ≥ 24 mm and high systolic annular velocities of >10 cm/s. High systolic annular velocities in the RV appear to correlate with exercise performance suggesting that this is a measure of enhanced RV diastolic function [5]. As such, an athlete with an enlarged RV, with a small fractional area change but a TAPSE of >14 mm, a systolic annular velocity of >9 cm/s and a large LV cavity size would indicate physiological RV enlargement rather than ARVC in the absence of symptoms or a family history.

In contrast, findings suggestive of RV pathology include regional wall motion abnormalities or RV aneurysms, which should trigger more comprehensive investigation including CMR

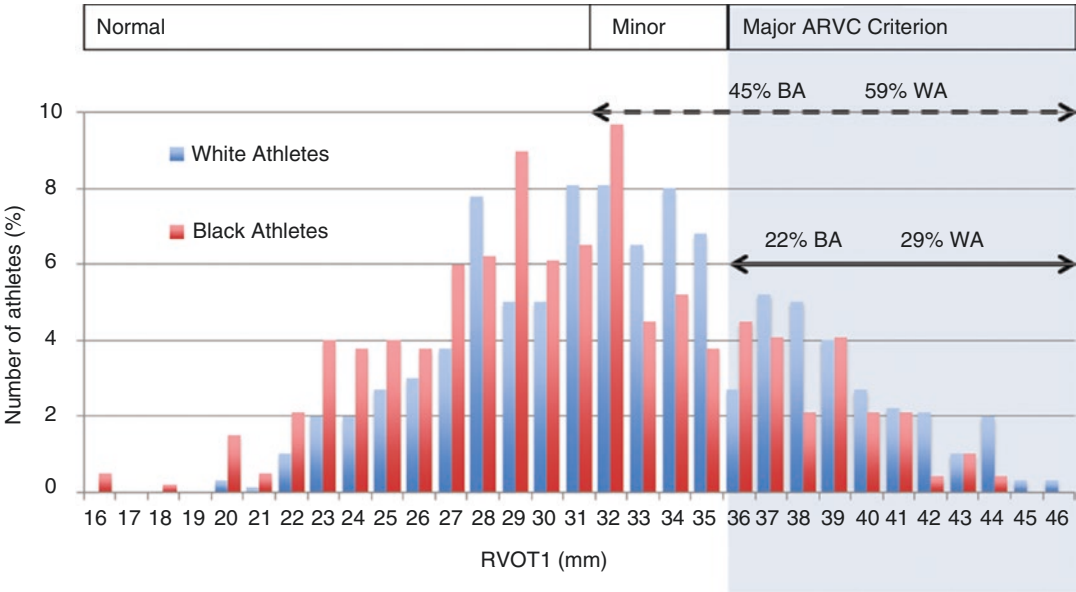


Fig. 37.16 Right ventricular outflow tract dimensions in a cohort of 300 black highly trained athletes and 375 white highly trained athletes. *RVOT1* right ventricular out-

flow tract measured from the parasternal short axis view. Reproduced with permission from Zaidi et al. [3]

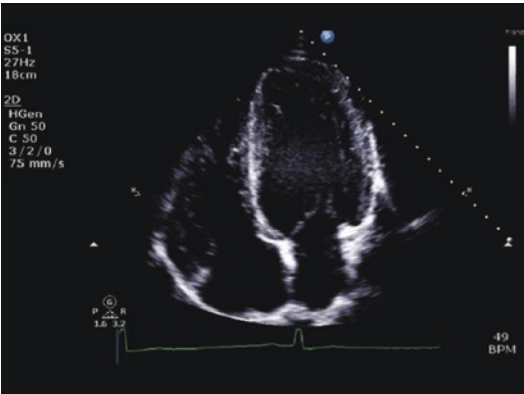


Fig. 37.17 Athlete's heart on echocardiography with symmetric LV and RV enlargement shown in the four chamber view

(Fig. 37.18). CMR has added value in the diagnosis of ARVC in athletes as it has the ability to assess RV structure and function as well as demonstrating myocardial fibrosis (Fig. 37.19).

The Role of the ECG

The ECG may be useful in the differentiation between physiological RV enlargement and ARVC. In general, anterior T wave inversion beyond V_2 with an isoelectric or downward shift of the ST segment is extremely rare in athletes, irrespective of ethnicity, and favours the diagnosis of ARVC. Other features in support for the diagnosis of ARVC include epsilon waves or multiple polymorphic ventricular extrasystoles of RV origin (Fig. 37.20).

Athlete's Heart versus Isolated Left Ventricular Non Compaction (LVNC)

Finally, worthy of mention is the detection of numerous and prominent trabeculations within the LV myocardium of the athlete (Fig. 37.21).

Regional Wall Motion Abnormalities in ARVC

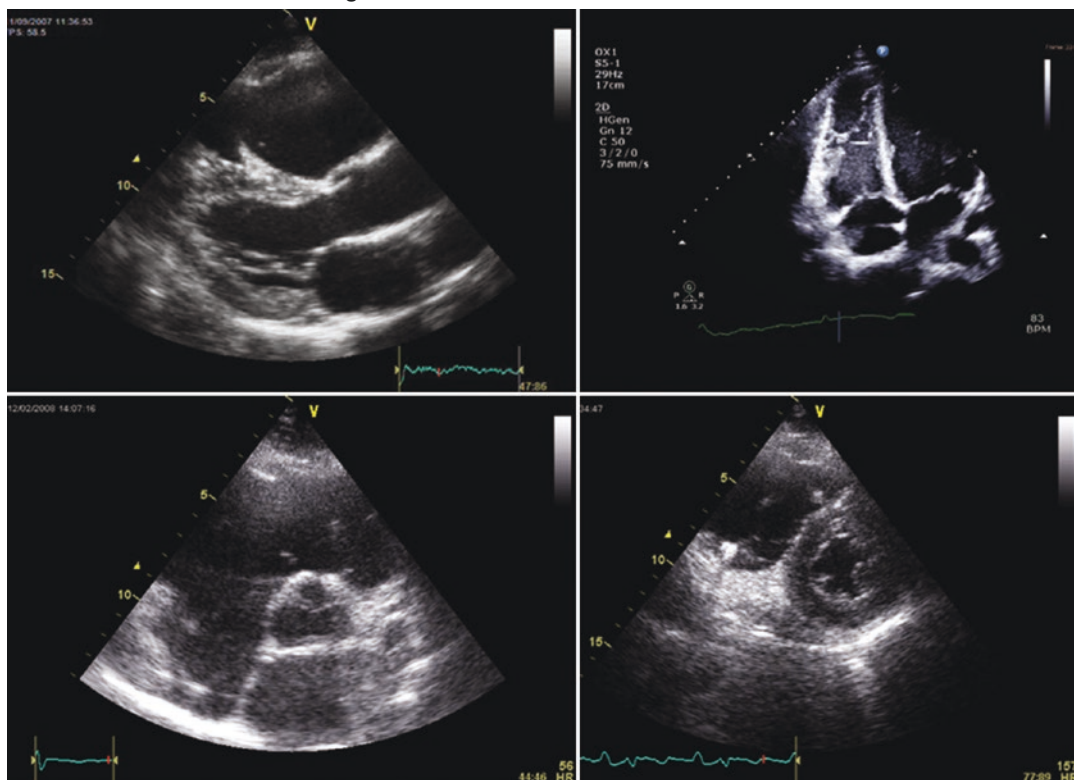


Fig. 37.18 Arrhythmogenic right ventricular cardiomyopathy on echocardiography. Clockwise from top left; the parasternal long-axis view, the apical four-chamber view and the parasternal short axis view at the level of the

papillary muscles and the parasternal short axis view at the level of the aortic valve. These show right ventricular dilatation and abnormal right ventricular morphology

A cross-sectional study of over 1000 athletes reported that 18% of athletes exhibited increased LV trabeculations that were > 2 standard deviations above the population mean. Moreover, 8% of athletes fulfilled echocardiographic criteria introduced by Chin et al. [27] and Jenni et al. [28], which were developed for the diagnosis of LVNC. These athletes were asymptomatic and had no clinical features associated with LVNC, such as heart failure, thromboembolic events or arrhythmias [29].

It is unlikely that such a high proportion of athletes express a mild form of LVNC. One hypothesis is that an increase in cardiac preload

may cause increased LV trabeculation as part of a benign remodeling process akin to increased LV thickening (an epiphenomenon). This process of LV trabeculation increasing at a time of elevated cardiac workload has been described in a prospective study of 104 pregnant women with morphologically normal left ventricles who underwent serial echocardiography in the first trimester, third trimester and 6 months post partum. Of these, 25% developed de novo LV trabeculations and 8% fulfilled echocardiographic criteria for LVNC. One year post-delivery, the increased LV trabeculations regressed in almost all women [30].

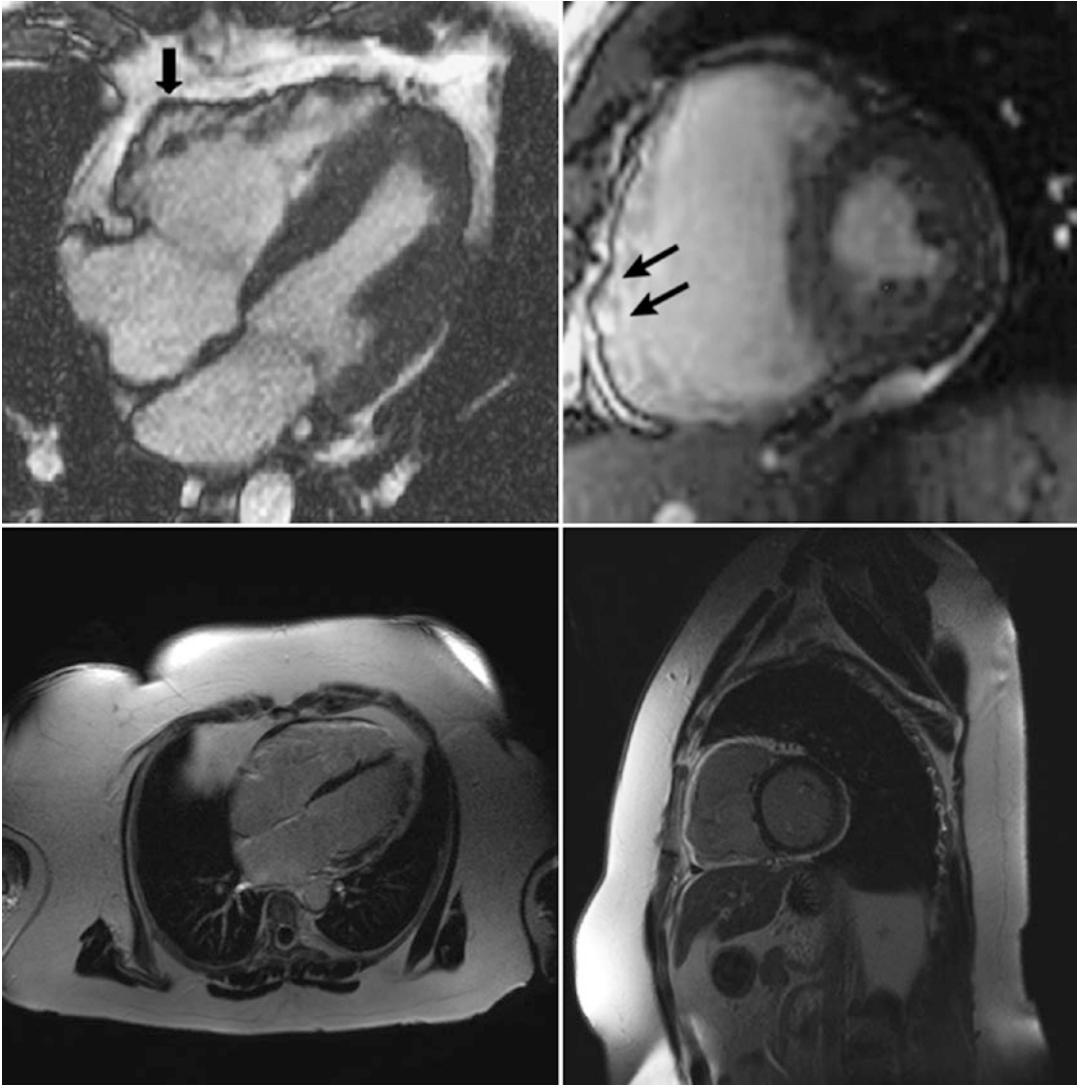


Fig. 37.19 Cardiac MRI images of two different patients with arrhythmogenic right ventricular cardiomyopathy. The top panels demonstrate aneurysms of the RV free wall in four chamber view (top left) and short axis view at the

level of the papillary muscles (top right). The bottom panels show diffuse RV fibrosis and wall thinning in four chamber view (bottom left) and short axis view at the level of the mitral valve (bottom right)

It is recognized that 0.9% of athletes have shown a triad of increased LV trabeculation, reduced LV systolic function and repolarization changes, comprising of T wave inversion, which raises the possibility of isolated LVNC [29]. In such individuals the presence of cardiac symptoms, family history of LVNC, T wave inversion in the lateral leads, failure of LV function to improve with exercise, exercise induced

arrhythmias and a low peak oxygen consumption may suggest LVNC (Fig. 37.22).

In conclusion, athletic training is associated with structural changes that may mimic cardiomyopathy, the differentiation between the athlete's heart and cardiomyopathy is possible using a methodical and clinical approach but it can be challenging even for those in the field who evaluate athletes frequently (Fig. 37.23).

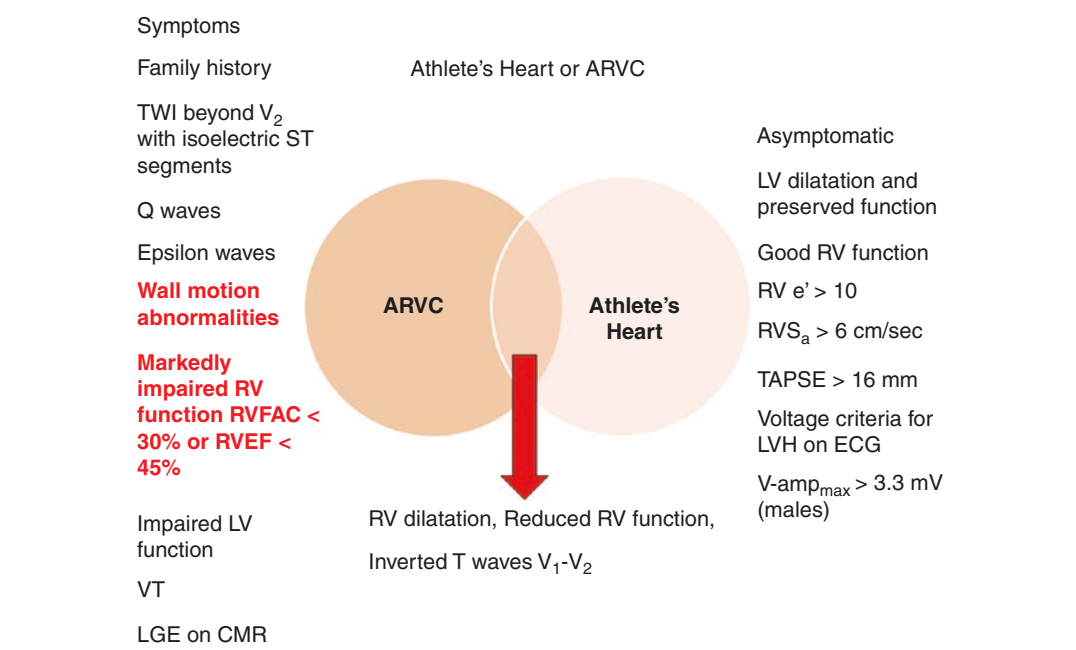


Fig. 37.20 Algorithm summarizing how to distinguish between physiological right ventricular adaptation of the athlete's heart and arrhythmogenic right ventricular cardiomyopathy. *ARVC* arrhythmogenic right ventricular cardiomyopathy, *CMR* cardiac magnetic resonance, *ECG* electrocardiogram, *LBBB* left bundle branch block, *LGE* late gadolinium enhancement, *LV* left ventricle, *LVH* left ventricular hypertrophy, *RV* right ventricle, *RVEF* right ventricular ejection fraction, *RVFAC* right ventricular fractional area change, *TAPSE* tricuspid annular plane systolic excursion, *TWI* T wave inversion, *V-amp_{max}* maximal QRS amplitude in the precordial leads, *VT* ventricular tachycardia

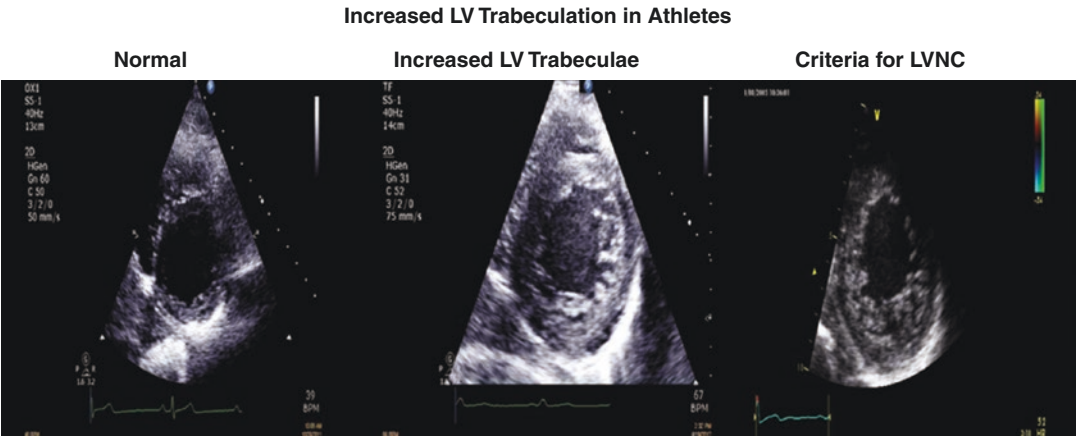


Fig. 37.21 Increased LV trabeculations on echocardiography in athletes demonstrating the challenge of distinguishing between normal and LVNC

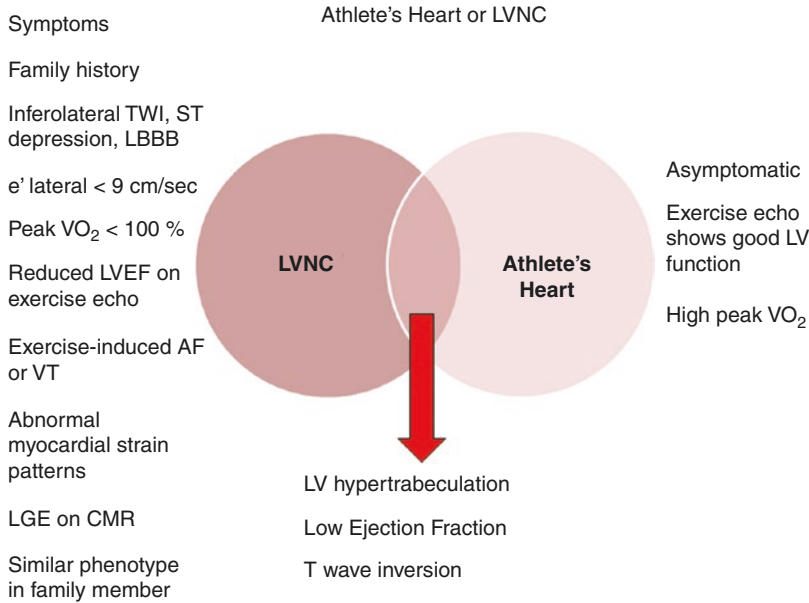


Fig. 37.22 Algorithm summarizing how to distinguish between physiological increased left ventricular trabeculation of the athlete's heart and left ventricular non-compaction cardiomyopathy. *AF* atrial fibrillation, *CMR*

cardiac magnetic resonance, *LBBB* left bundle branch block, *LVEF* left ventricular ejection fraction, *LGE* late gadolinium enhancement, *LVNC* left ventricular non-compaction cardiomyopathy, *VT* ventricular tachycardia

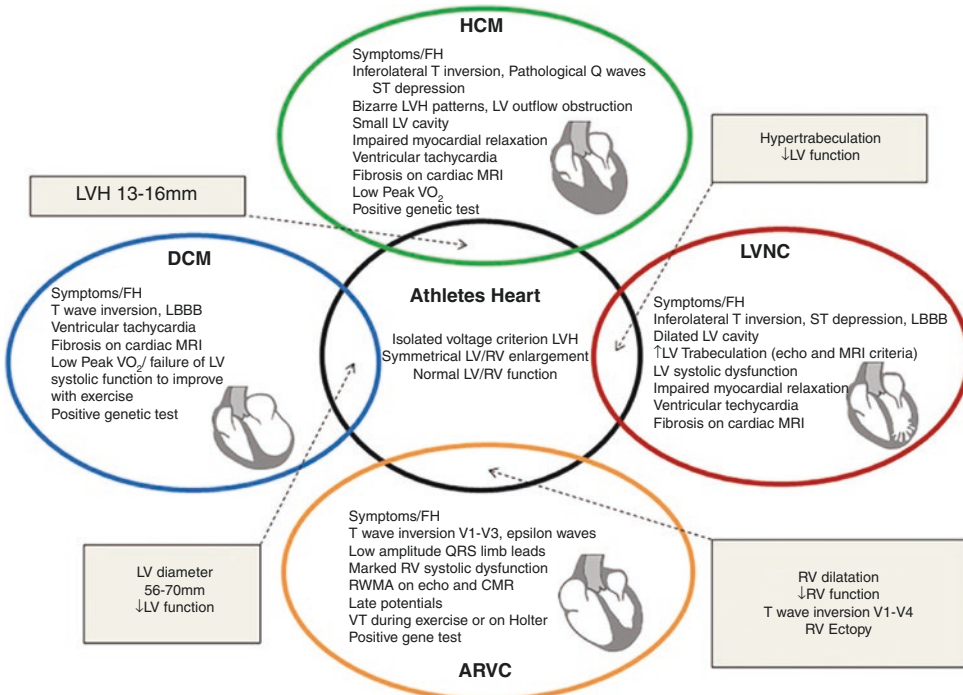


Fig. 37.23 Differentiating features between physiological cardiac changes and cardiomyopathy in athletes. *ARVC* arrhythmogenic right ventricular cardiomyopathy, *CMR* cardiac magnetic resonance, *DCM* dilated cardiomyopathy, *FH* family history, *HCM* hypertrophic cardio-

myopathy, *LV* left ventricle, *LVH* left ventricular hypertrophy, *LVNC* left ventricular non-compaction cardiomyopathy, *RWMA* regional wall motion abnormalities, *VT* ventricular tachycardia. Reproduced with permission from Sharma et al. [9]

References

- Mitchell JH, Haskell W, Snell P, Van Camp SP. Task force 8: classification of sports. *J Am Coll Cardiol*. 2005;45(8):1364–7.
- Maron BJ. Structural features of the athlete heart as defined by echocardiography. *J Am Coll Cardiol*. 1986;7(1):190–203.
- Zaidi A, Ghani S, Sharma R, Oxborough D, Panoulas VF, Sheikh N, et al. Physiological right ventricular adaptation in elite athletes of African and Afro-Caribbean origin. *Circulation*. 2013;127(17):1783–92.
- Oxborough D, Sharma S, Shave R, Whyte G, Birch K, Artis N, et al. The right ventricle of the endurance athlete: the relationship between morphology and deformation. *J Am Soc Echocardiogr*. 2012;25(3):263–71.
- D'Andrea A, Caso P, Sarubbi B, Limongelli G, Liccardo B, Cice G, et al. Right ventricular myocardial adaptation to different training protocols in top-level athletes. *Echocardiography*. 2003;20(4):329–36.
- Rodriguez CJ, Diez-Roux AV, Moran A, Jin Z, Kronmal RA, Lima J, et al. Left ventricular mass and ventricular remodeling among Hispanic subgroups compared with non-Hispanic blacks and whites: MESA (Multi-ethnic Study of Atherosclerosis). *J Am Coll Cardiol*. 2010;55(3):234–42.
- Maron BJ, Pelliccia A. The heart of trained athletes: cardiac remodeling and the risks of sports, including sudden death. *Circulation*. 2006;114(15):1633–44.
- Pelliccia A, Culasso F, Di Paolo FM, Maron BJ. Physiologic left ventricular cavity dilatation in elite athletes. *Ann Intern Med*. 1999;130(1):23–31.
- Sharma S, Merghani A, Mont L. Exercise and the heart: the good, the bad, and the ugly. *Eur Heart J*. 2015;36:1445.
- Zaidi A, Sharma S. Exercise and heart disease: from athletes and arrhythmias to hypertrophic cardiomyopathy and congenital heart disease. *Futur Cardiol*. 2013;9(1):119–36.
- Pelliccia A, Maron BJ, Spataro A, Proschan MA, Spirito P. The upper limit of physiologic cardiac hypertrophy in highly trained elite athletes. *N Engl J Med*. 1991;324(5):295–301.
- Basavarajaiah S, Boraita A, Whyte G, Wilson M, Carby L, Shah A, et al. Ethnic differences in left ventricular remodeling in highly-trained athletes relevance to differentiating physiologic left ventricular hypertrophy from hypertrophic cardiomyopathy. *J Am Coll Cardiol*. 2008;51(23):2256–62.
- Papadakis M, Carre F, Kervio G, Rawlins J, Panoulas VF, Chandra N, et al. The prevalence, distribution, and clinical outcomes of electrocardiographic repolarization patterns in male athletes of African/Afro-Caribbean origin. *Eur Heart J*. 2011;32(18):2304–13.
- Rawlins J, Carre F, Kervio G, Papadakis M, Chandra N, Edwards C, et al. Ethnic differences in physiological cardiac adaptation to intense physical exercise in highly trained female athletes. *Circulation*. 2010;121(9):1078–85.
- Sheikh N, Papadakis M, Carre F, Kervio G, Panoulas VF, Ghani S, et al. Cardiac adaptation to exercise in adolescent athletes of African ethnicity: an emergent elite athletic population. *Br J Sports Med*. 2013;47(9):585–92.
- Sheikh N, Papadakis M, Schnell F, Panoulas V, Malhotra A, Wilson M, et al. Clinical profile of athletes with hypertrophic cardiomyopathy. *Circ Cardiovasc Imaging*. 2015;8(7):e003454.
- Caselli S, Maron MS, Urbano-Moral JA, Pandian NG, Maron BJ, Pelliccia A. Differentiating left ventricular hypertrophy in athletes from that in patients with hypertrophic cardiomyopathy. *Am J Cardiol*. 2014;114(9):1383–9.
- Butz T, van Buuren F, Mellwig KP, Langer C, Plehn G, Meissner A, et al. Two-dimensional strain analysis of the global and regional myocardial function for the differentiation of pathologic and physiologic left ventricular hypertrophy: a study in athletes and in patients with hypertrophic cardiomyopathy. *Int J Cardiovasc Imaging*. 2011;27(1):91–100.
- Schnell F, Riding N, O'Hanlon R, Axel Lentz P, Donal E, Kervio G, et al. Recognition and significance of pathological T-wave inversions in athletes. *Circulation*. 2015;131(2):165–73.
- Sharma S, Elliott PM, Whyte G, Mahon N, Virdee MS, Mist B, et al. Utility of metabolic exercise testing in distinguishing hypertrophic cardiomyopathy from physiologic left ventricular hypertrophy in athletes. *J Am Coll Cardiol*. 2000;36(3):864–70.
- Abernethy WB, Choo JK, Hutter AM. Echocardiographic characteristics of professional football players. *J Am Coll Cardiol*. 2003;41(2):280–4.
- Claessen G, Schnell F, Bogaert J, Claeys M, Pattyn N, De Buck F, et al. Exercise cardiac magnetic resonance to differentiate athlete's heart from structural heart disease. *Eur Heart J Cardiovasc Imaging*. 2018.
- La Gerche A, Burns AT, Mooney DJ, Inder WJ, Taylor AJ, Bogaert J, et al. Exercise-induced right ventricular dysfunction and structural remodelling in endurance athletes. *Eur Heart J*. 2012;33(8):998–1006.
- Lang RM, Bierig M, Devereux RB, Flachskampf FA, Foster E, Pellikka PA, et al. Recommendations for chamber quantification: a report from the American Society of Echocardiography's guidelines and standards committee and the Chamber Quantification Writing Group, developed in conjunction with the European Association of Echocardiography, a branch of the European Society of Cardiology. *J Am Soc Echocardiogr*. 2005;18(12):1440–63.
- Marcus FI, McKenna WJ, Sherrill D, Basso C, Baucé B, Bluemke DA, et al. Diagnosis of arrhythmogenic right ventricular cardiomyopathy/dysplasia: proposed modification of the task force criteria. *Circulation*. 2010;121(13):1533–41.
- Zaidi A, Sheikh N, Jongman JK, Gati S, Panoulas VF, Carr-White G, et al. Clinical differentiation between physiological remodeling and Arrhythmogenic right ventricular cardiomyopathy in athletes with marked electrocardiographic repolarization anomalies. *J Am Coll Cardiol*. 2015;65(25):2702–11.

27. Chin TK, Perloff JK, Williams RG, Jue K, Mohrmann R. Isolated noncompaction of left ventricular myocardium. A study of eight cases. *Circulation*. 1990; 82(2):507–13.
28. Jenni R, Oechslin E, Schneider J, Attenhofer Jost C, Kaufmann PA. Echocardiographic and pathoanatomical characteristics of isolated left ventricular non-compaction: a step towards classification as a distinct cardiomyopathy. *Heart*. 2001;86(6):666–71.
29. Gati S, Chandra N, Bennett RL, Reed M, Kervio G, Panoulas VF, et al. Increased left ventricular trabeculation in highly trained athletes: do we need more stringent criteria for the diagnosis of left ventricular non-compaction in athletes? *Heart*. 2013;99(6): 401–8.
30. Gati S, Papadakis M, Papamichael ND, Zaidi A, Sheikh N, Reed M, et al. Reversible De Novo left ventricular Trabeculations in pregnant women: implications for the diagnosis of left ventricular non-compaction in low risk populations. *Circulation*. 2014; 130:475.

Introduction

Cardiac toxicity by chemotherapeutic agents was first described more than 50 years ago, after the introduction of Daunomycin as an antimetabolic agent [1]. The early recognition of heart failure as a side effect of anthracyclines, led the oncologists to limit its cumulative dose, and prompted them to serially monitor heart function looking for left ventricular dysfunction [2]. Initial tools included voltage reduction in electrocardiograms and measurement of systolic ejection time assessed by “sphygmo-recording” [3]. Nevertheless, endomyocardial biopsy and the echocardiographic evaluation of the left ventricular ejection fraction (LVEF) evolved as the methods more commonly used for the identification of anthracycline-induced cardiomyopathy [4, 5]. The importance of endomyocardial biopsy decreased over time due to cost, risks inherent to its invasive nature and more importantly the important advances made in noninvasive cardiac imaging. As a result, noninvasive calculation of LVEF became the most widely used tool for monitoring cardiac function during and after cancer therapy [6].

J. C. Plana
Baylor St. Luke’s Medical Center,
Baylor College of Medicine, Houston, TX, USA
e-mail: Juan.PlanaGomez@bcm.edu

Side Effects of Chemotherapeutic Agents and Cardiac Complications Following Chemotherapy

Chemotherapeutic agents may affect the cardiovascular system in different ways. Table 38.1 summarizes the most common side effects.

Historically, the term cardio-toxicity was used indistinctly to refer to all types of cardiotoxicity, although more commonly referring to left ventricular dysfunction.

The expert consensus on the multi-modality imaging of the adult patient during and after cancer therapy coined the new term of

Table 38.1 Most common side of effects of different chemotherapeutic agents in the cardiovascular system

Agent	Most frequent toxicity
Anthracyclines	Heart failure, myopericarditis, arrhythmias
Trastuzumab	Heart failure
Cyclophosphamide	Heart failure, myopericarditis, arrhythmias
Taxanes	Heart failure, ischemia, arrhythmias
Fluoracil	Myocardial ischemia and infarction
Cisplatin	Hypertension
Methotrexate	Ischemia, arrhythmias
Tamoxifen	Venous thrombosis
Radiotherapy	Restrictive heart disease, accelerated atherosclerosis, pericardial effusion

cancer therapeutics related cardiac dysfunction (CTRCD) to specifically refer to left ventricular dysfunction caused by chemotherapeutic agents. CTRCD was defined as a confirmed drop (by repeated cardiac imaging performed 2–3 weeks following the study showing the initial drop) of greater than 10 absolute points of LVEF to a value less than 53%. Drops may be further categorized as symptomatic or asymptomatic, or with regard to reversibility, i.e., reversible (to within 5% points of baseline) partially reversible (improved by at least 10% points, but remaining more than 5% points below baseline) irreversible (remaining within 10% points of the nadir) or indeterminate (patient not available for re-evaluation due to death or refusal to undergo further imaging [7].

Classification of Cardio-Toxic Drugs

Although there are more than 200 chemotherapeutic agents with different mechanisms of action and toxicity, for the sake of day to day clinical practice the expert consensus breaks CTRCD down in two types: Type I and II. Table 38.2 summarizes the differences using anthracyclines and trastuzumab as the prototypes for type I and II CTRCD. The understanding of the mechanisms of toxicity is essential, as it will give the clinicians the knowledge needed to know what to look for during surveillance of toxicity.

Mechanisms of Toxicity

Anthracyclines

Anthracycline cardiac toxicity has been for long attributed to the production of reactive oxygen species. Nevertheless, in the last decade the role of the enzyme topoisomerase 2 has gained significant relevance [8]. There are two topoisomerase 2 iso-enzymes in mammal species: Top2 α and Top2 β . It has been demonstrated that the anti-tumoral effect of doxorubicin is mediated by the formation of a ternary complex between Top2 α , doxorubicin and the DNA double helix [9]. Top2 α is only expressed in cells with a high mitotic rate like neoplastic cells, which explains the high efficacy of anthracyclines. In contrast, Top2 β is only expressed in normal tissue like cardiac cells. It was recently demonstrated in a Top2 β knockout animal model that dexrazoxane, a known cardio-protectant against doxorubicin cardiotoxicity, is active through the inhibition of Top2 β , which supports the role of Top2 β in anthracycline-induced CTRCD [10].

The incidence of heart failure fluctuates between 2.2 and 5.1% depending on the series [11]. The curves elaborated by Von Hoff and Swain showed that heart failure incidence is relatively low until a cumulative dose of 450 mg/m² is achieved [12]. This finding promoted the common belief that CTRCD was unlikely with doxorubicin doses lower than 450 mg/m².

Table 38.2 Characteristics of type I and type II CTRCD

	Type I	Type II
Characteristic agent	Doxorubicin	Trastuzumab
Clinical course and typical response to antiremodeling therapy (β -blockers, ACE inhibitors)	May stabilize, but underlying damage appears to be permanent and irreversible; recurrence in months or years may be related to sequential cardiac stress	High likelihood of recovery (to or near baseline cardiac status) in 2–4 months after interruption (reversible)
Dose effects	Cumulative, dose related	Not dose related
Effect of rechallenge	High probability of recurrent dysfunction that is progressive; may result in intractable heart failure or death	Increasing evidence for the relative safety of rechallenge (additional data needed)
Ultrastructure	Vacuoles; myofibrillar disarray and dropout; necrosis (changes resolve over time)	No apparent ultra structural abnormalities (though not thoroughly studied)

Adapted with permission from Plana JC, Galderisi M, Barac A. Expert consensus for the multi-modality imaging of the adult patient during and after cancer therapy. J Am Soc Echocardiogr : 2014;27:911–39

Nevertheless, animal data reported by Neilan et al. showed that CTRCD is produced with doses as low as 20 mg/kg of doxorubicin, after detecting a 75-fold increase in cardiac cell apoptosis only 24 h after exposure [13]. The actual theory of anthracycline-induced CTRCD, supports the concept of an early and cumulative-dose dependent myocyte apoptosis. The later drop in LVEF follows the heart failure bio-mechanic model associated with negative left ventricular remodeling with subsequent secondary neuro-hormonal activation [14]. Anthracycline-induced CTRCD has been linked to a very poor prognosis, with 2-year mortality as high as 60% [15].

Trastuzumab

The amplification of the HER2/neu (ErbB2) gene identifies a group of breast cancer patients with very poor prognosis. Trastuzumab (Herceptin®) is a humanized monoclonal antibody that targets the tyrosine kinase receptor encoded by ErbB2 gene [16]. The development of this monoclonal antibody has been one of the most significant breakthroughs in the history of translational research after its approval in 1998. Multiple large-scale studies have proven that trastuzumab significantly reduces the risks of recurrence and early death in patients with HER2-positive breast cancers. However, symptomatic heart failure has been reported in 4% of treated patients and sub-clinical LV dysfunction in up to 10% of treated patients [17].

Combined Chemotherapy

The addition of trastuzumab to anthracyclines therapy increases the toxicity risk. Slamon et al. compared three chemotherapy regimens in patients with metastatic HER2 positive breast cancer, reporting a rate of 27% drop in LVEF in the group of combined trastuzumab-anthracycline, 13% in the trastuzumab-paclitaxel protocol and 8% in the trastuzumab free group. The incidence of severe cardiac dysfunction with

New York Heart Association (NYHA) class III or IV was the highest with 16%, in the patients who received trastuzumab and anthracycline, compared to 3% in patients who received anthracyclines without trastuzumab and 2% of those who received trastuzumab and paclitaxel [18].

Animal studies done using a cardiac stress model mediated by hemodynamic overload (aorta ligation), showed that ErbB2 knockout mice were significantly more susceptible to cardiac toxicity and heart failure. These findings support the crucial role of the ErbB2 as a cardio-protective pathway, that permits myocyte survival during acute stress signaling activation [19]. A blockade in this cardio-protective pathway after anthracycline exposure, creates the substrate for apoptosis during subsequent exposure to trastuzumab. This premise is consistent with clinical findings showing evidence of increased CTRCD after exposure to trastuzumab in patients with underlying myocardial disease in which the cardiac stress signals are presumably already activated [17].

Methods for Early Detection

LVEF is a major predictor of outcome in CTRCD, and the most common method used to evaluate cardiac function at baseline and during cancer treatment [6]. Although different imaging modalities have been used, LVEF is most commonly evaluated with echocardiography [20].

2D Echocardiography

Echocardiography has been established as the cornerstone in the imaging evaluation of patients in preparation for, during, and after cancer therapy. This is due to its wide availability, versatility, lack of radiation exposure, and low cost when compared to other modalities (nuclear medicine, magnetic resonance imaging). In addition to the evaluation of left and right ventricular dimensions, systolic and diastolic function at rest and during stress, it also allows a comprehensive evaluation of cardiac valves, aorta and pericardium, making it the imaging modality

of choice in the evaluation of the cancer patient [21–25]. However, the technique is affected by the quality of the acoustic window, the use of geometric assumptions in the calculation of left ventricular (LV) volumes, load dependency and operator expertise [26]. Thavendiranathan et al., reported that the 95% upper confidence interval for 2D LVEF is 10% when sequentially following cardio-oncology patients. This is problematic as this is the magnitude of change in LVEF that is looked for to adjudicate CTRCD [7, 27]. Additionally, the reported intra and inter-observer variability is significantly high, with ranges that fluctuate between 6–11% and 8–16% respectively, depending on the series [28].

Contrast Enhanced Echocardiography

The use of contrast agents is crucial for the assessment of LV volumes and function when the endocardium is not well defined, as it opacifies the LV and enhances the endocardial border definition [29]. This is particularly important as endocardial border dropout is frequently encountered in the imaging of patients with breast cancer due to prior mastectomy, chest radiation, insertion of breast expanders and breast reconstruction surgery. The American Society of Echocardiography and the European Association of Cardiovascular Imaging recommend the use of ultrasonic contrast agents when ≥ 2 contiguous LV segments are not seen on non-contrast images [7, 30, 31]. Nahar et al. compared LVEF quantification by radionuclide angiography with four different 2D echocardiography techniques (fundamental, fundamental with contrast, harmonic, and harmonic with contrast), reporting incremental correlation with each method. However, harmonic imaging with contrast provided the closest correlation [32]. Also, when compared with standard 2D imaging, contrast enhancement increased the feasibility of biplane volume analysis from 79 to 95%, and narrowed the limits of LVEF agreement between echo and CMR from -18.1

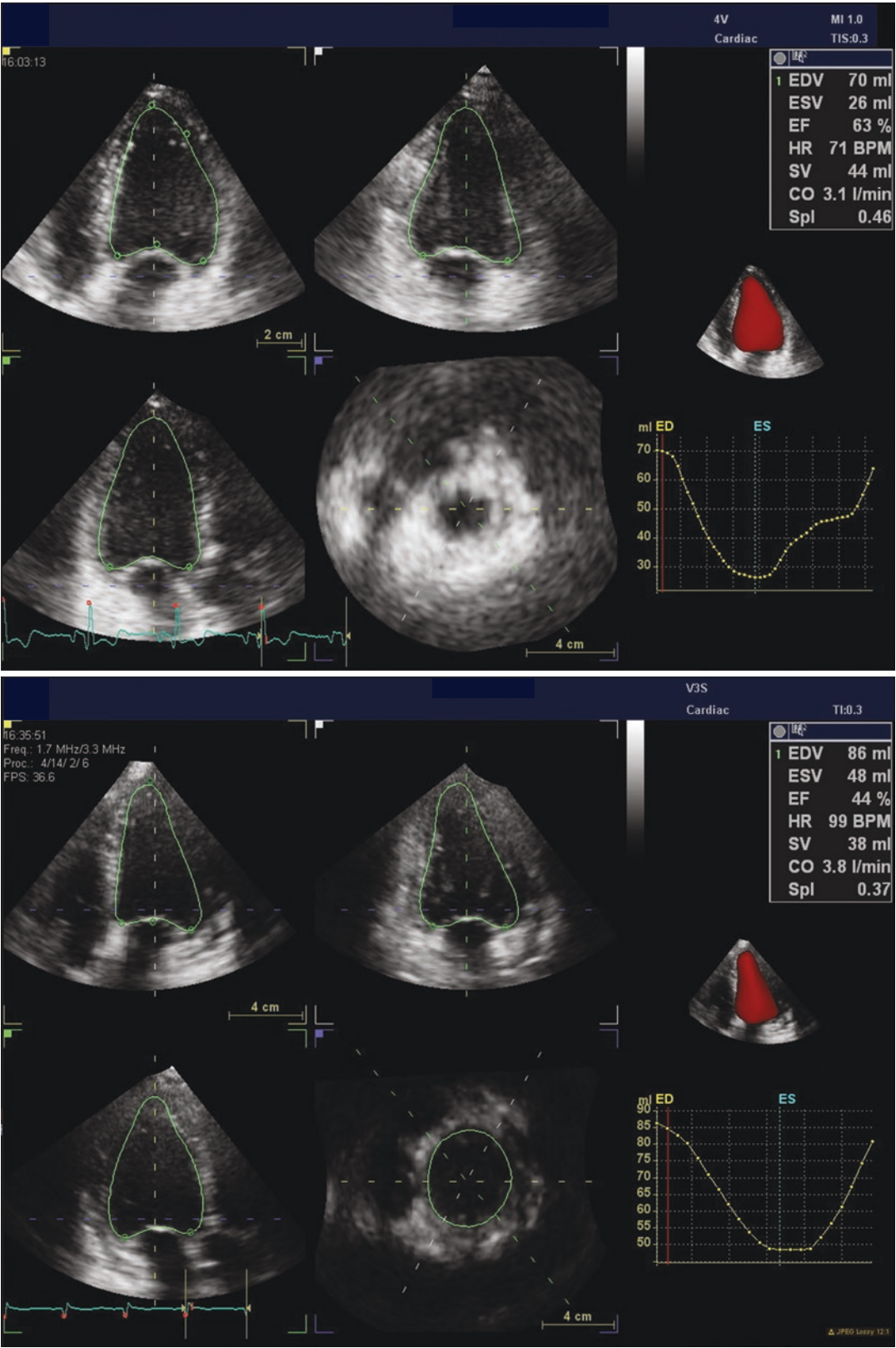
to 8.3% to -7.7 to 4.1% [33]. Intra and inter-observer reproducibility also benefited from contrast use, achieving correlation indices (r) of >0.9 [29].

To obtain the best enhancement echocardiographic contrast, it is crucial to optimize the 2D images in the 4-chamber view; bringing the mechanical index to 0.15–0.3 to decrease the amount of bubble destruction and adjust the probe frequency for best penetration. Once the injection of contrast starts, the rate of injection needs to be decreased if attenuation is present or increased swirling is observed.

3D Echocardiography

The main pitfalls of 2D echocardiography in the calculation of ventricular volumes and LVEF quantification are the geometrical assumptions made, and the common foreshortening of the left ventricle. Real time 3D echocardiography emerged as an alternative because of its ability to capture full ventricular volumes with no geometrical assumptions and allowing easy identification of the true apex of the heart [34]. Jacobs et al. compared the accuracy of 2D and 3D imaging against CMR for measuring end diastolic volume, end systolic volume, and LVEF. 3D measurements had a higher correlation with CMR ($r = 0.96, 0.97$ and 0.93 for EDV, ESV and EF respectively) [35].

Real time 3D has also proven to be a reproducible tool, making it the ideal method for the sequential calculation of LVEF required in chemotherapy patients. A comparison of four techniques (2D bi-plane, 2D tri-plane and 3D echocardiogram with and without contrast) in patients undergoing chemotherapy and stable LV function showed that non-contrast 3D volume and LVEF had the best intra and inter-observer as well as the lower test-retest variability giving the operator the possibility of identifying changes of 6 absolute point of LVEF (below the 10 point threshold that would adjudicate CTRCD). 3D LVEF provided an upper CI limit of 4.9 [27] (Fig. 38.1).



Contrast Enhanced 3D Echocardiography

There is contradictory data regarding the advantages of contrast enhanced 3D echocardiography, currently preventing its use on daily clinical practice.

Corsi et al. compared contrast 3D imaging with CMR, reporting not only an improvement in the accuracy and reproducibility of LV volume measurements in patients with poor image quality, but also an enhancement in the assessment of regional wall motion assessment from 3D datas-

ets [36]. In contrast, Jenkins et al. reported that contrast enhanced 3D echocardiography was not superior to a contrast 2D approach for LVEF measurement when compared to CMR. However contrast 3D was superior to other contrast and non-contrast modalities in patients with previous infarction [37]. Following the same line, a recent study performed in cancer patients undergoing chemotherapy did not show advantage of contrast 3D over standard 3D imaging for determination of LV volumes and LVEF in terms of reproducibility and temporal variability [27] (Fig. 38.2).

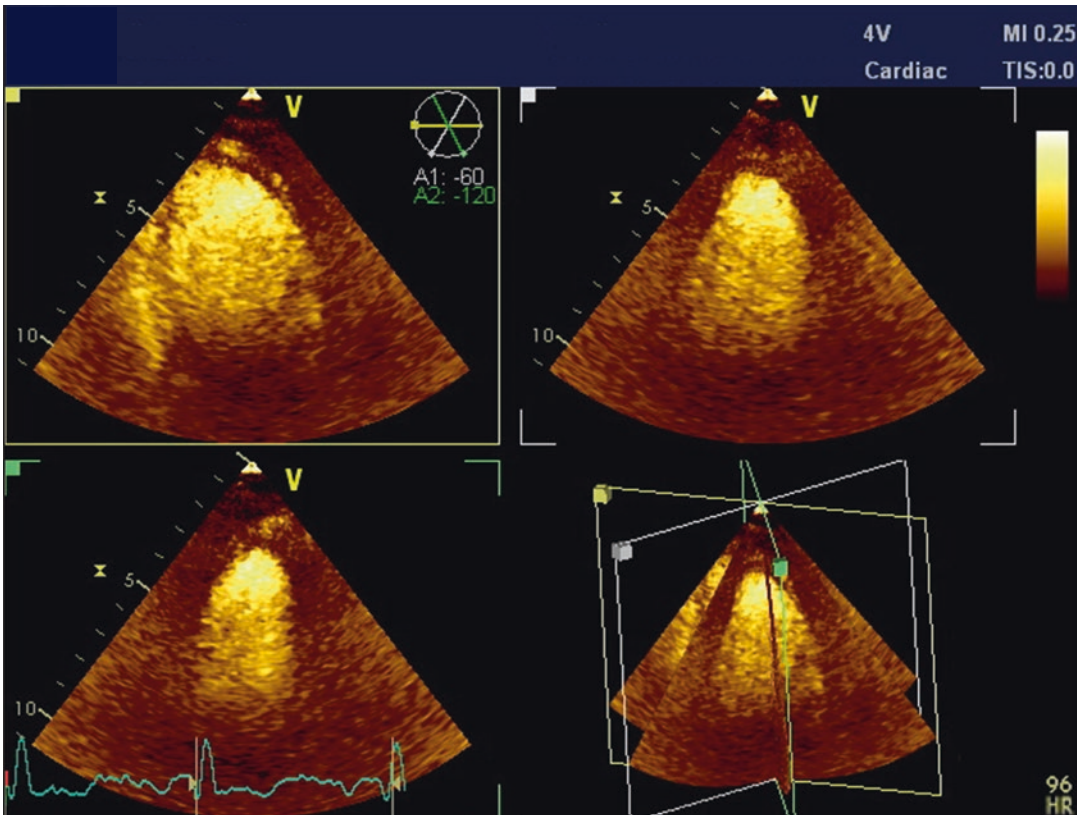


Fig. 38.2 3D LVEF with echocardiographic contrast enhancement

2D Based Left Ventricular Strain

Although LVEF is the most common method of monitoring cardiac function during cancer treatment, it is not optimal due to its inherent variability (>10%) [27], and as a result inability to detect early subtle changes in ventricular function [38]. Evaluation of left ventricular mechanics using 2D speckle-tracking have emerged as a reproducible and more accurate method for evaluation of systolic function [39–41], and the detection of detect subclinical left ventricular dysfunction [42–45].

Global longitudinal strain (GLS) is calculated as the percentage of shortening or lengthening of an individual segment and is reported as a mean of the 18 cardiac segments.

GLS also has a lower inter-observer variability as reported by Marwick et al. [46]. The authors studied the GLS inter-observer variability in 242 normal subjects, reporting a mean difference 0.24% and a 95% CI of −9.6 to +9.7%.

GLS has proven to be an early independent predictor of subsequent reduction in LVEF after exposure to chemotherapeutic drugs. Negishi et al. evaluated the optimal myocardial deformation index to predict CTRCD at 12 months in 100 breast cancer patients that received chemotherapy (46 with simultaneous anthracyclines and trastuzumab). They assessed them at baseline, 6 months and 12 months and found that a 11% drop in GLS (95% CI, 8.3–14.6%) was the strongest predictor of later cardiotoxicity with an area under the curve of 0.87, a sensitivity of 65% and a specificity of 94% [47] (Fig. 38.3).

In clinical practice, GLS should be used in all patients exposed to cardio-toxic regimens where available. When baseline strain measurement is available a GLS reduction $\geq 15\%$ when compared to baseline is considered of clinical significance.

If a baseline strain assessment is not available, the reader is referred to the JUSTICE study defining abnormality as 2 SD below the mean for vendor, gender and age (Table 38.3) [48].

Stress Echocardiography

Exercise and dobutamine stress echocardiography have been used in the identification of anthracycline-induced CTRCD. In 31 cancer patients studied before, during and after 6 months chemotherapy therapy, low dose dobutamine did not provide additional value for the early detection of cardiotoxicity [49, 50]. A prospective study of LV contractile reserve by repeated low-dobutamine stress echocardiograms in 49 women with breast cancer showed that a reduction in LVEF with dobutamine >5%, appeared to be a threshold that discriminate the risk of a future drop in LVEF [51].

It is reasonable to assess the presence of ischemia in patients with risk factors or known history of CAD who will receive regimens associated with ischemia induction (i.e. 5FU and anti-VEGF inhibitors).

Cardiac Complications Following Radiotherapy

Evidence of dose dependent increase in cardiovascular disease after chest radiotherapy has been documented in several studies, especially in the field of breast cancer and lymphoma. Ionizing radiation causes micro and macro-vascular damage in all cardiac tissues (pericardium, valves, heart muscle and coronary arteries). Primary radiation fibrosis is not related to the primary effect of the radiation, but rather to a reparative response of the heart tissue to injury in the micro-vascular system.

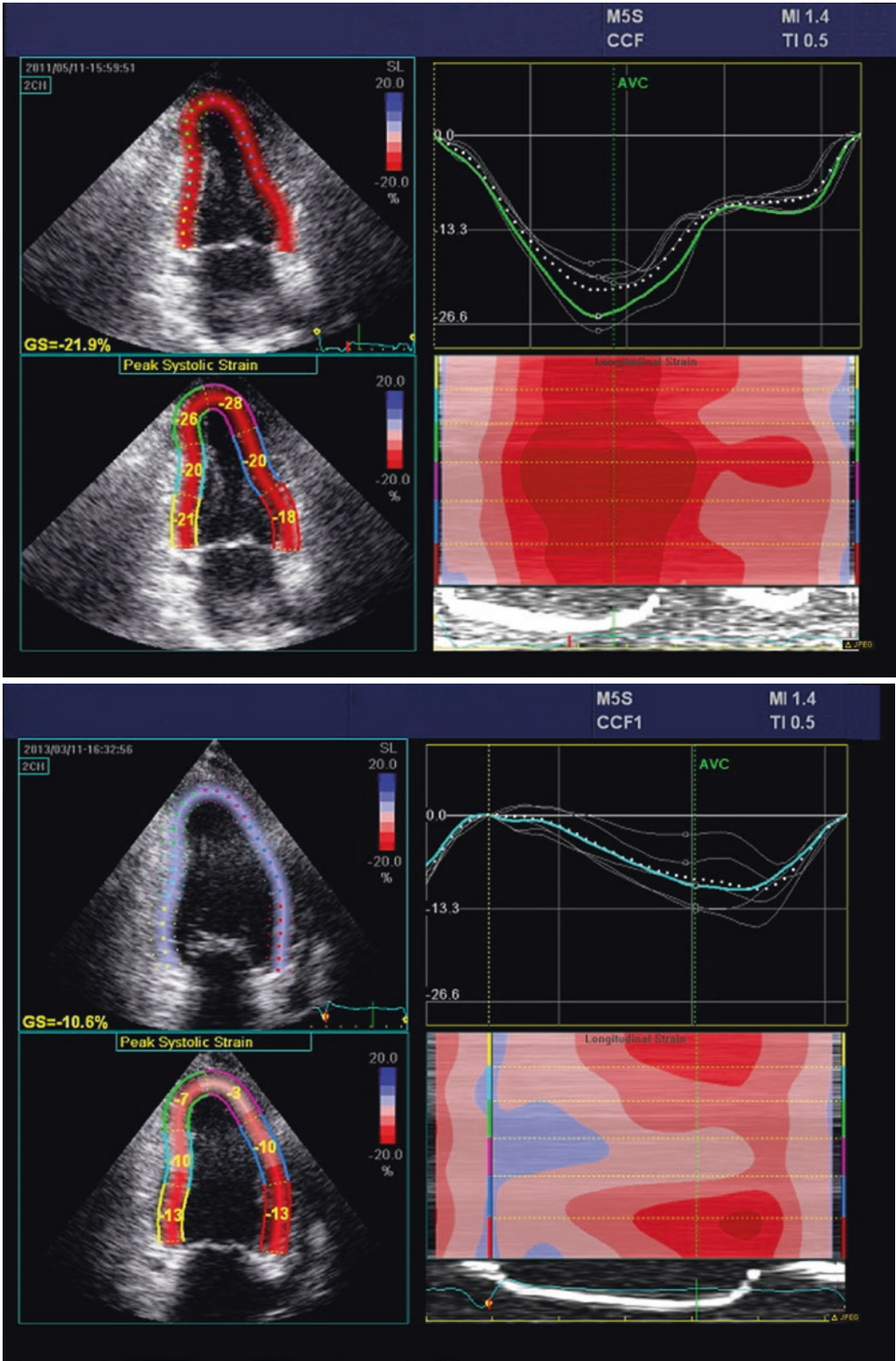


Fig. 38.3 Global longitudinal strain pre and post exposure to anthracyclines. Sub-clinical LV dysfunction is present as GLS has fallen 46%

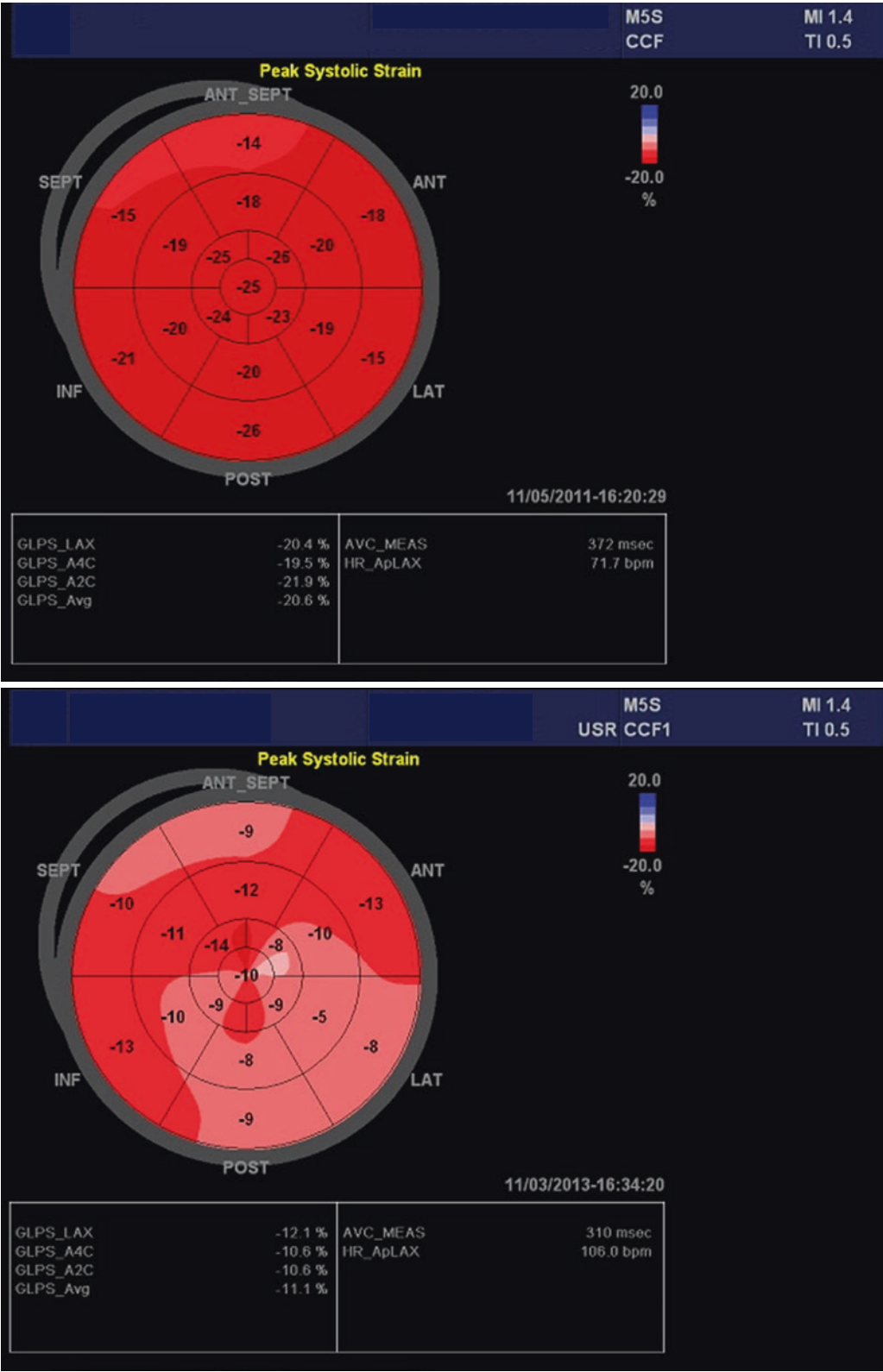


Fig. 38.3 (continued)

Table 38.3 Definition of sub-clinical LV dysfunction by global longitudinal strain measurement

<i>Cardiotoxicity by changes in global longitudinal strain (GLS)</i>	
Change in GLS	Reduction $\geq 15\%$ from baseline
Absolute number of GLS	Drop below the lower limit of normal for vendor, gender and age when baseline is not available [48]

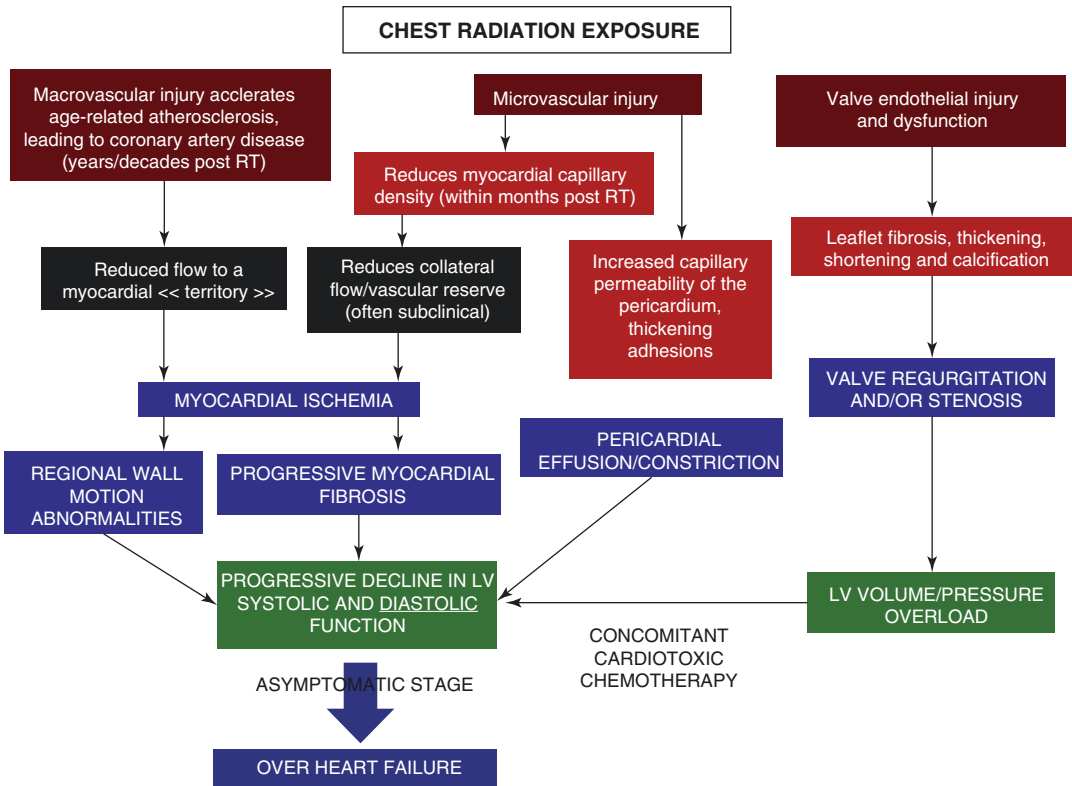


Fig. 38.4 Pathophysiology of radiation-induced heart disease. Reproduced with permission from [53]

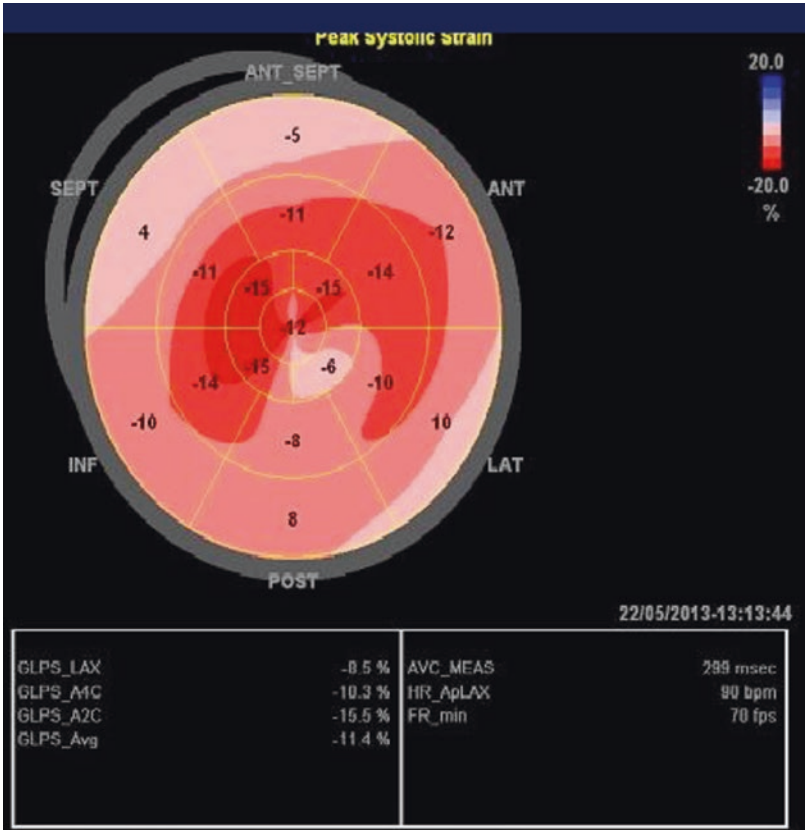
Echocardiography continues to be the working horse in the evaluation of pericardial and valvular heart disease in these patients. Strain imaging has emerged as a very useful tool unveiling the presence of myocardial injury not previously recog-

nized with 2D echocardiography [52] (Fig. 38.4). A summary of cardiac changes noted after radiation therapy are noted in Fig. 38.5. Global strain values can also be significantly reduced following radiation (Fig. 38.6).

Acute	Long-term
Pericarditis <ul style="list-style-type: none"> Acute exudative pericarditis is rare and often occurs during radiotherapy as a reaction to necrosis/inflammation of a tumour located next to the heart. Delayed acute pericarditis occurs within weeks after radiotherapy and can be revealed by either an asymptomatic pericardial effusion or a symptomatic pericarditis. Cardiac tamponade is rare. Spontaneous clearance of this effusion may take up to 2 years. 	Pericarditis <ul style="list-style-type: none"> Delayed chronic pericarditis appears several weeks to years after radiotherapy. In this type, extensive fibrous thickening, adhesions, chronic constriction, and chronic pericardial effusion can be observed. It is observed in up to 20% of patients within 2 years following irradiation. Constrictive pericarditis can be observed in 4–20% of patients and appears to be dose-dependent and related to the presence of pericardial effusion in the delayed acute phase.
Cardiomyopathy <ul style="list-style-type: none"> Acute myocarditis related to radiation-induced inflammation with transient repolarization abnormalities and mild myocardial dysfunction. 	Cardiomyopathy <ul style="list-style-type: none"> Diffuse myocardial fibrosis (often after a > 30-Gy radiation dose) with relevant systolic and diastolic dysfunction, conduction disturbance, and autonomic dysfunction. Restrictive cardiomyopathy represents an advanced stage of myocardial damage due to fibrosis with severe diastolic dysfunction and signs and symptoms of heart failure
Valve disease <ul style="list-style-type: none"> No immediate apparent effects. 	Valve disease <ul style="list-style-type: none"> Valve apparatus and leaflet thickening, fibrosis shortening, and calcification predominant on left-sided valves (related to pressure difference between the left and right side of the heart). Valve regurgitation more commonly encountered than stenosis. Stenotic lesions more commonly involving the aortic valve. Reported incidence of clinically significant valve disease: 1% at 10 years; 5% at 15 years; 6% at 20 years after radiation exposure. Valve disease incidence increases significantly after >20 years following irradiation; mild AR up to 45% ≥moderate AR up to 15%, AS up to 16%, mild MR up to 48%, mid PR up to 12%.
Coronary artery disease <ul style="list-style-type: none"> No immediate apparent effects. (Perfusion defects can be seen in 47% of patients 6 months after radiotherapy and may be accompanied by wall-motion abnormalities and chest pain. Their long-term prognosis and significance are unknown.) 	Coronary artery disease <ul style="list-style-type: none"> Accelerated CAD appearing in the young age. Concomitant atherosclerotic risk factors further enhance the development of CAD. Latent until at least 10 years after exposure. (Patients younger than 50 years tend to develop CAD in the first decade after treatment, while older patients have longer latency periods.) Coronary ostia and proximal segments are typically involved. CAD doubles the risk of death; relative risk of death from fatal myocardial infarction varies from 2.2 to 8.8.
Carotid artery disease <ul style="list-style-type: none"> No immediate apparent effects. 	Carotid artery disease <ul style="list-style-type: none"> Radio therapy-induced lesions are more extensive, involving longer segments and atypical areas of carotid segments. Estimated incidence (including sub-clavian artery stenosis) about 7.4% in Hodgkin's lymphoma.
Other vascular disease <ul style="list-style-type: none"> No immediate apparent effects. 	Other vascular disease <ul style="list-style-type: none"> Calcification of the ascending aorta and aortic arch (porcelain aorta). Lesions of any other vascular segments present within the radiation field.

Fig. 38.5 Acute and chronic manifestations of radiation-induced heart disease. Reproduced with permission from [53]

Fig. 38.6 Global longitudinal strain in patient with radiation-induced restrictive heart disease



Conclusions

Echocardiography is the mainstay for the evaluation of the patient during and after cancer therapy (chemo or radiotherapy). Three-dimensional echocardiography is the method choice for the evaluation of LVEF where available, as it has the lowest inherent variability, therefore allowing the adjudication of CTRCD. If the technique is unavailable, the enhancement of 2D echocardiograms with contrast is an acceptable alternative. It is essential to use strain imaging during the surveillance of patients receiving potentially cardiotoxic chemotherapeutic agents due to its ability to recognize subtle changes in cardiac function that prognosticate downstream CTRCD.

References

1. Tan C, Tasaka H, Yu KP, Murphy ML, Karnofsky DA. Daunomycin, an antitumor antibiotic, in the treatment of neoplastic disease. Clinical evaluation with special reference to childhood leukemia. *Cancer*. 1967;20:333–53.
2. Lefrak EA, Pitha J, Rosenheim S, Gottlieb JA. A clinicopathologic analysis of adriamycin cardiotoxicity. *Cancer*. 1973;32:302–14.
3. Greco FA, Brereton HD, Rodbard D. Noninvasive monitoring of adriamycin cardiotoxicity by “Sphygmo-Recording” of the pulse wave delay (QKd interval). *Cancer Treat Rep*. 1976;60:1239–45.
4. Ramos A, Meyer RA, Korfhagen J, Wong KY, Kaplan S. Echocardiographic evaluation of adriamycin cardiotoxicity in children. *Cancer Treat Rep*. 1976;60:1281–4.

5. Billingham ME, Bristow MR, Glatstein E, Mason JW, Masek MA, Daniels JR. Adriamycin cardiotoxicity: endomyocardial biopsy evidence of enhancement by irradiation. *Am J Surg Pathol*. 1977;1:17–23.
6. Lenzhofer R, Dudczak R, Gumhold G, Graninger W, Moser K, Spitzky KH. Noninvasive methods for the early detection of doxorubicin-induced cardiomyopathy. *J Cancer Res Clin Oncol*. 1983;106:136–42.
7. Plana JC, Galderisi M, Barac A, Ewer MS, Ky B, Scherrer-Crosbie M, Ganame J, Sebag IA, Agler DA, Badano LP, Banchs J, Cardinale D, Carver J, Cerqueira M, DeCara JM, Edvardsen T, Flamm SD, Force T, Griffin BP, Jerusalem G, Liu JE, Magalhaes A, Marwick T, Sanchez LY, Sicari R, Villarraga HR, Lancellotti P. Expert consensus for multimodality imaging evaluation of adult patients during and after cancer therapy: a report from the American Society of Echocardiography and the European Association of Cardiovascular Imaging. *Eur Heart J Cardiovasc Imaging*. 2014;15:1063–93.
8. De Graff WG, Myers LS Jr, Mitchell JB, Hahn SM. Protection against Adriamycin cytotoxicity and inhibition of DNA topoisomerase II activity by 3,4-dihydroxybenzoic acid. *Int J Oncol*. 2003;23:159–63.
9. Tewey KM, Rowe TC, Yang L, Halligan BD, Liu LF. Adriamycin-induced DNA damage mediated by mammalian DNA topoisomerase II. *Science*. 1984;226:466–8.
10. Lyu YL, Kerrigan JE, Lin CP, Azarova AM, Tsai YC, Ban Y, Liu LF. Topoisomerase II β -mediated DNA double-strand breaks: implications in doxorubicin cardiotoxicity and prevention by dexrazoxane. *Science*. 2007;67:8839–46.
11. Von Hoff DL, Layard MW, Basa P, Davis HL Jr, Von Hoff AL, Rozencweig M, Muggia FM. Risk factors for doxorubicin-induced congestive heart failure. *Ann Intern Med*. 1979;91:710–7.
12. Ewer MS, Von Hoff DD, Benjamin RS. A historical perspective of anthracycline cardiotoxicity. *Heart Fail Clin*. 2011;7:363–72.
13. Neilan TG, Jassal DS, Perez-Sanz TM, Raher MJ, Pradhan AD, Buys ES, Ichinose F, Bayne DB, Halpern EF, Weyman AE, Derumeaux G, Bloch KD, Picard MH, Scherrer-Crosbie M. Tissue doppler imaging predicts left ventricular dysfunction and mortality in a murine model of cardiac injury. *Eur Heart J*. 2006;27:1868–75.
14. Mann DL, Bristow MR. Mechanisms and models in heart failure: the biomechanical model and beyond. *Circulation*. 2005;111:2837–49.
15. Felker GM, Thompson RE, Hare JM, Hruban RH, Clemetson DE, Howard DL, Baughman KL, Kasper EK. Underlying causes and long-term survival in patients with initially unexplained cardiomyopathy. *N Engl J Med*. 2000;342:1077–84.
16. Baselga J, Norton L, Albanell J, Kim YM, Mendelsohn J. Recombinant humanized anti-HER2 antibody (Herceptin) enhances the antitumor activity of paclitaxel and doxorubicin against HER2/neu over-expressing human breast cancer xenografts. *Cancer Res*. 1998;58:2825–31.
17. Chien KR. Herceptin and the heart—a molecular modifier of cardiac failure. *N Engl J Med*. 2006;354:789–90.
18. Slamon DJ, Leyland-Jones B, Shak S, Fuchs H, Paton V, Bajamonde A, Fleming T, Eiermann W, Wolter J, Pegram M, Baselga J, Norton L. Use of chemotherapy plus a monoclonal antibody against HER2 for metastatic breast cancer that overexpresses HER2. *N Engl J Med*. 2001;344:783–92.
19. Crone SA, Zhao YY, Fan L, Gu Y, Minamisawa S, Liu Y, Peterson KL, Chen J, Kahn R, Condorelli G, Ross J Jr, Chien KR, Lee KF. ErbB2 is essential in the prevention of dilated cardiomyopathy. *Nat Med*. 2002;8:459–65.
20. Jannazzo A, Hoffman J, Lutz M. Monitoring of anthracycline-induced cardiotoxicity. *Ann Pharmacother*. 2008;42:99–104.
21. Jurcut R, Wildiers H, Ganame J, D’Hooge J, Paridaens R, Voigt JU. Detection and monitoring of cardiotoxicity—what does modern cardiology offer? *Support Care Cancer*. 2008;16:437–45.
22. Schwartz RG, McKenzie WB, Alexander J, Sager P, D’Souza A, Manatunga A, Schwartz PE, Berger HJ, Setaro J, Surkin L, et al. Congestive heart failure and left ventricular dysfunction complicating doxorubicin therapy. seven-year experience using serial radionuclide angiocardiology. *Am J Med*. 1987;82:1109–18.
23. Ng R, Better N, Green MD. Anticancer agents and cardiotoxicity. *Semin Oncol*. 2006;33:2–14.
24. Swain SM, Whaley FS, Gerber MC, Weisberg S, York M, Spicer D, Jones SE, Wadler S, Desai A, Vogel C, Speyer J, Mittelman A, Reddy S, Pendergrass K, Velez-Garcia E, Ewer MS, Bianchini JR, Gams RA. Cardioprotection with dexrazoxane for doxorubicin-containing therapy in advanced breast cancer. *J Clin Oncol*. 1997;15:1318–32.
25. Batist G, Ramakrishnan G, Rao CS, Chandrasekharan A, Gutheil J, Guthrie T, Shah P, Khojasteh A, Nair MK, Hoelzer K, Tkaczuk K, Park YC, Lee LW. Reduced cardiotoxicity and preserved antitumor efficacy of liposome-encapsulated doxorubicin and cyclophosphamide compared with conventional doxorubicin and cyclophosphamide in a randomized, multicenter trial of metastatic breast cancer. *J Clin Oncol*. 2001;19:1444–54.

26. Stanton T, Leano R, Marwick TH. Prediction of all-cause mortality from global longitudinal speckle strain: comparison with ejection fraction and wall motion scoring. *Circ Cardiovasc Imaging*. 2009;2:356–64.
27. Thavendiranathan P, Grant AD, Negishi T, Plana JC, Popovic ZB, Marwick TH. Reproducibility of echocardiographic techniques for sequential assessment of left ventricular ejection fraction and volumes: application to patients undergoing cancer chemotherapy. *J Am Coll Cardiol*. 2013;61:77–84.
28. McGowan JH, Cleland JG. Reliability of reporting left ventricular systolic function by echocardiography: a systematic review of 3 methods. *Am Heart J*. 2003;146:388–97.
29. Yu EH, Sloggett CE, Iwanochko RM, Rakowski H, Siu SC. Feasibility and accuracy of left ventricular volumes and ejection fraction determination by fundamental, tissue harmonic, and intravenous contrast imaging in difficult-to-image patients. *J Am Soc Echocardiogr*. 2000;13:216–24.
30. Mulvagh SL, Rakowski H, Vannan MA, Abdelmoneim SS, Becher H, Bierig SM, Burns PN, Castello R, Coon PD, Hagen ME, Jollis JG, Kimball TR, Kitzman DW, Kronzon I, Labovitz AJ, Lang RM, Mathew J, Moir WS, Nagueh SF, Pearlman AS, Perez JE, Porter TR, Rosenbloom J, Strachan GM, Thanigaraj S, Wei K, Woo A, Yu EH, Zoghbi WA. American Society of Echocardiography consensus statement on the clinical applications of ultrasonic contrast agents in echocardiography. *J Am Soc Echocardiogr*. 2008;21:1179–201. quiz 1281.
31. Senior R, Becher H, Monaghan M, Agati L, Zamorano J, Vanoverschelde JL, Nihoyannopoulos P. Contrast echocardiography: evidence-based recommendations by European Association of Echocardiography. *Eur J Echocardiogr*. 2009;10:194–212.
32. Nahar T, Croft L, Shapiro R, Fruchtman S, Diamond J, Henzlova M, Machac J, Buckley S, Goldman ME. Comparison of four echocardiographic techniques for measuring left ventricular ejection fraction. *Am J Cardiol*. 2000;86:1358–62.
33. Malm S, Frigstad S, Sagberg E, Larsson H, Skjaerpe T. Accurate and reproducible measurement of left ventricular volume and ejection fraction by contrast echocardiography: a comparison with magnetic resonance imaging. *J Am Coll Cardiol*. 2004;44:1030–5.
34. Badano LP, Boccacini F, Muraru D, Bianco LD, Peluso D, Bellu R, Zoppellaro G, Iliceto S. Current clinical applications of transthoracic three-dimensional echocardiography. *J Cardiovasc Ultrasound*. 2012; 20:1–22.
35. Jacobs LD, Salgo IS, Goonewardena S, Weinert L, Coon P, Bardo D, Gerard O, Allain P, Zamorano JL, de Isla LP, Mor-Avi V, Lang RM. Rapid online quantification of left ventricular volume from real-time three-dimensional echocardiographic data. *Eur Heart J*. 2006;27:460–8.
36. Corsi C, Coon P, Goonewardena S, Weinert L, Sugeng L, Polonsky TS, Veronesi F, Caiani EG, Lamberti C, Bardo D, Lang RM, Mor-Avi V. Quantification of regional left ventricular wall motion from real-time 3-dimensional echocardiography in patients with poor acoustic windows: effects of contrast enhancement tested against cardiac magnetic resonance. *J Am Soc Echocardiogr*. 2006;19:886–93.
37. Jenkins C, Moir S, Chan J, Rakhit D, Haluska B, Marwick TH. Left ventricular volume measurement with echocardiography: a comparison of left ventricular opacification, three-dimensional echocardiography, or both with magnetic resonance imaging. *Eur Heart J*. 2009;30:98–106.
38. Stapleton GE, Stapleton SL, Martinez A, Ayres NA, Kovalchin JP, Bezold LI, Pignatelli R, Eidem BW. Evaluation of longitudinal ventricular function with tissue Doppler echocardiography in children treated with anthracyclines. *J Am Soc Echocardiogr*. 2007;20:492–7.
39. Korinek J, Wang J, Sengupta PP, Miyazaki C, Kjaergaard J, McMahon E, Abraham TP, Belohlavek M. Two-dimensional strain—a Doppler-independent ultrasound method for quantitation of regional deformation: validation in vitro and in vivo. *J Am Soc Echocardiogr*. 2005;18:1247–53.
40. Yeon SB, Reichek N, Tallant BA, Lima JA, Calhoun LP, Clark NR, Hoffman EA, Ho KK, Axel L. Validation of in vivo myocardial strain measurement by magnetic resonance tagging with sonomicrometry. *J Am Coll Cardiol*. 2001;38:555–61.
41. Urheim S, Edvardsen T, Torp H, Angelsen B, Smiseth OA. Myocardial strain by Doppler echocardiography. Validation of a new method to quantify regional myocardial function. *Circulation*. 2000;102: 1158–64.
42. Hare JL, Brown JK, Leano R, Jenkins C, Woodward N, Marwick TH. Use of myocardial deformation imaging to detect preclinical myocardial dysfunction before conventional measures in patients undergoing breast cancer treatment with trastuzumab. *Am Heart J*. 2009;158:294–301.
43. Ho E, Brown A, Barrett P, Morgan RB, King G, Kennedy MJ, Murphy RT. Subclinical anthracycline- and trastuzumab-induced cardiotoxicity in the long-term follow-up of asymptomatic breast cancer survivors: a speckle tracking echocardiographic study. *Heart*. 2010;96:701–7.
44. Poterucha JT, Kutty S, Lindquist RK, Li L, Eidem BW. Changes in left ventricular longitudinal strain with anthracycline chemotherapy in adolescents precede subsequent decreased left ventricular ejection fraction. *J Am Soc Echocardiogr*. 2012;25:733–40.
45. Sawaya H, Sebag IA, Plana JC, Januzzi JL, Ky B, Tan TC, Cohen V, Banchs J, Carver JR, Wiegers SE, Martin RP, Picard MH, Gerszten RE, Halpern EF, Passeri J, Kuter I, Scherrer-Crosbie M. Assessment of echocardiography and biomarkers for the extended prediction of cardiotoxicity in patients treated with anthracyclines, taxanes, and trastuzumab. *Circ Cardiovasc Imaging*. 2012;5:596–603.
46. Marwick TH, Leano RL, Brown J, Sun JP, Hoffmann R, Lysyansky P, Becker M, Thomas JD. Myocardial

- strain measurement with 2-dimensional speckle-tracking echocardiography: definition of normal range. *JACC Cardiovasc Imaging*. 2009;2:80–4.
47. Negishi K, Negishi T, Hare JL, Haluska BA, Plana JC, Marwick TH. Independent and incremental value of deformation indices for prediction of trastuzumab-induced cardiotoxicity. *J Am Soc Echocardiogr*. 2013;26:493–8.
48. Takigiku K, Takeuchi M, Izumi C, Yuda S, Sakata K, Ohte N, Tanabe K, Nakatani S, JUSTICE Investigators. Normal range of left ventricular 2-dimensional strain: Japanese ultrasound speckle tracking of the left ventricle (JUSTICE) study. *Circ J*. 2012;76:2623–32.
49. Bountiokos M, Doorduijn JK, Roelandt JR, Vourvouri EC, Bax JJ, Schinkel AF, Kertai MD, Sonneveld P, Poldermans D. Repetitive dobutamine stress echocardiography for the prediction of anthracycline cardiotoxicity. *Eur J Echocardiogr*. 2003;4:300–5.
50. Cottin Y, L'Huillier I, Casasnovas O, Geoffroy C, Caillot D, Zeller M, Solary E, Guy H, Wolf JE. Dobutamine stress echocardiography identifies anthracycline cardiotoxicity. *Eur J Echocardiogr*. 2000;1:180–3.
51. Civelli M, Cardinale D, Martinoni A, Lamantia G, Colombo N, Colombo A, Gandini S, Martinelli G, Fiorentini C, Cipolla CM. Early reduction in left ventricular contractile reserve detected by dobutamine stress echo predicts high-dose chemotherapy-induced cardiac toxicity. *Int J Cardiol*. 2006;111:120–6.
52. Lancellotti P, Nkomo VT, Badano LP, Bergler-Klein J, Bogaert J, Davin L, Cosyns B, Coucke P, Dulgheru R, Edvardsen T, Gaemperli O, Galderisi M, Griffin B, Heidenreich PA, Nieman K, Plana JC, Port SC, Scherrer-Crosbie M, Schwartz RG, Sebag IA, Voigt JU, Wann S, Yang PC, European Society of Cardiology Working Groups on Nuclear Cardiology and Cardiac Computed Tomography and Cardiovascular Magnetic Resonance; American Society of Nuclear Cardiology; Society for Cardiovascular Magnetic Resonance; Society of Cardiovascular Computed Tomography. Expert consensus for multi-modality imaging evaluation of cardiovascular complications of radiotherapy in adults: a report from the European Association of Cardiovascular Imaging and the American Society of Echocardiography. *Eur Heart J Cardiovasc Imaging*. 2013;14:721–40.
53. Lancellotti P, Nkomo V, Badano L. Expert consensus for Multi-Modality Imaging Evaluation of Cardiovascular Complications of Radiotherapy in Adults: A Report from the European Association of Cardiovascular Imaging and the American Society of Echocardiography. *J Am Soc Echocardiogr*. 2013;26:1013–32.

Pocket-Size Hand-Held Echocardiography

39

Vasileios F. Panoulas and Petros Nihoyannopoulos

Introduction

Cardiac ultrasound is currently the most widely used and cost-effective diagnostic imaging tool in cardiology [1]. Miniaturization and digital techniques recently resulted in the development of high-resolution battery powered small hand held ultrasound devices with excellent gray scale and color blood flow imaging capabilities. Examples of such devices include the V-scan (GE Healthcare) and the Acuson P10 (Siemens) (Fig. 39.1).

Current Equipment

Currently available echo machines may be classified into four main categories (Table 39.1).

Current PSE devices offer diagnostic quality 2D and color Doppler imaging in real-time. They come with a broad-bandwidth, phased array

probe (1.7–3.8 MHz). The flow sector represents blood flow within an angle of 30°. Images and videos (automatic auto cycle without the need for ECG trace) can be stored in examination folders, recalled via a gallery function, and transferred to PC or USB throughout a docking station. Their technical characteristics may be summarized as:

(1) grey-scale images have a 2D sector angle <75°, depth <25 cm; (2) color flow imaging (available in one product only) has a fixed color box size and a fixed pulse repetition frequency; (3) measurements are restricted to distances and areas; (4) options for patient identification are limited, albeit feasible; (5) connectivity requires dedicated software tools.

Technical characteristics and image quality are usually sufficient for the qualitative evaluation of: left and right ventricular structure [2] and function [3, 4], pericardial [5] and/or pleural effusion [6], B-lines evaluated by lung ultrasound as a sign of extravascular lung water, size and respiratory changes of inferior vena cava, and extent of calcification and motion of aortic cusps [7, 8]. If available, valve regurgitation can be assessed by color Doppler.

Electronic Supplementary Material The online version of this chapter (https://doi.org/10.1007/978-3-319-71617-6_39) contains supplementary material, which is available to authorized users.

V. F. Panoulas
Department of Cardiology, Royal Brompton and
Harefield NHS Foundation Trust, London, UK
e-mail: v.panoulas@imperial.ac.uk

P. Nihoyannopoulos (✉)
Imperial College London, Hammersmith Hospital,
London, UK
e-mail: petros@imperial.ac.uk

Terminology

Recently the American Society of Echocardiography (ASE) have released a document on Focused cardiac ultrasound (FCU) [9, 10], defined as a



Siemens Acuson P10	V-scan
<ul style="list-style-type: none">• Dimensions:<ul style="list-style-type: none">– Display unit: 142 x 97 x 54 mm– Probe: 137 x 47.8 x 31.8 mm• Weight: 725 g• Display: 3.7 in.<ul style="list-style-type: none">– 640 x 480 pixels resolution• Field of black/white 2D view<ul style="list-style-type: none">– 78° with maximum depth of 24 cm• Color flow<ul style="list-style-type: none">– none• Broad bandwidth array probe<ul style="list-style-type: none">– From 2 to 4 MHz• Data stored on removable 1GB SD card (up to 2GB)• Recharge time for device battery<ul style="list-style-type: none">– 1 h for 75% battery capacity• Price: \$4,676.	<ul style="list-style-type: none">• Dimensions:<ul style="list-style-type: none">– Display unit: 135 x 72 x 28 mm– Probe: 120 x 33 x 26 mm• Weight: 390 g• Display: 3.5 in.<ul style="list-style-type: none">– 240 x 320 pixels resolution• Field of black/white 2D view<ul style="list-style-type: none">– 75° with maximum depth of 25 cm• Color flow sector<ul style="list-style-type: none">– blood flow within an angle of 30°• Broad bandwidth array probe<ul style="list-style-type: none">– From 1.7 to 3.8 MHz• Data are stored on 4GB microSD or microSDHC card (up to 32 GB)• Recharge time for device battery:<ul style="list-style-type: none">– 1 h for 90% battery capacity• Price \$7,900
	

Fig. 39.1 Currently available pocket-size hand-held echo devices

Table 39.1 Classification of currently available echo machines according to their size and functions

Echo machines	Echo machines capabilities
<i>Stationary high-end systems</i> Full range of standard echo	Full range of standard echo modalities and measurements (MM, 2D, PW, CW, Colour, TVI, TEE), and advances modalities (3D, contrast)
<i>Mobile systems</i> Smaller machines on wheels, middle range technology	Full range of standard echo modalities and measurements (MM, 2D, PW, CW, Colour, TVI, TEE)
<i>Portable systems</i> Small machines that can be carried by a person	Basic, standard echo modalities and measurements (MM, 2D, PW, CW, Colour)
<i>Pocket-size hand-held devices</i> Fit in a lab coat pocket	Limited functions (2D, Colour) and measurement package

2D two-dimensional, 3D three-dimensional, *Colour* colour doppler, *CW* continuous doppler, *MM* M-mode, *PW* pulsed doppler, *TVI* tissue velocity imaging

focused examination of the cardiovascular system performed by a physician using ultrasound as an adjunct to the physical examination to recognize specific ultrasonic signs that represent a narrow list of potential diagnoses in specific clinical settings. In their guidelines authors aim to clarify

the terminology surrounding PHE devices. In particular they distinguish two types of echocardiography: (1) “complete” or “comprehensive” and (2) “limited” echocardiography. FCU belongs to the latter subdivision and can be carried out using PHE devices. Synonyms to PHE in the literature

include “hand-held echocardiography,” “hand-carried echocardiography,” “ultrasound stethoscope”, “bedside cardiac ultrasound”, “quick look cardiac ultrasound”, “pocket-size echocardiography”, “point of care echocardiography,” and “directed echocardiography.”

FCU extended physical examination may be performed primarily from the parasternal and subcostal acoustic windows, which is consistent with two published ultrasound examinations that involve cardiac imaging as a part of their protocols. Both the Cardiopulmonary Limited Ultrasound Exam (CLUE) and Focused Abdominal Sonography in Trauma (FAST) examinations image the heart from these two windows. This however should not limit more experienced operators capable to obtain and interpret apical views.

Limitations of Pocket-Size Echocardiography

The transducer technology is not the same, and the complex image enhancement and artifact reduction abilities cannot be reproduced on a PHE. In addition, the images are visualized on a screen with significantly lower resolution and size compared with those available with state-of-the-art echocardiography. Commonly performed acquisition modifications, such as the ability to zoom, alter the ultrasound beam focus, narrow sector width, adjust dynamic range, use harmonic imaging, use settings optimized for contrast, change gray-scale maps, or optimize transducer frequency, are lacking. These restrictions make identification of subtle abnormalities inappropriate for PHE scope of practice. Despite these limitations, PHE devices generate clinically useful images.

PHE devices have been miniaturized to improve functionality at the bedside and reduce cost. The compromise of smaller devices is loss of features, including spectral Doppler, tissue Doppler, and 3D.

Lack of spectral Doppler renders PHE devices inappropriate for the assessment of pericardial constriction, pulmonary hypertension and dia-

stolic dysfunction. Quantitation of regurgitant or stenotic valvular lesion severity is also not feasible with PHE. However, the morphology of stenotic valves and secondary findings, such as chamber enlargement/volume load and hypertrophy, may provide cues to an experienced user. Color Doppler is also available on most systems and has been used to qualitatively assess for potentially severe regurgitant lesions (Fig. 39.2 and Video 39.1).

In an attempt to distinguish the limitations of PSE devices from the skill of the operator, the writing group of the ASE reviewed studies that included at least 50 patients in which a small platform was compared with traditional echocardiography, with all images acquired and interpreted by experts to determine which pathologies PHE devices are capable of detecting [9, 11]. Cardiac abnormalities that have been accurately detected included left ventricular (LV) and right ventricular (RV) enlargement, LV and RV systolic function, LV hypertrophy, LA enlargement, pericardial effusion and inferior vena cava (IVC) size.

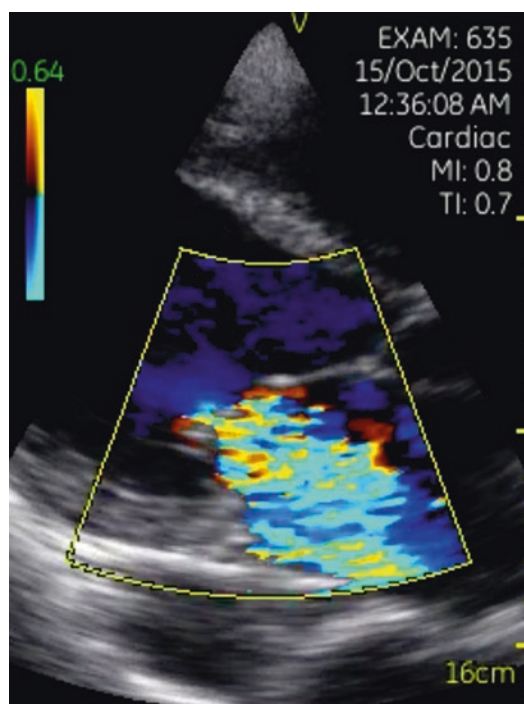


Fig. 39.2 Severe mitral regurgitation in a patient with dilated cardiomyopathy

The most commonly studied pathology that was adequately detected by using PHE was LV systolic dysfunction, in which sensitivities of 73–100% and specificities of 64–96% have been demonstrated. Most importantly, although the ability to detect abnormalities at the bedside by PHE users is lower than having a comprehensive TTE, it is clearly better than traditional bedside assessment [9]. In other words, PHE use allows detection of cardiac pathology more accurately than physical examination, which supports its use as an adjunct to physical examination [8, 12, 13], but not as a replacement for echocardiography [9].

Clinical Use of Pocket-Size Hand-Held Echocardiography

Pocket-size devices complement the physical examination in various settings:

1. *Emergency setting*, including a rapid initial assessment of critically ill patients in emergency units, intensive care units, coronary care units or in the coronary catheter laboratories.

In the *emergency room* PHE can be a useful tool in screening for pericardial effusion (Fig. 39.3 and Video 39.2) in trauma or arrested patients, assessing the left ventricular (LV) function in shocked patients, visualizing the right ventricular size and function in patients presenting with suspected large pulmonary embolism.

In *cardiac intensive care* units PHE can control for the presence of pericardial effusion/haematoma, regional wall motion abnormalities or valvular abnormalities in decompensated patients post cardiac surgery. In general intensive units LV assessment is often a requirement for shocked patients or those difficult to wean from the ventilator. Bread and butter during cardiology on-calls in tertiary care centers are the primary calls for patients with ST segment elevation (Videos 39.3 and 39.4). In this setting, PHE can be useful in (1) aiding diagnosis in equivocal ECG changes, by identifying regional wall motion abnormalities and presence or not of

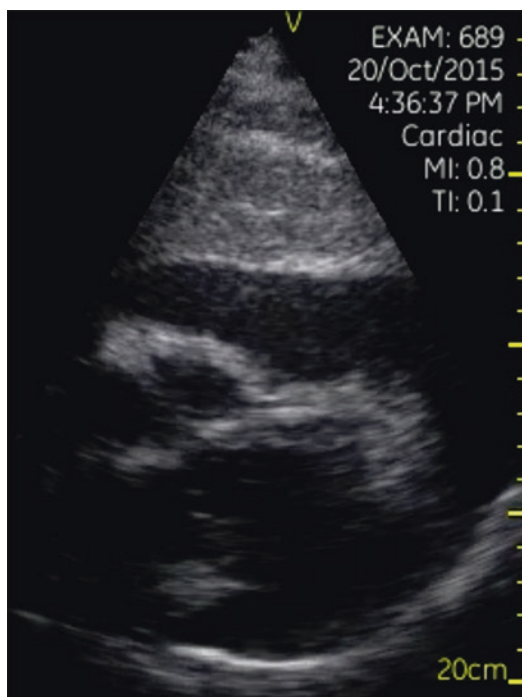


Fig. 39.3 V-scan echo subcostal view demonstrating large pericardial effusion with tamponade

viable/non-scarred myocardium, (2) assessing the severity of LV systolic dysfunction which can lead to better procedural planning (i.e. need for circulatory support) and (3) identifying alternative diagnoses that cause confusing ECG changes in post-arrest patients.

2. *Outpatient clinics*, during cardiology consultations in- or outside health-care facilities and hospitals. When physical examination raises the suspicion of underlying pathology, PHE can confirm the diagnosis in question and trigger appropriate further imaging/testing (comprehensive echocardiography). A typical example is the detection of clinical aortic stenosis. PHE can confirm the presence of calcified aortic cusps with reduced opening (Fig. 39.4 and Video 39.5) and trigger referral for comprehensive imaging. Furthermore in expert hands, PHE can exclude any structural abnormalities (Video 39.6) in cases with atypical or benign sounding symptoms (e.g. young patient with benign sounding palpitations) and hence reduce the number of referrals for comprehensive echocardiography.



Fig. 39.4 Heavily calcified aortic valve with markedly reduced cusp mobility on parasternal long axis view, suggestive of severe aortic stenosis



Fig. 39.5 Athlete with abnormal ECG with lateral T-wave inversions found to have asymmetric septal hypertrophy on the parasternal long axis of V-scan hand-held echo

3. *Prehospital setting*, where they can be used for first cardiac evaluation in ambulances attending to trauma patients (pericardial effusion, collapsing LV walls suggestive of marked hypovolaemia, valvular abnormalities caused by blunt trauma etc), out of hospital arrests or haemodynamically unstable patients
4. *Community setting*, where PHE have proven to be a useful tool for screening programmes in schools, industries, and other community activities. Examples include screening for athletes with abnormal ECG changes for hypertrophic cardiomyopathy (Fig. 39.5 and Video 39.7) [14, 15] or remote communities [16–19] with high incidence of rheumatic fever.

Medical schools; PHE devices may become a valuable teaching tool in medical schools. A recent study [8] by Panoulas et al. has shown that with limited training, medical students increased their diagnostic accuracy when using PHE on top of physical examination. Furthermore, what greater way of learning when you can visualise the cause of your clinical finding (e. g. aortic stenosis in a patient

with ejection systolic murmur and absent second sound, severe LV systolic impairment and mitral regurgitation in a patient with fluid overload and a pan systolic murmur at the apex—Fig. 39.1 and Video 39.1).

5. *Monitoring of an echocardiographic finding*. PHE is often used as a tool to allow frequent serial examination of an ultrasound finding. LV systolic function in patients undergoing chemotherapy could be monitored in this way as long as there is a baseline comprehensive study. In a similar fashion, a patient with pericardial effusion not requiring drainage, can be monitored on a frequent basis in a cost effective manner.

Training Requirements

Expert (accredited) echocardiographers do not need any training for the use of PHE devices. Conversely, echocardiography societies recommend specific training for cardiologists not fully conversant with echocardiography [20]. For non-

cardiologists and/or other medical professionals, a dedicated training and revision of basic cardiac physiology and pathology knowledge should be mandatory. This appears to be the only way to avoid abuse and potential harm to patients due to both over- and under-diagnosis of serious heart diseases. The European Association of Echocardiography (EAE) promotes the idea of a training specifically tailored to the information that can be obtained from this new class of devices as mandatory part of a certification process [21, 22]. This would ensure a widespread use of this new technology with certified competence, avoiding abuse and potential misuse [23]. Recommendations for cardiac ultrasound training for non-echocardiographers include three core components: didactic education, hands-on image acquisition, and image interpretation experience.

Didactic Education

The training could potentially be delivered as hybrid learning modules with a combination of traditional class lectures and online interactive modules. The online module should end with an exam to ensure that all trainees are prepared for hands-on practice. For spatial training, the use of imaging aids such as 3D cardiac models, phantom imaging, and simulation mannequins may expedite the understanding of scanning planes and their corresponding anatomy. Review of digital-video loops and still frames of normal cases, which show the recommended scanning views and normal variants should be included. The trainee should be familiarized with different chest conformations and possible deviations from the typical scanning windows.

Hands On

The majority of hands-on experience should be acquired on real patients, preferably in the clinical setting. Initially imaging of normal subjects

who have excellent windows and are cooperative in their positioning and respiration is a good way to learn acoustic windows, imaging planes, transducer manipulation, and basic anatomy. However, imaging at the bedside in real-life settings with real-time feed back from a proctor is an invaluable experience. Although most guidelines recommend independent image acquisition, as a core component of training, there is often ambiguity in the setting in which this occurs. The ASE recommends that a significant number of examinations should be performed with the PHE device (or device with similar capabilities) that the physician will be using for FCU and performed on patients in clinical settings typical of the trainee's scope of practice.

Image Interpretation

Trainees should keep a logbook of documented cases where they performed and reported the echocardiogram. The logbook images and reports should subsequently be reviewed by an accredited sonographer, who will provide feedback on all aspects (image acquisition and interpretation).

Future Perspective

Pocket size echocardiography has already infiltrated our daily medical practice, particularly in the emergency setting. The expanding uses and reducing cost of PHE devices will enable a more universal uptake of PHE from cardiology and non-cardiology physicians and general practitioners in both hospital and community settings. Appropriate training, starting as early as medical school will ensure certain standards are met and will avoid potential patient harm and misuse of the available technology. Worldwide cost-effective screening programs will enable reduction in the burden of cardiovascular disease at a global level.

References

1. Roelandt JR. Seeing the heart; the success story of cardiac imaging. *Eur Heart J*. 2000;21(16):1281–8.
2. Senior R, Galasko G, Hickman M, Jeetley P, Lahiri A. Community screening for left ventricular hypertrophy in patients with hypertension using hand-held echocardiography. *J Am Soc Echocardiogr*. 2004;17(1):56–61.
3. Fukuda S, Shimada K, Kawasaki T, Fujimoto H, Maeda K, Inanami H, et al. Pocket-sized transthoracic echocardiography device for the measurement of cardiac chamber size and function. *Circ J*. 2009;73(6):1092–6.
4. Liebo MJ, Israel RL, Lillie EO, Smith MR, Rubenson DS, Topol EJ. Is pocket mobile echocardiography the next-generation stethoscope? A cross-sectional comparison of rapidly acquired images with standard transthoracic echocardiography. *Ann Intern Med*. 2011;155(1):33–8.
5. Galderisi M, Santoro A, Versiero M, Lomoriello VS, Esposito R, Raia R, et al. Improved cardiovascular diagnostic accuracy by pocket size imaging device in non-cardiologic outpatients: the NaUSiCa (Naples ultrasound stethoscope in cardiology) study. *Cardiovasc Ultrasound*. 2010;8:51.
6. Biais M, Carrie C, Delaunay F, Morel N, Revel P, Janvier G. Evaluation of a new pocket echoscopic device for focused cardiac ultrasonography in an emergency setting. *Crit Care*. 2012;16(3):R82.
7. Prinz C, Voigt JU. Diagnostic accuracy of a hand-held ultrasound scanner in routine patients referred for echocardiography. *J Am Soc Echocardiogr*. 2011;24(2):111–6.
8. Panoulas VF, Daigeler AL, Malaweera AS, Lota AS, Baskaran D, Rahman S, et al. Pocket-size hand-held cardiac ultrasound as an adjunct to clinical examination in the hands of medical students and junior doctors. *Eur Heart J Cardiovasc Imaging*. 2013;14(4):323–30.
9. Spencer KT, Kimura BJ, Korcarz CE, Pellicka PA, Rahko PS, Siegel RJ. Focused cardiac ultrasound: recommendations from the American Society of Echocardiography. *J Am Soc Echocardiogr*. 2013;26(6):567–81.
10. Spencer KT. Focused cardiac ultrasound: where do we stand? *Curr Cardiol Rep*. 2015;17(3):567.
11. Coletta C, De Marchis E, Lenoli M, Rosato S, Renzi M, Sestili A, et al. Reliability of cardiac dimensions and valvular regurgitation assessment by sonographers using hand-carried ultrasound devices. *Eur J Echocardiogr*. 2006;7(4):275–83.
12. Giannotti G, Mondillo S, Galderisi M, Barbati R, Zaca V, Ballo P, et al. Hand-held echocardiography: added value in clinical cardiological assessment. *Cardiovasc Ultrasound*. 2005;3:7.
13. Brennan JM, Blair JE, Goonewardena S, Ronan A, Shah D, Vasaiwala S, et al. A comparison by medicine residents of physical examination versus hand-carried ultrasound for estimation of right atrial pressure. *Am J Cardiol*. 2007;99(11):1614–6.
14. Weiner RB, Wang F, Hutter AM Jr, Wood MJ, Berkstresser B, McClanahan C, et al. The feasibility, diagnostic yield, and learning curve of portable echocardiography for out-of-hospital cardiovascular disease screening. *J Am Soc Echocardiogr*. 2012;25(5):568–75.
15. Wyman RA, Chiu RY, Rahko PS. The 5-minute screening echocardiogram for athletes. *J Am Soc Echocardiogr*. 2008;21(7):786–8.
16. Choi BG, Mukherjee M, Dala P, Young HA, Tracy CM, Katz RJ, et al. Interpretation of remotely downloaded pocket-size cardiac ultrasound images on a web-enabled smartphone: validation against workstation evaluation. *J Am Soc Echocardiogr*. 2011;24(12):1325–30.
17. Singh S, Bansal M, Maheshwari P, Adams D, Sengupta SP, Price R, et al. American Society of Echocardiography: remote echocardiography with web-based assessments for referrals at a distance (ASE-REWARD) study. *J Am Soc Echocardiogr*. 2013;26(3):221–33.
18. Beaton A, Okello E, Lwabi P, Mondo C, McCarter R, Sable C. Echocardiography screening for rheumatic heart disease in Ugandan schoolchildren. *Circulation*. 2012;125(25):3127–32.
19. Kobal SL, Lee SS, Willner R, Aguilar Vargas FE, Luo H, Watanabe C, et al. Hand-carried cardiac ultrasound enhances healthcare delivery in developing countries. *Am J Cardiol*. 2004;94(4):539–41.
20. Zamorano JL, Moreno R, Alburquerque C. Echocardiography performed by physicians outside of echolabs - is it possible? *Eur Heart J*. 2002;23(11):908–9.
21. Popescu BA, Andrade MJ, Badano LP, Fox KF, Flachskampf FA, Lancellotti P, et al. European Association of Echocardiography recommendations for training, competence, and quality improvement in echocardiography. *Eur J Echocardiogr*. 2009;10(8):893–905.
22. Nihoyannopoulos P, Fox K, Fraser A, Pinto F, Laboratory Accreditation Committee of the EAE. EAE laboratory standards and accreditation. *Eur J Echocardiogr*. 2007;8(1):80–7.
23. Sicari R, Galderisi M, Voigt JU, Habib G, Zamorano JL, Lancellotti P, et al. The use of pocket-size imaging devices: a position statement of the European Association of Echocardiography. *Eur J Echocardiogr*. 2011;12(2):85–7.

Part XI

Interventional Echocardiography

Intraoperative Echocardiography

40

William J. Stewart and Robert M. Savage

Intraoperative echocardiography (IOE) is an important component in the management of patients undergoing cardiac surgery [1–3]. It provides information about valve structure and function, ventricular size and function, and hemodynamics that is crucial to contemporary management decisions in modern heart surgery [4–6]. Although IOE is used to monitor cardiac patients in the setting of non-cardiac surgery [7], that topic is outside the scope of this chapter. Intraoperative echo is an essential element in basic procedures such as valve repair, and also contributes substantially in cases where the surgical mission is more challenging or the patient's perioperative risk is higher.

Epicardial Versus Transesophageal Echocardiography

Transesophageal echo (TEE) is the chosen modality for IOE [8, 9] because it does not interrupt car-

diac surgery, and is performed by someone other than the surgeon, usually a cardiologist or anesthesiologist [10]. Epicardial echocardiography can be performed using a standard transthoracic transducer placed directly on the heart. Sterility is maintained by placing the probe within a sterile sheath, with ultrasonic gel to eliminate the air. This method was the primary mode of IOE in the mid 1980s, but was displaced in the last 20 years by transesophageal echocardiography (TEE). Epicardial echo is still a useful option in instances when TEE is unable to provide adequate imaging, more common for anterior structures, ascending aortic atheroma [11], and left ventricular (LV) outflow tract obstruction. Epicardial echo is also the procedure of choice in a situation where the surgeon prefers to do the transducer work.

Essentials of the IOE Exam

It is essential that the echocardiographer be well versed in the process of cardiac surgery, the hemodynamic effects of anesthesia and the heart-lung machine, as well as the diagnostic elements of echocardiography and Doppler echocardiography. It is important to have equipment available which is of sufficient diagnostic quality to achieve the diagnostic agenda. In addition, the echocardiographer should be familiar with previous images stored in digital format, to compare with the current ones. It is essential

W. J. Stewart (✉)
Department of Cardiovascular Medicine,
The Cleveland Clinic Foundation,
Cleveland, OH, USA
e-mail: Stewartw@ccf.org

R. M. Savage
Cardiothoracic Anesthesia and CVICU, Heart and
Vascular Institute, McLeod Regional Medical Center,
Florence, SC, USA

Table 40.1 Objectives of intraoperative echocardiography

Pre-pump TEE
• Redefine primary surgical target(s) <ul style="list-style-type: none">– Severity and mechanism of valve dysfunction
• Evaluation of other valves, unexpected lesions
• Define ventricular function <ul style="list-style-type: none">– Baseline under anesthesia– Global and segmental wall motion
• Assist with cannulation, instrumentation <ul style="list-style-type: none">– Atheroma, thrombi, anatomic variants
Post-pump TEE
• Safety net on results <ul style="list-style-type: none">– Define success of primary surgery– Evaluation for residual regurgitation or stenosis
• Assess complications of surgery
• Assess intraoperative myocardial ischemia/infarction
• Assess residual intracardiac shunting

to generate a report from the diagnostic IOE study, so that the results can be factored into the patient’s subsequent clinical management.

In most cases, cardiac surgery utilizes cardio-pulmonary bypass. Exceptions include off-pump coronary bypass and pericardial stripping. Therefore, most IOE is done in two portions, the *pre-pump* and the *post-pump* examinations. Each has its purposes (Table 40.1).

Pre-pump IOE

It is important to have the patient fully evaluated prior to entering the operating room. IOE should not be a substitute for good preoperative clinical evaluation. An exception to this is extremely emergent surgery [12], where death hangs in the balance of minutes, such as aortic dissection with impending tamponade [13–15], or acute aortic or ventricular rupture. Therefore, it should be a rare circumstance where the pre-pump IOE is relied upon as the sole determinant of the cardiac operation. However, IOE does provide a last-minute update on the status of the heart and cardiovascular hemodynamics in the operating room [16]. It can provide a substantial “quality control”, especially in cases where some of the

patient’s pathology was not understood fully preoperatively.

Many patients come to the operating room without transesophageal echo done preoperatively, and TEE is a more sensitive tool for defining many intracardiac abnormalities. Additional diagnostic features leading to changes in the operative mission are found from 6 to 19% of the time.

Particular care should be paid to the difference between ambulatory hemodynamic conditions and the anesthetic state. Compared to “street conditions,” the anesthetized patient may have less sympathetic tone, altered intravascular volume status, interval treatment, or different heart rate and rhythm. Many patients have less mitral or tricuspid regurgitation on the pre-pump TEE than was found in the echo lab or the cath lab. Quantitative Doppler techniques to accurately measure the severity of the regurgitation are very feasible with high quality TEE images (Fig. 40.1).

Whenever the pre-pump IOE makes a substantive change in the surgical plan, the patient’s clinical physicians should be contacted to discuss the proposed changes in light of preoperative impressions. Tricuspid regurgitation, dynamic LV outflow tract obstruction, and myocardial ischemia are the most common examples where loading conditions can erroneously suggest that certain goals of surgery need to be altered.

Post-pump IOE

The TEE study after cardio-pulmonary bypass is a golden opportunity to evaluate the success of the surgical missions and provide a “safety net” for its objectives. It allows the surgical team to determine if the elimination of valve dysfunction is complete and if new valvular or other complications have developed. It also provides an immediate evaluation of both overall and segmental myocardial function, and to check for intraoperative ischemia or infarction at a time when additional bypass surgery can be done. New or residual intracardiac shunts can be identified and defined.

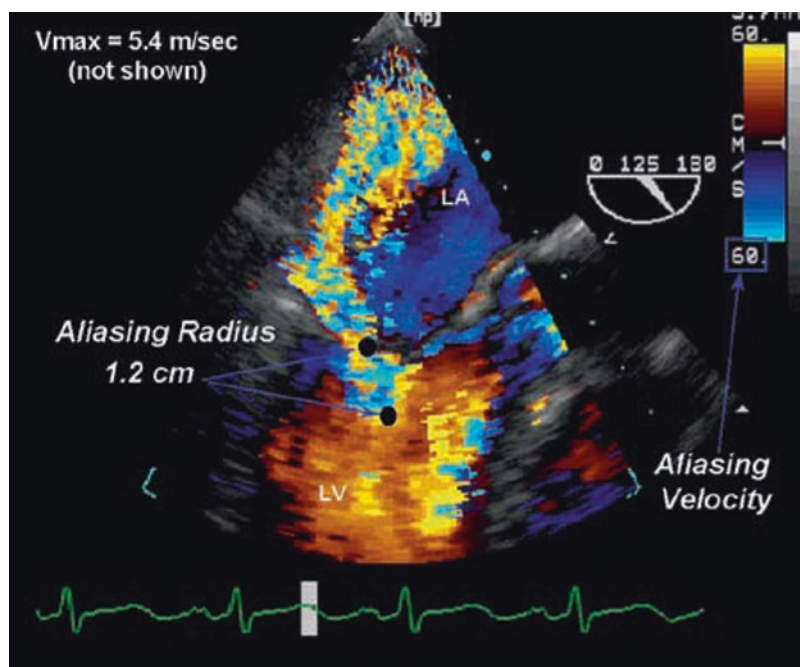


Fig. 40.1 Mid-esophageal long axis view at 125° multiplane angle of a patient with severe *mitral regurgitation (MR)* from *anterior leaflet prolapse*, with the jet deflected posteriorly, showing the measurement of a 1.2 cm aliasing radius (R) within the flow convergence zone (measured between the black dots). Note that the aliasing velocity

(Va), is 60 cm/s. Using the formula to calculate regurgitant orifice area (ROA) of $2 \pi R^2 Va/V_{max}$, and knowing that the maximum MR velocity (V_{max}) by continuous wave Doppler was 5.4 m/s, the calculated ROA is 1.0 cm². An ROA over 0.4 cm² is considered severe for MR

It is unwise to ignore the information defined by post-pump intraoperative echo. Residual valve dysfunction on postpump echo has been associated with substantially higher early post op complications (86% vs 15%) and higher mortality rate (43% vs 5%) when these findings are not corrected.

Our guidelines for doing further surgery during a second run of cardio-pulmonary bypass, a *second pump run*, is as follows: When there is no residual valve regurgitation or stenosis or it is mild (1+ on a scale of 4+), no further surgery is done. When there is moderately severe to severe (3+ to 4) residual valve regurgitation or stenosis after attempted repair, then further repair or replacement during a second pump run is done. When there is moderate (2+) residual valve dysfunction, further surgery should be done if there is no contraindication. In this latter case, we often try to observe the situation for a few minutes without decannulating or giving protamine.

In many circumstances, this time provides the opportunity to observe the amount of valve dysfunction further, while allowing transient myocardial problems to resolve. In this circumstance, we often challenge the patient to unmask latent regurgitation, using increased blood pressure to a mean pressure of 100–110 mm Hg, using 100 mcg boluses of intravenous phenylephrine, and using volume loading. In addition, postpump findings such as systolic anterior motion (SAM) with outflow obstruction after mitral valve repair should warrant a second pump run to correct the SAM, or replace the valve [17].

Process and Completeness of the IOE Study

It is important to approach the echo examination with efficiency and completeness. In evaluating a patient with a single abnormality, we first look

at the valve or structure in question, the one that will be addressed by the operation. This has been called “Willie Sutton’s law, *going for the money*.” If the patient suddenly becomes unstable thereafter, at least the most important questions have been answered. Both structural imaging (black and white) and color Doppler images of that structure are recorded from multiple long and short axis views. Because each structure has three-dimensional anatomy, a single plane with often miss important structural or flow patterns that will be covered by using numerous orthogonal planes. After addressing the most important questions for that case, a complete echo survey is done, looking at all four chambers, all four valves, pulmonary and systemic veins and arteries. A digital or video tape record is made of each structure, for later side-by-side comparison with the post-pump images, useful particularly if there are new abnormalities.

Indications for Intraoperative Echo

The most common uses of IOE are listed in Table 40.2. The most important patients to use intraoperative echo are those in whom the study leads more commonly to changes in the surgical or anesthetic management. In *valve repair*, the most common pre-pump contributions of the IOE is the detailed understanding of the *mechanism* of the valve dysfunction, based on the echo (Fig. 40.2), which is key to knowing what specific surgical maneuvers are needed to correct the problem. Esophageal pathology (strictures or tumors) are a contraindication to intraoperative TEE, as they increase the risk of complications [18].

IOE in Mitral Valve Repair

The most common indication for IOE is *valve repair for mitral regurgitation* (MR). The pre-pump echo evaluates the structure and flow abnormalities of each component of the mitral valve (annulus, leaflets, chordae, papillary mus-

Table 40.2 Indications for intraoperative echo

• Repair of any valve
– Mitral, aortic, or tricuspid valve repair
• Left ventricular function; global and segmental
– Location and persistence of ischemia
• Complex congenital heart surgery
• Complex infection-abscess, prosthetic endocarditis
• Peri-prosthetic regurgitation
• Dissection, aortic root surgery
– Especially with aortic valve resuspension
• Myectomy-hypertrophic cardiomyopathy
• Ongoing myocardial ischemia
• Cardiac tumor
• Minimally invasive procedures (MIP)
1. Hemi-sternotomy, port access,
• Off-pump coronary bypass (OPCABG)
• Alternative valve replacements (stentless)
– Homograft, Ross, Stentless bioprosthesis
• Implantable LV assist devices
• High risk coronary bypass
– Guidance in cannulation (atheroma)

cles, left ventricle, and left atrium) in multiple mid-esophageal planes, and a short axis view from a trans-gastric probe position [19–22]. Each plane is imaged in color and 2D echo (Fig. 40.3a, b). Pulsed and continuous wave Doppler is used to characterize the antegrade velocity profile. Pulsed Doppler of pulmonary vein velocity is also useful to assess for velocity waveforms, especially systolic reversal, a common finding in severe MR (Fig. 40.4).

In particular, which leaflet is abnormal is determined in various long axis views [23], such as the mid-esophageal transverse view of the mitral valve at 0° multiplane angle, and the mid-esophageal long axis view of the mitral valve at 120–150°. The mid-esophageal inter-commissural view of the mitral valve at about 60°, aligned parallel to the line between the medial and lateral commissures, is particularly helpful in learning the medial-versus-lateral locations of the structural and flow abnormalities of the most involved leaflet [24]. For example this helps to distinguish which scallop of the posterior leaflet is abnormal. Three dimensional echo [25–27] is also useful to visualize medial versus lateral aspects of mitral valve pathology and flow (Fig. 40.5).

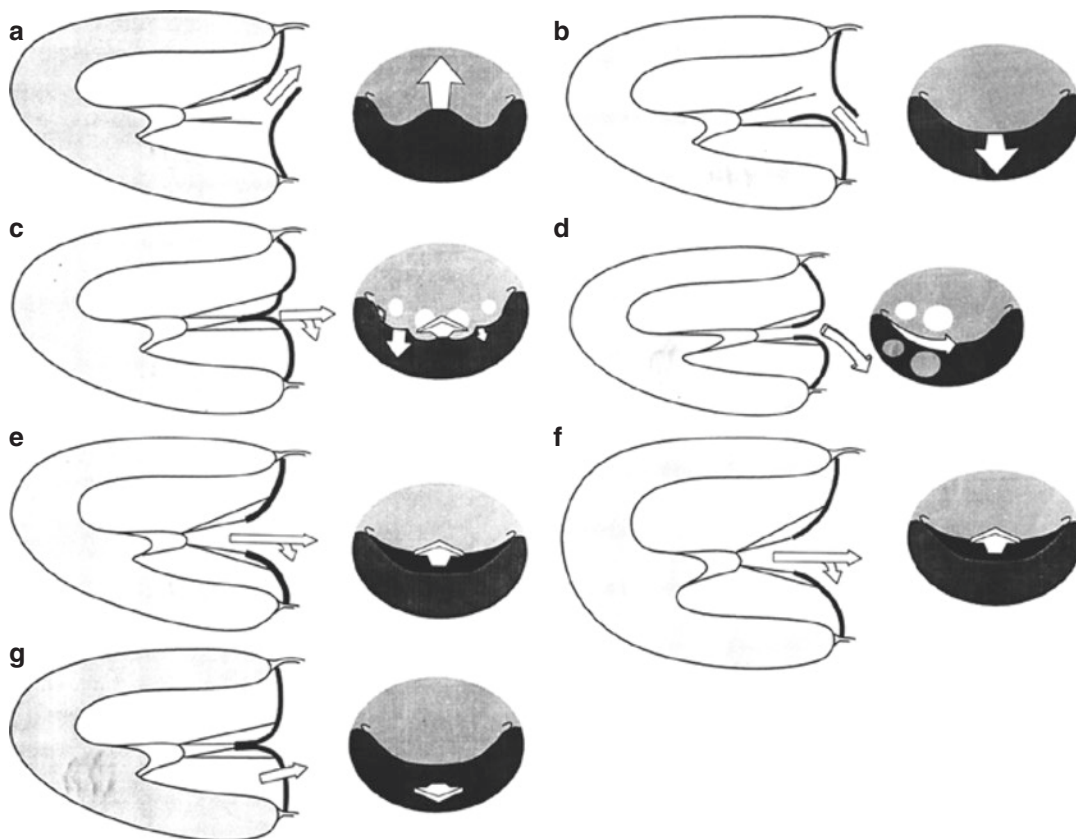


Fig. 40.2 Composite diagram of seven types of *mitral regurgitation (MR) mechanisms* based on mitral leaflet motion and jet direction (see arrows), determined respectively by echo imaging and color Doppler imaging. Each pair indicates leaflet and jet characteristics in long axis (left) and short axis (right) images. **(a):** posterior prolapse

or flail. **(b):** Anterior prolapse or flail. **(c):** Bileaflet prolapse of flail. **(d):** Commissural chordal elongation or papillary muscle disruption. **(e):** Restricted leaflet motion. **(f):** Relative restriction and apical tethering of normal leaflets caused by left ventricular enlargement and dysfunction. **(g):** Leaflet perforation or congenital cleft

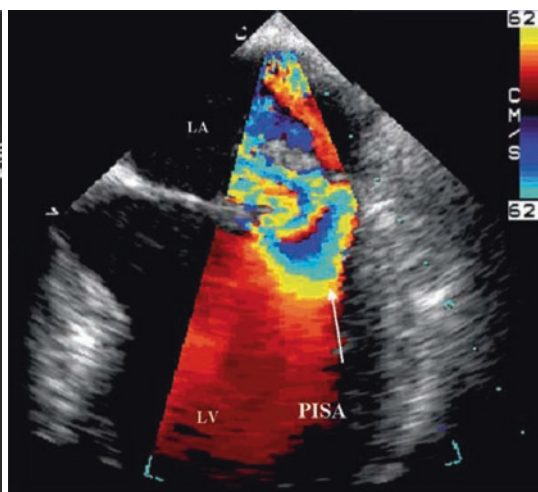
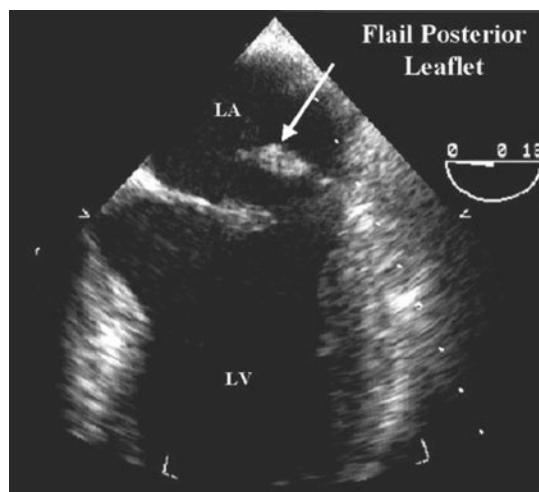


Fig. 40.3 Mid-esophageal long axis view at 0° multiplane angle of a patient with severe mitral regurgitation (MR). *Left:* posterior leaflet flail (arrow), within the left

atrium (LA). *Right:* the jet is deflected posteriorly and there is a large flow convergence (arrow), also called the proximal isovelocity surface area (PISA)

Fig. 40.4 Pulse wave Doppler spectrum (grey scale contours) recorded by TEE from the left upper pulmonary vein in a patient with MR, showing *reversal of systolic flow* (RSF), indicating that the MR is severe. Superimposed is a directly measure left atrial pressure (thin line waveforms), illustrating, on a scale of 0–40 mm Hg large 45 mm “V” waves during each ventricular systole, which transiently exceed pulmonary parenchymal pressure, causing the flow reversal

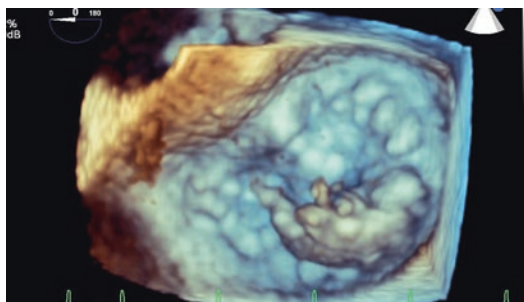
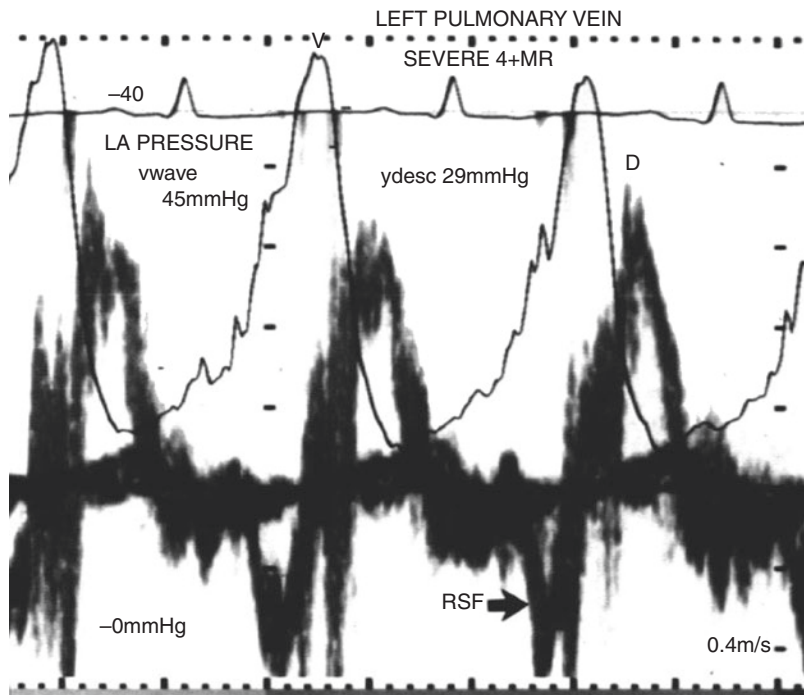


Fig. 40.5 Three dimensional echo from intraoperative TEE, using the “surgeon’s view from the left atrial side of the mitral valve, in a patient with mitral regurgitation due to posterior mitral prolapse with ruptured chordae to the middle scallop. This imaging helps the surgeon to visualize the pathology in motion and to determine which parts of mitral leaflet anatomy are abnormal

IOE in Left Ventricular Outflow Tract Surgery

In aortic valve disease and dynamic LV outflow tract obstruction, a similar approach is made using imaging and color Doppler views from multiple imaging planes [28]. The short axis of the aortic valve is best viewed from a mid-

esophageal view at about 45–60°. The long axis view of the aortic valve and LV outflow tract should be evaluated at an angle of about 125–140°, approximately 90° from where the short axis view was ideal. Antegrade aortic valve velocity is recorded using the deep transgastric views, aligning the cursor through the flow convergence in the LV outflow tract seen on the color image. Most patients with aortic valve disease undergo aortic valve replacement, for which IOE is less essential because the likelihood of changes in operative management based on IOE are low. For the patient with severe aortic regurgitation (AR), *valve repair* is most feasible if the mechanism of dysfunction (definable by IOE) is a prolapsing non-calcified bicuspid aortic valve (Fig. 40.6a, b). The maneuver needed to correct the AR is triangular exclusion of a portion of the conjoined leaflet edge. This reduces the length of its edge to the length equal to that of the non-conjoined leaflet. The pledgetted commissural sutures at the commissures bring the suspension points of the valve inward to enhance coaptation [29]. After repair, residual regurgitation is the most common abnormality.

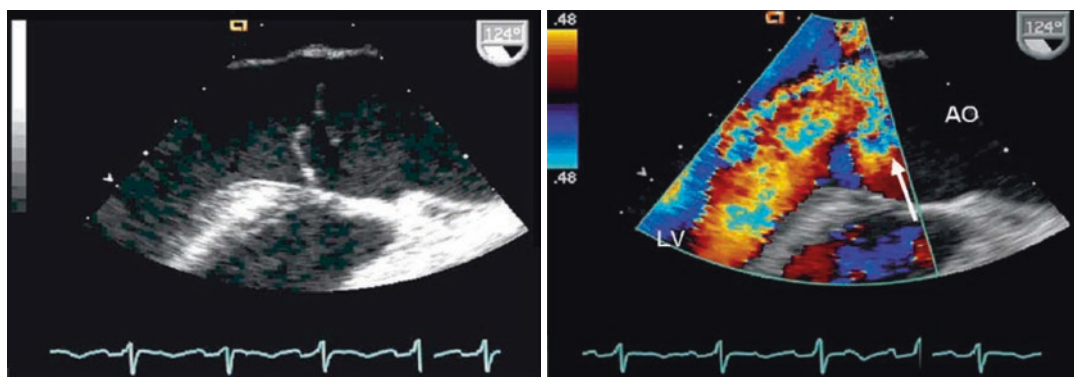
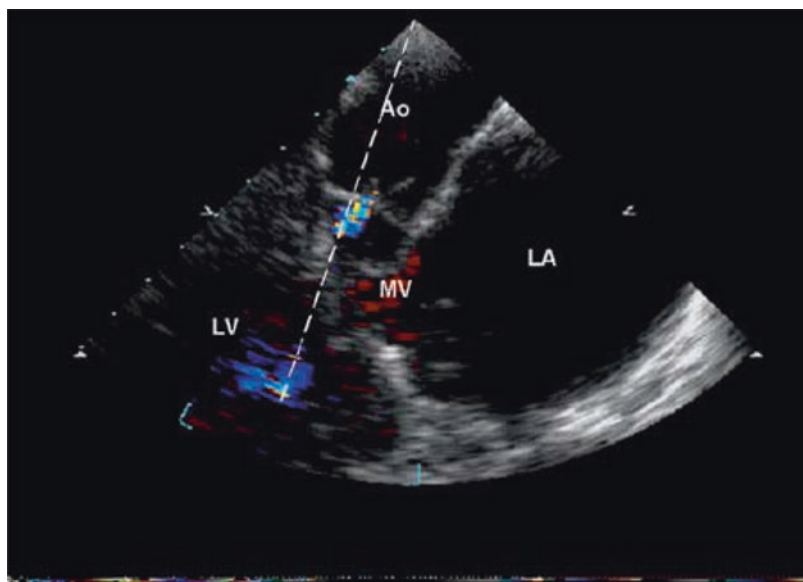


Fig. 40.6 Mid-esophageal long axis view of the aorta (AO) at 124° multiplane angle, in a patient with severe aortic regurgitation (AR). *Left:* prolapse of the conjoined right-left cusp of a non-calcified *bicuspid* valve. *Right:* color Doppler image, showing that the AR jet is deflected

posteriorly within the left ventricular (LV) outflow tract. Note the large flow convergence (arrow), allowing calculation of regurgitant orifice area by the proximal isovelocity surface area method. An ROA over 0.3 cm² is considered severe for AR

Fig. 40.7 Color flow image recorded by *epicardial imaging* in a patient with hypertrophic cardiomyopathy undergoing myectomy to relieve dynamic subaortic obstruction. A transthoracic transducer within a sterile sheath is used to place a continuous wave Doppler cursor (dashed line) directly through, and parallel to, the high velocity flow located at the point of apposition of the mitral valve (MV) leaflets against the hypertrophied interventricular septum



Myectomy for hypertrophic cardiomyopathy is an important role for IOE [30, 31]. On the pre-pump TEE we define the thickness of the septum to plan the location of the myectomy, the farthest point of contact of the mitral systolic anterior motion (SAM) with the septum, and the locations of the papillary muscles [32]. This helps the surgeon to know the extent of resection, as the thickness of the septum cannot be determined by the surgeon through the aortotomy. In addition, it is important to distinguish mitral regurgitation resulting from SAM,

versus MR resulting from intrinsic disease of the mitral valve such as prolapse or flail. The LV outflow gradient can often be recorded by TEE using a deep transgastric view for continuous wave Doppler. If not, epicardial echo (Fig. 40.7) may be useful to record the highest velocity at the point of SAM-septal contact. After myectomy, we look for persistent SAM and MR, or a persistent gradient of over 40 mmHg at rest or with Isoproterenol infusion, which is the most common reason mandating a second run of cardiopulmonary bypass. Although unusual, we

also look for a new ventricular septal defect at the location of the myectomy.

IOE in Coronary Atherosclerosis

In any patient undergoing cardiac surgery, but especially in those with significant *coronary disease*, we look for segmental abnormalities of the left (and right) ventricles. Prior to surgery, we store a digital clip of each standard view of the left ventricle, including mid esophageal views from multiplane angles of 0°, 60° and 120° (Fig. 40.8), and trans-gastric short and long axis views, at 0° and 90° respectively. After surgery these same views can be obtained, and juxtaposed with the pre-pump images to accurately diagnose new ischemia or infarction.

One of the most common and devastating complications of coronary bypass surgery is atherosclerotic embolization to the brain, kidneys, liver, etc. [33]. This occurs more commonly in patients with *atheroma of the thoracic aorta* (Fig. 40.9). Because it is very sensitive, epicardial echo would find atheroma on many elderly patients undergoing cardio-pulmonary bypass [34]. In some, epicardial echo helps define the location and method of arterial cannulation. Transesophageal echocardiography is not as good for imaging atheroma in the ascending aorta because it is in the far field, and partly hidden in the blind spot for TEE, where the tracheal bifurcation blocks the imaging access. However, in practice, epicardial echo is used more selectively for this purpose, favoring cases when there are clinical suspicions of severe ascending atheroma, known severe carotid disease, or heavy aortic knob calcification by chest X-ray. When a TEE is done for another purpose prior to cannulation for cardio-pulmonary bypass, information about the presence and severity of atheroma of the thoracic aorta [35] may be the reason for deciding to do epicardial echo for ascending atheroma. It is known that atheroma typically get worse as one proceeds distally, so severe mobile atheroma are unlikely in the ascending aorta if they are not found distally.

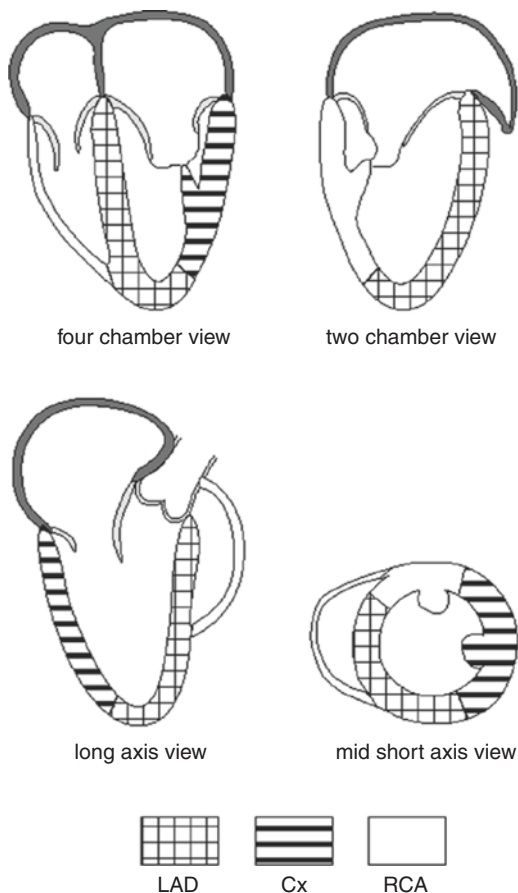


Fig. 40.8 Diagrams of typical *coronary artery perfusion* beds as they are distributed in standard TEE image planes, mid-esophageal images at 0° (four chamber), 60° (two chamber), and 120° (long axis) multiplane angle, and the transgastric image plane at 0° multiplane angle. The shadings depict the left anterior descending (LAD) territory with a checked pattern, the circumflex (Cx) territory in a striped pattern, and the right coronary artery territory in a plain white pattern. Individual patients' coronary distributions vary substantially

IOE in Other Cardiac Conditions

In *congenital heart disease*, the primary goal is to define the location and size of septal defects and exclude additional abnormalities [36]. The challenge of very little babies is the unavailability of TEE probes that are small enough. One solution is to use intracardiac echo (ICE) probes either in the esophagus or on the surface of the heart. We utilize intravenous contrast echo frequently after

shunt surgery to verify the elimination of the septal defect. Continuous wave Doppler from the epicardial window is useful for determination of LV and RV outflow tract obstruction.

In *endocarditis*, and especially peri-prosthetic regurgitation and peri-valvular abscesses, IOE is an essential element for planning the degree of resection as well as the location of infection-related fistulas. After surgery, excluding peri-prosthetic leakage is similar to other valvular lesions, but there is the additional issue of



Fig. 40.9 Transesophageal echo image at 0° multiplane angle of the aortic arch in a patient with *severe protruding atheroma*. When these are large and/or mobile, the likelihood of embolization increases, especially with more manipulation of the aorta during heart surgery

determining the exclusion of persistent fistula. The use of the aortic homograft is an essential surgical tool in peri-aortic infection. After implantation of a *homograft* (Fig. 40.10a, b), *Ross procedure*, or *stentless valve*, the post-pump echo is important in verifying competency, and determining that the leaflets are suspended well without prolapse.

A similar set of statements can be made about patient's undergoing aortic valve surgery together with surgery for an ascending *aortic aneurysm*. The pre-pump IOE is helpful in defining if the aortic valve leaflets are inherently abnormal, and the diameters of the aortic annulus, sinuses, and sino-tubular junction. If the valve is re-suspended using a supra-coronary conduit, or with a David procedure, the post pump TEE is used to look for residual aortic regurgitation.

Lastly, in *minimally invasive or robotic surgery*, done through a limited thoracotomy [37–39], IOE is important to make up for some limitations caused by a less optimum visualization of the heart by the surgeon. Most patients undergoing repair or replacement of a single valve (aortic or mitral) can have a hemi-sternotomy. However, this smaller incision induces some limitations on the operative team. It is harder to follow heart size and therefore to judge the adequacy of volume filling from the

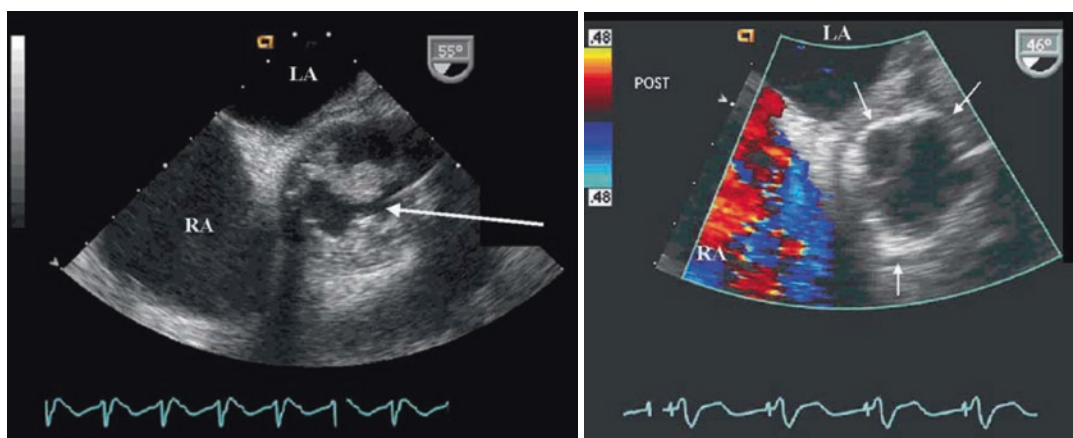


Fig. 40.10 Mid-esophageal short axis views of the aortic valve in endocarditis. *Left:* Pre-pump TEE image showing a *peri-aortic abscess*, causing regurgitation adjacent to an aortic prosthesis. *Right:* Post pump TEE image shows a

normal aortic homograft, with a concentric double density with a thin clear space (arrows) between the donor aortic annulus (homograft inclusion cylinder) and the recipient's aortic annulus. RA right atrium

pump. In addition, intracardiac air is more difficult to remove, because the LV apex cannot be lifted up for needle de-airing. IOE helps to optimize management of these issues.

Complications of Heart Surgery Definable by IOE

Persistence of valvular regurgitation is the most common problem encountered on the post-pump intraoperative echocardiogram. However new valvular regurgitation of a valve not previously abnormal is problem that occurs occasionally. The most common surprise is new MR resulting from worsened LV enlargement. Peri-prosthetic regurgitation (Fig. 40.11), after a new prosthesis is implanted is not uncommon [40], particularly in patients with peri-valvular infection or a calcified mitral annulus. A stitch from the mitral prosthesis placed all the way through to the aortic valve is a rare complication of which to be aware. A new atrial septal defect has been found on some post-pump IOE studies, especially when the mitral valve is approached via the right atrium and the interatrial septum. Iatrogenic aortic dis-

section is a rare result of aortic cannulation, the aortic vent, or a proximal vein graft anastomosis.

Pitfalls of IOE

The most important problem encountered in the practice of intraoperative echo is inexperience, see Table 40.3. It is a daunting task to apply all the diagnostic acumen needed for accurate outpatient TEE to the operating room environment. It is challenging to have persons on hand who have sufficient echo experience who also are familiar with and available in the operative environment. It is recommended that the practitioner of IOE have at least level 2 training in TEE as defined by the American Society of Echocardiography [41]. This includes training under supervision for at least 300 echo studies. This educational agenda is therefore long, and difficult to accomplish without a concentrated period of fellowship in a formal training environment.

The persons doing intraoperative TEE studies are often cardiology or cardio-thoracic anesthesiology physicians. Each has a substantial learning curve that is often not facilitated in a standard fel-

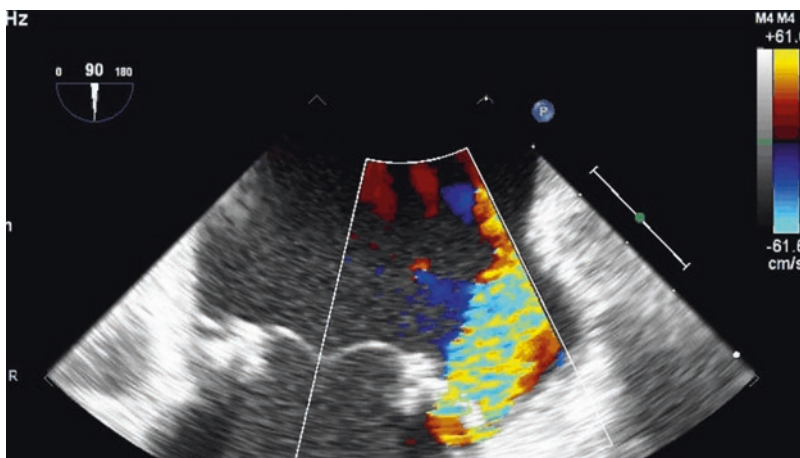


Fig. 40.11 Mid-esophageal two chamber color Doppler image of the left atrium and left ventricle at 90° multi-plane angle, immediately after mitral valve replacement for endocarditis, showing *peri-prosthetic mitral regurgitation*, with the color jet located anterior and superior to the

bioprosthetic mitral sewing ring. Afterward this patient underwent a second pump run, adding a few stitches, with no peri-prosthetic MR seen by TEE immediately afterward

Table 40.3 Intraoperative echo pitfalls

• Inexperience
• Inadequate study
– Imaging time too short
– Imaging planes too few
– Coupling (sleeving, contact)
• Hemodynamic instability: hypotension, hypovolemia
• Interference to imaging
– Electronic (electrocautery, environment)
– Room lights on

lowship without personal initiative. For example, a cardiology fellow may lack experience with the process of cardiac surgery, or be uncomfortable engaging in diagnostic studies in the operative environment, with changing hemodynamic conditions. The anesthesiology fellow often has inadequate exposure to ultrasound technology, intra-cardiac anatomy, and the diagnostic process inherent in imaging and flow analysis.

In many hospitals, the ideal IOE team includes both cardiologists and anesthesiologists, working together to provide coverage of the various patients presenting for cardiac surgery. The team also involves the echo competence of the cardiac surgeon(s). Even if the surgeon does not *perform* the study, understanding the flavor of the information of the imaging and flow analysis takes a substantial learning curve, which should be included in the agenda of cardiac surgical training.

Conclusion

Care of the patient undergoing cardiac surgery is enhanced substantially by a careful and selective program of intraoperative echocardiography. This enhances patient outcomes by giving up to the minute information about the patient's cardiac performance before and after the corrective procedure.

References

1. Grimm RA, Stewart WJ. The role of intraoperative echocardiography in valve surgery. *Cardiol Clin*. 1998;16(3):477–89.
2. Mahmood F, Shernan SK. Perioperative transoesophageal echocardiography: current status and future directions. *Heart*. 2016;102(15):1159–67. <https://doi.org/10.1136/heartjnl-2015-307962>. Epub 2016.
3. Thys DM, Abel M, Bollen BA, Stewart WJ, Pearlman S, American Society of Anesthesiologists and the Society of Cardiovascular Anesthesiologists Task Force on transesophageal Echocardiography, et al. Practice guidelines for perioperative transesophageal echocardiography. *Anesthesiology*. 1996;84:986–1996.
4. Click RL, Abel MD, Schaff HV. Intraoperative transesophageal echocardiography: 5-year prospective review of impact on surgical management. *Mayo Clin Proc*. 2000;75(3):241–7.
5. Cosgrove DM, Stewart WJ. Mitral valvuloplasty. *Curr Probl Cardiol*. 1989;14:359–415.
6. Taylor BS, Brady MB. Echo, the Cardiac Operating Room, and Intraoperative Echocardiography. *J Am Soc Echocardiogr*. 2015;28(7):32A.
7. DeBruijn NP, Clements FM, Kisslo JA. Intraoperative transesophageal color flow mapping: initial experience. *Anesth Analg*. 1987;66:386–90.
8. Shanewise JS, Cheung AT, Aronson S, Stewart WJ, Weiss RL, Mark JB, Savage RM, Sears-Rogan P, Mathew JP, Quinones MA, Cahalan MK, Savino JS. ASE/SCA guidelines for performing a comprehensive intraoperative multiplane transesophageal echocardiography examination: recommendations of the American Society of Echocardiography Council for Intraoperative Echocardiography and the Society of Cardiovascular Anesthesiologists Task Force for Certification in Perioperative Transesophageal Echocardiography. *J Am Soc Echocardiogr*. 1999;12(10):884–900.
9. Sheikh KH, de Bruijn NP, Rankin JS, et al. The utility of transesophageal echocardiography and doppler color flow imaging in patients undergoing cardiac valve surgery. *J Am Coll Cardiol*. 1990;15:363–72.
10. Markin NW, Gmelch BS, Griffie MJ, Holmberg TJ, Morgan DE, Zimmerman JM. A review of 364 perioperative rescue echocardiograms: findings of an anesthesiologist-staffed perioperative echocardiography service. *J Cardiothorac Vasc Anesth*. 2015;29(1):82–8.
11. Wareing TH, Davila-Roman VG, Barzilai B, Murphy SF, Kouchoukos NT. Management of the severely atherosclerotic ascending aorta during cardiac operations. A strategy for detection and treatment. *J Thorac Cardiovasc Surg*. 1992;103:453–62.
12. Kratz T, Steinfeldt T, Exner M, Dell Orto MC, Timmesfeld N, Kratz C, Skrodzki M, Wulf H, Zoremba M. Impact of Focused Intraoperative Transthoracic Echocardiography by Anesthesiologists on Management in Hemodynamically Unstable High-Risk Noncardiac Surgery Patients. *J Cardiothorac Vasc Anesth*. 2016;31(2):602–9. <https://doi.org/10.1053/j.jvca.2016.11.002>. pii: S1053-0770(16)30524-9.

13. Erbel R, Oelert H, Meyer J, et al. Effect of medical and surgical therapy on aortic dissection evaluated by transesophageal echocardiography. Implications for prognosis and therapy. The European Cooperative Study Group on Echocardiography. *Circulation*. 1993;87:1604–15.
14. Simon P, Owen AN, Havel M, et al. Transesophageal echocardiography in the emergency surgical management of patients with aortic dissection. *J Thorac Cardiovasc Surg*. 1992;103:1113–7.
15. Thorsgard ME, Morrisette GJ, Sun B, Eales F, Kshetry V, Flavin T, Tyberg R, Garberich RF, Harris KM. Impact of intraoperative transesophageal echocardiography on acute type-A aortic dissection. *J Cardiothorac Vasc Anesth*. 2014;28(5):1203–7. <https://doi.org/10.1053/j.jvca.2014.05.012>.
16. Secknus MA, Klein AL, Smedira NG, Cosgrove DM, Stewart WJ. Does prepump intraoperative echocardiography change operative plans in mitral valve repair? *J Am Soc Echocardiogr*. 1996;9:374.
17. Freeman WK, Schaff HV, Khandheria BK, et al. Intraoperative evaluation of mitral valve regurgitation and repair by transesophageal echocardiography: incidence and significance of systolic anterior motion. *J Am Coll Cardiol*. 1992;20:599–609.
18. Purza R, Ghosh S, Walker C, Hiebert B, Koley L, Mackenzie GS, Grocott HP. Transesophageal echocardiography complications in adult cardiac surgery: a retrospective cohort study. *Ann Thorac Surg*. 2017;103(3):795–802. <https://doi.org/10.1016/j.athoracsur.2016.06.073>.
19. Mahmood F, Matyal R. A quantitative approach to the intraoperative echocardiographic assessment of the mitral valve for repair. *Anesth Analg*. 2015;121(1):34–58.
20. Poelaert JJ, Bouchez S. Perioperative echocardiographic assessment of mitral valve regurgitation: a comprehensive review. *Eur J Cardiothorac Surg*. 2016;50(5):801–12. Epub 2016 Jun 3.
21. Shah PM, Raney AA, Duran CM, Oury JH. Multiplane transesophageal echocardiography: a roadmap for mitral valve repair. *J Heart Valve Dis*. 1999;8(6):625–9.
22. Sheikh KH, Bengtson JR, Rankin JS, de BN, Kisslo J. Intraoperative transesophageal Doppler color flow imaging used to guide patient selection and operative treatment of ischemic mitral regurgitation. *Circulation*. 1991;84:594–604.
23. Stewart WJ, Currie PJ, Salcedo EE, et al. Intraoperative doppler color flow mapping for decision-making in valve repair for mitral regurgitation. Technique and results in 100 patients. *Circulation*. 1990;81:556–66.
24. Stewart WJ, Currie PJ, Salcedo EE, et al. Evaluation of mitral leaflet motion by echocardiography and jet direction by Doppler color flow mapping to determine the mechanisms of mitral regurgitation. *J Am Coll Cardiol*. 1992;20:1353–61.
25. Calleja A, Poulin F, Woo A, Meineri M, Jedrzkiewicz S, Vannan MA, Rakowski H, David T, Tsang W, Thavendiranathan P. Quantitative modeling of the mitral valve by three-dimensional transesophageal echocardiography in patients undergoing mitral valve repair: correlation with intraoperative surgical technique. *J Am Soc Echocardiogr*. 2015;28(9):1083–92.
26. Kapoor PM, Muralidhar K, Nanda NC, Mehta Y, Shastri N, Irpachi K, Baloria A. An update on transesophageal echocardiography views 2016: 2D versus 3D tee views. *Ann Card Anaesth*. 2016;19(Supplement):S56–72. <https://doi.org/10.4103/0971-9784.192624>.
27. Mahmood F, Jegannathan J, Saraf R, Shahul S, Swaminathan M, Mackensen GB, Knio Z, Matyal R. A practical approach to an intraoperative three-dimensional transesophageal echocardiography examination. *J Cardiothorac Vasc Anesth*. 2016;30(2):470–90. <https://doi.org/10.1053/j.jvca.2015.10.014>. Epub 2015 Oct 23.
28. Currie PJ, Stewart WJ. Intraoperative echocardiography for surgical repair of the aortic valve and left ventricular outflow tract. *Echocardiography*. 1990;7:273–88.
29. Cosgrove DM, Rosenkranz ER, Hendren WG, Bartlett JC, Stewart WJ. Valvuloplasty for aortic insufficiency. *J Thorac Cardiovasc Surg*. 1991;102:571–6.
30. Marwick TH, Stewart WJ, Lever HM, et al. Benefits of intraoperative echocardiography in the surgical management of hypertrophic cardiomyopathy. *J Am Coll Cardiol*. 1992;20:1066–72.
31. Grigg LE, Wigle ED, Williams WG, Daniel LB, Rakowski H. Transesophageal doppler echocardiography in obstructive hypertrophic cardiomyopathy: clarification of pathophysiology and importance in intraoperative decision making. *J Am Coll Cardiol*. 1992;20:42–52.
32. Sonny A, Sale S, Smedira NG. Abnormalities of mitral subvalvular apparatus in hypertrophic cardiomyopathy: role of intraoperative 3D transesophageal echocardiography. *Anesth Analg*. 2016;123(5):1094–7.
33. Blauth CI, Cosgrove DM, Webb BW. Atheroembolism from the ascending aorta: an emerging problem in cardiac surgery. *J Thorac Cardiovasc Surg*. 1992;103:1104–12.
34. Davila-Roman VG, Phillips KJ, Daily BB, RM D, Kouchoukos NT, Barsilai B. Intraoperative transesophageal echocardiography and epiaortic ultrasound for assessment of atherosclerosis of the thoracic aorta. *J Am Coll Cardiol*. 1996;28(4):942–7.
35. Kouchoukos NT, Wareing TH, Daily BB, Murphy SF. Management of the severely atherosclerotic aorta during cardiac operations. *J Card Surg*. 1994;9:490–4.
36. Muhiudeen IA, Roberson DA, Silverman NH, Haas GS, Turley K, Cahalan MK. Intraoperative echocardiography for evaluation of congenital heart defects in infants and children. *Anesthesiology*. 1992;76:165–72.
37. Cosgrove DR, Sabik JF. Minimally invasive approach for aortic valve operations. *Ann Thorac Surg*. 1996;62:596–7.
38. Secknus MA, Scalia GM, Asher CR, Savage RM, Cosgrove DM, Stewart WJ. Intraoperative trans-

- esophageal echocardiography in minimally invasive cardiac valve surgery. *Circulation*. 1996;94:1–442.
39. Secknus MA, Asher CR, Scalia GM, Cosgrove DM 3rd, Stewart WJ. Intraoperative transesophageal echocardiography in minimally invasive cardiac valve surgery. *J Am Soc Echocardiogr*. 1999;12(4):231–6.
40. Konoske R, Whitener G, Nicoara A. Intraoperative evaluation of paravalvular regurgitation by trans-esophageal echocardiography. *Anesth Analg*. 2015;121(2):329–36.
41. Cahalan M, Abel M, Goldman M, Pearlman A, Sears-Rogan P, Russell I, Shanewise J, Stewart W, Troianos C. American Society of Echocardiography and Society of Cardiovascular Anesthesiologists task force guidelines for training in perioperative echocardiography. *Anesth Analg*. 2002;15(6):647–52.

Role of Echocardiography in Transcatheter Aortic Valve Implantation

41

Rafal Dworakowski, Mehdi Eskandari,
and Mark J. Monaghan

Introduction

Transcatheter aortic valve implantation (TAVI) represents one of the most significant technological advances made in cardiovascular medicine in the last decade. Since Alan Cribier performed the first TAVI in 2002, the valve design and the delivery systems have been refined. The new devices have lower delivery profiles, are repositionable and retrievable and have features to prevent paravalvular aortic regurgitation (PAR). While TAVI can be done with favourable outcomes in selected patients by skilled multidisciplinary teams, the technique remains challenging and associated with potentially serious complications. Imaging plays a key role in selection and risk stratification of TAVI candidates. Echocardiography is the modality of choice for diagnosis of aortic stenosis (AS) and, along with other imaging modalities, is used for screening patients for TAVI. Furthermore, it can be used for pre-procedural planning and intra-procedural guidance and plays a pivotal role in post-procedural follow-up.

In this chapter we discuss the role of echocardiography in TAVI from the diagnosis of severe AS to the long term follow up.

Current TAVI Valves

Current guidelines emphasize a multidisciplinary team approach to TAVI and since echocardiographers are an important member of the team, they need to be familiar with the design of different TAVI valves, as each valve has specific characteristics resulting in different anatomic requirements.

There is a fundamental difference between the TAVI and surgical valves. Unlike surgical valves, they don't have a sewing ring and thus create a higher effective orifice area [1, 2]. It also means that there could be potentially a space around the valve resulting in PAR.

Whilst there are several TAVI valves under development or in clinical evaluation, there are two models supported by the largest body of evidence and experience in use: balloon expanding Edwards Sapien Valve (Edwards Lifesciences Irvine, CA, USA) and self expanding Medtronic CoreValve (Medtronic, Minneapolis, MN, USA). They have different characteristics, anatomical requirements and echocardiographic appearance but both provide excellent outcome with their latest generations. The most recent generations of these two valves, Sapien 3 and Evolute R, are the dominant valves in use currently.

R. Dworakowski · M. Eskandari (✉) · M. J. Monaghan
Kings College Hospital, London, UK
e-mail: mehdi.eskandari@nhs.net

The original Edwards Sapien valve was a balloon expandable device that had a stainless steel support frame with a bovine pericardial valve and a fabric skirt within it. This device was implanted via a transfemoral (TF) or trans-apical/trans-aortic approach. The Sapien XT (made of a cobalt-chromium alloy) was delivered on a more sophisticated, lower-profile delivery system (Fig. 41.1a). The third generation of the Edwards Sapien valve, Sapien 3 has an additional outer skirt that has minimized PAR (Fig. 41.1b). It also has the advantage of an even smaller and ‘double flexing’ delivery system. The anchoring of the Edwards Sapien valves and function of the valves are both intra-annular. Edward Salien valves are deployed under rapid pacing.

The self-expanding CoreValve is self-centering and partially repositionable. It is made of a nitinol stent with porcine pericardial leaflets (Fig. 41.1c). The nitinol stent has three zones. The lower zone that applies high radial forces within left ventricular outflow tract (LVOT) and annulus anchoring the valve, the middle zone that carries a controlled force to avoid jailing the coronary ostia and an upper zone with low radial forces which functions to orient the valve in the direction of aortic root axis [3]. The valve is intended to seat in a supra-annular position. The second generation, Evolut R valve, has a smaller delivery system, a lower frame height, and is fully recapturable and repositionable. Because of the supra annular position of the leaflets of the

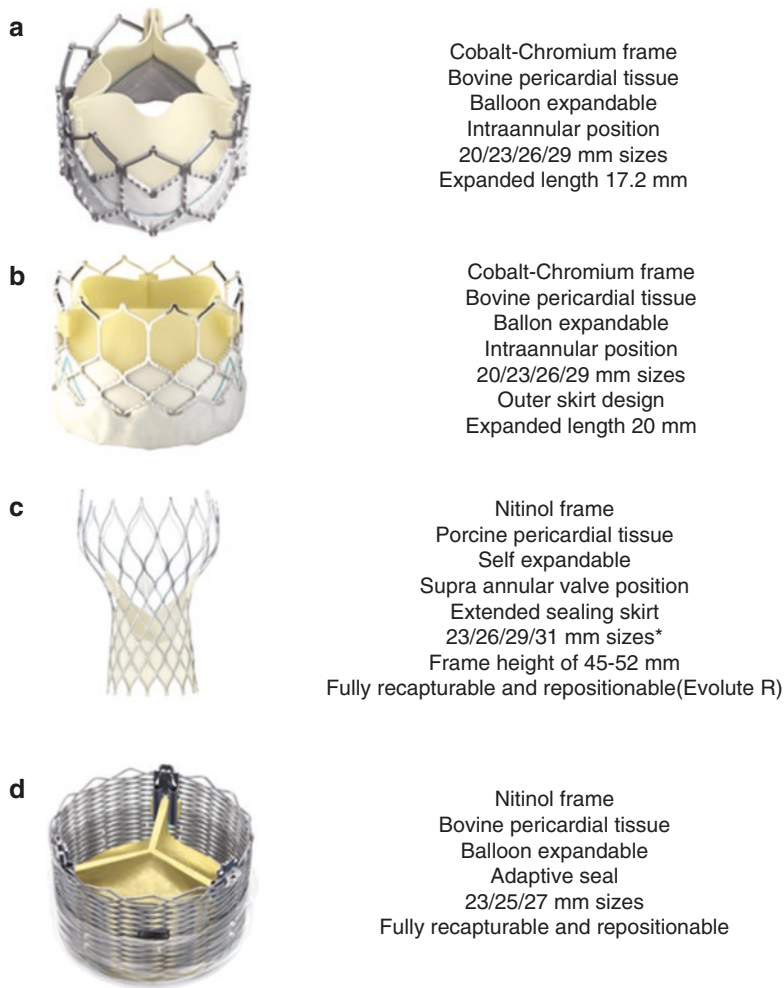


Fig. 41.1 Commonly used TAVI valves

CoreValve and Evolut R, they will result in lower gradients in small annuli [4]. They can be inserted through transfemoral or trans aortic routes.

The Lotus Valve (Boston-Scientific, Natick, Massachusetts, USA) (Fig. 41.1d) is pre-mounted on the delivery system. It can be retrieved, repositioned and redeployed any time prior to release. It is delivered via the trans-femoral approach only and consists of a woven nitinol frame with valve leaflets of bovine pericardium. The ventricular portion of the valve is surrounded by an adaptive seal [5]. On deployment, it shortens mechanically in a controlled way, providing additional radial strength comparing to traditional self-expandable nitinol devices. The Lotus valve carries a higher rate of post procedural pacemaker requirement [5].

The Direct Flow (Direct Flow Medical, Santa Rosa, CA, USA) is a self-expanding valve with a novel metal free ‘double ring’ design with two aortic (upper) and ventricular (lower) inflatable rings. The rings contain noncompliant angioplasty balloon technology and are connected by a tubular bridging system. Each ring can be pressurised (through the normal saline/contrast injections) independently allowing inflating/deflating the rings and hence retrieval before deployment. After obtaining the optimal position, the rings are filled with a polymer [6]. The bovine pericardial valve is attached to a cuff that conforms to the annulus. Owing to the speed of deployment, Direct Flow does not require rapid pacing. It provides excellent sealing but suffers from higher gradients [4]. Direct Flow is available only for transfemoral approach.

The Portico valve (St. Jude Medical, Minneapolis, Minnesota) is a nitinol self-expanding re-sheathable device which consists of bovine pericardial leaflets and a porcine pericardial sealing cuff [7]. It is similar to the Evolut R and provides open stent cell design to allow access to coronary arteries.

The Symetis Acurate (Symetis SA, Ecublens, Switzerland) is another self-expanding nitinol stent valve with porcine pericardial leaflets which is available for both transapical and transfemoral approaches. This valve has an upper crown for supra-annular anchoring to minimize protrusion

into LV and a lower crown that is designed to protrude only minimally into the LVOT. It has inner and outer pericardial skirts to minimize PAR [8].

The JenaValve (JenaValve Technology GmbH, Munich, Germany) is a self-expanding valve consisting of porcine pericardial leaflets attached to a crown shaped self expanding nitinol stent. It has three ‘feelers’ that will be based in the aortic sinuses at the base of native leaflets. The feelers in combination with the stent arms in the lower part of the prosthesis allows clipping the native valve leaflets enabling the operators to accurately position the prosthesis in the anatomically correct position. Rapid pacing is not required during prosthesis positioning and release. It can be used with both transfemoral and transapical approaches [9]. The clipping mechanism is particularly useful in noncalcified valves or those whose primary pathology is aortic regurgitation (AR) than AS.

Given the rapid technology advances in the TAVI field, valve designs are sure to undergo further refinements and improvements in the coming years.

Pre-procedural Echocardiography

Patient selection is of paramount importance to achieve a successful TAVI procedure with a good long-term outcome. Selection of potential candidates is complex and involves a multidisciplinary team evaluation and multimodality imaging approach in order to fully delineate the anatomy of the aortic valve, aorta and peripheral vasculature.

Diagnosis of Severe Aortic Stenosis

Transthoracic echocardiography (TTE) remains the modality of choice to establish the presence of severe AS with Doppler assessment of peak and mean gradients and calculation of aortic valve area (AVA) by the continuity equation. According to the current guidelines, severe AS is defined by an AVA of $\leq 1 \text{ cm}^2$ ($\leq 0.6 \text{ cm}^2/\text{m}^2$) or a mean aortic valve gradient of $\geq 40 \text{ mmHg}$. It is

important to note that continuity equation is based on the presumption that the LVOT is a circular structure and therefore its area can be calculated from the LVOT diameter obtained in a long axis view of the aorta. We have learned from the 3D imaging on TAVI patients that the LVOT in fact is an elliptical structure and that the measurements from the long axis view of the aorta reflects the shortest diameter. Thus the calculated LVOT area will be often underestimated resulting in underestimation of the AVA by continuity equation. For this reason, when applicable, use of 3D derived LVOT area in the continuity equation will increase the accuracy of the AVA measurements.

Severe AS can be classified into four groups. (1) Preserved left ventricular (LV) ejection fraction (EF), normal flow and high gradient (2) low EF, low flow and low gradient (3) preserved EF, low flow and low gradient or so called paradoxical AS and (4) preserved EF, normal flow but low gradient. The latter carries the best prognosis comparable with moderate AS and reflects either measurement errors or it can be related to the small body surface area where the indexed AVA would not fall within severe AS. However, it may also imply inconsistencies in guidelines as some studies have shown that an AVA less than 1 cm^2 is not necessarily expected to generate gradients more than 40 mmHg and that in a subgroup of patients, gradients less than 40 mmHg may still be indicative of a severely stenosed valve [10].

Stroke Volume index is the parameter to determine the flow with values $>35 \text{ ml/m}^2$ being considered as normal.

Groups 2 and 3 pose diagnostic and therapeutic challenges:

Low EF, Low Flow and Low Gradient This may pose the dilemma of distinguishing between true severe AS and pseudo-severe AS in which reduced stroke volume contributes to the reduction in calculated valve area from continuity equation. Valve dobutamine stress echocardiography can help distinguish between these two in the majority of cases (in those who fail to increase

the stroke volume by dobutamine the test will be non-diagnostic) and provides useful information concerning contractile reserve.

Preserved EF, Low Flow and Low Gradient This entity is characterized by marked LV concentric remodeling and a reduction in compliance (mimicking restrictive physiology) and also subclinical LV dysfunction, identified by more sensitive parameters such as reduction in global longitudinal strain. It's more common in the elderly, female gender and those with systemic hypertension. These patients have a worse prognosis than moderate AS or those with preserved EF, normal flow and high gradient severe AS. The key here is to distinguish this group of patients from the group of severe AS, *normal* flow but low gradient who lack features of restrictive physiology and carry a better prognosis [10].

It's important to note that like any other valvular pathology; diagnosis of severe AS requires a multi parametric approach. In cases that TTE is indeterminate in assessment of severity of AS, transoesophageal echocardiography (TOE) should be used. A multi parametric approach including 3D derived LVOT area (that is much easier with TOE) and direct planimetry using 3D guided 2D multiplanar reconstruction of the aortic valve will likely determine the severity of AS.

Once the diagnosis of severe AS is made, the next step will be to determine if aortic valve anatomy is suitable for TAVI and what prosthetic valve should be chosen to fit the given anatomy.

Assessment of Aortic Complex

In contrast to conventional valve surgery, when aortic valve anatomy is not so important for the procedural planning, a successful TAVI procedure depends fully on an appropriate patient selection. Pre-procedural imaging and assessment of aortic complex anatomy, including LVOT (composed of the basal ventricular septum and the subaortic mitral valve curtain), aortic annulus,

aortic valve cusps, sinuses of Valsalva, and sinotubular junction plays a pivotal role in the process of patient selection. Initial TTE not only is used for the diagnosis of severe AS but also is useful in anatomical assessment of aortic complex and co-existing pathologies.

After consideration of a patient for TAVI, multi-slice computed tomography (MSCT) and 3D TOE are preferred modalities in preparation for the procedure. MSCT does have advantage over echocardiography in the assessment of calcification and lumen visualization, has better lateral resolution and offers assessment of the iliac arteries. However, it is missing functional assessment that can be offered by the TOE and requires the use of contrast media which may be disadvantageous in patients with renal insufficiency. TOE although suffers from low lateral resolution (sub-optimal coronal view) and blooming artefact from the presence of calcium, has superior temporal resolution, allows visualization of the valve hinge points, provides physiological information, eliminates motion based artifacts and allows one to visualize adjacent structures. In addition, MSCT is contraindicated in severe renal impairment and also poses a radiation risk that although accepted in elderly patients, it will become a more concerning factor as evidence supporting use of TAVI in lower risk and younger patients are emerging.

Although all cardiac structures should be assessed prior to the procedure, the TAVI-specific TOE typically begins with an assessment of the aortic complex.

Aortic Valve Anatomy

A pre-procedural understanding of the anatomy allows interventional cardiologists and echocardiographers to plan the procedure and decide on the type and the size of the TAVI valve.

Bicuspid aortic valve is a relative contraindication to TAVI mainly because of elliptical valvular orifice and asymmetric calcification, which may increase the risk of incomplete and incorrect deployment of the prosthetic valve causing

PAR. Presence of bicuspid aortic valve very often coincides with aortopathy and dilated aortic root, which itself can interfere with the valve anchoring mechanism and/or increase the risk of aortic dissection, due to abnormal arterial wall structure. However recent studies have shown that TAVI in bicuspid aortic valve is feasible with favourable short and intermediate outcome [11, 12].

Distribution of calcification on the aortic valve is another very important factor, which influences decision making on the type and the size of the TAVI valve that is going to be used. Using the short-axis views of the aortic valve, calcifications could be described as central or eccentric and further the severity, location, and symmetry of the aortic valve calcification can accurately be assessed (Fig. 41.2). Eccentric calcification is a known risk factor for the PAR. In addition, the combination of eccentric calcification and elongated leaflets can increase the risk of coronary obstruction during valve deployment.

Stroke is one of the major TAVI complications. The primary responsible mechanism is the traumatic injury of the calcified valve by the delivery system. Other mechanisms are embolization from atheroma in the aorta or related atrial fibrillation. The improvement in delivery systems, increase in operators' experience, and minimizing valve manipulation or balloon valvuloplasty before valve deployment has significantly reduced the rate of stroke in TAVI [4].

Cerebral embolic protection devices, although not clinically proven, may be justified in certain clinical situations. Presence of mobile structures on the aortic valve is not uncommon and should be identified during pre or intra procedural TOE as a potential source of a cerebral event that may be prevented by use of cerebral embolic protection devices.

Annulus Diameter Measurements

Annular dimensions are key measurements in the TAVI valve sizing. Choosing the correct valve size is important as undersizing the prosthesis can result in device migration and embolisation

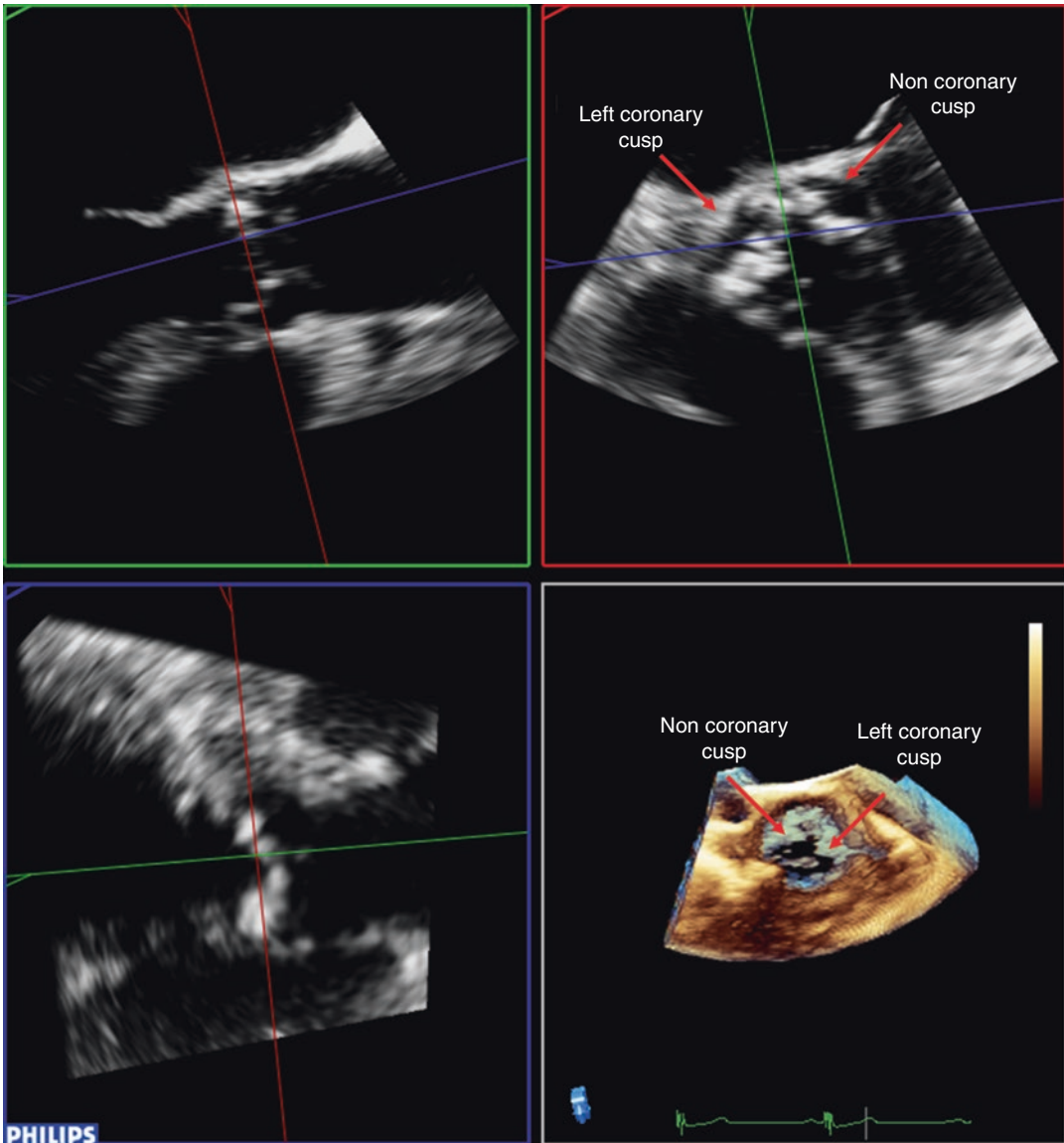


Fig. 41.2 Multiplanar reconstruction of a zoomed 3D dataset of the aortic valve obtained by TOE showing eccentric calcification of non and left coronary cusps in

the transverse view. Note the transverse view (upper right) is a mirrored image and hence inverted non and left coronary cusps

or significant PAR. On the other hand, oversizing increases the risk of life threatening complications such as annular rupture and also the risk of vascular injury, as bigger delivery systems are needed. The other problem with inaccurate valve sizing is associated with valve mechanics. Consequent under- or over-expansion of the valve leads to redundancy of leaflet tissue or leaflet non-coapta-

tion resulting in transvalvular regurgitation. In addition, leaflet malfunctioning can create regions of compressive and tensile stress and may result in a reduction of valve durability.

Unlike the mitral valve, the aortic valve lacks an actual annulus. The Aortic valve annulus is defined as a virtual plane at the level of the hinge points of the three cusps. It is also important to

note that the aortic annulus (like LVOT), in the majority of cases, is elliptical with the shortest diameter in sagittal (anterior-posterior) and the longest diameter in coronal (right-left) planes. Thus, use of a 3D imaging modality that allows measurements of the annulus diameter in two orthogonal planes as well as measurements of the perimeter and area (that then allows calculation of the annulus diameter) is essential. The measurement is taken at the point of insertion of the aortic valve cusps, from tissue–blood interface to blood–tissue interface—trailing edge to leading edge regardless of the degree of calcification of the aortic cusps. There has been a debate as to which measurement should be taken for valve sizing—area, perimeter or an average of orthogonal diameters? Whilst the minimum diameter is associated with valve undersizing, the maximum diameter can potentially increase the risk of annular rupture. The Annulus is a dynamic structure with changes in dimension during the cardiac cycle. Thus for the TOE sizing, we advocate the use of annulus perimeter which is not affected by the change in shape and geometry of the annulus during cardiac cycle, or how elliptical the annulus is, as opposed to area. Annular measurements should be performed in mid-systole to ensure that the largest dimensions are obtained. Figures 41.3 and 41.4 depict the schematic view of the virtual aortic annulus and its area and perimeter measurements by 3D TOE respectively.

It's important to note that the annular dimensions are not the only values in deciding on the valve size or the type of the valve. Factors such as calcification, aortic sinuses and sinutubular junction diameters, plus the height of the left and right coronary ostia all play an important role.

LVOT/Septum Assessment

The other important anatomic feature, which should be taken into account when deciding what valve type and size should be used, is a sigmoid septum and asymmetrical septal hypertrophy. Both are frequent in the elderly patients with hypertension and severe AS. The presence of a

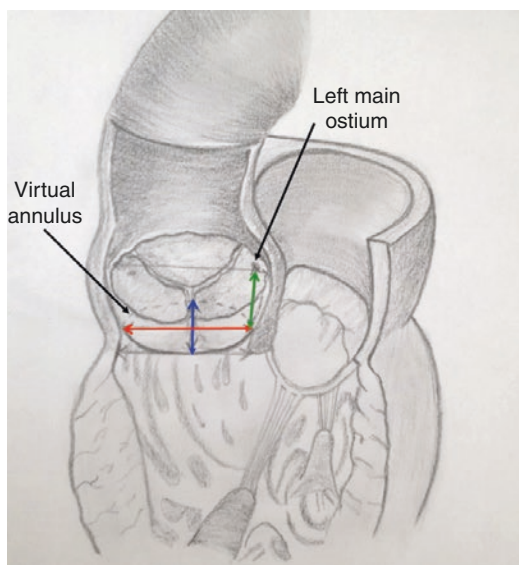


Fig. 41.3 Schematic view of the virtual annulus of the aortic valve that is defined as the plane at the level of basal attachment of the aortic valve cusps

protruding sigmoid septum can cause subvalvular gradients that can be a contraindication to the TAVI [13]. It also increases the risk of complete heart block after procedure and can be responsible for valve misplacement and upward movement during deployment. Attention should also be given to the presence of calcification into the LVOT that increases the chance of PAR and aortic rupture (Fig. 41.5).

Distance to Coronary Arteries

From the very beginning of the TAVI development, the risk of obstruction of the coronary arteries has been a concern. The risk depends not only on the distance of coronary ostia from the annulus but also on the size of aortic sinuses and the extent of aortic cusp calcification. The 3D zoom dataset of the aortic valve and aortic sinuses can be used for multiplanar manipulation and reconstruction to allow derivation of the coronal plane for measurement of the annulus-to-left main and annulus to right coronary artery distance (Fig. 41.4h). The length of the right and left coronary cusp and distribution of calcium should

not be ignored in risk assessment of coronary artery occlusions (Fig. 41.6). In general, a distance of >10 mm is desirable for most of the valves available on the market.

Aortic Sinus, Ascending Aorta and Sino-Tubular Junction Anatomy

Attention should be paid to the size of aortic sinuses and sinotubular junction (Fig. 41.4f, g).

Small aortic annulus coinciding with a small aortic root might increase the risk of coronary ostia obstruction and aorta-left atrium fistula. On the other hand, a very dilated root increases the risk of valve embolization. For some self-expandable valves, the long multi-staged frame is anchored not only within the aortic annulus but also extends superiorly into the supracoronary aorta. The supra-coronary portion serves to self-centre the valve and provides an additional point of fixation. In a dilated aortic root this mechanism can be impaired

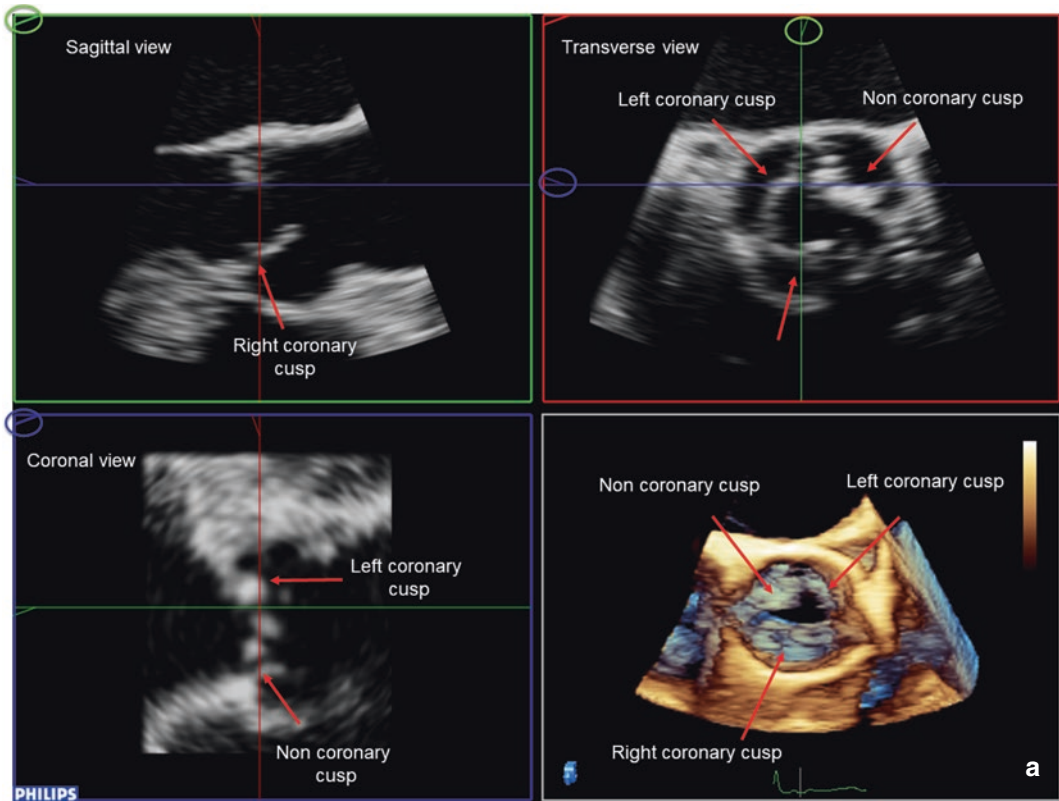


Fig. 41.4 (a) Multiplanar reconstruction of a zoomed 3D TOE dataset of a stenotic aortic valve. A mid systolic frame when the aortic valve is at maximum of its opening is chosen. Note that the transverse view in this panel is a mirrored image and hence inverted non and left coronary cusps. The small triangles in the corner of each panel help with anatomical orientation. (b) Alignment of the sagittal and coronal planes (by rotating the blue and green line in sagittal and coronal views) to bisect the the long axis of the aorta. (c) The red line is then moved such that it crosses the hing point of the right coronary cusp (red arrow), and roughly the left coronary cusp (blue arrow) and the non coronary cusp (yellow arrow) hinge points. In the transverse view that now shows the cross section of the virtual annulus, the green plane can be rotated in left and right directions to ensure that the right coronary cusp

has been crossed at the hing point. (d, e) Thereafter the blue line in the transverse view is rotated through the other two cusps to ensure that they have also been bisected at the level of the hing point. The perimeter, area and shortest and longest dimension of the annulus then can be measured on the transverse view. (f) The red line is moved to the level of sinuses of Valsalva. Measurements can be done in the transverse view (yellow lines). (g) The red line now is moved to the level of sinutubular junction where its dimensions can be measured in transverse view (yellow lines). (h) Measuring distance of the left main from the annulus. The red line is moved from annulus toward the sinuses of Valsalva where the left main is usually visible around 10 o'clock in the transverse view. Either blue or green plane (in this case blue plane) can be rotated across the left main. The yellow line shows the left main height

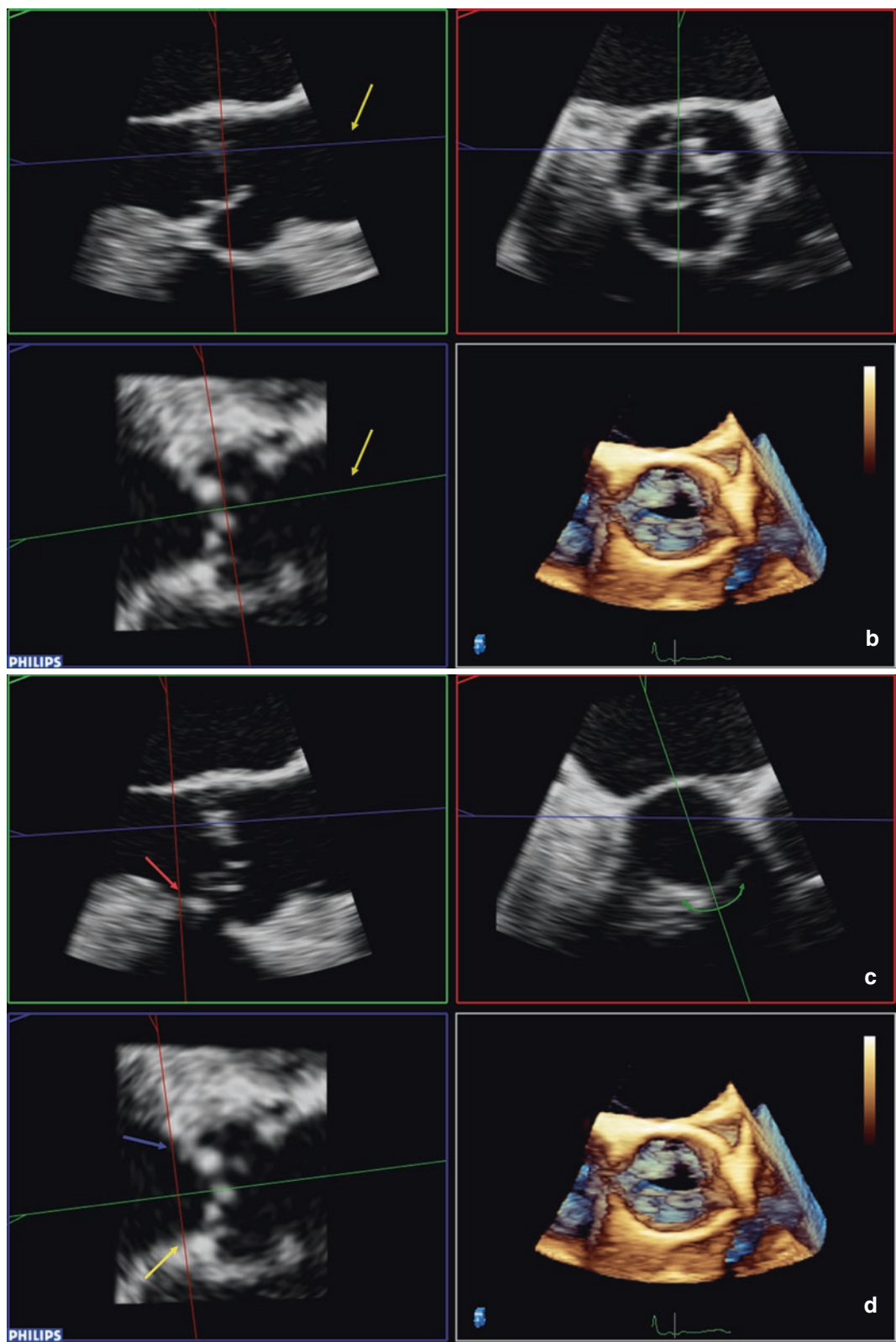


Fig. 41.4 (continued)

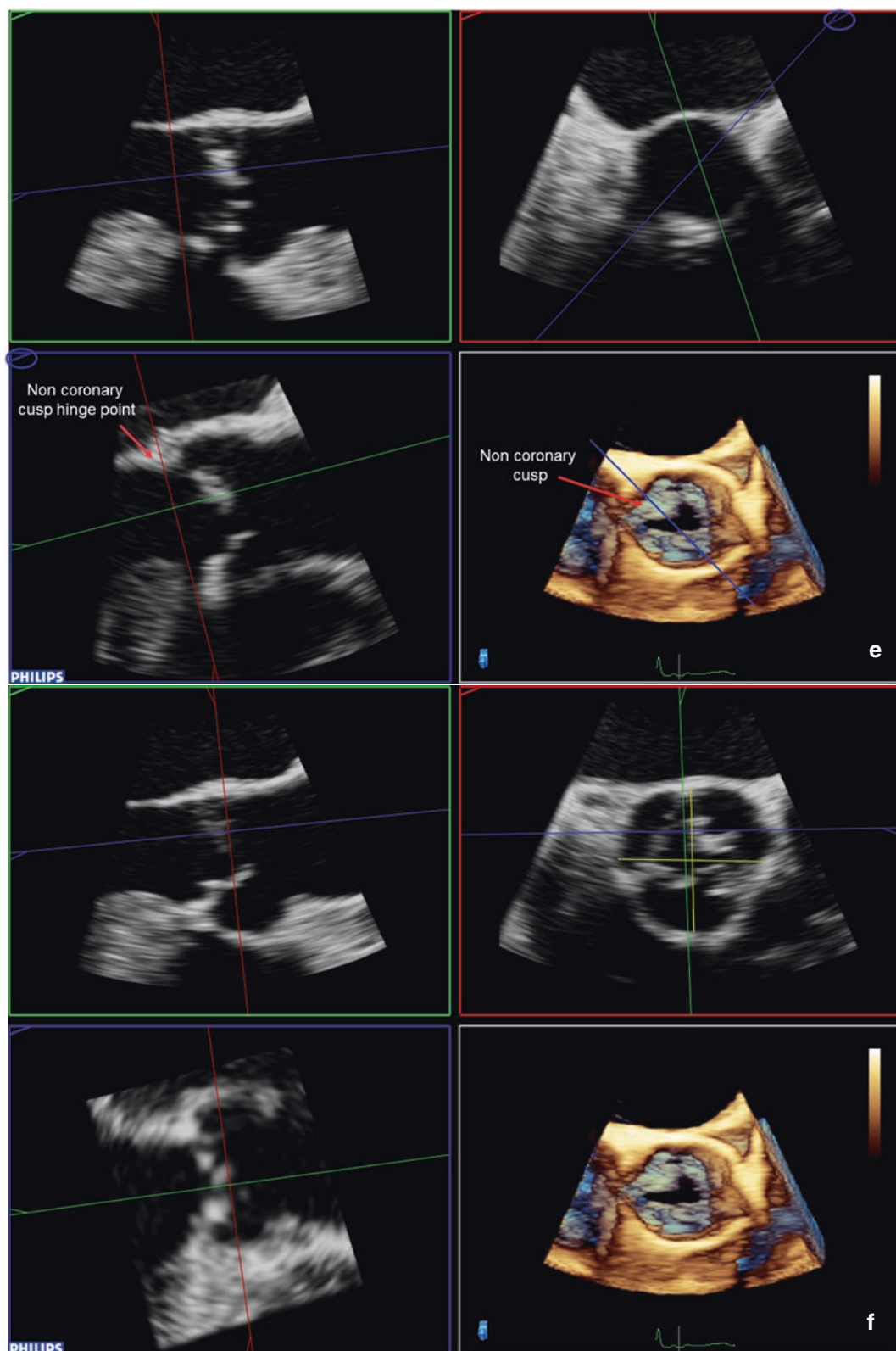


Fig. 41.4 (continued)

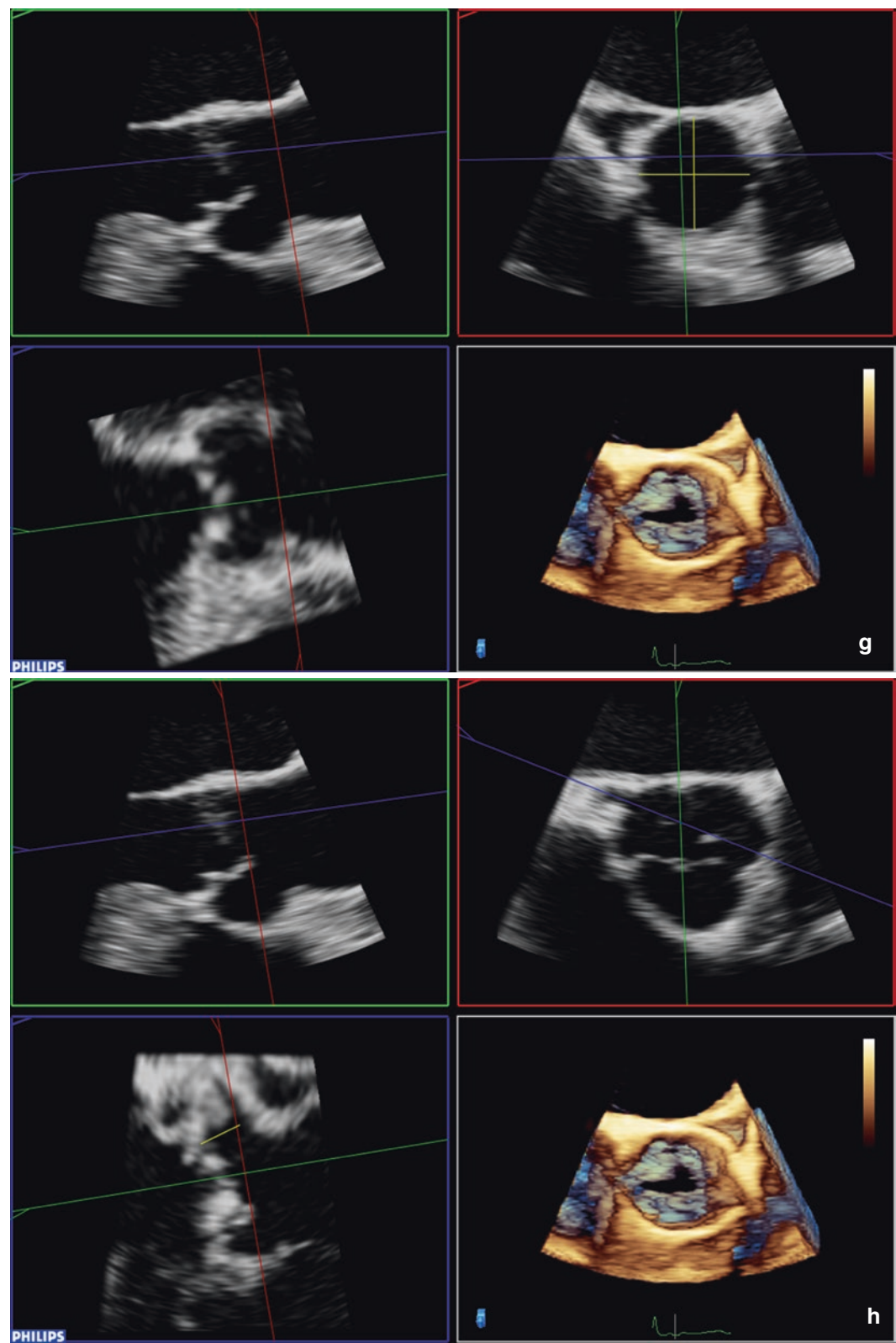


Fig. 41.4 (continued)

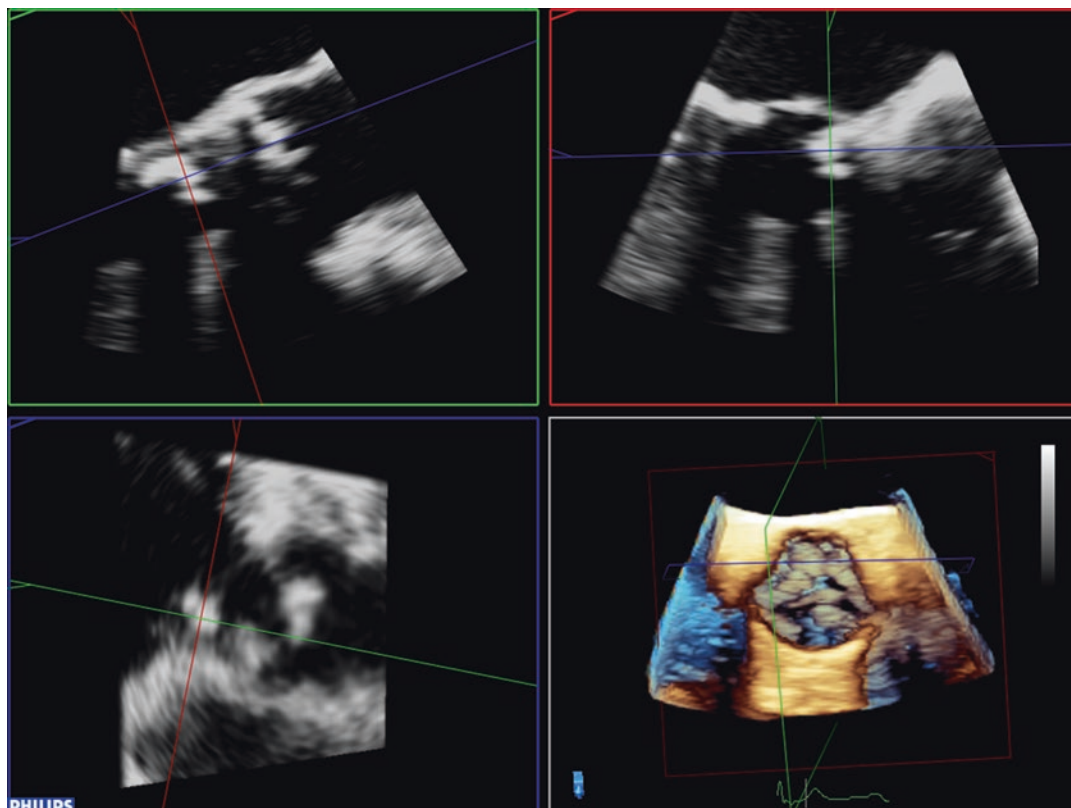


Fig. 41.5 Multiplayer reconstruction of a zoomed 3D TOE dataset of the aortic complex showing significant calcification of the LVOT

and result in imperfect valve position. Ascending aorta/aortic arch could be easily assessed during the pre-operative phase TOE. Presence of atheroma/thrombi in the ascending aorta might influence the access site for TAVI owing to the potential risk of stroke. Assessment of descending aorta should also be a part of TAVI work up as presence of atheroma/thrombus is not uncommon in the elderly TAVI patients (Fig. 41.7).

Assessment of Coexisting Pathologies

Pre TAVI echocardiography should not be limited to only assessment of aortic complex. Assessment of other co-existing pathologies with potential impact on post procedural morbidity and mortality plays a pivotal role in TAVI patient selection.

Presence of left ventricular dysfunction, although unlike surgical aortic valve replacement is unlikely to elicit further investigation to assess the contractile reserve, is important because of adverse prognostic implications [14]. Of note presence of LV thrombus is a contraindication to TAVI as during the procedure a wire is positioned in the LV apex.

Presence of mild mitral regurgitation (MR) is common in the TAVI population but carries low concern. Moderate-severe MR however is associated with adverse morbidity and mortality. Mechanism of MR should be carefully examined although it's often difficult to fully differentiate between the primary and secondary MR owing to the relatively common leaflet calcification in the elderly group of patients undergoing TAVI. Primary MR is unlikely to diminish after TAVI but in the case of functional MR, improvement can be expected. It appears that MR improves in roughly

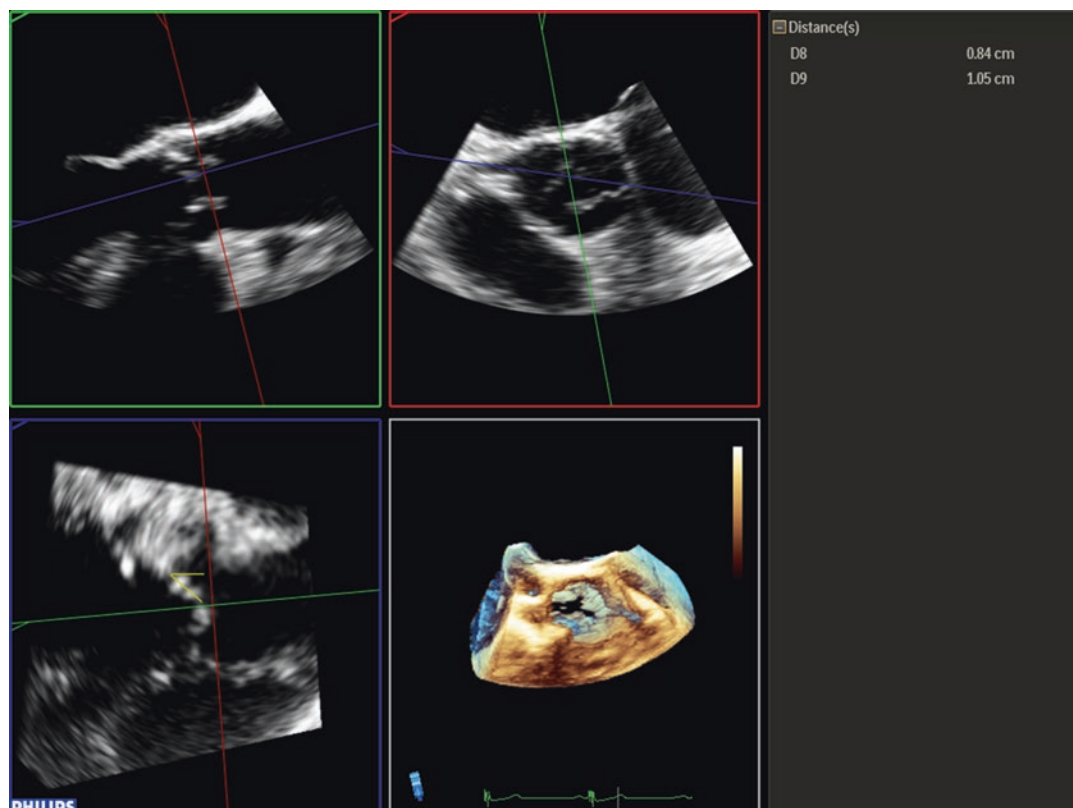


Fig. 41.6 A 3D guided 2D multiplanar reconstruction of the 3D dataset of a case with severe AS that was referred for TAVI. Note the low left main height (8.5 mm) and the approximate length of the left coronary cusp (10.5 mm) that

poses the major risk of left main obstruction. After taking into the account the extent of calcification and size of the sinuses of Valsalva and after discussion in the heart team meeting the case was considered not suitable for TAVI

half of the TAVI population with moderate –severe MR and deteriorates in a small proportion of these patients [15]. It should also be noted that moderate to severe MR may cause a reduction in gradients across the aortic valve resulting from a reduction in forward flow, due to the leaking mitral valve.

Right ventricular dysfunction, tricuspid regurgitation and pulmonary hypertension all have prognostic significance and although not influencing the procedural success, can alter the outcome and should be carefully discussed in a multidisciplinary meeting.

Prevalence of atrial fibrillation in the population of patients with severe AS is about 10% [16]. Thromboembolic risk due to paroxysmal atrial fibrillation is high in this group. Left atrial appendage thrombus should be excluded in the work up phase. In the presence of thrombus in the left

atrial appendage, a valve which does not require rapid pacing for deployment, or a periprocedural embolic protection device can be used.

A summary of preprocedural echocardiography assessment is shown in Table 41.1.

Intra-Procedural Echocardiography

Echocardiography is routinely used during TAVI. Use of TOE is associated with the perceived need for general anesthesia. Although general anesthesia was the favourable approach in the early years of TAVI, recently there has been a trend towards a simpler procedure by means of conscious sedation or local anesthesia and a transfemoral approach which limits the use of intra procedural TOE. In such patients, TTE

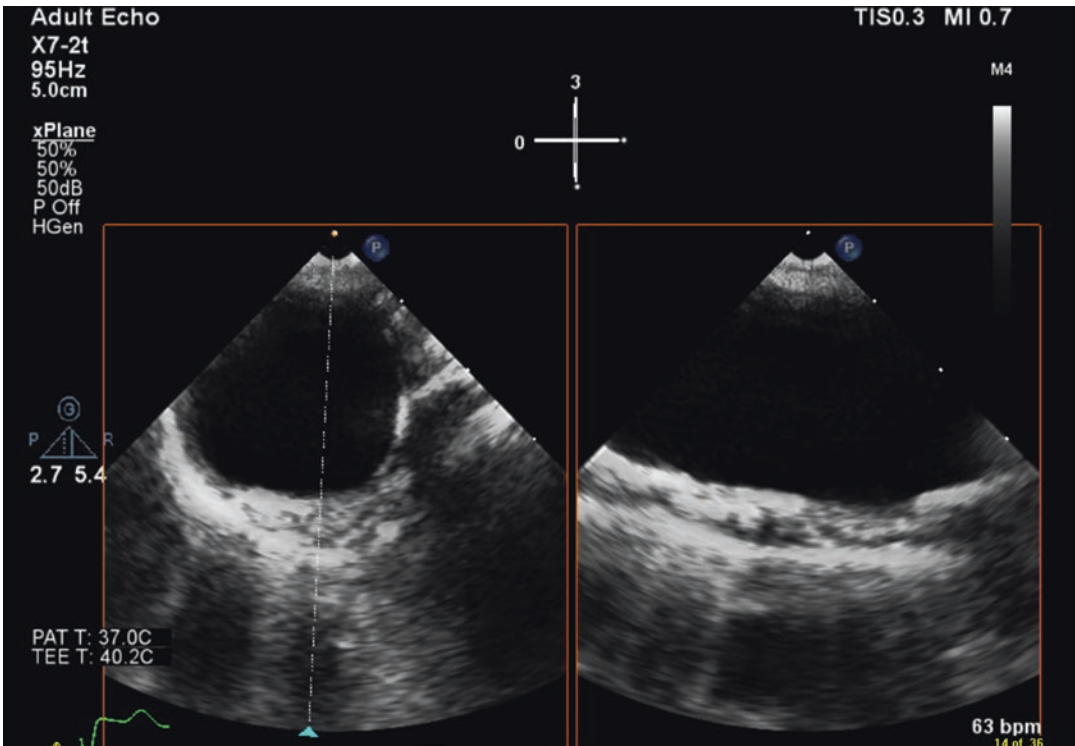


Fig. 41.7 Significant descending aorta atheroma diagnosed by TOE

may have a role in guiding the procedure and in particular identifying PAR at the end of the procedure. If TTE is to be used, a brief study before the procedure is needed to confirm adequacy of imaging windows. However; in the absence of robust evidence against general anesthesia, it's still the preferred approach in many centers. As TAVI moves towards the lower-risk patient population and outcomes are expected to improve, TOE will likely to continue to play an important role in optimizing TAVI procedural results.

In patients undergoing TAVI via a transapical approach, TTE is helpful in locating and marking the LV apex in order to guide the thoracotomy. The apex should be checked in two orthogonal planes, by the use of bi-plane imaging if available, in the presence of the cardiothoracic surgeon so that the optimal access point can be marked on the chest wall. Once the skin is marked with the optimal position, it is essential that the patient and/or the skin are not moved. Optimal location of the

LV puncture can then be further assessed and confirmed by TOE. A mid oesophageal plane (again, preferably biplane imaging) whilst the surgeon pushes the apex gently with their finger will assure the optimal puncture site such that the wire and catheters will be aligned with the aortic valve avoiding the mitral valve apparatus.

Intra-procedural TOE starts with assessment of baseline LV function, regional wall motion, pericardium, baseline aortic valve gradients and the function of other valves as well as left atrial appendage especially in patients with atrial fibrillation. Transgastric views are particularly important for assessment of baseline left ventricular regional motion and pericardial space. This is important in order to detect new wall motion abnormalities or pericardial effusion after deployment of the valve. Aortic valve anatomy including distribution of calcification can be reviewed again at the beginning of the procedure. Deep transgastric views help measuring gradients across the

Table 41.1 Pre-procedural transoesophageal echocardiography

Pre-procedural transoesophageal echocardiography
<i>Aortic valve morphology</i>
Aortic valve morphology
Bicuspid versus tricuspid
Degree and location of calcification
Annular dimensions
Minimum and maximum diameters
Perimeter
Area
Aortic valve haemodynamics
Aortic valve gradients and area
Stroke volume
Left ventricular outflow tract
Extent and distribution of calcium
Presence of sigmoid septum
Aortic root dimensions and calcification
Diameter of the sinuses of Valsalva
Sinotubular junction diameter and calcification
Location of coronary ostia and risk of obstruction
<i>Mitral valve</i>
Severity of mitral regurgitation
Mitral valve/annulus calcification
<i>Left ventricular size and function</i>
Wall motion assessment
Exclude intra-cardiac thrombus
Hypertrophy and septal morphology/Cavity size
<i>Right heart</i>
Right ventricular size and function
Tricuspid valve morphology and function
Estimate of pulmonary artery pressures
<i>Left atrial appendage</i>
Exclude thrombus

aortic valve and assessment of AR after deployment of the valve. A checklist for intra procedural TOE assessment is summarised in Table 41.2.

After establishing the access and insertion of the temporary pacing wire, the first part of the TAVI procedure is crossing the aortic valve and placing a support wire in the LV apex. Interventional cardiologists normally rely on fluoroscopy for this part but real time 3D TOE imaging of aortic valve showing the opening orifice of the valve leaflets might help in crossing a tightly narrowed aortic valve.

TOE is able to identify malposition of the stiff wire if it is caught in the mitral valve apparatus

Table 41.2 Intra-procedural TOE checklist

Procedural step	Imaging recommendation
Pacing wire position	Confirm the wire positing in the right ventricle
Stiff wire position	Confirm the wire position in the left ventricle apex without entanglement in the mitral apparatus and worsening of mitral regurgitation
Balloon aortic valvuloplasty (BAV)	Image during and immediately following BAV for aortic leaflet motion in relation to coronary ostia and for assessment of aortic regurgitation after BAV Assess the location of the displaced calcified leaflets for possible deformation of the aortic wall and the risk of annular rupture
Valve positioning	Balloon-expandable valve: cover the native leaflets while being below the sinotubular junction. Optimal final position covers the native leaflets Self-expanding valve: higher edge of the stent should be 3–5 mm below the annulus
Post deployment	Assess stent positioning, shape, and leaflet motion; perform comprehensive hemodynamic measurements including effective orifice area Assess paravalvular regurgitation relying on short-axis images of the LVOT just below the inflow edge of the valve stent (gastric views are helpful in the detection of paravalvular aortic regurgitation) Assess coronary artery patency and ventricular function; Assess mitral valve morphology and function Assess TR velocities and estimate pulmonary artery pressures Exclude perforation and pericardial effusion

causing MR (or worsening of existing MR). This is not uncommon and can potentially interfere with the stability of the TAVI valve or can result in haemodynamic instability (Fig. 41.8). Perforation of either the left or right ventricle by the stiff wire or temporary pacing wire has been reported and should be monitored during the procedure.

Occasionally, the stenotic native aortic valve needs to be predilated using a balloon catheter.

This is usually for two reasons. First, the virtual annulus diameter is borderline and balloon valvuloplasty helps to decide on the valve sizing. In addition, when the risk of coronary artery obstruction has been identified on pre-procedural TOE/MSCT, further assessment can be performed during balloon valvuloplasty. A biplane TOE image at the time of balloon valvuloplasty will allow assessment of the sinuses and the left main in relation to the balloon size. Visualisation of the inflated balloon in the sinuses will allow one to decide on the size of the TAVI valve in the

case of borderline annulus and aortic sinuses diameters. Assessment of the left main coronary ostia is done in the short axis view when the relation of the inflated balloon to the left main ostia can be seen on the echo image. Second, balloon dilatation of a severely stenotic valve will facilitate the delivery of the TAVI valve. It's important to note that the presence of more than mild AR is a relative contraindication to balloon valvuloplasty as it may cause deterioration of the AR and sudden haemodynamic compromise. The same concern also applies to a heavily calcified valve.

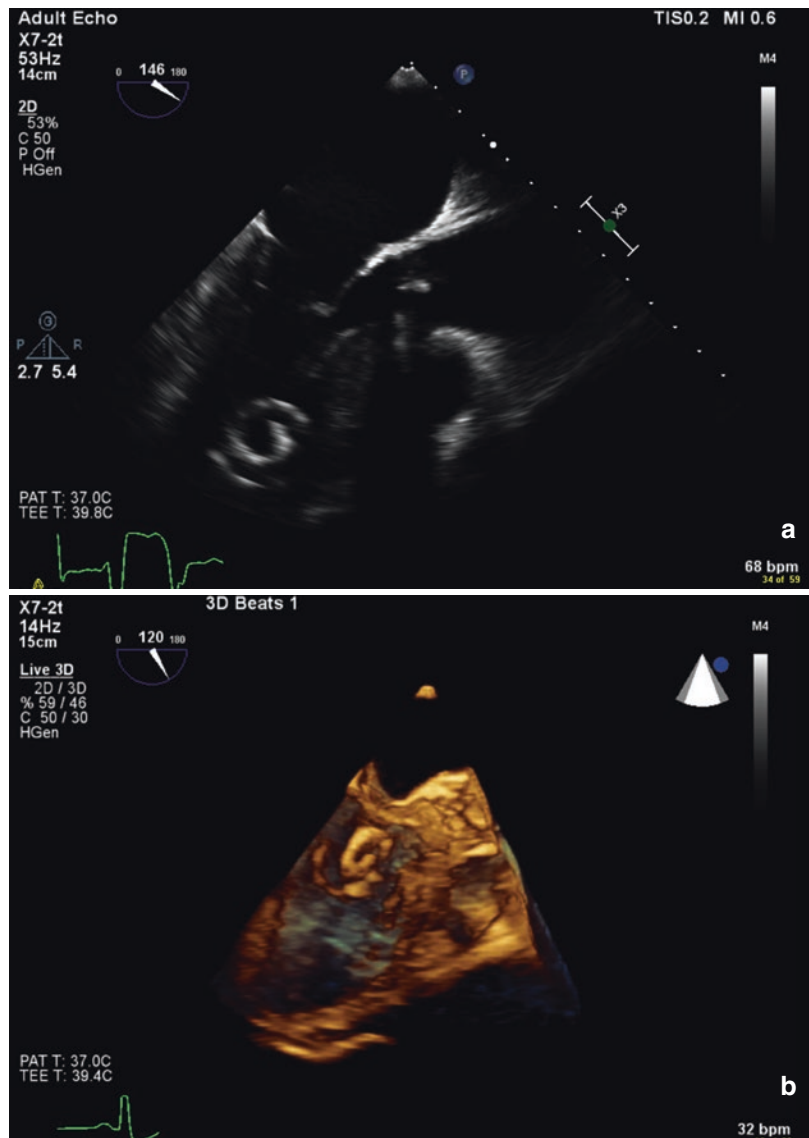
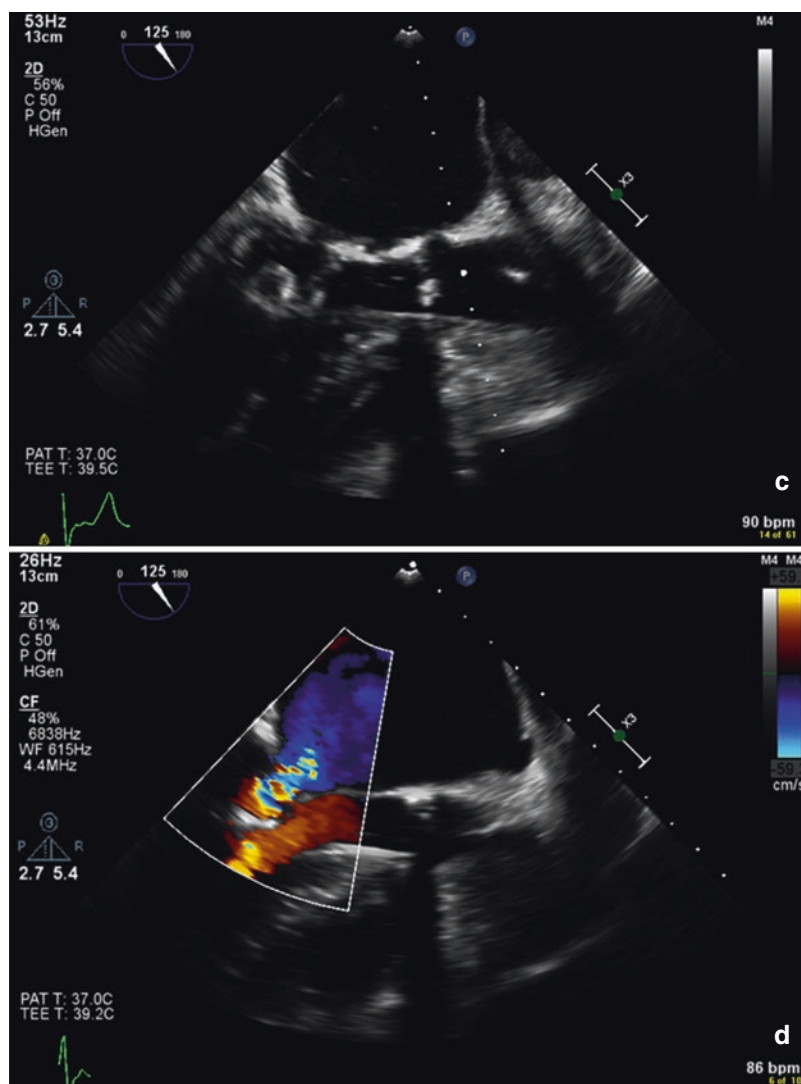


Fig. 41.8 (a) Proper position of the stiff wire in the left ventricle apex. (b) Real time 3D TOE imaging of the aorta and left ventricle showing improper position of the stiff wire underneath the mitral valve. (c, d) Mitral regurgitation due to entanglement of the stiff wire in the mitral valve apparatus

Fig. 41.8 (continued)

Therefore, immediate echo assessment of the aortic valve after balloon valvuloplasty is crucial. A longer loop (usually 10–20 beats) should be captured to allow assessment of the aforementioned details during balloon valvuloplasty.

An appropriate valve position is essential for a successful TAVI procedure. A TAVI valve that is placed too deep into the LVOT can restrict anterior mitral leaflet opening or may result in complete heart block requiring permanent pacing. A prosthesis that is delivered excessively antegrade, toward the aortic sinuses of Valsalva, apart from PAR can obstruct the coronary ostia or embolise distally into the aorta. When the prosthesis is

positioned too low, the native aortic valve cusps may fold over the top of the prosthesis and impede its function.

TOE can be used as an adjunctive imaging tool for positioning the TAVI valve, potentially reducing the need for contrast injection during deployment and the fluoroscopy time. It can be particularly helpful when the native valve is not heavily calcified and hence not easily visible on fluoroscopy.

Echocardiography considerations differ between deployment of balloon and self expandable valves, with the latter being primarily performed by the use of fluoroscopy. In case of balloon

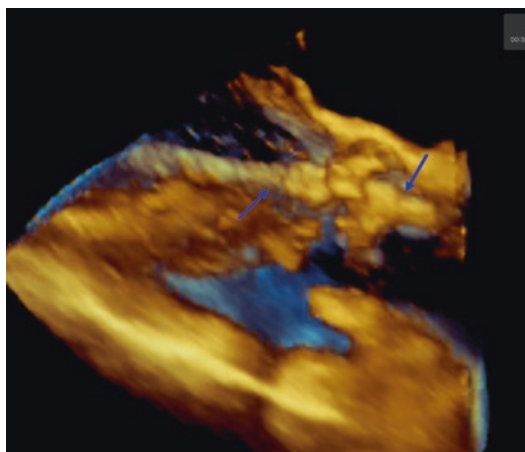


Fig. 41.9 Positioning of a Sapien 3 valve by 3D TOE. The focus here is on the aortic side of the crimped valve that should cover the entire native leaflet

expandable valves, it's important to note that for the first and the second generations of the valve, there is an upward movement in both ventricular and aortic sides due to the shortening of the crimped valve that is more in the ventricular side of valve or valve inflow (by about 3–4 mm). Given that for these iterations of the Edward SAPIEN valves, an ideal deployed position of the valve inflow (lower edge) would be 2 mm below the annulus, therefore, the optimal echocardiographic position of the crimped valve during pacing deployment should be 5–6 mm below the annulus [17]. The ventricular and aortic edges of crimped valve are visible on 3D echocardiography although it requires considerable experience. Reducing 3D gain may help differentiating the crimped valve from the balloon. In the case of the Sapien 3 valve, the focus should be on the aortic side of the crimped valve ensuring it covers the native leaflets but remains below the sinotubular junction, as this iteration only shortens from the ventricular side and not the aortic side [17] (Fig. 41.9).

Deployment of the self expanding valves is a slower process that does not require rapid pacing and is primarily dependent on fluoroscopy. In the case of Corevalve, deployment starts with slight misalignment of the valve in relation to the longitudinal axis of the aorta. The posterolateral portion of the valve that corresponds to the non and left coronary cusp on echo, lies slightly higher

than the anterolateral. This edge should be at least 4 mm below the annulus (and not more than 10 mm). This is because the skirt, in the lowest 4 mm of the valve is intermittent, rather than continuous and therefore leaving less than 4–5 mm of the valve below the annulus increases the chance of PAR. Thus, the optimal position for the ventricular edge of the valve should be 4–10 mm below the annulus. For the second generation Evolute R, that has an extended sealing skirt, this distance should be around 3–5 mm. During the final deployment the valve will correct its misalignment [17]. Further post balloon dilatation is required if the valve appears to be under expanded or remains malposed.

Immediate Post Valve Deployment Echocardiography

Immediate assessment of the shape (circularity) and the position of the valve (in relation to the LVOT and native annulus), impact of the TAVI valve on the mitral valve leaflets and haemodynamic performance of the TAVI valve is crucial. Presence of AR may necessitate treatment with balloon dilatation or rarely even a valve in valve procedure. In event of a sudden clinical deterioration, echocardiography plays an important role in detecting the potential causes. Although, TOE is preferred, TTE can be an alternative in patients undergoing TAVI with conscious sedation.

Assessment of the Position and Function of the TAVI Valve

The long axis view of the aortic valve should be obtained immediately after valve deployment to assess its position, leaflet motion and presence of AR. The position of the TAVI valve in relation to the LVOT and the mitral valve should be carefully studied. The short axis views (either via bi plane imaging or using a separate acquisition) are then used to assess the circularity of the valve, its relation to the coronary ostia and sinuses and assessment of AR.

TOE provides the most rapid and accurate assessment of AR immediately after valve deployment. Some degree of transvalvular regurgitation is common, when the delivery apparatus and/or guide wire remains across the valve. It usually improves after their removal or repositioning. Assessment of PAR starts with the aortic valve long axis view. If biplane imaging is available, a transverse image can be obtained at different levels without moving the TOE probe allowing identification of the regurgitant jet. Otherwise the transverse views should be obtained at different levels from the leaflets to the level of annulus and down to the level of the LVOT. Transgastric views, although not recommended for quantification of PAR, are helpful in detection of the regurgitant jets, particularly those originating from the anterior part of the valve that are prone to acoustic shadowing in the mid oesophageal view [17]. Continuous-wave, pulsed-wave, and colour Doppler study of the aortic valve to confirm satisfactory prosthetic valve function is also done in the transgastric position. Whilst an undersized prosthesis is expected to be associated with PAR, in contrast, an oversized prosthesis may result in suboptimal stent expansion, impaired cusp mobility, and central AR. Transvalvular AR can also be caused by damage to the leaflets because of the crimping process or aggressive balloon inflation [15]. Quantification of post procedural PAR will be discussed in detail in the next section.

When TTE is used for assessment of the valve function and AR, it's important to check the parasternal short and long axis as well as three and five chamber views, as often one of these and not all provides adequate image quality. In each view the TTE probe should be tilted in different angles so that the valve cusp is most visible in order to detect any PAR.

Potential TAVI Complications Diagnosable by Echocardiography

Left Ventricular Dysfunction

Left ventricular dysfunction with acute wall motion abnormalities may be secondary to coro-

nary ostial occlusion by fragment embolization or by an obstructive portion of the valve frame, or a native cusp. It's usually associated with severe drop in blood pressure. Although this complication may be fatal, successful management of ostial occlusions with percutaneous angioplasty or bypass surgery has been reported. Other potential causes of new regional wall motion abnormality are new left bundle branch block and localised haemopericardium compressing the LV [18].

Pericardial Effusion

It is difficult to identify and be sure about exact cause of pericardial effusion but in case of temporary wire perforation, haematoma can be identified or even the wire exit can be seen.

Aortic Trauma

Tear or rupture of the aortic root may be observed during the procedure after balloon valvuloplasty or prosthesis deployment (mainly with the balloon expandable valves), especially in the presence of extensive annular calcification or prosthesis oversizing. Aortic haematoma is the result of microperforation of all the layers of the vessel. Aortic dissection (i.e. intimal tear) can also happen both during valve deployment or by the delivery catheter particularly in an unfolded or stiff aorta. Both aortic haematoma and aortic dissection requires close observation and surgical repair in case of expansion (Fig. 41.10) [18].

Sudden worsening of mitral regurgitation is another possible complication of TAVI that may occur due to right ventricular pacing (LV asynchrony) or as a consequence of prosthetic misplacement with pressure on the anterior mitral leaflet or by the direct damage or distortion of the subvalvular apparatus during the wire and catheter manipulation. The latter is more common with the antegrade apical approach that may cause temporary or, in the case of chordal or leaflet rupture, permanent distortion and severe MR. Careful echocardiographic monitoring of the mitral valve during and after implantation can help avoid this complication. Changes in LV pressure, for example in cases of new LV dysfunction, can also cause mitral regurgitation.

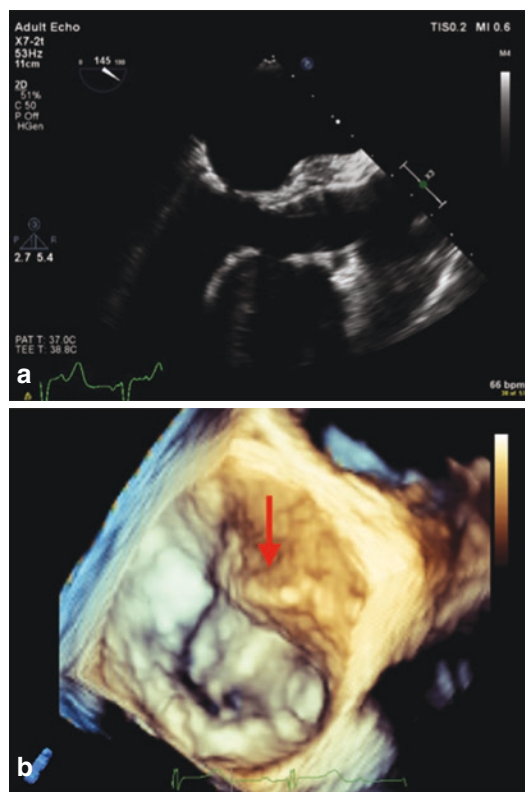


Fig. 4.110 (a) A Long axis aortic view obtained by intra-procedural TOE suggestive of an aortic tear/haematoma. (b) 3D TOE view of the same case showing bulging aortic haematoma into the left atrium (red arrow). The patient was haemodynamically stable and observed for a short period in the cath lab with no progression of the haematoma

Ventricular Septal Defect

Ventricular septal defect during TAVI procedure is a rare but potentially life-threatening complication. Thin membranous septum and extension of calcification to LVOT are considered as risk factors [18]. It can be identified with TOE and an attempt at treatment can be made if this is identified early.

Other Echocardiography Approaches to TAVI

Performing TOE by use of a trans nasal probe has been described in sedated patients. However, the lack of 3D imaging, limited probe availability and poor tolerability by some patients has limited

its use. Intracardiac echo (ICE) has also been introduced to the field of the TAVI, however it poses additional challenges in securing adequate visualization and adds extra cost to an already expensive procedure.

Follow-Up Echocardiography

Like surgically replaced valves a baseline echocardiography (usually at 1 month) is recommended for future reference if needed. Thereafter annual studies are currently recommended [19] although this approach lacks evidence and is likely to change as we learn more about the TAVI valves through the clinical trials and registries.

Aortic Regurgitation

PAR is an important complication of the TAVI that has been shown to be associated with increased mortality for both balloon-expandable and self-expanding valves. Moreover, in early series, TAVI was associated with PAR in more than 80% of patients. Thus, presence of PAR has become an important method for determining the effectiveness of various valve iterations or designs. The incidence of moderate or severe PAR has been reported to be between 2 and 17% in randomized trials and major registries [20] and is significantly associated with adverse outcome and mortality. Although to a lesser degree, even mild PAR is independently associated with increase in all-cause mortality [21].

The underlying contributing mechanisms for PAR include: (a) undersized TAVI valve (b) inappropriate low or high stent position (c) presence of heavy calcification on the valve, at the level of annulus or LVOT. In all cases, the annulus fails to be completely sealed, resulting in PAR.

Accurate assessment of severity of the PAR is difficult in the absence of validated methods. PAR jets are often multiple, eccentric, irregularly shaped, confined to the LVOT wall, and may be masked partially or totally as a result of acoustic shadowing from the calcifications of the native aortic annulus or from the TAVI valve stent.

The circumferential extent of the PAR jet(s) estimated in the short-axis view is the main parameter that has been proposed in major society guidelines for semiquantitative assessment of the PAR severity. Assuming the transverse view as a clock screen, this parameter is assessed by estimating visually the approximate number of minutes occupied by the PAR jet(s) according to the face of a clock and by dividing this number by 60 min. The circumferential extent is then expressed as a percentage and, according to the 2009 ASE guidelines, a value between 10 and 20% would correspond to moderate PVR, and a value >20% to severe PVR. These cut-off values have been revised in the 2012 Valve Academic Research Consortium 2 recommendations and an extent of between 10 and 30% corresponds to moderate PAR, and >30% to severe PAR. PAR circumferential extent may vary substantially depending on the plane of interrogation. It is thus important to scan the entire height of the stent and use the short-axis plane where the vena contracta of the jet is the smallest. An image plane that is too high (above the stent or upper portion of the stent) may underestimate the regurgitation, whereas a plane that is too low in the LVOT may overestimate the regurgitation severity. The circumferential extent of the jet becomes even more complex and less reliable when multiple and/or eccentric jets are present. In the case of multiple-jet PAR, the vena contracta may be at different levels depending on the jets, and this may, therefore, require several image planes to assess the overall circumferential extent of the PAR. Moreover, the PAR jets, and particularly the anterior jets may be very eccentric and in such case, the jet may be directed across the short-axis plane (instead of long axis), which may lead to an overestimation of the circumferential extent and thus of the severity of the PAR. Thus, grading of PAR should not rely solely on the examination of the short-axis view and estimation of the circumferential extent. This measure should be integrated with other views and parameters. However, this technique provides a rapid tool for assessment of the PAR in cath lab, immediately after deployment of the valve (Fig. 41.11).

The width of the jet at its origin is probably the most important parameter to consider for grading the severity of PAR. It is assessed visually in the parasternal and apical views, and an estimate of the ratio of the jet width to the LVOT diameter may be provided and expressed in percentage. However this validated technique is most suited for transvalvular AR [15]. Besides the size and circumferential extent of the jet at its origin, other characteristics may be used to grade the severity of the PAR, including the number of jets and the visualization of the jet path along the stent and/or of the proximal flow convergence. Nevertheless, a single jet can be severe if it has a large vena contracta. On the other hand, three mild jets may correspond to moderate PAR or more. When the path of the PAR jet is clearly visible along the whole length of the stent, this is often associated with moderate or greater PAR.

Doppler parameters, including the signal intensity and pressure half-time of the continuous-wave envelope of the regurgitant jet(s) and the timing and velocity of the diastolic flow reversal in the descending aorta, may also be determined to corroborate PAR severity. However, the accuracy of these parameters is limited in the early post-procedural period because of the acute nature of PAR and the frequent coexistence of moderate-severe diastolic dysfunction. Furthermore, pressure half-time is highly heart-rate dependent. The flow reversal in the descending aorta and the end-diastolic velocity measured by pulsed-wave Doppler is strongly influenced by aorta compliance, and increased arterial stiffness may result in false-positive results. Quantitative methods such as the proximal isovelocity surface area (PISA) method are rarely applicable to PAR. The regurgitant volume may, however, be estimated by comparison of stroke volumes across the aortic valve (representing total stroke volume) and a non-regurgitant valve (either mitral or pulmonary) and can be used for prosthetic valves. Although total stroke volume (regurgitant and forward volumes) can be measured by subtracting LV end-systolic volume from end-diastolic volume, the more common method is to calculate the stroke volume across the LVOT. Three-dimensional echocardiography may become the method of choice for

assessing aortic regurgitant volume and effective regurgitant orifice area (EROA). Validation of this technology for quantitating native AR is growing, although the utility of 3D echocardiography for the assessment of prosthetic regurgitation has yet to be determined (Table 41.3).

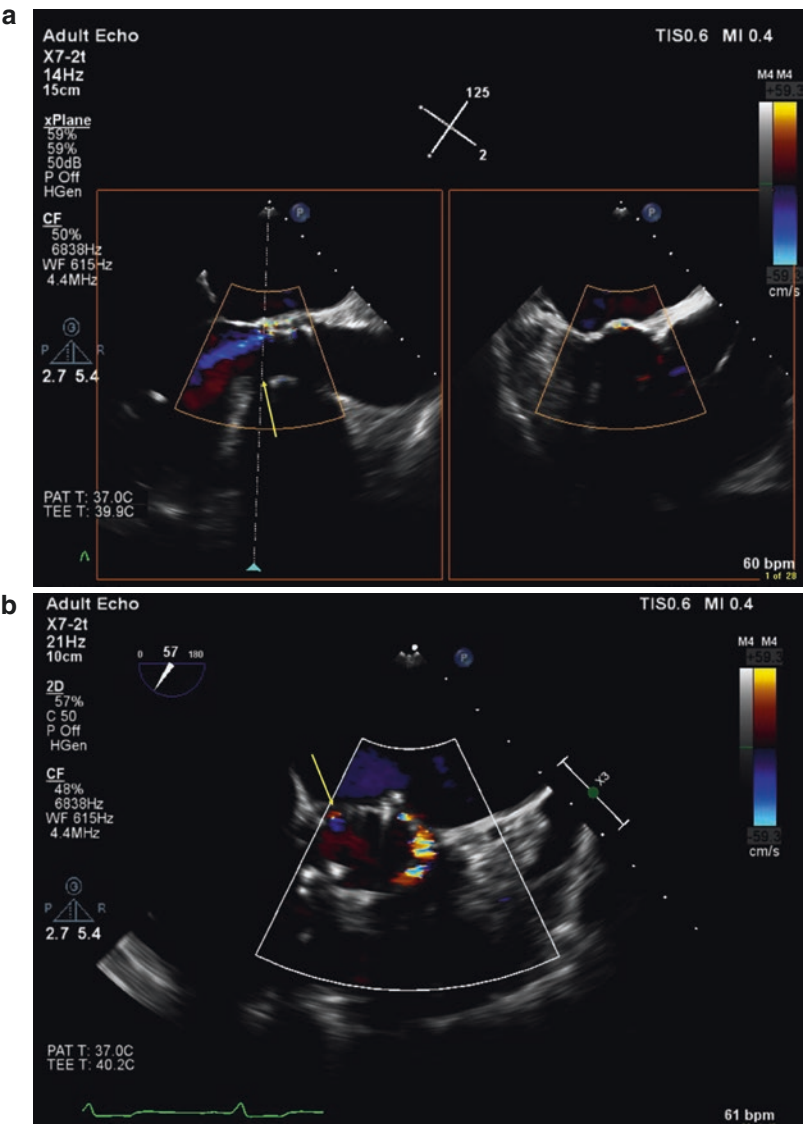
As for native AR, the use of regurgitant jet area and length of the jet in the LVOT are no longer recommended because these parameters are unreliable indicators of AR severity, given their dependence on blood pressure and aortic and ventricular compliance.

Notably, cardiac MRI studies have shown that TTE underestimates the severity of PAR and further imaging by TOE or MRI should be undertaken if clinically appropriate.

TAVI Valve Dysfunction

A baseline TTE study following TAVI is essential for future reference in case a newly detected high gradient occurs. This allows differentiation of a pre-existing patient prosthesis mismatch from

Fig. 41.11 Assessment of PAR in the cath lab by TOE after valve deployment. (a) An example of mild PAR however it's important to note that the shadow at the anterior part of the valve (yellow arrow) may obscure other regurgitant jets. Gastric views could be helpful in detecting other potential PAR jets. (b) An example of severe PAR. The small jet that is visible in non coronary cusp (yellow arrow) appeared to be more significant in a different plane that is shown in (c). (d) More accurate assessment of PAR can be done by measurement of the 3D vena contracts area using multiplanar reconstruction of a zoomed 3D colour Doppler dataset



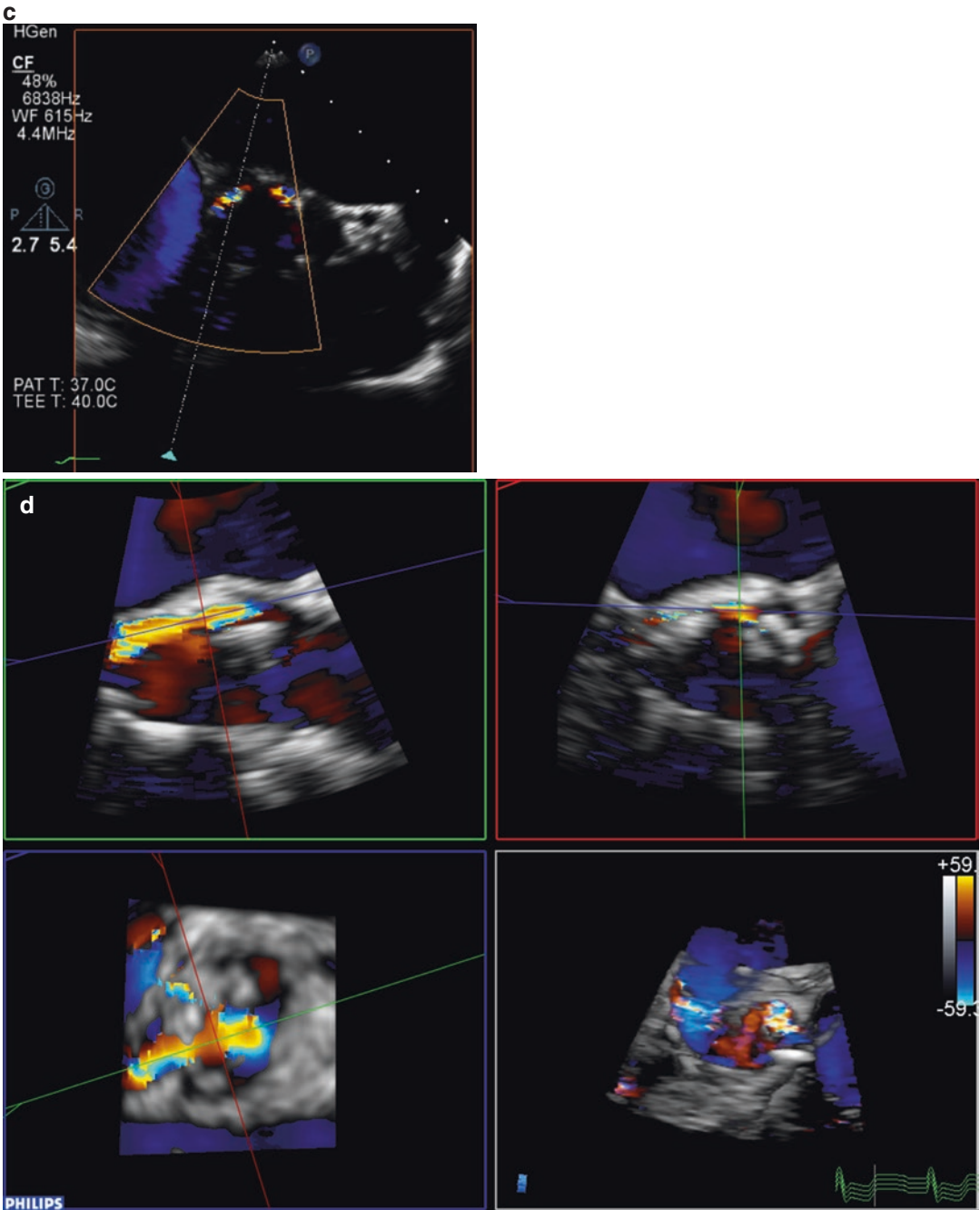


Fig. 41.11 (continued)

other causes of high gradient such as thrombus formation. Performing a baseline study is particularly important as currently there are no well-established normal gradients and EOA for TAVI valves [22]. Thrombus formation, although not

visible on the aortic valve by TTE, can be suspected of by an unexpected increase in gradients. TOE is the modality of choice to assess leaflet mobility and to confirm thrombus formation, however MSCT can also be used (Fig. 41.12).

Table 41.3 Assessment of paravalvular aortic regurgitation

	Mild	Moderate	Severe
<i>Structural parameters</i>			
Valve stent	Normal	Usually abnormal	Usually abnormal
<i>Qualitative/Semiquantitative parameter</i>			
Wide/extensive jet origin	Absent	Present	Present
Jet path visible along the stent	Absent	Often present	Present
Proximal flow convergence visible	Absent	Often present	Present
Diastolic flow reversal	Absent	Intermediate	Holosystolic
Vena contracta (mm) color doppler	<4	4–6	>6
Circumferential extent of prosthetic PVR (%)	<20%	20–29%	>30%
<i>Quantitative parameters</i>			
Regurgitant volume (mL/beat)	<30 ml	30–59 ml	>60 ml
Regurgitant fraction (%)	<30%	30%–49%	>50%
Effective regurgitaion orrifice area (cm ²)	0.10 cm ²	0.10%–0.29 cm ²	>0.3 cm ²

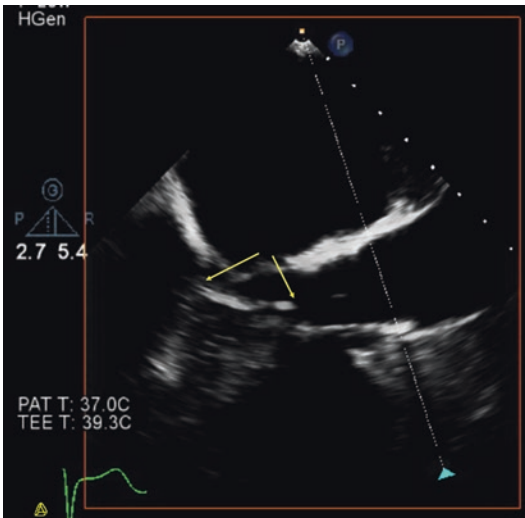


Fig. 41.12 A TOE long axis aortic view that shows a thrombosis on a TAVI valve (yellow arrows). The patient had high gradients on her 1-year follow up TTE

If an increase in transvalvular gradients post TAVI is caused by thrombus formation, anticoagulation could resolve this issue [23]. The potential role of valve thrombosis in valve degeneration is unknown but possibly by early detection, valve durability could be extended.

Patient prosthesis mismatch, although frequent in early surgical aortic valve replacement series, it seems to be less frequent in the TAVI population, especially in those with a small annulus, in comparison with equivalent surgical aortic valve replacement [15].

Other potential causes of TAVI valve dysfunction that can be identified by follow up echocar-

diography include: TAVI valve migration that has been reported as late as a year, structural valve failure and endocarditis. Unlike surgical valves, TAVI valve leaflet degeneration, calcification or pannus formation has been rarely reported. These cases would present with an unexpected increase in gradients, new onset AR or both [15].

Measurement of TAVI valve EOA (by continuity equation) is essential in suspected valve dysfunction. It's important to take care to measure the LVOT pulse wave Doppler just beneath the valve stent instead of within the stent (below the leaflets) as there is often flow acceleration within the stent, resulting in higher pulse wave Doppler velocities that may lead to overestimation of EOA. Therefore the LVOT diameter should also be measured at the level of pulse wave Doppler measurements.

In the case of co-existing pathologies such as left ventricular dysfunction and mitral regurgitation at the time of TAVI, follow up TTE would help to study the impact of TAVI on the left ventricular reverse remodeling and to assess if the degree of mitral regurgitation has changed or not.

Future Directions

Despite the success and rapid technical advances of TAVI procedures, limitations remain. The future of TAVI will also include imaging improvements. Integrated imaging consoles in hybrid theaters are a reality in many centers. Co-registration

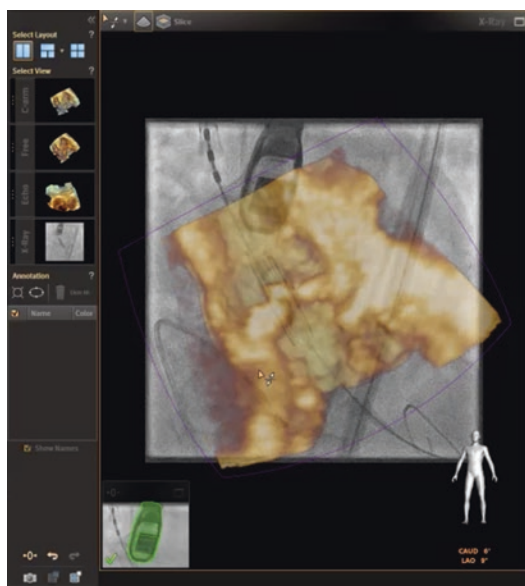


Fig. 41.13 An example of fusion of 3D TOE image of aortic valve on fluoroscopy screen during positioning of a Sapien 3 valve

of real time 2D and 3D echocardiography with fluoroscopy has become commercially available (Fig. 41.13). Such techniques allow online determination of the co-planar view and can improve precision in TAVI valve positioning with the aim to reduce contrast use and to improve patients' outcome. Studies are required to assess if fusion imaging can result in an improvement in patients' outcome. Real time hybrid imaging can also help performing TAVI with minimal contrast volume in patients at high risk of acute kidney injury.

References

1. Clavel MA, Webb JG, Pibarot P, et al. Comparison of the hemodynamic performance of percutaneous and surgical bioprostheses for the treatment of severe aortic stenosis. *J Am Coll Cardiol*. 2009;53:1883–91.
2. Pibarot P, Weissman NJ, Stewart WJ, et al. Incidence and sequelae of prosthesis-patient mismatch in transcatheter versus surgical valve replacement in high-risk patients with severe aortic stenosis: a PARTNER trial cohort—a analysis. *J Am Coll Cardiol*. 2014;64:1323–34.
3. Piazza N, de Jaegere P, Schultz C, Becker AE, Serruys PW, Anderson RH. Anatomy of the aortic valvar complex and its implications for transcatheter implantation of the aortic valve. *Circ Cardiovasc Interv*. 2008;1:74–81.
4. Figulla HR, Webb JG, Lauten A, Feldman T. The transcatheter valve technology pipeline for treatment of adult valvular heart disease. *Eur Heart J*. 2016;37:2226.
5. Meredith IT, Hood KL, Haratani N, Allocco DJ, Dawkins KD. Boston Scientific Lotus valve. *EuroIntervention*. 2012;8(Suppl Q):Q70–4.
6. Schofer J, Colombo A, Klugmann S, et al. Prospective multicenter evaluation of the direct flow medical transcatheter aortic valve. *J Am Coll Cardiol*. 2014;63:763–8.
7. Willson AB, Rodes-Cabau J, Wood DA, et al. Transcatheter aortic valve replacement with the St. Jude Medical Portico valve: first-in-human experience. *J Am Coll Cardiol*. 2012;60:581–6.
8. Mollmann H, Diemert P, Grube E, Baldus S, Kempfert J, Abizaid A. Symetis ACURATE TF aortic bioprosthesis. *EuroIntervention*. 2013;9(Suppl):S107–10.
9. Rudolph TK, Baldus S. JenaValve—transfemoral technology. *EuroIntervention*. 2013;9(Suppl):S101–2.
10. Pibarot P, Dumesnil JG. Low-flow, low-gradient aortic stenosis with normal and depressed left ventricular ejection fraction. *J Am Coll Cardiol*. 2012;60:1845–53.
11. Perlman GY, Blanke P, Dvir D, et al. Bicuspid aortic valve stenosis: favorable early outcomes with a next-generation Transcatheter Heart valve in a multicenter study. *JACC Cardiovasc Interv*. 2016;9:817–24.
12. Mylotte D, Lefevre T, Sondergaard L, et al. Transcatheter aortic valve replacement in bicuspid aortic valve disease. *J Am Coll Cardiol*. 2014;64:2330–9.
13. Kronzon I, Jelnin V, Ruiz CE, et al. Optimal imaging for guiding TAVR: transesophageal or transthoracic echocardiography, or just fluoroscopy? *JACC Cardiovasc Imaging*. 2015;8:361–70.
14. Eleid MF, Goel K, Murad MH, et al. Meta-analysis of the prognostic impact of stroke volume, gradient, and ejection fraction after Transcatheter aortic valve implantation. *Am J Cardiol*. 2015;116:989–94.
15. Fryearson J, Edwards NC, Doshi SN, Steeds RP. The role of TTE in assessment of the patient before and following TAVI for AS. *Echo Res Pract*. 2016;3:R19–34.
16. Urena M, Hayek S, Cheema AN, et al. Arrhythmia burden in elderly patients with severe aortic stenosis as determined by continuous electrocardiographic recording: toward a better understanding of arrhythmic events after transcatheter aortic valve replacement. *Circulation*. 2015;131:469–77.
17. Hahn RT, Little SH, Monaghan MJ, et al. Recommendations for comprehensive intraprocedural echocardiographic imaging during TAVR. *JACC Cardiovasc Imaging*. 2015;8:261–87.
18. Hahn RT, Gillam LD, Little SH. Echocardiographic imaging of procedural complications during self-expandable transcatheter aortic valve replacement. *JACC Cardiovasc Imaging*. 2015;8:319–36.
19. Holmes DR Jr, Mack MJ, Kaul S, et al. ACCF/AATS/SCAI/STS expert consensus document on transcatheter aortic valve replacement. *J Am Coll Cardiol*. 2012;59:1200–54.

20. Bax JJ, Delgado V, Bapat V, et al. Open issues in transcatheter aortic valve implantation. Part 2: procedural issues and outcomes after transcatheter aortic valve implantation. *Eur Heart J*. 2014;35:2639–54.
21. Kodali S, Pibarot P, Douglas PS, et al. Paravalvular regurgitation after transcatheter aortic valve replacement with the Edwards sapien valve in the PARTNER trial: characterizing patients and impact on outcomes. *Eur Heart J*. 2015;36:449–56.
22. Kappetein AP, Head SJ, Genereux P, et al. Updated standardized endpoint definitions for transcatheter aortic valve implantation: the valve academic research Consortium-2 consensus document. *J Thorac Cardiovasc Surg*. 2013;145:6–23.
23. Descoux J, Gautier-Pignonblanc P, Innorta A, et al. Effectiveness of anticoagulant therapy in the treatment of post-TAVI bioprosthetic thrombosis. *J Cardiothorac Surg*. 2015;10:50.

Echocardiography in Mitral Valve Repair

42

Michael Bellamy and Christopher Baker

Introduction

Surgical mitral valve repair remains the gold-standard for operable patients with symptomatic severe MR with very good outcomes in centres with expertise in repair techniques.

Echocardiography plays an essential role in the patient's pre-operative assessment, helping to guide decisions in multi-disciplinary /heart team discussions. The utility of 3D trans-oesophageal echo in particular, can provide unique mitral valve imaging to correctly identify mitral valve pathologies and help plan for successful surgical repair.

Transoesophageal echo is also used peri-operatively to assess the immediate results of valve repair and diagnose any complications that may arise.

In high risk or very elderly patients turned down for surgery, echocardiography is also essential in percutaneous mitral valve interventions. Echo plays a key part in patient screening, detailed valve assessment, procedural guidance and follow up.

(A) Surgical Mitral Valve Repair

A comprehensive echocardiographic assessment in patients for mitral valve surgery should combine both transthoracic and transoesophageal imaging prior to the operating room. The assessment of mitral valve disease, in both chronic primary and secondary MR, is described in the earlier chapter. This includes anatomical relationships, Doppler echocardiography and 3D imaging. The principles and use of transoesophageal and intra-operative echocardiography are described elsewhere in this textbook.

The comprehensive pre-operative assessment includes:

1. Transthoracic echocardiography
 - a. Left ventricular (LV) function and the consequences of LV volume overload (LV ejection fraction, LV end-diastolic and end-systolic dimensions, left atrial size and left atrial volume)
 - b. Aetiology of mitral valve disease and the mechanism of MR, either primary, secondary or mixed aetiology
 - c. Quantitation of MR
 - d. Mitral annulus assessment for presence and degree of calcification
 - e. Right ventricular assessment
 - f. Tricuspid valve assessment, measurement of the tricuspid annulus, quantitation of any tricuspid regurgitation and estimation of pulmonary pressures

M. Bellamy (✉) · C. Baker
Department of Cardiology, Imperial Healthcare NHS
Trust, Hammersmith Hospital, London, UK
e-mail: michael.bellamy@imperial.nhs.uk

- g. Identification and assessment of any other valve pathology
2. Transoesophageal echocardiography
 - a. For more detailed and supplementary anatomic assessment
 - b. Confirmation of the aetiology and mechanism of MR
 - c. Confirmation of MR severity/further quantitation
 - d. Assessment of atrial septal anatomy, left atrial appendage and pulmonary veins
 - e. Assessment of the ascending aorta and any aortic pathology prior to surgery
 - f. Tricuspid valve assessment and annulus
 - g. Acquisition of 3D left atrial surface (surgical) views of the mitral valve
 - h. Measurement of the mitral annulus (3D anatomic modelling if available)

The display of three-dimensional left atrial surface mitral valve images is particularly helpful when presenting and discussing surgical repair options and in determining the suitability for valve repair.

3D Echocardiography in Primary Mitral Valve Disease (Degenerative)

The complexity and success of surgical repair will be determined by the extent of mitral leaflet prolapse, degree and quality of excess leaflet tissue, single or multiple MR jets, degree of annular dilatation, presence of calcification and involvement of the commissures [1]. Left atrial surface (en face) views obtained by 3D TOE allow direct visualisation of the mitral valve from a 'surgical perspective'. Examples of typical 3D TOE images are illustrated as follows:

1. *Anterior mitral leaflet (AML) pathology*: see Figs. 42.1, 42.2, and 42.3
Case examples are shown for prolapse with flail segments secondary to chordal rupture (arrows). In Fig. 42.1, the chordal rupture is localised to the lateral segment, A1. In Fig. 42.2, chordal rupture is seen centrally at A2 (multiple chords) and in Fig. 42.3, the medial segment is affected with flail of the

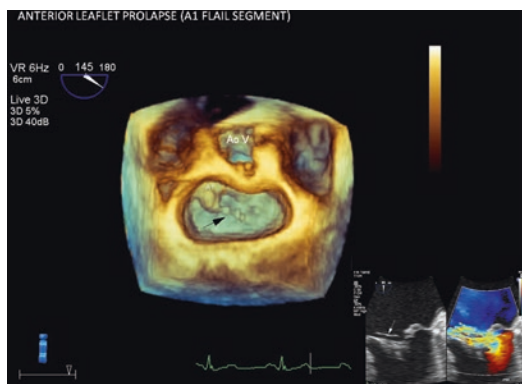


Fig. 42.1 Anterior leaflet (A1). Transoesophageal 3D left atrial *en face* view in primary MR of a lateral (A1) segment flail with a ruptured chord. The aortic valve (AoV) is seen at 12 o'clock. 2D imaging is shown in the bottom right panel with an eccentric posteriorly directed MR jet on colour Doppler with a large proximal isovelocity surface area (PISA). The ruptured chord (arrow) is visible in the left atrium above the posterior mitral leaflet

A3 segment. The MR jet is directed posteriorly in all cases with an eccentric jet on colour Doppler. The prolapse may of course affect more than one segment depending on the extent of pathology leading to more diffuse jets and affecting a larger area of the valve.

The anterior leaflet segments are less well defined than the posterior leaflet. However, left atrial 3D echo visualisation is usually able to define anatomy and localise the pathology for the surgeon. Left atrial 3D *en face* views are the easiest and quickest method to identify which segments are affected.

More detailed assessment of leaflet thickness, length, coaptation and orientation requires standard 2D imaging using multi-plane angles. The mid-oesophageal angles for identifying central AML pathology include 0° and 135°. Medial scallop pathology (A3) is visualised between 30° and 50° (see Fig. 42.3) and lateral pathology (A1) (see Fig. 42.1) at 90–100°. The left atrial appendage can serve as a lateral landmark.

The degree of MR should be quantified using recommended guidelines [2] but from a practical viewpoint, proximal isovelocity surface area (PISA) measurement techniques work

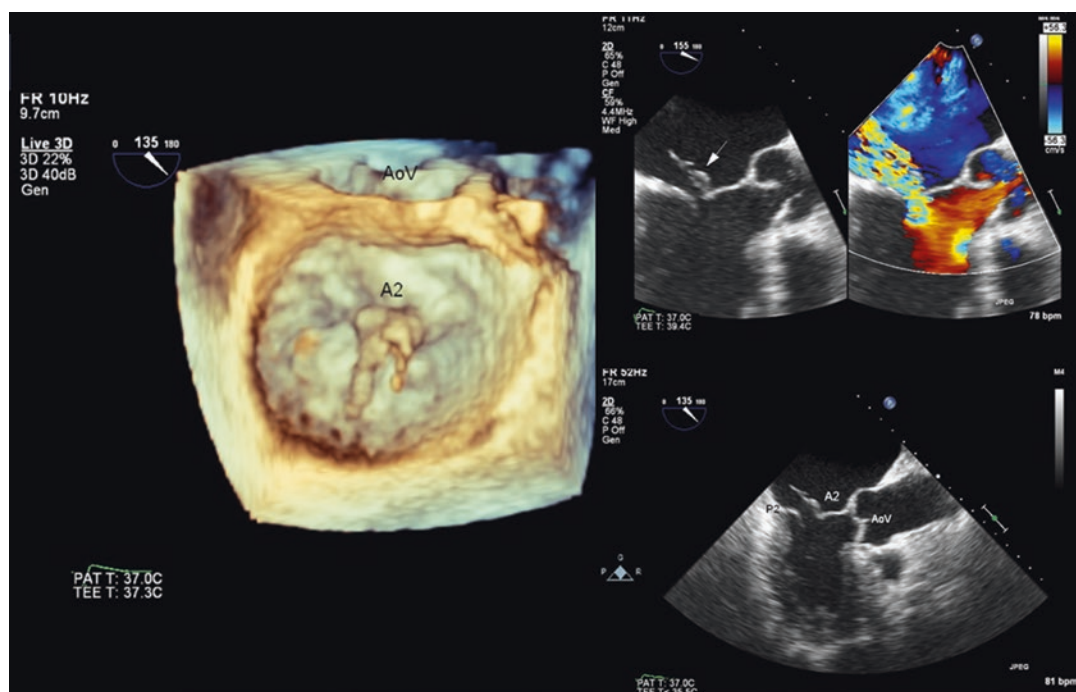


Fig. 42.2 Anterior leaflet (A2). Left panel shows 3D left atrial view of a middle (A2) segment flail and multiple ruptured chordae. 2D imaging with colour Doppler is

shown in the right panel. The flail middle segment and chords can be clearly visualised in the left atrium using a multi-plane probe angle of 135–155°

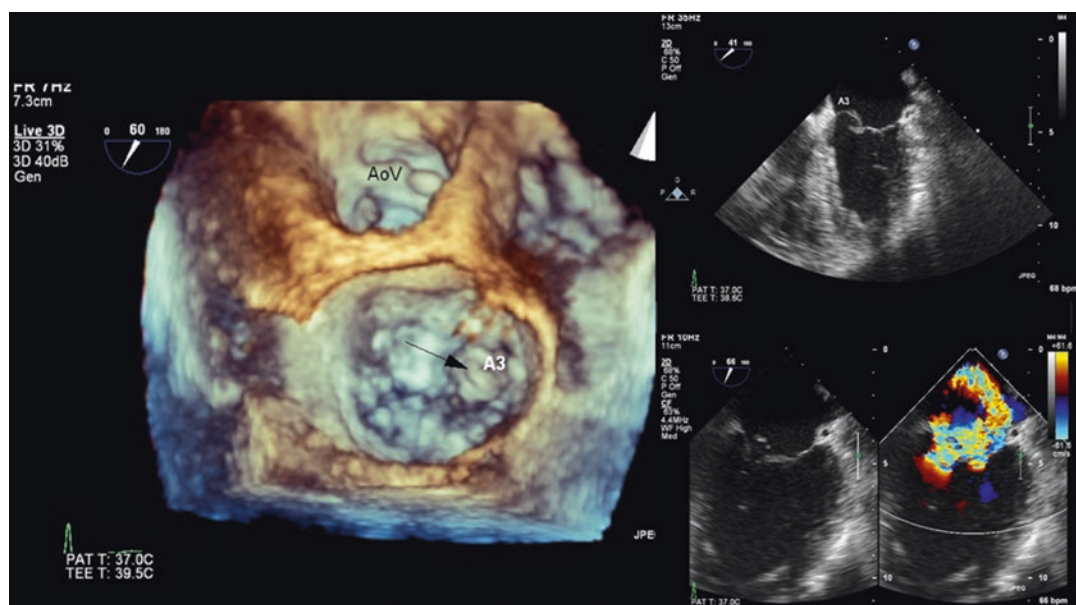


Fig. 42.3 Anterior leaflet (A3). Left panel—3D left atrial view of anterior medial segment (A3) prolapse. Right panel—2D TOE multi-plane imaging at 40–45° identifies

A3 prolapse medially. The resulting MR jet is directed posteriorly and laterally and has a wide vena contracta

well with the caveat that continuous wave Doppler for peak MR velocity (MR Vmax) and MR VTI are sometimes best obtained via combined transthoracic imaging for very eccentric and wall hugging MR jets. Vena contracta area using colour Doppler multi-plane reconstruction is another method that may prove useful for determining the regurgitant orifice area, particularly for multiple jets [3]. 3D PISA techniques are in development but remain to be validated.

2. *Posterior mitral leaflet (PML) pathology*: see Figs. 42.4, 42.5, 42.6, 42.7, 42.8, 42.9, and 42.10

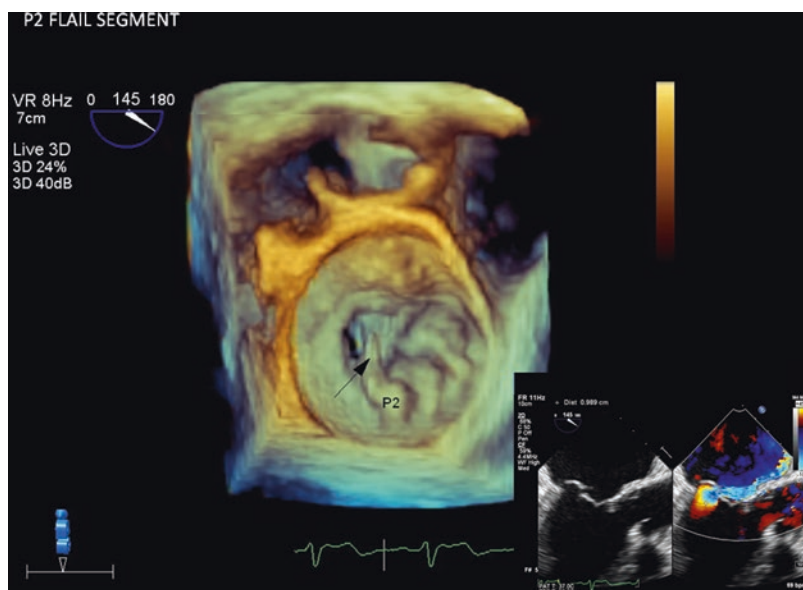
The middle scallop (P2) of the PML is the most commonly affected segment leading to a typical eccentric, anteriorly directed MR jet. Figures 42.4 and 42.5 show typical examples of flail P2 scallops with ruptured chords (arrows). The flail segments are easily identified in the anterior-posterior mid-oesophageal TOE projections at multi-plane angles of 0° and 135° (left ventricular outflow tract view). Isolated P3 segment (Fig. 42.6) and P1 segment prolapse are much less common and more often arise in combination with P2

pathology (Figs. 42.7 and 42.8) or with multi-segment involvement in Barlow-type valves (Fig. 42.9). It is essential to identify and report mitral valve pathology affecting multiple scallops as this is likely to increase the complexity of successful repair, with Barlow-type valves being the most challenging. It is also important to correctly identify when mitral valve prolapse extends to the commissures (see Fig. 42.10—anterolateral commissure with A1, P1 and P2 involvement).

3. *Bileaflet prolapse/Barlow-type pathology*: see Figs. 42.9 and 42.11

Classically this involves typical bowing of both leaflets with excess leaflet tissue and annular dilatation. TOE 2D imaging shows both leaflets prolapsing beyond the plane of the mitral annulus often with more marked leaflet thickening and redundancy. Multiple segments may be involved and typically there is more than one MR jet on colour Doppler, which can be best appreciated in the medial-lateral multi-plane views (bicommissural at 55–70°). Full-volume 3D colour acquisitions can also be helpful. Mitral valve repair may still be feasible but with a much lower chance of success.

Fig. 42.4 Posterior leaflet (P2). 3D left atrial view of classic P2 prolapse with flail due to chordal rupture (arrow). Bottom right panel shows the TOE 2D LVOT view, MR colour jet and PISA. The MR is very eccentric and directed anteriorly in the left atrium towards the aortic root. The pansystolic murmur on clinical examination commonly radiates into the aortic area



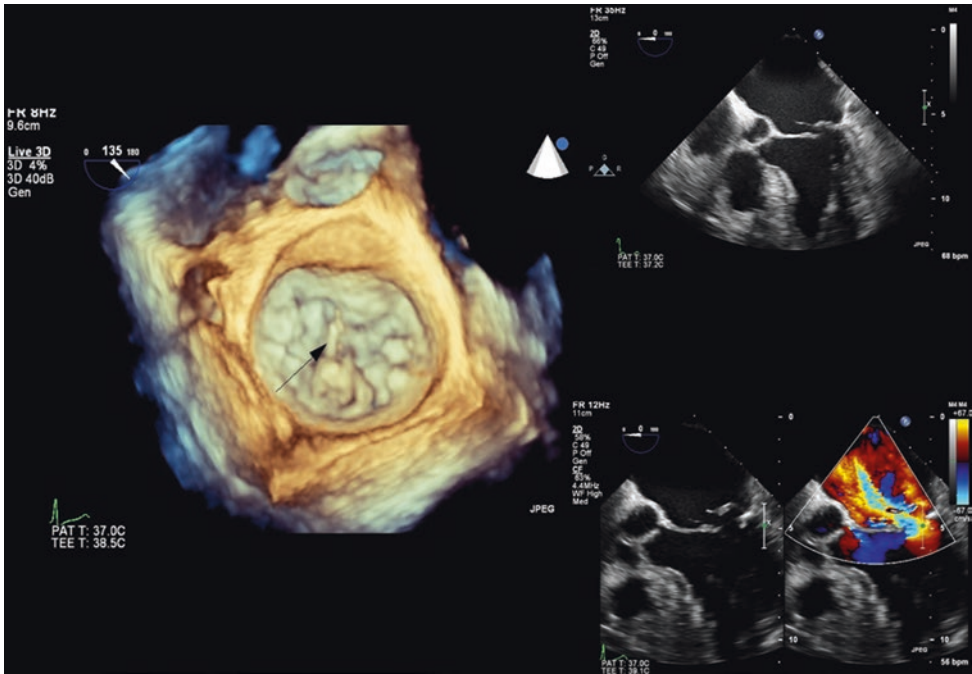


Fig. 42.5 Posterior leaflet (P2). Another typical example of localised posterior leaflet prolapse and flail seen on 3D imaging. There are two ruptured primary chords (arrow).

This example shows the TOE 2D appearance at a multi-plane angle of 0° with the posterior leaflet on the right and a flail height of <10 mm

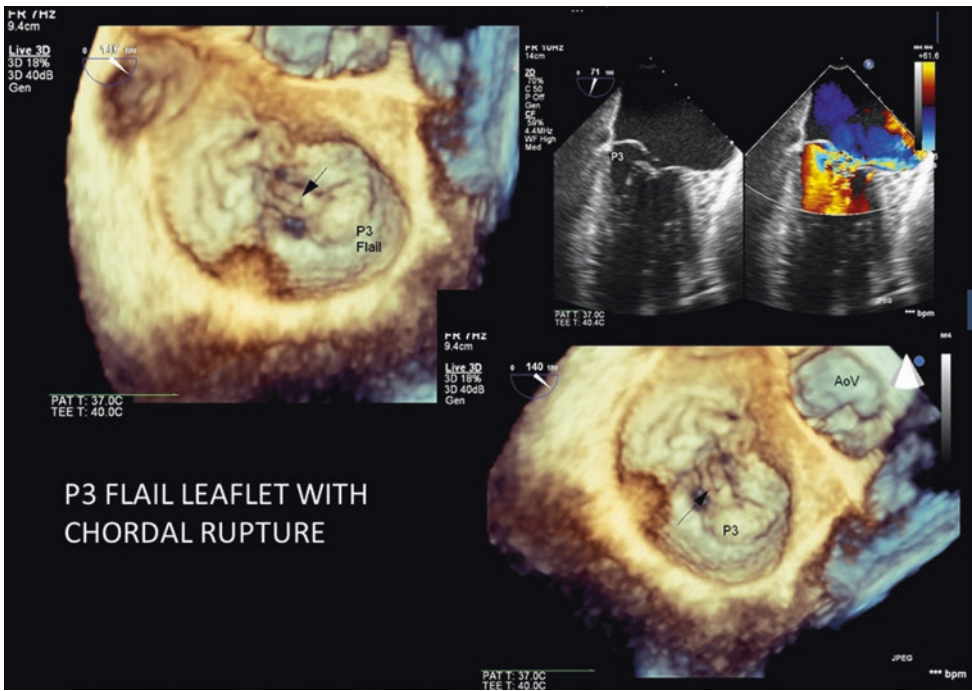


Fig. 42.6 Posterior leaflet (P3). A medial posterior segment flail is shown in the upper left panel with 2 visible ruptured chords (arrow). The P3 segment is best seen on 2D TOE imaging at 70° (upper right panel)

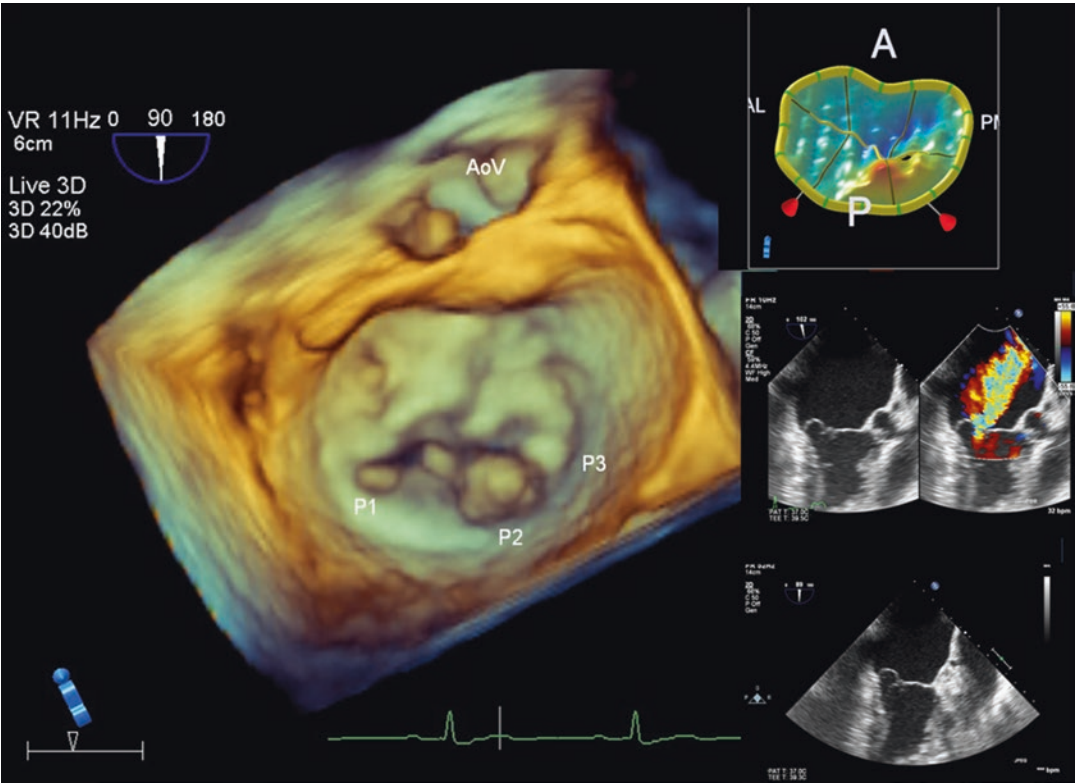
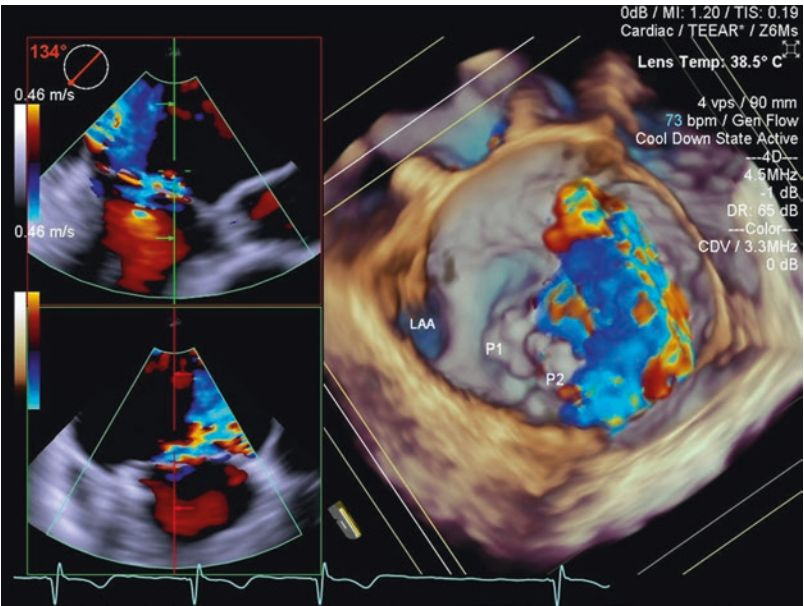


Fig. 42.7 Prolapse extending from P2 into P3 segment. In this example, prolapse of the middle segment of the posterior mitral leaflet (P2) extends into the medial segment (P3). The segments affected can be more easily visu-

alised by mitral valve modelling using Mitral Valve Quantification (MVQ™ by Philips) (top right panel). The prolapse also involves the posteromedial commissure

Fig. 42.8 Prolapse extending from P2 into P1 segment - 3D Colour. Primary/degenerative mitral regurgitation with a colour jet arising from the middle (P2) and lateral (P1) posterior segments. The MR jet is directed anteriorly and medially when visualised in the left atrium



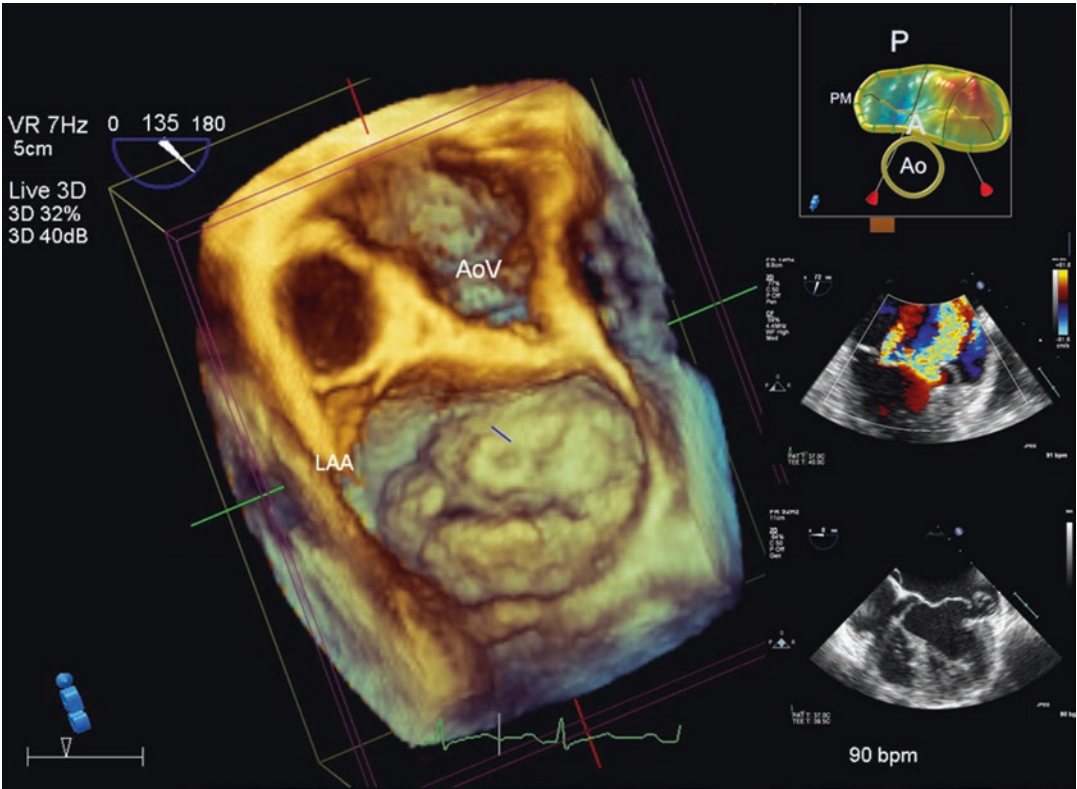
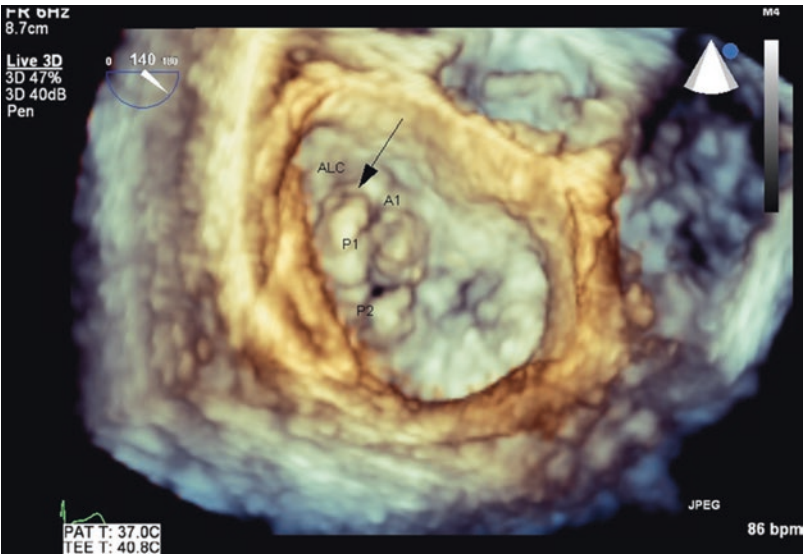


Fig. 42.9 Myxomatous mitral valve disease (Barlow-type). TOE 3D imaging showing extensive bileaflet mitral valve prolapse (LA view). The segments most affected include the lateral and middle scallops, A1, P1, A2 and P2 with the left atrial appendage being a lateral landmark.

The resulting MR jets are best visualised in a medial-lateral (bicommissural) view at 70° (right middle panel). A durable mitral valve repair is extremely challenging in Barlow-type valves

Fig. 42.10 Multi-segment involvement extending to the anterior commissure. Myxomatous mitral valve disease with prolapse involving the middle and lateral segments of the posterior leaflet (P2, P1) and the lateral anterior segment (A1). The prolapse also extends into the anterolateral commissure (ALC), increasing the complexity of mitral valve repair



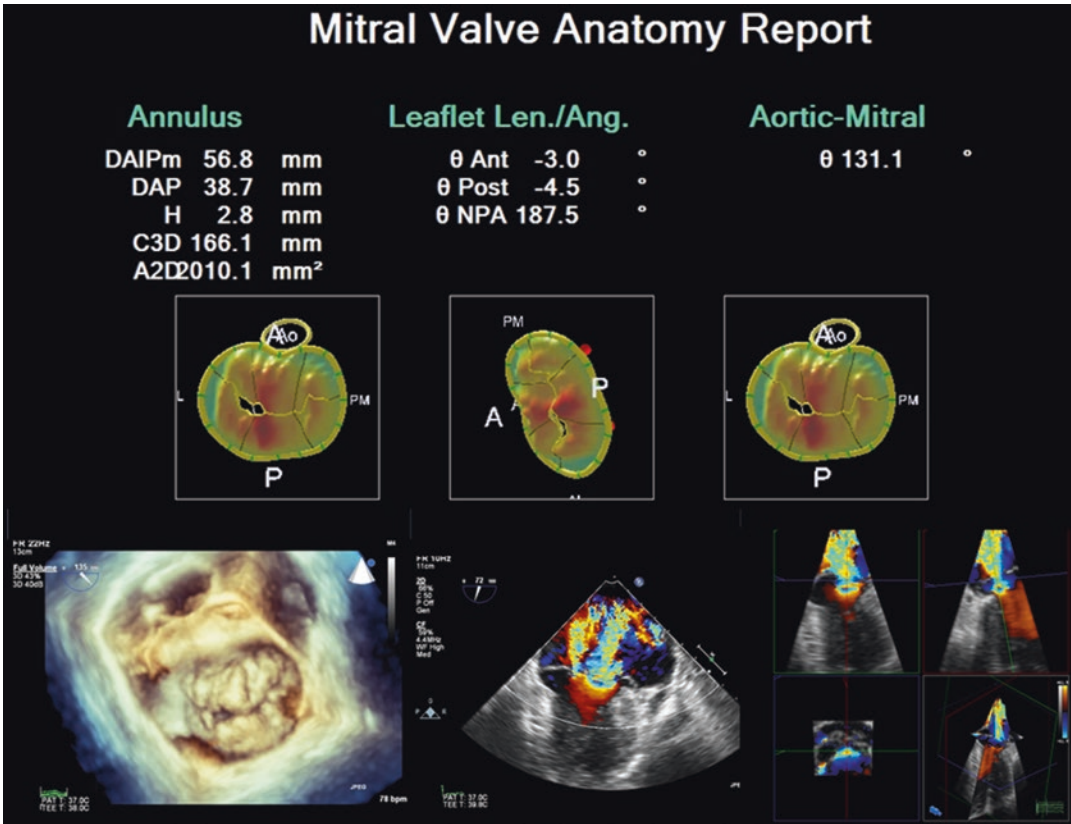


Fig. 42.11 Mitral Valve Quantification (MVQ™)-derived anatomical modelling in Barlow's disease. Multi-segment prolapse in a Barlow valve with all six segments billowing above the plane of the mitral annulus (coded red). The respective TOE-derived images for (1) 3D LA view (bottom left panel) (2) 70° -bicommissural colour

Doppler (bottom middle panel) and (3) 3D colour multi-plane reconstruction (MPR), 3D vena contracta (bottom right panel) are shown. Mitral valve annular measurements are labelled as follows:- *DAIPm* lateral-medial diameter (mm), *DAP* anterior-posterior diameter (mm), *C3D* circumference (mm)

Mitral Valve Quantification:

Figs. 42.11, 42.12, 42.13, 42.14, and 42.15

Commercial software has been developed by industry to allow modelling of the mitral valve to display regions of prolapse above the level of the annulus or regions of tethering below the annulus. This is typically done using a colour coded format (red above and blue below the annulus). Figure 42.11 (MVQ—Mitral Valve Quantification™, Philips) illustrates the type of mitral valve model that can be generated. This has been replaced with an updated software version on newer echo machines by the same vendor (MVN™—Mitral Valve Navigation™—Fig.

42.12), that uses speckle technology to improve leaflet tracing and annular tracking.

An example of another mitral valve modelling package (eSie Valves™ by Siemens) is shown in Figs. 42.13, 42.14, and 42.15. This utilises a more automated approach by tracking leaflet movement during the cardiac cycle and generates a colour coded analysis which can be superimposed on the 3D mitral valve image. Other software packages are available from other vendors.

Mitral valve anatomical modelling can help to provide a clearer visual representation of the regions of leaflet prolapse [4]. The calculation of mitral annular dimensions may be helpful for surgeons in planning valve repair. The usefulness of

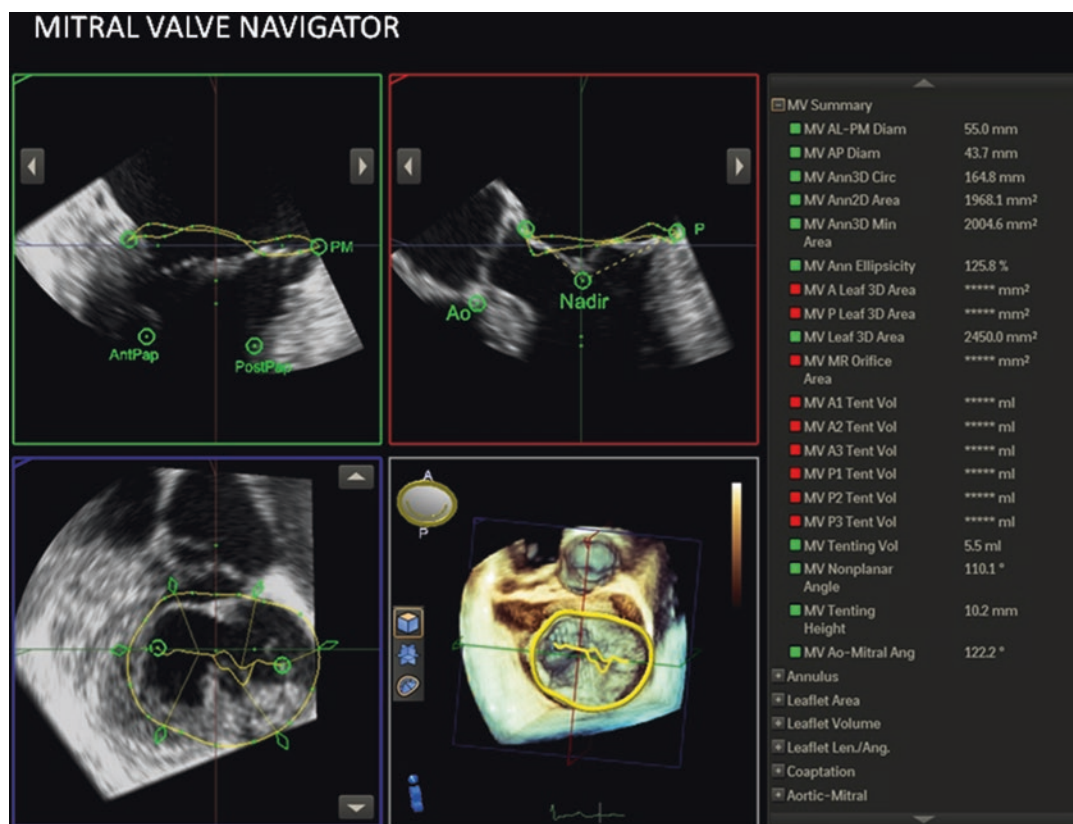


Fig. 42.12 Mitral valve navigation (MVN™). MVN is a Philips QLAB application that allows anatomic modelling of the mitral valve using speckle technology for annulus tracking and leaflet tracing to improve workflow effi-

ciency. An example of the modelling software images is shown. Data output for mitral annular dimensions is similar to MVQ

the additional measurements that can be obtained using this software remains to be more clearly defined.

3D Echocardiography in Secondary Mitral Valve Disease (Functional)

The outcomes of mitral valve repair in secondary MR are less predictable than in primary MR and longer term durability less certain. There also remains a continuing debate between mitral valve repair versus replacement (with sub-valvular preservation) [5].

Surgical annuloplasty is often used to repair secondary/functional MR (FMR) whereby an undersized ring is inserted at the mitral annulus with the aim of restoring normal leaflet coapta-

tion and MR reduction. The type of ring (complete, partial, ischaemic or band, etc) will vary according to the MR aetiology (ischaemic or non-ischaemic) and surgical preference/experience.

Mitral valve surgery is considered reasonable by current guidelines (AHA/ACC 2014/ESC 2012) for patients with chronic severe secondary MR (stages C and D) who are undergoing coronary artery bypass grafting or AVR (Class IIa recommendation). It may also be considered for patients with symptomatic (NYHA III-IV) severe MR who have persistent symptoms despite guideline directed optimal medical therapy for heart failure (Class IIb recommendation). It may also be considered for patients with chronic secondary moderate MR (Stage B) who are undergoing other cardiac surgery.

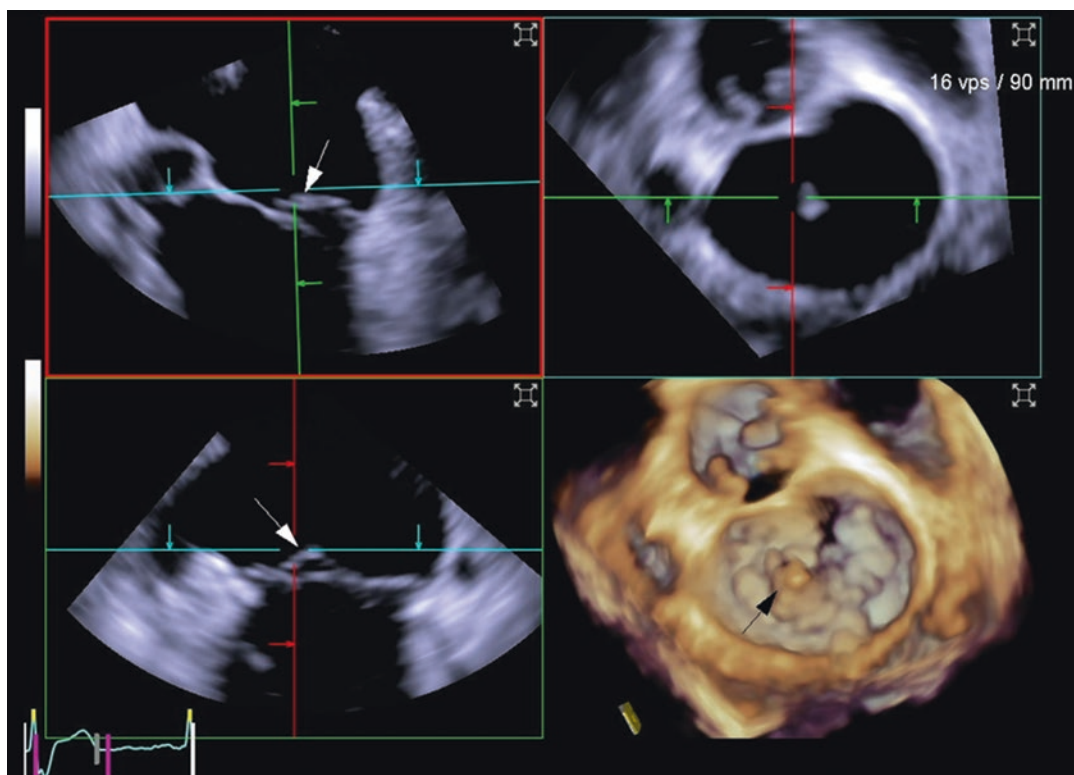


Fig. 42.13 3D TOE imaging using Siemens SC2000—single beat full volume imaging. Typical quad view showing multi-plane reconstruction images in a patient with posterior middle segment (P2) prolapse/flail. The *en face* left atrial view is obtained from a single beat full volume

acquisition. This technology can be very useful compared to standard 4 beat acquisitions, particularly in patients with frequent irregular ectopic beats or atrial fibrillation, where significant ‘stitching’ artefacts can affect image quality

Echocardiography allows the mechanism of secondary MR (ischaemic versus non-ischaemic) to be determined. TOE allows for improved quantitation using 3D colour techniques (3D vena contracta area) as the regurgitant orifice is usually wider and more crescentic in shape in functional compared to primary MR. Differences in MR aetiology may also lead to differences in mitral leaflet orientation with symmetric or asymmetric leaflet tethering [6].

Some pre-operative echocardiographic parameters have been proposed that may impact on the likely success of surgical repair. These include leaflet systolic tenting area >2.5 – 3.0 cm², a posterior leaflet angle $>45^\circ$ (indicating a high posterior leaflet restriction), coaptation depth >1 cm, complex jets amongst others [7].

Examples of 3D images in chronic secondary MR:

1. *Annular dilatation/Non-ischaemic cardiomyopathy*: see Fig. 42.16a–d

Changes in mitral annular size from either left atrial or left ventricular dilatation leads to malcoaptation of the mitral leaflets and a central MR jet (Fig. 42.16a). The MR jet is usually wide and positioned across the central scallops (Fig. 42.16b). The colour Doppler jet may appear narrower in the anterior-posterior projection (Fig. 42.16a) (TOE mid-oesophageal 0° and 135°) but the medial-lateral/bicommissural view (TOE 70°) (Fig. 42.16b) reveals the true width of the jet across A2-P2 and may sometimes extend out to the medial and lateral segments and both commissures.

The 3D vena contracta area is demonstrated in Fig. 42.16c (bottom left—see blue line posi-

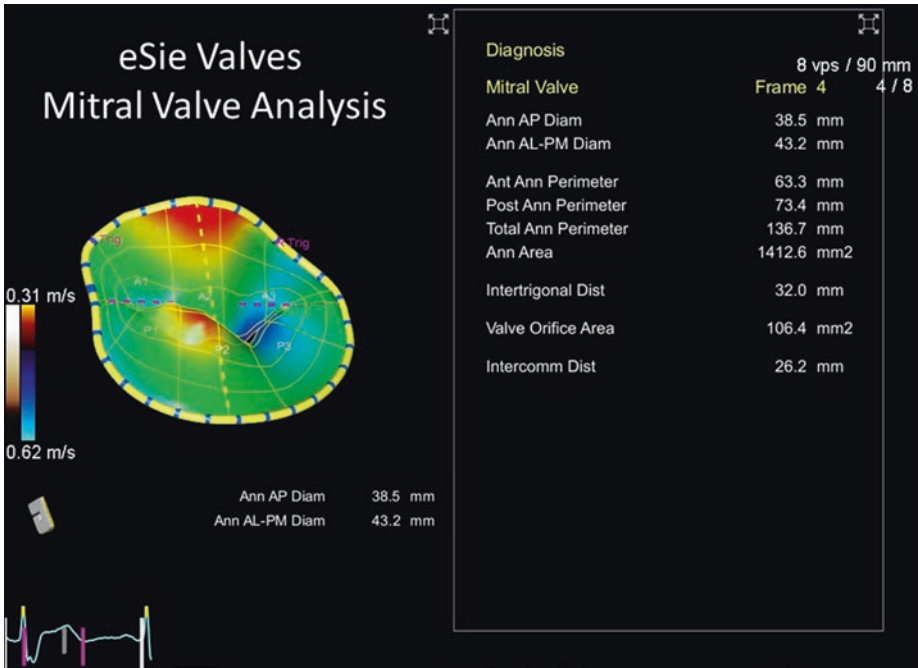


Fig. 42.14 eSie Valves™ mitral modelling. Siemens *eSie Valves* is an algorithm used for automated mitral valve analysis. The left panel shows the modelling for

mitral valve prolapse affecting the lateral and middle posterior segments (P1 and P2). Annular dimensions are listed on the right panel similar to other vendor systems

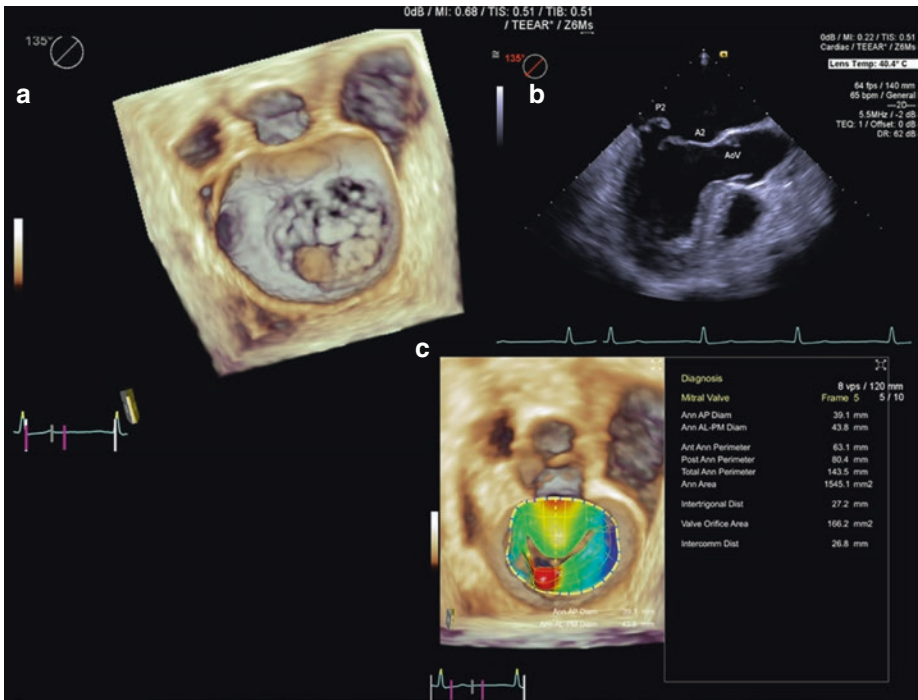


Fig. 42.15 2D, 3D and eSie Valve assessment of posterior leaflet prolapse. (a) 3D left atrial view demonstrating P2 prolapse (b) 2D LVOT view and (c) eSie Valve ana-

tomical model superimposed on 3D mitral valve image for enhanced visual representation of the mitral valve pathology

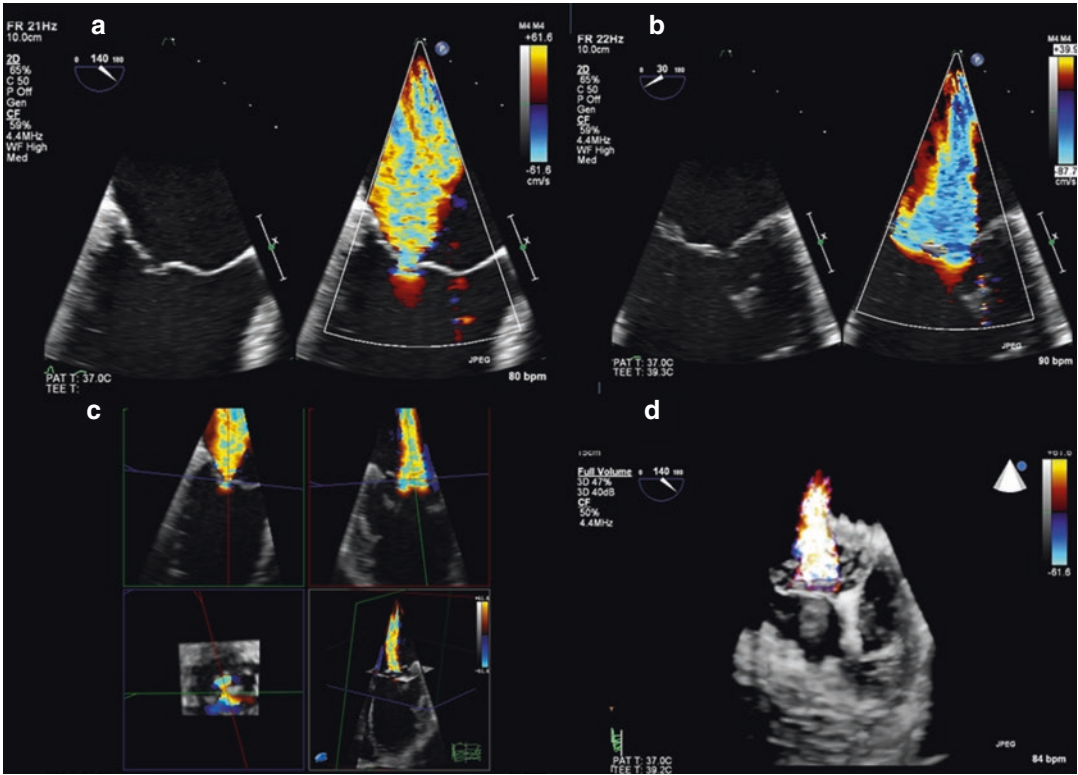


Fig. 42.16 Functional mitral regurgitation (non-ischaemic). (a) TOE 2D LVOT view with central MR arising at A2-P2. The MR jet appears narrow at the point of malcoaptation (b) TOE medial-lateral view showing true

width of MR jet (c) 3D colour multi-plane—3D vena contracta area is seen in the bottom left panel (blue plane) and (d) 3D full volume colour acquisition still image showing the wide central MR jet

tioned at the MR vena contracta itself). The shape of the orifice is typically a crescent and not circular. Full volume colour acquisitions (Fig. 42.16d) may also be helpful in visually interpreting the size of the colour jet. Eccentric jets are also possible depending on the resulting mitral leaflet orientation and angle of malcoaptation.

Mitral valve models (Fig. 42.17) can also be used for illustrating the valve tethering (coded blue below the level of the annulus) and for mitral annular dimensions. Annular dilatation is present when the ratio annulus/anterior leaflet is >1.3 or when the diameter is >35 mm. The presence and extent of annular calcification is an important parameter to describe.

2. Functional-ischaemic MR: see Figs. 42.18 and 42.19

Frequently, there is asymmetric tethering due to restriction of the posterior leaflet. Figure 42.18a illustrates a case of chronic severe functional-ischaemic MR with more extreme leaflet tethering (Fig. 42.18b) and a large tenting area (Fig. 42.18c—below the white line). The anterior leaflet overrides the posterior leaflet resulting in an eccentric posteriorly directed MR jet. The MR jet is wide across the central scallops. However, the jet direction can vary depending on wall motion abnormalities and how remodelling of the left ventricle affects mitral leaflet orientation. A more central jet in ischaemic MR is illustrated in Fig. 42.19.

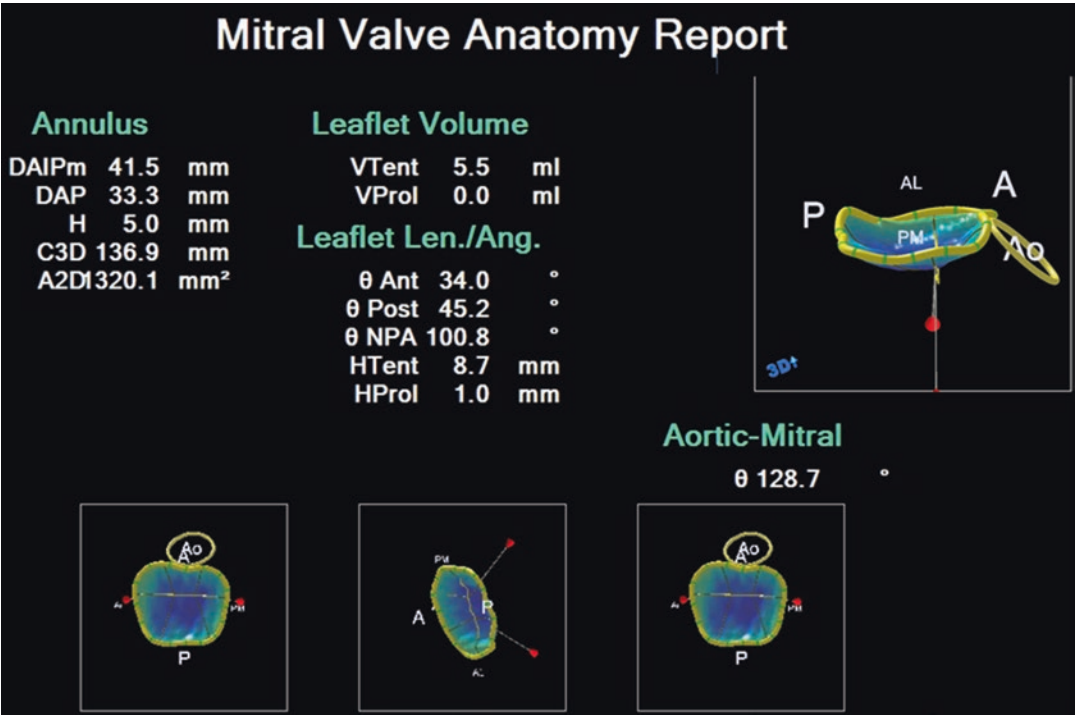


Fig. 42.17 Mitral Valve Anatomic Model—Functional MR. Leaflets coded blue when positioned below the level of the mitral annulus. The specific mitral annular mea-

surements are listed in the top left panel. See Fig. 42.11 legend for abbreviations

Tricuspid Valve and Annulus Assessment

A comprehensive pre-operative assessment should also include an evaluation of tricuspid regurgitation and tricuspid annular dilatation. The TR grade and pulmonary systolic pressure are best assessed by transthoracic echo. The tricuspid annulus can be measured in the apical four chamber view using 2D imaging as recommended in the ACC/AHA 2014 Valvular Heart Disease Guidelines [8]. The annulus can also be measured during TOE examination from a longitudinal mid-oesophageal long axis view at 0°.

The normal tricuspid valve annulus diameter in adults is 28 ± 5 mm in the four chamber view. Significant tricuspid annular dilatation is defined by a diastolic diameter of >21 mm/m².

Surgical intervention with tricuspid annuloplasty is usually recommended for an annulus ≥40 mm [8].

(B) Trans-Catheter Mitral Valve Repair

High risk or very elderly patients with primary mitral valve (MV) disease and those with secondary MR and poor left ventricular function can be treated with MitraClip [9]. A detailed description of the role of echo during other trans-catheter techniques for mitral valve repair such as NeoChord for primary MR and direct and indirect annuloplasty devices for secondary MR is beyond the scope of this chapter.

Echocardiography plays an important role in (1) patient selection, (2) peri-procedural guid-

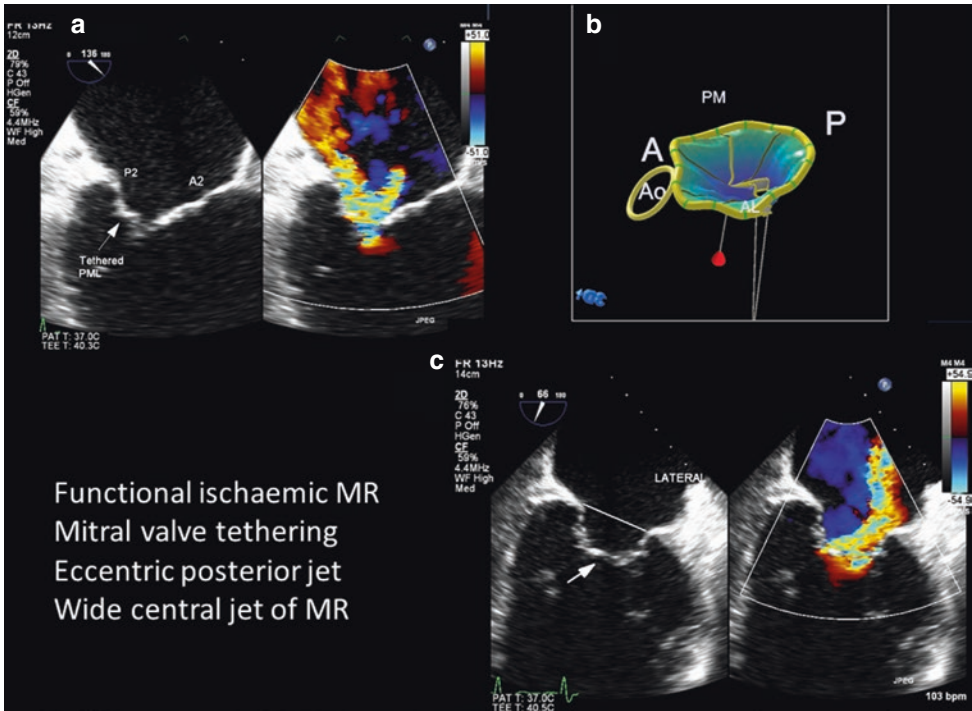


Fig. 42.18 Leaflet tethering in chronic functional-ischaemic MR—assymmetric. (a) Tethered posterior leaflet due to inferior wall akinesis and malcoaptation of the anterior leaflet resulting in an eccentric posterior MR jet (b) mitral valve model with pronounced tenting and a central regurgitant orifice (c) large tenting area (below white line). Wide central jet seen on colour Doppler in the bicommissural projection

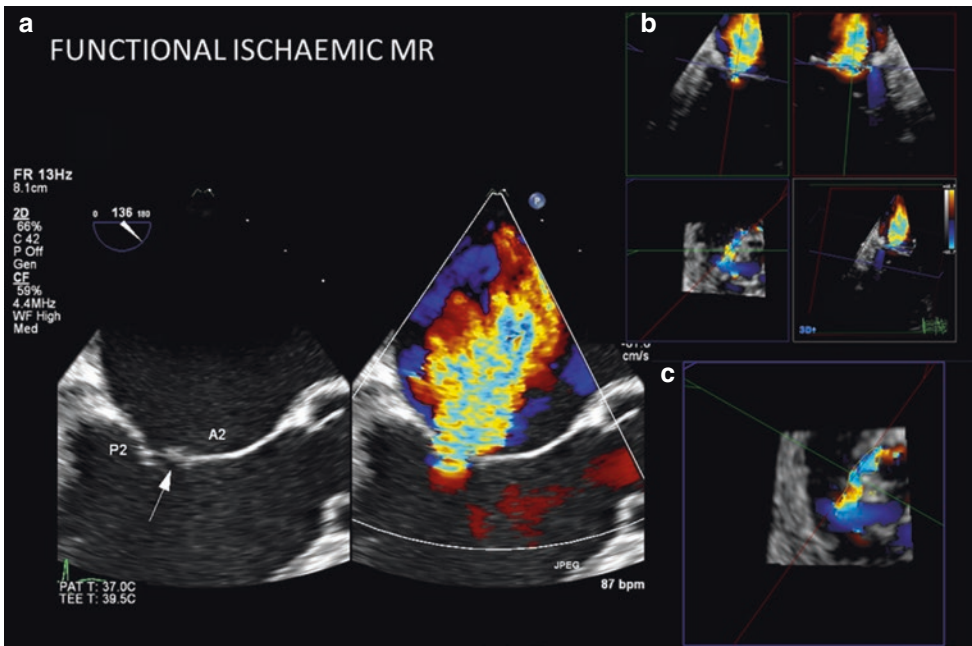


Fig. 42.19 Functional ischaemic MR—central jets. (a) 2D TOE case example of central MR jet in LVOT view. (b) mitral regurgitant orifice is wide and crescentic in appearance. (c) 3D vena contracta

ance and acute outcome in MR reduction, and (3) ongoing MR surveillance and left ventricular remodelling at follow-up.

Edge-to-Edge Mitral Repair Using MitraClip

Percutaneous edge-to-edge repair using MitraClip (Fig. 42.20) is the most commonly used technique with the largest worldwide experience (over 40,000 implants). MitraClip has the advantage that it can be used in both primary and secondary MR.

The MitraClip device (Abbott Vascular, Menlo Park, CA) replicates the surgical Alfieri double orifice, stitch repair [10] whereby the mitral leaflets are sutured together to keep the two valve leaflets more closely opposed during systole, so reducing regurgitation. The device, a 4 mm wide polyester coated cobalt chromium clip, is delivered to the valve via the femoral vein and a transseptal puncture and “clips” the leaflets together over a limited area (Fig. 42.21). The procedure is conventionally performed under a general anaesthetic to allow transoesophageal echocardiographic guidance and

there is no need for a sternotomy or cardiopulmonary bypass.

Indications

Selection Criteria for Optimal Results

Patient selection needs to be on an individual basis and should be undertaken by a Mitral Valve Heart Team; comprising mitral surgeons, interventionists, and imagers. The decision regarding suitability for percutaneous repair should follow the European Guidelines [9] and established clinical trials/registries [11–13] and will be based on:

- (1) Symptoms
- (2) Surgical risk
- (3) Cause and severity of mitral regurgitation
- (4) Anatomical suitability
- (5) Left ventricular function

Anatomic Considerations

The Mitraclip procedure is an echo guided procedure and careful evaluation of the valve anatomy as well as the mechanism and quantitative assessment of severity of regurgitation is mandatory using both transthoracic and 2/3D transoesopha-

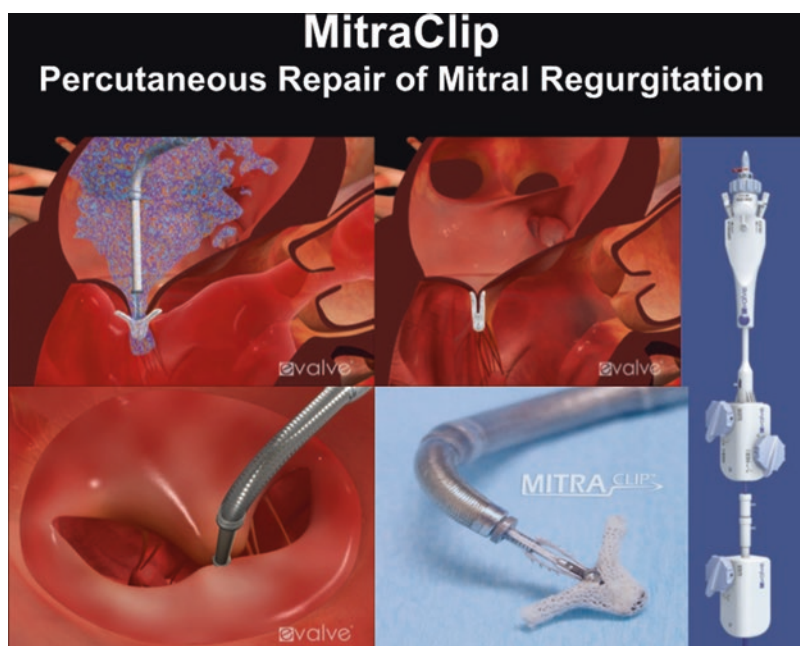


Fig. 42.20 Edge-to-edge mitral valve repair using MitraClip device (Abbott Vascular)

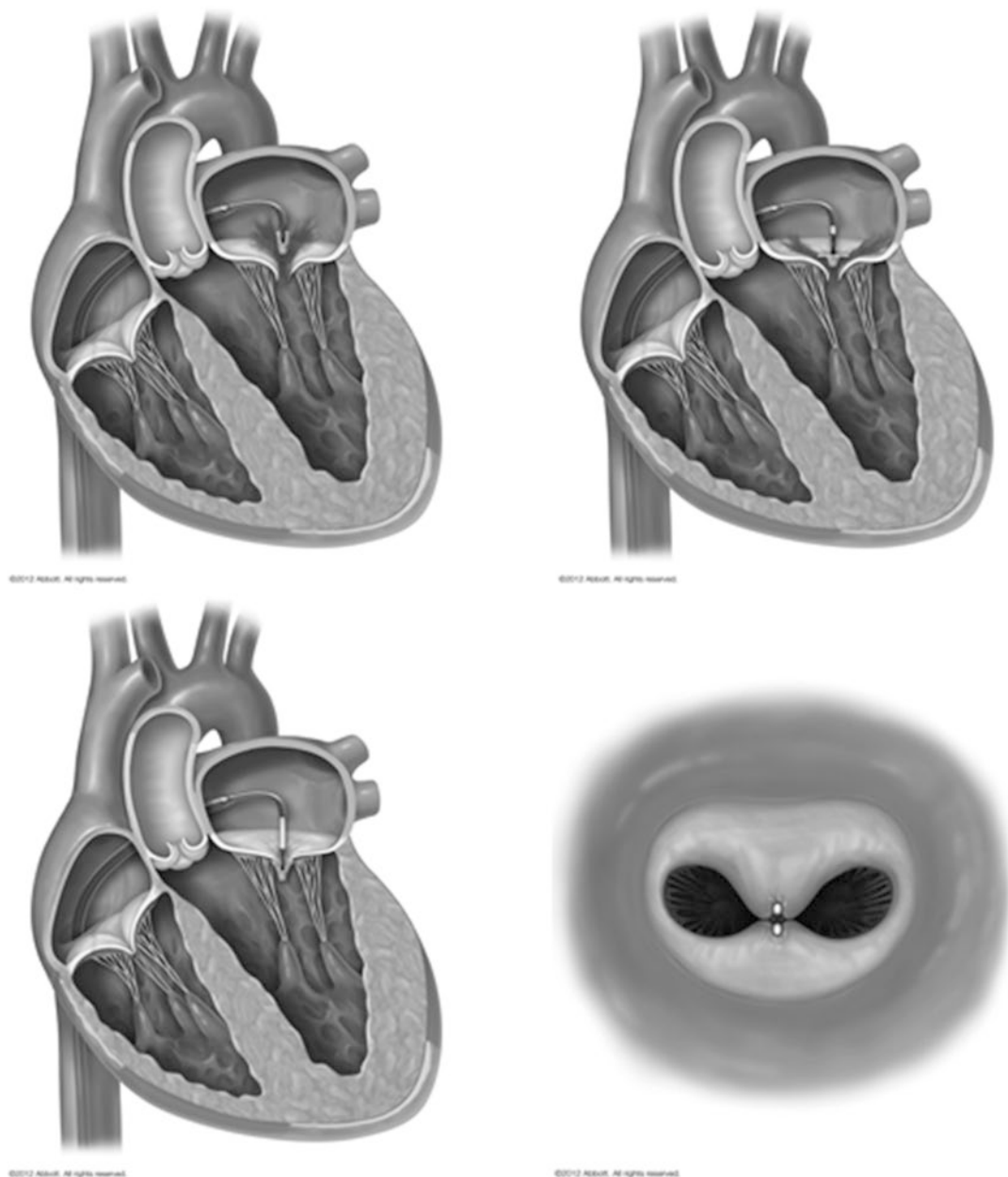


Fig. 42.21 MitraClip double orifice replicating the surgical Alfieri stitch repair. MitraClip is performed from right femoral vein access using a trans-septal approach under TOE guidance

geal echocardiography. The application of 3D techniques and models that provide the equivalent of a surgical left atrial view, can help in the pre-procedure assessment to better define the mitral pathology in the same way as already discussed and illustrated above for patients being considered for surgical repair.

In primary MR a number of criteria, largely taken from the EVEREST II study [11], are indicative of a likely optimum outcome (Fig. 42.22, Table 42.1). These are based on some simple principles; a valve large enough not to become stenosed following clipping, the absence of a cleft(s), the absence of leaflet thickening/calcification

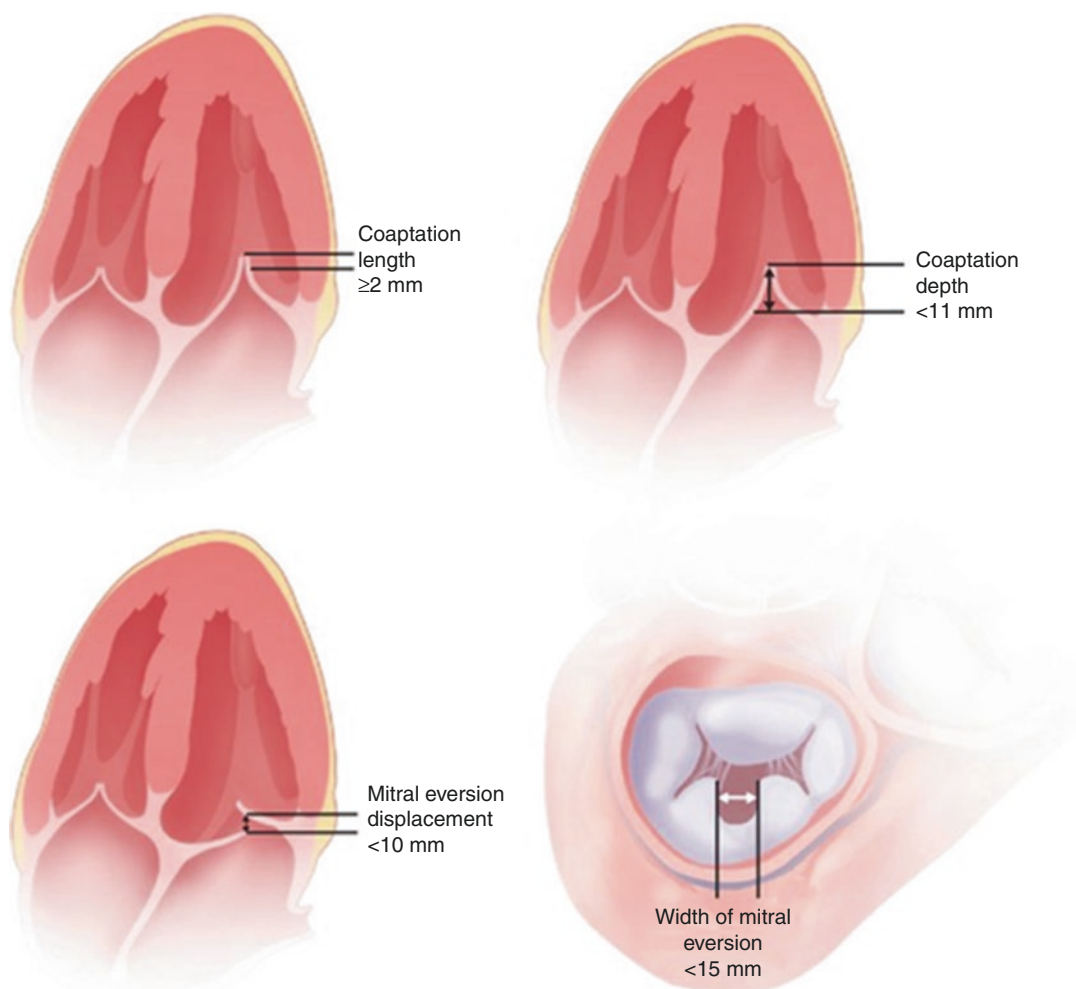


Fig. 42.22 MitraClip selection criteria. Top panel—functional (secondary) MR. Bottom panel—degenerative (primary) MR

which would prevent clip closure and leaflets that are thin enough, long enough and close enough to be grasped by a clip with arms of 9 mm in length. Optimal anatomy is focused on a central A2-P2 regurgitant orifice that is not too wide (Fig. 42.23). In the case of primary MR due to leaflet prolapse or flail, the width or extent of the affected segments can have a significant bearing on acute procedural success and longer-term durability of repair. Residual areas of prolapsing leaflet may lead to progression of MR over time. All the disease should be covered and engaged by the clip or clips. Excessive flail height (>10 mm) or a lack of secondary chordal support can also make grasping the leaflets extremely challenging. This is not to

say that patients with more challenging anatomy have not been treated by the technique, though success rates inevitably fall with increasingly complex valve disease.

Secondary MR is proving to be an expanding area for the use of the Mitraclip, driven in part by the lack of success of conventional surgical techniques. Some features applicable to primary MR will be important in patient selection including the presence of clefts and a small mitral orifice. However, more often the issue is one of (a) the width of the MR jet, (b) the coaptation length where there is leaflet malapposition due to posterior leaflet tethering and override of the anterior leaflet (c) an actual coaptation gap where the leaf-

Table 42.1 Selection criteria for MitraClip according to mitral valve anatomy [20]

Optimal valve morphology	Conditionally suitable valve morphology	Unsuitable valve morphology
Central pathology in segment 2	Pathology in segment 1 or 3	Perforated mitral valve leaflet or cleft
No leaflet calcification	Mild calcification outside of the grip-zone of the clip system: ring calcification, post annuloplasty	Severe calcification in the grip-zone
Mitral valve opening area >4 cm ²	Mitral valve opening area >3 cm ² with good residual mobility	Haemodynamically significant mitral stenosis (valve opening area <3 cm ² , MPG >5 mmHg)
Mobile length of the posterior leaflet ≥10 mm	Mobile length of the posterior leaflet 7 mm to <10 mm	Mobile length of the posterior leaflet <7 mm
Coaptation depth <11 mm	Coaptation depth ≥11 mm	
Normal leaflet strength and mobility	Leaflet restriction in systole (Carpentier IIIB)	Rheumatic leaflet thickening and restriction in systole and diastole (Carpentier IIIA)
Flail width <15 mm Flail gap <10 mm	Flail width >15 mm only with a large ring width and the option for multiple clips	Barlow’s syndrome with multisegment flail leaflets

Morphological suitability criteria for the MitraClip intervention; modified according to the Everest criteria and the Crossroads training experiences on patient selection. ‘Optimal morphology’ is well-suited for implantation, ‘conditionally suitable valve morphology’ should be preferably treated in experienced centres and ‘unsuitable valve morphology’ is contraindicated to therapy. The PMR with flail leaflet is determined in the intercommissural 2-chamber view; the flail gap is determined in the long axis view as the distance of the end of the flail leaflets in the LA to the opposite-lying leaflet
MPG mean pressure gradient, *PMR* primary mitral regurgitation, *LA* left atrium

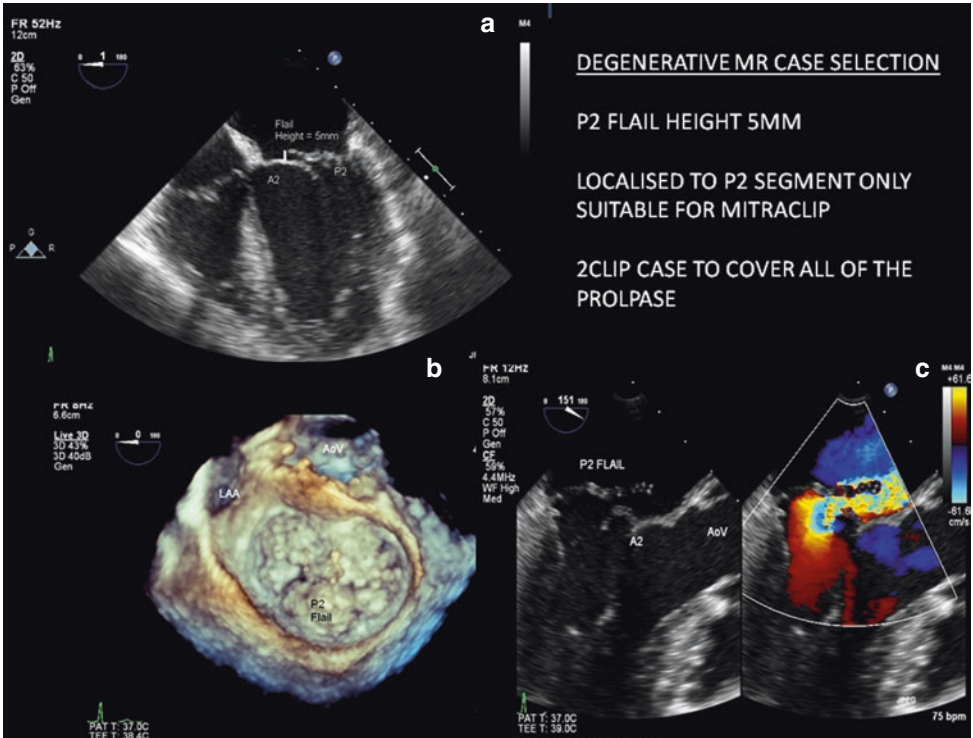


Fig. 42.23 MitraClip case selection in primary MR (EVEREST II criteria). **(a)** Flail height (vertical distance from opposite leaflet) <10 mm **(b)** Prolapse is localised to the middle (P2) segment only—ideally width of affected tissue <15 mm. One or two central clips can be used to

cover / enclose ALL of the prolapsing segment to prevent recurrence of MR **(c)** Leaflets are not excessively thickened or calcified with good potential for grasping. There is good secondary chordal support

lets do not meet at all (d) the tenting height that reflects the extent of leaflet tethering from left ventricular dilatation and (e) any under curling of the posterior leaflet resulting in restriction of mobility and often shortening of the leaflet length available for grasping. In particular, care must be taken to recognize where the leaflet ends and where a taught primary chord begins. An example of suitable anatomy in functional MR is shown in Fig. 42.24.

Indicators of Success

Primary MR

- Flail height /gap <10 mm
- Flail width <15 mm
- Absence of leaflet cleft in grasping area
- Mitral valve area >4 cm²
- Absence of leaflet thickening and/or calcification
- Posterior leaflet length ≥10 mm

Secondary MR:

- Absence of leaflet cleft in grasping area
- Mitral valve area >4 cm²
- Absence of leaflet thickening and/or calcification
- Posterior leaflet length ≥10 mm
- Coaptation length ≥2 mm
- Tenting height /coaptation depth <11 mm

Role of Echocardiography During the MitraClip Procedure

The Mitraclip procedure is a transoesophageal echo-guided technique and is conventionally performed under a general anaesthetic. Although not mandatory, the availability of live 3D echo imaging is advantageous.

Useful TOE views.

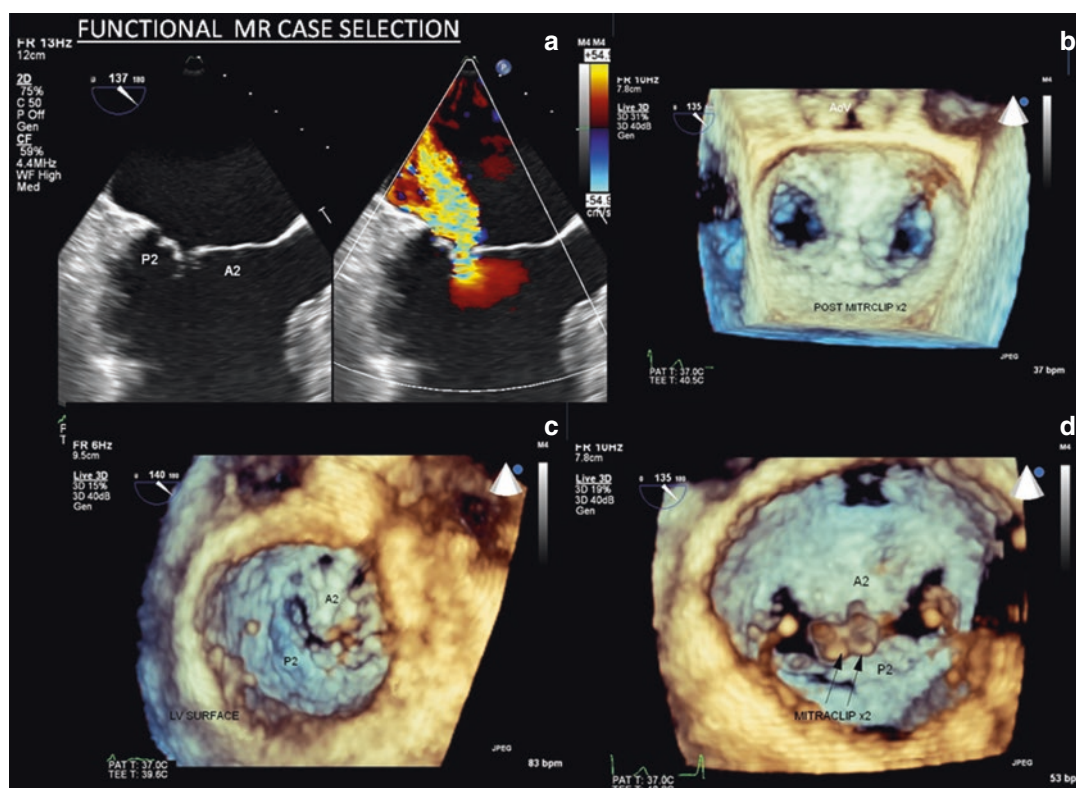


Fig. 42.24 MitraClip case selection in secondary MR (EVEREST II criteria). (a) 2D TOE LVOT view showing structurally normal leaflets with a central coaptation defect. The coaptation length is ≥2 mm and coaptation depth <11 mm (b) 3D mitral view from left ventricle

showing central defect at A2-P2 (c) Successful MitraClip deployment with 2 central clips required to achieve adequate reduction in MR grade. Image shows clips from the left atrial projection and (d) from the left ventricular projection

1. Mid-oesophageal short axis (45–60°) and bicaval (90–110°)
2. Long axis view (135°)
3. Bicommisural view (55–70°)
4. Surgical *en face* 3D LA view

Transoesophageal Echo-Guided Transseptal Puncture

This is a crucial initial part of the MitraClip procedure, the aim being to cross the interatrial septum superiorly and posteriorly, thus allowing a perpendicular approach to the mitral valve.

Our approach is to use a Cooke SLO catheter consisting of a sheath and dilator with a Brokenbrough XS (extra sharp) transseptal needle.

Following a right femoral vein puncture, the SLO catheter is placed in the superior vena cava over a guidewire. Many operators give a small initial dose of heparin at this stage (e.g. 2,500U) to prevent wire/catheter associated thrombus formation. The wire is then removed and the transseptal needle advanced to approximately 1 cm from the tip of the dilator. Under ultrasound and radiographic control, the sheath and needle are withdrawn into the right atrium facing the tip of the catheter towards the septum. This will usually see the transseptal needle's arrow facing between 4 and 7 o'clock, generally the more clockwise the larger the left atrium. The transseptal catheter assembly will be seen to make two movements as it is withdrawn inferiorly first over the aorta and then into the fossa ovalis.

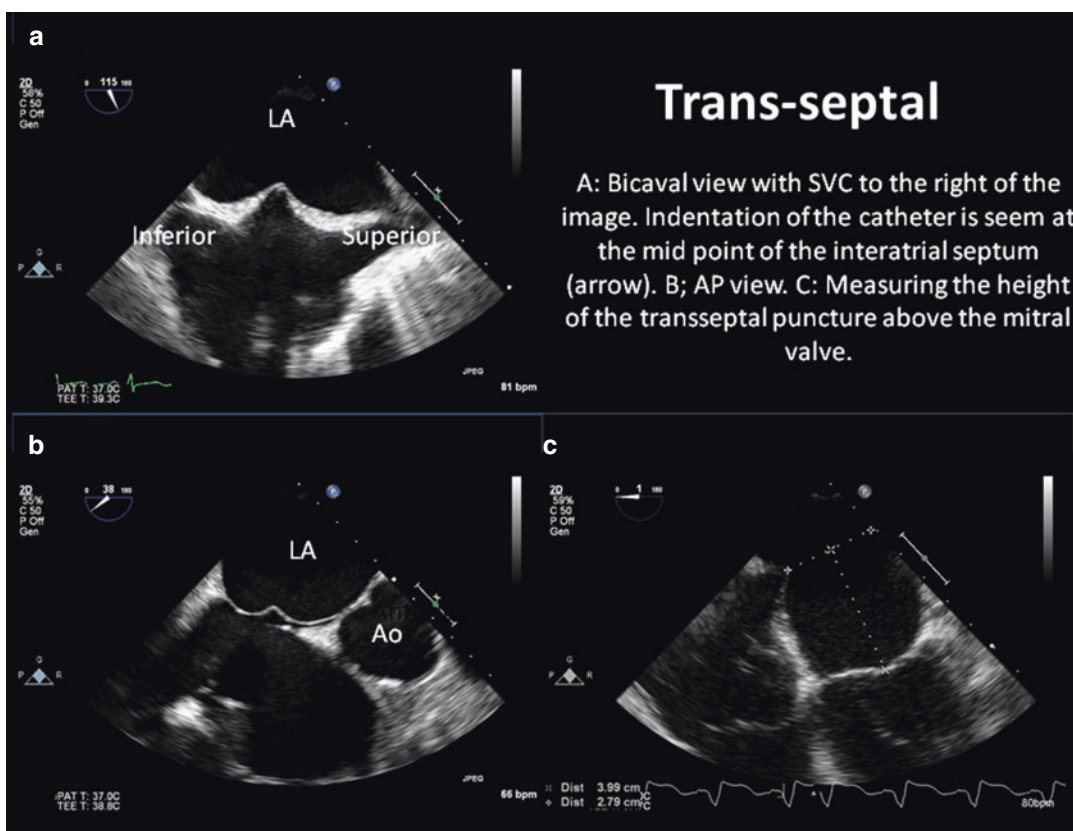


Fig. 42.25 TOE guided trans-septal puncture. Bicaval view (a) with superior vena cava (superior) to the right of the image and inferior vena cava (inferior) to the left. Indentation of the transseptal catheter is seen at the mid point of the interatrial septum. The anteroposterior (AP)

view (b) demonstrates the aorta (Ao) located anteriorly on the right and posterior septum to the left. The catheter indentation is clearly seen in the middle of the atrial septum. The height of the transseptal puncture site is measured in the 4 chamber view (c)

The passage of the catheter is followed on TOE in the 90° view until indentation of the superior portion of the septum is identified (Fig. 42.25a). The anterior-posterior position of the catheter is confirmed in a 30° view (Fig. 42.25b). The catheter can be manipulated anteriorly—anticlockwise rotation or posteriorly—clockwise rotation.

The distance from the intended puncture site to the valve is measured in a 0° view aiming to cross the septum 3.5–4 cm from the mitral annulus (Fig. 42.25c). Where there is significant leaflet prolapse a higher puncture may be helpful (up to 5 cm). Conversely, where there is significant leaflet tethering, a lower puncture may be advantageous. The catheter is manipulated anteriorly and/or inferiorly to come closer to the valve.

The septal puncture is performed by advancing the needle out of the SLO catheter and across the septum under haemodynamic monitoring. Once crossed, the dilator and sheath are passed into the left atrium (LA) keeping the needle fixed in position. Heparin is administered to maintain an activated clotting time (ACT) >250 s. The needle and dilator are removed and the sheath directed towards the left upper pulmonary vein (LUPV). The sheath is then used to place an Amplatz super stiff guidewire into the LUPV using TOE to remain clear of the left atrial appendage.

The sheath is then withdrawn and the femoral access site dilated with an 18F dilator, taking care not to displace the wire from its position in the LUPV at all times.

Positioning of the Steerable Guiding Catheter

The 24F MitraClip steerable guide catheter is advanced over the wire into the right atrium. Septal crossing is achieved with continuous forward pressure and gentle rotation as required. Once the guide catheter is across the septum, the catheter is placed in the stabilizer and the dilator removed into the catheter.

Once prepared, the clip delivery system (CDS) is keyed (blue on blue) into the guide and is advanced through the guide and so into the left atrium.

Advancing and Steering the CDS

The clip is then directed towards the mitral valve using medial torque (clockwise rotation of the medial ‘M’ knob) and posterior rotation of the guide catheter. This is often easiest to do under 3D TOE control (Fig. 42.26). Once in line with the valve, the clip is translated backwards and forwards using the clip handle to remove stored torque and assess the direction of clip travel. This should be towards the apex of the left ventricle and can be assessed both radiographically and on echo.

The clip position can be manipulated in the anterior-posterior plane using counterclockwise and clockwise rotation of the guide catheter respectively. Medial and lateral movement is made using the medial ‘M’ knob of the CDS.

Correct Positioning and Trajectory Above the MV Regurgitant Orifice Along with the Orientation of Clip Arms

The antero-posterior orientation of the clip relative to the valve is seen in the left ventricular outflow tract view (LVOT, 135°) view (Fig. 42.27a) and the medial-lateral orientation assessed in a bi-commissural (60–70°) view (Fig. 42.27b). In general, the aim is to initially position the clip at the zone of maximal flow convergence of the mitral regurgitation.

Orientation of Clip Arms

The clip is then unlocked and opened to 180° and the grippers raised. The clip arms are then rotated to be perpendicular to the line of coaptation. This is often best seen using live 3D imaging (Fig. 42.27—LA surface view) and when placing the clip at A2-P2, will mean the arms are of equal length when seen in the LVOT view. Conversely, the arms are not seen in the bi-commissural view.

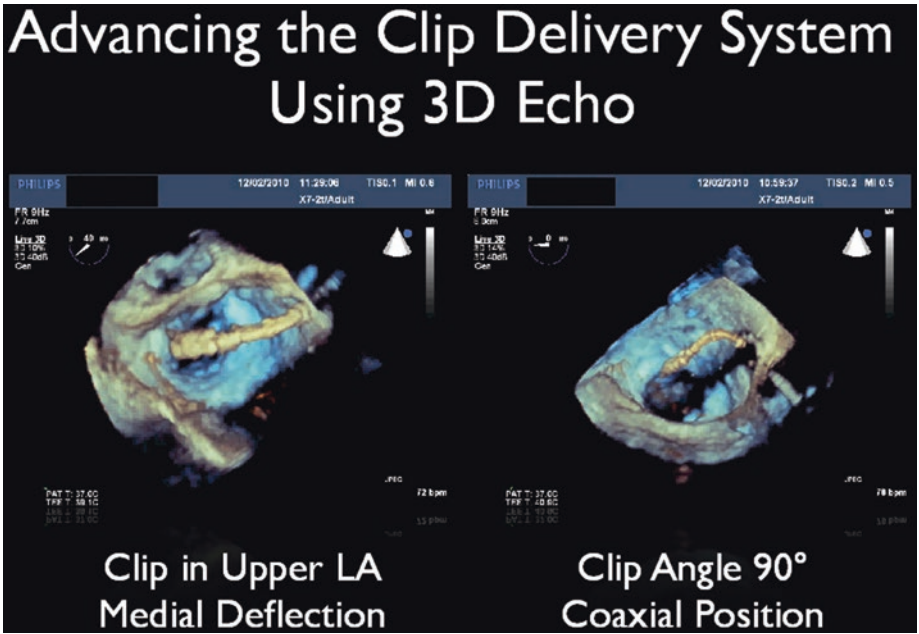


Fig. 42.26 3D TOE guidance of steerable guide and clip delivery system. Posterior guide rotation and medial deflection (clockwise turning of the ‘M’ knob) of the clip

delivery system advances the clip towards the mitral valve aiming for a central coaxial position with a clip angle of 90° above the MR jet

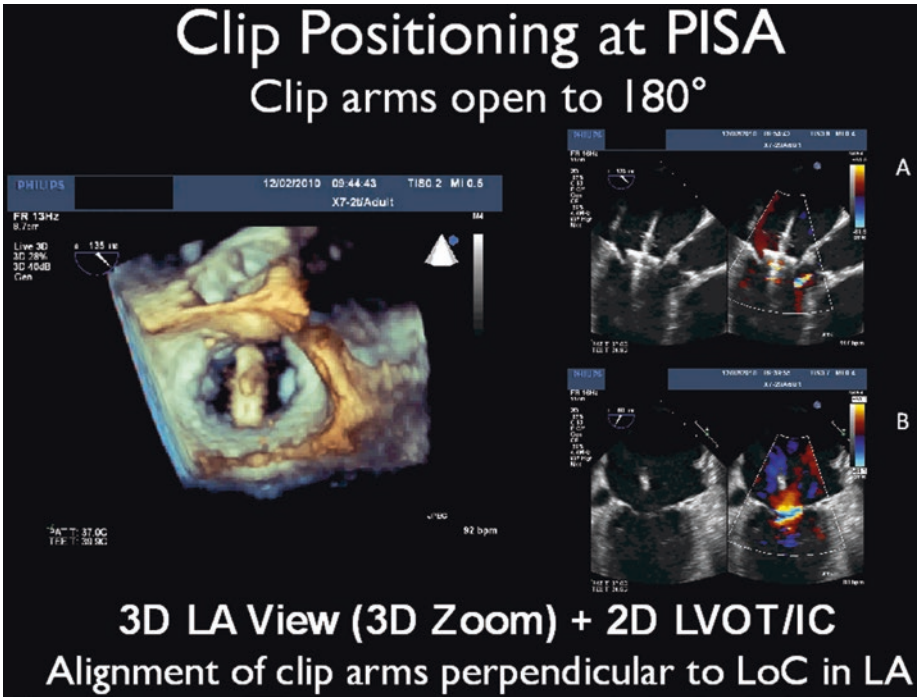


Fig. 42.27 Positioning of the MitraClip with alignment of the clip arms perpendicular to the line of coaptation (LoC). Left panel—3D zoom left atrial view with clip arms open to 180°. Clip arms seen at 12 o’clock and 6

o’clock. Right panel—2D imaging required for perception of height from the valve. Both clip arms should be of equal length in the LVOT view (if correctly aligned) and not seen in the inter- or bi-commissural (IC) 60–70° view

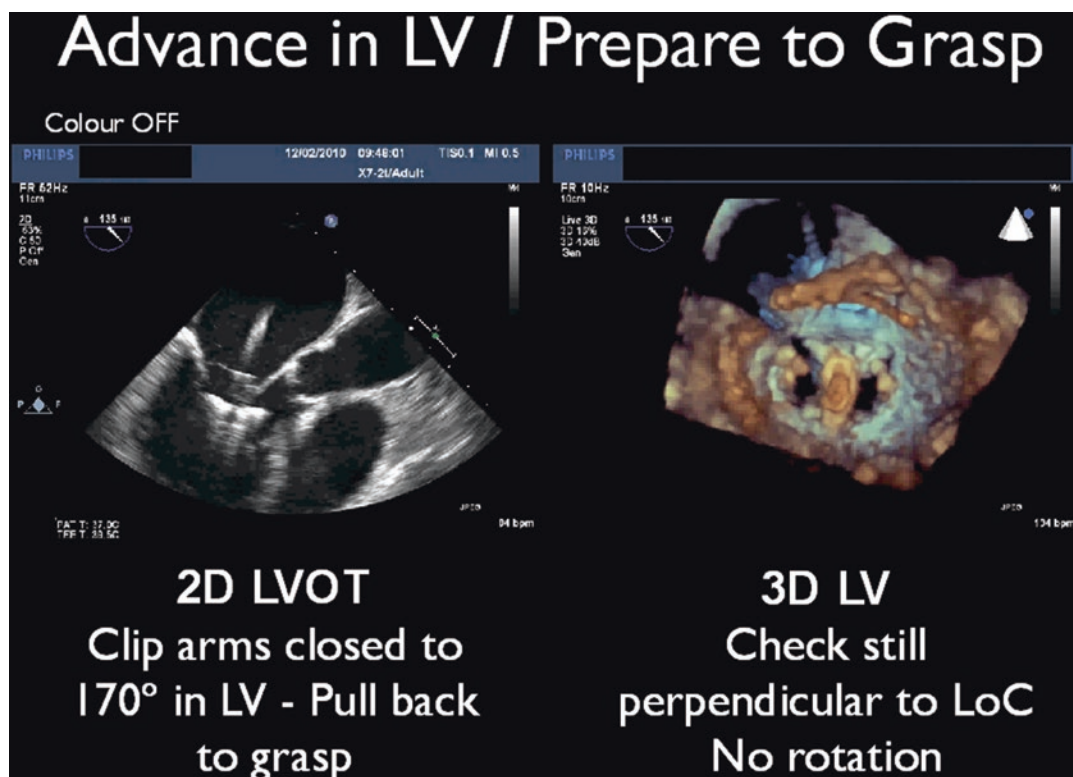


Fig. 42.28 Advancing the MitraClip into the left ventricle. Left panel—both clip arms should remain of equal length in the LVOT projection otherwise the clip may have rotated due to stored torque. If rotation occurs, the clip arms will no longer be perpendicular to

the line of coaptation and thus incorrectly orientated for grasping. Left panel—3D zoom left ventricular (LV) surface imaging can help to check orientation in the LV

Entry into the LV and Leaflet Grasp

The clip is then advanced smoothly into the LV so it is positioned below the valve leaflets (Fig. 42.28). Careful rotation of the clip handle can be made to correct any displacement though care must be taken to avoid entanglement with the subvalvular apparatus, especially if working towards either commissure.

The clip is closed to 120° and withdrawn slowly whilst observing the leaflets and their position within the clip arms in the LVOT view. Once both leaflets are in position the grippers are dropped securing the leaflets and the clip closed to 60° (Fig. 42.29). Failure to capture both leaflets is frequently due to rotation of the clip so the arms are no longer perpendicular to the leaflet edges or if the clip is being withdrawn at a disadvantageous angle.

Assessing the Acute Result and Clip Deployment

Verification of satisfactory leaflet grasp is assessed echocardiographically by observation of:

- Length of leaflet insertion at the moment of gripper deployment
- Leaflet immobilization and absence of leaflet lift
- Limited leaflet mobility relative to the tips of both clip arms
- Adequate MR reduction

If the clip position proves to be unsatisfactory then the clip can be opened, inverted, the grippers raised and the clip withdrawn carefully back into the left atrium.

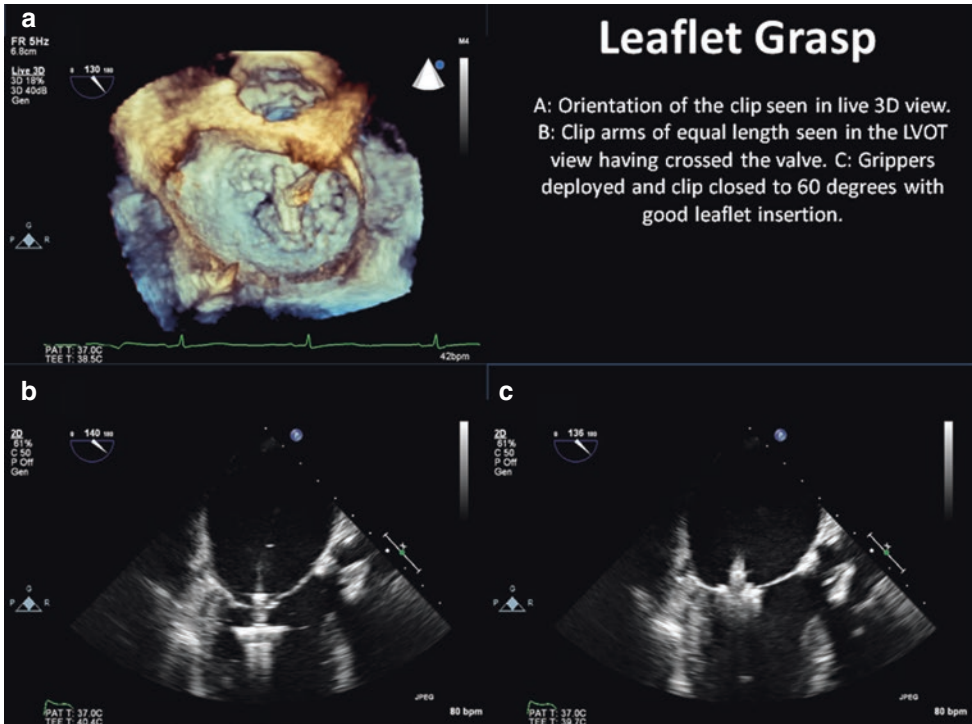


Fig. 42.29 2D and 3D echo guidance for leaflet grasping

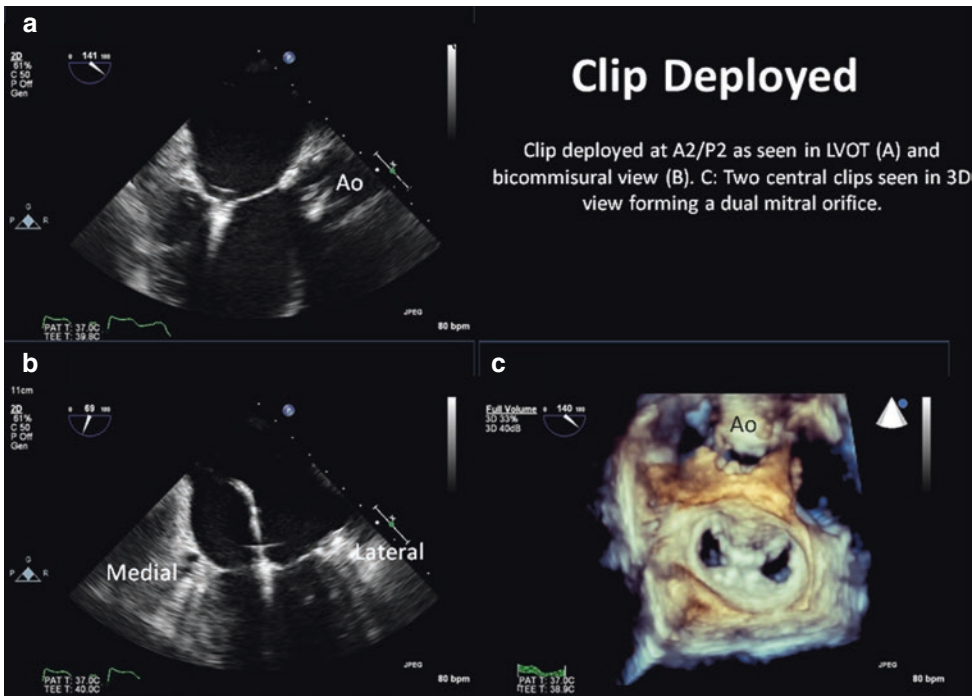


Fig. 42.30 MitraClip deployment and final clip release

Once a satisfactory clip position has been achieved (Fig. 42.30), the clip is fully closed and deployed as per the instructions for use.

Following clip deployment the degree of residual MR and mitral valve area/transmitral gradient are assessed.

Further clip(s) can be deployed for residual MR or to ensure anatomical coverage of the prolapse/flail segment in primary MR where the aim should be for a surgical quality result. Crossing the valve should now be performed with the clip closed to prevent displacement or damage to the clipped valve. Further clip deployment should not occur in the presence of iatrogenic mitral stenosis (mean mitral gradient >5 mmHg or mitral valve area by planimetry of <1.5 cm²). The final deployment can be well visualised using the LA surface 3D TOE view (Fig. 42.30c).

Assessment of Residual Mitral Regurgitation

The echocardiographic assessment of residual MR is not straightforward post clip implantation and can be challenging. Quantitative assessment using the PISA method has not been validated in the presence of multiple jets of MR, which are not infrequent and can be very eccentric. Equally, standard quantitative techniques are not validated in Alfieri-type double orifice valves. Furthermore, the assessment takes place under general anaesthetic with altered loading conditions, which will affect the degree of MR visualised on colour Doppler.

With these pitfalls in mind, the simplest approach remains the measurement of MR jet area relative to the left atrial area (MRJA/LAA) pre and post-clip implantation but this will be affected by changes in jet direction and multiple jets.

The MR grading parameters used by the Echo Core Lab in the EVEREST Trials (Table 42.2) [14] included (1) colour flow Doppler jet area, (2) pulmonary venous flow pattern, (3) regurgitant volume (RVol) and (4) regurgitant fraction (RF). It must be remembered that the RVol and RF values for grading MR in this study apply specifically for primary MR. Secondary MR cut off values for ERO and RF are quoted to be half of those stated for primary MR [15].

Beyond the change in size of the jet on colour flow mapping, our approach has been to pay particular attention to jets that have a significant zone of flow convergence (PISA) below the mitral valve leaflets or are associated with residual areas of prolapse or anatomical defects seen on 2D/3D imaging.

Full volume 3D colour acquisitions, where technically feasible, can be helpful in assessing the location and significance of residual MR jets. Using multiplane 3D reconstruction (MPR) software on the Philips iE33 or EPIQ echo machine, residual jets can be interrogated to determine their vena contracta area and thus effective regurgitant orifice (ERO) and MR regurgitant volume (RVol = ERO × MR VTI), although this can be time intensive and problems arise with stitching

Table 42.2 Mitral regurgitation grade criteria

Variable	Mild (1+)	Moderate (2+)	Moderate to Severe (3+)	Severe (4+)
Colour flow Doppler jet area	Small central <4 cm ² or <10% of LA area	Moderate central 4–6 cm ² or 10%–30% of LA area	Large central >6 to <8 cm ² or >30% to <40% of LA area or eccentric to first PV	Large central >8 cm ² or >40% of LA area or eccentric to second PV
Pulmonary vein flow	Systolic dominant	Diastolic dominant	All diastolic	Systolic reversal
Regurgitant volume (ml)	<30	30–44	45–59	≥60
Regurgitant fraction (%)	<30%	30–39%	40–49%	≥50%

From: Foster E et al. Am J Cardiol. 2007;100:1577–83

Data based on American Society of Echocardiography published guidelines for the quantitation of native valvular regurgitation that have not been previously applied in a therapeutic trial

LA left atrial, PV pulmonary vein

artefact due to irregular rhythms. The regurgitant fraction can also be calculated but requires additional measurement of the aortic outflow stroke volume. Use of 3D PISA [16, 17] and automated 3D PISA algorithms using single beat 3D acquisitions may also provide another useful method to assess residual MR but this technique remains to be validated in future studies.

Mitral Stenosis

Although isolated reports of mitral stenosis have been made [18], long term follow up data confirms that the technique does not lead to the development of mitral stenosis [12]. This is providing the initial mitral valve area is adequate and meets the appropriate selection criteria. It is very important to adequately measure the mitral valve area at the screening TOE, even in patients without any obvious commissural fusion. This is particularly relevant in smaller women or where there is primary leaflet disease other than myxomatous/floppy valves. There is no validated gold standard on how to measure mitral valve area pre and post MitraClip, but a number of different methods have been investigated and compared [19].

There is general agreement that clip implantation should be avoided in the presence of a mean transmitral gradient >5 mmHg. The transmitral gradient is easily measured by continuous wave Doppler.

Our practice is to measure both the transmitral gradient by CW Doppler and the maximal MV opening area at the leaflet tips by 3D multi-plane reconstruction (MPR) techniques. 3D MPR allows planimetry of the largest valve opening area. Valve areas close to or below 4 cm^2 will have a much higher chance of developing post clip mitral stenosis (mean gradient >5 mmHg) and may prevent a two clip implantation strategy best suited to wider secondary MR jets or wider prolapsing segments where it is important to cover all the prolapsing tissue for durability of repair.

Complications

Despite the procedural complexity, older age, comorbidity and high-risk of patients referred for Mitraclip, the technique has proven to be safe and

the complication rate remarkably low for such a patient population. The procedural risk for major adverse cardiac events from the published trials and registries is in the region of 1–3%. Possible complications may include:

- Pericardial tamponade
- Transseptal complications to adjacent cardiac structures (although this is unusual with correct TOE guidance)
- Left atrial or appendage perforation
- Mitral valve leaflet tears
- Chordal damage or rupture with progressive MR
- Clip partial detachment
- Clip full detachment and embolization
- Infection
- Larger iatrogenic atrial septal defect due to septal trauma or tear
- Air embolism
- Stroke
- Myocardial infarction
- Major haemorrhage

Summary

In patients with mitral regurgitation, echocardiography is the imaging modality of choice for planning mitral valve repair. It allows a comprehensive analysis of mitral valve anatomy and pathology using a combination of 2D and 3D techniques. The surgeon is now able to have a unique ‘surgical perspective’ on the challenges of any planned repair with the availability of 3D *en face* mitral valve images. Examples of different mitral pathologies in primary and secondary MR have been illustrated. A comprehensive echo assessment should also include the mitral annulus and 3D anatomic models are available that can provide more accurate annular measurements.

Secondary MR poses many challenges for durable mitral repair, both in non-ischaemic and ischaemic aetiologies. Case examples have been used to highlight the differences between these two patient groups along with the importance of accurate MR quantitation and the methods that can be used.

Percutaneous mitral valve repair with MitraClip is an option for selective patients turned down for conventional surgery. There are many challenges remaining in this field but good outcomes can be achieved in both primary and secondary MR using 2D and 3D echocardiography to select patients, guide the procedure, assess acute procedural success and determine longer term durability, left ventricular modelling and any progression of MR during follow-up.

In the future, newer trans-catheter repair devices will provide the much needed alternatives when mitral anatomy is unfavourable for any one device, providing the safety and cost-effectiveness are up to the challenge in an ever expanding area. Echocardiography is likely to remain an essential part of these procedures.

Take Home Messages

- Pre-operative assessment of patients for surgical mitral valve repair requires both comprehensive transthoracic and transoesophageal echocardiography prior to the operating room.
- Two-dimensional imaging is required for anatomic assessment of leaflet morphology, thickness, calcification, tethering, mechanism and quantitation of mitral regurgitation. Adverse features for repair can be identified.
- Three-dimensional left atrial (en face) TOE views are most helpful in confirming the location and extent of leaflet prolapse when planning surgical repair. It provides a quick and easy method to visualise mitral anatomy from the *'surgical perspective as illustrated by the examples presented in this chapter.'*
- Mitral valve anatomic modelling provides a method for more detailed measurement of the mitral annulus.
- The tricuspid valve and annulus should also be fully assessed
- Percutaneous edge-to-edge mitral valve repair using MitraClip is a well established treatment option for anatomically suitable patients turned down for surgical repair. It can be used to treat both primary and secondary MR.
- Echocardiography is key to appropriately selecting suitable patients for MitraClip
- MitraClip is an echo-guided procedure under general anaesthesia and requires a combination of 2D and 3D techniques for each stage of the intervention (trans-septal, clip passage through the left atrium, clip positioning and leaflet grasping). Success depends on good imaging.
- Echo continues to have a key role in the assessment of residual MR and ongoing patient follow-up post repair.

References

1. Omran AS, Woo A, et al. Intraoperative transesophageal echocardiography accurately predicts mitral valve anatomy and suitability for repair. *J Am Soc Echocardiogr.* 2002;15:950–7.
2. Lancellotti P, Moura L, et al. European Association of Echocardiography recommendations for the assessment of valvular regurgitation. Part 2: mitral and tricuspid valve disease. *Eur Heart J Cardiovasc Imaging.* 2010;11(4):307–32.
3. Hyodo E, Iwata S, et al. Direct measurement of multiple vena contracta areas for assessing the severity of mitral regurgitation using real-time 3D TEE. *J Am Coll Cardiol Img.* 2012;5:669–76.
4. Chandra S, Salgo I, et al. Characterisation of degenerative mitral valve disease using morphologic analysis of real-time three-dimensional echocardiographic images. Objective insight into complexity and planning of mitral valve repair. *Circ Cardiovasc Imaging.* 2011;4:24–32.
5. Mick SL, Keshavamurthy S, Gillinov AM. Mitral valve repair versus replacement. *Ann Cardiothorac Surg.* 2015;4(3):230–7.
6. Agricola E, Oppizzi M, et al. Echocardiographic classification of chronic ischemic mitral regurgitation caused by restricted motion according to tethering pattern. *Eur J Echocardiography.* 2004;5(1):326–34.
7. Lancellotti P, Marwick T, Pierard LA. How to manage ischaemic mitral regurgitation. *Heart.* 2008;94:1497–502.
8. Nishimura RA, et al. 2014 AHA/ACC guideline for the management of patients with valvular heart disease. *Circulation.* 2014. <https://doi.org/10.1161/CIR.0000000000000031>.
9. Joint Task Force on the Management of Valvular Heart Disease of the European Society of Cardiology, European Association for Cardio-Thoracic Surgery, Vahanian A, Alfieri O, Andreotti F, Antunes MJ, et al. Guidelines on the management of valvu-

- lar heart disease (version 2012). *Eur Heart J*. 2012;33(19):2451–96.
10. Alfieri O, De Bonis M. The role of the edge-to-edge repair in the surgical treatment of mitral regurgitation. *J Card Surg*. 2010;25(5):536–41.
 11. Feldman T, Foster E, Glower DD, Kar S, Rinaldi MJ, Fail PS, et al. Percutaneous repair or surgery for mitral regurgitation. *N Engl J Med*. 2011;364(15):1395–406.
 12. Feldman T, Kar S, Elmariah S, Smart SC, Trento A, Siegel RJ, et al. Randomized comparison of percutaneous repair and surgery for mitral regurgitation: 5-year results of EVEREST II. *J Am Coll Cardiol*. 2015;66(25):2844–54.
 13. Maisano F, Franzen O, Baldus S, Schafer U, Hausleiter J, Butter C, et al. Percutaneous mitral valve interventions in the real world: early and 1-year results from the ACCESS-EU, a prospective, multicenter, nonrandomized post-approval study of the MitraClip therapy in Europe. *J Am Coll Cardiol*. 2013;62(12):1052–61.
 14. Foster E, Wasserman HS, Gray W, Homma S, Di Tullio MR, Rodriguez L, et al. Quantitative assessment of severity of mitral regurgitation by serial echocardiography in a multicenter clinical trial of percutaneous mitral valve repair. *Am J Cardiol*. 2007;100(10):1577–83.
 15. Grigioni F, Enriquez-Sarano M, Zehr KJ, Bailey KR, Tajik AJ. Ischemic mitral regurgitation: long-term outcome and prognostic implications with quantitative Doppler assessment. *Circulation*. 2001;103(13):1759–64.
 16. Buck T, Plicht B. Real-time three-dimensional echocardiographic assessment of severity of mitral regurgitation using proximal isovelocity surface area and vena contracta area method. Lessons we learned and clinical implications. *Curr Cardiovasc Imaging Rep*. 2015;8:38.
 17. Schmidt FP, Gniewosz T, et al. Usefulness of 3D-PISA as compared to guideline endorsed parameters for mitral regurgitation quantification. *Int J Cardiovasc Imaging*. 2014;30(8):1501–8.
 18. Cockburn J, Fragkou P, Hildick-Smith D. Development of mitral stenosis after single MitraClip insertion for severe mitral regurgitation. *Catheter Cardiovasc Interv*. 2014;83(2):297–302.
 19. Biaggi P, Felix C, Gruner C, Herzog BA, Hohlfeld S, Gaemperli O, et al. Assessment of mitral valve area during percutaneous mitral valve repair using the MitraClip system: comparison of different echocardiographic methods. *Circ Cardiovasc Imaging*. 2013;6(6):1032–40.
 20. Boekstegers P, Hausleiter J, Baldus S, von Bardeleben RS, Beucher H, Butter C, et al. Percutaneous interventional mitral regurgitation treatment using the Mitraclip system. *Clin Res Cardiol*. 2014;103(2):85–96.

Echocardiography in Device Closure and Paravalvular Leaks

43

Rosita Zakeri and Nilesh Sutaria

Atrial Septal Defects

Background

Atrial septal defect (ASD) is a persistent inter-atrial communication, which occurs in approximately 1 in 1,000 live births. The most common type is the ostium secundum defect, which involves the region of the fossa ovalis and accounts for 75% of cases, followed by the ostium primum, sinus venosus defect (superior [SVC] or inferior vena cava [IVC] type) and an unroofed coronary sinus. Although the sinus venosus does not form part of true atrial septum, it is an adjacent structure, involving the SVC and often right upper pulmonary vein (RUPV), through which an ASD may occur. The unroofed coronary sinus is rare and represents an absence of the thin wall of tissue separating the coronary sinus from the left atrium (LA). Overall, ASDs account for up to 40% of clinically significant intra-cardiac shunts in adults. Depending on the size of the ASD, degree of shunting, and associated cardiac abnormalities, the clinical presentation varies widely from asymptomatic to right

ventricular failure (volume overload), pulmonary arterial hypertension, atrial arrhythmias, and paradoxical thromboembolism.

Echocardiography is the primary modality for the diagnosis of an ASD, assessment of the right heart, pulmonary artery pressures, demonstration of left-to-right shunting, and for exclusion of associated valvular and structural defects. Current indications for closure include: a significant shunt causing right ventricular enlargement (with or without symptoms), paradoxical thromboembolism or, rarely, orthodeoxia-platypnoea syndrome. Generally, only the secundum-type ASD is considered suitable for percutaneous closure.

Patent Foramen Ovale

A patent foramen ovale (PFO) differs from an ASD in that it comprises an inter-atrial flap rather than a true structural deficiency of the inter-atrial septum. The foramen ovale has a tunnel-like appearance and remains closed as long as LA pressure exceeds right atrial (RA) pressure; thus right-to-left inter-atrial communication occurs intermittently, for example during a Valsalva manoeuvre or on deep diving. PFOs are present in 20–25% of the general population and are only considered to be of clinical importance in the presence of right-to-left shunting precipitating paradoxical embolism and stroke. Migraine,

R. Zakeri (✉)
Royal Brompton Hospital, London, UK
e-mail: rosita.zakeri@doctors.org.uk

N. Sutaria (✉)
Imperial College Healthcare NHS Trust, St Mary's Hospital, London, UK
e-mail: nsutaria@nhs.net

Caisson's disease and platypnoea-orthodeoxia syndrome are other less common, but potentially relevant considerations.

Detection and Assessment

The initial diagnosis of an ASD or PFO is frequently made on transthoracic echocardiography (TTE). Comprehensive echocardiographic evaluation of an ASD or PFO should include quantification of the defect size, a description of its shape, rims, degree and direction of blood shunting, atrial and ventricular chamber dimensions, and estimated pulmonary artery pressures. Intra-cardiac shunting can be demonstrated on colour Doppler imaging or bubble study with agitated saline. If no shunting is observed at rest, it is important to repeat the bubble study following release of Valsalva manoeuvre to detect the potential for right-to-left shunting when RA pres-

ures are elevated. If closure is planned, transoesophageal echocardiography (TOE) is often required to provide anatomical details for selection of a percutaneous closure device or surgical planning. Although several nomenclatures exist to describe the anatomy of a secundum ASD, frequently, five distinct rims are identified and named after their adjacent structures (Fig. 43.1). Defects in one or more rims may occur. In one large series, a deficiency of the aortic rim was the most common defect observed (42%) [1]. Multiple defects may also occur (Fig. 43.2).

Echocardiography for Device Closure of ASD/PFO

Pre-procedure

The immediate pre-procedure echocardiographic study should confirm the pathological findings, detect any anomalous pulmonary venous drain-

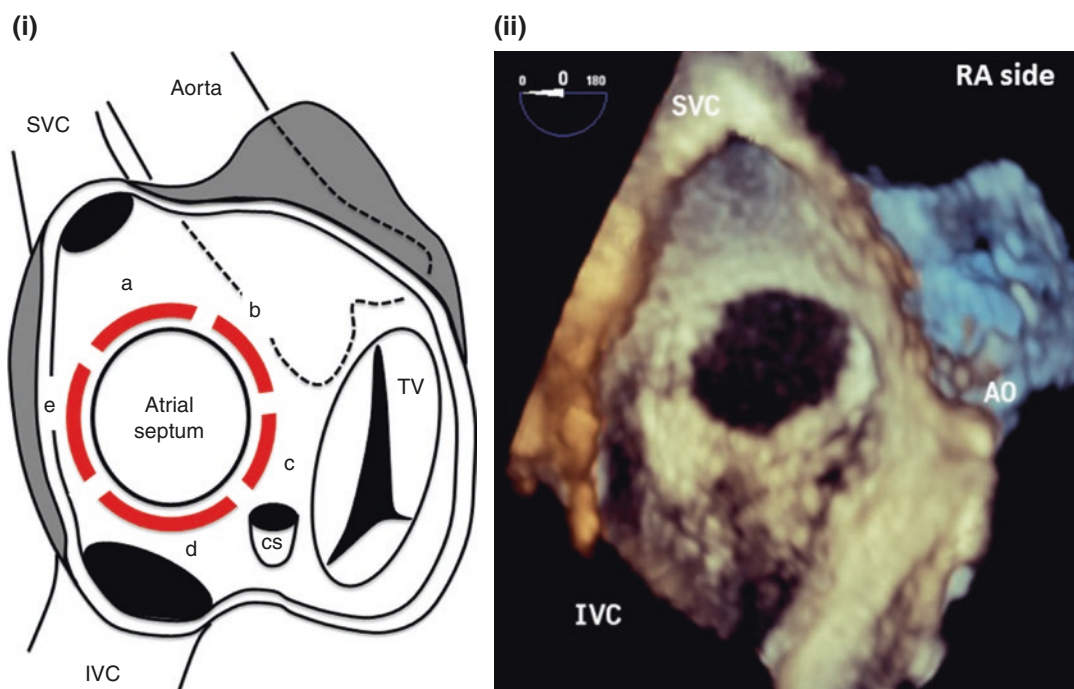


Fig. 43.1 Secundum atrial septal defect. (i) Anatomical schematic: in a clockwise direction, when viewed from the right atrium, the rims of an atrial septal defect consist of: (a) a superior rim, adjacent to the superior vena cava; (b) an aortic rim, adjacent to the aortic valve; (c) an atrioventricu-

lar valve rim, adjacent to tricuspid valve (or mitral valve in the left atrium); (d) an inferior rim, adjacent to the inferior vena cava, (e) a posterior rim, formed by the posterior free wall of the atria. (ii) Corresponding 3-dimensional transoesophageal echocardiography 0° view from right atrium

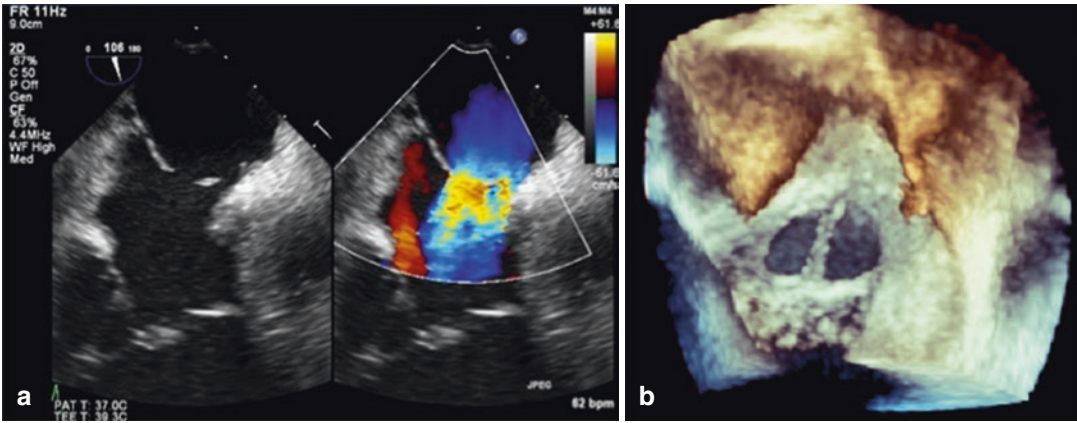


Fig. 43.2 Fenestrated atrial septal defect. (a) Mid-oesophageal modified bicaval view. A wide area of left to right atrial shunting with more than one origin can be seen on colour flow Doppler, (b) 3D transoesophageal echocardiography demonstrates the fenestration

Table 43.1 Transoesophageal echocardiography views of ASD rims

	ASD rims visible
<i>Mid-oesophageal level</i>	
0–20° high level view	SVC-atrial junction and ascending aorta
0–20° mid-level view (Fig. 43.3a)	Atrioventricular valves – Mitral or tricuspid rim
30–45° mid-level view, turn probe to the left (Fig. 43.3b)	– Aortic rim – Posterior rim This view often provides the maximum size of the defect
90–110° bicaval view (Fig. 43.3c)	– Superior rim (SVC) – Inferior rim (IVC; occasionally visible) Rotate clockwise to measure the distance between the ASD and the right upper pulmonary vein
<i>Low oesophageal level</i>	
0°	The inferior rim is difficult to image with conventional TOE. The probe should be advanced into the stomach, retroflexed, and slowly withdrawn into the lower oesophagus, to allow the ultrasound beam to lie perpendicular to the IVC

age (which would require surgical correction) and exclude the presence of left atrial appendage (LAA) thrombus.

Eligibility for Device Closure

The entire rim of the ASD should be visualised to ensure an adequate platform for device placement (Table 43.1, Fig. 43.3a–c). The minimum eligible rim size is device-specific, though, as a general rule, a circumferential rim of 5 mm is necessary for stability. An inferior rim of less than 5 mm is a contraindication for device closure. A deficient, or even absent, aortic rim, on the other hand may still be amenable to percutaneous closure if a selected

ASD occluder device is splayed to encompass the aortic bulb. The presence of complex, challenging variants should also be demonstrated e.g. inter-atrial septal (IAS) aneurysm, fenestrated or multiple defects, prominent Eustachian apparatus stretching into the RA or a long tunnel, which would affect the choice of device.

Sizing of the Device

ASD dimensions should be measured in a minimum of two planes and, preferably real-time 3DE should be used to verify the largest diameter (Fig. 43.4). Device selection is based on the measured diameter of the defect and should not

Fig. 43.3 Atrial septal defect rims. (a) The atrioventricular and posterior rims of an ASD can be visualised in the mid-oesophageal 4-chamber (0° – 20°) view; (b) the aortic and posterior rims of an ASD can be visualised in the mid-oesophageal (30– 45°) view; (c) the superior and inferior rims of an ASD can be visualised in the bicaval view (approx. 90° – 110° ; here 120°). *Key:* (a) superior rim; (b) aortic rim; (c) atrioventricular valve rim; (d) inferior rim; (e) posterior rim. IVC, inferior vena cava; SVC, superior vena cava; TV, tricuspid valve

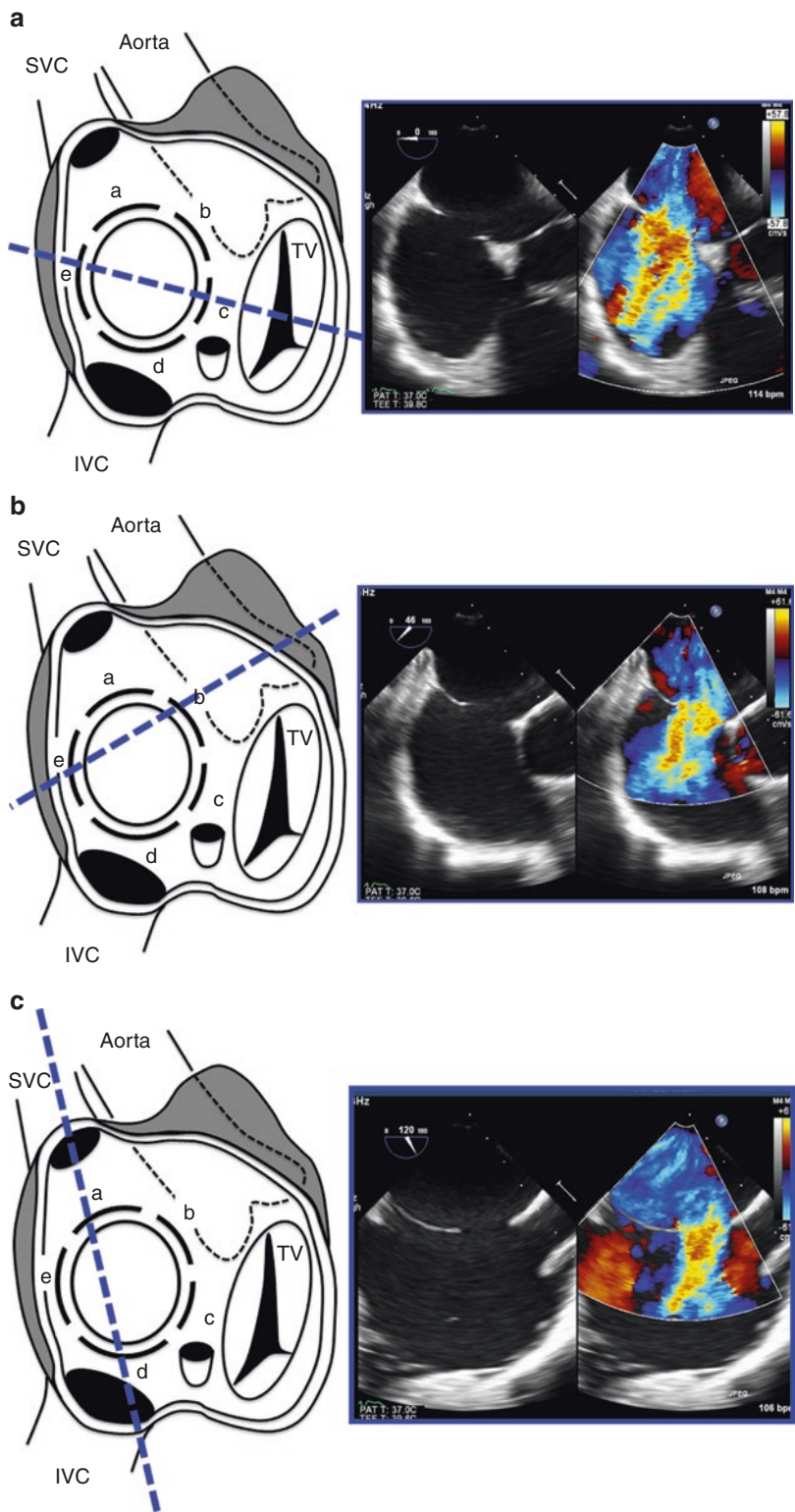
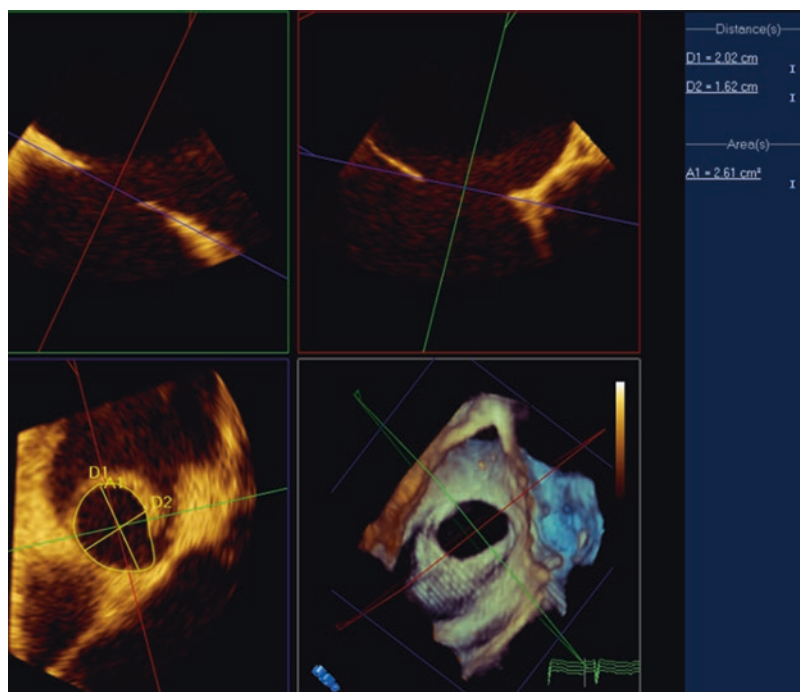


Fig. 43.4 3-dimensional multiplanar reconstruction of an atrial septal defect with a deficient aortic rim



exceed the manufacturer-specified cut-off value. Current devices allow closure of defects of less than 40 mm in diameter.

The Role of 3D Echocardiography

The main advantage of 3DE is to provide an *en face* view from the RA perspective (Fig. 43.1), which demonstrates all the rims, size and shape of the septal defect, and relationship with the aortic root, great veins and relevant associated structures such as a prominent Eustachian ridge, which may impede device deployment. 3DE with multiplanar reconstruction also allows precise measurement of the maximum diameter (Fig. 43.4). The key limitation, however, is signal dropout, particularly with thin, aneurysmal IAS tissue.

Intraprocedural

ASDs and PFOs are closed via a transvenous approach, typically via the femoral vein. 3DE optimally displays the defect *en face*, device positioning and deployment (Fig. 43.5), however two-dimensional echocardiography (2DE) remains essential for detecting the presence of any small clots on the guidewire and complications such as a pericardial effusion. TOE permits

continuous visualisation of the guidewire and facilitates its placement in the pulmonary vein, avoiding LAA perforation. A sizing balloon is advanced over the guidewire and across the defect. In the modified bicaval view (90–100°) an image of the defect and both atria can be obtained, and the position of the balloon in its long-axis confirmed. Prior to inflation, it must be ensured that the balloon is at a safe distance from the mitral valve leaflets in order to prevent inadvertent valve obstruction. The balloon is subsequently inflated until a ‘waist’ appears; colour Doppler should be used to confirm absence of flow between the balloon and ASD margins (stop-flow method; Fig. 43.5a). At this point, balloon size can be assessed on echocardiography or fluoroscopy. Of note, the balloon rounds the defect, thus balloon sizing may yield slightly larger dimensions than direct ‘un-stretched’ TOE measurements of the defect size.

Once the appropriate device has been selected, the delivery catheter (with collapsed closure device) is passed over the guidewire and into the LA. It is important to visualise the tip of the catheter and ensure it is mobile within the LA body prior to release of the LA disc, in order to avoid

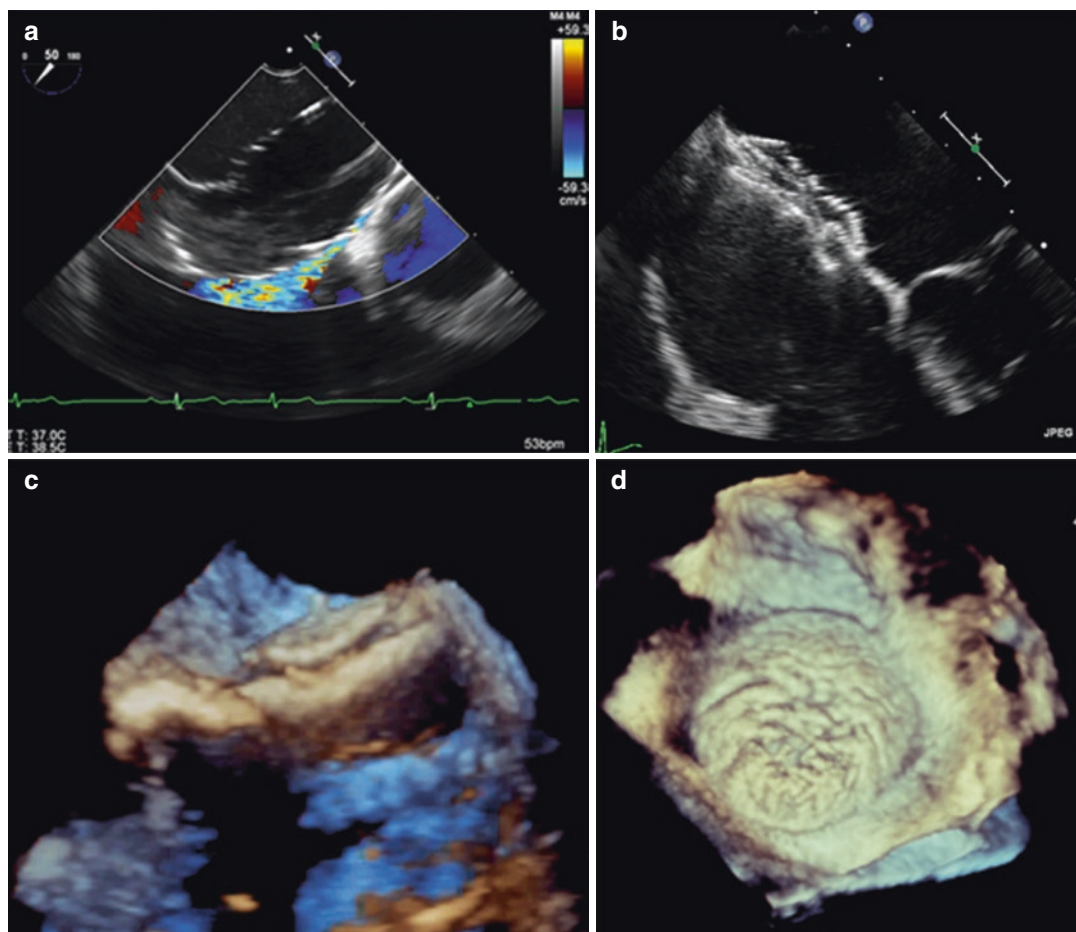


Fig. 43.5 Amplatzer atrial septal occluder device: (a) 2-dimensional mid-oesophageal four chamber view with colour Doppler during sizing balloon inflation, (b) 2-dimensional mid-oesophageal four chamber view with

occluder device in situ, (c) 3-dimensional view from the left atrium, (d) 3-dimensional view across the interatrial septum (the left atrial disc of the occluder device is seen in the near field)

entrapment of the LAA, mitral valve or subvalvular apparatus. The LA disc is released first and apposed against the LA side of the defect. The RA disc is then released. Both discs must be seen to be fully expanded and with sufficient rim caught between them (Fig. 43.5b). Prior to removal of all catheters, a comprehensive assessment should be made of the device stability and position, including any excess angulation, impingement of the LA wall or aortic root, and residual interatrial shunt. This is performed via a combination of echocardiography, fluoroscopy and manual manoeuvring ('pull' or 'wiggle' test). Residual leak may require upsizing of the device or the placement of additional occluder devices (Fig. 43.6).

Throughout the procedure it is important to scrutinise guidewires and catheters for development of thrombus or fibrin deposition. Rarely, inferior ST elevation may be noted on electrocardiography and inferior wall motion abnormalities have been detected on TOE, related to air embolization from catheters to the right coronary artery.

Immediate Post-procedure

A final assessment of device position should be made including identification of any residual inter-atrial shunt, cardiac perforation or intrapericardial haemorrhage. Mitral valve function should be assessed to exclude structural injury.

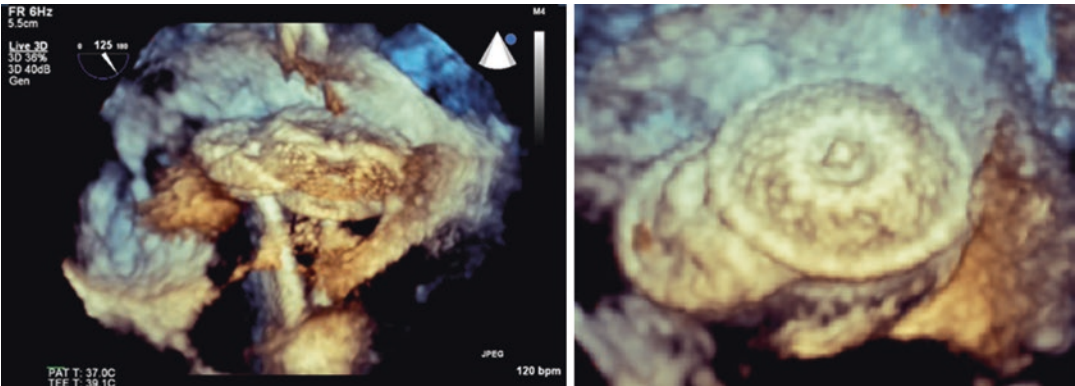


Fig. 43.6 Atrial septal defect closure requiring placement of two overlapping devices

Table 43.2 Echocardiography checklist for ASD device closure

<i>Pre-procedure</i>
– Define ASD location, size, number, rim size, distance from mitral valve/right upper pulmonary vein
– Identify left to right shunting
– Identify associated abnormalities e.g. mitral valve prolapse, prominent Eustachian ridge
– Define functional consequences (right atrial and ventricular enlargement)
<i>Intraprocedural</i>
– Visualise guidewire placement in the LA/LAA
– Confirm appropriate location (away from mitral valve apparatus) for balloon inflation
– Confirm correct positioning of the device discs and satisfactory incorporation of rims
– Detect residual shunting
<i>Immediate post-procedure</i>
– Check device position
– Assess for residual shunting
– Exclude pericardial effusion
<i>Follow up</i>
– Check device position
– Assess for residual shunting
– Quantify any change in right atrial and right ventricular size

Follow-Up

Repeat TTE echocardiography at 6–12 weeks should be performed to exclude device displacement or erosion and document any residual inter-atrial shunt (Table 43.2).

Paravalvular Leaks

Background

Paravalvular leak (PVL) refers to one or more regurgitant jets arising outside of an implanted valvular prosthesis, between the surgical ring and the surrounding native cardiac tissue. PVLs may

arise at any time after surgery, and may be precipitated by surgical technical factors, progressive tissue degeneration, annular calcification, or infection (Fig. 43.7). The reported incidence varies widely between studies, however mechanical mitral valve prostheses are more susceptible, with 7–17% of all surgically implanted mitral valves exhibiting PVL, compared with 2–10% of implanted aortic valves [2, 3]. Indications for PVL intervention include symptomatic heart failure, progressive LV dilatation or impairment, and haemolysis requiring recurrent transfusion. Surgery is the treatment of choice for patients with very large PVLs associated with valve dehiscence, infective endocarditis, or concomitant

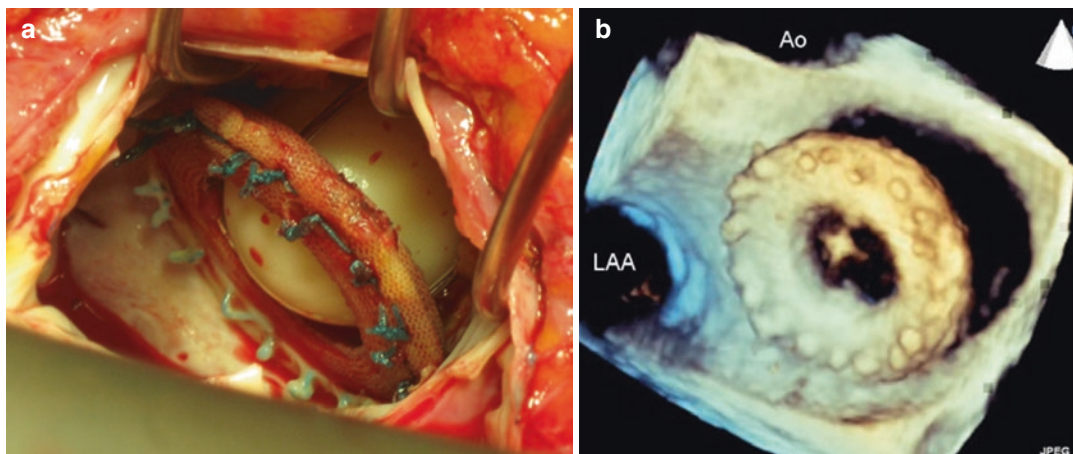


Fig. 43.7 Severe dehiscence of a mitral valve prosthesis. (a) Surgical view, (b) perioperative 3-dimensional transoesophageal echocardiography

indications for surgery including valvular or ischaemic heart disease. However, in this group of patients who are often older and more frail, the risk of adverse outcomes following re-do surgery is high and surgical success rates are limited. For selected patients with isolated PVL or prohibitive surgical risk, percutaneous transcatheter closure has emerged as first line therapy [4].

Mitral PVL

Detection and Assessment

An initial TTE can demonstrate mitral regurgitation and provide relevant information regarding prosthetic valve function, mean gradient, and left ventricular size and function. However, artefact from mechanical mitral valve prostheses commonly obscures the regurgitant jets. TOE can clearly define the jet origin and extent in the left atrium; 3D TOE in the LA surgical view can also demonstrate the size and location of the leak. Therefore a screening TOE, and in particular 3DTOE, are required for clear characterisation of the defect(s).

On TOE, the mitral valve is conventionally described as a clock-face viewed from the left atrium, i.e. 'the surgeon's view' (Fig. 43.8). 3D images should be rotated to position the anterior mitral ring (adjacent to the aortic valve) at the 12 o'clock position, and the left atrial appendage at the 9 o'clock position. A PVL appears as an area

of echo drop out outside the sewing ring and its origin can be described as its position on the clock-face and relationship to the aortic valve and LAA. Common locations for a mitral PVL are anteromedial (between 10 and 11 o'clock) or posterolateral (between 5 and 6 o'clock) in the surgical view [5].

The associated regurgitant jet should be confirmed with colour Doppler imaging, and 3D colour in particular has proved invaluable to avoid falsely diagnosing areas of echo drop out as PVL. The entire sewing ring should be systematically imaged in multiple long-axis planes from 0° to 180° and, whenever possible, a transgastric view of the valve ring 'en face' with colour Doppler should also be attempted.

Severity

It is recommended to use both a qualitative and quantitative approach to describe the severity of mitral regurgitation, albeit few quantitative parameters have been validated for PVL assessment (Table 43.3). Regurgitant jet area and jet density are imprecise; proximal flow convergence radius, i.e., proximal isovelocity surface area (PISA), is also not validated in PVL, although a large PISA radius does support severe PVL. The accuracy of transvalvular quantitative Doppler is questionable as the prosthesis may alter antegrade flow, however pulsed Doppler assessment of pulmonary vein flow is useful and the presence of pulmonary vein systolic flow reversal is a reliable and specific

Fig. 43.8 Surgeon’s view of the mitral valve on 3-dimensional echocardiography. The aortic valve (12 o’clock) and left atrial appendage (LAA; 9 o’clock) are used for orientation. The anterior mitral valve leaflet is in the near field; the posterior leaflet is in the far field

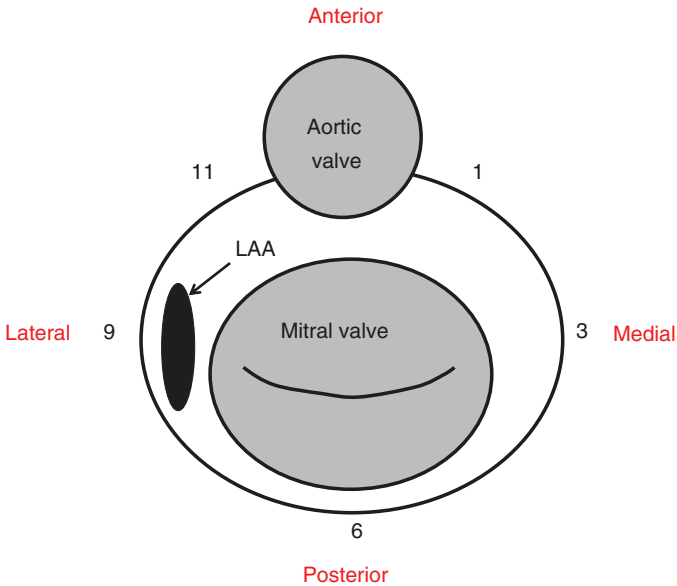


Table 43.3 Echocardiographic parameters used to quantify mitral regurgitation severity (Adapted from [6] for prosthetic valve regurgitation)

Parameter	Grade of mitral regurgitation		
	Mild	Moderate	Severe
<i>Qualitative</i>			
Left ventricular size	Normal/mildly dilated	Mildly/moderately dilated	Moderately/severely dilated
Extent of regurgitant jet	Small jet (approx. <20% LA area)		Large jet (approx. >40% LA area) or any size wall-impinging jet
Doppler signal of regurgitant jet (CW Doppler)	Parabolic	Usually parabolic	Early peaking ‘triangular’ Multiple jets
Proximal flow convergence radius, mm ^a	Minimal (<4)	Intermediate (4–8)	Large (≥9)
Systolic flow reversal in the pulmonary veins ^b (PW Doppler)	Absent	Absent	Present
<i>Semi-quantitative</i>			
Vena contracta width, mm (colour Doppler)	<3	2–5	≥6
<i>Quantitative</i>			
Effective regurgitant orifice area, mm ²	<20	20–49	≥50

In general, the more concordant parameters obtained, the more confidence in the evaluation grade

^aBaseline shift at a Nyquist limit of 40 cm/s; cutoffs for eccentric jets may be higher

^bSpecific but not sensitive

sign of severe mitral regurgitation [6]. Locating the largest vena contracta by 2D colour Doppler along with X-plane to provide minor and major planes for estimation of the regurgitant orifice is useful. However, the most accurate assessment of mitral PVL severity may be obtained using advanced 3D post-processing software, which

allows multiplanar reconstruction and planimetry of the true regurgitant orifice area (Fig. 43.9a–d). Additionally, 3D volume sets should be acquired to assess the area of dehiscence. An area exceeding 25% of the ring circumference is likely to require multiple devices if percutaneous closure is attempted.

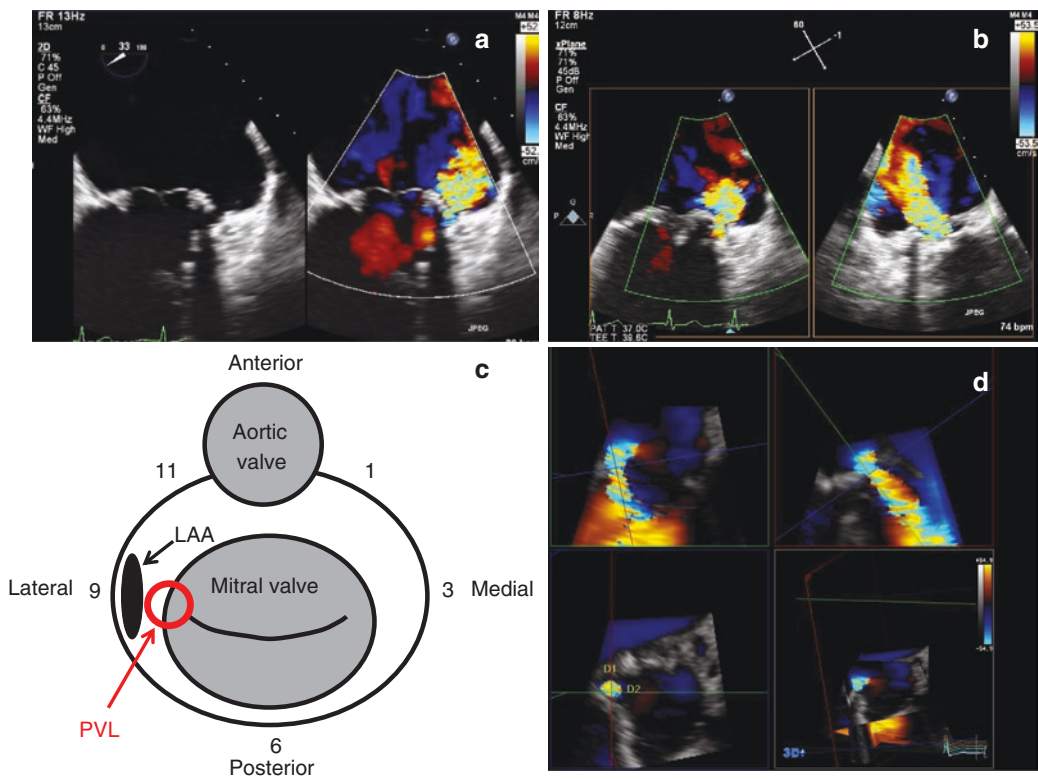


Fig. 43.9 Mitral prosthesis paravalvular leak. (a) Mid-oesophageal 30° view with and without colour flow Doppler, (b) x-plane with colour flow Doppler, (c) schematic representation of the position of the PVL at 9 o'clock, (d) 3-dimensional multiplanar reconstruction with assessment of vena contracta. LAA left atrial appendage, PVL paravalvular leak

tation of the position of the PVL at 9 o'clock, (d) 3-dimensional multiplanar reconstruction with assessment of vena contracta. LAA left atrial appendage, PVL paravalvular leak

Aortic PVL

Detection and Assessment

An initial TTE can demonstrate aortic regurgitation, aortic valve prosthesis function, mean transvalvular gradient, and left ventricular structure and function. Acoustic shadowing and reverberation artefacts from the prosthesis can limit visualisation. TOE is equally susceptible to artefact, particularly for anterior aortic pathology, and in these cases TTE may offer superior guidance. However TOE may reveal posterior PVLs that were not visible on surface imaging or difficult to distinguish from mitral flow, thus a combined TTE/TOE approach is necessary. It is important to examine the entire perimeter of the aortic valve, using x-plane functions and 3DE, with and without colour, in order to map the origin of a PVL and full extent of valve dehiscence.

For bioprostheses resembling native aortic valve anatomy, the location of a PVL may be described relative to the cusp(s) involved. Alternatively, the location may be described using the 'clock-face' nomenclature with the aortic valve in a short axis view and confirmed relative to the anterior or posterior positions in the long-axis view (Fig. 43.10). Often both terminologies are used. Case series have demonstrated that aortic PVLs most frequently occur between the right and non-coronary cusps, between the 7 and 11 o'clock position [7, 8].

For aortic PVL assessment, it is essential to include examination of coronary artery origins. With 3DE it may also be possible to measure the distance between the aortic annulus and coronary ostia. A coronary ostium that is anatomically low in the aortic root and close to the valve ring may be at risk of occlusion during

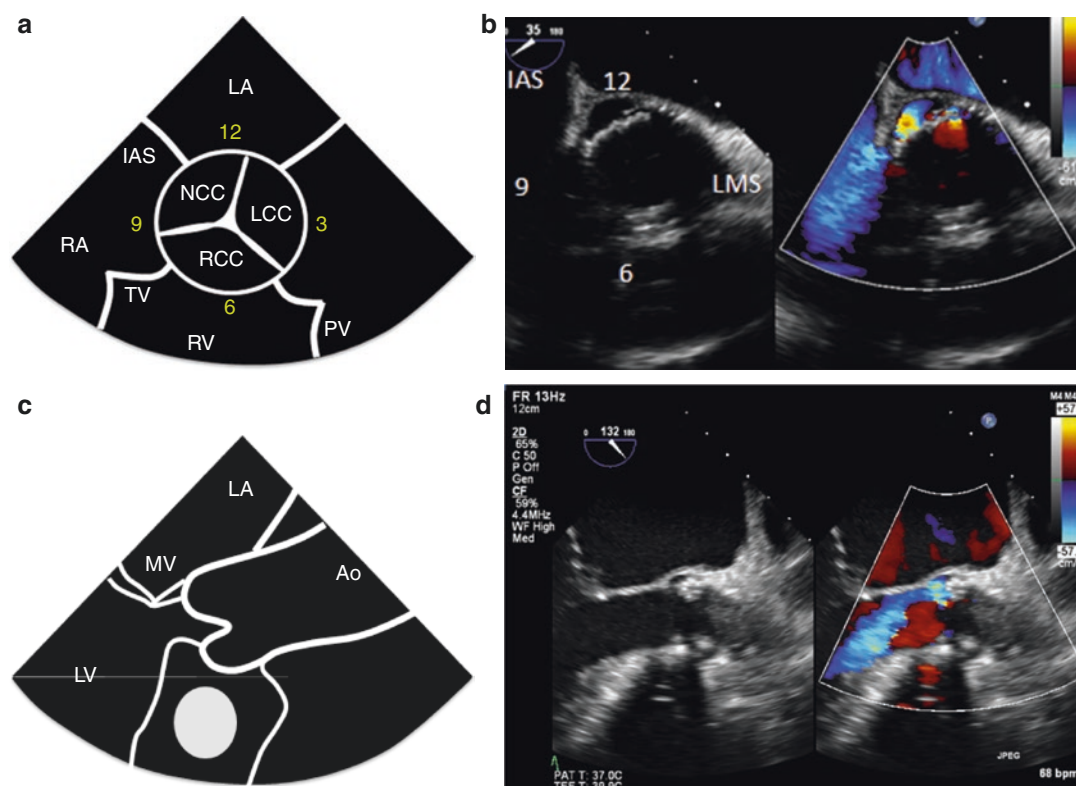


Fig. 43.10 Aortic paravalvular leak on transoesophageal echocardiography. (a) Clock-face schematic of the aortic valve (60° view), (b) aortic paravalvular leak in the 11 o'clock position on 2D TOE with colour Doppler, (c) schematic of a mid-oesophageal aortic valve long-axis view (130°) including the ascending aorta (Ao), (d) poste-

rior aortic paravalvular leak on 2D TOE with colour Doppler. *IAS* interatrial septum, *LA* left atrium, *LCC* left coronary cusp, *LMS* left main stem coronary artery, *LV* left ventricle, *MV* mitral valve, *NCC* non-coronary cusp, *RA* right atrium, *RCC* right coronary cusp, *RV* right ventricle

percutaneous PVL closure and thus influence the device selection.

Severity

Assessment of the severity of aortic PVLs should include a combination of qualitative and quantitative parameters, similar to those used to assess native aortic valve regurgitation. However, because of the nature of PVL jets and associated artefact, it may be difficult to apply usual parameters of aortic regurgitation severity. A region of flow convergence in the aortic root should be sought and, if present, suggests the regurgitation is significant. Jet width at its narrowest point (vena contracta) can be measured and compared with the LVOT diameter, however, the circumferential extent of

regurgitation is often a more useful descriptor of PVL severity. Importantly, because the circumferential extent may vary significantly depending on the plane of interrogation, 3DE is helpful to find the short axis plane with the smallest vena contracta. In the case of an eccentric jet or multiple jets (Fig. 43.11), diastolic flow reversal in the descending aorta is perhaps the most reliable measure of severe regurgitation. In cases where mechanical valve artefact impedes assessment, transgastric TOE may offer the best view of the aortic regurgitation jet origin and extent. Several different grading systems for aortic PVL severity have been proposed; a 3-class grading scheme (mild/moderate/severe) is the most commonly employed (Table 43.4).

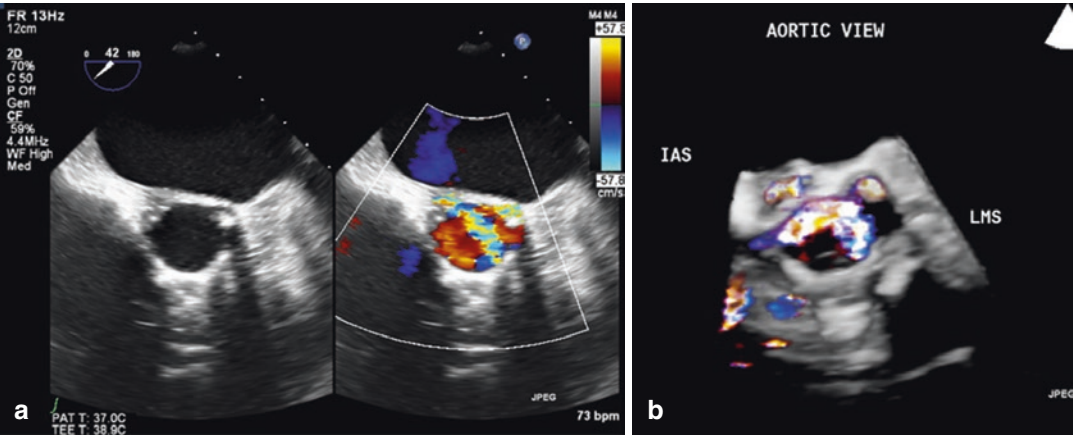


Fig. 43.11 Multiple aortic paravalvular leaks (11 o'clock and 2 o'clock positions). (a) Short axis 2D view (40°–60°), (b) Short axis 3D view with colour

Table 43.4 Echocardiographic parameters used to grade aortic paravalvular regurgitation severity (adapted from [6, 9])

Parameter	Grade of aortic paravalvular regurgitation		
	Mild	Moderate	Severe
<i>Qualitative</i>			
Left ventricular size	Normal/mildly dilated	Mildly/moderately dilated	Moderately/severely dilated
Doppler signal of regurgitant jet (CW Doppler)	Narrow jet origin	Narrow or wide jet origin	Wide jet origin Multiple jets Proximal flow convergence visible
Diastolic flow reversal in the descending aorta ^a (PW Doppler)	Absent	Intermediate	Holodiastolic (end-diastolic velocity >25 cm/s)
<i>Semi-quantitative</i>			
Jet width at origin, % LVOT diameter (colour Doppler)	<15%	15–60%	>60%
Vena contracta width, mm (colour Doppler)	<2	2–6	>6
Vena contracta area, mm ² (3D)	<10	10–40	>40
Jet deceleration rate, (pressure half time), ms (CW Doppler)	Slow (>500)	Variable (>200)	Steep (<200)
Circumferential extent of PVR, % ^a	<10	10–30	>30
<i>Quantitative</i>			
Effective regurgitant orifice area, mm ²	<10	10–30	>30

CW Doppler continuous wave, LVOT left ventricular outflow tract, PVR paravalvular regurgitation, PW Doppler pulsed wave Doppler

^aParameters that are most frequently applicable

Echocardiography for Device Closure of PVL

Pre-procedure

Assuming a comprehensive diagnostic TTE or TOE has already been performed, the immedi-

ate pre-procedure study should confirm the pathological findings, exclude LAA thrombus, and record the baseline transvalvular gradient. For aortic PVL closure it is also vital to identify the coronary ostia before proceeding (Table 43.5).

Table 43.5 Echocardiography checklist for PVL device closure

<i>Pre-procedure</i>
– Location and severity of PVL
– Location of coronary ostia (aortic PVL)
– Exclude prosthetic and intracardiac thrombi or vegetations
<i>Intraprocedural</i>
– Facilitate guidewire and catheter placement
<i>Immediate post-procedure</i>
– Seating of the closure device
– Coronary artery flow (aortic PVL)
– Ensure normal functioning of the prosthetic valve
– Residual PVL
– Exclude pericardial effusion
<i>Follow up</i>
– Seating of the closure device
– Residual PVL
– Changes in chamber remodelling

Intra-Procedural

Mitral PVL Closure

For mitral PVLs, a transapical approach provides retrograde direct access to the mitral valve and is most useful for a single posterior or septal PVL

or where multiple PVL closure is attempted. More frequently, a transseptal approach, via antegrade femoral artery access, is used and facilitates easier guidewire positioning across anterior and lateral PVLs as well as carrying a lower risk of bleeding complications.

When a transseptal antegrade approach is used, TOE should be used to visualise the catheter tip in real time and guide safe transseptal puncture, with both antegrade and retrograde approaches, real time 3DE in the LA surgical view greatly assists the interventional cardiologist to achieve optimal guidewire and catheter placement and device positioning and orientation across the defect before deployment (Fig. 43.12). The device should always be deployed under echocardiographic guidance and an immediate assessment made of the position and any impingement of prosthetic valve leaflet/disc function, prior to release. Once released, it is necessary to confirm there has been no migration of the device, prosthetic valve function is unrestricted and determine the presence of any residual PVL. Any of these out-

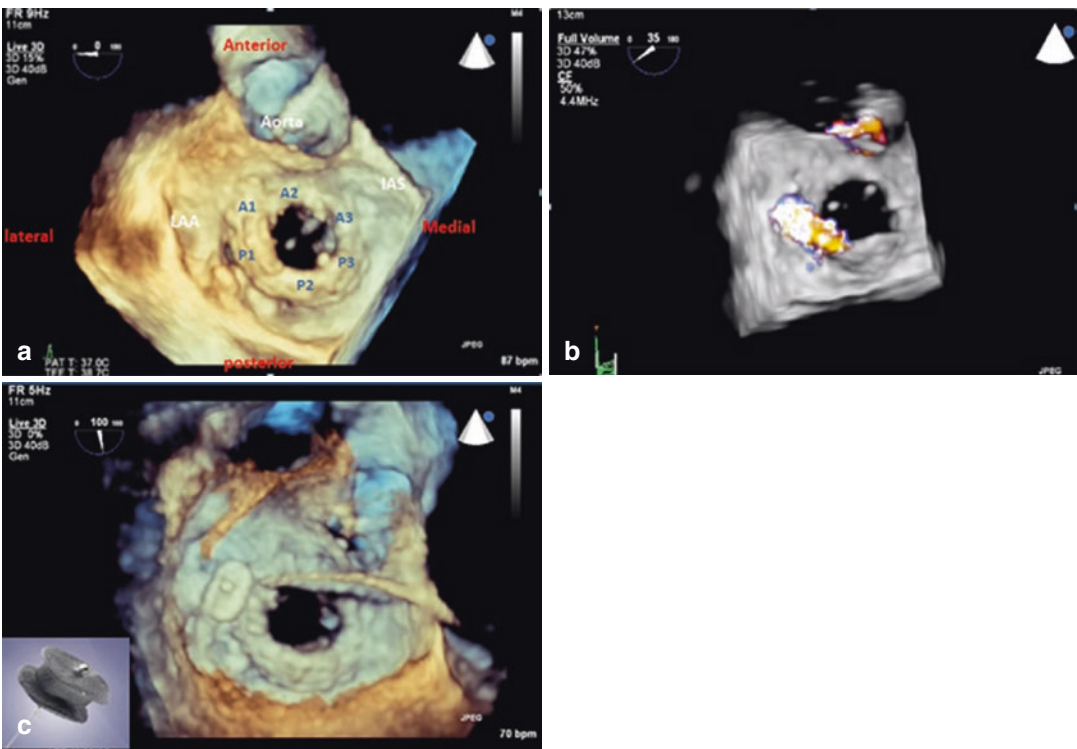


Fig. 43.12 Mitral paravalvular leak in the lateral (9 o'clock) position on: (a) 3-dimensional transoesophageal echocardiography, (b) with colour flow Doppler, (c) after device closure (inset shows the occluder device)

comes warrant reposition of the device or removal with a subsequent attempt. In some cases of large or multiple PVLs, more than one closure device is often required.

Aortic PVL Closure

A retrograde transaortic approach (via femoral artery access) is most frequently used for aortic PVL closure. However if the patient has both mitral and aortic prostheses, or a previous failed transaortic attempt, a transapical approach may be utilised. For both cases, 2D and 3D TOE and fluoroscopy may be used to confirm the position of the guidewire and device prior to deployment. After deployment, echocardiography should be used to confirm normal functioning of the aortic valve prosthesis, identify any residual regurgitation and, of critical importance, ensure that there has been no impingement of the mitral subvalvular apparatus or obstruction of coronary artery ostia. Any concerns about coronary flow should prompt coronary angiographic assessment.

Immediate Post-procedure

A final assessment of device location, prosthetic valve function and any residual PVL should be performed and the results documented for later comparison. The presence of a new or worsening pericardial effusion, even if small, should alert the operator to the possibility of a haemopericardium.

Long-Term Follow Up

There are no formal recommendations regarding post-procedure surveillance. However, serial assessment is required to assess the stability or progression of any residual PVL or to detect further valve dehiscence even after successful closure. Complementary information regarding anatomical changes and chamber volumes may be obtained from other imaging techniques such as magnetic resonance imaging or computed tomography.

Conclusions

Echocardiography has a pivotal role in the case selection, guidance and follow-up of patients undergoing transcatheter intervention. TTE in the

awake state remains the primary modality for diagnosis, evaluation of associated LV and RV disease and haemodynamic assessment of valve lesions and pulmonary artery pressures, which may alter under general anaesthesia. A careful baseline TOE at the onset of any procedure is essential and a combination of 2D and 3D TOE is invaluable for defining anatomy and guiding intervention. At all times, it is important that there is a close working relationship between the interventionalist and imager so that image orientation is clearly understood and real-time feedback can be provided, including immediate detection and communication of complications. As such, the echocardiographer needs to be aware of the wide range of devices available and have an in-depth knowledge of each step of the interventional procedure. Advances in imaging technology continue to facilitate the expansion of more complex structural intervention; including fusion imaging which allows overlay of 3D echocardiographic data onto the fluoroscopic image. Specific practice guidelines, training and accreditation should now be considered for specialists in structural imaging in order to maintain high standards and safe practice in this exciting field.

References

1. Podnar T, et al. Morphological variations of secundum-type atrial septal defects: feasibility for percutaneous closure using Amplatzer septal occluders. *Catheter Cardiovasc Interv.* 2001;53(3):386–91.
2. Hammermeister K, et al. Outcomes 15 years after valve replacement with a mechanical versus a bioprosthetic valve: final report of the veterans affairs randomized trial. *J Am Coll Cardiol.* 2000;36(4):1152–8.
3. Ionescu A, Fraser AG, Butchart EG. Prevalence and clinical significance of incidental paraprosthetic valvar regurgitation: a prospective study using transoesophageal echocardiography. *Heart.* 2003;89(11):1316–21.
4. Calvert PA, et al. Percutaneous device closure of paravalvular leak: combined experience from the United Kingdom and Ireland. *Circulation.* 2016;134(13):934–44.
5. De Cicco G, et al. Mitral valve periprosthetic leakage: anatomical observations in 135 patients from a multicentre study. *Eur J Cardiothorac Surg.* 2006;30(6):887–91.
6. Zoghbi WA, et al. Recommendations for evaluation of prosthetic valves with echocardiography and doppler ultrasound: a report from the American Society of Echocardiography's guidelines and

standards committee and the task force on prosthetic valves, developed in conjunction with the American College of Cardiology Cardiovascular imaging committee, cardiac imaging committee of the American Heart Association, the European Association of Echocardiography, a registered branch of the European Society of Cardiology, the Japanese Society of Echocardiography and the Canadian Society of Echocardiography, endorsed by the American College of Cardiology Foundation, American Heart Association, European Association of Echocardiography, a registered branch of the European Society of Cardiology, the Japanese

Society of Echocardiography, and Canadian Society of Echocardiography. *J Am Soc Echocardiogr*. 2009;22(9):975–1014. quiz 1082–4.

7. De Cicco G, et al. Aortic valve periprosthetic leakage: anatomic observations and surgical results. *Ann Thorac Surg*. 2005;79(5):1480–5.
8. Ruiz CE, et al. Clinical outcomes in patients undergoing percutaneous closure of periprosthetic paravalvular leaks. *J Am Coll Cardiol*. 2011;58(21):2210–7.
9. Pibarot P, et al. Assessment of paravalvular regurgitation following TAVR: a proposal of unifying grading scheme. *JACC Cardiovasc Imaging*. 2015;8(3):340–60.

Echocardiography in Electrophysiology

44

Francesco F. Faletra, Giovanni Pedrazzini,
Laura Anna Leo, Romina Murzilli, Elena Pasotti,
Tiziano Moccetti, and Siew Yen Ho

Introduction

Two-dimensional transthoracic echocardiography (2D TTE) plays a major role in the field of the electrophysiology. In general, before any electrophysiological (EP) procedure, electrophysiologists need a 2D TTE to evaluate left (LV) and right ventricular size and function, LV wall thickness, atrial size and, of course, valve morphology and function. 2D TTE is also the first line imaging modality in several myocardial diseases generating life-threatening arrhythmias such as arrhythmogenic right ventricular dysplasia, dilated, ischemic, hypertrophic, and non-compaction cardiomyopathies. Moreover, it has an important role in the care of patients with heart failure treated with cardiac resynchronization therapy (CRT). Indeed, to assess LV dyssynchrony and, indirectly, to predict a favourable response to CRT several echocardiographic techniques have been proposed from m-mode echocardiography in early days [1], to tissue Doppler imaging velocities and strain [2], from two-dimensional speckle tracking strain [3], to real

time three-dimensional transthoracic echocardiography [4], or, finally, to three-dimensional speckle tracking strain. Despite of the huge amount of studies and a plethora of measurements, there is no consensus yet on which echocardiographic parameter/s should be used to quantify dyssynchrony and identify patients who will respond to CRT. Likely a more integrate approach with other imaging techniques (such as magnetic resonance imaging and computed tomography) that define the location and extent of LV scar tissue as well as anatomy of coronary veins may optimize the selection of patients who benefit from CRT.

On the other hand, two-dimensional transesophageal echocardiography (2D TEE), is the imaging technique of choice to visualize the complex morphology of left atrial appendage (LAA) and rule out thrombi or spontaneous contrast (sludge or smoke-like formation) into LAA before electrical cardioversion or any other ablation procedures.

However, as for other structural heart disease (SHD) percutaneous interventions, 2D/3D TEE may be very useful in a context of invasive electrophysiological (EP) laboratory. Indeed, complex ablations require a deep knowledge of cardiac anatomy of target structure/s: unexpected anatomical variants or anatomical barriers may cause difficulties in catheter's manipulation or in catheter stability, prolonging the procedural time or causing inadequate ablation. Although 2D

F. F. Faletra (✉) · G. Pedrazzini · L. A. Leo · R. Murzilli
E. Pasotti · T. Moccetti
Department of Cardiology, Fondazione Cardiocentro
Ticino, Lugano, Switzerland
e-mail: francesco.faletra@cardiocentro.org

S. Y. Ho
Cardiac Morphology, Royal Brompton Hospital and
Imperial College, London, UK

TEE may recognise some of these variants (for example a long Eustachian valve), the tomographic nature of this technique allows imaging cardiac structures only in cross-sectional planes making it difficult to reconstruct mentally the actual 3D aspect of any cardiac structure (and therefore anatomical variants) based on the interpretation of multiple tomographic planes. Recently, in combined work with pathologists, we have shown that 3D TEE may display cardiac structures in format similar to anatomic specimens [5, 6]. Because of this ability, 3D TEE may play a new role: a pre-procedural assessment of the anatomy of target structures. 3D TEE in fact, may identify *before the procedure* unusual and important anatomical variants that alert electrophysiologists to tailor the interventional strategy according to individual patient's anatomy.

Another potential use of 2D/3D TEE may be that of guiding electrophysiologist *during* EP ablation. What the electrophysiologists really need during any ablation are: first, precise anatomical details of the 'terrain' where the ablation takes place; second, an imaging tool that may guide in "real time" catheter/s navigation in any step of the ablation, and finally, an immediate alert of any potential complication.

Intracardiac echocardiography (ICE) may fulfill these requirements [7, 8]. It has the advantage of not requiring prolonged esophageal intubation or general anesthesia. Moreover, the same electrophysiologist can perform both ablation procedure and ICE imaging without the need of an echocardiographer for imaging acquisition and interpretation. However, 2D ICE has the same limitations of 2D TEE, being a tomographic technique it cannot image in a single plane curved catheters. Whenever a catheter shaft crosses the ultrasound beam, it may appear to represent the catheter tip. Moreover, a precise understanding of spatial position of catheters in relation to other cardiac structures need multiple planes and image adjustments that may distract the electrophysiologist during ablation. This additional work requires a specific technical skill (different in orientation compared to standard echocardiography) and ability to manipulate the catheter within

the heart to obtain proper views. If done by the same electrophysiologist who perform the ablation, the use of ICE may prolong the procedure. In principle, 3D ICE should overcome some of the above-mentioned limitations; however, as far as we know, at this time experience with real time 3D ICE are limited to a very few institutions and no clinical investigations are available on this technique yet. Finally, ICE requires a dedicated system and disposable catheters. These requirements produce additional costs to the procedure.

3D TEE has the potential to become a new, anatomy-driven navigational guide for EP procedures. Indeed, better than 2D TEE, it may visualize long segments of catheters, catheter's tip positions and movements through chambers and across atrial septum, clarify the spatial relationship between catheters and anatomic structures and, of course, alert electrophysiologists to any complications during the procedure. However, while the use of 3D TEE for SHD interventions is well established and include almost all the SHD procedures [9, 10], this is not the case for ablation procedures.

In the first part of the chapter, we present 3D TEE images of atrial anatomical variants relevant for electrophysiologists. In the same section, we discuss the strengths and limitations of the technique during two of the most frequent ablation procedures: cavo-tricuspid isthmus (CVTI) ablation in patients with typical atrial flutter and pulmonary veins (PVs) isolation in patients with atrial fibrillation. In the second part of the chapter, we discuss of the role of 2D/3D TEE during occlusion of left atrial appendage (LAA), a percutaneous procedure, which is performed by both electrophysiologists and interventional cardiologists.

The Role of 2D/3D TEE in Ablation of CVTI and PVS

Anatomic Variants of Right Atrium

Several anatomical variants may complicate a relatively simple EP procedure such as the ablation of cavo-tricuspid isthmus (CVTI) for typical

atrial flutter. Long diastolic isthmus or an angulation between IVC and CVTI close to 90° as well as a very prominent and rigid EV may make catheter manipulations difficult [11, 12]. The posterior part of the CVTI nearest to a tall EV may be more difficult to reach for good contact. The CVTI surface may be rather irregular with recesses and prominences. In presence of large and deep sub-Eustachian pouch-like recess, the catheter tip-atrial wall contact may not occur in the deepest area of the recess, resulting in an incomplete ablation line. Finally, pectinate muscles may occasionally cross the terminal crest encroaching to some extent on the CVTI. Their presence may also create gaps in the ablation line [13]. A pre-procedural 2D/3D TEE study (usually performed for ruling out thrombi) may alert on the presence of one or more of such variants allowing electrophysiologists tailoring the ablation strategy according the specific anatomy encountered. For example, a long guide sheath may help manoeuvring the catheter in presence of prominent and rigid EV. A medial ablation line, closer to the coronary sinus ostium, or more lateral may avoid sub-Eustachian pouch or pectinate muscles. 3D TEE better than 2D TEE may illustrate these anatomical variants (Fig. 44.1).

Anatomical variants from the usual pattern of four pulmonary veins (PVs) may also occur. It is non-infrequent to find a short or long common venous trunk on the left side, or more than two veins on the right side (Fig. 44.2).

However, while 3D TEE may visualize CVTI in almost all patients, imaging the four pulmonary veins in any patient undergoing ablation for atrial fibrillation is more challenging. While the entire contour of the upper PV ostia are visible in almost 90% of cases, the ostia of the lower PVs may be explored in about 30–40% of cases. The difficulty in consistently imaging the lower pulmonary veins may be due to the different angulations by which the lower veins drain into the left atrium, making them less favourable for 3D TEE visualization. Thus, electrophysiologists often refer to other imaging techniques such as CT scan or MRI to define pre-procedural anatomy and variant of the PVs.

3D TEE During CVTI Ablation

An effective use of 3D TEE as a guidance imaging modality during CVTI ablation requires several assumptions. First, 3D TEE images of the target structures should be immediately and intuitively comprehensible by the electrophysiologists. This implies, when possible, that the 3D TEE imaging of target structures should have perspectives similar to X-ray projections (Fig. 44.3).

Second, 3D TEE should be able to follow fast catheter movements and, at the same time, the acquisition of the volumetric pyramid data set should be large enough to include the entire area of CVTI. Unfortunately, a large pyramidal data set implies a low frame rate, which, in turn, makes it difficult to track reliably catheter movements. An acceptable compromise between the largest possible field and the highest possible frame rate is the acquisition of a pyramidal data set of $60^\circ \times 60^\circ$ that allows a frame rate of 9–10 Hz. Third, the 3D TEE resolution should be high enough to recognize the catheter tip-tissue contact point during energy delivery. Once again, a high spatial resolution requires an increased number of scan lines per volume, which, in turn, reduces the frame rate. However, during ablation with the catheter at a fixed position, the 3D volume data set can be reduced in size (focusing on the catheter tip and immediate surrounding structures) to increase the frame rate while maintaining a high enough spatial resolution.

The widespread use of the 3D TEE during a simple, straightforward procedure (such as a CVTI ablation of 3D TEE) remains limited by the need of deep sedation or even general anaesthesia (which implies an additional time for induction, intubation, extubation and recovery) and the presence of an experienced operator with a fully equipped echo-machine. Recently we have shown that combination of 3D TEE imaging with the traditional fluoroscopy-guided approach may significantly reduce the fluoroscopy time and radiation exposure [14]. Thus in selected cases, (such as during pregnancy or in young female at childbearing age) 3D TEE may be useful as additional imaging tool for minimizing the risk of radiation.

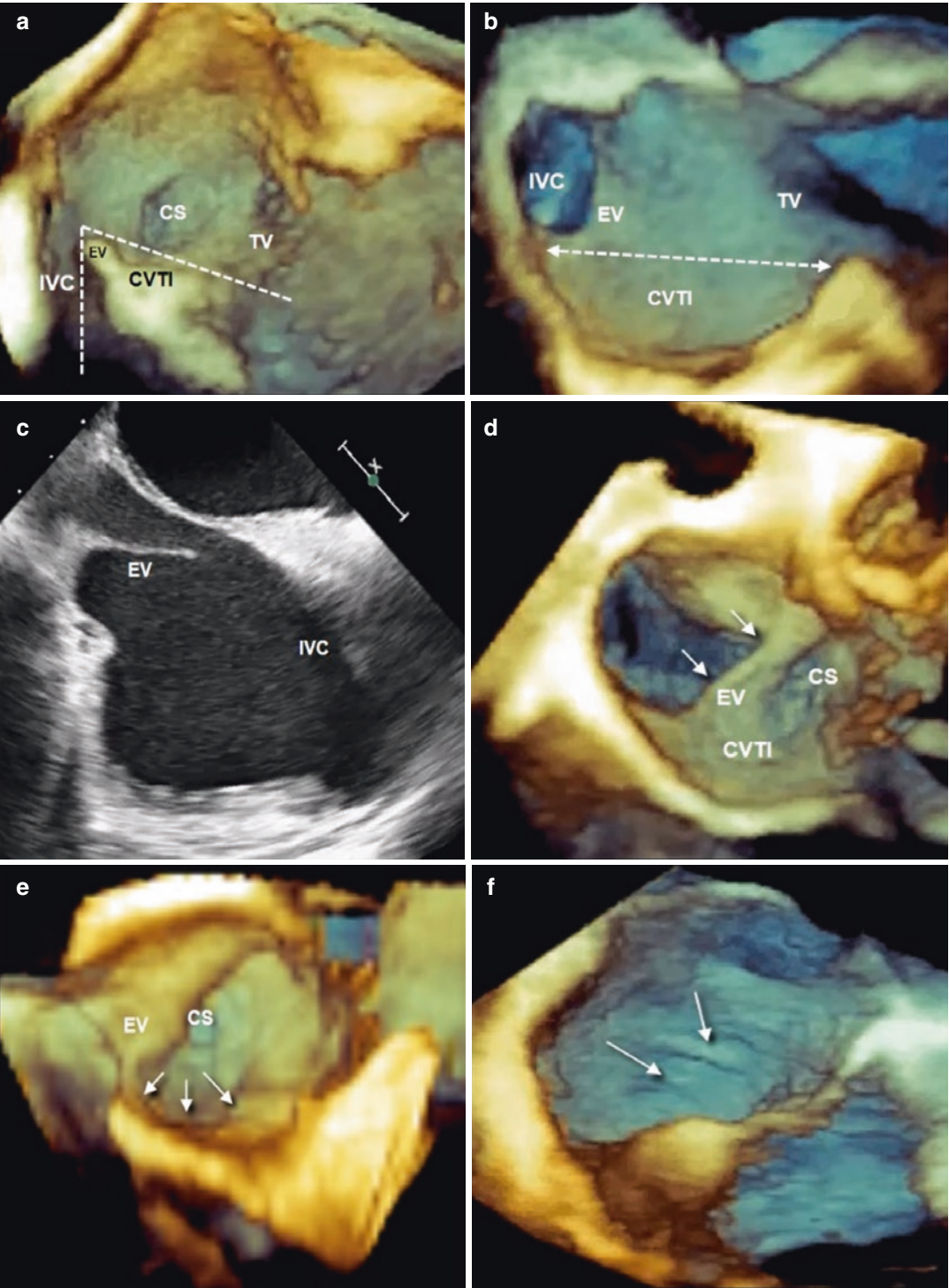


Fig. 44.1 (a) 3D TEE image in a RAO-similar projection, showing the angle between inferior vena cava (IVC) and cavo tricuspid isthmus (CVTI). (b) Diastolic length of CVTI measured on the 3D image. (c) 2D TEE image of a long Eustachian valve (EV). (d) Same case in 3D

TEE. The image show the EV (arrow), the cavo-tricuspid isthmus (CVTI) and the coronary sinus (CS). (e) Deep pouch (arrows) of CVTI. (f) Pectinate muscles (arrows) encroaching the CVTI

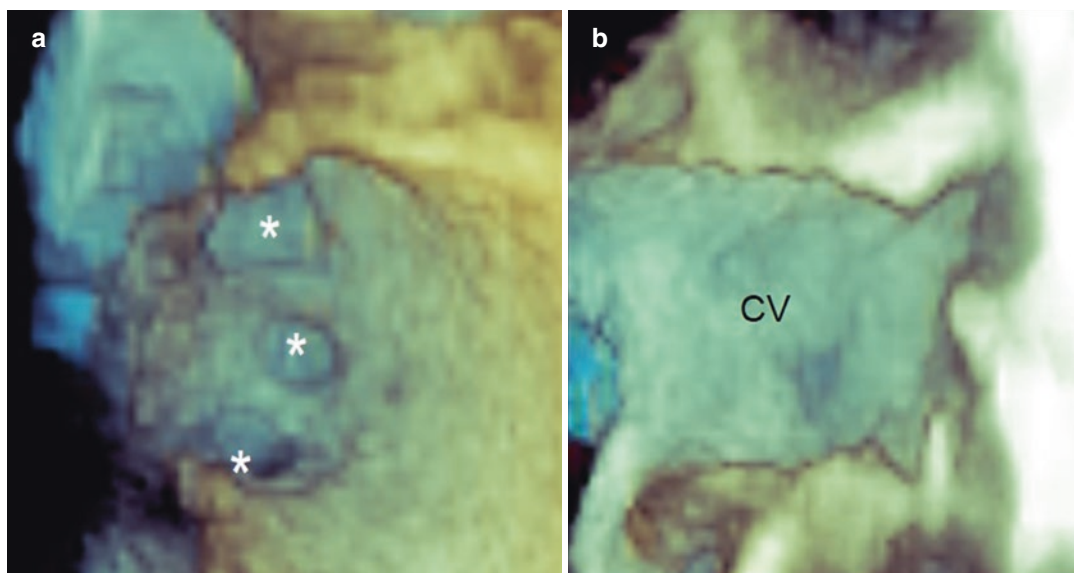


Fig. 44.2 (a) 3D TEE image of three right pulmonary veins (*asterisks*) and (b) a left common vein (CV)

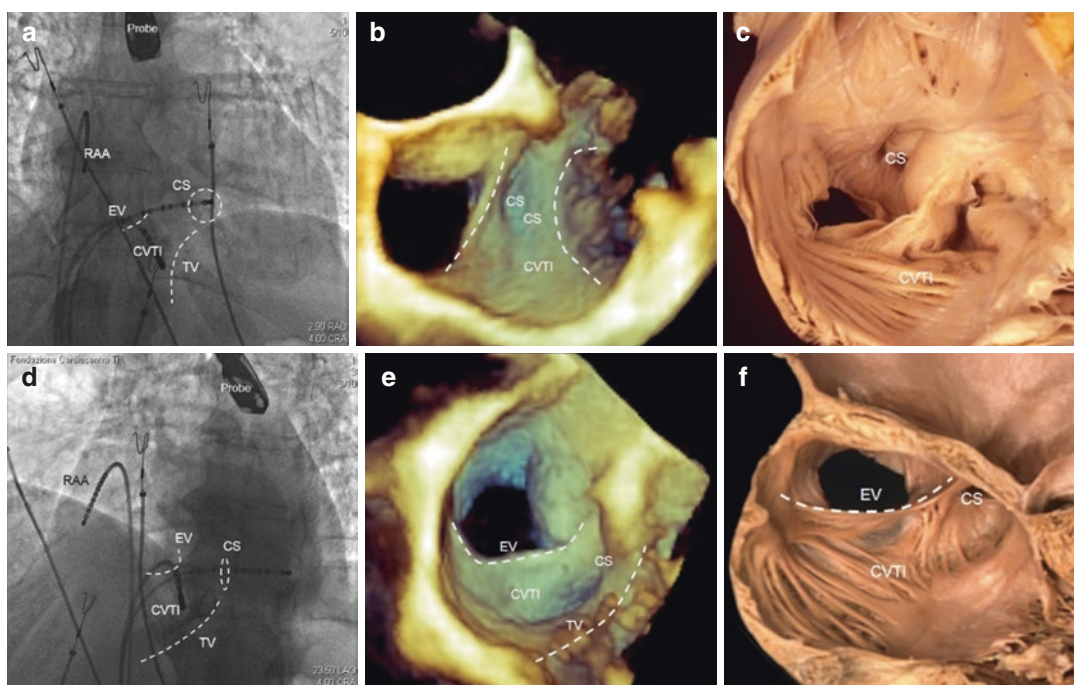


Fig. 44.3 (a) Right oblique anterior fluoroscopic projection (RAO). The dotted lines mark the border of Eustachian valve (EV) and tricuspid (TV) hinge line. The dotted circle marks the orifice of coronary sinus (CS). Corresponding

3D TEE image (b) and (c) anatomic specimen. (d) Left oblique anterior fluoroscopic projection (LAO); (e) the corresponding 3D TEE image and (f) anatomic specimen

Figure 44.4 shows two different moments of CVTI ablation monitored by 3D TEE with favourable outcome.

3D TEE During PV Ablation

The first step of ablation of PVs requires transseptal crossing of two catheters (i.e. mapping and ablation catheters). Although experienced operators may perform the double puncture using only fluoroscopy, nowadays most electrophysiologists require 2D TEE at least for complicated punctures (i.e. extreme rotation of cardiac axis, repeat transseptal punctures, small size or aneurysm of fossa ovalis). 3D TEE may have the additional advantages compared with 2D TEE of imaging both catheters crossing the atrial septum in a single perspective (Fig. 44.5).

Although theoretically feasible (Fig. 44.6) 3D TEE guidance of PV ablation is more challenging than CVTI ablation for the following reasons: first, rarely 3D TEE visualizes all four PVs orifices in the same patient. Second, despite their different shapes, discrimination between mapping and ablation catheter may be difficult especially when they are close each other. Third, when compared with electro-anatomic mapping system, 3D TEE has

limited sensitivity in exactly identifying the catheter tip location [personal data].

Finally, there are at least two reasons of concern regarding the use of 3D TEE during ablation of PVs. First, oesophageal displacement required for visualization of the pulmonary veins may deform atrial geometry and interfere with catheter manipulation. Second, the 3D TEE probe produces heat that may augment the heating produced by the procedure when radio frequency energy is used. Whether this new source of heat may increase the risk of potential injury to the oesophageal wall or affect the efficacy of the procedure is still unknown.

In conclusion, because of the above-mentioned reasons, we cannot suggest, at this time, the widespread use 3D TEE during PVs ablation. New ultrasound imaging modalities (see below X-ray-echo fusion imaging) may renovate the interest of 3D TEE during EP procedures.

Percutaneous Closure of Left Atrial Appendage

Introduction

Atrial fibrillation (AF) is the most common sustained cardiac arrhythmia with a prevalence of 0.4–

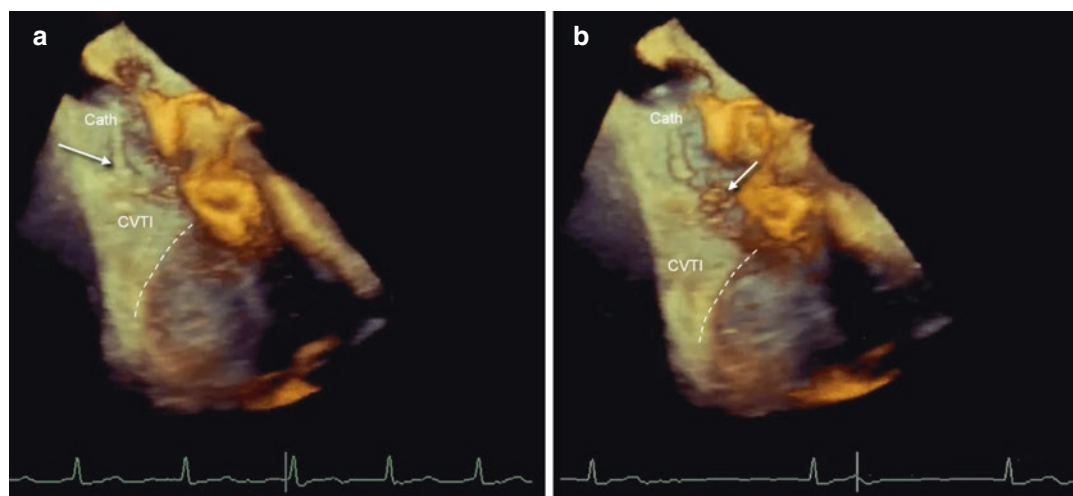


Fig. 44.4 (a) 3D TEE image showing the CVTI in LAO-similar perspective. The arrows points at the tip of catheter (Cath). The EKG shows a typical atrial flutter. (b)

Micro bubbles caused by the cavitation phenomenon produced by tissue heating during energy delivery (arrow). The EKG show the recovery of sinus rhythm

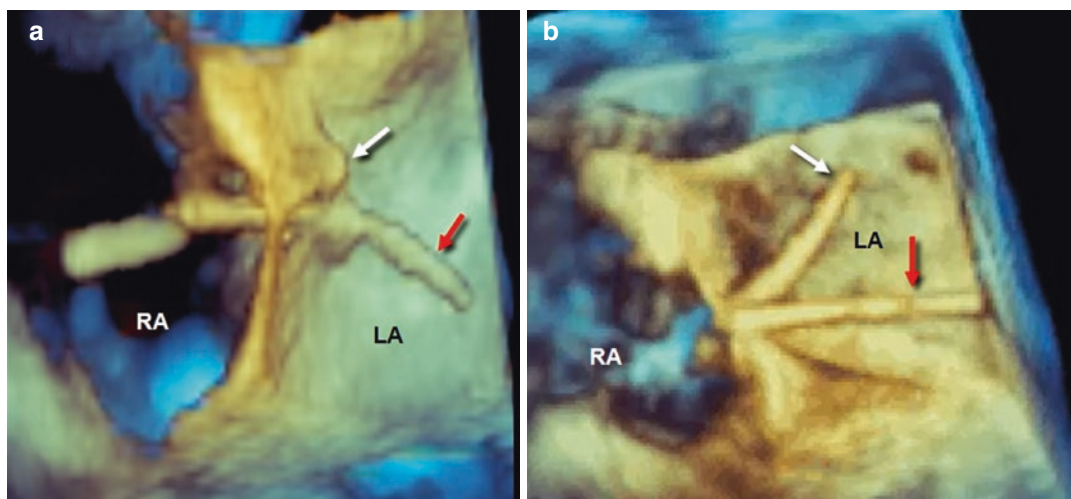


Fig. 44.5 (a) 3D TEE image in LAO-similar perspective showing one catheter already in left atrium (LA) (red arrow) and one catheter forcing against the atrial septum

from right atrium (RA) causing the so-called “tenting” (white arrow). (b) Both catheters in LA (red and white arrow)

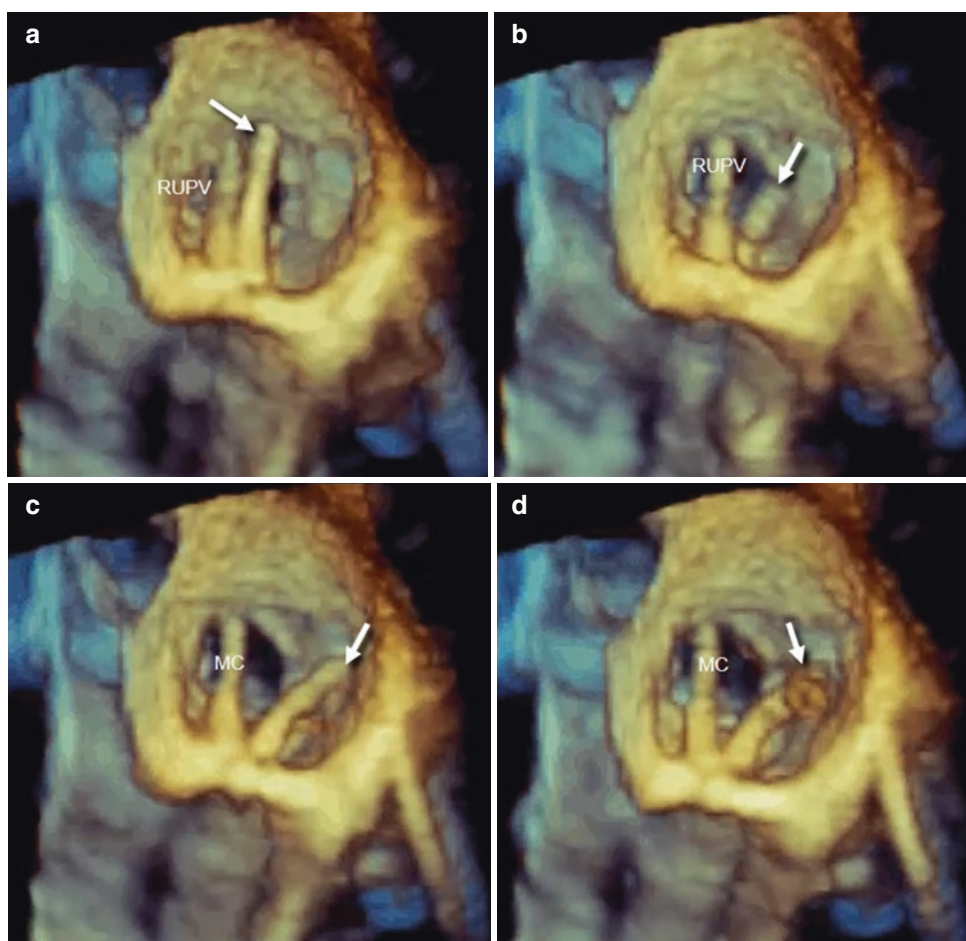


Fig. 44.6 Consecutive 3D TEE images of the ablation of the right upper pulmonary vein (RUPV). The arrow points at the tip of the ablating catheter, which moves from the

(a) 12 o’ clock to (b, c) 2 o’ clock position. (d) Microbubble due to cavitation flowing from the point of energy delivery (arrow). MC mapping catheter

1.0% of the general population. The lifetime risk of developing AF is as high as 26% for men and 23% for women [15]. The prevalence of AF in individuals aged 65–75 years is of 3–5% and rises up to 9% in patients older than 80 years. Unfortunately, AF is associated with a significant mortality and morbidity, due to heart failure and fatal or disabling stroke. Indeed, AF accounts for 15–20% of stroke in general population and up to 30% in patients >80 year old [16]. Accordingly, the medical treatment focuses on rate and/or rhythm control and prevention of thromboembolism. Anticoagulation therapy is effective in reducing the risk of stroke particularly in patients with AF and high stroke risk (i.e. patients with congestive heart failure, hypertension, diabetes mellitus, previous stroke or transient ischemic attack and age >75 years ($\text{CHADS}_2 > 1$)). On the other hand anticoagulation remains an *iatrogenically induced disease* especially for patients exposed to the therapy for decades. Difficult balance between efficacy and risk of bleeding, drug-drug interactions and risk of major bleeding in case of traumatic events remain, in fact, the major drawbacks for a long-term anticoagulant therapy. Although the new oral anticoagulant (NOACs) appear to have a wider therapeutic window, less drug-drug interactions and no need for frequent blood tests, a bleeding risk remains with any anticoagulant therapy and, though reduced, the risk of cerebrovascular embolism is not totally abolished. In addition, a significant percentage of patients with AF (from 10% to 30%) have contraindications to anticoagulation.

Rational for Percutaneous Occlusion of LAA

The rapid and uncoordinated muscular atrial tissue contraction leads to blood stasis particularly pronounced in the left atrial appendage (LAA) due to its particular “cul-de-sac” configuration and a narrow entry orifice. 2D TEE studies have shown that in non-valvular AF more than 90% of thrombi formation occur in in LAA [17]. Thus, percutaneous LAA closure with specifically designed devices has emerged as an appealing option for stroke preventions. Clinical trials have shown that this procedure is non-inferior to anticoagulation with respect to the primary endpoint of stroke, cardiovascular death or systemic embolism [18].

The Role of 2D/3D TEE in Pre-procedural Assessment

The LAA has a complex and extremely variable structure: muscular bundles (pectinate muscles) partially divide the main cavity into cubicles of variable sizes. Secondary cavities (lobes) may extent out from the main cavity in different directions. Because the type and size of occluder is strictly dependent on the size and shape of LAA, understanding this complex anatomy is of paramount relevance. 2D TEE is the first line imaging technique before the procedure to exclude pre-existing thrombi and to assess the suitability for LAA closure. In particular, 2D TEE allows an accurate sizing LAA. A 180° rotation of the transducer located at mid-esophageal level ensures a complete scanning of LAA and accurate measurements of the maximum dimensions of the orifice, landing zone (measured immediately below the circumflex artery) and length of main lobe (Fig. 44.7).

On the other hand, 3D TEE appears to be particularly appropriate for imaging LAA. First, the LAA is a relatively small structure positioned roughly at the same depth as the mitral valve. This favorable combination provides images of exquisite quality (due to the high line density) and with high frame rate (due to the small volume scanned). Second, the LAA orifice may be visualized in “en face” and diameters, circumference and area of the LAA orifice can be reliable measured [19]. Finally, appropriate longitudinal cuts may reveals the presence, site and size of secondary lobes arising from the main LAA body. Because of its complex anatomy, it is likely that measurements taken from 3D TEE are more accurate than the corresponding 2D measurements [19]. Dedicated software allows measuring of diameter of LAA orifice and landing zone and maximum depth using either multi-planar reconstruction or directly on 3D images (Fig. 44.8).

2D/3D TEE Guidance During the Procedure

The procedure consists of the following steps:

- (a) A trans-septal puncture in the middle portion of the fossa ovalis (which allows a coaxial

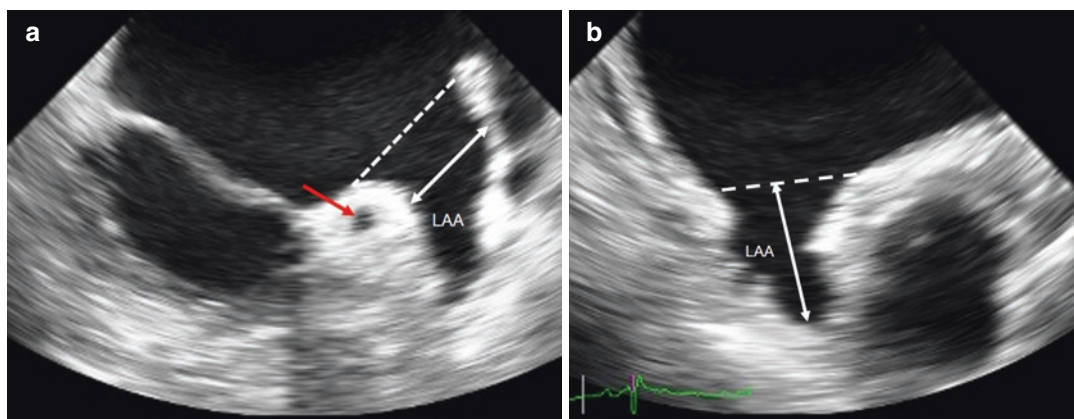


Fig. 44.7 2D TEE image of left atrial appendage (LAA) in two perpendicular planes. (a) The image shows where to measure the diameter of the LAA orifice (*dotted line*) and

the diameter of the “landing zone” (*double head arrow*). The red arrow point at the circumflex artery. (b) The double head arrow indicates the maximum depth of the main lobe

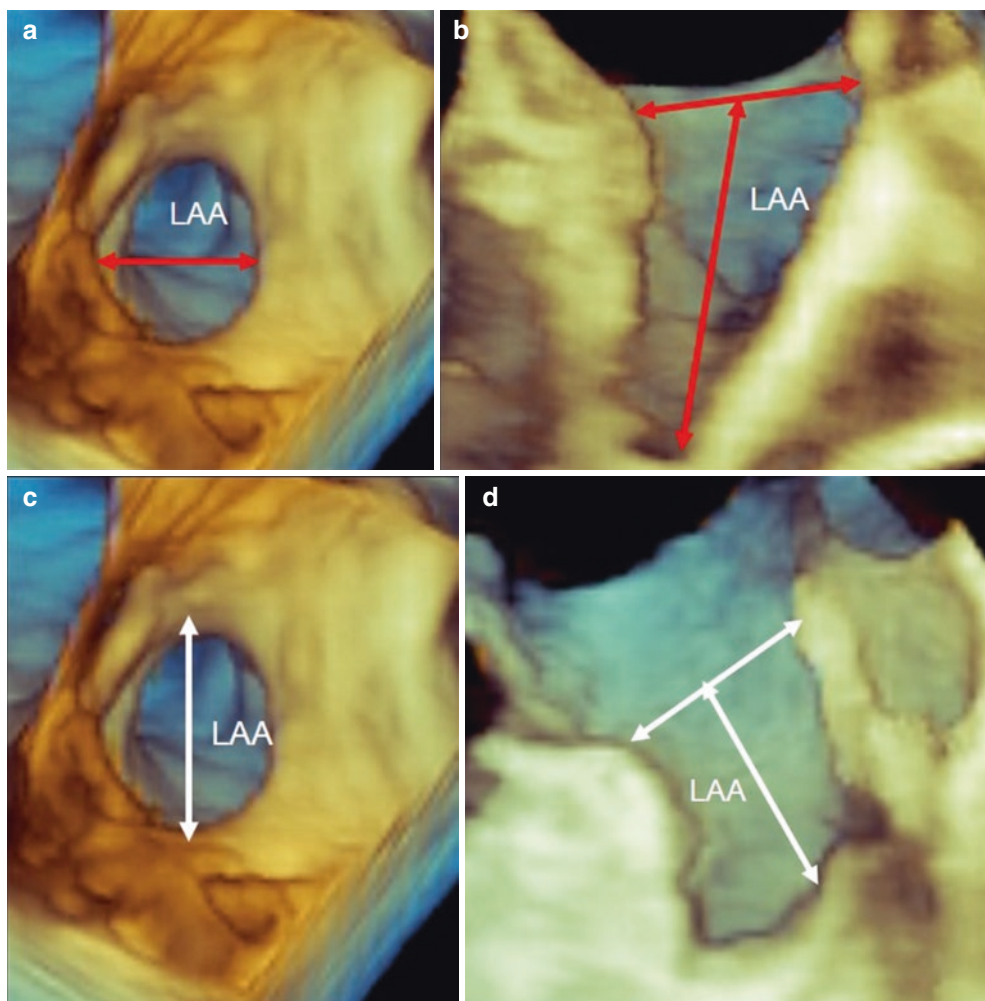


Fig. 44.8 3D TEE image of left atrial appendage in “en face view” (panel a, c) and in long axis views (Panel b and d). Showing the minimum (red double head arrow in

panel a) and maximum diameter (white double head arrow in panel c) of the orifice and the depth in two longitudinal cuts

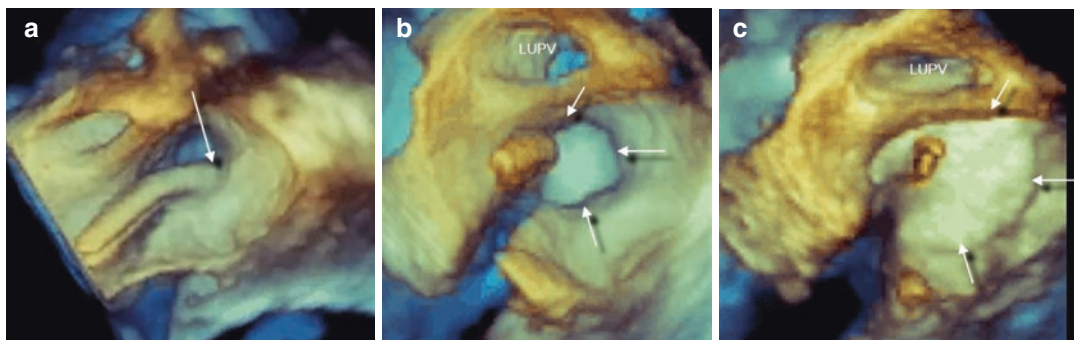


Fig. 44.9 3D TEE image of consecutive steps of the LAA occlusion. (a) catheter inside the LAA (arrow). (b) The act of opening the lobe (arrows) and (c) the disc. LUPV left upper pulmonary vein

engagement of the LAA). The ‘tenting’ of the fossa ovalis marks the site of the puncture.

- (b) Advancement of the tip of guide catheter into the LAA
- (c) Deploying the device in the LAA
- (d) Pull-push maneuver
- (e) Withdrawal of delivery system

Images presented in the following pages refer to the deployment of an Amplatzer occluder.

Fluoroscopy with 2D or, more recently, with 3D TEE can follow each of these steps with the same efficacy. Of course, 3D TEE, providing panoramic 3D images that including long segments of catheters, allows a better understanding of spatial relationship between catheter and LAA (Fig. 44.9).

However, once the catheter is inside the LAA both 2D and 3D TEE are effective in following the deployment of the lobe and the disc of the occluder.

Fusion Imaging

As seen above, fluoroscopy and 2D/3D TEE are the imaging modalities for guiding LAA occlusion. Recently a new system of X-ray-echo live fusion, which combines the excellent instrument imaging of X-ray with the high-quality soft tissue imaging of ultrasound, emerges as a new imaging tool for guiding percutaneous SHD procedures. There are several reasons because this new system will work.

First, both fluoroscopy and 2D/3D TEE are well suited for merging since both are real-time imaging modality and have complementary abilities. Echocardiography perfectly displays soft tissues, but has a narrow field of view including only narrow sectors of the heart. Moreover, echocardiographic images suffer from reverberations and shadowing caused by catheters and devices. On the other hand, while soft tissue are almost invisible to fluoroscopy and it is difficult to orient in three-dimensional space using only fluoroscopy, fluoroscopic images embrace the entire heart and the chest and may transitorily display chamber and vessel cavities filled with contrast. Moreover, fluoroscopy perfectly defines all types of wires, catheters and metallic devices since this interventional equipment have been originally designed for X-rays.

Second, the system aligns 2D/3D TEE images into X-ray fluoroscopic coordinate system. Any time the C-arm of fluoroscopy moves, the 3D TEE image automatically rotates according to the new X-ray projections (the so-called image-based tracking). Moreover, by means of a mouse, the echocardiographer may crop, rotate or make more transparent the 3D TEE images. Interventional cardiologists (or electrophysiologists) are accustomed to fluoroscopic projections such as antero-posterior (AP), right anterior oblique (RAO) left anterior oblique (LAO) with various degrees of angulation, and cranial or caudal tilting. Since the system adapts echo

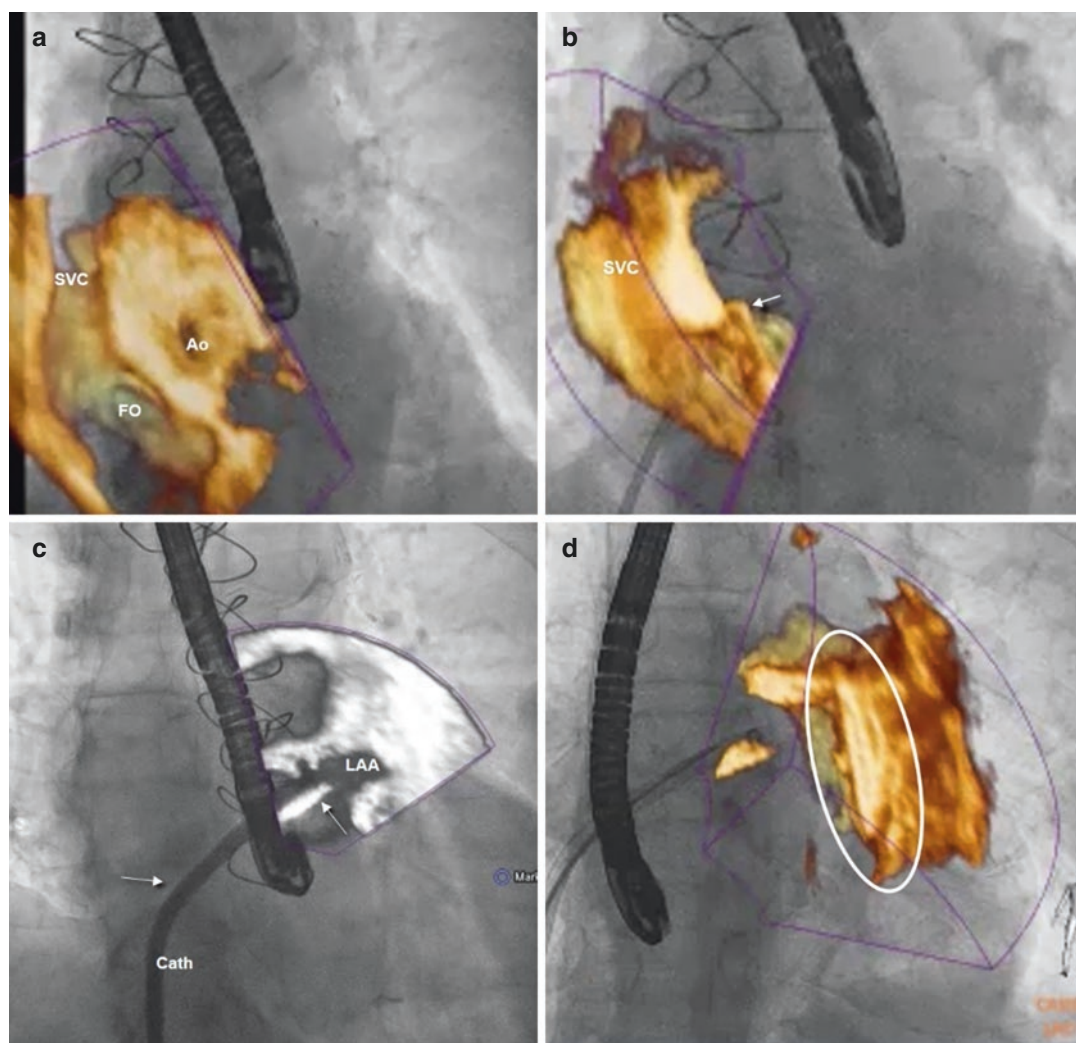


Fig. 44.10 X-ray-echo fusion imaging of consecutive steps of the LAA occlusion. (a) Delineation of fossa ovalis (FO) and superior vena cava (SVC), (b) catheter inside

the LAA (arrow). (c) The act of opening the lobe (arrows) and (d) the disc

images to X-ray projections, fused images provides a high degree of confidence to the interventionists in understanding various 2D/3D echo perspectives.

Third, interventionists may focus only in one screen during catheter manipulations instead of looking at a large quad-screen monitor with that displays multiple images simultaneously and there is no more need for a mental effort to integrate very different perspectives of ultrasound and X-ray data.

The following figure show different steps of LAA occlusion guided by X-ray-echo fusion (Fig. 44.10).

Conclusion

Currently, fluoroscopy coupled with 2D/3D TEE imaging is the state-of-art to guide LAA occlusion. The novel imaging processing territory opened with X-ray-echo fusion will likely trans-

form the way of guiding percutaneous procedure. Whether this new modality will improve the workflow and catheter navigation, reducing procedural time, increasing patient's safety and improving outcomes needs to be determined.

References

1. Pitzalis MV, Iacovello M, Romito R, et al. Cardiac resynchronization therapy tailored by echocardiographic evaluation of ventricular asynchrony. *J Am Coll Cardiol*. 2002;40:1615–22.
2. Penicka M, Bartuken J, De BB, et al. Improvement of left ventricular function after cardiac resynchronization therapy is predicted by tissue Doppler imaging echocardiography. *Circulation*. 2004;109:978–83.
3. Delgado V, Ypenburg C, Van Bommel RJ, et al. Assessment of left ventricular dyssynchrony by speckle tracking strain imaging comparison between longitudinal, circumferential and radial strain in cardiac resynchronization therapy. *J Am Coll Cardiol*. 2008;51:1944–52.
4. Kapetanakis S, Kearney MT, Siva A, et al. Real-time three-dimensional echocardiography a novel technique to quantify global left ventricular mechanical dyssynchrony. *Circulation*. 2005;112:992–1000.
5. Faletra FF, Ho SY, Auricchio A. Anatomy of right atrial structures by real-time 3D transesophageal echocardiography. *JACC Cardiovasc Imaging*. 2010;3:966–75.
6. Faletra FF, Nucifora G, Ho SY. Imaging the atrial septum using real-time three-dimensional transesophageal echocardiography: technical tips, normal anatomy, and its role in transseptal puncture. *J Am Soc Echocardiogr*. 2011;24:593–9.
7. Martin RE, Ellenbogen KA, Lau YR, et al. Phased-array intracardiac echocardiography during pulmonary vein isolation and linear ablation for atrial fibrillation. *J Cardiovasc Electrophysiol*. 2002;13(9):873–9.
8. Fergusson JD, Helms A, Mangrum JM, et al. Catheter ablation of atrial fibrillation without fluoroscopy using intracardiac echocardiography and electro-anatomic mapping. *Circ Arrhythm Electrophysiol*. 2009;2(6):611–9.
9. Faletra FF, Pedrazzini G, Pasotti E, et al. 3D TEE during catheter-based intervention. *JACC Cardiovasc Imaging*. 2014;7:292–3.
10. Perk G, Lang RM, Garcia-Fernandez MA, et al. Use of real time three-dimensional transesophageal echocardiography in intracardiac catheter-based interventions. *J Am Soc Echocardiogr*. 2009;22:865–82.
11. Lim KY, Murray C, Liu H, Weerasooriya R. Pre-ablation magnetic resonance imaging of the cavotricuspid isthmus. *Europace*. 2007;9:149–53.
12. Kirchhof P, Ozgun M, Zellerhoff S, et al. Diastolic isthmus length and “vertical” isthmus angulation identify patients with difficult catheter ablation of typical atrial flutter: a pre-procedural MRI study. *Europace*. 2009;11:42–7.
13. Asirvatham SJ. Correlative anatomy and electrophysiology for interventional electrophysiologist: right atrial flutter. *J Cardiovasc Electrophysiol*. 2009;20:113–22.
14. Regoli F, Faletra FF, Nucifora G, et al. Feasibility and acute efficacy of radiofrequency ablation of cavotricuspid isthmus-dependent atrial flutter guided by real-time 3D TEE. *JACC Cardiovasc Imaging*. 2011;4:716–26.
15. Lloyd-Jones DM, Wang TJ, Leip EP, et al. Lifetime risk for development of atrial fibrillation: the Framingham Heart Study. *Circulation*. 2004;110:1042–6.
16. Psaty BM, Manolio TA, Kuller LH, et al. Incidence of and risk factors for atrial fibrillation in older adults. *Circulation*. 1997;96:2455–61.
17. Blackshear JL, Odell JA. Appendage obliteration to reduce stroke in cardiac surgical patients with atrial fibrillation. *Ann Thorac Surg*. 1996;61:755–9.
18. Bayard YL, Omran H, Neuzil P, et al. PLAATO (Percutaneous Left Atrial Appendage Transcatheter Occlusion) for prevention of cardioembolic stroke in non-anticoagulation eligible atrial fibrillation patients: results from the European PLAATO study. *EuroIntervention*. 2010;6:220–6.
19. Nucifora G, Faletra FF, Regoly F, et al. Evaluation of the left atrial appendage with real-time 3-dimensional transesophageal echocardiography. Implications for catheter-based left atrial appendage closure. *Circ Cardiovasc Imaging*. 2011;4:514–23.

Index

A

- Abscess, 360
- Acceleration time (AT), 421
- Acquisition rates, 859
- Acute aortic syndromes, 193
- Acute chest pain
 - medicolegal implications, 468
 - problem, 467–468
 - work-up in, 468–469
- Acute coronary syndromes, non-ST elevation, 460
- Acute myocardial infarction (AMI), 452, 457–458
 - contrast echocardiography, 566
 - echocardiography usage, 470
 - global left ventricular function, 475–476
 - global left ventricular shape, 476–477
 - infarct expansion, 476
 - left ventricular diastolic function, 480–482
 - left ventricular spatial flow pattern, 482–483
 - quantitating left ventricular function, 477–478
 - remote asynergy, 475
 - silent complications, 485
 - V-HeFT trials, 477
- Acute pulmonary embolism, echocardiography, 416–417
- Adenosine, 493
- Adults with congenital heart disease (ACHD)
 - associated anomalies, 819
 - atrial situs, 818
 - atrioventricular valve morphology, 819
 - cardiac morphology, 819
 - cardiac position, 818
 - ccTGA (*see* Congenitally corrected transposition of the great arteries (ccTGA))
 - complications, 817
 - double switch operation, 831
 - D-type ventriculo arterial discordance, 819
 - echocardiographic assessment in patients after surgical repair, 831
 - follow up, 817
 - L-type ventriculo arterial discordance, 819
 - palliative surgery, 831
 - physiologic REPAIR, 831
 - segmental analysis, 818–819
 - sequential segmental approach, 818
 - spectrum of, 817
 - TGA (*see* Transposition of the great arteries (TGA))
 - thoraco-abdominal status, 818
 - TOF (*see* Tetralogy of Fallot (TOF))
 - transesophageal/three dimensional echocardiography, 831–832
 - transthoracic echocardiography, 818
 - ventricular topology, 818–819
 - ventriculo-arterial relationships, 819
- Albunex, 542
- American Society of Echocardiography (ASE), 141, 937
- Amyloid heart disease, 609
- Amyloidosis, 874, 875
- Anaphylactic reaction, treatment, 570
- Anemia, 330
- Aneurysm, 360
- Annulo-leaflet mitral band, 296
- Anterior mitral leaflet (AML) pathology, 988–990
- Anterior mitral valve leaflet (AMVL), 204, 210
- Anterior wall ischaemia, 458
- Anterolateral muscle, 208
- Anthracyclines, 604
 - cardiac toxicity, 922–923
 - global longitudinal strain, 928
 - three-dimensional LVEF, 925
 - trastuzumab and, 923
- Anti-anginal therapy, 502
- Anti-ischemic therapy, 491
- AoCoA, *see* Coarctation of the aorta (AoCoA)
- Aorta, echo assessment, 191
- Aortic aneurysm
 - aortic rupture, 722–723
 - definition, 722
 - etiologies, 722
 - imaging, 723
 - pseudoaneurysms, 722
- Aortic arch (AA), 40
- Aortic atheroma, 762
- Aortic atheromatous disease
 - classification, 733
 - clinical significance, 733–734
 - imaging, 734–735
 - pathophysiology, 732
 - transthoracic imaging, 720

- Aortic coarctation, 735–736
 Aortic diastolic flow reversal, 108
 Aortic disease, 167–168, 633
 Aortic disorders
 annular size, 721
 aortic root dimensions, 723
 aortic trauma, 732
 DeBakey and Stanford classification systems, 726
 descending thoracic aorta, 722
 imaging, 731–732
 intramural hematoma, 728–731
 parasternal views, 719
 penetrating aortic ulcers, 731–732
 suprasternal view, 720
 transesophageal imaging, 721–722
 transthoracic imaging, 719, 720
 Aortic dissection, 193–194
 aortic regurgitation, 728
 classification, 726
 clinical presentation, 726
 coronary arteries, 727–728
 echocardiographic findings, 726–727
 etiologies, 724–726
 false lumen, 727
 imaging, 724
 intimal flap, 727
 pathophysiology, 724
 pericardial effusion, 728
 risk factors for, 725
 surgery, 728
 Aortic leaflet, 66
 Aortic position, 330, 342
 Aortic regurgitation (AR), 52, 101, 106–109, 191, 318, 633
 bicuspid aortic valve with, 837
 causes, 187
 clinical decision making in, 189
 continuous wave Doppler, 189
 echo assessment of, 187
 flow reversal in thoracic/abdominal aorta, 189
 masses on aortic valve, 190
 pathophysiology, 185–187
 quantification of, 187–188
 quantification of flow, 188–189
 quantitative analysis of, 190
 surgical management, 190
 TVI (TVIAR), 107
 Aortic root, 177
 Aortic rupture, 722
 Aortic sinuses, 177, 968
 Aortic stenosis (AS), 102–103, 151, 177–179
 anatomy and physiology, 783
 asymptomatic patient with, 316
 cautions, 785
 changes in LV function, 315
 clinical decision making in, 184
 continuity equation, 184
 echo assessment of, 179–184
 examination, 783
 exercise echocardiography, 315
 exercise testing, 314–315
 impact on management, 315
 with impaired LV function, 184–185
 low flow/low gradient, 315–318
 mean gradient, 315
 morphology, 179–182
 pathophysiology, 179
 with preserved LV function, 185
 quantification of, 182–185
 systolic pulmonary artery pressure, 315
 3D echocardiography, 785
 transcatheter aortic valve implantation, 963
 transesophageal echocardiography, 784–785
 2D transthoracic echocardiography, 784
 Aortic syndrome, acute, 193–196
 Aortic trauma, 732
 Aortic valve, 163
 anatomy, 65, 177
 aortic leaflet, 66–70
 ventriculoarterial junction, 65
 hypertrophic cardiomyopathy, 590
 masses on, 190
 Aortic valve area (AVA), 100, 184
 Aortic valve closure (AVC), 869
 Aortic valve disease, 185
 AR, *see* Aortic regurgitation (AR)
 Arcade lesion, mitral valve, 292
 Arrhythmic right ventricular cardiomyopathy (ARVC)
 apical four-chamber view, 614, 615
 athlete's heart *vs.*, 912
 definitions and pathophysiology, 612
 diagnosis, 612–614
 echocardiographic characteristics, 614–615
 right ventricle enlargement from, 913–914
 triangle of dysplasia, 615
 Arterial shunt, 838
 Arterial switch operation (ASO), 808, 826
 AS, *see* Aortic stenosis (AS)
 Ascending aorta, 721
 ASD, *see* Atrial septal defect (ASD)
 Asymmetric septal hypertrophy (ASH), 584
 Atherosclerotic ulcer, 195
 Athlete's heart
 arrhythmic right ventricular cardiomyopathy, 912–913, 915, 916
 cardiac adaptation, 899–900
 cardiac dimensions in, 900–903
 cardiopulmonary exercise testing, 909–911
 diastolic function, 907–908
 vs. dilated cardiomyopathy, 911–912
 dynamic training, 899
 echocardiogram, 904
 echocardiographic upper reference limits, 903
 electrocardiogram, 909, 914
 end-diastolic left ventricular cavity size, 903
 history and demographics, 904
 vs. hypertrophic cardiomyopathy, 903
 vs. isolated left ventricular non compaction, 914–919
 left ventricular hypertrophy

- cavity size, 906–907
 - magnitude, 904–906
 - outflow tract obstruction, 907
 - pattern, 906
 - multi-faceted assessment, 904
 - physiological adaptation, 901
 - physiological cardiac changes, 918
 - QRS voltages, 910
 - repeat assessment after detraining, 909
 - right ventricular outflow tract dimensions, 914
 - static training, 900
 - sudden death, 899
 - systolic function, 908–909
 - Atrial arrhythmias, 167, 759
 - Atrial ejection force, 668
 - Atrial electromechanical interval (AEMI), 749
 - Atrial fibrillation, 167, 740
 - Atrial pouch, 85
 - Atrial redirection procedures, 808
 - Atrial septal aneurysm (ASA), 740, 757
 - anatomy, 756
 - echocardiographic assessment, 761
 - echocardiography impact on patient management, 762
 - potential mechanisms of stroke, 758
 - thoracic aortic atheroma, 760
 - treatment, 759
 - Atrial septal defect (ASD)
 - anatomy and physiology, 768
 - cautions, 771
 - color Doppler image, 769
 - detection and assessment, 1016
 - device closure, 1017
 - diagnosis, 1015
 - echocardiography checklist, 1021
 - fenestrated, 1017
 - follow-up, 1021
 - imaging and recognition, 771
 - immediate post-procedure, 1020
 - intraprocedural, 1019–1020
 - multiplanar reconstruction, 1019
 - overlapping devices, 1021
 - pre-procedure, 1016–1017
 - rims, 1018
 - secundum, 1016
 - sizing of device, 1017–1019
 - transoesophageal echocardiography, 770–771, 1017, 1019
 - 2D transthoracic echocardiography, 768–770
 - Atrial septectomy, 837
 - Atrial situs, 818
 - Atrial switch operation, 825
 - Atrioventricular (AV) delay, 653, 655
 - Atrioventricular (AV) septal defect
 - anatomy and physiology, 778
 - cautions, 779
 - echocardiographic evaluation, 778
 - partial, 778
 - surgical intervention, 778
 - transesophageal echo, 779
 - 2D transthoracic echocardiography, 778–779
 - Atrioventricular compliance, 318
 - Atrioventricular groove, 160
 - Atrio-ventricular septum, 207
 - Atrioventricular valve morphology, 819
 - Automated endocardial border tracking, 462
 - Axial computed tomography, 444
- B**
- Bacterial endocarditis, 703
 - Bacterial vegetations, 704
 - Balloon atrial septostomy, 825
 - Barlow-type pathology, 990
 - Beamformers, 848
 - Bernoulli equation, 29, 126
 - Bicuspid aortic valve, 192, 837, 965
 - Bicuspid valves, 180, 187, 192
 - Bileaflet prolapse, 990
 - Biological valves, 326
 - Biplane Simpson's method, 129
 - Biplane volumetric assessment, 115
 - Bjork modification, 838
 - Blalock–Taussig (BT) shunt, 821
 - Bleeding, 330
 - Blood clots, 431
 - Body surface area (BSA), 99
 - Bolus injections, 549
 - Brock procedure, 821
- C**
- CAD, *see* Coronary artery disease (CAD)
 - Cancer therapeutics related cardiac dysfunction (CTRCD), 922
 - Capillary de-recruitment, 561
 - Carbomedics, 326
 - Carcinoid disease, 300
 - Cardiac allograft vasculopathy (CAV), 636
 - Cardiac amyloidosis, 589, 606, 622
 - Cardiac chamber collapse, 432
 - Cardiac electrical activity, 876
 - Cardiac magnetic resonance (CMR)
 - imaging, 137, 522
 - Cardiac masses, 168
 - abdominal cavity, 707
 - anterior myocardial infarction, 687–689
 - anterolateral muscle bundle, 706
 - artifacts, 712–713
 - atrial appendage, 710
 - bacterial endocarditis, 703
 - bi-leaflet mitral prosthesis, 711
 - central tendon of diaphragm, 706–707
 - clinical context, 685–686
 - Denver shunt, 715, 716
 - diagnosis reemphasized, 686
 - etiologies, 685
 - inferior vena cava, 707, 714
 - interventricular septum, 715
 - intracavitary, 685, 714
 - intramural, 685

- Cardiac masses (*cont.*)
- inverted atrial appendage, 708–709
 - left atrial appendage thrombi, 690
 - mitral regurgitation, 694
 - mitral valve repair/replacement, 709–712
 - MRI/CT images, 686
 - multi-lobulated vegetative mass, 705
 - muscle bundle, 706
 - myxoma, 692–698, 713
 - non-bacterial thrombotic endocarditis, 704–706
 - papillary fibroelastoma, 699, 702, 703
 - parasternal long axis, 694
 - prosthetic mitral ring, 704
 - rhabdomyoma, 698, 700
 - ruptured papillary muscle, 707–708
 - serial diastolic frames, 693
 - superior and inferior venae cavae, 705
 - suspicious mass lesion, 712, 713
 - thrombi, 687–691
 - transducer, 714
 - transesophageal echocardiogram, 712
 - transesophageal four-chamber view, 717
 - ultrasound imaging, 686
- Cardiac morphology, 819
- Cardiac resynchronization therapy (CRT), 76, 150, 643, 1031
- imaging integration, 655–657
 - optimization, 653–655
- Cardiac situs, 791
- Cardiac structural disorders, 621
- Cardiac tamponade, 432
- Cardiac toxicity, 604, 921
- Cardiac ultrasound, 937
- normal cardiac anatomy, 33–34
 - standard imaging planes, 34
 - apical window, 36–38
 - Doppler basics, 40–42
 - left parasternal window, 34–36
 - subcostal window, 38–39
 - suprasternal window, 39–40
 - transducer, 33
- Cardio-embolic events, 756, 763
- Cardioembolic strokes, 166–167
- Cardiomyocytes, 526
- Cardiomyopathies, 577
- amyloid deposition, 607
 - cardiac amyloidosis, 608
 - causes, 578–579
 - classification, 579
 - parasternal short axis, 610
 - peripartum, 605
 - restrictive, 612
 - systemic amyloidosis, 608
- See also specific Cardiomyopathies*
- Cardio-oncology
- contrast enhanced 3D echocardiography, 926–927
 - echocardiographic contrast enhancement, 926
 - radiotherapy, 927–930
 - strain imaging, 930
 - stress echocardiography, 927
 - 3D echocardiography, 924–926
 - 2D based left ventricular strain, 927
 - 2D echocardiography, 923–924
- Cardio-toxicity, 921–922
- Cardiovascular disease, myocardial deformation, 150
- Cavotricuspid isthmus (CVTI), 75
- 2D/3D TEE in, 1032
 - 3D TEE during, 1033
- CHADS2-VASc score, 749
- Chagas Disease, 875, 876
- Chemotherapeutic agents, side effect, 921–922
- Chiari's network, 398
- Chordae tendineae, 62–63
- CHRISTMAS (Carvedilol Hibernation Reversible Ischemia Trial: Marker of Success) trail, 538
- Chronic ischemic dysfunction, 529
- Circumferential uniformity ratio estimate (CURE), 649
- Circumflex artery, 508
- Coanda effect, 226
- Coarctation of the aorta (AoCoA), 735
- anatomy and physiology, 785–786
 - cautions, 787
 - diagnosis, 785
 - 3D echocardiography, 787
 - transoesophageal echocardiography, 787
 - 2D transthoracic echocardiography, 786–787
- Color Doppler imaging, 300
- analysis, 97
 - display, 53
- Color flow Doppler, 40, 41, 96, 104, 107, 187, 497
- Color flow imaging
- advantages, 24
 - limitations, 25–26
- Color tissue Doppler imaging, 135, 136
- Colour-coded TDI, 668, 669
- Complex aortic atheroma, 749
- Congenital absence, pericardium, 443
- Congenital anomaly, mitral valve, 286–296
- Congenital heart disease (CHD), 168
- abdominal vessels, 793–796
 - atrial appendages, 792
 - atrioventricular septal defect, 799
 - building blocks, 791
 - cardiac apex, 797
 - case study, 890
 - characteristic features, 793, 795
 - crab view, 799
 - discordant atrioventricular connections, 798
 - double orifice mitral valve, 800
 - ductal cut, 803
 - Ebstein's anomaly, 795, 801
 - follow-up after atrial redirection procedures, 808
 - Fontan circulation, 808–815
 - functionally single ventricle circulation, 814
 - left ventricle, 792
 - malformations, 767–771
 - mitral valve, 792
 - neo-aorta, 808
 - normal and parachute mitral valves, 800
 - outflow tracts, assessment, 795–799
 - parasternal long axis view, 797, 802

- parasternal short axis view, 802
- pre and post cardiac catheterization, 890
- pulmonary veins, 797
- sequential segmental approach, 791–793
- single ventricle, 795
- sonographic window, 794
- specific cardiac lesions, 801
- strain analysis in, 892–895
- suprasternal coronal view, 803, 804
- surgical repair, 804
- tetralogy of Fallot, 802–807
- transoesophageal echocardiography, 792
- transposition of the great arteries, 807
- tricuspid regurgitation caused by, 300
- tricuspid valve, 792
- two-dimensional strain analysis, 891
- Z-scores in growing patients, 799–801, 804
- Congenital isolated pulmonary valve, 307
- Congenitally corrected transposition of the great arteries (ccTGA)
 - anatomy and physiology, 829
 - aortic arch sidedness, 831
 - assessing ventricular function, 831
 - associated lesions, 829–830
 - atrioventricular and ventriculoarterial discordance, 829
 - AV valve morphology and function, 830
 - cardiac position and atrial situs, 830
 - LVOT obstruction, 831
 - transthoracic echocardiography, 830–831
 - ventricular morphology and atrioventricular connection, 830
 - ventriculoarterial connection, 830
- Congestive heart failure, 271
- Constrictive pericarditis, 611
 - causes of, 437
 - circumferential pericardium, 443
 - clinical features, 438
 - diastolic assessment, 440
 - echocardiographic findings, 438
 - etiologies, 437
 - intrathoracic and intracardiac pressures, 438–440
 - longitudinal systolic strain, 441
 - Mayo Clinic diagnostic criteria, 441–442
 - mid-ventricular septal M-mode recording, 439
 - pathology and pathophysiology, 437
 - pulsed-wave Doppler recording, 438, 439
 - strain imaging, 440
 - test performance characteristics, 442
- Constrictive pericarditis (CP), 151
- Continuity equation, 99–100, 126–127
 - aortic stenosis, 184
 - clinical applications of, 100–101
- Continuous wave (CW) Doppler, 40, 42, 121, 188, 189, 223, 301
- Continuous wave (CW) spectral Doppler, 29
- Contrast echocardiography
 - acute coronary syndrome, 566
 - acute myocardial infarction, 566–567
 - attenuation, 559
 - bolus injections, 549–550, 562–563
 - clinical indications, 551
 - commercially available, 542
 - constant infusion, 550
 - destructive imaging techniques, 545
 - dobutamine stress echo, 558, 565
 - Doppler signals, 556
 - free gas bubble, 543
 - global and regional left ventricle function, 550
 - global left ventricular function, 554
 - harmonic imaging, 546–547, 553
 - high MI MCE, 564–566
 - infusion, 563
 - interventional therapy, 829
 - intracardiac masses, 554–555
 - left ventricular apical thrombus, 553–554
 - low MI MCE, 563–564
 - low MI real-time perfusion imaging, 564
 - LVO image quality, 552
 - microbubbles, 542–545, 549
 - molecular imaging, 570–571
 - myocardial perfusion, 559–560
 - myocardial viability studies, 567–569
 - non-destructive imaging techniques, 547
 - power modulation, 548, 556
 - power pulse inversion, 548–549
 - pulse inversion Doppler, 547
 - quantitative contrast colour kinesis, 555
 - second harmonic imaging, 545
 - side effects, 570
 - sonothrombolysis, 570
 - stress echocardiography, 556–559
 - stress MCE, 560–562
 - therapeutic applications, 570
 - 3D contrast studies, 571
 - transpulmonary passage, 542
 - types of, 541–542
 - ultra harmonics, 545–546
- Conventional colour Doppler mapping, 404
- Cor triatriatum, 295
- CoreValve, 962, 963
- Coronary angiography, 637
- Coronary angioplasty, 629
- Coronary arteries, 177, 727–728
- Coronary artery bypass graft (CABG), 521
- Coronary artery disease (CAD), 150
 - diagnosis, 507
 - echocardiography, 451
 - etiological factor, 620
 - progression, 452
 - regional wall motion abnormality, 451–452
 - severity and prognosis, 451
 - ultrasound technology, 451
 - wall motion vs. systolic wall thickening for assessment, 452–453
- Coronary atherosclerosis, 954
- Coronary CT, stress echocardiography vs., 511
- Coronary sinus (CS), 75–78, 177, 213
- Coronary sinus septal defect, 768
- Coronary vasodilator stress, 493
- Crista supraventricularis (CSV), 87
- Cytoskeletal proteins, 526

D

Deformation imaging
 in cardiac chambers
 assessment of RV deformation, 144–146
 right ventricle, 144
 tissue Doppler imaging derived velocities, 144
 velocity and displacement, 131–132
 Degenerative disease, 187
 Dehiscence, 330
 Delayed-enhanced cardiac magnetic resonance (DE-cMR), 537
 Denver shunt, 715, 716
 Destination therapy, 632
 Destructive imaging techniques, 545
 Di George syndrome, 820
 Diastolic dysfunction, 623–624
 Diastolic function
 assessment, 123
 left ventricular, assessment of, 120
 Didactic education, 942
 Dilated cardiomyopathy (DCM), 150
 apical four-chamber view, 602
 athlete's heart vs., 911
 cardiac toxins, 604
 Doppler echocardiography
 family screening, 603
 intracardiac flow and risk of embolisation, 602
 LV pressures estimation, 601–602
 mitral regurgitation, 601
 tissue Doppler imaging, 602–603
 echocardiography role, 600–601
 familial/genetic DCM, 600
 idiopathic, 599–600
 isolated left ventricular non-compaction, 605
 myocarditis, 603
 pregnancy and parturition, 604–605
 with reduced contraction, 604
 Dipyridamole, 492, 493
 Direct Flow, 963
 Dobutamine, 318, 492–493
 in dysfunctional segments, 529, 530, 532
 echocardiography, 489, 514, 637
 Dobutamine stress echocardiography (DSE), 185, 317, 471, 535, 829
 Doppler assessment, hemodynamics, 96
 Doppler basics, 40
 Doppler compression, 55
 Doppler echocardiography, 95, 125
 diastolic events, 590
 family screening, 603
 intracardiac flow and risk of embolisation, 602
 intraventricular flow velocity, 592
 LV pressures estimation, 601
 mitral regurgitation, 592, 601
 principles, 18–20
 systolic events, 591
 tissue Doppler imaging, 602
 Doppler effect, 19, 40, 51
 Doppler frequency, 19
 Doppler modes, 24, 28
 Doppler of pulmonary veins, 105
 Doppler principle, 95–97

Doppler shift, 19, 27, 95
 Doppler tissue imaging (DTI), 123
 Doppler velocity tracings, 626
 Ductal cut, 798
 Dyssynchrony
 atrioventricular node, 877
 cell-to-cell conduction, 879
 characteristic hypocontractility, 875
 CRT device, 876
 ECG, 883
 electrical activation-contraction coupling, 878–880
 functional abnormalities, 871
 functional patterns, 869–874
 Kaplan–Meier curves, 884
 LBBB and, 876
 localized posterior wall infarction, 874
 mitral insufficiency, 872
 parasternal long axis, 873
 parasternal long axis, 872
 regional strains, 886
 specialized conducting system, 877–878
 timing patterns, 876, 880–883

E

Ebstein's anomaly, 789
 anatomic severity, 833
 anatomy and physiology, 787–788, 832
 associated anomalies, 832
 associated lesions, 834
 cautions, 788
 echocardiographic evaluation
 TV repair and replacement, 834
 in unrepaired cases, 832–834
 surgical valve repair/replacement, 834
 transesophageal/three dimensional echocardiography, 834
 3D TTE, 788
 2D echocardiography, 832
 ventricular function, 833
 Echo assessment of aorta, 191–196
 Echocardiographic deformation imaging, 134
 Echocardiographic tissue tracking, 134
 Effective orifice area (EOA), 184
 Effective regurgitant orifice (ERO), 106
 Effective regurgitant orifice area (EROA), 224, 226
 Effusive-constrictive pericarditis, 442–443
 Ejection fraction (EF), 116, 129
 Electric impulses, 4
 Electrical activation-contraction coupling, 878
 Electrical alternans, 431
 Electrophysiological (EP) procedure, 1031–1032
 CVTI ablation, 1033–1036
 left atrial appendage, 1036–1041
 PV ablation, 1036
 right atrium, anatomical variants, 1032
 Embolus
 during aortic manipulation, 762
 epidemiology, 739–740
 investigation algorithm, 741
 left atrium

- anatomy, 742–744
- appendage Doppler, 744–745
- echocardiographic assessment of, 745–748
- myxoma, 750–751
- spontaneous echo contrast, 749–750
- thromboembolism, 748–749
- thrombus, 748
- tumors, 750
- left ventricle
 - echocardiographic identification, 751–752
 - embolization, 752
 - thrombus, 751
- potential cardiovascular sources, 740–742
- prosthetic valves, 753–754
- transthoracic vs. transesophageal
 - echocardiography, 742
- valvular vegetations, 752
- Endocardial border, 113
- Endocardial border tracking, automated, 462
- Endocardial definition, 460
- Endocardial dysfunction, 151
- Endocardial fibers, 131
- Endocarditis, 166, 275, 330, 340, 341, 955
- Endomyocardial biopsy (EMB), 603
- Enterococcus faecalis*, 350
- Epicardial echocardiography, 947
- Epicardial fat pad, 431
- Epicardial scanning, 719
- eSie Valves™ mitral modelling, 997
- European Association of Echocardiography (EAE), 141, 942
- Eustachian valve, 398
- Evolut R valve, 962, 963
- Exercise, 151
 - aortic stenosis, 314, 315
 - capacity, 318
 - echocardiography, 313, 508, 509
 - echo tests, 492
 - stress, 318, 492, 508, 562
- F**
- False lumen, 727
- False-positive perfusion, 555
- Familial thoracic aortic aneurysm, 725
- Fibrillation, atrial, 167
- Fibrinous strands, 754
- Fibrosis, 274
- Fistula, 360
- Flow assessment principle, 97–99
- Flow convergence method, 188, 302
- Fontan circulation
 - arterial switch operation, 809
 - atrial flow, 811
 - challenges, 810
 - failure, 815
 - hypoplastic left heart syndrome, 812
 - obstruction, 812
 - pulmonary arteries, 810, 813
 - total cavopulmonary connection, 808
 - valvar regurgitation, 814
 - ventricular function, 814
- Fontan operation, 838, 840
- Fossa ovalis (FO), 78, 398
- Fourier's theorem, 15
- Fractional area change (FAC), 419
- Fractional shortening, 129
- Frank-Starling mechanism, 414
- Free wall rupture, 483–485
- Fusion imaging, LAA, 1040
- G**
- Gamma-glutamyltransferase, 604
- Ganglioma, 715, 716
- Glenn operation, 838
- Global longitudinal strain (GLS), 316, 630, 631, 637
 - amyloidosis, 864
 - apical four-chamber view, 851, 854, 856
 - calculations, 854, 856, 859
 - cardiac valvular disease, 845
 - Chagas Disease, 865
 - clinical use, 846
 - comparisons, 859–860
 - complex mathematics, 851
 - congenital heart disease, 845
 - determination, 866
 - diffuse ischemic cardiomyopathy, 873
 - display components, 853
 - ejection fraction, 848
 - formula for, 848
 - frame rate, 857
 - functional abnormalities, 863
 - functional patterns, 862–864
 - global vs. regional strain, 846–847
 - heart failure, 845
 - hypocontractile segmental strain values, 862
 - interventricular septum, 852
 - intra- and interobserver reproducibility, 860
 - ischemic heart disease, 845
 - Lagrangian strain, 847
 - length of line, 864–866
 - lines and thicknesses, 854–856
 - longitudinal regions, 850–854
 - longitudinal shortening, 857
 - longitudinal strain, 847, 850
 - measurement, 845
 - natural strain, 847
 - non-uniform speckle, 861
 - numbers, 859
 - peak systolic strain, 858
 - position in image, 859
 - raw/DICOM, 857–859
 - resolution affecting, 860–862
 - simplifying process, 846
 - speckle tracking, 848–849, 859
 - strain algorithms, 859
 - strain curves, 858
 - timing in image, 859
 - two-chamber view, 855
 - type, 852, 859
 - ultrasound image, 849, 859
 - utility of, 845–846

Grading left ventricular diastolic function, 125
Great artery, 34

H

Harmonic imaging, 460–461
Harmonic power Doppler, 546
Hatle formula, 332
Heart failure, 619
 clinical staging, 619–622
 diastolic dysfunction, 623–624
 Doppler velocity tracings, 626
 echocardiography in critical care units, 631
 flow propagation, 626
 left atrial pressure, 627
 LV diastolic function, 626
 LV systolic dysfunction, 622–623
 mitral annular velocities, 626
 mitral inflow velocities, 624
 myocardial mechanics, 151, 627–628
 non-compaction of left ventricle, 621
 peri-implantation TEE, 633
 predominant circumferential/longitudinal dysfunction, 628
 pre-procedure evaluation, 632–633
 preserved longitudinal strain, 630
 pulmonary venous Doppler velocities, 625–626
 remodeling, 619
 screening, 637–638
 therapeutic and surgical interventions, 631–632
 with transmural dysfunction, 628–631
 ventricular assist devices, 632–635
Heart failure with preserved ejection fraction (HFpEF), 151
HeartMate II left ventricular assist device, 634
Hemodynamics, 95
 and flow, 125
 Doppler assessment of, 96
High PRF PW Doppler, 23
Hinge point, 474
HMGCo-A reductase inhibitors, 762
Homograft valves, 328
Hydroxyethyl glutaryl coenzyme A (HMG-CoA), 734
Hypertension, 724
Hypertrophic cardiomyopathy (HCM), 151, 577
 abnormal fiber arrangement, 580
 angulated septum, 588
 aortic valve, 590
 apical four-chamber projection, 596
 and athletes, 589–590, 903–904
 cardiac amyloidosis, 589
 causes, 587
 characterisation, 583
 colour flow mapping, 594
 concentric hypertrophy, 589
 congenital heart disease, 588
 diagnosis, 581
 diastolic filling pressures, 598
 Doppler echocardiography, 590

 diastolic events, 590–591
 intraventricular flow velocity, 592
 mitral regurgitation, 592–594
 systolic events, 591–592
 echocardiography role, 581–584
 familial, 579
 fibrosis, 580
 hypertrophic cardiomyopathy, 593
 left ventricular false tendons, 587–588
 LV hypertrophy patterns, 584–585
 mild/absent ventricular hypertrophy, 587
 mitral apparatus, 590
 M-mode echocardiography, 582, 593
 myocardial velocity gradients, 599
 oblique measurements, 588
 papillary muscles, 579
 parasternal long-axis projection, 601
 parasternal long/short-axis view, 582, 584–586
 pathology, 577–580
 pathophysiology, 580
 posterior wall thickness ratio, 588–589
 predictors of prognosis, 598–599
 pulsed wave sample volume, 595
 right ventricular moderator band, 588
 short-axis parasternal view, 583
 tissue Doppler imaging, 594–595
 assessing longitudinal function, 596–597
 assessing radial LV function, 597
 diastolic function and LV filling pressures, 597–598
 differentiation from athlete's heart, 598
 mitral annular velocities, 595–596
 transmitral velocity profile, 591
 troponin T mutation, 587
 two-dimensional echocardiography, 582
 ventricular hypertrophy, 581
Hypoplastic left heart syndrome, 294

I

Idiopathic restrictive cardiomyopathy, 609
Infective endocarditis (IE), 166, 345, 633
 abscess, 360, 361
 AHA recommendations, 367
 aneurysm and pseudoaneurysm, 360
 biplane two-dimensional echocardiograms, 351
 clinical diagnosis of, 347
 clinical presentation, 345
 diagnosis of, 347–350
 Duke criteria for, 347, 348
 echocardiography, 345, 346, 365–366
 ESC recommendations, 366
 fistula, 360–363
 guideline recommended algorithms, 365
 incidence, 345
 inter-observer agreement, 368
 intracardiac device, 358–360
 M-mode sweep, 346
 native valve perforation, 362–363

- necropsy specimen, 348
 - new valvular/paravalvular regurgitation, 355
 - paired parasternal long axis, 356
 - parasternal long axis, 347, 352–355
 - pathologic necropsy specimen, 345
 - perforation, 364
 - PET/CT reveals infection, 358
 - prognosis, 366–367
 - prosthetic valve dehiscence, 363
 - pseudoaneurysm, 362
 - S. aureus*, 346
 - sensitivity/specificity of TTE/TEE, 363–364
 - sequential TEE long axis views, 363
 - thoracic endovascular aortic repair, 358
 - three-chamber still frames, 348
 - three-dimensional echo, 355
 - transesophageal echocardiography
 - mitral valve, 357
 - still frames, 364
 - three-dimensional still frames, 359
 - views, 351
 - transesophageal two-dimensional zoom views, 359
 - valvular dehiscence, 365
 - vegetation, 350–355, 358
 - Infective vegetative endocarditis, 275
 - Inferior vena cava (IVC), 38, 120
 - assessment of, 120
 - dilatation and loss, 419
 - plethora of, 433
 - proximal, 417
 - subcostal projection, 417, 421
 - Interatrial septum (IAS), 78, 85, 164, 207
 - Intervention related cardio-embolic events, 763
 - Interventional therapy
 - arterial switch operation, 826
 - biventricular size and function, 827
 - dobutamine stress/contrast echocardiography, 829
 - echocardiographic evaluation
 - after arterial switch operation, 827
 - after Rastelli operation, 828
 - neoaortic root dilatation, 827
 - palliative procedures, 825
 - pulmonary hypertension, 827
 - Rastelli operation, 827
 - RVOT stenosis, 827
 - transesophageal/three dimensional echocardiography, 828
 - transthoracic echocardiography, 825–826
 - venous pathway, 826
 - Interventricular delay, 653
 - Interventricular septum (IVS), 775
 - extension, 770
 - leftward shift of, 421
 - Intimal flap, 727, 729
 - Intracardiac echocardiography (ICE), 358, 1032
 - Intracardiac masses, 554
 - Intracardiac shunt, 168, 633
 - Intracavitary masses, 685, 714
 - Intramural hematoma, 194
 - atherosclerotic plaque, 731, 733, 734
 - clinical significance, 731
 - continuous wave Doppler, 735
 - development, 730
 - imaging, 730–731
 - luminal surface, 730
 - transesophageal echo views, 730
 - Intraoesophageal transducer, 84
 - Intraoperative echocardiography (IOE), 947
 - aortic aneurysm, 955
 - bicuspid valve, 953
 - complications, 956
 - coronary artery perfusion, 954
 - coronary atherosclerosis, 954
 - endocarditis, 955
 - epicardial imaging, 953
 - epicardial vs. transesophageal echocardiography, 947
 - essentials of, 947–948
 - indications, 950
 - in left ventricular outflow tract surgery, 952–954
 - in mitral valve repair, 950–952
 - myectomy, 953
 - objectives, 948
 - peri-aortic abscess, 955
 - peri-prosthetic mitral regurgitation, 956
 - pitfalls, 956–957
 - post-pump, 948–949
 - pre-pump, 948
 - process and completeness, 949–950
 - protruding atheroma, 955
 - robotic surgery, 955
 - second pump run, 949
 - three dimensional echo, 952
 - Intra-procedural echocardiography, 973–978
 - Intrathoracic/intracardiac pressures, 438
 - Inverted atrial appendage, 708–709
 - Ischaemic cascade, 452
 - Ischemic mitral regurgitation, 478
 - Isolated left ventricular non compaction (LVNC), 914
 - Isolated pulmonary valve stenosis, 307
 - Isovolumic contraction (IC), 134
 - Isovolumic relaxation time, 404
- J**
- Jena Valve, 963
- L**
- Lambl's excrescences, 754
 - Lateral mitral annulus, Doppler imaging, 124
 - LBBB, *see* Left bundle branch block (LBBB)
 - Lead Zirconate Titanate, 4
 - Leaflets, 177
 - LeCompte, 826
 - Left anterior descending artery (LAD), 454
 - Left atrial (LA)

- Left atrial appendage (LAA), 1031
 - detection of, 742
 - Doppler flow pattern, 746, 748
 - evidence, 749
 - fusion imaging, 1040–1041
 - intravenous microbubble contrast, 744
 - location, 745
 - mobility, 749
 - normal Doppler appearance, 745
 - orifice challenges, 748
 - percutaneous closure of, 1036
 - percutaneous occlusion of, 1038
 - pulsed-wave Doppler, 747
 - size, 748
 - sludge, 749
 - thrombus formation, 752
 - X-ray-echo fusion imaging, 1041
- Left atrial isthmus (LAI), 78
- Left atrial myxoma, 280–286
- Left atrial thrombi, 690–691
- Left atrial volume index (LAVI), 120
- Left atrium (LA), 78–85, 123
 - anatomy, 661–662
 - area, 664
 - assessment, 667
 - atrial phasic volumes, 667
 - booster pump function, 667, 669
 - conduit function, 667
 - deformation, 671
 - echocardiographic assessment, 663
 - ejection force, 668
 - end-systole, 664
 - enlargement, 661
 - left lateral aspect, 662
 - measurement, 662–664
 - mural thrombus, 747
 - myocardial deformation imaging, 146, 671–673
 - myxoma, 751
 - outcome data, 665
 - phasic function, 667
 - prognostic significance, 665
 - reservoir function, 667, 670
 - RT3DE measurements, 666
 - size, 118–120, 661, 662
 - spectral Doppler indices, 667–668
 - strain, 671, 672
 - three-dimensional measurements, 665–666
 - 3D speckle tracking echocardiography, 673
 - tissue Doppler imaging, 668–671
 - transmitral and pulmonary venous flow, 667–668
 - in ventricular filling, 661
 - volume, 664–665
- Left bundle branch block (LBBB), 508, 643, 876
 - and dyssynchrony, 876
 - QRS morphology, 644
 - strict ECG criteria, 883–886
- Left circumflex artery (LCx), 455
- Left lateral ridge (LLR), 78
- Left upper pulmonary vein (LUPV), 204
- Left ventricular (LV), 89
 - apical thrombus, 553
 - cavity, 111, 113
 - chamber size, volumetric assessment
 - three-dimensional method, 114–117
 - two-dimensional method, 113–114
 - contrast echocardiography, 550–553
 - diastolic function, 120–123, 626–627
 - deformation, three-dimensional, 131
 - dysfunction, 522, 979
 - eccentricity index, 403–404
 - filling pressures, 625
 - hypertrophy, 509
 - mass, 115
 - morphological abnormalities, 632
 - myxoma, M-mode echocardiogram, 286
 - papillary muscles, 400
 - rotation and twist, 133–134
 - size and systolic function, 632
 - systolic dysfunction, 622
 - thrombus, 485–487, 687–690, 740
- Left ventricular assist device (LVAD)
 - HeartMate II, 634
 - immediate post-operative complications, 634
 - inflow and outflow cannula, 634
 - mechanical circulatory support with, 632
 - peri-implantation TEE, 633–635
 - post-implantation follow-up, 635
 - post-operative evaluation of recipient, 636–637
 - pre-procedure evaluation, 632–633
 - pump speed, 633
- Left ventricular dyssynchrony
 - assessment, 643, 644, 646
 - cardiac magnetic resonance, 649
 - distinct patterns, 643
 - gated myocardial perfusion SPECT, 650
 - lead position, 650–651
 - magnetic resonance imaging, 647
 - with MDCT, 651
 - myocardial scar, 651–653
 - nuclear imaging, 649–650
 - three-dimensional echocardiography, 647, 648
 - two-dimensional speckle tracking echocardiography, 644
- Left ventricular ejection fraction (LVEF), 126, 550, 643, 921
- Left ventricular end diastolic pressure (LVEDP), 125
- Left ventricular hypertrophy (LVH), 179
- Left ventricular noncompaction of the myocardium (LVNC), 605–606
- Left ventricular opacification (LVO), 451, 461, 552–553
- Left ventricular outflow tract (LVOT), 117, 179, 952
- Left ventricular systolic function, 116
 - biplane methods for quantification of, 117
 - linear methods for quantification of, 117
 - three-dimensional method for quantification of, 117–120
- Loeys-Dietz syndrome, 193, 725
- Löffler's endocarditis, 607
- Lotus Valve, 963
- Low-dose dobutamine echocardiography, 487, 488

M

- Magnetic resonance imaging (MRI)
 - LV dyssynchrony, 647–649
 - stress echocardiography vs., 511
- Marfan's syndrome, 187, 192, 330, 724, 725, 729
- Mayo Clinic diagnostic criteria, 441
- McConnell sign, 420
- Mechanical dyssynchrony, 889
- Mechanical valves, 325, 326, 756
- Medico-legal implications, 468
- Mild hemolysis, 330
- Mitraclip procedure
 - advancing into left ventricle, 1009
 - advantage, 1001
 - anatomic considerations, 1001–1005
 - antero-posterior orientation, 1007
 - CDS, advancing and steering, 1007
 - clip arms orientation, 1007
 - clip deployment, 1009–1011
 - complications, 1012
 - deployment, 1010
 - echocardiography role, 1005–1006
 - indicators of success, 1005
 - leaflet grasping, 1009, 1010
 - mitral stenosis, 1012
 - positioning, 1008
 - residual mitral regurgitation, 1011–1012
 - selection criteria, 1001, 1003–1005
 - steerable guiding catheter, 1007
 - transoesophageal echo-guided transseptal puncture, 1006–1007
 - trans-septal approach, 1002
- Mitral annular calcification (MAC), 275–280, 755
- Mitral annular tissue Doppler, 123
- Mitral annular velocities, 626
- Mitral annulus, 60
- Mitral aortic intervalvular fibrosa (MAIVF), 360
- Mitral apparatus, 590
- Mitral inflow, 121
- Mitral inflow velocities, 624–625
- Mitral leaflets, 35, 62
- Mitral orifice, 276
- Mitral position, 332, 342–343
- Mitral regurgitant jets, 224
- Mitral regurgitation (MR), 101, 151, 279, 284, 478–479
 - asymptomatic patient, 320
 - changes in, 321
 - classification, 257
 - and congestive heart failure, 271–274
 - contractile reserve, 321
 - grade criteria, 1011
 - hypertrophic cardiomyopathy, 592
 - impact on management, 321
 - indication for stress testing, 321
 - ischemic, 322
 - management, 321–322
 - primary, 319
 - secondary, 321
 - severity, 1023
- Mitral stenosis (MS), 101–102, 108–109, 223, 243–256, 318, 755
- Mitral valve, 60, 163
 - anatomy, 214–220
 - arcade lesion of, 292
 - congenital anomalies of, 286
 - repair/replacement, 709
- Mitral valve annulus (MAC), 274
- Mitral valve disease
 - cardiac anatomic relationships
 - apical views, 207–211
 - parasternal long axis, 199–205
 - parasternal short axis, 205–207
 - surgical view, 211–214
 - color flow Doppler controls, 231–232
 - altered Nyquist (scale factor), 236
 - effect of frame rate and persistence, 236–237
 - excess image gain, 237–239
 - hints from spectral Doppler, 241–243
 - jet duration, 239–241
 - system setting variability, 239
 - use of color gain, 232–236
 - cyclical mitral valve movement, 220–221
 - functional anatomic segments, 214–215
 - functional nomenclature, 215–220
 - mitral prolapse, 256–257
 - classification of mitral regurgitation, 257–260
 - typical type II, A2 leaflet prolapse, 266–268
 - typical type II, P2 leaflet prolapse, 260–266
 - visualization of other mitral procedures, 268–271
 - mitral regurgitation evaluation, 224–226
 - jet severity calculations, 226–227
 - mitral timing relationships, 227
 - relationships of spectral Doppler, 227–231
 - mitral stenosis, 243–249
 - mean mitral gradient by Doppler, 253
 - planimetry of mitral orifice, 249–253
 - normal Doppler mitral profiles, 221–224
- Mitral valve navigation (MVN™), 995
- Mitral valve prolapse (MVP), 256–258, 263, 275, 285, 756
- Mitral Valve Quantification (MVQ™), 994–995
- Mitral valve repair
 - annular dilatation/non-ischaemic cardiomyopathy, 996–998
 - anterior leaflet, 988, 989
 - anterior mitral leaflet, 988
 - bileaflet prolapse/barlow-type pathology, 990
 - functional mitral regurgitation, 998
 - functional-ischaemic MR, 998
 - intraoperative echocardiography in, 950
 - leaflet tethering, 1000
 - Mitraclip (*see* Mitraclip procedure)
 - myxomatous, 993
 - posterior leaflet, 990, 991
 - posterior mitral leaflet pathology, 990
 - pre-operative assessment, 987
 - surgical, 987–999
 - 3D echocardiography, 988–990, 995–998
 - 3D TOE imaging, 996
 - trans-catheter mitral valve repair, 999–1001
 - transoesophageal echocardiography, 988
 - transthoracic echocardiography, 987
 - tricuspid valve and annulus assessment, 999

- Mixed aortic valve disease, 185
- M-mode method, 111
- Moderator band (MB), 87
- Multi-detector computer tomographic (MDCT) angiography, 415
- Multivessel ischemia, 501
- Myocardial blood flow (MBF), 452
- Myocardial contrast echocardiography (MCE), 472, 514, 534, 560
 - diagnostic and prognostic utility, 569
 - high MI MCE, 564
 - low MI MCE, 563
 - myocardial blood flow, 568
 - safety of, 569–570
 - stress MCE, 560
- Myocardial deformation, 129, 130, 137
 - assessment, 142
 - in cardiovascular diseases, 150
 - echocardiographic assessment of, 134
 - echocardiographic measurements used to assess, 132
 - imaging, 129, 465–466, 671–673
 - anatomical basis and basic measurements, 129–131
 - clinical applications, 149–151
 - clinical applications in chambers, 151–156
 - deformation imaging in cardiac chambers, 144–146
 - left atrium, 146–148
 - myocardial mechanics in heart failure, 151
 - principal strain, 144
 - right atrium, 148
 - segmental vs. global Strain, 143–144
 - timing of mechanical events, 143
 - values and variability, 148–149
- Myocardial fibers, 129, 130
- Myocardial functions, 129
- Myocardial hibernation, 460, 522
- Myocardial infarction (MI), 467
 - acute chest pain, 467–469
 - AP2CH, 484
 - AP4CH, 483, 486
 - clinical recommendations and implications, 489–490
 - complications, 484
 - developments, 489
 - diagnosis of, 469–470
 - echocardiography usage, 488
 - emergency room, 468
 - endocardial border detection, 472
 - extent of, 470–471
 - factors influencing prognosis, 473
 - infarct expansion, 476
 - ischemic mitral regurgitation, 478
 - left ventricular dilatation, 477
 - left ventricular filling, 482
 - mechanisms, 479–480
 - mitral inflow patterns, 481
 - prognosis after, 473
 - prognostic reassessment after, 516–517
 - regional left ventricular function, 473–475
 - regional wall motion score index, 474, 475
 - residual myocardial ischemia, 488–489
- Myocardial ischemia, 453, 499
 - degree and duration of, 452
 - residual, 488
- Myocardial mechanics, heart failure, 151
- Myocardial performance index, *see* Tei index
- Myocardial perfusion imaging, 559
- Myocardial perfusion scintigraphy, 509
- Myocardial revascularization, 521
- Myocardial scar, 651, 652
- Myocardial velocity, 131, 464
- Myocardial velocity gradient (MVG), 597
- Myocardial viability, 487–488
 - akinetic anteroseptal and apex wall, 535
 - alterations, 524–526
 - animal models, 527
 - biphasic response, 536
 - cardiac magnetic resonance imaging, 522
 - CD31 staining, 524
 - characteristics of, 531
 - chronic reversible ischemic dysfunction, 527–528
 - clinical identification, 531–532
 - clinical role, 538–539
 - contrast echocardiography, 567
 - definition and clinical relevance, 511–512
 - detection, 499, 513–515, 521
 - diagnosis of, 514
 - extracellular matrix, 526–527
 - flow reserve, 522
 - functional recovery, 512–513
 - hibernating cardiomyocytes, 527
 - historical perspective, 522
 - inotropic reserve, 522–524
 - left ventricular dysfunction, 523
 - microcirculation, 524
 - molecular mechanism, 526
 - myocardial contrast echocardiography, 534–535
 - negative stress echocardiogram, 515–516
 - normal cardiomyocytes, 525
 - pathological changes, 527
 - perfusion-contraction matching, 522
 - physiological spectrum, 528–531
 - positive stress echocardiogram, 516
 - positron emission tomography, 522
 - prognostic value of, 515
 - real time 3D echocardiography, 537–538
 - rest echocardiography, 533–534
 - stress echocardiography, 511, 535–537
 - structural modifications, 524
- Myocarditis, dilated cardiomyopathy, 603
- Myxoma
 - atrial, 695–698
 - cardiac masses, 692–698, 713
 - left atrial, 280
 - left atrium, 750–751
 - left ventricular, 699
 - parasternal long axis, 692
 - right ventricular inlet view, 715
 - transesophageal echo, 695

N

Native valve perforation, 362
 Natural strain (SN), 847
 Necropsy section, 361
 New oral anticoagulant (NOAC), 763–764, 1038
 Non-bacterial thrombotic endocarditis (NBTE), 705
 Non-destructive imaging techniques, 547
 Non-ST elevation acute coronary syndromes, 460
 Nuclear imaging, LV dyssynchrony, 649–650
 Nyquist shift, 236
 Nyquist's Theorem, 22

O

Obstruction, causes, 333
 Optimal pharmacologic stress, 508
 Optison, 557
 Organic tricuspid valve regurgitation, 826
 Oscillating masses, 277
 Outflow tracts, assessment, 795–799

P

PA banding, 838
 Pannus, 330, 335
 Papillary fibroelastoma, 699–703, 754–755
 Papillary muscle rupture, 483
 Papillary muscles (PMs), 36, 62
 Paraprosthetic leaks, 337
 Paravalvular aortic regurgitation (PAR), 961
 Paravalvular leak (PVL), 1021–1022
 aortic, 1025, 1026
 detection and assessment, 1024–1025
 intra-procedural, 1028
 severity, 1025–1026
 device closure, 1027
 grade aortic paravalvular regurgitation severity, 1026
 immediate post-procedure, 1028
 long-term follow up, 1028
 mitral, 1027
 detection and assessment, 1022
 intra-procedural, 1027–1028
 severity, 1022–1024
 mitral prosthesis, 1024
 pre-procedure, 1026–1027
 Patent ductus arteriosus (PDA)
 anatomy and physiology, 779–780
 cautions, 782
 diagnosis, 781
 identification, 780
 quantification, 780
 3D echocardiography, 782
 transoesophageal echocardiography, 782
 2D transthoracic echocardiography, 780–782
 Patent foramen ovale (PFO), 168, 418, 740, 1015
 anatomy, 756–758
 echocardiographic assessment, 761
 echocardiography impact on patient management, 762–763
 detection and assessment, 1016

 device closure, 1017
 with embolic events, 759
 follow-up, 1021
 immediate post-procedure, 1020
 intraprocedural, 1019
 potential mechanisms of stroke, 758
 pre-procedure, 1016–1017
 sizing of device, 1017–1019
 thoracic aortic atheroma, 760–761
 3D echocardiography, 1019
 treatment, 759–760
 Pedunculated masses, 685
 Pencil probe, 29
 Penetrating aortic ulcers, 731
 Perfusion scans, 416
 Perfusion scintigraphy, 510
 Perfusion-contraction matching, 522
 Pericardial cyst, 445
 Pericardial effusion (PEff)
 cardiac chamber collapse, 432–433
 cardiac tamponade, 432
 clinical features, 430–431
 Doppler findings, 434
 echocardiographic features, 431–432
 echocardiographically guided pericardiocentesis, 435–437
 etiology, 430
 procedural steps, 436
 respiratory variation, 433
 subcostal view, 446
 Pericardium
 anatomy and function, 429–430
 axial computed tomography, 444
 congenital absence, 443–445
 echo-bright coagulum, 431
 fibrous, 430
 frontal chest radiograph, 443
 right atrial and left atrial compression, 432
 swinging motion, 431
 tumors, 445–446
 Peri-implantation TEE, 633
 PFO, *see* Patent foramen ovale (PFO)
 Pharmacologic stress, 492, 502, 508
 PHE, *see* Pocket-size hand-held echocardiography (PHE)
 Piezo-electric crystal, 5
 PISA, *see* Proximal isovelocity surface area (PISA)
 Plethoric inferior vena cava, 303
 Pocket-size hand-held echocardiography (PHE)
 cardiac intensive care units, 940
 classification, 938
 clinical use, 940–941
 community setting, 941
 current equipment, 937
 currently available, 938
 didactic education, 942
 emergency room, 940
 emergency setting, 940
 expanding uses and reducing cost, 942

- Pocket-size hand-held echocardiography (PHE) (*cont.*)
 - hands-on experience, 942
 - heavily calcified aortic valve, 941
 - image interpretation, 942
 - image quality, 937
 - limitations, 939–940
 - medical schools, 941
 - mitral regurgitation, 939
 - monitoring, 941
 - outpatient clinics, 940
 - prehospital setting, 941
 - technical characteristics, 937
 - terminology, 937–939
 - training requirements, 941–942
- Point of maximum impulse (PMI), 36, 37
- Porcine bioprosthesis, 270
- Porcine mitral valve, 219
- Portico valve, 963
- Posterior descending artery (PDA), 453
- Posterior mitral leaflet (PML) pathology, 990
- Posterior mitral valve leaflet (PMVL), 204
- Potts shunt, 821
- Power Mode (Amplitude) Imaging, 27
- Power modulation, 548
- Power pulse inversion, 548
- Predictors of Response to CRT (PROSPECT) trial, 643, 645
- Pregnancy
 - and aortic dissection, 726
 - and parturition, 604–605
- Pressure half-time (PHT), 107
- Primum ASD, 768
- Principal strain (PS), 144
- Prosthetic heart valves, 633
 - dehiscence, 363
 - evaluation of, 166
- Proximal isovelocity surface area (PISA), 103–104, 188
 - clinical applications of, 104–106
 - radius, 302
- Pseudoaneurysm, 360, 485, 722
- Pulmonary angiography, 415, 416
- Pulmonary arterial end-diastolic pressure (PEDP), 402
- Pulmonary artery, 417
- Pulmonary artery pressure, 304
- Pulmonary circulation hemodynamics, 389
- Pulmonary embolism (PE), 413
 - acute, 414, 416
 - blood gas analysis, 415
 - chronic, 413
 - classification, 415
 - detection of thrombus, 417–418
 - diagnosis, 413, 415–416
 - echocardiography in, 416
 - four-chamber projection, 417
 - haemodynamic consequences, 414
 - haemodynamic response, 414
 - high-risk, 415
 - management, 424
 - parasternal long-axis projection, 419
 - parasternal short-axis view, 422
 - pathophysiology, 414–415
 - risk factors for, 413
 - RV dysfunction, 418–421
 - RV systolic pressures, 421–424
 - symptoms and signs, 415
 - tricuspid regurgitation, 422
 - ventilation-perfusion lung scanning, 415
- Pulmonary hypertension (PH), 826
 - changes in, 399
 - guidelines in, 410–411
 - outcomes in, 410
 - pressure vs. volume right ventricular overload, 401
 - protocol, 406–407
 - real-time three-dimensional echocardiography, 405–406
 - two-dimensional echocardiography, 399
- Pulmonary position, 332
- Pulmonary regurgitation (PR), 822
 - assessment of severity, 309–310
 - carcinoid heart disease, 309
 - etiology, 308–309
 - moderate, 309
 - steep deceleration slope, 310
- Pulmonary stenosis (PS)
 - anatomy and physiology, 782
 - assessment of severity, 306–307
 - cautions, 783
 - CW Doppler, 308
 - echocardiography, 307
 - etiology and mechanisms, 306
 - indirect findings with, 308
 - levels of, 837
 - RVOT obstruction, 306
 - systolic peak, 307
 - therapeutic guidance, 307–308
 - 3D echocardiography, 783
 - 2D transthoracic echocardiography, 782–783
- Pulmonary valve (PV)
 - apical 5-chamber view, 305
 - anatomy, 72–73
 - cardiac output and resistance, 409–410
 - echocardiography, 305
 - parasternal long-axis projection, 305
 - parasternal short axis view, 305
 - qualitative evaluation of, 306
 - real-time 3D echocardiography, 305
 - subcostal short-axis view, 305
 - 3D TEE during, 1036
 - TOE role, 305
 - 2D TTE standard views, 305
- Pulmonary veins (PV), 83, 124, 1032
- Pulmonary venous Doppler velocities, 625
- Pulmonary venous inflow, 123–125
- Pulsatile system, 97
- Pulse inversion Doppler, 547
- Pulse repetition frequency (PRF), 22
- Pulsed mode tissue Doppler imaging, 404
- Pulsed wave Doppler (PWD), 20–21, 40, 41, 52, 56, 121, 163

aliasing effect, 21–22
 analyses, 302
 clinical applications, 22–23
 high PRF PW Doppler, 23–24
 recording, 438
 Pulsed-wave TDI, 668
 PVL, *see* Paravalvular leak (PVL)

R

Range-Velocity Product, 22
 Rashkind procedure, 825
 Rastelli classification, 778, 827
 RCM, *see* Restrictive cardiomyopathy (RCM)
 Real time three-dimensional echocardiography (RT3DE), 59, 298, 537, 665
 Region of interest (ROI), 131
 Regional functional assessment, 129
 Regional scoring, 498
 Regional wall motion
 abnormality, 451, 458–460
 acute ST-elevation myocardial infarction, 457
 analysis, 456–457
 anatomy and echocardiographic findings, 453–456
 automated endocardial border tracking, 462–463
 left ventricular opacification using contrast agents, 461–462
 myocardial deformation, 465
 non-ST elevation acute coronary syndromes, 460
 vs. systolic wall thickening, 452
 three-dimensional echocardiography, 463–464
 tissue Doppler imaging, 464
 Regional wall motion abnormalities (RWMA), 451
 Regurgitant jet size, 107
 Relative wall thickness (RWT), 116
 Remote asynergy, 475
 Replacement heart valve
 aortic malfunction, 331
 aortic position, 330–332, 342
 aortic regurgitation, 339
 bileaflet mechanical valve, 334, 340
 biological valves, 326–329
 bleeding, 330
 cause of obstruction, 333–335
 complications, 329–330
 dehiscence, 330
 deterioration of valve, 329
 diagnosis of high velocities, 331
 echocardiography, 325
 endocarditis, 330, 340
 failure of biological mitral valve, 338
 mechanical valves, 325–326
 mild hemolysis, 330
 minimum dataset for echocardiography, 330
 mitral position, 332, 342–343
 mitral regurgitation, 339
 mitral valve, 334
 normal ranges for, 342–343
 pannus, 330
 patient-prosthesis mismatch, 332, 333
 pulmonary obstruction, 334
 pulmonary position, 332
 regurgitation
 colour mapping, 335–337
 patterns, 336
 quantification, 337
 valve rock, 335
 stented biological valves, 327
 thromboembolism, 329
 thrombosis, 329
 thrombus, 335
 timing of echocardiography, 341
 postoperative, 340–341
 preoperative, 340
 tricuspid position, 332–333
 tricuspid valve, 334
 types, 325
 Residual RVOT obstruction, 822
 Respiratory variation, right/left-heart
 filling, 433–435
 Rest echocardiography, 533–534
 Restricting orifice, 29–30
 Restrictive cardiomyopathy (RCM), 437, 438, 442, 606
 cardiac amyloidosis, 606–607
 vs. constrictive pericarditis, 151, 611–612
 endomyocardial fibrosis, 607–609
 eosinophilic cardiomyopathy, 607
 idiopathic restrictive cardiomyopathy, 609
 restrictive physiology, 611
 Rhabdomyoma, 698–700
 Rheumatic mitral valve disease, 181, 740, 755
 Right atrial appendage (RAA), 75
 Right atrium (RA), 73–78
 air and volume, 403
 American Society of Echocardiography
 guidelines, 678
 anatomical variants, 1032–1033
 anatomy, 397–398, 673
 apical 4-chamber view, 674, 676
 area, 674–675
 assessment, 673–677
 collapse, 433
 CT and 3D transoesophageal echocardiographic
 reconstructions, 674
 echocardiographic assessment, 675
 linear measurements, 673–674
 phasic volumes, 677
 physiology, 399
 pressure, 120, 402, 677–678
 RT3DE guided triplane, 676
 speckle tracking imaging, 677
 structural and functional aspects, 673
 3D volume assessment, 676–677
 tissue Doppler imaging, 677
 2D volume assessment, 675–676
 volume index, 403
 Right coronary artery (RCA), 456
 Right oblique anterior fluoroscopic projection, 1035
 Right pulmonary artery (RPA), 40

- Right ventricle (RV), 85–89
 anatomy, 397
 anatomy and function, 373–375
 arrhythmogenic dysplasia, 377
 arterial supply, 373
 assessment, 823
 collapse, 432
 contractility, 402
 diastolic dysfunction, 404
 diastolic function, 392
 dilatation, 401, 418
 dilatation and dysfunction, 822
 dimensions assessment, 375
 distal diameter, 376
 dysfunction, 418, 632
 ejection fraction, 381–383
 end-diastolic, 376
 factors influencing, 375
 failure, 414
 four-chamber projections, 421
 four-chamber view, 400
 fractional area change, 381–383, 403
 free wall, 400
 function assessment, 381
 heart rate and body surface area, 409
 hypertrophy, 401
 inflow region, 373
 inflow tract, 399–400
 knowledge-based reconstruction, 383
 linear dimensions, 379
 McConnell sign, 420
 muscular fibres, 374
 myocardial performance index, 385, 405
 non-invasive assessment, 383–384
 normal, 398
 normative values, 378, 382
 outflow tract acceleration time, 402–403
 physiological features, 398–399
 physiology, 398
 pressure gradient, 423
 pressure-loading, 399, 401
 proximal diameter, 376
 and pulmonary circulation hemodynamics, 389–391
 pulsed wave Doppler, 423
 septal aspect of, 373
 speckle tracking, 389, 390, 408, 420
 subcostal view, 400
 systolic function, 384, 387–388
 systolic pressure, 391, 402, 421
 thickness, 374, 378
 three-dimensional echocardiography, 379–381, 406
 3D strain imaging, 388–389
 3D transthoracic echocardiography, 382
 tissue Doppler velocity imaging, 385–387
 trabeculated apical segment, 373
 transesophageal echocardiographic assessment, 377
 transthoracic echocardiographic assessment, 376
 tricuspid inflow, 404
 tricuspid annular plane systolic excursion, 384
 ventriculo-infundibular fold, 373, 374
 volume assessment, 379
 volume-loading, 401
 volumes and function, 381
 wall thickness and linear dimensions, 375–379
 Ross procedure, 329, 955
 Ruptured papillary muscle, 707
 RVFWS, 419
- S**
 S' wave velocity, 405
 Sapien XT, 962
 Scintigraphy
 myocardial perfusion, 509
 stress echocardiography vs., 510
 Second harmonic imaging, 545
 Secundum ASD, 768
 Segmental analysis, 818
 Segmental longitudinal strain assessment, 150
 Semi-supine exercise, 314
 Septal leaflet, 70
 Septal shudder, 439
 Septomarginal trabeculation (SMT), 374
 Septum primum (SP), 88
 Septum secundum (SS), 78, 88
 Sequential segmental analysis, 791
 Serous membrane, 429
 Sessile attachment, 685
 Shear deformation, 129
 Simpson's biplane approach, 664
 Sinotubular junction, 69, 72
 Sinus of Valsalva aneurysms (SVAs), 195
 Sinus venosus ASD, 768
 Sonomicrometry, 867–869
 Sound (pressure) waves, 3
 Specialized conducting system, 877
 Speckle tracking
 global longitudinal strain, 848
 protocol, 407–408
 region of interest (ROI) used for, 138
 strain, 407
 3D imaging, 409
 two-dimensional, 408–409, 466
 Speckle tracking echocardiography (STE), 139, 628
 Spectral Doppler analysis, 96
 Spectral Doppler indices, 667–668
 Spectral pulsed tissue Doppler imaging, 135, 136
 Spontaneous echo contrast (SEC), 748, 749
 examples, 750
 in LA cavity, 753
 and thromboembolism, 750–756
 Standard stress test, 509
 Steady-State Free Precession (SSFP), 911
 Stentless heterograft valve, 327
 Stentless valve, 955
 Strain, 132–133
 Strain rate (SR), 133
 Stress echocardiography, 535–537
 accuracy, 504–508
 advantages and disadvantages, 509
 apical 2-chamber views, 503
 application, 503

availability and trained staff, 473
 contents, 501
 contrast imaging, 494–495, 556
 vs. coronary CT, 511
 digital image acquisition, 495
 ECG signal, 496
 in emergency room, 471
 exercise ECG, 497, 508
 exercise vs. pharmacologic stress, 508
 false negative results, 502
 false positive results, 500–502
 gain settings, 495, 496
 harmonic imaging, 494
 implications of, 491
 indications, 492
 initial imaging step, 496
 interpretation of exercise, 498
 left anterior descending ischemia, 500
 low-dose dobutamine, 505
 LV opacification, 494
 vs. magnetic resonance imaging, 511
 magnitude of ischemia, 500
 multivessel ischemia, 501
 myocardial contrast echocardiography, 472, 560, 566
 myocardial ischemia, 499–500
 myocardial regions, 495
 myocardial viability, 511–515
 in non-coronary heart disease, 518
 non-exercise stress, 491
 optimal pharmacologic stress, 508
 optimizing endocardial definition, 497
 pathophysiology, 491
 performance, 495–496
 vs. perfusion scintigraphy, 510
 peri-operative use, 517–518
 pitfalls, 471–472
 pitfalls in standard performance, 500–502
 post-stress images, 496
 pre- and post-stress images, 496
 preparation, 491
 protocols, 313
 qualitative interpretation, 497–498
 quantitative interpretation, 502–504
 regional scoring, 498
 regional wall motion abnormalities, 498
 report, 498
 risk stratification, 473, 517
 vs. scintigraphy, 510–511
 segmental analysis, 498
 selection of method, 491–492
 semi-quantitative interpretation, 497
 strain and strain-rate imaging, 506
 stress Doppler studies, 497
 stressor, 492
 structured review, 498
 subgroups for standard exercise testing, 508–509
 testing, indications, 313
 tissue Doppler imaging, 504
 true apical 2-chamber view, 495
 in valvular heart disease, 518
 wall thinning, 499

Stroke, 739
 cardioembolic, 166
 potential mechanisms of, 758
 thoracic aortic atheroma and, 761
 Stroke volume (SV), 127, 409, 964
 Structural heart disease (SHD), 1031
 Subclinical myocardial dysfunction, 150
 Subcostal four-chamber view, 38
 Subcostal long-axis of inferior vena cava, 38
 Subcostal short axis-left ventricular level, 39
 Subendocardial fibers, 131
 Subepicardial fibers, 131
 Sudden cardiac death (SCD), 598
 Suprasternal aortic arch view, 39
 Surgical annuloplasty, 995
 Surgical Treatment for Ischemic Heart Failure (STICH)
 trial, 538, 539
 Symetis Acurate, 963
 Symptom-limited test, 313
 Synchronicity, 92
 Systemic hypertension, 725
 Systolic anterior motion (SAM), 230, 590, 953
 Systolic pulmonary artery pressure, 315

T

Tamponade, 432
 clinical diagnosis of, 434
 hepatic venous Doppler profile in, 435
 in mitral E velocity, 434
 pericardial effusion causing, 433
 with right ventricular compression, 432
 with ventricular septal shift, 434
 TAPSE, *see* Tricuspid annular plane systolic excursion (TAPSE)
 Teardrop configuration, 444
 TEE, *see* Transesophageal echocardiography (TEE)
 Tei index, 384, 404–405
 Terminal crest (TC), 73–75
 Tetralogy of Fallot (TOF)
 anatomy, 820
 aortic override and valve, 820
 associated lesions, 820
 atrioventricular valve morphology and function, 820
 congenital heart disease, 802–807
 coronary artery anomalies, 821
 palliative procedures, 821
 physiology, 820
 postoperative evaluation, 806, 807
 preoperative checklist, 805
 proximal branch PAs, 822
 pulmonary valve function, 821
 RVOT obstruction, 820
 sequential segment analysis, 820
 surgical repair, 821–822
 surgical therapy, 821
 three dimensional echocardiography, 823–824
 transthoracic echocardiography, 822–823
 after palliative procedures, 821
 in unoperated patients, 820
 tricuspid valve dysfunction, 822

- Thoracic aorta, 187, 189, 191, 192
 Thoracic aortic atheroma, 760–762
 Thoracic endovascular aortic repair (TEVAR), 358
 Thoracic trauma, 725
 Thoraco-abdominal status, 818
 Three-dimensional echocardiography (3DE), 205, 406
 aortic stenosis, 785
 atrial septal defect, 771
 atrioventricular septal defect, 779
 coarctation of the aorta, 787
 Ebstein anomaly, 788
 LV dyssynchrony, 647
 patent ductus arteriosus, 782
 pulmonary stenosis, 783
 ventricular septal defect, 777
 Three-dimensional LV deformation, 131
 Three-dimensional speckle tracking echocardiography (3D-STE), 133, 137, 673
 Three-dimensional transthoracic echocardiography (3D TEE)
 CVTI ablation, 1032, 1033
 guidance during procedure, 1038
 LAO-similar perspective, 1036, 1037
 pre-procedural assessment, 1032, 1038
 PV ablation, 1032, 1036
 RAO-similar projection, 1034
 right pulmonary veins, 1035
 right upper pulmonary vein, 1037
 Thrombi-in-transit, 417
 Thromboembolism, 329, 750–756
 Thrombolysis, 335
 Thrombosis, 329
 Thrombosis in situ, 759
 Thrombus, 335
 Thrombus-in-transit, 418
 Time gain compensation (TGC), 552
 slider, 45
 ultrasound, 8
 Time velocity integral (TVI), 97–98
 Tissue Doppler imaging (TDI), 26–27, 134, 594, 668
 advantages, 136
 assessing radial LV function, 597
 color, 135, 136
 colour-coded, 465
 derived velocities, 144
 diastolic function and LV filling pressures, 597
 differentiation from athlete's heart, 598
 limitations, 465
 longitudinal function, 596
 mitral annular velocities, 595
 myocardial dysfunction, 602
 myocardial velocity, 464–465
 pitfalls of, 136
 precautions, 136
 spectral, 135
 spectral pulsed, 136
 velocity imaging, 385
 Tissue tracking, 137
 by assessment, 137
 deformation imaging, 137–143
 echocardiographic methods used for, 134
 Total cavopulmonary connection (TCPC), 808, 838
 Trabecula septomarginal (TSM), 87
 Transcatheter aortic valve implantation (TAVI)
 annulus diameter measurements, 965–967
 aorta atheroma diagnosed by, 974
 aortic complex assessment, 964–965
 aortic regurgitation, 980–982
 aortic sinus, 968–972
 aortic stenosis, 963–964
 aortic trauma, 979
 aortic valve anatomy, 965
 assessment of PAR, 982
 assessment of position, 978–979
 co-existing pathologies, 972–973
 coronary arteries, 967–968
 current valves, 961–963
 dysfunction, 982–984
 follow-up echocardiography, 980
 imaging, 961
 immediate post valve deployment
 echocardiography, 978
 insertion, 763
 intra-procedural TOE checklist, 975
 left ventricular dysfunction, 979
 long axis aortic view, 984
 LVOT/septum assessment, 967
 multiplanar reconstruction, 966, 968
 multiplayer reconstruction, 972, 973
 paravalvular aortic regurgitation, 984
 pericardial effusion, 979
 pre-procedural echocardiography, 963
 pre-procedural transoesophageal
 echocardiography, 975
 Sapien 3 valve, 985
 thromboembolic risk, 973
 ventricular septal defect, 980
 Transcatheter aortic valve implantation (TAVI), 179, 763
 Transcatheter valves, 329, 337
 Transducer, 4, 5, 848
 transoesophageal, 18
 See also specific transducer
 Transesophageal echocardiography (TEE), 59, 159, 219,
 246, 263, 266, 275, 276, 281, 284, 288,
 289, 296
 angulated view, 362
 aortic stenosis, 784
 aortic valve, 163–164
 atrioventricular septal defect, 779
 clinical applications, 166–170
 complications, 172
 for delineating atrial septal aneurysm, 168
 epicardial vs., 947
 mitral valve, 163
 patient preparation and instrumentation, 159–163
 peri-implantation, 633
 perioperative and TEE during procedures, 169–170
 pitfalls, 170–172
 right ventricle, 165
 sensitivity and specificity of, 363
 transthoracic vs., 742
 tricuspid valve, 165

- Transesophageal imaging, 721
 - Transesophageal M-mode echocardiogram, 159
 - Transient pericardial constriction, 442
 - Transoesophageal echocardiography (TOE), 179, 298, 417
 - atrial septal defect, 770
 - coarctation of the aorta, 787
 - congenital heart malformations, 767
 - indications for, 341
 - mid-oesophageal cava view, 773
 - mid-oesophageal four chamber view, 776
 - mid-oesophageal view, 772
 - necessary, 341
 - patent ductus arteriosus, 782
 - Transoesophageal transducer, 18
 - Transposition of the great arteries (TGA), 807–808
 - anatomy and physiology, 824
 - associated lesions, 824
 - atrioventricular concordance, 824
 - echocardiographic assessment of unrepaired cases, 824–825
 - postoperative checklist, 810
 - preoperative checklist, 807
 - Transthoracic echocardiography (TTE), 59, 115, 169, 179, 632
 - Ebstein anomaly, 788
 - parasternal long axis view, 775
 - sensitivity and specificity of, 363
 - Tetralogy of Fallot, 822
 - thrombus, 417
 - vs. transesophageal echocardiography, 742
 - Transthoracic imaging, 719–721
 - Trastuzumab (Herceptin®), 923
 - Tricuspid annular plane systolic excursion (TAPSE), 144, 319, 384–386, 405, 419
 - Tricuspid annulus diameter, 300
 - Tricuspid position, 332
 - Tricuspid regurgitant velocity, 402
 - Tricuspid regurgitation (TR), 106, 299
 - assessment of severity, 300–304
 - consequences, 302
 - echocardiographic assessment, 304
 - functional/secondary, 300
 - iatrogenic damages, 300
 - PISA method, 302
 - primary, 300
 - rheumatic involvement, 300
 - velocity, 125
 - Tricuspid stenosis (TS)
 - assessment of severity, 304–305
 - etiology and mechanisms, 304
 - Tricuspid valve (TV), 165, 297–299
 - anatomy, 70–72
 - morphology analysis, 300
 - planimetry of, 305
 - prolapse, 300
 - standard TOE views, 299
 - standard TTE views, 298
 - three-dimensional transthoracic echocardiography, 299–301
 - Tricuspid valve closure opening time (TCO), 385
 - Two-dimensional (2D) chest wall echocardiogram, 33
 - Two-dimensional (2D) Doppler methodology, 98
 - Two-dimensional (2D) imaging, 43, 44
 - Two-dimensional echocardiography, 34, 98
 - Two-dimensional method, 111
 - Two-dimensional speckle tracking echocardiography (2D-STE), 137, 139–140
 - advantages and strengths, 140–141
 - image acquisition, 140
 - LV dyssynchrony, 644–647
 - potential pitfalls and technical considerations, 141–142
 - Two-dimensional transthoracic echocardiography (2D TEE), 298, 768
 - in ablation of CVTI and PVS, 1032–1036
 - aortic stenosis, 784
 - atrioventricular septal defect, 778
 - coarctation of the aorta, 786
 - electrophysiology, 1031
 - guidance during procedure, 1038–1040
 - left atrial appendage, 1039
 - life-threatening arrhythmias, 1031
 - patent ductus arteriosus, 780
 - in pre-procedural assessment, 1038
 - pulmonary stenosis, 782
 - ventricular septal defect, 774
- U**
- Ulcerated atherosclerotic lesion, 195
 - Ultra harmonics, 545
 - Ultrasound, 3
 - artifacts, 10–12
 - attenuation, 7
 - concepts of, 3–4
 - depth, 48
 - focal zone, 47–48
 - harmonics, 50–56
 - imaging modalities
 - contrast harmonic, 14–15
 - grey scale, 14
 - harmonic imaging, 14–17
 - M-mode, 7
 - parallel processing, 12–14
 - real-time 3D imaging, 18
 - tissue harmonic imaging, 15–17
 - 2-D sector scan, 5–7
 - ultrasound beam, 4–5
 - measurements, 49–50
 - monitor setup, 44
 - patient identification, 43
 - preparation, 43–56
 - preset, 43
 - reflection, 7
 - resolution, 8–10
 - safety, 30
 - time gain compensation, 8
 - transducer, 39, 43
 - transesophageal imaging, 17–18
 - 2D imaging and basic image manipulation, 44–47
 - waves, 4

- Univentricular heart
 - anatomy and physiology, 835
 - associated lesions, 835
 - atrioventricular valve atresia, 836
 - definition, 835
 - double inlet ventricle, 836
 - echocardiographic evaluation, 839–840
 - pulmonary stenosis, 837
 - quantitative assessment of ventricular function, 837
 - surgical interventions, 837–839
 - transesophageal/three dimensional echocardiography, 841
 - in unrepaired cases, 836–837
 - ventricular arterial connection, 837
 - ventricular morphology and function, 836
- Unroofed coronary sinus, 768
- V**
 - Valsalva sinuses, 68
 - Valve anatomy, 301, 308
 - Valve dobutamine stress echocardiography, 964
 - Valve repair, 950
 - Valve stenosis, 633
 - Valvular heart disease, 151
 - aortic regurgitation, 318
 - aortic stenosis, 314–318
 - exercise stress echocardiography protocols, 314
 - mitral regurgitation, 319–322
 - outcome with exercise testing and imaging, 317
 - stress protocols, 313–314
 - stress testing, 313
 - Valvular lesions, 107
 - Valvular regurgitation, 355–358, 633
 - Vascular Ehlers-Danlos syndrome, 725
 - Vasculitis, 725
 - Vegetation
 - echocardiographic features, 752–753
 - embolism, 753
 - infective endocarditis, 350, 353, 358
 - valvular, 752
 - Vegetative endocarditis, 275, 277
 - Velocity time integral (VTI), 184
 - Vena contracta, 107, 188, 225–227, 301
 - Ventilation-perfusion (V/Q) lung scanning, 415
 - Ventricular assist devices, 632
 - Ventricular hypertrophy, 589
 - Ventricular septal defect (VSD)
 - anatomy, 771–774
 - cautions, 777–778
 - characterization, 774
 - determination, 774
 - hemodynamic burden, 776
 - identification, 825, 830
 - inlet, 775, 777
 - juxta-arterial, 775
 - mid-oesophageal four chamber view, 777
 - muscular, 777
 - nonrestrictive, 776
 - outlet, 777
 - perimembranous defects, 775
 - perimembranous, 775
 - physiology, 771–774
 - restrictive, 776
 - right ventricular pressure, 777
 - size and location of, 837
 - sub-tricuspid, 775
 - 3D echocardiography, 777
 - 2D transthoracic echocardiography, 774–776
 - Ventricular septal rupture, 483
 - Ventricular topology, 819
 - Ventriculoarterial junction, 65
 - Ventriculo-infundibular fold (VIF), 373, 374
 - Vitamin K antagonist (VKA), 763
- W**
 - Wall motion score (WMS) index, 474
 - pre-thrombolytic period, 475
 - thrombolytic and primary PCI era, 475
 - Waterston shunt, 821
 - Willie Sutton's law, 950